American Society of Biomechanics

34th Annual Meeting

Providence, RI
August 18–21, 2010

BROWN

Rhode Island Hospital
A Lifespan Partner

NIBIB

NIAMS
National Institute of Arthritis and Musculoskeletal and Skin Diseases

RIH Orthopaedic Foundation, Inc.
an
test facility


AMTI
FORCE AND MOTION


ATI
INDUSTRIAL AUTOMATION
www.ati-ia.com


BERTEC


DELSYS


INSTRON


KISTLER
measure. analyze. innovate.


MotionAnalysis


MOTEK
MEDICAL


NDI
Northern Digital Inc.
RESEARCH-GRADE MOTION CAPTURE


NORAXON
EMG & Sensor Systems


POLHEMUS
INNOVATION IN MOTION


QUALISYS
Motion Capture Systems


C-Motion


Tekscan


ViSiON
RESEARCH
An AMETEK Company


SIMULIA


CORTECH
SOLUTIONS


The
Motion Monitor
...The Total Solution in Motion Capture


MTS


novel


VICON


Xcitex


BIOMOMENTUM


PTI
Phoenix Technologies
3D real-time active optical mocap systems


Mixed Sources
FSC

HOW TO USE THIS PROGRAM:
- Use the links in the Table of Contents to view each Program Section
- Use the provided Bookmarks to view each ABSTRACT

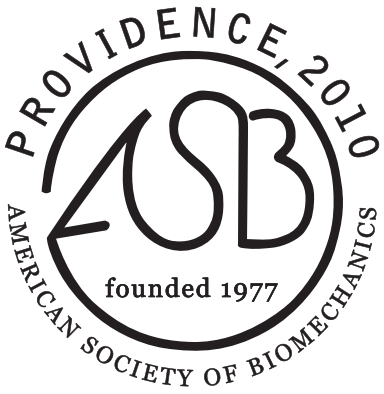

Table of Contents

Wednesday, August 18

Hall C

- Tutorial 1 Grant Writing for NIH
- Lab Tour 1 Neuro-Rehab. Lab Gait and Motion Analysis
- ASB Executive Board Meeting (Rm 554)
- ASB Executive Board and Exhibitor Reception (RISD)
- Opening Reception Museum of Art Rhode Island School of Design (RISD) (6:00–7:30)

Hall E

- Tutorial 2 X-ray Recon. of Moving Morphology
- Lab Tour 2 Facility for X-Ray Recon. of Movement (XROMM)

Thursday, August 19

Hall C

- Breakfast
- Rehabilitation
- Break and Exhibits
- Neuro-Rehabilitation
- Break and Exhibits
- Box Lunch and Exhibits
- Motor Control
- Break
- Machines Inspired by Animal Locomotion
- Poster Sessions (odd numbers) and Exhibits
- Break
- Junior Faculty Mentoring Roundtable (Rm 555)

Hall A

- Tissue Mechanics
- Break and Exhibits
- Muscle
- Break and Exhibits
- Keynote Address *George Lauder, PhD* Harvard University
- Knee
- Break
- Biomech App of Biplane Fluoroscopy
- Student Mentoring Roundtable (Rm 557)

Hall E

- Past Presidents Breakfast (Rm 554)
- Methods
- Break and Exhibits
- Injury
- Break and Exhibits
- Diversity Luncheon (Rm 557)
- Bone
- Break and Exhibits

Friday, August 20

Hall C

- Breakfast
- Orthopaedics
- Break and Exhibits
- Comp. Modeling
- Break and Exhibits
- Box Lunch and Exhibits
- Borelli Award Lecture *Farshid Guilak, PhD* Duke University
- Break
- Robotic Lower Limb Orthoses and Prostheses
- Poster Sessions (even numbers) and Exhibits
- Banquet The Herreshoff Marine Museum & America's Cup Hall of Fame Bristol, RI (6:00–10:00)

Hall A

- Neuro-mechanics
- Break and Exhibits
- Joint Mechanics
- Keynote Address *James J Collins, PhD* Boston University
- 3D Models of Muscle-Tendon Behavior

Hall E

- Women in Science Breakfast (Rm 557)
- Gait
- Break and Exhibits
- Pathological Gait
- Keynote Address *James J Collins, PhD* Boston University
- ASB Business Meeting (Hall E)

Saturday, August 21

Hall C

- 5k River Run
- Breakfast
- Imaging
- Break
- Upper Extremity
- Break
- Young Scientist Predoctoral Award
- Young Scientist Postdoctoral Award
- James J. Hay Memorial Lecture *Darren Stefanyshyn, PhD* University of Calgary
- Closing Ceremony and Awards
- ASB Executive Board Meeting (Rm 554)

Hall A

- Sports
- Award Finalists J Biomed Clin Biomech

Hall E

- Locomotion Energetics
- Posture & Balance

Night on the town

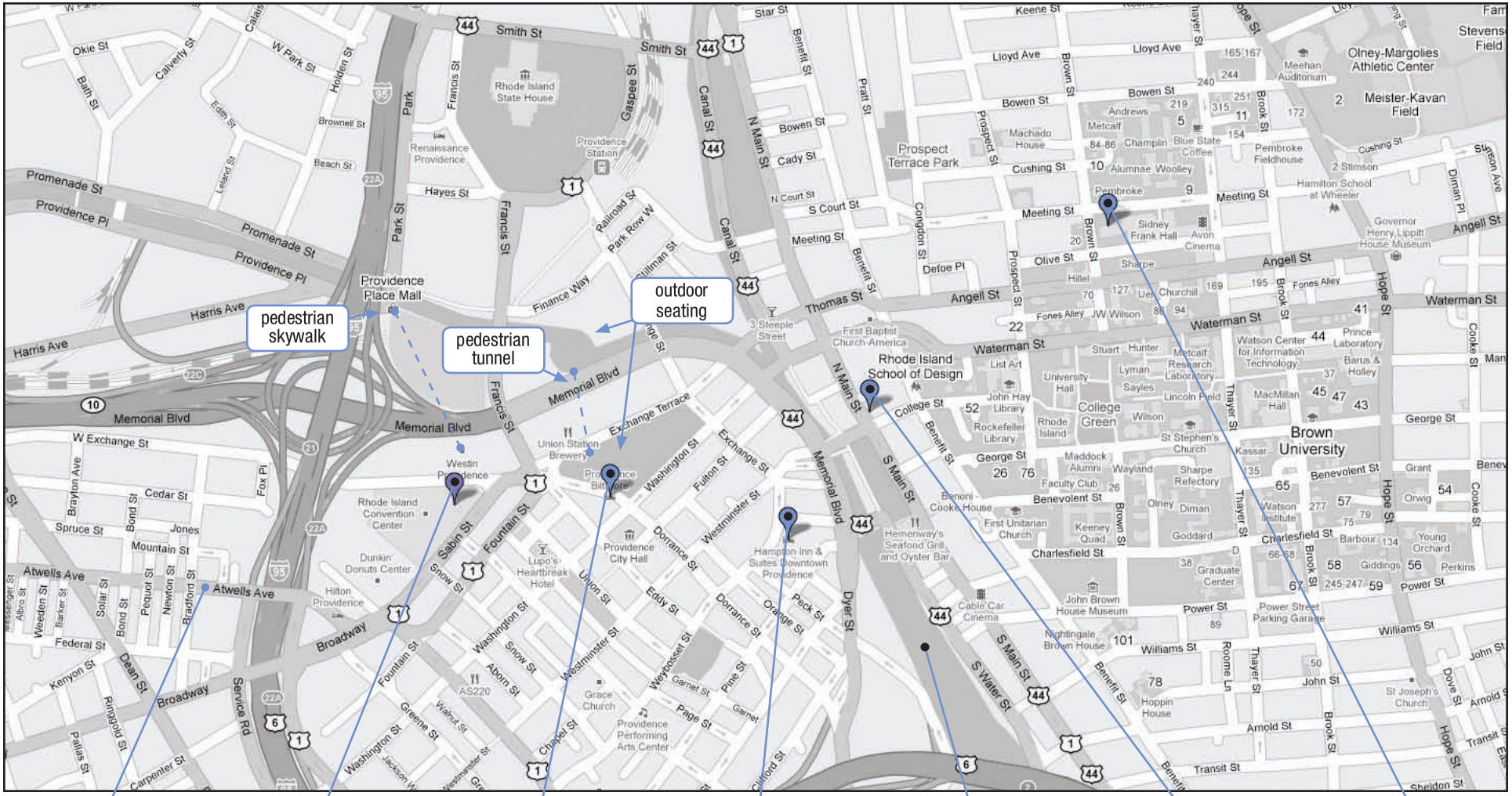

Federal Hill on Atwells Ave

ASB 2010 Meeting Venue Rhode Island Convention Center

Providence Biltmore Hotel

Hampton Inn & Suites

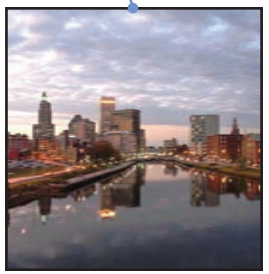

Downtown Providence from Providence River

Opening Reception RISD Art Museum

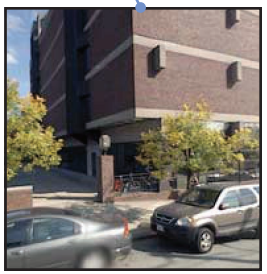

Tour 2: XROMM Facility and Comparitative Biomechanics at BioMed Center

PROVIDENCE RESTAURANTS
2010 American Society of Biomechanics
August 18-21, 2010

COFFEE

- **Starbucks (in Biltmore Hotel)**
  11 Dorrance St. (401) 490-4495
- **Dunkin' Donuts (1 block from Convention Center)**
  66 Fountain St. (401) 521-6913
- **Tazza Caffe (also serves food and alcohol; 3 blocks from Convention Center)**
  250 Westminster St. (401) 421-3300

BREW PUBS

- **Trinity Brewhouse (2 blocks from Convention Center)**
  186 Fountain St. (401) 453-2337
- **Union Station Brewery (1 block)**
  36 Exchange Terrace (401) 274-2739
- **RiRa Irish Pub (1 block)**
  50 Exchange Terrace (401) 272-1953
- **The Wild Colonial (12 blocks; pool & darts)**
  250 South Water Street (401) 621-5644
- **Harry's Bar & Burger (4 blocks)**
  121 North Main Street (401) 228-7437

PROVIDENCE PLACE MALL (1 block from, and connected to, RI Convention Center through Westin Hotel on Third Level)

- **Food Court,** 3rd Level (burgers, pizza, Indian, Chinese, Japanese, Italian, Subway, etc.)
- **Joe's American Bar & Grill**
  Ground level (401) 270-4737
- **Fire + Ice**
  Ground level (401) 270-4040
- **Cheesecake Factory**
  Ground level (401) 270-4010
- **Uno Chicago Grill**
  Ground level (401) 270-4866

OTHER RESTAURANTS CLOSE TO CONVENTION CENTER

- **Agora (in Westin Hotel; breakfast, lunch and dinner)**
  One W. Exchange St. (401) 598-8011
- **Fleming's Prime Steakhouse & Wine Bar (in Westin Hotel; expensive)**
  One W. Exchange St. (401) 533-9000
- **Luxe Burger Bar (1 block)**
  5 Memorial Boulevard (401) 621-5893
- **McCormick & Schmick's Seafood (in Biltmore Hotel)**
  11 Dorrance St. (401) 351-4500
- **Murphy's Deli & Bar (1 block from Convention Center)**
  100 Fountain St. (401) 621-8467
- **Capital Grille (1 block; very expensive)**
  One Union Station (401) 521-5600
- **Ardeo (Mediterranean; 1 block; somewhat expensive)**
  One Union Station (401) 351-1400
- **Fatty McGee's Dublin Pub (2 blocks)**
  55 Union St. (401) 831-3288

ECLECTIC

- **Cuban Revolution (3 blocks from Convention Center)**
  50 Aborn St. (401) 331-8829
- **The Restaurant at AS220 (4 blocks)**
  113 Empire St. (401) 831-3663
- **The Red Fez (6 blocks)**
  49 Peck St. (401) 272-1212
- **Tini (4 blocks)**
  200 Washington St. (401) 383-2400

FINE DINING

- **Pot Au Feu (5 blocks from Convention Center)**
  44 Custom House Street (401) 273-8953
- **Bacaro (12 blocks from Convention Center)**
  262 South Water Street. (401) 751-3700
- **Gracie's (4 blocks from Convention Center)**
  194 Washington St. (401) 272-7811
- **Local 121 (4 blocks)**
  121 Washington St. (401) 274-2121
- **Bravo Brasserie (4 blocks)**
  123 Empire St. (401) 490-6112
- **New Rivers (8 blocks)**
  7 Steeple St. (401) 751-0350
- **Mill's Tavern (8 blocks)**
  101 North Main Street (401) 272-3331
- **Hemenway's Seafood Grill and Oyster Bar (10 blocks)**
  121 South Main Street (401) 351-8570
- **Ten Prime Steak and Sushi (6 blocks)**
  55 Pine St. (401) 453-2333
- **Cav (1 mile from Convention Center)**
  14 Imperial Place (401) 751-9164
- **Al Forno (1.2 miles from Convention Center)**
  577 South Main St. (401) 273-9760

FEDERAL HILL

A superb Italian restaurant district is located on Atwells Ave. and Spruce St., just west of the Convention Center (all price ranges). Federal Hill is close in distance, but on the other side of the Rte. 95 highway. Really worth a trip by taxi or on foot.

BROWN UNIVERSITY AREA

Many eateries are clustered around Brown University, particularly on Thayer and Hope Streets (1.2 miles from Convention Center). Notable eateries: Kabob and Curry (Indian) at 261 Thayer St. (401) 273-8844, East Side Pockets (Middle Eastern) at 278 Thayer St. (401) 453-1100, Nice Slice (Pizza) at 267 Thayer St. (401) 453-6423, and Sawadee (Thai) at 93 Hope St. (401) 831-1122. Wickenden St. (0.5 mi south of Brown, 1.2 mi from Convention Center) has many restaurants and art galleries.

OTHER RESOURCES

- **7-Eleven Convenience Store (3 blocks from Convention Center)**
  25 Dorrance St (401) 351-6287
- **CVS Pharmacy (Providence Place Mall; 1 block from, and connected to, RI Convention Center)**
  Ground level (401) 270-4440

Check out the "Program" section of the website for a detailed map of Providence restaurants and bars:
http://brown.edu/Conference/American_Society_of_Biomechanics/index.php

Welcome Fellow Biomechanists

On behalf of the ASB executive board, Brown University, Rhode Island Hospital, and the many people who have worked to make this conference happen, we would like to wish you a very hearty welcome to Providence! We are delighted to host the 34th Annual Meeting of the American Society of Biomechanics!

Participation in this year's conference has been strong following a trend that reflects the growing strength of the Society and of biomechanics research. Nearly 500 abstracts were submitted from researchers across the U.S. and 20 countries, from which 104 were selected for podium presentations and 357 for poster presentations. The meeting also includes four timely symposia, exciting keynote and award presentations, networking opportunities, interactive tutorials and lab tours. It is sure to be a stimulating, fun and productive four days – a moveable feast for biomechanists!

Brown University and Rhode Island Hospital are delighted to host this year's meeting. In Providence, biomechanics research is a collective enterprise with ongoing collaborations between investigators at several institutions, including Brown University, Rhode Island Hospital, and the Providence VA Medical Center. The interdisciplinary nature of the field is reflected in the diversity of departments with active biomechanics research programs, ranging from Orthopedics, to Ecology and Evolutionary Biology, to Computer Science. We hope you will have a chance to visit the campus and tour a lab while you are here. We are excited to bring such an important event to our community.

The Society and its Annual Meeting are run solely with volunteer labor. Each year, members' efforts allow us to enjoy conferences that are home-grown, friendly, and accessible – "the NPR of meetings," as one member put it. Many people and institutions deserve our heartfelt gratitude for making this conference possible.

First, the ASB Executive Board and the staff at Brown Conference Services provided invaluable advice and support regarding the mechanics of conference planning and organization, abstract reviewers spent many hours evaluating submissions, and numerous student volunteers have graciously (if not willingly) agreed to provide support before and during the meeting. We are grateful for all of their efforts.

In addition, several local institutions provided critical financial support: The Department of Orthopaedics, the Warren Alpert School of Medicine at Brown University, the Center for Restorative and Regenerative Medicine at the Providence VA Medical Center, and Rhode Island Hospital. We also gratefully acknowledge support from NIAMS and NBIB at the NIH.

And finally, it is you, the meeting participants, who make the event a worthwhile endeavor. We thank you for submitting abstracts, presenting talks and posters, participating, and enjoying this event!

We're confident you'll enjoy our Renaissance City, as well as the stimulating company of your fellow biomechanists. Enjoy Providence – take a Gondola ride, dine *al fresco* on Federal Hill, visit Brown's green, hug a Mr. Potato Head. We are glad to have you here, and we hope the week provides you with inspiration, companionship, and lifelong memories.

Sincerely,

J.J. Trey Crisco and Thomas Roberts	Douglas Moore	Darryl Thelen
Meeting Co-Chairs	**Head Local Organizing Committee**	**Program Chair**

The Meeting and Program Committees

ASB Meeting Committee

Elizabeth L. Brainerd, Ph.D. • Susan E. D'Andrea, Ph.D. • Alena Grabowski, Ph.D. • Sharon Swartz, Ph.D.

ASB Local Committee

Emily Abbott • Koosha Aslani • Liz Drewniak • Arlene Garcia • Nick Gidmark • Michelle Gosselin • Eni Halilaj • Cally Harper • Robert Kambic • Sarath Koruprolu • Dennis Kwon • Scott McAllister • Andrew Matson • Danny Miranda • David Paller • Tara Patterson • William Pfaff • Emilia Raimondo • Mike Rainbow • Dale Ricks • Joel Schwartz • Matt Shalvoy • Jody Soares • Beth Therrien • Natalie Wilhelm • Matt Williams

ASB Program Committee

Ahmet Erdemir • Ajit Chaudhari • Alaa Ahmed • Alejandro Espinoza Orías • Amy Silder • Andrew Karduna • Anita Vasavada • Brian Umberger • Chris Hass • Craig McGowan • Daniel Herman • Don Anderson • Elizabeth Hsiao-Wecksler • Eric Kennedy • Erika Nelson-Wong • Fan Gao • Francisco Valero-Cuevas • Gregory King • Gregory Sawicki • Heidi-Lynn Ploeg • Huub Maas • Jae Kun Shim • Jason Scibek • Jian Liu • Jill McNitt-Gray • Jill Schmidt • Jinger Gottschall • Katherine Saul Holzbaur • Kimbery Edginton Bigelow • Kotaro Sasaki • Kristian O'Connor • Kurt Manal • Laura Wojcik • Laurel Kuxhaus • Martin Tanaka • Michael Hahn • Michael Madigan • Michael Pavol • Naira Campbell-Kyureghyan • Nils Hakansson • Patrick Sparto • Paul Ivancic • Richard Hughes • Rob Siston • Samuel Ward • Sang Wook Lee • Silvia Blemker • Srinivas Tadepalli • Steven McCaw • Tamara Bush • Walter Herzog • William Ledoux • Yu Shu

Assistants to the Program Chair

Robert Bradford • Laura Chernak • Carrie Francis • Amy Lenz • Jen Sanfilippo • Anne Schmitz

ASB Executive Committee

President: Tom Buchanan, University of Delaware

President-Elect: Jill McNitt-Gray, University of Southern California

Past-President: Irene Davis, University of Delaware

Treasurer: Paul DeVita, East Carolina University

Treasurer-Elect: Gary Heise, University of Northern Colorado

Secretary: Michael Madigan, Virginia Tech

Program Chair-Elect: Wendy Murray, Northwestern University

Education Committee Chair: Nick Stergiou, University of Nebraska at Omaha and University of Nebraska Medical Center

Communications Committee Chair: Zong-Ming Li, Cleveland Clinic

Meeting Chairs: J.J. Trey Crisco and Thomas Roberts

Program Chair: Darryl Thelen

Newsletter Editor: Michelle Sabick, Boise State University

Student Representative: Becky Fellin, University of Delaware

Meeting Sponsor

The Society gratefully acknowledges the support of the following Corporate Members.

Meeting Information at a Glance

Conference Location

All of the academic meeting events (podium presentations, posters, mentoring sessions, etc.) will be held on the fifth floor of the Rhode Island Convention Center (RICC). Only the welcome receptions, banquet, and lab tours will be held off-site.

Registration

The registration desk is located on the 4th floor of the RICC. Registration will be staffed on Wednesday from 10:00 a.m. to 6:00 p.m., and Thursday and Friday from 8:00 a.m. to 5:00 p.m.

ASB Executive Board/Exhibitor's Reception

Wednesday, August 18, 5:30–6:00 pm

Danforth Room, RISD Museum

Attendance limited to ASB Executive Board, Exhibitor Representatives, and Organizers of the 2010 and 2011 Annual Meetings of the ASB.

General Opening Reception

Wednesday, August 18, 6:00–8:00 pm

Main Gallery, RISD Museum

Attendance is open to all meeting delegates, staff and exhibitor representatives

See Social Program (next page) for details.

Exhibitor Booths

Exhibitor booths will be located in the foyer of the main Ballroom (Halls A, C & E).

Exhibitors' Presentations

The exhibitors will be afforded the opportunity to make brief, technical presentations highlighting the use of their devices/technologies for basic biomechanics research. All exhibitor presentations will be held in Room 555A. The schedule for the exhibitor presentations will be posted at the meeting, and a paper copy will be included in the handouts distributed at registration.

Poster Presentations

There will be two formal poster sessions: **Thursday, from 4:30 p.m. to 6:00 p.m. and Friday from 4:30 p.m. to 6:00 p.m.** Odd-numbered posters will be presented on Thursday afternoon and even-numbered posters will be presented on Friday afternoon. At least one named author is required to be present at each poster during its designated poster session. Light refreshments (antipasto, cheeses, veggies, crackers, fresh fruit) and a cash bar will be available during the two formal poster sessions.

Podium Presentations

Each presenter is allotted 10 minutes for the presentation and 5 min for discussion. *Due to time constraints, speakers will not be allowed to use their own computers for podium presentations.* Speakers must upload their presentations to conference computers on the day prior to their talk. The speaker ready room (558B) is available from 10:00 a.m.–5:00 p.m. on Wednesday, and from 8:00 a.m. to 5:00 p.m. on Thursday and Friday.

Breakfasts

7 a.m. Thursday, Friday and Saturday

Seasonal fruit bowl, freshly baked muffins, English muffins and bagels served with butter, cream cheese, jellies and peanut butter. Coffee, decaf, tea, orange and apple juice.

Coffee Breaks

AM (Thursday, Friday and Saturday)

Coffee, decaf, tea, orange and apple juice, and assorted pastries.

PM (Thursday and Friday)

Assorted snack bars, whole fruit and fresh coffee.

Lunches

12:30 Thursday and Friday

Box lunches will be provided. There will be a choice of turkey, ham or grilled vegetable wrap. All lunches will include chips, whole fruit, a jumbo cookies for dessert and a beverage.

Banquet

Friday, August 20, 6:00–10:00 pm

A traditional Rhode Island Lobster Boil will be held at the Herreschoff Marine Museum and America's Cup Hall of Fame in Bristol, Rhode Island (see page 5 for more details).

Buses will depart from Sabin Street in front of the Rhode Island Convention Center (RICC) starting at 5:45 p.m., and will return to the RICC at approximately 10:30 p.m.

Internet Access

Free wireless access will be available in two "hotspots" within the Rhode Island Convention Center (RICC): The Terrace Café and Rotunda (see RICC map on page 40). If you want the abstracts with you during the meeting you are encouraged to download the Proceedings ahead of time.

Networking and Professional Development

Diversity Luncheon

(Thursday, August 19, Room 557, 12:30–1:30 pm)

An open discussion regarding diversity-related issues and personal experiences and how they impact the careers of minority biomechanists. Reservations are required as seating is limited. Contact: Sai Vikas Yalla (yalla@uwm.edu).

Student Mentoring Roundtable

(Thursday, August 19, Room 557, 6:15–7:15 pm)

This session is designed to create a casual atmosphere where students can ask questions and gain insight from world-class researchers. Past mentoring sessions have included discussions about CVs, finding the right job, contract negotiation, networking at ASB, and research in industry versus academia. This session is separate from ASB's one-on-one mentoring programs, and students may attend this session without participating in the mentor program. Contact: Becky Fellin (fellin@udel.edu)

Junior Faculty Mentoring Roundtable

(Thursday, August 19, Room 555B, 6:15–7:15 pm)

This mentoring session is intended to provide junior faculty and postdocs "best practice" tips for being successful in research, teaching, and service (and life away from the lab). A panel of distinguished senior faculty members representing diverse fields within biomechanics and a variety of career stages will help lead discussions. Contacts: Liz Hsiao-Wecksler (ethw@illinois.edu) and Kim Edginton Bigelow (bigeloke@notes.udayton.edu)

Women in Science Breakfast

(Friday, August 20, Room 557, 7:00–8:00 am)

This breakfast is an informal, enjoyable gathering with other women members of ASB. Come and catch up with old friends and meet some new ones! Reservations are required as seating is limited to 100 conference attendees. Contact: Becky Fellin (fellin@udel.edu)

Social Program

Opening Reception – RISD Museum

(Wednesday, August 18, 6:00–7:30 pm)

- Located at 20 North Main Street, **The Museum of Art at the Rhode Island School of Design**, also known as the **RISD Museum**, is Rhode Island's leading museum of fine and decorative art, housing a collection of 84,000 objects of international significance. It is southeastern New England's only comprehensive art museum and is accredited by the American Association of Museums.
- The Opening Reception will be presented by the Artists at RISD Caterers, and will feature a selection of locally-inspired hors d' oeuvres, wine, beer and non-alcoholic beverages.
- During the reception the entire Museum will be available to ASB Meeting Attendees

Banquet – Herreshoff Marine Museum

(Friday, August 20, 6:00–10:00 pm)

- **Herreshoff Marine Museum/America's Cup Hall of Fame** Bristol, RI
- The **Herreshoff Marine Museum/America's Cup Hall of Fame** is dedicated to the education and inspiration of the public through presentations of the history and innovative work of the Herreshoff Manufacturing Company and the America's Cup competition.
- The Museum, bordering beautiful Narragansett Bay, in Bristol, Rhode Island, is one of the nation's most important historic maritime treasures. The museum regularly hosts classic yacht regattas, sponsor symposia on classic yacht design and restoration, and operates an outstanding sailing school for youth and adults.
- The banquet will include a classic Rhode Island Lobster Boil, prepared by legendary Newport caterer T.R. McGrath. The menu will include Quahog chowder, "stuffies," steamers, mussels, assorted vegetables and dip, garden salad, lobster, barbecued chicken, potato salad, watermelon, brownies and cookies (and a vegetarian pasta option), as well as free beer, wine, soda and water.
- Busses depart from the RICC, 1 Sabin Street, beginning at 5:45 p.m.

5k River Run

(Saturday, August 21, 7:00 am)

Join us Saturday, August 21st at 7 am for the 2nd Annual ASB 5k race. The course will take you on a tour through the historic streets and along the waterfront of Downtown Providence. The run will start and finish in the same location within walking distance of the conference hotel and convention center. Check out the website for course details and get ready for some friendly competition. See the ASB Providence 2010 web site for updates.

Instructions for Presenters

Poster Presentations

Posters can be mounted on free-standing poster boards with either push pins or Velcro tabs (please bring your own pins or tabs). Posters should be mounted by 8:00 a.m. on Thursday, August 19th. Posters are to be removed by 2:00 p.m. on Saturday, August 21st. Any posters not removed will be discarded.

There will be two formal poster sessions: **Thursday, from 4:30 p.m. to 6:00 p.m. and Friday from 4:30 p.m. to 6:00 p.m.** Odd-numbered posters will be presented on Thursday afternoon and even-numbered posters will be presented on Friday afternoon. At least one named author is required to be present at each poster during its designated poster session. Light refreshments (antipasto, cheeses, veggies, crackers, fresh fruit) and a cash bar will be available during the two formal poster sessions.

Podium Presentations

Each presenter is allotted 10 minutes for the presentation and 5 min for discussion. During the discussion please approach a microphone, and state your name and affiliation before asking your question.

Due to time constraints, speakers will not be allowed to use their own computers for podium presentations. **Speakers must upload their presentations to the conference computers in the speaker ready room on the day prior to their talk.** The speaker ready room (558B) is available from 10:00 a.m.–5:00 p.m. on Wednesday, and from 8:00 a.m. to 5:00 p.m. on Thursday and Friday.

Speaker Ready Room (558B)

Wednesday, August 18, 10:00 am–5:00 pm
Thursday & Friday, August 19 & 20, 8:00 am–5:00 pm

Speakers must upload their presentations to the conference computers in the speaker ready room on the day prior to their talk.

Tutorials

Wednesday, August 18

🕓 12:30–2:00 pm, Hall C

Tutorial 1: Grant Writing for the NIH: New Guidelines, Old Tricks

Presenters: Thomas Buchanan, PhD and Nick Stergiou, PhD

In this tutorial, two members of the ASB Executive Board will present (1) the new guidelines adopted by the NIH for writing and reviewing applications, and (2) what stays always the same in these applications like writing good hypotheses!

Wednesday, August 18

🕓 12:30–2:45 pm, Hall E

Tutorial 2: X-ray Reconstruction of Moving Morphology (XROMM): Hardware, Software, and Validation Procedures for Model-Based X-ray Motion Analysis

Presenter: Beth Brainerd, PhD

The past few years have seen rapid growth in the use of biplanar videoradiography (fluroscopy) combined with model-based motion analysis for measuring 3D skeletal kinematics. At Brown University we have been developing a set of model-based motion analysis methods we are calling X-ray Reconstruction of Moving Morphology (XROMM; see our web site www.xromm.org). This tutorial will include an overview of hardware and software development, and demonstrations of software for marker-based XROMM (also called dynamic RSA) and markerless XROMM. Methods for measuring precision and accuracy and for validating markerless XROMM will be discussed.

Lab Tours

Wednesday, August 18

Tour 1: 2:00–5:00 pm

The Gait and Motion Analysis Laboratory and the Neurorehabilitation Lab, The Center for Restorative and Regenerative Medicine, Providence Veterans Administration Medical Center.

The Gait and Motion Analysis Laboratory is a part of the Center for Restorative and Regenerative Medicine, a collaboration between the Providence VA Medical Center (VAMC) and Brown University. The mission of the Center is to improve function for individuals with limb trauma by developing technologically advanced solutions for the restoration of limb function. The research program in the Gait and Motion Analysis Lab is directed towards developing advanced technology assessment tools to complete the restoration of function by advanced rehabilitation. Currently, the lab is focused on the evaluation and development of prostheses to improve function in lower extremity amputee patients, osteoarthritis and the use of virtual reality in rehabilitation. Participants will also tour the Neurorehabilitation Lab at the Center for Restorative and Regenerative Medicine. The Neurorehabilitation Lab is focused on upper extremity rehabilitation post-stroke and lower extremity rehabilitation in individuals with Multiple Sclerosis and Parkinson's disease. The lab uses the Lokomat, Anklebot robots, MIT-Manus robots, Armeo robots, Near-Infrared Spectroscopy, and GAITRite instrumented electronic walkway to study and evaluate subjects.

- There will be two opportunities to tour the Providence VAMC.
  - After Tutorial 1, buses will leave the Rhode Island Convention Center (RICC) at 2:15 pm. After visiting the VAMC, this bus will then transport attendees to Tour 2. You will return to downtown Providence by a 10 min. walk. Those wishing not to attend Tour 2 will be transported back to the RICC on this bus.
  - After Tutorial 2, buses will leave the RICC at 3:30, visit the VAMC, and then this bus will return to the RICC at 5:00 pm.

Tour 2: 3:15–5:00 pm

Brown University facility for X-ray Reconstruction of Moving Morphology (XROMM) and Comparative Biomechanics.

This lab tour will feature new technology for three-dimensional imaging of rapid skeletal motions, XROMM. Participants will also tour comparative biomechanics labs at Brown, including laboratories that study fish feeding and biomechanics, bat flight, and frog jumping.

See the web site www.xromm.org for more details of the facility. This tour complements Tutorial 2.

- The lab tour will begin at 3:15 at the Biomed Building (171 Meeting St.) on the campus of Brown University (see map on inside back cover). Participants have two options:
  - Take Tour 1 first (see Tour 1) after Tutorial 1 and then get transported to the XROMM and Comparative Biomechanics Laboratory. You will return to downtown Providence by a 10 min. walk.
  - After Tutorial 2, walk up to the XROMM and Comparative Biomechanics Laboratory. You will return to downtown Providence by a 10 min. walk.

Plenary and Awards Sessions

Thursday, August 19

🕙 11:30 am–12:30 pm, Hall A

Keynote Address

Fish Robotics and Biomechanics

George Lauder, PhD, Harvard University

There are over 28,000 species of fishes, and a key feature of this remarkable evolutionary diversity is a great variety of propulsive systems used by fishes for maneuvering in the aquatic environment. Fishes have numerous control surfaces (fins) which act to transfer momentum to the surrounding fluid. Most fishes are unstable and use several control surfaces simultaneously for propulsion and to maintain body position. In this presentation I will discuss the results of recent experimental kinematic and hydrodynamic studies of fish fin function, and their implications for the construction of robotic models of fishes. Recent high-resolution video analyses of fish fin movements during locomotion show that fins undergo much greater deformations than previously suspected. Experimental work on fin mechanics shows that fishes possess a mechanism for actively adjusting fin surface curvature to modulate locomotor force. Fish fin motion results in the formation of vortex rings of various conformations, and quantification of vortex rings shed into the wake by freely-swimming fishes has proven to be useful for understanding the mechanisms of propulsion. Experimental analyses of propulsion in freely-swimming fishes have lead to the development of three self-propelling robotic models: a pectoral fin robotic device, a robotic fish tail, and a flapping flexible foil robotic model of fish body deformation; I will discuss the design of each robotic model along with recent results and their implications for understanding the biomechanics of underwater propulsion.

About the Speaker

Dr. Lauder is a world leader in the study of the form, function and evolution of the musculoskeletal system of fish. His work has produced some of the major insights into the mechanical function of the locomotor and feeding apparatus of fish. Current projects in his lab pioneer the use of robotics to explore the mechanical design of fins, the mechanisms of hydrodynamic propulsion, and the potential for bio-inspired robotic swimming devices

Plenary Sessions continued

Friday, August 20th

11:30 am–12:30 pm, Hall A

Keynote Address

From Vibrating Insoles to Synthetic Gene Networks

James J. Collins, PhD, Boston University

In this talk, we describe how nonlinear dynamical approaches can be used to study, mimic and improve biological function at multiple scales, ranging from whole-body dynamics to gene networks. We describe, for example, how input noise can be used to enhance human sensory function and motor control. Specifically, we show that touch sensation and balance control in young and older adults, patients with stroke, and patients with diabetic neuropathy can be improved with the application of sub-sensory mechanical noise, e.g., via vibrating insoles. We describe how this work has led to the creation of a new class of medical devices to address complications resulting from diabetic neuropathy, restore brain function following stroke, and improve elderly balance. We also describe how techniques from nonlinear dynamics and molecular biology can be used to model, design and construct engineered gene networks, leading to the development of the field of synthetic biology. We discuss the implications of synthetic gene networks for biotechnology, biomedicine and biocomputing.

About the Speaker

Dr. Collins is a renowned bioengineer and inventor. His use of nonlinear dynamics to model and mimic biological function has led to several medical devices, including noise-based sensory prosthetics that improve locomotor function and balanced in the elderly and patients with compromised neuromotor control. He is a pioneer in systems biology, and currently developing methods and applications for reverse engineering gene regulatory networks. Dr. Collins has received numerous awards and distinctions, including a MacArthur Foundation "Genius Award" and an NIH Director's Pioneer Award. He is also a past recipient of the ASB Young Scientist Post-Doctoral Award.

Friday, August 20th

2:00 pm–3:00 pm, Hall A

Borelli Lecture

The Role of Biomechanics in the Health, Degeneration, and Repair of the Synovial Joint

Farshid Guilak, PhD

Laszlo Ormandy Professor of Orthopaedic Surgery, Duke University Medical Center

Osteoarthritis is a painful and debilitating disease of the joints that is characterized by progressive degeneration of the articular cartilage that lines the joint surfaces. The etiology of osteoarthritis is poorly understood, although it is now well accepted that biomechanical factors play an important role in the onset and progression of this disease. The primary goal of our studies has been to determine the mechanisms by which mechanical loading affects the physiology of our joints. Using a hierarchical approach to span different systems ranging from clinical studies and in vivo animal models to studies of tissue, cellular, and subcellular mechanics, we have identified specific mechanical signaling pathways that appear to play a role in cartilage physiology as well as pathology. These pathways may provide novel pharmacologic targets for the modification of inflammation or cartilage degeneration in osteoarthritis. Additionally, our studies have focused on tissue engineering approaches for repairing cartilage damage with osteoarthritis. Using novel textile processes that allow weaving of biomaterial fibers in three dimensions, we have created functionalized bioactive scaffolds that can recreate many of the complex biomechanical properties and anatomic features of articular cartilage. In combination with a multipotent population of stem cells isolated from subcutaneous fat, we have developed a tissue-engineering approach for resurfacing osteoarthritic joint surfaces. Taken together, these studies emphasize the critical role that biomechanics plays in the physiology as well as pathology of the joint, and demonstrate the importance of biomechanical factors in functional tissue engineering of cartilage and other joint tissues.

About the Borelli Award Recipient:

Dr. Guilak's research has focused on cellular mechanics and tissue engineering of articular cartilage in the context of osteoarthritis. He is a true pioneer in the investigation of chondrocyte biomechanics and mechanotransduction, having been the first to characterize its mechanical properties in situ and ex situ, in health and disease, using a variety of exquisite testing methods. He has also played a critical leadership role in the development of the field of "Functional Tissue Engineering".

His research in this area has focused on the regeneration of articular cartilage using novel 3D biomaterial structures that are explicitly designed to mimic the biomechanical properties of native articular cartilage.

Plenary Sessions continued

Saturday, August 21st

9:30 am–10:45 am, Hall A

Journal of Biomechanics Award Finalists

The mechanical properties of the endomysium affect propensity for muscle fiber injury near the myotendinous junction

Sharafi B, Blemker S
University of Virginia

How do step width and arm swing affect energetic cost and lateral balance during running?

Arellano C, Kram R
University of Colorado

Clinical Biomechanics Award Finalists

Patients with patellofemoral pain exhibit elevated bone metabolic activity at the patellofemoral joint

Draper C, Besier T, Frederickon M, Beau G, Delp S, Quon A, Gold G
Stanford University

Virtual pre-operative reconstruction planning for comminuted articular fractures

Thomas T, Anderson D, Willis A, March J, Brown T.

University of Iowa.

11:00 am–11:15 am, Hall A

Young Scientist Predoctoral Award

Theoretical Analysis of Limitations to Maximum Sprinting Speed Imposed by Muscle Mechanical Properties

Ross Miller, University of Massachusetts Amherst

11:15 am–11:30 am, Hall A

Young Scientist Postdoctoral Award

A Phenomenological Muscle Model to Assess History Dependent Effects in Human Movement

Craig McGowan, PhD, University of Texas at Austin

Saturday, August 21st

11:30 am–12:15 pm, Hall A

James J. Hay Memorial Lecture

Sport Biomechanics: Equipment and Performance

Darren Stefanyshyn, PhD,
University of Calgary

From a performance perspective, it is very important to optimize the energy transfer between athlete and equipment. This is generally achieved by: maximizing the (conservative) energy which is returned, minimizing the (non-conservative) energy which is lost and/or optimizing the musculoskeletal system. While these are rather simple mechanical concepts, the complex interaction between the athlete and the piece of equipment requires a detailed understanding of sport biomechanics. Additionally, how the uniqueness of each individual athlete relates to specific equipment properties must be understood. Over the past 30 years, sport biomechanists and sport equipment manufacturers have investigated ways of improving athletic equipment to enhance performance. The result is equipment that is stronger, lighter, more durable and more pleasant to use. Consequently, sport performances are faster, higher, longer and more accurate than ever before.

About the Hay Award Recipient:

Dr. Stefanyshyn's contributions to the biomechanics community have been virtually exclusively in the area of sports biomechanics, specifically work related to improving performance through optimizing shoe design in track sprinters, golf club design for average and world class golf players, hockey sticks for improving the accuracy and speed of slap shots, and a variety of research related to the aerodynamic design and musculoskeletal support of sportswear in athletes ranging from downhill skiers to speed skaters and runners.

12:15 pm -12:45 pm, Hall A

ASB Travel Grant

Zifchock R, Motion Analysis Laboratory, Hospital for Special Surgery

Gao F, Department of Health Care Sciences, UT Southwestern Medical Center at Dallas

Symposia

Thursday, August 19, 3:15–4:30 pm

Machines Inspired by Animal Locomotion

organized by Rodger Kram, PhD, University of Colorado

Hall C

Biologically inspired design is a remarkably active and fruitful area of interdisciplinary collaboration among engineers, computer scientists, and comparative biologists. Active areas of research in this field include the development of robots that draw on principles of animal locomotion to improve their swimming, flying, walking or running performance. Speakers in this symposium will present their latest ideas and machines. These talks will complement the presentation by one of the keynote speakers, George Lauder, who has been using robotic fish to explore principles of fish locomotion.

3:15 Experiments with Robotic Birds and Perching Planes

Russ Tedrake, Ph.D.
Computer Science and Artificial Intelligence Lab
Massachusetts Institute of Technology

3:35 BigDog and PETMAN: Legged Robots Inspired by Animals

Marc Raibert, PhD
Boston Dynamics

3:55 Bio-inspired Robot Design for Legged Locomotion

Sangbae Kim, PhD
Biomimetic Robotics Lab
Massachusetts Institute of Technology

4:15 Panel Discussion

Applications of Bi-Plane Fluoroscopy/ X-Ray Technology in Basic and Applied Biomechanics Research

organized by Michael R. Torry, PhD, Steadman-Philippon Research Institute

Hall A

The purpose of this ASB symposia is to present novel techniques and data regarding the uses of bi-plane fluoroscopy/ x-ray in 3D motion analysis. The focus of these talks will be applied in nature with emphasis placed on summary of knowledge gained from this new technology with regard to shoulder, knee, foot/ankle and animal kinematics.

3:15 Applications of Biplane Videoradiography and X-Ray Reconstruction of Moving Morphology (XROMM) to Comparative Biomechanics Research

Elizabeth Brainerd, PhD
Brown University

3:30 Biplane X-Ray Analysis of In-Vivo Shoulder and Tendon Function

Michael Bey, PhD
Henry Ford Hospital

3:45 Using Biplane Fluoroscopy to Quantify Foot Bone Motion

William Ledoux, PhD
VA Puget Sound

4:00 Applications of Dynamic Stereo X-Ray to in vivo Knee Research

Scott Tashman, PhD
University of Pittsburgh

4:15 Panel Discussion

Symposia continued

Friday, August 20, 3:15–4:30 pm

Robotic Lower Limb Orthoses & Prostheses

organized by Dan Ferris, PhD, University of Michigan

Hall C

Advances in robotic technology have led to new designs for powered lower limb orthoses and prostheses. The technological advancements will continue to accelerate in coming years, making innovative commercial products viable by the end of the decade. Key hurdles that still need to be overcome include maximizing device efficiency, developing controllers that facilitate user control, and achieving adaptability for different environments and tasks. This symposium will bring together experts in the field to discuss their recent accomplishments and outline how major challenges can be overcome in the near future. This symposium will complement ongoing research at the Center for Restorative and Regenerative Medicine at the Providence VA Medical Center, affiliated with Brown University.

3:15 Work and Energy for Mobile Human Walking Assistance

Art Kuo, PhD
University of Michigan

3:35 Robotic Lower Limb Orthoses: Goals, Obstacles, and Current Research

Dan Ferris, PhD
University of Michigan

3:55 Powered Ankle-Foot Prosthesis Improves Metabolic Demand of Unilateral Transtibial Amputees during Walking

Hugh Herr, PhD
Massachusetts Institute of Technology

4:15 Panel Discussion

3D Models of Muscle-Tendon Behavior

organized by Silvia Blemker, PhD, University of Virginia

Hall A

The last several decades have brought significant advances in computational modeling of skeletal muscle. Several groups have developed techniques for simulating the complex three-dimensional morphology and behavior of muscle and tendon. These models have provided many insights into the complex and nonuniform interactions between tendon, aponeurosis, and muscle during movement. The goal of the symposium is to bring together leaders in this area to discuss the applications, approaches, experimental validation, challenges, and future opportunities for 3D muscle-tendon models.

3:15 Dynamic Simulation of Musculoskeletal Biomechanisms in 3D

Dinesh Pai, PhD
University of British Columbia

3:30 3D Model of Skeletal Muscle to Predict Intramuscular Pressure

Kenton Kaufman, PhD
Mayo Clinic

3:45 Modeling to Study Muscular Mechanics Within the Context of Fascial Integrety: Linked Fiber-Matrix Mesh Model

Can Yucesoy, PhD
Bogaziçi University

4:00 3D Muscle Modeling with Application to Muscle Strain Injury

Silvia Blemker, PhD
University of Virginia

4:15 Panel Discussion

Podium Sessions

Thursday, August 19, 8:00–9:15 am

	Hall C	Hall A	Hall E
	Rehabilitation	**Tissue Mechanics**	**Methods**
Session chairs	Kurt Manal, PhD *University of Delaware* Nils Hakansson, PhD *University of Delaware*	Don Anderson, PhD *The University of Iowa* Mark Carl Miller, PhD *University of Pittsburgh.*	Tamara Reid Bush, PhD *Michigan State University* Elizabeth T. Hsiao-Wecksler, PhD *University of Illinois at Urbana-Champaign*
8:00	**Compensatory Step Training of Unilateral, Above-Knee Amputees: a Potential Intervention for Reducing Trip-Related Falls** Crenshaw J, Kaufman K, Grabiner M University of Illinois at Chicago	**Optimization-Based Assessment of the Transverse Compresssive Mechanical Properties of the Digital Flexor Tendons and the Median Nerve** Main E, Goetz J, Rudert M, Goreham-Voss C, Brown T *University of Iowa*	**Improving Regions of Deviation Gait Symmetry Analysis with Pointwise T-Tests** DiBerardino L, Ragetly C, Hong S, Griffon D, Hsiao-Wecksler E *University of Illinois at Urbana-Champaign*
8:15	**Are the Effects of Gait Retraining Similar Between the Trained and the Untrained, Contralateral Limb of Runners?** Fellin R, Davis I *University of Delaware*	**An Experimental Platform for Measuring the Mechanical Behaviour of Tendons in Torsion** Martin L, Buckley P, Zavatsky A *University of Oxford*	**Comparative Assesment of Bone Pose Estimation Using Point Cluster Technique and OPENSIM** Lathrop R, Thompson J, Chaudhari A, Siston R *Ohio State University*
8:30	**Effect of Hip Muscle Strengthening on Frontal Plane Gait Mechanics in Patients with Knee Osteoarthritis** Park S, Pohl M, Lloyd C, Baxter J, Wiley P, Ferber R *University of Calgary*	**An Objective Quantitative Comparison of Structural Damage from Differing Rabbit OA Models** Goreham-Voss C, Tochigi Y, McKinley T, Brown T *University of Iowa*	**Human Gait Recognition Performance Prediction from 3D Resolution Simulation Using Ground Truth Motion Capture Data** Fullenkamp A, Campbell B, Bowden D, Hess C *711th Human Performance Wing*
8:45	**Weight-Bearing Asymmetry and Clinical Measures of Impairment and Function Before and After Total Knee Arthroplasty** Christiansen C, Robertson T, Stevens-Lapsley J *University of Colorado Denver*	**AFM Analysis of Cartilage Degradation in a Rat Model Following ACL Transection** Waller K, Darling E, Jay G *Brown University*	**Segmental Kinematic Analysis Using a Tridimensional Reconstruction of Rat Hindlimb: Comparison Between 2D and 3D Joint Angles** Joao F, Amado S, Armada-da-Silva P, Maurício A, Veloso A *Technical University of Lisbon*
9:00	**Joint Loads in ACL-Deficient Individuals After Neuromuscular Training** Gardinier E, Manal K, Buchanan T, Snyder-Mackler L *University of Delaware*	**The Orientation of Collagen Fibers of the Transverse Carpal Ligament** Prantil R, Xiu K, Kim K, Gaitan D, Sacks M, Woo S, Li Z *University of Pittsburgh*	**A Novel Technique Quantifying Phalangeal Interface Pressures at the Hand-Handle Interface** Sinsel E, Gloekler D, Wimer B, Warren C, Wu J, Buczek F *National Institute for Occupational Safety and Health*

Podium Sessions

Thursday, August 19, 9:45–11:00 am

	Hall C	Hall A	Hall E
	Neurorehabilitation	**Muscle**	**Injury**
Session chairs	Jinger Gotschall, PhD *Pennsylvania State University* Keith Gordon, PhD *Rehabilitation Institute of Chicago*	Gregory Sawicki, PhD *North Carolina State University* Dominic Farris, PhD *North Carolina State University*	Chris Powers, PT, PhD *University of Southern California* Irene Davis, PhD, PT *University of Delaware*
9:45	**Elliptical Exercise Improves Walking Mechanics in Multiple Sclerosis Patients** Huisinga J, Stergiou N *University of Nebraska at Omaha*	**Decoupling of Muscle Shortening and Joint Kinematics During Frog Jumping** Astley H, Roberts T *Brown University*	**Kinetic and Kinematic Differences in Female Runners with Iliotibial Band Syndrome: The Effects of Fatigue** Zifchock B, Brown A, Hillstrom H *Hospital for Special Surgery*
10:00	**Relationships Between Muscle Contributions to Walking Subtasks and Functional Walking Status in Persons with Post-Stroke Hemiparesis** Hall A, Peterson C, Kautz S, Neptune R *University of Texas at Austin*	**The Effects of Denervation and Self-Reinnervation in the Guinea Fowl Lateral Gastrocnemius** Carr J, Chao L, Biewener A *Harvard University*	**Patellar Tracking Measures Correlate with Vastus Medialis Onset Delay in Maltracking Patellofemoral Pain Subjects** Pal S, Draper C, Fredericson M, Gold G, Delp S, Beaupre G, Besier T *Stanford University*
10:15	**Mechanical Recovery Influenced by Dorsiflexor Not Plantarflexor Stimulation in Post-Stroke Gait** Hakansson N, Kesar T, Reisman D, Binder-Macleod S, Higginson J *University of Delaware*	**Limb Muscle Function During High-Powered Energy Absorption** Konow N, Azizi E, Roberts T *Brown University*	**Altered Knee Muscle Reflex Activity During a Cutting Maneuver is Influenced by Motor Learning Not Neuromuscular Training** Kipp K, Brown T, McLean S, Palmieri-Smith R *University of Michigan*
10:30	**Constant Speed Practice on a Treadmill Can Maintain Lower Extremity Kinetics for People Post Stroke** *Wutzke C, Lewek M* *University of North Carolina at Chapel Hill*	**Passive Properties of Muscle Fibers Are Velocity Dependent** Rehorn M, Blemker S *University of Virginia*	**Approximate Entropy of Stride-To-Stride Intervals Following ACL Injury** Rhea C, Kiefer A, D'Andrea S, Warren W, Aaron R *Brown University*
10:45	**Muscle Contributions to Propulsion in Post-Stroke Hemiparetic Subjects Following Locomotor Training** Allen J, Kautz S, Neptune R *University of Texas at Austin*	**Regional Stiffening of Mouse Tibialis Anterior Tendons with Age** Wood L, Arruda E, Brooks S *University of Michigan*	**Quadriceps Strength and Neuromuscular Strategies Continue to Improve Two Years After ACL Reconstruction** Roewer B, Di Stasi S, Snyder-Mackler L *University of Delaware*

Podium Sessions

Thursday, August 19, 1:45–3:00 pm

	Hall C	Hall A	Hall E
	Motor Control	**Knee**	**Bone**
Session chairs	Alaa Ahmed, PhD *University of Colorado* Helen Huang, PhD *University of Colorado*	Ajit Chaudhari, PhD *The Ohio State University* Joe Seay, PhD *U.S. Army Research Institute of Environmental Medicine*	Heidi-Lynn Ploeg, PhD *University of Wisconsin-Madison* Jill Schmidt, PhD *University of Wisconsin-Milwaukee*
1:45	**Motor-Unit Pool Properties Contribute to Continuous and Discrete Force Variability** Hu X, Newell K *Pennsylvania State University*	**The Effect of External Loading on the 3D Patellar Tendon Moment Arm Measured with Dynamic MRI** Schmitz A, Westphal C, Thelen D *University of Wisconsin-Madison*	**An Integrated Modeling Method for Bone Strain Analysis** Leib D, Wang H, Dugan E *Boise State University*
2:00	**Rotational Object Perturbations Result in Characteristic Types of Kinematic Grip Responses** De Gregorio M, Santos V *Arizona State University*	**Open Knee: A 3D Finite Element Representation of the Knee Joint** Sibole S, Bennetts C, Borotikar B, Maas S, van den Bogert A, Weiss J, Erdemir A *Cleveland Clinic*	**Finite Element Prediction of Surface Strain and Failure Load at the Distal Radius Using Simplified Boundary Conditions** Edwards W, Troy K *University of Illinois at Chicago*
2:15	**Biomechanical and Experimental Confounds to the Detection of Neurally-Generated Muscle Synergies** Kutch J, Kurse M, Hentz V, Lightdale N, Fassola I, Valero-Cuervas F *University of Southern California*	**Position of the Quadriceps Muscle Actuator Influences Knee Loads During Simulated Squat Testing** Hast M, Piazza S *Pennsylvania State University*	**Does Frequency Effect Fatigue Fracture of Spine Motion Segments During Repetitive Loading?** Yalla S, Campbell-Kyureghyan N *University of Wisconsin-Milwaukee*
2:30	**Prehension Control while Performing Circular Arm Movements** Slota G, Latash M, Zatsiorsky V *Pennsylvania State University*	**Associations Between Anterior Knee Pain and Patellofemoral Kinematics in Cerebral Palsy** Sheehan F, Behnam A, Alter K *National Institutes of Health*	**Mechanical Loading of the Mouse Tibia Stimulates Localized Bone Adaptation** Bhatia V, Troy K *University of Illinois at Chicago*
2:45	**Maximal Voluntary Force, But Not Submaximal Steadiness, is Limited by a Low-Friction Condition During Index Finger Pressing Tasks** Keenan K, Collins J, Massey W, Walters T *University of Wisconsin-Milwaukee*	**The Association Between Patella Alignment and Femoral Trochlear Geometry** Teng H, Chen Y, Powers C *University of Southern California*	**Validation of a Micro-CT Approach for Characterization of Murine and Human Bone in Osteogenesis Imperfecta** Jameson J, Slavens B, Molthen R, Smith P, Harris G *Marquette University*

Podium Sessions

Friday, August 20, 8:00–9:15 am

	Hall C	Hall A	Hall E
	Orthopedics	Neuromechanics	Gait
Session chairs	Rob Siston, PhD *The Ohio State University* Richard Hughes, PhD *University of Michigan*	Francisco Valero-Cuevas, PhD *University of Southern California* Wendy Murray, PhD *Northwestern University*	Amy Silder, PhD *Stanford University* Ray Browning, PhD *Colorado State University*
8:00	Three Dimensional Fracture Mechanics of Ceramic Total Hip Bearings Elkins J, Pedersen D, Callaghan J, Brown T *University of Iowa*	Higher Antagonist Co-Contraction in Hand Osteoarthritis Leads to Detrimental Joint Mechanics Lee S, Schnitzer T, Kamper D *Rehabilitation Institute of Chicago*	Vertical Ground Reaction Forces Increase Over Time During 60 Minutes of Forced-Cadence Marching Seay J, Gutekunst D, Frykman P *U.S. Army Research Institute of Environmental Medicine*
8:15	Mason II Fractures with Three Millimeter Displacement Require Reduction Drushel M, Palmer G, Baratz M, Miller M *Allegheny General Hospital*	Proprioceptive Acuity in the Frontal and Sagittal Planes in Knee Osteoarthritis Cammarata M, Dhaher Y *Northwestern University*	Relative Sensitivity of Net Muscular Moments to Changes in Walking Speed and Body-Weight Support Goldberg S, Stanhope S *Hofstra University*
8:30	Design of a 1st Metatarsophalangeal Hemi-Arthroplasty Implant Based on Morphometric Data Kumar A, Donley B, Cavanagh P *University of Washington*	Role of Proprioception and Foot Somatosensation in Detecting Slipping Accidents Beschorner K, Redfern M, Cham R *University of Wisconsin-Milwaukee*	Positive and Negative Muscle Work in Lean and Obese Adults During Incline and Decline Walking DeVita P, McNally M, Rider P, Copple T, Long B, Kulas A, Hortobagyi T *East Carolina University*
8:45	The Biomechanical Effects of Variability in Femoral and Tibial Component Rotational Alignment During Total Knee Arthroplasty in a Simulated Oxford Rig Thompson J, Hast M, Granger J, Piazza S, Siston R *Ohio State University*	Learning Uncertain Dynamics for Postural Control Ahmed A, Wolpert D *University of Colorado at Boulder*	Moving and Shaking: Soft Tissue Work in Human Walking Zelik K, Kuo A *University of Michigan*
9:00	Tibial Tuberosity Medialization Alters Tibiofemoral Kinematics Along with Patellofemoral Pressure Distribution Elias J, Mani S, Saranathan A, Kirkpatrick M, Gump L, Cosgarea A *Akron General Medical Center*	Neuronal Noise Influences Gait Variability and Fall Risk in a Dynamic Walking Model Roos P, Dingwell J *University of Texas at Austin*	Gait Characteristics of Simulated Lunar Locomotion Hanson A, Gilkey K, Weaver A, Perusek G, Thorndike D, Kutnick G, Grodsinsky C, Rice A, Cavanagh P *University of Washington*

Podium Sessions

Friday, August 20, 9:45–11:00 am

	Hall C	Hall A	Hall E
	Computational Modeling	**Joint Mechanics**	**Pathological Gait**
Session chairs	Jeff Reinbolt, PhD *University of Tennessee* Ahmet Erdemir, PhD *Cleveland Clinic*	Paul Ivancic, PhD *Yale University* Michael Rainbow *Brown University*	Michael E. Hahn, PhD *University of Washington* Todd D. Royer, PhD *University of Delaware*
9:45	**Evaluation of Different Projectiles in Matched Experimental Eye Impact Simulations** Weaver A, Kennedy E, Duma S, Stitzel J *Virginia Tech-Wake Forest University Center for Injury Biomechanics*	**Simulated Contact Forces in the Triquetrum-Hamate Joint Driven with Subject Specific In-Vivo Kinematics** Rainbow M, Schwartz J, Kamal R, Akelman E, Crisco J *Brown University*	**Kinematic Gait Deviations, Center of Mass Power, and the Metabolic Demands of Gait for Individuals with Cerebral Palsy** Schwartz M, Rozumalski A, van der Krogt M *University of Minnesota-Twin Cities*
10:00	**The Capsule's Contribution to Total Hip Construct Stability -- a Finite Element Analysis** Elkins J, Rudert M, Tochigi Y, Pedersen D, Ellis B, Callaghan J, Weiss J, Brown T *University of Iowa*	**3D in Vivo Cervical Spine Kinematics: Preliminary Comparison of Fusion Patients and Control Subjects** McDonald C, Chang V, Bachison C, Bartol S, Bey M *Henry Ford Hospital*	**Stair Climbing Adaptations to Reduce Quadriceps Demand in Patients with Knee Osteoarthritis Are Not Associated with Pain** Asay J, Boyer K, Andriacchi T *Department of Veterans Affairs Bone and Joint Center*
10:15	**Development and Validation of a Finite Element Model of the Superior Glenoid Labrum** Gatti C, Maratt J, Palmer M, Hughes R, Carpenter J *University of Michigan*	**In Vitro Description of Foot Bony Motion Using a Cadaveric Robotic Gait Simulator** Whittaker E, Aubin P, Ledoux W *Veterans Health Administration Rehabilitation Research and Development Center of Excellence for Limb Loss Prevention and Prosthetic Engineering*	**Decreased Complexity in Leg Motion Patterns During Walking in Knee Osteoarthritis** Tochigi Y, Segal N, Vaseenon T, Brown T *University of Iowa*
10:30	**A Comparison of the Performance of Hexahedral and Tetrahedral Elements in Bone-Soft Tissue Finite Element Models** Tadepalli S, Erdemir A, Sett S, Cavanagh P *University of Washington*	**In Vivo Load-Relaxation of the Trunk with Prolonged Flexion** Toosizadeh N, Bazrgari B, Hendershot B, Muslim K, Nussbaum M *Virginia Polytechnic Institute and State University*	**Use of Neuromechanical Redundancy for Locomotor Compensation in Able-Bodied and Transtibial Amputee Subjects** Herrin K, Toney M, Chang Y *Georgia Institute of Technology*
10:45	**A Three-Dimensional Inverse Finite Element Analysis of the Heel Pad** Chokhandre S, Halloran J, Sirimamilla A, van den Bogert A, Erdemir A *Cleveland Clinic*	**Division of Labor Among Limbs and Joints of the Cat During Level and Slope Walking** Klishko A, Hodson-Tole E, Prilutsky B *Georgia Institute of Technology*	**Center of Rotation Position in Non-Articulated Prosthetic Feet: Implications for Prosthetic Foot Kinetics** Sawers A, Hahn M *University of Washington*

Podium Sessions

Saturday, August 21, 8:00–9:15 am

	Hall C	Hall A	Hall E
	Imaging	**Sports**	**Locomotion Energetics**
Session chairs	Frances T. Sheehan, PhD *National Institutes of Health* Amy Silder, PhD *Stanford University*	Kris O'Connor, PhD *University of Wisconsin-Milwaukee* Rick Hinrichs, PhD *Arizona State University*	Craig McGowan, PhD *University of Idaho* Carrie Peterson *University of Texas at Austin*
8:00	**Contact Differences Between Medial and Lateral Tibial Plateau Compartments Accompany Weight-Bearing** Dubowsky S, Allen J, Gade V, Barrance P *Kessler Foundation Research Center*	**Longitudinal Increases in Knee Abduction Moments During Maturation** Hewett T, Myer G, Ford K *Cincinnati Children's Hospital Medical Center*	**Metabolic Energy and Muscle Activity Required for Normal, Exoskeletal, and Added Weight Hopping** Grabowski A, Briner H, Shields B, Herr H *Massachusetts Institute of Technology*
8:15	**Altered Knee Arthrokinematics After Medial Meniscus Root Tear** Tashman S, Martin D, Antonino M, Harner C *University of Pittsburgh*	**Home-Based Instructional Program to Reduce Biomechanical Risk Factors for Knee Injury** Milner C, Tate J, Westlake C, Zhang S, Fairbrother J *University of Tennessee*	**Mechanics and Energetics of Human Hopping with a Passive-Elastic Ankle Exoskeleton** Sawicki G, Farris D *North Carolina State University and University of North Carolina at Chapel Hill*
8:30	**Combining Registration with Cine-PC Data in Order to Create Accurately Animated Subject-Specific Knee Joint Models.** Sipprell W, Borotikar B, Gavelli F *National Institutes of Health*	**Whole Body Biomechanical Modifications During Landings with a Secondary Horizontal Momentum Redirection Task** Held L, McNitt-Gray J, Flashner H *University of Southern California*	**Pendular Dynamics Applied to Obese Gait** Russel E, Hamill J *University of Massachusetts Amherst*
8:45	**Effect of Initial Manual Registration on the Final Results of Image Registration on Kinematics and Contact Analyses in the Radiolunate Joint** Johnson J, Fischer K *University of Kansas*	**Alterations in Knee Laxity During the Menstrual Cycle Change Muscle Activation Patterns During Selected Athletic Movements** Park S, Stefanyshyn D, Fukuchi C, Küpper J *University of Calgary*	**Walking Downhill: The Trade-Off Between Energetics and Stability** Hendrix E, Hunter L, Dean J *Medical University of South Carolina*
9:00	**Activation and Aponeurosis Width Affect Measured Strain in the Biceps Femoris Muscle** Fiorentino N, Rehorn M, Handsfield G, Epstein F, Blemker S *University of Virginia*	**Do Impacts Cause Running Injuries? A Prospective Study** Davis I, Bowser B, Mullineaux D *University of Delaware*	**Effect of Rigid Shoe Shape on Energetic Cost of Human Walking** Adamczyk P, Kuo A *Intelligent Prosthetic Systems, LLC*

Podium Sessions

Saturday, August 21, 9:30–10:45 am

	Hall C	Hall A	Hall E
	Upper Extremity	**Awards Session**	**Posture and Balance**
Session chairs	Katherine Saul, PhD *Wake Forest University* Jason J. Kutch, Ph.D. *University of Southern California*	Irene Davis, PhD, PT *University of Delaware*	Kimberly Edginton Bigelow, PhD *University of Dayton* Angela DiDomenico, Ph.D. *Liberty Mutual Research Institute for Safety*
9:30	Glenohumeral Muscle Forces During Wheelchair Activities Morrow M, Kaufman K, An K *Mayo Clinic*	*Journal of Biomechanics Award Finalist* The Mechanical Properties of the Endomysium Affect Propensity for Muscle Fiber Injury Near the Myotendinous Junction Sharafi B, Blemker S *University of Virginia*	Adaptation and Form of the Unconstrained Lateral Compensatory Stepping Response Hurt C, Earnest L, Grabiner M *University of Illinois at Chicago*
9:45	Muscle Function During the Push Phase of Wheelchair Propulsion Rankin J, Kwarciak A, Richter W, Neptune R *University of Texas at Austin*	*Journal of Biomechanics Award Finalist* How Do Step Width and Arm Swing Affect Energetic Cost and Lateral Balance During Running? Arellano C, Kram R *University of Colorado at Boulder*	A Musculoskeletal Model of Postural Control: Simulated Aging of Muscle Mechanical Properties Hasson C, van Emmerik R, Caldwell G *Northeastern University*
10:00	Relationship Between Clinical Measurements of Shoulder Motion and Strength and Baseball Pitching Mechanics Hurd W, Morrey B, Kaufman K *Mayo Clinic*	*Clinical Biomechanics Award Finalist* Patients with Patellofemoral Pain Exhibit Elevated Bone Metabolic Activity at the Patellofemoral Joint Draper C, Besier T, Fredericson M, Beaupre G, Delp S, Quon A, Gold G *Stanford University*	The Effects of an Unexpected Stance Foot Inversion Perturbation and Neuromuscular Loop Delay on Next Step Width in Healthy Adults Kim H, DeMott T, Strauss R, Richardson J, Ashton-Miller J *University of Michigan*
10:15	Net Torques Vary Across MCP Joints During a Text Typing Task Asundi K, Dennerlein J *Harvard University*	*Clinical Biomechanics Award Finalist* Virtual Pre-Operative Reconstruction Planning for Comminuted Articular Fractures Thomas T, Anderson D, Willis A, Marsh J, Brown T *University of Iowa*	Properties of Step Initiation in Parkinson's Disease Suggest Different Involvement of Saggital and Frontal Preparatory Movements Yungher D, Creath R, Rogers M *University of Maryland, College Park*
10:30	Evaluating the Importance of Including the Carpometacarpal Joints When Modeling the Hand Buffi J, Murray W *Northwestern University*		Perturbation-Based Balance Training in Older Adults at Increased Risk for Falls Bieryla K, Madigan M *Bucknell University*

Poster Sessions

Thursday, August 19, 4:30–6:00 pm

Clinical

1 **Development of Motorized Facilitated Ankle Stretching**
Gao F
UT Southwestern Medical Center at Dallas

3 **Ipsilateral and Contralateral Reaching in Persons with Chronic Stroke**
Finley M, Combs S
University of Indianapolis

5 **The Use of a Flexible, Non-Heel and Inexpensive Footwear Decreases Knee Loads in Elderly Women with Osteoarthritis**
Trombini-Souza F, Kimura A, Butsugan M, Ribeiro A, Aoki P, Passaro A, Arnone A, Sacco I
University of Sao Paulo

7 **Differences in Muscle Activation, Joint Kinematics and Kinetics During a Step Compared to Elliptical Exercise Pattern while Using the Precor AMT Trainer**
Rogatzki M, Kernozek T, Willson J, Greany J, Hong D, Porcari J
University of Wisconsin-La Crosse

9 **Perturbation Training Improves Gait Patterns in ACL Deficient Females**
Di Stasi S, Snyder-Mackler L
University of Delaware

11 **Biomechanical and Gait Improvements After Passive Stretching and Active Movement Training in Children with Cerebral Palsy**
Wu Y, Hwang M, Ren Y, Gaebler-Spira D, Zhang L
Rehabilitation Institute of Chicago

13 **The Influence of a Neuromuscular Training Program on Landing Mechanics while Fatigued**
Greska E, Cortes N, Ringleb S, Onate J
Old Dominion University

15 **Simulation Detects Changes in Muscle Activation in Post-Stroke Gait After a Functional Electrical Stimulation Intervention**
Knarr B, Kesar T, Helm E, Reisman D, Binder-Macleod S, Higginson J
University of Delaware

17 **Effects of Continuous Passive Motion on Lower Extremity Hypertonia in Children with Cerebral Palsy**
Cheng H, Ju Y, Guan P
Chang-Gung University

Friday, August 20, 4:30–6:00 pm

Clinical

2 **Feasibility of Group Kickboxing to Improve Balance and Gait in Patients with Multiple Sclerosis**
Jackson K, Bigelow K
University of Dayton

4 **Quantitative Examination of Core Muscle Activation During Isometric Exercises**
Oliver G, Stone A, Plummer H, Keeley D
University of Arkansas

6 **Examining the Dose Response Relation for Neuromuscular Electrical Stimulation and Recovery Following Total Knee Arthroplasty**
Marmon A, Petterson S, Snyder-Mackler L
University of Delaware

8 **Comparative Gait Analysis of Ankle Arthrodesis and Arthroplasty: Initial Results of a Prospective Study**
Hahn M, Wright E, Segal A, Orendurff M, Ledoux W, Sangeorzan B
Veterans Health Administration Rehabilitation Research and Development Center of Excellence

10 **Improvement in Off-Axis Neuromuscular Control During Functional Tasks Following Six-Week of Pivoting Elliptical Training**
Lee S, Ren Y, Geiger F, Chang A, Press J, Zhang L
Northwestern University

12 **Stroke Rehabilitation: A Kinematic Analysis of Device-Assisted and Clinician-Assisted Sit-To-Stand Transfers**
Hueftle A, Balogh B, Taylor A, Goldman A, Buster T, Burnfield J
Madonna Rehabilitation Hospital

14 **Lateral Wedges Reduce Medial Knee Loading in Asymptomatic, Obese Women**
Russel E, Hamill J
University of Massachusetts Amherst

16 **Deficits in the Heel-Rise Test in Patients with Achilles Tendon Rupture Can Be Explained by Tendon Elongation and Muscular Weakness**
Silbernagel K, Manal K
University of Delaware

18 **Altered Inter-Joint Coordination During Walking in Patients with Total Hip Arthroplasty**
Chiu S, Chou L
University of Oregon

Poster Sessions

Thursday, August 19, 4:30–6:00 pm

Clinical continued

19 **Kinematic Analysis of Five Cardiovascular Exercises**
Buster T, Taylor A, Frazier M, Burnfield J
Madonna Rehabilitation Hospital

21 **Neuro-Mechanical and Clinical Outcome of Stroke Rehabilitation of Ankle Impairments Through Passive Stretching and Active Movement Training**
Waldman G, Wu Y, Ren Y, Li Y, Wang L, Guo X, Roth E, Zhang L
Northwestern University

23 **The Impact of Stochastic Resonance Electrical Stimulation and Knee Sleeve on Impulsive Loading During Gait in Knee Osteoarthritis**
Collins A, Blackburn J, Olcott C, Jordan J, Grewal B, Yu B, Weinhold P
University of North Carolina at Chapel Hill

25 **Efficacy of Gait Training with Real-Time Biofeedback in Correcting Knee Hyperextension Patterns in Young Women**
Teran-Yengle P, Singh B, Yack H
University of Iowa

27 **Trunk Movement in Manual Wheelchair Propulsion in Various Overground Conditions**
Worobey L, Koontz A, Boninger M
University of Pittsburgh

29 **A Reward System for Altering Distribution of Effort in Multi-Limb Exercise**
Skinner N, Ferris D, Kuo A
University of Michigan

31 **Variability of Clinical Examination Techniques Used to Assess Laxity of the Anterior Cruciate Ligament**
Jacobs C, Branch T, Siebold R
ERMI, Inc.

33 **The Effect of Foot Type on Plantar Loading**
Kraszewski A, Chow B, Frey J, Lenhoff M, Backus S, Deland J, Demp P, Song J, Heilman B, Rajan S, Woodley A, Hillstrom H
Hospital For Special Surgery

Friday, August 20, 4:30–6:00 pm

Clinical continued

20 **Is Ankle Instability a Central Or Peripheral Issue?**
Gutierrez G, Kaminski T
New York University

22 **Do Those with Perceived Ankle Instability Have Associated Mechanical Instability?**
Liu K, Gustavsen G, Kaminski T
University of Delaware

24 **Comparison of Lower Extremity Electromyographic (EMG) Demands During ICARE Training and Walking**
Burnfield J, Shu Y, Buster T, Taylor A, Merriman L
Madonna Rehabilitation Hospital

26 **Compensatory Movement Strategies Among Subjects with Hip Fracture During a Sit to Stand Task**
Kneiss J, Bukata S, Puzas J, Houck J
University of Rochester Medical Center

28 **Step Length Variability During Gait Initiation in Parkinson's Disease**
Roemmich R, Nocera J, Vallabhajosula S, Amano S, Hoover B, Hass C
University of Florida

30 **Abdomen-Thigh Contact Forces During Functional Reaching Tasks in Obese Individuals**
Singh B, Brown T, Callaghan J, Yack J
University of Iowa

32 **The Use of the EMG Integral and Kinematic Analysis for Evaluation of Spastic Hemiplegic Patients**
Silva C, Vanderlei F, Carvalho A, Kuriki H, Polito L
University Estatual Paulista

34 **Abstract Withdrawn**

Poster Sessions

Thursday, August 19, 4:30–6:00 pm

Comparative

35 Computational Modeling of Ardipithecus Ramidus: A Revolution in Evolution
McGuan S
LifeModeler,Inc.

37 Study of Propulsion Mechanisms in Leech Anguilliform Swimming
Chen J, Iwasaki T, Friesen W
University of Virginia

39 Kinematic Modeling of the Seahorse Tail
Praet T, Van Cauter S, Adriaens D, Kannan S, Masschaele B, Srigiriraju S, De Beule M, Verhegge B
Ghent University

41 Finite Element Simulation of a Porcine Temporomandibular Joint
Dalne S, Sindelar B, Cotton J
Ohio University

43 The Effects of Differential Wing Stroke Amplitude and Stroke Offset on Insect Body Moments During Perturbed Flight Conditions
Vance J, Faruque I, Humbert J
University of Maryland, College Park

Computational Modeling

45 Computed-Tomography-Based Finite-Element Models of Long Bones Can Accurately Capture Strain Response to Bending and Torison
Varghese B, Hangartner T
Wright State University

47 Bone Fracture Analysis Using the Extended Finite Element Method (XFEM) with ABAQUS
Liu X, Qin X, Du Z
Dassault Systemes Simulia Corp

49 Using Subject-Specific Muscle Parameters to Compare Muscle Forces Between an EMG-Driven and OPENSIM Musculoskeletal Model
Olchowski D, Buchanan T, Higginson J
University of Delaware

51 Development of a Three-Dimensional Finite Element Model of the Hand and Wrist
Gong M, Oliver M, Dony R, Semechko A
University of Guelph

Friday, August 20, 4:30–6:00 pm

Comparative

36 Skeletal Muscle Architecture of the Goat Hindlimb
Arnold A, Eng C, Biewener A
Harvard University

38 Study of Motor Control of Leech Anguilliform Swimming
Chen J, Friesen W, Iwasaki T
University of Virginia

40 Animal-Robot Interaction Forces As a Measure of Locomotor Function Following Spinal Cord Injury
Nessler J, Duhon J, Keller R, Thys T
California State University, San Marcos

42 Functional Morphology of Dorsal Fins in Two Shark Species
Maia A, Wilga C
University of Rhode Island

44 A Biomedical Perspective on Variation in the Human Clavicle, with Particular Reference to LB1 from Flores, Indonesia
Eckhardt R, Weller A
Pennsylvania State University

Computational Modeling

46 Development of a Hybrid Model Simulating the Vibration Characteristics of a Human Hand-Finger System
Wu J, Dong R, Xu Y, Welcome D
National Institute for Occupational Safety and Health

48 Testing and Modeling the Nonlinear Behavior of UHMWPE Used in Orthopaedic Implants
Gomaa S, Leisinger S
DePuy Orthopaedics, Inc.

50 Equivalence of Elastic Contact and Finite Element Models of Patient-Specific Contact Stress Exposure in the Human Ankle
Kern A, Anderson D, Brown T
University of Iowa

52 Sensitivity of Strains in the Femoral Neck to Variations in Muscle Forces
Anderson D, Madigan M
Virginia Polytechnic Institute and State University

Poster Sessions

Thursday, August 19, 4:30–6:00 pm

Computational Modeling continued

53 **Influence of In-Vivo Tendon Force-Strain Relationship for Different Loading Rates into EMG-Driven Model**
Gerus P, Rao G, Manal K, Buchanan T, Berton E
Aix-Marseille University

55 **Abstract Withdrawn**

57 **Dynamic Simulation of Movement Based on OPENSIM and Matlab/Simulink**
Mansouri M, Reinbolt J
University of Tennessee

59 **Simulation of Subject-Specific Bone Remodeling**
Sonar A, Issen K, Kuxhaus L, Carroll J
Clarkson University

61 **Unique Representations to Analyze Three Dimensional Movements**
Vrongistinos K, Jung T, Wee S, Costello T, Hwang Y, Stylianides G
California State University, Northridge

63 **Small Chest Impactors at High Accelerations: Assessing Thorax Injury Potential from a Finite Element Model**
Danelson K, Bolte J, Stitzel J
Wake Forest University

65 **Reliable Finite Element Modeling of Osteoporotic Bone Augmentation**
Basafa E, Armiger R, Kutzer M, Sutter E, Mears S, Belkoff S, Armand M
Johns Hopkins University

67 **Biodynamic Modeling of Stair-Ascent by PCL-Deficient Patients**
Li K, Tashman S, Harner C, Zhang X
University of Pittsburgh

Friday, August 20, 4:30–6:00 pm

Computational Modeling continued

54 **Peak Contact Stress in Human Hip Joint - Biomechanics Or Mechanobiology?**
Daniel M, Hornova J, Iglic A
Czech Technical University in Prague

56 **On the Role of Lipid Anisotropy in the Transition Between Lamellar and Inverted Hexagonal Lipid Phases**
Perutkova S, Daniel M, Iglic A, Kralj-Iglic V
Czech Technical University in Prague

58 **Finite Element Modeling of Intraneural Ganglion Cysts of the Common Peroneal Nerve**
Elangovan S, Odegard G, Morrow D, Wang H, Hebert-Blouin M, Spinner R
Michigan Technological University

60 **Subject-Specific, Group-Mean, and Generic Musculoskeletal Models for Predicting Isometric Ankle Dorsiflexion Torque**
LaBoda M, Gidley A, Hasson C, Caldwell G, Umberger B
University of Massachusetts Amherst

62 **Evaluation of Stepping Task Biomechanics Using OPENSIM**
Malineni S, King G
University of Missouri - Kansas City

64 **A Complete, Universal, and Verifiable Set of Upper Body Segment Parameters for Three-Dimensional Dynamic Modeling**
Vette A, Yoshida T, Thrasher A, Masani K, Popovic M
University of Toronto

66 **Sensitivity of Predicted Peak Isometric Ankle Dorsiflexion Torque to Musculoskeletal Model Parameter Values**
Gidley A, Laboda M, Umberger B
University of Massachusetts Amherst

68 **Accuracy of Bone and Cartilage Models Obtained from CT and MRI**
Thorhauer E, Miyawaki M, Illingworth K, Holmes J, Anderst B
University of Pittsburgh

Poster Sessions

Thursday, August 19, 4:30–6:00 pm

Ergonomics

69 **Grip Surface Friction Affects Maximum Tip Pinch Force**
Engel A, Enders L, Keenan K, Seo N
University of Wisconsin-Milwaukee

71 **The Box and Block Test Score is Dependent Upon Block Surface**
Cary D, Enders L, Seo N
University of Wisconsin-Milwaukee

73 **Correlation Between Guided Grip Force and Perceived Exertion for Males**
Li K
Chung Hua University

75 **A Flexed Wrist Results in Larger Muscle Stresses During Tapping**
Chen H, Asundi K, Dennerlein J
Harvard University

77 **Joint Contribution to Fingertip Movement During Directional Tapping**
Qin J, Trudeau M, Dennerlein J
Harvard University

79 **Assessment of Arm Dynamics in Experienced Workers while Operating Right-Angle Torque Tools**
Ay H, Sommerich C, Luscher A, Gumpina R
Ohio State University

81 **Verbal Estimation of Peak Dynamic Hand Forces in Experienced and Novice Manual Material Handlers**
Andrews D, Phillips A, Weir P
University of Windsor

83 **Individual Determinants of Stability During Lifting**
Lussier B, Delisle A, Berrigan F, Plamondon A
University of Sherbrooke

Gait

85 **Center of Mass Power Profiles for Individuals with Cerebral Palsy**
Schwartz M, Rozumalski A
University of Minnesota-Twin Cities

87 **Can a Novel Virtual Environment Mobility Platform Replicate the Biomechanical and Physiological Effects of Overground Walking?**
Boynton A, Kehring K, White T
U.S. Army Research Laboratory

Friday, August 20, 4:30–6:00 pm

Ergonomics

70 **Slip-Resistance and Abrasion of New & Used Shoe Soles**
Li K
Chung Hua University

72 **Hand Support Reduces Peak L5/S1 Moments in One-Handed Lifting**
Faber G, Kingma I, van Dieën J
VU University, Amsterdam

74 **Vibration Frequency Influences Foot to Leg Transmission**
Smith G, Bressel E, Nash D
Utah State University

76 **Acute Biomechanical Responses to a Prolonged Standing Exposure: Implications for Job Rotation Design**
Nelson-Wong E, Howarth S, Callaghan J
Regis University

78 **Biodynamic Modeling and Physical Capacity Assessment of Human Arm Response in Experienced Torque Tool Operators**
Ay H, Sommerich C, Luscher A, Gumpina R
Ohio State University

80 **Thumb Motor Performance Varies by Movement Orientation and Direction During Mobile Phone Use**
Trudeau M, Udtamadilok T, Dennerlein J
Harvard University

82 **Pressure on the Knee while Performing a Lateral Lift from Kneeling Postures**
Mayton A, Pollard J, Porter W, Moore S
National Institute for Occupational Safety and Health

84 **Quantification of Dynamic Human Seated Spinal Curvatures**
Leitkam S, Bush T
Michigan State University

Gait

86 **Habituation to Galvanic Vestibular Stimulation During Gait**
Roche J, Steed D, Redfern M
University of Pittsburgh

88 **Asymmetry, Limb Dominance and Foot Orientation During Walking Gait**
Polk J, Rosengren K
University of Illinois at Urbana-Champaign

Poster Sessions

Thursday, August 19, 4:30–6:00 pm

Gait continued

89 **Joint Powers Are Affected by Age and Peripheral Arterial Disease.**
Koutakis P, Myers S, Pipinos I, Johanning J, Stergiou N
University of Nebraska at Omaha

91 **Effects of Load Carriage on Foot Anthropometrics**
Goffar S, Reber R, Christiansen B, Miller R, Naylor J, Rodriguez B, Walker M, Teyhen D
U.S. Army-Baylor University

93 **Frontal Plane Kinetics and EMG Activity During Stair Ambulation**
Hall M, Stevermer C, Gillette J
Iowa State University

95 **Biomechanics of Uphill Walking in Moderately Obese Adults**
Reynolds M, Ehlen K, Dannecker K, Carter C, Browning R
Colorado State University

97 **Vascular Occlusion Affects Gait Variability Patterns of Healthy Younger and Older Individuals**
Myers S, Johanning J, Pipinos I, Stergiou N
University of Nebraska at Omaha

99 **Dynamic Stability of a 3D Dynamic Walking Model with Simulated Neuronal Noise**
Roos P, Dingwell J
University of Texas at Austin

101 **Neuromuscular Control Adaptation in Gait due to Injury: A Motivating Study Using a Simplified Dynamic Model**
DiBerardino L, Dankowicz H, Hsiao-Wecksler E
University of Illinois at Urbana-Champaign

103 **Increasing Paretic Leg Extension in Pre-Swing is Important for Increasing Forward Propulsion During Walking**
Peterson C, Kautz S, Neptune R
University of Texas at Austin

105 **Hip Joint Moments Using a Greater Trochanter Method of Locating the Hip Joint Center**
O'Connor K, Weinhandl J
University of Wisconsin-Milwaukee

107 **Dynamic Stability of Walking During Anterior-Posterior and Medio-Lateral Support Surface and Visual Field Translations**
McAndrew P, Dingwell J, Wilken J
University of Texas

Friday, August 20, 4:30–6:00 pm

Gait continued

90 **Effects of Handrail Use on Healthy Treadmill Walking**
Zahradka N, Reisman D, Higginson J
University of Delaware

92 **Reliability of Regional Plantar Pressure During Walking, Stair Ascent and Descent**
Chen Y, Lo O, Iannuzzi L, Mroczek K, Rao S
New York University

94 **Load Carriage Increases Mechanical Loading Rates During Walking**
Wang H, Frame J, Ozimek E, Reedstrom C, Leib D, Dugan E
Ball State University

96 **Human Ankle Mechanics During Able-Bodied and Pathological Gait**
Dutta A
Rehabilitation Institute of Chicago

98 **Gait After Unilateral Total Knee Arthroplasty: Frontal Plane Analysis**
Alnahdi A, Zeni J, McGinnis K, Snyder-Mackler L
University of Delaware

100 **The Effect of Foot Type on Temporal-Distance Gait Parameters in Healthy Individuals**
Frey J, Zifchock R, Chow S, Kraszewski A, Patel V, Lenhoff M, Backus S, Deland J, Demp P, Song J, Heilman B, Rajan S, Woodley A, Hillstrom H
Hospital for Special Surgery

102 **Effect of a Supervised Hip Flexor-Stretching Program on Gait in Healthy Elders**
Watt J, Jackson K, Franz J, Dicharry J, Della Croce U, Kerrigan D
University of Virginia

104 **Braking and Propulsive Impulses Positively Relate to Walking Speed During Accelerated and Decelerated Walking**
Peterson C, Kautz S, Neptune R
University of Texas at Austin

106 **A Passive-Elastic Ankle Exoskeleton Using Controlled Energy Storage and Release**
Wiggin B, Collins S, Sawicki G
North Carolina State University and University of North *Carolina at Chapel Hill*

Poster Sessions

Thursday, August 19, 4:30–6:00 pm

Gait continued

109 The Effect of Various Thong Flip-Flops on Gait Kinetics
Shroyer J, Weimar W
University of Louisiana at Lafayette

111 Over-Striding During Fixed-Cadence Load Carriage Leads to Increased Ground Reaction Forces
Gutekunst D, Frykman P, Seay J
Washington University

113 Human Postural Model That Captures Rotational Inertia
Dutta A, Goswami A
Rehabilitation Institute of Chicago

115 Gait Biomechanics in Hip Arthroplasty Patients and Control Subjects: Effect of Big Femoral Head and Surface Replacement Protheses
Bouffard V, Nantel J, Therrien M, Vendittoli P, Lavigne M, Prince F
Université de Montréal

117 Foot Forces During Exercise on the International Space Station
Genc K, Gopalakrishnan R, Kuklis M, Maender C, Rice A, Bowersox K, Cavanagh P
University of Washington

119 Assessing Performance of Three Types of Biomechanical Models Applied to Normal Human Gait
Buczek F, Rainbow M, Cooney K, Bruening D, Schmitz A, Thelen D
National Institute for Occupational Safety and Health

121 Temporal & Spatial Gait Characteristics During Prolonged Exposure to a Normal Surface in Workboots
Garner J, Wade C
Auburn University

123 Gravitational Impulse Model Predicts Collision Dynamics During Gait
Yeom J, Park S
Korea Advanced Institute of Science and Technology

125 Fifteen Observations on the Structure of Optimal Gaits for Various Simple Bipedal Models
Srinivasan M
Ohio State University

Friday, August 20, 4:30–6:00 pm

Gait continued

108 Walking on an Oscillating Treadmill: Two Paths to Functional Adaptation
Brady R, Peters B, Bloomberg J
Wyle Integrated Science and Engineering Group

110 The Effect of Sustained Static Kneeling on Knee Joint Gait Parameters
Kajaks T, Costigan P
McMaster University

112 Changes in Gait Kinematics at Preferred Walking Speed in People with Multiple Sclerosis
Busa M, Jones S, Remelius J, House J, Sugumaran K, Eve J, Van Emmerik R
University of Massachusetts Amherst

114 Symmetry of Plantar Pressure During Self-Selected Walking, Fast Walking, Heel Raise and Sit-To-Stand Activities
Lo O, Iannuzzi L, Mroczek K, Rao S
New York University

116 Limb Kinematics Predict Emotion Recognition with Walking Speed Modifications in Biomechanical Animations
Gross M, D'Angelo J
University of Michigan

118 Assessing Spatiotemporally Complex and Coupled Gait Patterns Using Temporal Cross-Correlation
Park K, Dankowicz H, Hsiao-Wecksler E
University of Illinois at Urbana-Champaign

120 A Limb Suspension Model to Describe Leg Stiffness Change with Gait Speed
Kim S, Park S
Korea Advanced Institute of Science and Technology

122 Ankle & Knee Musculature Co-Contraction Following Extended Durations of Walking in Workboots
Wade C, Garner J
Auburn University

124 The Effect of Heel Height on Peak Tibial and Head Accelerations and Shock Attenuation During Walking
Barkema D, Derrick T, Martin P
Iowa State University

Poster Sessions

Thursday, August 19, 4:30–6:00 pm

Gait continued

127 Ground Reaction Forces Scale to Ramp Angle During Transitions
Sheehan R, Gottschall J
Pennsylvania State University

129 The Effect of Foot Type of Normal Subjects on Foot Contact Dynamics
Mootanah R, Frey J, Zifchock R, Chow S, Kraszewski A, Lenhoff M, Backus S, Deland J, Demp P, Song J, Hillstrom H
Anglia Ruskin University

131 The Effects of a Downhill Grade on the Biomechanics of Walking in Obese Adults
Dannecker K, Ehlen K, Reynolds M, Browning R
Colorado State University

133 Multi-Segment Foot Model Kinetics During Normal Gait
Bruening D, Cooney K, Buczek F
Shriners Hospitals for Children - Erie

Lower Extremity

135 Three-Dimensional Position Capture of the Lower Extremity Mechanical Axis Correlates Significantly with Radiographical Measurement in Patients with Knee OA
Foxworth J, Renner J
Winston Salem State University

137 Comparison of Bilateral Kinematics and Kinetics During Sit-To-Stand and Stand-To-Sit Between Healthy Subjects and Unilateral Knee Osteoarthritis Patients
Burnett D, Campbell-Kyureghyan N, Topp R, Quesada P
University of Louisville

139 The Influence of Patella Cartilage Thickness on Patella Bone Stress in Females with and Without Patellofemoral Pain
Ho K, Yang N, Farrokhi S, Powers C
University of Southern California

141 Preferred Frequency During a Simple Bouncing Task
Merritt K, Raburn C, Dean J
Medical University of South Carolina

Friday, August 20, 4:30–6:00 pm

Gait continued

126 Joint Contact Force Comparisons Between Healthy Subjects and Those with Medial Compartment Knee Ostearthritis
Manal K, Kumar D, Buchanan T, Rudolph K
University of Delaware

128 Discrete Frequency Adjustment of Walking Above and Below Preferred Stride Frequency Causes an Increase in the Metabolic Cost of the Movement
O'Halloran J, Remelius J, van Emmerik R, Hamill J
University of Massachusetts Amherst

130 Natural Ankle Pseudo-Stiffness During Gait Initiation
Guinn L, Takahashi K, Razzook A, Stanhope S
University of Delaware

132 Collision Compensation by Active Push-Off with Gait Speed
Park H, Yeom J, Park S
Korea Advanced Institute of Science and Technology

134 People Walking on Treadmills Control Speed, Not Position
Cusumano J, John J, Dingwell J
Pennsylvania State University

Lower Extremity

136 A Comparison of Experimental and Simulated Patellofemoral Contact Mechanics Before and After Trochlear Osteotomy
Bennetts C, Fening S, Colbrunn R, Andrish J, Erdemir A
Cleveland Clinic

138 Increase Patellofemoral Joint Stress with Internal Femoral Rotation: A Finite Element Analysis
Yang N, Ho K, Farrokhi S, Powers C
University of Southern California

140 Curve Inflection and Modification of the Anterior Knee Laxity Compliance Index: Specific Variables to Assess Anterior Cruciate Ligament Integrity
Wordeman S, Paterno M, Quatman C, Bates N, Hewett T
University of Cincinnati

142 Minimizing Variability of Anterior Tibial Translation Measures Duirng Knee Laxity Testing
Jacobs C, Branch T, Browne J, Campbell J
ERMI, Inc.

Poster Sessions

Thursday, August 19, 4:30–6:00 pm

Lower Extremity continued

143 **Does Quadriceps Moment Arm Dysfunction Exist in Cerebral Palsy?**
Sheehan F, Behnam A, Alter K
National Institutes of Health

145 **Drop Landings in Military Boots**
Oliver G, Booker J, Stone A, Plummer H
University of Arkansas

147 **Tibial Acceleration and Slope Contributions to ACL Loading During a Simulated Landing Impact**
McLean S, Oh Y, Palmer M, Ashton-Miller J, Wojtys E
University of Michigan

149 **The Effects of Single-Leg Landing Technique on ACL Loading**
Laughlin W, Weinhandl J, Kernozek T, O'Connor K
University of Wisconsin-Milwaukee

151 **Examining the Kinematics of the Knee During a Side Step Cutting Task Using the Helical Axis Method**
Samaan M, Ringleb S, Choisne J, Bawab S, Cortes N, Greska E, Onate J
Old Dominion University

153 **Biomechanical Analysis of Stepping Down in Continuous Gait Following Ankle Evertor Fatigue: A Pilot Study**
Pozzi F, Gutierrez G, Moffat M
New York University

155 **Lower Extremity Kinematic Sequence During the Single Leg Hop Test Following ACL Reconstruction**
Orishimo K, McHugh M, Kremenic I, Mullaney M, Nicholas S
Nicholas Institute of Sports Medicine and Athletic Trauma

157 **Effect of Impulsive Transverse Plane Tibial Torques and Frontal Plane Moments on in Vitro ACL Relative Strain During a Simulated Jump Landing**
Oh Y, Lipps D, Ashton-Miller J, Wojtys E
University of Michigan

Friday, August 20, 4:30–6:00 pm

Lower Extremity continued

144 **Estimation of Anterior Tibial Translation and Ligament Loading in Healthy and ACL-Deficient Knees During Walking**
Shao Q, MacLeod T, Manal K, Buchanan T
University of Delaware

146 **A Line Profile Approach to Quantify PTOA Using T1rho MRI**
Klocke N, Thedens D, Martin J, Amendola A, Brown T
University of Iowa

148 **Load Response of Articular Cartilage and Ligaments to Valgus Loading: A Fibril-Reinforced Model of the Knee**
Kazemi M, Gu K, Li L
University of Calgary

150 **Predicting Knee Valgus During Landing from a Jump from a Field Test in a Fatigued Condition**
Afifi M, Hinrichs R
University of Calgary

152 **Dynamic Knee Joint Stiffness and Knee Joint Moments After Unilateral TKA**
McGinnis K, Zeni J, Alnahdi A, Snyder-Mackler L
University of Delaware

154 **Ankle Actuator Deficits in the Presence of Achilles Tendinopathy**
Chang Y, Siemienski A, Gregor R, Kulig K
University of Southern California

156 **A Comparison of Maximal Knee Moments Generated During Single Joint Knee Extension and Leg Press Tasks**
Gordon M, Schulz B, Ashton-Miller J
University of Michigan

158 **Effects of Ankle Immobilization on Knee Joint Biomechanics During an Unanticipated Cutting Maneuver**
Boros R, Plumlee E
Texas Tech University

Poster Sessions

Thursday, August 19, 4:30–6:00 pm

Methods

159 Filtering GRF Data Affects the Calculation and Interpretation of Joint Kinetics and Energetics During Drop Landings
McCaw S, Gardner J, Barlow L
Illinois State University

161 Experimental and Modeling Investigation of SEMG Spike Analysis
Gabriel D, Christie A, Inglis J, Kamen G
Brock University

163 Variability of Gait Kinematic Data Associated to Observer and Marker Placement Technique
Moniz-Pereira V, Carnide F, Agostinho R, Amado S, Veloso A
Technical University of Lisbon

165 Longitudinally Assessed Change in Stature and Segment Length
Ford K, Myer G, Shapiro R, van den Bogert A, Hewett T
Cincinnati Children's Hospital Medical Center

167 Analysis of Gait Cycle Shapes Using Parallel Factor Analysis
Helwig N, Hong S, Polk J, Lague M
University of Illinois at Urbana-Champaign

169 Modeling Nonlinear Errors in Surface Electromyography due to Baseline Noise: A New Methodology
Law L, Krishnan C, Avin K
University of Iowa

171 Locating the Hip Joint Center Using a Greater Trochanter Method
Weinhandl J, O'Connor K
University of Wisconsin-Milwaukee

173 The Use of Dynamical Systems Theory Methods to Refine Kinematic Movement Data As an Input to an Artificial Neural Network
O'Halloran J, Anderson R
University of Massachusetts Amherst

175 Normalization of EMG Amplitude: A Comparison of Different Methods Used to Test Individuals with Arthritis of the Hand
Calder K, Galea V, Wessel J, MacDermid J, MacIntyre N
McMaster University

Friday, August 20, 4:30–6:00 pm

Methods

160 Effects of Experimental Setup and Modeling Assumptions on Predicted Trunk Properties Using a System Identification Method
Bazrgari B, Nussbaum M, Madigan M
Virginia Polytechnic Institute and State University

162 A Comparison of Vibration Acceleration Measured with High Speed 3-D Motion Capture and Triaxial Accelerometers
Bressel E, Smith G, Nash D
Utah State University

164 Is Subjects' Joint Torque Variability Related to Joint Torque Error?
Riemer R
Ben-Gurion University of the Negev

166 A Framework for Studying Underactuation in the Human Hand
Balasubramanian R, M. Dollar A
Yale University

168 Human Attribute Recognition from Optimized 2D Viewing Angle Simulation
Bowden D, Santez D, Fullenkamp A, Campbell B
711th Human Performance Wing

170 A Cadaveric Robotic Gait Simulator with Fuzzy Logic Vertical Ground Reaction Force Control
Aubin P, Whittaker E, Ledoux W
Veterans Health Administration Rehabilitation Research and Development Center of Excellence for Limb Loss Prevention and Prosthetic Engineering

172 Effect of Scientist Experience on the Repeatability of Palpation of Scapular Landmarks
Hooke A, Kaufman K, An K
Mayo Clinic

174 Can Hip and Knee Kinematics Be Improved by Eliminating Thigh Markers?
Schulz B, Kimmel W
Veterans Health Administration Health Services Research and Development Center of Excellence

176 Soft Tissue Artifact Has Inter-Subject and Inter-Motor-Task Similarities: A New Concept for Its Compensation
Gao B, Banks S, Zheng N
University of Florida

Poster Sessions

Thursday, August 19, 4:30–6:00 pm

Methods continued

177 **Evaluation of an Inertial and Magnetic Measuring System As a Method of Collecting Kinematics of Wheelchair Propulsion**
Daigle S, Rampurawala Z, Hsiao-Wecksler E, Sosnoff J
University of Illinois at Urbana-Champaign

179 **Estimation of Stride Variability from Foot-Mounted Inertial Sensors**
Rebula J, Kuo A
University of Michigan

181 **New Approach to Characterize Trunk Neuromuscular Responses During Rapid Voluntary Extremity Movement**
Mehta R, Cannella M, Wattananon P, Henry S, Silfies S
Drexel University

Motor Control

183 **Stabilization of the Total Force in Multi-Finger Pressing Tasks Studied with the 'inverse Piano' Technique**
Martin J, Budgeon M, Zatsiorsky V, Latash M
Pennsylvania State University

185 **Computational Model to Predict the Effects of Cognitive and Neuromuscular Impairments on Driving**
Long B, Gillespie I, Tanaka M
Wake Forest University

187 **Planarity of Force Distribution in a 4-Finger Force Space During Multi-Finger Prehension and Its Implication for Inverse Optimization**
Niu X, Terekhov A, Latash M, Zatsiorsky V
Pennsylvania State University

189 **Trial-To-Trial Adaptation of Multi-Digit Forces to Texture for Object**
Zhang W, Gordon A, McIsaac T, Santello M
Arizona State University

191 **Exploiting Redundancy in Generalized Reaching Tasks**
Smallwood R, Dingwell J
University of Texas

193 **Multi-Finger Synergies During Isometric Force Production Task in Index Finger Amputees**
Karol S, Shim J
University of Maryland, College Park

Friday, August 20, 4:30–6:00 pm

Methods continued

178 **Reliability and Validity of Accelerometer-Based Smartphones to Assess Physical Activity**
Saha I, Dirik A, Topkara U, Memon N, Guitierrez G, Rao S
New York University

180 **Time Normalizing Gait Data Based on Gait Events**
Morris E, Hsiao-Wecksler E
University of Illinois at Urbana-Champaign

182 **A Kinematic Method for Strike Pattern Detection**
Altman A, Davis I
University of Delaware

Motor Control

184 **Prehension Synergy: Principle of Superposition During Multi-Finger Torque Production on Mechanically Fixed- and Free-Objects**
Park J, Zatsiorsky V, Kim Y, Kim Y, Shim J
Pennsylvania State University

186 **Trunk Segment Coordination During a Jumping Task in Elite Dancers: An Exploration Using Vector Coding**
Smith J, Siemienski A, Popovich J, Kulig K
University of Southern California

188 **Adaptive Changes in Finger Force Variance in Response to Index Finger Fatigue in a Multi-Finger Task**
Singh T, Zatsiorsky V, Latash M
Pennsylvania State University

190 **Nonlinear Smooth Orthogonal Decomposition Identifies Local Muscle Fatigue Dynamics in Sawing Motion**
Segala D, Gates D, Dingwell J, Chelidze D
University of Rhode Island

192 **Differences in Grip Characteristics Between Younger and Older Females**
Irwin C, Sesto M
University of Wisconsin-Madison

194 **Adaptations of Multi-Finger Interactions Through Fatigue Exercise**
Shim J, Huang J, Karol S, Kim Y, Yoon B
University of Maryland, College Park

Poster Sessions

Thursday, August 19, 4:30–6:00 pm

Motor Control continued

195 **Limitations to Synchronization of Coordinated Finger Movement**
Gu Y, Hiley M, Pain M
Loughborough University

197 **Variable Stiffness Shoe Alters Muscle Activations and Knee Joint Moments.**
Boyer K, Andriacchi T
Stanford University

199 **Directional Characteristics of Fingertip Force Production After Hemiparetic Stroke**
Towles J, Triandafilou K, Stoykov M, Kamper D
Rehabilitation R&D Service, Edward Hines Jr. VA Hospital

Muscle

201 **Dependence of Muscular Mass in the Origin of Inguinal Hernia**
Susín A, Herrera B, López-Cano M, Fortuny G
Universitat Rovira i Virgili

203 **Gastrocnemius Atrophies Preferentially in Post-Stroke Plantar Flexors**
Ramsay J, Buchanan T, Barrance P, Higginson J
University of Delaware

205 **Variability in Biceps Femoris Long Head Muscle-Tendon Morphology**
Handsfield G, Fiorentino N, Blemker S
University of Virginia

207 **A Unique Method of Measuring Dynamic Rate of Torque Development: Comparison of Explosive Power Athletes and Controls**
Tillin N, Pain M, Oguz H, Lewis G, Folland J
Loughborough University

209 **Variation in Muscle Model Output Using Cadaver-Specific Model Parameters**
Infantolino B, Challis J
Pennsylvania State University

211 **A 3D Model Demonstrates the Effects of Increased Activation on Nonuniform Strains in Muscle**
Rehorn M, Blemker S
University of Virginia

Friday, August 20, 4:30–6:00 pm

Motor Control continued

196 **Biomechanical Constraints on the Control of Endpoint Stiffness**
Hu X, Murray W, Perreault E
Northwestern University

198 **Interlimb Coordination for Force Control During Human Hopping**
Yen J, Chang Y
Georgia Institute of Technology

200 **Active Joint Position Sense: Effects of Elevation Angle, Arm Dominance and Proximal vs Distal Joints**
Hyler J, Harding E, Karduna A
University of Oregon

Muscle

202 **Characterization of Upper Limb Muscle Volume in Female Older Adult Subjects Following Resistance Exercise Training**
Vidt M, Daly M, Eggebeen J, Simpson W, Marsh A, Saul K
Virginia Tech–Wake Forest University School of Biomedical *Engineering and Sciences*

204 **Muscle Activity During Running Scales Non-Uniformly Across Phases of the Gait Cycle**
Silder A, Thelen D
Stanford University

206 **Active Force Enancement As a Source of SSC Enhancement**
Pain M, Buckeridge E, O'Brien T, Forrester S
Loughborough University

208 **Mechanical Maladaptations to Eccentric Exercise Result in Sustained Hypertrophic Signaling in Skeletal Muscle Cells**
Abshire S, Best T, Butterfield T
University of Kentucky

210 **Tracking Non-Contractile Material in Muscle**
Infantolino B, Hughes J, Neuberger T, Challis J
Pennsylvania State University

212 **Lifting Capacity and Fatigue Recovery in Healthy Young Adults and Elderly Individuals**
Annick C, Annie N, Danik L
Université de Montréal

Poster Sessions

Thursday, August 19, 4:30–6:00 pm

Muscle continued

213 Spring-Loaded Ankle Exoskeletons Reduce Metabolic Cost and Alter Gastrocnemius Fascicle Behaviour in Human Hopping
Farris D, Sawicki G
North Carolina State University and University of North Carolina at Chapel Hill

215 Predicting the Effect of Pulse Duration on Fatigue During Electrically Stimulated Non-Isometric Contractions
Marion S, Hull M, Wexler A
University of California

217 Joint-Specific Power Production, Fatigue, and Recovery During Submaximal Exercise
Elmer S, Grisham J, Hahn S, Martin J
University of Utah

Posture and Balance

219 Do Children Use a Different Strategy in Adapting to a Tendon Vibration Perturbation During Standing?
Wu J, McKay S, Angulo-Barroso R
Georgia State University

221 Effect of Arm Restriction on Upper Body Response to a Slip
Jayadas A, Boros R
Texas Tech University

223 Postural Stiffness Model and Outdoor Falls in Older Adults: The Mobilize Boston Study
Kang H, Quach L, Li W, Lipsitz L
California State Polytechnic University Pomona

225 Affect of Intensive Environmental Noise of Human Postural Control
Bateni H, Vaizasatya A, Blaschak M
Northern Illinois University

227 Foot Placement and Seat Height Effects on Sit-To-Stand Joint Moments
Gillette J, Stevermer C
Iowa State University

229 The Effect of a Subject-Specific Dual-Task on Standing Balance
Sukits A, Chambers A, Cham R, Nebes R
University of Pittsburgh

Friday, August 20, 4:30–6:00 pm

Muscle continued

214 Evaluation of Neuromuscular Dynamics of Hyperactive Reflexes at the Elbow Poststroke
Liu J, Ren Y, Xu D, Chung S, Rymer W, Zhang L
Northwestern University

216 Incorporating Velocity Characteristics into Cost Functions Does Not Alter Optimal Muscle Forces in Normal Walking
Gopalakrishnan A, Hakansson N, Higginson J
University of Delaware

Posture and Balance

218 Age-Related Modifications in Forward Reach Movement Patterns
Lin S, Liao C
National Cheng Kung University

220 The Effect of Obesity on Balance Recovery Using an Ankle Strategy is Dependent on Perturbation Type
Matrangola S, Madigan M
Virginia Polytechnic Institute and State University

222 Sensitivity and Specificity of a Clinical Screening Tool for Fall Risk
Bigelow K
University of Dayton

224 Postural Stiffness Model and Dual Task in Older Adults: The Mobilize Boston Study
Kang H, Lipsitz L
California State Polytechnic University Pomona

226 What Aspects of Postural Transitions Affect Balance Control Upon Standing?
DiDomenico A, McGorry R
Liberty Mutual Research Institute for Safety

228 Comparison of Alternate Stair Descent Patterns
Stevermer C, Hall M, Gillette J
Des Moines University

Poster Sessions

Thursday, August 19, 4:30–6:00 pm

Posture and Balance continued

231 **Is There a Tradeoff Between Stabilization and Maneuverability During Whole-Body Movements?**
Huang H, Ahmed A
University of Colorado at Boulder

233 **Fall Risk Does Not Depend on Body Mass Index**
Rosenblatt N, Premier D, Grabiner M
Univeristy of Illinois at Chicago

235 **Multiscale Entropy Identifies Complexity Changes in Postural Control of Adolescent Idopathic Scoliosis**
Busa M, Gruber A, Gorton G, Masso P, Hamill J, Van Emmerik R
University of Massachusetts Amherst

237 **Trunk Kinematics Discriminate Multidirectional Falls and Recoveries Following Large Postural Disturbances**
Cain J, Crenshaw J, Kaufman K, Grabiner M
University of Illinois at Chicago

239 **Dynamic Balance Control During Sit-To-Stand Movement: An Examination with the Center of Mass Acceleration**
Fujimoto M, Chou L
University of Oregon

241 **An Experimental Study of Postural Control During Downward Reach and Pick-Up Movements: Effects of Age and Limiting the Length of the Base of Support**
Hernandez M, Ashton-Miller J, Alexander N
University of Michigan

243 **Proactive Postural Adjustments During Multiple Exposures to Trips**
Coley B, Cham R, Nelson C
University of Pittsburgh

245 **Whole-Body Local Dynamic Stability During Walking and Running**
Qiao M, Jindrich D
Arizona State University

247 **Experimental Analysis of Kinematic Variables Associated with Biomechanical Sit-To-Stand Movement**
Mughal A, Iqbal K
University of Arkansas at Little Rock

Friday, August 20, 4:30–6:00 pm

Posture and Balance continued

230 **Lower Extremity Coordinated Mobilization and Stabilization During Static Stance: The Unique Role of the Vasti Muscles**
MacLeod T, Manal K, Snyder-Mackler L, Buchanan T
University of Delaware

232 **Spinal Cord Injury and Time to Instability in Seated Posture**
Shin S, Sosnoff J
University of Illinois at Urbana-Champaign

234 **Minimizing Postural Instability When Carrying Load: The Effects of Carrying Grocery Bags on the Elderly**
Sutton E, Bare D, Taylor M, Kinor D, Schaeffer J, Jules A, Bigelow K
University of Dayton

236 **Time-To-Contact Identifies Differences in Postural Control in Adolescent Idiopathic Scoliosis**
Gruber A, Busa M, Gorton G, Van Emmerik R, Masso P, Hamill J
University of Massachusetts Amherst

238 **Fall Risk Estimation of Community-Dwellering Elderly Using Invariant Density Analysis**
Hur P, Kang H, Lipsitz L, Hsiao-Wecksler E
University of Illinois at Urbana-Champaign

240 **Application of Augmented Reality for the Elderly Fall Risk Prediction**
Chang C, Yang S, Tsai Y, Hsieh
National Yang-Ming University,

242 **The Effect of Increased Inertia on Balance Using an Ankle Strategy**
Costello K, Matrangola S, Madigan M
Virginia Polytechnic Institute and State University

244 **Age Effects on Lateral Stability During Stepping**
King G, Akula C
University of Missouri - Kansas City

246 **Dynamic Stability During Successful and Failed Compensatory Stepping Responses**
Crenshaw J, Cain J, Grabiner M
University of Illinois at Chicago

Poster Sessions

Thursday, August 19, 4:30–6:00 pm

Prosthetics

249 Biomechanical Analysis of a Unilateral Transfemoral Amputee During Hill Walking Transitions: A Case Study
Stern K, Gottschall J
Pennsylvania State University

251 Failed Trip Recoveries of Above-Knee Amputees Suggest Possible Fall-Prevention Interventions
Crenshaw J, Kaufman K, Grabiner M
University of Illinois at Chicago

253 Differences in Sagittal Plane Angular Momentum Between Below-Knee Amputees and Non-Amputees Across a Range of Walking Speeds
Silverman A, Neptune R
University of Texas at Austin

255 Lower Extremity Mechanical Work of Different Prosthetic Feet: An Immediate Response Case Study
Allen A, Heise G, Smith J
University of Northern Colorado

257 Relationships Between Amputee Independent Prosthesis Properties and Gait Performance: A Preliminary Study
Major M, Twiste M, Kenney L, Howard D
University of Salford

259 Contribution of Toe- Off Kinematics to the Prosthetic Knee Flexion During Swing Phase of Transfemoral Amputee Gait
Dabiri Y, Najarian S, Eslami M, Zahedi S, Moser D, Shirzad E, Moradihaghighat R
Amirkabir University of Technology (Tehtan Polytechnic)

261 Response to Tripping Perturbations in Transfemoral Amputees
Sierra F, Zhang F, Huang H, D'Andrea S
Brown University

Running

263 Assessment of the Support Vector Machine for Detecting Age-Related Changes in Running Kinematics
Fukuchi R, Eskofier B, Ferber R, Duarte M
University of Calgary

265 Joint Moments During Walking and Running at Different Speeds
de David A, Stergiou P, Stefanyshyn D
University of Brasilia

Friday, August 20, 4:30–6:00 pm

Prosthetics

248 Knee Joint Forces and Moments in Below-Knee Amputees Across Increasing Steady-State Walking Speeds
Fey N, Neptune R
University of Texas at Austin

250 Individual Muscle Function in Below-Knee Amputee Walking
Silverman A, Neptune R
University of Texas at Austin

252 Virtual Prototyping Functional Characteristics of a Passive-Dynamic Ankle Foot Orthosis
Schrank E, Tierney J, Guinn L, Takahashi K, Razzook A, Stanhope S
University of Delaware

254 A Pneumatically Powered Portable Ankle-Foot Orthosis
Shorter K, Kogler G, Loth E, Durfee W, Hsiao-Wecksler E
University of Illinois at Urbana-Champaign

256 Ground Reaction Force Characteristics of Different Prosthetic Feet: An Immediate Response Case Study
Heise G, Allen A, Hoke M, Smith J
University of Northern Colorado

258 Roll-Over Shape Dynamics During Stance in Natural Gait
Takahashi K, Razzook A, Guinn L, Schrank E, Stanhope S
University of Delaware

260 Analysis of Ankle Muscle Co-Contraction in Trans-Tibial Amputees
Seyedali M, Morgenroth D, Czerniecki J, Hahn M
Veterans Health Administration Rehabilitation Research and Development Center of Excellence

Running

262 Effects of Using Heel Windows and Single Subject Analysis to Measure Rear Foot Motion During Running
Becker J, Osternig L, James S, Chou L
University of Oregon

264 Friction Demand During Running and Cutting
Blanchette M, Sigward S, Powers C
University of Southern California

Poster Sessions

Thursday, August 19, 4:30–6:00 pm

Running continued

267 Acclimation to Treadmill Running in Minimal Footwear
TenBroek T, Rodrigues P, Murphy S, Hamill J
New Balance Athletic Shoe, Inc.

269 Maximum Possible Quadriceps Force 50ms After Ground Contact
Domire Z, Boros R, Hashemi J
Texas Tech University

271 Variations in Running Form Among Female Sprinters, Middle, and Distance Runners
Cunningham R, Hunter I, Seeley M, Feland B
Brigham Young University

273 Step Width and Iliotibial Band Strain During Running
Meardon S, Campbell S, Derrick T
University of Wisconsin-La Crosse

275 Ankle Brace with a Heel Strap is Effective in Stablizing Ankle in Frontal Plane in Walking and Running
Zhang S, Wortley M, Freedman J, Carson D
University of Tennessee

277 Reducing Abnormal Alignment in Female Runners with PFPS Through Gait Retraining Using Mirror Feedback
Willy R, Noehren B, Davis I
University of Delaware

279 The Effects of Indoor Track Curve Radiuson Sprint Speed and Ground Reaction Forces
Tukuafu J, Hunter I
Brigham Young University

Friday, August 20, 4:30–6:00 pm

Running continued

266 High Plantar-Flexor Passive Stiffness Increases Achilles Tendon Loading During Landings
Whitting J, Steele J, McGhee D, Munro B
University of Wollongong

268 The Effect of Functional Fatigue and Ankle Bracing on Lower Extremity Response to Jump Landing Tasks
Stafford E, Gillette J
Iowa State University

270 Ground Contact Time and Running Speed in Elite Championship Distance Races
Hunter I, Cunningham R, Ingebretsen S, Butler D
Brigham Young University

272 A Prospective Study of Loading Rates in Female Runners Who Develop Plantar Fasciitis
Bowser B, Hamill J, Davis I
University of Delaware

274 Variation of Anatomical Parameters That Affect Estimated Anterior Cruciate Loading During Drop Landings
Koehler C, Lopez T, Kernozek T, Ragan R
University of Wisconsin-La Crosse

276 Metatarsophalangeal Joint Kinetics in Running and Jumping
Forrester S, Hofmans E
Loughborough University

278 Change in Medial Longitudinal Arch Stiffness After a Prolonged Run
Hageman E, Ward E, Derrick T
Iowa State University

280 Are the Vibram Fivefingers a Functional Alternative to Barefoot Running in Inexperienced Barefoot Runners?
Paquette M, Baumgartner L, Zhang S
University of Tennessee

Poster Sessions

Thursday, August 19, 4:30–6:00 pm

Spine

281 Neck Motion due to the Halo-Vest in Prone and Supine Positions
Ivancic P, Telles C
Yale University

283 Dynamic Modeling of Human Lumbar Spine Via Msc Adams
Tabesh M, Elahinia M
University of Toledo

285 Disturbances to Intrinsic Stiffness and Reflexive Muscle Responses Following Prolonged Trunk Flexion
Hendershot B, Bazrgari B, Muslim K, Toosizadeh N, Nussbaum M, Madigan M
Virginia Polytechnic Institute and State University

287 A New Surrogate Bone Model for Testing Intervertebral Devices
Au A, Aiyangar A, Anderson P, Ploeg H
University of Wisconsin-Madison

289 Inter-Examiner Comparisons of a Human Clinical Cervical Diagnosis Technique
Rutledge B, Reid-Bush T, Vorro J, DeStefano L, Francisco T, Gorbis S
Michigan State University

291 A Finite Element Study of Dual Bearing Surface Sliding Kinematics and Wear in the Charite Total Disc Replacement
Goreham-Voss C, Brown T
University of Iowa

293 Dynamic Response of the Trunk to Position Perturbations - Effects of Gender, Preload, and Trunk Angle
Miller E, Bazrgari B, Hendershot B, Nussbaum M, Madigan M
Virginia Polytechnic Institute and State University

295 The Quantitative Assessment of Contribution of Risk Factors to Overstress at Adjacent Segments After Lumbar Fusion: Removal of Posterior Ligaments Pedicle Screws
Kang K, Lee H, Kim K, Kim H, Jang J
Yonseisarang Hospital

Friday, August 20, 4:30–6:00 pm

Spine

282 Mechanisms of Whiplash Injury Prevention Attributable to Energy-Absorbing Seat
Ivancic P, Xiao M
Yale University

284 Identification of Hyperelastic Properties of Lumbar Multifidus
Koo T, Zheng Y
New York Chiropractic College

286 Load Bearing Capability of Annular Fibers is Affected by Their Incomplete Length: A Finite Element Model Analysis
Hussain M, Gay R, An K
Logan University

288 Assessment of Gender Variations in the Cervical Response to Rear Impacts
Fritz J, Harris G
Marquette University

290 Comparison of Energy Dissipation in Thoracolumbar Motion Segments due to Load Frequency Variation
Campbell-Kyureghyan N, Yalla S
University of Wisconsin-Milwaukee

292 Effect of Off-Axis Fluoroscopy Imaging on 2D Lumbar Spine Kinematics
Ben-Abraham E, Zhao K, Magnuson D, Shaw M, Berglund L, Gay R, An K
Mayo Clinic

294 Cervical Spine Center of Rotation During in Vivo Dynamic Flexion / Extension
Baillargeon E, Lee J, Donaldson W, Kang J, Anderst W
University of Pittsburgh

Poster Sessions

Thursday, August 19, 4:30–6:00 pm

Sports

297 **Quantative Analysis of SEMG of the Upper Extremity Musculature while Cutting Common Paddle Sport Entanglement Materials Using Two Different Tools**
Oliver G, Aldrich T, Moiseichik M
University of Arkansas

299 **Association Between Attributes of a Cyclist and Bicycle Seat Pressure**
Nash D, Bressel E, Dolny D
Utah State University

301 **Archery Biomechanics: A Kinematical Approach**
Ertan H, Irmak R
Anadolu University

303 **The Influence of Glove and Hand Position on Pressure Over the Ulnar Nerve During Cycling**
Slane J, Timmerman M, Ploeg H, Thelen D
University of Wisconsin-Madison

305 **Identifying Different Biomechanical Techniques - Technique Taxonomy Applied to Golf Putting.**
McLaughlin P, Best R
Victoria University

307 **The Influence of Tissue Masses on Lower Extremity Injuries and Reported Pain in Varsity Soccer Players**
Schinkel-Ivy A, Burkhart T, Andrews D
University of Windsor

309 **Effects of Equine Racetrack Surface Type, Depth, and Confining Area on Force and Displacement Measurements Using a Track-Testing Device**
Setterbo J, Yamaguchi A, Hubbard M, Upadhyaya S, Stover S
University of California, Davis

311 **Regulation of Angular Impulse During Golf Swings with Different Clubs**
McNitt-Gray J, Requejo P, Flashner H
University of Southern California

313 **A Kinematic Comparison of Three Different Volleyball Blocking Techniques**
Neves T, Seeley M, Johnson A, Myrer J
Brigham Young University

315 **Biomechanics of the Cross-Country Sit-Skier and Impact on Sit-Ski Design - a Top Secret 2010 Project**
Leblanc-Lebeau M, Rancourt D, Langelier E, Cyr M, Lessard J, Smeesters C
Universite de Sherbrooke

Friday, August 20, 4:30–6:00 pm

Sports

296 **Optimizing Position of the Horizontal Bench Press Using Surface Electromyography**
Jagessar M
University of Trinidad and Tobago

298 **Windmill Pitching Kinetics: Injury Implications in High School Softball Pitchers**
Plummer H, Keeley D, Oliver G
University of Arkansas

300 **Application of Spacesuit Glove Performance Tests to Athletic and Personal Protective Equipment**
England S, Benson E, Mesloh M, Thompson S, Rajulu S
MEI Technologies, Inc.

302 **The Influence of Sex and Maturation on Knee Valgus Moments During Cutting: Implications for ACL Injury**
Powers C, Pollard C, Lee S, Cesar G, Sigward S
University of Southern California

304 **A Model Predicting Anterior Shear Stress in the Shoulder During the Slide Step Delivery in High School Baseball Pitchers**
Keeley D, Oliver G, Hackett T, Torry M
University of Arkansas

306 **Two-Dimensional Sequential Analysis of the Front Snap Kick**
Weimar W, Madsen N, Garner J, Wang Y
Auburn University

308 **Frequency Response of the Wrist and Elbow Following Impacts with and Without Wrist Guards**
Burkhart T, Andrews D
University of Windsor

310 **Contribution of Trunk and Pelvis Rotation to Punching in Boxing**
Cabral S, João F, Amado S, Veloso A
Technical University of Lisbon

312 **A Framework for Measurement and Modeling of Human Climbing**
Russell S, Zirker C, Blemker S
University of Virginia

314 **Lumbopelvic Stability Correlates to Transverse Lumbar Spine Torque During the Golf Swing**
Yontz N, Jamison S, Chaudhari A
Ohio State University

Poster Sessions

Thursday, August 19, 4:30–6:00 pm

Sports continued

317 Variations in Climbing Strategies Between Experienced and Inexperienced Rock Climbers
Zirker C, Russell S, Blemker S
University of Virginia

319 Biomechanical Energetic Analysis of Pitching Motion of Professional Japanese Baseball Pitchers
Aoki K, Mochimaru M, Himeno R
National Institute of Advanced Industrial Science and Technology

Tissue Mechanics

321 Frequency Content of Cartilage Impact Signal Reflects Acute Histologic Structural Damage
Heiner A, Martin J, McKinley T, Goetz J, Thedens D, Brown T
University of Iowa

323 Localized Measures of Tendon Impingement on the Median Nerve Within the Carpal Tunnel
Kunze N, Goetz J, Thedens D, Baer T, Lawler E, Brown T
University of Iowa

325 Temperature Dependence on Porcine Internal Carotid Artery Vascular Mechanics
Fitzpatrick J, Capaldi F
Drexel University

327 A 3-D Breast Software Phantom to Investigate Breast Biomechanics During Ultrasound Strain Imaging Using Finite Element Modeling
Hashmi S, Keralapura M
San Jose State University

329 Testing for Material Properties of the Human Anterior Cruciate Ligament
Ren Y, Ahn C, Park H, Fang D, Zhang L
Rehabilitation Institute of Chicago

331 Changes in Cross Sectional Stress at the Distal Radius Following Short Term Mechanical Loading
Edwards W, Troy K
University of Illinois at Chicago

333 Understanding the Effects of Ligament Sectioning on the Stability of the Ankle and Subtalar Joint Using Euler Angles and the Rotation About a Helical Axis
Choisne J, Ringleb S, Samaan M, Bawab S, Naik D
Old Dominion University

Friday, August 20, 4:30–6:00 pm

Sports continued

316 Steady-State Handling Characteristics of a Bicycle
Cain S, Perkins N
University of Michigan

318 Velocity of the Taekwondo Axe Kick and Resultant Linear Acceleration of an Instrumented Head Form
Fife G, Kaminski T, O'Sullivan D, Pieter W, Shin I, Lim T
University of Delaware

Tissue Mechanics

320 Relationship Between Sacral Skin Blood Flow Oscillations and Vasodilatory Functions in People at Risk for Pressure Ulcers
Jan Y, Liao F, Garrison D, Anderson M
University of Oklahoma Health Sciences Center

322 Evaluation of Frost's 3-Way Rule Equation for Bone Adaptation to Mechanical Stimulation
Rastgar Agah M, Yingling V
Temple University

324 Relationships Between Dual Energy X-Ray Absorptiometry (DXA) and Computed Tomography (CT) Measures of Bone and Their Ability to Predict Fracture Load
Troy K, Edwards W
University of Illinois at Chicago

326 Effects of Posterior Capsule Attachment Status on Flexion Moment Resistance in the Hip
Stroud N, Rudert J, Baer T, Brown T
University of Iowa

328 Effects of Normal and Shear Loads on Blood Perfusion and Reactive Hyperemia in the Skin
Manorama A, Reid-Bush T, Baek S
Michigan State University

330 Viscoelastic Properties of Diabetic and Non-Diabetic Plantar Soft Tissue
Pai S, Ledoux W
University of Washington

332 ACL Length Changes During Robotic Simulation of Knee Laxity Tests
Lee A, Hagen J, Wahl C, Manner P, Cavanagh P
University of Washington

Poster Sessions

Thursday, August 19, 4:30–6:00 pm

Tissue Mechanics continued

335 Fatigue Properties of Proximal Humeral Fractures Fixed with Locked Plate System
Li J, Hymes R, Schulman J, Theiss M
Inova Fairfax Hospital

337 Simulation of a Percutaneous Aortic Valve Deployment into a Patient-Specific Aortic Root
Sirois E, Wang Q, Sun W
University of Connecticut

Upper Extremity

339 Elbow and Wrist Muscle Fiber Operating Ranges Throughout the Range of Motion for Flexion-Extension and Pronation-Supination
Dorman D, Warren R, Gonzalez R
LeTourneau University

341 Kinematic and Kinetic Analysis of Shoulder Motion During Tetraplegic Wheelchair Propulsion
Yarossi M, Dyson-Hudson T, Forrest G, Kwarciak A, Sisto S
Kessler Foundation Research Center

343 Effect of Concomitant Latissimus Dorsi Transfer on Joint Reaction Force for Reverse Total Shoulder Arthroplasty
Hansen M, Otis J, Ciccone W, Jacofsky M, Jaczynski A, Boyles A
SHRI-CORE Research Labs

345 Alterations in Shoulder Joint Perception Pre and Post Workday
Ettinger L, Kincl L, Karduna A
University of Oregon

347 Effect of Plication on Gleno-Humeral Translation: A Preliminary in Vitro Study
Rao S, Miana A, Lenhoff M, Backus S, Vanadurongwan B, Chen N, Brown A, Coleman S, Cordasco F, Altchek D, Fealy S, Imhauser C, Karduna A, Warren R, Wright T, Zifchock R, Hillstrom H
Hospital for Special Surgery

349 Shoulder External Rotation During Physical Assessment and Throwing Activity
Zheng N, Eaton K
University of North Carolina at Charlotte

Friday, August 20, 4:30–6:00 pm

Tissue Mechanics continued

334 A New Instrument for Assessing Heel Pad Mechanical Properties
Gales D, Challis J
Pennsylvania State University

336 The Use of Ultrasound Elastography to Assess Long-Term Tendon Remodeling and Mechanics Following Musculotendon Injury
Chernak L, Silder A, Lee K, Thelen D
University of Wisconsin-Madison

Upper Extremity

338 High Coefficient of Friction at the Hand-Object Interface Contributes to Increased Maximum Grip Force by the Phalanxes During Power Grip
Enders L, Engel A, Seo N
University of Wisconsin-Milwaukee

340 The Influence of Altering Push Force Effectiveness on Individual Muscle Demand During Wheelchair Propulsion
Rankin J, Kwarciak A, Richter W, Neptune R
University of Texas at Austin

342 Correlation Between Wrist Biomechanics and Median Nerve Health Parameters in Manual Wheelchair Users
Toosi K, Impink B, Collinger J, Yang J, Koontz A, Boninger M
University of Pittsburgh

344 Shoulder Kinematic Patterns During Execution of Circuit Resistance Training in Individuals with Paraplegia: a Case Series
Riek L, Ludewig P, Nawoczenski D
University of Rochester

346 The Effects of Noise and Inertia Distribution During a Planar Reaching Task
Nguyen H, Dingwell J
University of Texas at Austin

348 The Effect of Biceps Reattachment Site on Moment Arm
Weir D, Schmidt C, Wong A, Howard M, Miller M
University of Pittsburgh

350 A Dynamic CT Technique for Assessment of Wrist Joint Instability
Zhao K, Leng S, Qu M, McCollough C, An K
Mayo Clinic

Poster Sessions

Thursday, August 19, 4:30–6:00 pm

Upper Extremity continued

351 A Method of Geometric Description of the Glenoid Fossa
Gielo-Perczak K
Worcester Polytechnic Institute

353 Geometric Variability in the Subchondral Bone Surfaces of the First Trapeziometacarpal Joint
Halilaj E, Rainbow M, Patel N, Moore D, Crisco J
Brown University

Friday, August 20, 4:30–6:00 pm

Upper Extremity continued

352 Effects of Midcarpal Arthrodesis on Wrist Coupling and Performance
Garg R, Kraszewski A, Stocklein H, Backus S, Lenhoff M, Wolff A, Hillstrom H, Wolfe S
Hospital For Special Surgery

354 Effects of Crutch Type and Arm Dominance on Shoulder Joint Kinetics During Three Point Swing Through Gait
Singhal K, Casebolt J, Kwon M, Jackson E, Kwon Y
Texas Womans University

Rhode Island Convention Center 5th Floor

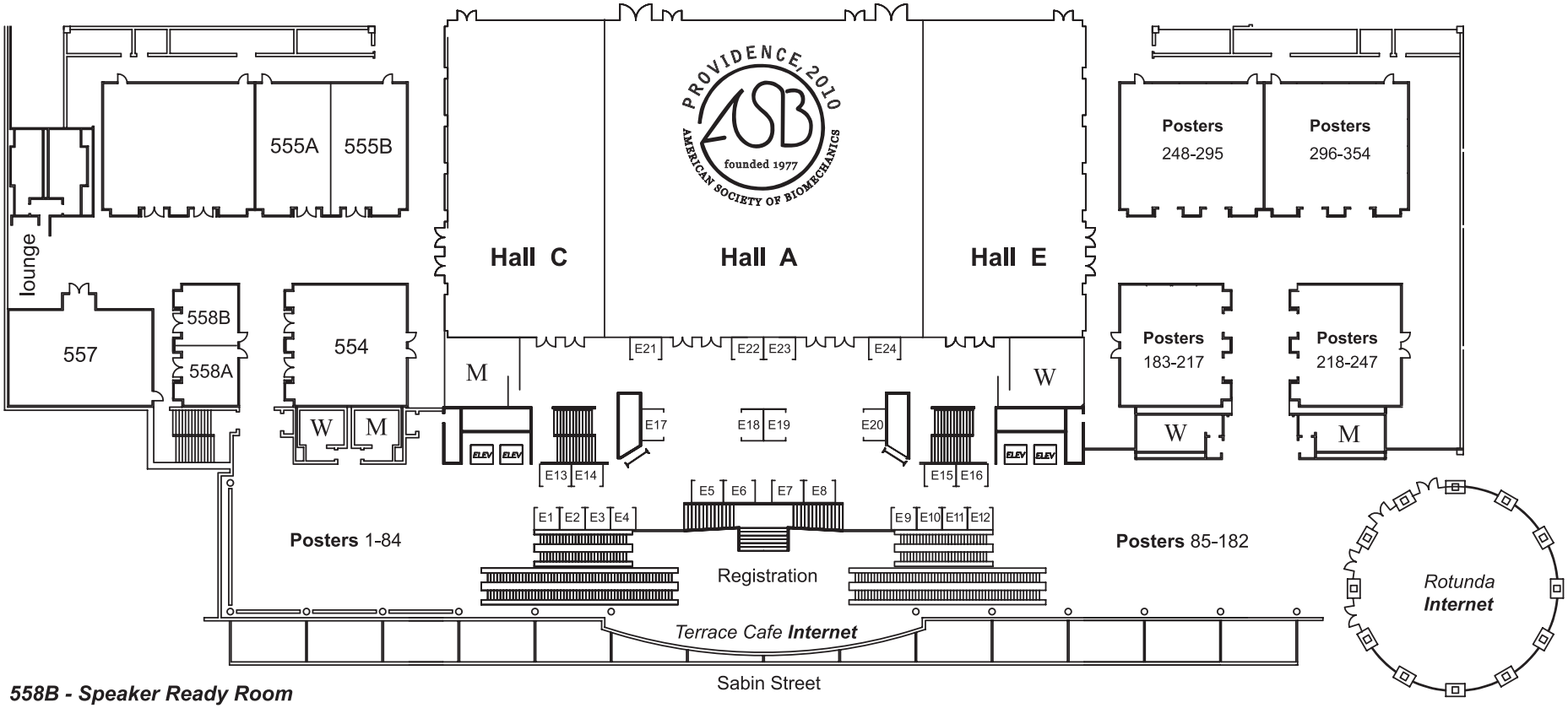

558B - Speaker Ready Room
555A - Exhibitors' Presentations

ASB Bus Stop at Street Level

Fish Robotics and Biomechanics

George Lauder, PhD
Alexander Agassiz Professor of Zoology, Department of Organismal and Evolutionary Biology, Harvard University

There are over 28,000 species of fishes, and a key feature of this remarkable evolutionary diversity is a great variety of propulsive systems used by fishes for maneuvering in the aquatic environment. Fishes have numerous control surfaces (fins) which act to transfer momentum to the surrounding fluid. Most fishes are unstable and use several control surfaces simultaneously for propulsion and to maintain body position. In this presentation I will discuss the results of recent experimental kinematic and hydrodynamic studies of fish fin function, and their implications for the construction of robotic models of fishes. Recent high-resolution video analyses of fish fin movements during locomotion show that fins undergo much greater deformations than previously suspected. Experimental work on fin mechanics shows that fishes possess a mechanism for actively adjusting fin surface curvature to modulate locomotor force. Fish fin motion results in the formation of vortex rings of various conformations, and quantification of vortex rings shed into the wake by freely-swimming fishes has proven to be useful for understanding the mechanisms of propulsion. Experimental analyses of propulsion in freely-swimming fishes have lead to the development of three self-propelling robotic models: a pectoral fin robotic device, a robotic fish tail, and a flapping flexible foil robotic model of fish body deformation; I will discuss the design of each robotic model along with recent results and their implications for understanding the biomechanics of underwater propulsion.

About the Speaker

Dr. Lauder is a world leader in the study of the form, function and evolution of the musculoskeletal system of fish. His work has produced some of the major insights into the mechanical function of the locomotor and feeding apparatus of fish. Current projects in his lab pioneer the use of robotics to explore the mechanical design of fins, the mechanisms of hydrodynamic propulsion, and the potential for bio-inspired robotic swimming devices.

From Vibrating Insoles to Synthetic Gene Networks

Jim Collins, PhD
Professor, Department of Biomedical Engineering, Boston University

In this talk, we describe how nonlinear dynamical approaches can be used to study, mimic and improve biological function at multiple scales, ranging from whole-body dynamics to gene networks. We describe, for example, how input noise can be used to enhance human sensory function and motor control. Specifically, we show that touch sensation and balance control in young and older adults, patients with stroke, and patients with diabetic neuropathy can be improved with the application of sub-sensory mechanical noise, e.g., via vibrating insoles. We describe how this work has led to the creation of a new class of medical devices to address complications resulting from diabetic neuropathy, restore brain function following stroke, and improve elderly balance. We also describe how techniques from nonlinear dynamics and molecular biology can be used to model, design and construct engineered gene networks, leading to the development of the field of synthetic biology. We discuss the implications of synthetic gene networks for biotechnology, biomedicine and biocomputing.

About the Speaker

Dr. Collins is a renowned bioengineer and inventor. His use of nonlinear dynamics to model and mimic biological function has led to several medical devices, including noise-based sensory prosthetics that improve locomotor function and balanced in the elderly and patients with compromised neuromotor control. He is a pioneer in systems biology, and currently developing methods and applications for reverse engineering gene regulatory networks. Dr. Collins has received numerous awards and distinctions, including a MacArthur Foundation "Genius Award" and an NIH Director's Pioneer Award. He is also a past recipient of the ASB Young Scientist Post-Doctoral Award.

The Role of Biomechanics in the Health, Degeneration, and Repair of the Synovial Joint

Farshid Guilak, PhD
Laszlo Ormandy Professor of Orthopaedic Surgery, Duke University Medical Center

Osteoarthritis is a painful and debilitating disease of the joints that is characterized by progressive degeneration of the articular cartilage that lines the joint surfaces. The etiology of osteoarthritis is poorly understood, although it is now well accepted that biomechanical factors play an important role in the onset and progression of this disease. The primary goal of our studies has been to determine the mechanisms by which mechanical loading affects the physiology of our joints. Using a hierarchical approach to span different systems ranging from clinical studies and in vivo animal models to studies of tissue, cellular, and subcellular mechanics, we have identified specific mechanical signaling pathways that appear to play a role in cartilage physiology as well as pathology. These pathways may provide novel pharmacologic targets for the modification of inflammation or cartilage degeneration in osteoarthritis. Additionally, our studies have focused on tissue engineering approaches for repairing cartilage damage with osteoarthritis. Using novel textile processes that allow weaving of biomaterial fibers in three dimensions, we have created functionalized bioactive scaffolds that can recreate many of the complex biomechanical properties and anatomic features of articular cartilage. In combination with a multipotent population of stem cells isolated from subcutaneous fat, we have developed a tissue-engineering approach for resurfacing osteoarthritic joint surfaces. Taken together, these studies emphasize the critical role that biomechanics plays in the physiology as well as pathology of the joint, and demonstrate the importance of biomechanical factors in functional tissue engineering of cartilage and other joint tissues.

About the Borelli Award Recipient

Dr. Guilak's research has focused on cellular mechanics and tissue engineering of articular cartilage in the context of osteoarthritis. He is a true pioneer in the investigation of chondrocyte biomechanics and mechanotransduction, having been the first to characterize its mechanical properties in situ and ex situ, in health and disease, using a variety of exquisite testing methods. He has also played a critical leadership role in the development of the field of "Functional Tissue Engineering". His research in this area has focused on the regeneration of articular cartilage using novel 3D biomaterial structures that are explicitly designed to mimic the biomechanical properties of native articular cartilage.

THEORETICAL ANALYSIS OF LIMITATIONS TO MAXIMUM SPRINTING SPEED IMPOSED BY MUSCLE MECHANICAL PROPERTIES

Ross H. Miller, Brian R. Umberger, and Graham E. Caldwell

University of Massachusetts, Amherst, MA, USA
email: rhmiller@kin.umass.edu, web: http://www.umass.edu/biomechanics

INTRODUCTION

Maximum running speed is an important parameter during many athletic competitions. Running speed is determined by stride length and stride frequency. While both increase directly with speed, maximum sprinting speed is reached when stride frequency can no longer be increased [1]. The force-velocity relation of skeletal muscle has thus been implicated as a critical limiting factor in speed achievement [2,3]. Other muscular properties such as force-length and activation dynamics have been shown to influence the control of walking [4] and jumping [5]. At maximal speed, lower extremity muscles undergo substantial length and activation changes; these properties may also influence running speed.

Thus, our purpose was to evaluate the effects of removing various muscle mechanical properties on the achievement of maximum sprinting speed. Since it is impossible to remove muscle mechanical properties *in vivo*, a computer simulation approach was used to systematically test the limiting effects of specific properties on sprint performance.

METHODS

A musculoskeletal model of the human body was developed to simulate running in the sagittal plane (Figure 1). The skeleton was comprised of seven rigid segments (trunk, 2 thighs, 2 legs, 2 feet). Each lower extremity was actuated by nine Hill-based muscle models. The model's state equations were:

$$\ddot{q} = f_1\left(q,\dot{q},A,L_{CC}\right) \quad \text{(Eq. 1)}$$

$$\dot{A} = f_2\left(E(t),A\right) \quad \text{(Eq. 2)}$$

$$\dot{L}_{CC} = f_3\left(A,L_{CC}\right) \quad \text{(Eq. 3)}$$

where q is a vector of generalized coordinates, and A and L_{CC} are vectors of muscle model activations and contractile component lengths. E is a vector of muscle model excitations, and t is time.

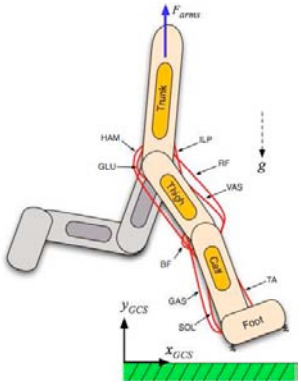

Figure 1. The seven-segment musculoskeletal model with nine muscles actuating each lower extremity; only the right muscle models are shown.

To simulate sprinting, equations 1-3 were solved simultaneously using a numerical ODE solver. Each excitation signal $E(t)$ was parameterized by nine nodal values over the time for one step. The 72 nodal E values were optimized to maximize the average speed of the model. The step duration was also allowed to vary as a control variable. Periodicity in the initial and final kinematic states was enforced with a penalty function, as was the constraint that the net horizontal ground reaction impulse must equal zero. A full stride was generated by assuming bilateral symmetry of the lower limbs. The initial kinematic state was taken from motion capture data of eight human runners sprinting at maximum effort.

To evaluate the effects of muscle mechanical properties, the optimization was repeated four times with different Hill model versions for all muscles. In the first, the force-length property was removed by assuming that L_{CC} was always at optimal length. In the second, the force-velocity property was removed by altering its traditional double-hyperbola to a straight line with a slight slope to avoid numerical indeterminacy. The excitation-activation property was removed in the third by optimizing $A(t)$ instead of $EXC(t)$. In the final model, all muscular properties were removed by optimizing the active joint torques. The outcome variable in all

five optimizations was the average horizontal speed of the model over the simulated step.

RESULTS AND DISCUSSION

In the initial optimization, the model achieved an average speed of 6.30 m s^{-1}, using a stride length of 3.15 m and a stride frequency of 2.00 Hz. These values were all within 8% of those measured from the human subjects.

Table 1 compares the speeds achieved in the optimizations when particular mechanical properties were removed from the muscle model algorithm. Removal of the force-length property increased the sprinting speed by only 2% above the speed of the initial optimization with all muscular properties. However, removing the force-velocity and the excitation-activation relationships increased speed by 16% and 8%, respectively. Moreover, the effect of muscular property removal was additive: when the optimization was performed with all muscular properties removed, the speed increased by 21%. In each simulation, at least 80% of the increase in speed was due to an increase in stride frequency (see Table 1). Stride length remained relatively constant during all conditions.

Of the tested muscular properties, removing force-velocity had the largest effect on speed, supporting previous conjectures that the force-velocity property plays a major role in the limitation of human running speed [2,3]. However, even small speed differences can have a large effect on the outcome of a race such as the 100-m dash. Therefore, the excitation-activation (8% speed changes) and force-length (2%) relations also could affect maximal running speed. Here we removed the properties to observe the largest possible effects. The exact influence of variations between runners is unknown, but our simulations indicate that differences in force-velocity and excitation-activation will have the largest effect. Physiologically, it is notable that both of these properties are strongly influenced by muscle fiber type ratios, which play a determinative role in athletic potential for power and endurance.

The removal of muscular properties also had an effect on the ability of the model to perform a periodic step. The smallest differences between the initial and final kinematic states were present when all muscular properties were included, while the largest differences were present with all muscular properties removed (see Table 1). Gerritsen *et al*. [4] found that muscular properties were important for stabilizing the body in response to perturbations during walking. It may be that muscle mechanical properties are needed for accurate spatio-temporal control of the limbs in preparation for stride events such as foot contact. However, the differences in angular positions and velocities between the optimizations were relatively small on an absolute scale (less than 1 deg and 10 deg s^{-1}).

CONCLUSIONS

Simulations of human sprinting support previous theories that the force-velocity relationship plays a critical role in the determination of maximum speed by limiting the maximum stride frequency. However, the excitation-activation relationship, and to a lesser extent the force-length relationship, may also play important roles, and the speed-limiting effects of these muscular relationships appear to be additive. Future work will address the extent that individual variation in muscular properties between runners impacts maximal speed, and the importance of the mechanical properties of individual muscles in limiting maximum speed achievement.

Table 1. Simulated sprinting performances when various muscle mechanical properties were removed. "Speed" is the horizontal speed during one step. SF and SL are the stride frequency and stride length. ε_θ and ε_ω are the average differences in the initial and final angular positions and velocities of segments.

Properties removed	Speed (m s^{-1})	SF (Hz)	SL (m)	ε_θ (°)	ε_ω (°/ s)
Full model	6.30	2.00	3.15	4.5	50.1
Force-Len	6.41	2.03	3.16	4.6	59.6
Force-Vel	7.30	2.29	3.19	4.6	60.5
Exc-Act	6.82	2.13	3.20	4.7	55.5
All	7.60	2.35	3.23	4.8	62.2

REFERENCES

1. Luhtanen K and Komi PV. *Biomechanics VI-B*, E Asmussen *et al*., 1978.
2. Chapman AE and Caldwell GE. *J Biomech* **16**, 79-83, 1983.
3. Weyand PG *et al*. *J Appl Physiol* **89**, 1991-1999, 2000.
4. Gerritsen KGM *et al*. *Motor Control* **2**, 206-220, 1998.
5. Van Soest AJ and Bobbert MF. *Biol Cybern* **69**, 195-204, 1993.

A PHENOMENOLOGICAL MUSCLE MODEL TO ASSESS HISTORY DEPENDENT EFFECTS IN HUMAN MOVEMENT

[1]Craig P. McGowan, [1]Richard R. Neptune and [2]Walter Herzog
[1]Department of Mechanical Engineering, University of Texas at Austin, Austin, TX, USA
[2]Faculty of Kinesiology, University of Calgary, Calgary, AB, Canada
email: cpmcgowan@mail.utexas.edu, web: www.me.utexas.edu/~neptune/

INTRODUCTION

In a recent study, we developed and validated a modified Hill-type muscle model that included shortening induced force depression based on the relationship with mechanical work [1]. The model was able to accurately reproduce *in-situ* experimental data when incorporated into a forward dynamics computer simulation and was used to examine the influence of force depression on dynamic cyclic movements. The results showed that in maximal power pedaling, force depression has the potential to substantially reduce the amount of muscle power produced. However, during pedaling, muscle contractions are predominately concentric. In contrast, in many activities muscles undergo repeated stretch-shorten cycles. It is not clear to what extent stretch induced force enhancement effects mechanical output, nor is it known to what degree force depression and force enhancement may offset one another during dynamic cyclic movements.

Therefore, the aims of this study were to 1) develop and validate a muscle model that includes stretch induced force enhancement, and 2) combine this model with our previous model of force depression to validate the cumulative effects during controlled stretch-shorten and shorten-stretch cycles. The model's ability to accurately reproduce force enhancement on the descending limb of the force-length curve and its ability to characterize the differences in cumulative effects between stretch-shorten and shorten-stretch cycles were evaluated by comparing the outputs from simulated *in-situ* experiments with actual experimental data from isolated cat soleus muscles [2, 3].

METHODS

A previously described muscle ergometer model was used to simulate the in-vivo experiments [1]. Briefly, the model consisted of two blocks mounted horizontally on a frictionless surface with a muscle governed by Hill-type intrinsic properties mounted between them. One block underwent prescribed linear motion in which position and velocity was controlled. Values for the optimal muscle fiber length (36 mm), tendon slack length (74 mm, including aponeurosis), maximum shorting velocity (3.3 lengths/sec) and maximum isometric force (28.6 N) were set to the approximate average values for a cat soleus muscle.

Simulations were developed to match a subset of the protocol from the experimental study [2]. The experiment was designed to compare the isometric force following constant velocity stretches of fully active muscles with the isometric force of a muscle that was not stretched. Individual stretches were made for three lengths (3mm, 6mm and 9mm) at three different velocities (3mm/s, 9mm/s and 27mm/s) for a total of nine stretches. To account for force-length effects, isometric contractions and all stretches ended at the same length (9 mm greater than optimal). A second set of simulations was developed to examine the model's ability to reproduce experimental data in stretch-shorten and shorten-stretch cycles. Stretch-shorten cycles consisted of a 4 mm contraction preceded by active stretches of 0 mm, 2 mm and 4 mm. Similarly, shorten-stretch cycles consisted of a 4 mm stretch preceded by contractions of 0 mm, 2 mm and 4 mm. All length changes occurred at 4 mm/s and ended at the muscle's optimal length. Results from these simulations were compared to data in the literature [e.g., 3].

Based on experimental data from cat soleus muscles [2], when the muscle was actively stretched on the descending limb of the force-length curve, the relationship between force enhancement (FE) and

muscle length change (ΔL) was best described by a second order polynomial equation ($R^2 > 0.99$). On the ascending limb of the force velocity curve, FE was considered to be independent of length change based on data from the literature [4]. Shortening induced force depression was included based on our previously described model [1]. Force enhancement was abolished as soon as the muscle began shortening such that the effects were not cumulative in stretch-shorten cycles. Whereas, force depression was maintained until the muscle was deactivated and the effects were cumulative in shorten-stretch cycles.

RESULTS AND DISCUSSION

On the descending limb of the force length curve, the simulations of single muscle active stretches accurately reproduced the experimental data for all conditions (e.g., 9 mm/s; Fig. 1). The average root mean square error (RMSE) between the simulations and experimental data while the muscle was active was 0.59 N (range: 0.45 – 0.85 N) for 3 mm/s stretches, 0.60 N (range: 0.36 – 1.05 N) for 9 mm/s stretches and 0.98 N (range: 0.68 – 1.42 N) for 27 mm/s stretches. Across all of the simulations on the descending limb, the average RMSE was 0.72 N.

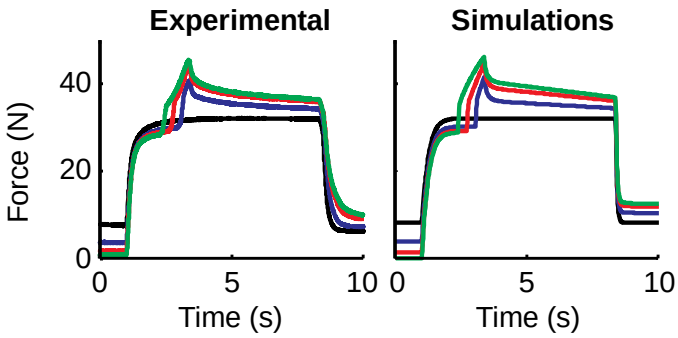

Figure 1. The simulations of *in-situ* experiments were accurately able to reproduce the experimental data. Constant velocity stretches (9 mm/s) are shown for 3, 6, and 9mm.

Simulations of stretch-shorten and shorten-stretch cycles were consistent with experimental data from the literature [e.g., 3]. The results also show the model was able to capture the cumulative effects of force depression and enhancement when the muscle underwent shorten-stretch cycles and the non-cumulative effects during stretch-shorten cycles (Fig. 2).

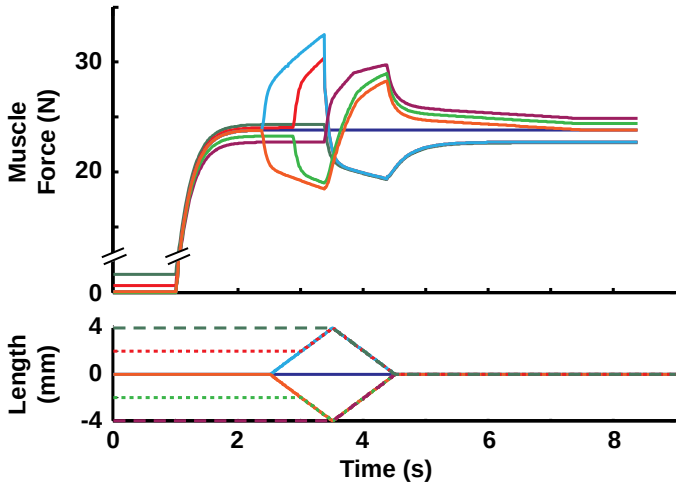

Figure 2. The simulations accurately characterized the cumulative effects of force enhancement and depression during stretch-shorten and shorten-stretch cycles.

Despite the general acknowledgement that history dependent effects are common in vertebrate skeletal muscles, their inclusion in models of muscular force is rare. However, in the *in-situ* simulations in this study, the modified Hill-type model matched the experimental data over 6 times better than the classic Hill-type model (RMSE: 0.72 N vs. 4.41 N) used in the majority of studies.

CONCLUSIONS

The results of this study show that a relatively simple phenomenological muscle model can accurately reproduce experimentally measured stretch induced force enhancement. When the model was combined with our previously described shortening induced force depression model, the combined model was able to reproduce the non-linear cumulative effects of force enhancement and force depression during stretch-shorten and shorten-stretch cycles. In future studies, the model will be incorporated into more complex musculoskeletal models to examine the influence history dependent effects have on human movement such as running.

REFERENCES

1. McGowan CP. et al. *J Biomech.* **43**, 449-454, 2010.
2. Herzog W and Leonard T. *J Exp Biol* **205**, 1275-1283, 2003.
3. Herzog W and Leonard T. *J Biomech.* **33**, 531-542, 2000.
4. Hisey et al, *J Biomech.* **42**, 1488-1492, 2010.

SPORT BIOMECHANICS: EQUIPMENT AND PERFORMANCE

Darren J. Stefanyshyn

Human Performance Laboratory, Faculty of Kinesiology, University of Calgary, Calgary, AB, Canada
email: darren@kin.ucalgary.ca, web: http://www.kin.ucalgary.ca/hpl

INTRODUCTION

Energy is the ability to do work. The more energy an athlete or piece of equipment has the more work an athlete can do. Increased work results in an increase in performance, for example a higher jump or a longer throw. From a performance perspective, it is very important to optimize the energy transfer between athlete and equipment. This is generally achieved by:

- maximizing the (conservative) energy which is returned,
- minimizing the (non-conservative) energy which is lost and/or
- optimizing the musculoskeletal system.

ENERGY RETURN IN SPORTS EQUIPMENT

There are many examples of energy storage and return in sports equipment. Vaulting poles, diving boards, trampolines, ice hockey sticks, tennis racquets and other pieces of equipment are successful examples of energy storage and return. In all of these cases, performance in the sport is highly dependent on the energy stored in the equipment. The extra energy returned by the diving board increases a diver's height and flight time allowing the diver to perform more complex dives. The extra energy stored in a hockey stick allows the athlete to shoot the puck faster. In these sports, the objective is to maximize the energy returned, to ensure it occurs in the right location, at the right time and with the right frequency.

ENERGY LOSS IN SPORTS EQUIPMENT

The concept of minimizing the loss of energy attempts to minimize the use of energy, which is not related to performance but would be available to enhance performance if it would not have been spent unnecessarily. Many athletic activities like swimming and skating can be characterized as physical endeavors to overcome external resistance forces. Energy is used to overcome these resistive forces. If the magnitudes of these external resistive forces can be reduced, the amount of energy that is lost combating these forces can be decreased. The net result is that an athlete can perform a given task while expending less energy or use the saved energy to enhance performance. Some examples of such energy loss can include loss due to friction, drag and energy dissipation in materials.

OPTIMIZING THE MUSCULOSKELETAL SYSTEM WITH SPORTS EQUIPMENT

Optimizing the musculoskeletal system utilizes the inherent properties of muscle to maximize performance. By placing muscles into favorable positions where force or power output are maximized, performance can be increased. Subtle changes in equipment can lead to large differences in muscle output and the resulting performance. The position of an athlete on a bicycle, for example, can be adjusted in order to optimize the range in which muscles work to maximize power output

SUMMARY

For the most part, these are rather simple mechanical concepts. However, the complex interaction between the athlete and the piece of equipment requires a detailed understanding of sport biomechanics. Additionally, how the uniqueness of each individual athlete relates to specific equipment properties must be understood.

Over the past 30 years, sport biomechanists and sport equipment manufacturers have investigated ways of improving athletic equipment to enhance performance. The result is equipment that is stronger, lighter, more durable and more pleasant to use. Consequently, sport performances are faster, higher, longer and more accurate than ever before.

BIOMECHANICS OF GOAT AND DOG LOCOMOTION: BIOINSPIRATION FOR BIGDOG

[1]Andrew A. Biewener, [1]Ivo G. Ros, [1]Edwin H. Yoo, and [2]David V. Lee

[1]Harvard University, CFS, Bedford, MA, USA
University of Nevada, Las Vegas, NV, USA
email: abiewener@oeb.harvard.edu, web: http://www.oeb.harvard.edu/affiliates/cfs/

INTRODUCTION

To ensure stability, animals must control the pitch, roll and yaw moments exerted about their body center of mass (CoM). Terrestrial animals exert time-varying forces on the ground that result in a net resultant ground reaction force (GRF) that acts from a center of pressure (CoP) under the animal. Moments about the animal's CoM depend on the location of the CoP and orientation of the GRF relative to the animal's CoM. With the goal of informing the design of BigDog^{TM}, a large quadrupedal robot constructed by Boston Dynamics to move quickly over uneven and variable grade terrain, we sought to examine how the CoP and net GRF of dogs and goats track their whole-body CoM during trotting and galloping gaits. These data were used to assess the magnitude of CoM pitch, roll and yaw through time. We hypothesized that pitch moments would be greatest during galloping due to asymmetrical fore versus hind limb ground contact and that roll moments would be greatest during trotting due to misalignment of CoM position relative to net GRF and CoP produced by the in-phase contralateral fore-hind support of this gait. We also examined how goats produce forces with their forelimbs versus their hindlimbs when climbing a 65 degree instrumented wall.

METHODS

Four dogs (BM=41 kg) and four goats (BM=32 kg) were trotted and galloped over a series of force platforms (2 AMTI and 2 Kistler) that enabled ground reaction forces to be collected from all four limbs over full strides for both gaits. Trunk kinematics were recorded from infrared markers (Qualysis, Inc. 240 Hz) along with digital video (30 Hz) gathered in lateral view. CoM position was determined from integration of $GRF_{x,y,z}$ and initial conditions for velocity and body position. Speed was determined from motion capture of the animal's horizontal movement. Measurements of CoP and net GRF exerted through time were then used to calculate the temporal patterns of pitch, roll, and yaw moments about the animal's CoM. Limb GRFs were also obtained for four goats during running jumps and climbing against a 65^{o} wall (2.5m height) instrumented with two AMTI force plates mounted on cinder blocks. Infrared motion capture (Qualysis, 240 Hz) was used to carry out joint kinematics and inverse dynamics of joint moments.

RESULTS AND DISCUSSION

Consistent with our hypothesis, pitch moments were largest during level galloping compared with trotting for both dogs and goats (Fig. 1). Though smaller in magnitude, pitch moments about the CoM were larger than either roll or yaw moments at

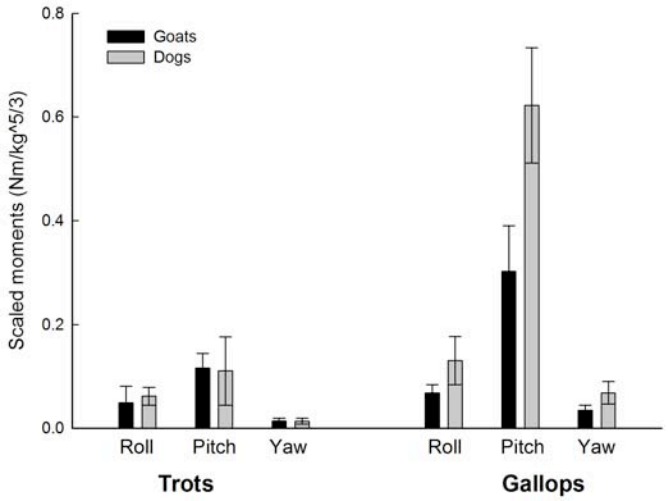

Fig. 1: Peak CoM moments (mean±SD) developed during trotting versus galloping in goats and dogs. Moments are normalized to $BM^{5/3}$ due to size differences between the two species.

a trot as well. Given the animals' straight movement, it is not surprising that yaw moments

were small for both gaits. The peak magnitudes of pitch and roll moments were minimized by the animals maintaining a remarkably close alignment of the net whole-body GRF to the position of their CoM, despite the time-varying location of individual limb contact and GRFs. Pitch moments in dogs were significantly greater than in goats at a gallop. This likely reflects the greater vertebral body-axis flexibility of dogs compared with goats, as well as the fact that the dogs galloped at a faster speed than goats (6.6 vs 4.3 m/s).

During wall ascent, the fore and hind limbs both produced positive work to elevate the animal's CoM to gain PE during the initial running jump. However, during the subsequent climbing stride on the wall, the forelimbs produced little force to avoid unwanted pitch away from the wall. Instead, the hind limbs produced all of the propulsive force and work for continued ascent. The forelimbs instead provided a 'follow-the-leader' target for the hind limbs' position of ground contact.

The close alignment of net GRF and tracking of CoP with respect to CoM position that we observed during steady level terrestrial gaits for dogs and goats is not surprising given the importance of avoiding large CoM pitch and roll moments that would otherwise cost additional metabolic and mechanical energy to control and likely lead to decreased locomotor stability. This is exemplified by the much-improved performance of BigDog compared with a previously developed quadrupedal robot that produced forces using in-line limb actuation and prismatic springs [1], inspired by the spring-loaded inverted pendulum mechanics that has been successfully used to model a variety of legged running animals [2, 3], but which suffered large CoM pitching moments.

By adopting a more compliant limb design [4], together with mass-spring mechanical energy savings [2,3], animals are able to reduce their energy expenditure and smooth the motion of their trunk relative to their limbs by minimizing CoM moments during running gaits. This reduces the mechanical and metabolic energy requirements for locomotion, as well as improving the stability of the animal's movement. These features are incorporated in the design of BigDog, which has significantly improved its performance compared with an earlier first-generation quadrupedal robot [1].

CONCLUSIONS

Despite the time-varying pattern of fore and hind limb contact and individual limb ground reaction forces, the phasing of limb support in quadrupeds during trotting and galloping gaits results in remarkably close tracking of the animal's net center of pressure and whole-body ground reaction force relative to its body CoM, which keeps CoM moments and trunk inertial rotations low. These features of quadrupedal limb design and time-varying ground force distribution have been successfully implemented in BigDog, enabling it to achieve exceptional speed and stability for its size when moving over rugged terrain. The varying use of fore versus hind limbs during steep ascent is also critical for maintaining CoM pitch control, while at the same time achieving the propulsive work needed for ascent.

REFERENCES

1. Raibert MH. J Biomech **23**, 79-98, 1990.
2. McMahon, TA and Cheng, GC. *J Biomech* **23**, 65-78, 1990.
3. Farley, CT, Glasheen, J, McMahon, TA. *J Exp Biol* **185**, 71-86, 1990.
4. Lee, DV, McGuigan, MP, Biewener, AA. *J Appl Physiol* **104**, 130-141, 2008.

ACKNOWLEDGEMENTS

Supported by DARPA BioDynotics (BAA #01-42).

Bio-inspired robot design for legged locomotion

Sangbae Kim,
Massachusetts Institute of Technology
Cambridge, Massachusetts 02139
email: sangbae@mit.edu, web: http://web.mit.edu/sangbae/www/research.html

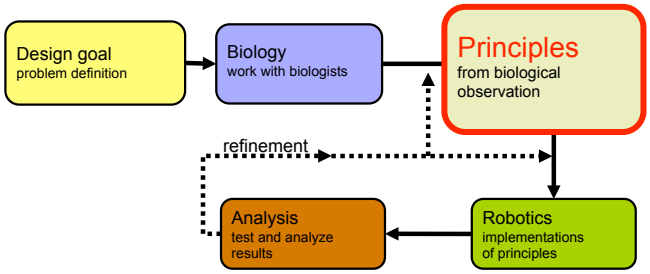

Fig. 1: A design process for bio-inspired robots

I. Learning from biology

Mobile robot designers are increasingly searching for inspirations and design cues from biological models. Although animals are great model for mobile robots, the process of implementation is often ambiguous. The direct implementation of biological features and morphology often becomes ineffective and misleads engineers due to various reasons. Firstly, engineers investigate animals to achieve a few particular functions whereas features of animals may serve for multiple functions or often remains unknown. Biological system are believed to evolves for many functions. Animals need to adapt to various natural environments, reproduce themselves, eat, digest, and grow. When it comes to robotics platforms, the requirements are much simpler and based on the applications. Secondly, difference between engineering building blocks and biological mechanisms prevent engineers from direct replication. Biological systems grows whereas mechanical systems are manufactured. Control system, actuators, structures, energy sources and mechanical properties in biological systems differ from artificial counterparts in a great extent.

II. Design process

For effective implementation of ideas, a design process is introduced. The design process begins with seeking a function from biological systems. Often locomotive functions of animals become target function that engineers seek to achieve. Next step undergoes extensive observation of related behaviors in collaboration with biologists. Conversations with biologists are invaluable for identifying a range of animal examples and for pointers to the literature concerning their morphology and operation. Although the animal examples are generally impressive, it is important to remember that nature does not produce optimal solutions in any formal sense. Rather, nature works on the principle of what is "good enough"

Fig. 2: Stickybot, a bio-inspired robot capable of climbing smooth surfaces. Inset: detail of toes curling to facilitate detachment

to afford a competitive advantage. Through comparative analysis and careful abstraction, hypothesizing principles follows. Sometimes, comparing homologous features among several species helps to remove bias from the interpretation. Through cautious observation and reasoning, we can extract hypotheses about the principles that govern the animals' behavior and performance. The principles includes design principles behind detail features, simplified model of certain behaviors, and physical principles of a phenomenon. Hypothesized principles can be verified by biologists and engineering tools such as simulations and experiments. The next step is, selectively, to implement the principles in a robot. Since mechanical components differ from biological organisms, the principles need to be adapted in an artificial design space. The underlying functional principles need to be extracted from biology, digested by the designer and reincarnated. Modification of the principles through subsequent experimentations and analysis will ultimately provide refinement of the principles, and will accordingly improve the final design.

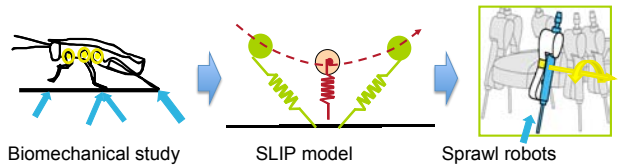

Fig. 3: Bio-inspired robot design based on principles from biological study.

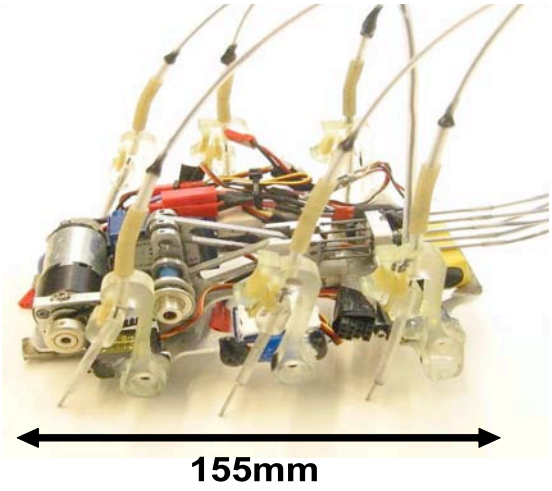

Fig. 4: iSprawl is a small (0.3 Kg) autonomous, bio-inspired hexapod that runs at 15 body-lengths/second(2.3 m/s).

III. Bio-inspired robots

Introduction of three successful bio-inspired robots exemplify the process: a) iSprawl is a cockroach-inspired hexapod with compliant, under-actuated legs and runs at 15 body-lengths per second, b)Spinybot is a hexapod that uses its toes with microspines to climb rough surfaces, including stucco, concrete and brick walls. Stickybot is a gecko-inspired quadruped that climbs smooth vertical surfaces using the worlds first directional adhesive, directional polymeric stalks (DPS) inspired by the directional setae and lamellae of the gecko. The design principles of Stickybot include hierarchical compliance, directional adhesion, and distributed force control.

IV. Future work

The future research direction of the biomimetic robotics lab includes obtaining principles behind highly dynamic behaviors of the animals and implementing on robotic platforms. Extensive study on biological runners such as dogs and cheetahs will inspire the morphologic design of the galloping robot capable of the fast traverse on rough and unstructured terrains. Figure 5 shows a potential concept platform that enables research on hyper dynamic robotics. This new field of study will focus on qudrupeds' behavior such as jumping, high speed running with gallop gait, and energy efficient running with trotting gait. Agile mobility of the robotic platform requires high acceleration capability with dynamic stability, jumping over large obstacles, and landing with the flexible

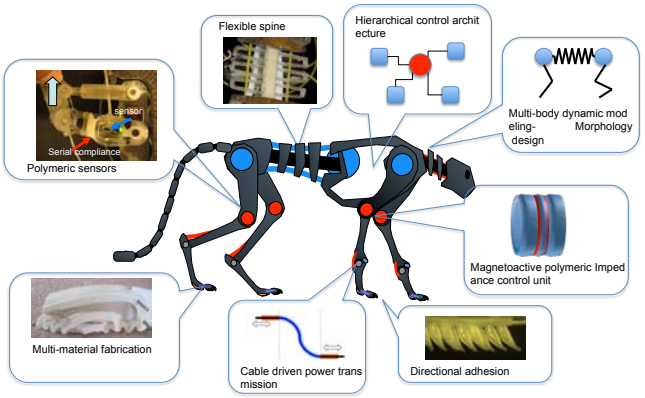

Fig. 5: A schematics of new quadruped running robotic platforms. This platform will be capable of basic locomotive functions for hyper dynamic robotic research.

body articulation. These highly dynamic behaviors involve multi-body dynamics of the dynamic control with tunable mechanical impedance. Based on the mechanical properties of actuators, the actuator allocation and actuation scheme can be optimized in order to achieve maximum performance. The first key thrusts include the development of high power density actuators with impedance control in pursuit of optimized force coordination of multi-degree of freedom legs and effective energy storage. Second research thrust seek to achieve a new control architecture that allows discrete impulse control of each stride to transition from one state to another and maintain a certain steady state. The final research thrust focuses on development of manufacturing techniques that allows light-weight resilient structure capable of dynamic locomotion.

APPLICATIONS OF BIPLANE VIDEORADIOGRAPHY AND X-RAY RECONSTRUCTION OF MOVING MORPHOLOGY (XROMM) TO COMPARATIVE BIOMECHANICS RESEARCH

[1]Elizabeth L. Brainerd, [2]David B. Baier and [1]Stephen M. Gatesy

[1]Brown University, Providence, RI, USA
[1]Providence College, Providence, RI, USA
email: brainerd@brown.edu, web: http://www.xromm.org

INTRODUCTION

Skeletal motion in diverse vertebrate animals from fish to horses can be imaged with high-speed, biplane videoradiography. Skeletal landmark points or implanted radio-opaque beads can be tracked in 3D, but videoradiography becomes more powerful when combined with detailed data on bone morphology from CT or laser scans. X-ray Reconstruction of Moving Morphology (XROMM) is a set of marker-based and markerless techniques for 3D animation of polygonal mesh bone models to match skeletal motion from biplane X-rays with high precision and accuracy [1-2].

XROMM methods for comparative biomechanics research are similar to techniques in human biomechanics, such as marker-based Dynamic RSA [3] and markerless model-based motion analysis [4-5]. However, work on non-human animals poses distinct challenges and opportunities for these 3D X-ray methods.

Marker-based XROMM [1] is particularly well suited to animal research because surgical implantation of radio-opaque bone markers is often possible. Surgical implantation of radio-opaque beads into muscles and tendons is also practical, making it possible to capture 6 degree-of-freedom skeletal kinematics, tendon strain, and muscle fascicle strain simultaneously.

Implantation of radio-opaque beads into small and fragile bones is not always possible. Scientific Rotoscoping [2] is a form of manual, markerless XROMM in which individual bone models or articulated skeletal models are manually aligned to sets of 2D X-ray and standard external video images. Combining marker-based and markerless XROMM can be a powerful approach for comparative biomechanics research.

METHODS

We have developed two sets of biplane X-ray hardware at Brown University. One system is based on refurbished, relatively inexpensive mobile C-arm fluoroscopes (Fig. 1). Mobile C-arms are suitable for studies of locomotion in animals up to about the size of a domestic cat, and for feeding studies in larger animals. There are now at least four biplane C-arm systems dedicated to comparative biomechanics research in the USA, and the relatively low cost makes the technology potentially available to many researchers.

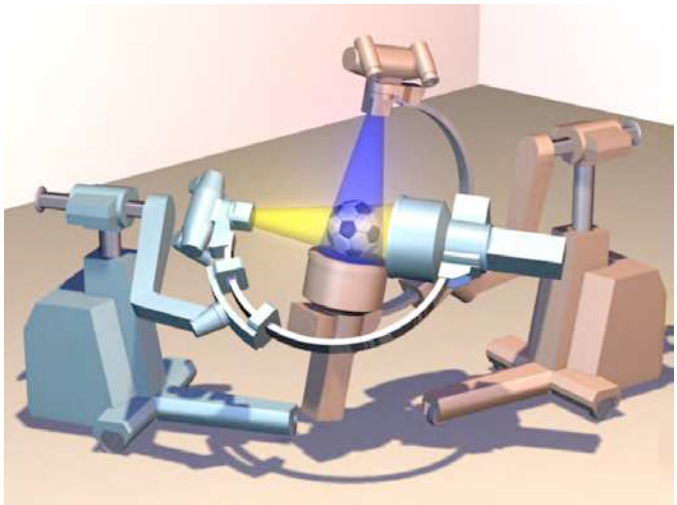

Figure 1: Mobile C-arm fluoroscopes retrofitted with 30-cm image intensifiers and high-speed video cameras. Systems refurbished and retrofitted by Radiological Imaging Services, Hamburg PA, USA (www.risinc1.com).

We have also developed a large scale biplane system that is suitable for larger animals (including humans) and can generate higher X-ray energies.

The X-ray tubes are mounted on tube cranes hanging from the ceiling (Fig. 2). The 40-cm IIs are mounted on mobile bases made from C-arm stands. The source-to-image distance for each system can be as large as 2 m, and independent movement of the four components gives the system outstanding flexibility in physical configuration.

Figure 2: A large-scale biplane videoradiography system with flexible imaging configuration for animals up to the size of horses. Mobile II supports built by Radiological Imaging Services, Hamburg PA, USA (www.risinc1.com); X-ray system designed and integrated by Imaging Systems and Service, Painesville OH (issi-na.com).

Image intensifiers (IIs) introduce severe image distortion. We image a standardized sheet of perforated metal and then use the idealized geometry of the perforations to correct the fluoroscopic images. The perforated metal is a steel sheet, 1.20 mm thick with 3.18 mm diameter holes spaced 4.76 mm apart in a staggered pattern (part number 9255T641, McMaster-Carr, Robinson NJ, USA). We use a local weighted mean (LWM) distortion correction algorithm, implemented in MATLAB (code available through xromm.org). For 3D calibration, we use an acrylic calibration object with 64 steel spheres. Direct linear transformation (DLT) and marker tracking are implemented in MATLAB [6]. Precision and accuracy for marker-based tacking are ±0.1 mm or better for both biplane systems [1,7].

Computational methods for marker-based XROMM [1] and markerless Scientific Rotoscoping [2] have been published previously. We use Autodesk Maya software as the primary tool for skeletal animation and for exploring and measuring data from XROMM animations.

RESULTS AND DISCUSSION

Two mobile C-arm fluoroscopes, retrofitted with high-speed video cameras, form an effective system for measuring 3D skeletal kinematics of small to medium-sized animals. For example, we have used mobile C-arms to record jaw movements during feeding in minipigs, leg kinematics in jumping frogs, wing motion during flap-running in birds, and oral jaw kinematics during feeding in carp.

The large-scale system (Fig. 2) produces higher quality images due to greater X-ray intensities (lower II noise). For studies of fish and other aquatic animals, C-arms can be used for marker-based studies. However, when shooting through water, higher energies are necessary to produce images of sufficient quality for Scientific Rotoscoping (markerless XROMM).

In the future, marker-based animation for large, proximal bones combined with markerless Scientific Rotoscoping for fragile distal elements may become a powerful approach for XROMM animation of complex, articulated skeletal models of non-human animals. The biplane radiography, distortion correction, calibration, and MATLAB and Maya methods that we have developed lend themselves well to this hybrid approach.

REFERENCES

1. Brainerd EL, et al. *J Exp Zool* **313A**, 2010.
2. Gatesy SM, et al. *J Exp Zool* **313A**, 2010.
3. Tashman S, et al. *Clin Ortho Rel Res* **454**, 66-73, 2007.
4. Banks SA, Hodge WA, *IEEE Trans Biomed Eng* **43**, 638-648, 1996.
5. Bey MJ, et al. *J Biomech Eng* **128**, 604-609, 2006.
6. Hedrick, TL, *Bioinsp and Biomim*, **3**, 2008.
7. Miranda, DL, et al. *Transactions of ORS'10*, New Orleans, LA, USA, 2010.

ACKNOWLEDGEMENTS

Sponsors: W.M. Keck Foundation, Bushnell Faculty Research Fund, RIH Orthopaedic Foundation, Autodesk, and U.S. National Science Foundation, grant numbers 0552051, 0532159 and 0840950.

BIPLANE X-RAY ANALYSIS OF IN-VIVO SHOULDER AND TENDON FUNCTION

[1]M. Bey, [1]K. Ciarelli, [1]P. Kolowich, [1]T. Lock, [1]V. Moutzouros, [2]A. Baker, [2]J. Iannotti, [2]K. Derwin

[1]Henry Ford Hospital, Bone and Joint Center, Detroit, MI USA
[2]Cleveland Clinic, Department of Biomedical Engineering, Cleveland, OH USA
email: bey@bjc.hfh.edu

INTRODUCTION

Rotator cuff tears are common and have a major impact on function, comfort, and medical care costs. Surgical repair of a torn rotator cuff relies implicitly on the belief that restoring normal glenohumeral joint (GHJ) mechanics is necessary to obtain a satisfactory outcome, but the extent to which surgery restores normal GHJ mechanics is not known. Furthermore, surgical outcomes are typically assessed with measures of muscle strength, range of motion, and pain, but these do not directly assess tendon function. To address this complex clinical problem, we are pursuing complementary studies aimed at understanding: 1) glenohumeral joint motion after rotator cuff repair in human patients, and 2) in-vivo tendon function in a canine model of tendon injury and repair.

METHODS

Human Study: Following IRB approval, 32 rotator cuff repair patients (age: 61.9±11.4) and 32 healthy, asymptomatic control subjects (age: 29.3±5.8) enrolled in this study. Each patient had arthroscopic surgical repair of a rotator cuff tear and an asymptomatic contralateral shoulder. All subjects were positioned with their shoulder centered within a biplane x-ray system [1]. Biplane x-ray images were acquired for each shoulder during abduction from full adduction to 120°. Testing was conducted at 3, 12, and 24 months post-surgery for the patients, and at one time point for the control subjects. Bilateral CT scans of the humerus and scapula were acquired for each subject.

The 3D positions of the humerus and scapula were tracked from the biplane x-ray images using an accurate (±0.4 mm, ±0.5°) model-based tracking technique [2]. GHJ contact patterns were calculated by combining joint motion measured from the biplane x-ray images with the patient-specific bone models [3]. The contact center was determined by calculating the centroid of the distance between humerus and glenoid surfaces for each frame. The contact center was calculated over the entire trial and normalized to the anterior/posterior (A/P) and superior-inferior (S/I) glenoid dimensions.

Canine Study: Following IACUC approval, the superior two-thirds of the infraspinatus (INF) tendon was detached from the humerus and adjacent tendon and repaired in 2 experimental dogs. Tantalum beads were implanted in the humeral head at the repair site and on the surface of the INF tendon. Beads were implanted in the same locations of a control dog, but no tendon injury was created. Standard x-rays obtained at surgery and 2 weeks post-surgery revealed that one experimental dog had an intact repair and one dog had a failed tendon repair. Thus, the dogs used in this feasibility study represent an intact repair, a failed repair, and a control dog without injury or repair. Tendon function during trotting was assessed by measuring the 3D position of the implanted beads from biplane x-ray images. Testing was conducted at 2-to-4 week intervals starting at 2 weeks post-surgery.

To assess in-vivo tendon function, we calculated repair tissue deformation as the 3D distance between the tendon and humerus beads. From these data we then determined both the range and the baseline position (i.e., mean) of tissue deformation. A decrease in the range suggests that repair compliance is decreasing over time (i.e., the repair is getting stiffer). A decrease in the baseline (or mean) of tissue deformation suggests that repair contracture may be occurring over time. In addition to the range and mean, we normalized the range by the mean to obtain a deformation parameter that is independent of the initial distance between the tantalum beads (which can not be precisely controlled). This normalized range can be used to compare between individual dogs at any time point.

RESULTS AND DISCUSSION

Human Study: The S/I contact center was significantly different between repaired and contralateral shoulders ($p<0.001$, Fig. 1), and the standard deviation of the contact center was smaller in the repaired shoulder than in the contralateral shoulder ($p=0.02$). No significant differences were detected between shoulders in terms A/P contact center ($p=0.08$), A/P contact center range ($p=0.98$), S/I contact center range ($p=0.56$), or A/P contact center standard deviation ($p=0.81$).

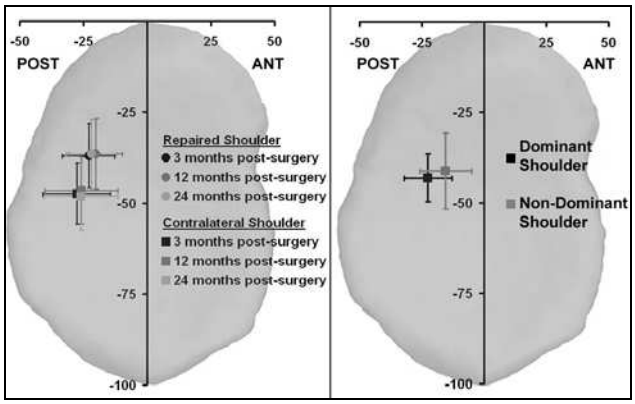

Fig. 1: Average (±sd) joint contact center during abduction in rotator cuff repair patients (left) and control subjects (right).

The data indicated that the humerus in the repaired shoulder was positioned more superiorly on the glenoid than the contralateral shoulder. Although it is unclear if this represents an etiologic factor contributing to the injury or a result of the surgical repair, this finding suggests that restoring normal GHJ mechanics may not be necessary to achieve a satisfactory clinical outcome. The data failed to demonstrate significant differences over time in the joint contact patterns (Fig. 1), but the variability between patients was high. This high variability supports the use of an alternative analyses, and therefore future efforts will investigate the relationship between dynamic joint stability and shoulder strength in both subject populations.

Canine Study: The mean repair tissue deformation decreased over time in the intact repair ($p=0.003$, Fig. 2), suggesting that the tendon repair contracted approximately 19% over 28 weeks. In contrast, changes in mean repair tissue deformation over time were not detected for the failed repair ($p=0.96$, Fig. 2) or control dog ($p=0.06$, Fig. 2).

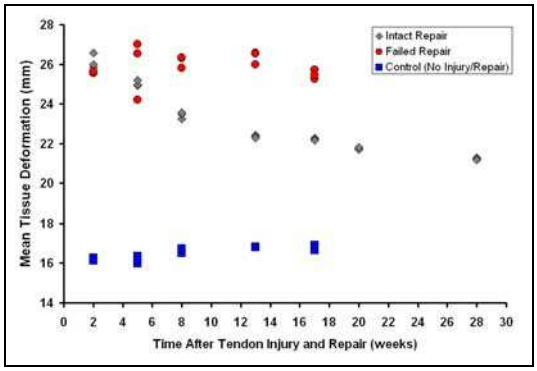

Fig. 2: Mean tissue deformation vs. time for an intact repair (♦), failed repair (●), and control dog (■). For each dog, there are 3 trials per time point.

The range of repair tissue deformation decreased significantly with time in the intact repair ($p=0.001$), suggesting that the healing tendon repair became 70% stiffer over 28 weeks. The range of repair tissue deformation also decreased significantly over time in the failed repair ($p=0.05$), suggesting a stiffening or maturation of scar tissue. In the control dog, the range of repair tissue deformation did not depend on time ($p=0.49$). The normalized range of repair tissue deformation significantly decreased over time in the intact ($p=0.001$, Fig. 3) and failed ($p=0.04$, Fig. 3) tendon repairs, reaching normal control levels only in the intact tendon repair by 17 weeks of healing.

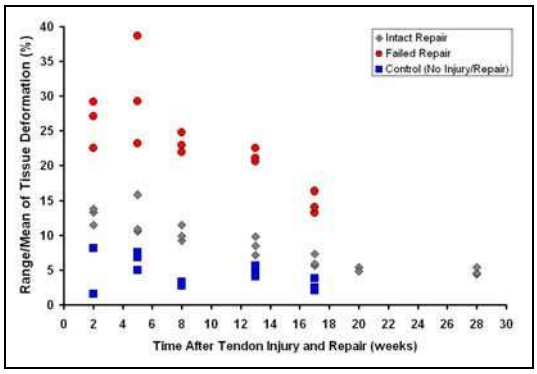

Fig. 3: Normalized range of repair tissue deformation vs. time for intact repair (♦), failed repair (●), and control dog (■). For each dog, there are 3 trials per time point.

REFERENCES

1. Bey et al. J Biomech 41(3), 2007.
2. Bey et al. J Biomech Eng 128(4), 2006.
3. Bey et al. Trans Orthop Res Soc 33:247, 2008.

ACKNOWLEDGEMENTS

These projects were supported by grant AR051912 from NIH/NIAMS, Henry Ford Hospital, and the Cleveland Clinic.

USING BIPLANE FLUOROSCOPY TO QUANTIFY FOOT BONE MOTION

[1,2,3]William R. Ledoux, [1]Richard Tsai, [1]Michael Fassbind, [1,3]Bruce J. Sangeorzan, and [4]David R. Haynor

[1]VA RR&D Center of Excellence for Limb Loss Prevention and Prosthetic Engineering, Seattle, WA
Departments of [2]Mechanical Engineering, [3]Orthopaedics & Sports Medicine, and [4]Radiology,
University of Washington, Seattle, WA
Email: wrledoux@u.washington.edu, web: http://www.amputation.research.va.gov/

INTRODUCTION

Tracking the motion of the bones of the foot is technically challenging. Computerized infrared camera systems with surface markers can be used, but skin motion artifact is a problem and small foot bones necessitate grouping. X-ray stereophotogrammetry has also been used in controlled static positions [1], but these methods are invasive and dynamic foot motions were not reported. Others have also evaluated the orientations of the bones of the foot using time-sequence MRI [2]; this requires positioning the feet in static locations which does not necessarily represent bone motion during gait. More recently, retro-reflective markers with bone pins have been used to quantify foot bone motion [3]. These studies represent the gold standard for *in vivo* foot bone motion, but the invasiveness limits its utility. Single plane fluoroscopy has been used to study hindfoot kinematics [4]; while the flexibility and utility is obvious and attractive, the complex anatomy of the foot with many small, occluding bones limits this system. Others have used dual C-arms to study ankle motion [5-7]; however, this setup required quasi-dynamic data collection as subjects were not able to walk unfettered through the field of view. Despite this progress, the ability to use a biplane fluoroscopy system to study foot bone motion remains incompletely explored to date.

METHODS

The hardware for our biplane fluoroscope has been modeled after an existing system [8]. In v1.0, two BV Pulsera C-arms (Philips Medical Systems) were positioned to optimally image a foot (Fig. 1). As medial/lateral floor height camera angles will lead to bone occlusion, the optimal images were obliquely oriented. Each system has an optional laser installed that projects a light crosshair towards the flat detector entrance plate, indicating the center of the X-ray beam and enabling alignment of the C-arm without turning on the X-ray. Additionally, each system has custom designed exposure control boards installed, which allow the two C-arms to function as a 'master-slave' system. Preliminary validation demonstrated that current was applied to the two X-ray generators within 80 microseconds.

Figure 1: v1.0 of the biplane fluoroscope.

One concern with v1.0 is the low sampling rate (8 Hz); this was addressed in v2.0 by replacing the existing Philips cameras with high-speed cameras (Vision Research Inc), which we have purchased and synchronized. Another concern is that the position of the C-arms prevents normal walking. This was addressed in v2.0 by removing the X-ray generators and image intensifiers from the C-arms and mounting them to four custom designed support structures. After collecting the data described below with v1.0, we constructed the support structures and disassemble the C-arms. To date, we have mounted both image intensifiers (II) and both X-ray sources, and attached the high-speed video cameras (Fig. 2).

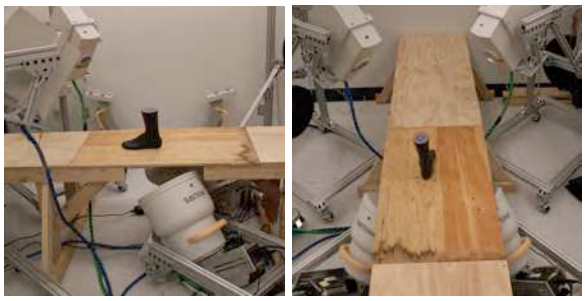

Figure 2: v2.0 of the biplane fluoroscope with the foot phantom on a temporary walkway.

There are four phases of custom software development for our biplane system. Phase I encompasses calibration, including distortion correction, bias correction and 3-D calibration. Phase II includes the generation of digital reconstructed radiographs (DRRs) from a CT scan. Phase III entails the implementation of the similarity and comparison measures between the fluoroscope images and the generated DRRs. Phase IV consists of speed and memory optimizations, including migrating the software from Matlab to C/C++ and graphics card processing with CUDA.

RESULTS AND DISCUSSION

To date, we have completed Phase I and II, and begun Phase III of the custom software development. To achieve Phase I, we have constructed a precisely machined aluminum grid for distortion correction and a 3-D calibration frame with 36 metal balls. We compared the distortion corrected data points to the aluminum grid and found an average RMS error for both C-arms of 0.082mm (Fig. 3). We then conducted the 3-D calibration by boot strapping each of the 36 points; the average RMS error was 0.102mm.

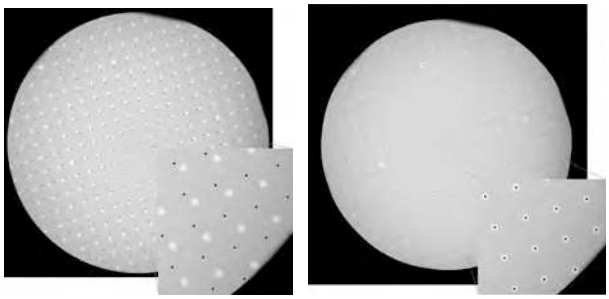

Figure 3: Distortion correction.

We have collected data with v1.0 of the biplane fluoroscope with a foot phantom (Phantom Labs) with metal balls embedded on 3 bones (tibia, calcaneus and first metatarsal) (Fig. 4). The foot phantom was also CT scanned. The metal balls were used to embed fixed coordinate systems in the first metatarsal and calcaneus. Using the CT scan of the foot phantom as the gold standard, we obtain a bone-to-bone Cardan angle relationship of [-155.61, 8.03, -32.13]. Using the biplane system, we calculated the same bone-to-bone angular relationship as [-155.73, 8.00, -32.07], or within 0.15˚ of the gold standard. Additionally, DRRs of the foot phantom were generated and a preliminary, manual alignment with the fluoroscope data was conducted (Fig. 5).

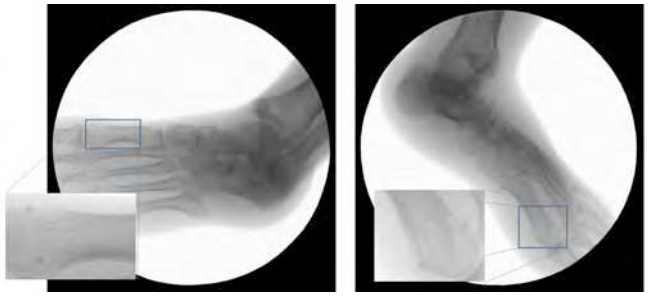

Figure 4: The metal balls on the first metatarsal.

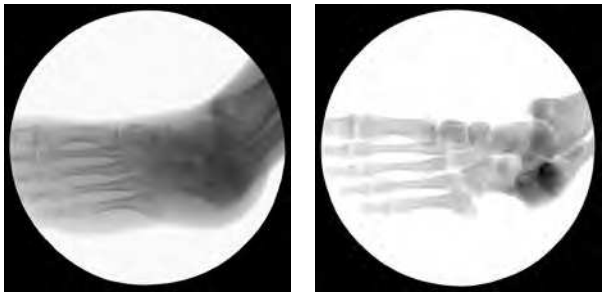

Figure 5: Fluoro data and DRR of foot phantom.

CONCLUSIONS

We have successfully built and implemented v1.0 of our biplane fluoroscopy system; v2.0 has been constructed, but not yet used. We have completed several phases of the custom software development and conducted complete calibrations. Our preliminary validation demonstrated sub-millimeter and sub-degree accuracies (0.1mm and 0.15˚), which compares well to other existing biplane systems. In the immediate future, we will complete the construction of v2.0 of the biplane system and continue the development of Phase III and IV of the custom biplane software. Extensive data collection and analysis will then be conducted, first with the foot phantom and then with living human subjects.

REFERENCES

1. Lundberg, A., et al., Foot and Ankle, **9**, 1989.
2. Siegler, S., et al., J Biomech, **38**, 2005.
3. Nester, C., et al., J Biomech, **40**, 2007.
4. Yamaguchi, S., et al., Foot Ankle Int, **30**, 2009.
5. de Asla, R.J., et al., J Orthop Res, **24**, 2006.
6. Li, G., et al., J Biomech, **41**, 2008.
7. Wan, L., et al., J Orthop Res, **26**, 2008.
8. Giphart, J.E., et al., *55th ORS*, Las Vegas, 2009.

ACKNOWLEDGEMENTS

Research has been supported by VA RR&D service.

Applications of Dynamic Stereo X-Ray to In Vivo Knee Research

Scott Tashman and William Anderst

University of Pittsburgh, Pittsburgh, PA, USA
email: tashman@pitt.edu

INTRODUCTION

Injuries to nearly any of the major structural tissues in the knee, such as the ACL, PCL or menisci, are associated with significantly increased risk for early osteoarthritis (OA). Effective treatments have been developed for alleviating pain and restoring function after these injuries. Unfortunately, most recent evidence suggests that these treatments may have at best limited efficacy for preventing long-term joint degeneration. Existing knowledge on the pathogenesis of knee OA is insufficient to identify specific factors responsible for the initiation and progression of disease after knee injury. Thus, developing treatments capable of preventing OA has been especially challenging.

Over the past 15 years, we have studied the mechanics of injured/repaired joints and how mechanics are related to joint degeneration. We have focused primarily on the ACL (we have investigated PCL and meniscal injuries as well). Though there are almost certainly biological factors that contribute to OA development after joint injury, a basic premise of our work is that joint mechanics must be restored to a state where joint homeostasis can be achieved. Therefore, our work has focused on three questions: How are joint mechanics disrupted by injury? How effective are existing treatments for restoring pre-injury joint mechanics? What specific mechanical abnormalities are associated with degenerative changes in the joint? This paper will briefly describe some of the studies we have performed to address these questions.

METHODS

Assessing in vivo joint mechanics is a significant challenge. In order to determine joint function at a level relevant to specific joint structures, high accuracy (±1 mm or better) is essential. Video-motion analysis cannot achieve this level of accuracy, due to skin motion artifacts. Additionally, to understand the mechanical environment the joint must endure under daily use, measurements must be made during dynamic, functional activities driven by muscular forces and with joint stresses relevant to the lifestyle of the patient. Thus, for an athlete with an ACL injury, studies of running or jumping would be appropriate. Alternatively, for a less active individual concerned most about activities of daily living, gait and stair ascent/descent might be more relevant tasks. Conventional MRI and radiographic systems constrain motion to confined spaces and/or are incapable of achieving frame rates adequate for these kinds of studies.

To address these shortcomings, we designed a system specifically for high-accuracy dynamic joint studies. This system (Figure 1) combines two x-ray sources (driven by cardiac cine-angiography generators capable of 1 ms pulses at 180 Hz) with two x-ray detectors (40 cm image intensifiers coupled to 4 Mpixel, 14-bit, 500 Hz cameras) with a custom-built gantry system that allows flexible positioning along with an open geometry for freedom of movement. A well-developed software system enables 3D kinematic tracking using either implanted tantalum markers (Dynamic Radio-Stereophotogrammetric Analysis, or D-RSA)[1] or a automated model-based tracking system for matching 3D bone models (from CT) to the stereo radiographs without markers.[2] Validated accuracy for dynamic, in vivo joint studies is ±0.1-0.7 mm.[2,3]

Figure 1: Dynamic Stereo X-Ray (DSX) system, configured for knee imaging during treadmill running.

RESULTS/DISCUSSION

We will discuss primarily our work related to ACL injury and repair. We have shown that conventional ACL reconstruction fails to restore normal knee kinematics during functional activities.[4] This leads to altered contact paths (Figure 2), exposing cartilage to unanticipated loads and potentially placing it at risk for OA.

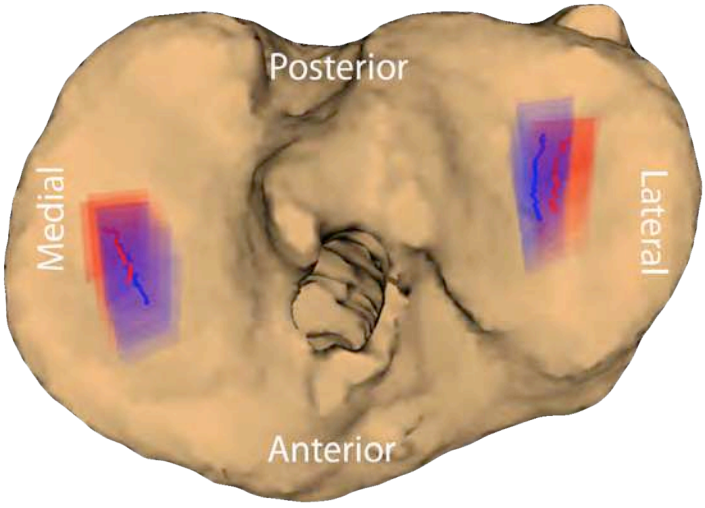

Figure 2: Tibial contact paths for the ACL-reconstructed limb (red) are shifted relative to the contralateral, uninjured limb (blue).

The most commonly used procedure for ACL reconstruction fails to locate the graft within the anatomical footprint of the native ACL. Thus, we have begun a study investigating a more anatomical approach to ACL reconstruction (developed by Freddie Fu, M.D.), utilizing two separate grafts placed within the footprint of the native ACL insertions. Preliminary data suggest that this technique may more effectively restore dynamic knee function than traditional techniques. This research is ongoing to evaluate both biomechanical and clinical benefits of this new surgical procedure.

We have also performed a series of studies using a ligament-deficient canine model to evaluate specific mechanical factors related to OA development and progression after ACL loss. We have shown that shifts in contact areas, as well as increased relative velocities of the joint surfaces, were associated with more severe OA development. [5,6]

We believe that these canine studies support our hypotheses that the abnormal mechanics resulting from non-anatomical ACL reconstruction may

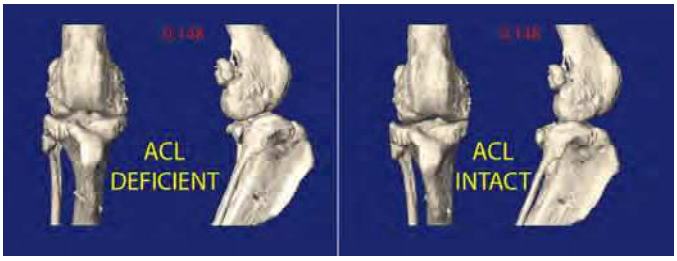

Figure 3: Canine knee kinematics, 150 ms after paw-strike (one frame extracted from a 250 frame/s motion sequence). Note that tibia is shifted anteriorly in the ACL-deficient limb (left), compared to the ACL-intact state (right).

contribute significantly to the development and progression of osteoarthritis. Thus, our imaging and anlysis techniques can provide a kinematic basis for the development and evaluation of new treatments that may be more effective for preventing OA after knee injury.[7]

We have performed similar studies of in vivo, dynamic knee function on patients with other knee injuries (PCL, medial meniscus), and in each case have found distinct patterns of abnormal joint kinematics. These kinematic patterns vary with load and activity, reinforcing the need to evaluate joint function during tasks specific to the anticipated activity level of the targeted population.

REFERENCES

1 Tashman, S. & Anderst, W. In Vivo Measurement of Dynamic Joint Motion Using High Speed Biplane Radiography and CT: Application to Canine ACL Deficiency. *Journal of Biomechanical Engineering* **125**, 238-245 (2003).

2 Bey, M. J., Zauel, R., Brock, S. K. & Tashman, S. Validation of a new model-based tracking technique for measuring three-dimensional, in vivo glenohumeral joint kinematics. *J Biomech Eng* **128**, 604-609 (2006).

3 Anderst, W., Zauel, R., Bishop, J., Demps, E. & Tashman, S. Validation of three-dimensional model-based tibio-femoral tracking during running. *Med Eng Phys* **31**, 10-16 (2009).

4 Tashman, S., Kolowich, P., Collon, D., Anderson, K. & Anderst, W. J. Dynamic Function of the ACL-reconstructed Knee during Running. *Clin Orthop Relat Res* **454**, 66-73 (2007).

5 Anderst, W. J., Les, C. & Tashman, S. In vivo serial joint space measurements during dynamic loading in a canine model of osteoarthritis. *Osteoarthritis Cartilage* **13**, 808-816 (2005).

6 Anderst, W. J. & Tashman, S. The association between velocity of the center of closest proximity on subchondral bones and osteoarthritis progression. *J Orthop Res* **27**, 71-77 (2009).

7 Tashman, S., Kopf, S. & Fu, F. The Kinematic Basis of ACL Reconstruction. *Operative Techniques in Sports Medicine* **In Press** (2009).

ACKNOWLEDGEMENTS

Primary funding received from NIH/NIAMS: R01AR046387, R01AR043860

WORK AND ENERGY FOR MOBILE HUMAN WALKING ASSISTANCE

Arthur D. Kuo

University of Michigan, Ann Arbor, MI, USA
email: artkuo@umich.edu, web: http://hbcl.engin.umich.edu

INTRODUCTION

Recent interest has sparked the development of robotic exoskeletons, orthoses, and prostheses to assist human gait and other functions. Assistance can restore walking function to persons with reduced abilities, for example due to amputation, stroke, or spinal cord injury. Alternatively, assistance can potentially improve performance for healthy individuals, perhaps to improve endurance, speed, or load carrying ability. Although prototype devices have shown early promise for several of these applications, many require tethering for delivery of electrical or hydraulic power. A considerable challenge for further development is a means to provide assistance in a mobile form, with the power supply carried onboard. Here we will examine the constraints due to the actuation requirement and ways to reduce them, by either making the power supply economical or finding ways to assist locomotion with low power.

ACTUATION REQUIREMENTS

The mechanical power needed for human locomotion may be estimated in a variety of ways. One estimate is the power delivered at each of the leg joints, which could be treated directly as motor specifications for an external assist device.

Much lower power requirements may be obtained if the joints are ignored and only the net power of each leg is considered. One such estimate is the rate of work performed on the body center of mass (COM), which shows that push-off is accomplished with a concerted action of the entire leg (Kuo et al., 2005), in amount less than the summed contributions of individual joints.

An even lower requirement may be obtained by considering the total power requirements for steady gait. On level ground, steady gait actually requires zero net work from the entire body over a stride. Perhaps an external assistance device could be designed to store and return mechanical energy in such a way as to reduce the net power requirements to nearly zero.

POWER SUPPLY

The actuation requirements contribute to the total amount of source power that must be supplied. At present, the most viable solution is the electric battery, but its relatively lower energy density results in either limited endurance or a considerable battery load to be carried.

Power requirements become even more critical when the efficiency of conversion and control are considered. There are considerable transmission losses due to the need to amplify torque. More difficult to quantify are losses associated with closed-loop control, as many exoskeletons require high-gain, high-bandwidth control to reduce the inertia and frictional loads felt by the user. An informal survey of recent devices suggests that the electrical power supplied to devices is often several times the mechanical power they produce. Mobile power supply constraints therefore greatly limit powered assistance of the individual joints.

ECONOMICAL ASSISTANCE STRATEGIES

Perhaps assistance can be provided with reduced power requirements. Instead of assisting each of the joints, it may be possible to assist the overall mechanical action of the body while requiring much less power. For example, it may be possible to provide assistance to push-off of the leg as whole, with less power than would otherwise be required of the individual joints.

Greater savings are perhaps possible by obtaining energy not from an external source, but from the human user. One possibility is to have the user supply the power directly at one joint, and then apply it to augment a different joint. Such a redistribution of power has some potential to

improve function, but is also likely to come at substantial energy cost to the user. It is therefore most sensible to obtain power by harnessing the negative work performed by the user. We will discuss two such applications, for generating electrical power (Donelan et al., 2008) or capturing mechanical power directly (Collins et al., 2010).

OUTLOOK FOR MOBILE ASSISTANCE

We identify several challenges for future development. Assuming that practical devices will remain battery powered for the foreseeable future, it is likely that electric motors will produce the work, and this technology is unlikely to experience revolutionary changes. It is therefore incumbent on designers to tackle two remaining issues: economical assistance strategies that avoid simply enhancing individual joints, and control methodologies that reduce the high-gain, high-bandwidth, and therefore high energetic cost of performing that assistance. Another issue not addressed here is that assistive devices to be worn by the user are subject to severe usability constraints, because it is difficult to attach a device to the body that bears forces comparable to body weight without inducing discomfort. Aside from shoes, few objects are worn for long durations while bearing such weight. The body interface problem must then be integrated with the design of assistance strategy. Fortunately, the pace of technology development has never been faster. Provided it is directed toward realistic and practical goals, there is no reason why mobile locomotion assistance cannot succeed.

REFERENCES

1. Kuo, A. D. et al. (2005). Energetic consequences of walking like an inverted pendulum: step-to-step transitions. *Exerc Sport Sci Rev* 33, 88-97.
2. Donelan, J. M. et al. (2008). Biomechanical energy harvesting: generating electricity during walking with minimal user effort. *Science* 319: 807-810.
3. Collins, S. H. & Kuo, A. D. (2010) Recycling energy to restore impaired function during human walking. *PLoS One* 5: e9307.

ROBOTIC LOWER LIMB ORTHOSES: GOALS, OBSTACLES, AND CURRENT RESEARCH

Daniel P. Ferris

University of Michigan, Ann Arbor, MI, USA
email: ferrisdp@umich.edu, web: http://www-personal.umich.edu/~ferrisdp/UMHNL.html

INTRODUCTION

Recent advances in robotic technology have made wearable powered devices for assisting human movement commercially viable. Press releases, news media, and blogs continually highlight examples of prototype robotic devices in development. These range from military funded exoskeletons for soldiers (e.g. Berkeley Bionics' BLEEX and Raytheon Sarcos' XOS) to industry initiated powered orthoses for individuals with mobility impairments (e.g. Honda's Stride Management Assist and Argo Medical Technologies' ReWalk) to academic research projects for gait rehabilitation (e.g. University of Tsukuba's HAL and MIT's AnkleBot). The expansion of research in this field is occurring at exponential rates, leading to the possibility for extensive use of the devices in the coming decades.

At present, however, it is difficult to know how close society is to having robotic lower limb orthoses/exoskeletons in everyday use. Researchers building commercially viable robotic lower limb orthoses/exoskeletons usually have one of three purposes in mind: human performance augmentation for healthy individuals, mobile assistive technology for disabled individuals, or therapeutic motor re-learning in the clinic for neurologically impaired individuals. In all three cases, there is little positive evidence that the devices are working as well as intended. In many cases, companies work to protect industry trade secrets and minimize negative perceptions of the devices. This is understandable given the potential commercial profits from the devices, but it makes it impossible to predict how long-term use of the devices will impact human health. In other cases where published data are available, the results have been generally disappointing. For example, there has been no evidence that robotic lower limb orthoses or exoskeletons can actually reduce the metabolic cost of walking or running compared to unaided locomotion.

The purpose of this presentation is to highlight ongoing research in the University of Michigan Human Neuromechanics Laboratory on robotic limb orthoses and exoskeletons, and identify goals and obstacles to future development of similar devices.

METHODS

In the University of Michigan Human Neuromechanics Laboratory, we have focused on building robotic lower limb orthoses and exoskeletons to provide insight into human locomotion biomechanics. We have primarily used artificial pneumatic muscles (sometimes called McKibben muscles) to actuate our exoskeletons. The artificial pneumatic muscles have activation dynamics similar to human muscle. We have built exoskeletons for the ankle, knee, and hip as well as for the whole limb combined. The control methods we have used include proportional myoelectric control, hand held pushbutton control, and kinematic based footswitch control. Experimental studies have included both neurologically intact healthy subjects and neurologically impaired subjects.

RESULTS AND DISCUSSION

Based on the results from the studies, we have identified some key principles governing the human-machine interface for lower limb robotic orthoses and exoskeletons. First, adaptation to the orthoses results in motor learning that can be stored and recalled. Second, myoelectric based controllers produce different biomechanical adaptations than kinematic based controllers. Third, there are unequal metabolic impacts for mechanical assistance at the respective lower limb joints (e.g.

hip, knee, ankle). Fourth, the strength of the mechanical assistance from the orthosis impacts the rate of motor learning. Fifth, the nervous system puts a priority on maintaining consistent net muscle moments during walking as a control strategy.

CONCLUSIONS

Ongoing technology advancements will continue to increase the viability of powered orthoses and exoskeletons for helping healthy and disabled individuals walk and run. The limiting factor in making the devices successful appears to be a lack of biomechanical understanding on how humans adapt and benefit from powered mechanical assistance. More studies need to identify the biomechanical, neural, and metabolic consequences of mechanical assistance to the lower limbs during human movement so that the knowledge can aid engineers in designing and refining exoskeleton devices.

ACKNOWLEDGEMENTS

The work presented represents the sweat and devotion of many Human Neuromechanics Laboratory members over the years, including Steve Cain, Mike Cherry, Keith Gordon, Pei-Chun Kao, Catherine Kinnaird, Cara Lewis, and Greg Sawicki. We also thank Ammanath Peethambaran, Mark Taylor, Jake Godak and Anne Manier for help with designing and fabricating the orthoses. The research was supported by the National Science Foundation (BES-0347479), National Institutes of Health (NS045486 and NS062119), and Christopher Reeve Paralysis Foundation (FAC2-0101).

POWERED ANKLE-FOOT PROSTHESIS IMPROVES METABOLIC DEMAND OF UNILATERAL TRANSTIBIAL AMPUTEES DURING WALKING

[1, 2]Hugh M. Herr, [1, 2]Alena M. Grabowski

[1]Massachusetts Institute of Technology, Cambridge, MA, USA
[2]Department of Veterans Affairs, Providence, RI, USA
email: alenag@mit.edu, web: http://media.mit.edu/~alenag

INTRODUCTION

When using conventional prostheses, people with transtibial amputation typically require 10-30% more metabolic energy to walk at the same speeds as non-amputees and this metabolic discrepancy becomes more pronounced at faster walking speeds [1]. A greater metabolic demand implies that amputees fatigue sooner and more often, and are not able to sustain the same walking speeds as non-amputees. Therefore it is not surprising that amputees' preferred walking speeds are typically 30-40% slower than non-amputees [1]. The elevated metabolic demand and slower preferred speeds of transtibial amputees are likely due to the inability of their conventional passive prostheses to produce power at the ankle.

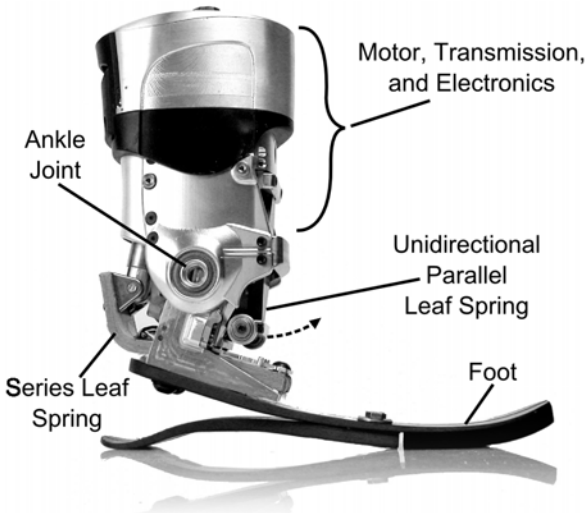

Figure 1: Powerfoot Prosthesis

The restoration of near-normal biological walking in amputees has not been previously demonstrated with any mechanical device [2]. The biological human ankle performs greater positive than negative work during each stance period of walking, especially at fast walking speeds [3,4] and generates nearly 80% of the mechanical power required during a gait cycle [3]. During ground contact, conventional prostheses behave as passive springs and therefore cannot provide the net positive work normally done by the biological leg muscles during terminal stance in walking.

The MIT Biomechatronics Group and iWalk, Inc. have designed a novel, powered ankle-foot prosthesis (Powerfoot) that supplies positive work at the prosthetic ankle joint (Fig. 1). The purpose of this pilot study was to determine how use of the Powerfoot affects metabolic cost during walking across a wide range of velocities. We predicted that amputees using the Powerfoot would have a lower metabolic cost of transport and faster preferred walking speed compared to using a conventional prosthesis.

METHODS

Three healthy adult male unilateral transtibial amputees gave informed written consent and participated in the study. All amputees were at least 1 year post-amputation, and at or above a K3 level of ambulation as defined by Medicare. We utilized high functioning amputee subjects with no known cardiovascular, pulmonary, or neurological disease or disorder, and no musculoskeletal problems. Each amputee completed an acclimation session and two experimental sessions.

During the acclimation session, a certified prosthetist adjusted and aligned the Powerfoot for each subject. Then, a technician tuned the Powerfoot to each subject by adjusting the spring stiffness, magnitude of power, and timing of power delivery during walking. We tuned the Powerfoot so

that the prosthetic ankle angle and torque matched biomimetic data across a range of walking speeds.

During the experimental sessions, we measured and compared rates of oxygen consumption and carbon dioxide production using a portable metabolic analysis system (Cosmed K4b^2, IT) while subjects stood in place and walked at five constant speeds (0.75, 1.00, 1.25, 1.50, and 1.75 m/s) on a treadmill. We averaged steady-state metabolic rates from minutes 4-6 of each standing and walking trial and then used a standard equation to calculate the metabolic cost of transport. Subsequently, we measured each subject's preferred walking speed on the treadmill. Each subject completed one experimental session using his own prosthetic foot and a subsequent session using the Powerfoot.

RESULTS AND DISCUSSION

Compared to using a conventional prosthesis, amputees using the Powerfoot had 6, 7, 10, 13, and 16% reductions in metabolic cost of transport to walk at 0.75, 1.00, 1.25, 1.50, 1.75, respectively. The minimum metabolic cost of transport shifted from 1.25 m/s while subjects used their own foot to 1.35 m/s while subjects used the Powerfoot. Preferred walking speeds were 1.09 m/s while using a conventional prosthetic foot, and 1.37 m/s while using the Powerfoot.

CONCLUSIONS

Supplying biomimetic power at the prosthetic ankle joint reduced the metabolic cost of transport and improved preferred walking speed in three unilateral transtibial amputees. Future studies are planned that target a larger sample size.

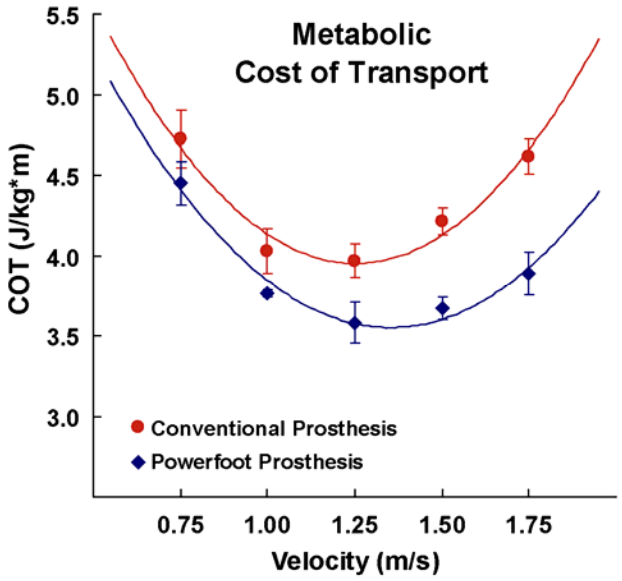

Figure 2: Average metabolic cost of transport (error bars ± SEM) for amputees using their own conventional prosthesis (red circles) and the Powerfoot prosthesis (blue diamonds) to walk 0.75-1.75 m/s. Using the Powerfoot prosthesis reduced cost of transport by 6-16% compared to using a conventional prosthesis to walk at all speeds.

REFERENCES

1. Hsu MJ et al. *Arch Phys Med Rehab* **87**, 123-129, 2006.
2. Collins DM et al. *Crit Rev in Biomed Eng* **34(5)**, 379-436, 2006.
3. Winter DA. *Clin Ortho & Rel Research* **175**,147-154, 1983.
4. DeVita P et al. *J Exp Biol* **210**, 3361-3373, 2007

ACKNOWLEDGEMENTS

This research was funded by a Career Development Award from the Department of Veterans Affairs.

Dynamic Simulation of Musculoskeletal Biomechanisms in 3D

Dinesh K. Pai

Sensorimotor Systems Laboratory, Department of Computer Science
University British Columbia, Vancouver, BC, Canada

email: pai@cs.ubc.ca, web: http://www.cs.ubc.ca/~pai

INTRODUCTION

Our approach to biomechanical modeling is motivated by the long term goal of developing a precise and constructive understanding of how the central nervous system (CNS) controls movement. The dynamics of the biomechanical plant could potentially account for many features of movement and coordination that should not be attributed to neural control. I discuss what is needed for this task, and describe our solution, using biomechanical strands.

REQUIREMENTS

It is helpful to first discuss the constraints imposed on biomechanical models used for motor control.

Complexity. Even simple natural movements, such as reaching for an object, involve large numbers of muscles in the body. A long standing challenge of neural control is to understand how the CNS coordinates these large numbers of muscles, perhaps organizing them in a flexible way into a small number of synergies. To test hypotheses of motor control it is essential to model large scale biomechanical systems, with a large numbers of muscles. Robust algorithms are required to simulate these large scale systems efficiently, preferably at interactive rates.

Biomechanisms. Frequently, muscles do not simply insert on a bone but terminate in a complex network of tendons and connective tissues. It is well known that the tendons of many muscles span multiple joints resulting in complicated mechanical coupling between joints, and that fascia could couple the action of different muscles. Particularly striking is the insertion of the extensor muscles of the hand, which terminate in a complex mechanism. Perhaps most suprising is the relatively recent discovery that even the apparently simple extraocular muscles (EOMs) of the eye are held in the orbit by pulley-like structures made of connective tissue and smooth muscle. We will call such biomechanical networks of tendon, connective tissues, and muscle ``biomechanisms," to suggest a role similar to that played by mechanisms in engineering. Even though it is generally believed that biomechanisms are functionally important, their precise functions are not very well understood. For instance, it has been proposed that orbital pulleys may help implement Listing's law and make rotations of the eye appear commutative, but this has not been shown with dynamic simulations with realistic anatomy.

Realistic dynamics. A series of remarkable papers from the laboratories of McMahon, McGeer, Ruina and others have shown that many features of walking, in both humans and robots, could be generated by ballistic movements. This suggests that it is important to simulate the dynamics of biomechanical systems, and not just statics or kinematics. But this is complicated for two reasons: (1) Biomechanisms significantly modify the dynamics of a plant, since they could couple the mass of a muscle in one body segment to distant body segment. (2) Constitutive models of active muscles that can accurately predict the action of muscles in normal use are not yet known.

Proprioception. Neural control and learning of movement requires proprioceptive information from muscle spindles and golgi tendon organs. To model these mechanoreceptive sense organs, it is important to not only simulate the gross behavior of muscle but also the strains, strain rates, and stresses within muscle.

METHODS

In my laboratory we have developed a new approach to biomechanical simulation that addresses these requirements and combines the advantages of solid mechanics models with the efficiency and scalability of line-of-force models.

Unlike standard FEM models of solid mechanics that discretize muscles into tetrahedral elements, we discretize into thin rod-like elastic elements called **strand** elements, that can curve in three dimensions [1]. A strand has distributed mass, physiological cross sectional area (PCSA), and elastic properties that can vary along its length. Each strand receives a single neural activation signal that affects its constitutive properties; thus a strand is a unit of motor action. A strand could represent either an entire musclulotendon, a compartment within a muscle, or a single motor unit - this is a choice a user can make based on the level of detail required for a specific investigation.

RESULTS AND DISCUSSION

Hand [1]. We developed a model of the hand and forearm with 54 musculotendon strands and 17 bones (see Figure). Musculotendon paths were constructed based on standard textbook models in the literature. The simulation currently runs at interactive rates on ordirnary PCs. To test the utility of the model for motor control, we developed an inverse activation algorithm that estimates motor commands from a given target hand movement.

Oculomotor System [2]. We developed a model of the human orbit with realistic anatomy, including the EOMs, connective tissue pulleys, ligaments, and constraints due to contact between tendons and the globe. The resulting model generates realistic gaze positions and saccade trajectories given EOM innervations, and can simulate pathologies such as acute superior oblique palsy.

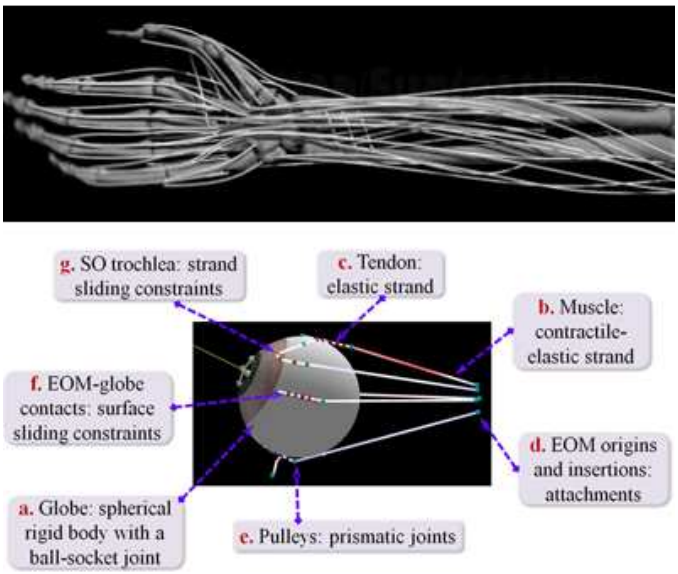

Above: strand model of the hand and arm [1]. **Below**: model of the human orbit [2].

CONCLUSIONS

The key advantage of our approach is that a strand represents in detail the mechanical actions of muscles that are most useful for motor control, while ignoring other effects in the transverse directions. Thus a strand is not a general purpose model of muscle (for instance, it would be unsuitable for simulating palpation or surgical incision of muscle). It was specifically designed for motor control. A second advantage is that we can model constraints such as tendon sheaths in a dynamically consistent way, with constraint forces computed using Lagrange multipliers. This is makes it possible to simulate complex biomechanisms.

REFERENCES

1. S. Sueda, A. Kaufman, D. K. Pai, “Musculotendon Simulation for Hand Animation,” in ACM Transactions on Graphics (Proc. SIGGRAPH), 27(3), 2008. Article 83.
2. Q. Wei, S. Sueda, D. K. Pai ``Biomechanical Simulation of Human Eye Movement," *Proceedings of ISBMS10*, January 23-24, 2010.

ACKNOWLEDGEMENTS

This work was made possible by all the members of my lab, especially S. Sueda and Q. Wei, and the support of PWIAS, NIH, CIHR, HFSP, NSERC and the Canada Research Chairs Program.

3D MODEL OF SKELETAL MUSCLE TO PREDICT INTRAMUSCULAR PRESSURE

[1]Kenton R. Kaufman, [1]Duane A. Morrow, [2]Gregory M. Odegard, [2]Tammy L. Haut Donahue, [3]Patrick J. Cottler, [4]Samuel Ward, [4]Richard Lieber

[1]Mayo Clinic, Rochester, MN, [2]Michigan Technological University, Houghton, MI, [3]Luna Innovations, Roanoke, VA, [4]University of California, San Diego
email: kaufman.kenton@mayo.edu

INTRODUCTION

Human movement depends on the ability of muscles to generate sufficient force. Manual muscle testing, the most common method for measuring muscle strength, only detects weakness when muscle strength is less than ~40% of normal[1]. Measurement of intramuscular pressure (IMP) is emerging as an improved method for quantifying muscle force in-vivo. IMP is well-correlated with muscle force for isolated[2] and intact muscle[3], as well as during gait[4, 5].

Atraumatic in-vivo measurement of IMP is becoming practical in the clinical setting. Advances in sensor design have resulted in a 250μm diameter microsensor, which demonstrates accuracy better than 2% full-scale output (FSO) with repeatability and hysteresis better than 1% FSO[6].

Mathematical models, critical for understanding the structure and function of muscles, have evolved over that past century. Blix observed that muscle force varies with sarcomere length[7]. Investigators have used Hill-type muscle models to predict individual muscle forces. However, these models don't account for mechanical equilibrium[8] or muscle curvature during contraction. Most recently, 3-D continuum mechanical muscle models have started to emerge that address these deficiencies[9-13]. However, these models have not been fully validated. The goal of this research is to create a model that will aid in the understanding of muscle force production and advance clinical applications of IMP.

METHODS

Our work is focused on developing a fully 3D, continuum mechanics-based model of skeletal muscle. The model represents muscle as a transversely isotropic, hyperelastic, and isovolumetric material, characterized by the following strain energy density function[14]:

$$\psi = \sum_{i=1}^{3} a_i \left(I_1 - 3\right)^i + \sum_{j=1}^{3} b_j \left(I_2 - 3\right)^j + \sum_{k=2}^{6} c_k \left(I_4 - 1\right)^k + (\mathrm{J}-1)^2 / d$$

where a_i, b_j, c_k, and d are material parameters; J is the Jacobian, and I_1, I_2, I_4 are scalar invariants of the Green deformation tensor. The material parameters have been determined from material tests of New Zealand white (NZW) rabbits skeletal muscle under longitudinal extension, transverse extension, and longitudinal shear[15]. Muscle active stress is given by[16]:

$$\psi_a = +\gamma q \phi \mathbf{M}$$

where γ is a material constant; $q\ \{q \in R : 0 \le q \le 1\}$ is the scalar muscle activation parameter, $\mathbf{M}$ is the structural tensor for transverse-isotropic materials, and ϕ is the time-independent evolution of loss in actin/myosin interaction[16] given by

$$\phi = \exp\left[-\kappa \frac{\left(I_4 - I_4^0\right)^2}{\left(I_4^0\right)^2}\right]$$

where I_4^0 is the value of I_4 for the optimized activation length and κ is a shape parameter that affects the steepness of the ascending/descending limbs of the active length-tension relationship. When ϕ=1, actin/myosin interaction is maximized and ϕ decreases as the muscle shortens or extends from the optimized length.

A 3D finite element method (FEM) model has been created from magnetic resonance images of a NZW rabbit hindlimb. Scans were manually segmented using Analyze (Mayo Clinic, Rochester, MN) to determine representative muscle geometry. The muscle geometry was meshed in ANSYS (ANSYS, Inc., Canonsburg, PA) using 852 8-noded brick elements. A mixed u-p formulation was used to simulate incompressibility. Displacement boundary

conditions were used to simulate experimental trials. Active stress was simulated in the model through the application of a compressive load on each element surface normal to the fiber axis. For each displacement, resultant forces from proximal tendon area nodes were summed vectorially to create the length-tension comparison. IMP was modeled as the hydrostatic pressure calculated from the dilatational component of the Cauchy stress tensor. IMP was taken from an element in the deep muscle belly representative of the microsensor location in the experimental trials.

RESULTS AND DISCUSSION

The FEM approach was compared with previously published experimental data of muscle length-tension-IMP[2]. The model accurately predicts the toe and linear regions of the passive muscle length tension (Fig. 1) and length pressure relationships (Fig. 2). The model also accurately predicts the active length-tension relationship (Fig. 3). Current efforts are underway to accurately model the active length-IMP relationship.

This model marks the first time a 3D FEM model of muscle has been validated against experimental muscle force and IMP data. Further, this model is based on experimentally measured muscle material properties. The largest uncertainty in all 3D models of this type may be the assumption that muscle contracts isovolumetrically. This assumption is based on the experiments conducted by Swammerdam in 1667[17]. Incorporation of this phenomenon into constitutive relationships is at its infancy. As 3D muscle models grow in complexity, more effort will also need to be devoted to establishing appropriate boundary conditions and methods for interaction with surrounding tissues.

ACKNOWLEDGEMENTS

NIH Grant R01 HD31476

REFERENCES

1. W. C. Beasley, *Archives of Physical Medicine and Rehabilitation*, 1961, 42, 398-425, 1961
2. J. Davis, K. R. Kaufman, et al., *Journal of Biomechanics*, 2003, 36, 505-12, 2003
3. T. M. Winters, G. S. Sepulveda, et al., *Muscle Nerve*, 2009, 40, 79-85, 2009
4. K. R. Kaufman and D. H. Sutherland, *Operative Techniques in Sports Medicine*, 1995, 3, 250-255, 1995
5. J. U. Baumann, D. H. Sutherland, et al., *Clinical Orthopaedics & Related Research*, 1979, 145, 292-299, 1979
6. P. S. Cottler, W. R. Karpen, et al., *Ann Biomed Eng*, 2009, 2009
7. M. Blix, *Scandanavian Archives of Physiology*, 1894, 5, 149-206, 1894
8. B. J. J. J. Van der Linden, H. F. Koopman, et al., *Clinical Biomechanics*, 1998, 13, 256-260, 1998
9. S. S. Blemker, P. M. Pinksy, et al., *Journal of Biomechanics*, 2005, 38, 657-665, 2005
10. A. W. J. Gielen, C. W. J. Oomens, et al., *Computer Methods and Biomechanics in Biomedical Engineering*, 2000, 3, 231-244, 2000
11. T. Johansson, P. Meier, et al., *Journal of Theoretical Biology*, 2000, 206, 131-149, 2000
12. J. A. C. Martins, E. B. Pires, et al., *Computer Methods in Applies Mechanics and Engineering*, 1998, 151, 419-433, 1998
13. C. A. Yucesoy, B. Koopman, et al., *Journal of Biomechanics*, 2002, 35, 1253-1262, 2002
14. D. A. Morrow, T. L. Donahue, et al., *Computer Methods and Biomechanics in Biomedical Engineering*, 2010, 13, 1-10, 2010
15. D. A. Morrow, T. L. Haut Donahue, et al., *Journal of the Mechanical Behavior of Biomedical Materials*, 2010, 3, 124-129, 2010
16. G. M. Odegard, T. L. Haut Donahue, et al., *Journal of Biomechanical Engineering*, 2008, 130, 2008
17. M. Cobb, *Nature Reviews Neuroscience*, 2002, 3, 395-400, 2002

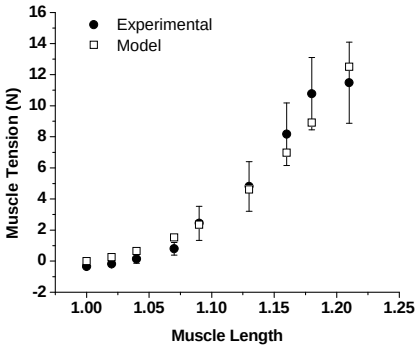

Figure 1. Muscle passive length-tension relationship

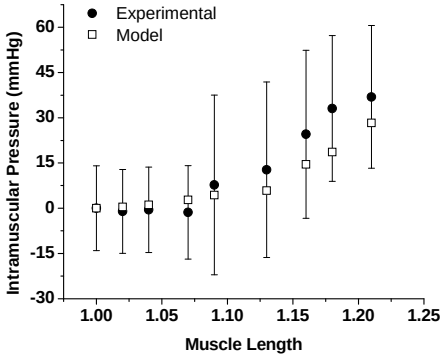

Figure 2. Muscle passive length-pressure relationship

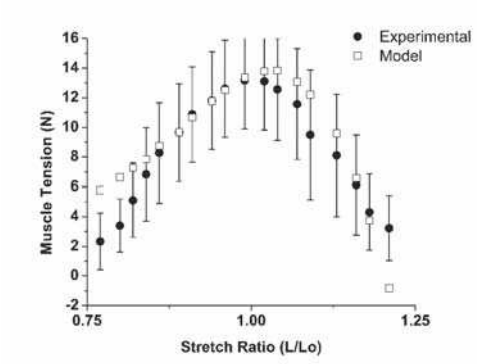

Figure 3. Muscle active length-tension relationship

MODELING TO STUDY MUSCULAR MECHANICS WITHIN THE CONTEXT OF FASCIAL INTEGRETY: LINKED FIBER-MATRIX MESH MODEL

[1]Can A. Yucesoy and [2]Peter A. Huijing

[1]Boğaziçi University, Istanbul, Turkey
[2]Vrije Universiteit, Amsterdam, the Netherlands
email: can.yucesoy@boun.edu.tr, web: http://www.bme.boun.edu.tr/bmewebg/profiles/yucesoyc.asp

INTRODUCTION

Quantification is central to scientific understanding of phenomena and performing experiments is clearly the fundamental approach in doing that. Experiments in vitro and in situ allow determining muscle tissue mechanical properties and gross muscle physiological properties (e.g. length-force characteristics). However, mechanics of the actual donor structure may remain unattended and it is often of interest also to determine the mechanisms producing the function. If limitations in accessing muscular structures can be eliminated, experiments in vivo are highly informative. However, e.g., using imaging, the analysis remains only kinematic.

On the other hand, mathematical models can enhance immensely insights gained experimentally: (i) effects of diverse parameters can be studied inexpensively, (ii) experimentally generated hypotheses can be tested, (iii) new hypotheses for experiments can be generated, (iv) conditions impossible to create experimentally can be addressed and (v) mechanisms producing tissue function can be isolated.

Using analytical models, nonlinear material properties and large deformations can be handled; and solutions of the equilibrium equations are possible, but typically within a definite material domain only. In contrast, with at least similar capabilities, the finite element method has a great advantage that geometrically highly complex structures can be modeled. The value of finite element model may be substantial, provided that it is developed with a specific and well defined purpose determining (1) the extent to which the actual problem can be simplified, (2) the modeling assumptions to be made and (3) the relevant model output parameters and their interpretation. In studies in which this approach has been applied successfully to skeletal muscle [e.g., 1], as well as in Hill type models, muscle was not modeled as operating within the context of a fascial integrity: (1) elements have been used in which both active and passive properties of muscle tissue are lumped, hence, the roles of intramuscular connective tissues and their interaction with the contractile apparatus were not accounted for explicitly. (2) Muscle was considered as an isolated entity hence, the continuity of ***intramuscular*** fascia (e.g., epimysium, perimysium, endomysium) and ***epimuscular*** fascia such as collagen reinforced neurovascular tracts or compartmental boundaries were not accounted for.

LINKED FIBER-MATRIX MESH MODEL

In contrast, the linked fiber-matrix mesh (LFMM) model was designed specifically to study muscular mechanics within the context of fascial integrity [2]. The mechanical roles played by such muscle-related fascia has been referred to as ***intra- and epimuscular myofascial force transmission*** [e.g., 3]. Major effects of such force transmission include differences in muscle forces exerted by muscle at its origin and insertion, as well as the length range of muscle active force exertion being dependent on actual mechanical conditions imposed (e.g. muscular relative positions). The following concepts determined the modeling approach of the LFMM model: (I) Peripheral multi-molecular connections between the muscle fiber and the extracellular matrix (ECM) are capable of transmitting force. Therefore, the force balance determining the length of a sarcomere is much more complex than just the interaction between sarcomeres arranged in series within the same muscle fiber: it also includes ***intramuscular myofascial loads*** i.e., forces exerted by i) the ECM and ii) sarcomeres located in neighboring

myofibers. (II) In vivo, muscle is not an isolated entity, since direct collagenous linkages between epimysia of adjacent muscles and indirect connection between muscles (via epimuscular fascia) form an integral mechanical system. Therefore, also ***epimuscular myofascial loads*** take part in the balance of forces determining the length of a sarcomere.

LFMM model for isolated muscle

Intracellular and ECM domains of skeletal muscle are considered explicitly as two separate domains that are linked elastically. Two new elements were introduced into ANSYS 9.0: (1) The ***ECM element*** represents the collagen reinforced ECM, including the basal lamina and connective tissue components such as endomysium, perimysium and epimysium. (2) The ***muscle fiber element*** representing myofibers.

The geometry of the LFMM model was defined as the contour of a longitudinal slice at the middle of the belly of an isolated rat EDL muscle, but can be made to fit any muscle architecture. The ECM domain is represented by a mesh of ECM elements (***matrix mesh***). In the same space, a separate mesh of muscle fiber elements is built to represent the intracellular domain (***fiber mesh***). The two meshes are rigidly connected to single layers of elements representing proximal and distal aponeuroses: a node representing myotendinous connection sites is the common node of ECM, myofiber and aponeurosis elements. At the intermediate nodes, fiber and matrix meshes are linked elastically to represent the trans-sarcolemmal attachments of the (intracellular) cytoskeleton and ECM.

The ECM element incorporates a strain energy density function that accounts for the non-linear and direction dependent material properties, as well as the constancy of muscle tissue volume during length changes and contraction. For the muscle fiber element, the total stress acting exclusively in the local fiber direction is the sum of the active stress of active sarcomeres and the stress due to intracellular passive tension.

LFMM model within the context of fascial integrity

The LFMM model was extended to take into account the epimuscular connections: (I) ***Extramuscular connections***. Nodes of the matrix mesh located at one-third of the fascicle length from its proximal end were linked fixed nodes (modeling bone). This represents all extramuscular connections (i.e. the collagen reinforcement of blood vessels and nerves and compartmental boundaries). (II) ***Direct intermuscular connections***. The corresponding nodes of the matrix meshes of two muscle models were linked elastically.

CONTRIBUTION OF LFMM MODEL TO MUSCLE MECHANICS

This model allows (1) quantifying muscle forces exerted at the proximal and distal tendons, for which agreement with experimental data is achieved by using suitable stiffness values selected for epimuscular links and even more important, (2) studying factors that cannot experimentally be observed: e.g., myofiber strain and stress distributions in the fiber direction. Note that such fiber strains quantify sarcomere length distributions both serial (within the same muscle fibers) and parallel (in different parts of the muscle) whereas, fiber stresses indicate myofibers' local capability of force exertion. Assessing such model parameters in association with muscle length-force characteristics provides explanations for the mechanisms causing proximo-distal force differences and those causing the dependency of muscle length force characteristics on mechanical conditions. For example, increased sarcomere length heterogeneity (both serial and parallel) due to epimuscular myofascial loads causes a shift in muscle optimum length to a higher length [4]. Therefore, in agreement with the modeling goals, the LFMM model has provided an important contribution to our understanding of the mechanisms and key effects of epimuscular myofascial force transmission. Offering new insights for muscle mechanics, this has important implications regarding muscle function in health and disease, as well as treatment of pathologies.

REFERENCES

1. Blemker SS, et al. ***J Biomech*** **38**, 657-665, 2005.
2. Yucesoy CA, et al. ***J Biomech*** **35**, 1253-1262, 2002.
3. Yucesoy CA, et al. ***J Biomech Eng*** **127**, 819-828, 2005.
4. Yucesoy CA, et al. ***J Electromyog & Kinesiol,*** **17**, 664-679, 2007.

3D MUSCLE MODELING WITH APPLICATION TO MUSCLE STRAIN INJURY

[1,2]Silvia S. Blemker, [2]Michael R. Rehorn, and [1]Niccolo Fiorentino

Departments of [1]Mechanical and Aerospace Engineering and [2]Biomedical Engineering,
University of Virginia
E-mail: ssblemker@virginia.edu Web: http://www.mae.virginia.edu/muscle

INTRODUCTION

Advances in computational mechanics have inspired a new class of three-dimensional (3D) muscle models that allow us to explore complex structure-function relationships in skeletal muscle and tendon [e.g., 2,8]. These models have expanded the applications of muscle modeling, motivated the need for new types of experimental validation, generated new hypotheses, and provided a bridge between whole muscle mechanics and muscle fiber mechanics.

This presentation will describe the integration of 3D muscle models of the hamstrings muscles with novel medical imaging techniques to understanding how internal muscle morphology influences muscle injury susceptibility. Future directions of 3D muscle models will also be discussed.

3D MODELING FRAMEWORK

We have created three-dimensional models from magnetic resonance image (MRI) data of individual subjects. Muscles, external tendons, aponeuroses, and bones are all manually segmented (Fig. 1A), and three-dimensional volumetric hexahedral meshes are generated from the segmentations (Fig. 1B). Representations of the muscle fiber geometry (Fig. 1C) are created by morphing template fiber geometries to each 3D model [2]. In the simulations, a transversely isotropic, incompressible, hyperelastic constitutive model is used to describe the active and passive stress-strain relationship in the muscle and tendon tissue [1]. Additionally muscle-muscle and muscle-bone contact can be resolved using a penalty formulation. These models allow us to analyze muscle tissue strains, whole fiber strains, and whole muscle strains during a given set of joint movements and activation patterns. As an example, simulations of active lengthening contractions performed with 3D models of the biceps femoris long head muscle (Fig. 1D) demonstrate that peak strains are localized near the proximal myotendinous junction of the muscle.

In addition to creating models directly from MRI data, we have also created simplified models that allow us to perform systematic sensitivity studies and explore how specific features of a given muscle's internal muscle-tendon morphology affect the muscle behavior.

IMAGING AS VALIDATION

In order to test predictions from 3D models, we have employed dynamic MRI techniques to measure strains within muscles during passive and loaded joint motion conditions. For example, we are using cine Displacement ENcoding with Stimulated Echoes (DENSE) to determine the displacements and strains [7,9] of tissues in the biceps femoris long head (BFLH) muscle during both passive and eccentric contractions. We compared the strain distributions determined using cine DENSE with those determined by a 3D model of the BFLH (Fig. 1D-E). Strains predicted by the model were similar to the dynamic imaging data. The region of largest strain was concentrated near the medial border of the muscle, which corresponds to the proximal muscle-tendon junction.

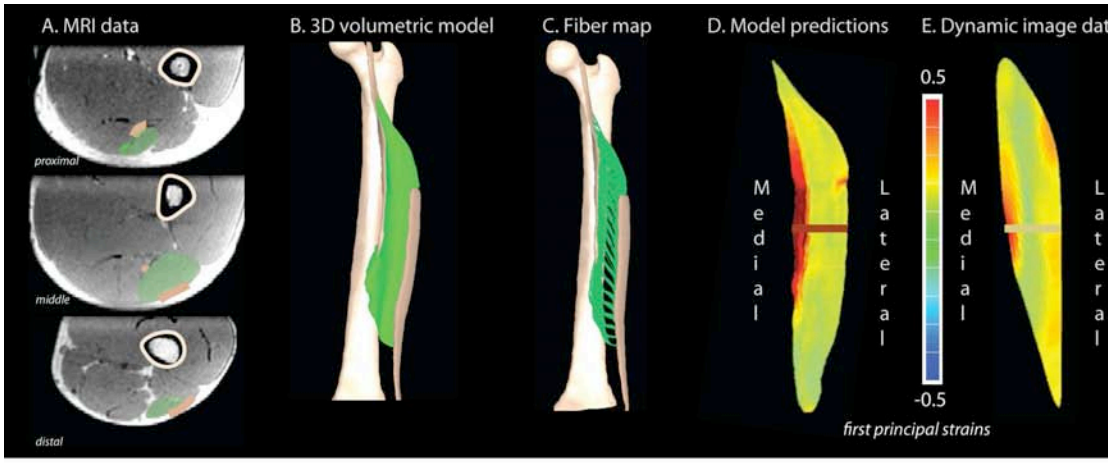

Figure 1. 3D models and experimental strain data. Static MRI data (A) is used to created 3D volumetric meshes (B) of muscles, aponeuroses, and tendons (B) and a corresponding fiber map (C). Strains predicted by the model in a given plane (D) are compared to strains determined from dynamic MRI data (E).

APPLICATION TO MUSCLE INJURY

Hamstring strain injury is a significant problem for many athletes. Of the hamstrings muscles, the biceps femoris longhead (BFLH) is the most commonly injured and reinjured, with the injury most frequently localized along the proximal muscle-tendon junction [3], which corresponds precisely with the region of peak localized strains which we measured with cine DENSE imaging as well as that we predicted by the 3D model.

A sensitivity study performed with the 3D model showed that the relative widths of the proximal and distal aponeuroses greatly affect the magnitude and location of the peak strain in the BFLH muscle [6]. Decreasing the width of the muscle's proximal aponeurosis increased the magnitude of the strains localized near the proximal myotendinous junction. MR images of 14 healthy volunteers demonstrated a significant variation in the dimensions of the proximal aponeurosis [5]. Dynamic MR images of these same volunteers [4] showed that muscles with narrow proximal aponeuroses had higher peak strains as compared to muscles with narrow proximal aponeuroses. These results support the predictions made by the 3D models and suggest that variations in internal muscle-tendon morphology may be a factor that influences muscle injury susceptibility.

FUTURE DIRECTIONS

There are several fruitful areas of modeling extensions that we are currently exploring. Areas that will be discussed during this presentation include: micromechanical models to appropriately model the myotendinous junction; incorporation of passive and active velocity-dependent effects in the constitutive formulation, and simulating muscle tissue behavior during complex loading situations such as running.

REFERENCES

1. Blemker SS.,et al. *J Biomech* 38,657-665, 2005.
2. Blemker, S.S., and Delp, S.L., *ABME*, 33, 661-673, 2005.
3. De Smet, A.A and Best, T.M.. *Am J Roentgenol* 174, 2000.
4. Fiorentino, N. et al., *34th Annual ASB Meeting*, 2010.
5. Handsfield G, et al. *34th Annual ASB Meeting*, 2010.
6. Rehorn MR and Blemker SS. *J Biomech* in press, 2010.
7. Spottiswoode B, et al. *IEEE TMI* 26, 15-30, 2007.
8. Yucesoy CA, et al. *J Biomech* **35**, 1253-1262, 2002.
9. Zhong X, et *a*l**.** *Mag Res Med* **61**, 981-988, 2009.

ACKNOWLEDGEMENTS

We would like to thank Darryl Thelen and Amy Silder. Funding sources for this work was provided by NIH RO1 AR056201.

COMPENSATORY STEP TRAINING OF UNILATERAL, ABOVE-KNEE AMPUTEES: A POTENTIAL INTERVENTION FOR REDUCING TRIP-RELATED FALLS

[1] Jeremy R. Crenshaw, [2] Kenton R. Kaufman and [1] Mark D. Grabiner

[1] University of Illinois at Chicago, Chicago, IL, USA
[2] Mayo Clinic, Rochester, MN, USA
email: jcrens2@uic.edu, web: http://www.uic.edu/ahs/biomechanics/

INTRODUCTION

With a yearly fall incidence of 66% [1], above-knee (AK) amputees can benefit from rehabilitation methods aimed at fall prevention. For older, non-amputee adults, practicing a compensatory stepping response (CSR) on a modified treadmill improved the recovery response to treadmill disturbances [2] and overground trips [3]. Previously, we reported that, after six CSR training sessions, a unilateral, AK amputee demonstrated longer step lengths, decreased trunk flexion, and increased dynamic stability when responding to treadmill disturbances [4]. Unpublished data from our laboratory has identified low hip vertical height (z_{pelvis}), short recovery step lengths (L_{step}), delayed recovery step times, and large trunk flexion velocities (*TFV*) as important mechanisms of failed trip recoveries by unilateral, AK amputees. The purpose of this study was to evaluate the ability of CSR training to improve these mechanisms. We hypothesized that, compared to the first training session, the sixth training session would be characterized by the following:

- Improved success in recovering from postural disturbances.
- A higher z_{pelvis} at the first recovery step completion.
- A longer first L_{step} and a shorter step time after disturbance onset (t_{step}).
- Smaller trunk flexion angle (*TFA*) and *TFV* at the first recovery step completion.

METHODS

Three women and two men (age: 43±10.7 years, height: 172±12 cm, mass: 79.7±22.3 kg) with unilateral, AK amputations participated in this study. Four subjects used prostheses with a microcomputer controlled knee (C-Leg®, Otto Bock, Minneapolis, MN), and one subject used a prosthesis with a hydraulic knee (Mauch SNS®, Ossur, Aliso Viejo, CA).

The training protocol consisted of a sequence of progressively challenging disturbances eliciting CSRs. For each trial, the subjects stood on a custom treadmill (Active StepTM, Simbex, Lebanon, NH), and a posteriorly-directed treadmill acceleration necessitated the subject to execute an anterior-directed CSR of multiple steps to avoid falling. The initial belt accelerations lasted 0.5 sec, and ranged from 1.5 m/s^2 to 6.25 m/s^2. After the initial acceleration, the treadmill decelerated at a constant rate of -0.375 m/s^2. For small disturbances (≤2.25 m/s^2), peak treadmill velocity was maintained so that the minimum belt displacement was 2 m.

All subjects participated in six training sessions over the course of two to three weeks. For each session, the subjects performed two series of CSRs, once taking the initial step with the non-prosthetic limb (NPL), and once taking the initial step with the prosthetic limb (PL). Time permitting, each series progressed in difficulty until the subject could not recover from the disturbance or the subject recovered from the most challenging disturbance. For all trials, motion capture data was collected at 120 Hz. In order to determine the effects of training day (DAY) and stepping limb (LIMB) on each of the independent variables (z_{pelvis}, L_{step}, t_{step}, *TFA*, and *TFV*), a mixed model ANOVA was used with fixed (DAY & LIMB) and random (subject) factors. If significant correlations of the independent variable with the initial treadmill belt acceleration (a_{belt}) existed, a_{belt} was included in the ANOVA as a covariate.

RESULTS AND DISCUSSION

Success of CSRs

During the sixth session, three of the five subjects successfully recovered from disturbances that had resulted in a fall during the first session. The two other subjects either had not progressed to failure on the first session, or successfully recovered from all disturbance magnitudes on the first day. Initially stepping with the PL resulted in falls at lower disturbance accelerations than when stepping with the NPL.

Hip Elevation

z_{pelvis} was not significantly correlated with a_{belt} ($p<0.05$). The main effect of DAY ($p=0.067$) and the DAY*LIMB interaction ($p=0.390$) were not significant, suggesting no training effect. A significant main effect of LIMB ($p<0.001$) suggested that z_{pelvis} was higher when stepping with the PL (EMM ± SE = 52.4±0.012 %BH) than when stepping with the NPL (50.4±0.012 %BH).

Step Kinematics

t_{step} and L_{step} were significantly correlated with a_{belt} ($p<0.001$). A significant main effect of DAY ($p<0.001$) and LIMB ($p<0.001$) suggested a decrease in t_{step} with training, and an increase of t_{step} when stepping with the PL (Figure 1). A larger LIMB discrepancy in t_{step} was apparent at disturbances with low a_{belt} (LIMB*a_{belt} $p<0.001$). The largest training improvement in L_{step} occurred when stepping with the PL in response to the most challenging disturbances (DAY*LIMB*a_{belt} $p<0.001$, Figure 1).

Trunk Kinematics

TFA and *TFV* were significantly correlated with a_{belt} ($p<0.001$ & $p=0.039$, respectively). For both stepping limbs, the largest training effect on *TFA* was apparent for large disturbances (DAY*a_{belt} $p<0.001$). The largest training effect on TFV was observed when stepping with the PL in response to the most challenging disturbances (DAY*LIMB*a_{belt} $p<0.001$).

CONCLUSIONS

With CSR training, unilateral, AK amputees improved their ability to recover from large postural disturbances. The subjects improved their CSR by taking longer initial steps in less time, and reducing their trunk flexion. The largest improvements were observed when stepping with the PL in response to the most challenging disturbances.

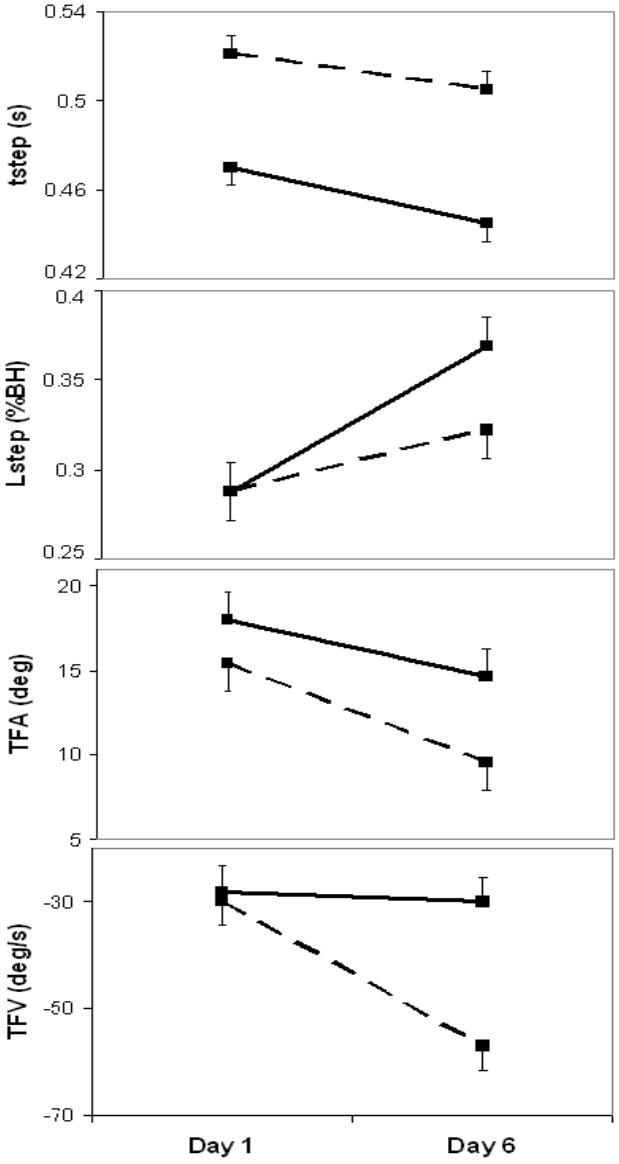

Figure 1: Estimated marginal means (± SE, evaluated at a_{belt}=3.6 m/s^2) of L_{step}, t_{step}, *TFA*, and *TFV* for each combination of DAY and LIMB (NPL = solid, PL = dashed). Positive trunk angles denote flexion from upright (0 deg).

REFERENCES

1. Miller WC, et al. *Arch Phys Med Rehabil* **82**, 1031-1037, 2001.
2. Owings T, et al. *Clin Biomech* **16**, 813-819, 2001.
3. Bieryla K, et al. *Gait Posture* **26**, 208-213, 2007.
4. Crenshaw JR, et al. *Proceedings of ASB'09*, State College, PA, USA, 2009.

ACKNOWLEDGEMENTS

Funding by Otto Bock Healthcare, Minneapolis, MN

ARE THE EFFECTS OF GAIT RETRAINING SIMILAR BETWEEN THE TRAINED AND THE UNTRAINED, CONTRALATERAL LIMB OF RUNNERS?

[1]Rebecca E. Fellin and [1,2,3]Irene S. Davis

[1]Biomechanics and Movement Science Program, University of Delaware, Newark, DE, USA
[2]Department of Physical Therapy, University of Delaware, Newark, DE, USA
[3]Drayer Physical Therapy Institute, Hummelstown, PA, USA
email: fellin@udel.edu

INTRODUCTION

Over 32 millions Americans run for exercise, and many are injured every year. Stress fractures are among the most serious of these injuries, with the tibia being the most common site [5]. Stress fractures have an alarmingly high re-injury rate of 36% [2]. Excessive vertical impact loading, including vertical impact peak (VIP), instantaneous and average vertical loading rates (IVLR and AVLR) as well as peak positive tibial acceleration (PPA), have been linked to tibial stress fractures [4].

We have demonstrated that runners with high vertical loading can be retrained to land softer and reduce their loading on the trained limb [1]. However, loading is often high on both limbs. A transfer of the effects of the gait training to the contralateral limb would have an added benefit in these cases. Previous studies of unilateral upper extremity strengthening found bilateral strength gains with lower gains in the untrained limb [3].

Therefore, the purpose of this study was to compare changes in vertical impact loading between the trained and contralateral limb following gait retraining. We hypothesized that loading (VIP, AVLR, IVLR) would be reduced in the contralateral limb, but to a lesser degree than in the trained limb.

METHODS

This is an ongoing study of which 8 subjects (28.0 ± 8.5 yrs) have been collected, to date. For inclusion, all subjects were running >10 miles/wk, currently injury free, and exhibited PPA > 8g's at a screening. This value was 1 standard deviation above the mean of a database of 400 runners.

A tri-axial accelerometer (PCB Piezotronics, Depew, NY, USA) was attached to the anteromedial aspect of subject's distal tibia. Subjects ran at 3.35 m/s on an instrumented treadmill (AMTI, Watertown, MA, USA) A VICON (Oxford, UK) motion analysis system captured kinetic data at 1000 Hz.

Subjects completed 8 sessions of retraining using real-time visual feedback of their PPA. They ran at a self-selected speed on a treadmill (AMTI, Watertown, MA) with a tri-axial accelerometer on their distal tibia. Subjects were instructed to land softer and keep their PPA <50% of their baseline value, depicted as a line on the monitor.

Run time increased from 15 minutes in the first session to 30 minutes in the final session. A faded feedback paradigm [6] was used whereby subjects received 100% visual feedback the first four sessions, and it was gradually removed over the last four sessions. Subjects were prohibited from running outside the laboratory during the training. After the final training session, subjects completed a second kinetic analysis.

Forceplate and accelerometer data were filtered at 50 and 75 Hz, respectively. Variables of interest, IVLR, AVLR, and VIP, were compared pre and post gait retraining on the training limb (TL) and the contralateral limb (CL). PPA was also analyzed on the TL. Due to the current sample size, data were analyzed descriptively. Means, standard deviations, percent changes and effect sizes were calculated.

RESULTS AND DISCUSSION

The results suggested that the gait retraining was successful as PPA decreased from 8.9 ± 3.1 g to 6.1 ± 3.2 g on the TL, which was a 31.3% decrease across subjects. All impact loading variables decreased post retraining (Table 1), with average decreases of 28.1% and 19.4% on the TL and CL, respectively. The effect sizes associated with these changes ranged from 0.9-1.4, which indicated large effects of the intervention in both limbs.

VIP was reduced in both limbs following training, but the TL demonstrated a 20.5% decrease, while a 13.2% reduction was seen on the CL. This finding was also true for IVLR, where decreases of 36.5% and 22.6% were noted on the TL and CL, respectively. Finally, reductions in AVLR were 27.5% and 20.3% in the TL and CL, respectively. These results support those reported by Lee et al. [3] in which cross training effects to the CL were less than the effects seen in the TL.

Table 1: Loading variables pre and post gait retraining (mean(SD)). Units: VIP (BW), AVLR and IVLR (BW/s)

	TL		CL	
Variable	Pre	Post	Pre	Post
VIP	1.8 (0.3)	1.4 (0.2)	1.7 (0.3)	1.5 (0.2)
IVLR	98.2 (23.2)	66.0 (19.2)	97.2 (31.1)	71.6 (23.2)
AVLR	79.5 (19.7)	56.2 (14.3)	79.8 (27.4)	61 (21.5)

The individual responses of the eight subjects demonstrate the trend of reductions bilaterally (Figures 1-3). Reductions in the CL were generally either similar to or less than reductions in the TL across subjects. Most subjects (5/8) demonstrated reductions of at least 15% in the CL for at least one variable.

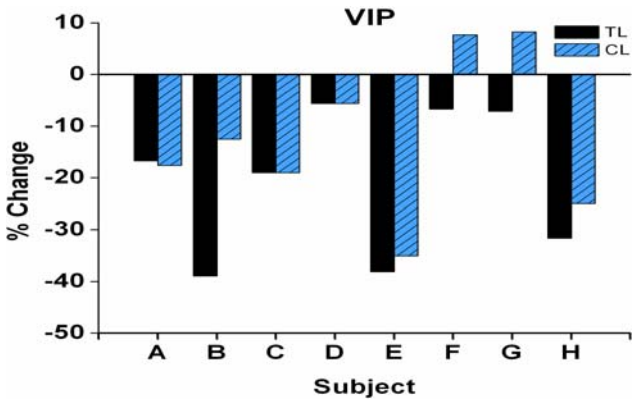

Figure 1: VIP % change after retraining for TL and CL.

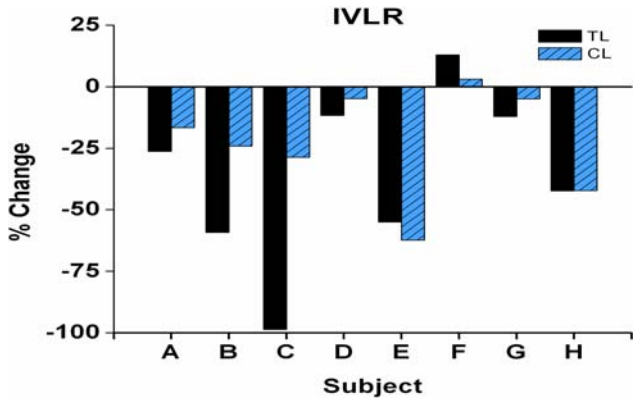

Figure 2: IVLR % change after retraining, TL and CL.

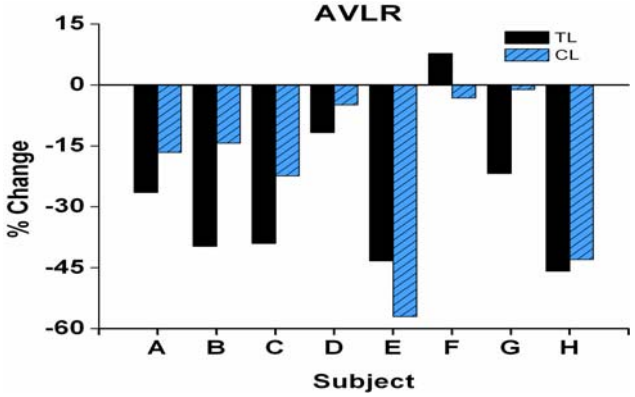

Figure 3: AVLR % change after retraining, TL and CL.

These preliminary results are very promising for several reasons. Subjects who undergo retraining often exhibit excessive loading bilaterally. The average values at baseline were similar between the two groups (Table 1). These values for both the TL and CL would place a runner at increased risk for a stress fracture [4]. As people have difficulty focusing on concurrently changing their mechanics in both limbs, the limb with higher loading for the variable of interest (PPA in this study) is chosen for retraining. Despite that the reduction in CL loading was less than in the TL, the mean values for impact loading all fell within normal limits of healthy control subjects following the intervention [4]. Therefore, training one limb had a reduced, but still important, cross training effect on the contralateral limb, reducing its risk for injury.

CONCLUSIONS

These preliminary data suggested that reductions in loading observed on the contralateral limb were a result of gait retraining. These reductions were not as large as those observed on the training limb. However, mean values for this cohort were within normal limits in the contralateral limb (as well as the training limb) following the retraining.

REFERENCES

1. Crowell, H and Davis I. *Proceedings of ASB, Blacksburg, VA, USA, 2006.*
2. Hauret, K et al. *Mil Med* **166**, 820-6, 2001.
3. Lee, M et al. *Clin Neurophysiol* **120**,802-8, 2009.
4. Milner, C et al. *Med Sci Sports Exerc* **38**, 323-8, 2006.
5. Taunton, J et al. *Br J Sp Med* **36**, 95-101, 2002.
6. Winstein, C. *Phys Ther* **71**, 140-9, 1991.

ACKNOWLEDGEMENTS

This study was supported by: DOD W911NF-05-1-0097, DOD W81XWH-07-1-0395 and NIH 5R01HD50679-2.

EFFECT OF HIP MUSCLE STRENGTHENING ON FRONTAL PLANE GAIT MECHANICS IN PATIENTS WITH KNEE OSTEOARTHRITIS

[1]Sang-Kyoon Park, [1]Michael Pohl, [1]Chandra Lloyd, [1]Jill Baxter, [2]Preston Wiley, [1]Reed Ferber

[1]Running Injury Clinic, Faculty of Kinesiology, University of Calgary, AB, CANADA
[2]Sport Medicine Centre, Faculty of Kinesiology, University of Calgary, AB, CANADA
email: spark@kin.ucalgary.ca, web: www.runninginjuryclinic.com

INTRODUCTION

Knee osteoarthritis (OA) is the most common joint disease with the medial compartment being the most effected [1]. It has been suggested that frontal plane joint mechanics such as asymmetric movement and an increased knee abduction moment during walking have been associated with the progression of medial knee OA [2, 3]. Thus, an improvement in these mechanics may have a beneficial disease-modifying effect. It has been proposed that weakness of the hip abductor muscles may lead to additional pelvic drop in the contralateral swing limb, which shifts the body's centre of mass (COM) toward the swing limb [2]. This shift may have an influence on increased loading across the medial compartment of the knee. Therefore, strengthening lower extremity muscles, focusing on the hip abductors may be beneficial. However, studies on the effect of muscle strengthening on changes in pain and frontal plane kinematics in knee OA have not been well studied. The purpose of this study was to investigate the effect of a 6-week hip strengthening program on frontal plane gait kinematics and knee OA pain.

METHODS

Nine patients over age 40 (7 females, 2 males, age: 54.8±5.6years, weight: 72.1±9.7kg, height: 170.5±10.2cm) who had been diagnosed with mild-to-moderate medial knee OA (K-L grade 1-3) were recruited from the Knee OA Clinic at the University. Biomechanical, strength and knee pain data were collected both prior to and following a 6-week hip muscle strengthening protocol. The strengthening program included strengthening the hip abductor, external rotator, and extensor muscles. Biomechanical data were collected using an eight camera motion analysis system (Vicon, USA) during treadmill walking (Figure 1). Maximum isometric muscle strength was measured using a force dynamometer (Lafayette instrument, USA). Knee pain was quantified using a visual analog scale (VAS). One examiner conducted all measurements to maintain consistency in the testing. An intraclass correlation coefficient (ICC) of within-day hip abductor strength on 9 patients showed good repeatability (ICC=0.98; $p<0.01$).

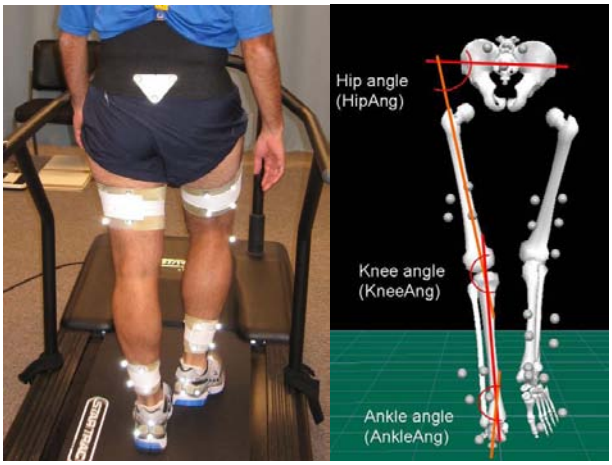

Figure 1: Experimental set up (left: treadmill walking, right: marker sets from a rear view).

Paired t-tests were performed to investigate any changes in frontal plane gait mechanics, muscle strength, and pain following a 6-week program.

RESULTS

After the 6 week program, the OA patients demonstrated 9.0%, 8.5%, 3.1% increase in abductor, rotator, and extension strength, respectively in maximal isometric measurements. Pain was reduced 46% ($p=0.001$). Significant changes in frontal plane kinematics were measured with decreased hip adduction and ankle inversion angles at heel contact ($p<0.05$; Table 1).

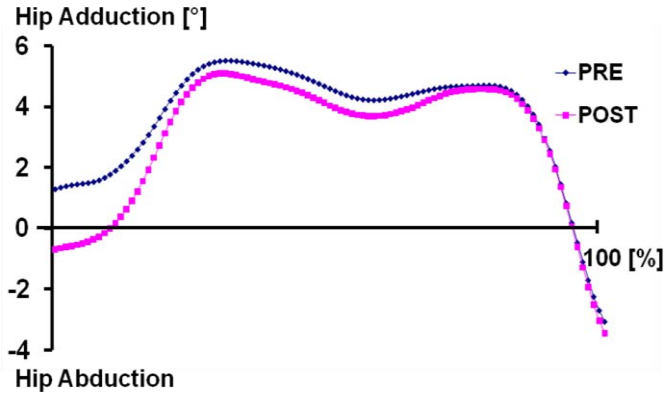

Figure 2: Hip adduction/abduction angles in knee OA patients during the stance phase of walking (pre vs. post exercise).

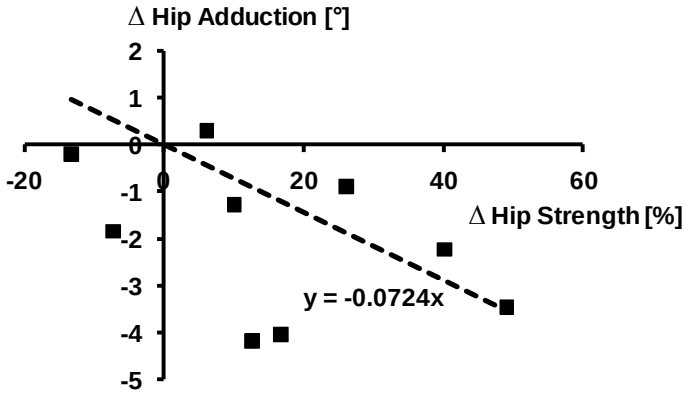

Figure 3: Linear regression using increases in hip strength to predict changes in hip adduction angle at heel contact during walking.

DISCUSSION/ CONCLUSIONS

These results suggest that a hip based strengthening program can effectively change joint kinematics during walking in addition to improving the pain associated with knee OA. Figure 2 shows that the hip adduction angle at heel contact underwent a greater reduction on the more affected side of the lower extremity following the 6-week exercise protocol. Additionally, the ankle inversion angle at heel contact was also decreased. These results indicate that strengthening musculature may play an important role in providing frontal plane stability and controlling medial and lateral loading at the knee during walking [4]. It is plausible that strengthening the hip abductors decreases hip adduction and ankle inversion which might lead to decreased external loading on the medial compartment of the knee [5]. Furthermore, a regression analysis indicated that increases in hip strength are negatively correlated with changes in hip adduction angle at heel contact (Figure 3; R=-0.45, p=0.22). This information would be useful to develop more effective individualized or subject specific interventions for medial knee OA.

Further research including the measurement of joint loading and electromyography (EMG) of the lower extremity is under investigation to better understand the effect of hip strengthening exercises on the progression in knee OA to develop optimal rehabilitation protocols.

REFERENCES

1. Felson DT, *Ann Intern Med* **133,** 635-646, 2000.
2. Chang A, *Arthr Rheum* **52,** 3515-9, 2005.
3. Mündermann A, *Arthr Rheum* **50,** 1172-8, 2004.
4. Pohl M, *Annals Rheumatic Diseases* **68,** S478, 2009.
5. Briem K & Snyder-Mackler, *J Orthop Res* **27**, 78-83, 2008.

ACKNOWLEDGEMENTS

Alberta Innovates Health Solutions Team Grant

Table 1: Summary of pain, hip abductor strength, and frontal plane joint angles between pre and post exercise training in knee OA patients.

	Pain (VAS)	Hip Abd Strength (Kg)	Frontal Plane Joint Angle (°)					
			Peak Ankle Eversion	Ankle Inv@HC	Peak Knee Adduction	Knee Add@HC	Peak Hip Adduction	Hip Add@HC
Pre Exercise	3.03 (2.15)	23.02 (10.10)	-9.12 (2.83)	2.72 (3.32)	7.24 (4.82)	2.71 (3.99)	6.14 (3.37)	1.29 (2.53)
Post Exercise	1.61** (1.40)	25.11* (7.15)	-9.59 (1.18)	1.32** (3.29)	8.00 (4.20)	3.26 (3.23)	5.62 (3.74)	-0.69** (2.50)

* indicates p<0.1, ** indicates p<0.05 compared with values in pre exercise, HC: heel contact

WEIGHT-BEARING ASYMMETRY AND CLINICAL MEASURES OF IMPAIRMENT AND FUNCTION BEFORE AND AFTER TOTAL KNEE ARTHROPLASTY

Cory L Christiansen, Tasia C Robertson, and Jennifer E Stevens-Lapsley

Department of Physical Medicine & Rehabilitation, Physical Therapy Program,
University of Colorado Denver, Aurora, CO, USA
email: cory.christiansen@ucdenver.edu

INTRODUCTION

It is known that weight-bearing asymmetry (WBA) occurs in individuals with unilateral knee osteoarthritis, characterized by preferential unloading of the affected limb. Even after total knee arthroplasty (TKA) intervention, WBA has been identified during common weight-bearing tasks such as walking [1] and sit-to-stand transitions [2]. It is possible that altered movement patterns created by WBA may impede rehabilitation progression following TKA, by reducing the demand on the surgical limb during daily function.

The purpose of this study was to examine the course of change for WBA, measured during transitions between sitting and standing, in individuals with unilateral knee OA before and after TKA. Secondly, the relationships between WBA and clinical measures of knee impairment and physical function were evaluated over the course of rehabilitation.

METHODS

Fourteen people with unilateral knee OA participated (age: 62.6 (7.5) years; BMI: 30.8 (4.9) kg/m^2; sex: 7 women and 7 men). Participants in this group underwent TKA and participated in standardized rehabilitation for 9 weeks after surgery. Seventeen people of similar ages to the TKA group (age: 66.8 (6.5) years; BMI: 27.2 (3.5) kg/m^2; sex: 8 women and 9 men) were enrolled in a control (CTL) group to allow comparison of WBA.

All participants performed a Five Times Sit-to-Stand Test (FTSST), consisting of a timed sequence of transitions between sitting and standing. During the test, vertical ground reaction force (vGRF) was measured with separate force platforms (PASCO scientific, Roseville, CA) under each foot.

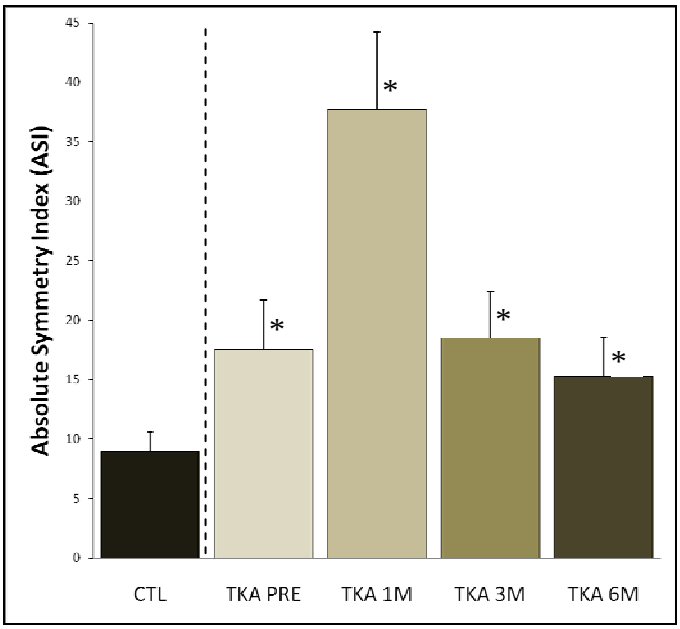

Figure 1: Absolute symmetry index (ASI) for the control (CTL) group and total knee arthroplasty (TKA) group pre- and post-operatively for vertical ground reaction force during transitions between sitting and standing. A value of zero would indicate perfect symmetry. Post-operative months 1, 3, and 6 are indicated by 1M, 3M, and 6M, respectively. *Significant difference compared to CTL group ($p < 0.05$).

Average vGRF during the FTSST was used as the measure of limb loading. An absolute symmetry index (ASI), using absolute limb loading difference, allowed comparison of WBA between TKA and CTL groups.

For the TKA group, measures of knee impairment and physical function were obtained at 1 month, 3 months, and 6 months post-operatively. Knee impairment was assessed using pain, motion, and strength measures. Pain was measured for the involved knee using an 11-item self-report numerical pain rating scale (NPRS) directly following the FTSST. Knee motion was assessed using a manual goniometer to measure degree of active knee extension motion with participants in

supine. Knee extension strength was assessed as maximum knee extension torque using an electromechanical dynamometer (CSMI, Stoughton, MA) with participants seated, hips flexed to 85° and knees flexed to 60°.

Physical function was assessed with two standardized clinical measures: a Six-Minute Walk Test (6MWT) and Stair Climb Test (SCT). The 6MWT measured the total distance walked on a level course in 6 minutes. The SCT measured time to ascend and descend one stair flight (12 steps).

Independent t-tests were used to identify differences in WBA between CTL and TKA groups. Pearson correlation coefficients were used to examine relationships between WBA and all other outcome measures across the time course of rehabilitation. To examine these correlations, a direction specific symmetry value was required. This was calculated as a simple symmetry ratio (SR) of the surgical limb value divided by the non-surgical limb value. A SR was calculated for vGRF during the FTSST as well as knee motion and strength impairment measures.

RESULTS AND DISCUSSION

Figure 1 illustrates WBA for the TKA group in comparison to the CTL group. Differences were present for WBA between the CTL group and TKA group at all time points. This finding agrees with previous studies for people with TKA [2,3].

Table 1 provides the TKA group correlations of WBA with all outcome measures at all time points. Significant correlations with WBA were identified pre-operatively for knee extension motion and knee extension strength. At all time points after surgery, the SCT was significantly correlated with WBA and the 6MWT was not.

These results indicate that factors related to WBA change from before to after TKA. Pre-operatively, greater WBA (i.e., lower symmetry ratio) was correlated with less symmetry in knee extensor strength and greater symmetry in knee extension motion. After surgery, correlations between WBA and these knee impairment measures were not significant. Interestingly, knee pain was not correlated with WBA at any time point.

In regards to physical function, relationships with WBA also change from before to after TKA. While no correlations with WBA were present prior to surgery, greater WBA was correlated with poorer function after surgery for the SCT. At all post-operative time points, SCT time was moderately correlated with WBA such that greater WBA was related to worse performance (i.e., longer time for stair ascent and descent). There was no significant correlation between 6MWT and WBA at any time point.

CONCLUSIONS

WBA during transitions between sitting and standing is greater for people with unilateral knee OA prior to and following TKA, when compared to healthy adults of similar age. In addition, relationships between WBA and select measures of knee impairment and physical function change across the course of rehabilitation. Further research is required to determine the viability of targeting WBA for intervention during TKA rehabilitation.

REFERENCES

1.Harato K, et al. *J Arthroplasty* **25,** 225-29, 2010.
2.Boonstra MC, et al. *Phys Ther* **90**, 149-56, 2010.
3.Mizner RL, et al. *J Orthop Res* **23**, 1083-90, 2005.

Table 1: Pearson product moment correlations between weight-bearing asymmetry and outcome measurements at progressive time points in relation to surgery.

	PAIN	EXT MOTION SR	STRENGTH SR	6MWT	SCT
Pre-operative	-0.25	**-0.47***	**0.51***	0.20	-0.34
1M post-operative	<0.01	-0.23	0.05	0.31	**-0.49***
3M post-operative	0.04	-0.28	0.42	0.42	**-0.61***
6M post-operative	0.09	0.15	0.36	0.44	**-0.50***

6MWT = Six-Minute Walk Test, SCT = Stair Climb Test, PAIN = Pain rating on numerical pain rating scale for surgical knee after sit-stand transitions, EXT MOTION SR = Symmetry ratio for extension range of motion, STRENGTH SR = Symmetry ratio for isometric knee extension strength, 1M = 1 month, 3M = 3 month, 6M = 6 month. * $p < 0.05$ (critical value of r for significance was 0.46)

JOINT LOADS IN ACL-DEFICIENT INDIVIDUALS AFTER NEUROMUSCULAR TRAINING

Emily Gardinier, Kurt Manal, Thomas S. Buchanan and Lynn Snyder-Mackler

University of Delaware, Newark, DE, USA
email: smack@udel.edu

INTRODUCTION

Early-onset osteoarthritis (OA) occurs in approximately every second ACL-injured knee within 10-20 years of injury, and may be related to altered knee loading patterns. The majority of individuals fail to dynamically stabilize their knee after injury ("non-copers"). Their neuromuscular compensation after injury includes truncated knee motion and altered muscle activity, which may culminate in loading insult to articular cartilage.

A specialized type of neuromuscular training called perturbation training was designed to increase dynamic stability and neuromuscular awareness in the lower extremity [1]. Perturbation training was first shown in ACL-deficient (ACL-D) individuals to improve function and elucidate changes in lower extremity muscle activities [2]. This type of training may also promote coordinated muscle strategies in non-copers more successfully than pre-operative strengthening programs alone. Insight into the effect of rehabilitation on joint loading will aid our understanding of the effect of neuromuscular strategies on degenerative changes which follow ACL injury.

The purpose of the present study was to estimate joint loading in ACL-D non-copers pre- and post-training to investigate the effect of standard quadriceps strength training (STR) versus quadriceps strength with perturbation training (PERT) on joint contact forces during gait. We hypothesized that joint contact forces would be greater in the ACL-D limb for all subjects at screening and that PERT training would produce more symmetrical loading than STR training alone.

METHODS

Seven individuals with acute unilateral ACL rupture (4 men, 3 women) participated in the study (Table 1). All underwent functional screening [1] and were classified as non-copers. All participants were athletes, 18-37 years old and acutely injured (<6 months). All demonstrated full knee range of motion, minimal effusion, ≥70% quadriceps index and ability to hop on the injured limb without pain. Participants were randomly chosen to undergo aggressive quadriceps strength training (STR; n=3) or quadriceps strength with perturbation training (PERT; n=4). Training consisted of 10 physical therapy sessions administered 2-5 times per week at the University of Delaware Physical Therapy Clinic. This study was approved by Institutional Review Board and all subjects provided informed consent prior to testing.

Table 1. Subject demographics.

Age (yrs)	28.1	±	7.4
Height (m)	1.74	±	0.08
Mass (kg)	88.3	±	18.3
Walking Speed (m/s)	1.49	±	0.09
Time from Injury (wk)	11.4	±	7.6
Training Comp. (wk)	3.9	±	1.8

Stance phase kinematics and kinetics were collected with the use of standard motion analysis methods (i.e., video cameras & force platform) and analyzed with Visual3D (C-motion, Inc). Electromyography (EMG) was collected for 7 lower extremity muscles. Subjects performed isolated maximum voluntary isometric contractions for validation of electrode placement and normalization of EMG amplitudes among subjects and between testing sessions.

Muscle forces were estimated using an EMG-driven model [3]. EMGs and joint kinematics were input to a modified Hill-type muscle model to estimate muscle forces. The muscle forces were applied to a frontal plane moment-balancing algorithm with contact forces as the unknowns. Contact forces for the medial and lateral compartments were time-normalized to 100 samples and normalized by bodyweight (BW). Three trials per subject were averaged in this manner.

RESULTS AND DISCUSSION

As a group, subjects walked with similar medial and lateral compartment loads in both limbs (Fig 1) at screening. We expected to observe asymmetrical medial joint loading at this time point, based on the knowledge that ACL-D non-copers exhibit asymmetrical muscle activations and sagittal plane excursions and moments. However, several different loading strategies may be present in this cohort, obscuring group differences. Recent assessment of the wide-ranging functional response to treatment and surgery among non-copers has demonstrated this cohort to be more variable than previously speculated [4].

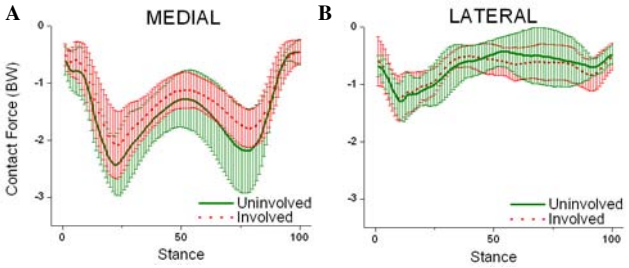

Figure 1: Medial (A) and lateral (B) compartment joint contact forces for involved and uninvolved limbs at screening. (Bars are standard deviations.)

Individuals who received STR training increased their peak medial contact force in both limbs after training (Fig 2a). This increase may be detrimental to articular cartilage health, and in the unstable ACL-D knee with altered contact mechanics, over-loading of normally un-loaded areas of cartilage may initiate degenerative changes.

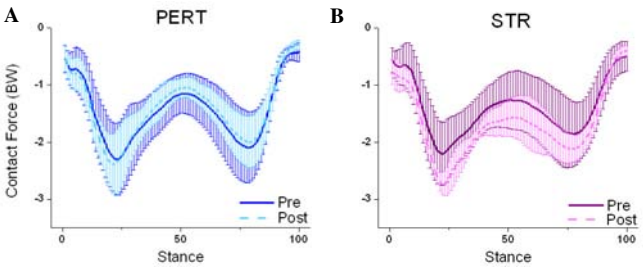

Figure 2: Medial compartment joint contact forces for (A) PERT and (B) STR training groups pre- and post-training.

Individuals who received PERT training in addition to strength/agilities maintained similar peak medal contact forces in both limbs after training (Fig 2b).

Similar results were found for the lateral compartment. Lateral joint loading did not change after training in the PERT group (Fig 3a). However, those who received STR training increased lateral joint contact forces post-training, when compared to screening (Fig 3b).

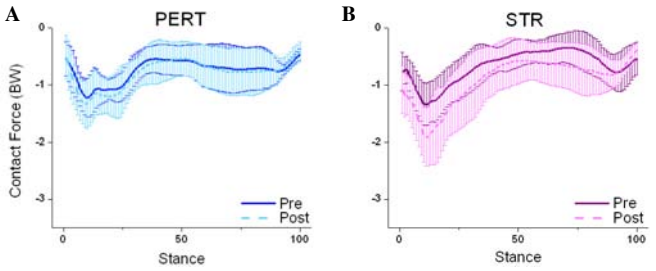

Figure 3: Lateral compartment joint contact forces for (A) PERT and (B) STR training groups pre- and post-training.

We lack loading analyses for non-copers who received no training intervention prior to surgery. However, pre-operative strength is predictive of knee function after surgery [5], and aggressive quadriceps strengthening is our current standard of care for ACL-injured individuals.

CONCLUSIONS

Joint loading was not different between limbs in ACL-D non-copers at screening. This may be due either to the presence of several loading strategies within the group, or it may reflect a truly normally-loaded ACL-D knee acutely after injury.

Joint loading increased with strength training alone, but when training was augmented with a neuromuscular training protocol, joint loading did not increase. These results suggest that perturbation training after ACL injury may be protective against increases in joint loading.

REFERENCES

1.Fitzgerald GK et al. *Knee Surg, Sports Traumatol, Arthrosc* **8**, 76-82, 2000.
2.Chmielewski TL, et al. *J Electromyogr Kinesiol* **12**, 267-74, 2002.
3.Buchanan TS, et al. *J Appl Biomech* **20**, 367-95, 2004.
4.Hartigan EH et al. *J Orthop Sports Phys Ther* **40**, 141-54, 2010.
5.Eitzen I, et al. *Br J Sports Med* **43**, 371-376, 2009.

ACKNOWLEDGEMENTS

Supported by NIH: R01 AR048212, AR046386, and S10 RR0223

OPTIMIZATION-BASED ASSESSMENT OF THE TRANSVERSE COMPRESSSIVE MECHANICAL PROPERTIES OF THE DIGITAL FLEXOR TENDONS AND THE MEDIAN NERVE

[2]Erin K Main, [1,2]Jessica E Goetz, [1]M James Rudert, [1,2]Curtis M Goreham-Voss & [1,2]Thomas D Brown

[1]Department of Orthopaedics & Rehabilitation, University of Iowa, Iowa City, IA, USA
[2]Department of Biomedical Engineering, University of Iowa, Iowa City, IA, USA
email: erin-main@uiowa.edu, web: http://poppy.obrl.uiowa.edu

INTRODUCTION

Carpal tunnel syndrome is a common chronic peripheral nerve entrapment disorder caused by mechanical insult of the median nerve, which may occur in part as a result of impingement by the surrounding digital flexor tendons. Finite element (FE) analysis provides a method to model the potentially pathological contact stresses between the flexor tendons and the median nerve [1]. Realistic FE simulations depend upon using physiologically accurate transverse compressive material properties for the digital flexor tendons and the median nerve. In this work, a custom-designed transverse testing apparatus was used to measure the transverse compressive stiffness of these structures. An FE model, used in conjunction with an optimization routine, allowed these transverse material properties to be inferred from the experimental transverse stiffness data.

METHODS

The (nine) digital flexor tendons and the median nerve were dissected from each of three normal cadaver hands ranging in age from 50 to 65 years old. The nerve and tendon diameters in the region of the carpal tunnel were determined using a purpose-developed device, which constrained the tissues to a circular cross-sectional area. This same section of the specimen was then used as the testing region.

The specimens were mounted in a specially designed transverse testing apparatus, using serpentine clamps (Fig. 1). Hollow cylindrical Delrin collars matching the specimen's diameter were placed around the tendons and nerves outside of the serpentine clamps, to prevent tissue flattening due to clamping. The preparation included a 37˚C saline bath. During testing, the specimens were held under a constant axial load (15N for flexor tendons, 5N for the median nerve), which was applied through a pneumatic cylinder controlled by a precision regulator. Transverse compression of the flexor tendons and median nerves was applied quasistatically (0.5 mm/sec) via convex Delrin platens 10 mm in diameter. The platens were connected to bearing slides with their displacement driven by an MTS 810 actuator. Each specimen's major axis was assessed based on the displacement at which initiation of load uptake occurred. Specimens were then compressed 40% of their major cross-sectional axis. Throughout testing, the load was measured with an 11.3 kg load cell.

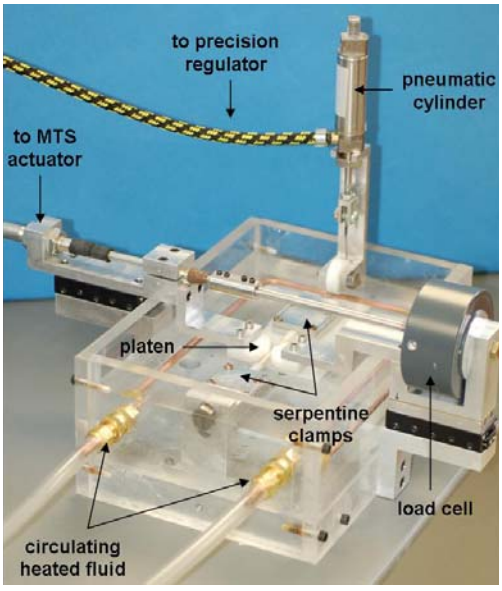

Figure 1: Transverse compression testing device.

FE models corresponding to each physical test were run in ABAQUS 6.91 (Fig. 2). The cylindrical platens were modeled in ABAQUS CAE as rigid surfaces, meshed with rigid body (R3D4) elements. Each tissue structure was modeled as an ellipse,

based on the experimentally measured cross-sectional area and major axis dimension. The tendon and nerve structures were meshed with hybrid hexahedral continuum elements using TrueGrid, with increased mesh refinement in the contact region.

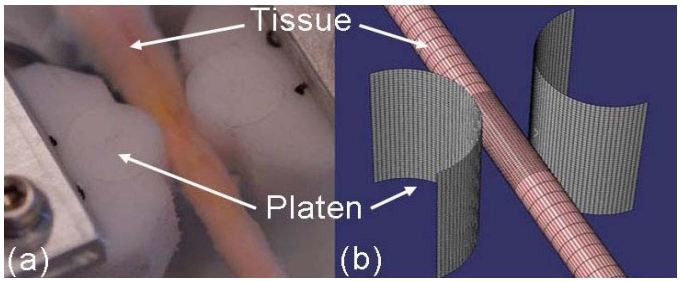

Figure 2: (a) Transverse testing apparatus with convex platens. (b) FE model corresponding to the experimental set up.

A first-order Ogden hyperelastic constitutive definition was used for the tendon and the nerve. For this constitutive model, strain energy W is a function of deviatoric principal stretches (λ_n):

$$W(\lambda_1,\lambda_2,\lambda_3) = \frac{\mu}{\alpha}(\lambda_1^{\alpha} + \lambda_2^{\alpha} + \lambda_3^{\alpha} - 3)$$

The FE models were used in conjunction with a Matlab optimization routine. Initial values for the two Ogden hyperelastic coefficients (μ and α) were selected for the first FE iteration. Transverse force and displacement data from the FE analysis were interpolated with the experimental results, allowing for force values to be obtained for the same set of displacement values. The sum of the squared error was then determined based on the difference in the force values between the experimental and the FE results. The material coefficient fitting routine utilized a least squares nonlinear optimization function to minimize this error, by iteratively adjusting the Ogden coefficients in subsequent FE runs.

RESULTS AND DISCUSSION

The optimization routine yielded well-convergent Ogden coefficients for the digital flexor tendons and median nerve (Figure 3). The average value of the coefficients for all of the finger tendons was 24.8 kPa for μ and 6.5 for α. The nerve was less stiff, with average coefficient values of 8.8 kPa for μ and 2.3 for α. The flexor pollicis longus (FPL) tendon tended to have a lower μ coefficient and a higher α coefficient as compared to both the deep (D) and superficial (S) finger tendons (Table 1).

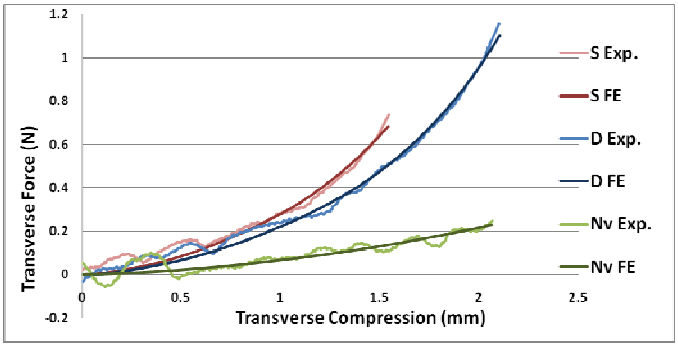

Figure 3: Experimental transverse force vs. compresssion data and optimized FE results, for illustrative superficial (S) and deep (D) tendons and the median nerve (Nv). Specimens were compressed 40% of their major axis.

Table 1: Average Ogden coefficients of the individual flexor tendons and the median nerve.

	μ (kPa)		**α**	
	Average	*St Dev*	**Average**	*St Dev*
D2	**22.9**	*4.20*	**6.20**	*0.60*
D3	**31.4**	*6.70*	**5.60**	*3.00*
D4	**18.8**	*3.20*	**4.50**	*3.20*
D5	**19.8**	*0.00*	**11.0**	*0.00*
S2	**25.8**	*18.5*	**4.00**	*1.90*
S3	**19.5**	*4.30*	**5.90**	*2.60*
S4	**31.4**	*9.90*	**6.00**	*2.30*
S5	**38.7**	*10.5*	**6.30**	*4.60*
FPL	**14.7**	*6.10*	**9.20**	*6.20*
Nerve	**8.80**	*2.50*	**2.30**	*0.60*

CONCLUSIONS

The Ogden hyperelastic material property definition provided a reasonable means to describe the transverse compressive behavior of the flexor tendons and the median nerve. The digital flexor tendons on average were nominally 3 to 4 times stiffer than the median nerve.

REFERENCES

1.Ko C & Brown TD. *Comput Methods Biomech Biomed Engin* **10**(5), 343-349, 2007.

ACKNOWLEDGEMENTS

Funding provided by NIH AR05389. Dr. Yuki Tochigi provided helpful assistance.

AN EXPERIMENTAL PLATFORM FOR MEASURING THE MECHANICAL BEHAVIOR OF TENDONS IN TORSION

Lisa M Martin, C Paul Buckley and Amy B Zavatsky

Department of Engineering Science, University of Oxford, Oxford, UK
email: amy.zavatsky@eng.ox.ac.uk, web: http://www.eng.ox.ac.uk

INTRODUCTION

Although the mechanical behavior of tendons in tension is well characterized, significantly less is known about their behavior in torsion. An understanding of tendon behavior in torsion would prove useful in applications such as anterior cruciate ligament (ACL) reconstruction, as the ACL twists as much as 76.0˚ ± 20.1˚ about its long axis *in vivo* [1]. Although the torsional behavior of the scapholunate ligament has been characterized [2], no other attempts appear to have been made to measure the torsional response of either tendons or ligaments. The acquisition and analysis of such data for tendons similar to those used in ACL reconstruction would allow for more accurate characterization of ACL grafts in finite element models and, in turn, might lead to improved surgical techniques. Furthermore, such data can be used as a benchmark by tissue engineers. The aim of this study was to develop an experimental platform for characterizing the torsional response of tendons.

METHODS

This experimental approach uses bovine digital extensor tendons, shown to be excellent mechanical representatives of double-bundle semitendinosus-gracilis ACL grafts [3]. Bovine feet are acquired the day of slaughter, frozen at -18˚C, and thawed overnight prior to testing. The medial digital extensor, common digital extensor (prior to branching), and lateral digital extensor tendons are then dissected. After soaking in 10% sucrose for one hour, each tendon is measured every 5 mm along its length using an image-based, non-contact technique [4] to obtain its cross-sectional shape (Fig. 1). The tendons are then soaked overnight in 10% sucrose.

On the following day, one end of each tendon is fixed between two ribbed rubber sheets using cyanoacrylate glue, and a braided Spectra® line (PowerPro®) is laced through the sheets and tendon for additional fixation. A second line is laced through the opposite end of each tendon to create a suture which distributes tensile loads through the tendon. The sutured end of each tendon is pulled through a Dural® tube ("tendon tube") within which it is fixed in axial alignment using tissue paper soaked in cyanoacrylate. The result is an axially centered tendon with rigidly fixed ends. The tendons are then soaked in 10% sucrose for one hour.

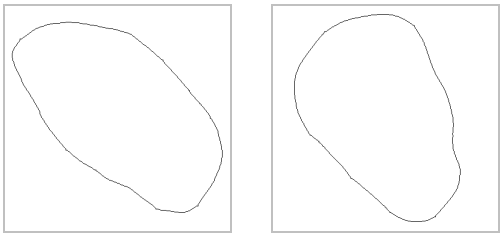

Figure 1: Two cross-sections of a sample tendon (each square is 8 mm x 8 mm).

Tests are conducted using a torsion pendulum (Fig. 2) suspended in a Zwick/Roell tension/compression testing machine with spring-activated grips (Zwick Roell AG). The tendon tube is inserted into a brass "cap" with holes through which the suture is threaded. The tube and cap are positioned relative to each other using a steel cross-pin, and the suture is pulled taut and tied off. The cross-pin is removed and then used to secure the subassembly inside the receiver bolted to the inertia bar. Grub screws prevent rotational slip. The assembly is suspended from Kevlar® strands, chosen for their low torsional stiffness, low damping, and high tensile strength. The assembly without the tendon has a moment of inertia about its axis of 629 g cm^2. The addition of ball bearings of known mass at discrete locations allows for controlled increases in inertia. Finally, a draft shield is placed around the tendon. This setup ensures that tension is transmitted directly to the tendon; that the test axis, tendon longitudinal axis,

and inertia bar axis of rotation are co-axial; and that there is no rotational slip of the tendon.

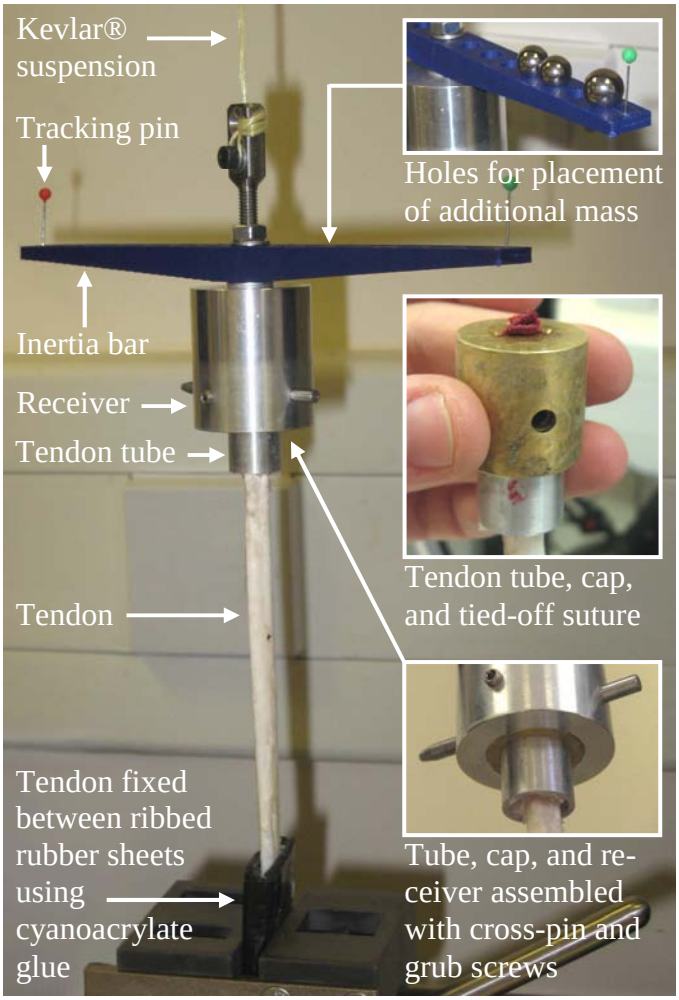

Figure 2: Torsion pendulum assembly.

A nominal tensile load is applied to remove slack. Rotational oscillations of the torsion pendulum assembly are initiated manually and recorded on digital video using a PlayStation® Eye camera (Sony) at 640x480 px resolution and 30 fps using the CL-Eye Platform Driver (Code Laboratories, Inc.). The oscillation video is processed through the color-based tracking of a red pin on the inertia bar, yielding a plot of angle vs. time to which an exponentially decaying sine wave is fit to determine the frequency and damping coefficient (Fig. 3). Initial oscillations are excluded from the fit to minimize the influence of the manual start. The stress function and shear strain distributions are computed numerically for each of the measured cross-sections. Integration of the stress function then provides the torsion constant. Using the length of the tendon, the positions of the cross-sections along its length, and the individual torsion constants, an effective torsion constant for the entire tendon is calculated. The complex shear modulus is then calculated from the oscillation frequency and damping coefficient. Although air resistance has been found to be negligible, the effect of the suspension strands is taken into account. All test data are processed in MATLAB (The MathWorks™).

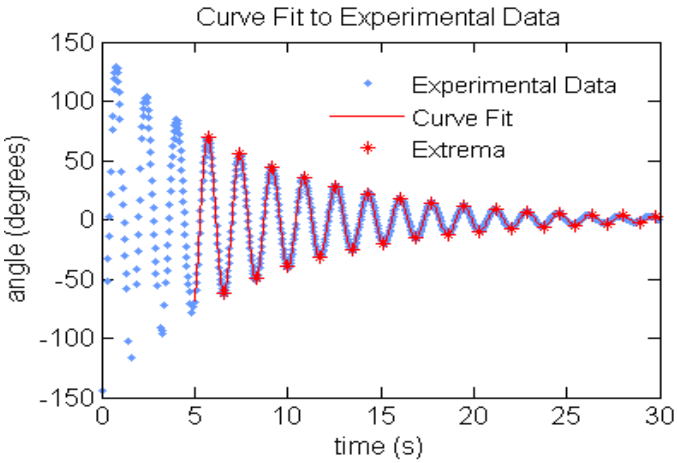

Figure 3: Exponentially decaying sine wave fit to experimental data.

RESULTS AND DISCUSSION

For the sample tendon with test results in Figure 3, the tendon length which underwent torsion was 110 mm, the effective torsion constant was J = 118 mm^4, the maximum shear strain was 0.055, and the complex shear modulus was G^* = 0.78 + j0.058 MPa.

CONCLUSIONS

This experimental platform may be used for efficient testing of tendons in torsion using a wide range of inertias and tensile loads.

REFERENCES

1.Jordan SS, et al. *Am J Sports Med* **35**, 547-551, 2007.
2.Zdero R, et al. *Proc Inst Mech Eng Part H J Eng Med* **222**, 907-914, 2008.
3.Donahue TLH, et al. *J Biomech Eng* **121**, 162-169, 2001.
4.Salisbury ST, et al. *Meas Sci Technol* **19**, 045705, 2008.

ACKNOWLEDGEMENTS

Lisa M. Martin is funded by a Marshall Scholarship.

AN OBJECTIVE QUANTITATIVE COMPARISON OF STRUCTURAL DAMAGE FROM DIFFERING RABBIT OA MODELS

[1]Curtis Goreham-Voss, [1]Yuki Tochigi, [1]Todd McKinley and [1]Thomas Brown

[1]University of Iowa, Iowa City, IA, USA
email: curtis-voss@uiowa.edu

INTRODUCTION

Structural damage within the extra-cellular matrix (ECM) of cartilage is a well-recognized feature of osteoarthritis (OA). Elevated chondrocyte death has been shown to occur in proximity to cartilage cracks [1, 2], and the importance of ECM damage is recognized by its inclusion in OA grading scores by Mankin and OARSI [3, 4]. However, to date, little attention has been paid to the specific morphology of cartilage cracks. Careful quantification of crack morphology would provide an additional source of information to compare different OA models. In this study, an image analysis computer program is developed which automatically calculates several morphologic parameters of cracks as seen in digitized cross-sectional histologic sections. This program is then applied to a large series of histology slides from rabbit OA models involving ACL-transection, an osteochondral defect, or both, to invoke OA. Structural damage and crack morphology are compared among the different models, and between 8 week versus 16 week sacrifice times.

METHODS

A Matlab program was designed to quantify crack morphology. For each slide, the user sets a grey-level threshold, which auto-segments the cartilage from the background. The user then identifies the articular surface and the tide-mark. Isolated regions in the cartilage are identified, and a threshold on region area is used to remove cracks too small to quantify. For each remaining crack region, thinning operations are used to reduce the region to a series of branches. The largest branch is identified as the centerline, and for surface cracks the centerline is constrained to pass through the center of the crack opening. Based on the crack region, centerline, articular surface and tidemark, several morphologic characteristics are calculated: (1) **Type –** 'Flaw' if number of branches is greater than 4 or ratio of opening width to crack length is greater than 0.8, 'Crack' otherwise, (2) **Opening Width –** absolute width of the crack at its opening to the articular surface, (3) **Angle –** angle between the local articular surface and a line fit to the centerline, (4) **Location –** 'Surface' if crack breaches the articular surface, 'Subsurface' otherwise, (6) **Affected Area –** immediate area likely to be significantly structurally compromised by crack, calculated as convex hull area of the region, (7) **Area** – total area of the crack, (8) **Center Length** – length of the centerline only, (9) **Total Length –** combined length of all crack branches, including centerline, (10) **Tortuosity –** a measure of the linearity of the crack, calculated here as 1-Chord/(Center Length), where Chord is the distance between the start point and endpoint of the centerline, (11) **Relative Depth –** the normalized distance the crack extends through the cartilage thickness.

The crack morphology program was run on a series of slides from a study of three rabbit OA models. In that study, OA was induced by a partial or complete transection of the ACL, by an osteochondral defect created in one of the femoral compartments, or by both a transection and a defect. Several non-operative control specimens were also processed. For each specimen, four mid-compartmental sagittal plane histologic sections were taken, one from each compartment (medial and lateral, tibial and femoral). The slides were Safranin-O/fastgreen-stained and digitized for processing. A total of 569 slides were processed (the complete slide, which would include the entire weight-bearing region within the sectioned plane), with 840 individual cracks identified and quantified. Significant differences between crack morphology parameters were tested using ANOVA on means (ordinal data) or t-tests of proportions (categorical data).

RESULTS AND DISCUSSION

Morphologic characteristics of individual cracks, comparing 8 week and 16 week timepoints and comparisons between control and the different OA models are shown in Figure 1. No statistically significant variation in crack morphology was found between the two time points. However, several statistically significant differences were found between the OA models, particularly in lengths and areas. There was little difference in morphology between cracks found in the control specimens and those in ACL transection specimens. Figure 2 shows the variation of total damage per specimen. Again, there is no difference between 8 and 16 week groups. Increases in total crack area and affected area are seen with different OA models, although the differences in total affected area between individual OA models do not reach statistical significance.

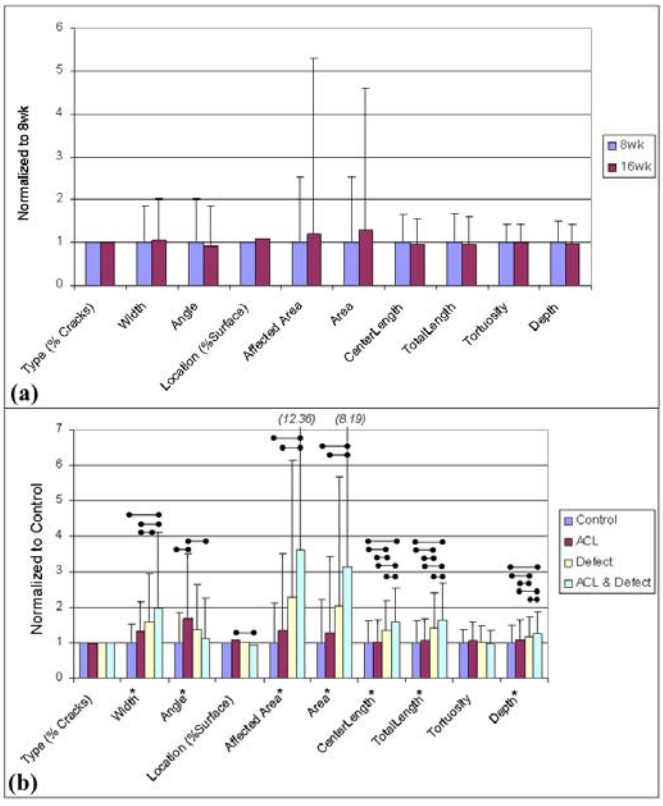

Figure 1. Relative changes in crack morphology parameters between (a) time points, and (b) OA models. Asterisks by categories indicate statistically significant differences among all groups; bars above values indicate statistically significant differences between specific groups ($p<0.05$)

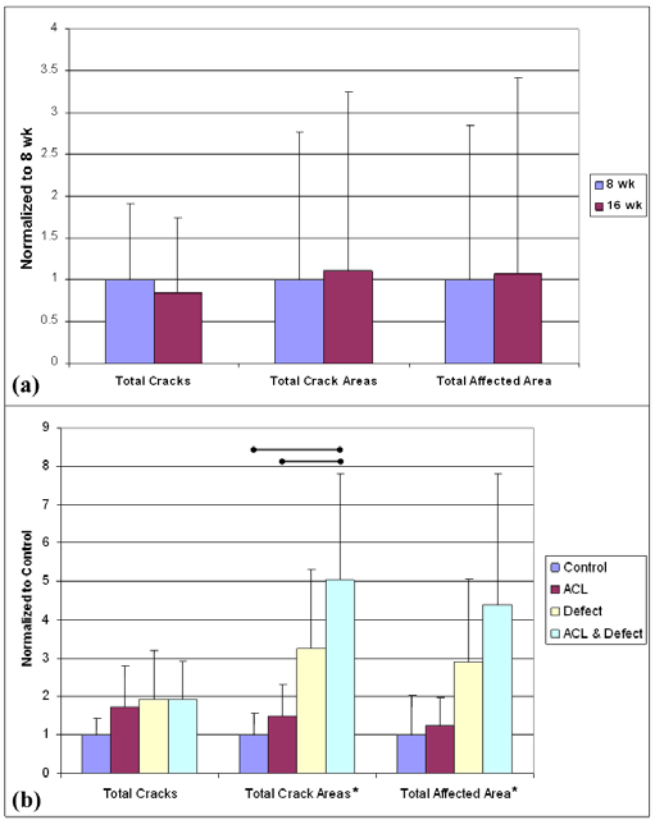

Figure 2. Relative changes in total damage across all four slides per specimen. Statistical power and annotations are the same as Figure 1.

CONCLUSIONS

The data presented in this study suggest that there is little difference in mechanical damage between 8 week and 16 week sacrifice times. There are, however, significant differences between different OA models, with the ACL model causing the least severe damage, followed by the defect model, and with the most damage from the combined model. It is likely that mechanical damage occurs differently in different clinical patient groups as well. The program developed here can be used to help ensure that OA models are relevant to the injury population under study. Future applications of this program will investigate the mechanical damage in impact specimens, as well as clinical specimens.

REFERENCES

1. Démarteau et al. OAC 14(6):589-96, 2006.
2. Lewis et al. JOR 21(5):881-7, 2003.
3. Mankin et al. JBJS 53A(3):523-37, 1971.
4. Pritzker et al. OAC 14(1):13-29, 2006.

ACKNOWLEDGEMENTS

This study was supported by a grant from the NIH (5 P50 AR055533)

AFM ANALYSIS OF CARTILAGE DEGRADATION IN A RAT MODEL FOLLOWING ACL TRANSECTION

[1]Kimberly Waller, [1]Eric Darling, PhD and [1,2]Gregory Jay, MD, PhD

[1]Brown University, Providence, RI, USA
[2]Rhode Island Hospital, Providence, RI, USA
email: Kimberly_Waller@brown.edu

INTRODUCTION

Anterior Cruciate Ligament (ACL) injury is a common sports-related injury associated with degenerative cartilage changes that present as osteoarthritis (OA) due to altered biomechanics, biological pathways and decreased boundary lubrication. While the exact progression of OA is unknown, its early presence is often marked by the loss of glycosaminoglycans (GAG) in the cartilage matrix and a discrete fibrillation of the surface and loss of superficial zone chondrocytes [2]. There is currently no treatment for OA to repair the breakdown of cartilage.

Using Atomic Force Microscopy (AFM), Stoltz, et al. demonstrated that the superficial zone stiffness properties reflecting the collagen network differ from the properties of the entire thickness of the cartilage, as well as changes in the superficial zone stiffness before the loss of GAG and bulk mechanical properties of articular cartilage in the femoral head of a collagen IX knockout mouse [1].

This study aims to detect the early signs of OA in the femoral condyles of a rat following ACL transection.

METHODS

Skeletally mature male Lewis rats underwent ACL transection of the right hind leg, as described previously [2]. Control rats were sacrificed on day 0 and underwent no surgical procedure. At 19 and 40 days post operatively, the limbs were harvested and kept at 4°C in a protease inhibitor cocktail (Roche).

Following the isolation and separation of the femoral condyle into femoral and medial compartments, the samples underwent AFM testing in three load bearing regions of the cartilage, using two probe types to analyze microstiffness and nanostiffness. Samples were kept fresh in PBS and protease inhibitor throughout the study and used within two days of harvest. Prior to testing, specimens were mounted on petri dishes and remained hydrated throughout testing. Testing was complete within 48 hours of harvest.

The stiffness measurements of articular cartilage were performed by indentation in three 20 micron x 20 micron areas of the cartilage. Load-displacement curves were recorded in contact mode at a trigger point that corresponds to the maximum applied load, of 1.8nN for the sharp pyramidal tips (115 mm long SiN cantilevers, nominal cantilever spring constant of 0.32 N/m; Veeco, Santa Barbara, CA) and 100nN for the microspheres (Si02 Glass Particle 5µm in diameter, mounted on a cantilever, nominal spring constant 7.5 N/m; Novascan, Ames, IA). Nanostiffness and microstiffness were determined by fitting an elastic model to the experimental data. Images of the cartilage surface were taken in tapping mode using the sharp pyramidal probe.

RESULTS AND DISCUSSION

Three weeks following ACL transection, a drop in both nanostiffness and microstiffness was apparent compared to control. After 40 days, the surface of the cartilage was rough and the microstiffness decreased from the 19 day time point (Figure 1).

At the nanoscale, the cartilage stiffness decreased from approximately 16 kPa across the femoral condyle to 7 kPa, 19 days postoperatively. Forty days postoperatively, another decrease in stiffness was observed in the lateral condyle, to about 1.5kPa (Figure 2).

We observed a dramatic decrease in microstiffness at the day 19 time point, followed by a further decrease at day 40 (Figure 3). It is hypothesized that the decrease in stiffness of the bulk cartilage matrix is due mainly to the loss of GAG, which is a common symptom of OA and is irreversible.

The mechanical properties of the medial condyle were generally higher than that of the lateral condyle (Figures 2 and 3). This observation is likely due to the fact that the medial condyle sees a higher load *in vivo* than the lateral condyle, and as a result, naturally shows a more robust matrix. The increased degree of softening is likely caused by a number of changes in the joint including altered biomechanics, down-regulation of GAG and possibly lubricin [2], as a result of inflammation.

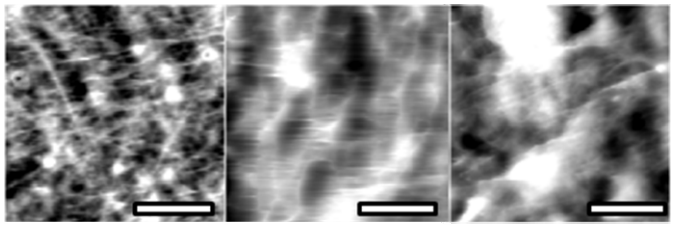

Figure 1: AFM Images taken with a sharp probe. (left) No surgery. The collagen matrix is intact with clear, intersecting fibrils. **(middle)** 19 days post-operatively the matrix has begun to break down. Fibers still show connections, but with a clear breakdown. **(right)** 40 days post-operatively, the matrix shows increased degradation. Scale bar represents 5 µm.

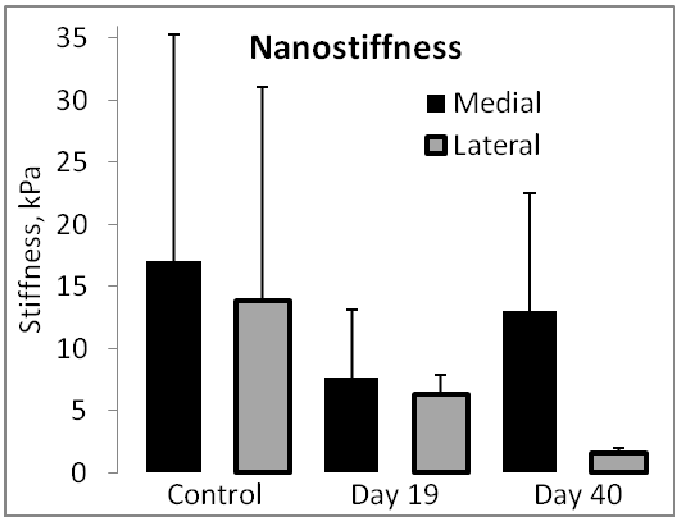

Figure 2: Nanostiffness observed in the medial and lateral compartments of the femoral condyle following ACL transection.

The observed decrease in elastic modulus and collagen breakdown indicate a loss in cartilage integrity and an increase in fibrillation and cartilage surface disruption, which is seen in histological studies of ACL transection in rat models [2].

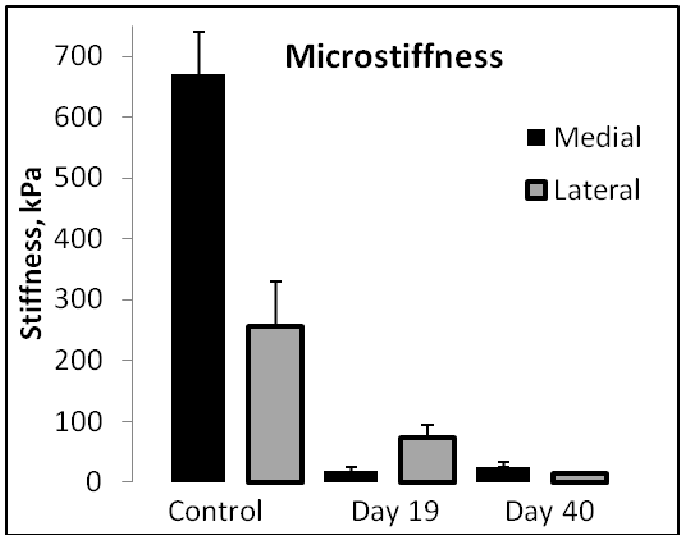

Figure 3: Microstiffness observed in the medial and lateral compartments of the femoral condyle following ACL transection.

CONCLUSIONS

An early change in mechanical properties seen in the superficial zone may serve as further indication of cartilage degradation and could indicate early chondrocyte death and collagen network breakdown, which have been hypothesized to occur prior to significant cartilage damage and significant loss of GAG. Subsequent studies may employ this method as a technique to test preventative OA treatments for patients with ACL tears, meniscal disruption, or other traumas associated with articular cartilage damage.

REFERENCES

1. Stoltz M, et al. *Nature Nanotechnology* **4**,186-192, 2009.
2. Elsaid KA, et al. *Arthritis & Rheumatism* **60(10)**, 2997-3006, October 2009.

ACKNOWLEDGEMENTS

This research was funded by NIH/NIAMS R21AR055937, RO1AR050180, R41AR057276 and NCRR COBRE P20 RR024484.

THE ORIENTATION OF COLLAGEN FIBERS OF THE TRANSVERSE CARPAL LIGAMENT

[1]Prantil, R K; [1]Xiu, KH; [1]Kim, KE; [1]Gaitan, D; [1]Sacks, M S; [1]Woo, SL; [2]Li, ZM
[1]Department of Bioengineering, University of Pittsburgh, Pittsburgh, PA
[2]Departments of Biomedical Engineering, Physical Medicine and Rehabilitation, and Orthopaedic Surgery, Cleveland Clinic, Cleveland, OH
E-mail: liz4@ccf.org

INTRODUCTION

Currently, carpal tunnel syndrome (CTS) affects 1% of America's population. CTS is classified as a compression neuropathy of the median nerve which, in turn, causes pain. To treat CTS, surgeons transect the transverse carpal ligament to release pressure off the median nerve.

The transverse carpal ligament (TCL) is located at the palmar roof of the carpal tunnel. Gross observation shows that the ligament appears to be a dense collagenous matrix with fibers roughly oriented along the transverse direction [1]. However, an anatomical investigation on the configuration of the TCL shows that there are fibers orienting in the oblique (unlar/radial oblique) and the transverse directions [2]. The mechanical properties of the ligament could be largely affected by the fiber orientation within the matrix. Thus, knowledge of the TCL's fiber orientation is needed to better understand its mechanical properties and its role in regulating carpal tunnel biomechanics.

Therefore, the purpose of this study was to quantify collagen fiber orientation within the TCL using the small angle light scattering (SALS) technique which has shown to be effective in quantifying fiber structure in connective tissue [3].

METHODS

Eight TCL samples, removed from human cadaver hands (53±13 years), were used in this study. The TCL tissue was fixed in 10% formalin solution for 24 hours. Two tiny holes were drilled along the connection line between the midpoints of the distal and proximal edges of the TCL. These two holes were used as the reference for quantifying fiber orientation. The TCL's thickness was measured with calipers. Individual 20μm sections were cut evenly along the thickness of the TCL in a cryostat (Microm®). Sections of three thickness levels (25%, 50% and 75%) were collected from each TCL referenced at its dorsal face. SALS was used to scan the fiber orientation for each section [3].

The orientation index (OI) and the preferred fiber direction were used to describe the fiber distribution on each scanned area [3]. The OI is a value that measures the sparsity of fibers over the area while the preferred fiber direction is the average measurement for fiber orientation. Fiber areas were included in locations where their OIs were less than 45º [4]. Fibers were grouped in the following orientation ranges: Radial-Oblique [23º, 67º], Transverse [0º, 22º] & [158º, 180º], Ulnar-Oblique [113º, 157º], and Longitudinal [68º, 112º] (Fig. 1). In the left hand, the oblique ranges are switched to match with the anatomical descriptors for the right side.

The Watson-Williams test on the angular dispersion was used to investigate the differences of the fiber orientation with respect to the tissue slice depth. In addition, a two-way ANOVA was used to analyze differences along the slice depth and the fiber orientation type. Thereafter, Bonferroni post-hoc analyses were ran for each factor and the interaction term between

factors to if significant differences were found (α=0.05).

RESULTS

The fiber percentages in each orientation range along the 25%, 50% and 75% thickness of the TCL are shown in Fig. 2 that the transverse fibers increased as the depth increased. The predominance of the transverse fibers seemed to increase as the depth increased. In contrast, the radial-oblique and longitudinal fiber areas seemed to stay relatively constant while the ulnar-oblique fiber areas decreased as the slice depth increased. Although there appears to be an increasing amount of transverse fibers as the depth increases, the Watson-William test revealed this change to be insignificant ($P > 0.05$).

In contrast, the two-way repeated measures ANOVA found that the fiber percentages in individual orientation types were significantly different ($P < 0.05$). Post-hoc testing for the fiber percentages indicated that the transverse fibers are the predominant orientation type, followed by oblique and longitudinal fibers (Fig. 2).

DISCUSSION

The predominant fiber within the TCL was found to be transverse followed by oblique and longitudinal fibers. It was also found that this arrangement of fibers doesn't significantly change from the surface to the deeper portion of the TCL. The data are in contrast with those in the past [2]. But, we believe that the current technique is more quantitative.

Also the TCL was found to have a preferred degree of fiber alignment suggesting material anisotropy, namely transverse isotropy because the predominant, fiber direction is transverse while there are marginal, orthogonal fibers. These findings are validated by our laboratory; tensile testing of the TCL showed that the tangent modulus of the transverse direction was 38 times respectively higher than those in the longitudinal direction.

REFERENCES

[1] Rotman et al. 2002 Hand Clin 18:219-230
[2] Isogai et al. 2002 J Orthop Sci 7:79-83
[3] Sacks et al. 1997 Ann Biomed Engin 25: 678-689
[4] Debski et al. 2006 J Shoulder Elbow Surg 12(3): 247-252

ACKNOWLEDGEMENTS

NIH T32EB0039-01 (MSS), NIH R03AR054510 (ZML), and Center for Biological Imaging (CBI).

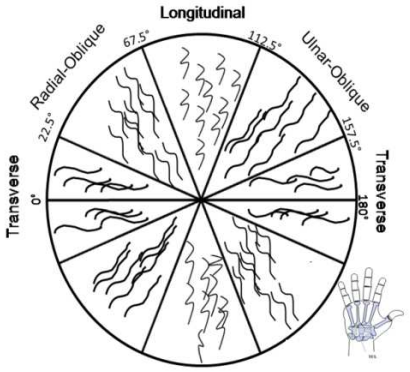

Figure 1: Displays fiber ranges that were considered (palmar view of right hand).

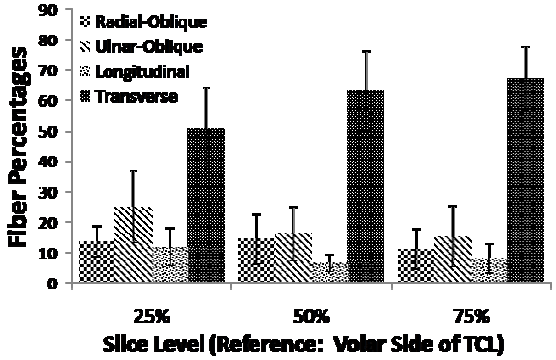

Figure 2: Shows the fiber percentages throughout the depth of the TCL.

IMPROVING REGIONS OF DEVIATION GAIT SYMMETRY ANALYSIS WITH POINTWISE T-TESTS

Louis A. DiBerardino III, Chantal A. Ragetly, Sungjin Hong, Dominique J. Griffon and Elizabeth T. Hsiao-Wecksler

University of Illinois at Urbana-Champaign, Urbana, IL, USA
email: diberard@illinois.edu, ethw@illinois.edu

INTRODUCTION

Pathological and injured gaits often produce limb asymmetry, which can be used to identify and track problems [1]. Shorter et al. addressed this by developing the Regions of Deviation (ROD) method for identifying regions of the gait cycle where joint angular displacements deviated from normative data [2]. To statistically identify differences, Shorter et al. performed a *t*-test at single points during stance and swing. Our goal was to extend their statistical analysis by utilizing point-wise *t*-tests on the deviation data throughout the entire gait cycle to get a sense of the true regions for which the movement patterns deviated from normal. We demonstrate these methods on canine gait data of Labrador Retrievers without and with naturally occurring cranial cruciate ligament disease (CCLD) in the hind limb. The CCL is a critical stifle (knee) stabilizer and CCLD is the leading cause of pelvic lameness in dogs. ROD methodology results on these dogs were then compared to the kinematic peak difference analysis described in [3].

METHODS

Twenty-one adult pure bred Labrador Retrievers (36.6 ± 8.5 kg, 81 ± 30 months, 13 females/8 males) were used. Twelve were healthy and 9 had unilateral hind limb CCLD. Data collection and inverse dynamics computation were previously described [3,4]. Sagittal-plane projections of joint angular displacements for the hip, stifle (knee), and hock (ankle) joints of both hind limbs were examined. Data were linearly time normalized from 0-100% gait cycle at 1% increments, and separated into stance and swing. Both phases were normalized again so that toe-off consistently occurred at 46% GC, which was the healthy group average.

Since this work focused on deviations from symmetry, analysis was performed on the magnitude of differences between the left (*l*) and right (*r*) joint angles (*V*). The absolute difference for each joint (*j*) of subject *i* was defined as

$$\Delta V_{j,n}^{(i)} = \left| V_{j,n}^{(i,l)} - V_{j,n}^{(i,r)} \right| \quad (1)$$

for each *n*, corresponding to percent gait cycle. The deviation from normative data (*D*) was defined as

$$D_{j,n}^{(i)} = \begin{cases} \Delta V_{j,n}^{(i)} - N_{j,n} & \text{if } \Delta V_{j,n}^{(i)} > N_{j,n} \\ 0 & \text{if } \Delta V_{j,n}^{(i)} \le N_{j,n} \end{cases}, \quad (2)$$

where $N_{j,n} = \Delta\bar{V}_{j,n} + \mathrm{SD}_{j,n}$, such that the corresponding healthy group mean and standard deviation are $\Delta\bar{V}_{j,n}$ and $\mathrm{SD}_{j,n}$, respectively. Paired *t*-tests were performed ($\alpha = 0.05$) at every point *n* (1% GC) of *D* between groups for each joint. All points *n* found to be significant were then considered to fall within a region of deviation from symmetry for joint *j*.

Discriminant function analysis (DFA) was used to validate that these discrete regions of deviation were better discriminators of differences between healthy and CCLD behavior than using the entire cycle. Subjects were classified with the holdout method as either healthy or having CCLD. These classification results were then compared to similar results using all time points (rather than just regions of deviation) to see whether the ROD methodology improved the classification.

RESULTS and DISCUSSION

Average CCLD affected and contralateral limb joint angle patterns were qualitatively quite different from the average normal limb (Fig.1a-c). The major peaks previously analyzed by [3] are labeled for reference and comparison. The asymmetries induced by CCLD were also readily apparent; significant regions of deviation from symmetry, as compared to the healthy group, are indicated by shading (Fig.1d-f).

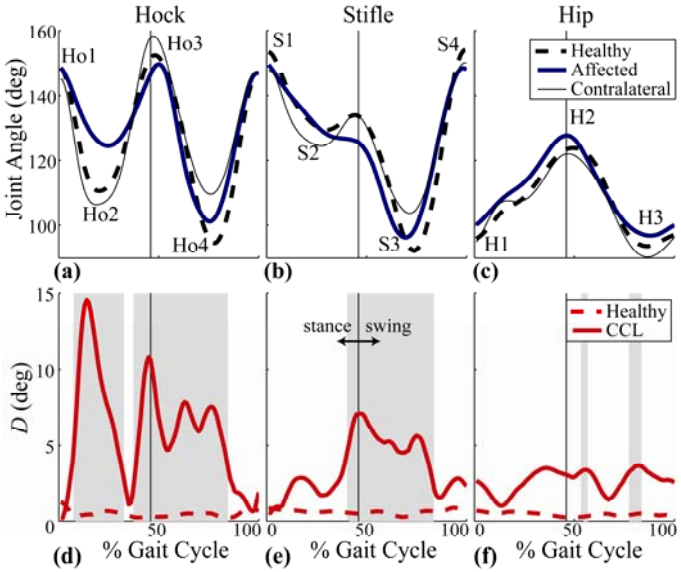

Figure 1: Group averaged joint angles (a-c) and corresponding deviations from normal, *D* (d-f). Regions of deviation are shaded. Stance/swing transition is at 46% GC.

Comparing significant peak differences from [3] to the shaded regions of deviation was the first step in assessing the additional information provided by the new ROD methodology. Significant peak differences (between affected and contralateral limbs) found in [3] were hock flexion in stance (Ho2) and stifle flexion in swing (S3). Current results found regions of deviation at those peak locations, as well as at peak swing-phase extension and flexion of the hock (Ho3 and Ho4, respectively), and peak swing extension and flexion of the hip (H2 and H3, respectively). These additional peaks within the regions of deviation suggested that their asymmetry was significantly affected, while peak values between individual limbs were not. Thus, studying differences of limb asymmetry between healthy and CCLD groups (rather than differences between affected and contralateral limbs of the injured group) uncovers additional insight to the effects of the disease.

An additional benefit to using the ROD methodology is to provide the assessment of symmetry beyond that of traditionally only examining peak values such as in [3]. This was especially prevalent in the hock and stifle angle differences, where the regions of deviation encompassed wide areas around the significant peaks. Timing offsets (in addition to those compensated for by normalizing stance and swing) can also be uncovered in these regions. For example, the shaded region around peak S3 appears to be caused by a timing shift between the affected and contralateral limbs.

DFA was used to assess whether the regions of deviation were truly areas of the gait cycle needing focus. DFA using only the identified regions of deviation as input classified all but two subjects correctly (one from each group), whereas DFA using all time points throughout the gait cycle classified four subjects incorrectly (one healthy and three CCLD). Therefore, using the regions of deviation data, instead of all time points, decreased the DFA classification error, suggesting that the ROD methodology is a viable approach for distinguishing differences in motion patterns.

CONCLUSIONS

ROD analysis using *t*-tests provides a unique opportunity to focus gait analysis on regions of the gait cycle that demonstrate significant asymmetry. This study successfully demonstrated how the new method expanded analysis outside of predetermined areas of interest such as peak differences, thus identifying regions of significance throughout the gait cycle. Further focusing on asymmetry magnitudes between limbs, rather than only assessing unilateral group means, may provide new insight into abnormal gait patterns. This work suggests that these sections (regions) during gait should be examined more thoroughly. These significant times and asymmetry magnitudes can then help researchers and clinicians understand the mechanisms behind lameness and compensation.

REFERENCES

1.Griffin MP, et al. *Gait Posture* **3**, 132-42, 1995.
2.Shorter KA, et al. *Clin Biomech* **23**, 459-67, 2008.
3.Ragetly CA, et al. *Vet Surg*, in press, 2010.
4.Ragetly CA, et al. *Am J Vet Res* **69**, 1188-96, 2008.

ACKNOWLEDGEMENTS

National Science Foundation, grant #0727083, and American Veterinary Medical Foundation.

COMPARATIVE ASSESSMENT OF BONE POSE ESTIMATION USING POINT CLUSTER TECHNIQUE AND OPENSIM

[1] Rebecca L. Lathrop, [1]Julie A. Thompson, [1,2]Ajit M.W. Chaudhari and [1,2]Robert A. Siston
Departments of [1]Mechanical Engineering and [2]Orthopaedics, The Ohio State University
Email: lathrop.16@osu.edu

INTRODUCTION

Human movement analysis through the use of non-invasive, in-vivo motion capture aims to recreate skeletal motion and joint kinematics from the 3D position of markers placed on subjects' skin. Markers placed on the skin are subject to soft tissue artifact, which can result in misrepresentation of skeletal movement and joint kinematics [1]. Techniques known as bone pose estimators have been developed in an attempt to minimize the effects of soft tissue artifact from motion capture data and to more accurately represent rigid body motion [2].

Many laboratories have begun to use the bone pose estimator known as the Point Cluster Technique (PCT) to estimate tibio-femoral motion, which uses eigenvalues and eigenvectors of a virtual inertia tensor to minimize soft tissue artifact using evenly distributed and weighted clusters of markers on the femur and shank in order to estimate non-rigid movement of the soft tissue [3]. The estimated rigid body motion is then represented by 4 virtual markers which form a coordinate system at the center of the cluster which is used for subsequent analysis. However, other researchers have proposed bone pose estimators using a singular-value decomposition method as an alternative that may work better in some cases [2].

Other laboratories have begun to perform gait analyses and simulations of movement with the open-source software package OpenSim [4]. OpenSim computes kinematics using a least squares approach to minimize the difference between experimental marker locations and virtual markers on the model while maintaining joint constraints [4]. Because motion capture data is often collected using the marker placement conventions of PCT before being input to OpenSim, it is important to determine the differences in results that would come from performing inverse kinematics simulations with the actual markers versus the virtual markers generated by the PCT algorithm. Therefore, the purpose of this study was to evaluate the differences in knee kinematics obtained with three methods: 1) the standard PCT approach, 2) the least squares approach applied to the actual marker set placed on the subject and 3) the least squares approach applied to the virtual markers representing the output of the PCT algorithm.

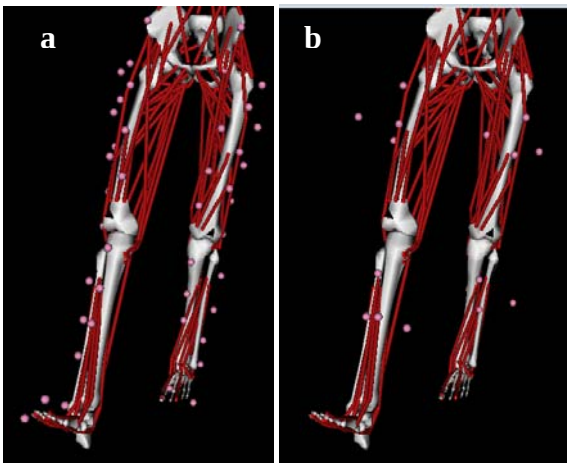

Figure 1: The PCT marker convention (a) and the resultant 4-marker coordinate system representing rigid body motion in OpenSim (b).

METHODS

Gait data was obtained for 3 healthy subjects while walking at a self-selected speed in our motion analysis laboratory (8 Vicon MX-F40 cameras). Reflective markers were placed on the skin following PCT convention, with additional markers on the pelvis and foot. Thigh clusters consisted of the greater trochanter and lateral femoral epicondyle markers plus nine markers evenly distributed across the anterior and lateral thigh. Shank clusters consisted of the lateral maleolus marker plus six additional markers evenly distributed across the anterior and lateral shank. Four virtual markers were generated according to the PCT algorithm to describe the cluster coordinate system for each segment, and

using custom scripts in Matlab and Vicon Bodybuilder, joint angles between the femoral coordinate system and the tibial coordinate system were calculated using a standard Euler method (*Mocap* results).

In order to determine kinematics using a least squares approach, a generic musculoskeletal model of the lower extremities was scaled in OpenSim using static calibration data obtained in the gait laboratory. The model was represented as a 30-degree-of-freedom linkage. The pelvis was defined with six degrees of freedom with respect to the ground. Hip joints were modeled as ball-and-socket joints; knees were modeled with six uncoupled degrees of freedom. Each ankle joint, subtalar joint, and metatarsophalangeal joint was modeled as a frictionless revolute joint [5].

The inverse kinematics problem was then solved in OpenSim using both the resultant 4-marker coordinate systems from the PCT (*coordinate* approach) and also on the entire 46-marker PCT marker set (*cluster* approach). Additionally, because OpenSim relies on the user-specified weighting of individual markers [4], both the *coordinate* and *cluster* trials were run with two sets of marker weights for a total of four inverse kinematics simulations for each data set. The two marker weighting conditions were: 1) *equal weight:* each marker is assigned an equal weight 2) *body weighted: e*ach marker is assigned a weight so that all markers on a given body have equal weighting and add up to 1000; for example, in the *cluster* approach 11 markers are tracked on the femur, so each marker is assigned a weight of 1000/11. Resultant Root Mean Squared (RMS) differences in knee kinematics between the five approaches were calculated.

Table 1: Average Root Mean Squared (RMS) differences in estimated tibio-femoral angles (°) for three subjects between different bone pose estimation techniques.

Flexion-Extension	MoCap	Coord Equal	Coord Body	Cluster Equal	Cluster Body
MoCap					
Coord Equal	4.8271				
Coord Body	4.8087	0.0436			
Cluster Equal	3.3117	1.8998	1.8940		
Cluster Body	3.4376	1.6992	1.6915	0.2706	
Varus-Valgus	MoCap	Coord Equal	Coord Body	Cluster Equal	Cluster Body
MoCap					
Coord Equal	3.3402				
Coord Body	3.3434	0.0250			
Cluster Equal	3.3407	1.1568	1.1591		
Cluster Body	3.3779	1.1836	1.1833	0.2794	
Internal-External	MoCap	Coord Equal	Coord Body	Cluster Equal	Cluster Body
MoCap					
Coord Equal	3.9953				
Coord Body	3.9125	0.2253			
Cluster Equal	5.3012	2.3384	2.3678		
Cluster Body	5.0565	2.2175	2.1842	0.7097	

RESULTS AND DISCUSSION

Minimal differences were observed due to changes in marker weighting within OpenSim. Knee flexion-extension angles exhibited similar patterns for all OpenSim approaches as well as for the Mocap results. Results from the *cluster* and *coordinate* approaches in OpenSim were often different from each other and from the *MoCap* results. However the largest differences were seen between the *MoCap* and OpenSim results. Even when results exhibited similar patterns, an offset was typically observed between the *MoCap* results and all OpenSim results, which is reflected in the RMS errors reported in Table 1. This offset may be due to marker placement error, scaling error in OpenSim, or differences in the methods by which anatomical reference frames are determined.

CONCLUSIONS

This work illustrates the variability in resulting kinematics between different approaches for bone pose estimation in gait analysis. Future work is needed to minimize these differences to allow for comparisons across multiple gait analysis platforms. For OpenSim users, this work also suggests that kinematic results at the knee are relatively insensitive to changes in OpenSim parameters.

REFERENCES

1. Holden, J.P., et al., Gait & Posture, 1997. **5**(2): 217-227
2. Cereatti, A., et al., J Neuroeng Rehabil, 2006. **3**: 7.
3. Andriacchi, T.P., et al., J Biomech Eng, 1998. **120**(6): 743-9.
4. Delp, S.L., et al., IEEE Trans Biomed Eng, 2007. **54**(11): 1940-50.
5. Delp, S.L., et al., IEEE Trans Biomed Eng, 1990. **37**(8): 757-67.

HUMAN GAIT RECOGNITION PERFORMANCE PREDICTION FROM 3D RESOLUTION SIMULATION USING GROUND TRUTH MOTION CAPTURE DATA

[1]Adam M. Fullenkamp, [2]Brian Campbell, [1]David Bowden and [1]Christopher Hess

[1]711th Human Performance Wing (711 HPW/RHPA), WPAFB, OH, USA
[2]Bowling Green State University, Bowling Green, OH, USA
email: Adam.Fullenkamp@WPAFB.AF.MIL

INTRODUCTION

Human gait recognition algorithms are traditionally presented and tested with image sources comparable to those that would be utilized in an operational setting (e.g. 2D surveillance video footage for a system intended to be used in a bank) [1]. Such reports provide an apt depiction of recognition performance for the particular image source and recognition algorithm combination, but it can be difficult to extrapolate and predict the performance of the same recognition approach with varying image fidelity (e.g. different pixel resolutions). Specifically, as in the case of a model-based recognition solution, it would be difficult to determine if the correct classification rate was most greatly affected by image resolution, silhouette extraction, model fitting, or match score selection. However, by utilizing the high-fidelity movement information provided by 3D motion analysis, different environmental conditions can be simulated to evaluate their impact on gait recognition performance. Accordingly, the purpose of this experiment was to study the effect of simulated pixel resolution on gait recognition performance using high-resolution motion capture data.

METHODS

A sample of 50 healthy adult subjects was used in this study (22±1 years, 175±10 cm, 75±15 kg). 3D motion analysis data were collected for each subject using a high-resolution passive optical motion capture system (MAC, Santa Rosa, CA). The marker set was chosen so that the major joint centers were identified and the 3D marker trajectories were temporally normalized to 100% of the gait cycle [2].

Six spatial resolution conditions were simulated by applying uniform noise to the raw motion capture data at magnitudes of 0cm, 2cm, 4cm, 6cm, 8cm, and 10cm. Gait recognition performance was evaluated using a Monte Carlo approach that involved 100 iterations of recognition testing at each level of uniform noise (600 total tests).

Each gait recognition test required the random selection of two different gait cycles from each subject which were then separated into two matching databases (template and unknown). Match scores were calculated between all gait cycles in the template database and all gait cycles in the unknown database to yield 50 true match scores and 2,450 non-match scores (50^2 total comparisons). To validly compare two different gait cycles from either the same or different subjects, 3D marker data were made local to the mid-pelvis, divided by mid-shoulder height, and rotated so that all subjects walked in the positive x-direction. Match scores were determined for each comparison of two gait cycles by calculating the sum Euclidean distance for all 3D landmarks at each percent of the gait cycle.

Gait recognition performance was quantified by using the true match scores and non-match scores from each test to calculate percent correct classification rates (%CCR), the area under the Receiver Operative Characteristic (ROC) curve (AUC), and the Cumulative Match Characteristics (CMC) (Figure 1 and Table 1). Additionally, all data are presented as averages of the 100 recognition tests at each noise level. CMC curves depict the percent of correct matches in the top *n* rank. Accordingly, the percent of correct matching in the top 1 rank corresponds to the %CCR. For ROC curves, an area of 1.0 indicates perfect discrimination and an area of 0.5 indicates that there is no discrimination power.

RESULTS AND DISCUSSION

The application of 0cm, 2cm, and 4cm magnitude uniform noise had little effect on gait recognition performance with %CCR's greater than 99.8% and AUC's greater than 0.998 (Table 1). These results indicate near perfect gait matching for this sample of subjects. Recognition performance began to drop substantially with the addition 6cm, 8cm, and 10cm of uniform noise resulting in %CCR's of 95.6%, 73.7% and 48.9%, respectively. Similarly, changes in AUC's indicated considerable reduction in discrimination performance at the higher noise levels.

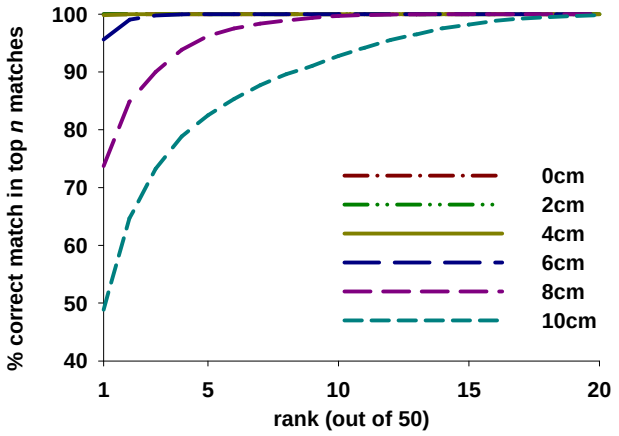

Figure 1: AVG CMC curves for each uniform noise level (Note: 0cm and 2cm curves start at 100% and follow the top edge of the figure).

The CMC curves for 0cm, 2cm, and 4cm noise levels indicate that the correct matches were in the top 2 rank for 100% of recognition tests (Figure 1). For the these conditions of smaller noise levels, the CMC measures show that the true match scores were always in the top 4% of match scores. 100% of correct matches for the 6cm, 8cm, and 10cm noise levels occurred at the 5, 19, and 30 ranks, respectively. These values correspond to true match scores that are consistently in the top 10%, 38%, and 60% of all match scores for a given recognition test.

Although a %CCR of 48.9% would seem to indicate that there is no minimal discrimination power for correct matching at the 10cm noise level, the associated AUC value of 0.869 demonstrates that the matching is significantly greater than chance ($p < 0.001$ compared to AUC of 0.5). Further, it should be noted that at noise levels approaching 10cm, there is still the appearance of overall gait motion throughout the gait cycle. Since it cannot be expected that joint centers will continue to align at this noise level, it may be more appropriate to evaluate the overall change in shape of the 'noisy' point cloud instead of attempting to identify individual body segments. This type of whole-body shape change analysis is more typical of motion-based gait recognition approaches [3].

CONCLUSIONS

This study demonstrates the utility of simulating different sensor and environmental conditions for gait recognition performance prediction using ground truth motion capture data. Similar analyses could be used to identify limitations associated with sensor viewing perspective, to compare the sensitivity of two competing systems, and to identify the conditions for which model-based or motion-based gait recognition solutions are most appropriate.

REFERENCES

1. Sarkar S, et al. *IEEE Trans PAMI*, **27**, 162-177, 2005.
2. Davis BL, et al. *Hum Mov Sci*, **10**, 575-587, 1991.
3. Ho MF, et al. *Proceedings of ICME'09*, New York City, NY, USA, 2009.

Table 1: Average gait recognition performance for each level of uniform noise simulation

	Uniform Noise Level (cm)					
	0	**2**	**4**	**6**	**8**	**10**
%CCR	100	100	99.8	95.6	73.7	48.9
AUC	> 0.999	> 0.999	0.998	0.983	0.936	0.869

SEGMENTAL KINEMATIC ANALYSIS USING A TRIDIMENSIONAL RECONSTRUCTION OF RAT HINDLIMB: COMPARISON BETWEEN 2D AND 3D JOINT ANGLES

[1]Filipa João, [1]Sandra Amado, [1]Paulo Armada [2]Ana Colette Maurício and [1]António Veloso

[1]Faculty of Human Kinetics, Technical University of Lisbon, Lisbon, Portugal
[2]Department of Veterinary Sciences, Biomedics Sciences Institute of Abel Salazar, Porto University, Portugal
email: filipajoao@fmh.utl.pt

INTRODUCTION

Functional recovery is one of the primary goals of therapeutic intervention in neuromuscular research. Animal models have been widely used to assess motor and sensory functions after induced lesion. Several spatial and kinematic parameters have been reported as sensitive outcome variables to quantify functional recovery: ankle angle, ankle-stance angle, stance/swing ratio, step length ratio, angle of the ankle joint at terminal stance, angle of the ankle joint at midswing, tail height, tail deviation and midline deviation. Eversion, dragging and exorotation of the foot during stance phase is referred by Meek [1] as an important aspect of walking quality. The rotation of the injured paw instead of dragging, contracture of toes, inversion of the feet and plantar flexion of the toes have been described as the main qualitative of abnormalities observed in foot placement during locomotion. Nevertheless there are few published studies where tridimensional kinematics is used to describe ratôs locomotor function [2,3]. What is, this approach is based on the vector dot product, which only enables us the computation of planar angles [4], moreover only sagital plane angular data has been reported. In order to better understand the effects of induced lesions in ratôs locomotor function, a more anatomical and functional approach should be considered. The purpose of the present study is: (1) to perform a segmental kinematic analysis using a tridimensional reconstruction of the rat hindlimb, regarding the morphology and the movement of each segment, (2) to calculate hip, knee, ankle and metatarsophalangeal planar angles (sagital, frontal and transverse planes) and (3) to compare both 3D (Cardan sequence x-y-z) and 2D angles for the peaks of flexion, extension, IC (initial contact), TO (toe-off), midstance, midswing, stance amplitude and swing amplitude in the sagital plane of motion.

METHODS

Eight adult male Sasco Sprague Dawley rats (Harlan, Barcelona, Spain) with approximately 250g and 0,23m of length were used in this study. Motion capture was collected with an optoeletronic system of 6 cameras Qualisys (Oqus-300) operating at a framerate of 200Hz. Animals walked on a Perspex track with length, width and height of respectively 120, 12 and 15 cm. 7 reflective markers with 2mm diameter were attached to 7 bony prominences on the right side of the rat: 4th finger, 5th methatarsal head, lateral malleolus, lateral knee joint, great trochanter, anterior superior iliac spine and ischial tuberosity. Three non collinear markers were attached to segments foot, shank and thigh. Seven virtual markers (placed medially to the attached ones) were generated by means of anthropometric and CT scans data, to obtain the correct joint diameter. Five body segments were reconstructed: pelvis, right thigh, right shank, right foot and right finger using Visual 3D software for biomechanics modeling. A a total of 42 gait cycles kinematics from 7 rats were obtained. Gait parameters were normalized to the gait cycle. Three-dimensional biomechanical analyses were carried out and hip, knee, ankle and metatarsophalangeal joint angular displacements were calculated.

RESULTS AND DISCUSSION

There were no significant differences when comparing averaged 2D and 3D angular displacements for the flexion/extension actions in the hip and ankle joint parameters (Fig.1). However,

extension peak and swing amplitude in the knee joint are significant different between 2D and 3D approaches, with a knee extension peak of 110˚ and 123˚ for the 3D and 2D methods, respectively. Knee angular amplitude in the swing phase was 69˚ and 50˚ for the 3D and 2D methods, respectively. Also, MF joint shows statistically significant differences in the extension peak (40˚ and 51˚ for 3D and 2D, respectively) and angular displacement at IC instant (9˚ and 18˚ for the 2D and 3D, respectively).

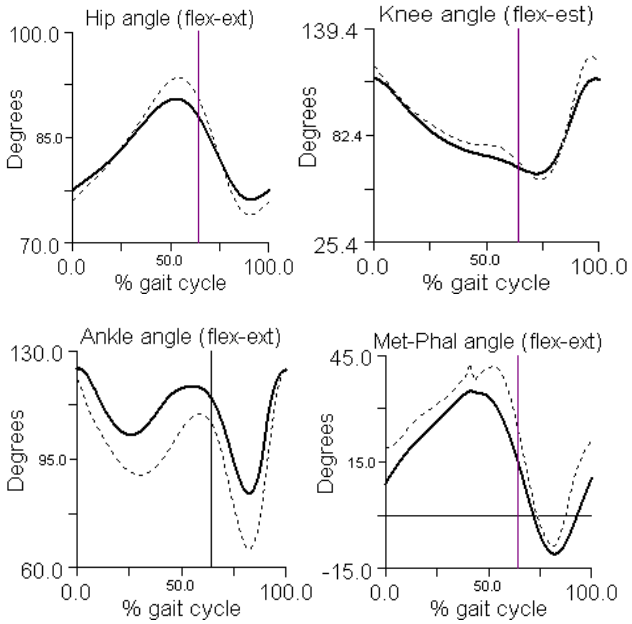

Figure 1: Averaged 3D angular displacement (solid line) of lower limb joints around the medio-lateral axe of rotation. Averaged 2D planar angle (sagital plane) (dotted line).Vertical line corresponds to toe-off instant.

Regarding 3D joint angular displacement around the anterior-posterior axe (Fig.2), hip adduction peak occurs at 17% of gait cycle with an angle of 9.7ę, while the abduction peak occurs at 70%, with an angle of 30ę. IC, midstance, midswing and TO occur with the hip at 18ę, 16˚, 28˚ and 13˚ of angular displacement, respectively. Stance amplitude is 13˚ and swing amplitude is 28˚. Knee abduction/adduction 3D curve reveals a pattern that suggests a more functional behavior, when compared with 2D curve. Ankle and MF joints show an eversion peak of 9˚ at 39% of gait cycle and an inversion peak of 15ę at 50% of gait cycle, respectively. Regarding segments axial rotation, foot segment has an external rotation peak of -20ę, occurring at 54% of gait cycle.

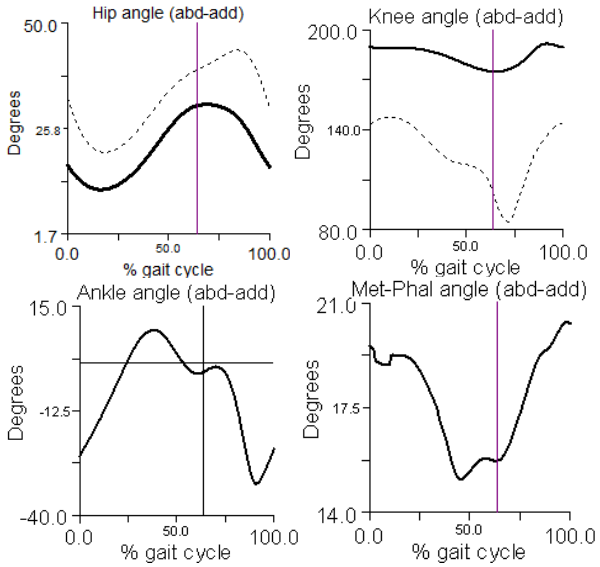

Figure 2: Averaged 3D angular displacement (solid line) of lower limb joints around the anterior-posterior axe of rotation. Averaged 2D planar angle (frontal plane) (dotted line). Vertical line corresponds to toe-off instant.

CONCLUSIONS

Angular displacement not just in sagital plane but also in frontal and transverse planes of motion seems to have an important functional meaning, due to the existence of a gait pattern where eversion of the foot and exorotation occur. Clinical conditions also refer toe angular deviations, so including toe segment in rat kinematics is extremely important. Moreover, adding segment´s axial rotation to kinematic data will allow the recognition of several dysfunctional events in gait patterns. Comparing 2D with 3D computing methods, it should be considered that rat joints are not always aligned in the same plane of motion, so computing planar angles can under/overestimate joint angular displacement. Nevertheless, the contribution of the Euler/Cardan rotations for the joint angular displacement cannot be neglected, in order to clarify which kinematics gait parameters are specially connected to functional recovery.

REFERENCES

1.Meek MF, et al. *Muscle Nerve* **24**, 753-759, 2001.
2.Canu MH, et al. *Exp Neur* **218**, 98-108, 2009.
3.Garnier C, et al. *Behavior Brain Res* **186**, 57-65, 2008.
4.Couto PA, eta al. *J Neurosci Methods* 173(2), 193-2.

A NOVEL TECHNIQUE QUANTIFYING PHALANGEAL INTERFACE PRESSURES AT THE HAND-HANDLE INTERFACE

Erik W. Sinsel, Daniel Gloekler, Bryan Wimer, Christopher Warren, John Z. Wu, Frank L. Buczek

National Institute for Occupational Safety and Health, Morgantown WV, USA
email: Erik.Sinsel@cdc.hhs.gov

INTRODUCTION

The forces and pressures experienced by the hand during tool use have been identified as important risk factors for hand related injuries and disorders such as hand-arm vibration syndrome, carpal-tunnel syndrome, and hand/wrist tendinitis [1]. Reliable phalangeal kinetics of the index through little finger are essential for inverse dynamics models of the hand during gripping [2]. Pressure sensor gloves and phalange sensors designed primarily for *in situ* use can suffer from migration, reduced range of motion, grip interference, restricted coverage, and unknown sensor position and orientation which precludes force vector calculation [3]. We present a novel technique to analytically allocate interface pressure cells to finger phalanges providing quantification of phalangeal pressures and forces during gripping.

METHODS

Subjects with dominant right hands performed gripping exertions on cylindrical aluminum handles instrumented with pressure sensor grids. Hand markers provided 6 degree-of-freedom phalangeal kinematics, recorded at 100 Hz with a 14-camera Vicon Nexus motion capture system with typical calibration error less than 0.5 mm; kinematic modeling was performed in Visual3D (C-Motion Inc.) [4]. Tekscan 5101 or 5101N thin-film pressure sensor grids (square cells 2.54 mm and 3.75 mm, respectively) were adhered to handles with rows manually aligned with right cross-sectional planes. Tracking markers were attached to cylinders at longitudinal ends and retro-reflective discs were adhered to pressure cells free of camera occlusion during trials. Pressure data were recorded at 10 Hz by Tekscan software on a separate computer, synchronized with the Vicon Nexus system. Anthropometric photographs were used to determine mediolateral widths at the finger joints and tips. Subsequent analysis was performed in MATLAB (The Mathworks Inc.) using standard and custom functions.

For each matching pressure and kinematic sample, cylinder tracking markers were used to create a standard cylindrical coordinate system and kinematic data were transformed into this system. Grid markers were used to estimate the local positions of pressure cells. Minimal cross-sectional misalignment of the grid was corrected by modeling rows as helical arcs with kinematically determined torsion. To mitigate the limiting effect of cell size relative to kinematic error, each cell was divided into a grid of equally sized sub-cells, assuming constant cell pressure distribution.

Each phalange was modeled as a frustum of a right circular cone with radii determined by the mediolateral widths described above [4]. A phalange silhouette was defined as the trapezoid created by the intersection of the frustum and a plane parallel to the cylindrical axis that contains the frustum's longitudinal axis (Figure 1).

An approximation of a radial projection of the silhouette onto the cylinder surface was created by intersecting the cylinder surface with vectors from silhouette points to the cylindrical axis. The projection vectors were constructed so as to be orthogonal to the cylindrical axis (Figure 1). The surface of a cylinder is developable in that the planar representation retains the geometric properties of surface curves [5], and a shortest-path helical arc on the surface is equivalent to a line segment in the planar representation. Projected points were linearly interpolated along corresponding silhouette edges, and sub-cells with bounded centroids formed the phalange region on the pressure grid.

The physical constraints of human anthropometry and cylindrical gripping tended to result in highly linear projected curves. However, to address potential extreme combinations of handle size, anthropometry, and phalange orientation, the longitudinal silhouette edges were defined with an arbitrary number of interval points which, when interpolated, could provide a better approximation of the projected curve.

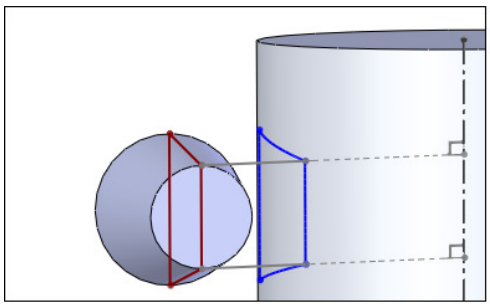

Figure 1: Example of phalange frustum with silhouette projected onto the cylinder surface by vectors orthogonal to the cylindrical axis.

Modeling phalanges as rigid body frusta resulted in interference between phalange silhouettes which produced projected surface regions imperfectly mated at interphalangeal joints. These regions were connected at the midpoints of respective medial and lateral vertices of adjacent transverse edges (Figure 2). Remaining contested sub-cell pressure was apportioned among contesting regions.

The pressure sub-cells of a region were integrated to provide total pressure, and surface normal force vectors were summed to calculate a resultant force vector applied to the corresponding phalange.

RESULTS AND DISCUSSION

Our technique produces pressure mappings which qualitatively correspond well with phalanges of the hand (Figure 2). Our method provides phalangeal pressures and resultant force vectors during gripping without the potential weaknesses described above. We conclude it is viable to pursue this approach for meeting the need for phalangeal kinetics data in techniques like inverse dynamics, and to help improve the understanding of injury mechanisms related to gripping.

Disclaimer: The findings and conclusions in this abstract have not been formally disseminated by the National Institute for Occupational Safety and Health and should not be construed to represent any agency determination or policy.

REFERENCES

1.NIOSH Publication No. 97-141, *Musculoskeletal Disorders and Workplace Factors*, 1997.
2.Wu JZ, et al. *Med Eng & Phys* **31**, 1214-18, 2009.
3.Lemerle P, et al. *Ergonomics* **51**, 168-191, 2008.
4.Buczek FL, et al. *Proceedings of GCMAS 15th Annual Meeting*, Miami, FL, USA, 2010.
5.Salomon D. *Transformations and Projections in Computer Graphics*, Springer-Verlag, Ltd., 2006.

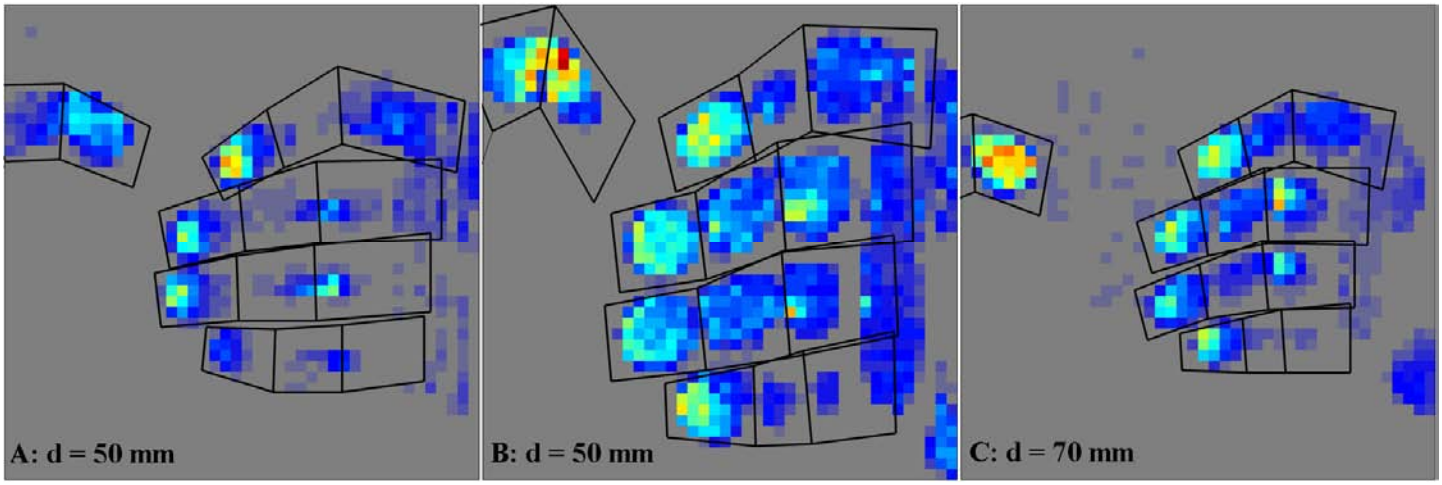

Figure 2: Projected phalange regions on pressure distributions for multiple subjects and handle diameters (d). Panels A and B are two subjects of markedly different hand size. Panels B and C are the same subject.

ELLIPTICAL EXERCISE IMPROVES WALKING MECHANICS IN MULTIPLE SCLEROSIS PATIENTS

Jessie M. Huisinga[1], and Nicholas Stergiou[1,2]
[1]Nebraska Biomechanics Core Facility, University of Nebraska at Omaha, Omaha, NE
[2]University of Nebraska Medical Center, College of Public Health, Omaha, NE
Email: jhuisinga@unomaha.edu URL: http://biomech.unomaha.edu

INTRODUCTION

Multiple Sclerosis is a progressive neurological disease that is associated with a wide range of symptoms including motor weakness, increased falls, exaggerated fatigue, poor balance, spasticity, vision problems, heat sensitivity, decreased physical activity, cognitive deficits, and depression [1]. Exercise has been shown to improve overall quality of life and mobility in MS patients [2, 3]. However, the most effective exercise modality to improve mobility in MS patients is unknown. In order to determine whether gait-simulating exercise training is a viable treatment option for MS patients, biomechanical analysis of gait is necessary to quantitatively determine whether changes in gait mechanics occurs as a result of the training. Therefore, the purpose of this study was to determine the effect of a short-term aerobic, gait-simulating exercise intervention on the functional movement status of MS patients. It was hypothesized that the training would result in joint torques and powers that were closer to those of healthy controls.

METHODS AND PROCEDURES

Eighteen MS patients (46.1 ± 10.1 yrs; EDSS 2.4 ± 0.7) and 18 healthy matched controls (40.7 ± 11.3 yrs) walked through a 10 meter walkway at their self-selected walking pace, while kinetics and kinematics were collected for 10 trials with a Kistler force plate (600Hz) and an 8-camera Motion Analysis system (60 Hz). Data collection was performed on the MS patients before and after individuals participated in a total of 15 exercise session over a period of six weeks. The exercise modality used by all patients was an elliptical exercise machine which allowed weight-bearing, sagittal plane motion with joint kinematics similar to walking [4]. Each training session consisted of 30 minutes of cumulative exercise. Healthy controls underwent only one gait analysis. Joint torques and powers were calculated from the ground reaction forces and the kinematics for each participant. Maximum flexor and extensor torques and maximum power absorption and generation were identified for the hip, knee, and ankle joints. Paired t-tests were used to compare within MS patients pre- and post-training while a linear mixed model was used to compare outcome measures between MS patients pre- and post-training to healthy controls with velocity as a covariate.

RESULTS

MS patients before training compared to healthy controls exhibited significantly decreased walking velocity, decreased ankle dorsiflexor torque (ADT), decreased ankle plantarflexor torque (APT), decreased knee extensor torque (KET), and decreased hip flexor torque (HFT). In addition MS patients had significantly decreased ankle dorsiflexor power absorption during early stance (A1), decreased ankle plantarflexor power generation during late stance (A2), decreased power absorption at the knee during early stance (K1), decreased hip extensor power generation during early stance (H1), and decreased power absorption of the hip flexors during late stance (H2) (Table 1). Velocity did not have a significant effect on any of these outcome variables. As a result of

training, within the MS patients significant increases occurred in APT, HET, A1, A2, and K1 such that after training, significant differences were not present for these variables between MS patients and controls.

DISCUSSION

Baseline differences between healthy controls and MS patients in joint torques and powers were present prior to the training which indicated that MS patients had significantly decreased flexor and extensor torques and decreased power generation and absorption at all three joints. Following the elliptical exercise training program, significant increases were found for both joint torques and powers such that the MS patients gait parameters moved closer to those of the healthy controls and were no longer significantly different. These results agree with our hypothesis and provide exhilarating support for the use of elliptical exercise training as a rehabilitation tool for MS patients. The significant improvements are occurring during early and late stance specifically. During early stance both ankle (A1) and knee (K1) power absorption are increased which indicates improved weight acceptance during the transition from double to single support. During late stance, there is increased plantarflexor torque (APT) as well as increased power generation at the ankle (A2). During late stance/pre-swing, muscle activity at the ankle enables the leg to enter the swing phase with sufficient propulsion to move the body mass forward. Clinicians refer to gait powered by ankle push-off as using an "ankle strategy", which is thought to be the preferred walking strategy for healthy young adults [5]. Thus, as a result of short term (6 weeks/15 sessions) elliptical training, MS patients seem to have adopted a gait strategy that is similar to the preferred strategy of healthy adults. These findings provide support for the use of an elliptical exercise machine, which is a gait-simulating exercise, as a tool to improve gait mechanics in MS patients in a relatively short amount of time.

REFERENCES

1. Noseworthy et al. (2000) *N Engl J Med* 343(13):938-52.
2. Snook & Motl (2009) *Neurorehabil Neural Repair* 23(2):108-116.
3. Motl & Gosney (2008) *Mult Scler* 14(1):129-35.
4. Burnfield et al (2010) *Phys Therapy* 90(2):289-305.
5. Kerrigan et al. (1998) *Arch Phys Med Rehabil* 79(3):317-22.

ACKNOWLEDGEMENTS

ASB Grant-In-Aid, the MARS Foundation and the Nebraska Research Initiative.

		Pre-training mean (S.D)	Post-training mean (S.D.)	Control mean (S.D.)	*p-value* pre-con; pre-post; post-con
	Velocity (m/s)	1.11 (0.22)	1.12 (0.24)	1.24 (0.26)	0.023*; 0.212; 0.023*
Joint Torques (N*m/kg)	ADT	-0.277 (0.076)	-0.2844 (0.082)	-0.412 (0.197)	0.013*; 0.571 0.018*
	APT	1.189 (0.140)	1.266 (0.127)	1.341 (0.264)	0.016*; 0.004*; 0.166
	KET	0.542 (0.176)	0.549 (0.188)	0.705 (0.273)	0.020*; 0.333; 0.050*
	KFT	-0.269 (0.145)	-0.274 (0.168)	-0.292 (0.232)	0.833; 0.837; 0.835
	HET	0.611 (0.201)	0.688 (0.158)	0.802 (0.273)	0.123; 0.006*; 0.333
	HFT	-0.781 (0.188)	-0.763 (0.028)	-1.048 (0.306)	0.007*; 0.568; 0.003*
Joint Powers (Watts/kg)	A1	-0.394 (0.035)	-0.477 (0.042)	-0.661 (0.243)	0.002*; 0.003*; 0.060
	A2	2.499 (0.118)	2.81 (0.134)	3.193 (0.869)	0.017*; 0.003*; 0.177
	K1	-0.711 (0.056)	-0.807 (0.072)	-1.068 (0.432)	0.013*; 0.040*; 0.146
	K2	0.457 (0.048)	0.458 (0.051)	0.561 (0.323)	0.430; 0.959; 0.502
	K3	-0.497 (0.038)	-0.480 (0.042)	-1.057 (0.646)	0.153; 0.572; 0.093
	H1	0.410 (0.038)	0.438 (0.032)	0.660 (0.325)	0.036*; 0.396 0.036*
	H2	-0.687 (0.037)	-0.652 (0.039)	-0.990 (0.429)	0.025*; 0.345; 0.008*
	H3	0.490 (0.025)	0.464 (0.025)	0.784 (0.340)	0.108; 0.229; 0.131

Table 1: Joint torque and joint power variables; *Sig ($p < 0.05$).

RELATIONSHIPS BETWEEN MUSCLE CONTRIBUTIONS TO WALKING SUBTASKS AND FUNCTIONAL WALKING STATUS IN PERSONS WITH POST-STROKE HEMIPARESIS

[1]Allison L. Hall, [1]Carrie L. Peterson, [2,3,4]Steven A. Kautz and [1]Richard R. Neptune

[1]Department of Mechanical Engineering, The University of Texas at Austin, Austin, TX, USA
[2]Brain Rehabilitation Research Center, Malcom Randall VA Medical Center, Gainesville, FL, USA
[3]Department of Physical Therapy, University of Florida, Gainesville, FL, USA
[4]Brooks Center for Rehabilitation Studies, University of Florida, Gainesville, FL, USA
email: allison.hall@mail.utexas.edu, web: http://www.me.utexas.edu/~neptune

INTRODUCTION

Walking speed is commonly used to predict stroke severity and assess functional walking status (i.e., household, limited community and community walking status) post-stroke [1]. The underlying mechanisms that limit walking speed (and functional walking status by extension) need to be understood to improve post-stroke rehabilitation. Previous experimental studies have shown correlations between paretic plantarflexor output during the pre-swing phase and walking speed and suggest that the paretic hip flexors can compensate in some hemiparetic subjects [e.g., 2]. Modeling and simulation studies of healthy walking have shown that the ankle plantarflexors, soleus (SOL) and gastrocnemius (GAS), and uniarticular hip flexors (IL) are essential contributors to the walking subtasks of forward propulsion, swing initiation and/or power generation during pre-swing [3,4]. However, the relationships between functional walking status and individual muscle contributions to these walking subtasks in hemiparetic walking are unknown. The goal of this study was to use 3D forward dynamics simulations to investigate the relationships between functional walking status in post-stroke hemiparetic walking and muscle contributions to forward propulsion, swing initiation and power generation.

METHODS

A previously developed 2D modeling and simulation framework [3] was modified to generate 3D forward dynamics walking simulations (from midstance to toe-off) that emulated the experimental kinematics and ground reaction forces (GRFs) of two representative hemiparetic subjects walking at their self-selected speed (limited community walker, 0.45 m/s; community walker, 0.90 m/s) and an age-matched healthy control subject walking at 0.6 and 1.0 m/s. Subjects walked on a split-belt instrumented treadmill (Tecmachine) for 30 seconds while kinematic, GRF and EMG data were collected. The EMG data were used to constrain the timing for each muscle excitation pattern in the optimization to ensure muscles were producing force in the appropriate phase of the gait cycle in the simulation. Excitation patterns for each muscle were defined using a bimodal Henning pattern and the patterns (timing and amplitude) and initial joint angular velocities were optimized using a simulated annealing algorithm [5] that minimized the differences between the simulated and experimental data. Muscle-induced acceleration and segment power analyses [3] were performed to quantify individual muscle contributions to forward propulsion (average horizontal pelvis acceleration), swing initiation (average power delivered to the leg) and power generation (average musculotendon power) during the pre-swing phase.

RESULTS AND DISCUSSION

Similar to the healthy control subject (Fig. 1A), the ankle plantar flexors (SOL, GAS) generated the majority of propulsion in the paretic leg in the community walker (Fig. 1B). However, in the limited community walker, the paretic leg muscles contributed little to forward propulsion and the non-paretic leg muscles (rectus femoris, RF and vastii, VAS) compensated for the reduced paretic leg output (Fig. 1B). This result is consistent with Bowden et al. [6] who showed that the non-paretic leg's contribution to the A/P GRF was increased in hemiparetic subjects who were more impaired. The

non-paretic leg muscles (primarily hamstrings, HAM) in the limited community walker increased their contributions to pelvis deceleration and the net effect from both legs (sum of Totals, Fig. 2B) was to decelerate the pelvis during pre-swing.

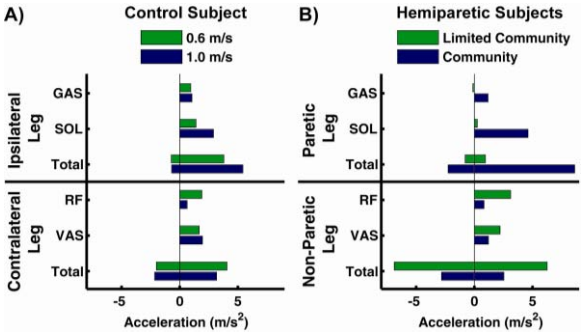

Figure 1: Primary muscle contributions to forward propulsion by A) the healthy control subject during ipsilateral pre-swing, and B) the hemiparetic subjects during paretic pre-swing, where *Total* is the positive and negative sums from all muscles for the respective leg.

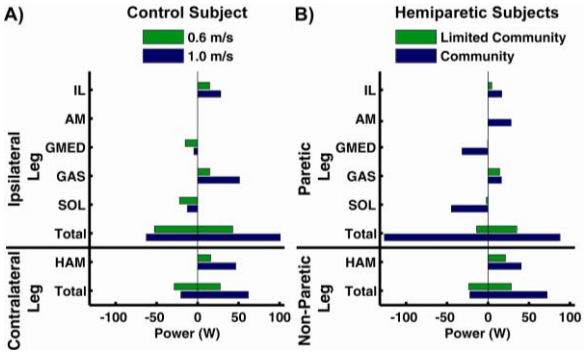

Figure 2: Primary muscle contributions to swing initiation by A) the healthy control subject during ipsilateral pre-swing, and B) the hemiparetic subjects during paretic pre-swing, where *Total* is the positive and negative sums from all muscles for the respective leg.

The community walker's muscle contributions to swing initiation were similar to those seen in the healthy control subject (Fig. 2A) with paretic GAS, IL and non-paretic HAM contributing to paretic leg swing initiation (Fig. 2B). Paretic adductor magnus (AM) and gluteus medius (GMED) also contributed positively and negatively, respectively, to swing initiation in the community walker (Fig. 2B). Clear deficits existed in the paretic and non-paretic leg muscle contributions to swing initiation in the limited community walker (Fig. 2B). This is consistent with previous studies showing reduced paretic leg kinetic energy at toe-off, which suggests impaired paretic leg swing initiation [e.g., 7]. The negative contributions from the paretic leg muscles (GMED and SOL) were also greatly reduced (Fig. 2B), allowing the leg to accelerate into swing.

Power generation by muscles in the community walker closely resembled those of the control subject. However, in the limited community walker, the paretic leg muscles, specifically GAS and IL, generated less power consistent with their reduced contributions to forward propulsion (GAS) and swing initiation (GAS and IL). Paretic SOL absorbed power in the limited community walker, reducing its contribution to forward propulsion.

CONCLUSIONS

The analyses showed that deficits in forward propulsion, swing initiation and power generation are related to functional walking status in hemiparetic walking. Increased contributions from the paretic leg muscles (i.e., plantarflexors and hip flexors) and reduced contributions from the non-paretic leg muscles (i.e., knee and hip extensors) to the walking subtasks were critical in achieving a higher functional walking status. Interventions targeting these muscle groups may improve rehabilitation outcomes and the functional walking status of persons with post-stroke hemiparesis.

REFERENCES

1.Bowden MG, et al. *Neurorehabil Neural Repair* **22**, 672-675, 2008.
2.Nadeau S, et al. *Clin Biomech* **14**, 125-135, 1999.
3.Neptune RR, et al. *Gait Posture* 28, 135-143, 2008.
4.Liu MQ, et al. *J Biomech* **41**, 3243-3252, 2008.
5.Goffe WL, et al. *J Econometrics* **60**, 65-99, 1994.
6.Bowden MG, et al. *Stroke* **37**, 872-876, 2006.
7.Chen G, et al. *J Biomech* **41**, 877-883, 2002.

ACKNOWLEDGEMENTS

This work was funded by NIH grant RO1 HD46820 and the Rehabilitation Research & Development Service of the VA.

Mechanical recovery influenced by dorsiflexor not plantarflexor stimulation in post-stroke gait

Nils A. Hakansson[1], Trisha Kesar[2], Darcy Reisman[2], Stuart Binder-Macleod[2] and Jill Higginson[1]
[1]Department of Mechanical Engineering, University of Delaware, Newark, DE, USA
[2]Department of Physical Therapy, University of Delaware, Newark, DE, USA
email: nilsh@udel.edu

INTRODUCTION

Stroke leads to gait impairments such as slower walking speeds, inter-limb asymmetry, and increased energy consumption [1]. Functional electrical stimulation (FES) applied to the dorsiflexor muscles of stroke survivors is commonly used to address foot-drop, [2] and therefore improve safety, speed, and efficiency of walking [3]. However, FES of the dorsiflexors alone does not address other critical gait deficits such as reduced ankle plantarflexor moment and push-off forces during terminal stance and decreased knee flexion angle during swing [4].

The mechanical recovery index (R), a measure of the mechanical energy exchange that is preserved through the pendulum-like motion of the whole-body center of mass (COM) during gait, can provide insights into the effects of FES on post-stroke gait mechanics and energetics. Therefore, the objective of this study was to test whether the immediate effects of applying FES to ankle dorsiflexors (DF) or to both plantar and dorsiflexors (PDF) improved mechanical recovery indices of post-stroke gait.

METHODS

All subjects gave informed consent to participate in the study which was approved by the University of Delaware Human Subjects Review Board. Gait data were collected from 8 chronic stroke subjects (2 female; mean age 60 ± 8 years; mean years since stroke 6.7 ± 6.4 years). All subjects could walk for at least 5 minutes continuously at their self-selected speed.

Surface electrical stimulation electrodes were applied over the dorsiflexor and plantarflexor muscles. A Grass S8800 stimulator and SIU8TB stimulus isolation unit (Grass Instrument Co, Quincy, MA) delivered the stimulation (30-Hz trains, pulse duration of 300μs, 300ms long) to both the dorsiflexor and plantarflexor muscles. Electrical stimulation timing was controlled by two compression-controlled footswitches attached to the sole of the forefoot and hindfoot of the subjects' shoes. DF stimulation was applied from when the forefoot footswitch left the ground until the hindfoot switch contacted the ground (paretic swing phase). PDF stimulation was applied from when the hindfoot switch left the ground until the forefoot switch left the ground (paretic terminal stance) [2, 4].

An 8-camera motion analysis system (Vicon 5.2, Oxford, England) recorded (100 Hz) the positions of 41 retroreflective markers placed on the bony landmarks of the foot, shank, thigh, pelvis, and trunk of the subjects as they walked on an instrumented treadmill (AMTI, Watertown, MA) at their self-selected speed. Data was collected as the subjects walked: (1) without FES (noFES), (2) with DF FES, and (3) with PDF FES.

Body segment masses were determined from anthropometric data [5] and COM positions were calculated from marker position data using Visual 3D (C-Motion, Rockville, MD). COM positions were low-pass filtered at 6Hz. Segment velocities and accelerations were calculated by taking derivatives of the limb COM positions relative to the whole-body COM and used to calculate segment kinetic and potential energies [6].

Mechanical recovery was calculated to assess the energy exchange between the vertical, anterior-posterior and medial-lateral directions of the whole-body COM during gait [6, 7]. Mechanical recovery (R) was calculated as:

$$R = \frac{W_v + W_{ap} + W_{ml} - W_{ext}}{W_v + W_{ap} + W_{ml}} * 100$$

where W_v, W_{ap}, and W_{ml} are the vertical, anterior-posterior, and medial-lateral components of the whole body external work, W_{ext}, respectively. W_v, W_{ap}, and W_{ml} were calculated by summing the positive changes in vertical, anterior-posterior, and medial-lateral components of energy, respectively, averaged over five consecutive gait cycles.

Paired-sample t-tests were performed to identify differences in the average mechanical recovery between noFES versus DF and noFES versus PDF. Significance was set at $p<0.05$.

RESULTS and DISCUSSION

The average mechanical recovery across subjects during noFES was 44.2% (range 35.3 to 59.1%), during DF FES was 48.0% (range 33.1 to 61.3%), and during PDF FES was 44.5% (range 27.5 to 56.1%) (Figure 1). The application of DF FES significantly increased mechanical recovery compared to noFES (p = 0.038). The application of PDF FES did not have a significant effect on mechanical recovery compared to noFES (p = 0.892). Overall, the average mechanical recovery across subjects was greatest for the DF, followed by the PDF and noFES conditions. Overall mechanical recovery was low relative to healthy adults walking at self-selected or slow speeds [6].

DF FES resulted in a significant increase in mechanical recovery as compared to the noFES condition. The observed increase in mechanical recovery with DF FES was likely produced because DF FES increased ankle dorsiflexion during swing phase [4]. As a result, during walking with DF FES, compensation by other muscles to improve swing phase dynamics may not have been required.

There was no significant difference in the mechanical recovery between the noFES and PDF FES conditions. It was expected that PDF FES would increase mechanical recovery due to the plantarflexors capacity to accelerate the COM forward. We hypothesize that because PDF FES was delivered only during terminal stance, it may have resulted in increased knee flexion [2] instead of COM forward acceleration, thereby causing minimal changes in mechanical recovery.

None of the subjects had much experience walking with FES and we did not provide time to adapt to walking with FES during the data collection session. Prolonged training with FES may enable the subjects to learn to adjust their muscle activity patterns to utilize the FES more efficaciously, and result in greater improvements in mechanical efficiency.

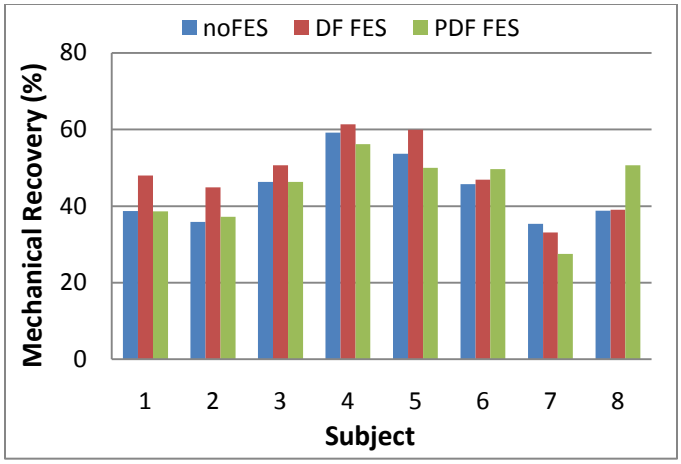

Figure 1. Mechanical recovery over three gait cycles for each of the subjects as they walked with noFES, DF FES, and PDF FES.

In summary, the immediate effect of FES applied to the dorsiflexors demonstrated an improvement in mechanical recovery in post-stroke gait whereas FES applied to both the dorsiflexors and plantarflexors did not.

REFERENCES

1. Zamparo, P., et al., *Scand J Med & Sci Sports*, 1995. **5**(6): p. 348-352.
2. Kesar, T.M., et al., *Stroke*, 2009. **40**(12): p. 3821-3827.
3. Taylor, P.N., et al., *Arch Phys Med Rehab*, 1999. **80**(12): p. 1577-1583.
4. Kesar, T.M., et al., *Phys Ther*, 2010. **90**(1): p. 55-66.
5. Winter, D.A., Biomechanics and Motor Control of Human Movement. 4th ed. 2009, Hoboken: Wiley. 370.
6. Cavagna, G.A., et al., *J. Physio*, 1976. **262**(3): p. 639-657.
7. Detrembleur, C., et al., *Gait & Posture*, 2003. **18**(2): p. 47-55.

ACKNOWLEDGEMENTS

The authors are grateful to Ben Roewer for his help with Visual 3D. This study was funded by NIH NS 055383 and NIH NR 010786.

CONSTANT SPEED PRACTICE ON A TREADMILL CAN MAINTAIN LOWER EXTREMITY KINETICS FOR PEOPLE POST-STROKE

Clinton J. Wutzke, Michael D. Lewek

University of North Carolina at Chapel Hill, Chapel Hill, NC, USA
email: mlewek@med.unc.edu

INTRODUCTION

Over 780,000 people experience a stroke each year [1] with less than 30% of people post stroke capable of walking faster than 0.8 m/s [2]. High intensity practice is necessary to elicit appropriate neuro-motor changes [3]. Because the paretic side produces smaller joint moments and powers than the non-paretic side, we believe that maintaining limb kinetics as large as possible will produce the greatest training effect. Unfortunately, during continuous overground walking, individuals post-stroke continuously reduce gait speed and walking distance throughout the session [4], implying reduced lower extremity joint kinetics.

Locomotor training on a treadmill is a common component of a conventional rehabilitation program. Importantly, such training can ensure constant speeds that are high intensity to improve locomotion in people post-stroke. In this way, we anticipate limb kinetics will not decrease throughout a training session, despite the profound weakness and incoordination that occur following stroke.

The purpose of this study was to characterize the changes in hip and ankle kinetics, as well as propulsive forces throughout a 20 minute treadmill training session. We hypothesized that use of a treadmill to ensure a constant walking speed would counteract the expected reduction in kinetics from the beginning to the end of the training session.

METHODS

All participants read, understood and signed an IRB approved consent form. Ten individuals with resultant hemiplegia from chronic stroke (5 male, 5 female, $\bar{x}$ age 56.9 $\pm$ 9.1 years, $\bar{x}$ time since CVA 62.1 $\pm$ 59.5 months) completed a single 20 minute treadmill training session at a constant walking speed on a split belt treadmill with two embedded force platforms (Bertec Inc). All participants wore a safety harness during training which was attached to a dynamic body weight support system. Rest breaks were provided, as necessary. Treadmill speed was determined by a licensed Physical Therapist.

Three dimensional lower extremity kinematics (120 Hz) and ground reaction forces (1080 Hz) were collected throughout training with an eight camera motion capture system (Vicon/Peak). Peak moments (normalized to height and body weight) and powers (normalized to body weight) at the ankle and hip during late stance, and anterior/posterior propulsive forces were measured for each step and averaged over each minute of the training session.

Comparisons of propulsion and ankle and hip kinetics were conducted using repeated measures ANOVAs. Specifically, comparisons were made between early (first five minutes) and late training (last five minutes) for all variables, with an α=0.05.

RESULTS AND DISCUSSION

Training speed ($\bar{x}$ speed=0.8 m/s, range: 0.45 - 1.0 m/s) averaged 118% of subject's self selected overground velocity ($\bar{x}$ speed=0.71 m/s, range: 0.37 - 1.1 m/s). All subjects took at least one break during the training session ($\bar{x}$ = 1.6 breaks).

Moments and powers at the ankle were significantly lower on the paretic side compared to the nonparetic side (all $p \leq 0.05$) at each time interval (minutes 1-5, minutes 16-20) (see Table 1). Propulsive forces from the paretic limb were lower than those from the non-paretic limb during both time epochs ($p<0.05$).

Overall, participants managed to maintain consistent limb kinetics throughout training. Specifically, peak ankle and hip moments on the paretic side during the first five minutes were not different compared to the final five minutes of the session (p=0.464; p=0.695 respectively). Peak ankle and hip powers also remained consistent on the paretic side between the first and last five minutes (p=0.327; p=0.650 respectively).

Although we were concerned about increased 'use' of the non-paretic limb as a compensatory mechanism, we observed no significant increase in either ankle moments or powers, or hip moments or powers on the non-paretic side throughout training (all $p \geq 0.400$).

Finally, peak propulsive forces did not differ significantly between the time intervals for either the paretic or non paretic limbs (p=0.088; p=0.500 respectively).

CONCLUSIONS

Despite substantial reductions in limb kinetics on the paretic side compared to the non-paretic side, people post stroke are able to maintain consistent ankle and hip kinetics in both limbs throughout a 20 minute treadmill training session. We believe that ensuring limb kinetics are not reduced is important for maintaining high intensity practice. Maintaining consistent paretic limb kinetics throughout a treadmill training session suggests that treadmill training is an effective method to increase the volume of stepping practice while ensuring high 'effort' steps. The use of treadmill training as part of a rehabilitation program following stroke appears to ensure no decrement of limb kinetics for the greatest training effect.

REFERENCES

1. Rosamond W, et al. *Circulation*, **115**(5), e69-171, 2007.
2. Hill K, et al. *Aust J Physiother;* **43**(3), 173-180, 1997.
3. Pohl M, et al. *Stroke*; **33**, 553-558, 2002
4. Sibley KM, et al. *Gait Posture*; **27**(3), 387-92, 2008.

ACKNOWLEDGEMENTS

This work was supported in part by a grant from the Foundation for Physical Therapy, Inc. Geriatric Endowment Fund (to Lewek).

Table 1: Lower extremity ankle and hip kinetics and propulsion of the paretic and nonparetic limbs.

	First 5 Minutes		Last 5 Minutes	
	Paretic	NonParetic	Paretic	NonParetic
	Mean ± (SD)	Mean ± (SD)	Mean ± (SD)	Mean ± (SD)
Peak Ankle Moment (Nm/kgm)	0.58 ± 0.12*	0.68 ± 0.10	0.58 ± 0.12*	0.67 ± 0.10
Peak Hip Moment (Nm/kgm)	0.29 ± 0.11	0.27 ± 0.11	0.30 ± 0.14	0.28 ± 0.12
Peak Ankle Power (W/kg)	0.85 ± 0.57*	1.69 ± 0.66	0.84 ± 0.55*	1.66 ± 0.72
Peak Hip Power (W/kg)	0.59 ± 0.29	0.77 ± 0.25	0.61 ± 0.30	0.74 ± 0.24
Peak Propulsion (N)	51.11 ± 39.62*	96.56 ± 38.08	59.28 ± 44.08*	98.04 ± 40.25

* = $p \leq 0.05$ compared to non-paretic limb (during the same time period)

MUSCLE CONTRIBUTIONS TO PROPULSION IN POST-STROKE HEMIPARETIC SUBJECTS FOLLOWING LOCOMOTOR TRAINING

[1] Jessica L. Allen, [2,3,4] Steven A. Kautz and [1] Richard R. Neptune

[1] Department of Mechanical Engineering, The University of Texas at Austin, Austin, TX, USA
[2] Brain Rehabilitation Research Center, Malcolm Randall VA Medical Center, Gainesville, FL
[3] Dept of Physical Therapy and [4] Brooks Center for Rehabilitation Studies, University of Florida
email: jessica.allen@mail.utexas.edu; web: http://www.me.utexas.edu/~neptune

INTRODUCTION

Increased walking speed, which is generated by increasing muscle contributions to the anterior posterior ground reaction forces (A-P GRFs), is an important goal in post-stroke rehabilitation. However, because of poor coordination of the paretic leg, walking speed is often increased through compensatory effort by the non-paretic leg. A recent study identified percent of paretic propulsion (PP = paretic / [paretic + non-paretic] propulsion, 0.5 = perfect symmetry) as an effective propulsion symmetry measure that is related to the level of coordination of the paretic leg and predicts walking performance [1].

While individual muscle contributions to forward propulsion are well understood in healthy subjects [2, 3], gait impairments and compensatory strategies used to generate propulsion can vary dramatically among post-stroke hemiparetic subjects. Although two studies have analyzed individual muscle function in multiple post-stroke hemiparetic subjects [4, 5], no study has compared individual muscle contributions to forward propulsion in post-stroke subjects who increased their walking speed following rehabilitation. Therefore, the purpose of this study was to use 3D modeling and simulation analyses to assess whether different mechanisms are used to generate propulsion in post-stroke subjects who increased their fastest-comfortable walking speed following rehabilitation training using different levels of propulsion symmetry.

METHODS

Two subjects greater than six months post-stroke completed a 12-week body weight supported treadmill locomotor training program. Both subjects walked at approximately the same speed pre-therapy and increased speed by the same amount post-therapy with different levels of propulsion symmetry (Table 1). Each subject was analyzed post-rehabilitation as they walked on a split-belt instrumented treadmill while bilateral kinematics, EMG and GRFs were collected. A previously developed 2D model and optimization framework [2] were modified to simulate 3D walking and used to perform the simulation analyses. Muscle excitation patterns were defined using a modified gaussian shape that consisted of 4 parameters: onset, offset, amplitude, and shape factor. A simulated annealing algorithm optimized the excitation parameters for each muscle to minimize the difference between the simulated and experimentally collected kinematics and GRFs. Individual muscle contributions to the paretic and non-paretic A-P GRFs were calculated as described in [2] and then integrated within the paretic and non-paretic propulsive phases (approximately equal to the second half of stance in each leg).

Table 1: Pre- and post-rehabilitation speed and PP.

		Speed (m/s)	PP (%)
Subject 1	Pre	0.70	5.8
	Post	1.00	33
Subject 2	Pre	0.80	48
	Post	1.10	44

RESULTS AND DISCUSSION

The primary contributors to non-paretic leg propulsion were similar in both subjects, with only minor differences in magnitude (Fig 1A) while there were large differences in the primary contributors to paretic leg propulsion (Fig 1B). Consistent with previous studies of healthy walking [2, 3], the soleus and gastrocnemius were among the largest contributors to propulsion in both subjects.

However, their contributions were much lower in Subject 2. While the paretic leg gastrocnemius (GAS_P) was the largest contributor to paretic leg propulsion for Subject 1, the largest contributor for Subject 2 was the paretic leg gluteus medius (GMED_P). The positive contribution of GMED_P to propulsion is consistent with previous simulation analyses [3]. The magnitude of this contribution was much higher in Subject 2 due to high GMED_P and low paretic leg plantarflexor (SOL_P and GAS_P) excitation, which was consistent with the collected EMG data.

The hamstrings also played a role in propulsion generation. The non-paretic leg hamstrings (HAM_NP) were a primary contributor to non-paretic leg propulsion in both subjects with the contribution exceeding that from the non-paretic leg soleus (SOL_NP) in Subject 2. In addition, the paretic leg hamstrings (HAM_P) were among the largest contributors to paretic leg propulsion for Subject 2. The high HAM_P contribution to propulsion is consistent with the subject's prolonged EMG activity into late stance, which has been observed in other hemiparetic subjects [6]. In healthy walking, the hamstrings are active and contribute positively to the A-P GRFs from the beginning to mid-stance when forward propulsion begins. Thus, the prolonged hamstring activity appears to be an effective compensatory mechanism to increase propulsion from the paretic leg in response to the low output from the ankle plantarflexors.

Subject 1 relied largely on the plantarflexors for propulsion generation in both legs, which is indicative of an ankle strategy used to increase speed by increasing PP towards symmetry following rehabilitation. In contrast, Subject 2 relied less on the plantarflexors to generate propulsion and instead utilized muscles crossing the hip, indicative of a hip strategy to increase speed and may explain the small decrease in PP following rehabilitation.

CONCLUSIONS

The results of this study highlight the importance of including symmetry measures in addition to walking speed when developing rehabilitation interventions and monitoring their outcomes. Despite similar increases in walking speed, the contributions to forward propulsion differed between the two subjects; Subject 1 relied largely on an ankle strategy for increased propulsion generation from the paretic leg while Subject 2 utilized a hip strategy to increase speed. These different mechanisms to generate propulsion may be related to impairments pre-therapy. Further simulation analyses comparing these subjects pre- and post-rehabilitation are needed to further understand the different propulsion mechanisms related to speed increases and to better understand the relationship between PP and individual muscle contributions to propulsion.

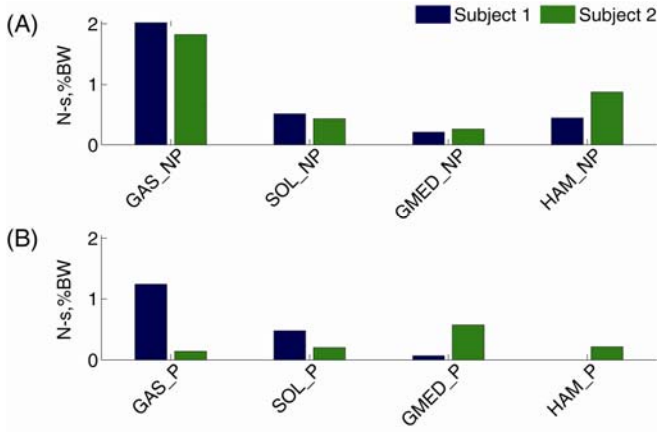

Figure 1: Top muscle contributors to the AP GRFs for subject 1 (blue) and 2 (green) during the (A) non-paretic and (B) paretic propulsion phases.

REFERENCES

1.Bowden, MG, et al. *Stroke* **37,** 872-6, 2006.
2.Neptune RR, et al. *Gait Posture* **19**, 194-205, 2004.
3. Liu MQ, et al. *J Biomech* **39**, 2623-2630, 2006.
4. Peterson CP, et al. *J Biomech*, 2010 (in review).
5. Hall AL, et al. *Gait Posture* 2010 (in review).
6. Den Otter, et al. *Gait Posture* **25**, 342-52, 2007.

ACKNOWLEDGEMENTS

This work was supported by NIH grant R01 NS55380 and the Rehabilitation Research & Development Service of the VA.

DECOUPLING OF MUSCLE SHORTENING AND JOINT KINEMATICS DURING FROG JUMPING.

[1]Henry Astley and [1]Thomas Roberts

[1]Brown University, Providence, RI, USA
email: Henry_Astley@brown.edu

INTRODUCTION

Elastic tendons can decouple changes in muscle length from changes in joint angle, allowing the muscles to operate over lengths and velocities which are favorable for contractile performance. While the role of elastic tendons has been well-studied in steady-speed locomotion, their role in acceleration is not well understood. The remarkable jumping ability of anurans is an excellent system for addressing this issue due to well-characterized muscle physiology, extensive prior work, static pre-jump posture, and recent data suggesting that elastic energy storage in tendons may occur[1]. We hypothesized that during strong accelerations (jumping), a frog muscle with a significant tendon would be decoupled from movement at its joint due to tendon stretch and recoil.

METHODS

In order to test this hypothesis, we quantified simultaneous joint movement and muscle strain in the ankle of leopard frogs (*Rana pipiens*) during jumping (24 jumps from 4 frogs). The ankle is extended primarily by the plantaris, a large pennate muscle with a prominent tendon. Joint movement and muscle fascicle strain were quantified using X-ray Reconstruction Of Moving Morphology (XROMM) [2], a high-speed biplanar cinefluoroscopy system with sub-millimeter accuracy (Fig. 1).

Radiopaque beads were surgically affixed to the tibiofibula and fused tarsal bones (the proximal and distal bones of the ankle joint, respectively), four in each bone. To track muscle fascicle lengths, two beads were inserted into the muscle along a single fascicle plane, at either end of the fascicle. After recovering from surgery, frogs were induced to jump from between two calibrated orthogonal image intensifiers fitted with high speed cameras set to 500 fps and 90 kVp X-ray sources.

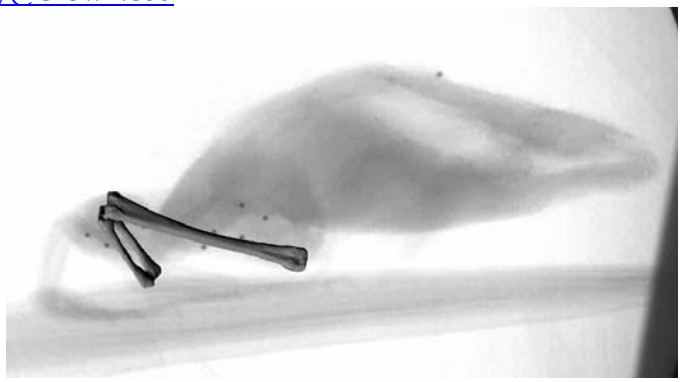

Figure 1 – A frame of X-ray video of a representative jump at the onset of ankle extension, superimposed with CT-scan models of the bones.

Digitized points were registered to CT-scanned models of the bones and markers (Fig. 1). Digitized muscle marker positions were used to calculate instantaneous fascicle length. Bone models were then animated using the digitized data, allowing characterization of the bone movement in six degrees of freedom.

Only rotation in the flexion/extension axis was considered, as this is the primary movement of the plantaris. Onset of ankle extension was defined as the point where the ankle angle reached 5% of peak extension (arrow, Fig. 2A). Internal moment arm at the ankle joint in flexion/extension was determined by tendon travel [3].

RESULTS AND DISCUSSION

In all jumps, muscle fascicle strain was strongly decoupled from joint movement (Fig. 2). More than half (53%±3% SE, N=24) of total fascicle strain occurred prior to onset of ankle extension. Following this, rapid joint movement occurs with little fascicle strain (Fig. 2). The muscle strain-joint angle relationship (Fig. 2B) depicts periods of substantial muscle shortening and no joint movement, followed by a period of substantial ankle motion accompanied by little fiber strain. We interpret this pattern to reflect the role of tendons,

which stretch to absorb muscle shortening early in the jump, and recoil to power joint ankle extension later in the jump.

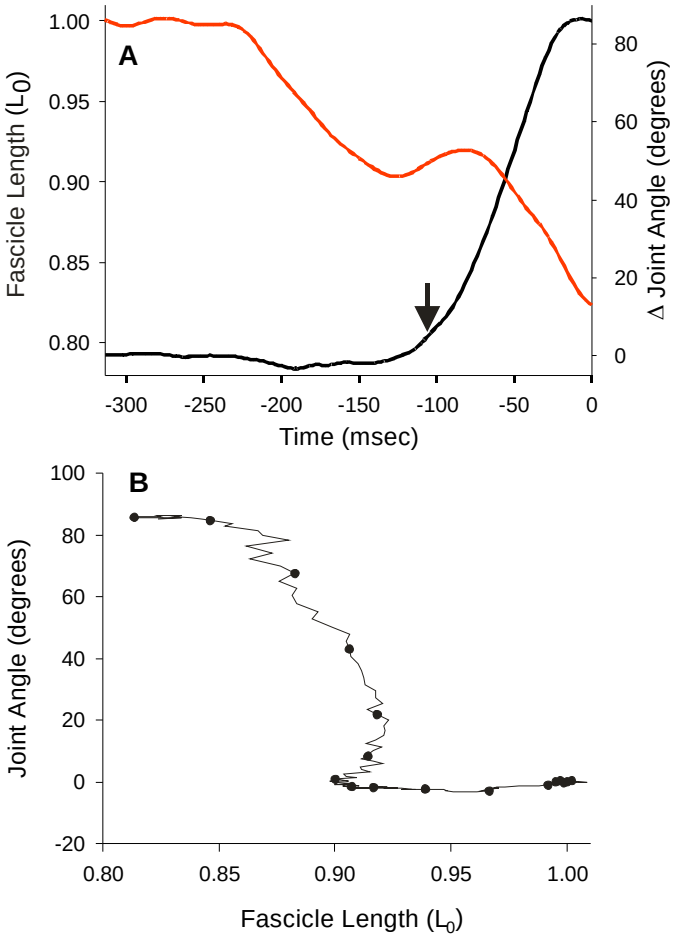

Figure 1 – For a representative jump. A) Muscle fascicle strain (red) and joint angle (black) vs. time before toe-off (zero). Arrow indicates onset of ankle extension. B) Fascicle strain vs. joint angle for the same jump. Points occur every 20 ms.

The relationship between muscle strain and joint angle cannot be explained by muscle moment arm, as measurements in isolated limbs show it to be constant across the entire range of motion. While the plantaris crosses the knee at the origin, this does not substantially alter our conclusions. Knee extension would result in proximal displacement of the muscle belly, adding to (rather than cancelling out) the effects of the initial fascicle shortening.

The observed pattern of muscle-joint decoupling is consistent with storage of strain energy in elastic tendons in order to amplify power output. During the initial muscle shortening without joint movement, the plantaris tendon would be stretched. Subsequently, the muscle remains nearly constant in length, while the joint moves substantially, suggesting that this joint movement is produced by tendon recoil. This is supported by the high angular velocity and acceleration that occurs without corresponding muscle shortening. Frog jumping provides a particularly striking illustration of the influence of elastic tendons on muscle length trajectory that is likely an important determinant of locomotor performance in vertebrates.

REFERENCES

1. Peplowski MM & Marsh RL. *J. Exp. Biol.* **200**, 2861-2870, 1997
2. Brainerd, EL, et al. *J. Exp. Zool.* **313A**, in press, 2010
3. Calow LJ & Alexander, RM. *J. Zool., Lond.* **171**, 293-321, 1973

ACKNOWLEDGEMENTS

Funded by NSF Grant 064242. Many thanks to Emily Abbott, Manny Azizi, and Megan Dawson for assistance with surgery, and to Elizabeth Brainerd, Dale Ritter, Allyce Sullivan, David Baier, Megan Dawson, and Nick Gidmark for help with XROMM operation and data processing.

THE EFFECTS OF DENERVATION AND SELF-REINNERVATION IN THE GUINEA FOWL LATERAL GASTROCNEMIUS

Jennifer Carr, Linda Chao and Andrew Biewener
Harvard University, Cambridge, MA, USA
email: carr@fas.harvard.edu

INTRODUCTION

Running and walking require that animals be able to negotiate variable terrain and recover from unexpected perturbations. Reflex responses that monitor and respond to changes in muscle force and length play an important role in controlling how an animal stabilizes its center of mass and produces ground reaction forces during locomotion [1, 2, 3]. One method of studying the role of muscle reflexes during locomotion is to eliminate reflex responses by performing surgical self-reinnervation. Self-reinnervation experiments have demonstrated that motor innervation can be restored to a muscle, but not sensory afferents [4, 5, 6].

Self-reinnervation studies have been performed on several species of quadrupedal mammals. Our study was performed in part to validate a bipedal model that could be used to study the function of reflexes during different types of locomotion. Guinea fowl (*Numida meleagris*) were used as experimental animals because they are bipedal, they are excellent runners and have been used in other experiments so our data can be compared with other studies.

The goals of this study were two-fold. We wanted to determine whether self-reinnervation in the Lateral Gastrocnemius (LG) caused the loss and subsequent reestablishment of motor innervation and the permanent loss of sensory afferents. Secondly, we wanted to determine whether during locomotion there were differences in muscle activity and joint kinematics between the self-reinnervated limb and the opposite unaltered limb.

By demonstrating a loss of function followed by the recovery of motor function we will validate a bipedal model for studying the role of reflexes during locomotion. We will then use that model to study the role of reflexes on both steady and unsteady locomotion.

METHODS

In order to validate guinea fowl as a bipedal model we studied the effects of denervation and subsequent self-reinnervation in three animals. Prior to surgery kinematic measurements were taken at the hip, knee, ankle and tarsometatarsal-phalangeal (TMP) joint using high-speed video during level locomotion. Denervation of the right LG muscle was performed by making an incision in the popliteal region of the right hindlimb to expose the tibial nerve. In order to denervate the limb an incision was made in the popliteal region of the right hindlimb to expose the tibial nerve. The branch innervating the LG was identified proximal to its entry to the muscle. The LG nerve bundles were transected and immediately sutured using 6-0 non-absorbable silk and secured with fibrin glue (Bovine Thrombin in $CaCl_2$, Fibrinogen, and Fibronectin from Bovine plasma). Subsequently, the opened fascia and skin were sutured closed. Function of the LG was monitored at three and six weeks post denervation by recording joint kinematics using high-speed video and by recording muscle electrical activity using electromyography (EMG) electrodes during treadmill locomotion. We also tested for self-reinnervation of sensory afferents by measuring the presence or absence of a calcaneal tendon reflex.

To determine whether there were differences in muscle activity and/or joint kinematics between the self-reinnervated limb and the unaltered limb the same surgery as described above was performed on four additional guinea fowl. Approximately a year after self-reinnervation the LG on the right (self-reinnervated) and left (unaltered) side of the guinea fowl were implanted with EMG electrodes to measure muscle activity. The four birds were run and walked on a level and over obstacles on a treadmill while muscle activity and joint kinematics were recorded. The presence or absence of sensory

afferents was again tested by measuring a calcaneal tendon reflex.

RESULTS AND DISCUSSION

Three weeks post surgery we were able to demonstrated that the LG had been effectively denervated (Fig.1). Denervation significantly ($p<0.05$) affected joint kinematics at the hip, knee, ankle and TMP joint during both walking and running.

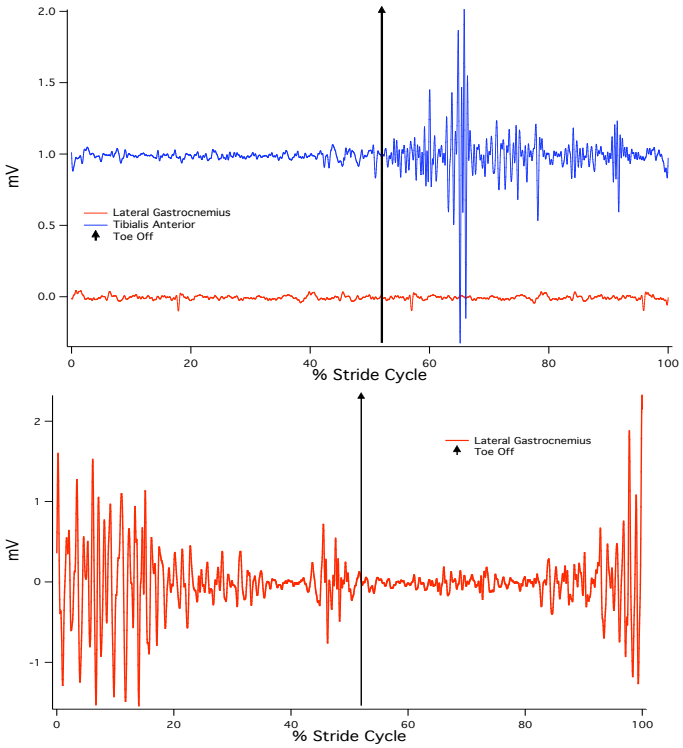

Figure 1: This figure demonstrates the electrical activity measured throughout a running stride in the right denervated LG (red) and the tibialis anterior (blue) three weeks (top) and six weeks (bottom) after the denervation surgery.

By six weeks post-surgery self-reinnervation of the motor nerves had occurred and electrical activity in the LG was reestablished. Joint kinematics at six weeks post-surgery of the hip, knee and ankle were not significantly different from those measured prior to surgical denervation. The sensory afferents at six weeks, however, did not demonstrate self-reinnervation, with no evidence of a calcaneal tendon reflex.

At one year after self-reinnervation there was still no demonstrable self-reinnervation of sensory afferents to the LG based on the continued absence of a reflex response in the muscle. Despite this, no significant differences were measured in duty factor, stride time or stance time between the right (self-reinnervated) limb and the left (unaltered) limbs. There was however a significant difference ($p<0.05$) in the frequency characteristics of the EMG waveforms between the right and left LG. The intact left LG EMG measurements demonstrated a greater average frequency and a greater maximum frequency than EMGs recorded from the right LG during all locomotor (level and obtacle) conditions measured (Fig. 2).

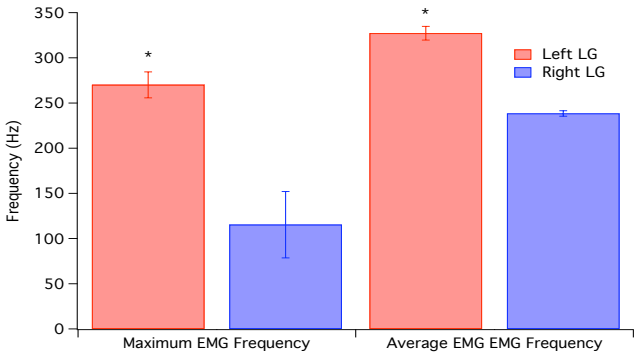

Figure 2: This figure demonstrates the maximum EMG frequency and average EMG frequency of the left and the right LG during locomotion.

CONCLUSIONS

Our study validates guinea fowl as a bipedal model for self-reinnervation of the lateral gastrocnemius. Using guinea fowl we were able to successfully denervate the LG and measure self-reinnervation of the motor efferents but not the sensory afferents. We also demonstrated significant effects of self-reinnervation on various parameters of level and obstacle treadmill locomotion.

REFERENCES

1. Daley, M. A., Felix, G. and Biewener, A. A. *J. Exp. Biol.* **210**, 383-94. 2007.
2. Daley, M. A., Usherwood, J. R., Felix, G. and Biewener, A. A. *J. Exp. Biol.* **209**, 171-87. 2006.
3. Loeb, G. E. *Conf. Proc. IEEE Eng. Med. Biol. Soc.* **17**, 1393-1394. 1995.
4. Cope TC, et al. *Journal of Neurophysiology*. **71**, 817-820. 1994.
5. Cederna PS, et al. *Plastic and Reconstructive Surgery*. **105**, 2003-2009. 2009.
6. Wasserschaff M. *Brain Research*. **515**, 241-246. 1990.

LIMB MUSCLE FUNCTION DURING HIGH-POWERED ENERGY ABSORPTION

Nicolai Konow, Emanuel Azizi and Thomas J. Roberts
Dept. of Ecology and Evolutionary Biology, Brown University, Providence RI, USA
email:nkonow@brown.edu

INTRODUCTION

Energy absorption *via* active lengthening of muscle is a part of most locomotor tasks and the essential function of muscles during decelerations. Our understanding of muscle function during energy absorption remains limited. An important aspect of understanding the mechanism of active muscle lengthening in absorbing the energy of high-powered activity is to quantify the influence of series elastic elements (i.e. tendon and aponeurosis) on the behavior of the muscle contractile element (i.e. fascicles). Wild turkeys have calcified tendons in their distal hind limb muscle tendon units. This trait permits measurements of muscle-tendon unit force, simultaneous with measurements of fascicle length and activity and skeletal kinematics. Turkeys also have a propensity towards ground locomotion coupled with good flight landing performance. By quantifying fascicle behavior in the turkey lateral gastrocnemius muscle-tendon unit during landing, which is a high-powered energy absorption event, we wanted to answer the question: how is energy absorbed during high-powered *in-vivo* muscle contractions? We expected the pronounced leg flexion following a landing-impact to result in considerable fascicle lengthening during a period of rapid force-rise in the muscle tendon unit. We also predicted much higher muscle tendon unit forces compared with running [1]. The combination of rapid lengthening and high forces should translate into high rates of energy absorption by the fascicles.

METHODS

In *N*=6 wild turkeys (BM=3.0-3.4kg) the lateral gastrocnemius (23-30g) was studied *in vivo* and *in situ*. Sonomicrometry crystals and EMG electrodes were implanted surgically along a fascicle, to measure fascicle length and activity, and strain gages were bonded to both aspects of the ossified tendon to measure muscle force [1]. Following recovery, animals performed landings from heights

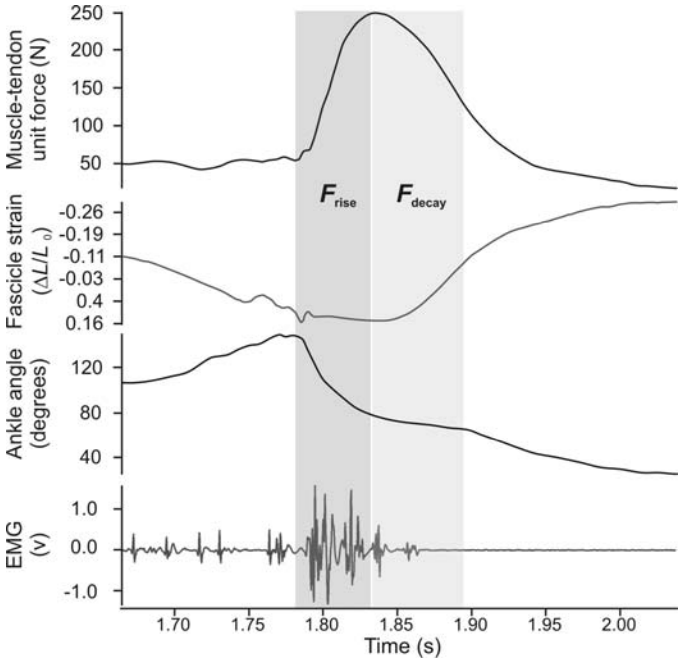

Figure 1. Data from a representative 1.5m landing, with definition of the force-rise and -decay periods (shaded columns) based on the profile of muscle-tendon unit force. Landing is at left margin of dark column.

of 0.5, 1 and 1.5m. High-speed video was recorded in lateral view of all *in vivo* trials. Following *in vivo* experiments, strain gages were calibrated to force *in situ*. Muscle power was calculated as the product of muscle force and fascicle velocity as measured by sonomicrometry. Changes in ankle angle were measured via motion-analysis of high-speed videos.

RESULTS AND DISCUSSION

Prior to landing, gastrocnemius fascicles shortened actively to extend the ankle (Fig. 1). Following impact, there was a sharp rise in muscle-tendon unit force, which approached three-fold the stance phase force during 2.5 m s^{-1} level-running [1], as expected. We divided analysis into two periods, separated by the timing of peak force. Our results showed an unexpected decoupling of fascicle length change and ankle kinematics during high-powered energy

absorption. Most of the impact-absorbing ankle flexion occurred during force-rise (i.e. prior to peak force) and this pattern remained constant across drop heights (Fig. 2A). During force rise and ankle flexion, the fascicles remained quasi-isometric, or shortened slightly (Fig. 2B). Most of the fascicle lengthening occurred during the period of force decay, when little ankle flexion occurred (Fig. 1). The amount of fascicle lengthening during force-decay increased with height to an average of 25% of L_0 (Fig 2A). This considerable fascicle lengthening acted as a significant energy-sink, absorbing more than 20J/kg muscle during 1.5m landings (Fig. 3).

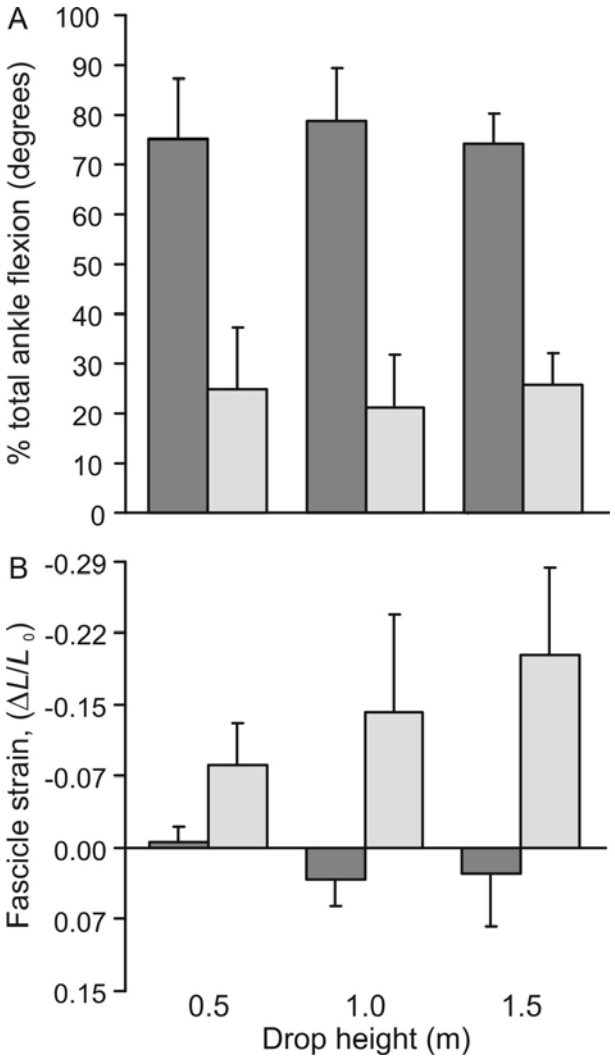

Figure 2. Decoupling of ankle kinematics (A), predominating during force-rise (dark grey), and fascicle strain (B), predominating during force-decay (light grey) of high-powered energy absorption events. Negative strain is fascicle lengthening. Error bars indicate S.E.M.

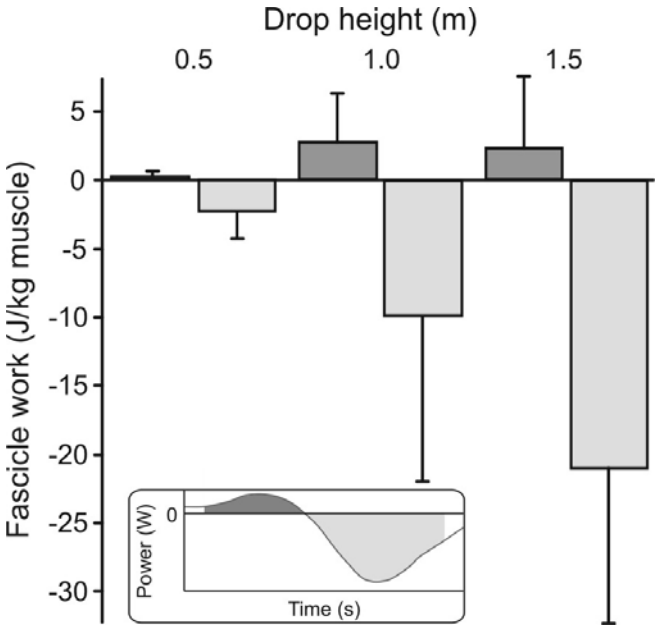

Figure 3. Work done by muscle fascicles, calculated from the integrated area of muscle power during the period of force rise (dark grey) and force decay (light grey). Fascicle lengthening during force decay acts as significant energy sink, absorbing >20J/kg muscle during 1.5m landings. Energy absorption is lower during less challenging landings.

CONCLUSIONS

The observation that most muscle lengthening occurred when there was limited joint flexion, and most of the joint flexion occurred when there was limited muscle lengthening, supports the idea that elastic elements function to decouple fascicle length changes from joint movements. These data suggest that in an energy-absorbing event, energy stored transiently in elastic elements can be released to do work on muscle contractile elements. This decoupling mechanism may allow for higher rates of energy absorption during high-power activities, ultimately providing a mechanism that may protect against muscle damage during fascicle lengthening.

REFERENCES

1. Gabaldon, A. et al., *J Exp Biol* **207**, 2277-2288 2004.

ACKNOWLEDGEMENTS

Supported by NIHAR055295 to TJR.

PASSIVE PROPERTIES OF MUSCLE FIBERS ARE VELOCITY DEPENDENT

Michael R. Rehorn, Silvia. S. Blemker

University of Virginia, Charlottesville, VA, USA
email: mrr6r@virginia.edu, web: http://mae.virginia.edu/muscle

INTRODUCTION

The passive properties of skeletal muscles determine an important component of the total force generated within a muscle fiber [1]. While it is known that muscle fibers behave viscoelastically in passive tension [2], to date, most studies have focused on quantifying the passive stress-strain relationship of single muscle fibers during quasi-static loading conditions despite the fact that human movement is a dynamic process. Moreover, most models of skeletal muscle assume that the passive properties of the tissue are purely elastic, thus ignoring the transient effects due to the rate of loading [3]. While these assumptions allow for the accurate description of intramuscular stresses during static loading, it is unclear how the viscoelastic properties of muscle may impact transient stresses over a physiologic range of lengthening velocities. Therefore, the goal of this work was to analyze the effects of lengthening velocity on the peak stresses measured within single muscle fibers to determine how passive behavior changes over a given range of lengthening rates.

METHODS

Tibialis anterior muscles were dissected from two four-month-old male ICR wild-type mice after euthanization with an IP injection of Sodium Pentobarbital in accordance with the guidelines set out by the Animal Care and Use Committee at the University of Virginia. Immediately following dissection, muscle tissues were placed in room temperature relaxing solution and later kept in storage solution at -20^{o}C [4].

Skinned muscle fibers were manually dissected while immersed in relaxing solution and secured to two wires using four 10-0 nylon sutures. One wire was attached to a high-speed length controller (ASI, model no. 322C) and the other was secured to a force transducer (ASI model no. 405A, 1.0mN/volt). The entire experimental apparatus was mounted on the stage of an inverted microscope so that fibers could be imaged during the course of the experiments (Fig. 1A). All mechanical tests were conducted in relaxing solution at 37^{o}C.

A total of 4 fibers were tested (n=4). Each fiber was subjected to a standard protocol as to ensure structural integrity of the specimen and to provide a consistent initial configuration for all experiments. Initial fiber length (L_o) was set to the length at which the fiber began to resist passive extension, ensuring that there was no slack length left in the fiber. Fibers were imaged at both 10X and 40X optical zoom in order to measure L_o and to examine them for any obvious signs of damage (Fig. 1B).

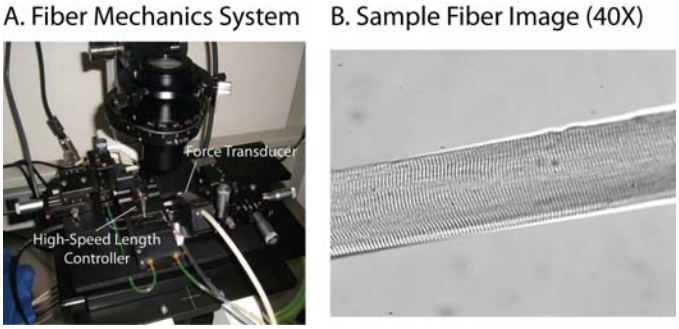

Figure 1: Isolated fibers were secured to a high-speed length controller and force transducer (A) and were imaged (B) to check for obvious signs of damage and to measure sarcomere lengths and diameters.

All fibers were preconditioned by applying a 2Hz sinusoidal length change with maximum amplitude $1.4L_o$ for 10 seconds. Hysteresis loops were plotted for each cycle. Fibers were considered preconditioned once multiple hysteresis loops overlapped. This generally happened after 12-16 cycles.

Ramp hold tests were conducted by stretching fibers to $1.4L_o$ at 13 different velocities ranging from 0.1 to 10 fiber-lengths-per-second (L_o/s) (Fig. 2A). 40X images were acquired at fiber lengths L_o and $1.4L_o$ for each ramp hold test in order to measure

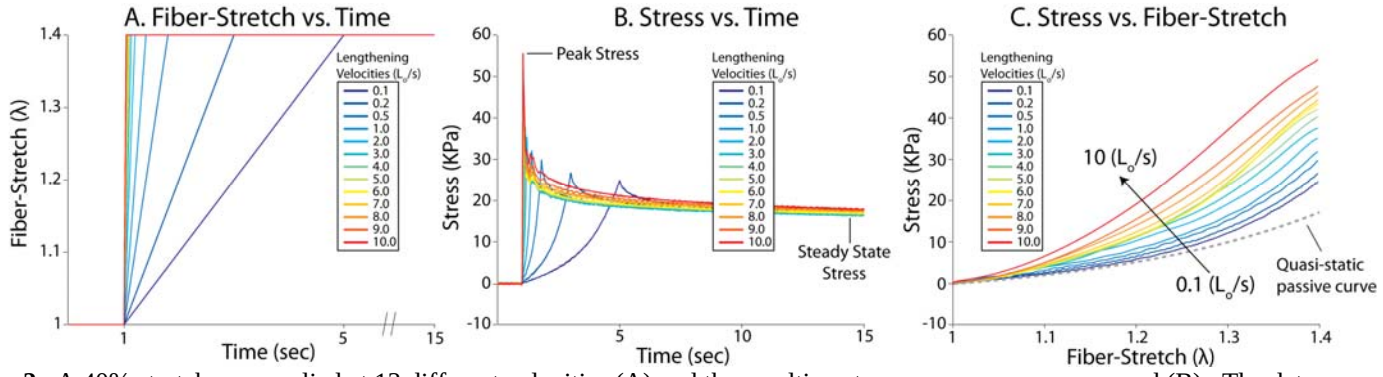

Figure 2. A 40% stretch was applied at 13 different velocities (A) and the resulting stress response was measured (B). The data were used to determine how the transient stress-stretch behavior of the muscle fiber varies with loading velocity.

sarcomere lengths and fiber diameters (Fig. 1A). Average sarcomere lengths were calculated from the images using an Autocorrelation/FFT algorithm implemented in MATLAB (Mathworks) and were then used to calculate fiber-stretch on a sarcomere level: $\lambda=L/Lo$, where L is the current sarcomere length and Lo is the initial sarcomere length. Fiber cross-sectional areas were calculated assuming the fiber had a cylindrical shape and that fiber volume was preserved throughout the experiment. Stress was calculated by dividing measured force by cross-sectional area. Data were analyzed by averaging the peak stress and steady state stress for all fibers (n=4). Steady state stresses were measured at the end of 15 seconds of relaxation and used to determine quasi-static properties. Peak stress was determined to be the maximum stress measured during the ramp phase of the individual test (Fig. 2B).

RESULTS AND DISCUSSION

The quasi-static stresses measured in this study were in the range of previously reported values [5] and were independent of loading rate (Fig. 2B). Peak stress within the fiber increased as lengthening velocity increased (Fig. 2B). Similarly, the stress-strain relationship was dependent on lengthening velocity (Fig. 2C). Even at relatively slow velocities (e.g. $0.1L_o/s$), the transient peak stress within the muscle fiber was over 100% larger than the peak quasi-static stress (Fig. 3).

CONCLUSIONS

These results demonstrate that the passive properties of skeletal muscle fibers are velocity dependent and that viscoelastic effects may be important in determining muscle fiber forces at physiologic rates of lengthening.

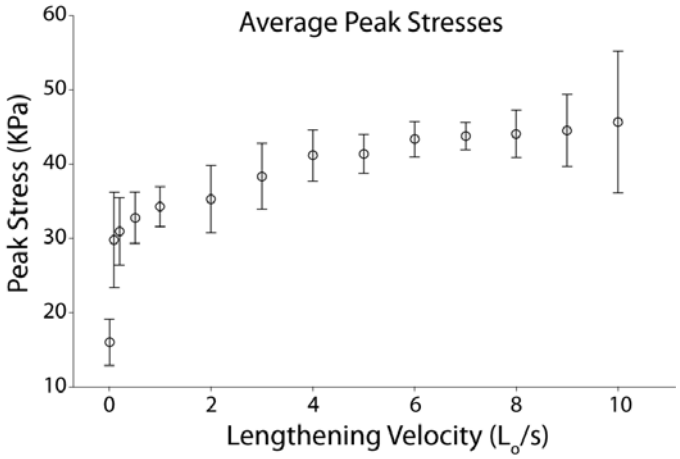

Figure 3. Average peak stresses ± one standard deviation for all fiber tests (n=4).

Future work will include measuring viscoelastic properties of both fibers and fiber bundles. These results will be used to develop a viscoelastic muscle model that characterizes the relaxation response in order to examine how these properties affect predictions of muscle force during dynamic movements.

REFERENCES

1. Proske, U, and Morgan, D, *J Muscle Res Cell M*, 20(5) 433-442, 1999
2. Wang, K, et al. *Biophys J*, 64 1161-1177, 1993
3. Zajac, FE, *Crit Rev Biomed Eng*, 17(4) 359-411, 1989
4. Friden, J, et al. *Muscle Nerve*, 27(2) 157-164, 2003
5. Bensamoun, S, et al. *J Biomech*, 39(3) 568-578, 2006

AKNOWLEDGEMENTS

Funding for this work was provided by NIH grant R01 AR 056201, the Funds for Excellence in Science and Technology at the University Virginia, and the National Skeletal Muscle Research Center at UC San Diego.

REGIONAL STIFFENING OF MOUSE TIBIALIS ANTERIOR TENDONS WITH AGE

Lauren K. Wood, Ellen M. Arruda, and Susan V. Brooks

University of Michigan, Ann Arbor, MI, USA
email: svbrooks@umich.edu

INTRODUCTION

The incidence of tendinopathy increases markedly with age although the mechanisms for the increase are unknown [1]. Tendons interact with muscle contractile elements to transmit forces to the skeleton to generate movement. Thus, injury or dysfunction of tendons has serious implications for immobility, a major contributor to decreased quality of life among the elderly. Although tendons have typically been treated as homogenous structures for studies of mechanical properties, tendons actually demonstrate functionally graded behaviors along their length [2]. The impact of aging on these local properties remains entirely unexplored. The objective of this study was to examine age-related changes in the regional mechanical properties of tendons. We hypothesized that the region of the tendon nearest the muscle would stiffen with age, leading to a stiffer tendon overall.

METHODS

Tibialis anterior (TA) muscle-tendon units (MTUs) were extracted from young (3-4 month old, n=12), adult (8-12 month old, n=10) and old (28-30 month old, n=5) male C57BL/6 mice. MTUs were gripped at the 1st metatarsal and TA muscle in our custom-made tensile tester, and 25 μm polystyrene beads were brushed along the entire length of the tendon to serve as optical markers for strain measurements. The MTUs were immersed in PBS, and the cross-sectional area (CSA) was determined at six points along the tendon. Tendons were subjected to a sequence of load-unload cycles of 10% (2x), 15% (1x), and 20% (3x) grip-to-grip strain at a constant strain rate of 0.01% per second. Synchronized force and image recordings were obtained during testing. Bead positions were tracked using Metamorph software, and nominal strains in the proximal (near the muscle), central and distal (near the bone) tendon regions were calculated as the change in separation between beads in each region divided by their initial separation. Regional nominal stress was determined by dividing raw load data by the local CSA. Overall tendon strain and stress were calculated using the most proximal and distal beads and average tendon CSA, respectively.

In each tendon region, maximum stiffness (defined as the maximum slope of the stress-strain response) was determined for the first load-unload cycle. Stiffness at 1.5% strain was also calculated for the overall tendon response. Regional mechanical data were compared using a two-way ANOVA, with age and tendon region as independent factors, and Dunn's *post hoc* test as necessary. Significance was set a priori at $p < 0.05$. All animal procedures were approved by the University committee on the use and care of animals.

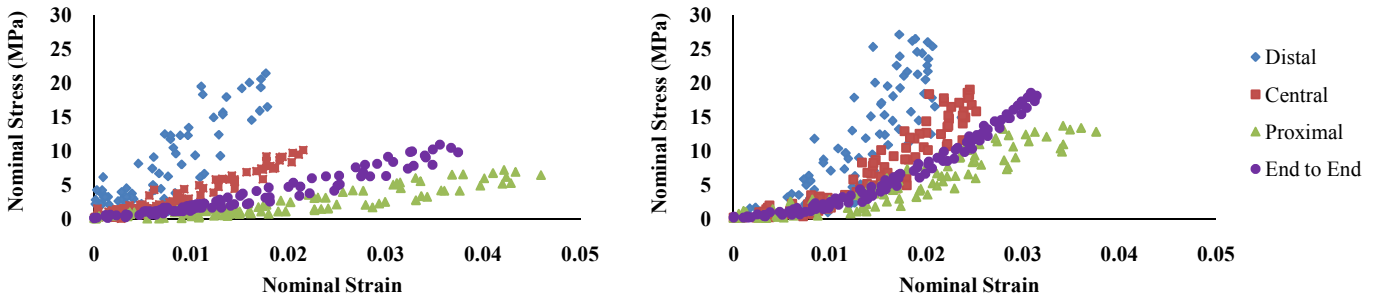

Figure 1: Representative stress-strain responses of TA tendons from young (left) and old (right) mice undergoing a 10% strain load-unload cycle. Response of the distal (blue diamonds), central (red squares) and proximal (green triangles) regions of the tendon differ significantly from the overall tendon response (purple circles). For both age groups, tendon stiffness is greatest in the distal region and smallest in the proximal region of the sample. Tendons of old mice show dramatic stiffening of the central and proximal regions, leading to a stiffer tendon.

RESULTS AND DISCUSSION

Cyclical mechanical testing demonstrated that tendons of all age groups possess large differences in their stress-strain response along the length of the tendon (Fig. 1). Strain was greatest in the proximal region and decreased towards the distal end of the tendon. Tendons of old mice showed decreased strain in the proximal region when compared to tendons of young and adult mice (Table 1). Average forces significantly increased from 0.79 ± 0.15 N and 0.82 ± 0.19 N for the young and adult groups, respectively, to 1.07 ± 0.25 N for tendons of old mice. The tendons of old mice also showed significantly larger stresses in the proximal region when compared with young mice (data not shown).

Table 1: Nominal strain data for all age groups. Superscripts indicate significant difference from young (a) and adult (b) age groups ($p < 0.05$).

	Nominal Strain			
	Distal	**Central**	**Proximal**	**End to End**
Young	0.018 ± 0.005	0.024 ± 0.006	0.041 ± 0.005	0.033 ± 0.005
Adult	0.016 ± 0.004	0.023 ± 0.007	0.043 ± 0.008	0.032 ± 0.009
Old	0.018 ± 0.006	0.021 ± 0.005	0.030 ± 0.011[a,b]	0.023 ± 0.001[a]

The greater stresses and lower strains in the proximal region of tendons of old compared with young or adult mice resulted in a dramatic increase in stiffness in that region (Fig. 2). Stiffness was 124% and 75% greater in the proximal region for tendons of old compared with young and adult mice, respectively. Higher stiffness was also present to a lesser extent in the distal and central regions of tendons of old mice. When combined, stiffening in all regions of the tendon resulted in a significant increase with age in end to end stiffness across all age groups. Stiffness increased from 527 ± 91 MPa for young mice, to 799 ± 157 MPa for adults and 1419 ± 126 MPa for old mice. There was also a significant increase in stiffness at the physiological level of 1.5% strain for tendons of old mice compared with the other age groups (Table 2).

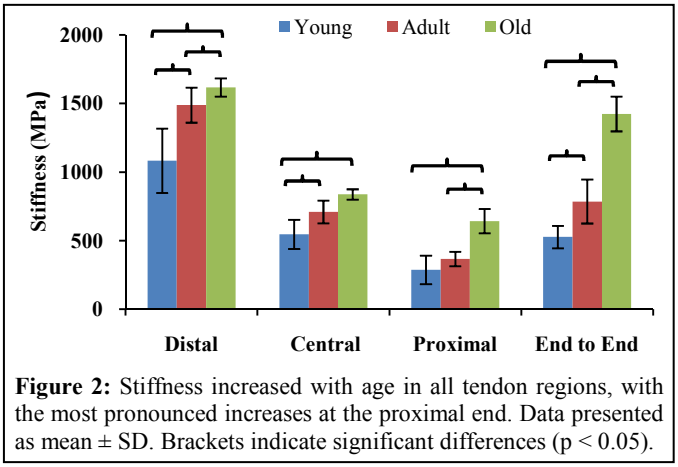

Figure 2: Stiffness increased with age in all tendon regions, with the most pronounced increases at the proximal end. Data presented as mean ± SD. Brackets indicate significant differences ($p < 0.05$).

Table 2: Stiffness at 1.5% strain for all age groups. * denotes significant difference from young and adult age groups ($p < 0.05$).

	Young	**Adult**	**Old**
Stiffness (MPa)	306 ± 62	377 ± 137	798 ± 104*

These data show that tendon stiffens with age. Furthermore, the stiffening is not a result of uniform stiffening along tendon. Rather, it is largely due to pronounced stiffening in the proximal region of the tendon, and amplified by increases of a lesser extent in the distal and central portions. Age-related stiffening is also present at physiologically relevant strains. Human TA tendons function between 0 and 2.5% strain during normal activity [3], and our data demonstrate a marked increase in stiffness within that range. These findings agree with *in vivo* reports of increased joint stiffness and impaired mobility in the elderly population [4].

Given the dramatic regional variation in mechanical properties along tendons, constructing meaningful structure-function relationships will also require analysis of underlying composition and structure to be performed regionally. Clarifying mechanisms underlying changes with aging in the structure and function of muscle-tendon units will improve the likelihood of developing treatments aimed at preventing the onset and progression of age-related tendinopathy and physical frailty.

REFERENCES

1. Milgrom C, et al. *J Bone Joint Surg Br* **77**, 296-298, 1995.
2. Arruda EM, et al. *J App Physiol* **101**, 1113-1117, 2006.
3. Maganaris CN. *J Biomech* **35**, 1019-1027, 2002.
4. Hortobagyi T and DeVita P. *J Electromyogr Kinesiol* **10**, 117-126, 2000.

ACKNOWLEDGEMENTS

Financial support by NIH #AR0556242.

KINETIC AND KINEMATIC DIFFERENCES IN FEMALE RUNNERS WITH ILIOTIBIAL BAND SYNDROME: THE EFFECTS OF FATIGUE

Becky Avrin Zifchock, Allison Brown, Howard Hillstrom
Hospital for Special Surgery, New York, NY
email: zifchockr@hss.edu

INTRODUCTION

Iliotibial band syndrome (ITBS) is the second most common chronic running injury [1], and a leading cause of knee pain in runners [2]. While a clear understanding of the cause of ITBS would elucidate proper treatment protocols, the literature is not conclusive. Work by Noehren et al [3] has shown that runners who go on to develop ITBS tend to have increased hip adduction and knee internal rotation angles. They suggest that this posture may increase the strain on the fibers of the iliotibial band, and may also increase the friction with the contact surface of the lateral femoral epicondyle. While this work is useful for understanding dynamic malalignment that may lead to ITBS, its usefulness in understanding gait mechanics in runners currently experiencing symptoms may be limited. As pointed out by Miller et al [4] fatigue is a likely component of abnormal gait mechanics and is likely to play a role in running injury, particularly one such as ITBS whose symptoms typically worsen with fatigue. Miller et al. showed that runners with ITBS had larger foot adduction and knee flexion values pre-fatigue and larger foot inversion and knee flexion values post-fatigue as compared to healthy runners. However, in light of the findings of Noehren et al., and the physiological pull of the iliotibial band across the hip and knee joints, frontal and transverse kinetics and kinematics at these joints may be more closely related to the injury mechanism. Therefore, the purpose of this study was to compare hip and knee kinetics and kinematics between runners with ITBS and healthy runners before and after a fatiguing run. Following a fatiguing run, as compared to the healthy runners, runners with ITBS were expected to exhibit larger increases in hip and knee angles and moments.

METHODS

As part of an ongoing study, data from 14 female runners were included in this analysis. Gait mechanics from seven healthy runners (28.6±8.3 yrs; 1.6±0.1 m; 56.9±5.8 kgs) and seven ITBS runners (31.9±9.0 yrs; 1.7±0.1 m; 59.3±5.2 kgs) were measured during overground running. Data were collected before and after a treadmill run to fatigue. Subjects were prompted to run on the treadmill at a speed that approximated their 5K race pace and were asked to stop when they reached a self-reported Rating of Perceived Exhaustion of 17/20 or a Pain Score of 6/10 [5].

Hip and knee kinetics and kinematics were collected from a standard 6-degree-of-freedom marker set using a 12-camera motion capture system (Motion Analysis; Santa Rosa, CA) and four forceplates (Bertec; Columbus, OH and AMTI; Watertown, MA). Subjects ran through the data collection volume as they traversed a 25 m runway. Analog and video were smoothed at 50Hz and 8Hz, respectively, using a fourth-order Butterworth filter. Peak values of the following parameters were identified from the stance phase of each of five trials and averaged: hip adduction and internal rotation angles, knee abduction and internal rotation angles, hip abduction and external rotation moments, and knee adduction and external rotation moments. Data from the dominant limb was used for the healthy runners, and data from the involved limb was used for the ITBS runners.

Statistical analyses were carried out in SPSS 16.0 (Chicago, IL). Two-way mixed-factor ANOVAs were used to test for any effects of injury status (between factor) and fatigue status (within factor) for each variable. Due to the preliminary nature of this work, significance was set at $p < 0.10$ for all analyses.

RESULTS AND DISCUSSION

Healthy runners and ITBS runners fatigued after approximately 25±7 min and 26±8 min of treadmill running, respectively.

The results of this study were not supportive of the hypotheses. As a result of fatigue, the ITBS runners were expected to demonstrate larger increases in all of the variables of interest, as compared to the

healthy runners. Yet there was only one significant interaction between group and time, and this showed that peak hip internal rotation angles were significantly decreased in ITBS runners as a result of fatigue ($p = 0.03$, Figure 1A). This equated to an average difference of 53.5% between pre and post-fatigue.

There were a significant main effect of time, which suggested that both groups demonstrated decreases in peak hip adduction angles ($p = 0.08$, Figure 1B) and peak hip abduction moments ($p = 0.03$, Figure 1C). This is contrary to the expectation that these parameters would increase with fatigue. It should be noted, however, that these differences tended to be small. On average there was a 9.1% difference in peak hip adduction angle and a 4.2% difference in peak hip abduction moment between pre and post-fatigue.

A significant main effect of group was demonstrated for knee adduction moment ($p = 0.01$, Figure 1D), which suggested that ITBS runners have increased values both pre and post-fatigue. The average difference in peak knee adduction moment between groups was 46.4%.

CONCLUSIONS

These findings suggest that, with increased fatigue, ITBS runners do not tend to exhibit changes hip and knee gait patterns that place higher strains on the iliotibial band. Only one variable demonstrated large changes as a result of fatigue. The unexpected tendency of the ITBS runners to decrease hip internal rotation may be a neuromuscular attempt at reducing iliotibial band strain as the body begins to fatigue. This theory is also supported by the fact that the ITBS runners exhibited increased knee adduction moments as compared to the healthy runners. These findings suggest that runners with ITBS may adopt dynamic postures that avoid excessive strain on the iliotibial band, or excessive contact friction with the lateral femoral epicondyle. It is also possible that these avoidance postures are exaggerated with repetitive motions and the onset of fatigue.

REFERENCES

1. Taunton, *Br J Sports Med* 2003
2. Fredricson, *Clin J Sport Med* 2000
3.Noehren, *Clin Biomech* 2007
4. Miller, *Gait Posture* 2007
5. *Borg's Perceived Exertion and Pain Scales* 1998

ACKNOWLEDGEMENTS

The authors gratefully acknowledge New Balance for providing the footwear for our subjects.

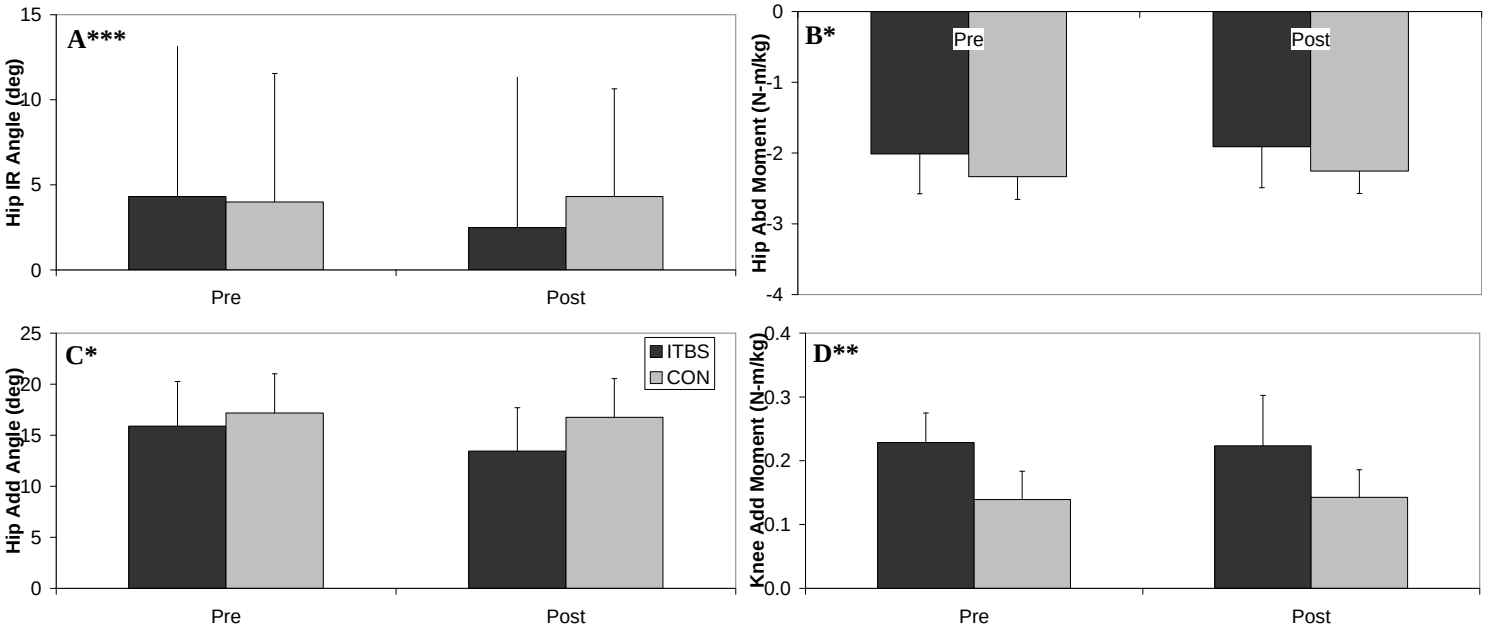

Figure 1: Comparisons of hip and knee kinetics and kinematics between ITBS runners and healthy control runners in the pre and post-fatigue state, where * indicates an effect of time, ** indicates an effect of group, and *** indicates an interaction

PATELLAR TRACKING MEASURES CORRELATE WITH VASTUS MEDIALIS ONSET DELAY IN MALTRACKING PATELLOFEMORAL PAIN SUBJECTS

[1]Saikat Pal, [1]Christine Draper, [1]Michael Fredericson, [1]Garry Gold,
[1]Scott Delp, [1,2]Gary Beaupre, and [1]Thor Besier
[1]Stanford University, Stanford, CA; [2]VA Palo Alto Health Care System, Palo Alto, CA
email: spal5@stanford.edu

INTRODUCTION

Patellofemoral pain (PFP) syndrome accounts for a large fraction of knee disorders seen in sports medicine clinics [1]. A possible mechanism of pain is elevated stress at the cartilage-bone interface due to excessive lateral tracking of the patella. Delayed onset of vastus medialis (VM) activation in comparison to vastus lateralis (VL) is reported to cause lateral tracking of the patella [2], but evidence relating muscle activation delay to patellar maltracking is sparse. Broad categorization of diverse PFP subjects into a single group may be insufficient to explain the variability observed in VM onset delay [2]. The purpose of this study was to determine if precise classification of PFP subjects based on maltracking measures would lend insight into the effect of VM onset delay on maltracking of the patella. We hypothesized that two measures of patellar tracking, patellar tilt and bisect offset, correlate with VM onset delay in PFP subjects classified as maltrackers.

METHODS

We analyzed 15 (7M, 8F) healthy control subjects and 40 (21M, 19F) PFP patients with chronic pain (longer than 3 months) but no prior surgery or traumatic knee injuries. All subjects were between 18-42 years of age. The PFP subjects were diagnosed by an experienced clinician. Each subject was analyzed performing walking and jogging trials at self-selected speeds, and electromyography (EMG) recordings of the VM and VL muscles, 3D motion, and ground reaction forces were measured simultaneously in a gait lab. Anticipatory EMG activations during the swing phase prior to heel strike were evaluated (Figure 1). A muscle's activation onset threshold was defined as the greater of 3 standard deviations (SD) of its resting value [3] and 2% of the larger of VM or VL muscles' peak

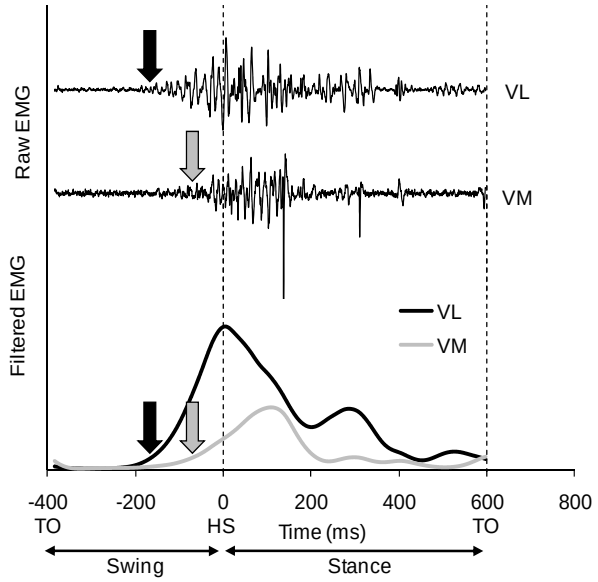

Figure 1: EMG activity of the VL & VM muscles during a walk trial. Toe off (TO, at left) marks the initiation of swing phase, and trial time was adjusted to represent heel strike (HS) as time zero. The arrows indicate measured EMG onset times.

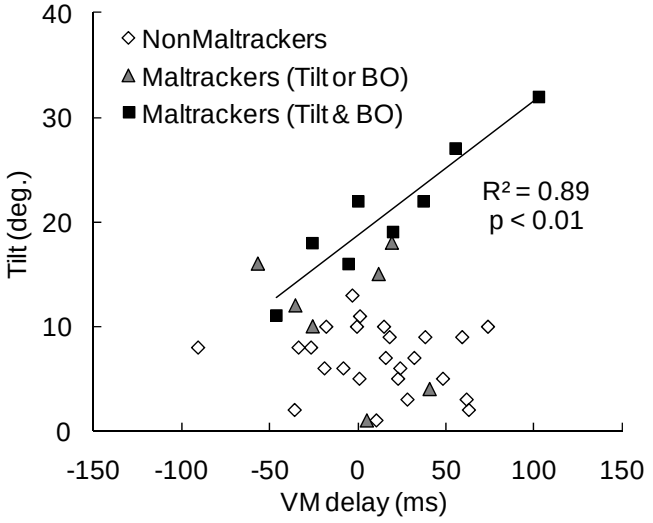

Figure 2: Relationship between VM onset delay & tilt in PFP subjects classified based on maltracking measures for walking trials. The regression line represents a significant relationship in subjects with both abnormal tilt and abnormal bisect offset.

activations; this provided a consistent method to record muscle activation onset prior to heel strike.

The PFP subjects were classified based on maltracking measures acquired from weight-bearing magnetic resonance (MR) imaging [4]. Images were obtained using a 0.5T Signa SP open-MRI scanner (GE Healthcare) fit with a backrest to stabilize a subject in an upright position (knee flexed ~5°). The scan parameters were described previously [5]. From an MR volume, an oblique-axial plane intersecting the center of the patella and the most posterior points of the femoral condyles was created to measure patellar tilt and bisect offset values. Patellar tilt is the measure of the angle formed by lines joining the posterior femoral condyles and the maximum width of the patella; bisect offset describes the percentage of the patella lateral to the midline of the femur [4]. Due to the non-Gaussian distribution of the data, a standard two-parameter Weibull distribution was fit to gender-specific tilt and bisect offset values and associated 75% confidence intervals were defined as maltracking thresholds; a PFP subject was classified as a maltracker if his/her tilt or bisect offset values were in the highest quartiles of the measured data.

RESULTS AND DISCUSSION

The thresholds for abnormal patellar tracking were 11.0° (tilt) and 68.1% (bisect offset) for males, and 15.3° (tilt) and 72.3% (bisect offset) for females. Approximately 38% (15/40) of PFP subjects were classified as maltrackers. Eight (4M, 4F) subjects had both abnormal tilt and abnormal bisect offset.

Only maltracking PFP subjects with both abnormal tilt and abnormal bisect offset displayed significant relationships with VM onset delay; $R^2 = 0.89$ ($p < 0.01$) with tilt for walking (Figure 2, Table 1), and $R^2 = 0.75$ ($p = 0.01$) with bisect offset for jogging (not shown). Vastus medialis onset delays varied substantially among subjects. For walking trials, mean (SD) delays were 18 (57) ms and 9 (39) ms for the control and PFP groups, respectively, with no statistically significant difference between the means of the groups ($p = 0.52$).

CONCLUSIONS

The results demonstrate significant relationships between VM onset delay and patellar tracking only in maltracking subjects with both abnormal tilt and abnormal bisect offset. The other subject groups demonstrated large ranges of onset delays and maltracking values, but with no significant relationship between the two measures. A possible explanation is that VM onset delay is one of several factors affecting patellar tracking. Trochlear geometry and tension of the surrounding soft-tissue structure may also affect patella tracking. Further, differences in VM onset between studies [2] may be due to selection of PFP subjects; a study with a large number of subjects with high tilt and bisect offset values would likely measure significant delay in mean VM onset compared to healthy subjects.

A clinical intervention such as VM retraining may be effective in only a subset of PFP subjects, those with excessive tilt and excessive bisect offset measures. The results highlight the importance of appropriate classification of PFP subjects prior to selection of a clinical intervention.

REFERENCES

1. DeHaven KE, et al. *Am J Sports Med* **14**, 218-24, 1986.
2. Wong YM. *Phys Ther Sport* **10**, 71-4, 2009.
3. Cowan SM, et al. *Arch Phys Med Rehab* **82**,183-9, 2001.
4. Draper CE, et al. *J Orthop Res* **27**, 571-7, 2009.
5. Besier TF, et al. *J Orthop Res* **26**, 1627-35, 2008.

ACKNOWLEDGEMENTS

VA Rehabilitation R&D Service (#A2592R), NIH (EB005790-05).

Table 1: Relationship between VM onset delay and patella maltracking measures for walking trials.

Group	# of subjects	Tilt		Bisect Offset (BO)	
		R^2	p-value	R^2	p-value
Controls	15	< 0.01	0.86	0.01	0.74
PFP	40	0.02	0.33	0.02	0.36
NonMaltrackers-PFP	25	0.02	0.50	0.08	0.17
Maltrackers-PFP (Tilt or BO)	7	0.12	0.45	0.37	0.14
Maltrackers-PFP (Tilt & BO)	8	0.89	< 0.01	0.43	0.08

ALTERED KNEE MUSCLE REFLEX ACTIVITY DURING A CUTTING MANEUVER IS INFLUENCED BY MOTOR LEARNING NOT NEUROMUSCULAR TRAINING

Kristof Kipp, Tyler Brown, Scott McLean, and Riann Palmieri-Smith

University of Michigan, Ann Arbor, MI, USA
email: kristof@med.umich.edu

INTRODUCTION

Anterior cruciate ligament (ACL) injuries may result from a lack of neuromuscular control during dynamic tasks. In particular, it has been suggested that an extended and abducted knee during dynamic movements may precipitate injury through increased strain within the ACL [1].

Despite the wide use of neuromuscular training protocols that focus on improving knee joint motions and stability during dynamic activities, the mechanisms that are associated with decreased incidence of ACL injury are not well understood [2].

Short-latency reflex activation of muscles may increase joint stability by effectively stiffening the joint, thus protecting against deleterious joint motions during dynamic movement [3]. The primary purpose of this was study was to determine if neuromuscular training affects knee joint motions and reflex activation during a dynamic landing task. A secondary purpose was to determine if changes in reflex activation could account for changes in knee joint motion.

METHODS

Twenty-three healthy un-trained young adults were randomized into one of two groups (Training and Control). Training occurred three times a week over a six-week period, for a total of 18 sessions. Successful completion of the training program required completion of at least 16 training sessions. Control subjects were asked to continue their normal daily activities during the six-week period.

Neuromuscular training included the following components: core strength and balance, plyometrics, resistance, and speed training, which were derived from previous prevention techniques touted to be effective at reducing the biomechanical measures associated with ACL injury. Each training session was composed of three specific 30-minute components. Core strength and balance training was performed first in every session. The remaining components systematically varied to limit disinterest and/or fatigue of components occurring later in the session. Early training sessions were used to develop proper technique. After establishing proper technique during the initial sessions, the training protocol progressively increased the volume, duration, and intensity.

Kinematic data and EMG were recorded during pre and post-training testing sessions. Knee joint kinematics and EMG of the medial and lateral quadriceps (MQ & LQ) and hamstring (MH & LH) muscles were quantified during subject initiated jump landings that required subjects to take-off one meter behind a force platform, jump over a 17 cm, and land on their dominant foot and then aggressively jump laterally to the side away from their landing foot. Four to five successful landing trials were collected for analysis.

Kinematic data were filtered with a fourth-order Butterworth filter at 12 Hz and processed in Visual 3D software to calculate knee flexion and abduction rotations. Peak knee joint angles between heel strike and toe-off were calculated relative to the subject's static posture. EMG data were bandwidth filter (10-500Hz), rectified, smoothed with a 50ms moving-average, and normalized to % MVIC. Short-latency stretch-reflex (SLSR) activation was calculated as the average EMG activity between 30-60 ms after heel strike.

Statistical analyses consisted of separate general linear models with repeated measures that were used to test for the effects of the training protocol

on peak joint angles and short-latency stretch-reflex activations. Correlation analyses were to be used as follow-up for significant treatment interactions to establish associations between variables. The α-level was set at 0.05.

RESULTS AND DISCUSSION

No significant interaction or main effects were noted for knee joint flexion and abduction angles (Table 1). Further, no significant interactions were noted for any of the short-latency stretch reflexes. The analysis did, however, indicate significant main effects between pre and post-training sessions for all short-latency stretch reflexes (Table 1). In the absence of any significant interactions, no statistical correlation analyses were performed.

The results indicate that the neuromuscular training program used in this study did not affect knee joint kinematics during the observed landing task. Surprisingly, both groups showed greater short-latency stretch reflex activations during the post-testing session. Greater reflex activation during the impact phase immediately after landing is typically associated with higher joint stiffness [4]. Lacking any changes in knee motion it is thus likely that both groups demonstrated greater knee joint stiffness after landing.

While various levels of the central nervous system could underlie the enlargement of the short-latency stretch reflexes component, it has been shown that fast segmental spinal mechanisms can mediate long-term plasticity of the sensorimotor system in response to perturbation training [5]. It was suggested that these adaptations essentially reflect the process of motor learning [5]. Since increases in the short-latency stretch reflex components were observed in both groups, it is thus likely that a learning effect mediated changes in reflex activation levels such that upon second exposure to the landing task both groups performed the task with similar joint motions, but greater short-latency stretch reflexes to increase joint stiffness and stability.

CONCLUSIONS

The neuromuscular training program did not affect knee joint kinematics. Although we observed greater short-latency stretch reflex activations during the post-testing sessions in all muscles, the fact that this effect was noted in both groups likely indicates a learning effect.

REFERENCES

1. Griffin LY, et al. *Am J Sports Med* **34**, 1512–1532, 2006.
2. McLean, SG. *J Athl Train* **43**, 538-540, 2008.
3. Sinkjaer, T, et al. *J Neurophysiol* **60**, 1110-1121, 1988.
4. Horita T, et al. *Eur J Appl Physiol Occup Physiol* **73**, 393-403, 1996.
5. Meyer-Lohmann J, et al. *Exp Brain Res* **64**, 393-399, 1986.

ACKNOWLEDGEMENTS

We would like to thank Priya Venkatasubramanian for help with data processing and acknowledge support from the National Institutes of Health (NIH) Grant # NIH Grant T32 HD007422-19.

Table 1: Pre and post-training knee joint angles (º) and short-latency stretch reflexes (%MVIC) for the control and experimental group.

	Control Group		Training Group	
	Pre-training	**Post-training**	**Pre-training**	**Post-training**
Knee Flexion	54.8 ± 7.2	53.8 ± 6.6	59.2 ± 5.9	59.1 ± 7.7
Knee Abduction	13.6 ± 7.2	13.8 ± 5.0	12.6 ± 5.0	12.7 ± 4.9
LQ	2.0 ± 0.6	3.4 ± 3.3*****	2.3 ± 0.7	3.7 ± 2.1*****
MQ	2.2 ± 0.6	3.3 ± 2.3*****	2.6 ± 1.5	4.5 ± 2.9*****
LH	0.5 ± 0.4	1.2 ± 1.0*****	0.4 ± 0.2	1.0 ± 0.8*****
MH	0.4 ± 0.2	0.8 ± 0.7*****	0.4 ± 0.3	0.8 ± 0.7*****

***** $p < .05$ vs. Pre-training

Approximate entropy of stride-to-stride intervals following ACL injury

[1,2]Christopher K. Rhea, [1]Adam W. Kiefer, [1,2]Susan E. D'Andrea, [1,2]William H. Warren and [1,2]Roy K. Aaron

[1]Brown University, Providence, RI, USA
[2]Center for Restorative and Regenerative Medicine, VA Medical Center, Providence, RI, USA
email: christopher_rhea@brown.edu

INTRODUCTION

The anterior cruciate ligament (ACL) is the most commonly torn knee ligament, resulting in decreased knee stability. Biomechanical deficits during gait following an ACL tear have been documented [1], however it is unclear whether the deficits affect gait adaptability. Since the goal for any rehabilitation program is to restore functional mobility following injury, an evaluation of gait adaptability is needed to track patient progress. Examining the variability in gait is potentially one way to assess adaptability. An optimal pattern of variability is desired – too regular (stereotyped) and gait becomes less adaptable, whereas too random and gait becomes unstable. For this reason, a complex hybrid of a regularity and variability in gait is desired. Healthy adults show this complex pattern [2], however a more regular pattern emerges following an ACL tear, indicating that the injury leads to a less functional form of gait [3].

Approximate entropy (ApEn) has been used to characterize the regularity of continuous gait dynamics of healthy controls and ACL-injured or ACL-reconstructed subjects by analyzing knee kinematics over 80-100 strides [3, 4]. Conversely, an interval method has been employed to characterize gait dynamics over many more strides by examining stride duration (i.e. stride-to-stride intervals; see methods) [2]. The purpose of this project was to examine whether a torn ACL affected the regularity (using ApEn) of stride-to-stride intervals over hundreds of strides compared to healthy controls. Additionally, the unaffected leg of the ACL subject was examined to determine whether a decrement in gait dynamics was present due to compensation for the injured leg.

METHODS

Five subjects with a unilaterally torn ACL (4 females, 1 male; 27.2 ± 7.8 yrs, 1.67 ± 0.10 m, 66.4 ± 13.2 kg) and five healthy dominant leg-matched controls (4 males, 1 female; 27 ± 2.6 yrs, 1.73 ± 0.09 m, 72.2 ± 11.6 kg) were tested after informed consent. All ACL-injured subjects injured their right leg and testing occurred prior to ACL-reconstruction. Subjects walked at a self-selected pace for 20 minutes on a treadmill, resulting in approximately 500 strides for each leg. Digital force sensors (Delsys, Boston, MA) were taped to the heel of both the right and left foot to capture heel strike data. The stride-to-stride intervals for each leg were calculated by determining the time between heel contacts of the same leg using a customized routine in MATLAB (Mathworks, Inc., Natick, MA). Means and standard deviation of the intervals were calculated, as well as the ApEn of the interval time series using the input parameters of r = 0.2 and m = 2, consistent with previous ApEn analyses on gait dynamics [3,4]. ApEn for each leg in both groups (healthy and ACL-injured) were analyzed with a 2 × 2 (leg × group) between-within ANOVA. Follow-up pair-samples t-tests were used when appropriate

RESULTS AND DISCUSSION

Preferred walking speed was not different between groups (M = 2.2 ± 0.5 m/s), nor was the mean or standard deviation of the duration of the stride-to-stride intervals between groups or legs different (all $p > 0.05$). A leg × group interaction was observed for ApEn (see Figure 1), $F(1,8) = 6.514$, $p = .034$. A lower ApEn was observed for the injured leg of the ACL-injured group (M = 1.12 ± 0.18) compared to the matched leg of the control group (M = 1.43 ±

0.06). No within group leg differences were observed ($p > 0.05$).

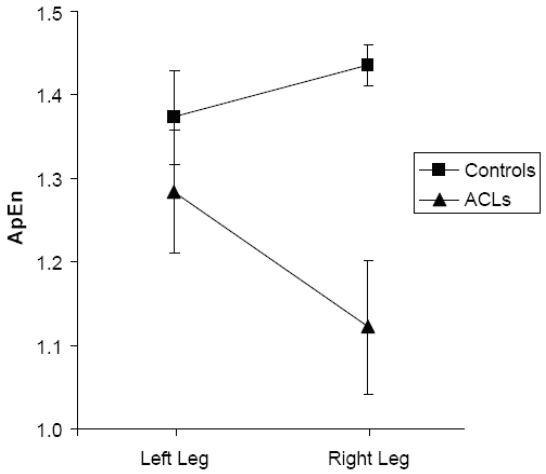

Figure 1: Leg × group interaction for ApEn. The ACL-injured group injured their right leg.

While the duration mean and standard deviation of the stride-to-stride intervals did not differ, ApEn captured revealed differences in regularity. The ACL-injured group exhibited lower ApEn for the injured leg compared to the matched leg of healthy controls. No leg differences were observed in the ACL-injured group, showing that the effect of the ACL tear is present in the stride duration of both the injured and unaffected legs. The healthy controls showed no leg difference in regularity, as one may expect.

An appropriate pattern of variability – not too regular, but not random – is desirable in adaptive gait. If the stride-to-stride intervals are too regular, it may reflect a stereotyped gait that fails to adapt to normal variation in context (e.g. center of gravity position at heel strike, ground irregularities). Therefore, gait dynamics should exhibit a regular pattern with adaptive variation – a complex combination of regularity and variability. It has been suggested that an ACL deficient leg does not exhibit an appropriate level of complexity, evidenced by lower ApEn (less complexity; more regularity) of knee kinematics over 80 steps compared to the contralateral limb [3]. The results of the current study show that more regularity was observed in the ACL deficient leg when compared to the same side leg of the controls. These findings support previous research suggesting that an ACL injury leads to the emergence of a more stereotyped, regular form of motion [3]. One might assume that a less stable knee due to injury would lead to more random, as opposed to more regular, gait dynamics, perhaps due to decreased neuromuscular control. However, in compensating for the knee instability caused by the torn ACL, co-contraction of the muscles crossing the knee may occur, leading to a less flexible knee joint and a more stereotyped motion. This stereotyped motion has been hypothesized to be a less adaptable form of movement [3]. The lack of leg differences in the ACL-injured group indicates that the regularity of the contralateral stride duration is also influenced by the injury. This is not surprising, considering that both left and right stride durations include support phases by the affected and unaffected leg. Previous data show changes in muscle strength in both the injured and unaffected leg [1], although other results indicate leg differences in gait dynamics following ACL injury [3].

CONCLUSIONS

Mean and standard deviation of the duration of stride-to-stride intervals between groups or legs was not different, but ApEn showed: 1) more stereotyped, regular stride durations in the ACL deficient leg compared to healthy controls, 2) no difference in regularity between the ACL deficient leg and the contralateral leg and 3) no difference in regularity between legs for controls. The results suggest that a unilateral ACL tear causes a change toward less adaptable gait dynamics in both limbs.

REFERENCES

1. Urbach D et al., *Med Sci Sports Exerc*, **31**, 1691-1696,
2. Hausdorff JM et al., *J Appl Physiol* **88**, 2045-2053, 2000.
3. Georgoulis AD et al., *J Clin Monit Comput,* **20**, 11-18, 2006
4. Moraiti, CO et al., *Arthroscopy,* **25**, 742-749, 2009

ACKNOWLEDGEMENTS

Funded by the Department of Veterans Affairs, Rehabilitation Research and Development.

QUADRICEPS SRENGTH AND NEUROMUSCULAR STRATEGIES CONTINUE TO IMPROVE TWO YEARS AFTER ACL RECONSTRUCTION

Ben Roewer, Stephanie Di Stasi and Lynn Snyder-Mackler

University of Delaware, Newark, DE, USA
email: broewer@udel.edu, web: http://www.udel.edu/PT/

INTRODUCTION

After anterior cruciate ligament (ACL) rupture, some individuals demonstrate the ability to dynamically stabilize their injured knee (potential copers). The majority of ACL deficient individuals, however, are classified as non-copers; they have knee instability with daily activities, exhibit quadriceps weakness, and have altered movement patterns. Prior to surgery, non-copers have been shown to make initial contact with less knee flexion on their involved side, achieve less peak knee flexion, and exhibit reduced knee power absorption during weight acceptance [1]. These non-copers customarily undergo ACL reconstructive surgery (ACLR) to repair the damaged ligament.

Quadriceps weakness is ubiquitous following surgery. Restoring quadriceps strength post-ACLR has been shown to increase knee angles and moments at peak knee flexion (PKF) during gait [2]. However, no one has evaluated the performance of this non-coper cohort two years post-ACLR. Loss of quadriceps strength and limb symmetry could result in long-term changes in movement patterns. Additionally, aberrant joint motion has been proposed as a mechanism for articular degeneration [3]. Therefore, it is imperative to understand how this non-coper cohort behaves after leaving a formal post-ACLR training protocol. The goal of this study was to determine whether altered neuromuscular control strategies, evident acutely after injury, resolved over time.

METHODS

Fifteen athletes who underwent ACL reconstructive surgery were recruited for this study (Table 1). Subjects were included in the study if they were 13-55 years old with no concomitant ligament injury in the ipsilateral limb, had no articular cartilage damage, and had >1 giveway episodes prior to surgery. Each subject was tested for maximal volitional quadriceps strength normalized to BMI before surgery and at 6 and 24 months post-ACLR. They also participated in a motion analysis session during each of the three testing sessions in which they walked overground across an embedded force plate. Kinematic and kinetic data reduction was performed with custom software programming. We analyzed quadriceps strength, and knee/hip angles, moments, and powers during the weight acceptance phase of gait (first 25% of stance). Paired t-tests were used to compare outcome variables between limbs and over time ($p<.05$).

Table 1: Subject demographics (Mean ± SD)

	Male (n=9)	Female (n=7)
Age (yr)	27.8 ± 9.1	32.5 ± 12.0
BMI (kg/m^2)	31.2 ± 5.0	25.1 ± 2.5

RESULTS AND DISCUSSION

Prior to surgery, quadriceps strength was greater in the uninvolved limb compared to the involved limb (Table 2). These strength asymmetries resolved over time as quadriceps strength in the involved limb improved at 24 months. Quadriceps strength in the uninvolved limb did not significantly change over time. While PKF angles were symmetrical prior to surgery, asymmetries emerged at 6 months because the PKF angle of the uninvolved limb increased. These asymmetries resolved at 24 months as the PKF angle of the involved limb significantly increased. Differences in knee extensor moment at PKF between limbs were detected prior to surgery and at 6 months. These asymmetries also resolved at 24 months as the moment at PKF in the

involved limb significantly improved. At 24 months, no differences in quadriceps strength or knee angles and moments at PKF were detected between limbs.

Prior to surgery, the uninvolved hip appeared to compensate for the involved knee by absorbing power early in stance (Figure 1). This behavior persisted at 6 months, but eventually resolved at 24 months. At 24 months, hip power in both limbs was positive early in stance, suggesting improved gait behaviors between limbs.

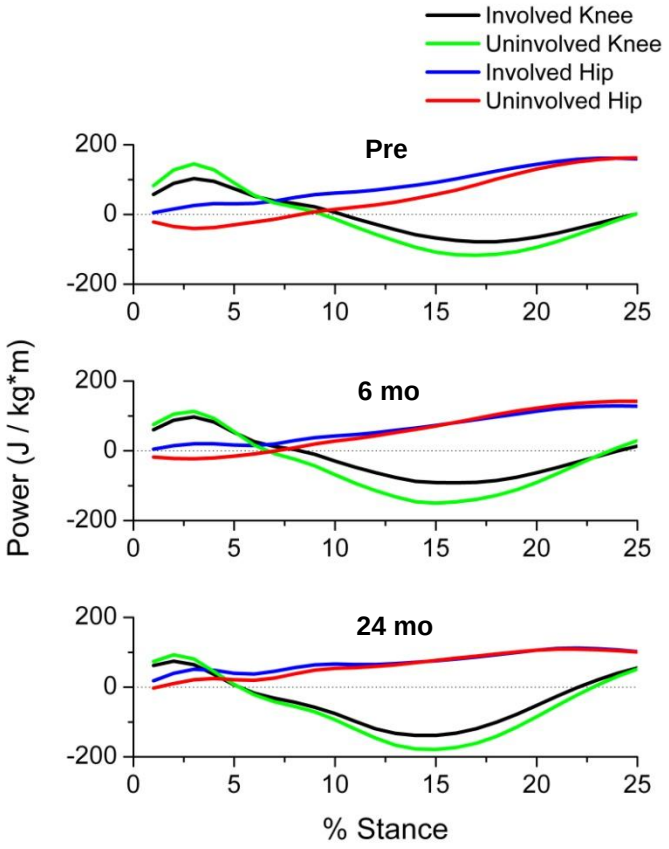

Figure 1: Knee and hip power of the involved and uninvolved limbs at three time points: pre surgery, 6 months post-ACLR, and 24 months post-ACLR. Data is presented from heel strike to 25% of stance. Positive values = power generation. Negative values = power absorption.

Knee power was also positive early in stance, but it appeared to diminish at 24 months. The involved and uninvolved knees appeared to absorb power more symmetrically over time; they also began to absorb power earlier in stance. Peak negative knee power also improved over time and appeared more symmetrical at 24 months.

CONCLUSIONS

Long term outcomes of the non-coper cohort have not been previously described. Our results suggest that non-copers have the capacity to improve their quadriceps strength and weight acceptance strategies long after ACLR. Six months post-ACLR is a common time for surgeons to clear their patients to return to sport. While quadriceps strength became symmetrical at 6 months, differences in kinematics and kinetics were still present. This suggests that six months of intensive physical therapy might not be long enough to resolve all strength and movement asymmetries prior to returning to sport for some non-copers. Although limb differences were evident 6 months after surgery, recovery of symmetrical movement patterns 2 years after ACLR was noted. Our results suggest that non-copers have the capacity to improve their quadriceps strength and neuromuscular strategies long after ACLR.

REFERENCES

1.Rudolph KS, et al. *Journal of Electromyography and Kinesiology*, **8**, 349-362, 1998.
2.Lewek M, et al. *Clinical Biomechanics*, **17**, 56-63, 2002.
3.Andriacchi, et al. *Journal of Bone and Joint Surgery*, **91 Suppl 1**, 95-101, 2009.

ACKNOWLEDGEMENTS

This work was funded by R01AR048212 and S10RR022396.

Table 2: Quadriceps strength, PKF, and moment at PKF were compared between limbs and across time. Mean ± SD are shown with significant differences between time points (*) and between limbs (shaded) ($p < 0.05$).

	Quad Strength (N/kg/m^2)		**Peak Knee Flexion** (deg)		**Moment at PKF** (Nm/kg*m)	
	Involved	Uninvolved	Involved	Uninvolved	Involved	Uninvolved
Pre	34.9 +/- 12.4	42.5 +/- 13.0	24.3 +/- 5.7	26.6 +/- 5.4	0.33 +/- 0.16	0.40 +/- 0.12
6 mo	40.5 +/- 13.0	42.6 +/- 10.3	24.9 +/- 7.0	30.0 +/- 5.9*	0.42 +/- 0.10*	0.53 +/- 0.12*
24 mo	45.9 +/- 14.7*	45.3 +/- 9.6	27.5 +/- 6.4*	29.4 +/- 5.8	0.58 +/- 0.15*	0.62 +/- 0.12

MOTOR-UNIT POOL PROPERTIES CONTRIBUTE TO CONTINUOUS AND DISCRETE FORCE VARIABILITY

Xiaogang Hu and Karl M. Newell
Department of Kinesiology, The Pennsylvania State University
Email: xxh120@psu.edu

INTRODUCTION

Isometric force exhibits variability that scales with force level. The proportional relation between force and force variability tends to vary in different isometric force tasks. In continuous constant force production, the variability (SD) increases at an accelerating rate (quadratic scaling) with force level. In contrast, the trial-to-trial peak force variability in discrete force pulse task increases at a negatively accelerating rate (square-root scaling) with force level. The mechanisms of contrasting variability scaling function in discrete and continuous isometric force have not been addressed.

Muscle force is mediated by properties of motor-unit (MU) pool including unit recruitment, rate coding, and synchronization of MU. Through simulations with the MU pool model [1], this study investigated the properties of the motor-unit pool that lead to the different force variability functions in continuous and discrete contractions.

METHODS

The MU pool model consisted of 120 MUs with systematic variations in recruitment range, firing rate patterns, synchronization characteristics, and amplitudes and durations of twitch forces. A prescribed excitatory drive (E) was used as the model input to produce the desired force output in arbitrary unit (AU). The recruitment range and firing properties (peak firing rate and synchronized firing of MU) of the MU pool were manipulated. All the values of the variables were the same as the original model, except the variables manipulated here.

The continuous force comprised 9 force levels in response to 9 steady state levels of E from 10% to 90% of maximum E with 10% increment. The same 9 excitation levels were used in the discrete force pulse. The time-to-peak of E was adjusted such that the time-to-peak of force output was slightly longer at higher peak force, E increased linearly from 0 to the corresponding peak and then decreased to zero.

Three ranges of recruitment were chosen. When the recruitment range was 20 fold, MU 1 was recruited at E of 1 AU and MU 120 was recruited at E of 20 AU. The narrow range was set at 20 fold comparing with moderate range of 40 fold and wide range of 70 fold. Three sets of peak firing rate (PFR) were used in the simulations. The low PFR ranged from 25 Hz for MU 1 to 15 Hz for the MU 120, the moderate PFR: 35-25 Hz, and the high PFR: 45-35 Hz. Three synchronization levels (no synchrony, moderate, and high synchrony) were selected. The moderate level involved synchrony of 10% of the action potentials discharged by the reference MU and 25% in the high synchrony.

The duration of each force level was 10 s for continuous force and 1 s for discrete force. In continuous force 1 trial was simulated at each force level, and 200 trials were simulated in the discrete force. The SD of force was calculated over the simulated trials at each force level. The quadratic, linear, and square-root functions were fit to the force and force variability function and the best fit is shown in the graphs.

RESULTS AND DISCUSSION

In the continuous task (Fig. 1A) the narrow recruitment range led to high variability, especially at moderate force levels. However, the level of variability at the three recruitment ranges tended to converge at high force levels. The different recruitment ranges also led to distinct variability scaling functions in the continuous task; whereas the same qualitative function was evident at all the recruitment ranges in the discrete task (Fig. 1B).

When the PFR was varied in the continuous force (Fig. 1C), the low PFR resulted in high force variability, that was more pronounced at higher force levels. The scaling relations changed from quadratic (low and moderate PFR) to linear (high PFR) with increasing PFR. In the discrete force (Fig. 1D), the level of variability diverged at the moderate force levels. The scaling functions changed from quadratic (low PFR) to square-root (moderate and high PFR) with increasing PFR. However, the differences were not as pronounced as in the continuous force.

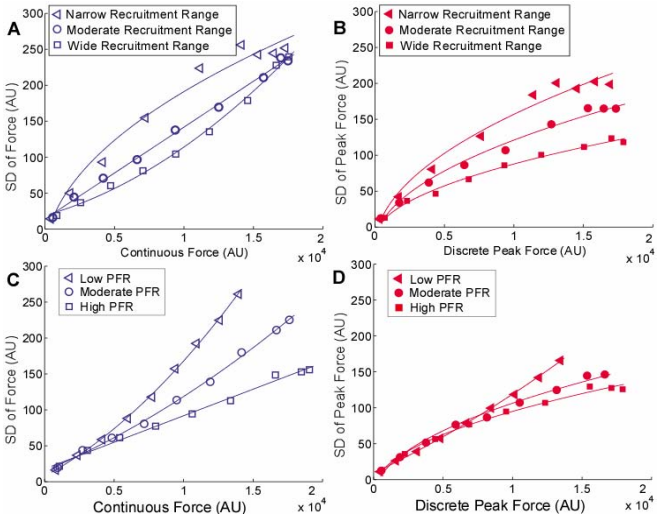

Figure 1: Variability in forces at different recruitment ranges and peak firing rates (PFR). (AU: arbitrary unit).

As shown in Fig. 2, the synchronized firing had a stronger effect on variability in the continuous as opposed to the discrete force. The variability in the continuous force showed a quadratic increase over force level regardless of the synchronization level, whereas the variability in the discrete force followed a square-root increase over the peak force.

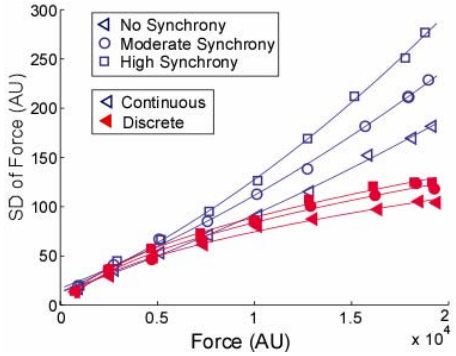

Figure 2: SD of force at three synchronization levels.

A series of discrete forces with four peak force levels and three time-to-peak force constraints were also simulated. The results (figures not shown) showed that the SD and coefficient of variation (CV) of force decreased with longer time-to-peak force at all force levels. The results also showed that force level had a stronger effect than the time constraints on force variability, which is consistent with the experimental finding that the force variability was scaled up as a square-root function of force level and down with a quarter power function of time-to-peak [2]. The results also verified the validity of the MU pool model for discrete force variability.

The different firing properties of the MU pool were shown to contribute differently to the variability in discrete and continuous force production. The firing properties (i.e. lower peak firing rate and higher synchronization of MUs) led to greater variability in the continuous than in the discrete force output. The range of recruitment also changed the scaling functions in the continuous force production.

CONCLUSIONS

The general outcome of the simulations was that the range of recruitment, the peak firing rate, and the synchrony between MUs contributed to the different variability functions in continuous and discrete contractions. The simulation results suggest that the MU pool model can produce the distinct force variability functions of continuous and discrete isometric force production. The simulations also revealed that the model can produce outcomes that are consistent with properties of the force output other than the amount of variability (SD), such as time-to-peak force in the discrete pulse. Thus, the MU pool model generates a much broader set of task relevant force variability findings than has previously been shown. The simulation results provide preliminary insight into the neuromuscular mechanisms of the contrasting force and force variability functions in continuous and discrete isometric forces.

REFERENCES

1. Fuglevand AJ, et al. *J Neurophysiol* **70**: 2470-2488, 1993.
2. Carlton LG, Newell KM. *Variability and motor control*, Human Kinetics, Champaign, IL, 1993.

Rotational Object Perturbations Result in Characteristic Types of Kinematic Grip Responses

Michael De Gregorio, M.S. and Veronica J. Santos, Ph.D.

Biomechatronics Lab, Arizona State University, Tempe, AZ, USA
email: michael.degregorio@asu.edu

INTRODUCTION

Reflex-like corrective responses have been observed in precision grip tasks that involve translational perturbations of the grasped object [1]. The translational perturbations primarily elicited flexion and extension responses. This study investigates grip responses to rotational object perturbations that elicit abduction and adduction of the fingers as well as flexion and extension.

METHODS

This IRB-approved study used a Vicon motion-capture system to collect kinematic data from both the thumb and index finger of the dominant hand of an unimpaired subject (24 markers) and an instrumented test object (3 markers) (Fig. 1). The timing of the first dorsal interosseous (FDI) muscle response was measured for all subjects (n=22) using surface EMG (Biopac EMG 100C). The rigid test object housed two six degree-of-freedom load cells (ATI Nano-25 F/T), each attached to an independent grip plate -- one each for the thumb and index finger. Subjects held the object in midair using a precision grip with each digit centered on its grip plate. The test object was then subjected to an unannounced rotational perturbation imposed by a mass (100g or 150g) and pulley system attached to one of five attachment points on the object. The attachment points induced clockwise and counterclockwise rotations about the x- and y-axes, and a forward tilt about the z-axis (Fig. 1). Subjects were instructed to right the object back to its original orientation after detecting the perturbation, which would occur at a random time point during each five second trial. All data were processed using MATLAB.

RESULTS AND DISCUSSION

A preliminary kinetic analysis for perturbations about the x-axis suggested that for clockwise

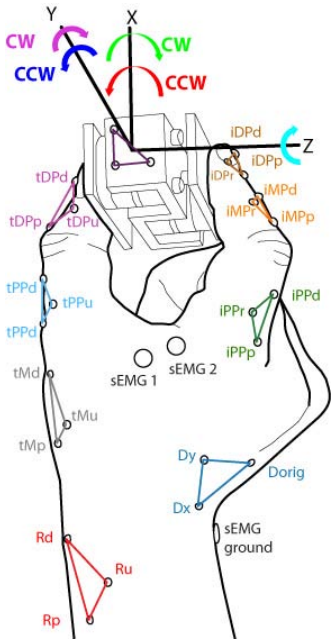

Figure 1: Experimental Setup. Triads of markers were used to track the motion of the thumb, index finger, and object. Arrows indicate the five perturbation directions. Surface EMG was used to record the FDI response.

perturbations the thumb acts as a pivot point and the index finger acts as the primary corrective agent. The opposite trend holds true for perturbations in the counterclockwise direction [2]. These results were further verified via a more expansive analysis here. The trends held across all subjects and trials (five per perturbation direction and magnitude).

A preliminary kinematic analysis for perturbations about the x-axis revealed that abduction/adduction responses were elicited in the thumb and index finger in addition to flexion/extension. The analysis revealed that peak index finger joint angles were well synchronized with peak object rotation angles (~65-80ms after perturbation) while thumb joint angles lagged behind [2]. New results verified the synchronization of peaks that was seen previously. However, the time from perturbation onset to maximum object rotation (start of the correction) ranged from 130 to 278 ms (averaged across all trials for each perturbation direction and

magnitude). Some individual trials were as fast as 65 ms. Further investigation is needed to determine how much of the correction is due to the passive structure of the hand and how much is active.

The kinetic analysis for perturbations about the y-axis suggested that the mode of correction was not as well defined. Both clockwise and counterclockwise cases displayed similar trends. The grip forces (z-direction thumb and index finger forces) were relatively large (peaks typically range from 1.5 to 4 lbf) in comparison to the other force components. The x-direction forces related to the corrective rolling action of the fingertips were smaller, having magnitudes of 0.5 lbf or less.

Simultaneous coordination of adduction/abduction and flexion/extension degrees of freedom was observed in perturbations about the y-axis. The average time from perturbation onset to maximum object rotation ranged from 79 to 294 ms. No joint angles appeared to synchronize with the maximum object rotation. Figure 2 shows the relationship between abduction/adduction and flexion/extension degrees of freedom in the thumb carpometacarpal joint. Trials across each rotation direction were fairly well grouped, suggesting that different perturbation directions result in characteristic types of corrective responses. Responses for perturbations about the y-axis overlapped one another possibly because the range of motion for rolling of the fingertips is somewhat limited for the task's grip posture.

Joint angle velocities were also plotted in the same manner. The velocities for each perturbation direction and magnitude were grouped together and shared the same region of joint angle velocity space. This suggests that, regardless of perturbation direction or magnitude, reflex-like corrections occur at similar rates.

CONCLUSIONS

For rotational perturbations about the x-axis, each digit appears to play a specific role (pivot or primary corrective agent). For rotational perturbations about the y-axis, the primary corrective action is to grip harder along the z-axis. The corrective forces along the x-axis are relatively small and do not seem to be dependent upon perturbation direction.

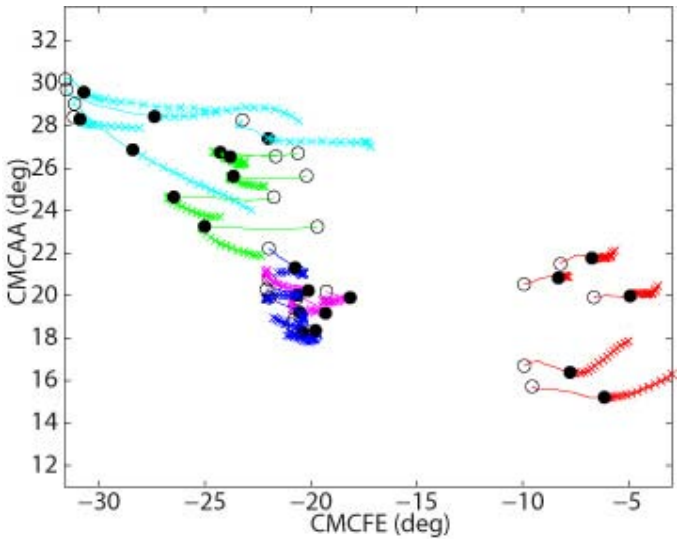

Figure 2: Thumb carpometacarpal joint angles for adduction/abduction vs. flexion/extension (150g case). The colors correspond to the five perturbation directions from Fig. 1. Open circles mark perturbation onset. Closed circles mark the time of maximum object rotation. X's correspond to 0 to 75ms after max. object rotation.

The thumb and index finger react with both adduction/abduction and flexion/extension corrective responses. These responses are clustered by perturbation direction as well as by perturbation magnitude. The perturbation direction groups exist even when comparing two different finger joints. The joint angle velocities group together well and are nearly equal. This suggests that subjects employ reactive corrective responses at similar speeds independent of perturbation direction and magnitude. We plan to use the joint angle space as one domain for characterizing the type of perturbation to which the system is subjected. If we could detect and identify these perturbations properly in an artificial system, the appropriate bio-inspired corrective grip response could then be implemented in a robotic or prosthetic hand.

REFERENCES

1. Johansson, R.S. and Flanagan, J.R. "Tactile sensory control of object manipulation in humans," in *Handbook of the Senses: Somatosensation*, **6**, San Diego: Academic Press, 2008, 67-86.
2. De Gregorio, M., Bair, K., and Santos, V.J., *Proc. of the Robotics Science and Systems Conf.*, Seattle, WA, USA, 2009.

BIOMECHANICAL AND EXPERIMENTAL CONFOUNDS TO THE DETECTION OF NEURALLY-GENERATED MUSCLE SYNERGIES

[1]Jason J Kutch, [1]Manish U Kurse, [2]Vincent R Hentz, [1]Nina Lightdale, [1]Isabella Fassola, and [1]Francisco J Valero-Cuevas

[1]University of Southern California, Los Angeles, CA, USA
[2]Stanford University School of Medicine, Stanford, CA, USA
email: kutch@usc.edu, web: bbdl.usc.edu

INTRODUCTION

A hypothesis that has received considerable attention is that the CNS activates muscles in patterns (synergies) so as to reduce the number of control degrees-of-freedom (DOF). Such covariation has been detected as a reduction in the dimensionality of muscle activations in a number of experimental paradigms, including cat postural control [1], human postural control [2], human arm control [3]. While such dimensionality reduction in muscle activations is commonly observed, there exist counterexamples [4, 5], and the non-neural sources that could contribute to such covariation (e.g., plant biomechanics, task constraints, and the choice of motor outputs selected by the experimenter) have received little rigorous study. Here we set out to establish the extent to which non-neural sources enforce muscle synergies.

More specifically, several studies have attempted to control for these confounds by requiring the production of circular or spherical (i.e., omnidirectional) force output (e.g. [3, 6]). Unfortunately, a rigorous computational geometric analysis proves that, for many realistic distributions of muscle mechanical action across multiple joints, omnidirectional force tasks are an insufficient test of neural synergies. This is because omnidirectional outputs unavoidably constrain muscle activity patterns to a low-dimensional subspace, even in the absence of any neural constraints.

METHODS

We analyzed the transformation from tendon tension to endpoint force of the human index finger measured in cadaveric specimens. In this experimental paradigm [7, 8], we rigidly attach the fingertip to a 6 degree-of-freedom load cell and apply known tensions to each of the 7 tendons of the index finger (FDS, FDP, EI, EDC, FDI, FPI, LUM). We apply every one of the 128 possible combinations of 10 and 1 N tension across tendons in random order. We linearly regress the resulting endpoint forces against the tendon tensions to determine the 3×7 *action matrix* for the finger, whose *i*th column is the 3-dimensional endpoint force resulting from applying 1 N to the *i*th tendon.

Applying established methods in computational geometry [9, 10] to the action matrix, we compute the set of all muscle activation patterns that can feasibly produce endpoint forces on a circle in the plane of finger flexion-extension. We then calculate the dimensionality of these muscle activations using principal components analysis (PCA).

RESULTS AND DISCUSSION

The action vectors for all 7 muscles were distributed over endpoint force space so as to enable the production of force in any direction (Figure 1A). For a set of forces spanning all directions in the plane of finger flexion-extension (Figure 1B), we computed the dimensionality of the set of muscle activations that could have feasibly generated these forces (Figure 1C). We found that the requirements of this task and the distribution of the action vectors suffice to constrain the feasible muscle activations to a low dimensional subspace of the 7-dimensional muscle activation space. Three principal components explain > 80% of the muscle activation space variance (Figure 1C).

These results challenge the tendency in sensorimotor neuroscience to attribute low-dimensionality in muscle activation to neural

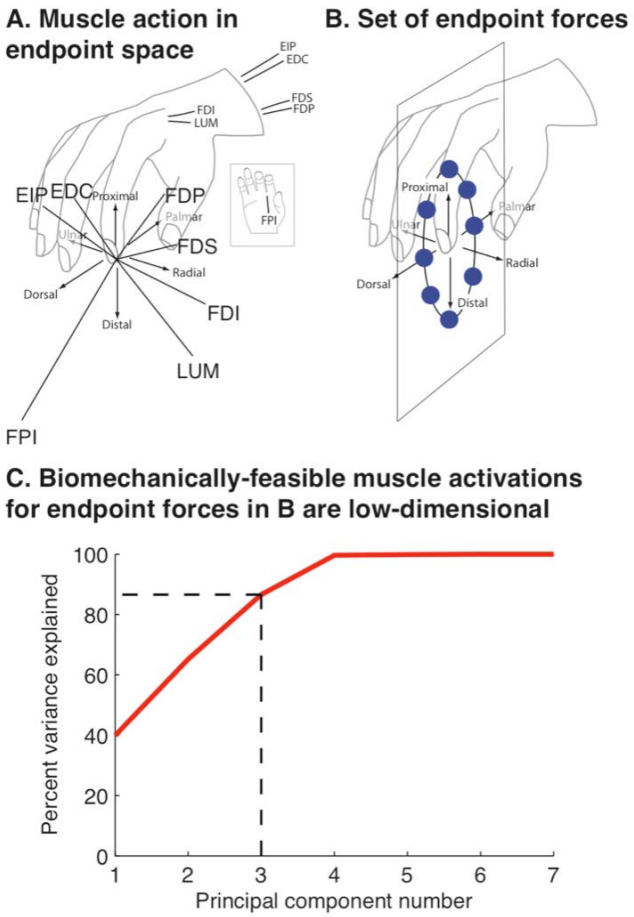

Figure 1: A. Action vectors for all muscles. B. Target endpoint forces. C. Dimensionality of feasible activation set.

constraints. Experiments that exhaustively explore omnidirectional force production in a circle (or sphere, Figure 1B) *do not* necessarily remove non-neural confounds.

The non-neural confounds described in this study show the need to look beyond structure in average muscle activations. Recent studies have suggested that natural variability produced by humans during motor tasks may be rich in information about neurally-generated muscle synergies [4, 5, 11].

These results compel us to develop novel experimental approaches that can conclusively establish the neural contributions to muscle synergies. Dimensionality reduction of neural origin can only be advocated after removing non-neural confounds [12]. Given that generating sufficiently many force outputs is likely to be experimentally prohibitive, leveraging experimental data with computational models can help establish the amount of dimensionality reduction attributable to the neural controller.

REFERENCES

1. Torres-Oviedo, G., et al., *Journal of Neurophysiology*, **96**, 1530-1546, 2006.
2. Krishnamoorthy, V., et al., *Experimental Brain Research*, **152**, 281-292, 2003.
3. d'Avella, A., et al., *Journal of Neuroscience*, **26**, 7791-7810, 2006.
4. Kutch, J.J., et al., *J Neurophysiol*, **100**, 2455-71, 2008.
5. Valero-Cuevas, F.J., et al., *Journal of Neurophysiology*, **102**, 59, 2009.
6. Torres-Oviedo, G., et al., *Journal of Neurophysiology*, **98**, 2144, 2007.
7. Valero-Cuevas, F.J., et al., *J Biomech*, **33**, 1601-9, 2000.
8. Kutch, J.J., et al. *Proceedings of Neural Control of Movement*, Waikoloa Beach, HI, 2009.
9. Avis, D., et al., *Discrete & Computational Geometry*, **8**, 295-313, 1992.
10. Valero-Cuevas, F.J., et al., *Journal of Biomechanics*, **31**, 693-703, 1998.
11. Tresch, M.C., et al., *Current Opinion in Neurobiology*, 2009.
12. Keenan, K.G., et al., *Journal of Neuroscience*, **29**, 8784, 2009.

ACKNOWLEDGEMENTS

This material is based upon work supported by NSF Grants EFRI-COPN 0836042, BES-0237258, and NIH Grants AR050520 and AR052345 to FVC.

PREHENSION CONTROL WHILE PERFORMING CIRCULAR ARM MOVEMENTS

[1]Gregory P. Slota, [2]Mark L. Latash and [1]Vladimir M. Zatsiorsky

[1]Biomechanics Laboratory, Pennsylvania State University, University Park, PA, USA
[2]Motor Control Laboratory, Pennsylvania State University, University Park, PA, USA
Email: GSlota@psu.edu web: http://www.biomechanics.psu.edu

INTRODUCTION

Multifinger prehension during object manipulation has been studied previously in single motion paths (vertical, horizontal, diagonal) [1,2]. Human control of internal force has been shown to be coupled with the manipulation force. In contrast, the decoupling of internal and manipulation forces has been utilized in robotics [3].

When humans manipulate handheld objects through 2D space (picking up an object from one spot on a table and placing it down at another), trajectories tends to follow fluid movement patterns. This movement path is a combination of two sub-movements, lifting/lowering vertically and transporting horizontally. How this combination of movements affect the control of prehension forces has not been fully studied.

The purpose of this study was to quantify the force sharing patterns of normal forces during the prehension control of holding onto an object while performing complex arm movements. Our interests were in seeing whether and how the grasping force (i.e. the internal force) is coupled with the vertical and horizontal manipulations.

METHODS

An instrumented handle (Fig. 1a) was used to collect data consisting of handle orientation (3 DoF rotation), accelerations (linear 3 DoF), and applied forces/moments (five digits × 6 forces/moments). This study used a wireless data collection system which allowed for unrestricted movement over a subject's complete range of motion.

The test protocol consisted of holding the handle with a five digit precision grip (finger tips only). Instructions were to apply natural effort to maintain grip of the handle while maintaining an upright orientation and moving the object along the prescribed moment path. The area of movement was defined by two sets of parallel strings (vertical, horizontal) (Fig. 1b). Subjects were instructed to move the handle in a circular path using the guide strings as vertical and horizontal boundaries. A metronome provided a beat for subjects to follow and perform cyclic patterns at 0.5, 1, 1.5, and 2 Hz.

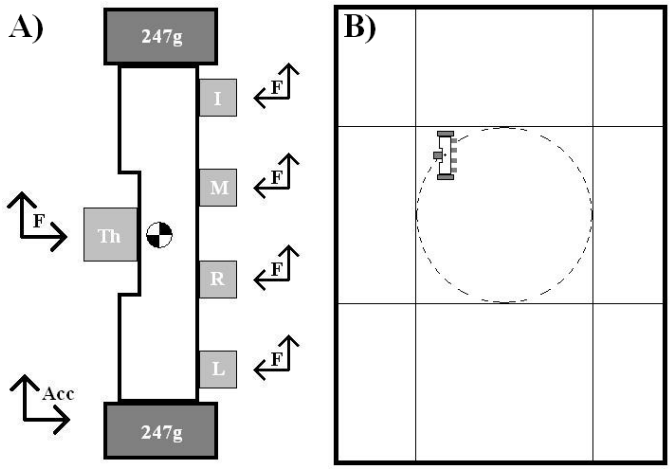

Figure 1: A) Instrumented handle with 6-DoF force sensors, 3-DoF accelerometer, 3-DoF orientation. B) Movement path as defined by a grid of guide strings.

RESULTS AND DISCUSSION

Normal forces of the thumb (Th) and virtual finger (Vf = sum of index, middle, ring, little fingers) were recorded and compared to the handle's accelerations. The results show that for circular movements, all four parameters—horizontal forces of the Th and Vf and the vertical and horizontal accelerations of the handle— changed as sine waves of the same frequency but different phases (Fig. 2).

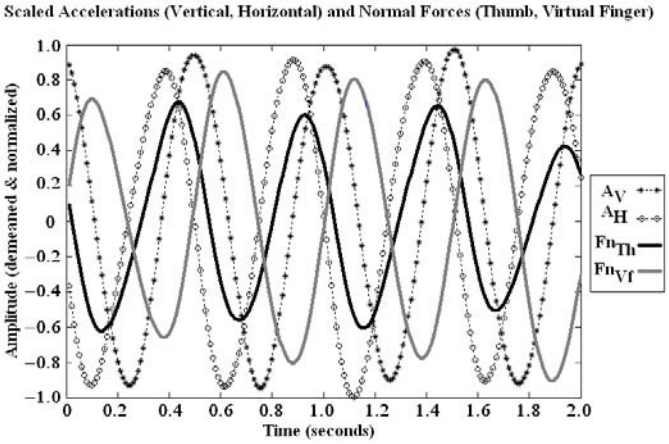

Figure 2: Normalized sine wave patterns of normal forces (Fn_{Th},Fn_{Vf}) and accelerations (A_V,A_H) during a counter clockwise circular movement. Shown parameters: A_V lags A_H, Fn_{Vf} lags Fn_{Th}, and no two are in phase.

A model for the superposition of the normal forces (Fn) includes the forces due to vertical manipulation of the object (F_{VM}), forces due to horizontal manipulation of the object (F_{HM}), and internal grasping forces due to holding onto the object (F_G) (Equ. 1).

$$Fn = F_{VM} + F_{HM} + F_G \quad (1)$$
$$Fn_{Th} = (k*M*|A_V|) + (M*A_H*(0.5 + C)) + F_G \quad (2)$$
$$Fn_{Vf} = (k*M*|A_V|) - (M*A_H*(0.5 - C)) + F_G \quad (3)$$

$$A_V = A_{Vo} \sin(wt) + G \quad (4)$$
$$A_H = A_{Ho} \sin(wt \pm \pi/2) \quad (5)$$
(+ counter clockwise, – clockwise)

The definition of other terms used include: M=mass of the handle, k=scaling factor (dependent on friction), C=scaling of Th-Vf ratio, A_{Vo}=amplitude of vertical acceleration, A_{Ho}=amplitude of horizontal acceleration, w=frequency, t=time, G=gravity.

Equations 2 and 3 represent the normal forces for the Th and Vf, respectively. The VmFs are in phase and equal in magnitude. The value of k is dependent on the surface friction as well as any self imposed safety margin. The HmFs are 180° out of phase (±) and are not required to be of equal magnitude. The net force between the Th and Vf controls in the horizontal movement. The F_G parameter represents the baseline forces required to hold onto the static object as well as any excessive gripping force or safety margins.

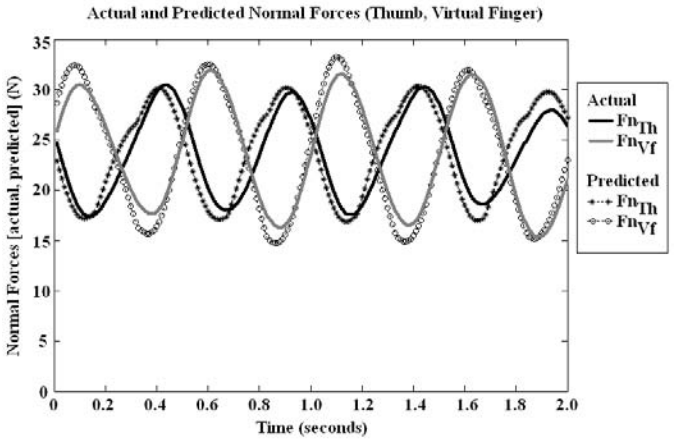

Figure 3: Comparison between actual normal forces (Th,Vf) and predicted values. Shown example data set: 2 Hz counter-clockwise movement, k=0.141, C=-0.073, F_G=22.3 N, VAF=98.9%.

The values of k, C, and F_G are subject and trial dependant and were estimated for a best fit of the model to the actual data (Fig. 3). Validity of the model was assessed in terms of the variance accounted for (VAF) when compared with the actual normal forces.

$$VAF = 100*(1-(sum(diff(t)^2))/(sum(actual(t)^2))) \quad (6)$$
$$diff(t) = actual(t)-predicted(t)$$

CONCLUSIONS

The results of this study have shown that the effects of complex movement patterns on prehension control can be explained by the superposition of the effects of vertical and horizontal manipulation forces in addition to internal forces. Future iterations of this model will include movement along the third axis as well as accounting for non-vertical handle orientations.

REFERENCES

1. Gao F, Latash ML, Zatsiorsky VM. *Exp Brain Res* **165**, 69-83, 2005.
2. Smith MA, Soechting JF. (2005). J Neurophysiol **93**(1): 137-45.
3. Zou B-R, Qian W-H. *IEEE Trans Syst Man Cybern* **30**, 185-192, 2000.

ACKNOWLEDGEMENTS

NIH grants AG-018751, NS-035032, AR-04856

MAXIMAL VOLUNTARY FORCE, BUT NOT SUBMAXIMAL STEADINESS, IS LIMITED BY A LOW-FRICTION CONDITION DURING INDEX FINGER PRESSING TASKS

Keenan KG, Collins JD, Massey WV, & Walters T [1]
[1]University of Wisconsin-Milwaukee, Milwaukee, WI, USA
email: keenan@uwm.edu

INTRODUCTION

The index finger is a critical contributor to the successful performance of activities of daily living (e.g., buttoning a shirt, typing, etc) and many investigators have studied its biomechanics and neuromuscular control [1,2,3]. Pressing tasks with the index finger are common in the field of motor control, although previous experimental approaches have almost exclusively focused on the production of force magnitudes irrespective of accurately directed forces. This may be problematic; however, as manual dexterity tasks require not only the production of precise force magnitudes, but also well-directed forces. For example, Cole [1] reported that older adults have an inability to produce well-directed submaximal forces during force-matching tasks. While it is unclear what mechanisms might lead to an inability to accurately direct forces, or whether these impairments influence daily function, assessing its potential influence on manual dexterity is a logical next step.

The directional accuracy requirements of a pressing task can be altered by changing the coefficient of friction between the fingers and the object being manipulated. Specifically, a low-friction interface requires well-directed forces perpendicular to the surface being manipulated or the finger will slide along the surface. Conversely, a high-friction interface allows a wider range of force directions without slipping. Using a high- and low-friction interface between the thumb and a force-sensor, Valero-Cuevas and colleagues [2] found that maximal voluntary force production (MVC) was not altered for the two friction conditions. However, it was not reported if the actual force direction differed across conditions, which may be important as a similar force direction might lead to similar MVC forces. Also, muscle activity increased in two thumb muscles for the low-friction condition, which may have helped to preserve MVC force.

The purpose of the current study was to manipulate the friction constraints of a novel index finger pressing task [3] to examine its influence on two commonly investigated motor outputs: i) MVC force magnitude, and ii) fluctuations in force during submaximal force-matching tasks.

METHODS

Subjects (n=21; 21.4±3.8 years old) pressed straight downward with the tip of their right index finger onto an aluminum surface (3cm x 3cm) that was attached to a 6-axis force/torque sensor (ATI Industrial Automation, Nano17). A thermoplastic cast was formed around the tip of the participant's index finger to allow maximal force production while reducing pain (Figure 1). Subjects received visual feedback of the force perpendicular to the aluminum surface (i.e., Fz) on a 24-inch LCD monitor and no information on force direction was supplied. Each subject performed MVCs with the contact point at the tip of the finger on two different surfaces: Teflon and sandpaper. Following the MVCs, subjects were instructed to hold a constant force at 2.5% and 10% of their MVC for 13 seconds. Subjects were instructed to keep the force trace as close as possible to the target line at 2.5%

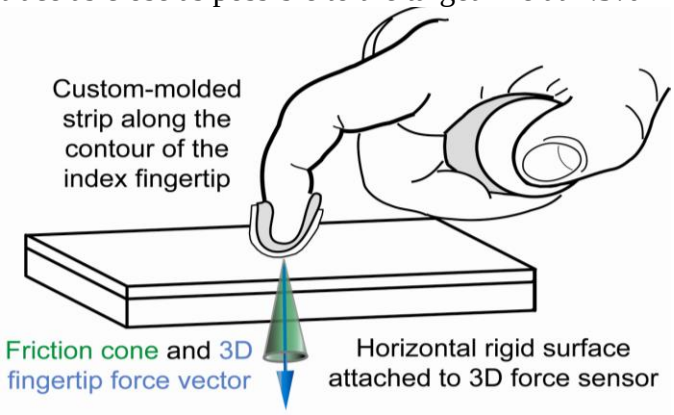

Figure 1: Subjects pressed with their finger into a rigid horizontal surface. The horizontal surface was attached to a force sensor and the surface was covered with either sandpaper or Teflon to establish a high- and low-friction condition, respectively. The size of the friction cone (i.e., allowable force directions without slipping off the surface) is decreased by a decrease in the coefficient of friction between the surfaces.

and 10% of MVC. Two trials were performed for each condition. The static steadiness trials were performed with and without visual feedback, though as no differences were found between visual conditions the results were combined. Muscle activity was estimated using surface electromyography (EMG) recorded from first dorsal interosseous, extensor digitorum communis, and flexor digitorum superficialis. EMGs were filtered, normalized, and processed as in [3]. Significant differences between friction conditions for MVC force magnitude and direction, submaximal force variability, and EMG amplitude were examined using t-tests ($p<0.05$).

RESULTS AND DISCUSSION

MVC force declined ($p<0.01$) by 14.6% when pressing on Teflon (38.4±17.5 N) compared to sandpaper (44.9±21.1 N, Figure 1). This force magnitude decline cannot be explained by a change in MVC force direction. Fingertip forces in the proximal/distal direction were calculated when Fz was maximal. Forces were directed distally for both sandpaper (2.0±6.6 N) and Teflon (0.4±2.4 N), although the difference was not significant ($p=0.11$). Interestingly, EMG amplitude dropped by 16.3% in FDI ($p<0.05$), but there were no significant differences in EDC ($p=0.47$) and FDS ($p=0.12$). Although it is unclear why EMG amplitude decreased in first dorsal interosseous, it is possible that after practice trials subjects adapted a control strategy to limit pressing as hard as possible to avoid slipping on the low-friction surface.

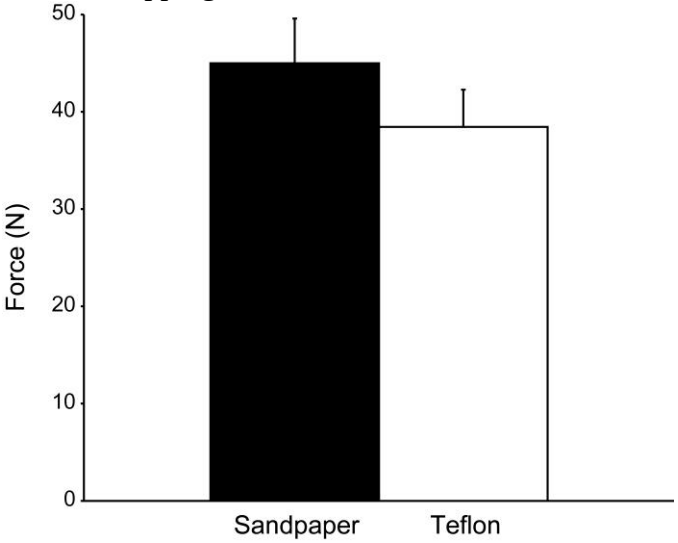

Figure 2: Maximal voluntary force production was reduced when pressing into a force sensor covered with a low-friction Teflon surface compared to a high-friction sandpaper surface. Bars are grouped means ± SE.

In contrast to MVC force, fluctuations in force during submaximal force-matching tasks were not different across friction conditions (Figure 3). Specifically, the coefficient of variation in force was similar at 2.5% (sandpaper = 34±5%; Teflon = 36±4%; $p=0.25$) and 10% (sandpaper = 21±2%; Teflon = 22±2%; $p=0.38$) MVC force.

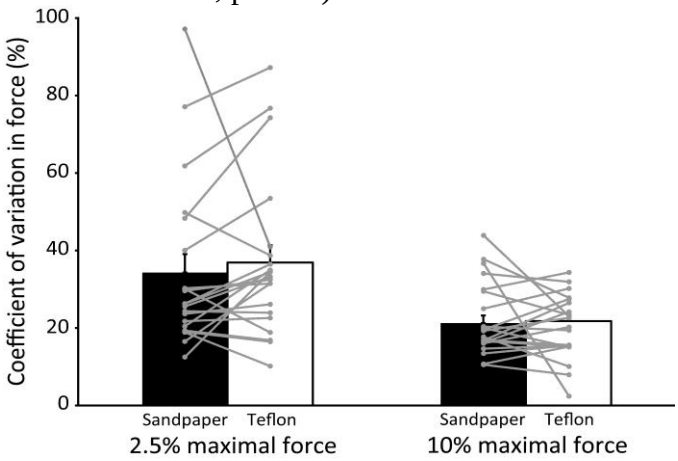

Figure 3: Performance on submaximal force-matching tasks was not influenced by the friction condition. The coefficient of variation in force (in the direction perpendicular to the surface being pressed against) was similar regardless of pressing into a sandpaper- or Teflon-covered surface. Bars are grouped means ± SE and individual data are also represented by gray dots connected by lines.

CONCLUSIONS

Maximal voluntary fingertip force was influenced by the friction condition. Thus, for those tasks performed at high levels of force the coefficient of friction may be an important determinant of manual dexterity performance. However, for submaximal forces, there was no impairment in motor performance during force-matching tasks. It should be noted that these findings are generalizable to young healthy adults, it is unclear if the same results will be found in clinical or older populations.

REFERENCES

1. Cole KJ. *Exp Brain Res*, 285-291, 2006.
2. Johanson ME et al. *J Hand Surg*, 698-705, 2001.
3. Keenan et al. *J Neurosci*, 8784-8789, 2009.

ACKNOWLEDGEMENTS

We acknowledge the University of Wisconsin Research Growth Initiative and the Judd Leighton Foundation for their support of this project and to Hillary Gruska, John Hubbard and Ryan Kern for their assistance in data collections.

The Effect of External Loading on the 3D Patellar Tendon Moment Arm Measured with Dynamic MRI

Anne Schmitz, Christopher Westphal, and Darryl G. Thelen

University of Wisconsin-Madison, Madison, WI, USA
email: ambaus@wisc.edu, web: http://www.engr.wisc.edu/groups/nmbl/

INTRODUCTION

Muscle forces are an important determinant of the knee cartilage contact loads that arise during movement. However, models used to estimate muscle forces often rely on a generic description of knee musculoskeletal geometry [1] in which moment arms are assumed invariant with load. Recent dynamic imaging studies have shown that moment arms can vary under functional loading conditions [2]. For example, a recent fluoroscopic study found significant variation in the patellar tendon moment arm with quadriceps contraction [3]. However, the analysis was limited to the sagittal plane and thus could not account for three-dimensional effects [2,4]. The goal of this study was to compare the 3D patellar tendon moment arms between movements that involved active shortening and lengthening quadriceps contractions.

METHODS

High resolution static MR images were used in conjunction with dynamic MR imaging to compute subject-specific patellar tendon moment arms about the knee finite helical axis. Eight healthy subjects (four male, four female, ages 22-28 years) participated. Each subject performed cyclic knee flexion-extension (30 cycles per minute) through ~35 degrees of motion within the bore of a MR scanner (Fig. 1a). A MRI compatible loading device was used to apply either elastic or inertial loads about the knee [5], which induced quadriceps activity with knee extension or flexion, respectively (Fig. 1c). Subjects performed three trials for each loading condition.

CINE phase contrast imaging [6] was used to measure 3D tissue velocities within a sagittal-oblique imaging plane (pixel size of 0.94 x 0.94 mm) that bisected the femur, tibia, and patella (Fig. 1b). At each frame of the cyclic movement, linear least squares was used to calculate the translational and angular velocity of the femur, tibia, and patella that best agreed with measured pixel velocities. Forward-backward and Fourier integration of the rigid body velocity data was then performed to compute the 3D translations and rotations of the tibio-femoral and patella-femoral joints [7].

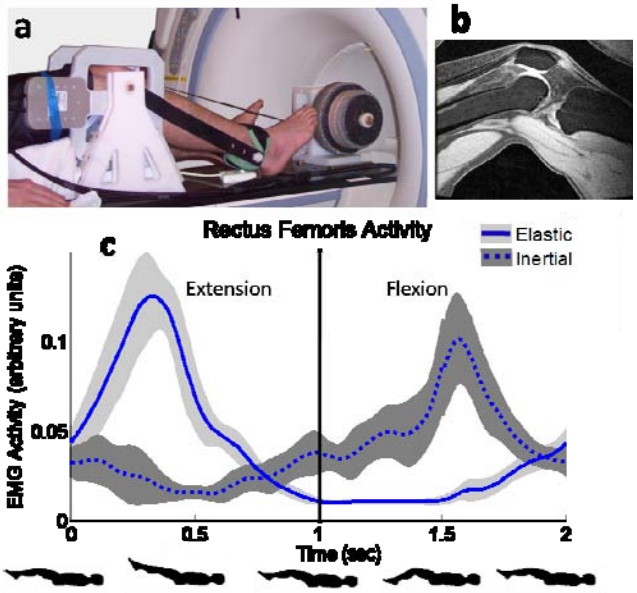

Figure 1: (a) MR compatible loading device, (b) Sagittal-oblique imaging plane, (c) Quadriceps activity (shown for one representative subject) was induced during either knee extension (elastic loading) or flexion (inertial).

The static MR images were segmented to create subject-specific knee models in which the origin and insertion of the patellar tendon could be identified. Anatomical landmarks were then co-registered between the dynamic and static image data [8]. Tibiofemoral kinematics were used to compute the instantaneous finite helical axis (FHA) of the tibia with respect to the femur at each frame (Fig. 2) [2,8]. The patellar tendon moment arm was then determined as the shortest distance between the

patellar tendon line of action and the joint axis [2]. We did not compute moment arms near the ends of the knee range of motion since small joint velocities at these phases introduce error into the finite helical axis calculation [8]. A two-tailed paired Student *t*-test was used to compare the moment arms between elastic and inertial loading conditions at 5 degree increments during both the knee extension and flexion phases (Fig. 1c).

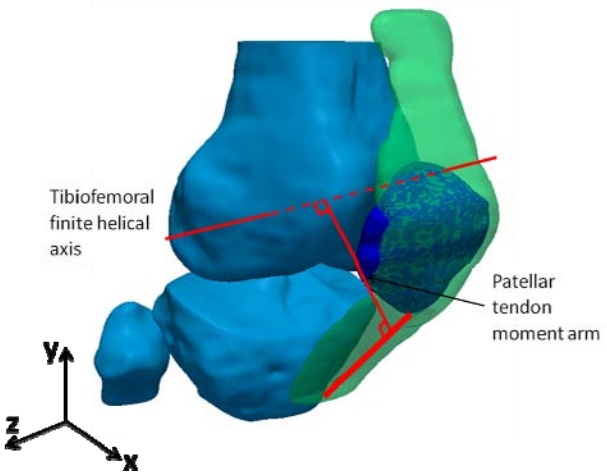

Figure 2: The patellar tendon moment arm was the shortest distance between the tendon's line of action and the tibiofemoral finite helical axis.

RESULTS AND DISCUSSION

Patellar tendon moment arms varied significantly with loading. During the knee extension phase, the inertial load induced a significantly smaller moment arm than elastic loading between 20 and 40 degrees of knee flexion, with differences ranging from 14-34% at angles where at least seven subjects were represented (Fig. 3). Similar results were seen during the flexion phase. The load-dependent variation in moment arms can arise from changes in patellofemoral kinematics and/or tibiofemoral kinematics. Further analysis revealed that the FHA in the inertial case was significantly more anterior (~5 mm) near full knee flexion, thereby contributing to the decreased moment arm. Anterior translation of the tibia due to quadriceps activity with knee flexion likely induced this change [9].

The quadriceps undergo lengthening contractions during the loading phase of gait, making the inertial case relevant to consider in the context of functional movement. The inertial loads used in this study induced peak knee extension moments of ~0.5 Nm/kg [9], which is comparable to that seen in the loading phase of gait [10]. Hence, a reduction in the patellar tendon moment arm could necessitate greater muscle forces during gait than would be estimated using kinematic knee models [1]. Further analysis is required to determine the net effect on knee cartilage contact patterns, given that articular surface geometry and ligament stretch are also important to consider.

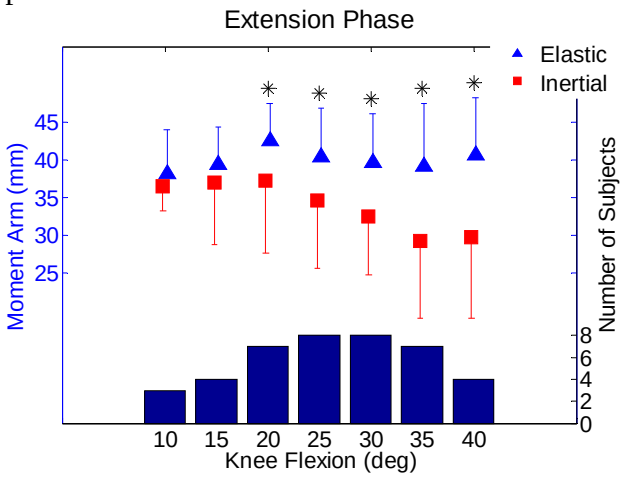

Figure 3: Patellar tendon moment arms for elastic and inertial loads. *p<0.05 for load effect

CONCLUSIONS

Eccentric loading of the quadriceps can reduce the patellar tendon moment arm, which may be important to consider when using models to estimate internal knee loads during locomotion.

ACKNOWLEDGEMENTS

NIH T32 AG000213 (P.I. Sanjay Asthana)
DoD DR080326

REFERENCES

1.Koehle, M. J., et al. *J Biomech* **41**, 1143-1146, 2008.
2.Sheehan, F. *J Biomech* **40**, 1968-1974, 2007.
3.Tsaopoulos, D. E., et al. *J Biomech* **40**, 3325-3332, 2007.
4.Tsaopoulos, D. E., et al. *Eur J App Physiol* **105**, 809-814, 2009.
5.Silder, A., et al. *J Med Devices* **3**, 1-5, 2009.
6.Sheehan, F., et al. *J Biomech Engr* **121**, 650-656, 1999.
7.Pelc, N., et al. *J MRI* **5**, 339-345, 1995.
8.Sheehan, F. *J Biomech* **40**, 1038-1047, 2007.
9.Westphal, C., et al. *Proceedings of American Society of Biomechanics*, State College, 2009.
10.Whittington, B., et al. *Gait & Posture* **27**, 628-634, 2008.

OPEN KNEE: A 3D FINITE ELEMENT REPRESENTATION OF THE KNEE JOINT

[1,2]Scott Sibole, [1,2]Craig Bennetts, [3]Bhushan Borotikar, [4]Steve Maas, [2]Antonie J. van den Bogert, [4]Jeffrey A. Weiss and [1,2]Ahmet Erdemir

[1]Computational Biomodeling Core and [2]Dept. of Biomed. Eng., Cleveland Clinic, Cleveland, OH, USA
[3] Dept. of Rehab Medicine, Clinical Center, NIH, Bethesda, MD
[4]Department of Bioengineering, University of Utah, Salt Lake City, UT, USA
e-mail: erdemira@ccf.org, web: http://simtk.org/home/openknee

INTRODUCTION

Finite element (FE) analysis has become an important tool in knee biomechanics to explore joint and tissue function, to understand injury mechanisms, study pathological joint mechanics and evaluate surgical performance. Numerous models have been developed and used (a recent PubMed search reveals 382 publications) and in many cases, multiple models were constructed independently to investigate similar questions [1,2]. If disseminated, computational tools and models can avoid the duplication of research effort and provide a means for investigators to reproduce the results from other laboratories [3].

The typical process for generating a validated, specimen-specific FE model involves: 1) imaging of a cadaver specimen, 2) gathering kinetic and kinematic data for the intact specimen, 3) material testing of the substructures, 4) reconstruction of anatomical geometry, 5) mesh generation, 6) constitutive modeling, 7) definition of boundary conditions, loads, and constraints, 8) mesh convergence analysis, and 9) validation and sensitivity analysis. The entire process can be a laborious task and often presents barriers for isolated research groups due to limited access to experimentation tools and/or engineering expertise. Subsequent scientific investigations with the validated model are usually a small fraction of the research time and resources. Our long-term research goal is to develop a knee joint model to describe and predict the passive kinematics of the knee, and provide an initial platform to investigate more detailed mechanics of joint substructures after modifications to address specific research questions. The objective of this presentation is to describe our initial efforts to develop a freely distributable model of passive knee mechanics, while providing the research community with all data that was used for model development as well as the model itself.

METHODS

Magnetic Resonance (MR) images of a right cadaver knee (70 y. o. female donor) were collected using a 1.0 Tesla extremity scanner (Orthone, ONI Medical Systems, Inc., Wilmington, MA) with the joint at full extension [4]. Robotic testing was performed using a hexapod (Rotopod R2000, Parallel Robotic Systems Corp., Hampton, NH) to collect passive load-displacement and torque-rotation data for the tibiofemoral joint in all six degrees of freedom [4].

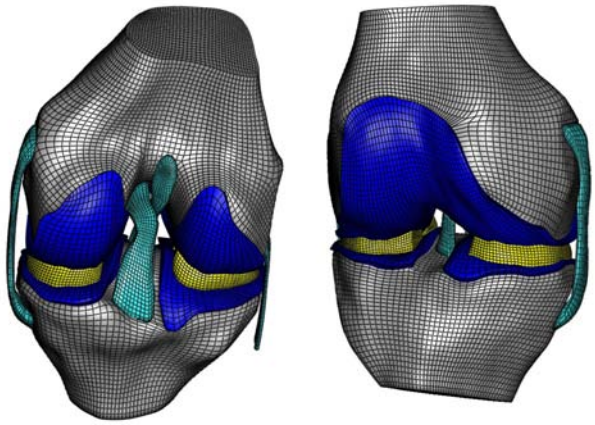

Figure 1: Hexahedral mesh of the tibiofemoral joint. Left-posterior view. Right - anterior view.

The geometries of the femur, tibia, anterior & posterior cruciate ligaments, medial and lateral collateral ligaments, articular cartilage, and menisci were extracted from MR images manually using VolSuite (http://www.osc.edu/archive/VolSuite). Spline curves represented the boundaries, and were used to generate parametric surfaces in Rhinoceros (McNeel, Seattle, WA). The surfaces were imported to TrueGrid (XYZ Scientific Applications, Livermore Inc., CA) and meshed with 133,295 hexahedral elements (Fig. 1). The mesh density may

be adjusted later pending a mesh convergence study.

The femur and tibia were rigid. Cartilage and menisci were nearly-incompressible neo-Hookean materials [6]. Ligaments were nearly-incompressible, transversely isotropic, hyperelastic materials [6,7]. Ligament insertion areas were constrained to move with the rigid bone. Frictionless contact was defined between all structures that may come into contact. To test the solution process, a passive flexion was simulated by fixing the tibia and prescribing a 90° rotation of the femur about an approximate mediolateral axis, while leaving all other degrees of freedom free. For pre-processing, simulation, and post-processing, free and open-source software were employed: PreView, FEBio [5], and Postview, respectively (http://mrl.sci.utah.edu/software).

An open access philosophy was adapted for model construction to allow anyone to utilize and/or modify the model at all stages of development. The use of an open-source pre-processor and solver strengthens the capacity for others to use the model, and incorporate changes based on their scientific question. Documentation and dissemination for the experimentation and modeling are available at https://simtk.org/home/openknee, including a wiki, forums, and source code repository. This provides the scientific community a pathway to test, assess validity, provide recommendations, and implement new features.

RESULTS AND DISCUSSION

A preliminary tibiofemoral joint model was developed and is available at the site, including MR images, geometries, and mesh. Currently, the model is capable of simulating passive knee flexion from full extension to approximately 75 degrees of flexion (Fig. 2). It should be noted that, the purpose of this simulation was to test model robustness and no merit should be given to the output as additional simulations for validation are warranted.

FE representations of the knee will have limitations, depending on the scientific question. A rigorous verification and validation process needs to be employed. For example, if one is interested in ligament stresses, estimation of the in situ ligament strain at reference model configuration may become important [7]. Simplifications can be conducted on a need basis, i.e. if overall joint response is the variable of interest, the ligaments can be represented as line elements. The presented FE model of the knee joint is currently in a stage of infancy. Making it publicly available at this early stage is important for testing of the open-source development philosophy in the field of biomechanical modeling.

The research team not only seeks to provide a model which can be extended and modified to meet a particular researcher's need, but also to benefit from the expertise of numerous investigators who may use the model and provide feedback during its development. In return, model quality can be enhanced by wide-spread suggestion and criticism.

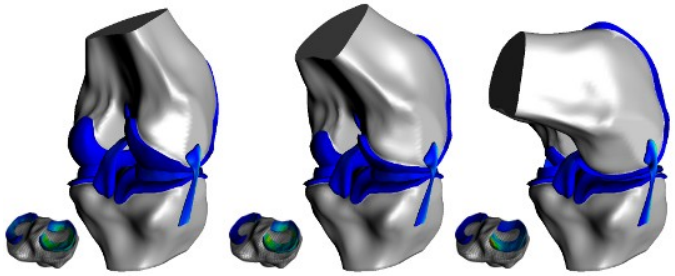

Figure 2: Simulation of knee flexion of approximately 75 degrees using FEBio. Von Mises stress distribution at 23°, 45°, and 75° flexion, from left to right.

REFERENCES

1. Vaziri A, et al. *Annals of Biomed Eng*. **36**, 1335-1344, 2008.
2. Zielinska B, et al. *J Biomech Eng.* **128**, 115-123, 2006.
3. Delp S, et al. *IEEE Transactions on Bio-Medical Engineering.* **54**, 1940-1950, 2007.
4. Borotikar BS. *Doctoral Dissertation, Cleveland State University.* 2009.
5. Maas S, et al. SCI Institute Technical Report #UUSCI-2009-009, 2009.
6. Peña E, et al. *J Biomech,* **38**, 1686-1701, 2006.
7. Gardner JG, et al. *J Orthop Res,* **21**, 1098-1106, 2003.

ACKNOWLEDGEMENTS

This study funded by NIH grants R01EB009643, R01GM083925, and R01AR049735. Hosting provided by Simbios, National Center for Biomedical Computing at Stanford.

POSITION OF THE QUADRICEPS MUSCLE ACTUATOR INFLUENCES KNEE LOADS DURING SIMULATED SQUAT TESTING

Michael W. Hast and Stephen J. Piazza

The Pennsylvania State University, University Park, PA, USA
email: piazza@psu.edu

INTRODUCTION

Since the introduction of total knee replacement (TKR) in the 1970s, a variety of devices have been created to test the mechanics of prosthetic knee components. One of these, the 'Oxford Rig' simulates knee flexion with a universal joint at the hip, a ball joint at the ankle, and pelvis stage that slides on vertical rails. This simulator provides an indication of knee function during everyday activities that occur under quadriceps load, such as rising from a chair or climbing stairs, while permitting six degrees of freedom each at the tibiofemoral and patellofemoral articulations [1]. Several investigators have published studies of knee mechanics using variants on the original Oxford Rig design. While these design iterations have maintained 12 degrees of freedom for the knee joint, the fixation point of the actuator intended to stand in for quadriceps muscles has often been varied. While the actuator in the original Oxford Rig was attached to the femur [2], quadriceps actuators have also been fixed to the moving pelvis stage [3] and to the ground [4].

The purpose of the present study was to use a forward-dynamic computer simulation to examine how TKR kinematics and kinetics differ in the Oxford Rig depending on how the actuator is mounted. Simulations of loaded knee flexions were carried out with the actuator mounted on the femur segment, on the pelvis stage, and fixed to the ground while pulling in two different directions-vertical and horizontal (Figure 1).

METHODS

We based our computational model on a physical Oxford Rig in our laboratory. This rig employs a mechanical leg, consisting of steel rods for the femur and tibia. Custom-made aluminum mounting blocks attach to the steel rods and are fitted with Scorpio PS (Stryker Orthopaedics) Size 3 TKR components. The patella mounts on a 2.54 cm wide by 0.2 cm thick strip of nylon webbing. A custom-made aluminum swivel connects the patellar tendon to a nylon coated steel cable, which attaches to a linear actuator (Northern Tool, Burnsville, MN). Medial and lateral collateral ligaments are represented by rubber bands.

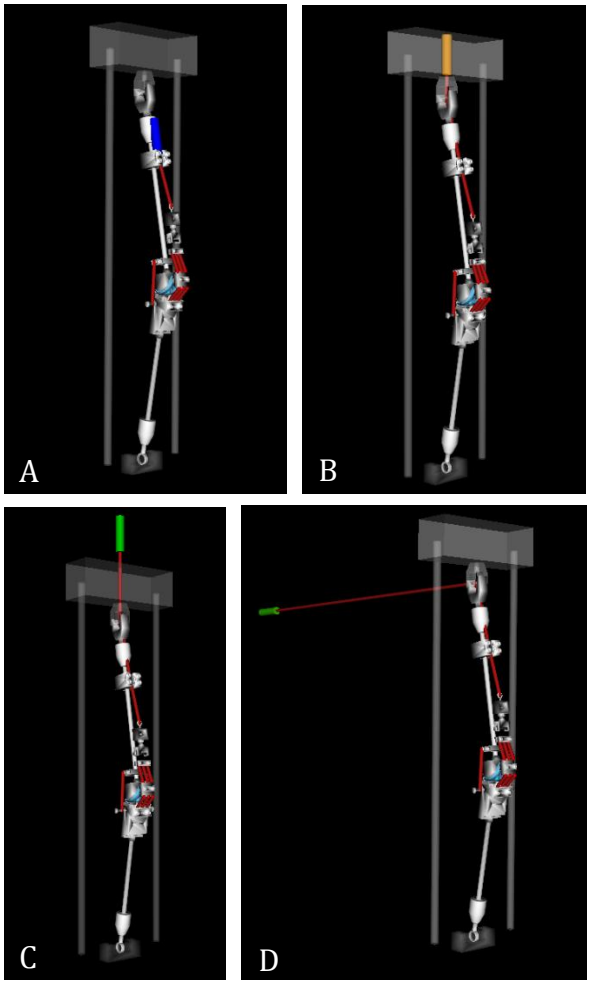

Figure 1: Models of Oxford Rigs with the quadriceps actuator fixed to (A) the femur and (B) the pelvis stage. Actuators were also attached to the ground with actuator displacement in the (C) vertical and (D) horizontal directions. Knee flexion occurred as the pelvis stage was lowered under quadriceps control.

The ten-segment forward dynamic model was created using the SIMM/Dynamics Pipeline (MusculoGraphics, Inc., Santa Rosa, CA) and SD/FAST (Parametric Technologies, Inc., Needham, MA) software packages. A CAD model of the rig was created in SolidWorks (Concord, MA), which was used to determine the inertial properties of the segments. The quadriceps cable, patellar tendon, and collateral ligaments were modeled as springs with appropriate linear force-deformation relationships. Varied demands on the knee extensors were simulated by placing 10 and 20 kg masses at the pelvis stage. The quadriceps cable routing, with respect to the femur, was consistent across simulations. Simulated linear actuators were massless. Knee flexions from 30° to 100° were simulated over 20 s to minimize inertial effects. Contact between the implants was modeled using a rigid body spring model [5]. Knee flexion angles were determined using the convention described by Grood and Suntay [6].

RESULTS AND DISCUSSION

Quadriceps Muscle Force

Large quadriceps forces that increased with knee flexion were required when the actuator was mounted on the femur or the pelvis stage (Figure 2). Mounting the actuator on the ground segment, however, significantly reduced required quadriceps force and quadriceps force did not consistently increase with flexion. Orienting the actuator horizontally resulted in less of this reduction of required quadriceps force.

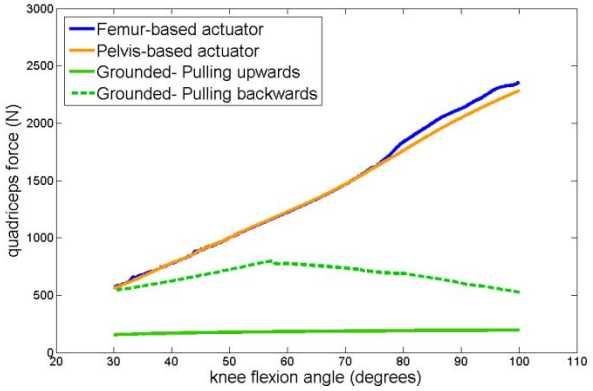

Figure 2: Required quadriceps force plotted versus knee flexion angle with 20 kg of pelvis mass.

Contact Forces

No significant differences in patellofemoral or tibiofemoral contact forces were found between simulations with femur-based and pelvis-based actuators. Similar to required quadriceps force, simulations with grounded actuators had contact forces with smaller magnitudes, and proportional changes in contact forces (and quadriceps force) occurred when pelvis masses were changed from 10 kg to 20 kg.

Kinematics

Despite large differences in loading of the knee joint, the method of actuation did not substantially affect TKR implant kinematics during knee flexion simulations. Differences in internal/external rotation of the knee during flexion was less than 1°, and initial cam-post mechanism contact occurred at approximately the same knee flexion angle (between 71°-73°).

CONCLUSIONS

The results of this study will be useful for tailoring future knee simulators to varied design constraints and scientific questions. For example, space limitations may prevent the actuator from being mounted on the femur, but our results show that mounting the actuator on the pelvis stage produces substantially the same knee loading and motions. It was found that when the quadriceps actuator is grounded, muscle and contact forces were reduced, perhaps making this choice less suitable for studying internal knee forces. Knee joint kinematics, however, were largely unaltered by this reduced loading, suggesting that useful investigations of implant motions, if not forces, may be possible with less powerful ground-fixed actuators.

REFERENCES

1. Zavatsky, A.B. *J Biomech* **30,** 277-280, 1997.
2. Bourne, R. *Trans. Orthop Res. Soc.* **24,** 160, 1978.
3. Quentelier, J. *Acta Bioeng & Biomech* **10,** 23-28, 2008.
4. Singerman, R. *Trans. ASME* **117,** 8-14, 1995.
5. Landon, R.L. *Comp Meth in App. Mech & Eng* **198,** 2339-2346, 2009.
6. Grood, E.S., Suntay, W.J. *J Biomech Eng* **105,** 136-144, 1983.

ACKNOWLEDGMENTS

This work was supported in part by Stryker Orthopaedics.

Associations Between Anterior Knee Pain and Patellofemoral Kinematics in Cerebral Palsy

[1]Frances T. Sheehan, [1]Abrahm J. Behnam and [1,2]Katharine E. Alter

[1]Rehabilitation Medicine, National Institute of Health, Bethesda, MD, USA
[2] Mount Washington Pediatric Hospital, Baltimore, MD,USA
email: fsheehan@cc.nih.gov, web: http://pdb.cc.nih.gov

INTRODUCTION

Flexion contractures and anterior knee pain (AKP) can severely limit function for individuals with Cerebral Palsy (CP). To date most studies evaluating AKP in patients with CP have focused on the radiographic findings of patellar fragmentation. Unfortunately, neither patellar fragmentation nor flexion contractures have been shown to be predictive of AKP in CP [1,2]. Therefore, the purpose of this study was to quantify the role that patellofemoral (PF) kinematics may play in the development of AKP in patients with CP. To accomplish this, complete 3D PF kinematics were quantified in a group of patients diagnosed with CP, but varied in their report of AKP and compared to the PF kinematics in an asymptomatic able-bodied (control) population.

METHODS

Fifteen volunteers with CP and 50 asymptomatic controls provided informed consent (or assent) prior to participating in this IRB approved study. If appropriate and time permitted, both knees were studied, creating a total study enrollment of 18 knees in the CP cohort (9M/8F, age=21.9 ± 10.8years, height = 166.4± 8.6cm, mass=57.1±10.1kg) and 60 knees in the control cohort (28M/32F, age = 26.5 ± 8.6 years, height = 170.9 ± 9.6 cm, mass = 69.0 ± 15.8kg). All participants were placed supine in an MR imager (1.5 T, GE Medical Systems, Milwaukee, WI, USA or 3.0 T, Philips Medical Systems, Best, NL) and were asked to cyclically flex and extend their knee while a dynamic cine-phase contrast (PC) MR image set (x,y,z velocity and anatomic images frames) was acquired [3]. In order to establish anatomical coordinate systems dynamic cine images (anatomic images only) were acquired in three axial planes. Integration of the velocity data enabled accurate (<0.5mm [3]) quantification of 3D PF and tibiofemoral (TF) kinematics throughout the motion cycle.

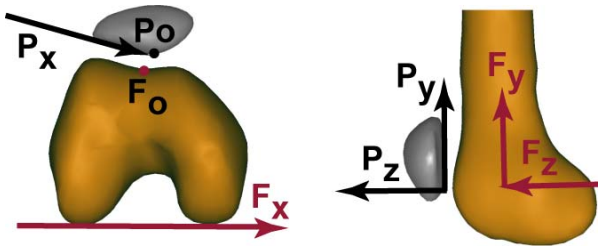

Figure 1: Schematic of the patellar and femoral coordinate systems, defined such that x,y, and z were positive in the medial, anterior, and superior directions, respectively. Flexion, medial tilt and varus rotation were in the positive x,y, and z directions, respectively.

A two-way ANOVA (α=0.05) was used to compare kinematics between groups at single knee-angle increments from 40° to 10° knee extension (only 5 subjects with CP were able to extend beyond 10° and few controls could flex beyond 40° due to the closed-bore environment). For the CP cohort Spearman's ρ was used to identify associations between PF kinematics and two discrete variables: pain (yes/no) and GMFCS score (I-V). The GMFCS score indicates the level of function. A score of I indicates full independence in all mobility and a score of V indicates complete dependence for all mobility. The PF kinematics for the correlations were taken from a single knee angle (20°), which was the angle closest to full extension that all subjects with CP could reach. Discriminate analysis was used to determine if PF kinematics could predict AKP in CP.

RESULTS AND DISCUSSION

The patellae of the CP cohort were superiorly and posteriorly displaced, extended, and in varus rotation, as compared to the control population

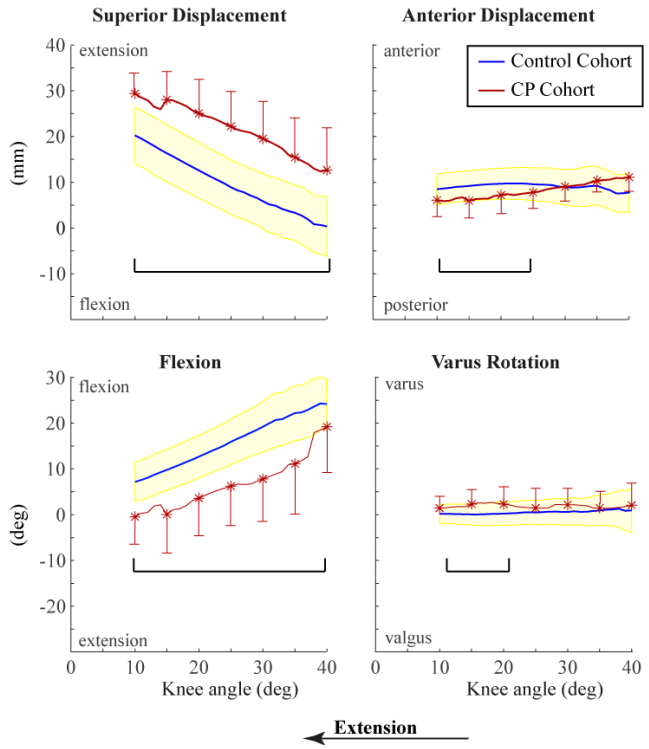

Figure 2: The four kinematic variables demonstrating significant differences between cohorts. The black lines with end caps indicate the range of knee angles where significance was found. The control population (blue) is presented with 1SD range shaded in yellow; whereas the CP cohort (red) had 1SD bars every five degrees.

(Figure 1). The CP cohort did not demonstrate significant lateral shift or tilt. In addition, the four variables demonstrating significant differences from the control population were moderately correlated to each other (superior–posterior, r = 0.70, p=0.002; superior-extension, r=0.77, p<0.001; superior-varus, r=0.67, p=-0.003). All 4 kinematic variables were significantly increased in the CP cohort with AKP (n=7), compared to the CP cohort without AKP (n=11). PF lateral displacement and tilt were not different between cohorts.

AKP and GMFCS both correlated with PF kinematics (Table 1), as well as with each other (ρ=0.57, p=0.01). Combined, PF extension and superior displacement discriminated patients with CP and AKP and those without AKP (94.4%).

This study, for the first time, identified kinematic markers that discriminated AKP in patients with CP. Interestingly, patella alta (increased PF superior displacement) has been documented in both individuals with CP and individuals without CP, but diagnosed with AKP and PF maltracking ("maltrackers"). A recent study suggested that patella alta may encourage PF dislocation in maltrackers by removing the patella from the constraints of the femoral groove (hyper-mobility) in terminal extension [4]. Yet, for the patients with CP, this was not the case. It is likely that RF tightness or spasticity, or both reduces PF lateral mobility (hypo-mobility), while pulling the patella superiorly and rotating it back onto the femoral shaft (increased extension). This promotes contact between the patellar cartilage and the femoral shaft during terminal extension. This contact may lead to excessive cartilage wear and pain. Therefore, reducing both patella alta and PF extension in patients with CP and AKP may be key to long term knee joint health.

CONCLUSIONS

Patients with higher GMFCS rating have more pronounced deformities at the knee. Specifically these individuals have increased patella alta and extension. These findings predicted the higher level of pain in this group. PF extension was also accompanied by hypo-mobility. The greater the severity of these kinematics alterations, the more likely it is for these patients with CP to experience AKP. Therefore, re-aligning the patella in patients with CP and AKP may be critical to long term knee joint health. When addressing patella alta as a cause of knee pain, it is important to consider how alterations in patellar alignment may affect other dynamic and static knee joint parameters.

REFERENCES

1.Topoleski TA, et al. *J Ped Orthop* **20**, 636-9, 2000
2.Senaran H, et al. *J Ped Orthop*, **27**, 12-6, 2007
3.Sheehan FT, et al. *J Biomech* **31**, 21-26, 1998
4.Sheehan FT, et al. *J. Orthop Res* **27**, 266-275, 2009

Table 1: Spearman correlation coefficients (ρ)

	Superior	Posterior	Extension	Varus
Pain	0.69(p=0.001)	0.53(p=0.02)	0.71(p<0.001)	0.49(0.03)
GMFCS	0.70(p=0.001)	-	0.69(p=0.002)	-

THE ASSOCIATION BETWEEN PATELLA ALIGNMENT AND FEMORAL TROCHLEAR GEOMETRY

[1]Sharon Hsiang-Ling Teng, [1]Yu-Jen Chen, and [1]Christopher M Powers

[1]University of Southern California, Los Angeles, CA, USA
email: hsianglt@usc.edu, web: http://pt2.usc.edu/labs/mbrl/

INTRODUCTION

Altered patella alignment has been proposed as an etiologic factor associated with patellofemoral pain. Previous studies have suggested the geometry of femoral trochlea plays an important role in determining patellar kinematics [1,2]. More specifically, the depth of the trochlear groove as well as the height of the lateral anterior femoral condyle are thought to be important structural features that contribute to patella stability. The purpose of the current study was to determine which anatomical characteristic of the distal femur (the depth of the trochlear groove or the height of the lateral anterior femoral condyle) better correlates with patella alignment (lateral patella displacement and lateral patella tilt) as assessed using MRI.

METHODS

Thirty-six females participated in this study. Eighteen of the participants had a diagnosis of patellofemoral pain, while the remaining subjects were pain-free. A 1.5T MR system (General Electric Medical Systems, Milwaukee,WI) was used to obtain axial plane images of the patellofemoral joint, using a fat suppressed FSPGR pulse sequence. The image field of view was 20 cm x 20 cm and the slice thickness was 2 mm. Each subject was imaged at four knee flexion angles (0^o, 20^o, 40^o, 60^o). A nonferromagnetic loading device permitted imaging to be performed during unilateral knee extension in the supine position (25% of body weight).

Measures of patellar alignment and femoral trochlear geometry were examined on the image containing the widest patella. Lateral patella displacement was quantified using the bisect offset (BSO; Figure 1a) [3]. Lateral patella tilt was assessed using the patella tilt angle (PTA; Figure 1b) [4].

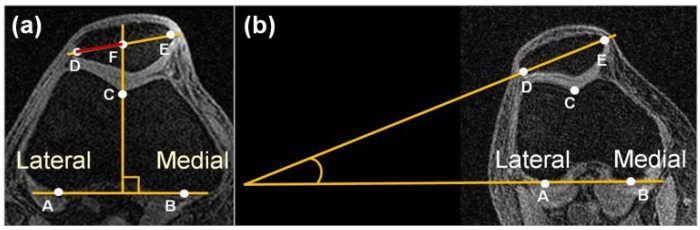

Figure 1: Measurements of patellar alignment. (a) Bisect offset. (b) Patella tilt angle

The depth of the trochlear groove was measured using the sulcus angle (SA; Figure 2a) [5]. The height of the lateral anterior femoral condyle was measured using the lateral trochlear inclination angle (LTI; Figure 2b) [6]. The within-day and between-day intra-rater reliability for all the measurements was determined to be excellent (ICC's ranging from 0.90-0.99).

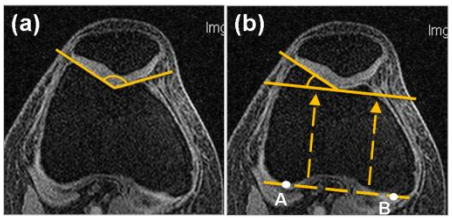

Figure 2: Measurements of femoral trochlear geometry: (a) Sulcus angle. (b) Lateral trochlear inclination.

Pearson correlation coefficients were used to examine the association between measures of patella alignment and femoral trochlear geometry. This analysis was performed at each knee flexion angle.

RESULTS AND DISCUSSION

Pearson correlation coefficients revealed significant correlations between LTI and patellar alignment across all flexion angles (Table 1). No significant correlations were observed between the SA and measures of patellar alignment for any knee flexion angle (Table 2).

The association between LTI and patellar alignment was stronger at higher knee flexion angles. This finding can be explained by the fact that the contact between the patella and the lateral femoral trochlea increases as the knee flexes. In contrast, the sulcus angle takes into consideration the shape of the entire femoral trochlea (including the medial anterior femoral condyle). The fact that the patella gets pulled laterally with quadriceps contraction (owing to the quadriceps angle), suggests that the lateral femoral is more important than the medial anterior femoral condyle in providing patella stability.

CONCLUSIONS

The findings of this study suggest that the geometry of the lateral anterior femoral condyle is better associated with patellar alignment than the geometry of entire trochlear groove. As such, the lateral trochlear inclination angle should be used to evaluate potential structural factors that may underlie patella malalignment in persons with patellofemoral pain.

REFERENCES

1.Powers CM. *Phys Ther* **80**, 965-973, 2000.
2.Harbaugh CM, et al. *J Orthop Res*, DOI 10.1002/jor.21101, 2010.
3.Brossmann J, et al. *Radiology* **187**, 205-212, 1993.
4.Sasaki T, et al. *Int Orthop* **10**, 115-120, 1986.
5.Brattstrom H. *Acta Orthop Scand* **68**,85-138, 1964.
6.Carrillon Y, et al. *Radiology* **216**, 582-585, 2000.

Table 1: Pearson correlation coefficients (*r*) for lateral trochlea inclination and patellar alignment

	Knee flexion angle			
	0°	**20°**	**40°**	**60°**
BSO	-0.48**	-0.60**	-0.61**	-0.62**
PTA	-0.37*	-0.50**	-0.52**	-0.69**

BSO: bisect offset; PTA: patellar lateral tilt angle; *$p < 0.05$; **$p < 0.01$

Table 2: Pearson correlation coefficients (*r*) for sulcus angle and patellar alignment

	Knee flexion angle			
	0°	**20°**	**40°**	**60°**
BSO	0.17	-0.04	-0.02	0.13
PTA	0.09	0.01	-0.05	0.25

BSO: bisect offset; PTA: patellar lateral tilt angle

AN INTEGRATED MODELING METHOD FOR BONE STRAIN ANALYSIS

[2]Daniel Leib, [1]He Wang, [2]Eric L. Dugan
[1]Ball State University, Muncie, IN, USA
[2]Boise State University, Boise, ID, USA
email: danleib@boisestate.edu

INTRODUCTION

Stress fracture is a common overuse injury experienced by participants of activities involving repetitive loading such as running and loaded walking. One population especially susceptible to this type of injury is US ARMY recruits. The incidence of stress fracture during basic training is about 6% in recruits [1] with the most common site of fracture being the tibia; these tibial stress fractures account for more than 40% of total stress fractures in the military [2,3].

The precise cause of tibial stress fracture remains elusive despite considerable research on the subject [4]. One cause of this ambiguity may be the use of surrogate variables instead of the root mechanical causes of bone microdamage such as deformation. Since gathering bone strain data *in vivo* in large populations has inherent limitations, it is useful to explore musculo-skeletal modeling techniques that can be used to investigate changes in bone strain response across different individuals. The goal of this project was to develop a set of methods capable of generating strain data for large cohorts of subjects.

METHODS

Five subjects (demographics) were used from a larger cohort of subjects whose data were collected for a concurrent project. Walking data were collected for unloaded walking at 1.67 m/s on an AMTI force instrumented treadmill with kinematics collected using 12 Vicon F-series cameras at 120Hz and ground reaction forces collected at 2400Hz (AMTI, Watertown, MA, Vicon, Oxford, UK). Bone geometries were obtained using computed tomography (CT). These images were segmented and 3D geometry files were generated in Materialise MIMICS 13.0 (Materialise, Leuven, Belgium).

These 3D surface geometries were used in MD MARC 2008 (MSC.Software, Santa Anna, CA) to build hexmesh finite element (FE) models with generic linear isotropic material properties of elastic modulus 17GPa, density 1.9g/cm^3, and Poisson's ratio of 0.3. These tibia models were then imported into a scaled LifeMOD musculo-skeletal model.

Once positioned, spatial coordinates of muscle model markers representing origins and insertions as well as joint positions relative to the tibia were exported. The exported position data were used to build new FE tibias incorporating massless rigid body links between muscle and joint attachment points using a custom Python script (version 3.0). Boundary conditions were assigned as rotational and translational degrees of freedom of the nodes representing the ankle and knee joint centers and flexible bodies (modal neutral files) were generated for use in LifeMOD.

For a full description of LifeMOD modeling methods and the use of flexible bodies, see Al Nazer [5]. Key differences between the current study and that of Al Nazer et al include a larger number of muscle actuators on the leg that includes the flexible tibia , subject specific segment scaling based on joint center calculations, ground reaction forces, and subject specific tibial geometries generated from CT scans.

In order to build a muscle and joint actuated subject specific model, a static lower body model was first built using subject sex, mass, and height as scaling inputs into the GeBOD [6] database incorporated into LifeMOD. Segments and joint locations and orientations were then scaled using joint center data calculated in Visual3D. Once a scaled model was built, experimental kinematic data were then used to perform an inverse

kinematic (IK) analysis. The results of this analysis were used to "train" the muscle (right leg) and joint (left leg) PID controllers used to actuate the model in a forward dynamics (FD) analysis. Flexible tibias were then imported into LifeMOD.

A FD analysis was then performed with the addition of ground reaction forces applied to both feet and motion capture kinematics disabled. Maximum principle, minimum principle, and maximum shear strain values were then calculated using the Durability plug-in for MD ADAMS/View for the nodes most closely representing the location of the strain staples used in *in vivo* studies [5,7,8,9] (MSC. Software, Santa Ana, CA).

RESULTS AND DISCUSSION

The averaged results for a preliminary analysis of 5 subjects are presented in Table 1. Maximum principle and minimum principle strains and strain rates appear to be consistent with previously reported values, though maximum shear strain and strain rate values for these 5 subjects are markedly lower. Further analysis is needed to determine if these differences are due to modeling methods or to differences in experimental protocols, specifically treadmill versus over-ground walking.

In summary, the methods used in this study provide a promising means of investigating tibial strain and strain rate across individuals and conditions. Since these methods do not require the use of invasive bone staples, more diverse populations and conditions can be studied in the future.

REFERENCES

1.Brukner, P., et al. *Stress fracture*, 1999
2.Beck, T.J., et al. *J. of Bone and Mineral Res.* **11**, 645-653, 1996.
3.Winfield, A.C., et al. *Military Medicine*. **162**, 698-702, 1997.
4.Brukner, P., et al. *Stress Fractures*, Blackwell Science Asia Pty Ltd, 1999
5.Al Nazer, R., et al. *Multibody Systems Dynamics* **20**, 287-306, 2008.
6.Cheng, H., et al. *Proceedings of the 15th Southern Biomedical Engineering Conference*, Dayton, OH, USA, 1996.
7.Lanyon, L.E., et al. *Acta Orthop. Scand.* **46,** 256-268, 1975.
8.Burr, D.B., et al. *Journal of Bone and Joint Surgery* **82**, 591-594, 2000.
9.Milgrom, C., et al. *Journal of Biomechanics* **40**, 845-850, 2006.

ACKNOWLEDGEMENTS

Funding source: Department of the Army #W81XWH-08-1-0587

Ed Rezer of Device Analytics for FE analysis support

Table 1: Averaged Strains and Strain Rate Comparisons

	Strain (Microstrain)			**Strain Rate (Microstrain/s)**		
	Max Prin	**Min Prin**	**Max Shear**	**Max Prin Rate**	**Min Prin Rate**	**Max Shear Rate**
Lanyon et al[7]	395	-434	829	Not reported	-4000	Not reported
Burr et al[8]	437	-544	871	11006	-7183	16162
Milgrom et al[9]	840	-454	1183	3955	-3306	10303
Al Nazer et al[5]	305	-645	948	4000	-7000	10000
Present Simulation	526	-531	426	5042	-2548	3062

FINITE ELEMENT PREDICTION OF SURFACE STRAIN AND FAILURE LOAD AT THE DISTAL RADIUS USING SIMPLIFIED BOUNDARY CONDITIONS

W. Brent Edwards and Karen L. Troy

[1]University of Illinois at Chicago, Chicago, IL, USA
email: edwardsb@uic.edu, web: http://www.uic.edu/ahs/biomechanics

INTRODUCTION

In an effort to improve bone strength and prevent fracture at the distal radius, we have developed a mechanical loading intervention in which females cyclically load their forearm. To relate the applied stimulus with the bone adaptation response, an accurate characterization of the mechanical environment within the bone must be known. Finite element (FE) models have been an effective tool for both strain and fracture-risk assessment. An ideal model would simulate physiological loading scenarios with simplified boundary conditions, allowing for computationally efficient strain determination for numerous subjects. We are also interested in the ability of the FE method to predict fracture strength as a means to assess the effectiveness of our loading protocol. Here, we compared experimental surface strains and fracture loads with specimen-specific FE models for the purpose of validating our simplified boundary conditions and model generating algorithm.

METHODS

Five freshly frozen female cadaver forearms (mean age 78 yrs, range 59-93 yrs) were obtained for this study. Specimens were stored at -20 °C, but thawed to room temperature for: 1) computed tomography (CT) data acquisition (voxel size: 625 x 234 x 234 µm), 2) specimen preparation, and 3) testing.

Specimens had radial/ulnar osteotomy 14 cm proximal to Lester's Tubercle; the proximal most 8 cm of the forearms were embedded in polymethylmethacrylate (Fig 1). Six strain gage rosettes (Micro-Flextronics Ltd, Coleraine, N. Ireland) were adhered circumferentially to the periosteal surface of the radius (3 distal & 3 proximal; Fig 1). Prior to strain gage attachment the periosteum was removed, the surface was cleaned with isopropyl alcohol, sanded, and recleaned with isopropyl alcohol.

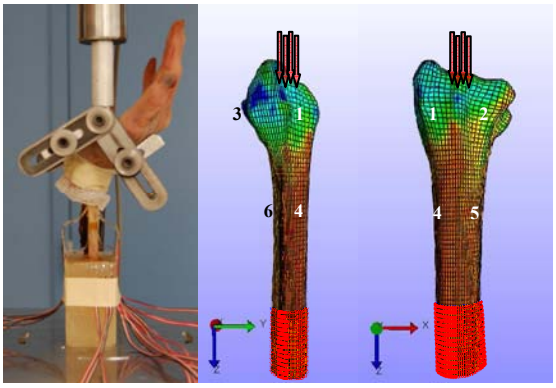

Figure 1: Left – experimental set-up. Center and Right – sagittal and frontal views of FE model illustrating strain gage locations and simplified boundary conditions.

For strain assessment, specimens were loaded in compression under displacement control (0.1 mm/s), to 300 N (MiniBionix 858, MTS Systems, Eden Prairie, MN). Force was applied to the palm with the hand extended 60° to simulate falling conditions [1]. Following five trials to 300 N, the specimens were loaded in the same configuration until failure occurred, as indicated by a rapid decrease in the force/displacement curve and (usually) an audible crack. After testing, dissected cross-sections were overlaid with CT images to determine FE nodes associated with strain gage location.

Stereolithographic models based on segmented CT data were imported into IA-FEMesh (University of Iowa, Iowa City, IA) for FE model creation. The models consisted of 15,763 ± 2,478 8-node hexahedral elements with 18,198 ± 2,700 degrees of freedom depending on specimen size. A nominal element size of 1 mm^3 was chosen in accordance with a mesh convergence analysis. Models were assigned inhomogeneous linearly-isotropic material properties based on relationships between Hounsfield units, apparent density, and Young's modulus [2]. Moduli were binned to 230 ± 4 values

ranging from 0.02 to 20,900 MPa, each having a Poisson's ratio of 0.4.

Finite element analyses were performed using FEBio software (Musculoskeletal Research Laboratories, Salt Lake City, UT). The proximal end of the radius was fully constrained at the location of potting. A ramped quasi-static load of 300 N was distributed over four nodes in the center of the radial articular surface. The unit vector of the applied load was based on an unsymmetrical beam theory analysis using proximal strain gage rosette information and CT data. Modeled and experimentally determined principal strains at 300 N were compared using simple linear regression.

Failure was simulated with a ramped load to 3 kN. Failure was predicted using distortion energy (DE) failure theory [3]:

$$(\sigma_{1i}-\sigma_{2i})^2+(\sigma_{2i}-\sigma_{3i})^2+(\sigma_{3i}-\sigma_{1i})^2 \geq 2\sigma_{yi}^2,$$

where σ_{1i}, σ_{2i}, and σ_{3i} are the principal stresses and σ_{yi} is the yield strength for the i^{th} element. Element yield strengths were proportional to Young's modulus [4]. Fracture was assumed after a contiguous volume of 350 mm^3 had failed [3].

RESULTS AND DISCUSSION

A significant correlation between modeled and experimental strains was observed (r = 0.82, SE = 140 με, $p < 0.001$). When separate regressions were run for proximal and distal gage locations, a strong correlation was observed for proximal locations (r = 0.97, SE = 51 με, $p < 0.001$; Fig 2). The respective correlation for the distal locations was more moderate (r = 0.79, SE = 171 με, $p < 0.001$; Fig 2).

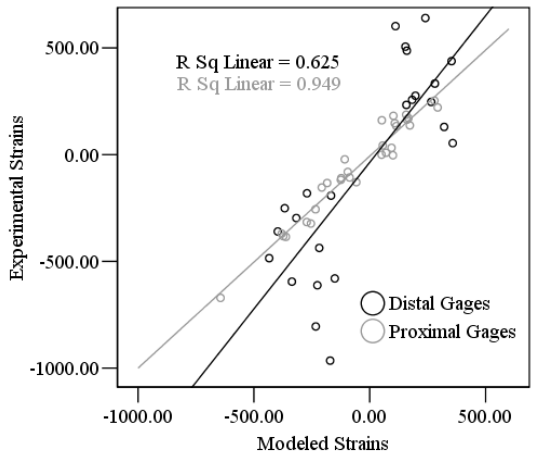

Figure 2: Experimental vs. Modeled strains (με).

The accuracy in predicted strain is dependent on how well our FE model represents both the structural characteristics and boundary conditions of the radius. The distal radius predictions were more sensitive to the simplified loading scenario because of their close proximity to the articular surface. However, distal strain gages would also be more influenced by bony imperfections that can act as stress risers. In these circumstances the FE model could be more indicative of the general strain environment underneath the gage locations.

Of the five specimens loaded until failure, three fractured at the distal radius (mean failure load 999 ± 202 N). The DE theory overestimated failure by 163 ± 76 %. Similar overestimations were obtained using other stress- and strain-based failure theories such as Coulomb-Mohr, modified Mohr, max normal strain, and strain energy density. In an effort to determine radius failure load under non-physiological loading conditions, the ulna and all soft tissue were removed from one of the unfailed radii. Epoxy putty was formed over the distal articular surface of the radius and left to harden. This allowed for a subsequent mechanical test until failure with a distributed load over the entire distal articular surface. In this scenario, the radius failed at 2,344 N and FE analysis with DE theory estimated failure at 2,266 N; a 3 % difference.

CONCLUSIONS

The present study has shown that simplified boundary conditions, along with our model generating algorithm, provides realistic measures of radius bone strain under physiological loading conditions. Unfortunately, these simplified boundary conditions can lead to an overestimation in radius fracture strength during a simulated fall due to potential disagreements in distal strain distributions. The DE failure theory does however predict fracture under non-physiological loading conditions (e.g. a distributed load over the entire distal articular surface) and can be used as an outcome measure to predict failure strength.

REFERENCES

1.Troy KL & Grabiner MD. *Clin Biomech* **22**, 1088-1095, 2007.
2.Wirtz DC, et al. *J Biomech* **33**, 1325-1330, 2000.
3.Keyak JH, et al. *J Biomech* **33**, 209-214, 2000.
4.Rohl, L, et al. *J Biomech* **24**, 1143-1149, 1991.

DOES FREQUENCY EFFECT FATIGUE FRACTURE OF SPINE MOTION SEGMENTS DURING REPETITIVE LOADING?

[1,2]Sai Vikas Yalla, [1]Naira H Campbell-Kyureghyan

[1]University of Wisconsin-Milwaukee, Milwaukee, WI, USA
[2]email: yalla@uwm.edu

INTRODUCTION

While typical manual material handling (MMH) tasks have lifting rates ranging from 1 to 15 lifts/min, fatigue failure tests of spine motion segments (MSs) were typically performed at frequencies that resulted in equivalent lifting rates from 15 to 120 lifts/min [1,2]. The comparison of frequency effects between prior studies is complicated due to differences in specimen preparation, variation in preload values and loading rates during compressive strength measurement. Moreover, for repetitive tests, between 37 and 100% of the ultimate monotonic compressive strength was used as the repetitive load.

Most previous studies on MS failure due to repetitive loading, performed at relatively high loading rates, found compressive fractures at the end plate intruding into the trabecular bone. The current study investigates the effects of lower frequency loading on the location and type of fracture occurrence in cadaveric spine MSs.

METHODS

38 fresh thoracolumbar spine MSs were dissected from 12 human cadavers whose age ranged from 53 to 91 years. The intervertebral disc grades were classified using a system similar to Friberg and Hirsch 1949 [3]. MSs were positioned at Harrison angles to account for their natural alignment [4]. 18 segments were tested for monotonic compressive failure, defined by a drop in the sustained force, at a rate of 4 mm/hr. Repetitive testing was performed on two randomized groups of 10 segments each (20 MSs total). Each group was tested at one of two frequencies, 0.1 and 0.2 Hz, for a period of 8 hours.

The repetitive load magnitude for each segment was set at 50% of the failure stress from the compressive failure test on a MS from the same spine.

After repetitive loading, the MSs were CT scanned with a slice distance of 0.06 mm by an Actis 220/225 FFi CT/DR system (Bio-Imaging Research. Inc.). CT scans were converted to 3D models using Mimics (Materialise) software. MSs tested for failure and fatigue strength were later dissected by careful incision to the mid transverse plane of the intervertebral disc. The disc was carefully removed and the specimen was examined and inked for any visible fractures on the end plates (Figure 1).

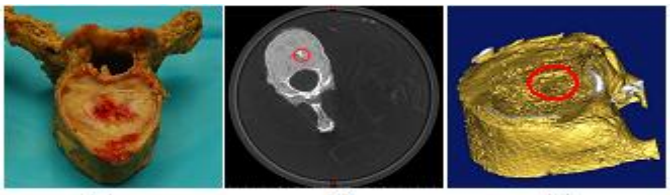

Figure 1. (a) Inked MS with identified damage areas, (b) CT scan, (c) 3D model of MSs showing intrusion of the endplate

Discs, endplates and fractures were photographed, classified and analyzed using a method similar to that used in a fatigue fracture study by Brinckmann 1988 [1]. The location of end plate fracture was determined similar to Adams et al., 2006 [5]. A nested model, which is a special case of a mixed model, was used for statistical analysis at α=0.05.

RESULTS AND DISCUSSION

Visual inspection of 20 MSs prior to the repetitive tests revealed that 55% of the MSs were of Grade 0, 30% were Grade 1 and the remainder were of Grade 2 (mild degeneration).

The majority of superior vertebrae (60%) and inferior vertebrae (80%) in the 0.2 Hz test group had compressive fractures (Table 1) at Location 5. The remaining MSs cycled at 0.2 Hz displayed signs of depression, edge, and anterior-posterior fractures within the superior or inferior sections at Locations 1, 8 and 2. In the 0.1 Hz test group, 70% of both superior and inferior vertebrae had compressive fractures (Table 1) at Location 5. The remaining MSs in that group displayed signs of ring and intrusion fractures within the superior or inferior sections at Locations 2, 8, 6 and 7.

In more than 90% of the MSs, end plate fractures were found on both the superior and inferior endplates at both loading frequencies. The most frequent fracture location in both frequency groups (~70%) was the mid region of the end plate (Location 5). Considering the structure and composition of the intervertebral disc and the end plate, since the applied repetitive loads were at low frequencies, the pressure applied by the nucleus pulposus on the annulus fibrosus and the end plate would result in fractures to the relatively weaker end plate close to the vicinity of the nucleus pulposus.

While all MSs tested for repetitive loading show signs of compressive fractures on the end plate, mixed model analysis of the effect of frequency was found to have no significant ($p>0.05$) effect on either type or location of fracture. Although the fracture types were similar to prior studies, the fractures themselves were not identical to fractures found in prior studies. At the high rates of loading used in prior studies, complete failure or fractures clearly protruding into the cancellous bone were observed, while fractures in the current study were restricted to only the end plate. This could be explained by the reduced velocity effects in the nucleus due to low frequency loading, including lower stiffness and strength, rendering the nucleus unlikely to produce fractures in the bone.

CONCLUSIONS

Loading MSs at typical lifting frequencies found in industry resulted in fractures to the mid-region of the endplates. No significant difference was found between the fracture locations for the frequencies of 6 and 12 lifts per minute. However, a potentially important difference was found when the fracture locations were compared to the results of previous research conducted at higher loading frequencies. At higher frequencies, fractures were found in the cancellous bone as well as the endplate. A recent study by Henschke et al. 2008 [6] on the available literature for screening fractures in patients with low back pain suggest inadequate diagnostics or methodology in accordance with Deyo et al. 1996 [7]. Since endplate fractures are difficult to identify using standard imaging techniques, the current study results suggest that different diagnosis methods may be required for injuries due to activities at typical industrial lifting rates.

REFERENCES

1. Brinckmann P, *Fatigue Fracture of Human Lumbar Vertebrae*. Butterworth, 1988.
2. Gallagher S, *Spine* **32**, 1832 2007.
3. Friberg S, *Acta Orthopaedica* **19**, 222 1949.
4. Harrison DE, *Spine* **26**, e235 2001.
5. Adams MA, *Journal of Bone and Mineral Research* **21**,1409 2006.
6. Henschke N, *Journal of Clinical Epidemiology* **61**, 110 2008.
7. Deyo RA, *Spine* **21**, 2826 1996.

Table 1: Percentage of types of CFT MS fractures with respect to the inferior or superior vertebrae.

Type	0.1 Hz		%	0.2 Hz		%
	Superior	Inferior		Superior	Inferior	
Stellate	2	0	11.1	1	1	11.8
Lateral	0	0	0.0	2	2	23.5
Soft Endplate	1	1	11.1	0	0	0.0
Ring	1	0	5.6	0	0	0.0
Anterior posterior	3	2	27.8	2	3	29.4
Intrusion	3	5	44.4	2	2	23.5
Depression	0	0	0.0	1	0	5.9
Edge	0	0	0.0	1	0	5.9

MECHANICAL LOADING OF THE MOUSE TIBIA STIMULATES LOCALIZED BONE ADAPTATION

[1] Varun A. Bhatia, [1,2]Karen L. Troy
[1]Bioengineering Department, University of Illinois at Chicago
[2]Department of Kinesiology and Nutrition, University of Illinois at Chicago
email: vbhati2@uic.edu, web: http://www.uic.edu/ahs/biomechnics

INTRODUCTION

Mechanical loading of bone stimulates an adaptive response that can result in bone being added or removed from specific regions. Importantly, this type of adaptation can confer greater mechanical benefits to the bone structure than would be expected based on simple measures of bone mineral content or density [1]. This suggests that much of the adaptation occurs on a local structural and material level and may be targeted to mechanically important regions.

Our previous work with a mouse tibia model of bone adaptation has shown that mice experience an acute and temporary decrease in whole bone mineral content (BMC) and mechanical stiffness 10-14 days after initiating a regular novel mechanical loading regime [2]. Our purpose was to detect the specific locations of bone apposition and resorption within the tibiae of mice using micro computed tomography (μCT) imaging. We expected adaptation to occur first in the cancellous regions at the knee and ankle, due to the relatively large surface area available for remodeling. We also expected to observe changes in the mid-diaphysis, due to the natural curvature of the bone.

METHODS

With protocols approved by the Institutional Animal Care and Use Committee, 16 female C57BL/6 mice (age: 18 weeks) were divided into three loading groups: 3-day (8 mice), 7-day (4 mice) and 10-day (4 mice). Prior to any mechanical loading and after sacrifice, both tibiae were scanned using a small animal DEXA (pDXA, Norland, Ft. Atkinson, WI) to measure whole bone BMC. A custom fabricated loading apparatus was used to axially compress the left tibia of each mouse for 50 cycles a day at 0.5Hz (Figure 1), three days per week for the respective number of days. Based on previous data indicating that a rest period between loading cycles can be osteogenic [3], a 15 second rest period was inserted between each loading cycle. The right tibia acted as a within-subject control. After sacrifice, the loaded and the contra-lateral tibiae were dissected for mechanical testing. Whole-bone stiffness was measured in axial compression by applying a ramped load up to 15 N at 8 μm/s.

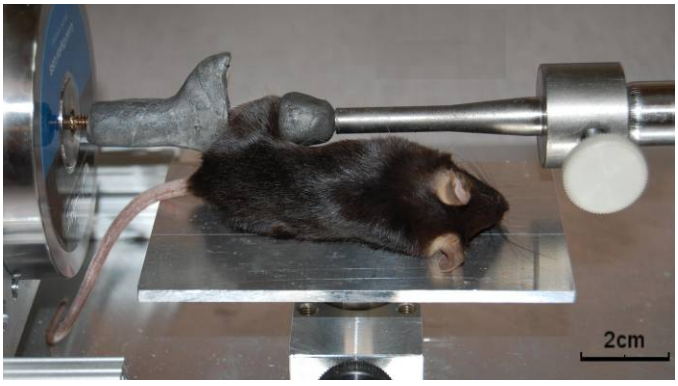

Figure 1 The loading device applies an axially-directed compressive load to the tibia of the mouse

All bones were imaged using a μCT machine (Scanco μ40, Scanco Medical AG, Switzerland) with a 20 μm voxel size. The μCT images were analyzed using Scanco analysis software to obtain whole bone mineralized tissue density (ρ_{tiss}; g/cm^3), BMC (g), trabecular number (1/mm), trabecular thickness (mm) and trabecular spacing (mm). Sectional BMC, ρ_{tiss}, volume (mm^3) and bone volume fraction (BV/TV; mm^3/mm^3) were calculated for 1 mm thick sections through the length of the bone and the principal mass moments of inertia were calculated for the whole bone using a custom code in Matlab (MathWorks, MA).

Planned comparisons included paired t-tests for post-loading loaded versus non-loaded limb for the different parameters for the 3-day group. Due to the small sample size, Cohen's d (effect size) rather than a t-statistic was calculated in the loaded versus non-loaded limbs for the 7- and 10-day groups.

RESULTS AND DISCUSSION

Whole bone BMC of the loaded limb measured using DXA, decreased 1mg compared to the non-loaded limb (d=-1.225) for the 10-day group. Loaded limb stiffness decreased 12.7N/mm compared to non-loaded limb in the 7-day group (d=-1.335) and 7.1N/mm in the 10-day group (d=-0.898). This is in agreement with our previous data [2] which showed a decrease in both BMC and stiffness around 10 days after the start of loading.

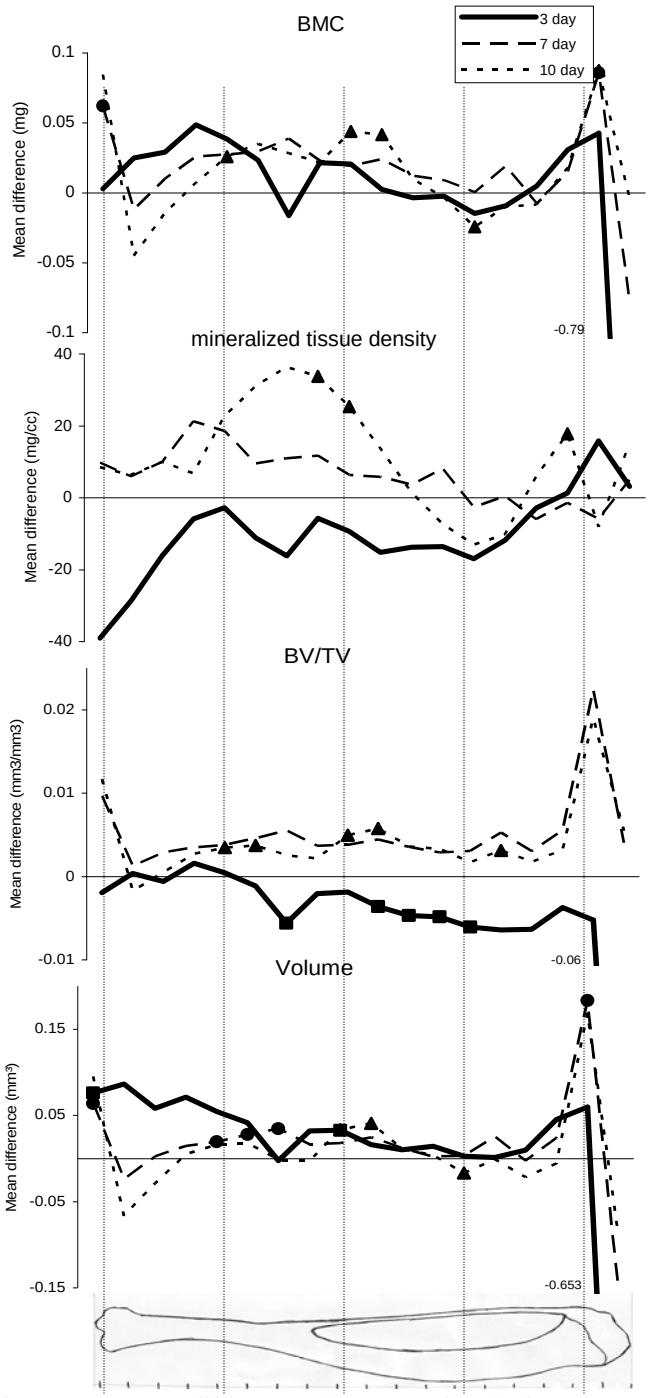

Figure 2 Mean difference between loaded and non-loaded limbs for BMC, ρ_{tiss}, BV/TV and volume, at different sections of the bone, for the three groups. ■, ● and ▲ indicate effect sizes greater than 0.7 for the 3, 7, and 10-day groups.

The largest changes appeared to be localized to the trabecular regions of the bone. The 3-day loaded limb showed a significant increase in trabecular spacing (p=0.034) compared to the non-loaded limb. In the 10-day group we observed a 0.1/mm increase in trabecular number (d=0.927) and a 0.17mm decrease in trabecular spacing (d=-0.854) for the loaded vs. non-loaded limbs. Together, this indicates that the initial response to mechanical loading is trabecular thinning and resorption (3 days), followed by thickening and the formation of additional trabeculae during the following week.

Figure 2 shows the mean difference between loaded and non-loaded limbs at serial locations within the bone as measured by μCT. Although the 3-day mice did not show any changes in BMC or ρ_{tiss} there was a marked decrease in the BV/TV of the loaded bones. For the 10 day group, we observed an increase in BMC, ρ_{tiss} and BV/TV for the loaded limb. The changes were observed either at the distal and proximal ends where there is a large amount of trabecular bone, which has a greater surface area available for turnover, or regions that would be expected to experience larger strains during the mechanical loading intervention due to the inherent shape of the bone.

We observed no correlation between mechanical stiffness and any of the other measured parameters in the loaded limb. It is unclear what gives rise to the decrease in mechanical stiffness observed around 10 days. The mid-diaphyseal changes in ρ_{tiss} and especially BV/TV suggest endosteal resorption in the 3-day group, but cortical thickening in the 10-day group at this location. Micro-finite element analysis in the future will be useful to link the magnitude of mechanical strain experienced by each region of the bone with a local adaptive response.

REFERENCES

[1] Robling AG, et al. *J Bone Miner Res* **17**, 1545–1554, 2002
[2] Bhatia VA, et al. Proceedings of the Orthop. Res. Soc. #685, 2010
[3] Srinivasan S, et al. J Bone Miner Res **17**, 1613-1620, 2002.

VALIDATION OF A MICRO-CT APPROACH FOR CHARACTERIZATION OF MURINE AND HUMAN BONE IN OSTEOGENESIS IMPERFECTA

[1,2]John Jameson, [1-3]Brooke Slavens, [1,2,4]Robert Molthen, [2,3]Peter Smith, and [1-3]Gerald Harris

[1]Department of Biomedical Engineering, Marquette University, Milwaukee, WI, USA
[2]Orthopaedic and Rehabilitation Engineering Center (OREC), Milwaukee, WI, USA
[3]Shriners Hospitals for Children, Chicago, IL, USA
[4]Zablocki VA Medical Center, Milwaukee, WI, USA
email: john.jameson@marquette.edu, web: http://www.orec.org

INTRODUCTION

Osteogenesis imperfecta (OI) is a rare genetic, musculoskeletal disease characterized by mutations in type I collagen, ultimately leading to abnormal collagen synthesis and assembly [1]. Although it is highly heterogeneous, common symptoms include frequent bone fractures, decreased stature, and progressive spinal and limb deformities. Currently patients are classified into eight clinical groups, where Type III is the most severe form compatible with life. To date, there is little biomechanical data of OI bone. Because of the limited availability and small size of human OI specimens, most research has focused on animal models. One commonly studied murine model of Type III OI is the homozygous *oim* B6C3Fe *a/a-Col1a2*^{oim}/J strain (*oim/oim*). The goal of this study was to validate a system for the evaluation of *oim/oim* and human OI bone samples using micro-computed tomography (μCT).

METHODS

Animals. All animals were obtained from Jackson Laboratory (Bar Harbor, ME) and studies were performed under approval of an Institutional Animal Care and Use Committee (IACUC) protocol. Five *oim/oim* and five wild type (+/+) femora were harvested from male mice and fresh frozen at -70°C until μCT evaluation. Average ages for the *oim/oim* and +/+ strains at tissue dissection were 9 and 10 weeks, respectively.

Imaging. All scans were performed using a μCT system developed at the Zablocki VA Medical Center (Milwaukee, WI) [2]. The system is composed of a 100.50 X-ray source (3-mm focal spot; Comet North America), an AI-5830-HP image intensifier (North American Imaging) coupled to a Silicon Mountain Design SMD1M-15 CCD camera (DALSA), and a specimen micromanipulator stage, all mounted on a precision rail. Femora were thawed, placed in 1.5-mL Eppendorf tubes filled with saline, mounted on the specimen stage, and scanned in continuous mode (33 kVp, 242 μA, 7-frame average) at two magnification levels. Reconstructions were performed using a standard Feldkamp algorithm, with resulting voxel sizes of 17 and 34 μm, corresponding to high and low magnification, respectively.

Geometrical analysis. Cortical and trabecular regions of interest (ROIs) were isolated and analyzed for several structural morphometric parameters using ImageJ (v1.42; NIH) and MicroView (v2.1.2; GE Healthcare). Femoral length was measured using MicroView's line tool. Longitudinal cortical regions were selected from the low magnification scans, where each ROI extended distally 2.5 mm from the femoral midpoint. These regions were analyzed for cross-sectional area (CSA) and cortical thickness (Ct.Th). Cylindrical trabecular regions were located in the high magnification scans just proximal to the distal femoral growth plate, extending proximally 1.5 mm with a diameter of 1 mm. After applying a local threshold (determined using MicroView's auto-threshold option), trabecular ROIs were evaluated for bone volume fraction (BV/TV) and trabecular number (Tb.N), thickness (Tb.Th), and spacing (Tb.Sp).

Statistical analysis. Data from each genotype was pooled and compared for statistical significance using an unpaired student's t-test.

RESULTS AND DISCUSSION

Structural data. Femoral length was not significantly different between the two groups. However, *oim/oim* cortical and trabecular indices were generally inferior to controls (Table 1) and agreed well with OI mouse literature [3,4]. *Oim/oim* cortical geometry was more flattened and ellipsoidal in appearance (Figure 1B). Mid-shaft o*im/oim* cortices showed a 16% reduction in CSA, suggesting decreased resistance to bending loads, as found in a prior study [3]. *Oim/oim* trabecular regions appeared more open in structure (Figure 1B). This was confirmed by our findings of significantly reduced BV/TV and Tb.N, with a corresponding increase in Tb.Sp (Table 1). These results agree with prior findings that OI mice have decreased trabecular bony tissue that is also of reduced mechanical viability [3,4].

Extension to human OI bone. After establishing agreement with murine literature, we applied our methods to a human OI bone specimen. Pediatric OI patients suffer frequent fractures that require routine surgical intervention. Small bone fragments are often removed during these procedures. One such specimen was collected (under written consent and IRB approval) and fresh frozen until μCT imaging was conducted. The bone was scanned at 24-μm voxel resolution and analyzed using similar methods to the animal study. The wedge-shaped sample was composed almost exclusively of trabecular bone (Figure 2); thus, only applicable parameters were calculated. Surprisingly, the specimen showed increased BV/TV and Tb.N, but decreased Tb.Sp (Table 1) compared to healthy femoral head tissue [5]. One possible explanation is that this patient was treated with bisphosphonates, which have been shown to have similar effects in murine studies [3,4]. To our knowledge, this is the first application of μCT to determine morphometric parameters in human OI bone.

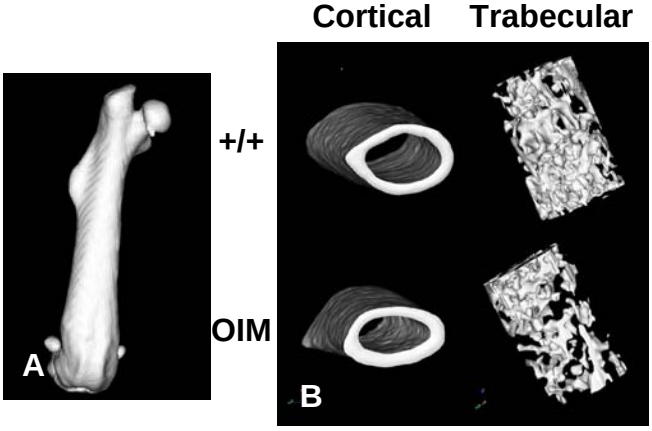

Figure 1: Representative surface-shaded renderings of mouse femora from μCT data. (A) Whole femur. (B) Cortical and trabecular ROIs.

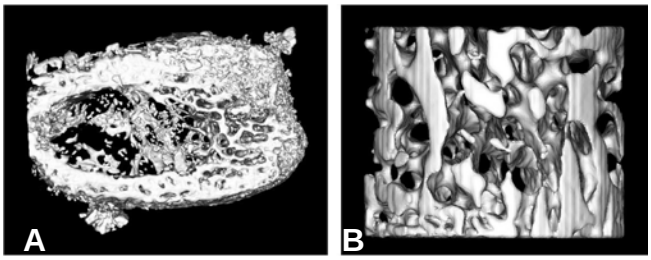

Figure 2: Human OI bone sample. (A) Wedge-shaped specimen with dimensions 10.5 x 6.25 x 5.56 mm. (B) Cylindrical trabecular ROI with 3-mm diameter and 2.5-mm height.

REFERENCES

1. Chiasson RM, et al. *Interdisciplinary treatment approach for children with osteogenesis imperfecta,* Shriners Press, 2004.
2. Karau KL, et al. *Am J Physiol* **281**, H1447-H1457, 2001.
3. Misof BM, et al. *Bone* **36**, 150-158, 2005.
4. Uveges TE, et al. *JBMR* **24**, 849-859, 2009.
5. Hildebrand T, et al. *JBMR* **14**, 1167-1174, 1999.

ACKNOWLEDGEMENTS

This work was supported by OREC, the Dr. Ralph and Marian Falk Medical Research Trust, and NIDRR Grant H133G050201.

Table 1: Summary of calculated bone parameters.

Genotype	Morphometric Parameters					
	CSA (mm^2)	*Ct.Th (mm)*	*BV/TV*	*Tb.N (mm^{-1})*	*Tb.Th (mm)*	*Tb.Sp (mm)*
Control (+/+)	0.87 ± 0.15	0.20 ± 0.03	0.25 ± 0.05	6.89 ± 1.71	0.036 ± 0.006	0.12 ± 0.04
Oim/oim	**0.73 ± 0.10**[*]	0.19 ± 0.01	**0.14 ± 0.03**[†]	**3.67 ± 1.03**[†]	0.038 ± 0.005	**0.28 ± 0.09**[†]
Healthy Human [5]	-	-	0.26 ± 0.08	1.60 ± 0.29	0.194 ± 0.033	0.64 ± 0.11
Human OI	-	-	0.45	2.90	0.154	0.19

[*] $p < 0.06$ between +/+ and *oim/oim*.
[†] $p < 0.05$ between +/+ and *oim/oim*.

THREE DIMENSIONAL FRACTURE MECHANICS OF CERAMIC TOTAL HIP BEARINGS

[1,2]JM Elkins; [1]DR Pedersen; [1,3]JJ Callaghan; [1,2]TD Brown

[1]Department of Orthopaedics, University of Iowa, Iowa City, IA; [2]Biomedical Engineering, University of Iowa, Iowa City, IA; [3]Iowa City Veterans Administration Medical Center, Iowa City, IA

INTRODUCTION

Due to concerns over particle generation in conventional metal-on-polyethylene hip bearings used in total hip arthroplasty (THA), interest in advanced low-wear bearing alternatives, such as ceramic-on-ceramic (CoC) couples has reemerged. While ceramics demonstrate excellent compressive strength, the brittle nature of the material reduces bending strength, sometimes leading to catastrophic fracture when material loads exceed tensile limits. Impingement events lead to stress concentrations at both the site of contact between the neck and liner, as well as the head egress-site (Fig 1). Fractures of ceramic liners have been associated with both these sites [1]. Toward understanding the key biomechanical factors involved, a non-linear 3-D finite element (FE) model for crack growth was thus developed to investigate the effects of malpositioned components on fracture growth propensity during impingement in CoC THAs.

METHODS

FE models were built for two separate kinematic challenges associated with posterior dislocation. The FE models consist of femoral component (28 mm), acetabular liner, rigid metal backing and hip capsule (Fig. 1).

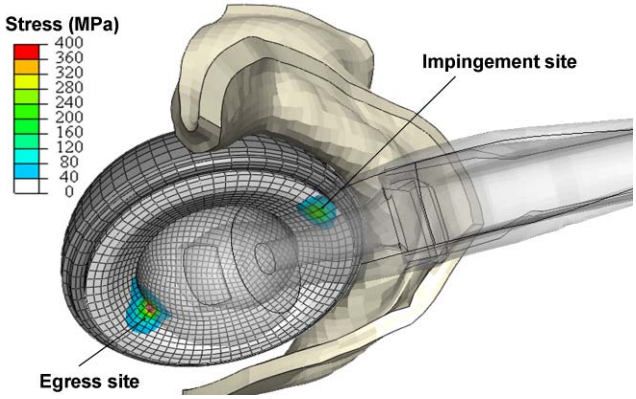

Figure 1: Liner von Mises stresses developed during impingement of a right hip in flexion.

The cup liner and femoral head were modeled as linearly elastic alumina (E=380MPa, ν=0.23) while the femoral neck was modeled as CoCr (E=210MPa, ν=0.3). A total of 92 FE models were run, simulating either a stooping challenge or a sit-to-stand challenge from a normal height (SSN) for various combinations of cup tilt and version. An additional six models were developed for a single orientation (40° inclination, 10° anteversion) simulating additional dislocation-prone maneuvers with inverse-dynamics derived subject kinematics and joint contact forces [2]. These additional maneuvers include rolling over in bed (ROLL), seated leg crossing (SXLG), a sit-to-stand from a low position (SSL), standing shoe-tie (TIE), and a low squatting position (SQUAT) noted to cause CoC fracture in studies of Asian THA patients [3]. Nodal displacements from these 98 models were passed to a fracture-mechanics submodel.

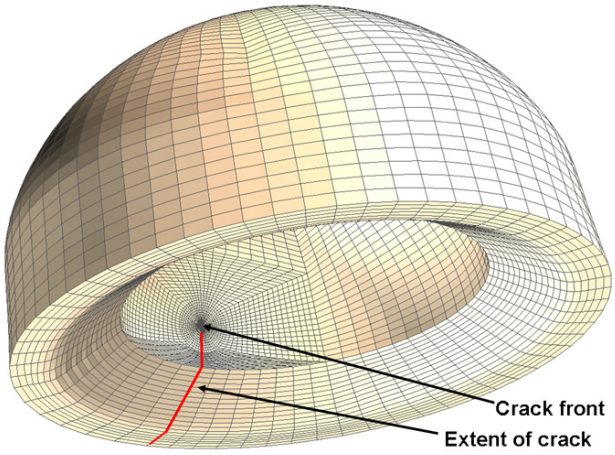

Figure 2: Ceramic liner with fracture located at the egress site, featuring a rosette element structure with singular elements surrounding the entire crack front.

The fracture submodel (Fig. 2) was meshed using Truegrid and custom written Mathcad code to capture the singular stress field at the crack tip using collapsed 20-noded brick elements with quarter-point node spacing. Global models were run with ABAQUS/Explicit while the quasi-static

fracture analysis was analyzed with an ABAQUS/Standard submodeling routine. J-integral contours were evaluated from the interior-most 5 layers of rosette elements around the crack front, from which mixed-mode stress intensity factors (SIFs: K_I, K_{II} and K_{III}) were determined.

RESULTS AND DISCUSSION

Calculated values of tensile-mode stress intensity factor (K_I) were seen to vary approximately linearly with respect to cup inclination and version (Figs. 3-5). Cups with at least 40° of inclination were seen to exceed the reported critical stress intensity factor (K_{IC}) required for crack growth in alumina [ISO 6474].

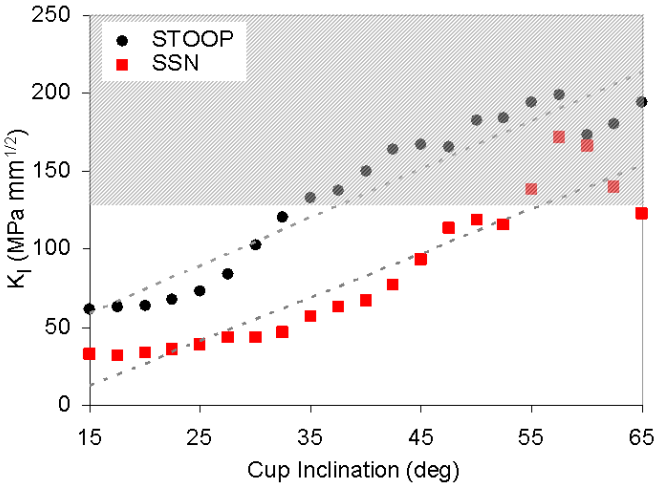

Figure 3: K_I stress intensity factors for both the stoop and sit-to-stand challenges as a function of tilt for a 10° anteverted cup. Gray zone represents critical K_I (K_{IC}) for crack propagation

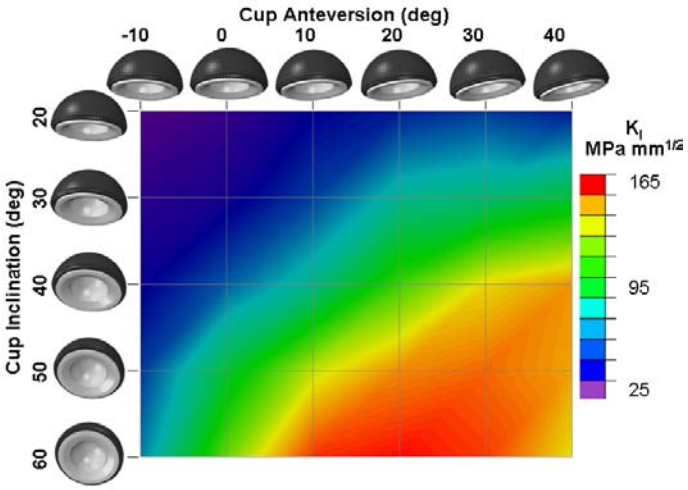

Figure 4: K_I stress intensity factors for the SSN challenge for various combinations of cup inclination and anteversion.

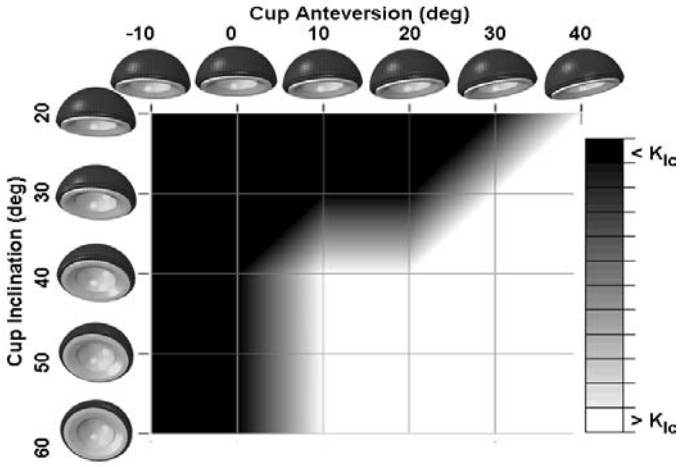

Figure 5: K_I stress intensity factors vs K_{IC} for the stoop challenge. White indicates computed K_I stress intensity factors that exceeds K_{IC}

Three kinematic challenges were seen to cause K_{IC} to be exceeded for a neutral cup orientation (Fig. 6).

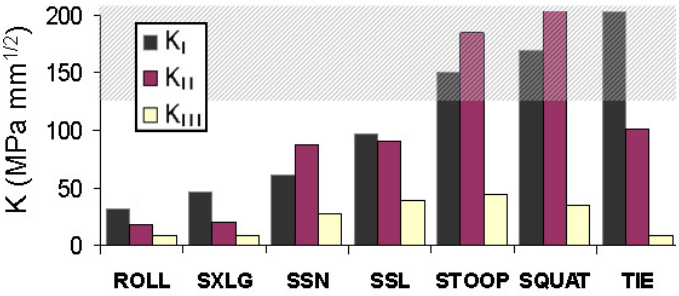

Figure 6: Mixed mode stress intensity factors for 7 dislocation-prone maneuvers.

CONCLUSIONS

Stresses developed during impingement of THA components are seen to be sufficient for crack propagation for CoC bearings, especially for extreme cup orientations. The stoop, squat and shoe-tie maneuvers were particularly deleterious. To the authors' knowledge, this is the first 3D FE fracture analysis of physiologically realistic impingement/dislocation for a CoC THA.

REFERENCES

1. Park YS et al. JBJS 88A: 780-787, 2006.
2. Nadzadi ME et al. J Biomech 36, 577-591, 2003.
3. Ha YC et al. CORR 458, 106-110, 2006.

ACKNOWLEDGEMENTS

Financial support was provided by NIH AR53553 and by the Department of Veterans' Affairs. We appreciate assistance from Drs. Lu Kang and John Yack and Mr. Bhupinder Singh.

MASON II FRACTURES WITH THREE MILLIMETER DISPLACEMENT REQUIRE REDUCTION

[1]Michael Druschel, [1]Gregory Palmer, [1]Mark E Baratz, [1,2]Mark Carl Miller

[1]Allegheny General Hospital, Pittsburgh PA, USA
[2]University of Pittsburgh, Pittsburgh, PA, USA
email: mcmiller@wpahs.org

INTRODUCTION

Open questions remain in the treatment of radial head fractures; in particular, the severity of Mason II fractures requiring operative treatment remains uncertain. Current practice suggests that any Mason II fracture with a displacement of greater than 2 mm requires operative treatment because of deficits in the range of motion, but little evidence documents this thinking. Thus, if a fracture displacement of greater than 2mm does not cause a range of motion deficit, the treatment rationale will require further examination. The Biomechanics Laboratory at Allegheny General has developed the capability of replacing the native radial head with morphometrically correct plastic models. Furthermore, these radial head models can include anatomically appropriate Mason II fracture fragments that can be adjusted to replicate fragment displacements from 1 to 4 mm with or without periosteal attachment. The current research first tested pronation/supination motion with the native radial head, followed by tests of three radial head fracture models with 3 mm displaced fragments. The null hypothesis was that no kinematic differences in pronation/supination would occur.

METHODS

Five cadaveric elbows were tested in a physiologic elbow simulator to study blockage of pronation/supination after Mason II fractures. The simulator applied loads through the tendons of the five major muscles crossing the elbow and operated under servocontrol to actuate the elbow in any combination of pronation/supination and flexion/extension. Load cells monitored all actuation forces, an inclinometer measured flexion angle and a potentiometer quantified pronation - supination.

Radial heads for the recreation of Mason II fractures were formed from CT scans. Using software (Mimics, Materialise Inc.), the radial head was segmented, including the cartilage. The image was imported into SolidWorks (Dassault Sytemes) for manipulation and placement of the virtual fractures. Fracture fragments consisting of one-third of the head and extending past the distal border of the lateral cartilaginous surface were split from the head every 120 degrees around the circumference. Teeth formed on the mating fracture surfaces ensured that the fragment could be positioned 0 – 4 mm distal to the foveal surface and held in place.(s. Figure) A small screw, covered by bone wax after its insertion, held the fragment in place. The three virtual heads (one for each 120 degree increment of fracture location) were then fabricated in a rapid prototyping machine.

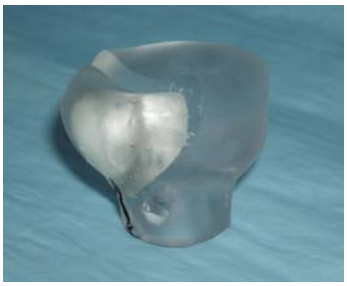

Radial head from rapid prototyping machine with displaced fragment

To replace the native head with an anatomically correct plastic part and preserve the functional native anatomy, a longitudinal osteotomy to remove the lateral half of the distal humerus was performed. The osteotomy extended six centimeters proximally from the lateral border of the trochlear groove. This osteotomy preserved the annular ligament. The osteotomy fragment was returned to its original position by two 2.5 mm screws inserted through lateral-medial holes drilled prior to the osteotomy.

To mount the plastic head in place of the native head, the neck of the radial head fragment included a hole aligned with the canal of the radius for insertion of a short, stepped shaft. A small cross-lock pin held the shaft to the radial head. The native head was removed, carefully identifying its orientation and length, using the surface of the saw cut to assist in placement. The plastic head with the short shaft was inserted into the bone cement-filled canal of the native radius in the exact position as the native head, preserving the original length. After the bone cement set and closure of the osteotomy site, the specimen was ready for testing.

Two types of Mason II fracture were examined. First, a three millimeter displaced fracture that had healed and united was modeled and tested. The fragment was displaced 3 mm, with the rotation constrained by the teeth on its face, and fixed to the radial head with the screw. Second, the experiment modeled and tested a three millimeter displaced fracture that was held in place by incompletely fractured bone and a distal slip of the periosteum. The periosteal fracture model introduced a gap between the fragment and the radial head body by inclusion of a 1 mm spacer over a loosely tightened screw holding the fragment to the head. To model the periosteal attachment, the fragment was also held by a 4-0 suture looped through the fragment's screw hole and tied to the distal rim of the fragment through a 1.8 mm hole.

Fracture sites 120 degrees apart were tested in the five elbows. The first fragment was located just proximal to the biceps tuberosity. The triangle in the accompanying figure shows the orientation of a fragment relative to the tuberosity.

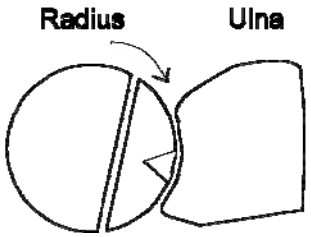

Circumferential location of the fracture

Before replacing the radial head, each elbow was first mounted in the simulator for testing of pronation/supination of the native case. The simulator held the humerus in a clamp while control algorithms caused the forearm to move. The same algorithms worked on the native and the fracture model cases so that identical conditions existed for all tests. The elbow was held at 90 degrees of flexion by the brachialis with a low level of triceps co-contraction. Pronation then occurred with a maximum of 66 Newtons applied to the pronator teres, followed by supination with a maximum of 66 Newtons load applied to the biceps. The test began at neutral, fully pronated, then fully supinated, fully pronated and finally returned to neutral. Three trials of each test were performed. If the load reached 66 Newtons, movement in the current direction ceased, the direction of movement was reversed and the cycle continued until completed.

After testing the native case, the elbow was removed from the simulator, the native head was excised and a model head with no displacement was inserted in order to determine if use of the model itself created a kinematic deficit. The periosteal models were then tested. Finally, the elbow was again dismounted from the simulator, and the models with only the 3 mm displacement were tested. Three trials were performed for all cases.

RESULTS AND DISCUSSION

Kinematic deficits resulted in three elbows. In the three elbows, the average loss of motion was 30 degrees, with supination in two elbows in and pronation in one. In one supination case, an increase in force overcame catching that had occurred. The capitellum was scuffed in two cases. Causes of the deficit were abutment of the fracture face on the ulnar notch and catching on the capitellum.

That three out of five showed functional loss indicates that a fracture with a 3 mm fragment displacement requires surgical intervention. Although it is unclear whether any repair without open reduction is possible, conservative treatment with immobilization might not result in complete functional recover. More specimens and other fracture displacements should be tested to further elucidate the consequences of these fractures.

ACKNOWLEDGEMENTS

The partial support of the Albert J. Ferguson Foundation for Orthopaedic Research is gratefully acknowledged.

DESIGN OF A 1ST METATARSOPHALANGEAL HEMI-ARTHROPLASTY IMPLANT BASED ON MORPHOMETRIC DATA

[1,2]Atul Kumar, [3]Brian Donley, [1]Peter R. Cavanagh

[1]Department of Orthopaedics and Sports Medicine, University of Washington, Seattle, WA, USA
[2]Chemical and Biomedical Engineering Department, Cleveland State University, Cleveland, OH, USA
[3]Department of Biomedical Engineering, Cleveland Clinic, Cleveland, OH, USA
Email: cavanagh@uw.edu

INTRODUCTION

The first metatarsophalangeal joint (MTPJ1) plays a crucial role in many human locomotor movements [1]. When conservative treatments of MTPJ1 pathology fail, a number of surgical options are available including arthroplasty [2-3]. In most MTPJ1 arthroplasty procedures, the distal articulating surface (the proximal 1st phalanx) is maintained, and it is important that the geometry of any metatarsal head replacement be designed with close fidelity to the original metatarsal head. The alignment of the replacement must also be accurate to ensure optimal functionality. In this study, we present a quantitative approach to the design of "hemicap" replacements for the articular surface of the 1st metatarsal head based on an analysis of 3-D scans of osteological specimens.

METHODS

Osteological specimens of the 1st metatarsal and 1st phalanx from the Hamann-Todd collection at the Cleveland Museum of Natural History were scanned using a 3D desktop laser scanner (NextEngine 3D Scanner HD). A total of 97 adult bone sets were scanned (48 male and 49 female sets; age range: 30-50; mean ± SD age: 39.5 ± 5.69 yrs for males and 37.0 ± 5.32 yrs for females; body weight ± SD: 130.2 ± 12.29 lbs for males and 127.0 ± 15.89 lbs for females). Scanned data of bones were aligned to a common reference frame using a two stage process of initial and secondary alignment. During *initial alignment*, three landmark points were identified on each specimen with respect to the anatomical position to create an initial local reference frame (Fig. 1a) for each bone. Template bones were then chosen for men and women separately. From the initial local reference frame of template bones, optimal fit ellipsoids were found for each template bone. This was achieved through the use of an unconstrained non-linear optimization method with a minimization of the cost function; which was calculated from the sum of the squared distance between each point on an ellipsoid and the closest point on the bone. The initial local reference frames for the template bones were then aligned to the local reference frame of the obtained ellipsoid to generate the final local reference frame of template bone. For the *secondary alignment*, the anterior 40% of individual target bones were then aligned to the appropriate template bone using unconstrained non-linear optimization as described above (after first transforming the target bones from the contralateral side by a reflection in the X-Z plane of the initial reference frame) . Each entire target bone was then transformed according to the rotations and translations calculated from the optimization.

The metatarsal head was identified by successive truncation of proximal regions. Radial slices of the MTH were obtained, with cutting planes rotating in increments of 1°, from -10° to 180° with respect to the z-axis, around an axis perpendicular to the X-Z plane at the midpoint of the line between the most superior and inferior points on the metatarsal head (Fig. 1b). Separate rules for trimming the surface were followed in different sectors of the MTH to segment the articular patch. From +10° to 180° on the medial and lateral side, 14% of slice width was trimmed. From -10° to +9°, on lateral side, 14 % of slice width was trimmed. At each degree of increment from -10° to +9°, on the medial side, (100-5× (n-1)) % of slice width was trimmed, where n=1 to21. A quadratic curve was then fitted to each slice. The root mean square (RMS) error, calculated only in the middle one-third of the slice, was

compared with critical residuals from 0.25 mm to 0.65 mm on all slices to identify the inferior extent of the surface. The patch created at the maximum critical residual value, before the crest region begins, was selected as the superior articular surface. An optimal fit sphere was found for each articular patch. The normal distribution curve was then fit to the distribution of the radii of the spheres. Based on the z-score from this fit, bones were divided into three groups for males and females separately: Small (<-1z), Medium (≥-1z and ≤+ 1z), and Large (>+1z). Data from each group were compiled into one set, and a best fit ellipsoid was obtained for each set using the same unconstrained nonlinear optimization method as described above (Fig. 1c). The final step involved extraction of a region from the ellipsoid surface that contained the median of patch dimensions found in a group (Fig. 1d).

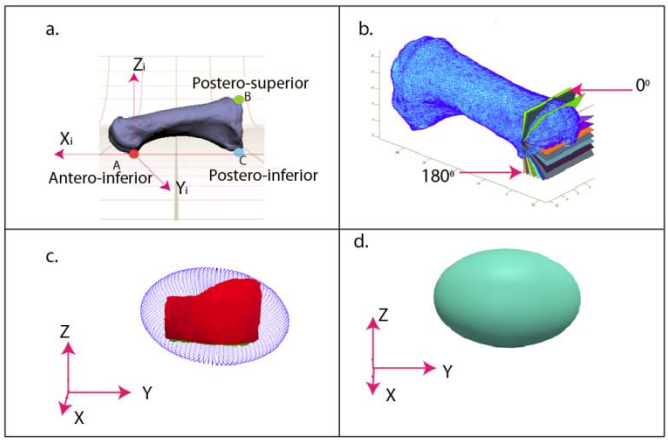

Figure 1: a) Coordinate system of initial alignment b) Cutting planes for metatarsal head. c) Ellipsoid fitted to one of the size group. d) Final implant surface.

RESULTS AND DISCUSSION

The mean radii of the spheres used to divide the size groups were 12.04 ±1.56 mm and 11.12 ±1.25 mm for males and females, respectively.

The final implant on the scanned image of a medium male specimen is shown in Fig. 2. The parameters of ellipsoid, obtained for male and female, are presented in Table 1.

The ellipsoid articulation provides a good contact area through the available arc of motion [4]. The optimization program, used for the secondary alignment and to find the best fit ellipsoid, requires initial parameters which should be close to the actual data values.

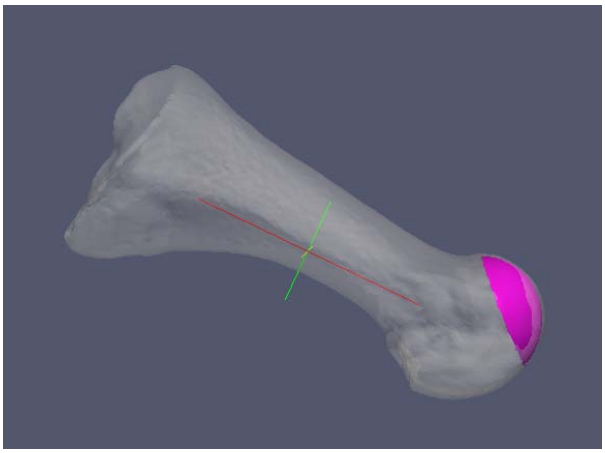

Figure 2: The final implant shown on the scanned image of a medium male specimen.

Table 1: Three semi-axes length (in mm) of ellipsoid for male and female.

	Semiaxis-x	**Semiaxis-y**	**Semiaxis-z**
Male			
Small	7.34	10.65	8.60
Medium	8.11	11.99	9.12
Large	8.47	14.36	10.69
Female			
Small	7.84	9.81	6.85
Medium	7.88	10.61	7.12
Large	8.56	12.78	7.26

CONCLUSIONS

A new method for the design of a partial MTPJ1 arthroplasty was identified based on the congruity of the implant and bones from an osteological collection. This method can be extended to the design of implants for other joints.

REFERENCES

1. Stokes IA et al. *J Anat* 1979; **129**(Pt 3):579-590.
2. Schneider W et al. *Foot Ankle Int* 2002; **23**(4):321-329.
3. Raikin SM et al. *J Bone Joint Surg Am* 2007; **89**(9):1979-1985.
4. Grosland NM et al. *Clin Orthop Relat Res.* 2004 ; **421**:134-142.

THE BIOMECHANICAL EFFECTS OF VARIABILITY IN FEMORAL AND TIBIAL COMPONENT ROTATIONAL ALIGNMENT DURING TOTAL KNEE ARTHROPLASTY IN A SIMULATED OXFORD RIG

[1]Julie Thompson; [2]Michael Hast; [1]Jeffrey Granger, M.D.; [2]Stephen Piazza; [1]Robert Siston

[1]The Ohio State University, Columbus, OH, USA
[2]Pennsylvania State University, University Park, PA, USA
email: thompson.1288@osu.edu

INTRODUCTION

Although total knee arthroplasty (TKA) is generally considered to be an effective intervention for joint diseases such as osteoarthritis (OA), many patients face functional limitations post-operatively [1]. The success of TKA depends on many factors, but it has been suggested that errors in surgical technique are the most common cause for revision TKA and can lead to suboptimal functional performance [2]. Despite this importance of surgical technique, there is significant variability associated with femoral and tibial component rotational alignment in the transverse plane, with errors for femoral component rotation ranging from 13° internal rotation to 16° external rotation [3] and errors for tibial component rotation ranging from 44° internal rotation to 46° external rotation [4]. While malrotation of the femoral and tibial components is a major cause of patellofemoral complications [5] and pain [6], it remains unknown how alignment variability impacts TKA patients' ability to perform activities they deem important.

The purpose of this study was to determine the effects of femoral and tibial component rotational alignment in TKA on quadriceps force, ligament forces, and knee kinematics for two different implant designs during a simulated squatting motion using a forward-dynamic computer simulation of an Oxford Rig.

METHODS

We created a forward-dynamic model of an 'Oxford Rig,' a commonly used cadaveric test, which simulated controlled knee flexion from 20°-120°. The Oxford Rig permits 6-degrees-of-freedom for both the tibiofemoral and patellofemoral joints [7]. Muscular architecture and limb lengths were based on the model described by Delp [8], and a 30 kg mass was placed at the pelvis to simulate ½ body weight. The quadriceps muscles were represented by a single muscle acting along the line of action of the vastus intermedius, and the force necessary to lower the pelvis in a controlled manner was determined using a proportional derivative controller. The PCL was modeled as 10 fibers with slack lengths and attachment points that begin to generate forces at 80° of flexion of a natural knee motion [9]. Contact between the implants was modeled using a rigid body spring model [10]. Knee flexion angles were determined using the convention described by Grood and Suntay [11].

Cruciate-retaining (CR) and posterior-substituting (PS) versions of the same implant (Scorpio; Stryker Orthopaedics) were used in the simulations. Femoral rotational alignment was varied between 15° external rotation and 15° internal rotation in 5° increments. Tibial rotational alignment was varied between 20° external rotation and 20° internal rotation in 5° increments. We investigated the effects of variability in rotational alignment on quadriceps muscle force, collateral ligament forces, and tibiofemoral anterior/posterior translation.

RESULTS AND DISCUSSION

Femoral component alignment, in general, had a much greater effect on all variables of interest than the tibial component alignment or choice of implant design. Additionally, internal rotation of the femoral component yielded more undesirable results than external rotation.

Quadriceps Muscle Force

The quadriceps force required to perform the squatting motion was greatest for the internally aligned femoral and tibial components (Figure 1). For externally aligned femoral components, the

tibial component alignment has little effect on quadriceps force.

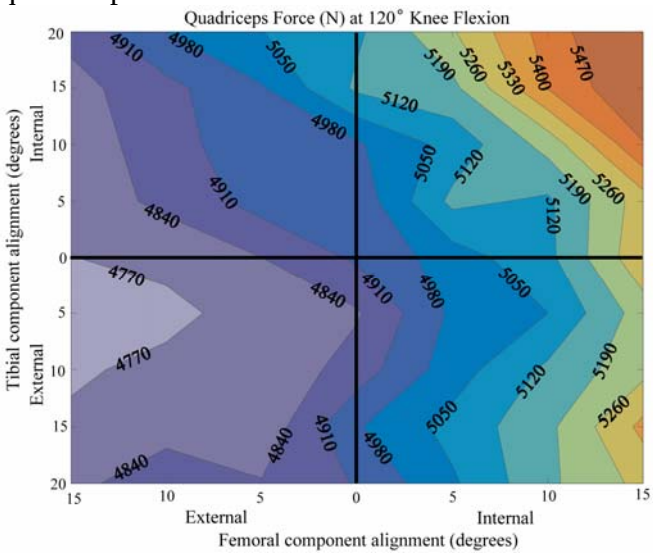

Figure 1: Effect of femoral and tibial component rotational alignment on quadriceps force at 120° knee flexion for the CR implant design. The quadriceps demand was greatest for internal femoral and tibial component alignments.

Ligament Forces

Forces in the Medial Collateral Ligament (MCL) were generated only for internal femoral component alignments of 10° or higher, regardless of tibial component alignment. The MCL force for both implant designs was above a published yield point value of 453 N [12] for the 15° internal femoral component alignment (Figure 2). In contrast, forces in the Lateral Collateral Ligament were never in danger of yielding at any component alignment.

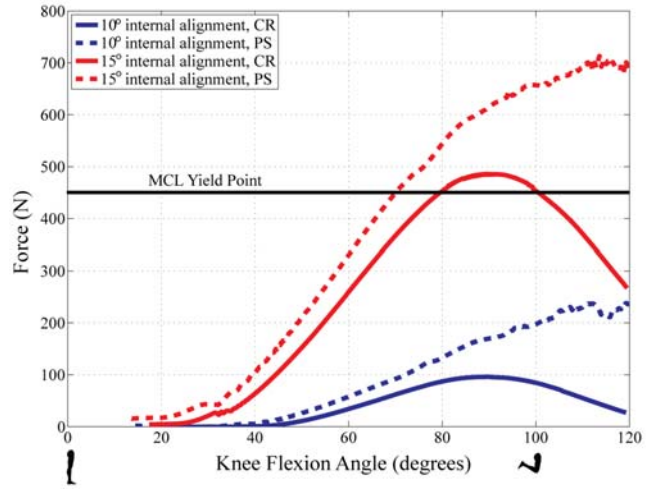

Figure 2: Effect of femoral component rotational alignment on MCL force for the CR and PS implant designs. Force is higher for the PS implant, but is above a yield point value for both implants at 15° internal alignment.

Kinematics

Internal femoral component alignment and external tibial component alignment induced paradoxical anterior femoral translation and also introduced a reversal of the natural "screw-home" motion of the knee (internal rotation of the tibia with respect to the femur during flexion).

CONCLUSIONS

Orthopaedic surgeons are taught to avoid internal rotational alignment of the components, and these results provide one of the first illustrations of how rotational alignment can potentially affect post-operative function. Our findings suggest that internal alignment of the femoral component of greater than 10°, regardless of the tibial component alignment, has a detrimental effect on function during a simulated squatting motion. We saw that large internal alignments of the femoral and tibial components place a greater demand on the quadriceps. Since OA and TKA patients experience significant quadriceps weakness [13], component alignments which increase the required quadriceps force could make functional tasks such as squatting more difficult. Additionally, internally aligned femoral components generated higher forces in the MCL, which would be felt as stiffness by the patients. Finally, our results provide a potential explanation for why a reduced screw-home motion and abnormal anterior femoral translation has been observed in knees following TKA [14]. We believe that a forward dynamic simulation may help us understand the relationship between surgical parameters and the ability to perform important functional tasks and is a key step towards improving patient satisfaction and post-operative performance.

REFERENCES

1. Weiss, J.M., et al. *CORR***,** 172-188, 2002.
2. Stulberg, S.D., et al. *JBJS Am* **84-A Suppl 2,** 90-98, 2002.
3. Siston, R.A.,et al. *JBJS Am* **87,**2276-2280, 2005.
4. Siston, R.A., et al. *CORR* **452,** 65-69, 2006.
5. Dennis, D.A., et al. *CORR***,** 168-176, 1992.
6. Barrack, R.L., et al. *CORR***,** 46-55, 2001.
7. Zavatsky, A.B. *J Biomech* **30,** 277-280, 1997.
8. Delp, S.L., et al. *IEEE Trans Biomed Eng* **37,** 757-767, 1990.
9. Makino,A.,et al. *Arthroscopy* **22,**684.e1-5, 2006.
10. Li, G., et al. *J Biomech* **30,** 635-638, 1997.
11. Grood, E.S., Suntay, W.J. *J Biomech Eng* **105,** 136-144, 1983.
12. Kennedy, J.C.,et al.*JBJS Am* **58,** 350-355, 1976.
13. Mizner, R.L., et al. *JBJS* **87,** 1047-53, 2005.
14. Siston, R.A., et al. *JOR* **24**, 1607-1614, 2006.

TIBIAL TUBEROSITY MEDIALIZATION ALTERS TIBIOFEMORAL KINEMATICS ALONG WITH PATELLOFEMORAL PRESSURE DISTRIBUTION

[1]John Elias, [1]Saandeep Mani, [1]Archana Saranathan, [1]Marcus Kirkpatirck, [1]Laura Gump and [2]Andrew Cosgarea

[1]Akron General Medical Center, Akron, OH, USA
[2]Johns Hopkins University, Baltimore, MD, USA
email: jelias@agmc.org

INTRODUCTION

Medialization of the tibial tuberosity is a popular surgical option for patellofemoral pain related to lateral malalignment. Medialization decreases the lateral component of the force applied to the patella by the patella tendon. In vitro, medialization has been shown to reduce excessive lateral shift and tilt of the patella, as well as decrease the pressure applied to cartilage on the lateral facet of the patella [1]. Reorienting the patella tendon also alters the force applied to the tibia. The current study was performed to characterize the influence of medializing the tibial tuberosity on tibiofemoral kinematics, while also characterizing variations in the pressure applied to medial and lateral patellofemoral cartilage.

METHODS

Tibiofemoral kinematics and patellofemoral pressures were measured in vitro with 10 knees. Each knee was secured to a testing frame with the femur horizontal (Fig. 1). A rod inserted into the tibia was passed through a slotted fixture on the frame to hold the knees at 40°, 60° and 80° of flexion, without constraining the other degrees of freedom for the tibia. The vastus medialis obliquus (VMO), vastus lateralis, vastus intermedius, and the medial and lateral hamstrings were loaded with loading cables and pulleys. The total quadriceps force was 590 N, with approximately 5% of the force applied by the VMO to represent the VMO weakness common in patients with patellofemoral pain [2]. The total hamstrings force was 200 N, divided equally between the medial and lateral hamstrings. For each knee, the tibial tuberosity was osteotomized and secured back onto the tibia with screws. The knees were tested with the tuberosity lateralized from its position on the intact tibia to represent a malalignment condition. The tuberosity was also medialized from the lateral position by 10 mm. The average Q-angles were 20° and 11° for lateral and medial tuberosity positions, respectively.

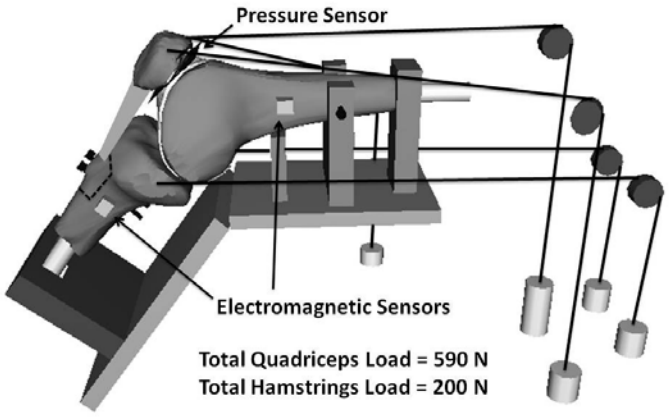

Figure 1: Schematic diagram of test set-up.

Tibiofemoral kinematics were measured with a set of electromagnetic sensors (trakSTAR, Ascension Technology), while the patellofemoral pressure distribution was measured with a thin pressure sensor (I-scan, Tekscan). Electromagnetic sensors were secured to the tibia and femur, with another sensor used to digitize landmarks on the bones to establish the standardized reference frame for quantifying tibiofemoral kinematics [3]. The pressure sensors, which were individually calibrated [2], were inserted into the patellofemoral joint after sectioning the lateral retinaculum. The position of the patellar ridge was palpated on the sensor for each test, in order to distinguish between medial and lateral pressures. At each flexion angle, translations, rotations, and maximum lateral and medial pressures were compared between the lateral and medial tibial tuberosity cases with paired t-tests, with p set to 0.05.

RESULTS AND DISCUSSION

Medializing the tibial tuberosity tended to increase the external rotation, decrease the valgus orientation and increase the lateral translation of the tibia (Table 1). The increase in the average external rotation was approximately 10°, and was significant at each flexion angle. The decrease in valgus orientation was less than 2°, and was significant at 40°. The increase in lateral translation was 1 to 2 mm, but was not significant at any flexion angle

Medializing the tibial tuberosity tended to decrease the maximum lateral patellofemoral and increase the maximum medial pressure (Fig. 2). The decrease in the average maximum lateral pressure was significant at 60° and 80°. The increase in the average maximum medial pressure was significant at 80°. With the tibial tuberosity medialized, the maximum medial pressure was still consistently smaller than the maximum lateral pressure.

The kinematic data complicates planning for tibial tuberosity medialization. The increased tibial external rotation and, to a lesser extent, the increased lateral shift increase the lateral orientation of the patella tendon. Therefore, with the knee loaded, the lateral orientation of the patella tendon is decreased less than planned. In addition, altered tibiofemoral kinematics could adversely influence tibiofemoral pressures. The decrease in valgus orientation could increase the pressure applied to medial tibiofemoral cartilage. The altered rotation will also alter points of tibiofemoral contact during function. Pressure could move into regions of cartilage that have not adapted to repetitive loading, possibly leading to cartilage degradation.

The tibiofemoral kinematic variations do not eliminate the benefit to the patellofemoral joint. Tibial tuberosity medialization reduces the maximum lateral pressure, and the elevated medial pressures do not exceed the lateral pressures. The tibiofemoral kinematic variations may prevent overcorrection of patellofemoral alignment and the pressure distribution.

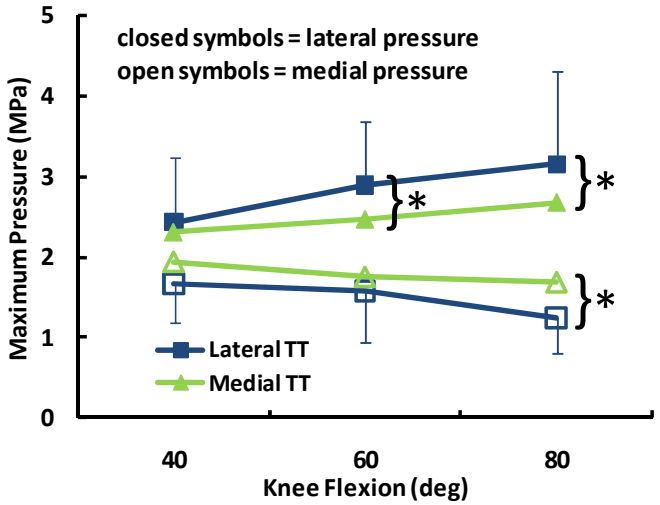

Figure 2: Maximum lateral and medial pressure (± standard deviation) at each flexion angle for the lateral and medial tibial tuberosity (TT) positions. Significant differences are marked with an asterisk.

CONCLUSIONS

Following tibial tuberosity medialization, tibiofemoral kinematic variations reduce surgically-applied changes in the orientation of the patella tendon. The kinematic changes could adversely influence tibiofemoral biomechanics, but do not eliminate the benefit for the patellofemoral joint.

REFERENCES

1. Ramappa AJ et al. *Am J Sports Med* **34**, 749-56, 2006.
2. Elias JJ et al. *J Orthop Res* **27**, 578-83, 2009.
3. Grood ES and Suntay WJ. *J Biomech Eng* **105**, 136-44, 1983.

ACKNOWLEDGEMENTS

NIH/NIAMS 1R03AR054910.

Table 1: Tibiofemoral kinematics (± standard deviation), * indicates significant difference at a flexion angle

	External Rotation (deg)		Valgus Orientation (deg)		Lateral Translation (mm)	
Flexion	**Lateral TT**	**Medial TT**	**Lateral TT**	**Medial TT**	**Lateral TT**	**Medial TT**
40°	-10.8 ± 5.7*	1.9 ± 7.3*	5.6 ± 5.9*	4.0 ± 6.3*	1.3 ± 5.3	3.3 ± 5.4
60°	-4.1 ± 6.8*	5.6 ± 8.0*	4.8 ± 4.4	4.2 ± 4.5	2.4 ± 5.2	3.3 ± 5.8
80°	0.7 ± 8.4*	7.7 ± 8.4*	3.7 ± 4.9	2.3 ± 5.0	0.4 ± 4.7	1.3 ± 6.0

HIGHER ANTAGONIST CO-CONTRACTION IN HAND OSTEOARTHRITIS LEADS TO DETRIMENTAL JOINT MECHANICS

[1]Sang Wook Lee, [2,3]Thomas J. Schnitzer, and [1,4]Derek G. Kamper

[1]Sensory Motor Performance Program, Rehabilitation Institute of Chicago, Chicago, IL, USA
[2]Department of Internal Medicine, Northwestern University, Chicago, USA
[3]Department of Physical Medicine and Rehabilitation, Northwestern University, Chicago, USA
[4]Department of Biomedical Engineering, Illinois Institute of Technology, Chicago, IL, USA
email: sanglee2@northwestern.edu

INTRODUCTION

Hand osteoarthritis (OA) is one of the most common joint disorders in elderly. It often has significant functional consequences, such as reduced mobility, force deficit, and pain [1]. In knee and hip OA, various neuromechanical changes were found to underlie OA development and progression, including muscle incordination [2] and joint malalignment. As of yet, however, many hand OA studies remain 'observational', focusing largely on gross systemic factors such as body weight and occupation. Thus neuromechanical pathways through which disease development or progression may occur remain largely unidentified in hand OA.

Therefore, the aim of this study was to elucidate potential changes in neuromechanics following hand OA and their effects on the disease progression. First, we identified the changes in muscle coordination patterns following hand OA, e.g. increased muscle co-contraction [2]. We then estimated the detrimental effects of the altered neuromechanics in hand OA patients on joint force, an important mechanical factor in OA development and progression.

METHODS

Muscle coordination of hand OA patients

Two subjects with hand OA and two control subjects with no history of arthritic disease participated in the study. Subjects were instructed to first perform maximal isometric finger flexion grasp. An electronic grip dynamometer (Fabrication Enterprise Inc., New York) recorded grip force. Subjects were then asked to generate 25%, 50%, and 75% of their maximal grip force (3 trials/level). Visual feedback of grip force was provided on a computer screen. Electromyographic (EMG) activities of the flexor digitorum superficialis (FDS) and extensor digitorum communis (EDC) muscles were recorded via surface electrodes (Delsys Inc., Boston, MA) throughout each trial. Each EMG signal was rectified and low-pass filtered to create an activation envelope. Activation levels of the two muscles at each task were then represented as a proportion of their maximum activation levels as measured during maximal voluntary contractions of each muscle.

Joint force estimation

For each subject, the proximal interphalangeal (PIP) joint force during the grip task was estimated using a normative biomechanical model that describes the location of the FDS tendon around the joint (Fig. 1) [3]. The PIP joint was chosen as hand OA usually affects the distal and proximal interphalangeal (DIP/PIP) joints of the fingers, as well as thumb carpometacarpal joints.

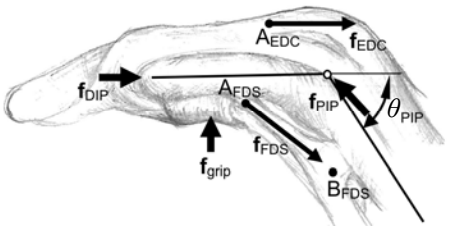

Figure 1: Finger biomechanical model describing tendon forces and grip force orientation and location

The magnitude of the grip force vector, $\|\mathbf{f}_{grip}\|$, was first determined from the recorded grip force. Since FDS and EDC muscle properties of each subject may vary (resulting in different grip force magnitudes), the corresponding muscle forces f_{FDS} and f_{EDC} could not be determined simply from the normative muscle cross-sectional area (CSA) values. We thus employed force and moment

equilibrium equations about the PIP joints in order to estimate tendon forces and joint reaction forces (Fig. 1). Here, we assume that the ratio of the two maximum force magnitudes ($||\mathbf{f}_{FDS}||_{max}$:$||\mathbf{f}_{EDC}||_{max}$) remains similar to the value estimated from their normative CSA values obtained from 21 forearms [4], which is 2.2:1. Tendon location points, A_{EDC}, A_{FDS}, and B_{FDS}, were determined from the normative biomechanical model [4], which also provided the basis for the orientation and application locations of the tendon force vectors, $\mathbf{f}_{EDC}$ and $\mathbf{f}_{FDS}$. The magnitudes of the tendon force vectors, $||\mathbf{f}_{FDS}||$ and $||\mathbf{f}_{EDC}||$, were represented as a proportion of their maximum force, i.e. $||\mathbf{f}_{FDS}||=r_1||\mathbf{f}_{FDS}||_{max}$, and $||\mathbf{f}_{EDC}||=r_2c||\mathbf{f}_{EDC}||_{max}$ (c = 0.5, representing EDC force distribution to central slip; at terminal slip $||\mathbf{f}_{DIP}||= r_2(1–c)||\mathbf{f}_{EDC}||_{max}$). Since the grip task that subjects performed mainly involves isometric flexion of the PIP joint, not the DIP joint, we did not include the contribution of the FDP muscle force to the joint force. Activation levels of the muscles, r_1 (FDS) and r_2 (EDC), were determined from the EMG data obtained from the isometric flexion experiments (e.g. see Fig. 2).

RESULTS AND DISCUSSION

OA patients generally demonstrated much higher co-contraction of antagonist muscle (EDC) across all grip force levels (Fig. 2). Although the subjects were not age-matched, increase in the co-contraction levels for OA subjects (100% – 300%) far exceeded any potential difference due solely to the younger age of control subjects (40% – 80%, [5]).

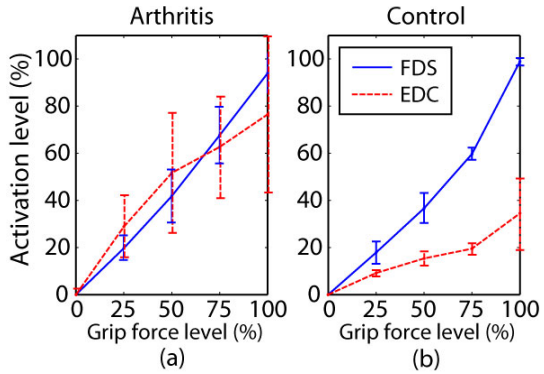

Figure 2: Muscle activation level of agonist (FDS) and antagonist (EDC) in (a) OA patients and (b) control subjects during power grasp.

For each subject, the PIP joint force was estimated from the estimated grip force based on the biomechanical model of the finger (Fig. 1). Even though grip forces generated by OA group were smaller, the estimated internal forces at their PIP joints were much greater compared to those of control subjects (Table 1). Interestingly, increase in joint force was greater at lower force levels; i.e. $||\mathbf{f}_{PIP}||$ increased by 53% at 25% grip force and by 38% at 50% grip force, but only by 3% at 100% grip force. Overall, higher antagonist co-contraction in OA subjects led to an inefficient strategy that created higher detrimental internal force while generating lower end-point (grip) force.

Table 1: Mean grip force magnitudes $||\mathbf{f}_{grip}||$ and the estimated joint force $||\mathbf{f}_{PIP}||$ (OA vs. control)

Grip force level (%)	$||\mathbf{f}_{grip}||$ (N)		$||\mathbf{f}_{PIP}||$ (N)	
	OA	Control	OA	Control
25	50.6	73.3	181	118
50	101.2	146.7	299	217
75	151.8	220.0	346	301
100	202.4	293.4	420	409

The results of this study provide possible explanation to the progressive nature of the disease [6]. Similarly, increased antagonist co-contraction was considered to be responsible for knee OA progression [2]. The reason for the increased co-contraction, however, still remains unclear, although some hypotheses, such as compensating joint laxity, have been postulated. This study suggests that interventions for hand OA should target this detrimental mechanism of increased antagonist co-contraction in order to effectively prevent disease development and stop progression.

Limitations of the study should be acknowledged. First, only a small number of subjects were tested and the two groups were not age-matched. Only the FDS and EDC muscles were considered in the current model. Additionally, some discrepancy could exist between musculoskeletal geometry of the subjects and that of the normative model. Muscle force ratio ($||f_{FDS}||$:$||f_{EDC}||$) might differ from the value estimated from the normative CSA values. A future study that addresses the current limitations would be necessary to confirm the findings of this study.

REFERENCES

1. Kjeken I, et al. *Ann Rheum Dis* **64**, 1633-38, 2005.
2. Lewek M, et al. *Arthritis Rhuem* **52**, 2845-53, 2005.
3. Lieber RL, et al. *J Hand Surg [Am]* **17**, 787-98, 1992.
4. An KN, et al. *J Biomech* **12**, 775-88, 1979.
5. Burnett RA, et al. *J Appl Physiol* **89**, 61-71, 2000.
6. Harris PA, et al. *Osteoar Cartilage* **2**, 247-52, 1994.

PROPRIOCEPTIVE ACUITY IN THE FRONTAL AND SAGITTAL PLANES IN KNEE OSTEOARTHRITIS

Martha Cammarata[1,2] and Yasin Dhaher[1,2]

[1] Department of Biomedical Engineering, Northwestern University, Chicago, IL, USA
[2] Sensory Motor Performance Program, Rehabilitation Institute of Chicago, Chicago, IL, USA
E-mail: m-cammarata@u.northwestern.edu

INTRODUCTION

The initiation and progression of knee osteoarthritis (OA) may be attributed in part to abnormal loading placed on the articular cartilage during everyday tasks. In particular, changes in frontal plane kinetics and kinematics at the knee may be especially detrimental to joint health [1,2]. These abnormal frontal plane loads may be due to decreased passive ligament-capsule stiffness as well as alterations in neuromuscular control. The latter is partially dependent on joint proprioception, or the perception or joint position and movement. Indeed, proprioceptive impairments to knee flexion and extension have been demonstration in people with knee OA [3] and this deficit has been identified as a risk factor for the progression of the disease [4]. However, despite the significant role that frontal plane loading may play in the progression of knee OA, joint proprioception in the frontal plane of the knee and its modulation with OA has not yet been examined. It is unknown if frontal plane knee proprioception is differentially affected by knee OA compared to sagittal plane proprioception.

Accordingly, the aim of this study was to quantify proprioception in both the frontal and sagittal planes of the knee in healthy and osteoarthritic knees. We hypothesize that proprioceptive acuity will be decreased in the knee OA population and that proprioceptive acuity will be increased in the frontal plane compared to the sagittal plane in both groups. If proprioceptive acuity is differentially modulated by knee OA across planes, it may indicate that the disease differentially affects the contribution of specific sensory afferents, which may be the result of disease induced changes in joint mechanics. This investigation may help to elucidate some of the neuromechanical factors that contribute to the progression of the disease.

METHODS

Thirteen persons with knee OA (7 males, 6 females, age mean (SD) 57 (10) years) and ten age-matched healthy control subjects (7 males, 3 females, age 55 (8) years) participated in the study after providing informed consent. Participants in the knee OA group had been diagnosed with unilateral or bilateral tibio-femoral knee OA according to American College of Rheumatology guidelines and presented radiographic evidence of OA in the symptomatic knee(s) with a Kellgren/Lawrence grade of 2 or higher.

The more affected limb of knee OA subjects and the right leg of control subjects were tested. For testing in the frontal plane, subjects were seated in an experimental chair with the knee fully extended. The ankle was placed in an inflated aircast and secured to a servomotor, which rotated into varus and valgus. Brackets were fastened around the knee to prevent translation. In the sagittal plane, subjects were seated in the chair with the knee at 30° of flexion and the servomotor center of rotation was aligned with the femoral epicondyles. Subjects wore headphones and an eyemask to reduce auditory and visual cues.

Proprioception was assessed in varus, vaglus, flexion, and extension using the threshold to detection of passive movement (TDPM), following a protocol similar to previously published reports [3,5]. From the initial posture, the servomotor rotated the knee at a velocity of 1°/s and subjects were instructed to press a handheld button as soon as movement of the limb was detected. TDPM was defined as the position difference between the onset of movement and the subjects' detection of movement. Following familiarization with the protocol, at least five trials were performed in each testing direction in a randomized order. The average

of all trials in each direction was used in further analysis.

To determined the effects of knee OA and movement direction on proprioception, a repeated measures Analysis of Variance (ANOVA) with one between factor (subject group) and one within factor (movement direction) was performed with alpha set a priori at 0.05. Post-hoc Tukey-Kramer comparisons were performed to determine specific differences between groups.

RESULTS

TDPM results indicated decreased proprioceptive acuity in the knee OA group compared to the control group (Figure 1). A significant effect of study group (P=0.02) was detected and post-hoc Tukey-Kramer comparisons showed that TDPM values were significantly larger (indicating decreased proprioceptive acuity) in the knee OA group for all directions tested.

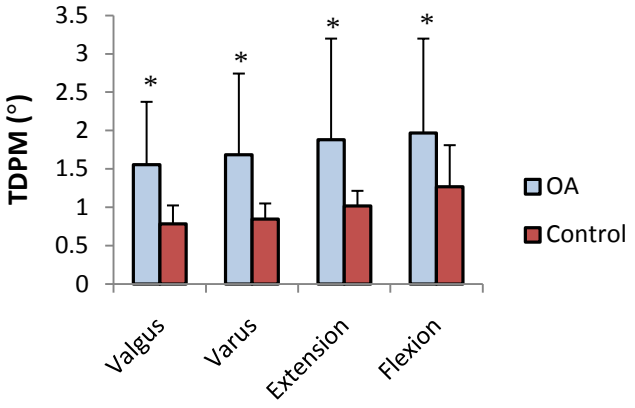

Figure 1: TDPM results (in degrees) for knee OA and healthy control subjects for each direction tested. Error bars represent standard deviation. *Significant difference between OA and control groups (P<0.05)

While on average, TDPM in the frontal plane was decreased compared to the sagittal plane, no significant differences (P>0.05) between movement directions were noted within each study group. Furthermore, the amplitude of difference between groups was consistent across all directions (Table 1).

DISCUSSION AND SUMMARY

Our results indicate that proprioceptive acuity is decreased in knee OA subjects compared to healthy age-matched control subjects equally in both the frontal and sagittal planes of the knee. However, within each group, there were no significant differences noted between movement directions. These results suggest that proprioceptive impairments associated with knee OA are not tissue specific, but rather represent a global decline in prorioceptive acuity. Further, this may signify that assessing TDPM solely in the sagittal plane is a sufficient metric to gauge proprioceptive decline in knee OA.

REFERENCES

1. Jackson, B. D., et al. (2004). *J Sci Med Sport* 7(3): 347-357.
2. Lewek, M. D., et al. (2004). *Osteoarthritis Cartilage* 12(9): 745-751.
3. Pai, Y. C., et al. (1997). *Arthritis Rheum* 40(12): 2260-2265.
4. Sharma, L., et al. (2003). *Arthritis Rheum* 48(12): 3359-3370.
5. Hurkmans, E. J., et al. (2007). *Arthritis Rheum* 57(8): 1398-1403.

ACKNOWLEDGEMENTS

This work was supported by funding from the National Institutes of Health (R01 AR049837), the Arthritis Foundation and the Alpha Omicron Pi Foundation.

Table 1: Difference in TDPM measures between knee OA and Control groups in degrees. Reported as Mean (95% Confidence Intervals)

Frontal Plane			Sagittal Plane		
Valgus	0.78	(0.06, 1.58)	Extension	0.89	(0.19, 1.59)
Varus	0.82	(0.13, 1.69)	Flexion	0.67	(0.04, 1.58)

ROLE OF PROPRIOCEPTION AND FOOT SOMATOSENSATION IN DETECTING SLIPPING ACCIDENTS

[1]Kurt Beschorner, Ph.D., [2]Mark Redfern, Ph.D. and [2]Rakié Cham, Ph.D.

[1]University of Wisconsin-Milwaukee, Milwaukee, WI, USA
[2]University of Pittsburgh, Pittsburgh, PA, USA
email: beschorn@uwm.edu, web: http://www4.uwm.edu/ceas/faculty_profiles/KEBeschorner.html

INTRODUCTION

Falls are a serious occupational and public health problem. Factors that contribute to the initiation and outcome of the slip include environmental (flooring, liquid contaminants, lighting) and person-specific (walking style, anticipation, slip detection and slip response). Generating a timely and effective response to a slip is critical to achieving recovery from the slip [1]. Prior to generating a postural response, the body must first detect that a slip is occurring. Previous research has indicated that degradation in the sensory system due to aging may increase slip risk [2]. The precise sensory systems responsible for detecting slipping, however, are unknown. The purpose of this project is to examine the role of sensory flow from foot somatosensation and lower-body proprioception to detecting slipping events.

METHODS

Data from 17 younger (aged 20-35) and 13 older adults (aged 50-65) was collected and analyzed. All subjects were consented prior to their participation and this research was approved by the University of Pittsburgh Institutional Review Board. Subjects donned a protective harness during all trials. Subjects were informed that the floor would be dry and then completed three dry trials followed by an unexpected slip trial. The unexpected slip was induced by applying a diluted glycerol fluid contaminant onto a force plate. Subjects had a set of 79 reflective markers during testing, which were recorded by motion capture cameras and allowed for the calculation of ankle, knee and hip angles. Slipping trials were categorized by slip severity using the maximum slipping velocity of the heel measured shortly after heel strike, with a threshold of 1.0 $m*s^{-1}$ [3]. Subjects walked across 2 force plates that measured ground reaction forces.

The primary variables of interest were the joint angles both ipsilateral and contralateral to the slip and the normal ground reaction force. The time that a joint angle during a slip deviated from normal walking conditions was determined, and interpreted as the initial time that a slip could be detected by the proprioceptors in that joint. The normal force deviations were interpreted as the time that foot pad somatosensation could detect a slip. The deviation time was calculated between the slip trial and the preceding dry trial. Thresholds for detection were set at 20% of the maximum for normal force, 10% of the range of motion during gait for hip and knee angles and 20% of the range of motion during stance for ankle angles. Deviation times (TimeDev) were calculated as the time after heel strike that the deviation exceeded these thresholds (Fig. 1). Occurrences when the deviation exceeded the threshold at the time of heel contact (pre-deviation; 3/210 occurrences) and when the deviation never exceeded the threshold during the first 450 ms after heel contact (no deviation; 12/210 occurrences) were excluded from the analysis.

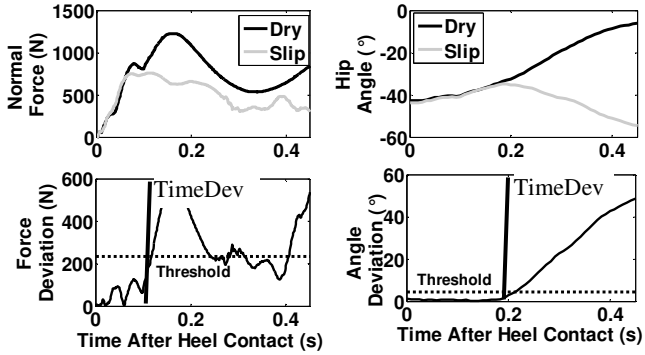

Fig. 1: Normal force (left) and hip angle (right) for a representative subject. The deviation graphs (bottom) indicate when the threshold was exceeded.

An ANOVA analysis was performed with TimeDev as the dependent variable, the sensory system in which the deviation occurred (i.e. joints and foot pad) as a fixed-factor independent variable and subject as a random-independent variable. For each subject, the sensory system that first deviated from baseline conditions was identified (i.e. the sensory system likely responsible for detecting the slip) and the time that the first deviation occurred across all of the sensory systems was identified ($TimeDev_{Initial}$). An ANOVA analysis was performed with $TimeDev_{Initial}$ as the dependent variable, subject as a random independent variable and age group, slip severity and their interaction as fixed-factor independent variables.

RESULTS AND DISCUSSION

Deviation time (TimeDev) differed across the sensory systems ($p<0.001$). Post-hoc (Tukey) analyses reveal that the normal force deviated prior to any of the joint angle measures (Fig. 2) ($p<0.001$). Therefore, foot somatosensation is the first opportunity for detecting a slip.

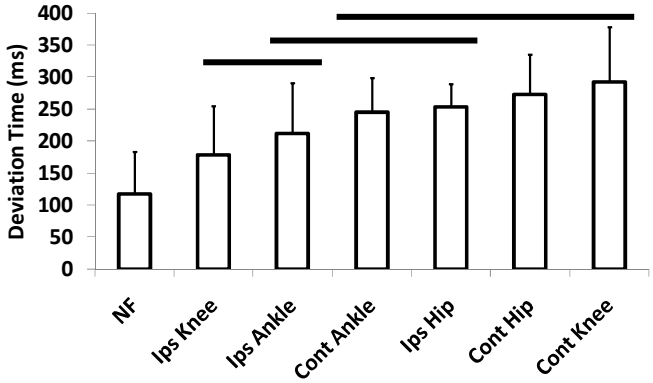

Figure 2: Average deviation times (with standard deviations) for normal force (NF), ipsilateral joint angles (Ips) and contralateral joint angles (Cont). Bars represent non-significant differences ($p<0.05$).

Inspection of the data revealed that 22 subjects experienced initial deviations in foot somatosensation; 4 subjects experienced initial deviations in the knee angle ipsilateral to the slip; 2 subjects experienced deviations in the ankle angle ipsilateral to the slip; 1 subject experienced deviations in the knee and another in the ankle contralateral to the slip.

Neither slip severity, age group or their interaction significantly contribute to the time in which the first system initially deviated from baseline conditions ($TimeDev_{Initial}$). Therefore, the timing in which the flow of sensory information first deviates is not dependent on slip severity or the age of the person.

While this study strongly indicates that foot somatosensation may be critical to the detection of slips, there are other contributing factors that could affect the detection of slipping accidents. This study did not examine other sensory systems that may also play a role in detecting slipping accidents such as the vestibular system. In addition, this study did not examine sensitivity among different sensory systems, which could have been used to define the thresholds for slip detection.

This research may be critical to identifying working conditions and pathologies that affect a person's ability to properly detect and respond to a slipping accident. In particular, cold working conditions may reduce foot somatosensation sensitivity or diseases such as diabetes are known to in some cases degrade foot sensations. Future research intends to focus on the affects of reduced foot somatosensation on the ability to properly respond to slipping accidents.

CONCLUSIONS

In this abstract, foot somatosensation was identified as being potentially critical to the process of detecting and responding to slipping accidents. Person's who have a limited ability to sense foot pressures may have a limited ability to detect a slip and generate an effective postural response.

REFERENCES

1. Tang and Woollacott, 1998, *J. Gerent. A, Biol Sciences Medical Sciences*. 53(6): p. M471-80.
2. Lockhart et al., 2002, *Safety Science*. 40(7-8): p. 689-703.
3. Brady et al., 2000, J. Biomechanics, 33(7): p. 803-8.

ACKNOWLEDGEMENTS

This research was funded by NIOSH grant (R03OH007533 and R01OH007592, PI: Rakié Cham, Ph.D.). Special thanks to Dr. Furman for conducting screenings.

LEARNING UNCERTAIN DYNAMICS FOR POSTURAL CONTROL

[1,2] Alaa A Ahmed and [2]Daniel M Wolpert
[1]Department of Integrative Physiology, University of Colorado at Boulder, USA,
[2]Department of Engineering, University of Cambridge, UK,
email: alaa@colorado.edu

INTRODUCTION

Skilled movement depends upon our ability to control for movement dynamics and predict the consequences of that control. For example, our everyday movements generate forces upon the environment, as well as forces upon our own bodies. When these forces are predictable, voluntary movement is usually preceded by anticipatory postural adjustments (APAs). But we are frequently called upon to make skillful movements in uncertain dynamic environments. It has been shown that, for arm movements, the central nervous system adapts by compensating for the average of the expected perturbations [1]. However, it is not known whether the postural control system will adapt to random dynamics in the same manner. In contrast to reaching movements, whole-body postural control is inherently unstable. Thus anticipatory postural compensation, if inappropriate, could lead to a loss of balance and potential fall. Indeed, it has been suggested that postural adaptation is scaled to the confidence in load dynamics [2], rather than the expected mean. In this study we investigate whether the postural control system will adapt to random perturbations with anticipatory control, despite the associated risk of instability.

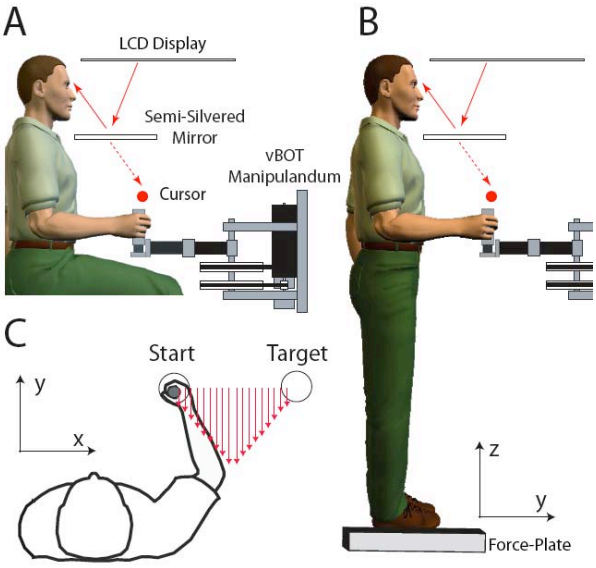

Figure 1: Experimental Setup; A: seated position; B: standing position; C: forces on FORCE trials.

We hypothesized that anticipatory postural adjustments will be significantly reduced in the presence of random perturbations (H1). This would imply that, in the presence of uncertainty and instability, subjects prefer a more conservative control strategy and scale their control to their confidence in the impending dynamics. We also hypothesized that uncertainty may inhibit transfer of learning between whole-body postures (H2).

METHODS

Thirteen right-handed participants (7M/6F) made planar reaching movements while standing postures. Experimental procedures were approved by the Local Ethics Committee.

Participants grasped the handle of a force-generating robotic manipulandum (vBOT) and moved a cursor to a target presented in the horizontal plane. Task relevant visual feedback was presented within the plane of movement via a semi-silvered mirror, reflecting the display of an LCD monitor suspended horizontally above (Figure 1A). When standing, participants stood with feet slightly apart on a 6-axis force-torque sensor (ATI Technologies, Apex, NC) (Fig. 1B).

Subjects were divided into two groups of equal size. In one group (CONSTANT), the magnitude of the perturbation was kept constant at 0.2 Ns/cm. In the other group (RANDOM), the magnitude of the perturbation was randomly drawn from a Gaussian distribution with a mean of 0.2 Ns/cm and SD 0.05 Ns/cm. Both groups initially performed 350 trials in the standing position. After 50 trials (*Baseline* Phase), robot forces were turned on for 300 trials (*Learning*). They then switched to a seated posture for 100 trials (*Transfer*), followed by 100 trials with the forces turned off to extinguish the adaptation

(*Washout*). In FORCE trials, the robot generated a force upon the hand proportional to its velocity, and perpendicular (clockwise) to its direction (Fig. 1C). Catch trials were inserted randomly, to measure the predictive force learned. Handle position, robot-generated forces, and forceplate forces were recorded at 500 Hz.

To assess learning of the dynamics we examined movement error on each trial, measured as the peak perpendicular deviation from the target vector (Fig 2A). To rule out the use of an impedance-based strategy, we examined the peak force generated into the force channel on catch trials as a measure of anticipatory control (Fig 2B). Anticipatory postural control in the standing configuration was measured as the velocity of the center of pressure 100 ms prior to the onset of hand movement. Movement of the center of pressure in the direction of the impending perturbing force would indicate an anticipatory postural adjustment (Fig 2C). Appropriate anticipatory control should lead to minimal reactive control, measured as peak COP velocity after movement initiation (Fig 2D).

RESULTS AND DISCUSSION

All participants learned to make accurate reaching movements to the target and significantly reduced their movement error from early to late in the *Learning* phase (Fig 2A). Both groups also generated significant anticipatory forces on catch trials of similar magnitudes by late *Learning* (Fig 2B). Although movement error was similar, error observed upon removal of the forces early in the *Washout* phase was lower in the RANDOM group (Fig 2A, $p < 0.05$). This suggests that subjects in the RANDOM group used an impedance control strategy, while also learning an internal model of the mean of the perturbations. By late in the *Learning* phase, participants in both groups developed similar anticipatory postural adjustments (H1; Fig 2C, $p>0.05$). Reactive control was also appropriately minimized from early to late *Learning* in both groups (Fig 2D, $p<0.05$). Movement performance, quantified as movement error, transferred from standing to sitting in both groups (H2; Fig 2B, $p > 0.05$), however the RANDOM group generated significantly less anticipatory force ($p < 0.05$).

CONCLUSIONS

Under conditions of uncertainty, the postural system adapts to the mean of the perturbations despite the threat of instability. However, uncertainty does appear to inhibit transfer of learning between postures.

REFERENCES

1.Scheidt et al. *JNP*, **86**, 971-985, 2001.
2.Toussaint et al. *EBR*, **120**, 85-94, 1998.

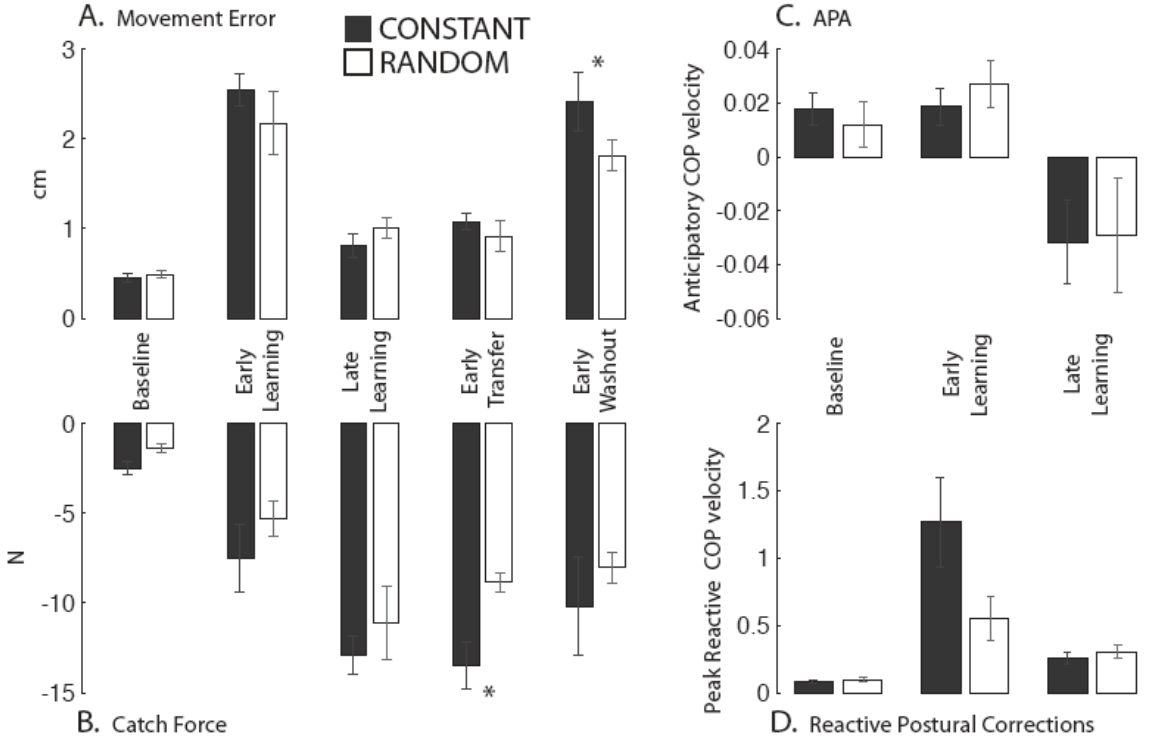

Figure 2
Results;
A: Movement error;
B: Anticipatory forces;
C: Anticipatory postural adjustments;
D: Reactive postural adjustments

NEURONAL NOISE INFLUENCES GAIT VARIABILITY AND FALL RISK IN A DYNAMIC WALKING MODEL

[1]Paulien E. Roos and [1]Jonathan B. Dingwell

[1]The University of Texas at Austin, Austin, TX, USA
email: jdingwell@mail.utexas.edu

INTRODUCTION

Older adults are at an increased risk of falling and exhibit increased gait variability [1, 2]. We do not know however if increased gait variability directly causes these falls. Neuronal noise increases with aging are likely to increase gait variability, which in turn might increase fall risk. Conversely, increased variability could reflect *appropriate* corrections for small perturbations and thereby indicated decreased fall risk. Thus, the relation between these factors needs to be better understood.

The aims of this study were to determine how increased neuronal noise affects gait variability and probability of falling, and if changes in gait variability directly predict fall risk. We hypothesized that with increasing neuromuscular noise amplitude 1) probability of falling and 2) gait variability would increase, and that 3) gait variability would significantly predict fall risk.

METHODS

We implemented an intrinsically laterally unstable 3D dynamic walking model (Fig. 1), adapted from [3]. To maintain lateral stability, this model included a lateral step controller. At each instant of ground contact this controller made small lateral adjustments to match the state variables to their 'noise free solution' values. The lateral adjustments were achieved by changing the splay angle of the legs (ϕ). The model otherwise walked passively down a gentle slope (4%), with gravity providing the forward propulsion [3].

To approximate the neuronal noise that is present in humans, we applied uniformly distributed random noise to the lateral step controller. The amplitude of this noise (j_{noise}) was varied between a very small amplitude that did not make the model fall over and a large amplitude for which the model always fell. For each condition, 100 simulations were run, each up to 125 steps or until the model fell over.

Fig. 1. Graphical representation of the 3D dynamic walking model.

The probability of falling ($\%_{FALL}$) was calculated for each j_{noise} and also the average number of steps the model took before falling (*STF*). Gait variability measures were calculated for each simulation. Step length (SD_{SL}), step width (SD_{SW}) and step time (SD_{ST}) variability were calculated as their respective standard deviations. Variability of the state variables was calculated for each state variable individually $MSD(q)$ (as in [4]) and combined in a single measure $MSD(\theta_{Tot})$ as the length of the vector containing all state variability measures.

The correlations between the gait variability measures and $\%_{FALL}$ or *STF* were approximated by sigmoidal fits. These sigmoidal fits were calculated using 'lsqcurvefit' in Matlab (Mathworks, R2008a). For each relationship variance accounted for (r^2) and statistical significance (p) were reported.

RESULTS AND DISCUSSION

The model fell over more often and after fewer steps when noise amplitude (j_{noise}) increased (Fig. 2). This confirmed our first hypothesis. Gait variability increased with j_{noise} in a sigmoidal manner (Fig. 3) and could predict fall risk ($\%_{FALL}$) significantly (Fig. 4). This confirmed our second hypothesis and partly confirmed our third.

The most important outcome from this study was that it showed how changes in gait variability

resulting from increased neuronal noise can directly affect fall risk. Gait variability increased with noise amplitude (Fig. 3) and the probability of falling increased in turn with increasing gait variability (Fig. 4).

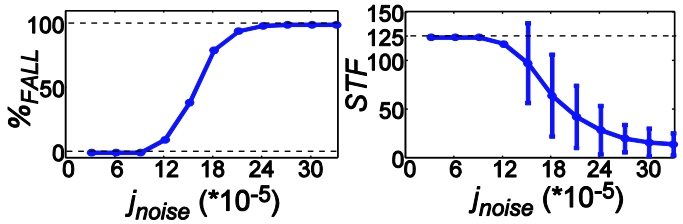

Fig. 2. $\%_{Fall}$ and STF against j_{noise}. Error bars represent ±1 standard deviations.

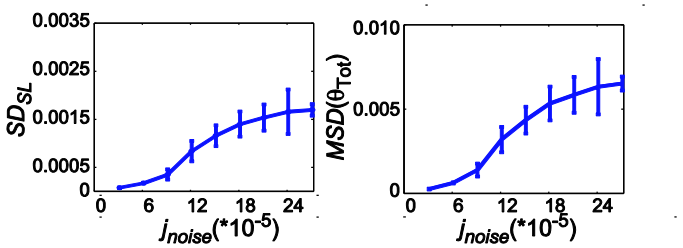

Fig. 3. j_{noise} against the variability in SD_{SL} and $MSD(\theta_{Tot})$. Error bars represent ±1 standard deviation. Similar figures for SD_{SW} and SD_{ST} showed the same trends.

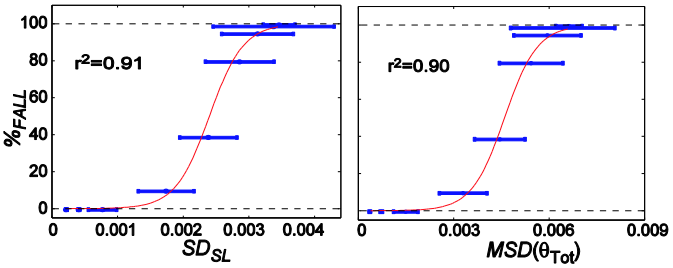

Fig. 4. SD_{SL} and $MSD(\theta_{Tot})$ against $\%_{FALL}$. Red lines are sigmoidal functions fitted to the average data. Error bars represent ±1 standard deviation. All r^2 values were very high ($r^2 \geq 0.87$; $p \leq 2.3*10^{-4}$). Similar figures for SD_{SW} and SD_{ST} showed the same trends and are therefore not shown.

Notably, the relationship between gait variability and the probability of falling was far from linear, as often assumed. At either low gait variability (which might correspond to healthy adults) or high gait variability (which might correspond to frequent fallers), small increases in noise amplitude and variability had only *minor* effects on probability of falling. Conversely, at intermediate noise and gait variability levels (which might correspond to healthy elderly), similar incremental increases resulted in *significant* increases in probability of falling. This is explained as follows. At very low noise amplitudes, the model was well within its limits, whereas at intermediate noise amplitudes, the model got close to its maximum ability to deal successfully with the perturbations applied to the controller. At the very high noise amplitudes the model was already beyond this maximum ability.

We used a very simplified model in this study that was sufficient to address our research aims, but it did not include many other factors that may also contribute to fall risk. The conclusions of our study therefore only relate to fall risk and neuronal noise. We were therefore able to show that there is a direct link between neuronal noise, gait variability and fall risk. The relationship we found between gait variability and fall risk may be specific to this model, however $\%_{FALL}$ has to be bounded between 0% and 100% and therefore some type of sigmoidal relationship has to be exhibited. Whether or not these findings will translate to predicting risk of falling in humans remains to be tested.

CONCLUSIONS

This study validated the concept that age-related increases in neuronal noise are likely to play a direct contributing role in increasing fall risk. Changes in gait variability resulting from increases in neuronal noise may predict fall risk. The relationship found between fall risk and gait variability was however not linear and therefore care needs to be taken when applying gait variability as a predictor in fall prevention practice.

REFERENCES

1. Hausdorff JM, Rios DA, Edelberg HK. *Arch Phys Med Rehab* **82**, 1050-1056, 2001.
2. Maki BE. *J Am Geriatr Soc* **45**, 313-320, 1997.
3. Kuo AD. *Int J Robot Res* **18**, 917-930, 1999.
4. Dingwell JB,Marin LC. *J Biomech* **39**, 444-452, 2006.

ACKNOWLEDGEMENTS

Funded by Grant #1-R21-EB007638-01A1 from the National Institutes of Health.

VERTICAL GROUND REACTION FORCES INCREASE OVER TIME DURING 60 MINUTES OF FORCED-CADENCE MARCHING

Joseph F. Seay, David J. Gutekunst, and Peter N. Frykman
U.S. Army Research Institute of Environmental Medicine, Natick, MA USA
e-mail: joseph.seay@us.army.mil

INTRODUCTION

During group marches, soldiers with a wide range of height must walk in step with one another at the same imposed step rate. This "fixed cadence" marching has been suggested as a possible cause for higher rates of lower-extremity injuries in women and shorter men due to over striding that can occur when taller recruits dictate marching step rate [1]. In-vivo tibial strains increase following an extended march [2], suggesting a possible role for fatigue-related biomechanical changes in the etiology of tibial stress fractures. Ground reaction forces (GRF) may also lend insight into mechanisms of lower extremity overuse injury; research on runners has associated higher peak impact GRF with a history of tibial stress fractures [3].

The purpose of this study was to assess the effects of fixed cadence walking at step frequencies above and below preferred step rate (PSR) on GRFs in individuals who were unaccustomed to cadence marching for extended periods of time. We hypothesized that step rates below PSR would lead to greater antero-posterior (A-P) and vertical GRFs during braking and propulsion portions of the stance phase. We also hypothesized that these effects would be exacerbated over the course of an hour-long bout under militarily relevant loading conditions.

METHODS

Five volunteers (1 woman, 4 men) with no military marching experience gave informed consent in accordance with AR 70-25 on the use of volunteers in research. Participants completed three 60-min bouts of walking on a treadmill on non-consecutive days. Treadmill speed was 1.34 m/s for all bouts, and presentation order was randomized between participants for preferred (PSR), slower (85%PSR), and faster (115%PSR) step rates. PSR was determined during a separate orientation visit, and investigators used a metronome during all three conditions to ensure adherence to step rates. In order to simulate basic combat training conditions, participants were provided military boots and carried 20 kg of equipment that included body armor vest, light backpack, and a simulated weapon.

Data were collected at 5, 35, and 55 min. GRF data were collected at 1200 Hz using a treadmill with a front-back force platform configuration (AMTI, Watertown, MA). An 8-camera Qualisys system collected 3-dimensional motion data at 120 Hz, which were synchronized with the force platform outputs and combined in Visual3D post-processing software (C-Motion, Germantown, MD).

Two-way repeated measures ANOVA (Cadence by Time) ($p < 0.05$) were performed for peak A-P and vertical GRF during braking (first 50%) and propulsion (final 50%) portions of stance. Effect size (ES) was also calculated to express differences relative to a pooled standard deviation [4].

RESULTS

Slower step rates resulted in greater (i.e., more negative) A-P braking GRF ($p < 0.001$, Table 1). Specifically, walking at 85%PSR resulted in significantly greater braking forces than walking at PSR, and both step rates resulted in significantly greater A-P braking forces than 115%PSR. Slower step rates also resulted in increased (i.e., more positive) A-P propulsion GRFs ($p = 0.028$). Only the A-P braking force differences were supported by large effect sizes ($ES > 0.8$), indicating that those differences were more clinically relevant.

There were no differences between step rates for peak vertical GRF during braking or propulsion. However, peak vertical braking GRF increased over time, regardless of step rate ($p < 0.001$, Figure 1). Post-hoc analyses revealed that peak vertical GRF

during braking increased from 5 min to 35 min, and remained at this level through the end of the bout (55 min). Large effect sizes (ES > 0.88 for both) strengthened findings from these comparisons.

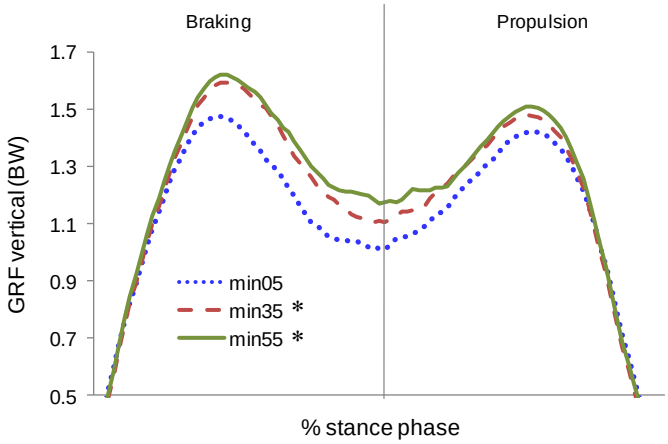

Figure 1: Average vertical GRF traces at different time points, normalized to body weight (BW) and averaged across step rate. "*" indicates significant peak braking differences from minute 5.

DISCUSSION AND CONCLUSIONS

Walking at 85%PSR increased A-P braking GRF an average of 4.7% over the range of step rates examined in this study (i.e., 85 to 115% PSR). Even the average 1.8% increase observed between 85%PSR and PSR would have a cumulative effect over a 9 to 12-week training period. This finding supports the idea that "over striding" may be related to the etiology of tibial stress fractures.

In our inexperienced participants, peak vertical braking GRFs increased an average of 6.3% toward the middle of the bout (minute 35), and had increased 6.8% by the end of the 60-minute bout (minute 55). This finding occurred across all step rates, suggesting that the participants acclimated to carrying the load in a potentially detrimental manner (i.e., increased forces at the same speed and step rate), increasing the mechanical demand placed on the lower extremities. Even if the vertical GRF stabilizes as a result of training and familiarity with carrying a load, the increase in vertical GRF may have implications for lower extremity injuries. This observation, combined with previously reported increased incidence of musculoskeletal overuse injuries during the second and third weeks of training [5] has implications for familiarization and work-rest cycles while recruits acclimate to load carriage and forced-cadence marching.

Based on our A-P GRF findings, increasing step rate during marching may mitigate the incidence of injury by shortening stride length and allowing shorter recruits to avoid over striding. Vertical GRF findings add to previously reported changes due to prolonged load carriage that have been implicated in lower extremity overuse injuries. However, further research will be needed to identify factors responsible for observed increases in vertical GRFs over time.

REFERENCES

1. Knapik JJ, et al. *Med Sci Sports Exer* **33:**946-54, 2001.
2. Milgrom C, et al. *J Biomech* **40:**845-850, 2007.
3. Milner CE, et al. *Med Sci Sports Exer* **38:**323-8, 2006.
4. Cohen, J. *Statistical power analysis for the behavioral sciences. (2nd ed.)* Earlbaum, New Jersey, 1988.
5. Almeida SA, et al. *Med Sci Sports Exerc* **31:**1176-1182, 1999.

ACKNOWLEDGEMENTS

The authors would like to thank Megan Coyne for her contributions to data collection and processing.

DISCLAIMER

The statements in this document are the private views of the authors and are not the official views of the Army or the Department of Defense.

Table 1: GRF peak means (±SD) collapsed across step rates. * = sig difference ($p<0.05$) compared to 85%, # = sig difference compared to 85% and PSR, † = large Effect Size (ES > 0.8), ‡ = main effect for time.

Peak Force	STEP RATES			Effect Size		
(BW)	85%	PSR	115%	85% v PSR	85% v 115%	115% v PSR
Vertical GRF braking ‡	1.56±0.1	1.59±0.1	1.58±0.1	0.06	1.03 †	0.07
Vertical GRF propulsion	1.46±0.1	1.52±0.1	1.54±0.1	0.41	0.34	0.75
A-P GRF braking	-0.25±0.03	-0.20±0.03 *	-0.16±0.02 #	2.51 †	4.07 †	1.56 †
A-P GRF propulsion	0.28±0.04	0.25±0.04 *	0.23±0.03 #	0.11	0.21	0.10

NOTE: 85% = 85% PSR, 115% = 115% PSR

RELATIVE SENSITIVITY OF NET MUSCULAR MOMENTS TO CHANGES IN WALKING SPEED AND BODY-WEIGHT SUPPORT

[1]Saryn R. Goldberg and [2]Steven J. Stanhope

[1]Hofstra University, Hempstead, NY, USA
[2]University of Delaware, Newark, DE, USA
email: saryn.goldberg@hofstra.edu

INTRODUCTION

Measuring relative muscle effort during a dynamic task is a challenge. This makes it difficult, in many clinical cases, to assess the muscular impairments that most limit an individual from being able to walk at a desirably fast speed. The data presented here from unimpaired individuals walking at multiple combinations of walking speeds and body-weight support levels show that different muscle groups exhibit different relative sensitivities to changes in each of these two factors. We envision that modulation of these and other variables during gait analysis could be used to develop a "biomechanical stress test" that would enable selective dynamic probing of how limited muscle strength may contribute to diminished walking ability in individuals with impairments.

METHODS

Motion capture and force platform data were collected from 8 unimpaired adult subjects as they walked on an instrumented, split-belt treadmill (Bertec Corp., Columbus, OH) while wearing a harness connected to a custom-designed, overhead body-weight support system (Intelligent Automation, Inc., Rockville, MD). The body-weight support system was specifically designed to maintain a constant support load throughout the gait cycle. Subjects walked with four different levels of body-weight support (0, 20, 40, and 60% of body weight) at each of three walking speeds (0.4, 0.6, and 0.8 statures/s, ranging on average from 0.7 to 1.4 m/s). Conditions were presented to subjects in a randomized order. Subjects were given 1.5 minutes to acclimate to each condition before data were collected for at least one minute.

Data were used to calculate hip, knee, and ankle net muscular moments for the left leg for all clean treadmill strides (i.e. neither foot fell on the opposite belt and the subject did not drift fore or aft.) Peak flexion and extension moments at the hip, knee, and ankle were averaged across trials within each condition for each subject. Average peak moments were scaled for each subject by the value measured when walking at 0.8 statures/s with zero body-weight support (i.e. after scaling, the peak moments for this condition had a value of 1.0). These scaled peak moment values were averaged across subjects for each condition. The relative sensitivity (S) of a muscle group to a change in walking speed (or body-weight support) was calculated at each body-weight support level (walking speed) as the difference in the scaled peak moment values at the lowest and highest walking speed (body-weight support level). Differences in sensitivities were evaluated using t-tests and the Holm-Bonferroni method for multiple comparisons with $p < 0.05$. These tests did not account for causal linkages across joints.

RESULTS AND DISCUSSION

As expected, in general, subjects' peak joint moments decreased with decreasing walking speed and with increasing body-weight support. However, the relative sensitivities of the moments at the hip, knee, and ankle to changes in speed and body-weight support were variable across muscle groups.

For example, when subjects walked with 40% body-weight support over a range of speeds, the ankle extensors showed a low relative sensitivity to changes in walking speed (dropping from a scaled mean peak moment value of 0.67 to 0.50 {$S = 0.17 \pm 0.07$} over a change in walking speed from 0.8 to 0.4 statures/s) as compared to the knee extensors ($p < 0.05$), which showed a high relative sensitivity to changes in speed (dropping from a scaled peak moment value of 0.80 to 0.34 {$S = 0.47 \pm 0.24$} over a change in walking speed from 0.8 to 0.4 statures/s) (Fig. 1). This was observed at other levels of support, and suggests that an increase in supported walking speed poses more of a relative

challenge to the knee extensors than to the ankle extensors.

Conversely, when subjects walked at 0.6 statures/s, the knee extensor moment showed a much lower relative sensitivity to changes in body-weight support than all other muscle groups ($p < 0.05$), with the knee flexors showing a higher relative sensitivity to changes in body-weight support than all other muscle groups ($p < 0.05$) (Fig. 2).

Previous studies have examined the contribution of joint moments [1] or individual muscles [2,3] to support and forward progression. Our work complements these studies, but examines the data from a different vantage point and towards a different goal. As opposed to elucidating muscle function, we aim to identify how conditions could be altered to selectively challenge individual muscle groups. This goal is well-served by our choice to scale peak moments by those observed at a control condition. However it is important to recognize that this approach may mask which muscle groups showed the largest absolute changes in peak joint moment with changes in either walking speed or body-weight support levels.

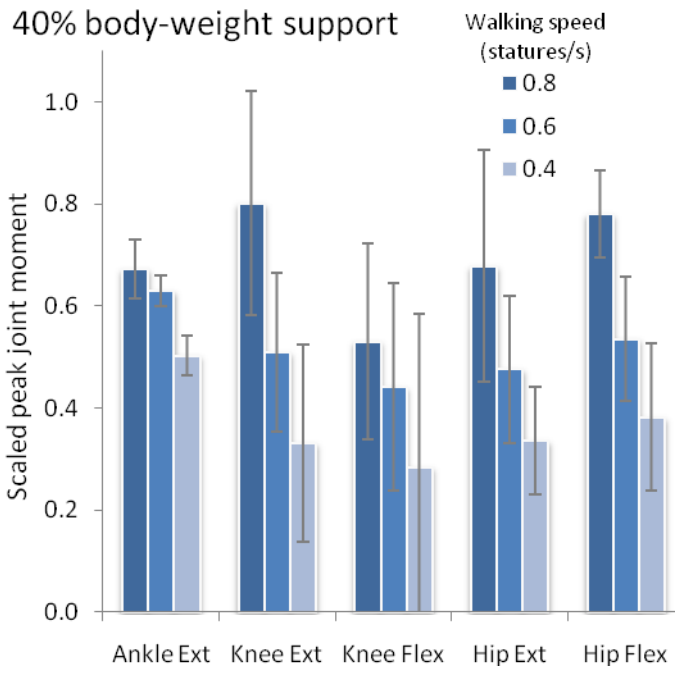

Figure 1: Scaled peak joint moments averaged for 8 unimpaired subjects walking with 40% body-weight support at a range of speeds. Error bars indicate ±1 standard deviation. The ankle extensor moment shows less relative change with walking speed than the knee extensors ($p < 0.05$).

By compiling these data for additional subjects over a broad range of walking speeds and support levels, we aim to provide a framework for selecting combinations of walking speed and body-weight support that could be used to effectively probe the biomechanical limits of an impaired gait strategy. Altering the level of body-weight support provided during sub-intervals of the gait cycle [4] could further differentiate the relative level of challenge provided to individual muscle groups.

REFERENCES

1.Kepple TM, et al. *Gait Posture* **6**, 1-8, 1997.
2.Liu MQ, et al. *J Biomech* **41**, 3243-3252, 2008.
3.McGowan CP, et al. *J Biomech* **42**, 850-856, 2009.
4.Franz JR, et al. *J Biomech* **40**, 3244-3250, 2007.

ACKNOWLEDGEMENTS

This research was supported by an Intramural Research Program of the National Institutes of Child Health and Human Development and the Clinical Center of the National Institutes of Health.

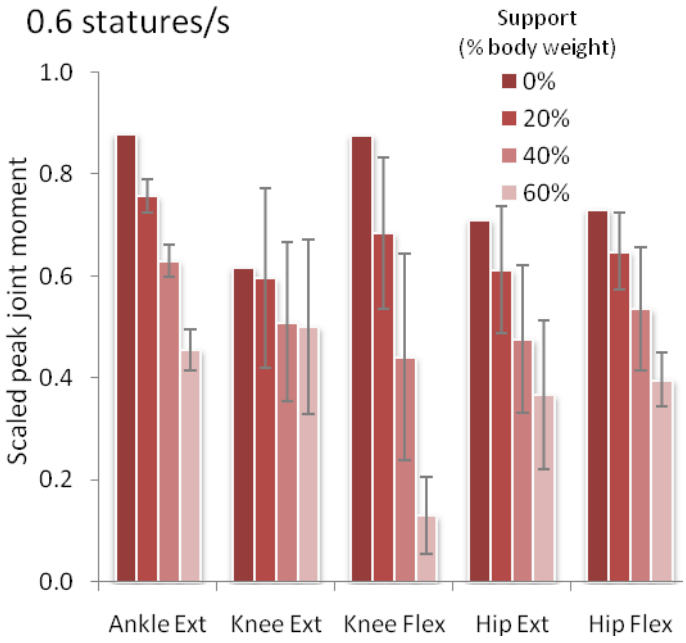

Figure 2: Scaled peak joint moments averaged for 8 unimpaired subjects walking at a speed of 0.6 statures/s at a range of body-weight support levels. Error bars indicate ±1 standard deviation. The knee extensor moment shows less relative change with body-weight support level than the other net muscle moments ($p < 0.05$), while the knee flexor moment shows more relative change ($p < 0.05$).

POSITIVE AND NEGATIVE MUSCLE WORK IN LEAN AND OBESE ADULTS DURING INCLINE AND DECLINE WALKING

[1]Paul DeVita, [1]Michael McNally, [1]Patrick Rider, [1]Tim Copple, [2]Ben Long, [1]Anthony Kulas, and [1]Tibor Hortobagyi

[1]East Carolina University, Greenville, NC, USA
[2]Winston-Salem State University, Winston-Salem, NC, USA
email: devitap@ecu.edu

INTRODUCTION

Skeletal muscles perform more work while ascending vs. descending both stairs and inclines [1]. This observation led us to the global hypothesis that skeletal muscles generate more mechanical energy in gait tasks that raise the center of mass compared to the mechanical energy they dissipate in gait tasks that lower the center of mass despite equivalent changes in total body mechanical energy. Subsequent tests have supported this hypothesis during incline and decline running [2] and have also shown the bias in positive over negative muscle work increases with running speed [3]. A hypothetical explanation for this bias toward positive work is that while only shortening (concentric) muscle contractions can generate mechanical energy needed in ascending gaits, all tissues can dissipate energy in descending gaits through vibrations caused by relatively large ground impact forces. Indeed, soft tissues motions dissipate large amounts of energy in impact-type movements [4]. It follows therefore that individuals with more soft tissue mass (i.e. obese vs. lean) would have a larger bias in muscle work in ascending vs. descending gaits thus providing a basis for further testing this hypothesis. The purpose of the study was to compare muscle work during incline and decline walking in lean and obese adults. We expected a significant group by gait direction interaction in muscle work: muscle work would be larger in incline vs. decline walking and this bias would be larger in obese vs. lean adults.

METHODS

3D motion capture and force plate systems were used to calculate lower limb joint powers during incline and decline walking on a 10° slope at 1.5 m/s in 20 otherwise healthy obese (mass=119 kg; BMI =40 kg/m²) and 20 lean (mass=71 kg; BMI=23 kg/m²) adults. Negative, positive and total muscle work throughout the stride were derived from the joint powers and compared between groups and gait directions with two-way repeated measures ANOVA ($p<0.05$). We verified that obese had larger soft tissue vibrations by comparing the accelerations of a marker in the region of the right anterior superior iliac spine. Average accelerations were 7.56 m/s² and 5.79 m/s² ($p<0.05$, t-test) in obese vs. lean.

RESULTS AND DISCUSSION

Significant group by gait direction interactions were observed for both stride length ($p=.015$, Figure 1) and the maximum resultant ground reaction force ($p=.020$, Figure 2). The significant increase in stride length from decline to incline gaits was significantly larger in lean vs. obese adults. Since stride length directly affected the amount of vertical displacement per step and subsequently muscle work we therefore normalized all work values by stride length to provide an analysis of work per unit distance and not per unit step. The significant increase in ground reaction force from incline to decline gaits was significantly larger in obese vs. lean adults.

Both incline and decline gaits had positive and negative phases of muscle work. Total muscle work however was positive and negative in incline and decline gaits. The magnitude of muscle work (i.e. $|J|$) was 21% larger in incline vs. decline walking ($p=.003$) and was 56% larger in obese vs. lean adults ($p<.001$, Figure 3). These data therefore provided further support for our global hypothesis that skeletal muscles generate more mechanical

energy in gait tasks that raise the center of mass compared to the mechanical energy they dissipate in gait tasks that lower the center of mass. They did not however support our expectation of a significant interaction between lean and obese adults during incline and decline gaits. We expected the bias towards positive over negative muscle work to be larger in obese vs. lean adults. This outcome is surprising also because the interaction in ground reaction force was considered to be a causative factor for an interaction in muscle work.

We observed previously that gait speed interacts with the positive bias in muscle work in non-level gaits [3]. Faster speeds have a larger positive bias. We now conjecture that the present walking speed was insufficient for eliciting a larger bias in the obese vs. lean adults and that a faster speed may reveal the expected interaction. Lastly, it is possible that the modeling techniques had sufficient error when applied to the obese adults to interfere with the biomechanical calculations [5].

CONCLUSIONS

These data supported our global hypothesis that skeletal muscles generate more mechanical energy in gait tasks that raise the center of mass compared to the mechanical energy they dissipate in gait tasks that lower the center of mass despite equivalent changes in total body mechanical energy. They did not however support our expectation that the bias towards positive muscle work would be larger in obese vs. lean adults. Obese and lean adults had statistically identical bias of 21% more positive muscle work in incline vs. negative muscle work in decline walking.

REFERENCES

1. DeVita P et al. *J Exp Biol*. 210, 3361-3373. 2008.
2. DeVita P et al. *J Biomech*, 41, 3354-3359, 2008.
3. Janshen et al, *Proc Gait & Clin Movt Analysis Soc*. Richmond, VA, 2008.
4. Pain M et al. *J Appl Biomech*, 231-242, 2002.
5. Chambers A et al. Clin Biomech, 25, 131-136, 2010.

ACKNOWLEDGEMENTS

This study partially supported by NIH AG16192.

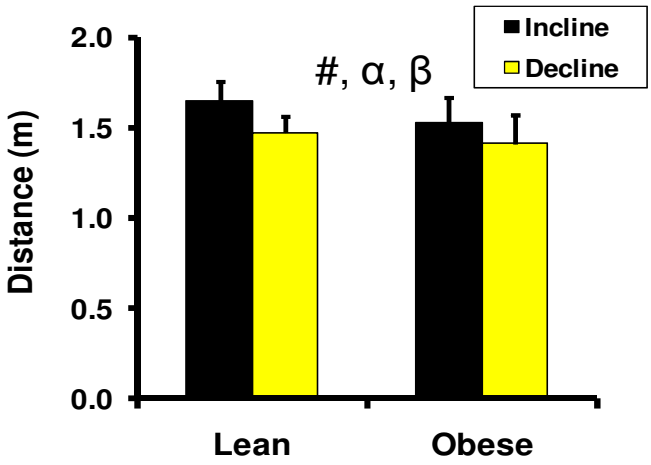

Figure 1. Mean (sd) stride lengths. #, α, β: significant interaction, group, & direction effects, p<.05.

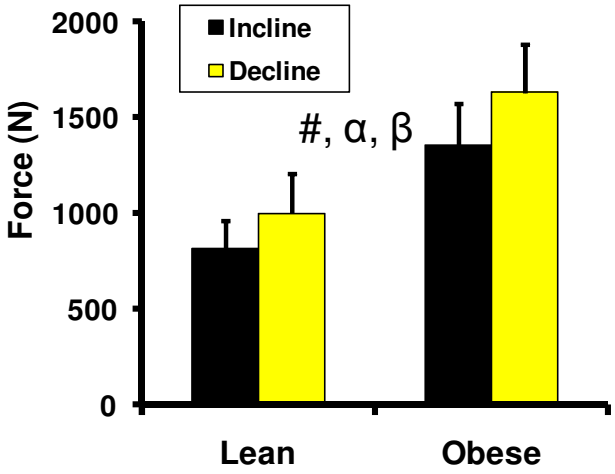

Figure 2. Mean (sd) first maximum ground reaction force. #, α, β: significant interaction, group, & direction effects, p<.05.

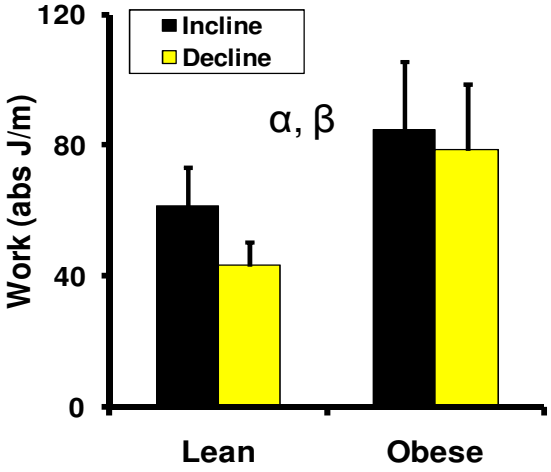

Figure 3. Mean (sd) absolute total muscle work. α, β: significant group & direction effects, p<.05.

MOVING AND SHAKING: SOFT TISSUE WORK IN HUMAN WALKING

Karl E. Zelik and Arthur D. Kuo

University of Michigan, Ann Arbor, MI, USA
email: kzelik@umich.edu, web: http://hbcl.engin.umich.edu

INTRODUCTION

Joint work performed by lower-limb muscles and tendons is considered the dominant energetic contributor to walking, but soft tissues elsewhere in the body may also do significant work. Steady level-ground walking requires zero net mechanical work per stride, yet less negative work is performed about the lower-limb joints than positive [1]. This suggests that joint work measures fail to capture some negative work performed by the body. This uncaptured work may be indicative of unmodeled soft tissue deformations, as is recognized in running and jumping impacts, but typically not in walking, when collisions occur after heelstrike. Soft tissue work could influence walking economy or the risk of tissue injury or degeneration. The purpose of this study was to investigate the energetic contributions of soft tissue in human walking. We hypothesized that (1) soft tissue performs significant negative work during the collision of the leg with the ground (Collision phase of gait), and (2) soft tissue dissipates more Collision energy at faster gait speed, as total Collision magnitudes increase.

METHODS

We propose that work performed on the body center of mass (COM), but not captured by rigid-body joint work estimates is an indicator of soft tissue deformations (Fig. 1). We performed standard gait analysis on subjects walking on an instrumented treadmill at various speeds (N=10, 0.7–2.0 m/s). We compared 3D mechanical work estimates from conventional inverse dynamics and COM work analysis during individual phases of the gait cycle, looking for indications of soft tissue work, specifically during Collision phase. The phases of gait – Collision, Rebound, Preload, Push-off, Swing – are defined by fluctuating regions of positive and negative COM work, beginning at heelstrike (Fig. 2). Inverse dynamics calculations were performed using commercial software (Visual3D, C-Motion). We computed COM work rate independently for each limb based on the 3D dot product of each limb's ground reaction force with COM velocity [2]. Statistical analysis of covariance was used to evaluate work trends across speed.

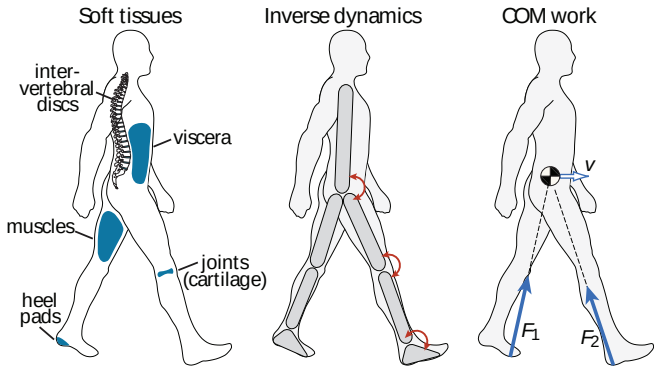

Figure 1: Soft tissues of the body and models for estimating work.

RESULTS AND DISCUSSION

We observed a strong correspondence between COM work rate and summed joint power of the ankle, knee and hip (Fig. 2). No COM vs. joint work differences were found for Pre-load or Push-off phases (P>0.05, Fig. 3). COM work of Collision and Rebound could be largely attributed to the knee joint, and Pre-load and Push-off to the ankle.

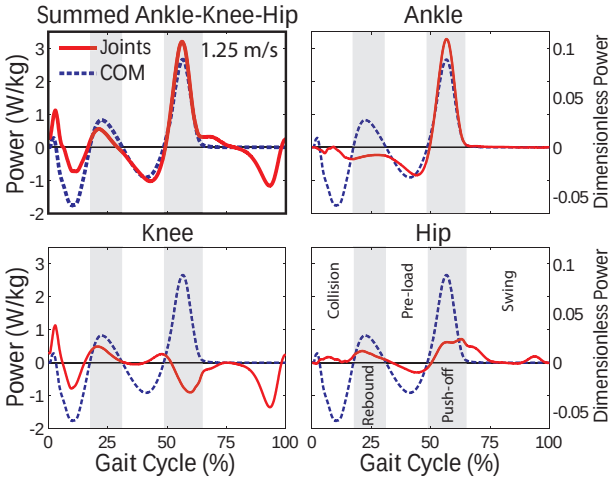

Figure 2: Average COM vs. summed ankle, knee and hip joint power. Gait phases are defined by alternating regions of positive/negative COM work.

The largest difference between COM and summed ankle-knee-hip work was during Collision, with 3.8 J less joint work at 0.7 m/s and 33.0 J less at 2.0 m/s (Fig. 3). These results suggest that substantial negative soft tissue work is performed during Collision, increasing with speed ($P<0.03$). At the nominal 1.25 m/s, ankle-knee-hip negative work fails to capture about 7.5 J during Collision, which amounts to about 31% of the negative work per stride and 60% of the negative Collision work [3].

Another substantial difference was in the positive work of Rebound. Summed ankle-knee-hip joint work was consistently less than COM by about 4 J across all speeds ($P=0.001$). At 1.25 m/s, this Rebound difference constitutes about 10% of the positive work per stride performed by the lower extremity joints. Soft tissue contributions to Rebound were not proportional to Collision work, but might nonetheless represent a damped elastic response that cannot be attributed to rotational contributions of the ankle-knee-hip joints.

A limitation of this study is in the degree to which joint work and COM work are comparable. The two types of work are not identical, but substantial energetic differences between them may still provide indirect evidence of soft tissue work. It is possible that the differences could also be attributed to contributions of unmeasured joints or errors in force and torque estimates induced by rigid body assumptions. However, we also observed less negative work about the lower extremity joints than positive work (e.g., -28 vs. +34 J at 1.25 m/s), a separate indicator of negative work by soft tissues, since steady gait requires zero net work per stride.

We believe that soft tissues play an underappreciated role in walking. Not only do they reduce peak impact loads, but they also dissipate, store and even return energy.

REFERENCES

1. DeVita P et al. (2007). *J Exp Biol* 210, 3361-73.
2. Donelan JM et al. (2002). *J Biomech* 35, 117-24.
3. Zelik KE & Kuo AD (2010). *J Exp Biol*, subm.

ACKNOWLEDGEMENTS

Supported in part by a National Science Foundation Graduate Research Fellowship (K.E.Z.), the Department of Defense & NIH H0055706 (A.D.K.).

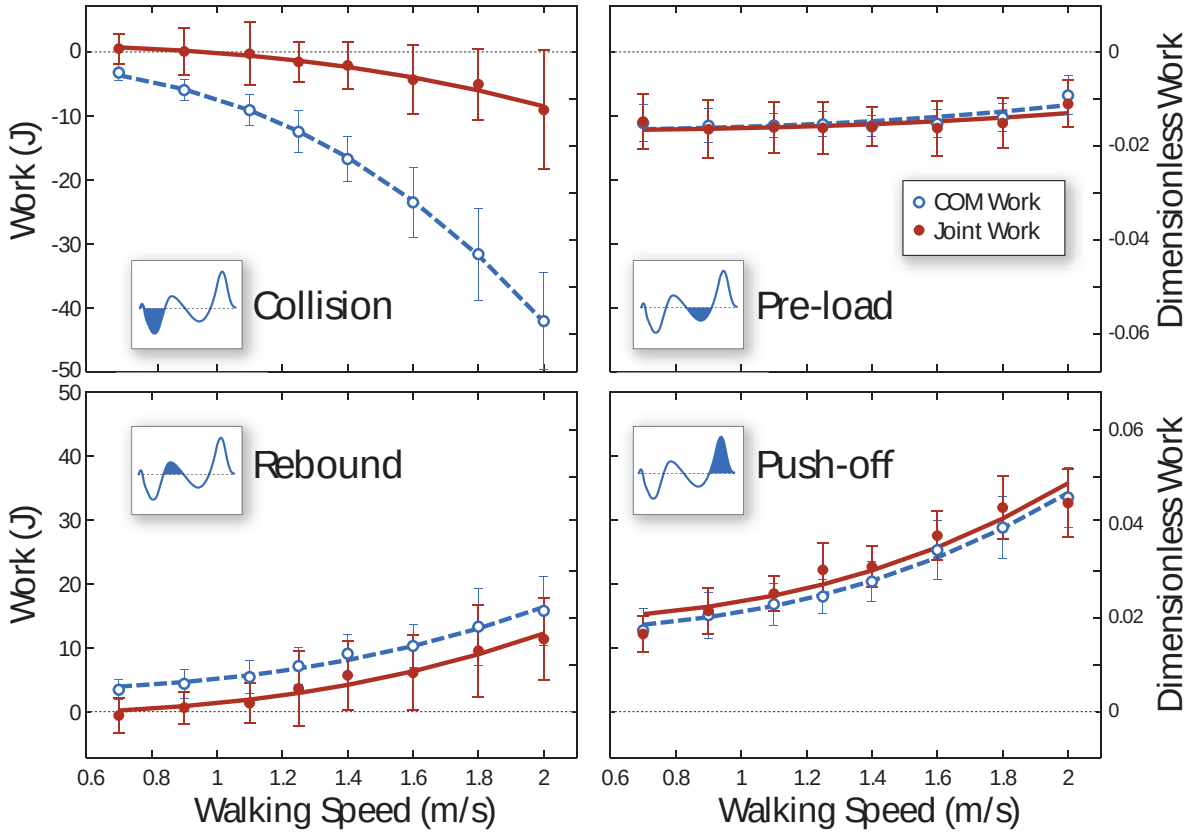

Figure 3: Average COM and summed ankle-knee-hip joint work vs. speed during phases of gait cycle. Work values were integrated from power plots (e.g., Fig. 2) during specified phases of gait.

GAIT CHARACTERISTICS OF SIMULATED LUNAR LOCOMOTION

[1]Andrea Hanson, [2]Kelly Gilkey, [2]Aaron Weaver, [2]Gail Perusek, [3]David Thorndike, [3]Gilead Kutnick, [3]Carlos Grodsinsky, [1]Andrea Rice, [1]Peter Cavanagh

[1]University of Washington, Seattle, WA, USA
[2]NASA Glenn Research Center, Cleveland, OH, USA
[3]ZIN Technologies, Inc., Cleveland, OH, USA
email: cavanagh@uw.edu

INTRODUCTION

During the Apollo missions, unique locomotion strategies were adopted to efficiently move across the lunar surface (e.g. lunar loping). Bone mass maintenance is thought to be dependent on load bearing activity but it is unclear to what extent the partial gravity (1/6*g)* environment for the moon will be osteoprotective or how the gait profile of new methods of locomotion affect skeletal loads. In this study, we aim to characterize gait parameters measured during simulated lunar locomotion to allow determination of potential efficacy on musculoskeletal health.

The use of accelerometry has evolved as a means of monitoring human activity [1,2] and more recently as an activity recognition tool [3,4]. Efforts are also being made to correlate the characteristics of accelerometer signals with associated changes in bone mineral density (BMD) [5,6]. It is our goal to develop a wireless, ambulatory device to remotely monitor parameters related to bone health of astronauts during lunar and Martian missions.

We have developed an accelerometer-based system, worn on the body and have tested the device with humans in a simulated lunar environment. Data were collected during a series of representative lunar activities. An artificial neural network (ANN) recognizes each activity from feature-characteristics. The equivalent mechanical load of each activity will be used in calculations of the enhanced daily load stimulus (EDLS) theory [7] to estimate overall bone health.

METHODS

Our bone health monitoring (BHM) system consists of two units, one positioned in the midsole of the subject's footwear and the other attached to the waist. On-board components consist of a tri-axial accelerometer (±12 g), a high-impact single axis accelerometer (±50 g), and a tri-axial rate gyro (±2000º/sec). An embedded microprocessor is programmed with custom software to performed on-board data decimation such that a sampling rate of 256 Hz and 1024 Hz is achieved at the hip and foot sensors, respectively. Data is transmitted wirelessly to a local CPU via Bluetooth radio. A 3.7V 230 mAh Li-poly battery currently supplies at least 4 hours of continuous use. A sleep mode minimizes power drain during periods of rest. Overall dimensions of the foot unit are 76 mm x 24 mm x 10 mm with a packaged mass of 25 grams. The hip unit is approximately half the length and twice the height of the foot unit and has a packaged weight of 21 grams.

Six subjects were recruited (3 female and 3 male) for participation in a pilot study conducted in the enhanced Zero Gravity Locomotion Simulator

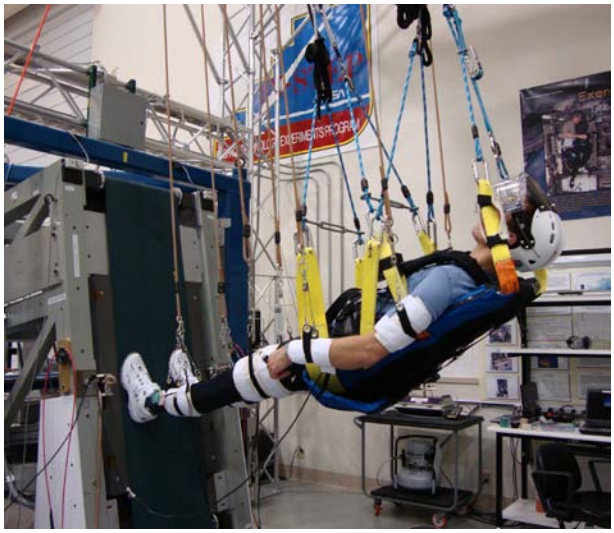

Figure 1: Subject suspended in the eZLS facility tilted to achieve 1/6 BW load at the feet.

(eZLS) facility (Fig. 1) at Glenn Research Center in Cleveland, OH. The eZLS simulates reduced gravity environments and locomotor activity on an instrumented treadmill. Subjects were instructed to walk (3 MPH), run (6 MPH), or lope (2 MPH) while loaded to 1/6 of their body weight (BW) and instrumented with BHM sensors. Force plate data allowed comparison of the ground reaction forces to accelerometer signals and provided verification that 1/6*g* BW loading was achieved.

The ANN inputs are derived from the statistical components of individual axes of accelerometer signal histograms (Fig. 2). The network was trained for pattern recognition. The mean, standard deviation, skewness, and kurtosis were calculated for acceleration peaks in the Z- (up/down) and Y-axis (forward/backward) for lunar walking, running, and loping [4]. The network is a two-layer feed-forward algorithm with 20 hidden neurons, and trained with scaled conjugate gradient back-propagation. Custom software (Matlab, Mathworks Inc.), was used for all data processing.

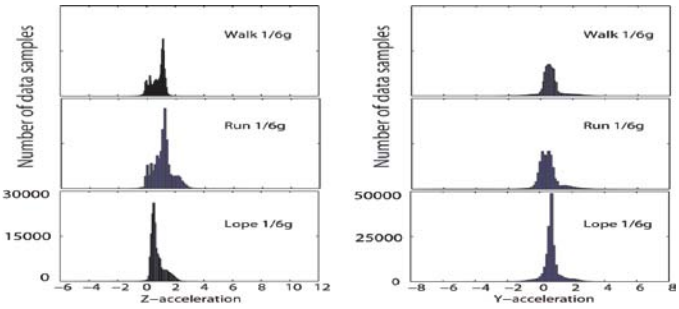

Figure 2: The histogram of accelerometer data in the Z-axis (left) and Y-axis (right) for 1/6g walking, running, and loping.

RESULTS AND DISCUSSION

Upon examination of ground reaction forces (GRFs), it was noted that 3 MPH was beyond the walk-run transition speed resulting in a flight-phase in 3 of 6 subjects (Fig. 3). There was not a strong correlation between flight-phase and subject gender or weight. With more subjects, an examination of the Froude number may provide insight into this gait characteristic [8].

The input array consisted of 8 inputs from 18 samples. Training of the network was successful with no misclassifications for any of the activities. A second pilot study is currently underway, from which new data will be generated and used to validate the trained network. In addition to walking, running, and loping, we plan to include additional surface activities (ladder climb, hopping, lift and carry tasks, etc.) and exercises (squatting, cycling, rowing, etc.) to our activity recognition library. Analysis of the angular rate data will be essential in characterizing dynamic vs. static activities. Additional signal characteristics will be drawn from the time and frequency domains for more robust characterization of activities.

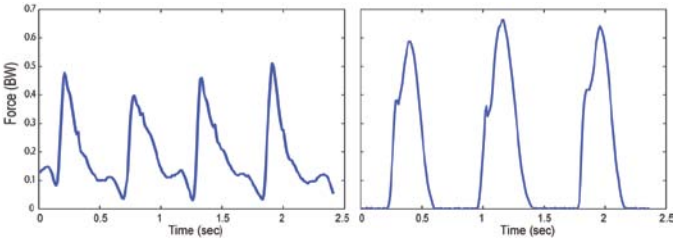

Figure 3: GRF at 3 MPH locomotion at 1/6*g* loading without a flight-phase (left) and with a flight-phase (right).

We have successfully developed an unobtrusive, wireless, ambulatory activity monitor and have tested it in simulated lunar gravity. Initial efforts in developing an activity recognition algorithm have been successful. Completion of this algorithm will result in an unobtrusive tool to identify task performance and to monitor bone health in astronauts during remote missions.

REFERENCES

1.Welk G, *Proceedings of ORS*, Las Vegas, NV, 2009.
2.Parka J, et al. *Proceedings of IEEE EMBS*, Lyon, France, 2007.
3.Sharma A, et al. *Proceedings of IEEE ICCHIT*, Busan, Korea, 2008.
4.Baek J, et al. *Lecture Notes in Computer Science*, Springer Berlin-Heidelberg, 2004.
5.Heikkinnen R, et al., *J Biomech*, **40**, 2967-2974, 2007.
6.Jamsa T, et al., *Clin Biomech*, **21**, 1-7, 2006.
7.Genc K, et al., *Aviat Space Environ Med*, **80**, 919-26, 2009.
8.Donelan J, et al., *J Exp Bio*, **203**, 2405-15, 2000.

ACKNOWLEDGEMENTS

This work supported by the National Space Biomedical Research Institute through NASA NCC 9-58. The authors also acknowledge the contributions of [2]Mark Savina, [2]Sergey Samorezov and [3]Hemal Shah.

EVALUATION OF DIFFERENT PROJECTILES IN MATCHED EXPERIMENTAL EYE IMPACT SIMULATIONS

[1,2]Ashley A. Weaver, [4]Eric A. Kennedy, [1,3]Stefan M. Duma, and [1,2]Joel D. Stitzel

[1]Virginia Tech-Wake Forest University Center for Injury Biomechanics, Winston-Salem, NC, USA
[2]Wake Forest University School of Medicine, Winston-Salem, NC, USA
[3]Virginia Polytechnic Institute and State University, Blacksburg, VA, USA
[4]Bucknell University, Lewisburg, PA, USA
Email: asweaver@wfubmc.edu

INTRODUCTION

There are over 1.9 million eye injuries each year in the United States with trauma being the second leading cause of visual impairment [1]. Common sources of eye trauma include motor vehicle crashes, military operations, and sporting events. Experimental eye impacts and computational simulations with a variety of blunt objects have been used previously to determine injury tolerance of the eye. The VT-WFU Eye Model is a finite element model of the eye validated to predict globe rupture for dynamic blunt impacts and is used in this study to model eye impact experiments with a variety of projectiles and loading conditions [2].

METHODS

A collection of experimental eye impact tests in the literature were computationally modeled using an FE model of the eye to analyze global and localized responses to a variety of blunt projectile impacts [2,3,4]. Eight projectile geometries were simulated to recreate the experiments, including varying sizes of several geometries, for a total of 79 cases. The geometries, material properties, and impact velocities of projectiles modeled are summarized in Table 1. A separate FE model was created for each projectile and impacts were simulated in LS-Dyna (LSTC, Livermore, CA) with the existing eye model surrounded by a simulated orbit and soft tissue. Lagrangian and Eulerian meshes in the eye model allow for analysis of the mechanics of solid and fluid interactions. Peak pressure in the center of the vitreous and maximum principal stress in the corneoscleral shell and associated element location were computed for each case. Statistical analyses were performed to investigate the eye response.

RESULTS AND DISCUSSION

Based on previously published globe rupture levels (stress: 23 MPa, pressure: 2.1 MPa), the computational results agreed well with the experimental results. Mean stresses and pressures were significantly higher and exceeded the rupture thresholds in simulations matched to experiments where globe rupture occurred (Table 2).

Table 2: ANOVA comparison of computational simulations grouped by experimental globe rupture

Metric, MPa	**Rupture**		**No Rupture**		*F Ratio*	*P*
	Avg	*SD*	*Avg*	*SD*		
Stress	24.2	6.1	10.0	5.1	120.7	<0.0001
Pressure	2.2	0.8	0.5	0.5	122.1	<0.0001

Peak stresses were located in different regions of the eye for different projectiles (Figure 1). Peak stresses occurred in the cornea for the BB and in the limbus for the plastic, foam, and some aluminum rods. Other projectiles such as the baseball and paintball caused peak stresses near the equator due to equatorial expansion of the eye.

Relationships between peak stress and pressure and projectile geometry, velocity, kinetic energy (KE), and area-normalized KE were investigated. Normalized KE had the highest Pearson correlation coefficients (stress: 0.89, pressure: 0.66) and was found to be a much better predictor of peak stress and pressure than KE alone (Figure 2). This supports previous findings that normalized KE is a better predictor of globe rupture [4].

The remainder of the difference between the normalized kinetic energy and peak stress is likely explained by two things: the bluntness versus

sharpness of the impactor and the relative size of the impactor versus the cross sectional area of the eye. A multiple regression analysis has shown incorporating the relative size of the projectile tightens the grouping of the stress response data.

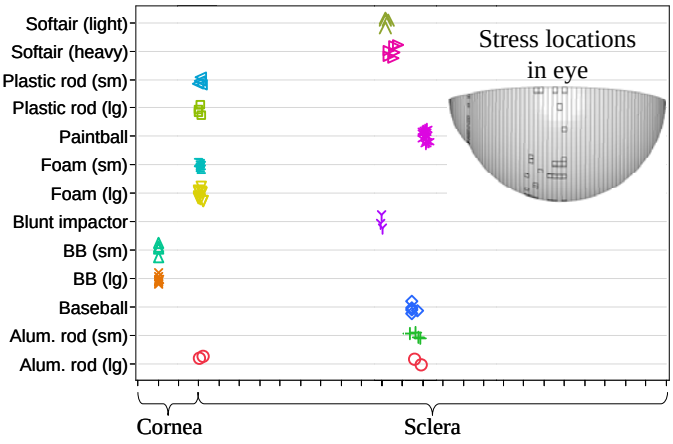

Figure 1: Locations of peak stresses in eye.

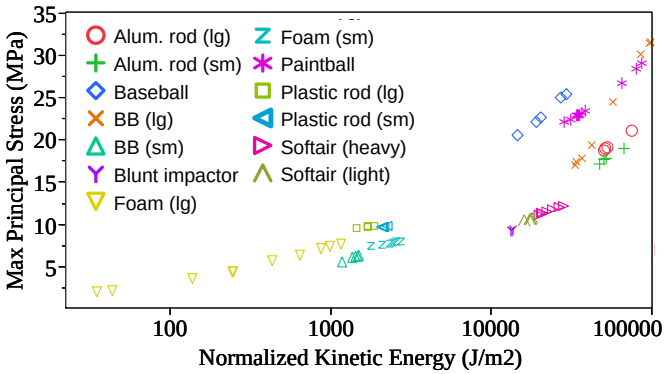

Figure 2: Area-normalized kinetic energy versus maximum principal stress for different projectiles.

CONCLUSIONS

This study determined the stress and pressure response of the eye through computational modeling of a variety of projectiles and loading conditions. Simulations predicted the region of the eye where injury is most likely to occur for a particular projectile. Normalized energy was highly correlated with peak stress and pressure and was the best single predictor of globe rupture. Incorporation of the projectile relative size reduced variability in the stress response and may be of importance in eye injury prediction.

In summary, the computational results agree strongly with the matched experimental results. This further validates the ability of the eye model to predict globe rupture in diverse loading conditions and scenarios and is of value in mitigating injury caused by blunt ocular trauma.

REFERENCES

1. McGwin G, et al. *Arch Ophthalmol* **123**, 970-976, 2005.
2. Stitzel JD, et al. *Stapp Car Crash J* **46**, 81-102, 2002.
3. Delori F, et al. *Invest Ophthalmol* **8**, 290-301, 1969.
4. Kennedy EA, et al. *Stapp Car Crash J* **50**, 651-671, 2006.

Table 1: Summary of Simulations

Object	# Cases	Dia. (mm)	Mass (g)	Modulus (N/mm^2)	Vel. Limits (m/s)		Average Max. Stress (MPa)	Average Max. Pressure (MPa)
					Lower	*Upper*		
Baseball	5	76.10	146.50	12	30.10	42.80	23.13	2.18
BB, lg	9	4.50	0.38	200000	53.00	122.40	26.16	1.12
BB, sm	5	4.37	0.34	200000	10.18	11.47	6.01	0.11
Paintball	12	17.30	3.13	12	65.50	112.50	24.14	2.70
Softair Pellet, heavy	7	6.00	0.21	1800	73.03	87.35	11.62	0.75
Softair Pellet, light	4	6.00	0.12	1000	88.32	117.80	10.64	0.70
Aluminum Rod, lg	4	11.16	5.19	70000	43.71	53.21	19.49	1.82
Aluminum Rod, sm	4	9.25	3.57	70000	42.13	59.20	17.93	1.61
Blunt Impactor	3	19.90	112.55	3000	8.53	8.72	9.37	0.56
Foam, lg	12	6.35	0.08	2	4.30	31.00	5.04	0.13
Foam, sm	6	4.50	0.04	2	38.06	47.23	7.78	0.19
Plastic Rod, lg	4	9.75	0.69	1000	17.83	20.16	9.74	0.41
Plastic Rod, sm	4	7.62	0.35	1000	23.50	24.46	9.72	0.36
Total Runs	**79**							

THE CAPSULE'S CONTRIBUTION TO TOTAL HIP CONSTRUCT STABILITY – A FINITE ELEMENT ANALYSIS

[1,2]JM Elkins; [1]MJ Rudert; [1]Y Tochigi; [1]DR Pedersen; [3]BJ Ellis; [1,4]JJ Callaghan; [3]JA Weiss; [1,2]TD Brown

[1]Department of Orthopaedics, University of Iowa, Iowa City, IA; [2]Biomedical Engineering, University of Iowa, Iowa City, IA; [3]Bioengineering, University of Utah, Salt Lake City, UT; [4]Iowa City Veterans Administration Medical Center, Iowa City, IA

INTRODUCTION

Instability/dislocation, a frequent complication following total hip arthroplasty (THA) has recently been identified as having surpassed mechanical loosening as the most common reason for revision THA surgery [1]. The hip capsule, a robust but intricate collection of soft tissue, stabilizes the hip joint during over a large range of motion by constraining motion between the acetabulum and proximal femur. Structural compromise of the capsule, either from pre-existing pathology or resulting from the surgical approach, is thus of particular concern following THA. To investigate the relationship between capsule structural integrity and THA instability, a finite element (FE) model was developed to parametrically explore the effects of capsular defects on dislocation resistance.

METHODS

A human cadaveric hemipelvis was carefully dissected of all non-capsular soft tissue. Fiber directions on the exposed, intact capsule were demarcated with silastic tubes filled with barium contrast, and the hemipelvis was CT-scanned (Fig 1A).

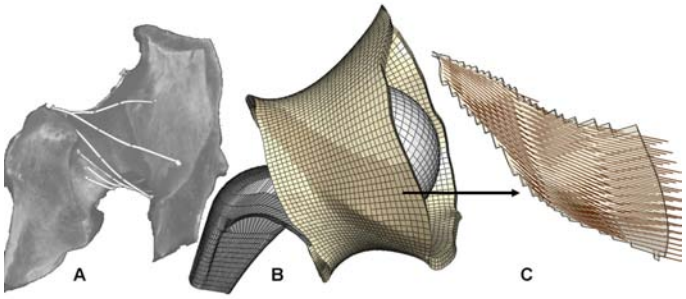

Figure 1: A): CT dataset for a native (left) cadaver hip hemi-pelvis. (B): Capsule representation in the corresponding FE model. (C): Fiber directions shown for a single fiber-direction family

The CT data set was segmented to include the marking tubes, capsule and bony structures. The segmented surfaces were meshed with TrueGrid (Fig. 1B). The capsule was modeled using a micromechanical fiber-based anisotropic strain energy potential developed by Holzapfel [2]. Material coefficients were inferred using load-displacement data for capsule distraction [3]. The capsule was incorporated into an existing THA FE model (Fig. 1B), which consists of 3 parts: Femoral component (28mm), liner and backing. A metal-on-metal bearing couple was chosen, with the head, neck and liner (all CoCr) modeled as linear elastic (E=210 GPa, ν = 0.3). A sit-to-stand motion sequence [4] was used to assess the influence of capsule integrity on dislocation resistance. Capsular defects, simulating surgical incisions or incisional repair, were postulated at various positions, indexed circumferentially (Fig. 2).

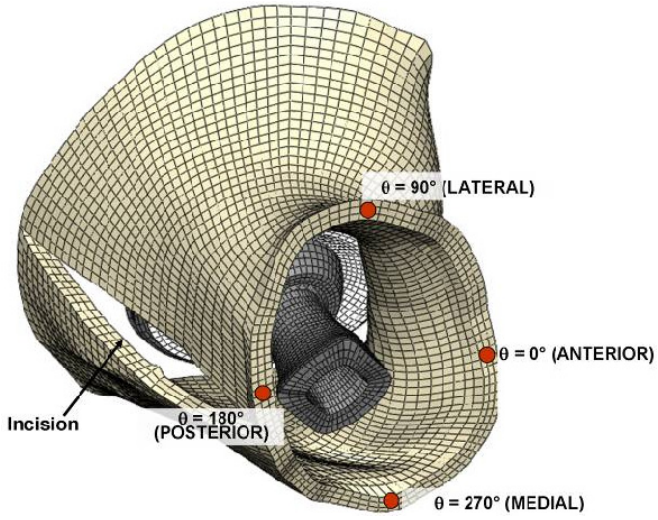

Figure 2: Coordinate conventions for specifying circumferential location, illustrated for a right hip in flexion. The anterior-most aspect of the capsule is assigned a value of θ=0° with θ increasing in a counter-clockwise fashion. Representatively, a longitudinal incision is shown, located at approximately 190°.

One-hundred-nine individual FE simulations were run (Abaqus Explicit 6.9), including the baseline case of an intact normal capsule, 22 cases of capsule thickness variation, and 86 specific situations of defect or defect + repair

RESULTS AND DISCUSSION

For all FE runs, the resultant moment that developed to resist dislocation (designated as the resisting moment) was tracked throughout the entire kinematic input sequence (Fig. 3). The initial rise in resisting moment is caused by progressive tautening of the capsule. For the most compromising case, the capsule provided virtually no resistance to dislocation, and the resisting moment was attributable to hardware interactions only. Repair of this defect returned construct stability to near baseline levels.

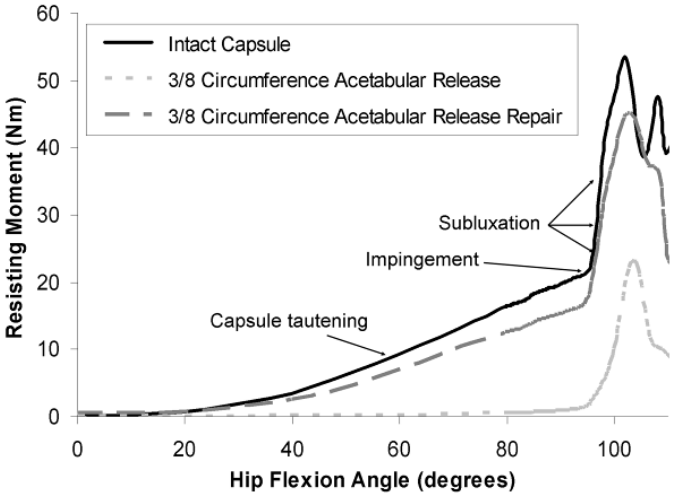

Figure 3: Resisting moment developed during impingement and dislocation.

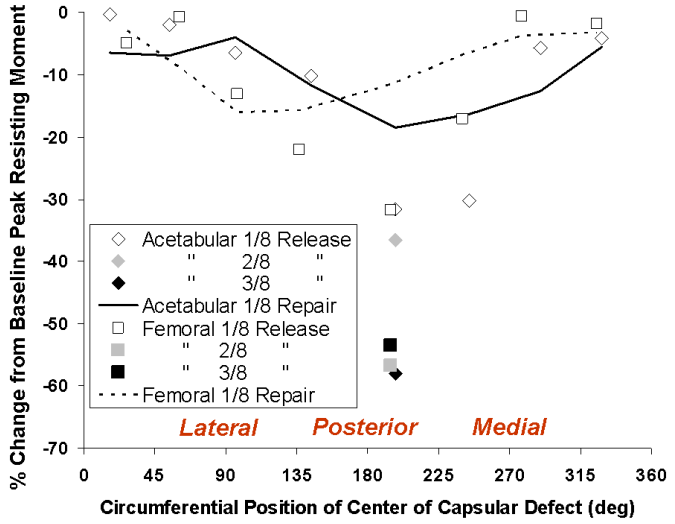

Figure 4: Effects of capsule detachment and repair.

Capsular release from both the acetabular and femoral attachment sites created a substantial drop in construct stability (Fig. 4). Again, repair of these defects returned stability to near base-line levels of dislocation resistance. Simulated suture tensile loads, arising from various repair techniques, were seen to be highly technique-and location-dependent (Fig. 5). Several suturing variants involved average tensile loads far exceeding the reported suture ultimate tensile strength (gray bar in Fig. 5).

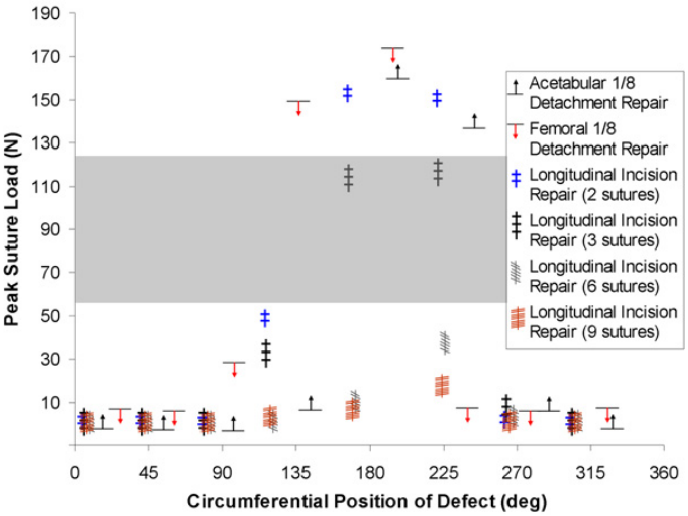

Figure 5: Peak suture tension developed for repairs of longitudinal slits with two, three, six, or nine sutures, and for single-site repairs of regional acetabular and femoral insertion detachments.

CONCLUSIONS

Localized compromise of capsule integrity can dramatically reduce construct stability. Appropriate repair of these capsule deficits can recover near-normal dislocation resistance, although repair-site failure is a concern. These finite element results underscore the benefit of retaining/repairing capsular structures in total hip arthroplasty, in order to maximize overall construct stability.

REFERENCES

1. Bozic KJ et al. JBJS 91A: 128-133, 2009.
2. Gasser TC et al. J Roy Soc Inter. 3, 15-35, 2006
3. Stewart KJ, et al. J Biomech 35, 1491-1498, 2002
4. Nadzadi ME, et al. J Biomech 36, 577-591, 2003

ACKNOWLEDGEMENTS

Financial support was provided by NIH AR53553 and by the Department of Veterans' Affairs

DEVELOPMENT AND VALIDATION OF A FINITE ELEMENT MODEL OF THE SUPERIOR GLENOID LABRUM

Christopher J Gatti, Joseph D Maratt, Mark L Palmer, Richard E Hughes, James E Carpenter

University of Michigan, Ann Arbor, MI, USA
email: rehughes@umich.com, web: www-personal.umich.edu/~rehughes/index.html

INTRODUCTION

The glenoid labrum is a common source of musculoskeletal pain and disability. Superior humeral head translation is one proposed mechanism of injury. The labrum is difficult to study in a laboratory setting because of its small size and articular location. The purpose of this study was to develop and validate a finite element model of the glenoid labrum for humeral head translation in order to understand the mechanical environment experienced by the labrum.

METHODS

The geometry of the glenoid, glenoid cartilage, labrum, and humeral head cartilage was obtained from μCT imaging (voxel size of 93 μm, reconstructed at 186 μm) and segmented using Mimics (Materialise NV). Boolean operations were used to distinguish the labrum from the glenoid cartilage and obtain accurate geometry of each tissue. Tetrahedral meshes were created in HyperMesh 9.0 (Altair Engineering, Inc.) using C3D4 elements for the glenoid labrum and cartilage (26,177 and 23,141 elements, respectively) and R3D3 rigid elements for the glenoid bone and humeral head cartilage (3,772 and 7,729 elements respectively) (Fig. 1).

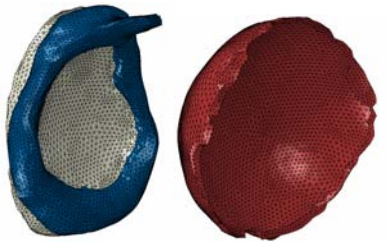

Figure 1: Finite element meshes of the labrum, glenoid cartilage, and humeral cartilage.

The labrum was modeled using a homogeneous, linear elastic, transversely isotropic material to represent the circumferentially-oriented fibrous composition of the labrum (E_p=0.24 MPa [1], E_θ=22.8 MPa [2], ν_p=0.33, $\nu_{\theta p}$=0.10, $G_{\theta p}$=2.0 MPa [3], where p defines the transverse plane and θ defines the circumferential direction of the labrum). The transversely isotropic material law was implemented using coordinate systems aligned to the circumferential orientation of the labrum. The glenoid cartilage was modeled as a homogeneous, linear elastic, isotropic material (E=1.7 MPa [1], ν=0.018 [4]), and the glenoid bone and humeral cartilage were modeled as rigid surfaces. The rigid glenoid surface was fixed in all degrees of freedom. The humeral head cartilage was oriented such that the humerus was positioned in 30° of glenohumeral abduction in the scapular plane with zero humeral rotation. The humeral cartilage was constrained from rotation and loaded with a 50N compression force directed into the glenoid. Quasi-static analyses were performed by translating the humeral head superiorly along the glenoid using displacement-control for 1, 2, and 3 mm above the center of the glenoid. Simulations were run using ABAQUS/Explicit v6.9 (SIMULIA, Inc.) with a critical time step of approximately 5e-6 seconds.

A validation experiment was performed on 6 shoulder specimens in a custom testing fixture. The boundary and loading conditions were set to be easily reproduced in the finite element model. The glenoid was fixed with the articular surface directed upward. A 50N compressive load was applied to the humerus directed into the glenoid, and the humerus was translated superiorly along the glenoid using computer-controlled motors. Radiopaque beads were placed along the superior labrum to determine the amount of movement of each bead in the plane of the glenoid. Radiographs were taken at 1, 2, and 3 mm of superior humeral head translation. The glenoid-plane movement of nodes along the superior labrum in the finite element model were then compared to the glenoid-plane movement of the beads in the validation experiment.

RESULTS AND DISCUSSION

The results of the model compared well to those from the validation experiment, especially in the superior and posterosuperior regions of the labrum (Fig. 2). The strains were greatest in 11-12 and 12-1 regions of the labrum and generally increased with greater humeral head translations (Fig. 3, 4).

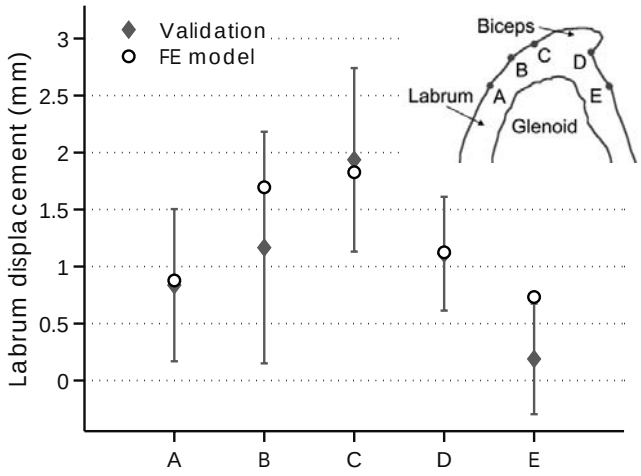

Figure 2: Labrum displacement for the finite element model and validation experiment for 3 mm of superior humeral head translation.

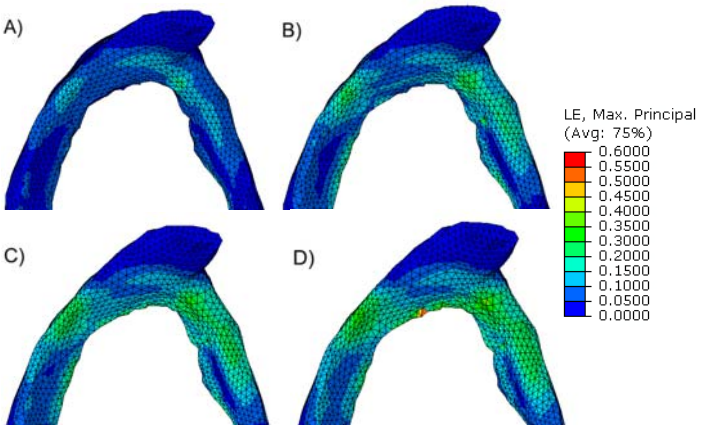

Figure 3: Strains in the labrum for 0, 1, 2, and 3 mm of superior humeral head translation (A, B, C, D, respectively).

The labrum and biceps attachment have high morphological variability which made standardizing a testing protocol between the model and validation experiment challenging [5]. Although the finite element model was based on a single specimen, the results of the validation experiment based on 6 specimens compared well to the model without optimizing model parameters. The displacement measures of the labrum were compared for movement only in the plane of the glenoid, and it is possible that there was movement out of this plane which was not measured due to the single radiograph technique. The model could be improved by using hexahedral elements and refining the integration of the biceps tendon, and this would likely extend the usability of this model.

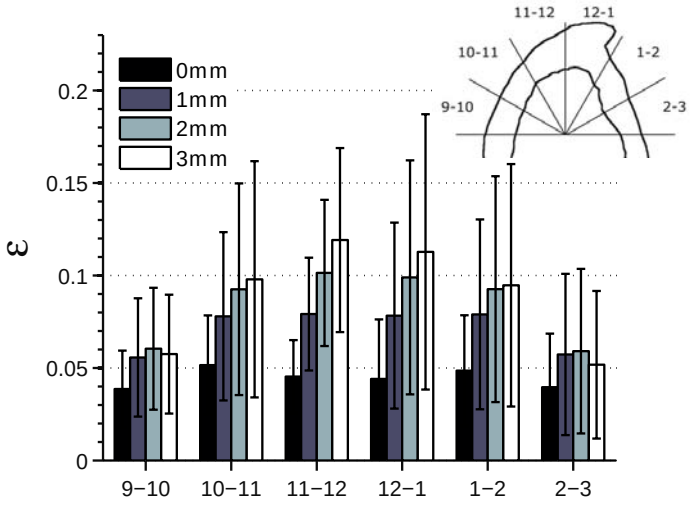

Figure 4: Mean (± 1 st. dev.) strains the superior labrum for 0, 1, 2, and 3 mm of superior humeral head translation.

CONCLUSIONS

A finite element model of the glenoid labrum was developed and validated for humeral head translation. This model could be used to better understand the local mechanical environment of the labrum and its relationship to pathology.

REFERENCES

[1] Carey J, et al. *J Biomed Mat Res* **51**, 711-716, 2000.
[2] Smith CD, et al. *J Anat* **212**, 49-54, 2008.
[3] Yao J, et al. *J Biomech Eng* **128**, 135-141, 2006.
[4] Cohen B, et al. *Transactions of ORS*, 1993.
[5] Smith C, et al. *Shoulder & Elbow* doi: 10.1111/j.1758-5740.2010.00050.x

ACKNOWLEDGEMENTS

This work was funded by the Department of Orthopaedic Surgery and the Valassis Endowed Research Fund. The authors thank all those who contributed to this study.

A COMPARISON OF THE PERFORMANCE OF HEXAHEDRAL AND TETRAHEDRAL ELEMENTS IN BONE-SOFT TISSUE FINITE ELEMENT MODELS

[1]Srinivas C. Tadepalli, [2]Ahmet Erdemir, [3]Subham Sett, [1]Peter R. Cavanagh

[1]University of Washington, Seattle, WA, USA
[2]Cleveland Clinic Foundation, Cleveland, OH, USA
[3]Dassault Systemes SIMULIA, Providence, RI, USA
email: cavanagh@uw.edu,

INTRODUCTION

Characterization of foot-ground or foot-shoe contact stresses provides significant insight into the biomechanics of the normal and pathological foot. The finite element method (FEM) is widely used in orthopaedic biomechanics for predictive simulations of joint contact stresses[1-2]. Due to the complex geometries of the anatomical structures, mesh generation accounts for most of the labor in model development. In FEM, hexahedral elements are generally preferred over tetrahedral elements because of their superior performance in terms of convergence and accuracy of solution[3,4]. This becomes more apparent as the convergence behavior of simulations are hindered by large deformation, material incompressibility, and contact with friction, mechanical features commonly seen in foot mechanics. Unfortunately, unlike tetrahedral meshing which is highly automated [5], hexahedral mesh generation is a time consuming process requiring considerable operator intervention. Despite their reputed advantages, the relative performance of tetrahedral meshes in contact models has not been well established; to our knowledge, there has not been a comprehensive study comparing the performance of hexahedral and tetrahedral elements when material and geometric nonlinearity are combined with material incompressibility and shear force loading conditions. Hence, the objective of the present study was to evaluate various types of meshes that can be used to model the interaction of a bone-soft tissue construct in contact with the rigid surface under compressive and shear loading.

METHODS

To assess the influence of the mesh type on the convergence and accuracy of the solution, a simplified geometric representation of a bone-soft tissue construct was used (a hollow sphere of inner and outer diameters of 20 mm and 30 mm, respectively). The model consisted of three components: bone, soft tissue and floor. Bone and the floor were modeled as rigid bodies to decrease computational time and the soft tissue was modeled as an incompressible hyperelastic material with a strain energy represented by a first order Ogden material model [6]. The bone and floor were meshed using 2D rigid shell elements (triangular and quadrilateral) while soft tissue was meshed using 3D continuum tetrahedral (linear and quadratic) and hexahedral (linear) elements [7]. A mesh convergence study was performed using both the models to assess the required mesh density (number of nodes and elements) for a converging solution. Tied contact was defined between the bone and the soft tissue so as to prevent any relative motion. Surface-to-surface contact was defined between the soft tissue and the floor. Two types of simulations were conducted using: 1) frictionless contact and; 2) contact with a coefficient of friction (0.3) between the floor and the soft tissue. The floor was completely fixed in all degrees of freedom while the bone and the soft tissue were allowed to move in the vertical direction (the direction of the applied load) and also horizontally along the direction of the applied shear force where appropriate. Two loading scenarios were considered. In the first case, a constant compressive load of 300N was applied to the bone. In the second case, the compressive load was increased to 700N and in addition, a shear force of 100N was also applied to the bone. Additional simulations also evaluated the effect of relaxation of the incompressibility assumption on tetrahedral mesh performance. For this purpose the Ogden material model parameter, was changed to reflect an

effective Poison's ratio of 0.45. In all simulations, the influence of the mesh type on the contact pressure predictions between the soft tissue and the rigid floor, and solution time was assessed. All the simulations were performed on a 16 processor computer with 64 GB RAM. Abaqus 6.10 beta [7] was used for the FE analysis.

RESULTS AND DISCUSSION

The peak pressure values, pressure distribution patterns, and the CPU times under the given loading conditions for hexahedral, linear and quadratic tetrahedral meshes are reported in Table 1. Contact pressure distributions for various conditions are shown in Figures 1, 2, and 3. Models consisting of hexahedral, linear and quadratic tetrahedral elements resulted in smooth and uniform pressure distribution in frictionless contact under compressive and shear loading conditions at full incompressibility [8]. When frictional contact was added between the soft tissue and the floor, the pressure distribution from the mesh consisting of linear tetrahedral elements was mesh dependent, as illustrated by many patches of locally elevated pressure indicating the phenomena of shear locking at full incompressibility (Figure 1b). Models consisting of hexahedral and quadratic tetrahedral elements resulted in smooth and uniform pressure distribution in frictional contact under compressive (Figure 2a, b) and shear loading conditions at full incompressibility (Figure 3a, b). In the most challenging simulation (700N compression, 100 N shear, contact with friction), both hexahedral and quadratic tetrahedral meshes resulted in similar pressure distributions.

CONCLUSIONS

Given the large amounts of time required for meshing complex anatomical structures using hexahedral elements, use of quadratic tetrahedral meshes appears to be a feasible alternative even in the setting of large-deformation hyperelastic contact. It should be noted that other FE solvers may have varying formulations to accommodate material and geometric nonlinearities and results from a test problem such as that presented here should always be examined.

REFERENCES

1. Li W, et al. *J Orthop Res* **26,** 1039-1045, 2008.
2. Shirazi R, et al. *J Biomech* **42,** 2458-2465, 2009
3. Cifuentes A, et al. *Finite Elements in Analysis and Design* **12,** 313-318, 1992.
4. Benzley S, et al. *4th*, *IMR*, 179-191, 1995.
5. CUBIT [http://cubit.sandia.gov/]
6. Erdemir A, et al. J Biomech **39,**1279-1286, 2006.
7. Abaqus 6.10 beta [http://www.simulia.com]
8. Tadepalli, SC et al. ASME SBC, 2010.

ACKNOWLEDGEMENTS

This study was supported by NIH grants 7 R01 HD037433-08 and R01 EB006735.

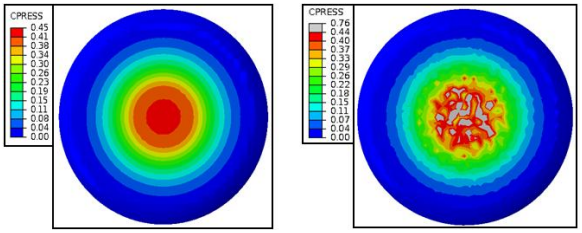

Figure 1: (a) Pressure distribution in hexahedral mesh as a result of compressive load (300 N) and contact with friction (μ=0.3) at full incompressibility. (b) Corresponding pressure distribution in linear tetrahedral mesh.

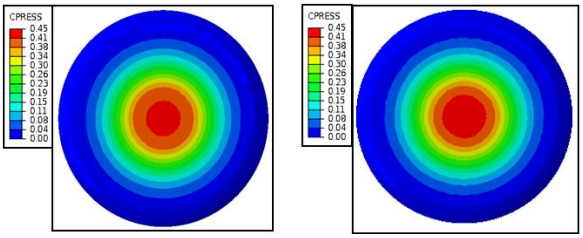

Figure 2: (a) Pressure distribution in hexahedral mesh as a result of compressive load (300 N) and contact with friction (μ=0.3) at full incompressibility. (b) Corresponding pressure distribution in quadratic tetrahedral mesh.

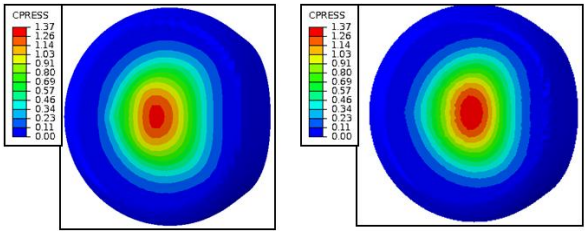

Figure 3: (a) Pressure distribution in hexahedral mesh as a result of compressive load (700N) combined with shear force (100N) and contact with friction (0.3) at full incompressibility. (b) Corresponding pressure distribution in quadratic tetrahedral mesh.

Type of Mesh	μ	ν	Load	Contact Pressure (KPa)	Time(Sec)
Hexahedral	0	0.5	300 (C)	450.5	5833
Tetrahedral (Lin)	0	0.5	300(C)	474.3	4018
Tetrahedral (Quad)	0	0.5	300(C)	462.0	8238
Hexahedral	0.3	0.5	300 (C)	440.4	13779
Tetrahedral (Lin)	0.3	0.5	300(C)	765.5	30964
Tetrahedral (Quad)	0.3	0.5	300(C)	450.4	19459
Hexahedral	0.3	0.5	700(C) + 100(S)	1303	64444
Tetrahedral (Lin)	0.3	0.5	700(C) + 100(S)	1593	75516
Tetrahedral (Quad)	0.3	0.5	700(C) + 100(S)	1371	64390

Table 1: Influence of mesh type on peak contact pressure prediction and computational time, coefficient of friction, Poisson's ratio, compressive (C) and shear (S) load, peak contact pressure and the simulation times.

A THREE-DIMENSIONAL INVERSE FINITE ELEMENT ANALYSIS OF THE HEEL PAD

[1,2]Snehal Chokhandre, [1,2]Jason Halloran, [3]Abhiram Pavana Sirimamilla, [2]Antonie J. van den Bogert and [1,2]Ahmet Erdemir

[1]Computational Biomodeling Core and [2]Dept. of Biomed. Eng., Cleveland Clinic , Cleveland, OH, USA
[3]Dept. of Biomed. Eng., Case Western Reserve University, Cleveland OH, USA

e-mail: chokhas@ccf.org web: https://simtk.org/home/multidomain

INTRODUCTION

Performing vital functions during locomotion and bearing significant loads, the foot is the primary interface between the body and the ground. Heel pad response can be used for biomechanical analysis of plantar tissue, which performs many important functions including shock absorption and distribution of contact loads [1]. To quantify plantar tissue behavior, previous computational studies have generally adopted two-dimensional representations and characterized nonlinear elastic parameters using compression dominant data only [1]. Hence, the goal of this study was to obtain material properties of the heel pad using a three-dimensional (3D) representation of specimen-specific heel pad geometry along with 3D loading response during compression dominated loading. Our follow-up objective was to compare optimized model predictions with data from a separate combined loading scenario including compression and shear. From diabetic foot ulceration to footwear design, the outcome of this work could be used to assess or improve many interventions or preventive treatment options utilizing computational modeling as an evaluation platform [2].

METHODS

Foot experimentation was previously performed on a specimen from a 58 year old male donor [3] (Fig. 1A). Computed tomography (CT) scans (Siemens s5vb20b, Medical Solutions USA, Inc., Malvern, PA) were collected for model development. The mechanical tests were conducted using a six degree of freedom robot (Rotopod R2000, Parallel Robotics Corp., Hampton, NH) using position control. A 25.4 mm diameter spherical indenter was used for compression testing of the heel which was followed by a combined compression and anterior-posterior shear loading [3]. During testing a foot specific coordinate axis was setup to approximately define the anterior axis from the posterior aspect of the heel to the second toe.

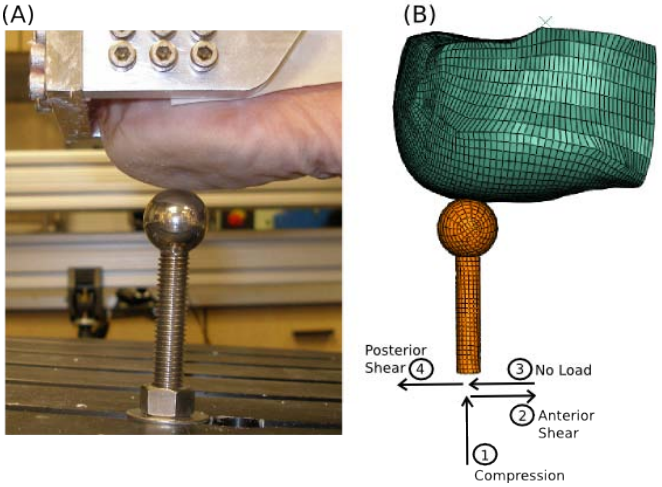

Figure 1: Heel pad indentation: (A) experimentation, and (B) 3D model with combined loading directions (B).

A 3D finite element (FE) heel pad model was developed to represent the foot specific geometry (Fig. 1B). The FE package Abaqus (Simulia, Providence, RI) was used to reproduce the experimental test conditions. The heel pad material (plantar soft tissue) was represented as a non-linear elastic material with an effective Poisson ratio of 0.475 to approximate near incompressibility. The strain energy function was defined as a first order Ogden form [4],

$$U=(2\frac{\mu}{\alpha^2})(\lambda_1^\alpha+\lambda_2^\alpha+\lambda_3^\alpha-3) \qquad (1)$$

Where, $\lambda_{1\text{-}3}$ are the principal stretches, and μ and α are the material properties representing the hyperelastic behavior. The experimental load-deformation data for the compression only cycle was used for the material parameter (μ and α) optimization and the combined loading (compression and shear) data was used to validate the model response.

For minimization of the sum of squared-errors between model predicted and experimental reaction forces, the Truncated Newton optimization algorithm available in SciPy (http://www.scipy.org) was utilized. Thirteen evenly spaced points along each directional loading curve were defined for the error calculation (anterior-posterior, medial-lateral, superior-inferior). Initial guess values were specified as μ = 0.1 kPa, α = 11. The optimized parameter values were then used to simulate the load response during a test in which the heel pad was compressed, and then additionally deformed in anterior and posterior shear. Simulations were compared to measured responses.

RESULTS

A total of 117 iterations were required to reach convergence with a corresponding root mean square error (RMSE) of 0.7136 N (0.61% max force magnitude) between model and experiment (Fig. 2A). Optimized material parameters were found as μ= 1.084 kPa and α = 9.780. Using the optimal parameters, it was observed that the overall trends and magnitudes were reproduced during combined loading (Fig 2B). The superior direction loading resulted in an RMSE of 10.54 N (3.0% max force magnitude) with the lateral and anterior directions realizing 21.67 N (6.38% max force magnitude) and 6.52 N (1.9% max force magnitude), respectively.

DISCUSSION

The study was successful in reproducing the 3D geometry and accurately predicted multi-axis response during the compression dominant indentation test (Fig. 1 and 2A). Using the optimized parameters, it was also observed that the model predicted load response was generally comparable in the dominant shear loading direction (anterior) with very good agreement in the superior loading direction (Fig. 2B). It is speculated that deviations in the lateral force behavior could be a result of registration errors between CT image set and experimental setup. Future sensitivity and optimization studies will assess this explanation. Further plantar tissue validation will also be performed for additional loading tools and loading scenarios [3]. Given the availability of data, this study could also be extended to include forefoot passive response, effectively modeling whole foot structural response. To the authors knowledge, this study is the first to optimize nonlinear elastic material parameters using dominant and off-axis loads in a 3D model and including a validation attempt with an additional dataset. The results have important implications for the accurate prediction of shear response in plantar tissue and lend more insight into the biomechanics of this important structure.

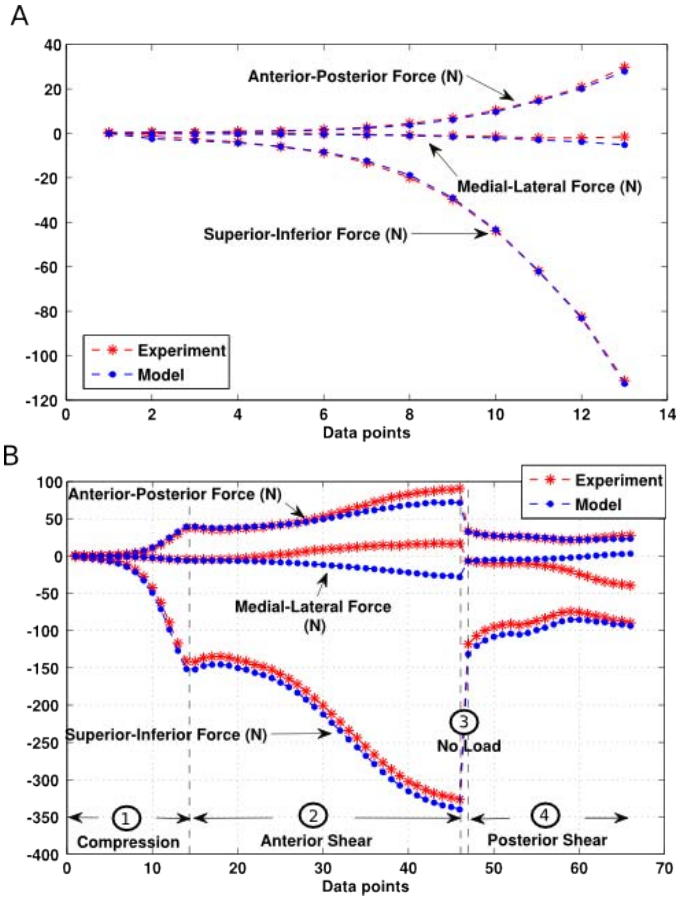

Figure 2: Comparison of experimental reaction forces with the model predicted values using the optimized material properties A) compression B) combined loading of compression and anterior-posterior shear.

REFERENCES

1. Erdemir et al. *J Biomech*, **39**, 1279-1286, 2006.
2. Budhabhatti et al. *JBME*, **129**, 750-756, 2008.
3. Erdemir et al. *JBME*, **131**, 094502, 2009.
4. *Abaqus User's Manual*, Version 6.7.1, 2007.

ACKNOWLEDGEMENTS

This study was funded by NIH R01EB006735.

SIMULATED CONTACT FORCES IN THE TRIQUETRUM-HAMATE JOINT DRIVEN WITH SUBJECT SPECIFIC *IN-VIVO* KINEMATICS

[1]Michael Rainbow, [2]Joel Schwartz, [2]Robin Kamal, [2]Edward Akelman, and [2]Joseph Crisco
[1]Brown University and [2]Department of Orthopaedics, The Warren Alpert Medical School of Brown University and Rhode Island Hospital, Providence, RI, USA
email: michael_rainbow@brown.edu, web: http://www.brownbiomechanics.org

INTRODUCTION

The articulation of the triquetrum on the hamate (TqH) has been alternatively described as a rotation on the saddle shaped surface of the hamate, a translation along a helicoidal or screw-shaped path, and a rotation on the convex oval surface of the hamate[1]. Recently TqH motion was studied along the dart thrower's path[2] (DTM), wrist motion from radial extension to ulnar flexion, that some suggest to be the most important functional motion of the joint[3]. It was shown that the articulation of the triquetrum on the hamate was roughly helicoidal as the triquetrum rotated around the convex surface of the hamate. It was qualitatively observed that the triquetrum maintains a distal course along the hamate until it reaches a prominent distal ridge at which point it begins a volar course. However it is difficult to determine whether or not the triquetrum is interacting with the distal ridge of the hamate using standard kinematic measures. The purpose of this study was to compute the orientation and location of the contact force between the triquetrum and hamate as the wrist moved along a dart thrower's path.

METHODS

Following IRB approval and informed consent, 3 male and 3 female, right-handed volunteers, average age 24.3 ± 2.8 yrs were screened for any injury or diseases that would affect carpal motion. The right wrist of each subject was CT scanned using a custom designed jig in the neutral wrist position and 5 static positions along a hammering path. Positions along the path included -40º (windup), -20º, 0º (hammer handle perpendicular to forearm), 20º, and 40º (impact). Separate tessellated 3-D bone surface models representing the outer cortical shell of the third metacarpal, radius, hamate, and triquetrum were generated through segmentation of the neutral CT scan in Mimics 9.11 (Materialize, Leuven, Belgium).

Six-degree-of-freedom global transforms describing the motion of each bone from the neutral wrist position to each hammering position were calculated using a previously established markerless bone registration technique[2]. Transforms describing the relative motion of the TRQ with respect to the HAM along the hammering path were then computed. Cartilage articular facets of the triquetrum and hamate bones were approximated using landmark features of the CT scans, verified by comparison with a high resolution μCT volume image of a cadaver triquetrum and hamate (age 62). The scans were generated at a resolution of 60 μm (isometric voxels) using a desktop micro-computed tomography system (μCT 40, Scanco Medical, CH). The soft tissue and bony surfaces were manually segmented using Mimics 13. A single three-dimensional (3-D) surface model was generated from the μCT datasets using minimal smoothing and point reduction. These surfaces were used to identify cartilage on the articular surfaces of the CT bone surfaces (**Fig. 1**). These regions were thickened between 0.5mm-0.75mm, based on known cartilage thickness and with the requirement that the articular surfaces were in contact throughout the entire range of motion studied. These modified models were then smoothed using Geomagic Studio 11 (Geomagic Inc, Durham, NC) and imported into LifeModeler (LifeModeler Inc, San Clemente, CA).

LifeModeler was used to compute the contact force between the triquetrum and hamate throughout the hammering path based on the amount of intersection of the two surface meshes. Contact force location and orientation were reported in a capitate-based inertial coordinate system because it aligned well with the dorsal-volar and proximal-distal directions of the hamate. Linear regression was then performed on both location and orientation of the force vector in the proximal-distal and dorsal-volar directions to examine the relationship of each

of these variables with the independent variable of wrist position along the hammering path.

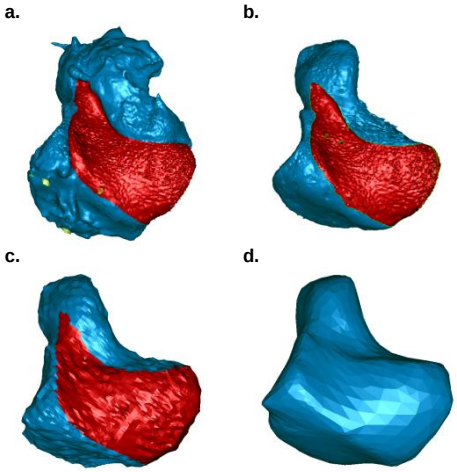

Figure 1. Smooth regions (red) of soft tissue segmented from μCT (**a**) were matched with the articular surfaces of the bone surfaces (**b**) to identify cartilaginous regions. Similar features on each subject's CT bone surface were used to identify the articular region (**c**). This region was then thickened between 0.5mm-0.75mm, and the entire body was smoothed for use in the LifeMOD simulation (**d**).

RESULTS AND DISCUSSION

As the wrist moved from radial-extension toward ulnar-flexion the contact force vector significantly ($P < 0.0001$) travelled 7.2 ± 2.1 mm in the distal direction and 4.2 ± 1.7 mm in the volar direction. The force vector swept through a mean angle of 58.1° ± 7.0° across subjects. The orientation of the force vector significantly ($P < 0.0001$) shifted from a more proximal (but still distal) orientation to a more distal orientation and from a dorsal to volar orientation as the triquetrum moved distally and volarly along the hamate. We qualitatively observed that at the strike position of the hammering task, the contact force vector was located on or near the distal ridge of the hamate (**Fig. 2**).

CONCLUSIONS

We measured the triquetrum-hamate articular contact force using a rigid body spring model driven by *in vivo* kinematics of the triquetrum with respect to the hamate along a dart throwers path. Our visual understanding of the triquetrum translating along an oblique path over the hamate from proximal and dorsal to distal and volar as the wrist moved along the dart throwers motion was confirmed by the changes in the computed articular contact forces. We found that as the triquetrum moved distally on the hamate the contact force shifted from its location on the oval articular surface of the hamate to the distal ridge. The orientation of the force vector also shifted from a more dorsal to a volar direction. These data suggest that the distal ridge of the hamate does indeed act as a guide for the triquetrum as the wrist moves through a dart thrower's motion. Primary limitations in this study include the imposed penetration of the articular surfaces of the triquetrum and hamate, as well the lack of adjacent carpal articulations and ligament constraints. Future work will include these structures and the use of kinematics to train a model for forward dynamics simulation.

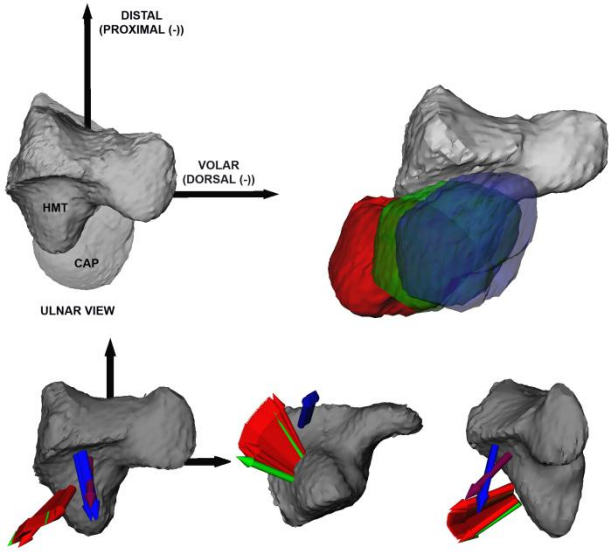

Figure 2. The hamate (HAM) in the capitate (CAP) coordinate system space (**Top left).** The positions of the TRQ (colored) on the HAM (grey) of a typical subject at the windup (red; wrist at -40º), neutral hammer (green; wrist at 0º), and impact (blue; wrist at 40º) wrist positions (**Top right)**. Three views of the contact force as it sweeps through the range of wrist positions (**Bottom Panel**). As the triquetrum moved distally on the hamate, the force vector shifted from a distal location and more dorsal orientation (red vector) to a proximal location and a more volar orientation (blue vector).

REFERENCES

1. Moritomo *et al.*, *J Hand Surg* [AM], 2003.
2. Kamal *et al*., *ORS Trans* **35**, *2010.*
3. Crisco *et al.*, *JBJS* [AM], 2005.

3D IN VIVO CERVICAL SPINE KINEMATIS: PRELIMINARY COMPARISON OF FUSION PATIENTS AND CONTROL SUBJECTS

[1]Colin P McDonald, [2]Victor Chang, [3]Casey C Bachison, [3]Stephen W Bartol and [1]Michael J Bey

[1]Bone and Joint Center, Henry Ford Hospital, Detroit, MI, USA
[2]Neurosurgery Department, Henry Ford Hospital, Detroit, MI, USA
[3]Orthopaedic Surgery Department, Henry Ford Hospital, Detroit, MI, USA
email: cmcdona2@hfhs.org

INTRODUCTION

Degenerative disc disease (DDD) of the cervical spine is a common condition that causes significant pain, disability, and medical expense. For example, treatment for DDD in 2000 exceeded 110,000 patients in the United States alone [1]. A common treatment for patients involves removal of the degenerated disc and fusion of the adjacent vertebral bodies. However, previous research has shown that as many as 25-92% of patients treated with fusion have disc degeneration at the adjacent levels within 10 years after surgery [2,3]. It has been hypothesized that this degeneration results from changes in motion at vertebral segments adjacent to the fusion site [2]. However, it is unknown if fusion patients have altered cervical spine motion. Thus, the objective of this study was to compare the dynamic, three-dimensional (3D) motion of the cervical spine in control subjects and cervical fusion patients.

METHODS

Following IRB approval, ten subjects were tested. Five subjects had no history of spine pathology or spine surgery (control subjects, mean age: 28±1.6 years) and five subjects had surgical fusion of the C5-C6 vertebrae (fused subjects, mean age: 49±5.1 years). The fused subjects were tested at a mean of 21 months post-surgery. Subjects were seated with their neck centered in a biplane x-ray system [4]. Biplane x-ray images were acquired at 60 Hz during two motion tasks: axial neck rotation and neck extension. For the axial neck rotation task, subjects rotated their neck from a position of maximal right rotation to maximal left rotation. For the neck extension task, subjects moved their neck from a position of full flexion (chin against chest) to full extension. 3D motion of the head relative to the torso was also recorded using a video-based motion capture system. Following testing, CT scans of the cervical spine were acquired.

Motion at C4-C5 and C6-C7 was measured for each subject, as these represented the vertebral motion segments above (C4-C5) and below (C6-C7) the fusion site for the fused subjects. To accomplish this, CT images of the vertebral bodies (C4-C7) were segmented from the surrounding soft tissues and reconstructed into 3D bone models. The 3D position and orientation of each vertebra was determined from the biplane x-ray images using a model-based tracking technique [5]. Briefly, this technique generates a pair of digitally reconstructed radiographs (DRRs) from the 3D bone model, and then optimizes the correlation between the DRRs and the corresponding biplane x-ray images. This technique has been previously validated and is accurate to within ±0.6mm and ±0.6°.

Using custom software, anatomic coordinate systems were created for each vertebra (Figure 1). Lateral bending was defined as rotation about the X-axis (directed in the anterior direction), flexion-extension was defined as rotation about the Y-axis (directed to the patient's left), and axial rotation was defined as rotation about the Z-axis (directed in the superior direction). Kinematic outcome measures were determined by calculating translations and rotations at the adjacent vertebral motion segments (C4-C5 and C6-C7) for each group [6]. For axial neck rotation, C4-C5 and C6-C7 total range of motion was calculated from 55° right rotation to 55° left rotation. For neck extension, C4-C5 and C6-C7 range of motion was calculated from 50° neck flexion to 50° neck extension.

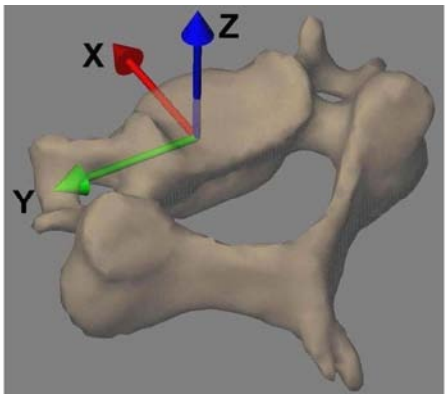

Figure 1: An anatomical coordinate system was created for each vertebra.

For each motion task (axial neck rotation and neck extension), a t-test compared control subjects and fused subjects in terms of the total range of motion about each anatomical axis above (C4-C5) and below (C6-C7) the fused segment.

RESULTS AND DISCUSSION

For the axial neck rotation motion task, rotation was evident about all three anatomical axes although the prominent rotation was in lateral bending. Rotation at C4-C5 and C6-C7 was greater in the fused subjects about all three anatomical axes, but this finding was statistically significant for only lateral bending ($p<0.03$, Figure 2).

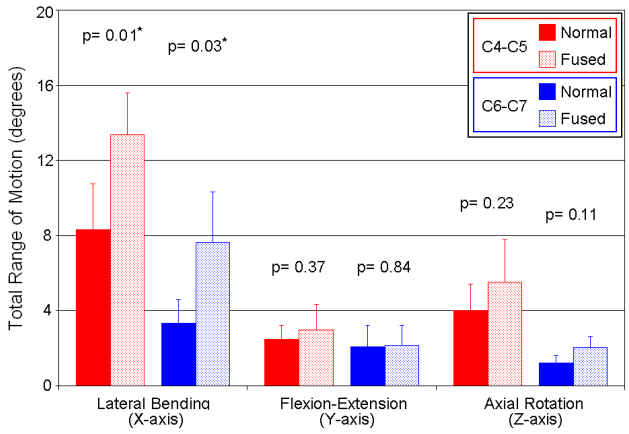

Figure 2: Range of motion for axial neck rotation.

For the neck extension task, flexion-extension was the dominant motion, with significant rotations in lateral bending and axial rotation. The data failed to detect any statistically significant differences between the control and fused subjects at each motion segment. This was consistent for rotations about all 3 anatomical axes ($p>0.14$, Figure 3).

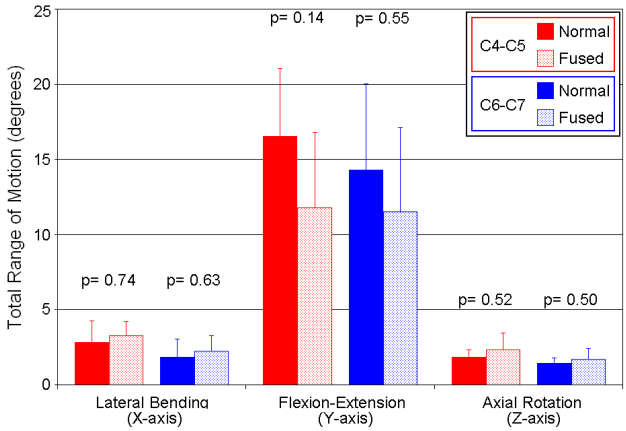

Figure 3: Range of motion for neck extension.

CONCLUSIONS

This study demonstrated differences in C4-C5 and C6-C7 motion between control subjects and patients who had undergone fusion of the C5-C6 vertebrae. In general, the fused subjects demonstrated greater range of motion about all anatomical axes than the control subjects for both axial neck rotation and neck extension motion tasks. However, the exception to this finding occurred during the neck extension motion task, where fused subjects demonstrated lower range of motion in flexion-extension than the control subjects. The significance of this finding is unclear, but on-going research will test additional subjects to more fully characterize kinematic differences following cervical spine fusion.

Cervical spine motion is complex, and a 3D dynamic in-vivo measurement technique is necessary to accurately quantify the rotations that occur about all three anatomical axes. An accurate measurement of adjacent segment motion following spinal fusion is an important step toward understanding the relationship between spinal fusion and adjacent level disc degeneration.

REFERENCES

1. Patil et al. Neurosurg 57, 2005.
2. Goffin et al. J Spinal Disord Tech, 17, 2004.
3. Hillibrand et al. J Bone Joint Surg Am, 81, 1999
4. Tashman et al. J Biomech Eng, 125, 2003.
5. Bey et al., J Biomech Eng, 128, 2006.
6. Stokes, Spine, 19, 1994.

IN VITRO DESCRIPTION OF FOOT BONY MOTION USING A CADAVERIC ROBOTIC GAIT SIMULATOR

[1]Eric Whittaker, [1,2]Patrick M. Aubin, and [1,3,4]William R. Ledoux

[1]VA RR&D Center of Excellence for Limb Loss Prevention and Prosthetic Engineering, Seattle, WA
Departments of [2]Electrical Engineering, [3]Orthopaedics & Sports Medicine, and [4]Mechanical Engineering, University of Washington, Seattle, WA
Email: wrledoux@u.washington.edu, web: http://www.amputation.research.va.gov/

INTRODUCTION

An accurate description of the bony motion of the foot during normal gait can aid in identification of foot abnormalities, injury prevention, and surgical correction. While *in vivo* foot models are common, they suffer from inaccuracies related to skin artifact and rigid body assumptions, and generally fail to account for the complexity of the foot. *In vitro* models used with dynamic gait simulators [1-3] allow for invasive techniques to access individual bones; however, accurate kinematics during gait simulations have been affected by non-physiologic ground reaction forces (GRFs) [2], low velocity [1,3], low vertical GRF magnitude (≤½ body weight (BW)) [1,2], exclusion of bones [1,3], and technically (rather than anatomically) based coordinate systems [1-3].

We have developed a ten-segment foot model with anatomically based coordinate systems for use with our robotic gait simulator (RGS). Simulations were performed at ¾ BW with a more biomechanically realistic GRF and velocity. This model provides a thorough and accurate description of the bony motion of the foot during gait.

METHODS

The foot model consisted of the following ten segments, each instrumented with four retro-reflective markers inserted into the respective bone: tibia/fibula (TIB), talus (TAL), calcaneus (CALC), navicular (NAV), cuboid (CUB), all three cuneiforms (grouped) (CUB), first (MET1), third (MET3), and fifth (MET5) metatarsals, and the proximal phalanx of the hallux (HAL). All of the segments used right-handed, anatomically based coordinate systems constructed from three markers or digitized bony landmarks. The additional fourth marker on each segment was used for redundancy and allowed for post-processing marker replacement in the case of marker dropout. Four of the segments (talus, navicular, cuneiforms, and cuboid) used three bony landmarks digitized with a four-marker stylus to create the segment's coordinate system. These points were tracked with a four-marker rod inserted into a screw placed in the bone. In general, the x-axis pointed anteriorly, the y-axis pointed superiorly, and the z-axis pointed laterally for right feet and medially for left feet. Kinematic data was collected with a six-camera Vicon MX system.

***Figure 1**: Fully instrumented specimen.*

Three neutral cadaveric specimens transected approximately 10 cm proximal to the ankle joint were prepared. The following nine tendons were dissected: Achilles (Ach), tibialis anterior (TA), tibialis posterior (TP), peroneus longus (PL), peroneus brevis (PB), flexor hallucis longus (FHL), flexor digitorum longus (FDL), extensor hallucis longus (EHL), and extensor digitorum longus (EDL). The RGS consisted of a Kistler force plate mounted to a 6-degree of freedom R2000 parallel

robot. The prescribed motion of the RGS was based on average *in vivo* tibia-to-ground kinematics from 10 healthy subjects [4]. The tendons were attached to force-controlled actuators, and muscles forces were prescribed from *in vivo* EMG data, or for the Achilles, *in vivo* measured force. Vertical GRF was scaled to ¾ of the donor's BW and adjusted with fuzzy logic real time control of the Ach and TA tendon forces and close loop iterative fuzzy logic control of the force plate position. *In vitro* GRF was achieved to an average of ±7.6%*BW of the *in vivo* data. Three stance-phase trials (heel-strike to toe-off) were performed in 2.7 sec each (four times slower than *in vivo* stance phase) for each foot.

RESULTS AND DISCUSSION

The ten-segment foot model provided repeatable kinematic data for the cadaveric specimens. Average standard deviations in sagittal plane segment angles across all three trials did not exceed 2° (Table 1). Sagittal plane range of motion (ROM) was greatest between the proximal phalanx and first metatarsal (avg: 63.98° for all specimens), and between the talus and the tibia (avg: 21.30°). In the midfoot, more motion was measured between the cuneiforms and navicular (avg: 13.45°) than between the navicular and talus (avg: 6.56°) or the metatarsals and cuneiforms (avg: 7.16°) (Table 1).

Table 1: *Avg ROM ± avg st. dev. for three trials; segment angle: CHILD_PARENT, read as "Child with respect to Parent"; all units in degrees;* ***bold*** *values indicate presence of multiple marker dropout*

	Specimen 1 (Left)	**Specimen 2 (Right)**	**Specimen 3 (Left)**
Segment Angle	*Avg. ROM ± Avg. St. Dev.*	*Avg. ROM ± Avg. St. Dev.*	*Avg. ROM ± Avg. St. Dev.*
TAL_TIB	20.95 ± 0.29	22.15 ± 1.76	20.79 ± 0.31
CALC_TAL	8.18 ± 0.32	4.68 ± 0.67	6.40 ± 0.15
NAV_TAL	6.96 ± 0.33	4.40 ± 0.46	8.32 ± 0.19
CUB_CALC	12.11 ± 0.84	7.67 ± 0.25	**21.45 ± 1.98**
CUN_NAV	13.63 ± 0.10	15.68 ± 0.78	11.03 ± 0.22
MET1_CUN	7.22 ± 0.33	10.36 ± 1.86	4.47 ± 0.09
MET3_CUN	8.49 ± 0.47	**6.79 ± 0.71**	5.65 ± 1.02
MET5_CUB	**20.00 ± 1.17**	11.78 ± 0.57	15.80 ± 1.19
HAL_MET1	63.10 ± 0.36	63.03 ± 0.79	65.82 ± 0.47

The anatomical coordinate systems proved beneficial in their ability to describe the initial position of each bone. For example, specimen 1 had a more adducted forefoot than the other two specimens as evidenced by the first metatarsal with respect to talus (Figure 2). First metatarsal motion relative to the talus is an important measure in assessing foot type, and repeatable data such as these demonstrate the utility of the foot model.

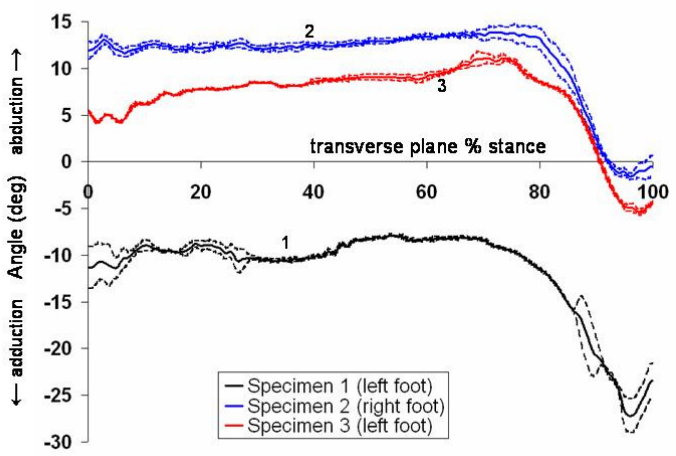

Figure 2*: Mean ± 1SD of three trials for transverse plane angles for first metatarsal with respect to talus; filtered with 15 Hz low pass filter*

CONCLUSIONS

This study provides an improvement in the understanding of foot bony motion during gait by providing anatomically based kinematic data during gait simulated with biomechanically realistic GRFs at both a higher velocity and load than is currently available. Efficacy of the data is limited only by the ability of the Vicon system to track the reflective markers during the dynamic trials. An extensive variety of kinematic interpretations can be made from the data presented in this study.

REFERENCES

1. Hurschler C, et al. *Foot & Ankle Int.* **24**(8)**,** 2003.
2. Nester CJ, et al. *J Biomech* **40**(9), 2007.
3. Okita N, et al. *Gait & Posture* **30**(1), 2009.
4. Bayomy AF, et al. *JBJS*. In press, 2010.

ACKNOWLEDGEMENTS

This work was funded in part by the VA RR&D, grants A3923 and A4843C.

IN VIVO LOAD-RELAXATION OF THE TRUNK WITH PROLONGED FLEXION

Nima Toosizadeh, Babak Bazrgari, Brad Hendershot, Khoirul Muslim and Maury A. Nussbaum

Industrial & Systems Engineering, Virginia Tech, Blacksburg, VA, USA
email: nussbaum@vt.edu

INTRODUCTION

Many occupational tasks require prolonged trunk flexion, and such exposures are associated with an increased risk of low back disorders (LBDs). Understanding the mechanical and physiological consequences of flexion is complicated by time-dependent responses to sustained trunk postures. As such, an accurate assessment of load partitioning among passive and active components of the human trunk, such as in biomechanical models, requires a realistic representation of rate-dependent passive properties. While creep and load-relaxation responses of the spine under axial loading have been extensively investigated [1-3], viscoelastic responses to prolonged trunk flexion, in particular load-relaxation behaviors, have not been sufficiently described.

Hence, the main purpose of this study was to quantify the load-relaxation response of the human trunk during prolonged flexed postures. Load-relaxation responses of the trunk were measured *in vivo* at different trunk flexion angles and exposure durations. Measured trunk responses were then fit using a viscoelastic model. We hypothesized that the trunk would exhibit nonlinear viscoelastic responses to prolonged flexion and that these would depend on the trunk flexion angle.

METHODS

Twelve participants, gender balanced, with mean (SD) age of 22.7 (3.7) years and body mass of 67.8 (11.3) kg, participated in the study. Trunk postures were monitored using electromagnetic sensors (Xsens, Los Angeles, CA, USA) on the T10 and S1 spinous processes, and bipolar surface electrodes were used to monitor activity of the bilateral erector spinae, internal obliques, external obliques and rectus abdominis muscles. Using these, initial measurements were obtained of flexion-relaxation (FR) angles. Participants then stood in a metal frame that restrained pelvic and lower limb motions. Participants' trunks were constrained at the T8 level using a harness-rod assembly (Fig. 1) and their legs were raised to achieve trunk flexions of 33, 66, and 100% of their FR angle; this was held (with minimal muscle activity) for durations of 2 and 16 min. Temporal variation of passive trunk resistance (i.e., trunk load-relaxation) to the induced flexion was measured using an in-line load cell (Interface SM2000, Scottsdale, AZ, USA) located on the rod-harness assembly.

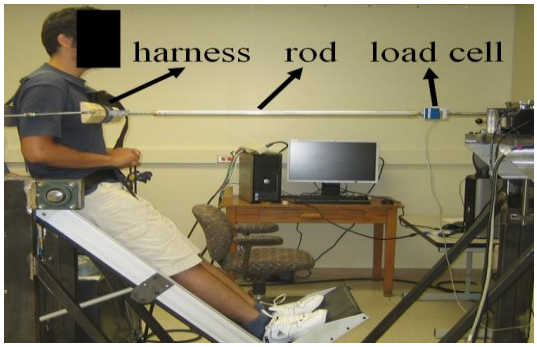

Figure 1: Experiment setup (33% of FR angle)

Load-relaxation responses of the trunk were modeled using a three-parameter model, based on Ponyting-Thomson's approach:

$$M(t) = \frac{\theta_0 k_2}{k_1 + k_2}\left(k_2 e^{-\left(\frac{k_1+k_2}{C}\right)t} + k_1\right)$$

where θ_0 is the initial angle, k_1 and c are torsional spring and damper components in parallel, and k_2 is an in-series torsional spring (Fig. 2). Passive moments, M(t), were calculated from measured forces and the vertical distance between the harness and S1. Model parameters were estimated for each trial (angle and duration) by minimizing least-squared errors in predicted moments. Mixed-factor analyses of variance (ANOVA) were used to assess the effects of gender, flexion angle, and duration on model parameters ($\alpha = 0.05$).

RESULTS AND DISCUSSION

Measured load-relaxation behaviors (i.e., decreases in moments) were significantly affected by exposure duration (p=0.037) and flexion angle (p<0.01), but did not differ between genders (p=0.25). Mean (SD) trunk moments decreased following 2 min. of exposure at 33, 66, and 100% of FR by 2.2 (3.6), 2.6 (4.5), and 21.6 (21.9) Nm, respectively. Following 16 min. of exposure, the respective decreases were 6.8 (5.9), 11.6 (11), and 26.1 (16.3) Nm. For each participant and condition, the Ponyting-Thomson models fit the measured load-relaxation behaviors closely (average relative error = < 3%).

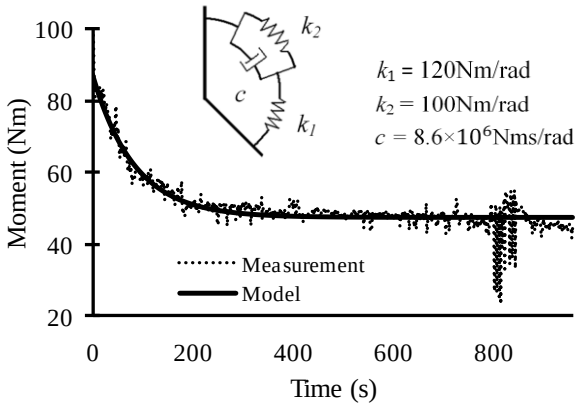

Figure 2: Sample results for measured and predicted passive trunk moment (angle = 100% of FR, duration = 16 min.).

Fitted model parameters indicated nonlinear viscoelastic behaviors during the sustained flexed postures. All three parameters were significantly (p<0.01) affected by flexion angle, with particularly large effects evident when flexion angle increased from 66 to 100% of FR (Fig. 3). Here, k_1 and c represent the time-dependent and k_2 the instantaneous responses to deformation. The larger values of k_1 and c at 100% of FR thus indicate a more pronounced load-relaxation response at this extreme flexion angle. No model parameters were affected by exposure duration (p>0.089), and these did not differ between genders (p>0.22). These findings suggest that a simple linear viscoelastic model can reasonably simulate trunk responses to prolonged flexion, but (as was anticipated) passive tissue responses are specific to flexion angle. The current experimental setup isolated the effects of trunk flexion angle and exposure duration independent of variation in gravitational loads and trunk muscle activity. Specified flexion angles were achieved by raising participants' legs, rather than by having them maintain forward flexion of the trunk. Any variability or potential confounding induced by muscle activity, inaccurate posture maintenance, or fatigue was thereby avoided.

CONCLUSIONS

Exposure to prolonged static trunk flexion is an important risk factor for occupational LBDs. The current work can facilitate a better understanding of how the load distribution among passive and active trunk components is altered during such exposures. Here, the angle-dependent, nonlinear, load-relaxation behavior of the human trunk was quantified. Future applications of these results to biomechanical models of the human trunk may provide better estimates of spinal loadings and stability under diverse occupational demands.

REFERENCES

1.Marta K, et al. *J Biomech* **39,** 1180-1190, 2005.
2.Holmes AD,et al. *Med Eng Phys* **18**,99-104, 1996.
3.Burns ML, et al. *J Biomech* **17**, 113-130, 1984.

ACKNOWLEDGEMENTS

This publication was supported by Cooperative Agreement Number R01-OH004089 from CDC-NIOSH. Its contents are solely the responsibility of authors and do not necessarily represent the official views of the CDC.

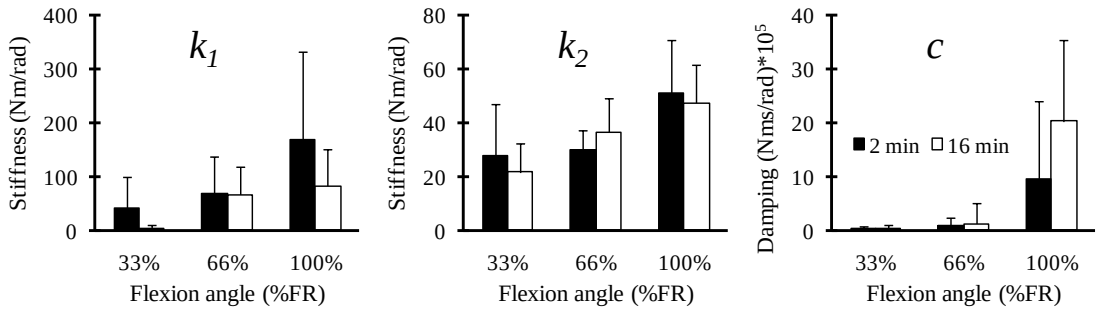

Figure 3: Summary of effects of flexion angle and duration on model parameters. Error bars are SD.

DIVISION OF LABOR AMONG LIMBS AND JOINTS OF THE CAT DURING LEVEL AND SLOPE WALKING

[1]Alexander Klishko, [2]Emma Hodson-Tole and [1]Boris Prilutsky

[1]Georgia Institute of Technology, Atlanta, GA, USA
[2]Manchester Metropolitan University, Manchester, UK
email: aklishko3@gatech.edu, web: http://www.ap.gatech.edu/Prilutsky

INTRODUCTION

The musculoskeletal system of quadrupedal animals is mechanically redundant. Redundancy gives rise to different gaits [4], various task-dependent patterns of muscle activity [8] and motor adaptation to injury [1]. Investigating motor tasks that can be accomplished by the animal in several different ways can help in understanding the physiological mechanisms guiding the process of motor strategy selection. The goal of this study was to investigate how external loads are distributed among limbs and major limb joints during level and slope walking in the cat. Our hypotheses were that different cats use similar division of labor among limbs and joints and that this division can be explained based on the distribution of muscle mass among limbs and limb segments.

METHODS

Four female cats (3.6±0.4 kg) were trained for several months to walk on a Plexiglas enclosed walkway (3.0 x 0.5 m) with three small force plates (0.16 x 0.11 m; Bertec Inc., OH, USA) embedded in the walkway floor. Locomotor tasks included level, downslope (-50% or -27^o) and upslope (50% or 27^o) walking. After training 28 small (6 or 9 mm) reflective markers were attached to cat's shaved skin over estimated joint center positions in 4 limbs by double-sided adhesive tape. Marker positions during level and slope walking were recorded by a 6-camera motion capture system (Vicon, UK) at 120 frames/s; ground reaction forces, at 360 Hz. Marker coordinates, ground reaction forces and known segment inertial parameters [5] allowed for calculations of moments of force at metatarsophalangeal (MTP), ankle, knee and hip joints of both hindlimbs as well as at metacarpophalaneal (MCP), wrist, elbow and shoulder joints of both forelimbs (for details see [3,6]). Ground reaction forces were normalized to body weight; joint moments, to cat body weight and hindlimb length. Ground reaction forces and normalized joint moments were averaged within a single cat and across cats for each percent of walking cycle. Peaks of ground reaction forces and joint moments were measured and tested for statistical differences between joints and walking conditions using repeated measures ANOVA. Significance level was set at 0.05.

RESULTS AND DISCUSSION

During level walking, peaks of vertical ground reaction forces exerted by forelimbs exceeded those of hindlimb by about 20% (Fig. 1; $p<0.05$). Similar results were reported for walking or running of other tetrapods: pigs, dogs, goats and horses (for review see [6]). During upslope walking, hindlimbs exerted substantially greater normal forces on the ground compared to forelimbs (Fig. 1; $p<0.05$). During downslope walking, forelimb forces were about 40% higher than hindlimb forces ($p<0.05$).

During quadrupedal level walking, constant speeds can be maintained with different distribution of decelerating and accelerating actions of fore- and hindlimbs. Cats choose to accelerate themselves more by hindlimbs (have greater positive horizontal force impulse) and decelerate more by forelimbs (greater negative impulse) during level walking (Fig. 1; $p<0.05$). This preference may be explained by relatively larger hindlimb segments and muscles and their greater ability to generate mechanical energy compared to forelimb muscles [5,7]. Although forelimbs experienced similar or greater forces and do similar absolute amount of mechanical work during body deceleration, the relatively weaker forelimbs can still effectively decelerate body because deceleration involves

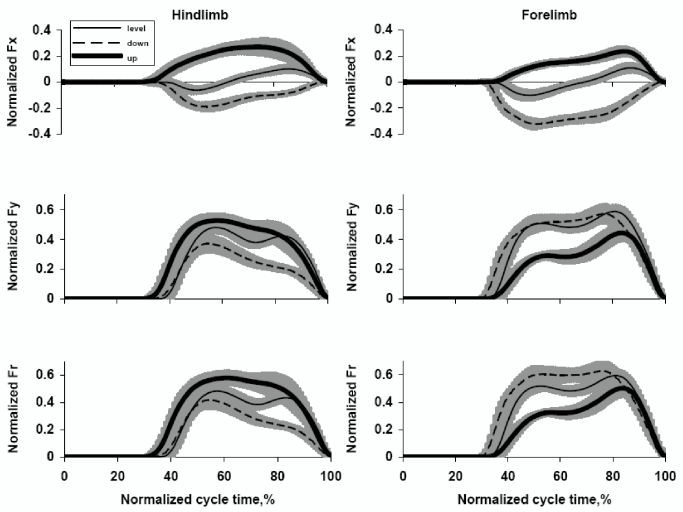

Figure 1. Ground reaction forces applied to hindlimbs (left panel) and forelimbs (right panel) during level, downslope and upslope walking as a function of normalized walking cycle. Mean ± SD of multiple trials of four cats. Fx, tangential force component; Fy, normal force component; and Fr, resultant force vector magnitude.

eccentric muscle action, which substantially enhances muscle force potential, reduces metabolic cost, and allows passive structures (ligaments, cartilage, bones) to absorb some of body energy. Horses that have a similar distribution of muscle mass across fore- and hindlimbs also accelerate themselves more with hindlimbs and decelerate with forelimbs during trotting at constant speeds [2].

During stance of cat level walking, hindlimb extensor moments dominate with a greatest contribution of knee and ankle extensors (Fig. 2, left panel). The forelimb support action during first half of stance is mostly provided by the elbow extensors, and during second half of stance by shoulder flexors (Fig. 2, right panel). Changing slope of locomotion from downslope to upslope modifies the contribution of joints to the support actions of hind- and forelimbs. For example, the largest hindlimb muscle group, hip extensors [7], became dominant among hind- and forelimb joints in upslope walking (Fig. 2), whereas in downslope walking a greatest contribution is provided by the large shoulder flexors (Fig. 2).

This specific division of labor between hind-

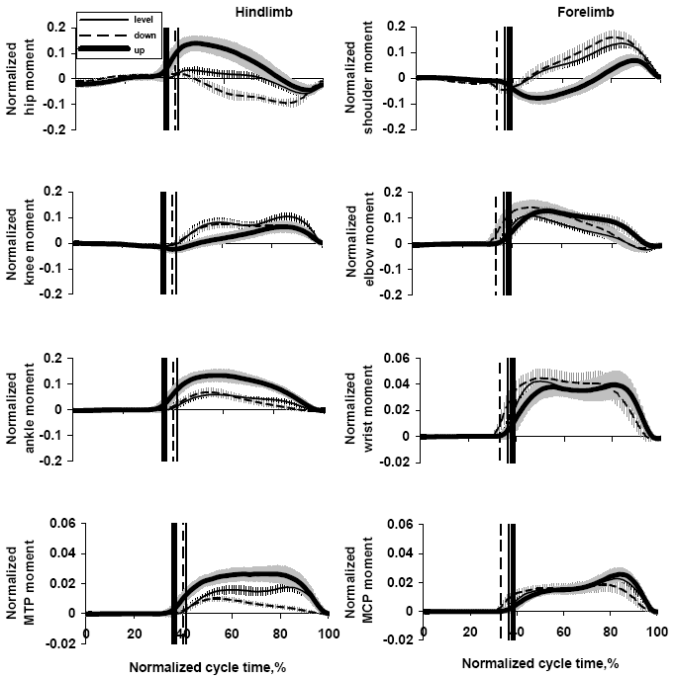

Figure 2: Normalized joint moments at fore- and hindlimb joints of multiple trials of four cats during level, downslope and upslope walking as a function of a walking cycle. Mean±SD. Extensor moments are positive. Vertical lines indicate swing-to-stance transitions

and forelimbs and among proximal and distal joints appears to be a common feature of quadrupedal (horses, goats, dogs) and bipedal (birds and humans) locomotion and reflects a specific distribution of muscle mass along hind- and forelimb segments.

REFERENCES

1.Chang YH, et al. *J Exp Biol*. **212**, 3511-3521, 2009.
2.Dutto DJ, et al. *J Exp Biol*. **207**, 3507-3514, 2004.
3.Gregor RJ, et al. *J Neurophysiol*. **95**, 1397-1409, 2006.
4.Hildebrand M. *Science* **150**, 701-708, 1965.
5.Hoy MG, Zernicke RF. *J Biomech*. **18**, 49-60. 1985
6.Prilutsky BI, Klishko AN. In: *Motor Control – Theories, experiments, and applications*. (Latash M, Danion F Eds) Oxford University Press, 2010.
7.Sacks RD, Roy RR. *J Morphol*. **173**,185-95. 1982
8.Smith JL, et al. *Ann N Y Acad Sci*. **860**, 452-455, 1998.

KINEMATIC GAIT DEVIATIONS, CENTER OF MASS POWER, AND THE METABOLIC DEMANDS OF GAIT FOR INDIVIDUALS WITH CEREBRAL PALSY

[1, 2] Michael H. Schwartz, [2] Adam Rozumalski, and [2] Marjolein van der Krogt

[1]University of Minnesota-Twin Cities, Minneapolis, MN, USA
[2]Gillette Children's Specialty Healthcare, St. Paul, USA

email: schwa021@umn.edu

INTRODUCTION

Increased metabolic power demand during gait is a significant concern for individuals with Cerebral Palsy (CP). It is common for children with CP to require metabolic power over 200% of their non-disabled peers. While this increased demand is the result of an atypical gait pattern, the precise mechanism by which gait deviations lead to increased power demand is not understood. It has been hypothesized that in normal gait, re-direction of the center of mass (COM) by the ground reaction forces, especially during step-to-step transitions, is a major determinant of the required energy [1].

Kurz observed differences in the COM power profiles of 10 subjects with CP compared to 10 typically developing controls [2]. In the CP group, the lead leg performed more negative work and the trail leg less positive work during double support. The excess negative work then had to be "recovered" through additional positive work performed by the stance limb during single support. Though metabolic energy was not measured in his study, Kurz postulated that these COM power deviations may account for the increased metabolic cost known to occur in children with CP.

In the present study we investigate the extent to which COM power and overall gait deviations explain the increased metabolic power required for gait in subjects with CP.

METHODS

Subjects with a diagnosis of diplegic CP, who had previously undergone gait and oxygen testing during the same visit, were identified from the clinical database at our center. Gait data was collected using a 12 camera optoelectronic system and 4 force plates, and was processed using the Vicon Plug-in-Gait model. Overall kinematic gait pathology was quantified using the gait deviation index (GDI) [2]. For the GDI, each 10-point decrement below 100 equates to one standard deviation from normal gait. Subsequent to gait testing, oxygen data was collected using a breath-by-breath oxymeter during either a 3 or 10 minute resting period, followed by a 6 minute walk. The mechanical COM power ($\dot{W}_{mech}$) was estimated from the gait data following Donelan. [1]. All data was nondimensionalized using body mass and leg length (mass/*body mass*, length/*leg length*, time/$\sqrt{leg\ length / g}$). Net metabolic power ($\dot{E}_{met}$) was calculated as the net nondimensional oxygen consumption [3]. A linear scaling of the COM power was used to correct for differences in walking speed between gait and oxygen testing. Data was grouped by $\dot{W}_{mech}$ (increments of 0.01) or GDI (increments of 10), and groups with N>9 were plotted, but all the data were used in the statistical calculations.

RESULTS AND DISCUSSION

There were 221 male and 183 female subjects, with a mean (sd) age of 13.2 (6.3) years, height of 1.49 (0.17) m, and mass of 47.0 (20.2) kg. The metabolic demand increased with COM power (r^2 = .28, $p<0.01$) [Figure 1]. Metabolic demand as percent of speed matched control increased with kinematic gait deviations measured by the GDI (r^2 = .25, $p<0.01$) [Figure 2]. A linear regression of metabolic demand vs. COM power yielded an efficiency of 19%.

$$\dot{W}_{mech} = 0.19\dot{E}_{met} - 0.01 \ (r^2 = .28). \qquad (1)$$

The relatively small variance in metabolic power accounted for by COM power (28%) suggests that in subjects with gait pathology, factors besides re-mechanical work on the COM may play a large role in creating metabolic demand. Such factors include spasticity, which can lead to co-contraction, and knee-hyperflexion, which can cause deviations from

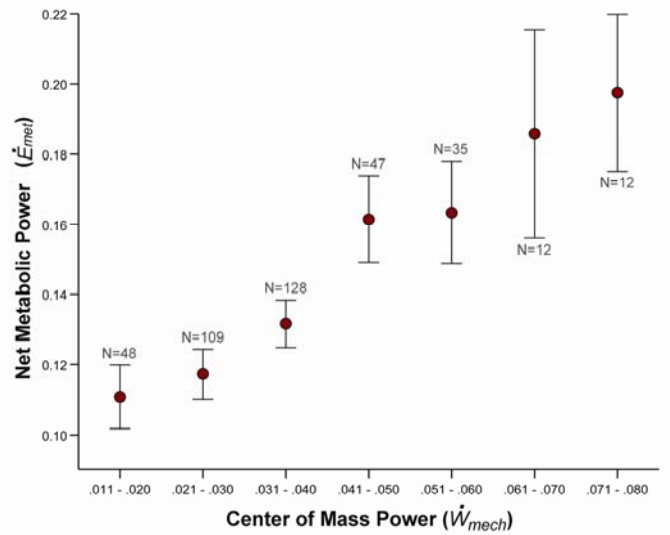

Figure 1. Metabolic demand increases with COM power.

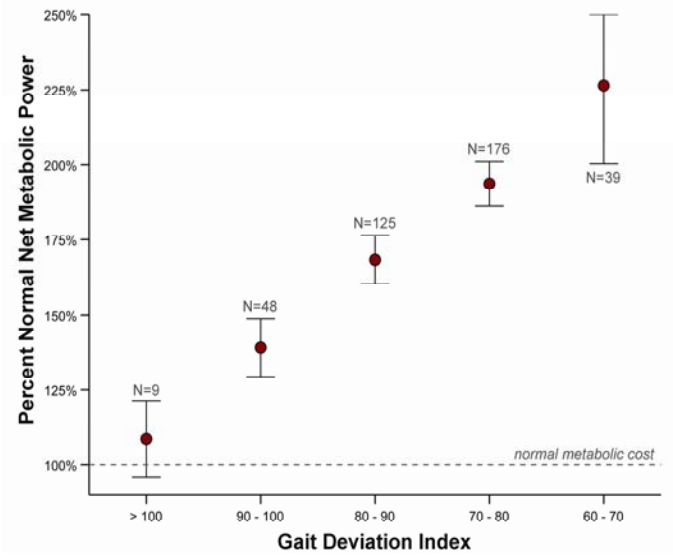

Figure 2. Metabolic demand increases with gait deviations.

an efficient pendulum gait. Interestingly, for a given level of COM power, metabolic power increases systematically with GDI [Figure 3]. That is, even when controlling for COM power, larger gait deviations lead to larger metabolic demand. This suggests that gait deviations are linked to the energy consuming mechanisms not accounted for by mechanical COM power. On the other hand, gait deviations alone account for only 25% of the variance in speed-matched metabolic power, indicating that simply walking atypically is not a sufficient explanation for increased power demand during gait in subjects with CP.

Experimental design and analytical compromises may have introduced variability into the results; lowering the explanatory capacity of either COM power or gait deviations. The most egregious of these is the fact that gait and metabolic data were collected asynchronously. This has two possible impacts on the results. The first is that the gait pattern may have varied between the tests. The second is that the gait speed during the two exams may not be matched. Although we corrected for the differences in speed, this may still have introduced some error due to the non-linear relationship between COM power and speed.

The specific mechanism for increased metabolic power demand in CP is not fully explained by either mechanical COM power, or by gait deviations. However, each of these measures may be clinically useful as a means of assessing sources of gait inefficiency, and for evaluating possible interventions aimed at lowering the metabolic cost of walking.

REFERENCES

1. Donelan JM *et al*. (2002) *J Exp Biol*, **205**:3717-27.
2. Kurz MJ *et al*. (2010) *Gait Posture*, **31**:347-50.
3. Schwartz MH *et al*. (2008) *Gait Posture*, **28**:351-7.
4. Schwartz MH, *et al*. (2006) *Gait Posture*, **24**:14–22.

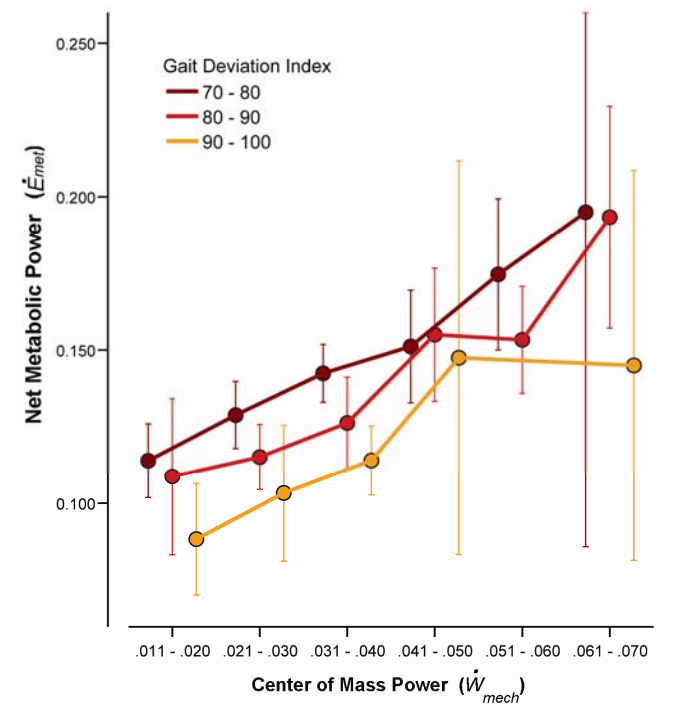

Figure 3. Metabolic demand increases with GDI for a given level of COM power.

STAIR CLIMBING ADAPTATIONS TO REDUCE QUADRICEPS DEMAND IN PATIENTS WITH KNEE OSTEOARTHRITIS ARE NOT ASSOCIATED WITH PAIN

[1]Jessica L. Asay, [1,2]Katherine Boyer and [1,2]Thomas P. Andriacchi

[1]Department of Veterans Affairs Bone and Joint Center, Palo Alto, CA, USA
[2]Department of Mechanical Engineering, Stanford University, CA, USA
email: asay@va51.stanford.edu

INTRODUCTION

Loss of quadriceps femoris function is a common clinical finding in patients with knee OA[1-2] and is consistent with reports that patients reduce the external knee flexion moments (net quadriceps moment) by increasing trunk flexion while climbing stairs[3]. Loss of quadriceps muscle strength may also be a risk factor in the initiation and progression of OA[2]. It remains unclear if the reduced quadriceps function during stair climbing is an adaptation to pain or associated with the disease process. Evaluating stair climbing biomechanics offers a potentially useful method for testing quadriceps function, patient function, and OA disease severity. The purpose of this study was to test the hypothesis that reduced quadriceps function during stair climbing is associated with pain in patients with knee OA and the compensatory mechanism to reduce quadriceps demand is reduced when pain is controlled with either and analgesic or anti-inflammatory medication.

METHODS

Six patients were randomized to one of six active treatment sequences with a single-blind washout. The treatments included placebo, oxycodone HCL, and celecoxib. Each patient was their own control using a placebo controlled double blind treatment, double dummy cross-over study design.

The patients met the following inclusion criteria: had been using non-steroidal anti-inflammatory medications 15 of the 30 days prior to enrollment for knee pain, had a Kellgren Lawrence (KL) grade 2 or 3, met the clinical classification criteria defined by the American College of Rheumatology (ACR), were in good general medical health, did not have concurrent conditions that indicated the patient is not a candidate for treatment with either opioid or a COX-2 inhibitor or did not have inflammatory arthritis or gout, and did not have a history of acute ligamentous or meniscal injury in the last year or significant changes in OA related treatments in the 3 months prior to screening. OA patients were matched according to age, body mass index, and gender to control subjects, and gait values were compared using analysis of variance and least significant difference post-hoc test ($\alpha = 0.05$).

Reflective markers were placed on anatomical landmarks of the lower body: iliac crest, greater trochanter, tibial plateau, lateral malleolus, heel, and fifth metatarsal. For trunk analysis, markers were placed on both iliac crests and shoulders. Marker data was captured at 120 Hz using nine Qualisys Oqus cameras. Ground reaction force was collected using a Bertec force platform placed under the first step. Lower limb kinematics and kinetics were calculated using inverse dynamics and the six-marker link system[4]. Moments were normalized to bodyweight and height (%Bw*Ht). Forward trunk lean was measured and defined as the sagittal plane projection of the angle between a line connecting the midpoint of the transacromion line and the midpoint of the trans-iliac crest line and the global vertical axis. The peak external moments and flexion angles for the ankle, knee, and hip and the maximum trunk flexion angles were calculated and averaged between trials.

RESULTS AND DISCUSSION

Patients with OA had significantly reduced knee flexion moments compared to controls when they were on a placebo washout (P=0.001) and active pain medications: celecoxib (P=0.001) and oxycodone (P=0.002). Patients on washout, celecoxib, and oxycodone also exhibited

significantly larger hip flexion moments when compared to the control subjects (P=0.017, P=0.008, and P=0.05, respectively). There were no significant differences between groups for trunk, hip, and knee flexion angles.

Similar to patients with radiographically severe OA compensating by exhibiting trunk flexion while ascending stairs[3], these radiographically moderate, but symptomatically severe, patients seem to adopt a different strategy to reduce the quadriceps demand and unload the knee joint. These patients are compensating through increased loading on their hips. They have yet to adopt the trunk lean strategy as seen in the radiographically severe OA patients.

There were no significant differences for joint angles or moments between OA treatments and placebo washout. Due to the strict inclusion criteria of this study, the number of eligible patients was limited and the sample size was small. Further analysis with a larger subject pool could potentially reveal differences in joint moments and angles when subjects are not taking pain medication compared to when they are on different types of pain medication.

CONCLUSIONS

Radiographically moderate, but symptomatically severe, patients with OA developed a compensation strategy to lower the external knee flexion moment on the knee and reduce the demand on quadriceps while ascending stairs. The patients displayed this compensation strategy when they were and were not on pain medication, which could indicate that the strategy is not related to increased pain, but rather due to functional limitations.

REFERENCES

1.Hurley MV. *Curr Opin Rheumatol* **10**, 246-250, 1998.
2.Slemenda C et al. *Ann Intern Med* **127**, 97-104, 1997.
3.Asay JL et al. *J Orthop Res* **28**, 325-9, 2009.
4.Prodromos CC et al. *J Bone Joint Surg Am* **67**, 1188-1194, 1985.

ACKNOWLEDGEMENTS

Funding provided by Pfizer Pharmaceuticals
Clinical assistance given by Dr. Carmo Trindade

Table 1: Difference between patients with OA while on a placebo washout, celecoxib, and oxycodone, and asymptomatic, non-OA control subjects. (* P<0.05 from Control)

	Age	BMI	Knee Flexion Moment (%Bw*Ht)	Hip Flexion Moment (%Bw*Ht)	Trunk Flexion Angle (°)
OA Washout	62.77±4.88	27.19±3.27	3.06±0.94*	6.41±1.56*	6.84±3.64
OA Celecoxib			3.24±0.77*	6.68±1.37*	8.60±7.25
OA Oxycodone			3.16±1.13*	6.00±1.40*	9.48±5.80
Control	61.17±5.19	26.23±3.47	5.05±0.46	4.40±0.90	7.76±2.94

DECREASED COMPLEXITY IN LEG MOTION PATTERNS DURING WALKING IN KNEE OSTEOARTHRITIS

Yuki Tochigi, Neil A. Segal, Tanawat Vaseenon, and Thomas D. Brown

The University of Iowa, Iowa City, IA, USA
email: yuki-tochigi@uiowa.edu, web: http://poppy.obrl.uiowa.edu/

INTRODUCTION

The theory of chaos considers homeostasis to be characterized by "chaotic" properties or complexity in a biologic system that provides the necessary flexibility to adapt to external stresses, as well as to physiological “noises” in biological systems [1]. This concept has led to the “loss of complexity hypothesis”, in which high system complexity is described as healthy, while decrease of system complexity is associated with pathology.

In the case of walking, flexibility in leg motion control presumably plays a crucial role in stable locomotion. Measurement of such motion control flexibility is anticipated to help understand the mechanisms of functional impairment associated with lower-extremity pathologies. In this study, we explored the chaotic property of leg motion patterns during walking by means of accelerometry, in older adults with symptomatic knee OA and in control subjects. It was hypothesized that those with symptomatic OA would exhibit less complexity in leg motion patterns than control subjects.

METHODS

A total of one-hundred and two volunteers (Table 1), including subjects with symptomatic knee OA (n = 55) and control subjects (n = 57), were recruited with IRB approval (#200907764). These subjects underwent a long distance corridor walking test. The OA subjects were asked to walk 400 meters (20 laps in a 20 meter walkway) at the quickest pace that he/she could maintain for that distance (or if he/she felt unable to walk 400 meters, then to walk for 2 minutes at his/her quickest pace). Control subjects completed two sessions of 200-meter walking test, one at a self-selected pace and the other at his/her quickest pace. Each walking test was timed, and the average speed was computed.

Leg motions during the walking test were measured using a light-weight wireless activity monitoring system (DigiTrac®, IM Systems Inc., Baltimore, MD), attached bilaterally just above each ankle using Velcro. This device measured/recorded tri-axial accelerations of the lower leg segment, at a sampling rate of 40 Hz. The data recorded were analyzed using a custom Matlab program, to compute a chaotic non-linear measure “sample entropy (SampEn)” [2]. SampEn (*m*, *r*, *N*) quantified the complexity of a time-series dataset consisting of *N* data points, by assessing the probability that equal sequences of length *m*, would remain similar after a time increment. The degree of similarity was determined by the tolerance *r*. The output was a unitless, non-negative number where lower values indicate more regular signal and higher values more complex signal. This measure of chaos was calculated for acceleration data in each axis (anterior-posterior, proximal-distal, or medial-lateral), as well as for the sagittal-plane 2D-acceleration data (combination of the anterior-posterior and proximal-distal data) and for the 3D acceleration data, at 10 second intervals ($N = 400$), with the other parameters set at typical values, “$m = 2$” and “$r = 0.2$”.

RESULTS AND DISCUSSION

In the control subject data (Figure 1), there was a trend that the SampEn measures became higher when a subject walked at a faster pace (1.3 ± 0.1 fold faster than the self-selected pace). Of the SampEn measures studied, the medial-lateral axis data (SampEn-ML) were least affected by walking speed (difference between sessions was 1.1 ± 0.1 fold), and data for each individual subject were well correlated between walking sessions ($r = 0.86$). In addition, SampEn-ML did not significantly differ by sex ($p = 0.31$).

Figure 2 is a scatter plot of SampEn-ML vs. age, in the control (at the self-selected pace) and OA subjects. In the control group, there was a weak (but significant) trend that SampEn-ML decreased with age ($r = -0.218$, $p < 0.001$). OA subject data appear to deviate from control data. Figure 3 shows a

statistical comparison between the control and OA groups in the subjects matched by age (53 – 79 years) and walking speed (1.2 – 1.6 m/sec). There was evidence that SampEn-ML in these selected OA subjects was significantly lower ($p < 0.001$) than in the matched controls, suggesting reduced complexity in medial-lateral leg motion patterns in OA subjects.

CONCLUSIONS

Leg motion patterns during walking in symptomatic OA subjects were characterized by decreased complexity (stride-to-stride variability) in the medial-lateral acceleration time sequence. Reduced motion pattern complexity associated with knee pathology is consistent with previous observations in patello-femoral pain syndrome [3] and ACL deficiency [4]. Given that OA knees often have coronal-plane malalignment, the reported abnormality may be associated with reduced ability to accommodate load re-distribution between medial/lateral compartments. The present leg motion complexity measurement technique does not require elaborate gait analysis equipment, and therefore lends itself to multi-institutional studies. As SampEn-ML provides a gait velocity-independent measurement of motion pattern complexity, this may be a valid and convenient clinical tool for intra-patient (before vs. after therapy) as well as inter-patient (screening for gait impairments) assessments.

REFERENCES

1. Lipsitz LA and Goldberger AL. Jama 267, 1806-09, 1992.
2. Richman JS and Mooran JL. Am J Physiol Heart Circ Physiol 278, H2039-49, 2000.
3. Hamill J et al. Clin Biomech 14, 297-308, 1999.
4. Moraiti CO et al. Knee Surg Sports Traumatol Arthrosc 15, 1406-13, 2007

ACKNOWLEDGEMENTS

NIH Grant 5 P50 AR055533
Foundation for PM&R Musculoskeletal Research Grant

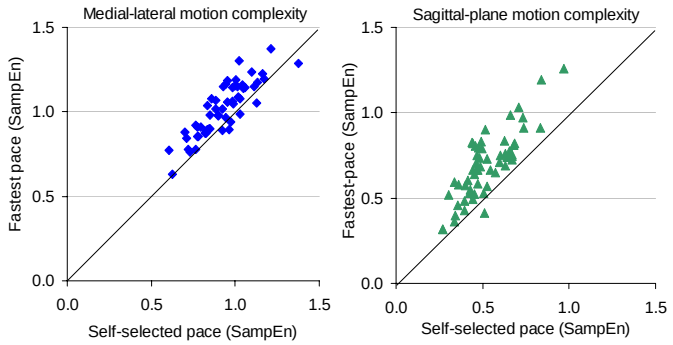

Figure 1. Correlation of SampEn values between walking sessions. Central lines indicate the "1 : 1" relationship.

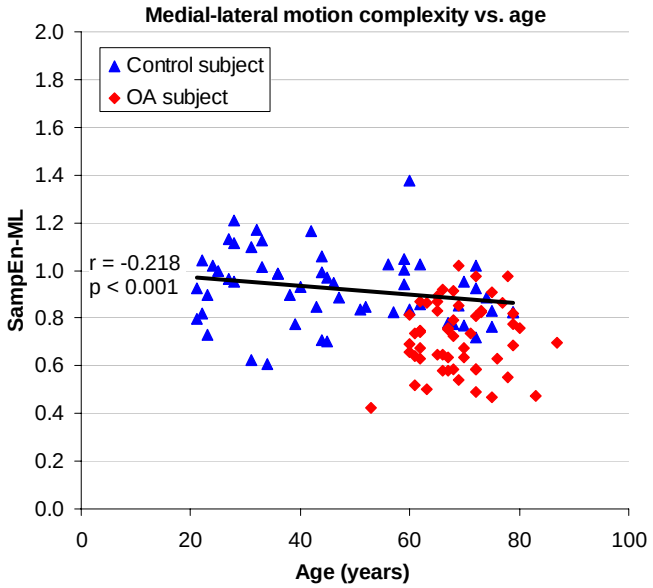

Figure 2. Relationship of SampEn-ML data with age.

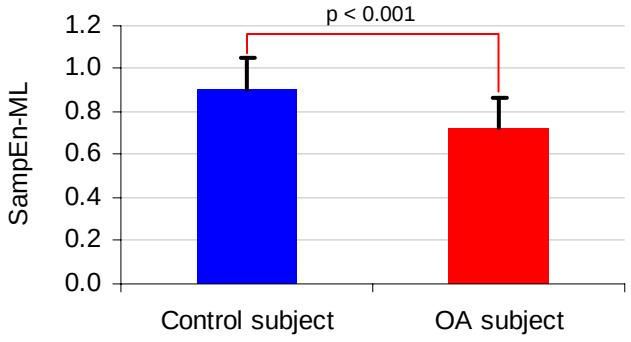

	Control subject	OA subject
Number (F : M):	22 (12 : 10)	27 (18 : 9)
Age (year):	67.1 ± 7.3	66.0 ± 6.0
Speed (m/sec):	1.4 ± 0.1	1.3 ± 0.1

Figure 3. Comparison of SampEn-ML between groups in matched subjects. Values are mean ± SD.

Table 1: Demographic of study participants and the walking speed data

Group	**Number** (female : male)	**Age** range (mean)	**Walking speed** (m/sec): range (mean ± SD) Self-selected pace	Fastest pace
OA subject	55 (37 : 18)	53 – 87 (68.8)	Not tested	0.4 – 1.6 (1.2 ± 0.2)
Control subject	57 (29 : 28)	21 – 79 (47.0)	1.0 – 1.7 (1.4 ± 0.1)	1.5 – 2.3 (1.9 ± 0.2)

USE OF NEUROMECHANICAL REDUNDANCY FOR LOCOMOTOR COMPENSATION IN ABLE-BODIED AND TRANSTIBIAL AMPUTEE SUBJECTS

Kinsey Herrin, MSPO, Megan Toney, BSE and Young-Hui Chang, PhD
Comparative Neuromechanics Laboratory, Georgia Institute of Technology, Atlanta, GA, USA
email: kinsey.herrin@gatech.edu, megan.e.toney@gmail.com

INTRODUCTION

Human locomotion is often characterized as a highly redundant system, with far more degrees of freedom available than necessary [1]. Kinematic deviations in a particular joint can be counteracted by appropriate changes at other joints, causing decreased variances of whole limb level variables, such as leg orientation (LO) [2-4]. In short, high variance among individual joints along with associated low variance in a task variable such as LO can be indicative of a step-to-step interjoint compensation mechanism during walking. The loss of a considerable portion of the locomotor system due to amputation leads to significant limb control adaptations to achieve a stable gait [5].

We hypothesized that otherwise healthy unilateral traumatic transtibial amputees would utilize the remaining motor redundancy of their legs to stabilize an invariant leg orientation trajectory. We directly tested this idea by comparing individual joint kinematics variances relative to LO variance within amputee subjects and also against AB (AB) control subjects. We further hypothesized that amputees would demonstrate greater interlimb asymmetries in joint variance compared to AB controls due to a greater reliance on the intact limb for controlling gait compensations due to the reduced motor redundancy on the amputated leg.

METHODS

Five unilateral, transtibial amputees and seven AB control subjects were asked to walk on a split-belt treadmill for three 30 second trials at two speeds (1.2 m/s and 1.4m/s). Kinematic data were collected using a six-camera motion analysis system (120 Hz, VICON). Walking speeds were randomized to prevent any accommodation effects. Subjects were instructed to walk looking straight ahead with one foot on each belt.

Individual joint and whole limb kinematics of both the sound and affected limbs of traumatic transtibial amputees were compared to AB control subjects with no history of injury or neurological impairments. Whole limb performance was measured with LO, which is quantified as the inclination angle of the vector connecting the anterior superior iliac spine and toe markers. LO control is critical for proper foot placement and orienting the ground reaction force vector to allow for successful and stable gait. The total variance of LO when compared to the average total variance of the joint angles provides insight into how joint deviations may counteract one another to lead to a stable LO trajectory.

RESULTS AND DISCUSSION

Mean joint kinematic trajectories in amputee gait during early- and mid-stance were remarkably similar to those found for AB individuals (Fig 1). However, significant differences ($p<0.05$) become apparent in terminal stance (50-60% of the gait cycle) and throughout swing phase (60-100%) for the ankle and knee between both the affected, prosthetic and sound limbs of the traumatic amputee when compared to the AB controls. The differences seen in the ankle angle during swing are not surprising, as the prosthetic ankle is mechanically fixed when no external force is applied. Despite the significant differences also observed in the knee angle, LO of the prosthetic limb does not differ from the LO of controls, implying that the overall whole limb performance of the prosthetic side is conserved in traumatic amputees. LO of the sound side, on the other hand, deviates from the mean LO trajectory observed in AB controls during swing phase, suggesting that amputees utilize their sound limbs to adjust for their contralateral deficits.

Averaged total variance per joint was similar for both amputee and control subjects (Fig 2). While the average total variance of individual joint angles was high for all subjects, we observed significantly less ($p<0.05$) total variance in LO. This suggests that despite large step-to-step deviations in individual joint kinematics, amputees likely structure this joint-level variance in a similar way as AB sub-

jects to maintain an invariant LO trajectory between each step cycle. As predicted, asymmetries in averaged total joint variance between the intact and affected legs were found in the amputee subjects, while control subjects showed symmetry in inter-limb joint variances (Fig 2). Interlimb asymmetries in average variance per joint in the amputee subjects were more pronounced at the slower walking speed ($p<0.05$), but disappear at the faster speed. This change suggests that traumatic amputees utilize

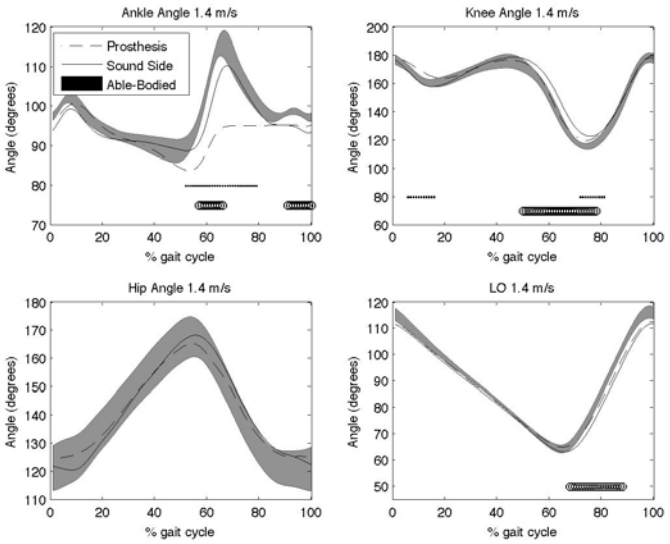

Figure 1: Mean ankle, knee, hip and LO kinematic trajectories over all subjects through a complete gait cycle at 1.4 m/s. Swing phase onset is at 60%. Solid dots indicate significance between prosthetic side and AB; open circles indicate significance between sound and AB ($\alpha=0.05$).

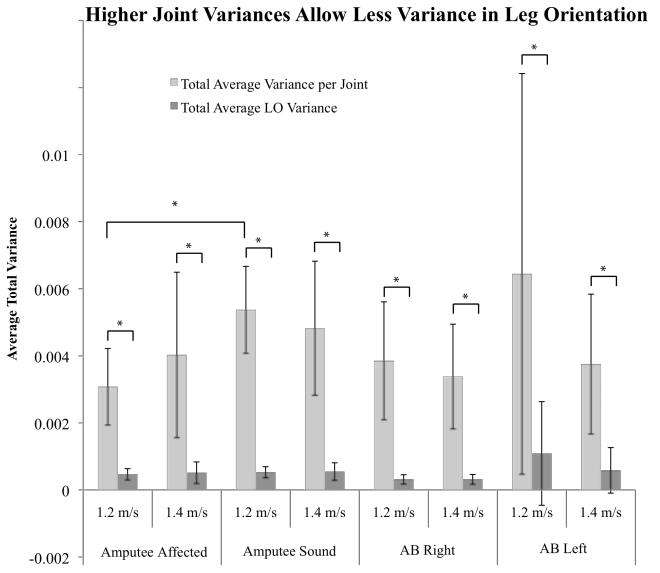

Figure 2: Average total variance per joint in each leg was high for both amputee and AB subjects, but variance for LO was much lower ($p<<0.05$).

some alternate motor control strategy at faster speeds [6], which needs to be further studied to obtain a complete understanding of amputee gait.

CONCLUSIONS

Mean joint kinematics of both the prosthetic and sound limbs in amputees differ from the AB controls, but mean LO trajectory differed for the sound side only. These differences imply that amputees utilize their intact limb to compensate for and control the changes resulting from the contra-lateral amputation. Significantly greater average total variances per joint ($p<0.05$) for all subjects did not result in correspondingly high variances in whole limb orientation, supporting our first hypothesis. This suggests that individual joints are regulated such that a deviation at one joint is counteracted at another joint, resulting in highly invariant whole limb performance between successive steps. Our results further suggest that amputees structure joint variance to perform similarly and predictably from step to step. Although the average joint kinematics for traumatic amputees differ from controls, amputee subjects still perform true to an invariant LO value over successive steps, resulting in stable, predictable whole limb behavior, which is critical for effective gait.

Understanding differences in how the joints are controlled during healthy and pathological gait can serve as a reference for evaluating the influence of different prosthetic components and their implementation on amputee gait. Characterizing for limb amputation can provide critical insight into the effectiveness of fundamental strategies for gait rehabilitation in individuals affected by other pathologies such as limb loss, stroke, and spinal cord injury.

REFERENCES

1. Srinivasan, M and Ruina A. *Nature*. **439(7072)**: 72-75, 2006.
2. Chang, YH, et al. *J. Exp. Biology*. **212**: 3511-3521, 2009.
3. Heiderscheit, BC *J. of Applied Biomechanics*. **2000(16)**: 419-427, 2000.
4. Auyang, AG, et al. *Experimental Brain Research*. **192**: 253-264, 2009.
5. Breakey, *J. Orthotics and Prosthetics*. **30(3)**: 17-24, 1976.
6. Bauman, J and Chang, YH. *J. Neuroscience Methods*. **186**: 18-24, 2010.

CENTER OF ROTATION POSITION IN NON-ARTICULATED PROSTHETIC FEET: IMPLICATIONS FOR PROSTHETIC FOOT KINETICS

[1,2]Andrew Sawers and [1,3]Michael Hahn

[1]RR&D Center of Excellence, Department of Veterans Affairs, [2]Departments of Rehabilitation Medicine, and [3]Mechanical Engineering, University of Washington, Seattle, WA USA,
email: sawera@u.washington.edu

INTRODUCTION

Joint kinetics have been estimated via inverse dynamics with link-segment models to analyze the performance of non-articulated energy storage and return (NA-ESR) prosthetic feet [1] and to examine the motor control strategies and compensations adopted by lower limb amputees [2]. A central assumption of the link-segment model commonly used in this application is that the ankle's axis of rotation acts as a fixed hinge; yet in NA-ESR prosthetic feet, no true ankle articulation exists, and the extent to which any axis remains fixed is unknown. Despite these concerns, this computational approach has been used to assess differences within and between amputees, and in comparison to non-amputees [1,3]; thus reports of estimated kinetics in NA-ESR prosthetic feet, and proximal joints may be in question [4]. Two groups have attempted to address this concern [4,5], yet neither reported the actual axis location. Additionally, the feet tested previously are not commonly prescribed in clinical use today. The overall objectives of our work are to discern the magnitude of ankle joint axis mis-location required to induce meaningful alterations in joint kinetics, evaluate the center of rotation position in a series of NA-ESR prosthetic feet, and quantify the effect of any differences in center of rotation position on prosthetic foot and proximal joint kinetics of a unilateral transtibial amputee. The primary focus of this paper is the quantification of the center of rotation position in NA-ESR prosthetic feet.

METHODS

To determine the magnitude of ankle joint axis mis-location required to induce meaningful alterations in joint kinetics, systematic error simulations were performed using previously collected gait data from one healthy non-amputee. Incremental adjustments of 10mm were made to the location of the ankle joint axis in the anterior-posterior direction (in the tibial coordinate system) by modifying a link-segment model in BodyBuilder™ (Vicon; Lake Forest, CA). Differences in kinetic output were examined at the ankle, knee and hip. Next, the position of the center of rotation for eight commonly prescribed NA-ESR prosthetic feet was estimated from kinematic gait data collected at 120 Hz from one unilateral transtibial amputee walking at self-selected walking speed. Using KineMat [6], a MATLAB™ (MathWorks, Natick, MA) software package, the sagittal plane position of the helical axis of motion [7] was estimated. Differences between the assumed fixed ankle axis and helical axis position were examined over stance phase.

RESULTS AND DISCUSSION

The systematic error simulations of ankle joint axis position resulted in substantial changes to knee and ankle kinematics, as well as ankle kinetics. Ankle powers are presented for an entire gait cycle in Figure 1.

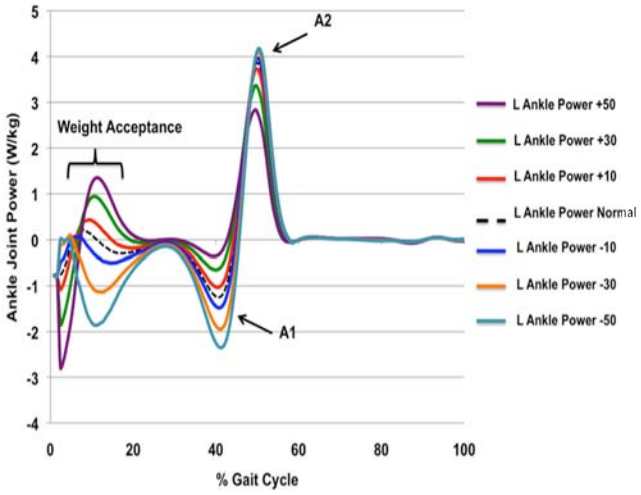

Figure 1: Changes in ankle joint power with alterations to A-P ankle joint axis position.

A posterior shift of the ankle joint axis resulted in greater power absorption during the A1 power burst, while anterior shifts generated a decrease in power absorption. During the A2 power burst shifting the axis posteriorly resulted in increased power generation, whereas power generation was reduced with an anterior shift. These results indicate that from weight acceptance to toe-off, a posterior shift in the ankle joint axis location from its traditionally assumed position near the lateral malleoli would induce an overestimation of power absorption and generation, while an anterior shift would result in an underestimation of power absorption and generation.

Using a helical axis of motion to estimate the center of rotation position across a series of NA-ESR prosthetic feet resulted in notable differences in the anterior, posterior, superior and inferior directions from the traditionally assumed fixed axis position. Tibial angle at the point of peak displacement (difference between fixed and helical axis positions) differed across directions and in some cases between feet within a direction. Peak anterior displacement of the helical axis compared to the assumed fixed axis position for eight NA-ESR prosthetic feet and the tibial angle at peak displacement are shown in Figure 2. Displacements ranged from slightly over 10 mm up to nearly 80 mm, occurring between mid-stance (4º tibial angle) and toe-off.

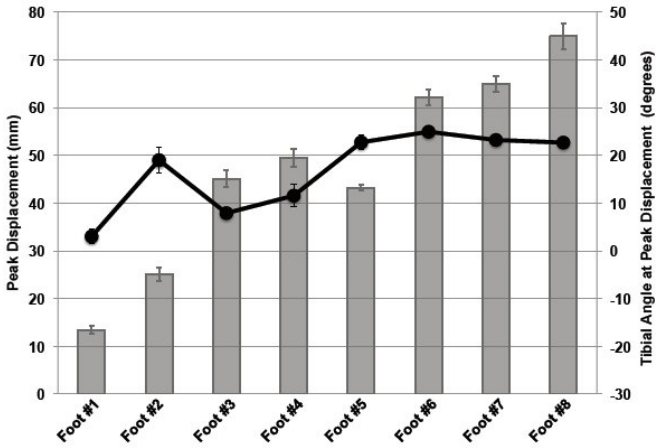

Figure 2. Peak anterior displacement of the helical axis from the fixed axis position for eight commonly prescribed prosthetic feet and the tibial angle at peak displacement; columns represent peak displacement, line represents tibial angle at peak displacement.

Based upon the results from the systematic error simulation, displacements of 10 mm in the anterior direction occurring near mid-stance (foot #1), would likely have little effect on estimates of power at the ankle, while a displacement of 80 mm occurring later in stance (foot #8), would grossly misrepresent power at the ankle. Our group is currently working on comparisons between joint kinetics estimated using the assumed fixed axis and helical axis positions respectively.

CONCLUSIONS

This paper represents the first effort to estimate the actual center of rotation position in NA-ESR prosthetic feet. Based on these results, the validity of calculating joint kinetics for NA-ESR prosthetic feet and the proximal joints may be in question if the ankle axis is assumed to act as a fixed hinge that mirrors the position of the intact contralateral ankle. The helical axis position may be utilized to more precisely account for the kinetics within prosthetic foot-ankle prostheses. Additionally, the differences in peak displacement of helical axis position between different prosthetic feet may have implications for how unilateral transtibial amputees utilize the energy storing capacity of these feet and subsequently how they should be trained during rehabilitation. The results from our first two aims validate the need to re-examine techniques commonly employed to estimate foot and ankle kinetics among individuals with lower limb loss.

REFERENCES

1. Barr AE, et al. *Phys Ther* **72**, 344-354, 1992
2. Underwood HA, et al. *Clin Biomech* **19**, 609-616, 2004.
3. Su PF, et al. *Arch Phys Med Rehabil* **89**, 1286-1394, 2000.
4. Geil MD, et al. *J Biomech* **33**, 1745-1750, 2000.
5. Prince F, et al. *IEEE Trans Rehab Eng* **2**, 247-255, 1994.
6. Reinschmidt C, et al. (http://www.isbweb.org/software/movanal/kinemat) 1997.
7. Woltring HJ, et al. *J Biomech* **18**, 379-389, 1985.

ACKNOWLEDGEMENTS

This study was supported by the ASB Graduate Student Grant in Aid, the Orthotic and Prosthetic Education and Research Fund (OPERF), the American Orthotic and Prosthetic Association (AOPA) and the Department of Veterans Affairs grant A4883C.

CONTACT DIFFERENCES BETWEEN MEDIAL AND LATERAL TIBIAL PLATEAU COMPARTMENTS ACCOMPANY WEIGHT-BEARING

[1]Sarah R. Dubowsky, [2]Jerome Allen, [2]Venkata Gade and [1, 2] Peter J. Barrance

[1]University of Medicine and Dentistry of New Jersey, Newark, NJ, USA
[2]Kessler Foundation Research Center, West Orange, NJ, USA
email: pbarrance@kesslerfoundation.org

INTRODUCTION

A number of studies have previously shown that lower-body muscle activity and knee joint loading in the supine, or recumbent positions, is quite different from that in fully upright, physiological load-bearing stance [1,2]. The use of MR imaging during upright, weight-bearing stance provides the benefits of identifying loading and contact position differences in a pathologic knee during functional activity. For example, after injury to the ACL, an investigation into knee kinematics and tibial plateau contact positions during functional loading may help identify why these injuries predispose individuals to the early onset of osteoarthritis (OA). Injury to the ACL is linked to the initiation and progression of OA, possibly by *changes in the local loading and contact area between joint cartilage surfaces* [3]. We recently reported significant changes in tibiofemoral positioning and cartilage contact locations accompanying the transition to weight-bearing in subjects with healthy knees [4]. In the current study, we further explored these relationships and how they may relate to functional anatomy.

METHODS

Six subjects (5m, 1f, age 32.83±7.36 years) without orthopaedic knee issues gave informed consent to participate in the MR imaging for this study. Scanning was performed in a 0.6T vertically open scanner (FONAR Corp., Melville, NY). Scans were acquired bilaterally at two levels of weight-bearing: *high weight-bearing* (HWB), during which the patient is nearly vertical, and *low weight-bearing* (LWB), during which the patient is reclined (85º and 20º from horizontal, respectively). Scanning protocols, image digitization, model creation, and data analysis have been previously described [4]. Anterior/posterior (A/P) translational displacement of the joint was calculated between tibial and femoral coordinate systems. Contact positions were calculated as the centroids of contact regions defined as areas of femoral cartilage lying within a threshold distance from tibial cartilage [4]. The positions of the centers of contact were calculated relative to the tibial plateau coordinate system (Figure 1). A mixed procedure repeated measures analysis of variance (ANOVA) was first run to investigate the effect of weight-bearing on kinematics and contact positions during the transition from LWB to HWB (alpha=0.05). We then explored the relationship between changes related to weight-bearing in joint kinematics and contact positioning in each compartment of the tibial plateau using linear regression analysis to calculate correlation and slope coefficients.

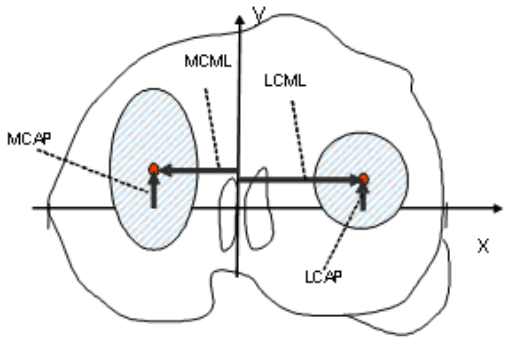

Figure 1: Variables defining tibial contact are anterior/posterior locations in the medial and lateral condyles (MCAP, LCAP), and the medial/lateral coordinates of these points (MCML, LCML).

RESULTS AND DISCUSSION

As previously reported, we observed significant anterior positioning of the tibia accompanying the transition to weight-bearing ($p<0.01$). Concomitantly, a medial ($p<0.05$) and posterior ($p<0.05$) shift in the lateral compartment contact points was observed. In the medial compartment, there were similar trends mimicking the lateral

compartment contact shift, although there was no significance in either the medial/lateral (M/L, p=0.16) or the A/P (p=0.50) directions.

In the lateral compartment, there is a clear association between tibial plateau contact and joint positioning (Figure 2, R^2=0.796). Upon weight-bearing, as the tibia moved anterior relative to the femur, the contact position on the tibial plateau shifted posteriorly (slope=-0.734). This relationship in the medial compartment of the tibial plateau is substantially less (Figure 3, R^2=0.429, slope =-0.259). The differences between compartments may be explained by the contact relationships between the curved geometry of the femoral condyles and the surface of the tibial plateau. The medial side of the tibial plateau has a shallow concave shape, conforming to the medial femoral condyle. Upon weight-bearing, compression between these two curved surfaces may result in a decreased translation in this compartment. However, the lateral side of the tibial plateau is flatter than the medial side. The lower congruency may allow greater motion between the two during the transition to weight-bearing.

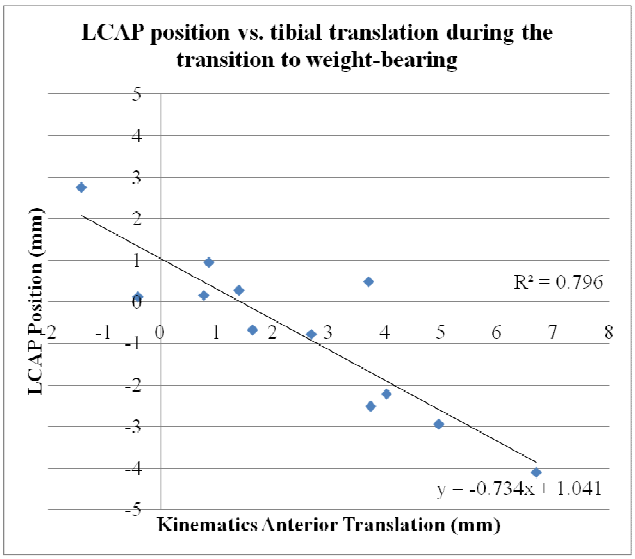

Figure 2: Relationships between anterior translation of the tibia and the posterior shift of the lateral femoral condyle contact on the tibial plateau during the transition to weight-bearing.

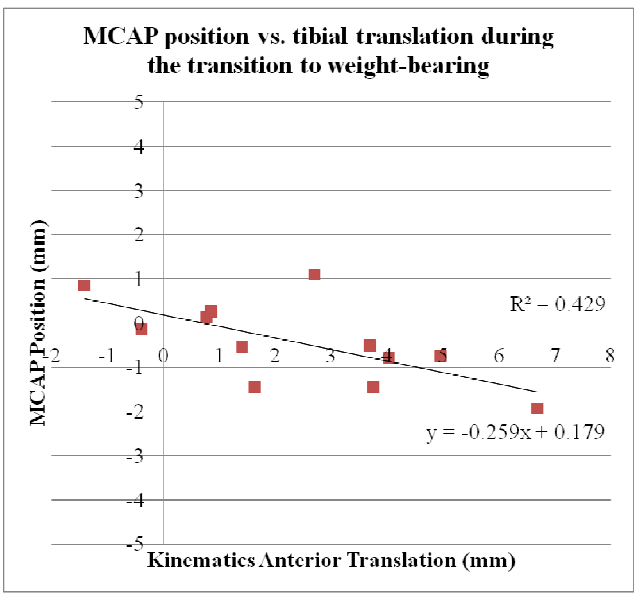

Figure 3: Relationship between anterior translation of the tibia and the posterior shift of the medial femoral condyle contact.

CONCLUSIONS

During the transition to weight-bearing, significant differences in tibiofemoral kinematics and contact positions have been observed. Weight-bearing MRI and computational modeling demonstrated that for a given amount of tibial translation, change in contact location differs between medial and lateral compartments. Differences in functional anatomy appear to offer an explanation for these differences. Such relationships are likely to be disrupted by ligamentous damage, and future explorations may shed light on why ACL injury predisposes an individual to the early development of OA.

REFERENCES

1.Maffiuletti NA, et al. *Med Sci Sports Exer* **35**, 1511-1516, 2003.
2.Chen G, et al. *J Biomech* **34**, 749-756, 2001.
3.Herzog WA, et al. *Arthritis Rheum* **49**, 239-47, 2003.
4.Dubowsky SR, et al. *Proceedings of ORS '10*, New Orleans, LA, USA, 2010.

ACKNOWLEDGEMENTS

Contents of this abstract were developed under two grants from the Dept of Education, NIDRR H133G080136 and H133P070007. However, those contents do not necessarily represent the policy of the Dept of Education, and you should not assume endorsement by the Federal Government. Support for the work was also provided by the Kessler Foundation.

ALTERED KNEE ARTHROKINEMATICS AFTER MEDIAL MENISCUS ROOT TEAR

Scott Tashman, Daniel Martin, Marisa Antonino and Christopher Harner

University of Pittsburgh, Pittsburgh, PA, USA
email: tashman@pitt.edu

INTRODUCTION

Meniscal injuries are the most common indication for knee surgery and are associated with high rates of knee osteoarthritis (OA) [1,2]. The meniscus functions to distribute loads and guide the contact path of the tibio-femoral joint, but little is known about the specific factors in meniscal injury that predispose patients to developing OA. Medial meniscus root tear (MMRT) completely disrupts meniscal hoop stresses and exposes cartilage to contact forces similar to those after total meniscectomy [3]. It has been hypothesized that shifted areas of joint contact after knee injury may predispose the joint to OA [4]. Therefore, studying arthrokinematics (joint contact kinematics) after MMRT may offer insights into the mechanisms for OA development after meniscal injury.

The purpose of this study was to analyze the effects of MMRT on joint contact kinematics during activities of daily living. We hypothesized that the loss of medial meniscus function resulting from this injury would alter the location of joint contact on the medial tibial plateau during squatting.

METHODS

Subjects with recent, isolated MMRT (MRI-confirmed) and capable of performing the study tasks without significant limitations or discomfort were recruited for this IRB-approved protocol. High-resolution CT scans of both knees were obtained, from which volumetric 3D models were reconstructed. Biplane radiographic images of the subjects' knees were obtained at 100 frames/s during the downward phase of squatting (Figure 1).

Using custom software, digitally reconstructed radiographs (DRRs) were generated from the 3D bone models. These DRRs were automatically correlated with the biplane radiographic images to determine 3D positions of the tibia and femur during squatting. This method tracks tibiofemoral kinematics with dynamic precision of 0.3-0.7 mm for translation and 0.3-0.9 degree for rotation or better [5]. The affected knee of each subject was compared to his or her unaffected contralateral knee. The location of joint contact on the medial and lateral tibial plateau was calculated as the location of closest bone-to-bone distance between the femur and the tibia (Figure 2). A repeated measures ANOVA was performed to compare contact path locations between the affected legs and the control legs. Significance was set to $\alpha = 0.05$.

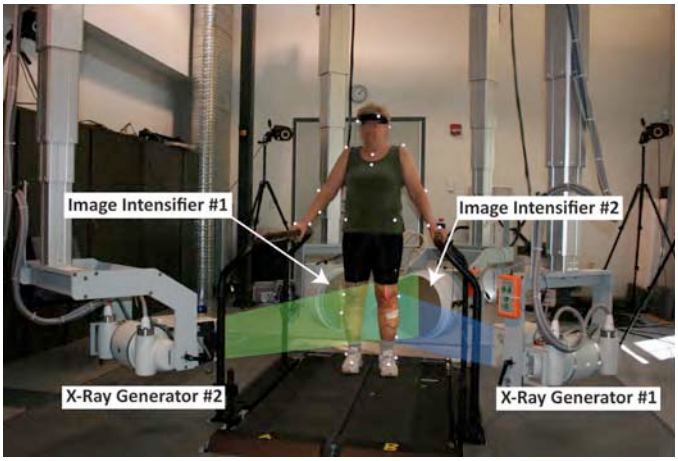

Figure 1: Laboratory set-up. X-ray generators and image intensifiers configured to image left knee.

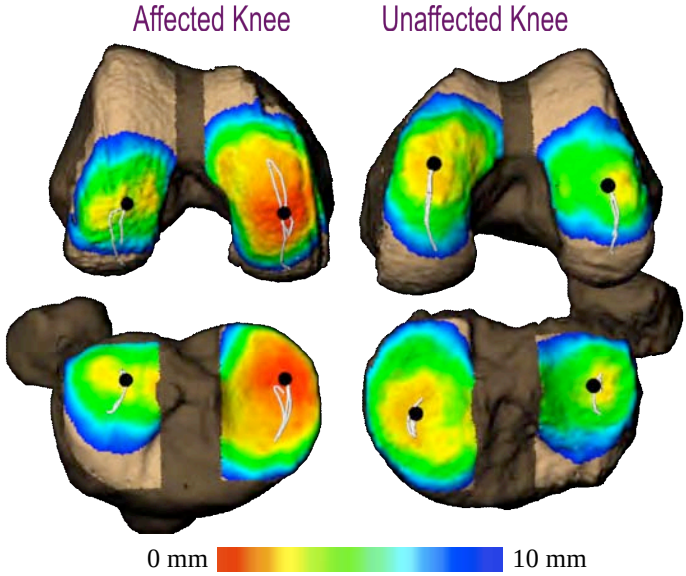

Figure 2: Contact paths estimated from centroids of bone-to-bone distance maps (representative trial)

RESULTS

Mean contact paths for 7 subjects during descending squat movement from 20° to 80° of knee flexion are shown graphically in Figure 3 and plotted as a function of knee flexion angle in Figure 4 (medial compartment only). Medial compartment paths were shifted posteriorly and medially (p=0.001) after medial meniscal root tear. Lateral compartment paths were unchanged.

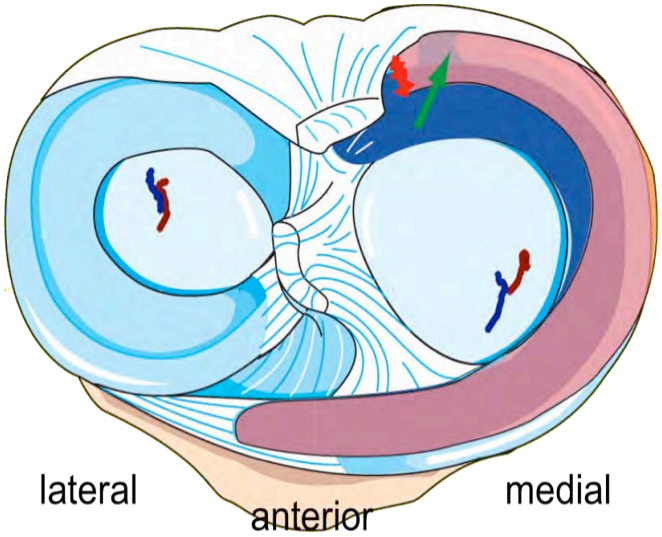

Figure 3: Mean joint contact paths for MMRT (red) and contralateral/uninjured (blue) knees, 7 subjects. Curves are superimposed over a generic drawing of the knee (scaled to average tibial size) for perspective. Contact paths in the medial compartment were shifted medially (ANOVA: p=0.001) and posteriorly (significant only at low flexion angles). Lateral compartment paths were unchanged. Arrow shows expected displacement of the medial meniscus from the uninjured (blue) to root tear (red) state, corresponding with shift in contact path.

CONCLUSIONS

Medial meniscal root tear consistently shifted contact points on the medial tibial plateau posteriorly and medially. This shift is consistent with the meniscal displacement expected with MMRT, as illustrated in Figure 2 (blue is original meniscal position; red shows estimated shift after injury). This clearly demonstrates that, in addition to its widely understood role for distributing load, the medial meniscus also plays an important role for guiding the contact path of the knee. Future investigations will include other injury types and the effectiveness of repairs for restoring normal knee function.

REFERENCES

1. Garret WE et al. JBJS Am. 2006;88:660.
2. Owings MF et al. Vital Health Stat 13 1996;139:1.
3. Allaire RB et al. JBJS Am. 2008;90:1922.
4. Andriacchi TP, et al. Ann Biomed Eng. 2004;32(3):447-57.
5. Bey MJ et al. J Biomech Eng 2006;128:604.

ACKNOWLEDGEMENTS

Funded by a grant from the Arthritis Foundation.

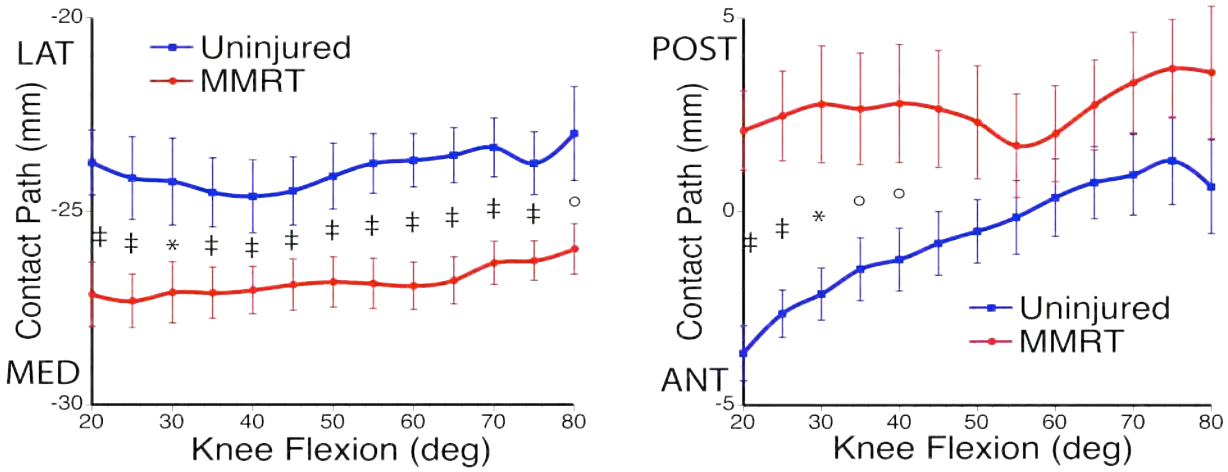

Figure 4: Mean medial-compartment joint contact paths for MMRT (red) and contralateral/uninjured (blue) knees: Left - medial/lateral path position; Right - anterior/posterior path position. Points are 7-subject means every 5°; vertical bars are ±1 standard error. Significance (paired t-test): ‡ p<0.01, * p<0.05, o p<0.10 (trend).

COMBINING REGISTRATION WITH CINE-PC DATA IN ORDER TO CREATE ACCURATELY ANIMATED SUBJECT-SPECIFIC KNEE JOINT MODELS.

[1]William Sipprell, [1]Bhushan S. Borotikar, and [1]Frances Gavelli

[1]Functional and Applied Biomechanics, Dept. of Rehabilitation Medicine, NIH, Bethesda, MD, USA
email: fsheehan@cc.nih.gov, web: http://pdb.cc.nih.gov/

INTRODUCTION

Patellofemoral pain syndrome (PFPS) is one of the most common causes of orthopaedic related physician visits each year [1], yet the etiology of the pain is still not fully understood. Although the PF pain has been demonstrated to be associated with altered PF kinematics, an actual variation in joint contact has yet to be demonstrated. Various techniques are currently available for quantifying *in vivo* 3D joint motion non-invasively. Cine-PC (CPC) MRI being one of them [2]. Despite its excellent accuracy (<0.33mm) and precision (<0.21°) [3], CPC is limited in its ability to provide 3D spatial data, due to subject stamina and time constraints.

Thus, the objective of the current study was to develop a method for accurately registering 3D MR images with dynamic multi-plane cine (MPC) images, acquired in a similar manner to the CPC images. While registration between the dynamic and static models at a single time frame is sufficient to relate the dynamic data to the static data, registration can be performed for all 24 time frames. The current study utilized this redundancy of information to evaluate the registration, wherein the patellar kinematics were defined for all time frames using the dynamic to static registration and then compared to the kinematics, derived through the integration of the CPC velocity data.

METHODS

Five healthy volunteers (2 males, 3 females) provided informed consent prior to participating in this IRB approved study. Each subject was asked to lay supine within the 3T (Philips Medical Systems, Best, NL) MRI bore with the fully extended knee placed in an 8-channel knee coil. The subjects were asked to remain still while a static 3D sagittal Gradient Recall (GRE) Image with fat-suppression was acquired with isotropic voxels of 1mm. Next, the subjects remained supine, but with their knee was placed in an MRI-compatible jig that enabled rhythmic knee flexion-extension exercise with flexible transmit-receive coils securely place around the knee. During this exercise a dynamic CPC MR image set (x,y,z velocity and anatomic images over 24 time frames) was acquired [2]. In addition, 2 MPC image sets (anatomic images only) datasets were acquire (a 4-plane axial and a 5-plane sagittal).

A static 3D patellar model was attained by first segmenting the 3D GRE images using an in-house program, MIPAV (Medical Image Processing and Visualization, NIH, Bethesda, MD). In a similar manner a sparse dynamic patellar model was acquired for each time frame by segmenting the patella from the MPC images. These segmentations resulted in point clouds which were then imported into model development program (Geomagic Inc., Research Triangle Park, NC). The 3D static point cloud was fit with a triangular polynomial surface and then smoothed (maximum smoothing set to 0.2mm). The dynamic point cloud for each time frame was fit to the 3D static triangular mesh model using an Iterative Closest Point algorithm. The transformation matrix (translation and orientation) of the dynamic to static fit was recorded and saved.

Patellar kinematics were first derived through integration of the CPC velocity data and were expressed relative to an anatomical coordinate system, defined in the time frame representing full extension. The kinematics were again defined using the transformation matrices from the 24 dynamic to static registrations. These kinematics were expressed relative to the same coordinate system as the CPC velocity data. Since integration provides a low-pass filter, the registration kinematics were filtered with a low-pass butterworth filter. The accuracy of the registration was determined by the average absolute error between the kinematics derived through registration and those derived from

integration. Since only a single registration is required to animate the static model, two accuracies were defined. The first incorporated all 24 times frames and the second incorporated only the quasi-static (QS) images representing full extension to full flexion (change in knee angle over the time frame was less than 2°).

RESULTS AND DISCUSSION

Average absolute errors using QS time frames were less than 1.0mm and 1.5° (Table 1), which is comparable to registration of a sparse static patellar model to a high quality 3D model (errors less than .88mm and 1.75° [4]). The errors averaged over the QS times frames were lower than those averaged over all 24 time frames. Errors for patellar tilt were considerably higher than other degrees of freedom, indicating that the fitting algorithm might not have enough dynamic data to get closer fit from the registration process for this degree of freedom.

At the current time CPC remains an analytically simpler and more accurate technique for tracking kinematics (0.33 mm and 0.9^{o}), as compared to the dynamic to static registration. Thus, for applications requiring rendering a 3D model throughout a movement, the most accurate approach is to register a single time frame (during the quasi-static periods of movement) and use the kinematics derived through integration to animate the model.

The patella was selected as the focus of this study because it is smallest bone in the knee joint and has complex kinematics especially in maltracking patients. When this technique is employed to track femoral or tibial movement, smaller errors are expected.

CONCLUSIONS

Combining accurate kinematics from the integration of the CPC data with the registration (shape matching) of a coarse dynamic patellar model from a single time frame to a high quality 3D model, allows for the accurate, non-invasive *in vivo* quantification of joint contact mechanics as well as other joint properties, such as ligament strains. The ability to non-invasively quantify these joint properties will greatly enhance our understanding of both healthy and pathological joint mechanics.

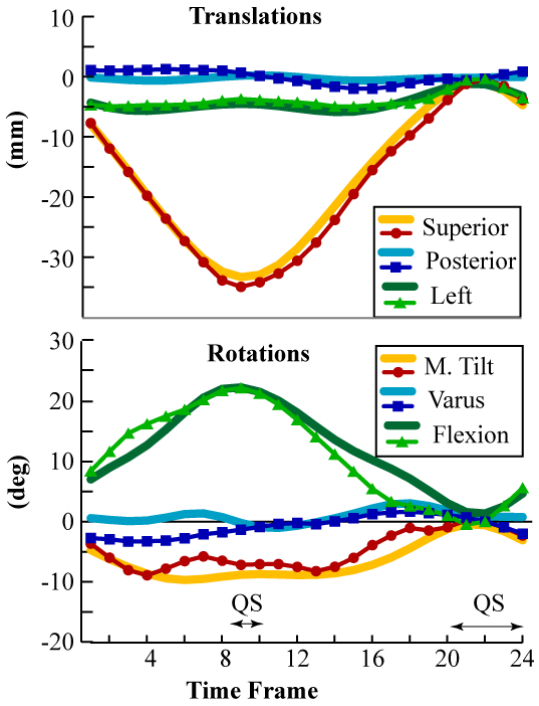

Figure 1: Patellar translations and rotations for one subject (3259L) during flexion/extension cycle over all (24) time frames. The QS time frames are delineated with a double arrow line.. Lines with no markers represent integration kinematics, and lines with markers represent registration kinematics. M. Tilt = medial tilt.

REFERENCES

1. Iwamoto J *et al. Gend.Med.* **5,** 405-414, 2009.
2. Sheehan FT, et al. *J Biomech* **31**, 21-16, 1998.
3. Behnam et al. ASB 2009.
4. Fellows RA, et al. *J Magn Reson Imaging* **22**, 145-153, 2005.

Table 1: Average absolute errors of the registration kinematics compared with integration kinematics. The first row represents the error averaged over all time frames and the second the error averaged over the QS frames.

	X (Medial)		Y (Posterior)		Z (Superior)		X (Extension)		Y (Varus)		Z (Tilt)	
	Avg	SD	**Avg**	SD	**Avg**	SD	**Avg**	SD	**Avg**	SD	**Avg**	SD
All	**1.05**	0.34	**0.74**	0.20	**1.53**	0.52	**2.11**	1.06	**2.38**	0.94	**2.31**	1.31
QS	**0.85**	0.19	**0.54**	0.34	**1.02**	0.36	**1.28**	0.58	**1.29**	0.93	**1.53**	0.95

EFFECT OF INITIAL MANUAL REGISTRATION ON THE FINAL RESULTS OF IMAGE REGISTRATION ON KINEMATICS AND CONTACT ANALYSES IN THE RADIOLUNATE JOINT

[1]Joshua E Johnson and [1]Kenneth J Fischer

[1]University of Kansas, Lawrence, KS, USA
email: fischer@ku.edu

INTRODUCTION

Kinematics are widely used in computational processes as input parameters for displacement driven models. Small errors in kinematics can lead to compounded errors in final contact results, and hence accuracy is of utmost importance [1]. When using registration to acquire kinematics from images, for instance magnetic resonance imaging (MRI), the initial conditions from manual registration may potentially influence accuracy of the final registration and resulting contact mechanics. Therefore this study investigated the effects of different initial conditions on lunate kinematics obtained from image registration and related contact mechanics (contact force, contact area and peak contact pressure). Kinematics and contact data were expected to differ with perturbations in initial manual registration.

METHODS

MR images of two cadaver forearm specimens were acquired. Images of the wrist were obtained without load as well as during simulated light grasp (loaded). The radius and lunate bones without cartilage were isolated from both sets to obtain kinematics by image registration.

Registration was performed using Analyze 5.0. The radius was chosen as the fixed reference and registration of the loaded radius image to the unloaded radius was used to align the image sets. The loaded lunate was then transformed into the unloaded image coordinate system. Registration of the unloaded lunate image to the transformed loaded lunate provided the final kinematic transformation. To investigate the effects of different initial conditions, firstly, manual registration was carefully performed to obtain standard initial conditions for both radius and lunate. A standard best match was then selected from 25 subsequent auto-registration iterations. Translation (1, 2, 3 pixels) and rotation (1°, 2°, 3°) perturbations in the X, Y and Z directions were applied to the manual registration standard to obtain altered initial conditions. Best matches were again selected after 25 auto-registration iterations, and the final results were compared to the standard best match using RMS errors for translation and rotation
In order to compare contact data, the standard kinematics and kinematics obtained from perturbed initial conditions were implemented with surface contact models of the radius and lunate in the Joint_Model program [2]. Based on effective cartilage modulus of 4 MPa and uniform thickness of 1 mm, local contact pressure is determined from local surface penetration while contact area is the area of surface penetration. Integration of contact pressures over the contact area provides the contact force.

RESULTS AND DISCUSSION

Table 1: Percent differences in average RMS error for translation (T) and rotation (R) perturbations for specimens 1 (S1) and 2 (S2).

Perturbation	% Difference in RMS Error (1 to 3)			
	Translation Vector		Rotation Vector	
	S1	S2	S1	S2
T (pixels)	10.8	11.2	0.5	4.0
R (degrees)	24.0	25.3	40.2	25.7

Auto-registrations after perturbations in the careful manual registration resulted in a qualitatively worse match between image sets. Looking at lunate kinematics for both specimens, average RMS error for translation and rotation vectors rotation perturbations resulted in higher errors than

translation perturations (Table 1). Generally, the average errors were highest for perturbations in the Z direction, perpendicular to the imaging plane (Table 2).

Looking at lunate contact mechanics data, perturbations in initial registration conditions had showed initial rise and then fall of contact measures for translations for Specimen 1, as opposed to a fall-rise-fall pattern for rotation perturbations (Fig 1, left). Contact data showed progressive decreases in all contact measures for Specimen 2 with increasing perturbations (Fig. 1, right). Perturbations in initial manual registration resulted in up to 50% differences in contact mechanics measures—particularly contact force for Specimen 1 with a 3° translation perturbation and contact force for Specimen 2 with a 3° rotation perturbation. Otherwise, contact mechanics differences were generally within about 30%.

From the kinematics results the out of plane direction appears generally to have higher differences. Since in plane resolution of MR images are usually higher than out of plane image thickness, resolution anisotropy may further compound errors. With increasing perturbations, contact model results appear to be generally underestimated in this study. While higher differences in kinematics in this study led to increased separation in radiocarpal contact, over-estimations errors could also be expected. Overall, initial manual registration clearly influences the final registration and contact mechanics. Care must be taken to manually align the image volumes as closely as possible prior to auto-registration to obtain the best overall registration possible.

ACKNOWLEDGEMENTS

This research was financially support by NIH Grant R01EB008709. We thank Dr. Sang-Pil Lee and Allan Schmidt for assistance acquiring images.

REFERENCES

1.Goto A, et al. *J Orthop Res* **23**, 750-6, 2005.
2.Kwak SD, et al. *Comp Meth Biomech Biomed Eng* **3**, 41-64, 2000.

Table 2: Average X, Y and Z translation and rotation vector RMS errors for translation (T) and rotation (R) perturbations for specimens 1 and 2.

Specimen	Perturbation	RMS Error					
		Translation Vector (pixels)			Rotation Vector (degrees)		
		X	Y	Z	X	Y	Z
1	T (pixels)	0.2778	0.2154	0.2832	0.0137	0.0127	0.0117
	R (degrees)	0.2153	0.2143	0.2230	0.0092	0.0102	0.0074
2	T (pixels)	0.3516	0.3179	0.3647	0.0117	0.0087	0.0120
	R (degrees)	0.4433	0.4218	0.4149	0.0112	0.0119	0.0130

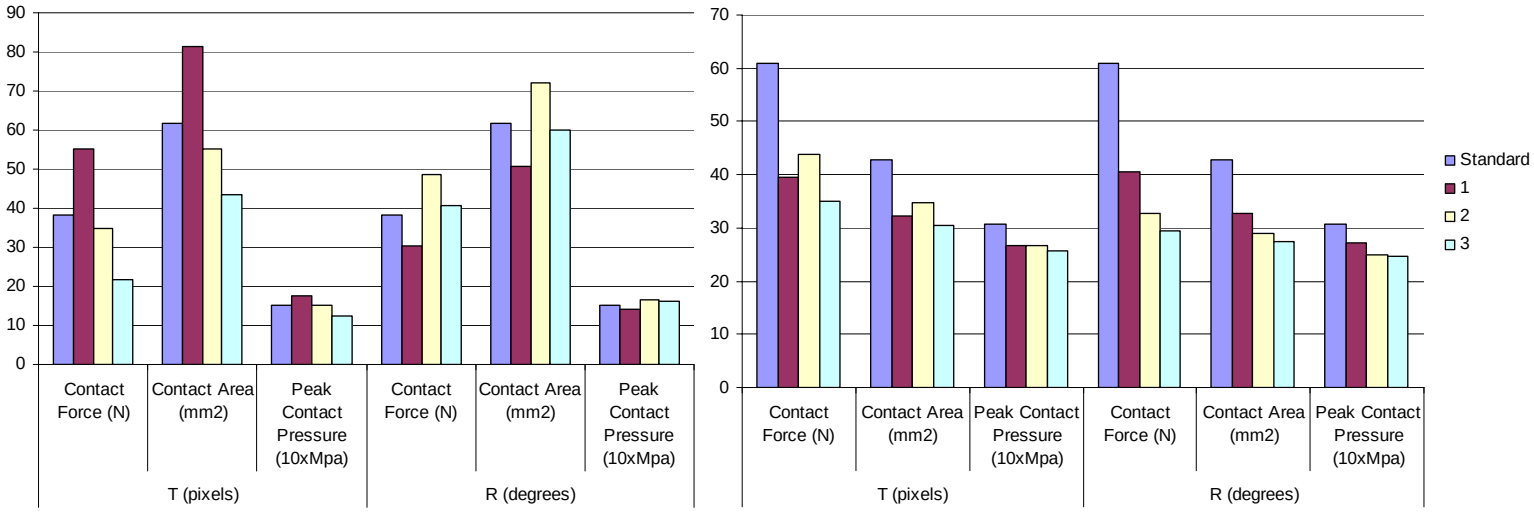

Figure 1: Average contact data for (a) specimen 1 and (b) 2 for translation (T) and rotation (R) perturbations

ACTIVATION AND APONEUROSIS WIDTH AFFECT MEASURED STRAIN IN THE BICEPS FEMORIS MUSCLE

[1]Niccolo Fiorentino, [2]Michael Rehorn, [2]Geoffrey Handsfield, [3]Fred Epstein, [1,2]Silvia Blemker

University of Virginia, Departments of [1]Mechanical & Aerospace Engineering, [2] Biomedical Engineering and [3]Radiology, Charlottesville, VA, USA
email: niccolo@virginia.edu, web: http://www.mae.virginia.edu/muscle

INTRODUCTION

Acute strain injury remains a prevalent problem in collegiate, professional, and recreational athletics. Hamstrings muscles are commonly the site of acute strain injury in the lower limb. Of the three hamstrings muscles, the biceps femoris long head (BFLH) muscle is injured most often, with injury frequently localized along the proximal aponeurosis [1].

Imaging studies [2] and computational models [3] have shown that strains are elevated in the muscle tissue neighboring the BFLH's proximal aponeurosis, which may explain why injury occurs in this region. Furthermore, the models have demonstrated that the decreasing width of the muscle's proximal aponeurosis [3] and increasing muscle activation level [4] both have the potential to increase the magnitude of the strains that are localized near the proximal aponeurosis. The goals of this study were to use functional MRI to measure mechanical strain *in vivo* in the BFLH muscle and to compare strain in the region surrounding the proximal aponeurosis i) during eccentric contraction and passive motion and ii) for subjects with narrow and wide proximal aponeuroses.

METHODS

Fourteen healthy subjects (nine male, five female) provided informed consent and were imaged in accordance with the University of Virginia's Institutional Review Board guidelines. Subjects were placed in the head-first prone position inside a 3T Siemens Trio MR scanner (Fig. 1A). Right knee flexion-extension was repeated at a rate of one cycle every two seconds and was performed using a MR-compatible exercise device designed to ensure repeatable motion inside the scanner bore as well as to load the hamstrings eccentrically [5]. In a separate acquisition, each subject's leg was moved for them to study the kinematics of passive motion.

High-resolution images were used to define the functional imaging plane through the BFLH's proximal and distal aponeuroses and through the muscle belly (Fig. 1B,C). Displacement ENcoding with Stimulated Echoes (DENSE) images were acquired during 2.5 minutes of repeated knee flexion-extension [6] with the following imaging parameters: 3.125 x 3.125 mm^2 in-plane resolution, 5 mm slice thickness, 51 ms temporal resolution, and 0.08 cycles/mm displacement-encoding frequency.

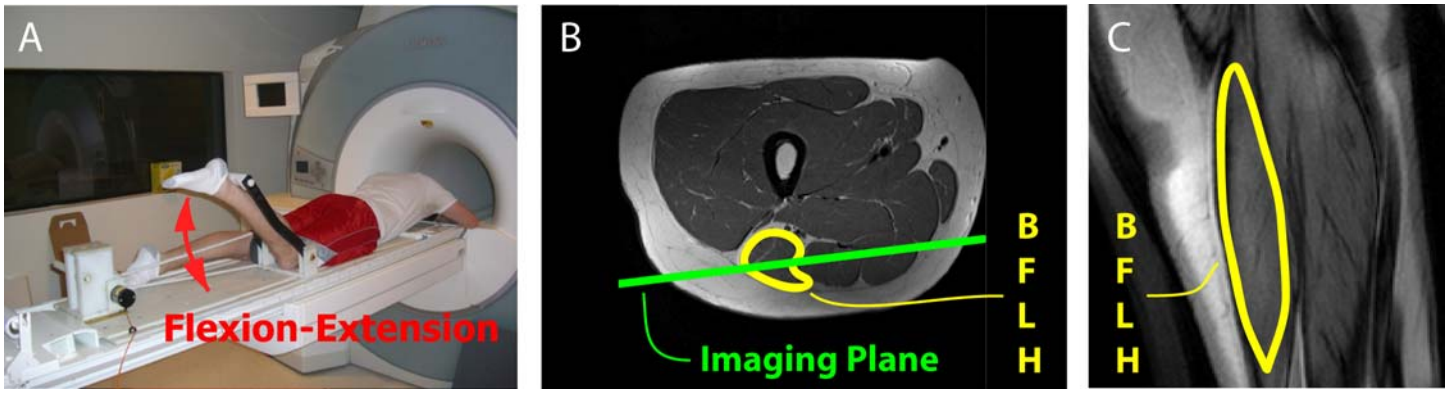

Figure 1. Experimental setup and imaging plane definition. Subjects repeated knee flexion-extension during DENSE image acquisition (A). The functional imaging plane was defined on high-resolution axial images such that it passed through the proximal and distal aponeuroses of the biceps femoris long head muscle (B, C).

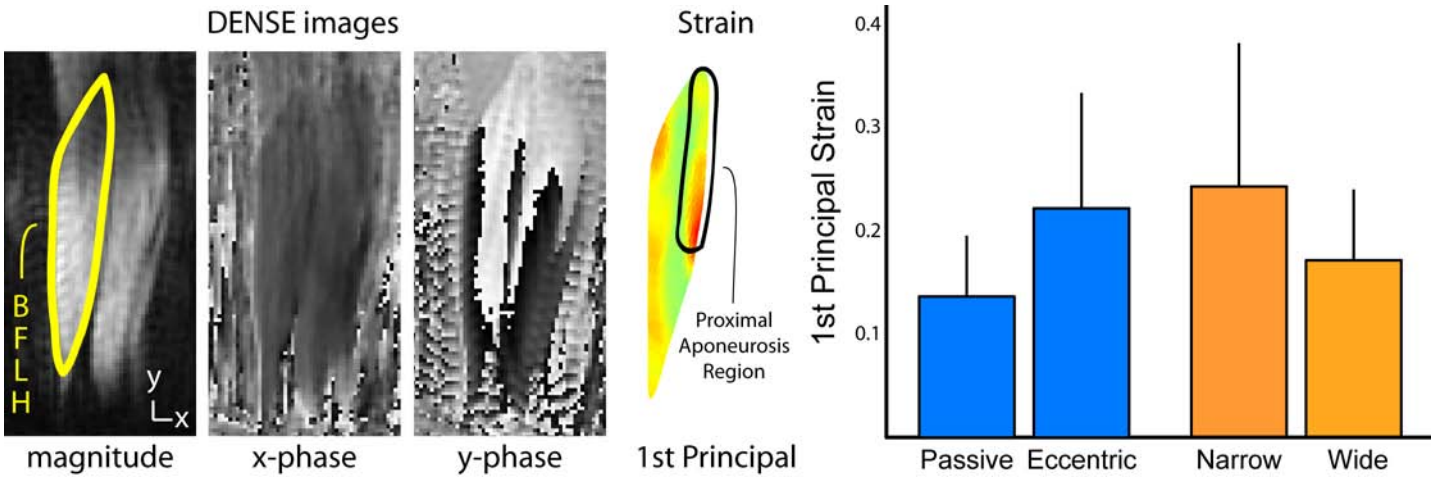

Figure 2. Example images and strain results. Example DENSE magnitude image with the BFLH outlined and phase images (including phase wrap). Lagrangian strain tensors were found at a pixel-wise resolution, decomposed into principal strains, and averaged over the medial third of the muscle adjacent to the proximal aponeurosis. Average 1st principal strains are reported i) during eccentric contraction and passive motion and ii) for subjects with a wide (> 5 mm, N=8) and narrow (< 5 mm, N=6) proximal aponeurosis.

DENSE images were imported into Matlab (MathWorks, Inc., Natick, MA, USA) and analyzed with custom-built software [7]. DENSE phase images (Fig. 2), where image intensity is proportional to displacement, were used to track tissue positions over time. Image data sets with a mean through-plane displacement greater than 20% of in-plane displacement were discarded. Lagrangian strain tensors were calculated at a pixel-wise resolution, and 1st principal strains (most positive eigenvalue) were averaged along the medial third of the muscle adjacent to the proximal aponeurosis (Fig. 2). To compare subjects with different proximal aponeurosis morphologies, subjects were grouped into two categories according to proximal aponeurosis width: wide > 5 mm (N=8) and narrow ≤ 5 mm (N=6). Aponeurosis width measurements are described and reported in [8].

RESULTS AND DISCUSSION

Average first principal strain in the region near the proximal aponeurosis was 0.14 ± 0.06 during passive motion and found to be higher (0.22 ± 0.11) during eccentric contraction (Fig. 2). For the group of subjects with a narrow aponeurosis width, average 1st principal strain was 0.24 ± 0.14 and found to be lower for the wider aponeurosis width group (0.17 ± 0.07).

Elevated strains along the proximal aponeurosis during eccentric contraction support the hypothesis that higher strains are present in the region where injury is normally observed. Moreover, the smaller strain magnitudes seen during passive motion illustrate that the kinematics associated with knee flexion-extension cannot be solely responsible for higher strains along the proximal aponeurosis. Thus, muscle activation likely contributes to regions of higher localized strains.

Results comparing subjects with different aponeurosis widths (Fig. 2) confirm previous computational model findings [3] that muscles with narrower widths experience higher localized strains adjacent to the proximal aponeurosis. Therefore, aponeurosis dimensions could potentially serve as a preliminary marker for acute strain injury susceptibility.

REFERENCES

1. De Smet AA and Best TM. *AJR Am J Roentgenol* **174**, 393-399, 2000.
2. Silder A and Thelen DG. *Proceedings of the ASB'09,* State College, PA, USA, 2009.
3. Rehorn MR and Blemker SS. *J Biomech,* in review, 2010.
4. Rehorn MR and Blemker SS. Submitted to ASB, 2010.
5. Silder A, et al. *J Med Devices* **3**, 034504, 2009.
6. Zhong X, et al. *Mag Res Med* **61**, 981-988, 2009.
7. Spottiswoode B, et al. *IEEE TMI* **26**, 15-30, 2007.
8. Handsfield G, et al. Submitted to ASB, 2010.

ACKNOWLEDGEMENTS

We would like to thank Darryl Thelen, Amy Silder, and Christopher Westphal. Funding sources for this work were provided by NIH RO1 AR056201, NIH R01 EB001763 and the National Science Foundation Graduate Research Fellowship Program.

LONGITUDINAL INCREASES IN KNEE ABDUCTION MOMENTS DURING MATURATION

[1,2,3]Timothy E. Hewett, [1]Gregory D. Myer & [1,2]Kevin R. Ford
[1]Cincinnati Children's Hospital Medical Center, Cincinnati, OH, USA
[2]University of Cincinnati, Cincinnati, OH, USA
[3]University of Kentucky, Lexington, KY, USA
email: tim.hewett@cchmc.org, web: http://cincinnatichildrens.org/sportsmed

INTRODUCTION

Knee abduction moment (*KAM)* may increase during adolescent growth [1]. This injury risk factor has been demonstrated to coincide with pubertal development [2] Specifically, following an adolescent growth spurt, increased body mass, height of the center of mass and length of lower extremity segments may lead to increased *KAM* [2]. The primary purpose of this study was to determine the relationship between skeletal growth and increased KAM (Figure 1).

The secondary purpose of this study was to determine when females diverge from males in *KAM*. The first tested hypothesis was that females would demonstrate peak KAM at peak height velocity (PHV). The second tested hypothesis was that females would demonstrate divergent KAM at peak height velocity (PHV).

METHODS

The subject sample consisted of pre-pubertal, pubertal and post-pubertal female and male athletes. Each subject participated in a pre-season testing session immediately prior to their basketball or soccer season. Multiple subjects were tested longitudinally for multiple years using the same methods. The drop vertical jump (DVJ) from a total of 1648 subject visits, 1296 female, 352 male were analyzed with 3D motion analysis. Prior to motion analysis, 37 retro-reflective markers were placed on each subject. The subjects were positioned for a static pose trial in a standardized position. Subjects performed three box DVJ trials. Trials were collected with a motion analysis system consisting of ten digital cameras (Eagle cameras, Motion Analysis Corporation, Santa Rosa, CA)

The analyses of 3D motion data were performed in Visual3D (C-Motion, Inc., Germantown, MD). 3D marker trajectories of the static trial were used to calculate each segment joint center. Peak *KAM* was determined during the landing phase of each trial of the DVJ. Segment lengths were calculated as the distance between the proximal and distal joint center (e.g. thigh segment distance was equal to the distance between the hip joint center to knee joint center). Percent of adult stature was estimated using the Khamis-Roche method. ANOVA was used to test for differences in change in tibial length and *KAM* between screening years (Figure 1). A two-way ANOVA was used with maturation measured as % adult stature and sex as the independent variables and knee abduction moment (KAM) as the dependent variable (Figure 2).

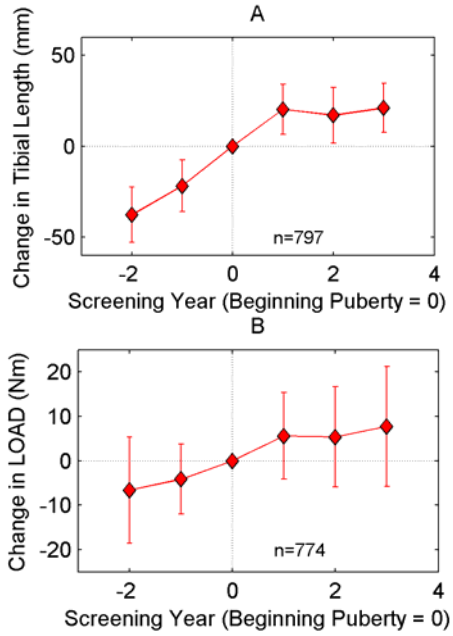

Figure 1 Longitudinal change in tibia length (A) compared to change in *KAM* (B) in only female subjects with longitudinal measures.

RESULTS AND DISCUSSION

LE Lever Length Increases in Athletic Adolescent Females.

The 3D motion analysis methods to measure tibia length and *KAM* described in the Methods section above were used to calculate change in tibia length and change in *KAM* from 862 girls and 1653 screenings relative to their test at beginning puberty (Figure 1A and 1B). Pubertal and post-pubertal girls displayed increased tibia length and *KAM* relative to both pre-pubertal females (p=0.001).Change in tibia length associated with change in *KAM* (p=0.001, Figure 1).

Post-pubertal females displayed increased *KAM* and tibia length relative to both pre-pubertal and pubertal females (p=0.001). Reliability of our measures of tibia length and *KAM* was high.

Timing of Knee KAM increases with maturation in female, but not male, athletes.

Figure 2 shows the relationship between % adult stature and *KAM* in females and males.

The plots in Figure 2 indicate a strong relationship between maturation as measured by % adult stature and KAM in females, but not males. A significant sex by maturation interaction ($p < 0.001$) was observed. Maturation resulted in greater *KAM* in females, but not males.

Post-hoc analyses showed consistent sex differences in groups greater than 88% of adult stature. Hence, sex differences in *KAM* appear to coincide with PHV.

The high *KAM* cut-off score, as reported by Myer et al. [3] is transposed over the data points and demonstrates that females exceed the cut score related to increased risk of ACL injury at or near peak height velocity.

CONCLUSIONS

Sex differences in *KAM* during and following PHV appear to contribute to the increased risk of ACL injury in pubertal females. Longitudinal increases in *KAM* occurred in female, but not male athletes. Increased *KAM* may be useful for the identification of individual female athletes at increased risk of ACL injury. Finally, neuromuscular training designed to decrease *KAM* and to prevent ACL injury may be best instituted just prior to or during PHV that occurs at approximately 92% of adult stature.

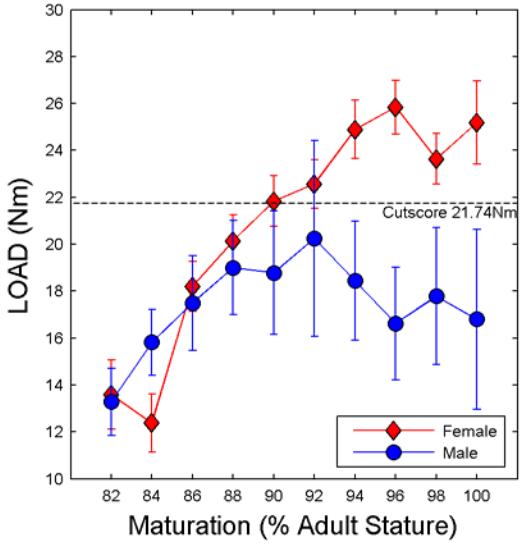

Figure 2: Relationship between % adult stature and knee abduction moment (*KAM or LOAD*) in both female and male subjects.

REFERENCES

1. Hewett TE. et al. *J Bone Joint Surg Am.* **86**, 1601-1608. 2004.
2. Ford KR. et al. *Med. Sci. Sports Exerc.* **42,** 2010 *in press.*
3. Myer GD et al. *Am J Sports Med.* 2010; *in press.*

ACKNOWLEDGEMENTS

The authors would like to acknowledge funding support from NIH Grant R01-AR049735, R01-AR055563 and R01-AR05

HOME-BASED INSTRUCTIONAL PROGRAM TO REDUCE BIOMECHANICAL RISK FACTORS FOR KNEE INJURY

Clare E. Milner, Jeremiah J. Tate, Carolyn G. Westlake, Songning Zhang and Jeffrey T. Fairbrother

University of Tennessee, Knoxville, TN, USA.
Email: milner@utk.edu

INTRODUCTION

Knee injuries are a major cause for concern in female athletes who participate in sports which involve jumping, such as basketball, volleyball and soccer. Non-contact ACL injuries are potentially preventable and have, therefore, been the target of specialized instructional programs developed for jumping athletes. Many of these programs are comprehensive and attempt to address several aspects of performance that may be related to injury risk, such as strength, balance, plyometrics, and technique. While effective, these programs typically require a large time commitment. It has been suggested recently that future research should focus on identifying the components of these multi-dimensional programs which contribute directly to reducing biomechanical risk factors for injury [1].

Therefore, the aim of this study was to determine whether a home-based technique training program was effective in modifying landing biomechanics in female athletes at risk of knee injury. We hypothesized that knee biomechanics and peak ground reaction force post-training and at follow-up would be different from baseline in the intervention group and unchanged in a control group.

METHODS

As part of an ongoing study, 24 young, healthy female recreational athletes (basketball, volleyball, soccer) were recruited. The study was approved by the Institutional Review Board and all subjects provided informed consent to participate. Following a 5 minute warm-up, maximum jump height was determined as the highest of three countermovement jumps using a vertical jump measuring device. Participants were video screened for excessive knee valgus during landing from a countermovement jump while performing a basketball rebounding task. Jump height was set using a basketball on a retractable cord placed at 80% of the individual's maximum jump height. Those who landed with the kneecap medial to the great toe in all three trials were considered to be at increased risk of knee injury [2] and continued in the study. Sixteen participants who exhibited excessive valgus were randomly assigned into experimental (n = 8) and control (n = 8) groups. Baseline performance of countermovement jumps during the rebounding task was recorded. Lower extremity position and force data were recorded using an optoelectronic motion capture system at 240 Hz and synchronized force platforms at 1200 Hz.

Baseline testing was followed by an investigator-led instructional session which focused on reducing medial knee displacement during landing. The short instructional program was developed according to motor learning principles [3] and consisted of both demonstration and instruction. Participants were instructed to focus on their image in a mirror and minimize any inward movement of the knees. Participants practiced modified jumps in three blocks of five jumps in front of a full-length mirror, which they used to receive feedback. Control participants were instructed simply to practice jumping with the same block and trial structure in a sham intervention.

Participants were then provided with materials outlining a one-week home-based program of technique training, with a faded feedback design. Two training sessions were conducted in front of a mirror on non-consecutive days of the week with a faded feedback design. Control participants completed the sham intervention of maximum height jumping practice only. Participants returned to the laboratory for a post-training assessment of landing biomechanics. Further assessment of retention was conducted one week later.

Variables of interest were determined during the landing phase, from ground contact to peak knee flexion. These were: peak knee valgus angle (V-ANG), peak external knee valgus moment V-MOM), peak vertical ground reaction force (GRF), and peak knee flexion angle (FLEX). Effect sizes were used to compare variables from baseline to post training and to follow up in each group [4].

RESULTS AND DISCUSSION

Following the instructional program, we expected to find changes from baseline in the experimental group reflecting a reduction in those variables associated with knee injury risk. No change from baseline was expected in the control group. These hypotheses were partially supported (Table 1). Instruction provided to the experimental group focused on a frontal plane modification to landing biomechanics to reduce knee valgus. V-ANG during landing was reduced slightly after training (ES = 0.42) and unchanged at follow up (ES = 0.03) compared to baseline in the experimental group. V-MOM was reduced slightly at both time points in the experimental group (ES = 0.29, 0.49). The magnitude of change was comparable to a comprehensive program [5]. Both V-ANG (ES = 0.35, 0.83) and V-MOM (ES = 0.81, 0.61) increased in the control group.

Although not targeted in the instructional program, two other variables associated with knee injury risk were positively influenced by the instructional program. GRF was reduced slightly compared to baseline at both time points in the experimental group (0.21, 0.16 BW; ES = 0.47, 0.33), while unchanged in the control group (ES = 0.17, 0.11). This reduction is about half that found in a comprehensive program [6]. FLEX showed no change post training (ES = 0.08), but a small increase from baseline at follow up in the experimental group (4.8°; ES = 0.21). FLEX was reduced slightly post training (ES = 0.30) and unchanged from baseline at follow up (ES = 0.08) in the control group.

These data are part of an ongoing study and, thus, are limited by small sample size. As additional participants are enrolled into both groups, statistical analysis of the data will indicate whether the small positive changes seen here are significant. The transfer of any positive effects of the countermovement jump instructional program to other jumping tasks will also be investigated.

REFERENCES

1. Hewett TE, et al. *Am J Sports Med* **34**, 490-498, 2006.
2. Ekegren CL et al. *J Orthop Sports Phys Ther* **39**, 665-674, 2009.
3. Schmidt RA & Lee TD. *Motor Control and Learning: A Behavioral Emphasis*, *4th Ed* 2005.
4. Cohen J. *Statistical Power Analysis for the Behavioral Sciences,* 1988.
5. Myer GD, et al. *BMC Musculoskel Disord* **8**, 39, 2007.
6. Hewett TE, et al. *Am J Sports Med* **24**, 765-773, 1996.

Table 1: Knee variables and ground reaction force in at each time point, mean (sd)

Control	**Peak knee valgus (°)**	**Peak external valgus moment (Nm/kg)**	**Peak vertical GRF (BW)**	**Peak knee flexion (°)**
Baseline	7.3 (4.6)	0.48 (0.17)	1.72 (0.46)	74.4 (14.4)
Post training	8.9 (4.5)	0.62 (0.18)	1.79 (0.42)	70.4 (12.1)
Follow up	11.3 (5.0)	0.59 (0.21)	1.76 (0.39)	73.3 (13.1)
Experimental				
Baseline	11.2 (3.9)	0.58 (0.24)	1.77 (0.43)	87.3 (19.2)
Post training	9.7 (3.3)	0.52 (0.20)	1.56 (0.44)	89.2 (26.3)
Follow up	11.3 (3.3)	0.48 (0.16)	1.61 (0.50)	92.1 (26.2)

WHOLE BODY BIOMECHANICAL MODIFICATIONS DURING LANDINGS WITH A SECONDARY HORIZONTAL MOMENTUM REDIRECTION TASK

L. Held[1], J. L. McNitt-Gray [1,2,3], and H. Flashner [4],
[1]Department of Biomedical Engineering, [2]Kinesiology, [3]Biological Sciences
[4]Aerospace and Mechanical Engineering
University of Southern California, Los Angeles, CA, USA
email: held@usc.edu

INTRODUCTION

Landing tasks are common in many sports and the loads experienced are often associated with an increased risk of lower extremity injury. In volleyball, as in most sports, athletes are required to generate horizontal momentum in various directions immediately after landing. To satisfy these task requirements, athletes must effectively distribute large reaction forces experienced immediately after contact (impact) and redirect their vertical momentum at touchdown into horizontal momentum as quickly as possible.

Previous landing studies have investigated the three-dimensional kinematics and kinetics during landing using a drop landing task [1, 2]. While drop landings provide a repeatable task from a research perspective, the land and stop task does not reflect the task requirements of most landings performed during competition [3], with the exception of gymnastics [4].

The purpose of this study was to determine how systematic modifications of a secondary task at the whole body level affect preparation and execution of a sport-specific land and go task. We hypothesized that changes in secondary task direction would result in modifications of the roles of the right and left legs during impact and the subsequent ground contact phase. Block, land and go tasks with increasingly more posterior secondary task direction requirements were hypothesized to involve redistribution of the ground reaction forces (GRF) and impulse generation between legs to accommodate for increasingly more rotation of the whole body prior to push.

METHODS

Six female collegiate Division I volleyball players cleared for participation provided written informed consent in accordance with the Institutional Review Board. The participants ranged in age from 19-22 years (mean 20.5 years, SD 1.05 years) with a mean height of 1.89 m (SD 0.03 m) and a mean weight of 775.5 N (SD 43.12 N).

Each subject performed a series of volleyball block landing tasks along a net followed immediately by a secondary task (STOP; LEFT: 90˚/parallel to net, DIAG: 135˚ to back and left, BACK: 180˚/ perpendicular to net) using standard three-step footwork. Subjects were informed of the go direction prior to each trial and performed the task at a self-selected speed. One representative trial of each task was analyzed.

Figure 1. Modifications in landing strategy for a block and go diagonal task are evident, including modifications in foot position prior to contact and via pivoting during post-impact.

Three-dimensional kinematics using high-speed cameras (200 Hz, NAC Visual Systems, Burbank, CA, USA) and reaction forces (dual force plates, 1200 Hz, Kistler, Amhurst, MA, USA) were collected simultaneously during the performance of each task. GRF was normalized to body weight and used to define the phases during the ground contact. Reflective tracking markers were placed on body landmarks and digitized (Vicon Motus, Centennial, CO, USA) during a standing calibration frame and all movement trials. Markers on the second metatarsal and calcaneus were used to define the longitudinal axis of the foot. Digitized three-dimensional coordinates of tracking markers were individually filtered with a quintic spline filter (8 Hz) and visually confirmed with video records. The foot orientation was calculated by finding the projection of the foot vector onto the horizontal plane of the plate. All calculations were performed using a custom Matlab (The Mathworks Inc, MA) routine for processing.

RESULTS AND DISCUSSION

Load distribution between right and left legs during the impact phase (plate contact to first local minimum of vertical GRF curve) varied across tasks (Fig. 1). During LEFT, the right leg accounted for 85.8±7.4% of the peak impact force, whereas it accounted for 56.5±7.2% and 55.0±11.8% of the peak impact force during STOP and DIAG, respectively, and even less than 50% during BACK.

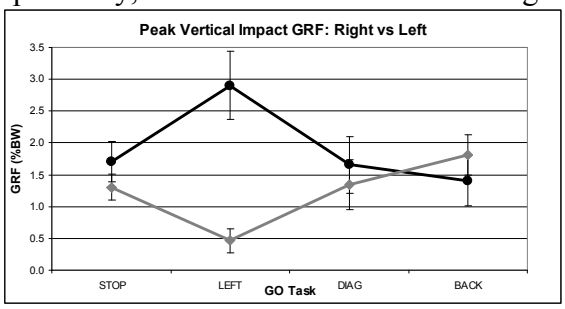

Figure 1: Mean (SD) between-leg distribution of vertical ground reaction forces during the impact phase of a land and go tasks (STOP, LEFT, DIAG, BACK). Reported peak force magnitudes were calculated as the average vertical force during the 10ms prior to and after peak impact force (near the time of heel contact).

Timing and distribution of horizontal impulse generation between right and left legs varied across tasks (Fig. 2). The left leg only contributed to horizontal impulse during BACK, and did so during impact, not the push phase (duration of ground contact when only right foot was on the ground).

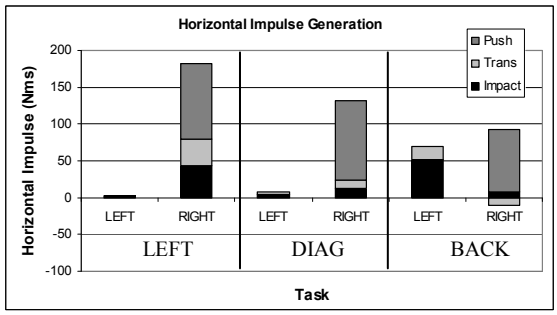

Figure 2: Horizontal impulse generation during the ground contact phase for an exemplar subject. During the left and diagonal tasks, the left leg did not generate any horizontal impulse in the direction of travel.

Between task differences in orientation, as indicated by right foot orientation, were observed prior to phases involving large forces (impact, push). Foot placement was modified during the flight phase prior to contact. Foot orientation prior to the push phase was modified after impact via a pivoting action (Fig. 3). These observed modifications in lower extremity orientation relative to the reaction force are expected to affect the distribution of mechanical demand imposed on joints and between axes of the same joint (flex/ext vs. add/abduction).

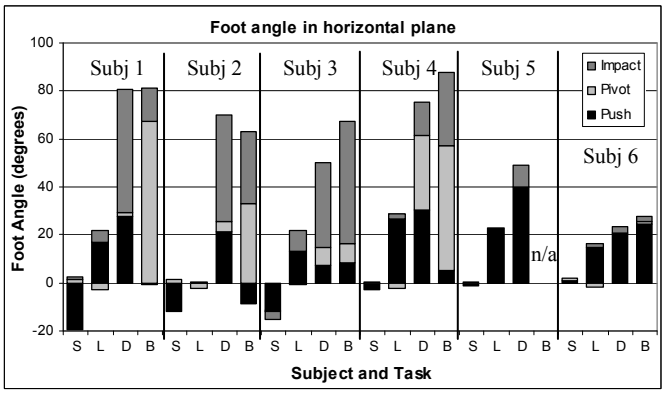

Figure 3. Foot angle in the horizontal plane at the end of impact, transition, and pivot, for each subject. All subjects demonstrate between task modifications in foot orientation during impact. During post-impact phase, subjects 1-4 demonstrate a pivoting strategy prior to the push, whereas subjects 5-6 do not. (S=STOP, L=LEFT, D=DIAG, B=BACK)

CONCLUSIONS

Secondary task requirements following a landing affect lower extremity kinematics and between-leg force distribution during the impact phase of a landing task. In this study, block, land and go tasks with increasingly more posterior secondary task direction requirements involved redistribution of load between legs to accommodate for increasingly more rotation of the whole body prior to push. Modification of the GRF relative to lower extremity segments is expected to influence the net joint moments at the ankle, knee, and hip [5]. When developing models of effective landing technique, secondary tasks must be taken into account.

REFERENCES

1. Ford KR, Myer GD, Hewett TE. *Med Sci Sports Exer* **35(10)**, 1745-1750, 2003.
2. Gehring D, Melnyk M, Gollhofer A. *Clin Biomech* . **24(1)**, 82-7, 2009.
3. Edwards S, Steele JR, McGhee DE. *Scand J Med Sci Sports*, 2009.
4. McNitt-Gray JL. et al. *International Journal of Sport Biomechanics* **7(2)**, 201-224, 1991.
5. McNitt-Gray, J.L. et al., *J of Biomech***, 34**, 1471–1482, 2001.

ACKNOWLEDGEMENTS

USC Women's Volleyball Team

ALTERATIONS IN KNEE LAXITY DURING THE MENSTRUAL CYCLE CHANGE MUSCLE ACTIVATION PATTERNS DURING SELECTED ATHLETIC MOVEMENTS

[1, 2] Sang-Kyoon Park, [2] Darren Stefanyshyn, [2, 3] Claudiane Fukuchi, [4] Jessica Küpper

[1] Running Injury Clinic, Faculty of Kinesiology, University of Calgary, [2] Human Performance Laboratory, Faculty of Kinesiology, University of Calgary, [3] Sport Medicine Centre, University of Calgary, [4] Schulich School of Engineering, University of Calgary, Calgary, Alberta, CANADA
Email: spark@kin.ucalgary.ca, web: www.runninginjuryclinic.com

INTRODUCTION

Female athletes experience a much higher incidence of anterior cruciate ligament (ACL) injuries during sporting activities compared to their male counterparts [1]. Epidemiology studies have found a relationship between a high number of ACL injuries and a certain phase of the menstrual cycle [2]. Biomechanical studies have investigated the ACL injury mechanism behind this relationship, speculating that changes in female hormones during the cycle may have an impact on dynamic joint function of the knee, which may lead to more injurious situations [3, 4]. A recent study has found that increased knee joint laxity (KJL) during the menstrual cycle leads to increased knee joint loads [5]. However, whether alterations in knee joint laxity during the menstrual cycle are also associated with alterations in muscle activations of the lower extremity during athletic movements has not been studied. Therefore, the purpose of this study was to investigate whether altered KJL during the menstrual cycle has an influence on different neuromuscular control of the lower extremity.

METHODS

Twenty-six healthy females (height, 170.1±7.1cm; mass, 65.0±9.3kg; age, 22.7±3.3years) participated in the study. They had been actively involved in sporting activities (8.7±4.4 h/wk). Inclusion criteria required that the subject have a normal menstrual cycle (28.9 ± 2.7days), no history of oral contraceptive use, and no knee injury during the previous six months. Each subject performed a series of tests (blood sample, KJL and electromyography (EMG)) at three different phases of the menstrual cycle (Follicular Phase: 6.1±1.4, Ovulation: 16.1±3.0, Luteal Phase: 22.8±3.2days, $p<0.001$) [5]. The timing of data collection was confirmed with a blood sample and ovulation predictor kit (Clearblue, UK). Blood samples were sent to a local laboratory to determine levels of estradiol and progesterone. Passive KJL was measured at a load of 89N using the KT-2000 (MEDmetric Corp, USA). After completion of blood sample and KJL tests, EMG was collected using round bipolar surface electrodes (Biovision, Germany). EMG electrodes were placed on the skin overlying the muscle belly of the medial head of the gastrocnemius (GAS), the biceps femoris (BF) vastus medialis (VM) and the vastus lateralis (VL) on the right leg (Figure 1). Muscle activation onsets before heel contact (HC) as indicated from a force plate (Kistler, Switzerland) were calculated. Co-contraction between lower extremity muscles using correlation coefficients (CC), and time (%) to reach peak EMG in each muscle during the stance phase (100%) were calculated using a Matlab7.6 (Mathworks, USA). The subject performed ten trials of cutting at 3.5m/s within ±10% range (Figure 1). A repeated measure analysis of variance determined whether there was a laxity effect on muscle activations with SPSS (SPSS Inc., USA) at $p<0.05$.

Figure 1: Experimental set up (left: placements of EMG electrodes, right: cutting on a runway).

RESULTS

This study found that increased KJL during ovulation changes muscle activations, showing delayed VM onset and decreased CC during movement. Increased KJL was observed during ovulation (Table 1). Figure 2 shows delayed onset of VM activation during ovulation and the luteal phase compared to the follicular phase. In addition, delayed onset of VL activation was found during the luteal phase compared to ovulation (Figure 2). A lower level of co-contraction between GAS and VM was found during ovulation compared to the luteal phase (Table 1). However, there were no significant differences in time to reach peak EMG between the three phases.

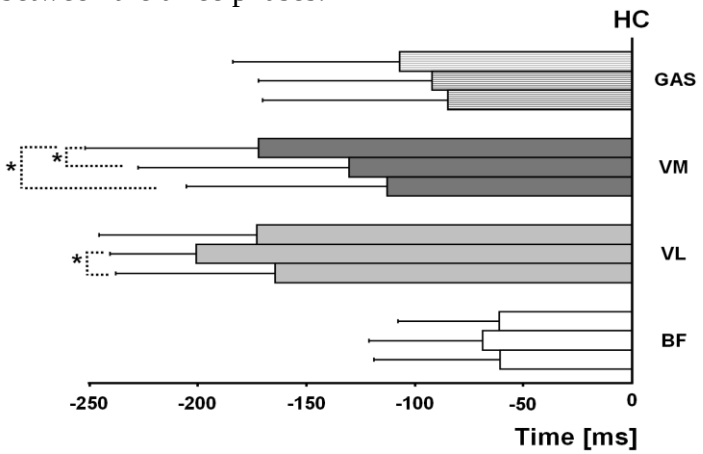

Figure 2: Onset of muscle activations (pre-activation) between follicular phase (top), ovulation (middle) and luteal (bottom) phase (* indicates significant difference at $p<0.05$).

DISCUSSION/CONCLUSIONS

Studies have found that greater KJL in females delays timing of muscle reflex [6] and increases knee joint load [5]. This greater KJL in females is known to be a strong risk factor for a high incidence of ACL injuries during sports. Furthermore, increased KJL during ovulation has been observed in several studies [5]. However, the links between increased KJL during the menstrual cycle and changes in muscle activations during movement has not been well understood.

Current findings suggest that increased KJL during ovulation may increase the risk of ACL injury by delayed muscle activations and possibly, decreased muscle co-contraction during movement. Pre-activation or onset of muscles is required to prepare the body for high rates of loading during landing. Appropriate co-contraction between antagonistic muscles surrounding the knee such as quadriceps and hamstrings or quadriceps and gastrocnemius reduce the strain on the ACL and provide dynamic stability during movement. However, a difference in co-contraction of GAS/VM between ovulation and luteal phase is small. Whether this difference is clinically meaningful is questionable. Further investigation will be required in this relationship. Our previous study found that increased KJL during the menstrual cycle leads to increased knee joint load in healthy females [5]. Thus, the findings of different EMG activation, influenced by an increased KJL during the menstrual cycle, may provide important information toward creating an overall picture of the ACL injury mechanism in females.

REFERENCES

1. Arendt et al., *Am J Sports Med* **23,** 694-701, 1995.
2. Wojtys et al., *Am J Sports Med* **26,** 614-9, 1998.
3. Chaudhari et al., *Am J Sports Med* **35,** 793-800, 2007.
4. Dedrick et al., *J Electromyogr Kinesio* **18**, 68-78, 2008.
5. Park et al., *Am J Sports Med* **37**, 1169-77, 2009.
6. Shultz et al., *J Electromyogr Kinesio* **14**, 475-483, 2004.

ACKNOWLEDGEMENTS

The institute of Gender and Health (IGH) of the Canadian Institutes of Health and Research (CIHR)

Table 1: Changes in KJL and muscle activations during the menstrual cycle.

	Laxity	Time to Peak EMG (%)				Muscle Co-contraction (CC: Correlation Coefficients)					
	(mm)	GAS	VM	VL	BF	VM/BF	VL/BF	GAS/VM	GAS/VL	VM/VL	GAS/BF
Follicular Phase	4.72 (1.66)	47.9 (34.7)	61.1 (31.5)	50.8 (31.0)	38.0 (33.5)	0.005 (0.267)	0.020 (0.241)	-0.061 (0.160)	0.014 (0.148)	0.481 (0.176)	0.261 (0.183)
Ovulation	5.13* (1.73)	33.9 (28.7)	58.7 (37.1)	54.8 (41.8)	54.9 (34.6)	-0.041 (0.160)	0.029 (0.133)	-0.059* (0.149)	-0.002 (0.145)	0.462 (0.133)	0.244 (0.196)
Luteal Phase	4.55 (1.53)	38.9 (34.4)	46.5 (36.5)	47.7 (34.5)	43.2 (34.9)	0.018 (0.202)	0.051 (0.182)	0.041 (0.162)	0.049 (0.156)	0.496 (0.149)	0.247 (0.187)

* indicates significant difference from Luteal Phase at $p<0.05$ with Bonferroni correction.

DO IMPACTS CAUSE RUNNING INJURIES? A PROSPECTIVE INVESTIGATION

[1,2]Irene S. Davis, [1]Bradley Bowser and [3]David Mullineaux

[1]Department of Physical Therapy, University of Delaware, Newark, DE, USA
[2]Drayer Physical Therapy Institute, Hummelstown, PA, USA
[3]Department of Kinesiology and Health Promotion, University of Kentucky, Lexington, KY
email: mcclay@udel.edu

INTRODUCTION

During running, the foot collides with the ground approximately 1000 times per mile. These collisions vary significantly by the strike pattern that the runner adopts. A rearfoot strike pattern results in a very distinct vertical impact peak that is missing in a midfoot or forefoot strike landing (Figure 1) [1]. The impact peak of a rearfoot strike is associated with higher rates of loading compared with a forefoot strike pattern. Impact peak magnitudes are also positively correlated to tibial shock. Interestingly, increased vertical impact peaks, loading rates and tibial shock have been associated with a history of tibial stress fractures [2], plantar fasciitis [3], and more recently, patellofemoral pain syndrome [4].

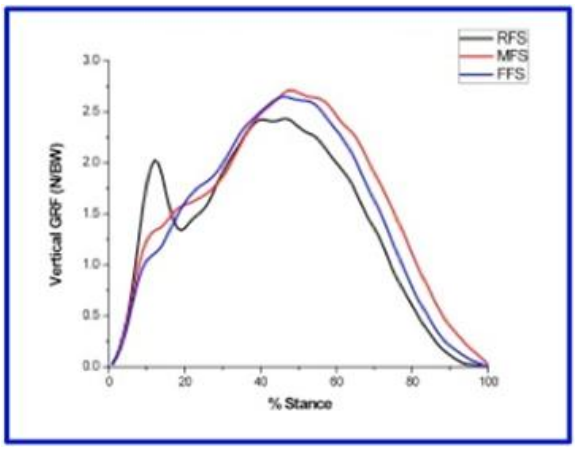

Figure 1. Vertical ground reaction force of a rearfoot, midfoot and forefoot strike landing.

Barefoot runners strike with a mid or forefoot strike pattern [5] as it hurts to land on their heels. Thus, it is possible that we were designed to run with a mid or forefoot strike pattern that is absent of this impact peak, thus lessening the impact loads to the body.

Up to 79% of runners sustain an injury in a given year [6]. Approximately 80% of shod runners are rearfoot strikers [7]. It is plausible that rearfoot strikers with increased impact loads, may be at greater risk for the development of an injury than those with lower loads.

In summary, previous studies have documented higher impact loading in runners with a history of injury. However, these studies were retrospective in nature and cannot establish causative relationships. Therefore, the purpose of this prospective study was to compare the impact loads of rearfoot strike runners who go on to develop a running injury to those who have never been injured. It was hypothesized that runners who went on to develop a running-related injury would have higher vertical impact peaks, vertical average loadrates, vertical instantaneous loadrates and peak tibial shock.

METHODS

240 female rearfoot strike runners, aged 18-40 years and running a minimum of 20 miles per week were recruited. Tibial accelerometry and ground reaction force data were collected at 1080 Hz as subjects ran overground at 3.5 m/s. The vertical impact peak (VIP), vertical average loadrate (VALR), vertical instantaneous loadrate (VILR) and peak tibial shock (TS) were extracted from 5 trials and averaged for each subject. In addition to the impact variables, peak vertical force (FZ) was assessed.

Running mileage and injuries were reported monthly for 2 years. Only injuries diagnosed by a medical professional were included. The impact loading variables were analyzed in the runners who went on to sustain an injury. These values were then compared to those of a group of runners who had never sustained a running related injury. Outliers were removed using a boxplot analysis. Independent t-tests were used to statistically assess the data. In addition, the four dependent variables (VIP, VILR, VALR, PPA) were entered separately into a forward binary logistic regression with the constant included. The odds to be injured were then calculated.

RESULTS AND DISCUSSION

A total of 242 female runners have been analyzed, to date (Figure 2). 139 (57%) sustained a prospective

injury. 70 (50%) of these sought medical attention and served as the injured (INJ) group. Of the 103 runners who did not sustain a prospective injury, only 22 had not been injured retrospectively either. This group served as the uninjured (UNINJ) group.

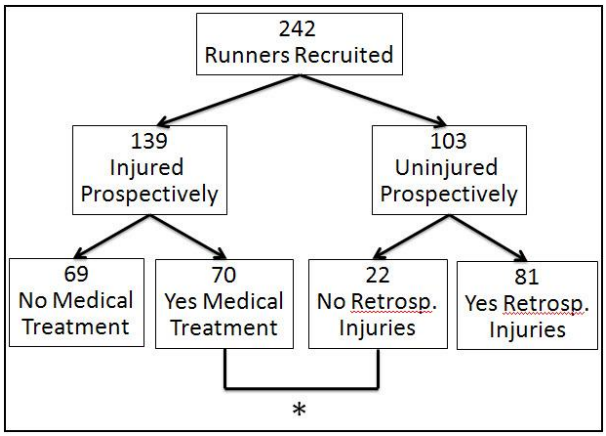

Figure 2. Breakdown of injured and uninjured groups. The '*' indicates the two groups that were compared in this study.

The subjects were well-matched for age (INJ: 26.8±9.8 yrs; UNINJ: 25.5±10.3 yrs) and monthly mileage (INJ:107.6±43.1 miles; UNINJ: 97.0±30.9 miles). 125 injuries were medically diagnosed in the 70 INJ subjects. The top 5 prospective injuries are presented in Table 1.

Table 1. Top 5 injuries sustained prospectively

Injury	No.	% Total
Iliotibial Band Syndrome	14/125	11.2
Anterior Knee Pain	12/125	9.6
Tibial Stress Fracture	6/125	4.8
Tibial Stress Syndrome	6/125	4.8
Plantar Fasciitis	6/125	4.8
Total	44/125	35.2

Following the boxplot analysis, 1 subject was removed from the UNINJ group for TS, 1 for VALR. For the INJ group, 1 subject was removed for VILR, 2 for VIP and VALR, and 3 for TS. The resulting comparison of impact loading between the UNINJ and INJ groups is presented in Table 2

Table 2. Comparison of variables of interest between groups

Variable	UNINJ	INJ	P
TS (g)	4.8 (1.5)	5.9 (2.7)	0.018
VIP (bw)	1.5 (0.24)	1.7 (0.26)	0.041
VALR (bw/s)	62.4 (14.1)	72.1 (18.1)	0.028
VILR (bw/s)	77.0 (18.1)	84.5 (22.4)	0.157
FZ (bw)	2.5 (0.17)	2.5 (0.19)	0.961

Due to their significant contributions to distinguishing between groups, VIP and AVLR were entered together into the logistic regression. Owing to shared variance, VIP was omitted and the final model was Odds = 1.035*AVLR*0.318 (1.035; 95%CI 1.003 to 1.069). Applying this to the AVLR group means resulted in odds to be injured of 3.2 times higher for the injured group than for non-injured group.

Our injury findings were consistent with previous literature. It has been reported that between 20-80% of runners get injured in a given year [6], and 57% of our runners sustained a prospective injury. In terms of injury distribution, iliotibial band syndrome, anterior knee pain, tibial stress syndrome and plantar fasciitis were also among the top five injuries in a much larger study of 2002 runners [8].

As hypothesized, all impact loading was greater in the injured runners compared with the never-injured group. All impact variables were significantly higher, except for VILR. Interestingly, FZ, the peak value of the vertical force, was identical between groups. This further underscores the importance of impact loads in the development of these injuries.

The fact that all running injuries were included increases the significance of these results. While it is recognized that the etiology of running injuries is multi-factorial, this suggests that impact loading may be a global indicator for the development of an injury. Based upon the odds ratio for VALR, reducing impacts is likely to result in an overall reduction of injury risk. Based on previous reports, adopting a midfoot or forefoot strike pattern will reduce these impacts. However future studies of injury patterns in midfoot and forefoot strike runners are needed.

CONCLUSIONS

Based upon the preliminary results of this study, it appears that an increase in impact loading amplifies the risk of developing a running-related injury.

REFERENCES

1. Cavanagh, PR et al., *JOB*, **13**:397-406, 1980.
2. Milner, C et al., *Med Sci Sports Exerc* **38**, 323-8, 2006.
3. Pohl, MB et al., *Clin J Sp Med*, **19**(5):372-376, 2009.
4. Davis, IS et al, *Proc of ACSM Mtg*, 2010.
5. Lieberman, D, et al., *Nature*, **463**:531-535, 2010.
6. Lun, V et al., *Br J Sports Med* **38**:576-580, 2004.
7. Hasegawa, H et al., *J Str Cond*, **21**(3):888-893, 2007.
8. Taunton, J et al., *Br J Sp Med* **36**, 95-101, 2002.

ACKNOWLEDGEMENTS

This study was supported by: DAMD17-00-1-0515

METABOLIC ENERGY AND MUSCLE ACTIVITY REQUIRED FOR NORMAL, EXOSKELETAL, AND ADDED WEIGHT HOPPING

[1]Alena M. Grabowski, [1]Hazel Briner, [2]Beth Shields, & [1]Hugh Herr
[1]Massachusetts Institute of Technology, Cambridge, MA, USA
[2]Harvard University, Cambridge, MA, USA
email: alenag@mit.edu, web: http://media.mit.edu/~alenag

INTRODUCTION

During bouncing gaits such as hopping, the human musculoskeletal system is integrated such that the body behaves like a simple spring-mass system [1], where changes in leg stiffness are primarily achieved by modulating ankle stiffness [2]. Elastic energy storage and return in the compliant musculo-skeletal structures of the leg greatly reduces the metabolic demands needed to achieve bouncing gaits [3]. However, leg muscles must generate force during each stretch-shorten cycle to compensate for energy losses due to damping, which requires metabolic energy. Previous research indicates that Triceps Surae muscle activity is largely responsible for maintaining leg stiffness during hopping [4].

A recent study [5] has shown that use of a springy leg exoskeleton, comprised of fiberglass leaf springs placed in parallel with the biological legs, can substantially decrease the metabolic demands of hopping. However, the mechanism for this metabolic reduction has not been completely elucidated. The exoskeleton allows storage and return of elastic energy in the leaf springs such that body weight is transferred through the exoskeleton directly to the ground instead of this force being completely sustained by the biological legs.

We sought to determine metabolic power and leg muscle activity during two-legged hopping at 2.2-3.2 Hz normally, using an exoskeleton, and with added weight (equal to the exoskeleton's weight). We hypothesized that metabolic demand and Triceps Surae muscle activity would decrease during exoskeletal hopping and increase during added weight hopping compared to normal hopping.

METHODS

Nine healthy recreational runners [5 F, 4 M; 23 (6) yrs; 64.0 (7.2) kg] gave informed written consent and participated. Subjects hopped in place to the beat of a metronome at 2.2, 2.4, 2.6, 2.8, 3.0, and 3.2 Hz during each experimental session. Sessions were separated by at least 2 days.

During sessions 1, 2, and 3, subjects hopped normally, using the SLE exoskeleton previously described in [5], and with added weight (58 N), respectively. For each session, we measured rates of oxygen consumption and carbon dioxide production (Cosmed K4b^2, IT) while subjects stood and hopped in place at the frequencies listed above. Each trial was 5 minutes followed by at least 3 minutes rest. We determined average steady-state metabolic rates from minutes 2.5-4.5 of each trial and calculated metabolic power (in Watts) using a standard equation. Net metabolic power was calculated by subtracting standing from gross metabolic power.

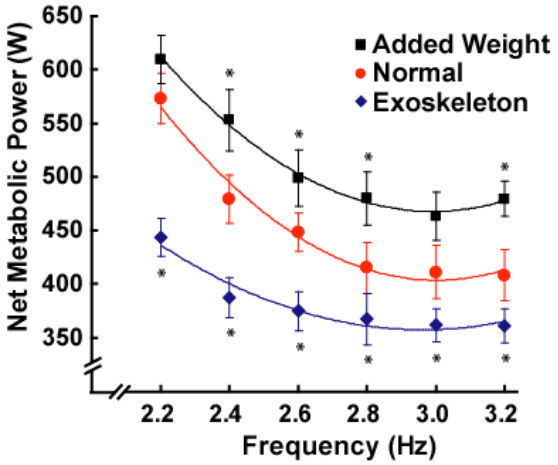

Figure 1: Average (+/-SEM) net metabolic power for added weight (black squares), normal (red circles), and exoskeletal (blue diamonds) hopping. *indicates significantly different from normal hopping (P<0.05).

During session 4, we measured ground reaction forces and electromyography (EMG) at 2520 Hz from the Lateral Gatrocnemius (LG), Medial Gastrocnemius (MG), Soleus (Sol), Tibialis Anterior, Rectus Femoris, Biceps Femoris,

Semitendinosus, Gluteus Maximus, and Iliopsoas. Subjects hopped in place normally, using an exoskeleton and with added weight at all frequencies, for a total of 18 trials. Each trial was approximately 30 seconds.

Raw EMG data were band pass filtered (10-500 Hz), rectified, and low pass filtered (10 Hz cut-off). Then, the processed EMG signals were normalized to maximum voluntary isometric contractions. We determined stance and aerial phases from the vertical GRF data for 15 steps using a 10N threshold. Then, we calculated mean stance and aerial phase integrals (iEMG) of the normalized EMG for each subject using trapezoidal integration.

RESULTS AND DISCUSSION

Using an exoskeleton decreased net metabolic power by 23, 19, 16, 12, 12, and 12%, whereas hopping with added weight increased net metabolic power by 6, 15, 11, 16, 13, and 18% compared to hopping normally at 2.2, 2.4, 2.6, 2.8, 3.0, and 3.2 Hz, respectively (Fig 1). For all conditions, hopping at 3.0 Hz required the least metabolic power.

LG and MG muscle activity were lower using an exoskeleton compared to normal hopping at all frequencies (Fig 2). LG iEMG were 8-29% lower during the stance phase and 24-44% lower during the aerial phase. MG iEMG were 2-24% lower during the stance phase and 36-45% lower during the aerial phase. At slow hopping frequencies, Sol iEMG were also significantly lower while using the exoskeleton compared to normal and weighted hopping. We found no other significant differences between exoskeletal and normal hopping in stance phase iEMG for any of the other muscles analyzed.

Contrary to our hypothesis, LG, MG, and Sol iEMG were not significantly greater for weighted compared to normal hopping. During weighted hopping, ground contact time was significantly longer and aerial time was significantly shorter than normal hopping, but none of the muscles that were analyzed had significantly greater iEMG. Hoppers may have altered their body position, recruited muscles that were not analyzed in the present study or adopted different individual muscle activity strategies to hop with added weight. But, further analysis is necessary to understand the mechanism responsible for the greater metabolic demand incurred when hopping with added weight.

CONCLUSIONS

Using an exoskeleton during hopping requires much less metabolic power than hopping normally. This metabolic reduction is likely due to decreased Triceps Surae muscle activity. In contrast, hopping with added weight incurs much greater metabolic demands than hopping normally but does not elicit greater Triceps Surae muscle activity. Thus, exoskeletons designed for bouncing gaits such as hopping and running, may further improve metabolic economy by reducing the device weight.

REFERENCES

1. Blickhan R. *J Biomech* **22**, 1217-1227, 1989.
2. Farley CF & Gonzalez O. *J Biomech* **29**, 181-186, 1996.
3. Biewener AA. *Am Zool* **38**, 703-717, 1998.
4. Hobara H, Kanouse K, & Suzuki S. *Neurosci Lett* **418**, 55-59, 2007.
5. Grabowski AM & Herr HM. *J Appl Physiol* **107,** 670-678, 2009.

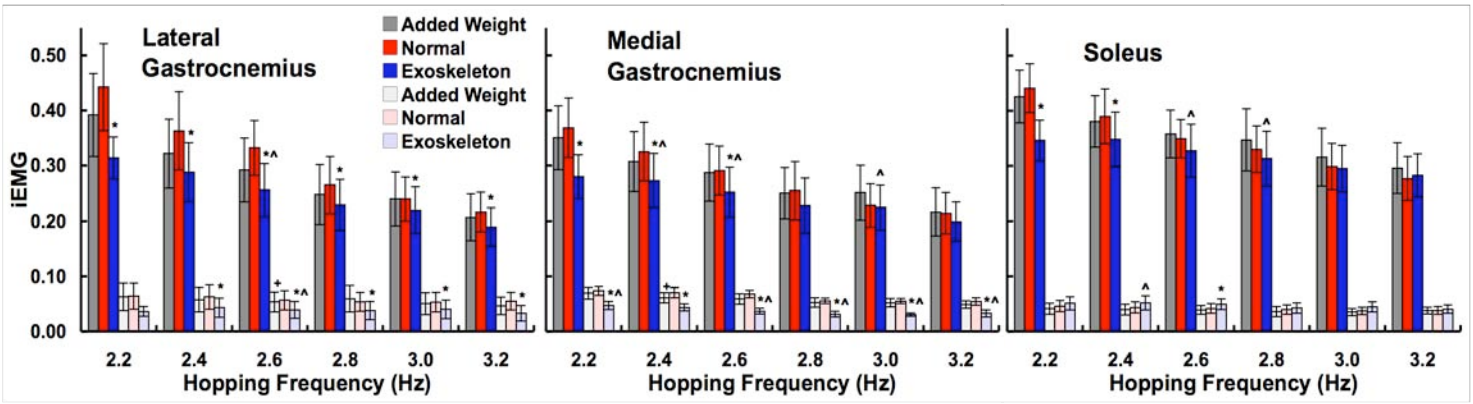

Figure 2. Average (+/-SEM) iEMG during stance (dark colors) and aerial (light colors) phases for added weight (gray), normal (red), and exoskeletal (blue) hopping. *, ^, and + show significant differences between normal and exoskeletal, weighted and exoskeletal, and normal and weighted hopping, respectively (P<0.05).

MECHANICS AND ENERGETICS OF HUMAN HOPPING WITH A PASSIVE-ELASTIC ANKLE EXOSKELETON

Gregory S. Sawicki[1], Dominic J. Farris[1]

[1]Joint Dept. of Biomedical Engineering, North Carolina State University and University of North Carolina-Chapel Hill, Raleigh, NC, USA
e-mail: greg_sawicki@ncsu.edu

INTRODUCTION

A major goal of powered lower-limb exoskeletons is to act in parallel with the user's leg muscles and reduce metabolic energy consumption during locomotion. One approach is to deliver power to the limbs using attached motors/actuators to perform net mechanical work and help drive the lower-limb joints. An alternative is to use passive elastic elements (i.e. springs) to recycle center of mass energy, storing it at one phase of the gait and returning it later.

The passive, 'energy-neutral' approach is appealing because it requires no outside power source and can still reduce the mechanical demands placed on biological muscle-tendon units. In fact, Ferris et al. showed significant reductions in triceps surae EMG when humans hopped on one-leg with an elastic ankle exoskeleton over a range of hopping frequencies [1]. That study did not measure metabolic energy consumption.

A recent study by Grabowski et al. was the first to our knowledge to document a reduction in metabolic cost during human locomotion with a passive exoskeleton. They showed that when humans hop on two-legs with assistance from bilateral leaf springs attached from hip to heel user's reduced net metabolic power by up to 27% [2].

Our goal in this study was to determine whether providing mechanical assistance with parallel springs acting at the ankle joint *only* could reduce the metabolic cost of two-legged hopping. Based on the results of Grabowski et al. [2] we hypothesized that (1) net metabolic power would be lower in the springs versus no springs condition, independent of hopping frequency (2) reductions would be larger for more compliant springs and (3) peak reductions would be less than 27% because our device only provides assistance at the ankle rather than over the whole leg.

METHODS

We constructed a pair of custom-made carbon fiber elastic ankle exoskeletons for a single subject (mass=63 kg, height= 170 cm) following [1]. To spring-load the ankle we attached linear tension springs (Mc Master-Carr Inc.) between two metal brackets on the posterior of the exoskeletons. To vary ankle exoskeleton compliance we used springs with different linear stiffness values (compliant=2.1 kN/m; stiff = 5.1 kN/m). The moment arm length for the spring attachment was 14.0 cm, yielding ankle exoskeleton torsional stiffness values of 0.71 N-m/deg (compliant) and 1.75 N-m/deg (stiff). The subject hopped on two-legs at 2.0, 2.2 and 2.4 Hz donning exoskeletons without springs (NS), with compliant springs (CS) and with stiff springs (SS). Each trial lasted 4 minutes with 7 minutes rest between trials. To test our primary hypotheses, we calculated the net metabolic power (gross minus resting) (watts) using rates of oxygen consumption and carbon dioxide production measured with indirect

calorimetery. We used inverse dynamics to calculate the ankle muscle-tendon average positive mechanical power over the hopping cycle (watts). To assess the mechanical contribution of the exoskeletons we used force recordings from a load cell attached in series with the springs to determine the average positive mechanical power delivered during recoil (watts)

RESULTS

Preliminary results (n =1) indicate that bilateral elastic ankle exoskeletons can reduce net metabolic power over a wide range of two-legged hopping frequencies and exoskeleton stiffness values. Net metabolic power was reduced in *all* hopping conditions with parallel exoskeleton springs (CS and SS) when compared to no springs (NS) (Fig. 1, top). Metabolic savings ranged from 8% (at 2.4 Hz, CS) all the way up to 25% (at 2.0 Hz, SS). Contrary to our hypothesis, our largest reduction (25% at 2.0 Hz, SS) was close to what Grabowski et al. reported (27%) in similar conditions with a *compliant*, *full-leg* exoskeleton. Our mechanics data support the result that stiff springs are more effective than compliant ones. The biological muscle-tendon contribution to ankle positive work was always lower in the SS versus CS condition (Fig. 1, bottom).

DISCUSSION

Our device provides parallel stiffness at the ankle joint *only*, but can achieve reductions in metabolic cost that are similar to a full-leg exoskeleton. It is possible that assistance at one joint could cause postural changes and influence the mechanical demands at other joints. In addition, the effective exoskeleton stiffness seems to be a critical design variable that deserves further attention. Other future work will attempt to extend the concept of 'energy-neutral' passive exoskeleton assistance to other locomotion tasks (e.g. running, walking).

REFERENCES

1. Ferris DP et al., *J Appl Physiol*, **100(1)**, 163-70, 2005.
2. Grabowski AM et al., *J Appl Physiol*, **107(3)**, 670-8, 2009.

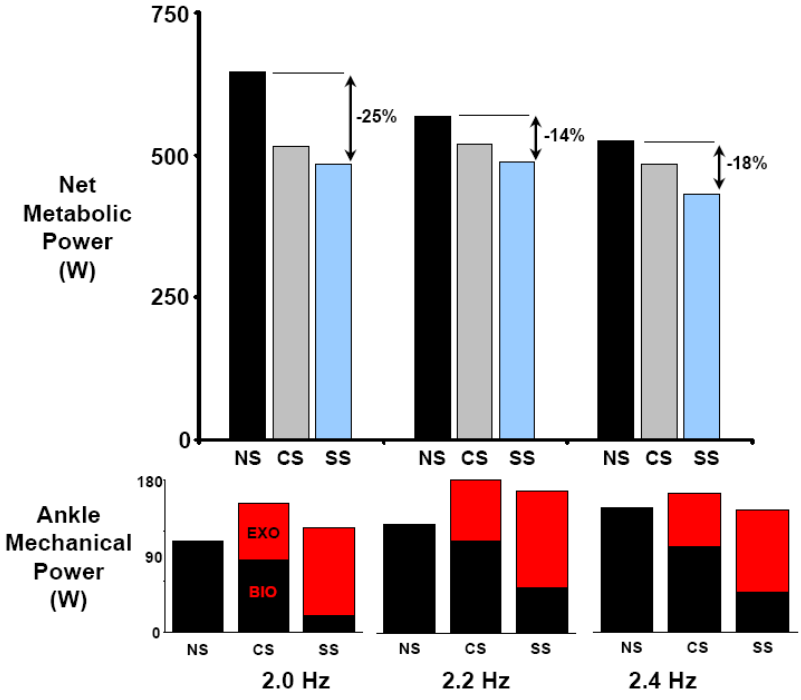

Figure 1: (**Top**) Net metabolic power (W) for one subject during two-legged hopping at 2.0, 2.2. and 2.4 Hz (left to right) in three conditions: wearing bilateral elastic exoskeletons without springs (black, NS), with compliant springs (gray, CS) and with stiff springs (light blue, SS). Percentages are reductions between NS and SS conditions. (**Bottom**) Average ankle positive mechanical power (W) over a hopping cycle. In each condition, red portion of the bar is the exoskeleton contribution and black portion is the biological muscle-tendon contribution to the overall ankle joint power output. The stiff exoskeleton delivered more positive mechanical power (on recoil) and reduced net metabolic power more than compliant at all frequencies.

PENDULAR DYNAMICS APPLIED TO OBESE GAIT

Elizabeth M. Russell and Joseph Hamill

University of Massachusetts, Amherst, MA, USA
email: erussell@kin.umass.edu

INTRODUCTION

Biological systems self-optimize to perform at the least metabolic cost [1]. Humans select walking speed to minimize the metabolic cost per distance. Deviations from the two components comprising speed, stride frequency (SF) and stride length (SL), increase metabolic cost [2] in a U-shaped fashion with the minimum at the preferred SF-SL combination. Therefore, over-striding (long, slow steps) or under-striding (short, quick steps) increases the aerobic demand compared to the preferred gait.

An oscillator operating at its resonant frequency requires a minimum driving force to maintain its period. Therefore, a limb oscillating at or near its resonant frequency should require minimal internal work performed by the body segments and produce the lowest metabolic cost, compared to other periods. Holt et al. [2] found that the periods of limb oscillations are predicted by modeling the limb as a simple force-driven pendulum.

It is possible that the increased metabolic cost in some populations may be partially attributable to limb oscillations that veer away from resonance. The gait characteristics in obese populations differ from non-obese populations. Specifically, obese individuals have greater hip abduction during swing [3], which may lead to limb oscillations less than predicted by a force-driven pendulum.

The purpose of this study was to determine if the limbs of obese women operate at the predicted resonant frequency, and if metabolic cost is minimized at that frequency. We hypothesized that non-obese women would display limb oscillations operating near resonance when metabolic cost was minimized and that secondary plane movement in obese women would cause the limbs to operate at a frequency below their predicted frequency.

METHODS

Ten obese (age = 35.2 ± 10.8; BMI = 37.9 ± 4.9 $kg \cdot m^{-2}$) and 10 controls (age = 21.0 ± 1.9; BMI = 22.2 ± 1.5 $kg \cdot m^{-2}$) consented to participate in the study. Participants were free of lower extremity injury and had not experienced a change in body weight greater than 9 kg within the past five years.

Preferred speed was found by increasing and decreasing treadmill belt speed until subjects consistently identified the same preferred speed six times. Preferred SF (PSF) was the number of counted strides taken during 1 min of walking. Preferred SL was found as the product of preferred speed and PSF^{-1}. At a constant preferred speed, subjects walked at ±0%, ±5%, ±10%, ±15%, ±20% of their PSF, as paced by a metronome.

Metabolic cost was measured through indirect calorimetry with 15-sec averaging. Participants walked for 6 minutes with the final 2 minutes averaged to assess steady state VO_2. Retroreflective markers were placed on anatomical landmarks of the right lower extremity and recorded (240 Hz) during the final 30 seconds of walking at the given SF condition.

Kinematic data were filtered at 8 Hz. 3D lower extremity joint angles were calculated over ten consecutive strides and time-normalized to the gait cycle. Predicted frequencies were assessed using the approach described by Holt et al. [2]. The length of the limb was measured from the marker on the right greater trochanter to the lateral maleollus. Dempster's [4] body segment parameters were used to find center of mass locations. Plagenhoef's [5] limb inertial characteristics were used.

Data are presented as group means and standard deviations. A two-way (group x condition) ANOVA was done ($p<0.05$) to compare differences between

and among groups and conditions. Tukey's post hoc test assessed significant differences within main effects where appropriate. Effect sizes were calculated as per Cohen [6].

RESULTS AND DISCUSSION

Metabolic cost was minimized at or just above the PSF (Figure 1). PSF matched predicted SF near the minimum metabolic cost in the Obese group, but the Control subjects preferred to walk with longer steps than predicted at the frequency where cost was minimized (Figure 2). Metabolic cost, however, was not significantly different between +5% (minimal cost) and -5% (predicted SF) PSF.

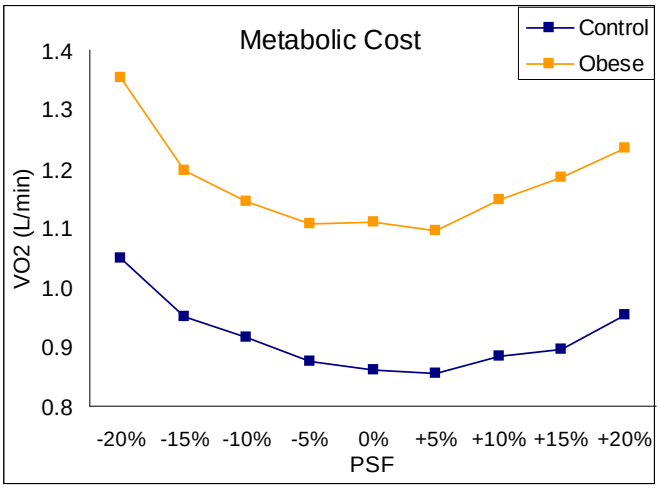

Figure 1: Ensemble averages of steady state metabolic cost over 9 SF conditions.

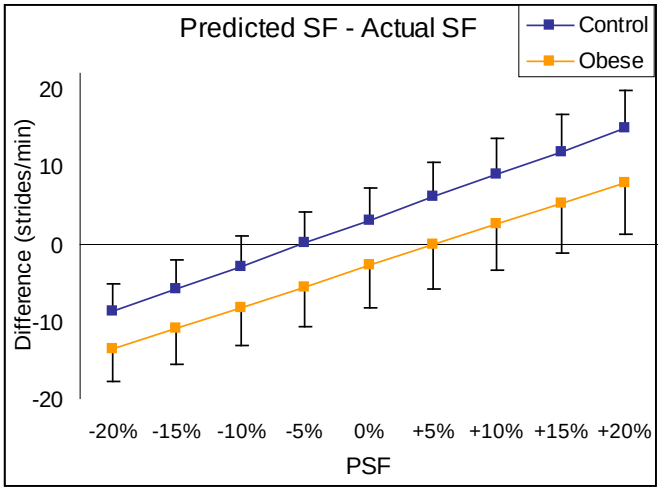

Figure 2: The difference between the predicted and actual SF over 9 conditions. At a baseline of 0 the subjects used a walking SF equal to the predicted.

Interestingly, both groups operated near resonance. However, at constant preferred speed, the Control group preferred shorter strides and a higher SF than predicted (56.2 ± 2.3 vs. 59.2 ± 1.7 strides/min) while the Obese preferred longer strides and a lower frequency of oscillation than predicted (56.8 vs. 53.7 strides/min). Note: at a constant speed, as SF increases, SL decreases.

Preferred speeds were lower in the Obese group (2.6 ± 0.4 mph vs. 3.1 ± 0.3 mph for the Control group). Despite walking at a lower speed, the metabolic cost was still greater for the Obese group across every SF condition (Effect size > 0.9). Limb lengths were longer in the Control group (0.71 ± 0.24 m vs. 0.65 ± 0.27 m).

CONCLUSIONS

Contrary to our hypothesis, predicted SF closely matched the SF at which metabolic cost was minimized in the Obese group, but not in the Control group. The Control subjects were able to walk with a higher SF than predicted and still minimize metabolic cost. These differences in metabolic cost were small and there were no significant differences in cost between the SF at with cost was minimized (+5% in both groups) and the SF closest to that predicted by the force-driven oscillator (-5% in the Control and +5% in the Obese). We conclude that the overall higher cost of walking in the Obese group necessitates that they adhere to strict optimization of SL-SF combinations to minimize cost, while non-obese subjects can utilize higher frequencies of limb oscillations, even if doing so requires more energy.

REFERENCES

1.Wilke JT. *Int J Neurosci*, **7**, 125-143, 1977.
2.Holt KG. et al. *Med Sci Sports Exer* **23**, 491-498, 1991.
3.Spyropoulos P. et al. *Arch Phys Med Rehabil* **72**, 1065-1070, 1991.
4.Cohen J. *Statistical Power Analysis of the Behavioral Sciences (2nd Ed.)*, Erlbaum, 1990.
5.Dempster WT. *Space Requirements of the Seated Operator*, 1955.
6.Plagenheof SC. *Res Q Amer Assoc Health Phys Ed*, **37**, 103-112, 1966.

WALKING DOWNHILL: THE TRADE-OFF BETWEEN ENERGETICS AND STABILITY

Emily Hendrix, Lindsay Hunter, and Jesse Dean

Medical University of South Carolina, Charleston, SC, USA
email: deaje@musc.edu

INTRODUCTION

Humans tend to choose walking patterns that minimize energetic cost [1], but must also maintain stability. We used model simulations and experiments to investigate the potential trade-off between energetic economy and stability during downhill walking, a context in which gravitational potential energy will reduce the need for active powering but may also contribute to instability.

One method of keeping energetic cost low is to take advantage of the body's passive mechanics, as evidenced by the development of dynamic walkers. These simple devices can walk with low energetic demand when powered by a downhill slope or push-off impulses [2, 3] and can produce typical human kinematics by actuating the swing leg with passive springs [4]. In comparison to human walking, however, these devices are quite unstable.

We hypothesized that when walking downhill, humans prefer to increase stability rather than minimize energetic cost by behaving like a dynamic walker. In simulations of a dynamic walking model, we anticipated that increased slope would decrease the required actuation and decrease stability. Similarly, we expected that instructing subjects to walk more like dynamic walkers would decrease both energetic cost and stability.

METHODS

Model Simulations
Our dynamic walking model is actively powered by push-off impulses, with the hip and knee joints actuated by bi-articular springs (Fig. 1A) [4]. For a range of downhill slopes, we quantified the push-off and spring stiffness values that produced gait limit cycles (at 1.25 m/s), the stride period, and the model stability (using the gait sensitivity norm metric [5]).

Experimental Procedure
Twelve subjects walked on a treadmill for 6 minutes at 1.25 m/s. The treadmill was set to one of four slopes (0, 0.05, 0.10, and 0.15 grade decline), and subjects were instructed either to walk normally (*normal* walking) or to allow gravity to assist their walking and use as little muscle activity as possible (*relaxed* walking). One *normal* and one *relaxed* walking trial were performed at each slope.

Metabolic cost and foot-ground contact data were collected. All data were analyzed during the last 3 minutes of each trial to ensure subjects reached a steady state. Paired 2-way ANOVAs ($p<0.05$) were performed to determine if metabolic cost, average stride period, or stride period variability were significantly influenced by slope or walking strategy (i.e. *normal* or *relaxed*).

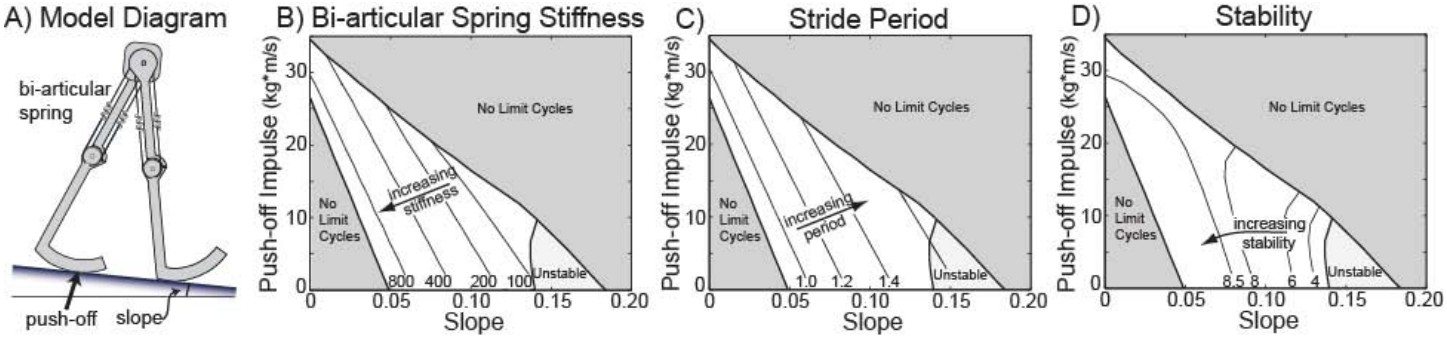

Figure 1. A dynamic walking model (A) was able to walk down a range of slopes. Steeper slopes allowed a decrease in push-off impulse and spring stiffness (B), increased stride period (C), and decreased stability (D).

RESULTS AND DISCUSSION

As hypothesized, subjects did not prefer the energetically optimal gait when walking downhill. Subjects were able to voluntarily reduce energetic cost by walking more like our simple model, but this was accompanied by decreased stability.

In our dynamic walking model, steeper slopes required less push-off and weaker springs (Fig. 1B). The decreased spring stiffness at steeper slopes caused an increase in stride period (Fig. 1C) and a decrease in stability (Fig. 1D).

Experimentally, walking using a *relaxed* strategy decreased energetic cost by 16% at the steeper slopes (Fig. 2A). The *relaxed* strategy increased stride period (Fig. 2B) and stride period variability (Fig. 2C), a measure associated with instability [6].

While the dynamic walking model was able to walk down a range of slopes, it did not predict the *normal* gait strategy used by human subjects. The model predicted that steeper slopes would reduce the required actuation (both push-off impulse and spring stiffness) and increase stride period. In contrast, the experimentally measured energetic cost of walking reached a plateau at a relatively shallow slope (~0.05), and stride period actually decreased at steeper slopes.

The discrepancy between our model predictions and *normal* walking behavior may be explained by the decrease in model stability at steeper slopes. In order to maintain stability, humans may prefer a gait strategy that requires more active control and is thus more energetically costly.

The importance of stability in determining the preferred gait pattern is supported by the *relaxed* walking data. Simply by changing their gait strategy to behave more like a dynamic walker, subjects were able to voluntarily reduce the energetic cost of walking. Despite the improvement in energetic economy, this gait is likely not preferred because of the decrease in stability, as evidenced by increased stride period variability [6].

CONCLUSIONS

When walking downhill, humans prefer a gait strategy that increases stability rather than minimizing energetic cost. This may partially explain the increased cost of locomotion in older adults and patients with gait disorders. While some of the increased energetic cost may be due to changes in cardiovascular or muscular properties, an additional portion may be attributable to the goal of ensuring stability. Additionally, the development of assistive devices may require the assurance of stability as an important first step in encouraging subjects to prefer a gait with reduced energetic cost.

REFERENCES

1. Alexander RM. *Am J Hum Biol* **14**, 641-8, 2002.
2. McGeer T. *Int J Robot Res* **9**, 62-82, 1990.
3. Collins S, et al. *Science* **307**, 1082-5, 2005.
4. Dean JC, Kuo AD. *J Roy Soc Int* **6**, 561-73, 2009.
5. Hobbelen DGE, Wisse M. *IEEE Trans Robotics* **23**, 1213-24, 2007.
6. Hausdorff JM. *Hum Move Sci* **26**, 555-89, 2007.

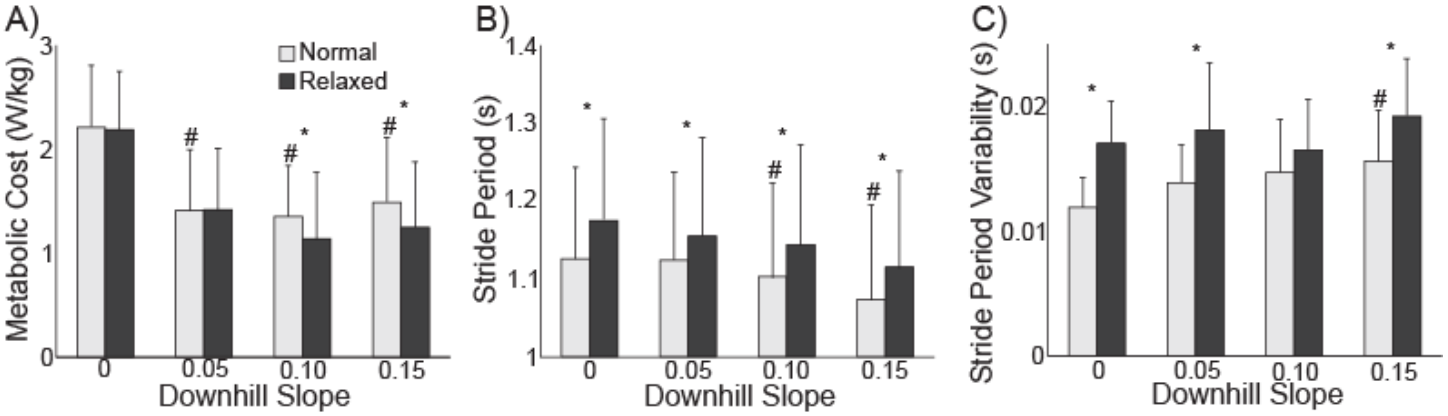

Figure 2. Walking using the relaxed strategy decreased energetic cost at the steeper slopes (A), increased stride period (B), and increased stride period variability (C). #Significantly different from walking on level ground. *Normal and relaxed values are significantly different.

EFFECT OF RIGID SHOE SHAPE ON ENERGETIC COST OF WALKING

Peter Adamczyk[1,2] and Arthur Kuo[2]

[1]Intelligent Prosthetic Systems, LLC, Ann Arbor, MI; [2]University of Michigan, Ann Arbor, MI
email: p.g.adamczyk@gmail.com

INTRODUCTION

Shoes with rocker bottoms and other shapes are commonly used in rehabilitation, for example in walking boots and diabetic or orthopedic footwear. Although such shapes may increase walking comfort or alter plantar pressure and ankle joint moment, they may also have positive or negative effects on the energetic requirements of walking, that are thus far unknown. Humans walking in normal shoes coordinate the leg so that it resembles a rolling segment with a radius of curvature about 30% of leg length, a parameter that is maintained across variations in speed, slope and load [1]. It is unclear whether rocker bottom shoes alter this motion, or whether they cause humans to adjust their gait. We therefore measured the biomechanical and energetic effects of rigid rocker bottoms on the gait of healthy adults.

METHODS

We attached rigid arc shapes to the bottoms of modified walking shoes, and compared metabolic energy expenditure and leg mechanics during walking with arcs of different radii. We expected that perturbations to the shape of the bottom of the foot would lead to changes in the body's control of the ankle and the mechanics of center of mass (COM) motion, with repercussions for the energy consumed in walking. We hypothesized that increasing radius would lead to decreases in the work performed on the COM by reducing the collision loss in each landing. We also hypothesized that very small- and large-radius arcs would lead to the highest metabolic cost, with a minimum between. Both of these predictions are motivated by the results of our prior study with immobilized ankles and similar arc shapes [2].

Seven healthy human subjects gave their informed consent to walk on an instrumented treadmill while wearing shoes with different rigid arcs attached to the bottom. We constructed 5 pairs of rigid convex arc shapes from wood and stiff foam rubber, having radii of curvature 0.05, 0.15, 0.30, 0.50 and 1.00 m (Fig 1). We attached these shapes interchangeably to walking shoes using Velcro and straps. Subjects walked for 7 minutes per condition while we used indirect calorimetry to estimate energy expenditure..

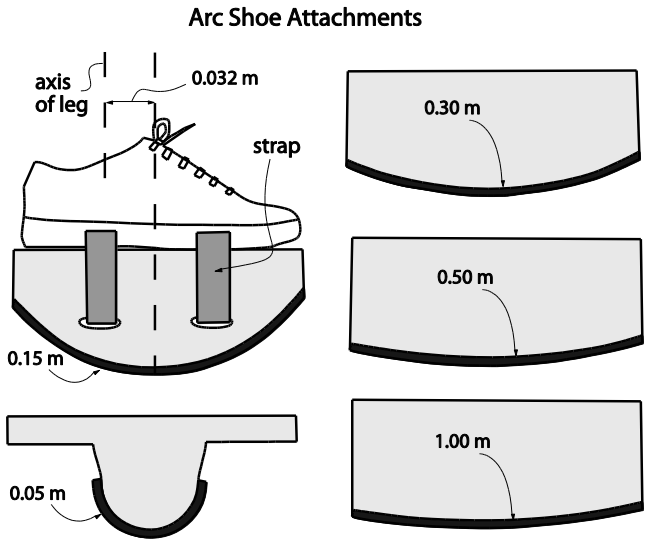

Figure 1: Five arc shapes of different radius were attached to the bottom of a shoe by velcro and straps in order to experimentally manipulate foot-ground interaction mechanics.

For four subjects, we also measured lower body mechanics, using motion capture data and ground reaction forces (GRF) from an instrumented treadmill. We estimated the rate of work performed on the COM by each leg (COM work) by the dot product of that leg's GRF with COM velocity, as determined from integrated GRF [3]. We integrated negative portions of the COM work rate curves and divided by step time to obtain the mean rate at which negative work is performed on the COM [3]. We also computed lower body joint motions and inverse dynamics.

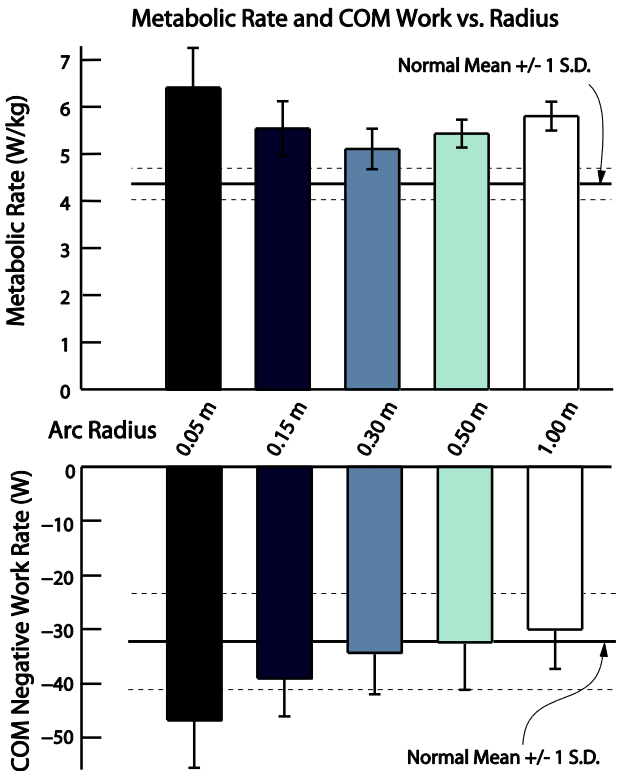

Figure 2: Gross metabolic rate was minimized by an arc of radius 0.30 m, similar to the effective rollover shape observed in normal walking. COM work decreased steadily with increasing radius of curvature of the foot bottom arc.

RESULTS and DISCUSSION

Gross metabolic rate exhibited a minimum for arcs of radius 0.30 m, with smaller and larger radii leading to increased energy expenditure (Fig 2). Values ranged from 17.5% (for 0.30 m arcs) to 47% (0.05 m arcs) above the rate measured during normal walking. This trend is consistent with prior results using a fixed-ankle apparatus [2]. This finding suggests that even with the ankle free to compensate, the body incurs a penalty for an unusual foot shape.

Mean COM work rate decreased with larger arcs, with the smallest radius resulting in 45% more work than normal and the largest radius resulting in 7% less than normal (Fig 3). This result is also consistent with prior results using a fixed-ankle apparatus [2], in which COM work declined consistently for larger radii, even while metabolic cost exhibited a minimum and increased again. We suspect that there are costly features of joint control are accentuated by small- and/or large-radius arcs.

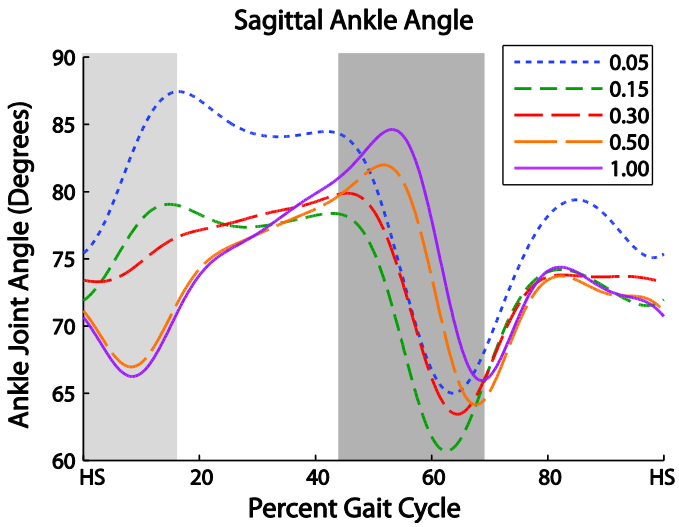

Figure 3: Ankle motion was dramatically different in early stance, as a forward center of pressure (COP) forced the foot into dorsiflexion (light gray). In late-stance, the angular excursion during plantarflexion was similar across all conditions (dark gray).

Ankle motion was dramatically different for large- and small- radius arcs in early stance, but remarkably similar during ankle plantarflexion (Fig 3). With small arcs, the GRF passed in front of the ankle joint immediately upon landing, forcing the foot into dorsiflexion instead of its usual early plantarflexion. The ankle did not reach the same position in mid-late stance, but the subsequent dorsiflexion excursion was nearly constant across conditions. Thus, ankle push-off was kinematically similar across all the conditions, despite wide variation in early-to-mid stance. A possible alternative strategy for adapting to small arcs would have been to plantarflex the ankle much more during the single-stance period, in an attempt to preserve the rollover shape. That this adaptation was not observed might be because it is helpful to preserve ankle push-off, which might reduce negative COM work in the subsequent collision [3].

REFERENCES

1.Hansen AH. *J Pros Orth* **17 (4S)**, 23ff, 2005.
2.Adamczyk PG, et al. *J Exp Bio* **209**, 3953ff, 2006.
3.Donelan JM, et al. *J Biomech* **32**, 117ff, 2002.

ACKNOWLEDGEMENTS

Partially supported by NIH grant 2R44HD055706.

GLENOHUMERAL MUSCLE FORCES DURING WHEELCHAIR ACTIVITIES

Melissa Morrow, Kenton Kaufman and Kai-Nan An

Biomechanics and Motion Analysis Laboratories, Division of Orthopedic Research
Mayo Clinic, Rochester, USA
email: an.kainan@mayo.edu , web: http://mayoresearch.mayo.edu/biomechanics/

INTRODUCTION

Shoulder pain associated with impingement syndrome is a common complaint in the manual wheelchair population. A major determinant of impingement is the balance of muscle forces about the glenohumeral joint. The wrong combination of muscle activation patterns can result in increased compression between the acromial arch and humeral head. To investigate muscle contributions, EMG offers valuable information on activation patterns and magnitudes, but it does not provide individual muscle forces. Currently, musculoskeletal modeling is employed to analyze the distribution of muscle effort about a joint. The purpose of this study was to apply a previously validated upper extremity musculoskeletal model utilizing an optimization algorithm to predict glenohumeral muscle force distribution during manual wheelchair activities to assess if there are detrimental muscle forces that could contribute to shoulder impingement syndrome.

METHODS

Twelve manual wheelchair users were recruited for this study. Subjects performed three trials of two propulsion tasks (level, 1:12 ramp) and a weight relief task. Kinematics were recorded with a 10-camera system (Motion Analysis Corp.). Three dimensional handrim forces and moments were collected with bilateral SmartWheels (Three River Holdings, LLC). Intersegmental joint forces and moments were calculated using inverse dynamics.

Glenohumeral muscle forces for each wheelchair activity were determined using an optimization algorithm developed in MATLAB (Mathworks, Inc.) minimizing the neuromuscular activation [1]. A Hill-type musculoskeletal model was used consisting of thirteen muscle bundles crossing the shoulder complex. Model input variables included intersegmental forces and moments calculated in Visual3D (C-motion, Inc.), muscle parameters from the literature [2], and muscle orientations for known joint orientations (SIMM, Musculographics, Inc.).

The peak forces of the rotator cuff, deltoid and pectoralis major muscle groups were identified for each activity and averaged over all subjects. The peak forces were normalized to maximum muscle force for statistical analysis. A two-factor (subject, condition) ANOVA with one repeated measure (condition) was performed for each peak normalized muscle force. When significant main effects were identified for condition (α=.05), post hoc Bonferroni-adjusted pair wise comparisons were performed.

RESULTS AND DISCUSSION

The peak normalized (Fig. 1A) and absolute (Fig. 1B) forces of the rotator cuff, deltoid and pectoralis major muscle groups were investigated in this study to address the muscle imbalance concerns associated with shoulder impingement. In the rotator cuff, the ramp condition peak muscle force was greater than both level propulsion and weight relief in the supraspinatus muscle ($p=.0012$, $p=.0006$; respectively) and greater than level propulsion in the subscapularis ($p=.0307$). In the deltoid muscle group, ramp propulsion peak muscle force was greater than level and weight relief in the middle ($p<.0001$, $p=.0008$; respectively) and anterior ($p=.0015$, $p=.0011$; respectively) sections. Additionally, the peak normalized forces of the ramp and weight relief conditions were greater than level propulsion in pectoralis major ($p<.0001$, $p<.0001$; respectively).

To maintain repeated muscle contractions for an hour or more without inducing fatigue, muscle

activations must remain below 25.1% maximum voluntary contraction [3]. Based on the model estimated muscle force activities in this study, the ramp condition shows the greatest potential for rotator cuff fatigue due to high activations of the subscapularis (100%) and supraspinatus (92%) (Fig. 1A). If the cuff stabilizers are fatigued, they will have a decreased ability to counter the forces of the larger deltoids [4]. The potential for superior migration of the humeral head is high for all conditions based on high forces in the deltoid muscles and is especially likely during the ramp condition where the peak normalized forces are large for the anterior (94%), middle (68%) and posterior (47%) groups (Fig. 1A). In addition to significant deltoid muscle activity, the ramp condition was predicted to cause superior glenohumeral contact forces more than two times that predicted for level propulsion [5]. The potential for the supraspinatus tendon to be rotated under the acromion is high due to pectoralis major peak normalized forces above 40% for all conditions (level = 41%, ramp = 100%, and weight relief = 94%) (Fig. 1A).

The rotator cuff muscles, being smaller muscle groups than the deltoid and pectoralis major groups, will experience higher muscle stress at similar high peak force magnitudes due to smaller cross-sectional areas. This increased stress can contribute to a greater likelihood of fatigue in the cuff muscles in comparison to the larger, higher capacity deltoid and pectoralis major muscle groups. It may be likely, based on the data presented here, that the rotator cuff muscles could not stabilize against the deltoids, especially in the high peak force ramp condition. These results suggest manual wheelchair users would benefit from a strengthening rehabilitation program that targets increasing rotator cuff strength and, at the same time, pays particular attention to muscle strength imbalance between the internal and external rotators of the humerus.

REFERENCES

1. Kaufman KR, et al. *Neuroscience* **40**, 781-792, 1991.
2. Langenderfer J, et al. *Clin Biomech* **19**, 664-670, 2004.
3. Hagsberg M. *J Applied Phys* **51**, 1-7, 1981.
4. Mulroy SJ, et al. *APMR* **77**, 187-193, 1996.
5. Morrow MM et al. *Proceedings of ASB'09*, State College, PA, USA, 2009.

ACKNOWLEDGEMENTS

Work supported by NIH Grant R01 HD 48781.

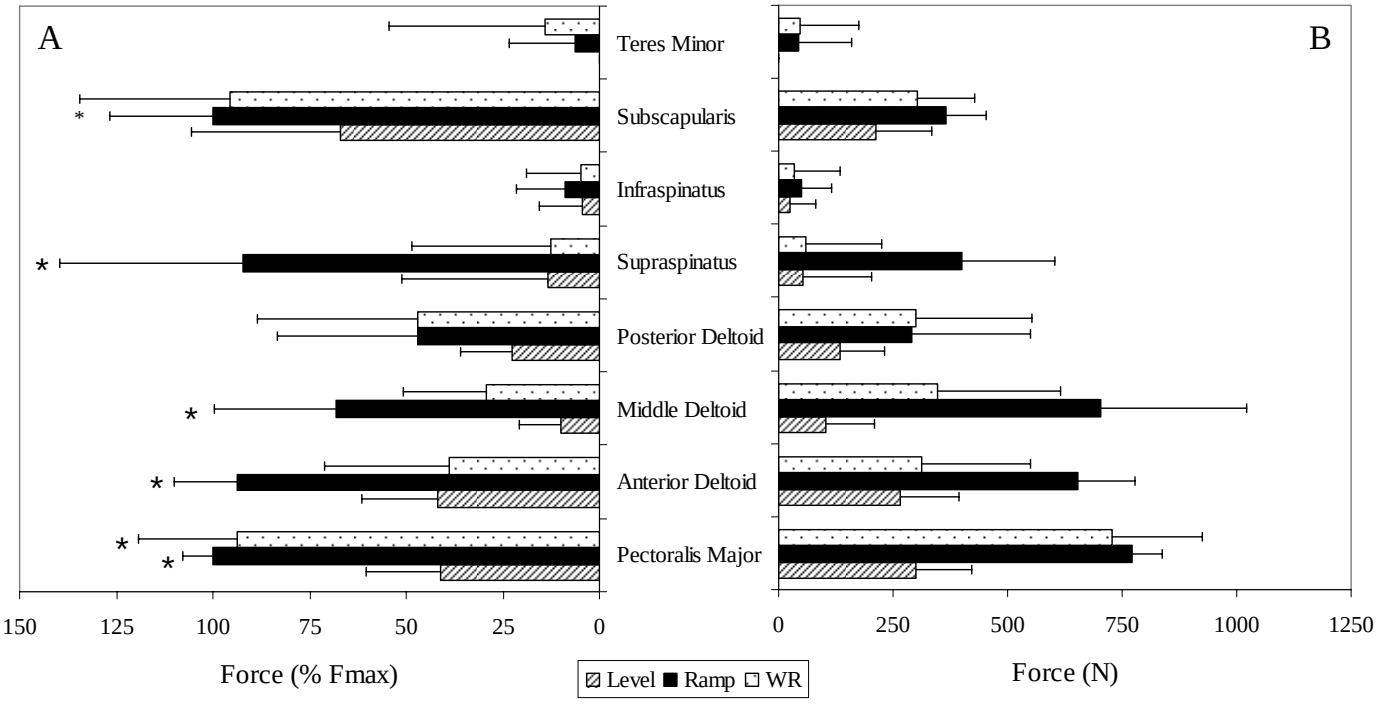

Figure 1. **A**: Model predicted peak muscle forces normalized to maximum muscle forces (Fmax). **B**: Model predicted peak muscle forces. *Ramp or weight relief forces significantly greater than level propulsion.

MUSCLE FUNCTION DURING THE PUSH PHASE OF WHEELCHAIR PROPULSION

[1]Jeffery W. Rankin, [2]Andrew M. Kwarciak, [2]W. Mark Richter and [1]Richard R. Neptune

[1]Department of Mechanical Engineering, The University of Texas at Austin, Austin, TX, USA
[2]Max Mobility LLC, Antioch, TN, USA
email: jwr383@mail.utexas.edu, web: http://www.me.utexas.edu/~neptune

INTRODUCTION

The majority of manual wheelchair users will experience upper extremity injuries and/or pain [1], which have been linked to the considerable physical demand placed on the upper extremity during wheelchair propulsion. As a result, much effort has been devoted to developing propulsion techniques that reduce upper extremity demand. However, the functional roles of individual muscles and how they work in synergy to satisfy the mechanical energetic demands of wheelchair propulsion are poorly understood. Understanding muscle function is a prerequisite for identifying how different propulsion techniques influence upper extremity demand and potential injury mechanisms.

Previous wheelchair propulsion studies have used EMG analyses to examine muscle function, which classified muscles broadly as either having push or recovery functions [e.g., 2]. Others have used joint power analyses to examine function based on net joint power [3]. However, how individual muscles contribute to the power flow that generates wheelchair propulsion is not well understood. Therefore, the purpose of this study was to use a forward dynamics simulation of the push phase of wheelchair propulsion to identify muscle function based on how individual muscles generate, absorb and/or transfer mechanical power to overcome the external workload.

METHODS

An upper extremity musculoskeletal model and forward dynamics simulation of wheelchair propulsion was used within a dynamic optimization framework that identified the muscle excitation patterns required to produce a simulation of normal wheelchair mechanics. The cost function used in the optimization minimized the difference between the simulation and experimentally collected push phase joint kinematics and handrim forces of a representative wheelchair user.

The upper extremity model was developed based on the work of Holzbaur et al. [4] and consisted of six rotational degrees of freedom representing trunk, shoulder, elbow and forearm articulations. Trunk lean and hand translations were prescribed over the entire stroke based on experimental kinematic data. Twenty-six Hill-type musculotendon actuators governed by intrinsic muscle force-length-velocity relationships were used to drive the model. Muscle excitation-activation dynamics were modeled using a first order differential equation with muscle specific activation and deactivation time constants.

Following the optimization, individual muscle contributions to the mechanical power of each body segment and the external handrim power were determined using a segment power analysis [5]. Individual body segments were combined into a single group representing the upper body.

RESULTS AND DISCUSSION

The optimization framework successfully identified muscle excitation patterns that reproduced the experimental data, with average joint kinematic and handrim differences of 0.6 degrees and 2.7 N, respectively, which were within one standard deviation of the experimental data. The segment power analysis showed that the proximal muscles (e.g. shoulder flexors) generated most of the mechanical power during the push phase, with the anterior deltoid (ADELT) being the primary contributor (Fig. 1A). During the first half of the push phase, ADELT provided similar amounts of power to the body and handrim (Fig. 1A; dotted and

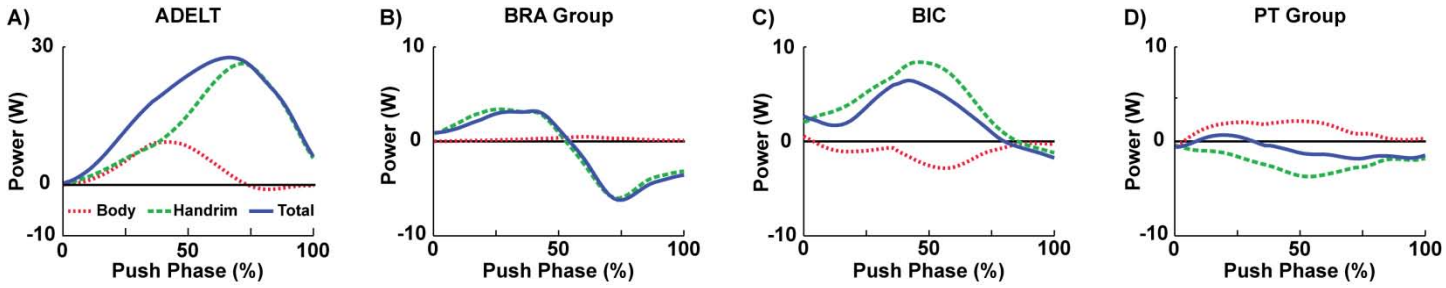

Figure 1: Muscle contributions to body and handrim power during the push phase. Note the change in scale with ADELT. *Total* is the total musculotendon power, which is the sum of the *Body* and *Handrim* power.

dashed lines equal). During the second half, ADELT delivered most of its power directly to the handrim (Fig. 1A; dashed line). The functional role of the proximal muscles as the primary power generators is consistent with a previous study showing the net shoulder flexion moment increases the mechanical energy of the arm and hand/handrim during the push phase [3].

The brachioradialis and brachialis muscles (BRA group), which are elbow flexors that do not cross the shoulder joint, were active over a large portion of the push phase. These muscles provided power to the handrim during the first half of the push phase (Fig. 1B; dashed line positive), but then absorbed power from the handrim in the second half (Fig. 1B; dashed line negative). The biceps brachii (BIC), elbow flexors that also cross the shoulder, acted to transfer power from the arm (Fig. 1C; dotted line negative) to the handrim (Fig. 1C; dashed line positive) as well as generate power directly to the handrim (Fig. 1C; solid line positive).

The most distal upper extremity muscles (e.g., pronator teres and pronator quadratus, PT Group) did not generate or absorb power from the handrim or body for most of the push phase (Fig. 1D; solid line near 0). Instead, these muscles acted primarily to transfer power from the handrim to the body (Fig. 1D; dashed line negative, dotted line positive). Similar energy transfer mechanisms have been shown in other movement tasks such as pedaling and walking [e.g., 6].

CONCLUSIONS

Identifying individual muscle function during wheelchair propulsion is challenging due to the multi-articular and multi-muscle nature of the upper extremity. However, the forward dynamics simulation and segment power analysis framework used in this study is ideally suited to quantify muscle contributions to the mechanical energetics of wheelchair propulsion and identify muscle function.

ADELT was found to be the primary contributor to mechanical power during the push phase. This muscle also acts to elevate the humeral head in the glenohumeral joint, which requires high activity from antagonistic muscles to stabilize the joint. This may explain why overuse injuries (e.g., in the rotator cuff muscles) and pain (e.g., due to glenohumeral joint inflammation) at the shoulder are common among wheelchair users. The elbow flexors (BIC and BRA Group) generated power directly to the handrim as well as transferred power from the arm to the handrim. Although these muscles provide almost as much energy as ADELT early in the push phase, the prevalence of elbow injuries is much lower. This may be due to the lower muscle co-contraction required to stabilize the elbow joint.

REFERENCES

1. Finley, MA, et al., *J Rehabil Res Dev* **41,** 385-394, 2004.
2. Mulroy, SJ, et al., *Arch Phys Med Rehabil* **85,** 925-934, 2004.
3. Guo, LY, et al., *Clin Biomech* **18,** 106-114, 2003.
4. Holzbaur, KR, et al., *Ann Biomed Eng* **33,** 829-840, 2005.
5. Fregly, BJ, et al., *J Biomech* **29,** 81-90, 1996.
6. Zajac, FE, et al., *Gait Posture* **16,** 215-232, 2002.

ACKNOWLEDGEMENTS

This work was supported by NIH grant R01 HD053732.

RELATIONSHIP BETWEEN CLINICAL MEASUREMENTS OF SHOULDER MOTION AND STRENGTH AND BASEBALL PITCHING BIOMECHANICS

[1]Wendy J. Hurd, [1]Bernard F. Morrey, and [1]Kenton R. Kaufman
[1]Mayo Clinic, Rochester, MN, USA
email: hurd.wendy@mayo.edu

INTRODUCTION

Elbow injuries in the youth athlete are a serious problem. The incidence of elbow pain in youth baseball pitchers age 9-14 years is reported at 26%, and shoulder pain at 32% [1]. The most common elbow injury involves damage to the ulnar collateral ligament, while two of the most common shoulder injuries include anterior glenohumeral instability and tendonitis of the posterior rotator cuff [2]. At this point, relationships between clinical presentation and pitching biomechanics have not been described. Furthermore, the role of the shoulder in the development of elbow injuries has not been elucidated. Such information may provide insight to identifying individuals at risk for developing injury, and development of evidence based injury prevention and rehabilitation programs.

METHODS

27 uninjured baseball pitchers participated in the study. Subjects were on average 16 years old (Range, 15-19 years), were 1.8 m tall (Range, 1.7-2.0), and weighed 82 kg (Range, 61-105). The cohort consisted of 22 right-handed pitchers and 5 left-handed pitchers. All study participants were participating in baseball, listed pitching as their primary position, and had pitched competitively for a minimum of three consecutive years. The absence of injury was confirmed through evaluation by a board certified sports physical therapist.

Passive shoulder range of motion of the dominant limb was measured clinically using a goniometer with the throwing arm abducted to 90 degrees and the subject supine. Maximum voluntary isometric shoulder strength of the throwing limb internal and external rotators was measured with a hand-held dynamometer while subjects were seated, and the limb abducted to 90 degrees and the shoulder in neutral rotation. Two trials were performed for each motion and strength measured, with the average of the trials used for subsequent analysis.

Kinematics were recorded with a 10-camera Motion Analysis EVa RealTime system (Motion Analysis Corp., Santa Clara, CA). Reflective markers were placed on anatomical landmarks on the subject's trunk and throwing arm. Calculations were based on a 3-D kinematic model previously described [3]. A three-dimensional model of the upper extremity was developed using Visual3D (C-Motion Inc., Germantown, MD, USA). The model consisted of rigid body segments, including the trunk, upper arm, lower arm, and hand. Helical angles were used to describe transverse plane shoulder kinematics, and Euler angles to describe horizontal plane shoulder kinematics. Joint kinetics were derived using inverse dynamics. The inertial properties of the hand, forearm, and upper arm and the force of the baseball, modeled as a 142-g mass, with the point of force application on the hand assumed to be the mid-point between the second and fifth metacarpal heads.

Clinical variables of interest included shoulder passive external (ERROM) and internal rotation (IRROM). Strength measures of interest included maximum isometric shoulder external (ERSTR) and internal rotation (IRSTR) muscle force of the dominant limb normalized to subject body weight. Biomechanical variables of interest were selected based on their potential insight to injury risk: The elbow adduction moment was selected to represent stress across the medial elbow, which may contribute to the risk of ulnar collateral ligament injury. The shoulder internal rotation moment was chosen to represent stress to the anterior glenohumeral joint which may contribute to functional anterior shoulder instability. The shoulder external rotation moment was selected to represent stress to the posterior aspect of the shoulder, potentially contributing to increased

activity of the posterior rotator cuff musculature (the external rotators) and tendonitis in pitchers. Regression analysis was performed using the clinical and biomechanical variables to determine the influence of shoulder motion and strength on pitching characteristics. Bivariate correlations were performed to investigate coupling between the biomechanical variables.

RESULTS AND DISCUSSION

Results for clinical measures are in Table 1. Significant results from regression analysis are in Figure 1. Correlations between biomechanical variables indicated a strong, positive relationship between the peak elbow adduction moment and the peak shoulder internal rotation moment ($P<0.01$; $R=0.90$). There were no other significant correlations between biomechanical variables.

This is the first study to evaluate the relationship between clinical presentation of the thrower's shoulder and pitching mechanics. The negative relationship between ERROM, and the elbow adduction and shoulder internal rotation moments, suggests that individuals with limited shoulder motion may be at increased risk for injury to both the shoulder and elbow. Consequently, rehabilitation and injury prevention programs that incorporate ERROM stretching may be effective in lowering joint moments and reducing injury risk.

The coupling between the shoulder internal rotation and elbow adduction moments is a consequence of limb positioning and geometry as the arm is accelerating during the pitching motion. The same external forces contributing to an adduction moment at the elbow are simultaneously producing an internal rotation moment at the shoulder. Consequently, individuals may be equally vulnerable to injury to both the shoulder and elbow. This may provide insight to why athletes who return to play after injury at one site subsequently experience injury to the adjacent joint.

Higher internal rotation moments were associated with greater internal rotation strength. As the primary muscle group responsible for accelerating the arm, hypertrophy of the internal rotators is considered a normal finding in the baseball pitcher. An increase in internal rotation strength without a concomitant gain in external rotation strength, however, has been associated with shoulder injury. It is possible that among this cohort of uninjured athletes the range of external rotation strength was not adequate to provide insight to the relationship between these two variables.

CONCLUSIONS

This study has demonstrated that inadequate shoulder external rotation motion may place baseball pitchers at risk for both shoulder and elbow injuries as a consequence of increased joint stress. Future studies that prospectively evaluate this population will be necessary to confirm the relationship between biomechanical variables and injury risk, and to elucidate physical and biomechanical characteristics that result in throwing-related injury.

REFERENCES

[1] Lyman S. et al. *Med Sci Sports Exercise*, 1803-10, 2001.
[2] Collins C. et al. *Pediatrics*, 1181-7, 2008.
[3] Morrow, M. et al. *J Electromyogr Kinesiol*, 61-7, 2010.

ACKNOWLEDGEMENTS

Funding provided by MLB. Consulting support provided by Kerlan-Jobe Orthopedic Clinic.

Table 1

Clinical Measures	Mean (SD)	*Biomechanical Measures*	Mean (SD)
ERROM	127° (10)	Peak Elbow Adduction Moment	0.559 Nm/Ht*mass (0.09)
IRROM	59° (9)	Peak Shoulder IR Moment	0.609 Nm/Ht*mass (0.08)
ER Strength	17% (3)	Peak Shoulder ER Moment	0.078 Nm/Ht*mass (0.04)
IR Strength	25% (6)		

Figure 1

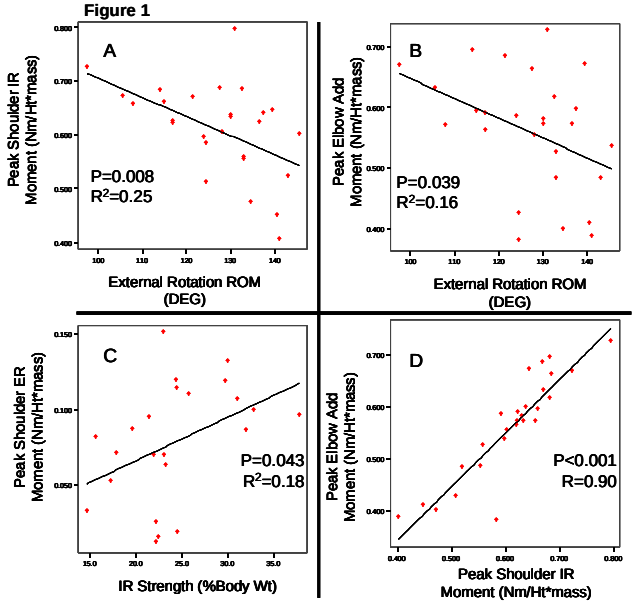

NET TORQUES VARY ACROSS MCP JOINTS DURING A TEXT TYPING TASK

[1]Krishna Asundi and [1,2]Jack Dennerlein

[1]Harvard School of Public Health, Boston, MA, USA
[2]Brigham and Women's Hospital, Boston, MA, USA
email: kasundi@hsph.harvard.edu

INTRODUCTION

The most consistent finding among epidemiologic studies evaluating computer use and musculoskeletal outcomes is the association between hours keying and hand/arm health outcomes [1]. While peak forces applied to the keyboard are low (~3 N [2]), keying is a highly repetitive activity where a proficient typist may strike the keys over 20,000 times per hour.

Previous studies have measured keyboard reaction forces during typing [2] and dynamic joint loads during single finger tapping [3], however, no study to our knowledge, has characterized loads of the fingers and upper extremity joints during multi-finger typing. Quantifying finger and upper extremity joint dynamics during typing will help inform the design of keyswitches and keyboards aimed at reducing the biomechanical loads associated with computer use.

In this preliminary study, we assessed individual keystrike forces and the net external torques across the first 4 metacarpal-phalangeal (MCP) joints during a continuous multi-finger typing task. We also evaluated how key-strikes from each digit affect joint torques at the wrist.

METHODS

Three participants (2 female, 1 male) completed a one minute typing task. Participants completed the task on a standard keyboard with the "J" key set at elbow height when seated. Informed consent was obtained, and all protocols were approved by the Harvard School of Public Health Institutional Review Board.

A six degree of freedom force transducer (F/T Sensor Gamma, ATI Industrial Automation, Apex, USA) secured underneath the keyboard measured force and moment at 100 samples/s.

An infrared 3-D motion analysis system (Optotrak Certus, Northern Digital, Waterloo, Canada) tracked upper extremity trajectories at 100 samples/s. Modeling the trunk, arm, forearm and hand as rigid bodies, the location of specific bony landmarks, relative to clusters of three infrared light emitting diodes (IREDs), were tracked and used to define segment local coordinate systems and joint centers.

A local coordinate system for the thumb was defined using 3 IREDs, one fixed to the thumbnail and 2 fixed to a rigid plate. The rigid plate was secured to the 1st MCP, such that one IRED was directly over the joint and the second was lateral to it and perpendicular to the long axis of the thumb. The thumb joint center was assumed to be at the IRED placed directly over the 1st MCP.

Local coordinate systems for the index, middle and ring fingers were defined using IREDs secured to each fingernail and locations of the 2nd and 5th MCP, tracked as bony landmarks associated with the hand IRED cluster. Joint centers for each digit were calculated as a proportion of the distance between the 2nd and 5th MCP.

Individual finger key-strikes were identified using center of pressure (COP) values and the 3D location of each fingertip IRED. COP was calculated using force and moment data, assuming all moment data were due to off-axis loads. Key-strikes were defined as periods where force exceeded the 60th percentile of all applied forces. A key-strike was attributed to a finger when its IRED was the closest to the COP and it was at least 25% closer than any other IRED.

Peak force, COP and segment kinematics at peak force during each key-strike were then input into an inverse dynamics link segment model to calculate joint torques at the MCP of the digit striking the

key. Torques at the wrist were also calculated for each key-strike.

RESULTS

From a one minute typing task, an average of 16 to 35 key-strikes were identified for each finger (Table 1). Peak key-strike forces were greatest for the middle finger, and lowest for the ring finger. Forces were similar between the thumb and index fingers.

	Thumb	Index	Middle	Ring
Key-strikes	35 (2)	26 (3)	16 (13)	20 (8)
Force [N]	1.6 (0.3)	1.6 (0.1)	1.7 (0.2)	1.4 (0.2)
Torque [Nmm]	72 (22)	77 (12)	96 (11)	76 (10)

Table 1. Mean (SD) number of identified key-strikes, peak force and MCP joint torque magnitude during key-strikes with the associated digit (n=3).

Torque magnitude was greatest at the middle MCP and smallest at the thumb MCP (Table 1). Torque at the thumb MCP was shared across extension and abduction, while torques at the index, middle and ring MCPs were primarily in extension (Figure 1). Adduction and pronation MCP torques were largest for the thumb, while extension torques were greatest for the middle finger.

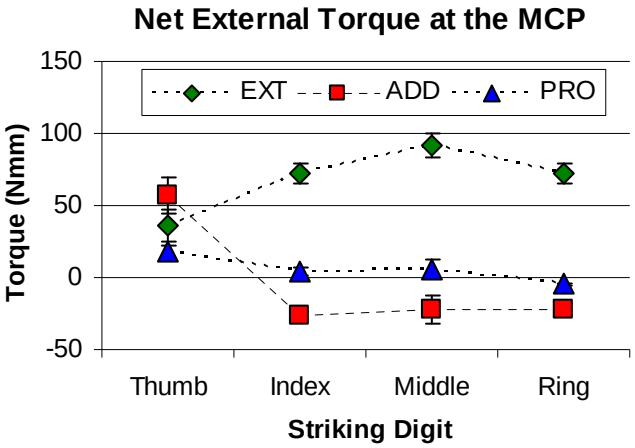

Figure 1. Mean net external torques at the MCP joints during key-strikes with the first four digits of the hand. Positive values indicate torques in extension (EXT), adduction (ADD) and pronation (PRO). Vertical bars indicate +/- 1 SD, n=3.

Flexion torque at the wrist (negative extension values) was greatest when fingers were not striking the keys, while suppination torque (negative pronation values) was greatest during thumb key-strikes (Figure 2). As key-strikes moved laterally from the thumb to the middle finger, flexion and suppination (negative pronation values) torques at the wrist decreased while adduction torques increased.

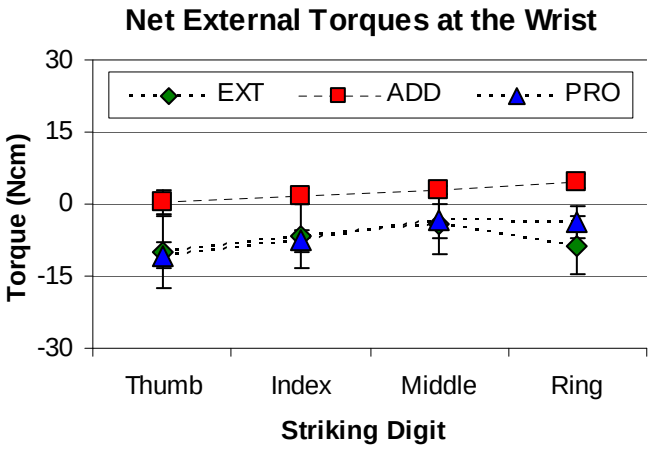

Figure 2. Mean net external torques at the wrist joints during keystrikes with the Thumb, Index Middle and Ring finger as well as during no keystrikes (None) . Positive values indicate torques in extension (EXT), adduction (ADD) and pronation (PRO).

DISCUSSION

This is the first study to characterize individual key-strike forces and torques at the MCP joints during a text typing task. Our results indicate joint torques at the MCP vary by the digit striking the keys. Furthermore, fingers strikes affect wrist torques differentially. These findings suggest keyboard design features, such as keyswitch make force and split keyboard angles should take into account which fingers will be striking the keys.

Finally, in addition to evaluating keyboard design features, the methods reported here can also be used to characterize hand and finger functionality among computer workers with disorders such as osteoarthritis.

ACKNOWLEDGEMENTS

NIOSH Grant R01 OH008373.

REFERENCES

1. Gerr, F., et al. *J Occup Rehabil* **16** 265-77. (2006).
2. Asundi, K. R., et al. *X2009*, Boston, MA. 2009.
3. Dennerlein, J. et al. *J Biomech* **40** 3013-22. 2007

EVALUATING THE IMPORTANCE OF INCLUDING THE CARPOMETACARPAL JOINTS WHEN MODELING THE HAND

[1,3]James Buffi and [1,2,3,4]Wendy M. Murray

Departments of [1]Biomedical Engineering and [2]PM&R, Northwestern University, Chicago, IL
[3]SMPP, Rehabilitation Institute of Chicago, Chicago, IL; [4]VA Hines, Hines, IL
email: jamesbuffi2013@u.northwestern.edu
web: http://www.smpp.northwestern.edu/Murray/index.shtml

INTRODUCTION

Though a principle means of interaction with the outside world and invaluable to human function, the human hand presents a challenge to study. The intricacy of hand motions, as well as the small size and close proximity of the bones of the hand complicate our ability to characterize hand kinematics during functional tasks.

The study of complex hand motions links motion capture data to a kinematic model of the hand. Most kinematic models include the metacarpophalangeal (MCP), proximal interphalangeal (PIP), and distal interphalangeal (DIP) joints of the fingers [1]. The MCP joints are generally described as orthogonal and intersecting, allowing for ab-adduction and flexion-extension. The DIP and PIP joints are described with a single flexion-extension degree of freedom. The thumb is generally described with 4 non-intersecting joints.

Recent kinematic hand models have also added a metacarpal arch degree of freedom [1], however, it is not always included [2]. The carpometacarpal (CMC) joints of digits 2 through 5 allow the metacarpals of the hand to move from a flat surface to an arch, facilitating the opposition of the little finger (digit 5) and the thumb (digit 1). Evidence has shown that the metacarpal arch is important for prehensile hand movements [3].

This study investigated to what extent including the metacarpal arch in a kinematic model of the hand improves the ability to recreate motions that include opposition of digits 1 and 5. An Immersion Cyberglove was used to record a simple motion, and then the motion was recreated using two kinematic models: one that included the metacarpal arch, and one that did not.

METHODS

To evaluate the influence of the metacarpal arch, kinematic descriptions of digits 3 through 5 were added to an existing model of the upper limb [4] that includes kinematic models of digits 1 and 2 (the thumb and index finger) only. First, the metacarpal bone segments in the model were re-oriented to lie in a single plane. Second, kinematics of the DIP, PIP, and MCP joints of digits 3 through 5 were defined based on the literature [5]. Finally, one degree of freedom, involving simultaneous motion at the CMC joints for digits 2 through 5, was added to simulate the metacarpal arch. The joint kinematic functions were based on the literature [6].

In five subjects, an Immersion Cyberglove (San Jose, CA) was used to record a simple motion involving opposition of digits 1 and 5. Each subject donned the Cyberglove and was instructed to touch the tip of digit 5 to the thumb tip and then cyclically extend and flex the finger and thumb while maintaining contact between the distal segments. A single, 20-second trial of data was collected per subject at a rate of 90 Hz.

The raw voltage data collected during each testing session were converted to joint angles using an optimization routine that solved for the gains for each Cyberglove sensor. Assuming a specific kinematic model, the joint angles that result from this process minimize the distance between the “pad” of digit 1 and the “pad” of digit 5 over the entire 20-second trial. This approach was adapted from a calibration method originally developed for

robotic hand telemanipulation [7]. The optimization was performed in MATLAB (Natick, MA).

For each subject, the raw voltage data were transformed using this optimization method assuming (1) a kinematic model of the hand that included the metacarpal arch, and (2) the same model without this degree of freedom. To estimate the effect of the arch, the distance between the "pads" of digits 1 and 5 was defined geometrically and calculated as a function of time over 5 full cycles of the motion for each data set using both kinematic models. In both cases, the average distance over 5 motion cycles was calculated. In addition, the average distance during the last 10% of each cycle (when the thumb and finger were flexed and closest to the palm) was calculated. The results for each model were compared using matched pair t-tests. Results were considered significant for $p < 0.05$.

RESULTS AND DISCUSSION

As evaluated based on the proximity of the distal segments of digits 1 and 5, including the metacarpal arch in the kinematic model of the hand improved the overall performance of the model. When the motion data from 5 subjects were analyzed and reconstructed over 5 complete cycles, the pad of the little finger was an average of 0.33 cm from the pad of the thumb when the metacarpal arch was included (Fig. 1). The average distance between the thumb and the index finger ranged from 0.13 cm to 0.84 cm across subjects. Without a metacarpal arch, the distance between the thumb and finger was significantly longer after the same analysis (average = 2.1 cm; range = 1.40 cm to 2.98 cm).

The distance between the thumb and index finger varies considerably within a movement cycle when the metacarpal arch is not modeled (cf., Fig. 1, green curve). A significant difference between models was observed even for the last 10% of each cycle (i.e., the portion of the cycle where the distance between the pads of the thumb and finger is the least for the model without a kinematic arch).

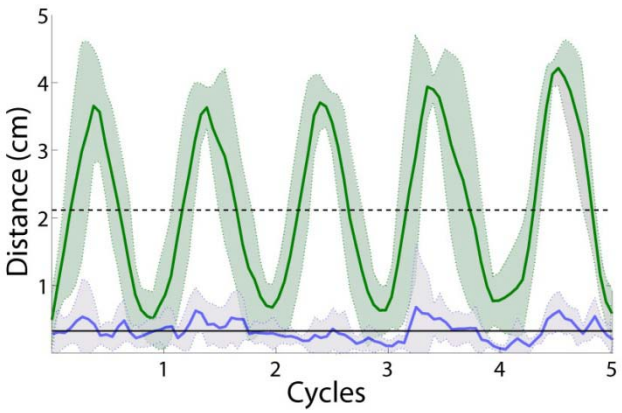

Figure 1: The distance between the pads of digit 1 and 5 versus motion cycle, both with (blue) and without the metacarpal arch (green). Shaded areas represent one standard deviation from the mean; black lines indicate the overall mean for 5 cycles.

CONCLUSIONS

Excluding the metacarpal arch in a kinematic hand model limits the ability of the model to recreate motions involving opposition of the small finger and thumb. Excluding the arch may also limit modeling of power grip because CMC flexion contributes to grip strength during this posture [8].

REFERENCES

1. Metcalf, C.D., et al. *Ieee Trans on BME* **55**, 1199-1210, 2008.
2. Veber, M., et al. *Meccanica* **42**, 451-463, 2007.
3. Sangole, A.P. and M.F. Levin. *J Biomech* **41**, 829-837, 2008.
4. Holzbaur, K.R.S., et al. *Ann of Biomed Eng* **33**, 829-840, 2005.
5. Degeorges, R., et al. *Surgical and Radiologic Anatomy* **27**, 43-50, 2005.
6. El-shennawy, M., et al. *J Hand Surgery-American Vol* **26A,** 1030-1035, 2001.
7. Friedman, J. and T. Flash. *Cortex* **43**, 444-460, 2007.
8. Bora, F.W. and N.H. Didizian. *J Bone and Joint Surgery-American Vol* **A 56**, 1459-1463, 1974.

ACKNOWLEDGEMENTS

This work was funded by NIH R01 HD046774.

THE MECHANICAL PROPERTIES OF THE ENDOMYSIUM AFFECT PROPENSITY FOR MUSCLE FIBER INJURY NEAR THE MYOTENDINOUS JUNCTION

Bahar Sharafi and Silvia S. Blemker
University of Virginia, Charlottesville, VA
email: Bahar@virginia.edu, website: http://www.mae.virginia.edu/muscle/

INTRODUCTION

The myotendinous junction (MTJ) is a common site of injury in skeletal muscles. This has been observed in whole muscles [1] as well as single fiber preparations [2]. The extent of muscle injury is correlated with strain [3] and regions of high localized strain within tissue have been shown to be the sites of injury [4]. The stress-strain properties reported for tendon are much stiffer than those reported for muscle fibers [5], which may give rise to large strains within the fiber near the myotendinous junction.

It is thought that the endomysium plays a role in protecting fibers from injury [6]; however, the mechanisms underlying this hypothesis are unclear. The purpose of this study was to create micromechanical models of the MTJ to explore this hypothesis by determining the potential effects of endomysium mechanical properties on strain distributions (and therefore likelihood of injury) within muscle fibers near the myotendinous junction.

METHODS

We created a three-dimensional finite element (FE) model of a tapered muscle fiber ending at the MTJ, based on published images [7]. We represented the end of the fiber as an ellipsoid, while the rest of the fiber is modeled as a cylinder. The fiber is covered in a layer of endomysium connective tissue, which is also surrounded by other muscle fibers (Fig. 1). To represent the interdigitation between the fibers and the tendon, the end of the fiber is surrounded in tendinous tissue. One end of the model is constrained from moving in the fiber direction. The other end is given a prescribed displacement in order to simulate a 15% lengthening of the muscle. A hyperelastic, nearly incompressible, transversely isotropic material was used to represent all the tissues [8], where each material is represented by an along-fiber tensile modulus, an along-fiber shear modulus, a cross-fiber shear modulus, and a bulk modulus. For the fiber material these parameters are 37.5 kPa, 1.25 kPa, 1.25 kPa, and 2.5 MPa respectively. The tendon is assumed to be ten times stiffer than the fiber, that is, all moduli for the tendon are 10 times those of the fiber. The preferred direction for the transversely isotropic constitutive model used for all materials is assumed to be the direction of the muscle fiber. The constitutive model for the muscle fiber includes activation, which changes between 0 (for passive fiber) and 1 (for maximally active fiber) [8]. The transition region of the tendon that interdigitates with the fibers is assigned material moduli that vary linearly from endomysium moduli values to tendon moduli values, as a function of distance between the endomysium and the tendon.

Simulations were performed over a range of endomysium moduli, and we analyzed the effects of varying the endomysium moduli on the peak along-fiber strain (peak tensile strain in the direction of the fiber).

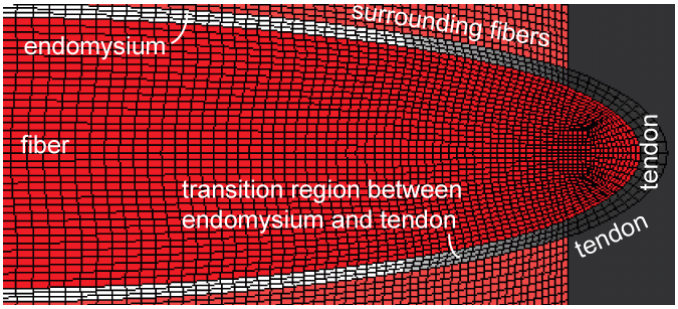

Figure 1: We created a finite element mesh of a fiber tapering and inserting into the myotendinous junction.

RESULTS

The models predict that tensile strains within the fiber are concentrated near the myotendinous junction (Fig. 2). Moreover, peak strains are highly dependent on endomysium moduli and activation (Figs. 2 and 3). Peak localized tensile strains were substantially higher than the average strain for the whole fiber. The peak localized tensile strains were considerably higher for lower endomysium moduli (Fig. 3) and higher for active rather than passive stretch (Fig. 3). The average strain was 15% for all cases. In the passive case the peak strain was 17% for the most compliant endomysium modeled and 27% for the stiffest endomysium modeled. In the active case, the corresponding values were 24% and 36%.

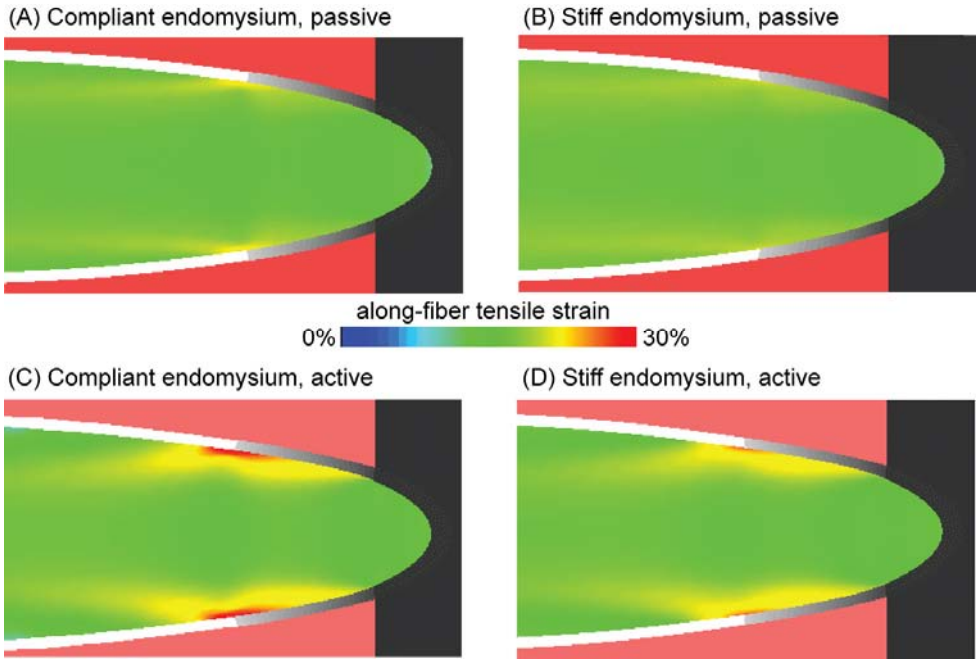

Figure 2: Strain contour plots show the distribution of along-fiber tensile strain within the muscle fiber during passive and active stretches of 15% for a model with endomysium moduli that are 1/100 of the tendon moduli (A and C) and a model with endomysium moduli that are 1/10 of the tendon moduli (B and D).

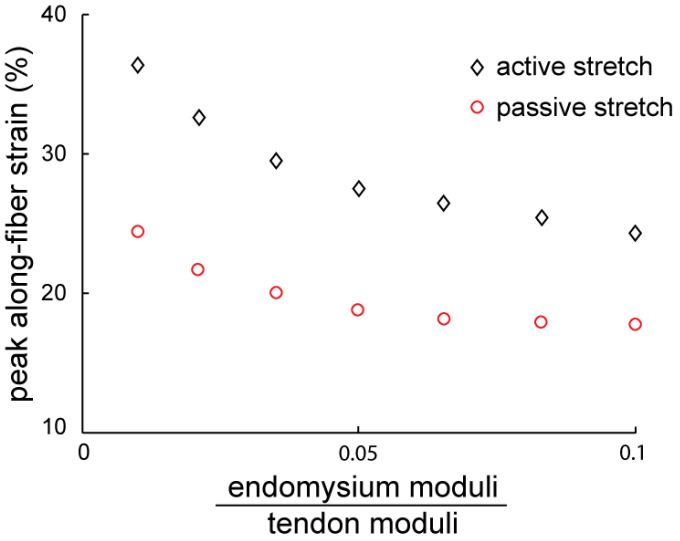

Figure 3: Peak along-fiber tensile strains within the fiber are plotted as a function of the ratio of endomysium moduli to tendon moduli, for an average fiber strain of 15%.

CONCLUSIONS

Endomysium mechanical properties have a significant effect on the strain concentrations near the myotendinous junction. A stiffer endomysium results in lower strains within the fiber, and therefore lower propensity for injury. This conclusion supports the hypothesis that the endomysium plays a role in protecting fibers from injury [6] and indicates that muscles with a compromised endomysium or compromised mechanical linkage between fiber and endomysium due to disease may be more susceptible to injury. For example, a higher susceptibility to lengthening contraction-induced injury has been observed in muscles affected by Duchenne muscular dystrophy [9] where the linkage between the fiber and endomysium is impaired [8]. Moreover, we found as much as a 66% increase in peak strains during active stretch compared to passive stretch. This finding is consistent with the higher incidence of injury that is observed during active lengthening [10].

REFERENCES

1. Garrett WE,Jr, et al. *Am.J.Sports Med.* **16,** 7-12, 1988.
2. Tidball JG, et al. *J.Appl.Physiol.* **67,** 1063-1069, 1989.
3. Lieber RL, et al. *J.Appl.Physiol.* **74,** 520-526, 1993.
4. Best TM, et al. *J.Biomech.Eng.* **117,** 262-265, 1995.
5. Zajac FE. *Crit.Rev.Biomed.Eng.* **17,** 359-411, 1989.
6. Pasternak C, et al. *J.Cell Biol.* **128,** 355-361, 1995.
7. Barrett B. *Acta Anat.(Basel)* **48,** 242-257, 1962.
8. Blemker SS, et al. *Journal of Biomechanics* **38,** 657-665, 2005.
9. Moens P, et al. *J.Muscle Res.Cell.Motil.* **14,** 446-451, 1993.
10. Lieber RL, et al. *Am.J.Phys.Med.Rehabil.* **81,** S70-9, 2002.

ACKNOWLEDGEMENTS

Funding for this work was provided by NIH grant R01 AR 056201, the Funds for Excellence in Science and Technology at the University Virginia, NSF grant #0734262, and the National Skeletal Muscle Research Center at UC San Diego.

HOW DO STEP WIDTH AND ARM SWING AFFECT ENERGETIC COST AND LATERAL BALANCE DURING RUNNING?

Christopher J. Arellano and Rodger Kram

Locomotion Laboratory, University of Colorado, Boulder, CO USA
email: arellanoc@gmail.com

INTRODUCTION

In walking, humans maintain lateral balance by varying step width [1] but prefer a moderate step width that minimizes metabolic cost. Walking with step widths that are narrower or wider than the preferred step width is metabolically more expensive [2]. In comparison to walking, humans prefer to run with much narrower step widths which would seem to present a challenge for maintaining lateral balance.

McClay et al. [4] speculated that medio-lateral (M-L) foot placement during running may be important in minimizing the muscular effort needed to maintain lateral balance. This implies that like in walking, there may be a preferred (and energetically optimal) step width in running that minimizes metabolic cost. Swinging the arms is also thought to improve "balance" and possibly reduce the energetic cost of running [3]. We tested these ideas experimentally to gain insight into the energetic cost and balance during running.

To understand the roles of step width and arm swing in human running, we tested 4 specific hypotheses as follows: The *rate of O_2 consumption* will be greater 1) at step widths greater or less than preferred and 2) when arm swing is eliminated. *Step width variability* will be greater 3) at step widths greater or less than preferred and 4) when arm swing is eliminated.

METHODS

Ten healthy young subjects (5M/5F, 24.4 ± 4.2 yrs, 65.4 ± 11.7 kg, Leg Length (LL) = 93.1 ± 5.6 cm; mean ± SD) ran at 3 m/s on a force measuring treadmill for randomized conditions of target step widths (i.e. 0%, 15%, 20%, and 25% LL), at preferred step width with arm swing (Arms), and at preferred step width without arm swing (No Arms).

During each 7-minute trial, we measured the 3-D motions of the legs (Motion Analysis Corp.), ground reaction forces (AMTI), and rates of O_2 consumption ($\dot{V}O_2$) using expired gas analysis (Parvo Medics). During the target step width conditions, we provided real-time visual feedback of foot placement using a computer monitor positioned in front of the subject (Fig. 1). Reflective markers were placed on the heel, mid-foot, and toe of each shoe. Subjects were instructed to place each heel on the respective virtual lines at the instant of heel-contact. The 0% LL trial was achieved by projecting a single virtual line. During the No Arms condition, subjects crossed their arms in front of their chest.

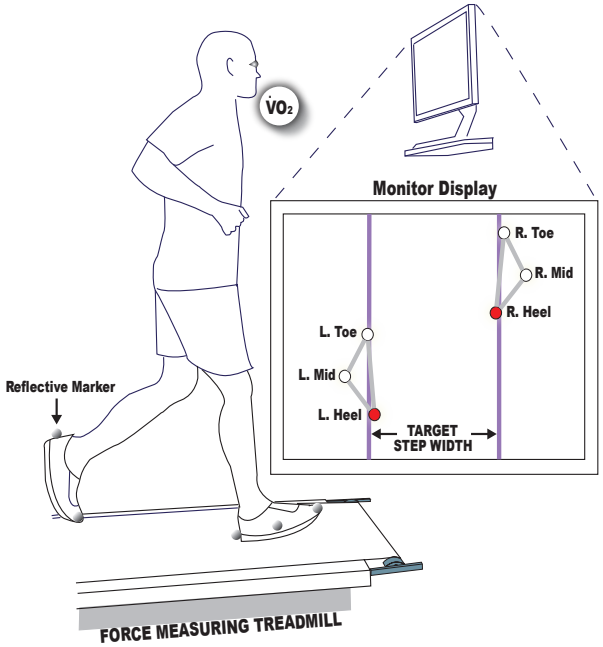

Figure 1: Real-time visual feedback displaying top-down view of reflective markers and virtual lines.

We measured the average step width (%LL) during the last 3 minutes of each trial. Step width was defined as the M-L distance between the heel markers for successive steps. Initial-contact was identified at the instant that the vertical GRF

reached a threshold of 10%BW. Step width variability was defined as the standard deviation about the average step width [1]. An increase in step width variability signified a decrease in lateral balance while running.

The net rate of O_2 consumption (ml/kg/min) was calculated by subtracting the average standing rate of O_2 consumption from the total rate of O_2 consumption during the last 3 minutes of each running condition. For each dependent measure, we used repeated measures ANOVA with *a priori* comparisons between the Arms conditions and the target step width conditions using a Bonferroni correction (α = .0125). To compare between Arms and No Arms, we used paired t-tests with statistical significance set an α level of .05.

RESULTS AND DISCUSSION

Rate of O_2 Consumption: Subjects consumed O_2 more rapidly when running at target step widths greater or less ($p < .001$) than the preferred step width (Arms). Compared to the Arms condition, the rate of O_2 consumption was 4, 8, 11, and 15% greater at target step widths of 0, 15, 20, and 25% LL, respectively (all p's < .0125, Fig. 2). When arm swing was eliminated, the rate of O_2 consumption was 8% greater than running with normal arm swing ($p < .001$, Fig. 2).

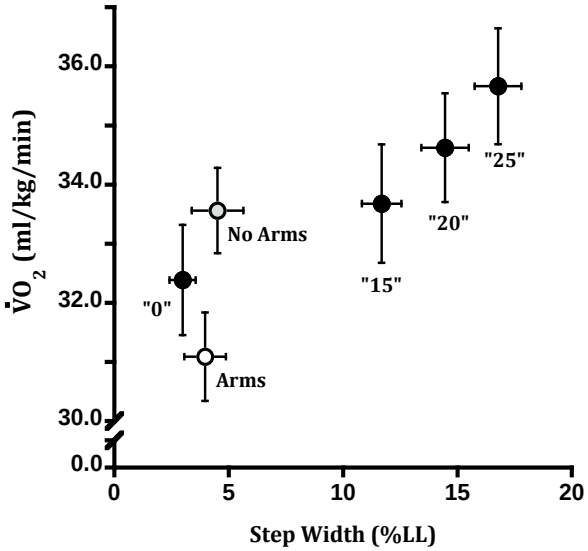

Figure 2: $\dot{V}O_2$ (mean ± SEM) versus target step width (% LL). Arms denotes preferred running. Quotation marks indicate that subjects were unable to match the target step widths (" %LL ").

Step Width Variability: Step width variability was greater when subjects ran at target step widths greater ($p < .001$) than the preferred step width. Compared to the Arms condition, step width variability increased by 38, 48, and 69% at target step widths of 15, 20, and 25% LL, respectively (all p's < .0125, Fig. 3). Mean step width variability at the 0% target step width was 7% greater than the Arms condition but the difference was not statistically significant ($p = .09$). During No Arms, step width variability was 9% greater ($p = .012$) than the Arms condition. In general, running with step widths other than preferred or without arm swing decreased lateral balance as indicated by an increase in step width variability.

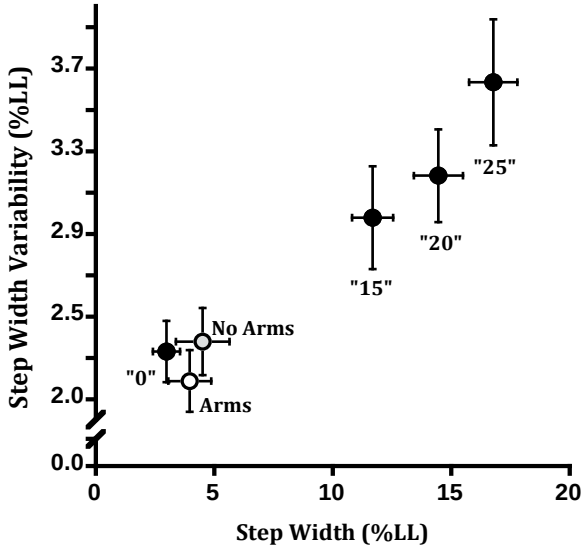

Figure 3: Step width variability (mean ± SEM) versus target step width (% LL).

CONCLUSIONS

While running, humans appear to choose their step width and swing their arms so as to minimize metabolic cost and optimize for lateral balance.

REFERENCES

1. Bauby CE & Kuo AD. *J Biomech* **33**, 1433-1440, 2000.
2. Donelan JM, et al. *Proc. R. Soc. Lond.* B **268**, 1985-1992, 2001.
3. Hinrichs RN. *Multiple Muscle Systems:* In J. Winters & S.L.Y. Woo (Eds.), 1990.
4. McClay IS & Cavanagh PR. *Clin Biomech* **9**, 117-123, 1994.

ACKNOWLEDGEMENTS

The NASA Harriett G. Jenkins Fellowship awarded to C.J.A. and the Colorado Diversity Initiative supported this study.

PATIENTS WITH PATELLOFEMORAL PAIN EXHIBIT ELEVATED BONE METABOLIC ACTIVITY AT THE PATELLOFEMORAL JOINT

[1]Christine E. Draper, [1]Thor F. Besier, [1]Michael Fredericson,
[1,2]Gary S. Beaupre, [1]Scott L. Delp, [1]Andrew Quon, and [1]Garry E. Gold
[1]Stanford University, Stanford, CA, [2]VA RR&D Center, Palo Alto, CA
email: cdraper@stanford.edu

INTRODUCTION

Patellofemoral pain accounts for a large fraction of knee disorders seen in sports medicine clinics [1]. Despite the prevalence of this disorder, the specific cause of pain remains unclear. One possible mechanism of pain is elevated subchondral bone stress at the patellofemoral joint.

Bone remodeling in response to mechanical stress or injury can be visualized using modalities such as ^{99m}Tc-MDP bone scanning and ^{18}F NaF Positron Emission Tomography/Computed Tomography (PET/CT). These techniques can detect alterations in tissue metabolism that may accompany or precede pathological changes in tissue structure. Bone scans have revealed increased bone activity in 52% of patients with patellofemoral pain [2]; however, because it is difficult to quantify bone activity in specific regions of the joint using this technique, the relationship between bone metabolic activity and pain remains unclear. ^{18}F NaF PET/CT provides improved anatomic localization of metabolic activity. In this technique, the tracer, ^{18}F NaF, becomes incorporated into the bone at sites of bone remodeling with high metabolic activity.

The goal of this study was to characterize regions of increased bone metabolic activity in patients with patellofemoral pain and to evaluate whether metabolic activity correlates with pain.

METHODS

We examined the knees of 20 subjects (12M, 8F) diagnosed with chronic patellofemoral pain by a sports medicine physician. Subjects were between 20-42 years of age, had no prior knee surgery, injury, or other knee joint pathology. Four subjects had unilateral pain.

^{18}F NaF PET/CT scans were taken of both knees of all subjects. Subjects received 5-10mCi of ^{18}F NaF intravenously (0.08mCi/kg). To minimize the effects of physical activity and blood flow on tracer distribution, subjects rested in a seated position for 30 minutes prior to tracer injection and for 60 minutes between the tracer injection and the scan. During the scan, subjects lay in a supine position with their legs secured by straps around the ankles. This minimizes movement, facilitating PET and CT image registration. The following parameters were used to acquire the PET images: Axial FOV: 18cm, pixel size: 4.3mm, slice thickness: 4.25mm, 5 min acquisition per bed position, OSEM iterative reconstruction. The CT images used for anatomical registration were acquired with the following parameters: 140kVp, 90mAs, slice thickness: 5mm, FOV: 50cm, reconstruction matrix: 512x512.

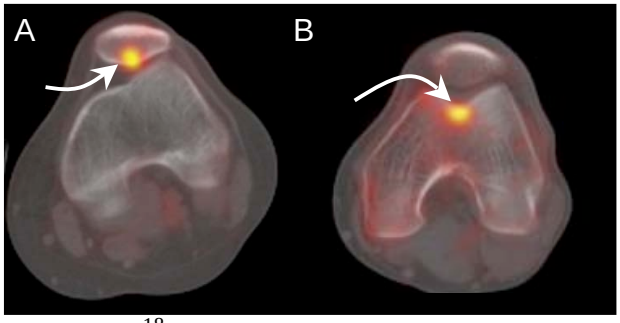

Figure 1: ^{18}F NaF PET/CT image showing increased tracer uptake (arrows) in the patella (A) and trochlea (B).

Tracer uptake corresponds to bone metabolic activity and was quantified by measuring the standardized uptake value (SUV):

$$\text{SUV (g/ml)} = \frac{\text{pixel value (Bq/ml)*patient weight (g)}}{\text{dose corrected by tracer half-life and duration between injection and scan (Bq)}}$$

To account for differences in overall tracer uptake among subjects, each patient's SUV measurements were normalized by his/her bone background SUV. Since all subjects were free of tibial pathology, an

axial slice through the tibial epiphysis, just proximal to the tibial tuberosity, was chosen to be representative of background tracer uptake. The mean SUV in the tibial slice was used to normalize all SUV measurements of the patellofemoral joint.

Increased uptake was defined to be an SUV greater than twice the bone background. The peak SUV in the patellofemoral joint and the mean SUV of the region of increased uptake were measured. The maximum pain experienced during the previous year was recorded on a scale from 0-10 and the location of pain (medial/lateral facet, etc) was assessed during the clinical exam.

RESULTS AND DISCUSSION

We detected regions of increased tracer uptake in 17 of the 20 painful knees and two of the four non-painful knees. Increased uptake occurred in 15 patellae and four trochleae (Figure 1). The lateral patellar facet was the most common location of tracer uptake (10 knees). There were 15 subjects with increased uptake who could localize pain to either the medial or lateral side of the joint. In 11 of the 15 subjects, the side of maximum pain was consistent with the side of peak tracer uptake.

The mean and peak normalized SUV were significantly greater in the painful patellofemoral joints compared to the pain-free knees (Figure 2).

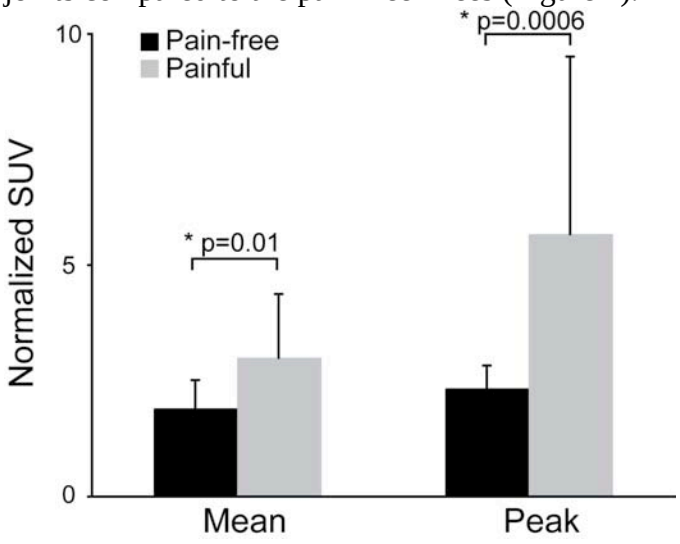

Figure 2: Comparison of mean and peak normalized SUV between pain-free (n=4) and painful knees (n=20).

Increasing mean and peak normalized SUV correlated with increasing pain experienced by the patients (Figure 3; mean: $r^2 = 0.55$, $p = 0.0005$; peak (not shown): $r^2 = 0.29$, $p = 0.02$).

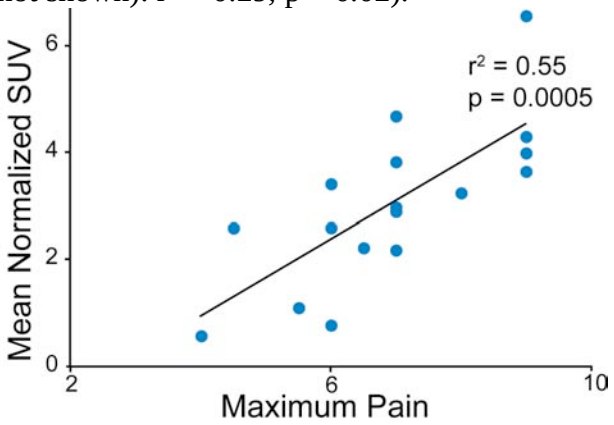

Figure 3: Relationship between mean normalized SUV and maximum pain.

CONCLUSIONS

These results suggest that patellofemoral pain may be related to increased bone metabolic activity indicative of accelerated bone remodeling in the patellofemoral joint. One possible explanation for this relationship could be related to the fact that areas of mineralized bone with high metabolic activity receive rich sensory innervation [3].

While the increase in bone metabolic activity might be due to elevated mechanical stress in the tissue, a study investigating this relationship is needed.

One implication of this study is that ^{18}F NaF PET/CT may be useful to characterize regions of increased bone activity in patients, indicating potential sources of pain. This information could guide treatment decisions by identifying the affected regions of the joint. Furthermore, treatments that reduce bone metabolic activity in the joint may alleviate pain in some patients.

REFERENCES

1. Devereaux and Lachmann. *Br J Sports Med* **18**, 18-21, 1984
2. Naslund, et al. *Br J Sports Med* **39**, 162-5, 2005
3. Mach, et al. *Neuroscience* **113**, 155-66, 2002

ACKNOWLEDGEMENTS

VA Rehabilitation R&D Service (#A2592R), NIH (EB002524-01, EB005790-05).

Virtual Pre-Operative Reconstruction Planning for Comminuted Articular Fractures

[1]Thaddeus P. Thomas, [1]Donald D. Anderson, [2]Andrew R. Willis,
[1]J. Lawrence Marsh, and [1]Thomas D. Brown
[1]Department of Orthopaedics and Rehabilitation, The University of Iowa, Iowa City, IA
[2]University of North Carolina at Charlotte, Charlotte NC
email: thaddeus-thomas@uiowa.edu

INTRODUCTION

Highly comminuted articular fractures (Fig 1.a) are complex injuries to treat. Successful clinical outcomes are most likely when the anatomy is precisely restored. Virtual pre-operative reconstruction planning using three-dimensional (3D) puzzle solving methods offers new capabilities for achieving this objective with less surgical insult.

3D puzzle solving methods for this purpose were previously developed utilizing surrogate specimens [1]. Accurate fracture reconstructions were obtained by interactively matching native fragment surfaces to an intact template. While successfully piloted in a clinical case, more automated methods will be required in order for this approach to be practical in a clinical setting [2]. Surrogate geometries were obtained from high resolution laser scans, but in vivo geometries were segmented from CT data using fairly laborious methods. Additional complexity is present in vivo, as the structure of peri-articular bone makes it more susceptible to plastic deformations (i.e., crush).

The objective of the present study was to develop and apply new automated bone segmentation and 3D puzzle solving algorithms to obtain fracture reconstructions in a clinical series of highly comminuted tibial plafond fractures.

METHODS

Ten tibial plafond fracture cases were retrospectively analyzed. A novel and mostly automated image analysis technique was developed to segment bone geometries from pre- and post-surgical reduction CT scans (Figure 1). A modified 3D watershed segmentation algorithm that iteratively propagated regions from cortical seeds into cancellous bone regions was implemented in

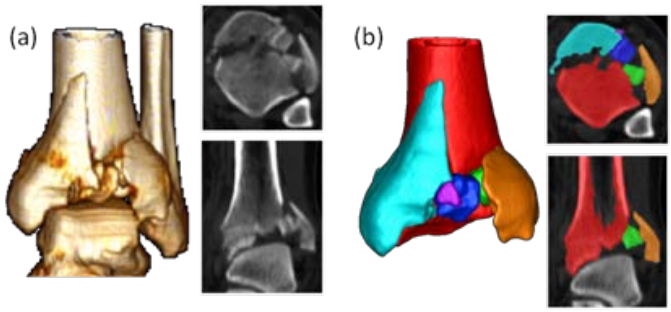

Figure 1. CT data are segmented into discrete objects using a semi-automated watershed method.

MATLAB. Propagation speed was controlled by a combined image intensity and distance transform function. Whereas prior methods required 8-10 hours per case, this new method enabled the processing of each case in < 20 minutes with minimal user guidance.

Each tibia was then methodically reconstructed by matching fragment native (periosteal and articular) surfaces to an intact template that was created from a mirror image of the healthy contralateral limb. Fragment native surfaces were identified using a region-growing algorithm that propagated discrete surface patches to boundaries of high curvature [2]. As a consequence of the tibia's shape and fracture behavior, the surface patch with the largest area was reliably identified as the native surface.

Distal tibia geometries were reconstructed using Geomagic Studio software. Reconstruction started by aligning the intact template to the intact diaphyseal segment of the fractured tibia. Next, the algorithm proceeded by individually aligning the remaining fragments' native surfaces to the template, from largest to smallest, using an iterative closest point (ICP) algorithm. The accuracy and speed of alignment was improved by iteratively reducing the ICP search space as each new template/fragment match was achieved.

Puzzle solution accuracies were quantified by calculating distances between the intact template and the reduced tibia's native surface. Since the articular surface is the most important to precisely restore to forestall joint degeneration, it was isolated from the periosteal surface and separately compared to the intact anatomy. To illustrate the clinical utility of 3D puzzle solving, virtual reconstructions were compared to those achieved in surgery.

RESULTS AND DISCUSSION

Computational surface alignment yielded precise geometric reconstructions for ten clinical cases, with average distance differences of 0.39 mm relative to their intact templates. The articular surfaces were generally congruent. However, five cases displayed some crush from the impact event. These cases had an average articular alignment error of 0.63±0.17 mm, while cases without crush averaged 0.4±0.11mm.

Virtual pre-operative reconstruction planning holds great potential for improving articular fracture treatment. Provided this blueprint for restoring the original anatomy, the surgeon can minimize surgical insult while still achieving accurate fracture reconstructions. Furthermore, the ideal reconstruction can be used to plan for intra-operative complexities in order to avoid further complications.

Figure 2 shows three illustrative cases. The surgically reduced tibia in Case A was shortened by more than 2.5cm, an outcome with likely mechanical effects. Knowledge of the puzzle solution could have enabled the surgeon to better restore anatomic limb length. In case B, there was an obvious articular defect in the puzzle solution. While perfectly repairing that defect is unlikely given the plastic deformation, its detection could have allowed for the pre-operative preparation of biological interventions or engineered tissues to mitigate the incongruity. For case C, a metaphyseal void in the puzzle solution highlights a loss in bone. This structural instability could have been recognized virtually, giving the surgeon the opportunity to have either planned an alternate fragment configuration, a different fixation technique, or a tissue grafting solution. Unfortunately, the outcome was less than ideal, with the joint surface angulated approximately 30° anteriorly.

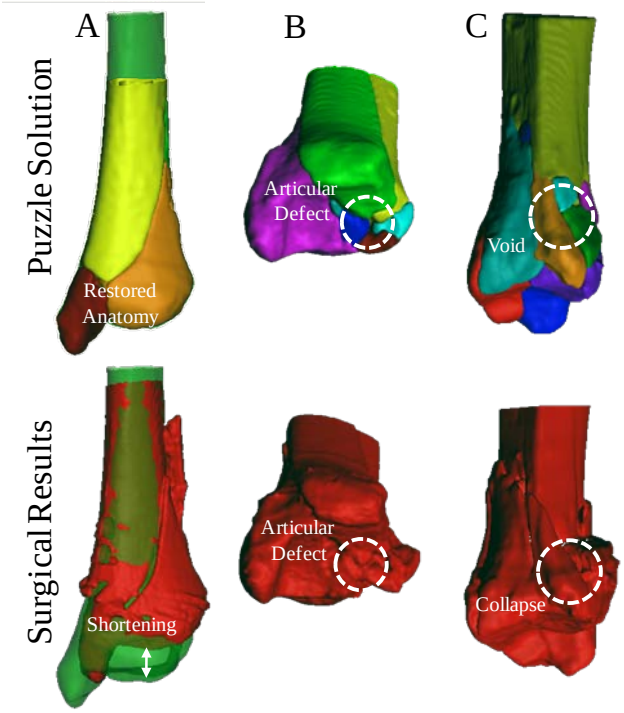

Figure 2. Three puzzle solutions are compared to what was achieved surgically.

Of course, challenges remain to be addressed. Particularly, clinical execution of a planned reconstruction needs to respect broader anatomic constraints: the surgical access site, the presence of nearby neurovascular structures, the sequence in which fragments can be optimally reduced, etc. Despite such limitations, the results from this study suggest that 3D puzzle solving methods offer a powerful new tool for enhancing the surgical reconstruction of complex peri-articular fractures.

REFERENCES

[1] Thomas TP, et al. ASB #1045, 2009.

[2] Thomas TP, et al. *A computational/experimental platform for investigating three-dimensional puzzle solving of comminuted articular fractures.* Computer Methods in Biomechanics and Biomedical Engineering (in Press).

ACKNOWLEDGEMENTS

Funded by the NIH (P50AR055533 and R21AR054015), the AO Foundation, Switzerland, and by a MRIG from the Roy J. Carver Charitable Trust at The University of Iowa.

Adaptation and form of the unconstrained lateral compensatory stepping response

[1]Christopher P. Hurt, [1]Laura Earnest, [1]Mark D. Grabiner
[1]Department of Kinesiology and Nutrition, University of Illinois at Chicago, Chicago, IL, USA
churt2@uic.edu, URL:http://www.uic.edu/ahs/biomechanics

INTRODUCTION

Maintaining dynamic stability requires regulation of the relationship between the kinematics of the center of mass (COM) and the base of support (BOS). If this relationship is disrupted a compensatory step may be required to re-establish stability. The compensatory stepping response (CSR) to fore-aft disturbances is a whole body skill which can be quickly and effectively adapted [1].

Stability can be challenged in all directions however, and accumulating evidence suggests that age-related differences of the compensatory stepping response (CSR) may be accentuated with respect to medio-lateral stability [2]. Little research currently exists, however, on the CSR following lateral disturbances. Descriptively, three different types of compensatory steps have been reported in response to lateral disturbances: the sidestep sequence (SSS), the loaded leg sidestep (LLS) and the crossover step (COS). One study reported that younger adults prefer performing a COS to extend the lateral base of support [3]. It should be noted however that in this study subjects were instructed to resist stepping and were discouraged from using their arms to aid in their recovery. Although these constraints provide greater experimental control over the study, it is presently unknown to what extent the unconstrained CSR differs. Further, this study did not report how subjects CSR adapted to repeated lateral disturbances of the same magnitude.

The purpose of this study was to characterize the unconstrained stepping response to unpredictable lateral disturbances in younger adults. We were also interested in understanding how subjects adapted their stepping response to repeated exposures of the same disturbance.

METHODS

Ten healthy young adults (6 females, age 24± 2.0 years, 172.5±9.3mm, 67.9±12.4 kg) participated in this study. Subjects were exposed to 30 lateral disturbances (15 each direction) which were delivered via a microprocessor controlled platform (Simbex, Lebanon NH).

The disturbance waveform comprised a 240 ms approximately square-wave acceleration pulse followed by a 240 ms deceleration pulse. Acceleration for the lateral disturbances was 4.1 m/s^2 (peak velocity 1.0 ms^{-1} and total displacement of 0.24 m), which was chosen because it was similar to a previous study [3] and it elicited a stepping response in all trials. Direction of the disturbance (i.e. left-right) was randomized to minimize the ability of subjects to preplan their response. Initial stance width was standardized to the horizontal distance between the ASIS markers. Subjects were instructed to "do whatever it takes to recover your balance".

Frontal plane kinematics of the compensatory stepping response was captured using an eight camera motion capture system (Motion Analysis, Santa Rosa, CA). The COM for each subject was estimated based on a ten segment model and anthropometric estimations [4]. A measure, margin of stability (MOS) was utilized to quantify the quality of the CSR. The more positive the number the greater stability afforded by the step.

The equation for margin of stability [modified from Hof [5]]: $MOS = d - \left(v/\sqrt{g/l}\right)$

- d=the distance from the BOS (most lateral foot marker (toe or heel) of the stepping limb) to the COM; $d = BOS - COM$
- $v = v_{COM} - v_{belt}$; v_{belt} is the velocity of the treadmill belt; g = 9.81 m/s^2; l is the distance in the frontal plane between the stepping ankle and the COM.

Recovery strategies were documented for each subject. First-step kinematics was quantified with respect to the foot used to extend the lateral BOS. Foot displacement was calculated as the difference between the COM of the recovery foot sampled at footoff and footstrike. COM position at recovery footstrike was quantified as the distance between the foot COM and whole body COM. Values for lateral trunk flexion were extracted at heelstrike. The

difference between the minimum and maximum values of trunk lateral flexion was used to calculate trunk excursion. MOS at footstrike and minimum MOS (MOS_{min}), which occurs coincidently with or shortly after footstrike was also quantified. We assumed that subjects performing an unconstrained CSR would be equally as likely to perform COS as they would a SSS which was tested using a chi-square test. Adaptation to the task was tested using repeated measures ANOVA in which the recovery responses for each subject were broken up into 3 blocks of 10. Bonferroni adjustments were utilized for post hoc comparisons.

RESULTS AND DISCUSSION

Table 1: Recovery strategy utilized by each subject: **SSS** is a sidestep sequence **LLS** is a loaded leg sidestep and **COS** is a crossover step

	Recovery Strategy		
Subject	SSS	LLS	COS
1	14	14	1
2	18	8	4
3	--	--	30
4	11	--	19
5	17	--	13
6	30	--	--
7	30	--	--
8	14	--	16
9	14	--	15
10	28	1	--
Total	175	24	98

Subjects most often performed a SSS (175/ 297) to recover stability (Table 1, $p<0.05$). This is not in agreement with previous research [3, 6]. We suggest that the difference in these findings relate to an absence of constraints on the recovery response. Of interest is the varied responses utilized by subjects. For instance 3 out of 10 subjects utilized the same limb to extend the BOS regardless of disturbance direction suggesting the potential role of a preferred limb in recovering stability to these disturbances. Statistically the adaptation in the CSR took place between block 1 and block 2. Adaptations included a significant decrease in MOS_{fs} ($p<0.05$) and MOS_{min} ($p<0.05$). There was also a reduction in the total angular excursion of the trunk ($p<0.05$, table 2).

It is not intuitive that subjects would establish a smaller MOS as the result of repeated exposures to the same disturbance. One possibility is that reduced angular excursions of the trunk were related to the change in MOS that was observed. It is also possible that as subjects became more familiar with the task they understood their limits of stability which allowed them to optimize their CSR to these disturbances by achieving a MOS which was still sufficient in re-establishing lateral stability but may have been more energetically favorable.

CONCLUSIONS

In the unconstrained stepping response younger adults prefer to utilize a SSS to recover stability, although 3 out of 10 subjects used the same limb to extend their BOS regardless of disturbance direction. Currently we are investigating the role of limb in the compensatory stepping response. Also, as part of the adaptive process, subjects produced a CSR which although sufficient to re-establish stability produced a significantly smaller MOS. It would be of interest to investigate whether older adults would adapt their CSR similarly to younger adults. An inability of older subjects to adapt their CSR to lateral disturbances has been prospectively related to an increased fall-risk [7].

REFERENCES

1. Owings GS. *Clin Biomech* **16**, 813-819, 2001.
2. McIlroy WE. J Gerontol **51**, M289-M296, 1996.
3. Maki BE. *J Biomech,* **29**, 343-353, 1996.
4. Winter DA. *Biomechanics and Motor Control of Human Movement,* John Wiley & Sons, Ltd., 2005.
5. Hoff A. et al. J Biomech **38**, 1-8, 2005.
6. Maki BE. J Gerontol **55**, M27—M277, 2000.
7. Hilliard .MJ. *Arch.of Phy sMed Rehab* **89**, 1708-1713, 2008.

Table 2: Key variables relating the compensatory stepping response compared across the first ten and last ten lateral disturbances. fs=footstrike *p<0.05 between blocks 1&2, 1&3

	MOS_{fs} (mm) *	**MOS_{min} (mm)***	**COM Position $_{fs}$ (mm) ***	**Foot Displacement (mm)**	**Lateral Trunk Flexion $_{fs}$ (deg)**	**Trunk Angular Excursion (deg) ***
Block 1	141.1 ± 33.7	121.0 ± 29.3	214.5 ± 62.9	302.2 ± 42.2	7.3 ± 3.8	13.9 ± 4.0
Block 2	109.6 ± 29.6	87.9 ± 32.1	185.6 ± 60.6	286.7 ± 58.9	5.6 ± 3.4	11.0 ± 4.3
Block 3	100.0 ± 21.8	79.7 ± 28.4	185.1 ± 47.9	296.9 ± 59.4	5.2 ± 2.9	9.9 ± 3.6

A MUSCULOSKELETAL MODEL OF POSTURAL CONTROL: SIMULATED AGING OF MUSCLE MECHANICAL PROPERTIES

[1,2]Christopher J. Hasson, [1]Richard E.A. van Emmerik, and [1]Graham E. Caldwell

[1]University of Massachusetts Amherst, Amherst MA, USA
[2]Northeastern University, Boston MA, USA [E-mail: cjhasson@neu.edu]

INTRODUCTION

Recent work has implicated age-related changes in muscular properties as detrimental to postural stability [1, 2]. However, prospective studies are usually constrained to follow subjects for only a few years, rather than over a human life span [3]. Also, the numerous age-related anatomical, physiological, and neural changes make it difficult to draw causal relationships between specific neuromuscular changes and their effect on postural control. An alternate approach is to use a musculoskeletal model, where simulated age-related changes can be applied independently and evaluated systematically.

Previous modeling studies have investigated the ability of different neural controllers to regulate posture and the effects of ankle joint stiffness [4, 5]. Here we extend this work with an inverted pendulum postural dynamics model incorporating muscle mechanical properties derived from young and older adults. A feedback-based neural controller is used to activate Hill muscle models, with upright stance simulated by finding optimal controller gains. The muscle model properties are then systematically altered to investigate how age-related changes affect postural control.

METHODS

Equations of motion were derived with Autolev™ for a 2-segment sagittal plane inverted pendulum model powered by individual ankle muscles. A frictionless hinge ankle joint linked the skeletal segments; the foot-floor interaction was modeled with 21 spring-damper elements (Figure 1). A variable step-size integrator was used to integrate the model state equations to simulate upright stance.

Three Hill muscle models representing the dorsiflexors (DFs) and plantarflexors (PFs; individual gastrocnemius and soleus muscles) actuated the skeletal model. Each muscle model included a contractile component (CC) with non-linear excitation-activation, force-length (*FL*) and force-velocity (*FV*) properties, and a series elastic component (SEC) with a non-linear force-extension relationship ($F\Delta L$). The properties were defined by 9 parameters: maximal isometric force (P_0), optimal CC length (L_0), *FL* width (W), SEC slack length (L_S) and stiffness coefficients (α, β), and Hill *FV* constants (a/P_0, b/L_0, ε). Ankle passive stiffness was represented by a non-linear torque-angle relation. Muscle kinematical models were based on SIMM™ [6].

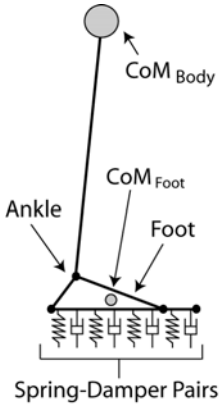

Figure 1. Model.

Two age-specific postural models were created using the average muscle parameter values from 6 young and 6 older male subjects [1]. Motor commands for postural stabilization were generated using proportional-derivative (PD) feedback control based on existing torque-generator models [4], modified to control individual muscle models. A genetic numerical optimization algorithm was used to find optimal DF and PF controller gains (K_D and K_P) to minimize center-of-mass (CoM) motion and muscular force while maintaining upright stance. A penalty was applied if the model fell.

Next, simulations were performed with the optimized young model controls while independently changing each of the nine PF muscle parameters to the mean value of the older male subjects. We focused on the PFs because they provide the majority of ankle torque during quiet stance. Here, the young controller gains were kept at their optimized levels, however in the face of a sudden muscle property alteration, it is likely that neural control would adapt to maintain stability. Therefore, a sensitivity analysis was performed in which each PF muscle parameter was altered separately and the model control gains re-optimized. Each muscle parameter was varied from optimal across 6 levels (±5%, ±10%, and ±15%). Because some older

parameters were outside this range, more optimizations were performed with parameters set to the older values.

RESULTS AND DISCUSSION

Both young and old models were able to achieve stable posture and qualitatively reproduced basic CoM and center-of-pressure (CoP) dynamics during quiet stance; however, the older model needed higher controller gains and greater muscle excitation than the younger model (Figure 2).

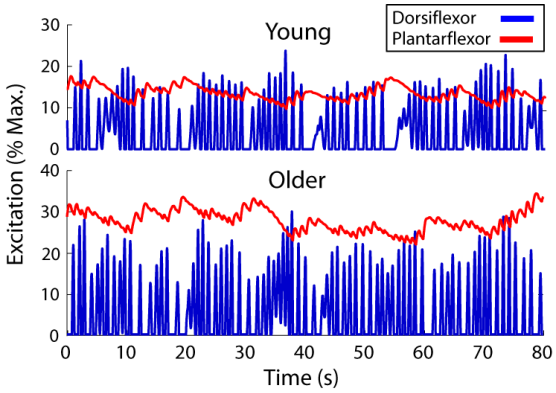

Figure 2. Optimized muscle model excitations.

Replacing all nine PF muscle parameters with older values resulted in the young optimized model promptly falling forward. When each parameter was "aged" independently, the model fell when P_0, L_0, and L_S were changed to older values, but remained standing when the other 6 were changed.

In the sensitivity analysis with re-optimized controller gains, the model was more robust to changes in muscle mechanical properties, and achieved stable balance in most cases. However, the model's behavior was sensitive to changes in P_0, L_0, and L_S, with changes in K_P needed for optimal balance. In some cases, the model was unable to balance no matter what the control adjustments.

Changes in PF P_0 were inversely related to the optimal PF K_P (Figure 3), because weaker muscles require more excitatory drive. Nevertheless, the young model was able to remain standing even with the 42% lower older P_0, provided the control gains were allowed to increase sufficiently. This suggests that quiet stance performance is robust to changes in P_0 (at least until a lower limit is reached).

Changes in L_0 and L_S had nonlinear effects on the controller gains (Figure 3). The PF K_P gains were close to their minimum values using the original set of young muscle mechanical properties, but increased as L_0 and L_S shifted from the young optimum. The young model fell when the older L_0 was used. Together, this suggests that the L_0 and L_S combination in the young subjects was close to optimal for minimizing muscle excitatory drive. Conversely, the young model's control of quiet stance was not sensitive to changes in the *FV* parameters or the *FΔL* stiffness coefficients (α, β).

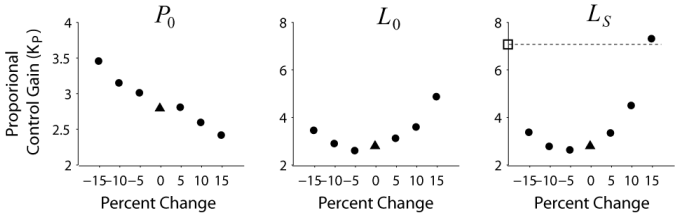

Figure 3. (●): Sensitivity analysis for K_P. (▲): Optimized young model with experimentally estimated muscle properties. (□): Model with older parameters. Older result not shown for P_0 (-42%, K_P = ~5), model fell using the older L_0 value (0.30%).

We also observed a negative relation between the mean model CoP speed and L_S. As the *FL* parameters were not changed in concert with L_S, decreasing L_S caused the CC to operate at longer lengths. This shifted the CC into a weaker/unstable *FL* position, resulting in greater control inputs and a larger CoP speed. This may explain age-related increases in CoP speed [1], as the older subject's L_S was 20% shorter than the young.

CONCLUSIONS

We developed age-specific versions of a feedback-driven postural control model that included DF and PF muscle properties estimated from young and older adults. The model was able to balance using either set of properties, and predicted age-related changes in muscle activity consistent with experimental studies [1]. A sensitivity analysis showed that P_0, L_0, and L_S had the most influence on the model's selection of neural controller gains, with the latter two properties being close to optimal when experimentally measured values were used. This is important, since our previous work [1] has shown age-related differences in L_0 and L_S.

REFERENCES

1. Hasson CJ. Dissertation, Univ. of Mass. Amherst, 2009.
2. Onambele GL, et al. J App Physiol **100**: 2048-56, 2006.
3. Brauer SG, et al. J Gerontol A **55**: M469-476, 2000.
4. Perteka RJ. J Neurophysiol **88**: 1097-1118, 2002.
5. Winter DA, et al. J Neurophysiol **80**: 1211-1221, 1998.
6. Delp et al. IEEE Trans Biomed Eng **37**: 757-767, 1990.

ACKNOWLEDGEMENTS

Supported by NIH R03AG026281.

THE EFFECTS OF AN UNEXPECTED STANCE FOOT INVERSION PERTURBATION AND NEUROMUSCULAR LOOP DELAY ON NEXT STEP WIDTH IN HEALTHY ADULTS

Hogene Kim, Trina DeMott, Rachel Strauss, James K. Richardson, James A. Ashton-Miller
Biomechanics Research Laboratory
University of Michigan, Ann Arbor, Michigan
Email: hogenek@umich.edu, Website: http://me.engin.umich.edu/brl/

INTRODUCTION

Many falls in the elderly occur while walking on an irregular surface [1]. It has been shown that an irregular surface increases the level of challenge during gait, as reflected by increased step width (SW) variability [2]. This SW variation may reflect the need to control stability in the frontal plane [3]. An underfoot perturbation under the medial aspect of the stance foot, akin to stepping on a pebble, has been shown to cause a cross-over step (the first post-perturbation step crosses the midline in order to recover balance) [4]. Since loop delays adversely affect the ability of a feedback control system to reject perturbations, we tested the hypothesis that, following an unexpected medial underfoot perturbation of the right stance foot, a longer delay in the myoelectric latency (τ) of the right peroneal ankle muscle would decrease the post-perturbation step width.

METHODS

We recruited six healthy active elderly (three males, three females, age 66.8±8.6 yrs). Each subject wore a pair of custom sandals equipped with hinged flippers concealed within the medial and lateral aspects of the shoe sole, just behind the metatarsal heads [5]. With the medial flipper deployed, the resultant sandal sole inversion inclination in the frontal plane was 16^{o}.

Subjects performed 15 gait trials walking along a 6-m level walkway equipped with a staggered pair of AMTI force plates. They walked at a purposeful speed "as though they were crossing a busy street". Randomly, in four of the 15 trials, after 3 or more steps of normal gait, a flipper was covertly deployed once during the swing phase under the right medial forefoot. Approximately 25 msec after the next (right) heel strike the subject then had to counter the effect of the resulting inversion perturbation during that stance phase and adjust the subsequent first post-perturbation SW so as not lose balance. The flipper was retracted immediately after the perturbed stance phase.

3-D kinematics of foot, leg, pelvis and trunk (including ankle inversion angle, step length, step width were collected at 100 Hz using an optoelectronic Certus system and 28 markers. The ground reaction force on the perturbed step and the first post-perturbation step were collected at 1 kHz using the AMTI force plates. The myoelectric muscle activity of the right peroneus longus were measured at 2 kHz using a Delsys Trigno wireless EMG system. SW was normalized by unperturbed step width. Peroneal τ was measured from heel strike to the onset of peroneus longus response to the inversional perturbation. Within-subject analyses of post-perturbation SW variability, after normalization by unperturbed SW, was examined using a F-test, and the correlation of the first perturbation step width with peroneal response time was examined using Pearson's correlation coefficient, with $p<0.05$ considered significant.

RESULTS AND DISCUSSION

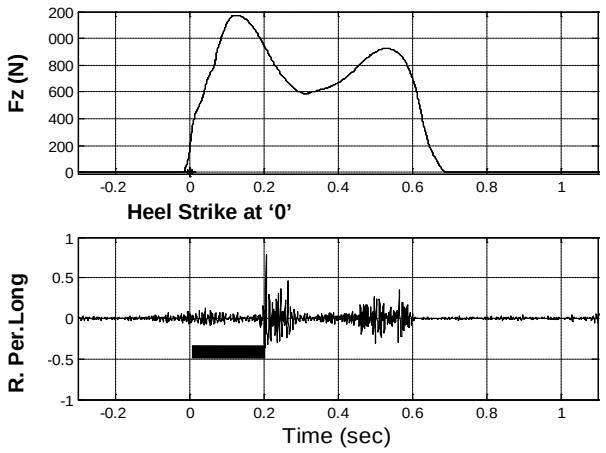

Figure 1. (Top) A typical time history of the vertical ground reaction force. (Bottom) Corresponding myoelectric activity in peroneus longus. The peroneal τ is shown by the thick bar.

In the four perturbation trials the mean (±SD) onset of ankle inversion caused by the flipper was 25.5±16.6 ms following heel strike.

Figure 2 shows the typical history of stance phase ankle inversion with and without the medial perturbation. Examples of three different peroneal responses (short, average, and long **τ**) to that perturbation are shown below for the same subject.

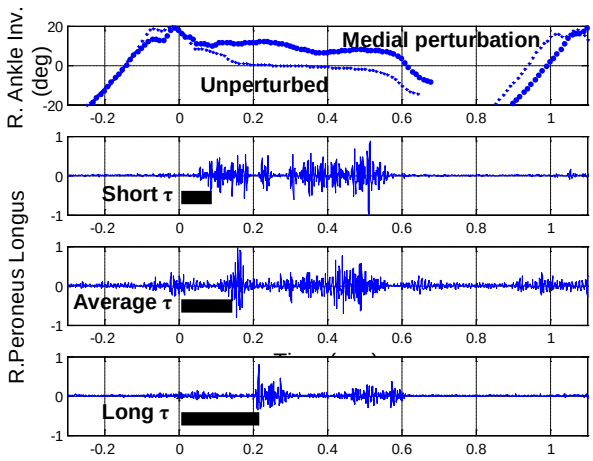

Figure 2: Comparison of ankle eversion ankle versus time history (top) and examples of short, average and long peroneus longus τ from the same subject.

A scatter plot of the normalized 1st post-perturbation SW plotted against the resulting myoelectric latencies in peroneus longus shows a significant inverse correlation (R=-0.8512, P<0.0001, Figure 3).

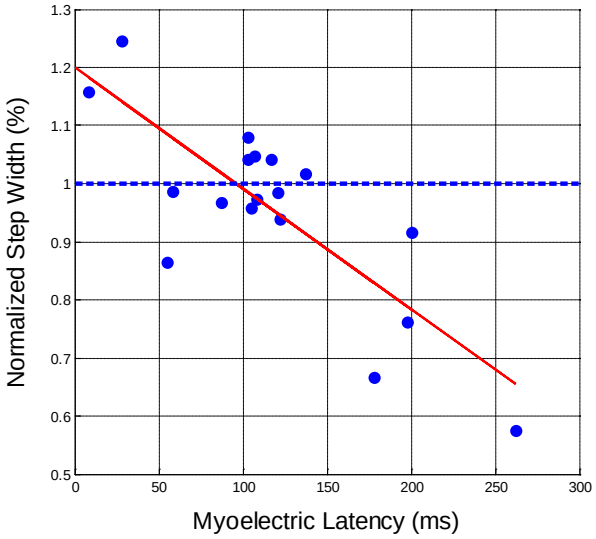

Figure 3 Scatter plots of 1st post-perturbation SW and regression line for the right medially-perturbed trials SW and τ in 6 subjects

If we replot the Figure 3 data as box whisker plots (with median, upper and lower 25th centile quartiles, and maximum and minimum values) we see greatest SW variation for the post-perturbation SW of the first of the four perturbation trials. The variance of this SW in the 1st (#1) of the four trials was significantly greater than that of subsequent perturbation trials #3 and #4 (F=4.69, where $F_{.05}$=4.06) (Figure 4). This is evidence of habituation to the stimulus, meaning that the greatest challenge to stability is on the first perturbation trial, particularly with a slowed peroneal response.

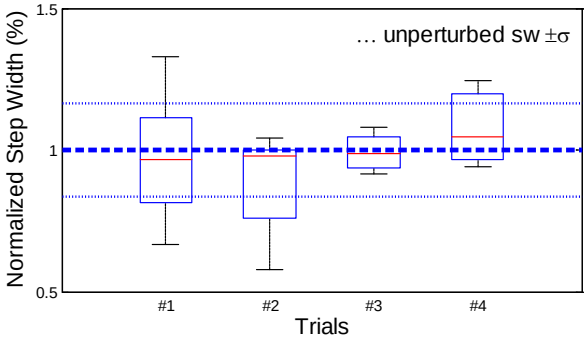

Figure 4: Control chart, with boxplots, of the post-perturbation SW for the post-perturbation step from each of the four perturbation trials showing evidence of habituation. The light broken lines represent ±1 SD of unperturbed SW. Data are from 6 subjects.

CONCLUSIONS

1) In these healthy older individuals, the longer it takes the stance limb peroneus longus to respond to the unexpected inversional perturbation, the narrower the 1st post-perturbation step width will be.

2) Evidence of habitation was found over four trials.

REFERENCES

1. Berg K, et al., *Age and Aging*; **6**:2612-8, 1997
2. Thies SB, et al., *Gait & Posture*, **22**:26-31, 2005
3. Bauby CE, et al., *J Biomech*, **33**:1433–40, 2000
4. Thies SB, et al. *Gait & Posture*, **26**:156-160, 2007
5. Kim H, et al., ASB Annual Meeting, State College PA, 2009

ACKNOWLEDGEMENT

PHS grants R01 AG 026569 & P30 AG 0248

PROPERTIES OF STEP INITIATION IN PARKINSON'S DISEASE SUGGEST DIFFERENT INVOLVEMENT OF SAGGITAL AND FRONTAL PREPARATORY MOVEMENTS

Don Yungher, Robert Creath and Mark W. Rogers

University of Maryland School of Medicine, Baltimore, MD, USA
email: mrogers@som.umaryland.edu

INTRODUCTION

When healthy persons initiate a voluntary forward step, a series of biomechanical events occur prior to the first step. In the mediolateral direction (M-L), the center of pressure (CoP) moves towards the swing foot which propels the center of body mass (CoM) towards the single stance foot. The CoP also shifts backwards in the anteroposterior direction (A-P), which propels the CoM forwards [1]. While the association between the CoP motion and stepping is biomechanically evident [2], the control relationship between M-L and A-P CoP movements has not yet been well-defined.

Persons with Parkinson's disease (PD) typically show hesitation of gait initiation, a form of akinesia, which may be attributable to difficulties with CoP control prior to stepping [3]. It is unknown whether the abnormally prolonged duration and reduced amplitude of CoP shifts accompanying impaired step initiation in PD may represent a disruption in the control that affects A-P and M-L CoP movements.

We have developed an intervention for gait initiation in PD aimed at improving the coupling of postural and locomotive components of stepping [4]. When a participant's loading forces begin to change to generate M-L CoP displacement, the floor beneath the stance leg suddenly drops (1.5 cm) which enhances the M-L CoP movement prior to first-step lift-off. This represents a form of posture assisted locomotion (PAL) training.

In this study, we determined: 1) the extent to which the properties of M-L and A-P CoP movements are temporally and spatially related prior to step initiation in people with PD; and 2) the relationship between early CoP changes and first step characteristics. Analyses were performed prior to, immediately after, and six weeks after PAL training.

METHODS

Seven subjects with clinically moderate PD participated in the study. PAL training was conducted twice a week for six weeks and included sixty repetitions of rapid self-initiated gait in each session. Pre-, post- and retention tests were conducted. CoP characteristics prior to stepping were determined from ground reaction forces, and step characteristics were identified from kinematic analysis.

Correlation analyses were performed for the timing and magnitude characteristics of the A-P and M-L CoP displacements prior to first step onset. Associations between first step characteristics (step length and peak velocity) and CoP parameters were also calculated. The kinetic and kinematic variables were compared between test sessions to determine the effects of PAL training.

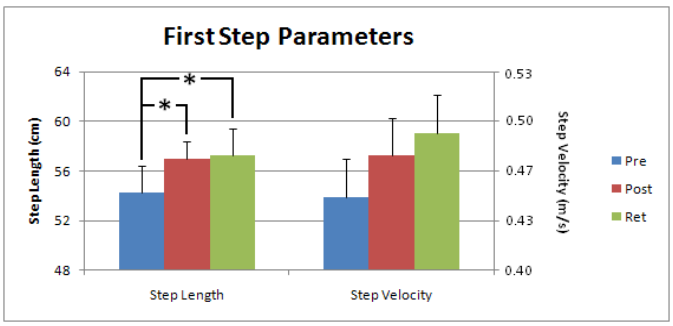

Figure 1: Improvement of step initiation by PAL training, sustained through retention test. *: $p<0.05$

RESULTS AND DISCUSSION

Step length showed improvement immediately post training and remained greater at the six-week

retention test (Mann-Whitney, $p<0.05$). Similar trends were observed for step velocity (Figure 1).

The A-P and M-L CoP shifts prior to the first step were poorly correlated ($r<0.5$) with stepping performance in pre- and post-tests. During the retention test, however, there were higher correlations between peak CoP amplitudes, and the step length and velocity (Table 1).

Pre-training, the correlation between M-L and A-P CoP shifts were better for duration ($r=0.56$) than for peak amplitude ($r=0.32$). Post training, timing and amplitude of CoP shifts were well correlated ($r>0.75$). In the retention test, the correlation between A-P and M-L shift durations decreased ($r=0.36$), while the correlation between the peak amplitudes remained high ($r=0.81$) (Figure 2).

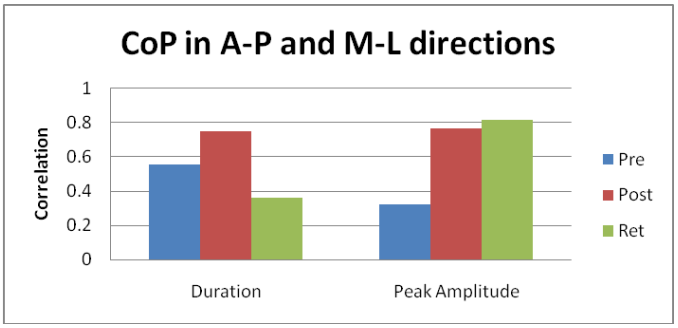

Figure 2: Correlation between A-P and M-L CoP parameters.

A-P and M-L peak CoP amplitudes feature prominently in the improvement of step initiation. In the post-test, CoP shifts are better correlated than in the pre-test both in timing and amplitude, and the first steps are faster and longer. After six weeks retention, the improved temporal relationship between the A-P and M-L CoP shifts diminished, but the correlation between CoP amplitudes persisted, as did the association between CoP amplitudes and step parameters (Table 1). Improving step initiation was concomitant with increased coupling of the amplitudes of A-P and M-L CoP shifts. While the correlation of CoP shift durations also improved, the durations did not correlate with step parameters (Table 1). Six weeks after training, the duration correlation decreased, yet the first steps were long and fast.

Stepping behavior in PD allows for the exploration of the relationship between M-L and A-P CoP shifts and step initiation. Healthy persons generate CoP shifts in the M-L and A-P directions for different control purposes; promoting balance utilizing M-L CoP shifts and propelling the center of mass through A-P shifts [1,2]. Thus, it is likely that the relationships identified here - 1) Prioritization of CoP displacement magnitude, and 2) Independence of step properties from the direction of CoP shift - are part of the mechanism used by PD participants in PAL training.

The PAL rehabilitative training approach, in which step initiation is enhanced by mechanically altering limb loading to affect CoP changes prior to stepping, is effective for improving step length and velocity, with lasting effects.

REFERENCES

1.Jian,Y., et al. *Gait and Posture*, **1**, 9-22. (1993).
2.Rogers,M.W., et al. *Arch Phys Med Rehabil*, **82**(5), 619-624 (2001).
3.Schaafsma, J.D., et al. *Eur J Neurol*, **10**(4), 391-8. (2003).
4.Mille, M.L., et al. *Movement Disorders*, **22**(1), 20-27. (2006).

Table 1: Correlation between step and CoP parameters, pre- and post- PAL training

	Step Length vs M-L		Step Length vs A-P		Step Speed vs M-L		Step Speed vs A-P	
	Dur	Amp	Dur	Amp	Dur	Amp	Dur	Amp
Pre-test	0.34	0.50	0.13	0.20	0.40	0.40	-0.03	0.15
Post-test	-0.06	0.27	-0.06	0.28	0.20	0.29	0.05	0.15
Retention	0.05	0.47	0.01	0.55	0.12	0.61	-0.15	0.61

PERTURBATION-BASED BALANCE TRAINING IN OLDER ADULTS AT INCREASED RISK FOR FALLS

[1]Kathleen Bieryla and [2]Michael Madigan

[1]Bucknell University, Lewisburg, PA, USA
[2]Virginia Tech, Blacksburg, VA, USA
email: k.bieryla@bucknell.edu

INTRODUCTION

Approximately one in three adults 65 years and older fall each year [1]. Many falls in older adults result from to some type of postural perturbation (e.g., trips, slips, etc.). As such, the ability to recover balance from a postural perturbation without falling is an important skill for fall prevention. Older adults may be able to improve their ability to recover from a postural perturbation through perturbation-based balance training (PBBT), similar to the way other motor skills can be improved through training.

Most falls, however, occur in older adults who are at an increased risk of falling due to physical and/or cognitive impairment. The effectiveness of PBBT may be dependent upon fall risk. Therefore, the purpose of this study was to investigate the efficacy of PBBT in older adults at an increased risk for falls.

METHODS

Five older adults from a local nursing home completed this study (85 ± 6.5 years). The study was approved by the Virginia Tech Institutional Review Board, and written consent was obtained from all participants prior to participation.

A single subject experimental design was used where participants served as their own controls using multiple baseline measurements prior to training. Testing consisted of four baseline tests, each separated by one week, four weeks of training, and two follow-up tests, one week and one month after the end of the training.

Testing and training were performed on a pneumatic instrumented moving platform (Figure 1) while participants stood on the platform relaxed and looking straight ahead. Prior to the first baseline test, each participant's maximum displacement that could be withstood without stepping was determined. Subsequent baseline and follow-up tests consisted of six trials using this maximum displacement (including three forward and three backward translations). Training consisted of three sessions per week for four weeks, and 50 trials per session. Throughout the training, the direction and distance of the platform movement was varied randomly, and the distance was gradually increased as each participant's performance improved.

Figure 1: Experimental set-up of the pneumatic platform which translated a maximum of 0.08m forward and 0.13m backward at an average velocity of 0.25m/s. A force platform is integrated with the moving platform and used to quantify balance.

During all testing, ground reaction forces were sampled at 1000 Hz from a force platform mounted on the platform, and the center of pressure (COP) was determined. Balance was quantified using the time to stabilization of the center of pressure (TTS COP) [3]. TTS COP was defined as the time for the COP velocity to return below a threshold velocity that was common across all participants. This threshold was based upon the mean and standard deviation of COP data prior to platform movement from all participants. Prior to statistical analysis, TTS was normalized to the displacement of the platform (nTTS) to account for variability in the

platform displacement due to the pneumatic actuation. A log transform was performed on the data to yield normal homogeneous residuals. A one-way mixed-model ANOVA was conducted to determine the effect of session (before training, one week post-training, one month post-training). In the event of a significant main effect, pair-wise comparisons were completed using Tukey's HSD.

RESULTS AND DISCUSSION

An initial ANOVA on the baseline tests revealed no effect of baseline session ($p=0.60$) on nTTS. As such, the participants exhibited a consistent baseline prior to training on the moving platform.

All participants were able to decrease their nTTS after training (Figure 2). The percent changes ranged from a 12.7% decrease from baseline to one week post-training to a 57.2% decrease from baseline to one week post-training. On average, participants decreased their nTTS by 41.6% from baseline to one week post-training.

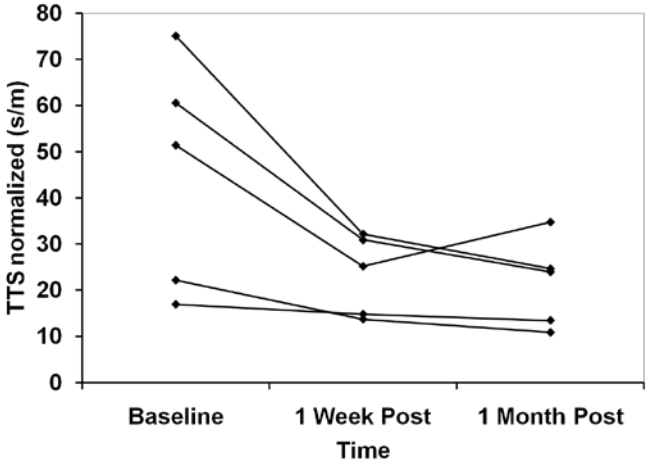

Figure 2: Mean nTTS for each participant during the last baseline session, one week post-training, and one month post-training.

When comparing nTTS of the last baseline test with the one-week and one-month tests, there was a main effect of session ($p<0.001$). Post-hoc comparisons indicated nTTS for the last baseline test (44.8 ± 28.3 s/m) was significantly higher than nTTS for one-week post training (24.2 ± 12.1 s/m; $p<0.001$). nTTS for the last baseline test was also significantly higher than nTTS for one-month post training (22.0 ± 15.4 s/m; $p<0.001$).

Changes in nTTS before training to one week post-training quantified improvements in balance from motor learning. Differences, or lack thereof, in nTTS before training to one month post-training quantified the ability of participants to retain improvements from motor learning for one month. Our results show that older adults at an increased risk for falls were able to decrease their nTTS (indicative of an improvement in balance), and were able to retain these improvements for at least one month without further training.

Similar studies have also demonstrated the ability for both young and older adults to improve balance after exposure to a postural perturbation although distinct differences do exist. For example, Pavol et al. [3] exposed young and healthy older adults to a single session of five simulated slips and both groups experienced a similar exponential decrease of fall incidence within a single day. Few studies have examined older adults at a high-risk for falls. Shimada et al. [4] showed after six months of PBBT on a treadmill, frail older adults were able to improve reaction time to an auditory stimulus during perturbed walking. Although the current study and Shimada et al. [4] both used high-risk older adults, key difference exist including training regiment, length, and intensity.

CONCLUSIONS

In conclusion, the results provide evidence that PBBT can improve balance in older adults at an increased risk for falls. Future studies should investigate as to whether these improvements translate to reduced risk of falls outside of the laboratory.

REFERENCES

1. Rubenstein LZ. *Age and ageing* **35 Suppl 2**, ii37-ii41, 2006.
2. Vearrier LA, et al. *Gait Posture* **22**, 153-163, 2005.
3. Pavol MJ, et al. *J Gerontol A Biol Sci Med Sci* **57**, M496-503, 2002.
4. Shimada H, et al. *Am J Phys Med Rehabil* **83**, 493-499, 2004.

ACKNOWLEDGEMENTS

KAB was supported by an American Association of University Women Selected Professions Fellowship.

DEVELOPMENT OF MOTORIZED FACILITATED ANKLE STRETCHING

Fan Gao

UT Southwestern Medical Center at Dallas, TX, USA
email: fan.gao@utsouthwestern.edu, web: http://www.utsouthwestern.edu/findfac/

INTRODUCTION

Proprioceptive neuromuscular facilitation (PNF) was first proposed by Herman Kabat for the purpose of rehabilitation of polio patients with paralysis [1]. The technique was mainly based on the principles of Sherrington's laws of irradiation, successive induction and reciprocal innervation. Under tendon loading the Golgi tendon organs which is located in the musculotendinous junction will be fired and result in neurological inhibition and muscle relaxation. In facilitated stretching, a strong isometric contraction of the target muscle will trigger the Golgi tendon organs and relax the target muscle to facilitate lengthening and increasing range of motion. Due to its effect and ease to implement, PNF has become popular for physical therapist and athletic trainers to facilitate joint flexibility. Klein et al. found that PNF treatment in elderly will significantly improve flexibility, ROM, strength and ADL function [2]. The PNF is even found effective to increase muscle volume and alter muscle fiber types [3] and compared to static stretching PNF technique is more effective [4].

Stroke induced contractures and/or spasticity around ankle joint can severely limit the mobility of stroke survivors. Currently, few effective treatments for contracture and/or spasticity are available. One treatment option is passive movement of the joint. Clinically, a physical therapist (PT), [5-7] passively stretches the joint by manually moving the joint through the range of motion (ROM) to reduce spasticity and/or contracture. Continuous passive motion (CPM) devices are widely used in clinics and in patients' homes to prevent postoperative adhesion and reduce joint stiffness. More recently, a motorized device with intelligent control has been developed [8]. Though intelligent stretching provides promising treatment intervention there are still some limitations. For example, the treatment is purely passive with muscles totally relaxed. Due to the lack of voluntary participation the effects induced by intelligent stretching are limited to improvement in passive joint properties instead of muscle strength and coordination which are more related to functional performance. PNF technique combines both passive and active stretching and significant improvement on muscle strength and coordination has been reported [2-4]. Therefore PNF technique will be an excellent candidate as a more effective intervention strategy. The goal of this study is to develop a single degree of freedom motorized device which could successively implement PNF hold-relax technique on the ankle joint.

METHODS

Development of motorized device

The motorized device consists of a servo motor (Danaher motion Inc., USA) and an inline gear box with a 25:1 gear ratio which increases the loading capacity of the motor up to 50 Nm. One uniaxial torque sensor was mounted on the motor shaft to register the torque signal. The motor was controlled by a drive and speed mode was chosen to control the speed and direction of the motor rotation. A built-in rotation encoder was used to provide the current position of the motor shaft (figure 1).

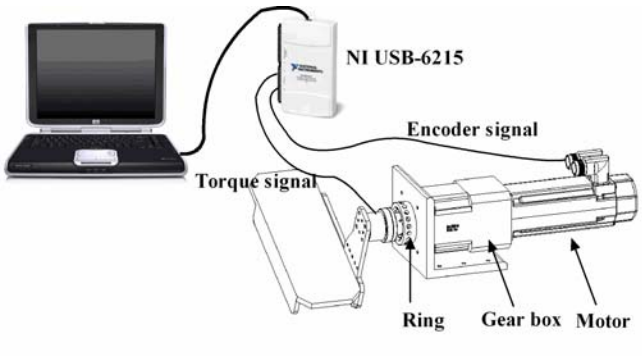

Figure 1: Illustration of motorized device

Implementation of intervention strategies

The motor drive and torque sensor are interfaced with custom LABVIEW program (National instrument Inc., USA). The control and encoder signals from the motor drive were connected with a National Instrument USB data acquisition card (NI USB-6215). Surface EMGs of the muscles were fed into the LABVIEW program. An illustration of foot-ankle was shown and updated on the front panel based on the current ankle position. With PNF technique, direct and indirect hold-relax (HR) were implemented. The ankle joint is first held at dorsiflexion which is adjusted for individual and the subject isometrically resists the movement of the motor by matching the prescribed muscle activation level (normalized EMG) for ~10 seconds. The motor slowly moved further toward dorsiflexion if the subjects could not match the prescribed muscle activation. The motor will then relax and move the ankle into a new dorsiflexion. The muscle groups activated depended on the selected technique. With direct HR (DHR) the calf muscle will be activated while the tibia anterior muscle will be activated with indirect HR (IDHR) (figure 2). Each short session will last ~5 min with one min break thereafter. The dorsiflexion position was updated after each short session and in total there were twelve short sessions.

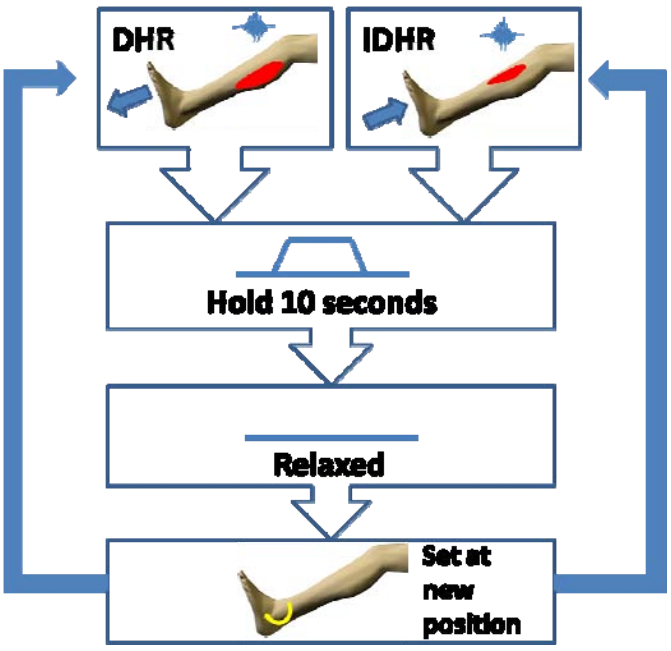

Figure 2: Flow chart of HR intervention

RESULTS AND DISCUSSION

Pilot study showed successful implementation of facilitated ankle stretching using a motorized device. Outcome measurements including ankle range of motion, muscle power, locomotion are underway to evaluate the effects of the intervention. It is expected that the motorized facilitated ankle intervention will be more effective in increasing ankle joint range of motion and neuromuscular function. It will be a promising intervention for treating spastic joint in stroke survivors. However, stroke survivors might have difficulties in voluntary muscle contraction and maximal effort might be challenging. With PNF hold-relax intervention, the target level of muscle activation could be set submaximal instead of maximal and previous study comparing the effects using submaximal and maximal effort in a PNF intervention observed equally improvements in range of motion [9].

REFERENCES

1.H. Kabat, M. Knott, *Phys Ther Rev* **33**, 53 (1953).
2.D. A. Klein, W. J. Stone, W. T. Phillips, J. Gangi, S. Hartman, *JOURNAL OF AGING AND PHYSICAL ACTIVITY* **10**, 476 (2002).
3.N. Kofotolis, I. S. Vrabas, E. Vamvakoudis, A. Papanikolaou, K. Mandroukas, *Br J Sports Med* **39**, e11 (Mar, 2005).
4.D. C. Funk, A. M. Swank, B. M. Mikla, T. A. Fagan, B. K. Farr, *The Journal of Strength and Conditioning Research* **17**, 489 (2003).
5.R. W. Bohannon, P. A. Larkin, *Phys Ther* **65**, 1676 (Nov, 1985).
6.M. L. Dombovy, B. A. Sandok, J. R. Basford, *Stroke* **17**, 363 (May-Jun, 1986).
7.A. M. Moseley, *Phys Ther* **77**, 240 (Mar, 1997).
8.L. Q. Zhang *et al.*, *IEEE Trans Neural Syst Rehabil Eng* **10**, 149 (Sep, 2002).
9.J. B. Feland, H. N. Marin, *Br J Sports Med* **38**, e18 (August 1, 2004, 2004).

ACKNOWLEDGEMENTS

American Heart Association National Scientist Development Award

FEASIBILITY OF GROUP KICKBOXING TO IMPROVE BALANCE AND GAIT IN PATIENTS WITH MULTIPLE SCLEROSIS

[1]Kurt Jackson and [1]Kimberly Edginton Bigelow

[1]University of Dayton, Dayton, OH, USA
email: jacksokj@notes.udayton.edu, Kimberly.Bigelow@udayton.edu

INTRODUCTION

Multiple Sclerosis (MS) affects an estimated 200,000 individuals in the US, causing gait and balance impairments from the earliest stages of the disease [1,2]. Martin et al. found that compared to healthy controls, MS patients with minimal impairment walked with reduced speed and stride length and performed poorer on the functional reach task using to measure balance, even those exhibiting no pyramidal signs [2]. Impairment of balance and gait contribute to the higher prevalence of falls in this population, reducing quality of life [3].

Research efforts have sought to identify effective interventions that can reduce functional impairment in patients with multiple sclerosis. For example, it has been found that a tailored balance rehabilitation program improved patient's performance on clinical balance tests [4]. Kickboxing appeals as a possible intervention due to the required movements, coordination, and weight shifts that are required, as well as the ability to work with groups of patients at one time. However, there is very limited work to determine whether a kickboxing program is feasible for this population and whether it may prove helpful in improving gait and posture.

The aim of this pilot study was to determine if clinical measures of gait and balance, as well as posturography measures improved based on participation in kickboxing. A secondary aim was to determine the feasibility of training five individuals at once and make recommendations for future adaptation of such a program.

METHODS

Five subjects (mean age: 57 ± 11, mean Expanded Disability Status Scale: 3.2 ± 2.5, 1 male and 4 females) participated in this pilot study. Prior to beginning kickboxing training, all subjects completed a series of clinical tests, including: Timed Up & Go, Berg Balance Scale, Dynamic Gait Index, and Ten Meter Walk Test. Subjects also completed the Activities of Balance Confidence Scale (ABC). Postural sway data was also collected for all subjects using a force-measuring platform. Subjects completed static balance trials: Eyes Open, Flat Surface; Eyes Closed, Flat Surface; Eyes Open, Foam Surface; Eyes Closed, Foam Surface. Center of pressure was collected for 30 seconds at 1000 Hz. Anterior-Posterior and Medial-Lateral Sway Range was calculated for each trial. Subjects also completed at least two trials of the Limits of Stability task.

Subjects then participated in an eight week kickboxing training led by a certified kickboxing instructor. The group training was held twice a week for 60 minutes each time. During participation all subjects wore harnesses anchored into the ceiling. The kickboxing exercises increased in difficulty throughout the eight weeks and required coordinated movements as well as balance to stand on one leg, while kicking with the other.

At the completion of the program, all subjects repeated the series of tests that they had done prior to participation. To analyze the effectiveness of the intervention, Minimal Clinically Important Difference (MCID) values for the associated tests were used.

RESULTS AND DISCUSSION

The most notable improvement post-training was for the Dynamic Gait Index task. All subjects improved after completion of the kickboxing program. Results are shown in Figure 1. The MCID for the Dynamic Gait Index task, where the maximum possible score is 24 points, is reported to

be 3 points [5]. Three subjects had a change of 2 and one had a change of 4 points, suggesting meaningful improvement. It is felt that the kickboxing program improved the Dynamic Gait Index scores because participants demonstrated improvements in the tasks that were similar to those experienced during kickboxing such as rotational movement between head and trunk, pivot turning and single leg stance.

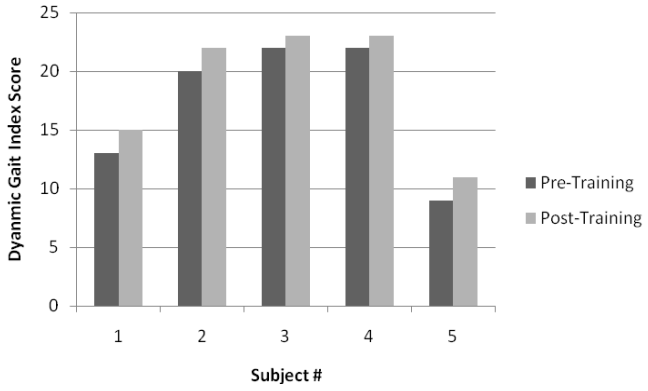

Figure 1. Changes in Dynamic Gait Index Score

Improvement in the Berg Balance Scale was also observed. Two subjects improved by 5 points, nearing the MCID value of a change of 6 points [6]. Another subject improved by 4 points. The two subjects with the highest starting scores did not approve additionally, however this is likely due to a ceiling effect (maximum score 56). Figure 2 shows these results. Similar to the Dynamic Gait Index, it is felt that the kickboxing program improved the Berg Balance Scale scores because participants showed the most consistent improvement in the categories requiring single leg stance, narrow base of support and alternate stepping and turning which are routinely challenged during kickboxing.

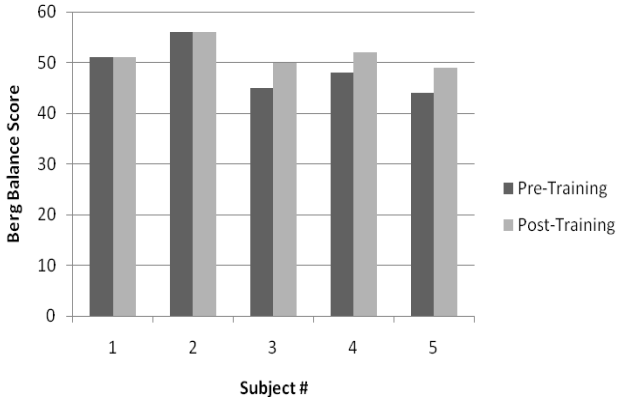

Figure 2. Changes in Berg Balance Scale Score

Interestingly, despite these functional improvements, subjects did not generally express increased balance confidence according to the ABC. In fact, three subjects reported lower scores after the participation in the kickboxing training. This may be because kickboxing challenged the subjects more than typical activities, and as such they better recognized their own imbalance. Future research will be needed to examine this disconnect and how to prevent it in the future.

Posturography results demonstrated that subjects tended to exhibit increased postural sway during quiet standing in the anterior-posterior and medial-lateral directions, and decreased ranges during the limits of stability task. It is possible that these decreased limits of stability ranges, where subjects lean as far in each direction as they feel they can without losing balance, were tied to the decreased balance confidence observed.

Though more work is needed to better quantify the effectiveness of kickboxing training, this pilot study suggests that this innovative intervention has potential. The general trend of improvement in the clinical tests suggests that this may be effective in improving balance and gait. Subjective feedback also demonstrated that subjects enjoyed the experience and camaraderie of participating in a group setting. The use of multiple overhead harnesses was important in providing stability to subjects during training and allowed one trainer to work with multiple participants. Currently a follow-up study is underway to examine the effects of kickboxing at a larger-scale.

REFERENCES

1.Noonan CW, et al. *Neurology* **59**, 136-138, 2002.
2.Martin CL, et al. *Multiple Sclerosis* **12**, 620-628, 2006.
3.Cattaneo D, et al. *Arch Phys Med Rehabil* **83**, 864-867, 2002.
4.Cattaneo D, et al. *Clin Rehabil* **21**, 771-781, 2007.
5. Marchetti G, Whitney C. *Poster at 2010 APTA CSM*, San Diego, CA, 2010.
6. Stevenson T. J Aust Physio **47**, 29-38, 2001.

ACKNOWLEDGEMENTS

We wish to acknowledge Camille Bowshire, Ember Grant, Melissa Weston, and Alexander Jules.

IPSILATERAL AND CONTRALATERAL REACHING IN PERSONS WITH CHRONIC STROKE

[1]Margaret A. Finley, [1]Stephanie Combs

[1]University of Indianapolis, Krannert School of Physical Therapy, Indianapolis, IN, USA
email: finleym@uindy.edu, web: http://pt.uindy.edu/

INTRODUCTION

Stroke is the leading cause of severe, long-term disability in the U.S. Over 800,000 strokes occur annually with 80% of individuals experiencing residual impairment.[1] Abnormal upper extremity flexion synergy patterns in the paretic arm after stroke interfere with isolation of motion and accomplishment of complex actions. Specifically, reaching across the trunk with humeral adduction and elevation and concomitant elbow extension is altered in the paretic limb.

Reaching movements of the paretic limb in individuals with impairment from stroke have been described as "less smooth."[2] However, limited literature exists comparing the kinematics of reaching to ipsilateral targets compared with targets placed contralateral to the paretic side. Additionally, little information on the kinematics of these tasks in the "less impaired" nonparetic limb exists.

The purpose of this project was to describe and compare the kinematics of ipsilateral and contralateral reaching in the paretic and nonparetic limbs of individuals with impairment from chronic stroke. The focus of this presentation will be the movement smoothness of these tasks. It was hypothesized that interlimb differences would exist for both reaching directions as well as differences would be found for the paretic limb between ipsilateral and contralateral movement kinematics.

METHODS

Ten individuals with upper extremity impairment from chronic stroke participated (Table 1). Following informed consent, the upper extremity section of the Fugl-Meyer Motor Assessment (FMA) was performed to clinically document level of impairment in the paretic limb. Three-dimensional kinematic data of upper extremities and trunk was collected (MotionMonitor™ Minibirds, 100Hz) during unilateral reaching (paretic and nonparetic limbs) to targets located ipsilateral and contralateral to the limb. International Society of Biomechanics International Shoulder Group recommendations for definition of global and local coordinate systems as well as Euler rotation sequences for segmental and joint motions were followed.[2] Order of target location and reaching limb were randomly presented. Participants were instructed to reach to the target at a self-selected, comfortable speed. Data were exported and processed with custom routines in Matlab™ to determine scapulohumeral, trunk and elbow kinematics in addition to mean speed, peak speed, smoothness metric (mean/peak velocity)[2] and movement duration. Movement initiation was defined as the time when tangential velocity exceeded 5% of maximal velocity and end of movement defined when the velocity dropped below this 5% threshold.[5] Only the velocity metrics will be presented here.

Pearson correlations (r, $p \leq 0.05$) determined if relationships existed between the FMA and the paretic and nonparetic limb movement kinematics during ipsilateral and contralateral reaching. Paired t-test ($p \leq 0.05$) compared the paretic to nonparetic limb movement variables in ipsilateral and contralateral reaching. ANOVA ($p \leq 0.05$) compared ipsilateral and contralateral reaching kinematics between limbs. Given the small sample size, effect sizes were calculated for all comparisons.

RESULTS AND DISCUSSION

Peak speed and movement duration of the paretic limb during ipsilateral reaching had a significant

correlation to the FMA. Nonparetic limb ipsilateral reaching had significant correlations of the FMA to mean speed, peak speed and movement duration, while during contralateral reaching the FMA was significantly related to all movement variables (mean speed, peak speed, smoothness ratio, duration). Regardless of the limb or reaching direction, decreased velocity and increased movement duration were associated with greater impairment in the paretic limb.

Table 1: Demographics of participants (n=10)

Age	61.6 ± 11.2 years
Stroke Onset	5.3 ± 2.9 years
Gender	Males = 6; Females = 6
Fugl-Meyer UE (max = 66)	44.0 ± 13.9

Paretic and nonparetic limb smoothness (p= 0.049) and movement duration (p=0.007) were different for ipsilateral reaching. Although not significant, large to very large effect sizes were found for mean speed, peak speed and movement smoothness ratio as well. Contralateral reaching revealed significant differences between limbs for peak speed (p=0.037) with large to very large effect sizes for mean speed, smoothness and movement duration. No difference was found between paretic limb ipsilateral and contralateral reaching in any of the variables with medium effect sizes found among all meaures.

Overall, reaching movement velocity and movement smoothness was reduced in the paretic limb compared with the nonparetic limb for ipsilateral and contralateral reaching with a strong inverse relationship to clinically measured impairment level in the paretic limb. Figure 1 illustrates the reduced smoothness, noted as multiple peaks in movement velocity, of three levels of impairment during ipsilateral reaching, paretic limb (1a) and nonparetic limb(1b).

CONCLUSIONS

Although reaching movement kinematics were different between the paretic and nonparetic limbs in persons with chronic stroke, greater impairment in the paretic limb was related to altered movement patterns in the nonparetic limb.

REFERENCES

1.Bhogal SK, et al *Top Stroke Rehabil.* Summer 2003.
2.Rohrer B, et al. *J Neurosci.* Sept 15 2002.
3.Wu G, et al. I. *J Biomech.* May 2005.
4. Wagner, J.M, et al, *Phys Ther.* May 2008.

ACKNOWLEDGEMENTS

Funding provided by the University of Indianapolis InQuery Collaborative Grant

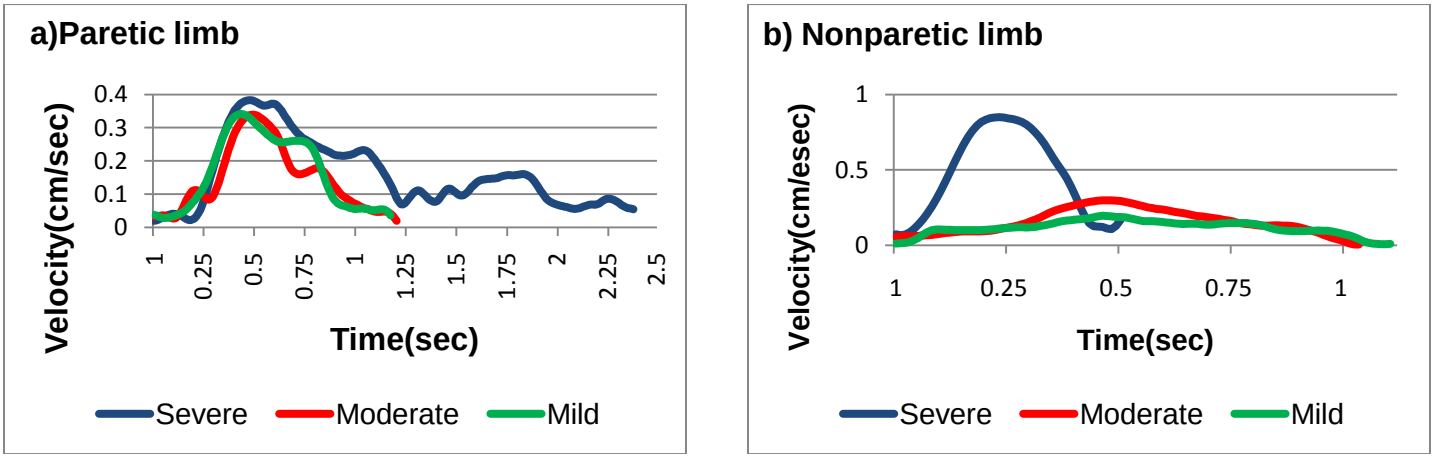

Figure 1: Ipsilateral reaching of three participants with varied impairment levels: a) paretic limb, b) nonparetic limb

QUANTITATIVE EXAMINATION OF CORE MUSCLE ACTIVATION DURING ISOMETRIC EXERCISES

Gretchen Oliver, Audrey Stone, Hillary Plummer and David Keeley

University of Arkansas, Fayetteville, AR, USA
email: goliver@uark.edu

INTRODUCTION

Emphasis has previously been placed on performing various types of abdominal crunches in attempt to target the anterior abdominals. Recently, improved understanding that the core is composed of the entire lumbo-pelvic-hip complex (LPHC) has resulted in an increase in popularity of core stability routines focused on recruiting the anterior, medial, lateral and postural musculature that supports the LPHC. In attempt to target the core in its entirety, many choose to include core exercises that result in isometric contractions. Thus, with the increased popularity of these isometric core exercises, it was the purpose of our study to quantitatively examine the muscle activations of three common isometric core stability exercises (abdominal bridge, abdominal bridge with leg lift, and superman) along with a newly introduced core exercise (flying squirrel) and determine if muscle activations differed among the exercises. We hypothesized that all exercises would activate core musculature and that there would be differences in muscle activations among the exercises.

METHODS

Thirty healthy collegiate graduate students (age: 23.4 ± 1.4yr, height: 171.3 ± 10.3cm, mass: 73.3 ± 16.2kg), regardless of gender, consented to participate in the current study. Participants reported no lower extremity, or back, injury within the past six months. Testing protocols for the current study were approved by the University of Arkansas Institutional Review Board. Prior to participation the approved procedures, risks, and benefits were explained to all participants.

Participants reported for testing prior to engaging in any vigorous activity that day. Location of core musculature which included bilateral gluteus maximus, gluteus medius, external oblique, and the multifidus were identified through palpation. Adhesive 3M Red-Dot bipolar surface electrodes (3M, St. Paul, MN) were attached over the muscle bellies and positioned parallel to muscle fibers using techniques described by Basmajian and Deluca.[1] Manual muscle tests (MMTs) were used to identify the maximum voluntary isometric contraction (MVIC) following the techniques described by Kendall et al.[2] Each MMT was conducted to establish baseline readings for each participant's maximum muscle activity to which all sEMG data could be compared.

Electromyographic data were collected via a Noraxon Myopac 1400L 8-channel amplifier. The signal was full wave rectified. Signals were smoothed based on the smoothing algorithms of root mean squared at windows of 100ms. Throughout all testing, sEMG data were sampled at a rate 1000Hz.

Participants were provided examples of proper techniques for each of the exercises, and the order in which participants completed the exercises was randomized. Individual participants performed each exercise as a warm-up trial before data were collected. During the test trials, participants were instructed on proper posture through verbal cues. The exercises that the participants performed were the following: *superman* (prone with arms and legs extended off the floor), *flying squirrel* (prone with arms and legs extended off the floor, shoulders externally rotated, and hips internally rotated), *abdominal bridge* (supine with knees flexed and feet on the floor with torso and pelvis raised off the floor), *abdominal bridge with one leg support* (abdominal bridge with one foot lifted off the floor and knee extended. Participants performed each exercise for 10s three times with a 30s rest between

repetitions and a 1-minute rest between the various exercises.

RESULTS AND DISCUSSION

The flying squirrel (left 55.3 ± 29.9, right 55.2 ± 21.1 %MVIC) and superman (left 55.3 ± 29.9, right 55.2 ± 21.1 %MVIC) exercises produced significantly greater muscle activation in the multifidi than any of the bridge exercises (bridge: left 31.2±17.7, right 30.9±13.7; bridge with right leg lift: left 34.5±20.0, right 38.5±16.5; bridge with left leg lift: left 38.0±22.7, right 34.0±13.1 %MVIC). The bridge exercise produced significantly lower muscle activation in the gluteus maximus (left 20.2±14.5, right 16.2±10.7 %MVIC), and the bridge with leg lift produces significantly lower %MVIC of the gluteus maximus on the same side as the lifted leg (bridge with right leg lift: left 32.6±19.3, right 6.8±4.1; bridge with left leg lift: left 7.2±4.8, right 26.3±17.4 %MVIC). Similarly, the bridge exercise produced significantly lower muscle activation in the gluteus medius (left 17.4±8.9, right 16.1±9.6 %MVIC), and the bridge with leg lift produces significantly lower muscle activation of the gluteus medius on the same side as the lifted leg (bridge with right leg lift: left 35.6±16.0, right 11.5±13.0; bridge with left leg lift: left 9.4±13.5, right 31.1±14.7 %MVIC). The bridge exercise (left 9.6±8.9, right 8.3±8.3 %MVIC) produced significantly lower muscle activation in the obliques than the bridge with leg lift exercises (bridge with right leg lift: left 16.3±11.8, right 14.1±11.2; bridge with left leg lift: left 16.6±12.2, right 14.4±11.2 %MVIC).

The purpose of this study was to quantitatively examine the muscle activations of three common isometric core stability exercises (abdominal bridge, abdominal bridge with leg lift, and superman) and a newly introduced core exercise (flying squirrel). The data revealed that the flying squirrel and the superman exercises produced the greatest overall muscle activations. In addition the abdominal bridge with the leg lift displayed increased muscle activation of the gluteal group especially the gluteus medius of the support leg (opposite the leg lifted).

CONCLUSIONS

The flying squirrel, abdominal bridge, abdominal bridge with leg lift and superman exercises all provided muscle activations in what we previously defined as the primary musculature of the core. Overall the flying squirrel and superman exercises provide the greatest overall muscle activation of the core. The findings of this study demonstrate that any of these exercises may be incorporated into a core stability program or be used as adjuncts to supplement a currently implemented core stability program.

REFERENCES

1.Basmajian, JV, et al. *Muscles alive, their functions revealed by electromyography (5th ed.).* 1985.

2. Kendall, FP et al. *Muscles: Testing and Function (4th ed).* 1993.

THE USE OF A FLEXIBLE, NON-HEEL AND INEXPENSIVE FOOTWEAR DECREASES KNEE LOADS IN ELDERLY WOMEN WITH OSTEOARTHRITIS

[1]Francis Trombini-Souza, [1]Aline A. Kimura, [1]Marco K. Butsugan, [1]Ana Paula Ribeiro, [1]Paula M. H. A. Aoki, [1]Anice C. Pássaro, [2]Antônio C. Arnone and [1]Isabel C.N.Sacco.

[1] Physical Therapy, Speech and Occupational Therapy Dept, School of Medicine, University of Sao Paulo; [2]University Hospital, University of Sao Paulo, Sao Paulo, SP, Brazil
email: trombinisouza@usp.br

INTRODUCTION

A recent study [1] found that about 27 million of Americans are affected by osteoarthritis (OA) - the degenerative joint disease most common of the musculoskeletal system [2]. The knee joint is the most affected of the lower limbs [3]. One of the most important treatment is to reduce load on this joint, because the overload increases the process of joint degeneration, and hence loss of functionality for daily activities. Based on the pioneering studies of Robbins and Hanna (1987) [4] and recent results obtained by Shakoor and Block (2006, 2008) [5,6], it is believed that the use of shoes that mimic the barefoot condition may reduce the overload on the knee during gait. The purpose of this study was to evaluate and compare the influence of a commercial flexible/ non-heeled/ inexpensive footwear, with a modern high-heeled modern shoe and barefoot condition on the knee adduction moments during gait in elderly women with and without OA knee.

METHODS

We evaluated the gait of 45 elderly women: 21 with OA grade 2 or 3 [7] (OAG) [65±4 yrs, 64,8±8,4 kg, 1,57±0,06 m, 26,2±2,9 kg/m^2 and 24 asymptomatic control individuals (CG) [65 ± 5 yrs, 68,9 ± 7,8 kg, 1,54 ± 0,05 m, 28,8 ± 3,2 kg/m^2]. The three-dimensional angular displacement was evaluated by six infrared cameras (Optitrack FLEX: V100, Natural Point, USA) and ground reaction forces were evaluated using a force plate embedded in the middle of a 10m walkway (AMTI OR-6-7-1000). The subjects walked in a self-selected cadence in 3 conditions: barefoot, Moleca® (flexible women's footwear, made of canvas, anti-slip rubber sole and no-heel, costs around USD 9.00; Calçados Beira Rio® S.A, Novo Hamburgo – RS, Brazil) and modern women´s shoes with heels at maximum 5cm high (Fig. 1).

Figure 1: (A) Moleca®; (B) High-heeled shoe.

The synchronized data were collected at 100 Hz (A/D card, AMTI, 12 bits). Software Visual3D (C-motion, Ontario, Canada) was used to calculate the knee adduction moment. Moment peaks at the initial and final stance phase and the knee angular impulse in the three conditions were calculated by custom-written matlab function. Comparisons were performed by two-way ANOVAs for repeated measures, where conditions were within factor, and groups were between factor ($\alpha = 0.05$).

RESULTS AND DISCUSSION

The acute effect of Moleca's use significantly reduced the 1st adduction moment peak (initial stance) in the CG in 10.8% and in the OAG in 12.0%, compared to the modern shoe. And also, Moleca's acute use significantly reduced the 2nd adduction moment peak (final stance) in the CG in 15.7% and in the OAG in 12.0%, compared to the high-heeled shoes. There was no statistical difference between the effect of the Moleca® and the barefoot condition in the 1st moment peak and in the 2nd moment peak (final stance) on both groups [(CG, p=0.114; OAG, p=0.393); CG, p=0.746; OAG, p=0.574) respectively]. Moreover, the use of high-heeled shoes significantly increased the 1st moment peak in the CG in 16.0% and in the OAG in 14.4%, compared to the barefoot condition.

Also, the high-heeled shoe significantly increased the 2nd adduction moment peak in CG in 14.3% and in OAG in 9.7%, compared to the barefoot condition. The acute use of Moleca® also produced a significantly greater decrease in the adduction moment peak during midstance in both groups [CG (27.8%) and OAG (27.0%)], compared to modern high-heeled shoe. The barefoot gait also showed minimum adduction moment (midstance) significantly lower than the high-heeled shoe, with a reduction of 29.7% in CG and 17.1% in the OAG, compared to high-heeled shoe. Among several satisfactory results, what was the most surprising one was that the Moleca's use provided a significant decrease of 12% of the minimum adduction moment compared to barefoot condition in the OAG. These results can be attributed to the greater flexibility of the Moleca® that can mimic the kinetic patterns of barefoot gait. Moreover, the absence of heel in Moleca® prevents the heel contact with the ground soon and with greater impact, as seen in high-heeled shoes. This characteristic may change the loads on the knee, especially at the initial contact. Knee higher overloads are already described when using high-heeled shoes, that has greater sole rigidity. These moderns shoes' characteristics may have contributed to the results observed when comparing to the flexible footwear and barefoot gait.

CONCLUSIONS

The acute effect of the use of a commercial flexible, non-heel and inexpensive footwear (Moleca®) in elderly women with knee OA provided adduction moments not different from barefoot gait and a relevant reduction in the knee loads compared modern female shoes. The Moleca® can also, in some gait phases, provides a further decrease in knee adduction moment compared to the barefoot condition, with the advantage, however, to give external protection to the feet while walking.

REFERENCES

1. Lawrence RC, et al. *Arthritis Rheum*. **58**(1), 26-35, 2008.
2. Scott DL et al. *Br J Rheumatol*. **37**(5), 546-54, 1998.
3. Pecina M, et al. *Arh Hig Rada Toksikol*. **52**(4), 429-39, 2001.
4. Robbins SE, et al. *Med Sci Sports Exerc*. **19**(2),148-56, 1987.
5. Shakoor N, et al., *Arthritis Rheum*. **54**(9), 2923-7, 2006.
6. Shakoor N, et al. *Arthritis Rheum*. **59**(9), 1214-20, 2008.
7. Kellgren JH, el al. *Ann Rheum Dis.*16(4):494-502, 1957.

ACKNOWLEDGEMENTS

Brazilian Government Funding Agencies (CNPq - 480209/2007-3, CAPES and FAPESP - 2008/03335-5) for financial support.

Table 1: Means, standard deviations and *p*-values of the knee adduction moments during barefoot gait (B), Moleca® (M) and high-heeled modern shoe (H) of the control group (CG) and osteoarthritis group (OAG).

Variable	Condition	CG (*n* = 24)	OAG (*n* = 21)	*P* CG x OAG	*p* CG	*p* OAG
1st adduction moment peak (inicial stance)[&]	Barefoot	2.10 ± 0.91	2.51 ± 1.53	0.928	0.114 (B-M)	0.393 (B-M)
	Moleca®	2.23 ± 0.86	2.58 ± 1.45	0.953	**<0.001** (B-H)	**<0.001** (B-H)
	High-heeled	2.50 ± 1.04	2.93 ± 1.43	0.919	**<0.001** (M-H)	**<0.001** (M-H)
Minimum adduction moment (midstance)[&]	Barefoot	0.76 ± 0.94	1.51 ± 1.73	0.842	0.839 (B-M)	**0.017** (B-M)
	Moleca®	0.78 ± 0.89	1.33 ± 1.67	0.726	**<0.001** (B-H)	**<0.001** (B-H)
	High-heeled	1.08 ± 0.88	1.82 ± 1.60	0.743	**<0.001** (M-H)	**<0.001** (M-H)
2st adduction moment peak (final stance)[&]	Barefoot	1.45 ± 1.23	1.97 ± 1.64	0.915	0.746 (B-M)	0.574 (B-M)
	Moleca®	1.43 ± 1.12	1.92 ± 1.64	0.922	**0.002** (B-H)	**0.004** (B-H)
	High-heeled	1.69 ± 1.22	2.18 ± 1.59	0.924	**0.002** (M-H)	**0.002** (M-H)
Angular impulse of adduction moment[#]	Barefoot	68.77 ± 46.58	100.26 ± 79.47	0.888	0.195 (B-M)	0.278 (B-M)
	Moleca®	72.15 ± 45.44	97.43 ± 79.38	0.744	**<0.001** (B-H)	**<0.001** (B-H)
	High-heeled	85.28 ± 46.50	115.60 ± 77.81	0.814	**<0.001** (M-H)	**<0.001** (M-H)

[&] N.m; [#] N.m/ms

EXAMINING THE DOSE RESPONSE RELATION FOR NEUROMUSCULAR ELECTRICAL STIMULATION AND RECOVERY FOLLOWING TOTAL KNEE ARTHROPLASTY

[1]Adam R. Marmon, [2]Stephanie C. Petterson, [1]Lynn Snyder-Mackler

[1]University of Delaware; Department of Physical Therapy, Newark, DE, USA
[2]University of East London; School of Health and Biosciences, London, England
email: marmon@udel.edu

INTRODUCTION

The frequency of total knee arthroplasty (TKA) procedures performed in the United States for end-stage osteoarthritis has increased substantially over the past decade to approximately half a million per year and will continue to increase in the coming years [1]. However, consensus among therapists on the treatment regimens following TKA remains equivocal. One of the aims of physical therapy must be to minimize the weakness of the involved limb, which can cause patients to rely on the non-operative limb, in turn increasing peak knee joint moments [2]. Improvements in quadriceps strength and voluntary activation of the surgical limb have been demonstrated with the use of progressive quadriceps strength training interventions, but remain impaired when compared to the uninvolved limb[3]. Short-term improvements in quadriceps strength and voluntary activation have been enhanced following a rehabilitation protocol that combines standard strength training with neuromuscular electrical stimulation (NMES) [4]. However, identification of the appropriate NMES dosage necessary to achieve clinical and functional improvements had not been systematically examined. The goal of the current project was to determine if a dose response curve could be constructed for patients who received NMES as part of their physical therapy treatment following TKA.

METHODS

Seventy patients (41 men; 65.3 ± 8.7 yrs), who participated in a clinical trial designed to enhance quadriceps muscle recovery following unilateral TKA were initially examined 6 weeks after surgery. The patients were then enrolled in a 6-week rehabilitation program that combined standard progressive strength training protocols with NMES. Strength training protocols were customized for each patient; the prescribed exercises targeted quadriceps strengthening. In general, the strength training protocols consisted of 2 sets of 10 repetitions, progressed to 3 sets of 10 repetitions.

A stimulation paradigm was concurrently implemented with each strengthening protocol and comprised electrically evoked quadriceps muscle contractions (Table 1). The target dosage for each session was 30% of the subject's maximal voluntary contraction (MVC), with the training intensity adjusted to the maximum tolerated each session. Dosage was tracked by recording the average mechanical force produced during the evoke contractions (Figure 1). Additionally, magnetic resonance images of the quadriceps muscle group were used to calculate lean muscle cross sectional area (LCSA) from 29 of the 70 patients. MVC, levels of voluntary muscle activation (central activation ratio; CAR), and LCSA were examined at baseline and after 3 and 6 weeks of treatment.

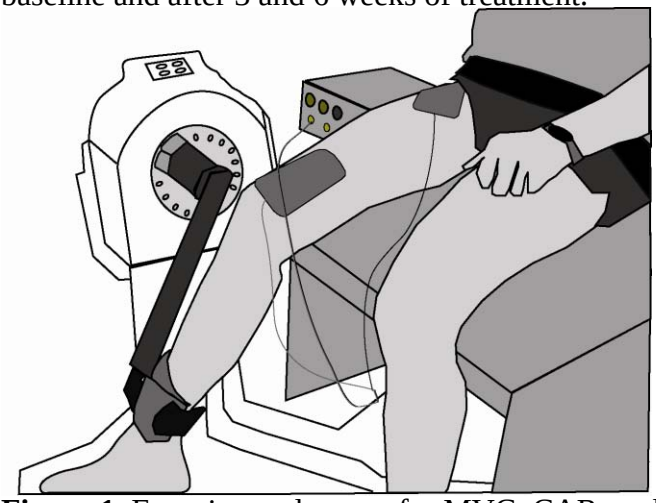

Figure 1. Experimental set-up for MVC, CAR, and NMES.

RESULTS AND DISCUSSION

The improvements in strength and voluntary activation ($p<0.001$) were significantly correlated

A

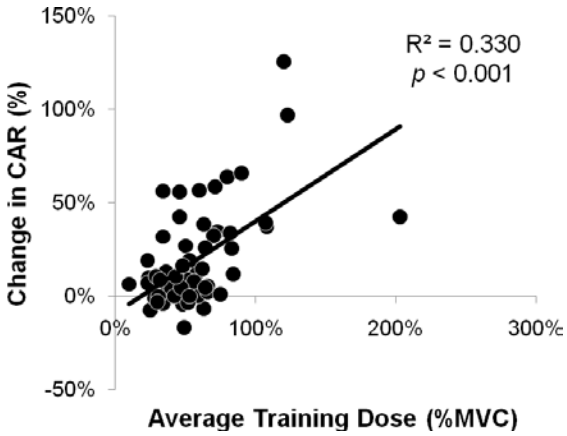

B

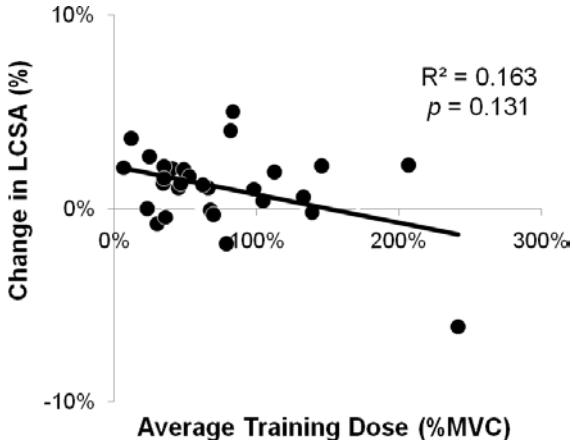

C

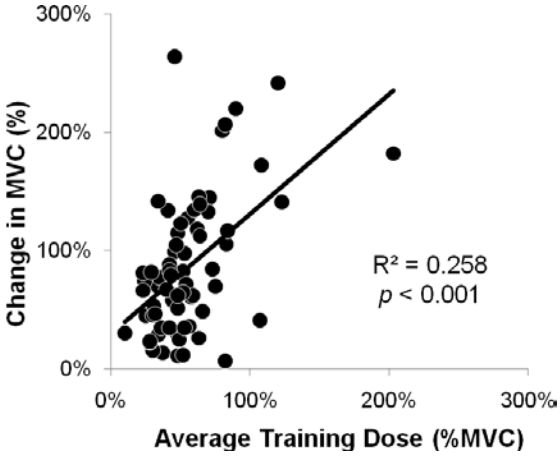

Figure 2. Changes in MVC (A), CAR (B), and LCSA (C) from initial evaluation through 6 weeks of standard rehab and NMES.

with the dose of NMES (Figure 2 A,B) from the initial evaluation through the 6-weeks of treatment ($r = 0.508$ and $r= 0.574$ respectively; $p \leq 0.001$). The LCSA of the quadriceps for the 29 subjects was reduced ($p<0.001$), and was not significantly correlated ($r = -0.287$) with the dose of NMES (Figure 2C).

CONCLUSIONS

Considering the functional importance of strength, voluntary activation, and muscle size on recovery from TKA, the current findings suggest that the maximizing the electrically elicited training force during rehabilitation will enhance short-term recovery following TKA.

REFERENCES

1. Murphy, et al. Arthritis & Rheumatism 59(9): 1207-13, 2008.
2. Milner, et al. Arch Phys Med Rehabi 89(10): 1965-9, 2008.
3. Petterson, et al. Arthritis & Rheumatism 61(2): 174-183, 2009.
4. Petterson, et al. J Orthop Sport Phys Ther 36(9)678-85, 2006.

ACKNOWLEDGEMENTS

Supported by NIH: R01-HD041055

Table 1. NMES Treatment Parameters

Carrier Frequency	2.5 KHz
Burst Rate	75
On Time	10 s + 2 s ramp
Off Time	80 s
Current Amplitude	Patient Tolerance
Dose	10 contractions
Treatment Frequency	3 per week
Treatment Duration	6 weeks

Differences in Muscle Activation, Joint Kinematics and Kinetics during a Step compared to Elliptical Exercise Pattern while using the PRECOR AMT Trainer

Matthew J. Rogatzki, Thomas W. Kernozek, John D. Willson, John F. Greany, Di-An Hong and John P. Porcari

University of Wisconsin-La Crosse, La Crosse, WI, USA
e-mail: kernozek.thom@uwlax.edu

INTRODUCTION

Cardiovascular response has been shown to be similar when using a step or elliptical exercise machine [1]. There has been limited research examining the differences in lower extremity joint kinetics and kinematics or muscle activation patterns between these two motions. Our purpose was to compare these factors while using a step and elliptical pattern performed on the PRECOR AMT Trainer.

METHODS

Twenty subjects performed both the step and elliptical pattern on the same PRECOR AMT trainer at 80% of their maximal heart rate reserve (HRR). A standardized warm-up was employed in determining the workload needed to obtain an 80% maximal HRR at a 120 steps/min pace. The PRECOR AMT allows either a step or elliptical movement pattern. Three-dimensional kinematic data and pedal based ground reaction force (GRF) from the right leg and pelvis were measured at 120 Hz and 720 Hz, respectively, over 10 cycles and synchronized to a common frequency of 120 Hz. Sagittal joint angles and internal moments (normalized to BW and height) were calculated using custom software based on the coordinate data synchronized with the GRF from the right pedal. Electromyography (EMG) data were measured at 1080 Hz from the rectus femoris, biceps femoris, gluteus maximus, and erector spinae muscles. Maximum voluntary isometric contraction data were collected prior to the exercise session. Dependent t-statistics were used to compare the discrete variables from the two exercise motions (alpha=0.05).

RESULTS AND DISCUSSION

Exercise performed using the step pattern resulted in greater peak hip flexion (p=0.016), greater knee extension (p=0.043), and less plantar flexion (p=0.046) than the elliptical pattern. Peak hip flexor moments (p=0.038) and knee extensor moments (p=0.001) were found to be greater during the step motion than the elliptical motion (Fig. 1 & 2).

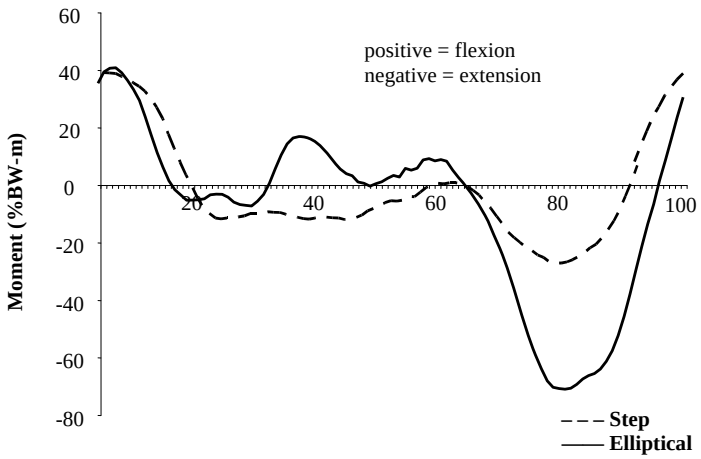

Figure 1: Ensemble average hip moment normalized to the percentage of the movement cycle (% cycle).

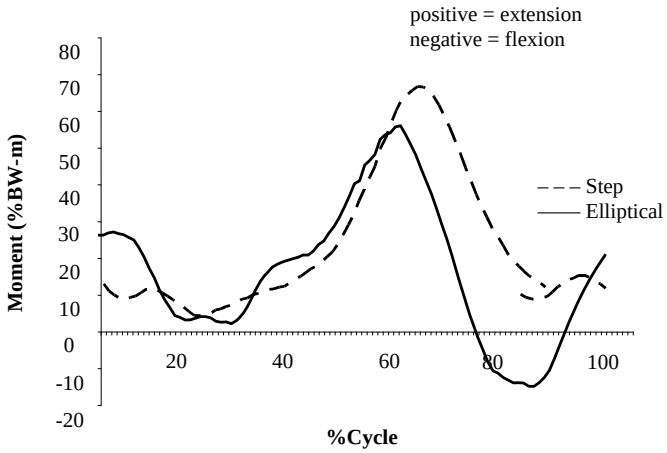

Figure 2: Ensemble average knee moment normalized to the percentage of the movement cycle (% cycle).

There was primarily a posterior shear joint reaction force at the shank during both motions (Fig. 3). However peak shear force became anterior with the elliptical motion (p=0.005), but remained posterior throughout the cycle for the step motion.

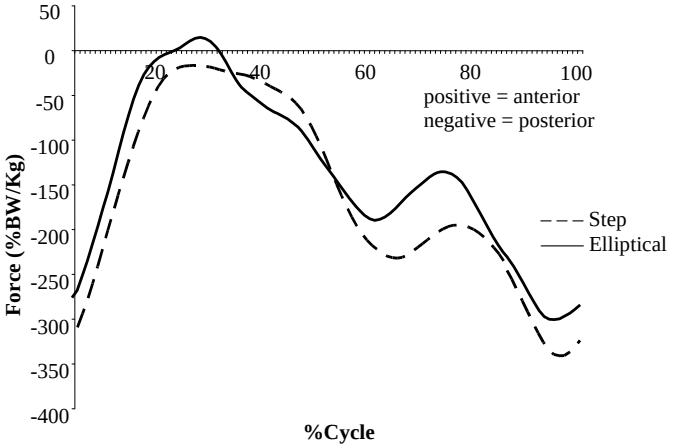

Figure 3: Ensemble average shear force normalized to the percentage of the movement cycle (% cycle).

Muscle activation (Table 1) for the biceps femoris and gluteus maximus were similar during both motions. There was decreased activation in the rectus femoris and erector spinae while performing the step pattern (p=0.000 and 0.003, respectively) in comparison to the elliptical pattern.

Results in performing the step and elliptical motion of the current study differs from the reports of other studies. Knutzen et al. [2] reported lower shear joint reaction force at the knee, yet greater moments at the hip and knee than the PRECOR AMT. Lu et al. [3] found greater knee shear joint reaction force and lower moments at the hip, knee, and ankle than the PRECOR AMT. Similar methods as the current study were used by Knutzen et al. [2] and Lu et al. [3] suggesting there may be differences due to the type of elliptical machine being used. D'Lima et al. [4] reported similar in vivo average peak forces at the tibia for both a stair stepper and elliptical trainer, whereas we showed differences in these forces at the shank between these motions on the same trainer. Based on the literature and our data, it appears that different exercise trainers allow different movement patterns and loading scenarios.

CONCLUSIONS

Differences in kinematic, kinetic and muscle activation appear to be present between the step and elliptical exercise pattern when using this machine. The step pattern resulted in greater hip flexion and knee extension, while the elliptical pattern resulted in greater ankle plantar flexion. Primarily a hip flexor and knee extensor moment was produced with the step pattern, whereas hip extensor and knee flexor moments were greatest during the elliptical exercise pattern. Knee anterior shear joint reaction force along with activation of the rectus femoris and erector spinae were greater during the elliptical pattern than during the step pattern. Understanding the mechanical load undertaken by the lower extremities during the step and elliptical pattern may be useful to rehabilitation professionals and others who use these machines to prescribe therapeutic exercise for injured patients that need to increase or maintain cardio respiratory fitness levels.

REFERENCES

1.Egana M. & Donne B. *J Sports Med Phys Fitness*, **44**, 141-146, 2004.
2.Knutzen K., et al. *RQES* **78**, A14-A15, 2007.
3.Lu, T.W., et al. *MSSE*, **39**, 1651-1658, 2007.
4.D'Lima, D.D., et al. *Clin Orthop Relat. Res*., **466**, 2605-2611, 2008.

Table 1: Means (SD) for maximum muscle activation (% MVIC) during the step and elliptical exercise pattern across all subjects while using the PRECOR AMT trainer. * Difference between motions.

	Step	Elliptical	
Muscle	**Mean (SD)**	**Mean (SD)**	**P-value**
Rectus Femoris	23.7 (9.5)	34.3 (11.9)	*0.000
Biceps Femoris	23.3 (12.8)	23.7 (12.2)	0.946
Gluteus Maximus	33.6 (14.2)	36.0 (16.2)	0.540
Erector Spinae	12.2 (9.2)	22.2 (11.5)	*0.003

COMPARATIVE GAIT ANALYSIS OF ANKLE ARTHRODESIS AND ARTHROPLASTY: INITIAL RESULTS OF A PROSPECTIVE STUDY

[1,2]Michael Hahn, [1]Elise Wright, [1]Ava Segal, [4]Michael Orendurff, [1-3]William Ledoux and [1,3]Bruce Sangeorzan

[1]RR&D Center of Excellence, Department of Veterans Affairs; Departments of [2]Mechanical Engineering, and [3]Orthopaedic and Sports Medicine, University of Washington, Seattle, WA, USA
[4]Texas Scottish Rite Hospital for Children, Dallas, TX, USA
email: mehahn@u.washington.edu, web: http://www.amputation.research.va.gov/

INTRODUCTION

Ankle osteoarthritis (OA) has been reported to affect 6% of the general population [1]. The condition is characterized by pain, decreased range of motion (ROM), reduced quality of life, and general disability. Standard surgical treatment for end-stage ankle OA has been tibiotalar arthrodesis, however follow-up studies have reported the development of OA in surrounding joints due to altered motion and loading [2-3]. Tibiotalar endoprostheses have been shown as a functional alternative to arthrodesis [4]. A limited number of studies have reported biomechanical outcomes of ankle arthroplasty [5-7]. Only one study compared the post-surgery outcomes of ankle arthrodesis and arthroplasty, however their study design involved a mix of non-paired samples rather than a within-subject paired sample [8]. The purpose of this prospective study was to compare pre-/post-surgery gait between arthrodesis and arthroplasty patients. It was hypothesized that at 12 months post surgery, patients with arthroplasty would have improved temporal-distance parameters, and increased ankle ROM, peak internal plantar flexor moment, and power compared to their pre-surgery condition and compared to patients with arthrodesis.

METHODS

Sixteen patients (58.4 +/- 10.0 years, 1.7 +/- 0.1 m, 89.7 +/- 17.1 kg) scheduled for surgical treatment of end-stage ankle OA were recruited for a prospective pre-/post-surgery gait analysis protocol. The protocol was approved by the Institutional Review Board. Written informed consent was obtained prior to each subject's participation. Patients were considered to have end-stage ankle OA based on their decision to undergo either arthrodesis or arthroplasty as a primary intervention to treat their OA condition. Potential participants were excluded if they had experienced a recent (<1 year) surgical, neurological, metabolic or lower limb musculoskeletal problem in the lower extremities, or had experienced multiple correction surgeries.

Eight patients received tibiotalar arthrodesis (FUSE), and eight received tibiotalar arthroplasty (TAR) (Salto® Talaris, Tornier, Edina, MN). All patients were evaluated prior to surgery and 12 months post surgery. Standard anthropometric measures were taken. Sixteen retro-reflective spherical surface markers were placed according to a standard bilateral lower extremity marker set. Patients were asked to walk across a 10m walkway at a self-selected walking speed, while barefoot. Three trials were analyzed for the affected limb in each condition. Ground reaction force data were recorded at 1200 Hz from embedded force platforms (AMTI BP400600, Watertown, MA; Bertec FP4060-NC, Columbus, OH). Marker trajectories were recorded at 120 Hz with a 12-camera Vicon MX system (Vicon, Lake Forest, CA) and filtered with the Woltring setting of MSE = 20. The Plug-In Gait model (Vicon) was used to calculate joint kinematics and net internal joint kinetics using standard inverse dynamics.

A mixed effects linear model was used to compare temporal-distance parameters, sagittal plane ankle ROM, peak ankle moments, and peak ankle powers between pre- and post-surgery conditions for both groups. Kinematic and kinetic comparisons included gait velocity as a covariate. Pre-/post-surgery changes were tested for group effects. Statistical tests were run using R (v.2.9.1).

RESULTS AND DISCUSSION

Temporal-distance measures of gait improved across both groups at 12 months post-surgery, with no significant group effect. Self-selected gait velocity increased from 0.97 to 1.17 m/s (p=0.002), stride length increased from 1.10 to 1.25 m (p=0.002), stride time decreased from 1.17 to 1.10 s (p=0.020), and cadence increased from 104.3 to 110.2 steps/min (p=0.021). Compared to pre-surgery conditions, TAR patients showed a trend of increased ankle ROM (3.4 deg; p=0.051), whereas FUSE patients showed no trend (Figure 1).

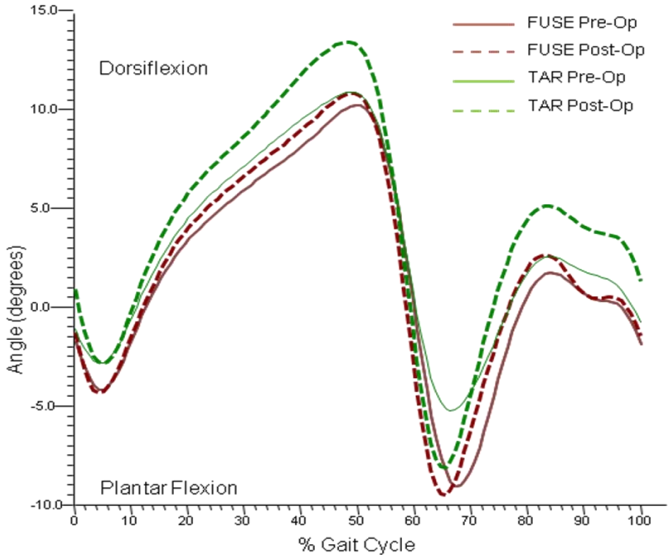

Figure 1: Group ensemble averages for ankle angle.

Pre-/post-surgery changes were different between groups for peak internal plantar flexor moment (p=0.032); increasing 0.18 Nm/kg for FUSE, and decreasing 0.14 Nm/kg for TAR (Figure 2).

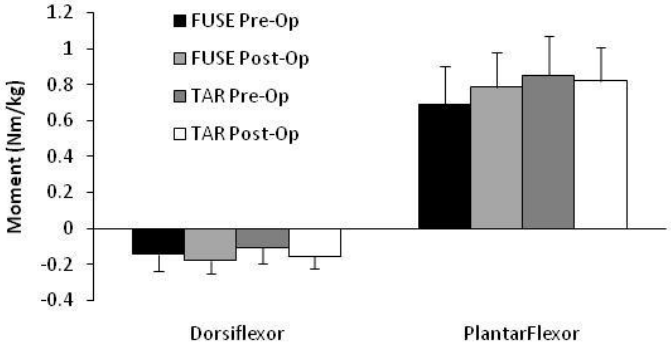

Figure 2: Sample means (SD error bars) of internal ankle moments; pre- and post-surgery.

Considering gait velocity as a covariate, both groups increased ankle power absorption from -0.42 to -0.56 W/kg (p=0.039, see Figure 3), however there was not a significant group effect.

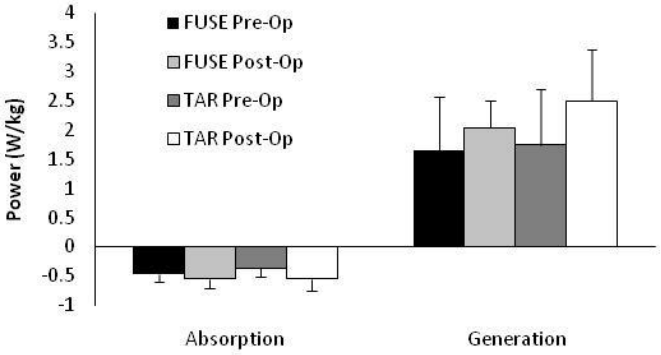

Figure 3: Sample means (SD error bars) of ankle power; pre- and post-surgery.

Though plantar flexor moment decreased in the TAR group, increased ROM and subsequently greater angular velocity during push-off resulted in large power generation. The combined effect allows sustained gait velocity and improved gait function overall. These findings are in agreement with those of Piriou et al. [8].

CONCLUSIONS

From the initial findings of this long-term study it appears that overall gait function is improved at 12 months post-surgery for both surgery types (as seen in improved temporal-distance measures). However, tibiotalar arthroplasty appears to retain more natural ankle joint function. Long term follow up should reveal more significant functional outcomes.

REFERENCES

1. Huch K et al., *Semin Arthritis Rheum* **26**, 667-674, 1997.
2. Fuchs S et al., *J Bone Joint Surg Br* **85**, 994-998, 2003.
3. Morrey BF et al., *J Bone Joint Surg Br* **62**, 777-784.
4. Bonnin M et al., *Clin Orthop Relat Res* **424**, 6-18, 2004.
5. Doets HC et al., *Foot Ankle Int* **28**, 313-322, 2007.
6. Dyrby C et al., *Foot Ankle Int* **25**, 377-381, 2004.
7. Valderrabano V et al., *Clin Biomech* **22**, 894-904, 2007.
8. Piriou P et al., *Foot Ankle Int* **29**, 3-9, 2008.

ACKNOWLEDGEMENTS

This study was supported by Department of Veterans Affairs grant A4513R.

PERTURBATION TRAINING IMPROVES GAIT PATTERNS IN ACL DEFICIENT FEMALES

[1]Stephanie Di Stasi and [2]Lynn Snyder-Mackler
[1]University of Delaware, Newark, DE, USA
email: smack@udel.edu

INTRODUCTION

Research has well established that women are at higher risk for ACL injury than men. Outcomes of a functional screening examination that classifies athletes with ACL injury showed that women were more likely to be classified as non-copers than men.[1] Knee instability is characteristic of non-copers, and these athletes present with the poorest functional performance acutely after injury. The movement strategies of men and women classified as non-copers have not been compared.

Perturbation training is a specialized neuromuscular training paradigm that normalizes movement behaviors in ACL-deficient athletes who have recurrent knee instability.[2] The capability of non-copers to improve knee function and resolve aberrant movement patterns suggest that this cohort possesses a more malleable neuromuscular system than previously thought.[2] Uninjured athletic females have also shown positive adaptations to perturbation training.[3]

Investigations of healthy control subjects suggest little difference between the sagittal plane kinematics and kinetics of men and women. Observed differences in movement patterns between genders acutely after ACL injury or after perturbation training can therefore be attributed to a gender-specific response. We hypothesized that females and males would have asymmetrical gait kinematics and kinetics after injury, and that these differences would resolve with pre-operative perturbation training.

METHODS

21 ACL-deficient athletes (9 females, 12 males; ages 15-50) were classified as non-copers using a validated functional screening examination.[4] All athletes participated in cutting, pivoting, or jumping activities for more than 50 hours/year. Subjects were selected for this study from an ongoing randomized controlled trial if they received a combination of pre-operative perturbation training and progressive strength training. All testing procedures were approved the University of Delaware Institutional Review Board and all subjects provided written informed consent prior to study participation.

Table 1. Subject Demographics

	Men	Women
Age (years)	25 ± 8.7	33.7 ± 12.6
BMI (kg/m^2)	30.5 ± 5.1	28.4 ± 7.2
Training (wks)	3.5 ± 1.7	3.5 ± 1.9

Three-dimensional gait data were collected using standard motion analysis techniques before (PRE) and after (POST) 10 sessions of perturbation training. Five walking trials at a controlled, self-selected speed, were collected and analyzed for each limb. Kinematic and kinetic data were processed using custom software programming (Visual3D and LabVIEW). Sagittal plane hip and knee angles and moments at peak knee flexion PKF), and knee excursions from initial contact to PKF were calculated.

To evaluate limb symmetry between men and women, we used an ANOVA with one repeated measure of time. Paired t-tests were used to determine where limb differences existed. A priori significance level was set at 0.05.

RESULTS AND DISCUSSION

Prior to perturbation training, only the women demonstrated kinematic differences between limbs both at the knee (Figure 1) and the hip (Figure 2). After perturbation training, knee ($p = 0.134$) and hip ($p = 0.515$) angles at PKF were similar.

We hypothesized that men and women would present acutely after injury with asymmetrical limb movement, as aberrant motion is the hallmark of this cohort. In support of these findings, a recent investigation of non-copers' return to sport capabilities after ACL reconstruction suggests that there may be larger variability within this group than initially described.[5]

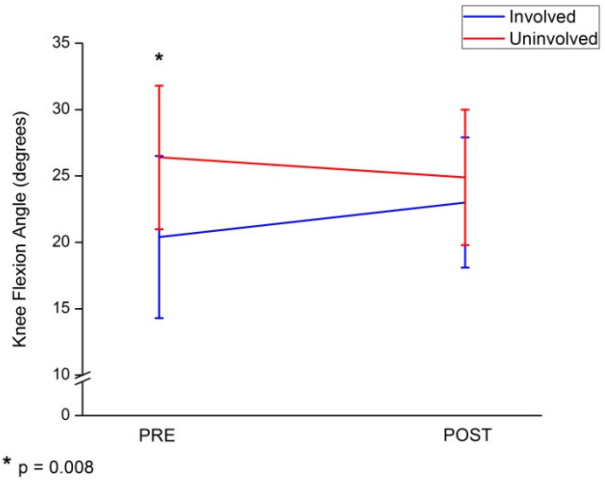

Figure 1. Women's knee flexion angles at PKF, before and after perturbation training. Bars = standard deviation.

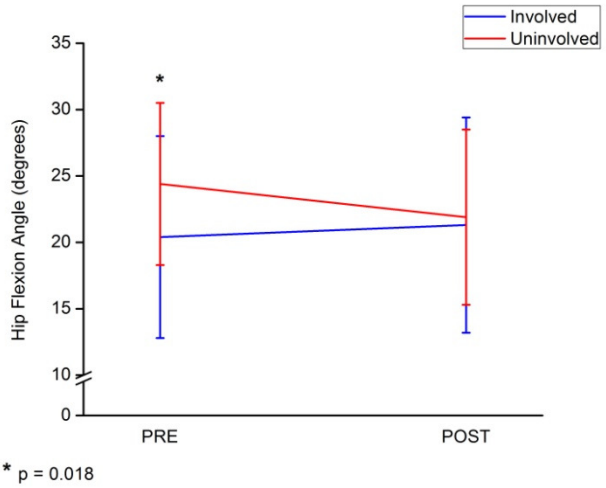

Figure 2. Women's hip flexion angles at PKF, before and after perturbation training.

Pre-training limb asymmetries in knee flexion excursion (Involved: 14.3° ± 5.8; Uninvolved: 18.2° ± 5.7) and hip flexion excursion (Involved: 11.5° ± 4.7; Uninvolved: 6.9° ± 4.2) also resolved after perturbation training (Knee - Involved: 14.8° ± 5.8; Uninvolved: 16.8° ± 5.9; Hip – Involved: 9.7° ± 3.8; Uninvolved: 7.9° ± 4.3).

Men demonstrated symmetrical knee and hip kinematics acutely after injury, and perturbation training did not alter their movement behaviors (Table 2). Asymmetrical hip and knee moments between genders were not found between pre- to post-training.

Table 2. Men's hip and knee joint angles at PKF, before and after perturbation training.

	PRE	POST
Involved Knee	24.7° ± 7.8	24.8° ± 6.6
Uninvolved Knee	26.4° ± 5.4	28.1° ± 5.1
Involved Hip	25.4° ± 6.5	27.3° ± 5.6
Uninvolved Hip	26.2° ± 5.4	28.1° ± 6.1

CONCLUSIONS

Differences in gait characteristics of male and female non-copers have not been previously described. Our findings provide evidence to support that non-copers are a variable group, and more specifically, that gender is a meaningful subgroup in this population. A differential response to ACL reconstruction and post-operative rehabilitation may also be evident. Future investigations into the gait characteristics and functional performance of non-copers should consider the effects of gender.

REFERENCES

1.Hurd WJ, et al. *J Orthop Sports Phys Ther* **38**, 36-41, 2008.
2.Hartigan EH, et al. *J Orthop Res* **27**, 724-729, 2009.
3.Hurd WJ, et al. *Knee Surg Sports Traumatol Arthrosc* **14**, 60-69, 2006.
4.Fitzgerald GK, et al. *Knee Surg Sports Traumatol Arthrosc* **8**, 76-82, 2000.
5.Hartigan EH, et al. *J Orthop Sports Phys Ther* 40, 141-154, 2010.

ACKNOWLEDGEMENTS

This research is supported by the NIH, RO1 AR048212 and S10 RR0223, and the Foundation for Physical Therapy (PODS I).

Improvement in off-axis neuromuscular control during functional tasks following six-week of pivoting elliptical training

[1,2]Song Joo Lee, [2]Yupeng Ren, [2]Francois Geiger, [1]Alison H. Chang, [2]Joel Press and [1,2]Li-Qun Zhang

[1]Northwestern University, Chicago, IL, USA
[2]Rehabilitation Institute of Chicago, Chicago, IL, USA

email: l-zhang@northwestern.edu, web: http://www.ric.org/research/centers/smpp/Staff/index.aspx

INTRODUCTION

Although knee movements are mainly about the major axis of flexion/extension, knee injuries such as ACL injuries most commonly occur in pivoting sports, which involve strong and potentially excessive off-axis loads to the knee(knee valgus/varus and tibial rotation). Current research and training mostly focus on sagittal plane movement and there is a lack of research and training protocols for off-axis control and movements, which are closely related to potential injuries to the knee. The purpose of this study was to investigate off-axis neuromuscular control and conduct six-week off-axis training during functional tasks and evaluate the outcome.

METHODS

A novel pivoting and sliding elliptical machine was developed (1) to train individuals' off-axis neuromuscular control (2) to evaluate training outcome in terms of the subject's off-axis neuromuscular control and stability. Sixteen subjects without any musculoskeletal disorder participated in the study. Among them, 9 subjects in the study group participated in 18 sessions of off-axis training (3 times/week for six weeks). At the beginning, middle and after the trainings, off-axis neuromuscular control properties were evaluated quantitatively in terms of off-axis stability and off-axis energy, strength, proprioception, and EMG activities from muscles crossing the knee. Seven healthy individuals served as the control group and participated in only the 3 evaluation sessions at the same intervals.

All the subjects gave informed consent (approved by the Institute of Review Board at Northwestern University) prior to the beginning of the training program. All participants were examined for their physical condition, particularly the knee to insure that their knees had a normal range of laxity, muscle strength, and free of any significant knee symptoms. After completing the clinical screening, individuals who did not have any other knee symptoms participated in the research program. Individuals in the control group were age and physical-activity level matched to the study group.

During the pre, mid and post training evaluation sessions, rotational stability, lateral stability, proprioception, and muscle activations were evaluated using the pivoting/sliding elliptical machine, with the EMG signals measured from the Biceps femoris, Semitendinosus, Medial Gastrocnemius, Lateral Gastrocnemius, Vastus Medialis Obliquus and Vastus Lateralis.

During each training session, the subject was asked to complete tasks under two different modes at several intensity levels at both lower limbs. In the first mode, the footplates were free to rotate with low friction (free rotation mode) or with assistive spring force. In the second mode, the footplates were perturbed to rotate with 1 Nm peak sinusoidal perturbation torque and 5 Nm offset torque in internal or external rotation. The subject was asked to maintain both footplates straight (aligning the second toe with the knee cap) during the functional stepping movement. In each training session, the subjects were first asked to do a few minutes of regular elliptical stepping movements without any pivoting movements, as a way of warming up and preparation for the training.

All footplate kinematic, kinetic and EMG data from the pre, mid, and post evaluations were analyzed in Matlab (Version 7.8). All data were segmented and time-normalized into percents of the elliptical cycle. Generally, data from 20-30 elliptical cycles per trial

were analyzed to make comparisons between different conditions including different modes of tasks and different evaluation sessions. Energy in pivoting for each foot was computed using the following equation.

$$Pivoting\ energy = \frac{1}{n}\sum_{i=1}^{n} |\, torque(i) * rotation\ angle(i) \,|$$

where n=1000 is the number of the data points in a trial. Since the tasks were "maintaining footplate straight", ideally the pivoting energy should be zero.

Independent samples t-tests were used to compare between the groups per each evaluation session. One-way ANOVA tests were used to compare between evaluations per group with post hoc tests.

RESULTS AND DISCUSSION

Pivoting stability of the study group improved significantly following the six-week pivoting training (Fig. 1), while the control group did not show significant improvement ($p<0.01$). Pivoting energy reduced significantly after the 6-week training and the subjects better dealt with the perturbing torque in pivoting and maintained both feet straight during elliptical movements (Figure 2 and Table 1).

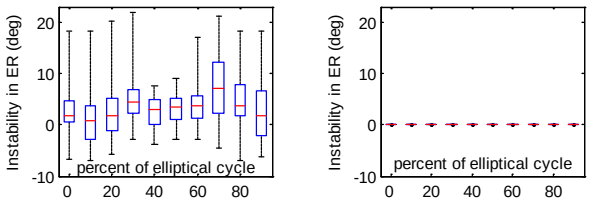

Figure 1: Representative data (from 30 elliptical cycles) showing improvement in rotational stability following the six-week pivoting training during free rotation mode (Left: Pre training evaluation, Right: Post training). The 2 tails indicate the max and min values and the box plot range indicates 25 and 75% of data. The red bar indicates the median values at 0, 10, 20, 30, 40, 50, 60, 70, 80 and 90% of the elliptical cycle.

Following the training, individuals in the study group showed reduced pivoting energy during the elliptical walking compared to the control group ($p<0.01$, Table 1).

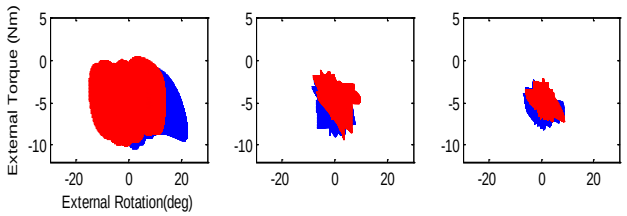

Figure 2: Reduction in pivoting energy following the 6-week training during forward elliptical walking under the external sinusoidal perturbations. The blue and red colors correspond to data from the left and right foot respectively (1st column: Pre training eval-uation, 2nd column: Mid training, 3rd column: Post training).

CONCLUSIONS

Subjects in the study group improved their off-axis stability in tibial rotation significantly. Their improved off-axis neuromuscular control was associated with reduced pivoting energy during the elliptical stepping movements, indicating they could better perform the off-axis control with reduced energy/work involved.

Although muscle activation patterns are not reported here due to limited space, the reduced pivoting energy may be associated with more skilled but less muscle activities throughout elliptical cycles for trained subjects to maintain the footplates positions. Overall, the pivoting elliptical training (combining sagittal and transverse movements) can help healthy individuals to improve their off-axis stability and neuromuscular control with reduced energy/effort, which may help them to better deal with potential injuries associated with pivoting sports.

ACKNOWLEDGEMENTS

The authors would like to acknowledge the support of NIH and NSF.

Table 1: Reduction in pivoting energy (Nm*rad*%elliptical cycle^{-1}) during forward elliptical walking in the free rotation mode before/after the six week training. Reported values are in mean (±1STD). * indicates P<0.01 between the control and the training groups. Ψ indicates P<0.01 between evaluations.

Group	Pre training Evaluation	Mid training Evaluation	Post training Evaluation	P value (between evaluations)
Training (N=9)	7.11 (3.80)	1.42 (1.35) *	1.48 (1.09)*, Ψ	<0.001
Control (N=7)	4.31 (2.56)	4.54 (1.03)	4.12(1.60)	0.921
P value (between groups)	0.118	<0.001	0.002	

BIOMECHANICAL AND GAIT IMPROVEMENTS AFTER PASSIVE STRETCHING AND ACTIVE MOVEMENT TRAINING IN CHILDREN WITH CEREBRAL PALSY

[1]Wu, Y-N; [1]Hwang, M; [1]Ren, Y; [1,2]Gaebler-Spira, D; [1,2]Zhang, L-Q

[1]Rehabilitation Institute of Chicago, Chicago, IL, USA
[2]Northwestern University, Chicago, IL, USA
email: l-zhang@northwestern.edu

INTRODUCTION

Cerebral palsy (CP) is the most prevalent physical disability in children, with an estimated 764,000 children and adults in the United States with this diagnosis. Mobility is important in functional independence and participation for children with CP. Different from adults with disabilities, children with disabilities risk losing functional mobility during adolescence because of the still growing musculoskeletal system and ongoing secondary impairments such as soft tissue shortening, weakness, and bony deformity [1], and those children also experience a loss of independence much sooner [2].

Ankle impairment with spasticity, contracture, muscle weakness, and/or insufficient selective motor control is a frequent cause of functional including gait limitations [3]. There is a lack of effective and convenient treatment of stretching and motor control training for children with CP and ankle impairment. We incorporated the therapeutic rationale into an advanced and portable rehabilitation robot with biofeedback computer game to increase joint functional range of motion (ROM) and improve motor control in children with CP. The aim of this study was to investigate the efficacy of the robotic rehabilitation on the biomechanical properties of ankle joint and ambulation in the children with CP.

METHODS

Twelve children with spastic CP (Table 1.) participated in the study. The participants came to our laboratory in a rehabilitation hospital three sessions a week for six weeks. The same training protocol was used for each session. It consisted of four parts: 20 minutes of warm-up passive stretching, 15 minutes of assisted-active movement, 15 minutes of resisted-active movement and 10 minutes of final passive stretching. All participants completed the 18 sessions of hourly training successfully.

Before and after the 18-session intervention, biomechanical properties including the passive ROM (PROM), active ROM (AROM), muscle strength, and simple gait were evaluated. Insole pressure sensors (F-Scan®, Tekscan Inc., South Boston, USA) were used to investigate the gait pattern. The flexible sensors were trimmed to fit the participant's feet and placed in the shoes. Step calibration was adopted to calibrate the sensor. The participant walked continuously at their comfortable speed for 30 seconds. The distance of trajectories of center of force (COF) during stance phase was calculated to represent the foot progression. The ratios of swing phase (stance phase) of trained side to swing phase (stance phase) of non-trained side were derived to evaluate gait symmetry. A ratio close to one indicates the two sides are more even during walking. For statistics analysis, paired *t*-tests were conducted, with significance levels of $p<0.05$.

RESULTS AND DISCUSSION

Significant increases were observed in dorsiflexion PROM (p=0.002), AROM (p=0.02), and dorsiflexor muscle strength (p=0.001) (Figure 1). Figure 2 shows the typical example of COF before and after 18-session intervention. The distance of COF trajectory of the trained side increased significantly (7.5 ± 3.8 cm before training vs. 8.8 ± 4.2 cm after, p=0.04). The increased force progression during stance might have improved gait efficiency. The participants walked more evenly on the two sides during both stance phase and swing phase after the intervention (p=0.01).

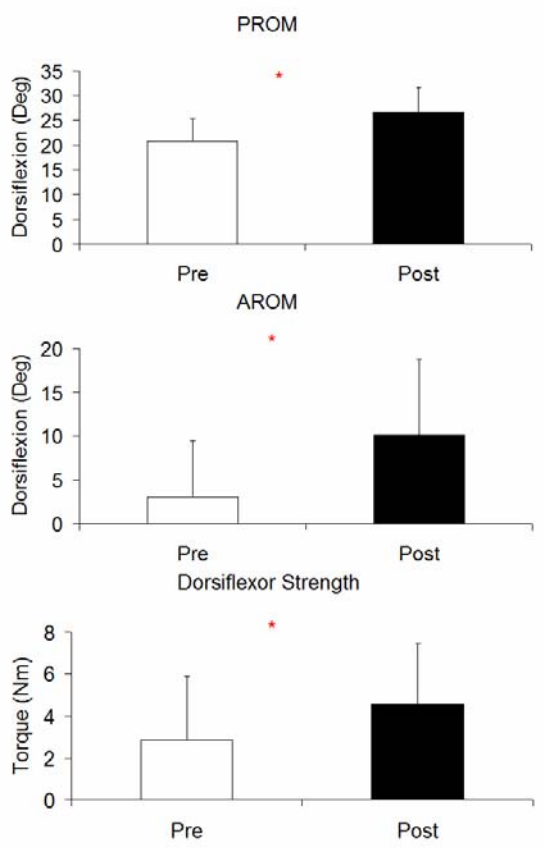

Figure 1: Biomechanical properties of the ankle joint before and after the intervention. Asterisk (*) denotes $p<0.05$.

CONCLUSIONS

Passive stretching combined with active movement training through motivating game-playing benefits children with CP and ankle impairment. It increased the PROM, AROM and muscle strength, and improved the gait with more even swing/stance phases on the two sides, and increased force progression during the stance phase. Frequent and convenient rehabilitation based on the approach may benefit larger populations over long term.

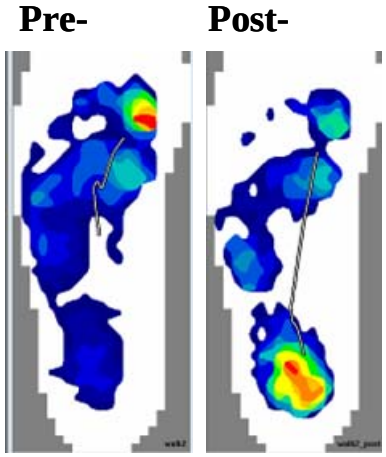

Figure 2: A representative case of the foot contact pressure and COF trajectory.

REFERENCES

1. Gajdosik CG, et al. *Phys Occup Ther Pediatr,* **21**:49-68, 2001.
2. Bottos M, et al. *Dev Med Child Neurol,* **43**:516-28, 2001.
3. Meinders M, et al. *Scand J Rehabil Med*, **30**:39-46, 1998.

ACKNOWLEDGEMENTS

We acknowledge gratefully the support from the participants and their families. We also acknowledge the funding supports of the NIH and NIDRR.

Table 1: Participants Characteristics

Subject no.	Gender	Age	Subtype	Treated side	GMFCS	Dorsiflexion	Ankle MAS
1	F	5 y	Diplegia	R	II	15.4	3
2	F	8y 8m	Diplegia	R	II	18.3	3
3	M	6y 1m	Diplegia	R	II	11.2	3
4	F	5y 4m	Diplegia	R	III	21.0	2
5	M	10y	Diplegia	R	II	26.0	3
6	F	9y 4m	Diplegia	R	II	20.0	3
7	F	7y 7m	Hemiplegia	R	I	24.9	1+
8	M	5y	Hemiplegia	L	I	24.1	2
9	F	8y 9m	Hemiplegia	L	I	22.0	3
10	M	8y 4m	Hemiplegia	L	I	26.5	2
11	M	15y 11m	Hemiplegia	R	I	16.7	2
12	M	10y	Hemiplegia	L	I	22.0	3

STROKE REHABILITATION: A KINEMATIC ANALYSIS OF DEVICE-ASSISTED AND CLINICIAN-ASSISTED SIT-TO-STAND TRANSFERS

[1,2]Aaron M. Hueftle, [1,2]Bradley J. Balogh, [1]Adam P. Taylor, [1]Amy J. Goldman, [1]Thad W. Buster, [1,2]Judith M. Burnfield
[1]Madonna Rehabilitation Hospital, Institute for Rehabilitation Science and Engineering, Lincoln, NE
[2]Biological Sciences and Biological Systems Engineering, University of Nebraska – Lincoln, Lincoln, NE
email: jburnfield@madonna.org, web: http://madonna.org/research_institute

INTRODUCTION

Work injuries arising from manually transferring patients during rehabilitation are concerning [1]. Although mechanical sit-to-stand transfer devices are frequently available to lessen clinician's physical effort, many rehabilitation therapists hesitate to use devices owing to concerns that device-assisted transfers may promote abnormal patient movement patterns. Our previous research documented significant differences in kinematic patterns between a device-assisted and normal sit-to-stand transfer in individuals without known pathology [2]. However, it was unclear from this work whether a clinician-assisted transfer would more closely simulate "normal" movement than a device-assisted transfer when patient weakness and movement control problems were present. The purpose of the current study was to compare sagittal plane kinematics during device-assisted and clinician-assisted transfers in patients participating in an acute stroke rehabilitation program.

METHODS

Ten adults (50-82 years; 7 males) engaged in acute inpatient stroke rehabilitation participated. A single physical therapist (36 years of age, 8 years acute stroke rehabilitation experience) provided all physical and verbal patient assistance. A Vancare VeraLift (V) power-driven sit-to-stand unit was used for device-assisted trials. Twelve-camera motion analysis (Qualisys) documented sagittal plane kinematics of the trunk, pelvis and thigh (each expressed relative to vertical), as well as knee and ankle angles. Participants performed three device-assisted conditions: 1) giving best effort (V-BE); 2) providing no effort (V-NE); and 3) physical therapist guided motions using physical assistance and verbal cues (V-PT). A fourth trial, with only a physical therapist's assistance (PT), was performed. INITIAL (0% movement cycle; seated), PEAK (maximum flexion or extension achieved), and FINAL (100% movement cycle; standing) joint angles were quantified. Independent t-tests identified differences in INITIAL, PEAK and FINAL angles between each condition (PT, V-PT, V-BE, and V-NE) and a normative database [2] of unassisted sit-to-stand movements in individuals without pathology (CONT). Coefficient of multiple correlations (CMC) quantified similarities in movement profiles between each condition and CONT.

RESULTS AND DISCUSSION

CMC values comparing each activity's movement pattern to CONT data are provided in Table 1. Movement profiles for activities studied are displayed in Figure 1. Significant differences between CONT and each test condition's INITIAL, PEAK and FINAL kinematic positions are summarized for key body regions in Table 2.

Table 1: Coefficients of multiple correlation values comparing sagittal plane sit-to-stand kinematic profiles during each condition tested to control group angles.

Region	Condition			
	PT	V-PT	V-BE	V-NE
Trunk	0.93	0.48	0.38	0.43
Pelvis	0.90	0.66	0.49	0.74
Thigh	0.98	0.96	0.96	0.91
Knee	0.99	0.98	0.97	0.96
Ankle	0.45	0.38	0.30	0.44

The greatest similarity in movement patterns between all conditions and CONT data occurred at the thigh and knee as evidenced by the high CMCs (≥ 0.91). In contrast, relatively fixed ankle postures across test conditions poorly simulated CONT ankle motion (CMC ≤ 0.45). At the trunk and pelvis, the PT condition simulated CONT data most closely; however, the trunk was more flexed and the pelvis more anteriorly tilted at the beginning and end.

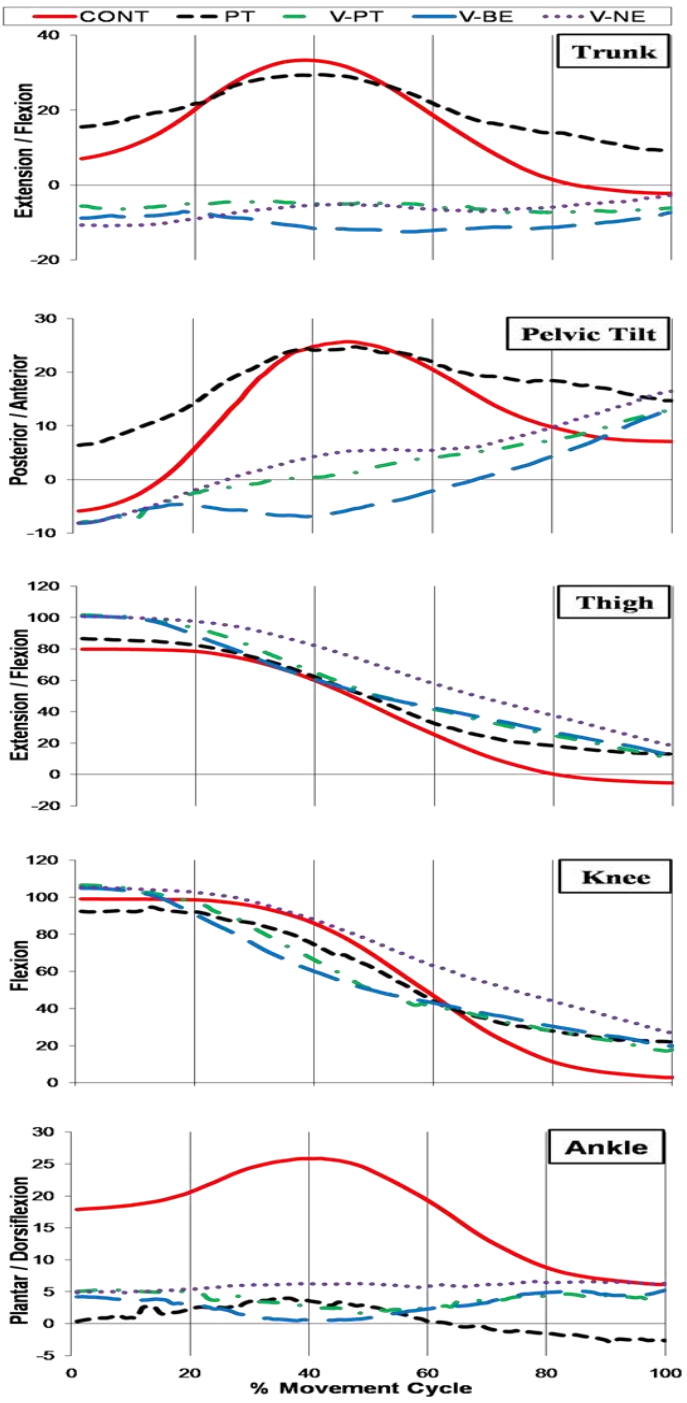

Figure 1: Sagittal-plane mean joint motion of the trunk, pelvis, thigh, knee and ankle during four conditions tested in patients recovering from a stroke. Normative sit-to-stand movement pattern displayed in RED.

Although the comparison of CMC values suggested that the PT condition most closely simulated CONT movement patterns at all joints compared to the device-assisted conditions, significant peak joint angle differences were identified in 10 of the 15 positions analyzed (Table 2). Within device-assisted conditions, the level of active participation of the clinician and patient primarily influenced movement profiles of the trunk, pelvis and ankle. CMC values suggest that the V-PT condition better approximated CONT trunk postures compared to V-BE and V- NE. The V-NE condition more closely simulated CONT pelvis and ankle postures compared to V-BE and V-PT.

CONCLUSIONS

Sit-to-stand movement patterns of individuals recovering from an acute stroke most closely simulated normal (CONT) when transfers were facilitated by the experienced clinician without use of the device. Further research is required to explore how movement patterns are influenced by use of alternate mechanical lift devices and clinicians of varying experience, fatigue levels, and anthropometrics. Additionally, the level of task-specificity (movement biofidelity) and repetition required to help patients relearn to move from a seated to standing posture independently has yet to be quantified. Given previous research indicating a 2.55 fold greater risk of back injury for clinicians performing >10 transfers/day [1], it is essential that techniques are identified to minimize clinician's risk while ensuring optimal patient outcomes.

REFERENCES

1. Campo M et al. *Phys Ther, 88,* 608-619, 2008.
2. McBride MM et al. *Online Proceeding ASB Annual Meeting:http://www.asbweb.org/ conferences/2009/pdf/931.pdf.*

ACKNOWLEDGEMENTS

This work was funded, in part, by Undergraduate Creative Activities and Research Experiences (UCARE) Program grants to AMH and BJB.

Table 2: Comparison of INITIAL, PEAK and FINAL joint positions during each condition to data recorded from individuals without pathology (CONT). Alpha level set at $p < 0.05$ (***** = No Significant Difference).

	Trunk	Pelvis	Thigh	Knee	Ankle
Start	PT>CONT>V-PT, V-BE, V-NE	PT>CONT	ALL>CONT	*	CONT>ALL
Peak	CONT>V-PT, V-BE, V-NE	CONT>V-PT, V-BE, V-NE	V-PT, V-BE, V-NE>CONT	*	CONT>ALL
Stop	PT>CONT	ALL>CONT	ALL>CONT	ALL>CONT	CONT>PT

The Influence of a Neuromuscular Training Program on Landing Mechanics while Fatigued

[1]Eric Greska, [1]Nelson Cortes, [1]Stacie Ringleb and [2]James Onate

[1]Old Dominion University, Norfolk, VA, USA
[2]Ohio State University, Columbus, OH, USA
email: egreska@odu.edu

INTRODUCTION

Anterior cruciate ligament (ACL) neuromuscular training programs have demonstrated positive effects in reducing ACL injuries. These studies included strength, flexibility, agility, and plyometric training to alter landing mechanics. Neuromuscular control strategies and biomechanical parameters are further altered when the effects of fatigue are present [1]. However, there is a lack of information regarding how training programs affect the neuromechanical aspect under a fatigued status. Therefore, the purpose of this study was to determine the effects of a neuromuscular training program on landing mechanics during a fatigued status while performing a sidestep cutting task.

METHODS

Lower extremity biomechanics of 12 female collegiate soccer athletes (19.2±0.8 years, 1.67±0.06 m, 60.2±6.5 Kg) were obtained after completion of a fatigue protocol at two sessions: pre and post training. The fatigue protocol consisted of four sets of a functional circuit that included: L-Drill, agility ladder, vertical jumps (80% of their maximum), and step-ups onto a 20-cm box. For the testing sessions, participants performed five trials of a sidestep cutting task at pre and post-training sessions. The task was displayed in a randomly unanticipated order through custom-made software. Twelve high-speed VICON cameras (Vicon Motion Systems Ltd, Oxford, UK) sampling at 270Hz and two Bertec Force Plates (Model 4060-NC, Bertec Corporation, Columbus, OH, USA) sampling at 1080Hz were used to track marker trajectory and ground reaction forces, respectively. From the standing (static) trial, a lower body kinematic model was created for each participant using Visual 3D (C-Motion, Rockville MD, USA). The kinematic model was used to quantify the motion at the hip, knee, and ankle joints. The standing trial with a circular motion of the pelvis was used to estimate a functional hip joint center [2]. Based on a power spectrum analysis, marker trajectory was filtered with a fourth-order Butterworth zero lag filter with a 7 Hz cutoff frequency, whereas ground reaction force data were filtered with a similar filter with a 25 Hz cutoff frequency. The training program spanned 10 weeks and consisted of resistance training twice a week, and agility and plyometric training twice a week, on non-consecutive days. Paired samples *t*-tests were conducted to assess fatigue differences between pre and post training for multiple instances during the stance phase of the sidestep cutting task. Alpha level set *a priori* at .05

RESULTS AND DISCUSSION

Multiple significant differences in kinematic data were presented over the instances of the stance phase (Table 1). A significant difference was found for hip flexion during initial contact (IC), peak knee flexion (PKF), peak vertical ground reaction force (PVGRF), peak posterior ground reaction force (PPGRF), and peak stance, displaying a greater amount of flexion about the hip post training while in a state of fatigue. A significant difference was displayed for the knee abduction angle at initial contact, changing from an abducted position prior to training, to an adducted position after training. Ankle flexion also demonstrated a significant difference from pre to post training during PKF, PVGRF, and PPGRF. The ankle presented was plantarflexed at pre training, and significantly increased its plantarflexion post training. Significant differences for kinetic variables are presented in Table 2. Posterior ground reaction force significantly increased from pre to post training during both the PVGRF and PPGRF stance phases. The knee extension moment at peak stance was

found to significantly increase between testing sessions.

The alterations in kinematic patterns demonstrates that the training program utilized within this study was able to elicit positive changes in relation to reducing the risk for incurring an ACL injury, even while in a fatigued status. This is an important factor as it has been pointed out that fatigue may negate any biomechanical changes brought about by neuromuscular training program aimed at preventing ACL injuries [3]. The increase in posterior ground reaction forces at PVGRF and PPGRF may be seen as a negative factor in preventing ACL injuries, but the overall increases were less than one times bodyweight. These kinetic increases may not increase the risk of incurring an ACL injury when coupled with the kinematic changes that occurred, allowing for an attenuation of the increased kinetic factors through neuromuscular control.

CONCLUSIONS

The neuromuscular training program demonstrated an effect on landing mechanics during a sidestep cutting task while in a state of fatigue. Decreased hip flexion and a heel-to-toe foot strike have both been implicated as factors that increase the risk of incurring an ACL injury [4]. Post training, the participants demonstrated increased hip flexion, as well as an increased plantarflexed ankle position, which may demonstrate that the training was successful in decreasing at-risk motion patterns even in a fatigue status.

REFERENCES

1. Mclean SG, Samorezov JE. *Med Sci Sports Exerc* **41**, 1662-1673, 2009.
2. Schwartz MH, Rozumalski A. *J Biomech* **38**, 107-116, 2005.
3. Renstrom P, et al. *Br J Sports Med* **42**, 394-412, 2008.
4. Cortes N, et al. *J Appl Biomech*. **23**, 289-299, 2007.

Table 1. Significant differences for kinematic variables. Angles measured in degrees.

	Pre-Training Mean±SD	Post-Training Mean±SD	*t*-score	Sig.	Effect Size (*d*)
Initial Contact					
Hip Flexion (+)/Extension (-)	27.91±8.89	41.10±10.02	-2.654	.022	1.39
Knee Abduction (-)/ Adduction (+)	-1.63±3.71	0.71±2.99	-2.459	.032	0.69
Peak Knee Flexion					
Hip Flexion (+)/Extension (-)	19.41±9.81	33.39±11.23	-2.673	.022	1.33
Ankle Dorsiflexion (+)/ Plantarflexion (-)	-4.18±2.95	-9.21±3.40	4.301	.001	1.58
PVGRF					
Hip Flexion (+)/Extension (-)	22.61±10.25	38.77±11.06	-3.117	.010	1.52
Ankle Dorsiflexion (+)/ Plantarflexion (-)	-1.54±3.57	-4.85±3.36	2.762	.018	0.96
PPGRF					
Hip Flexion (+)/Extension (-)	25.96±9.36	40.74±10.67	-2.886	.015	1.47
Ankle Dorsiflexion (+)/ Plantarflexion (-)	-2.30±4.95	-5.66±4.07	2.964	.013	0.74
Peak Stance					
Hip Flexion (+)/Extension (-)	29.15±9.21	42.57±10.63	-2.590	.025	1.35

Table 2. Significant differences for kinetic variables. Posterior ground reaction force measured in multiples of body weight.

	Pre-Training Mean±SD	Post-Training Mean±SD	*t*-score	Sig.	Effect Size (*d*)
PVGRF					
Posterior Ground Reaction Force	0.32±0.11	0.66±0.49	-2.594	.025	0.97
PPGRF					
Posterior Ground Reaction Force	0.68±0.16	0.95±0.37	-2.471	.031	0.98
Peak Stance					
Knee Extension (+)/ Flexion (-) Moment	1.91±0.31	2.21±0.54	-2.256	.045	0.67

LATERAL WEDGES REDUCE MEDIAL KNEE LOADING IN ASYMPTOMATIC, OBESE WOMEN

Elizabeth M. Russell and Joseph Hamill

University of Massachusetts, Amherst, MA, USA
email: erussell@kin.umass.edu

INTRODUCTION

Obesity is the primary modifiable risk factor for knee osteoarthritis [1]. The knee joint is the most frequent location for osteoarthritis due to its load-bearing requirements and osteoarthritis typically develops when the joint cannot respond to the magnitude or intensity of the loading stresses [2]. Increased body weight beyond "healthy limits" magnifies the loads on the knee joint and can lead to knee osteoarthritis [3], particularly at the medial compartment of the knee where the loads are greatest [4,5].

The external adduction moment is the biomechanical variable most frequently studied with knee osteoarthritis due to its strong correlation with the medial compartment load [5]. Laterally-wedged insoles are designed to shift the center pressure under the foot laterally and decrease this adduction moment arm. Even small (1 mm) shifts in the center of pressure under the foot can significantly decrease adduction moments and peak medial compartment loads by redistributing a portion of the load to the lateral compartment [6]. While lateral wedges have been used in a variety of populations with knee osteoarthritis, their efficacy for reducing risk factors for the disease has never been determined in asymptomatic, high-risk populations.

The purpose of this study was to examine if lateral wedges could reduce biomechanical risk factors for knee osteoarthritis in a high risk population: that is, obese women. We hypothesized that an 8^o lateral wedge would significantly reduce the peak external knee adduction moment and impulse of the adduction moment during walking.

METHODS

Eight obese (age = 26.9± 10.5; BMI = 34.8 ± 4.1 $kg{\cdot}m^{-2}$) and eight control women (age = 27.0 ± 8.9; BMI = 22.3 ± 1.2 $kg{\cdot}m^{-2}$) consented to participate in the study. Subjects were free of lower extremity injury and had not experienced a change in weight greater than 9 kg in the past five years.

Standing frontal plane knee angles were measured [7] to assess alignment. Subjects with moderate-severe varus or valgus malalignments were excluded from the study. Retroreflective markers were placed on anatomical landmarks of the right lower extremity and recorded (240 Hz) while subjects walked 10 times across a force platform (1200 Hz) at a standard speed of 1.25 $m{\cdot}s^{-1}$.

All subjects wore standard walking shoes and performed the 10 walking trials with and without a laterally-wedged insole. The insole was comprised of EVA material that was wedged 8^o along the entire length of the insole. All subjects wore the insole for 1 hour before data collection began.

Kinematic data were filtered at 8 Hz and kinetic data at 50 Hz. The externally-applied adduction moment and the impulse of the adduction moment were calculated as surrogates of medial compartment joint loading. Rather than only examining and making conclusions based on a discrete instance of the stride cycle, angular impulse gives a more complete overview of the time during which the medial compartment is loaded. For presentation, data were time-normalized to the stance phase of gait. Data are presented as group means and standard deviations. A two-way (group x condition) ANOVA was done ($p<0.05$) to compare differences between and among groups and conditions.

RESULTS AND DISCUSSION

The use of an 8° laterally-wedged insole significantly reduced the peak external knee adduction moment (Figure 1). The Control group reduced their average moment by 0.6 Nm ($p<0.01$) and the Obese group by 1.68 Nm ($p=0.025$).

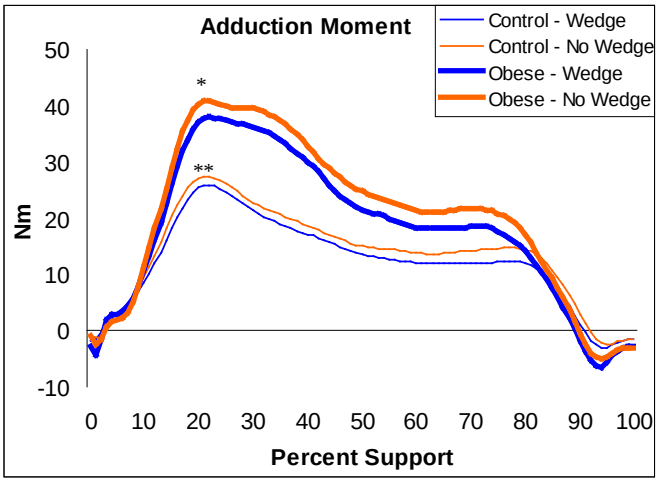

Figure 1: External knee adduction moment. * indicates significant differences between the wedge and no wedge conditions.

The lateral wedge also produced benefits over the course of the stance phase by reducing the angular impulse of the external knee adduction moment for the Control ($p<0.01$) and Obese ($p=0.016$) groups. (Figure 2). Thorpe et al. (8) reported higher values in individuals with knee osteoarthritis, even when peak moments did not differ.

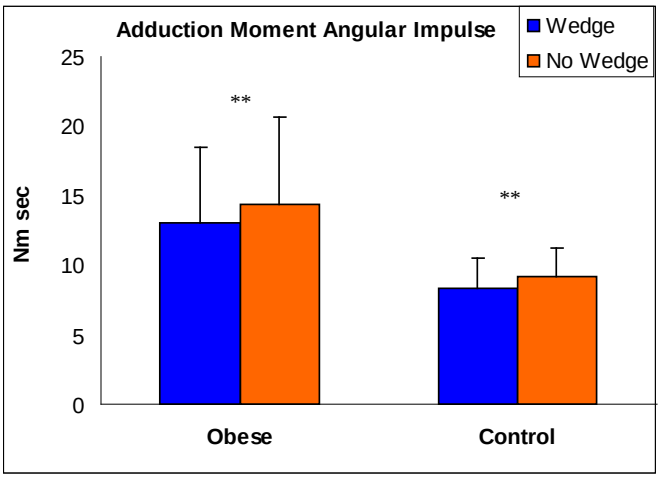

Figure 2: Angular impulse of the external knee adduction moment. Bars represent SD.

The obese group had significantly greater peak adduction moment and impulse values compared to the control group. This increased peak loading and increased load over the course of stance have been shown to contribute to knee osteoarthritis [8,9].

CONCLUSIONS

The goal of this study was to apply a prophylactic orthotic to reduce risk factors reported to influence the course of knee osteoarthritis in the most high-risk populations. An 8° lateral wedge was effective at reducing two of the suggested biomechanical risk factors for knee osteoarthritis. Given the susceptibility of obese, female populations to knee osteoarthritis and the efficacy of lateral wedges, particularly in the early stages of the disease, this protocol may be effective for unloading the medial compartment of the knee joint. These results serve as a foundation for future research designed to use laterally-wedged insole interventions as preventative strategies for knee osteoarthritis instead of temporary treatments.

REFERENCES

1.Felson DT, et al. *Ann Int Med* **109**, 18-24, 1988.
2.Radin EL, et al. *J Biomech* **15**, 487-492, 1982.
3.Felson DT, et al. *Arth Rheum* **41**, 1343-1355, 1998.
4.Andriacchi TP. *Orthop Clin North Amer* **25**, 395-403, 1994.
5.Zhao D, et al. *J Orthop Res* **25**, 789-797, 2007.
6.Shelburne KB, et al. *Clin Biomech* **23**, 814-821, 2008.
7.Vanwanseele B, et al. *Clin Orthop Rel Res* **467**, 504-509, 2009.
8.Thorp LE, et al. *Arth Rheum* **54**, 3842-3849, 2006.
9.Miyazaki T, et al. *Ann Rheum Dis* **61**, 617-622, 200.

ACKNOWLEDGEMENTS

The authors would like to thank Kasey Carley, Mia Santos and Stephanie Stark for help with data collection and analysis. Funding for this work was supported by an American Society of Biomechanics Grant-in-Aid Award.

Simulation detects changes in muscle activation in post-stroke gait after a functional electrical stimulation intervention

[1]Brian A. Knarr, [2]Trisha M. Kesar, [1]Erin Helm, [1,2]Darcy S. Reisman, [1,2]Stuart A. Binder-Macleod, [1,3]Jill S. Higginson
[1]Biomechanics and Movement Science, [2]Dept of Physical Therapy,
[3]Dept of Mech. Engineering, University of Delaware, Newark, DE, USA
email: bknarr@udel.edu

INTRODUCTION

Functional electrical stimulation (FES) has the capacity to alter muscle function when used as a tool for gait retraining in post-stroke individuals[1]. Typically, FES is applied to the ankle dorsiflexors (DF) during the swing phase of gait[2,3]. More recently, the use of FES has been extended to the ankle plantarflexors (PF) during pre-swing to increase pushoff forces[1]. A goal of the FES gait retraining program tested in the current study was to improve push off forces during pre-swing and foot clearance during swing, two common deficits in post-stroke gait, by delivering FES to ankle plantar- and dorsiflexors, respectively. Computer simulation studies can demonstrate the function of individual muscles in healthy[4,5] and post-stroke gait[6]. Identifying the functions of specific muscles during the gait cycle can be a useful method to assess and enhance gait retraining tools such as FES. Comparison of pre- versus post-training simulations can provide insights into the mechanisms by which gait retraining produces improvements in post-stroke gait function. Additionally, we posit that correlation between simulation results and clinical outcomes can provide validation for the accuracy of simulations a predictive tool. The objective of this study is to use subject-specific simulations to determine the changes in activation of the ankle plantar and dorsiflexor muscles in stroke patients after an FES gait retraining program.

METHODS

Eight subjects (age 63±8.6, 3 men, >6 months post-stroke) were recruited to participate in a 12-week FES gait retraining intervention, involving both plantar and dorsiflexor stimulation. All subjects signed informed consent forms approved by the Human Subjects Review Board at the University of Delaware. Self-selected speed walking data were collected on an instrumented split belt treadmill (Bertec Corp.) using an 8-camera Motion Analysis system pre- and post-intervention. Three-dimensional, forward dynamic simulations were created from walking trials using OpenSim[7]. The muscle activations and forces required to reproduce the experimentally measured gait kinetics and kinematics were computed using the Computed Muscle Control algorithm[8].

The medial gastrocnemious (MG), soleus, tibialis posterior (TP) and tibalis anterior (TA) muscles were analyzed in this study. For each muscle, we calculated percent activation (relative to full activation) for the full gait cycle and during the double support and swing phases. Differences between pre- and post-intervention for each muscle were evaluated using paired t-tests. Changes in percent activation post-intervention were tested for correlation with changes in peak knee flexion.

RESULTS AND DISCUSSION

Two simulations per subjects (16 total) were built from the trials at self-selected speed at the time of collection. Average post-intervention self-selected speed was 0.15 m/s faster than pre-intervention.

Soleus muscle activation for a single subject is shown in Figure 1. For this subject, a clear increase in peak activation during double support can be seen post-intervention. During the rest of the gait cycle, there is decreased activation of the soleus post-intervention. This new post-intervention muscle activation pattern is consistent with the timing of PF FES used during the intervention, which stimulated PFs only during pre-swing.

Averaged data for all 8 subjects was calculated for all four muscles during the gait phase of interest, i.e. during double support for the PFs and during swing phase for TA (Figure 2). Although there was an average increase in the total activation during the

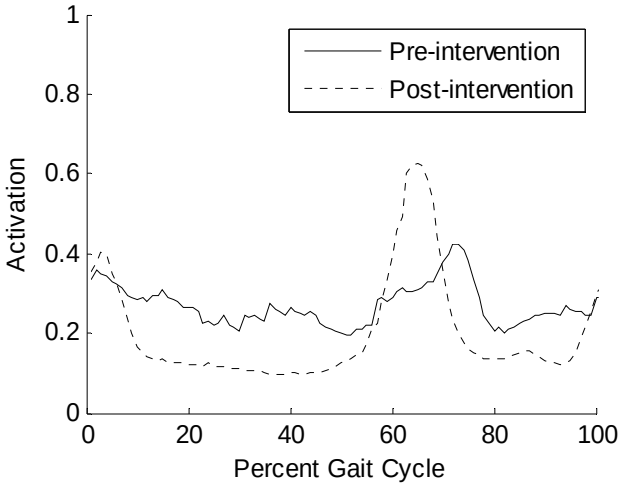

Figure 1. Average activation of the soleus muscle over the gait cycle for pre- and post-intervention.

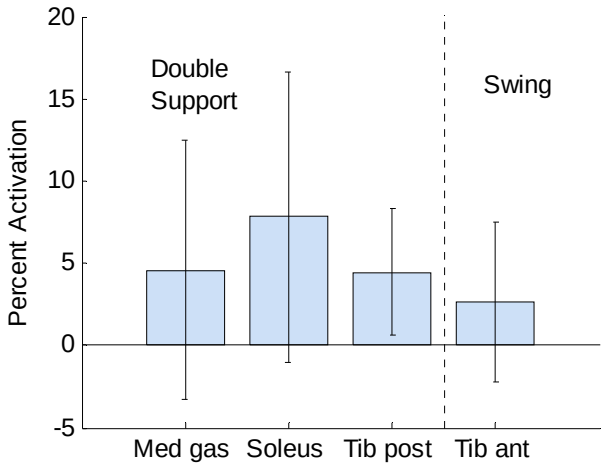

Figure 2. Change in activation percentage during double support / swing phase of gait from pre- to post-intervention.

gait phase of interest, this change is not significant, potentially due to innate variability between stroke subjects and a limited sample size. Soleus experienced the largest average change across subjects, at 7.8%, followed by 4.58%, 4.45% and 2.56% in the medial gastrocnemius, tibialis posterior, and tibialis anterior muscles, respectively. These average changes correspond to the application of FES during training. Although a trend of an average increase in activation was seen in the three PF muscles during double support (16.82% total increase), only a small average change was seen for these muscles over the full gait cycle (1.3% total). This suggests a change in the PF control pattern across the entire gait cycle, not just during the period of FES application.

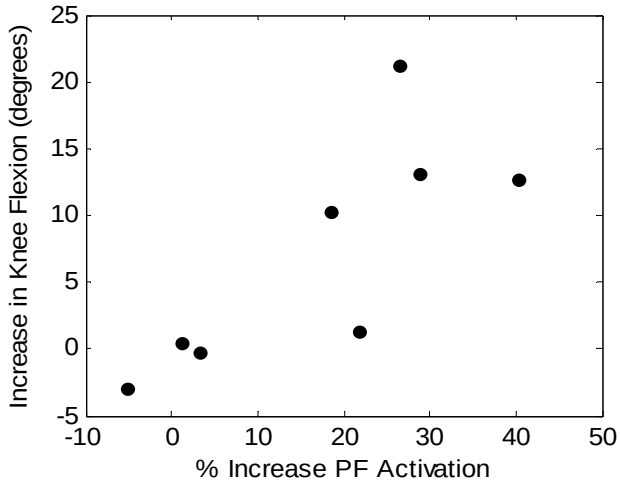

Figure 3. Increase in PF activation vs. increase in peak knee flexion from pre- to post-intervention.

Peak knee flexion during swing is hypothesized to increase with increases in PF activation during pre-swing as a result of greater forward propulsive forces[1]. Although no relationship was found between propulsive forces and changes in activation, those subjects who exhibited the greatest increases in knee flexion also had the largest percent increase in PF activation (Figure 3). This is noteworthy, as it demonstrates a correlation between model predictions and a clinically relevant gait variable measured pre- and post-intervention.

CONCLUSIONS

Notable differences can be seen in the control pattern used by stroke subjects as a response to FES intervention. Evidence of an improved control strategy during gait was seen in the activation of the PF muscles and is consistent with kinematic measures of gait performance. For the first time, muscle-actuated simulations were used to detect the effect of a gait retraining intervention on post-stroke muscle activation patterns.

REFERENCES

1. Kesar TM. *Stroke*. 2009;**40**:3821-3827.
2. Kottink AI. *Artificial organs*. 2004;**28**(6):577-86.
3. Kesar TM. *Physical Therapy*. 2010;**90**(1):55-66.
4. Neptune RR. *J Biomech.* 2001;**34**(11):1387-98
5. Zajac FE. *Gait and Posture*. 2002;**16**:215-232.
6. Higginson JS. *J Biomech*. 2006;**39**(10):1769-77.
7. Delp SL. *IEEE transactions on bio-medical engineering*. 2007;**54**(11):1940-50
8. Thelen DG. *J Biomech.* 2006;**39**(6):1107-15.

ACKNOWLEDGEMENTS

NIH NS 055383 NIH NR 010786

DEFICITS IN THE HEEL-RISE TEST IN PATIENTS WITH ACHILLES TENDON RUPTURES CAN BE EXPLAINED BY TENDON ELONGATION AND MUSCULAR WEAKNESS

[1]Karin Grävare Silbernagel, [1] Kurt Manal

[1]University of Delaware- Newark, DE, USA
Email: kgs@udel.edu

INTRODUCTION

Achilles tendon ruptures are common, especially in middle-aged individuals, and the incidence in both men and women is rising. Regardless if the tendon is treated surgically or non-surgically the calf musculature is found to have a strength deficit of 10-30% and this appears to become permanent. Another major complication is the tendon heals in an elongated position causing disproportionate weakness in the end-range of plantar flexion. Gait abnormalities have also been found 24 months after injury and believed to be associated with strength deficits and tendon elongation.

The heel-rise test is an often used measure of muscular endurance in clinical trials [1]. This test is simple, can easily be performed in the clinical setting and has been shown to be responsive to improvements over time as well as to discriminate between various treatment protocols. When combined with a portable device that measures heel-rise height and the number of repetitions the total amount of work performed can be calculated. In a recent study using this device we found that patients had significant deficits in the heel-rise after one year [2]. However it is important to understand if the deficit found is due to tendon elongation, muscle weakness or a combination since the suggested treatment is different.

We have begun to investigate if the deficit in muscular endurance during the heel-rise test is due to plantar flexion strength deficits and/or tendon elongation. Of interest is to determine if the results from the different parameters such as heel-rise height, repetitions and endurance can be used to determine the cause of the deficit.

METHODS

Two patients with Achilles tendon ruptures were evaluated with Ultrasound (US) and motion analysis for measuring the Achilles tendon length. Furthermore plantar flexion strength was evaluated using a dynamometer and muscular endurance was evaluated using our portable device during a heel-rise test. In addition data for 4 healthy adults subjects were included for comparison.

Measurement of Achilles tendon length

Achilles tendon length was defined as the distance between the insertion to the calcaneus (OTJ) and the musculotendinous junction (MTJ). An 8 camera Qualysis motion analysis system was used to record the position of markers attached on the US probe. US images were acquired using a 60 mm linear transducer (Aloka SSD-5000, Tokyo, Japan).

Measurement of strength

Plantarflexion (PF) strength was evaluated using a Biodex System 3 (Biodex Medical Systems, Shirley, New York) dynamometer. Data were sampled at 1000 Hz and analyzed off-line. The patients were seated in the dynamometer with the knee fully extended. Three volitional maximal isometric PF efforts of 3 second duration were collected at 10° dorsiflexion (DF) and 10° PF.

Measurement of heel-rise

The heel-rise test was performed with the participant standing on an incline placing the ankle in 10° DF Figure 1). The subject was instructed to go as high as possible on each heel-rise and then lower the heel to the starting position at a frequency of 30 repetitions/min. The subject was asked to perform as many heel-rises as possible. The MuscleLab (Ergotest Technology) measurement system was used for the evaluations. A linear encoder with a spring-loaded string is connected to a sensor inside of the unit was attached to the heel

(Figure 1). The maximal height of the heel-rise was documented as well as the total work in joules.

Figure 1: The heel-rise test with the linear encoder attached to the heel of the shoe.

RESULTS AND DISCUSSION

Both patients had a heel-rise endurance deficit (69% and 56%) on the injured side compared to the uninjured side. The maximal heel-rise height was less on the injured sides (7.8 and 5 cm respectively) and the side to side differences in the number of repetitions were 5 and 12 respectively. The Achilles tendon had healed in an elongated position for both patients with a side to side difference of 4 cm (Figure 2). For the patient with the greater difference in heel-rise height but less of a difference in number of repetitions the strength evaluation revealed no deficit in 10° of dorsiflexion (Figure 3). For the other patient who had less of a heel-rise height difference but a greater difference in heel-rise repetition the strength test revealed a 30% deficit in 10° of dorsiflexion (Figure 3). Both patients had strength deficits (31%) in 10° of plantarflexion (Figure 2). For healthy individuals there were no differences in tendon length, heel-rise height or endurance (Figure 2).

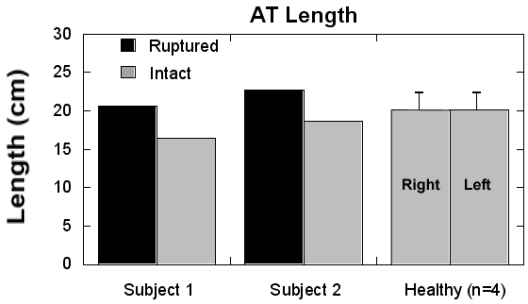

Figure 2. Measure of Achilles tendon length in patients and healthy individuals.

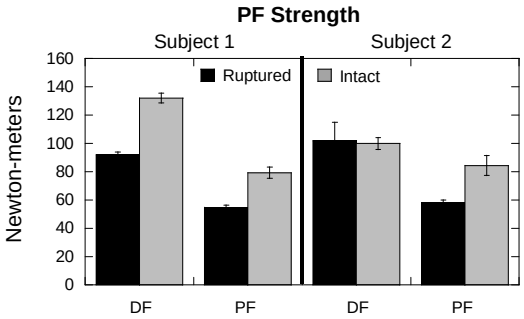

Figure 3. Plantarflexion strength in 10° of dorsiflexion and 10° of plantarflexion.

Our results indicate that the deficit in heel-rise endurance for subject 1 could be explained by tendon length but not due to a strength deficit while subject 2 a combination of tendon elongation and strength deficit are likely associated with the deficit. It appears that differences in the heel-rise height parameter are primarily explained by tendon length whereas the heel-rise repetition parameter is primarily explained by muscle strength.

CONCLUSIONS

Evaluating the height, repetition and muscular endurance during a heel-rise test provides valuable information regarding the reasons for deficits seen in patients with Achilles tendon rupture. Using this heel-rise test method in clinical trials might then give further information regarding the reasons for the short and long term outcomes. Future treatments can then be designed specifically to address the patients' deficits.

REFERENCES

1. Hébert-Losier K. *J Sci Med Sport* **12**, 594-602, 2009.
2. Silbernagel KG: *Knee Surg Sports Traumatol Arthrosc* **18,** 258.264, 2010.

EFFECTS OF CONTINUOUS PASSIVE MOTION ON LOWER EXTREMITY HYPERTONIA IN CHILDREN WITH CEREBRAL PALSY

[1]Hsin-Yi Kathy Cheng, [2]Yan-Ying Ju and [1]Pao-Wen Guan

[1]Graduate Institute of Early Intervention, Chang-Gung University, Tao-Yuan, TAIWAN
[2]Graduate Institute of Physical Therapy, Chang-Gung University, Tao-Yuan, TAIWAN
email: kcheng@mail.cgu.edu.tw

INTRODUCTION

Statistics showed that 70 to 80 percent of patients with cerebral palsy have spastic clinical feature, and the affected limbs often demonstrated muscular hypertonia and abnormal gait [1]. To avoid musculoskeletal deformities and improve gait characteristics in children with cerebral palsy, managing muscular hyperactivity is an important treatment goal. Recently researchers have found decrement of muscle hypertonia after continuous passive motion (CPM) treatment in patient with stroke and spinal cord injuries [2, 3]. Similar to stroke and spinal cord injury, cerebral palsy was also characterized with upper motor neuron lesion. However to date, no such application has been applied to children with cerebral palsy. The purpose of this study was to investigate the effects of CPM on lower extremity hyperonia in children with cerebral palsy. We hypothesized a decrease in muscle hypertonia and an improvement in ambulatory function could be found following CPM intervention.

METHODS

This study implemented a quasi-experimental design. A total of 10 children with spastic cerebral palsy with six–minute walking ability with or without assistive devices between ages 6-12 were included. All the subjects had hypertonia confirmed by Modified Ashworth Scale (MAS) scores at knee extensors greater than 1. Subjects were recruited from local hospitals and the informed consent was in accordance with institutional review board procedures at Chang-Gung Memorial Hospital. Subjects with the following conditions were excluded: 1) received lower extremity operation within 6 months; 2) received lower extremity Botox injection within 6 months; 3) knee joint contracture over 10 degree. Those who were taking oral anti-hypertonia medication such as baclofen were asked not to take any within 24 hours before the experiment.

All subject received CPM to the knee joints with angular velocity of 15 and 0 degree per second for 20 minutes, with a one-week interval between the two CPM interventions. Angular velocity of 15°/s was the experimental condition. The cyclic knee excursion was set between flexion 20° to 100°. For the control condition, subjects sat on the CPM device with both knees rested at 60° flexion for 20 minutes. The orders of the tests were counter-balanced. The control group could help distinguish a real tone-reducing effect caused by CPM movement from an effect caused by merely a 20-minute muscle relaxation. Variables measured included the Relaxation Index (RI) of the pendulum test of knee joints, the MAS scores, passive range of motion (PROM) of the knee joints, plus the timed up-and-go (TUG) and the 6-minute walking test (6MWT) for lower extremity functional evaluation. Electromyography (EMG) of the leg muscles were monitor during the intervention to ensure no active muscle involvement. The knee joint angle was monitored by electrogoniometer (SG65, Biometrics Ltd. USA) and collected via Biopac system with further analysis with Acqknowledge software (Biopac system, Inc., Santa Barbara, CA, USA). Each of these variables was measured before and after each CPM intervention.

All data were analyzed using SPSS version 17.0 (SPSS Inc., Chicago, IL, USA) statistical software. Descriptive statistics were used to calculate the means and standard deviations of the subject's demographics. Friedman two-way analysis of variance (ANOVA) by ranks was used to analyze if the MAS scores have changed. All other measurements were analyzed with two-way ANOVAs with repeated measures on velocity (15°/s and 0°/s) and timing (pretest and posttest). The level of significance was set at $p < 0.05$.

RESULTS AND DISCUSSION

Five girls and five boys participated this study, with an average age of 8.28±2.42 years, height 135.62± 10.23 cm. As expected, the EMG of leg muscles revealed that the muscles did not participate actively during the intervention. The Friedman ANOVA by ranks showed a statistically significant decrease of MAS scores (χ^2=9.25, $p<0.05$). The MAS score after CPM at 15°/s was 1.08±0.51. The minimum significant difference for all pairwise contrasts indicated that differences existed between the MAS score measured after CPM at 15°/s and the MAS scores measured at three other timings.

Statistical significances were also found for RI values (Fig. 1). Post-hoc Tukey test revealed that the differences existed between the RI measured after CPM at 15°/s and three other RIs. No significant difference was found among PROM measurements. As for the ambulation tests, both TUG (Fig. 2) and 6MWT (Fig. 3) demonstrated statistically significant improvements ($p<0.05$). Post-hoc Tukey also revealed that the differences were found between the values measured after CPM at 15°/s and three values measured at other timings.

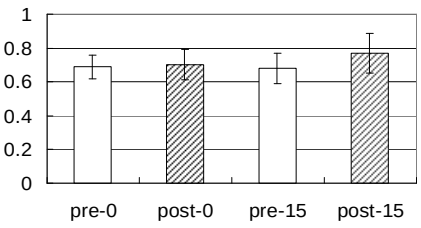

Fig.1 RI values for 4 measurement timings

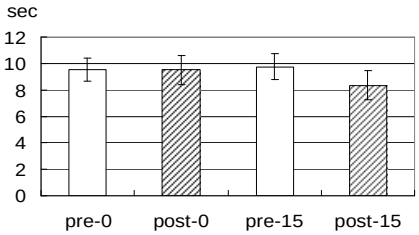

Fig.2 TUGs for 4 measurement timings

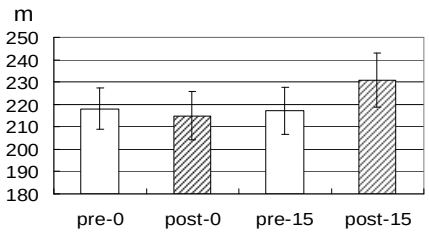

Fig.3 6MWT for 4 measurement timings

The MAS evaluates overall hypertonia and is commonly used for testing the efficiency of treatment in clinics. Our results demonstrated that CPM on the knee joint reduced the MAS score in the children with cerebral palsy. In stroke patients, it was also demonstrated that repeated passive movement induced a decrease in spastic hypertonia through a combination of reflexive and mechanical factors [4]. Since a good correlation was found between the severity of spasticity measured by the MAS and the RI measured with pendulum test [5], the significantly improved RI scores found in this study, like the results for MAS scores, supported that CPM could be effective in managing hypertonia.

No difference was found for PROM in the current study. The authors intended to avoid CPM excursion to the end range of knee joint to avoid the involvement of stretch effects. Therefore the results of PROM indicated that CPM at 15°/s did not contribute to muscle lengthening.

The authors included the TUG and 6MWT for the purpose of evaluating the immediate effect of CPM intervention on subject's ambulation. Since existing hypertonia of the lower extremity in children with cerebral palsy often disturbed their gait characteristics and performance, it was expected that decreased hypertonia would improve ambulatory function. The results of TUG and 6MWT provided a direct evidence of the contribution of hypertonia and its influence on ambulation.

CONCLUSIONS

The current study demonstrated that CPM to the knee joint at an angular velocity of 15°/s for 20 minutes decreased muscular hypertonia and improved ambulatory function in children with cerebral palsy. Whether the effects would last for a longer period of time and demonstrate clinical significance need further investigation.

REFERENCES

1.Krigger KW. *Am Fam Physician* 73, 91-100, 2006.
2.Wu CL, et al. *Kaohsiung J Med Sci* 22(12), 610-616, 2006.
3.Chang YJ, et al. *Clin Rehabil* 21, 712-718, 2007
4.Davies JM, et al. *Disabil Rehabil* 18, 83–90, 1996.
5.Fowler EG, et al. *Dev Med Child Neurol* 42, 182-189, 2000.

ALTERED INTER-JOINT COORDINATION DURING WALKING IN PATIENTS WITH TOTAL HIP ARTHROPLASTY

Shiu-Ling Chiu and Li-Shan Chou

Department of Human Physiology, University of Oregon, Eugene, OR, USA
E-mail:chou@uoregon.edu

INTRODUCTION

Total hip arthroplasty (THA) is a common surgery for a deteriorated hip joint to effectively regain its functions. Patients underwent THA are reported to have a higher risk of falling due to the residual deficits in balance control and joint function [1]. Previous gait analyses of THA patients were mainly focused on the kinematics and kinetics of individual joint. However, human gait is a complex task requiring a precise end point motor control that is accomplished by a multi-joint coordination. Inconsistency in such coordination may induce gait deviations [2]. Investigating the inter-joint coordination during gait would help us to identify changes in neuromuscular control strategies due to hip joint dysfunction. The purpose of this study was to investigate the patterns and variability of inter-joint coordination for both surgical and non-surgical limbs of THA patients during walking.

METHODS

Thirty adults were recruited and divided into two groups in this study. Twenty patients underwent unilateral THA (15 male, 5 female, age = 56.5 ± 5.4 yrs, BMI = 32.6 ± 4.0 kg/m^2), and 10 subjects served as age-matched controls (5 male, 5 female, age = 59.9 ± 5.3 yrs, BMI = 26.3 ± 3.9 kg/ m^2). THA patients were tested three times at pre-surgery, 6-weeks and 16-weeks post surgery, respectively. All patients received the same un-cemented Zimmer hip implants and followed the same physical therapy regimens during the study period. Control subjects were tested twice with one month apart.

An eight-camera motion analysis system (Motion Analysis Corp., Santa Rosa, CA) was used to collect the whole body motion during level walking at self selected pace. A total of 29 reflective markers were placed on bony landmarks. Joint kinematics of the bilateral lower extremities was calculated by using OrthoTrak kinematic analysis software (Motion Analysis Corp).

Continuous related phase (CRP), which is derived from the phase portraits of two adjacent joints, was used to investigate the inter-joint coordination pattern and variability [3]. Between groups differences in CRP pattern were examined by using cross-correlation measures and root-mean-square (RMS) difference to compare the ensemble mean curves of THA group to the controls. The variability of coordination for each subject was calculated as average standard deviation of every point on the ensemble CRP curve over a stride, namely deviation phase (DP). A mixed-model analysis of repeated measures was used to analyze the effects of groups and time on DP. If significant differences are detected, a post-hoc analysis with gait velocity as a covariate was performed to further examine the role walking speed on detected group differences. Significance level was set at 0.05.

RESULTS AND DISCUSSION

At pre-surgery and 6-week post surgery, gait velocities of THA group (1.05 ± 0.25 m/s and 1.09 ± 0.22 m/s, respectively) were significantly slower than that of the controls (1.29 ± 0.17 m/s) ($p<0.01$). However, no significant differences were detected between two groups at 16-week post surgery. Significant time effects on gait velocity were detected in THA patients at 16-week post surgery (1.23 ± 0.15 m/s) when compared to pre-surgery and 6-week post surgery ($p<0.005$).

RMS differences for hip-knee and knee-ankle CRP decreased gradually after THA surgery for both surgical and nonsurgical limbs (Fig. 1). The surgical limb remained a greater RMS difference than nonsurgical limb at 6- and 16-week post surgery.

Cross-correlation measures were overall strong for CRP patterns of both limbs, with r^2 values greater than 0.94, and were improved after surgery (Fig. 2).

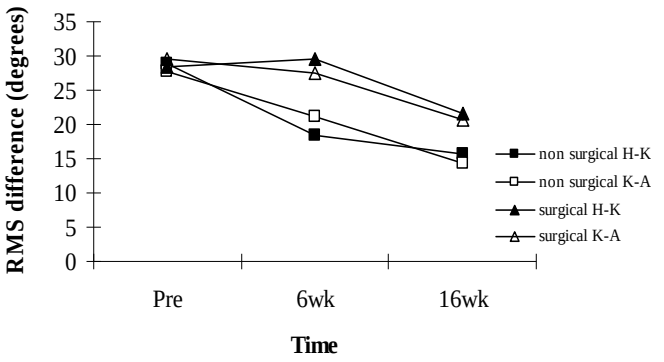

Figure 1: RMS differences (degrees) for CRP patterns between controls and THA.

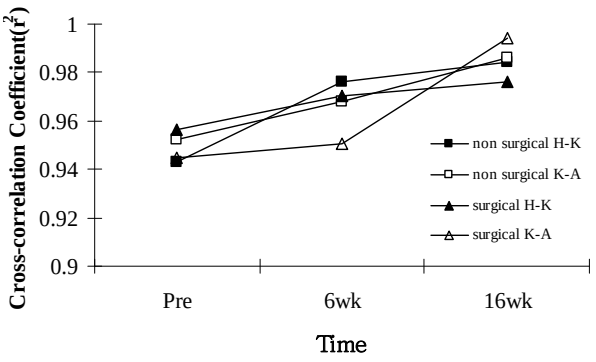

Figure 2: Cross-correlation (r^2) for CRP patterns between controls and THA

The variability for CPR is shown in Table 1. The surgical and nonsurgical limbs of THA group had higher DP values comparing to the controls at pre-surgery and 6-week post surgery. Of the surgical limb, significant group differences in hip-knee DP values were detected at pre-surgery, and significant group differences in knee-ankle DP values were detected at both pre-surgery and 6-week post surgery. Compared to pre-surgery, significant time effects on THA patients were detected in hip-knee DP values at 16-week post surgery for both limbs, and in knee-ankle DP values at 16-week post surgery for surgical limb.

CONCLUSIONS

Our results suggest that adjustments in inter-joint coordination of THA patients occurred at both surgical and nonsurgical limbs in responses to a deteriorated hip joint. The hip-knee and knee-ankle coordination demonstrated a higher variability to compromise this constrained hip joint, especially in the surgical limb. Asymmetric changes in accommodations and variability of bilateral lower extremities may contribute to the residual gait problems observed in THA patients. Therefore, clinical efforts may exert to improve the inter-joint coordination in this population.

REFERENCES

1.Majewski, M., et al. *J Bone Joint Surg [Br]* **87**, 1337-1343, 2005.
2.Winter, DA. *Phys Ther*. **72**, 45-53, 1992.
3.Burgess-Limerick, R, et al. *J Biomech* **26**, 91-94, 1993.

ACKNOWLEDGEMENTS

Assistances from Hao-Ling Chen, Ph.D., Ms. Crystal Mills, Brian Jewett, MD, and Dennis Collis, MD are greatly appreciated.

Table 1: DP values for CRP curves of controls and THA

	Controls	THA					
		Non surgical			Surgical		
		Pre-surgery	6-week post surgery	16-week post surgery	Pre-surgery	6-week post surgery	16-week post surgery
Hip-Knee	30.63 (7.22)	41.14 (17.87)	40.05 (28.79)	26.98 †# (10.63)	53.38 * (25.83)	45.44 (25.17)	30.98 †# (11.30)
Knee-Ankle	38.47 (6.32)	48.32 (18.93)	47.14 (25.65)	37.81 (21.58)	63.76 * (27.23)	53.59 * (21.04)	42.62 †# (15.52)

* significant group difference; † comparing to pre-surgery; # comparing to 6-week post surgery

KINEMATIC ANALYSIS OF FIVE CARDIOVASCULAR EXERCISES

[1]Thad W. Buster, [1]Adam P. Taylor, [2]Mathew Frazier, [1]Judith M. Burnfield
[1]Madonna Rehabilitation Hospital, Institute for Rehabilitation Science and Engineering, Lincoln, NE
[2]Creighton University, Omaha, NE
email: jburnfield@madonna.org, web: http://madonna.org/research_institute

INTRODUCTION

Cardiovascular (CV) exercise remains a key component of national health efforts aimed at preventing chronic and secondary medical complications in people of all abilities. While there are several equipment options available for use, a variety of individual factors (e.g., fitness goals, physical impairments) can complicate selection of appropriate training devices. A clear understanding of the biomechanical demands imposed by common CV exercise equipment should help guide device selection. In our previous work [1-3], we highlighted how muscle effort (peak, mean, duration) varied across five commonly performed cardiovascular exercises. The purpose of the current study was to explore lower extremity sagittal plane kinematic demands arising during the same cardiovascular exercises.

METHODS

Ten individuals (19-31 years of age; 6 male) with no known musculoskeletal or neurological disorders participated in a multi-session study. During the first three sessions, subjects walked and jogged on a treadmill (**TW** and **JG**; Life Fitness™ 97Ti) and trained on an elliptical cross-trainer (**EL**; Life Fitness™ 95Xi), recumbent bicycle (**RB**; Life Fitness™ 95Ri), and stairstepper (**SS**; Life Fitness™ 95Si) for familiarization purposes. During the fourth session, dominant limb lower extremity kinematics (Motion Analysis, Santa Rosa, CA) were recorded as subjects performed each exercise at a self-selected speed. All activities were performed for three minutes in a randomized order and data were recorded during the final minute. Footswitch (TW and JG) and footplate kinematics (EL, RB, and SS) defined movement cycle (MC) phasing. MCs were defined by the instant of heel contact to the next ipsilateral heel contact (TW & TJ) and the most anterior (EL), posterior (RB), and superior (SS) footplate positions to their next respective positions. Peak flexion and extension angles that occurred throughout the movement cycle were identified for each activity at the hip, knee and ankle.

STATISTICAL ANALYSIS

Separate one-way analysis of variance (5 x 1 ANOVAs) with repeated measures determined if peak angles varied significantly across the five conditions at each joint.

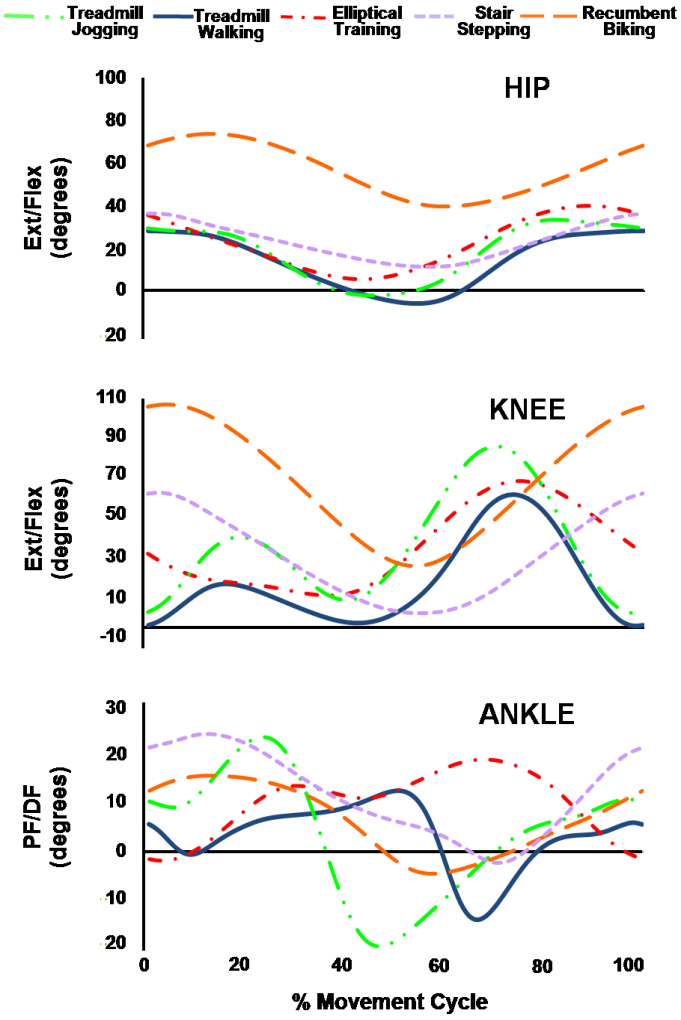

Figure 1. Ensemble averaged (mean) kinematic plots of sagittal plane hip, knee, and ankle motion while performing cardiovascular exercises (n=10).

RESULTS AND DISCUSSION

Kinematic profiles for each exercise activity are presented in Figure 1. At the *hip,* all activities started in flexion which lessened to a nadir during the middle of the MC and then progressively increased prior to the MC's termination. The hip's arc of motion was greatest during EL (49º) and shallowest during SS (34º). Peak hip flexion and extension demands varied significantly across activities (Table 1). At the *knee,* three movement patterns were apparent. TJ and TW displayed characteristic bimodal profiles. Following near full extension at initial contact, rapid flexion preceded the first flexion peak during early stance that approximated ½ to ⅓ the amplitude of the respective second peak that occurred during swing. Nearly full knee extension was achieved prior to the next initial contact. In contrast, RB and SS displayed unimodal patterns. Peak flexion occurred close to onset of the MC. Maximal extension was achieved at approximately ⅔ of the MC. The EL movement profile was a hybrid of the two previous patterns. The knee started in approximately 35º of flexion and then extended until approximately 36% of the MC at a rate more gradual than that occurring during the single limb support period of TW and TJ. Knee flexion in the latter half of the MC most closely approximated that of walking. The largest arc of knee motion occurred during TJ (78º), while EL required the smallest arc (59º). Peak knee flexion and extension demands varied significantly across exercises (Table 1). *Ankle* movement profiles appeared disparate across activities although a close examination suggests some similarities. TJ and TW cycles were initiated with brief motion towards plantar flexion, followed by progressive dorsiflexion as body weight progressed across the foot. A rapid plantar flexion wave characterized the stance-swing transition followed by achievement of a dorsiflexed ankle during swing. SS and RB demonstrated unimodal patterns. Maximal dorsiflexion occurred in early stance and maximal plantar flexion was achieved in the latter half of the MC. During EL, the ankle remained primarily in DF, with the pattern in early stance somewhat approximating that achieved during walking. TJ necessitated the greatest arc of sagittal plane ankle motion (44º), while RB required the shallowest (22º). Peak plantar flexion and dorsiflexion demands varied significantly across activities (Table 1).

CONCLUSIONS

The significant variations in motion demands documented across cardiovascular exercises in the current study provide empirical data to guide selection of exercise interventions to promote therapeutic goals. For example, if full hip extension induces undesirable pain, then RB and SS may provide opportunities to achieve cardiovascular goals while minimizing pain. Alternatively, the gentle repetitive stretch on anterior capsule structures during EL may offer a means for progressively elongating a flexible hip flexion contracture. Further research exploring the application of select cardiovascular exercises on reducing range of motion impairments is warranted.

REFERENCES

1. Takahashi S et al. *Supp to MSSE,* 39(5): S255.
2. Burnfield JM et al. *Supp to MSSE,* 41(5): S568-569.
3. Buster TW et al. *Supp to MSSE,* 41(5): S569.

ACKNOWLEDGEMENTS

The authors are grateful for the support provided by the Daniel's Fund (Denver, CO).

Table 1. Comparison of peak flexion/extension angles achieved at hip, knee and ankle during cardiovascular exercise. Note: positive values (+) = flexion or dorsiflexion; negative values (-) = extension or plantar flexion.

	Peak Position	RB	EL	SS	TJ	TW	Significant Main Effect
HIP	Flexion	96 (13)	54 (5)	48 (8)	44 (3)	38 (4)	RB > TJ, TW; EL > TW
	Extension	51 (10)	5 (4)	14 (6)	-4 (6)	-9 (5)	TW, TJ, EL > RB; TW > SS
KNEE	Flexion	107 (5)	71 (3)	66 (10)	87 (9)	65 (4)	RB > TJ > EL, SS, TW
	Extension	29 (9)	12 (4)	6 (8)	6 (4)	-2 (4)	TW > SS, TJ, EL > RB
ANKLE	Dorsiflexion	17 (10)	25 (6)	25 (7)	24 (3)	13 (3)	EL, SS > TW
	Plantar Flexion	-5 (6)	-4 (4)	-4 (7)	-20 (7)	-15 (5)	TJ, TW > RB, EL, SS

IS ANKLE INSTABILITY A CENTRAL OR PERIPHERAL ISSUE?

[1]Gregory M. Gutierrez and [2]Thomas Kaminski

[1]New York University, New York, NY, USA
[2]University of Delaware, Newark, DE, USA
email: gmgutierrez@nyu.edu

INTRODUCTION

Lateral ankle sprains are among the most common orthopedic injuries and typically involve a hyper-supination of the ankle. The disruption of the lateral ligament complex is a frequent corollary to residual symptoms, including mechanical instability, pain, weakness, swelling, and/or recurrent sprains, which can affect up to 72% of the patients [1]. These individuals are considered to have a subsequent pathology known as ankle instability (AI). AI is a costly public health concern and has been studied for many years, yet we know little about the mechanism behind it.

AI was first described by Freeman et al. [2] and they proposed that the mechanism was one of articular deafferentation from the initial injury, which would theoretically affect closed-loop (feedback/reactive) neuromuscular control, but recent research has called that theory into question. It has been speculated that open-loop (feedforward/preparatory) mechanisms may play a more significant role in the development of AI [3]. To further complicate the issue, it is also unknown whether these deficits occur in the central (eg. central inhibition) or peripheral (eg. damage to the peripheral structures) nervous system. There is evidence of altered peripheral nervous function [4], but recent research has suggested the deficits are central in nature [5]. Therefore, the purpose of this work was to evaluate individuals with bilateral and unilateral AI, those with a history of sprains with no AI, and uninjured controls, in terms of open- and closed-loop neuromuscular control when subjected to a supinating perturbation during landings.

METHODS

Twenty subjects (Table 1) gave informed consent to participate in this research and were placed into one of 4 groups dependent on ankle health history, as follows: 5 individuals with bilateral ankle instability (BIAI), 5 individuals with unilateral ankle instability (UNIAI), 5 individuals who have a unilateral history of ankle sprain without AI (UNILAS), and 5 bilaterally uninjured controls (CONT). Ankle health was determined with a ankle injury history questionnaire and the Cumberland Ankle Instability Tool (CAIT) [6].

To assess preparatory and reactive neuromuscular control during dynamic activity, a kinematic and EMG analysis of a landing on a specially designed supinating platform was performed. The device and jump landing technique are described elsewhere [7]. Electrodes were placed on the tibialis anterior (TA), peroneus longus (PL), rectus femoris (RF), and biceps femoris (BF) bilaterally. Retro-reflective markers were placed directly on the skin of the lower extremities in order to establish anatomical coordinate systems for the pelvis, thighs, shanks, and feet. The heel counters of several pairs of shoes were cut out so that proximal and distal calcaneal markers could be fastened directly to the skin, which allowed better monitoring of subtalar motion, specifically in the frontal plane.

Subjects performed a total of 22 drop landings on both limbs, with the test limb landing on the supinating device, including 6 supinating and 16 non-supinating trials, in a specified order (to maximize time between supinating trials) unknown to the subject. Both limbs were tested in all subjects, with the more affected limb tested first (coin flip used to determine first test limb for the CONT group). All EMG data were bandpass filtered (2^{nd} order, zero-lag, Butterworth filter, with f_c = 20-300 Hz), rectified, and smoothed with a low-pass filter (2^{nd} order, zero-lag, Butterworth filter, with f_c = 7 Hz). EMG data were normalized to the maximum activity during the non-supinating trials

in each respective muscle. The pre-touchdown (preparatory) time period was defined as 200 ms prior to touchdown, while the post-touchdown (reactive) time period was defined as 200 ms following the instant of touchdown. Dependent variable included: preparatory and reactive average EMG for the TA & PL, and ankle joint angles at touchdown and at 200 ms post touchdown. A 4 x 2 x 2 (Group x Condition x Limb) mixed MANOVA was used.

RESULTS AND DISCUSSION

The statistical test revealed a significant main effect for condition. Specifically, the supinating platform caused significantly more plantarflexion (~5°), abduction (~5°), and inversion (~9°) at the ankle 200 ms post touchdown, which coincided with significantly more activity of the PL (~8%). This demonstrates the stretch reflex in action, which responded to the perturbation by increasing activation in an attempt to control excessive rotation.

Contrary to current theories [3], no differences were noted in preparatory activity between groups. Several trends were noted which may result in significance with more statistical power (ie. more subjects). Subjective questioning of the subjects indicated that the experimental protocol was novel. Therefore, there is a distinct possibility that subjects were behaving in a protective fashion (especially those with AI), due to the potential risk of injury associated with a forced supination, even though they moved within a normal range-of-motion. This theory is partially supported by a Condition x Group interaction noted for reactive PL activation, which indicates the groups responded to the perturbation differently. Specifically the BIAI and UNIAI groups had significantly greater reactive PL activity in the supinating trials than the UNILAS and CONT groups (Figure 1). When combined with the fact that both limbs in both AI groups behaved similarly, these results support the theory that AI is a centrally derived dysfunction. More specifically, the UNIAI group behaved similarly to the BIAI group with both their limbs (ie. including their "non-affected" limb), which suggests that there may be central inhibition in these individuals. Further, the UNILAS group behaved similarly to the CONT group, which signifies this group deserved future research, as they may hold the key to understanding how to rehabilitate individuals following an ankle sprain, such that they do not develop AI.

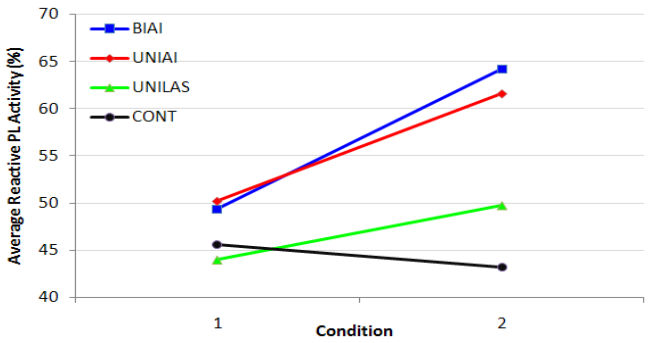

Figure 1: Group x Condition interaction for reactive PL activity; Condition 1 = non-supinating trials, Condition 2 = supinating trials.

REFERENCES

1. Hertel J. *Sports Med*, **29**, 361-371, 2000.
2. Freeman MA et al. *J Bone Joint Surg Br*, **47,** 678-685, 1965.
3. Gutierrez GM et al. *PM R*, **1**, 359-365, 2009.
4. Kleinrensink GJ et al. *Med Sci Sports Exerc*, **26**, 877-883, 1994.
5. Hass CJ et al. *Am J Sports Med*, [ePub], 2010.
6. Hiller CE et al. *Arch Phys Med Rehabil*, **87**, 1235-1241, 2006.
7. Gutierrez GM & Kaminski TW. *J Appl Biomech*, **26**, 114-121, 2010.

ACKNOWLEDGEMENTS

Matthew Hinsey, Brittany Kozitzki, and On-Yee Lo are acknowledged for the assistance with data collection and processing.

Table 1: Subject Demographic Information (mean ± SD)

Group	Gender Distribution	Age (yrs)	Height (m)	Weight (kg)	Exercise Participation (hrs/day)
BIAI	2M / 3F	20.2 ± 1.5	1.76 ± 0.07	71.1 ± 8.1	2.0 ± 0.7
UNIAI	0M / 5F	19.8 ± 0.8	1.63 ± 0.07	62.1 ± 5.4	1.3 ± 0.4
UNILAS	1M / 4F	21.2 ± 3.8	1.67 ± 0.09	66.6 ± 9.6	1.2 ± 0.7
CONT	2M / 3F	19.8 ± 1.3	1.69 ± 0.12	67.5 ± 18.9	1.2 ± 0.3

Neuro-mechanical and Clinical Outcome of Stroke Rehabilitation of Ankle Impairments through Passive Stretching and Active Movement Training

[1]Genna Waldman, [1]Yi-Ning Wu, [1]Yupeng Ren, [2]Yue Li
[3]Liang Wang, [1]Xin Guo, [1,2]Elliot J. Roth, [1,2] Li-Qun Zhang

[1]Northwestern University, Chicago, IL, USA
[2]Rehabilitation Institute of Chicago, Chicago, IL, USA
[3]Illinois Institute of Technology
Email: l-zhang@northwestern.edu

INTRODUCTION

Spasticity, contracture and motor impairment are major sources of disability in neurological disorders including stroke, spinal cord injury, multiple sclerosis, and cerebral palsy [1-2]. Treatment of these pathological conditions presents a constant challenge to the medical rehabilitation community. Physical therapy is important and effective in treating joints with limited mobility, spasticity and/or contracture [2-3]. Manual stretching used in physical therapy may be laborious to the therapists and the outcome is dependent on the experience and the subjective "end feeling" of the therapists. There is a need for an effective and convenient method of therapy for stroke survivors with impaired ankles. The objective of this study is to investigate the neuromuscular/biomechanical changes and clinical outcome in stroke survivors induced by controlled passive stretching and active movement training of the impaired ankle using a portable rehabilitation robot.

METHODS

Seven stroke survivors are participants in this study (Table 1). The first four subjects have completed the study protocol and the last three are currently going through the training intervention. The study consists of 18 one hour sessions (3 times a week over 6 weeks) using a custom portable ankle rehabilitation robot. Neuromuscular/biomechanical as well as clinical evaluations are done before and after the training.

The training sessions includes both passive stretching and active movement training. During each session the subjects will sit with their leg in an extended position (so that gastrocnemius as well as soleus muscles would be stretched) and their foot secured in the footplate of the portable rehabilitation robot (Figure 1). Stretching limits are based on manual measurements of the subject's range of motion at the beginning of each training session, with extra room allowed for potential improvement through the passive and active movement treatment. The device stretches the ankle safely throughout the range of motion (ROM) to extreme dorsiflexion and plantarflexion until a specified peak resistance torque is reached with the stretching velocity controlled based on the resistance torque (the higher the resistance, the slower the stretching). The ankle is held at the extreme position for a period of time to let stress relaxation occur before it is rotated back to the other extreme position.

Figure 1. Experimental Setup.

After a period of stretching of about 20 minutes, the subject will use the loosened calf muscles immediately in voluntary movement training for about 30 minutes. They use the ankle rehabilitation robot to play biofeedback computer games, which help motivate them and facilitate motor recovery. On the one hand, if the patients cannot finish the active movement task, the robot will provide

assistance and keep the patients engaged in the training. On the other hand, if the patient can do a task easily, resistance will be provided by the robot to challenge them and also help improve their muscle strength as well as motor control. The last 10 minutes of the session is another period of stretching.

Before and after the 18 session intervention, biomechanical properties are evaluated including dorsi-flexion passive ROM (PROM) and active ROM (AROM), Achilles tendon reflex, and muscle strength. The clinical evaluations include Modified Ashworth Scale (MAS), Stroke Rehabilitation Assessment of Movement (STREAM), time up and go (TUG) test and 6-minute walk test.

RESULTS AND DISCUSSION

The preliminary results from the four subjects who have completed the training show an improvement trend in all the outcome measures (Figure 2). AROM increased from 33.9 degrees to 42.7 degrees. PROM averaged from 4.4 degrees in dorsiflexion to 4.9 degrees. The average MAS improved from an average of 2.25 to 1.75 and the STREAM score increased from 26.5 to 29. TUG times for the subjects decreased from 18 seconds to 17.6 seconds. Subject's 6-minute walk increased from 282.7 meters to 288.3 meters.

Our rehabilitation protocol including passive stretching and active movement training using a portable ankle rehabilitation robot can benefit stroke survivors that have impaired ankles.
The results showed a trend of increased range of motions that improved functional mobility shown by the improved MAS, STREAM score, TUG time and 6-minute walk.

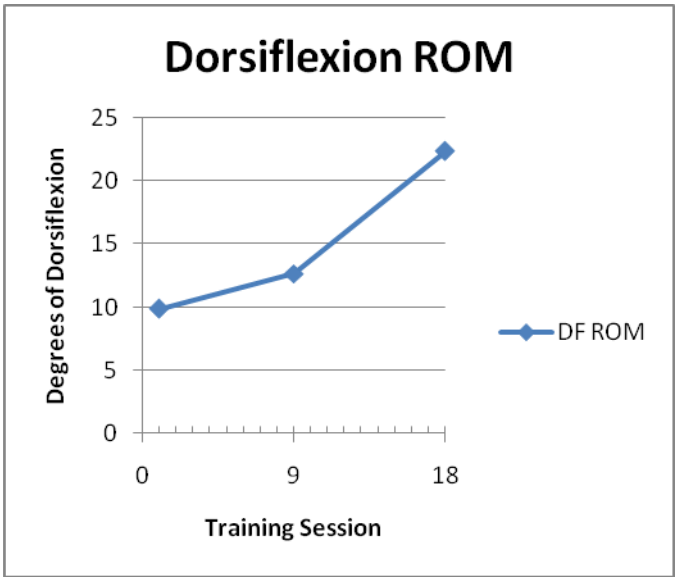

Figure 2: Improved dorsiflexion ROM from a typical stroke survivor.

REFERENCES

[1] N. J. O'Dwyer, L. Ada, and P. D. Neilson, "Spasticity and muscle contracture following stroke," *Brain*, **119**, pp. 1737–1749, 1996.

[2] M. Stokes, *Neurological Physiotherapy*. London: Mosby Int. Limited, 1998. [7] J. Carr and R. Shepherd, *Neurological Rehabilitation: Optimizing Motor Performance*. Oxford: Butterworth-Heinemann, 1998.

[3] M. L. Dombovy, B. A. Sandok, and J. R. Basford, "Rehabilitation for stroke: A review," *Stroke*, **17**, pp. 363–369, 1986.

ACKNOWLEDGEMENTS

We acknowledge the support of NIH.

Table 1: Participant Demographics

Subject	Gender	Age	Stroke Duration	Affected Side	MAS
1	F	39	3.6 years	L	3
2	M	60	2.1 years	L	1
3	M	52	4 years	L	3
4	M	55	4.3 years	L	2
5	F	52	5.8 years	L	3
6	M	45	11.7 years	L	1+
7	M	60	3.2 years	L	1+

Do Those with Perceived Ankle Instability have Associated Mechanical Instability?

K. Liu, G. Gustavsen & T. Kaminski

University of Delaware, Newark, DE, USA
Email: kathyliu@udel.edu

INTRODUCTION

The ankle is the most commonly injured joint in the body while sprains comprise 85% of all ankle injuries [1]. The most common risk factor for an ankle sprain is a previous sprain event. With recurrent sprains, the chance of residual symptoms of ankle instability increases dramatically. Ankle instability, defined as a "giving way", has been categorized into mechanical instability (MI) and functional instability (FI) [2]. There lacks evidence as to whether both are present in ankle instability or if they are independent from one another. Therefore, the purpose of the current study is to determine if there are differences in MI as measured by ankle arthrometry between ankles that have been categorized as stable or unstable by the Cumberland Ankle Instability Test (CAIT).

METHODS

A total of 60 healthy Division I collegiate athletes participated in this study. All subjects have not had an ankle sprain within the past 6 months. All subjects filled out the CAIT, a questionnaire used to determine perceived instability (PI) by self-reported symptoms [4]. The CAIT is scored on a 30-point system where a score of 28 and above is considered functionally "stable" while a score of 24 and below is considered functionally "unstable". Subject's ankles that scored between the 25-27 range were not used in the analysis. Therefore, a total of 46 subjects (21 females and 25 males, age= 18 ± 1, height= 178.8 ± 9.5 cm, mass= 77.2 ± 13.2 kg) contributed 73 ankles that were included in the final analysis.

Measurements for inversion and eversion rotation, along with anterior displacement of the ankle were obtained using an instrumented ankle arthrometer (Blue Bay Research, Inc., Milton, FL). The ankle arthrometer was interfaced to a computer with a custom written software program using Labview (National Instruments, Austin, TX). Subjects were positioned supine on a table with the foot extended over the edge of the table. A strap was placed above the malleoli, securing the lower leg, preventing any movement. The foot was then secured to the arthrometer using the heel and dorsal clamps. The tibial pad was secured onto the lower leg. Once the arthrometer was secured, the ankle was placed in a neutral position for all tests. To measure anterior displacement, an anterior load of 125N was placed on the ankle. For inversion-eversion rotation, a 4Nm load was placed on the ankle starting in the neutral position, rotating it to the left then the right. An indicator bar on the computer was used as a gauge to help the researcher identify the appropriate load for each measure.

Data were analyzed using an independent t-test comparing each of the ankle arthrometer measurements between the stable and unstable groups as determined by the CAIT. Statistical significance was set at $p \leq 0.05$.

RESULTS AND DISCUSSION

There were significant differences in inversion rotation between the stable and unstable groups as categorized by the CAIT. Subjects with CAIT scores 24 and below (unstable) demonstrated more inversion laxity than those with scores 28 and higher (stable) (Table 1). There were no significant differences in eversion rotation and anterior displacement between the stable and unstable ankles.

When compared with the results by Hubbard et al., our combined inversion and eversion rotations are similar [3]. However, they did not examine inversion and eversion rotation separately as was done in this project. We contend that inversion rotation, measured separately, is an important value because a majority of ankle sprains occur with an inversion mechanism [1]. Intuitively, it makes sense that those with perceived levels of ankle instability would have greater levels of ligament laxity, especially in the inversion direction.

Ankle instability often affects those who have had previous ankle sprains. The CAIT has been found to be a reliable questionnaire to measure FI [4]. The CAIT is a short 9-question survey that can be easily administered to assist the clinician with categorizing ankle instability. Additional research is needed to examine the relationship between mechanical and functional instability.

CONCLUSION

Based on the results of this study, those individuals who subjectively report as having unstable ankles have an associated increase in inversion laxity as compared to those with stable ankles.

REFERENCES

1. Garrick J. *Amer. J. Sports Med.* **5(6),** 241-242, 1977.
2. Hertel J. *J Athletic Training.* **37(4),** 364-375, 2002.
3. Hubbard T, et al. *Med. Sci. Sports Exerc.* **36(5)**, 760-766, 2004.
4. Hiller C, et al. *Arch. Phys. Med. Rehabil.* **87**, 1235-1241, 2006.

Table 1: Ankle arthrometer measurement between stable and unstable groups.

	Group	N	Mean ± St. Dev.	*p*-value
Inversion Rotation (^{o})	Stable	38	32.7 ± 8.5	0.01*
	Unstable	35	38.7 ± 10.7	
Eversion Rotation (^{o})	Stable	38	22.1 ± 6.8	0.72
	Unstable	35	22.7 ± 6.7	
Anterior Displacement (mm)	Stable	38	8.3 ± 3.2	0.87
	Unstable	35	8.2 ± 3.9	

* Indicates a significant difference between the groups.

THE IMPACT OF STOCHASTIC RESONANCE ELECTRICAL STIMULATION AND KNEE SLEEVE ON IMPULSIVE LOADING DURING GAIT IN KNEE OSTEOARTHRITIS

[1]Amber Collins, [1]J. Troy Blackburn, [1]Chris Olcott, [1]Joanne Jordan, [1]Bikramjit Grewal, [1]Bing Yu, [1]Paul Weinhold

[1]The University of North Carolina at Chapel Hill, Chapel Hill, NC, USA
email: amcollin@email.unc.edu

INTRODUCTION

Walking patterns of persons with knee osteoarthritis (OA) are increasingly being studied as a way of better understanding the role of joint mechanics in the development and progression of knee OA. Specifically, heightened impulsive loading is one biomechanical feature demonstrated in these patients [1,2]. Proprioceptive deficits with OA [3] may contribute to elevated impulsive loading, and it has been proposed that correcting these deficits may help to slow disease progression. While the use of knee braces and sleeves has produced a moderate improvement in proprioception, stochastic resonance (SR) stimulation, which has been shown to enhance mechanoreceptor sensitivity [4], may enhance these effects [5]. By improving sensitivity and therefore proprioception, it may be possible to positively alter gait biomechanics. Altering gait may therefore enable a person to more appropriately load their joint, thus delaying the progression of disease. Our goal is to determine whether impulsive loading rates during weight acceptance of gait are altered when subjects are presented with a subthreshold level of electrical stimulation at the knee in combination with a knee sleeve.

METHODS

Following approval by the Institutional Review Board, 22 subjects (7 males, 15 females) with minimal to moderate (KL grade 1-3) medial knee OA were recruited for testing.

Gait kinetics and kinematics were measured using an electromagnetic tracking system and force plate during four conditions combining the use of a neoprene knee sleeve and SR electrical stimulation (bipolar, Gaussian white noise). Each subject's threshold for detecting the stimulation was determined prior to gait analysis and a level of 75% of threshold was used during subsequent testing in combination with a neoprene knee sleeve (E75:S). The four testing conditions were: no stimulation/no sleeve (control1 NE/NS1), counterbalance of two conditions: E75/S and NE/S, and no stimulation/no sleeve (control2 NE/NS2). Each subject was instructed to walk at a fast, self-selected speed barefoot down a 10 meter, level walkway. Five trials were completed for each of the four testing conditions. Ground reaction forces were acquired (1440Hz) unfiltered and normalized to subject's body weight (N). Loading rate was calculated from the vertical ground reaction force (Fz) three ways over increasing time domains: 1.) **Fz LR max (BW/s):** Max slope from the 1st derivative of polynomial fit between initial ground contact and the peak heel strike transient HST 2.) **Fz LR HST (BW/s):** linear slope between initial ground contact and the peak HST and 3.) **Fz LR to Peak (BW/s):** linear slope between initial ground contact and the overall peak ground reaction force (Fz) (Figure 1).

Differences between the two control condition means (NE:NS1 and NE:NS2) were assessed followed by computing an average (NE:NSave) for subsequent analysis. One-way repeated measures analysis of variance was conducted to determine overall significant differences between the measured variable within the four treatment conditions ($p<0.05$). Tukey's post hoc analysis was performed to determine further differences between conditions.

RESULTS AND DISCUSSION

No difference between the control conditions was found for any of the outcome measures. Walking speed was also not found to differ across conditions. While the loading rate from initial contact to overall

peak Fz (Fz LR to Peak) was not statistically different between conditions, both the Fz LR HST and Fz LR max demonstrated trends toward overall significance (p=0.093, p=0.084, respectively, Fig.2).

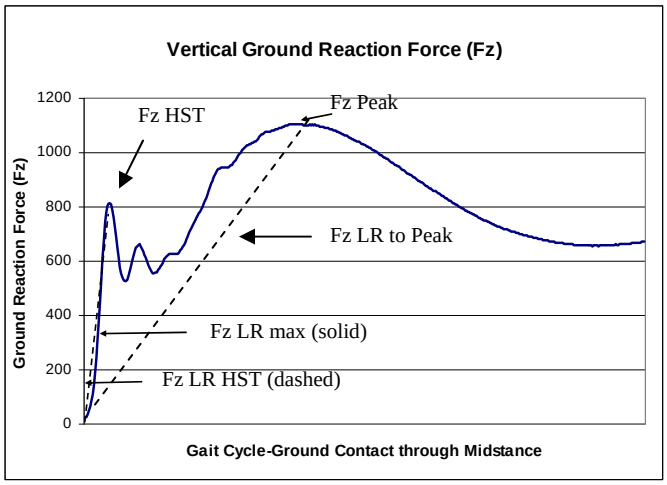

Figure 1: Vertical component of ground reaction force from a test subject, demonstrating outcome measures with respect to the generated data plot.

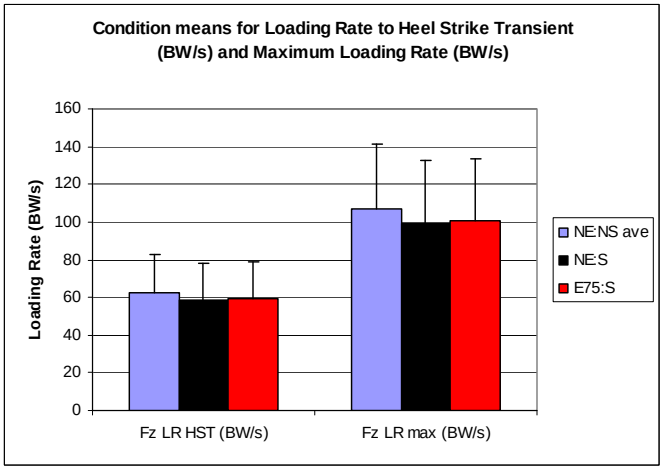

Figure 2: Loading Rate to Heel Strike Transient and Maximum Loading Rate averaged across subjects for the three testing conditions.

The trend for a decreased loading rate demonstrated in both the E75:S and NE:S conditions may be the result of a higher average knee flexion angle ($p<0.001$) seen at contact (13.2^o and 12.9^o, respectively) compared to that of the average control condition (11.1^o). However, knee flexion angle at contact for the E75:S and NE:S groups did not significantly differ from each other. Our previous studies demonstrating an improvement in joint position sense with the stimulation and sleeve conditions in knee OA subjects [5] suggests the increased flexion at contact may result from enhanced proprioception with these conditions though we can not discount that passive tension of the sleeve may also have contributed to this response. The amount of knee flexion excursion from initial contact to maximum knee flexion of midstance was found to be significantly more for the average control (NE:NSave), though the maximum knee flexion of midstance was found to be equivalent among the conditions.

CONCLUSIONS

The NE:S and E75:S conditions demonstrated a trend toward decreasing loading rates and with additional planned subjects these differences may become statistically significant. This trend may be a result of increased knee flexion at contact as demonstrated in both of the treatment conditions. It is possible that the increased knee flexion seen at contact was improved by enhanced proprioception as a result of the knee sleeve and SR stimulation treatments. The current configuration of SR stimulation did not demonstrate an ability to enhance the effects of a sleeve alone.

REFERENCES

1. Mundermann et al. *Arthritis & Rheumatism*. **52:9**, 2005.
2. Radin et al. *Journal of Orthopaedic Research*. **9:3**, 1991.
3. Barrett et al. *The Journal of Bone and Joint Surgery*. **73(B)**, 1991.
4. Collins, JJ, et al. *Nature*. **383**, 770, 1996.
5. Collins, AT, et al. *Journal of Orthopaedic Surgery and Research*. **4:3**, 2009.
6. Collins, AT, et al. Tran Ortho Res Soc. vol 56. # 1985

ACKNOWLEDGEMENTS

We would like to thank the Arthritis Foundation for financial support.

COMPARISON OF LOWER EXTREMITY ELECTROMYOGRAPHIC (EMG) DEMANDS DURING ICARE TRAINING AND WALKING

[1,2]Judith M. Burnfield, [1]Yu Shu, [1]Thad W. Buster, [1]Adam P. Taylor, [1]Larry Merriman, [2]Carl A. Nelson
[1]Madonna Rehabilitation Hospital, Institute for Rehabilitation Science and Engineering, Lincoln, NE
[2]University of Nebraska – Lincoln, Lincoln, NE
email: jburnfield@madonna.org, web: http://madonna.org/research_institute

INTRODUCTION

Physical activity is essential to improve function, yet many individuals face barriers to maintaining an active lifestyle due to muscle weakness. Resources used during formal rehabilitation (e.g., robotic therapy) are rarely available in the community. Over the past two years, our team addressed the need for an affordable, accessible tool to help individuals with physical disabilities improve walking and cardiovascular fitness by developing **ICARE**, an **I**ntelligently **C**ontrolled **A**ssistive **R**ehabilitation **E**lliptical trainer and therapeutic program. ICARE includes an intelligently controlled motor to assist leg movements.[1,2] Similarities of kinematic and electromyographic (EMG) patterns between walking and elliptical training[3] suggest that ICARE training also could help individuals regain or retain flexibility and strength required for walking, particularly if the muscle demands could be customized to those with weakness. The current study compared muscle demands across three levels of ICARE motor assistance and while walking. We hypothesized that the Active Assist ICARE mode would reduce muscle demands compared to other activities.

METHODS

Nine individuals without known pathology (mean age, 47 years) and five with varying medical conditions (diabetes, traumatic brain injury, total knee arthroplasty, transfemoral amputation, and hip fracture; mean age 48 years) participated. All ambulated independently. Surface EMG quantified muscle demands of gluteus maximus (**GMax**), gluteus medius (**GMed**), lateral hamstring (**LH**), vastus lateralis (**VL**), soleus (**SOL**) and tibialis anterior (**TA**) across ICARE and walking (**W**) conditions. Simultaneous 12-camera motion analysis and footswitches determined cycle timing for ICARE and walking, respectively. Participants walked at a self-selected speed across a 6-m walkway and then ICARE trained using three levels of motor assistance at similar self-selected speeds: 1) *Active Assist* (**AA**; motor provided adequate force to help client's legs move at self-selected speed); 2) *Active Assist Plus* (**AAP**; motor disengaged whenever client's speed exceeded motor's threshold speed; clients exerted effort at level that maintained elliptical training speed ~2 RPM higher than targeted speed); and 3) *Resistive* (**R**; motor not engaged and not assisting). EMG data were normalized to each muscle's maximal voluntary contraction and expressed as a percentage of maximal voluntary contraction (% MVC).

STATISTICAL ANALYSIS

Separate 4 x 1 ANOVAs with repeated measures identified significant differences in peak and mean amplitude of EMG activation across conditions.

RESULTS AND DISCUSSION

Electromyographic profiles for each muscle are presented in Figure 1. At the hip, **GMax** and **GMed** activation patterns during walking and ICARE training demonstrated notable similarities with the greatest activity occurring in early stance. Peak and mean **GMed** demands diminished in the AA mode compared to AAP (Table 1). Mean **GMed** demands also decreased during AA compared to R. Peak activity of **LH** diminished during AA training compared to walking, while mean **LH** activity reduced during all ICARE modes compared to walking. At the knee, peak and mean **VL** demands were lower during walking compared to R training. Use of the AA mode reduced mean **VL** demands compared to the other two ICARE training modes. At the ankle, the **SOL** demonstrated a similar gradual increase in activity during the first portion of the ICARE movement cycle to that documented during walking, except the maxima occurred earlier. Peak **SOL** activity during W exceeded AA and R levels, and mean W activity also exceeded AAP. Peak and mean **TA** activity were greater during walking than AA and AAP. While mean R was less than walking, it exceeded demands during AA.

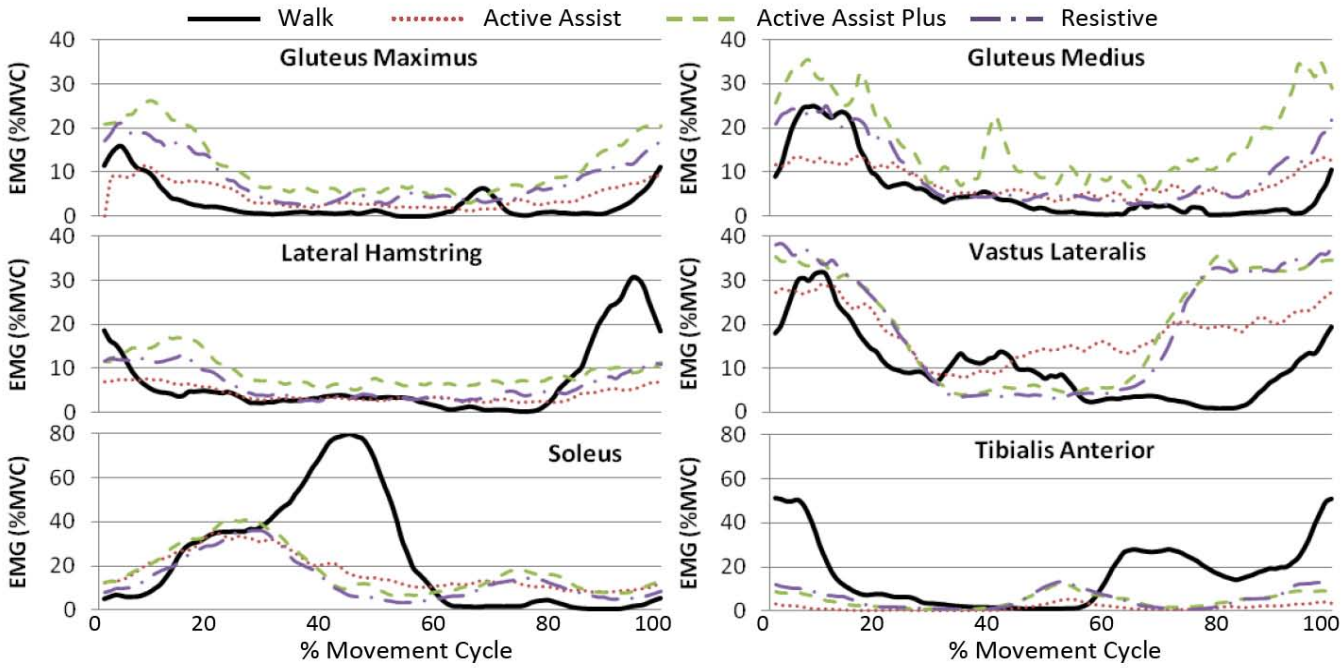

Figure 1. Ensemble averaged (mean) electromyographic (% MVC) plots of select muscles while walking and ICARE training (N=14).

CONCLUSIONS

Individuals with weakness often confront challenges with exercising due to a lack of equipment that appropriately accommodates to the needs of the compromised muscles. Consistent with our initial hypothesis, exercising in the Active Assist ICARE mode decreased muscle demands in 9 of 12 comparisons. Only **GMAX** (peak and mean) and **VL** (peak) demands failed to register significant reductions in amplitude during AA training. The current study's findings suggest that the addition of an intelligent motor system did broaden the range of muscle demands that could be accommodated during ICARE training. Our current research is evaluating practical use of the ICARE trainer during inpatient and outpatient rehabilitation and at a fitness facility.

REFERENCES

1. Burnfield JM et al. (2010). *Accepted, RESNA 2010 Annual Conference.*
2. Shu Y et al. (2010). *Accepted, RESNA 2010 Annual Conference.*
3. Burnfield JM (2010). *Phys Ther.* 90(2): 289-305.

ACKNOWLEDGEMENTS

This work was supported in part by a grant from the Department of Education NIDRR grant number H133G070209.

Table 1. Peak and mean electromyography activity (expressed as % MVC) recorded during walking and ICARE training (n=14)
Key: AA = Active Assist, AAP = Active Assist Plus, R = Resistive, W = Walk

		Walk	Active Assist	Active Assist Plus	Resistive	P values	Main Effect
Gluteus Maximus	Peak	23(24)	21(23)	33(30)	31(23)	0.046	No Significant Difference
	Mean	11(11)	9(9)	15(13)	13(10)	0.069	No Significant Difference
Gluteus Medius	Peak	26(22)	18(18)	40(31)	33(24)	0.034	AA<AAP
	Mean	13(10)	7(6)	14(8)	14(8)	0.019	AA<R,AAP
Lateral Hamstring	Peak	41(26)	15(20)	33(36)	27(26)	0.006	AA<W
	Mean	17(10)	6(8)	13(13)	11(9)	0.003	AA,R,AAP<W
Vastus Lateralis	Peak	34(26)	37(22)	48(19)	52(16)	0.022	W<R
	Mean	15(10)	15(8)	22(9)	24(7)	<0.001	AA<AAP,R; W<R
Soleus	Peak	92(21)	49(25)	59(29)	51(26)	0.002	AA,R<W
	Mean	41(12)	20(10)	24(13)	20(11)	<0.001	R,AA,AAP<W
Tibialis Anterior	Peak	66(26)	12(13)	25(21)	31(26)	<0.001	AA,AAP<W
	Mean	26(11)	6(6)	11(8)	15(13)	<0.001	AA<R,W; AAP,R<W

EFFICACY OF GAIT TRAINING WITH REAL-TIME BIOFEEDBACK IN CORRECTING KNEE HYPEREXTENSION PATTERNS IN YOUNG WOMEN

P Teran-Yengle, B Singh, and HJ Yack
University of Iowa, Iowa City, IA, USA
Email: patricia-teranyengle@uiowa.edu

INTRODUCTION

Knee hyperextension is thought to be associated with increased stress to the posterior joint capsule of the knee [1] and anterior cruciate ligament (ACL) [2] and increased contact stress on the anterior compartment of the tibial-femoral joint [3]. Abnormal stress to these tissues can be detrimental to the knee joint [4,]. Compared to men, women demonstrate greater incidences of knee hyperextension [5]. Methods to correct for knee hyperextension such as taping, bracing, muscle strengthening, and neuromuscular training [6] have shown limited success. Several studies support training, using biofeedback, to affect performance and learning of motor skills [7] and in teaching patients to regulate their movements [8]. The aim of this study was to investigate the efficacy of real-time biofeedback, provided during treadmill gait training, for correcting knee hyperextension patterns in young female subjects while walking.

METHODS

Ten healthy women, ages 18 to 39 years, with asymptomatic knee hyperextension underwent a three-week (6 sessions) treadmill gait retraining program. Clinical measures of knee hyperextension greater than 5° were used as the inclusion criteria. Participants underwent a physical and gait evaluation. The physical evaluation assessed muscular strength and passive range of motion in each subject's lower limbs using standard techniques. The gait evaluation was conducted along an 8 m walkway using a three-dimensional motion analysis system (Optotrak, NDI; Kistler) with subjects walking at their self selected (SS) speed and at 3 mph. Gait data was processed using Visual 3D software (C-Motion). After the initial evaluation, subject participated in supervised treadmill training twice a week for three weeks. Each training session lasted one hour and consisted of three eight-minute sessions with three-minute rest periods in between training sessions. Real-time biofeedback (Visual 3D) was provided on a computer screen placed on a table (150 cm in height) about 1m in front of subject. Participants received real-time biofeedback (Fig. 1) for the knee that showed the greater knee extension (involved knee) at either initial contact or toe off. Once subjects gain proficiency controlling their more involved knee, real-time biofeedback was also provided for correction of hyperextension pattern on the less involved knee. Treadmill gait data were collected, without feedback, at the beginning (pretraining) and end (posttraining) of each training session. A final overground gait evaluation, following initial evaluation protocol, was performed at the end of the three weeks of training.

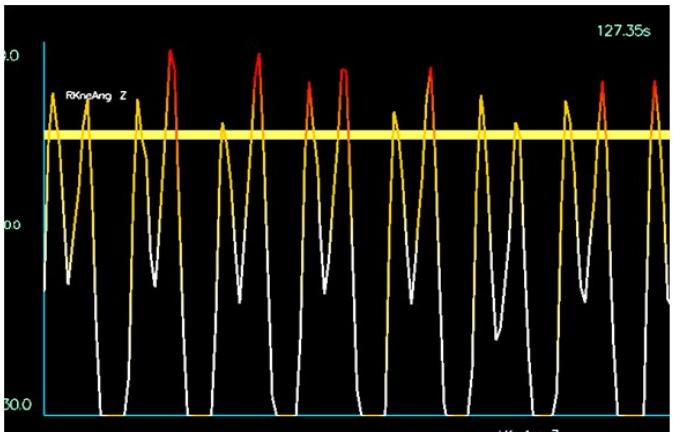

Figure 1: Real-time biofeedback: Horizontal band represents the target area where subjects attempted to center motion (5° flexion). Vertical lines represent the movement of the knee in the sagittal plane.

RESULTS AND DISCUSSION

Ten women (age 26.2 $\pm$ 5.4; weight 71 $\pm$ 14 Kg; height 1.6 $\pm$ 0.1 m) took part in this study. Initial muscular testing showed normal values for knee extensors (145 $\pm$ 12 N), and flexors (129 $\pm$ 25 N). The passive range of motion showed 9.7 $\pm$ 3.2°

(from 6° to 14°) of knee extension. Initial gait evaluation showed that seven subjects had greater knee extension in their right knee. Maximum knee extension occurred at initial contact in seven subjects and at toe off in 3 subjects.

A paired T-test showed significant evidence that treadmill gait training intervention reduced knee hyperextension pattern in involved (Fig. 2) and less involved knees (Fig.3). As shown in Figure 3, the greatest reduction of knee extension pattern occurred between the third (TM3) and fourth (TM4) treadmill training sessions. Figure 3 also shows the within-session training effects (pre and posttraining) and intersession training effects (carryover in between training sessions) of the augmented type feedback provided. Data also show evidence of some loss in ability to control knee extension patterns, in the involved knee, during the final over ground gait evaluation at self selected speed (p <0.05) and 3 mph (p <0.06) walking.

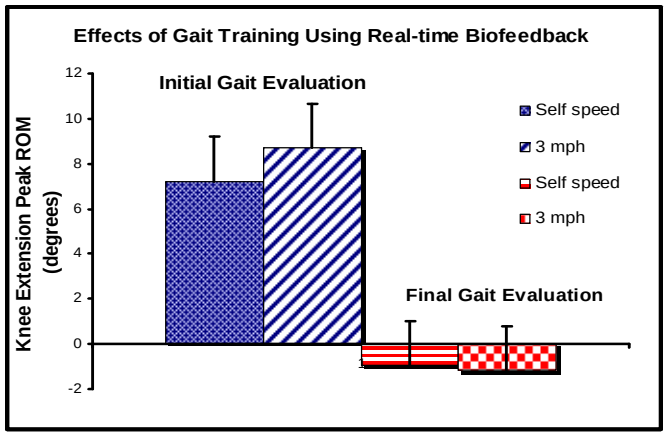

Figure 2: Peak knee extension at initial and final gait evaluations. Treadmill gait retraining intervention, using real-time biofeedback, significantly reduced knee hyperextension patterns during over ground walking at self-selected (SS) (p<0.01) and 3 mph (p<0.01).

SUMMARY & CONCLUSIONS

The results of this study indicate that subjects in this study showed decreased knee hyperextension during treadmill gait retraining intervention. Subjects showed greatest improvement in decreasing knee hyperextension during the first and third treadmill training sessions. When working on correcting the knee hyperextension patterns in the involved knee, subjects demonstrated simultaneous reduction in peak knee extension in the less involved knee. Subjects demonstrated gradual improvements that continued over the three-week training program. Gained proficiency, controlling knee hyperextension patterns during treadmill training, was evident for over ground walking at and self selected speed. There was some loss in proficiency controlling knee extension between treadmill training and walking over ground at 3 mph. Improvements in decreasing knee hyperextension during walking may help to relieve constant stress in the knee joint. The present study showed that knee sagittal plane kinematics can be influenced with dynamic gait training using real-time biofeedback.

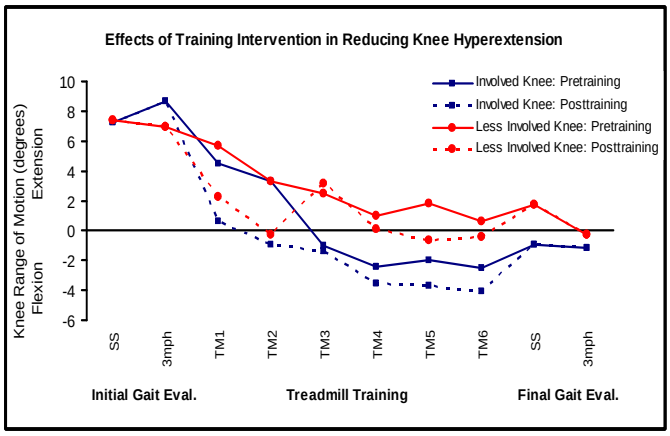

Figure 3: Data showing training's effect in involved and less involved knee hyperextension. Trend lines indicate change over time toward less knee hyperextension in involved and less involved knee (p<0.01) and loss of proficiency between posttraining session (TM6) and final gait evaluation at SS (p <0.05) and 3 mph (p <0.05).

REFERENCES

1. Oatis CA. Kinesiology.: Mechanics & Pathomechanics of human movement (2004).
2. Senter, C., & Hame, S. L. (2006). Biomechanical analysis of tibial torque and knee flexion angle: Implications for understanding knee injury. *Sports Medicine (Auckland, N.Z.)*, 36(8), 635-641.
3. Nisell R et al (1986). Joint Forces in Extension of the Knee *Acta Orthop Scand* 57; p. 41- 46.
4. Sharma L. et al. (2008). Relationship of meniscal damage, meniscal extrusion, malalignment, and joint laxity to subsequent cartilage loss is osteoarthritic knees. *Arthritis & Rheumatism*, 58(6), 1716-1726.
5. Medina McKeon J M et al. (2009). Sex Differences and Representative Values for 6 Lower Extremity Alignment Measures. *Journal of Athletic Training*, 44(3); p.249-55.
7. Mandelbaum, B. R. et al. (2005). Effectiveness of a neuromuscular and proprioceptive training program in preventing anterior cruciate ligament injuries in female athletes. *The American Journal of Sports Medicine*, 33 (7), 1003-1010.
8. Wulf, G., Shea, C., & Lewthwaite, R. (2010). Motor skill learning and performance. *Medical Education, 44*(1), 75-84.
9. Coker CA. (2006). *Motor Learning & Control for Practitioners.* Holcomb Hathaway, Publishers, Inc.

COMPENSATORY MOVEMENT STRATEGIES AMONG SUBJECTS WITH HIP FRACTURE DURING A SIT TO STAND TASK

[1,2] Janet Kneiss, Susan Bukata,[2] J.Edward Puzas,[2] Jeff Houck [1,2]
[1]Ithaca College-Rochester, Rochester, NY, [2] University of Rochester Medical Center, Rochester, NY
email: Janet_Kneiss@URMC.Rochester.edu

INTRODUCTION

After a hip fracture elderly populations (>65) experience a loss of physical function (>50% loss of lower extremity function) and increased risks of falls despite return of functional independence[1]. Asymmetrical limb loading (lower limb loading of the involved limb) noted in hip fracture subjects may contribute to decreased function and falls risk[2]. However, which knee or hip kinetic patterns explain altered limb loading are not known[3]. Global decreases in joint kinetics (both knee and hip may occur) or joint specific strategies (higher knee dependence) may underlie altered limb loading. Understanding the typical patterns may facilitate targeted rehabilitation programs and improve outcomes. Therefore the purpose of this study was to compare hip and knee kinetics during a sit to stand task in subjects with hip fracture (HF) to elderly controls (EC). The two initial hypotheses are: 1) Hip fracture subjects would demonstrate lower involved side joint kinetics (hip/knee moments/powers), indicating a global decrease (global strategy) in limb function compared the uninvolved side and controls. And 2) hip fracture subjects would demonstrate similar uninvolved side kinetics (hip/knee moments/powers) to the controls. Indicating a higher dependence on the uninvolved limb to achieve rising.

METHODS

Fifteen subjects (3 male, 12 female; age=77 ± 6) post hip fracture and 15 controls (4 male, 11 female; age=73 ± 5) participated in this study. All subjects were community dwelling and recently discharged from home care physical therapy. An Optotrak Motion Analysis System (Northern Digital Inc, CAN) and Motion Monitor Software (Innsport Training Inc, USA) collected kinetic and kinematic data at a sample rate of 60 Hz and a low pass filter rate of 6 Hz. Angles were then produced and calculated from a Cardan angle Z-X-Y sequence of rotations. Hip and knee moments and powers calculated from the appropriate angles and ground reaction force (collected at 1000 Hz using Kistler force plates under each foot). Subjects were asked to perform sit to stand "as fast as possible" three times. Time to rise was calculated from seat off to upright posture. Data were averaged over the three trials and statistically compared across side (involved/uninvolved) and groups (hip fracture/control).

RESULTS AND DISCUSSION

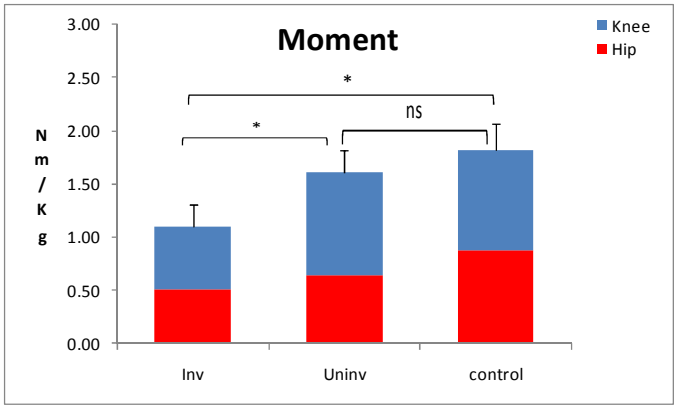

Figure 1: Hip and knee moments for for the involved, uninvolved and control limb.

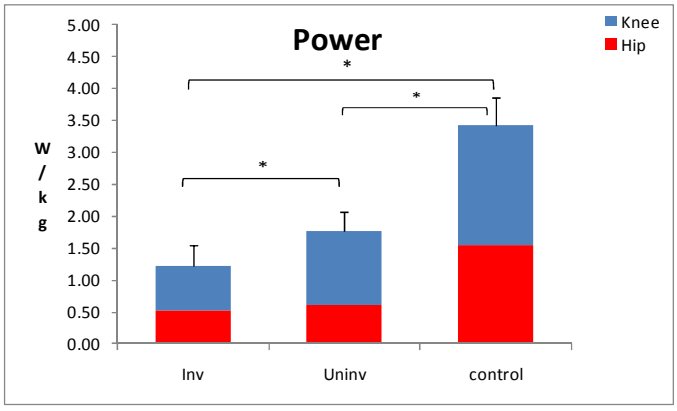

Figure 2: Hip and knee powers for the involved, uninvolved and control limb.

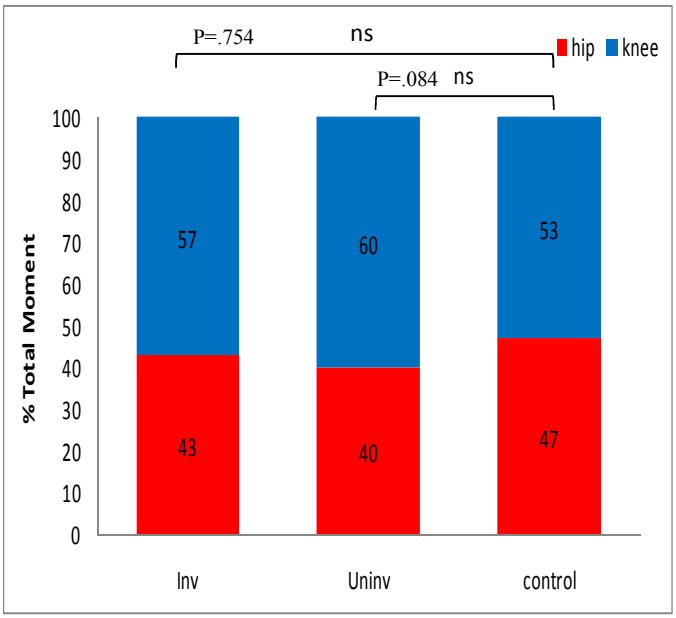

Figure 3. Percent total (hip and knee) moment for the involved, uninvolved and control limb.

Subjects with HF have a significantly slower time to rise compared to controls ($p<0.001$, HF = 1.2 s ± .41 vs EC = 0.72s± .19). The new findings of our study show that individuals with hip fracture have significantly lower hip/knee moments (Figure 1) on the involved limb ($p<0.001$, HF = 1.0 Nm/Kg ± .23 vs EC = 1.7Nm/Kg ± .23) but not the uninvolved limb ($p=0.113$, HF = 1.63 Nm/Kg ± .29 vs EC = 1.83Nm/Kg ± .31) compared to elderly controls. Additionally, the HF group had lower hip/knee powers on both the involved ($p<0.001$, HF = 1.2 W ± .45 vs EC = 3.2W ± .81) and uninvolved limb ($p<0.001$, HF = 1.8 W ± .71 vs EC = 3.4 W ± .83) (Figure 2). To evaluate the contribution of each joint the percent of the total moment or power was also evaluated (Figure 3). This analysis suggested equal contributions of each joint, irrespective of which limb was assessed (involved, uninvolved, controls). Further, HF subjects tend to use a movement strategy that is reliant on the uninvolved limb (figure 3).

CONCLUSIONS

Subjects with hip fracture employed movement strategies that included lower contributions of both the hip and knee on the involved limb supporting the first hypothesis. Because both hip and knee contributions were similar (figure 3) a global strategy (of the involved limb) was used to achieve a sit to stand. This suggests that decreases of the involved limb are interdependent between both the hip and knee joints rather than isolated to only deficits of the hip joint (i.e knee dominant strategy). A higher dependence on the uninvolved limb was shown partially supporting the second hypothesis. Hip and knee contributions were significantly higher on uninvolved limb but this was not equal to controls (Figure 2). The significant decrease in bilateral power suggests the movement strategy employed by subjects with hip fracture is associated with decreased speed to achieve rising during a sit to stand. This finding that global deficits of the involved limb limit overall sit to stand performance may be important in directing rehabilitative care post hip fracture by focusing on global performance of both the hip and knee. Future studies should focus on understanding the interdependence of the hip and knee joints rather than isolated joint specific deficits such as strength.

REFERENCES

1. Magaziner, J., W. Hawkes, and J.R. Hebel, Recovery from hip fracture in eight areas of function. *J.Gerontol.A Biol.Sci.Med.Sci*., 2000. 55: p. M498.
2. Portegijs, E., et al., Asymmetrical lower extremity power deficit as a risk factor for injurious falls in healthy older women. *Journal of the American Geriatrics Society*, 2006. 54(3): p. 551-3.
3. Talis, V.L., et al., Asymmetric leg loading during sit-to-stand, walking and quiet standing in patients after unilateral total hip replacement surgery. *Clin Biomech* 2008. 23(4): p. 424-33.

ACKNOWLEDGEMENTS

The authors are grateful for support from the National Institute of Aging; Center for Research Translation,Grant#:1P50AR054041-02).

ROLE OF TRUNK MOVEMENT IN MANUAL WHEELCHAIR PROPULSION IN VARIOUS OVERGROUND CONDITIONS

Lynn Worobey, BS, Alicia Koontz, PhD, Michael L Boninger, MD
Human Engineering Research Laboratories, VA Center for Excellence for Wheelchairs and Associated Rehabilitation Engineering, Highland Drive VA Medical Center, Pittsburgh, PA
University of Pittsburgh, Department of Bioengineering, Department of Rehabilitation Science and Technology, and Department of Physical Medicine and Rehabilitation, Pittsburgh, PA
E-mail: law93@pitt.edu Web: www.herlpitt.org, www.herl.research.va.gov

INTRODUCTION

Previous studies have found that paradoxical movement (e.g. trunk moving in opposition to the arms) during propulsion on a dynamometer was associated with lower mef values [1,2]. Mef is the contribution of tangential force to overall resultant force (Ft^2/F_R^2). Thus, low mef values may indicate that propulsion technique is suboptimal. Paradoxical movement is believed to occur when the trunk is not stable or strong enough (e.g. due to paralysis) to brace itself against the forces that are imparted onto the pushrim. Prior studies describing paradoxical trunk motion have all been performed using a propulsion simulator. We have found that propulsion on a simulator does not perfectly emulate the range of natural overground surfaces encountered in daily living [3]. This study evaluated trunk paradoxical movement during propulsion over three surfaces: carpet, linoleum, and ramp. We hypothesized: (1) paradoxical movement would increase as the difficulty of the traversed surface increased (2) excursion would decrease as individuals approached steady state (3) increased paradoxical movement would correlate with slower self-selected velocities and a lower mef.

METHODS

Subjects: Ten male manual wheelchair users without history of limb fractures of dislocations that they had not recovered from gave informed consent to participate in this study. The average age and years post injury of the group were 48±10.4 and 10.5±7.8 years respectively. In this group there were seven individuals with spinal cord injury (2 cervical, 4 thoracic, 1 lumbar), one transfemoral amputee, and two bilateral transtibial amputees.

Experimental Protocol: Subjects used their own wheelchair with two SmartWheels (Three Rivers Holdings, Inc., Mesa, AZ) attached which measure three-dimensional forces and moments on the pushrim. Data was collected from nondominant side with the second SmartWheel used only for balancing weight. Unilateral non-dominant kinematic data were collected using a six camera Vicon MX motion capture system (Vicon, Lake Forest, CA). Subjects completed three trials over each of three surfaces: linoleum, high pile carpet and ramp (5º grade). Surfaces were completed in a random order and all subjects started from rest and propelled up to a self-selected velocity.

Data Analysis: Kinematic data were collected at 60Hz and kinetic data were collected at 240Hz. Linear interpolation was performed to synchronize the two data sets. Only start up strokes (strokes 1-3) were examined. Propulsion was divided into push and recovery phases by visual inspection based on when the propulsive moment curve crossed baseline (e.g. y=0). Using MATLAB, we determined the maximum resultant force (F_R), maximum moment about the hub (Mz), average velocity, and mef for each stroke and averaged across the three trials. Forces were normalized by combined body and chair weight. Percentage of the phase the trunk was moving backward and trunk forward/backward linear excursion were determined for push and recovery. Kinematic variables were calculated using markers on the sternum and center of the hub.

Statistical Analysis: Kinetic and kinematic variables were compared across conditions and separately for each stroke using a Freidman's test with post hoc comparisons performed using Wilcoxon signed rank tests. A correlation between propulsion (Mz, F_R, velocity, mef) and trunk movement variables (backward and forward excursion during push and recovery) was investigated using Spearman's correlation.

RESULTS AND DISCUSSION

During the push phase, the most trunk rearward excursion occurred on the ramp, followed by carpet

and lastly linoleum (Table 1). Rear excursion averages during push and recovery (Table 1) were higher than the average found in a previous study for dynamometer propulsion at 0.9m/s (15.7mm) [1]. Forward and backward trunk excursion during recovery remained relatively consistent for all strokes. For all conditions, trunk excursion in both directions decreased as the number of strokes increased during push phase. The percentage of time the trunk moved backward during push and recovery (37.1-49.1% and 46.5-63.9%) was in accordance with a previous study conducted on a dynamometer (42.6% and 59.4%) [1].

As rearward excursion during the push phase increased, Mz and velocity decreased indicating the ability to generate effective forces was lower (R: -0.66 to -0.86, $p<0.05$) More forward trunk excursion during the push phase was correlated with slower self-selected velocity and lower mef (R: -0.56 to -0.79, $p<0.05$) Combined, these findings indicate that less overall trunk excursion during the push phase resulted in better biomechanics. In a sub-analysis of the dataset, subjects with higher levels of trunk impairment had more rearward excursion during the push phase on all surfaces (62.7, 70.5, and 46.9 mm on carpet, ramp, linoleum respectively) as compared to those with lumbar spinal cord injuries or amputations (42.6, 61.5, 40.6 mm). In contrast to push phase, it was found that during recovery more forward (R: 0.73 to 0.84, $p<0.05$) and backward (R: 0.67 to 0.75, $p<0.05$) excursion produced better biomechanics (increased F_R, Mz, and velocity).

CONCLUSIONS

This is the first paper to report trunk excursion for a diverse group of wheelchair users with mobility impairments on natural surfaces. Paradoxical motion became more pronounced as surface difficulty increased. Greater trunk excursion in both directions during the push phase correlated with a decreased ability to generate forces and moments and a lower self-selected velocity. The findings suggest that using a rigid back support, strengthening residual core muscles, and/or applying functional electrical stimulation during the push phase when forces are imparted to the rim may be helpful for improving propulsion biomechanics.

REFERENCES

1. Koontz AM. *Proceedings of ASB'04*, Portland, OR, USA, 2004.
2. Rice I. *Proceedings of RENSA'04*, Orlando, FL, USA, 2004.
3. Koontz AM, et al. *J Appl Biomech*, In press.

ACKNOWLEDGEMENTS

This material is based upon work supported by the National Institutes of Health (Grant Number: 1 R03 HD049735-01A1). This material is the result of work supported with resources and the use of facilities at the Human Engineering Research Laboratories, VA Pittsburgh Healthcare System. The contents of this paper do not represent the views of the Department of Veterans Affairs or the United States Government.

Table 1: Magnitude of excursion (mm) during push and recovery (mean+SD)

		Forward /Push	Backward / Push	Forward /Recovery	Backward /Recovery
Carpet	stroke 1	87.2 (34.6) *	73.9 (24.4)	25.9 (24.0)	29.3 (28.4) *
	stroke 2	65.1 (41.1) *	52.1 (24.0) +	18.5 (16.7)	39.4 (32.2)
	stroke 3	56.2 (33.6) *+	40.6 (21.6) *	17.0 (16.8) *	32.7 (24.0)
Ramp	stroke 1	118.8 (57.4) *	91.9 (26.5) #	25.3 (19.0) #	64.0 (57.6) *
	stroke 2	106.4 (57.4) *#	56.4 (20.7) #	17.1 (20.2)	53.3 (50.8)
	stroke 3	97.2 (51.0) *#	62.5 (23.0) *#	28.2 (20.9) *#	39.2 (44.4)
Linoleum	stroke 1	102.7 (49.5)	70.9 (19.9) #	17.6 (17.9) #	40.9 (32.2)
	stroke 2	63.0 (45.9) #	37.1 (15.2) +#	14.0 (10.7)	42.9 (29.5)
	stroke 3	28.8 (20.2) +#	28.5 (8.4) #	13.7 (10.3) #	33.4 (20.5)

Symbols indicate significant difference ($p<0.05$) between carpet-ramp (*), carpet-linoleum (+), ramp- linoleum (#)

STEP LENGTH VARIABILITY DURING GAIT INITIATION IN PARKINSON'S DISEASE

Ryan Roemmich, Joe Nocera, Srikant Vallabhajosula, Shinichi Amano, Brian Hoover, and Chris Hass

University of Florida, Gainesville, FL, USA

rroemmich@ufl.edu

INTRODUCTION

Parkinson's disease (PD) is associated with several changes in motor tasks including postural control and gait. As such, patients with PD are more likely to experience a fall than their aged-matched peers. In fact, 80 percent of patients with PD fall during the course of their disease with 30 percent falling weekly. Recent research suggests gait variability may be an important predictor of both mobility impairment and falls, which is particularly relevant to PD as instability is a key characteristic of the disease. Among the various spatiotemporal parameters used to evaluate gait variability, step length has been shown to be among the most reliable [1].

Gait initiation is a vital component to mobility as it challenges the postural system by transitioning the body from a stable base of support during standing to the dynamic act of locomotion. In healthy older adults, GI step length variability is demonstrated as an important predictor of postural problems. Due to degradation of the postural control system demonstrated in PD, falls may be provoked during gait initiation and variability in the length of the first step (rather than step-to-step variability) may be important in predicting these falls.

Recent research suggests that first-step length variability in elderly fallers is more than twice as great as first-step length variability seen in elderly non-fallers, while elderly non-fallers did not differ from young non-fallers[2]. Thus, consistency of foot placement during stepping while initiating gait appears to be significant in the prevention of falls and in fall recovery. For steady-state walking, patients demonstrating a coefficient of variation greater than 7 percent have been defined to be at high risk of falling[3].

To date, however, research has yet to examine variability during gait initiation (GI) in PD. Therefore, this study sought to preliminarily investigate GI variability in patients with PD when compared to their aged-matched peers.

METHODS

Seventy-five participants, 57 persons with Parkinson's disease (65.65±9.63yr, 171.46±8.82cm, 83.48±16.25kg, 2.3±.5 Hoehn and Yahr stage) and 18 age-matched healthy older adults (65.11±12.41yrs, 168.08±10.79cm, 75.23±19.96kg) participated. Persons with PD were tested while clinically "ON" approximately 1 hour after taking their antiparkinsonian medication. At the time of testing, no patients exhibited dyskinesias or other non purposeful movements.

Gait initiation trials began with the participant standing quietly on a force platform (Bertec, Columbus Ohio) mounted flush with the laboratory floor. Initial positioning of the feet was self-selected. In response to an auditory signal, the participants initiated walking and continued to walk for several steps. For each participant, at least 3 data collection trials were collected at a self-selected pace.

Kinematic data were collected using an 3D Optical Capture system (Vicon Peak, Oxford, UK) collecting at 120Hz. Thirty-nine passive reflective markers were attached to the body in accordance with the Vicon Plug-in-Gait marker system. The length of the first step for each trial was calculated as the displacement of the heel marker from initial heel-off to the subsequent heel-strike. Step length variability was then evaluated using the coefficient of variation while analyzing across trials.

RESULTS AND DISCUSSION

Patients with PD showed increased first-step length variability when compared to healthy elderly adults. Increased step variability during GI may have important implications as a predictor of falling and/or freezing in PD and may provide insight into the general impaired mobility and motor control frequently seen in PD. When combined with the results of previous research which have shown alterations in the GI motor program in patients with PD, more research is needed to investigate the effects of GI variability on postural instability and falling in Parkinson's disease.

REFERENCES

1. Brach, J.S., S. Perera, S. Studenski, and A.B. Newman. The Reliability and Validity of Measures of Gait Variability in Community-Dwelling Older Adults. *Archives of Physical Medicine and Rehabilitation* **89,** 2293-2296, 2008.

2. Mbourou, G.A., Y. Lajoie, N. Teasdale. Step Length Variability at Gait Initiation in Elderly Fallers and Non-Fallers, and Young Adults. *Gerontology* **49**, 21-26, 2003.

3. Nakamura T, K. Meguro, H Sasaki. Relationship between falls and stride length variability in senile dementia of the Alzheimer type. Gerontology **42,** 108–113, 1996.

Table 1: Coefficient of variation (CV) of first-step length in elderly adults with PD and healthy elderly adults.

	N	Mean CV (p = .02)	SD CV
PD	57	.0989	.06166
Healthy Elderly	18	.0656	.03197

A REWARD SYSTEM FOR ALTERING DISTRIBUTION OF EFFORT IN MULTI-LIMB EXERCISE

Nathaniel E. Skinner[1], Daniel P. Ferris[2], Arthur D. Kuo[1]
[1]Department of Mechanical Engineering, [2]Department of Kinesiology
University of Michigan, Ann Arbor, MI, USA
email: nskinner@umich.edu, web: http://hbcl.engin.umich.edu

INTRODUCTION

Robotic devices for rehabilitation are intended to improve patient outcomes while simultaneously reducing the demands placed on therapists. Devices such as the Lokomat aid the patient's ability to walk, but provide little incentive for patients to actively participate and exercise the weakened limbs.[1,2] Robotic rehabilitation should simultaneously provide resistance for exercise while incentivizing a desired distribution of effort between limbs.

Patient participation can be elicited by making the task self-driven.[3] There remains the hurdle of giving a patient incentive to exercise a weakened limb, especially when only using stronger limbs may fulfill the exercise task. We propose to reward the user with a variable weighting of limb work contributions to create an incentive for exercising designated limbs or limb combinations.

METHODS

We propose that users allocate limbs to a multi-limb exercise task based on a sense of subjective effort that is a quantifiable function of the power generated by the arms and legs (Fig.1A). The overall shape of the effort function is unknown, but we expect it to generally increase with greater power from any limb. The function should also yield combinations of arms and legs powers that are perceived as equal effort (contours in Fig. 1A). By presenting subjects with a task that rewards contributions from the arms and legs differently, we hope to quantify the subjective effort function.

We designed exercise task constraints such that the limbs are disproportionately rewarded. The user receives greater reward for using some limbs than others. We call these weightings "reward biases" (Fig.1B).

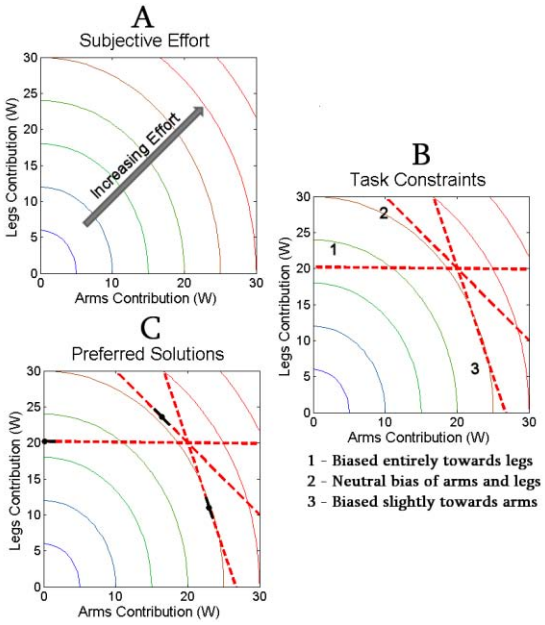

Figure 1: (A) Hypothetical subjective effort function, shown with lines of equal effort, where effort increases with greater power from either arms or legs. (**B)** An exercise task may be viewed as a constraint line, which the user may satisfy with a combination of arms and legs. The task may be biased to reward arms or legs disproportionately, thereby favoring one set of limbs. (**C)**Users are expected to select the combination satisfying the task with least subjective effort (dark lines). This provides a means of identifying the effort function.

The subject is given visual feedback similar to a power meter, with a desired power goal for each task. Users may explore possible ways to achieve the task, and their preference is used to as an indicator of the subjective effort function (Fig. 1C). This approach is analogous to constrained optimization, where the effort function is to be minimized, and the imposed exercise task is a constraint. The optimal solution is thus the intersection of the constraint line with a contour of least effort.

We used the NuStep recumbent stepper to measure subjective effort for healthy adults (N = 10) performing cyclical exercise with their arms and legs. We provided 11 distinct tasks with varying

reward biases, ranging from rewarding arms alone to legs alone, with several combinations rewarding both at separate levels. We measured the power produced by the arms and legs, and used the preferred combination as a measure of what we call their "performance bias". Subjects provided their informed consent according to University procedures.

RESULTS AND DISCUSSION

Data suggest that the effort function increases with greater power from the arms and legs (Fig.2). Randomized task combinations were applied repeatedly, and show that the effort function is consistent and repeatable.

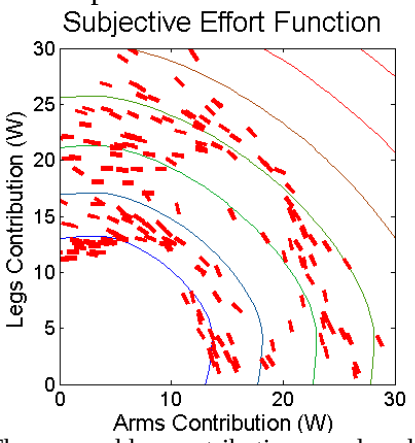

Figure 2: The arm and leg contributions produced by all subjects, with an average effort function determined by fitting contours to performance data. Each mark indicates the power from arms and legs in a task, with a slope corresponding to the task constraint.

To characterize the effort function, we compared the performance bias against the reward bias. We fitted their relationship with a modified generalized logistic function in the form:

$$PB = A + \frac{K - A}{1 + e^{-B*(IB-M)}}, (1)$$

The best-fit equation yielded parameter values A= 0.13, K= 0.83, M= -0.12, and B = 4.2. This fit confirms the consistency and repeatability of subjective effort (R^2=0.80, Fig. 3). Even though subjects were unaware of the particular reward bias for each task, they were consistent in their selection of arm and leg contributions to satisfy that task.

The bias towards using the legs more than the arms is indicated by the performance vs. reward curve. When given a neutral reward bias, where effort from their arms and legs are counted equally, subjects still used their legs to produce 57.2% of the work.

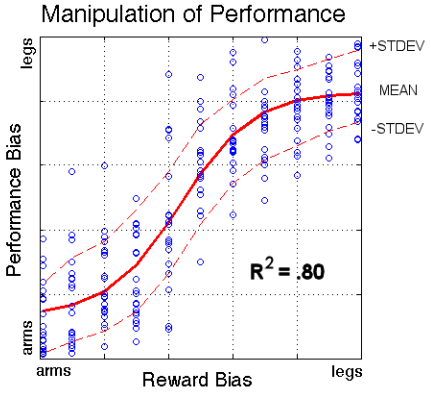

Figure 3: Performance bias (arms vs. legs) of healthy subjects (N = 10) performing exercise tasks with varying amounts of reward bias (also arms vs. legs). The performance bias follows an approximately sigmoidal curve, favoring arms or legs consistently if the task reward favors arms or legs.

There were few cases of subjects using solely the arms or legs. This could be partially accounted for from our stipulation that they keep both arms and legs in steady contact with NuStep, even if they preferred to perform little or no work with some limbs. Even with the limbs exerting little force, this would lead to some non-zero work on the machine.

It is unknown whether or how much the subjective effort functions corresponds to physiological variables such as applied force or metabolic energy expenditure. We expect that factors such as discomfort, fatigue, or strength discrepancies would cause subjective effort not to be determined only by energy expenditure.

A possible application of reward biases is to neurological rehabilitation. For example, if a patient with weak legs tends to favor their arms, a reward bias could be used to incentivize greater leg contributions. In many tasks, the reason for unequal performance bias may thus be sensible in terms of the short-term goal of minimizing subjective effort. The reward bias can be used to favor a longer term goal of exercising a weakened limb. Robotic rehabilitation has potential to systematize the incentivizing of exercise for a designated limb.

REFERENCES

1. Reinkensmeyer DJ. et al. *Proc IEEE Int. Conf.* 1009-1015, 2007.
2. Lunenburger L. et al. *Engineering in Medicine and Biology Society*, **2(1)**, 4888–4891, 2004.
3. Huang HJ. Ferris DP. *J Applied Physiology*, **97**, 1299–1308, 2004.

ABDOMEN-THIGH CONTACT FORCES DURING FUNCTIONAL REACHING TASKS IN OBESE INDIVIDUALS

[1]Bhupinder Singh, [2]Thomas D. Brown, [3] John J. Callaghan, [1] H John Yack
[1]Program in Physical Therapy & Rehabilitation Science
[2]Orthopedic Biomechanics Laboratory
[3] Department of Orthopedic Surgery
University of Iowa
email: bhupindersingh@uiowa.edu

INTRODUCTION

Thirty-four percent of adults in the United States are overweight and an additional 32.2% are obese (BMI >30.0) [1]. Obesity has been associated with an increased risk of disability through a range of mechanisms, including skeletal stress. In this population, the effect of mechanical stress on various joints during different activities has been documented.

Sibella (2003) [2] introduced a model of the fat mass to explain limited trunk lean in obese subjects during sit to stand activity. Thigh-calf [3] and heel-gluteus [4] contact forces during kneeling and squatting have been recently reported in normal weight subjects, but no study has been done to investigate the pressure exerted by abdomen on the thigh during functional activities.

The purpose of our study was to investigate the contact forces exerted by the abdomen on the thigh during functional reaching activities e.g. shoe tying in adult obese individuals.

METHODS

Six obese subjects, 4 female and 2 male, without current neurological or orthopedic ailments, aged between 40-70 years, mean BMI 39.8 kg/m^2 (range 32.6- 47) were included in this study.

Contact pressure between abdomen and thigh was measured using the Tekscan conformat pressure mapping sensor (model #5330, Tekscan, South Boston, MA, USA) during forward leaning task. The subject started from the erect seated position from a custom normal height chair, then leaned over to reach their right foot (e.g. shoe tying) and were instructed to hold the position. The activity was performed three times and a maximum pressure value documented for each subject.

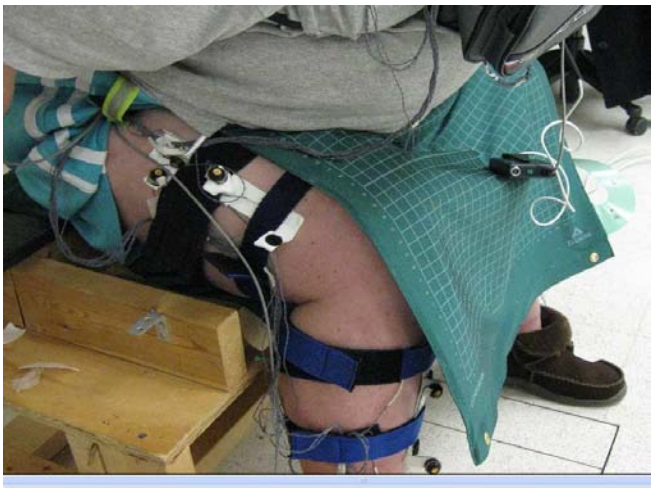

Figure 1: Experimental set-up. The reflective markers and the conformat pressure mapping sensor seen as the subject leans during a reaching task from a normal height wooden chair.

Triads of infrared emitting diode markers were placed on the pelvis, trunk and bilaterally on the thigh, leg, and foot. Kinematic data were collected using the Optotrak motion analysis system (Model 3020, Northern Digital Inc., and Waterloo, Ontario, Canada).Force plate data under the right foot was obtained from Kistler force plate.

Tekscan supplied software was used to calculate the centers of pressure and total forces due to abdomen-thigh contact area. A water bladder, to simulate the abdominal tissue and weights, were used to calibrate the thigh mat. Trunk flexion angle, in reference to lab axis system, was determined using the marker positions of the triad mounted on cervical vertebrae C7.

Regression analyses were performed to determine the association between measures.

RESULTS AND DISCUSSION

Contact forces were maximal when the trunk was maximally flexed in all subjects. The mean abdomen-thigh contact force was 10.17 +/- 5.18 % body weight. Subject A exerted 56.7 N (4.32% body weight) and Subject B exerted 189.1 N (19.96 % body weight). (Fig 2). The magnitude of the contact force and the area of contact varied across individuals, however there was a fairly broad dispersion of pressure on the thigh for all subjects.

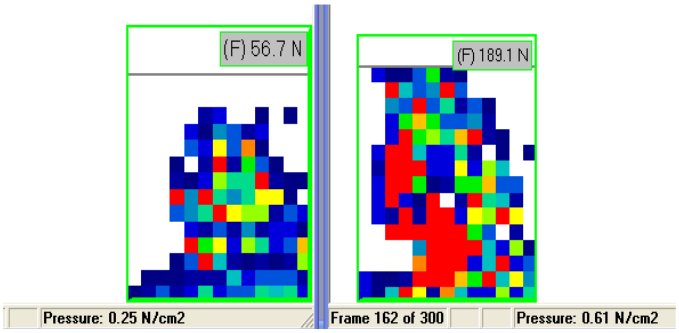

Subject A: BMI 47 Subject B: BMI 32.6

Figure 2: Examples of abdomen-thigh contact pressure distributions of two subjects with extreme BMI values captured at maximal trunk flexion angle during a reaching, shoe tying task.

About 32% of the variability in the force exerted by the abdomen is explained by the body mass index (fig 3).

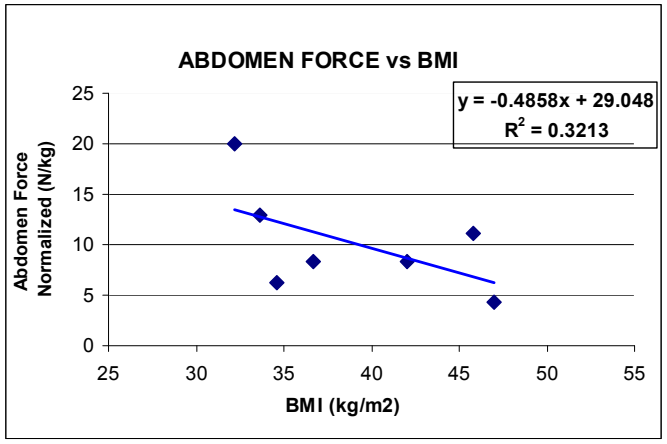

Figure 3: Regression plots for relationship between the force exerted by abdomen (normalized to individual body weight) and BMI.

Results show that considerable forces are exerted by the abdomen on the femur, which will potentially affect the forces at the hip joint. One subject with the highest BMI (47 kg/m^2) reported the lowest force among the six subjects, indicating possible restriction by the extra abdominal mass while reaching for the right shoe. Obese subjects show limited trunk flexion during normal sit to stand movement [2] and similar trends are seen for this reaching task (fig 4). No relationship is seen for trunk lean and abdomen force (R= 0.06)

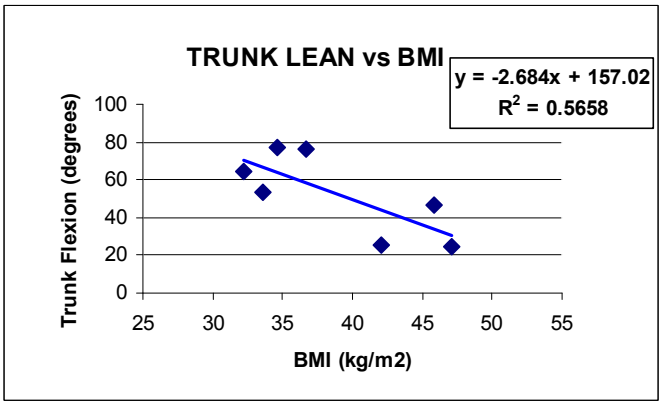

Figure 4: Regression plot for relationship between the Trunk flexion angle and BMI. 56% of the variability in the trunk lean is explained by the body mass index (R-value 0. 748)

CONCLUSIONS

A considerable amount of force is exerted by the abdomen on the thigh, mean 10.17 % body weight during forward trunk lean activities. This segment contact force should be included in the biomechanical analysis of obese subjects. Further work is being done to find possible implications of this contact force and how it may affect the forces and moments across the hip joint.

REFERENCES

1.Ogden CL, *JAMA* 2006;295:1549–55
2.Sibella F ,Clinical Biomechanics 18 (2003) 745–750
3. Zelle J, Clinical Biomechanics 22 (2007) 821–826
4. Pollard JP, Proceedings *of ASB,* Penn State *2009*

ACKNOWLEDGEMENTS

Department of Veterans Affairs-ICVMC

VARIABILITY OF CLINICAL EXAMINATION TECHNIQUES USED TO ASSESS LAXITY OF THE ANTERIOR CRUCIATE LIGAMENT

[1]Cale A Jacobs, [2]Thomas P Branch and [3]Rainer Siebold

[1]ERMI, Inc., Atlanta, GA
[2]University Orthopaedic Clinic, Decatur, GA
[3]ATOS Hospital, Heidelberg, Germany
email: calejacobs@hotmail.com

INTRODUCTION

Recent literature comparing different anterior cruciate ligament (ACL) reconstruction techniques have used the Lachman and Pivot Shift tests to quantify surgical outcomes, suggesting that double-bundle techniques may provide a more stable reconstruction when compared to single-bundle techniques [1,2]. However, during clinical examination of knee joint laxity, surgeons may place their hands or position the patient differently from one another, which affects the force delivered to the knee and the surgeon's ability to interpret laxity [3]. The subjective nature of clinical tests inherently limits the ability to generalize results from a single surgeon or single facility to the entire orthopedic community. The purpose of this study was to quantify the variability of these tests in a group of experienced surgeons in order to better understand the .

METHODS

Twenty-one board-certified orthopaedic surgeons specializing in sports medicine volunteered for the study (mean age = 47.7 y, years experience = 20 y), and data collection for this IRB-approved protocol was completed over a 2-day period. A single subject with no history of traumatic knee injury was evaluated by all 21 surgeons. The Lachman and pivot shift tests were instrumented with an electromagnetic joint evaluation system sampling at 120 Hz (3D Evaluator^{TM}, ERMI, Inc., Atlanta, GA; Figure 1). For both tests (Lachman and pivot shift), surgeons performed 1 trial of 3 repetitions in succession. The order of testing was consistent for each examiner, and testing was solely performed on the left knee. Kinematics were calculated using the ISB recommendations, with the hip joint center calculated using a spherical best-fit approach[4].

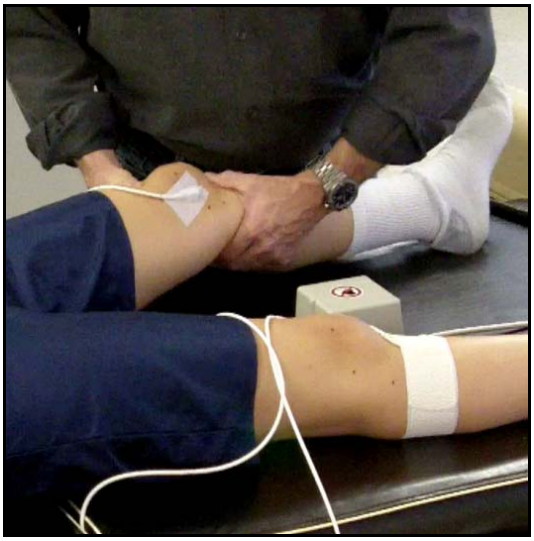

Figure 1: Performance of the Lachman test with an electromagnetic joint evaluation system.

The coefficient of variation over 3 trials was calculated for each surgeon, as well as the Minimum Detectable Change (MDC), which is defined as the minimum amount of difference that can be considered clinically significant. All analyses were performed with SPSS Statistics v17.0 (Chicago, IL), with $p < 0.05$ being considered significant.

RESULTS

For the Lachman test, the mean translation of the tibia relative to the femur was 8.3 ± 3.7 mm. These results are not unlike previous KT1000 testing of this subject, which demonstrated 7 mm of displacement with an applied force of 134 N. However, while the mean value was similar to an instrumented test, the amount of total anteroposterior translation ranged from 3.3 to 17.9

mm between the 21 surgeons during manual testing.(Figure 2)

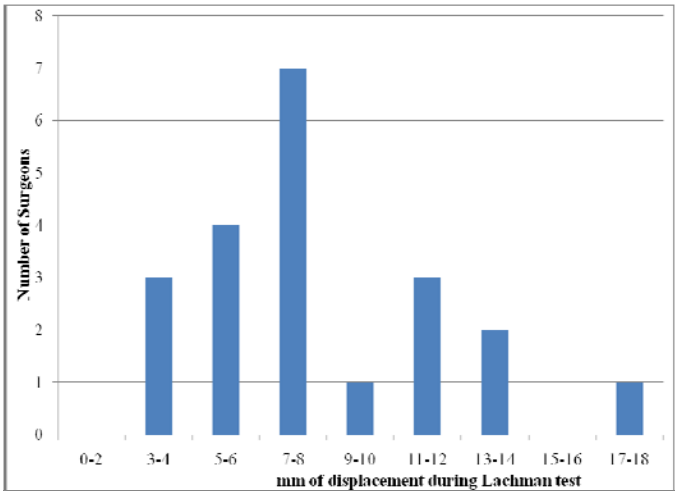

Figure 2: Distribution of anterior displacement measurements taken by the 21 surgeons during the instrumented Lachman test.

Only 5 of 21 surgeons had a coefficient of variation value of less than 10%, and the mean coefficient of variation was 22.8% for the group. The MDC was 5.0 mm between surgeons, and 9 of 21 surgeons demonstrated differences of more than 3 mm between their 3 repetitions.

The Pivot Shift movement patterns demonstrated even more variable results. For example, 3 surgeons started with the knee fully flexed whereas the others started in full extension, and 1 surgeon externally rotated the knee while going into flexion, which dramatically differed from the others. By definition, these surgeons were not performing a true pivot shift exam, and it has become apparent through this experience that the nomenclature surrounding the pivot shift test differs between surgeons based on where and with whom that surgeon trained as well as technique modifications that they have incorporated through their own professional experiences.

The magnitude of posterior translation during reduction of the tibia during the pivot shift, as well as the acceleration of posterior translation have been previously used to describe the pivot shift phenomenon [5]. In this sample of surgeons, both the magnitude and acceleration of posterior translation significantly correlated with the surgeon's years of clinical experience.

DISCUSSION/CONCLUSIONS

The results of common tests of joint laxity vary greatly between surgeons. The results of these tests are influenced by hand placement, the amount and direction of force applied, as well as the rate at which the force is applied. Even when using an electromagnetic joint laxity measurement system to quantify the clinical exam, the results of manual testing performed by one surgeon cannot be generalized to the entire orthopaedic community. As such, the validity of these utilizing these tests to quantify surgical outcomes is questioned.

REFERENCES

1. Siebold, R, Dehler, C, and Ellert, T. Prospective randomized comparison of double-bundle versus single-bundle anterior cruciate ligament reconstruction *Arthroscopy* **24**, 137-145, 2008.
2. Muneta, T, Koga, H, Mochizuki, T, Ju, Y-J, Hara, K, Nimura, A, Yagishita, K, and Sekiya, I. A prospective randomized study of 4-strand semitendinosus tendon anterior cruciate ligament reconstruction comparing single-bundle and double-bundle techniques *Arthroscopy* **23**, 618-628, 2007.
3. Floyd, RT, Peery, DS, and Andrews, JR. Advantages of the prone Lachman versus the traditional Lachman *Orthopedics* **31**, 671-675, 2008.
4. Gamage, SSHU and Lasenby, J. New least squares solutions for estimating the average centre of rotation and the axis of rotation J Biomech 35, 87-93, 2002.
5. Hoshino, Y, Kuroda, R, Nagamune, K, Yagi, M, Mizuno, K, Yamaguchi, M, Muratsu, H, Yoshiya, S, and Kurosaka, M. In vivo measurement of the pivot-shift test in the anterior cruciate ligament-deficient knee using an electromagnetic device Am J Sports Med 35, 1098-1104, 2007.

THE USE OF THE EMG INTEGRAL AND KINEMATIC ANALYSIS FOR EVALUATION OF SPASTIC HEMIPLEGIC PATIENTS

[1]Cristiano Rocha da Silva, [1]Franciele Marques Vanderlei, [1]Augusto Cesinando de Carvalho, [2]Heloyse Uliam Kuriki and [2]Leonardo Ferreira Polito

[1]Universidade Estadual Paulista, Presidente Prudente, SP, Brazil
[2]Universidade de São Paulo, São Carlos, SP, Brazil
email: cristiano.rsilva@ymail.com

INTRODUCTION

In hemiplegics individuals, the spasticity hinders the functional range of motion (FRM), causing an alteration in the reflex mecanism of the reciprocal inibition motor control, provoking an agonist-antagonist cocontraction, followed by hardening and slow movements on the affected member [1]. Surface electromyography (sEMG) and kinematics can provide data that complement the clinical evaluation of a hemiplegic indivual's motor function, contributing to a more effective terapeutical course elaboration.

METHODS

Twenty four individuals were evaluated. Twelve post-stroke individuals with average age of 59,28±7,01 years, injury time of 7.21±4.87 years, and twelve helathy individuals (control group) with average age of 64.51±9.30 years. The research was aproved by the UNESP Research Ethical Committee. The individual, after being informed about the research participation, signed an informed consent term.

For the sEMG signal aquisition, two pairs of AgCl electrodes, 10mm diameter, were used. The electrodes were placed parallely, 20mm afar from each other, in the Biceps Brachii (BB) and Triceps Brachii (TB). A Lynx EMG 1000 signal conditioner module was used for signal capture. A digital camera was used to the image acquisition, using one calibration plan and three 25mm sphere styrophoam markers, placed in anatomical reference points: acromion, medial epicondyle of the humerus and styloid process of the radius. The acquisition software used was the Ariel Performance Analysis System (APAS). The placement and the movement made by the subjects is showed in Figure 1. The movements were made using the plegic and the non-plegic side, in the hemiplegic subjects, and in the healthy subjects the superior dominant member was selected. To syncronize the systems a device made by a LED (Light Emitter Diode) was used.

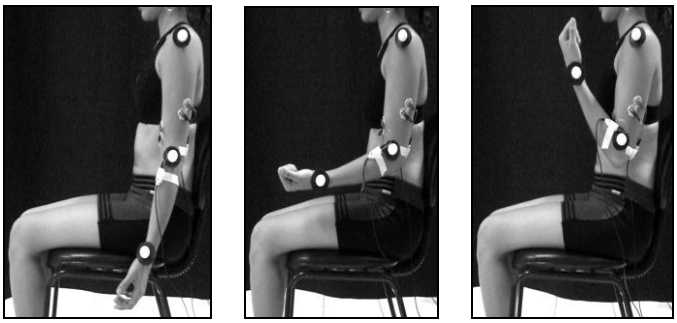

Figure 1: Subject position, electrode and styrophoam markes placement, during elbow flexion movement

The sEMG signals were analyzed in the AqDAnalysis software and the APAS software was used to obtain the FRM. The MatLab software was used to processing selected data, using an algorythm that was developed for such matter. The parameter used in the sEMG evaluation was the signal integral (IEMG). For the statistical analysis, the Kolmogorov-Smirnov test was applied to assess data normality, and then a Kruskal-Wallis test was applied to variable comparison, with a 5% significance level.

RESULTS AND DISCUSSION

The IEMG values, shown on Table 1, of the BB unloaded flexion movement, allows to observe that the control group was significantly greater in relation to hemiplegic subjects. In the loaded movement, this order inverts, the non-plegic side of

the hemiplegic subjects presented an IMEG value significantly greater than the control group and than the plegic side. This finding allows the understanding that, possibly, there is a greater demand in the non-plegic side, resulting in an overload to compensate the lack of strenght and muscular recruitment that exists in the plegic side. Olney and Richards [2] report that the sEMG activity on the plegic side is smaller than on the non-plegic side. The IEMG values of the TB do not show differences between unloaded movement, although, in the loaded, the plegic TB was different than the others.

When comparing the FRM, shown in Table 2, of the hemiplegic subjects and the control group it can be observed that both sides presents FRM decrease, however, only the plegic side presented a significantly difference.

Therefore, otherwise than most studies showed, a neurological injure is not exclusive in the contralateral hemibody, the hemiplegia settles contralatterally to the brain injury, but ipsilatteral side to the injury is also affected [3,4].

CONCLUSIONS

The results allowed to observe an increased fiber recruitment and the strenght generation of the non-plegic member in relation to the plegic side. The hemiplegic individual presents a FRM loss in the plegic side as well as in the non-plegic side, showing that a functional loss after a stroke occurs in both sides, but in different proportion. So, there must emphasyzed that a more effective intervention, with terapeuthical proposals for both sides of the hemibody of the hemiplegic, prioritizing the coordination and functionality.

REFERENCES

1. MACHADO, A.B.M. **Neuroanatomia Funcional.** 2ª edição. São Paulo: Atheneu, 1993, 359p.
2. OLNEY, S.J, RICHARDS, C.L. Hemiparetic gait following stroke. Part II: Recovery and phsical therapy . **Gait & Posture**. 1996; 4:149-62.
3. LENT, R**. Cem bilhões de neurônios: Conceitos fundamentais de neurociências**. São Paulo: Atheneu 2004.
4. LUNDY-EKMAN, L. **Neurociência: fundamentos para a reabilitação**. Rio de Janeiro: Guanabara Koogan, 2000.

ACKNOLEDGEMENTS

The authors thanks CAPES and FAPESP (process nº 2007/08397-6) for financial support.

Table 1: IEMG (u.n) signal values from flexion of elbow movement groups.

		Control	Plegic	Non-plegic
Elbow flexion – unloaded	BB	3,34 ± 2,07	2,55 ± 1,44	2,88 ± 1,48
	TB	1,52 ± 0,61	1,32 ± 1,09	1,51 ± 0,80
Elbow flexion –loaded	BB	3,84 ± 2,19	2,60 ± 1,68	4,42 ± 2,70
	TB	1,56 ± 0,98	1,02 ± 0,81	1,68 ± 1,17

Table 2: FRM (degree) values from flexion of elbow groups.

	Control	Plegic	Non-plegic
Elbow flexion – unloaded	119,18 ± 8,83	98,99 ± 21,50	115,05 ± 13,57
Elbow flexion – loaded	124,98 ± 7,69	93,94 ± 23,67	115,44 ± 15,73

THE EFFECT OF FOOT TYPE ON PLANTAR LOADING

[1]Andrew Kraszewski, [1]Betty Chow, [1]Jocelyn Frey, [1]Mark Lenhoff, [1]Sherry Backus, [1]Jonathan Deland, [2]Phillip Demp, [2]Jinsup Song, [2]Benjamin Heilman, [1]Sonali Rajan, [1]Andrea Woodley, [1,2]Howard Hillstrom

[1]Leon Root, MD, Motion Analysis Laboratory, Hospital for Special Surgery, New York, NY USA
[2]Gait Study Center, Temple University School of Podiatric Medicine, Philadelphia, PA, USA
email: kraszewskia@hss.edu

INTRODUCTION

Improved understanding of the pathomechanics that afflict individuals with pes planus *(e.g. hallux valgus, hallux limitus, osteoarthritis, tendonitis, plantar fasciitis, neuroma, posterior tibial dysfunction, chronic keratomata, collapsing pes valgus, etc.)* and pes cavus *(e.g. hammertoes, tailor bunion, metatarsalgia, diabetic neuropathy, etc.)* feet is needed[1]. Most of these pathologies involve aberrant plantar loading. The specific aim of this project is to compare plantar loading parameters during gait for asymptomatic healthy individuals across foot type (i.e. pes planus, pes rectus, and pes cavus).

METHODS

The investigators hypothesized that asymptomatic healthy individuals with pes planus, rectus, and pes cavus foot types will show differences in plantar loading measures. Asymptomatic healthy test subjects were evaluated at the Leon Root, MD Motion Analysis Laboratory at the Hospital for Special Surgery (HSS). Enrollment included 61 test subjects which were stratified, according to resting calcaneal stance position (RCSP) and forefoot to rearfoot (FF-RF) relationship, into pes planus, pes rectus, and pes cavus sub-groups. Dynamic plantar pressure measurements were recorded with an Emed-X system (Novel, Munich, Germany). Subjects walked barefoot across the sensor mat at their preferred speed; five steps per side were collected and analyzed with Novel masking software. The program divided each footprint into anatomical regions and calculated each measure within a region (see Figure 1). Pressure measures of interest were peak pressure (PP), maximum force (MF), pressure-time integral (PTI), force-time integral (FTI), and contact area (AREA). The hypothesis was evaluated with a univariate mixed effect analysis of variance (ANOVA). Foot type was a fixed effect and replication was a random effect. Significance was set at $p \leq 0.05$. Post hoc t tests were evaluated using Bonferroni correction with significance set at $p \leq 0.017$.

RESULTS AND DISCUSSION

Table 1 summarizes a subset of the results from this investigation, tabulating peak pressure and maximum force along with walking velocity and clinical foot type classification measures (FFRF & RCSP). Most plantar regions of the foot were sensitive to foot type. For example, hallux (M01) PP and MF values were significantly higher for pes planus foot types. PP and MF beneath the first metatarsal head (M04) in pes planus feet were significantly lower than both pes rectus and pes cavus feet. This data supports the "hyper-mobile 1st-ray theory" suggesting that load is supported by the 2nd and 3rd metatarsal heads in the pes planus foot. PTI and FTI (not shown) corroborate this observation. This may seem paradoxical because individuals with pes planus feet have a medially-shifted ground reaction force vector. At the 5th metatarsal head (M08) PP and MF values were significantly higher in the pes cavus foot compared to pes planus as anticipated. Unexpectedly PP and MF was lowest in the lateral arch for pes cavus feet. The medial and lateral heel had similar loading across foot types. Cavus feet were distinguished by higher PP at the lateral aspect of the heel yet displayed lower PP at the lateral arch. The medial arch has a substantially greater contact area (not shown) than both rectus and cavus feet while the rectus foot has substantially greater area than cavus feet.

CONCLUSIONS

Several measures of plantar loading are sensitive to foot type in this asymptomatic healthy cohort. This data may serve a normative reference for future investigations of pedal pathology, the design of improved treatments, and the demonstration of the efficacy of those treatments.

REFERENCES

1.Song J. *J APMA,* **86**(1) 16-23, 2006.

ACKNOWLEDGEMENTS

NIH Grant: 1R03HD053135-01.

TABLE 1. Plantar pressure measurements across foot types. Peak pressure (PP) and maximum force (MF) are listed for region masks hallux, metatarsals 1-5, medial and lateral arch and heel; RCSP, FFRF and walking velocity (Vel) are listed along with ANOVA p-values and significant post-hoc comparisons.

	Peak Pressure(N/cm^2), *Mean(SD)*				
	Planus N=27	**Rectus** N=22	**Cavus** N=12	**ANOVA**	**Post Hoc***
RCSP(deg)	-6.21(0.23)	-0.77(0.2)	0.04(0.31)	0.000	1,2
FFRF(deg)	6.50(0.4)	2.54(0.35)	-1.79(0.53)	0.000	1,2,3
Vel(m/s)	1.33(0.02)	1.28(0.02)	1.31(0.03)	0.138	
PP-M01	43.9(6.9)	37.1(5.6)	32.5(5.8)	0.000	1,2
PP-M04	28.1(8)	35.8(6.6)	37.3(6.8)	0.000	1,2
PP-M05	51.1(5.8)	37.7(4.8)	38.8(4.9)	0.000	1,2
PP-M06	40.4(4.3)	34.2(3.6)	34.8(3.6)	0.000	1,2
PP-M07	27.8(3.6)	26(3)	25.6(3.1)	0.084	
PP-M08	20.1(5.8)	26.3(5.2)	25.3(5.3)	0.000	1,2
PP-M09	33.8(4)	33.6(3.3)	38.4(3.4)	0.000	1,3
PP-M10	37.2(4.8)	36.5(4)	38.8(4.1)	0.304	
PP-M11	11.5(1.7)	10.9(1.4)	7.7(1.5)	0.000	1,3
PP-M12	20.1(5.8)	26.3(5.2)	25.3(5.3)	0.001	1,3
	Maximum Force(N), *Mean (SD)*				
	Planus	**Rectus**	**Cavus**	**ANOVA**	**Post Hoc***
MF-M01	135(17.1)	108.8(14.1)	91.5(14.5)	0.000	1,2,3
MF-M04	134.9(23.4)	148.2(19.2)	157.2(19.7)	0.006	1
MF-M05	177.1(16.2)	151.1(13.3)	152.1(13.6)	0.000	1,2
MF-M06	172.6(17.8)	150.7(14.6)	152.3(14.9)	0.000	1,2
MF-M07	104.6(14.9)	98.9(12.3)	100.8(12.6)	0.329	
MF-M08	41(10.7)	51.6(8.8)	58.4(9)	0.000	1,2
MF-M09	221.2(19.4)	215(15.9)	207.1(16.3)	0.065	
MF-M10	265.4(21.6)	255.6(17.7)	241.7(18.2)	0.002	1
MF-M11	107(25.8)	79.7(20)	52.7(20.5)	0.000	1,2,3
MF-M12	26.8(7.7)	13.7(6.3)	6.2(6.5)	0.000	1,2,3
**Bonferonni post-hoc significance set if p < 0.017*					
1 = Cavus vs. Planus; 2 = Rectus vs. Planus; 3 = Cavus vs. Rectus					

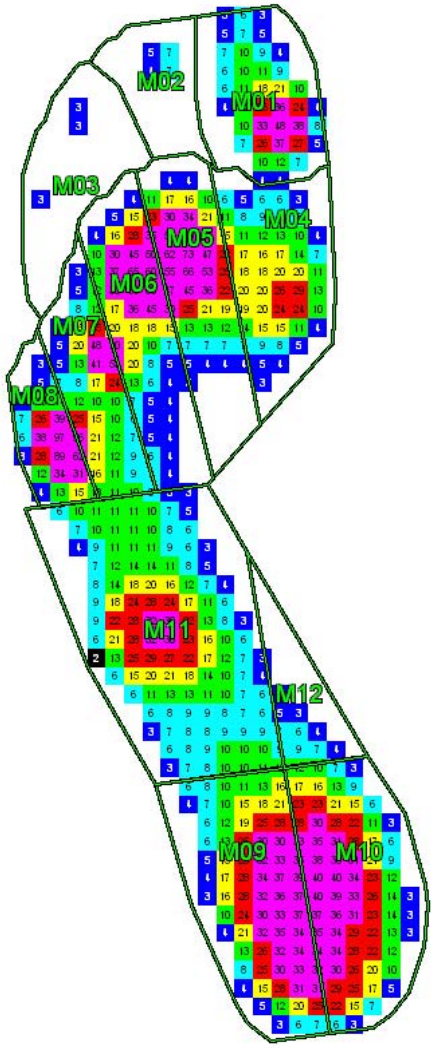

Figure 1: Plantar pressure masking. This mask was implemented in Novel software. Plantar pressure parameters during self-selected walking speed was calculated and tabulated for each masked region of each trial across all subjects.

M01 = Hallux
M02 = 2nd toe
M03 = 3rd, 4th, and 5th toes
M04 = sub metatarsal head 1
M05 = sub metatarsal head 2
M06 = sub metatarsal head 3
M07 = sub metatarsal head 4
M08 = sub metatarsal head 5
M09 = Lateral Heel
M10 = Medial Heel
M11 = Lateral Arch
M12 = Medial Arch

Computational Modeling of Ardipithecus Ramidus: A Revolution in Evolution

Shawn McGuan

Founder/CEO/CTO LifeModeler, Inc.
email: smcugan@lifemodeler.com, web: http://lifemodele.com

INTRODUCTION

The discovery of the 4.4 million year old Ardipithecus Ramidus (Ardi) was termed the "Most Significant Scientific Breakthrough" by the Journal of Science in 2009. The scientific effort involved 15 years of research, 47 scientists and 9 nations and represented one of the largest collaborative efforts of its kind. LifeModeler is proud to be one of these scientific organizations, providing significant evidence to the mobility and social behavior of this fascinating creature.

This work describes the odyssey of discovery in how the scientific team used computational biomechanics tools to reconstruct locomotion and other patterns of behaviors from the fossil record. It presents the succession of computational models which incorporate the various theories of joint articulations, muscle attachments and segment positions to provide additional evidence to the question which has been troubling Ardi scientists for years: "How can a foot that can grasp a branch, also walk efficiently?"

It concludes will detail the methodology of mapping the motion of Ardi from the computational models derived from the fossil record into the motion of a human subject which led up to the animation sequences seen in the Discovery Channel special "Discovering Ardi" in December 2009.

METHODS

The bones gathered from the fossil record were used build (Fig.1) the computational biomechanics model of the lower limb in LifeMOD®. Kinematic axes and range of motion between each bone segment were established by examining the articular surfaces (Fig.2).

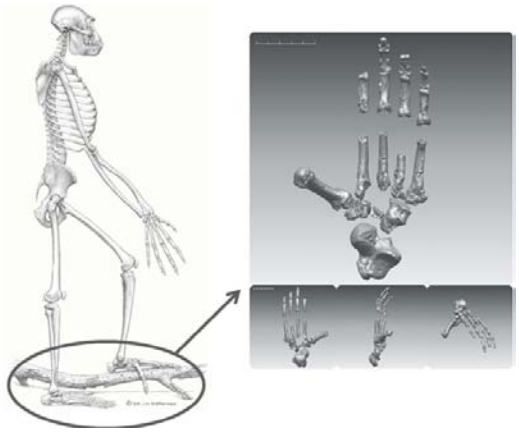

Figure 1: Ardipithecus Ramidus foot bones

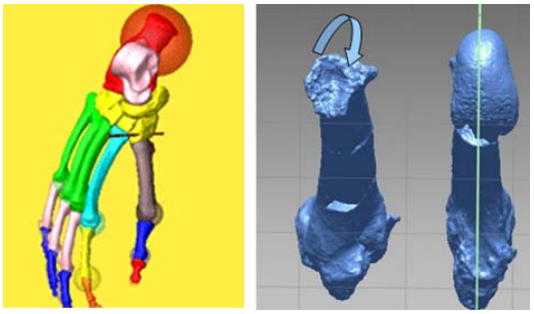

Figure 2: Segment axes and ROM were established by examining the articular surfaces of the bones.

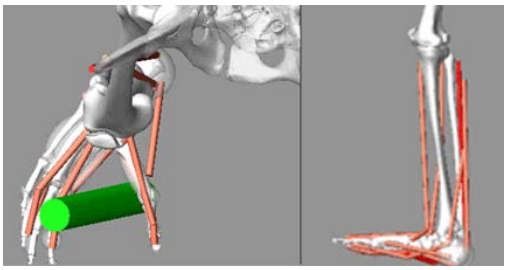

Figure 3: Dual purposed lower limb model; grasping and walking.

Muscles were then laced through the lower limb model using a variety of wrapping and scaffolding techniques. The lower limb model was then used to model two distinct activities of the limb; grasping and walking. The combination of segment geometry, joint axes, muscular attachment and

activations produced very specific motions at the hip and knee.

The hip/knee/ankle motion patterns were then morphed into full body model derived from a motion capture experiment with a test subject.

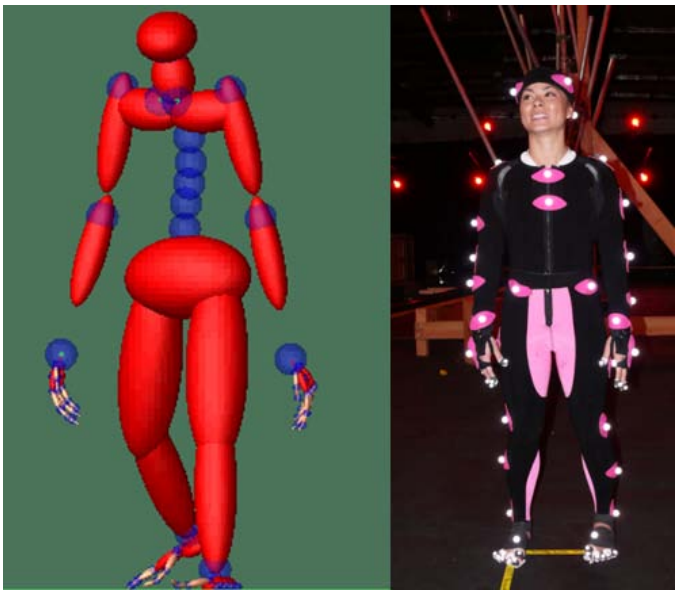

Figure 4. Mapping the motion derived from the lower limb model onto a full body model

RESULTS AND DISCUSSION

The modeling of functional behaviors of Ardipithecus Ramidus amounted to a forensic study of a creature that existed 4.5 million years ago. The biomechanical model was created from the partial set of bones from the fossil record, guidance from the team of evolutionary biologists and knowledge of human and chimpanzee anatomy [1,2].

The model was used to support various theories regarding physical behaviors of the creature postulated by the evolutionary biologists of the scientific group. The key to the discovery was the dual purpose foot; a foot that can grasp a branch yet effectively fulcrumate during locomotion.

One of the key components in the model was the attachment location of the peroneus longus (PL) muscle. From the fossil record, scientists determined that the PL muscle in Ardi was quite large. In addition the distal attachment of the muscle was on the medial aspect at the base of the first metatarsal, instead of the medial cuneiform as it is in modern humans. This attachment location had a very distinct effect of adducting and internally rotating the great toe. This motion coupling facilitated the grasping action as well as to provide a stable platform for locomotion. It was also determined from the fossil record, that Ardi fulcrumated of the second ray instead of the first ray as in modern humans. These kinematic couplings and action along with the location of the talocrural and subtalar joint axes in Ardi, provided information on tibial axial motion during walking and climbing. The lordosis of the lumbar spine in Ardi, provided information on the necessary muscular activity of the hip flexors and extensors during locomotion.

This knowledge provided a “dynamic template” which was used to adapt the motion from a modern human (of similar stature to Ardi). In reproducing the motion and activity patterns of Ardi, all muscular activity was guided by the physical limitations of each active muscle.

CONCLUSIONS

The computational biomechanics model lead to new insights of walking and grasping behaviors of Ardi. It functioned as a platform for the evolutionary biologists to test theories about motion while being restricted to the physical limitations of the creature as dictated by the fossil record.

The model will be extended to explore more complex activity patterns of Ardi.

REFERENCES

1. Lovejoy, C.O., et al. Combining Prehension and Propulsion: The Foot of Ardipithecus Ramidus, October 2009, Science 326, 72
2. Keith, A., The history of the human foot and its bearing on orthopedic practice, J Bone Joint Surg Am. 1929;11:10-32.

ACKNOWLEDGEMENTS

Professor Owen Lovejoy, Kent State University.

SKELETAL MUSCLE ARCHITECTURE OF THE GOAT HINDLIMB

Allison S. Arnold, Carolyn M. Eng and Andrew A. Biewener

Concord Field Station, Harvard University, Bedford, MA, USA
email: asarnold@alum.mit.edu, web: www.oeb.harvard.edu/affiliates/cfs

INTRODUCTION

With the increased availability of software for generating muscle-driven simulations [e.g., 1], many investigators are creating biomechanical models and simulating movements, with the hope of preventing injuries or improving the efficacy of treatments. However, very few are validating the predictions of their models by comparing results to key parameters, such as the muscle forces and fascicle length changes measured *in vivo*. These parameters are difficult to quantify in humans, since they generally involve invasive techniques. Simulation-based studies of animals — which could be compared, for example, to sonomicrometry, EMG, or tendon force buckle measurements during *in vivo* experiments [e.g., 2] — are needed to test and refine techniques for modeling and simulation.

With this aim in mind, we have characterized the skeletal geometry, segment masses and inertias, joint kinematics, and muscle force-generating properties of the hindlimb of a goat *(Capra hircus)*, as necessary to create a 3D musculoskeletal model. This abstract describes new insights gained from analyzing the muscle architecture.

METHODS

Dissections were performed on the formalin-fixed pelvis and right hindlimb of one adult male specimen (mass = 46 kg). After measuring the specimen's joint angles at their fixed orientations, the origins and insertions of all the major hindlimb muscles (divided into 43 muscle-tendon units) were digitized. The muscles were removed and their architectural properties determined as described by Lieber *et al.* [e.g., 3]. For each muscle unit, we isolated 2-3 fascicle bundles, measured raw fiber length with a digital caliper, and averaged these data. Under magnification, we freed 5-8 small fiber bundles from each fascicle, and we assessed bundle sarcomere length using laser diffraction (VHK circular beam diode laser, wavelength = 635 nm, power = 4.9 mW, *Coherent Inc.*). We calculated the physiological cross-sectional area (PCSA) of each muscle unit from its measured mass (m), density (ρ = 1.056 g/cm^3 [4]), optimal fiber length (l_o^f), and surface pennation angle (α) as follows:

$$PCSA = \frac{m}{\rho * l_o^f} * \alpha$$

We estimated the optimal fiber length of each muscle unit from its raw fiber length (l_{raw}^f), bundle sarcomere length (l_{raw}^s), and optimal sarcomere length (l_o^s) as follows:

$$l_o^f = \frac{l_{raw}^f}{l_{raw}^s} * l_o^s$$

The measured sarcomere lengths of the muscles, after averaging across fiber samples, ranged from 1.78 – 3.18 μm. We assumed an optimal sarcomere length of 2.4 μm; this is similar to the optimal lengths reported for cat and monkey [5], and it appears consistent with our laser diffraction data.

RESULTS AND DISCUSSION

Examination of the muscles' architectural features is informative (e.g., Fig. 1). These data reveal, for example, that the goat's biarticular rectus femoris (RF) has the largest PCSA, and thus the greatest force-generating capacity of all the hindlimb muscles. The massive gluteobiceps (GBi) and gluteus medius (GMED) also have substantial force-generating capacity. At the ankle, the goat's biarticular gastrocnemius (LG and MG), the short-fibered fibularis tertius (FibT), and the superficial and deep digital flexors (SDF and the combined heads of DDF) are the strongest muscles.

The goat's hamstrings (SM, ST, and BF), by contrast, have the longest optimal fiber lengths. The sartorius (SAR) and adductor (ADD) also have

relatively long fiber lengths; these muscles are presumably designed to undergo large excursions.

Comparison of the PCSAs for groups of muscles indicates that the goat's ankle plantarflexors are substantially stronger than the ankle dorsiflexors (i.e., the plantarflexors have a greater total PCSA). Also, the goat's knee extensors, as a group, are stronger than the knee flexors. These results are consistent with analogous data derived from human studies [6], and likely reflect the important anti-gravity function of these muscle groups. At the hip, the goat's flexors and extensors have similar total PCSAs; this result differs from human studies.

Analyses of the goat's muscle architecture, in combination with musculoskeletal modeling and simulation tools, may offer new insights in comparative biomechanics studies. For instance, in bipedal humans, Ward and colleagues [6] have argued that soleus is the most important force generator at the ankle (due to its exceptionally large PCSA), and vastus lateralis is the most important force generator at the knee. However, the quadrupedal goat does not have an equivalent soleus at the ankle, and its rectus femoris is substantially stronger than any of its vasti. Observations such as these may help guide future studies aimed at elucidating general principles of musculoskeletal function and design. Also of note, Eng and colleagues [7] have examined whether architectural features of selected muscles scale with body mass; in their study, data from mouse, rat, cat, human and horse were included. The goat data reported here help "fill the size gap" between cat and human, and thus could make a contribution to future scaling studies.

CONCLUSIONS

We have analyzed the architectural features of all the major muscles in the goat hindlimb. Our next step is to incorporate these data into a detailed, 3D model that characterizes the muscles' force- and moment-generating capacity over a functional range of limb positions.

ACKNOWLEDGEMENTS

We gratefully thank Carlos Moreno, Maria deBoef, Jennifer Carr, James Wakeling, Sabrina Lee, and Pedro Ramirez for their assistance.

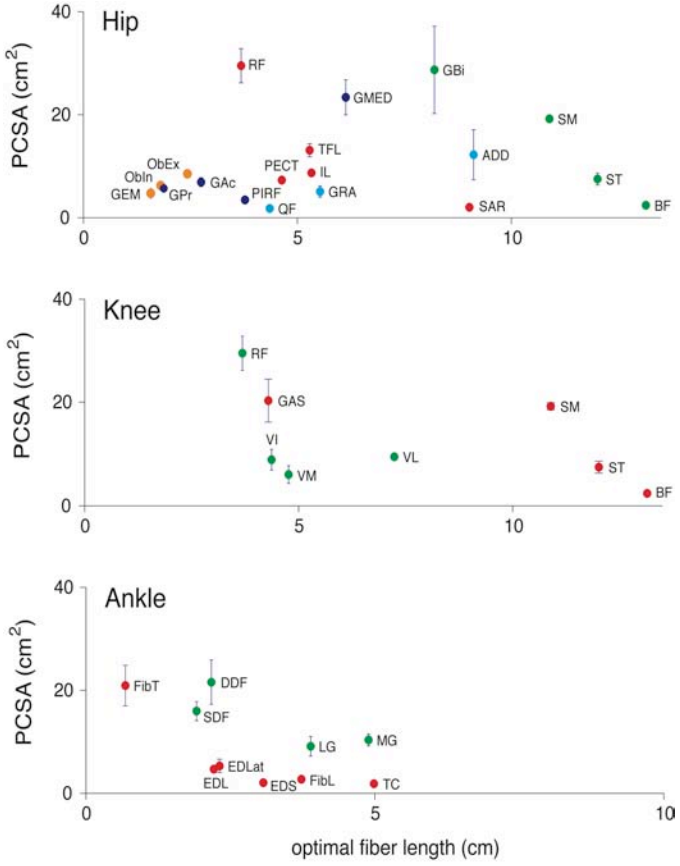

Figure 1: Plots of PCSA vs optimal fiber length for selected goat muscles at the hip, knee, and ankle. Error bars (± 1 SD) reflect variability in the lengths obtained from sampling 2-3 regions per muscle-tendon unit; some muscles that were divided into multiple units (e.g., gluteobiceps, gluteus medius, gastrocnemius, and deep digital flexors) have been combined here for clarity. To aid interpretation, muscles that primarily extend a joint are shown in green, muscles that primarily flex are shown in red, and the hip abductors, adductors, and rotators are shown in blue, cyan, and orange, respectively.

REFERENCES

1. Delp SL, et al. *IEEE Trans Biomed Eng* **54**, 1-11, 2007.
2. McGuigan MP, et al. *J Exp Biol* **212**, 2092-2104, 2009.
3. Lieber RL, et al. *J Hand Surg Am* **15**, 244-250, 1990.
4. Ward SR and Lieber RL. *J Biomech* **38**, 2317-2320, 2005.
5. Burkholder TJ and Lieber RL. *J Exp Biol* **204**, 1529-1536, 2001.
6. Ward SR, et al. *Clin Orthop Relat Res* **467**, 1074-1082, 2009.
7. Eng CM, et al. *J Exp Biol* **211**, 2336-2345, 2001.

STUDY OF PROPULSION MECHANISMS IN LEECH ANGUILLIFORM SWIMMING

[1]Jun Chen, [2]Tetsuya Iwasaki and [1]Wolfgang Otto Friesen

[1]University of Virginia, Charlottesville, VA, USA
[2]University of California, Los Angeles, CA, USA
Email: jc6cd@virginia.edu, tiwasaki@ucla.edu, wof@virginia.edu

INTRODUCTION

The swimming gait of the leech is anguilliform, with rearward traveling waves that propel the animal forward. We analyze this motion with a simple fluid model that combines Taylor's resistive and Lighthill's reactive forces, and fix the drag coefficients by fitting model predictions to trajectory data derived from video recordings. The fluid force on the body, the power supply from the muscle, and its dissipation to the fluid are predicted by the model. Thrust generation and power transmission mechanisms along the body of swimming leeches are investigated. The model for body-fluid interactions developed in this study will be an essential element of our integrated model for anguilliform swimming, comprising the central pattern generator (CPG), muscle activation dynamics, body-fluid interactions, and sensory feedback.

METHODS

The leech body is modeled by a chain of eighteen rigid links on a plane, subject to fluid forces and joint torques generated by muscle contractions. We adopted the equations of motion developed in [3] with a modification on the description of the environmental (fluid) force. Our simple fluid model combines Taylor's resistive force [1] and Lighthill's reactive force [2], and is given, for each link, by

$$\begin{aligned} \gamma_t &= c_t\left(5.4l\sqrt{\rho\mu d|v_n|}v_t\right) \\ \gamma_n &= \text{sign}(v_n)c_p\rho dlv_n^2 + c_a\rho\pi d^2 l a_n/2 \end{aligned} \quad (1)$$

where γ_t and γ_n are the fluid forces in the body coordinates, the subscripts t and n represent, respectively, the tangential and normal components, ρ and μ are the density and viscosity of the fluid, d and l are the width and half length of the body link, v_t and v_n are the link velocities in body coordinates (the implicit assumption is that the fluid is static), c_p and c_t are the drag coefficients, c_a is the added mass coefficient and a_n is the acceleration of the link in the normal direction.

The model was decoupled as described in [3] into two sets of equations: (Dynamics A) one from the muscle torques to the resulting body shape change, and (Dynamics B) the other from the shape change to the inertial movements of the body. The inertial movements refer to the translation of the center of gravity and the overall rotation, which is defined as $\theta_o := (\sum_{i=1}^{18}\theta_i)/18$, where θ_i are the link angles with respect to the direction of locomotion, which is fixed to the horizontal axis in this study.

The body movements during steady swimming were recorded via a high-speed camera, and the video images were processed to generate time courses of kinematic variables. Fig. 1 illustrates the data processing of the measured joint angles.

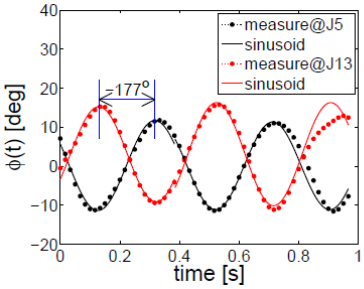

Figure 1: Measured joint angles ϕ_5 and ϕ_{13} during swimming. Joint angles change sinusoidally. The posterior joint ϕ_5 lags anterior joint ϕ_{13}.

We simulated Dynamics B by enforcing the measured body shape change, and determined the fluid drag coefficients c_p, c_t and c_a by minimizing the root-mean-square error between the simulated trajectory of the center of gravity and the video data. The joint torques were then predicted by inverting Dynamics A using the shape change data and the estimated drag coefficients.

RESULTS AND DISCUSSION

The fluid drag coefficients were found to be $c_p = 3$, $c_t = 0.6$ and $c_a = 0$, indicating that the resistive force is dominant over the reactive force in leech swimming (Re=500~1000). Video data of eight swim episodes and simulated swimming were compared in terms of the trajectory of the gravity center (GC) and the overall body rotation (θ_o). The result (see Fig.2 for a sample) shows that the simple fluid force model (1) captures the essence.

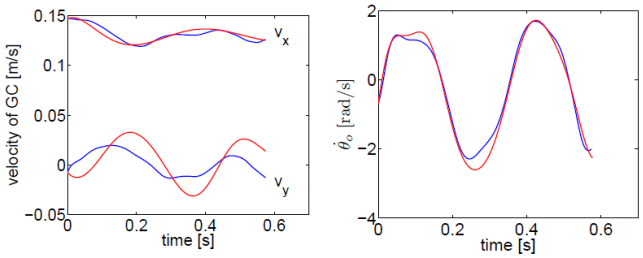

Figure 2: Comparisons of a simulated swimming (blue curves) with the video data (red curves).

We computed the distribution of thrust and drag along the body (Fig. 3), where the thrust and drag on each link are calculated by the projection of normal and tangential fluid forces, respectively, in the direction of swimming averaged over one cycle. Thrust is generated all along the body and increases towards the tail; drags experienced by the links are roughly uniform over the body.

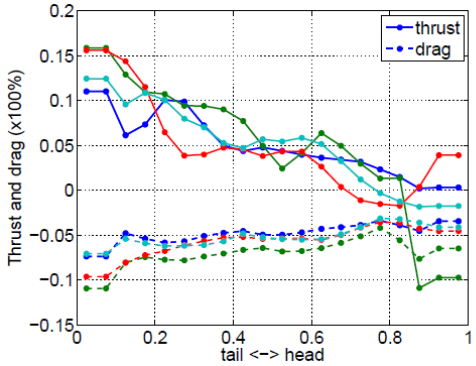

Figure 3: Thrust and drag generated along the body. The values are normalized by total thrust. The abscissa is the body location, "0" denotes the tail tip and "1" denotes the head tip. The colored curves represent four swimming episodes.

We also calculated the energy supplied to the body by muscle in one cycle and its dissipation to the fluid along the body (Fig. 4). The power from the muscle is mainly supplied in the mid-body and is dissipated into the fluid mostly at the tail link.

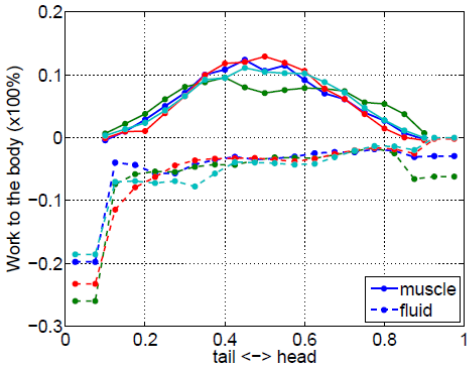

Figure 4: Energy supplied at 17 body joints in one cycle (upper curves) and its dissipation into the fluid (lower curves). The values are normalized by the total work of 17 joint muscles in one cycle.

The time courses of muscle power input at joints show that mid-body muscles always supply power, whereas the muscles near the tail region both supply and absorb power during each cycle. Correlating the negative power stroke with the muscle strain, we found that the energy supplied by the mid-body muscles is transmitted to the elastic energy of the posterior muscles through body kinematics. The elastic energy stored in the muscles near the tail region acts on the fluid and generates large fluid forces.

CONCLUSIONS

A simple static model appears to capture the hydrodynamic forces during leech swimming. More generally, our results suggest that, in anguilliform swimming, thrust is generated all along the body but increases towards the tail. Power from muscles is generated primarily in the mid-body and is dissipated to the fluid at the tail tip.

REFERENCES

1.Taylor SG. *Proc R Soc Lond A* **214**, 158-183, 1952.

2.Lighthill MJ. *J Fluid Mech* **44**, 265-301, 1970.

3.Saito M, et al. *IEEE Control Syst Mag* **22**, 64-81, 2002.

STUDY OF MOTOR CONTROL OF LEECH ANGUILLIFORM SWIMMING

[1]Jun Chen, [1]Wolfgang Otto Friesen and [2]Tetsuya Iwasaki

[1]University of Virginia, Charlottesville, VA, USA
[2]University of California, Los Angeles, CA, USA
Email: jc6cd@virginia.edu, wof@virginia.edu, tiwasaki@ucla.edu

INTRODUCTION

The propagation speed of motor unit activation along the body of anguilliform swimmers, such as eel and lamprey, can be recorded using electromyographical techniques and compared with the wave of mechanical body curvature. Model-based analysis is a necessary tool to reveal the underlying mechanisms. We use models of body-fluid interactions and muscle activation dynamics, which were developed from video recordings of swimming leeches and experimental data on muscle activation dynamics, to predict the motorneuron (MN) impulse frequency and muscle tension. The propagation speeds of MN activation wave along the body, the tension wave and the body curvature wave are compared. The mechanisms that give rise to faster tension waves from the slower MN activation waves are discussed.

METHODS

The leech body is modeled by a chain of eighteen rigid links. At each joint, the muscle torque and MN impulse frequency are related by

$$u(t) = r\big(T_v(t) - T_d(t)\big),\ \ T_*(t) = T(f_*, x_*) \quad (1)$$

where the subscript $*= d$ or v, representing the dorsal and ventral muscles, respectively, u is the joint torque from the muscle, r is the half of body thickness, T is the muscle tension, f is the MN impulse frequency, and x is the muscle strain. The torque $u(t)$ during swimming was predicted from the video shape data and the fluid force predicted from body-fluid system equations. Tension model T has the form $T = a(f)h(x)$, where $a(\cdot)$ and $h(\cdot)$ are the muscle activation and basic tension-length relation functions. With x determined from the swimming video, T is a linear function of muscle activation a. Expressed as discretized time courses $u(t)$, $a_d(t)$, $a_v(t)$, $h_d(t)$ and $h_v(t)$, given as column vectors of dimension n=17, (1) turns into the system of n linear equations with $2n$ unknowns. To eliminate the redundancy of the solution $a_d(t)$ and $a_v(t)$, we look for the unique solution such that the quantity

$$\sqrt{\frac{1}{t_1}\int_0^{t_1} f_d^2(t) + f_v^2(t)\,\mathrm{d}t}, \quad (2)$$

is minimized subject to:

$$T_d(t) \geq 0, T_v(t) \geq 0 \quad (3)$$

where $f_d(t)$ and $f_v(t)$ are related to $a_d(t)$ and $a_v(t)$ by the dynamic function $a(\cdot)$ and t_1 is the duration of the swimming episode. $a(\cdot)$ is a first-order low pass filter with a time delay unit. Discrete approximation of (1)-(3) leads to minimization of a quadratic cost function over an Euclidean vector of $a_d(t)$ and $a_v(t)$, subject to linear equality and inequality constraints, which can be solved efficiently using MATLAB LMI control toolbox. $f_d(t)$, $f_v(t)$, $T_d(t)$ and $T_v(t)$ are then obtained from $a_d(t)$ and $a_v(t)$. We also used the tension and the activation variable $a_d(t)$ and $a_v(t)$ as the cost function, but they did not give solutions of MN impulse frequency close to the observed values. Thus it seems reasonable to consider MN impulse frequency to be positively correlated to energy costs.

RESULTS AND DISCUSSION

The predicted time courses of MN activity on the ventral side (for example) during intact swimming are shown in Fig. 1, where the ordinate is the impulse frequency of a firing MN. Only five out of seventeen body joints are shown. MN activities at the head (J17) and tail (J1) joints are very small. The sequence of mid-body frequency peaks (arrows in Fig. 1) illustrates a propagating wave from anterior to posterior. The propagation of the MN activation is slower than the propagation of tension (Fig. 2). The magnitude of impulse frequency approximates the observed values (80~100Hz).

The negative impulse frequency implies accelerated tension-reduction. This prediction suggests that inhibitory MNs accelerate muscle relaxation. Tension (Fig. 2) is near zero during a portion of the cycle, suggesting that inhibitory MNs not only accelerate the muscle relaxation, but further reduce the intrinsic tonus tension.

Another prediction is that both MN impulse frequency and muscle tension are larger on the ventral side than that on the dorsal side, perhaps due to the effects of gravity.

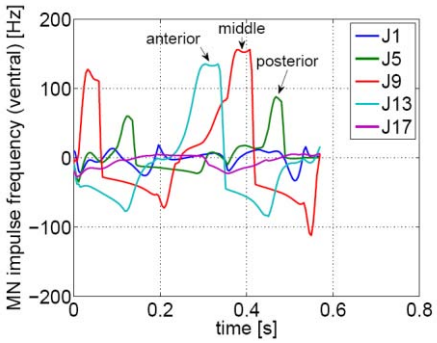

Figure 1: The predicted MN impulse activation along the body during intact swimming from the measured kinematic data of swimming videos.

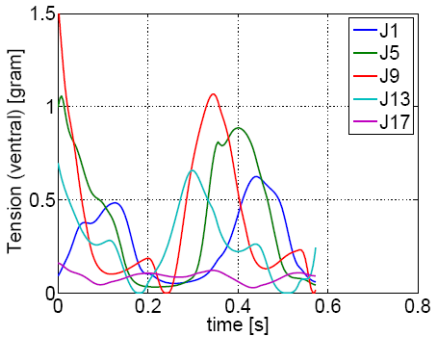

Figure 2: Predicted tension of five joint muscles during intact swimming.

The phase of MN activation and muscle tension in the strain cycle are shown in Fig. 3. The tension and strain of muscles in the tail region are nearly in phase. Together with the prediction that the MN activities at the tail joint are very small (Fig. 1), it suggests the tail behavior is passive. The slope of the phase curves in Fig. 3 is inversely proportional to the propagation speed of the corresponding waves, showing that MN activation speed is close to the body curvature wave; nevertheless, the tension wave is twice as fast as either.

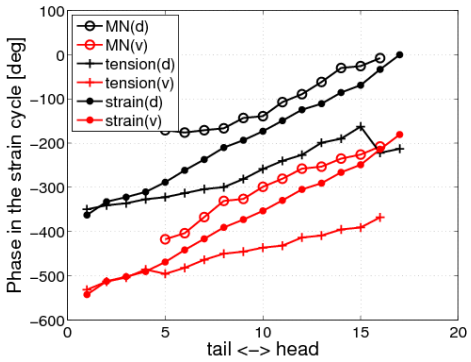

Figure 3: The phase of MN impulse activation and muscle tension in the strain cycle.

To uncover the mechanisms of how faster tension waves can result from slower MN activation waves, we did a simple calculation of the product of two same-speed slow waves of sinusoidal oscillations with the same oscillation amplitude, bias and phase as the fundamental harmonic of the predicted muscle activation variable $a_v(t)$ and tension-length function $h_v(t)$ on the ventral side. The product comprises a bias term, a term with twice the frequency and a term with the fundamental frequency. The wave speed of the fundamental component is found to be about twice as fast as $a_v(t)$ and $h_v(t)$. It means it is possible to generate a faster tension wave with slow MN activation and body curvature waves through the multiplicative structure of the tension, i.e., $T(f,x) = a(f)h(x)$, if the amplitude, bias and phase of two slow waves are appropriately set.

CONCLUSIONS

The data-based model results provide the following conclusions and predictions about leech anguilliform swimming: 1) MN impulse frequency appears to be positively correlated to energy costs; 2) MN activities are relatively large in the mid-body and very small in both head and tail regions; 3) Inhibitory MNs not only accelerate the muscle relaxation, but also reduce the intrinsic tonus tension to nearly zero; 4) The tail moves passively during swimming; and 5) The propagation speed of MN activation along the body is close to the observed body curvature wave, nevertheless the tension wave is twice fast. The multiplicative structure of tension model provides an explanation.

KINEMATIC MODELING OF THE SEAHORSE TAIL

[1]Tomas Praet, [1]Sofie Van Cauter, [2]Dominique Adriaens, [3]Srikanth Kannan, [4]Bert Masschaele, [3]Srikanth Srigiriraju, [1]Matthieu De Beule and [1]Benedict Verhegghe

[1]Institute Biomedical Technology (IBiTech-bioMMeda), Ghent University, Ghent, Belgium
[2]Evolutionary Morphology of Vertebrates (Dept. of Biology), Ghent University, Ghent, Belgium
[3]SIMULIA HQ, Providence, RI, USA
[4]Centre for X-ray Tomography (UGCT), Ghent University, Ghent, Belgium
email: tomas.praet@ugent.be

INTRODUCTION

Through billions of years of natural selection, nature has produced elegant and efficient solutions to a whole range of real-world problems. The evolutionary adaptation of an organism to its environment is in a lot of ways comparable to the design cycle in engineering: changes in functionality are tested on their fitness and are thereafter reinforced or rejected.

A seahorse (belonging to the genus *Hippocampus*) is one example of an animal that underwent remarkable adaptations to its environment. Due to a relatively weak caudal fin, the seahorse is hardly able to escape from predatory fish. For defensive purposes, the seahorse is covered by bony plates instead of scales, acting like a sort of armor against bites of predators. Despite the 'armor plating', this fish has still a remarkable tail bending flexibility. The seahorse can use its tail as a prehensile organ, grasping onto plants and other object on the seafloor.

The unique combination of strength and flexibility of the seahorse tail structure is very interesting from an engineering point of view. The tail bending mechanism has been studied in vivo [1], but details of the mechanics and kinematics involved remain largely unknown. Modeling the seahorse tail will hopefully provide a profound insight in the mechanics and kinematics of the different chains of the tail skeleton.

METHODS

A micro-CT scan (spatial resolution 21 µm) of a seahorse (species *Hippocampus reidi*) with curled tail was performed by the Centre for X-ray Tomography of Ghent University. Segmentation and 3D-mesh generation was carried out using Amira 5.2 (Visage Imaging, Inc.) (Fig.1, left). For two tail segments, the five skeletal elements (a central vertebral element, surrounded by four dermal plates) were exported as individual triangular surface meshes (Fig.1, right). Two other segments were combined into a single surface mesh in order to act as a constraining structure during the kinematic analyses.

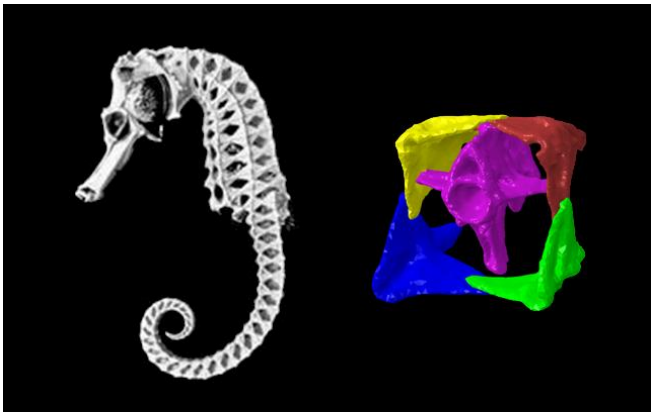

Figure 1: Micro-CT scan of a seahorse (left) and a single tail segment (right)

The musculoskeletal system of the seahorse tail was modeled with Abaqus/CAE 6.9-EF1. The geometry was simplified by replacing the different elements with rigid beam connections between the centre of mass of each element and the attachment points (Fig.2). The mass of each part was approximated by multiplying its volume with 1800 kg/m³ [2]. Muscles and joints between the elements were modeled by creating connectors. The joints were given constraints according to their physiology and stability considerations. They included sliding joints

and ball and socket joints. The entire model is demonstrated in Fig.3.

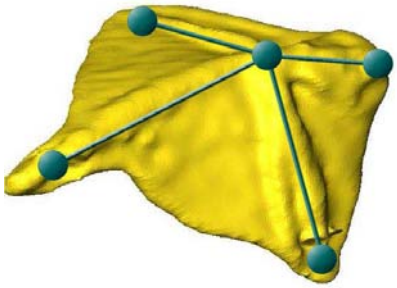

Figure 2: Beam connections on a dermal plate

The attachment points of the muscles were determined with pyFormex, an open-source software package intended for generating, manipulating and operating on large geometrical models of 3D structures (www.pyformex.org). As the different segments of the tail skeleton appear to have a highly uniform shape, the determination of the attachment points was automated within pyFormex, which has proven to be well suited as a dedicated pre-processor for finite element modeling.

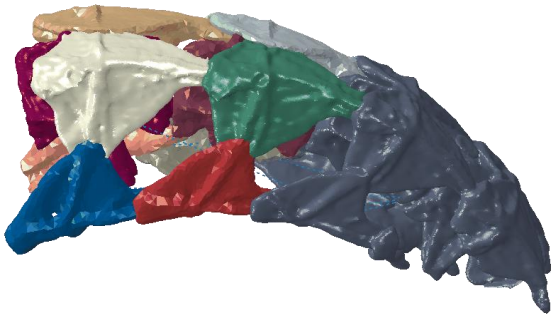

Figure 3: Tail model with the different skeletal segments

RESULTS AND DISCUSSION

The main muscles that seem to be involved in the ventral curving of the caudal system are the myomere muscles and the median ventral muscles (Fig.4). The myomere muscles are biarticulate, spanning three vertebrae. They can bend the tail both ventrally (bilateral contraction) and laterally (unilateral contraction). The median ventral muscles are uniarticulate and connect the ventral processes of two consecutive vertebrae. Contraction of these muscles causes a ventral bending of the system.

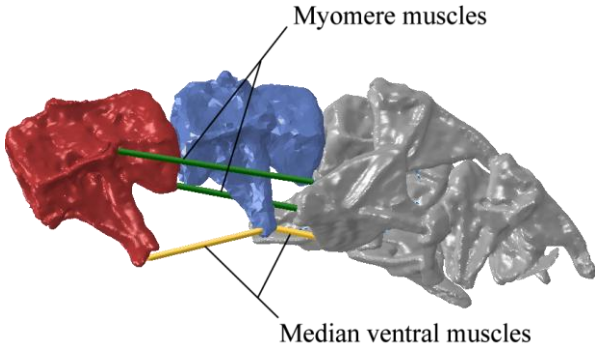

Figure 4: Modeled tail bending muscles

Two different sets of kinematic constraints were applied to the model. In the first simulation, the caudal segments were stretched, while measuring the connector motions. The second analysis used the connector motions of the median ventral muscles. As the tail stretches, the different elements of the tail segments enlarge while the overlapping joints between the dorsal and ventral plates become shorter.

CONCLUSIONS

Some segments of the musculoskeletal system of the tail of a seahorse were modeled. As the tail stretches the joints between the vertebrae, dorsal and ventral plates move in a complex way to allow the motion. The model holds promise to provide a keen insight in the kinematics involved.

REFERENCES

1. Hale, M. E., "Functional Morphology of Ventral Tail Bending and Prehensile Abilities of the Seahorse, Hippocampus kuda", *Journal of Morphology*, **227**, 51-65, 1996.
2. Biltz R. M., Pellegrino E. D., "The Chemical Anatomy of Bone: I. A Comparative Study of Bone Composition in Sixteen Vertebrates", *The Journal of Bone and Joint Surgery*, **51**, 456-466, 1969.

ACKNOWLEDGEMENTS

This research is funded by the Fund for Scientific Research Flanders, Belgium (*FWOVlaanderen*). The authors would like to thank Subham Sett, Victor Oancea and Gaetan Van Den Bergh from Simulia for their valuable support.

ANIMAL-ROBOT INTERACTION FORCES AS A MEASURE OF LOCOMOTOR FUNCTION FOLLOWING SPINAL CORD INJURY

Jeff A. Nessler, Jessica Duhon, Robert Keller and Thomas Thys

California State University San Marcos, San Marcos, CA, USA
email: jnessler@csusm.edu

INTRODUCTION

Rodent models are commonly used to study spinal cord injury (SCI). Previously, a system of robotic devices was developed for research into the recovery of locomotor function in these animals [1-3]. This device was designed to serve both as a means to apply locomotor training to bipedal stepping animals and as an assessment tool for the recovery of hindlimb function [4]. Originally, this device consisted of a body weight support mechanism, bilateral hindlimb manipulators, and a small, motorized treadmill [1]. More recently, the motorized treadmill has been replaced by two reciprocating platforms. This configuration was shown to result in greater stepping activity in adult rats following spinal contusion [2]. Detailed descriptions of both versions of the device can be found in [1-2].

Recently, a new version of the device was fabricated with four 6DOF force/torque sensors (Nano17, ATI Automation) positioned at the points of interaction between the animal and robotic device. Two sensors were placed in series with the hindlimb manipulators, and two sensors were placed beneath the sliding platforms to measure ground reaction forces (Fig 1). Detailed measurement of interaction forces between the robot and animal will be useful for a variety of reasons. First, these data may provide a sensitive and precise method by which locomotor recovery might be assessed. Second, these data may provide an accurate assessment of animal effort and may therefore be used as a method to dose training intensity. Finally, these data may be useful for designing assist as needed training algorithms in this animal model. The purpose of this study was to determine if differences in locomotor function could be detected for animals at 20 vs. 42 days post SCI through evaluation of animal-robot interaction forces. These data will provide a preliminary evaluation of the feasibility of recording continuous force data from an animal stepping in the robotic device following SCI.

METHODS

Mid-thoracic spinal cord transection surgery was performed on 5 female, Sprague-Dawley rats at 5 days of age. Following surgery, the animals were returned to their mothers and allowed to recover for 20 days. At 25 days of age, the animals were placed on the robotic device. A specialized harness was used to attach each animal to the weight support system. Small strips of neoprene were wrapped around the animal's ankle and an alligator clip was used to hold the ends of each strip together. The alligator clip was attached in series to the force/torque sensor and hindlimb manipulator, and was allowed to rotate about a mediolateral axis via revolute joint. For all animals, body weight support was set to approximately 90% of the animal's body weight.

Following setup, the rats underwent a brief period of automated locomotor training, during which time robot interaction forces were measured. The training algorithm was designed to alternate pulls of each hindlimb into extension while the stance limb was held directly beneath the animal's body. When swing was detected, the animal's limb was released and allowed to swing forward while the contra-lateral limb was then pulled into extension. This training algorithm is also described in greater detail in [2]. Each animal was trained for a period of 5 minutes, and force data were collected for 2 one minute intervals during this time at 1000Hz. As a preliminary analysis, raw data were first filtered (4^{th} order Butterworth filter, 8 Hz cutoff), and then the overall mean and peak forces were identified from each trial. Data from the right and left limb were

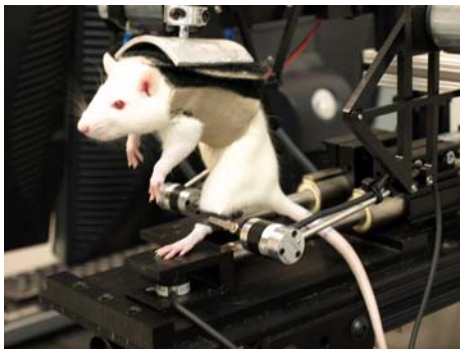

Figure 1: Instrumented robotic device.

averaged, and 3 measures of force were identified for each animal: resultant force in the sagittal plane between the animal and hindlimb manipulator, ground reaction force in the vertical direction (GRF_Z), and propulsive ground reaction force (GRF_X). Forces were analyzed both raw and following normalization to animal body weight.

RESULTS AND DISCUSSION

While stepping in the robotic device, animal-robot interaction forces were successfully recorded from all 5 animals (Fig 2). Overall, both mean and peak raw forces increased from day 20 to day 42 (Fig 3). For example, peak vertical ground reaction force (GRF_Z) increased from 1.35±0.31N to 2.40±1.33N, peak propulsive ground reaction force (GRF_X) increased from 0.71±0.15N to 2.07±1.38N, and peak hindlimb interaction force increased from 0.76±0.07N to 1.40±0.71N. Each of these increases was significant.

When forces were normalized to animal body weight, animal-robot interaction forces were reduced at day 42 when compared to performance at day 20 post SCI (Fig 3). For example, peak vertical ground reaction force decreased from 2.52±0.58% to 1.97±1.09%. One exception was peak propulsive ground reaction force, which increased from 1.33±0.28% to 1.70±1.14%, though this increase was not significant.

These data provide preliminary evidence that animal-robot interaction forces can be recorded with sufficient resolution for use in the assessment of locomotor function and for the design of locomotor training algorithms. In particular, these data may provide an in-vivo measure of muscle function following extended periods of disuse in severely impaired animals. Though initial results are promising, additional study is needed to further characterize the hindlimb force capabilities of various rodent models following SCI.

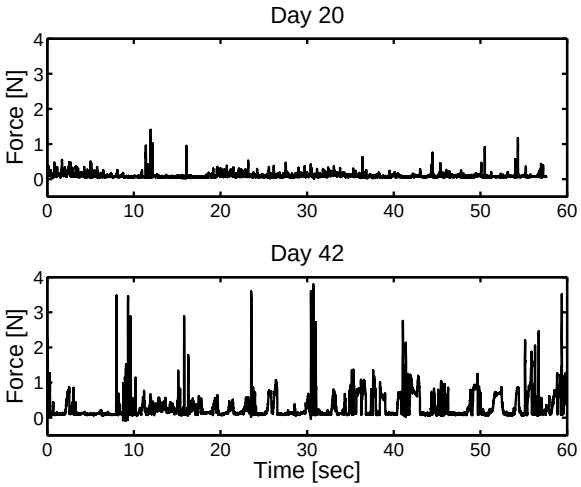

Figure 2: Raw vertical ground reaction force at 20 and 42 days post injury for a representative animal.

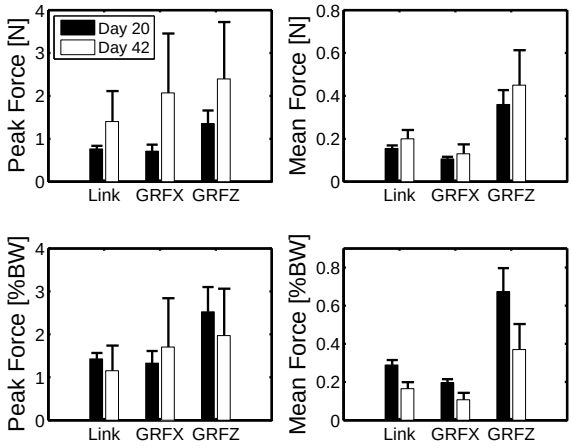

Figure 3: Mean and peak animal-robot interaction forces at 20 and 42 days post injury. Link: sagittal plane resultant force measured at hindlimb manipulator, GRF_X: propulsive ground reaction force, GRF_Z: vertical ground reaction force. Bars represent standard deviation (n=5).

REFERENCES

1. Nessler, JA, et al. *IEEE Trans Neural Sys Rehab Eng*, **13**(4): p. 497-506, 2005.
2. Nessler, JA, et al. *J Neurosci Meth*, **159**: p. 66-77, 2007.
3. Nessler, JA, et al., in *25th annual IEEE EMBS*, Cancun, Mexico. p. 1629-1632, 2003.
4. Nessler, JA, et al. *J. Neurotrauma*, **23**(6): p. 882-896, 2006.

ACKNOWLEDGEMENTS

This work was supported by NSF 0850516.

FINITE ELEMENT SIMULATION OF A PORCINE TEMPOROMANDIBULAR JOINT

[1]Sarang Dalne, [1]Betty Sindelar and [1]John Cotton

[1]Ohio University, Athens, OH, USA
email: cotton@ohio.edu, web: http://oak.cats.ohiou.edu/~cotton/

INTRODUCTION

Temporomandibular joint (TMJ) disease effects up to 20 to 25% of the population resulting in pain dysfunction and arthritis. Many computational simulations of human TMJ mechanics using the finite element (FE) method have been demonstrated including [1-4].

The pig is a useful model to study TMJ mechanics due to its structural and mechanical similarity to humans, as well as its relatively low expense. A FE model of the pig TMJ will be useful for comparing joint mechanics of the two species. Additionally, as the pig is a more flexible experimental model, an experimentally verified porcine FE model could increase confidence in human models using similar FE techniques. We demonstrate here the first FE model of the pig TMJ.

METHODS

We used CT scans of a Hanford pig [5] to create the geometry of the TMJ and surrounding bone. The mandible and temporal bones were segmented with Amira (Visage Imaging, Carlsbad, CA, USA). Extracted surfaces were exported into Marc (MSC Software, Santa Ana, CA, USA). We created superior and inferior disc surfaces from the bone's articulating surfaces while estimating disc sides manually.

Surface meshes were converted to a solid mesh of linear tetrahedra. We added linear springs to represent the superior and inferior posterior retrodiscal ligaments and TMJ ligaments at their anatomic locations. The resulting FE mesh (Figure 1) had over 40,000 degrees of freedom.

Materially, we defined the TMJ disc as a Mooney-Rivlin material with constants C_{10} and C_{01} of 27.9 and -20.8 MPa respectively, after Chen [1]. Bone was modeled as isotropic and linear elastic with a modulus of 1.5 GPa, reflecting the dense cancellous bone of the CT scans. The ligaments were assigned a stiffness of 2.7 N/cm [1]. This stiffness value carries considerable doubt, so a parametric study was performed to examine its impact on the results. The disc was assigned frictionless contact with both the temporal fossa and the mandible.

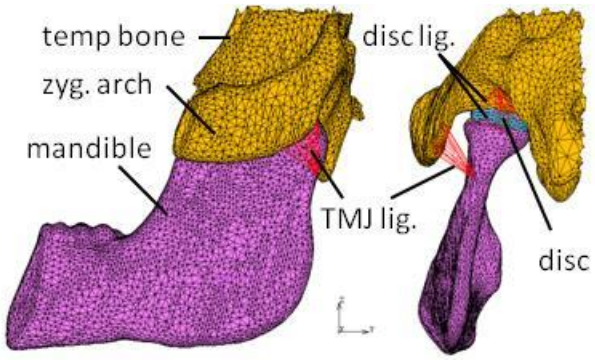

Figure 1: Lateral and posterior views of the FE model geometry showing skull (yellow), mandible (purple) and disc (blue), with ligaments in red.

Muscle loads estimated from [5-7] were added to simulate clenching (Figure 2). All outer boundaries of the skull, as well as the anterior portion of the zygomatic arch, were fixed.

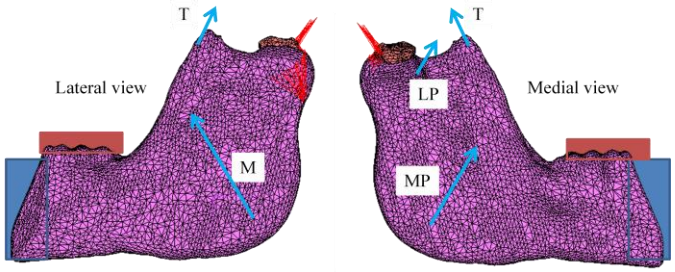

Figure 2: The masseter (M, 304 N); medial (MP, 227 N) and lateral (LP, 100 N) pterygoid; and temporalis (T, 212 N) were applied as forces. The tooth surface (red box) was constrained against superior and anterior motion, while the blue box is constrained against medial/lateral motion.

The model was simulated using a gradually applied quasi-static load with an automatic adaptive step procedure, due to the nonlinearities from the disc material and contact. The model was checked for approximation error in both mesh and force step discretization.

RESULTS AND DISCUSSION

The model resulted in an expected pattern of the disc being compressed except for the posterior-most portion where tension was realized by the pulling of retrodiscal ligaments. Values of maximum disc stresses are presented in Table 2. Maximum stresses were seen in the lateral portions of the central zone (Figure 3).

Table 2. Results of this model's maximum stresses (tensile, compressive, and von Mises) compared to reported FE models [1-4] for humans.

FE subject	Load case	Maximum stress (MPa)		
		σ_T	σ_C	σ_{vm}
Porcine	clench	1.9	13.3	3.6
Human [3]	clench			0.85
Human [4]	clench	0.25	0.7	
Human [1]	closing	3.7	8.0	8.0
Human [2]	closing			2.8

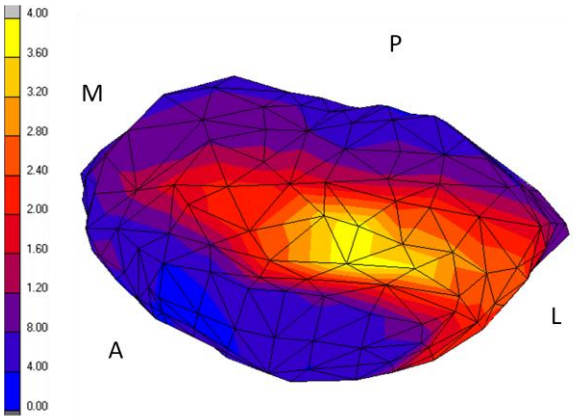

Figure 3. Superior view of von Mises stresses (MPa) in the TMJ disc.

Simulations with ligament stiffness multiplied by factors of 100 and 0.01 resulted in similar patterns and maximum σ_{vm} in the disc changing only -25% and +2%, respectively. This indicates that, at least for our clenching load, ligament stiffness plays a relatively minor role on disc stress.

We also compared our FE results at the subcondylar mandible and zygomatic arch to experimental data of feeding pigs [8]. Our magnitudes of maximum and minimum principal stresses largely fell within one standard deviation of data recorded from strain gauges. However, the orientation of the stress tensor showed significant differences.

CONCLUSIONS

Stresses were found to be in the general range of what is reported in human (Table 2). The (di)similarities between human and pig models could be due to geometric differences between the species, as well as both actual or modeled differences between loads and material properties. We did find that the maximum stresses were in the lateral central zone which is consistent with human TMJ studies and theories.

REFERENCES

1. Chen J, et al. *Medical Engineering & Physics*, **20**, 565-572, 1998.
2. Beek M, et al. *Journal of Biomechanics*, **33**, 307-316, 2000.
3. Hirose M, et al. *European Journal of Oral Sciences*, **114**, 441-448, 2006.
4. Perez del Palomar A, et al. *Annals of Biomedical Engineering*, **36**, 1014-1023, 2008.
5. Tickhill J. *The Virtual Pig Head*, www.oucom.ohiou.edu/virtualpig/pig_head.htm
6. Herring SW. *Journal of Mammalogy*, **66**, 603-617, 1985.
7. Langenbach GEJ, et al. *Journal of Anatomy*, **201**, 383-389, 2002.
8. Herring SW, et al. *The Anatomical Record*, **266**, 152-166, 2002.

FUNCTIONAL MORPHOLOGY OF DORSAL FINS IN TWO SHARK SPECIES

[1]Anabela Maia and [1]Cheryl D Wilga
[1]University of Rhode Island, Kingston, RI, USA
email: amaia@mail.uri.edu, web: http://www.uri.edu/cels/bio/maia

INTRODUCTION

Contrary to most teleost fishes, sharks lack a gas bladder and despite high lipid content in the liver are negatively buoyant [1]. Shark fins also lack the fine motor control of teleost fins [2]. Shark dorsal fins are composed of basals, radials and ceratotrichia [3, 4]. We investigate the functional morphology of shark dorsal fins in white spotted bamboo sharks, *Chiloscyllium plagiosum*, and spiny dogfish, *Squalus acanthias*, two unrelated species that inhabit different habitats and have strikingly different dorsal fin morphology. We hypothesize that the benthic bamboo shark is going to use the dorsal fins to augment thrust during steady swimming and will have fine control of the fins during maneuvering. The spiny dogfish with spines in front of each fin will use these fins as stabilizers in steady swimming and as a pivot in turning.

METHODS

We swam four sharks of each species in a flow tank at $0.5BL.s^{-1}$ and $0.75BL.s^{-1}$ while recording dorsal and lateral views using high speed video with electromyographic data. Later, we induced turning in a circular tank with objects to simulate a complex environment and induce spontaneous turning, while gathering the same type of data. Electrodes were bilaterally implanted into three regions along the dorsal fin muscle on the first and second dorsal fins and unilaterally in the left red epaxial musculature just below each fin for reference. We also investigated fin skeletal and muscular anatomy.

RESULTS AND DISCUSSION

The dorsal fin anatomy of benthic white-spotted bamboo sharks and benthopelagic spiny dogfish reflects swimming habit. Differences are apparent in external and internal anatomy. Bamboo sharks have a larger second dorsal fin area and proportionally more muscle extending into both dorsal fins than spiny dogfish. Skeletal elements are composed of a variable number of basals and radials that are almost indistinguishable and lack a clear arrangement in spiny dogfish (Fig 1 top). In contrast, bamboo sharks have a single row of multiple plate-like elongated basals followed by a row of shorter radials that fans out into the fin web (Fig.1 bottom). Between each basal and radial is a cartilaginous pad, indicating a movable joint. Bamboo fin muscle bundles are discrete and correspond with the radials. Spiny dogfish fin muscles have a more compact structure and lack discrete bundles. Dorsal fin complexity in spiny dogfish is increased by the presence of an anterior spine. The spines are wrapped in thick collagen fibers pointing posteriorly, which insert into the skin near the middle portion of the fin base. Similar bundles of collagen fibers run in the opposite orientation from the middle to the end of the fin base. The collagen fibers appear to make the fin more rigid but also create bending planes in the middle of the fin.

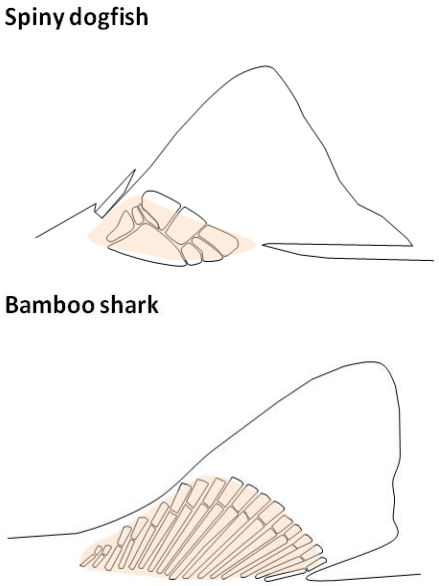

Figure 1: Schematic representation of the skeletal and muscular anatomy of bamboo shark first dorsal fin. Shaded area represents the area occupied by the dorsal fin muscle.

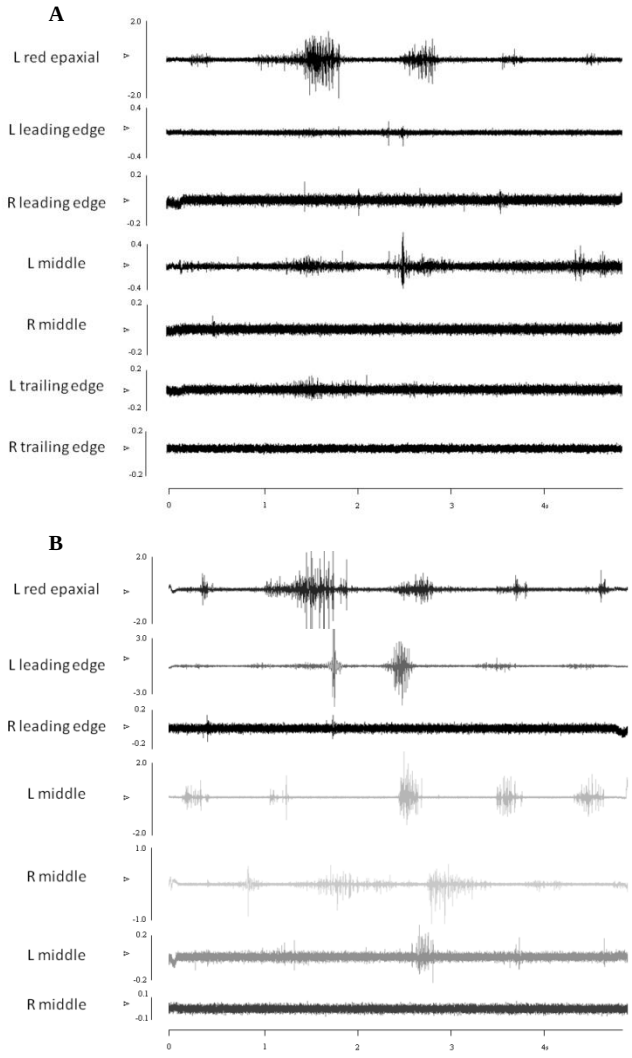

Figure 2: Representative traces of muscle activity along the first (A) and second (B) dorsal fins of a bamboo shark during a left turn.

During steady swimming, the spiny dogfish first dorsal fin moves independently of the body with higher amplitude at lower speeds, indicating a stabilizing function to counter increased instability. The first dorsal fin has a three dimensional conformation at maximum displacement. The second dorsal fin appears to move passively with the caudal portion of the body, although it cannot be ruled out at this point that the dorsal fin may augment thrust. This will be later tested using particle image velocimetry. Bamboo shark dorsal fins move in synchrony with the trunk, showing relatively higher amplitude of movement compared to dogfish at both speeds. First and second dorsal fins show a similar kinematic pattern with comparable displacements when corrected for axial displacement and appear independent of speed. This indicates a different function of the dorsal fins during steady swimming in the two species. The first dorsal fin in spiny dogfish likely contributes to stability while the second dorsal fin, as well as both dorsal fins in bamboo sharks, appears to contribute to added thrust. Preliminary electromyography data corroborates these conclusions.

During turning maneuvers, the first and second dorsal fins were active in both species, with contralateral and ipsilateral musculature showing bursts throughout the turn. There appears to be independent control of the different muscle bundles along the fin, since onset, offset and duration varied among the three implanted regions for both species. Muscle fin activity suggests that there is a thrust component to bamboo dorsal fins during maneuvers (Figure 2). Spiny dogfish dorsal fins revealed variable muscle activation patterns and might be more versatile than first thought.

CONCLUSIONS

Dorsal fin bending in dogfish may play a role in stabilizing forces, while the complex structure of bamboo shark fins imparts greater mobility to redirect thrust forces, as corroborated by anatomical, kinematic and electromyography analyses.

REFERENCES

1.Jobling M. *Environmental biology of fishes*, Chapman & Hall, 1995.
2.Lauder GV. *Amer. Zool.* **29**, 85-102, 1989.
3.Compagno LJV. Endoskeleton, in *Sharks, Skates and Rays: The Biology of Elasmobranch Fishes*, John Hopkins University Press, 1999.
4. Liem KF and Summers AP. Muscular System, in *Sharks, Skates and Rays: The Biology of Elasmobranch Fishes*, John Hopkins University Press, 1999.

ACKNOWLEDGEMENTS

The authors would like to acknowledge Jason Ramsay, Shannon Gerry, Jocelyne Dolce, Matt Lotti, Stacey Sakai, Andrea Scott and Ashley Stoher for help with experiments and animal care, and the undergraduates that participated in this project Bonnie Witte, Ashley Heinze, Britt McGee and Kim Arbonies. The experiments were approved under the IACUC protocol # AN05-07-001. A. Maia is funded by MCTES/FCT/SFRH/ BD/36852/2007

THE EFFECTS OF DIFFERENTIAL WING STROKE AMPLITUDE AND STROKE OFFSET ON INSECT BODY MOMENTS DURING PERTURBED FLIGHT CONDITIONS

[1]Jason T Vance, Imraan Faruque, and J Sean Humbert

[1]University of Maryland, College Park, MD, USA
email: jvance@umd.edu, web: http://www.avl.umd.edu/

INTRODUCTION

The extraordinary flight behavior of insects is characterized by robust flight performance in heterogeneous environments, which consist of gusts and turbulence that form around natural and man-made landscapes. Recent investigations have revealed that insects quickly respond to perturbations by employing asymmetric wing strokes. Here, we investigate the kinematic strategies used by the European honey bee, *Apis mellifera*, in response to a simple wind gust, and we characterize how variation in the differential stroke amplitude and stroke offset between the right and left wings affects insect body moments.

METHODS

Honey bee foragers were flown in a 25-L cylindrical flight chamber. A small-diameter (1mm) port was plumbed into the wall of the flight chamber to administer a simple, low pressure (5 psi) gust of air. Three high-speed (6006 fps) video cameras, oriented orthogonal to each other, recorded free-flight during the gust perturbation. Six morphological landmarks (head, tip of abdomen, left and right wing hinges, and left and right wingtips) were digitized from the video sequences using custom software [1]. A wireframe model of the honey bee wing planform [2] was superimposed over the wing image and rotated for best fit to determine the wing angle. From these landmarks, the following kinematics were calculated: body attitude (roll, pitch, and yaw); wing stroke position within the stroke plane (ϕ); stroke-averaged angle of attack ($\alpha_{r,avg}$); stroke amplitude (Φ); and, the mean position of stroke amplitude, stroke offset (ϕ_{off}). Differential stroke amplitude (Φ_d) and stroke offset ($\phi_{off,d}$) were calculated as the difference between the right and left wings for each of these two parameters.

Artificial wing stroke kinematics were created using stereotyped honey bee kinematics [2] that were scaled to produce variation in Φ_d and $\phi_{off,d}$ similar to the range observed in the honey bee gust response. The reference flight kinematics were: $\Phi = 90°$; $\phi_{off} = 30°$ (dorsal); $\Phi_d = 0°$; $\phi_{off,d} = 0°$; wingbeat frequency = 225 Hz. A quasi-steady model [3] was used to estimate aerodynamics and body moments about the roll, pitch, and yaw axes for $\Phi_d \in [0°, 50°]$ and $\phi_{off,d} \in [0°, 40°]$.

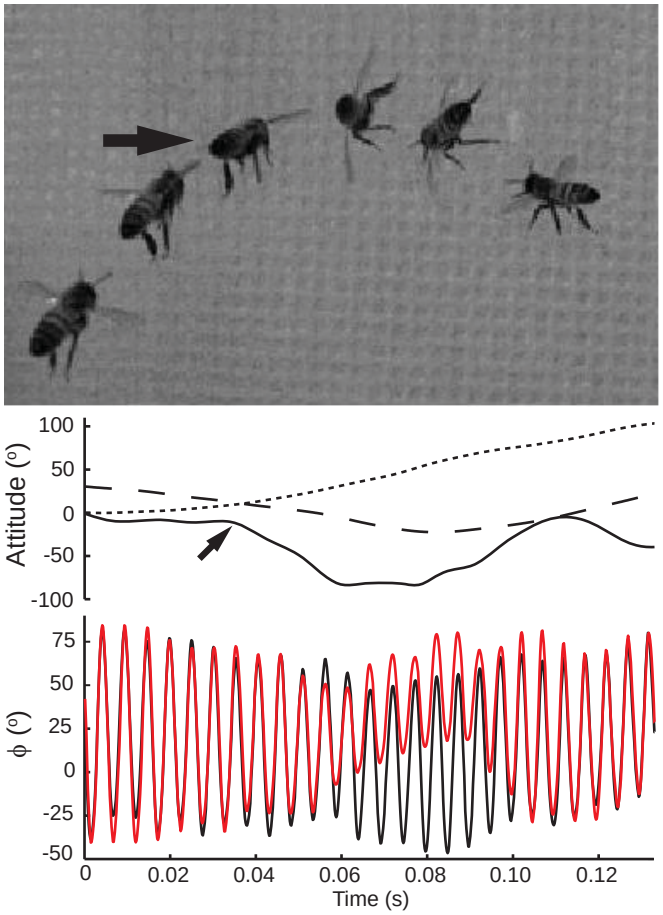

Figure 1: Body attitude (roll, solid line; pitch, dashed line; and yaw, dotted line), and wing stroke position (ϕ; right wing, red; left wing, black) during honey bee flight in response to wind gust perturbation (indicated by arrow).

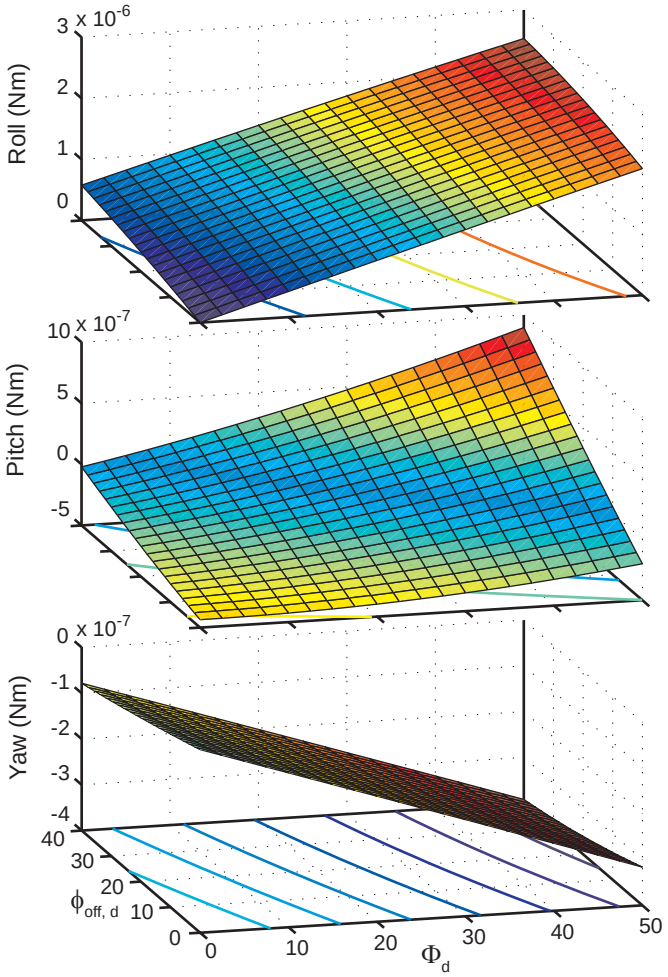

Figure 2: The effects of differential stroke offset ($\phi_{off,d}$) and amplitude (Φ_d) on body moments: roll, pitch, and yaw (positive values are moments about clockwise direction).

RESULTS AND DISCUSSION

The gust perturbation (Fig. 1) caused a counter-clockwise (CCW) rotation (2723 deg s^{-1}) about the bee's roll axis. The bee employed an asymmetric kinematic regime 19.3 msec after the onset of the roll rotation. Right wing Φ decreased 55% and ϕ_{off} shifted 26 degrees dorsally, whereas left wing Φ decreased 15% and ϕ_{off} shifted 9 degrees in the ventral direction. In total, the asymmetric kinematic regime lasted 53 msec (approximately 10 wing strokes) before the bee reverted back to a symmetric stroke pattern. The $\alpha_{r,avg}$ varied during the gust perturbation, particularly at max roll; however, right and left $\alpha_{r,avg}$ were not different**.**

The symmetric Φ and ϕ_{off} of the reference flight kinematics (Φ_d = 0; $\phi_{off,d}$ = 0) produced no roll or yaw moments, but the dorsally-biased ϕ_{off} produced a CCW moment about the pitch axis suitable to maintain body angle (Fig 2). Roll moments increased in the clockwise (CW) direction, and yaw moments increased in the CCW direction, in proportion to Φ_d and $\phi_{off,d}$; these moments resulted from the increasing left-wing dominance across this kinematic variation. Deviations in either Φ_d or $\phi_{off,d}$ away from the reference flight kinematics reduced the bee's pitch moment to nearly zero. However, combinations of high Φ_d and $\phi_{off,d}$ produced large CCW pitch moments which would tend to incline the body angle. During the gust perturbation, the high Φ_d and $\phi_{off,d}$ strategy was observed during horizontal body angle and maximum CCW roll (Fig. 1). Thus, the modeled moments are congruent with the restorative body motions that followed.

Bees employ asymmetric wing strokes in response to gust-induced perturbations. The combination of Φ_d and $\phi_{off,d}$ produces simultaneous moments about the roll, pitch, and yaw axes, arresting and reversing the perturbed body motions over a relatively few wing strokes. Although the observed kinematics suggest a strategy that maximizes moments about all three axes, it is not known whether bees are able to independently control Φ_d and $\phi_{off,d}$; or, whether $\phi_{off,d}$ is simply a consequence from the active manipulation of Φ_d, which would be evidence of a simplified control architecture. Finally, for the purpose of this investigation, our aerodynamic model ignores body motions due to the gust and kinematic response, yet the local changes to wing motion - forced by body rotation [3,4] and translation [3] - contribute significantly to aerodynamic force production, even if the wing strokes are symmetric. Future research that investigates the coordination of passive and active aerodynamic mechanisms will be valuable in characterizing the scope of insects' ability to mitigate the effects of gusts and other environmental turbulence.

REFERENCES

1. Fry, S.N., et al. *J. Exp. Biol.*, **208**, 2303-2318, 2005.
2. Altshuler, D. L., et al. *Proc. Natl. Acad. Sci. USA*, **102**, 18213-18218, 2005.
3. Faruque, I. and Humbert. J.S. *J Theor Biol.*, In Press.
4. Hedrick, T.L., et al. *Science*, **324**, 252-255, 2009.

A BIOMEDICAL PERSPECTIVE ON VARIATION IN THE HUMAN CLAVICLE, WITH PARTICULAR REFERENCE TO LB1/5 CLAVICLE FROM FLORES, INDONESIA

[1]Robert B. Eckhardt, [1] Alex Weller

[1]Laboratory for the Comparative Study of Morphology, Mechanics and Molecules
Department of Kinesiology | The Pennsylvania State University | University Park, PA
eyl@psu.edu

INTRODUCTION

In 2004 a small sample of skeletal remains discovered in Liang Bua Cave on the island of Flores, Indonesia was described as representing an entirely new species of humans that existed and evolved in isolation on the island from more than 800,000 years ago until approximately 15,000 years ago.[1] Supposed evidence for this new species was its possession of a constellation of reportedly unique attributes. These features comprised short stature (reconstructed as 1.06 m) and a brain that not only was extremely reduced in volume (approximately 400 ml), but markedly smaller than would have been expected from any applicable scaling factor in humans. In addition, numerous other skeletal features, from dentition through the humerus to the foot, were said to be outside the range known for members of our own species, *Homo sapiens*. Jacob, et al.[2] showed that nearly all of the known features of the Flores skeletons could be accounted for in terms of variation normal for populations in that geographic region (Australomelanesia). In the specimen called LB1, there were few skeletal characteristics in the sample that were not explicable as normal regional variants; LB1 is represented by the only one known skull plus about half of its postcranial elements.

Following the publication of Jacob, et al. (2006), supporters of the unique species status of the Flores skeletons have continued to discover new "uniquenesses." As one recent example, Larson, et al.[3]have said the clavicle of LB1 is unique due to its peculiar morphology: "…modern humans are distinct in displaying a single inferior curve of the clavicle in posterior [i.e. dorsal] view…" while LB1/5 "…retains the primitive double curvature seen [in] African apes and all hominins except modern humans (Voisin, pers. comm.)"

METHODS

A 27 year old female subject who is thought to have a developmental disorder-not otherwise specified-was identified. It is most probable that the patient has Laron Syndrome (Primary Growth Hormone Insensitivity Syndrome) With the fully informed consent of the subject, a full body, thin bone CT (Siemens/Sensation 40, 120 kv, 51 mAs, 1.000mm slice interval—transverse plane) was obtained. Segmentation and isolation of the clavicle was completed using Mimics (Materialise—Leuven Belgium). An ASCII STL file of each of the clavicles generated and imported into Geomagic Studio (Geomagic—Research Triangle Park, NC). As necessary, smoothing, manual segmentation and triangle reduction processes were completed.

Following methods as described by Voisin[4] measurements of the clavicle curvature in subject A were obtained through creating a 2D projection of the dorsal and cranial views.

RESULTS AND DISCUSSION

Subject A's clavicle shows an inferior curvature index of 10.9, more than 2 standard deviations above the reported human mean of 5.1, and scarcely below the mean of common chimpanzees (Pan troglodytes) at 10.7.

As an even more striking test (and refutation) of the anatomical uniqueness hypothesis, our developmentally abnormal human patient manifests a clearly visible superior curvature with an index of 5.08, which is less than one sd below that of common chimpanzees (mean = 7.6).

CONCLUSIONS

In extant humans, the observed range of skeletal variation is known to be influenced by various factors that lead usually to normal development, and less frequently to abnormal development, thereby creating an expanded range of variation. Biomedical investigators do not, however, characterize developmentally unusual individuals as nonhuman, which is equivalent to their assignment to a species other than our own. Instead, we accept that abnormal variation expands the known spectrum of development in various dimensions. There is no reason for believing that earlier human populations were free from developmental anomalies; this realization suggests as a corollary that unusual variants, past as well as present, do not necessitate the creation of novel species, particularly when they can be matched explicitly in our own.

REFERENCES

1. Brown, P, et al., *Nature*, **431**, 1055-1061, 2004.
2. Jacob, T, et al., *Proc Natl Acad Sci, USA* 103, 13421-13426, 2006.
3. Larson, S, et al., *J Hum Evol*, **55**, 1-16.
4. Voison, J. *The Anatomical Record Part A* 288A, 944-953

ACKNOWLEDGEMENTS

This research has been reviewed and approved for compliance with the policy of the human subjects Institutional Review Board on November 13, 2008. Approval # 28014

COMPUTED-TOMOGRAPHY-BASED FINITE-ELEMENT MODELS OF LONG BONES CAN ACCURATELY CAPTURE STRAIN RESPONSE TO BENDING AND TORISON

Bino Varghese, Thomas Hangartner

Wright State University, Dayton, OH, USA
email: varghese.2@wright.edu, web: http://www.wright.edu/academics/bmil/bmil.htm

INTRODUCTION

Finite element (FE) models constructed from computed tomography (CT) data are emerging as an invaluable tool in the field of bone mechanics [1]. Their clinical application has been limited due to the lack of high level of automation and reliable estimation of accuracy [2].

METHODS

In this study, a combined numerical–experimental study is performed comparing FE-predicted surface strains with strain gauge measurements. 40 major, cadaveric, long bones (humerus, radius, femur and tibia), which cover a wide variety of geometries, are tested under both three-point bending and torsion. The FE models are constructed from trans-axial volumetric CT scans, and a generalized mathematical relationship between bone density and the Young's modulus is used for the trabecular region of all bones [3,4].

RESULTS AND DISCUSSION

The calculated maximum principal strains at the nodes corresponding to the sensing area of each strain gauge were averaged and compared to the strains obtained from the attachment sites on the bones. Strain graphs of a representative femur are displayed in bending (Fig.1A) and in torsion (Fig.1B). The calculated FE strain is represented as a solid line, and the experimentally measured strain values are represented as points.

The exact positions of the strain gauges on all bones for both loading configurations are tabulated in Table 1. As a rule, the strain gauges were applied in regions of the bone containing trabecular bone and also providing high maximum principal strain values under three-point bending and torsion.

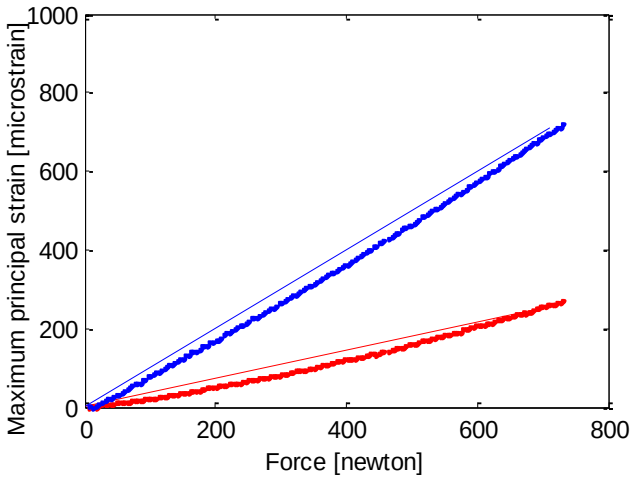

A

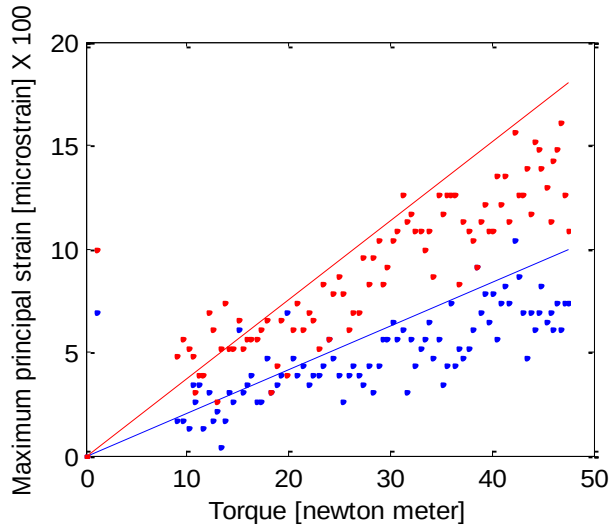

B

Figure 1: Measured strains from mechanical testing (points) and calculated strains from FE-models (solid lines) for three-point bending (A) and torsion (B) of a sample femur. The lines and data points with the higher slope in (A) represents the strains at the mid-diaphysis (B_{100}); those with the lower slope represent the strains relating to the epiphyses (B_{50}). Similarly in (B), the higher slopes relate to T_{50} and the lower slopes to T_{25}.

To assess the performance of the FE models in capturing the true bone response for bending, only loading beyond 100 N was considered. In the case of torsion, the lower limit of the linear region was set at 2 Nm and the upper limit at the end of the linear range (due to the destructive nature of the test). Within this range, the R^2 values of the measured strains versus load under three-point bending are 0.96 – 0.99 in all bones. Under torsion, the R^2 values range from 0.61 – 0.99 in all bones; however, the majority (88%) of the bones have an R^2 value ranging from 0.82 – 0.95. These R^2 values are reasonable to claim linearity [2], which is indicative of the validity of the experiments.

To quantify the error of the FE-calculated strains from the measured strains, the error between the line fit through the measured strains and the line represented by the FE-calculated strains was computed for all bones under all loading conditions (Table 1). The errors for all bones ranged from -13 to 27% under bending and from -61 to 30% under torsion. For the purpose of comparison, the errors recorded in the literature between FE-calculated and measured strain range from 27 - 60% for bending of the proximal femur [4,5,6]. Therefore, the error range of 5 – 14% found in the femurs of this preliminary study is an improvement.

Further, to the best of our knowledge, comparison of the strains calculated from FE-torsion analysis and strains measured from torsion experiments have not been recorded in any published studies. We compared FE-calculated and strain-gauge-measured maximum principal strains, and the results are quite encouraging, Additionally, in this study, long bones other than the femur i.e., the tibia, the radius and the humerus have been considered. These bones were included in the study to evaluate the accuracy of the FE technique over a wide range of bone geometries and material properties in 3-D.

CONCLUSIONS

In summary, we have shown that the method of constructing 3-D FE models from CT data predicts strain-gauge-measured surface-strains on major long bones, tested under three-point bending and torsional loads *in-vitro*, reasonably well. In subsequent studies, the material properties will be optimized to minimize the errors of the FE models across all bones.

REFERENCES

1.Schileo E, et al. *J Biomech* **41**, 2483-2491, 2008.
2.Taddei F, et al. *J Biomech* **39**, 2457-2467, 2006.
3.Morgan EF, et al. *J. Biomech* **36**, 897-904, 2003.
4.Taddei F, et al. *Med. Eng. Phys* **29,** 973-979, 2007.
5.Taddei F, et al. *Clin. Biomech* **23**, 1192-1199, 2008.
6.Bessho M, et al. *J Biomech* **40**, 1745-1753, 2007.

Table 1: Range of R^2 values for various strain gauge locations (location indicated in parentheses) obtained by fitting a linear model to the measured strains over the linear range for all bones under three-point bending and torsion. The range of percent errors recorded between the measured strains and the FE-calculated strains are displayed beside the range of R^2 values. Positions of the strain gauges, B for bending and T for torsion, are also tabulated. The subscript number indicates approximately the percentage of maximum strain recorded at that site. N: number of samples. The notation P_{end} indicates proximal end and D_{end} indicates distal end.

FEMUR (N=10)	**B_{50}** (18% from P_{end})	**B_{100}** (50% from P_{end})	**T_{25}** (15% from P_{end})	**T_{50}** (17% from P_{end})
	0.96 - 0.99, 6 - 14%	0.97 - 0.99, 5 - 11%	0.61 - 0.99, -2 - 16%	0.82 - 0.99, -61 - 16%
TIBIA (N=10)	**B_{50}** (18% from D_{end})	**B_{100}** (50% from D_{end})	**T_{25}** (11% from D_{end})	**T_{50}** (14% from D_{end})
	0.98 - 0.99, -11.3 - 12%	0.98 - 0.99, -4 - 19%	0.90 - 0.92, -30 - 30%	0.90 - 0.92, -40 - 20%
HUMERUS (N=10)	**B_{50}** (20% from P_{end})	**B_{100}** (50% from P_{end})	**T_{25}** (13% from P_{end})	**T_{50}** (15% from P_{end})
	0.99, -10 - 14%	0.99, -11.9 - 17%	0.64 - 0.95, -28 - 22%	0.95 - 0.97, -7 - 9%
RADIUS (N=10)	**B_{50}** (20% from D_{end})	**B_{100}** (50% from D_{end})	**T_{25}** (15% from D_{end})	**T_{50}** (18% from D_{end})
	0.96 - 0.99, -10 - 13%	0.96 - 0.99, -9 - 3%	0.73 - 0.97, -5 - 16%	0.75 - 0.97, -15 - 3%

DEVELOPMENT OF A HYBRID MODEL SIMULATING THE VIBRATION CHARACTERISTICS OF A HUMAN HAND-FINGER SYSTEM

John Z Wu, Ren G Dong, Xueyan S Xu, and Daniel E Welcome
National Institute for Occupational Safety and Health, Morgantown, WV, USA
Email: jwu@cdc.gov

INTRODUCTION

It is well known that prolonged, intensive exposure to hand-transmitted vibration could cause a series of disorders in the sensorineural, vascular, and muscular systems of the fingers. Since the mechanical stress and strain are known to be the essential factors that modulate the growth, remodeling, morphogenesis of the biological system, it has been proposed that the immediate effects of the vibration on the fingers should be evaluated by quantifying vibration-induced stress, strain, and power absorption in the soft tissues [1,2]. Because it is technically difficult to directly quantify the stress and strain in the fingers, biomechanical modeling would be applied for such analysis. Traditionally, two types of models have been applied to simulate the responses of the human hand-arm system to vibration: lumped mass model and finite element (FE) model. The lumped mass model can only simulate the global biodynamic response of the hand-arm systems. Although FE method can be applied to model detailed anatomical structures of the biological system, it is technically difficult to model the entire hand-arm system using a FE method. In the current study, we propose a hybrid modeling method for analyzing the biodynamic responses of a fingertip, taking advantage of both modeling approaches.

METHODS

The hand-finger system is simulated by using a hybrid model, which combines a lumped parameter model with a two-dimensional (2D) FE model, as illustrated in Fig. 1. The fingertip is simulated using a 2D FE model, while the effective mass of the hand-finger is represented by the mass element *m*. The coupling between the fingertip and hand-finger is represented by the spring and damping element (*k1* and *c1*). The contact between the fingertip and the vibrating plate is simulated in the FE modeling, while the coupling between the hand and the vibrating plate is represented by another spring/damping unit *(k3* and *c3*). The coupling between hand, forearm, and ground is represented using a spring/damping unit (*k2* and *c2*). The fingertip model was assumed to be composed of skin layers, subcutaneous tissue, bone, and nail. The biquadral, plain-strain elements were used in the FE

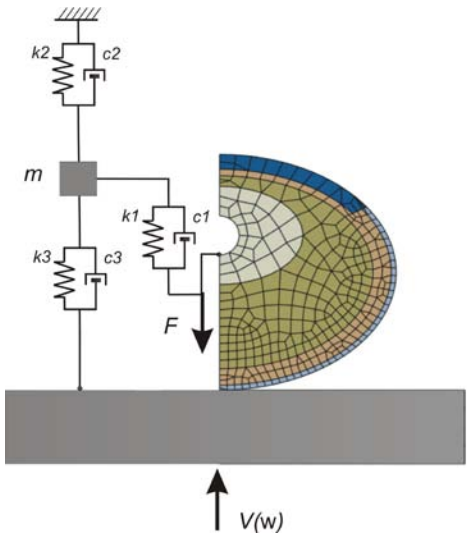

Figure 1: The vibration of a fingertip is simulated by 2D FE model combined with lumped elements.

models and the commercial FE software package, ABAQUS (version 6.8), was utilized for the analyses. The skin is assumed to be composed of two layers: the outer skin (0.10 mm thick) and inner skin (1.26 mm thick). The outer skin layer contains stratum corneum and a part of the viable epidermis, and is considered as linearly elastic; while the inner skin layer is composed of dermis and a part of the viable epidermis, and is characterized as nonlinearly elastic. The bone and nail are assumed to be linearly elastic [3]. Two-term Mooney-Rivlin models are applied to characterize the nonlinearly elastic behaviors, and the Rayleigh formula is applied for the frequency-dependent viscous damping characteristics of the soft tissues, as described in our previous studies [4,5]. The lumped element parameters were determined by fitting the model to experimental measurements during human subject testing. The vibration transmissibility of the fingertip was measured using a laser vibrometer (Polytec PSV-300-H). The basic measurement method and testing setup were similar to those reported in a previous study [6]. Briefly, a flat, rectangular aluminum platform (21.6 x 12.7 cm, 1.09 kg) connected to a single-axis vibration testing system (Unholtz-Dickie, TA250-S032-PB) was used to deliver the vibration. The subjects pushed

against the plate with an open hand at a given static force during the measurement.

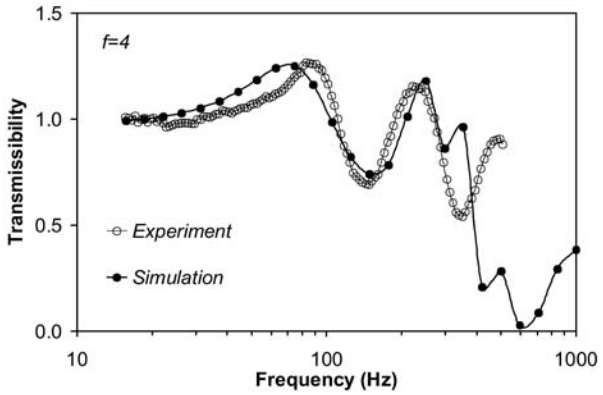

Figure 2: The magnitude of the vibration transmissibility calculated using the model is compared with the experimental data.

RESULTS AND DISCUSSION

By adjusting the lumped parameters (*k1-k3*, *c1-c3*, and *m*), the model predictions of the magnitudes of the vibration transmissibility are fitted to the experimental data; representative results are shown in Fig. 2. The transmissibility (Fig. 2) is defined as the ratio of the vibration magnitude at the nail to that at the vibration plate. It is seen that the model predictions for the first and second resonant responses agree well with the experimental measurements.

Typical results for the distributions of vibration magnitude and velocity along the central line of the fingertip model are depicted in Fig. 3. The spatial distances of the plots refer to the fingertip in the undeformed state. The frequency-dependent characteristics of the vibration penetrations into the soft tissues are quantitatively analyzed in these figures. At the tissue/plate contact surface, the vibration velocity is constant at 8 mm/s, and the corresponding vibration magnitude decreases with increasing frequency. However, the distributions of the vibration within the soft tissue depend on the frequency; especially when the frequency is equal to or greater than 125 Hz, the distribution patterns of the vibration in the soft tissue varied suddenly: the gradients of vibration displacement and velocity across the tissue become substantially greater.

CONCLUSIONS

The proposed modeling approach can effectively take into account both local and global responses, such that the vibration-induced tissue stress, strain, and power absorption density in the fingertip, as well as the global driving point biodynamics can be predicted. The static stress and strain due to the static compression of the fingertip can also be predicted using this model. Although only the fingertip biodynamic responses were simulated in the current study, such a modeling approach can be generalized to predict the detailed biodynamic responses of other anatomical substructures of the hand-arm system. The proposed method is a practical and efficient approach to simulate the detailed biodynamic responses of a complex biological system, which is exposed to vibration.

REFERENCES

1. Bovenzi M. *Scand J Work Environ Health* **24**, 138-44, 1998.
2. Miwa T. *Ind Health* **5**, 213-20, 1967.
3. Yamada H. *Strength of biological materials*, Williams and Wilkins Co., Baltimore, 1970.
4. Wu JZ, Welcome DE, Dong RG. *Comput Methods Biomech Biomed Eng* **9**, 55-63, 2006.
5. Wu JZ, Dong RG, Welcome DE. *Med Eng Phys* **28**, 816-26, 2006.
6. Concettoni E, Griffin M. *J Sound Vib* **325**, 664-78, 2009.

DISCLAIMER

The findings and conclusions in this report are those of the authors and do not necessarily represent the official position of the National Institute for Occupational Safety & Health. The mention of trade names, commercial products, or organizations does not imply endorsement by the US Government.

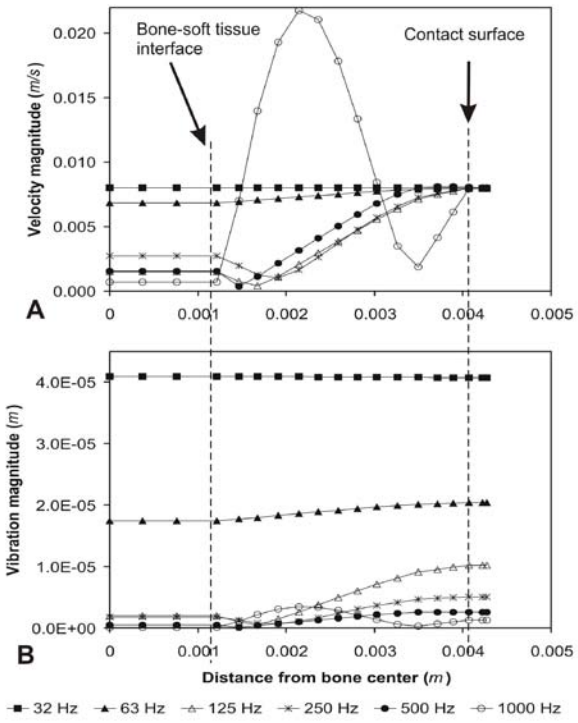

Figure 3: The simulated distributions of vibration velocity and magnitude within the tissues of a fingertip.

BONE FRACTURE ANALYSIS USING THE EXTENDED FINITE ELEMENT METHOD (XFEM) WITH ABAQUS

Xiangyi (Cheryl) Liu, Xiaoliang Qin and Zhen-zhong Du

Dassault Systemes Simulia Corp, Providence, RI, USA
email: Cheryl.LIU@3ds.com web: www.simulia.com

INTRODUCTION

The bones of elderly people with osteoporosis are susceptible to either traumatic fracture as a result of external impact, such as what happens during a fall, or even spontaneous fracture without trauma as a result of muscle contraction [1, 2]. Understanding the fracture behavior of bone tissue will help researchers find proper treatments to strengthen the bone in order to prevent such fractures, and design better implants to reduce the chance of secondary fracture after receiving the implant.

A number of fracture criteria have been proposed for bone tissue and many of the studies used FEA models to correlate critical values of the proposed criteria with bone fracture patterns observed in experiments [3, 4]. However, simulation of actual crack initiation and growth has been hard to achieve using the conventional FEA approach. With the new extended finite element method (XFEM) available since Abaqus 6.9, researchers can simulate crack initiation and growth more easily. In this study we demonstrate how XFEM can be used to predict proximal femur fracture due to impact.

METHODS

Modeling stationary discontinuities, such as a crack, with the conventional finite element method requires that the mesh conform to geometric discontinuities. Therefore, considerable mesh refinement is needed in the neighborhood of the crack tip to capture the singular asymptotic fields adequately. Modeling a growing crack is even more cumbersome because the mesh must be updated continuously to match the geometry of the discontinuity as the crack progresses.

The extended finite element method was first introduced by Belytschko and Black [5]. It is an extension of the conventional finite element method based on the concept of the partition of unity by Melenk and Babuska [6], which allows local enrichment functions to be easily incorporated into a finite element approximation. The presence of discontinuities is ensured by the special enriched functions in conjunction with additional degrees of freedom. However, the finite element framework and its properties such as sparsity and symmetry are retained [7].

The geometry of an intact human femur was imported into Abaqus/CAE and meshed with linear tetrahedron elements (C3D4). The bone density distribution (Fig. 1) was obtained using a bone remodeling algorithm implemented with Abaqus subroutine USDFLD [8].

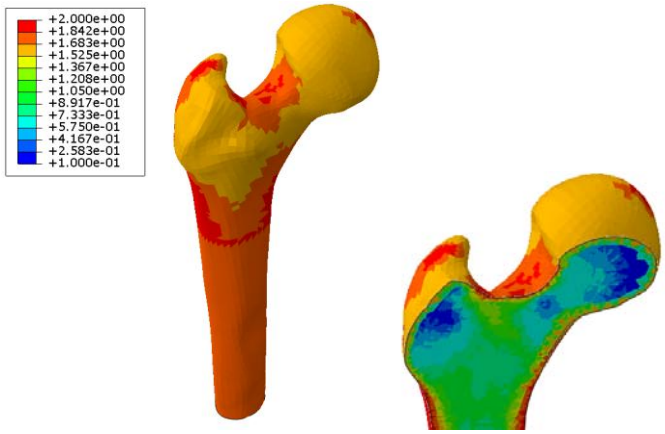

Figure 1: Bone density distribution predicted by bone remodeling theory.

The bone density is incorporated into the model as a field variable. The bone material is assumed to be isotropic linear elastic with Young's modulus as a cubic function of bone density. Similarly, the damage initiation and damage evolution parameters are also defined as functions of bone density. Maximum principal strain is used as the damage

initiation criterion. Damage evolution is assumed to follow the energy dissipated during the process.

A femur fracture test is simulated using the Abaqus implicit dynamic procedure with the top plate fixed, the distal end of the femur and the bottom supporting plate moving up toward the top plate at the same speed (Fig. 2).

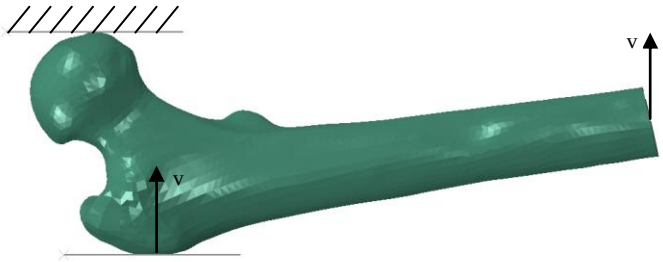

Figure 2: Boundary conditions of the FEA model.

RESULTS AND DISCUSSION

The Abaqus XFEM analysis predicted crack initiation in the femur neck just below the femur head (Fig. 3a). The crack grew toward the femur head (Fig. 3b, 3c) and eventually crossed from the femur neck into the femur head (Fig. 3d).

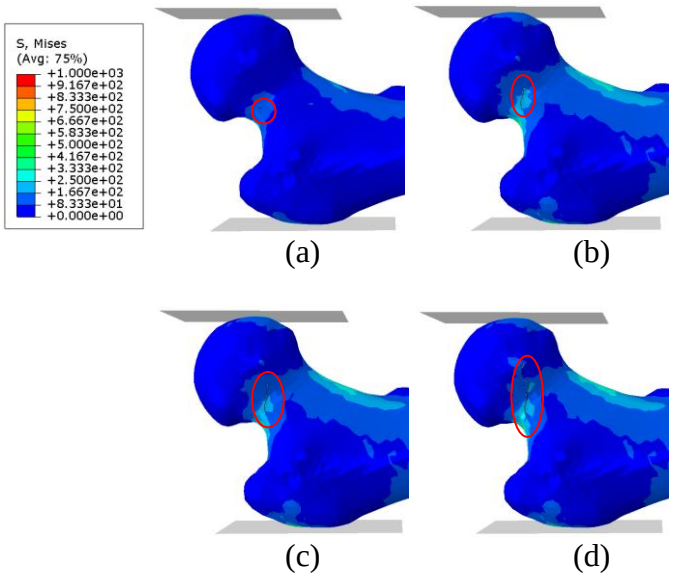

Figure 3: Analysis results.

Since no physical testing was performed for this specific femur, we were not able to validate the analysis results. However, similar bone fracture patterns were observed in experiments [9]. To properly validate such an analysis, the initial bone density should be calculated based on CT data.

CONCLUSIONS

Bone, as a biological tissue, possesses a very complex hierarchical structure. From a mechanical point of view, it is transversely isotropic with a higher modulus in the longitudinal direction. It is asymmetric with higher strength in compression than in tension and shear. The fracture and failure properties of bone tissue are even more complex. Various theories have been proposed including stress or strain-based criteria, von Mises or maximum principal invariant-based criteria, and more recently composite failure criteria.

What we implemented in this study is a very simplified version of bone material properties. Our goal was to demonstrate the new XFEM technology and how it may be used to study bone fracture and failure properties. In Abaqus 6.10-EF1, a new user subroutine permitting user-defined damage initiation criteria will be available for Abaqus XFEM, which will provide greater flexibility in implementing new failure criteria. In future studies, we will demonstrate how composite failure criteria may be implemented using this user subroutine to study bone fracture.

REFERENCES

1. Sloan J, et al. *Injury* **13**, 230-2, 1981.
2. Horiuchi T, et al. *Orthopedics* **11(9)**, 1277-80, 1998.
3. Keyak JH, et al. *J Biomech*, 31, 125-33, 1998.
4. Oden ZM, et al. *J Orthop Res*, 17(5), 661-7, 1999.
5. Belytschko, et al. *Int J Numer Meth Eng*, 45, 601-20, 1999.
6. Melenk J, et al. *Comput Method Appl M*, 39, 289-314, 1996.
7. Abaqus 6.9 Documentation, Analysis User's Manual, Section 10.6.1.
8. Liu X, et al, *ASME Summer Bioengineering Conference*, Naples, FL, 2010 (under review).
9. Shaw MN, et al. *Mater Sci Tech*, 3, 1457-1467, 2007.

TESTING AND MODELING THE NONLINEAR BEHAVIOR OF UHMWPE USED IN ORHTOPAEDIC IMPLANTS

Said T. Gomaa and Steve Leisinger

DePuy Orthopaedics, Inc, Warsaw, IN, USA
email: sgomaa@its.jnj.com, web: http://www.depuy.com

INTRODUCTION

Ultra High Molecular Weight Polyethylene (UHMWPE) is the material of choice for the bearing components of orthopaedic implants since its first clinical usage in 1962 by Sir John Charnley. It has been successfully implanted in millions of people to replace natural knee, hip and shoulder articulating surfaces. New varieties of UHMWPE are developed periodically by manufacturers of orthopaedic implants in order to improve the longevity of such components. The nonlinear strain-rate sensitivity, creep and relaxation behaviors of Marathon®, a brand name of UHMWPE produced and commercialized by DePuy Orthopaedics, were explored through strain-rate controlled experiments at room temperature. These nonlinear behaviors were modeled using the Three Network Model (TNM) developed by Jorgen Bergstrom [3]. The Three Network Model showed excellent modeling capabilities for the nonlinear deformation of UHMWPE.

METHODS

A MTS servo-hydraulic testing machine, with direct measurement of load and strain was used to test cylindrical specimens subjected to monotonic tensile loading and unloading [1]. Cylindrical specimens having a 0.5 in. diameter and 1.5 in. gage length were machined and a 1.0 in. gage length clip-on extensometer was used. Three types of tests were performed, strain-rate sensitivity, creep and relaxation. For strain-rate sensitivity studies, tension tests were conducted using three engineering strain rates, 1×10^{-1} s^{-1}, 1×10^{-2} s^{-1} and 1×10^{-3} s^{-1}. The specimens were loaded to 50% engineering strain, then unloaded to zero stress at the same strain rate magnitude. The creep tests were performed by loading the specimens using a 1×10^{-3} s^{-1} strain rate up to engineering stress levels of 12.5, 12.3 and 15.8 MPa. The stress was held constant while the strain was recorded. The relaxation tests were performed by straining the specimens up to 5% engineering strain using three strain-rates, and the strain value was held constant while the stress was allowed to relax for one hour.

RESULTS AND DISCUSSION

UHMWPE shows nonlinear strain rate sensitivity with almost equidistant flow stress curves as shown in Fig. 1. The curves for the three tensile tests show overlap up to a strain of about 1% beyond which they start to diverge. Above a strain of approximately 10%, the stress-strain curves are mostly equidistant. The unloading parts of the stress-strain curves are nonlinear; however, all of the specimens unload to the same strain value irrespective of the strain-rate used.

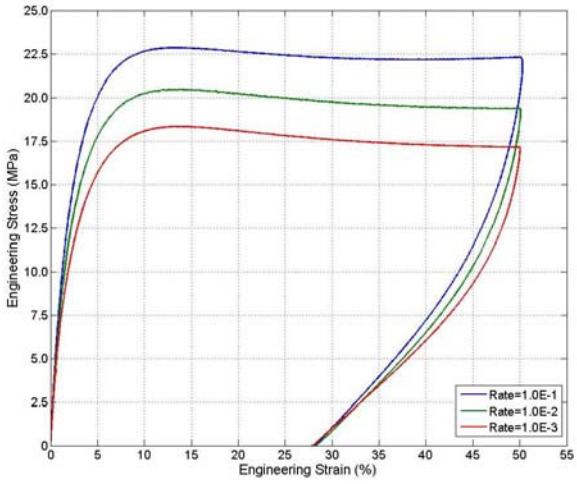

Figure 1: Nonlinear rate sensitivity of UHMWPE.

Figure 2 shows the three creep tests performed with a prior strain rate of 1×10^{-3} s^{-1}. The figure shows that for stress levels far below the yield strength, (10.5 and 12.3 MPa), the specimens experience primary creep, and for stress levels close to the

yield strength, (15.8 MPa), the specimens experience tertiary creep. Continuation of the creep tests at 15.8 MPa would have resulted in fracture.

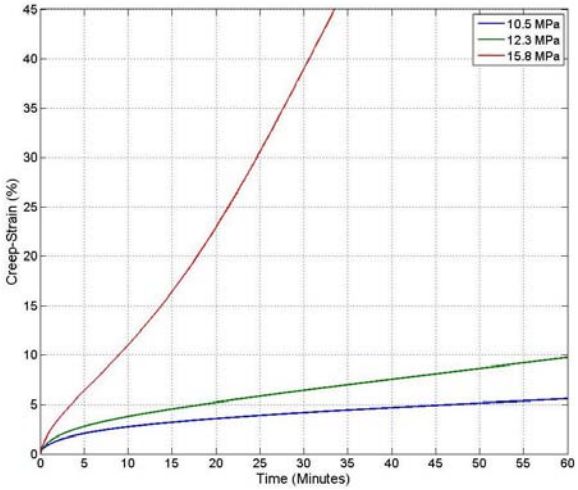

Figure 2: Creep curves for UHMWPE.

Figure 3 shows the stress drop in one-hour relaxation tests for specimens strained to 5% strain. Although the specimens experienced different maximum stresses due to the different strain rates during loading, all of them relax, approximately, to the same stress value.

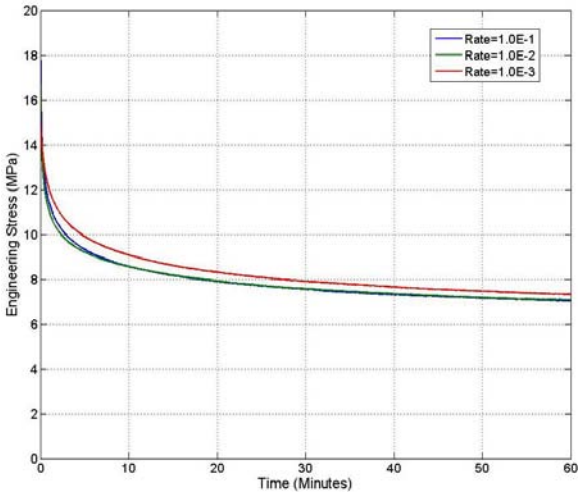

Figure 3: Relaxation curves for UHMWPE.

The TNM [3] was used to model the nonlinear behavior of UHMWPE. Figure 4 shows a comparison between stress-strain curves obtained from experiment with that obtained from TNM for the case of monotonic loading and unloading using a strain rate of 1×10^{-3} s^{-1}. The true values of stress and strain were used because the model parameters will be fed into a finite element program. As shown in this figure, the model predicts the nonlinear monotonic loading fairly well. Also, the model prediction of the nonlinear unloading is satisfactory.

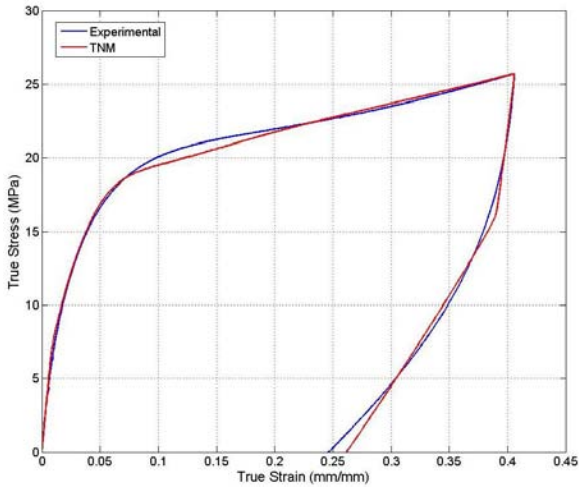

CONCLUSIONS

The experimental nonlinear rate-dependent behavior, creep and relaxation of UHMWPE, were presented. The UHMWPE exhibits highly nonlinear rate dependent behavior during loading and unloading. The Three Network Model predicts the nonlinear loading/unloading behavior of UHMWPE quite well. Modeling the UHMWPE using rate independent plasticity models can be gross approximation to the material behavior and it should be avoided since more refined constitutive models are now available [2,3].

A new set of experiments that allow for longer creep and relaxation periods might be needed to fully characterize the creep/relaxation behavior. Also, performing the experiments at body temperature rather than room temperature will make them more clinically relevant.

REFERENCES

1.Khan F, *Ph.D. thesis, Rensselaer Polytechnic Institute*, Troy, NY, USA, 2002.
2.Krempl E et al, *Int. J Plasticity* **19**, 1069-1095, 2003.
3.Bergstrom J, *Biomaterial*, **25**, 2171-2178, 2004.

USING SUBJECT-SPECIFIC MUSCLE PARAMETERS TO COMPARE MUSCLE FORCES BETWEEN AN EMG-DRIVEN AND OPENSIM MUSCULOSKELETAL MODEL

[1]David G. Olchowski, [1]Thomas S. Buchanan, and [1]Jill S. Higginson

[1]University of Delaware, Newark, DE, USA
email: dgolchow@udel.edu

INTRODUCTION

Individual muscle forces cannot be calculated from experimental data because the number of muscles that cross a joint create an indeterminate system. Many different optimization approaches exist to solve this problem. Previous studies have used EMG to derive subject-specific muscle parameters that match inverse dynamics [1], while others use a generic model but redistribute loads between muscles crossing the joint [2].

The aim of our study was to incorporate optimized subject-specific parameters from an EMG-driven model to be used in place of OpenSim's generic values. Muscle forces were compared to determine how well OpenSim matched the EMG-driven output. Using subject-specific parameters may enhance the utility of forward dynamic simulations for designing individualized interventions.

METHODS

Three dimensional kinematic and kinetic data were collected from 2 healthy young male subjects walking on a split-belt, motorized treadmill at self-selected speeds (Bertec Corp. Columbus, OH). An 8-camera Motion Analysis system was used to record locations of 23 markers in dynamic trials while EMG data were collected on one lower limb from 4 muscles (TA, Sol, MG, LG). The walking trials were normalized to MVC data that was collected using a Biodex dynamometer.

The generic OpenSim model was scaled to match the anthropometry of each subject [2]. Inverse dynamics was performed to determine the ankle joint moment. Moment arms and musculotendon lengths were calculated based on the kinematics. This data was input to the EMG-driven model along with maximum isometric force (MF) values and subject scaled parameters of tendon slack length (TSL) and optimal fiber length (OFL).

The EMG-driven model describes the relationship from neural command to muscle force and joint moment. The model incorporates a simulated annealing algorithm [3] while constraints are put on muscle parameters to optimize within a physiologically relevant range. The forward dynamics joint moment is calibrated to the inverse dynamics and the differences are minimized [1].

Table 1: Scaled and optimized subject-specifc muscle parameters for Subject 1.

Muscle	Scaled	Optimized	% Diff.
Tendon Slack Length (m)			
MG	0.393	0.394	0.21
LG	0.383	0.380	-0.74
Sol	0.253	0.276	8.76
TA	0.220	0.209	-4.94
Optimal Fiber Length (m)			
MG	0.060	0.061	1.30
LG	0.065	0.067	3.76
Sol	0.051	0.051	0.48
TA	0.097	0.101	5.00
Max. Isometric Force (N)			
MG	1558	3114	99.86
LG	683	1365	99.86
Sol	3549	7098	100
TA	905	1810	100

The optimized subject-specific muscle parameters (MF, TSL, and OFL) from the EMG-driven model are changed in the OpenSim scaled model. Symmetry was assumed since we were using healthy subjects with no known pathologies. A reduced residual algorithm was applied to make the generalized coordinates more dynamically consistent with experimental moments and GRF [2].

Finally, a computed muscle control algorithm is applied which uses static optimization and a proportional-derivative control to predict muscle excitations that reproduce experimental kinematics [4]. Computed muscle forces were compared with those from the EMG-driven model.

RESULTS AND DISCUSSION

Optimized values TSL and OFL for both subjects resulted in percent differences within 9% of generically scaled values (Table 1). Muscle force data from the OpenSim model showed a similar pattern to the EMG-driven model. Magnitude of muscle force during stance phase was comparable across all muscles (Fig. 1). Differences in peak force values between the models were all within 425N (Table 2). The timing of muscle activity from both models also showed a strong similarity.

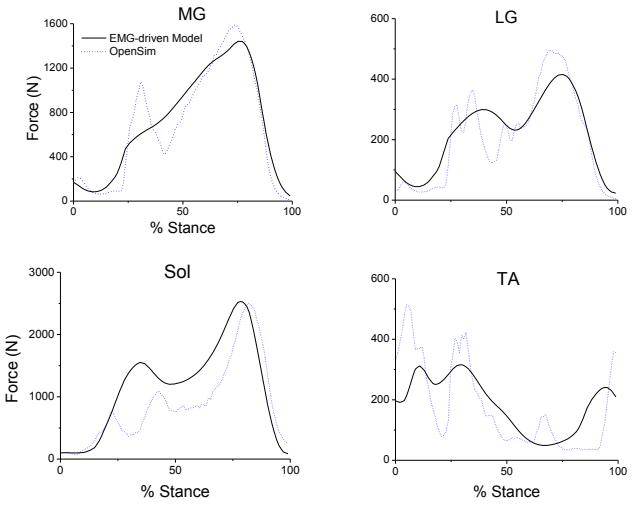

Figure 1: Ankle muscle forces in Subject 1 as determined from an EMG-driven model and OpenSim.

OpenSim determines muscles excitations that minimize the weighted sum of muscle forces as it reproduces experimental kinematics. The EMG-driven model determines muscle parameters that allow the forward dynamic joint moment to closely match the input inverse dynamics. With these differences, it is encouraging that our results show that the two models can still produce similar muscle forces in both magnitude and timing.

Table 2: Averaged difference in peak ankle forces between subjects.

Muscle	MG	LG	Sol	TA
Diff. in Peak Force (N)	425	150	25	150

In this study we perturbed a total of 12 parameters across 4 muscles. Previous studies have looked at the sensitivity of perturbing one parameter and calculating the resulting differences in muscle forces [5]. Because the parameters were optimized in an EMG-driven model, they may better represent actual physiological values for this individual. Changes in TSL (± 10%) and OFL (± 5%) were constrained for each muscle and applied across functional muscle groups (i.e. plantarflexors, dorsiflexors). To account for differences in strength between subjects, gain factors were allowed to vary over a much larger range (-50/+100%). We believe this will reflect the diversity among healthy and pathological subjects.

CONCLUSIONS

Our study has shown that using subject-specific muscle parameters, forces in the ankle muscles are similar with an EMG-driven model and OpenSim. Our future work will incorporate subject-specific parameters based on EMG data into OpenSim to better capture muscle impairments in an individual with pathological gait.

REFERENCES

1.Buchanan TS, et al. *J Appl Biomech*. **20**, 367-395, 2004.
2.Delp SL, et al. *IEEE Trans Biomed Engn*. **54**, 1940-1950, 2007.
3.Goffe WL, et al. *J Econometrics*. **60**, 65-100, 1994.
4.Thelen DG, et al. *J Biomech*. **36**, 321-328, 2003.
5.Ming X, et al. *J Appl Biomech*. In Press.

ACKNOWLEDGEMENTS

NIH Grant NS 055383 and AR 046386

EQUIVALENCE OF ELASTIC CONTACT AND FINITE ELEMENT MODELS OF PATIENT-SPECIFIC CONTACT STRESS EXPOSURE IN THE HUMAN ANKLE

[1]Andrew M. Kern, [1]Donald D. Anderson and [1]Thomas D. Brown

[1]Orthopaedics and Rehabilitation, The University of Iowa, Iowa City, IA, USA
web: http://poppy.obrl.uiowa.edu ; e-mail: andrew-kern@uiowa.edu

INTRODUCTION

Elevated articular contact stress exposure associated with incongruity following articular fracture reduction provides a direct explanation for the development of post-traumatic osteoarthritis (PTOA). Prior assessment of chronic contact stress exposure in the ankle following articular fracture reduction used patient-specific finite element (FE) analysis[1]. FE contact analysis is expensive both in computational and in analyst time, limiting its usefulness in multi-center studies involving large numbers of subjects. By contrast, elastic contact modeling is a much less computationally expensive method than FE. The purpose of this study was to establish the equivalence of contact stresses computed in the ankle using elastic contact methods versus FE models.

METHODS

Model geometries were taken from prior patient-specific FE studies of the relationship between contact stress exposure and PTOA development[1]. Eleven models of intact ankles were used, with CT data providing the underlying bone geometry. Since cartilage was not visible on CT images, a 1.7mm uniform cartilage thickness was assumed.

The elastic contact model was implemented in MATLAB utilizing methods as described by Bei et al.[2]. The elastic contact modeling approach treated the apposing cartilage surfaces of an articular joint as a system of linear springs with an underlying rigid bone foundation. Each tibial surface patch was assigned a linear spring capable of exerting force along the polygon normal, and connected to a nearest neighbor talar surface point. Surface facets were deemed in contact when the tibial surface overlapped the talar surface node. The deformation for each spring was computed based on the overlap. Areas of the associated polygons were then used to calculate the applied forces, subject to a given joint apposition. A force-balancing algorithm was used to drive the ankle through a flexion-extension arc, while the joint was allowed free motion in all other degrees of freedom, except for the talus that was fixed against vertical displacement. Contact stress distributions were computed over 13 steps of a simulated gait cycle[1].

Contact stresses were examined in eleven intact cases for which solutions had previously been obtained using ABAQUS 6.5-1 FE software[1]. For ease of comparison, the models used for elastic contact in the present study were identical to the FE models. Contact stresses computed with the elastic contact modeling approach were compared on a site-by-site basis with the FE results. The computed rigid body kinematics were also compared.

RESULTS AND DISCUSSION

Run time for the elastic contact model was approximately 1 hour to complete all 11 models, as compared to 10-20 hours per model to compute the FE solutions. Similar contact stress distributions were obtained with the two methods (Figure 1). The mean difference between elastic contact and FE contact stresses was 0.42 (±0.41) MPa across all 11 cases, differing mainly in regions of high pressure and near the margin of contact.

The majority of the differences in computed contact stresses were less than 1 MPa (Figure 2). There was a slight bias towards the elastic contact having higher contact stress than FE, as seen by the normal fit (red line, Figure 2). When the difference between the FE and elastic model was greater than 1 MPa, it was generally in a region along the edge of contact, where only one methodology predicted contact. This is most likely attributable to slight

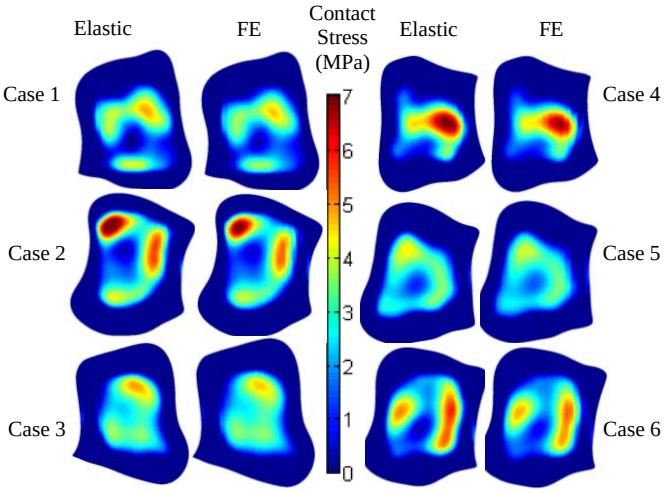

Figure 1: Elastic contact model stress compared to FE contact stress for 6 of 11 cases in the distal tibia. Instantaneous contact stresses were averaged over the gait cycle for comparison.

discrepancies in the computed kinematics as well as the continuum-vs-discrete modeling.

The mean translational differences between elastic and FE contact model computations in the inferior-superior, medial-lateral, and anterior-posterior directions were 0.02(±0.01), 0.14(±0.07) and 0.49(±0.16) mm, respectively (Figure 3). The mean rotational differences in inversion/eversion and internal/external rotation were 0.11(±0.02) and 0.05(±0.09) degrees, respectively across all 11 cases. Flexion-extension rotations are not shown because they were both controlled as part of the gait cycle to be identical.

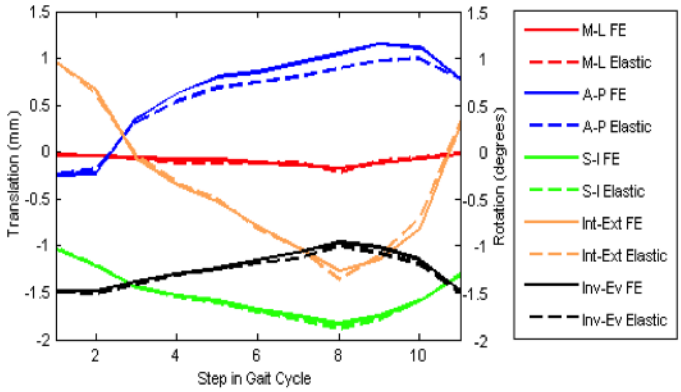

Figure 3: Comparison of medial-lateral (M-L) anterior-posterior (A-P) superior-inferior (S-I) translations and internal/external (Int-Ext) inversion/eversion (Inv-Ev) rotations in FE and elastic contact models over case 3.

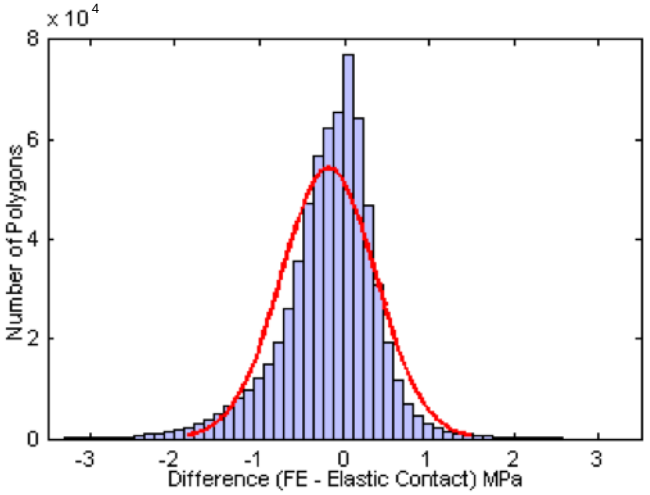

Figure 2: Histogram of contact stress differences between FE and elastic contact modeling on a site-by-site basis, across 13 gait cycle steps of 11 cases. Only sites deemed to be in contact are compared.

CONCLUSION

The elastic contact model implemented provides reasonably close contact stress and kinematic solutions to those of FE analysis, while drastically reducing the amount of computational and investigator time required to achieve these results.

REFERENCES

1. Li W, Anderson DD, Goldsworthy JK, Marsh JL, Brown TD. *J Orthop Res*. 26(**8**),1039-1045, 2008.

2. Bei Y, Fregly BJ. *Med Eng Phys*. 26(**9**):777-789, 2004.

ACKNOWLEDGEMENTS

This project funded by NIH/NIAMS #AR055533

DEVELOPMENT OF A THREE-DIMENSIONAL FINITE ELEMENT MODEL OF THE HAND AND WRIST

Max Gong, Michele Oliver, Robert Dony and Anton Semechko

School of Engineering, University of Guelph, Guelph, ON, Canada
email: mgong@uoguelph.ca, web: http://www.soe.uoguelph.ca

INTRODUCTION

Repetitive strain injuries (RSI) are injuries that can develop as a result of repetitive movement, sustained loading, working in awkward postures, and other risk factors [1]. These types of injuries generally inflict damage to the soft, muscular, and bony tissues of an anatomical structure. There are numerous RSI's of the upper limb including carpal tunnel syndrome, tenosynovitis, and osteoarthritis (OA) of the hand-wrist [1].

Tasks that lead to RSI can be as simple as using a kitchen knife or more complex such as using the hydraulic-actuation joystick for controlling heavy vehicles. As an example, hydraulic-actuation joysticks are used to control many mobile North American construction, forestry and mining vehicles. Operators using these controllers may perform 20000 or more repetitive actions in a 10-hour shift [2]. It has been shown that these repetitive actions combined with static loading on the upper limb musculature of the operators can lead to discomfort and pain [2].

Using data from a previously imaged cadaveric specimen, the objectives of the current work were: 1) To use finite element (FE) modeling to quantify the stress distributions in the bones of the upper limb and the contact stresses at the joints; 2) To investigate possible bones and joints in the hand and wrist, prone to injury, which may become areas of high risk for developing osteoarthritis; and 3) To create a more complete FE model of the hand and wrist, and to explore the roles of cancellous bone during load transmission.

METHODS

The bony geometry for the FE model was developed from computed tomography (CT) images of a cadaveric left upper limb specimen (N=1). The CT images were segmented using MeVisLab 1.6.1 (MeVis Research GmbH, Bremen, Germany). The cortical and cancellous layers were delimited separately for 29 bones (14 phalanges, 5 metacarpals, 8 carpals, radius, and ulna).

The segmented bones were converted into 3D surfaces using MeVisLab and imported into Mimics 12 (Materialise NV, Leuven, Belgium) to create FE meshes. A total of 58 meshed parts (29 for cortical bone and 29 for cancellous bone) were created consisting of a total of 312264 second-order, tetrahedral elements.

Cartilage and ligaments were added to the bony geometry in ABAQUS 6.8 (Dassault Systemes Simulia Corp., Providence, RI, USA). Cartilage thickness was extruded using the Edit Mesh toolkit. Ligaments were modeled as non-linear, tension only springs [3]. The material properties for the bony and soft tissues were acquired from the literature.

A 54.3 N load was applied to the palm of the hand with the wrist in a neutral position. The load was intended to provide a rough approximation of the hand-wrist loading which might occur from using a joystick or other hand tool. This low-level load was static and compressive in the axial direction. The proximal ends of the radius and ulna were constrained as they were confined during the CT imaging process. Contact between bones was simulated using the General Contact formulation in ABAQUS. A sensitivity analysis was conducted to assess the impact of varying cartilage density on joint contact stress.

RESULTS AND DISCUSSION

It was shown that a static, compressive load applied to the wrist in a neutral position results in load transmission primarily to the scaphoid and lunate (Fig. 1), as well as high peak contact stresses at the

radioscaphoid and radiolunate articulations. These bones and articulations are areas of high risk for OA initiation and progression by means of the scaphoid lunate advanced collapse and scaphoid non-union advanced collapse injury mechanisms. The scaphotrapeziotrapezoid articulation was also identified as an area with high contact stress and subsequently, an area for high risk of injury and possible development of OA.

The results also demonstrated that there is load transfer between cortical and cancellous bone during load transmission, whereby the roles of cancellous bone may be to de-localize stress away from the joints and to transfer stress to the stronger shaft of the cortical shell. This would effectively reduce the risk of injury to the joints where OA initiates and progresses.

In addition, the sensitivity analysis showed that under a static load higher peak contact stress exists at a joint with cartilage in higher density (Fig. 2). This suggests that higher density cartilage may be more susceptible to injury under repetitive loading as they are subjected to consistently high mechanical stress.

FUTURE WORK

While these results demonstrate the potential of the technique for a single specimen, further work is required to generalize the results across a larger sample population. Future research will concentrate on creating statistical shape models of the bony geometry to characterize the variations across a population set. Further work will also include the development of methods to extract cartilage and anatomical features such as ligament and tendon attachment sites directly from volumetric imaging data since the current work assumes uniform cartilage density and atlas-derived ligament attachment locations.

CONCLUSIONS

The current study has provided insight into areas of hand and wrist FE analysis not explicitly studied in previous research: possible risk areas for developing OA in the hand and wrist from low-level loading, possible roles of cancellous bone during load transmission from low-level loading, and cartilage tissue injury in relation to cartilage density.

The current study has also made important contributions to the development of FE models of the hand and wrist such as outlining the methods used to create a complete bony model of the upper limb.

REFERENCES

1. Yassi A. L*ancet* **349**, 943-947, 1997.
2. Golsse JM. *Technical Note TN-134*, Pointe Claire, Quebec, Canada, 1989.
3. Carrigan SD, et al. *Annals of Biomedical Engineering* **31**, 718-725, 2003.

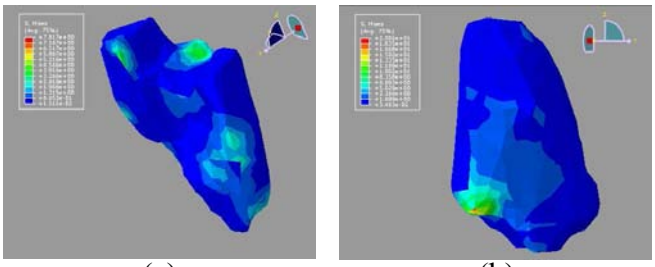

(a) (b)

Figure 1: Stress distribution in the cortical bone of the (a) scaphoid and (b) lunate. The lunate has the highest peak stress of 20.0 MPa. Each sub-figure uses its own von Mises stress scale.

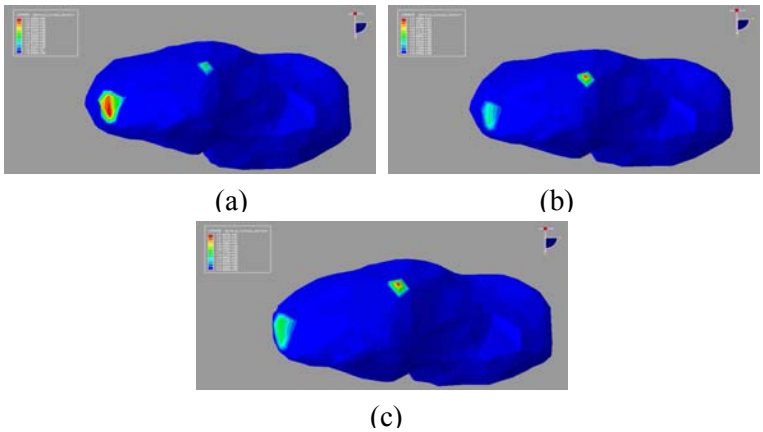

(a) (b)

(c)

Figure 2: Peak contact stress at the radioscaphoid articulation for the three cartilage densities, as indicated on the proximal end of the scaphoid: (a) 11.0 MPa for1.1 g/cm^3, (b) 13.9 MPa for 1.2 g/cm^3, (c) 14.7 MPa for 1.3 g/cm^3. All images are in axial view. Each sub-figure uses its own von Mises stress scale.

SENSITIVITY OF STRAINS IN THE FEMORAL NECK TO VARIATIONS IN MUSCLE FORCES

Dennis E. Anderson and Michael L. Madigan

Virginia Polytechnic Institute and State University, Blacksburg, VA, USA
email: dennisa@vt.edu, web: http://www.biomechanics.esm.vt.edu/

INTRODUCTION

Muscle forces play a role in the health and strength of the femur, both through stimulating remodeling processes [1] and by reducing shear and bending in the bone [2] which reduces the risk of material fatigue [3]. Older adults display differences in joint kinetics during gait [4], which may indicate age-related changes in normal muscle forces. Such changes may influence bone loading and therefore have a role in age-related changes in bone strength. Because of the high incidence of hip fractures in older adults, and the connection between muscle forces and bone strength, understanding the effect of muscle forces on strains in the proximal femur is of interest. This study examined the effects of individual muscle forces on strains in the femoral neck using a finite element model.

METHODS

Body motion and ground reaction force data were collected during a single gait trial while a participant (82 year old female, height 157.5 cm, mass 62.1 kg) walked at 1.1 m/s with a step length of 0.65 m. The study was approved by the IRB at Virginia Tech, and the participant provided informed consent prior to participation. Muscle forces during gait were estimated with static optimization and a musculoskeletal model in OpenSim [5]. A finite element model was obtained from the public dataset of the VAKHUM project [6] and geometrically scaled to match the size of the participant. The estimated muscle forces were applied to the finite element model.

Strains were examined at four locations on the femoral neck: superior, anterior, inferior and posterior. Baseline loads were those at 55% and 86% of gait cycle, which corresponded to peaks in maximum principal (MP) strains in early and late stance phase. Muscle forces were perturbed by ±10% and ±20%, and the resulting MP and maximum shear (MS) strains determined. The muscles investigated included those that attached to the femur and crossed the hip joint. To examine the relative importance of muscles forces to strain, percent change in strain versus percent change in muscle force was determined.

RESULTS AND DISCUSSION

The highest MP strain among the four locations investigated occurred on the superior side of the femoral neck, and the highest MS strain occurred on the inferior side, both at 86% of gait (Table 1).

Table 1: Strains (με) in the femoral neck of the femur with baseline muscle forces applied.

Location	55% Gait Cycle		86% Gait Cycle	
	MP	MS	MP	MS
Superior	2202	1454	2508	1657
Anterior	336	400	202	367
Inferior	985	2074	1076	2258
Posterior	422	768	299	517

Five muscles, gluteus maximus (GMAX), gluteus medius (GMED), gluteus minimus (GMIN), iliopsoas (IP) and piriformis (PIR) produced changes in strain of more than 1% in the femoral neck with a 20% force perturbation (Figure 1). Increasing GMAX force increased strains on the anterior and posterior femoral neck at 55% of gait cycle. Increasing GMED force decreased strains on the superior, anterior and inferior sides of the femoral neck, but increased strain on the posterior side. GMIN followed a similar pattern to GMED, but had a smaller effect. Increasing IP force only had an effect at 86% of gait cycle, when it decreased strains in the posterior femoral neck, but increased strains at the other locations. Increasing PIR force caused small increases in strains in the anterior and

posterior femoral neck at 55% of gait cycle, but a small decrease in MP strain in the posterior femoral neck at 86% of gait cycle.

While the relationship between muscle force and strain was typically linear, the anterior and posterior femoral neck at 86% of gait cycle showed nonlinear variation with GMED force. This was due to the direction of MP strain changing from along the length of the femoral neck (caused by bending) to along the radius of the femoral neck (caused by compression). The effect of the muscles on strain was also not consistent between the two time points investigated. The hip angle was 21.7° flexion at 55% of gait cycle and 14.3° extension at 86% of gait cycle. These differences in hip angle can change the directions of the muscle forces applied to the femur, changing their effect on strains.

CONCLUSIONS

Results indicate that strains in the femoral neck were affected by several muscles, particularly the GMED and IP. Understanding the importance of various muscles to strains in the proximal femur may aid in future efforts to understand and prevent hip fractures in older adults.

REFERENCES

1. Turner, CH. *Bone* **23**, 399-407, 1998
2. Duda, GN, et al. *J Biomech* **31**, 841-846, 1998
3. Taylor, D, et al. *J Biomech* **36**, 1103-1109, 2003.
4. DeVita, P, et al. *J Appl Physiol* **88**, 1804-1811, 2000.
5. Delp, SL, et al. *IEEE Trans Biomed Eng* **54**, 1940-1950, 2007.
6. Van Sint Jan, S. *The VAKHUM Project*, accessed from http://www.ulb.be/project/vakhum/, 2008.

ACKNOWLEDGEMENT

This work was supported by Award Number F31AG030904 from the National Institute on Aging. The content is solely the responsibility of the author and does not necessarily represent the official views of the National Institute on Aging or the National Institutes of Health.

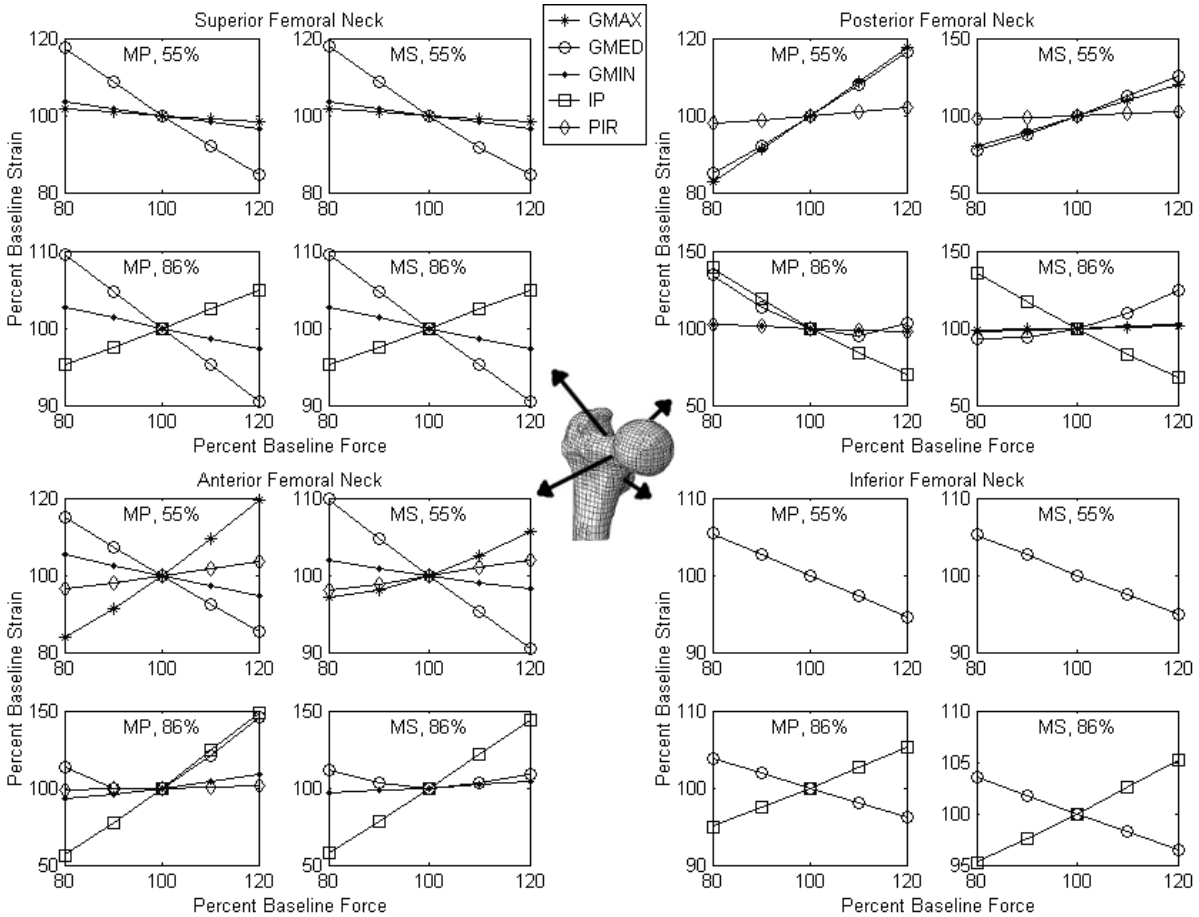

Figure 1: Percent change in baseline strains in the femoral neck relative to percent change in baseline muscle forces. Results are shown for both MP and MS strains at 55% and 86% of the gait cycle.

INFLUENCE OF *IN-VIVO* TENDON FORCE-STRAIN RELATIONSHIP FOR DIFFERENT LOADING RATES INTO EMG-DRIVEN MODEL

[1]Pauline Gerus, [1]Guillaume Rao, [2]Kurt Manal, [2]Thomas S. Buchanan and [1]Eric Berton

[1] Aix-Marseille University, FRANCE
[2]University of Delaware, DE, USA
email: pauline.gerus@univmed.fr

INTRODUCTION

Neuromusculoskeletal modeling combines experimental measurements and mathematical models to estimate forces produced by the muscle-tendon complex. Hill-type models are widely used to represent musculotendon contraction dynamics assuming a purely elastic tendon. A generic force-strain relationship for the tendon is often used based on *in-vitro* tests [1]. Recent developments using ultrasound has shown a high inter-subject variability of *in-vivo* force-strain relationship and higher strain than previously reported [1]. In addition, current elastic models of tendon do not account for strain-rate dependence.

In this present study we investigated the influence of *in-vivo* force-strain relationships of the medial gastrocnemius (MG) tendon estimated by ultrasound (US) imaging and obtained during different loading rates on the estimation of muscle forces through an EMG-driven model. We hypothesize that the tendon force-strain relationship influences the estimation of muscle forces.

METHODS

An *in-vivo* MG tendon force-strain relationship was estimated for ten healthy male subjects. Experimental data were collected using a Biodex System 3 dynamometer with the right ankle dorsiflexed at 20° (0°=neutral position) and knee fully extended. Subjects were instructed to develop ramp-up and down contractions (from rest to 100% of maximal voluntary moment) at three different target speeds: C1 (ramp time = 1 sec), C4 (4 sec) and C8 (8 sec). Tendon strain for the MG was estimated by combining motion capture and US imaging. Myotendinous junction (MTJ) displacement was recorded with US (30Hz) and tracked manually. MTJ elongation was divided by the initial tendon length computed from markers placed on the probe and on the calcaneum. Normalized MG force was estimated from the ankle net joint moment. Finally, an Ogden hyperelastic model was used to fit each force-strain relationship for each subject and condition.

Additional dynamic trials, walking and one-leg hopping at 2 Hz were performed by each subject. Movement data were sampled at 100 Hz using a Qualisys Oqus 500 system, while EMG and force plate data were sampled at 2000 Hz. EMG were collected for MG, LG, SOL, and TA for both the isometric dynamometer and dynamic (walk / hop) trials.

An EMG-driven model [2] was used to estimate muscle forces. The force-strain relationship for tendon was represented by: (1) generic values often used in musculoskeletal modeling applications (Zajac), and (2) the subject specific *in-vivo* tendon force relationships described earlier. The tendon was modeled using a force-strain relationship, normalized to resting tendon length and maximal isometric force [2].

The EMG-driven model calibration process was performed using one trial for each of the isometric, walking and hopping tasks and for the different force-strain relationships. The force-strain relationship obtained for C1 (1 second ramp time) was used for the isometric and walking trials because the tendon velocity was more similar than for the C4 and C8 ramp conditions. EMG, kinematic and dynamic data were used as input into EMG-driven model. Finally, the two different calibrations (*in-vivo* condition vs. generic Zajac condition) were compared in order to test the influence of force-strain relationship.

RESULTS AND DISCUSSION

The tendon behavior through different loading rates revealed that tendon strain was greater when contraction speed decreased with forces greater than 30% of normalized force. This finding demonstrates the loading rate dependence of tendon (Figure 1), a

property not generally considered in the contraction-dynamics of Hill-type models.

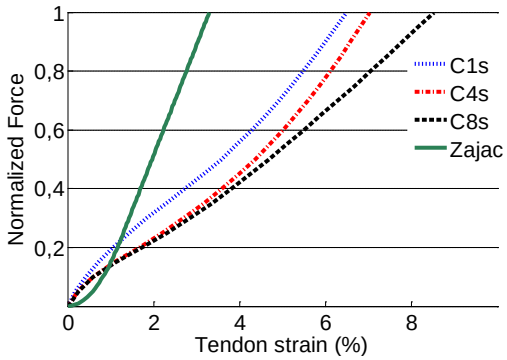

Figure 1: Group averaged force-strain relationship of the MG tendon according to the experimental conditions. Zajac's generic EMG-driven model curve is also presented.

For isometric tasks, muscle-related variables presented in Table 1 were significantly higher for *in-vivo* condition compared to Zajac condition, and in agreement with data reported by [3]. However, this difference between the two conditions was not observed in the estimation of muscle forces.

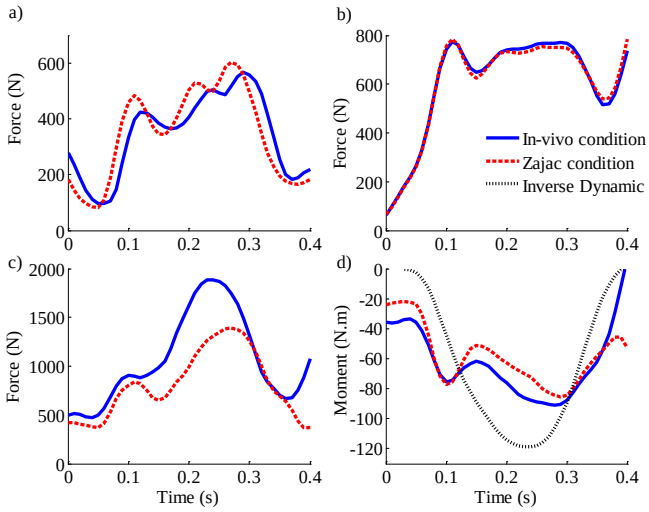

Figure 2: Muscle forces for a) LG, b) MG, c) SOL, and d) the net joint moment estimated by the model and by inverse dynamics for one subject on hopping task. Note the difference in muscle forces for LG and SOL.

For walking task, no difference was observed between the two conditions. This similarity could be explained by low muscle forces and thus no difference in tendon strain between the two conditions (see Figure. 1). For hopping tasks, higher amplitude of tendon strain (3.3% ± 2.1% vs. 1.5% ± 0.6%) were observed for *in-vivo* condition. Higher mean forces of MG (697N ± 246N) and SOL (1095N ± 392N) for *in-vivo* condition compared to Zajac condition (648N ± 256N and 968N ± 319N) (see Fig. 2). Hopping is a movement where the tendon undergoes high strain. The difference in muscle forces between the two conditions demonstrates the importance of accurately characterizing the tendon for highly dynamic tasks.

CONCLUSIONS

Muscle fiber behavior for our EMG-driven model agreed more closely with experimental observations [3] when *in-vivo* force-strain relationships obtained under different loading rates were used rather than the generic Zajac tendon-strain relationship. Muscle force estimates using the different tendon-strain relationships only differed for the hopping tasks where tendon strain is high. The tendon force strain relationships shown in Figure 1 are easily incorporated into existing Hill-type muscle models. This may be important when investigating ballistic movements or tasks that take advantage of elastic energy storage. Further, it would be interesting to estimate *in-vivo* force-strain relation of tendon-aponeurosis and not only tendon as previous studies have shown difference between the tendon and aponeurosis behaviors.

REFERENCES

1. Zajac FE. C*rit Rev Biomed Eng* **17**, 359-411,1989.
2. Buchanan TS, et al. *J Appl Biomech* **20**, 367-395, 2004.
3. Arampatzis A, et al. *J Biomech* **40**, 1946-1952, 2007.

Table 1: Average value for amplitude of fiber length and maximum tendon strain obtained on isometric tasks according to the two conditions (*In-vivo* condition vs. Zajac condition)

	Amplitude of fiber length (mm)		**Max tendon strain (%)**	
	***In-vivo* condition**	**Zajac condition**	***In-vivo* condition**	**Zajac condition**
LG	21.5 ± 1.0	7.9 ± 0.2	5.6 ± 2.4	2.4 ± 0.3
MG	20.0 ± 0.9	7.1 ± 0.2	4.9 ± 2.1	2.2 ± 0.2
SOL	12.2 ± 0.5	4.4 ± 0.1	5.0 ± 2.0	2.3 ± 0.2

PEAK CONTACT STRESS IN HUMAN HIP JOINT– BIOMECHANICS OR MECHANOBIOLOGY?

[1,2]Matej Daniel, [1]Jana Hornová, [2]Aleš Iglič

[1]Czech Technical University in Prague, Prague, Czech Republic
[2]University of Ljubljana, Ljubljana, Slovenia
email: matej.daniel@fs.cvut.cz, web: http://www.biomechanics.cz

INTRODUCTION

The hip contact stress is considered an important factor influencing the development of the hip joint cartilage [1]. The hip contact stress has been measured using several approaches and also estimated on the basis of mathematical models [2,3]. A detailed description of various methods for measurement and estimation of contact stress distribution can be found in Brand et al, 2002 and Brand, 2005 .

Generally, the values of the peak contact stress p_{max} measured experimentally, regardless of the method used, are considerably higher than the values obtained from mathematical models. On the other hand, these mathematical models successfully predicted clinical status of the hip [4,5]. Considering results of experiments as more precise, the question arises how to explain the clinical relevance of the mathematical models. As suggested by Mann, 2002, the differences between the theoretical predictions and the experimental results can be caused by unrealistic assumptions in the mathematical models where the regional variations in geometry of subchondral bone, thickness, and stiffness of the cartilage are neglected. Therefore, it is the aim of this study to determine how the regional variations in the local geometry of the hip joint influence the hip stress distribution.

METHODS

Mathematical models used in this study are based on data acquired from the Visible Human Project [6]. Two models are created: simplified mathematical model used in clinical studies and more precise three-dimensional model based on CT data.

The first model is based on analysis of standard anteroposterior radiogram as this method is used in the clinical studies mostly. Radiogram image was created by projection of filtered CT images to frontal plane as described in Daniel et al, 2005. Method HIPSTRESS [4] was used to calculate hip joint contact pressures. Within this method, it is assumed that femoral head and acetabulum are ideally spherical and congruent while the elastic layer of cartilage completely fills the articular gap. Size of the femoral head is defined by its radius r and inclination of the acetabulum is defined by the center-edge angle of Wiberg ϑ_{CE}.

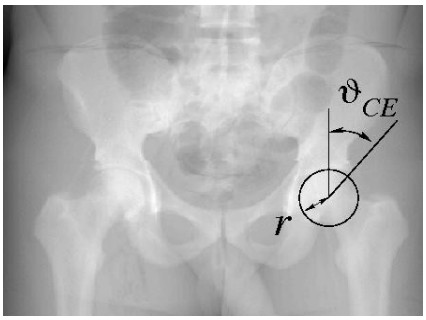

Figure 1: Simulated radiogram from CT images showing parameters describing geometry of the hip.

The second model is based on CT data analysis. Contours of bony structures were segmented manually and custom-made software has been used to create a surface triangular network using a Delaunay triangulation. In this model, upon loading the hip by the resultant hip force ***R***, the femoral head is assumed to moved towards the acetabulum and the cartilage layer is squeezed. Since the cartilage is considered to be an ideally elastic continuum, the stress is a function of the local cartilage deformation. The displacement of the femoral head that generates force ***R*** transmited through the hip joint was determined using a Levenberg-Marquardt algorithm.

Static loading is assumed within this study: the constant resultant hip force ***R*** has the magnitude 2.5

times the body weight (BW), it lies in the frontal plane (e.g. 2000 N for a 80 kg man) and it is inclined for an angle 5 degrees medially from the vertical axis. The radius of the femoral head is 26 mm and the center-edge angle of Wiberg is 40°.

RESULTS AND DISCUSSION

Biomechanical parameters describing the hip joint contact stress distribution in the model based on plain radiogram and CT data are shown in Tab. 1. The former model predicts more than two times lower peak contact stress than the latter one. This confirms that simplified articular surface shape predicts too low maximum contact stress. The stress estimated from CT images is closer to the values measured experimentally [2] and this method may be considered to be more accurate.

The peak contact stress describes loading at one point only and does not describe how the load is distributed over the articular surface. Hence, parameters other than p_{max} were evaluated as well. These parameters are the mean contact stress, standard deviation of the stress, and the size of the area of non-zero stress, .i.e. the weight-bearing area *A*. Tab. 1 shows that there are considerably lower differences in these parameters between both models as in the case of p_{max} indicating similar overall stress distribution in both models.

Fig 2 shows absolute value of difference of contact stress between both models. It can be seen, that both mathematical model predict very similar stresses over most of the articular surface.

Model	p_{max} **[MPa]**	**mean** *p* **[MPa]**	**stdev** *p* **[MPa]**	A **[mm²]**
CT	3.6	0.77	0.75	2274
Radiogram	1.7	0.67	0.55	2784

Table 1: Parameters describing hip joint pressure distribution.

CONCLUSIONS

Based on the presented results, it can be conluded that the ability of the simple model to asses exact value of the peak contact stress p_{max} is disputable. The peak contact stress estimated by using simple model can be considered as a parameter related to overall contact but not as the exact value of the stress. Clinical studies have shown that a peak contact stress determined using simplified models is relevant parameter to estimate the long-term cartilage development and can therefore be described as a mechanobiological parameter in clinical studies.

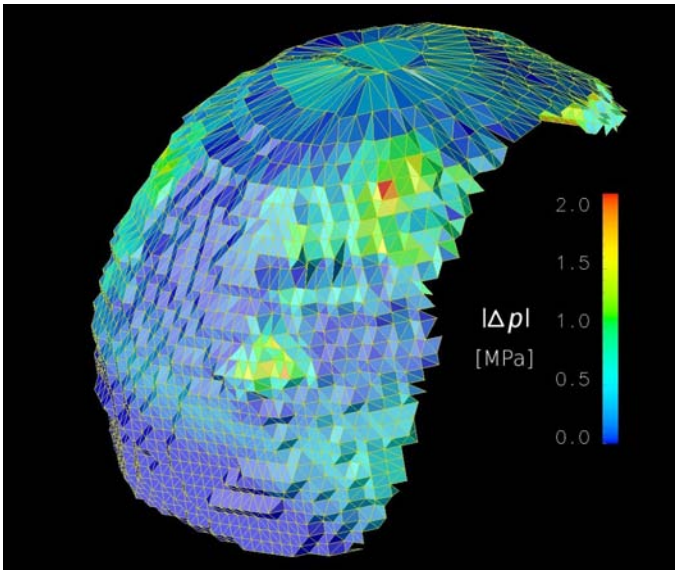

Figure 2: Absolute values of difference between contact stress estimated from CT images and from AP radiogram.

REFERENCES

1. Brand RA. *Iowa Orthop J*, **25,** 82–94, 2005
2. Brand RA et al. *Hip Int.* **11**, 117–126, 2001.
3. Mann R.W. *J Biomech* **35**, 1291–1292, 2002.
4. Mavčič B et al. *J Orthop Res* **20**, 1025–1030 2002.
5. Mavčič B et al. *Clin Biomech* **19**, 939–943, 2004.
6. Ackerman MJ. D-Lib Magazine, 1995.
7. Daniel et al. *Comp Meth Biomech Biomed Eng* **8,** 25-29, 2005.

ACKNOWLEDGEMENTS

Research is supported by project MSM 6840770012.

ON THE ROLE OF LIPID ANISOTROPY IN THE TRANSITION BETWEEN LAMELLAR AND INVERTED HEXAGONAL LIPID PHASES

[1]Šarka Perutkova, [2]Matej Daniel , [1]Aleš Iglič, [3]Veronika Kralj-Iglič

[1]Laboratory of Biophysics, Faculty of Electrical Engineering, University of Ljubljana, Slovenia
[2]Laboratory of Biomechanics, Faculty of Mechanical Engineering, CTU in Prague, Czech Republic
[3] Laboratory of Clinical Biophysics, Faculty of Medicine, University of Ljubljana, Slovenia
email: matej.daniel@gmail.com, web: http://www.biomechanika.cz/

INTRODUCTION

Phospholipids in aqueous solution undergo a self-assembling process and form various structures. The driving force of this process is predominantly the hydrophobic effect. The most common and biologically the most relevant phase is the fluid lamellar lipid bilayer phase (L_α). Nevertheless, nonlamellar model membranes are becoming a subject of increasing interest, due to their importance in living organisms and due to their promising technical applications such as in drug delivery, gene transport and nanotechnology. The direct L_α-H_{II} phase transition in POPE takes place upon increasing the temperature of the system over 74 °C. Structural data on POPE layers obtained by high-resolution small-angle X-ray diffraction [1] was taken into account to validate our model. It was assumed that the intrinsic shape of the POPE molecule favors the inverted cylindrical configuration within the lipid monolayer and that the intrinsic anisotropy increases with increasing temperature.

METHODS

The equilibrium configuration is determined by the minimum of the free energy of the system. We consider for the total free energy of the hexagonal phase two energy contributions: the energy of local bending and the interstitial energy. Starting from a single molecule energy and applying the methods of statistical physics, the free bending energy of a lipid monolayer was derived taking into account the anisotropy of the lipids [2]:

$$f_b = \int \left[(h-h_m)^2 + \left(d^2 + d_m{}^2\right)\right] d\tilde{l} - \kappa \int \ln\left(2\cosh((1+\tilde{k}/kT)\upsilon 2 d d_m)\right) d\tilde{l},$$

where h is the local mean curvature, d the local curvature deviator, h_m the intrinsic mean curvature, d_m the intrinsic curvature deviator (all quantities are normalized with respect to z_0), $\kappa = 1/\upsilon = 2kTz_0{}^2$, k is Boltzmann constant, T is absolute temperature, ξ is the constant describing the strength of the interaction between a single lipid molecule and the surrounding membrane continuum and $\tilde{k}$ is the constant describing the direct interaction between lipid molecules.

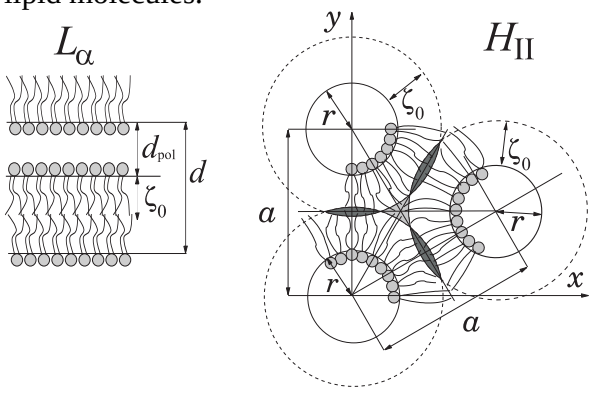

Figure 1. Geometry of L_α and H_{II} phases. Cylinders of radius r are within a distance of a. The parameter ζ_0 denotes the equilibrium length of hydrocarbon chains, while d_{pol} is the lattice repeat distance. As the distance between the cylinders is not constant, stretching or compressing of some hydrocarbon chains (shown by shading) is required in order to fill the voids (adapted from [3]).

We assume in the model that the interstitial energy is equal to the stretching energy of the lipid chains which should be stretched in order to fill the voids in the H_{II} lattice (Fig.1). The stretching energy of the single lipid chain can be expressed within the harmonic spring model as: $f_i = \tau(\zeta - \zeta_0)^2$, where ζ is the length of the single lipid molecule and τ is the corresponding stretching modulus. The

minimization was performed numerically using Monte Carlo simulated annealing method.

RESULTS

We calculated the equilibrium configuration of the system in which an inverted central phospholipid cylinder is embedded in two adjacent lipid bilayers. In Fig. 2, snapshots of the equilibrium configurations for anisotropic molecules $D_m = |H_m|$ and different values of model constants are displayed. From left to right, the intrinsic lipid curvature is increased. The top row presents the L_α phase. Below, from top to bottom, the stretching modulus of the lipids is increased. The value of the equilibrium free energy f is given for the L_α phase, while the values of the difference between the energy of the H_{II} phase and the L_α phase $\Delta f = f_{HII} - f_{L\alpha}$ are depicted for the H_{II} phase.

CONCLUSION

Our results indicate that including the phospholipid anisotropy in the expression for the local bending energy can explain the experimentally observed stability of the H_{II} phase and the L_α-H_{II} transition at higher temperatures. Moreover, adding of the interstitial energy to the total monolayer energy is also needed. We show that with increasing absolute values of intrinsic curvature deviator D_m of lipid molecules (which was assumed to increase with increasing temperature), the L_α-H_{II} phase transition, which is observed in experiments [2] takes place beyond a certain threshold temperature. Finally, by using our model, we could also reproduce realistic lipid configurations (Fig. 2) in good agreement with experimental results [1, 2]. In conclusion, we have shown that lipid anisotropy plays an important role in the stability of the H_{II} phase and in the L_α-H_{II} phase transition.

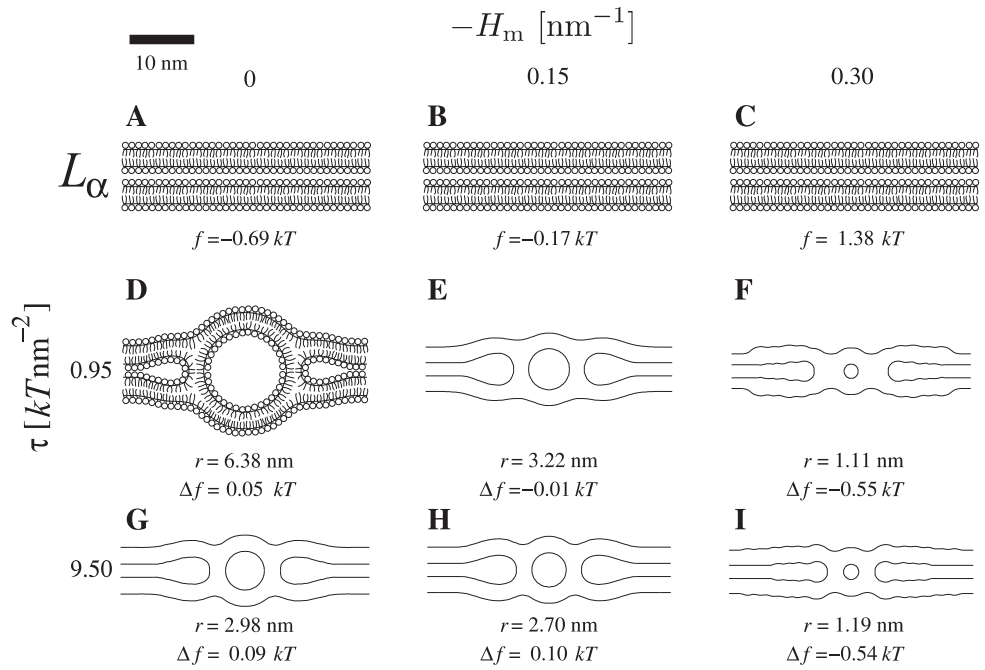

Figure 2. Configuration of the lipid monolayers adjacent to a central cylinder representing a nucleation line in the L_α-H_{II} transition for different intrinsic curvatures of the lipid molecules H_m and different stretching modula of the phospholipid chains τ. It is considered that $D_m = |H_m|$. The free energy per lipid molecule and the radius of the central cylinder are given for each configuration; $\tilde{k}/kT = 1$ (adapted from [3]).

REFERENCES

1. Rappolt M. et al. *Biophys J* **84,** 3111-3122, 2003.
2. Kralj-Iglič V. et al. *J Stat Phys* **125**, 727-752, 2006.
3. Mareš T. et al. *J Phys Chem B* **8**, 16575-16584, 2008

DYNAMIC SIMULATION OF MOVEMENT BASED ON OPENSIM AND MATLAB®/SIMULINK®

Misagh B. Mansouri and Jeffrey A. Reinbolt

University of Tennessee, Knoxville, TN, USA
email: misagh@utk.edu, web: http://rrg.utk.edu

INTRODUCTION

Numerical simulations are playing an important role in solving complex problems and have the potential to revolutionize medical decision making and treatment strategy. Musculoskeletal conditions cost the U.S. economy alone over $849 billion per year (7.7% of the U.S. Gross Domestic Product) and place great demands on healthcare systems worldwide [1]. This area could greatly benefit from computational tools offering greater understanding of human movement and predictive capabilities for optimal treatment planning.

Currently there is no freely available, open-source computational tool providing an interface between software packages for robust design and control as well as modeling and simulating neuromusculoskeletal systems. Others [2] have tools to convert musculoskeletal and kinetics models from commercial software [3] to Simulink® blocks. Simulink® extends MATLAB®, the leading mathematical computing software for engineers and scientist, with a graphical environment for rapid design, control, and simulation of dynamic systems. However, this package has limited resources for modeling and simulating neuromusculoskeletal systems. On the contrary, OpenSim [4] is a popular open-source platform for modeling, simulating, and analyzing these systems, but it is lacks the robust design and control tools of MATLAB®/Simulink®.

Our goal was to develop an interface between MATLAB®/Simulink® and OpenSim that combines their relevant strengths (e.g., rapid model-based design, control systems, numerical simulation, and human movement dynamics). The MATLAB®/Simulink® and OpenSim integrated platform contributes to the overall understanding of human movement and has the potential to improve surgical and rehabilitation treatment planning.

METHODS

We developed and demonstrated the MATLAB®/ Simulink® and OpenSim interface (Fig. 1) using a three step process.

Figure 1: New S-function (system function) interface linking rapid design and control tools of MATLAB®/Simulink® with neuromusculoskeletal dynamic simulation tools of OpenSim.

First, we developed a MATLAB® S-function (system function) based on an OpenSim model as a Simulink® block. This block interacts with the Simulink® engine, similar to built-in Simulink® blocks. The S-function works with any OpenSim model regardless of the number of input controls (e.g., muscle excitations or joint torques) or output states (e.g., kinematics).

Second, we created a generic open-loop Simulink® model that loads and executes the OpenSim-based S-function developed in the first step (Fig.2). To demonstrate the open-loop characteristics of this model, we used a simple human arm model with 2 degrees of freedom and 6 muscle-tendon actuators. Kinematics resulting from a Simulink® simulation of elbow flexion were directly compared with those from OpenSim forward dynamics.

Figure 2: Generic open-loop Simulink® model using the OpenSim-based S-function interface to generate output states (e.g., kinematics) from input controls (e.g., muscle excitations or joint torques).

Third, we created an example closed-loop Simulink® model by adding a proportional, integral, and derivative (PID) controller with feedback to extend the open-loop model created in the second step (Fig. 3). The open-loop model is limited to using fixed controls that cannot be changed by the resulting motion. On the other hand, many human movement applications require closed-loop control systems. To demonstrate the closed-loop characteristics of this Simulink® model, we used a human arm model balancing a pole free to rotate about the hand. This biomechanical system had 2 degrees of freedom, a constraint on elbow angle as a function of shoulder angle to reduce the number of controls, and 1 shoulder torque actuator.

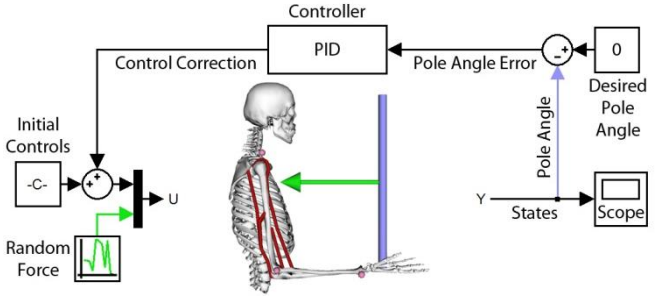

Figure 3: Example closed-loop Simulink® model extending the open-loop case with proportional, integral, and derivative (PID) control of a human arm balancing a pole despite force disturbances.

A PID controller was used to balance a pole above the hand by adjusting the torque at the shoulder (Fig. 3 & 4a). The controller gains were tuned using the classic Ziegler–Nichols method. The desired pole angle (measured from vertical) was 0 and it was used to compute a pole angle error and then a control correction. The initial controls, computed from inverse dynamics, were used to maintain arm position before control correction was necessary. The combination of control correction and initial controls is analogous (but not identical) to the human brain's output for the arm to balance a pole. Random force disturbances were added to the pole and the pole angle error was observed.

RESULTS AND DISCUSSION

The new interface between MATLAB®/Simulink® and OpenSim allowed rapid model-based design and numerical simulation of human movement using both open-loop (Fig. 2) and closed-loop (Fig. 3) control systems. For the open-loop case, Simulink® generated elbow flexion angle matched OpenSim within 0.39º RMS. This result indicated an OpenSim model and its controls behave similarly in Simulink® and OpenSim. For the closed-loop case, the PID controller successfully rejected random force disturbances (Fig. 4b) and balanced the pole above the hand with a maximum pole angle from vertical of 0.0177º (Fig. 4c).

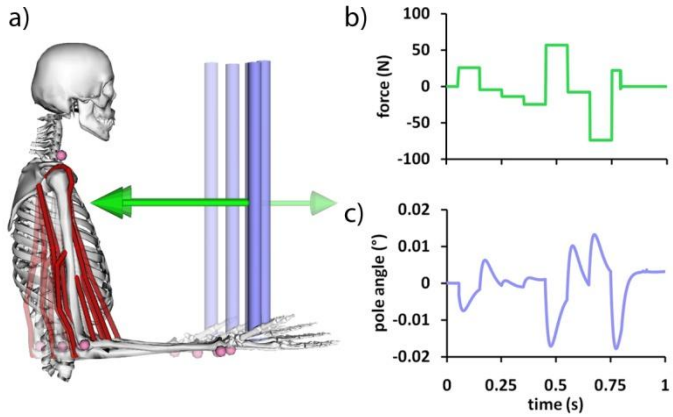

Figure 4: Dynamic simulation generated in Simulink® of (a) PID controlled human arm model balancing a pole (five time frame series from 0.54s to 0.74s shown). (b) Random force disturbances were added to the pole and (c) the pole angle measured from vertical remained small.

The potential to use integrated computational tools to better understand human movement and optimally design treatments is exciting. We have posted all source code, Simulink® model examples, and user documentation related to this work on a SimTK.org project dedicated to the interface (https://simtk.org/home/opensim_matlab). Once this project is complete and made public, it will not only integrate software tools, but also allow integration of neuroscientists, physiologists, biomechanists, and physical therapists to adopt, adapt, and generate new solutions for musculoskeletal conditions.

REFERENCES

1. Jacobs JJ, et al., *Burden of Musculoskeletal Diseases in the US*, 1st ed. AAOS, 2008.
2. Davoodi R, et al., *Med. Eng. Phys.*, **25**, 3–9, 2003.
3. Delp SL and Loan JP, *Comp. Science Eng.*, **2**, 46-55, 2000.
4. Delp SL, et al., *IEEE Trans. Biomed. Eng.*, **54**, 1940-1950, 2007.

ACKNOWLEDGEMENTS

Supported by a subaward from NIH Roadmap for Medical Research U54 GM072970.

FINITE ELEMENT MODELING OF INTRANEURAL GANGLION CYSTS OF THE COMMON PERONEAL NERVE

[1]Shreehari Elangovan, [1]Gregory Odegard, [2]Duane Morrow, [2]Huan Wang, [2]Marie-Noëlle Hébert-Blouin and [2]Robert Spinner

[1]Michigan Technological University, Houghton, MI, USA
[2] Mayo Clinic, Rochester, MN, USA
email: gmodegar@mtu.edu

INTRODUCTION

Intraneural ganglion cysts (IGC) are mucinous cysts which form within the epineurium of peripheral nerves, most commonly the common peroneal nerve (CPN), and are known to produce neurologic deficit

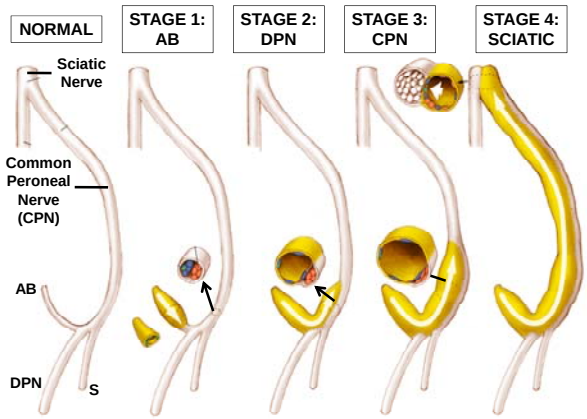

Figure 1: Stages of Intraneural Ganglion Cyst Propagation

(e.g. a foot drop with CPN involvement). There has been much debate amongst clinicians about their origin and treatment. Previous research [1] supports the theory that synovial fluid from the superior tibiofibular joint enters the articular branch (AB) of the CPN subsequent to joint capsule disruption through injury or degeneration. The increased pressure caused by continuous influx of fluid compresses nerve fascicles, expands the nerve radially (Fig. 1 - stage I) and causes further propagation proximally into the CPN (Fig. 1 - stages II, III and IV). To effectively treat IGC and eliminate the common situation of postoperative recurrence, surgeons would benefit from an understanding of the underlying mechanics that influence cyst growth. It has been recently suggested [2] that Finite Element Analysis (FEA) be used to predict the growth behavior of cysts. The objective of this study is to use FEA to study proximal cyst propagation at the AB/Deep Peroneal Nerve (DPN) junction just before it reaches the CPN.

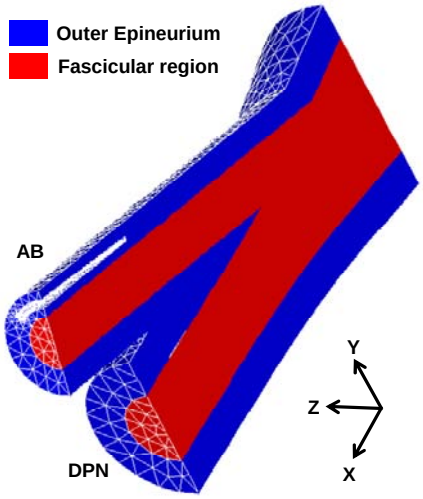

Figure 2: Finite Element Model

METHODS

A three-dimensional finite element model of the junction between the AB and DPN branches of the CPN was constructed, as shown by the cut-away mesh shown in Fig. 2. The AB meets the DPN at an acute angle of 16.5˚, as measured with cadaveric studies. The negative X-axis represents the proximal direction and the positive X-axis represents the distal direction. The model contained two regions: red elements representing the fascicular region, surrounded by blue elements representing the epineurium. Due to the high degree of morphological similarity between nerve and human ligament, each region was modeled as a Mooney-Rivlin hyperelastic isotropic material with transverse properties of the human medial collateral ligament [3]. Dimensions were taken from

cadaveric studies. The cyst is represented by the hollow crescent-shaped region along the length of the articular branch, as shown in Fig. 3. The model was meshed with tetrahedral elements using ANSYS. The boundary conditions included translational restraints at the two ends A and B (Fig. 3) and the application of a pressure load of 1 MPa, corresponding to that estimated to be exerted by the cyst fluid onto the interior faces of the cyst in the AB.

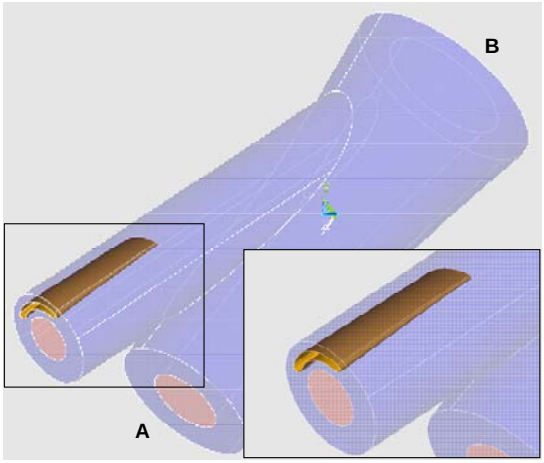

Figure 3: Cyst Geometry

RESULTS AND DISCUSSION

The FEA modeling with the material properties and boundary conditions as described above produced a contour plot of the von Mises stress on the cyst left face where the magnitude varied between 19.29 to 33.75 MPa (Fig. 4). The stress distribution on the right face was similar since the model is symmetric about the XY plane (Fig. 2). Similarly, the von Mises stress distribution on the cyst tip varied between 3.78 to 22.62 MPa. The distortion energy theory failure criteria were applied and the volume of all elements in which the von Mises stress exceeded the ultimate tensile stress of the tissue (assumed value 1.44 MPa) was determined. The material encompassed by the volume of failed elements was removed and the geometry of the cyst was remodelled as shown in Figure 5, where cyst dimensions have increased by Δl and $\Delta\theta$ in the length and arc angle, respectively. After the growth of the cyst, the pressure was again applied and the cyst growth cycle was repeated. Such remodeling steps indicate that the cyst predominantly wants to propagate along the sides, circumferentially, as opposed to along the AB. However, when it is assumed that side face material failure strength is much higher than that at the cyst tip, remodeling steps indicate that the cyst propagates along the AB towards the junction which matches the clinically observed growth pattern.

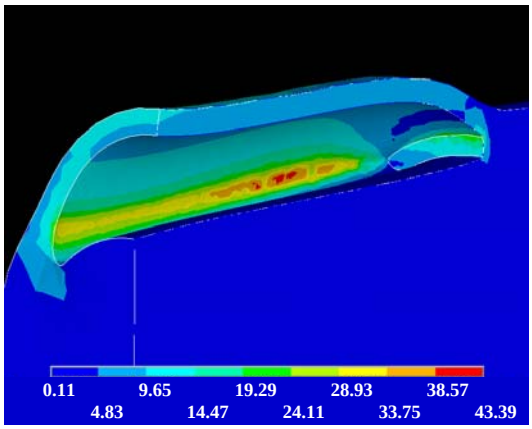

Figure 4: von Mises stresses on the Cyst Left Face

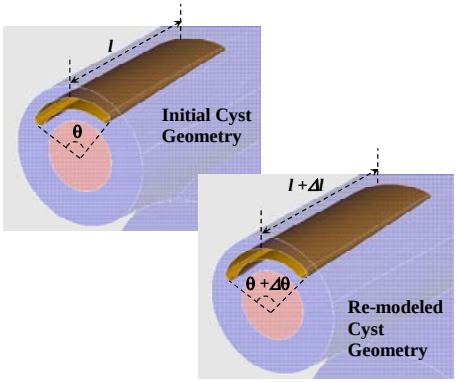

Figure 5: Initial and Re-modeled Cyst Geometries

REFERENCES

1. Spinner, R.J., et al., Peroneal intraneural ganglia: the importance of the articular branch. A unifying theory. Journal of Neurosurgery, 2003. 99(2): p. 330-343.
2. Elangovan, S., et al., Intraneural ganglia: a clinical problem deserving a mechanistic explanation and model. Neurosurgical Focus, 2009. 26(2).
3. Quapp, K.M. and J.A. Weiss, Material characterization of human medial collateral ligament. Journal of Biomechanical Engineering-Transactions of the ASME, 1998. 120(6): p. 757-763.

SIMULATION OF SUBJECT-SPECIFIC BONE REMODELING

[1]Ajay V. Sonar, [1]Kathleen A. Issen, [1]Laurel Kuxhaus and [1]James J. Carroll

[1]Clarkson University, Potsdam, NY, USA
email: jcarroll@clarkson.edu, web: http://clarkson.edu

INTRODUCTION

Bone is a living, growing tissue. The architecture of the inner porous (trabecular) bone that gives bone its strength is continually changing as a result of mechanical adaptation to the external loads. The aging process can be mathematically modeled to simulate the process of adaptive bone remodeling. The idea proposed in this research is to use realistic mechanical loading to simulate the structural change in trabecular bone over time. Realistic mechanical loading data was used to calculate the forces on the joints. These calculated mechanical forces were then used in a remodeling algorithm to predict the future geometry of the trabecular bone.

METHODS

The long-term goal of this work is to use real-world motion data as the driving factor for the bone remodeling algorithm, outlined in Figure 1. Virtual human modeling and simulation software (LifeMOD, LifeModeler, Inc.) is used to calculate the forces at various joint locations or at specific marker location. The force data is then used in the remodeling algorithm to alter the geometry which follows the mechanical adaptation principal. The modified geometry is then imported back in to LifeMOD's virtual human model to calculate the new set of force data. The highlighted sections in Figure 1 indicate the focus of this work.

In this experiment, μCT scans of the 4th lumbar vertebrae with a resolution of 18μm X 18μm X 36μm were used. Subsequent calculations were performed in MATLAB (The MathWorks). These images were thresholded with at 22.4% of the maximal grayscale value to separate bone from the marrow [1]. A 3D geometry was constructed from these images using an isosurface algorithm. A set of parameters that characterize the bone structure were calculated. Comparing these parameters with the values published based on clinical studies validates one aspect of the simulation.

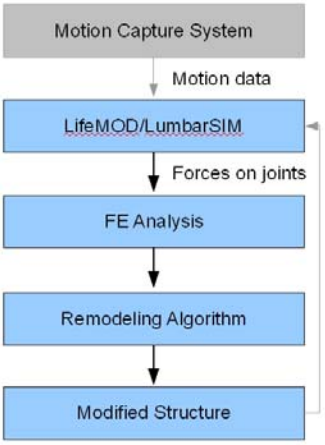

Figure 1: Proposed remodeling cycle.

Osteocyte cell locations were randomly distributed within the 3D reconstruction [3]. Strain Energy Density (S.E.D) rate triggers the remodeling process [2]. The S.E.D. ($R_i(t)$) at an osteocyte location is proportional to the product of strain and stress tensors at that location (Eqn 1). The effective mechanical stimulus on the surface of the bone at a location is the sum of the effect of all the osteocytes within its vicinity whose intensity reduces exponentially (function $f_i(x)$) with distances ($d_i(x)$ and D) (Eqn 2) [3].

$$R_i(t) = \frac{1}{2}\sigma_i\varepsilon_i \quad \begin{cases} \sigma_i = Strain\,tensor \\ \varepsilon_i = Stress\,tensor \end{cases} \tag{1}$$

$$P(x,t) = \sum_{i=1}^{N} f_i(x)\mu_i R_i(t)$$
$$fi(x) = e^{-(di(x)/D)} \tag{2}$$
$$\mu_i = Mechanosensitivity\,of\,osteocyte\,i$$

The final change (dm/dt) in relative density at location on the surface is proportional (by τ) to the effective mechanical stimulus (P), the bone formation threshold (k_{th}) and the relative amount of bone resorbed per day (r_{oc}) [2]. This was modeled using the equations as described in (Eqn 3).

$$\frac{dm}{dt} = \begin{cases} \tau\{P(x,t) - k_{th}\} - r_{oc} & for\ P(x,t) > k_{th} \\ -r_{oc} & for\ P(x,t) \le k_{th} \end{cases} \quad (3)$$

RESULTS AND DISCUSSION

An example of image processing on one slice is shown (Fig. 2). The set of images are stacked and stitched using MATLAB to produce a 3D geometry.

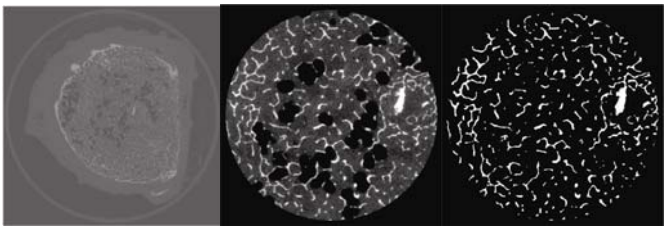

(a) (b) (c)

Figure 2: (a) Original CT (b) ROI (c) Binary image

An important intermediate calculation is that of the mid-axis of the structure and the orientation of each trabeculae with respect to the horizontal plane (Fig. 3). The parameters were calculated on several small sections about $3mm^3$ selected randomly from the vertebrae and compared (Table 1) with previously-reported values [4]. Loads calculated from LifeMOD were used to mathematically simulate bone remodeling on these sections. An example result of the remodeling algorithm is shown (Fig. 4).

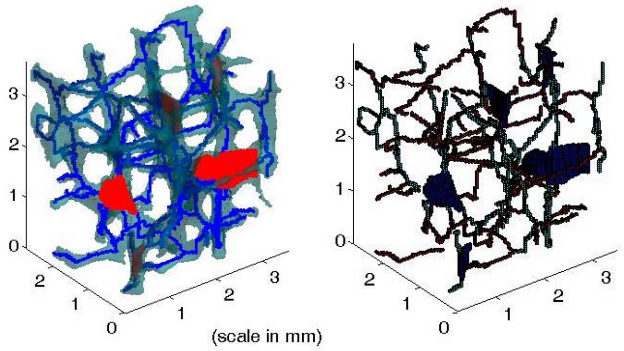

(a) (b)

Figure 3: (a) Mid-axis overlapped on the structure and (b) Orientation.

Future work will parallelize the remodeling algorithm to gain ability to run the simulation on whole vertebrae.

Table 1: Calculated parameter and the clinical data.

Parameters	Samples	Clinical Study
	Range (min – max)	Mean (SD)
rTb.Th (mm)	0.092 – 0.120	0.139 (0.028)
pTb.Th (mm)	0.103 – 0.150	0.139 (0.028)
Tb.Sp (mm)	0.070 – 0.130	0.854 (0.143)
Tb.N (mm^{-1})	2.788 – 4.990	1.161 (0.181)
BV/TV (%)	12.2 – 33.6	8.7 (0.033)
BS/BV (mm^{-1})	9.71 – 30.29	21.17 (3.59)

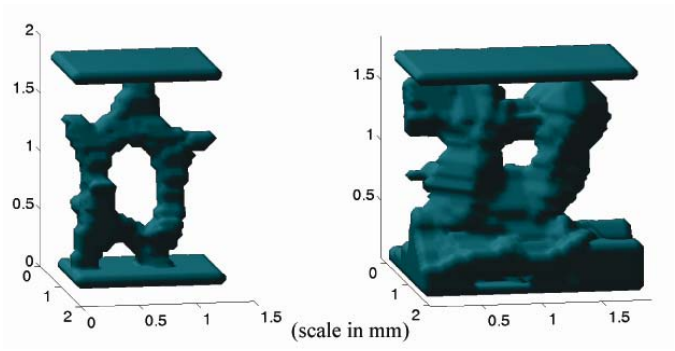

(a) (b)

Figure 4: Example Result: (a) Original geometry (b) After 14 iterations of remodeling.

CONCLUSIONS

We have implemented the algorithm which uses real-world motion data to drive a remodeling algorithm in vertebral bone. Clinically, these results could be used to adapt the lifestyle to sustain stronger bones for longer period of time. Future work collecting more diverse motion data will give insight to activity-related bone remodeling.

REFERENCES

1.Ruegsegger P, et al. *Calcif Tiss Int* **58**, 24-9, 1996.
2.Huiskes R, et al. *Nature* **405**, 704-06, 2000.
3.Mullender M, et al. *Bone* **22**, 125-31, 1998.
4.Hildebrand T, et al. *J Bone Miner Res* **14**, 1167-74, 1999.

SUBJECT-SPECIFIC, GROUP-MEAN, AND GENERIC MUSCULOSKELETAL MODELS FOR PREDICTING ISOMETRIC ANKLE DORSIFLEXION TORQUE

[1]Michelle D. LaBoda, [1]Alexis D. Gidley, [1,2]Christopher J. Hasson, [1]Graham E. Caldwell & [1]Brian R. Umberger
[1]Department of Kinesiology, University of Massachusetts, Amherst, MA, USA
[2]Department of Biology, Northeastern University, Boston, MA, USA
email: umberger@kin.umass.edu

INTRODUCTION

Computer models of the musculoskeletal system have become common tools in biomechanics research. Most applications involve using a generic (Gen) musculoskeletal model, perhaps with some gross scaling to body size. In these cases, the model parameter values may not be applicable to the subject(s) being studied. However, advances in non-invasive imaging techniques have made it possible to obtain large sets of model parameters on specific populations [1]. These parameters can then be used to develop highly-tailored subject-specific (SS) models, or averaged to develop a group-mean (GM) model. However, it is not yet clear how the results obtained with SS models compare to GM or Gen models.

One of the key tests for a musculoskeletal model is how well it can predict the joint torque - joint angle relation for a particular subject or group of subjects. In order to gain more insight into the performance of SS musculoskeletal models, compared to GM and Gen models, we evaluated the ability of all three types of models to predict active isometric dorsiflexion torques in a group of healthy, young adult subjects. We hypothesized that SS predictions would be better than GM predictions, which would in turn be better than Gen model predictions.

METHODS

Nine male subjects (age 28±4 yrs; height: 1.78±0.06 m; mass: 76.6±9.3 kg) provided informed consent and participated in this study. Peak, maximal effort dorsiflexion torques were measured for the left ankle at joint angles of -30°, -15°, 0°, and +15° (plantar flexion is negative, dorsiflexion is positive) on a dynamometer (Biodex). Subjects also performed a slow, ramped contraction at the -15° joint angle. During the ramped contraction, an ultrasound (US) probe (Acuson L7384) was used to image the superficial and deep aponeuroses of the tibialis anterior. Subjects also underwent axial and sagittal T1-weighted MRI scans of the lower limb.

The lower limb, distal to the knee joint, was modeled using two rigid bodies (shank and foot) that articulated at a frictionless hinge joint (ankle). Active torque was produced by a two-component Hill-type model that represented the muscles in the anterior compartment: tibialis anterior, extensor digitorum longus, and extensor hallucis longus. Model parameter values were acquired from the experimental data. Muscle volumes and moment arms were determined from the MRI data. To account for retinacular stretch, the modeled moment arms increased linearly with force from the resting (measured) values, by up to 35% at peak torque [2]. Dorsiflexion torque was converted to muscle force using the moment arms. The US images from the ramped contraction were used to quantify the stiffness of the series elastic element. Contractile element lengths and pennation angles were extracted from the US data with the muscles at rest. The only model parameter that was ‘tuned’ was the slack length of the series elastic element. This parameter, for which no direct measurements are possible, was adjusted for each subject to minimize the differences between measured and simulated dorsiflexion torques. Individual subject model parameter values were used to create nine SS models, and average parameter values were used to create a single GM model.

Active isometric dorsiflexion torque predicted by each model was compared to the measured values at the four joint angles. Dorsiflexion torques predicted using the GM model and a popular Gen model [3] were compared with the average measured torque, while the SS model torques were compared to the measured torques for the corresponding subject. GM and Gen model predictions were also compared

to the individual subject measured torques. Model performance was evaluated by computing the root-mean-square difference (RMSD) between the measured and predicted dorsiflexion joint torques.

RESULTS AND DISCUSSION

Dorsiflexion torques predicted using the GM model agreed well with the average measured values (Fig. 1A, RMSD = 1.2 N m). The torques predicted using the Gen model were of the correct average magnitude, but did not capture the trend in the measured data (Fig. 1A, RMSD = 5.7 N m).

The quality of the SS model predictions varied among subjects, with the best and worst SS model predictions shown in Fig. 1B and 1C, respectively. Averaged across all subjects, the SS models yielded the best SS torque predictions (RMSD = 6.2±3.5 N m), with the GM model (RMSD = 8.0±3.5 N m) and the Gen model (RMSD = 9.5±3.7 N m) resulting in poorer predictions of individual subject joint torques.

The comparisons of GM and Gen models to the average dorsiflexion torque data (Fig. 1A) demonstrate that a model based on parameter values unique to a specific population more accurately predicts group responses compared to a Gen model. This is important to consider when using musculoskeletal models to understand differences in movement capabilities among different populations (e.g., young versus old, able-bodied versus movement-impaired).

On average, the SS models yielded better predictions of individual subject joint torques than either the GM or Gen models. However, the quality of the SS model predictions varied among subjects. In the cases with larger RMSD values (e.g., Fig. 1C), the trends in the data were still reproduced, and the errors tended to be greatest at one of the two extreme joint angles. RMSD values could be further reduced, if desired, by adjusting one or more additional model parameters through optimization, using the variability in the GM data as constraints on the allowable range of values.

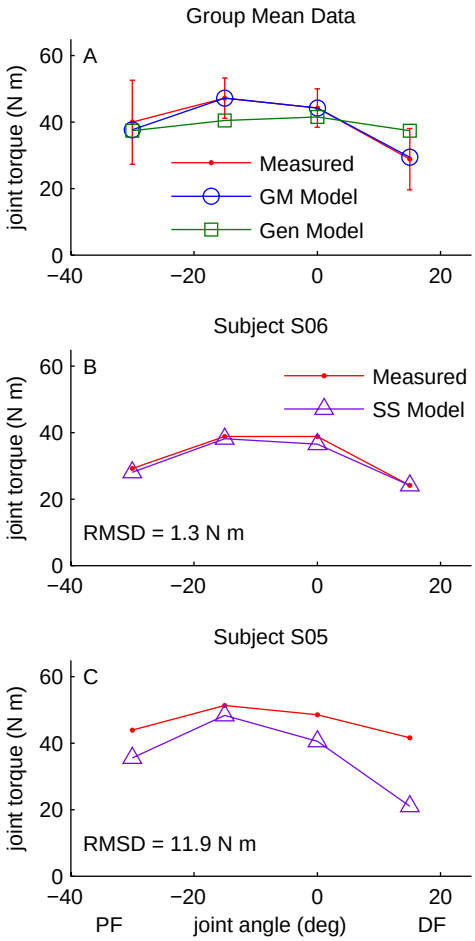

Figure 1: Measured joint torque - joint angle curves compared with predictions from the SS, GM, and Gen models.

CONCLUSIONS

This study demonstrated the greater accuracy of SS and GM models over a Gen model for predicting dorsiflexion joint torques. However, care must be used with SS models, as the quality of predicted joint torques can vary from subject-to-subject.

REFERENCES

1. Hasson, CJ, et al. *Proceedings of ASB '09*, State College, PA, USA, 2009.
2. Maganaris, CN. *J Biomech*, **33**, 375-379, 2000.
3. Delp SL, et al. *IEEE Trans Biomed Eng* **37**, 757-767, 1990.

ACKNOWLEDGEMENTS

Supported by a grant from the UMass Amherst Research Office.

UNIQUE REPRESENTATIONS TO ANALYZE THREE DIMENSIONAL MOVEMENTS

[1]Konstantinos Vrongistinos, [1]Taeyou Jung, [1]S. O. Wee, [1]T. Costello, [2]Y. Hwang and [3]G. Stylianides

[1]California State University, Northridge, CA, USA
[2]California State University, San Bernardino, CA, USA
[3] The University of Scranton, PA, USA

email: kv61497@csun.edu web: http://www.csun.edu/~kv61497

INTRODUCTION

Motion analysis measurements include errors from different sources. The purpose of this paper is to clarify the use of Euler Parameters (a.k.a. unit quaternion) in the analysis of three dimensional movements especially in smoothing techniques. A smoothing technique in three dimensional space is presented to demonstrate that Euler parameters have a significant advantage over single dimensions smoothing techniques.

METHODS

Simulated data were analyzed with two different methods. The first method was a traditional Butterworth smoothing technique on each individual dimension (B1D) and the second method used a Butterworth filter on the Euler parameters (B4D) that in essence is a smoothing technique of the transformation matrices [1]. Both methods were based in a fourth-order zero-lag Butterworth filter. The first set of data consists of simulation data, of a pendulum that moves in three dimensions and three markers were used to track the movement of the pendulum. Three different noise levels 1% and 2.5% were superimposed over the simulated trajectories. The MSE of each noise level on the linear and angular kinematics were calculated and compared between the methods.

In order to have control over the measured values, the angular velocity of a simple pendulum was calculated from surrogate data generated with computer simulation (see Figure 1). The cylinder had radius 0.05, height 0.26m, mass=1.31 kg, principle mass moments of inertia 0.0079, 0.0079, 0.0011 kg.m2, and initial angular velocity T 5.236, 17.453, 52.359 rad/sec. The three non-collinear points defined a local reference frame. Data were collected at 50 Hz for 24s for total 1200 3D data points. The pendulum was free to rotate in three dimensions, but it was not allowed to slide. The only forces that acted on the pendulum were gravity and the reaction forces at the spherical joint.

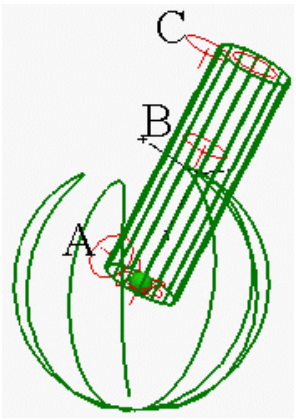

Figure 1. Trajectory of simulated pendulum data collected at 50Hz

The second data set consisted of simulated gait data with Helen Hayes marker set. The second data set were used to compare different methods of calculating angular velocities on different joints. There were three different methods that used to calculate the angular velocities, (a) an Euler angle method of XYZ rotations, where velocities are calculated from differentiation of Euler angles (EAD) (b) a tensor matrix method where velocities are calculated from equation 1

$$\omega = \dot{A}^{21}A^{12} = \begin{vmatrix} 0 & -\omega_3 & \omega_2 \\ \omega_3 & 0 & -\omega_1 \\ -\omega_2 & \omega_1 & 0 \end{vmatrix} \quad \text{equation 1.}$$

and (c) a quaternion method where velocities are calculated from the Euler parameters [2].

RESULTS AND DISCUSSION

The results demonstrated that the B4D method using Euler parameters is more robust relative to B1D method (See Table 1), where consistently had smaller mean square errors.

The results from the gait simulation demonstrated that when there is minimal error the Tensor and Quaternion methods calculate the exact same results and EAD is quite close with the result

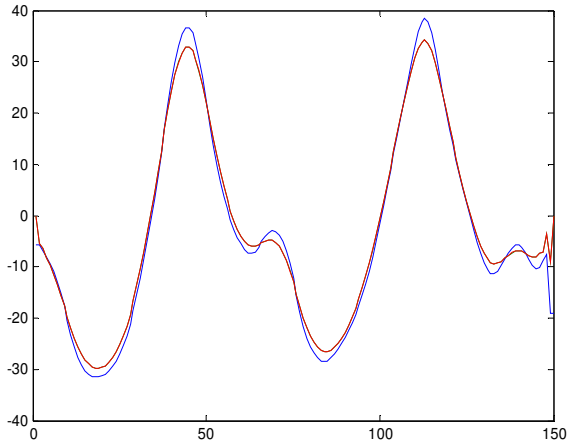

Figure 2. Flexion velocities in deg/s with three different methods of the thigh relative to pelvis with simulated data. EAD differs from other methods.

However when error of 2% where superimposed to the simulated data the traditional EAD method showed increased problems to preserve the smoothness of the data (see Figure 3)

CONCLUSIONS

Smoothing in individual dimensions maybe acceptable for two dimensional analysis, but in 3D creates significant errors in the orthogonality of the transformation matrices.

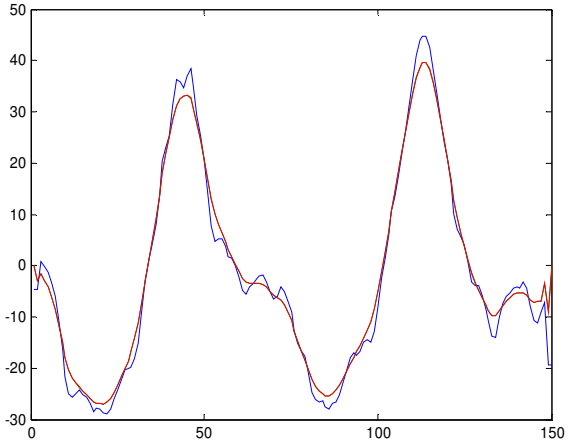

Figure 3. Flexion velocities in deg/s with three different methods of the thigh relative to pelvis with error superimposed to simulated data. Euler angle differentiation is not smooth.

The interesting observation is that the differences on the pendulum simulation are more profound on the linear derivatives. The reason is that the angular derivatives were calculated with the quaternion methods that are very robust. That is verified with the gait data where the quaternion and tensor methods kept the integrity of the velocities better than the EAD method

REFERENCES

1. Vrongistinos et al. Wheelchair propulsion using quaternions. *Proceedings of ASB'01,* San Diego, CA, USA, 2001, 257-258.
2. Wittenburg, J. (1977). Dynamics of systems of rigid bodies. Stuttgart, Germany

Table 1: Mean square errors for one dimensional smoothing B1D and Euler Parameter Smoothing B4D.

Percent Noise		Linear Velocities m/s			Angular Velocities rad/s		
		X	Y	Z	X	Y	Z
0%	B1D	.3277	.3266	.4559	.6447	2.4329	2.4734
	B4D	.1878	.2006	.2005	1.2573	2.4884	2.5435
1%	B1D	.4071	.4097	.5274	1.4857	2.4425	2.5206
	B4D	.1867	.1995	.1984	1.2601	2.4877	2.5428
2.5%	B1D	.4078	.4013	.5284	1.4808	2.4431	2.5212
	B4D	.1878	.2006	.2005	1.2573	2.4884	2.5435

EVALUATION OF STEPPING TASK BIOMECHANICS USING OPENSIM

Sai M. Malineni and Gregory W. King

University of Missouri – Kansas City, Kansas City, MO, USA
email: smmxz4@umkc.edu, web: http://sce.umkc.edu/cme/

INTRODUCTION

To quantitatively evaluate biomechanical risk factors for age-related falls, laboratory-based methods are often used for assessment of kinetic and kinematic characteristics of balance and locomotion. Interventions to improve such risk factors often involve exercise or physical therapy. However, they do not always result in balance improvement [1], possibly due to lack of task specificity [2,3]. To help bridge the gap between biomechanical assessment and intervention, we propose subject-specific, task-specific musculoskeletal modeling of balance activities. Such an approach could be used to (1) identify age- and fall-related balance deficiencies and (2) identify targets for exercise-based balance rehabilitation through simulation, thus removing the need for repetitive experimental testing. As a preliminary step in developing such a tool, the purpose of this study was to investigate the feasibility of performing model-based analysis of a stepping maneuver, similar to that used during balance recovery, using the OpenSim architecture [4].

METHODS

One healthy adult male participant performed a stepping task consisting of voluntary, rapid forward steps with the right leg. Two different step lengths were considered, including a short step representing the participant's natural step length (78 cm), and a long step representing a larger-than-natural (96 cm) step length. The participant performed 5 trials of the task for each step length condition in a randomized order to minimize anticipation and learning effects. Ground reaction forces and moments were captured from two force plates (AMTI, Watertown, MA, USA) placed at the initial (stance) and final (landing) locations of the stepping foot. Tape was placed on the landing force plate to identify targets for the two step lengths. Lower extremity motion was measured with motion capture equipment (Vicon, Los Angeles, CA, USA) tracking reflective markers placed on the sacrum and bilaterally on the anterior superior iliac spine, thigh, knee, tibia, lateral malleolus, calcaneous, and second metatarsal. Force and motion data were imported into OpenSim (Figure 1), where a generic lower extremity model was scaled to the participant's anthropometry based on calculated distances between pairs of markers.

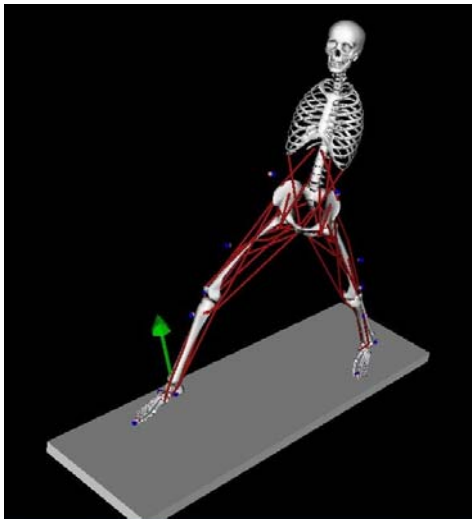

Figure 1: Representative trial depicting stepping task landing phase in OpenSim

Inverse kinematics and inverse dynamics algorithms were applied to the scaled model in order to extract joint kinematics and torques, respectively. Saggital plane joint torque time series were exported from OpenSim, and MATLAB (The MathWorks, Natick, MA, USA) was used to extract maximal landing phase joint torques in the stepping leg: ankle plantarflexion/dorsiflexion, knee flexion/extension, and hip flexion/extension. Means of outcome variables in each testing condition were compared graphically, as is generally accepted for single-subject designs [5].

RESULTS AND DISCUSSION

Maximal joint torques occurred in ankle dorsiflexion, knee extension, and hip flexion for all trials. Graphical analysis of torques (Figure 2) suggested that long steps, compared to short, required larger knee extension and hip flexion torque, but similar ankle dorsiflexion torque .

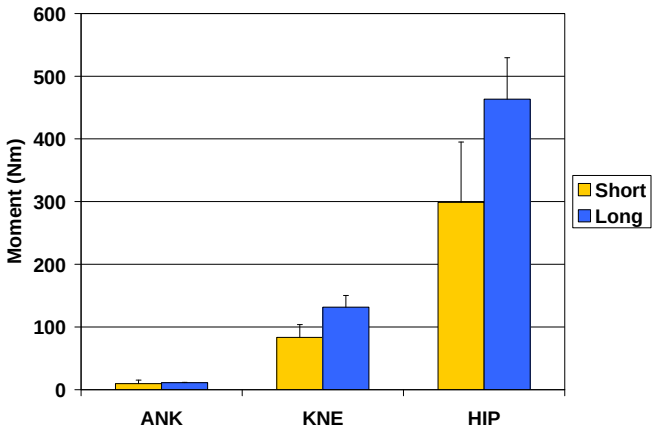

Figure 2: Maximal landing phase ankle dorsiflexion, knee extension, and hip flexion torque for long and short steps

These results indicate that maximal landing phase joint torques during a stepping task are sensitive to step length, a commonly-reported risk factor for falls [6]. This finding is in agreement with previous work reporting age-related reductions in lower extremity joint dynamics and their correlation to step length during similar stepping tasks [7,8]. This may help to explain age-related differences in step length during balance recovery maneuvers, as age-related declines in strength likely reduce the maximal joint torque required for larger steps. Furthermore, small steps may not effectively arrest a faller's momentum in a single step, necessitating a multiple step response also considered to be a common predictor of fall risk [9]. Our lack of observed task-related differences in maximal ankle dorsiflexion torque suggests equivalent ankle strength requirements for both step length conditions. Although maximal ankle torque would be expected to occur in plantarflexion to decelerate forward body rotation [8], the larger dorsiflexion torques observed here suggest an emphasis on eccentric activity to slow downward foot rotation at landing. This effect may be task- or subject-specific; more testing is required to determine if similar effects extend to other participants and tasks. This study also addresses the possibility of using the OpenSim environment to investigate subject-specific interventions for improving balance recovery effectiveness. While the sample results reported here suggest that knee extensors and hip flexors may be potential targets for interventions designed to increase step length, it is not clear what effect an exercise-based intervention would have on step length without further testing or simulation. Future studies should (1) investigate joint power in order to evaluate whether interventions should focus on concentric or eccentric muscle activation; (2) utilize OpenSim's Computed Muscle Control feature to predict muscle activation associated with sub-optimal balance recovery performance; and (3) utilize OpenSim's forward dynamics capability to investigate intervention effectiveness without the need for repetitive experimental testing.

CONCLUSIONS

This preliminary study reports differences in lower extremity peak joint torque between short and long step lengths during a stepping task similar to that used for balance recovery. Long steps, compared to short, were characterized by larger maximal knee extensor and hip flexor torque. Maximal ankle dorsiflexor torque was similar between the step length conditions. This work also demonstrates the use of OpenSim as a platform for biomechanical evaluation of fall-related balance deficiencies, and shows promise for its use in development of exercise-based interventions to reduce fall risk.

REFERENCES

1.Jensen J, et al. *Aging Clin Exp Res* **16**, 283-292, 2004.
2.Maki BE, et al. *Age Ageing* **35 Suppl 2**, ii12-ii18, 2006.
3.Mansfield A, et al. *BMC Geriatr* **7**, 12, 2007.
4.Delp SL, et al. *IEEE Trans Biomed Eng* **54**, 1940-1950, 2007.
5.Kinugasa T, et al. *Sports Medicine* **34**, 1035-1050, 2004.
6.Koski K, et al. *Age Ageing* **25**, 29-38, 1996.
7.Schulz BW, et al. *Clin Biomech (Bristol, Avon)* **22**, 689-696, 2007.
8.Madigan ML, et al. *J Gerontol A Biol Sci Med Sci* **60**, 910-914, 2005.
9.Hilliard MJ, et al. *Arch Phys Med Rehabil* **89**, 1708-1713, 2008.

Small Chest Impactors at High Accelerations: Assessing Thorax Injury Potential from a Finite Element Model

[1,2]Kerry A Danelson, [3]John H. Bolte and [1,2]Joel D. Stitzel

[1]Wake Forest University School of Medicine, Winston-Salem, NC, USA
[2]Virginia Tech – Wake Forest University Center for Injury Biomechanics, Winston-Salem, NC, USA
[3]Ohio State University, Columbus, OH, USA
email: jstitzel@wfubmc.edu

INTRODUCTION

Finite element models (FEMs) of the human body are used extensively to simulate impacts and predict the likelihood of injury given these loading conditions. For this study, a total body FEM was used to simulate the interaction between a NASA suit umbilical connector (UC) and the body in high acceleration landing conditions. The intent was to determine possible sources of injury with a variety of loading conditions and device designs. An advantage of using a total body FEM over an anthropometric test device (ATD) to conduct these tests is the ability of the user to query the model for additional data about anatomical regions of interest, such as strain data for each rib. Injury metrics were selected and analyzed for each simulation. From these injury metrics, the optimal configuration of the UCs to minimize risk of injury was determined.

METHODS

The FEM of the occupant used in this analysis was a modified version of the Total HUman Model for Safety (THUMS, version 1.61c, Toyota Technical Development Corporation, Nagoya, Japan). This model was developed for use in automotive testing and it has been extensively validated using post mortem human subject (PMHS) data [1]. The modifications implemented in the THUMS stabilized the model response in inferior/superior acceleration configurations.

The THUMS model was seated in a basic rigid seat and 24 simulations were conducted with variations in UC type, offset distance, UC location, and countermeasure design. The two UCs that were modeled were a 2.27 kg (5 lb) rectangular block and a 3.17 kg (7 lb) cylinder. To simulate the potential effects of various suit thicknesses, these UCs were offset to 1 mm, 15 mm, and 30 mm from the THUMS outer shells. The location of the UC was also varied between the chest and the thigh. The direction of the acceleration pulse varied with the location of the UC. For the chest UC, the acceleration pulse was in the anterior to posterior direction. For the thigh UC, the pulse was in the inferior to superior direction. In addition to UC models, chest plate models were created to distribute the load of the UC across a wider area of the chest. This design was intended to minimize local chest deflections. As a comparison for all UC simulations, the chest and thigh acceleration pulses were simulated using the same model with no UC present. Figure 1 illustrates the rectangular UC placed on the chest with the implementation of the countermeasure plates.

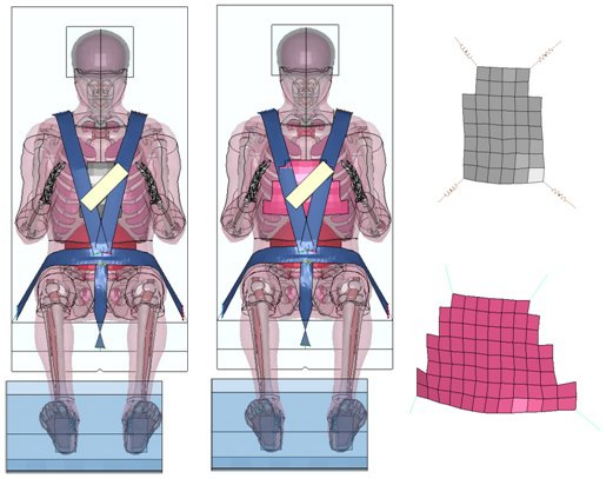

Figure 1: The model with a 2.27 kg (rectangular) UC placed on the chest with a small plate (left) and a large plate (center). Additionally, the plate geometry of the small (top right) and large (bottom right) plates that were created to conform to the shape of the THUMS chest.

Once the simulations were complete, the potential risk of injury to the occupant was quantified with selected injury metrics. For the chest placement scenarios, the injury metrics were: maximum first principal strain in the ribs, sternal deflection, chest deflection, and viscous criterion (V*C). The first principal strain metric measured potential fracture risk to the ribs [2]. The sternal deflection and chest deflection assessed risk for a variety of thoracic injuries [3]. The V*C measured possible risk of injury to thoracic organs [4]. For the thigh placement scenarios, the maximum strain in the femur was compared between the configurations. This metric predicted risk of femur fracture.

RESULTS AND DISCUSSION

For chest placement simulations, the results of the model indicated localized chest compression due to the weight of the UC impacting the chest. In comparison, the thigh placement of the UC demonstrated little change in the model response with minimal contribution of the UC to strain values in the femur. The individual injury metrics further defined the advantages and disadvantages of specific UC, offset, and countermeasure configurations.

Sternal and chest deflection calculations indicated that deflection increased with increasing mass of the UC and varied little with increased offsets. Additionally, the large plate was the most effective countermeasure tested for deflection. The maximum strain value increased with increased weight and increased offset. All rib strain values were below the approximate failure limit of 2.4% strain. The countermeasure design that was most effective for reducing rib strain was the small plate. Figure 2 illustrates the locations of high and low strain values in the ribs for one simulation. Similar to the strain values, the viscous criterion values also increased with an increase in mass and offset distance. The most effective countermeasure design for V*C was the large plate.

For the thigh placement, the strain values demonstrated little change with variations in the UC type and offset. Additionally, the femur strain values were an order of magnitude below the rib strain values.

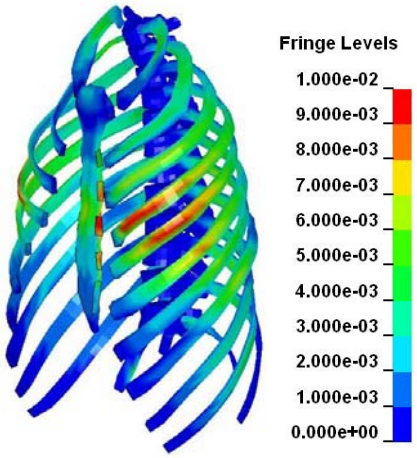

Figure 2: First Principal strain in the rib cage for the 3.17 kg (cylinder) UC and 30 mm offset. The areas of high strain, shown in red, are located along the lateral aspect of the ribs.

CONCLUSIONS

The femur load cases had the lowest risk of injury to the occupant. Additionally, unlike the thorax, the thigh area does not contain critical organs such as the heart and lungs.

The lighter, rectangular UC was less likely to cause injury to the chest than the heavier, circular UC. Also, smaller offsets generally resulted in lower injury metric values. Based on these trends, if the UC is required to be attached to the chest it was recommended that the smaller UC be closely coupled to the suit. Finally, the use of a chest plate or another countermeasure to distribute the loading of the UC connector reduced the risk of chest injury.

REFERENCES

1. Iwamoto M, et al. *Proceedings of IRCOBI '02*, Munich, Germany, 2002.
2. Stitzel JD, et al. *Stapp Car Crash J* **47**, 243-265, 2003.
3. Eppinger R., et al. *NHTSA report*, 1999.
4. Viano DC, et al. *Proceedings of 30th Stapp Car Crash Conference*, 1986.

ACKNOWLEDGEMENTS

The authors would like to acknowledge the assistance of the Orion Task 1 team, specifically Brad Granderson and Jeff Sommers.

A COMPLETE, UNIVERSAL, AND VERIFIABLE SET OF UPPER BODY SEGMENT PARAMETERS FOR THREE-DIMENSIONAL DYNAMIC MODELING

[1,2]Albert H Vette, [1,2]Takashi Yoshida, [3]T Adam Thrasher, [2]Kei Masani, and [1,2]Milos R Popovic

[1]University of Toronto, Toronto, ON, Canada
[2]Toronto Rehab, Toronto, ON, Canada
[3]University of Houston, Houston, TX, USA
email: a.vette@utoronto.ca, web: www.toronto-fes.ca

INTRODUCTION

Dynamic models of the human trunk have been extensively used to investigate the biomechanics of lower back pain and postural instability in different populations. Despite their diverse applications, these models rely on intrinsic upper body segment parameters (UBSP), e.g., each segment's mass-inertia characteristics. However, a comprehensive UBSP set allowing state-of-the-art, three-dimensional (3D) dynamic modeling does not exist to date. Therefore, our objective was to establish a UBSP database that is accurate, complete, and universal, i.e., independent of pre-defined (lumped) trunk portions such as upper and lower trunk. Potential applications include the study of (1) spinal pathologies; and (2) the relation between muscle activation patterns, spinal loadings, and upper body kinematics of different populations. Besides many other benefits, the gained theoretical insights can assist in assessing the feasibility of developing a neuroprosthesis for trunk stability [1].

METHODS

Based on high-resolution, transverse color images from the Male Visible Human (MVH) [2], anatomical structures were digitally reconstructed via commercial software. Subsequently, we identified a complete set of UBSP (3D spinal joint and 3D center of mass coordinates, the mass, and the moment of inertia tensor) for 24 vertebral trunk and head segments and 2 × 2 upper limb segments. The trunk was divided into 5 lumbar segments (L1 to L5), 12 thoracic segments (T1 to T12), 6 cervical segments (C2 to C7), and the head (HD). Note that cervical and head segment parameters are needed for studying whiplash [3] and the control of head-trunk dynamics during external perturbations [4]. The upper limbs were divided into upper arm (UA) and forearm-hand (FA-H) segments.

To demonstrate the practicality of the UBSP, they were finally implemented in a 3D dynamic model of the upper body [5] to predict lumbar joint torques from experimental kinematics during perturbed sitting. The horizontal force had a Gaussian profile (200 N), was applied just inferior to the axilla, and perturbed the subject with MVH anthropometrics in the anterior-left direction (five trials).

RESULTS AND DISCUSSION

Figure 1 depicts the surface reconstructions of the MVH body shell and spine. The identified joint centers were used to define the vertebral trunk segments and upper limb segments for which respective mass-inertia characteristics were calculated using the geometric method.

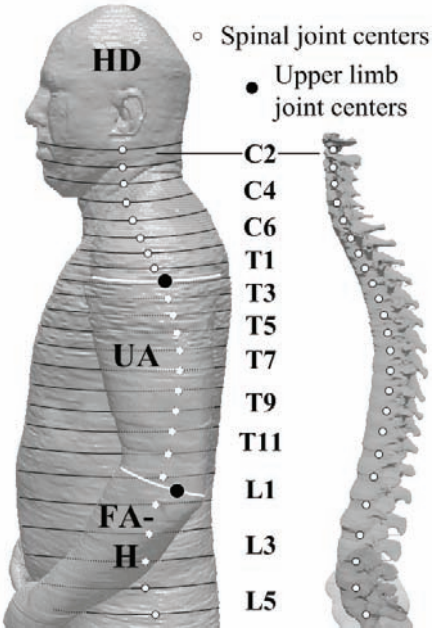

Figure 1: MVH body shell and segmentation.

Figure 2 depicts the results of the inverse dynamics method using the identified UBSP set. Shown are the anterior-posterior (AP) trunk angle and joint torques for an anterior-left diagonal perturbation during sitting (average of five trials). A visual inspection suggests, for example, that the torque traces are affected by the AP curvature of the spine.

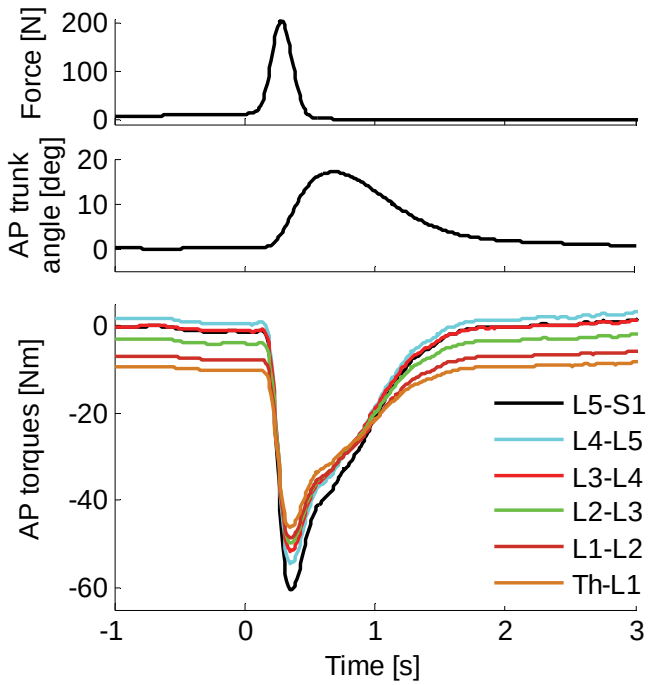

Figure 2: Inverse dynamics results for perturbed sitting.

One of the main objectives of the present study was to obtain a set of parameters that is uniquely independent of any pre-defined (lumped) body segmentations. This goal was accomplished by identifying the parameters for all transverse trunk segments in between the intervertebral discs of the spine. Since the resultant UBSP database is *universal* with respect to potential model definitions and, hence, model applications, it should become an important resource for researchers working on different challenges and in different areas (e.g., basic, sports, and surgical biomechanics, rehabilitation engineering, and ergonomics).

The acquired parameters can be easily combined for different model segmentations. In our inverse dynamics application, for example, we used the obtained parameters in a model that features five lumbar and a head-arms-thorax segment [5]. Additional models for which the database could be harvested have been used to study spinal loads during various tasks, whiplash injuries, and the coordination of head-trunk dynamics. While most studies on UBSP do not have this level of flexibility, others report parameter sets that are incomplete when needed for state-of-the-art 3D dynamic modeling (see below).

Another advantage of the obtained dataset is the fact that the utilized MVH images are freely available from the National Library of Medicine (NIH, USA). Consequently, the obtained UBSP are entirely *verifiable* when applying the utilized identification procedure. Note that this property represents a unique feature as the data used in other UBSP reports (e.g., CT, MRI, or cadaver data) are study-specific and generally not accessible to the scientific community. Moreover, the freely available MVH images allow researchers to *expand* the UBSP database to include respective parameters of the lower body.

Due to the availability of high-resolution color photographs of the MVH, we could obtain accurate 3D surface models of the body shell and spine. The voxels on which the 3D surface reconstructions were based had a size of 0.144 mm × 0.144 mm × 1 mm [2]. This resolution allowed us not only to minimize errors in boundary tracing, but also to acquire an accurate stack along the longitudinal body axis. Since all identified UBSP are based on the 3D surface models, their quality was essential for identifying *accurate* parameters. In addition, the present study obtained a *complete* set of UBSP as needed for 3D dynamic modeling (3D joint coordinates, segment mass, 3D COM location, and moment of inertia tensor) – and this for 24 vertebral trunk segments (HD to L5) and 2 × 2 upper limb segments.

REFERENCES

1. Masani K, et al. *Clin Biomech* **24**, 176-182, 2009.
2. Spitzer V, et al. *J Am Med Inform Assn* **3**, 118-130, 1996.
3. Garcia T, Ravani B. *ASME J Biomech Eng* **125**, 254-265, 2003.
4. Fard MA, et al. *ASME J Biomech Eng* **125**, 533-539, 2003.
5. Wilkenfeld AJ, et al. *J Rehabil Res Dev* **43**, 139-152, 2006.

Reliable Finite Element Modeling of Osteoporotic Bone Augmentation

[1]Ehsan Basafa, [2]Robert Armiger, [2]Michael Kutzer, [1,3]Edward Sutter, [3]Simon Mears, [1,3]Stephen Belkoff and [1,2,3]Mehran Armand

[1] Department of Mechanical Engineering, Johns Hopkins University, Baltimore, MD, USA
[2]Johns Hopkins University Applied Physics Laboratory, Laurel, MD, USA
[3]Department of Orthopedic Surgery, Johns Hopkins Medicine, Baltimore, MD, USA
email: basafa@jhu.edu

INTRODUCTION

Osteoporosis is a major factor in reducing the bone strength and consequently increasing the risk of fracture. Femoral augmentation, i.e. injecting bone cement into weakened areas of the osteoporotic femur, is a potential therapeutic approach to reduce the risk of fracture due to falls in an elderly individual who has already experienced a contralateral hip fracture [1]. Effective bone augmentation, however, requires detailed planning, biomechanical analysis and precise control of the procedure to avoid cement extravasation into unintended regions causing osteonecrosis and/or areas of stress concentration. We present a comprehensive framework for patient-specific heterogeneous and anisotropic finite element model generation and analysis of the femur for the purpose of studying the effects of cement injection on bone mechanics. We also compare the simulation using this framework with the experimental results obtained from mechanical testing of the augmented femora.

METHODS

Ten pairs of fresh-frozen osteoporotic human femora were obtained and one femur from each pair was randomly chosen for femoroplasty and was manually injected by 15-20 mL of bone cement into the intertrochanteric region of the femur. CT scans were taken from all the specimens before and after the injection. The femora were then mechanically tested in a configuration simulating lateral falls on the greater trochanter [1]. Load and displacement data were recorded until complete failure of the bone. The linear part of the resulting force-displacement curves before yielding was isolated and the stiffness and the absorbed energy values were calculated. A customized MATLAB (Mathworks Inc.) user interface semi-automatically segmented the bone in CT images and created a finite element mesh model of combined 15-node wedge and 20-node quadratic brick elements. Each bone model had a total of 10500 elements and 42646 nodes. Bone density was calibrated to the CT Hounsfield intensity values (HU) using a combination of six phantoms having known material densities and piecewise linear interpolation. The resulting ash densities were then converted to apparent densities [2] and, using a combination of the mathematical relationships described in the literature [3,4], the HU intensity inside each mesh element was used to determine its density, orthotropic elastic moduli, and Poisson ratios. Normal vectors to the planes of slices, which were defined in the segmentation step by the user, were used to define a local axis of anisotropy for the elements of different regions of the bone (Fig. 1).

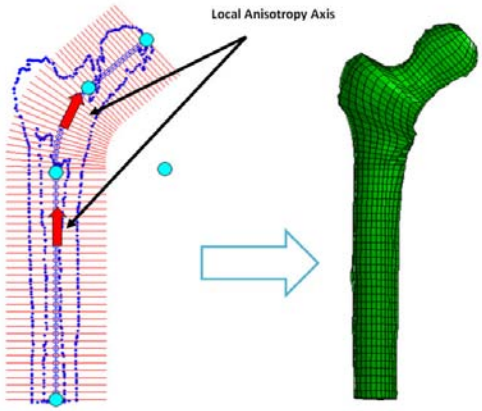

Figure 1: Slices defined for segmentation and local axis of anisotropy determination

For augmented specimens, the CT scans obtained before and after the injection were registered based on mutual image volume intensity information. Voxel intensity thresholds were used to identify

elements that were injected with the cement. These elements were then assigned an isotropic elastic modulus of 1800 MPa and a Poisson ratio of 0.4 [5]. Boundary conditions similar to the mechanical testing were applied to the models with the forces being the loads at the end of the linear force-displacement curves of the experiments. ABAQUS/Standard (Simulia Inc.) was used to analyze the finite element models. The resulting displacements were recorded and the stiffness values were calculated as the ratio of the forces over displacements. Additionally, the sum of the elastic energies stored in all the elements were calculated.

RESULTS AND DISCUSSION

The experimental data from one of the specimens was excluded, since there was no detectable linear force-displacement region. For the remaining 19 femora, average errors between the experiments and simulation results were 22% and 28% for stiffness and energy values respectively. Three of the models had an error larger than 40%. High correlations of R=0.70 and R=0.89 were observed between the experimental and simulation values of the stiffness and energies, respectively (excluding these "outliers" the correlations increase to 0.90 and 0.98, respectively.). There are several possible sources of error in the experiments and simulations, including errors in positioning of the specimens when applying the loads and also errors in converting from HU intensities to elastic moduli. Fig. 2 compares the experiments and simulations.

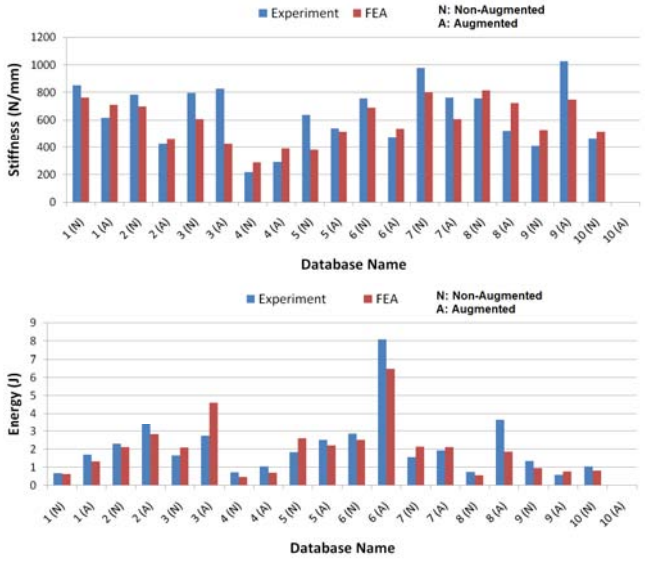

Figure 2: Comparison of stiffness (top) and energy (bottom) values. The data for 10(A) was discarded.

Both simulations and experiments showed a significant ($P<0.05$) increase in the absorbed energy for the augmented specimens relative to the non-augmented ones (Table 1). The increase in absorbed energy in these specimens is lower than our previous experiment [1], likely due to the smaller injection volumes (15-20 mL compared to 40-50 mL). No significant difference between the stiffness values was observed, but this was consistent in our FE simulation, current experiment, as well as previously reported work [1].

Table 1: Comparison between augmented and non-augmented groups

Parameter	Non-augmented mean±SD	Augmented mean±SD	P-value
Energy (experiments)	1.510±0.749 J	2.840±2.210 J	0.026
Energy (FE)	1.557±0.888 J	2.542±1.896 J	0.037
Stiffness (experiments)	687.6±235.7 N/mm	609.3±227.4 N/mm	0.227
Stiffness (FE)	618.8±187.0 N/mm	568.0±135.3 N/mm	0.190

CONCLUSIONS

Patient-specific finite element models were generated from CT scans of femur bones with and without cement augmentation. The models were analyzed and their results showed close agreement with the results of mechanical tests performed on the real specimens. The described framework therefore provides a reliable foundation for pre-planning of osteoporotic bone augmentation procedures.

REFERENCES

1.Sutter EG, et al. *J Orthop Trauma* **24**, 95-99, 2010.
2.Keyak JH, et al. *J Biomed Mater Res* **28**, 1329-1336, 1994.
3.Wirtz DC, et al. *J Biomech* **33**, 1325-1330, 2000.
4.Peng L, et al. *Med Eng Phys* **28**, 227-333, 2006.
5.Lee C. *The Well-Cemented Total Hip Arthroplasty*, Springer, 2005.

ACKNOWLEDGEMENTS

This work is supported by grant 5 R21 EB0077747-02 form National Institute of Health.

SENSITIVITY OF PREDICTED PEAK ISOMETRIC ANKLE DORSIFLEXION TORQUE TO MUSCULOSKELETAL MODEL PARAMETER VALUES

Alexis D. Gidley, Michelle D. LaBoda, and Brian R. Umberger

University of Massachusetts, Amherst, MA, USA
email: umberger@kin.umass.edu

INTRODUCTION

Musculoskeletal models are commonly used in biomechanics research. While many studies use generic models, non-invasive imaging techniques have made it possible to obtain large sets of model parameter values in specific populations (e.g., young versus older) for creating representative, group-mean (GM) models. However, the process of obtaining model parameter values from imaging modalities is laborious and costly, and it is not always clear which of the many model parameters researchers should focus their efforts on for obtaining highly-accurate estimates.

Sensitivity analysis [1-3] is a tool that can help guide the creation of GM musculoskeletal models. Among other uses, a sensitivity analysis can help in prioritizing which of the many parameter values require the best estimates. Therefore, the purpose of this study was to determine the sensitivity of predicted isometric dorsiflexion joint torques to variations in model parameter values, using a GM musculoskeletal model with parameter values obtained from healthy, young adults. These results will help guide data collection efforts for future applications of the musculoskeletal model.

METHODS

The distal part of the lower limb was modeled as two rigid bodies (shank and foot) articulating at a frictionless hinge joint (ankle). Active torque was produced by a two-component Hill-type model consisting of a contractile element (CE) and a series elastic element (SEE). The Hill-type model represented the muscles in the anterior compartment: tibialis anterior, extensor digitorum longus, and extensor hallucis longus. Model parameters values were determined using a combination of ultrasound, magnetic resonance imaging, and dynamometer measurements in a group of nine male subjects (28±4 yr; 1.78±0.06 m; 76.6±9.3 kg) [4]. Peak, active isometric dorsiflexion torques were measured on the dynamometer at ankle joint angles of -30°, -15°, 0°, and +15° (plantar flexion is negative, dorsiflexion is positive). The average model parameter values were used to create a GM musculoskeletal model for predicting active isometric dorsiflexion torques at the same four joint angles.

The sensitivity of ankle dorsiflexion torque to the model parameter values was assessed by systematically varying the parameter values and computing the change in the predicted torque [1]. The specific model parameters included in the sensitivity analysis were: peak CE isometric force (F_0), optimal CE length (L_0), width of the CE force-length curve (w), CE pennation angle (pen_0), SEE slack length (L_S), SEE extension at F_0 (U_0), and the coefficients in a fourth-order polynomial used to represent muscle-tendon length (L_{MT}) as a function of ankle joint angle (A_0-A_4). To facilitate comparisons across parameters, normalized sensitivity coefficients (S) were computed as

$$S = \frac{\Delta T / T_0}{\Delta p / p_0}$$

where T_0 and p_0 are a nominal torque and a nominal parameter value, and ΔT represents the change in torque resulting from the change, Δp, in the parameter value. The sensitivity coefficients were evaluated for each model parameter at each of the four joint angles. Averages of the absolute values of the sensitivity coefficients were computed across joint angles for each parameter, and across parameters for each joint angle. Absolute averages were used to avoid cancelation of coefficient values.

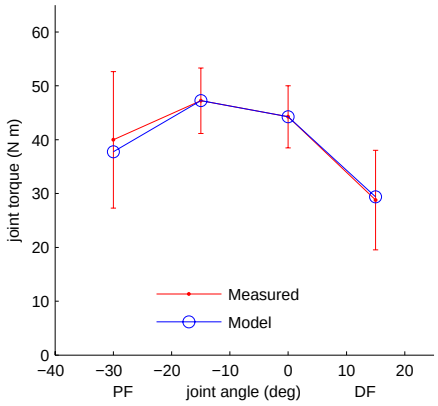

Figure 1: Measured and modeled joint torque - joint angle curves.

RESULTS AND DISCUSSION

There was good agreement between the measured dorsiflexion joint torques and the joint torques predicted using the musculoskeletal model (Figure 1). The model parameters that had the highest sensitivity coefficients (Table 1), averaged across joint angles, were L_S, L_0, F_0, and A_0 (in the L_{MT} polynomial, A_0 is the 0th-order term, representing *MT* length when joint angle is 0°). The large sensitivity for L_S is consistent with prior reports in the literature [2,3]. A_0 also had a large sensitivity, of similar magnitude to L_S; however, these two parameters are highly interrelated [2]. Thus, L_S and A_0 do not represent two independent sensitivities of the model. L_0 exhibited a moderately large sensitivity; this parameter has previously been reported to have a small or large sensitivity, depending on the application [2,3]. The sensitivity coefficient for F_0 (1.00) is dictated by the direct relation between muscle force and joint torque. The remaining model parameters (w, U_0, pen_0, A_1-A_4) all had small sensitivities.

Averaging the coefficients across parameters at each joint angle (Table 1) revealed that the sensitivities were greater at the two extreme angles (-30° and +15°) than at the two intermediate angles (-15° and 0°). Less sensitive torque predictions at the intermediate joint angles is an important result, as most applications of the model would involve joint angles within this narrower range. However, some parameters still had sizeable sensitivities at the intermediate joint angles (e.g., L_S at 0°).

As in prior studies [2,3], L_S was found to be a key parameter affecting musculoskeletal model performance. This represents a challenge, as L_S can not be measured *in vivo*. Fortunately, nearly every other model parameter can be estimated non-invasively, allowing L_S to be determined numerically [4]. A_0 had a similar sensitivity to L_S, but the two are not independent, and compared to L_S, estimating A_0 is relatively straightforward.

Table 1: Sensitivity coefficients (*S*)

	Ankle Angle				Abs
	-30	**-15**	**0**	**15**	**Avg**
L_s	7.16	-0.50	-6.47	-14.25	7.10
L_0	1.85	-0.11	-1.18	-2.10	1.31
F_0	1.00	1.00	1.00	1.00	1.00
w	0.26	<0.01	0.27	1.12	0.41
U_0	0.34	-0.03	-0.30	-0.56	0.31
pen_0	<0.01	<0.01	<0.01	<0.01	<0.01
A_0	-8.48	0.58	7.63	16.96	8.41
A_1	-0.61	0.02	<0.01	-0.62	0.31
A_2	0.04	<0.01	<0.01	-0.02	0.01
A_3	0.02	<0.01	<0.01	<0.01	0.01
A_4	<0.01	<0.01	<0.01	<0.01	<0.01
Abs Avg	0.14	0.09	0.09	0.14	

CONCLUSIONS

Of the parameters with the highest coefficients, only L_S can not be measured *in vivo*. However, if values for the other parameter with large sensitivities (e.g., F_0) are obtained accurately, it should be possible to determine reasonable estimates for L_S numerically.

REFERENCES

1. Lehman, SL. *Math Biosci*, **62**: 107-122, 1982.
2. Out, L. et al. *J Biomech Eng*, **118**: 17-25, 1996.
3. Scovil, CY. *J Biomech*, **39**, 2055-2063, 2006.
4. LaBoda, MD, et al. *Proceedings of ASB*, Providences, RI, USA, 2010.

ACKNOWLEDGEMENTS

We thank C.J. Hasson, Graham Caldwell, and Adam Iwanski for their assistance. Supported by a grant from the UMass Amherst Research Office.

Biodynamic modeling of stair-ascent by PCL-deficient patients

[1]Kang Li, [1,2,3]Scott Tashman, [1]Christopher Harner and[1,2,3]Xudong Zhang
[1]Departments of Orthopaedic Surgery, [2]Mechanical Engineering & Materials Science,
[3]Bioengineering, University of Pittsburgh, PA, USA
email: xuz9@pitt.edu

INTRODUCTION

Although numerous studies have been conducted to examine biomechanical consequences after posterior cruciate ligament (PCL) injuries [1], there are still numerous unknown or unresolved issues surrounding how PCL injuries affect movements and functions. Jonsson and Karrholm [2] observed no difference in kinematics between normal and PCL-injured knees. A recent study [3] showed that PCL-deficient patients had significantly larger anterior-posterior (AP) translations as compared to the contralateral non-injured knees during stair-ascent. However, whether such kinematic changes are associated with deleterious joint and tissue mechanical responses has never been evaluated. In this study, we began to study in an integrative manner the differences in knee joint kinematics, ground reaction force, and muscle force between the PCL-injured and non-injured knees during stair-ascent. We hypothesized that knee muscle forces and ground reaction force observed on the injured side were different from those on the noninjured side.

METHODS

Nine patients diagnosed with unilateral, isolated grade II PCL instability performed stair-ascent activities in our laboratory. Knee joint kinematics were measured using a biplane X-ray system while the whole-body kinematic data were acquired using a surface-based motion capture system. Ground reaction force data were collected using two ATMI force plates. We employed a computational modeling framework recently developed to incorporate the whole-body kinematics, the biplane X-ray knee kinematics, and the ground reaction measurements as the input. The framework includes OpenSim and a series of custom programs, which integrate the input data and create patient-specific musculoskeletal dynamic models (Figure 1). The patient-specific models predicted joint and tissue mechanical variables including muscle forces estimated based on an optimization algorithm with the cost function of minimizing the total muscle stress.

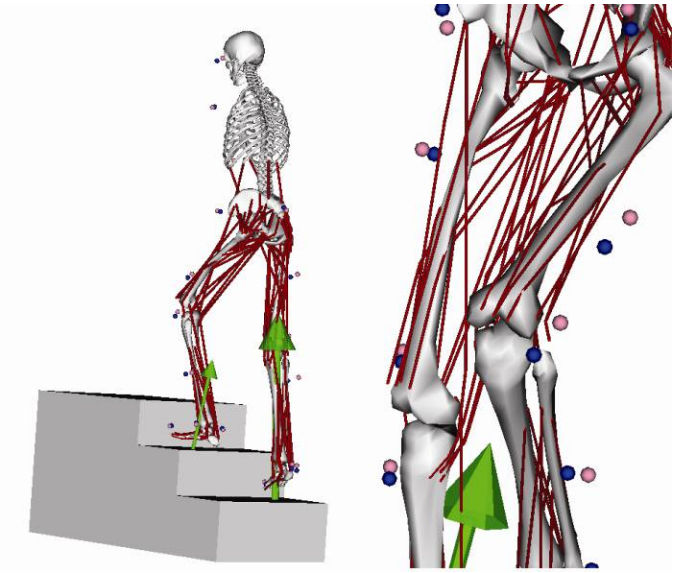

Figure 1: A 27-DOF 92-muscle biodynamical model created in OpenSim. The knee joint of the leading leg has two translational DOFs (anterior-posterior and proximal-distal translations) and three rotational DOFs (flexion-extension, adduction-adduction, and internal-external rotations). The contra-lateral knee has two translational DOFs (the anterior-posterior and proximal-distal translations) and one rotational DOF (flexion-extension rotation). The green arrows represent the ground reaction force vectors. The blue spheres represent the measured surface markers, and the pink spheres represent the virtual markers defined in the OpenSim.

RESULTS AND DISCUSSION

Figure 2 shows some sample outputs from the modeling. The AP translation of the injured knee was much greater than that of the intact knee. Both

intact and injured legs were exposed to transient impulsive forces, which have been implicated as a risk factor or potential marker for long-term joint degeneration [6]. However, when the difference in AP translation at the initial contact between the injured and non-injured knees was small (<3-4mm), the transient impulsive force experienced by the injured leg was greater than that by its contra-lateral leg (Figure 2b); otherwise, the force for the injured side was comparable to or lower than the contra-lateral side (Figure 2a). These findings, though preliminary, reflect the complex nature of even the isolated PCL injury: the increased joint laxity may be accompanied by a protective response to attenuate the transient impulsive forces. This trade-off may offer some insight into the mechanism and treatment of isolated PCL injuries.

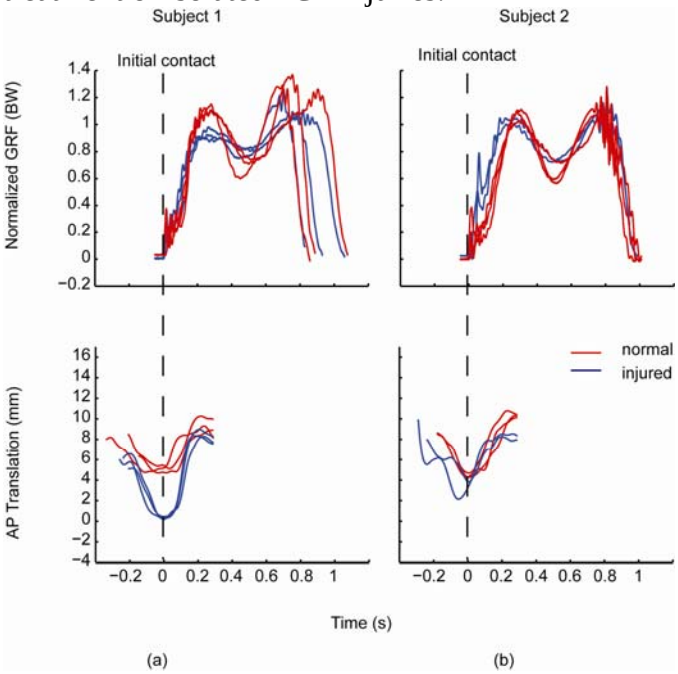

Figure 2: Comparisons of the AP translations (relative to the tibia) and ground reaction forces during stair-ascent between the injured and contra-lateral normal knees.

As expected, the AP translation in the injured knees could not be detected by the surface-based system. Surface markers had significant movements relative to the bones. This suggests that surface markers based system may be insufficient for detecting subtle but important changes in joint mechanics caused by injuries.

The muscle forces during stair ascent were derived based on the accurate kinematics (Figure 3). The muscle force patterns of normal knees are similar to the EMG pattern reported in the literature [7]. However, it remains a challenge to determine the muscle forces for the PCL-deficient knees using the current model in OpenSim. In the modeling process, it was required significant large forces of additional actuators in order to find the feasible solutions, which could result in unrealistic muscle force estimates. We are currently working to overcome this limitation by exploring various hypothesized scenarios of muscle activation or ligament restraining deficits.

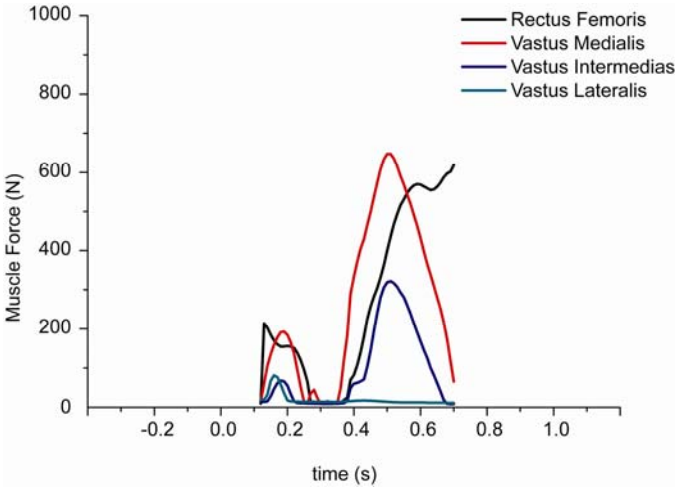

Figure 3: A sample set of quadriceps muscle forces for the non-injured knee.

REFERENCES

1. Grassmayr et al. (2008). J Sci Med Sport 11:433-443.
2. Jonsson and Karrholm(1999) JOR 17:185-191.
3. Tashman (2010). Proc ORS Annual Meeting.
4. Delp et al. (2007) IEEE Trans Biomed Eng. 54:1940-50.
5. Delp et al. (1990) IEEE Trans Biomed Eng. 37(8):757-67.
6. Radin et al.(1991). JOR 9:398-405.
7. Ciccotti et al. (1994). AJSM 22(5):645-650.

ACKNOWLEDGEMENTS

This work was supported in part by a grant from the NFL Charities.

ACCURACY OF BONE AND CARTILAGE MODELS OBTAINED FROM CT AND MRI

[1]Eric Thorhauer, [2]Motoko Miyawaki, [2]Ken Illingworth, [3]J. Andrew Holmes and [2]William Anderst

[1]University of Pittsburgh, Department of Mechanical Engineering, Pittsburgh, PA, USA
[2]University of Pittsburgh, Department of Orthopaedic Surgery, Pittsburgh, PA, USA
[3]University of Pittsburgh, Swanson Center for Product Innovation, Pittsburgh, PA, USA
email: anderst@pitt.edu

INTRODUCTION

Accurate three-dimensional (3D) models of bone and cartilage are required to estimate joint surface interactions, such as cartilage-to-cartilage contact patterns and to evaluate tissue response to load, intervertebral disc strain or cartilage strain, during in vivo movement. Information obtained from these highly accurate 3D models can be used to evaluate the efficacy of different surgical techniques and to track disease progression, for example cartilage thinning in osteoarthritis.

This project is part of a larger effort to evaluate the accuracy of different segmentation and 3D reconstruction techniques. This study is an initial evaluation of the accuracy of 3D models created from one segmentation software technique. The purpose of this project was to evaluate the accuracy of 3D bone and cartilage models using image acquisition, segmentation and reconstruction tools commonly used in biomedical research.

METHODS

This study used two fresh cadaveric knees (male, age 23 and female, age 41). Fiducial markers were fabricated from WaterShed XC11122 resin on a stereolithography machine as hollow spheres 8 and 12 mm in diameter with a 1 mm wall thickness. The spheres were filled with Radiance® multimodality fluid (Beekley) and sealed with press-fit septum rubber stoppers. The spheres were attached to the heads of PEEK screws, five of which were inserted into each bone (Figure 1). MRI images using 3T Sagittal 3D DESS WE sequences (slice thickness of 0.70mm, pixel spacing 0.39 and 0.52 mm/pixel) were collected for each knee on a Siemens 3T scanner. CT sequences on a GE Lightspeed 64 slice scanner were also collected with a slice thickness of 1 mm and pixel spacing of 0.75 and 0.80 mm/pixel. The MR and CT images were manually segmented using Mimics (Materialise, Leuven, Belgium). The bones, cartilage, and markers were rendered as point clouds in Mimics.

Following MRI and CT scan, the knee joints were disarticulated and soft tissue was removed, leaving the native cartilage structure intact. The specimens were then laser scanned as has been done previously [1] using a FARO arm with an accuracy of 0.025mm and scan resolution of .254mm to produce point clouds that included the bone and cartilage surfaces. Each bone was spray-coated with talcum power to improve laser scan data acquisition. The cartilage was then removed by soaking in a 6.5% sodium hypochlorate solution for at least 4 hours. Bone surfaces were again spray-coated with talcum powder. Laser scanning was repeated for the specimens without cartilage. Prior to each laser scan, fiducial markers were identified via hard probing with the FARO arm. Point clouds from laser scanning, CT and MR data were imported into Geomagic Studio software (Geomagic, Durham, NC). Geomagic was used to create 3D surfaces from all point cloud data. All models were coregistered using a best-fit of the centroids of the fiducial markers.

Bone model accuracy was defined as the average deviation between laser scan and CT bone models at the articulating surfaces. Cartilage model accuracy defined as the difference in cartilage thickness between laser scan and MR cartilage models.

Figure 1: Knee specimen with fiducial markers.

Figure 2: Laser scanning (A) and marker probing (B) with FARO arm.

RESULTS AND DISCUSSION

Fiducial markers were coregistered with an average accuracy of .675 mm, .482 mm, .200 mm for MR to FARO, CT to FARO, and both FARO scans, respectively.

CT-based surfaces deviated on average less than 0.5 mm from FARO-based surfaces (Figure 3). Average deviation was 0.25 mm for regions where CT surfaces were larger than FARO surfaces and 0.44 mm for regions where CT surfaces were smaller than FARO surfaces. Average standard deviation of all bones was 0.512 mm.

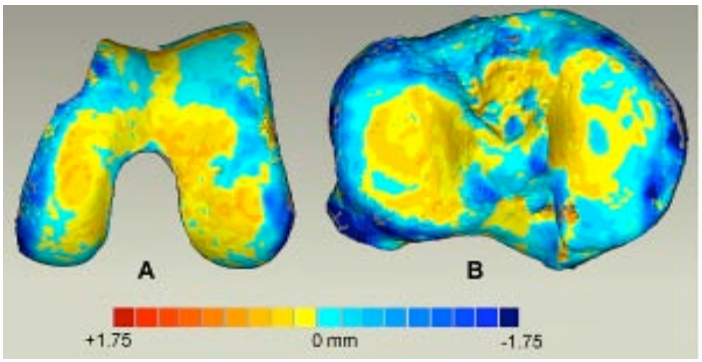

Figure 3: Color map of deviations in femur (A) and tibia (B) bone models: segmented CT relative to FARO scan.

In areas in where MR cartilage models were thicker than FARO cartilage models, the average deviation was 1.15 mm on average. In areas in where MR cartilage models were thinner than FARO cartilage models, the average deviation was 0.38 mm. As seen in Figure 4, areas where MR cartilage was thicker than FARO cartilage were more prevalent.

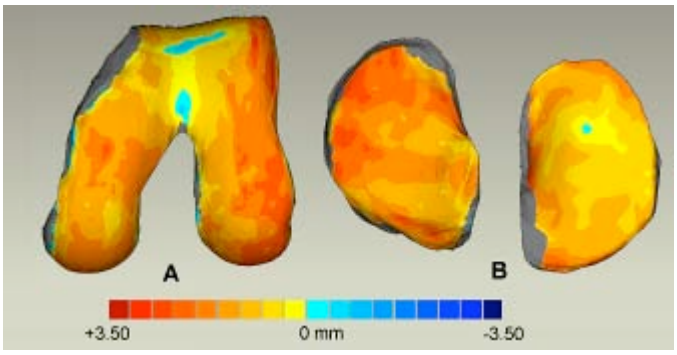

Figure 4: Color map of difference in cartilage thickness of femur (A) and tibia (B): segmented MR relative to FARO scan.

CONCLUSIONS

Bone surfaces generated from manually segmented CT scans provide accurate models. However, cartilage surface models segmented from MR tended to over-estimate cartilage thickness for both femur and tibia by 1.15 mm, similar to previous reports [2]. Such deviation is significant, considering overall cartilage thickness between femur and tibia at the joint is about 6 mm.

REFERENCES

1.Koo,S., et al. Osteoarthritis and Cartilage **13**, 782-9, 2005.
2.Bowers, M.E., et al. Osteoarthritis and Cartilage **16**, 1167-1173, 2008.

ACKNOWLEDGEMENTS

This project was funded by The Albert B. Ferguson Jr., MD, Orthopaedic Fund of The Pittsburgh Foundation.

GRIP SURFACE FRICTION AFFECTS MAXIMUM TIP PINCH FORCE

Alexander K. J. Engel, Leah R. Enders, Kevin G. Keenan and Na Jin Seo

University of Wisconsin-Milwaukee, Milwaukee, WI
email: seon@uwm.edu

INTRODUCTION

Pinch grip is used in many daily activities such as picking up small objects and writing. Although pinch grip has been extensively studied, the friction condition between the fingers and grasped object has not been considered as a contributing factor to individuals' pinch strength. The maximum pinch grip force may vary with grip surface friction as described below.

The finger slips against a fixed object surface when the digit force is directed such that the ratio of shear to normal forces is greater than the coefficient of friction between the finger and the object [1]. To prevent slip, the digit has to generate force within an allowed range determined by the friction coefficient between the digit and grip surface [2] as illustrated in Fig. 1. A low-friction surface limits the digit force direction to a narrower range compared to a high-friction surface. In other words, a low-friction surface requires the digit force to be closer to the direction perpendicular to the grip surface than a high-friction surface does.

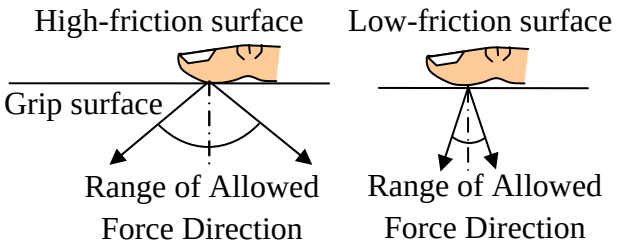

Figure 1: To prevent finger-object slip, the digit force has to be directed such that the ratio of shear to normal forces is less than the coefficient of friction between the finger and the object [1-2]. A high-friction surface allows a wider range of pinch force direction compared with a low-friction surface while not resulting in finger slip.

Generation of well-directed digit force requires precise coordination of all muscles of the finger [2-5]. When the requirement of precise control of digit force direction is lessened (such as in gripping a high-friction surface allowing a large shear to normal force ratio), the number of muscle coordination patterns to successfully complete the task [3,4] will also increase. This may result in increased pinch force. It was hypothesized that individuals will be able to produce greater pinch force when gripping objects with a high coefficient of friction between the fingers and the grip surface than when gripping objects with a low coefficient of friction.

METHODS

Twelve healthy subjects (5 males and 7 females, age = 21-30 years old, all right-handed) were seated with the forearm resting on a table. They performed maximum isometric tip pinch grip exertions (between the tips of the thumb and index finger) for 5 seconds on two fixed parallel flat surfaces (Fig. 2). Two grip surfaces – smooth rubber and paper – were tested to simulate high- and low-friction surfaces, respectively (coefficient of friction = 0.9 between rubber and skin [6] and 0.3 between paper and skin [7]). Each grip surface was connected to a load cell (Nano17, Mini40; ATI Industrial Automation, Inc.; Apex, NC) that measured pinch force (in the direction perpendicular to the grip surface) for the thumb and index finger separately.

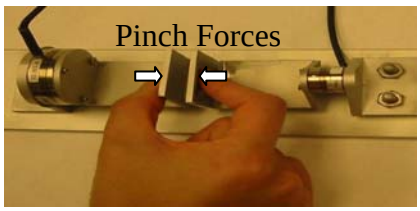

Figure 2: Subjects gripped two fixed parallel flat surfaces covered either with high-friction rubber or with low-friction paper. The grip surfaces were connected to load cells that measured pinch force.

Both hands were tested with each surface condition three times (for a total of six grip exertions per subject) to compute the means. The two flat surfaces were separated by a distance of 3.8 cm for both rubber and paper conditions. The maximum pinch force for each finger was defined as the maximum mean pinch force across a two-second period. Analysis of variance was performed to determine whether maximum pinch force was significantly affected by the grip surface (paper vs. rubber), the subject, hand (right, left) and finger (thumb, index finger) as blocking factors.

RESULTS AND DISCUSSION

The maximum tip pinch force for the rubber surface was 13% greater than that for the paper surface (p=0.017, Fig. 3). The data support the hypothesis that subjects can produce greater pinch force when gripping objects with a high coefficient of friction between the fingers and the grip surface than when gripping objects with a low coefficient of friction.

The increased pinch force for the rubber surface may be attributable to a greater range of pinch force direction allowed without slippage for high friction surfaces than for low friction surfaces (Fig. 1). Well-coordinated muscle activation patterns are needed to direct digit force within a narrow range of force direction [4-5]. This may have reduced the subjects' ability to generate maximum pinch force for the low-friction paper surface compared with the high-friction rubber surface.

Consistent with a previous study [8], the maximum pinch force was greater for the dominant right hand (58.3 N, standard error, SE, = 5.0 N) than for the non-dominant left hand (52.3 N, SE = 3.5 N). Greater force was recorded for the thumb (57.8 N, SE = 3.9 N) than for the index finger (52.8 N, SE = 5.5 N) most likely due to the thumb being stronger than the index finger [9].

CONCLUSIONS

Maximum tip pinch force increased 13% by changing the grip surface from paper (coefficient of friction of 0.3 with finger skin) to rubber (coefficient of friction of 0.9 with finger skin). This effect of the grip surface on maximum pinch force has not been shown previously. Thus for daily living tasks that require high pinch force, use of a high friction surface may be beneficial. Future studies investigating pinch grip forces should control for the surface interface between the measuring device and the fingers.

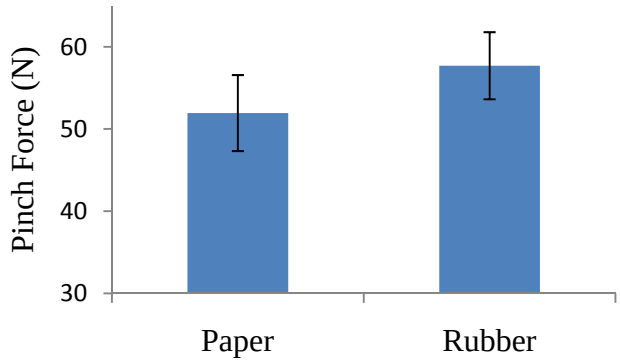

Figure 3: Mean ± standard error maximum pinch force for the two grip surfaces (index finger and thumb, left and right hand, and subjects pooled)

REFERENCES

1. MacKenzie CL, Iberall T. *The Grasping Hand* **104**, North-Holland, 1994.
2. Cole, KJ. *Exp Brain Res* 175, 285-291, 2006.
3. Valero-Cuevas FJ, Zajac FE, Burgar CG. *Journal of Biomechanics* **31**, 693-703, 1998.
4. Johanson ME, Valero-Cuevas FJ, Hentz VR. *The Journal of Hand Surgery* **26**, (4) 698-705, 2001.
5. Milner, TE and Dhaliwal SS. *Exp Brain Res* **146**, 197-204, 2002.
6. Seo NJ, Armstrong T J. *Ergonomics* **52**, 609-16, 2009.
7. Buchholz B, Frederick LJ, Armstrong TJ. *Ergonomics* **31**, 317-25, 1988.
8. Mathiowetz V, et al. *Archives of Physical Medicine and Rehabilitation* **66**, 69-72, 1985.
9. Paivinen M, Haapalainen M, Mattila M. *Occupational Ergonomics* **2**, 163-177, 1999/2000.

ACKNOWLEDMENTS

This project was funded by the University of Wisconsin-Milwaukee College of Engineering and Applied Sciences Fostering Undergraduate Research Program and by the University of Wisconsin System Administration.

SLIP-RESISTANCE AND ABRASION OF NEW & USED SHOE SOLES

Kai Way Li

Chung Hua University, Hsin-Chu, Taiwan, ROC
email: kai@chu.edu.tw

INTRODUCTION

The significance of slipping and falling has been well-established in the literature [1-3]. The factors affecting the slip-resistance of footwear such as footwear and floor materials, floor surface conditions, and shoe sole tread design have been discussed in the literature [4, 5]. However, most of the investigations were conducted using new footwear and floor materials. The new and used footwear may have different slip-resistance and other features. The objective of this study was to compare the coefficient of friction (COF) and abrasion of new and used outsoles for two types of footwear.

METHODS

Two type of footwear commonly worn both at workplace and daily activities were tested. One was a work shoes with hard rubber soles. The soles of rubber-soled shoes have a high Shore-A hardness value of 79.9 (±1.5). The other type of footwear was a sneaker with a shoe sole material of EVA with a shore-A hardness of 28.4 (±1.5).

Twenty adult male subjects were recruited for footwear usage test. These subjects were split into two groups. One group included office staffs in an organization. The other group comprised of college students. The age, stature, and body weight for the office clerks were 42.8 (±9.7) yrs, 168.7 (±7.7) cm, and 73.7 (±2.7) kg, respectively. The age, stature, and body weight for the college students were 22.0 (±1.1) yrs, 168.6 (±6.6) cm, and 73.7 (±17.3) kg, respectively.

The experiment involved the human subjects encompassed a longitudinal study. Each subject received one pair of shoes which fitted his feet size. The rubber-soled shoes with leather topping were distributed to the office clerks and the EVA-soled sneakers were distributed to the college students. The subjects were required to wear the experimental shoes for eight hours per day and three says per week (or equivalent to 24 hours per week) for 26 weeks. Each subject have worn the test shoes for at least 624 (26 week *3 day *8 hour) hours during the experiment. The subjects returned the shoes at the end of the test period. Ten shoe sole samples of each type of the used were prepared for the abrasion and COF measurements. Ten shoe sole samples for each type of new shoes were also prepared for the COF and abrasion measurements.

A NBS Shoe Sole Abrasion Tester was used to measure the abrasion of the sole samples. Measurement of abrasion followed those in the ASTM-D1630 standard [6]. Friction measurements of the shoe soles were conducted on both the terrazzo and vinyl floors. The R_a, also known as the center line average of surface heights (CLA), for the vinyl and the terrazzo floors were 0.66 (±0.23) μm and 1.12 (±0.33) μm, respectively. The surface conditions were either dry or wet. A Brungraber Mark II slipmeter was used for friction measurements. The standard test method published by the American Society for Testing and Materials [7] was adopted. The measurement protocol refined by Chang [8] was also used.

RESULTS AND DISCUSSION

Figure 1 show the mean (±std) COF for the new and used shoe soles under the floor, footwear, and floor surface conditions. Pair-wised student t-tests were conducted to compare the differences in COF between the new and used shoe soles for each floor-footwear-surface condition. The results of all the t-tests were statistical significant ($p<0.001$). The new shoe soles had significant higher COF then those of the used ones except for the wet vinyl and terrazzo floors tested using the rubber soles.

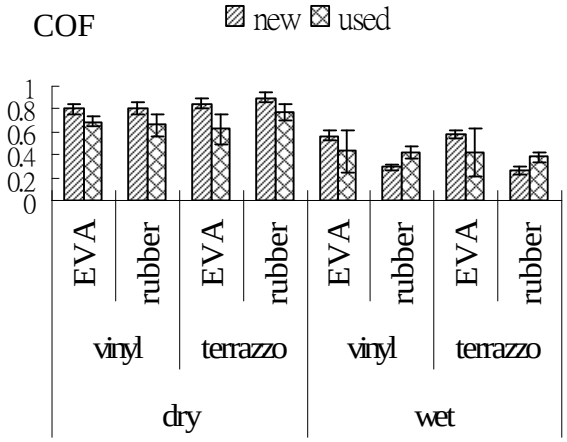

Figure 1: COF for the new and used shoe soles under floor, shoe sole, and surface conditions.

The abrasive indexes of the sole samples are shown in Figure 2. Pair-wised student t-tests were conducted to compare the difference in abrasive index between the new and used shoe sole for both of the rubber- and EVA-soled samples. The results for both tests did not reach the α=0.05 significance level. The difference between rubber and EVA samples for both the new and used samples were also tested. For both the new and used samples, the abrasive indexes for rubber were significantly (p<0.0001) higher than those of the EVA samples.

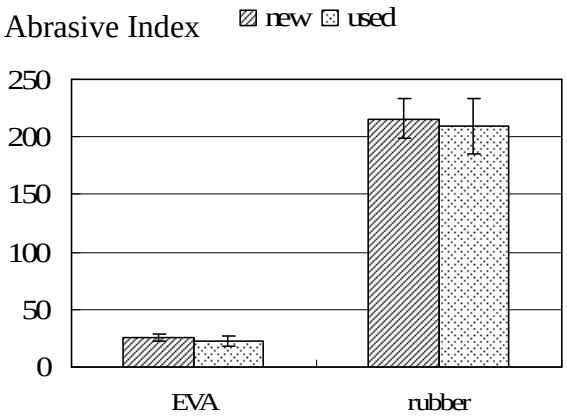

Figure 2: Abrasive index for new and used shoe soles for the types of footwear materials tested.

On dry vinyl and terrazzo floors tested, the COF values decreased after a six month usage for both of the rubber and EVA samples. The COF values also decreased for the same period for EVA samples under wet conditions on both floors. The COF of the used rubber samples increased, however, on wet vinyl and terrazzo floors as compared to their new counterparts.

CONCLUSIONS

The differences of abrasion between new and used shoe soles were not statistically significant. The used shoe soles, however, had significant lower COF values than the new ones except the rubber soles tested on wet vinyl and terrazzo floors.

REFERENCES

1.Leamon TB, Murphy, PL, *Ergonomics* **38(3)**, 487-498, 1995.
2.Tisserand M. *Ergonomics* **28**, 1027-1042, 1985.
3.Strandberg L.*Ergonomics* **28**, 131-147, 1985.
4.Li KW et al., *Saf Sci* **42**, 547-565, 2004.
5.Li KW, Chen CJ, *Saf Sci* **43(7)**, 391-405, 2005.
6.American Society for Testing and Materials, F-1630-07, *Annual Book of ASTM Standards.* West Conshohochen, PA, 2007.
7.American Society for Testing and Materials, F-1677-05, *Annual Book of ASTM Standards*. 15.07. West Conshohochen, PA, 2005.
8.Chang WR, *Saf Sci* **40**, 593-611, 2002.

ACKNOWLEDGEMENTS

This research was financially supported by the National Science Council of the ROC under grant NSC 97-2221-E-216-027.

The Box and Block Test Score is Dependent upon Block Surface

Daniel T. Cary, Leah R. Enders, Na Jin Seo

The University of Wisconsin-Milwaukee, Milwaukee, WI, USA
E-mail: dtcary@uwm.edu

INTRODUCTION

The ability to grip and manipulate objects is essential in performing various activities of daily living. Various clinical assessments of hand grip function have been developed and frequently used to identify individuals with sensorimotor impairment and to quantify their functional ability [1, 2]. One of the common clinical tests used to assess individuals' hand grip function is the Box and Block Test [1, 2]. First developed in 1957 [3], the Box and Block Test has been used to evaluate gross manual dexterity not only for healthy individuals [4], but also for individuals with disorders such as Cerebral Palsy [3].

An individual's ability to grip and manipulate objects is affected by many factors including hand strength [5], sensorimotor impairment [5], and frictional coupling between hand and object [6]. In particular, increases in the coefficient of friction (COF) between the fingers and an object reduce the minimum required grip force for individuals to successfully grip and lift the object [7]. An increase in finger-object COF also allows for greater deviation and variance of digit force direction from the direction perpendicular to the grip surface [8]. This study was performed to investigate if grip objects' frictional surfaces affect individuals' hand grip function. It was hypothesized that increasing hand-object COF improves hand grip function assessed using the Box and Block Test.

METHODS

Thirteen young healthy subjects (5 male, 8 female, 20-30 years of age) performed the Box and Block Test in a seated posture using their non-dominant hand for the following three sets of blocks: the commercially-available original blocks with the painted wood surface (COF 0.5 with skin [9]), blocks covered with a smooth sheet of rubber (COF 0.9 with skin [10]), and blocks with a paper surface (COF 0.3 with skin [11]) All three types of blocks had the same dimensions and weight (within ± 1 mm and 1 g). Subjects were instructed to move as many blocks as possible from one side of the container to the other for a period of 60 seconds [1]. The Box and Block Test score was determined by the total number of blocks that the individual moved in 60 seconds.

The Box and Block Test was repeated twice per block surface. The three block surface conditions were presented to subjects in a randomized order. Two minute rest breaks were allowed between tests to prevent muscle fatigue.

Analysis of variance was performed to determine if the within-subject variable of block surfaces (paper, painted wood, and rubber) significantly affected the Box and Block Test score. A post-hoc pair-wise comparison was performed to examine the Box and Block Test scores between the three block surfaces. The p-value of .05 was considered significant.

RESULTS AND DISCUSSION

The mean Box and Block Test scores for the three block surfaces are shown in Fig. 1. The effect of the block surface condition on the Box and Block Test score was found to be significant ($p<.01$). The Box and Block Test score was higher for the rubber-finished blocks than for both the paper- and painted wood-finished blocks ($p<.01$). The score was not significantly different between the painted wood blocks and the paper-finished blocks ($p>.05$).

Subjects were able to move 10% more blocks when gripping rubber-finished blocks compared to the painted wood- or paper-finished blocks. The results partially support the hypothesis that increasing hand-object frictional coupling improves hand grip function.

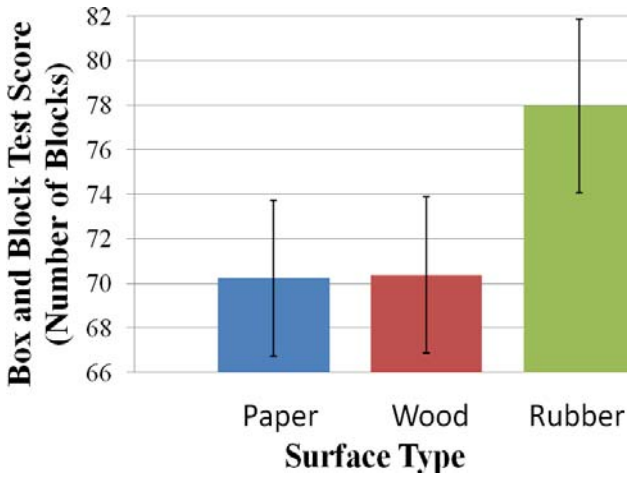

Figure 1: The mean ± SE Box and Block Test scores (the number of blocks moved in 60 seconds) for the three block surfaces (the thirteen subjects' data pooled). The effect of the block surface was significant (p<.01).

Improvement in hand grip function for the rubber surface may first be due to reduction in the minimum required grip force. Increase in COF between the fingers and blocks allows individuals to successfully grip and lift the blocks with less grip force [7]. Secondly, high finger-object COF allows individuals to generate digit force in a wider direction but may prevent the finger from slipping from the object surface, compared with low finger-object COF [8]. This increase in finger-object COF may lessen the requirement for digit force direction control and thus may reduce the need for individuals to precisely control hand muscles [12]. The contribution of these two mechanisms may be more pronounced for a high COF condition such as between rubber and skin than for medium and low COF conditions (Fig. 1).

In addition, the blocks sometimes slid across the container floor when the finger came in contact with the block, which could also have contributed to the Box and Block score. Specifically, sliding occurred more for the painted wooden blocks compared to the other block surfaces. This sliding may have reduced the Box and Block Test score particularly for the painted wooden blocks.

CONCLUSIONS

Higher coefficients of friction can increase hand-object frictional coupling [6]. The present study demonstrates that increasing the frictional coupling between the hand and grip objects can improve individuals' performance in the Box and Block Test. This finding has significant implications in rehabilitation as well as in ergonomics. A simple intervention of modifying grip object surfaces may be beneficial in improving hand grip function for people with weakness and for people with sensory and motor impairments. In addition, future investigations and clinical testing should recognize that the measurement of hand grip function is affected by grip objects' frictional surfaces.

REFERENCES

1. Mathiowetz V, et al. *American Journal of Occupational Therapy*. **38,** 386-391, 1985.
2. Trombly CA: *Occupational Therapy for Physical Dysfunction*, Williams and Wilkins, 1983.
3. Cromwell FS: *Occupational Therapist's Manual for Basic Skill Assessment; Primary Prevocational Evaluation*, Fair Oaks Printing, 1976.
4. Desrosiers J, et al. *Archives of Physical Medicine and Rehabilitation*. **75**,751-755, 1994.
5. Boissy P, et al. *Clinical Rehabilitation.* **13**, 354-362, 1999.
6. Seo NJ et al. *Human Factors* **50**, 227-236.
7. Johansson RS and Westling G. *Experimental Brain Research*. **56**, 550-64, 1984.
8. MacKenzie CL, Iberall T. *The Grasping Hand*, North Holland, 1994.
9. Bullinger HJ, et al. 1979.
10. Seo NJ and Armstrong TJ. *Ergonomics*. **52**, 609-616, 2009.
11. Buchholz B, et al. *Ergonomics*. **31**,317-25, 1988.
12. Milner, et al. *Exp Brain Res* **146**, 197-204, 2002.

ACKNOWLEDMENTS

This project was funded by the University of Wisconsin-Milwaukee College of Engineering and Applied Sciences Fostering Undergraduate Research Program and by the University of Wisconsin System Administration.

HAND SUPPORT REDUCES PEAK L5/S1 MOMENTS IN ONE-HANDED LIFTING

Gert S. Faber, Idsart Kingma and Jaap H. van Dieën

Research Institute MOVE, Faculty of Human Movement Sciences, VU University Amsterdam, The Netherlands;
email: g.faber@fbw.vu.nl, web: http://www.move.vu.nl/members/gert-faber/

INTRODUCTION

Manual lifting can result in high low back loading [1] which is probably the reason that lifting is a an important risk factor for low back pain [2]. In one-handed lifting, low back loading could be reduced by using the free hand to support the upper body. This study investigates the effect of hand support on back loading in one-handed lifts of a pencil and a heavy weight, using a self-selected and a weightlifters' technique (wide foot placement and straight back). It is hypothesized that hand support reduces back loading and that the effects of hand support are larger when lifting a heavier load and when using a weightlifters' instead of a self-selected technique.

Figure 1: Subject performing supported lifts of a pencil (top) and a 25kg weight (bottom) using a self-selected (left) and weight lifters technique (right).

METHODS

Nine healthy subjects performed supported and unsupported one-handed lifts. Hand support forces exerted on the left thigh were measured using a 6-DOF force/moment transducer (Fig. 1). These support forces were used together with ground reaction forces, lower body anthropometrics and kinematics of the lower body segments and the force/moment transducer in a bottom-up 3D inverse dynamics model [3] to calculate peak total L5/S1 moment (PTM). Repeated measures ANOVAs were used to test the effects of hand support, object weight and lifting technique and their interactions.

RESULTS AND DISCUSSION

In line with the hypothesis peak support forces were higher when lifting the 25kg weight instead of the Pencil. However, no effect of lifting technique was found (Fig. 2).

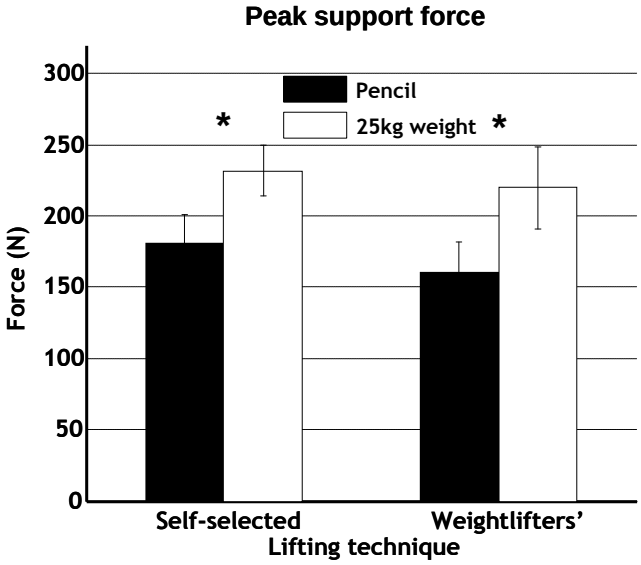

Figure 2: Peak support forces. * indicate significant differences between the lifts of the pencil and 25 kg weight. Error bar = 1 SEM.

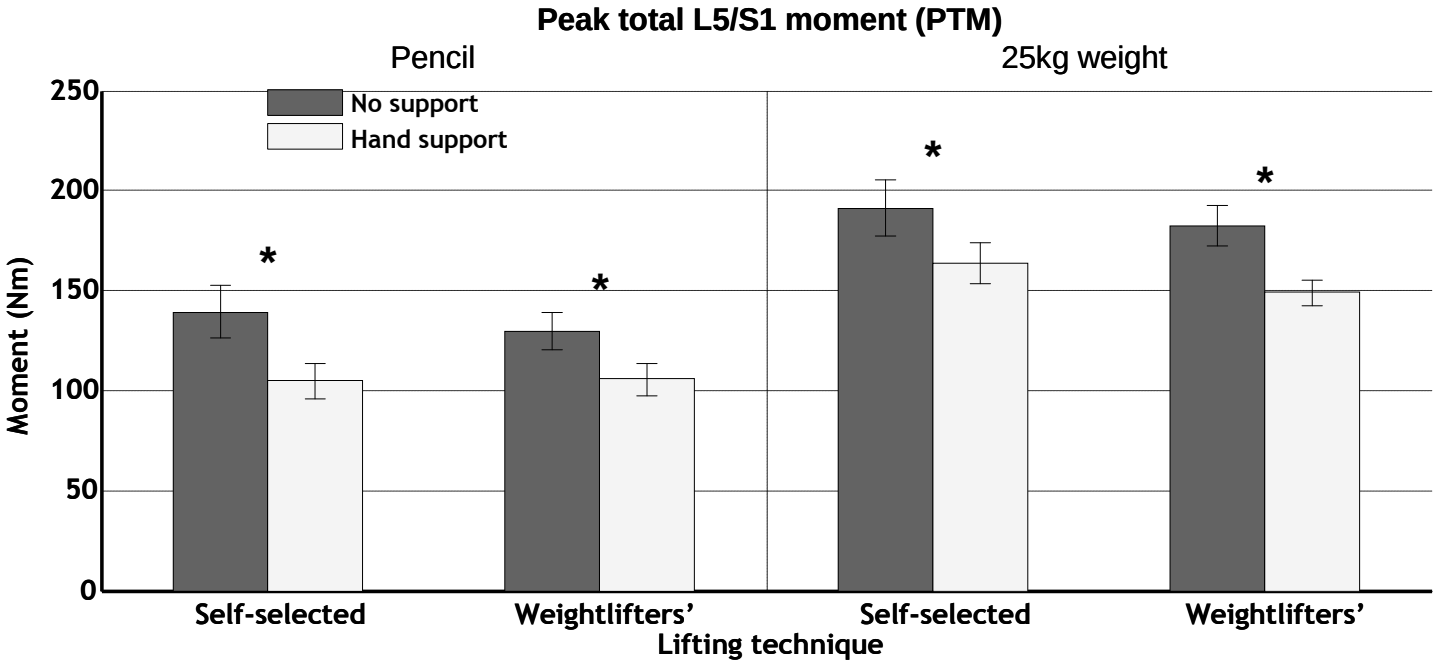

Figure 3: Peak total L5/S1 moments. * indicate significant effects of hand support. Error bar = 1 SEM.

Because the heavier lifts resulted in larger support forces, it was expected that the effect of hand support on the peak total L5/S1 moments would be larger in the 25kg lifts than in the pencil lifts. However, the ANOVA did not reveal any significant interactions indicating that the effect of hand support was independent of load mass and lifting technique (Fig. 3). On average, the effect of hand support was about 30Nm (20%). This effect appears to be low when considering the magnitude of the peak support forces (about 200N): when assuming a 0.5m moment arm of the support force, an effect of about 100Nm would be expected. The reason that the peak support forces did not result in such a large effect is because the peak total L5/S1 moment usually occurred slightly after the peak support force. At this instant in time support forces were considerably lower (around 70N). In addition, no effects of load weight or lifting technique were found at this instant in time (Fig. 4).

CONCLUSIONS

In conclusion, we found that using one hand to support the upper body during one-handed manual lifting reduced back loading by about 20%. Furthermore, the effect of hand support appeared to be independent of load weight and lifting technique.

REFERENCES

1. Faber GS, et al. *Ergonomics*, **52**, 1104-1118, 2009
2. Kuiper JI, et al.. *Int J Ind Erg*, **24**, 389-404, 1999.
3. Kingma I, et al.. *Hum Mov Sci*, **15**, 833-864, 1996.

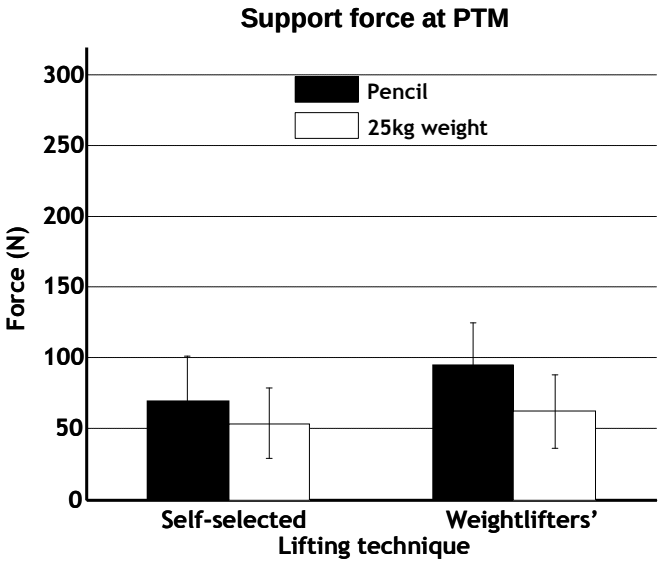

Figure 4: Support forces at the instant of PTM. * indicate significant differences between the lifts of the pencil and 25 kg weight. Error bar = 1 SEM.

CORRELATION BETWEEN GUIDED GRIP FORCE AND PERCEIVED EXETION FOR MALES

[1]Kai Way Li

[1]Chung Hua University, Hsin-Chu, Taiwan, ROC
email: kai@chu.edu.tw

INTRODUCTION

The study of perceived effort has long been dominated by Borg's concept of perceived exertion [1]. Borg's ratings of perceived exertion (RPE) scale (ranged from 6 to 20) have been widely used in analyzing various manual tasks as well as in many physical works [1] as a supplementary measure in addition to physiological measures. In addition to the RPE scale, Borg [2] has constructed another subjective scale, called CR-10 scale. Borg [2] claimed that the advantage of the CR-10 scale over the RPE scale is that the former lacks of an inter-subjective unit for direct determinations of intensity levels while the latter provides direct level estimates for determinations of ratio relationships between perceptual responses. Both the RPE and the CR-10 scales may be used to measure muscular exertion and physical workload for whole body or specific body segment.

Even though the Borg's RPE and CR-10 scales have been claimed function well, investigations and discussions on the design, function, and requirement of calibration are still continued. Buchholz *et al.* [3] examined the agreement of subjective ratings of upper extremity exposures with corresponding direct measurements obtained simultaneously from workers. Psychophysical ratings of exposure, based on the Borg CR-10 scale, were obtained for the period of time in which direct measurements were acquired using electro-goniometers, electro-inclinometers and electromyography. Subjects from workers at two automobile manufacturing plants were selected. Significant relationships between subjective ratings of wrist position and measured wrist posture or motion and between ratings of shoulder position and measured shoulder posture were not found.

In the study of Spielholz [4], twenty subjects applied power grip forces corresponding to their perceptions of different Borg CR-10 scale levels using both ''grip-to-scale'' and ''guided-grip'' procedures. These data were used separately to define relationships between scale ratings and actual force application. Two gripping tasks were performed and corresponding subjective hand force ratings were calibrated using the grip-to-scale calibration data. The results showed that the mean estimation error for a 44.5 N power grip task was significantly reduced from 142.8 to 62.3 N. The guided-grip calibration method also significantly reduced rating error for the power grip task. Spielholz's [4] study indicated that calibration of hand force ratings using the grip-to-scale procedure may improve the accuracy of hand exertion measurements using the Borg CR-10 scale.

Handgrip is a fundamental element in performing many tasks. The Borg's CR-10 has been discussed in the literature [1,2,3]. The objective of this study were to examine the relationship between the grip force of the dominant hand and the Borg's CR-10 ratings and to report the deviation of predicted grip force from measured force based on a linear regression model developed in the study.

METHODS

Twenty males were recruited as human subjects in the study. All the subjects were free from musculoskeletal injuries. Their age, gender, stature, and body weight were 22.1 (±2.5) yrs, 172.3 (±5.3) cm, and 69.8 (±12.5) kg, respectively. All the subjects received payment and had signed informed consent forms for their participation in the study. All the subjects, except one, were right-handlers.

In the experiment, each subject was required to grip a dynamometer under one of the four Borg CR-10

scale levels: 2, 5, 7, and 10. The scores of 2, 5, 7, and 10 on the CR-10 scale were assumed to represent 20%, 50%, 70% and 100% of perceived maximum voluntary contraction (MVC), respectively. The grip forces of the dominant hand of the subjects were measured. The upper arm of the subject was straight down and the lower arm was horizontal, or at 90° with the upper arm. The span of the dynamometer was 5 cm. Each subject will take a break for five minutes or more after he finished one measurement at the 5, 7, or 10 levels so as to avoid the effects of fatigue on the measurement.

Descriptive statistical analysis was performed. In addition, a linear regression model was built to describe the relationship between the grip force and the Borg's CR-10 scale. The statistical analyses were performed using the SPSS® 12.0 computer software.

RESULTS AND DISCUSSION

The means (±standard deviations) of the grip force corresponding to the scores of 2, 5, 7, and 10 on the CR-10 scale were 10.0 (±2.8), 23.5 (±4.2), 32.8 (±3.5), and 43.3 (±5.3) N, respectively. The Pearson's correlation coefficient between the CR-10 rating and the grip force was 0.95 (p<0.0001). A linear regression model was established to describe the relationship between the CR-10 score and grip force:

$$\text{Grip force} = 2.29 + 4.18 \times \text{CR-10 score} \qquad (1)$$

This model is statistically significant at p<0.0001 with an R^2, or coefficient of determination, of 0.90 and a root mean square error of 4.11. The intercept (2.29) and the slope (4.18) of the regression model were statistically significant at p<0.032 and p<0.0001, respectively. The scatter plots and regression line of (1) are shown in Figure 1. To assess the deviations of the measured grip force and the predicted values using (1), a mean absolute deviation (MAD) was defined using the following equation:

$$\text{MAD} = \frac{1}{n}\sum_{i=1}^{n} |\text{measured value} - \text{predicted value}|$$

where n is the sample size. The MAD was 3.02 N.

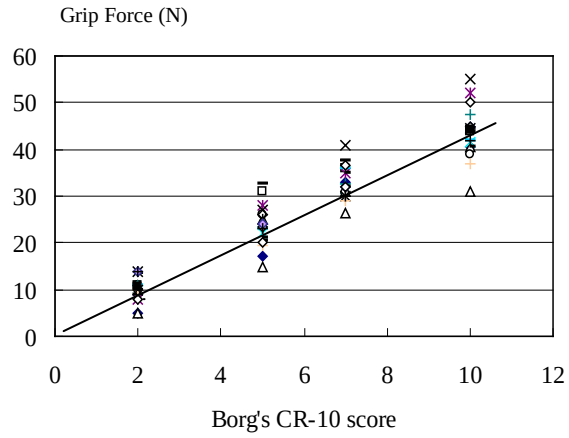

Figure 1: Scatter plots and regression line

In the regression model, the CR-10 score was highly correlated with the grip force. The linear regression model in (1) may be used to describe and predict the grip force of the dominant hand for the male subjects. The results of this study were consistent with the findings in the literature [4].

REFERENCES

1. Borg A. *Scand J Work Environmental Health* **16**, 55-58, 1990.
2. Borg A. *Medicine and Science in Sports and Exercise* **14**, 377-381, 1982.
3. Buchholz B., et al. *Ergonomics* **51**, 1064-1077, 2008.
4. Spielholz P. *Applied Ergonomics* **37**, 615-618, 2006.

ACKNOWLEDGEMENTS

This research was financially support by the National Science Council of the ROC under grant NSC 98-2221-E-216-01.

VIBRATION FREQUENCY INFLUENCES FOOT TO LEG TRANSMISSION

Gerald Smith, Eadric Bressel, and Dustin Nash
Biomechanics Laboratory, Utah State University, Logan UT, USA
email: Gerald.Smith@usu.edu

INTRODUCTION

Whole body vibration induced for training and therapy purposes is thought to positively stimulate muscle and bone. Potential therapeutic or detrimental effects of such vibration are likely dependent on the oscillation characteristics experienced by various tissues of the body. Whole body vibration is often described primarily in the vertical direction with characteristics including amplitude of the vibration, peak acceleration, RMS acceleration, and transmission ratio from instrument to person. Several studies have evaluated these characteristics across a range of frequencies [1, 2] but with focus on vertical direction only. However, vibration input at the foot can induce skeletal vibrations in multiple dimensions. This study evaluates the three-dimensional transmission characteristics from a vibration plate through the foot to the leg.

Most vibration studies ignore motion details of the vibration plate and typically report acceleration characteristics which are directly measured using accelerometers (usually only vertical direction). Recent technological advances of motion analysis instrumentation have increased the sampling frequency and resolution sufficiently to be capable of measuring moderate frequency vibration. This project made use of such instrumentation to measure three-dimensional transmission of vibration through a range of frequencies.

METHODS

Fifteen healthy males and females from a university population were recruited for this study. Low-mass reflective markers were placed on each subject's right tibial tuberosity and on the surface of a vibration plate immediately lateral to the subject's midfoot. The vibration plate was a model developed by Bosco Systems (Nemes) which includes a test mode which progresses through frequencies from about 25 to 55 Hz in 5 Hz increments and with durations of 5 s. Marker position-time data were recorded at 500 Hz using seven T-20 model cameras and Vicon Nexus software. 3-D position data were exported to MatLab for analysis.

Position data were first filtered using a double-pass Butterworth filter with cutoff frequency of 75 Hz. Acceleration was calculated using first central-difference formulas. Peak accelerations were determined for 50 cycles at each test frequency. Root-mean-square acceleration was determined through the same 50 cycles. Finally, transmission in each direction was characterized as the ratio of RMS acceleration at the tibia to that at the vibration plate. Paired t-tests were used to compare accelerations of plate and tibia at each frequency.

Like other vibration platforms [3], the Bosco System plate combined both horizontal and vertical motions of the surface. Representative oscillation patterns are shown in Figure 1 below. Relatively little medial-lateral motion was observed.

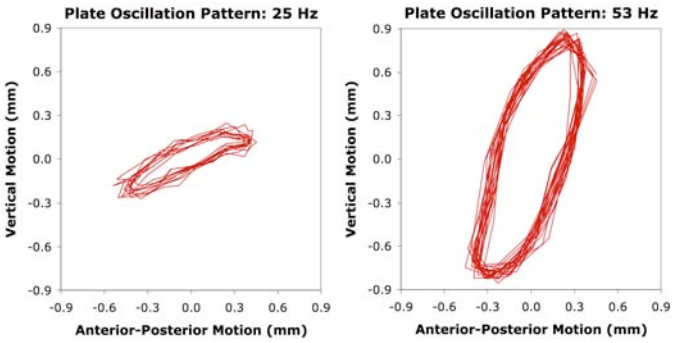

Figure 1: Sagittal plane motion of the vibration plate surface for multiple cycles at 25 and 53 Hz frequencies. Considerable anterior-posterior motion of the plate was observed. Amplitude of vertical motion changed with frequency and systematically shifted from about 0.5 mm peak-to-peak to more than 1.5 mm.

RESULTS AND DISCUSSION

Tibial motion characteristics were considerably different from the vibration plate. Each subject stood with feet flat on the surface and knees comfortably flexed, but small fluctuations of tibial position were evident combined with vibration patterns which included considerable medial-lateral vibration (Figure 2).

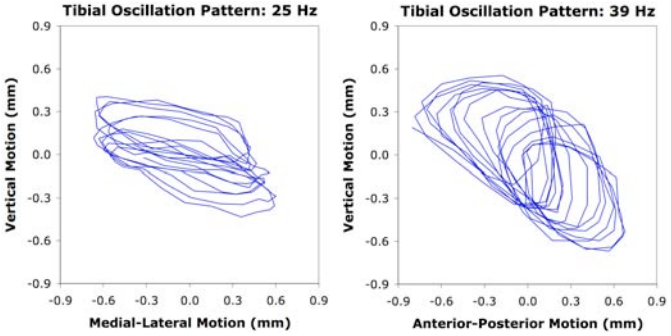

Figure 2: Frontal and sagittal plane motion of the tibial marker for multiple cycles at 25 and 39 Hz frequencies. Considerable medial-lateral and anterior-posterior motion of the tibia was observed.

Peak accelerations in the vertical direction ranged from about 0.9 ± 0.2 g at 25 Hz to 6.3 ± 0.5 g at 53 Hz. Anterior-posterior acceleration of the plate also increased with frequency up to about 3.8 ± 0.4 g at 53 Hz (Figure 3). Medial-lateral accelerations were all less than 1 g at the plate but consistently greater at the tibia (as much as 1.9 ± 0.8 g at 53 Hz). Transmissibility ratios comparing tibia to plate vibration based on RMS acceleration, generally decreased with frequency (Figure 4).

CONCLUSIONS

Human body vibration is a three-dimensional response with considerable acceleration in all directions. Substantial attenuation of vibration was observed from foot to leg–particularly at higher frequencies.

REFERENCES

1. Kiiski J, et al. *J Bone Min Research* **23**, 1318-1325, 2008.
2. Rubin C, et al. *Spine* 28, 2621-2627, 2003.
3. Branscomb, et al. *Proceedings of ASB 2009*, State College, PA, 2009.

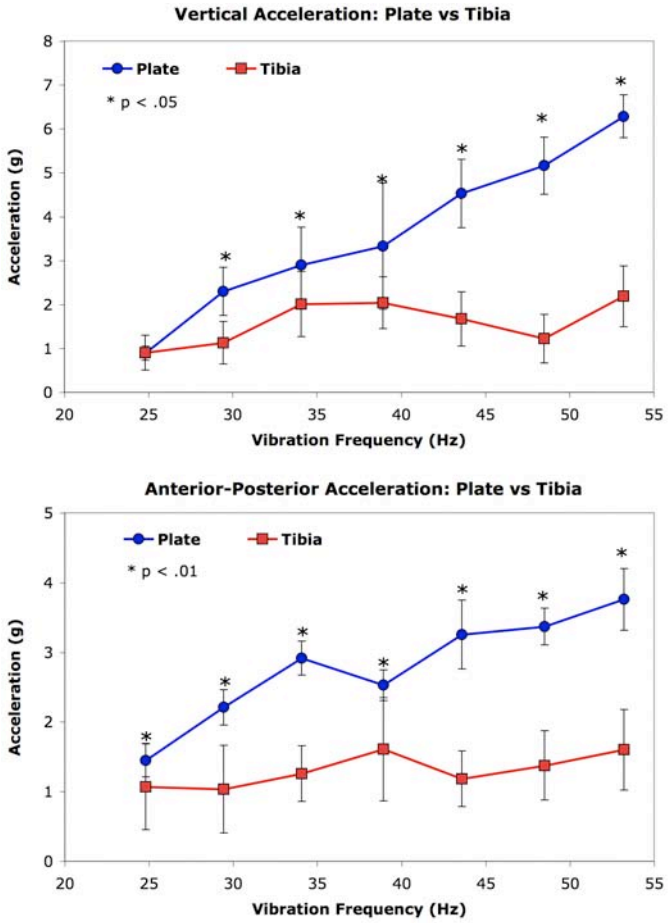

Figure 3: Peak acceleration in vertical and anterior-posterior directions. Tibial accelerations were significantly less than vibration plate accelerations across frequency.

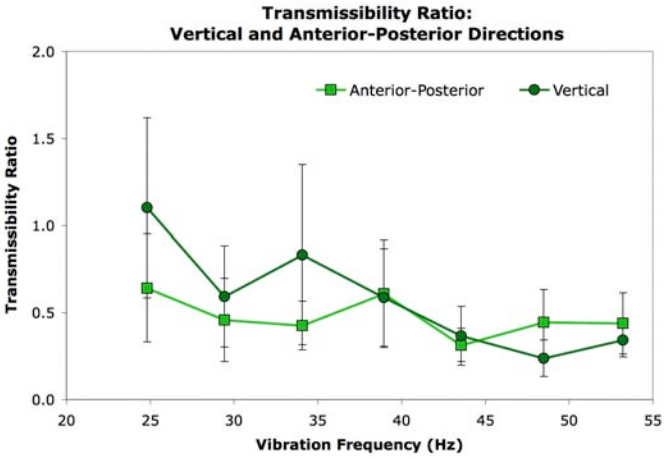

Figure 4: Vibration transmission from plate to tibia across frequencies. The reduced transmission observed for higher frequencies is due to nearly constant tibial acceleration across frequencies while plate acceleration increased with frequency.

A FLEXED WRIST RESULTS IN LARGER MUSCLE STRESSES DURING TAPPING

[1]Hua Chen, [1]Krishna Asundi and [1]Jack T. Dennerlein
[1]Harvard University School of Public Health, Boston, MA, USA
email: jax@hsph.harvard.edu

INTRODUCTION

Sustained non-neutral wrist postures during computer use have been identified as a risk factor for tendon injuries. A possible mechanism for injury may be that these non-neutral postures lengthen muscles and thus increase passive loads.

Three non-neutral wrist postures, adduction, extension, and flexion, are common during typing. Adducted and extended wrist postures have been observed during keyboard intensive tasks [1]. Typing on a negatively tilted keyboard, which is intended to reduce wrist extension and thus the risk of musculoskeletal disorders, could result in flexed wrist postures [2].

Non-neutral postures lengthen muscles selectively. Wrist adduction, extension, or flexion lengthens the abductor, flexor, or extensor muscles, respectively. The lengthened muscles develop passive stresses as a function of excursion and muscle elasticity [3].

This study compared hand and forearm muscle stresses during index finger tapping across four wrist postures using a computational model. We hypothesized that non-neutral wrist postures would lead to larger muscle stresses than in neutral posture due to the influence of passive stresses.

METHODS

Ten subjects participated in tapping experiments to measure forearm motion and fingertip force. Informed consent was obtained, and all protocols were approved by the Harvard School of Public Health Institutional Review Board.

During measurements, subjects tapped with the index finger on the F6 key of a keyboard. Keyboard angle and location were adjusted to create four unsupported wrist postures: neutral (NTL, subjects' right acromion was aligned with the key), adducted (ADD, subjects' midline was aligned with the key), extended (EXT, keypad was positively tilted 18^{o}), and flexed (FLX, keypad was negatively tilted 18^{o}). Subjects were asked to tap in sync with a 3 Hz metronome while maintaining the elbow and shoulder in a fixed posture. A 3D active marker motion analysis system (Optotrak, Northern Digital, Ontario, CN) tracked trajectories of the trunk, upperarm, forearm, hand, and index finger. A six-axis loadcell secured underneath the keypad measured fingertip force during keystroke. All data were collected at 100 Hz and saved to a computer.

Segment trajectories and force data were then inputted to an inverse dynamic model to compute flexion and abduction torques at the wrist and 2nd metacarpophalangeal (MCP) joint, as well as flexion torques at proximal and distal interphalangeal joints (PIP and DIP, respectively). Net joint torques represented the combined effects of the following muscles: the extensor digitorum and extensor indicis (LE), flexor digitorum superficialis (FDS), flexor digitorum profundus (FDP), dorsal interossei (DI), palmar interossei (PI), and lumbricales (LUM) crossing the finger joint(s), and the LE, FDS, FDP, extensor carpi radialis (ECR), extensor carpi ulnaris (ECU), flexor carpi radialis (FCR), and flexor carpi ulnaris (FCU) crossing the wrist joint.

Computed joint torques and segment trajectories, collapsed into one average tap, were used in an optimization model. The model predicted muscle stresses required to internally generate the equal torques, through the joint moment arms. The model sought the minimal combined muscle stresses that achieved the torques while complying with physiological constraints, including muscle passive mechanics [3], active mechanics, and index extensor hood mechanisms. Net internal torques, individual muscle stress, and active and passive stress components were computed for all subjects. Also sum of all muscle stresses was computed by summing the time integral of ten individual muscle stresses. Repeated measure ANOVA was used to

compare the torques and muscle stresses across the four wrist conditions.

RESULTS AND DISCUSSION

Unsupported wrist postures during tapping matched the four targeted conditions. Mean wrist flexion, extension, and adduction were largest during the FLX, EXT, and ADD conditions, respectively. Net torques acted to support the wrist and counter gravity. The NTL and FLX condition had the greatest extension torques of 0.24 N-m (Table 1).

Flexor muscles, FDS, FDP, FCR, and FCU, had the largest stress in EXT condition; extensor muscles, LE, ECR, and ECU, had the largest stress in FLX condition (data not shown). This was because passive muscle stresses developed as flexor and extensor muscles were stretched at EXT and FLX conditions, respectively.

FLX and ADD conditions showed the largest active and passive stress, respectively. The largest passive stress in ADD did not convert to the largest sum of muscle stresses as we hypothesized. Only one of the non-neutral postures, FLX, led to a significantly larger sum of muscle stresses compared to neutral posture, NTL (Table 1). This was in partial agreement with our hypothesis.

As muscles act to counteract net external torques, larger torques are expected to result in larger muscle stresses. Here NTL and FLX conditions were expected to result in the largest stresses due to their equally large torques. However, FLX led to a significantly larger sum of muscle stresses than the NTL condition (Table 1).

The larger stresses found for the FLX condition were not due to the posture dependent muscle passive properties. The FLX condition resulted in similar passive stresses compared to NTL, and passive components were small compared to active components for all conditions (Table 1).

Instead, those large stresses were due to changes in muscle moment arms at the wrist between the two conditions. Because net torque is the product of muscle forces and muscle moment arms, large moment arms allow a large torque to be produced by small forces. The wrist extensor moment arms decreased as the wrist changed from NTL to FLX condition [4], so larger extensor forces and stresses were required to produce a similar wrist torque at the FLX, compared to the NTL condition.

CONCLUSIONS

Tapping with an unsupported flexed wrist resulted in larger muscle stresses compared to other wrist postures, which demonstrated the adverse effect of typing at non-neutral postures. The large stresses were mostly due to the muscle active component rather than the passive components.

While both the NTL and FLX conditions led to similar wrist torque, muscle forces required to produce the torque were larger in the FLX condition due to the smaller muscle moment arms. This indicated the crucial role of moment arms in the wrist motions.

REFERENCES

1. Dennerlein, J. T. and P. W. Johnson (2006). Ergonomics **49**(1): 45-61.
2. Simoneau, G. G. and R. W. Marklin (2001). Hum Factors **43**(2): 287-98.
3. Qin,J.,etal., Journal of Biomechanics (2010), doi:10.1016/j.jbiomech.2010.01.014
4. Lemay, M. A. and P. E. Crago (1996). J Biomech **29**(10): 1319-30

Table 1: Mean (SD) wrist angles, torques, and the muscle stresses due to passive and active muscle mechanics. The superscript letter attached to the values reports the results from the Tukey post-hoc analysis. Values with different letters are ranked such that A>B>C. Levels not connected by same letter are significantly different.

Wrist Posture	NTL	ADD	EXT	FLX
Flexion, Abduction Angle [°]	-7^{B} (9), -4^{A} (4)	-7^{B} (10), -21^{C} (4)	-22^{C} (9), -2^{A} (4)	18^{A} (11), -10^{B} (7)
Flexion, Abduction Torque [N-m]	-0.24^{B} (0.08), 0.10^{A} (0.05)	-0.20^{A} (0.07), 0.10^{A} (0.06)	-0.22^{A} (0.08), 0.09^{A} (0.05)	-0.24^{B} (0.09), 0.09^{A} (0.05)
Sum of Muscle Stresses [N/cm^2]	11.97^{B} (2.46)	13.75^{AB} (2.80)	12.21^{B} (2.11)	14.81^{A} (2.91)
Passive Component [N/cm^2]	3.38^{B} (0.62)	4.72^{A} (1.24)	3.62^{B} (0.65)	3.35^{B} (0.68)
Active Component [N/cm^2]	8.58^{B} (2.41)	9.03^{B} (2.10)	8.59^{B} (1.94)	11.46^{A} (2.81)

ACUTE BIOMECHANICAL RESPONSES TO A PROLONGED STANDING EXPOSURE: IMPLICATIONS FOR JOB ROTATION DESIGN

[1]Erika Nelson-Wong, [2]Samuel J. Howarth and [2]Jack P. Callaghan

[1]Regis University, Denver, CO, USA
[2]University of Waterloo, Waterloo, ON, Canada
email: enelsonw@regis.edu

INTRODUCTION

Rotation between jobs is commonly used to reduce the incidence of workplace injuries [1]. Many tasks that are included in job rotation schemes have standing postures as a necessary and unavoidable component. Typically job rotation design has focused on alternating between jobs with high and low physical demands [2]. While prolonged standing may be classified as a task component with low physical demand, there may be adverse effects of moving from a sustained static posture to a more dynamic activity [1]. Epidemiology studies have shown a strong association between prolonged standing and low back pain (LBP) [3]. It is possible that including a period of prolonged standing in a job rotation cycle may have detrimental effects. The purpose of this study was to investigate the impact of a prolonged standing exposure on biomechanical profiles (trunk muscle activation, joint stiffness and kinematics) during 3 functional movements.

METHODS

Forty-three volunteers (22 male, 21 female) participated in this study. A set of 3 functional movements that incorporate base elements of common occupational tasks (squatting, forward bending from the hips, and single leg standing) were performed pre- and post- a 2-h standing exposure. Continuous electromyography was collected from 8 bilateral muscle groups (latissimus dorsi, thoracic and lumbar erector spinae, rectus abominis, internal and external oblique, gluteus maximus and medius). An 8-segment (trunk, pelvis, bilateral thigh, shank and foot) bottom-up inverse dynamic rigid link model was created from kinematic data (Optotrak Certus, Northern Digital Inc., Waterloo, ON) using Visual3D software (C-Motion Inc, Kingston, ON) and kinetic data from in-floor force platforms positioned under each foot (Advanced Medical Technologies Inc, Newton, MA). Primary outcome measures of interest included Flexion Relaxation Ratios (FRRs) during forward bending, Center-of-Pressure (COP) excursion during single leg standing (SLS), and active vertebral joint rotation stiffness (VJRS) during SLS and squatting.

FRRs for the thoracic and lumbar erector spinae and gluteus maximus muscles were calculated as a ratio between the linear enveloped EMG signals in upright standing and fully flexed positions. Anterio-posterior and medio-lateral COP (COP_{AP} and COP_{ML}) were calculated from the force platform data and maximum excursion over the 10-s SLS trial was calculated as the difference between the minimum and maximum COP values for each direction and each lower extremity. VJRS was calculated for each axis and each lumbar motion segment using an existing anatomical model in combination with distributed moment equations [4,5] for the eccentric and concentric phases of the squat and the SLS tasks.

Statistical analyses were conducted using multifactorial general linear models in SPSS version 17.0 (SPSS, Inc, Chicago, IL) with a significance criterion of $p \leq 0.05$.

RESULTS

There were significant changes from pre-post standing exposure in two of the outcome measures for the SLS task. During right SLS, there was a significant decrease ($F_{1,32} = 4.473$, $p < 0.05$) in active vertebral stiffness about the lateral bend axis at the L_2L_3, L_3L_4 and L_4L_5 motion segments

following the standing exposure (Fig. 1). Participants increased their relative trunk lateral bending angle (trunk relative to pelvis) during right SLS following standing exposure ($F_{1,38}$ = 8.63, p < 0.05) (Fig. 2). There was also a significant interaction between gender and standing exposure for COP_{AP} ($F_{1,39}$ = 4.201, p < 0.05) and COP_{ML} ($F_{1,39}$ = 8.506, p < 0.01) during SLS, with males demonstrating increased and females demonstrating decreased COP excursion in both directions following standing exposure. There were no significant pre-post standing differences for FRR during forward bending or VJRS during the squat task.

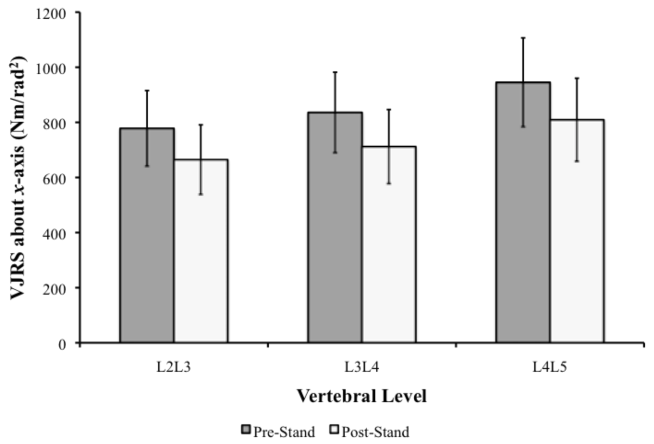

Figure 1: There was decreased vertebral rotation stiffness about the lateral bend axis from L_2 – L_5 during right SLS following standing exposure.

DISCUSSION

Results from this study indicate that there are biomechanical changes that take place during functional movement performance in response to a prolonged standing exposure, including a decrease in vertebral rotation stiffness, increased COP excursion and increased trunk lateral bend during a simple balance challenge.

The decreased stiffness observed in lateral bending during SLS could be an issue if the task being rotated to following prolonged standing included the necessity for resisting a side-load in combination with a balance activity, as might be seen in occupations such as construction, where workers spend most of their day in standing conditions and are also manipulating heavy loads, often at heights or on unstable/uneven surfaces.

It is unclear whether the increased COP observed in males would translate to greater difficulty with higher-level balance challenges or imply a balance deficit, as the magnitude of COP excursion remained relatively small (on the order of a 2-4 centimeters). This small decrease in postural stability could potentially have an impact on an individual's ability or safety in performing balance-intensive tasks following a period of standing, particularly if the task in question involved high risk (walking a narrow beam, working on unstable surfaces). Individuals who already have some balance deficit may be negatively impacted by a period of prolonged standing, and this should be a consideration when designing and implementing task rotation in the workplace.

The increase in right lateral bending of the relative trunk angle during RSLS following standing exposure may have been a compensation to decrease the moment arm for the right gluteus medius by centering the trunk mass more directly over the stance limb.

CONCLUSIONS

Prolonged standing exposures may have a negative impact on balance responses and the ability to resist lateral bending loads during balance challenges. These findings may not preclude prolonged standing from being a viable task component of job rotation except in certain high-risk scenarios. These factors should be considered when designing job rotation order.

REFERENCES

1. Meijsen & Knibbe. *AORN*, **86**, 2007.
2. de Oliveira Sato et al. *Applied Ergo*, **40**, 2009.
3. Andersen et al. *Arthritis & Rheum*, **56**, 2007.
4. Cholewicki & McGill. *J Biomech Eng*, **117** 1995.
5. Brown & Potvin. *Hum Movement Sci*, **26**, 2007.

JOINT CONTRIBUTION TO FINGERTIP MOVEMENT DURING DIRECTIONAL TAPPING

[1]Jin Qin, [1]Matthieu Trudeau and [1]Jack T. Dennerlein

[1]Harvard University, Boston, MA, USA
email: jax@hsph.harvard.edu

INTRODUCTION

Computer use has often been associated with upper extremity musculoskeletal disorders (UEMSDs). The prevalence of UEMSDs in the shoulder and neck region among computer users is even higher than the hand/arm region [1,2,3]. Previous biomechanical studies of computer users have been limited to the study of finger and wrist joint, movement in the sagittal plane, or tapping on a single key switch [4,5,6]. The goal of this study was to compare the biomechanical loading on the proximal vs. distal joints by calculating the contribution from the finger, wrist, elbow and shoulder joints to fingertip directional movements in three-dimensional (3-D) space.

METHODS

Six young (mean (sd) age 28.3 (±2.0) years) adults, three women and three men tapped on a stand-alone number keypad with their right index finger at the speed of 3 taps per second. Participants tapped in three conditions: (1) on a single key-switch (the number key 5); (2) in a left-right direction (back and forth on the number key 4, “left”, and 6, “right”); (3) in an up-down direction (back and forth between the number key 2, “down”, and 8, “up”). No forearm or palm support was provided.

Three-dimensional kinematics of the upper extremity were recorded using an active-marker infrared motion analysis system (Optotrak Certus System, Northern Digital, Ontario, CN). Four clusters of three markers secured on a rigid plate were mounted on the hand, forearm, upper arm and torso. A single marker was attached on the fingertip of the right index finger. Locations of these markers in 3-D space were recorded at 200 samples per second. All kinematic data were low pass filtered digitally using a forth order Butterworth filter with a cutoff frequency of 10 Hz and a zero phase shift. The finger was approximated as a single segment with the length spanning the metacarpophalangeal (MCP) joint center to the fingertip.

The MCP, wrist, elbow and shoulder joint contributions to the fingertip movement were calculated by multiplying the relevant joint excursion with the effective moment arm of the fingertip about the joint axes. First the vector from the joint rotation center to fingertip was calculated, and the effective moment arm was the vector projection to the plane that was perpendicular to the rotating axis. The coordinate axes orientations were as follows: anterior (+) and posterior (-) of the x axis, medial (+) and lateral (-) of the y axis, and superior (+) and inferior (-) of the z axis. Fingertip movement was defined as the distance moved in 3-D axis from the maximum position on the z axis to the maximum force applied on the key switch.

RESULTS AND DISCUSSION

Joint contributions to fingertip movement in the z direction (vertical) were similar between single key and left-right tapping, and the wrist contributed the most among all the joints (Figure 1). Joint contributions to fingertip movement changed substantially for up-down tapping. The shoulder and the MCP joints produced the most fingertip vertical movement for the “down” keystrokes. The wrist and elbow joints contributed positively (fingertip movement due to the joint was in the same direction as the measured fingertip movement) while the shoulder contributed negatively to the fingertip vertical movement for the “up” keystrokes. For fingertip movement in the y direction, shoulder and wrist were the major contributing joints, while the shoulder was the dominant contributing joint for fingertip movement in the x axis.

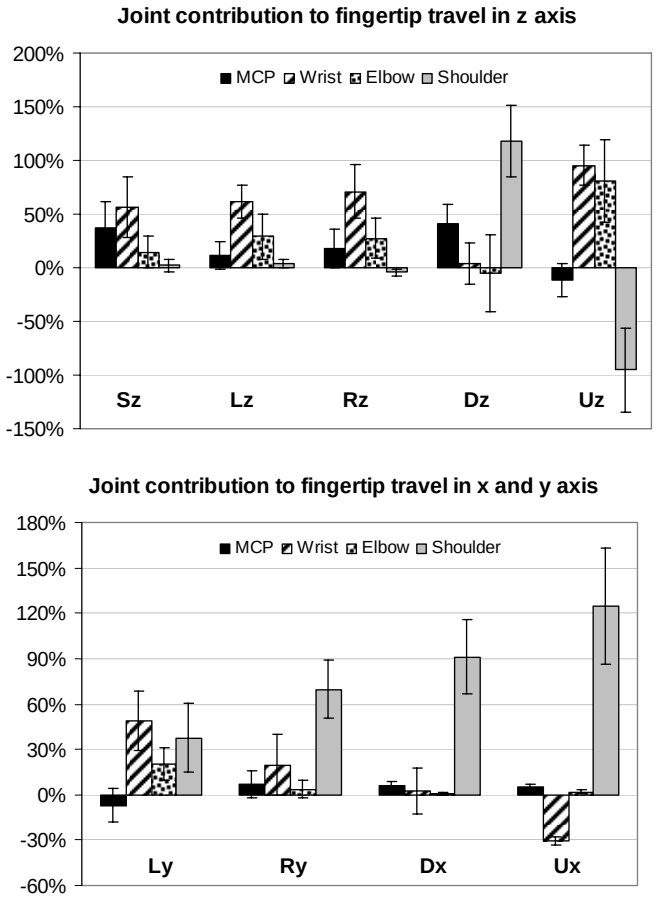

Figure 1: Percentage of joint contribution to fingertip three-dimensional movement averaged across subjects for the three experimental conditions. S – single key switch, L – left, R – right, D – down, U – up.

The various contributions across the different tapping conditions were consistent with the joint constraints and anthropometric characteristics of the upper extremity kinematic structure. We have modeled the upper extremity with four rigid segments with joints that limit the degrees of freedom to nine. In the typing postures with the forearm fully pronated and the elbow flexed at a right angle, all joints contribute to almost pure vertical movement of the fingertip through flexion and extension except for the shoulder, which produced both vertical and forward/backward motion in the x axis of the fingertip. During the up-down movements, the system takes advantage of the shoulder flexion/extension to move the finger along the x axis.

During the "down" keystrokes, the wrist contributed very little to the vertical movement but the shoulder contributed significantly. During the "up" keystrokes, pure shoulder flexion contributed to fingertip movement in the positive x and z directions, therefore the wrist and the elbow joints flexed in order to keep the fingertip on the same horizontal level as the keypad. For the left-right movements, abduction/adduction of the wrist and shoulder as well as internal/external rotation of the shoulder moved the fingertip to the two locations.

CONCLUSIONS

This study determined the MCP, wrist, elbow and shoulder joint contribution to fingertip movements in 3-D space. The upper extremity was modeled as a nine-degrees-of-freedom system while tapping at three conditions. During single key switch tapping, MCP and wrist contributed the most to fingertip vertical movement, while the shoulder joint became the dominant contributing joint during directional tapping, especially in up-down movements. These findings provide evidence for the increased biomechanical loading on the proximal joint from single key tapping to directional tapping.

REFERENCES

1.Gerr F, et al. *Am J Ind Med* **41**, 221-235, 2002.
2.Klussmann A, et al. *BMC Musculoskel Dis* **9**, 96-112, 2008.
3.Eltayeb S, et al. *BMC Musculoskel Dis* **8**, 68-79, 2007.
4.Serina ER, et al. *Ergonomics* **42**(7), 938-951, 1999.
5.Baker NA, et al. *Clin Biomech* **22**, 32-43, 2007.
6.Dennerlein JT, et al. *J Biomech* **40**, 3013-3022, 2007.

BIODYNAMIC MODELING AND PHYSICAL CAPACITY ASSESSMENT OF HUMAN ARM RESPONSE IN EXPERIENCED TORQUE TOOL OPERATORS

Haluk Ay[1], Carolyn M. Sommerich[2], Anthony F. Luscher[1], Rajiv Gumpina[2]
[1] Department of Mechanical Engineering
[2] Department of Integrated Systems Engineering
The Ohio State University

INTRODUCTION

The objective of this study was to develop and validate a new methodology for characterizing the human arm's response to impulsive pulling forces based on a single degree-of-freedom, second-order, linear model. Such forces are encountered while operating right-angle torque tools, and are thought to pose a risk of injury [1,2]. Previously published research involved human testing in which subjects, instructed to stabilize an underdamped mechanical system released from a non-equilibrium initial position, were subjected to an oscillating torque input [3]. This task differs from using a torque tool where the input is an impulsive torque with typical durations of 35 - 1000 *ms*, depending on stiffness of the fastened joint. Because human arm viscoelasticity is task-dependent [4], the new parameter assessment method was designed to more closely mimic right-angle torque tool operation. Testing was conducted with experienced torque tool operators. Effects of gender and working posture were examined.

METHODS

In order to validate the model and assess effective stiffness (*k*), mass (*m*) and damping (*c*) parameters, a novel apparatus (Fig. 1) and protocol were developed to test human subjects.

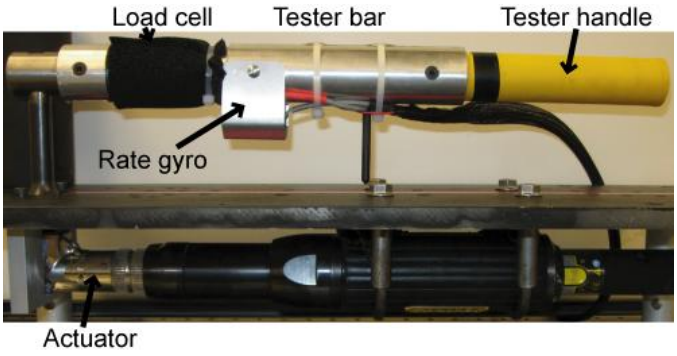

Figure 1: Physical appearance of the test apparatus.

A tester bar with textured handle on one end was connected to a fixed rotational actuator at the other end. The tester bar was instrumented with strain gages and a rate gyro in order to measure handle force and angular velocity, respectively.

Subjects were instructed to hold the handle stationary and prevent its horizontal rotation to the best of their ability, while a software-controlled sinusoidal torque pulse of 24 *Nm* amplitude and 233 *msec* duration was generated at the actuator and applied to the tester bar. Input torque, handle force and handle displacement data were sampled simultaneously. The angular displacement and acceleration of the handle were calculated using numerical integration and differentiation of the velocity signal, respectively.

Human arm response was modeled as a linear, single degree-of-freedom, second-order system with effective *k*, *m*, and *c* elements to be identified (Fig. 2).

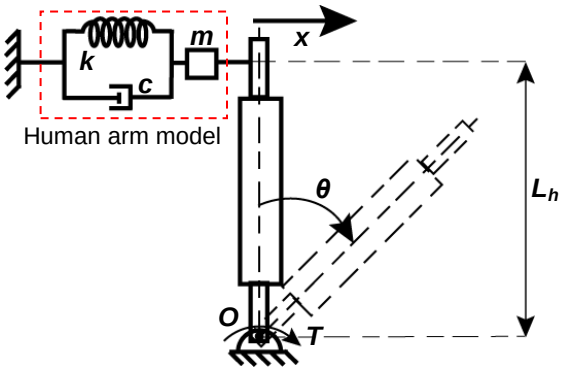

Figure 2: Description of the system model.

Equations (1) through (4) describe the system dynamics of the model:

$$T = K\theta + C\dot{\theta} + M\ddot{\theta} \quad (1)$$

$$K = kL_h^2 \ (2), \quad C = cL_h^2 \ (3), \quad M = mL_h^2 + I_O \ (4)$$

The system identification problem was set up with the torque applied by the actuator (*T*) as input and

handle angular displacement (θ) as output. *K*, *C*, and *M* denote the stiffness, damping, and mass values of the combined system of human and the tester bar. These parameters are related to the human arm *k*, *c*, and *m* through the measured tester bar handle length (L_h) and mass-moment of inertia with respect to the fixed pivot point *O* (I_O). The least-squares method in the time domain was used to identify system parameters based an input-output relationship-type approach [5].

The identified model parameters were validated in two ways. (a) The identified model was simulated with the same torque input in order to reproduce handle displacement. The reproduced handle displacement was then compared to the experimentally measured handle displacement data. (b) The handle reaction force (F_r) profile was calculated using equation (5) and compared to the strain gage measurement.

$$F_r = L_h\left(k\theta + c\dot{\theta} + m\ddot{\theta}\right) \quad (5)$$

As a first test of the newly developed parameter assessment methodology, physical capacity assessment experiments were performed with experienced tool operators. Subjects were asked to apply maximum effort in order to minimize horizontal rotation of the tester bar while standing in five different working postures.

RESULTS AND DISCUSSION

The reproduced displacement and calculated force profiles compared well with the experimental data. The linear model was appropriate for 93% of the 897 test trials; average difference in displacement peak time was 2.8 ms (sd=2.6; max. difference limit set to +/-12 ms = 10% of displacement duration). Average relative peak force error was 6.1% (sd=4.6%); an additional 5 trials were excluded because the force error was 20-25%. Fig. 3 provides sample results comparing measured handle force and displacement profiles to those calculated based on the identified model. In this example, the difference between measured and reproduced peak handle displacement times was 2 *msec*. The measured and calculated peak handle forces were 63.09 *N* and 66.77 *N*, respectively.

As expected, (*k*, *m*, *c*) parameters were affected by gender and posture. Peak handle displacement was found to vary with respect to *k*, *m*, and *c*, whereas peak handle force was not.

Additionally, the newly developed parameter identification methodology is directly applicable to characterize arm response while using an actual DC-torque tool, if instrumented with a rate gyro.

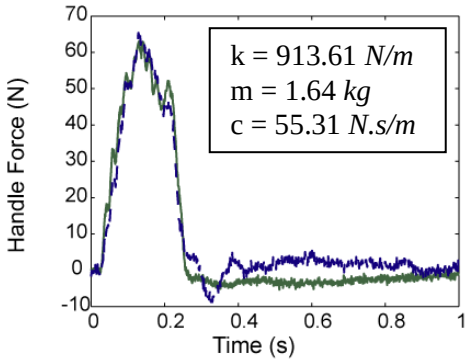

(a) Measured (green-solid) and calculated (blue-dashed) handle force.

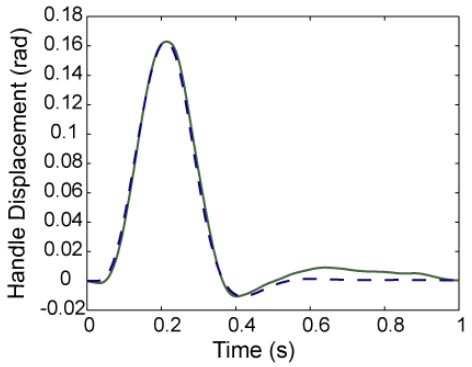

(b) Measured (green-solid) and reproduced (blue-dashed) handle displacement.

Figure 3: Sample results showing model validation**.**

REFERENCES

1. Kihlberg S, Kjellberg A, Lindbeck L. Discomfort from pneumatic tool torque reaction. *International Journal of Industrial Ergonomics*. 1995; 15: 417-26.

2. Ku C-H, Radwin R-G, Karsh B-T. Power hand tool kinetics associated with upper limb injuries in an automobile assembly plant. *Journal of Occupational and Environmental Hygiene*. 2007; 4: 391-399.

3. Lin J-H, Radwin R-G, Richard T-G. A single-degree-of-freedom dynamic model predicts the range of human responses to impulsive forces produced by power hand tools. *J Biomech*. 2003; 36: 1845-52.

4. Frolov A-A, Prokopenko R-A, Dufossè M, Ouezdou F-B. Adjustment of the human arm viscoelastic properties to the direction of reaching. *Biol Cybern*. 2006; 94: 97-109.

5. Eykhoff, P., 1974, *System Identification: Parameter and state estimation*. (London: John Wiley & Sons).

ASSESSMENT OF ARM DYNAMICS IN EXPERIENCED WORKERS WHILE OPERATING RIGHT-ANGLE TORQUE TOOLS

Haluk Ay[1], Carolyn M. Sommerich[2], Anthony F. Luscher[1], Rajiv Gumpina[2]
[1] Department of Mechanical Engineering
[2] Department of Integrated Systems Engineering
The Ohio State University

INTRODUCTION

The objective of this study was to identify the parameters of a single degree-of-freedom, linear, second-order model describing human arm dynamics while operating right-angle DC torque tools. A newly developed and validated assessment methodology for characterizing arm response to impulsive pulling forces was employed [1], in order to better understand the risk to workers who use these tools in repetitive, assembly line manufacturing operations [2].

Previously published research investigating the same problem used an underdamped mechanical system to estimate tool operator effective stiffness (k), mass (m) and damping (c) parameters in physical capacity assessment experiments [3], and then scaled the stiffness parameter based on normalized muscle activity in the forearm [4].

In the current study, k, m, and c parameters were directly calculated based on experiments conducted with experienced operators using commercially available, computer-controlled DC-type torque tools. Bundled with their computer controllers, these tools enabled closed-loop, microprocessor-based torque and speed control. The controllers could implement a variety of programmable tightening algorithms and they could also output the spindle torque and position signals for external use.

Effects of target torque, tightening algorithm, joint rate, gender, and working posture on arm response were examined.

METHODS

Experienced operators from the automobile industry were tested with three different Stanley™ brand DC-type tools in order to determine their k, m, and c while using right-angle torque tools. The tools' properties are given in Table 1. The mass moment of inertia of each tool with respect to its head (I_H) was determined using the bifilar pendulum method. Tools A and B were instrumented with a rate gyro to measure tool angular velocity; tool C (Fig.1) was instrumented both with a rate gyro and a custom load cell to measure handle reaction force as well.

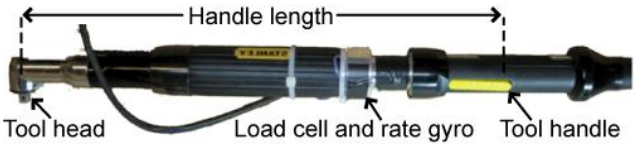

Figure 1: The physical appearance of tool C.

In the experiments, subjects were asked to tighten joints while holding the tool with one hand at either end of the tool (tool rotated away from the operator in the horizontal direction; Fig. 2); five standing work postures were tested. Medium-hard (MH: 90-100 deg.) and medium (M: 300-320 deg.) joint rates were achieved with a custom designed oil-filled joint simulator attached to a stand configurable in three-dimensional space (Fig. 2).

Figure 2: Joint simulator (left), configurable stand (middle) and the appearance of a male subject tested (right).

The method implemented in order to determine and validate k, m, and c parameters is described in Ay *et al.* [1]. It is based on providing a torque impulse (Fig. 3a) which the test subject reacts against while trying to minimize rotational handle displacement. The validation is in terms of the reproduced handle displacement and calculated force based on the identified model parameters, and for tool C measured force.

The input torque was measured with the respective tool's embedded torque transducer and sampled by the tool controller. The output handle displacement was calculated using numerical differentiation of the handle velocity signal, measured with a rate gyro affixed to the tool. Both input and output data were sampled simultaneously.

RESULTS AND DISCUSSION

Reproduced handle displacement and calculated peak force compared well to experimental data within the displacement build-up period (marked in Fig. 3b). Evaluation criteria, time to peak displacement, peak displacement and peak force values (latter calculations only available for tool C), were within 10%, 1% and 10% relative error, respectively.

A sample result comparing measured and reproduced displacement profiles is given (Fig. 3b). Subjects were observed to tend to pull the tool handle towards them during the joint run-down phase before the tool torque started building up.

Sample results of measured and calculated peak force values are provided (Table 2). While peak handle displacement was found to correlate with *k* and *c*, peak handle force was not affected by identified model parameters for the same joint rate and tightening algorithm.

Subjects operated the tools with 50% to 80% of both stiffness and damping capacities assessed in a previous phase of the research. This was contrary to the previously published research that assumed only stiffness scaled with respect to that of maximum capacity [4]. The *k*, *m*, and *c* parameters were affected by gender and posture, consistent with prior research.

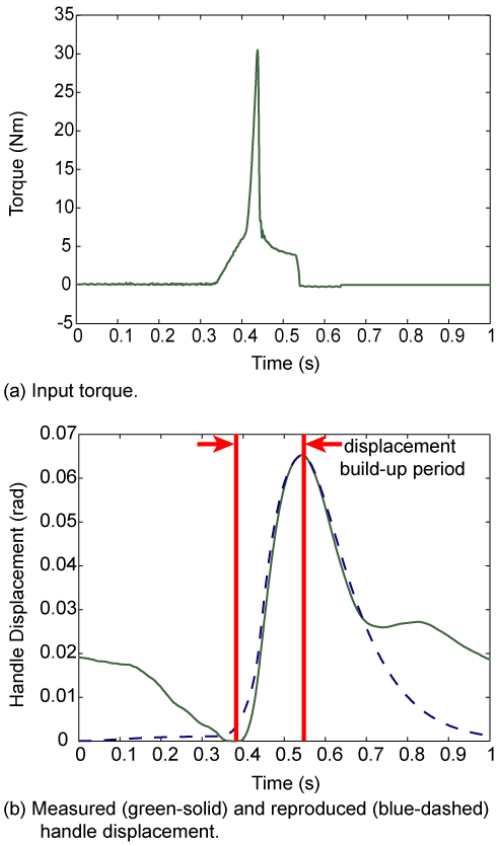

Figure 3: Sample result showing (a) input torque, (b) model validation based on displacement.

REFERENCES

1. Ay, H., Sommerich, C.M., Luscher, A.F. and Gumpina, R, 2010, Biodynamic modeling and physical capacity assessment of human arm response in experienced torque tool operators. *34th Annual Meeting of the ASB* (submitted).
2. Ku C-H, Radwin R-G, Karsh B-T. Power hand tool kinetics associated with upper limb injuries in an automobile assembly plant. *Journal of Occupational and Environmental Hygiene*. 2007; 4: 391-399.
3. Lin, J.H., Radwin, R.G. and Richard, T.G., 2001, Dynamic biomechanical model of the hand and arm in pistol grip power handtool usage. *Ergonomics*, **44,** 295-312.
4. Lin, J.H., Radwin, R.G. and Richard, T.G., 2003, Handle dynamics predictions for selected power hand tool applications. *Human Factors*, **45,** 645-56.

Table 1: Physical properties of the DC torque tools used in the experiments.

Tool Name	Model	Target Torque (*Nm*)	Handle Length (*m*)	Mass Moment of Inertia with Respect to Tool Head (*kg.m^2*)	Instrumentation
A	E44LA19-70	60	0.454	0.154	Rate gyro
B	E33LA14-33	33	0.400	0.070	Rate gyro
C	E33LA14-33	33	0.463	0.093	Load cell and rate gyro

Table 2: Sample results of measured and calculated peak force values together with the identified model parameters.

Estimated Model Parameters					Peak handle force (*N*)	
Stiffness (*N/m*)	Mass (*kg*)	Damping (*N.s/m*)	Joint rate	Tightening Algorithm	Measured	Calculated
278.27	1.576	50.20	MH	ATC™	66.69	63.76
889.41	3.524	60.20	MH	ATC™	65.78	66.30
1501.6	4.231	23.72	MH	ATC™	63.52	60.83

Thumb Motor Performance Varies by Movement Orientation and Direction during Mobile Phone Use

[1]Matthieu Trudeau, [1]Tawan Udtamadilok and [1, 2]Jack Dennerlein

[1]Harvard School of Public Health, [2]Harvard Medical School, Boston, MA, USA
email: mtrudeau@hsph.harvard.edu

INTRODUCTION

Mobile phone subscribers have increased by 25% annually over the past 8 years, but gains in quantifying and addressing issues with usability have not made as much progress [1]. Karlson et al. [1] assessed the difficulty of one-handed cell phone tapping tasks by calculating the time it takes to move the thumb from one area of a device to another. However, a user's performance in a task is dependent not only on speed but also on precision [2]. This study aims to determine the effects of movement orientation and direction during single handed mobile phone use on motor performance of the thumb as described by Fitts's Law metrics [2, 3]. These findings could be used to inform placement of interaction targets to improve overall usability by increasing accuracy and input efficiency.

METHODS

Twenty right-handed participants (15 male, 5 female) completed a reciprocal thumb tapping task on four mock ups of typical mobile phone designs (Small, Flip, Large, PDA). The keys were 15 mm in diameter. For each trial, participants tapped between two keys on the phone as quickly as possible for 5 seconds. Different travel distances were achieved by skipping over one or more keys. Different orientations were defined by the location of the two keys specified for each trial and were categorized as left-right (LR), northeast-southwest (NESW), northwest-southeast (NWSE), and up-down (UD). In addition, each movement was categorized by direction of the thumb movement. "Outward" movements of the thumb were defined as abduction and extension movements, and included the following directions: D→U, SE→NW, R→L, and NE→SW. "Inward" movements of the thumb were defined as adduction and flexion movements, and included the following directions: U→D, NW→SE, L→R, and SW→NE.

The 3-D position of the tip of the thumb relative to the mobile phone was measured using an active-marker motion capture system (Optotrak, Northern Digital Inc.). Based on this data, taps were identified as the minimums of the thumb's vertical position. For each tap, the movement time (MT) was defined from the previous tap to the current tap and the movement distance (A) was defined as the vertical distance between the current tap and the previous tap. For each movement orientation and direction, participant mean values for MT and A were calculated. In addition, the precision was defined as the effective width (W_e) of the target as

$$W_e = 4.133(SD)$$

where SD is the standard deviation of the thumb marker location about the mean value for all the taps associated with a movement orientation and direction [3]. From the movement times (MT), distances (A) and effective widths (W_e), the effective index of difficulty ($ID_e = \log_2(2A/W_e)$) and index of performance ($IP_e = ID_e/MT$) were calculated. In addition, the average speed of the movement (MS = A/MT) was calculated.

A 1-way repeated measures ANOVA was used to determine the main effects of device, movement orientation and movement direction on the motor performance parameters. A post-hoc Tukey's HSD test was used to determine if differences between the parameters for each orientation were significant.

RESULTS AND DISCUSSION

The motor performance parameters varied significantly across the orientations with the NESW movement providing the best metrics overall. MT

was found to be significantly higher for the NWSE orientation compared to the NESW orientation (Table 1). Thumb performance (IP_e) was found to be significantly higher for the NESW orientation compared to all the other orientations, and therefore it yielded the best results when both precision and speed were accounted for. This result suggests that thumb performance is significantly higher for abduction/adduction orientations as opposed to flexion/extension orientations, which could be explained by the fact that fewer degrees of freedom are involved in performing abduction/adduction, leading to greater efficiency.

In addition, the performance varied across target direction with "outward" movements of the thumb (either extension or abduction) performing better. Movements that involved an "outward" movement of the thumb had a significantly higher IP_e (14.2(0.48)) compared to "inward" movements (13.1(0.48)). Some of the "inward" movements often required a large amount of flexion of the thumb's IP & MCP joints and extension of the CMC joint. This posture may require more co-contraction of agonist and antagonist muscles due to influence by passive properties of muscles and connective tissues. As a result the capability of fine motor control in this awkward posture may be slightly compromised. The "outward" movements may be associated with more neutral postures, where the motor control is assisted by the conservative nature of passive forces to restore posture back to neutral. The difference in IP_e between "inward" and "outward" movements was smaller for the movement orientations that rely on more abduction/adduction of the CMC joint (NESW: 15.20(0.49) and UD: 13.95(0.48)) than on flexion/extension (NWSE 13.16(0.49) and LR 12.46(0.49)). This further supports the idea that the reciprocal flexion/extension posture of the thumb may be the reason for poorer performance.

CONCLUSIONS

Diagonal movements of the thumb that rely primarily abduction/adduction of the thumb provide the best overall performance whereas the "inward" movements that require reciprocal flexion/extension movements with more multi-articulate musculature provided the least performance.

REFERENCES

1. Karlson et al., *National Research Council of Canada Institute for Information Technology*, **1**, Hershey, PA, USA, 86-101, 2008.
2. Fitts, P. M., *Journal of Experimental Psychology*, **47**(6), 381-391, 1954.
3. Douglas et al. *Proceedings of the ACM conference on Human Factors in Computing Systems '99*, New York, NY, USA, 1999.

ACKNOWLEDGEMENTS

This study was funded in part by NIOSH R01 OH008373, and the NIOSH ERC at Harvard University-grant (T42 OH008416-05). The authors also thank Amy K. Karlson and Benjamin B. Bederson from the University of Maryland (USA) for contributing the data that was used in this study.

Table 1: Mean (and Standard Error) values of motor performance metrics

Direction	LR ↔	NESW ⧄	NWSE ⧅	UD ↕	Interpretation
Movement distance (mm) [5th, 95th percentile]	20.3 [4.4, 33.7]	34.0 [20.5, 61.4]	29.2 [15.7, 57.4]	27.7 [12.8, 63.4]	Large is difficult
Movement Time (s)	0.29 (0.01)^{A}	0.30 (0.01)^{B}	0.32 (0.01)^{C}	0.29 (0.01)^{B}	Small is better
Movement Speed (mm/s)	73.2 (5.3)^{D}	116.5 (5.3)^{A}	90.8 (5.3)^{C}	94.0 (5.3)^{B}	Large is better
Effective Width W_e (mm)	4.0 (0.2)^{B}	3.8 (0.2)^{A}	3.8 (0.2)^{A}	3.8 (0.2)^{A}	Small is better
Index of Performance (bits/s)	12.5 (0.5)^{D}	15.2 (0.5)^{A}	13.2 (0.5)^{C}	14.0 (0.5)^{B}	Large is better

^{ABC} Performance measures are ranked where A>B>C>D. Observations not connected by the same letter are significantly different.

VERBAL ESTIMATION OF PEAK DYNAMIC HAND FORCES IN EXPERIENCED AND NOVICE MANUAL MATERIAL HANDLERS

David M. Andrews, Amber Phillips and Patricia L. Weir

University of Windsor, Windsor, ON, Canada
email: dandrews@uwindsor.ca, web: http://uwindsor.ca/kinesiology/dr-david-andrews

INTRODUCTION

Many biomechanical models require hand forces as inputs for determining various joint moments and forces resulting from work (e.g. spine compression). Quantifying hand forces during work using direct techniques (e.g. force transducers) can be intrusive and interfere with the work at hand or require mockups of actual tasks to be performed off-line. Previous work by Marshall et al. (2004) [3] evaluated the potential for having workers verbalize their exerted hand forces as a percent of their maximal effort following training on hand-intensive grasping tasks. Pushing and pulling tasks that involved gross trunk and upper extremity movements that were more representative of those characteristic of manual material handling (MMH) tasks have also been studied using verbalized hand forces [2] but only for novice manual material handlers. Therefore, the purpose of this study was to determine the accuracy of verbally reported peak dynamic hand forces for a variety of pushing and pulling tasks and to quantify the effect of training on performance for both novice and experienced manual material handlers.

METHODS

After training, 32 participants (16 novice (8 M, 8 F); 16 experienced (8 M, 8 F)) performed symmetric and asymmetric pushes and pulls at 3 different force levels (low (10%-30% MVC), med. (40%-60% MVC) and high (70%-90% MVC)) and three heights (knee, waist and head), against a wall-mounted pneumatic cylinder in series with a force gauge attached to a handle (Fig.1). Air pressure within the cylinder was adjusted via a solenoid, which controlled the magnitude of the hand forces required to move the handle. Participants were assigned to one of four training groups: 1) Novice MMHs, feedback on 50% and 100% MVC exertions for 16 push and pull tasks; 2) Experienced MMHs with same feedback and tasks as group 1; 3) Novice MMHs, same feedback as groups 1 and 2, but for only 4 tasks; 4) Experienced MMHs, same feedback as groups 1, 2, and 3, but for only 4 tasks. During training, visual feedback of exertion levels during ramped contractions was provided on a monitor and each task was performed twice. After training, participants performed all 16 tasks without feedback and were asked to estimate their exertion levels and report them verbally as a % of maximal effort at the point when the handle began to move. Differences between the verbally estimated and the actual hand forces were quantified.

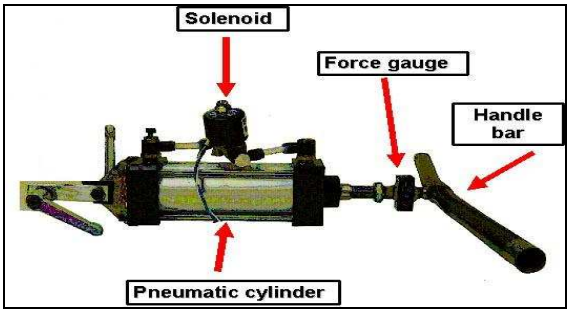

Figure 1: Dynamic hand force apparatus.

RESULTS AND DISCUSSION

Verbally estimated hand forces were similar across all four groups, even though two groups received training on 4 times the number of tasks (groups 1 and 2), and two groups consisted of participants with at least one year of MMH experience (groups 2 and 4) (Fig. 2). Participants were significantly more accurate at verbalizing pushes than pulls for two-handed tasks, but there was no difference for one-handed exertions. Participants were most accurate when reporting hand forces at the low force level for one-handed and two-handed tasks (errors of 10.2 %MVC and 9.4 %MVC, respectively). Eight regression equations were developed (e.g. Fig. 3) to

enable the prediction of actual peak dynamic hand forces from verbally estimated hand forces during one and two-handed push and pull tasks. Separate equations were generated for men and women, however, no significant differences were found in absolute error between the sexes. A strong relationship between actual and verbally estimated hand forces was indicated by the fairly high adjusted R^2 values (range from 0.55 for female two-handed pulls and 0.79 for male one-handed pulls).

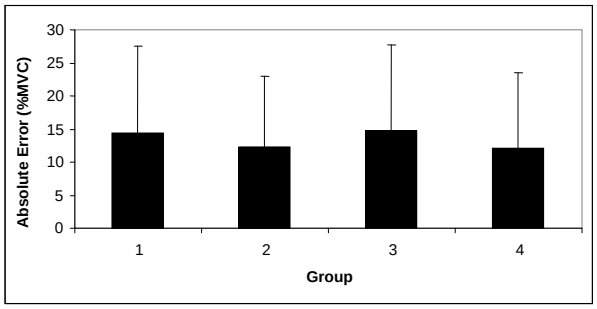

Figure 2: Mean (SD) absolute error (%MVC) between actual and verbally estimated peak dynamic hand forces for the four training groups.

The amount of error in verbalized hand forces did not improve with more feedback during training. While it is generally agreed that some level of training is a necessary step in psychophysical methods [1], the results here suggest that less training was sufficient for this type of activity. Less training makes this method more practical for field use.

The experience level of the participants also didn't have any significant effect on verbalized hand force estimates. The experts had a mean of 6.4 (4.6) years (range 2-20 years) of experience in MMH (job titles included general labourer, factory worker, and landscaper). It is possible that the unique and constrained nature of the lab-based pushing and pulling tasks used in this study were actually fairly novel for all participants, such that the participants in the experienced groups were not able to utilize the expertise they have developed over time. Additional training beyond what was provided here might be necessary before clear differences are seen between novice and experienced participants using this methodology.

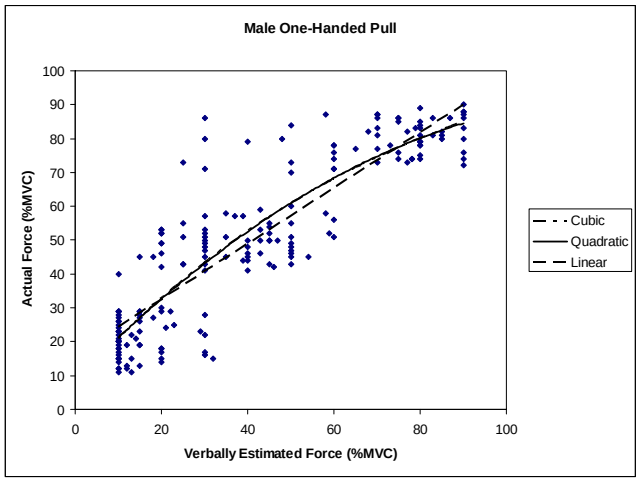

Figure 3: Scatter plot of actual and verbally estimated peak dynamic hand forces (% MVC) for male one-handed pulls.

CONCLUSIONS

This study suggests that less training is as effective as more training for obtaining verbalized peak dynamic hand forces using the developed system. Having workers verbalize their hand forces using this technique may be more convenient and less obtrusive than other more direct methods in the field and may help facilitate biomechanical analyses of tasks that are not feasible currently without physically interfering with the workers (e.g. nurses performing patient transfers). Establishing correction factors to adjust for errors in reported loads in field collections is an important next step.

REFERENCES

1. Andrews DM, et al., *Int J Ind Ergo*. **38**, 193-201, 2007
2. Burkhart TA, et al. *Proceedings of ISB 2009*, Cape Town, South Africa, 2009.
3. Marshall M, et al. *Human Factors*, **46(4)**, 697-710, 2004.

ACKNOWLEDGEMENTS

Thanks to AUTO21 for funding this project and to Don Clarke for his technical expertise.

PRESSURE ON THE KNEE WHILE PERFORMING A LATERAL LIFT FROM KNEELING POSTURES

Alan G. Mayton, CMSP, PE, Jonisha P. Pollard, MS, William L. Porter, MS, Susan M. Moore, PhD

National Institute for Occupational Safety and Health (NIOSH)
Office of Mine Safety and Health Research, Pittsburgh, PA
email: AMayton@cdc.gov, web: http://www.cdc.gov/niosh/mining

INTRODUCTION

Mine workers are restricted to kneeling, squatting, stooping, or crawling postures throughout their entire shift in low-seam (<42") and mid-seam (43" to 60") coal mines. In 2007, the Mine Safety and Health Administration (MSHA) database reported 84 knee injuries for seam heights between 30" and 54" which translates to an estimated $1.1 million using cost data from low-seam mine injury claims [1]. Significant injury risk is apparent when performing work with prolonged kneeling with sustained high forces on the knees [2]. Forces applied to the knees may also rise and decline rapidly when working (e.g. reaching for tools, moving materials) in kneeling postures. Moreover, the measurement of static pressure does not adequately reflect the high forces experienced during dynamic kneeling work tasks [2]. To enhance understanding of occupational kneeling and provide data to be used in the design of interventions (e.g. kneepads), mean pressures on the knee were estimated for kneeling and transferring a load laterally, a common mining practice.

METHODS

Seven subjects (5 male, 2 female), with no prior kneeling experience, volunteered to simulate three kneeling postures for a lateral lifting task that required twisting at the waist. Subject age varied from 20 to 60 years with a mean age (± SD) of 36 (±18) years. Subjects were screened for knee conditions, and no subject reported ever having serious injury or knee surgery. The test postures were kneeling: in full flexion (Near Full – sitting on heels), at 90° knee flexion (Near 90), and with only the right knee down (One Knee). These postures were simulated for work performed at a 48" vertical height, which restricted the subjects' posture.

A custom-made capacitive pressure sensor with 196 sensing units (0.22" by 0.48") was used (PPS, Los Angeles, CA). The sensor was pre-shaped to the knee at 90° flexion, 7" wide by 13.8" long with an active area of 4.6" by 8.3". Gaps between sensing units ranged from 0.065" to .322" with larger gaps in the curved portion of the sensor. Pressure data were collected at a variable sampling rate of approximately 5 Hz. Subjects were instrumented with reflective markers and motion data were recorded at a frequency of 60 Hz using the motion capture system (Motion Analysis Corporation, Santa Rosa, CA). Ground reaction forces were measured at a frequency of 1020 Hz using a force plate (AMTI, Watertown, MA), read through an analog-to-digital board (National Instruments, Austin, TX), and recorded using the motion capture software (EvaRT, Motion Analysis Corporation, Santa Rosa, CA). Pressure, force and motion data were synched through the motion capture software.

This data collection process was part of a larger study in which static postures were also investigated [3]. The peak pressures observed for these lateral lifting tasks, however, far exceeded the maximum calibrated pressure (35 psi) of the individual sensing units. Thus, to estimate the mean pressure applied to the knee, the ground reaction force at the right knee was divided by the active contact area of the sensor (total area of sensing units for pressure greater than the sensor threshold of 0.4 psi). Similarly, knee pressure was estimated for a 10 second static trial.

Prior to each trial, the pressure sensor was placed in a reference position and zeroed to eliminate any pressure artifact associated with the stretching of the sensor. Subjects were instructed to reach to their right to retrieve a 25 lbs block (shaped like a stopping/cinder block), bring it in front of their body, and then set it down on their left side in one

smooth motion. The block was instrumented with reflective markers to track its position.

Three stages of interest were isolated from these lifting tasks; when the block was picked up from their right side (BPU), when the block was directly in front of the subject (Block At Front - BAF), and when the block was placed down (BPD).

RESULTS AND DISCUSSION

Estimated mean pressure versus posture is shown in Figure 1 for the static trials that were collected as part of the larger study [3] and the three lifting stages. Similar results were found for the Near 90 and One Knee postures for all trials, as expected considering postural similarities. Estimated pressures increased in all postures when performing the lifting trial compared to the static trial. Drastic increases were noted in the Near Full posture during the lifting task. Highest mean pressures were seen at the BPU stage where estimated pressure exceeded 20 psi, which was more than four times the pressures estimated for the other postures. One reason for the notable differences in estimated mean pressure is smaller mean contact area. While forces for the Near Full posture were within 0.8 to 1.4 times the measured mean forces of the Near 90 and One Knee postures, the mean contact areas were 1.8 to 4.7 times *lower* for the Near Full posture. This is likely due to the contact of the tibial tubercle with the force plate when kneeling in full flexion.

When normalized to the static posture, estimated mean pressures for the Near Full posture exceeded those for the static trials by factors of 11, 8, and 5 for BPU, BAF, and BPD, respectively. An ANOVA showed posture was statistically significant ($p=0.003$) for normalized mean pressure. Differences in subject anthropometry and tubercle prominence may explain the wide variation in contact area, and thereby the variation in knee pressure for the Near Full posture.

Figure 1 also suggests the Near 90 and One Knee postures are preferred for lateral lifting. The mean pressure magnitudes during each stage of lift for these postures are similar to those during static kneeling. In considering a postural rotation strategy, these findings suggest that, in moving supplies with a lateral lift technique, workers should limit using the Near Full posture and instead use Near 90 or One Knee whenever possible. Observations have shown low-seam coal miners to most often use the Near Full posture. These miners routinely wear kneepads, which have been shown to aide in minimizing peak stresses on the knee while the mean pressure is not greatly affected [3]. Some limitations of this study included the effect on contact area estimates due to the size of the sensing units and associated gaps of the sensor and the inability to report peak pressures.

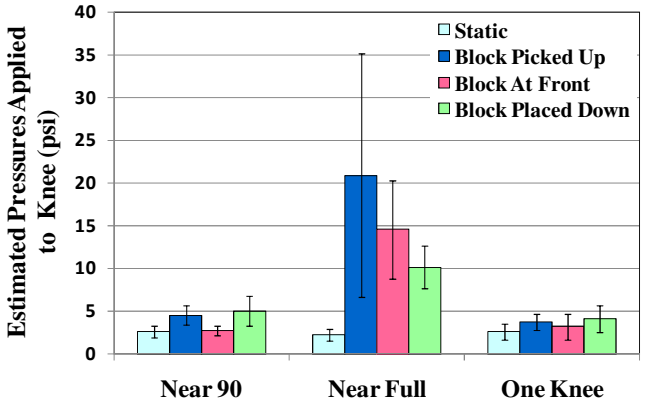

Figure 1: Estimated mean pressure for static trial and three stages of lifting task for each posture.

REFERENCES

1. Gallagher S et al. *Jour of Saf Res* **40**, 233-237, 2009.
2. Sharrard WJW. *Ann R Coll Surg Engl* **36**, 309-324, 1965.
3. Moore SM et al. *Proceedings - 33rd Annual Meeting of ASB '09*, Penn State University, August 26-29, 2009.

ACKNOWLEDGEMENTS

The authors thank Sean Gallagher of NIOSH for statistical support with this work.

DISLCAIMER

The findings and conclusions in this study are those of the authors and do not represent the views of NIOSH.

INDIVIDUAL DETERMINANTS OF STABILITY DURING LIFTING

Benoit Lussier, Alain Delisle, Felix Berrigan, André Plamondon and IRSST MMH research
University of Sherbrooke, Sherbrooke, Quebec, CAN
IRSST, Montreal, Quebec, CAN
email: alain.delisle@usherbrooke.ca

INTRODUCTION

Manual material handling (MMH) strategies adopted by workers are determinant for their safety. It could be postulated that workers not suffering from injuries have succeeded in adopting safe handling strategies through experience. Maintaining balance while handling a load, which can be seen as an external disturbance, is one important element for safe handling. High body mass index (BMI), because of its negative effects on balance control, imposes constraints on goal-directed movements [2] and should be taken into account when comparing subjects performing MMH. The aim of this study is to document the effect of experience in MMH on stability, while considering the influence of BMI on stability.

METHODS

Fifteen male experienced workers (age: mean = 38.1 yrs, SD = 9.8; years of experience in MMH: mean = 15.4 yrs, SD = 9.3) and 15 male novices (age: mean = 25.0, SD = 5.9; years of experience: mean = 0.5 yr, SD = 0.4) were volunteer for the study. There were 10 overweight (BMI>25 kg/m^2) experienced workers (BMI range: 25.1-33.7 kg/m^2), and 6 overweight novices (BMI range: 26.2-31.5 kg/m^2). All other workers' BMI was between 20 and 25. The task consisted of transferring four different types of box (3 boxes of 15 kg and one of 23 kg) from a conveyor to a hand trolley. Only the transfer of the 23 kg box on the pile of the three other boxes (96 cm high) was analyzed here. The distance between the conveyor and the trolley was 1.50 m. The handlers were free to choose their lifting techniques and there was no restriction on how to move. The only instruction given to the subjects was to handle the load the way they usually do. A large force plate and an optoelectronic system were used to measure ground reaction forces and whole body kinematics. Stability was assessed using the destabilizing force (F_d) that would need to be applied to the subject's centre of gravity in order to bring his center of pressure out of his base of support [1] expressed as:

$$F_d = \left| \frac{F_z}{H_{cg}} \right| B ,$$

where F_d is the destabilizing force, F_z the vertical ground reaction force, H_{cg} the height of the center of gravity including the load, and B the minimal distance of the centre of pressure to the contour of the base of support. A higher destabilizing force means a more stable subject. We computed the mean F_d during two distinct phases of the lift: the lifting phase and the deposit phase, delimited by the midpoint duration of the task.

RESULTS

During the lifting phase, there was no difference between groups on the mean F_d (Table 1, Fig. 1). Subjects with a smaller BMI showed a smaller mean F_d (less stable). There was no interaction between BMI and experience (Fig. 1).

Table 1: Group mean (SD) of the average F_d during the lifting phase

	Experienced	Novice	Total
Control	75.3	96.4	88.9
	(14.3)	(30)	(27)
Overweight	109.6	100.6	106.3
	(34.7)	(20.6)	(29.8)
Total	98.2	98.1	98.2
	(33.4)	(25.9)	(29.4)

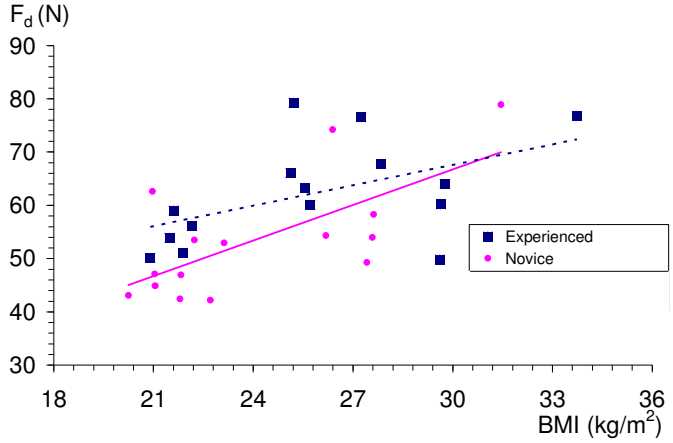

Figure 1: Mean destabilizing force (F_d) during the lifting phase in relation with body mass index (BMI).

During the deposit phase, there was a tendency for a larger F_d amongst experienced workers (Table 2, Fig. 2). Subjects with a larger BMI showed a larger mean F_d. However, a small interaction could be observed between BMI and experience (Fig. 2).

Table 2: Group mean (SD) of the average Fd during the deposit phase

	Experienced	Novice	Total
Control	54.1	48.4	50.4
	(3.6)	(6.8)	(6.3)
Overweight	66.4	61.5	64.6
	(9.1)	(12.1)	(10.2)
Total	62.3	53.7	58
	(9.7)	(11.1)	(11.1)

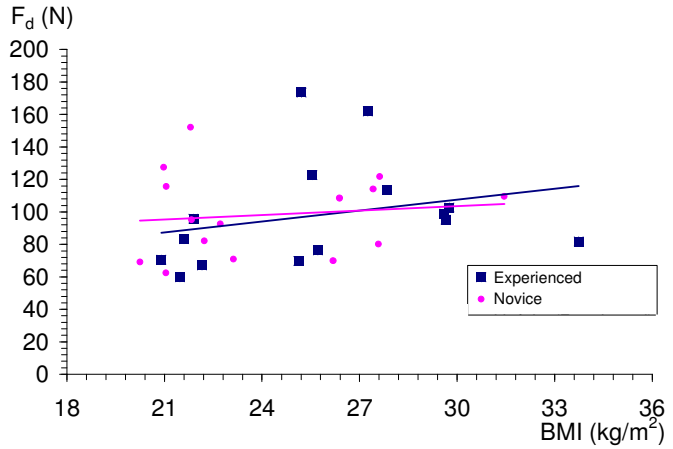

Figure 2: Mean destabilizing force (F_d) during the deposit phase in relation with body mass index (BMI).

DISCUSSION

The results from this study show that, although experienced workers appear to be more stable, their body mass index is a contributing factor to this stability. A larger body weight, a lower center of gravity, and a larger base of support all contribute to improve stability. Strategies adopted by workers while handling could influence both their base of support and the height of their center of gravity. Experience certainly determines these strategies, which can also be modified through training, but being overweight could also be determinant when adopting a lifting strategy.

The fact that overweight subjects are more stable, as assessed by the destabilizing force computed here, says nothing about the difficulty of controlling their balance neither about the difficulty that these subjects would face for recovering from a real loss of balance. Obviously, results observed from subjects with overweight can not be generalized to subjects with a BMI over 25 and especially obeses, which are more unstable than normal BMI subjects [3].

CONCLUSIONS

Both experience and body mass distribution could influence the handling strategy adopted by workers and are important for ensuring postural stability. Further research should address this issue.

REFERENCES

1.Delisle A., et al. *Clinical Biomech* **13**, 506-514, 1998.
2.Berrigan F., et al. *Intl J of Obesity* **30**, 1750-1757, 2006.
3. Hue O., et al. *Gait & Posture* **26**, 32–38, 2007

QUANTIFICATION OF DYNAMIC HUMAN SEATED SPINAL CURVATURES

Sam Leitkam, Tamara Reid Bush, PhD

Michigan State University, East Lansing, MI, USA
email: leitkams@msu.edu, reidtama@msu.edu

INTRODUCTION

Lower back pain (LBP) is a prevalent musculoskeletal dysfunction and costly societal problem [1]. Research has shown that the incidence of LBP caused by static seated postures can be reduced by promoting dynamic postural changes [2]. These postural changes are facilitated by chairs that support the human body through ranges of seated dynamic movement.

To develop chairs that support dynamic seated movements, a quantitative understanding of the interface between the human and the chair is required. One area of seat interaction is the seatback and of particular interest is the interface at the lumbar region. While several methods exist for quantifying lumbar curvature of a human in static standing postures, few exist for seated postures. Even fewer methods have the capability of capturing dynamic measurements while the subject's back is obscured by a seatback without requiring modification to the seat. One such method [3] was shown to predict lumbar curvatures from an anterior measure of the relative positions of the ribcage and pelvis for static postures.

The purpose of this research was to utilize the previously reported method to quantify the full range and trajectory of dynamic seated postures. These data can then be used to inform chair design and provide a means to test commercially available chairs that support dynamic postural change.

METHODS

Fifteen subjects (11 female, 4 male, with an average age of 23 (1.6) years) with no reported back pain or spinal injuries volunteered to participate in the research. Each subject was informed of the process and voluntarily provided signed consent.

A three-dimensional motion capture system (Qualisys, Gothenburg, Sweden) was used to quantify two different measures, the relative angular orientation of the subject's ribcage and pelvis, and the lumbar curvature of the subject. The measure between the ribcage and pelvis was referred to as the openness angle [4] while the lumbar curvature, quantified through a measure of a 3 point arc, was referred to as the lumbar angle (Figure 1).

To measure openness and the lumbar curvature, retro-reflective markers were attached to skin superficial to the sternum, anterior superior iliac spines (ASIS), lateral femoral condyles, seventh cervical vertebra (C7), twelfth thoracic vertebra (T12), and one midway between the posterior superior iliac spines (MidPSIS). Additionally, between T12 and the MidPSIS, markers were placed with a spacing of approximately 1 inch along the spinal column. The most eccentric marker between the T12 and MidPSIS markers was identified as LU.

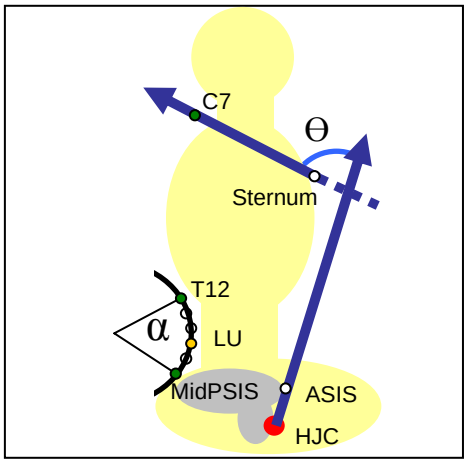

Figure 1. Diagram of seated subject showing markers at C7, T12, LU, MidPSIS, ASIS, and the sternum. Also showing the openness angle (Θ) and lumbar angle (α).

Subjects were seated on a stool and verbally queued through a continuous motion that started in a self-selected comfortable position. Upon initiation of

the test, subjects were asked to move to their maximum lordotic posture, then to their maximum kyphotic posture, and back to their original position in one continuous motion. Data were collected at 30 Hz for a total of 20 seconds.

For each subject, a time trace of the openness angles and lumbar angles were plotted with the openness angle as the independent variable and the lumbar angle as the dependent variable, Figure 2. A linear regression analysis was then performed on each subject's data.

The maximum and minimum values of openness angle and lumbar angle for each subject were also taken for comparison to previously collected static data.

RESULTS AND DISCUSSION

For the fifteen subjects the average r^2 value was 0.841. Figure 2 shows the same positive trend as the static data reported previously [3], i.e. a larger openness angle corresponds to a larger lumbar angle.

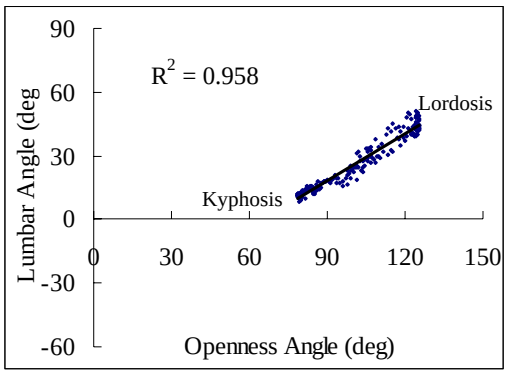

Figure 2. Sample plot of the dynamic motion occurring during seated postural change. The solid line represents a linear regression analysis of Openness vs. Lumbar Angle for a single subject.

However, it should be noted that while the data suggest the relationship between the two measures is linear, there were exceptions. Some subjects displayed a "loop" as seen in Figure 3. This suggests that while a linear relationship can generally fit the dynamic motion, in a practical sense, more elaborate models are necessary, and may need to occur on a subject by subject basis.

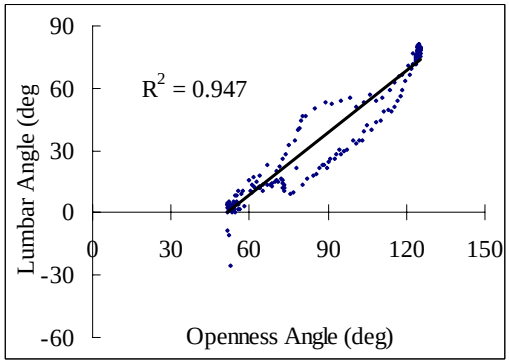

Figure 3. Sample Regression Analysis of Openness vs. Lumbar Angle for a single subject showing a "loop".

In addition, the ranges of motion for the dynamic tests were compared to the maximum kyphotic and lordotic data collected from static positions. Data in Table 1 show that in both the previous static and current dynamic cases, the openness and lumbar angles cover similar respective ranges. This shows that the dynamic data are consistent with previous findings while providing more information about the path of motion between maximum kyphotic and lordotic positions.

Table 1. Static and dynamic average range values for openness and lumbar angle

	Openness Angle (deg)			Lumbar Angle (deg)		
	Max	**Min**	**Range**	**Max**	**Min**	**Range**
Static Avg	**113.8**	**60.8**	**53.1**	**25.5**	**-16.0**	**41.5**
SD	16.4	15.4	15.4	25.6	6.9	25.3
Dynamic Avg	**110.3**	**62.0**	**48.3**	**32.7**	**-13.1**	**45.7**
SD	13.1	11.0	15.9	24.1	14.9	29.0

CONCLUSIONS

Results demonstrated that the lumbar angle as defined can measure and quantify a lumbar curvature through a dynamic range of motion. Additionally, the relationship between the openness angles and lumbar curvatures across a dynamic range of motion for a given subject can be approximated by a linear approximation. This work allows further characterization of the body seat interface for informing the design of seats.

REFERENCES

1. Lis A, et al. *Eur Spine J* **16**, 283 – 298,2007
2. van Dieen JH, et al. *Ergonomic* **44**, 739-750, 2001
3. Leitkam S, Bush TR *ASB, Penn State University*, 2009
4. Bush TR, et al. *Human Factors* **50**, 629-642, 2008

CENTER OF MASS POWER PROFILES FOR INDIVIDUALS WITH CEREBRAL PALSY

[1, 2] Michael H. Schwartz, [2] Adam Rozumalski

[1]University of Minnesota-Twin Cities, Minneapolis, MN, USA
[2]Gillette Children's Specialty Healthcare, St. Paul, USA

email: schwa021@umn.edu

INTRODUCTION

The mechanical work done by the trailing and leading leg on the body center of mass (COM) is an important determinant of the metabolic demands for normal gait [1]. Individuals with cerebral palsy (CP) require greater power to walk than their unimpaired peers, but little is known about the mechanical work performed by the legs of these individuals. Kurz observed differences in the COM power profiles of 10 children with CP compared to 10 typically developing matched controls [2]. In the CP group compared to the control group, he found that the lead leg performed more negative work and the trail leg less positive work during double support and the lead leg performed more positive work during single support. The purpose of the present study is to expand on the work of Kurz by examining the COM power profiles of a large group of individuals with CP walking at a wide range of self-selected speeds, and compare these to speed-matched controls.

METHODS

Subjects with a diagnosis of diplegic CP who had previously undergone barefoot gait analysis with consecutive force plate strikes were identified from the clinical database at our center. The barefoot control data had also been previously acquired for a study examining the effects of walking speed on gait [3]. Gait data had been collected using a 12 camera optoelectronic system and 4 force plates, and processed using the Vicon Plug-in-Gait model. The mechanical COM power was estimated from the gait data following Donelan [1]. Only trials with balanced positive and negative power (±15%) were analyzed. All data was nondimensionalized by $L^{nd} = L / L_{leg}$, $m^{nd} = m / m_{body}$, $t^{nd} = t \Big/ \sqrt{L_{leg} / g}$. Trials were categorized as belonging to one of three speed bins (v^{nd} = .300-.375, .375-.450, .450-.525) reasonably described as slow, free, and fast gait. Multiple trials within one speed bin from a single subject during a single test session were averaged.

Five components of the power profiles were selected for further examination, and computed as follows. For the lead leg, *collision* was computed as the negative work (integral of power) performed prior to 40% of the step, *pre-load* as the negative work done after 40%, *rebound* as the positive work done before70%, and *pre-push* (push-off preceding double-support) as the positive work done after 70%. For the trailing leg *push-off* was computed as the positive work performed during double support. *Total push* was computed as *pre-push* + *push-off*. A

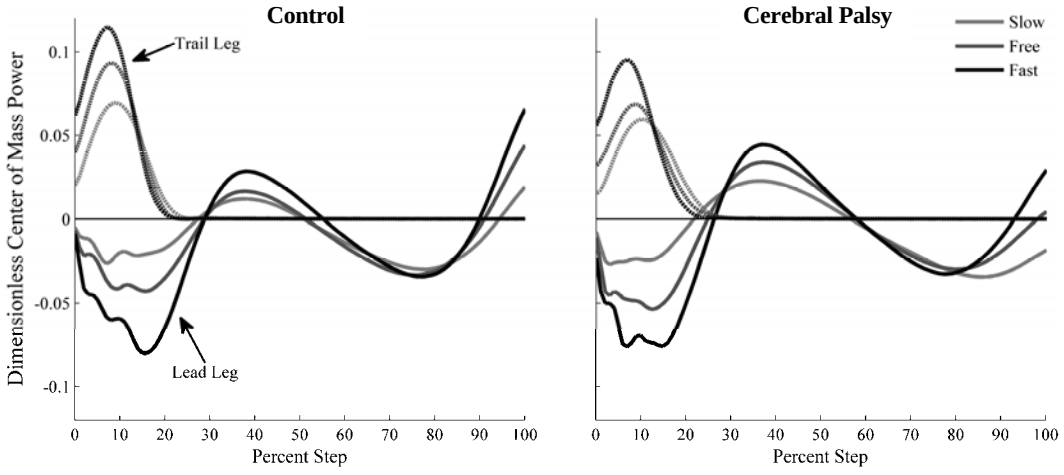

Figure 1. Power profiles at slow, free, and fast speeds for individuals with CP and speed matched controls. In the CP group, there is diminished lead leg power generation in late single stance (pre-push), and similarly reduced trailing leg push-off in double support. A larger than normal rebound work can be clearly seen, as well as subtle differences in the shape/timing of the collision power; with a more rapid onset of collision in the CP group.

general linear model with a Sidak adjustment for post hoc tests was performed to examine effects of group (CP vs. control), speed, and interactions between group and speed. Independent samples t-tests were then performed for each work component at each speed to assess differences between the CP and control groups controlling for speed.

RESULTS AND DISCUSSION

There were and 349 trials from 308 testing sessions involving 284 individuals (155 male, 129 female) in the CP group, with a mean (sd) age of 13.3 (5.9) years, height of 1.49 (0.17) m, and mass of 47.5 (20.0) kg. There were 123 trials from 83 individuals (48 male, 35 female) in the control group, with a mean (sd) age of 10.5 (3.5) years, height of 1.56 (0.21) m, and mass of 34.2 (9.6) kg.

The COM power profiles of the individuals with CP differed qualitatively from those of the control subjects [Figure 1]. Of particular interest was that individuals with CP lacked lead leg power generation prior to double support (pre-push) and had a more rapid onset of collision power.

The general linear model revealed significant main effects for all work components except pre-load. This unsurprisingly confirms that power profiles differ between individuals with CP and controls, and that speed affects power profiles. More interesting was the finding that total push and rebound had a significant interaction effect, implying a difference in speed dependency between the CP and control groups. Comparing work components between groups revealed that the CP group had a smaller pre-push, push-off and total push, and a larger rebound and total work at every speed [Table 1]. In contrast, collision work was only larger for the CP group during fast gait, and pre-load was only larger for the CP group at slow gait. These findings contrast slightly with those of Kurz. The current study examined faster speeds than Kurz's study. Also, in the previous study, the individuals with CP (and presumably the controls) walked in shoes; whereas all individuals in the present study walked barefoot. There is an intriguing implication that better shoe and/or orthosis designs could reduce collision work for individuals with CP.

The results of this study show that mechanical work done by the trailing and leading legs in children with CP differs from normal. Some of the differences may lead to an inefficient gait. For example, the failure of individuals with CP to generate push-off just prior to double support may necessitate a costly active rebound phase [1]. It is particularly intriguing and challenging to devise methods to test this hypothesis.

The reasons for the power profile differences between the CP group and controls are not clear. Possible causes include presence of kinematic gait deviations secondary to selective motor control deficits, weakness, instability, and poor proprioception. Future research should focus on finding the causes of the power profile differences, better understanding how these differences lead to increased metabolic demand for gait, and developing interventions (gait training, orthoses, etc…) that can correct the power profiles.

REFERENCES

1. Donelan JM *et al*. (2002) *J Exp Biol*, **205**:3717-27.
2. Kurz MJ *et al*. (2010) *Gait Posture*, **31**:347-50.
3. Schwartz MH *et al*. (2008) *J Biomech*, **41**:1639-50.

Table 1. Positive and Negative Independent Limbs Work Components as a Function of Dimensionless Speed

Walking Speed	Slow (.300 - .375)			Free (.375 - .450)			Fast (.450 - .525)		
Group	CP	Control	p	CP	Control	p	CP	Control	p
Trials	N=129	N=37		N=150	N=43		N=70	N=43	
Pre-Push (sngl. supp)	.001	.005	<.001	.004	.011	<.001	.009	.016	.001
Push-Off (dbl. supp)	.026	.033	.002	.029	.041	<.001	.036	.048	<.001
Total Push	.027	.037	<.001	.033	.052	<.001	.044	.064	<.001
Rebound	.031	.010	<.001	.045	.013	<.001	.066	.024	<.001
Collision	-.024	-.020	.192	-.045	-.037	.067	-.076	-.059	.041
Pre-Load	-.033	-.028	.047	-.032	-.030	.432	-.032	-.029	.447
Total Neg	-.057	-.048	.001	-.078	-.067	.001	-.108	-.088	.004
Total Pos	.058	.047	<.001	.078	.065	<.001	.110	.088	<.001

HABITUATION TO GALVANIC VESTIBULAR STIMULATION DURING GAIT

Jennica L. Roche, Daniel P. Steed and Mark S. Redfern

Human Movement and Balance Laboratory
University of Pittsburgh, Pittsburgh, PA, USA
email: jlr59@pitt.edu, web: http://hmbl.bioe.pitt.edu

INTRODUCTION

Balance requires the integration of proprioceptive, visual, and vestibular sensory inputs. Contributions from the vestibular system are increasingly important when other sensory signals are lacking or erroneous [1]. Galvanic vestibular stimulation (GVS), the application of a small electrical current across the mastoid processes, has been used to apply a stimulus to the vestibular system independent of vision and proprioception, thus allowing relatively easy isolation and control of the vestibular inputs into the postural control system.

When GVS is applied during stance, a whole-body lean towards the anode is observed due to a subconsciously perceived acceleration that results from firing rate changes at the vestibular nerve; however, adaptation as well as short-term and long-term habituation occurs as the stimulus is presented over prolonged periods [2, 3]. During gait, GVS produces a veering towards the anode, analogous to the response during stance, but the ability to adapt to such a vestibular stimulus during gait has not been clearly defined. We hypothesized that a habituation or adaptation process would occur within the dynamics of gait, similar to that seen in standing. Thus, the primary aim of this study was to identify the habituation processes to GVS during gait, and more specifically, to identify the effects of repeated exposure to GVS during gait.

METHODS

Nine healthy young adults (2F, 7M; mean age 25 ± 3.7 years) participated in this study. Subjects were free of neurological and vestibular disorders. Subjects were outfitted with tight fitting clothing, standardized 3/4 inch heeled shoes, and a safety harness.

Self-adhering stimulating electrodes (Superior Silver®, 3.17cm diameter) were affixed over each mastoid process in a binaural-bipolar configuration. Subjects were exposed during walking to a GVS stimulus consisting of two separate 5s square waves of alternating polarity (1mA), separated by 1s of no current. Only data during the first 5s of the current were analyzed. Prior to the gait trials, subjects were exposed to the same stimulus during quiet stance with their eyes closed at levels of increasing current (0.25, 0.5, and 1.0mA).

Subjects walked along an 8.5m walkway. Three-dimensional motion data were captured (120 Hz) by an eight M2-camera Vicon 612 motion capture system (Vicon Peak–UK). A forty-marker full body modified Helen Hayes marker set, including an additional reflective marker placed on top of the head, was employed ([4]; Vicon Motion Systems).

Kinematic marker data were used to calculate segmental angles and translations as dependent variables. A Vicon plug-in-gait model was utilized to determine the inter-segmental angles at the neck and lower spine as well as global segmental orientations of the head, thorax, and pelvis. Segmental deviations were calculated for the head, thorax, and pelvis in the frontal plane.

The independent variables included: GVS direction, gait phase of GVS trigger, and repetition. GVS direction was either anode right (R^+) or anode left (R^-). GVS trigger was either at heel contact (HC) or mid-stance (MS) with respect to the right foot. A total of four conditions were collected: R^+/HC, R^-/HC, R^+/MS, and R^-/MS. The order of the conditions was randomized within repetition.

RESULTS AND DISCUSSION

Analysis was performed using a four-way repeated measures ANOVA, with the model comprised of GVS direction (R^+, R^-), GVS phase trigger (HC, MS), trial order (1, 2, 3, 4), and repetition number (1, 2, 3). GVS direction was found to be significant for thorax tilt, pelvis tilt, and translations of the head, sternum, and pelvis (Table 1).

Table 1: Directional Significance

Angles		*Translations*	
Measure	P-value	Measure	P-value
Head	0.0612	Mid-Head	0.0465*
Thorax	0.0002*	Sternum	0.0305*
Pelvis	0.0175*	Mid-Pelvis	0.0302*
Neck	0.0970		
Spine	0.5329		

* indicates significance ($p<0.05$)

Despite pre-exposure to GVS, repetition effects were seen throughout the four conditions. The first repetition of each condition displayed a larger translational and rotational response than the second and third trials. However, no trial order effect was evident in any variable. The within-subject global deviations of the head, sternum, and pelvis were significantly larger in the first trial ($p < 0.05$), while the second and third trials showed no difference (Figure 1).

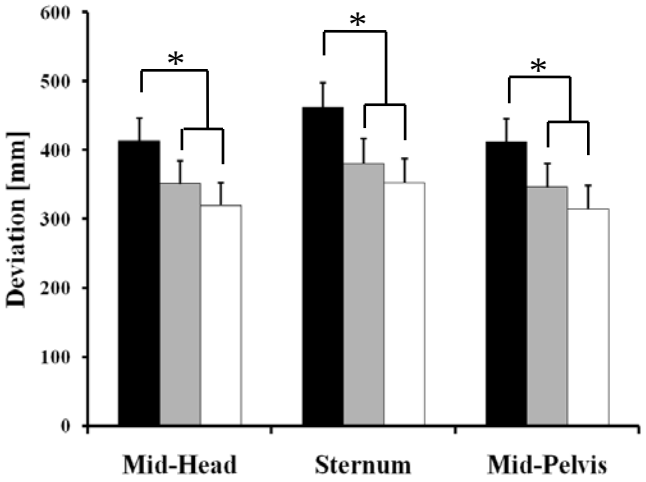

Figure 1: Translational responses to GVS in space. Repetition 1 is shown in black. Repetition 2 is shown in gray and repetition 3 is shown in white ($p<0.05$).

The head and thorax global mediolateral tilts were significantly greater in the first repetition of each condition, while repetitions two and three displayed no significant difference. The pelvis showed only significant difference between repetitions one and three (Figure 2). The first repetition of each condition had significantly greater neck mediolateral tilt, while the second and third repetitions were not significantly different. The spine mediolateral tilt was not significantly different between repetitions (Figure 2).

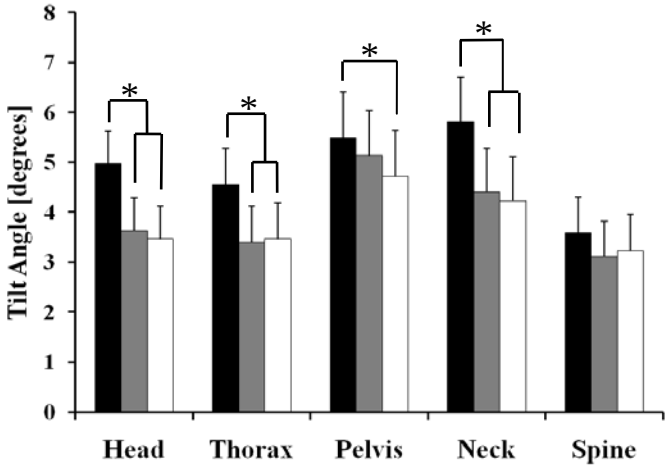

Figure 2: Within subject and condition least squares mean mediolateral segmental tilts. Values are recorded as all positive angles, where black represents repetition 1. The gray bars are repetition 2 and the white bars depict repetition 3.

An interaction effect between GVS direction and the gait phase of GVS trigger was seen in head, thorax, and pelvis deviations. The interaction effect may be due to the biomechanical limitation of crossing legs while walking if the stimulation pushed the subject towards support leg.

CONCLUSIONS

Habituation was observed after the first exposure to GVS in each gait condition. Thus, habituation appears to be specific to the conditions of exposure (i.e. timing and direction). The fact that no trial order effect was observed reinforces the hypothesis that habituation to vestibular sensory inputs during gait are task and perturbation-specific. .

REFERENCES

1. Cenciarini, et al. J *Neurophysiol* **95**, 2733-2750, 2006
2. Balter, et al. *Acta Otolaryngol* **124**, 262-271, 2004
3. Balter, et al. *Acta Otolaryngol* **124**, 941-945, 200.
4. Kadaba et al. *J. Orthop. Res.* **8,**383–392, 1990

CAN A NOVEL VIRTUAL ENVIRONMENT MOBILITY PLATFORM REPLICATE THE BIOMECHANICAL AND PHYSIOLOGICAL EFFECTS OF OVERGROUND WALKING?

[1,2]Angela Boynton, [1]Kathy Kehring and [1]Timothy White

[1]U.S. Army Research Laboratory, Aberdeen Proving Ground, MD, USA
[2]University of Delaware, Newark, DE, USA
email: aboynton@arl.army.mil

INTRODUCTION

Technological advances in computer graphics combined with the development of large rear-projection surround displays have enabled the creation of virtual environments that visually immerse the user into a sense of real-world presence. Over the years, more complex mobility platforms have been developed, attempting to achieve greater equivalence between the user's motions and those used in the real environment. The Omni-directional Treadmill (ODT) is one such mobility platform. The 8-ft x 8-ft working surface of the ODT, made up of 80 mini-belts that move perpendicularly to a main belt, allows the user to walk, jog, or even crawl in any direction. As the user navigates through the virtual environment, clusters of reflective markers attached to a rigid plate on the back of a neoprene waist band are tracked in real-time and used by the control system to determine how the belts of the ODT should move in order to return the user to the center of the workspace. The ability of this system to impose biomechanical and physiological effects on the user that are similar to those experienced in the real world is unknown. The purpose of this investigation was to determine the effect of terrain type (ODT versus overground) on select biomechanical and physiological variables.

METHODS

Ten healthy subjects (6 M / 4 F, age: 40.5 ± 7.8 yrs) walked for 5 minute periods at 1.12 and 1.34 $m \cdot s^{-1}$ along a circular course (4.27 m radius) overground (OG) and on the ODT. For the OG trials, the course was marked on the floor in black paint and the subject followed an investigator pushing a pacing wheel at the appropriate speed. During the ODT trials, the subject followed an avatar moving at the appropriate speed along the course through a virtual environment displayed on four screens enclosing the ODT (Fig. 1).

The 3-D motion of retroreflective markers on the subject's lower extremities was recorded at 120 Hz every 45 seconds for 10 second periods using a 6 camera motion capture system (overground: Motion Analysis Corp, Santa Rosa, CA; ODT: Vicon Motion Systems Inc, Lake Forest, CA) and then filtered at 6 Hz. A portable cardiopulmonary system (Cosmed USA, Chicago, IL) continuously sampled expired gases throughout each trial.

Figure 1: The subject follows an avatar through the virtual environment during the ODT trials.

Heel strike and toe-off events were identified using a velocity based algorithm applied to the heel marker trajectories in the pelvic coordinate system [1]. Mean temporal-spatial variables and sagittal plane joint excursions were calculated bilaterally for a minimum of six gait cycles per trial. Cadence and stride length were normalized to leg length [2]. Raw oxygen consumption data were normalized to body mass and then averaged over the final minute of data from each trial.

Separate multivariate analyses of variance with *post hoc* tests were performed to determine the effect of terrain on the temporal-spatial variables, joint excursions and normalized oxygen consumption values. OG and ODT conditions were considered significantly different for $p<0.05$.

RESULTS AND DISCUSSION

Terrain was found to have a significant effect on the temporal-spatial variables only at the faster walking speed (p=0.038). *Post hoc* analyses further revealed that left and right swing time (p=0.011 and 0.024) and left stride length (p=0.029) were significantly lower on the ODT than OG. As a consequence of the decreased left stride length, left leg cadence was also found to be significantly higher on the ODT (p=0.006). The magnitudes of these differences, however, are relatively small and consistent with the findings of previous studies comparing walking overground and on conventional treadmills (for example, see [3]).

A significant effect of terrain on sagittal plane joint excursions was found only at the faster walking speed (p=0.032). *Post hoc* analyses further revealed overall left knee and left and right ankle motion during the ODT trials to be significantly smaller (p=0.04, 0.03 and 0.009) than OG. The reduction in ankle excursion appears to be primarily related to a decrease of 5 to 10 degrees in peak plantarflexion following toe-off. A similar tendency was also observed for the slower walking speed and appears to be unique to walking on the ODT as it has not been reported in previous studies involving conventional treadmills (for example, see [3]). Although overall joint excursions at the hip and knee were similar between the two terrain conditions, there was a tendency for the joints to be more flexed throughout the gait cycle during walking on the ODT. An increase in overall joint flexion has also been observed for walking over slippery terrain and may reflect an attempt by the subject to increase stability by lowering their center of gravity towards their base of support [4].

Metabolic cost was found to be more than 20% greater for the ODT trials than OG (Fig. 2). This substantial increase may be due to differences in mechanical work, magnitude of muscle activation and cocontraction, and regulation of whole body angular momentum during walking on the ODT.

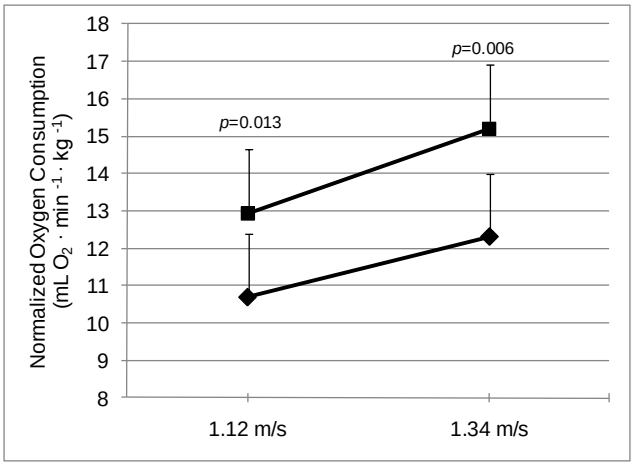

Figure 2: Normalized metabolic cost of walking overground (diamond) and on the ODT (square) at two speeds.

While the ODT provides a means for realistic navigation of virtual environments, the observed difference in metabolic cost must be taken into account when comparing the results of training or research studies using the ODT to those of real-world activities. Future studies should seek to identify and develop a better understanding of the mechanisms behind the increased physiological demand. Such studies would provide insight not only into the differences between locomotion in the real-world and on the ODT, but also serve to deepen our understanding of the mechanisms associated with the energetics of walking in general.

CONCLUSIONS

The ODT permits the user to walk through a virtual environment in a relatively natural way, but with a significant increase in physiological demand as compared to overground walking.

REFERENCES

1.Zeni JA, et al. *Gait Posture* **27**, 710-714, 2008.
2.Hof AL. *Gait Posture* **4**, 222-223, 1996.
3.Lee SJ and Hidler J. *J Appl Physiol* **104**, 747-755, 2008.
4.Marigold DS and Patla AE. *J Neurophysiol* **88**, 339-353, 2002.

ASYMMETRY, LIMB DOMINANCE AND FOOT ORIENTATION DURING WALKING GAIT

[1]John Polk, [2]Karl Rosengren

[1]University of Illinois, Urbana, IL, USA
[2]Northwestern University, Evanston, IL, USA
Email: jdpolk@illinois.edu

INTRODUCTION

Although healthy gait is often considered to be characterized by symmetric movement patterns, asymmetries in the early acquisition of gait have been thought to reflect differing balancing vs. propulsive roles for the limbs [1]. In adults, asymmetries have been linked to limb dominance [2,3]. Seeley et al. [3] tested for effects of limb dominance on support and propulsive roles, and found only moderate effects at higher speeds, however they did not examine medial and lateral force components or impulses. The goal of our study was to (i) test for the presence of asymmetries in foot orientation, temporal components, and force components; (ii) evaluate the hypothesis that foot posture can be used to discriminate functional roles for the limbs and (iii) determine whether the dominant limb plays more of a balancing or propulsive role during walking gait.

METHODS

Thirty-six adult subjects (17 F; 19 M) walked along a 24' level walkway with a force platform (Model 600900; AMTI, Watertown, MA) placed in the center. Subjects were asked to walk: (i) as they normally would along the platform [Normal]; (ii) with their foot externally (laterally) rotated approximately 45º [Outward]; (iii) with feet oriented in their direction of motion (0º) [Straight] along the walkway. Comfortable walking speeds were used. Consistency was maintained using a metronome (39-44bps). Ten trials (5 right; 5 left) were collected for each task and subject. Markers placed on the medial surface of the ball of the foot, and medial surface of the heel. Marker positions were recorded using standard photogrammetric methods. Foot orientation was calculated as the inverse cosine of the (apparent/actual) distances between the foot markers while the foot was flat on the force platform. Stride duration was calculated as the elapsed time between consecutive heelstrike events for the same limb. The following data were obtained from ground reaction force components: stance duration, peak vertical force and vertical impulse, peak braking and propulsive forces, braking and propulsive impulses, peak medial and lateral forces, peak medial and lateral impulses. Impulses were calculated using the trapezoid method. Forces were standardized by body weight; impulses were standardized by mass*(tibia length/gravity)$^{0.5}$[4]. A subject's dominant limb was the one preferred for kicking a ball. All subjects were right-limb dominant. Gait symmetry was assessed by symmetry ratios (L/R). Task effects were analyzed using one-way ANOVA.

RESULTS AND DISCUSSION

Stance and stride durations did not differ significantly across the tasks implying that locomotor speeds were comparable.

Asymmetry: As predicted, only angular deviation, and ML force components (and impulses) show significant asymmetry (Table 1). Foot asymmetry is greater during normal gait than during tasks where subjects deliberately alter foot posture. However, this deviation is small. Right feet (dominant limbs) have significantly higher medial and lower lateral peak forces than the left feet. All other variables did not deviate from symmetry.

Foot Orientation: Outward walking showed significantly higher medial and lateral peak forces,

and lateral impulses, than normal or straight walking. Outward walking also showed lower propulsive peak forces and impulses than normal or straight foot orientation, although the straight-outward comparison did not achieve statistical significance (p=0.056). Braking peak forces did not differ significantly across the task groups, but braking impulses were significantly larger for the outward walking group.

Dominant Limbs: Dominant (right) limbs were slightly more outwardly rotated, and generated significantly higher medially-directed, and lower laterally-directed forces and impulses.

CONCLUSIONS

Asymmetries exist in foot orientation (slight), and in medial and lateral GRF characteristics (significant).

Externally rotated foot postures result in higher lateral and medially directed forces and impulses than straight or normal walking. Straight foot postures do not produce different GRF characteristics than normal walking.

Dominant limbs produced higher medial and lower lateral forces and impulses, implying a greater role for the dominant limb in balancing functions during gait.

Increased external rotation of the foot leads to increased balancing and decreased propulsive roles.

REFERENCES

1. Ledebt et al. *Infant Behav Dev* **27,** 163-172, 2004.
2. Sadeghi et al. *Gait & Posture* **12**, 34-45, 2000.
3. Seeley et al. *Gait & Posture* **28**, 24-28, 2008.
4. Hof *Gait and Posture* **4**, 222-3, 1996.

ACKNOWLDEGEMENTS

Data processing assistance provided by: R. Perry, C. Sell, V. Prokuski, C. Rasmussen, M. Downen, L. Monaghan, P. Achille, C. Murphy. Funded by the Dept. of Anthropology, UIUC.

Table 1. Symmetry ratios (L/R). Bold values indicate greater than 10% asymmetry.

Task	Stride Dur.	Stance Dur.	Foot Angle	Peak Ground Reaction Forces					Impulses				
				Vert.	Prop.	Brake	Med.	Lat.	Vert.	Prop	Brake	Med	Lat
Normal	1.011	1.013	**0.881**	0.988	0.997	0.982	**0.566**	**1.588**	1.019	0.996	1.009	**0.411**	**1.984**
Straight	1.012	1.008	0.960	0.991	1.001	0.969	**0.559**	**1.759**	1.000	0.984	0.983	**0.347**	**2.211**
Outward	0.987	0.998	0.984	0.992	1.015	0.974	**0.636**	**1.377**	0.998	1.036	0.961	**0.494**	**1.767**

JOINT POWERS ARE AFFECTED BY AGE AND PERIPHERAL ARTERIAL DISEASE.

[1]Panagiotis Koutakis, [1]Sara A. Myers, [2]Iraklis I. Pipinos, [2]Jason M. Johanning, [1]Nicholas Stergiou

[1] Nebraska Biomechanics Core Facility, University of Nebraska at Omaha, Omaha, NE
[2]Dept of Surgery, University of Nebraska Medical Center, Omaha, NE
email: koutakisp@unmc.edu, web: http://biomech.unomaha.edu/

INTRODUCTION

Peripheral arterial disease (PAD) affects over 8 million people in the US and is a manifestation of atherosclerosis leading to decreased blood flow to the legs [1]. The result is ischemic pain known as claudication, a cramping that is induced by physical activity and impairs walking ability. Recent studies from our laboratory have identified abnormal neuromuscular alterations that affect gait in patients with PAD [2]. However, since many PAD patients are also elderly, the independent effects of age and the disease are unknown. Thus, the current study investigated PAD joint torques and powers in younger and older subjects.

METHODS

Twenty nine patients with PAD (PAD; 17 younger Y-PAD, age: 57.3 ± 5.29 years, body mass: 81.2 ± 18.4 kg, body height: 171.8 ± 8.02 cm, walking velocity: 1.25 ± 0.09 m/s; 12 older O-PAD, age: 74.0 ± 6.85 years, body mass: 81.4 ± 18.5 kg, body height: 171.3 ± 5.38 cm, walking velocity: 1.22 ± 0.15 m/s) diagnosed with Rutherford Class 2/Fontaine Class II arterial occlusive disease with classic Rose intermittent claudication and eighteen gender, age, height, and body mass matched healthy control subjects (CON; 9 younger Y-CON, age: 54.5 ± 6.19 years, body mass: 92.4 ± 20.17 kg, body height: 175.6 ± 7.19 cm, walking velocity: 1.30 ± 0.14 m/s; 9 older, age O-CON, 74.3 ± 6.54 years, body mass: 68.5 ± 12.5 kg, body height: 168.8 ± 6.74 cm, walking velocity: 1.24 ± 0.08 m/s) walked over a Kistler force platform to acquire kinetics (60 Hz), while joint kinematics (600 Hz) were recorded simultaneously with a 8-camera motion capture system (Motion Analysis, Santa Rosa, CA). Five trials were collected for each limb in the pain free. To ensure patients did not experience pain, a one minute rest period was required between each trial. Patients and healthy controls were matched post-hoc for their self-selected gait velocity. Joint kinetics were calculated during the stance phase of gait. Group means were compared with two by two ANOVAs (PAD versus CON; Younger versus Older). For significant interactions, independent t-tests were used for post-hoc analysis to identify significant differences between the group/age combinations.

RESULTS AND DISCUSSION

Joint Torques: There was a significant main effect of age for hip extensor torque (HET; Table 1) during early stance. Older subjects had significantly decreased hip extensor torque as compared with the Younger subjects. A significant interaction demonstrated that Y-PAD, O-PAD and O-CON groups had significant decreases in hip extensor torque as compared to Y-CON subjects. No significant differences were found in the other joints.

Joint Powers: Several differences were found between groups (PAD versus CON) for the joint powers (Table 1). PAD patients had significantly decreased ankle power generation (A2) in late stance, knee power absorption (K1) in early stance, knee power generation (K2) in mid stance, knee power absorption (K3) in late stance and hip power absorption (H2) in mid stance as compared to CON (Table 2). When comparing the age groups, (Younger versus Older), the Older group had significantly decreased K3 in late stance, H2 in mid stance, and hip power generation (H3) in late stance as compared to the Younger group (Table 1). In addition, a significant interaction was found between group and age for hip power generation (H1) in early stance. Specifically, O-CON and Y-PAD patients had a significantly reduced H1 in early stance as compared to Y-CON (Table 1).

It has been demonstrated in the literature that elderly joint torques and powers are affected by walking velocity. Specifically, ankle plantarflexor power and hip flexor and extensor powers were increased when walking velocity was increased [3]. Thus, we selected PAD subjects that had the same walking velocity as the control subjects in order to identify true differences in our clinical population. DeVita and Hortobagyi [4] had elderly subjects walk at the same velocity as young subjects and found that elderly are exhibiting power redistribution towards the hip joint. This power redistribution is compensating the power deficits of the ankle plantarflexors. However, our results did not demonstrate a similar pattern. In PAD subjects, the major limitation of walking is the reduced ankle plantarflexor power [2]. Matching for walking velocity this difference remained significant and was independent of aging. This suggests that ankle plantarflexor power can severely limit PAD subjects walking ability. Additional, age caused significant decreases of knee and hip joint powers during late stance. These results are in contradiction with other studies [3, 4] that demonstrated that elderly are increasing their knee and hip joint powers in late stance and further reveals the severity of PAD.

CONCLUSIONS

Joint kinetics are significantly altered in PAD patients during pain free locomotion. Symptomatic PAD produces locomotor abnormalities that are consistent for both age groups, with older subjects further demonstrating a significant dysfunction at the knee and hip joint. Our results are suggesting that PAD can severely limit the functional locomotor ability of both older and younger subjects.

REFERENCES

1.McDermott MM et al. *Cleve Clin J Med.* **73,** Suppl 4:S2-7, 2006.
2.Koutakis P et al. *J Vasc Surg.* **51**, 80-8, 2010.
3.Graf A et al. *Arch Phys Med Rehabil*. **86,** 2177-83, 2005.
4.DeVita P and Hotorbagyi T. *J Appl Physiol*. **88,** 1804-1811, 2000.

ACKNOWLEDGEMENTS

American Geriatrics Society's Hartford Foundation Dennis W. Jahnigen Award to [JMJ], the Onassis Public Benefit Foundation to [PK] and the Nebraska Research Initiative to [NS].

Table 1. Group means for significant joint kinetics for younger (Y) and older (O) Peripheral Arterial Disease (PAD) and Control (CON) groups.

	Y-PAD (N=17)		O-PAD (N=12)		Y-CON (N=9)		O-CON (N=9)		Significance
HET(N*m/kg)	0.84	± 0.16	0.84	± 0.22	1.01	± 0.19	0.76	± 0.16	†, ‖,¶,§
A2 (Watts/kg)	2.64	± 0.55	2.43	± 0.53	3.03	± 0.67	2.84	± 0.68	*
K1 (Watts/kg)	-0.82	± 0.32	-0.70	± 0.31	-1.04	± 0.41	-0.94	± 0.41	*
K2 (Watts/kg)	0.36	± 0.18	0.39	± 0.22	0.59	± 0.23	0.45	± 0.34	*
K3 (Watts/kg)	-0.76	± 0.17	-0.60	± 0.25	-0.96	± 0.30	-0.84	± 0.37	*,†
H1 (Watts/kg)	0.49	± 0.20	0.62	± 0.20	0.68	± 0.24	0.48	± 0.16	‖,§
H2 (Watts/kg)	-0.80	± 0.19	-0.67	± 0.30	-1.01	± 0.29	-0.89	± 0.23	*,†
H3 (Watts/kg)	0.66	± 0.17	0.60	± 0.27	0.78	± 0.21	0.62	± 0.23	†

* $p < .05$, significant differences between groups (CON vs. PAD), † $p < .05$, significant differences between age groups (Y vs. O), § $p < .05$, significant interaction between Y-CON and O-CON, ‖ $p < .05$, significant interaction between Y-PAD and Y-CON.

Effects of handrail use on healthy treadmill walking

[1]Nicole Zahradka, [2]Darcy Reisman and [1]Jill Higginson

[1]Department of Mechanical Engineering, University of Delaware, Newark, DE, USA
[2]Department of Physical Therapy, University of Delaware, Newark, DE, USA
email: zahradka@udel.edu

INTRODUCTION

Upper extremity movements and forces have important implications for rehabilitation of pathological gait. Patients with impaired gait due to stroke often rely on an outside source (such as a cane or handrail) to assist them. When performing treadmill studies with stroke patients, a handrail is often used. Stephenson et al. found that when handrails were present, a small amount of weight was borne through the upper limbs in healthy and stroke subjects which affected the activity of the proximal leg muscles [1]. The amount of force used on the handrail varies between subjects and may influence loads on the lower extremity. Therefore, it is important to consider whether the weight applied to the handrail significantly alters the ground reaction forces.

The objective of this study was to evaluate the effect of handrail use on the kinetics during treadmill walking in healthy subjects. We will (1) compare magnitudes of handrail and ground reaction forces and (2) compare left and right handrail forces when only one handrail is used.

METHODS

Three healthy subjects between 18 to 40 years of age with no history of muscle, bone or nervous system disorders were recruited. Potential subjects were asked to complete a physical activity readiness questionnaire and sign an informed consent prior to participating in this study.

The subjects walked at a self-selected speed in the hallway for 10 meters to assess their comfortable speed. This speed was used during the treadmill trials. All trials were recorded in Cortex (version 1.0.0.198) by eight cameras (Motion Analysis Corp., Santa Rosa, CA) that capture motion of reflective markers attached to the body segments at 60 Hz. Two force plates (embedded in the treadmill) and two force transducers (embedded in the handrails) (Bertec Corp., Columbus, OH) captured the ground reaction forces and handrail forces, respectively, at 1080 Hz.

Table 1. Subject Information (mean ± st dev)

Age	23
Gender	2 F, 1 M
Height (m)	1.67 ± .06
Weight (kg)	59.87 ± 15.89
Walking Speed ($m*s^{-1}$)	1.37 ± .2
Hand Dominance	Right

The subjects were asked to walk under four conditions (no hands on handrail (NHR), both hands on the handrail (BHR), left hand only on the handrail (LHR), and right hand only on the handrail (RHR)). The order of these trials was randomized and each trial was recorded for 30 seconds.

A model was created in Visual 3D including feet, legs, torso, arms and hands with segments scaled to subject height and weight. The handrail data was imported into Visual 3D, converted from volts to newtons and normalized to body weight. A Butterworth lowpass filter with a cutoff frequency of 25 Hz was used on the force plate and handrail data. Gait events were identified and trials were averaged over gait cycles and normalized to 101 points. The maximum ground reaction and handrail forces in the vertical direction were extracted for each trial.

RESULTS AND DISCUSSION

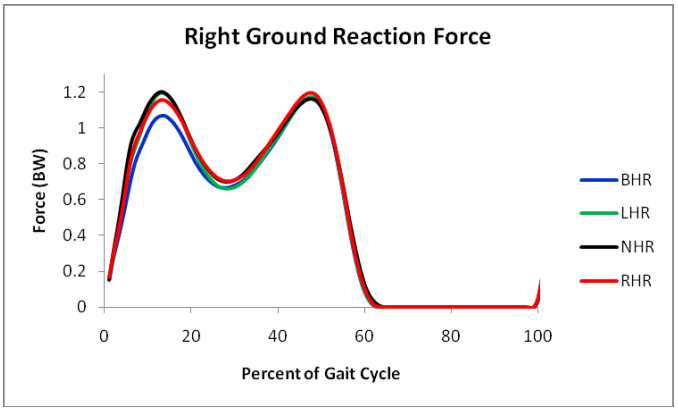

Figure 1: Differences noted in the first peak but not the second peak of the right vertical GRF.

The first peak force ranged from 1.19 ± .06 BW (NHR) to 1.0 ± .07 BW (BHR). The LHR and RHR conditions had a peak ground reaction force of 1.14 ± .1 BW. At the second peak, all four conditions reached a force 1.19 BW (Figure 1). The four conditions had varying peak forces during the first 30 percent of the gait cycle (foot flat to the local minima) and then had approximately the same peak force before right toe off. The left ground reaction force followed in a similar pattern. This suggests that force was applied to the handrail for balance after heel strike and no longer needed once stabilized.

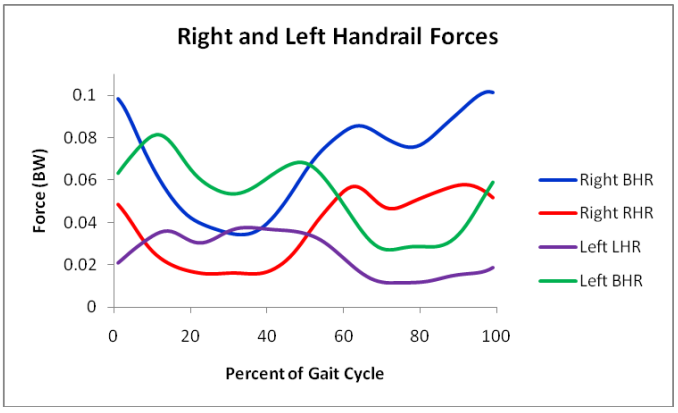

Figure 2: The left and right hands exert different peak forces on the handrails.

The handrail forces for the BHR condition were approximately twice as great as the handrail forces when only one of the handrails were held. This may be due to the subjects resting on the handrails. When the left handrail forces were plotted from LHS to LHS, they followed a similar trend to the right handrail forces. The right handrail was out of phase with the right ground reaction force, similar to arm swing.

The right arm exerted a higher peak force than the left arm under each comparable condition (Figure 2). The right BHR peak was .1 ± .12 BW while the left BHR peak was .08 ± .09 BW. Similarly the right RHR peak was .06 ± .04 BW and the left LHR peak was .04 ± .03 BW. It is important to note that all three subjects were right handed, which may suggest that hand dominance is a factor in the amount of force exerted on the handrails. To determine if hand dominance does play a role, more subjects with varying hand dominance will be collected.

Handrail forces ranged up to 10% of body weight and type of handrail usage affects the magnitude of the vertical GRF which will have implications for inverse dynamics calculations. It is likely that subjects with a pathological gait pattern who use handrails have altered joint loads which should be considered during rehabilitation and other treadmill studies.

REFERENCES

1.Stephenson JL, et al. *Gait & Posture* **31**, 109-115, 2010.

EFFECTS OF LOAD CARRIAGE ON FOOT ANTHROPOMETRICS

Stephen Goffar, Rett Reber, Bryan Christiansen, R Benjamin Miller, Jacob Naylor, Brittany Rodriguez, Michael Walker, Deydre Teyhen

U.S. Army-Baylor University, Fort Sam Houston, TX, USA
E-mail: Stephen.Goffar@us.army.mil

INTRODUCTION

Lower extremity overuse injuries are reportedly the most common injuries in the military. The heavy loads commonly carried by military personnel in training and combat environments increase the risk of lower extremity overuse injuries [1]. Moderate evidence links extremes of arch height (AH) with increased risk of lower extremity injuries. Understanding how military load carriage influences AH and other foot anthropometrics, may influence the development of military footwear and orthoses. These developments could potentially help mitigate the effects of load carriage and reduce the incidence of injuries related to military operations and training. The purpose of this study was to explore the effects of increasing levels of load carriage on foot anthropometrics.

METHODS

Subjects for this study were recruited from the active duty military population. Potential subjects were excluded if they weighed less than 70kg, were not between the ages of 18 and 45 years, did not speak fluent English, or had current pain or a condition which limited their ability to carry 40kg. After obtaining informed consent, heel-toe length (HTL), midfoot width (MFW), and AH were measured on the right foot in four conditions: non-weight bearing (NWB), weight bearing (WB), 20 kg load (20kg), 40 kg load (40kg). Measurements were obtained with the Foot Assessment Platform System (FAPS) [2]. To simulate the field environment, subjects wore the standard field uniform, and the load conditions included an M16, body armor, helmet, and a weighted ruck sack. The reliability of the foot measurements had an ICC $(2, 1) \geq 0.94$.

Subjects were divided into groups based on arch height index (AHI; high, normal, and low) and arch mobility (hypomobile, normal, hypermobile) for analysis. AHI was calculated by dividing the dorsal AH of the foot (taken at 50% of HTL) by HTL [2]. Arch mobility was calculated by subtracting AH in WB from AH in NWB. For both measures, values greater than 1.0 standard deviation from the mean delineated group membership.

Descriptive statistics, kappa, and percent agreement were calculated to explore the relationship between AHI and arch mobility. To determine the impact of load on foot anthropometrics, multiple 3×4 mixed model ANOVA's were calculated. A Greenhouse-Geisser correction was used when Mauchly's test for sphericity was significant. Bonferroni adjusted paired t-tests were used for post hoc analyses.

RESULTS AND DISCUSSION

Subjects included 117 service members (18 female) with mean age of 31.2 ± 5.5 years, height of 177.2 ± 7.0 cm, weight of 86.2 ± 11.0 kg, and BMI of 27.4 ± 2.9. Classifications by AHI resulted in 28 high (AHI > .267), 61 normal, and 28 low (AHI < .229). Classifications by arch mobility resulted in 20 hypomobile (< 8.4mm), 77

normal, and 20 hypermobile (>13.8mm). The percent agreement between AHI and arch mobility groups was 52.1% (kappa=0.17; Table 1).

		AHI			
		Low	Normal	High	
Mobility	Hypermobile	9	9	2	20
	Normal	17	43	17	77
	Hypomobile	2	9	9	20
		28	61	28	117

Table 1: Agreement between AHI and Arch Mobility

The interaction between AHI and load condition was significant for AH ($F=7.15$, $p<.001$) and MFW ($F=5.72$, $p=.002$) but not for HTL ($F=2.27$, $p=.09$). The main effect of load was significant for HTL ($p<.001$). The interaction between arch mobility and load condition was significant for AH ($F=93.68$, $p<.001$) (Figure 1); and MFW ($F=7.35$, $p<.001$) but not for HTL ($F=.144$, $p=.91$) values. The main effect of load was significant for HTL ($p<.001$).

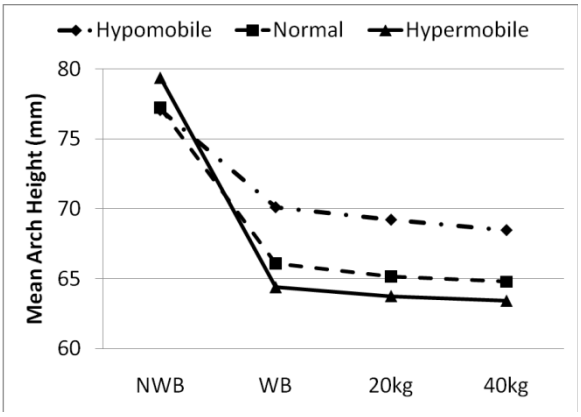

Figure 1: Changes in AH based on foot mobility

In general, as load increased AH decreased, MFW increased, and HTL increased, regardless of foot classification system. AH decreased significantly with each increase in load ($p<.014$) except in low arched and hypermobile feet between 20 and 40kg ($p>.47$). The mean decrease in AH was 12.4 ±2.7 mm from NWB to 40kg load condition. MFW increased significantly from NWB to WB and from WB to 40kg load ($p<.03$), regardless of foot classification system. The changes between WB and 20kg and 20kg and 40kg were more variable based on foot type and mobility. Independent of group, HTL increased from NWB to WB and WB to 40kg ($p<0.02$). The mean increase in HTL was 9.7 ±4.3 mm from NWB to 40kg load condition.

CONCLUSIONS

In stance, decreases in AH and increases in MFW appear to approach a maximal change with loads as small as 20 kg in most individuals. The greatest excursion in HTL occurred under the 40kg condition. Future research should assess characteristics of combat boot and orthotic design to determine how these devices might mitigate the impact of load. Although the impact of load was similar when analyzed based on AHI and arch mobility, the differences between the two classification systems warrant further research. The assumption that a high arched foot is hypomobile and a low arch foot is hypermobile is not supported by our findings. The impact of arch mobility on lower extremity injuries should be assessed.

REFERENCES

1. Bisiaux, M. *et al.* (2008). *Gait and Posture*, **28** (4), 693-8.
2. McPoil, T.G. *et al.* (2008). *The Foot,* **18**,220-7.

The opinions and assertions contained herein are the private views of the authors and are not to be construed as official or as reflecting the views of the Departments of the Army, Navy, Air Force or Defense.

Funding provided by U.S. Army Bone Health and Military Medical Readiness Program.

RELIABILITY OF REGIONAL PLANTAR PRESSURE DURING WALKING, STAIR ASCENT AND DESCENT

[1]YenWei Chen, [1]On-Yee Lo, [1]Louis Iannuzzi, [2]Kenneth Mroczek, [1]Smita Rao

[1]Department of Physical Therapy, New York University
[2]Department of Orthopedics, Hospital for Joint Diseases, New York University Langone Medical Center
E-mail for correspondence: smita.rao@nyu.edu

INTRODUCTION

Regional plantar pressure sustained at the foot-shoe interface is of considerable interest in a variety of clinical applications. While it is well established that regional plantar pressure is influenced by the activity being performed, specific changes that occur in regional plantar pressure during walking versus stair climbing are poorly understood. The issue is further confounded by the absence of reliability studies, examining the consistency of plantar pressure characteristics during stair ascent and descent. Reliability studies are essential, not only to establish reliable measures, but also to determine the number steps that need to be acquired and averaged in future studies. The purpose of this study was to assess the reliability of regional plantar pressure sustained during walking compared to stair ascent and descent, using intraclass correlation coefficients (ICC).

METHODS

All procedures were approved by the University Committee on Activities Involving Human Subjects at New York University. Seven asymptomatic subjects (Mean ± SD, age in years: 27.14 ± 3.72; BMI in kg/m^2: 23.5 ± 1.86, 4 male) participated in this study. All subjects were screened for musculoskeletal symptoms and pathology that may have influenced walking or other weight bearing activities of daily living.

Plantar pressure data were acquired using an in-shoe measurement system (Pedar Inc, Novel GMBH). Appropriately sized insoles were placed within subjects' footwear. Data were collected at 50 Hz as subjects performed the following activities at self selected speed: walking, stair ascent and stair descent. A mid gait protocol was used to eliminate the effects of acceleration and deceleration associated with initiation and termination of the walking trial.

Plantar pressure data were analyzed to obtain peak pressure sustained in the following six foot areas: heel, medial midfoot (m.mid), lateral midfoot (l.mid), medial forefoot (m.fore), lateral forefoot (l.fore) and great toe (g. toe). A minimum of ten mid-gait steps were analyzed for each activity.

Reliability was quantified using intraclass correlation coefficients (SPSS v16). ICC (2, k) was used to assess the reliability of the peak pressure of k measures, where k = 2 to 10 steps [1]. An ICC > 0.9 was operationally defined as indicative of acceptable reliability.

RESULTS AND DISCUSSION

Average ICC values for peak pressure sustained in the different regions of the foot during walking are summarized in Table 1.

Table 1: ICC (2,k) for peak pressure sustained in six foot regions during walking. Number steps needed to reach ICC≥0.9 are underlined.

Step	Heel	M. Mid	L. Mid	M. Fore	L. Fore	G. Toe
2	<u>0.96</u>	0.38	0.47	<u>0.93</u>	0.86	<u>0.96</u>
3	0.98	0.79	0.66	0.93	0.87	0.96
4	0.98	0.87	0.75	0.92	0.83	0.97
5	0.99	<u>0.91</u>	0.80	0.95	0.87	0.97
6	0.99	0.88	0.82	0.96	0.89	0.97
7	0.99	0.90	0.87	0.97	<u>0.91</u>	0.97
8	0.99	0.91	<u>0.90</u>	0.98	0.93	0.97
9	0.99	0.93	0.92	0.98	0.94	0.97
10	0.99	0.94	0.93	0.98	0.94	0.97

Average ICC values for peak pressure sustained in the different regions of the foot during stair ascent and descent are summarized in Table 2.

During self selected speed walking, ICC value suggests that 2 steps are needed to obtain ICC $\geq$ 0.9 at the heel, medial forefoot, and great toe. At the medial midfoot, lateral midfoot and lateral forefoot, five, eight and seven steps, respectively, are needed to reach acceptable reliability (ICC (2,k) $\geq$ 0.9). The results agree with the work of Putti et al (2006) and Bus et al (2005) that the measurements in heel are consistent between trials [2,3].

During stair ascent and descent, in contrast to walking, low reliability was noted at the heel and medial midfoot. This finding may be due to a subjects' rearfoot not contacting the ground consistently while climbing stairs. The peak pressure in medial forefoot displayed consistency between steps, while other foot masks showed more variation between steps. At the lateral midfoot, lateral forefoot and great toes, three, seven and four steps, respectively, are needed to reach acceptable reliability (ICC (2,k) $\geq$ 0.9).

Similarly, during stair descent, the results suggest that eight and nine steps are needed to obtain a reliable average measurement in heel and medial midfoot, respectively. Concerning lateral midfoot, medial forefoot, and great toe, two, three and four steps, respectively, were needed to obtain a reliable average measurement. The greater consistency of plantar loading in the forefoot compared to the rearfoot may also reflect the forefoot strike patterns used in stair descent versus walking.

CONCLUSIONS

Our results highlight that plantar pressure sustained during stair climbing may be more variable than that sustained during walking, particularly in the rearfoot. The variability in plantar loading may partially explain the contentious results reported by previous studies.

REFERENCES

1.Shrout, PE, & Fleiss, JL. *Psychological Bulletin*, **86**, 420-428, 1979.
2.Putti AB, et al. *Gait Posture* **25**, 401-5, 2006.
3.Bus SA, et al. *C Biomechanics* **20**, 892-899, 2005.

ACKNOWLEDGEMENTS

This study was supported in part by the New York Physical Therapy Association.

Table 2: ICC (2,k) for peak pressure sustained in six foot regions during stair ascent and descent. Number steps needed to reach ICC $\geq$ 0.9 are underlined.

	Stair Ascent						**Stair Descent**					
Step	**Heel**	**M. Mid**	**L. Mid**	**M. Fore**	**L. Fore**	**G. Toe**	**Heel**	**M. Mid**	**L. Mid**	**M. Fore**	**L. Fore**	**G. Toe**
2	-0.78	0.16	0.78	<u>0.96</u>	0.64	0.84	0.69	0.91	<u>0.93</u>	0.78	0.64	0.50
3	0.44	0.56	<u>0.90</u>	0.96	0.74	0.89	0.50	0.87	0.94	<u>0.90</u>	0.74	0.85
4	0.50	0.60	0.88	0.95	0.77	<u>0.91</u>	0.49	0.58	0.91	0.92	0.57	<u>0.91</u>
5	0.71	0.71	0.92	0.97	0.87	0.95	0.66	0.73	0.90	0.92	0.73	0.92
6	0.75	0.78	0.95	0.98	0.88	0.96	0.76	0.81	0.93	0.92	0.75	0.94
7	0.80	0.78	0.95	0.98	<u>0.90</u>	0.97	0.79	0.82	0.92	0.92	0.79	0.94
8	0.80	0.83	0.96	0.98	0.93	0.97	0.89	<u>0.90</u>	0.92	0.92	0.85	0.96
9	0.83	0.83	0.96	0.99	0.94	0.97	<u>0.91</u>	0.91	0.92	0.93	0.87	0.96
10	0.80	<u>0.90</u>	0.96	0.99	0.95	0.98	0.91	0.93	0.93	0.93	0.89	0.97

FRONTAL PLANE KINETICS AND EMG ACTIVITY DURING STAIR AMBULATION

[1]Michelle Hall, [1]Catherine Stevermer and [1]Jason Gillette

[1]Iowa State University, Ames, IA, USA
email: mhall2@iastate.edu

INTRODUCTION

Investigations of stair use can provide insight toward understanding loads experienced on a daily basis. However, few researchers studying stair descent and ascent have examined the mechanics of the hip and knee joint in the frontal plane. Knee varus moments are widely associated with knee osteoarthritis [1]. Greater medial displacement of the resultant ground reaction force from the knee joint centre increases the compression force on the medial knee. This alteration in loading is believed to be a risk factor for articular cartilage degeneration. Furthermore, hip abductor moments potentially affect lower extremity alignment and knee joint loading in the frontal plane during stair descent and ascent. A reduced hip abductor moment increases pelvic drop during single-leg support of walking, shifting the body's centre of mass to increase medial knee compression [2]. To help understand whether this relationship also exists in stair ambulation, baseline measures for hip abductor moments during stair descent and ascent are needed. In addition, the thigh muscles have limited potential to restrict frontal plane movement due to the knee joint stabilizing functions of the quadriceps and hamstrings. Co-contraction of the hamstrings and quadriceps has been shown to resist knee varus and valgus loads 11-14%, thereby improving joint stability [3].

The purpose of this study was to compare knee and hip joint frontal plane kinetics along with quadriceps and hamstrings EMG activity during stair ambulation in healthy individuals. It was hypothesized that maximum knee joint varus moments, hip joint abductor moments, vastus lateralis EMG, and biceps femoris EMG would all significantly increase when comparing stair ascent to stair descent since the individual has to elevate their body mass against gravity.

METHODS

Ten healthy subjects (4M/6F, age 25.4 ± 3.9 years, height 1.73 ± 0.1 m, mass 66.6 ± 12.4 kg) participated in this study. The staircase consisted of three steps (step height 18.5 cm, tread length 29.5 cm). Participants performed three maximum voluntary contractions (MVC) for the knee extensors and flexors. Following a static trial, participants were instructed to ascend or descend the stairs at a self-selected pace using the step-over-step approach. Participants performed three ascending and three descending trials leading with the right and left leg, respectively. The stair ambulation speeds were maintained within ±5% of self-selected pace for each subject.

Kinematic and kinetic recordings were collected using an 8-camera motion analysis system (Vicon), and portable force platforms (AMTI) were positioned on the first and second stair steps. Reflective makers were placed on the lower extremities and trunk. Electromyography (EMG) data were collected from the vastus lateralis and biceps femoris (Delsys). Using inverse dynamics, internal hip abduction moments and external knee varus moments were calculated during the stance phase of two steps for stair ascent and descent. Moments were averaged across trials and normalized to body mass. A linear envelope (10 Hz low-pass filter) was used to determine maximum EMG values during the stance phase of each step. Maximum EMG values were averaged across three trials and normalized to the MVC. A co-contraction ratio was determined using: EMGS/EMGL, where EMGS was the level of activity in the less active muscle and EMGL was the level of activity in the more active muscle. Multivariate ANOVA was used to test for main effects of stair direction (ascent and descent) on maximum joint moments and EMG activity. Significance was set at $p<0.05$.

RESULTS AND DISCUSSION

Knee varus moments (Table 1) were significantly greater during stair ascent as compared to stair descent during the first step ($p = 0.003$), while the second step approached significance ($p=0.072$). No significant differences in hip abduction moments were observed between stair ascent and descent for the first step. However, hip abduction moments were significantly greater for stair descent than for stair ascent during the second step ($p<0.001$).

EMG activity levels (Table 2) of the vastus lateralis were significantly greater during stair ascent as compared to stair descent for the first step ($p<0.001$) and for the second step ($p=0.042$). Biceps femoris EMG activity was significantly greater for stair ascent than for stair descent during the second step ($p=0.006$), but no significant differences were found for the first step. No distinct differences were noted for the co-contraction ratio between vastus lateralis and bicep femoris when comparing stair ascent (0.53 ± 0.26 first step, 0.53 ± 0.25 second step) to stair descent (0.64 ± 0.27 first step, 0.57 ± 0.26 second step).

Table 1: Maximum Normalized Joint Moments

Step	Direction	Moments (Nm/kg) Knee Varus	Moments (Nm/kg) Hip Abduction
First	Descent	0.20 ± 0.14	0.85 ± 0.22
	Ascent	0.57 ± 0.18[a]	0.82 ± 0.14
Second	Descent	0.37 ± 0.21	1.15 ± 0.15[c]
	Ascent	0.55 ± 0.12[b]	0.57 ± 0.11

[a] stair ascent > stair descent ($p<0.05$)
[b] stair ascent > stair descent ($p<0.10$)
[c] stair descent > stair ascent ($p<0.05$)

Table 2: Normalized EMG Activity

Step	Direction	Muscle Activity (%MVC) Vastus Lateralis	Muscle Activity (%MVC) Biceps Femoris
First	Descent	0.29 ± 0.09	0.26 ± 0.15
	Ascent	0.65 ± 0.13[a]	0.35 ± 0.18
Second	Descent	0.31 ± 0.17	0.16 ± 0.05
	Ascent	0.57 ± 0.24[a]	0.27 ± 0.07[a]

[a] stair ascent > stair descent ($p<0.05$)

The observation that knee varus moments were greater during stair ascent as compared to stair descent is consistent with previous research [4]. Increases in knee varus moments are of concern due to their association with medial knee joint compression [1]. Hip abduction moments were significantly higher during the second step of stair descent, but not the first step. This suggests that it is important to analyze multiple steps when using stair analysis as a clinical tool. Changes in the generation of hip abductor moments are critical to quantify since these moments have been reported to protect against the progression of knee osteoarthritis [2].

Increases in vastus lateralis muscle activity during stair ascent are necessary to counteract the net external knee flexion moment associated with stair ascent [4]. Biceps femoris muscle activity was also greater during the second step of stair ascent as compared to descent. Previously, it has been shown that lateral thigh muscle activation aids in opposing knee varus moments [3]. Despite an increase in knee varus moments and vastus lateralis muscle activity during ascent, the co-contraction ratio did not increase concomitantly as a potential mechanism to stabilize the knee joint. Additional analysis of medial thigh muscle activity patterns may provide further insight into knee joint stabilization.

CONCLUSIONS

Understanding thigh muscle activity patterns and lower extremity frontal plane mechanics is important for delaying the onset or slowing the progression of knee osteoarthritis. Stair ascent results in greater knee varus moments and greater vastus lateralis muscle activity when compared to stair descent. In contrast, stair descent resulted in increased hip abduction moments, but only during the second step. Therefore, it is suggested that multiple steps of stair ascent and stair descent should be analyzed during clinical assessments.

REFERENCES

1. Butler RJ, et al. *Br J Sports Med* **43**, 366-370, 2009.
2. Chang A, et al. *Arthritis Rheum* **52**, 3515-3519, 2005.
3. Zhang LQ, and Wang G. *J Biomech* **34**, 1107-1115, 2001.
4. Kowalk DL, et al. *J Biomech* **29,** 383-388, 1996.

LOAD CARRIAGE INCREASES MECHANICAL LOADING RATES DURING WALKING

[1] He Wang, [1]Jeff Frame, [1]Elicia Ozimek, [1]Cara Reedstrom, [2]Daniel Leib, and [2]Eric Dugan,
[1]Ball State University, [2]Boise State University
email: hwang2@bsu.edu

INTRODUCTION

Stress fracture is an overuse bone injury. It is a result of excessively repetitive loads acting on the bone over time which leads to fatigue induced bone microdamage [1,2]. Mechanical loading and loading rate are two major factors related to stress fracture development.

Military personnel are commonly afflicted by stress fractures during basic training. The injury rate of stress fractures during basic training is approximately 6% in the US ARMY [3]. During basic training, new recruits have to take on strenuous training protocols including loaded long-distance walking. The lower extremities are therefore exposed to increased and repetitive ground reaction impact forces during basic training. It was found that the most common site of stress fracture in military recruits is the tibia [3], which accounts for more than 40% of total stress fractures in the military [4,5].

Load carriage has been found to alter gait kinematics, and increase ground reaction force proportionally [6,7]. However, the effect of load carriage on the risk of musculo-skeletal injuries such as tibial stress fracture is not fully understood. Specifically, the effect of load carriage on mechanical loading rate has not been investigated. It is not clear, if and how load carriage affects the ground reaction loading rates during walking. The purpose of the study was to investigate the effect of load carriage on ground reaction loading rates during walking. It was hypothesized that ground reaction forces and ground reaction loading rates would increase during loaded walking.

METHODS

Eighteen healthy male subjects (age: 21 ± 2 yr.; body mass: 79 ± 11 kg; body height: 181 ± 4 cm) participated in the study. Subjects wore military boots and performed unloaded walking and loaded walking with a 32 kg rucksack at 1.67 m/s on a force instrumented treadmill (AMTI). Ground reaction forces were collected at 2400 Hz. The following variables were analyzed: peak vertical and antero-posterior (braking) ground reaction forces, peak instantaneous and average vertical and braking loading rates during weight acceptance of walking. A one-way repeated measures MANOVA was used to determine differences in these variables between normal and loaded walking conditions. $\alpha = 0.05$.

RESULTS AND DISCUSSION

Compared to unloaded walking, the loaded walking exhibited a 49% increase of peak vertical GRF, a 48% increase of peak braking GRF, a 96% increase of vertical ground reaction loading rate, and a 72% increase of braking ground reaction loading rate during weight acceptance ($p<0.000$) (Table 1).

As we expected, carrying a 32 Kg load led to significant increases of ground reaction forces. As high-magnitude mechanical loads are associated with tibial stress fracture [1, 3, 8], the large increases of ground reaction forces during loaded walking may lead to an increase of tibial bone strain and possibly increase the chance of developing tibial stress fracture.

We also found that there were significant increases of ground reaction loading rates when walking with load. As repeated loading at higher loading rates is more damaging to the bone than at lower loading rates [9], it is possible that the great increase of vertical and braking ground reaction loading rates could expose the tibial bones to increased risk of stress fracture. Surprisingly, the increases of ground reaction loading rates outpace the increases of ground reaction forces during loaded walking. It is possible that it may be the great increase of the ground reaction loading rates leading to great increased risk of tibial stress fracture.

Walking with loads that could be as high as 60% of body weight is an inevitable part of the military basic training. During a twelve-week basic training, the combined running and walking distance could exceed 200 miles [1]. The increased ground reaction forces and ground reaction loading rates associate with every step during loaded walking could expose the military recruits to increased risk of tibial stress fracture. Future study should focus on in-vivo measurement of tibial bone deformation to confirm that load carriage would lead to increases of strain and strain rate during walking.

CONCLUSIONS

Load carriage results in greater increases of ground reaction force loading rates during walking.

REFERENCES

1.Jones, B.H., et al. *Exercise & Sport Sciences Rev.* 17: 379-322,1989.

2.Burr, D, et al. *Exercise & Sport Sciences Rev.* 25: 171-194,1997.

3.Brukner, P., et al. *Stress fracture*, 1999

4.Beck, T.J., et al. *J. of Bone and Mineral Res.* 11: 645-653, 1996.

5.Winfield, A.C., et al. *Military Medicine*. 162: 698-702, 1997.

6.Polcyn, et al., Technical Report, *USARIEM*. 2002

7.Harman, et al., Technical Report, USARIEM. 2000.

8.Grimston, S.K., et al., *Int. J. Sport Biomechanics* 7: 293-302, 1991.

9.Schaffler, M.B., et al., *Bone* 10: 207-214, 1989.

ACKNOWLEDGEMENTS

Funding source: Department of the Army #W81XWH-08-1-0587

Table 1: Peak vertical and braking GRFs and instantaneous vertical and braking ground reaction loading rates during weight acceptance of walking.

Variables	Unloaded walking	Loaded walking
Peak vertical GRF (BW)*	1.28 ± 0.07	1.90 ± 0.17
Peak braking GRF (BW)*	0.23 ± 0.03	0.34 ± 0.04
Instantaneous vertical ground-reaction loading rate (BW/s)*	17.58 ± 3.96	34.48 ± 10.73
Instantaneous braking ground-reaction loading rate (BW/s)*	8.34 ± 1.73	14.39 ± 5.12

Note. * indicates $p < 0.000$

BIOMECHANICS OF UPHILL WALKING IN MODERATELY OBESE ADULTS

Michelle Reynolds, Kellie Ehlen, Kathryn Dannecker, Cameron Carter, Raymond Browning

Colorado State University, Fort Collins, CO, USA.
email: browning@cahs.colostate.edu

INTRODUCTION

Walking is a popular form of exercise for the prevention and treatment of obesity. However, walking may be a source of biomechanical loads that link obesity and musculoskeletal injury and pathology, including knee osteoarthritis [4]. During level walking, moderately obese adults have greater lower extremity net muscle moments vs. their non-obese counterparts [1,2]. When non-obese individuals walk uphill, hip and knee net muscle moments are greater than during level walking [3], but the effects of obesity on the biomechanics of uphill walking are not known. An understanding of how incline affects the biomechanics of walking in obese adults may aid in the development of exercise recommendations that reduce the risk of musculoskeletal pathology.

The purpose of this study was to quantify the biomechanics of uphill vs. level walking in moderately obese adults. We hypothesized that obese individuals would walk with a more flexed posture and that hip and knee extensor moments would increase during uphill vs. level walking.

METHODS

Twelve obese adult volunteers participated in this experiment, mass = 100.5 (15.7) kg, BMI = 33.4 (2.6) kg/m^2, (mean (S.D.)). We measured ground reaction forces and three-dimensional lower extremity kinematics while subjects walked on a dual-belt force measuring treadmill at 1.25 m/s. Each subject completed a 6-minute trial with the treadmill grade set at 0, 3, 6 and 9° (four trials total), with 30 seconds of biomechanics data collected during the final minute of the trial. Kinematic parameters were collected at 60 Hz using eight optoelectric cameras. Ground reaction forces and moments were recorded at 1200 Hz by force platforms embedded under each treadmill belt. We calculated net muscle moments at the hip, knee and ankle via standard inverse dynamics techniques. Body segment parameters were estimated via DEXA and published regression equations [5]. Biomechanics variables were normalized as to represent a percentage of the stride. We calculated the mean of each variable of interest over 20-25 strides at each grade for each subject and the mean across subjects for each trial.

Repeated measures ANOVA determined how obesity affected temporal gait characteristics, mid-stance joint angles and peak net muscle moments. Necessary post-hoc comparisons using Holm-Sidak were performed. A criterion of $p<0.05$ defined significance.

RESULTS AND DISCUSSION

There were no significant temporal-spatial differences measured in uphill verse level walking, (i.e. stride length and stride frequency were similar). Participants walked uphill with a more flexed posture, characterized by greater knee and hip flexion. Anterior-posterior braking ground reaction forces decreased while propulsive forces increased as the grade became steeper. As a result, participants exhibited increased hip and knee extensor net muscle moments when walking uphill vs. level walking (Fig. 1). Peak hip and knee extensor moments increased ~70% and 125% as grade increased. Ankle net muscle moments were similar across the grades used in this study. The abduction moment at the knee decreased during uphill vs. level walking (Fig. 2). The increase in net muscle moments at the hip and knee suggest increased loads across these joints during uphill vs. level walking. In addition, the greater hip extensor moment is likely to increase knee flexor muscle force production and require greater knee extensor muscle force to extend the knee. The reduction in the knee abduction moment during uphill walking

suggests a relatively lower medial distribution of load across the knee joint, although the compressive loads may be much greater.

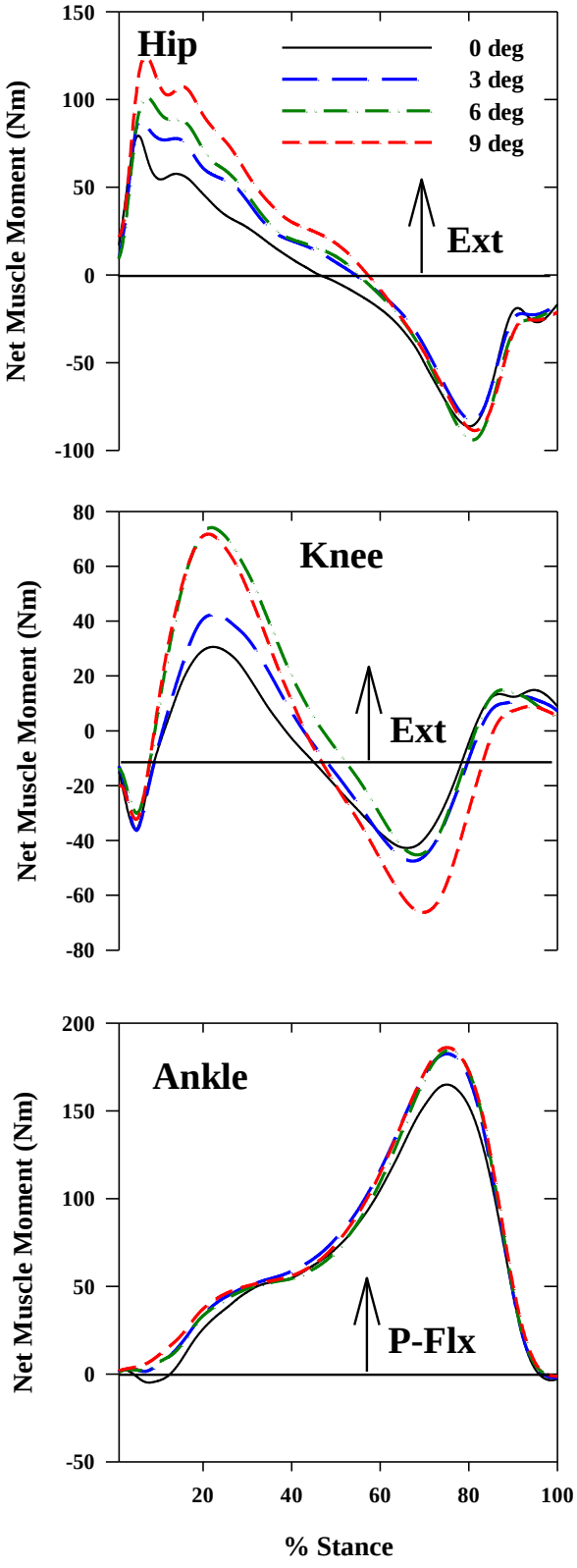

Figure 1. Mean hip, knee and ankle flexion/extension moments during level vs. uphill walking. Ext: extension, P-flex: plantarflexion.

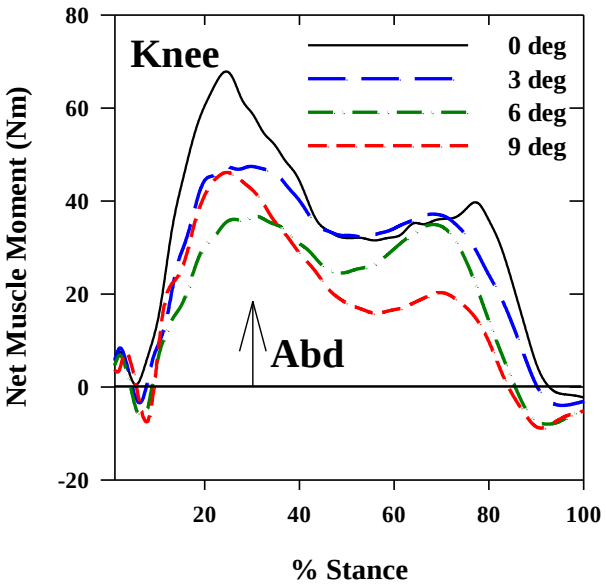

Figure 2. Mean knee abduction moment during level vs. uphill walking. Abd: abduction.

CONCLUSIONS

These results suggest that walking uphill at normal or typical walking speeds, while increasing energy expenditure, may not be ideal for obese adults as the risk of musculoskeletal injury/pathology is likely to be increased.

REFERENCES

1. Browning, R.C. et al. *Med Sci Sports Exerc*, **39**(9), 1632-41, 2007.
2. Lai, P.P., et al. *Clin Biomech*,. **23**, S2-6, 2008.
3. Lay, A.N., et al. *J Biomech*,. **39**(9), 1621-8, 2006.
4. Felson, D.T., et al. *Ann Intern Med*, **109**, 18-24, 1988.
5. Durkin, J.L., et al. *J Biomed Eng*, **125**, 515-522, 2003.

ACKNOWLEDGEMENTS

This research was supported by a grant from the CSU College of Applied Human Sciences and NIH grant R03AR059264.

HUMAN ANKLE MECHANICS DURING ABLE-BODIED AND PATHOLOGICAL GAIT

[1]Anirban Dutta

[1]Rehabilitation Institute of Chicago, Chicago, USA, a-dutta@northwestern.edu,

INTRODUCTION

Human ankle-foot complex plays an important role in absorbing/dissipating energy during foot-strike phase and injecting energy during push-off phase of walking, as it transforms from a relatively pliable state to a more rigid state [Nigg, 2007]. However, neuromuscular weaknesses can affect this critical function of ankle-foot complex and may have detrimental effect on the stability of walking. An active ankle-foot orthosis (AFO) was designed with a Stewart platform type mechanism with compliant linear actuators [Dutta and Dankowicz, 2003]. A relevant admittance matrix can be implemented by orienting the unloaded foot during swing phase (at minimal energy cost) [Piiroinen & Dankowicz, 2005] and constraining with passive mechanical elements [Goswami and Peshkin, 1999].

This paper investigated the mechanics of ankle joint during stance phase of gait with four able-bodied subjects and an incomplete spinal cord injured (ISCI) subject. Surprisingly, the net ankle-joint stiffness was found to be more 'statically' stabilizing (i.e., positive-definite) for ISCI that the able-bodied subjects. So the postulate that a biomimetic active AFO may play a stabilizing role in cases of pathological ankle could not be substantiated.

METHODS

The incomplete spinal cord injured subject (ISCI) was a 34 years old male with T1 motor incomplete spinal cord injury (ASIA D) that resulted in left hemiplegia, who could walk only short distances with rolling walker. Four able-bodied subjects who volunteered for this study had no known injury or pathology during the study. Informed consent was obtained from the subjects before their participation.

Retro-reflective markers were placed on the body segments according to the 'plug-in' gait marker set in the Vicon Workstation (Vicon Peak, USA) software to acquire lower-body kinematics data using a seven camera Vicon motion capture system. Two multi-axis force platforms (AMTI, USA) were embedded in the floor of the walkway. The mechanics of the left ankle (pathological for iSCI subject) was investigated for all subjects. Surface EMG was collected from Gastrocnemius (medial and lateral heads), Peroneus Longus, Soleus, and Tibialis Anterior following SENIAM guidelines [http://www.seniam.org/].

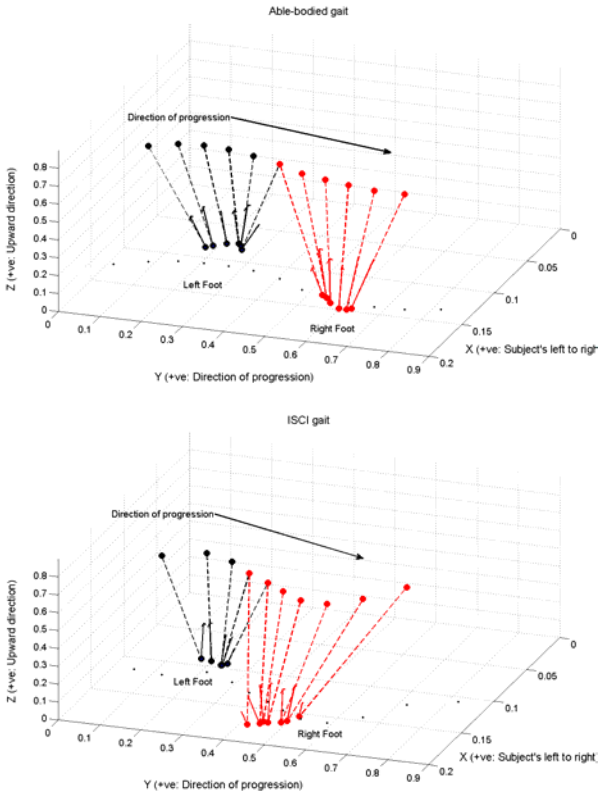

Figure 1: The figures show a typical able-bodied (top panel) and ISCI gait (bottom panel) with the global XYZ coordinate system.

The gait kinematics and ground reaction forces/moments data were digitally low-pass filtered at 10 Hz (5^{th} order zero-lag Butterworth) while the EMG data was band-pass filtered at 20Hz-500Hz (5^{th} order zero-lag Butterworth), rectified and low-pass filtered at 25 Hz (5^{th} order zero-lag Butterworth) before being analyzed with custom software developed in Matlab (The Mathworks, USA). Figure 1 shows the resultant ground reaction forces as arrows originating from the center of pressure (CoP) on force platform with black vectors showing left foot and red vectors showing the right foot. Also, the lean-line joining the CoM and the CoP is shown.

Joint torques (τ) and left-ankle joint-angle (θ) trajectory were found from VICON data. Assuming that the joint torque depends on joint-angle (θ) and muscle

forces (f), and muscle force (f) depends on muscle length (l) and neural drive (u) (ignoring the force-velocity dependence) [Hogan, 2007],

$$\frac{\partial \tau}{\partial \theta} = \Gamma(\theta) + j^T(\theta)\left(\frac{\partial f}{\partial l}\right) j(\theta) \qquad (1)$$

$$dl = j(\theta)d\theta$$

The muscle force is given by Mykin model [Shin et al., 2009]

$$l = (l_0 - l_1 u + \int j(\theta)d\theta) \text{ where } l_0 \text{ and } l_1 \text{ are parameters.} \qquad (2)$$

$$f = (k_0 + k_1 u)l \text{ where } k_0 \text{ and } k_1 \text{ are parameters}$$

The net joint stiffness $\left(\Gamma(\theta) + j^T(\theta)\left(\frac{\partial f}{\partial l}\right) j(\theta)\right)$ was estimated using multiple linear regression ('regress' in Matlab) from 40 able-bodied gait trials and 10 iSCI gait trials at each time-normalized data-point. The "kinematic stiffness" $(\Gamma(\theta))$ and "neuromuscular stiffness" $\left(j^T(\theta)\left(\frac{\partial f}{\partial l}\right) j(\theta)\right)$ were computed from neural drive (u) found from EMG data and jacobian ($j(\theta)$) found from muscle moment arms [Delp et al., 1990]. The net joint stiffness $\left(\Gamma(\theta) + j^T(\theta)\left(\frac{\partial f}{\partial l}\right) j(\theta)\right)$ was investigated for positive-definiteness.

RESULTS AND DISCUSSION

Figure 1 shows the movement planes and directions: X, Y, and Z. Figure 2 shows the ankle moment versus ankle angle plots for all the movement planes across all the trials for able-bodied and ISCI subjects. It can be seen in Figure 2 that the slow (~0.12 m/sec) ISCI gait speed created a hysteresis loop in all the plots which implied that the energy in the system was dissipated at the ankle. The hysteresis loop is almost absent for able-bodied subjects who are walking at their preferred speed (~1.4m/sec) (Figure 1).

We also analyzed the positive-definiteness of the net ankle-joint stiffness matrix by checking the eigenvalues as well as determinants of (1x1), (2x2), and (3x3) square sub-matrices (i.e., the principal minors) to see if they are all greater than zero. We found that the net ankle-joint stiffness was more 'statically' stabilizing (i.e., positive-definite) for ISCI that the able-bodied subjects. The ankle-moment verses ankle angle plots are consistent with the sagittal plane results presented in prior work [Hansen et al., 1990]. The hysteresis loop and energy dissipation could be explained by the slow walking speed in case of ISCI subjects.

SUMMARY

1. The energy in the locomotor system was dissipated more at the ankle joint incase of slower ISCI gait as compared to able-bodied gait – elucidated by the ankle moment versus ankle angle plots – in all the movement planes.
2. The net ankle-joint stiffness was more 'statically' stabilizing for ISCI that the able-bodied subjects, which need further investigation in terms of its constituents, "kinematic stiffness" matrix and "neuromuscular stiffness" matrix and how they affect the dynamical stability of gait.

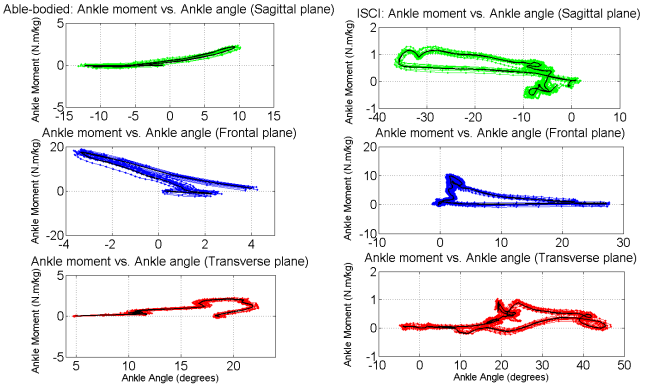

Figure 2: Ankle moment versus ankle angle plots for able-bodied subjects (left panel) and ISCI subjects (right panel).

REFERENCES

Nigg BM. *Biomechanics of the Musculo-skeletal System*, Wiley, 2007.

Dutta A and Dankowicz HJ. *BMES 2003 Annual Fall Meeting*, 2003.

Piiroinen, P and Dankowicz HJ. *International Journal of Bifurcation and Chaos*, 15(6), 1959-1974, 2005.

Goswami A and Peshkin M. *International Journal of Robotics Research*, 18(8), 1999.

Hogan N. Advances in Robot Control, 201-216, Springer Berlin Heidelberg, 2007.

Shin D, et al. *J Neurophysiol*, 101, 387-401, 2009.

Delp SL, et al. *IEEE Transactions on Biomedical Engineering*, 37, 757-767, 1990.

Hansen AH., et al. *Journal of Biomechanics*, 37, 1467-1474, 2004.

ACKNOWLEDGEMENTS

The concept for this work was developed when the author was working with Dr. Harry Dankowicz at the Engineering Science and Mechanics department of Virginia Polytechnic Institute and State University. The data-collection for this work was supported by Dr. Ronald Triolo's Merit Review project B2933R from the United States Department of Veterans Affairs at Loius Stokes Cleveland VA Medical Center.

VASCULAR OCCLUSION AFFECTS GAIT VARIABILITY PATTERNS OF HEALTHY YOUNGER AND OLDER INDIVIDUALS

[1]Sara A. Myers, [2,3]Jason M. Johanning, [2,3]Iraklis I. Pipinos, and [1,2]Nicholas Stergiou

[1]University of Nebraska at Omaha, Omaha, NE, USA
[2]University of Nebraska Medical Center, Omaha, NE, USA
[3]Veterans Affairs Medical Center, Omaha, NE, USA
email: sfagan@unomaha.edu, web: http://biomech.unomaha.edu

INTRODUCTION

Peripheral arterial disease (PAD) is a localized manifestation of systemic atherosclerosis, affecting the leg arteries and resulting in significantly reduced blood to the lower extremities. PAD affects eight to twelve million individuals in the US, with the majority of these being elderly[(1)]. Intermittent claudication, a cramping pain occurring in the lower extremity muscles with physical activity and relieved with rest, is the most common symptom of PAD. PAD has been shown to lead to poor health outcomes, immobility, physical dependence, and an increased risk for falling. Previous research in our laboratory indicates that PAD patients have altered gait variability patterns prior to the onset of claudication pain[(2)]. However, the specific mechanisms that contribute to these alterations in PAD patients are unclear. Potential mechanisms include insufficient blood flow, underlying neural and muscular abnormalities of the lower extremity, and systemic co-morbidities[(3)]. Therefore, our study sought to isolate and determine the impact of reduced blood flow on gait parameters by evaluating lower extremity gait variability before and after induced lower extremity vascular occlusion in healthy younger and older individuals. We hypothesized that a decrease in blood flow would result in significant gait variability alterations compared to baseline gait. Additionally, we hypothesize that age would augment the changes in gait variability following the vascular occlusion.

METHODS

Thirty healthy young subjects (Age: 22.8 ± 4.2 years) and 28 healthy older subjects (Age: 60.2 ± 8.2 years) walked on a treadmill while kinematics (60 Hz) were recorded using a Motion Analysis system. Participants walked at their self-selected speed for 3 minutes (Baseline). Next, vascular occlusion was induced by thigh cuffs placed bilaterally on the upper thighs and inflated to 200 mmHg for three minutes while subjects were standing. After three minutes of occlusion, the thigh cuffs were removed and the subjects immediately began walking on the treadmill (Post Occlusion). Relative joint angles of the ankle, knee, and hip were calculated for thirty strides from the Baseline and Post Occlusion conditions. Gait variability was assessed from the unfiltered joint angles using the largest Lyapunov exponent (LyE) and approximate entropy (ApEn). The LyE is a measure of the rate of divergence of neighbored state-space trajectories and it estimates the sensitivity of the locomotor system to perturbations. The ApEn quantifies the regularity or predictability of a time series. The Chaos Data Analyzer[(4)] was used to calculate the LyE. ApEn was computed using algorithms written by Pincus[(5)] implemented in Matlab. Gait variability was compared using a 2 X 2 ANOVA (Groups: Younger vs. Older, Conditions: Baseline vs. Post Occlusion). When a significant interaction was identified, independent t-tests were used for post-hoc analysis to identify significant differences between the group/condition combinations.

RESULTS AND DISCUSSION

There was a significant effect of condition for all variables tested. Specifically, the LyE and ApEn values were significantly higher Post Occlusion compared to the Baseline condition. There was also a significant effect of group, with the ApEn at the hip being significantly higher in the older group. Additionally, there was a significant interaction for the ApEn at the ankle. Specifically, the younger group had significantly higher values Post

Occlusion as compared with the older and younger groups at baseline. Also, the older group Post Occlusion had significantly higher ApEn at the ankle compared with the younger group at baseline.

Our results demonstrate significant gait variability alterations for all lower extremity joints Post Occlusion based on the LyE and ApEn in both healthy younger and healthy older individuals. The direction of differences are similar to a previous study comparing gait variability of healthy matched controls and patients with PAD[(2)]. Specifically, the differences indicated an increase in noise and irregularity while walking after vascular occlusion and may reflect a diminished capacity of the neuromuscular system to achieve a stable gait. However, direct comparison of the magnitude of change in LyE values show that interruption of blood flow does not account for the total amount of changes in gait variability exhibited by patients with PAD. To compare values directly, the mean differences from the healthy baseline condition (younger and older combined means) were expressed as percentage change averaged across all joints for the Post Occlusion condition and for PAD patients as compared to the healthy baseline condition. The Post Occlusion condition had an average increase in LyE values of 11.5%, while the PAD patients had an average increase of 41.3%[(2)]. Thus, our findings support the idea that interruption of blood flow results in significant gait alterations in otherwise healthy individuals, but patients with PAD experience additional alterations in variability that are likely due to underlying cellular abnormalitites in the lower extremity muscles and nerves that have been demonstrated in these patients[(6)]. As a result of age, there was only one significant group effect of the six variables tested, while restricted blood flow caused significant differences in all variables (Table 1). This suggests that altered blood flow status, as seen in PAD, is a greater determinant of gait function than age.

SUMMARY

Collectively, our study shows that reduced blood flow, in the absence of pathology significantly alters gait variability patterns. However, the change in the gait variability patterns was not as severe as previously documented in symptomatic patients with PAD during pain free ambulation. These results support the hypothesis that additional neuromuscular problems in the lower extremities of patients with PAD contribute to gait alterations in these patients. Nevertheless, blood flow is one mechanism contributing to altered gait variability patterns in patients with PAD and individuals with risk factors for PAD should be screened and treated immediately to prevent potential mobility problems (i.e. falls) and the development of more severe pathophysiological changes that have been observed in symptomatic PAD patients.

REFERENCES

1. American Heart Association, American Stroke Association. *Heart disease and stoke statistics*, 2007.
2. Myers S et al. *J Vasc Surg,* **49**, 924-31, 2009
3. McDermott M et al. *JAMA,* **286**,1599-606, 2001.
4. Sprott J, and Rowlands G. *Chaos data analyzer: The professional version*, American Institute of Physics, 1995.
5. Pincus S. *Chaos*, **5**, 110-7, 1995.
6. Pipinos I et al. *Vasc Endovascular Surg,* **42**, 101-12, 2008.

ACKNOWLEDGEMENTS

American Society of Biomechanics Graduate Student Grant-in-Aid, AAHPERD Graduate Student Grant-in-Aid, the Nebraska Research Initiative, and NIH (K25HD047194 and F31AG032788).

Table 1: Group means for the largest Lyapunov Exponent (LyE) and the approximate entropy (ApEn) for younger (Y) and older (O) groups during the Baseline (B) and Post Occlusion (PO) conditions. All values are reported mean ± standard deviation.

Condition	Ankle	Knee	Hip
LyE			
Y-B	.069 ± 0.02	.066 ± 0.02	.066 ± 0.02
Y-PO	.088 ± 0.02	.081 ± 0.02	.076 ± 0.02
O-B	.076 ± 0.02	.074 ± 0.02	.071 ± 0.02
O-PO	.080 ± 0.01	.084 ± 0.02	.080 ± 0.02
Significance	*	*	*
ApEn			
Y-B	.712 ± 0.13	.431 ± 0.08	.307 ± 0.06
Y-PO	.858 ± 0.17	.504 ± 0.08	.374 ± 0.08
O-B	.762 ± 0.14	.482 ± 0.08	.349 ± 0.08
O-PO	.822 ± 0.13	.527 ± 0.09	.406 ± 0.09
Significance	*, ‡, §, ‖,¶	*	*

* p<0.05, significant difference, B vs. PO
‡ p<0.05, significant difference, Y vs. O
§ p<0.05, significant interaction, Y-B vs. O-PO
‖ p<0.05, significant interaction, Y-B vs. Y-PO
¶ p<0.05, significant interaction, Y- PO vs. O-B

GAIT AFTER UNILATERAL TOTAL KNEE ARTHROPLASTY: FRONTAL PLANE ANALYSIS

[1,2]Ali H. Alnahdi, [1] Joseph A. Zeni, [1]Kevin McGinnis and [1]Lynn Snyder-Mackler
[1]University of Delaware, Newark, DE, USA
[2]King Saud University, Riyadh, Saudi Arabia.

INTRODUCTION

Total knee Arthroplasty (TKA) is a common surgical procedure for end stage osteoarthritis (OA). After unilateral TKA, OA progresses in a non-random fashion in which the side contralateral to the operated knee is more likely to show the progression of the disease more than the operated side [1]. This laterality in disease progression suggests that mechanical factors might be involved in the disease progression. Patients after TKA present with altered gait mechanics that either developed after surgery or retained from pre-surgery patterns. The altered gait mechanics may alter the loading on the contralateral side and predispose it to disease progression. The external knee adduction moment is the best predictor of OA progression and can be used as indirect measure of loading in the medial tibiofemoral compartment [2]. Based on that, examining the frontal plane mechanics is important in understanding loading in both limbs in subjects after TKA. The first aim of this study was to compare frontal plane kinematics and kinetics of the operated and non-operated knee in two groups, 6 months and 1 year after unilateral TKA. The second aim of this study was compare the mechanics of both sides in patients with TKA to a healthy control group.

METHODS

Thirty one subjects 6 months after unilateral TKA (10 women, Age 70.03± 7.6y, BMI 31.5±6.3) and forty four subjects 1 year after unilateral TKA (21 women, Age 63.25± 12.4y, BMI 30.5± 4.5) were recruited. The healthy control group consists of 20 subjects (11 women, Age 62.6± 6.5y, BMI 28.8± 5.1) who reported no knee pain or injury. All subjects signed informed consent forms prior to participation. Gait analysis was performed using a three dimensional, 8-camera motion capture system (VICON, Oxford Metrics, London, England) synchronized with two Bertec force platforms (Bertec Corp., Worthington, OH, USA). Spherical retro-reflective markers were placed bilaterally on anatomical landmarks and rigid thermoplastic shells with at least 3 markers were secured on the lower leg and thigh and pelvis. Subjects practiced walking until reaching a constant self-selected speed. The collected trials fell within 5% of the practiced speed with clear contact of only one foot on each force plate. Seven walking trials were collected for each subject and the mean of these trials was used in the analysis. Frontal plane knee joint angles were calculated using rigid body analysis and Euler angles. Joint moments were calculated using inverse dynamics and were expressed as external moments normalized to body mass and height using Visual 3D software (C-motion, Inc, Rockville, MD). Knee adduction impulse was calculated by integrating the knee adduction moment curve during stance phase. Spatial and temporal parameters of gait were also calculated. For the control group, the data of both sides were averaged and the average was used in the analysis. A two-way mixed model analysis of variance (time x side) was used to examine within subjects (operated versus non-operated) and between subjects (6 months versus 1 year) differences in patients with TKA. The operated and non-operated knees of TKA group (6 months and 1 year subjects grouped together) were compared independently with the control group using independent t-test. All statistical analyses were performed with SPSS 16. Significance level was set at 0.05.

RESULTS AND DISCUSSION

Kinematics, kinetics, and temporo-spatial parameters were examined (Table 1). Peak knee adduction moment (PKAM), and knee angle at PKAM showed no time by side interaction, no time effect, but effect of side was significant ($P<0.05$) with the non-operated knee being more adducted and having larger moment than the operated knee. Knee adduction impulse and stance time showed no

time by side interaction, no effect of side, but effect of time was significant (P<0.03) with the 6 months group having higher impulse and longer stance time. The 6 months group had higher impulse compared to the 1 year group because they spend more time in stance. The operated and non-operated knees have similar impulse but the non-operated knee have higher PKAM suggesting higher loading.

Comparing TKA group to the control group revealed no difference between both the operated and non- operated limbs and controls in knee angle at PKAM, knee adduction impulse, and stance time (P>0.05). The control group had longer step length compared to operated (P=0.006) and non-operated knee (P=0.001) of the TKA group. The control group PKAM was not different from the non-operated limb (P=0.094), but it was higher than operated limb (P=0.001) (Fig.1). Because the control group walked faster than the TKA group (P=0.001), we reanalyzed the PKAM data using one way ANCOVA using speed as a covariate. When controlled for speed, the non-operated knee PKAM was still not different from that of the control group (P=0.57), while the PKAM of the operated knee approached significantly lower values than that of the control group (P=0.056). Looking at the loading of the non-operated knee compared to healthy controls, the data suggests that both groups experience the same total exposure to the adduction moment, as indicated by the impulse data, and the same peak amplitude of the adduction moment. On the other hand, subjects with TKA walked with shorter step length compared to the control group. With shorter step length, TKA group will take more steps to cover the same distance compared to the control group. With increasing the number of steps, the exposure of the TKA group to repetitive loading will increase compared to the control group. The higher repetitive loading of the non-operated knee might explain the predictable progression of OA in that limb. PKAM and impulse data should be interpreted cautiously when there are differences in temporo-spatial parameters

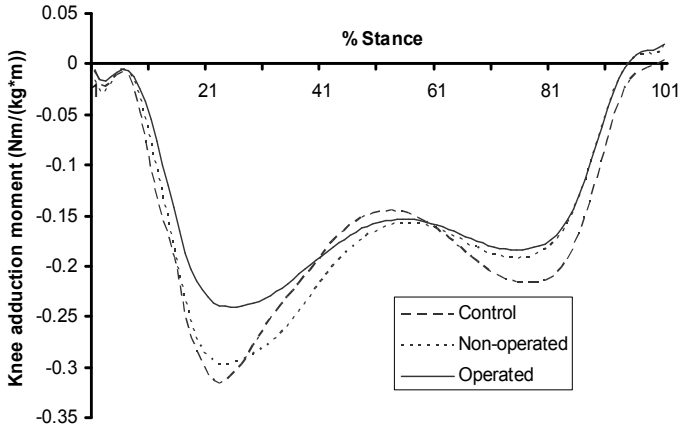

Figure 1. Average knee adduction moment curve.

REFERENCES

1. Shakoor, N, et al.. *Arthritis Rheum* **46,** 3185-9, 2002.
2. Miyazaki, T., et al.. Ann Rheum Dis **61** 617-22, 2002.

ACKNOWLEDGEMENTS

NIH grants (P20RR016458, S10RR022396) and a scholarship from King Saud University to Mr. Alnahdi.

Table 1: Gait parameters [mean (standard deviation)]; adduction angle is +ve; external adduction moment is -ve.

Variable	TKA 6mo		TKA 1 year		Control
	Operated	Non-operated	Operated	Non-operated	
Knee Angle (degree)	-0.14 (4.03)	2.65 (5.25)	0.58 (4.55)	2.7 (4.98)	2.26 (4.46)
PKAM (Nm/kg*m)	-0.26 (0.13)	-0.32 (0.14)	-0.28 (0.11)	-0.32 (0.15)	-0.37 (0.14)
Impulse ((Nm/kg*m)*s)	-0.11 (0.05)	-0.12 (0.05)	-0.09 (0.4)	-0.1 (0.05)	-0.12 (0.04)
Stance time (second)	0.7 (0.07)	0.7 (.07)	0.66 (0.06)	0.66 (0.05)	0.65 (0.06)
Step length (meter)	0.69 (0.08)	0.68 (0.08)	0.69 (0.06)	0.68 (0.06)	0.74 (0.07)
Walking speed (m/s)	1.27 (0.19)		1.31 (0.13)		1.43 (0.14)

DYNAMIC STABILITY OF A 3D DYNAMIC WALKING MODEL WITH SIMULATED NEURONAL NOISE

[1]Paulien E. Roos and [1]Jonathan B. Dingwell

[1]The University of Texas at Austin, Austin, TX, USA
email: jdingwell@mail.utexas.edu

INTRODUCTION

Fall risk increases in older adults and many risk factors have been identified [1]. Exercise programs can reduce falls in older adults. Typically, older adults enroll these programs having fallen. Early detection of increased fall risk will allow enrollment in preventative fall prevention programs. Several measures have been explored to identify those at risk of falling. Local and orbital stability are such measures, but initial studies to date on these measures were not conclusive on the application of these measures to predict fall risk [2, 3].

The aims of this study were therefore to determine how increased neuronal noise affects local and orbital stability, and if these measures can directly predict fall risk in a dynamic walking model. We hypothesized that 1) orbital stability would not change with increased neuronal noise, and therefore would not predict fall risk and that 2) short term, but not long term, local instability would increase with increased neuronal noise and therefore would be a predictor for fall risk.

METHODS

A 3D dynamic walking model (Fig. 1) was adapted from [4]. The model walked passively in the anterior-posterior direction, by walking down a gentle slope (4%) with gravity providing forward propulsion [4]. The model was inherently laterally unstable and included a lateral step controller to maintain lateral stability. This controller adjusted the splay angle of the legs (ϕ) at each instant of ground contact to match the state variables to their 'noise free' solution values. Neuronal noise, similar to that present in humans, was simulated by applying uniformly distributed random noise to the output of the lateral step controller. The amplitude of this noise (j_{noise}) was varied between a small amplitude that did not make the model fall over and a large amplitude for which the model always fell over. For each j_{noise}, 100 simulations were performed, each up to 125 steps or until the model fell over. For each j_{noise}, the probability of falling ($\%_{FALL}$) and the average number of steps the model walked before falling (*STF*) were calculated.

Fig. 1. Graphical representation of the 3D dynamic walking model.

For each separate simulation orbital stability (*maxFM*) and short term (λ_S) and long term (λ_L) local stability were calculated. Orbital dynamic stability was calculated by estimating the maximum Floquet Multiplier (*maxFM*) as in [3]. Local dynamic stability was calculated using the logarithmic divergence curve calculated as by Rosenstein et al. [5] and calculating the long-term (λ_L) and short-term (λ_S) Lyapunov exponents as in [6]. The λ_S were calculated over a range of 0 to 0.4 steps and λ_L over a range of 4 to 25 steps. To eliminate the influence of sample size on the outcomes [7], data were resampled to the average number of samples when no noise was applied to the model (881 samples/step). As accuracy of λ_S, λ_L and *maxFM* may increase with the number of steps used in the calculations [8], these variables were calculated over a consistent number of 50 steps for the first 20 trials of each j_{noise} that walked at least 55 steps.

RESULTS AND DISCUSSION

Orbital stability (*maxFM*) did not increase continuously or monotonically with noise amplitude (j_{noise}) (Fig. 2). It only increased significantly

($p<0.01$) at the highest noise amplitudes where the model fell over most of the time anyway and was therefore not a good predictor of fall risk ($\%_{FALL}$) (Fig. 2). This confirmed our first hypothesis.

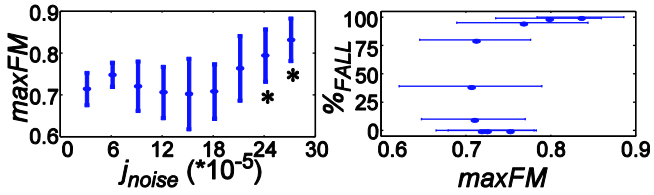

Fig. 2 Left: Local dynamic stability (*maxFM*) against noise amplitude (j_{noise}). Right: Probability of falling ($\%_{FALL}$) against *maxFM*. Error bars represent ±1 standard deviation. Significant differences ($p<0.01$) in *maxFM* from the value at $j_{noise} = 3*10^{-5}$ are indicated with a *.

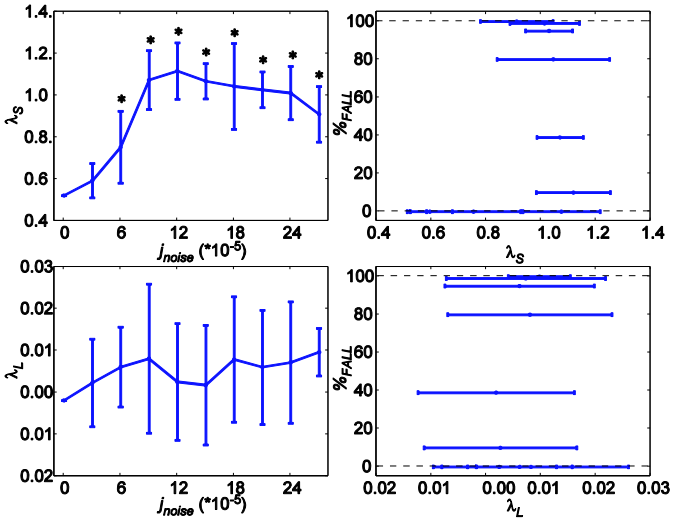

Fig. 3 Left: Short (λ_S) and long (λ_L) term local divergence exponents against noise amplitude (j_{noise}). Right: $\%_{FALL}$ against λ_S and λ_L. Error bars represent ±1 standard deviation. Significant differences ($p<0.01$) in λ_S and λ_L from the value at $j_{noise} = 3*10^{-5}$ are indicated with a *.

Short term local instability (λ_S) increased (more unstable) when noise was applied to the model, and leveled out at the higher noise amplitudes. λ_S started increasing before probability of falling ($\%_{FALL}$) even increased and was therefore a good early predictor for fall risk (Fig. 3). The long term local instability (λ_L) did not change with j_{noise} and was not correlated with fall risk ($\%_{FALL}$) (Fig. 3). This confirmed our second hypothesis.

The walking model used in this study only incorporated neuronal noise as a fall risk factor and did not include any other factors, such as strength, this does however not change our overall findings. The predictive behavior of short term local stability for fall risk may be specific to the model used in this study. Whether or not these findings will translate to predicting risk of falling in humans remains to be tested.

CONCLUSIONS

Short term local stability, but not long term local and orbital stability, was a good predictor for increased fall risk in a 3D dynamic walking model. This may have implications for fall prevention practice.

REFERENCES

1. Tinetti ME, Speechley M, Ginter SF. *New Engl J Med* **319**, 1701-1707, 1988.
2. Granata KP,Lockhart TE. *J Electromyogr Kinesiol* **18**, 172-178, 2008.
3. Su JL,Dingwell JB. *Trans ASME* **129**, 802-810, 2007.
4. Kuo AD. *Int J Robot Res* **18**, 917-930, 1999.
5. Rosenstein MT, Collins JJ, De Luca CJ. *Physica D* **65**, 117-134, 1993.
6. Dingwell JB,Kang HG. *Trans ASME* **129**, 586-592, 2007.
7. England SA,Granata KP. *Gait Posture* **25**, 172-178, 2007.
8. Bruijn SM, Dieen van JH, Meijer OG, *et al. J Neurosci Meth* **178**, 327-333, 2009.

ACKNOWLEDGEMENTS

Funded by Grant #1-R21-EB007638-01A1 from the National Institutes of Health.

THE EFFECT OF FOOT TYPE ON TEMPORAL-DISTANCE GAIT PARAMETERS IN HEALTHY INDIVIDUALS

[1]Jocelyn C. Frey, BS, [1]Rebecca A. Zifchock, PhD, [1]S. Betty Chow, PT, MA, OCS, [1]Andrew P. Kraszewski, MS, [1]Vishal Patel, BS, [1]Mark W. Lenhoff, BS, [1]Sherry I. Backus, PT, DPT, MA, [1]Jonathan T. Deland, MD, [2]Philip Demp, DPM, MS, PhD, [2]Jinsup Song, DPM, PhD, [2]Benjamin Heilman, MS, [1]Sonali Rajan, BS, MS, EdD, [1]Andrea Woodley, MS, [1]Howard J. Hillstrom, PhD

[1]Hospital for Special Surgery, NY, USA
[2]Temple University School of Podiatric Medicine, PA, USA
email: freyj@hss.edu

INTRODUCTION

An individual's foot structure is known to affect their injury patterns. McCluskey et al. [1] showed that people with pes cavus have conditions such as hammer toes, lateral ankle instability, and peripheral polyneuropathy, while those with pes planus tend to have conditions such as hallux valgus, posterior tibial tendon dysfunction, and plantar fasciitis [2]. Additionally, a study by Kaufman et al. showed that individuals with non-rectus foot structures had a higher incidence of overuse injuries than those with rectus feet [3]. This increased injury susceptibility may be related to differences in movement patterns caused by different foot types. A study by Hertel et al. looked at the effect of foot type on postural control [4]. However, there is little data in the literature describing the effect of foot type on temporal-distance gait parameters in healthy individuals.

Foot type is rarely accounted for in clinical gait analysis of healthy individuals. Yet, it is valuable to understand how an individual's foot structure affects their movement pattern. It may also be important to understand whether foot type should be considered when designing research studies as foot structure can vary within a population. Therefore, the purpose of this study was to determine if healthy individuals with different foot types have differences in temporal-distance gait parameters. It was hypothesized that foot type would have a significant effect on temporal-distance gait parameters.

METHODS

Sixty-one subjects were included in this study. Foot type was determined based on resting calcaneal stance position (RCSP) and forefoot to rearfoot alignment (FF-RF). Twenty-two were classified as having pes planus feet, 27 were classified as having rectus feet, and 12 were classified as having pes cavus feet.

Temporal-distance gait parameters were collected and analyzed using a GaitMatII (E.Q. Inc., PA) system. This device is a micro-computer controlled walkway comprising a matrix of binary switches to detect foot ground contact. Subjects completed 4 walks across the GaitMatII. The variables of interest were *step length, stride length, step time, swing time, stance time, single and double support time, velocity, and cadence*. All variables were normalized to each subject's height in meters.

Data from one foot were analyzed for each subject. For pes planus subjects, the foot (right or left) with the more valgus RCSP was included. For pes cavus subjects, the foot with the more valgus FF-RF value was included. For rectus subjects, the right foot was included.

The effect of foot type was tested separately for each variable using a one-way analysis of variance (ANOVA). Significance was set at $p<0.05$. A trend was operationally-defined at $p<0.1$. Post hoc t-tests were performed using the Bonferroni method.

RESULTS AND DISCUSSION

Table 1 summarizes the anthropometric characteristics of study subjects by foot type. There were no significant differences between the groups in terms of weight. To account for the trend that pes cavus subjects were taller than rectus subjects, all values were normalized to height. As expected, when compared to the rectus individuals, the pes

planus individuals exhibited more valgus RCSP and greater varus FF-RF values, while the pes cavus individuals exhibited more valgus FF-RF values.

Table 2 summarizes the study results. Contrary to the hypothesis, temporal-distance gait parameters were not significantly different between foot types.

Double support time and cadence exhibited a trend toward statistical significance. Post hoc t-tests indicated that there was a trend toward decreased cadence in the pes cavus as compared to the rectus individuals. There were no other statistical trends.

There were two parameters that exhibited a trend toward statistical significance. Both of these variables did exhibit moderately large differences between the different foot types. It is possible that a more evenly-distributed sample would have resulted in more statistically-significant differences. As opposed to grouping individuals, future studies could relate temporal-distance parameters to the precise degree of planus or cavus. These results only apply to temporal-distance parameters; the effects of foot type on full body kinetics and kinematics remains unclear. Additional research is needed before one could verify or refute that foot type is associated with differences in lower body motion parameters in healthy individuals.

CONCLUSIONS

The purpose of this study was to determine if healthy individuals with different foot types have differences in temporal-distance gait parameters. The results suggest that temporal-distance parameters are not affected by foot types. Therefore, foot type may not need to be considered when designing research studies of temporal-distance parameters in healthy individuals. However, more studies should be done to determine if this is true in individuals with pathology or deformity of the foot.

REFERENCES

1. McCluskey WP, et al. *Clin Orthop Relat Res* **247**, 27-37, 1989.
2. Giza E, et al. *Foot Ankle Clin* **12**, 251-271, 2007.
3. Kaufman KR, et al. *Am J Sports Med* **27**, 585-593, 1999.
4.Hertel J, et al. *J Athl Train* **37,** 129-132, 2002

ACKNOWLEDGEMENTS

NIH 1R03HD053135-01

Table 1: Test subject anthropometrics

	Pes Planus	Rectus	Pes Cavus	p-value
Number of Subjects	22	27	12	-
Males (Females)	10 (12)	8 (19)	6 (6)	-
Body Weight (N)	641.3 ± 128.1	662.8 ± 138.8	721.1 ± 155.1	0.38
Height (m)	1.71 ± 0.08	1.66 ± 0.11	1.74 ± 0.12	0.06
RCSP (°) (- valgus)	-6 ± 2	-1 ± 1	0 ± 1	>0.01
FF-RF (°) (- valgus)	7 ± 4	3 ± 1	-2 ± 1	>0.01

Table 2: Temporal-distance gait parameters (normalized to subject height)

	Pes Planus (SD)	Rectus (SD)	Pes Cavus (SD)	p-value
Step Length	0.40 (0.04)	0.39 (0.03)	0.39 (0.04)	0.72
Stride Length	0.80 (0.07)	0.79 (0.06)	0.77 (0.09)	0.64
Step Time (sec/m)	0.31 (0.02)	0.31 (0.02)	0.31 (0.04)	0.90
Swing Time (sec/m)	0.25 (0.02)	0.25 (0.02)	0.25 (0.03)	0.92
Stance Time (sec/m)	0.36 (0.03)	0.37 (0.03)	0.37 (0.04)	0.65
Single Support Time (sec/m)	0.25 (0.02)	0.25 (0.02)	0.25 (0.03)	0.98
Double Support Time (sec/m)	0.06 (0.01)	0.06 (0.01)	0.06 (0.01)	0.06
Velocity (sec)	0.77 (0.12)	0.78 (0.10)	0.72 (0.11)	0.38
Cadence (steps/sec*m)	67.7 (9.04)	71.3 (8.70)	64.7 (7.33)	0.08

NEUROMUSCULAR CONTROL ADAPTATION IN GAIT DUE TO INJURY: A MOTIVATING STUDY USING A SIMPLIFIED DYNAMIC MODEL

Louis A. DiBerardino III, Harry Dankowicz and Elizabeth T. Hsiao-Wecksler

University of Illinois at Urbana-Champaign, Urbana, IL, USA
email: diberard@illinois.edu

INTRODUCTION

Gait pathologies and injuries result in significant changes to the motion output [1]. The corresponding changes to the neuromuscular control system that generate these motions are more difficult to measure or interpret. For example, it has been shown through electromyography that control strategies can change even without significant kinematic or kinetic changes present [2]. The goal of this paper is to motivate the study of neuromuscular control adaptation due to injury using a simplified dynamic model. A fundamental hypothesis of this work is the existence of isolated discontinuous changes in the actuation strategies deployed by the neuromuscular control system in response to continuous changes in musculoskeletal physiology. Such discontinuous changes are common in nonlinear systems and could have immediate implications to rehabilitation strategies for maintaining functional gait.

To investigate the plausibility of this hypothesis, this work considers a multi-degree-of-freedom mechanical system that shares certain features with gait, such as periodicity, symmetry, coupled degrees of freedom, distinct phases of motion, and intermittent mechanical contact. The model's basic structure allows the possibility to study a periodic system response using simple inputs and equations of motion, while still capturing many of the advanced dynamical features found in gait.

METHODS

The simplified model used in this study is the periodically forced spring-mass-damper system shown in Fig. 1, where

$$F_i = A_{i,1}\cos\left(2\pi t + \phi_{i,1}\right) + A_{i,2}\cos\left(4\pi t + \phi_{i,2}\right) \qquad (1)$$

for $i \in \{3,5\}$ and $F_4 = -F_3 - F_5$, creating input similar to hip torques acting between the pelvis and thighs. Here, nonlinear spring constants emulate passive joint stiffnesses, where k_i increase from the given values (Table 1) at certain lengths of compression/extension, derived from [3]. Masses m_1 and m_7 are constrained to plastically impact the right wall (similar to foot impact) and to remain in sustained contact until the normal force becomes negative.

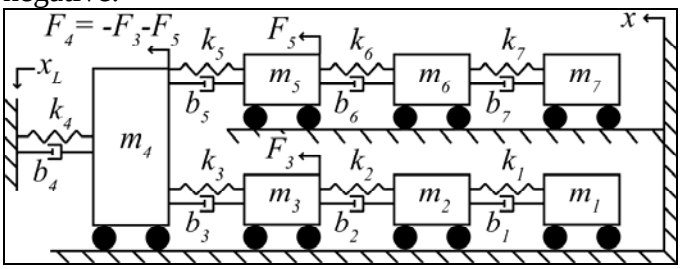

Figure 1: Coupled spring-mass-damper system.

The state-space equations for this system are then of the form

$$\frac{d\boldsymbol{x}}{dt} = \boldsymbol{A}_\sigma \boldsymbol{x} + \boldsymbol{F}\boldsymbol{u}, \qquad (2)$$

where the first seven components of state vector $\boldsymbol{x}$ are the positions of $m_1,\ldots,m_7$, and the remaining seven are the corresponding velocities. $\boldsymbol{A}_\sigma \in \mathbb{R}^{14\times 14}$ provides the relationships between the states and state derivatives (*i.e.*, combinations of k_i and b_i), where $\sigma \in \{1,2,3,4\}$ depends on the impact conditions. $\boldsymbol{F}\boldsymbol{u} \in \mathbb{R}^{14}$ provides the forcing described above.

The proposed procedure to investigate control adaptations due to 'injury' relies on numerical analysis and cost function optimization of (1) and (2). Specifically, we identify with the parameter values in Table 1 and with the left wall set to $x_L = 3$, a reference periodic solution found for

Table 1: Baseline parameters (l = natural spring length)

Index	m_i	k_i	b_i	l_i
1, 7	0.15	2.5	1	0.5
2, 6	0.5	5	2	1
3, 5	1	1	1	1
4	1	2.5	5	1

$$F_3 = 20\cos\left(2\pi t\right);\ F_5 = 20\cos\left(2\pi t + \pi\right) \qquad (3)$$

such that the motion of the lower masses is identical to that of the upper masses after a temporal shift of half a period. We proceed to increase k_6 and b_6 in 0.2 increments up to a maximal change of 2,

corresponding to a fully developed 'injury', and to subsequently reduce these parameters back to their reference values. After each change in the parameter values, optimization is applied to tune the forcing parameter values $A_{i,j}$ and $\phi_{i,j}$ (excluding $\phi_{1,1}$ without loss of generality) to minimize a suitably defined cost function applied to the asymptotic steady-state response.

Here, the cost function is a weighted combination of a measure of the degree of retained symmetry between the two sets of masses, quantified by the sum of $|x_1(t)-x_7(t-0.5)|$ across one period of oscillation, and a measure of the clearance of each end mass during the free-flight phase, quantified by the deviation in the maximal values of x_1 and x_7 from those found for the reference solution.

RESULTS and DISCUSSION

The equations of motion were numerically integrated using the *ode15s* routine in MATLAB. Optimization was performed using the *fmincon* routine in MATLAB. Overall control changes due to perturbation were assessed by comparing the baseline $A_{i,j}$ and $\phi_{i,j}$ values in (3) to the resulting control values after full perturbation, and upon return to baseline system parameters (Fig. 2).

As seen in Fig. 2, the perturbation necessitated control adaptation to maintain the prescribed goals of symmetry and clearance. More interesting was the result that the forcing did not return to the original form once the system configuration returned to the baseline state. This hysteresis demonstrated the ability for a system such as gait to settle onto some alternative control strategy during healing or rehabilitation.

Discontinuous changes in the (open-loop) control strategy throughout the parameter variation were assessed by plotting the optimized forcing variables versus the deviation in model parameters. The most interesting changes were found in amplitude $A_{3,2}$ (Fig.3). These are relatively large jumps in magnitude of the second forcing term for m_3 (Eq.1: i=3, j=2) at the third forward parameter iteration and first backward iteration. This suggests that controller sensitivity was quite large in certain regions of the model's parameter space. This implies that for systems with similar characteristics to gait, it is possible that certain phases of rehabilitation or healing could lead to discontinuous changes in control strategies. This is a plausible idea since the musculoskeletal system is a highly redundant system with infinitely many possibilities to achieve forward walking [4], allowing for the possibility of different control strategies exhibiting similar movement.

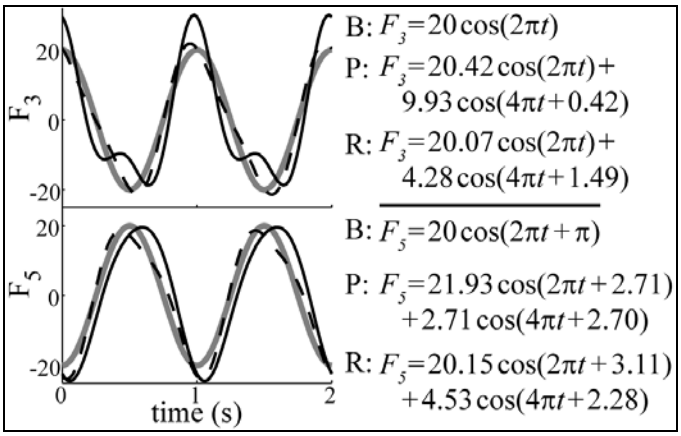

Figure 2: Baseline (B, grey), maximum perturbation (P, black) and return to baseline (R, dashed) forcing results

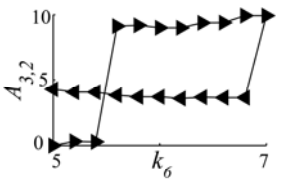

Figure 3: $A_{3,2}$ along perturbation of k_6 (and b_6)

Further work is needed for numerically implementing the controller goals to accommodate a broader range of system perturbations. A more detailed analysis of controller changes, and whether the resulting state outputs are discontinuously affected, is also needed. Work should extend to more realistic models of gait in order to better relate to the true control changes occurring with injury or rehabilitation. The present work certainly establishes that such phenomena may exist in dynamic systems sharing certain characteristics found in gait, and should be further explored to better understand the relatively unknown mathematics behind neuromuscular control with regard to injury.

ACKNOWLEDGMENTS

This work was funded by the National Science Foundation grant #0727083.

REFERENCES

1. Perry J. *Gait Analysis*, Slack, Inc., 1992.
2. Lindstrom M, et al. *Knee Surg Sports Traumatol Arthrosc* **18** (1), 106-114, 2010.
3. Yamaguchi GT. *Dynamic Modeling of Musculoskeletal Motion*, Kluwer Academic Publishers, 2001.
4. Bernstein, N. *The Coordination and regulation of movements*, Pergamon, 1967.

Effect of a Supervised Hip Flexor-Stretching Program on Gait in Healthy Elders

[1]J.R. Watt, [1]K. Jackson, [2]J.R. Franz, [1]J. Dicharry, [3]U. Della Croce, [4]D.C. Kerrigan.
[1]Department of Physical Medicine and Rehabilitation, University of Virginia, Charlottesville, USA
[2]Department of Integrative Physiology, University of Colorado, Boulder, USA
[3]Department of Biomedical Sciences, University of Sassari, Sassari, Italy
[4]JKM Technologies, LLC, Charlottesville, VA, USA

INTRODUCTION

We have previously shown, using 3-D motion analysis techniques, that reduced peak hip extension during walking is consistently found in elderly people when compared to young adults and is associated with hip flexion contracture [1, 2]. We have also previously shown moderate gait improvements from a twice-daily 10-week unsupervised hip flexor stretching program [3]. The purpose of this study was to evaluate the efficacy of a supervised, rigorous 10-week hip flexor stretching program in increasing passive hip extension and increasing hip extension, reducing peak anterior pelvic tilt and increasing stride length during walking in those with age-related reductions in peak hip extension.

METHODS

Eighty-two healthy elderly subjects (age 65-87 yrs) completed the study and were randomized to one of two study groups. A treatment group (n=43) completed a 10-week twice-daily hip flexor stretching program which was supervised twice weekly by a rehabilitation clinician. A control group (n=39) completed a 10-week shoulder stretching program. Pre- and post- intervention measures of passive hip extension range of motion and dynamic gait parameters during walking were taken. A 10-camera Vicon motion analysis system (Vicon Peak, Centennial, CO) and in-ground AMTI force plates (AMTI, Watertown, MA, USA) were used to collect kinematic and ground reaction force data during walking. The primary outcome parameters were passive hip extension range of motion, and peak hip extension, peak anterior pelvic tilt and stride length during walking. Paired samples *t*-tests were used to compare pre- and post-intervention values.

RESULTS AND DISCUSSION

The treatment group showed significant improvements in passive hip extension range of motion ($p = 0.007$) while the control group did not. Also, subjects in the treatment group who presented with limited pre-assessment peak hip extension during walking ($n_{treatment}=32$, $n_{control}=33$) had increased stride length ($p = 0.019$), peak hip extension ($p = 0.012$) and decreased anterior pelvic tilt ($p = 0.006$) during walking, while subjects in the control group showed only decreased anterior pelvic tilt ($p = 0.013$) (Table 1).

As hypothesized, a supervised hip flexor stretching program was effective in increasing stride length and peak hip extension and reducing anterior pelvic tilt during walking in healthy elderly adults with limited pre-intervention hip extension. The results of this study are in agreement with previous findings, which have indicated that stretches involving the hip can significantly alter hip extension, anterior pelvic tilt, stride length during walking [4-6]. However, this study demonstrates that a stretching program focused on a single muscle group can have the same or greater effects, and the results further implicate hip flexor tightness as a key to explaining age-related decline in gait function. This study also highlights the importance of supervision in achieving good results from a stretching program.

CONCLUSIONS

The results of this study support the use of a simple hip flexor stretching program in healthy elders with age related decline in gait function associated with hip flexor tightness

REFERENCES

1. Kerrigan, D.C., et al., *Arch Phys Med Rehab*, 2001. **82**, 26-30.
2. Kerrigan, D.C., et al., *Arch Phys Med Rehab*, 1998. **79**, 317-322.
3. Kerrigan, D.C., et al., *Arch Phys Med Rehab*, 2003. **84**, 1-6.
4. Christiansen, C.L., *Arch Phys Med Rehab*, 2008. **89**, 1421-1428.
5. Cristopoliski, F., et al., *Rev Bras Med Esp*, 2008. **14**, 139-144.
6. DiBenedetto, M., et al., *Arch Phys Med Rehab*, 2005. **86**, 1830-1837.

Table 1. Gait Parameters Pre- and Post- Intervention

	Treatment		Control	
Parameter	Pre	Post	Pre	Post
Passive Hip Extension (deg)	12.0 ± 6.2	15.3 ± 4.9*	14.5 ± 6.6	15.7 ± 6.9
Peak Hip Extension (deg)	7.6 ± 6.0	11.7 ± 8.5*	8.2 ± 5.6	11.2 ± 8.0
Peak Anterior Pelvic Tilt (deg	15.8 ± 5.6	11.9 ± 5.2*	13.7 ± 5.1	10.5 ± 5.3*
Stride Length (m)	1.41 ± 0.21	1.44 ± 0.20*	1.32 ± 0.18	1.33 ± 0.18

*indicates a value that is significantly different from the pre-intervention value, with $p<0.05$.

INCREASING PARETIC LEG EXTENSION IN PRE-SWING IS IMPORTANT FOR INCREASING FORWARD PROPULSION DURING WALKING

[1]Carrie L. Peterson, [2]Steven A. Kautz, and [1]Richard R. Neptune

[1] Dept. of Mechanical Engineering, The University of Texas, Austin, TX, USA
[2] Brain Rehabilitation Research Center, Malcom Randall VA Medical Center, Gainesville, FL
[3] Dept. of Physical Therapy and [4]Brooks Center for Rehabilitation Studies, Univ. of Florida, Gainesville.
email: clpeters@mail.utexas.edu; web: http://www.me.utexas.edu/~neptune

INTRODUCTION

Subjects with hemiparesis typically walk with asymmetric anterior-posterior ground reaction forces (AP GRFs) such that propulsive impulses (i.e. time integral of the positive AP GRF) generated by the paretic and non-paretic legs are not equal [1]. Large variability in paretic propulsion exists across hemiparetic subjects. Generally, most subjects generate less propulsion in the paretic leg compared to the non-paretic leg. However, there are some subjects who walk at slower speeds who consistently exhibit more paretic leg propulsion [2]. Underlying causes of variability in AP GRF impulses within hemiparetic subjects have been proposed such as: the inability to recruit muscles responsible for the generation of propulsion, increased activity in muscles that impair generation of propulsion, and indirect mechanics related to step length. Understanding mechanisms of propulsion generation within hemiparetic subjects would allow for the design of subject specific rehabilitation strategies and potentially improve intervention outcomes. Therefore, the goal of this study was to begin exploring the biomechanical predictors that best explain AP GRF impulses from mid to late stance.

METHODS

Kinematics and GRFs were recorded during three 30 s trials from 51 hemiparetic subjects (age 62.4 ± 12.0 yrs) walking at self-selected (SS) speed and from 21 age-matched control subjects (age 65.2 ± 9.6 yrs) walking at SS speed, 0.3 and 0.6 m/s on a split-belt instrumented treadmill. Standard inverse dynamics analysis determined intersegmental joint moments. Leg angle was computed as the angle between a line from the pelvis COM to the foot COM and vertical (positive when foot is posterior to the pelvis). The propulsive phase of the unimpaired stance phase was divided into two regions: early propulsion (i.e., second 50% of single leg stance) and pre-swing (i.e., second double support phase). Gait variables calculated within each region for each gait cycle included the AP impulse (time integral of the AP GRF), average leg angle and hip (flexor positive), knee (extensor positive) and ankle (plantar flexor positive) moment impulses (time integral of moment). Regression analyses were performed with two-level hierarchical models. In the first level, relationships between the AP impulses with each gait variable were determined with the contralateral AP impulse as an additional variable during pre-swing. In the second level, the relationships were examined to determine dependence on leg and asymmetry measured by the paretic step ratio (PSR = paretic step length/(non-paretic + paretic step length)). Hemiparetic subjects walking with PSR less than 0.47, between 0.47 and 0.53, and greater than 0.53 were classified in the low (n=9), symmetric (n=16) and high (n=26) PSR groups, respectively.

RESULTS AND DISCUSSION

Leg angle was positively related to the AP impulse in both regions for the paretic, non-paretic and control legs at each speed (Table 1) highlighting the importance of leg extension in achieving adequate propulsion. A simulation analysis of healthy walking found that the gluteus maximus, vasti and soleus muscles make substantial contributions to hip and knee extension during single limb support [3]. Thus, rehabilitation strategies aimed at increasing paretic propulsion should focus on these muscles to promote adequate paretic hip and knee extension.

The ankle moment impulse negatively related to the AP impulse during early propulsion for the paretic,

non-paretic and control legs at 0.3 and 0.6 m/s and related positively to the AP impulse during pre-swing for the controls (Table 1) and non-paretic legs for the low and symmetric PSR subjects (Table 2). These results are consistent with young healthy walking [4]. However, the paretic ankle moment was negatively related to the AP impulse during pre-swing for high PSR subjects (Table 2), suggesting different mechanisms of paretic AP impulse generation in this region for high PSR subjects. The contribution of the paretic ankle moment to the AP GRF likely depends on the paretic leg angle since high PSR subjects, who achieve less leg extension during pre-swing, demonstrated a negative relationship. The knee moment impulse was positively related to the AP impulse for the non-paretic leg at SS speed (Table 2) and control legs at 0.3 and 0.6 m/s in both regions (Table 1). However, the paretic knee moment impulse was negatively related during pre-swing (Table 2). The paretic, non-paretic and control leg hip moment impulses were negatively related to their respective AP impulses in both regions (Table 1). In healthy walking, the uniarticular hip flexors redistribute power from the trunk to the leg by decelerating the trunk and accelerating the leg forward during pre-swing [4]. While it has been hypothesized that the hip flexor moment compensates for the reduced ankle plantar flexor moment [5], we found that increased output from the uniarticular hip flexors from mid to late stance to advance the leg may have further decelerated the trunk with the net effect to decrease propulsion of the body COM.

During paretic pre-swing, the contralateral (non-paretic leg) AP impulses were negatively related to the ipsilateral (paretic leg) AP impulses in the hemiparetic and control subjects walking at 0.3 m/s, respectively (Table 1). Control subjects likely utilized the contralateral leg more to improve stability at the slow speed. Hemiparetic subjects had decreased weight bearing on the paretic leg requiring greater reliance on the non-paretic leg. Improving paretic leg weight bearing and stability may decrease the contribution from the contralateral leg AP impulse and be important for increasing paretic propulsion during paretic pre-swing.

Table 2: Significant second level coefficients of the hierarchical model: * ($p < .05$), and † ($p < .001$).

Early Propulsion Effect	**Coefficient**
Non-paretic knee moment	0.040†
Pre-swing Effect	
Paretic knee moment	-0.018*
Non-paretic knee moment	0.038*
High PSR, Paretic ankle moment	-0.024*
Low PSR, Non-paretic ankle moment	0.041†
Sym. PSR, Non-paretic ankle moment	0.048†

CONCLUSIONS

Increasing paretic leg extension and plantar flexor output and decreasing paretic hip flexor output from mid to late stance each have the potential to increase paretic propulsion in hemiparetic subjects.

REFERENCES

1. Bowden MG, et al. *Stroke* **37**, 872-6, 2006.
2. Balasubramanian CK, et al. *Arch Phys Med Rehabil* **88**, 43-9, 2007.
3. Arnold AS, et al. *J Biomech* **38**, 2181-9, 2005.
4. Neptune RR, et al. *Gait Posture* **19**, 194-205, 2004.
5. Nadeau S, et al. *Clin Biomech* **14**, 125-35, 1999.

ACKNOWLEDGEMENTS

Funded by NIH grant RO1 HD46820 and the VA Rehabilitation Research & Development Service.

Table 1: First level coefficients of the hierarchical model. Predictive variables were leg (e.g., paretic or non-paretic), average leg angle, and joint moment impulses. Significance indicated by * ($p < .05$), and † ($p < .001$).

	Early Propulsion				**Pre-swing**			
	Control			**Hemi.**	**Control**			**Hemi.**
	0.3 m/s	**0.6 m/s**	**SS**	**SS**	**0.3 m/s**	**0.6 m/s**	**SS**	**SS**
Leg	1.75	1.14	-0.15	2.67*	0.854	0.220	-3.509	13.95†
Leg angle	0.94†	1.32†	0.96†	0.86†	1.016†	1.457†	1.245†	0.95†
Hip moment	-0.055*	-0.065*	-0.0080	-0.038†	-0.059†	-0.067†	-0.090†	-0.063†
Knee moment	0.044†	0.028*	-0.056†	0.0028	0.057†	0.031*	0.010	-0.018*
Ankle moment	-0.023†	-0.031†	-0.010	-0.019†	0.024†	0.067†	0.107†	-0.024*
Contralateral AP					-0.147*	-0.034	0.014	-0.065*

BRAKING AND PROPULSIVE IMPULSES POSITIVELY RELATE TO WALKING SPEED DURING ACCELERATED AND DECELERATED WALKING

[1]Carrie L. Peterson, [2,3,4]Steven A. Kautz and [1]Richard R. Neptune

[1] Dept. of Mechanical Engineering, The University of Texas, Austin, TX, USA
[2] Brain Rehabilitation Research Center, Malcom Randall VA Medical Center, Gainesville, FL
[3] Dept. of Physical Therapy and [4]Brooks Center for Rehabilitation Studies, Univ. of Florida, Gainesville.
email: clpeters@mail.utexas.edu; web: http://www.me.utexas.edu/~neptune

INTRODUCTION

Daily mobility tasks are mainly comprised of short duration walking bouts. Approximately forty percent of all walking bouts for normal adult individuals in typical urban environments consist of less than twelve consecutive steps [1]. Thus, the ability to accelerate and decelerate is important for walking in daily life and is likely more demanding than maintaining a constant speed. Few studies have investigated acceleration and deceleration in walking and most were conducted at very fast walking speeds near the walk-to-run transition [2,3]. Only one study has been conducted at moderate speeds to examine joint kinetics associated with acceleration and deceleration [4]. However, only a small speed increase and decrease (1.0 to 1.4 m/s) could be investigated in this overground study due to the constraint of having to walk over two force plates. As a result, our current understanding of how healthy subjects modulate anterior-posterior ground reaction forces (AP GRFs) to increase and decrease speed over a wide range of moderate speeds is based on comparisons across steady-state speeds. Therefore, to further understand acceleration and deceleration in walking, the purpose of this study was to quantify AP impulses (i.e., time integral of the AP GRF), step length and step frequency in young healthy subjects accelerating and decelerating across moderate speeds.

METHODS

Kinematics and GRFs were recorded from eight healthy subjects (age 26 ± 2.9 yrs) walking on a split-belt instrumented treadmill at the VA Brain Rehabilitation Research Center and the University of Florida. Subjects first completed 30 second walking trials at their self-selected speed and at 0.4, 0.8, 1.2, 1.6 and 1.8 m/s. Subjects then completed trials during which they accelerated from 0 to 1.8 m/s, maintained a speed of 1.8 m/s for approximately 10 seconds, and then decelerated from 1.8 to 0 m/s. Three trials were conducted at acceleration and deceleration rates of 0.03, 0.06, 0.09 and 0.12 m/s^2. The order of constant speed trials and the rates for each acceleration and deceleration were randomized for each subject. Data were processed using Visual 3D and analyzed within the speed range of 0.4 to 1.8 m/s. Step length and step frequency were determined for each step from heel marker trajectories and GRF data. Braking and propulsive impulses (i.e., time integral of the negative and positive AP GRF, respectively) were computed for each step and were normalized by each subjects' body weight. Pearson correlation coefficients were determined between braking and propulsive impulses with walking speed to determine relationships at each rate of acceleration and deceleration.

RESULTS AND DISCUSSION

Braking and propulsive impulses were positively correlated with walking speed at each rate (Table 1). These results agree with a previous study that found braking and propulsive impulses to increase with steady-state speeds from 1.0 to 2.0 m/s [5]. Previously in overground walking, Orendurff et al. [4] found that acceleration (deceleration) was achieved by reducing (increasing) the braking impulse in early stance. However, in the current study across a wide range of walking speeds on a treadmill, the relationships between walking speed with braking and propulsive impulses were similar in magnitude and did not differ by rate (Table 1). Differences between studies may be due to subtle differences between treadmill and overground acceleration.

Table 1: Pearson coefficients of correlations between braking and propulsive impulses with walking speed at each rate. Significance indicated by † ($p < .001$).

Rate	Acceleration		Deceleration	
(m/s^2)	Braking	Propulsive	Braking	Propulsive
0.03	.703†	.699†	.789†	.609†
0.06	.529†	.559†	.716†	.659†
0.09	.576†	.661†	.741†	.552†
0.12	.549†	.664†	.545†	.541†

Step lengths and step frequencies systematically increased (decreased) with walking speed during acceleration (deceleration) (Fig. 1). Previously, systematic increases in peak AP forces with increasing step length were found in healthy walkers [6]. Increasing step length and corresponding peak AP forces increases AP impulses, whereas increasing step frequency decreases AP impulses. Thus, step length influenced AP GRFs more than step frequency during acceleration and deceleration such that AP impulses increased with walking speed.

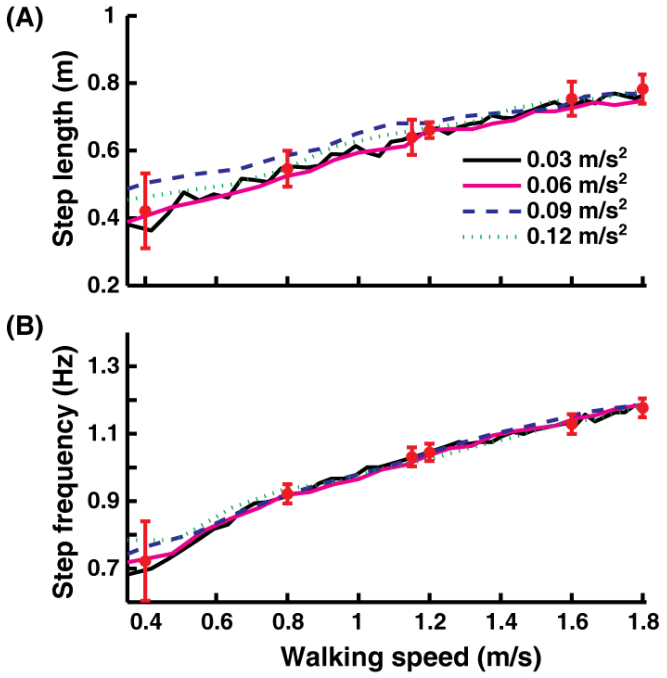

Figure 1: For a representative subject, (A) average step length (B) and step frequency during the acceleration trials for each rate. Also shown are the average step length and step frequency (error bars are ± 2 standard deviations) for each constant speed trial.

Subjects were able to modulate step length and frequency while accelerating and decelerating to attain step lengths and frequencies within ± 2 standard deviations of their average values during the constant speed trials (Fig. 1). Over this range of moderate constant speeds, healthy walkers have been shown to choose step frequencies that minimize the rate of metabolic energy expenditure [7]. Therefore, our results suggest that healthy subjects may modulate step frequency to minimize metabolic cost while accelerating and decelerating.

CONCLUSIONS

Braking and propulsive impulses were positively related to walking speed during acceleration and deceleration on a treadmill. Step length and frequency increased with walking speed and were near subjects' preferred step length and frequency at constant speeds suggesting economical energy expenditure by healthy subjects during non steady-state walking. Future work will determine relationships between joint moment and AP impulses during these non-steady state conditions. The outcomes of this work will provide the foundation to investigate motor coordination during acceleration and deceleration in pathological subjects in response to the increased task demands of non steady-state walking.

REFERENCES

1. Orendurff MS, et al. *J of Rehabil Research & Development* **45**, 1077-1090, 2008.
2. Diedrich FJ and Warren WH. *J Exp Psychol Hum Percept Perform* **21**, 183-202, 1995.
3. Segers V, et al. *Gait Posture* **24**, 247-54, 2006.
4. Orendurff MS, et al. *Gait Posture* **27**, 603-610, 2008.
5. Nilsson J and Thorstensson A. *Acta Physiol Scand* **136**, 217-27, 1989.
6. Martin PE and Marsh AP. *J Biomech* **25**, 1237-9, 1992.
7. Zarrugh MY and Radcliffe CW. *Eur J Appl Physiol Occup Physiol* **38**, 215-23, 1978.

ACKNOWLEDGEMENTS

We would like to thank researchers at the VA Brain Rehabilitation Research Center and the University of Florida for their assistance with data collection.

HIP JOINT MOMENTS USING A GREATER TROCHANTER METHOD OF LOCATING THE HIP JOINT CENTER

Kristian M. O'Connor & Joshua T. Weinhandl

Department of Human Movement Sciences
University of Wisconsin-Milwaukee, Milwaukee, WI, USA
E-mail: krisocon@uwm.edu Web: www.chs.uwm.edu/neuromechanics

INTRODUCTION

Accurate estimation of the hip joint center (HJC) is vital to the calculation of the hip joint moments. Inaccurate estimation of the HJC will result in inaccurate calculation of the distance from HJC to the thigh center of mass and hence hip joint moments. Holden & Stanhope [1] showed that a 2 cm anteroposterior displacement of HJC location resulted in a 33% change in peak flexor moments and a 2 cm medial-lateral displacement resulted in a 23% change in peak abductor moments.

HJC coordinates are typically estimated using functional approaches [2] or regression equations [3]. An alternative, yet unverified, predictive method that places the HJC coordinates at 25% of the distance from the ipsolateral to the contralateral greater trochanter (GT method) and is currently widely used in the biomechanics community. It is unkown how the moments generated by the GT method differ from the functional method, which has been suggested to be the best standard [2]. Therefore, the purpose of this study was to confirm that hip joint moments calculated using the GT method of locating the HJC produce comparable results to hip joint moments calculated using a functional method. A comparative analysis with hip joint moments calculated using the regression equations proposed by Bell et al. [3] was also performed.

METHODS

Ten healthy subjects volunteered to participate in this study. Each subject was asked to perform five walking trials and to repeat the testing procedure on a second day to assess the reliability of the methods.

Three-dimensional kinematic data were collected using a ten-camera Motion Analysis Eagle system (200 Hz), and force data were collected with an AMTI force platform (1000 Hz). HJC coordinates were estimated via the GT method, a functional (FUN) method [4], and the Bell et al. [3] regression equations based on pelvic width.

Three-dimensional hip joint moments were then calculated during the stance phase for each HJC estimate. Reliability of each method was quantified using the adjusted coefficient of multiple correlation (CMC) to evaluate the similarity between time series [5]. A 3×3 (method×plane) repeated measures ANOVA was used to assess potential differences in CMCs. Additionally, the average RMS difference was used to quantify differences in joint moments calculated using the FUN method and those yielded by the GT and BELL methods. These difference scores were then compared using a 2×2 (method×day) repeated measures ANOVA. Significance for all tests was set at $p<0.05$

RESULTS AND DISCUSSION

There were no differences in CMCs between methods, suggesting that all three methods yield repeatable hip joint moment calculations during walking. However, while the CMCs were excellent in all three planes (0.86-0.97), the CMCs for the frontal were significantly less than the sagittal and transverse planes.

Although the curves were repeatable for both the GT and BELL methods, RMS differences of hip joint moments were observed (Table 1 and Figure 1). These differences were due to the altered location of the HJC and mostly affected data in the frontal and transverse plane. In the sagittal plane the RMS difference was comparable for both the GT and BELL methods. However, the method×day interaction in the frontal and transverse planes was significant. Nevertheless, the RMS difference

associated with the GT method was less than the RMS difference associated with the BELL method in the both the frontal and transverse planes.

A potential cause for the increased RMS difference in frontal and transverse plane hip joint moments with the BELL method may be intra-examiner error in anatomical landmark identification. Della Croce et al. [6] reported intra-examiner errors in the medial lateral direction of 11.0 mm and 14.5 mm for the left and right ASIS respectively, compared to the 7.0 mm error in greater trochanter identification. Since the BELL method of relies exclusively on pelvic width (inter-ASIS distance), medial-lateral error in ASIS location will propagate to the anterior-posterior and vertical placement of the HJC. Seidel et al. [7] reported that HJC coordinates correlate strongly to pelvic width in the medial-lateral direction, but not in the vertical or anterior-posterior directions. They concluded that HJC location should not be determined as a function of pelvic width alone. The results of this study suggest that HJC estimates using the GT method are less vulnerable to errors in anatomical landmarks when compared to the BELL method and offer a viable option when calculating hip joint moments.

CONCLUSIONS

While all three methods of estimating the HJC yield repeatable joint moment calculations, the joint moments calculated using the GT method deviated less from the FUN method than those calculated using the BELL method. These results confirm the use of the GT method provide as a viable option when calculating hip joint moments during walking.

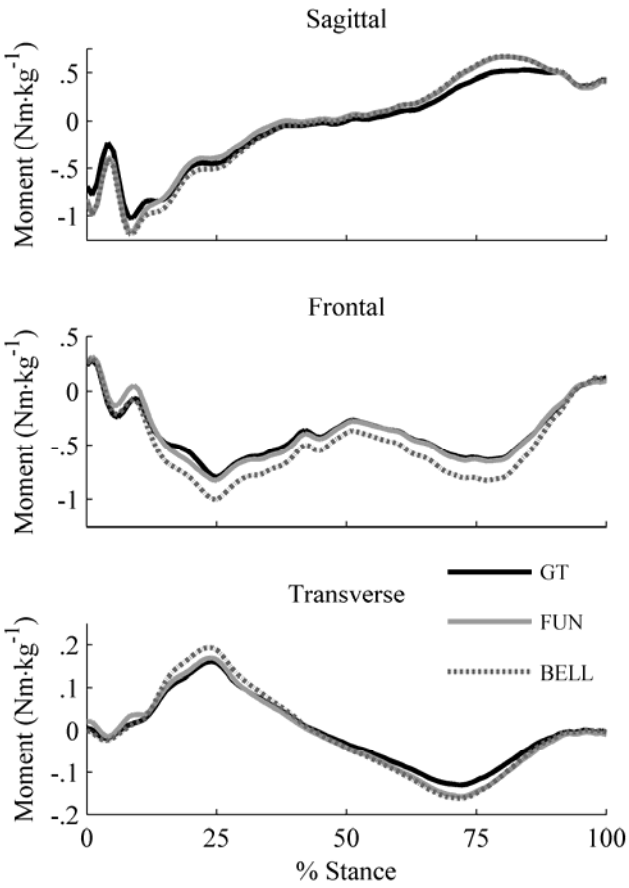

Figure 1. Hip joint moments in all three planes.

REFERENCES

1. Holden, JP & Stanhope, SJ. *Gait & Posture*, **11** 120-1, 2000.
2. Leardini, A et al. *J Biomech* **32,** 99-103, 1999.
3. Bell, AL et al. *J Biomech* **23**, 617-21, 1990.
4. Schwartz, MH & Rozumalski, A. *J Biomech* **38**, 107-16, 2005.
5. Kadaba, MP et al. *J Ortho Res*, **7**, 849-60, 1989.
6. Della Croce, U et al. *Med Biol Eng Comput*, **37**, 155-61, 1999.
7. Seidel, GK et al. *J Biomech*, **28**, 995-8, 1995.

Table 1. Coefficients of multiple correlation (CMC) and root mean square (RMS) error of hip joint moments using functional (FUN) method, greater trochater (GT) method, and Bell regression equations (BELL).

	Sagittal			Frontal			Transverse		
	CMC*	RMS		CMC	RMS†		CMC*	RMS†	
		Day 1	Day 2		Day 1	Day 2		Day 2	Day 2
FUN	0.97 ± 0.02	-	-	0.86 ± 0.10	-	-	0.95 ± 0.04	-	-
GT	0.97 ± 0.02	0.15 ± 0.08	0.09 ± 0.02	0.89 ± 0.06	0.11 ± 0.08	0.05 ± 0.02	0.96 ± 0.01	0.02 ± 0.02	0.01 ± 0.003
BELL	0.97 ± 0.02	0.12 ± 0.07	0.08 ± 0.03	0.92 ± 0.04	0.15 ± 0.06	0.15 ± 0.03	0.97 ± 0.02	0.02 ± 0.02	0.02 ± 0.003

† indicates significant method*day interaction ($p<0.05$).

* indicates significant difference from frontal plane ($p<0.05$).

A PASSIVE-ELASTIC ANKLE EXOSKELETON USING CONTROLLED ENERGY STORAGE AND RELEASE

Bruce Wiggin[1], Steven H. Collins[2], Gregory S. Sawicki[1]

[1]Joint Dept. of Biomedical Engineering, North Carolina State University and University of North Carolina-Chapel Hill, Raleigh, NC, USA
[2]Dept. of BioMechanical Engineering, Delft University of Technology, Delft, The Netherlands
e-mail: mbwiggin@ncsu.edu

INTRODUCTION

A major goal of powered lower-limb exoskeletons is to act in parallel with the user's leg muscles and reduce metabolic energy consumption during locomotion. Recent designs have focused on portable devices that can mimic the normal torque output of the lower-limb joints over the full gait cycle using large, powerful motors under high gain force control. Powerful motors are heavy, require bulky gears and mounting frames, and rely on even larger power sources. Furthermore, we are unaware of any study to date that demonstrates a metabolic savings during walking with a *portable* lower-limb exoskeleton.

On the other hand, a recent study indicates that when humans don tethered (i.e. non-portable), bilateral, lightweight, pneumatically powered ankle exoskeletons that replace *only* ~63% of the ankle muscle-tendon mechanical work during push-off, they reduce their metabolic energy consumption by 10-12% during treadmill walking [1]. Thus, supplying mechanical energy at a single joint (i.e. the ankle) during a key propulsive phase of walking (i.e. push-off) can have appreciable metabolic benefits.

Our goal in this study was to develop a *portable* device capable of providing ankle joint mechanical assistance during walking *without using external power from onboard actuators* (i.e. an 'energy-neutral' solution). Human walkers exploit a key passive dynamic principle of locomotion: elastic energy storage and return. Early in stance, strain energy is stored in the Achilles' tendon and then it is recovered later, providing up to 60% of the ankle joint mechanical work during push-off [1, 2]. We hypothesize that a passive wearable device using parallel elastic elements during the walking cycle is capable of recycling a significant portion of the ankle joint mechanical work and could reduce the metabolic cost of walking by up to 18% [1].

METHODS

Our goal was to provide all of the benefits of an actively powered exoskeleton [1] but in a portable framework without motors or an external energy source. We set out to develop a passive, 'energy-neutral' system with the following key design objectives: (1) deliver torque to the ankle following a pattern similar to the normal joint moment during walking and (2) recycle elastic energy during the stance phase while allowing free ankle rotation during swing.

In order to generate torque in parallel with the ankle joint center and match the normal ankle joint moment we centered our design around a pair of highly elastic (k_{eff}=13.2 kN/m), commercially available leaf springs (length=26.6 cm) (TAC 15, PSE Inc., Tucson, AZ). The resulting stiffness (k_{eff}=26.4 kN/m or ~5 N-m/deg) of the combined springs allowed for a design with a compact moment arm length (12.6 cm). We calculated a suitable spring origin

location; placing it below the ankle joint center (by ~1.5 cm) and forward (by ~14.0 cm), towards the ball of the foot (Fig. 1, top panel).

In order to store elastic energy and return it at the appropriate time during the gait cycle, we employed the principle of controlled energy storage and release [3]. We designed a system of springs, pins, and motion constraints to control the latch and release of a set of cams engaging and disengaging the leaf-springs during walking. This novel, adjustable 'smart-clutch' is advantageous because it uses the linear motion of the spring linkage, transmitted by changes in ankle joint angle, rather than electro-mechanical switching to set the timing of cam latch and release. In this way, we could disengage the springs at a critical ankle joint angle (i.e. max plantarflexion) to achieve free ankle rotation during swing.

RESULTS/DISCUSSION

Our design concept utilizes four key functional stages during walking gait to employ controlled energy storage and release: heel strike, foot flat, dorsiflexion, and push-off. At heel strike (Fig 1., orange) the clutch couples the cams to the spring linkage, but still allows for ratcheting upwards until foot flat. In stage 2, foot flat (Fig 1., green), the cams lock, allowing dorsiflexion to load the springs. During stage 3, the user's center of mass energy is stored as strain energy in the springs as the ankle dorsiflexes during mid stance (Fig 1., purple). During push-off, (stage 4) (Fig 1., light blue) energy is returned from the spring to propel the user's center of mass forward for the next step. Finally, the clutch releases the cams (Fig 1., dark blue), disengaging spring action for swing phase.

The current design configuration yields a maximum exoskeleton torque of ~105 N-m (Fig 1., red trace) and ~21 J of cycled spring energy. Future directions include device fabrication and human testing to determine whether an 'energy-neutral' passive elastic ankle exoskeleton using controlled energy storage and release can reduce metabolic cost during walking.

REFERENCES

1. Sawicki GS, et al. *Exerc Sport Sci Rev*, **37(3)**, 130-8, 2009.
2. Ishikawa M. *J Appl Physiol*, **99(2)**, 603-8, 2005.
3. Collins SH, et al. *PLoS One*, **5(2)**, e9307, 2010.

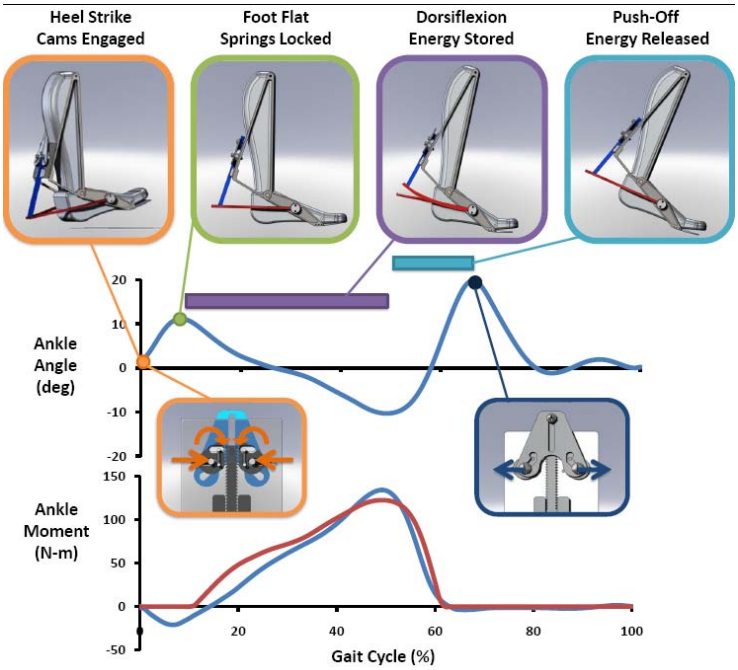

Figure 1: Passive-elastic ankle exoskeleton function during walking. Top row: Four key functional stages of controlled energy storage and release during stance (0-60%). Bottom rows: Light blue traces are representative walking data at 1.25 m/s for the ankle angle and ankle moment (plantar flexion +) over the stride from heel strike (0%) to heel strike of the same leg (100%). Red trace is the calculated torque contribution from the exoskeleton springs. Orange outlined panels show heel strike and cam/clutch engagement. Purple bar indicates period of spring energy storage. Light blue bar indicates period of spring energy recoil to aid push-off. Dark blue outlined panel shows cam/clutch release, disengaging the springs to allow for free swing.

DYNAMIC STABILITY OF WALKING DURING ANTERIOR-POSTERIOR AND MEDIO-LATERAL SUPPORT SURFACE AND VISUAL FIELD TRANSLATIONS

[1, 2]Patricia M. McAndrew, [2]Jonathan B. Dingwell, [3]Jason M. Wilken

[1]Department of Biomedical Engineering, University of Texas, Austin, TX, USA
[2]Nonlinear Biodynamics Lab, Dept. of Kinesiology, University of Texas, Austin, TX, USA
[3]Center for the Intrepid, Brooke Army Medical Center, Ft. Sam Houston, TX, USA
Email: mcandrew@mail.utexas.edu, Web: http://www.edb.utexas.edu/faculty/dingwell/

INTRODUCTION

Improving the ability to react to perturbations during daily activities like walking is a key to effective fall prevention training. Quantifying how walking stability changes in response to de-stabilizing events is critical for assessing how effective gait training interventions are. When small perturbations of increasing amplitude were applied to a dynamic model of walking, the model did *not* become orbitally more unstable, but *did* become locally more unstable [1]. In humans, healthy elderly were both orbitally and locally more unstable than healthy young adult subjects during *un*perturbed walking [2]. However, changes in orbital and local stability have not been assessed in humans during *perturbed* walking.

Virtual reality (VR) environments such as the Computer Assisted Rehabilitation ENvironment (CAREN) system (Fig. 1) provide a unique opportunity to understand how humans control gait stability. In such a system, we can apply well-controlled and repeatable visual and mechanical perturbations during gait. This study determined how continuous pseudo-random horizontal oscillations of the walking surface and visual field affected (local and orbital) dynamic gait stability.

METHODS

Twelve young healthy subjects participated with informed consent. Each subject completed five 3-min walking trials in the CAREN under each of 5 conditions: no perturbations (NOP), anterior-posterior platform (APP) or visual (APV) translations or mediolateral platform (MLP) or visual (MLV) translations. All translations were applied as a pseudo-random sum of sines with incommensurate frequencies of 0.16, 0.21, 0.24 and 0.49 Hz. Kinematic data for the head, trunk, pelvis and feet were collected using Vicon at 60 Hz.

Motions of a single marker placed on the seventh cervical (C7) vertebra were analyzed. Power spectral analyses confirmed that subjects responded to the applied perturbations [3].

Fig. 1. The CAREN is an immersive VR system with a six degree of freedom platform with a built-in instrumented treadmill.

To quantify stability, maximum Floquet multipliers (FM) and short-term (λ^*_s) and long-term (λ^*_l) local divergence exponents were calculated using standard techniques. State-spaces were generated using 3-D velocities and accelerations of the C7 marker. Maximum FM defines the amount by which small perturbations away from the mean reference trajectory grow or decay after one cycle. If the maximum FM has magnitude < 1, perturbations decay after successive strides, and the system is orbitally stable. Smaller FM indicate greater stability. Local divergence exponents quantify sensitivity to small perturbations *in real time* with larger values indicating increased instability. The results were analyzed using 2-factor ANOVA.

RESULTS AND DISCUSSION

The applied perturbations significantly altered each subjects' kinematics [3]. Conversely, subjects remained orbitally stable throughout the gait cycle for all experimental conditions. Maximum FM magnitudes did not increase significantly ($p \geq 0.104$; Fig. 2) for any perturbation condition. λ^*_s indicated increased local instability ($\lambda > 0$) during experimental conditions while λ^*_l indicated no changes in long-term local instability (Fig. 3). These results confirm previous modeling predictions [1].

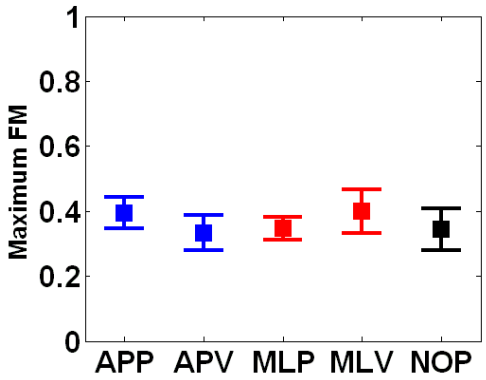

Fig. 2. Summary of average maximum FM by condition. Blue markers indicate AP perturbation conditions, red markers indicate ML perturbation conditions and the black marker indications the no perturbation condition. Note that all values are <1, indicating that subjects remained stable for all experimental conditions.

Even with substantial perturbations, subjects still maintained orbitally stable gait for all conditions. FMs theoretically reflect the inherent stability of the *system*, which should not depend strongly on the specifics of the perturbations applied [1] and this was reflected in these stable FM values.

Interestingly, there was a trend for subjects to be slightly less orbitally and locally stable during *platform* translations in the AP direction, whereas subjects were slightly less orbitally and locally stable during *visual field* translations in the ML direction.

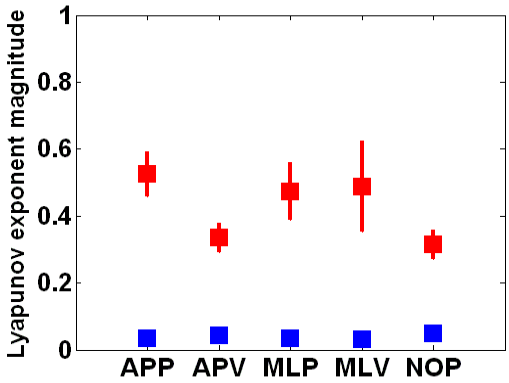

Fig. 3. Summary of average maximum local divergence exponents (λ^*). Red squares indicated short-term local stability (λ^*_s) and blue squares indicate long-term local stability (λ^*_l).

CONCLUSIONS

Our results indicate that inducing greater movement, and thus greater movement *variability* [3] does not necessarily induce greater orbital *instability* (Fig. 2) but does induce greater local instability (Fig. 3). What the FMs do not reflect is how people *achieved* stability, and while these FM appear to represent overall gait "stability", they may not in fact be sensitive enough to predict *risk* of falling. Despite no changes in orbital stability, subjects exhibited short-term local instability for all experimental conditions. This is consistent with the modeling results of Su and Dingwell [1].

ACKNOWLEDGEMENTS

Support provided by the Military Amputee Research Program (to JMW) and by National Institutes of Health Grant 1-R21-EB007638-01A1 (to JBD).

REFERENCE

1. Su, J. and J. Dingwell, *Dynamic stability of passive dynamic walking on an irregular surface.* Journal of Biomechanical Engineering, 2007. 129: p. 802-810.
2. Kang, H. and J. Dingwell, *Effects of walking speed, strength and range of motion on gait stability in healthy older adults.* J Biomech, 2008. 41: p. 2899-2905.
3. McAndrew, P., J. Dingwell, and J. Wilken, *Walking variability during continuous pseudo-random oscillations of the support surface and visual field.* J Biomech, In press.

WALKING ON AN OSCILLATING TREADMILL: TWO PATHS TO FUNCTIONAL ADAPTATION

[1]Rachel A. Brady, [1]Brian T. Peters and [2]Jacob J. Bloomberg

[1]Wyle Integrated Science and Engineering Group, Houston, TX, USA
[2]Neuroscience Laboratories, NASA Johnson Space Center, Houston, TX, USA
email: rachel.brady-1@nasa.gov

INTRODUCTION

Our laboratory is interested in treadmill training under novel sensorimotor conditions as a potential approach for mitigating space flight-induced ataxia. To investigate locomotor responses produced by healthy adults introduced to a novel walking condition, we mounted a treadmill on top of a motion base platform with six degrees of freedom. Subjects were classified into two groups according to how their stride times were affected by a laterally oscillating perturbation. Our data suggest that a person's choice of adaptation strategy is influenced by the relationship between his or her unique, natural stride frequency and the external frequency imposed by the motion base.

METHODS

Twenty healthy adults (12 men), average (± 1 S.D.) age 37 (± 9) years, walked at 4 km/h (2.5 mph) on a laterally oscillating treadmill that moved in a continuous sinusoidal pattern at a frequency of either 0.2 Hz or 0.3 Hz. Each subject's baseline stride time (BST) was determined during a period of normal treadmill walking before the onset of base motion. Stride time data for the perturbation portion of the exposure was normalized to this BST. Stride times did not vary between the 0.2 Hz and 0.3 Hz groups for either the baseline walk period ($p = 0.42$) or the perturbation period ($p = 0.22$), so the groups were combined.

Most subjects settled into a comfortable adapted walking strategy within the first 10 minutes of the 20-minute trial. To focus on the acute phase of adaptation, we restricted our stride time analysis to these first 10 minutes.

RESULTS AND DISCUSSION

Immediately after the support surface began to move, all participants rapidly decreased their stride times, presumably as a strategy for maintaining postural stability. After this initial decrease, stride times for some individuals (Return group, Fig. 1) trended back toward their baseline values while stride times for others (No Return group, Fig. 2) did not.

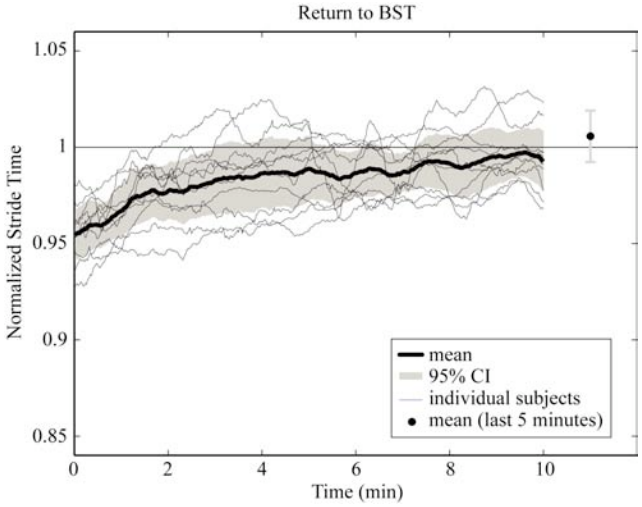

Figure 1: Return group. Stride times for 10 subjects trended toward their BSTs during the first 10 minutes of exposure.

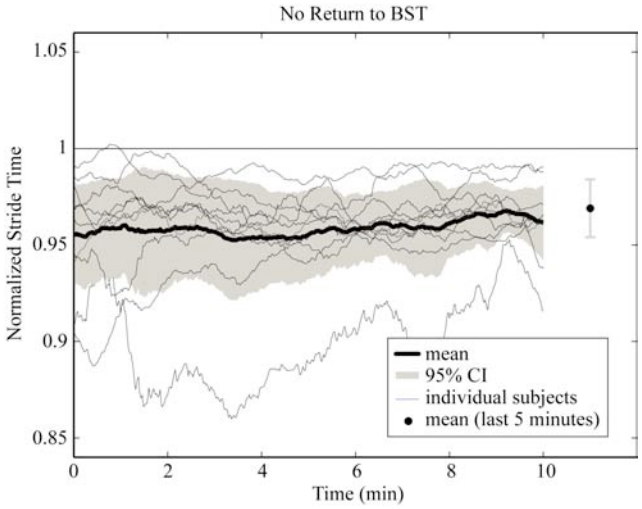

Figure 2: No Return group. Stride times for 10 subjects did not return to their BSTs.

An initial conclusion might be that the No Return group did not "adapt" to the base motion. However, functionally, participants in both groups appeared to be equally and fully adapted, and able to walk comfortably and effortlessly on the moving platform. A review of their stride time data suggested they accomplished this in different ways. To investigate, we looked at the relationship between a person's natural stride frequency and the external frequency imposed by the motion base.

Stride times that would result in an integer ratio between a subject's heel strike events and the lateral movement of the support surface were calculated and defined as entrainment stride times (ESTs). ESTs were stride times that would produce exactly three (3:1) or four (4:1) strides per support surface cycle. Due to variation in BSTs between subjects, the relationships between their BSTs and ESTs were also unique. A subject's nearest EST could have been higher (Fig. 3) or lower (Fig. 4) than his or her BST, or it could have been at the BST, which appears in the figures at 1 on the y-axis.

We believe that during adaptation, participants were influenced by two attractors, their natural stride frequency (BST) and the stride frequency required to achieve entrainment with the motion base (EST). For nine of ten subjects in the Return group, the nearest ESTs were at or above the BSTs, positioning both attractors in a positive direction that would draw a return toward the BST. For seven of ten subjects in the No Return group, the nearest ESTs were below the BSTs, positioning one attractor (BST) in a positive direction and the other (EST) in the negative. We believe these subjects were drawn away from the BST attractor by the EST.

CONCLUSIONS

Our data suggest that a person's stride time response while walking on a laterally oscillating treadmill is influenced by the relationship between the subject's unique, natural stride frequency and the imposed external frequency of the motion base. This relationship may be useful for checking the efficacy of gait training and rehabilitation programs. Preselecting and manipulating a person's EST could be one way to draw that individual out of a preferred "attractor well" during gait therapy or training.

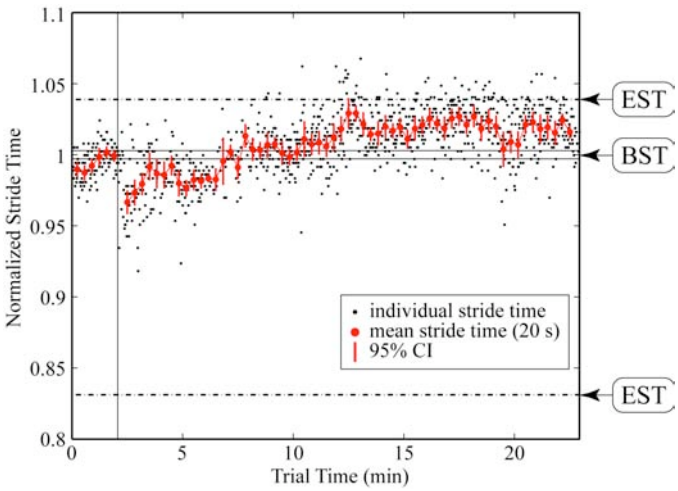

Figure 3: Example of normalized stride time data for a subject whose nearest EST was higher than his BST, represented on the y-axis at 1.

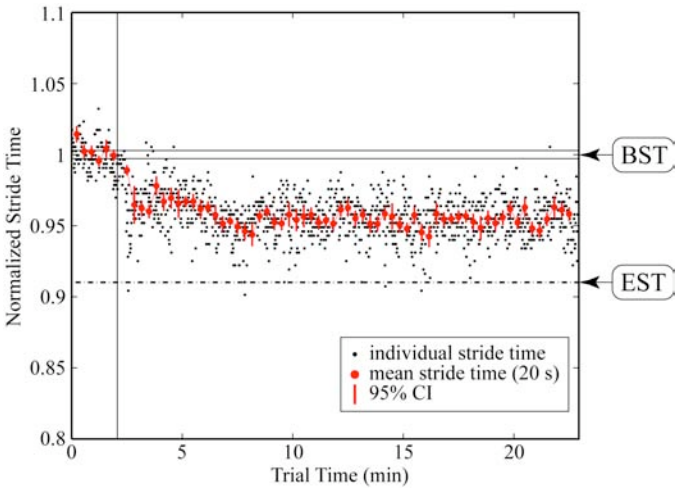

Figure 4: Example of normalized stride time data for a subject whose nearest EST was lower than his BST, represented on the y-axis at 1.

ACKNOWLEDGEMENTS

This work was supported by the National Space Biomedical Research Institute through NASA NCC 9-58.

THE EFFECT OF VARIOUS THONG FLIP-FLOPS ON GAIT KINETICS

Justin Shroyer[1] and Wendi Weimar[2]

[1] University of Louisiana at Lafayette, Lafayette, LA, USA
[2] Auburn University, Auburn, AL, USA
E-mail: jfs0725@louisiana.edu, Web: www.ull.edu

INTRODUCTION

Flip-flops are a common footwear option, and anecdotally, the general media is inundated with the opinions of podiatrist, chiropractors, and foot experts on the harmful affects that flip-flops have on the foot, lower leg and lower back. However, while still limited in quantity, research investigating the effects of flip-flops on gait parameters has recently been addressed in the scientific community [1,2,3].

Therefore, the purpose of this research study was to investigate the influence of various types of flip-flops with distinct structural properties versus barefoot on ground reaction forces (GRFs) at heel contact. It was hypothesized that individuals alter their gait when wearing flip-flops which results in a decreased attack angle, peak vertical forces, and anterior/posterior (ant/post) forces at heel contact when compared to walking barefoot.

METHODS

Seventy-eight females (21.5 ± 1.5 years, 1.65 ± .058 m, 63.53 ± 10.6 kg) served as participants. There were four footwear conditions: barefoot (BF), flip-flop 1 (FF1), flip-flop 2 (FF2), and flip-flop 3 (FF3) (Figure 1). FF1 had no arch support, FF2 had an arch support, and FF3 had an arch support, heel cup, midtarsal support, and wider straps.

On testing day, participants were asked to walk at a self-selected pace approximately 10 meters, across an AMTI force platform (OR6-7–Advanced Mechanical Technology, Inc. Watertown, MA.) in all four footwear conditions (BF, FF1, FF2, & FF3).

Figure 1: Flip-flop conditions; FF1, FF2, FF3 from top to bottom.

After the initial BF trial, participants were asked to walk in one of the flip-flop conditions; the order of the flip-flop conditions was randomized using a random order generator. After three flip-flop trials, participants were again instructed to perform a BF trial. This process was repeated until three trials for each footwear condition were obtained (BF, FF1, FF2, FF3).

The kinetic variables of interest were peak vertical force (F_V) at heel contact, the corresponding ant/post force (F_X), and attack angle at heel contact (θ_{AA}). Attack angle was calculated using F_V and F_X (Figure 2). Force variables were expressed as a percentage of body weight (%BW) and data were analyzed with a one-way repeated measures ANOVA for each dependent variable; F_V, F_X, and θ_{AA}.

RESULTS AND DISCUSSION

Results indicated a significant effect of footwear on both θ_{AA} and F_X; however, there was no significant effect on F_V (Table 1). A post hoc test indicated a significant difference between BF and FF2 (θ_{AA} p = .006, F_X p = .017) as well as BF and FF3 (θ_{AA} p = .003, F_X p = .007). FF2 and FF3 yielded a smaller θ_{AA} and a larger F_X than BF. There was no statistically significant difference between the flip-flop conditions for θ_{AA} or F_X.

The data suggests that the difference observed in the θ_{AA} was the result of the statically significant difference in F_X given there was no statistically significant difference in F_V.

CONCLUSIONS

Based on the current study, flip-flops do not have an affect on vertical GRFs at heel contact when compared to BF in college aged women; however, there was an effect on horizontal GRFs. The flip-flops with more structural components (FF2 & FF3) resulted in an increased ant/post GRF at F_V during heel contact and subsequently a decreased attack angle. This suggests that the design of the flip-flops had an affect on gait kinetics. For the variables F_V and θ_{AA}, the introduction of features such as an arch support and a heel cup in flip-flops resulted in kinetics that deviated from BF kinetics. Further research is needed to investigate the influence of flip-flops on other kinetic and kinematic variables.

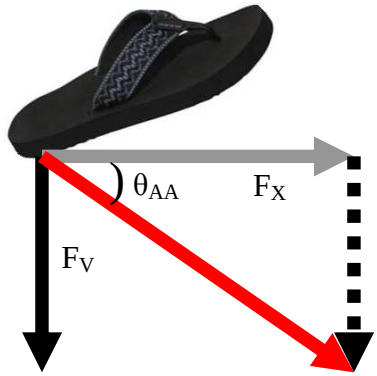

Figure 2: Calculation of Attack Angle (θ_{AA}) using the resultant vector of F_V and F_X.

REFERENCES

1. Shroyer, J., et al. Med Sci Sports & Exerc, **40**(5), S333, 2008.
2. Shroyer, J. & Weimar, W. *Proceedings of SEACSM*, Greenville, SC, USA, 2010
3. Carl, T. J., & Barrett, S. L. *J Am Podiatr Med Assoc*, **98**(5), 374-378, 2008.

ACKNOWLEDGEMENTS

The authors would like to thank both SOLE and Reef for the donation of the flip-flops used in this study.

Table 1: Effect of footwear on F_X, and θ_{AA} ($p \leq .05$). *†‡§ Statistical significance noted.

	Condition	N	Mean	SD	*F*	*p*	η^2	*Power*
F_X (%BW)	BF*†	78	-.1257	.0378	4.362	.005	.054	.867
	FF1		-.1332	.0343				
	FF2*		-.1362	.0380				
	FF3†		-.1369	.0380				
θ_{AA} (°)	BF‡§	78	-83.02	1.74	5.227	.002	.064	.925
	FF1		-82.67	1.53				
	FF2‡		-82.52	1.65				
	FF3§		-82.50	1.81				

THE EFFECT OF SUSTAINED STATIC KNEELING ON KNEE JOINT GAIT PARAMETERS

[1]Tara Kajaks, [2]Patrick A. Costigan

[1]McMaster University, Hamilton, ON, Canada
[2]Queen's University, Kingston, ON, Canada
email: kajakst@mcmaster.ca

INTRODUCTION

Epidemiological studies have identified kneeling as an occupational risk factor for knee joint osteoarthritis (KOA) [1], but direct biomechanical evidence for this relationship is lacking. A possible mechanism attributed to KOA onset is that prolonged static kneeling compromises the integrity of the knee joint ligaments resulting in knee joint instability, which would manifest itself as altered ambulatory loading profiles (Fig. 1). As a preliminary exploratory investigation, the purpose of this study was to investigate the effect of sustained static kneeling on knee joint gait parameters.

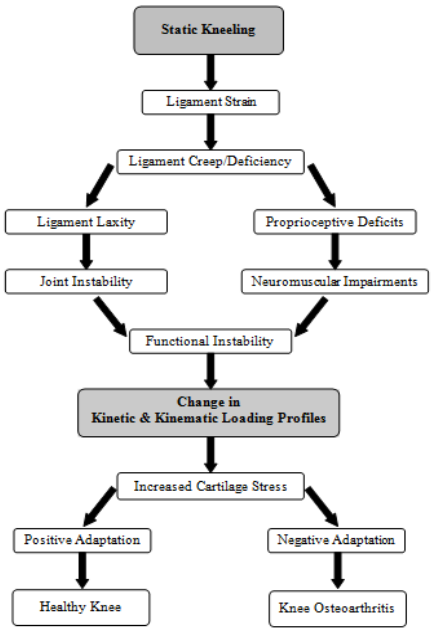

Figure 1: A hypothesized pathway for the relationship between static kneeling and KOA.

METHODS

Ten healthy male subjects (24.1 years ± 3.5, 1.80 m ± 0.06, 77.66 kg ± 7.68) with no history of knee injury volunteered for this study. Each subject's dominant leg and pelvis were instrumented with non-collinear infrared-emitting diode (IRED) clusters on rigid discs. The discs, with three IREDs each, were placed on the lateral side of the dominant foot, shank, and thigh, and over the posterior pelvis. Virtual markers from anatomical bone landmarks were also recorded via motion capture in the neutral posture using the tip of a six-IRED probe. The anatomical landmarks of interest on the dominant lower limb included the head of the first and fifth metatarsals, the medial and lateral malleoli, and the medial and lateral epicondyles, as well as bilateral heads of the greater trochanter and anterior superior iliac spines.

After a familiarization period, subjects performed ten walking trials at a self-selected normal pace over a force plate (AMTI, Watertown, MA, USA) embedded in the floor. Kinematic data was collected using two three-camera Optotrak Motion Tracking Systems (Northern Digital Inc., Ontario, Canada). A 16-channel Optotrak Data Acquisition Unit (Northern Digital Inc., Ontario, Canada) was used to collect the force plate at 1000Hz and motion data at 75Hz. Subjects then performed a static deep knee-flexion kneeling protocol consisting of three bouts of ten minutes of kneeling, each separated by a five minute seated rest period. Subsequently, a set of ten walking trials were performed after a one-minute rest and equipment verification period. The location of the anatomical virtual markers were then re-determined.

The ground reaction force and motion data were processed using Visual 3D software (Visual 3D, version 3.9, C-Motion Inc., MD, USA). The anatomical landmarks were used to define the proximal and distal ends of their respective anatomical segments, allowing for a single lower limb model to be created for each subject. A second-order lowpass Butterworth filter was used to filter the kinematic (6 Hz cutoff) and kinetic (25 Hz cutoff) data. Euler angles were used to calculate the

knee flexion angle (KFA) and knee adduction angle (KAA), and inverse dynamics was used to calculate the external knee adduction moment (KAM) and knee flexion moment (KFM) (normalized to body mass). Visual 3D's automatic gait detection function was used to extract the data from the stance phase of the gait cycle that occurred over the force plate, and these data were time normalized to 100% of the stance phase.

For each outcome measure (KFA, KAA, KAM, and KFM) statistical analysis involved calculating the within-subject root mean squared difference (RMSD) between the waveforms for each of the trials and the mean of the trials for each condition (pre-kneeling (PRE) and post-kneeling (POST)). The average RMSD was then determined for each subject. Additionally, the RMSD was calculated between each of the POST trials and the mean of the PRE condition. A paired t-test was used to determine if there was a significant difference between the RMSD calculated within respective conditions versus the RMSD of the POST condition against the mean of the PRE condition.

RESULTS AND DISCUSSION

No statistical difference was found between the RMSD calculated within conditions for the KFA, KAM, and KFM (Fig. 2) indicating that the variances within these outcome measures for the POST condition were similar to those during PRE gait, where the latter is considered to be the normal subject-specific stance-phase profile and therefore serves as the control condition. However, a significant difference was observed in the RMSD between these two conditions for the KFA ($p<0.05$), with an increase in RMSD in the POST condition. This indicates an increase in KFA variance in the POST gait trials. It is important to note, however, that this comparison does not address the shape of the waveforms, only their variance within each condition.

To test for differences in amplitude, the waveforms from the POST gait were compared with the average waveform of the PRE waveforms. The RMSD increased significantly for all outcome measures ($p<0.05$). This indicates a significant deviation in the POST condition from the PRE condition. While this measure does not speak to the direction of the deviation, this study sought only to determine if kneeling caused a change in gait waveform patterns. Indeed, we have shown that the within subject waveform variance does not change within conditions, but that it does increase in the POST condition relative to the PRE condition, indicating that static kneeling does have at least an acute effect on gait measures.

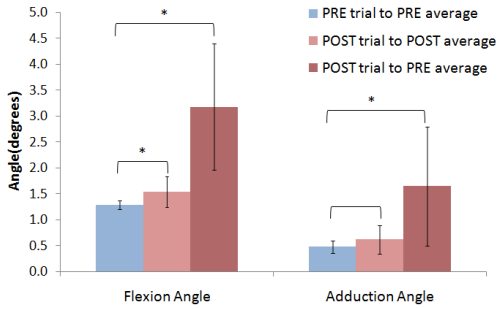

a)

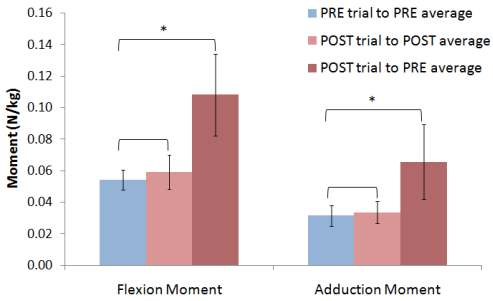

b)

Figure 2: RMSD averaged between subjects as calculated both between and within conditions for a) flexion and adduction angles and b) flexion and adduction moments. (* = $p<0.05$)

CONCLUSIONS

As changes in gait parameters have been associated with both knee joint instability and KOA (as reviewed in [2]), we believe that the findings of this study are evidence that the proposed pathway linking static kneeling to KOA may be viable and warrants further in-depth investigation.

REFERENCES

1.Baker P, et al. *J Rheumatol* **29**, 557-563, 2002.
2.Andriacchi TP, et al.. *Curr Opin Rheumatol*, **18**, 514-518, 2006

ACKNOWLEDGEMENTS

We would like to acknowledge the support and assistance of the Human Mobility Research Centre, Queen's University, Kingston, ON.

OVER-STRIDING DURING "FIXED-CADENCE" LOAD CARRIAGE LEADS TO INCREASED GROUND REACTION FORCES

[1]David J. Gutekunst, [2]Peter N. Frykman, and [2]Joseph F. Seay
[1]Washington University, St. Louis, MO, [2]U.S. Army Research Institute of Environmental Medicine, Natick, MA
email: djgutekunst@wustl.edu

INTRODUCTION

Military recruits undergo a structured regimen of training and exercise that yields a high incidence of lower-extremity injury [1]. Female sex [2] and shortness of stature [3] have been identified as independent risk factors for lower-limb overuse injuries; moreover it has been suggested that sex differences in lower-limb injury rates, especially tibial stress fractures, may be attributed to the shorter average leg length of females [3]. Recruits frequently march together at a "fixed cadence", i.e. the same step rate. When the marching speed and step rate are dictated by taller recruits, as occurs often during group marches, shorter recruits are forced to over stride [4]. Over-striding may increase lower-extremity loading and contribute to overuse injuries. For example, increased ground reaction force (GRF) loading rates and impact peaks have been linked to tibial stress fractures in runners [5].

In this analysis, we sought to assess the effects of fixed cadence marching at typical recruit training speeds across a range of step rates above and below each individual's preferred step rate (PSR). We hypothesized that faster speeds and slower step rates would correspond to greater (i.e. more negative) anterior-posterior (A-P) GRF during braking, higher A-P GRF during propulsion, and higher vertical GRFs during both braking and propulsion. Braking peaks were defined as occurring in the first 50% of stance, to encompass weight acceptance and early stance, whereas propulsive peaks were defined as maxima in the last 50% of stance.

METHODS

Five volunteers (1 woman, 4 men) participated after giving informed voluntary consent. Investigators adhered to AR 70-25 on the use of volunteers in research. Volunteers completed a series of six 10-minute treadmill bouts while carrying 20 kg of equipment (boots, body armor, and mock weapon) to mimic trainee marching. Subjects walked on a dual-forceplate treadmill (AMTI, Watertown, MA) with belts arranged in a fore-aft design. Each subject's preferred step rate (PSR) was assessed during a pre-testing familiarization session. The six bouts were conducted over two non-consecutive days, one for each speed (1.34 and 1.67 m/s). Three step frequencies (PSR, 85% PSR, and 115% PSR) were presented in random order for each speed. To limit effects of fatigue, a 10-minute break was provided after each bout.

Three-dimensional GRF data were collected at 1200 Hz using the dual forceplate treadmill. Measurements were collected over 5 consecutive strides 8 minutes into each 10 minute trial. Stance-phase events of initial contact and push-off were identified using Visual 3D (C-Motion, Germantown, MD) and data were normalized to stance time. Two-way repeated measures ANOVA (Speed by Step Rate) were performed for peak GRF values during braking and propulsion.

RESULTS AND DISCUSSION

Greater A-P braking and propulsive forces were observed with increased speed ($p<0.001$) and decreasing step rate ($p<0.001$), as shown in Table 1. The faster speed condition had 18% greater A-P braking force and 16% higher A-P propulsive force. When comparing across the step rate conditions, walking in the "over striding" condition (85% of PSR) led to a 28% increase in peak A-P GRF compared to PSR, whereas walking at 115% PSR led to a 25% reduction in peak A-P GRF compared to PSR (Figure 1). The effect during the propulsive phase was similar though less pronounced: walking at the 85% PSR "over-striding" condition led to a 19% increase in peak A-P GRF compared to PSR, and walking at 115% PSR led to a 19% reduction in peak A-P GRF compared to PSR.

Peak vertical GRF during the braking phase of stance (the first vertical GRF peak) was 13% higher at the faster speed (Table 1). In contrast to the findings for A-P GRF, in which maximum force

was negatively associated with step rate (i.e. highest force at 85% PSR), the lowest vertical GRF at both 1.34 and 1.67 m/s occurred at PSR. Compared to the PSR condition, peak vertical GRF was 6% higher at 85% PSR and 9% higher at 115% PSR (post-hoc $p<0.05$). Vertical GRF during propulsion was not different across speed or step rate.

One limitation of the current analysis is that there have not yet been enough volunteers to assess differences due to height. Previous work suggests that human gait follows patterns of a force-driven harmonic oscillator [6]. As more volunteers are analyzed, we will examine the possibility that grouping together individuals of similar height during fixed-cadence marches could eliminate over-striding in shorter recruits and thus lessen their injury risk.

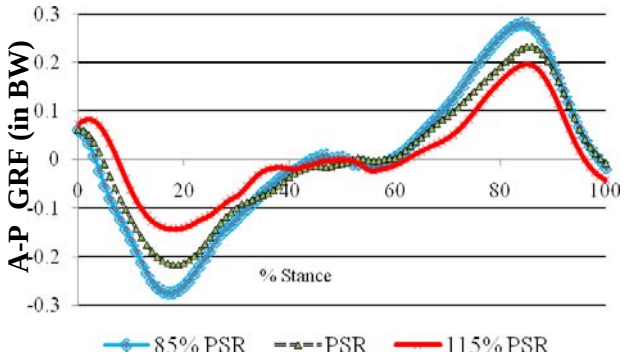

Figure 1: A-P GRF during stance, normalized to body weight (BW) and averaged across speeds.

CONCLUSIONS

The present study suggests that increased walking speed and lower step rate impose increased loads on the lower extremity, as measured by both vertical and A-P GRFs, thus increasing lower-extremity injury risk. The lack of statistical interaction between speed and step rate indicates that the effects of step rate on GRF are consistent across speeds typical of recruit training.

Our study design provided a model for the "over striding" hypothesis of lower extremity injuries, as the 85% PSR trials forced subjects to walk at a slower step rate and thus take longer steps to maintain speed. Our GRF findings supported the over striding hypothesis, which posits that long, slow steps increase biomechanical loading and the resulting risk of lower-extremity injuries. Slower cadences resulted in higher peak A-P GRFs during both the braking and propulsive phases of stance. Moreover, this effect was consistent across the two speeds tested. This increased force at the ground-foot interface translates to higher loads transmitted through the lower extremity, which may increase the risk of overuse injury when recruits carry loads over long distances.

Importantly, none of the kinetic outcomes was highest in the PSR condition, and vertical GRF during braking was minimized at PSR. Together, these results support a reduction in the use of "fixed cadence" marching that can lead to over-striding during recruit training.

REFERENCES

1. Knapik JJ, et al. *Mil Med* **166:**641-647, 2001.
2. Ozburn MS and JW Nichols. *Mil Med* **146:**332-334.
3. Finestone A, et al. *Mil Med* **156:**528-530, 1991.
4. Kelly EW, et al. *Mil Med* **165:**142-146, 2000.
5. Milner CE, et al. *Med Sci Sport Exer* **38:**323-8, 2006.
6. Holt KG, et al. *Hum Mov Sci* **9:**55-68, 1990.

ACKNOWLEDGEMENTS

The authors acknowledge Ms. Megan Coyne for her help with data collection and processing.

DISCLAIMER

The opinions or assertions contained herein are the private views of the authors and are not the official views of the Army or the Department of Defense.

Table 1: Peak ground reaction force values (in units of body weight, BW) in A-P and vertical directions.

	1.34 m/s			1.67 m/s		
Peak Force(BW)	**85% PSR**	**PSR**	**115% PSR**	**85% PSR**	**PSR**	**115% PSR**
A-P braking GRF*##	-0.24±0.04[a]	-0.20±0.02[b]	-0.14±0.03[c]	-0.34±0.05[a]	-0.26±0.03[b]	-0.20±0.03[c]
A-P propulsive GRF*##	0.27±0.03[a]	0.21±0.02[b]	0.19±0.02[c]	0.33±0.04[a]	0.30 ± 0.04[b]	0.26 ± 0.04[c]
Vertical braking GRF*#	1.55±0.10[a]	1.46±0.12[b]	1.62±0.17[a]	1.77±0.18[a]	1.66±0.05[b]	1.79±0.13[a]

*Speed main effect, $p<0.001$ # Step Rate main effect, $p<0.05$ ## Step Rate main effect, $p<0.01$
Differing letters (a,b,c) indicate significantly different values ($p<0.05$) in post-hoc comparisons within each Speed

CHANGES IN GAIT KINEMATICS AT PREFERRED WALKING SPEED IN PEOPLE WITH MULTIPLE SCLEROSIS

Michael A. Busa, Stephanie L. Jones, Jebb Remelius, Jordan D. House, Karthik Sugumaran, Julianna Eve, Richard E.A. Van Emmerik

University of Massachusetts Amherst, MA, USA
email: mbusa@kin.umass.edu , web: http://www.umass.edu/motorcontrol/

INTRODUCTION

Walking is an important activity of daily living and among people with Multiple Sclerosis (MS) is considered a significant determinant in assessing quality of life [1]. Previous studies have indicated that individuals with mild impairments due to MS have a slower preferred walking speed and altered stride characteristics such as shorter stride length and increased double support time [2,3]. These studies also found lower extremity kinematic changes in the joint angular excursions in individuals with MS compared to healthy controls.

These kinematic changes, however, could be driven by group differences in preferred walking speeds. In addition, the individuals tested had very mild mobility impairments (Expanded Disability Status Score [EDSS] 0-2.5), which may obscure the coordination changes that occur throughout the course of MS.

The purpose of this study was to determine the changes in gait kinematics at preferred walking speed in a group of individuals representing a wider range of mobility impairments due to MS (EDSS range 0-6) [4].

METHODS

Thirteen females and one male with mild to moderate impairment due to MS measured with the Patient Administered Expanded Disability Status Score [4] (median 4.0, range 3.0 to 6.0) and fourteen, age- and gender-matched, individuals without MS serving as controls (CON) volunteered for this study (Table 1).

Table 1: Participant Demographics.

	Age (yrs)	Height (cm)	Weight (kg)
CON	48.8 (10.3)	163.5 (6.8)	67.8 (10.7)
MS	48.6 (10.5)	156.7 (4.9)	70.0 (13.7)

All participants walked barefoot at preferred speed across a 2 x 0.5 meter instrumented walkway (RSscan International) set into the center of an 11.75 m boardwalk. Kinematic data were computed from a 13 segment biomechanical model (Visual 3D) constructed from 35 retro-reflective markers affixed to anatomical landmarks recorded during walking trials. Kinematic marker data were collected at 240 Hz (Qualisys Inc.) and filtered at 10 Hz using a 2^{nd} order recursive Butterworth filter and synchronized with RSscan data in Visual 3D (C-Motion).

Independent samples T-tests were used to compare MS and CON groups for differences in preferred walking speed and lower extremity (hip, knee and ankle joint) and trunk ranges of motion. (α=.05).

RESULTS

There was no significant difference (p=0.39) in preferred walking speed between MS and Control groups (Fig. 1). Individuals with MS significantly decreased ($p<0.05$) the range of motion (ROM) of both knee joints during the swing phase of gait (p=0.039 left and p=0.004 right) (Fig. 2), with a significant decrease in right knee ROM and a trend towards reduced left knee ROM across the entire gait cycle (p=0.007; Left p=0.08). The ROM of the trunk was decreased in the MS group (p=0.014) in the sagittal plane during the swing phase of gait. Both left and right knees were found to be in a significantly more flexed position at the time of heel strike (p=0.045 and p=0.014 respectively) in the MS group (Fig. 3). No other kinematic differences were found at the ankles or hips between the two groups.

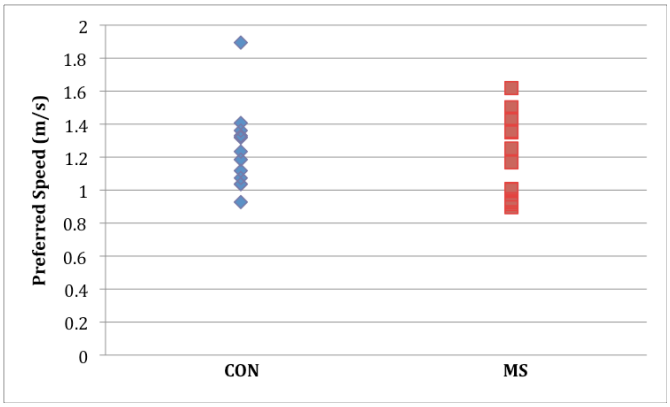

Figure 1: Preferred walking speed for MS and Control groups.

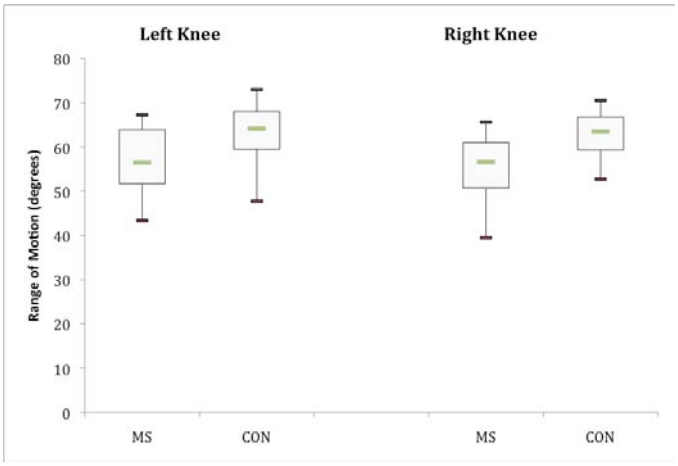

Figure 2: Knee range of motion during the swing phase of walking for MS and Control groups.

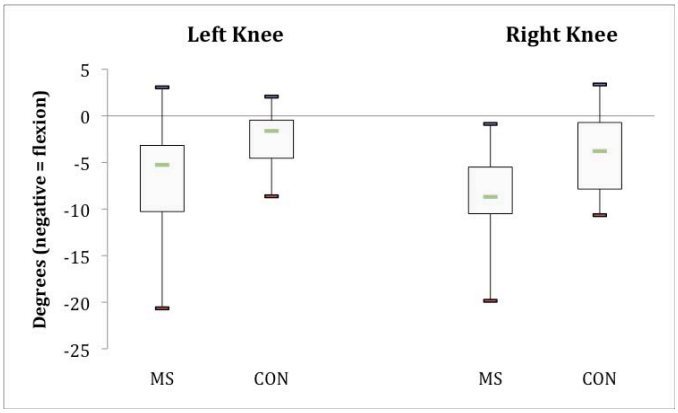

Figure 3: Knee angle (computed relative to angle during quiet stance) at heel strike for MS and Control groups.

DISCUSSION AND CONCLUSIONS

Contrary to previous reports [2,3], reduced preferred walking speeds relative to healthy controls were not observed in this cohort of individuals with MS, despite their greater level of mobility impairments. Even though preferred walking speed was similar, the MS group demonstrated altered lower extremity kinematics, namely a reduced knee ROM and increased knee flexion at heel strike. The range of motion in the upper body was also reduced in the MS group.

The flexed-knee gait pattern may serve to lower the body center of mass and reduce step length. These changes in knee joint motion, together with the reduced sagittal plane motion in the trunk, may improve gait stability in mild to moderately affected people with MS when walking at preferred speed.

REFERENCES

1. Heesen, C. et al. *Multiple Sclerosis*. 2008;**14**:988-991.
2. Benedetti MG et al. *Multiple Sclerosis*. 1999;**5**:363-368.
3. Martin CL et al. *Multiple Sclerosis*. 2006;**12**:620-628.
4. Bowen J et al. *Multiple Sclerosis*. 2001;**7(3):**201-206.

ACKNOWLEDGEMENTS

This research was supported by a National Multiple Sclerosis Society Research Grant RG 3974A2.

HUMAN POSTURAL MODEL THAT CAPTURES ROTATIONAL INERTIA

[1]Anirban Dutta and [2]Ambarish Goswami

[1]Rehabilitation Institute of Chicago, Chicago, USA
email: a-dutta@northwestern.edu
[2]Honda Research Institute, Mountain View, CA, USA
email: agoswami@honda-ri.com

INTRODUCTION

Inverted pendulum models have been very beneficial for the modeling and analysis of human gait and balance [Kuo, 2007]. These reduced models allow us to ignore the movements of the individual limbs, and instead, focus on two important points -- the center of pressure (CoP) and the center of mass (CoM) -- and the *lean line* that connects the two points. A limitation of the existing reduced models is that they represent the entire human body only as a point mass and do not characterize its moment of inertia. The rotational inertia is a property of the distributed masses of the limbs, and by ignoring it, un-natural constraints, such as zero angular momentum at the CoM and resultant ground reaction force (GRF) collinear with the lean line, are forced on to the model.

The Reaction Mass Pendulum (RMP) model [Lee & Goswami, 2007] extends the existing models by replacing the point mass with an extended rigid body – the abstracted 3D reaction mass – that characterizes the aggregate rotational inertia of the subject projected at the CoM. As the person moves through different limb configurations, the centroidal moment of inertia continuously changes, which is captured by the changing shape, size and orientation of the ellipsoidal reaction mass. We postulate that analysis of the rotational inertia especially in cases of pathological gait can provide additional insight. This is demonstrated with normative gait data from four able-bodied subjects and pathological gait data from one spinal cord injured subject.

METHODS

The incomplete spinal cord injured subject (ISCI) was a 34 years old male (weight: 66 Kgs, height: 1.68 m) with T1 motor incomplete spinal cord injury (ASIA D) that resulted in left hemiplegia, who could walk only short distances with rolling walker. Four able-bodied volunteers (age: 39.25±15.9 years, weight: 68±9 Kgs, height: 1.59±12 m), who had no known injury or pathology during the study. Informed consent was obtained from the subjects before their participation.

Retro-reflective markers were placed on the body segments according to the 'plug-in' gait marker set in the Vicon Workstation (Vicon Peak, USA) software to acquire lower-body kinematics data using a seven camera Vicon motion capture system. Two multi-axis force platforms (AMTI, USA) were embedded in the floor of the walkway. The subjects learned to step on the first force platform with their left foot and then step on the second force platform with their right foot after taking three over-ground strides at their preferred speed. The gait data was analyzed with custom software developed in Matlab (The Mathworks, USA). We projected the time-course of segmental CoM position and segmental orientation of thorax, pelvis, bilateral femur, bilateral tibia, and bilateral foot from both able-bodied and ISCI subjects on to an RMP model. All mass and length variables were normalized using subject's body mass and height, respectively.

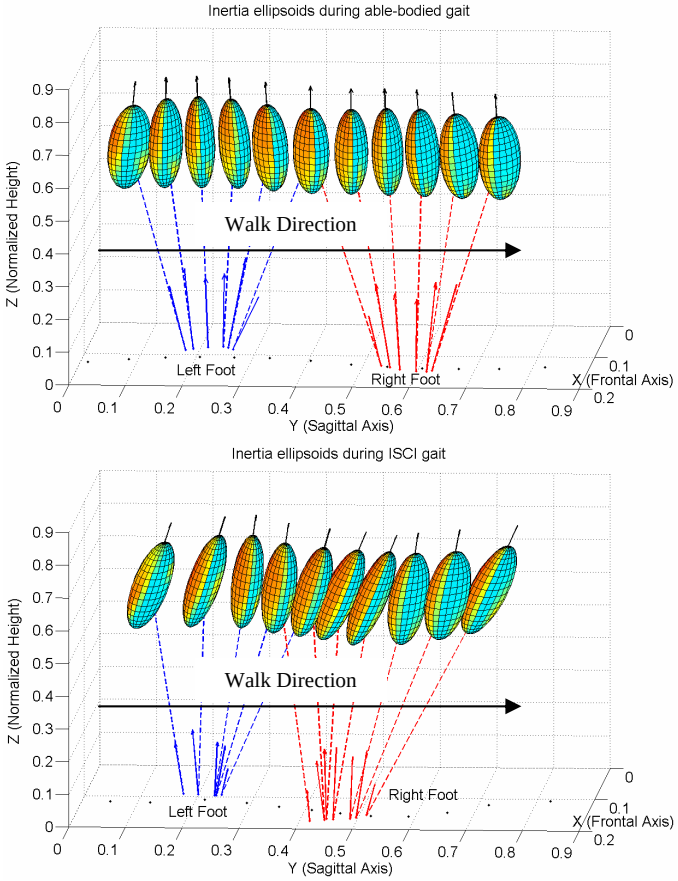

Figure 1: The figures show the evolution of RMP for able-bodied (top panel) and ISCI gait (bottom panel).

Figure 1 shows successive snapshots of the evolution of the RMP model of human gait. At each snapshot, the resultant GRF is shown by an arrow originating from the CoP on force platform, with blue arrow showing the left foot and red arrow showing the right foot GRF. Also shown are the corresponding lean line (in dashed) and the 3D inertia ellipsoid. The RMP model was constructed as follows: at every instant the inertia matrix of each body segment was

computed using anthropometric data [de Leva, 1996] and was projected to the aggregate body CoM using the corresponding spatial transformation matrix. All the projected segmental inertia matrices were summed to obtain the centroidal composite rigid body inertia (CCRBI) matrix. The semi-axes of the inertia ellipsoid were computed from the eigenvalues of CCRBI matrix while the orientation was given by its eigenvectors. The heel-strike and foot-off were lined up over multiple trials (able-bodied: 40 trials, ISCI: 10 trials) for ensemble averaging. Time abscissa was normalized by the duration from left heel-strike to right foot-off.

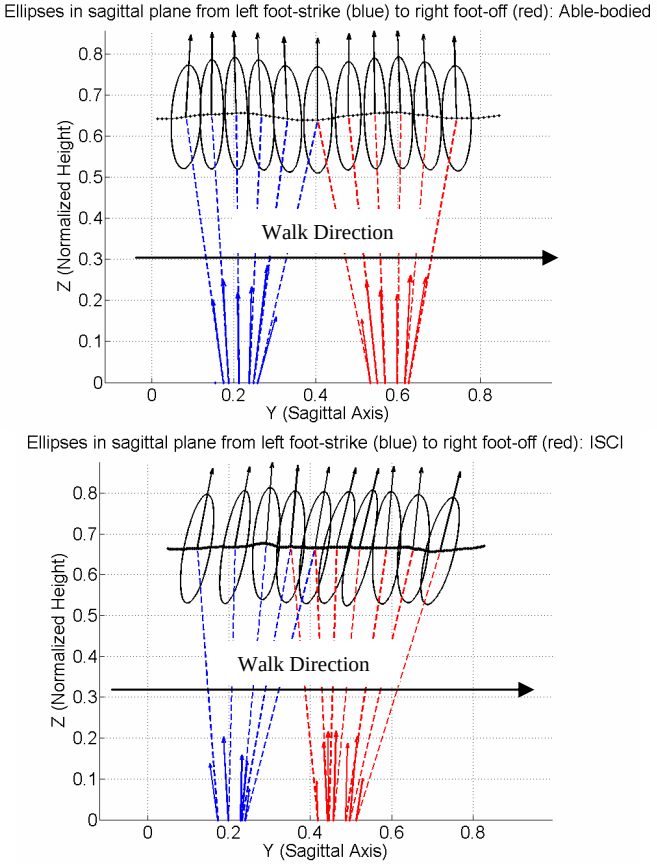

Figure 2: The figures show the evolution of RMP in sagittal plane for able-bodied (top panel) and ISCI gait (bottom panel).

RESULTS AND DISCUSSION

We analyzed the evolution of the RMP model in sagittal plane for able-bodied as well as ISCI gait. Figure 2 shows the GRF from the left-foot (blue) and right-foot (red), the lean line, inertia ellipses in sagittal plane, their centroids (i.e., CoM trajectory) and their orientation. Figure 2 clearly shows that the resultant GRF is not always collinear with the lean line, especially in the case of ISCI gait. This creates a Centroidal Moment (CM) about the CoM, as shown in Figure 3, row 3. Note that traditional point-mass pendulum models will incorrectly force the collinearity of the GRF and lean line, and will indicate a zero CM. Figure 2 shows a flatter CoM trajectory and a consistent forward tilt of inertia ellipse for ISCI's forward-flexed walker-aided gait when compared to able-bodied gait. Figure 3, row 1 shows that both gaits have similar pattern of the inertia ellipse shape and size. However the ISIC gait has a more pronounced vertical tilt in the sagittal plane (Figure 3, row 2). Figure 3 shows that the Centroidal Moment (CM) mostly counteracted the tilt of the ellipse in able-bodied gait except just prior to and during DS phase (tilt almost zero) while it is more complex for ISCI gait. The cost of pendular gait is largely focused on DS phase i.e., the step-to-step transition work, which may account for 60-70% of the overall metabolic cost [Donelan et al., 2002]. Point-mass pendulum models underestimate energy cost and favor shorter and faster steps in absence of rotational inertia [Kuo, 2007], which is accounted for in the RMP model.

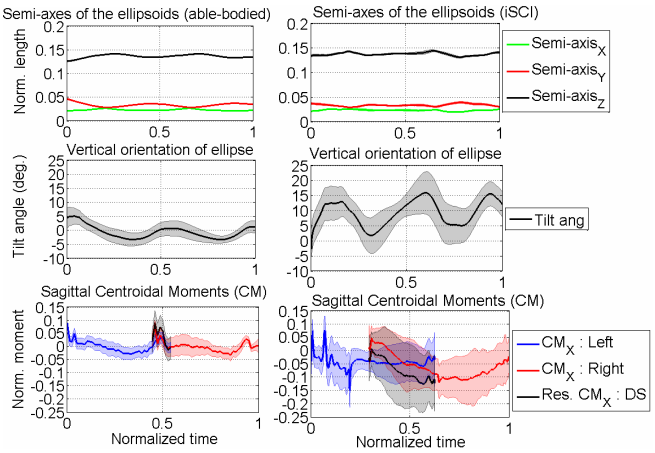

Figure 3: The figures show the semiaxes of inertia ellipsoid (first row), their sagittal plane orientation (second row: anterior tilt +ve) and the centroidal moment (CM) in sagittal plane (third row) for able-bodied (left panels) and ISCI gait (right panels). The shaded areas show ±1 standard deviation. DS: double-support phase of gait.

SUMMARY

1. RMP model augments the traditional point-mass pendulum model by capturing the shape, size and orientation of the aggregate rotational centroidal inertia.
2. RMP model captures the natural centroidal moment created by the GRF about the CoM which equals to zero in traditional point-mass pendulum models.

RMP model may provide insight into pathology and associated energy costs in cases of pathological gait. This however needs further investigation.

REFERENCES

Kuo, A. D. *Human Movement Science*, 26, 617-656, 2007.

Lee, S. H. and Goswami, A. *Proceedings of ICRA07*, 4667-4672, 2007.

De Leva, P. *J Biomech.*, 29(9), 1223-1230, 1996.

Donelan, J. M., Kram, R., and Kuo, A. D. *Journal of Experimental Biology*, 205, 3717-3727, 2002.

ACKNOWLEDGEMENTS

This work was supported by Dr. Ronald Triolo's Merit Review project B2933R from the United States Department of Veterans Affairs at the LS Cleveland VA Medical Center.

SYMMETRY OF PLANTAR PRESSURE DURING SELF-SELECTED WALKING, FAST WALKING, HEEL RAISE AND SIT-TO-STAND ACTIVITIES

[1]On-Yee Lo, [1]Louis Iannuzzi, [2]Kenneth Mroczek, [1]Smita Rao

[1]Department of Physical Therapy, New York University, [2] Department of Orthopedics, NYU Langone Medical Center. Email for correspondence: onyee.lo@nyu.edu

INTRODUCTION

High levels of asymmetry have been associated with musculoskeletal injury in activities such as running. [1] Symmetry of plantar pressure has been studied in walking [2] but not in activities of daily living (ADL) such as sit-to-stand. Current studies indicate that plantar loading is strongly influenced by activity. [3] Walking, sit-to-stand and heel raise are common weightbearing ADL as well as critical exercises for clinical intervention such as muscle strengthening, coordination and balance training.

An improved understanding of plantar pressure symmetry in ADL may provide useful information in designing footwear, preventing lower extremity injuries, and assessing the effectiveness of training programs. The purpose of this study was to determine the degree of symmetry for in-shoe plantar pressure between the left and right feet of healthy subjects during walking, heel-raise, and sit-to-stand in six foot regions.

METHODS

All procedures were approved by the Institutional Review Board. Eleven healthy adults (7 males: 30.3±3.5years, BMI: 26.4±3.67kg/m^2; 4 females: 29.5±3.70 years, BMI: 21.2±0.79 kg/m^2) participated in this study. All subjects were free from any musculoskeletal and neurological symptoms and able to perform the following four activities without any limit: self-selected walking (W), fast walking (F), heel raise (H), and sit-to-stand (S). The self-selected walking trials were collected first and the fast walking (15% higher than the self-selected speed) trials were collected subsequently.

In-shoe plantar pressures were collected by the Pedar-X system (Novel, Munich, Germany). Appropriately sized insoles were placed inside the subjects' own sneakers and were sampled at 50 Hz as the subjects performed four activities (W, F, H, S). Peak pressure (PP, kPa) and pressure-time integral (PTI, kPa/cm^2.s) were investigated at six foot regions: heel, midfoot, medial forefoot, central forefoot, lateral forefoot, and hallux. Absolute symmetry index (ASI, %) of PP and PTI for each activity and region were calculated based on the following formula [4]:

$$ASI = \frac{|X_R - X_L|}{\frac{1}{2}(X_R + X_L)} \times 100\%$$

where X_R indicates PP or PTI on right foot and X_L indicates PP or PTI on left foot.

The effect of activity and foot region on ASI of PP and ASI of PTI were determined by using a two way repeated measures ANOVA (SPSS Inc., Chicago, IL). If the interaction effect (activity x region) was significant ($\alpha < 0.05$), simple effects of activity on each foot region were assessed subsequently. In terms of post-hoc testing, ASI of PP and ASI of PTI during each activity were assessed using Bonferroni adjusted pair-wise comparisons.

RESULTS AND DISCUSSION

A significant activity-by-foot-region interaction was found for PP (p = 0.03), figure 1. Subsequently, significant simple effects were noted for PP at the lateral forefoot (p = 0.01) and hallux (p=0.005). Significant pair-wise differences compared to walking at self-selected speed are summarized in table 1.

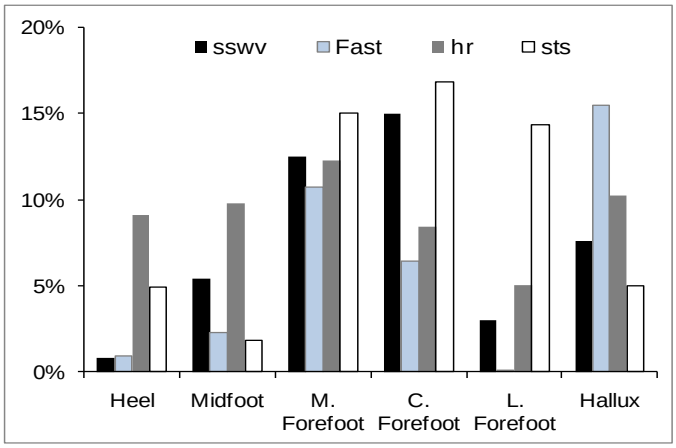

Figure 1. Summary of ASI for PP during self-selected (sswv) and fast (fast) walking, heel raise (hr) and sit-to-stand (sts) activities. Foot regions include heel, midfoot, medial forefoot, central forefoot, lateral forefoot and hallux.

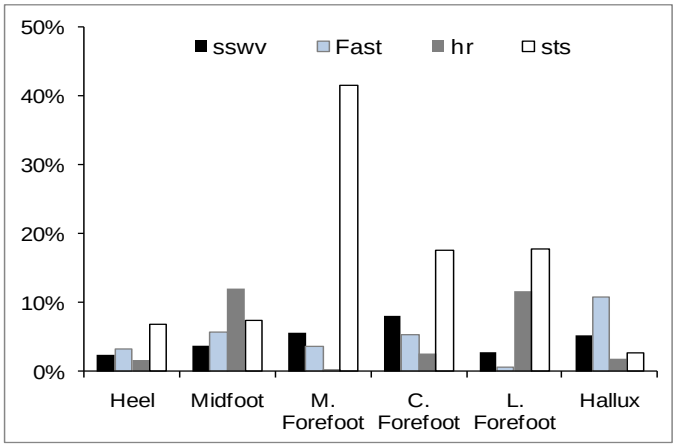

Figure 2. Summary of ASI for PTI during self-selected (sswv) and fast (fast) walking, heel raise (hr) and sit-to-stand (sts) activities. Foot regions include heel, midfoot, medial forefoot, central forefoot, lateral forefoot and hallux.

Significant activity-by-foot-region interaction was also found for PTI (p = 0.03). Significant simple effects were noted for PTI at the medial forefoot (p=0.016), central forefoot (p=0.012), lateral forefoot (p =0.001), and hallux (p =0.007). Significant pair-wise differences compared to walking at self-selected speed are summarized in table 1.

CONCLUSIONS

We sought to assess the degree of symmetry for in-shoe plantar pressure between the left and right feet of healthy subjects during walking, heel-raise, and sit-to-stand in six foot regions. The chief findings of our study indicate that bilateral activities such as heel raises and sit-to-stand may be accompanied by significant asymmetry in plantar loading. Additonal studies are indicated to examine patterns of asymmetry in clinical populations.

REFERENCES

1. Sadeghi, H., et al., Gait Posture, 12(1): 34-45,2000.
2. VanZant, R.S., et al., J Am Podiatr Med Assoc, 91(7): 337-42,2001.
3. Guldemond, N.A., et al., Diabetes Res Clin Pract, 77(2): 203-9,2007.
4. Zifchock, R.A., et al., J Biomech, 39(15): 2792-7,2006.

ACKNOWLEDGEMENTS

This study was partly supported by the New York Physical Therapy Association.

Table 1. Summary of PP (kPa) and PTI (kPa/cm2.s) during self-selected (sswv) and fast (fast) walking, heel raise (hr) and sit-to-stand (sts) activities. Foot regions include heel, midfoot, medial forefoot, central forefoot, lateral forefoot and hallux. ***** indicates significant difference compared to sswv based on Bonferroni adjusted pair-wise comparisons.

	PP	PP	PP	PP	PTI	PTI	PTI	PTI
Activity	sswv	fast	hr	sts	sswv	fast	hr	sts
Heel	0.8%	0.9%	9.1%	4.9%	2.4%	3.2%	1.6%	6.8%
Midfoot	5.4%	2.3%	9.8%	1.8%	3.7%	5.7%	12.0%	7.3%
M. Forefoot	12.5%	10.7%	12.3%	12.0%	5.6%	3.7%	0.4%	41.5%*
C. Forefoot	15.0%	6.4%	8.4%	16.8%	8.1%	5.3%	2.6%	17.5%*
L. Forefoot	3.0%	0.1%	5.0%	14.3%*	2.7%	0.6%	11.6%	17.8%*
Hallux	7.6%	15.5%*	10.2%	5.0%	5.2%	10.7%*	1.8%	2.7%

GAIT BIOMECHANICS IN HIP ARTHROPLASTY PATIENTS AND CONTROL SUBJECTS: EFFECT OF BIG FEMORAL HEAD AND SURFACE REPLACEMENT PROSTHESES

[1, 4]Vicky Bouffard, [1]Julie Nantel, [1]Marc Therrien, [3]Pascal-André Vendittoli, [3]Martin Lavigne and [1, 2, 4]François Prince

[1]Laboratoire Posture-Locomotion, Centre de Réadaptation Marie Enfant, Montréal, Qc, Canada
[2] Département chirurgie, Faculté de Médecine, Université de Montréal, Montréal, Qc, Canada
[3]Département d'orthopédie, Hôpital Maisonneuve-Rosemont, Montréal, Qc, Canada
[4]Département de kinésiologie, Université de Montréal, Montréal, Qc, Canada

Email: vicky.bouffard@umontreal.ca

INTRODUCTION

Since younger patients are now more frequently affected by osteoarthritis (OA) [1] hip arthroplasty expectations have changed. Indeed, patients not only want to be relieved from pain and stiffness but also wish to return as soon as possible to a higher level of physical activity [2].

Previous studies have reported that the hip abductor muscles of patients undergoing hip arthroplasty generate less strength compared to those of healthy subjects [3, 4]. This may explain the smaller hip abductor moment measured during gait [5]. One way to compensate for weaker hip abductor strength may be by shifting the body center of mass (COM) toward the hip prosthesis joint center (HPJC). This strategy implies a reduction of the moment arm length which consequently causes a decrease in the magnitude of the hip abductor moment and of the amount of strength needed from these muscles [6].

The purposes of this study are twofold: 1) to compare the distance between the COM and the HPJC during gait, and 2) to compare two types of prostheses: big femoral head (BFH) and surface replacement arthroplasty (SRA) at 12 months post surgery.

METHODS

All patients were diagnosed with hip OA and had a surgical intervention using a posterior approach. A control group was used for comparison. Groups' characteristics are shown in Table 1.

Table 1. Means (SD) of the groups' characteristics.

	BFH (n=12)	SRA (n=12)	Control (n=11)
Age (y)	50.8 (6.1)	52.8 (6.7)	47.7 (8.2)
Gender	5 F/ 7 M	6 F/ 6 M	7 F/ 4 M
Weight (kg)	75.3 (15.3)	74.1 (15.4)	73.5 (11.3)
Height (m)	1.68 (.04)	1.67 (.08)	1.67 (.09)
BMI (kg/m^2)	26.7 (4.7)	26.3 (3.8)	26.3 (3.0)

All subjects were asked to walk at their normal speed on a 10m walkway with two embedded force platforms (120Hz). Kinematics were recorded from an 8-Vicon cameras system (60Hz). The COM position was calculated from marker positions and anthropometric tables while the distance (in mm) from HPJC and COM was calculated in the frontal plane. Distances were normalized to the inter- ASIS distance for each individual (ratio = distance COM-HPJC/ distance inter-ASIS). The coefficient of variation (CV) ((SD/ average)* 100) was also calculated. Data were extracted for three different trials at five specific moments in the gait cycle heel contact (HC), maximum weight acceptance (MWA), mid-stance (MS), push-off (PO), and toe off (TO).

The results were then analysed using a one-way ANOVA. As required, the results were further analyzed with the Kruskal-Wallis test. All analyses were done with a level of significance set at 0.05.

RESULTS AND DISCUSSION

No difference was observed for the sociodemographic data.

No statistical significance was found for the COM-HPJC distance ratio (Table 2). These results suggest that our groups were similar to the healthy subjects.

Table 2. Mean (SD) of the HPJC-COM distance ratio

	BFH	SRA	Control
HC	0.344	0.331	0.333
	(.037)	(.027)	(.025)
MWA	0.357	0.339	0.359
	(.029)	(.027)	(.032)
MS	0.359	0.339	0.358
	(.033)	(.029)	(.026)
PO	0.363	0.348	0.363
	(.032)	(.026)	(.022)
TO	0.352	0.340	0.336
	(.039)	(.031)	(.025)

No statistical difference was found for the CV (Table 3). These results show, once again, that both prostheses groups did not differ from the control subjects.

Table 3. Mean (SD) of CV in %.

	BFH	SRA	Control
HC	3.3 (2.1)	3.1 (1.9)	4.3 (3.6)
MWA	2.8 (2.0)	3.2 (2.5)	3.5 (2.1)
MS	2.5 (2.4)	2.4 (1.5)	3.1 (1.4)
PO	3.4 (2.5)	2.4 (1.6)	3.5 (1.5)
TO	3.4 (2.9)	3.4 (2.6)	4.2 (1.0)

The absence of statistical significance between the two prostheses and the control subjects during a walking task, suggest that patients did not adapt their gait strategy. In fact, they did not decrease their moment arm length, by shifting more body weight on their affected limb to reduce constraints on their prosthetic hip joint and minimize the effort of their hip abductor muscles. One year post-surgery, patients who underwent hip arthroplasty control their COM the same way as that of the control subjects.

Furthermore, the absence of statistical significance between the CV revealed that our three groups were similar. In other words, the dispersion of data is the same between groups.

CONCLUSIONS

One year following surgery, patients undergoing hip arthroplasty do not seem to adapt their gait strategy by decreasing their moment of arm length, the COM-HPJC distance, in the frontal plane to compensate for their hip abductors weakness.

In this study, the predictive method was used to calculate the hip joint center. Recently, a new method known as the functional method was developed [7]. The latter method may be more efficient in this case because it takes into consideration the individual characteristics of patients. It could have an impact on the results.

REFERENCES

1. Loeser, RF., *Osteoarthritis cartilage* **17**, 971-979, 2009.
2. Mackichan F, et al. *Rheum Dis Clin North Am* **34**, 311-330, 2008.
3. Majewski M, et al. *J Bone Joint Surg Br* **87**, 1337-1343, 2005.
4. Trudelle-Jackson E, et al. J *Orthop Sports Phys Ther* **32**, 260-267, 2002.
5. Mont MA, et al. *J Arthroplasty* **22**, 100-108, 2007.
6. Asayama I, et al. *J Arthroplasty* **20**, 414-420, 2005.
7. Ehrig RM, et al. *J Biomech*. **39**, 2798-2809, 2006.

ACKNOWLEDGEMENTS

We would like to thanks the CIHR-MENTOR training program and the FRSQ for their financial and scholarship supports. The study was funded (unrestricted grant) by Zimmer, Warsaw, USA.

LIMB KINEMATICS PREDICT EMOTION RECOGNITION WITH WALKING SPEED MODIFICATIONS IN BIOMECHANICAL ANIMATIONS

Melissa Gross and Joshua D'Angelo

University of Michigan, Ann Arbor, MI, USA
email: mgross@umich.edu, web: http://www.umich.edu/~mgross

INTRODUCTION

Expression of emotion affects both posture and limb kinematics during walking [1,2]. Because gait speed also changes with emotion, speed-related changes in limb kinematics have confounded emotion-related kinematics in emotion recognition studies and in studies of individuals with mood disorders [2,3]. It is important to understand which gait kinematics are most sensitive to emotion to improve the design of clinical studies of movements in individuals with psychiatric disorders.

In this study, we used biomechanical animations to display emotionally expressive walking trials to observers. We manipulated the display speeds of walking with "slow" (i.e., sad) and "fast" emotions (i.e., anger and joy) to test the effects of modified limb velocities on emotion recognition. Because body postures remained the same while limb velocities changed across trials, we were able to separate the effects of posture and limb kinematics on emotion recognition and to determine which limb kinematics best predicted emotion recognition.

METHODS

Animated displays used in this study were created from a subset of walking trials generated in a larger study using motion capture [1]. The ten trials with the highest mean recognition rates for four target emotions, i.e., anger, joy, sadness and neutral (for simplicity, neutral was treated as a target emotion), were included in this study; these 40 trials were generated by 29 walkers (38% male; 19.8 ± 2.0 yrs).

Virtual markers were created to display the body during the walking trials [4]. Virtual markers were placed at joint centers of the shoulders, elbows, wrists, hips, knees, ankles, metatarsals and metacarpals, and on the heels. The trunk was modeled with markers placed at C5, T6 and L3 and three markers were placed on the head.

Gait cycle durations were modified to produce a range of modified walking speeds for a given target emotion that best approximated the original range of walking speeds for a different target emotion. Angry (1.55 ± 0.28 m/s), joyful (1.44 ± 0.18 m/s) and neutral (1.18 ± 0.11 m/s) trials were modified to produce angry-slow, joyful-slow and neutral-slow trials that were 36, 35 and 25% slower, respectively, and approximated the walking speeds of sad (0.93 ± 0.13 m/s) trials. Conversely, sad-fast trials were 60% faster than sad trials and approximated the walking speeds of angry trials. For example, the walking speeds in the "joyful-slow" trials ranged from 0.77-1.11 m/s, which was similar to the range of walking speeds in the sad trials (0.73-1.12 m/s).

Joint velocities were calculated in the original study using Visual3D software. Modified joint velocities were calculated by changing the time increments by the same factors that were used to change the display speeds for each target emotion condition.

Once the walking speeds were modified, each walking trial was looped so that it displayed three times in succession. The set of 80 (40 original speed; 40 modified speed) walking trials was ordered into three random sequences.

Observer subjects (n=31; 48% male; 20.1 ± 2.1 yrs) were recruited from the university community and gave informed consent before participating. After viewing each of the animated displays, observers selected one of ten emotions that they thought the walker was feeling. The mean recognition rate for each emotion item was calculated for each of the eight emotion-speed conditions (i.e., angry, joyful, sad, neutral, angry-slow, joyful-slow, neutral-slow, sad-fast). A mixed model with random observer

effects and fixed effects of emotion-speed, video sequence, and observer gender was used to test for differences between means ($p < .05$).

RESULTS AND DISCUSSION

Target emotion recognition rates were 56, 36, 23 and 38% in sad, angry, joyful and neutral trials, respectively. When display speeds were modified, the mean target emotion recognition rates decreased in sad-fast (21%) and angry-slow trials (11%) ($p<.001$), but did not change significantly in joyful-slow (22%) and neutral-slow (33%) trials.

Slowing down angry, joyful and neutral trials failed to produce emotion recognition patterns that were similar to sad. Sad was recognized in angry-slow trials, but at a much lower rate (16%) than in sad trials ($p<.001$); sad was not recognized in either joyful-slow or neutral-slow trials. Recognition of anger, joy and neutral was highest in angry-slow, joyful-slow and neutral-slow, respectively ($p<.01$), and anger, joy and neutral were not recognized in the sad trials.

Similarly, speeding up sad trials failed to produce emotion recognition patterns that were similar to anger, joy or neutral. Anger was recognized in both sad-fast (28%) and joyful (14%) trials, but at lower rates than in angry trials ($p<.01$). Sadness and joy were recognized only in sad-fast and joy trials, respectively. Sad-fast and neutral did not share recognition of any emotions.

Mean peak velocities at the hip, knee, shoulder and elbow were strongly correlated with emotion recognition in angry and sad trials (Table 1). Although angry and joyful trials shared the same range of limb velocities, joy recognition was not correlated with most limb velocities, suggesting that joy recognition depended more on posture than limb velocities. Like anger, sad recognition depended on limb velocities but unlike anger, sad recognition was associated with lower velocities. Recognition of neutral was not correlated with any joint velocity.

Although gait speeds were the same in angry and joyful trials, the relationship between emotion recognition and ankle and wrist kinematics differed (Table 1). Ankle velocity was associated only with anger recognition, so that higher ankle velocities predicted anger recognition, consistent with "heavy footed" walking with anger [5]. Wrist velocity was associated only with joy recognition, so that higher wrist velocities predicted joy recognition, consistent with "looser" movements associated with joy and "stiffer" movements associated with anger [6].

Table 1: Pearson correlation coefficients for target emotion recognition with peak flexor velocity

Joint	Target Emotion			
	Sad	Angry	Joyful	Neutral
Hip	-.601**	.847**	.058	-.153
Knee	-.586**	.748**	-.098	.068
Ankle	-.166	.473*	.265	-.095
Shoulder	-.558*	.834**	.312	-.135
Elbow	-.689**	.603**	. 286	.318
Wrist	-.637**	.339	.457*	.039

Note. Both natural and modified speed trials were used to calculate correlations for each target emotion (n = 20). Correlation coefficients for extensor velocities and recognition were very similar to those for flexor velocities shown here. **p < .01. *p < .05

CONCLUSIONS

The results of this study indicate that body posture and limb kinematics, and not just gait speed, are important when evaluating emotion expression in body movements in healthy individuals, and suggest that both posture and limb kinematics should be included in evaluations of therapeutic interventions in individuals with mood disorders.

REFERENCES

1. Crane EA. Dissertation, 2009.
2. Roether CL, et al. *Current Biology* **18**, R329-330, 2008.
3. Michalak J, et al. *Psychosomatic Medicine* **71**, 580-587, 2009.
4. Gross MM, et al. *Proc. American Society of Biomechanics*, State College, PA, USA, 2009.
5. Montepare J, et al. *Journal of Nonverbal Behavior* **11**, 33-42, 1987.
6. Montepare J, et al. *Journal of Nonverbal Behavior* **23**, 133-152, 1999.

ACKNOWLEDGEMENTS

Funded by NSF Grant (044430) to M. Gross.

FOOT FORCES DURING EXERCISE ON THE INTERNATIONAL SPACE STATION

[1,2]Kerim O. Genc, [3]Raghavan Gopalakrishnan, [3]Matthew M. Kuklis, [4]Christian C. Maender, [1]Andrea J. Rice, [5]Kenneth D. Bowersox and [1]Peter R. Cavanagh

[1]University of Washington, Seattle, WA, USA;
[2]Case Western Reserve University, Cleveland, OH, USA;
[3]Cleveland Clinic, Cleveland, OH, USA;
[4]NASA – Johnson Space Center, Houston, TX, USA; [5]Houston, TX.
email: cavanagh@uw.edu

INTRODUCTION

Bone mineral density (BMD), predicted bone strength, and muscle volume show decreases in the lower extremity and spine of crewmembers who fly long-duration missions on-board the International Space Station (ISS) [1,2]. These physiological changes are likely a result of a decrease in mechanical stimulus imparted on the musculoskeletal system while living in a microgravity environment [3]. Cavanagh et al. [4] demonstrated that exercise levels used during typical days on the ISS resulted in a 25% and 84% decrease in the magnitude and time duration of mechanical loading respectively. The purpose of the current study is to examine the full range of loading capabilities of the available exercise countermeasure devices and to compare these results with typical prescribed exercise days performed on Earth (1g) and on the ISS (0g).

METHODS

Four male crewmembers (age: 49.5 ± 4.7 years) who flew on long-duration missions aboard the ISS (mission duration: 181 ± 15 days) took part in this study. The study protocol was approved by the Committee for the Protection of Human Subjects at NASA's Johnson Space Center, Houston, TX, and by the local institutional IRBs. Each subject provided written informed consent.

Crewmembers performed data collection sessions during which the settings on the three exercise devices were varied throughout their available ranges. These devices include the Treadmill with Vibration Isolation and Stabilization (TVIS), the Cycle Ergometer with Vibration Isolation System (CEVIS), and the interim Resistance Exercise Device (iRED). On the TVIS, two crew members completed five trials each of walking (2 mph) and running (5.5 mph), one of whom also ran at 8 mph. Each trial had a loading configuration of 1-Bungee, 2-Bungees, SLD 120, SLD 170, or SLD 210. The SLD suffix represents the nominal load in pounds applied by a subject load device (SLD) to a harness worn by the runner. The bungee configurations refer to the number of bungee cords used to apply loads to the harness. Clips could be added in series to increase effective length without changing applied force. On the iRED, two crewmembers performed three trials each of bent-over rows, upright rows, straight-leg dead lifts, dead lifts, squats, single-leg squats, heel raises and single-leg heel raises, each with a different resistance setting. Each iRED trial consisted of approximately ten repetitions of the exercise. On the CEVIS, two crew members performed one minute trials at 60, 75 and 90 RPM at six different power settings.

In-shoe forces were monitored at 128Hz using capacitance-based force-measuring insoles (Novel Gmbh, Munich, Germany) placed inside the shoes of the crewmembers [5]. Custom software (Matlab, Mathworks Inc, Natick, MA) was used to extract peak forces from 30 seconds to 30 minutes of walking, running, and cycling and from individual resistance exercise activities. The data were then compared to the mean values for walking, running and cycling from the same subjects during typical days on Earth and on the ISS which were collected during a separate experiment [4, 5]. We also examined a hypothetical situation where crewmembers used the maximal exercise loading configurations from the current experiment as their typical exercise regimen.

RESULTS AND DISCUSSION

The average maximum single-leg loads for TVIS walking were 0.91 ± 0.19 times body weight (BW) at 2 mph and 1.77 BW for running at 8 mph, both at SLD 210 (Fig. 1). The average maximum available single-leg loads for iRED exercises were 0.32 ± 0.07 BW for bent-over rows, 0.23 ± 0.02 BW for upright rows, 0.30 ± 0.05 BW for straight-leg deadlifts, 0.41 ± 0.06 BW for deadlifts, 0.59 ± 0.03 BW for squats, 0.64 ± 0.09 BW for single-leg squats, 0.68 ± 0.08 BW for heel raises, and 0.72 ± 0.10 BW for single-leg heel raises. As both power and pedaling speed increased during CEVIS exercise, the peak in-shoe force during cycling increased from a minimum of 0.07 ± 0.02 BW at 75 watts to a maximum of 0.19 ± 0.04 BW at 210 watts.

All of the available external loading ranges during walking and running on TVIS resulted in foot forces that were substantially less than those during the same exercise performed on Earth (Fig. 1). However, the use of SLD 210 resulted in foot forces 38% greater than those experienced during typical regularly scheduled TVIS sessions on the ISS [4]. A major limiting factor to increasing SLD load on TVIS to Earth-like levels is the perceived discomfort of the harness that couples subject and subject load device.

There were no data from on-Earth performance of resistance exercise for comparison. The maximum available loads during iRED exercises were up to 50% greater than during typical exercise on the ISS. The data show that the variations in lower extremity loading as iRED settings changed were not always proportional. For example, when the canister settings for double-leg heel raises were increased from 200 lb to 300 lb (a 50% increase), the lower extremity load increased only 39%.

The loads from CEVIS are relatively small, rising only to a maximum of 0.19 BW at the most challenging setting studied (210 W), which is not different from the forces recorded on Earth (0.20 ± 0.086 BW). Even if substantial increases were available, this may not have a marked effect on the overall loading stimulus to bone.

When substituting the data from the typical loading configurations of TVIS, iRED and CEVIS [4] with the maximal data from the current experiment, we found a 5% increase in overall daily loading stimulus. This implies that if crewmembers had used the maximum load settings on the available devices during their typically prescribed exercise periods, they would still have experienced a 20% decrease in the magnitude of loading compared to Earth.

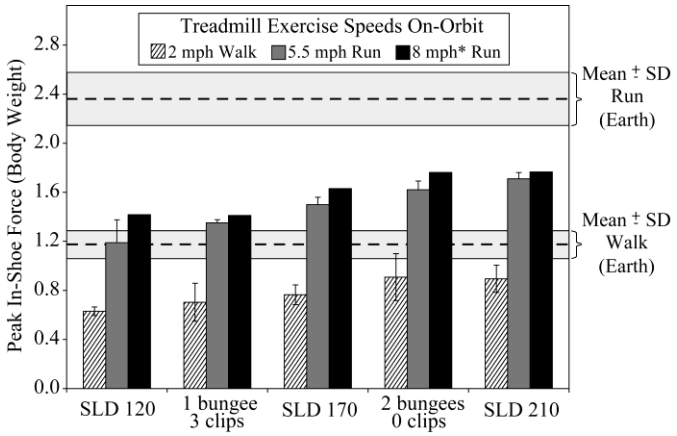

Figure 1: Mean peak in-shoe forces (in BW) during exercise on TVIS and in 1g. The data are mean values from 30 seconds of activity (± 1 SD) for 2 crewmembers.

CONCLUSIONS

The results from the current experiment indicate that exercise of typical duration at maximum loading on the available devices would not have provided sufficient mechanical loading to maintain bone health during long-duration missions on the ISS. Greater loading or duration of exercise will require improved SLD coupling for treadmill running and greater resistance exercise capability.

REFERENCES

1. Keyak JH et al. *Bone* **44**, 449-53, 2009.
2. Gopalakrishnan et al. *Aviat Space Environ Med* **81,** 91-102, 2010.
3. Lang TF et al. *J Bone Miner Res* **21,** 1224-30, 2006.
4. Cavanagh et al. *J Biomech* [In Press]
5. Cavanagh et al. *Aviat Space Environ Med* **80**, 870-81, 2009.

ACKNOWLEDGEMENTS

NASA cooperative agreement NCC 9 153. We also acknowledge Jess Snedeker, Ruth Ochia and the remarkable cooperation of the subjects.

ASSESSING SPATIOTEMPORALLY COMPLEX AND COUPLED GAIT PATTERNS USING TEMPORAL CROSS-CORRELATION

Kiwon Park, Harry Dankowicz and Elizabeth T. Hsiao-Wecksler

Department of Mechanical Science & Engineering
University of Illinois at Urbana-Champaign, Urbana, IL, USA
email: kpark31@illinois.edu

INTRODUCTION

Human gait is a spatiotemporally complex motion, where each segment and joint motion during gait is coupled across other joints. These spatiotemporal joint coupling patterns are closely associated with musculoskeletal injury mechanics, but previous tools used to examine human gait have mainly focused on univariate measures such as stride, step length, maximum range of motion, and the durations of stance and swing phases of gait. These tools are unable to capture the complex nature of human movement or assess correlated patterns of joint or segmental movement patterns within and between human limbs.

A temporal cross-correlation technique was used in the present study to characterize and detect the relative timing and shape of temporal signals across multiple joint variables (the spatial domain) during human gait. In particular, it was argued that spatial coupling across joints would manifest itself in characteristic delays (phase shifts) between significant events in distinct time signals. To highlight significant differences in spatiotemporally complex and coupled gait behaviors between different gait conditions, this technique was applied to the angular displacement and velocity histories across twelve lower extremity variables, for healthy subjects with a knee or ankle brace on the right leg and without brace. Bracing simulated knee or ankle injuries by restricting joint range of motion, and was used to provide a controlled experimental environment for simulating abnormal gait with known conditions. The goal of this study was to characterize different gait behaviors (unbraced, right knee braced, and right ankle braced) by using cross-correlation technique to investigate spatiotemporally complex and coupled joint parameters in gait.

METHODS

Gait data from a previous study were used [1]. Ten healthy male subjects (21 ± 2 yrs) walked for three minutes on a treadmill at a self-selected comfortable speed determined while wearing a knee or ankle brace on the right leg (DonJoy, Vista, CA; models 81099 and 82399, resp.). Each subject walked under three conditions: (1) normal (non-braced), (2) knee-braced, and (3) ankle-braced. Kinematic data were collected from a six-camera motion capture system (Vicon, Oxford, UK; 460 Datastation), and twelve lower extremity joint variables, viz., the bilateral hip, knee, and ankle angular displacements and velocities, were obtained. A custom-written MATLAB program was used to perform all calculations (R2008a, The MathWorks, Natick, MA).

In the present study, the normalized cross-correlation function was calculated [2]. Normalized cross-correlation values show the similarity in shape between two time-series signals as a scalar between -1 and 1. For this technique, the maximum cross-correlation values (Max CC) and phase shifts (PS) at which this maximum recorded were obtained for each cross-correlation function.

For each subject, normalized non-dimensional time-series data (z-score values) were analyzed for twelve joint variables. The temporal cross-correlation function was then computed for each pair of such joint variables at the hip, knee, and ankle joints, excluding the autocorrelation. Finally, for each subject, three 12×12 characteristic matrices (unbraced, right knee braced and ankle braced) were created, with rows and columns labeled by the twelve joint variables, such that the entries below the diagonal contained the Max CC for the corresponding pair of joint variables and the entries above the diagonal contained PS at which this maximum was recorded.

Next, to examine changes in max CC and PS of the entries of the characteristic matrices between different gait conditions (unbraced vs. knee or ankle braced), a paired t-test was performed on each entry across all ten subjects. A color-coded comparison matrix of the same size as the characteristic matrices was then created by coloring black those entries for which a significant difference ($p<0.01$) was found between the two conditions (unbraced vs. knee or ankle braced), and white those entries with no significant difference (Fig. 1).

RESULTS AND DISCUSSION

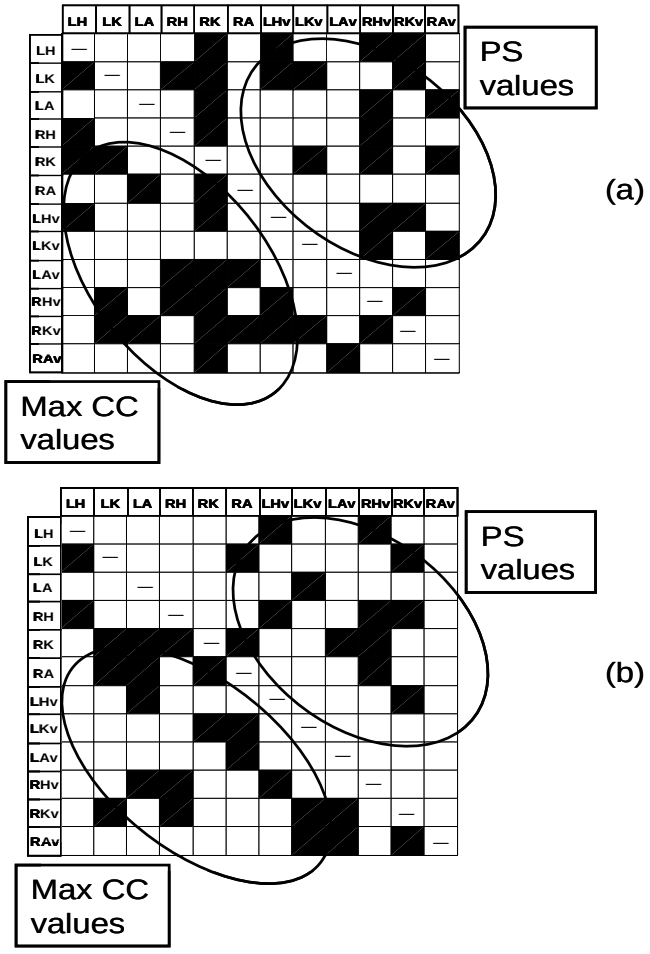

Figure 1: Characteristic diagrams showing differences between (a) unbraced vs. knee-braced, and (b) unbraced vs. ankle-braced. (LH = left hip angular position, LK = left knee angular position, RH = right hip angular position, etc., XX-v: angular velocity of XX).

The resultant characteristic diagram including colored squares, here referred to as a *signature*, highlighted those pairs of joint variables for which significant differences were found between the two conditions (unbraced vs. knee or ankle braced) in the relative timing and magnitude across the gait cycle. As might be expected, numerous cells indicating pairings of the restricted joint (RK in Fig. 1a, and RA in Fig. 1b) with other joint variables were found to be significantly different between the unbraced and braced condition. However, the characteristic diagram also indicates that significant changes were observed for couplings between other joint variables in addition to the braced joint parameters.

Knee bracing extensively affected these temporal joint couplings, such that there were a substantial number of black cells indicating that the Max CC and PS values for the respective variable pairing were significantly different between unbraced and knee-braced motions.

Ankle bracing did not influence the joint couplings as much as the knee bracing. The reduced number of affected variable pairing (black cells) could be due to the design of the ankle brace. The ankle brace in this study was a walking cast that had a convex rocker built into the sole. During stance, when restricting ankle motion should create the greatest perturbation, the rocker allowed the shank to smoothly roll over the ankle despite being locked at neutral, thus resulting in minimized impact to knee and hip motions with and without the brace.

CONCLUSIONS

This work investigated the nature of joint variable coupling for different simulated injured gait conditions. Statistical analyses of the results of a temporal cross-correlation technique were applied to characterize significant changes in the relative timing and magnitude of angular displacement and velocity profiles. More importantly, the signature diagram captured significant spatiotemporal changes and couplings not only of entries involving the affected right knee or ankle parameters, but among other joint variables.

REFERENCES

1. KA Shorter, et al. *Clin Biomech*, **23**:459-67, 2008
2. T Wren, et al. *J Biomech* **39**:2714-8, 2006.

ACKNOWLEDGEMENTS

The authors thank K. Alex Shorter for collecting the experimental data, and the National Science Foundation (#0727083) for partial funding.

ASSESSING PERFORMANCE OF THREE TYPES OF BIOMECHANICAL MODELS APPLIED TO NORMAL HUMAN GAIT

[1,2]Frank L. Buczek, [3]Michael J. Rainbow, [2]Kevin M. Cooney, [2]Dustin A. Bruening,
[4]Anne Schmitz, [4]Darryl G. Thelen

[1]National Institute for Occupational Safety & Health, Morgantown, WV, USA
[2]Shriners Hospitals for Children, Erie, PA, USA, [3]Brown University, Providence, RI, USA
[4]University of Wisconsin-Madison, Madison, WI, USA
email: fbuczek@cdc.gov

INTRODUCTION

Gait analyses provide clinical decision-makers with physical examination findings, joint kinematics and kinetics, and associated joint powers, leading to treatment recommendations. This last step is weakened by model-dependent inaccuracies in key gait analysis variables [1]. Yet, it is difficult to assess relative accuracy, because human motion capture is affected by soft tissue errors that mask true motion [2]. Direct methods to overcome this problem are invasive [3,4] and therefore clinically impractical. Forward dynamic simulations partially overcome this problem by providing a set of constrained bone-to-bone motions inferred from *in vivo* and *in vitro* studies [5], and by providing marker kinematics that exactly recreate these motions. The purpose of this study is to assess the performance of three types of biomechanical models using forward dynamic simulations, customized to individual gait patterns, as an estimate of true motion. In particular: **CGM** = conventional gait model; **OPT1** = CGM local reference frames [6] with six degree-of-freedom (6DOF) tracking; and **OPT2** = local reference frames based upon *in vivo* and *in vitro* studies [7], with 6DOF tracking. We hypothesize that OPT2 will match simulations better than OPT1 and CGM.

METHODS

Full-body data collection, using a ten-camera Vicon 612 system and three AMTI force plates, has been described in detail elsewhere [1]. Briefly, 25 normal volunteers were fitted with a hybrid marker configuration, allowing the identical stride to be analyzed in Visual3D (C-Motion, Inc.) using CGM, OPT1, and OPT2. Subject-specific gait simulations were generated for a subset of eight subjects for whom bilateral force plate data were available during double support. A generic whole body model was first scaled to match the measured segment lengths of each subject (Figure). We then used a least squares forward dynamics algorithm to compute the pelvic motion and joint kinematics that were optimally consistent with the experimentally acquired marker kinematics and ground reactions, while satisfying overall equations of motion. Simulated marker kinematics were generated assuming rigid fixation to each segment, and processed in Visual3D using the same algorithms as those for OPT2; associated gait data (twenty functionally relevant maxima and minima in joint angles, moments, and powers, see Table) were used as our best estimate of truth (**CLN**).

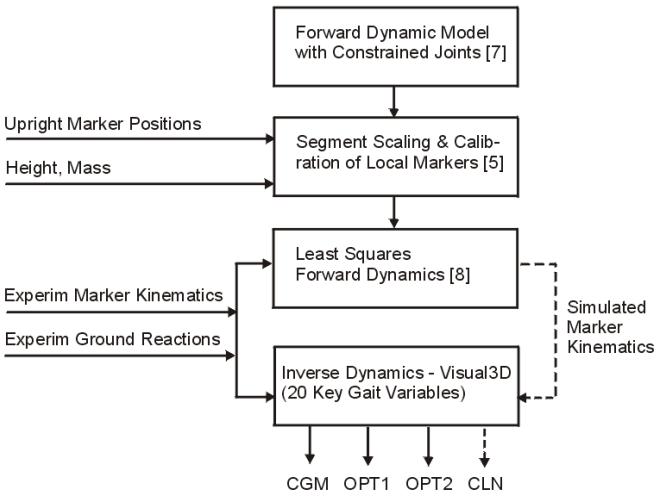

Figure. Forward and inverse dynamics processing.

Experimental marker kinematics, affected by noise (e.g., soft tissue errors), were processed in Visual3D according to CGM, OPT1, and OPT2 model criteria. Repeated measures ANOVAs, with Tukey HSD *post hoc* comparisons (Statistica 7), were used

to identify significant differences ($p<0.05$) between all pairs of models, for the twenty key gait analysis variables. Ensemble averages were also calculated for kinematic and kinetic data (not reported here.)

RESULTS AND DISCUSSION

Our primary hypothesis was supported, with no significant differences found between gait variables calculated using CLN and OPT2 models (Table). Six of twenty variables were significantly different between CLN and OPT1 models; nine of twenty variables were significantly different between CLN and CGM models. Significant differences between OPT1 and CGM were similar to, though not as many as, those reported by others [1]. OPT2 used joint centers different from those used identically in OPT1 and CGM. OPT2 and OPT1 both used 6DOF tracking, unlike the hierarchical tracking used in CGM. Given the pattern of significant differences across these models, it appears as though local reference frames (especially joint center locations) play a greater role in performance than does 6DOF tracking. Associated differences in gait variables for these normal subjects (per ensemble averages, not reported here) were more prominent than those reported between OPT1 and CGM [1], and may lead to different clinical interpretations. These differences may be exacerbated in a companion study of pathological gait not yet completed.

CONCLUSIONS

We conclude that differences in joint center locations play a greater role in the performance of biomechanical models applied to normal human gait, than does 6DOF tracking of body segments.

REFERENCES

1. Buczek FL, et al. *Gait Posture* **31**, 57-63, 2010.
2. Leardini A, et al. *Gait Posture* **21**, 212-225, 2005.
3. Lafortune MA, et al. *J Biomeh* **25**, 347-357, 1992.
4. Lundberg P, et al. *Gait Posture* **28**, 93-100, 2008.
5. Delp SL, et al. *IEEE Trans Biom Eng* **54**, 1940-1950, 2007.
6. Davis RB, et al. *Hum Mov Sci* **10**, 575-587, 1991.
7. Delp SL, et al. *IEEE Trans Biom Eng* **37**, 757-767, 1990.
8. Remy CD & Thelen DG. *J Biomech Eng* **131**, 031005, 2009.

ACKNOWLEDGEMENTS & DISCLAIMER

This work was funded by Shriners Hospitals for Children, Research Advisory Board grant #8510. The findings and conclusions in this report are those of the authors and do not necessarily represent the views of the National Institute for Occupational Safety and Health.

Table: Statistical comparison of key gait analysis variables across models (**bold** indicates significant at $p<0.05$).

		P-Values (Tukey HSD Post Hoc Comparisons)					
	Key Gait Variable	CLN OPT2	CLN OPT1	CLN CGM	OPT2 OPT1	OPT2 CGM	OPT1 CGM
1	maximum hip extension in late stance (deg)	1.0000	**0.0002**	**0.0002**	**0.0002**	**0.0002**	**0.0002**
2	maximum hip flexion moment in late stance (Nm/kg)	1.0000	**0.0026**	**0.0005**	**0.0026**	**0.0005**	0.8234
3	maximum hip flexion power absorption in late stance (W/kg)	1.0000	**0.0255**	**0.0003**	**0.0255**	**0.0005**	0.1828
4	maximum knee extension in late swing (deg)	1.0000	**0.0127**	**0.0002**	**0.0127**	**0.0002**	**0.0007**
5	maximum knee flexion moment in late swing (Nm/kg)	1.0000	0.8815	0.6525	0.8813	0.6528	0.2563
6	maximum knee flexion power absorption in late swing (W/kg)	1.0000	0.9232	0.1279	0.9242	0.1287	0.3561
7	maximum ankle plantarflexion at push-off (deg)	1.0000	**0.0002**	**0.0005**	**0.0002**	**0.0005**	**0.0009**
8	maximum ankle plantarflexion moment (Nm/kg)	1.0000	0.1167	0.1837	0.1167	0.1837	0.9942
9	maximum ankle plantarflexion power generation (W/kg)	1.0000	0.2446	0.8956	0.2446	0.8956	0.6136
10	maximum hip adduction in early stance (deg)	1.0000	**0.0016**	**0.0018**	**0.0016**	**0.0018**	0.9999
11	maximum hip abduction moment in early stance (Nm/kg)	1.0000	0.9646	0.9479	0.9646	0.9479	0.9999
12	maximum hip abduction power absorption early stance (W/kg)	1.0000	0.9634	0.6510	0.9635	0.6510	0.3749
13	maximum knee adduction moment at initial contact (Nm/kg)	1.0000	0.2176	0.7767	0.2178	0.7769	0.7212
14	maximum knee abduction moment in early stance (Nm/kg)	1.0000	0.3453	**0.0222**	0.3452	**0.0222**	0.4758
15	mean hip int/ext rotation across gait cycle (deg)	1.0000	0.9887	0.1455	0.9887	0.1455	0.0800
16	mean knee int/ext rotation across gait cycle (deg)	1.0000	0.4304	**0.0002**	0.4304	**0.0002**	**0.0007**
17	mean ankle int/ext rotation across gait cycle (deg)	1.0000	0.9945	**0.0080**	0.9945	**0.0080**	**0.0046**
18	maximum hip external rotation moment early stance (Nm/kg)	1.0000	0.9987	0.9833	0.9987	0.9833	0.9969
19	maximum knee external rotation moment late stance (Nm/kg)	1.0000	0.7800	0.1514	0.7800	0.1514	0.5917
20	maximum knee internal rotation moment early stance (Nm/kg)	1.0000	0.8271	0.8436	0.8271	0.8436	0.3596

A limb suspension model to describe leg stiffness change with gait speed

[1]Seyoung Kim and [1]Sukyung Park

[1]Korea Advanced Institute of Science and Technology, Daejeon, Republic of Korea
email: sukyungp@kaist.ac.kr, web: http://biomt.kaist.ac.kr

INTRODUCTION

A limb suspension model describing human steady state walking was developed for quantifying how humans change their lower limb stiffness as walking speed increases. It has been reported that vertical limb stiffness of the double support phase increases with walking speed [1]. However, the change of individual limb stiffness over a complete gait cycle with walking speed has not been quantified by a model, in the view of suspensions dealing with collision. Since one-segment inverted pendulum leg model has limitation describing ground reaction force profiles during gait [2], our model employed compliant leg with spring and damper to reproduce kinematics and kinetics of human's center of mass (CoM). The results indicated that the limb stiffness increased with gait speed and resulted in increased collision impact. Further examination of the stiffness change with various gait condition and/or subjects will be performed to quantify the gait strategy.

METHODS

Limb suspension model for human walking

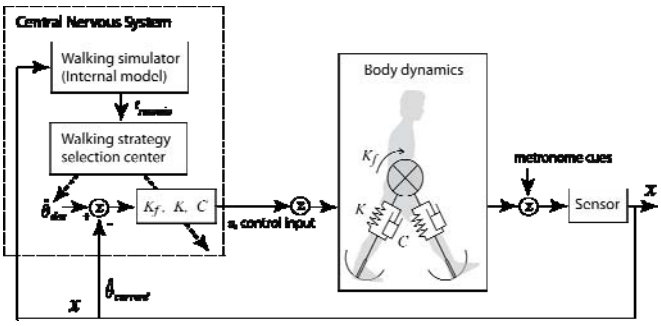

Figure 1: Schematic model of human steady state walking described by feedback control blocks.

Human body was modeled with two massless compliant legs with viscous damper and a concentrated CoM in sagittal plane [3,4]. Passive spring and damper provide suspensions to absorb collision impacts and to control excessive motion of CoM, respectively. A feedback control was used to swing torque generation to stabilize the gait (Fig.1). Hip torque feedback gains and suspension parameters (spring and damping constant) were obtained by optimization (Sequential Quadratic Program) using MATLAB®.

Experiment and data collection

Six healthy young (22.8±1.2 yrs.) subjects with no history of leg injuries participated in this study after signing the consent form approved by the IRB of KAIST.

Auditory gait frequencies ranged from 110-150 bpm (beats per minute) were given to the subject in order to maintain steady state walking by metronome sound. Five different frequencies were selected based on subject's natural and maximum walking speeds. Secondary size of gait frequency was the averaged self-selected frequency that he preferred in natural walking. The subject was instructed to walk on a straight 12 meter long, 1 meter wide walkway with steady speed guided by metronome's regular beat. The experiment consisted of total three sets of five randomly ordered gait frequencies. For each trial, ground reaction forces (GRFs) and kinematic data were recorded for 10 seconds using 3 force plates (AMTI, accugait®) and motion capture system (Motion analysis, hawk®), respectively. Velocities and trajectories of CoM were estimated by twice integrating the accelerations obtained from GRFs data [5,6].

RESULTS AND DISCUSSION

Model simulations reproduced the trajectories of CoM and GRFs with the goodness of fit (R^2=0.84) for one representative subject.

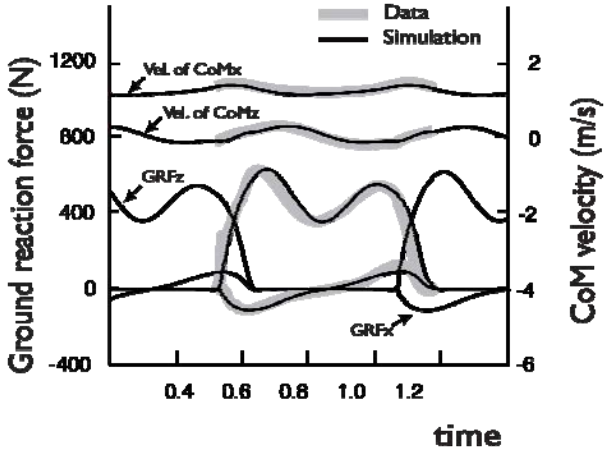

Figure 2: Velocities of CoM and GRFs data and model simulation with optimized spring constant, damping constant and hip torque feedback gain.

The vertical stiffness of lower limbs can be roughly calculated during double support phase under the assumption that both legs are considered as one linear spring [7]. CoM displacements decreased as walking speed increased, while mean value of total summed vertical GRFs from both legs significantly increased during the stance phase. By a simple approximation, the lower limbs' stiffness showed an increasing trend as walking speed increased (Fig.3).

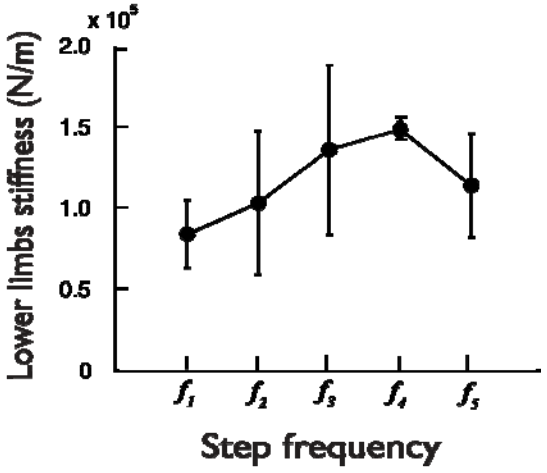

Figure 3: Averaged lower limbs' stiffness obtained from a simple approximation method.

Individual limb stiffness calculated by optimization increased as a function of gait speed. Similar to the lower limb stiffness estimated during the double support, the stiffness of each leg over a complete gait cycle significantly increased with gait speed ($p<0.05$) (Fig.4).

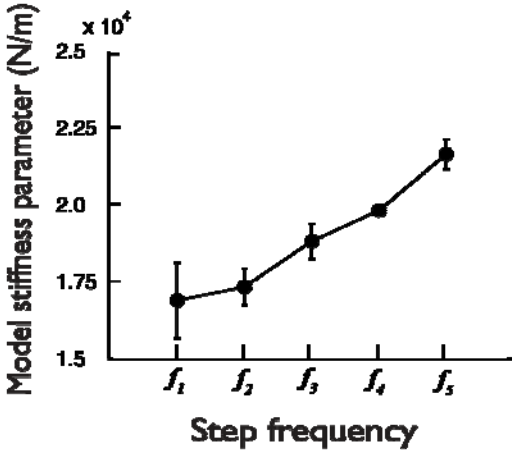

Figure 4: Averaged spring constant corresponding to each step frequency obtained from numerical optimization that minimizes the fitting error between the data and the model simulation.

The subject reduced suspensions with gait speed by increasing individual limb stiffness with the expense of increased collision impact. The change of individual limb stiffness as a function of walking speed could be used to quantify a gait strategy in response to a different walking conditions and/or subject groups.

REFERENCES

1.Rebular JR, et al. *Dynamic Walking* 4th Annual Meeting, 2009
2.Kuo AD. *Journal of biomechanical engineering*, **124**, 113-120, 2002
3.Geyer H, et al. *Proceedings of the Royal Society B*, **273**, 2861-2867, 2006.
4.Blum Y, et al. *Journal of biomechanics*, **42**, 2400-2405, 2009
5.Gard SA, et al. *Human Movement Science*, **22**, 597-610, 2004
6.Gutierrez-Farewik EM, et al. *Human Movement Science*, **25**, 238-256, 2006
7.Lipfert S, et al. *American Society of Biomechanics* 29th Annual Meeting, 2005

ACKNOWLEDGEMENTS

The work was supported by the Basic research fund of the Unmanned Technology Research Center, Agency for Defense Development of Korea.

TEMPORAL & SPATIAL GAIT CHARACTERISTICS DURING PROLONGED EXPOSURE TO A NORMAL SURFACE IN WORKBOOTS

John C. Garner[1], Chip Wade[2]

[1]Department of Health and Exercise Science, University of Mississippi, University, MS, USA
[2]Department of Industrial and Systems Engineering, Auburn University, Auburn, AL, USA
email: jcgarner@olemiss.edu, web: www.olemiss.edu/depts/hesrm/
email: cwade1@auburn.edu, web: http://www.eng.auburn.edu/department/ie/ose/

INTRODUCTION

There has been a tremendous amount of research that has investigated human gait on smooth level surfaces, with recent investigations extending gait analysis into ramps, stairs, steps, and while avoiding obstacles. However, much of the research is conducted in footwear that is typically used in activities of daily living (ADL) rather than in a work setting. The types of footwear worn for ADL are often designed primarily for comfort and/or aesthetics. Whereas footwear worn and designed for a work setting are often meant for safety and stability. These differences in footwear may potentially impact gait characteristics over time. The goal of this investigation was to identify changes in temporal gait characteristics over an extended duration of walking exposure in industry standard work boots.

METHODS

Sixteen healthy adult males (height: 176.18 ± 29.19 cm; mass: 84.08 ± 11.68 kg; age: 28.50 ± 9.63 years) were recruited based on an anthropometric blocked assignment for participation in this study. Written informed consent approved by the Institutional Review Board was obtained prior to participation. Exclusionary criteria included neurological, orthopedic, cardiovascular, pulmonary abnormalities as well as any other difficulties hindering normal gait and/or balance. Participants wore the same brand and model of steel toed work boots, which complied with the ANSI Z41-1991 standards; oil resistant soles, distinct heels, steel toes, and the ability to lace above 15.24 cm. Participants were instructed to walk at a self selected pace for a total of four hours along a flat hard vinyl surface which measured 25'x14'. The surface was of typical hardness as a worker would encounter in a manufacturing setting. Participants walked for the assigned incremented duration followed immediately by the testing protocol, with the cycle repeated for each exposure level. The participants were allowed no rest period between testing protocols and the following exposure period. The study used a repeated-measures design with exposure as a nine level independent variable: 1 hour, 2 hours, 3 hours, 4 hours of walking exposure, each associated with a pre-test (0 min).

The testing protocol consisted of the following. After preparations, participants were instructed to look straight ahead and walk naturally at a self-selected, comfortable pace across the assigned surface. Next, participants were allowed to practice walking as the researcher varied the starting point to ensure proper foot contact in the center of the force plates, which was used to determine a successful trial. Once the appropriate starting position was determined, participants were instructed to walk to the opposite end of the testing surface while data were recorded. Prior to each trial, participants returned to the starting position, waited for a period of one minute, and then were instructed to repeat the trial, for a total of 5 successful trials.

Full body motion and bilateral ground reaction forces were measured by a eight MX3-camera Vicon (Vicon Peak–UK) NEXUS motion measurement system recording three-dimensional motion data at a sampling rate of 120 Hz from 41 reflective markers placed on the boots and body [Helen Hayes configuration [1]. Ground reaction forces were measured on two AMTI (Advanced Mechanical Technology, Watertown, MA USA) type OR6-6 force plates embedded into the walkway. The GRF's data were recorded at a

sampling rate of 1080 Hz and synchronized with the motion data and video recordings. Video data were utilized to visually monitor each trial.

Data were collected, averaged and analyzed for the calculation of temporal gait characteristics. Gait cycle events [heel contact (HC) to toe off (TO)] were determined via force plate activation (20N force) and marked accordingly within the data to identify gait cycles. Gait characteristics of interest were cadence (steps/min); stride length (m), defined as the distance between sequential points of initial contact by the same foot; speed (m/sec); stance duration (sec), defined as the period during walking the foot is in contact with the floor; swing duration (sec), defined as the period during walking the foot is not in contact with the floor; double support (sec), defined as the period during walking that both feet are in contact with the floor; and single support (sec), defined as the period during walking that total weight bearing on a single foot occurs.

Dependent measures were evaluated using a 2 X 4 (test [pre v. post]) X (exposure level [1 hour v. 2 hours v. 3 hours v. 4 hours] repeated measures analysis of variance (ANOVA), independently for the seven temporal gait characteristics. Furthermore, statistical and practical differences between duration exposures would suggest that a post-hoc (paired sample t-test) would be appropriate for a univariate comparison to determine where the differences occur. For all analyses, a significance level of a = .05 was set.

RESULTS AND DISCUSSION

Overall, temporal gait parameters were significantly different as exposure duration increased (Table 1). The cadence significantly decreased as duration increased. Stride length (heel-toe) significantly decreased as duration increased. Speed significantly decreased as duration increased. Stance duration and double support duration characteristics increased as duration increased while swing duration and single support duration decreased as duration increased.

The results suggest a slower more pronounced gait as walking duration increased, potentially in anticipation of muscle fatigue or footwear characteristics. These progressive decreases in cadence, stride length, and speed and increases in support and duration measures indicates a more cautious gait over time.

CONCLUSIONS

The current findings are interpreted as being consistent with existing literature indicating a greater challenge to the gait control system as prolonged muscular activity is required; based on the understanding that work boot characteristics are more rigid than that traditional footwear, which would be utilized during activities of daily living.

REFERENCES

1.Kadaba, et al. *J Orth Research*, **7**, 849-860, 1989.

Table 1. Temporal gait measures

	Cadence	Stride Length	Speed	Stance Duration	Swing Duration	Double Support	Single Support
	steps/min	m	m/sec	sec	sec	sec	sec
Pre	97.3	1.36	72.9	59.3	40.1	22.6	38.4
	2.9	0.16	5.8	1.6	1.5	3.1	2.3
1 Hour	96.8	1.34	71.3	60.1	39.6	23.8	38
	3.1	0.21	5.1	1.7	1.7	2.7	3.1
2 hour	96.1	1.3	68.2	60.9	39	23.9	37.4
	4.2	0.18	7.6	1.8	2.1	2.1	2.6
3 hour	95.6	1.26	67.9	61.3	38.1	24.5	36.7
	4.8	0.26	8.6	2.1	1.6	2.9	1.8
4 hour	95.1	1.2	67.4	62.3	37.6	26.4	36.1
	5.3	0.19	7.9	2.6	2.2	1.8	2

ANKLE & KNEE MUSCULATURE CO-CONTRACTION FOLLOWING EXTENDED DURATIONS OF WALKING IN WORKBOOTS

Chip Wade[1], John C. Garner[2]

[1]Department of Industrial and Systems Engineering, Auburn University, Auburn, AL, USA
[2]Department of Health and Exercise Science, University of Mississippi Oxford, MS, USA
email: cwade1@auburn.edu, web: http://www.eng.auburn.edu/department/ie/ose/
email: jcgarner@olemiss.edu, web: http://www.olemiss.edu/depts/hesrm

INTRODUCTION

Much human gait research has been conducted on smooth level surfaces [1], for obvious reasons. A vast majority of activities of daily living occur on flat ground. However, much of the research is conducted in footwear that is typically used in activities of daily living (ADL) rather than in a work setting. The types of footwear worn for ADL are often designed primarily for comfort and/or aesthetics. Whereas footwear worn and designed for a work setting are often times meant for safety and stability. These differences in footwear would, in turn, potentially impact gait characteristics over time. The purpose of this study was to examine changes in muscle activity over an extended duration of walking exposure in work boots.

METHODS

Sixteen healthy adult males (height: 176.18 ± 29.19 cm; mass: 84.08 ± 11.68 kg; age: 28.50 ± 9.63 years) were recruited based on an anthropometric blocked assignment for participation in this study. Written informed consent approved by the Institutional Review Board was obtained prior to participation. Exclusionary criteria included neurological, orthopedic, cardiovascular, pulmonary abnormalities as well as any other difficulties hindering normal gait and/or balance. Participants wore the same brand and model of steel toed work boots, which complied with the ANSI Z41-1991 standards; oil resistant soles, distinct heels, steel toes, and the ability to lace above 15.24 cm. Participants were instructed to walk at a self selected pace for a total of four hours along a flat hard vinyl surface which measured 25'x14'. The surface was of typical hardness as a worker would encounter in a manufacturing setting. Participants walked for the assigned incremented duration followed immediately by the testing protocol, with the cycle repeated for each exposure level. The participants were allowed no rest period between testing protocols and the following exposure period. The study used a repeated-measures design with exposure as a nine level independent variable: 1 hour, 2 hours, 3 hours, 4 hours of walking exposure, each associated with a pre-test (0 min).

The testing protocol consisted of the following. After preparations, participants were instructed to look straight ahead and walk naturally at a self-selected, comfortable pace across the assigned surface. Prior to each trial, participants returned to the starting position, waited for a period of one minute, and then were instructed to repeat the trial, for a total of 5 successful trials.

EMG data were recorded from selected muscles in the dominant stance (right/leading) leg, including the Vastus Medialis (VM), Medial Hamstring (MH), Tibialis Anterior (TA), Medial head of Gastrocnemius (MG), Peroneus Brevis (PB), Flexor Hallucis Longus (FHL) using a Noraxon Telemyo 8-channel electromyography system with a hardware band pass filter (10–500 Hz). Proper electrode placement was confirmed using a sub maximal exertion test, followed by a Maximum Voluntary Contraction (MVC) test, which was utilized for normalization across subjects. EMGs were rectified and low-pass filtered at 50 Hz using a phaseless elliptical filter, then time normalized with respect to the stance leg with 0% being heel contact (HC) and 100% as toe off (TO). In addition, the EMG channels were peak normalized within subject using the MVC of each muscle. Gait cycle events [HC,,midstance (MS),and TO] were determined via force plate activation (20N force) and marked accordingly within the data to identify gait cycles. Co-contraction index (CCI) was calculated based on

the integrated ratio of the EMG activity (from -20% to 20% into stance, with HC being 0%; 30% to 70% into stance, with FF being 50%; from 80% to 120% into stance, with TO being 100%) of antagonist/agonist muscle pairs (TA/MG, VM/MH, PB/FHL) using the following equation [2]:

$$CCI = \int_{-20\%}^{20\%} \frac{Lower\ EMGi}{Higher\ EMGi} x(Lower\ EMGi + Higher\ EMGi)$$

Dependent measures were evaluated using a 2 X 4 (test [pre v. post]) X (exposure level [1 hour v. 2 hours v. 3 hours v. 4 hours] repeated measures analysis of variance (ANOVA), independently for the three CCI groups (TA/MG, VM/MH, PB/FHL). For all analyses, a significance level of a = .05 was set.

RESULTS AND DISCUSSION

Co-contraction was seen in the three antagonistic muscle pairs examined, and duration of walking had a significant effect on the co-contraction level (Figure 1). The CCI's were significantly different across exposure durations for ankle inversion/eversion (PB/FHL), ankle dorsiflexion/plantarflexion (TA/MG) and knee flexion/extension (VM/MH). These CCI changes were found consistently at the three times in the step cycle (HC, MS, and TO).

The EMG analysis found high co-contraction as duration of walking increased, providing insight into a possible underlying control mechanism while walking for extended durations in work boots. It has been noted in previous research that antagonist muscle co-activation assists in providing a defense against external impact forces. In addition, antagonist muscle co-activation has been shown to be important to ensure a systematic distribution of compression forces across the articular surface of the joint. Furthermore, individuals utilize co-contraction in order to perform activities with demands that are higher relative to their capability [3]. In this context, muscular co-contraction would simplify the task by reducing the amount of reactive forces within the musculoskeletal system.

CONCLUSIONS

Our findings are consistent with the exiting literature related to muscle activation patterns and co-contraction indices. It appears that walking for prolonged durations increases muscle activation to control the moments at the joints of the lower extremity, potentially increasing both localized muscle fatigue and the compressive loading on those joints.

Figure 1. Co-Contraction Index for ratios of the EMG activity of antagonist/agonist muscle pairs (VM/MH TA/MG, PB/FHL) at heel contact (HC), Mid-stance (MS) and Toe off (TO). *Pre to 4 hours from left to right on axis.

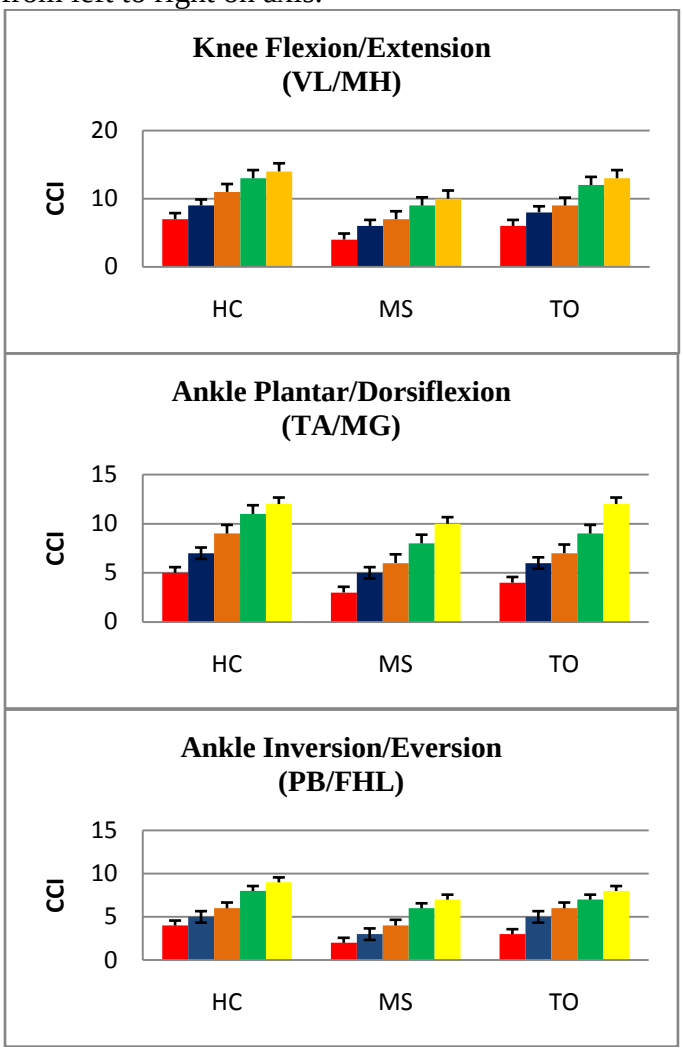

REFERENCES

1.Winter, D.A. *Biomechanics and motor control of human movement.* 3rd ed. Wiley, 2005.

2.Chambers, A. J., & Cham, R.. *Gait & Posture* **25**, 565-572, 2007.

3.Holt, et al.. *J Biomech* **36**, 465-471, 2003.

GRAVITATIONAL IMPULSE MODEL PREDICTS COLLISION DYANMICS DURING GAIT

Jin Yeom and Sukyung Park

Mechanical Engineering dept. KAIST, Daejeon, Korea
email: sukyungp@kaist.ac.kr, web: http://biomt.kaist.ac.kr

INTRODUCTION

Simplest walking model which assumes instantaneous collision with negligible gravity effect during step-to-step transition, though it successfully described the basic principles of gait dynamics, such as periodic gait cycles [1], and energetics of the actively powered gait [2], has limitation in representing the collision mechanics of human gait that lasts over a finite duration. As opposed to the instantaneous collision assumption employed in simplest walking model, step-to-step transition of human gaits occurs over a finite period by finite impulsive ground reaction forces that have the same order of magnitude to gravitational force. Along with the push-off and heel strike ground reaction impulses, therefore, gravitational impulse defined as a time integral of body weight over the duration of step transition, would contribute to momentum change as well. In this study therefore we proposed a new collision model that introduces the contribution of gravitational impulse to momentum change of the center of mass (COM) during step-to-step transition of gait and derived an averaged work-energy relationship to quantitatively analyze the collision mechanics.

METHODS

A new collision model includes the contribution of gravitational impulse *G*, along with the push-off (*P*) and heel strike (*H*) impulses, to the momentum change of COM during step-to-step transition. The gravitational impulse *G* is defined by the time integral of body weight (*mg*) over the collision duration Δt, which is reported to be inversely proportional to the gait speed [2] such that $\Delta t = \mu / v_{cm}^{-}$, where μ is the constant of proportionality. Mechanical work done by push-off, heel strike, and gravity during step-to-step transition, denoted as W_{push} W_{heel} and $W_{gravity}$, respectively, could be obtained by averaging the change of kinetic energy of the sequential application of each impulse in an order of *P*, *G*, and *H* and that of *H*, *G*, and *P* as follows

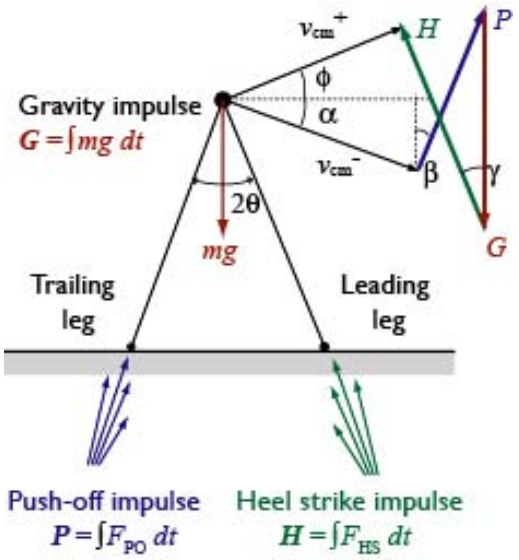

Figure 1: A new collision model that includes the contribution of gravitational impulse to momentum change of the COM during step-to-step transition.

$$\begin{cases} W_{push} = \dfrac{P}{2m}\left\{P + 2mv^{-}\sin(\beta-\alpha) + H\cos(\beta+\gamma) - G\cos\beta\right\} \\ W_{gravity} = \dfrac{G}{2m}\left\{G + 2mv^{-}\sin\alpha - P\cos\beta - H\cos\gamma\right\} \\ W_{heel} = \dfrac{H}{2m}\left\{H - 2mv^{-}\sin(\alpha+\gamma) + P\cos(\beta+\gamma) - G\cos\gamma\right\} \end{cases}$$

Being subject to the positive hip joint work constraint, the magnitude of optimal push-off that minimizes collision loss is obtained when push-off propulsion fully compensates the collision loss (Fig. 3), as predicted by the simplest model [3].

To validate the gravitational impulse model, we measured kinematic and kinetic responses of six healthy young (mean age 22.8 ± 1.2 yrs) subjects at five different walking speeds, controlled by step frequencies. The subjects reported no history of balance or gait disorder and signed the informed consent form approved by the IRB of KAIST prior

to the test. The average height and weight of the subjects were 1.7 ± 0.1 m and 66.5 ± 12.0 kg, respectively. Subjects walked on a 10 m long and 1 m wide walkway with three blocks of five different, randomly ordered gait frequencies ranging from approximately 88.5 ± 3.8 % to 134.3 ± 11.3 % of their self-selected natural gait frequencies (111.7 ± 6.0 bpm) over-ground. Lower limb kinematics and ground reaction forces were measured by an optical marker system (Motion Analysis, CA, US) and three force platforms (AMTI, MA, US), respectively, at a 200 Hz sampling frequency.

RESULTS AND DISCUSSION

Empirical data of collision dynamics and related energetics support the new collision model. The vector sum of collision impulses, including the gravitational impulse, induced the momentum change of the COM during the step-to-step transition. The newly introduced gravitational impulse modifies the previously predicted quantitative relationships of collision dynamics and their energetic (Fig. 2, 3).

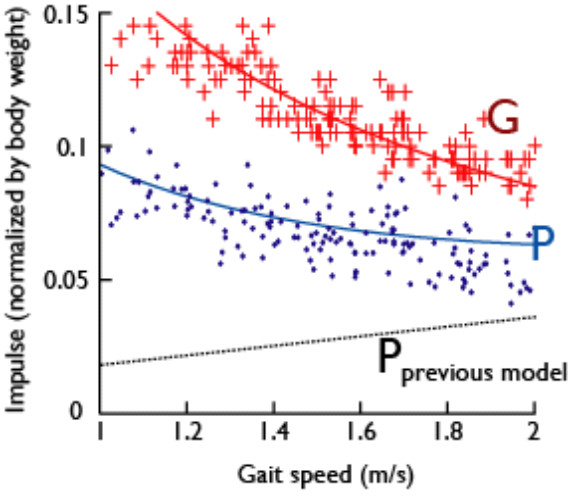

Figure 2: Model prediction (solid) and data (dots and crosses) of push-off impulse as function of gait speed. The magnitude of push-off and heel strike impulses greatly increases, compared to those predicted from instantaneous collision model, to compensate the gravitational impulse applied downward. Qualitatively, the optimal push-off decreases with gait speed, as opposed to the velocity-proportional increase predicted from the instantaneous collision model (dashed line).

Empirical data of mechanical cost were well approximated by the function of impulses as derived from the average of work-energy relationship.

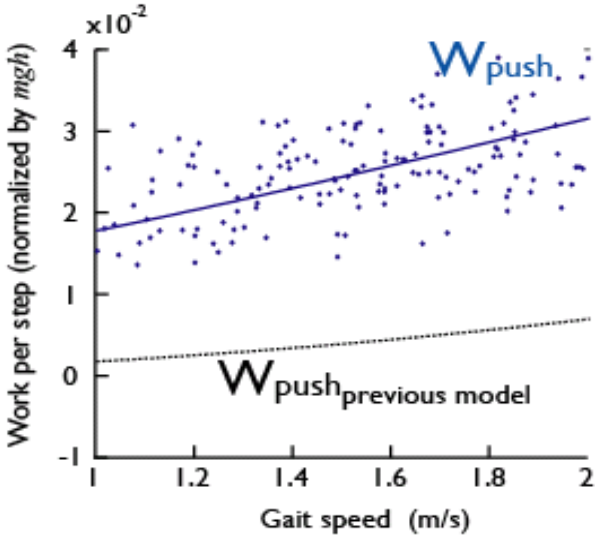

Figure 3: Model prediction (solid) and data (dots) of mechanical cost by push-off impulse as function of gait speed. The magnitude of mechanical work done by the ground reaction forces from the new collision model is approximately 5 folds greater than the previous model prediction (dashed line), which mostly attributes to 2~5 folds underestimated ground impulses from the instantaneous collision model.

The new gravitational collision model enables us to quantitatively analyze collision dynamics and energy cost for the step-to-step transition.

REFERENCES

1.McGeer, T., *Int. J. of Robotics Rech.* **9**, 62, 1990.
2.Kuo, A. D., *J. Biomechanical Engineering* **124**, 113, 2002.
3. Adamczyk, P. G.et. al., *J. Exp. Biol.* **212**, 2668-2678, 2009.

ACKNOWLEDGEMENTS

The work was supported by the Basic research fund of the Unmanned Technology Research Center, Agency for Defense Development of Korea.

THE EFFECT OF HEEL HEIGHT ON PEAK TIBIAL AND HEAD ACCELERATIONS AND SHOCK ATTENUATION DURING WALKING

Danielle D. Barkema, Timothy R. Derrick, and Philip E. Martin

Iowa State University, Ames, IA, USA
email: dbarkema@iastate.edu

INTRODUCTION

During normal walking, the body is subjected to impact forces at heel strike that transmit a shockwave up the musculoskeletal system. This repetitive axial loading has been shown to be important in joint degeneration [1, 2]. Most footwear designs supplement the body's natural shock absorbers by contributing to shock attenuation during walking. However, the design of high heeled shoes limits their ability to attenuate shock during walking as evidenced by greater peak tibial accelerations compared to flat shoes [3]. Our purpose was to determine the systematic effect of heel height on peak tibial and head axial accelerations and shock attenuation of the body during walking. It was hypothesized that peak tibial and head acceleration increase and shock attenuation decreases as heel height increases.

METHODS

Ten healthy women (age: 24.5 ± 5.0 yrs, height: 167.0 ± 7.8 cm, mass: 63.6 ± 9.1 kg), free from injury in the last 12 months, completed two test sessions. In session 1, anthropometric measures were taken and subjects were fitted with three shoes with heel heights of 1, 5, and 9 cm. Heel height was randomly ordered and preferred walking velocity was determined for each shoe condition as the average of 10 overground trials. Subjects then practiced overground walking at the experimental velocity of 1.3 $m \cdot s^{-1}$ for each of the three heel height conditions.

Session 2 was completed 1-7 days after session 1. Uniaxial accelerometers were securely mounted to the skin of the distal medial-anterior portion of the tibia and the center of the forehead and were stabilized with elastic bands. Reflective markers were placed on anatomical landmarks of the subject's trunk, pelvis and right lower extremity. Subjects completed shoe conditions in the same randomly determined order as used in session 1. Ten trials for each of the three heel height conditions were completed at each subject's preferred walking velocity (± 3%). Subjects then completed 10 trials for each heel height condition at 1.3 ± 0.04 $m \cdot s^{-1}$. Marker position and accelerometer data were sampled simultaneously at 200 Hz and 1000 Hz, respectively.

Acceleration data were analyzed in the time domain. Peak tibial and head accelerations (PTA and PHA, respectively) were identified. Shock attenuation (SA) was calculated as the percent decrease of the peak acceleration values:

$$SA = [1 - (PHA/PTA)] \cdot 100$$

In addition, stride length (SL), stride time (ST), and average walking velocity (V) were quantified from marker position data.

A one-way, repeated measures ANOVA was used to assess the effect of heel height on PTA, PHA, SA, and walking kinematics for both preferred and fixed walking velocity conditions.

RESULTS AND DISCUSSION

For both fixed and preferred walking velocities, PTA was significantly higher for the 5 cm heel height condition when compared to the 1 and 9 cm heel heights (Fig 1; Table 1). In addition, when walking at preferred velocities, PHA was higher for the 5 cm heel height than the 9 cm height. No differences were observed for SA for either preferred or fixed velocities.

Inconsistent with our hypothesis, PTA was highest for the 5 cm, intermediate heel height for both

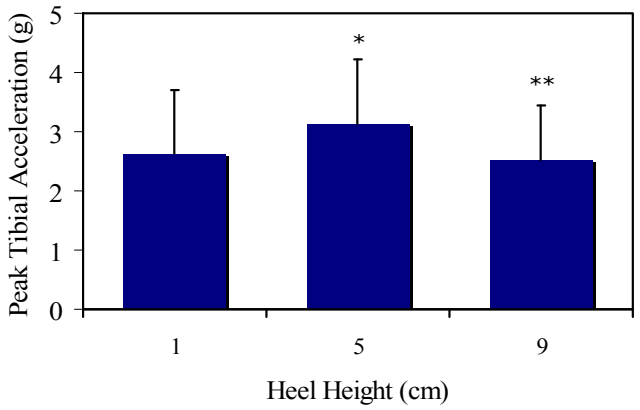

Figure 1. Mean (SD) peak tibial acceleration was highest for the intermediate (5 cm) heel height during fixed walking at 1.3 $m \cdot s^{-1}$. (* significantly different from 1 cm, ** significantly different from 5 cm)

preferred and fixed velocity conditions. Gait kinematics results help explain this counterintuitive outcome. Our results indicated average walking velocity, SL, and ST were similar for the 1 and 5 cm heels. However, average preferred walking velocity was lower for the 9 cm heel compared to the 1 and 5 cm conditions. This slower velocity contributes to lower PTA for the 9 cm heel height under preferred velocity conditions. In addition, SL was significantly shorter for the 9 cm heel height compared to the 1 and 5 cm heights for both preferred and fixed velocity conditions (Table 1). Higher heel heights limit ankle range of motion [5], thereby limiting the ankle plantarflexors' contribution to forward propulsion, resulting in shorter SLs. Shorter SLs reduce the vertical velocity of the foot, contributing to lower negative accelerations at heel strike and lower impact accelerations at the tibia [4]. PHA showed similar responses to heel height manipulation as PTA, but PHA responses were muted by the substantial SA that occurred between the tibia and head. Previous research has shown PHA to remain reasonably constant throughout a variety of gait alterations [4].

Voloshin and Loy [3] reported higher PTAs during walking in shoes with a 7.1 cm heel height compared to shoes with 1.4 cm heels. Tibial accelerations for higher heel heights have not been investigated. Higher PTAs, such as those observed for the 5 cm heel compared to the 1 and 9 cm heels, are indicative of greater axial loading, a key factor in joint degeneration [1, 2]. The somewhat counterintuitive results from our study underscore the interplay between heel height, gait kinematic adaptations, and lower extremity joint loading.

CONCLUSIONS

Highest PTAs during walking occurred for the 5 cm heel height compared to the 1 and 9 cm heights. Lower peak tibial accelerations for the 9 cm height were partially attributed to adaptations in gait kinematics reflected predominantly for the 9 cm heel condition. Further investigation of walking kinematics and kinetics in response to heel height is necessary in order to identify other possible adaptations that affect axial loading at heel strike.

REFERENCES

1.Radin EL, et al. *The Lancet,* 519-521, 1972.
2.Wosk J & Voloshin A J. *J Biomech* **4**, 261-267, 1981.
3.Voloshin AS & Loy DJ. *Gait & Posture* **2**, 117-122, 1994.
4.Derrick TR, et al. *Med Sci Sports & Exerc* **30,** 128-135, 1998.
5.Stefanyshyn DJ, et al. *J Appl Biomech* **16**, 309-319, 2000.

Table 1. Mean (SD) acceleration and kinematic variables in response to heel height at fixed and preferred walking velocities.

	Fixed Velocity (1.3 $m \cdot s^{-1}$)			Preferred Velocity		
	1 cm	**5 cm**	**9 cm**	**1 cm**	**5 cm**	**9 cm**
PHA (g)	0.66 (0.21)	0.72 (0.16)	0.61 (0.13)	0.68 (0.28)	0.74 (0.27)	0.56 (0.19)[b]
PTA (g)	2.62 (1.08)	3.14 1(0.08)[a]	2.52 (0.93)[b]	2.67 (1.24)	3.29 (1.38)[a]	2.52 (1.00)[b]
SA (%)	73.3 (9.5)	75.3 (7.2)	72.4 (11.7)	71.1 (11.2)	75.5 (7.8)	76.1 (7.1)
SL (m)	1.40 (0.08)	1.38 (0.06)	1.34 (0.06)[a b]	1.40 (0.11)	1.42 (0.11)	1.33 (0.12)[a b]
ST (s)	1.07 (0.06)	1.06 (0.05)	1.02 (0.05)[a b]	1.05 (0.04)	1.07 (0.07)	1.05 (0.09)
V ($m \cdot s^{-1}$)	1.31 (0.01)	1.30 (0.01)	1.30 (0.01)	1.33 (0.12)	1.33 (0.17)	1.28 (0.17)[b]

[a] = significantly different from 1 cm, [b] = significantly different from 5 cm

FIFTEEN OBSERVATIONS ON THE STRUCTURE OF OPTIMAL GAITS OF VARIOUS SIMPLE BIPEDAL MODELS

Manoj Srinivasan
Mechanical Engineering, Ohio State University, Columbus, OH, USA
email: srinivasan.88@osu.edu, web: http://movement.osu.edu

INTRODUCTION

It is thought that many aspects of steady human locomotion under normal conditions can be predicted by appealing to the hypothesis that healthy humans roughly move in a manner that minimizes the metabolic cost of locomotion [1,2,3,4,5]. While energy optimization with sufficiently realistic and complex models might be required for detailed quantitative predictions, we might obtain a deeper understanding of the qualitative effects of various model features on energetic optimal gaits by considering relatively simple models. Here, we consider four simple bipedal models with different leg architectures, combined with many different metabolic cost functions and muscle properties. Performing careful gait optimization on these many model permutations reveals simple underlying gait structure and similarity between the optimal gaits for substantially different models. We are also able to make a number of observations about the structure of the optimal gaits of the various models, many of which have not been previously noted.

METHODS

The four biped models are shown in Figure 1. All of them have point-mass upper bodies and massless legs; all four bipeds have uniarticular "muscles." However, the four bipeds differ in their detailed leg architecture, as shown in Figure 1. By discretizing the muscle forces as piecewise linear functions of time, we obtain the optimal muscle forces and initial conditions that produce to a periodic gait that minimizes a given metabolic cost function for various speeds and stride lengths. The metabolic cost function is one of many: related to mechanical work, force raised to some power, a quasi-steady model of muscle ATPase activity, or a generalization C_g involving a product of functions of a function force and a positive convex function of muscle contraction rate [1]. Different muscle properties are also considered. See [1] for details.

RESULTS AND DISCUSSION

The following observations follow from the many gait optimization permutations: 1) Even though the net joint mechanical work required in steady locomotion on level ground is zero in the absence of dissipation, joint mechanical work is unavoidable at non-zero gravity for most realistic bipeds; 2) Inverted pendulum walking and impulsive running are optimal for a vast number of metabolic cost modes for the springless models: for instance, the costs of the form Cg, and also the integral the knee-torque-squared; 3) The double humped ground

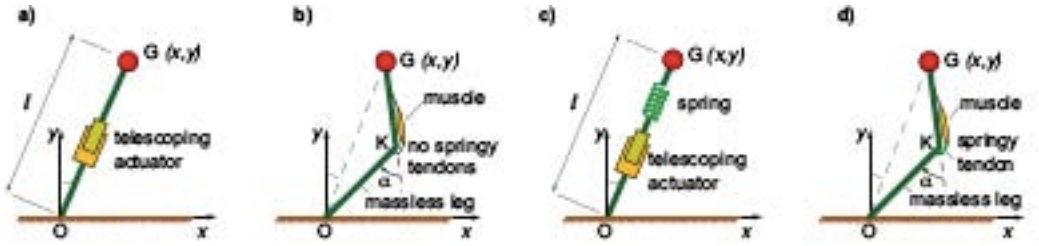

Figure 1: Four simple biped models, with a point-mass upper body and massless legs. The four bipeds are distinguished by the leg architectures: a) The leg is a telescoping actuator (muscle) with no spring in series. b) The leg has a knee and a uniarticular muscle, with no tendon is series. c) The leg has a telescoping actuator and a tendon is series. d) The leg has a knee and a uniarticular muscle in series with a tendon.

reaction force profile for walking arises as being optimal both in the spring-less models and in the springy models for a wide variety of tendon stiffnesses; 4) For the spring-less models, the optimal gaits have a bang-coast-bang optimal control, involving periods of large actuator forces interrupting periods of largely passive phases with either low actuator work (low force or isometric contractions); 5) More compliant gaits with roughly linear relationships between leg force and leg compression are obtained not only when the legs have compliant tendons but also when there is slow muscle activation even for the spring-less models. 6) All the models have both walking-like and running-like optimal gaits. The springless models have walking at low speeds and running at higher speeds. The springy models are similar to the spring-less models when the spring is stiff enough, but for more compliant tendons, running gaits can be optimal even at low speeds; 7) Almost all the optimal gaits obtained for almost all the models considered had a left-right asymmetry -- that is, the left stance is identical to the right stance. The springy models can have skipping-like asymmetric optimal gaits, but these go away when there is substantial cost for isometric muscle force; 8) Some of the gaits also have a time-reversal symmetry within a stance phase, as is approximately true for human walking and running stance phases; 9) Horizontal hip trajectory walking, sometimes thought to be optimal, is never optimal; 10) Almost all optimal gaits took advantage of the maximum leg length available; 11) Double stance in walking is optimal either when the tendons are sufficiently compliant, or when the muscle forces can increase only gradually; 12) Some animals have long tendons which appear to account for much of the leg work, while the muscle in series remains close to isometric, superficially looking like minimizing work. Because minimizing more general costs is almost identical to minimizing muscle work, some animals may *appear* to minimize muscle work even though they are minimizing something else (close isometric muscles in series with tendons doing negative and positive work). 13) Springs are not always energetically useful. If the springs are sufficiently stiff and the muscles are capable of only finite forces, the springs are essentially useless. 14) Springs are essentially useless energetically if minimizing a purely muscle-force dependent cost as used in many biomechanics (inverse dynamics and dynamic optimization) calculations. 15) Springs are useful energetically when the cost is substantially dependent on velocity (but in a plausible manner) -- for instance C_g [1]. 15) Minimizing simple robot electrical costs produces gaits identical to minimizing C_g for kneed springless bipeds. 16) Often, when the metabolic cost is a sum of two components, the cost component that determines the optimal strategy is a smaller fraction of the optimal cost. 17) Given the insensitivity of optimal solutions to some model perturbations, it may be that we get good predictions with a somewhat bad model; but it may be hard to infer good models from behavior.

CONCLUSIONS

We have considered numerous simple biped models in the context of gait optimization. However, we have been able to consider these model permutations only in limited parameter regimes. Therefore, while I believe that the results apply more generally than just for the parameter sets and model combinations they have been demonstrated for, it is possible that as these more extensive optimizations are performed with a greater coverage of the model space, some the specific results here will be subsumed into more general results. Nevertheless, the careful study of these simple models might be helpful in informing the construction of more complex models for the purposes of quantitative predictions.

REFERENCES

1. M. Srinivasan. Observations on the structure of energy minimizing bipedal gaits, based on gait optimization in many simple biped models *J. Royal Society Interface*, accepted, 2010.
2. M. Srinivasan and A. Ruina. *Nature*, **439**, 72-75, 2006.
3. M. Srinivasan. Optimal speeds for walking and running, and walking on a moving walkway. *CHAOS*, **19**, 026112, 2009.
4. F.C. Anderson and M.G. Pandy. *J. Biomechanical Engineering*, 123, 381-390, 2001.
5. A.E. Minetti and R.McN. Alexander. *J. theor. Biol.*, 186, 467-476.

JOINT CONTACT FORCE COMPARISONS BETWEEN HEALTHY SUBJECTS AND THOSE WITH MEDIAL COMPARTMENT KNEE OSTEARTHRITIS

Kurt Manal, Deepak Kumar, Thomas S. Buchanan and Katherine Rudolph

University of Delaware, Newark, DE, USA
email: manal@udel.edu

INTRODUCTION

The magnitude of the knee adduction moment has been shown to correlate with the severity and progression of knee osteoarthritis (OA) [1]. Walking speed is known to influence the magnitude of knee joint moments [2], and thus kinetic comparisons between subjects walking at different speeds can be difficult to interpret. Further, the relationship between knee moments and joint loading is not straightforward, particularly when agonist/antagonist muscles are co-activated. Co-activation is believed to be a neuromuscular strategy used by individuals with knee OA [3]. While greater co-contraction may help stabilize the knee, it may also increase the magnitude and duration of joint loading. Computational methods which account for subject specific neuromuscular activation patterns are important when studying articular loading. In addition, walking speed should be considered when making such comparisons. In this paper we present results of an EMG-driven modeling approach to predict articular loading for subjects with medial compartment knee OA and age-matched healthy control subjects. We hypothesized that subjects with medial compartment knee OA would exhibit greater medial compartment joint loading compared to healthy controls.

METHODS

Sixteen subjects (65 ± 10 years) with medial compartment knee OA and 12 age-matched healthy control subjects (60 ± 10 years) participated in this study. Standard motion analysis methods (ie., video cameras & force platform) and Visual3D (C-motion Inc.) were used to compute stance phase kinematics and kinetics for natural cadence walking. Medially and laterally offset segmental coordinate systems were constructed so that frontal plane knee moments could be expressed about the approximate centers of the medial and lateral condyles. These moments are balanced internally by forces from muscles and soft tissue, and by contact forces acting on the medial and lateral compartments. The location of the contact forces within the medial and lateral compartments was fixed within subject but varied between subjects according to individual anthropometry.

An EMG-driven musculoskeletal model was used to compute forces for 10 muscles crossing the knee: semimembranosus, semitendinosus, biceps femoris (longus & short head), medial and lateral gastrocnemius, rectus femoris and the vasti. EMGs were sampled at 1080 Hz using surface electrodes. EMG and joint kinematics were used as inputs to a Hill-type muscle model to compute individual muscle forces. Refer to [4] for specific details of the modeling approach. Muscle forces were applied to a frontal plane moment balancing algorithm leaving only the contact forces or soft tissue loads as the unknowns [5]. The contact forces for each trial were time normalized to 100 samples and normalized by bodyweight (BW) for data averaging. Three trials per subject were averaged in this manner.

RESULTS AND DISCUSSION

The preferred self-selected walking speed for the subjects with knee OA (1.34 ± 0.13 m/s) was significantly slower ($p < 0.05$) compared to the control subjects (1.55 ± 0.22 m/s). Mean peak contact force for both groups occurred during loading response (approximately 20% stance) and was greater for the OA subjects compared to controls. The difference however was not statistically significant (Table 1). Also included in

Table 1 are walking speeds and contact forces for 6 subjects with OA who walked at a similar speed as the controls. Peak contact force for these subjects was statistically greater compared to mean values for the healthy subjects (Table 1).

Table 1. Mean walking speed and medial compartment contact force during stance.

	Speed (m/s)	Force (BW)
OA (n=16)	1.34 ± 0.13 †	2.80 ± 0.54
OA (n=6)	1.48 ± 0.10	3.00 ± 0.46 †
Healthy (n=12)	1.55 ± 0.22	2.55 ± 0.44

(† = statistically different than healthy subjects)

The key point summarized in table 1 is that as a group (n=16) subjects with OA walked slower ($p < 0.05$) compared to healthy controls and peak loading was not statistically different. When matched by speed, subjects with OA (n=6) had significantly greater medial loading than healthy subjects (Table 1 & Figure 1).

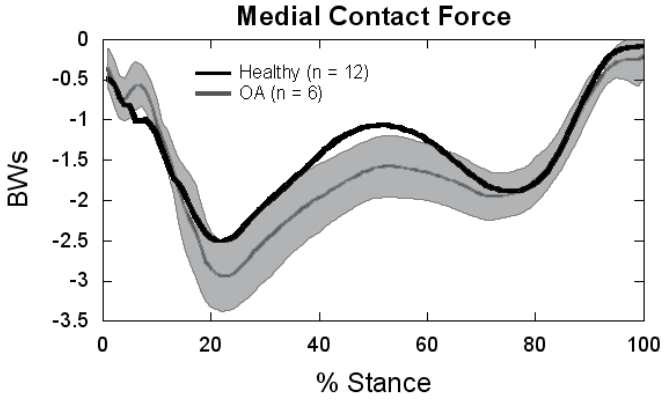

Figure 1. Medial compartment contact force for healthy subjects and those with OA walking at similar speeds. Peak loading was statistically greater for the OA subjects. The shaded region depicts ± 1 standard deviation for the OA subjects.

Although we did not specifically plan to compare walking speed and peak force, our results indicated such a relationship might exist and therefore it was examined as a secondary aim. We found a linear relationship between walking speed and peak medial contact force for subjects with OA. Those that walked faster tended to have larger medial compartment loading (Figure 2). A moderate correlation of r = 0.48 was observed and the linear trend approached statistical significance ($p = 0.06$). This relationship explains in part why differences in contact force between subjects with OA (n=16) and the healthy controls was not detected.

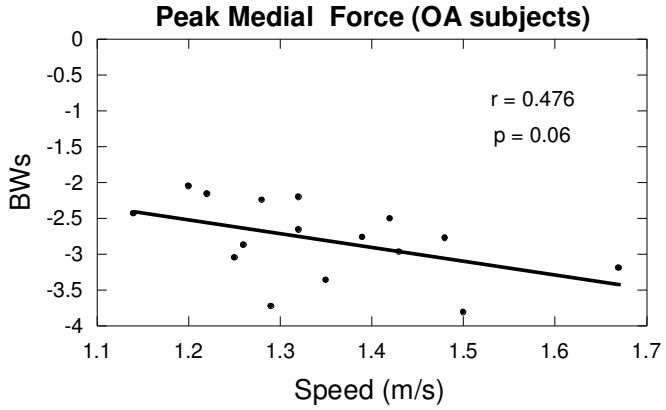

Figure 2: A moderate linear trend of increasing peak contact with walking speed was found for subjects with OA (n=16). The trend approached statistical significance ($p = 0.06$).

CONCLUSIONS

Some of our subjects with OA walked slower than age-matched controls. Slower walking was associated with smaller peak medial forces. Peak loading for the entire group of subjects with OA was not statistically different compared to the controls. However, comparisons between subjects walking at similar speeds indicated that those with OA experienced significantly greater loading than healthy controls. This finding has implications for clinicians and for those investigating dynamic loading of the knee.

REFERENCES

[1].Hurwitz et al., J Orthop Res. 20(1):101-7, 2002.
[2].Lelas et al., Gait & Posture. 17:106-112, 2003.
[3].Schmitt et al., J Orthop Res. 26(9):1180-5, 2008.
[4].Buchanan et al., J Appl Biomech. 20(4): 367-395, 2004.
[5].Winby et al., J Biomech. 42(14), 2294-2300, 2009.

ACKNOWLEDGEMENTS

Supported by NIH R01-AR48212 & P20-RR16458.

GROUND REACTION FORCES SCALE TO RAMP ANGLE DURING TRANSITIONS

Riley C. Sheehan & Jinger S. Gottschall

Department of Kinesiology, The Pennsylvania State University
University Park, PA 16802 USA
email: rcs241@psu.edu, http://www.biomechanics.psu.edu/nml/

INTRODUCTION

Throughout a normal day, we encounter a variety of slopes at various angles, from shallow accessibility ramps to steep natural slopes. We continually transition between level and hill surfaces while walking with a smooth and safe gait pattern. Our previous research indicates that these transition steps are a proactive anticipation of the demands of the next step[1,2]. Both Earhart & Bastian[3] and Prentice et al.[4] also documented these novel characteristics and concluded that the mechanical walking strategy is dependent upon the incline of the surface. Our goal was to expand our knowledge of surface transitions by evaluating the ground reaction forces prior to walking uphill and subsequent to walking downhill.

During level walking, the vertical component of the GRF is comprised of 2 separate peaks, the first peak occurs during weight acceptance in early stance while the second peak occurs during push off in late stance. The horizontal component of the GRF is negative from foot contact to midstance resulting in a braking impulse. Then, the GRF is positive until the end of stance resulting in a propulsive impulse. In this study, we focused on the second peak of the vertical GRF (V_{peak2}) and the propulsive impulse (I_{prop}).

Lay et al.[5] found that both the V_{peak2} and I_{prop} are greater during uphill walking, compared to level walking. They also observed that these modifications are dependent upon hill angle. Thus, because both the V_{peak} and the I_{prop} are larger during uphill walking, and the transition steps anticipate the demands of the next step, we hypothesized that V_{peak} and I_{prop} would be larger during the transition steps than during level walking and would increase with ramp angle.

In addition, Lay et al.[5] found that both the V_{peak2} and I_{prop} are less than level walking during downhill walking and also dependent upon hill angle. Likewise, because both the V_{peak} and the I_{prop} are smaller during downhill walking, we hypothesized that V_{peak} and I_{prop} would be larger during the transition steps than during level walking and would increase with ramp angle.

METHODS

Five healthy, college students (3 male, 2 female) completed the protocol consisting of level, uphill, and downhill walking trials at a self-selected velocity on a 25-m walkway. We utilized a custom-built ramp apparatus that we placed in series with two force plates within the walkway. A complete data set was the successful completion of 10 level walking trials with the left foot stance phase on each plate for 5 trials as well as 40 uphill and 40 downhill trials at different slopes (10 trials at each angle 7°, 15°, 23°, 31°) where the left foot stance phase was on the force plate closest to the ramp (FP1) for 5 trials and on the force plate furthest from the ramp (FP2) for 5 trials. Therefore, we collected the left foot forces during level walking, both 1 and 2 foot contacts prior to the uphill transition (L-UP), and 1 and 2 foot contacts subsequent to the downhill to level transition (DN-L). We calculated the magnitude of the V_{peak} and the I_{prop} for each condition, and normalized them to level walking values. The conditions were compared using a repeated-measures ANOVA followed by a Newman Keuls post hoc test with a significance of $p < 0.05$.

RESULTS AND DISCUSSION

Though our individual hypotheses were not all supported, our data supports our rationale that the magnitude of the force modifications leading to a

transition would scale with the ramp angle. Overall, our data indicate that both the magnitude and direction of force production is dependent upon the angle of the surface.

Figure 1. Second Vertical Peak

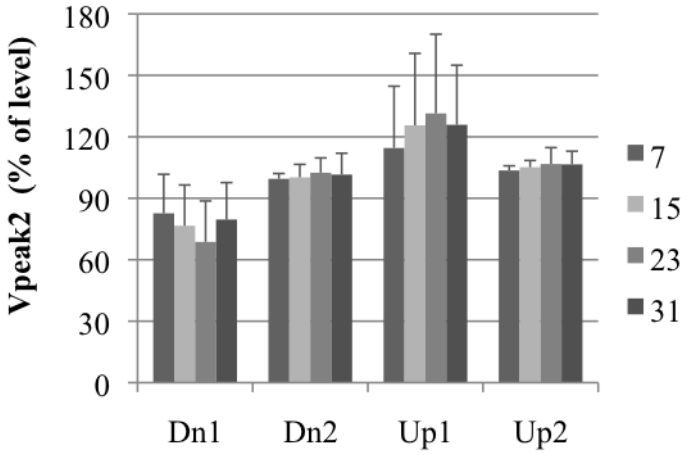

Figure 2. Propulsive Impulse

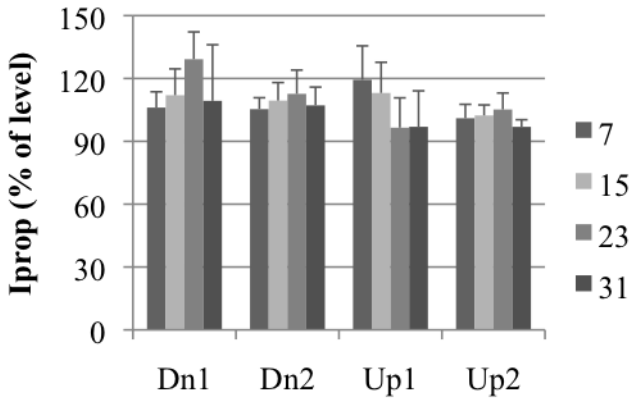

During the L-UP transition, there was a significant effect for ramp angle both V_{peak} and I_{prop} during the stance phase prior to the transition (Up1, Figure 1 and 2). In support of our hypothesis, the V_{peak} increased with ramp angle, except for the V_{peak} at 31° which was less than at 23°. Contrary to our hypothesis, the I_{prop} actually decreased with ramp angle. However, this coupled with the V_{peak} data suggest that as the angle of the ramp increases, the push-off angle also increases, trading horizontal force for vertical force. Also, though not as pronounced, there is a significant effect for ramp angle on V_{peak} and I_{prop} two steps from the transition (Up2). This is in contrast to the findings of Prentice et al.[4] who asserted that modifications to the walking pattern during a transition do not occur until the swing phase directly before contacting the new surface. Our data suggest that when transitioning from level ground to increasingly steep ramps, the participants attempted to prepare for the future demand of uphill walking by altering their push-off angle.

During the DN-L transition, there was a significant effect for ramp angle for V_{peak}, but not for the I_{prop}. However, for both V_{peak} and I_{prop} there was a significant difference from level walking for the 23°, but the 31° ramp did not follow the trend (Dn1, Figure 1, 2). Contrary to our hypothesis, the V_{peak} actually decreased with ramp angle. This may be due to the participants transferring the increased vertical force from the descent of a steep ramp to horizontal force. Though the trend of I_{prop} increasing with ramp angle is not significant, it does fit with our interpretation of the V_{peak} data and would support our hypothesis. The lack of significance may be due to a small sample size or the atypical results for the 31° ramp. While the V_{peak} values returned to level walking values by the second contact after the transition, there was still an increase in I_{prop} that scaled with ramp angle (Dn2). Our data suggests that when transitioning from increasingly steep ramps to level ground, the participants attempted to transfer the assistive vertical force from gravity to horizontal propulsive force to reduce the impact of the transition.

CONCLUSIONS

Our findings demonstrate that individuals modify their gait patterns at least two foot contacts prior to making a transition and that these strategies scale with the demands of the task. Additionally, the steps prior to uphill walking are modified to prepare for the forthcoming positive work while the steps subsequent to downhill walking are modified to reduce the impact of the transition.

REFERENCES

1. Sheehan & Gottschall. *Ergonomics,* (in press)
2. Sheehan & Gottschall. J Electromyogr Kinesiol. (in preparation)
3. Earhart & Bastian. *J Neurophysiol* 84, 605-615, 2000.
4. Prentice et al. *Gait Posture* 20, 255-265. 2004
5. Lay et al. *J Biomech* 39. 1621-1628. 2006

DISCRETE FREQUENCY ADJUSTMENT OF WALKING ABOVE AND BELOW PREFERRED STRIDE FREQUENCY CAUSES AN INCREASE IN THE METABOLIC COST OF THE MOVEMENT

Joseph O'Halloran, Jebb G. Remelius, Richard E.A. van Emmerik and Joseph Hamill

University of Massachusetts-Amherst, Amherst, MA, USA
email: josepho@kin.umass.edu

INTRODUCTION

Stride frequency is a parameter of locomotion that is sometimes chosen to maximize metabolic economy at preferred locomotory speeds. Humans have previously been shown to have the ability to choose movement patterns that minimize metabolic energy expenditure, a process that has been referred to as self-optimization [1]. Self-organizing systems tend to choose preferred states that show the most stable coordination and the least energy requirements. When stride frequency is varied above and below preferred, metabolic cost forms an inverted U-shape curve with the minimum at the preferred [1]. Self-organizing human systems tend to choose preferred states that show the most stable coordination and the least energy requirements. The respiratory system has, as its primary task, maintenance of adequate ventilation in order to supply the necessary amount of oxygen to and remove metabolic byproducts from the circulatory system.

The purpose of this study was to vary stride frequency from preferred to investigate the relationship between steady state metabolic cost (VO_2), and ventilatory efficiency (VE/VO_2) as well as to reveal how these relationships emerge over minute by minute time scales from rest.

It is hypothesized that heart rate response will be lowest and metabolic efficiency will be greatest at the preferred frequency

METHODS

Sixteen male subjects (age range 18-30 years) walked on a motorized treadmill (Accumill P, Pacer Fitness Systems, TX), at a self-selected speed. Sample size estimations were performed based on power analysis (80% statistical power and an alpha level of 0.05), using variability data from previously collected treadmill respiratory data [2].

Respiratory airflow was recorded by means of the differential pressure transducer in a TEEM 100 Portable Metabolic Analysis System (Medical Graphics Corp., MN). Respiratory flow was sampled continuously at 500 Hz. This system was also used to provide twenty-second averages of ventilatory and respiratory gas exchange variables during the experimental periods. Heart rate data was collected using a Polar wireless heart rate transmitter and receiver.

The stride frequency conditions consisted of walking at preferred stride frequency (PSF) first, followed by PSF-20%, PSF-10%, PSF +10%, and PSF +20% in a random order. Frequency was changed in a discrete manner. This set of frequency conditions was carried out during preferred walking speed (PWS). Each subject began a warm up period by walking on the treadmill for 5-10 minutes at a comfortable, self-selected pace after which their PWS and subsequently their PSF at PWS was determined. Each subject walked at a determined speed for that condition for five minutes. The treadmill belt was then stopped and the subject stood quietly for an additional 2.5 minutes. Metabolic, respiratory, kinematic, and stride data were collected continuously beginning at 2.5 minutes into the initial quiet stance period through to the end of the final quiet stance period. An additional rest period preceded all conditions when necessary, which concluded when the subjects heart rate dropped to the baseline PWS and the PSF at this speed were determined. Discrete conditions consisted of PSF performed first followed by the other conditions in a random order.

The subject's heart rate was recorded while in the standing position for use as a baseline resting measure between conditions. The experiment was

designed in order to investigate the steady state as well as the transitional dynamics of respiratory response to stride frequency manipulation.

RESULTS AND DISCUSSION

Analysis of stride frequency concludes that it increases linearly as the conditions increase. This confirms that the participants adhered to the protocol. Following this confirmation, the first result to be drawn is the number of breath cycles per minute at each frequency. This can be seen in Figure 1. PSF is significantly ($p<0.05$) lower than each of the other frequencies. The data forms a U-shaped curve.

The VE/VO_2 was also lowest at PSF. This is in agreement with the findings of [1]. However the curve is not U-shaped about PSF. PSF-20% shows a lower VE/VO_2 rate than PSF-10%.

Heart rate was lowest at PSF. However, variability was also greatest at this frequency (Table 1). The VO_2 measures are not in agreement with some of the previous findings. Steady state walking at PSF did not have the lowest VO_2 and but did have the greatest ventilatory efficiency (VE/ VO_2). Variability in VO_2 was similar across all conditions. Minute-by minute evaluations revealed that VO_2 and VE/ VO_2 reached steady rates near 90 seconds from the onset of walking.

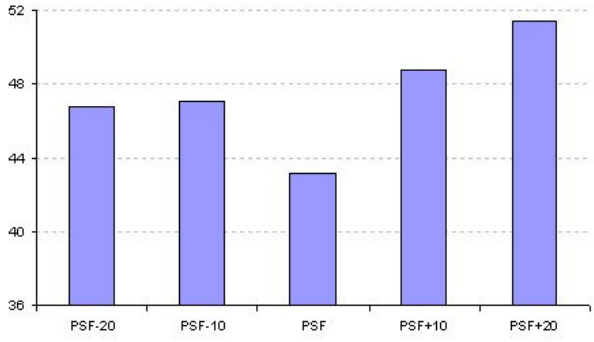

Figure 1: Number of breath cycles per minute.

CONCLUSIONS

Stride frequency is a critical parameter influencing metabolic cost of walking. Manipulation of this frequency while walking at preferred speed impacts on VE, VO_2, VCO_2 as well as heart rate measures. Some findings are not in agreement with previous literature which demand that this data be further explored, in conjunction with a kinematic analysis to explore possible influences of the metabolic cost of the movement established here on locomotor respiratory coupling. These findings provide evidence of the adaptability and efficiency and respiratory systems when perturbed by an influence in the form of stride frequency.

REFERENCES

1.Holt et. al. 1995. *Hum Mov Sci*, **14**, 45-60, 1995.
2.McDermott WJ, et al. *Eur J Appl Physiol* **89**, 435-444, 2003.

Table 1: Steady State Cardiovascular and Ventilatory Results

	PSF-20%	PSF-10%	PSF	PSF+10%	PSF+20%
HR(bpm)	88±14	88±10	84±17	89±12	93±12
$VO_2(l.min^{-1})$	0.93±.3	0.78±.3	0.88±.2	0.83±.3	0.93±.3
$VC0_2(l.min^{-1})$	0.94±.4	0.79±.3	0.89±.3	0.81±.3	0.94±.4
$VE(l.min^{-1})$	15.49±3.9	13.45±4.2	14.39±3.2	14.12±4.7	15.74±4.2
$VE/V0_2(l.min^{-1})$	14.93±1	15.14±.9	14.86±.7	15.05±.9	15.04±.8
$VE/VCO_2(l.min^{-1})$	6.07±1.9	5.90±1.9	6.16±1.7	5.96±1.8	5.98±1.8

THE EFFECT OF FOOT TYPE OF NORMAL SUBJECTS ON FOOT CONTACT DYNAMICS

[1,2]Rajshree Mootanah, [1]Jocelyn Frey, [1]Rebecca A. Zifchock, [1]S. Betty Chow, [1]Andrew P. Kraszewski, [1]Mark W. Lenhoff, [1]Sherry I. Backus, [1]Jonathan Deland, [1]Phillip Demp, [3]Jinsup Song, [1,2,3]Howard J. Hillstrom

[1]Hospital for Special Surgery, NY, USA
[2]Anglia Ruskin University, Chelmsford, Essex, UK
[3]Temple University School of Podiatric Medicine, PA, USA
email: rajshree.mootanah@anglia.ac.uk, MootanahR@hss.edu

INTRODUCTION

It is well documented that human movement is influenced by foot structure. Pes cavus is characterized by an excessively high arch and pes planus is characterized by the flattening out of the arch of the foot. Pes cavus is associated with clawing of the great and lesser toes [1, 2], and sometimes with pain. [3] Neurologic and idiopathic pes cavus have significantly different foot posture indices compared to the normal foot. [4] Pes planus is associated with increased plantar surface contact area and can be a risk factor in the development of overuse injuries [5, 6]. Foot type was found to affect the center of pressure excursion index (CPEI), which is the lateral displacement of center of the pressure curve from the line constructed between the initial and the final center of pressure values, normalized by the foot width at the anterior one third of foot. [7] Stance phase may be broken into three subphases: contact, midstance, and propulsion. Contact is the percentage of stance from heel strike (or initial contact) and the first midfoot/forefoot loading. Midstance is the percentage of stance from the end of contact to heel off (ie end of rearfoot loading). Propulsion is the percentage of stance from the end of midstance till toe-off (or final contact).

The effects of foot type on foot contact dynamics and function are not well understood. This information is important when planning treatment for pes cavus and pes planus feet. Hence, the aim of this study was to develop a normative dataset of temporal sequence of loading, CPEI, and the transverse foot angle of healthy subjects with pes planus, rectus, and pes cavus foot types. We hypothesized that subjects with different foot types have significant different temporal sequence of loading, CPEI, and transverse plane foot angles.

METHODS

Sixty-one healthy asymptomatic test subjects were recruited with the following inclusion/exclusion criteria: (1) no current symptoms of pain, (2) no other symptoms suggesting a pathology involving the foot and ankle, and (3) no hallux valgus or other visible pedal deformities (e.g. hammertoes). The foot type of each test subject was determined based on resting calcaneal stance position and forefoot-to-rearfoot alignment. The pes planus group had a (1) resting calcaneal stance position (RCSP) $\geq 4°$ of valgus, and (2) a forefoot-to-rearfoot relationship (FF-RF) $\geq 5°$ of varus. The rectus group had a (1) a RCSP between 0° and 2° of valgus, and (2) a FF-RF between 0° and 4° of varus. The pes cavus group had a (1) RCSP > 1° of varus and (2) a FF-RF > 1° of valgus. This resulted in a foot classification of 22 pes planus, 27 rectus and 12 pes cavus individuals (Table 1).

Temporal sequence of loading (contact, midstance and propulsion phases of stance), CPEI, and the transverse plane foot angle were calculated from plantar pressure distributions. The emed X system (Novel gmbh, Germany), consisting of 4 sensors per cm2 (475 mm x 320 mm) was employed to measure each individual's dynamic plantar pressure distribution. Custom software was developed in C++ to calculate each of these parameters.

The effect of foot type was tested for each parameter, using a mixed effect analysis of variance (ANOVA) model. The fixed effect was 'foot type' and the random effect was 'trial' (replications)

Significance was set at $p < 0.05$. A trend was operationally-defined at $p<0.1$. Post hoc t-tests were performed using the Bonferroni method ($P<0.0167$).

RESULTS AND DISCUSSION

The anthropometric information and clinical foot type classification of the subjects is summarized in Table 1. The temporal sequence of loading (contact, midstance, and propulsion) was not significantly different across foot type. Note that midstance on the left was nearly significant. CPEI demonstrated significant differences across pes planus and rectus as well as pes planus and cavus foot types. The transverse plane foot angle was significantly different across foot types on the right and was nearly significantly different on the left.

CONCLUSIONS

The temporal sequence of loading was not significantly different across foot types. CPEI and transverse plane foot angles did demonstrate differences between the rectus and planus and cavus and planus groups. No parameter in the study could distinguish the pes cavus from rectus foot types.

REFERENCES

1. De Doncker E, et al. ***Acta Orthop Belg*** **36**:383-559, 1970.
2. Sugathan HK, Sherlock DA. ***J Foot Ankle Surg***, **48** (6), 637-641, 2009.
3. Naudi S, et al. ***Rev Chir Orthop Traumatol*** **95**(4), 293-300, 2009.
4. Redmond et al. ***J Foot Ankle Res*** **1**:6, 2008.
5. Kaufman KR, et al. ***Am J Sports Med*** **27**: 585-593, 1999.
6. Levy JC. ***Foot Ankle Int*** **27**: 1060-1064, 2006.
7. Song J. ***JAPMA*** **86**(1):16-23, 1996.

ACKNOWLEDGEMENTS

NIH 1R03HD053135-01

Table 1: Test subject anthropometrics

	Pes Planus	**Rectus**	**Pes Cavus**
Subjects	22	27	12
Males (Females)	10 (12)	8 (19)	6 (6)
Body Weight (N)	641.3 ± 128.1	662.8 ± 138.8	721.1 ± 155.1
Height (m)	1.71 ± 0.08	1.66 ± 0.11	1.74 ± 0.12
BMI	22.2 ± 3.2	24.4 ± 4.1	24.0 ± 3.5
RCSP (°)	-6 ± 2	-1 ± 1	0 ± 1
FF-RF (°)	-7 ± 4	3 ± 1	-2 ± 1

Table: Foot Contact Dynamic Results

Parameters	Pes Planus	Rectus	Pes Cavus	ANOVA	Post Hocs
Contact (%St)-R	9.74(1.69)	9.81(1.54)	9.13(2.29)	0.137	
Contact (%St)-L	9.64(1.73)	9.71(1.55)	9.19(2.30)	0.330	
Midstance (%St)-R	49.93(5.64)	48.91(5.13)	50.25(7.67)	0.426	
Midstance (%St)-L	50.74(5.71)	49.03(5.14)	51.21(7,59)	0.096	
Propulsion (%St)-R	39.65(5.30)	41.36(4.82)	40.50(7.21)	0.176	
Propulsion (%St)-L	39.58(5.62)	41.16(5.03)	39.58(7.47)	0.189	
CPEI (%)-R	18.73(5.84)	22.08(5.16)	24.45(7.76)	<0.001	1, 2
CPEI (%)-L	18.57(5.65)	21.30(5.02)	24.01(7.47)	<0.001	1, 2
Foot Angle (°)-R	7.36(3.94)	9.81(3.48)	10.03(5.21)	<0.001	1, 2
Foot Angle (°)-L	7.22(4.86)	8.64(4.32)	9.35(6.43)	0.084	

Note: %ST = %Stance, CPEI=Center of Pressure Excursion Index
Bonferonni post-hoc significance set at $p<0.0167$
1 = Cavus vs Planus; 2 = Rectus vs. Planus; 3 = Cavus vs. Rectus

NATURAL ANKLE PSEUDO-STIFFNESS DURING GAIT INITIATION

[1]LaKisha D. Guinn, [1]Kota Takahashi, [1]Alexander R. Razzook, , [1,2,3]Steven J. Stanhope

[1]Biomechanics & Movement Science, University of Delaware, Newark, DE, USA
[2]Department of Mechanical Engineering, University of Delaware, Newark, DE, USA
[3]Department of Health, Nutrition and Exercise Sciences, University of Delaware, Newark, DE, USA
email: lguinn@udel.edu

INTRODUCTION

Understanding the mechanism of gait initiation is important for the design of lower limb prosthetics and orthotics and for improving gait in persons with neurological disorders inhibiting or delaying gait initiation. Natural ankle pseudo-stiffness (NAS) is a measure of the overall performance of the ankle system during gait as it is associated with the mechanical and neurological control. In this study NAS is defined as the slope of the ankle moment plotted as a function of ankle angle during gait initiation. Results of previous studies have indicated that NAS changes with walking speed [1,2]. In addition, the results of a recent study indicate that the characteristics of the ankle moment-angle curve at gait initiation change with steady-state walking speed [3]. These finding suggest that the modulation of ankle stiffness is an important function during gait initiation as well as normal walking. The aim of this pilot study was to quantify NAS in healthy individuals at gait initiation when accelerating to a normal walking speed.

METHODS

Six volunteers (2 females, 4 males) without neurological deficit or lower extremity deformity between the ages of 21 and 28 years (mean ± standard deviation: age,: 24.5 ± 2.59 years; height, 1.75 ± 0.069 m; weight, 80.8 ± 27.5 kg) were examined in this pilot study. Subjects were instructed to begin walking at a comfortable speed when given the "go" command. Prior to the beginning of the trial the subject was instructed of which foot to use to initiate gait. Two force plates and six cameras, sampling at rates of 360 and 120 Hz respectively, were used to examine kinetic and kinematic parameters. Ankle angle was calculated in the sagittal plane. Sagittal plane ankle moments were calculated using inverse dynamics (Visual 3D, C-Motion, Inc).

At the beginning of each trial, each foot was on a separate force plate to obtain the center of pressure (COP) for each foot. Four gait initiation trials were collected for each subject under both conditions of taking the first step with the right and left leg except for one subject in which three trials were collected for each leg. Therefore a total of 46 trials were collected. During the same session, kinematic and kinetic data were collected while the subject walked at four different speeds, normalized across subjects by height. Three trials were collected at each targeted velocity: 0.4, 0.6, 0.8 (normal), and 1.0 statures/s.

Natural ankle pseudo-stiffness values (NAS) were calculated by deriving the slope of ankle moment as a function of ankle angle between two events, end of anticipatory postural adjustment phase and the point of maximum ankle dorsiflexion of the trailing limb (Fig. 1). During this portion of the gait cycle the body is falling forward over the ankle joint and executing an eccentric contraction to control forward fall. Ankle moment data were normalized by body weight. The mean and standard deviation of NAS were averaged for all gait initiation trials and at each walking speed. NAS at gait initiation was compared to NAS during walking.

RESULTS AND DISCUSSION

The mean NAS at gait initiation was 0.137 ± 0.0184 Nm/deg BW, where BW is body weight (kg), during the phase of eccentric contraction (Fig. 2). NAS during normal walking increased with increasing velocity (Fig. 1, IV). This value was greater than NAS during walking at a normal velocity of 0.8 statures/s (difference = 0.0454 Nm/deg BW). There was an initial anticipatory

postural adjustment phase (Fig. 1, region a), during which the stiffness was typically low and highly variable across subjects. Following this period there was a region of increasing ankle moment as the body fell forward over the ankle and ankle angle increased to maximum ankle dorsiflexion (Fig. 1, region b). This was the region of the ankle moment-angle curve during which NAS was calculated. During this interval the leading limb lost contact with the ground and the trailing limb fully supported the body (Fig. 1, III) and controlled forward progression. At the end of this region the heel raised from the ground as the body continued to accelerate forward and another linear portion of the ankle moment-angle curve was initiated as the weight was transferred to the leading limb (Fig. 1, region c).

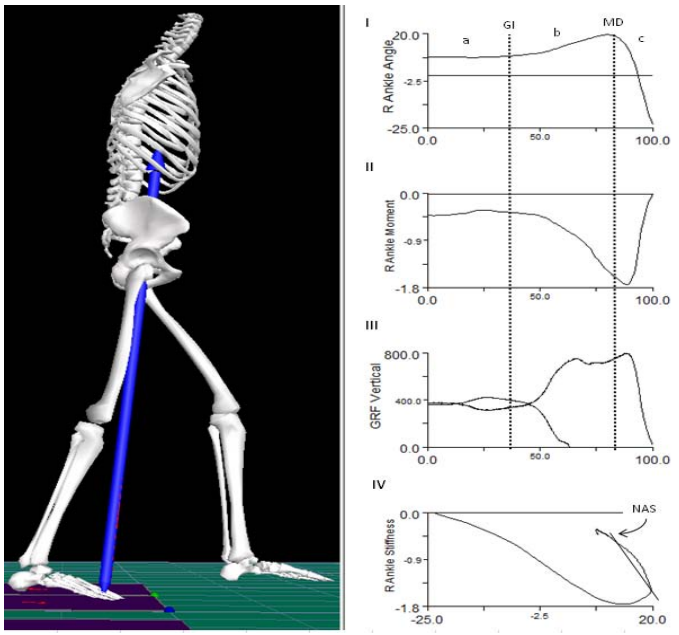

Figure 1. An example of a kinematic and kinetic patterns exhibited during gait initiation. Three distinct regions were identified: (a) anticipatory postural adjustment, (b) eccentric contraction as forward progression of the body is controlled, and (c) weight transfer. The ankle moment as a function of ankle angle curve, IV, demonstrates a clockwise progression, indicative of energy generation. (I, Ankle Angle v. Percent of Stance; II, Ankle Moment v. Percent of Stance; III, Vertical Ground Reaction Force v. Percent of Stance; GI, Gait Initiation; MD, Maximum Dorsiflexion Angle)

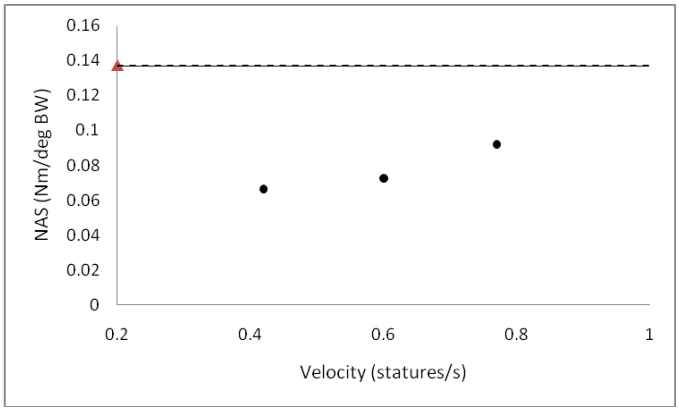

Figure 2. The x axis begins with gait initiation (GI). The (Δ) represents the mean natural ankle pseudo-stiffness (NAS) value at gait initiation. The (•) represents the mean NAS value at each walking velocity. The stiffness at gait initiation is greater than during normal walking (0.8 statures/s).

CONCLUSIONS

NAS was unexpectedly high during gait initiation**.** It was expected that the value at gait initiation would fit along the curve of NAS as a function of walking speed that was developed from the normal walking trials. This may indicate that a separate mechanism is utilized to initiate gait. This result may have important implications for patients such as those with Parkinson's disease who experience episodes of "start hesitation", a delay or complete inability to initiate gait. In addition it may also have implications for the design of lower limb prosthetics and orthotics.

REFERENCES

1.Hansen AH, et al. *J Biomech* **37,** 1467-1474, 2004
2.Razzook AR, et al. *Proceedings of ISPO '07,* Vancouver, Canada, 2007
3.Hansen AH, et al. *Gait & Posture* **31**, 13-17, 2010

THE EFFECTS OF A DOWNHILL GRADE ON THE BIOMECHANICS OF WALKING IN OBESE ADULTS

Kathryn Dannecker, Kellie Ehlen, Michelle Reynolds, Raymond Browning

Colorado State University, Fort Collins, CO, USA.
email: kldann@cahs.colostate.edu

INTRODUCTION

Walking is a common form of physical activity, and is an often prescribed form of exercise for obese individuals. During level walking, moderately obese adults have greater lower extremity net muscle moments vs. their non-obese counterparts [1,2]. However, individuals frequently encounter hills when walking in daily life. It is therefore important to also understand the impact of inclines and declines on the biomechanics walking. When non-obese individuals walk downhill, knee net muscle moments are greater than during level walking [3], but the effects of obesity on the biomechanics of downhill walking are not known. Downhill walking may be a source of biomechanical loads that link obesity and musculoskeletal injury and pathology, including knee osteoarthritis [4]. An understanding of how decline affects the biomechanics of walking in obese adults may aid in the development of exercise recommendations that reduce the risk of musculoskeletal pathology.

The purpose of this study was to quantify the biomechanics of moderate downhill vs. level walking in moderately obese adults. We hypothesized that obese individuals would walk with greater knee flexion and that knee extensor moments would increase during downhill vs. level walking.

METHODS

Ten obese adult volunteers participated in this experiment, mass = 100.5 (15.7) kg, BMI = 33.4 (2.6) kg/m^2, (mean (S.D.)). We measured ground reaction forces and three-dimensional lower extremity kinematics while subjects walked on a dual-belt force measuring treadmill at 1.25 m/s. Each subject completed a 6-minute trial with the treadmill grade set at 0 and 3° (two trials total), with 30 seconds of biomechanics data collected during the final minute of the trial. Kinematic parameters were collected at 60 Hz using eight optoelectric cameras. Ground reaction forces and moments were recorded at 1200 Hz by force platforms embedded under each treadmill belt. We calculated net muscle moments at the hip, knee and ankle via standard inverse dynamics techniques. Body segment parameters were estimated via DEXA and published regression equations [5]. Biomechanics variables were normalized as to represent a percentage of the stride. We calculated the mean of each variable of interest over 20-25 strides at each grade for each subject and the mean across subjects for each trial. Paired t-tests determined how obesity affected temporal gait characteristics, mid-stance joint angles and peak net muscle moments. A criterion of $p<0.05$ defined significance.

RESULTS AND DISCUSSION

There were no significant temporal-spatial differences measured in downhill verse level walking, (i.e. stride length and stride frequency were similar). Participants walked downhill with a slightly more flexed knee (Fig. 1).

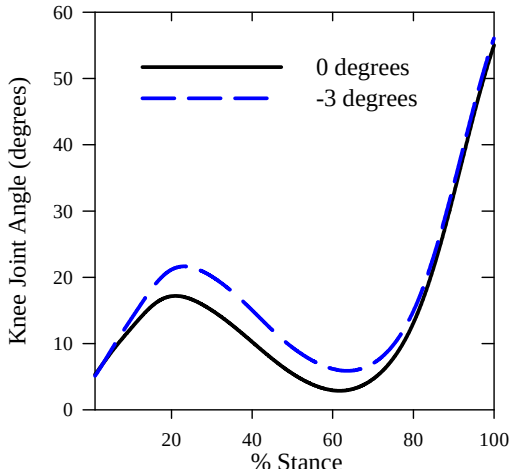

Figure 1. Mean knee flexion during stance during level vs. downhill walking.

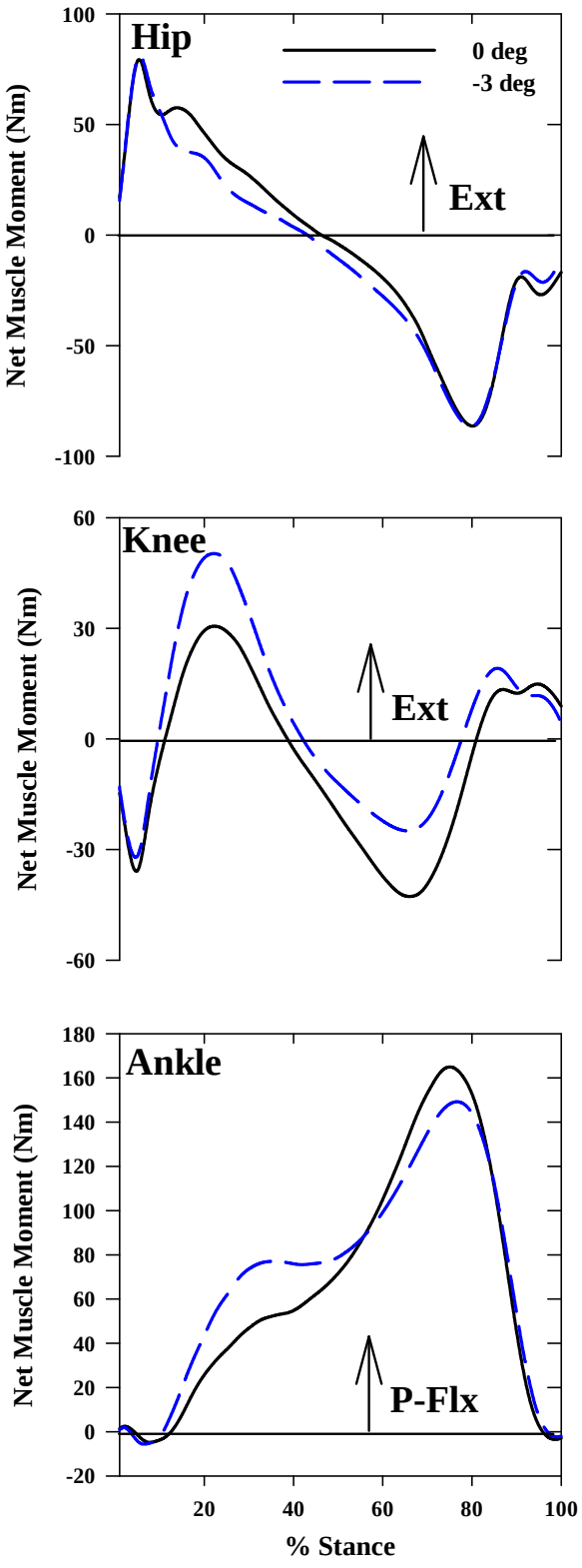

Figure 2. Mean flexion/extension moments during level vs. downhill walking. Ext: extension, P-flx: plantarflexion

Anterior-posterior braking ground reaction forces were greater while propulsive forces were smaller compared to level walking. As a result, participants exhibited increased knee extensor net muscle moments when walking downhill vs. level walking (Fig. 2). Peak knee extensor moments increased ~80% during downhill vs. level walking. Ankle net muscle moments were similar during downhill vs. level walking. The abduction moment at the knee was similar during downhill vs. level walking (Fig. 3). The increase in net muscle moments at the knee suggest increased joint loads during downhill vs. level walking and may increase the risk of musculoskeletal injury/pathology.

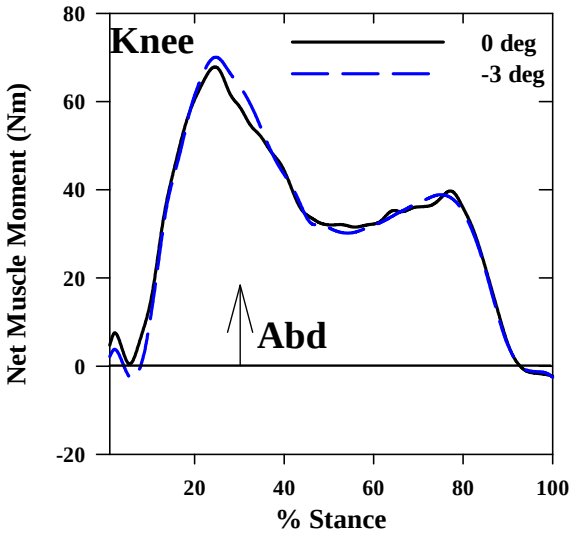

Figure 3. Mean knee abduction/adduction moments during level vs. downhill walking. Abd: Abduction

REFERENCES

1. Browning, R.C. et al. *Med Sci Sports Exerc*, **39**(9), 1632-41, 2007.
2. Lai, P.P., et al. *Clin Biomech*,. **23**, S2-6, 2008.
3. Lay, A.N., et al. *J Biomech*,. **39**(9), 1621-8, 2006.
4. Felson, D.T., et al. *Ann Intern Med*, **109**, 18-24, 1988.
5. Durkin, J.L., et al. *J Biomed Eng*, **125**, 515-522, 2003.

ACKNOWLEDGEMENTS

This research was supported by a grant from the CSU College of Applied Human Sciences and NIH grant R03AR059264.

COLLISION COMPENSATION BY ACTIVE PUSH-OFF WITH GAIT SPEED

[1]Heewon Park, Jin Yeom and Sukyung Park

Korea Advanced Institute of Science and Technology, Daejeon, Korea
email: Heewon_Park@kaist.edu, web: http://biomt.kaist.ac.kr

INTRODUCTION

Human walking can be divided into two phases: the single support phase and the double support phase. Despite the double support phase occurs over a short time which is only about 10% of one step duration, it is very important because step-to-step transition during this phase is a crucial event for the periodicity of human walking. Push-off and heel strike have a key role in propelling and maintaining a steady state gait. In this study, we examine how human maintain active propulsion under challenging gait condition.

METHODS

Eight healthy young subjects (eight male, 23.5±2.07) volunteered for this study. Written informed consent was obtained according to KAIST IRB protocols. Subjects participated in two test sessions of different load conditions: 1) unloaded and 2) loaded condition, in which subject walks carrying loads equal to 15% body mass positioned symmetrically about the trunk. Subjects walk on a 12 meter long, 1 meter wide walkway at five different gait frequency cued by a metronome. To minimize the effect of subject's fatigue, 5-10 minute resting session is given to the subject between each trial.

Three force plates were placed at the middle of the walkway to measure ground reaction force of three consecutive steps. Kinematic information of the subject was measured by motion capture system with six reflective markers attached on the at sacral position (L5 of vertebrae), each ankle joints, each knee joints, and root of the left little toe (Metatarsal-phalangeal joint). Ground reaction force and kinematic information is collected with 200Hz sampling frequency. These data filtered using Butterworth 5th low-pass filter with 5Hz cutoff frequency. For the force data, 30Hz cutoff frequency is used because meaningful data of ground reaction forces generally lies below 15Hz.

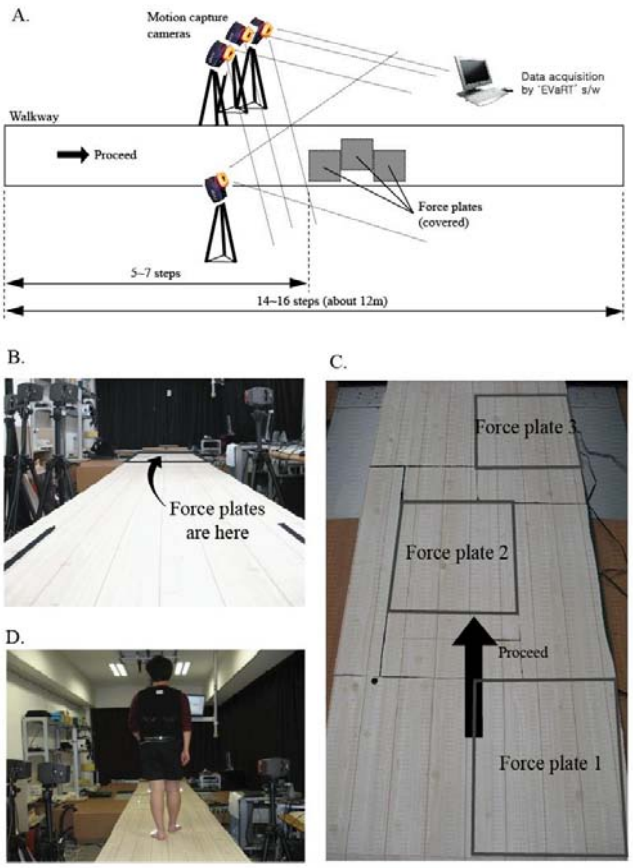

Figure 1: Walkway with motion capture system and force plates

RESULTS AND DISCUSSION

Empirically obtained average impulse forces of push-off and heel-strike tend to split from each other as the walking speed increases. The push-off force tends to decrease with increasing walking speed while the thee-strike force tends to increase.

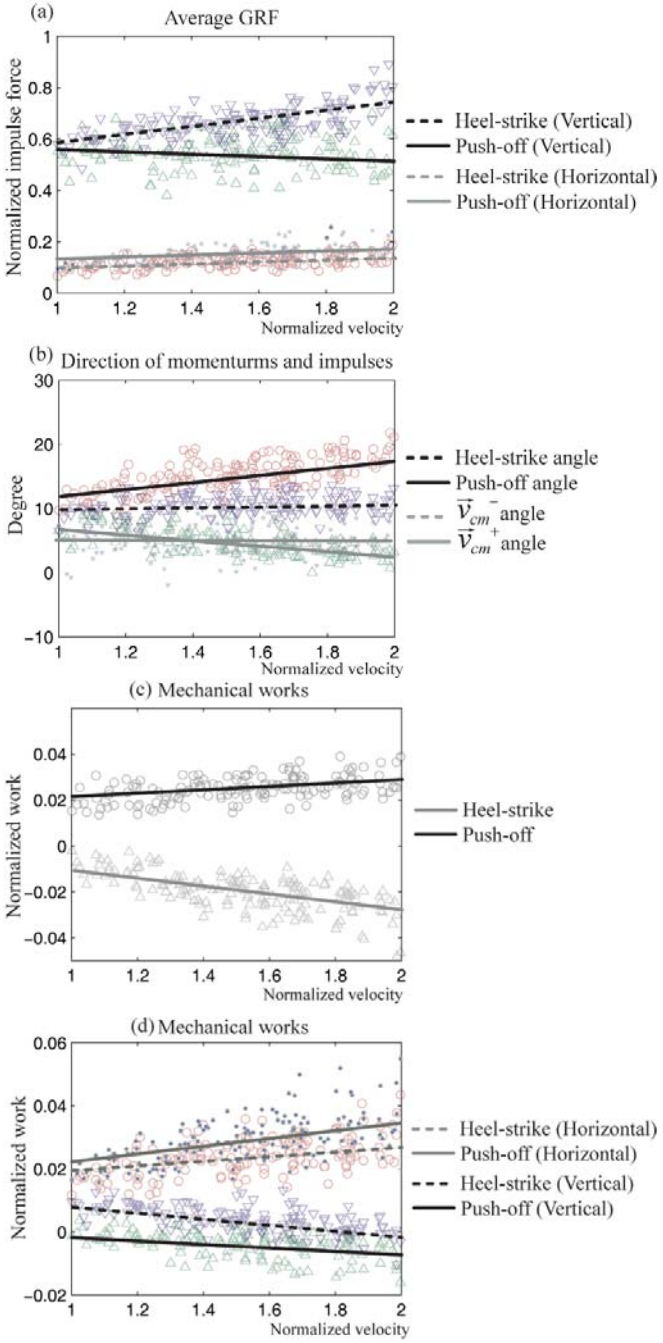

Figure 2: (a) Average impulse forces, (b) Mechanical work by push-off and heel-strike, (c) Axial components of mechanical works, and (d) Asymmetric vector direction occurred in the momentum changing process

Impulsive asymmetry was more highlighted in the horizontal mechanical cost, showing slightly greater positive work by horizontal propulsion of push-off than the heel strike collision loss. Although the vertical heel strike force was greater than the vertical push-offs, its mechanical cost does not show a significant difference as a function of gait speed, implying that the push-off propulsion was applied to energetically compensate the collision loss.

Also as increasing the gait speed, directions of push-off and heel-strike impulses were asymmetrically changed. Direction of momentums just before and right after the double support phase and the push-off and heel-strike impulses are shown in Fig2. The direction of heel-strike impulse was not significantly affected by gait speed, but that of push-off impulse increased as increasing gait speed, implying that the trailing leg configuration is adjusted to perform appropriate collision compensation.

Loading condition (15~20% of total body weight) did not a significantly change the collision compensation trends and gait parameters..

CONCLUSIONS

Although the push-off is more energetically more efficient than using hip torque actuation, humans may not fully compensate the collision loss using plantar flexion at various gait conditions. We observed the lack of push-off force at faster gait compared to those of heel strike.

Because of the limited capability to generate enough propulsion, the leg posture be adjusted to satisfy the challenging goals such as fast walking. Subjects changed the direction of the push-off impulse to minimize the energy loss due to heel-strike and maximize the force acting on moving their body forward.

REFERENCES

1.Kuo AD. *J Biomech Eng* **124**, 113, 2002.
2.McGeer T. *J Theor Biol* **163**, 277, 1993.
3.Cuccurullo SJ. *Physical Medicine and Rehabilitation Board Review*, Demos Medical Publishing, Inc., 2004.

ACKNOWLEDGEMENTS

The work was supported by the Basic research fund of the Unmanned Technology Research Center, Agency for Defense Development of Korea

MULTI-SEGMENT FOOT MODEL KINETICS DURING NORMAL GAIT

[1]Dustin A. Bruening, [1]Kevin M. Cooney, [1,2]Frank L. Buczek

[1]Shriners Hospitals for Children, Erie, PA
[2]National Institute for Occupational Safety & Health, Morgantown, WV,
Email: dbruening@shrinenet.org

INTRODUCTION

Kinematic multi-segment foot models have been increasingly used in clinical gait analysis and human movement research; however, the addition of kinetics has been hampered by unproven modeling assumptions and measurement difficulties. Specifically, ground reaction forces (GRFs) under subareas of the foot are difficult to measure [1], foot joint parameters have large inter-subject variability, and previously published kinetic models [2,3] are too complex for use in routine analysis [4,5]. Measurement limitations may be more readily overcome and model parameters more robustly implemented in a model that is simpler than those previously attempted. The purpose of this study was to calculate foot joint kinetics for a simple, three-segment foot model during normal gait. The model, measurement methodology, and results may be useful in future clinical analyses of foot and ankle pathologies, as well as for inputs to computer simulations and finite element models of the foot and ankle.

METHODS

The model joint centers and segment reference frames have been defined previously [6]. Briefly, the model consists of a Shank, Rearfoot, Forefoot, and Hallux segments, separated by ankle, midfoot (transverse-tarsal), and 1st metatarsal phalangeal (1MTP) joint centers. Due to the GRF measurement method used (see below), it was necessary to create two sub-models: 1- Midfoot (MFT) model, which included the Shank, Rearfoot, and Forefoot segments, and 2- Hallux (HLX) model, which included the Shank, Foot, and Hallux segments.

Nineteen markers were applied to the right foot of 17 normal pediatric subjects (9M, 8F), representing a range of ages (7-18, mean 12.6) and foot sizes. Subjects first walked at a self-selected speed across a floor containing 2 adjacent AMTI force platforms. Three trials with full foot/plate contacts were collected. Next, the subjects walked using a three-step targeting method, so that specified portions of the foot contacted the adjacent platforms. This was done for both of the sub-models, i.e. for the MFT model, the Rearfoot contacted one platform while the Forefoot (and toes) contacted the adjacent platform, with the platform division at approximately the midfoot joint center. For the HLX model, the division was just distal to the metatarsal heads, with the Hallux and toes isolated on the second platform. Subjects were instructed to walk as normally as possible and the starting position was adjusted until the appropriate placement, with a near normal gait pattern, was achieved. Trials were collected until at least three (for each model) were identified with accurate foot placement, which was verified visually by two video cameras located on either side of the plate division.

Marker trajectories were captured at 120 Hz, while GRF data was captured at 1560 Hz, filtered, and a threshold cutoff of 5N was applied. All data processing was performed using Visual 3D software. Spatiotemporal parameters, joint kinematics (Euler rotations), and single segment foot kinetics were compared between targeted and self-selected speed trials to help determine the extent to which targeting affected walking patterns. Ankle and midfoot joint kinetics were calculated from the MFT trials, while 1MTP joint kinetics were calculated from the HLX trials. All trials were time-normalized to % stance phase for kinetic comparisons, and a representative trial for each subject and each joint condition was chosen so to reduce differences due to targeting. The representative trials were used to calculate ensemble average kinetics across all subjects.

RESULTS AND DISCUSSION

Spatiotemporal parameters, kinematics, and rigid foot kinetics showed very few differences between targeted and self-selected speed trials, suggesting that the targeted results are reasonably representative of normal gait. When normalized by body mass, joint kinetics were consistent across subjects, and sagittal plane ensemble averages are shown below (Figure). In the sagittal plane, substantial midfoot power generation was noted during terminal stance. This is likely due to a combination of active muscle contractions, changes in midfoot joint(s) alignment, and ligamentous contributions. 1MTP power absorption slightly precedes midfoot power generation and suggests power transfer between segments (e.g. the windlass mechanism) to more efficiently plantarflex the midfoot and assist in propulsion. Non-sagittal plane results, although not presented here, may also improve understanding of foot and ankle function.

CONCLUSIONS

This study shows results from a novel kinetic model and measurement method. The targeted approach used in this study overcomes some of the previous measurement limitations, while at the same time introducing its own. It required targeted walking and multiple trials to achieve accurate foot placement. It also limited force analysis to two segments at a time, but the salient information from each of these analyses occurs at time periods where the third segment is not a prominent factor. The model is an improvement over previous kinetic models in its simplicity, and may be useful in clinical settings, whether with the GRF measurement method used here, a custom-built device [1], or a combined pressure mat/ force platform [7].

REFERENCES

1. Yavuz M., et al. *J Biomech* **40**, 3045-3049, 2007.
2. MacWilliams BA, et al. *Gait Posture* **17**, 214-224, 2003.
3. Scott SH and Winter, *J Biomech* **26**, 1091-1104, 1993.
4. Baker R and Robb, *Gait Posture* **23**, 399-400, 2006.
5. Buczek FL, et al. *Gait Posture* **23**, 519-522, 2006.
6. Bruening DA, et al. *Proceedings of JEGM '10*, Miami, FL, USA,2010.
7. Giacomozzi C and Macellari, *IEEE Trans Rehabil Eng* **5**, 322-330, 1997.

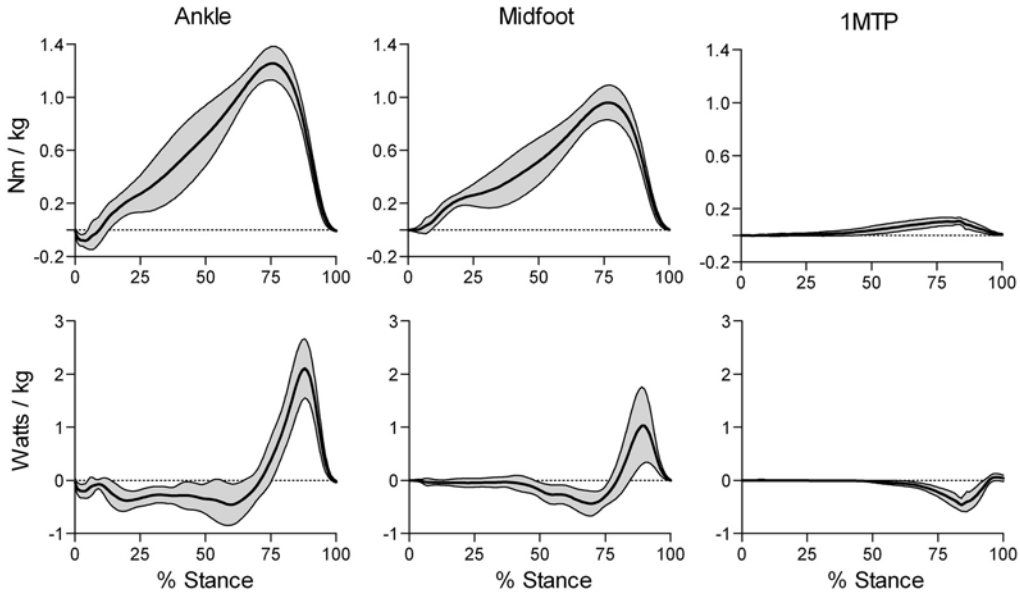

Figure: Ankle, midfoot, and 1st metatarsal-phalangeal (1MTP) ensemble average sagittal plane kinetics. Top row: plantarflexion (+) / dorsiflexion (-) moments; Bottom row: power generation (+) / absorption (-). (Mean ± stdev, n=17).

PEOPLE WALKING ON TREADMILLS CONTROL SPEED, NOT POSITION

[1] Joseph P. Cusumano, [1] Joby John, [2] Jonathan B. Dingwell
[1] Department of Engineering Science & Mechanics, Penn State University, State College, PA
[2] Nonlinear Biodynamics Lab, Department of Kinesiology, University of Texas, Austin, TX
E-mail: jpcusumano@psu.edu

INTRODUCTION

While both the vestibular and proprioceptive systems are known to be involved in the regulation of walking, visual optic flow has a dominant influence [1,2]. Altering visual optic flow induces changes in average preferred walking speeds [2]. However, it is not known how optic flow is used to control movements from each step to the next.

When subjects walk on a motorized treadmill in a static visual environment, they could try to maintain *exactly* the same scene (i.e., "absolute position control") at each consecutive step. Conversely, they could try to minimize optic *flow* at each step, such that they do not try to control small *changes* in the visual scene, but rather strive to make it stop *moving* (i.e., "speed control"). On average, these two strategies yield the same outcome: i.e., walking with the same average speed as the treadmill will keep the subject in the same average position. However, we demonstrate here that these two control strategies predict very different patterns of stride-to-stride *fluctuations* and show that humans adopt speed control, not position control.

METHODS

Seventeen healthy volunteers (age 18-28) walked on a level treadmill (Woodway USA) at their preferred speed. 3D movements of their feet were recorded continuously for 2 trials of 5 min each and used to compute stride times and lengths, T_n and L_n, for each stride, n.

Detrended fluctuation analysis (DFA) [3] was used to calculate stride-to-stride scaling exponents, α for stride speed S_n and treadmill absolute position D_n time series (Fig. 1). Uncorrelated white noise has α = 0.5, and α = 1.5 indicates Brownian motion. Values of α > 0.5 indicate statistical persistence (deviations likely go uncorrected over consecutive strides, indicating weak control), whereas α < 0.5 indicates antipersistence (deviations likely are corrected rapidly, indicating strong control).

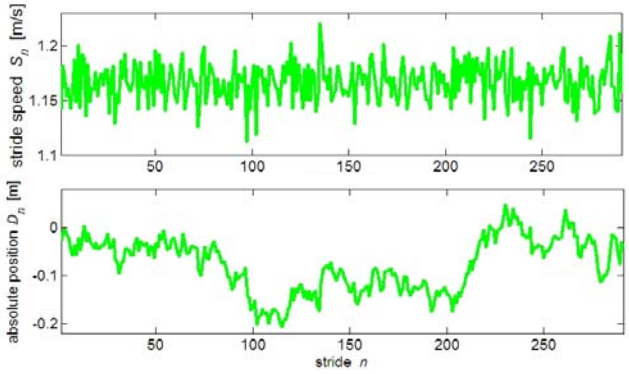

Figure 1: Typical time series for stride speed S_n (top) and stride absolute position D_n (bottom). The D_n data exhibits substantial statistical persistence, whereas the S_n data does not.

Walking on a treadmill with belt speed v simply requires that one stay on the treadmill. The absolute position after stride n is given by

$$D_n = \sum_{k=1}^{n} L_k - vT_k \,, \qquad (1)$$

where $[T_n, L_n]$ represent stride time and length, respectively. Any sequence $[T_n, L_n]$ for which $|D_N| < K/2$, where N is the total number of strides in a given trial and K is the length of the treadmill, will accomplish the task. Specific strategies are formulated using *goal functions* [4], F, which, when set to zero, provide a hypothesis on the strategy actually used for task execution. The absolute position satisfies $D_{n+1} = D_n + L_n - vT_n$, so we consider goal functions of the form

$$F = L_{n+1} - vT_{n+1} + cD_n \,, \qquad (2)$$

in which c is either 0 or 1, $[L_{n+1}, T_{n+1}]$ are viewed as controlled variables, and cD_n specifies the performance "target". The case c = 1 corresponds to *absolute position control*: subjects attempt to choose $[L_{n+1}, T_{n+1}]$ so that $F = D_{n+1} = 0$. The c = 0 case corresponds to *speed control*: the current absolute position is ignored, and the controller attempts to set $L_{n+1} - vT_{n+1} = 0$, so that the stride speed $S_{n+1} = L_{n+1}/T_{n+1} = v$.

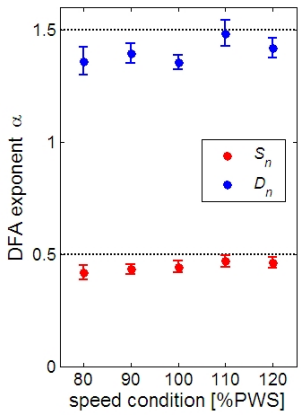

Figure 2: Experimental DFA exponents for stride speed (blue) and absolute stride position (red) showing that S_n is antipersistent, suggesting speed control, whereas D_n is persistent, suggesting no control. Error bars are 95% confidence intervals.

Stochastic control models [5] of the form

$$\mathbf{x}_{n+1} = \mathbf{x}_n + (I + N)\mathbf{u}(\mathbf{x}_n) + \boldsymbol{\eta}, \qquad (3)$$

were constructed, where $\mathbf{x}_n = [T_n, L_n]^T$, $\mathbf{u}(\mathbf{x}_n) = [u_1, u_2]^T$ was a vector of control inputs, N was multiplicative (motor output) noise, and $\boldsymbol{\eta}$ was additive (sensory and/or perceptual) noise. The controllers were found by minimizing the expected value of the cost function

$$C = \alpha F^2 + \beta p^2 + \gamma u_1^2 + \delta u_2^2, \qquad (4)$$

where the first term penalized error as specified by F, the second term penalized the distance, p, of the current state from the preferred operating point (POP), $[L^*, T^*]$, and the last two terms penalized the control inputs, $\mathbf{u} = [u_1, u_2]^T$.

RESULTS AND DISCUSSION

The absolute position time series D_n obtained in the experiments visibly exhibited strong persistence (Fig. 1, bottom), whereas the stride speed S_n appeared to have very low persistence (Fig. 1, top). This observation was confirmed quantitatively by the DFA results, which showed that across all conditions the scaling exponent for absolute position $\alpha(D_n) \approx 1.40$, corresponding to strong persistence approaching Brownian motion, whereas for the stride speed $\alpha(S_n) \approx 0.44$, indicating antipersistence. This suggests that it is speed, not position that is controlled.

This interpretation was supported by the simulations from the optimal control models (Eq. 3). Speed control (c = 0 in Eq. 2) gives D_n time series that mirror those observed in the experiments (Fig. 3). However, position control (c = 1 in Eq. 2) gives behaviors that are entirely different. Thus, the hypothesis that humans control speed while walking on a treadmill is supported The hypothesis that humans control absolute position is rejected.

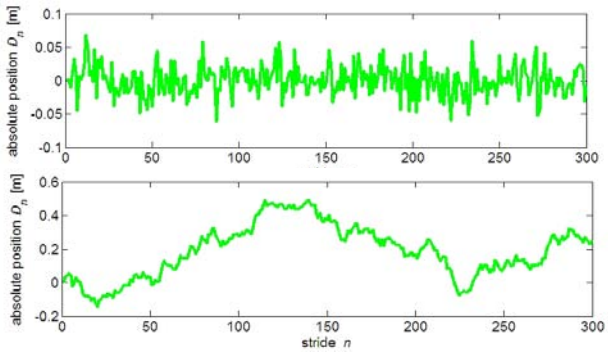

Figure 3: Typical simulated absolute position (D_n) time series from optimal control models (Eqs. 3 and 4): (top) position control (c = 1 in Eq. 2) with $\alpha \approx 0.44$; (bottom) speed control (c = 0 in Eq. 2) with $\alpha \approx 1.48$. Compare both to Fig. 1 (bottom).

CONCLUSIONS

Both speed and position control could be used to successfully walk on a treadmill. Indeed, based on average behavior alone it is impossible to distinguish between them. However, our analysis of stride-to-stride fluctuations has unequivocally demonstrated that humans use speed, and not position, to regulate walking. These results show that hypotheses on specific movement strategies formulated using goal functions, together with relatively simple stochastic optimal control models, allow one to successfully distinguish different movement regulation strategies.

REFERENCES

[1] Warren WH, et al., *Nature Neuroscience*, **4**(2): 213-216, 2001.
[2] Mohler B, et al., *Experimental Brain Research* **181**(2): 221-228, 2007.
[3] Peng C.-K. et al., *Nature*, **356**: 168-170, 1992.
[4] Cusumano JP & Cesari P, *Biological Cybernetics*, **94**: 367-379, 2006.
[5] Ogata, K. *Discrete-Time Control Systems* (2nd ed.). Prentice Hall. 1995.

ACKNOWLEDGEMENTS

Funded by Whitaker #RG-02-0354 (to JBD), NIH # EB007638 (to JBD), and NSF #0625764 (to JPC).

Three-dimensional Position Capture Of The Lower Extremity Mechanical Axis Alignment Correlates Significantly With Radiographical Measurement In Patients With Symptomatic Knee OA.

[1]Judy L. Foxworth and [2]Jordan B. Renner

[1]Winston Salem State University, Winston-Salem, NC, USA
[2]University of North Carolina, Chapel Hill, NC, USA
email: foxworthj@wssu.edu, web: http://www.biodynamicslab.org

INTRODUCTION

Osteoarthritis (OA) is the most prevalent form of arthritis affecting more than 27 million Americans [1] with the knee the most affected weight-bearing joint [2]. Static alignment of the lower extremity is used to determine the load distribution of the knee. The mechanical axis alignment (MAA) refers to the angle formed by a line drawn from the center of the femoral head to the center of the femoral intercondylar notch and a line drawn from the center of the tibial spines to the center of the ankle joint [3]. MAA is typically measured from frontal plane full length standing radiographs of the lower extremity. The purpose of this study was to determine if static standing measurements utilizing a three-dimensional motion capture system could estimate the MAA as compared to the gold standard (full length standing radiographs).

METHODS

Participants self-identified the more symptomatic knee, and all testing was performed on that knee. Participants completed self-report measures including the Western Ontario and McMasters Universities Osteoarthritis Index (WOMAC) and baseline visual analog scale (VAS) for current knee pain. In order to be eligible for the study, participants needed to report knee pain on most days, have a WOMAC pain subscore of 4 or more, report moderate pain on at least 1 listed activity in the WOMAC and demonstrate radiographic evidence of knee OA in the test knee (Kellgren-Lawrence (K-l) grading scale = 1 to 4).

Radiographic Exam: An anterior-posterior weight-bearing knee radiograph was used to identify presence of tibiofemoral OA. The participant's knee was flexed to 15 degrees, and the beam was centered on the joint space. Severity of tibiofemoral OA was measured using the K-L grading scale Participants with K-L score of 1 to 4 were eligible for the study.

Participants also completed a standardized full length lower extremity weight-bearing radiograph. The participant stood with equal weight on both lower extremities without footwear, positioned so that the tibial tubercles faced forward and the midheel and second digit of each foot were aligned with pieces of tape placed perpendicular to the frontal plane. The x-ray beam was centered on the test knee at a distance to allow visualization of the hip and foot. The same physician determined the K-L grade and measured the MAA of all participants.

Three-dimensional position capture: Participants performed standing static trials in bare feet. Participants were positioned with feet shoulder width apart and toes pointed forward. Passive reflective markers were placed by the same researcher on the following boney landmarks: sacrum, bilateral ASIS, mid thigh, medial and lateral epicondyle of the femur, mid tibia, medial and lateral malleolus, heel, and 2nd head of the metatarsal. Marker data was captured using ViconPeak motion analysis system and software (ViconPeak Performance Inc, Denver, CO). Eight infrared cameras recording at 60 Hz captured the position of the reflective markers during two 2-second trials. The average hip-knee-ankle (AVGHKA) angle was determined by Kin-Calc formula (Peak Performance) and defined as the angle between the hip joint center to the knee joint center, and a line from the knee joint center to the ankle joint center. Joint centers were determined by dividing half the distance between medial and

lateral markers taking into account the size of the marker.

All statistical computations were performed using SPSS 16.0 software (SPSS, Inc, Champaign, IL). Central tendencies were used to describe the sample. Simple linear regression was used to determine the correlation between the mechanical axis alignment as measured by radiograph (MAA) and the average hip-knee-ankle angle (AVGHKA) as measured by three-dimensional position capture.

RESULTS AND DISCUSSION

Thirty-nine individuals (26 females and 13 males) with varying knee OA severity (K-L grade 1 = 13; 2 = 4; 3 = 13 and 4 = 9) and mean BMI = 31.4 (29.4 – 33.3 CI) participated in this study. Intrarater reliability of radiographic measurement of the mechanical axis of the knee was very good (ICC = .98 - .99). A significant correlation was found between MAA and AVGHKA (R =.683, $p < .001$, Fig. 1). The MAA as measured on radiographs ranged from 11° valgus to 19° varus. The AVGHKA angle ranged from 11° valgus to 14° varus.

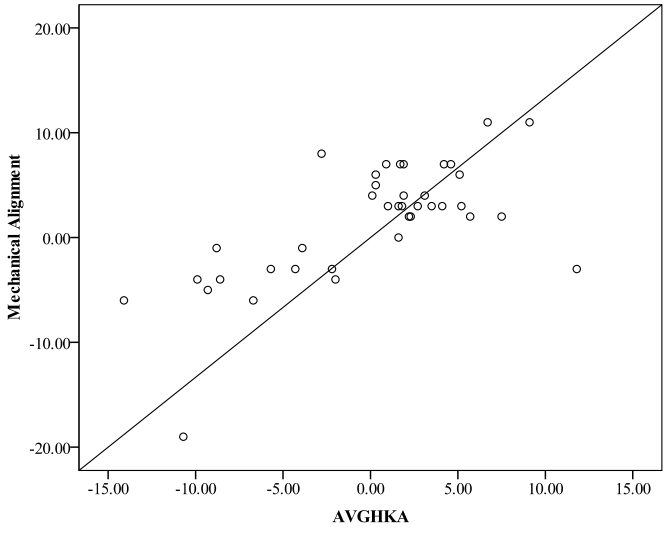

Figure 1: Mechanical axis alignment from radiographs (mechanical alignment) are moderately correlated with 3-D position capture (AVGHKA). Solid line depicts regression line.

The 3D position capture method was able to explain 47% of the variance in the mechanical axis alignment as measured by radiographs (R^2=.469; $p < .001$). The strength of the relationship found in this study between the two methods of mechanical axis measurement was not as strong as previously reported [4]. This may be a result of slightly higher BMI, the addition of valgus knee deformities and smaller sample size in the current study.

CONCLUSIONS

Three-dimensional position capture method of measuring lower extremity mechanical axis alignment in those with symptomatic knee OA is moderately correlated with the gold standard of radigraphically measured alignment. For those who routinely perform 3-D gait analysis, the position capture method is advantageous because it is time and cost effective as well and eliminates exposure to radiation for the subject. Further research with this new method needs to be performed using those with valgus knee alignment.

REFERENCES

1. Helmick CG, Felson DT, Lawrence RC, et al. *Arthritis & Rheumatism.*58 (1):15-25, 2008.

2 Messier S, Paul D, Cowan R, Seay J, Young H, Marsh A. *Arch Phys Med Rehabil.* April 86:703-709, 2005.

3.Kraus V, Vail TP, Worrell T, McDanial G. A *Arthritis & Rheumatism.* 52(6):1730-1735, 2005.

4. Mundermann A, Dyrby CO, Andriacchi TP. *The Knee.* 15:480-485, 2008.

ACKNOWLEDGEMENTS

This study was funded by the Winston Salem State University Research Initiative Program.

A COMPARISON OF EXPERIMENTAL AND SIMULATED PATELLOFEMORAL CONTACT MECHANICS BEFORE AND AFTER TROCHLEAR OSTEOTOMY

[1,2]Craig Bennetts, [2,3]Stephen Fening, [2,4]Robb Colbrunn, [3]Jack Andrish and [1,2]Ahmet Erdemir

[1]Computational Biomodeling Core, Departments of [2]Biomedical Engineering, and [3]Orthopaedic Surgery, and [4]BioRobotics and Mechanical Testing Core, Cleveland Clinic, Cleveland, OH, USA
e-mail: bennetc2@ccf.org, web: http://www.lerner.ccf.org/bme/cobi

INTRODUCTION

Femoral trochlear dysplasia is a morphological abnormality that can lead to patellar instability and dislocation [1]. A trochlear osteotomy, which raises the anterior surface of the lateral femoral condyle, is a viable intervention to prevent lateral patellar dislocation [2]. However, its effect on patellofemoral contact mechanics has not been established. This information will provide valuable clinical feedback to ensure that the procedure does not adversely affect the patellofemoral mechanics.

Finite element analysis (FEA) provides the capacity to evaluate patient-specific patellofemoral mechanics [3] and understand the influence of trochlear osteotomy on patellofemoral contact. Nevertheless, confidence in FEA results need to be established through comparison with experimental measurements. The goal of this study is to explore the credibility of FEA against a preliminary cadaver experimentation, where contact pressures can be measured before and after trochlear osteotomy.

METHODS

Experiments were performed using a non-pathological cadaveric knee from a 70 year old male. The procedures included magnetic resonance (MR) imaging of the knee at full extension (Orthone, ONI Medical Systems, Inc., Wilmington, MA) followed by mechanical testing of the patellofemoral joint (Rotopod R2000, Parallel Robotic Systems Corp., Hampton, NH). Holes were drilled on the tibia, femur and patella for registration between model and experimental tibiofemoral pose. A pressure sensor (K-Scan sensor 5051, Tekscan Inc., South Boston, MA) was placed between cartilage surfaces of the patella and femur to measure the contact pressure distribution. The femur was fixed to a stationary frame and the tibia to a moving platform. The quadriceps tendon was attached to a linear actuator using a freeze clamp.

Two tests were performed at approximate tibiofemoral flexion of 0° and 15°, at which the surgical correction is targeted to engage. At each angle, a quadriceps load was applied in 100 N increments, up to 600 N. At each increment, the reference hole locations and pressure sensor were manually digitized (Microscribe G2L, Immersion Corp, San Jose, CA) and the patellofemoral contact pressure distribution was recorded. All testing procedures were repeated before and after trochlear osteotomy. The surgical procedure was performed by cutting and raising the lateral side of the anterior femoral chondyle with an allograft bone wedge.

Finite element models of the patellofemoral joint were developed from the pre- and post-operative MR images. The models included the tibia, femur, femoral cartilage, patella, patellar cartilage and patellar tendon. Bones were modeled as rigid shells, cartilage was elastic [3], and the patellar ligament and quadriceps tendon were hyperelastic, with properties obtained from [4] . Frictionless contact between patellar and femoral cartilage was defined. The tibia was held fixed. The simulation included two steps: prescription of tibiofemoral kinematics and application of a 600 N quadriceps load. Contact pressures distributions between the femoral and patellar cartilage were extracted from the simulations.

For comparisons between model predictions and experimental data, various contact variables were derived from contact pressure distributions. These included total contact force, contact area, mean pressure, and peak pressure.

RESULTS AND DISCUSSION

Due to discrepancies in measured reference hole locations in images and during testing (> 5 mm), implementation of exact experimental tibiofemoral

kinematics in the models was not possible. Simulations at 0° tibiofemoral flexion were assumed to be the joint state during imaging. For 15° flexion, the femur was rotated about its epicondylar axis.

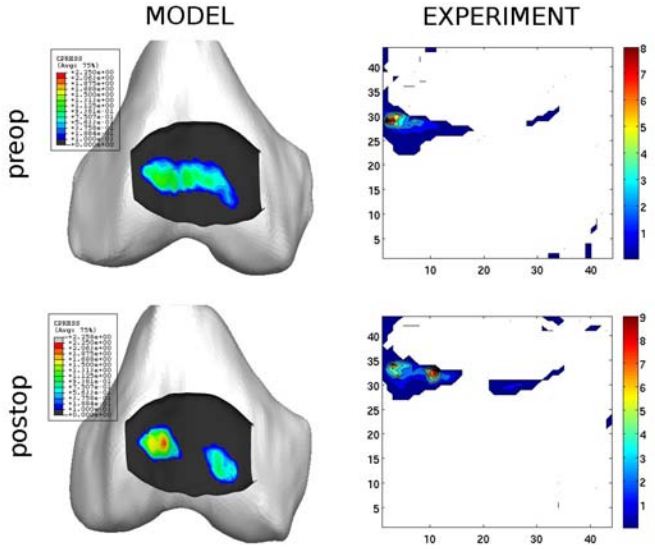

Figure 1. Contact pressures (MPa) for 0° tibiofemoral flexion at a quadriceps load of 300 N.

Trochlear osteotomy altered the contact pressures, as observed experimentally and predicted by modeling (Figure 1). Model predicted contact forces are similar pre- and post-operatively, but post-operative experimental forces are higher at 0° flexion (Figure 2). Relocation of patella due to surgery may affect the transmitted load. In experiments, joint angles were approximated, which may not be exactly the same, pre- and post-surgically. After osteotomy, contact area decreased experimentally at 15° flexion; for FEA this decrease was apparent at both joint angles. This may likely be the result of curvature change of the femoral cartilage, which caused redistribution of loading to two separate regions (Figure 1). As a consequence, mean and peak contact pressures both increased, as was measured by the experiments and predicted by FEA.

Our analysis suffered from many modeling assumptions, e.g. estimated tibiofemoral pose and orientation, and experimental limitations, i.e. sensor saturation and testing a non-pathological knee. Nonetheless, this preliminary study illustrates the potential of FEA for the evaluation of patient-specific patellofemoral surgery in regards to contact mechanics. Future experimentation and modeling studies to address current limitations of our procedures and to establish patient-specific FEA as a decision-making tool for patellofemoral joint care.

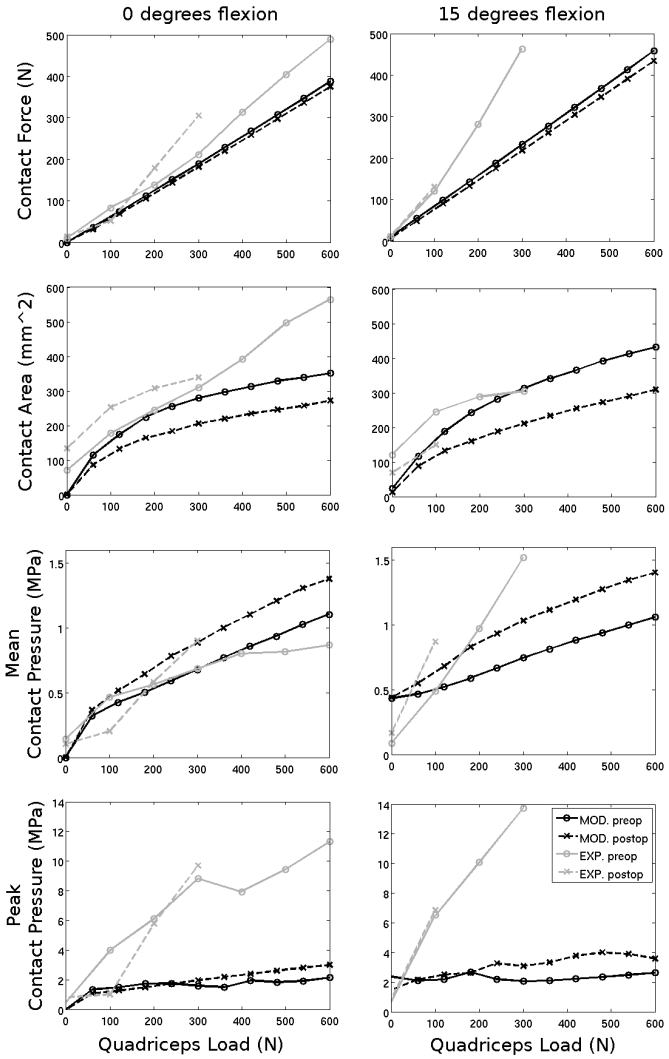

Figure 2. Contact variables versus quadriceps loading for the pre- and post-operative measurements and simulations. Experimental data points at which pressure sensor saturated (>15.28 MPa), are not shown.

REFERENCES

1. Pfirrmann et al. *J Radiology* 216, 858-64, 2000.
2. Koëter et al. *Knee Surg Sports Traumatol* Arthrosc, **15**, 228-232, 2007.
3. Besier et al. *Med Sci Sports Exerc*, **37**, 1924-1930, 2005.
4. Reeves et al. *J Physiol*, **548**, 971-981, 2003.

ACKNOWLEDGMENTS

This study was funded by the Shalom Foundation. The authors acknowledge Dr. John Elias and Dr. J. J. Stefancin for their initial contribution.

COMPARISON OF BILATERAL KINEMATICS AND KINETICS DURING SIT-TO-STAND AND STAND-TO-SIT BETWEEN HEALTHY SUBJECTS AND UNILATERAL KNEE OSTEOARTHRITIS PATIENTS

[1]David R. Burnett, MS, [2]Naira H. Campbell-Kyureghyan, PhD, [3]Robert V. Topp, PhD, [1]Peter M. Quesada, PhD

[1]Speed School of Engineering, University of Louisville; [2]College of Engineering and Applied Science, University of Wisconsin-Milwaukee; [3]School of Nursing, University of Louisville
email: drburn02@gwise.louisville.edu

INTRODUCTION

Common, yet essential, activities of daily living include the ability to rise from a seated position (sit-to-stand; SitTS) and sit from a standing position (stand-to-sit; StandTS), and these functions often precede or follow walking [1]. However, unlike studies of gait which have garnered a large amount attention, evaluations of SitTS and StandTS are more limited. While there is a moderate amount of literature concerning bilateral symmetry during SitTS, our knowledge is limited with respect to healthy or symptomatic individuals during StandTS. Additionally, even fewer studies have evaluated bilateral symmetry among subjects with joint pathologies such as knee osteoarthritis during SitTS and StandTS. The objective of this study is to quantify and compare bilateral kinematics and kinetics during SitTS and StandTS in healthy subjects and unilateral knee osteoarthritis (UKOA) patients.

METHODS

11 UKOA patients and 12 healthy controls participated in the study and signed the IRB approved consent form prior to participation. Demographic information is shown in Table 1. Reflective markers were placed in a modified Helen Hayes arrangement and marker spatial coordinates were obtained at 100 Hz with a Hawk Motion Tracking System (Motion Analysis Corp.). A force plate (Bertec Corp.) recorded ground reaction force at 1000 Hz. Subjects were instructed to rise and sit from an armless and backless bench at a comfortable pace with their arms at their sides in a natural position (Figure 1).

Figure 1: Marker arrangement and bench used to evaluate SitTS and StandTS

Differentiation between SitTS and StandTS phases was determined by examining the trunk vertical velocity (VEL_{TR}) as estimated by the offset marker. Since subjects started from a seated position, VEL_{TR} was initially 0 mm/s. Subsequently, VEL_{TR} would quickly increase and then decrease during completion of the SitTS phase until it ultimately settled around 0 mm/s, at which time the StandTS phase would commence and continue until VEL_{TR} once again reached 0 mm/s when the subject returned to the seated position. UKOA patients performed three full trials (SitTS & StandTS) with the affected (A) leg on the force plate and one trial with the non-affected (NA) leg on the force plate. Healthy subjects performed three trials each with their dominant (D) and non-dominant (ND) leg on the force plate. Sagittal plane kinematic variables included hip and knee angle maximum values and ranges of motion (ROM). Peak vertical ground reaction forces (VGRF) and flexion moments of the hip and knee were included in the kinetic analyses. A symmetry index (SI) was calculated by dividing the values for the A or ND side by the NA or D side, and a

value of 1 indicated perfect symmetry. Statistical differences between bilateral parameters were determined with t-tests (α=0.05).

RESULTS AND DISCUSSIONS

There were no statistically significant differences between parameters for the ND and D lower extremities among healthy individuals during SitTS and StandTS (Table 1). Sadeghi et al. [2] suggest that symmetry is achieved if no statistical differences exist between parameters that are measured bilaterally. Thus, SitTS and StandTS tasks in asymptomatic subjects can be considered symmetrical with respect to VGRF and kinematics and kinetics of the hip and knee. Jevsevar et al. [3] and Schenkman et al. [4] reported similar findings for sagittal plane kinematics and kinetics and VGRF during SitTS while this study is the first to report such findings during StandTS.

As can be seen in Table 1, all SI values for UKOA patients during SitTS and StandTS were less than 1 which signifies that the values for the A side were smaller than the NA side. These differences were statistically significant for hip and knee flexion ROM, VGRF, and peak knee moment. Essentially, it appears that the UKOA patients attempted to minimize lower extremity motion in their A limb and rely more on their NA limb to perform the SitTS and StandTS tasks. While evaluating only SitTS among UKOA patients, Su et al. [5] reported significant differences in hip and knee joint motion between the A and NA limbs while Mizner et al. [6] recently found significant differences between the A and NA limbs with respect to VGRF and peak knee moments. However, the current study is the first to report these findings during the StandTS phase in addition to SitTS.

A limitation of the current study is that healthy subjects and UKOA patients were not age or gender matched. Future studies could consider implementation of similar data collection techniques to assess bilateral biomechanical symmetry during SitTS and StandTS among a group of older individuals without UKOA.

CONCLUSIONS

Healthy subjects did not display any bilateral differences in kinematics and kinetics of the lower extremities during SitTS or StandTS while individuals with UKOA exhibited significant asymmetry in hip flexion ROM, VGRF, and knee flexion ROM and moments.

REFERENCES

1. Kralj A, et al., *J Biomechanics.* **30:**1123-1138, 1990.
3.Sadeghi H, et al., *Gait & Posture*. **12:**34-45, 2000.
3. Jevsevar D, et al., *Phys. Ther.* **73:**229-239, 1993.
4. Schenkman M, et al., *Phys. Ther.* **70:**638-648, 1990.
5. Su F, et al., *Clin. Biom.* **13:**176-181, 1998.
6. Mizner et al., *J. Ortho. Res.* **23:**1083-1090, 2005.

Table 1: Subject demographics and summary of biomechanical symmetry during SitTS and StandTS

							Symmetry Index						
	Demographics						Kinematics				Kinetics		
		Age (yr)	Height (cm)	Weight (kg)	Task		Peak hip flexion	Peak knee flexion	Hip flexion ROM	Knee flexion ROM	VGRF	Peak hip moment	Peak knee moment
Healthy	AVG	23.7	173.1	75.9	SitTS	AVG (SD)	0.991 (0.03)	0.998 (0.06)	0.995 (0.03)	1.026 (0.07)	1.038 (0.24)	1.099 (0.24)	0.896 (0.51)
						p	0.573	0.925	0.525	0.251	0.752	0.964	0.179
	SD	1.2	11.7	18.6	StandTS	AVG (SD)	1.002 (0.04)	0.997 (0.05)	1.003 (0.04)	1.029 (0.09)	1.035 (0.26)	1.059 (0.29)	1.014 (0.61)
						p	0.624	0.492	0.526	0.149	0.810	0.846	0.295
UKOA	AVG	63.0	170.8	99.9	SitTS	AVG (SD)	0.975 (0.05)	0.984 (0.07)	0.915 (0.07)	0.896 (0.11)	0.794 (0.12)	0.971 (0.36)	0.612 (0.19)
						p	0.585	0.641	*0.033**	*0.008**	*0.001**	0.994	*0.009**
	SD	10.0	11.3	16.4	StandTS	AVG (SD)	0.970 (0.04)	0.988 (0.06)	0.913 (0.06)	0.898 (0.09)	0.784 (0.17)	0.989 (0.42)	0.513 (0.24)
						p	0.497	0.756	*0.033**	*0.009**	*0.001**	0.929	*>0.001**

* Significant difference between A and NA limbs

Increase Patellofemoral Joint Stress with Internal Femoral Rotation: A Finite Element Analysis

Nicholas H. Yang[1], Kai-Yu Ho[1], Shawn Farrokhi[2], Christopher M. Powers[1]

[1]University of Southern California, Los Angeles, CA, USA
[2] University of Pittsburgh, Pittsburgh, PA, USA
email: powers@usc.edu, web: http://pt.usc.edu/labs/mbrl

INTRODUCTION

Disorders of the patellofemoral joint (PFJ) are among the most common and clinically challenging conditions encountered in orthopedic practice. Patellofemoral pain (PFP) affects a wide range of individuals, with higher incidence rates among women and those who are physically active.[1] The most commonly cited hypothesis as to the cause of PFP is related to abnormal patella alignment and/or tracking, which increases patellofemoral joint stress and subsequent articular wear.[2] Recent studies have shown that altered PFJ kinematics is the result of abnormal femoral internal rotation as opposed to abnormal patellar motion.[3] Internal rotation of the femur with respect to the patella has been shown to decreases the contact area and increases the stress at the patellofemoral joint in cadaver knees.[4] The objective of this pilot study was to compare the contact area, hydrostatic pressure and octahedral shear stress at the patella cartilage surface and at the cartilage-bone interface at 15 and 45° of knee flexion at different degrees of internal rotation of the femur.

METHODS

Subject-specific PFJ geometry of a female with PFP was obtained from high-resolution, sagittal plane MR images acquired with a 3.0 T MR scanner (General Electric Healthcare). Weight-bearing PFJ kinematics was acquired using sagittal plane MR sequence while the knee joint was loaded with 25% of body weight at 15 and 45° of knee flexion. Quadriceps muscle morphology was assessed from thigh MR images in coronal and axial planes. For biomechanical testing, lower extremity kinematics were collected using a Vicon (Oxford Metrics LTD.) 8-camera motion analysis system at 60 Hz. Ground reaction forces were recorded at 1560 Hz using 2 AMTI force plates. EMG signals of knee musculature were recorded at 1560Hz, using pre-amplified, bipolar, surface electrodes (Motion Lab Systems).

Input parameters for the FE model included: 1) joint geometry, 2) weight-bearing PFJ kinematics, and 3) quadriceps muscle forces (Fig. 1). The PFJ geometry was manually segmented on high-resolution MR images and the FE mesh of cartilage and bone was created using FE pre-processor (Hypermesh, Altair Engineering Inc.). The FE mesh was then registered to the position of each structure in the weight-bearing MR images. To estimate quadriceps forces, a previously described subject specific model of the PFJ was used.[5]

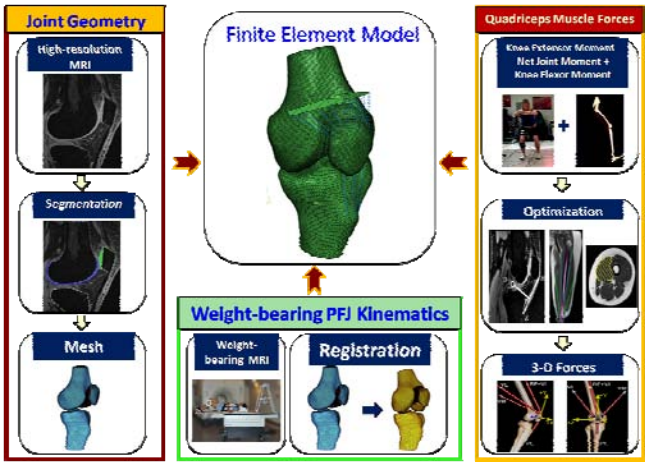

Figure1: Pipeline of patellofemoral joint FE model.

Quasi-static loading simulations were performed using a nonlinear FE solver (Abaqus, SIMULIA). Bone was modeled as rigid and the cartilage of the patella and femur was modeled as homogeneous isotropic tetrahedral continuum elements (elastic modulus of 4 MPa and Poisson ratio of 0.47). Quadriceps muscles were divided into 3 functional groups (rectus femoris/vastus intermedius, vastus medialis, and vastus lateralis) made up of 6 equivalent uniaxial connector elements. Patellar tendon was modeled as six uniaxial, tension-only

elements with stiffness of 4334 N/mm. Simulation were performed at 15 and 45° of knee flexion at 0 (neutral), 5 and 10° on internal femoral rotation. Since the soft tissues controlling the rotation of the patellofemoral joint were not included in the current model (i.e., ligaments and peripatellar retinaculum), the 3 rotational degrees of freedom of the patella were constrained.

RESULTS AND DISCUSSION

The hydrostatic pressure increased on the lateral facet of the patella with greater internal rotation of the femur (Fig. 2). Increased internal rotation led to decrease in contact area at the patellofemoral joint and increase in the peak hydrostatic pressure and octahedral shear stress at the cartilage surface and the cartilage-bone interface at both 15 (Table 1) and 45° (Table 2) of flexion.

Besier et al.[6] has reported that femoral rotation with the knee flexed at 60° increased PFJ stresses in one-third of their subjects. However, when simulating internal rotation, the patella was allowed to move with the femur. Kinematic MRI studies have shown the patella does not move with the femur as it rotates.[6] The results warrant further research over a larger group to determine the role of internal femur rotation on the contact area and stresses at the patellofemoral joint.

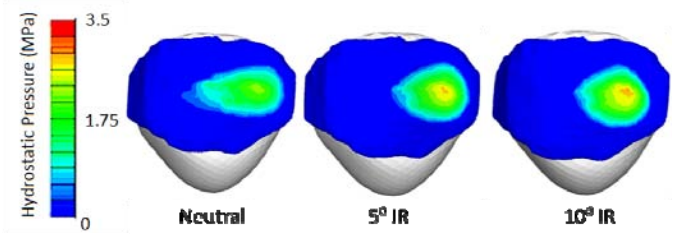

Figure 2: Hydrostatic pressure distribution at the patella cartilage surface at knee flexion of 45°.

REFERENCES

1. Almeida SA, et al. *Med Sci Sports Exerc* **31**, 1807-1812, 1999.
2. Fulkerson JP, et al. *Disorders of the patellofemoral joint*. Lippincott Williams & Wilkins, 2004.
3. Powers CM, et al. *J Orthop Sports Ther* **33**, 677-685, 2003.
4. Lee TQ, et al. *J Orthop Sports Phys Ther* **33**, 686-693, 1994.
5. Chen YJ, et al. *J Appl Biomech*, in press, 2010.
6. Besier TF, et al. *J Orthop Res* **26**, 1627-1635, 2008.

Table 1: Peak hydrostatic pressure and octahedral shear stress at the cartilage surface and cartilage-bone interface at 15° of knee flexion at different values of internal rotation of the femur

		Cartilage Surface		Cartilage-Bone Interface	
Internal Rotation	**Contact area (mm^2)**	**Hydrostatic Pressure (MPa)**	**Octahedral Shear Stress (MPa)**	**Hydrostatic Pressure (MPa)**	**Octahedral Shear Stress (MPa)**
Neutral	110	0.80	0.54	1.05	0.52
5°	72	0.91	0.63	1.27	0.58
10°	61	0.96	0.68	1.36	0.70

Table 2: Peak hydrostatic pressure and octahedral shear stress at the cartilage surface and cartilage-bone interface at 45° of knee flexion at different values of internal rotation of the femur

		Cartilage Surface		Cartilage-Bone Interface	
Internal Rotation	**Contact area (mm^2)**	**Hydrostatic Pressure (MPa)**	**Octahedral Shear Stress (MPa)**	**Hydrostatic Pressure (MPa)**	**Octahedral Shear Stress (MPa)**
Neutral	255	2.41	1.08	2.71	1.19
5°	219	2.92	1.35	3.33	1.37
10°	192	3.02	1.61	3.59	1.48

THE INFLUENCE OF PATELLA CARTILAGE THICKNESS ON PATELLA BONE STRESS IN FEMALES WITH AND WITHOUT PATELLOFEMORAL PAIN

[1]Kai-Yu Ho, [1]Nicholas H. Yang, [2]Shawn Farrokhi, [1]Christopher M. Powers

[1]University of Southern California, Los Angeles, CA, USA
[2] University of Pittsburgh, Pittsburgh, PA, USA
email: kaiyuho@usc.edu, web: http://pt.usc.edu/labs/mbrl

INTRODUCTION

It has been suggested that patellofemoral pain (PFP) is the result of increased pressure on highly innervated subchondral bone. Current literature suggests that individuals with PFP demonstrate thinner cartilage[1] and greater patellofemoral joint (PFJ) stress during functional activities (e.g., walking and squatting) [1,2]. Repetitive overloading of the PFJ is thought to adversely affect the shock absorption ability of articular cartilage thereby leading to subchondral bone damage [3].To date, the influence of patella cartilage thickness on bone stress (i.e. patella) is not fully understood. The purpose of this study was to quantify the influence of patella cartilage thickness on patella stress in persons with and without PFP.

METHODS

Two females with PFP (33.5 ± 5.0 years, 59.7 ± 5.7 kg, 1.65 ± 0.1 m) and 2 female pain-free controls (32.5 ± 5.0 years, 58.9 ± 8.4 kg, 1.64 ± 0.1 m) participated. Each subject underwent 2 data collection sessions: MR assessment and biomechanical testing. Subject-specific PFJ geometry was obtained from high-resolution, sagittal plane MR images acquired with a 3.0 T MR scanner (General Electric Healthcare). Weight-bearing PFJ kinematics were acquired using a separate sagittal plane MR sequence with the knee joint loaded to 25% of body weight at 45° of knee flexion. Quadriceps muscle morphology was assessed from thigh MR images in coronal and axial planes. Cartilage thickness was assessed using an axial plane MR sequence.

For biomechanical testing, subjects were asked to perform squatting at 45° of knee flexion. Lower extremity kinematics were collected using a Vicon (Oxford Metrics LTD.) 8-camera motion analysis system at 60 Hz. Ground reaction forces were recorded at 1560 Hz using 2 AMTI force plates. EMG signals of knee musculature were recorded at 1560Hz, using pre-amplified, bipolar, surface electrodes (Motion Lab Systems).

Input parameters for the FE model included: 1) joint geometry, 2) weight-bearing PFJ kinematics, and 3) quadriceps muscle forces (Fig. 1). The PFJ geometry was manually segmented on high-resolution MR images and the FE mesh of cartilage and bone was created using FE pre-processor (Hypermesh, Altair Engineering Inc.). The FE mesh was then registered to the position of each structure in the weight-bearing MR images. Three-dimensional quadriceps muscle forces were estimated using a previously described subject-specific, EMG driven model [4].

Quasi-static loading simulations were performed using a nonlinear FE solver (Abaqus, SIMULIA). Bone and cartilage of patella and femur were modeled as homogeneous isotropic tetrahedral continuum elements (bone: elastic modulus of 15 GPa and Poisson ratio of 0.3 [5]; cartilage: elastic modulus of 4 MPa and Poisson ratio of 0.47 [1]). The tibia was modeled as a rigid body. Quadriceps muscles were divided into 3 functional groups (rectus femoris/vastus intermedius, vastus medialis, and vastus lateralis) made up of 6 equivalent uniaxial connector elements. Patellar tendon was modeled as six uniaxial, tension-only elements with stiffness of 4334 N/mm [1].The peak compressive stress on the osseous-chondral interface of the bone was output for data analysis.

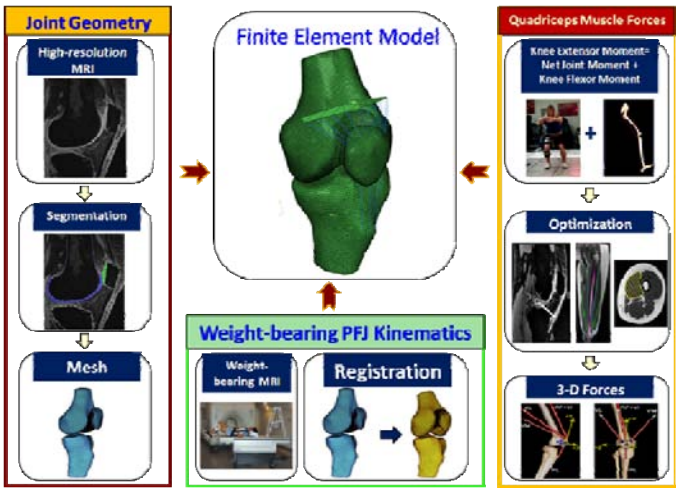

Figure1: Pipeline of patellofemoral joint FE model.

To obtain patella cartilage thickness, the cartilage was manually segmented on axial MR images. The thickness was quantified by computing the perpendicular distance between opposing voxels defining the edges of the patella cartilage. The average patella cartilage thickness obtained from all images was used for data analysis.

RESULTS AND DISCUSSION

Individuals with PFP demonstrated thinner cartilage (2.34 ± 0.16 mm) when compared to the pain-free controls (3.37 ± 0.05 mm) (Fig. 2a). Moreover, PFP subjects showed greater peak compressive patella stress (2.86 ± 0.43 MPa) when compared to the pain-free controls (1.04 ± 0.42 MPa) (Fig. 2b). Additionally, more concentrated stress was observed on the lateral facet in PFP subjects while a more evenly distributed stress pattern was observed in the control subjects (Fig. 3).

Previous literature has reported that bone compressive stress is correlated with bone tissue damage [6]. We hypothesize that the elevated bone stress observed in the current study may contribute to bone tissue injury (i.e. bone marrow lesions) and pain in persons with PFP. Future efforts will focus on increasing the sample size to better understand the influence of patella cartilage thickness on patella stress.

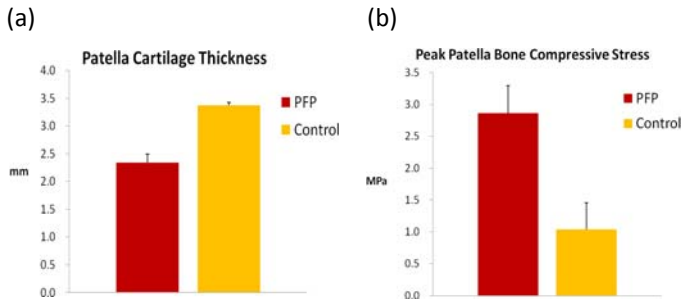

Figure 2: (a) Patella cartilage thickness, and (b) peak patella bone compressive stress of PFP subjects and pain-free subjects.

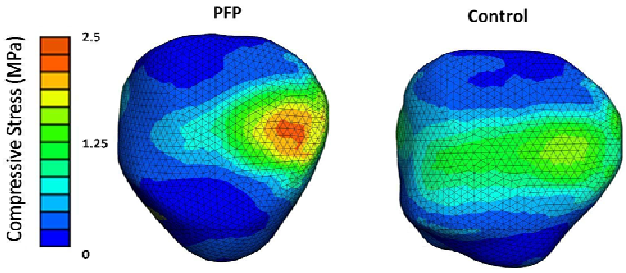

Figure 3: Compressive stress distribution in PFP and control subjects.

REFERENCES

1. Farrokhi S, et al., *Osteoarthritis Cartilage, In Review.*
2. Heino Brechter J & Powers CM. *Med Sci Sports Exerc* **34**: 1582-1593, 2002.
3. Karsdal M, et al. *Osteoarthritis Cartilage* **16**: 638-646, 2008.
4. Chen YJ, et al., *J Appl Biomech*, In Press.
5. Beillas P et al., *J Biomech* **37**: 1019-1030, 2004.
6. Nagaraja S et al., *J Biomech* **38**: 707-716, 2005.

CURVE INFLECTION AND MODIFICATION OF THE ANTERIOR KNEE LAXITY COMPLIANCE INDEX: SPECIFIC VARIABLES TO ASSESS ANTERIOR CRUCIATE LIGAMENT INTEGRITY

[1]Samuel C. Wordeman, [2]Mark V. Paterno, [3]Carmen E. Quatman, [1]Nathaniel A. Bates, and [1,2]Timothy E. Hewett

[1]University of Cincinnati, Cincinnati, OH, USA
[2]Cincinnati Children's Hospital Medical Center, Cincinnati, OH, USA
[3]University of Toledo, Toledo, OH USA
Email: wordemsc@mail.uc.edu

INTRODUCTION

Knee arthrometry is a common, reliable method to assess ACL integrity [1]. Current clinical techniques assess asymmetries in displacement at set arbitrary anterior forces as shown in **Figure 1**. The purpose of this study was to identify measures with greater sensitivity that could be used to assess ACL integrity in healthy (CTRL), ACL deficient (ACLD) and ACL reconstructed (ACLR) athletes.

METHODS

Anterior knee laxity curves were obtained using a CompuKT Knee Ligament Arthrometer from 230 limbs in 115 subjects (ACLD=15, ACLR=60, CTRL=50) by a single, highly reliable clinician (MVP; ICC=0.92). Displacements at 0, 67, 89 and 134 N of anterior force were identified using MATLAB. Linear portions of each curve were identified and the line of best fit was calculated.

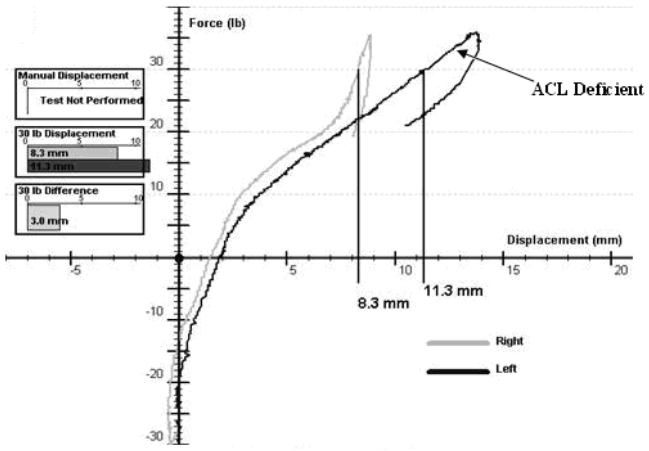

Figure 1: CompuKT laxity curves of ACL deficient and uninjured knee with side-to-side differences measured at 134 Newtons (30 lbf) anterior force.

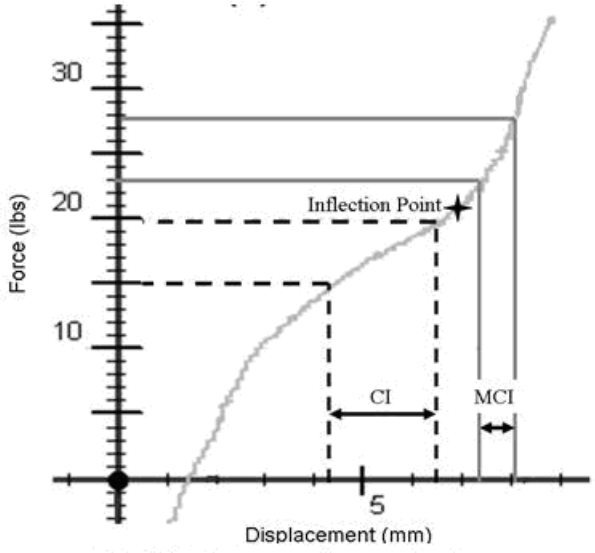

Figure 2: Force-displacement curve with Compliance Index (CI), Modified Compliance Index (MCI), and Inflection Point (┼).

Variables assessed included (1) inflection point, (2) compliance index (CI), and (3) modified compliance index (MCI). These variables are illustrated in **Figure 2**. Inflection point was defined as the point of intersection of the linear portions. CI was defined as the difference in displacements at 67 and 89 N of anterior force [2]. MCI was defined as the compliance of post-inflection stiffness over 22 N. If no inflection point was identified, MCI was defined as the compliance over 22 N. Statistical interactions were evaluated using 3x2 repeated measures ANOVA. A least significant difference test was used for multiple comparisons.

RESULTS AND DISCUSSION

Significant group-side interactions ($p<0.001$) were identified for displacement at inflection, CI, and

MCI. **Figure 3** shows boxplots of distributions by limb for all three subject groups for CI and MCI. Inflection points were identified in all ACLR and CTRL limbs. 40% of ACLD subjects exhibited no inflection on the deficient limb. CI demonstrated significant differences between CTRL and ACLR/ACLD groups ($p<0.0001$), however no differences were found between ACLR and ACLD ($p=0.135$). Post-hoc analyses of MCI demonstrated differences between all groups ($p<0.0001$). MCI > 1mm predicted ACL deficiency with 100% sensitivity (Sn) and 94.3% specificity (Sp) compared to 100% Sn and 58.8% Sp for CI>1. Asymmetry in AP laxity greater than 3mm at 134 N was 60% Sn and 100% Sp. 36.6% of reconstructed limbs had MCI greater than 1mm while 83.3% had CI greater than 1mm and 48.3% had asymmetry greater than 3mm.

The results from this study demonstrate the utility of analyzing arthrometric curve-shapes to better determine the status of the anterior cruciate ligament compared to currently applied criteria. Few studies to date have examined stiffness characteristics in arthrometric curves as a means of cruciate ligament assessment. Our results illustrate the need to take into account a commonly encountered range in arthrometric curves where the tangent stiffness is increasing. In doing so, the discrepancy in distributions between the healthy limbs of each group was vastly decreased. Liu et al conducted a modeling study in which a simulated KT arthrometric curve was obtained [3]. Their results indicated that in the event of a partial ACL tear, analysis of stiffness and rate of change of stiffness may be more sensitive to the condition of the ACL than displacement asymmetries [3]. The current study has adopted this methodology and applied it in a clinical setting while accounting for curve-shape variability from subject to subject, demonstrating the clinical validity of this approach.

CONCLUSIONS

Inflection point and modified compliance index scores of anterior knee laxity curves may serve as simple and accurate clinical diagnostic and outcome variables to assess ACL or graft integrity. The modified compliance index is useful for single leg data and may be more useful than displacement asymmetries in assessment of graft failure.

REFERENCES

1. Wroble RR et al. *Am J Sports Med* **18,** 396-99, 1990.
2. Daniel DM, et al. *Am J Sports Med* **13,** 401-407, 1985.
3. Liu W, et al. *J Biomech Engr* **124**, 294-301, 2002.

ACKNOWLEDGEMENTS

The authors would like to acknowledge funding from NFL Charities, NIH /NIAMS Grants R01-AR049735, R01-AR055563 and R01-AR056259, F32 AR 055844 and Dr. Marepalli B. Rao for his assistance.

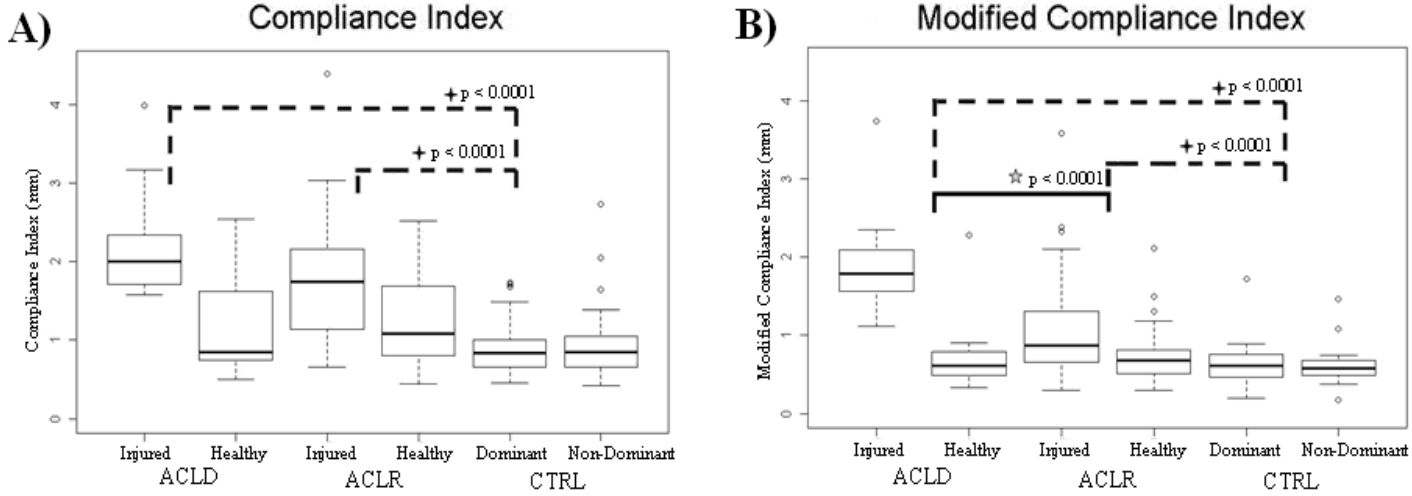

Figure 3:A) The distributions between groups and limbs of shows high variability even within healthy limbs. No significant difference was found between the ACL reconstructed and deficient groups.
B) The modified compliance index vastly reduces the variability between the healthy limbs of each population and demonstrated significant differences between reconstructed and deficient limbs.

PREFERRED FREQUENCY DURING A SIMPLE BOUNCING TASK

Kristen Merritt, Caroline Raburn and Jesse Dean

Medical University of South Carolina, Charleston, SC, USA
email: deaje@musc.edu

INTRODUCTION

Despite musculoskeletal system redundancy, humans tend to prefer stereotyped movement patterns during rhythmic motions such as walking or running. This preference may result from taking maximal advantage of the body's natural mechanics. In support of this idea, during pendular arm swing subjects prefer to move at the resonant frequency, at which small amounts of muscle activity can produce large displacements [1].

In the lower limb, the musculotendon complex crossing the ankle joint can be modeled as a damped mass-spring system [2]. By moving at the resonant frequency, mechanical energy will be stored in the elastic tendon, theoretically reducing the required muscular work.

We hypothesized that subjects will prefer to perform a simple bouncing task at the resonant frequency. We expected that the addition of mass will decrease both the preferred and resonant frequencies, while the addition of parallel stiffness will increase these measures.

METHODS

Six subjects performed a series of 30 second bouncing tasks. Subjects produced a rhythmic bouncing motion with no aerial phase while reclined 60^{o} on an instrumented TotalGym. The motion was powered by the ankle plantarflexors, and the knees were kept fully extended during the task.

Subjects bounced under three mechanical conditions: normal, with added mass (50% body mass), and with added parallel stiffness (3.2 kN/m). For each condition, subjects performed seven trials with bouncing frequency prescribed by a metronome (1, 1.5, 2, 2.25, 2.5, 2.75, 3Hz) and three trials at their preferred frequency. In each trial, subjects were given real-time visual feedback of their smoothed, rectified velocity, and a target level. Therefore, the positive work performed was constant across all trials within each mechanical condition.

We measured ground reaction force (GRF), displacement, and electromyographic (EMG) activity bilaterally from the soleus, medial, and lateral gastrocnemius. The *preferred frequency* for each mechanical condition was calculated from the last 10 seconds of displacement data for each preferred trial. The *resonant frequency* was calculated from the GRF and EMG data during the prescribed frequency trials. GRF and summed, rectified EMG data were smoothed and fit with sine waves. Gain and phase shift from EMG to GRF were then calculated at each prescribed frequency. Subsequently, a simple mechanical model (modified from [2]) was used to fit this data and identify the resonant frequency as that with the largest gain (Fig.1). A two-way repeated measures ANOVA ($p<0.05$) was performed to determine if the mechanical condition had a significant effect on preferred and resonant frequency, and if preferred and resonant frequency were significantly different.

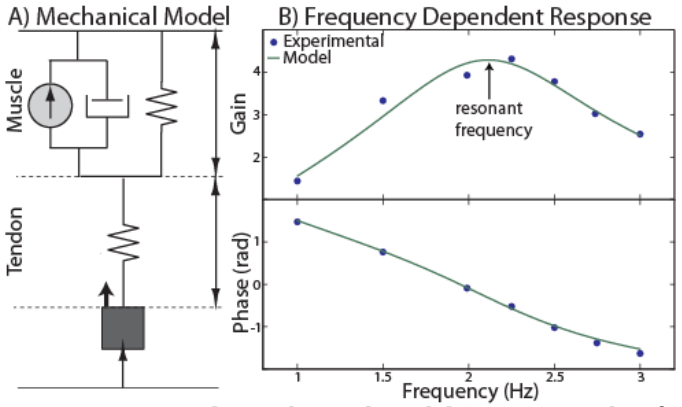

Figure 1. A simple mechanical model (A) was used to fit the EMG→GRF gain and phase values (B), predicting the resonant frequency.

To test the role of feedback in determining the preferred frequency, a single subject participated in an additional experiment. The subject performed preferred frequency trials (with 0, 25%, 50% added mass) before and during peripheral ischemia. Blood flow to the legs was cut off using cuffs inflated around the thighs. Ischemia was judged to be complete once the soleus stretch reflex, monitored using Achilles tendon taps, was eliminated [3].

RESULTS AND DISCUSSION

Contrary to our hypothesis, subjects did not prefer to bounce at the resonant frequency. This finding suggests that matching the body's natural mechanics is not the primary goal underlying the preferred bouncing pattern.

Both the preferred and resonant frequency scaled as expected under varied mechanical conditions. There was a significant main effect ($p=0.009$) of mechanical context on frequency, with added mass decreasing frequency and added stiffness increasing frequency (Fig. 2). However, the preferred frequency was significantly ($p<0.001$) lower than the calculated resonant frequency across mechanical conditions (Fig. 2).

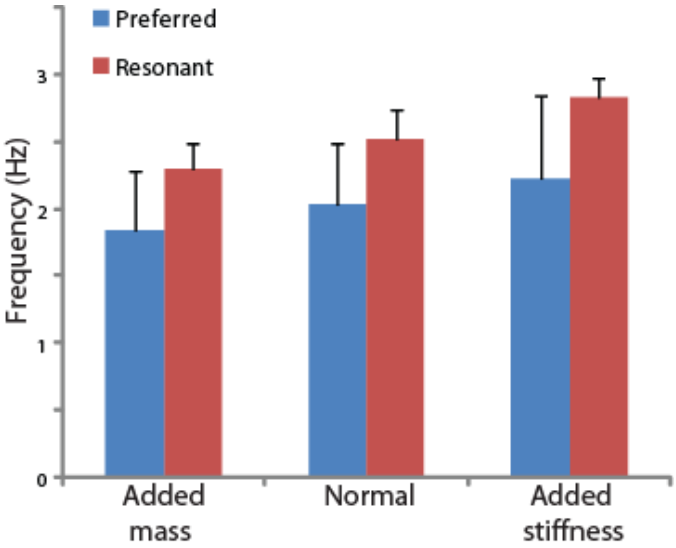

Figure 2. Mechanical condition influenced the movement pattern, while preferred frequency was lower than the resonant frequency.

Rather than matching the resonant frequency, humans may choose their preferred movement pattern by optimizing some other measure. For example, while energetic cost is related to muscular work [4], there is an additional cost of activating muscles at a high rate [5]. Therefore, energetic cost may actually be minimized by moving slower than the resonant frequency.

In the single tested subject, ischemia eliminated the effect of mechanical condition on preferred frequency. Prior to ischemia, the subject displayed the expected decrease in preferred frequency with added mass. Once the stretch reflex was eliminated, this mechanical dependence was no longer evident (Fig. 3). Therefore, the preferred frequency was likely influenced by sensory feedback, such as muscle length or velocity information from muscle spindles.

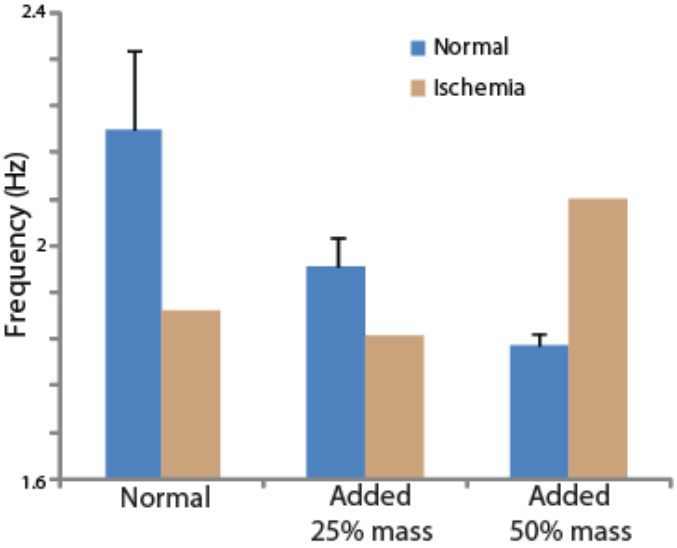

Figure 3. Peripheral ischemia eliminated the effect of mechanical condition on preferred frequency.

CONCLUSIONS

Subjects did not prefer to bounce at the resonant frequency, the movement pattern which would theoretically require minimal muscle work. The preference for slower frequencies may be due to the minimization of energetic cost. Preliminary results indicate that the choice of preferred frequency is dependent on sensory feedback, rather than being due to a learned feed-forward control strategy.

REFERENCES

1. Hatsopoulos NG, Warren WH. *J Motor Behav*, **28**, 3-14, 1996.
2. Bach TM, et al. *J Biomech* **16**, 85-90, 1983.
3. Gottlieb et al. *J Neurophys* **50**, 297-312, 1983.
4. Margaria R, et al. *J Appl Phys* **18**, 367-70, 1963.
5. Doke J, Kuo AD. *J Exp Biol* **210**, 2390-8, 2007.

MINIMIZING VARIABILITY OF ANTERIOR TIBIAL TRANSLATION MEASURES DUIRNG KNEE LAXITY TESTING

[1]Cale A Jacobs, [2]Thomas P Branch, [3]Jon E Browne, and [4]John C Campbell

[1]ERMI, Inc., Atlanta, GA
[2]University Orthopaedic Clinic, Decatur, GA
[3]Orthopaedic & Sports Medicine Clinic of Kansas City, Leawood, KS
[4]Bridger Orthopedic and Sports Medicine, Bozeman, MT
email: calejacobs@hotmail.com

INTRODUCTION

During clinical examination of knee joint laxity, surgeons may place their hands or position the patient differently from one another, which affects the force delivered to the knee and the surgeon's ability to interpret laxity [1]. Qualitative information can be gained, but manual tests are highly subjective as to the magnitude, direction, and rate at which the force is delivered, making it difficult for the surgeon to accurately and consistently interpret the direction and magnitude of motion that is produced [2].

Manual arthrometers were developed to decrease the variability of laxity examination by providing feedback as to the amount of force being applied as well as more consistent patient/joint positioning through the use of specialized bolsters. However, while improving upon the variability of the clinical exam, manual arthrometers have only demonstrated moderate reliability [3]. By controlling patient positioning and the magnitude, direction, and rate of force application during evaluation, automated testing systems may further improve the variability of knee laxity measures.

The purpose of this study was to determine if improving control of force and patient/joint positioning during evaluation of anterior knee stability would decrease variability in measures of anterior tibial translation (ATT).

METHODS

Ten healthy volunteers with no history of knee injury or surgery participated in this IRB-approved protocol (6 men, 4 women; mean age 33.9 y (range 23-47 y), height = 178.1 cm (range 154.9-190.5 cm, weight = 79.4 kg (range 51.8-111.4 kg)). Each subject was tested bilaterally using 3 different methods: instrumented clinical examination, manual arthrometer, and robotic knee testing (RKT).

The instrumented clinical exam was performed bilaterally by a single, board-certified orthopaedic surgeon. The test was instrumented with an electromagnetic joint evaluation system sampling at 120 Hz (3D Evaluator™, ERMI, Inc., Atlanta, GA). Kinematics were calculated using the ISB recommendations, with the hip joint center calculated using a spherical best-fit approach[4].

Figure 1: Simultaneous measurement of ATT with CompuKT and the electromagnetic systems.

Following the instrumented Lachman tests, each patient was bilaterally tested with a manual arthrometer (CompuKT, MEDmetric® Corp., San Diego, CA) by the same surgeon using well-accepted methods [5]. ATT measured at 134 N of force was used for all analyses. In order to compare

the agreement of the 2 measurement systems, data were also simultaneously collected with the electromagnetic system (Figure 1).

Subjects were then tested with the RKT system. The system applied an anteriorly-directed force at a constant rate of 1 mm/s, with both limbs being tested simultaneously. The amount of force applied was normalized to the subjects' height and weight, and represented 134 N in addition to the weight of the low leg. Once the target force threshold of 134 N was achieved, the system reversed direction until the 134 N threshold was achieved in the posterior direction. Data were collected using the previously described electromagnetic system, and all testing was performed by a single examiner. RKT testing was then repeated daily over 4 consecutive days.

ATT was collected during 3 trials of each test method, and the mean ATT of the 3 trials was used for analysis. Data collected simultaneously with the CompuKT and electromagnetic system were compared with a paired t-test. Reliability of the RKT system over the course of the 4 days was evaluated using an Intraclass Correlation Coefficient (ICC). Mean ATT and side-to-side differences in mean ATT were compared between the 3 methods with repeated measures ANOVAs, using Tamhane's post hoc analyses to assess paired differences. The variability of mean ATT and side-to-side differences in ATT were compared between the test methods using Levene's test of homogeneity of variances. All analyses were performed with SPSS Statistics v17.0 (Chicago, IL), with $p < 0.05$ being considered significant.

RESULTS

ATT collected simultaneously with the CompuKT and electromagnetic system did not statistically differ, with the mean difference between the 2 systems of 0.1 mm. Anteroposterior translation measured with the RKT demonstrated excellent reliability between days, with ICC = 0.87. ATT measured with the RKT was significantly greater ($p=.01$) than ATT measured with the CompuKT; however, did not differ from ATT measured during the Lachman tests (Table 1). No differences were noted in side-to-side ATT differences between the 3 methods. The use of the CompuKT significantly reduced the variability of side-to-side differences in ATT compared to the instrumented Lachman test ($p<.01$), and was significantly reduced with the RKT when compared with the CompuKT ($p=.01$).

DISCUSSION/CONCLUSIONS

In the current study of healthy subjects, the variability of side-to-side ATT differences was reduced from as the level of control was increased. Side-to-side differences in ATT > 3 mm have been used to identify unstable knees [5]. Minimizing the variability of ATT measurements may then reduce the number of knees falsely classified as unstable. Future cadaveric studies are needed to determine the magnitude of errors related to soft tissue artifact and muscle guarding, as well as to compare the accuracy of this electromagnetic system with surgical navigation systems. In conclusion, the variability of ATT measures was decreased with a manual arthrometer compared to an instrumented Lachman test, and was further reduced by controlling the magnitude, direction, and rate of force application with a robotic testing system.

REFERENCES

1. Floyd et al. *Orthopedics* **31**, 671-675, 2008.
2. Noyes et al. *Clin Orthop* **146**, 84-89, 1980.
3. Myrer et al. *Am J Sports Med* **24**, 104-108, 1996.
4. Gamage, SSHU and Lasenby, J. *J Biomech* **35**, 87-93, 2002.
5. Daniel et al. *Am J Sports Med* **22**, 632-644, 1994.

ACKNOWLEDGEMENTS

We would like to thank Edward Dittmar, Chris Madden, and Alex Sattler for their invaluable efforts in the development of the robotic testing system.

Table 1: Mean (± standard deviation) of anterior tibial translation (ATT) measured with the 3 test methods.

	Mean ATT	Side-to-Side Differences in ATT
Instrumented Lachman	8.67 ± 4.23 mm	2.92 ± 1.96 mm
CompuKT	6.61 ± 2.34 mm	1.96 ± 1.28 mm
Robotic System	10.59 ± 1.67 mm	0.99 ± 0.68 mm

DOES QUADRICEPS MOMENT ARM DYSFUNCTION EXIST IN CEREBRAL PALSY?

[1]Frances T. Sheehan, [1]Abrahm J. Behnam and [1,2]Katharine E. Alter

[1]Rehabilitation Medicine, National Institute of Health, Bethesda, MD, USA
[2] Mount Washington Pediatric Hospital, Baltimore, MD,USA
email: fsheehan@cc.nih.gov, web: http://pdb.cc.nih.gov

INTRODUCTION

Cerebral palsy (CP) is the most common disabling condition in childhood. It is a diverse group of movement and posture disorders of varying etiologies, the most common of which is believed to be injury to the developing brain during the prenatal period [1]. Motor impairments including muscle weakness can severely limit the functional abilities of individuals with CP. Moment arm (ma) dysfunction has been identified as another potential source of decreased joint torque in CP. Whether such a dysfunction affects the knee extensor mechanism is unknown. Therefore, the purpose of this study was to test if the patellar tendon ma (PTma) and the quadriceps relative ma (RelQma) are reduced in patients with CP.

METHODS

Sixteen volunteers with CP and 32 asymptomatic able-bodied volunteers (controls) provided informed consent (or assent) prior to participating in this IRB approved study. If deemed appropriate and time permitted, both knees were studied, creating a total study enrollment of 18 knees from patients with CP (9M/9F, age = 21.6±10.5 years, height = 166.0 ± 8.5cm, mass = 56.8 ± 9.8kg) and 40 knees from controls (19M/21F, age = 25.9 ± 8.6years, height = 171.0 ± 10.1cm, mass = 98.0 ± 12.9kg). All participants were placed supine in an MR imager (1.5 T, GE Medical Systems, Milwaukee, WI, USA or 3.0 T, Philips Medical Systems, Best, NL) and were asked to cyclically flex and extend their knee while a dynamic cine-phase contrast (PC) MR image set (x,y,z velocity and anatomic images frames) was acquired [2]. Dynamic cine images were also acquired in three axial planes to establish anatomical coordinate systems. The kinematics of each bone were quantified through integration of the velocity data, enabling the quantification of the 3D patellofemoral (PF) kinematics and tibiofemoral (TF) Instantaneous Helical Axis (IHA) and PTma, relative to the IHA, throughout the motion cycle [3]. Since the force of the patellar tendon acts directly on the tibia, the PTma can be directly calculated from the PF and TF kinematics (Fig. 1). In contrast, the quadriceps tendon acts through the patella to create a moment on the tibia. Thus, its relative ma, RelQma, is quantified based on the ratio of the patellar tendon to the quadriceps force (Fp/Fq), calculated using the moment balance equation for the patella relative to the PF point of contact (assumed to be the center of contact) [4]:

$$\sum M_{PC} = F_P * ma_P - F_Q * ma_Q = 0 \quad (1)$$

$$F_P = F_Q * ma_Q / ma_P \quad (2)$$

ma_P: ma of the patellar tendon, relative to PC
ma_Q: ma of the quadriceps tendon, relative to PC

Given that the moment on the tibia (relative to the IHA) created by the patellar tendon (M_{Tib_PT}) is:

$$M_{Tib\_PT} = PTma * F_P \quad (3)$$

Rearranging equation 3 and inserting F_P into equation 2 allows the moment on the tibia from the quadriceps (M_{Tib_Q}) to be calculated:

$$M_{Tib\_Q} = PTma * (ma_Q / ma_P) * F_Q \quad (4)$$

$$M_{Tib\_Q} = RelQma * F_Q \quad (5)$$

Therefore:

$$RelQma = PTma * (ma_Q / ma_P) \quad (6)$$

Since the RelQma requires a lengthy visual analysis of the images, all comparisons were done for a single knee angle (20°) using a Student's t-test, as the majority of the subjects with CP could not extend further than 20°. Interpolation was used,

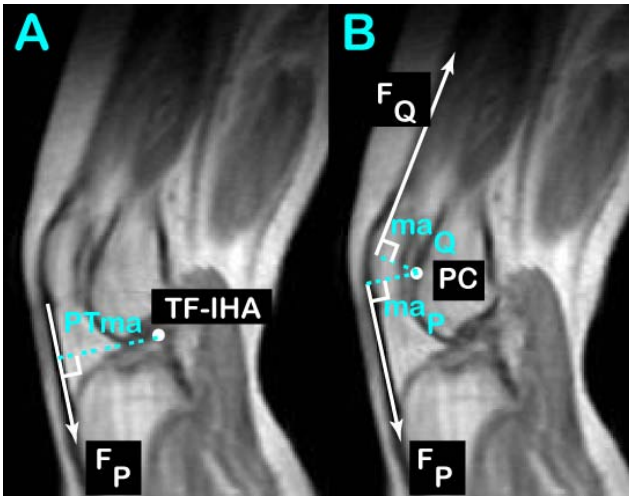

Figure 1: **A.** PTma was quantified by tracking the PT insertions into the patella and tibia and by defining the TF-IHA using the 3D TF kinematics. **B.** ma_Q and ma_P were defined through direct image-based measures at the time frame representing 20° knee extension.

when needed to ensure that all comparisons were done at 20° knee extension. In addition, correlations were calculated between the ma variables and both the PF kinematics and the GMFCS scores (level of function). A GMFCS score of I indicates full independence in all mobility and a GMFCS score of V indicates complete dependence for all mobility. A p-value < 0.05 was considered significant.

RESULTS AND DISCUSSION

The RelQma was 13.5% greater (44.7 mm vs. 39.4mm, p = 0.006) in the cohort with CP, relative to the control cohort. The increase in the RelQma was traced back to an 8% increase in ma_Q/ma_P (p=0.03) and an insignificant trend of increased PTma in patients with CP. For the CP population, a moderate inverse correlation was found between the GMFCS score and PTma (ρ=-0.49, p=0.05). Also for this cohort the PTma was moderately correlated with 2 other variables: PF anterior displacement (r = 0.50, p=0.05) and flexion (r=0.54, p=0.03). In combining both cohorts a weak correlation was found between relQma and PF superior displacement (r=0.322, p=0.02).

The current results are supported by earlier study, in which an asympomatic cohort with patella alta demonstrated an increase in ma_Q/ma_P and RelQma, compared to a control group [3]. As is common within the general CP population, the CP population within the current study demonstrated patella alta, a significant increase in PF superior displacement (13.3mm, p<0.001). Although patella alta appears to influence RelQma [3], only a weak correlation be found between RelQma and PF superior displacement when both the CP and control populations were combined. Therefore, further work is needed to more fully comprehend the factors influencing RelQma and PTma.

In the current study population, moment arm dysfunction did not exist for the knee extensor mechanism. In fact, just the opposite occurred. Although reduced extensor strength is typically noted in patients with CP, the increase in RelQma in patients with CP allowed these individuals to produce, on average, 13.5% more extensor moment for every unit of quadriceps force. Thus, any reduction in extensor torque indicates an even larger reduction in quadriceps strength for this patient group. The weak correlation between relQma and PF superior displacement suggests that interventions intended to reduce patella alta in the CP population may inadvertently reduce knee extensor torque. Since the CP population typically demonstrates severe losses in muscle strength, any loss of strength could be devastating to their mobility status. Thus, it important to recognize the trade-off between patella alta and knee extensor torque when planning procedures.

CONCLUSIONS

Although moment arm dysfunction has been hypothesized to cause reduce joint torque in individuals with CP, for the knee extensors the opposite occurs. The RelQma and PTma demonstrated and increase and no differences in this cohort of patients with CP, respectively, relative to a control population. This may have profound impact on the treatment of these patients in that surgeries aimed at improving function, may inadvertently result in reduced extensor strength.

REFERENCES

1.Bax M et al.: The Treatment of Gait Problems in Cerebral Palsy. Mac Keith Press, 2004, p. 9
2.Sheehan FT, et al. *J Biomech* **31**, 21-26, 1998
3.Sheehan FT, et al. *J Biomech* **40**, 1968-74, 2007
4.Ward SR et al. *J Biomech* **38**, 2415-22, 2005

ESTIMATION OF ANTERIOR TIBIAL TRANSLATION AND LIGAMENT LOADING IN HEALTHY AND ACL-DEFICIENT KNEES DURING WALKING

[1]Qi Shao, [1]Toran D. MacLeod, [1]Kurt Manal and [1]Thomas S. Buchanan

[1]Center for Biomedical Engineering Research
University of Delaware, Newark, DE, USA
email: shao@udel.edu, web: http:// www.cber.udel.edu

INTRODUCTION

Knowledge of internal knee-ligament loading is important for developing better surgical procedures and rehabilitation regimens of ACL-deficient patients. A few numerical models have been used to estimate ligament loading during walking [1,2]. However these models were not driven by measured EMGs, so they might have difficulty predicting the abnormal muscle activation patterns of ACL-deficient knees.

In this paper we describe an EMG-driven model that incorporates a knee-ligament model, and we apply this approach to estimate anterior tibial translation (ATT), anterior shear forces, and ligament loading in the knee joints of an ACL-deficient subject and a healthy subject during walking. The results of the ACL-deficient gait will be compared with those of the healthy gait to explain how the ACL-deficient subject compensated for the loss of the ACL.

METHODS

One male healthy subject (mass 60.5 kg, height 1.70 m) and one male subject without an ACL (mass 74.0 kg, height 1.72 m; right leg was the affected leg) gave informed consent before participating in this study. The experimental protocol was approved by the Human Subjects Review Board of the University of Delaware. The subjects were required to finish four walking trials with right foot striking the force plate, and another four walking trials with left foot striking the force plate. EMG, joint position and force plate data were collected during the trials. EMGs were collected from nine muscles of the leg of interest using surface electrodes, including RF, VL, VM, SM, BFL, MG, LG, Sol, and TA [3]. In this study we simulated the stance phase of both knees of the ACL-deficient subject, and the right knee of the healthy subject.

We calculated knee-ligament forces through a two-step procedure. First, an EMG-driven model [3,4] was used to estimate the muscle forces of the leg of interest to match the inverse dynamics calculated knee and ankle joint moments during stance phase of the walking trials.

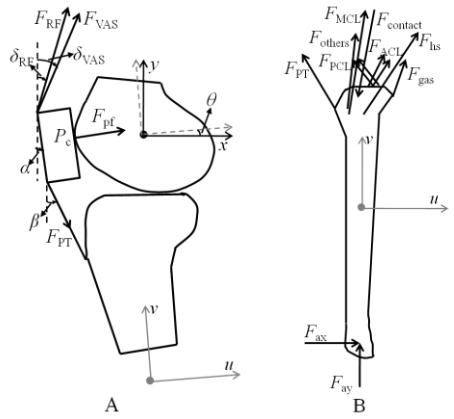

Figure 1: The knee joint model.

Second, a knee model that incorporated knee-ligaments was developed to calculate ATT and ligament loading. The model included the tibiofemoral and patellofemoral joints in the sagittal plane, and three segments: the femur, tibia and patella (Fig. 1A). The muscle forces and joint reaction forces calculated from the previous step were used as inputs. The approach used to model the patellofemoral joint was similar to that used by Liu and Maitland [2]. The contact and geometric compatibility conditions were required to be satisfied at the tibiofemoral joint. Knee ligaments were modeled as nonlinear elastic elements [1]. The ATT, knee joint contact force and ligament forces were solved through iterations until the force equilibriums of the tibia were satisfied (Fig. 1B).

RESULTS AND DISCUSSION

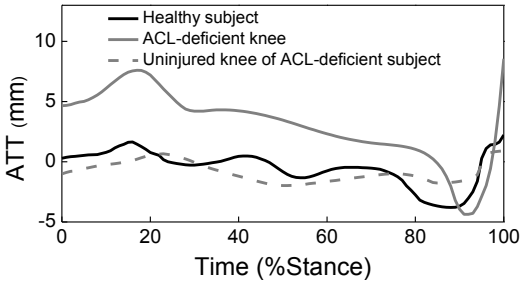

Figure 2: ATT comparison during stance phase.

The ACL-deficient knee had increased ATT compared to the contralateral uninjured side and the knee of the healthy subject (Fig. 2), and these calculated results were similar to previous findings of *in vivo* and *in vitro* experiments [5,6].

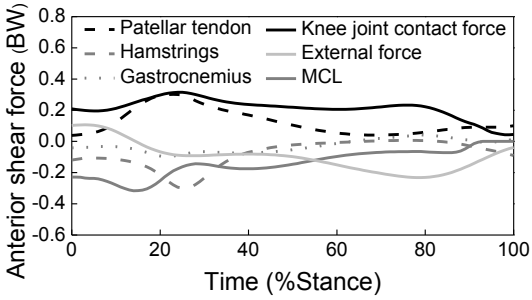

Figure 3: Anterior shear force distribution of the ACL-deficient knee.

For the ACL-deficient knee, the medial collateral ligament (MCL) was the major passive restraint of anterior shear force instead of the ruptured ACL (Fig. 3). We found strong co-contraction of the hamstrings and gastrocnemius, and these muscles functioned as active restraints to anterior shear force. However, co-contraction alone could not counteract the effect of ACL rupture, and the tibia of the ACL-deficient knee shifted more anteriorly during the stance phase.

For the healthy subject, the ACL was loaded for most of the stance phase, and the MCL, lateral collateral ligament and posterior capsule were also loaded (Fig. 4A). For the ACL-deficient subject, the MCL was loaded for most of the stance phase for the injured side (Fig. 4B), and both the ACL and MCL were loaded for the uninjured side (Fig. 4C).

CONCLUSIONS

This is the first time that an EMG-driven model has been used to estimate ligament loading in ACL-deficient patients. The approach could took into account the abnormal muscle activation strategies of ACL-deficient patients, and the results provided insights on how the patients compensated for the loss of the ACL. In future studies we will explore differences in ligament biomechanics associated with different rehabilitation protocols.

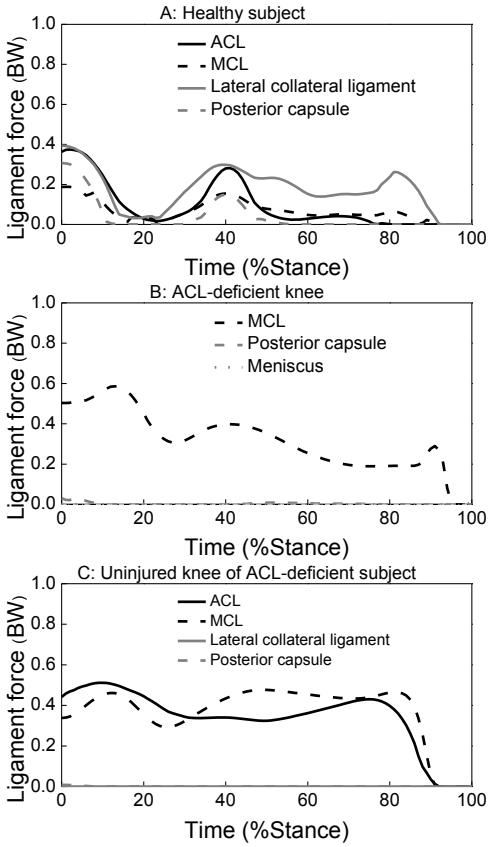

Figure 4: Knee-ligament loading comparison.

REFERENCES

1. Shelburne KB, et al. *J Biomech*, 37: 797-805, 2004.
2. Liu W, Maitland ME. *J Biomech*, **33**: 871-9, 2000.
3. Buchanan TS, et al. *J Applied Biomech*, **20**: 367-95, 2004.
4. Lloyd DG, Besier TF. *J Biomech*, **36**:765-76, 2003.
5. Kozanek M, et al. *J Biomech*. **42**:1877-84, 2009
6. Haimes JL, et al. *Am J Sports Med*. **22**:402-9, 1994

ACKNOWLEDGEMENTS

NIH R01-AR46386 and R01-AR48212.

DROP LANDINGS IN MILITARY BOOTS

Gretchen D. Oliver, Jackie Booker, Audrey J. Stone, and Hillary Plummer

University of Arkansas, Fayetteville, USA
email: goliver@uark.edu

INTRODUCTION

Drop landings are commonly used to evaluate predisposed risks of lower extremity injuries. It has been shown that forces exceeding 12 times a person's body weight can be experienced from these types of landings. Forces of that magnitude being repeatedly applied to the body can lead to a decrease in performance and injury [1]. Deployed military personnel often perform such landings when scaling obstacles in missions or dropping from a helicopter into a combat zone. Drops from helicopters can range anywhere from two feet if the helicopter is on the ground to six feet if the area is considered too dangerous to risk landing. The body's ability to absorb and control the forces involved in such extreme landings is critical to prevent injury [1]. Previous studies have shown that knee valgus, ankle eversion, and foot pronation are risk factors in lower extremity injuries [1,2]. The research is vast concerning drop landings and proper landing mechanics in relation to injury. However, there is a lack of research on military personnel and the effects that their boots on landing mechanics. Therefore it was the purpose of our study to examine military personnel performing a drop landing under three different footwear conditions.

METHODS

Sixteen male (n=13) and female (n=3) military personnel (21±3 yrs, 79±12kg, 172±10cm) volunteered to participate in the study. All participants were currently involved with the military and were deemed free from injury six months prior to testing. Participants reported for testing prior to participating in any resistance training or vigorous activity for that day. At the testing facility, participants were prepared so that kinematic data could be collected using The MotionMonitor™ electromagnetic tracking system (Innovative Sports Training, Chicago IL). Participants had a series of five electromagnetic sensors attached at the following locations: (1) medial aspect of the pelvis at S1, (2) the distal/posterior aspect of the right lower leg, (3) the distal/posterior aspect of the left lower leg, (4) the proximal/posterior aspect of the right upper leg, and (5) the proximal/posterior aspect of the right upper leg [3]. Sensors were affixed to the skin using double sided tape and secured using flexible hypoallergenic athletic tape. Following the attachment of the electromagnetic sensors, a sixth sensor was attached to a wooden stylus and used to digitize the palpated position of the bony landmarks. To accurately digitize the selected bony landmarks, participants stood in the neutral anatomical position during the digitization process.

Following all set-up and pre-testing protocols, the drop landing protocol was explained to the participants and they were given an unlimited amount of time to become accustom to the drop landing height and procedure. Once the participants were familiar with the landing height, they were given a random order of footwear conditions in which to perform the drop landing. The three footwear conditions were: bare feet, tennis shoes, and issued military boots. All conditions had the participants wearing their own footwear. Once the footwear was randomly assigned, each participant performed three drop landings for each of the three footwear protocols. Participants were instructed to drop down from a 47cm box as if they were dropping out of a helicopter in combat. Each participant was instructed to land on a 40 x 60 cm Bertec force plate (Bertec Corp, Columbus, Ohio) which was anchored into the floor.

Raw data describing sensor orientation and position were transformed to locally based coordinate systems for each of the respective body segments. Euler angle decomposition sequences were used to

describe both the position and orientation of the torso relative to the global coordinate system. The use of these rotational sequences allowed the data to be described in a manner that most closely represented the clinical definitions for the reported movements [3].

Data from the third drop landing of each footwear condition were selected for analysis. The third trial was selected to assure that the participant was accustomed to the different footwear and landing surface.

RESULTS AND DISCUSSION

A repeated measures analysis of variance (ANOVA) was performed to determine if there were any differences in the degree of knee valgus when performing jump landings in bare feet, tennis shoes, and boots. There were no significant differences in knee valgus among drop landings in different footwear ($p \geq .05$).

High risk activities such as landing from a jump have been linked to noncontact anterior cruciate ligament (ACL) injuries. The position of the lower extremity has been thought to be a major contributor to these injuries. It has been vastly reported that the position of knee valgus is the culprit of many noncontact ACL injuries. As previously discussed, limiting foot pronation has also been shown to decrease knee valgus. It is thought that by limiting the position of knee valgus during drop landings the incidence of injury could be reduced.

CONCLUSIONS

Our findings suggest that the rigid structure of military boots may not affect knee valgus during the drop landings. Previously, it has been stressed that athletes should be instructed on proper landing strategies in an attempt to decrease injuries, and this should be extended to all military personnel as well. Landing strategies are critical because the mechanics of landing direct the forces being absorbed. Improper transmission of forces up the kinetic chain may lead to lower extremity injury.

REFERENCES

1. Hargrave et al. *J Ath Train* **38**: 18-23, 2003.
2. Joseph et al. *Am J Sports Med* **36**: 285-289, 2008.
3. Myers et al. *Am J Sports Med* **33**: 263-271, 2005.

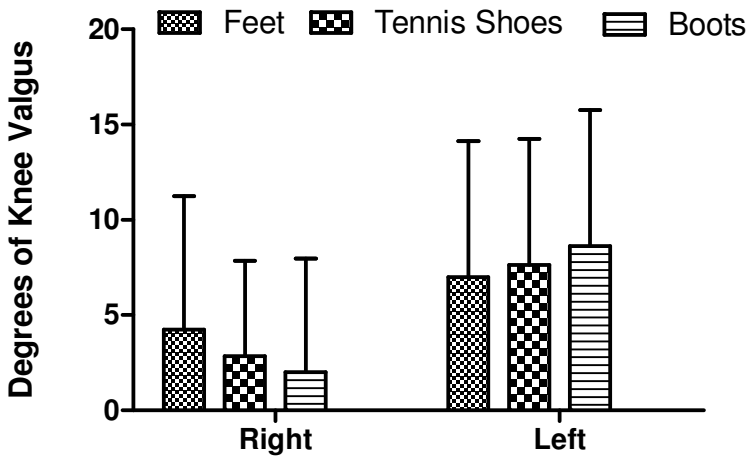

Figure 1. Degree of knee valgus for both the right and left sides when performing a drop landing in different footwear conditions.

A LINE PROFILE APPROACH TO QUANTIFY PTOA USING T1ρ MRI

NF Klocke, DR Thedens, JA Martin, A Amendola, TD Brown and DR Pedersen

University of Iowa, Iowa City, IA, USA
email: noelle-klocke@uiowa.edu, web: http://mnypt.obrl.uiowa.edu/

INTRODUCTION

Magnetic Resonance Imaging (MRI) has proven to be a non-invasive diagnostic tool for joint injury, with certain modalities (T1ρ) showing sensitivity to cartilage compositional changes [1]. However, distinguishing cartilage from surrounding tissues may be visually ambiguous in MRI, and observer variability may greatly affect the accuracy of cartilage assessment results. We here define an objective condyle-specific registration method, in which depth-dependent cartilage changes could be assessed for post-traumatic osteoarthritis (PTOA) development across patients' knees after acute ACL rupture using T1ρ and other MRI modalities.

METHODS

T1ρ MRI scans of five healthy subjects with no history of knee injury were acquired on three alternate days on a 3T Siemens TIM Trio scanner using a single channel transmit-receive extremity coil and a multi-slice protocol with a T1ρ spin-lock magnetization preparation block prepended to each fast spin-echo image acquisition. Sagittal slices through the trochlea, midline of the lateral femoral condyle (LFC), and 6mm lateral to the LFC midline slice were acquired. One ACL patient was imaged prior to surgery, and at 4 and 8 months post-surgery with the same protocol. Study protocol and informed consent documentation were approved by the Institutional Review Board.

Image analysis was developed in Matlab®. The direction-independent Canny filter was used to identify bone-cartilage boundaries, since edges found in an image and its negative would have the same location across MRI modalities [2]. A 20ms T1ρ sagittal slice with highlighted Canny-detected edges was displayed for user selection of two points demarcating anterior and posterior sulcus region boundaries (Fig. 1). Three anatomic landmarks were defined by locating the closest points on the Canny detected bone-cartilage interface (BCI) between them by next pixel progression. Inflections in the x-y positions of these pixels determined the sulcus midpoint, anterior ridge, and posterior ridge as anatomic landmarks. The posterior ridge became the specific anatomic reference point for region definitions, due to its clarity across subjects.

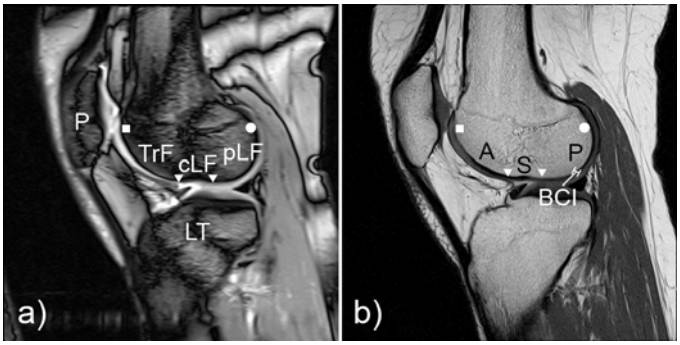

Figure 1: a) T1ρ image of regions in LFC [3] and b) its near negative proton density image shows regions used: *S*=sulcus between anterior and posterior ridges (triangles); *A*=anterior from sulcus; *P*=condyle posterior from sulcus.

A nearest neighbor line-growing protocol followed the posterior condyle BCI pixels (Fig. 2). An ellipse fit to the pixilated line using least-squares criterion defined a smooth BCI arc. Then sampling of the T1ρ relaxation times occurred in 0.5mm increments from the posterior ridge of the fitted BCI and along the osculating plane normals to create profiles at deep, radial, transitional and superficial layers (Fig. 3). Each assigned T1ρ value was the bilinear interpolation of the four nearest pixels. A circle fitted to the posterior condyle BCI delineated the weight-bearing region as 0-90° of knee flexion; radius was an anthropometric measure of knee size for normalization between subjects. The standard deviations for the measured radii from day to day for the five normal knees were 0.08-0.82 mm (0.5-5%) Data collection in the anterior and sulcus regions was performed similarly.

Variability of inter- and intra-user selection of anatomic landmarks was tested on three images. Three users were asked to pick the anterior and posterior bounds of the sulcus region four times. Then sensitivity of the program to the user's posterior boundary selection was tested by changing the posterior point to 49 possible pixels within a 7x7 grid (11 mm^2). The locations of these program-generated anatomic landmarks were recorded and compared for all validation tests. Repeatability of the BCI profiles' shape across time was also tested using analytical registration of the normal subjects' data. Registering the first point (posterior ridge) and the sixtieth point (30mm from posterior ridge) of the line profiles and performing an affine translation and rotation to align the curves in a common image allowed direct comparison between corresponding bone-cartilage interface points.

RESULTS AND DISCUSSION

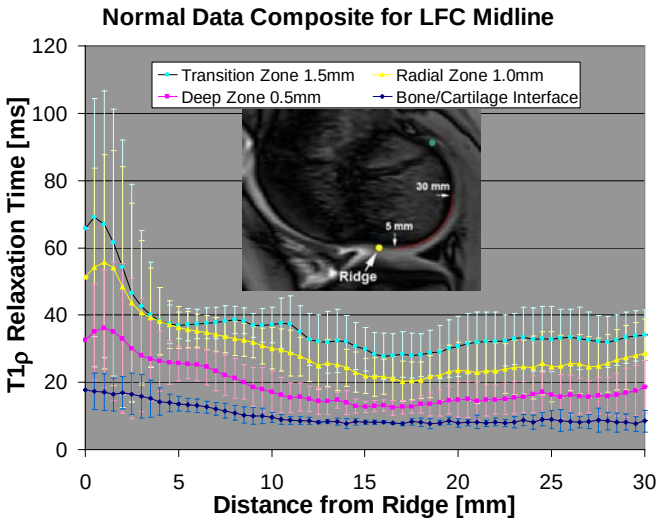

Figure 2: Normal subjects' composite average T1ρ relaxation times. Inset shows weight bearing region (5-30mm, approximately 90° flexion) Measured from the ridge (yellow) toward the green point.

User selection of anatomic landmarks varied from 2.95-6.24 mm agreement for the anterior ridge and 1.73-2.25mm for posterior ridge. The program's geometry-based criteria reduced the subjective user posterior ridge selections to a common pixel in all but two images (posterior ridge varied 0-2.25mm). The program's correction to user selection of the posterior ridge within an 11mm^2 area of 49 pixels reduced the bony landmark location to 1 of 3 pixels (maximum separation: 2.45 mm) compared to the maximum distance (4.64 mm) between the user-landmark selections. Slice location imprecision from different scanning sessions is inherent within the setup of the MRI, resulting in different geometries of the BCI interface and subsequent line profile curvatures, but this method yielded average differences in curvature geometry much less than 0.5 mm (1 pixel) between corresponding points.

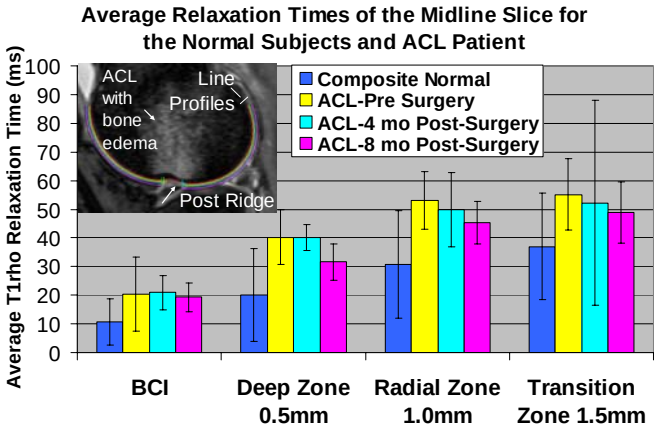

Figure 3: Average relaxation times within weight-bearing area (0-90° from posterior ridge). Line profiles are shown in the ACL patient's pre-surgery image. Higher relaxation times in ACL patients may indicate PTOA development [1].

An objective condyle-specific registration method has been developed for cartilage-specific T1ρ MRI. Validation tests confirm BCI registration reliability. Multiple-day imaging of normal knees demonstrates consistency of depth-dependent T1ρ imaging of cartilage, even near patient-specific posterior ridge geometry variations.

T1ρ MRI demonstrates sensitivity to cartilage composition changes during recovery from acute ACL trauma. Expanding this accurate objective registration of healthy subjects may determine normal cartilage relaxation times for this and future studies of knee homeostasis following ACL trauma and possible PTOA development.

REFERENCES

1.Blumenkrantz G, Majumdar, S. *European Cells and Materials* **13**, 75-86, 2007**.**

2.Canny, J. *IEEE Transactions on Pattern Analysis and Machine Intelligence*, **8**, 679-698, 1986.

3.Eckstein, F, et.al.. *Osteoarthritis Cartilage,* **14**, 974-983, 2006.

ACKNOWLEDGEMENTS

NIH grant P50 AR055533 provided funding.

TIBIAL ACCELERATION AND SLOPE CONTRIBUTIONS TO ACL LOADING DURING A SIMULATED LANDING IMPACT

[1]Scott McLean, [1]Youkeun Oh, [1]Mark Palmer, [1]James Ashton-Miller and [1]Edward Wojtys

[1]University of Michigan, Ann Arbor, MI, USA
email: mcleansc@umich.edu, web: http://www.kines.umich.edu/faculty/full-time/mclean.html

INTRODUCTION

Anterior cruciate ligament (ACL) injury is a potentially traumatic injury evoking substantial short and long-term debilitation. Current efforts aimed at preventing these injuries focus on modifying neuromuscular control elicited during landings, as it is amenable to training. Injury rates, however, remain largely unchanged.[1] We propose that by failing to consider factors additionally contributing to causality, the current prevention model is flawed. In single-limb landings, the large intersegmental accelerations arising at impact must be restrained by the internal joint structures and the pre-existing muscle-tendon loading across the joint. If an ineffective overarching neuromuscular strategy prevails, however, these accelerations may be large enough to compromise the passive restraint mechanism. This study aimed to demonstrate that impact-induced anterior tibial accelerations during single leg landings correlated with peak ACL strain. The impact of posterior tibial slope on this relation was additionally explored. This study was considered a critical initial step in determining whether this morphologic – mechanical interaction implicates within the ACL injury mechanism.

METHODS

An apparatus has been developed that simulates, in the presence of muscle forces, impulsive 3D loading during single limb landings (Fig 1A).[2] Using this device, 12 female cadaveric specimens (65.3 ± 10.5 years) were subjected to five consecutive impact load trials with a simulated impact load of 1299.1 ± 205.7 N. Each limb was initially fixed at 15º of knee flexion while quadriceps (180 N), hamstring (140 N), and gastrocnemius (140 N) muscle forces statically preloaded the joint. For each trial, 3D knee joint forces and moments were measured at 2 kHz via two 6 DOF load cells (AMTI, MA). Knee kinematic data were quantified based on the 3D positions of infrared (3 per segment) emitting diodes recorded at 400 Hz via a Certus system (Northern Digital, CN). Synchronous anteromedial bundle (AMB) relative strain was recorded at 2 kHz via a miniature DVRT (Microstrain, VT) inserted directly into the tissue. Lateral radiographs were taken of each specimen following testing, from which the lateral posterior tibial slope was calculated (Fig 1B).[3]

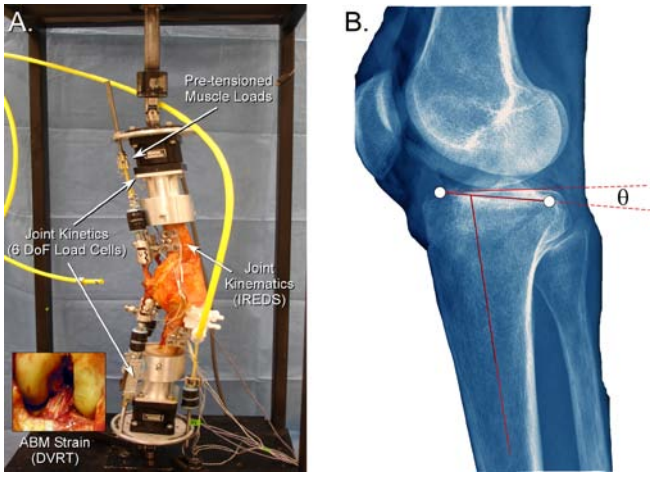

Fig 1: Knee kinetic and kinematic and AMB length changes were recorded for simulated impact trials (A). Posterior tibial slope was recorded via standard lateral radiographs (B).

Anterior tibial displacement data were filtered at 50 Hz and accelerations were quantified over the first 200 ms post-impact. Peak anterior tibial acceleration and AMB strain, the relative timings these peaks and posterior tibial slope measures obtained for all specimens were initially submitted to respective linear regression models to test for associations. Posterior tibial slope and peak tibial acceleration data were then submitted to a multiple linear step-wise regression model to examine their integrative association with peak AMB strain. Significance levels for inclusion and exclusion within this model were set at $p < 0.05$ and $p < 0.1$ respectively.

RESULTS AND DISCUSSION

Definitive peaks were evident in both tibial acceleration (7.87 ± 2.77 $m.s^{-2}$) and AMB strain magnitudes (3.35 ± 1.71 %) (Fig 2). The mean (± SD) lateral posterior tibial slope was 7.8 ± 2.1º.

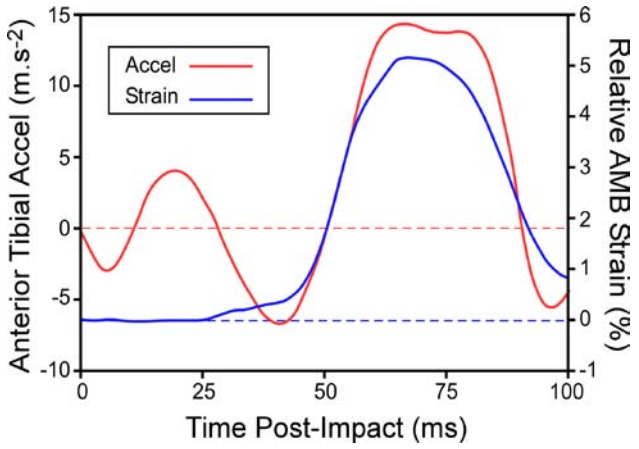

Fig 2: Sample impact-induced anterior tibial acceleration and relative AMB strain profiles.

Peak AMB strain significantly (p = 0.004) correlated with peak anterior tibial acceleration, explaining 62% of the variance (Table 1). The timing of the AMB strain peak (66 ± 4 ms) was also significantly (p = 0.001) correlated with peak tibial acceleration timing (66 ± 7 ms), explaining 67% of the variance. Peak anterior tibial acceleration was significantly (p = 0.004) correlated with posterior tibial slope, which explained 61.8% of the variance. Peak relative AMB strain also significantly (p = 0.007) correlated with posterior tibial slope, explaining 58% of the variance. Including both anterior tibial acceleration and posterior tibial slope within the step-wise regression model did not significantly (p = 0.304) improve AMB strain predictions. Specifically, the posterior tibial slope term only explained an additional 4.9% of the variance observed in AMB strain beyond that explained by peak anterior tibial acceleration alone.

We have shown that impact-induced peak anterior tibial acceleration elicited during simulated landings correlates with peak AMB strain. Considering extremely large tibiofemoral accelerations are possible during jump landings, ACL injury via this mechanism seems plausible. Impact-induced anterior tibial accelerations and hence the potential for ACL injury via this mechanism appear additionally dictated by tibiofemoral joint anatomy. Specifically, a larger posterior tibial slope appears to transfer high-rate compressive loading at impact to equally high anterior tibial shear loading rates, culminating in greater anterior tibial accelerations and AMB strains.[3] Further work is necessary to determine whether such associations extrapolate to explain actual injury causality. Current outcomes suggest improvements in ACL injury risk screening and intervention methods may be possible via non-invasive quantification of impact-induced tibial accelerations during landings. Understanding explicit relations between knee morphology and resultant joint mechanics appears equally critical to elucidating and countering the multi-factorial ACL injury mechanism. In particular, establishing prevention modalities that can successfully cater to individual joint vulnerabilities seems warranted. We intend to explore more complex relations between knee morphology and 3D mechanics with this specific goal in mind.

Table 1: Individual regression model coefficients associating peak AMB strain and peak anterior tibial acceleration, their respective timings, and lateral posterior tibial slope.

Variable / Predictor	SE	β	t	P
Peak AMB Strain / Peak Acceleration	0.000	0.787	4.041	0.004
Peak Acceleration / Tibial Slope	0.207	0.786	3.993	0.004
Peak AMB Strain / Tibial Slope	0.213	0.761	3.512	0.007
AMB Strain Timing / Acceleration Timing	0.000	0.819	4.124	0.001

CONCLUSIONS

Impact-induced peak anterior tibial acceleration is significantly correlated with peak AMB strain. This relation, and hence the potential for ACL injury via a tibial acceleration mechanism, is additionally governed by the posterior tibial slope. Improved understanding of the complex interactions between knee joint morphology and 3D knee mechanics during landings now appears warranted.

REFERENCES

1.Agel J, et al. *Am J Sports Med* **33**, 524-30, 2005.
2.Withrow T, et al. *Am J Sports Med* **34**, 269-74, 2006
3.Hashemi et al. Am J Sports Med **38**, 54-62, 2010

ACKNOWLEDGEMENTS

This work was funded by NIH (R01AR054821)

LOAD RESPONSE OF ARTICULAR CARTILAGE AND LIGAMENTS TO VALGUS LOADING – A FIBRIL-REINFORCED MODEL OF THE KNEE

Mojtaba Kazemi, Ke B Gu and LePing Li

Department of Mechanical and Manufacturing Engineering, University of Calgary, Alberta, Canada
Email: LePing.Li@ucalgary.ca

INTRODUCTION

The load response of knee joint is determined by functionalities of articular cartilage, menisci, bone and ligaments. The primary functions of articular cartilage are transmitting force across joint, minimizing stress concentration and providing a smooth surface for joint surfaces. The menisci act as load support and shock absorber. Ligaments connect articulating bones and act as stabilizer of knee movement [1].

Great progresses have been made in knee joint biomechanics. Due to high cost of experiments and technical difficulties in the measurement, finite element methods have been widely used to investigate the mechanical behavior of knee joint [2]. However, most anatomically accurate knee models only address the elastic behavior of the joint. The time-dependent load response of the knee associated with the fluid flow in the tissues is not well understood.

Articular cartilage and meniscus consist of proteoglycan (PG) matrix, collagen fiber network and fluid. These three constituents dominate the load response of the tissues in different loading conditions. Different models have been used to describe the mechanical behavior. One phase isotropic elastic models are usually used to study instantaneous or static response of the tissues. Biphasic models attempt to interpret the viscoelastic behavior associated with the fluid flow in the tissues [1]. Recently, the combined effect of site-specific fiber orientation and fluid flow was introduced in knee modeling [3]. Only simple compressive loadings were considered because the ligaments were not included in the model [3].

The long term goal of our research is to determine the contact mechanics of the knee under realistic loading conditions when the fluid flow and site-specific collagen orientations in the soft tissues are incorporated. Therefore, ligaments and patellar were added to the initial model. As a preliminary test of the finite element procedure, we investigated the load response of articular cartilage and ligaments in valgus loading.

METHODS

The solid model of knee (Fig. 1) was taken from an existing leg model of a healthy male [4]. The dimensions of articular cartilages, menisci and ligaments were determined from his MR images (femoral cartilage thickness 1.5-2.3mm; maximum thickness of menisci 6.6m). Bones were considered as linearly elastic because of their high stiffness in comparison with the soft tissues. The menisci and articular cartilages were modeled as fiber-reinforced fluid-saturated materials [5]. Linear elastic behavior was assumed for the non-fibrillar matrix (PGs). For collagen fibers, Young's modulus was taken to vary linearly with tensile strain but to be zero for compression. Collagen fibers in articular cartilage were assumed to follow the split-line pattern [6] while fiber orientation in medial and lateral menisci was aligned in radial and circumferential directions. Ligaments (Medial Collateral, Lateral Collateral, Posterior Cruciate and Anterior Cruciate) were assumed as linear elastic matrix reinforced by collagen fibers mainly aligned in longitudinal direction. Tibia and fibula were assumed fixed and a valgue torque was applied to the femur. The surface contact model in ABAQUS was used to simulate multiple mechanical contacts between the femoral cartilage and tibial cartilage or menisci as well as fibula cartilage with tibia. A user-defined material subroutine was incorporated in ABAQUS to define the 3D anisotropic and nonlinear properties of the collagen networks [5].

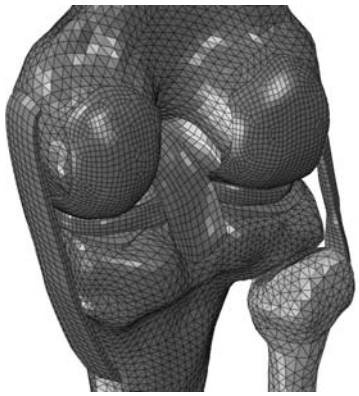

Figure 1: Finite element model of the knee, including distal femur, tibia, fibula, menisci, articular cartilages and ligaments. The meshed femur and tibia were, respectively, 104 and 80mm in length, about 1/3 longer than that shown here.

RESULTS AND DISCUSSION

As the first step to test the model, a unit valgus torque was applied to the femur. Two different cases were solved. In the first case, a steady state problem was solved to investigate the load support behavior of ligaments (Fig. 2). This solution also gave an approximation of articular cartilage response (Fig. 3). In the second case (not shown here), a transient analysis was solved to investigate the interaction of fluid and collagen network in articular cartilage.

Figures 2 and 3 show the results obtained in Lateral Collateral Ligament (LCL) and articular cartilage under valgus torque. A higher tensile stress was observed in the posterior part of the LCL (Fig. 2) while a moderate tensile stress appeared in the anterior part (not shown). The maximum principal stress occurred at the posterior region of the fibular insertion of the LCL.

Maximum principal stress in the femoral cartilage is shown in Fig. 3. The stress pattern was mainly due to contact between femoral cartilage and medial and lateral menisci. Due to valgus nature of loading, maximum values occurred on a cross line connecting medial and lateral menisci. The non-uniform stress pattern in cartilage was partially due to collagen fibers orientation. It was also observed that the collagen network significantly changed the patterns and magnitudes of tissue deformation and fluid flow in the femoral cartilage (not shown).

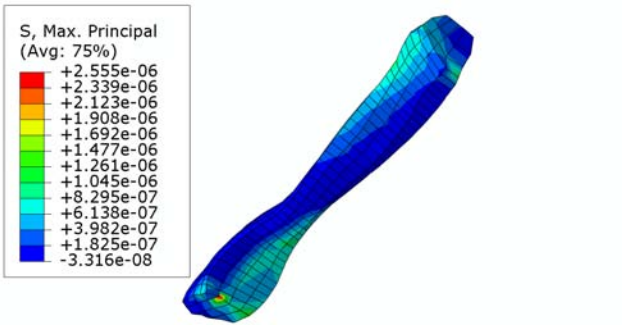

Figure 2: Maximum principal stress (MPa) in Lateral Collateral Ligament (LCL) due to unit valgus torque.

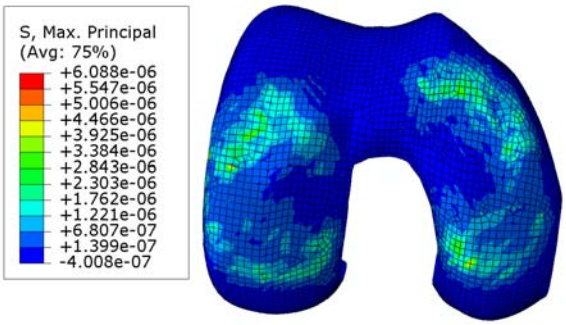

Figure 3: Maximum principal stress (MPa) in articular cartilage due to unit valgus torque.

REFERENCES

1. Fung YC. ***Biomechanics: Mechanical Properties of Living Tissues***, 2nd ed. Springer-Verlag, New York, 1993.
2. Bendjaballah MZ, Shirazi-Adl A, Zukor DJ. ***Knee* 2**, 69–79, 1995.
3. Gu KB, Li LP. ***Trans. Orthopaedic Research Society* 35**, 911, 2010.
4. Cheung JT et al. ***J Biomech* 38**, 1045-1054, 2005.
5. Li LP et al. ***Med Biol Eng Comput* 47**, 607-615, 2009.
6. Below S et al. ***J Arthrosc Relat Surg* 18**, 613-617, 2002.

ACKNOWLEDGEMENTS

Canadian Institutes of Health Research

THE EFFECTS OF SINGLE-LEG LANDING TECHNIQUE ON ACL LOADING

[1]Walter Laughlin, [1]Joshua Weinhandl, [2]Thomas Kernozek, and [1]Kristian O'Connor

[1]University of Wisconsin-Milwaukee, Milwaukee, WI, USA
[2]University of Wisconsin-LaCrosse, LaCrosse, WI, USA
email: laughlin@uwm.edu, Web: www.chs.uwm.edu/neuromechanics

INTRODUCTION

Anterior cruciate ligament (ACL) injury is one of the most debilitating and costly lower extremity injuries experienced by athletes [1]. It has been shown that over 70% of ACL ruptures occur in a non-contact situation [2], specifically during closed chain movements requiring rapid decelerations of the body's center of mass [2] such as; cutting, pivoting, stopping, or landing.

In an attempt to reduce ACL injury rates during landing tasks, neuromuscular and proprioceptive training programs have been developed to reduce an athlete's risk of injury. Decreases in ACL injury rates associated with these intervention programs have been attributed to a number of biomechanical changes during landing. In the sagittal plane, trained athletes show an increase in knee flexion angle at initial contact (IC) and throughout the range of motion of the knee [3]. This altered lower extremity position has been suggested to decrease ACL injury risk. However, no study has compared the change in ACL force that occurs as a result of sagittal plane knee mechanics. Therefore, the purpose of this study was to determine the effects of lower limb landing technique on ACL forces during single-leg drop landings.

METHODS

Eight physically active females (average mass = 63 kg), free from musculoskeletal injury volunteered to perform soft and stiff landings from a 37 cm box. The order in which these trials were performed was counterbalanced between subjects.

Three-dimensional kinematic data were collected using a ten-camera Motion Analysis Eagle system (200 Hz), and force data were collected with an AMTI force platform (1000 Hz). Surface electromyography (EMG) of the medial and lateral hamstrings and quadriceps were recorded using at 1000 Hz. Kinematic and kinetic data were used as inputs into a subject specific three-dimensional musculoskeletal model (Figure 1) [4,5,6]. The model then used a computed muscle control (CMC) algorithm to calculate muscle forces. These outputs were then used in a sagittal plane model of the knee [7] to calculate ACL force.

Dependent t-tests were assessed to determine potential differences in ACL force between the two landing conditions. Other variables of interest included hip and knee kinematics in the sagittal plane at IC as well as 200 ms post IC.

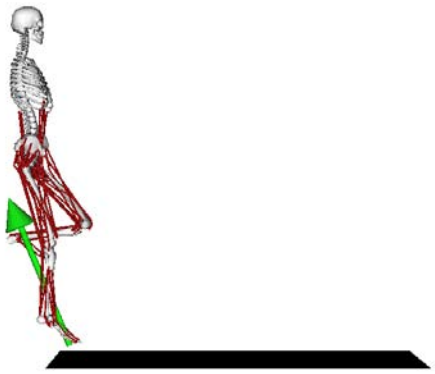

Figure 1. 19 degree-of-freedom, 92 actuator musculoskeletal model.

RESULTS AND DISCUSSION

The hip and knee kinematics (Figure 2) at IC and 200 ms post IC were different between the two landing conditions (Table 1). There was also a difference in the peak ACL force between the two landing conditions (Table 1). The stiff landing resulted in a 23% greater peak ACL force. In both landing conditions the peak ACL force occurred at ~10 to 20 ms post IC and dissipated to zero by 60 ms post IC (Figure 2).

Instructing subjects to land in a "soft" or "stiff" manner led to expected differences in maximum flexion angles and initial contact angle. The timing of the peak ACL force supports the theory that body position at contact is a critical determinant of ACL loading. This result suggests that a simple instructional cue may substantially decrease ACL loading. While the absolute forces were substantially lower than those believed to rupture the ACL (stiff = ~600 N), this estimation of ACL loading only accounts for sagittal plane mechanisms and does not account for other contributors to tension on the ACL. Reducing the sagittal plane contribution may serve to protect the ACL from excessive out of plane loading and reduce injury risk.

The individual contributors to the calculation of the ACL force were the shear components of the net joint force, tibiofemoral contact force, and the patellar tendon and hamstrings forces. The loading difference at the instant of peak ACL force was primarily due to a decreased posterior shear contribution by the hamstrings and secondarily due to an increased anterior shear by the tibiofemoral contact force. An increased shortening velocity of the hamstrings immediately after contact depressed the hamstrings force contribution.

Table 1. Hip and knee kinematics, and peak ACL forces.

		Soft	Stiff	p-value
Hip (°)	IC	29.1 ± 9.1	19.8 ± 8.8	0.003*
	200ms	65.1 ± 7.4	33.8 ± 15.6	<0.001*
Knee (°)	IC	16.5 ± 5.5	10.0 ± 3.4	0.007*
	200ms	81.7 ± 8.4	47.9 ± 19.1	0.001*
Peak ACL Force (BW)		0.80 ± 0.40	0.97 ± 0.47	0.046*

* Significantly different from soft ($p<0.05$)

CONCLUSIONS

The results of this study suggest that, when instructed to land in a soft manner, females show different single-leg landing mechanics at the knee and the hip as well as a decrease in the peak ACL force. Although the estimates of ACL forces did not reach magnitudes necessary to rupture the ligament, these findings support current research which suggests that changes in sagittal plane knee mechanics during landings may reduce an athlete's risk of ACL injury.

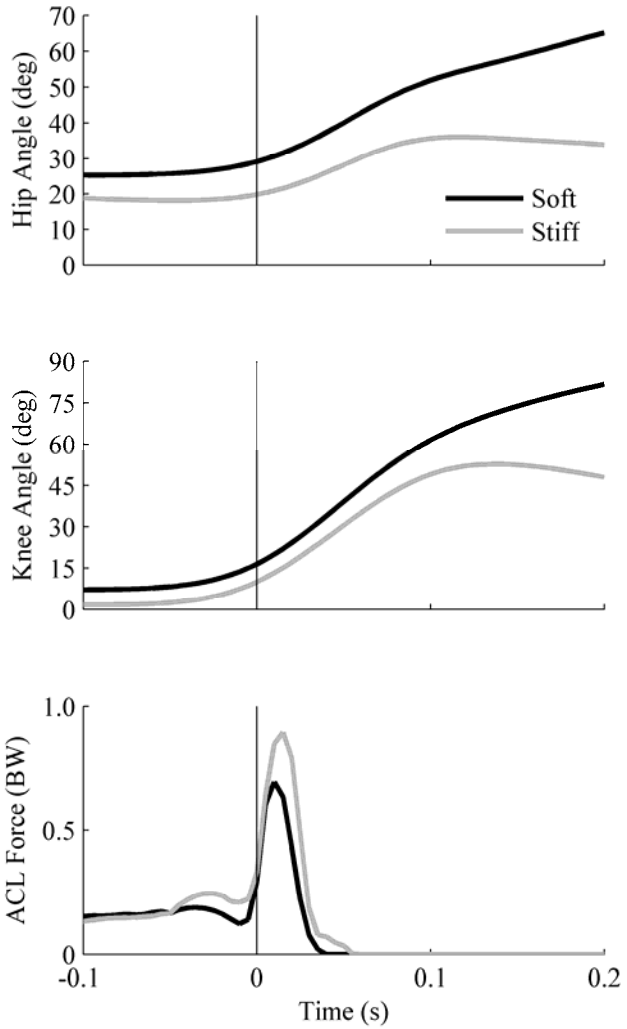

Figure 2. Hip and knee kinematics, and ACL forces. Zero time represents initial ground contact.

REFERENCES

1. Hewett, T. E. et al. *Am.J.Sports Med.*, **34,** 299-311, 2006.
2. Olsen, O. E. et al. *Am.J.Sports Med.*, **32**, 1002-12, 2004.
3. Mandlebaum, B.R. et al. *Am.J.Sports Med.*, **33**, 1003-10, 2005.
4. Thelen, D.G. & Anderson, F.C. *J Biomech*, **39**, 1107-15, 2006.
5. Delp, S.L. et al. *IEEE Trans.Biomed.Eng*, **37**, 757-67, 1990.
6. Thelen, D.G. et al. *J. Biomech*, **36**, 321-28, 2003.
7. Kernozek, T. W. & Ragan, R. J. *Clin Biomech*, **23**, 1279-86, 2008.

ACKNOWLEDGEMENTS

UWM College of Health Sciences Student Research Grant

PREDICTING KNEE VALGUS DURING LANDING FROM A JUMP FROM A FIELD TEST IN A FATIGUED CONDITION

[1,2]Mostafa Afifi and [2]Richard Hinrichs

[1]University of Calgary, Calgary, AB, Canada
[2]Arizona State University, Tempe, AZ, USA
email: mafifi@kin.ucalgary.ca

INTRODUCTION

It is imperative, when designing a test to detect an athlete's vulnerability to injury, that the test should be valid in both non-fatigued and fatigued situations. Detecting an athlete's potential for injury during later stages of athletic performances would allow coaches to make important decisions concerning whether or not to take a certain player out of a game.

Knee valgus has been identified as a non-favorable position during landing as it has been linked to ACL injuries [1]. In a recent study we found the change in distance between the knees experienced during landing could be predicted from that experienced during a squat in a group of active college students [2]. The distance between the knees was used as an indicator of knee valgus as it is a more practical measuring method if a field test is to be developed [3]. This was a good first step in an attempt to develop a field test to identify athletes with greater potential for ACL injuries. However, this was not tested in post-fatigue situations nor was a measure of true knee valgus used.

Thus, the purpose of this study was to establish if the quantity of true knee valgus observed after landing (Land) could be predicted from the valgus measurements during the downward movement of the takeoff (TO) phase of a jump and the downward movement of a squat (Squat) during both pre-and post-fatigued conditions.

METHODS

Twenty active college students (10 male, 10 female) participated in this study. Prior to testing participants read and signed an informed consent, which was approved by the Arizona State University Research Compliance Office. Participants were excluded if they had any orthopedic condition that would prevent them from performing a maximal vertical jump.

Position and orientation of all segments were recorded using 12-camera Vicon motion-capture system (240 Hz, Vicon, Oxford, UK). All participants were asked to perform three squats during which they squatted down and then back up to standing. Subjects were instructed to squat as if about to jump but to return to standing with the feet remaining in contact with the ground in order to replicate the first half of the takeoff phase of the jump. Subjects also performed three maximal countermovement vertical jumps while raising both arms as if to block a volleyball shot and land on both feet. Following the jumping and squatting tasks, participants underwent a fatiguing protocol, which consisted of the participants running on a treadmill at 10 km/h at a 10% uphill grade for 5 min.

Pearson product correlations were used to identify the relationship between knee valgus during Land, TO, and Squat. Linear regression analyses were conducted to identify the predictability of the knee valgus during Land from knee valgus during the TO and Squat.

RESULTS AND DISCUSSION

In the pre-fatigue condition, Pearson product correlations showed significant positive correlation between knee valgus experienced during TO, Land, and squat from both the right and left sides (Table 1). The strongest correlations were between TO and squat ($r = .948$ and $r = .860$, for the right and left sides, respectively). Similar results were seen in the post-fatigue condition as significant positive

correlations between knee valgus experienced during TO, Land, and squat from both the right and left sides were also observed (Table 2). The strongest correlations were also between TO and squat (r =.988 and r = .882, respectively).

Table 1 Relationship Between Knee Valgus Measured During TO, Land, and Squat (Pearson Product Moment Correlations) in the Pre-Fatigue Condition.

	Take off	*Landing*	*Squat*
Take off	1	.782*	.948*
Landing	.595*	1	.805*
Squat	.611*	.860*	1

Right side shown above the diagonal, Left side shown below the diagonal, * $p \leq .01$ level (2-tailed)

Table 2 Relationship Between Knee Valgus Measured During TO, Land, and Squat (Pearson Product Moment Correlations) in the Post-Fatigue Condition.

	Take off	*Landing*	*Squat*
Take off	1	.866*	.988*
Landing	.846*	1	.859*
Squat	.882*	.686*	1

Right side shown above the diagonal, Left side shown below the diagonal, * $p \leq .01$ level (2-tailed)

Knee valgus during Land showed correlations with knee valgus during Squat and TO for both the right and left sides that persisted during pre and post-fatigue conditions. As anticipated, correlations were not as strong as the Squat and TO correlations were for all but one measure (left knee Squat and TO had an r = .611, which is less than that between Squat and Land).

We believe there are two reasons why knee valgus during Squat and TO had a stronger relationship with each other than with Land. First, the start position for the Squat and TO was standing with the feet at shoulder width apart. Thus, the starting positions were almost identical. Although participants landed on two feet, the distance between the feet upon landing is not fully controlled considering the different possibilities of landing on any particular spot. The second reason is related to landing speed. The instructions given for the squat was to squat as if to jump but to return to stance without the feet leaving the ground. This assumes that the downward phases of each condition are performed at similar speeds. There may have been an inability to control the velocity of the upward phase in squatting and during the countermovement due to the different endpoints (airborne phase in the jump vs. stand in the squat) but that is irrelevant when comparing the downward phase. Land on the other hand was functionally different as maximum speed is reached just after the instant of touchdown and there is a continuous decrease in speed until a stop is reached. Despite these differences enough similarities existed between the three tasks to result in the significant positive correlations we found in both the right and left sides during the pre-fatigue and post-fatigue conditions.

A multiple step-wise linear regression analysis showed knee valgus during Squat to be the single best predictor for that during Land for both knees in the pre-fatigue condition with adjusted R^2 values of .648 and .374 for the right and left knees, respectively. Similar results were observed in the post-fatigue condition as right knee valgus during Squat was the single predictor with an R^2 value of .738. For the left side, knee valgus during the TO was the single predictor with an R^2 value of .715.

Regression analysis revealed that knee valgus experienced during landing is best predicted by either that observed during the downward phases of squatting or the takeoff prior to jumping with squatting being the better predictor.

CONCLUSIONS

Relationships found in this study have been consistent in both pre- and post-fatigue conditions. This suggests the ability of using knee valgus angle during squatting to predict the quantity of valgus that potentially may be experienced during landing which may prove to be a useful screening tool in determining which athletes would benefit from an ACL injuring prevention program. However, measuring knee valgus in a field setting may prove difficult. Future studies should investigate the relationship between true knee valgus during landing and the distance between the knees where participants would be allowed to land freely.

REFERENCES

1. Russel, KA, et al. *J Athl Train* **41**, 166-171, 2006
2. Afifi, M, et al. *Proceedings of NACOB'08,* Ann Arbor, MI, USA, 2008.
3. Noyes, FR, et al. *Am J Sports Med* **33**, 197-207.

EXAMINING THE KINEMATICS OF THE KNEE DURING A SIDE STEP CUTTING TASK USING THE HELICAL AXIS METHOD

[1]Michael Samaan, [1]Stacie I. Ringleb, [1]Julie Choisne, [1]Sebastian Bawab, [2]Nelson Cortes, [2]Eric Greska and [3]James Onate
[1]Mechanical Engineering, [2]Human Movement Science, Old Dominion University, Norfolk, VA, USA
[3]Ohio State University, Columbus, OH
email: SRingleb@odu.edu

INTRODUCTION

Knee injuries, particularly anterior cruciate ligament (ACL) injuries, are a common and potentially disabling sports related injury. Of the 80,000 annually reported ACL injuries, 70% are non-contact ACL injuries. Non-contact ACL injuries occur 5-7 times more frequently in females than males[1]. An example of a non-contact movement that may cause ACL injury is the side-step cutting task commonly performed in sports such as soccer and basketball.

In motion analysis, a common method used to study and understand these types of motions is Euler angles. Although this method is more clinically relevant, it may not appropriately describe 3-D motion due to the non-vectorial behavior of 3-D rotations [2]. Another method used to analyze 3-D motion data is the Helical Axis (HA). The main advantage of using the helical axis technique is that it provides information about the actual axes of rotation in a joint which cannot be obtained using Euler angles [3]. It has been stated that the helical axis or instantaneous axis of rotation of the knee joint is one of the most significant parameters quantifying these motion characteristics [4].

METHODS

The kinematic data studied in this work consisted of the stance phase of an unanticipated side step cutting task. Subject data was obtained from 9 female NCAA Division 1 soccer players. The subjects were of an average age, height and mass of 19.3±0.9 years, 1.68±0.05m, 61±8.4kg, respectively. All of the kinematic data was captured using a Vicon Motion System (Vicon-UK, Oxford, UK) in the Motion Analysis Laboratory at Old Dominion University with an IRB-approved protocol. The subjects were presented with an image of a rolling soccer ball which cut across the display screen thereby indicating to the subject to perform a side step cut in the direction of ball motion.

Using Visual 3D (Vis3D) (C-Motion Inc., Germantown, MD), Euler angles and the net rotation about the helical axis decomposed into all three directions (x, y and z) of the body fixed axis of the tibia measured with respect to the femur were calculated and exported for the right knee. The Euler angle data were exported using an order of rotation (XYZ) consisting of flexion/extension followed by add/abduction and concluding with internal/external rotation. The rotation matrix and translation vector were also exported from Vis3D and used to determine the unit vector and a point on the helical axis using the method developed by Spoor [5] in a custom written program in MATLAB (The Mathworks, Natick, MA). Another custom program was used to plot the helical axis at initial contact and peak knee flexion for each subject. The same program was used to plot both the Euler and helical angles for each of the planar motions mentioned in a similar manner as Woltring [2].

RESULTS AND DISCUSSION

The helical axis at initial contact was found to be oblique indicating a combination of all 3 planar motions in the task. The helical axis at peak knee flexion is extremely oblique for all nine subjects (Figure 1). This indicates that all three types of planar motion are heavily involved in this complex motion at this specific time frame. The Euler and decomposed helical angles are similar in the sagittal and transverse planes (Figure 2).

Side step cutting, in comparison to gait, is a more complex task involving large coupled motions. Analysis of the orientation of the helical axis during a flexion/extension motion in unconstrained cadaver

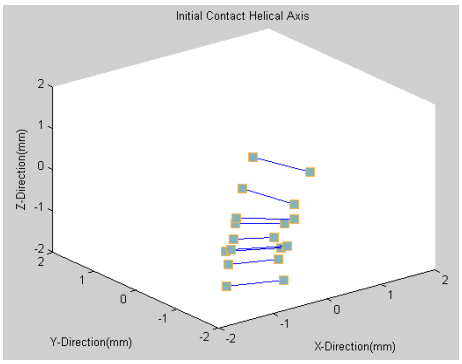

(a)

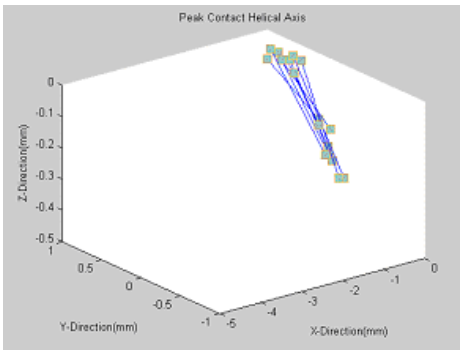

(b)

Figure 1: Helical axis orientation at a) initial contact and b) peak knee flexion

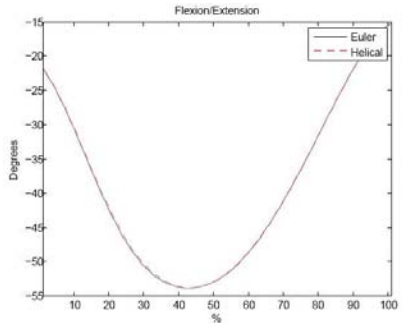

(a)

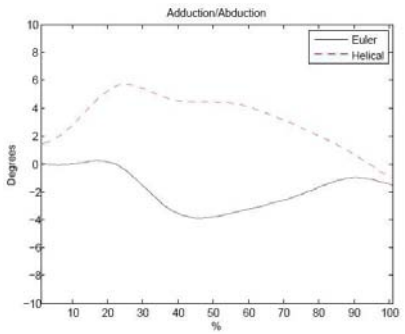

(b)

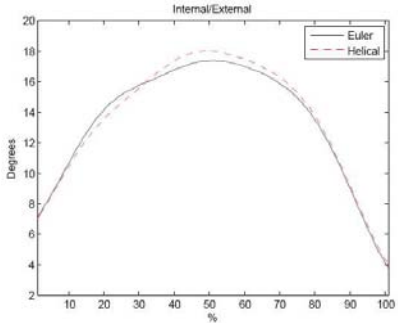

(c)

Figure 2: Euler & Helical angles for (a) flexion/extension (b) add/abduction and (c) internal/external rotation.

knees[4] were determined to be parallel to the trans-epicondylar axis. This same result was not seen in the side-step cutting task due to the coupled motions in all three planes. When comparing the Euler and decomposed helical angles, a high correspondence exists in flexion/extension yet there is variability in the other two motions particularly that of add/abduction, this variability was also observed in the coronal and transverse planes during gait [2].

The results presented here compared with an in vitro study designed to simulate knee flexion during gait demonstrate that the orientation of the helical axis (i.e., the axis of the rotation of the knee) varies with different motions. These results have implications in computational modeling and clinical treatment. Specifically, in dynamic modeling, the motion of the knee is typically defined as a one degree of freedom motion; however these data show that a one-degree of freedom motion is not sufficient in modeling complex knee. Additionally, with further study, this change in the orientation of the helical axis could provide orthopedic surgeons and rehabilitation specialists insight into how to operatively and non-operatively treat athletes who frequently perform complex motions, such as cutting tasks.

REFERENCES

1. McLean, S.G., et al. Clinical Biomech, **19**: p. 828-838, 2004.
2. Woltring, H.J. J Biomech, **27**, p. 1399-1414, 1994.
3. Nigg, B.M. et al *Biomechanics of the Musculo-skeletal System*. John Wiley & Sons Inc., 1999
4. Parks, S.A. 1997, Naval Post Graduate School: Monterey. p. 128.
5. Spoor, C.W. and F.E. Veldpaus. J Biomech, **13**, p. 391-393, 1980\

DYNAMIC KNEE JOINT STIFFNESS AND KNEE JOINT MOMENTS AFTER UNILATERAL TKA

[1]Kevin M. McGinnis, [1]Joseph A. Zeni, [1]Ali H. Alnahdi and [1]Lynn Snyder-Mackler
[1]University of Delaware, Newark, DE, USA.

INTRODUCTION

Total knee arthroplasty (TKA) is a widely used procedure in the management of knee osteoarthritis (OA). Over 500,000 TKA operations are performed each year, comprising nearly half of all total joint arthroplasties [1]. Return to normal gait is the main goal for patients after surgery [2]. Abnormal movement patters that persist after TKA could result in excessive loads on the operated and non-operated limb. This could expedite the progression of OA in the non-operated limb or contribute to the failure of the components of the knee prosthesis. Gait analysis is an important tool to measure biomechanical parameters before and after TKA. The purpose of this study was to compare sagittal plane kinetics and kinematics of the operated knee in patients 6 months and 1 year after surgery. The specific parameters that were compared are knee excursion, knee moment at peak knee flexion, and dynamic knee stiffness, all during early stance phase.

METHODS

Twenty-seven subjects were evaluated 6 months after unilateral TKA (8 women, Age 63.9±14.9, BMI 32.2±4.2) and thirty-eight subjects were evaluated 1 year after unilateral TKA (21 women, Age 67.6±7.3, BMI 31.0±5.5). Eighteen healthy adults (10 women, Age 61.6±6.4, BMI 29.6±5.0) with no reported knee pain also participated in the study and comprised a healthy control group. All subjects signed informed consent forms prior to participation in any facet of the study. Three dimensional gait analysis was performed using an 8-camera motion capture system (VICON, Oxford Metrics, London, England) synchronized with two Bertec force platforms (Bertec Corp., Worthington, Ohio, USA). Retro-reflective markers were placed bilaterally on anatomical landmarks and rigid thermoplastic shells were placed on the thigh, shank, and pelvis. Subjects walked at a self-selected speed. Seven walking trials were collected and the mean of these trials was used in the analysis. Sagittal plane angles were calculated using Euler angles. Inverse dynamics were applied to calculate joint moments, and were normalized to subject height and weight using Visual 3D software (C-motion, Inc., Rockville, Maryland, USA). Dynamic knee stiffness was calculated for each subject and was defined as the change in joint moment (M) divided by the change in joint angle (θ):

$$K_{joint} = \Delta M/\Delta\theta \quad (1)$$

Dynamic knee joint stiffness is plotted with the joint angle on the X-axis and joint moment on the Y-axis. An increase in joint moment represents an increase in the net external flexion moment [3]. Dynamic joint stiffness was measured over the linear region during loading phase, which begins when the average external knee flexion moment begins to increase and ends with peak knee flexion [3]. Data were linear fit over this phase and the slope of the line was defined as knee stiffness [(Nm/kg*m)/deg)]. Knee excursion was calculated as the difference in angle between the beginning and end of the time period mentioned above. Peak knee flexion moment was the maximum value for knee moment during this same time period. Quadriceps strength of the involved limb was collected on a Kin-Com Dynamometer (Chattecx Corp., Hixson TN). Quadriceps strength was operationally defined as the force output of the quadriceps during a maximal isometric contraction. Quadriceps strength in Newtons (N) was normalized to body mass index (BMI) and presented as N/BMI. Between group comparisons were made between 6 months and 1 year, 6 months and control, and 1 year and control group using independent t-tests.

RESULTS AND DISCUSSION

Knee stiffness was significantly higher in the 6 month group compared to the 1 year group (P=0.004). Subjects at 6 months had a knee stiffness value of K=0.0537 and subjects at 1 year had a knee stiffness value of K=0.0378 (Figure 1). Subjects in the control group had a knee stiffness of K=0.0413. No differences were found between the 1 year and control groups for knee stiffness, but differences between 6 months and control approached significant levels (p=0.085). Knee flexion moment significantly decreased between 6 months and 1 year post-surgery (Table 1) and the peak knee flexion moment at 1 year was also significantly lower than the control group. No differences were seen in knee excursion or self-selected walking speed between groups.

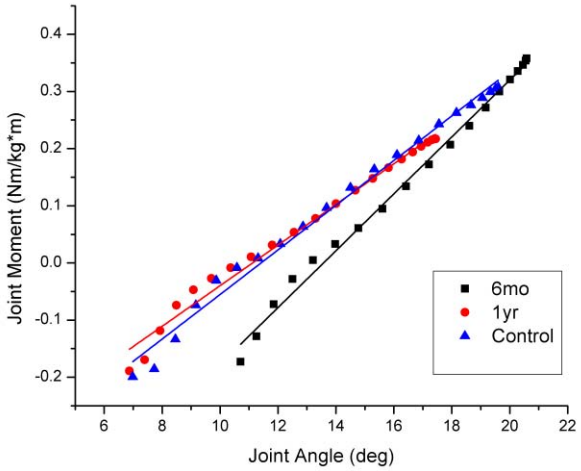

Figure1: Dynamic Knee Joint Stiffness after TKA

Because there was no difference in excursion between groups, the decrease in dynamic knee stiffness seen in the 1 year group occurred secondary to a reduction in the external knee flexion moment during the loading phase. These differences in joint moment occurred despite the fact that there were no differences in walking speed or peak knee flexion angle. Additionally, there were no differences between 6 months and 1 year for quadriceps strength.

Dynamic knee stiffness is an important parameter to evaluate because it is representative of how joint motions are controlled relative to the loads applied at the knee. Dynamic knee joint stiffness may be a useful tool to evaluate patients post surgery and may be related to higher levels of co-contraction that are found to exist pre- and post-operatively in persons with knee OA who undergo TKA. The results in this study are similar to previous work that showed improvements in temporo-spatial parameters within 3 months after surgery (stride length, walking speed, etc.), despite a significantly higher knee stiffness when compared to the control subjects [4]. This persistence of high values for knee stiffness can have negative long term effects, although based on our results, appears to dissipate 1 year after TKA [4]. Future work should examine clinical and biomechanical alterations that contribute to the reduction in knee moment and subsequent reduction in knee joint stiffness that occurs 1 year after TKA. Additionally, knee stiffness, joint excursions, and moments will be determined for the non-operated limb.

REFERENCES

1. Jacobs, JJ et al. *The Burden of Musculoskeltal Diseases in the United States*. American Academy of Orthopaedic Surgeons, 2008.
2. McClelland, JA et al. *The Knee* **14**, 253-263, 2007.
3. Zeni, AJ et al. *Clinical Biomechanics* **24**, 366-371, 2009.
4. Weatherly, K et al. Combined Sections Meeting of APTA 2010.

ACKNOWLEDGEMENTS

Funding for this study was provided by NIH P20 RR016458-08S2, NIH P20 RR016458 and NIH R01HD041055.

Table 1: Gait parameters [mean (standard deviation)];

Variable	TKA 6 months	TKA 1 year	Control
PKFM (Nm/kg*m)	0.35 (0.20)	0.21 (0.15)*†	0.31 (0.19)
Excursion (degrees)	10.34 (3.88)	10.70 (4.28)	12.46 (4.80)
Walking Speed (m/s)	1.36 (0.15)*	1.25 (0.17)*†	1.42 (0.15)
Quadriceps Strength (N/BMI)	17.98(6.75)	18.98(8.69)	

PKFM = peak knee flexion moment during loading response, * p>0.05 compared to controls, † p<0.05 compared to 6 month post-op TKA group

BIOMECHANCAL ANALYSIS OF STEPPING DOWN IN CONTINUOUS GAIT FOLLOWING ANKLE EVERTOR FATIGUE: A PILOT STUDY

Federico Pozzi, Gregory M. Gutierrez, and Marilyn Moffat

Department of Physical Therapy, New York University, NY, USA
email: fp485@nyu.edu, web: http://steinhardt.nyu.edu/pt/

INTRODUCTION

Everyday we are constantly challenged to step up and down from heights (eg. street curbs) during continuous gait. It has been proposed that during stepping down, the leading leg has to absorb the kinetic energy at landing, and a failure in energy absorption can lead to a loss of balance [1]. Additionally, muscle fatigue (MF) has been found to have an adverse effect on balance performance [2] and gait parameters [3], and thus may also be interpreted as a risk factor for falls. Therefore, the purpose of this pilot work is to evaluate the role of MF of the ankle evertors on kinematics, kinetics, and EMG of the lower extremity while stepping down during continuous gait.

METHODS

Six subjects (3M/3F, age = 27.0±2.3 yrs, height = 1.69±0.08 m, mass = 63.88±8.49 kg) gave informed consent and completed a physical screening form to assure that all subjects were free from any cardiovascular, neuromuscular, and musculoskeletal conditions that may affect movement patterns.

A custom 8.5 m walkway was built with a 15 cm step to simulate a street curb. A force plate (Kistler Instruments, Amherst, NY) was embedded in the lower walkway to capture data (sampling at 1200Hz) from the leading leg while stepping down. Subjects were asked to walk barefoot on the elevated walkway, step down with their test leg (determined by coin flip) on the ground level walkway, and keep walking until the end of the platform. Subjects performed one baseline measure (3 trials) and one post-fatigue measure (3 trials). Trials were discarded and performed again if subjects did not contact the force plates cleanly, targeted the plates, or if speed exceeded +/- 5% of their pre-determined self-selected speed.

Subjects were equipped with clusters of three markers on the first metatarsal, calcaneus, and shank and single markers on the pelvis (4), thigh (2), and lateral knee (1) on both legs. Kinematic data were acquired at 120Hz using five ProReflex cameras (Qualisys, Gothenburg, Sweden). EMG electrodes (DE-2.1, Delsys Inc, Boston, MA) were placed on the belly of the following muscles of the test leg: tibialis anterior (TA), peroneus longus (PL), peroneus brevis (PB), medial gastrocnemius (MG), vastus medialis, rectus femoris, and biceps femoris. EMG data were collected at 1200Hz using a Bagnoli 8 channel EMG system (Delsys, Inc., Boston, MA). The EMG signal was filtered (2^{nd}-order Butterworth; f_c = 10-300Hz), rectified, smoothed (2^{nd}-order Butterworth; f_c = 7Hz), and the signal was normalized to the maximal activation for each muscle during the gait trials.

The fatigue protocol was executed on the Biodex System III isokinetic dynamometer (Biodex Medical System, Shirley, NY). Subjects performed three maximal concentric (CON) and eccentric (ECC) eversion muscle actions at 90º/sec to calculate the maximal ECC eversion force. Then, they performed a fatigue protocol, which consisted of continuous CON-ECC eversion muscle actions at 90º/sec until fatigued. Subjects were considered fatigued when the ECC force output fell below 50% of the maximal ECC force for three consecutive ECC muscle actions. Due to the pilot nature of this work, only descriptive statistics were calculated.

RESULTS AND DISCUSSION

After the fatigue protocol, the PL and PB showed a 5-8% decrease in activation following touchdown. Surprisingly, the TA showed a similar decrease in activity (~10%) both before and after touchdown (Fig. 1). We believe that this result may be due to the inability to completely isolate the evertors on

the isokinetic dynamometer. Additionally, eversion is a complex movement, which also involves some degree of dorsiflexion, which may explain the decrease noted in the TA.

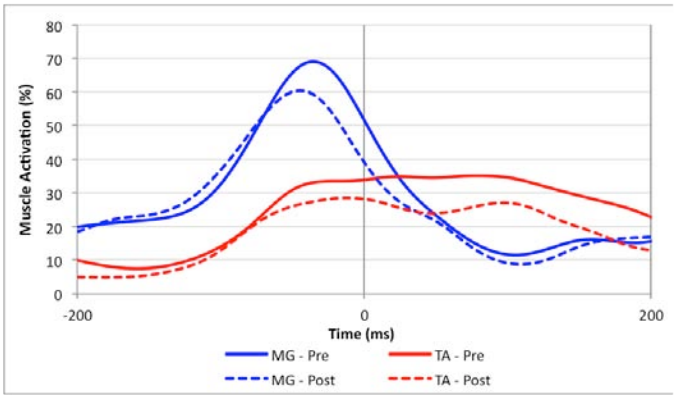

Figure 1: TA and MG EMG activation pre (solid) and post (dotted) fatigue. The vertical line represents touchdown.

It has been demonstrated that landing strategies (toe vs. heel) will change in relation to the height of the step [4]. According to the results of that study, we assumed that toe landing was the preferred strategy for our subjects, and that assumption was met. Van Dieen et al. investigated the mechanics of toe and heel lending and found that the leading leg absorbs more energy during toe landing [5]. This produces high dorsiflexion moments and negative power (increased energy absorption) at the ankle joint, which increases the demand on the ankle muscles to maintain joint stability. Our data showed similar patterns of moments and power after touchdown (Fig. 2). Toe landing produces a more anteriorly directed ground reaction force (GRF), which was responsible for generating the dorsiflexion moment at the ankle that was maintained throughout the first 200ms of stance. The peak negative power occurred right after touchdown, indicating high energy absorption at the ankle joint.

The isokinetically induced MF of the ankle evertors appeared to disrupt this pattern. We observed a decrease in both dorsiflexion moments and peak negative power (less negative in both cases; Fig. 2). This altered pattern may have been related to the decrease in the EMG activation of the TA, PL, and PB. Under normal conditions, the combined activation of these muscles in the first 200ms after touchdown may increase ankle stability, allowing more solid support for high moments and power generated by toe landing. Because the kinematics of the lower limb segments are similar pre and post fatigue, we hypothesized that a change in the alignment of the upper body during step down may alter the GRF direction, reducing the moment and power to compensate for the reduction in ankle muscle activity. Further studies are needed to support this hypothesis.

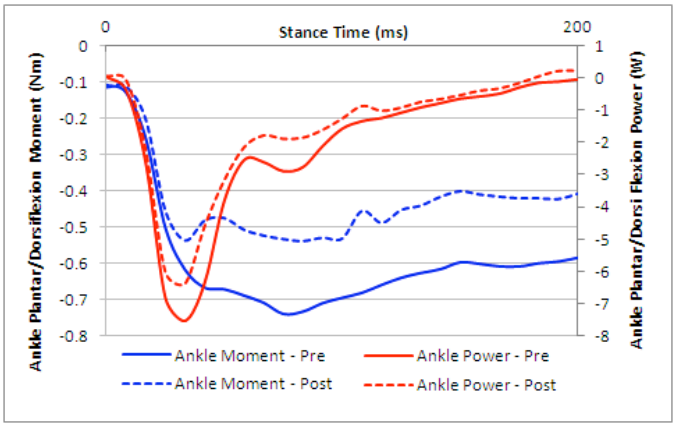

Figure 2: Ankle sagittal plane moment ([-] = dorsiflexion moment) and power ([-] = energy absorption) in the first 200ms of stance.

Our data also showed a decrease in the MG activation (~10%) immediately before and after touchdown following MF (Fig. 1). We believe that this change was likely made in anticipation of a decrease in peak negative power, rather than a direct consequence of MF. The convergence of MG activation and sagittal plane power (~50 ms post-touchdown) pre/post MF supported this hypothesis.

CONCLUSION

It appears that isokinetic fatigue at the ankle, which alters muscle activation, may change the biomechanics of gait to accommodate for the decreased activity.

REFERENCES

1.van Dieen JA, et al. *J Biomech* **40**, 3641-3640, 2007.
2.Reimer RC 3rd, et al. *J Sci Med Sport* **13**, 161-166, 2010.
3.Parijat P, et al. *Gait & Posture* **28**, 568-573, 2008.
4.van Dieen JA, et al. *Gait & Posture* **29**, 343-345, 2009.
5.van Dieen JA, et al. *J Biomech* **41**, 2417-2421, 2008.

ANKLE ACTUATOR DEFICITS IN THE PRESENCE OF ACHILLES TENDINOPATHY

[1]Yu-Jen Chang, [2]Adam Siemieński, [1]Robert J. Gregor and [1]Kornelia Kulig

[1] Jacquelin Perry Musculoskeletal Biomechanics Research Laboratory, Division of Biokinesiology and Physical Therapy, University of Southern California, Los Angeles, CA USA
[2] Department of Biomechanics, University School of Physical Education, Wrocław, Poland
email: changyuj@usc.edu, web: http://pt.usc.edu/labs/mbrl

INTRODUCTION

Tendon is the primary elastic energy storage-release structure actuated during the stretch-shortening cycle of the musculotendinous unit. An injured tendon, which is more compliant [1], may lead to an alteration in this energy modulation capability. The regulation of joint stiffness, however, is not achieved solely by the tendon, but is also controlled by the activation of skeletal muscle. During sub-maximal hopping, the ankle joint is the primary contributor to the leg stiffness [2]. We hypothesize that in the presence of Achilles tendinopathy, (1) the body will maintain ankle joint stiffness to preserve total leg stiffness; and (2) the tendinopathic Achilles tendon will not be able to exert the same amount of effort, determined by the net joint moment and net joint moment power, as the healthy tendon during the concentric phase of hopping.

METHODS

Twelve male subjects participated in this study, five with Achilles tendinopathy (46.8±9.0y/o), and seven without any known lower extremity pathology (44.6±8.2y/o). Lower extremity kinematics (Vicon 612 motion analysis system, Oxford, UK; 120Hz), and kinetics (AMTI force plate, Watertown, MA; 1,560Hz) were calculated during single-legged hopping at 2.2Hz (Fig. 1). Each subjects performed 20 hops, of which 8-20 were retained. Vertical ground reaction force (GRF_v, Fig.1A) data were used to calculate the leg stiffness (k_{leg}) at maximal GRF_v by the following equation:

$$k_{leg} = \frac{\dot{GRF_v}}{\int GRF_v} * m \qquad (1)$$

Where m is the body mass of the subject.

Sagittal plane Net Joint Moment (NJM) and Net Joint Moment Power (NJP) of the ankle joint were calculated using standard inverse dynamics (Fig. 1B and C). Angular stiffness of the ankle joint (k_{ankle}) at the interval of maximal GRF_v was defined using the following equation:

$$k_{ankle} = \left|\frac{\Delta\tau}{\Delta\theta}\right| \qquad (2)$$

Where τ is the NJM, and θ is the sagittal plane angular displacement of the ankle joint.

The concentric phase was defined as the time period when the ankle NJP is positive. Averaged ankle NJM and NJP during the concentric phase were calculated for each hop and averaged for each subject.

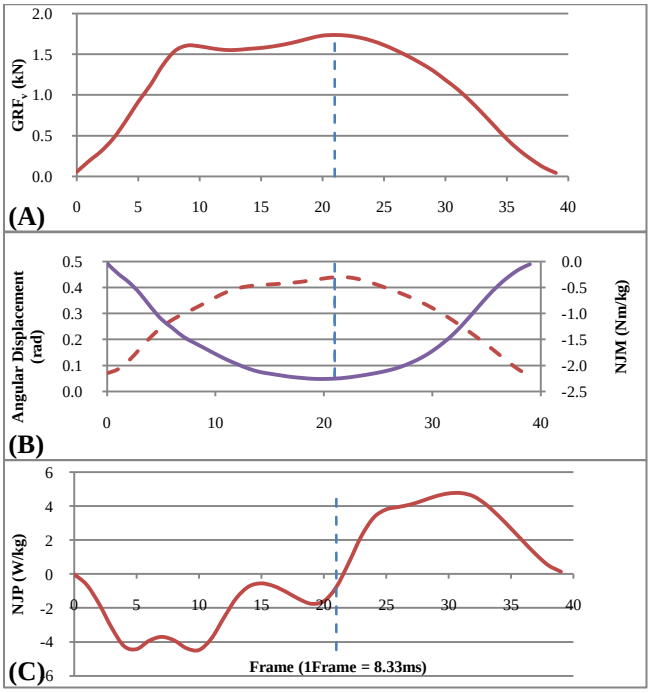

Figure 1. Vertical ground reaction force (A); sagittal angular displacement (dashed line) and net joint moment (solid line) at the ankle (B); and net joint moment power (C) at the ankle joint in the sagittal plane, from a typical hopping trial. Vertical dashed lines represent the instant of maximal ground reaction force.

RESULTS AND DISCUSSION

The analyses of leg stiffness at the time of maximal GRF_v showed no difference between Achilles tendinopathic subjects (AT) and healthy controls (HC) (Fig. 2A). Ankle joint stiffness also showed no difference between groups (Fig. 2B). This implies that humans attempt to maintain optimal leg stiffness through regulating the ankle stiffness, which can be achieved by modulating the muscle activations. In this study, we did not incorporate EMG to monitor the muscle activation. For future studies, EMG should be used to better understand the interaction between the tendon pathology and corresponding muscle activation.

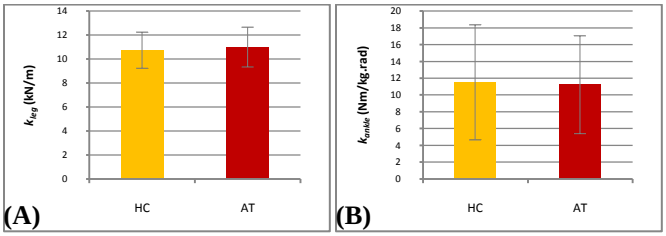

Figure 2. Leg stiffness (k_{leg}) and ankle joint stiffness (k_{ankle}) at the interval of maximal GRF_v in both groups. HC=healthy control, AT=Achilles tendinopathic, during hopping @ 2.2 Hz. Whiskers are SEM.

During the concentric phase, individuals with Achilles tendinopathy showed lower averaged ankle NJM and, though to a lesser extend, lower averaged ankle NJP (Fig. 3A and B). Human Achilles tendon is the primary structure designed to store and release elastic strain energy that ultimately reduces the metabolic costs during locomotion [3]. Lower NJM and NJP may indicate that the energy release during the concentric phase was down-modulated which may be attributed to the more compliant tendinopathic tendon.

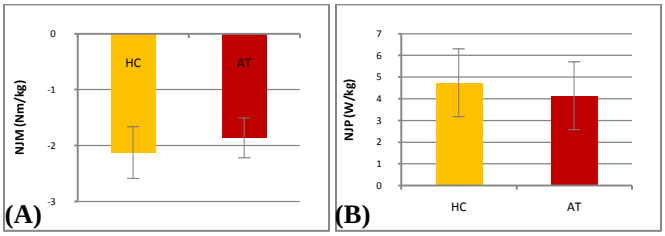

Figure 3. Averaged sagittal plane ankle net joint moment (NJM) (A), and net joint moment power (NJP) (B) during the concentric phase of hopping @ 2.2Hz. Whiskers are SEM.

These data also suggest that, during a novel unipedal ballistic activity, although the involved musculotendinous complex is able to maintain the joint and leg stiffness to prevent the body from collapse, the injured tendon cannot provide the desired power output during the concentric phase of hopping. This phenomenon might further alter the relationship between muscle and tendon and hence affect the motor control strategy. In sub-maximal hopping, this strategy is generally believed to be a force-dependent feed-forward control. Future studies need to address muscle activation and the role of the nervous system to clarify the impact of a local tendon injury on human movement control strategies.

REFERENCES

1. Arya S. & Kulig K. *J Appl Physiol.* 2009 Nov 5. [Epub ahead of print]
2. Farley CT, et al. *J Biomech* **32**, 267-273, 1999
3. Fukunaga T, et al. *Proc R Soc Lond* B **268**, 229-233, 2001

LOWER EXTREMITY KINEMATIC SEQUENCE DURING THE SINGLE LEG HOP TEST FOLLOWING ACL RECONSTRUCTION

Karl Orishimo, Malachy McHugh, Ian Kremenic, Michael Mullaney, Stephen Nicholas
Nicholas Institute of Sports Medicine and Athletic Trauma, New York, NY, karl@nismat.org

INTRODUCTION

The propulsive phase of a stretch-shortening cycle movement, such as a jump, is characterized by a proximal to distal transfer of joint velocities, with peak hip extension velocity preceding peak knee extension velocity, which in turn precedes peak plantarflexion velocity [1,2]. The purpose of this study was to examine this kinematic sequence during a single limb hop test in patients after ACL reconstruction.

METHODS

Thirteen patients who had undergone an ACL reconstruction (9 M, 4 F; Height: 174.5 ± 9.4 cm, Mass: 72.3 kg ± 11.9 kg, Age: 33 ± 10 yrs) performed maximal-effort single-leg horizontal hops on both the involved and noninvolved legs. All subjects were undergoing rehabilitation at our physical therapy clinic following a bone-patellar tendon-bone ACL reconstruction and had no history of injury to their noninvolved leg. Once subjects reached the point in their rehabilitation that they were able to successfully perform a clinically-normal single-leg hop test (85% of distance hopped on the noninvolved leg), they were tested for this study (a range of 4-12 months following surgery).

Kinematic data were recorded using six infared cameras (Qualysis) and 27 reflective markers. The motion data were then filtered with a fourth-order Butterworth low-pass filter with a cutoff frequency of 10 Hz in order to eliminate any high frequency noise.

Hop distance was measured from the toe in the starting position to the heel at landing. The propulsive phase of the jump was defined from the end of the counter-movement to takeoff. Sagittal-plane joint velocities (ankle, knee, hip) during the propulsive phase were calculated using specialized computer software (Visual 3D, C-Motion, Inc., Rockville, MD, USA). Ankle plantarflexion, knee extension and hip extension velocities were defined as positive values. For each subject, the velocity profile of each joint was normalized to the maximum velocity achieved by that joint during the propulsive phase. A paired t-test was used to compare hop distance and joint velocity profiles between the involved and noninvolved legs. $P < 0.05$ was considered significant.

RESULTS AND DISCUSSION

All subjects hopped further on the noninvolved leg (145.2 ± 30.6 cm) compared to the involved leg (135.8 ± 31.9 cm; $P < 0.001$). Hop ratios were greater than 85% and thus in the clinically normal range (87% to 99%; mean 93%).

Ensemble averages of the normalized joint velocities for the involved and noninvolved legs are shown in Figures 1 and 2. The arrow in each graph indicates the point where hip and ankle velocities are equal (hip decelerating, ankle accelerating) and is referred to here as the X-Point. The shaded area on the graphs illustrates the relationship between knee and ankle velocity immediately prior to peak ankle velocity.

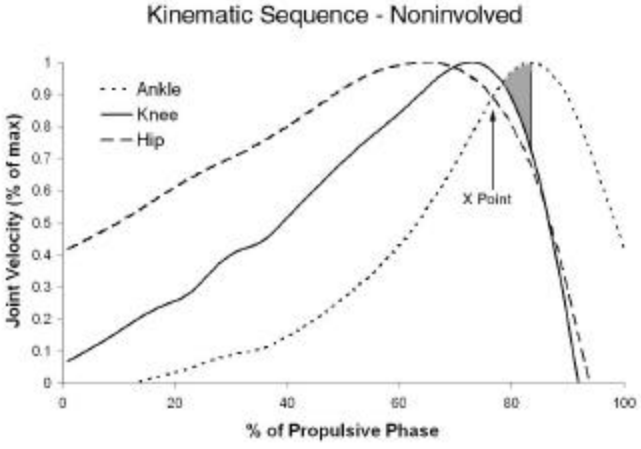

Figure 1: Kinematic sequence for the noninvolved leg

On the noninvolved side, hip and ankle velocities were 89% of peak at the X-Point and knee velocity was 97% of peak. On the involved side, hip and ankle velocities were 84% of peak at the X-Point and knee velocity was 91% of peak (lower relative velocities on the involved side $P<0.05$). With respect to the shaded areas, knee extension velocity at peak plantarflexion velocity on the noninvolved side was 75% compared with 29% for the involved side ($P<0.01$).

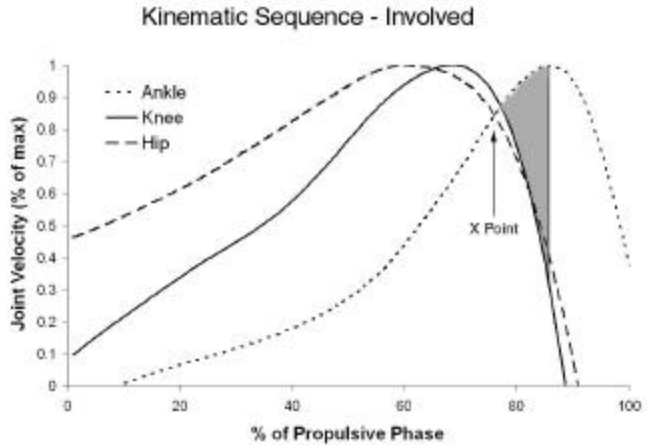

Figure 2: Kinematic sequence for the involved leg

These analyses indicate an impaired kinematic sequence on the involved side with an apparent disruption of the transfer of velocity from the knee to the ankle. Despite this disruption, hop distances on the involved and noninvolved legs were similar and the each patient's hop test was considered clinically within normal limits.

CONCLUSIONS

Although the mechanical stability provided the by ACL had been restored through surgical reconstruction, functional impairment of joint kinematics seems to persist during this high-demand activity. Methodologically, normalized proximal to distal to distal joint velocities may be a useful approach to studying stretch-shortening cycle kinematic sequences.

REFERENCES

1. Bobbert MF and van Soest AJ. *Exerc. Sport Sci. Rev*. **29**. 95-102. 2001

2. Rodacki A, *et al. Med. Sci. Sport Exerc*. **33**. 1157-1167. 2001

A COMPARISON OF MAXIMAL KNEE MOMENTS GENERATED DURING SINGLE JOINT KNEE EXTENSION AND LEG PRESS TASKS

[1]Mark T. Gordon, [2]Brian W. Schulz, and [1]James A. Ashton-Miller
[1]University of Michigan, Ann Arbor, MI, USA
[2]VA HSR&D/RR&D Center of Excellence, Maximizing Rehabilitation Outcomes,
James A. Haley VA Hospital, Tampa, FL, USA
email: mtgordon@umich.edu, web: http://me.engin.umich.edu/brl

INTRODUCTION

The peak knee extensor moment developed during an isolated knee extension exercise and a leg press exercise are often recorded under isotonic and/or quasi-isometric conditions [1,2]. From a training perspective it is important to know how those moments compare during the shortening and lengthening phases of exercises on such machines. So the present study compares the peak knee moment generated using a Biodex ('single joint') dynamometer with that on servo-controlled ('multi-joint') leg press machine (BLAST!, BioLogic Engineering, Inc., Dexter, MI) during the shortening and lengthening phases of quadriceps contraction.

METHODS

Seven male and seven female healthy younger adults (ages 20-35 years) were recruited to be part of the study. The average body mass was 74 (14) kg and the average height was 173 (11) cm. The data from one male subject was excluded from the study due to the subject stopping the Biodex machine during the trials. The data from the 90°/s and 120°/s trials shortening contraction of five additional subjects (2 male and 3 female) were excluded due to data recording errors.

Kinematic data were collected at 120 Hz using a Vicon camera system and 36 markers and were low pass filtered at 6 Hz. Force data were collected at 80 Hz from the BLAST! machine.

The knee extension exercise was performed on a 'single joint' BIODEX dynamometer. Trials were performed at three different velocities (60°/s, 90°/s, and 120°/s). The order of the velocities was randomized and the subjects completed the order three times for a total of nine trials. Each trial started with the subject's knee at flexed at ~90°. The subject first exerted maximal knee moment using a shortening quadriceps contraction to extend the knee, then exerted a maximal knee extensor moment while the dynamometer flexed the knee back to ~90° with a lengthening quadriceps contraction.

The leg press task was performed at three different knee angle velocities (15°/s, 25°/s, and 35°/s). The subject again started the trial with the knee at ~90° flexion. The subject then pushed on the foot plate with maximal force while the plate was driven distally at a prescribed rate, resulting in a quadriceps shortening contraction. Foot force was recorded normal to the foot plate. After 1-5 sec. rest, the subject pushed maximally against the foot plate as it returned towards them using a lengthening quadriceps contraction. The trials were randomized in the same manner as the knee extension trials. Single joint testing was completed one or more days prior to the leg press testing.

A subject-specific 3-D biomechanical model was generated in OpenSim. Positional data were used to scale a torso and leg musculoskeletal model and generate the kinematics of the leg press exercise. The force data was then combined with the kinematic data and inverse dynamics was used to solve for the knee joint moment. Knee joint moment data were normalized by dividing the joint moment by the subject's weight (N) and height (m) for both the knee extension and the leg press tasks.

Since there was a difference in knee joint rotational velocities on the BIODEX and leg press machines, the data could not be directly compared across machines at the same velocity. Instead the values were averaged to provide a peak knee extension moment for each apparatus during the quadriceps

shortening and lengthening phases. The peak 'leg press' knee moment was averaged across both knees to compare with the 'single joint' knee moment value after a 13% adjustment for the difference in knee joint velocities [3].

RESULTS AND DISCUSSION

The peak 'single joint' knee extensor moment was not a reliable predictor of the peak 'leg press' knee extensor moment in quadriceps shortening (Figure 1) or lengthening (Figure 2) contraction phases. This was surprising since each task involved a maximal exertion involving the knee joint. The bilateral deficit for the peak force during a leg press task is known to be approximately 80% [4] (dotted line in Figures 1 and 2). The data from the present study fall above that line and the peak knee extensor moment generated during the 'leg press' exercise proved significantly greater than during the 'single joint' knee extension exercise ($p \leq 0.05$).

On both machines, the quadriceps shortening phase peak knee moment could be used to predict the peak moment developed during the quadriceps lengthening phase (Figure 3).

Two limitations of this study include the modest sample size (n=13) and the leg press machine only recording the normal foot plate force. The latter is a relatively minor source of error based on unpublished data gathered on an earlier version of the machine equipped with a 6-axis force plate.

CONCLUSION

The peak knee joint extensor moment generated in a leg press task was significantly greater than the maximal knee extensor moment developed in the 'single joint' task. This has implications for the training and rehabilitation of the knee extensor muscles.

REFERENCES

1. Escamilla RF, et al. *Med&Sci in Sports Exercise* **39:4**, 556-569, 1998.
2. Wilk KE, et al. *Am J Sport Med* **24**, 518-527, 1996.
3. Tihanyi J, et al. *European J Appl Phys* **48**, 331-343, 1982.
4. Vandervoort AA, et al. *Phys Soc* 46-51, 1983.

ACKNOWLEDGEMENTS

This study was supported by a VA RR&D Career Development Award (E2964F) and Research Award Enhancement Program.

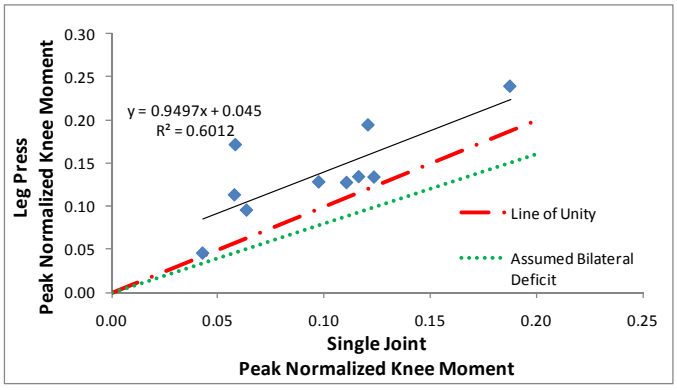

Figure 1: Comparison of peak knee moment data from both the 'single joint' and leg press machines during the quadriceps shortening contraction phase.

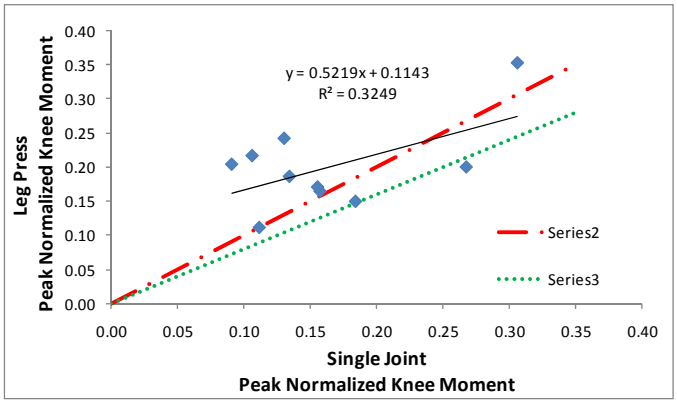

Figure 2: Comparison of peak knee moment data from both the 'single joint' and leg press machines during the quadriceps lengthening contraction phase.

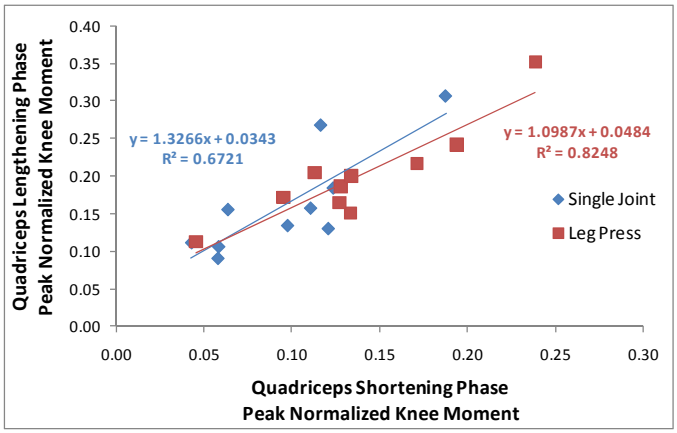

Figure 3: Peak knee extension moment during the quadriceps shortening and lengthening contraction phases for the knee extension and leg press tasks.

EFFECT OF IMPULSIVE TRANSVERSE PLANE TIBIAL TORQUES AND FRONTAL PLANE MOMENTS ON IN VITRO ACL RELATIVE STRAIN DURING A SIMULATED JUMP LANDING

[1]Youkeun Oh, [2]David Lipps, [1,2]James Ashton-Miller, [3]Edward Wojtys

[1]Mechanical Engineering Dept., [2]Biomedical Engineering Dept., [3]Orthopaedic Surgery Dept.,
University of Michigan, Ann Arbor, MI, USA
email: youkeun@umich.edu, web: http://me.engin.umich.edu/brl

INTRODUCTION

Non-contact ACL injuries frequently occur under multi-plane dynamic knee loadings. Previous studies have examined ACL loading under relatively modest quasi-static knee loads [2, 3, 4]. Ahmed et al. [1] provided early insight into how transverse and frontal plane moments in the presence of the anterior tibial translation can strain the ACL. For example, the ACL would be more strained if the tibia rotates about a point on the medial aspect of the tibia than on the lateral aspect of the tibia. We tested the hypothesis *in vitro* that, under the large impulsive loads associated with a simulated jump landing, that neither the direction of the applied axial tibial torque (i.e., internal vs external tibial torque) nor the direction of the frontal plane moment (i.e., varus or valgus) would affect anteromedial bundle anterior cruciate ligament (AM-ACL) relative strain.

METHODS

Nine fresh male cadaveric knees [mean (SD) age: 52.2 (16.0) years; five males] were mounted in a testing apparatus modified from Withrow et al. [4]. Under pre-impact quadriceps, hamstring and gastrocnemius muscle tensions, an impulsive force (~1 kN peaking at 50 ms) applied a peak flexion moment (~50 Nm peaking at 70 ms), varus or valgus moment (~ ±12 Nm peaking at 70 ms) and internal or external axial torque (~ ±25 Nm peaking at 70 ms) to the distal tibia with the knee initially in 15 deg of flexion. A 3-mm DVRT (Microstrain, Burlington, VT) was mounted on the AM-ACL to record relative strain. Tibiofemoral kinematics were recorded at 400 Hz, while 6-axis load cell, muscle forces and DVRT data were recorded at 2 kHz. After five pre-baseline (compression + flexion moment) trials ('A1'), four blocks of six trials were run on each specimen in an 'A1-B-C-D-E-A2' design, where the post-baseline block is 'A2'. The first experimental block ('B') was randomized to be either varus or valgus moment combined with either internal or external tibial torque. Then the direction of the frontal plane moment was reversed on each block, while the axial tibial torque direction was reversed for blocks 'D' & 'E'. A repeated measures ANOVA was used to test the hypotheses ($p<0.05$ being considered significant).

RESULTS AND DISCUSSION

The mean peak AM-ACL relative strain was 7.2 ± 4.4 % and 7.6 ± 5.1 % under internal tibial torque combined with varus and valgus moment, respectively. The corresponding values were 2.6 ± 2.7 % and 2.4 ± 3.0 % under external tibial torque combined with varus and valgus moment, respectively.

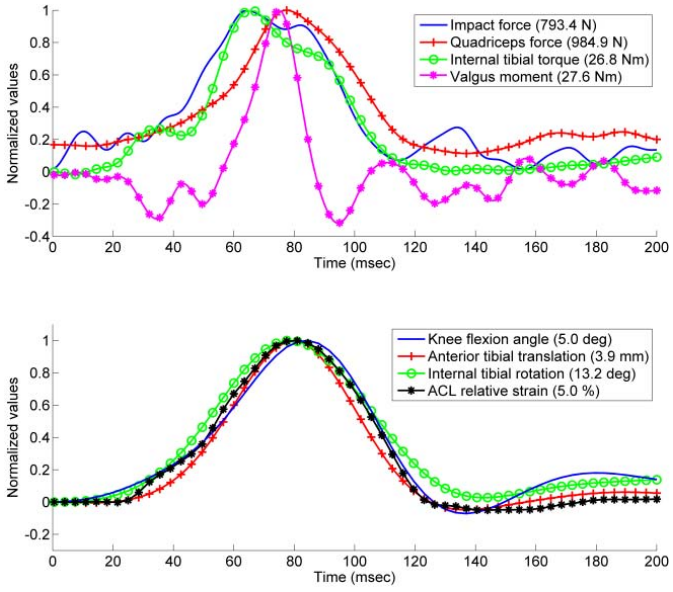

Figure 1: Sample temporal behavior of the applied impact force, resulting quadriceps force, internal

tibial torque, valgus moment, knee flexion moment, anterior tibial translation, internal tibial rotation, and AM-ACL relative strain. Measurements have been normalized to their peak values (see legends).

In a test of the hypothesis, the normalized mean peak AM-ACL relative strain was significantly greater under the internal than external tibial torque (p=0.004), regardless of the direction of the frontal plane moments (varus or valgus) (Fig. 2). This result corroborates, but extends the finding by Fleming et al. [3]. Their in-vivo quasi-static study suggested that the AM-ACL is not a restraint to varus-valgus moment.

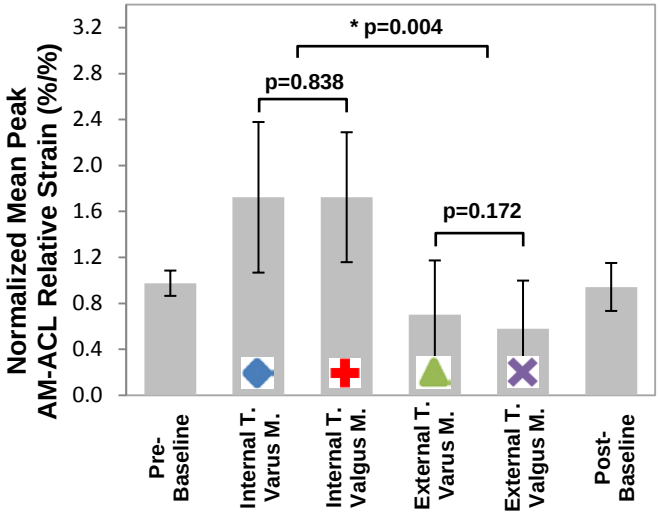

Figure 2: Normalized mean (SD) peak AM-ACL relative strain values under the frontal plane moments (M) and the axial tibial torques (T). Error bars represent ±1 standard deviation. The asterisk indicates a significant difference.

Under the internal tibial torque the tibia rotated about a medial center of rotation (COR), whereas under the external tibial torque it rotated about a lateral COR, regardless of whether a varus or valgus moment acted (Fig 3.). Ahmed et al. [1] suggested that the internal tibial torque would increase the ACL strain more when the tibia rotates about a medial COR than a lateral COR, and vice versa. Initially, we speculated that a varus and valgus moment would increase the compression on the medial and lateral aspects of the tibia, respectively, thereby guiding the location of the COR (i.e., a medial COR under a varus moment and a lateral COR under a valgus moment). However, because of the posterior translation of the femur relative to the tibia due to the large quadriceps force, the COR actually tends to occur on the medial and lateral aspects of the tibia for the internal and external tibial torque, respectively.

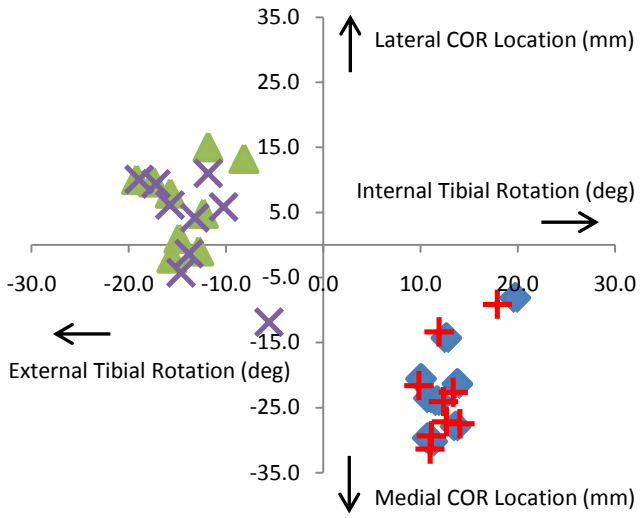

Figure 3: Axial tibial rotation angle vs. Center of rotation (COR) location under each compound impact loading (meaning of symbols shown in Fig. 2).

CONCLUSIONS

In the presence of muscle forces, the AM-ACL was strained the most under an impulsive internal tibial torque in the presence of compression and flexion moment, regardless of whether an impulsive varus or valgus moment acts during the simulated jump landing.

REFERENCES

1. Ahmed et al. JOR 1992;10:854-867
2. Durselen et al. AJSM 1995;23(1)
3. Fleming et al., J Biomech 2001;34(2):163-170
4. Kanamori et al. Arthroscopy 2002;18(4):394-398
5. Withrow et al. AJSM 2006;34(2):269-274.

ACKNOWLEDGEMENTS

This work was funded by NIH grant R01AR054821.

EFFECTS OF ANKLE IMMOBILIZATION ON KNEE JOINT BIOMECHANICS DURING AN UNANTICIPATED CUTTING MANEUVER

Rhonda Boros and Eric Plumlee

Texas Tech University, Lubbock, TX, USA
email: rl.boros@ttu.edu web: http://www.depts.ttu.edu/hess/biomechanics

INTRODUCTION

Ankle injuries, especially lateral sprains, are the most frequently sustained injury in sports and may account for as many as one-third of all sports injuries [1]. Because ankle sprains are recurrent in over 40% of cases, many athletes use ankle taping or bracing to try and prevent either initial ankle sprains or recurring ankle sprains [2, 3].

The effect of ankle immobilization on knee joint biomechanics is important because of the severity of knee injuries, specifically anterior cruciate ligament (ACL) injuries. ACL injuries negatively affect athletes in a number of ways, not the least of which is financially. While there is a large body of research on ankle immobilization (e.g. taping, bracing), there is considerably less regarding the effects of ankle immobilization on the motion of other lower extremity joints, especially the knee.

Landing studies that have investigated ankle immobilization have reported that vertical ground reaction forces tend to be consistent between braced and unbraced conditions, especially at initial contact (IC); however, it is difficult to associate landing tasks with cutting tasks, because landing from a vertical jump or drop does not require as much medial-lateral force as cutting does [4, 5].

The purpose of this study was to determine the effects of ankle immobilization on knee kinematics during an unanticipated 45° cutting maneuver.

METHODS

Four recreationally active, college-aged females (21.8±1.7 y, 1.7±0.0 m, 64.8±4.7kg) served as subjects in this pilot study to investigate the effects of brace use (ASO Ankle Stabilizers, Medical Specialties, Inc., Charlotte, NC) on knee joint kinematics during side-step cutting.

Participants were required to be between the ages of 18 to 25, recreationally active (i.e., exercise and participate in sport 3-5 days per week), have been former varsity high school basketball or soccer athletes, and currently free of any lower extremity injury at the time of testing. Potential subjects were turned away if they had ever suffered a lower extremity or back injury which required surgery. Participants wore their own “tight-fitting” clothes and athletic shoes. Upon arrival to the lab, subjects performed multiple trials of 45° cuts to the left and right. Motion analysis (300Hz, VICON-Nexus, Denver, CO) and force plate (1500Hz, AMTI, Advanced Mechanical Technology, Inc., Watertown, MA) data were utilized to obtain measures of peak vertical ground reaction force (VGRF) normalized to kg body mass, knee flexion at initial contact (FlexIC), peak knee flexion during contact (PKFlex), knee abduction angle at initial contact (AbdIC) and peak knee abduction angle during contact (PKAbd). Sixteen retro-reflective markers were attached to the subject, and the Nexus “plug in gait” served as the kinematic model for analysis. Statistical comparisons were made between braced and non-braced conditions via paired t-tests, with a significance level set at 0.05.

Subjects were instructed to sprint as fast as possible toward a lab assistant, who was acting as a “defender.” When the subject was approximately 2m away, the defender moved slightly to the right or left, forcing the subject to react and cut away (in the opposite direction) from the defender. Subjects had no prior knowledge of cut direction.

Brace condition (braced or non-braced) and cut direction (left or right) were determined using a random number generator. A successful cut trial resulted when the entire foot contacted the force plate. Trials continued until at least 14 successful trials (seven to the right and seven to the left) were

obtained. Braced and non-braced conditions were collected on separate days.

RESULTS AND DISCUSSION

Knee abduction angle at IC was significantly lower in the braced condition compared with the non-braced condition. No other statistically significant differences were observed. Summary results are presented in Table 1.

Table 1: Mean (SD) comparisons between braced and non-braced conditions. Positive abduction values denote knee adduction. * denotes statistically significant differences (P<0.05).

Condition	VGRF (N/kg)	FlexIC (deg)	PKFlex (deg)	AbdIC (deg)	PKAbd (deg)
Braced	26.8 (7.8)	21.5 (4.7)	47.5 (2.6)	-1.5 (6.1)*	-14.1 (10.8)
Non-braced	28.1 (8.6)	21.6 (5.2)	47.1 (5.7)	-7.8 (3.6)*	-19.1 (7.2)

CONCLUSIONS

Excessive knee abduction (i.e., valgus) at IC during landing has been reported to be potentially harmful to the ACL [6]. Our preliminary results suggest that the use of prophylactic ankle braces may actually reduce knee abduction during a cutting maneuver. Aside from the limited subject number, a possible explanation for these results may relate to the subject's experience with prophylactic brace use. Our subjects were healthy and uninjured, and generally did not have prolonged experience with brace use during their athletic careers. There have been some reports that athletes who utilize ankle braces or taping extensively during sports participation, either for prophylactic or joint instability reasons, may demonstrate altered joint mechanics during similar trials. In other words, perhaps our limited subjects altered their cutting strategy simply because they were wearing unaccustomed ankle braces. Further analysis is needed to determine the nature of this relation, and whether an accommodation period is warranted.

The reporting of knee abduction at IC is somewhat misleading, as the participants tended toward extremes. Two of the participants displayed knee abduction at IC, whereas the other two displayed slight knee adduction. The averaging of the data masks this polarity, and suggests an almost neutral knee position at IC. Examination of individual subject data reveals a positive relation between knee abduction at IC) and peak knee abduction during the cut. Two subjects demonstrated slight knee adduction (~1 to 5°) at contact, while the other two were abducted (~4 to 8°). These later two abducted subjects demonstrated peak knee abduction angles nearly four to seven times those of the other two (23.9° and 22.7° compared with 6.8° and 2.9°). It is unclear whether these extremes in frontal plane kinematics are a result of anatomy or are more neuromuscular and task specific in nature. Continued data analysis and increased subject population, to include males and athletes with prior brace experience and use, will ideally help illuminate the nature of this variability.

The use of the ankle braces had a lesser effect on stabilizing knee abduction (~3.5° reduction) in subjects demonstrating IC abduction compared with the IC adducted subjects (~8° reduction). These results suggest that the use of ankle braces, while possibly having a stabilizing effect on knee abduction, may have a relatively lesser protective effect in subjects who demonstrate excessive knee valgus and are more prone to ACL injury. The clinical relevance of this 3° to 8° reduction in abduction remains to be determined.

REFERENCES

1. Osborne MD, et al. *Sports Medicine*, **33**, 1145-1150, 2003.
2. Hughes T, et al. *Physical Therapy in Sport*, **9**, 136-147, 2008.
3. Venesky K, et al. *Journal of Athletic Training*, **41**, 239-244, 2006.
4. Hopper DM, et al. *British Journal of Sports Medicine*, **33**, 409-413, 1999.
5. Yi CH, et al. *Journal of Physical Therapy Science*, **15**, 81-85, 2003.
6. Hewett TE et al. *Am J Sports Med*, **33**, 492-501, 2005.

ACKNOWLEDGEMENTS

The authors would like to thank Larissa True, Dmitri Okorokov, and Kyle Litchfield for their help with collecting and analyzing data and recruiting participants.

FILTERING GRF DATA AFFECTS THE CALCULATION AND INTERPRETATION OF JOINT KINETICS AND ENERGETICS DURING DROP LANDINGS

Steven T. McCaw, Jacob Gardner and Lindsay Barlow
Illinois State University, Normal, USA
email: smccaw@ilstu.edu

INTRODUCTION

A joint kinetic and energetic analysis uses inverse dynamics to calculate joint moment of force (JMF), and joint mechanical power (JMP) as the product of JMF and joint angular velocity (ω) [6].

A kinetic and energetic analysis has been used to analyze contributions of the ankle, knee and hip joints to energy absorption during landing (i.e. [2, 3]) by integrating critical phases of the JMF and JMP data. However, compared to using unfiltered ground reaction force (GRF) data in the inverse dynamic analysis, digital filtering of the GRF causes dramatic differences in the JMF-time curves, especially at the hip and knee joints in the sagittal plane [1,4,5] where high frequency oscillations are attenuated. No project has quantified the altered JMF curves (integrals or peaks) and none has reported the effect of the altered JMF on subsequent calculation and integration of JMP.

We hypothesized that GRF filtering would decrease the calculated angular impulse (∫JMF) and negative work (∫JMP) at each joint, affecting the relative contribution of each joint to the total energy absorbed by the lower extremity.

METHODS

Six healthy, active, injury-free students (5 ♀, 1 ♂; age: 21.3±.7 y; ht: 1.67±.05 m; mass: 61.3±6.6kg) volunteered and provided informed consent. Subjects performed 5 soft and 5 hard (total 10 trials) two-legged landings off a 32 cm platform with the right foot landing on an AMTI forceplate (1000 Hz). Soft and hard landings differed in knee flexion range of motion during ground contact. Reflective markers, applied according to the *Plug-in Gait* template (Vicon), were tracked with 8 infrared cameras (200 Hz).

Hip, knee and ankle JMFs in the sagittal plane were calculated using two methods of data filtering (4th order low-pass Butterworth). In *Unfiltered*, marker data were filtered at 10 Hz, but the GRF were unfiltered. In *Filtered*, both GRF and marker data were filtered at 10 Hz. JMP was calculated as JMF • ω. Angular impulse and joint work were calculated for each trial by integrating the JMF and JMP time curves, respectively, between ground contact and maximum knee flexion. Total work was calculated as $\Sigma\ W_{Ank} + W_{Knee} + W_{Hip}$. The % of work by each joint was calculated as $Work_{Joint} / Work_{Total}$.

Five-trial mean values for each variable were entered into a 2x2 (style x filtering) repeated measures ANOVA (α=.05).

RESULTS AND DISCUSSION

There were no significant style x filtering interactions on the measures. There were significant main effects of both style and filtering. For brevity and to emphasize the effect of GRF filtering, results were pooled across the soft and hard landings (Table 1). For presentation clarity, grande ensemble averages were compiled from the linear envelopes of JMF and JMP data (Fig. 1) of individual subjects over the period between 10ms pre-contact and maximum knee flexion; only the grande ensemble curves for hard landings are presented.

GRF filtering attenuated the high frequency oscillations in the JMFs of the knee and hip, similar to [1,4,5]. The dominant, sharply peaked hip flexor JMF (15% of contact) and the rapid transition from a maximum to a minimum in the knee extensor JMF (15-25% of contact) were both eliminated. JMPs similarly exhibited reduced minima and maxima when JMF were calculated from filtered GRF data.

The extensor angular impulse and the negative work at all joints were significantly reduced compared to

using unfiltered GRF to calculate JMF (Table 1). Although total and joint works were reduced, relative joint contributions changed < 2%. Thus, although statistically significant, the alterations do not seem clinically meaningful.

Table 1. Descriptive statistics (Mean & SD) for angular impulse and work values calculated with and without filtering GRF data before the inverse dynamic analysis, pooled across soft and hard landings.

	Unfiltered GRF	Filtered GRF	
Moments($N \cdot m \cdot s \cdot kg^{-1}$): contact to max knee flexion			
Hip extensor impulse	0.093 0.059	0.081 0.055	*
Knee extensor impulse	0.289 0.077	0.285 0.077	*
Ankle Plantarflexor impulse	0.168 0.034	0.166 0.034	*
Powers ($J \cdot kg^{-1}$): contact to max knee flexion			
Work at hip	-0.20 0.16	-0.15 0.12	*
Work at knee	-1.37 0.37	-1.32 0.36	*
Work at ankle	-0.68 0.09	-0.65 0.09	*
Total Work	-2.26 0.50	-2.12 0.45	*
Relative Joint Contributions (% Total Work)			
Hip	7.8 4.2	5.8 3.7	*
Knee	59.2 4.0	60.8 5.1	*
Ankle	33.0 5.9	33.4 5.8	*

* p < .05

Of tremendous import is that GRF filtering altered *the fundamental patterns* of the JMF and JMP. Joint kinetics and energetics provide insight to the goals and strategies of the central nervous system [6]. The rapid oscillations in JMF and JMP calculated with unfiltered GRF data led to speculation on CNS strategies involving knee and hip joint trade-offs during landing [i.e. 2, 3] that may not be warranted with appropriate processing of GRF data.

CONCLUSIONS

Angular impulse and work values differ when JMF and JMP are calculated with and without filtering of GRF data, although the interpretation of individual joint contributions to total energy absorption is not affected. However, the attenuation of high frequency oscillations in both JMF and JMP time curves will influence interpretation of CNS strategies during landing.

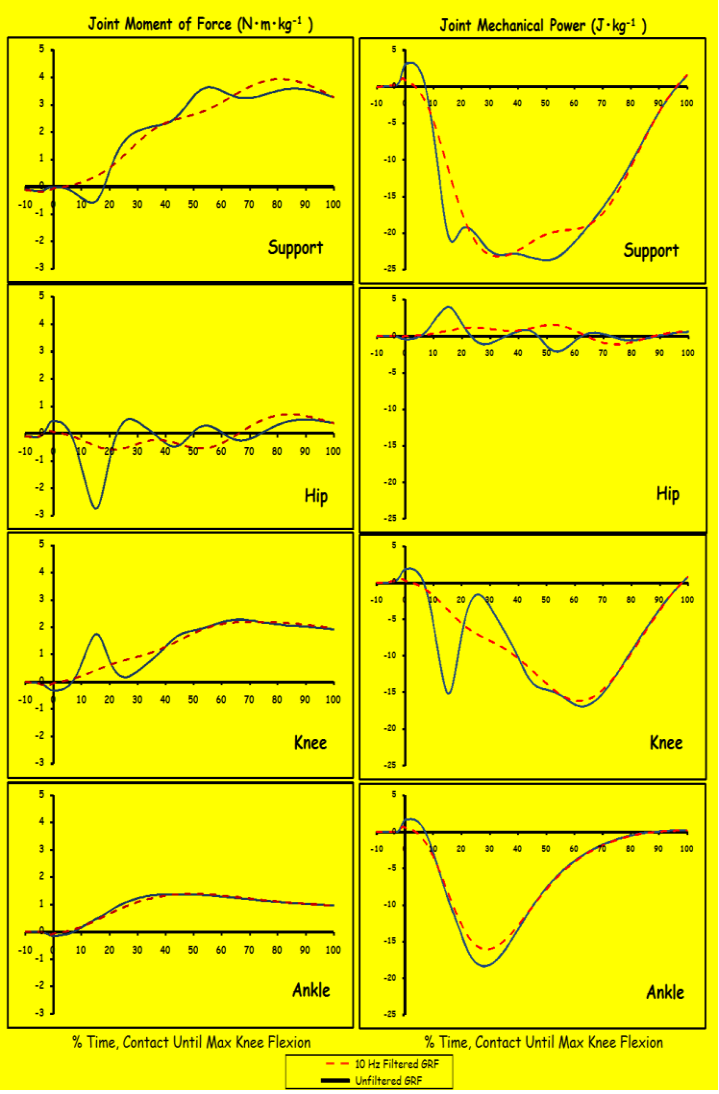

Figure 1. Grande ensemble average curves (n = 6, 5 trials) of JMFs (left) and JMPs (right) calculated with and without GRF filtering (10 Hz low-pass).
JMF: – flexor, + extensor
JMP: - Eccentric, + Concentric
(Hard Landing Data only)

REFERENCES

1. Bisseling, RW & Hof, AL. *J Biomech* **39**, 2438-2444, 2006.
2. DeVita, P & Skelly, WS. *MSSE* **24**, 108-115, 1992.
3. Madigan, ML & Pidcoe, PE. *J EMG & Kines*, **13**, 491-498, 2003.
4. van den Bogert, AJ & de Koning, JJ. *Proceedings of CSB*, Vancouver, 1996.
5. White, SC & Podraza, JT *Proceedings of ASB*, Stanford, 2007.
6. Winter, DA. *Biomechanics and motor control of human movement*. Wiley, 1979.

EFFECTS OF EXPERIMENTAL SETUP AND MODELING ASSUMPTIONS ON PREDICTED TRUNK PROPERTIES USING A SYSTEM IDENTIFICATION METHOD

Babak Bazrgari, Maury A. Nussbaum and Michael L. Madigan

Virginia Polytechnic Institute and State University, Blacksburg, VA, USA
email: nussbaum@vt.edu

INTRODUCTION

System identification methods have been used to estimate trunk mechanical properties (i.e., mass, stiffness, and damping) during sudden loading paradigms, as indirect measures of trunk neuromuscular control and to obtain information relevant to understanding and controlling low back pain. Despite an apparent sensitivity of these properties to several intrinsic and extrinsic factors, reported values have exhibited a wide range [1-3]. Such discrepancies may arise from sensitivities to experimental setup and modeling approaches. To address these issues, the present study investigated how trunk mechanical properties predicted with a system identification method are affected by: 1) positioning of the motion sensor; and 2) mechanical properties of elements between the trunk and the perturbing device (i.e., connecting rod, load cell, harness, and soft tissue below the harness).

METHODS

Six healthy individuals, gender balanced, with mean (SD) age of 23.2 (3.3) years and body mass of 69.3 (10.6) kg participated in the study. Participants stood in a custom metal frame designed to restrain pelvic and lower limb motions. A series of sudden, anteriorly-directed position perturbations were applied to the trunk at the T8 level via a rod-harness system. Each trial consisted of two 10-mm position perturbations at each of six different peak linear velocities (0.113, 0.232, 0.338, 0.457, 0.581, and 0.657 m/s). Displacements were measured at the motor and at the trunk surface. The former were obtained from a high-accuracy encoder (resolution ± 60 arcsec) attached to the servomotor shaft, while the latter were obtained from a high-accuracy (± 0.5 µm) laser displacement sensor (Keyence LK-G 150, Osaka, Japan) targeted at the midline of the dorsal aspect of the trunk immediately above the harness. Driving forces were measured using a load cell (Interface SM2000, Scottsdale, AZ, USA) in-line with the connecting rod. Two dynamic models (Fig. 1) were used to estimate trunk mechanical properties in response to the perturbations: 1) a one degree-of-freedom (1-DOF) mass-spring-damper system representing only the trunk; and 2) a two degrees-of-freedom (2-DOF) system that also included an extra mass-spring-damper element simulating passive responses of the connecting elements.

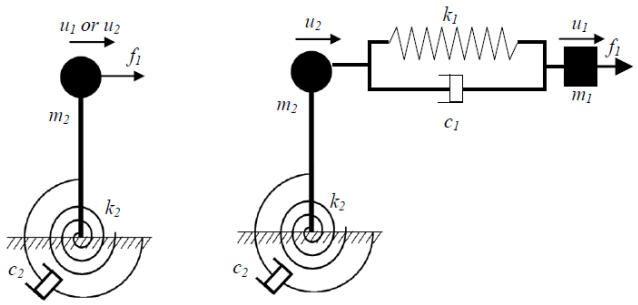

Figure 1. Schematic of the 1-DOF (left) and 2-DOF (right) models. u_1: kinematics from motor encoder; u_2: kinematics from laser sensor; f_1: kinetics from load cell; m, k and c: mass, stiffness and damping of the trunk and connecting elements.

Model parameters were determined by minimizing squared errors in estimated trunk kinetics (model output) given measured kinematics (model input). To investigate the effects of motion sensor positioning on model predictions, parameters of the 1-DOF system were evaluated using either kinematics from the motor encoder as input (1-DOF-M) or those from the laser sensor (1-DOF-L).

RESULTS AND DISCUSSION

Laser sensor readings revealed that the trunk started moving anteriorly ~ 10 ms after initiation of motor movement, in part due to initial deformation of soft tissues and harness padding. As a result, soft tissue deformation was erroneously considered part of

trunk motion in the 1-DOF-M model. Accordingly, the least-square curve fitting for the 1-DOF-M model simulated the trunk as a more damped structure. The 1-DOF-M was also not able to correctly capture the mass difference between males and females (Table 1). In contrast, parameters from the 2-DOF and the 1-DOF-L models were comparable, and these characterized the trunk as having more mass and less damping.

Predicted trunk mass was higher with the 1-DOF-L vs. 2-DOF models, reflecting inclusion of connecting element masses into predicted trunk mass in the former (Table 1). Other differences in predicted trunk stiffness and damping may as well be due to lumping of the properties of the connecting elements into the trunk properties in the 1-DOF-L model. Nonetheless, differences were small, mainly due to the use of relatively rigid connecting elements that resulted in a predominant contribution of trunk dynamic responses versus connecting elements to the measured force. Trunk stiffness in the current scenario (i.e., relaxed, upright posture) was predicted to be zero or negligible using all three models (Table 1).

Table 1. Predicted trunk mass (*m*), damping (*c*), and stiffness (*k*). Results are mean (SD) values over all trials, perturbing velocities, and participants.

		m (kg)	*c* (Nms/rad)	*k* (Nm/rad)
2-DOF Trunk	M	20.7 (1.4)	49 (4)	0 (0)
	F	16.2 (1.0)	18 (1)	0 (0)
	All	**18.5 (1.2)**	**34 (2)**	**0 (0)**
1-DOF-L	M	22.5 (1.5)	45 (4)	14 (25)
	F	18.4 (1.0)	15 (1)	100 (25)
	All	**20.5 (1.2)**	**30 (2)**	**57 (3)**
1-DOF-M	M	1.4 (1.9)	86 (4)	0 (0)
	F	2.8 (1.7)	48 (4)	0 (0)
	All	**2.1 (1.8)**	**67 (4)**	**0 (0)**

When the connecting rod was in tension (i.e., when pulling the trunk anteriorly), all three models predicted forces from measured kinematics similar to those measured ($r > 0.98$; Fig. 2). However, only the 2-DOF model provided reasonable representations of trunk kinetics when rod was under compression (i.e., when trunk motion is stopped). Reflexive muscle responses in the present study are likely to occur when the connecting rod is under compression, and are expected to unload the connecting rod slightly. As such, measured trunk kinematics should be less than model predictions that do not account for the reflexive component.

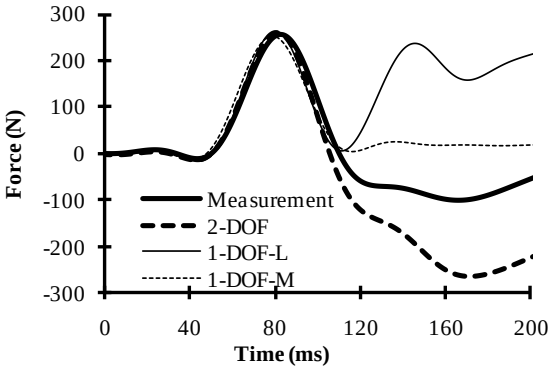

Figure 2. Sample predicted vs. measured forces during a trial with peak linear velocity = 0.338 m/s. Positive force = connecting rod in under tension.

CONCLUSIONS

The development of an effective method to assess trunk mechanical properties, as indirect measures of trunk neuromuscular control, may provide information relevant to the identification, control, and management of low back disorders. The results here suggest that more accurate estimates of trunk mechanical properties can be obtained by measuring kinematics at the trunk itself, and by modeling elements that connect the motor to the trunk.

REFERENCES

1. Granata KP and Rogers E. J *Electromyogr Kinesiol* **17**, 384-392, 2007.
2. Hodges P et al. *J Biomech* **42**, 61-66, 2009.
3. Gardner-Morse MG and Stokes IA. *J Biomech* **34**, 457-463, 2001.

ACKNOWLEDGEMENTS

This publication was supported by Cooperative Agreement Number R01-OH004089 from CDC-NIOSH. Its contents are solely the responsibility of the authors and do not necessarily represent the official views of the CDC.

EXPERIMENTAL AND MODELLING INVESTIGATION OF sEMG SPIKE ANALYSIS

DA Gabriel[1], A Christie[2], JG Inglis[1] and G Kamen[2]

[1]Brock University, St. Catharines, ON, Canada
[2]University of Massachusetts Amherst, Amherst, MA, USA
email: dgabriel@brocku.ca

INTRODUCTION

Problems in the traditional analysis of the surface electromyographic (sEMG) signal have been well documented [2]. Previous studies have described an alternative technique using a pattern classification method [4]. Five measures extracted from the sEMG signal are used to provide a unique characterization of the interference pattern for different motor unit behaviors. Simultaneous analysis of multiple sEMG measures allows for greater specificity in identifying changes in the sEMG interference pattern [6]. The purpose of this study was to investigate the sensitivity of the sEMG measures during the force gradation processes. The effects of tissue and electrode spatial filtering upon the sensitivity of each measure were further evaluated using a model of sEMG activity.

METHODS

Experimental data: Subjects (N=8) performed 5, 10-second isometric elbow flexion contractions from 0 to 100% MVC, increasing force at a rate of 10% MVC per second. Once subjects reached 100% MVC, they held the contraction for an additional second to ensure they achieved their maximum. The sEMG signals from the medial head of the biceps brachii were recorded with bipolar Ag/AgCl electrodes, amplified and band-pass filtered (10-2000 Hz). All signals were sampled by a 16-bit A/D converter at 25.6 kHz.

Model description: An inertial frame $A(x_0, y_0, z_0)$ placed at the muscle axis was used to locate each motor unit and the muscle fibres within its territory (**Figure 1**, top panel). A relative coordinate system was then placed at the motor endplate $B(x_{ep}^{'}, y_{ep}^{'}, z_{ep}^{'})$ of each muscle fibre within the motor unit. A bipolar impulse-response function was then convolved with the first derivative of the intracellular action potential to yield a single fibre action potential (SFAP) [1]. The SFAPs were summed to generate a single motor unit action potential (**Figure 1**, bottom panel). The physiologic properties from a well-known muscle model [5] and motor unit recruitment and firing rate schemes were combined to generate synthetic sEMG signals [3]. There were six simulation conditions corresponding to the combination of 3 radial electrode locations (y=0.1, 1, and 5 mm) and 2 inter-electrode distances (IED=1 and 2 cm).

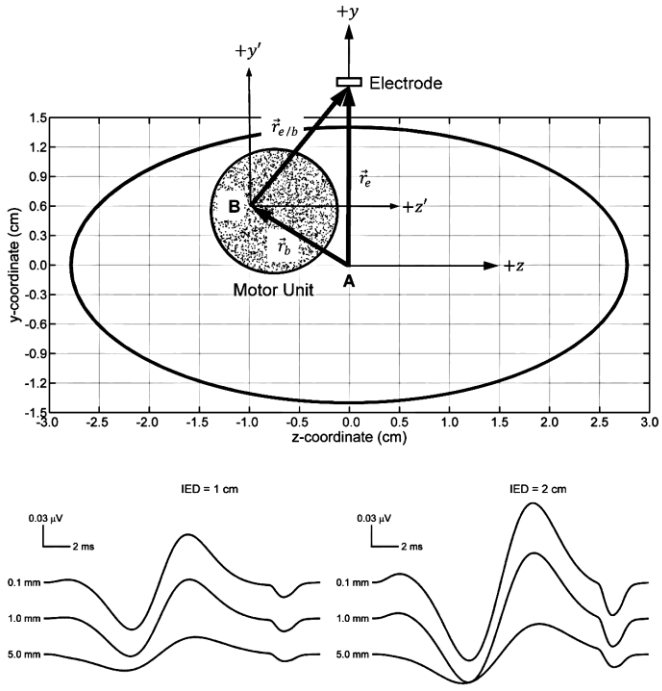

Figure 1. The coordinate systems for the muscle and motor unit territories used for the generation of muscle fiber action potentials.

The simulated and experimental sEMG signals were processed in the same way. The root-mean-square (RMS), mean power frequency (MNF), mean spike amplitude (MSA), mean spike frequency (MSF), mean spike slope (MSS), mean spike duration (MSD), and mean number of peaks per spike (MNPPS) were calculated from successive 500 ms epochs for the duration of the simulated contraction.

RESULTS AND DISCUSSION

The amplitude of sEMG exhibited a non-linear increase (**Figure 2**). While MSA was two-fold greater than RMS, there was no difference when normalized to the maximum values of their respective curves. There was a parabolic alteration for both frequency measures, but MSF was more sensitive than MNF to changes in force below 50% MVC. There was an inverse relationship between MSD and the frequency measures. The MNPPS exhibited a two-component response: it decreased rapidly from 5 to 30% MVC and gradually plateaued until 100% MVC.

The simulated sEMG was able to reproduce the essential features of the experimental data and the differences between the traditional and spike shape measures (**Figure 3**). Increasing the electrode distance from the source attenuated both the amplitude and frequency content of the signal. The differences between MNF and MSF were gradually eliminated at the farthest radial electrode location. The spatial filtering effect of increasing inter-electrode distance (IED) was more profound than increasing the electrode distance from the source. There was the expected increase in sEMG amplitude but the frequency content attenuated much more rapidly with increasing radial electrode distance. The same was true for differences between MNF and MSF.

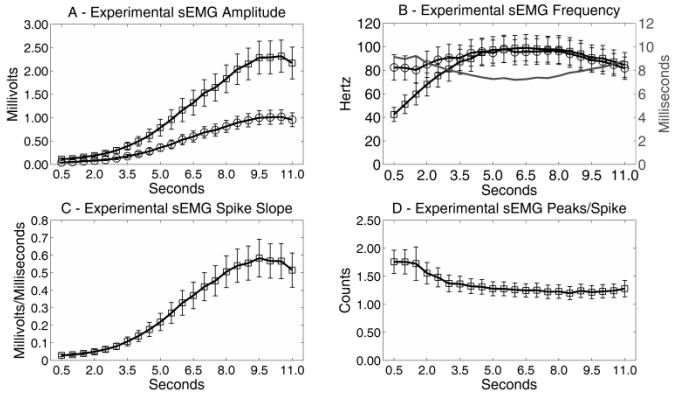

Figure 2. Experimental sEMG recordings. A: RMS (○) and MSA (□); B: MNF (○), MSF (□), and MSD (grey line); C: MSS; and D: MNPPS. Since subjects performed ramp contractions at 10% MVC per second, the x-axis in seconds also corresponds to percent MVC.

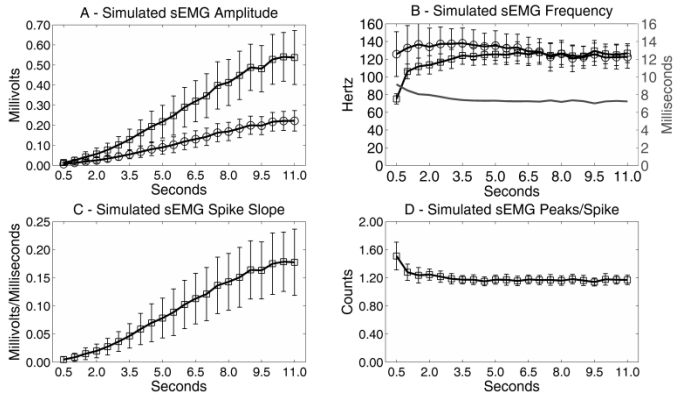

Figure 3. Simulated sEMG activity. Radial electrode location of 0.1 mm and an interelectrode distance of 1.0 cm. A: RMS (○) and MSA (□); B: MNF (○), MSF (□), and MSD (grey line); C: MSS; and D: MNPPS.

CONCLUSIONS

Taken together, the experimental data and modeling analysis showed that below 50% MVC, the sEMG spike measures were more sensitive to changes in force than traditional time and frequency analysis. However, there are additional limitations associated with electrode distance from the source that must be explored further. Future experimental work should ensure that the inter-electrode distance is no greater than 1 cm to mitigate the effects of tissue filtering.

REFERENCES

1. Dimitrov, GV, Dimitrova, NA (1989). *Med. Eng. & Phys*., **20**, 371-381.
2. Farina et al. (2002). *J. Appl. Physiol.*, **92**: 235–247.
3. Fuglevand et al. (1993). *J. Neurophysiol.*, **70**, 2470-2488.
4. Gabriel et al. (2007). *J. Neurosci. Meth.*,**159**: 146–152.
5. Keenan KG, et al. (2005). *J. Appl. Physiol.*, **98**,120-131.
6. Luttmann et al. (2000). *Int. J. Indust. Ergonom.*, **25**, 645-660.

ACKNOWLEDGEMENTS

Funded by the NSERC of Canada.

A COMPARISON OF VIBRATION ACCELERATION MEASURED WITH HIGH SPEED 3-D MOTION CAPTURE AND TRIAXIAL ACCELEROMETERS

Eadric Bressel, Gerald Smith, and Dustin Nash
Biomechanics Laboratory, Utah State University, Logan UT, USA
email: eadric.bressel@usu.edu

INTRODUCTION

To gain an appreciation of the adverse effects of whole body vibration (WBV) to the human body, researchers have traditionally mapped the vibration accelerations at various skeletal locations using skin mounted accelerometers (1, 2). Accelerometers mounted to the skin have been the preferred methodology because they avoid the traumatic alternative of bone mounted transducers and have sufficient sample rates to capture the motion (3). Camera technology has recently gained sufficient speed and resolution for measuring low amplitude high frequency vibrations and may be an alternative methodology for measuring vibration accelerations without some of the limitations of accelerometers. For instance, high speed camera systems may use low mass skin mounted markers (e.g., < 1 g) that are not tethered to a cable. Additionally, the possibility to map vibration accelerations of the entire skeleton three-dimensionally (3-D) is neither limited by the number of accelerometers available nor complicated by accelerometer orientation. While the advantages of using camera technology may allow for a better appreciation of the adverse effects of WBV to the entire skeleton, the methodology has not been compared against the more traditional accelerometer approach. The purpose of this study was to compare 3-D accelerations obtained with accelerometers and a high speed motion capture system during WBV.

METHODS

Fifteen healthy males and females (age = 23.0 ± 5.1 yrs; mass = 67.0 ± 10.9 kg) with no reported musculoskeletal injuries participated in the study. The experimental protocol required each participant to stand on a commercially available vibration platform (Nemes Bosco-system, Rome, Italy) with progressively greater frequencies of about29, 34, 39, 44, 49 and 53 Hz. Participants stood on the platform for approximately 5 s at each frequency with no shoes and knees slightly bent (i.e., 10-25º; Fig. 1).

Accelerations of the tibia were collected with a Vicon MX motion capture system and a triaxial accelerometer (PCB Inc.) using Nexus software (Fig. 1). The Vicon system was set-up with seven T-20 cameras that tracked low mass retro-reflective markers (1.2 g) while sampling at 500 Hz. The low mass accelerometer (5.4 g) sampled at 1000 Hz. Accelerations from marker position data were computed from 50 cycles of filtered position data (cutoff frequency = 75 Hz) using finite difference equations and expressed as root mean square (RMS). Accelerometer data across a similar 50 cycles of motion data were filtered (cutoff frequency = 150 Hz), down sampled, and then expressed with a RMS. RMS accelerations for each frequency were compared between collection techniques using a paired t-test; alpha = 0.05.

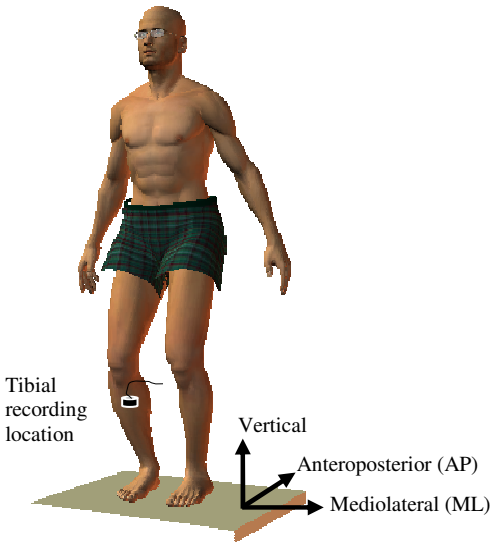

Figure 1. Vibration platform set-up, location for accelerometer and reflective marker, and sign convention for vibration direction.

RESULTS AND DISCUSSION

Vertical accelerations recorded with the camera system and accelerometer were similar at 29 Hz and 49 Hz, but different at other frequencies ($p < 0.01$; Fig 2). Anteroposterior and mediolateral accelerations were similar except for 39 Hz ($p < 0.02$; Fig 2).

These results suggest that accelerations measured separately with a camera system and accelerometer may not always be in agreement particularly for vertical measurements. There are numerous factors that could explain the disparity. Accelerometer orientation on the non-vertical tibia will produce "vertical" accelerations that are less than true vertical accelerations. The results in Fig. 2 support this contention for most frequencies tested. Other factors to consider include filtering characteristics, weight differences between marker and accelerometer, and how they are attached (wrapped vs double sided tape). These factors influence the potential skin resonance which is a limitation of any skin mounted device (3).

Practically speaking, the methodology of the camera system was superior to the accelerometer approach in terms of ease for data collection, but was far more expensive and required a more complex analysis to compute accelerations.

In conclusion, vertical tibial accelerations were greater when measured with a camera system than accelerometer at 34, 39, 44, and 53 Hz vibrations. Horizontal accelerations were more similar between methodologies with an exception at 39 Hz.

REFERENCES

1. Kiiski, J. et al. *J Bone Miner Res* **23**, 1318-1325, 2008.
2. Rubin, C. et al. Spine **28**, 2621-2627, 2003.
3. Lafortune, MA, et al. *J Biomech* **28**, 989-993, 1995.

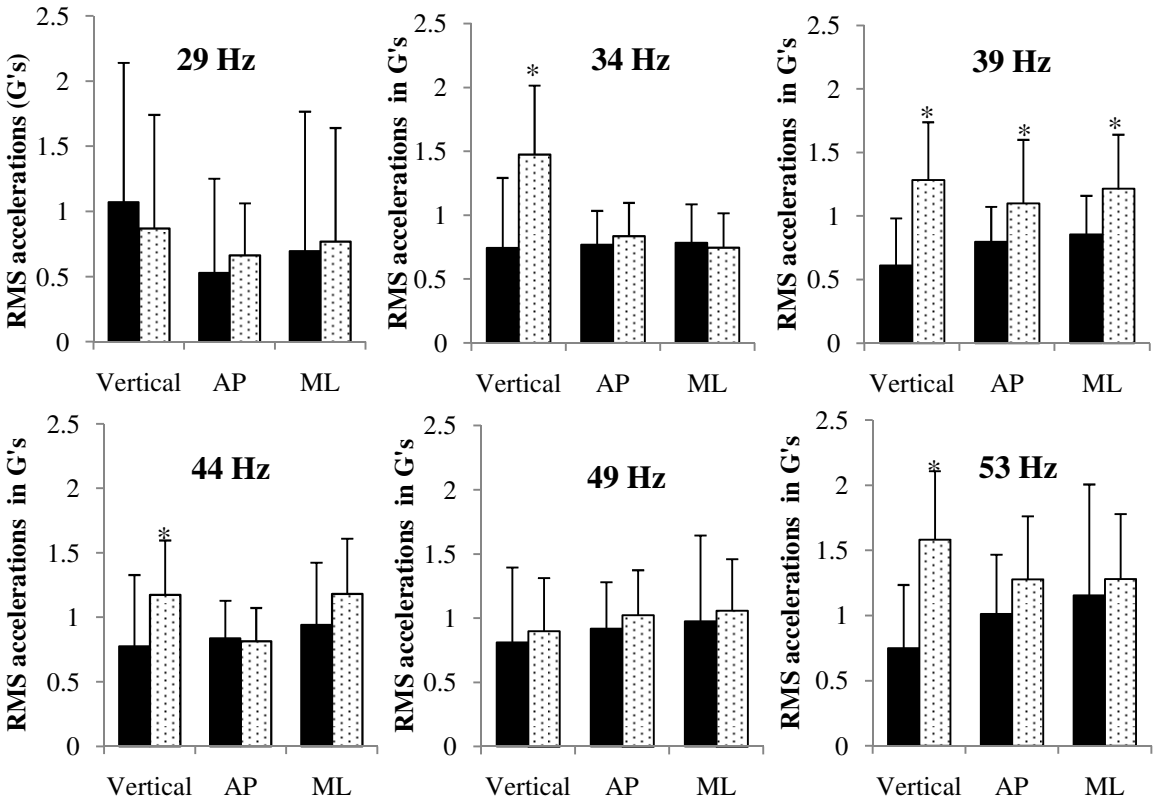

Figure. 2: Three-dimensional accelerations of the tibia recorded at different frequencies using a camera system (patterned bars) and accelerometer (solid bars). * significantly different from accelerometer; $p<0.02$.

VARIABILITY OF GAIT KINEMATIC DATA ASSOCIATED TO OBSERVER AND MARKER PLACEMENT TECHNIQUE

[1] Vera Moniz-Pereira, [1] Filomena Carnide, [1] Ruth Agostinho, [1] Sandra Amado, [1] António Veloso

[1] Neuromechanics of Human Movement Research Group
[1] Faculty of Human Kinetics, Technical University of Lisbon, Portugal
Email: veramps@fmh.utl.pt

INTRODUCTION

Gait is a complex motor pattern essential to the autonomy and quality of life, being therefore largely used as a physical function indicator in many different studies. For instance, gait analysis has been used to assess functional losses which occur with aging or with certain pathologies.

One of most used in vivo techniques to do such analysis implies the capture of skin markers instantaneous positions by optoelectronic sensors to reconstruct segment position and orientation. However, as any other technique, it has some error associated. It has been stated [1, 2] that this error might be instrumental or generated by Anatomical Landmark (AL) misplacement and markers movement dissociated from skeletal movement, which occur even in static conditions. While, nowadays, the estimation of instrumental errors is not problematic, the effect of AL misplacement and movement is much more complex, especially when considering soft tissue artifacts (STA). The variability generated by AL misplacement and movement has been attributed to three main sources: (1) the fact that palpable ALs are not points but surfaces, sometimes large and irregular; (2) the soft tissue layer of variable thickness and composition that covers the ALs; and (3) the palpation procedure that was used [3].

The purpose of this study was to assess the variability introduced by different observers and marker placement techniques (real AL, fixed on the skin (RAL), vs virtual AL, created with a digitizing pointer (VAL)) on gait kinematic data in order to guarantee data comparability in our Laboratory and between laboratories. Residual Analysis was done to measure the error associated with our laboratory motion capture (MOCAP) system to ensure data accuracy and precision.

METHODS

Twelve young (age: 21.60±2.3y) and active adults (measured through the short form of International Physical Activity Questionnaire, IPAC), with a Body Mass Index (BMI) of 22.0±2.2 Kg/m^2 and without any gait pathology, participated in the study.

Data collection included the following procedures: (1) demographic and physical activity monitoring; (2) anthropometric data assessment; (3) palpation and fixation of the real ALs; (4) trial I - static and dynamic (gait) motion capture with a 10 camera (Oqus 300) MOCAP system, from Qualisys Motion Capture System, at a sample frequency of 200Hz; (5) trial II -palpation and creation of the virtual ALs (2^{nd} static trial) using Visual 3D from C-motion inc; (6) repetition of steps 3 to 5 for the other two observers.

Kinematic data was obtained using Visual 3D where lower limb lengths, segment residuals and angular displacement in the sagittal plan were computed.

Statistical analysis was done with PASW Statistics 18.0 and included: (1) Descriptive statistics to determine central tendency and standard deviation; and (2) General linear model (GLM), with repeated measures to determine the influence of the method and the observer on the kinematic data. For those variables which did not met the GLM repeated measures assumptions (Kolmogorov-Sminorv test for standardized residuals for dependent variables and Machly's tests for sphericity), Friedman and Wilcoxon tests were applied to check for

differences between observers or methods, respectively. Differences between groups were consider statistically significant when p-value <0.05.

Immediately prior to data collection, all participants were informed about the study, accepted to participate and signed the informed consent. The Ethics Committee of Faculty of Human Kinetics approved the study protocol.

RESULTS AND DISCUSSION

In contrast with the results of our preliminary study [4], differences were found between observers for right foot, shank and thigh lengths. Effect size analysis (through the determination of partial ETA^2) showed for these variables that the observer can explain ~53%, 83% and 84%, respectively, of the results variability. Differences were also significant between observers when measuring left shank length with the RAL method and left thigh length with both of the methods. As both of these variables did not meet the sphericity assumption for the repeated measures, Friedman test was applied. It is also important to note that for almost all the other variables, for which no significant difference was found between observers, effect size values were high (between 0.276 and 0.441), meaning that the observer is responsible for approximately 28% to 44% of the results variability.

The method used (RAL vs VAL) didn't seem to introduce, as much as the observer, variability in the kinematic data analyzed. Differences were found for maximal residual of the right foot (partial ETA^2=0.76), right thigh segment length (partial ETA^2=0.51) and left thigh segment length for observer 1 (Wilcoxon test was used since the variable did not meet the sphericity assumption). For almost all the other variables, for which no significant difference was found between observers, effect size values were small (between 0.003 and 0.07), showing once again a lower contribution of the method for the data variability.

Residual analysis showed, as in our preliminary study, higher residuals for the foot (an average of 5.47 mm for right foot and 5.82 mm for left foot) followed by the thigh (an average of 4.46 mm for right thigh and 1.84 mm for left thigh) and finally the shank (an average of 1.75 mm for right shank and 1.32 mm for left shank). This led us to reconsidered camera step up, namely in what concerns the number of cameras at ground level, and marker step up, especially considering visibility and movement issues.

CONCLUSIONS

Agreeing with the literature [3] the observer seemed likely to introduce variability on the kinematic data studied. There was also some contribution of the method for the results variability, although lower than the contribution of the observer. This fact should be taken into account when comparing data, within or between laboratories, in order to guarantee its accuracy and meaning.

This work also points out the need, not only of determine the best data collection procedures for the specific task that is going to be studied, but also of assessing and reporting the inherent error in order to guarantee an harmonized understanding of data precision and accuracy levels.

REFERENCES

1. Chiari L, et al. ***Gait and Posture***, **21**, 197-211, 2005.
2. Cereatti A, et al. ***Journal of NeuroEngineering and Rehabilitation***, **3**, 2006
3. Della Croce U. et al. ***Gait and Posture***, **21**, 226-237, 2005.
4. Moniz-Pereira V, et al. ***Proceedings of ISB 09***, Cape Town, South Africa, 2009

IS SUBJECTS' JOINT TORQUE VARIABILITY RELATED TO JOINT TORQUE ERROR?

Raziel Riemer
Ben-Gurion University of the Negev, Beer Sheva, Israel
email: rriemer@bgu.ac.il

INTRODUCTION

In the analysis of human motion, the results of an individual are often compared to those of the normal population. This comparison is typically based on the expertise of the researcher and clinician or on statistical methods [1]. In such cases the size of variability among the test subjects is important, as it determines the ability to differentiate between various abnormalities. Previously it was shown that inaccuracies in body segment parameter (BSP) estimates, joint center of rotation locations, force plate, motion capture system measurements, and segment angle calculations can cause errors in the joint torque calculation. Furthermore it was shown that during walking these errors could be large relative to the joint torque [2]. This study builds on this previous work and examines if the estimated error (uncertainty) correlates to subject variability. If this holds true it might suggest that part of the subject variability is a result of the error in the joint torque estimation and not a real difference among the test subjects.

METHODS

Two models were used to represent the human body and were the base for the derivation of the joint torque equations. The first model was for the lower body and consisted of the foot, shank, and thigh. This model incorporated ground reaction force measurements and was derived using a recursive Newton-Euler method starting from the foot (bottom up). The second model consisted of two forearms, two upper arms, and the torso combined with the head, and was derived recursively starting from the hands (top down). An inverse dynamics solution was then computed for the joint torques at the ankle, knee, hip, bottom of the torso, shoulder, and elbow.

An error analysis method was used to compute the effects of input variable inaccuracies on the uncertainties in the joint torques calculated via inverse dynamics. The following formulation computes the upper bound of the possible error [3]:

$$U_j = \left|\frac{\partial \tau_j}{\partial x_1}\Delta x_1\right| + \left|\frac{\partial \tau_j}{\partial x_2}\Delta x_2\right| + \ldots\ldots + \left|\frac{\partial \tau_j}{\partial x_n}\Delta x_n\right|, \quad (1)$$

where U_j is the uncertainty in the torque value at joint j (τ_j), and Δx_i is the inaccuracy associated with input variable x_i. The magnitudes of the Δxi's reported values varied across the studies. Previously the range was represented by two sets: Set 1 (small Δx_i) and Set 2 (large Δx_i)[2]. I used the same values.

Five males and five females (weight: 75.98±14.74 kg; height: 1.69±0.06 m) walked at their normal speed, with the right foot landing on a force plate (AMTI), while a motion capture system (Vicon) recorded their movements. Their BSPs were calculated using the adjustments to Zatiorsky-Seluyanov's work by De Leva [4]. These parameters with motion and force measurements, and the Δx_i, were then put into Equation 1 to estimate the uncertainties in each joint torque. All calculated joint torque and uncertainty values were normalized in time as percentages of gait cycle, and then normalized by a subject's height and weight. Finally, correlations between the joint torque standard deviation and the average uncertainty of the subjects were calculated.

RESULTS AND DISCUSSION

The profiles of the subject's torque standard deviation show similarity to the uncertainty profiles (Fig 1&2). Moreover the variations in the torque values (3 standard deviations) were of similar magnitude to estimated uncertainty (U_1 or U_2). The coefficient of correlation (R^2) between the profiles of standard deviation (3σ) and the estimated uncertainties obtained using Set 1 were: 0.71, 0.64, 0.78, 0.41, 0.38, 0.49, in the ankle, knee, hip, bottom of the torso, shoulder, and elbow, respectively. The values obtained using Set 2 were: 0.71, 0.64, 0.78, 0.47, 0.38, 0.48 in the ankle, knee, hip, bottom of the torso, shoulder, and elbow, respectively. All the correlations were significant, with P value less than 0.01.

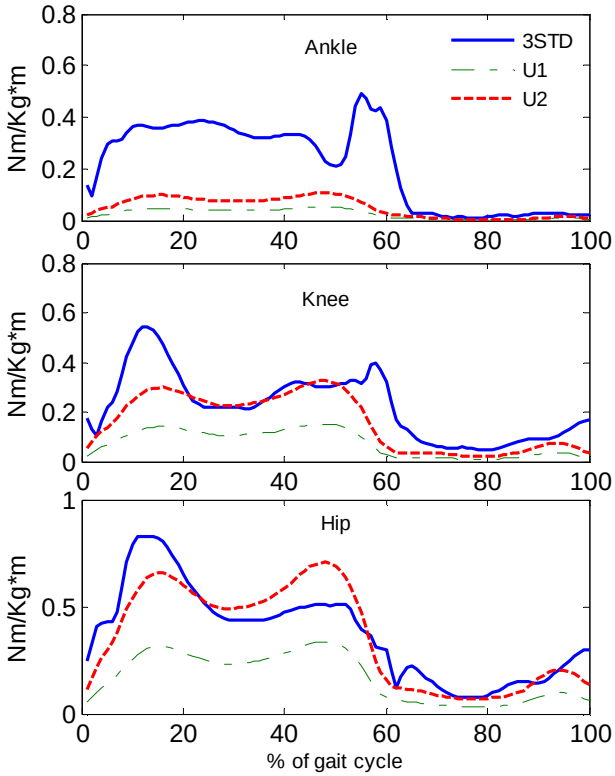

Figure 1: Leg joint torque: 3 standard deviations of the subject population vs. calculated uncertainty using the small (U1) and large (U2) set of Δx_i's

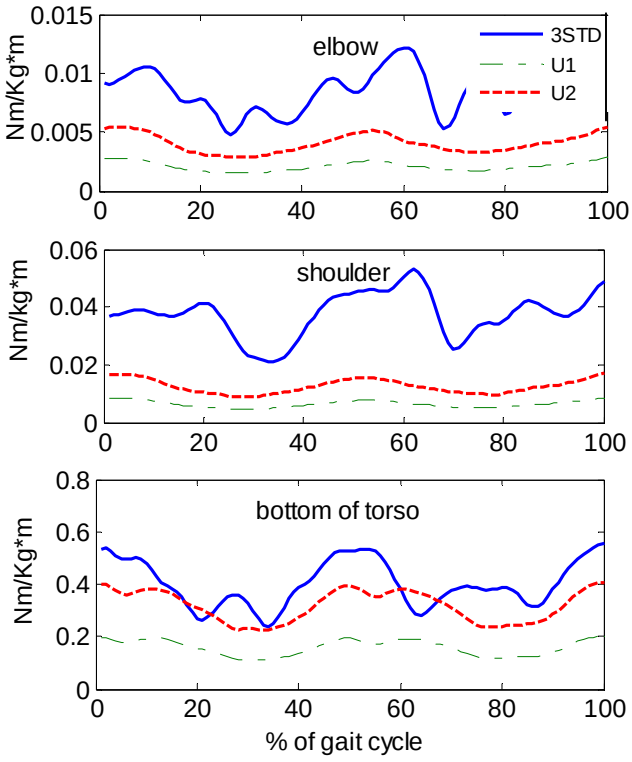

Figure 2: Upper body joint torque: 3 standard deviations of the subject population vs. calculated uncertainty using the small (U1) and large (U2) set of Δx_i's.

The medium to high correlations between the subject 3σ and the joint torque uncertainty suggest that subject variability is related to the uncertainty in the joint torque calculations. Further, for the knee and hip joint the magnitude of the uncertainty is close to the magnitude of the 3σ, and the correlation is relatively high. This suggests that a large portion of the variability in these joints might not be due to a real difference among the subjects but rather to an error in the joint torque estimations. In the ankle joint, although the correlation is high, the size of the uncertainty is small relative to the standard deviation. Therefore, it seems that this variation among the test subjects is less affected by the error in the joint torque estimations. For the upper body the correlations are lower than for the lower body, suggesting that less of the joint torque variation can be attributed to the uncertainty. This difference in the correlation values might be explained by the fact that for the lower model the error in the segment angle due to skin artifacts is the main source of uncertainty. However for the upper body (TD), the uncertainty is affected by additional factors, e.g., inaccuracies in segments angle, accelerations, and BSPs.

CONCLUSIONS

In this study it was found that the magnitude of the estimated error (uncertainty) has a medium to high correlation with subjects' 3σ. For the knee and hip joints these correlations are relativity high. The high uncertainty for these joints suggests that much of this joint torque variability might be due to the error in the estimations and not to real differences among the test subjects. This emphasizes a need for the use of error reduction methods (e.g., [5]). Further if possible during an analysis, more weight should be given to joints with smaller uncertainty e.g. ankle

REFERENCES

1. Shorter KA, et al**.** *Clin Biomech* **23,** 459-467, 2008.
2. Riemer R, *Gait Posture* **27** 578-588, 2008.
3. Taylor JR. *An introduction to error analysis: the study of uncertainties in physical measurements.* Sausalito, CA, University Science Books, 1997.
4. De Leva P, *J Biomech* **29,** 1223-1230, 1996.
5. Reinbolt JA, et al. *J Biomech* **38,** 621-626, 2005.

LONGITUDINALLY ASSESSED CHANGE IN STATURE AND SEGMENT LENGTH

[1,2]Kevin R. Ford, [1]Gregory D. Myer, [3]Robert Shapiro, [4]Antonie J. van den Bogert & [1,2]Timothy E. Hewett

[1]Cincinnati Children's Hospital Medical Center, Cincinnati, OH, USA
[2]University of Cincinnati, Cincinnati, OH, USA
[3]University of Kentucky, Lexington, KY, USA
[4] Cleveland Clinic Foundation, Cleveland, OH, USA
email:kevin.ford@cchmc.org, web: http://cincinnatichildrens.org/sportsmed

INTRODUCTION

Changes in body stature and segment lengths are important variables which may disrupt neuromuscular control during adolescent growth. Injury risk factors have been hypothesized to coincide with pubertal development. Specifically, following an adolescent growth spurt, increased body mass, height of the center of mass and length of lower extremity segments may contribute to altered movement patterns [1].

The purpose of this study was to compare the changes in body stature and individual segment lengths within one year of adolescent growth between pubertal and post-pubertal subjects. During pubertal growth, the overall change in stature should closely relate to the change in the combined length of the shank, thigh and trunk. Therefore, we aimed to validate the use of summated segment lengths calculated from a motion analysis static pose with the gold-standard assessment of height (stadiometer).

METHODS

The subject population consisted of 315 pubertal and post-pubertal subjects. Each subject participated in the first testing session immediately prior to their basketball or soccer season. Approximately one year after the initial testing session (mean 365.7 ± 14.7 days) the subjects were retested using the same methods.

Height was measured using a stadiometer (Figure 1, ShorrBoard, Olney MD) with the subject in bare feet and the subjects head positioned in the Frankfort plane. 37 retroreflective markers were placed on each subject. The subjects were placed for the static pose trial in a standardized position (Figure 1). Longitudinal trials were collected with a motion analysis system consisting of ten digital cameras (Eagle cameras, Motion Analysis Corporation, Santa Rosa, CA) positioned consistently in the laboratory over the multiple trials.

The analyses were performed in MATLAB (The Mathworks, Natick MA). 3D marker trajectories of the static trail were used to calculate each segment joint center. Segment lengths were calculated as the distance between the proximal and distal joint center (e.g. thigh segment distance was equal to the distance between the hip joint center to knee joint center). Segment center of mass (COM) were calculated based on sex-specific parameters from de Leva [1]. Right shank, right thigh and trunk segment lengths were summed for each subject and used in the analyses.

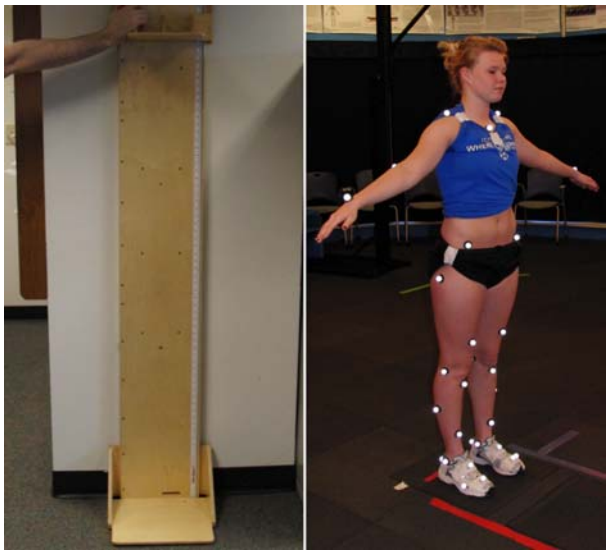

Figure 1: Left, stadiometer used for stature measurement. Right, retroreflective markers during static pose.

The summed segment length yearly changes (difference between first and second year) were validated against yearly stature changes from standard stadiometer measures using Intraclass Correlation Coefficients (ICC) and linear regression. Root mean square (RMS) fit error was also calculated between measures. One-way ANOVA was used to test for differences between pubertal groups.

RESULTS AND DISCUSSION

Pubertal subjects had significantly greater longitudinally increased change in each of the length measures compared to the post-puberal subjects (Table 1). The changes from year one to year two in subject height measured with a standard stadiometer were compared to yearly changes in length of the segments calculated from the motion analysis system (summed shank, femur, and trunk). The average difference in stature over all subjects measured with the stadiometer was not different compared to the change in summed segment length ($p > 0.05$). The RMS error was 1.71 cm between measurements. The calculated change in summated segment lengths from the first to second year demonstrated high reliability ($ICC_{(3,1)} = 0.83$) with measured changes in stature.

Figure 2 shows the relationship between stature and summed segment length calculated at the initial testing session (year 1). The linear regression indicates a strong relationship between the stature measure and segment length calculation (year 1: r2 = 0.943; year 2: r2 = 0.935). The relationship between vertical position of the body center of mass to stature was also high for each testing session (year 1: r2 = 0.918; year 2: r2 = 0.910).

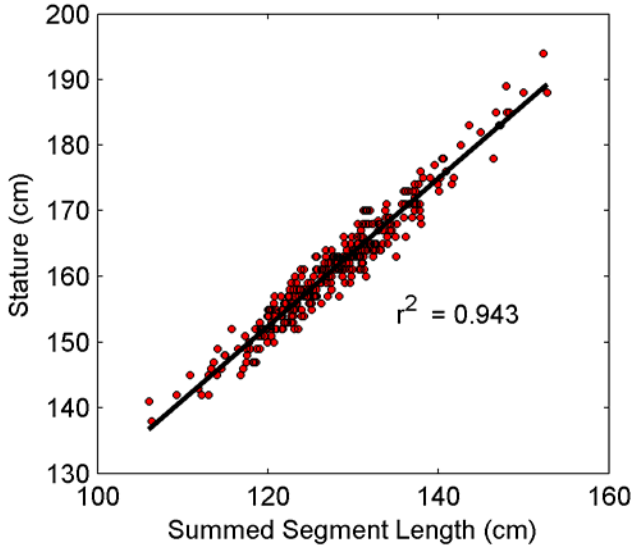

Figure 2: Relationship between stature and summed segment lengths.

CONCLUSIONS

Motion analysis techniques identified longitudinally increased segment lengths during puberty compared to post-puberty. Calculation of segment lengths, in conjunction with the analysis of dynamic tasks, may be useful to identify longitudinal changes that underlie altered movement mechanics and may place female athletes at higher risk of injury [3].

REFERENCES

1. Hewett TE. et al. *J Bone Joint Surg Am.* **86**, 1601-1608. 2004.
2. de Leva P. *J. Biomech* **29**, 1223-1230. 1996.
3. Hewett TE. et al. *Am. J. Sports Med.* **33**, 492-501. 2005.

ACKNOWLEDGEMENTS

The authors would like to acknowledge funding support from NIH Grant R01-AR049735, R01-AR055563 and R01-AR05625.

Table 1: Mean ± Standard Deviation for change in length measurements from first to second year.

	Pubertal (n=182)	**Post Pubertal (n=133)**	***p* value**
Stature (cm)	5.20 ± 2.59	0.90 ± 1.56	< 0.001
Summated Segment Length (cm)	4.76 ± 2.41	1.14 ± 1.64	< 0.001
Leg Length (cm)	2.73 ± 2.06	0.04 ± 1.59	< 0.001
Trunk Length (cm)	2.04 ± 1.88	1.10 ± 1.94	0.007
Vertical Height COM (cm)	3.14 ± 1.67	0.75 ± 1.13	< 0.001

A FRAMEWORK FOR STUDYING UNDERACTUATION IN THE HUMAN HAND

Ravi Balasubramanian and Aaron M. Dollar
Department of Mechanical Engineering, Yale University,
New Haven, CT.
{ravi.balasubramanian, aaron.dollar}@yale.edu

INTRODUCTION

While the human hand is capable of great dexterity enabled by intricate biomechanics and sophisticated neural control, it is underactuated, containing fewer actuation pairs than active degrees of freedom. While the exact numbers are debated, it has around 21 degrees of freedom and is driven by around 38 single-acting muscles which induce finger movement through a complex tendon web [1]. The additional degrees of freedom are actuated through some form of tendon coupling. One significant example of coupling in the human hand is the coupling between the distal and middle phalanxes of the four fingers, which are coupled through tendons that pull on both joints (see Fig. 1 and [2]). Simultaneously, this tendon routing is also adaptive—that is, the distal phalanx can curl inward even if the middle phalanx cannot move due to external obstruction. We are interested in understanding on how such adaptive underactuation in the human hand influences its grasping performance.

There are strong similarities between the flexion actuation of the human index finger's middle and distal phalanxes and the actuation mechanism of an underactuated robotic hand that we have built (the SDM Hand; see Fig. 2 and [3]). They are both driven by a single tendon that slides over idler pulleys and then inserts into the distal phalanx. Both systems also passively adapt to environmental geometric constraints. Recently we have proposed a framework to analyze the response of such underactuated hands to external disturbances [4]. When applied to the SDM Hand and an exemplar linkage-driven underactuated hand (see [5] for an example), we noticed that a tendon-driven underactuated hand offered strong advantages in grasping behavior. In this paper, we briefly present this framework and then apply it to analyze the stiffness of the human index finger resulting from underactuation.

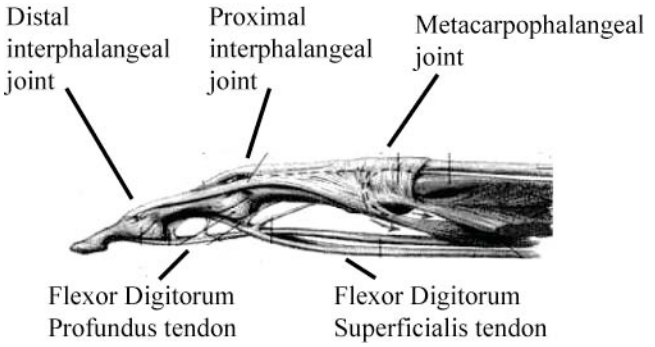

Figure 1: Biomechanics of the human index finger (reproduced from [2]).

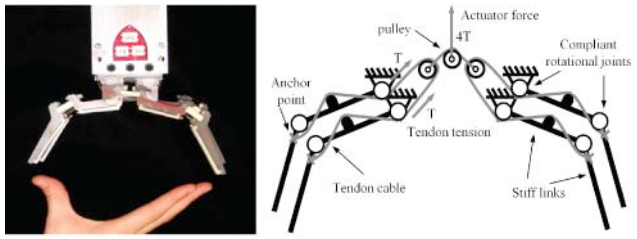

Figure 2: (a) The SDM Hand and (b) its transmission mechanism.

METHODS

The framework for studying underactuation consists of three elements:1) The static equilibrium equations that relate contact forces on the phalanxes with joint torques; 2) The kinematic coupling between joint motion and actuator motion; 3) The robot configuration change due to the external forces in the presence of joint coupling.

The relationship between the contact forces acting on the finger and the net joint torques may be expressed as $\tau = J_c^T f_e$, where $f_e = (f_1 \quad f_2)^T$ represents the normal contact force on the proximal and distal links, $\tau = (\tau_1 \quad \tau_2)^T$ the resulting torque at the joints, and $J_c \in R^{2\times 2}$ the contact Jacobian that maps between the two spaces [5].

The kinematics of a cable-driven underactuated mechanism can be expressed as first-order differential equation in the mechanism's

configuration $\theta = (\theta_1 \quad \theta_2)^T$ and actuator variable θ_a (the angle traveled by the pulley over which the tendon travels) as $J_a \Delta\theta = \Delta\theta_a$ where $J_a = (r_1 \quad r_2)^T$ represents the actuator Jacobian of the mechanism and r_i the actuator's moment arm for that joint.

The configuration change $\Delta\theta$ of the finger for external force f_e can be quantified using a Lagrangian view of the work done by the external forces and the energy stored in the springs in the presence of the actuation constraints. Indeed, the system response also depends on the control mode the hand is operated in. For example, if actuation (tendon) force is fixed, then the static balance may be expressed as $K\Delta\theta + J_c^T f_e + J_a^T f_a = 0$, where f_a represents the constant actuator force and K the joint stiffness matrix. In contrast, if actuator position (tendon length) is fixed, then the static balance may be expressed as

$J_a \Delta\theta = 0,$

$K\Delta\theta + J_c^T f_e + J_a^T \lambda = 0,$

where λ represents the actuator (tendon) force.

Taking the specific example of a precision grasp where there are forces only on the distal link, the mechanism stiffness Γ in the direction of a normal force f_2 on the distal link can be computed as $\Gamma = f_2 / \Delta d$. Here, $\Delta d \in R$ represents the deviation of the contact point in the force's direction and can be computed from $\Delta\theta$ using the forward kinematics of the finger.

RESULTS AND DISCUSSION

Using the framework, we computed the variation in passive stiffness of a point on the distal link of the human index finger as a function of finger configuration and force location (see Fig. 3). We used configuration-dependent joint stiffness estimates from [6] and moment-arm estimates from [7] (assuming MCP joint flexion and abduction-adduction were zero). We also estimated using the framework the coupled motion of the DIP and PIP joints when actuated internally. As expected, we notice that mechanism stiffness decreases as the contact location moves distal to the link. At the same time, we also notice the index finger stiffness increases as proximal joint flexes from zero.

We will build on these preliminary results and use the framework to analyze interesting human grasping tasks that are analogous to the control modes introduced in the previous section. Specifically, prior work has explored human tasks where muscle and tendon length are fixed (termed iso-metric tasks) as well as tasks with fixed fingertip force (iso-torque tasks) [8]. While these tasks have been studied previously in the context of overactuation of certain joints of the human hand, we would like to investigate how underactuation influences hand performance in these specific tasks. Through our framework developed for robotic hand design and grasping analysis, we are interested in gaining insight into human hand function.

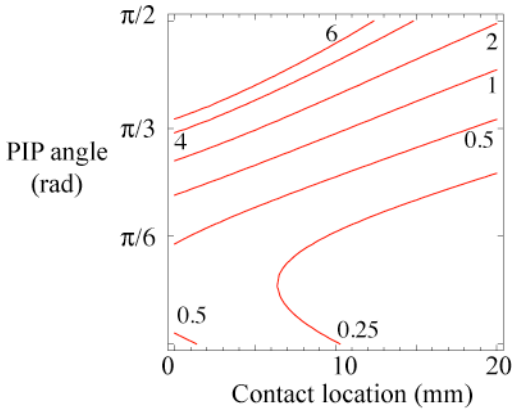

Figure 3: Contours of the passive stiffness (N/mm) of the middle and distal phalanxes of the human index finger resulting from underactuation.

REFERENCES

[1] Jones LA et al. *Human Hand Function*. Oxford Univ Press, 2006.

[2] Netter FH. *Atlas of Human Anatomy*. Rittenhouse Book Distrib, 1997.

[3] Dollar AM et al. *ASME/IEEE Trans on Mechatron* **11(2)**, 2006.

[4] Balasubramanian R, et al. In *Proc. of ASME IDETC/CIEC*. 2010. (submitted).

[5] Birglen L, et al. *Underactuated Robotic Hands*. Springer, 2008.

[6] Kamper DG et al. In *Proc. of IEEE EMBS*. 2001.

[7] Deshpande AD, et al. *Trans Biomed Eng* 2010. (In press).

[8] Balasubramanian R et al. In *Proc. of IEEE Internat. Conf. on Rob. and Automat.*, 4409–15. 2009.

ANALYSIS OF GAIT CYCLE SHAPES USING PARALLEL FACTOR ANALYSIS

[1]Nathaniel E. Helwig, [1]Sungjin Hong, [1]John D. Polk, [2]Michael R. Lague

[1]University of Illinois, Urbana, IL, USA
[2]The Richard Stockton College of New Jersey, Pomona, NJ, USA
Email: jdpolk@illinois.edu

INTRODUCTION

Gait data are typically collected in multivariate form, so multivariate analyses are often employed to quantify patterns of association between variables. Principal Component Analysis (PCA) is often used [1], but PCA is designed for two-mode data (subjects × variables), while many gait data are collected in higher-mode form (subjects × variables × conditions). Here, we present the benefits of analyzing gait data via Parallel Factor Analysis (PARAFAC) [2], which is designed for three- (or higher-) mode data. PARAFAC also overcomes the problem of rotational indeterminacy inherent in PCA. We apply PARAFAC to the analysis of gait data with the goal of distinguishing ankle and knee motion patterns in normal and perturbed gait.

METHODS

Ten healthy male subjects (21 ± 2 yrs.) walked on a treadmill under three walking conditions: (1) non-braced (normal), (2) knee-braced (with the right knee restricted to full extension), and (3) ankle-braced (with the right ankle restricted to neutral orientation) [3]. Sagittal plane ankle and knee displacement trajectories were divided into gait cycles (GC, from heel-strike to heel-strike), and the time axis of each GC was linearly transformed to represent % of the GC. Two-dimensional ankle and knee "GC shapes" were obtained (Fig. 1). Averages of 21 gait cycles for each subject and condition were calculated.

Generalized Procrustes Analysis (GPA) was used to determine consensus (i.e., average) normal ankle and knee shapes from the non-braced data. Subsequently, each shape from each subject in each experimental condition (non-braced, knee-braced, ankle-braced) was optimally aligned with its corresponding (ankle or knee) consensus via Procrustes Analysis (PA). After alignment, each shape was characterized by the signed x and y residuals for each % GC (from the corresponding % GC on the GPA consensus). This resulted in data arrays of 10 (subjects) x 200 (x and y residuals at each % GC) x 4 (conditions: brace right, brace left, normal right, normal left). PARAFAC was then used to decompose each three-mode array into weight matrices of subjects, % GC, and conditions.

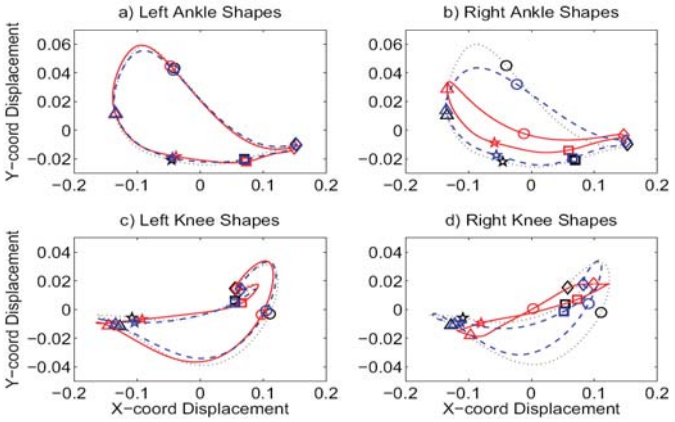

Figure 1. Average (over subjects) GC shapes in the non-braced (black dotted), knee-braced (red solid), and ankle-braced (blue dashed) conditions after alignment with GPA consensus. The symbols square, star, triangle, circle, and diamond represent 20%, 40%, 60%, 80%, and 100% of the gait cycle, respectively.

RESULTS AND DISCUSSION

Analysis of the effect of a right knee brace on ankle motion is presented here with brief summaries of the other three analyses. Subject weights did not reveal substantial patterning for any of the conditions in this study. Condition and % GC weights were both informative for all analyses.

Condition weights: The effects of the right knee brace on ipsilateral and contralateral ankle motion patterns are seen in the condition weights, with the right ankle (KB_R) weighted highly on Component 1 and the left ankle (KB_L) weighted highly on Component 2 (Fig. 2). The relative impact of these effects is quantified by the explained variance on each component.

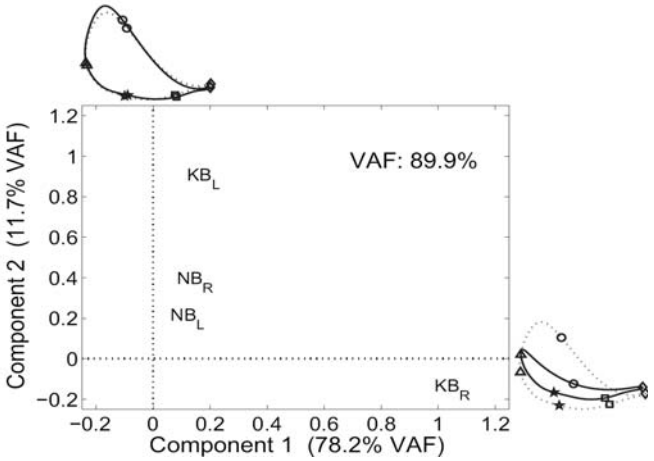

Figure 2. Condition weights for the effect of wearing a right knee brace on ankle motion patterns. KB=knee brace, NB=no brace. Hypothetical motion trajectories are shown for illustration. Dotted line= normal, Solid=braced. Symbols follow Fig.1.

The % GC weights assess the times during the gait cycle that best explain differences between normal and braced motion in x (anterior-posterior) and y (superior-inferior) directions (Fig. 3). For example, Component 1 had large positive weights on the x residuals and large negative weights on the y residuals at 80% GC (Fig. 3), indicating that a right knee brace caused the right ankle to deviate forward and downward relative to the non-braced consensus. Similarly Component 2 indicates that the brace caused the left ankle to move upward and backward relative to normal at 80% GC.

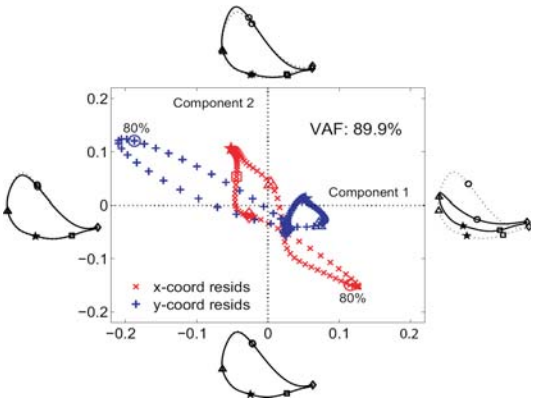

Figure 3. The % GC weights for x and y residuals. Symbols follow Fig 1&2.

Overall, the knee brace produced a flatter movement profile for the ipsilateral ankle. Ankle position was slightly elevated during stance phase but markedly lower during swing. The contralateral ankle was also affected by the restricted knee motion, but the effect was smaller with an elevated position being shown early in swing phase and a slightly depressed position just before and following heel-strike.

Similar PARAFAC decompositions were used to analyze 3 other bracing conditions. Ipsilateral knee motions were clearly affected by the knee brace throughout stance and swing; contralateral knee motions were also affected, but the effect was insubstantial. Restricted motion at the right ankle limited the motion of the ipsilateral knee and ankle but had a limited effect on the contralateral side.

CONCLUSIONS

PARAFAC is a descriptive model for gait analysis that allows for substantive parsimonious interpretation of shape differences between different data trajectories. This technique can be applied to many different types of gait data (e.g., joint moments, powers) and experimental designs. Specifically, PARAFAC allows for the identification of a few unique components that can discriminate the experimental conditions, identify the variables and time points that account for the differences between the experimental conditions, and quantify individual differences along each component.

ACKNOWLEDGEMENTS

Funding provided by NSF #0727083 and the Neer Disability Research Fund. Thanks to E. Hsiao-Wecksler, L. Diberardino III, K.A. Shorter and K. Rosengren.

REFERENCES

1. Deluzio et al. *Hum. Mov. Sci*. **16**, 201-217. 1997
2. Harshman & Lundy. In: Law et al. (Eds.), *Research methods for multimode data analysis*. New York: Praeger. pp. 122-215. 1984.
3. Shorter et al. *Clin. Biomech*., **23**, 459-467. 2008.

HUMAN ATTRIBUTE RECOGNITION FROM OPTIMIZED 2D VIEWING ANGLE SIMULATION

[1]David Bowden, [1]David Santez, [1]Adam M. Fullenkamp and [2]Brian Campbell

[1]711th Human Performance Wing (711 HPW/RHPA), WPAFB, OH, USA
[2]Bowling Green State University, Bowling Green, OH, USA
email: Adam.Fullenkamp@WPAFB.AF.MIL

INTRODUCTION

There are a variety of civilian and military applications for which it may be strategically advantageous to assess human attributes (e.g. identity, gender, injury status) from a distance. Of those recognition systems that utilize body segment motion, the majority have focused on individual gait recognition [1]. Many two-dimensional video-based gait recognition algorithms are developed under the presumption that saggital plane perspectives of gait provide the optimum viewing angle required for individual identification [1]. However, there have been few studies aimed at establishing multi-perspective baseline recognition performance from ground-truth motion capture data. In a novel approach to view-independent gait recognition, Zhang and Troje [2] tested the multi-perspective orthographic projection of 3D motion capture data to evaluate gait recognition from a set of varying training and testing 2D perspectives. While their approach was used to develop matching algorithms capable of robust gait recognition from multiple perspectives, this same concept can be exploited to establish discrimination content baselines and optimum sensor configurations. The purpose of this project was to develop an algorithmic design for the simulation of 2D video perspectives from the orthographic projection of 3D motion capture data and for the determination of viewing angles that offer enhanced human-attribute recognition.

METHODS

To demonstrate the function of the simulation architecture, the 3D gait motion of two pilot subjects were compared. Gait motion was captured using a high-resolution passive optical motion capture system (MAC, Santa Rosa, CA). The marker set employed for motion testing was comparable to that of Davis et al. [3], however, wand markers were eliminated and mid-segment markers were placed on the anterior aspects of the lower extremity segments.

Two gait cycles were taken from each pilot subject and all motion data were time normalized to a 100% gait cycle. To create gait-based match scores, all marker data were spatially normalized so that resulting body heights were uniform (arbitrary height of 1). This helped to avoid matching differences due to anthropometrics alone. Also, all motion data were aligned with the mid-pelvis as the common translational origin and the positive x-direction as the line of progression to allow for a point-to-point comparison of corresponding markers at each percent of the gait cycle. Match scores (λ) were then determined between two different gait cycles by calculating the sum Euclidean distance for all 3D landmarks at each percent of the gait cycle. To accomplish multi-view simulation of gait recognition performance, 3D motion data were rotated from an initial perspective of the yz plane (Figure 1a) about the y and z axes for all integer angles -90° to 90°:

$$R_y = \begin{bmatrix} \cos(\theta) & 0 & \sin(\theta) \\ 0 & 1 & 0 \\ -\sin(\theta) & 0 & \cos(\theta) \end{bmatrix} \qquad R_z = \begin{bmatrix} \cos(\theta) & -\sin(\theta) & 0 \\ \sin(\theta) & \cos(\theta) & 0 \\ 0 & 0 & 1 \end{bmatrix}$$

At each combination of y and z rotation, recognition performance scores (γ) were computed by

$$\gamma = \frac{\left(\frac{\left|\lambda_1^d + \lambda_2^d\right|}{2} - \frac{\left|\lambda_1^s + \lambda_2^s\right|}{2} \right)}{\left(\frac{\left|\lambda_1^d - \lambda_2^d\right| + \left|\lambda_1^s - \lambda_2^s\right|}{2} \right)},$$

where λ_1^d and λ_2^d are the match scores computed from the gait cycles of different subjects and λ_1^s and λ_2^s are the match scores computed from the gait cycles of same subjects.

RESULTS AND DISCUSSION

A surface mapping of the recognition performance scores calculated for each combination of y and z axis rotations is provided in Figure 2. The larger values (shown in red) represent 2D viewing perspectives for which gait recognition is improved and smaller scores (shown in black) represent 2D viewing perspectives for which gait recognition is diminished. The important observation to be made from Figure 2 is that gait recognition is weakest for 2D perspectives approaching the frontal plane and greatest for 2D perspectives depicting the saggital and transverse planes. This relationship is more clearly understood when the surface map is applied as an intensity map to a hemisphere to illustrate the optimum viewing perspectives in 3D (Figure 1). The hemisphere in Figure 1 is shown with a sample stick model to simulate the line-of-sight corresponding to each combination y and z rotation and associated gait recognition performance score.

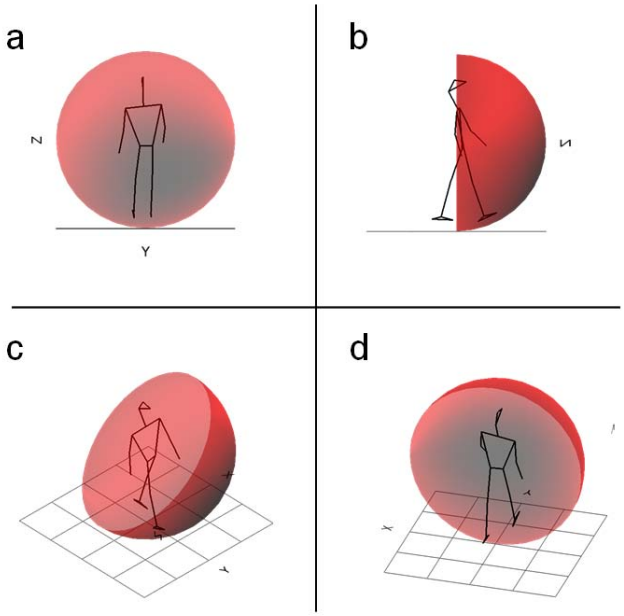

Figure 1: Intensity hemisphere based upon recognition performance at each 2D perspective (black = poorest recognition, red = greatest recognition); a) frontal plane perspective, b) sagittal plane perspective, c) rotations y = 40° and z = -80°, d) rotations y = 160°, and z = 170°

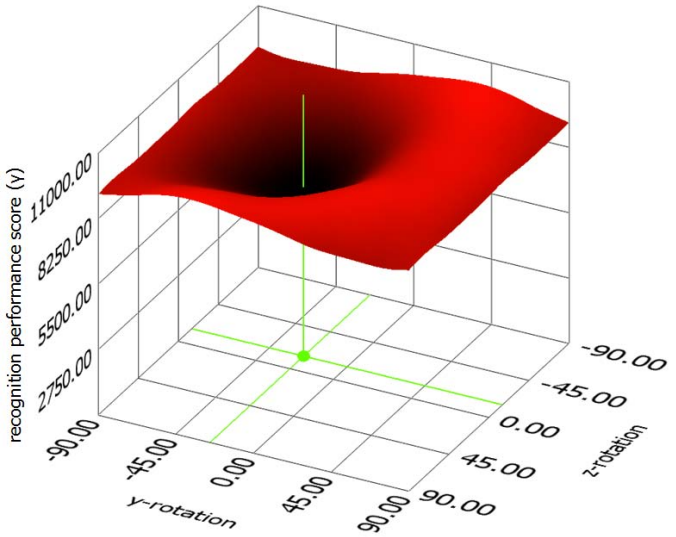

Figure 2: Surface mapping of recognition scores (γ) as a function of y-axis and z-axis rotations.

Figure 1a presents a frontal plane perspective and the darker shading in the line-of-sight indicated diminished gait matching performance. Based upon the iterative simulation, it was determined that the perspective denoted by a y-rotation of 160° and a z-rotation of 170° resulted in the poorest recognition performance (Figure 1d). Figure 1b and 1c also help to emphasize the improved recognition performance for perspectives that involve either saggital or transverse plane perspectives.

CONCLUSIONS

The greater purpose of this report has been to demonstrate the broad utility of 2D viewing angle simulation from 3D motion capture data. Analyses of this nature can be helpful in mission planning by informing operators of idealized sensor configurations and by providing intuitive visualizations of predicted system performance. Although it is not practical to employ traditional motion capture in the theater of operations, there is an obvious benefit to mission planning and system sensitivity analysis.

REFERENCES

1. Zhang R, et al. *Image and Vision Computing* **25**, 321-330, 2007.
2. Zhang Z & Troje NF. *Neurocomputing* **69**, 250-256, 2005.
3. Davis BL, et al. *Hum Mov Sci*, **10**, 575-587, 1991.

MODELING NONLINEAR ERRORS IN SURFACE ELECTROMYOGRAPHY DUE TO BASELINE NOISE: A NEW METHODOLOGY

[1]Laura Frey Law, [2]Chandramoulli Krishnan, and [1]Keith Avin

[1]University of Iowa, Iowa City, USA
[2]Rehabilitation Institute of Chicago, Chicago, IL, USA
email: laura-freylaw@uiowa.edu

INTRODUCTION

Surface electromyography (EMG) is extensively used to estimate muscle activation and force [1, 2]. Standard practice includes subtracting the baseline signal from the measured EMG signal prior to further analyses [2, 3]. However, to our knowledge this premise has not been verified experimentally. In particular, due to low signal-to-noise ratio for low-amplitude muscle contractions, such as antagonist muscle co-activation, baseline noise may be a potentially significant error source. Therefore, the purpose of this study was to model the influence of varying levels of random baseline noise on EMG signals of varying intensities, and determine an optimal method to account for baseline signal.

METHODS

A single burst of quadriceps muscle activity obtained during a maximal knee extensor contraction (60 deg/sec, ~1.4 sec) was isolated for the purpose of this study. The EMG signals were collected (Delsys Bagnoli, Boston, MA) at 1000 Hz with a 20 – 450 Hz band-pass anti-aliasing filter using custom Labview software (National Instruments) and a 16-bit data acquisition card (National Instruments). A 10-second zero-baseline vector was added to the EMG signals using a custom program written in Matlab (Mathworks, Natick, MA). The EMG signals were then halved three times and appended to create four EMG bursts of varying amplitude: 100%, 50%, 25% and 12.5% of maximum. Random noise was created using the "randn" command in Matlab, producing a signal with a mean of 0 and standard deviation of 1. This noise vector was then scaled to achieve random noise signals ranging from 5% to 50% of the burst EMG maximum. The noise signals were added to the simulated EMG bursts to create multiple trials of EMG data with varying levels of baseline noise (Figure 1A). The EMG data were rectified and low-pass filtered with a 200 ms moving average window (Figure 1B). The mean EMG activity was determined for each of the 4 bursts for each simulated baseline trial. The resulting error was calculated by subtracting the measured (corrected or uncorrected) mean EMG activity for each burst from its corresponding true value (i.e., 100%, 50%, 25% and 12.5% max).

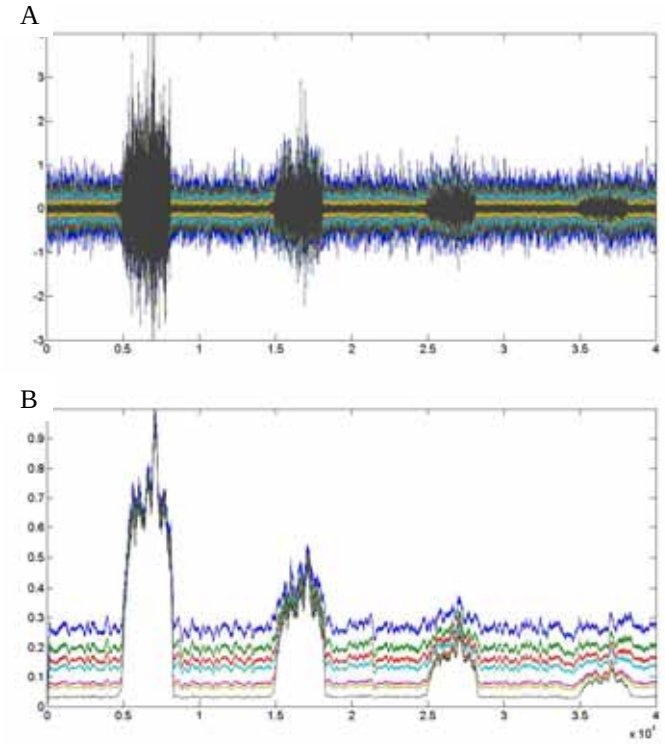

Figure 1: A) Raw and B) processed EMG bursts (100%, 50%, 25%, 12.5% maximum amplitude) with varying levels of added noise.

These error data were plotted (Figure 2) as a function of measured EMG and baseline noise. The resulting 3D surface was best fit (Table Curve 3D) to a three parameter equation:

$\ln(\text{error}) = A + B(\text{measured EMG}) + C(\ln(\text{noise}))^2$

The modeled errors were then removed from the measured values to calculate "corrected" EMG burst amplitudes. To validate this approach, a 2nd set of scaled EMG bursts with varying levels of simulated noise were created using EMG derived from a shoulder abductor muscle in a different subject. Corrected EMG burst amplitudes were assessed using both the constant baseline and the nonlinear modeled error (using prior a, b, and c values) subtraction methods. The resulting errors (measured relative to expected amplitude) were calculated for both methods.

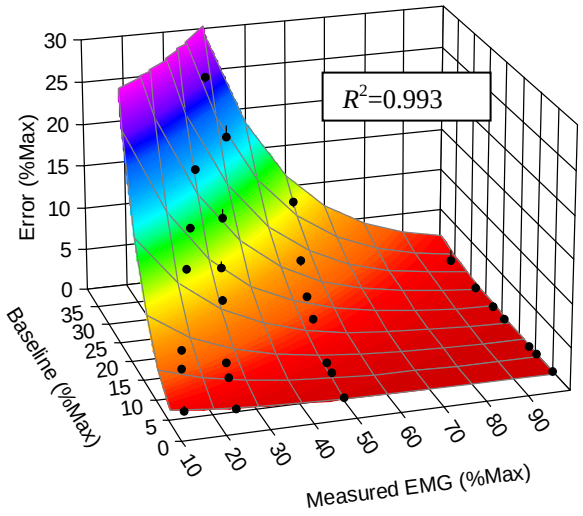

Figure 2: Model surface fit of errors (Measured – Actual) for mean EMG amplitude as a function of baseline noise and measured activation intensity.

RESULTS AND DISCUSSION

Baseline noise had minimal effects at max EMG amplitude, but increased nonlinearly (see Figures 1 and 2) with increasing baseline noise and decreasing signal amplitude. The nonlinear error model explained 99.3% of the variation in the measured error (Figure 2). The uncorrected EMG burst amplitudes overestimated actual EMG values as the signal to noise ratio decreased. Traditional baseline subtraction reversed this finding, consistently underestimating actual EMG amplitude (see Table 1) for low intensity bursts. The associated errors were relatively small for EMG amplitudes that were >50% of maximum, but on average resulted in errors approaching 100% of actual values for the lowest intensity bursts (either uncorrected or baseline subtraction methods). Using the nonlinear error model to correct EMG decreased errors to <1% max, in both test and validation EMG tracings (see Table 1 for validation EMG results).

CONCLUSIONS

Our results indicate that correcting baseline noise as a function of both baseline and measured signal amplitude ("true" + noise) produces highly accurate estimates of EMG amplitude when assessing mean activity during burst periods. Therefore, we recommend considering this approach when accounting for baseline noise during signal processing, particularly when the signal-to-noise ratio is low. It is to be noted the modeling coefficients are not universal, but would need to be estimated for each unique EMG processing algorithm using simulated EMG and noise data.

REFERENCES

1. Dowling JJ. *Sports Med.* **24**, 82-96, 1997.
2. Krishnan C, Williams GN. *Med Sci Sports Exerc*. **41**, 1652-60, 2010.
3. Hodges PW, Gandevia SC. *J Appl Physiol*. **89**, 967-76, 2000.

ACKNOWLEDGEMENTS

The authors were funded in part by the University of Iowa Graduate Program in Physical Therapy, the National Institutes for Health, K01AR056134-01A2 (LFL), NRSA 1 F31 AR056175-01 (KA), and the Foundation for Physical Therapy (KA).

Table 1: Mean corrected EMG activation assessments and the associated error following correction.

Baseline Noise (% max)	Constant Baseline Subtraction: mean EMG (% max)				Nonlinear Error Substraction: mean EMG (% max)			
	100%	50%	25%	12.5%	100%	50%	25%	12.5%
47.8	100.0	34.5	11.0	1.0	97.2	51.3	27.5	14.8
34.3	100.0	36.9	12.0	2.4	98.9	50.7	25.1	12.6
26.5	100.0	39.2	13.5	3.2	99.5	50.7	25.0	12.6
18.1	100.0	42.0	15.8	4.7	99.8	50.4	25.2	12.9
9.2	100.0	45.5	19.4	7.1	99.9	49.9	25.0	12.6
Ave Error	**0.0**	**-10.4**	**-10.7**	**-8.8**	**0.9**	**0.6**	**0.6**	**0.6**

A CADAVERIC ROBOTIC GAIT SIMULATOR WITH FUZZY LOGIC VERTICAL GROUND REACTION FORCE CONTROL

[1,2]Patrick M. Aubin, [1]Eric Whittaker, and [1,3,4]William R. Ledoux

[1]VA RR&D Center of Excellence for Limb Loss Prevention and Prosthetic Engineering, Seattle, WA 98108, Departments of [2]Electrical Engineering, [3]Orthopaedics & Sports Medicine, and [4]Mechanical Engineering, University of Washington, Seattle, WA 98195
Email: wrledoux@u.washington.edu, web: http://www.amputation.research.va.gov/

INTRODUCTION

Lower limb dynamic cadaveric gait simulators are useful to investigate the biomechanics of the foot and ankle but many systems, including earlier versions of ours, have several common limitations including, simplified tibial kinematics [1-4], greatly reduced velocities [1-4], and open loop trial and error vertical ground reaction force (vGRF) control [1, 2, 4]. To address these limitations, we have developed a high fidelity robotic gait simulator (RGS) capable of simulating the stance phase of gait by prescribing 6-degrees of freedom (DOF) tibial kinematics at biomechanically more realistic velocities, while controlling the vGRF via a novel multiple input multiple output (MIMO) fuzzy logic vGRF controller.

METHODS

The RGS simulated the stance phase of gait inversely in 2.7s by fixing a cadaveric specimen in place while a mobile force plate, articulated by a 6-DOF R2000 parallel robot, created the relative 6-DOF tibia to ground motion. Nine force controlled actuators prescribed tendon force to the peroneus longus (PL), peroneus brevis (PB), tibialis anterior (TA), tibialis posterior (TP), flexor hallucis longus (FHL), flexor digitorum longus (FDL), extensor hallucis longus (EHL), extensor digitorum longus (EDL), and the Achilles (Ach) tendons. The vGRF was controlled by altering the TA tendon force, Ach tendon force, and tibial kinematics via a MIMO fuzzy logic vGRF controller.

A MIMO fuzzy logic vGRF controller was designed with three inputs: $stance$, $vGRF_{error}$, and $\sum vGRF_{error}$, defined as the percent stance phase, the error between the target and actual vGRF, and the integral of the vGRF error, respectively. The input variable $stance$ was partitioned into four fuzzy sets: $heel\ strike$, $load\ response$, $midstance$, and $late\ stance$. The other two input variables, $vGRF_{error}$, and $\sum vGRF_{error}$, were partitioned into three fuzzy sets: negative (N), zero (Z), and positive (P). The controller had three outputs: ΔF_{Ach}, ΔF_{TA}, and Δx, defined as a change in Achilles tendon force, a change in TA tendon force, and a change in the mobile force plate position normal to its surface, respectively. A fuzzy rule base in the form of IF-THEN rules was designed for each output which stated the desired ΔF_{Ach}, ΔF_{TA}, and Δx for a given linguistic value of $stance$, $vGRF_{error}$, and $\sum vGRF_{error}$. During the gait simulation, ΔF_{Ach} and ΔF_{TA} were updated in real time, while Δx was added to the R2000's trajectory iteratively between gait simulations similar to an iterative learning controller previously developed by our group [5].

Three cadaveric lower limb specimens transected at approximately 10 cm proximal to the ankle joint had nine tendons dissected. Target tendon forces were estimated from a muscles' physiological cross sectional area, maximum specific isometric tension, and electromyography activity. A tibia coordinate system (TIB) was constructed from retro-reflective markers. The cadaveric foot was mounted into the RGS and the pose of TIB was determined via a 6-camera Vicon motion analysis system. The tibia was then repositioned into an optimal pose based on the results of an exhaustive search which found heel strike locations and TIB poses that would keep the R2000's trajectory inside its working volume and minimize its motor velocities. The target TIB with respect to ground kinematics and vGRF input into the RGS were previously collected from ten subjects performing four or five gait trials each.

During preliminary RGS trials, a superior-inferior offset to the R2000 trajectory and the Achilles tendon force were adjusted iteratively to slowly increase the first and second peak of the vGRF from zero to approximately three quarters body weight. Once the two vGRF peaks were roughly equal to their target peak forces, the fuzzy logic vGRF controller was enabled and a quartet of trials (three "learning" and one final trial) was performed with a recovery time of a few seconds between each learning trial. The four trials had the added benefit of allowing the foot tissues to precondition and the vGRF controller to account for the change in plantar tissue stiffness. During the recovery time the iterative fuzzy logic vGRF controller determined $\Delta x(t)$ for the next trial so that the *in vitro* vGRF would track the target *in vivo* vGRF. For each foot, three simulation quartets were collected, each containing three learning trials and one final trial.

RESULTS AND DISCUSSION

The fuzzy logic vGRF controller demonstrated its ability to achieve the vGRF with high fidelity (Fig. 1). The average RMS error between the target *in vivo* and actual *in vitro* vGRF was 7.6% body weight across all nine final trials. The sagittal, frontal, and transverse plane fixed angles of the tibia with respect to the ground were almost entirely within ± 1SD of those found *in vivo* for three feet (Fig. 2). The average RMS tracking error for PL, PB, TP, FHL, FDL, EHL, and EDL was 3.9N across all nine final trials. The mean peak Ach and TA tendon force was 1262 N at 80.4% stance and 119.4N at 15.1% of stance respectively. The trajectory optimization routine determined an 8.0% to 35.6% decrease in motor velocity was possible between the optimal and worst case pose of the TIB and heel strike location.

Close loop fuzzy logic vGRF control greatly improved the fidelity of the vGRF as compared to the trial and error tendon force adjustment method commonly used. An earlier version of the RGS with trial and error vGRF control had a vGRF RMS tracking error of 30.0% body weight and a 10s stance phase [1]. The trajectory optimization employed in this study decreased the stance phase to 2.7s, a substantial improvement compared to our previous system and most other gait simulators which range from 2s [2] to ~12s [3] to 60s [4]. One limitation of the study is the scaling of the vGRF to three quarters body weight. While full body weight simulations are within the working limits of the R2000 [5], frail cadaveric specimens often fail under larger forces. Performing the simulations at half body weight is a common limitation for many dynamic gait simulators [1-3].

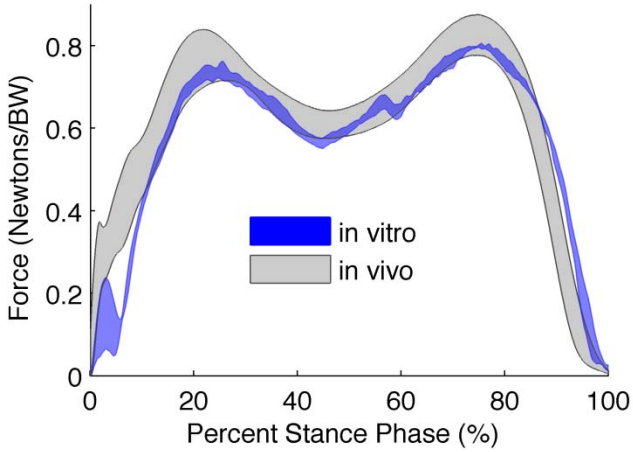

Figure 1: *In vitro* (gray) compared to the target *in vivo* (blue) vGRF.

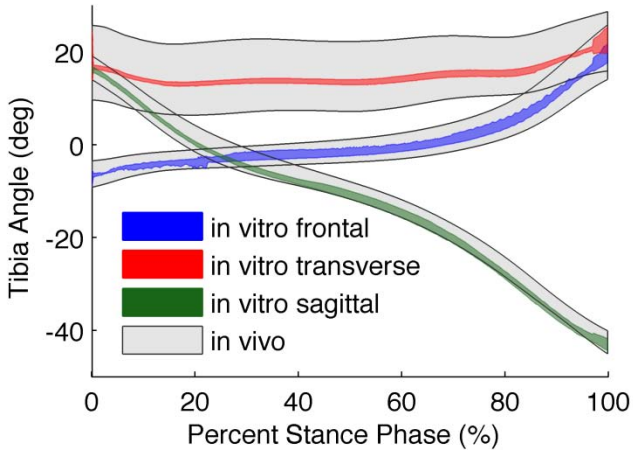

Figure 2: Mean *in vivo* ± 1SD tibia with respect to ground angles (gray) compared to mean *in vitro* ± 1SD tibia angles for the frontal (blue), transverse (red), and sagittal (green) planes for three feet.

REFERENCES

1. Bayomy, AF. *J. Bone Joint Surgery*, in press.
2. Nester, CJ. *J. of Biomechanics*, **40**(9), 2007.
3. Hurschler, C. *Foot & Ankle Int.* **24**(8)**,** 2003.
4. Okita, N. *Gait & Posture*, **30**, 2009.
5. Aubin, PM. *IEEE Trans Biomed Eng*. **55**, 2008.

ACKNOWLEDGEMENTS

This work was funded in part by the VA RR&D, grants A3923 and A4843C.

LOCATING THE HIP JOINT CENTER USING A GREATER TROCHANTER METHOD

Joshua T. Weinhandl & Kristian M. O'Connor

Department of Human Movement Sciences
University of Wisconsin-Milwaukee, Milwaukee, WI, USA
E-mail: weinhan2@uwm.edu Web: www.chs.uwm.edu/neuromechanics

INTRODUCTION

In the biomechanics literature, hip joint center (HJC) coordinates are commonly estimated using functional approaches [1] or regression equations [2]. Previous research has shown the functional approach to be potentially highly accurate yet dependent on the type of movement and range of motion of the joint. Furthermore, results of studies investigating the accuracy of the regression equations have been equivocal. An alternative, yet unverified, predictive method that places the HJC coordinates at 25% of the distance from the ipsolateral to the contralateral greater trochanter (GT method) is currently widely used in the biomechanics community. The purpose of this study was to confirm that this method is a viable option for estimating HJC coordinates. A comparative analysis with HJC coordinates estimated via the regression equations proposed by Bell et al. [3] was also performed.

METHODS

Ten subjects were fitted with reflective markers on the left and right greater trochanters, left and right anterior-superior iliac spines, and left and right posterior-superior iliac spines, as well as a rigid plate with four markers attached to the right thigh. Marker trajectories were collected at 200 Hz with a ten-camera Motion Analysis Eagle System (Santa Rosa, CA, USA) and filtered using a fourth-order, zero lag, recursive Butterworth filter with a cutoff frequency of 18 Hz. HJC coordinates were estimated via the GT method, a functional (FUN) method [4], and the regression equations based on pelvic width proposed by Bell et al. [3].

HJC coordinates for each of the three methods were reported in the pelvic anatomical coordinate system (Figure 1) and a 3×2 (method×day) repeated measures ANOVA was used to analyze potential differences between methods and test days. Additionally, the differences ($\Delta x, \Delta y, \Delta z$) between the FUN method and those yielded by the GT and BELL methods were calculated for each subject. These error scores were then compared using a 2×2 (method×day) repeated measures ANOVA. Significance for all tests was set at $p<0.05$.

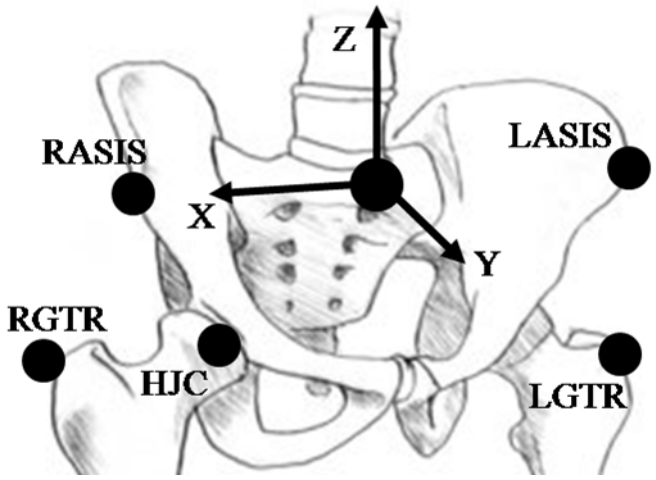

Figure 1. Pelvic anatomical landmarks and anatomical frame

RESULTS AND DISCUSSION

The FUN method was chosen as our baseline, "gold standard," measurement as it has been shown to approximate joint center locations to within one millimeter using computer simulation models and/or rigid mechanical linkage devices [4]. To maximize the accuracy of the FUN method used in the current study, we asked subjects to perform flexion/extension, abduction/adduction, and circumduction movements with a magnitude of $\pm 30^{o}$ while data was collected at 200 Hz for ten seconds (allowing a buffer to ensure a minimum of 500 valid samples).

The mean HJC coordinates in the pelvic ACS for all three methods and HJC error scores for the GT and BELL methods are presented in Table 1. Neither,

the method×day interaction nor main effect for between days was significant for HJC coordinates or error scores and therefore, the data is not presented in Table 1.

The absence of significant method×day interactions and day effects suggest that all three methods tested in the current study offer repeatable estimates of the HJC. Additionally, the HJC coordinates estimated using the BELL method agree with those reported by Leardini et al. [1]. The subjects in the current study had an average pelvic width ~13% greater than those used by Leardini et al. [1], resulting in a HJC estimate that was ~13% more medial, posterior and distal than reported by Leardini et al. [1]. It is possible that our subjects in fact did have wider pelvises than the subjects used by Leardini et al. [1]. However, these differences in pelvic width, and subsequent HJC coordinate estimates, are potentially due to a systematic difference in ASIS identification between the current study and Leardini et al. [1].

The results of this study suggest that the GT method offers repeatable estimates of the HJC coordinates that are comparable to those estimated using the FUN method. Even though the HJC coordinates estimated using the GT method were significantly different than the FUN method in the medial-lateral and anterior-posterior directions, the magnitudes of these errors were ~9.1 mm and ~11.6 mm respectively. Additionally, the error associated with the GT method was significantly less than the BELL method in the vertical and medial-lateral directions. In the current study, the GT method estimated the HJC location ~7.5 mm proximal to the FUN method, compared to the ~23.0 mm difference estimated by the BELL method. In the medial-lateral direction the GT method estimated the HJC location ~9.1 mm lateral to the FUN method, compared to a difference of ~14.5 mm estimated by the BELL method. While the GT method yielded a HJC estimate with smaller deviations from the FUN method than those estimated via the BELL method in the vertical and medial-lateral directions, there was no improvement in the anterior-posterior direction.

CONCLUSIONS

In summary, while all three methods tested in the current study offer repeatable estimates of the HJC, the GT method provides a HJC estimate with smaller deviation from the FUN method than those estimated via the regression equations proposed by Bell et al. [2]. Specifically, the GT method estimated HJC location with the decreased error in the medial-lateral and vertical directions. However, there was no difference in anterior-posterior direction errors (GT ~11.5 mm; BELL ~10.5 mm). Future work should examine if the GT method can be improved by incorporating an offset in the anterior-posterior direction as a function of pelvic depth. However, the results of this study confirm the use of the GT method as a viable option for estimating HJC coordinates.

REFERENCES

1. Leardini, A, et al. *J Biomech* **32,** 99-103, 1999.
2. Bell, AL et al. *J Biomech* **23**, 617-21, 1990.
3. Schwartz, MH, Rozumalski, A. *J Biomech* **38**, 107-16, 2005.
4. Ehrig, RM, et al. *J Biomech* **39**, 2798-809, 2006

Table 1. HJC coordinates (mm) and errors (mm) in the pelvic anatomical coordinate system pictured in Figure 1

	X		*Y*		*Z*		
	Coordinates*†‡	Error†	Coordinates*†	Error	Coordinates†‡	Error†	**Total Error**
FUN	80.7 ± 12.2	-	-39.8 ± 1.2	-	-102.4 ± 0.7	-	-
GT	89.9 ± 9.2	-9.1 ± 7.4	-51.4± 10.1	11.6 ± 9.7	-94.9 ± 17.8	-7.5 ± 17.5	23.5 ± 12.8
BELL	95.2 ± 8.5	-14.4 ± 3.8	-50.2 ± 4.5	10.4 ± 4.3	-79.3 ± 7.1	-23.0 ± 7.1	30.0 ± 5.5

* indicates FUN significantly different from GT (p <0.05).

† indicates FUN significantly different from BELL (p <0.05).

‡ indicates GT significantly different from BELL (p <0.05).

EFFECT OF SCIENTIST EXPERIENCE ON THE REPEATABILITY OF PALPATION OF SCAPULAR LANDMARKS

Alexander W. Hooke, Kenton R. Kaufman, and Kai-Nan An

Biomechanics and Motion Analysis Laboratories, Division of Orthopedic Research
Mayo Clinic, Rochester, USA
email: Kaufman.Kenton@mayo.edu, web: http://mayoresearch.mayo.edu/biomechanics/

INTRODUCTION

Scapular kinematics have historically been difficult to track using skin mounted markers due to its location beneath soft issue, translational ability, and its relatively amorphous shape. Both optical and electromagnetic tracking systems have been used in combination with bone pins to verify various measurement techniques [1-3], while others have measured how reliably skin mounted systems track scapular kinematics [4, 5]. In all cases, landmarks defining the scapular coordinate system, as specified by the ISB, were located using palpation and tracked either directly or via virtual marker digitization. Due to the unique properties of the scapula, scapular palpation is highly dependent on the skill and experience of the person performing the palpation. The purpose of this study was to assess the effect of a palpator's experience on the repeatability of a palpation dependent protocol for tracking scapular kinematics.

METHODS

Three physical therapists (PT) and three subjects (2 male, 1 female) with no history of shoulder pain were in this study. All PTs had experience in both general practice and manual palpation (Table 1).

Table 1:

	Years Experience	
	Certified	Motion Analysis Lab
PT 1	28	2
PT 2	30	14
PT 3	15	1.5

Kinematics were recorded with a 10-camera Motion Analysis EVa RealTime system (Motion Analysis Corp., Santa Clara, CA). Reflective markers were placed on 10 anatomical landmarks on the subject. A three-dimensional model of the right upper extremity was developed using Visual3D (C-Motion Inc., Germantown, MD, USA). The model consisted of three rigid body segments: trunk, right scapula, and right upper arm. All segments were defined using the ISB recommendations. Euler angles were used to describe the joint kinematics. Scapula orientation relative to the thorax was described as upward rotation, posterior tilting, and external rotation in the thorax coordinate system [6].

Scapular kinematics were captured by mounting a three marker triad on the flat, superior surface of the acromion process. The ISB recommended landmarks for scapular definition (angulus acromialis, trigonum scapulae, and angular inferior) were manually palpated, their locations were indicated using a digitizing pointer, and their locations were tracked relative to the marker triad on the acromion head.

With the subject in a neutral position, each physical PT completed two sessions of palpation and digitization of the scapular landmarks with each session consisting of three trials. This resulted in a total of 18 palpation trials being collected (3 PTs x 2 sessions x 3 palpation trials) for each subject. The sessions were separated by approximately one hour. All 10 markers were left on the subject so any differences appearing between trials could be attributed to differences in scapular definition.

The subject performed three tasks: shoulder abduction, flexion, and reaching across to the top of the opposite shoulder. Each task was performed in a single trial consisting of three repetitions.

The 18 different scapular definitions were applied to the three movement trials, so any differences appearing between trials would be attributed to differences in scapular definition. Inter-trial, inter-session, and inter-PT variability in scapular kinematics were calculated over the normalized

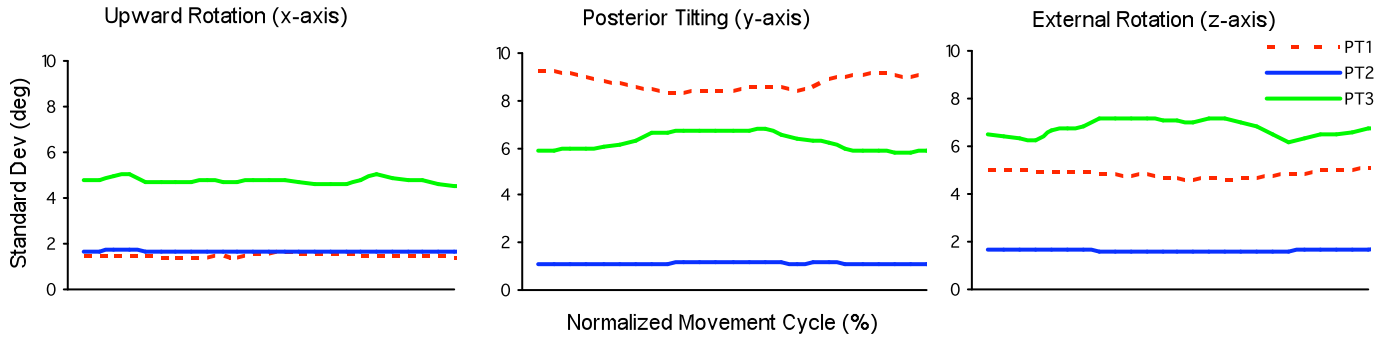

Figure 1: Variability of scapular kinematics during reach to opposite shoulder task. Intra-therapist variability is shown for each PT individually in the upward rotation, posterior tilting, and external rotation components. Data is normalized over one movement cycle.

movement cycle for each of the three tasks using the method described by Schwartz et al. [7].

The distance between a marker placed on the acromion head and the three scapular defining landmarks was calculated. Variability in these distances between trials, sessions and PTs was calculated to determine if kinematic variability was due to variations in the location of specific landmark(s).

RESULTS AND DISCUSSION

For all tasks, the mean inter-PT variability in scapular kinematics was over 6°. Looking at the intra-PT variability for each individual PT, prominent differences are noted. The variability in scapular kinematics using landmarks defined by PT 2 was less than 2° for all tasks, along all axes, averaged across all subjects, while variability using landmarks defined by PTs 1 and 3 was significantly higher and less consistent (Figure 1).

The variability in scapular landmark locations increased as the level of analysis expanded from inter-trial to inter-therapist. There were no significant differences in variability between landmarks (Figure 2).

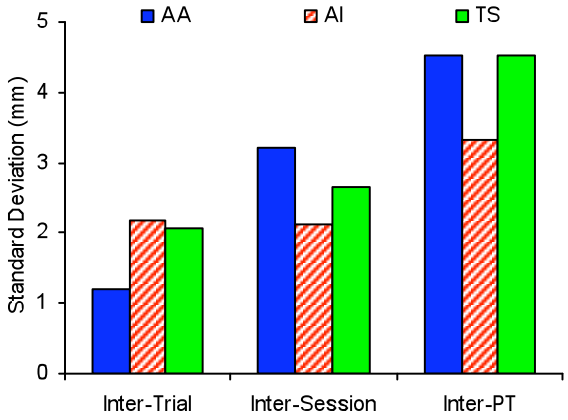

Figure 2: Variability in scapular landmark locations. Inter-trial, inter-session, and inter-PT variability is shown for the angulus acromialis (AA), trigonum scapulae (TS), and angular inferior (AI) landmarks.

CONCLUSIONS

Various techniques have been utilized for determining scapular position based on the palpation of scapular bony landmarks [1-5]. Based on the findings presented here, correct and repeatable palpation cannot be assumed and is highly dependent on the technique and experience of the palpator. Only the most experienced PT in this study was able to identify the landmarks recommended for definition of the scapula by the ISB reliably enough for clinical decision making. Deviations in landmark identification as small as 4mm are shown to have significant impacts on subsequent segments' kinematics. This suggests that palpators should take extra care in all landmark identification.

REFERENCES

1. Bourne, D., et al., (2009) Proc Inst Mech Eng H. 223: 349-61.
2. Bourne, D.A., et al., (2007) J of Shoulder Elbow Surg. 16: 150-62.
3. Karduna, A.R., et al., (2001) Trans Am Soc ME. 123: 184-190.
4. Myers, J., et al., (2006) J Sport Rehab. 15: 125.
5. Thigpen, C.A., et al., (2005) Res Sports Med. 13: 181-98.
6. Nawoczenski, D., et al., (2003) Arch of Phys Med Rehab. 84: 1293-1300.
7. Schwartz, M.H., J.P. Trost, and R.A. Wervey, (2004) Gait Posture. 20: 196-203.

ACKNOWLEDGMENTS

This project was supported by Grant Number R01 HD 48781 from NIH.

THE USE OF DYNAMICAL SYSTEMS THEORY METHODS TO REFINE KINEMATIC MOVEMENT DATA AS AN INPUT TO AN ARTIFICIAL NEURAL NETWORK

[1]Joseph O'Halloran and [2]Ross Anderson

[1]University of Massachusetts-Amherst, Amherst, MA, USA
[2]Biomechanics Research Unit, University of Limerick, Ireland
email: josepho@kin.umass.edu

INTRODUCTION

This paper outlines the development of a data format which optimizes the performance of an artificial neural network (ANN). Previous research has shown an ANN, designed for time series kinematic movement patterns, to be relatively successful in predicting the power output of rowers [1]. It is proposed that the use of dynamical systems theory (DST) methods can be used to refine this input data to improve the prediction capability and decrease the training time of the ANN. The DST data is designed to be complete in containing all the artifacts of the original time series kinematic data, while reducing its dimensionality. This ensures that the data contains all of the elements while reducing the time of training. DST methods have received increasing attention within biomechanics in recent years. The majority of these studies have focused on the use of DST in the examination of variability in data sets. While kinetics and kinematics of a movement pattern may not change, the higher order parameters contain much more information [2]. This implies that examining the derivatives (i.e. velocity and acceleration) will provide much more detail of the movement than simply examining the displacement data. Analysis of movement coupling is a relatively new area, which has been examined in a limited number of studies to date. DST methods have been used in the area of coordination of movement and also to examine the mechanisms of injury [3]. However, this research aims to examine the possible use of DST techniques in data refinement with the long term goal of employing the method chosen in an ANN. The 3 methods chosen for analysis are continuous relative phase (CRP), cross correlation (CC), and vector coding (VC). Each of the movement pattern data sets was investigated with an analysis of the output produced and of the possibility of use of each of these methods in the ANN. It is hypothesized that if the dimensionality of the data can be successfully reduced without removing any of the essential components of the signal, then this data can be used in the ANN to quantify the outcome measure of the movement patterns, with an improved prediction and with a reduced training time than that achieved in [1].

METHODS

Six rowers (5 novices, 1 experienced; age 23±2.9 yrs; height 165±7.7 cm; weight 68±7.5 kg) participated in the study. The participants performed a 2000m row on a RowPerfect ergometer (CARE RowPerfect, The Netherlands). This distance ensures that each participant would complete a large number of strokes (n>200). The distance of 2000 meters was completed in 357±59 strokes. Kinematic data was captured at 200Hz (Hawk Digital Real Time System, Motion Analysis Inc, USA). From the collected data 5 joint angles (ankle, knee, hip, shoulder, and elbow) for the entire movement could be identified.

Data analysis techniques used in DST were performed in this study. This involved angle-angle diagrams, phase plane plots, and subsequently CRP, CC, and VC. The refinement of the data for each of the three data sets used linked joint segments to compress the 5 joint angles into 4, 3 and 2 data curves. The data refinement techniques resulted in 9 series of data being individually tested on each ANN (Table1).

A fully connected feed-forward back-propagation network comprised of one input layer, one hidden layer and one output layer, trained with the Levenberg-Marquardt method was used. A separate ANN was designed (using Matlab V6.5 – The Mathworks, USA) for each participant to specifically reflect his or her joint kinematics.

One hundred strokes were randomly selected from the total number for each participant and used as training data for the ANN; the training data consisted of the DST data and the power output (obtained from the RowPerfect). The remaining data for each rower was then used as test data in the network.

RESULTS AND DISCUSSION

The results indicate that the correlation between the predicted power output and the actual power output was greatest for the CRP data. Within each method, the highest correlation occurred when 4 data sets, each comprising of 2 joint angles were used as input data. The best responding data is CRP with an average r^2 value of 0.83. The second responding data is CC with an average r^2 value of 0.74. VC performed poorly (Table2).

The time taken to train the network has also reduced dramatically from an average of 238(±30) to 37 (±20) minutes for the CRP data set A which was the fastest.

CONCLUSIONS

CRP provides a suitable method of data refinement for continuous movement pattern kinematic data. It retains the original data while providing information on the coordination involved in the movements. The data reduction method of CC also provides much possible benefit as a data refinement method for an ANN.

The use of CRP, especially within lower limb kinematics, is preferred as an input as it maintains the trends within 2 joints by compressing displacement and velocity of both joints into one time series variable. The use of 4 CRP curves, each a representation of linked segments within the body should provide a suitable input for the ANN without losing any information from the raw data.

Each technique brings its own benefit and the biomechanist must outline the demands of the study, the desired impact of the data reduction, and the future use of the reduced data before deciding on a particular method.

REFERENCES

1. O'Halloran J et al. *Proceedings of ISBS'06,* Salzburg, Austria, 2006.
2. Hamill J *Proceedings of ISBS'06,* Salzburg, Austria, 2006.
3. Stergiou N et al. *Gait and Posture* 6 (3): 177-185, 1997

Table 1: Data entered into ANN

CRP	CC	VC
2 joint angles (4 data curves) **(A)**	2 joint angles (4 data curves) **(D)**	2 joint angles (4 data curves) **(G)**
3 joint angles (3 data curves) **(B)**	3 joint angles (3 data curves) **(E)**	3 joint angles (3 data curves) **(H)**
4 joint angles (2 data curves) **(C)**	4 joint angles (2 data curves) **(F)**	4 joint angles (2 data curves) **(I)**

Table 2: r^2 results of amended input data

Participant	1	2	3	4	5	6
CRP						
A	0.9	0.87	0.79	0.86	0.79	0.81
B	0.8	0.63	0.67	0.67	0.6	0.71
C	0.3	0.5	0.27	0.42	0.38	0.56
CC						
D	0.79	0.76	0.64	0.76	0.77	0.70
E	0.74	0.53	0.53	0.71	0.57	0.61
F	0.19	0.14	0.2	0.4	0.15	0.13
VC						
G	0.63	0.40	0.43	0.43	0.46	0.51
H	0.4	0.31	0.32	0.46	0.39	0.46
I	0.13	0.09	0.21	0.23	0.16	0.21

CAN HIP AND KNEE KINEMATICS BE IMPROVED BY ELIMINATING THIGH MARKERS?

[1] Brian Schulz and [2]Wendy Kimmel

[1] VA HSR&D/RR&D Center of Excellence, Maximizing Rehabilitation Outcomes,
James A. Haley Veterans' Medical Center, Tampa, FL, USA
[2] Running Injury Clinic, Department of Kinesiology, University of Calgary, Calgary, AB, Canada
email: Brian.Schulz@va.gov

INTRODUCTION

Marker sets developed for gait analysis are often applied to more dynamic tasks with little or no validation, despite known complications of soft tissue artifact. To address this issue, here we present a comparison of the hip and knee kinematics of a single unimpaired male experimenter (height=1.7m, mass=84kg) as calculated by five concurrently-worn marker sets during eight different tasks.

METHODS

The first three tracking marker sets evaluated were Helen Hayes using 1) proximally-affixed thigh wands (HHprox), 2) distally-affixed thigh wands (HHdist), 3) patellar markers instead of thigh wands (HHpat). The remaining two marker sets used rigid four marker clusters on 4) shank & thigh (C-ST), and 5) shank only (C-S). Pelvis and foot segment definitions, joint centers, and segment coordinate systems were shared by all marker sets.

The first three tasks were femoral internal and external rotation tasks with 1) hip neutral and knee at full extension, 2) hip neutral and knee flexed to 90º, and 3) both hip and knee flexed to 90º. The remaining five tasks 4) walking along a straight path (walking), 5) walking in two clockwise or counterclockwise circuits of a 1m radius circle (turning), 6) running along a straight path (running), 7) maximal height jumping (jumping), and 8) maximal length out-and-back lunging (lunging).

RESULTS AND DISCUSSION

The shank-only marker set (C-S) was capable of detecting the most hip external-internal rotation, yet only did so during tasks where greater hip axial motions would be expected (Fig. 1). In general, few and small differences in knee and hip flexion-extension were observed between marker sets, while many and large differences in knee adduction-abduction and external-internal rotations at both the knee and hip were observed. These differences were greatest for more dynamic tasks and greater joint ranges of motion.

The femoral rotation test results were consistent with prior studies [1] and demonstrated that more distal markers were generally capable of capturing greater external-internal hip motions with C-S capturing the most (Fig.1). This was likely due to substantial proportions of hip external-internal rotations being detected as knee motions by the marker sets using thigh markers (HHprox, HHdist, and C-ST). For example, C-S captured 28-41º (68-242%) more femoral axial rotation than these marker sets, but when the hip external-internal rotation ROM was added to the knee external-internal rotation ROM for task 1 (knee locked) and to the knee adduction-abduction ROM for tasks 2 & 3 (knee flexed to ~90º), the combined ROMs for all five marker sets were within 4.1º, 2.1º, and 2.8º of each other for all three hip rotation tasks. These values were all less than the mean standard deviation for hip external-internal rotation ROM for all marker sets during the three hip rotation tasks (5º). The consistency of this combined knee and hip ROM across marker sets for the hip rotation tasks supports the hypothesis that substantial hip external-internal rotations are being detected at the knee by marker sets using thigh markers.

The femoral rotation tasks demonstrated that C-S was capable of capturing up to 242% more external-internal hip rotation ROM than the other tracking marker sets evaluated, but for the other dynamic

tasks C-S only detected substantially more for tasks (e.g. turning, jumping, & lunging) that would be expected to elicit greater external-internal rotations. C-S actually captured substantially less external-internal rotation ROM than HHprox and HHdist for running (Fig. 1), where thigh STA during the fast, bouncing gait pattern was likely to have artificially increased the ROM detected by thigh-mounted markers.

At the knee, all but C-S detected motions that were beyond established limits for external-internal rotation (>33º or <-23º) or adduction-abduction (>10º or <-10º) [2]. However, this study reports no 'gold standard' to define true skeletal motions. Considering that data from prior studies using intracortical pins have demonstrated substantial inter-subject and inter-study variation [3], no conclusions regarding which marker set most accurately represents true skeletal motions can be drawn from these data.

A consequence of the C-S definition of the thigh and knee segments is that the knee becomes a 2DOF joint. Flexion-extension is always detected, but the other DOF transitions between detecting 100% of knee external-internal rotation (and 0% of adduction-abduction) at 90º of knee flexion to detecting 100% of knee adduction-abduction (and 0% of external-internal rotation at full knee extension. This results in underestimation of knee external-internal rotation as the knee approaches full extension and underestimation of knee adduction-abduction as the knee approaches 90º of flexion (Fig. 5). For external-internal rotation, this property roughly corresponds to the movement permitted by the knee anatomy and to the data from [2]. For adduction-abduction, the underestimation caused by this DOF sharing may be preferable to the substantial hip motions interpreted by marker sets using thigh markers as non-physiologic (ROM>35º) knee adduction-abduction motion.

CONCLUSIONS

Marker set selection is critical to non-sagittal hip and knee motions. The shank-only marker set presented here is a viable alternative that may improve knee and hip kinematics by eliminating errors from thigh soft tissue artifact, particularly for tasks such as turning where hip external-internal rotations are anticipated and/or of interest. Furthermore, it is particularly well-suited to inertial measurement systems, as all lower limbs could be tracked using only five sensors rather than seven. This could substantially reduce the costs of portable gait analysis systems.

REFERENCES

1.Wren TAL, et al., *Gait & Posture*, **27**(3), 530-534, 2008

2.Blankevoort L, et al., *J Biomech*, 21(9), 705-720, 1988.

3.Reinschmidt C., et al.,
Gait & Posture, 6(2), 98-109, 1997. AND
J Biomech, 30(7), 729-732.

ACKNOWLEDGEMENTS

This study was supported by a VA RR&D Career Development Award (E2964F) and Research Award Enhancement Program.

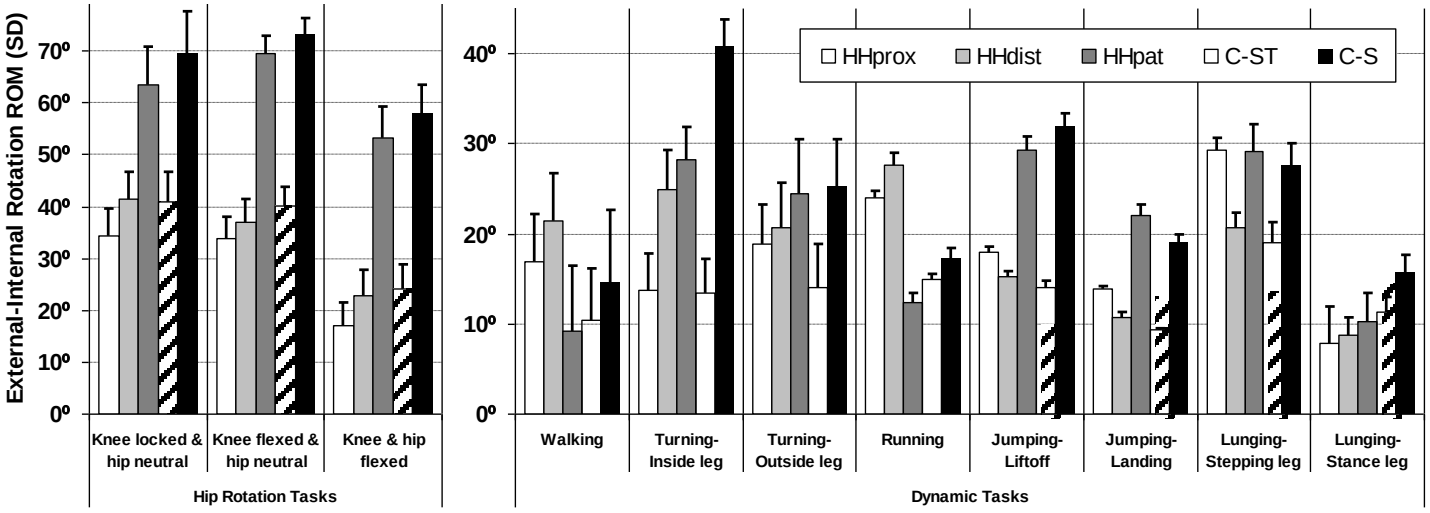

Figure 1: Mean (SD) hip external-internal rotation ROM for all tasks as calculated by all tracking marker sets.

NORMALIZATION OF EMG AMPLITUDE: A COMPARISON OF DIFFERENT METHODS USED TO TEST INDIVIDUALS WITH ARTHRITIS OF THE HAND

Kristina Calder[1], Vicki Galea[1], Jean Wessel[1], Joy MacDermid[1], and Norma MacIntyre[1]

[1]School of Rehabilitation Science, McMaster University, Hamilton, ON Canada
email: kcalder@mcmaster.ca

INTRODUCTION

Electromyography (EMG) is a technique used to measure muscle activity during voluntary and involuntary contractions. The use of surface EMG in the clinical decision-making process is becoming more prevalent in rehabilitation settings, where EMG signals between symptomatic and asymptomatic populations are being investigated. In order to compare activity between muscles, in the same muscle over time, and between individuals, the EMG should be normalized due to the high variability related to intrinsic and extrinsic factors [1]. Information regarding the use of EMG to study hand muscles in individuals with arthritis is sparse, and the best method to normalize the EMG in this population has not been investigated.

The overall aim of this study was to investigate two methods of normalizing EMG amplitude to determine the most appropriate normalization method to use in the hand arthritis population.

METHODS

Community-dwelling women over the age of 50 years without hand problems and those who met the American College of Rheumatology (ACR) clinical criteria for osteoarthritis (OA) or rheumatoid arthritis (RA) of the dominant hand were included in the study [2].

Dominant hand muscle activity was recorded using surface EMG from the thenar, first dorsal interosseous (FDI) and extensor digitorum communis (EDC) muscles. The surface EMG and force were recorded simultaneously during three maximum voluntary tripod pinch strength contractions (MVCs) and three reference voluntary tripod pinch strength contractions (RVCs) at 1kg of force using the NK tripod pinch device of the NK Hand Assessment System (Fig.1; NK Biotechnical Corporation, Minneapolis, MN, USA).

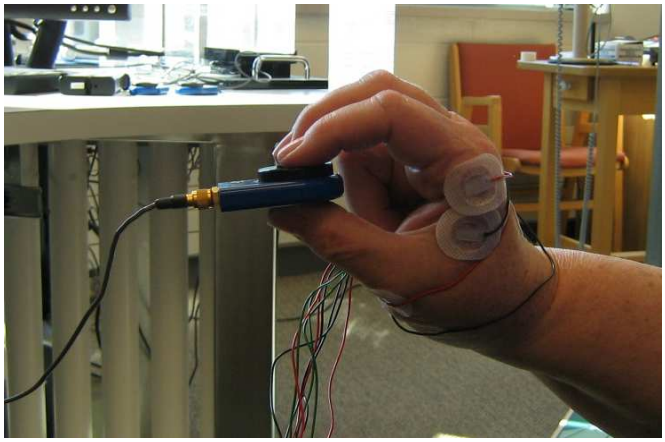

Figure 1: Experimental set-up showing the finger positioning on the tripod grip pinch device, and electrode placement on the thenar and FDI muscles (note: electrodes over EDC muscle not shown). Ground electrode positioned on dorsum of the hand.

Using a custom MATLAB software program (Mathworks Inc., Natick, MA), the raw EMGs from each of the contractions was bandpass filtered (20-450Hz), full-wave rectified and smoothed using a second order lowpass Butterworth filter (2Hz cutoff). The maximum EMG value from both the three MVCs and three RVCs were calculated for each subject in each muscle and used for the comparisons between methods.

A one-way analysis of variance (ANOVA) was performed to test for differences between the groups on subject characteristics (age, height, weight) and force values for the MVC and RVC tripod pinch tests. To test for group differences between the maximum EMG values obtained during the MVC and RVC for each muscle, one way ANOVAs were used. Post hoc analyses were performed using Tukey's pair-wise comparisons where appropriate.

Alpha level was set at 0.05 for all tests. Data in the text are reported as group means (SD), and were analyzed using SPSS statistical software (v.18).

RESULTS AND DISCUSSION

Subjects with no hand problems (n=9), hand OA (n=11) and hand RA (n=5) were recruited. Subject characteristics and mean force values for the tripod pinch strength conditions are shown in Table 1. No significant differences were found between the three groups for subject characteristics or force output scores ($p<0.05$). Therefore, the three groups were well matched in regards to subject characteristics, and since the subjects were instructed to exert 1kg of force with a visual aid for the RVC, the same force value for all three groups was expected. The finding that the MVC force value was not significantly different between the three groups is surprising. Previous research on the effect of hand strength in the osteoarthritis literature suggests that the disease leads to deficits in strength [3]. However, grip strength, not pinch strength, is the usual method used to assess hand strength. The authors of this study chose to use the tripod pinch strength testing device to evaluate normalizing EMG techniques because the overall objective is to record EMG of the hand muscles in individuals with arthritis when performing dexterity tasks. Performing the tripod pinch is more effective at isolating the thenar and FDI muscles, two muscles with a major role in movement of the first two digits of the hand.

When the MVC and RVC tripod pinch strength mean EMG values were compared between the groups, no significant differences were observed ($p>0.05$). A trend did exist for MVC pinch in the EDC muscle ($p=0.08$), where the control group had higher EMG activity [0.17(0.05] mV) compared to the OA [0.12(0.06) mV] and RA [0.09(0.05) mV] groups.

CONCLUSIONS

These findings suggest that when normalizing EMG data in the clinical hand arthritis population, either MVC or RVC contractions can be used. However, a limitation of this study was the small sample size and that the hand OA subjects had mild OA (based on a clinical examination of the hand by a physiotherapist). Considering previous studies have shown decreased strength in hand arthritis patients [3] and unpublished findings from our lab, using RVC to normalize EMG data may be more suitable. The idea of using RVCs in a clinical population has been used in studies where subjects have back pain [1]. The relevance for using an RVC in these studies is that a subject with a neuromuscular disorder will not give their true 100% effort when ask to perform a maximum contraction of the injured muscle due to pain inhibition, or fear of pain/injury. Therefore, using a reference task does not change between subjects or days so that any changes in myoelectric activity are biological [1]. Other methods of normalizing EMG in the hand arthritis population, such as using the peak EMG activity performed during a dynamic contraction or using M-waves have yet to be investigated.

REFERENCES

1. Lehman GJ and McGill SM. *J Manipulative Physiol Ther* **22**, 444-446, 1999.
2. Bellamy et al. *J Rheumatol* **26**, 2654-2658, 1999.
3. Bagis et al., Clin Rheumatol **22**, 420-424, 2003.

ACKNOWLEDGEMENTS

This study was funded in part by the Evelyn Mackin Grant for Research in Hand Therapy. Post-doctoral funding was gratefully supported by NSERC-Discovery Grant. We would also like to thank Jessica Lydiate and Alison Martin for their help with subject recruitment and data collection.

Table 1: Mean (SD) data for subject characteristics and force data (MVC and RVC) for the three groups.

Group	*n*	Age (yrs)	Height (cm)	Weight (kg)	MVC (kg)	RVC (kg)
Control	9	56.67 (5.5)	164.98 (6.40)	65.33 (8.72)	6.62 (1.23)	1.02 (0.06)
Hand OA	11	57.00 (5.33)	162.89 (5.02)	73.66 (14.24)	5.55 (1.81)	1.01 (0.05)
Hand RA	5	59.80 (5.81)	164.58 (5.50)	80.14 (15.41)	6.09 (3.02)	1.03 (0.06)

SOFT TISSUE ARTIFACT HAS INTER-SUBJECT AND INTER-MOTOR-TASK SIMILARITIES – A NEW CONCEPT FOR ITS COMPENSATION

[1,3]Bo Gao, [1]Scott Banks, and [2]Nigel Zheng

[1]University of Florida, Gainesville, FL, USA
[2]University of North Carolina at Charlotte, NC, USA
[3]Exactech Inc. Gainesville, FL, USA

Email: nzheng@uncc.edu

INTRODUCTION

Skin marker-based motion analysis has been widely used to study normal functions and pathological conditions of the human musculoskeletal system. A major source of errors associated with this technique is referred to as soft tissue artifact (STA), which is defined as the relative movement between skin markers and the underlying bone. Currently, a current opinion about STA is that it is a subject-specific and motor-task-specific artifact [1]. Under this premise, STA is not likely to be compensated using any comprehensive approaches. Instead, subject-specific techniques are considered necessary for effective STA compensation [2].

However, the major source of STA is muscle contraction and skin stretching, which are not random but are related to the adjacent joint motions. Considering most people have similar anatomical structure and motor coordination, muscle and skin movement are expected to have certain inter-subject similarities. This opinion was supported by a recent study revealing inter-subject common patterns of soft tissue deformation during walking [3]. Our hypothesis was that STA have inter-subject similarity as well as inter-motor-task similarity. This hypothesis was tested in the present study by examining STA *in vivo* using a simultaneous fluoroscopy and motion analysis. Similarities of STA behavior across different subjects and across different motor tasks were evaluated.

METHODS

Six male subjects (65.0 ± 3.0 yrs, 84.0 ± 8.8 kg, 1.72 ± 0.06 m) who had undergone a primary total knee arthroplasty (TKA) were tested. All subjects received the TKA at least 12 months ago and stayed physically active. Signed consent forms were obtained. Clusters of retro-reflective markers covered large area of the anterolateral sides of the thigh and the shank. Additional markers were placed on the pelvis, foot, patella and the C-arm (Fig.1). A motion capture system (MAC, CA) was used to track the skin marker motions at 60 Hz. A fluoroscopic system (SIEMENS AXIOM-Artis) was used to capture a series of X-ray images simultaneously at 7.5 Hz (Fig. 1). The markers on the fluoroscope image intensifier together with a custom made L-frame were used to establish the spatial relationship between the two systems; the patella marker was used to establish temporal synchronization between the two systems. A neutral standing posture was taken to obtain the transformation between implant and anatomical coordinate systems, and to define the initial positions of markers relative to the bone. The tested motor tasks included a series of knee flexion/extension movements at different hip flexion angles (-15°, 15°, 30°, 45°, and 60°) and a stepping-up activity.

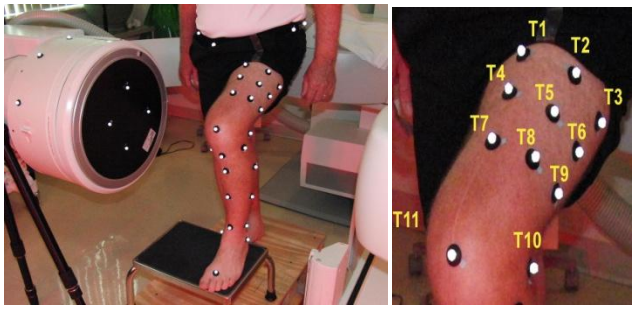

Figure 1: Test setup (left) and marker placement on the thigh (right).

A custom-developed program (JointTrack) was used to reconstruct 3D poses of the TKA prostheses from 2D fluoroscopic images. STA on the thigh and shank was then computed as markers' movement relative to the underlying prosthesis/bone. STA of each marker along each direction was examined

across subjects to evaluate inter-subject similarity. To evaluate inter-motor-task similarity, STA during the five trials of flexion/extension movements was compared. In addition, a set of "predicted" STA during stepping up activity was computed from the STA data obtained from the series of flexion/extension movements by matching adjacent joint flexion angles (hip and knee flexion angles for the thigh; knee and ankle flexion angles for the shank) with a multilinear regression approach. The "predicted" STA was then compared to the experimentally "measured" STA during stepping up activity, and the similarity between the two sets of data reflected the common behavior of STA during two totally different motor tasks.

RESULTS

Although the magnitudes of STA had some variability among different subjects, the general profiles of most markers' STA exhibited apparent similarity across subjects, especially for markers on the thigh where STA was much higher than that on the shank. Fig.2 shows the common patterns of STA on the thigh along proximal/distal (PD) direction of all subjects during stepping up. Most thigh markers moved distally while the knee flexed during the first half of the motor task, and then moved proximally while the knee extended during the second half of the motor task. When the subject concluded the motor task as standing, all STA became back to be close to zero. It was also noticed that markers on the same PD level exhibited even closer STA profiles. Markers on the knee (T10 and T11) exhibited opposite direction of STA compared to other markers, and relatively larger variability due to higher sensitivity of STA to skin location at the joint.

STA also exhibited apparant inter-motor-task similarity. First, the five trials of knee flexion/extension movements showed very similar STA patterns, with systematic changes indicating the influence of hip angle changes. In addition, the "predicted" STA computed from the series of knee flexion/extension movements exhibited very similar profiles comparing to the actually "measured" STA during stepping up activity, especially for thigh markers (Fig. 3). The prediction errors were much smaller than STA itself.

DISCUSSION

Contrary to some opinions, this *in vivo* study demonstrated that STA has both inter-subject and inter-motor task similarities. This new concept could lead to more effective approaches for STA compensation. The existence of inter-subject similarity means that STA models could be set up from one group of subjects and used for other subjects. Inter-motor-task similarity additionally opens the possibility comprehensive STA models that may be applicable for many different activities. The implementation of these concepts has been explored in recent work [4].

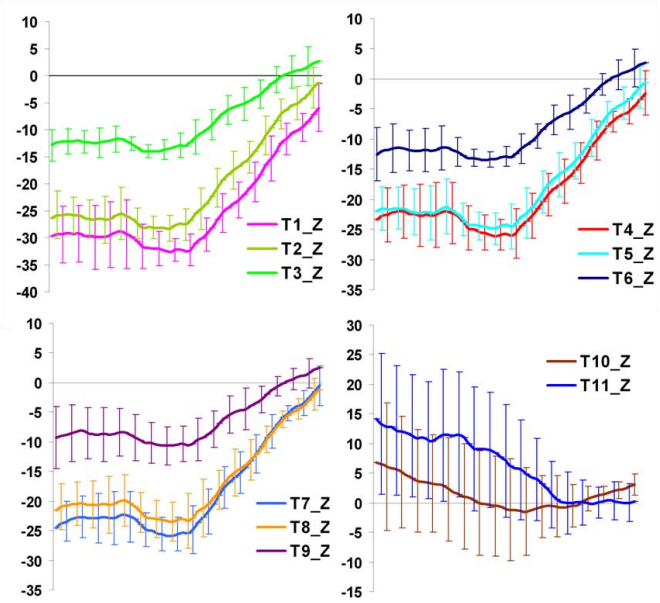

Figure 2: Inter-subject STA patterns (mean ± std) of individual markers on the thigh along PD direction during stepping up. (Unit: mm).

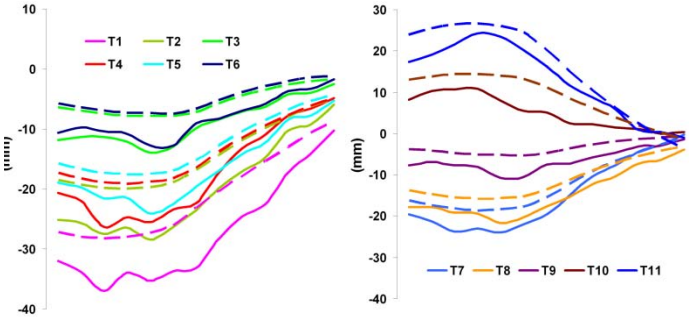

Figure 3: "Predicted" (dashed lines) and "Measured" (solid lines) PD component of thigh STA during stepping up activity.

REFERENCES

1.Leardini A. et al., *Gait Posture* **21** (2), 2005
2.Cereatti, A., et al., *J Neuroengi Rehabil*, **3**, 2006
3.Gao B. and Zheng N., *J Biomech* **41** (15), 2008
4.Gao B. Ph.D dissertation, 2009

EVALUATION OF AN INERTIAL AND MAGNETIC MEASURING SYSTEM AS A METHOD OF COLLECTING KINEMATICS OF WHEELCHAIR PROPULSION

Scott C. Daigle, Zahid M. Rampurawala, Elizabeth T. Hsiao-Wecksler, Jacob J. Sosnoff

University of Illinois at Urbana-Champaign, IL, USA
email: jsosnoff@illinois.edu

INTRODUCTION

There are an estimated 1.5 million manual wheelchair users in the United States. Manual wheelchair users depend on their upper limbs for mobility and activities of daily living. In previous wheelchair propulsion studies, propulsion has commonly been measured using traditional motion capture systems consisting of a set of high speed, infra-red cameras connected to a computer. Though accurate, these systems are expensive and limited to a laboratory setting. A possible substitute for such a system could be inertial and magnetic measuring systems (IMMSs). These devices are relatively cheap, portable and easy to use.

Although kinetic differences in wheelchair propulsion have been observed between laboratory and non-laboratory settings [2], there have been few examinations of kinematics outside a laboratory. IMMSs could be an effective way to measure kinematic differences in wheelchair propulsion outside of a laboratory setting. This study was carried out to determine the potential use of IMMS in obtaining propulsion kinematics of manual wheelchair users. The upper arm segment angle was recorded using an IMMS and data were compared to that obtained by a motion capture system.

METHODS

Three regular wheelchair users were asked to propel a Quickie (Phoenix, AZ) Titanium wheelchair on a roller system. Propulsion was carried out at a speed of ≈1.1m/s. Kinematic data were collected using two systems simultaneously; a 10 camera motion capture system (Motion Analysis, Santa Rosa, CA) and an IS-300 Pro (InterSense Inc, Billerica, MA) IMMS. Two minutes of data were collected for each subject, and the first 20 cycles of propulsion were analyzed using MATLAB to calculate upper arm segment angles, average range of motion (ROM) per cycle, cross correlation, and a fast Fourier transform of each trial. All subject testing procedures were approved by the University's Institutional Review Board.

The IMMS used in this experiment consists of four sensing units (SUs). Each sensing unit integrates an inertial measurement system, comprised of one 3D accelerometer and one 3D gyroscope along with a 3D magnetometer in order to compensate for gyro drift. IMMSs have the potential to estimate joint kinematics when a sensing unit is attached to each body segment of interest. In this study, we followed the sensor placements used by Cutti et al. [1] with SUs at the thorax, scapula, humerus and forearm. In order to initialize the system and adjust for sensor placement differences, subjects were asked to keep his/her arms at his/her sides and elbows bent at 90 degrees flexion. To determine the upper arm segment angle, we only needed the sensing unit attached to the humerus, however, the other three units were utilized to record kinematic data that will be analyzed in future studies. For the motion capture system, several retro-reflective markers were attached to bony landmarks on each subject. Markers attached to the glenohumeral center of rotation, acromion process, lateral epicondyle and medial epicondyle were used to measure upper arm segment angle.

RESULTS AND DISCUSSION

As seen in Table 1, the IMMS recorded upper arm segment angles that closely follow that of the motion capture system. Indeed, when the IMMS measurements are cross correlated with the motion capture measurements, average cross correlation coefficients at zero lag are 0.957 which indicates a nearly perfect match.

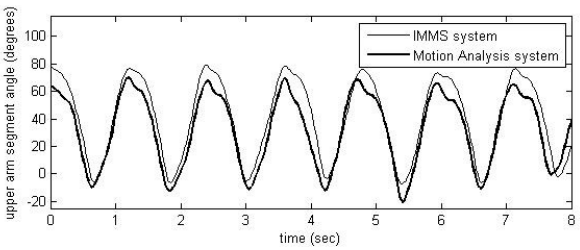

Figure 1: Subject 1 upper arm segment angle

The two systems generally report similar movement patterns (See Figure 1). However there were a few occasions when an appreciable shift in the segment angle was observed. Table 1 shows the average and standard deviation of segment angles calculated by both systems. On average, the segment angles calculated by the IMMS are shifted 11.1 degrees lower than what was calculated in the Motion capture system. This can be due to three factors: sensor placement, skin artifact, and magnetic interference. Both systems are subject to errors from sensor placement. The IMMS is more sensitive to skin artifact because it is attached with a cuff on the bicep, whereas the reflective markers used by the motion capture system are attached to bony landmarks. Additionally, the IMMS is sensitive to magnetic interference which is an inherent limit of the system.

In order to compare the timing of each signal, the amplitude spectrum of data from both systems is plotted for Subject 1 in Figure 2. This plot shows a nearly perfect match of the frequency composition of both signals.

Since these sensors provide a relatively reliable estimate of segment angle, we can be confident in utilizing them in traditional analyses of kinematics. Figure 3 shows the average cycle ± 1 standard deviation, where the time has been normalized so all cycles are the same length. These analyses were used to report the average ROM per cycle for each subject in Table 1. These quantities also experience minor shifts in mean positions of 3.93 degrees between the two systems.

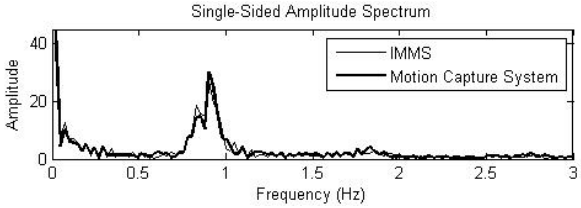

Figure 2: Subject 1 Amplitude Spectrum

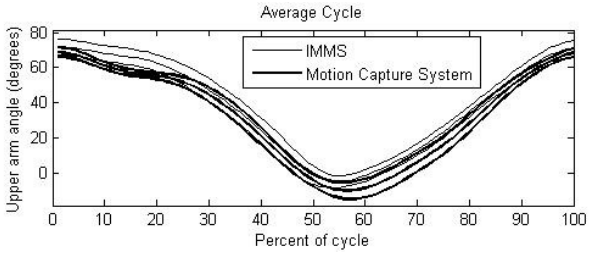

Figure 3: Subject 1 Average Cycle ± 1 SD (SD = standard deviation)

CONCLUSIONS

By comparing an IMMS with the gold standard in kinematic analyses, a motion capture system, we have shown that IMMSs are a promising technology for measuring the kinematics of wheelchair propulsion. Upper arm segment angle differences were shown to be minimal with average cross correlation coefficients at zero lag of 0.957. In future studies, IMMSs should be utilized to measure a whole range of segment angles rather than just one. The benefit of these systems is that they are not limited to the confines of a laboratory. With further evaluation and testing, it is likely that they can be used to collect kinematic data outside the laboratory.

REFERENCES

1.Cutti AG, et al. *Med Bio Eng Comput* **46**, 169-178, 2008.
2.Koontz AM, et al. *J Rehab R&D* **42**, 447-458, 2005.

ACKNOWLEDGEMENTS

National Center for Super Computing Applications and Peter Bajscy for technical assistance.

Table 1: Comparison of IMMS to motion capture system measurement of upper arm segment angle

	Subject 1	Subject 2	Subject 3
Cross Correlation Coefficient at Zero Lag	0.960	0.952	0.960
IMMS Mean Angle (deg) (±1SD)	38.0±27.0	40.1±24.0	33.9±29.3
Motion Capture System Mean Angle (deg) (±1SD)	32.7±27.1	22.2±23.0	23.8±34.2
IMMS Average ROM per cycle (deg)	49.5±22.8	48.7±25.2	48.0±18.9
Motion Capture System Average ROM per cycle (deg)	48.4±21.5	38.6±15.7	47.4±13.6

ESTIMATION OF STRIDE VARIABILITY FROM FOOT-MOUNTED INERTIAL SENSORS

John R. Rebula and Arthur D. Kuo

Department of Mechanical Engineering, University of Michigan, Ann Arbor, MI, USA
email: [jrebula|artkuo]@umich.edu, http://hbcl.engin.umich.edu

INTRODUCTION

Laboratory measures of stride distance and variabilities during walking can provide indicators of mobility and balance. For example, high stride width variability can indicate a person's fall risk [1]. Measurement of spontaneous walking during daily living may be preferable to laboratory measures, but are difficult to obtain without motion capture equipment. Body-worn inertial measurement units (IMUs), consisting of gyroscopes and accelerometers, are increasingly used to detect motion and speed. But current IMU methods do not yield measures of stride variability, due to position drift from integrated IMU signals. We propose that, with proper drift correction and identification of the direction of motion, a foot mounted IMU can be used to estimate stride length and width variability.

METHODS

Our proposed method reduces drift by correcting errors from ground contact information. Current methods [1] use integrated angular velocities from calibrated gyroscope measurements, as well as zero velocity updates during detected ground contact. We extend those methods by correcting angular velocities based on the accelerometers during the stance phase of gait. Instead of simply updating velocities to zero during ground contact, we perform a Zero Velocity Correction that also adjusts velocities at prior times to be compatible with available information. Stride information is then decomposed into length and width components for estimation of variabilities.

The gyroscopes are integrated during swing to estimate orientation, and the gyroscopes and accelerometers are fused during stance to estimate the orientation of the foot. This represents the discrete differences between the stance and swing phases. The accelerations are double integrated to yield positions. Assuming that the IMU is stationary during stance, the accelerometer can effectively act as an inclinometer to provide corrections to the gyroscope data.

A Zero Velocity Correction ensures that the foot returns to rest after each step. Due to sensor errors, the integrated velocity usually drifts from zero by the end of each swing. The Correction assumes a linear model of velocity drift that is subtracted from the estimated velocity throughout the swing to smoothly reset the velocity to zero. The corrected velocities are then double integrated to yield position trajectories in the IMU reference frame. Using the average heading from multiple steps, each stride is decomposed into length and width (Fig 1). The motion capture position trajectories are similarly decomposed along the direction of travel.

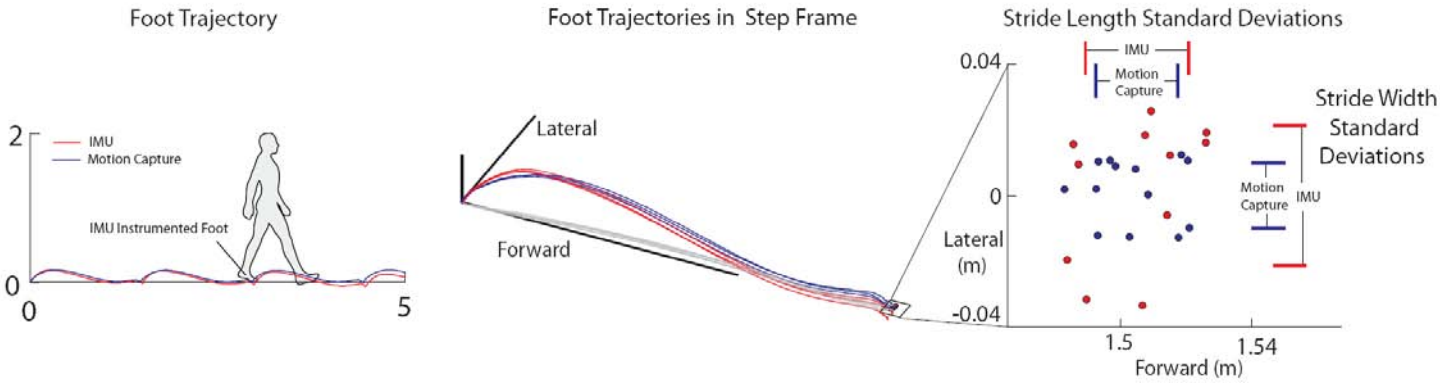

Figure 1: Example walking foot trajectories using a foot mounted IMU (left). Each stride is transformed into the stride-specific reference frame (middle). The standard deviations of the trajectory end points are used as the measure of variability (right). The stride length and width standard deviations for the IMU estimations are compared to those from motion capture.

To test our method, we measured healthy subjects (N = 6) walking on a treadmill with motion capture to yield proof data, and compared that to simultaneously collected data from a foot mounted IMU. One motion capture marker was placed on the IMU. Subjects each walked at four speeds: 1.03, 1.25, 1.47, and 1.7 m/s for one minute. A wireless IMU was attached to the right shoe. The IMU consisted of a 3 axis accelerometer and 3 gyroscope axes sampled at 1kHz [3]. We used a simple threshold of gyroscope magnitude to determine swing and stance phases [2]. To test our methods, we calculate stride length, and stride length and width variability from the IMU, and fit them to a calibration line using the motion capture data. The R^2 values of these fits quantify the performance of the IMU integration in predicting gait measures.

RESULTS AND DISCUSSION

Linear fits for the IMU estimates of mean stride length, and variabilities of stride length and width for 23 trials are fit to the same quantities calculated from motion capture, with an R^2 of 0.96, 0.52, and 0.39, respectively (Fig. 2). The mean IMU estimated stride lengths are within 3% of the proof stride lengths on average. The IMU processing estimates strides reasonably well. The IMU yields higher stride variabilities than motion capture, which we attribute to a higher noise floor inherent in IMU signals (Fig 2). The linear fits characterize the additional noise from the IMU processing. Although IMUs have good potential for resolving gait variability, considerable improvements are needed for stride variability, for example through improved IMU calibration and heading correction.

A limitation of the current approach is the assumption of straight walking. We will explore heuristic detection of periods of straight walking within a larger dataset, and calculate gait variability for those time periods. For non-straight walking during daily living, stride lengths and widths may be regarded as less meaningful. We also expect to improve the performance of the algorithm with a careful calibration of the gyroscope nonlinearity and temperature sensitivity. We expect this to add to the efficacy of these methods for modeling general ambulation.

CONCLUSIONS

We have shown results of foot mounted IMUs measuring level ground walking, suggesting that it can indicate some measures of gait variability. Unobtrusive, mobile gait measurement can potentially provide measures of mobility and fall risk, during *in vivo* walking data.

REFERENCES

1. JS Brach. *J Neuroengineering Rehabil.* 2005; 2: 21
2. Ojeda and Borenstein. *Proceedings of Safety, Security and Rescue Robotics'07,* Roma, Italy, 2007.
3. King K, et al. *Sensors and Actuators A: Physical* **141**, 619-630, 2008.

ACKNOWLEDGEMENTS

This work was supported in part by NIH AG03081.

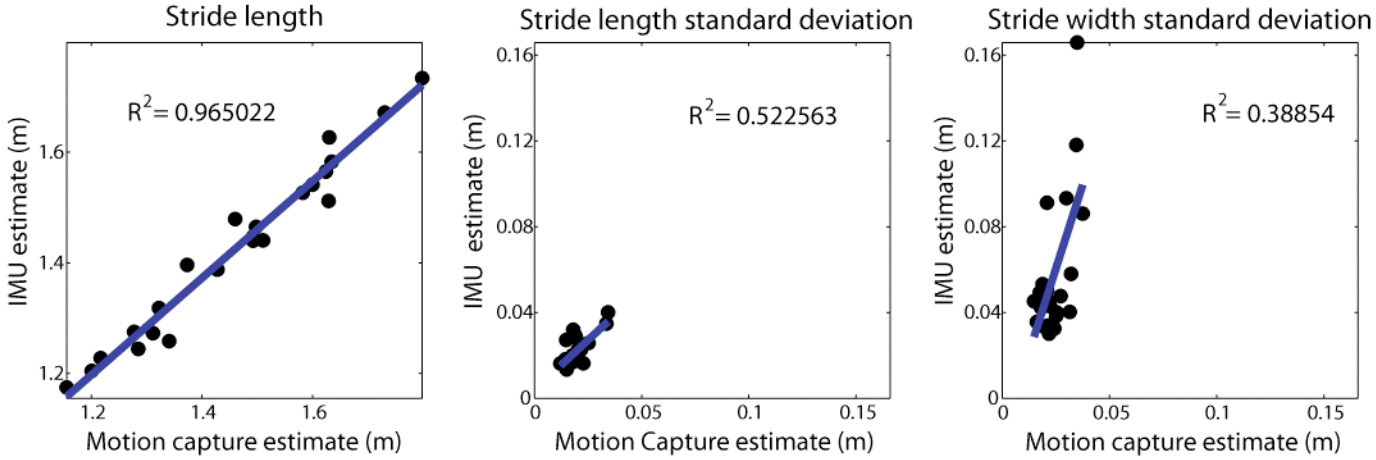

Figure 2: Mean stride length, and variability of stride length and width are estimated using IMU (vertical axis), and motion capture (horizontal axis) for 23 walking trials. The IMU stride length estimate closely approximates motion capture, and the fits of IMU to motion capture estimates for all three gait parameters are roughly linear.

TIME NORMALIZING GAIT DATA BASED ON GAIT EVENTS

Emily A. Morris and Elizabeth T. Hsiao-Wecksler
University of Illinois at Urbana-Champaign, Urbana, IL, USA
ethw@illinois.edu, http://www.mechse.illinois.edu/research/hsiao-wecksler/

INTRODUCTION

Time normalization of kinematic, kinetic and/or EMG gait data to % gait cycle is a common practice of assessing average behavior over several gait cycles or comparing gait patterns from different populations. This process assumes that gait cycles are periodic and assigns consecutive ipsilateral heel-strikes to 0 and 100% gait cycle. This approach however generally ignores timing variability in movement patterns both between and within gait cycles, e.g., variations in peak value times or toe-off times. Thus movement data averaged over multiple gait cycles may express reduced peak magnitudes and increased standard deviations due to inter- and intra-cycle variability in timing [1,2].

Although gait researchers often acknowledge these alignment problems, relatively few studies have attempted to address them. If used, separation between stance and swing phases by aligning data to toe-off is the most common approach. A few have tried aligning gait data at multiple instances throughout the gait cycle, such as peak values [1], arbitrary states [2], or across the entire gait cycle [3]. These works did not consider alignment based on clinically-relevant gait events that identify subphases of the gait cycle. Alignment by gait events could also allow comparison across joints and gait parameters, which may not be possible with the other techniques. Further, these works were interested in reducing temporal differences in order to better explore intensity differences in gait parameter magnitudes. They did not consider that added information about the system may be obtained by examining the temporal shifts necessary to make these alignments.

We recently explored multiple methods for time normalizing gait data and have found piecewise linear length normalization (PLLN) to be a preferable technique for removing timing variability between discrete points of interest throughout the gait cycle [4]. PLLN is essentially curve registration that compresses or expands the time axis of a cycle to-be-aligned with a target data set. Alignments are done using linear interpolation between specified points of interest along the gait cycle.

In this paper, we time normalized gait data using PLLN to specific gait events (based on subphases of the gait cycle). We also illustrate the potential utility of examining temporal shift signatures, i.e., temporal differences which highlight the direction and magnitude of temporal shifts necessary for alignment.

METHODS

Walking data from [5] were used in this study. In these experiments, ten healthy males, ages 19-23, walked for three minutes on a treadmill under two conditions: (1) normal, non-braced, and (2) braced right knee. The addition of a knee brace simulated an injury or other irregular gait pattern by preventing knee flexion. Sagittal-plane joint angles were calculated from motion capture data (Vicon, Oxford, UK). For each subject, one gait cycle of the right leg per condition was used. Right ankle angle data for eight subjects are reported here.

We defined only the subphases of stance phase due to the relative ease and repeatability in determining these events. Five subphases were identified from six gait events [6]: (i) loading response: ipsilateral heel strike (IHS^1) to contralateral limb toe-off (CTO^1), (ii) mid-stance: CTO^1 to limb alignment (LA, i.e., bilateral hip and knee alignment), (iii) terminal-stance: LA to contralateral heel strike (CHS^1), (iv) pre-swing: CHS^1 to ipsilateral toe-off (ITO^1), and (v) swing: ITO^1 to IHS^2.

A consensus data set was created from the unbraced ankle angle data by determining the average timing, in % gait cycle, for each gait event. Each of the individual unbraced cycles was then aligned to these average timings using PLLN. The average of these aligned unbraced data sets became the consensus curve (Fig. 1).

PLLN was then applied to ankle angle data from each knee-braced gait cycle relative to the consensus timings. The aligned knee-braced curves

were averaged. Individual temporal and intensity differences for the aligned cycle relative to the consensus cycle were also recorded from each braced and unbraced cycle. Finally average temporal and intensity differences were determined.

RESULTS AND DISCUSSION

Average timings for the gait events based on unbraced data were: 12 ± 1.4 (SD) %GC for CTO[1], 25 ± 2.0 %GC for LA, 51 ± 0.9%GC for CHS[1] and 64 ± 0.9 %GC for ITO[1] (Fig. 1). Bracing resulted in noticeable time variation from normal unbraced motion in the ankle angle (solid vs. dotted curves in Fig. 1). By using curve registration through PLLN of the braced data to the gait event timings in the consensus data, alignment of motion patterns was improved (red dashed vs. dotted curves in Fig. 1). This alignment allowed for examination of intensity differences in ankle angle magnitudes throughout the gait cycle (Fig. 2), rather than at individual specific points as is commonly reported.

PLLN allowed for the calculation of the temporal shifts associated with all points in a gait cycle. By examining the temporal differences, it can be easily observed that events in the braced data generally occurred before, or lead, comparable events in the consensus data (Fig. 2). The greatest timing variation occurred at toe-off, ITO[1] (9.4 ± 5.1 %GC); however by examining the temporal differences throughout the gait cycle, we also observe that timing variations occur at other gait events but with reduced variability (e.g., CHS[1] at 4.4 ± 2.0 %GC).

It is interesting to note that by selecting gait events as the points of interest for alignment, the peak magnitudes of the average aligned data did not increase (Fig. 1), as was observed in [1] which aligned to peak values. Therefore, the choice in alignment points will be affected by the motivation of the research question.

CONCLUSIONS

By specifically selecting clinically-significant gait events, it may be possible to provide improved interpretation of gait behaviors, especially behaviors that deviate from normative patterns. By capturing and examining the temporal differences that were necessary to expand or contract the given cycle relative to the consensus pattern, we also are provided with greater insight into more subtle timing differences within the gait cycle. These subtle timing differences may further provide added information about impaired control mechanisms of gait.

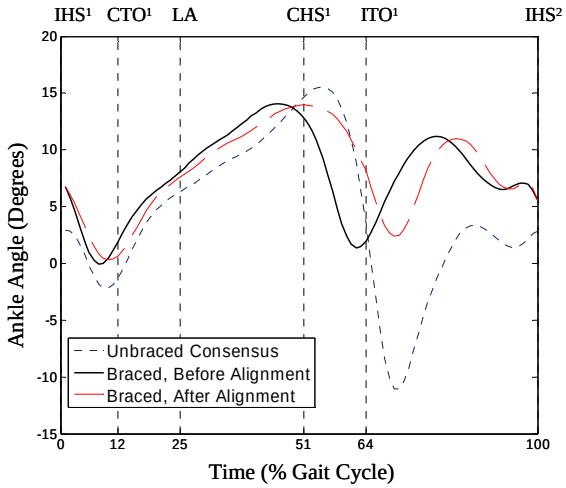

Figure. 1: Average ankle angle trajectories for right leg with knee brace before and after alignment with the consensus by PLLN. Average timings for key gait events based on unbraced motions are noted with vertical lines.

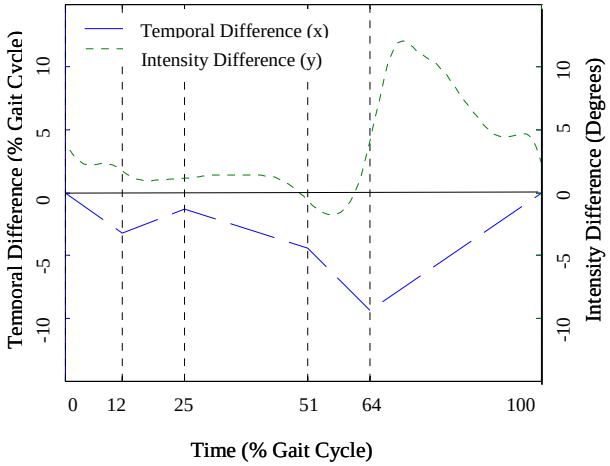

Figure 2: Average temporal and intensity differences

REFERENCES

1. Sadeghi H, et al. *Gait Posture* **12**:257-264, 2000
2. Forner-Cordero A, et al. *J Biomech* **39**:948-957, 2006
3. Chau T, et al., *J Neuroeng Rehabil*, **2**:22, 2005.
4. Helwig NE, et al. *ASB'09*, State College, PA, August, 2009
5. Shorter KA, et al. *Clin Biomech* **23**:459-467, 2008
6. Perry, J. *Gait Analysis*, Slack, Inc., 1992.

ACKNOWLEDGEMENTS

The authors thank K. Alex Shorter, Louis DiBerardino, Nate Helwig, John Polk and Sungjin Hong for assistance on this paper. This study was partially funded by a grant from the National Science Foundation (#0727083).

New Approach to Characterize Trunk Neuromuscular Responses During Rapid Voluntary Extremity Movement

[1]Rupal Mehta, [1]Marco Cannella, [1]Peemongkon Wattananon, [2]Sharon Henry, and [1]Sheri Silfies

[1]Drexel University, Philadelphia, PA, USA
[2] University of Vermont, Burlington, Vermont, USA
Email: rm335@drexel.edu web: http://www.drexel.edu/cnhp/rehab_sciences

INTRODUCTION

Assessing trunk muscle postural responses to perturbation is important for detecting neuromuscular dysfunction in patients with lumbopelvic pain. During rapid voluntary extremity movement, anticipatory activation of trunk muscles is a fundamental postural strategy for controlling center of mass and trunk stability.

Traditionally anticipatory activation is defined based on standard electromagnetic delay (EMD) of 40-60ms (time between onset of extremity muscle activation and initiation of movement or force generation). However, not everyone has an EMD in this range. Therefore use of a standard EMD (e.g., 50ms) could bias the interpretation of anticipatory activation. Details about the kinematics of the extremity may be a key factor in interpreting trunk muscle responses and expanding the characterization of trunk neuromuscular control during a self-perturbation task. For example, muscle responses have been largely characterized by latency alone; however, knowing muscle latency alone does not fully describe trunk postural control during this task.

The purposes of this study are to 1) determine test-retest reliability of extremity kinematic parameters during an arm self-perturbation task and 2) describe a method for determining and classifying trunk muscle timing (Turn On and Off) responses based on kinematics of the extremity.

METHODS

Seven subjects (4 female; age= 36±8; BMI= 24±3) performed 6 repetitions of the dominant upper extremity shoulder flexion in response to an auditory stimulus. Surface EMG activity was recorded at 2400 Hz (Band pass 10-500 Hz) from 6 trunk muscles bilaterally (IO/TrA, EO, RA, LM, LES, TES) and the anterior deltoid of the dominant arm. Dominant arm and trunk displacement were also collected simultaneously by an electromagnetic device (120Hz). EMG data was heart rate striped, and RMS filtered (20Hz). Onset and offset times of the trunk muscle phasic responses were determined by computer algorithm. The axis of rotation and the angular velocity of the humerus (arm) with respect to the trunk were calculated for each trial. The component of the angular velocity orthogonal to the plane of movement (sagittal) was segmented by an optimal linear piecewise algorithm [1] into four phases: initial resting (Phase I), rapid increase (Phase II), relative plateau (Phase III) and rapid decrease (Phase IV) to zero velocity (arm max elevation) (see Figure 1).

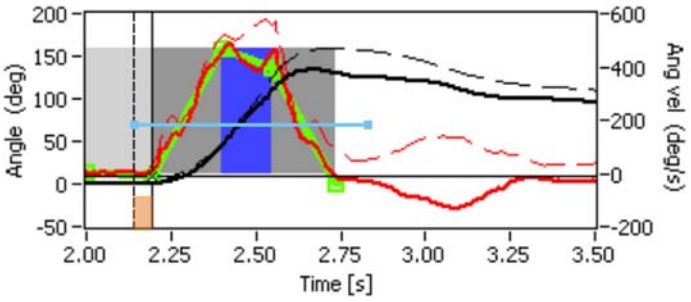

Figure 1: Schematic represents the four kinematic phases (shaded areas) determined with the optimization algorithm (green line), the anterior deltoid timing (blue line) and the EMD (dashed to solid vertical lines) during a single trial of rapid voluntary arm flexion. The black line represents arm angular rotation intensity (---- total, — sagittal). Red line is the angular velocity (---- total, — sagittal).

Trunk muscle timing was classified according to these kinematic phases. The EMD (defined as the

time from onset of anterior deltoid EMG to initial change in sagittal angular velocity of the arm) was determined for each subject. Anticipatory activation was defined for each subject as onset of trunk muscle activity during Phase I.

Test-retest reliability of extremity kinematics and anterior deltoid onset time was calculated using $ICC_{(2, 6)}$.

RESULTS AND DISCUSSION

Individual differences in EMD (86±28ms; range 39-110ms) were found. EMD was not correlated to maximum arm angular velocity (529±62°/s). For each phase, the mean time duration and maximum flexion of the arm were: Phase I- 293±59ms, 0°; Phase II- 458±24ms, 45±11°; Phase III- 617±34ms, 123±16°; and Phase IV- 719±23ms, 143±17°. Based on our classification, all muscles, across all subjects and trials functioned in an anticipatory manner (Phase I- initial resting).

Our data (Table 1) suggest that the EMD times typically used to determine anticipatory activation (40-60ms) may actually be an under estimation. This could result in misrepresentation of anticipatory activation as voluntary activation.

CONCLUSIONS

This approach provides a tool by which to customize analysis of trunk neuromuscular control based upon the actual kinematics of the perturbation and can advance our diagnostic analyses and interventions for patients with lumbopelvic pain.

REFERENCES

1. Nguyen T.B., Oommen B.J., Moment Preserving Piecewise Linear Approximations of Signals and Images, **IEEE Transactions on Pattern Analysis and machine Intelligence**, Vol. 19, No1, Jan 1997.

ACKNOWLEDGEMENTS

This study was supported in part by a grant from the National Institute of Child Health and Human Development (K01HD053632).

Table 1: Test-Retest Reliability of Extremity Kinematics and Deltoid Onset

	Test	Retest	SEM	95% CI	$ICC_{(2,6)}$
Onset of Deltoid (ms)	208 ±41	223 ±38	31	86.5	0.37
Onset of arm movement (ms)	293 ±59	307±50	23	63.5	0.82
Max Velocity (degree/s) (max1)	529 ±62	523 ±57	20	54.9	0.89
Max Velocity (degree/s) (max2)	485 ±109	452± 99	35	96.6	0.89
Max Displacement of arm (degree)	143± 17	133 ±14	6	16.9	0.85
Electromechanical Delay (ms)	86± 28	84± 25	8	21.1	0.92

A KINEMATIC METHOD FOR STRIKE PATTERN DETECTION

[1]Allison R. Altman and [1,2,3] Irene S. Davis

[1]Biomechanics and Movement Science, University of Delaware
[2]Drayer Physical Therapy, Hummelstown, PA
[3]Department of Physical Therapy, University of Delaware
email: aaltman@udel.edu

INTRODUCTION

Footstrike patterns are defined by the part of the foot that first makes contact with the ground. A rearfoot strike (RFS) is one in which the heel hits the ground first. In a midfoot strike (MFS), the foot lands flat at contact. Finally, a forefoot strike (FFS) is one in which the ball of the foot strikes the ground first. Hasegawa et al. [1] reported that 75% of distance runners are RFS, 24% are MFS and the remaining 1% are FFS. These results were based upon subjective visual inspection of videotaped recordings of 415 runners taken during a half marathon race.

However, in the laboratory, strike patterns are typically quantified by the strike index (SI) using a force plate [2]. SI is determined by locating the center of pressure (COP) at the moment of footstrike along the long axis of the foot. This distance is then normalized to the total length of the foot and multiplied by 100%. (Figure 1). A SI of 0-33% classifies one as a RFS, 34-67% as a MFS and 68-100% as a FFS.

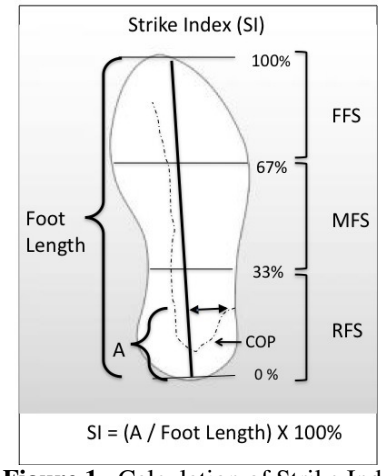

Figure 1. Calculation of Strike Index

However, force data are needed in order to make this calculation. This is not always possible in the natural running environment, or when running on conventional treadmills. While instrumented treadmills are becoming more available, they introduce considerably more noise to force data than those that are floor-embedded. This noise adds significant error to the calculation of COP, especially at footstrike when the forces are low.

Therefore, the purpose of this study is to determine whether a kinematic measure of the foot angle at footstrike can be used as a surrogate for SI. It was hypothesized that the footstrike angle (FSA) will be significantly correlated to the SI across a range of footstrike patterns.

METHODS

This is an ongoing study of which 8 healthy runners (3 M, 5 F) between the ages of 18 and 35 yrs, running more than 10 miles per week, have been recruited to date. 4 subjects were RFS, 2 were MFS and 2 were FFS. Each subject had 5 anatomical and 5 tracking markers placed on their right foot (Figure 2). Anatomical markers were removed following the standing calibration. Calcaneal markers were placed directly on the rearfoot through windows cut into the heel counter of the shoes. Subjects ran across a forceplate (Bertec, Columbus, OH) until 5 good trials were collected at 1000 Hz for each condition. Each subject ran utilizing a RFS, MFS, and FFS. Marker data were also recorded at 1000 Hz using an 8 camera Nexus System (Vicon, Oxford, UK). This high kinematic frame rate was chosen to provide exact synchronization between the force and kinematic data.

Kinematic and kinetic data were processed using Visual 3D (C-Motion, Rockville, MD). Marker data were filtered at 8 Hz and force data at 50 Hz. The SI was calculated as shown in Figure 1. The FSA was defined as the angle between the AP axis of the lab and vector formed between the distal heel marker (A) and the marker on the dorsum of the

second metatarsal (B) (Figure 2). The angle during standing was subtracted from the angle at footstrike resulting in 0° corresponding with a flat foot.

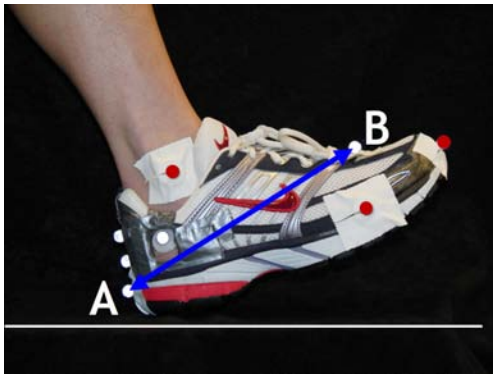

Figure 2 – Anatomical (red) and tracking (white) markers on the shoe. FSA was calculated as the angle between the vector AB and the AP lab axis.

The median value of SI from the 5 trials, and the corresponding FSA were used in the analysis. A correlation and linear regression were calculated comparing the SI values to their corresponding FSA values. Cut-off criteria were determined for RFS, MFS, and FFS using the regression model.

RESULTS AND DISCUSSION

The data were all normally distributed and displayed homogeneity of variance. The FSA was significantly correlated with SI with a Pearson's R = 0.9 ($p < 0.01$) (Figure 3).

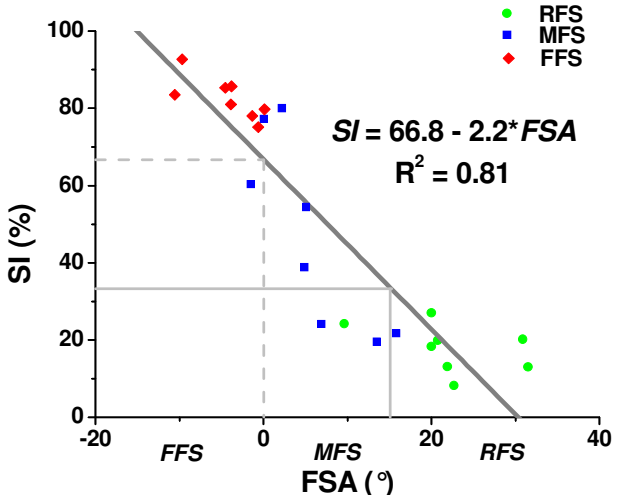

Figure 3. Relationship between SI vs. FSA with the regression line indicated in black. The solid line indicates the division between a RFS and a MFS. The dashed line indicates the division between a MFS and a FFS. *A positive FSA is in the direction of dorsiflexion.*

Based upon these preliminary data, a RFS corresponds with a FSA greater than 15.1°, a MFS with a FSA between 15.1° and 0.1°, and a FFS with a FSA less than 0.1°. These values generally confirm that the boundaries have been defined appropriately. However, in an ideal MFS, the foot should be completely flat on the ground, with a FSA of 0°. However, based upon the SI results, only 3 individuals landed with a true MFS pattern. Landing with a MFS pattern has been shown to be more difficult than a RFS or FFS pattern when it is not one's natural style [3]. The FSA values of the true MFS were indeed close to 0°.

This model allows for the convenient conversion from FSA to SI. For example, using the regression equation, a FSA of -10° (a plantarflexed foot) results in a SI of 88.8%, a FFS. A FSA of +10° (a dorsiflexed foot) results in a SI of 44.8%, or a MFS.

The gold standard for determination of strike pattern is the SI measure. However, the very strong correlation found in this study suggests that FSA may be a practical surrogate for SI. Having a method to obtain strike index when force data are not available can be extremely useful in a number of ways. While a motion analysis system was used in this study, this method can be easily translated into community settings. Using only a high-speed video camera, studies of strike patterns of runners during races can be conducted. Alterations in strike patterns as a result of gait retraining can be measured in the clinic using a camera and treadmill. The regression equation provides a way to translate any FSA into a SI measure.

Additional subjects who are natural RFS, MFS and FFS, are currently being collected. We plan to repeat this analysis using the natural strike patterns for each subject to further validate these findings.

CONCLUSIONS

These preliminary data suggest that the FSA can serve as a surrogate measure for SI in the absence of force data. Based upon the linear regression, cut-off values can be established to classify footstrike patterns based upon the angle of the foot at contact.

REFERENCES

1. Hasegawa H, et al. *J Str Cond Res* **21(3),** 888-893.
2. Cavanagh PR et al. *J Biomech* **13**, 397-406, 1990.
3. Altman, AR et al. ASB Mtg, State College, PA, 2009.

ACKNOWLEDGEMENTS

NIH 1 S10 RR022396

STABILIZATION OF THE TOTAL FORCE IN MULTI-FINGER PRESSING TASKS STUDIED WITH THE 'INVERSE PIANO' TECHNIQUE

[1]Joel R. Martin, [1]Mark K. Budgeon [1]Vladimir M. Zatsiorsky and [1]Mark L. Latash
[1]The Pennsylvania State University, University Park, PA, USA
email: jrm496@psu.edu

INTRODUCTION

One of the central problems in motor control is the problem of motor redundancy [1]. This problem emerges when the number of variables at a selected level of analysis is higher than the number of constraints defined by the task such that an infinite number of solutions are possible. Recently, this problem has been addressed using the concept of a synergy as a neural organization of elemental variables that stabilizes a required value (or time profile) of a potentially important performance variable by co-varying adjustments of the elemental variables [2].

When one finger changes its force, other fingers of the hand can show unintended force changes either in the same direction, called enslaving [3, 4, 5], or in the opposite direction, called error compensation [6, 7]. We tested a hypothesis that externally imposed changes in finger force predominantly lead to error compensation effects in other fingers thus stabilizing the total force. A novel device, the "inverse piano" (IP), was used to impose controlled displacements to one of the fingers over different levels of displacement magnitudes and rates.

METHODS

Ten male subjects participated in the study. The IP device (Fig. 1) consisted of four uni-directional force sensors mounted on linear actuators that could produce smooth movements in the vertical direction. The collection of force data and control of device was done using custom made LabVIEW software. The task was to press naturally with all four fingers to match a target force on a computer monitor for the first 5 s. Force feedback was removed for the next 5 s, at which point one of the force sensors was unexpectedly raised and lowered back to its initial position. Force feedback and target force then were returned to the monitor for the remaining 3 s. Subjects were told return to the target force, if they had deviated during the non-feedback phase. The instruction given during key raising was to "don't pay attention to changes in finger forces, rather maintain the same effort of fingers as prior to the perturbation." The target force was scaled to measured values of maximum voluntary contraction (MVC), which were collected at the beginning of the experiment. Surface electromyogram (EMG) was recorded from the flexor digitorum superficialis (FDS) during trials. EMG was collected to determine whether there was a change in muscle activity during key raising.

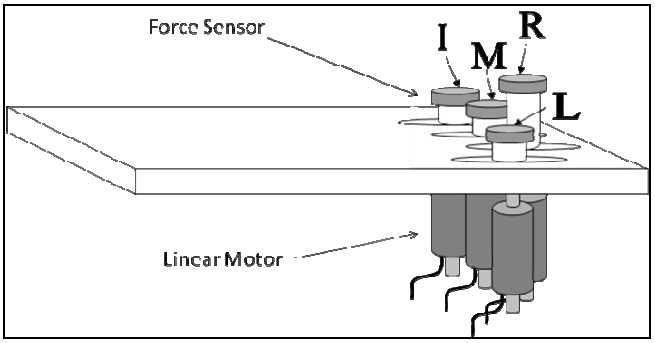

Figure 1: Schematic of the inverse piano device.

The final vertical displacement of key raised, speed of key raising, initial pressing force, and finger raised were the experimental variables. Two levels of final vertical displacement (1 cm and 2 cm), speed (1 cm/s and 3 cm/s), and initial target pressing force (5 % MVC and 20 % MVC) were used. There were four levels of finger raised (I, M, R, L).

The data of interest were the change in finger forces during the key raising. The change in finger force was defined as the difference between finger forces at the end of motor movement (to the raised position) minus the background force at the beginning. For each trial the force changes were calculated for all four fingers. The finger force changes were computed in terms of magnitude of force change and percent MVC of a given finger.

The force changes were then analyzed in several ways. First, for each combination of displacement, MVC, and speed, the data were averaged across subjects. Averaging was not performed across fingers. Further data analysis was performed on the sum of all finger force changes and the effect of proximity of non-raised fingers to the raised finger on their force change.

A four-way repeated measures MANOVA was performed to test for the effects of INITIAL FORCE (2 levels: 5% and 20%), DISPLACEMENT (2 levels: 1 cm and 2 cm), SPEED (2 levels: 1 cm/s and 3 cm/s), and FINGER (4 levels: I, M, R, and L). The responses tested were change in raised finger force, in terms of both N and % MVC, change in total non-raised finger force, change in total force (sum of individual finger force changes), and the % compensated values for each trial. A paired t-test was used to evaluate the difference in average EMG amplitude before and during key movement. To check whether proximity effects were significant a one-way ANOVA with three levels of proximity was applied.

RESULTS AND DISCUSSION

The force exerted by the raised finger always increased. The changes were from 1.39 ± 0.13 N (R-finger, INITIAL FORCE 5% of MVC, DISPLACEMENT 1.0 cm, SPEED 1.0 cm/s) to 8.00 ± 1.00 N (L-finger, INITIAL FORCE 20% of MVC, DISPLACEMENT 2.0 cm, SPEED 3.0 cm/s). In percent of the MVC, the changes ranged from 4.66 ± 0.38 % (I-finger, INITIAL FORCE 5% of MVC, DISPLACEMENT 1.0 cm, SPEED 1.0 cm/s) to 31.88 ± 2.19 % (L-finger, INITIAL FORCE 20% of MVC, DISPLACEMENT 2.0 cm, SPEED 3.0 cm/s). All the main effects, with the exception of the SPEED effect on the FORCE and % of the MVC change were statistically significant. There was no significant difference in muscle activity (EMG) during and before the key movement.

In all trials the total force of the non-raised fingers decreased. Hence, synergic mechanisms favoring negative force co-variation dominated over possible finger enslaving. The force changes ranged from –9.12 ± 1.49 N (L-finger, INITIAL FORCE 20% MVC, DISPLACEMENT 2.0 cm, SPEED 1.0 cm/s) to –0.29 ± 0.10 N (I-finger, INITIAL FORCE 5% MVC, DISPLACEMENT 1.0 cm, SPEED 1.0 cm/s). On a finger by finger comparison, the higher INITIAL FORCE level always resulted in a larger decrease in the total force of the non-raised fingers. For all other factors (FINGER, INITIAL FORCE, SPEED) being equal, the larger DISPLACEMENT level also always resulted in a larger decrease in the force of non-raised fingers. SPEED did not have a significant effect on the non-raised finger forces ($p > 0.50$). The proximity effect was found to be significant ($p < 0.005$) and showed a trend of a larger negative change in force by non-raised fingers with closer proximity to the raised finger.

Table 1: Statistical results on effect of experimental factors on finger force changes. P-values are given and significant values bolded.

Factor	Δ Raised Finger Force	Δ Non-Raised Finger Forces	Δ Total Force
INITIAL FORCE	**0.001**	**0**	**0.041**
DISPLACEMENT	**0.004**	**0.002**	0.845
SPEED	0.118	0.139	0.065
FINGER	**0.008**	**0.012**	0.255

CONCLUSIONS

The experiment produced two main results, reproducible across subjects: 1) a positive force change of raised finger and 2) a negative force change of non-raised fingers. In summary, these results showed that finger force adjustments during lifting of one of the fingers were dominated by synergic effects, not enslaving effects. These adjustments reduced the effects of the force change of the raised finger on total force, which may be interpreted as stabilization of the total force. We observed no signs of voluntary intervention by the subjects and hence interpret the data as resulting from involuntary synergic adjustments of finger forces.

REFERENCES

1. Bernstein NA. *The co-ordination and regulation of movements.* Pergamon Press, 1967.
2. Gelfand IM & Latash ML. *Motor Control* **2**, 206-313, 1998.
3. Schieber MH. *J Neurophysiol* **65**, 1381-1391, 1991.
4. Kilbreath SL & Gandevia. *J Physiol* **479**, 487-497, 1994.
5. Zatsiorsky VM, et al. *Biol Cybern* **79**, 139-150, 1998.
6. Latash ML, et al. *Exp Brain Res* **141**, 153-165, 2001.
7. Scholz JP, et al. *Biol Cybern* **86**, 29-39, 2002.

PREHENSION SYNERGY: PRINCIPLE OF SUPERPOSITION DURING MULTI-FINGER TORQUE PRODUCTION ON MECHANICALLY FIXED- AND FREE-OBJECTS

[1,2]Jaebum Park, [1]Vladimir M. Zatsiorsky, [2]You-Sin Kim, [5]Yoon-Hyuk Kim and [2,3,4,5]Jae Kun Shim

[1]Department of Kinesiology, The Pennsylvania State University, University Park, PA, USA
[2]Department of Kinesiology, University of Maryland, College Park, MD, USA
[3]Department of Bioengineering, University of Maryland, College Park, MD, USA
[4]Neuroscience and Cognitive Science (NACS) Graduate Program, University of Maryland, College Park, MD, USA
[5]Department of Mechanical Engineering, Kyung Hee University, Global Campus, Korea 130-701
email: jzp12@psu.edu, web: http://www.kinesiology.psu.edu/research/laboratories/mcl

INTRODUCTION

In order to maintain a stable static grasp of hand-held objects, the central nervous system (CNS) needs to satisfy a set of external static constraints [1]. In this study we used a free-object and mechanically fixed-object to investigate the effect of static constraints during a multi-digit prehension and to investigate how the CNS controls digits' forces and moments against the imposed static constraints within tasks. Specifically, we were interested in whether the principle of superposition (i.e., decoupling of grasping force control and rotational equilibrium control) is valid in fixed-object prehension when the scalar sums of individual finger (IF) normal forces and the total sum of the tangential forces are not necessarily required to be equal to the thumb normal force and the weight of object, respectively [1-3]. If the grasping stabilization, which is achieved via a high correlation between the normal forces of thumb and fingers in trial-to-trial changes, is still maintained, and the other elemental variables are grouped into an independent subset, then the principle of superposition in static human hand prehension is valid regardless of static constraints within tasks.

METHODS

Equipment: Five six-component transducers (three force and three moment components) were attached to an aluminum handle to measure forces/moment produced by individual fingers and thumb. One six-component (three position and three angle components) magnetic tracking device was mounted to the top of the handle in order to provide real-time feedback on linear and angular movements of the handle.

Experimental Procedure: There were twelve experimental conditions: 2 prehension types (fixed- and free-objects) × 6 torque conditions (supination efforts: –0.70, –0.47, –0.24 Nm; pronation efforts: 0.24, 0.47, 0.70 Nm). For the fixed-object condition, the handle was mechanically fixed to a vertical aluminum plate so that the handle could not be translated or rotated. The subjects were instructed to produce an assigned torque for 6-s while watching the feedback of torque being produced on a computer screen. For the free-object condition, the task for the subjects was to hold the handle while maintaining its pre-set constant linear and angular position against the given external torques. The task for the subjects was to hold the handle while maintaining the handle at equilibrium (i.e., quasi-static grasping). For a given condition, twenty five consecutive trials were performed.

Model: For a static prehension, the following three task constraints (i.e., mechanical constraints) in a two-dimensional grasping plane should be satisfied during a free-object prehension.

$$-F_{th}^{n} = F_{i}^{n} + F_{m}^{n} + F_{r}^{n} + F_{l}^{n} \quad (1)$$

$$F_{th}^{t} + F_{i}^{t} + F_{m}^{t} + F_{r}^{t} + F_{l}^{t} = -w \quad (2)$$

$$\sum_{k} (M_{k}^{n} + M_{k}^{t}) = -Tq, k = \{th, i, m, r, l\} \quad (3)$$

where F and M represent the force and moment, respectively; n and t refer to the normal and tangential force components; w and Tq represent the weight of the object and external torque; subscripts th, i, m, r, and l indicate the thumb, index, middle,

ring and little finger, respectively. Eq. 3 (i.e., rotational constraint) should be satisfied in both fixed- and free-object conditions while Eq. 1 and 2 should additionally be satisfied in the free-object condition.

Analysis: For the 25 trials in each condition, Pearson's coefficients of correlation between selected experimental variables were calculated. The analysis was performed at the virtual finger (VF) level. The variables at the VF level (e.g., F_n^{vf} and F_n^{th}) were computed as the vector sums of individual fingers' variables. The variables at the VF level included $F_n^{th}, F_n^{vf}, F_t^{th}, F_t^{vf}, F_t, M_n^{vf}, D_n^{vf}$,and M_t, where D_n^{vf} stands for the moment arm of the VF normal force. A principal component analysis (PCA) with a variance maximizing rotation (varimax) was performed.

RESULTS AND DISCUSSION

For both free- and fixed-object conditions, the thumb normal force was highly correlated with the VF normal force across the 25 trials for each condition (r > .8, pairs of variables F_n^{th} *vs* F_n^{vf} ; r = {0.87, 1.00}: range of correlation coefficients across all experimental conditions), while the VF normal force was not significantly correlated with the moment of VF normal force (r < .3, pair of variables F_n^{vf} *vs* M_n^{vf} : r ={0.04, 0.32}) in any of the torque conditions (Fig. 1). In addition, the thumb and VF normal forces had large loadings (|loading| > 0.7) in the same PCs and small loadings in other PCs for both fixed- and free-object conditions (Table 1). Although the large loadings in the same PCs for other variables (e.g., thumb and VF tangential forces and the moment arm of VF normal forces) were only observed in the free-object condition (PC2), it was commonly observed that normal forces and tangential forces were decoupled during both fixed- and free-object conditions (Table 1).

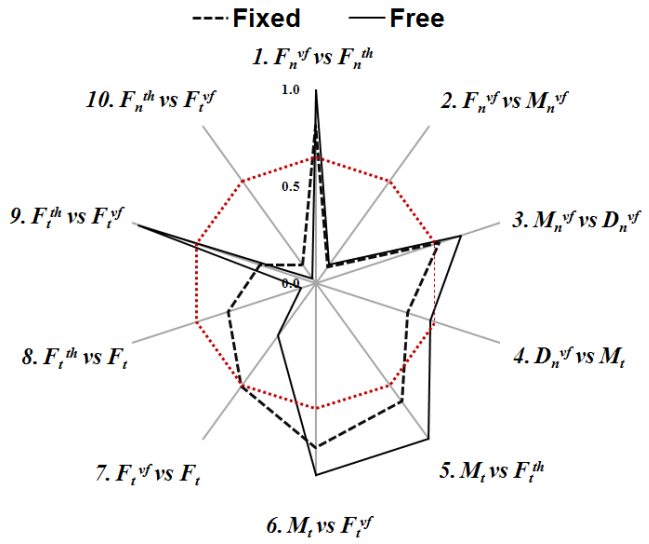

Figure 1: The correlation coefficients between ten pairs of elemental variables at the VF level. Averaged data across subjects and experimental conditions in prehension types (i.e., fixed- and free-objects) are presented. Red dotted line indicates the significant level of correlation coefficients (r = .5) with 25 of sample size.

Table 1: Groups of elemental variables at the virtual finger (VF) level which showed high loadings (|loading| > 0.7) on the same PCs.

	PC1	PC2	PC3	PC4
Free	$\{F_n^{th}, F_n^{vf}\}$	$\{F_t^{th}, F_t^{vf}, D_n^{vf}\}$		
Fixed	$\{F_n^{th}, F_n^{vf}\}$	$\{F_t^{th}, D_n^{vf}\}$ or $\{F_t^{vf}, D_n^{vf}\}$	$\{F_t^{vf}\}$ or $\{F_t^{th}\}$	$\{D_n^{vf}\}$

CONCLUSIONS

The independent controls of grasping stability (normal forces) and rotational equilibrium (moment of force) are not affected by the mechanical constraints within tasks. The data support the validity of principle of superposition in human hand static grasping tasks.

REFERENCES

1. Zatsiorsky VM, et al. *Robotica* **22**,231-234, 2004.
2. Shim, JK. and J. Park, *Exp Brain Res* **180**, 541-556, 2007
3. Shim, JK, et al. *J Neurophysiol* **93(6)**, 3649-3658, 2005.

COMPUTATIONAL MODEL TO PREDICT THE EFFECTS OF COGNITIVE AND NEUROMUSCULAR IMPAIRMENTS ON DRIVING

Benjamin L. Long[1,3], A. Isabella Gillespie[2,3], Martin L. Tanaka[2,3]

[1]Department of Physical Therapy, Winston-Salem State University, Winston-Salem, NC
[2]Department of Orthopaedic Surgery, Wake Forest University, Winston-Salem, NC
[3]Human Performance and Biodynamics Laboratory, a collaboration between
Wake Forest University School of Medicine and Winston-Salem State University
Email: mtanaka@wfubmc.edu

INTRODUCTION

Motor vehicle accidents are the leading cause of death for United States citizens age four through 34 years[1]. Mental distractions and physical impairments can further increase the risk of accidents by affecting a driver's ability to control the vehicle and react to various distractions. In this study, cognitive challenges and physical impairments were imposed and their affect on cognitive, neuromuscular, and total reaction time was evaluated. From these measured results, we developed a linear mathematical model that may be used to quantitatively predict drivers' performance under a variety of possible driving conditions. Predictions were not limited only to conditions tested, but rather, our model may be used to predict reaction speed for any linear combination of these test conditions. We believe that this is the first model to use this linear combination approach to predict drivers' reaction speed.

METHODS

Experiment

Twenty-four (8 female, 16 male) participants from the university and surrounding area volunteered to participate in the study. Group one (n=12) was tested to evaluate the effects of dual cognitive tasks on driving reaction speed, cell phone talking and texting. Group two (n=12) was used to evaluate the effects of a physical impairment on reaction speed, a fixed knee brace (FKB). Group two was also tested with a FKB and while talking a cell phone. This condition did not go into the development of the model but instead was used for model verification.

All trials were performed on a custom built driving reaction speed tester (DRST). A data acquisition card (National Instruments, Austin, Texas) installed in a personal computer was used to record (1000 Hz) the voltage associated with the positions of the gas, brake, and clutch pedals. After testing was completed, the test files were accessed using Matlab software (MathWorks; Natick, Massachusetts). Full braking time (FBT) was calculated from the sum of the cognitive reaction time (CRT), foot movement time (FMT), and break travel time (BTR).

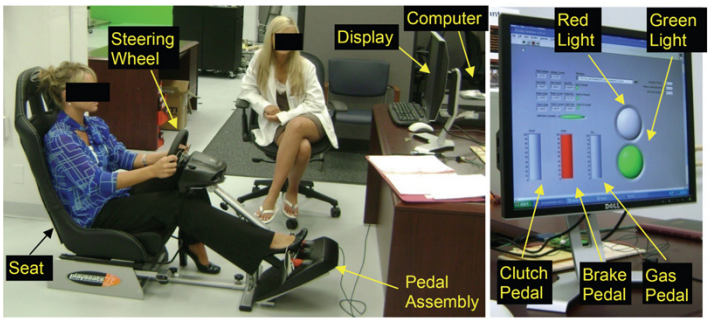

Figure 1: Driver Reaction Speed Tester (DRST).

Computational Model

A linear mathematical model was developed to predict the reaction speed under various testing conditions. The predicted full braking time, *PT*, for a specific set of test conditions was,

$$PT = N_j + \sum_{m=1}^{n} A_m + \sum_{m=1}^{n} B_m + \sum_{m=1}^{n} C_m$$

where N_j is the average FBT under normal conditions for participant *j*. A_m, B_m, and C_m are the effects of each modifier on the CRT, FMT and BTT, respectively. The applied modifying factor is *m*, and *n* is the total number of modifying factors. In this study, conditions primarily affecting cognitive reaction speed were talking (*m*=1) or texting (*m*=2) on a cellular phone. The main

modifier associated with musculoskeletal reaction speed was the physical impairment of a FKB (m=3).

A one-way ANOVA was used to determine the individual effect of cell phone talking, cell phone texting, and a fixed knee brace on CRT, FMT, BTT, and FBT. All statistics were analyzed using SPSS software (SPSS Inc.; Chicago, Illinois) with significance set as $p<.05$ for all tests.

RESULTS AND DISCUSSION

A threshold detection method was used to automatically find the time when each pedal was released and depressed (Figure 2). The net effect of each test condition on CRT, BTT, and FMT was calculated from the experimental results by subtracting the mean value for the test condition from the mean value for normal driving. These net effects were used as calibration parameters in the mathematical model (Table 1).

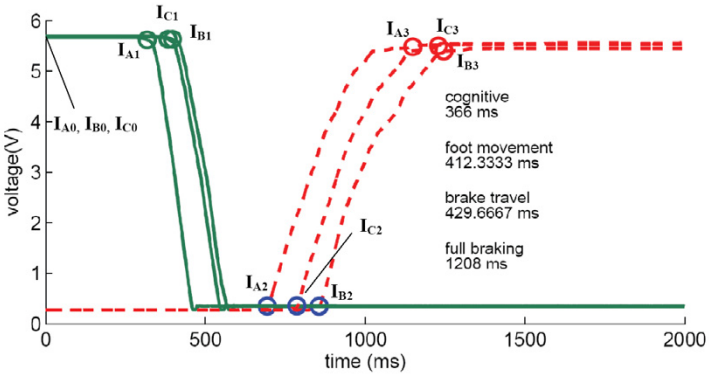

Figure 2: Reaction speed data. I_{A0}, I_{B0}, and I_{C0} mark the beginning of each individual reaction speed test within the trial. The second subscript, 1, 2, or 3, indicate the end of the cognitive, foot movement, and brake travel portion of the reaction speed test, respectively.

Table 1: Mathematical Model Calibration Parameters

Condition	Symbol	Reaction Speed Cost
Cell Phone Talking	A_1	122 ms
	B_1	0 ms
	C_1	0 ms
Texting	A_2	268 ms
	B_2	34 ms
	C_2	25 ms
Fixed Knee Brace	A_3	16 ms
	B_3	49 ms
	C_3	55 ms

The model was used to predict driving reaction speed for an untested condition, talking on a cell phone while wearing a FKB. This test condition was measured experimentally and the accuracy of the model evaluated. Recall that this condition was not used in the development of the model. The model predicted full braking time within 3% of the measured value (Figure 3).

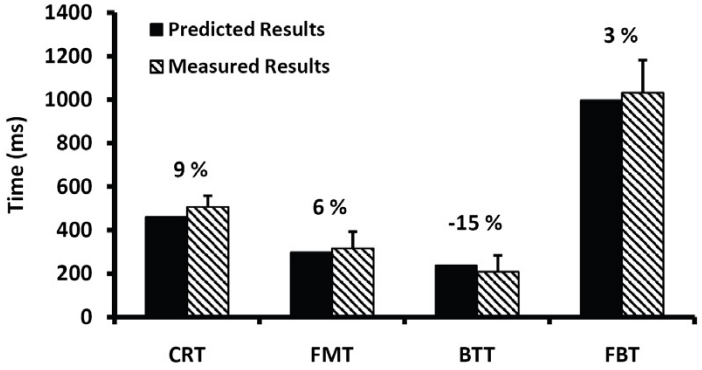

Figure 3: Comparison of model predicted and actual measured results for drivers' reaction time. The linear model was able to predict the full braking time within 3% of the actual measured value.

The use of the linear model is limited by its' inability to account for complex interactions that may occur between modifying variables. In addition, little information is known about the effect of participant learning under various testing conditions. These limitations will be addressed in future versions of the model.

CONCLUSIONS

This abstract presents a mathematical model that may be used to predict driving reaction speed for a variety of influencing conditions. Although only a few influential conditions were evaluated, we present a general approach that may be expanded to include other types of distractions, impairments, and environmental conditions.

REFERENCES

1. NHTSA. (2008). *Motor Vehicle Traffic Crashes As a Leading Cause of Death in the United States, 2005*. Washington, DC 20590: National Highway Traffic Safety Administration.

TRUNK SEGMENT COORDINATION DURING A JUMPING TASK IN ELITE DANCERS: AN EXPLORATION USING VECTOR CODING

[1]Jo Armour Smith, [2]Adam Siemienski, [1]John M. Popovich, Jr., [1]Kornelia Kulig
[1]Jacquelin Perry Musculoskeletal Biomechanics Research Laboratory, Division of Biokinesiology and Physical Therapy, University of Southern California, Los Angeles, CA.
[2]Department of Biomechanics, University School of Physical Education, Wroclaw, Poland.
Email: joannesm@usc.edu, web: http/pt2.usc.edu/labs/mbrl/

INTRODUCTION

Coupling analysis is a method of characterizing relative motion (coordination) between limbs, joints, or body segments during motor tasks. Coupling behavior is determined by factors such as joint morphology, muscle activation, and task constraints. It is significant because it is altered by neuro-musculoskeletal pathology [1] and may also be a function of skill level. The vector coding technique is one method of quantifying inter-segmental coordination. To date, it has not been used to characterize trunk motion. The purpose of this study was to use vector coding to quantify coordination of the thoracic and lumbar regions of the spine during a sub-maximal jumping task in elite dancers.

METHODS

Four healthy female collegiate dancers with an average of 14 years of dance training (range 12-17) were tested. Each subject performed consecutive double-legged vertical jumps at 95 b.p.m. The aesthetic demands of this type of dance jump resulted in several additional task constraints. The trunk remained vertical, the hips were externally rotated and the arms were held in front of the body at chest height throughout the jumps (Figure 1). Trunk kinematics and ground reaction force data were collected at 250Hz and 1500Hz respectively (Vicon 612 motion capture system, Oxford, UK; AMTI force plates, Watertown, MA). In addition to standard lower extremity markers, a marker array on L1 and individual markers on the sacrum, sternum, acromioclavicular joints and C7 were used to construct a three-segment trunk model. The duration of each jump was normalized to 101 time points, and then subdivided into three task-specific phases: propulsion (bottom of squat to toe-off); flight; and landing (touchdown to bottom of squat). Ground reaction force data and the sacral marker were used to identify phase transitions.

Sagittal angular displacement of the thoracic and lumbar segments with respect to the pelvis at each time interval were calculated for 10 jumps for each subject (Visual 3D™ software). The coupling angle (0-360°) for each time interval was derived as the angle from the right horizontal of a vector connecting two consecutive data points on the angle-angle plot of lumbar and thoracic motion. Mean coupling angles were then calculated as mean directions across 10 jumps using circular statistics [2]. The length of the mean vector was also calculated using circular statistics to give a ratio between 0 and 1. This ratio indicates the consistency of the data, with greater consistency as values approach 1. Mean coupling angles at time intervals with mean vector length greater than 0.4 were retained for further analysis.

For each time interval, coordination was categorized as in-phase (both spinal regions flexing or extending), anti-phase (one region flexing and the other extending), lumbar phase (predominantly lumbar spine motion) and thoracic phase (predominantly thoracic spine motion) using the coupling angle (Table 1). The relative frequency of each coordination category during the time intervals constituting the three phases of the jump was calculated for each subject to give a predominant pattern of coordination for each phase.

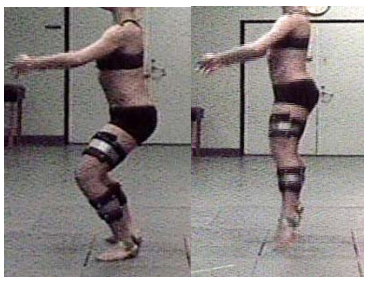

Figure 1: Double-legged dance specific vertical jump

Table 1: Bin widths for coordination category determination*

Coupling angle (degrees)	Coordination category	Coupling angle (degrees)	Coordination category
0-22.5	Lumbar phase	202.5-247.5	In-phase
22.5-67.5	In-phase	247.5-292.5	Thoracic phase
67.5–112.5	Thoracic phase	292.5-337.5	Anti-phase
112.5-157.5	Anti-phase	337.5-360	Lumbar phase
157.5-202.5	Lumbar phase		

*As described by [1]

RESULTS and DISCUSSION

All of the subjects were able to complete the jump task within the constraints outlined above. Graphs of mean trunk displacement, mean coupling angle and mean vector length across the time period of the jump for one subject are presented in Figure 2. All of the subjects demonstrated in-phase coordination during flight (Table 2). This is despite inter-subject differences in magnitude and direction of spinal displacement during this task-specific phase of the jump. In-phase coordination was also most common during propulsion and landing. However, these task-specific phases also had frequent lumbar and thoracic coordination phases, with no consistent pattern between subjects.

Despite the highly constrained task and the similarity of the dancers' skill level, some differences in strategies used to achieve successful task performance were observed. The variety of coordination patterns during propulsion and landing may be a result of different strategies employed by subjects to sustain a vertical trunk as the hips were flexing and extending. A maximal effort task may produce more stereotypical coordination across all subjects.

Coupling analysis of the trunk using the vector coding technique permitted quantification of trunk coordination during a rapid, complex task and identified similarities and differences between subjects that were not evident from displacement data alone. Following identification of normal task-specific trunk coordination, the vector coding technique has the potential to assist in discriminating between subjects of different skill levels, and in identifying injury mechanics.

REFERENCES

1.Chang R, et al. *J Biomech* **41**, 3101-3105, 2008.

2.Hamill J, et al. *J Appl Biomech* **16**, 407-418, 2000.

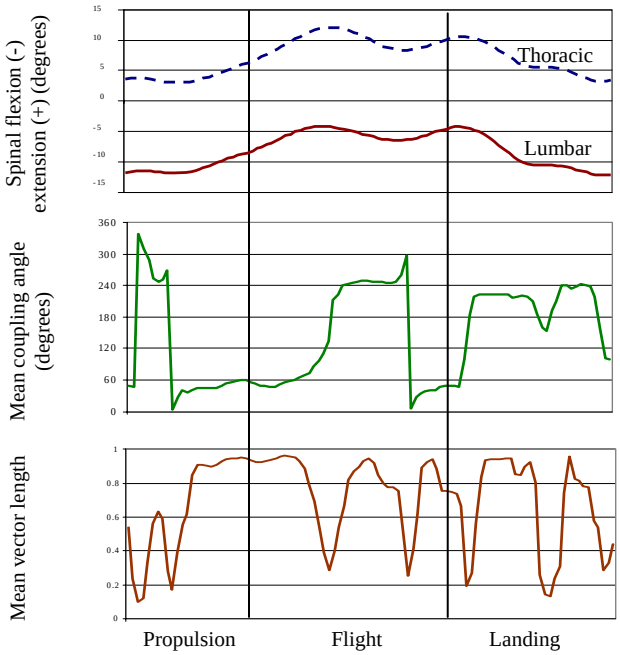

Figure 2: Mean angular displacement (top), mean coupling angle (middle), and mean vector length (bottom), for one subject (10 trials)

Table 2: Predominant coupling behavior (and % contribution) during each jump phase

	Task-specific phase of the jump		
	Propulsion	**Flight**	**Landing**
Subject 1	In-phase (85)	In-phase (73)	In-phase (96)
Subject 2	In-phase (65)	In-phase (55)	In-phase (38)
Subject 3	Lumbar phase (55)	In-phase (92)	Lumbar phase (50)
Subject 4	Thoracic phase (40)	In-phase (58)	In-phase (41)

PLANARITY OF FORCE DISTRIBUTION IN A 4-FINGER FORCE SPACE DURING MULTI-FINGER PREHENSION AND ITS IMPLICATION FOR INVERSE OPTIMIZATION

[1, 2] Xun Niu, [1,3]Alexander V. Terekhov, [1]Mark L. Latash and [1]Vladimir M. Zatsiorsky
[1]Kinesiology Dept., [2] Statistics Dept., The Pennsylvania State University, University Park, PA, USA
[3]Institut des Systèmes Intelligents et de Robotique, CNRS-UPMC, Pyramide ISIR, Paris, France
email: xun100@psu.edu

INTRODUCTION

The inverse optimization problem deals with determining an unknown objective function that is used by the controller for optimizing performance in a certain task. The solution consists in finding: (a) a parameterized class of objective functions (e.g. linear or quadratic) and (b) function parameters. Commonly, the cost function class is assumed by researchers *a priori* and the parameters (coefficients) are estimated from experimental data [1]. Recently, a new method of Analytical Inverse Optimization (ANIO) was developed [2.3]. The method allows reconstructing both the class of the cost function and its parameters from experimental recordings. The core of the method is a Uniqueness Theorem, which provides sufficient conditions for the uniqueness of the cost function. In this study, the ANIO method was applied in human multi-finger prehension (grasping) tasks to determine the cost function presumably used by the central controller to share activity among fingers.

METHODS

Experiment. Eight healthy male subjects held an instrumented handle using a prismatic grasp statically in the air. The forces and moments of force exerted by individual digits were recorded Four loads, 0.25, 0.5, 0.75, and 1.0 kg were attached at different points along the horizontal bar attached to the handle, thus generating four external torques of ±0.2 Nm, ±0.4 Nm plus zero torque. The experiment had two phases: (1) the subjects were instructed to hold the handle vertically with minimal normal force (calibration); (2) the computer recorded the forces and then set target forces on the computer screen, at 100%, 125%, 150% and 175% of the calibration force. Subjects were instructed to squeeze the handle and to match the target force level.

Analytical Inverse Optimization (ANIO). The ANIO method is a mathematical method that can be applied to problems with linear constraints. Its only assumption about the cost function is that this function is additive and twice differentiable. Such a method allows for reconstructing the unknown cost function from experimental recordings. The optimization problem is defined as:

Minimize:

$$J(F_{in}^n, F_{mi}^n, F_{ri}^n, F_{li}^n)=g_{in}(F_{in}^n)+ g_{mi}(F_{mi}^n)+ g_{ri}(F_{mi}^n)+ g_{li}(F_{li}^n) \quad (1)$$

subject to constraints on the total force and moment:

$$CF^n = \begin{pmatrix} 1 & 1 & 1 & 1 \\ Y_{in} & Y_{mi} & Y_{ri} & Y_{li} \end{pmatrix} F^n = \begin{pmatrix} F_{total}^n \\ M^n \end{pmatrix}$$

where g_i is an unknown scalar differentiable function with g'(·)>0 in the feasible region.

The pivotal idea in finding the objective function J is to approximate the spaces formed by the experimental data and the optimal solutions satisfying $\breve{C}KF = 0$, where $\breve{C} = I - C^T(CC^T)^{-1}C$ and K is a 4×4 orthogonal matrix composed of the coefficients of the highest order terms in the objective function J.

RESULTS AND DISCUSSION

The experimental data were mainly on a 2-dimensional hyperplane (experimental plane) in a 4-dimensional space of finger normal forces: 93.53±0.43% of the total variance was accounted for by the first two principal components with the larger eigenvalues. The planarity of the experimental observations is not a direct consequence of the task mechanics. Instead, it is a non-trivial finding indicating that the finger forces are specified in such a way by certain motor control mechanisms, which could be revealed by

optimality principles. The 'mechanical' hyperplanes defined by the "pure mechanical" constraints with the specific values of F^n and M^n were also determined. Each data point lied onto its own 'mechanical' hyperplane. In this experiment, the dihedral angle between experimental hyperplane and "mechanical" hyperplane equaled 83.7° ± 4.5° across subjects.

The planarity of the distribution of the experimental data demonstrates that the derivatives of the cost function with respect to individual finger forces have to be linear and hence the cost function is quadratic. The cost function was computed for each subject by minimizing the dihedral angle between experimental plane and the plane of optimal solutions determined from the Uniqueness Theorem. The approximation angle was 2.53±0.74°. The new ("optimal") plane contained 93.76±0.37% variance of the raw data. An objective function for an exemplary subject was

$$J = \frac{1}{2}\left(\left(F_{in}^n\right)^2 + 1.59\left(F_{mi}^n\right)^2 + 1.82\left(F_{ri}^n\right)^2 + 2.73\left(F_{li}^n\right)^2\right)$$
$$- 0.32F_{in}^n + 0.48F_{mi}^n + 0.1F_{ri}^n - 0.26F_{li}^n$$

The functions had a similar form across subjects; the second-order terms k_i were positive for all subjects and the relations $k_{in}<k_{mi}=k_{ri}<k_{li}$ were maintained. The absolute error value between the experimental data and optimization results were 0.30±0.01, 0.41±0.02, 0.40±0.02, 0.30±0.01 N for the each finger across subjects.

CONCLUSIONS

The inverse optimization problem for the force sharing among fingers was successfully solved by the ANIO method with good agreement with the experimental observations. The reconstructed function—a quadratic function with the non-zero linear terms— is unique, i.e. if there is another objective function fitting the same data with reasonable precision then it must be essentially similar to the reconstructed one (up to essential similarity and unknown linear terms).

REFERENCES

1.Prilutsky BI, Zatsiorsky VM. *Exerc Sport Sci Rev* **30**: 32-38, 2002.

2.Terekhov VA, Pesin YB, Niu X, Latash ML, Zatsiorsky VM. *J Math Biol*, 2009 (in press)

3.Niu X, Terekhov VA, Latash ML, Zatsiorsky VM. (under review).

ACKNOWLEDGEMENTS

The study was partially supported by NIH grants AG-018751, NS-035032, and AR-048563 and NSF grant DMS-0503810.

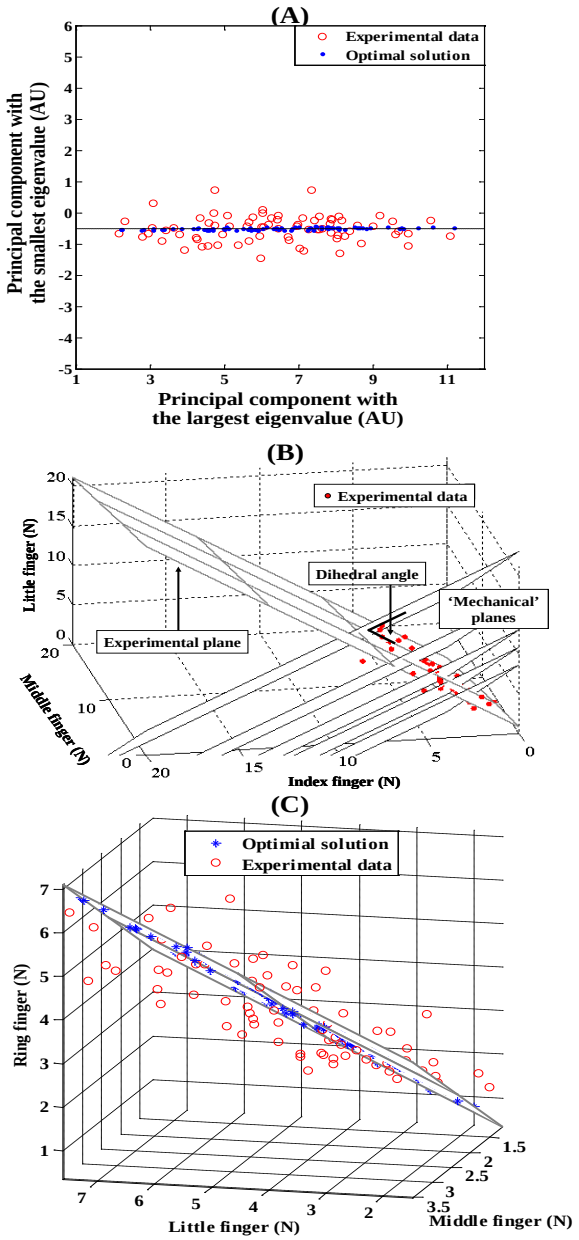

Figure 1: Illustration of planarity of finger forces and the optimal solutions computed from ANIO method. (A) PC with the smallest eigenvalue vs. PC with the largest eigenvalue; (B) 'mechanical' planes and experimental plane; (C) Projection onto the three-dimensional space: Middle finger – Ring finger–Little finger.

ADAPTIVE CHANGES IN FINGER FORCE VARIANCE IN RESPONSE TO INDEX FINGER FATIGUE IN A MULTI-FINGER TASK

Tarkeshwar Singh, Vladimir M. Zatsiorsky and Mark L. Latash

Pennsylvania State University, University Park, PA, USA
Email: tarkesh@psu.edu

INTRODUCTION

Muscle fatigue causes a drop in the maximal voluntary contraction (MVC) force and also in the accuracy (measured as an increase in intra-trial variability) of force production by the fatigued elements. On the other hand, accuracy of tasks performed by redundant sets of elements may be relatively preserved. We hypothesized that this is achieved by the less affected elements showing an increased variance of their outputs accompanied by a strong negative co-variation among the outputs of all the elements. To quantify the change in performance due to fatigue, we used the framework of the uncontrolled manifold (UCM) hypothesis [1]. The hypothesis assumes that the controller organizes covariation among elemental variables (finger modes (**m**) in our study) to stabilize a certain value of a performance variable (total force). We quantified variance in two sub-spaces within the **m** space, one corresponding to a fixed value of total force (UCM) and the other leading to changes in the total force (orthogonal to the UCM).

METHODS

Ten right-hand dominant subjects participated in the study. The participants performed four blocks of trials, the MVC by each finger and four fingers acting together (I,M,R,L and IMRL); one-finger accurate force ramp production trials (to estimate the enslaving matrix [2]); force ramps between 5 and 25% MVC as *discrete tasks*, and rhythmic force production at 0.9 Hz between 5% and 25% of the MVC as *cyclic tasks* (performed by IMRL and by I). Visual feedback of the force output was provided. To look at the effects of fatigue, the same four blocks of trials were repeated before and after a one-minute MVC fatiguing exercise by the I finger. To maintain the level of fatigue, the exercise was repeated for 20 s after each trial. For the cyclic task, the cycles were normalized to 100 data points, force data were transformed into **m** data, and the cycle-to-cycle mode variance at each time instant was decomposed into the variance within the UCM space (V_{UCM}) and orthogonal to it (V_{ORT}). V_{UCM} and V_{ORT} per degree of freedom were compared; $V_{UCM} > V_{ORT}$ was interpreted as a multi-finger synergy stabilizing the total force. A similar analysis was performed on the discrete force ramps. The RMS error was computed with respect to the average (across trials) performance ($RMSE_{mean}$). The index was normalized by the average force value over the task. Force variance was computed for individual fingers during the IMRL task; it was normalized to the squared MVC of the particular fingers. A synergy index, ΔV was computed reflecting the relative amount of V_{UCM} in the total variance (V_{TOT})

$$\Delta V = \frac{V_{UCM} - V_{ORT}}{V_{TOT}} \qquad (1)$$

This index was z-transformed before running statistical analysis on $Z_{\Delta V}$.

RESULTS AND DISCUSSION

After fatiguing the I finger, the peak MVC of the I, M, R and IMRL finger combinations dropped significantly. The I finger force dropped by about 34%. The drop in the MVC of the other fingers was smaller. During fatigue, the enslaving between the fingers increased by about 10% and this increase approached significance ($p=0.09$). Fatigue led to an increase in the RMS error by 47% for the discrete task and by 18% for the cyclic task (Fig 1). A two way ANOVA (*fatigue-condition* and *task* as factors*)* on absolute $RMSE_{mean}$ showed that $RMSE_{mean}$ for the I *combination,* but not for IMRL, increased significantly ($p<0.01$). The variance of the individual finger forces in the IMRL task increased

during fatigue. on average by about 50%. A three-factor ANOVA showed a main effect for *fatigue-condition* ($p<0.05$) and *task* ($p<0.001$) but not for individual fingers. Fatigue led to an increase in both V_{UCM} and V_{ORT}. However, V_{UCM} increased significantly more than V_{ORT} (Fig. 2). ANOVA on V_{UCM} showed main effects for *fatigue-condition* ($p<0.01$) and *task* ($p<0.05$). In contrast, ANOVA on V_{ORT} showed a main effect for *task* ($p<0.001$) but not for *fatigue-condition* ($p=0.37$). For the discrete and cyclic tasks, $Z_{\Delta V}$ increased by about 10% and by about 35%, respectively, during fatigue. A two way ANOVA showed significant effect of *fatigue-condition* ($p<0.05$) and *task* ($p<0.001$).

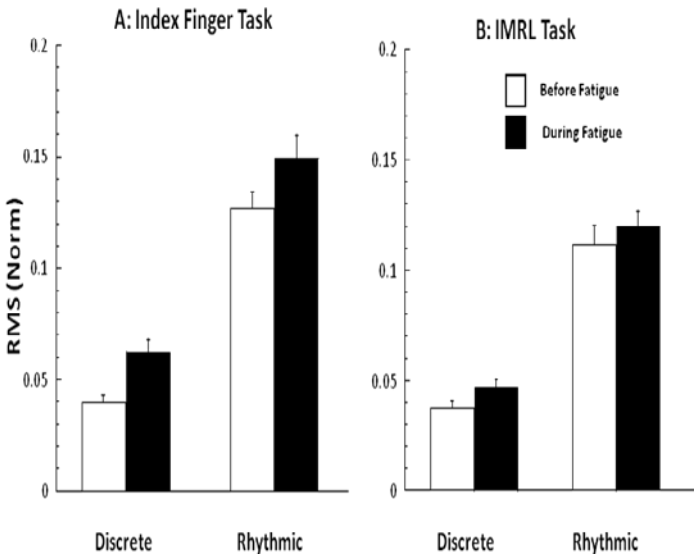

Figure 1: Normalized RMS error for the discrete and rhythmic tasks.

We did not observe differences between effects of fatigue on accuracy of multi-finger task performance ($RMSE_{mean}$ for the IMRL task did not change). This was expected and is in line with studies showing that goal-relevant features of performance are relatively preserved during fatigue in tasks involving redundant sets of elements [3].

Our findings provide support for the hypothesis offered in the Introduction. Fatigue of the index finger resulted in an increase in force variance of all four fingers. However, total force variance in the four-finger task showed minor changes during fatigue, which was due to an increase in negative co-variation among finger modes. In the framework of the UCM hypothesis, V_{UCM} increased more than V_{ORT} and this contributed to a significant increase in the index of force-stabilizing synergy (ΔV). If we view fatigue as an intrinsic perturbation into the ability of a finger to produce accurate force, strengthening the multi-finger force stabilizing synergy allows to avoid major detrimental effects of fatigue on the accuracy of force production in four-finger tasks. Strengthening a synergy (that is, increasing the relative amount of V_{UCM} in total variance) requires parallel changes in the variances of individual elements. There are two components of changes in characteristics of finger force variability, an increase in variance of commands to individual fingers and an increase in their negative co-variation to maintain accuracy of task performance. The former could be due to higher motor unit synchronization across flexor digitorum profundus (FDP) compartments [4] while the latter requires an explanation at a hierarchically higher level of the organization of multi-digit synergies.

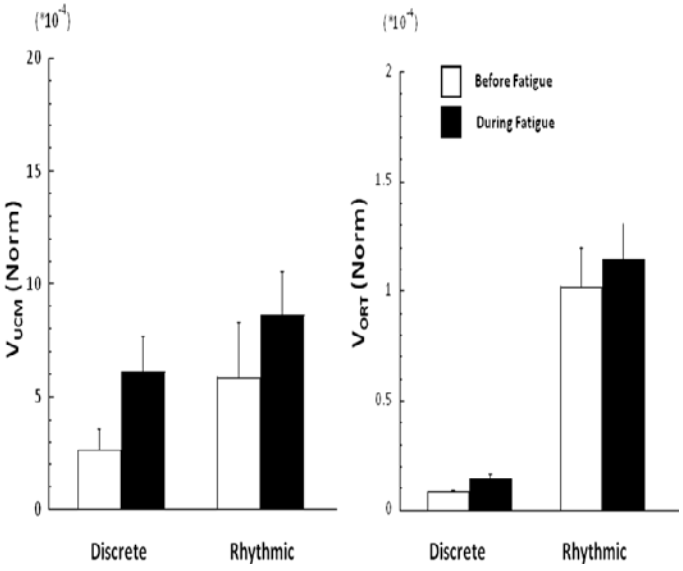

Figure 2: Normalized V_{UCM} and V_{ORT} for the discrete and rhythmic tasks.

REFERENCES

1.Scholz et al. *Exp Brain Res,***126**, 289-306, 1999
2.Zatsiorsky et al. *Biol Cybern* **79,** 139-150, 1998
3.Gates et al, *Exp Brain Res,* **187**, 573-585, 2008
4.Reilly et al. *J Neurophysiol,* **92**, 734-742, 2004

TRIAL-TO-TRIAL ADAPTATION OF MULTI-DIGIT FORCES TO TEXTURE FOR OBJECT MANIPULATION

[1]Wei Zhang, [2]Andrew M. Gordon, [2]Tara L. McIsaac, and [1]Marco Santello

[1]Arizona State University, Tempe, AZ, USA
[2]Columbia University, New York, New York, USA
email: wzhang70@asu.edu, Marco.Santello@asu.edu

INTRODUCTION

Tactile signals from the fingertips play a crucial role in the planning and control of object manipulations [1]. Specifically, digit force sharing patterns adapt to different object properties, such as texture between the digits and the object surface, to preventing slipping and dropping the grasped object [2]. The effect of texture on multi-digit force sharing patterns has been mostly studied during static tasks such as object hold [3,4]. However, little attention has been paid to the modulation of multi-digit forces to object texture that occurs within trial (from contact to onset of object manipulation) and from trial-to-trial. Here we addressed both of these questions by changing texture on the thumb and/or finger side of the object. We hypothesized that subjects would exhibit force adaptation to texture within each trial, hence before the onset of object manipulation.

METHODS

Ten right-handed volunteers (5 males and females, age: 24-45 yrs) participated in this study. During the experiment, subjects sat facing a vertically oriented handle (mass: 720 g) with five 6-component force/torque transducers (NANO 17/25; ATI inc.) that recorded individual digit forces and local moment of forces. The handle position and orientation were measured by an electromagnetic position tracking sensor (Polhemus Fastrak). We studied four texture conditions (R-R, S-S, S-R and R-S) by using contact surfaces covered with either 100-grit sandpaper (S) or rayon (R) between the thumb (TH) and/or the fingers (VF) and the grip surface. The virtual finger (VF) is an imagined digit that produces a mechanical action equivalent to that of the actual fingers of the hand [5]. Six consecutive trials were performed for each texture condition. The average static friction coefficient (*u)* across subjects was 0.48 ± 0.03 for the rayon and 1.08 ± 0.02 for the sandpaper.

During the experiment, subjects were instructed to use all five digits of the right hand to complete the task of grasping, lifting, steadily holding for 7s and replacing an object. Meanwhile, subjects were required to keep the handle upright throughout the task.

Data analysis was performed at the virtual finger – thumb level (VF-TH), which is considered as a higher control hierarchical level during human prehension tasks. To investigate multi-digit force adaptation to texture within trial, we measured digit normal force (F_n), tangential force (F_{tan}), center of pressure (CoP), and safety margin (SM) at the onset of object lift-off.

RESULTS AND DISCUSSION

We analyzed digit safety margin as a global variable to quantify the subjects' force strategy changes with local texture changing on TH and VF. As a result, digit local SM changed according to the texture conditions on the specific digit before the object lift onset (Fig 1A). Specifically, SM on both TH and VF increased when contacting sandpaper and decreased on rayon. Furthermore, subjects preferred to use higher SM at the TH than VF in symmetric texture conditions (R-R and S-S), and kept SM unchanged for each digit when it contacted the same texture, regardless of the texture at the opposing digit. Similar SM patterns were observed at object lift onset and hold from the first object lift and throughout the following trials (Fig 1B). These findings imply that subjects were able to adjust their forces according to the information received based on local tactile inputs and before lifting the object.

The digit force patterns at these two time points were highly correlated as indicated by large r-values ($r > 0.9$), indicating that the solution chosen before object lift-off was kept unchanged during later stages of the manipulation.

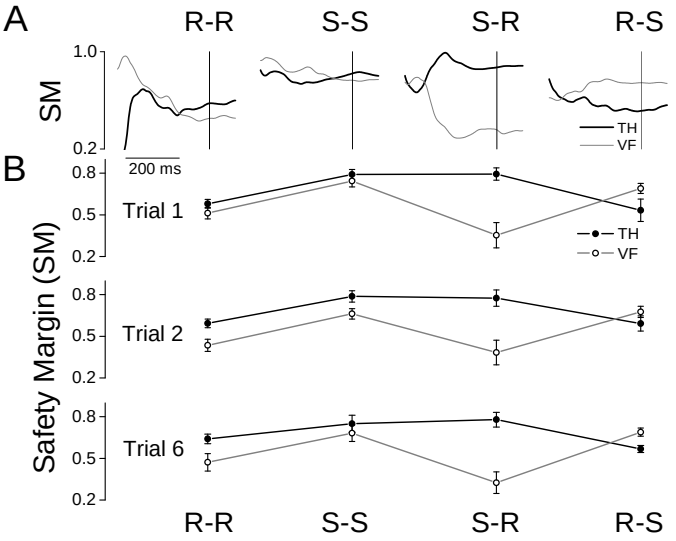

Figure 1: Typical and average performance of safety margin at lift onset. A: shows the typical safety margin time traces by TH and VF of the first trial from a representative subject. Grey vertical line denotes the object lift onset. B: shows the average safety margin at lift onset by TH and VF of the first trial (trial 1), an intermediate trial (trial 2) and the last trial (trial 6) in all four texture conditions.

Subjects significantly increased digit F_n when texture at the VF changed from sandpaper to rayon, regardless the texture changes on TH, i.e., F_n produced at lift onset in conditions of R-R and S-R are significantly larger than of S-S and R-S ($P<0.0001$). Similarly, subjects modulated distance between digits' CoP (ΔCoP) depending on the texture on VF, i.e., larger distance between digit positions for less slippery texture (S) on VF. Moreover, subjects exhibited the smallest and largest F*tan* differences between digits at S-R and R-S, respectively. These results might suggest that subjects preferred to plan and modulate digit forces based on the texture experienced by the VF. This might be driven by subjects' preference of contacting VF prior to TH during object grasping, which may thus provide tactile inputs to VF earlier than TH.

CONCLUSIONS

Subjects modulated multi-digit forces to texture prior to the onset of object manipulation within each trial, thus exhibiting no trial-to-trail adaptation. This quick force adaptation allowed subjects to generate a force distribution that was then used for the actual manipulation, hence reducing the need for continuous monitoring of sensory feedback at later stages of the manipulation.

REFERENCES

1. Johansson RS, et al. *Nat Rev Neurosci* **10**, 345-359, 2009.
2. Johansson RS, et al. *Exp Brain Res* **56**, 550-564, 1984.
3. Aoki T, et al. *Exp Brain Res* **172**, 425-438, 2006.
4. McIsaac TL, et al. *Exp Brain Res* **194**, 79-90, 2009.
5. Arbib MA, et al. *Hand function and the neocortex*, Springer, 1985.

ACKNOWLEDGEMENTS

This research was supported in part by NSF grant BCS 0819547 "Collaborative Research: Dexterous Control of Multi-Digit Grasping".

NONLINEAR SMOOTH ORTHOGONAL DECOMPOSITION IDENTIFIES LOCAL MUSCLE FATIGUE DYNAMICS IN SAWING MOTION

[1]D. B. Segala, [2]D. Gates, [2]J. B. Dingwell, and [1]D. Chelidze

[1]University of Rhode Island, Kingston, RI, USA
[2]University of Texas at Austin, Austin, TX, USA
email: chelidze@egr.uri.edu, web: http://mcise.uri.edu/chelidze/nld/

INTRODUCTION

Mean (MNF) and median (MDF) power frequencies of *electromyography* (EMG) signals of individual muscles have been shown to be a good indicators of local muscle fatigue. These signals are recorded one of two ways: using indwelling needles or surface electrodes. However, while indwelling needles are very invasive, both are not realizable in out-of-laboratory settings. Previously, it was shown that *smooth orthogonal decomposition* (SOD) has the distinct ability to extract smooth deterministic coordinates (i.e., separate signals according to their dominant time scale) from a vector-valued time series. We hypothesized that a nonlinear extension of SOD would find more optimal coordinates (smoother in time and requiring fewer dimensions) to characterize local physiological dynamics than its linear counterpart. By comparing kinematics smooth coordinates to EMG trends in the least squares sense, cross subject variability indicated that nonlinear SOD extracts more optimal coordinates that are in almost one-to-one relationship with actual EMG-based markers. It was shown that a 4-dimensional slow-time manifold can track and predict local muscle fatigue dynamics.

METHODS

A nonlinear form of SOD was used extract smooth coordinates from a vector-valued features space constructed from noninvasive movement kinematics data. Ten healthy right-handed subjects (27 ± 2.8 years; 1.71 ± 0.10 m height; and 69.91 ± 18.26 kg body mass) performed a sawing motion by pushing a weighted handle back and forth until voluntary exhaustion. Three sets of joint kinematic angles were measured from the elbow, wrist and shoulder, in addition to, surface EMG recordings from nine different muscle groups [1].

In general, when a muscle fatigues, a shift in the power spectrum to lower frequencies is observed, which can be attributed to many physiological phenomena [2]. The concept of PSW describes the deformation—change in the geometry—of a dynamical system's phase space when its parameters drift [3, 4]. Short-time measures of this deformation are shown to be in one-to-one relationship with actual parameter drifts and are used to develop corresponding feature vectors. SOD is a multivariate analysis tool that extracts low-dimensional, smooth, and deterministic trends from high-dimensional data (time series) [5]. In [3, 4], PSW and linear SOD based methodologies were able to extract smooth deterministic trends from movement kinematic time series which reflected both local (individual muscle) and global (systemic) EMG-based fatigue markers for stationary cyclist, load carriage walking US soldiers, and sawing subjects.

Muscle fatigue is viewed as evolving in a hierarchical dynamical system where slow-time fatigue accumulation and fast-time motion dynamics are coupled through parameters of the fast-time kinematic system. A fast-time kinematic phase space trajectory is reconstructed using time delay coordinate embedding. These trajectory is split into several consecutive data records. All records are

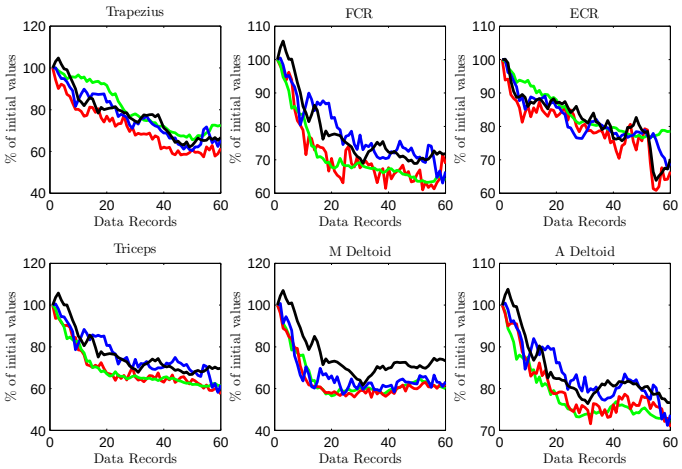

Figure 1: Nonlinear SOD projected trends onto MNF (red) indicators for elbow flexion/extension angle (green), humeral head angle (blue), and humeral head elevation (black) for subject 11. FCR/ECR: flexor/extensor carpi radialis.

partitioned into fixed hyper-boxes. A *PSW tracking metric* measures the short-time difference in the evolution of a trajectory starting from the same phase space point in the current and reference (i.e. the first) data records. Concatenating the weighted average of all tracking metrics from each hyper-box forms a feature vector for each data record. The time sequence of all these feature vectors form a multivariate time series Y.

Physiologic fatigue is treated as a smooth, deterministic process, which is captured by the vector-valued time series Y. SOD is used to reconstruct fatigue as the temporally smooth trends embedded in Y by solving a generalized eigenvalue problem of the auto-covariance matrices for Y and DY, where D is the discrete differential operator. The resulting eigenvalues are called *Smooth Orthogonal Values* (SOVs) and eigenvectors *Smooth Orthogonal Modes* (SOMs). *Smooth Orthogonal Coordinates* (SOCs) are obtained by projecting the feature space onto the subspaces spanned by the SOMs. The smoothness of the SOC is described by the magnitude of the corresponding SOVs. The higher the value of SOVs, the smoother in time are the corresponding SOCs. Deterministic fatigue is expected to be embedded in these dominant SOCs. The nonlinear SOD is accomplished by Taylor series expanding the smooth coordinates to include 2nd order terms. If a slow subspace is span by $\phi_{i i=1}^{n}$ SOMs, then new extended time series is $Y_{new} = \sum_i^n Y\phi_i + \sum_i^n \sum_j^n Y\phi_i\phi_j$.

Kinematic data was sampled at 60 Hz using an 8-camera Vicon-612 motion analysis system (Oxford Metrics,Oxford, UK). EMG signals were recorded at 1080 Hz using a Delsys Bagnoli-8 system integrated with the Vicon-612 system. Particulars about kinematic analysis can be found in [3], however, in all cases, 5 dominant SOMs were reserved for the nonlinear SOD analysis. Coefficient of determination R^2 values were used in conjunction with an ad hoc F-Test to determine how many smooth coordinates are needed to track conventional EMG indicators.

RESULTS AND DISCUSSION

All subjects demonstrated considerable muscle fatigue, as evidenced by decreased MNF and MDF [1]. Fig. 1 shows the fixed number of smooth coordinates for elbow flexion/extension (green line), humeral head angle (blue line), and humeral head elevation (black line) projected onto the EMG (red line) in the least squares sense. In the best case, only 2 coordinates from humeral head elevation were needed for the triceps muscle. An average of only 4 nonlinear coordinates were needed to track EMG. This result shows that using noninvasive easily obtainable movement kinematics we can construct a 4 dimensional manifold that can track and predict traditional EMG-based trends.

REFERENCES

[1] Gates, D.H. & Dingwell J.B., 2010. *J. Biomech.,* **43***(5)*, pp. 913–919.
[2] DeLuca, C., 1997. *J Appl Biomech,* **13**, pp. 135–163.
[3] Segala, D.B., et al., 2009. *Proc of IDETC/CIE*, San Diego, CA
[4] Song, M., et al., 2009. *J Biomech Eng,* **131**, 021004.
[5] Chelidze, D. & Zhou, W., 2006. *J Sound Vib,* **292**, pp. 461–473.

EXPLOITING REDUNDANCY IN GENERALIZED REACHING TASKS

[1]Rachel F. Smallwood, [2]Jonathan B. Dingwell

[1]Department of Biomedical Engineering, University of Texas, Austin, TX, USA
[2]Nonlinear Biodynamics Lab, Dept. of Kinesiology, University of Texas, Austin, TX, USA
Email: r.smallwood@mail.utexas.edu, Web: http://www.edb.utexas.edu/faculty/dingwell/

INTRODUCTION

Many daily tasks are redundant, such that there is an infinite number of ways to complete the task. For precisely defined tasks, this redundancy can take the form of a manifold in the space defined by the primary movement variables for the task [1,2]. We refer to this subspace as a "Goal Equivalent Manifold" (GEM) [1]. When performing physical tasks like aiming, throwing to a target, or reaching in time with a metronome, subjects exhibit more task-*ir*relevant variability (i.e., *along* the GEM, where deviations do not affect performance) than the task-relevant variability (i.e., perpendicular to the GEM, where deviations will directly cause errors in task performance) [1-3].

However, it is not known how generalizable these motor control processes are or if learning to exploit task redundancies requires having such a physical task to perform. The purpose of this study is to determine whether subjects can learn to adopt GEM-based control when presented with a generalized reaching task and only given feedback based on their performance relative to a GEM.

METHODS

Two different GEM functions were defined *a-priori*. Both GEMs were variations of the equation

$$D^m \cdot T^n = C \quad (1)$$

where D was total reaching distance, T was total reaching time, m & n were scaling exponents and C was a constant that defined the "goal" or target. For the first GEM, we defined $m = +1$ and $n = -1$ so that subjects had to achieve the same average *speed* (D/T = 45 cm/s) for each consecutive movement. For the second GEM, we defined $m = n = +1$ to obtain a second GEM ($D \times T$ = 45 cm·s) that was orthogonal to the first GEM (Fig. 2).

Four young healthy right-handed subjects participated. Subjects sat in a chair (Fig. 1) and made straight line reaching movements. They were not told what the specific goal for the movements was, only that there was a goal. After each reach, they were given feedback based on their performance in the form of an error (percent over or under the goal) and a graph that displayed their movement distance and time with color-coded points. Subjects were instructed to make their errors as close to zero as possible.

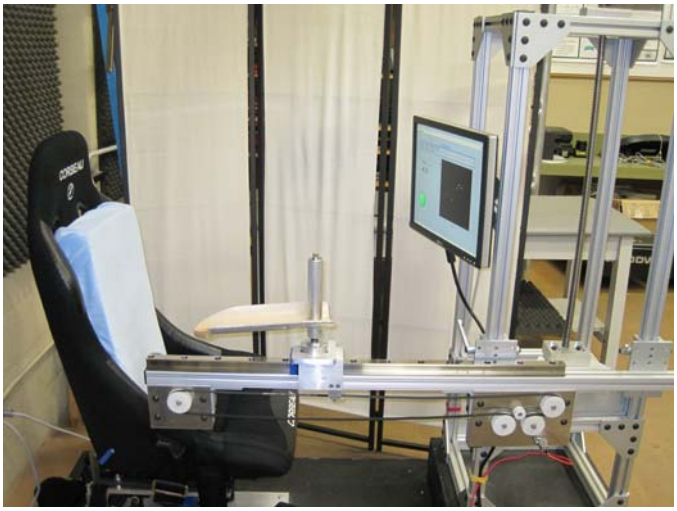

Figure 1: Subjects made straight line reaching movements with the handle, which recorded movement distance (D) and time (T). Visual feedback was provided on the video monitor.

All subjects were given the exact same instructions and the same type of visual feedback for both reaching tasks defined by each GEM. Likewise, both reaching tasks made use of reaching movements within the same regions of the workspace (i.e., same combinations of D & T).

For each GEM, subjects were given time to accustom themselves to the task and an opportunity

to visualize areas on the graph corresponding to low and high errors. Then they completed a set of 400 reaches that was used for analysis. Subjects completed this protocol for each of the two different GEMs in random order at least 3 days apart.

For each trial, the [*D*, *T*] data were first normalized to unit variance. The normalized [*D*, *T*] for each movement were then transformed into coordinates corresponding to deviations tangent to and perpendicular to the GEM [δ_P, δ_T]. We then calculated the standard deviations of δ_P and δ_T.

Linear regressions were performed to define the stability multiplier for each time series, λ, using:

$$X_{N+1} = \lambda \cdot (X_N) + \xi_N \quad (2)$$

where X corresponded to either δ_P or δ_T and ξ_N is a noise term. Values of $0 \le |\lambda| < 1$ correspond to stable movements, with smaller values of λ indicating more rapid corrections of cycle-to-cycle deviations.

A two-factor ANOVA for GEM (*D*/*T* vs. *D*×*T*) × Direction (δ_P vs. δ_T) was performed, as well as a one-way ANOVA for Direction for each GEM.

RESULTS AND DISCUSSION

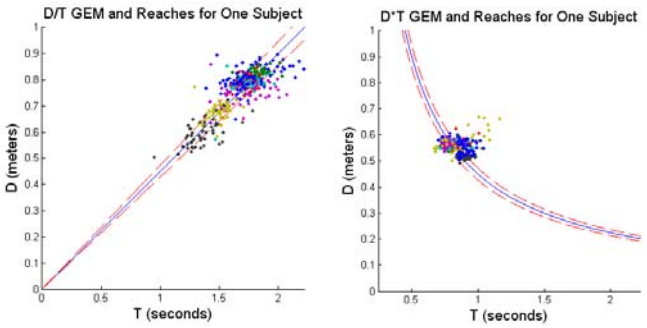

Figure 2: Representative data for both the velocity (*D*/*T*) and *D*×*T* GEMs. Solid lines are the GEM. Dashed lines indicate ±5% error bounds.

Significant interaction effects were found with the 2-factor ANOVA. For GEM 1 (*D*/*T*), standard deviations were significantly larger ($p << 0.0001$) in the δ_T direction than in the δ_P direction. In addition, λ was significantly higher for δ_T than for δ_P ($p = 0.001$). Thus, subjects were more variable in the task-irrelevant direction than in the direction where variability would lead to task errors, and subjects corrected deviations in the task-relevant direction much more rapidly than in the task-irrelevant direction. No significant differences were found for standard deviation or λ between the tangent and perpendicular directions for the *D*×*T* GEM.

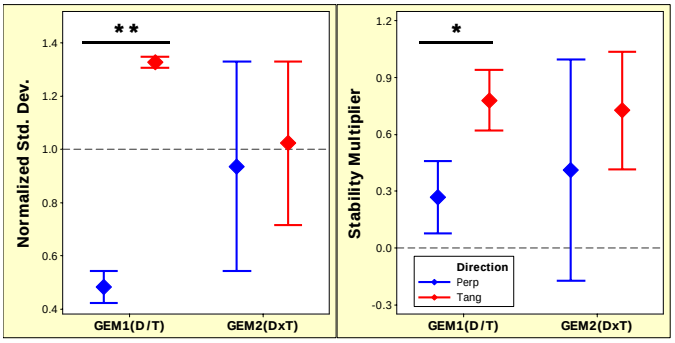

Figure 3: Normalized standard deviations and stability multipliers (λ) for both GEM's tested for both directions (δ_P='Perp'; δ_T='Tang'). Error bars indicate ±95% confidence intervals. Significant differences: ** $p << 0.0001$; * $p = 0.001$.

CONCLUSIONS

For GEM 1, subjects allowed their trial-to-trial movements to vary along the GEM, while controlling and minimizing deviations that would cause errors. Thus, these subjects clearly exploited the redundancy available in this task. For GEM 2, however, subjects appeared to find a single point along the GEM and did *not* exploit the redundancy available. This suggests that not all redundant tasks are equally learnable. In particular, the *D*/*T* GEM may have been easier to learn because muscle spindles can provide direct sensory feedback of movement velocity, whereas there are no sensory receptors that provide direct feedback of *D*×*T*.

REFERENCES

1. Cusumano JP and Cesari P. *Biol Cybern* **94**(5): 367-379, 2006.
2. Cohen R and Sternad D. *Exp Brain Res* **193**(1): 69-83.
3. Gates DH and Dingwell JB. *Exp Brain Res* **187**(4): 573-585, 2008.

ACKNOWLEDGEMENTS

Funded by Grant #1-R03-HD058942-01 from NIH.

DIFFERENCES IN GRIP CHARACTERISICS BETWEEN YOUNGER AND OLDER FEMALES

Curt Irwin, Mary Sesto

University of Wisconsin-Madison, Madison, WI, USA
email: msesto@wisc.edu

INTRODUCTION

Previous research indicates people lose strength as they age, including strength in the hands [1]. In addition to strength loss, recent work in our lab demonstrates that people also lose the ability to rapidly develop force in the hands, mirroring age-related force development deficiencies in other muscle groups [2]. Muscles of the upper extremity which are important for grip strength and RFD include extrinsic finger flexors, such as the Flexor Digitorum Profundus and Flexor Digitorum Superficialis, and intrinsic hand muscles such as the lumbricals. Focusing on just the intrinsic and extrinsic flexors, it has been theorized that aging may affect these muscle groups differently. Research in the hand and other muscle groups suggests that aging adversely affects the strength of distal muscles (e.g. hand intrinsics) to a greater extent than proximal muscles (e.g. extrinsic hand flexors)[3]. However, the tasks performed in these studies were relatively artificial and not generalizable to typical tasks performed with the hands [3].

The purpose of the current study was to determine whether differences exist in finger force orientation between younger and older females during a power grip, a typical hand function task. Differences in the force orientations may be attributable to alterations in the intrinsic – extrinsic muscle contribution.

METHODS

A total of 20 female participants took part in the study. Participants were grouped as > 65 years (n=10, mean age =74, SD=7.7) and < 30 years (n=10, mean age=24.5, SD=3.7). All participants were right-hand dominant, free of impairments which would affect grip and lived independently in the community. Informed consent was obtained in accordance with the University of Wisconsin guidelines for the protection of human subjects.

The Multi-Axis Profile (MAP) dynamometer was used for data collection. It was affixed with a 6.35cm diameter cylindrical plastic cover. The MAP measures a grip force vector (Figure 1) with magnitude (F) and angle (θ). This device has demonstrated very high test-retest reliability in younger and older adults [4].

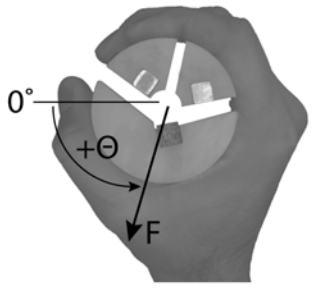

Figure 1: Overhead view of the MAP displaying resolved overall grip force vector with magnitude (F) and angle (θ)

Participants were seated for grip testing in the posture recommended by the American Society of Hand Therapists. The metacarpal-phalangeal joint was aligned with a landmark on the MAP to ensure the repeatability of the hand placement. Participants were instructed to squeeze the handle "as hard as you can and as fast as you can and hold for 5 seconds".

A grip profile (Figure 2) was acquired for each grasp at 1000Hz. The vector angle was examined at onset of grip force, during the force development phase at 25, 50 and 75% of maximal voluntary contraction (MVC) as well as during sustained MVC (plateau phase). Analysis of variance (ANOVA) was used to evaluate differences in grip strength, RFD and vector angle between younger and older groups.

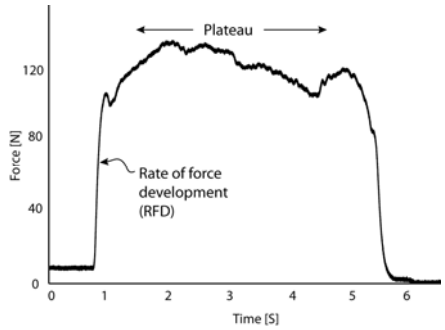

Figure 2: Representative grip force profile

RESULTS AND DISCUSSION

Both grip strength and rate of force development were decreased in older females ($p<0.05$). The overall grip force vector angle was also significantly shifted in the proximal direction (greater vector angle) for older females as compared to younger at the onset of grip, 25%, 50%, 75% and at maximal grip force ($p<0.05$). Table 1 displays vector angle results.

Figure 3 displays the average grip force vector magnitude and angle data.

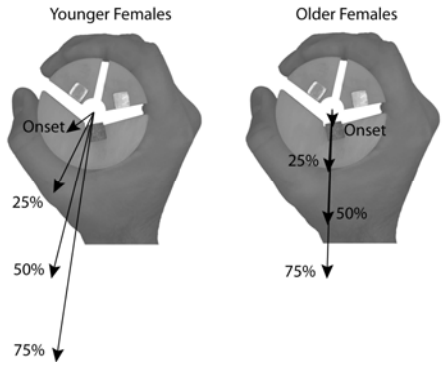

Figure 3: Force vector magnitude and angle for both younger and older females

CONCLUSIONS

It has been hypothesized that distal muscles are more affected by age than proximal muscles. This hypothesis has been successfully tested in the muscles controlling the hand using non-functional tasks [4,5] but has yet to be studied during power grip. One explanation for the results of the current study is a selective weakening of the intrinsic hand muscles, in particular the lumbricals. The lumbricals aid in flexion of the metacarpal-phalangeal (MCP) joint which could result in vector angles closer to 0°. In the current study, younger females produced vectors much closer to 0° than older females, especially at initiation of force production. This possibly indicates a higher level of intrinsic muscle contribution in the younger participants. Although these results support differential weakening of the intrinsic muscles as compared to the extrinsic muscles, further research is needed to determine the specific contributions of these particular muscle groups.

Another possible explanation for altered force angles would be differences in hand lengths between groups but the average hand lengths differed by less than 0.1cm (total SD=0.88cm) which is likely insufficient to significantly affect vector angles.

Of note, the participants in the current study were all free of impairments affecting the hand. It is possible that impaired individuals, such as those with osteoarthritis, may have even more significantly altered grip characteristics.

REFERENCES

1. Jansen CW et al. *J Aging Phys Act* **16**, 24-41, 2008.
2. Irwin, CB et al. *Proceedings of HFES'10*, San Francisco, CA, USA, Submitted for publication.
3. Shinohara, M et al. *J Appl Physiol*,. **95**, 1361-9, 2003.
4. Irwin, CB et al. *J Hand Therapy*, In Press.
5. Cole, K.J. *Experimental Brain Research*, **175**, 285-291, 2006

ACKNOWLEDGEMENTS

The contents of this paper were developed under grant 1UL1RR025011 from the Clinical and Translational Science Award (CTSA) program of the National Center for Research Resources, National Institutes of Health and grant T32 AG000265 Women's Health and Aging Research and Leadership Training Grant from the National Institute on Aging.

Table 1: Vector angle results

	Vector Angle [degrees]									
	Onset		25% MVC		50% MVC		75% MVC		MVC	
	Mean	(SD)	Mean	(SD)	Mean	(SD)	Mean	(SD)	Mean	(SD)
Younger	36.2	(9.3)	63.6	(11.6)	75.7	(8.4)	81.4	(7.1)	82.1	(8.8)
Older	92.7	(33.1)	86.4	(12.1)	87.7	(7.7)	88.2	(6.4)	90.3	(6.6)

MULTI-FINGER SYNERGIES DURING ISOMETRIC FORCE PRODUCTION TASK IN INDEX FINGER AMPUTEES

[1]Sohit Karol and [1,2]Jae Kun Shim

[1]University of Maryland, College Park, MD, USA
[2]Department of Mechanical Engineering, Kyung Hee University, Global Campus, Korea
email: skarol@umd.edu, web: www.sph.umd.edu/KNES/faculty/jkshim/neuromechanics

INTRODUCTION

The human hand is an excellent example of both kinetic as well as kinematic redundancy. Each finger of a hand can be considered as a force generator and all the daily manipulation and prehension tasks can be viewed as highly redundant, because the total force and total moment of forces needed to hold/press an object can be achieved by numerous combinations of forces/moments generated by individual fingers.

The problem of redundancy attains special significance in the case of finger amputees. With one or more amputee fingers, the kinetic degrees of freedom reduce considerably. However, it has been observed that loss of a digit usually reduces manual dexterity and interferes greatly with the person's Activities of Daily Living (ADL). Previous studies have reported that although considerable plasticity occurs in the primary motor cortex within the first ten days of index finger amputation the central pathways associated with amputated peripheral nerves retain some sensory and motor function even after three years of amputation [1]. Apart from the neuromuscular factors, passive biomechanical coupling also affects the finger independence and synergies [2]. However, the combined effect of all these factors after amputation of one finger on the maximum voluntary force (MVF) and synergies among other fingers is still unknown, and has a huge relevance in understanding the behavioral outcomes of cortical plasticity.

The purpose of this study was to compare the maximum voluntary force (MVF) and multi-finger synergies in index finger amputees with healthy age matched adults. Based on the decline in dexterity after amputation, we hypothesized that the MVF as well as multi-finger synergies in finger amputees would be less than those in the normal healthy adults.

METHODS

Sixteen right handed healthy volunteers without any history of neurological disorders participated in the experiments. Eight young subjects having an index finger amputation for more than eight years were assigned to the first group. Eight age and gender matched subjects were assigned to the control group

Details of the experimental setup have been described elsewhere [3]. The subjects were asked to rest the distal phalange of each finger (middle, ring and little, in case of the amputee group and all four fingers in case of the controls), in a thimble attached to the force sensors, such that all joints were slightly flexed and formed a dome shape with the hand.

In the first experiment, subjects performed four conditions of the maximum voluntary force (MVF) task in flexion: middle, ring, little and all the three fingers together (M, R, L, MRL). The individual finger MVF values were used to adjust the target force (20% of three-finger MVF) for the constant force production experiment. In the second experiment, a target force line representing 0% of MVF for the first three seconds and 20% of MVF for the next twelve seconds for a particular subject was displayed on the computer screen. After this initial phase of three seconds, the subjects were asked to press the sensors with the task fingers and trace the path of the 20% MVF lines using the task-finger force feedback. The total length of each trial was 15 seconds. Twelve trials were performed for each finger combination.

Data was analyzed under the framework of the Uncontrolled Manifold (UCM) hypothesis, details

can be described elsewhere [4].

RESULTS AND DISCUSSION

The MVF for the three finger task in the index finger amputees was significantly less than those in the control group. The results were supported by between factors ANOVA with a significant effect of group [$F_{[1,\ 15]} = 2.7$, $p<.05$]. This result confirmed our first hypothesis. After amputation, significant changes in muscle control strategies occur both at the cortical level as well as the peripheral level. Since index finger is the strongest one, loss of this digit does not seem to compensate for the hand strength even many years after amputation.

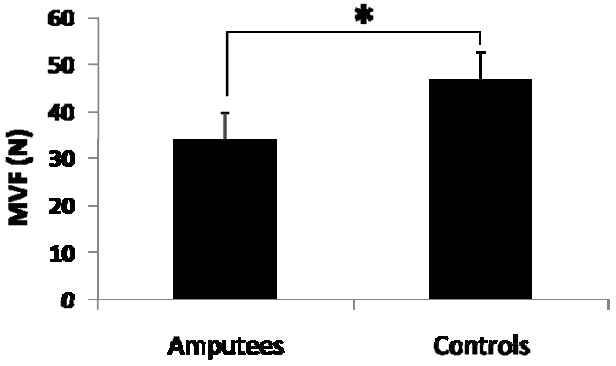

Figure 1 Maximum Voluntary Force (MVF) values for the index finger amputees and controls, with middle, ring and little fingers acting together. Means and standard errors are shown across all subjects. *$p<.05$

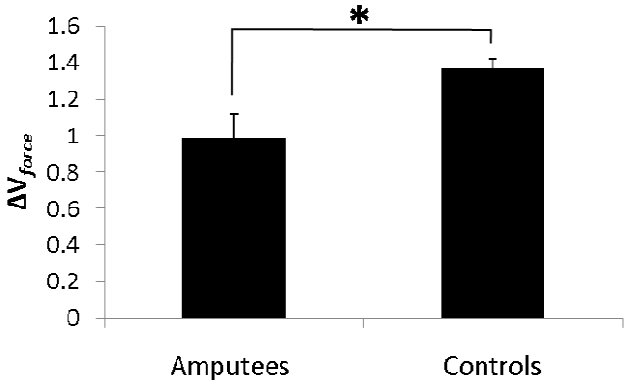

Figure 2 ΔV_{force} for the index finger amputees and the controls, with middle, ring and little fingers acting together. Means and standard errors are shown across all subjects. *$p<.05$

The values of ΔV were significantly lower in index finger amputees than in the control group. The results were supported by between factors ANOVA with a significant effect of group [$F_{[1,\ 15]} = 2.5$, $p<.05$]. Significant differences were also found between the two groups for V_{UCM} [$F_{[1,\ 15]} = 3.2$, $p<.05$], , however no significant differences were found for $V_{ORT.}$

Differences in the values of ΔV and V_{UCM} suggest that the inter-finger synergies decrease with finger amputation and the subjects might not be able to attain the same level of dexterity even after many years of amputation. On the other hand, no differences for V_{ORT} indicate that the amputee subjects produce the same amount of errors as their healthy counterparts. These results point towards a decreased ability of the amputees to use the flexible solutions to the degree of freedom problem at the level of control. Results from this study could lead to design of finger specific training for amputees, aiming to increase the finger strength as well as the inter-finger synergies.

REFERENCES

1. Dhillon GS, Kruger TB, Sandhu JS, Horch KW (2005) Effects of short-term training on sensory and motor function in severed nerves of long-term human amputees. *J Neurophysiol* 93: 2625-2633
2. Schieber MH, Lang CE, Reilly KT, McNulty P, Sirigu A (2009) Selective activation of human finger muscles after stroke or amputation. *Adv Exp Med Biol* 629: 559-575
3. Shim JK, Hsu J, Karol S, Hurley BF (2008) Strength training increases training-specific multifinger coordination in humans. *Motor Control* 12: 311-329
4. Scholz JP, Schoner G (1999) The uncontrolled manifold concept: identifying control variables for a functional task. *Exp Brain Res* 126: 289-306

ACKNOWLEDGEMENTS

This project was supported by the Graduate Research Initiative Project (GRIP), Department of Kinesiology, University of Maryland, College Park, USA.

ADAPTATIONS OF MULTI-FINGER INTERACTIONS THROUGH FATIGUE EXERCISE

[1,2]Jae Kun Shim, [1]Junfeng Huang, [1]Sohit Karol, [1]You-Sin Kim, [3]BumChul Yoon

[1]University of Maryland, College Park, MD, USA
[2]Department of Mechanical Engineering, Kyung Hee University, Global Campus, Korea
[3]Department of Physical Therapy, Korea University, Seoul, Korea
email: jkshim@umd.edu web: http://www.sph.umd.edu/KNES/faculty/jkshim/neuromechanics

INTRODUCTION

The human hand is one of the primary tools through which the central nervous system (CNS) physically interacts with the external world, either by pressing, grasping, or manipulating objects. Previous studies on multi-finger actions have identified multi-finger synergies, finger independence, finger force sharing, finger strength, and finger force deficits as important factors that influence motor performance of manipulation tasks [1]. However, little is known how these factors experience adaptations when the neuromuscular system undergoes "weakening" or "strengthening". This study investigates the effect of fatiguing exercise, used as a mode to "weaken" the neuromuscular system, on finger strength, finger independence, finger force sharing, force deficits, and multi-finger synergy. Many previous studies on multi-finger synergies have employed the Uncontrolled Manifold (UCM) analysis or variance analysis to investigate how individual fingers act together in multi-dimensional spaces during multi-finger pressing and prehension. These methods are designed to provide overall error compensations by all fingers, but they are limited in terms of quantifying individual fingers' contributions for the overall error compensations. In this study, we also quantified individual fingers' contributions to overall error compensations in order to assess the individual finger adaptations through fatigue exercise. We hypothesized that the adaptations of multi-finger synergies through fatigue exercise would be finger specific. When the neuromotor system is fatigued, we expected that the fingers conventionally thought to be most and least dexterous (i.e., index and ring fingers) would be used for more error compensation and less error compensation, respectively.

METHODS

Subjects: Fourteen right-handed healthy volunteers (age: 27.7±5.1 yrs; height: 177.3±7.3 cm; weight: 75.7±9.6 cm; hand length: 17.7±1.3 cm; hand width: 8.4±0.4 cm) without any history of neurological disorders participated in the experiments.

Apparatus: Details of the experimental setup have been described elsewhere [1]. The subjects were asked to rest the distal phalange of each finger in a thimble attached to the force sensors, such that all joints were slightly flexed and formed a dome shape with the hand.

Experiments: In the first experiment, subjects performed five conditions of the maximum voluntary force (MVF) task in flexion: index, middle, ring, little, and all four fingers together (I, M, R, L, IMRL). The four-finger MVF values were used to adjust the target force (20% of three-finger MVF) for the constant force production experiment. In the second experiment, a target force line representing 0% of MVF for the first three seconds and 20% of MVF for the next twelve seconds for a particular subject was displayed on the computer screen. After this initial phase of three seconds, the subjects were asked to press the sensors with the task fingers and trace the path of the 20% MVF lines using the task-finger force feedback. The total length of each trial was 15 seconds. Twelve trials were performed for the constant force production experiment. Subjects had the same tests before and after the finger flexion exercise and the order of the tests was balanced across subjects. For the fatigue exercise, subjects were asked to perform finger flexion exercise over the whole range of motion of index, middle, ring, and little metacarpophalangeal joints: 3 sets of 10 repetitions with the load of 70% 1-repetition maximum.

Analysis: Maximum voluntary force (MVF), finger independence, finger force sharing, force deficits were measured and calculated form the MVF tasks [1]. Data from the constant force production task were analyzed under the framework of the UCM analysis [2]. V_{UCM} (variance of error compensations among all fingers; "good" variance) and V_{ORT} (error variance; "bad" variance) were calculated. The individual finger components of V_{UCM} was also calculated.

RESULTS AND DISCUSSION

The MVF values for the four-finger task and individual finger tasks decreased after finger fatigue exercise (p<.001 for each pair; Fig 1). After the fatigue exercise, the MVF values decreased about 30-40% from the values without fatigue.

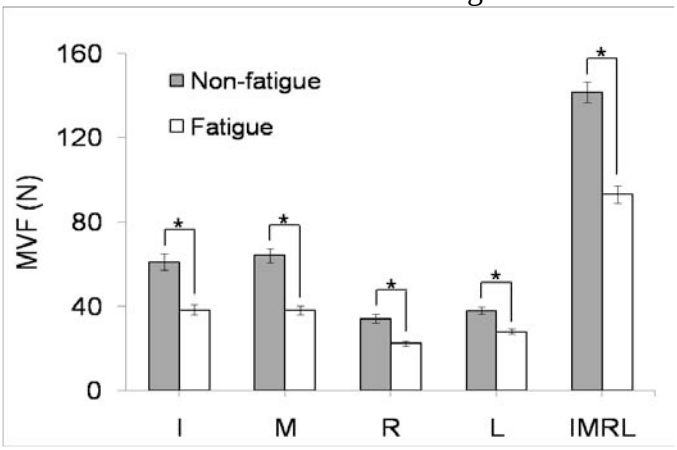

Figure 1. Maximum Voluntary Force (MVF) values from with and without fatigue, with index, middle, ring, little, and all four fingers. * p<.001.

The finger independence, finger force sharing, force deficits did not change after fatigue exercise. As one could easily expect, the ability to compensate each finger's errors (V_{UCM}) decreased (p<.05) and the performance error (V_{ORT}) increased (p<.05) after the fatigue exercise (Figure 2).

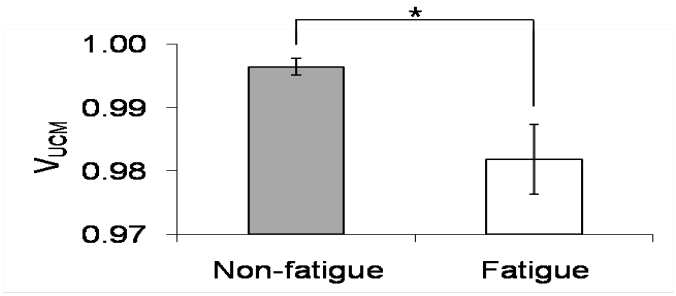

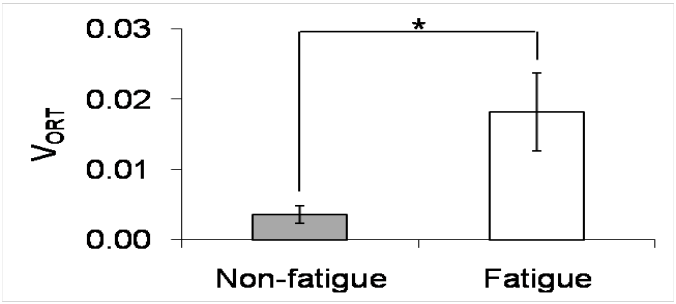

Figure 2. V_{UCM} and V_{ORT} with and without fatigue in finger flexor muscles. * p<.05.

One interesting finding was that the index finger, assumed to be the most dexterous finger, increased its contribution to V_{UCM} (p<.01) while the ring finger, assumed to be the least dexterous finger, decreased its contribution (p<.05) (Fig 3). Other fingers did not show statistically significant differences between fatigue conditions.

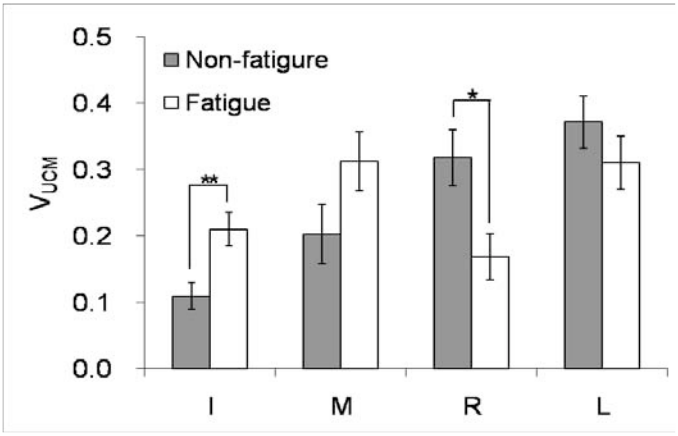

Figure 3. Individual finger contributions to V_{UCM} with and without fatigue in finger flexor muscles. ** p<.01; * p<.05.

REFERENCES

1. Shim JK, Hsu J, Karol S, Hurley BF (2008) Strength training increases training-specific multifinger coordination in humans. *Motor Control* 12: 311-329

2. Scholz JP, Schoner G (1999) The uncontrolled manifold concept: identifying control variables for a functional task. *Exp Brain Res* 126: 289-306

ACKNOWLEDGEMENTS

This project was supported in part by *Korea University Grants* and *Maryland Industrial Partnerships (MIPS) Award*.

LIMITATIONS TO SYNCHRONIZATION OF COORDINATED FINGER MOVEMENT

Yanjia Gu, Michael J. Hiley and Matthew T.G. Pain

Sports Biomechanics and Motor Control Research Group, Loughborough University, Leicestershire, UK
email: y.gu@lboro.ac.uk, web: www.lboro.ac.uk/departments/sses/

INTRODUCTION

Learnt movements have been characterised by aspects such as their reaction time, speed and accuracy [1]. Extensive experiments using finger tapping have been studied in periodic bimanual rhythmic movements [2,3]. However, relatively little research has been carried out on the manner in which the most simple skilled movements are executed. Even something as fundamental as the limits with which movements, such as single stroke finger taps, can be coordinated has not been determined. Further to this, the effects of different types of practice and task performance orientation have not been described in the literature. This study aimed to evaluate how accurately people can coordinate two index fingers in various simple tapping tasks and how the amount and quality of practice affects the measured limits of coordination.

METHODS

Twenty-four healthy adults gave informed consent (age 28±5 years) in accordance with Loughborough University's ethical advisory committee. During testing each participant performed simple index finger downbeats in three different conditions (left and right simultaneously, left then right, and right then left). In each case, participants' intrinsic stimulus triggered the initiation of two finger movements, and the participant was instructed to time the downbeats as closely as possible. Data were collected from force transducers positioned 5 mm below the underside of the index fingers. Participants were randomly divided into three groups (Control Group (CG), Practice (P), and Instructed Practice (IP)), each designed to undergo different amounts and quality of practice relevant to the tasks. The start and trip buttons of a classic three-button stopwatch were utilized for practicing normal single action timing. This allowed for instant feedback, but with poor accuracy and resolution. Given the system delays it is possible to start and trip the stopwatch so that it is running but displays 0.00.00 which may indicate a timing of below 10 ms but testing of the watch showed it was at least 20 ms.

The experiment consisted of two sessions. In the first session participants undertook different amounts of practice and performed 10 different measurement trials, each consisting of 10 to 20 taps per trial on the force transducers. In addition to this groups P and IP were allowed to practice with the stopwatch, trying to stop the watch as close to 0.00.00 as possible. The P group were left alone to practice, whilst the IP group were requested to accomplish the task of displaying 0.00.00 three times in a row and given advice on achieving this. In the second session all participants undertook the same practice as the IP group prior to testing. Data were collected through a common ADC sampling at 5000 Hz. Force onset was determined automatically when the value exceeded 3 stdev of the resting level. Significant differences were identified using T-test and ANOVA were used with a significance level of $p = 0.05$.

RESULTS AND DISCUSSION

Inter-tapping interval (ITI) was calculated by subtracting left index finger contact time from right index finger contact time, or vice versa. A small ITI indicated less time had elapsed between two closing downbeats. The force onset timings of left and right index finger in left then right taping are shown separately in Figure 1. A summary of the best, worst, and average ITI performance of each group are given in Table 1. For each participant, improvement ratios were calculated and pooled by group (Table 2). The shortest ITI in all groups for simultaneous tapping was 4.8 ms, whilst for non-synchronized tapping 11.1 ms for left then right and 6.9 ms for right then left. Significant improvement was observed in the second session for CG. As

might be expected, in the second session the IP group were observed to show the least improvement, and in some cases a decrease in performance. 'Instructed practice' seemed have no effect on synchronized movements.

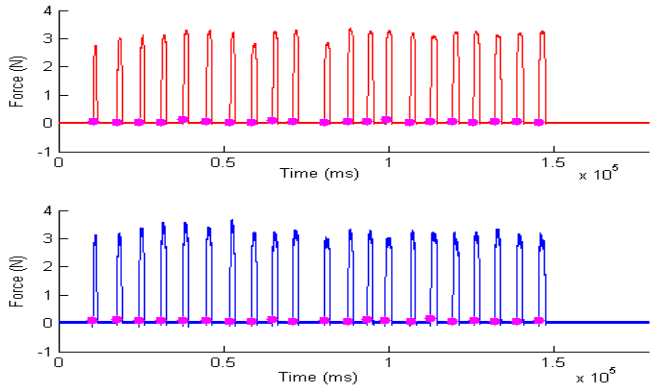

Figure 1: Force onsets in L/R tapping. Top, left finger; bottom, right finger. The solid circles denote finger contacts with the force transducer.

There was 99.8% confidence that the instructed practice led to a significant improvement in performance, and only one session was required if the training was appropriate. It should also be noted task performance was highly subject specific with a very wide range of abilities (Table 1).

Table 2: Mean ITI performance improvement

	L/R(ms)	R/L(ms)
Control Group	28.8	30.3
Practice	25.3	15.9
Instructed Practice	5.2	-2.4

CONCLUSIONS

In this study, we investigated the coordination of bimanual tapping with single discrete taps; the analysis was centered on the fundamental human temporal coordination limits between the two index fingers in various conditions. The present study demonstrated that there is a limit with which people can perform closing activities, even if it is spatial-response compatible and without any reaction factor involved. The limit for performing a simultaneous synchronized task seems to be around 5 ms for the best performers in the group. For a staggered task the best performances were between 7 and 11 ms. The values may vary between different conditions due to asymmetric control of muscle force.

Due to the psychological refractory period, the perception and action of closing movement are extremely limited, this is so-called dual-task interference. Some researchers have addressed the group processing theory which showed better performance when the stimulus onset asynchrony is less than 50 ms. However, the limit of this 'better performance' is still an issue. Our statistical data are essential to build a fundamental base of bimanual coordination movement.

The improvement in performance came from a change in the subject's perception of the task in terms of the level of information processing required to co-ordinate two independent limbs. Participants went from waiting to receive tactile feedback on the first tap before starting the second tap to not waiting and initiating the later one immediately after they triggered the first finger.

REFERENCES

1.Fitts PM. *Journal of Experimental Psychology*, **47**, 6, June, 381-391, 1954.
2.Kelso JAS. *American Journal of Physiology*, **240**, R1000-R1004, 1984.
3 Ivry, R.B. & Richardson, T. *Brain and Cognition*, **48**, 117-132, 2002.

Table 1: Results of the finger tapping coordination sessions.

	Shortest ITI	Longest ITI	Average ITI
		First Session	
CG	6.0 / 37.4 / 40.2	15.3 / 72.2 / 111.7	9.5 / 58.6 / 65.7
P	6.0 / 29.4 / 15.8	11.6 / 82.5 / 73.5	9.2 / 54.4 / 52.1
IP	5.2 / 19.4 / 6.9	20.3 / 85.8 / 59.5	12.1 / 40.1 / 34.9
		Second Session	
CG	4.8 / 13.3 / 15.8	13.1 / 44.5 / 55.7	9.1 / 30.8 / 32.9
P	5.8 / 11.1 / 19	24.8 / 46.8 / 86.9	11.7 / 29.0 / 36.2
IP	4.8 / 14.2 / 33.3	21.8 / 67.5 / 54.2	14.3 / 38.8 / 41.3
	Simultaneously / Left then Right / Right then Left (ms)		

BIOMECHANICAL CONSTRAINTS ON THE CONTROL OF ENDPOINT STIFFNESS

[1,3]Xiao Hu, [1,2,3,4]Wendy M. Murray and [1,2,3]Eric J. Perreault
Departments of [1]Biomedical Engineering and [2]PM&R, Northwestern University, Chicago, IL
[3]SMPP, Rehabilitation Institute of Chicago, Chicago, IL; [4]VA Hines, Hines, IL
Email: xiaohu2011@u.northwestern.edu

INTRODUCTION

Humans regulate arm mechanics to allow for stable interactions with the environment across a broad range of tasks. Understanding how this regulation occurs is an essential problem in motor control. The steady state mechanical properties of the arm can be characterized by endpoint stiffness, the relationship between externally applied displacements of the hand and the steady state forces generated in response [1]. Endpoint stiffness is directional, resisting perturbations in certain directions more than others [1, 2]. The ability to modulate the orientation of maximum stiffness provides a mechanism for tuning arm mechanics to the requirements of a specific task. However, there are conflicting results regarding how much voluntary control exists over the orientation of maximum stiffness [2, 3].

The control of stiffness orientation may be constrained neurally or biomechanically. Neural constraints include the ability or inability to activate muscles independently [4]. Biomechanical constraints pertain to the geometric properties of the musculoskeletal system and the strength of the muscles within. Biomechanical constraints can be assessed through modeling, but the few modeling studies that have addressed this question either also incorporated neural constraints [5] or used models that did not represent the geometric and muscular complexity of the human arm [6]. The purpose of this study was to determine whether the musculoskeletal system significantly constrains the ability to regulate endpoint stiffness orientation. This was accomplished using a realistic musculoskeletal model of the human arm [7] coupled with a scalable model of muscle stiffness [8]. This approach allows us to identify biomechanical constraints on stiffness orientation control separately from those that may also come from neural structures.

METHODS

Modeling

The musculoskeletal model used in this study was reported previously and shown to characterize the endpoint stiffness of the human arm over a wide range of conditions [9]. In summary, the model had two components: a muscle model characterizing short-range stiffness, and a realistic musculoskeletal model of the human arm with 37 muscle compartments and 4 kinematic degrees of freedom. Muscle stiffness scaled with muscle force, and was transformed to endpoint stiffness based on the kinematic parameters of the musculoskeletal model.

Simulations

The musculoskeletal model was used to predict endpoint stiffness at an arm posture and endpoint force matched to previously published data [2]. In the published experiment, subjects were instructed to rotate the orientation of maximal endpoint stiffness as much as possible in both the clockwise and counterclockwise directions. Endpoint forces in the horizontal plane were required to remain at zero, and postures were fixed (Fig. 1) throughout the experiment and in our simulations. The endpoint force constraints were implemented by requiring the flexion (Flex) torques about the shoulder and elbow to be zero. In the simulations, constrained optimization was used to determine the biomechanically feasible range of stiffness orientations given these mechanical constraints. This optimization was used to select the muscle activations that generated the maximum clockwise and counterclockwise rotations of stiffness orientation.

In addition to zero endpoint force, two additional constraints were evaluated. The first was the influence of supporting the arm against gravity, as was partially required in the initial experiments. This support required subjects to generate shoulder abduction (Abd) and axial rotation (Rot) torques. To evaluate how these additional torque requirements

affect the ability to control stiffness orientation, similar requirements were added to our simulation. These were estimated assuming typical segment masses for an average American adult male (86 kg) [10]. The second constraint assessed the influence of submaximal muscle contractions. The previous experimental trials lasted for approximately 1 minute, making maximum activation in any muscle unfeasible for the entire trial. We evaluated the influence of reduced muscle activation by computing the range of stiffness orientations that could be achieved at full activation and when the maximum activation of all muscles was constrained to be less than 30%, a value that can be sustained for at least 1 minute across a range of muscle groups [11].

RESULTS AND DISCUSSION

The control of endpoint stiffness orientation was constrained biomechanically. Unconstrained control of stiffness orientation would have allowed for solutions orthogonal to the stiffness estimated for the rest condition (blue, small ellipses). When constraining only the shoulder and elbow flexion torques, stiffness orientation could be rotated 20° counterclockwise and 73° clockwise, relative to the orientation of passive endpoint stiffness (Fig. 1A). This range decreased substantially when the maximal muscle forces were restricted to 30% of that maximum strength (Fig. 1B). The largest changes were in the ability to rotate stiffness orientation clockwise, which was reduced to 51°.

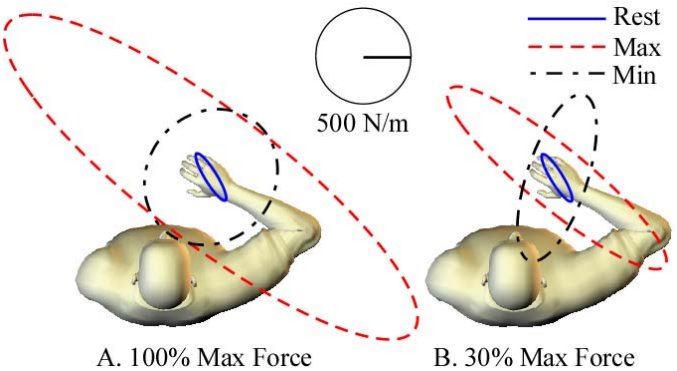

Figure 1: Range of stiffness orientations at different levels of maximal muscle force. Simulations considered a fully supported arm.

The achievable range of endpoint stiffness orientations was further reduced by adding constraints on the shoulder Abd and Rot torques to simulate supporting the arm against gravity (Fig. 2). These effects were observed only when muscle activations were limited to 30% of maximum. When the additional constraints were added to better reflect experimental conditions, the range of achievable stiffness orientations approached that reported experimentally, although remained larger. At the moment, it is not possible to determine whether these small differences are due to the additional presence of neural constraints not included in our model or simply variations in our model that do not reflect the variability of the experimental results. The latter are currently being assessed.

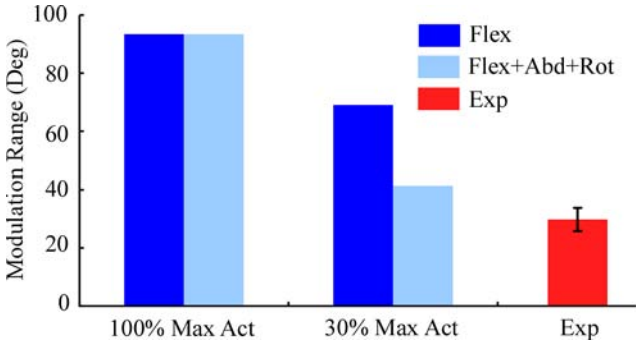

Figure 2: Control range of endpoint stiffness from simulations and one previous experimental study [2]. .

Our results demonstrate how a realistic musculoskeletal model can be used to explore how biomechanical constraints influence the ability to regulate arm mechanics. When constraints such as the need to support the limb against gravity or the maximum achievable muscle force are not considered, a wide range of stiffness orientations can be achieved, as has been reported previously using less realistic simulations [6]. Differences between our results and experimental findings may provide insight to the neural constraints on stiffness modulation [5] and how these constraints may be softened with appropriate training.

REFERENCES

1. Mussa-Ivaldi FA, et al, *J Neuroscience* **5**, 2732-43, 1985.
2. Perreault EJ, et al. *J Neurophysiol* **87**, 2808-2816, 2002.
3. Franklin DW, et al. *J Neurophysiol* **92**, 3097-3105, 2004.
4. Gribble PL, et al. *Exp Brain Res* **123**, 355-360, 1998.
5. Darainy M, et al. *J Neurophysiol* **92**, 3344-3350, 2004
6. Tee KP, et al. *Biol. Cybern* **90**, 368-375, 2004.
7. Holzbaur KRS, et al. *Ann Biomed Eng* **33**, 829-840, 2005
8. Cui L, et al. *J Biomech* **41**, 1945-1952, 2008
9. Hu X, et al. *33th Annual Meeting of ASB*, State College, PA, USA, 2009.
10. Ogden C, et al. *Adv Data* **347**, 1-17, 2004
11. Avin KG, et al. *Med Sci Sports Exerc*, Published Ahead-of-Print, Feb 2010

ACKNOWLEDGEMENTS

This work was supported by NIH R01 NS053813.

VARIABLE STIFFNESS SHOE ALTERS MUSCLE ACTIVATIONS AND KNEE JOINT MOMENTS.

[1,2]Katherine Boyer, [2,1]Tom Andriacchi
Stanford University, Stanford, CA, USA.
VA Palo Alto Bone and Joint Center, VAPAHCS, Palo Alto, CA, USA.
kboyer@stanford.edu

INTRODUCTION

Medial compartment knee osteoarthritis (OA) is nearly 10 times more common than lateral compartment OA [1] and develops in approximately 20-40 % of adults over the age of 60 [2]. A high maximum knee adduction moment in walking has been associated with OA rate of progression, treatment outcome, and disease severity. The use of a shoe intervention with a more rigid lateral compared to medial midsole, referred to as a variable stiffness shoe (VS), can reduce the knee adduction moment magnitude in both healthy persons [3] and osteoarthritis patients[4]. Initial investigations with this VS shoe have also found that only a small portion of the variability in the absolute change in the maximum knee adduction moment is explained by the peak magnitude in a neutral shoe and that secondary changes in the hip and ankle frontal plane moments accompany changes in the knee adduction moment [3; 5]. These results suggest that an important dynamic response by the lower extremity muscles may be involved in the adaptation to this intervention and thus the reduction of the knee adduction moment during walking.

Changes in both joint kinetics and lower extremity muscle activation patterns in response to athletic footwear with subtle design variations in midsole density, stiffness or in combination with wedged inserts have previously been reported [6; 7]. These results suggest investigations into the effects of shoe interventions should consider muscle in addition to joint mechanics. With respect to the VSS shoe, the mechanism linking the specific variation in shoe mid-sole properties with the changes in joint mechanics remain unclear. Therefore the purpose of this study was to quantify the effect of a VS shoe on muscle activity in the lower extremity during walking. It is hypothesized that increases in the mean EMG intensity will occur in response to walking the VS shoe compared with a neutral control shoe.

METHODS:

Gait analysis was performed on five healthy volunteers (24 +/- 2 yrs; 1.63+/- 0.05 m; 56.2 +/- 10.3 kg). Lower extremity joint kinematics were captured at 120 Hz using an 8 camera motion analysis system synchronized with an in-floor force platform to measure external ground reaction forces (GRF). Each subject performed three trials at their self-selected normal walking speed. Three dimensional net joint reaction moments were calculated using inverse dynamics. Two shoe conditions were tested: a control shoe with a uniform sole stiffness and an intervention variable stiffness shoe (VS) similar in construction to the control but with a midsole that is stiffer on the lateral compared to the medial side.

Bipolar surface EMG electrodes were placed on the gluteus medius (GM), biceps femoris (BF), tibialis anterior (TA), gastrocnemius medialis (MG) and lateralis (LG), and peroneus longus (PL) muscles according to the SENIAM recommendations[8]. Data were collected at 1200 Hz. The mean EMG intensities were determined for three time windows: a pre-activation phase (100 ms prior to heel-strike); a loading (0-50% of stance) phase; and a propulsion phase (50-100% of stance) of the gait cycle using wavelet techniques[9]. For each subject and muscle the EMG intensity was normalized to the average mean EMG intensity for the stance phase of the walking stride from the control shoe.

Statistics: Wilcoxon-sign rank tests were used to identify differences in the joint kinetics, GRFs and EMG intensities between the two tested shoe conditions. A confidence level of 90% was selected.

RESULTS

Kinetics: A reduction in the 1st peak adduction moment at both the knee and hip was found for the VS shoe compared to the control shoe (mean reductions of 12 and 13% respectively). Increases in both the ankle eversion and inversion moments were found for the VS shoe (18 and 45% respectively).

Forces: No differences in the total GRF magnitudes were found between the two shoe interventions. Small, but not statistically significant, reductions in the peak medial and peak lateral GRFs were found with the VS shoe.

EMG: Changes in the lower leg muscle EMG intensity were found in the pre-activation and loading phase time windows with VS shoe ($p < 0.1$). In the propulsion phase time window changes in the upper leg muscle EMG intensities were found ($p < 0.1$) (Fig. 1 a, b, c).

DISCUSSION

The preliminary results indicate changes in lower extremity muscle EMG intensities occur in response to a VS shoe. In agreement with previous results, reductions in the 1st peak knee and hip adduction moments and increases in both the ankle inversion and eversion peak moments were found.

The GRF vector direction and thus the joint moment magnitudes, are influenced by the relative position of the body center of mass with respect to the center of pressure. Increases in lateral muscle EMG intensity in stance, in particular the hip abductor and extensor (gluteus medius and biceps femoris) muscles, in response to the VS shoe suggest that a change in pelvic motion and contribute to the reduction in both the hip and knee adduction moments. The changes in EMG pre-activation intensities could produce a lateral rotation of the tibia at touchdown, or "toe-out" gait, and again contribute to the reduction of the knee adduction moment.

Interventions that result in a reduction of the knee adduction moment in walking are of interest because of the strong connections between the adduction moment magnitude and osteoarthritis disease status. The changes in selected muscle EMG intensities during the gait cycle for the VSS shoe suggest this intervention does not work in a purely passive mode, but that an active adaptation to the high lateral midsole stiffness occurs. It is not known how changes in the neuromuscular system in OA patients may impact the efficacy of this intervention. Our future work will aim to determine the specific relationships between EMG changes and changes in the frontal plane joint moments and to determine if similar muscle reactions are present in OA patients.

REFERENCES

(1) Ahlback,S *Acta Radiol.Diagn.(Stockh)*, Suppl- 72 1968.
(2) Felson,DT *Semin.Arthritis Rheum.*, **20**, 42- 50 1990.
(3) Fisher,DS et al. *J Orthop Res*, **25**, 540- 546 2007.
(4) Erhart,JC et al. *J Orthop.Res*, 2010.
(5) Erhart,JC et al. *J Biomech*, **41**, 2720- 2725 2008.
(6) Murley,GS et al. *Gait Posture*, **29**, 172- 187 2009.
(7) Mundermann,A et al. *Clin.Biomech*, **18**, 254- 262 2003.
(8) SENIAM group http://www.seniam.org/, 2010.
(9) von Tscharner,V *J.Electromyogr.Kinesiol.*, **10**, 433- 445 2000.

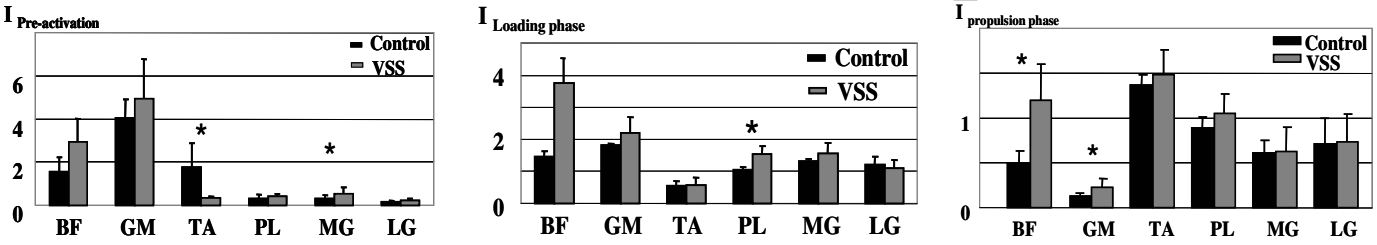

Fig 1: Mean EMG intensities for the selected muscles for a) pre-activation, b) loading phase, and c) propulsion phase time windows. * indicates a statistically significant difference between shoes $p < 0.1$.

INTERLIMB COORDINATION FOR FORCE CONTROL DURING HUMAN HOPPING

[1]Jasper T. Yen and [1]Young-Hui Chang

[1]Georgia Institute of Technology, Atlanta, GA, USA
email: jaspery@gatech.edu, web: http://www.ap.gatech.edu/Chang/CNL.php

INTRODUCTION

Mounting evidence in the biomechanics and neurophysiology literate suggests that motor control is made simple through control of just a few task variables. This suggests that for bouncing gaits such as hopping and running, controlled variables may include force applied on the ground as opposed to many individual joint torques. The rational for this hypothesis is that for bouncing gaits the force applied on the ground and center of mass displacement are like that of a bouncing ball. Joint torques of the lower limb act together such that the limb as a whole functions like a simple linear spring [1, 2]. Therefore, control of locomotion may operate in a low-dimensional space appropriate to the task.

Is force applied on the ground a controlled task variable during human hopping? Our previous studies on one-legged hopping in place showed that intralimb coordination of joint torques stabilize vertical force, implicating vertical force as a controlled task variable [3, 4]. In this current study, we investigated whether joint torques are coordinated across limbs to stabilize total vertical force generated by both legs during two-legged hopping. Alternatively, joint torques may be only coordinated within a single limb such that each leg's force production is stabilized independently.

METHODS

10 healthy subjects (ages 21 to 35 years) hopped in place following the 2.2 Hz beat of an audible metronome. Subjects hopped for three 30-second trials on their right leg and for three 30-second trials on two legs. Sagittal plane ankle, knee, and hip joint torques (net muscle-tendon moments) were calculated from kinematics and ground reaction forces recorded by a motion capture system (Vicon, UK; sampling rate 120 Hz) and two force plates (AMTI, USA; sampling rate 1080 Hz; Fig. 1). Approximately 150 hops were analyzed for each subject and hopping condition.

Figure 1: Sagittal plane ankle, knee, and hip joint torques (blue arrows) and vertical ground reaction force (black arrow) for one-legged hopping. The lower limbs were estimated as three-link planar systems.

We used the Uncontrolled Manifold (UCM) analysis method to determine if vertical force is controlled [3, 4, 5]. For each subject and hopping condition, the total joint torque variance across hops was divided into two components: 1) goal-equivalent variance (GEV), or variance that does not contribute to vertical force variance, and 2) non-goal-equivalent variance (NGEV), or variance that does contribute to vertical force variance. The normalized difference between the two components, or Index of Motor Abundance (IMA, Eq. 1), quantifies the degree vertical force is stabilized by the structure of joint torque variance.

$$IMA = \frac{GEV - NGEV}{GEV + NGEV} \qquad (1)$$

A positive IMA indicates task-level control of vertical force, while a zero or negative IMA indicates vertical force is not controlled.

For two-legged hopping, we determined if the right leg's vertical force, left leg's vertical force, and total vertical force of both legs were controlled as task

variables. We also investigated if vertical force was controlled for one-legged hopping.

RESULTS AND DISCUSSION

For one-legged hopping, the vertical force stability metric IMA was significantly greater than zero at discrete times during landing, mid-stance, and takeoff (Fig. 2A, $p < .05$). For two-legged hopping, however, vertical force stability of one leg decreased and was not significantly greater than zero during mid-stance (Fig. 2B and C). In contrast, total vertical force stability of both legs considered together was significantly greater than zero during mid-stance (Fig. 2D). The total vertical force stability signature of two-legged hopping was qualitatively similar to that of the stability signature for one-legged hopping.

CONCLUSIONS

Results indicated that total force, as opposed to individual leg forces, was a controlled task variable during two-legged hopping. Interlimb coordination of joint torques stabilized total force generation on the ground. The force generated by one leg was not an important control variable. Therefore, the locomotor system did not control individual limb forces during two-legged hopping, suggesting a minimization principle for the number of task-specific controlled variables during locomotion.

REFERENCES

1. Blickhan R, *J Biomech* **22**, 1217-1227, 1989.
2. McMahon TA and Cheng GC, *J Biomech* **23 Suppl 1**, 65-78, 1990.
3. Yen JT and Chang Y-H, *J R Soc Interface* Published online October 14, 2009.
4. Yen JT, Auyang AG, and Chang Y-H, *Exp Brain Res* **196**, 439-451, 2009.
5. Scholz JP and Schöner G, *Exp Brain Res* **126**, 289-306, 1999.

ACKNOWLEDGEMENTS

The authors thank Arick Auyang for obtaining a portion of the data used in this study.

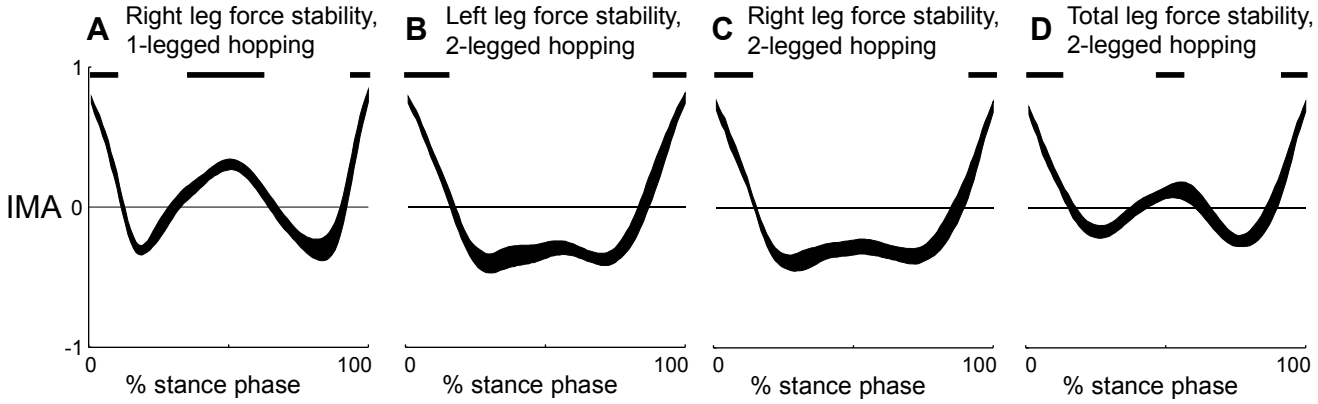

Figure 2: Mean (± SEM) vertical force stabilization for one-legged hopping (A) and two-legged hopping (B-D) during stance phase. Stance phase duration was normalized across hops, where 0% stance phase is initial contact with the ground and 100% stance phase is liftoff from the ground. Positive IMA indicates if and when vertical force was controlled. Vertical force of the right leg during one-legged hopping was controlled at landing, mid-stance, and takeoff (A). The right and left legs' individual vertical forces during mid-stance were not controlled during two-legged hopping (B, C). The two legs' total vertical force, however, was controlled during mid-stance, as it was for one-legged hopping. Black bars above the curves indicate when IMA was significantly greater than zero ($p < .05$).

DIRECTIONAL CHARACTERISTICS OF FINGERTIP FORCE PRODUCTION AFTER HEMIPARETIC STROKE

[1]Joseph D. Towles, [2]Kristen M. Triandafilou,[3]Mary Ellen Stoykov, [2]Derek G. Kamper

[1]Rehabilitation R&D Service, Edward Hines Jr. VA Hospital, IL, USA
[2]Dept. Biomedical Engineering, Illinois Inst Technology, Chicago, IL, USA
[3]Dept. Occupational Therapy, Rush University, Chicago, IL, USA
email: towles@northwestern.edu

INTRODUCTION

Post-stroke hemiparesis is often marked by persistent hand impairment [1], which adversely affects the ability to explore and manipulate the environment and thus quality of life. In a mechanical sense, the impairment can be described by an inability to exert appropriate grasp forces and/or position the hand correctly for grasp. As many everyday tasks require only limited grasp force production, the main difficulty often has more to do with generating proper force direction than magnitude. Only a few studies [2, 3] have explored the directional characteristics of fingertip force production and the effects of posture following hemiparetic stroke. These studies, however, did not fully characterize postural effects across the kinetic workspace. Thus, the goal of this study was to explore more fully the directional characteristics of fingertip force production, attempting to determine a basis for the feasible fingertip force set, and the effects of posture in stroke.

METHODS

Protocol

Nine individuals with chronic, hemiparetic stroke and severe hand impairment (as indicated by a rating of 2 or 3 for the Stage of Hand section of the Chedoke-McMaster Stroke Assessment [4]) participated in the study. Each subject was seated with his/her arm in a standard posture. The forearm and wrist were placed in a fiberglass cast and clamped to a table to prevent movement. The tip of the index finger was coupled to a 6-axis load cell in either a flexed (0^o adduction, 60^o flexion at the metacarpophalangeal joint; 45^o flexion at the proximal interphalangeal joint; 5^o-10^o flexion at the distal interphalangeal joint) or an extended (0^o adduction, 5^o flexion at the metacarpophalangeal joint; 5^o flexion at other joints) posture. Each subject was instructed to produce maximal force in one of six orthogonal directions at the fingertip (Fig. 1) without directional feedback. Three trials, each 10 sec. in length, were completed for each direction in random order. Force data were filtered at 225 Hz prior to sampling at 1000 Hz. In each subject, both index fingers were tested in the flexed and extended postures; and force produced by the ipsilesional finger served as the control (72 trials per subject).

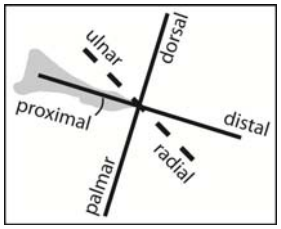

Figure 1: Fingertip force reference frame

Data Analysis

Maximal 3D fingertip force in each attempted direction was calculated by finding the average force in a 250 ms window centered about the peak force value for each of the 3 trials. The mean of the 3 trials was computed. This was repeated for each posture and index finger for each subject. Unit vector directions for the mean 3D force vectors produced (u_f) were calculated. Angular deviation of the produced vector (θ), relative to the target (u_t), was computed ($\theta = \cos^{-1} u_f^T u_t$) for each target force direction in the flexed and extended postures and for the contralesional and ipsilesional index fingers. For each posture, a two-way ANOVA was performed to explore the effects of finger and target direction on angular deviation (α = 0.05, PSAW, Chicago, IL). If significance resulted, post-hoc analyses using one-way ANOVAs (α = 0.05, PSAW) and boxplots (α = 0.05, Matlab, Natick, MA) were performed as well.

RESULTS AND DISCUSSION

As expected, subjects produced fingertip force significantly less accurately (p = 0.05) on the contralesional than the ipsilesional side. For example, in the flexed posture, subjects produced force in the ulnar direction 30^o less accurately. In the extended posture, they produced force 41^o less accurately in the same direction.

On the ipsilesional side, in the flexed posture, the accuracy with which subjects produced fingertip force, relative to the target direction, was divided into 2 statistical groups (p = 0.05, Table 1). Subjects produced fingertip force most accurately in the distal direction (16^o) and least accurately in the palmar (32^o), dorsal (40^o) and radial (47^o) directions. On the contralesional side, in the flexed posture—in which angular deviations were larger, more variable and spanned a larger space—the accuracy with which subjects produced fingertip force were divided into 3 statistical groups (p = 0.05, Table 1). Subjects produced fingertip force most accurately in the palmar (40^o) direction, and least accurately in the radial (100^o) and dorsal (103^o) directions.

Table 1: Post-hoc analysis

Flexed Posture

IPSI				CONTRA			
dis	a			pal	a		
uln	a	b		uln	a	b	
prox	a	b		prox	a	b	
pal		b		dis		b	c
rad		b		rad			c
dor		b		dor			c

Extended Posture

IPSI				CONTRA			
dis	a			prox	a		
prox	a			pal		b	
uln	a	b		uln		b	c
pal	a	b		dis		b	c
rad		b		rad			c
dor		b		dor			c

Groups arranged in increasing order of angular deviation, i.e., *a* is less deviated than *b*.

On both sides, in the extended posture, the accuracy with which subjects produced fingertip force was divided into the same number of groups as in the flexed posture with many members, per group, in common. On both sides, the directions in which fingertip force was produced with the least accuracy were the same as in the flexed posture. Of note, the accuracy with which subjects produced proximal force on the contralesional side significantly increased (i.e., angular deviation decreased) from the flexed (52^o) to the extended (38^o) posture (p = 0.05, transition from "a-b" to "a," Table 1).

Given that the statistical groups represent levels of directional accuracy, the observation that the number of levels was greater on the contralesional than the ipsilesional side may reflect limitations in the ability to activate or coordinate muscles to properly direct fingertip force. In fact, subjects produced highly misdirected forces on the contralesional side (e.g., 103^o from dorsal target direction). Previous studies have reported deficits in voluntary muscle activation deficits following stroke [3, 5].

The observation that the number of statistical groups remained the same across postures could be due to attempted compensation by the nervous system to meet task requirements despite posture-induced changes in musculoskeletal properties. Likely, muscle coordination strategy changed between postures [2, 3].

REFERENCES

1. Nakayama H, et al. *Arch Phys Med Rehab* **75**, 394-398.
2. Seo NJ, et al. *Exp Brain Res*, 2010 [Epub].
3. Cruz EG, et al. *Brain* **128**, 1112-1121, 2005.
4. Gowland C, et al. *Stroke* **24**, 58-63.
5. Lang CE, et al. *J Neurophys* **91**, 1722-1733, 2004.

ACKNOWLEDGEMENTS

Supported by Dept. of VA (#B6302R)

ACTIVE JOINT POSITION SENSE: EFFECTS OF ELEVATION ANGLE, ARM DOMINANCE AND PROXIMAL VS DISTAL JOINTS

Jacqlyn Hyler, Elizabeth Harding and Andrew Karduna
Department of Human Physiology, University of Oregon, Eugene, OR, USA
Email: karduna@uoregon.edu, web: http://biomechanics.uoregon.edu/obl/

INTRODUCTION

The conscious control of limb movement without visual input is important for maintaining joint stability and muscular control. A decrease in proprioception may predispose a person to injury. Previous studies have investigated proprioceptive acuity in the upper extremity in relation to elevation angle, arm dominance or proximal versus distal joint location[1-5]. The purpose of the present study was to comprehensively examine these issues, employing an active-active joint positioning and repositioning task. Joint position sense for the shoulder improves as flexion angles approach 90 degrees[1]. However, no similar studies have been conducted with the elbow. Findings centering on position sense asymmetry have been inconsistent. Some studies show a dominant limb advantage, others a non-dominant limb advantage and still others no difference between the limbs[2-4]. However to our knowledge, no previous studies have employed an active-active ipsilateral remembered paradigm to address this question. Proprioceptive studies on the lower extremity have identified increasing errors when moving from a more proximal joint to a distal joint. This trend has only loosely been established in the upper extremity. The shoulder demonstrates an advantage over the wrist, however no significant difference exists between the shoulder and elbow[5]. Again to our knowledge, no previous studies have employed an active-active ipsilateral remembered paradigm to address this question.

METHODS

A total of six subjects (1 male, 5 females), with a mean age of 25.3 years (± 6.9 years) participated in the study. All subjects were right hand dominant and had no history of elbow or shoulder pathology. Subjects followed a standard warm-up procedure before being fitted with a head-mounted display to inhibit any extraneous visual cues (Fig 1). Subjects remained seated on a kneeling chair throughout the experiment to avoid any tactile cues and provide for a complete return of arm to the side. Kinematic data were collected via the Polhemus Fastrak magnetic tracking system with receivers placed on the thorax and dorsal side of the wrist. Bony landmarks were digitized in order to establish anatomical standard coordinate systems[6].

Figure 1. Experimental Set-up

Testing involved a four-part protocol: right elbow (RE), right shoulder (RS), left elbow (LE) and left shoulder (LS). Three target positions at 50˚, 70˚, and 90˚ of flexion were presented in the sagittal plane. Positions were presented via custom-made Labview® software through the head-mounted display. Once the target position was reached, the display turned black and remained so for the remainder of the trial. Subjects held the position for three seconds, and returned their arm to their side. Subjects then attempted to replicate the target position in the absence of visual cues. Target positions and protocols were presented in a randomized order. Four trials at each flexion angle were completed. Error scores were defined as the repositioned angle minus the presented angle. Both the constant error (mean of the error scores) and

variable error (standard deviation of the error scores) were calculated.

RESULTS AND DISCUSSION

ELEVATION ANGLE**:** Constant error and variable error revealed that under all four conditions (RE, RS, LE, LS), there was a trend for joint position sense to improve as flexion angles increased. Previous literature indicates that joint position sense at the shoulder joint improves as elevation approaches 90 degrees[1]. This study demonstrates that the elbow joint follows this same progression.

PROXIMAL TO DISTAL: Both the right and left limb demonstrated decreased errors in joint position sense moving from the shoulder joint to the elbow joint. This trend was displayed for both variable error (Fig 2) and constant error (not shown). Previous studies have determined no difference in proprioceptive acuity between the shoulder and elbow joints. Perhaps this variance arises from the novelty of the present protocol. Preceding studies employed a threshold to detection of passive motion paradigm to determine proprioception[5].

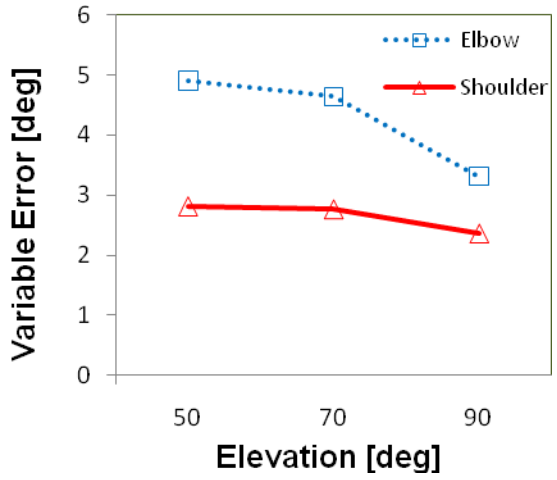

Figure 2. Right Shoulder vs Elbow

DOMINANT VS. NON-DOMINANT: Joint position sense errors were found to be lower at the dominant limb compared to the non-dominant limb. This trend was observed in both the shoulder (Fig 3) and elbow in an analysis of the constant error and variable error. These data may help to shed light on the conflicting contentions surrounding position sense asymmetry[2-4].

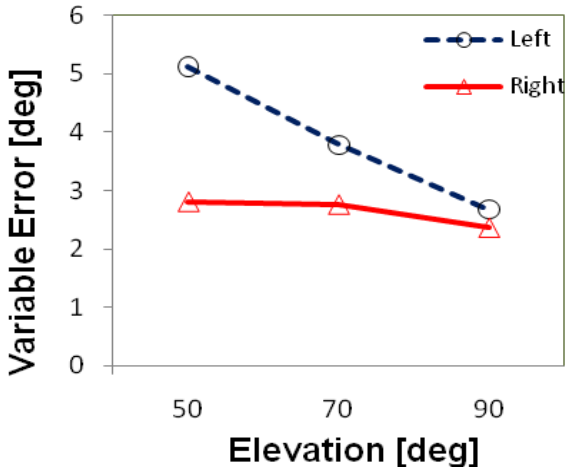

Figure 3. Left vs Right Shoulder

CONCLUSIONS

The results of this study indicate that joint position sense at the elbow improves as flexion angles approach 90 degrees. Errors at the proximal shoulder joint are smaller than at the distal elbow joint. Lastly, the dominant limb displays greater proprioceptive acuity than the non-dominant limb during joint positioning tasks. These results are preliminary. After a greater number of subjects are tested, the aforementioned trends will be analyzed for significance.

REFERENCES

1. Suprak DN, et al. *J Orthop Res* **24**(3), 559-568, 2006.
2. Adamo DE, Martin BJ. *Exp Brain Res* **192**(1), 87-95, 2009.
3. Sainburg RL. *Exp Brain Res* **142**(2), 241-258, 2002.
4. Goble D, Lewis C, Brown S. *Exp Brain Res* **168**(1), 307-311, 2006.
5. Sturnieks DL, Wright JR, Fitzpatrick RC. *J Physiol* **585**(3), 833-842, 2007.
6. Wu, et al. *J Biomech* **38**, 981-992, 2005.

ACKNOWLEDGEMENTS

Carl Erickson, for technical assistance

DEPENDENCE OF MUSCULAR MASS IN THE ORIGIN OF INGUINAL HERNIA

[1]Gerard Fortuny, [2]Manuel López-Cano, [1]Blas Herrera and [3]Antonio Susín

[1]Universitat Rovira i Virgili, Reus, Spain
[2]Universitat Autònoma de Barcelona, Barcelona, Spain
[3]Universitat Politècnica de Catalunya, Barcelona, Spain
email: gerard.fortuny@urv.cat, web: http://deim.urv.cat/~gerard.fortuny/

INTRODUCTION

We are interested in studying the genesis of a very common pathology: the human inguinal hernia. The way it appears is not definitively clear, but it is accepted that a combination of mechanical and biochemical alterations is the reason why this pathology occurs, and that muscular simulation plays an important role in this.

To study the dynamics of the region the oblique internal muscle has been simulated because this is the most important dynamic element, especially given its position in Hessert's triangle. The vertex of this triangle is the inguinal internal orifice; the triangle's side are the oblique internal muscle with the aponeurotic arch of the transverse muscle and the inguinal ligament; and the triangle's base is the aponeurotic edge of the straight muscle. We can consider the side of the inguinal as a fixed ligament and the side of the aponeurotic tissue as dynamically passive. The side of the oblique internal muscle is the dynamically active element in the triangle. This triangle is covered by the transversalis fascia, which is dynamically passive and the last element of protection before the appearance of hernias

METHODS

There are several studies on the simulation of the muscular movements but basically, the most popular model is that proposed by A. F. Huxley, known as the cross bridges theory [1]. The visco-elastic model proposed [2] uses the Hill-Maxwell mechanical model which is theoretically based 1n [1]. Thus a differential model can establish the control of the muscular contraction for every point.

The Hill-Maxwell model that we use to simulate the muscular unit consists of 3 elements, one contractile and two elastic. The contractile element EC is activated by a device *u(t)*, which represents the active force-generating capacity. The elastic element ES models the mechanical isometric response of muscle and EP accounts for the resistance to stretch. The formulation of the model took into account the strain of each element ($\varepsilon_c, \varepsilon_s$ and ε_p) and the associated stresses (σ_c, σ_s and σ_p), so that the lengths of each time moment t (l_c, l_s and l_p) can be calculated according to the initial lengths and strains per instant as $l_i = l_{i_0}(1+\varepsilon_i)$ where i= *c,s,p.*. Due to the structure of the Hill-Maxwell model, $\sigma_c = \sigma_p$ and the total stress is the sum of both ($\sigma = \sigma_c + \sigma_p$). The position of the muscle is obtained from the system:

$$\begin{cases} \dot{k}_c = -\left(|u| + |\dot{\varepsilon}_c|\right)k_c + k_{c_{\max}}|u|_+ \\ \dot{\sigma}_c = -\left(|u| + |\dot{\varepsilon}_c|\right)\sigma_c + k_c\dot{\varepsilon}_c + \sigma_{c_{\max}}|u|_+ \\ \rho\ddot{y} + c\dot{y} - div(\underline{\underline{F}} \cdot \underline{\underline{\sigma}}) = 0 \\ \sigma_c = k_s(\varepsilon - \varepsilon_c) \end{cases}$$

where k_c is the stiffness of the contractile element, the points indicate derivates regarding time and $\sigma_{c_{\max}}$ and $k_{c_{\max}}$ are empirically derived values. Moreover, the activation function *u(t)* is represented by $u(t) = |u(t)|_+ - |u(t)|_-$ with:

$$\begin{cases} |u(t)|_+ = k_{ATP} \cdot \mathrm{I}_{C_a(t) \geq \overline{C}} \\ |u(t)|_- = k_{RS} \cdot \mathrm{I}_{\overline{C} \geq C_a(t) \geq 0} \end{cases}$$

where $C_a(t)$ is the concentration of calcium for each point of time, $\overline{C}$ is the level that activates function, k_{ATP} and k_{RS} are two fixed values related

to properties of the sarcomeres, and finally, I_A is the indicatrix function.

RESULTS AND DISCUSSION

We submitted our model to muscular exposed contraction and then to several simulations from the state of reference, following the reference parameters in the literature. We measured the maximum strain in the fascia.

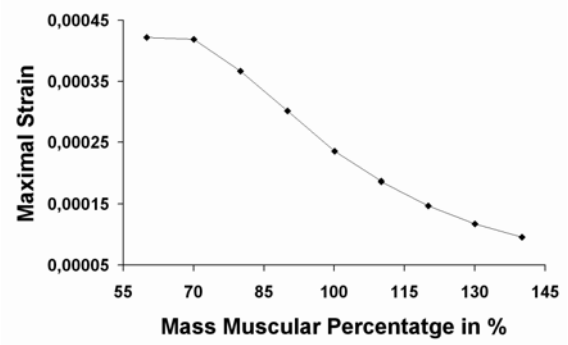

Figure 1: The vertical axis shows the maximum strain in the fascia. The horizontal axis shows the variation for the muscular mass in percentages.

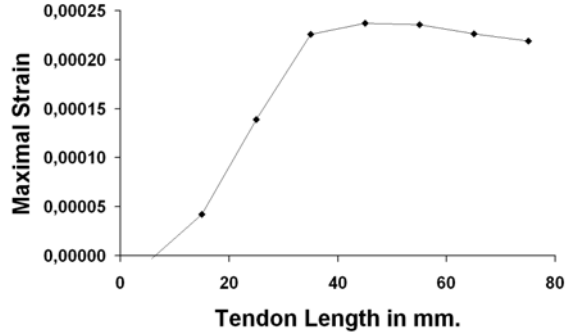

Figure 2: The vertical axis shows the maximum strain on the fascia. The horizontal axis shows the length of the tendinous tissue in mm.

In our study, we have varied the muscular mass in the direction orthogonal to the fibre. In this way we have varied the volume but not the length. The average muscular mass in our initial model was 100%, and we increased and decreased this mass by 40% in accordance with [3]. After subjecting the resulting models to muscular contraction, we measured the maximum strain on the fascia transversalis at the time of maximum contraction (Fig. 1).

Munhequete [3] showed that the average length of the lower fibres of the internal oblique muscle from the pubic tubercle is about 60 mm. (Fig. 3). In some cases the tendon can reach 90 mm and cover the whole triangle. In other cases it can be just 10 mm long.

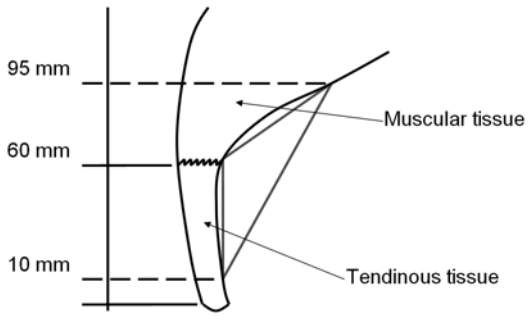

Figure 3: Scheme of the length of the tendinous tissue in the internal oblique muscle.

CONCLUSIONS

First, we demonstrate that Keith's conjectures are correct, that is, the risk of inguinal hernia diminishes when the volume of the muscular mass increases. This is shown by the maximum strain that can be place on the fascia transversalis.

Second, our model confirms the results obtained by Ajmani [4], which establish a direct dependence between the likelihood of suffering a hernia and the distance between the origin of the muscular fibres and the tubercle of the pubis. Ajmani states that individuals in whom this distance is greater are more likely to suffer from hernias, and this is corroborated by our model (Fig. 2).

REFERENCES

1.Huxley AF. *J. Physiol*. **243**, 1-43, 1974
2.Bestel J. *Modelè diffèntiel de la contraction muscularie contrôlée. Aplication au système cardiovasculaire*. Ph.D. disertation, Univesité Paris IX Dauphine, France, 2000
3.Munhequete E. "Estudio de las estructuras anatómicas relacionadas con la formación de hernias inguinales". PhD disertation, Universitat Autonoma de Barcelona, Spain, 2003..
4.Ajmani ML. et al. *Anat. Anz*. **153**, 245-248, 1983.

ACKNOWLEDGEMENTS

Support is obtained by Rovira i Virgili University, spanish grant: TIN2007-67982-C02-01 as well as additional support from the European Regional Development Fund (ERDF ERDF/FEDER).

CHARACTERIZATION OF UPPER LIMB MUSCLE VOLUME IN FEMALE OLDER ADULT SUBJECTS FOLLOWING RESISTANCE EXERCISE TRAINING

[1,2] Meghan E. Vidt, [1,2] Melissa Daly, [1] Joel D. Eggebeen, [1] W. Gregory Simpson, [1,2] Anthony P. Marsh and [1,2] Katherine R. Saul

[1]Wake Forest University, Winston-Salem, NC USA
[2]Virginia Tech – Wake Forest University School of Biomedical Engineering and Sciences
email: mvidt@wfubmc.edu, web: http://www.sbes.vt.edu/kholzbau/MoBL/index.html

INTRODUCTION

Previous studies have reported a positive correlation between isometric joint moment and muscle volume [1,2]. Muscle atrophy and strength loss occur with aging, but resistance exercise training in older adults increases muscle mass and strength [3]. In the upper extremity of young adults (24-37 y), individual muscle volumes and isometric joint moments at the shoulder, elbow and wrist have been measured [1,2]. However, there are no comparable data for older adults (age 65 and older). The aim of this study was to characterize muscle volumes and joint moments in older adults and to investigate the effect of a 6 week resistance exercise intervention on muscle volume and isometric joint moment. Therefore, our objective is to measure the individual muscle volume of older adults following a resistance exercise regimen and compare to a control group.

METHODS

Eight ostensibly healthy female subjects were evaluated (66-83 y; wt=49.9-83.9 kg; ht=154.9-167.6 cm). All study participants gave written informed consent. For each participant, muscle volume and isometric joint moment were measured at baseline and follow-up. Four subjects participated in resistance exercise training, while the other four were controls. Subjects in the exercise group met three times per week. Nine exercises for the upper limb were performed, six using machines and three with free weights. Each exercise was performed for 3 sets of 8 repetitions at 60% of the subject's 1 repetition maximum (1RM), and incrementally increased to 70% and 75% of 1RM at training sessions 6 and 7, respectively.

Subjects were imaged with a 1.5 T MRI scanner (GE Healthcare, Milwaukee, WI) using 3D spoiled gradient (SPGR) scans. The body coil was used to obtain images of the shoulder and upper arm, with a scan time of approximately 10 minutes. A flexed array long bone coil (Invivo, Orlando, FL) was used to obtain images of the upper limb with two successive scans, each lasting approximately 14 minutes.

The MR images were manually segmented (3D Doctor, Able Software Corp., Lexington, MA) to produce a three-dimensional reconstruction of the muscles of interest. A reproducibility study was performed, in which each muscle was segmented twice, showing repeatability within 5% muscle volume. The muscles of interest were selected from each of the main groups of action in the shoulder, elbow, and wrist. These muscles include the biceps brachii (BIC), triceps brachii (TRI), deltoid (DELT), pectoralis major (PEC), coracobrachialis (CBR), latissimus dorsi (LAT), brachioradialis (BRD), extensor carpi radialis (ECR), flexor carpi radialis (FCR), and flexor carpi ulnaris (FCU). Muscle volumes as a percent of total measured volume were calculated.

Maximum isometric joint moment was obtained at the wrist (flexion, extension), elbow (flexion, extension) and shoulder (abduction, adduction) joints using a KIN-COM isokinetic dynamometer (Isokinetic International, Harrison, TN). Analysis of covariance (ANCOVA), with a Bonferroni correction, was used to evaluate the group by time interaction for both muscle volume and isometric joint moment. A p-value of $p \leq 0.005$ was considered to be significant.

RESULTS AND DISCUSSION

Muscle volume measurements as a percent of total measured volume for all subjects, pre and post, are shown in Figure 1. On average, the change in volume was (mean±SD) 3.14±5.45% for the exercise group and 0.42±5.02% for controls. Group by time interactions were assessed for each of the muscles. The interaction for the FCR muscle volume was significant (p=0.003).

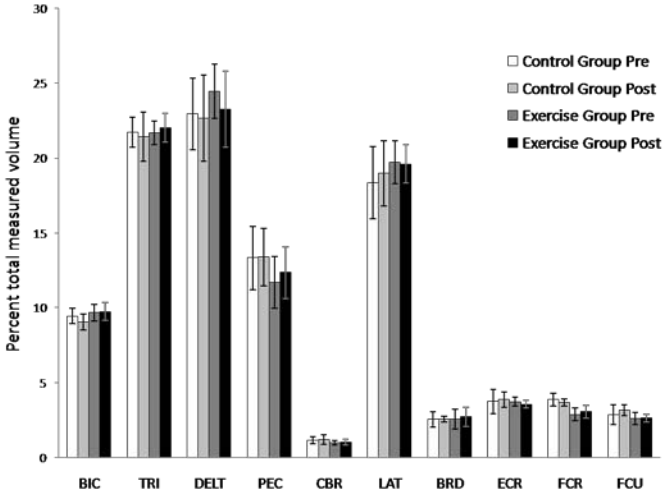

Figure 1: Muscle volume as a percent of total muscle volume measured (mean±SD) for exercise and control groups.

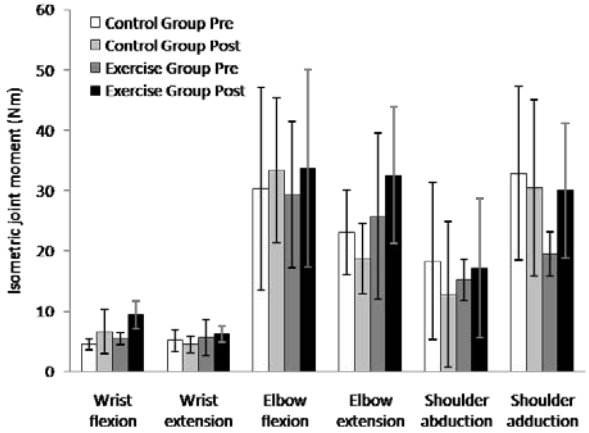

Figure 2: Isometric joint moment (mean±SD) for exercise and control groups, for pre and post testing.

Isometric joint moments from pre and post measurements for subjects in the exercise and control groups are shown in Figure 2. The group by time interaction for isometric joint moment was assessed, although none of the joint measures reached significance. We also summed the joint moments to obtain a composite measure of strength [4]. There was a significant group by time interaction (p=0.046), indicating a significant increase in strength in the exercise group. These data suggest that 6 weeks of resistance training are effective for increasing both composite and individual joint strength.

CONCLUSIONS

We conclude that female older adults exhibit a trend of increased strength following 6 weeks of resistance exercise. However, there were no significant increases in total muscle volume. The emerging trend toward increased strength with no muscle volume change may be explained by previous observations, where strength changes were a result of neural components, followed by a slower hypertrophic response [5]. Isometric joint moments tended to increase at all joints following resistance exercise, although our small sample size limited the statistical power to detect differences. These data represent a portion of a larger study that includes male older adults. Preliminary analysis of isometric joint moment measures in this larger group, which includes both male and female subjects, also shows a trend of increased strength following resistance exercise training. Muscle volume measurements and analyses are currently underway for the male subject group. Inclusion of these subjects may provide additional insight into the relationships between muscle volume, resistance exercise, and isometric joint moment in an older adult population.

REFERENCES

1. Holzbaur KR, et al. *J Biomech* **40**, 2442-2449, 2007.
2. Holzbaur KR, et al. *J Biomech* **40**, 742-749, 2007.
3. Strasser B, et al. *Wien Klin Wochenschr* **121**, 757-764, 2009.
4. Marsh AP, et al. *J Gerontol A Biol Sci Med Sci* **61**, 1186-1193, 2006.
5. Gabriel DA, et al. *Sports Med* **36**, 133-149, 2006.

ACKNOWLEDGEMENTS

Funding for This project was funded by the Wake Forest University Science Research Fund and Cross-Campus Collaborative Research Fund.

GASTROCNEMIUS ATROPHIES PREFERENTIALLY IN POST-STROKE PLANTAR FLEXORS

[1]John W. Ramsay, [1]Thomas S. Buchanan, [2]Peter J. Barrance, [1]Jill S. Higginson
[1]University of Delaware, Newark, DE, USA
[2]Kessler Foundation Research Center, West Orange, NJ, USA
email: jramsay@udel.edu

INTRODUCTION

Stroke annually affects nearly 795,000 people and is considered the leading cause of long-term disability in the United States [1]. On the paretic side, reduced strength and joint moments have been observed [2]. Whether post-stroke weakness is primarily due to muscle atrophy or impaired activation is unclear.

Plantar flexors function to support and propel the body during gait [3]. However weakness in these muscles has been related to various gait deficits in post-stroke populations, such as slow gait speed [4]. Therefore, the force generating capacity of post-stroke plantar flexors is of particular interest during rehabilitation.

Since muscle strength is a function of muscle size [5], the amount of atrophy a muscle undergoes is important in determining the overall force generating capacity of that muscle. Additionally, intramuscular fat content has also been shown to increase with age and some diseases [6], changing the mechanical properties of the muscle and altering its force generating capacity.

We expected that the paretic muscle volumes would be lower than the non-paretic volumes. The objective of this study was to quantify individual muscle volumes and intramuscular fat content in post-stroke plantar flexors.

METHODS

Eight subjects with post-stroke hemiparesis were recruited from the community and provided informed consent before participation. Axial MRI images were acquired of both paretic and non-paretic legs for each of the 8 subjects. Images were taken simultaneously from the ankle mortise to the iliac crest using a 1.5T Signa LX scanner (GE Medical, Milwaukee, WI). Five overlapping scan regions were used to reconstruct muscle volumes. Images taken from the lower leg (2 overlapping

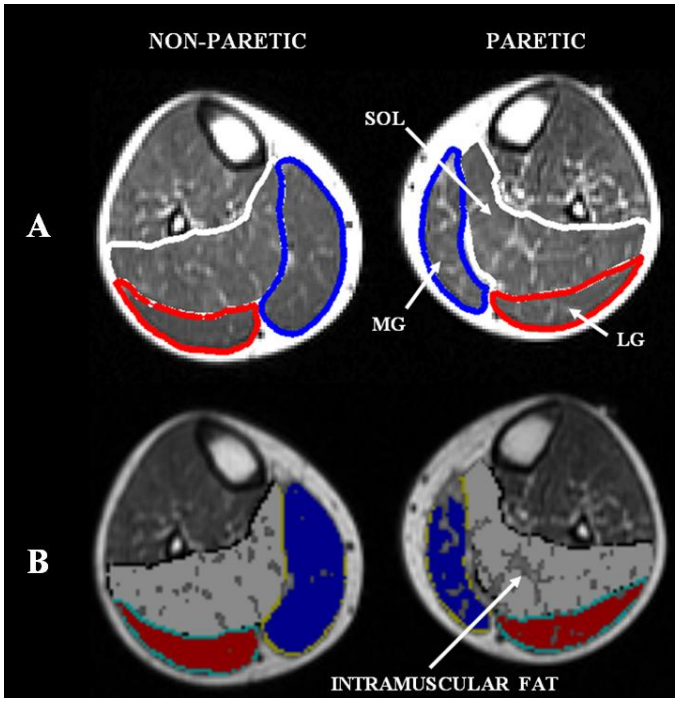

Figure 1. MRI images of non-paretic (L) and paretic (R) legs of a representative hemiparetic subject with (A) muscle boundaries and (B) intramuscular fat identified.

regions), thigh, and pelvis were scanned using a TR of 450 ms, TE of 10 ms, slice thickness of 10 mm and a space between slices of 11.5 mm. Knee images used the same TR and TE times, but the slice thickness was 5 mm and the space between slices was 6 mm. For all scans a 256 x 256 matrix size and FOV of 400 mm were used.

Digital reconstruction of the soleus (SOL), medial gastrocnemius (MG) and lateral gastrocnemius (LG) was performed by manually tracing each muscle boundary for the entire length of the muscle using IMOD software (Figure 1a) [7]. Next we created a surface mesh model of the individual muscles (Nuages, INRIA, Sophia-Antipolis, France) and muscle volume was calculated using the Visualization Toolkit (Kitware Inc., Clifton Park, NY). To eliminate intramuscular fat from the net muscle volume calculation, a pixel threshold was determined for each subject by visually inspecting each MRI scan (Figure 1b). Cross sectional areas

adjusted for fat were then summed over the length of each muscle and multiplied by slice thickness to obtain adjusted muscle volumes. The chosen threshold ranged from 180-280 out of 600 over the subject population.

Net paretic and non-paretic plantar flexor muscle volumes for each subject were calculated by summing the unadjusted volumes of the SOL, MG and LG from each side. Adjusted volumes to account for intramuscular fat were similarly calculated. Percent fat was calculated by comparing the adjusted volumes with the net volumes. Paired t-tests were used to determine whether there were any significant differences in the plantar flexor group and individual muscles between the adjusted paretic and non-paretic sides ($p<0.05$).

RESULTS AND DISCUSSION

For all subjects, adjusted plantar flexor muscle volumes were lower on the paretic side. Across subjects, total paretic muscle volumes (482 ±127.18 cm^3) were significantly lower than non-paretic volumes (642.19 cm^3 ±161.88) ($p<0.001$).

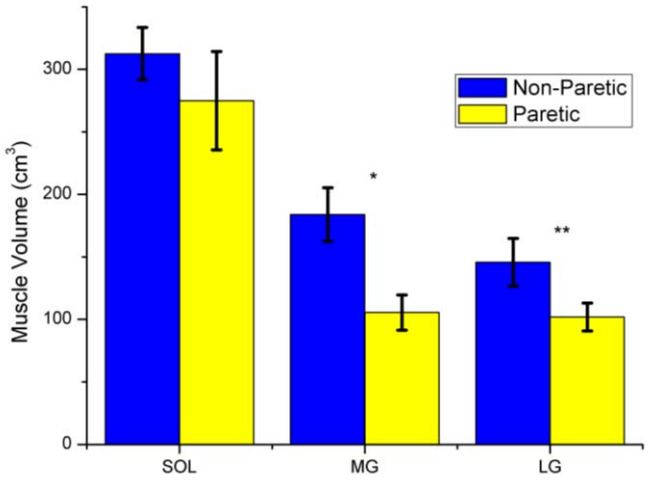

Figure 2. Mean adjusted muscle volumes (cm^3) with standard error bars for individual plantar flexor muscles. *p=0.034, **p=0.003

Gastrocnemius was significantly smaller on the paretic side (MG p=0.034 and LG p=0.003) but no differences were observed for soleus (Figure 2). The percent of intramuscular fat was significantly lower on the non-paretic side than the paretic side for all muscles ($p<0.05$) (Figure 3). For plantar flexors as a group, the paretic side had an average of 29% fat, compared to 18% on the non-paretic side ($p<0.001$).

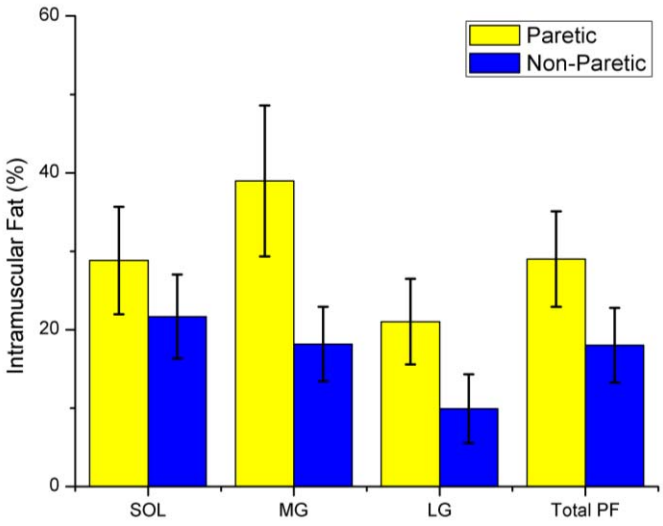

Figure 3. Intramuscular fat percentages for individual and group plantar flexor (PF) muscle volumes. SOL: p=0.014, MG: p=0.039, LG: p=0.002, Total PF: p<0.001

Although total plantar flexor volume is lower on the paretic side, the volume of the largest of the three plantar flexors (SOL) does not change significantly, suggesting that the gastrocnemius atrophies preferentially. Soleus includes more type I fibers and may atrophy at a slower rate. It is possible that uniarticular muscles like soleus serve as prime movers and may be spared while biarticular gastrocnemius is recruited less post-stroke.

Muscle weakness in post-stroke plantar flexors is in part due to muscle atrophy and intramuscular fat development. Future studies will address the relative contributions of impaired activation and muscle atrophy.

REFERENCES

1. Heart Assoc. *Stroke Statistics – 2009 Update*
2. Olney, SJ, and Richards, C. *Gait & Posture* 4, 136-148, 1996.
3. Neptune, RR. et al. *J Biomech* **34**, 1387-1398, 2001.
4. Nadeau, S, et al. *Clin Biomech* **14**, 125-135, 1999.
5. Leiber, RL, *Skeletal Muscle Structure, Function, and Plasticity, Lippincott Williams and Wilkins, 2009.*
6. Mitsiopoulos N, et al. *J Appl Physiol* **85**, 115-122, 1998.
7. Kremer, JR, et al. *J Struct Bio* **116,** 71-76, 1996.

ACKNOWLEDGEMENTS

NIH NS055383, DIA Omega Imaging, Newark, DE

MUSCLE ACTIVITY DURING RUNNING SCALES NON-UNIFORMLY ACROSS PHASES OF THE GAIT CYCLE

Amy Silder and Darryl Thelen

University of Wisconsin-Madison, Madison, WI, USA
email: silder@stanford.edu

INTRODUCTION

Following injury or surgery, runners may undergo clinical gait re-training to restore normal muscle activation and movement patterns. This type of rehabilitation would benefit from a better understanding of how muscle function changes with running speed. A number of studies have found that, when assessed across the entire gait cycle, muscle activity increases with speed [1,2]. However, considering the gait cycle as a whole is inherently less responsive to variance during discrete phases, when individual muscles differentially influence movement patterns [3]. One approach to investigate individual muscle function is to generate muscle-actuated simulations, which can directly compute a muscle's contribution to joint and center of mass (COM) motion [1,2]. Yet, such simulations remain challenging to generate and validate on a subject-specific basis. An important component of the validation involves comparison of the temporal muscle coordination patterns predicted by a model with experimental electromyographic (EMG) data. The purpose of this study was to quantify changes and variance in lower extremity muscle activity across speed during discrete phases of the gait cycle. These data provide a quantitative basis for validation of running simulations, and give insights into speed-related changes in muscle function that are relevant for clinical gait re-training and sports performance.

METHODS

Fourteen runners (9M, 5F; 32±9y; 1.78±0.07m; 69±9kg) participated in this study. Each subject ran on an instrumented treadmill at 70, 80, 90, 100 and 110% of his/her estimated 10km race pace ($3.8\pm0.4 ms^{-1}$). Trials were collected in random order, with 10 strides analyzed for each speed. EMG signals were measured on the right limb from the rectus femoris (RF), vastus lateralis (VL), biceps femoris (BF), medial hamstrings (MH), medial gastrocnemius (GAS), soleus (SOL), and tibialis anterior (TA). Signals were band-pass filtered at 20–500Hz, full wave rectified, and then low-pass filtered at 50Hz. Each signal was normalized to the root mean square (RMS) value for that muscle over the entire gait cycle from the 110% running speed. RMS activity was calculated for each phase and stride, and then averaged across strides. The gait cycle was divided into four phases: loading, propulsion, initial swing, and terminal swing. These phases were defined by initial contact, stance phase reversal, toe-off, and swing phase reversal, where stance phase and swing phase reversal were each defined as the transition from knee flexion to extension. Repeated measures ANOVA was used to assess the affect of speed on RMS activities across the entire gait cycle and within specific gait cycle phases. The affect of speed on peak vertical and fore-aft ground reaction forces were also determined.

RESULTS AND DISCUSSION

Average RMS muscle activity across the entire gait cycle increased significantly with speed for all muscles except the VL ($p=0.16$). Analysis of the four individual phases revealed that for all muscles except SOL, there was at least one phase during which activity did not increase with speed (Fig. 1).
Loading: Peak GRFs increased significantly with speed in both the vertical (8±4%, 2.42-2.62*body weight) and for-aft (54±17%) directions. RMS activities increased with speed for all muscles. Activity was largest during loading for the RF, VL, GAS, and SOL, when compared to the other three phases. Interestingly, the RF exhibited similar speed-related modulation as the VL, though running simulations predict that the vasti are primarily responsible for vertical support and deceleration during the first part of stance [3]. Additionally, GAS and SOL activities were largest during this phase, though propulsion is where these muscles typically receive most attention [3,5].

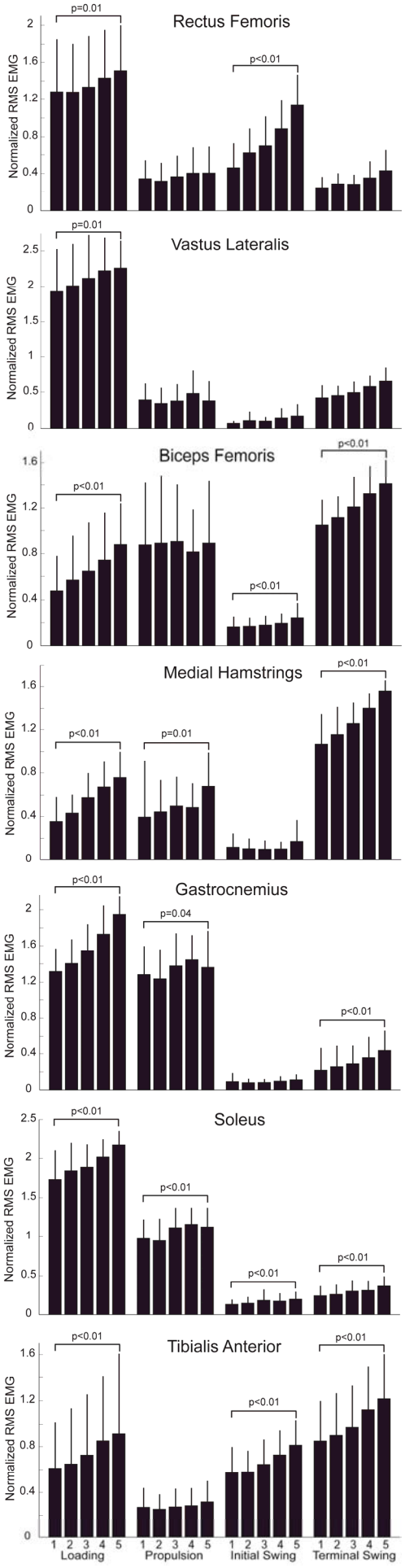

Figure 1. RMS values averaged within each phase of the gait cycle illustrate that activity does not increase uniformly with speed for all four phases.

Propulsion: Peak propulsion forces increased 34±12% across the speed range measured in this study. Muscle activity increased with speed for the GAS, SOL, and MH. Of these muscles, GAS and SOL muscles are thought to be the primary contributors to forward acceleration during running [3,5]. However, the average speed-related changes in GAS and SOL were notably smaller than changes in propulsion force and exhibited substantial variability across subjects (+9±33% and +19±27% for the GAS and SOL respectively).

Initial Swing: Muscle activity increased with speed for the RF, BF, SOL, and TA. However, when compared to the other phases, the magnitude of muscle activity was lowest during this phase for all muscles except the RF and TA.

Terminal Swing: Significant speed effects were measured for the MH, BF, GAS, SOL, and TA. Muscle activity remained relatively low during this phase for all muscles except the MH, BH, and TA. During terminal swing phase, the TA is likely active to maintain ankle dorsiflexion, while the hamstrings act eccentrically to decelerate the limb prior to foot contact [3].

CONCLUSIONS

The results of this study demonstrate that lower extremity muscle activity does not scale uniformly with speed across all phases of the gait cycle. This information can be directly used to assess the effectiveness of clinical gait re-training to restore normal coordination patterns, or to validate muscle-actuated simulations of running.

REFERENCES

1. Cappellini G, et al., *J Neurophysiol* **95**, 3426-37, 2006.
2. Mann RA, *Am J Sports Med*, **14,** 501-10, 1986.
3. Sasaki K and Neptune RR, *J Biomech*, **39,** 2005-13, 2006.
4. Nilsson J and Thorstensson, A., *Acta Physiol. Scand.* **136**, 217–27, 1989
5. Liu MQ, et al., *J Biomech*, **39**, 2623-30, 2006.

ACKNOWLEDGEMENTS

Kyle Gleason, MS.

Variability in Biceps Femoris Long Head Muscle-Tendon Morphology

[1]Geoffrey Handsfield, [2]Niccolo Fiorentino, and [1,2,3]Silvia S. Blemker

[1]Departments of Biomedical Engineering, [2]Mechanical and Aerospace Engineering, and [3]Orthopedic Surgery, University of Virginia, Charlottesville, VA, USA
email: gh8hq@virginia.edu, web: http://www.mae.virginia.edu/muscle/

INTRODUCTION

The biceps femoris long head, one of the muscles of the hamstrings group, is one of the most commonly injured lower-limb muscles. Previous studies have suggested that aponeurosis morphology influences injury susceptibility in muscle [1]. In that study, a model of the biceps femoris long head muscle predicted that the width of the muscle's proximal aponeurosis greatly affects localized tissue strains and therefore injury susceptibilities. However, it is currently unknown how much variability in aponeurosis morphology exists in the normal population. In the present work, we used magnetic resonance imaging (MRI) to characterize how muscle volume, proximal external tendon cross sectional area, and proximal aponeurosis width of the biceps femoris long head muscle vary across a group of healthy subjects.

METHODS

Eighteen volunteers (nine male and nine female, height range: 157.5-195.6 cm, weight range: 54.4-102.1 kg, age range: 21-39 years) were scanned on a 3T Siemens Trio MRI Scanner. The subjects were imaged head first in the prone position with the knee and hip extended, with three coils: one body coil was placed on the hip, one body coil on the knee, and one flex coil was wrapped around the subject's thigh. A proton density turbo spin echo protocol was used with the following imaging parameters: TE/TR/α: 29/6000/120˚, imaging matrix: 512×512, field of view: 250mm×250mm, slice thickness: 5mm, spatial resolution: 0.488mm×0.488mm. Axial slices were obtained from the origin of the biceps femoris at the ischial tuberosity to the insertion on the fibula.

MR images were imported into Materialise Mimics 13.1 medical contouring software. The biceps femoris long head (BFlh) was segmented, along with this muscle's proximal tendon and aponeurosis. Additionally, the semimembranosus, semitendinosus, and biceps femoris short head muscles were segmented. All segmentation was completed by one person.

Lengths and volumes of the muscles and tendons were found using the software's 3-D reconstruction feature. The muscle volume was plotted against the whole hamstring volume for each subject (Fig. 2). These data were then used to find a *gross cross-sectional area* (CSA) for each muscle and tendon:

$$CSA=(V_m/L_m)\,, \qquad (1)$$

where (V_m) is the volume measured for each muscle and (L_m) is the superior-inferior length measured parallel to the axis of the MRI scan. The physiological cross-sectional area (PCSA) for the BFlh was calculated as:

$$PCSA=(CSA)(L_m/L_f^0), \qquad (2)$$

where (L_m/L_f^0) is the muscle length to optimal fiber length ratio taken from literature [2].

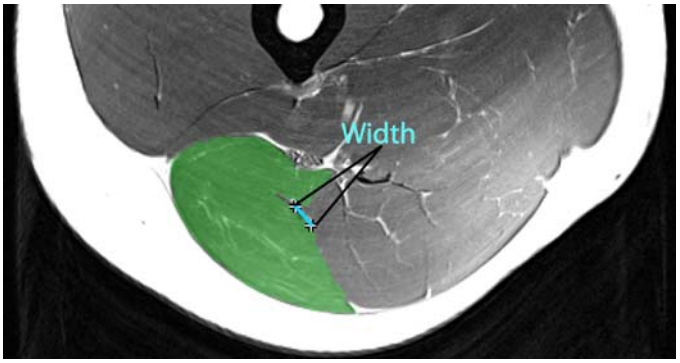

Figure 1: Axial MR image. The BFlh has been segmented (green). This slice was determined to be the representative slice. The BFlh proximal aponeurosis width (blue) was also calculated.

From each subject's image set we chose a representative slice, defined as the most distal slice at which the proximal BFlh aponeurosis was external of the BFlh (Fig.1). From this slice, we determined the width of the BFlh's proximal aponeurosis (Fig. 1).

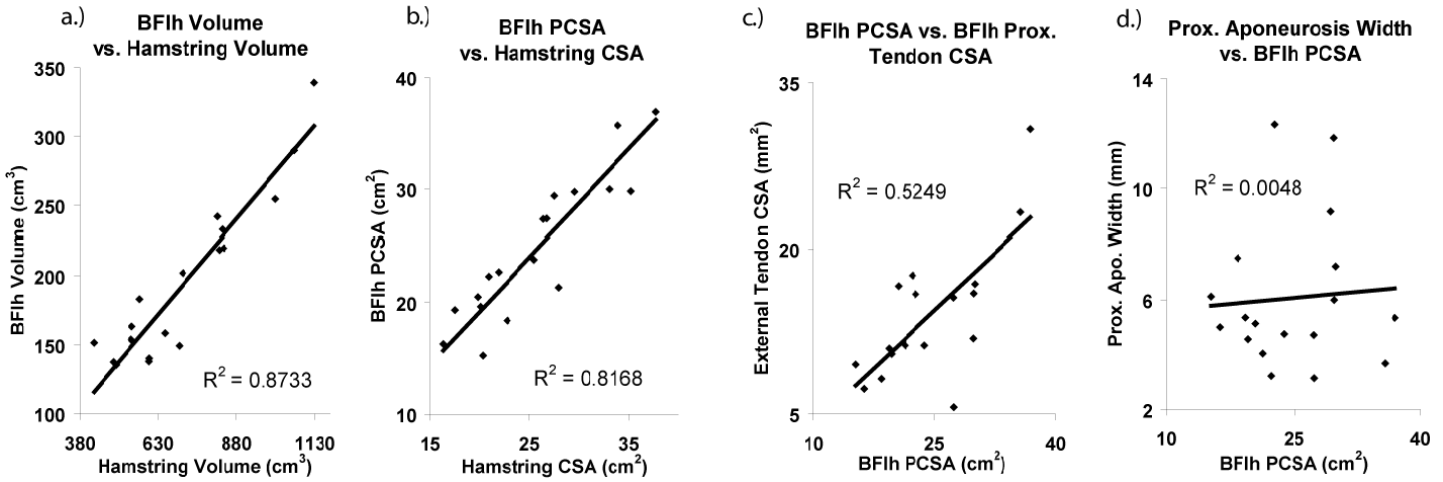

Figure 2: Morphological correlations between BFlh and hamstring (**a**. and **b**.) and between BFlh and tendons (**c**. and **d**.). **a.)** BFlh volume vs. whole hamstring volume for each subject (n=18). **b.)** BFlh PCSA vs. whole hamstring CSA for each subject (n=18). **c.)** Average CSA of the BFlh proximal external tendon vs. BFlh PCSA (n=17). **d.)** Proximal BFlh aponeurosis width vs. BFlh PCSA (n=18). Strong linear correlations were found for **a**.) and **b**.) with trend lines fixed to cross the origin (R^2=0.8733 and R^2=0.8168, respectively). Relationships shown in **c**.) and **d**.) show poor correlation (R^2=0.5249 and R^2=0.0048, respectively).

RESULTS

87% of the subjects' BFlh volumes could be predicted by a linear function of hamstring volume (Fig. 2a). 82% of the subjects' BFlh PCSAs could be predicted by the summed hamstring CSAs (Fig. 2b). The BFlh volume as a percentage of the whole hamstring volume (mean ± SD) was 0.275±0.034 while the BFlh PCSA as a percentage of the summed hamstring CSA was 0.312±0.035,

The relationships for tendon and aponeurosis measurements compared to BFlh PCSA show much less correlation. Average external tendon cross-sectional area exhibited a weak correlation with BFlh PCSA (R^2=0.52) (Fig. 2c). Proximal aponeurosis width showed no effective correlation with BFlh PCSA (R^2=0.005) (Fig. 2d).

CONCLUSIONS

Previous studies have found that muscles in a given muscle group scale linearly in volume and in PCSA with one another [4]. In this study, we also found that the volumes of the BFlh of healthy subjects scale linearly with whole hamstring volume and that BFlh PCSA is likewise scalable with hamstring CSA.

However, we observed that proximal external tendon and aponeurosis morphologies are variable across healthy subjects. It is commonly assumed that the average cross-sectional area of the tendon scales with the muscle PCSA [3]; however, we found only a weak correlation between tendon cross section and muscle PCSA.

It has been suggested that proximal aponeurosis morphology affects strain distributions within the muscle and therefore may be an indicator of muscle injury susceptibility [1]. In this study, we found a range of aponeurosis morphologies among 18 healthy subjects. This suggests that hamstring tissue strains and injury susceptibility may vary substantially across a normal population. A related study [5] explores the relationship between aponeurosis dimensions and localized strains in the muscle using functional MRI.

REFERENCES

1. Rehorn, MR and S.S. Blemker. *Journal of Biomechanics*, in review, 2010.
2. Ward, SR, et. al. *Clin. Orthop. Relat. Res.* **467**, 1074-1082, 2009.
3. Zajac, FE. *Crit Rev Biomed Eng*. **17**,4: 359-411, 1989.
4. Holzbaur, KRS et. al. *J Biomech* **40**, 742-749, 2007.
5. Fiorentino, NM et al., *Submitted to ASB*, 2010.

ACKNOWLEDGEMENTS

We would like to thank Micheal Rehorn, Amy Silder, and Darryl Thelen. Funding for this work was provided by NIH grant R01 AR 056201.

ACTIVE FORCE ENHANCEMENT AS A SOURCE OF SSC ENHANCEMENT

Matthew TG Pain[1], Erica Buckeridge[2], Thomas D O'Brien[3] and Stephanie E Forrester[4]

[1]SSEHS, Loughborough University. [2]Human Performance Group, Imperial College. [3]Sport, Health and Exercise Science, University of Hull. [4]STI, Loughborough University.
email: m.t.g.pain@lboro.ac.uk; web: www.lboro.ac.uk

INTRODUCTION

Force enhancement following active muscle stretch has a component characterized by an increase in isometric force, compared to an isolated isometric contraction, which decays exponentially with time, and is commonly called active force enhancement (AFE). It been observed in electrically stimulated muscle and under some voluntary conditions [1, 2].

The Stretch Shorten Cycle (SSC) occurs when an active muscle-tendon unit is forcibly stretched before it shortens, giving rise to increased levels of shortening force when compared to an isometric preload. Introducing a delay in the coupling time (CT) between the eccentric and concentric actions reduces SSC enhancement in an exponential manner [3] (Here CT is used to denote time after the eccentric has finished even if there is no concentric phase.). Different mechanisms for the SSC have been suggested (see review edition of the Journal of Applied Biomechanics, Issue 4 volume 13, 1997) however the exact contributions to overall performance remains equivocal. In this review Edman stated that AFE could not be a mechanism as a very small shortening of the muscle fiber removes AFE as reported in [4]. However, this mechanism has not been examined *in vivo.* This study aimed to determine whether SSC force enhancement could occur directly from the AFE state under sub-maximal voluntary and electrically stimulated conditions. Voluntary and electrical stimulation protocols were used to complement each other as there can be difficulty maintaining constant sub-maximal efforts and stimulation will not fully represent voluntary recruitment processes.

METHODS

Nine healthy subjects (4 female, 5 male; mean ± SD age = 28.6 ± 7.8 years; body mass = 70.5 ± 14.1 kg) gave informed consent. Seven subjects took part in the voluntary condition and six took part in the sub-maximal electrical stimulation condition. Subjects performed pure isometrics at five knee angles and eccentric-isometrics with a long isometric phase to look at AFE. They also performed sub-maximal knee extension SSC with six CT delays (0.07, 0.3, 0.6, 1, 2, 3 s) on a CON-TREX dynamometer for both conditions with 50^{o} of stretch at $60^{o}s^{-1}$, and the turnaround point at 90^{o} of knee flexion. Two types of SSC were performed in each condition, one with a concentric phase at $60^{o}s^{-1}$, and one with a fixed joint angle (SSCiso). In all cases, after the required CT subjects voluntarily went from sub-maximal to maximal effort extension as quickly as possible.

Stimulation trials involved taping two carbon-rubber electrodes thinly coated with conductive gel, over the skin covering RF, VL muscles and VM (7 x10 cm electrodes; cathode 8 cm proximal to patellar; anode 10 cm proximal to cathode). Tetanic contractions lasting the length of the SSC were evoked with a train of electrical impulses, square wave pulses, 0.1 ms duration at a frequency of 50 Hz. For voluntary trials quadriceps EMG was used to verify a constant level of activation and trials that did not conform were rejected. Data were normalized per subject and pooled for analysis.

RESULTS AND DISCUSSION

Subjects sub-maximally activated their quadriceps to 43.5 ± 9.7% of their MVC. Subjects were stimulated to produce torques at 25 to 40% of their MVC. All subjects were measured on the descending limb of their torque-angle curve.

Voluntary

Following an eccentric pre-stretch, AFE decayed exponentially with time and there was a significant increase in torque compared to an isolated isometric

for CT up to 0.6 s (Fig. 1). There was a significantly better exponential fit ($p < 0.05$) when CT=0 was removed, indicating at least a two stage process for the decrease in torque with increasing CT between the end of eccentric and an isometric. The fit without CT=0 gave a half life of 0.60 s:

$$Tn(t) = 0.56 + 0.34e^{-0.87CT} \qquad (R^2 = 0.979) \quad 1.$$

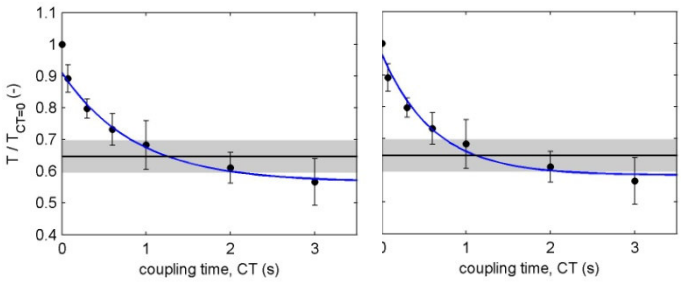

Figure 1. AFE group mean normalised torque versus CT. Fit without CT=0, left, and fit with CT=0, right. Black circles are mean ± SD, solid blue line is the exponential fit, shaded region is the mean ± SD for the pure isometric trials.

Torque increased, with no drop, when maximal effort was instigated during the SSCiso (Fig. 2). Similarly, torque increased and showed no drop during the SSC (Fig. 2) (once corrected for the small consistent drop seen in all trials, at all turnarounds including eccentric to isometric).

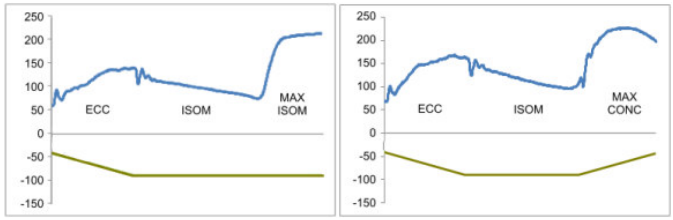

Figure 2. Example torque-time and angle-time profiles for SSCiso, left, and SSC, right.

During the SSC significantly greater torques were developed both at the start of the concentric phase and after 10° of extension for shorter CT. Concentric torques measured at 10° of extension decayed exponentially with increasing CT:

$$Tn(t) = 0.88 + 0.63e^{-0.85CT} \qquad (R2 = 0.938) \quad 2.$$

Average half life values for the exponential decay of AFE and SSC concentric at 10° were not significantly different (p=0.426).

Stimulated

Following an eccentric pre-stretch, AFE decayed exponentially with time and there was a significant increase in torque compared to an isolated isometric for CT up to 2 s. As observed in the voluntary trials, there was a significantly better exponential fit ($p < 0.05$) when CT=0 was removed. The fit, without CT=0 gave a half life of 0.56 s:

$$Tn(t) = 0.75 + 0.15e^{-0.81CT} \qquad (R^2 = 0.975) \quad 3.$$

A major difference compared to the voluntary results is that torque never dropped below the pure isometric level. Again torque increased, with no drop, when maximal effort was instigated during the SSCiso and the SSC. However, significant differences for torques measured during the concentric phases with respect to CT were only found at the start of the concentric phase not into the concentric phase. The torques into concentric, normalized to CT=0, were much greater in the stimulated condition compared to the voluntary condition. At 10^o of extension, or after 0.34 s, and at maximum, concentric torque values were similar for all CT and all tended to the same value. This could due to the superposition of different stimulated and voluntary recruitment strategies.

CONCLUSIONS

Whilst AFE decayed exponentially the onset of a maximal concentric contraction could increase directly from the AFE value, allowing higher concentric torques to be achieved when started from a shorter CT. This occurred in both voluntary conditions and in the better controlled stimulated conditions. For the voluntary condition decay patterns for AFE and SSC were not significantly different, and thus it appears that AFE could account for some of the SSC enhancement at sub-maximal to maximal effort levels.

REFERENCES

1.Edman KA, et al., *J Physiol* **281**, 139-155, 1978.
2.Lee E-J, & Herzog W, *J Physiol* **545**, 321-330, 2002.
3.Wilson et al. *Med Sci Sport Exerc* **23**, 364-370, 1991.
4.Piazzesi G. et al.. (1992). J. Physiol. **445**, 659-711

A UNIQUE METHOD OF MEASURING DYNAMIC RATE OF TORQUE DEVELOPMENT: COMPARISON OF EXPLOSIVE POWER ATHLETES AND CONTROLS

Neale A Tillin, Matthew TG Pain, Hannah E Oguz, Guy A Lewis, and Jonathan P Folland

[1]School of Sport, Exercise and Health Sciences, Loughborough University, Loughborough, UK
email: N.A.Tillin@lboro.ac.uk , web: http://www.lboro.ac.uk/departments/ssehs/

INTRODUCTION

Previous research has investigated the neural and mechanical determinants of rate of torque development (RTD) during isometric contractions [1,2]. However, functional activities where RTD is important are typically dynamic. Furthermore, the determinants of RTD in dynamic conditions may differ to those observed in isometric situations; yet no previous investigations have examined dynamic RTD. Torque production during dynamic contractions is greatly affected by changes in joint angle and velocity, so these variables must be controlled to effectively investigate the determinants of dynamic RTD. The current study employed a unique method of measuring RTD during concentric and eccentric contractions of the knee extensors, and investigated the neural and mechanical determinants of dynamic RTD in explosive power athletes, a group expected to have a high capacity for RTD, and untrained individuals.

METHODS

Ten elite male explosive power athletes (primarily sprinters and jumpers) and nine untrained males (controls) completed a series of fast voluntary and involuntary concentric and eccentric knee extensions on a CON-TREX dynamometer. In each trial the crank arm slowly moved to the start position for either a concentric (-81º from full knee extension) or eccentric (-14° from full knee extension) effort. On reaching the start position the crank arm accelerated from stationary at a constant 2000°/s^2 for 225 ms to 450°/s, moving 52°, before rapidly decelerating to stop at the end of the range of motion (67°). For the voluntary contractions participants were instructed to extend their knee as 'fast and hard' as possible at the start of the acceleration phase. Voluntary contractions with no discernable countermovement or pretension and where torque onset occurred at 2-6º into the acceleration phase were considered for analysis. For the involuntary contractions supramaximal octets (300 Hz) were evoked via electrical stimulation of the femoral nerve after 4 ± 1° of acceleration (at 125 ± 25°/s). Evoked supramaximal octets provide a measure of the maximal capacity of the muscle-tendon unit for RTD [1]. Participants completed 15-20 voluntary, and 3 evoked contractions in both concentric and eccentric conditions. To remove inertial affects of the shank the average torque-time profile of three passive trials (for either concentric or eccentric conditions) was subtracted from the torque-time profile of each contraction. Torque at 25 ms intervals from onset and peak RTD were assessed for all conditions. Electromyography (EMG) was also collected from the three superficial quadriceps muscles during the voluntary efforts. To determine agonist activation over different time intervals, root mean square EMG of each muscle was normalised to an evoked maximal M-wave, and averaged across the quadriceps. On a separate occasion participants completed a series of maximal isometric and isovelocity contractions of the knee extensors to determine their strength as a function of knee angle and velocity.

RESULTS AND DISCUSSION

During the evoked concentric contractions peak force and peak RTD was greater in the athletes (+22% and +29%, respectively; Fig. 1A); as was torque at 25 and 50 ms from onset in the evoked eccentric contractions (Fig. 1B). Collectively these results demonstrate a greater capacity of the muscle tendon-unit for both concentric and eccentric RTD in the athletes. Surprisingly, there was no difference between the groups in torque achieved at any time point during the voluntary concentric efforts (Fig. 2A), suggesting that the athletes were unable to utilize their enhanced capacity for RTD in these

conditions. On the other hand, the athletes torque at 150 ms from onset during the voluntary eccentric contractions was greater (+28%; Fig. 2B), suggesting that discrepancies in dynamic RTD between athletes and controls are more pronounced during eccentric than concentric contractions.

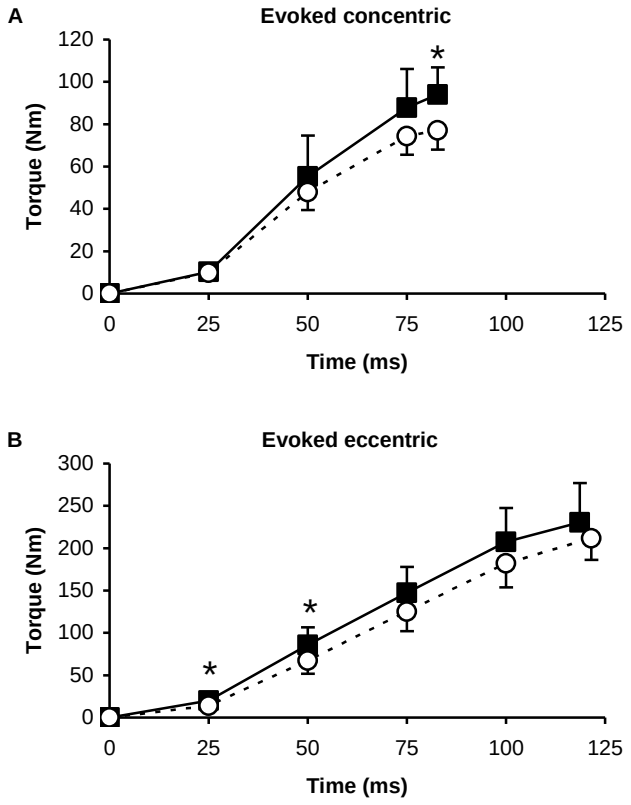

Figure 1: Torqe-time curves of athletes (filled squares) and controls (open circles) achieved during evoked concentric (A) and eccentric (B) knee extensions. *(P<0.05).

Volitional agonist activation during either the concentric or eccentric contractions was similar in both groups, which may explain the limited differences in voluntary RTD. This is in contrast to a recent study which showed greater agonist activation of athletes in 0-50 ms of explosive isometric contractions [2]. The dynamic conditions of the current study are likely to require greater coordination than isometric situations which may have reduced the possibility of observing group differences. Nevertheless, when the data were collapsed across both groups torque achieved at 100 ms was correlated with agonist activation over the same time period, in both concentric (R=0.563; P<0.05) and eccentric contractions (R=0.468; P<0.05). This suggests that initial agonist activation is an important determinant of dynamic RTD. Further analysis should involve normalizing torque to strength, as a function of joint angle and velocity, to establish the contribution of all neural and mechanical determinants.

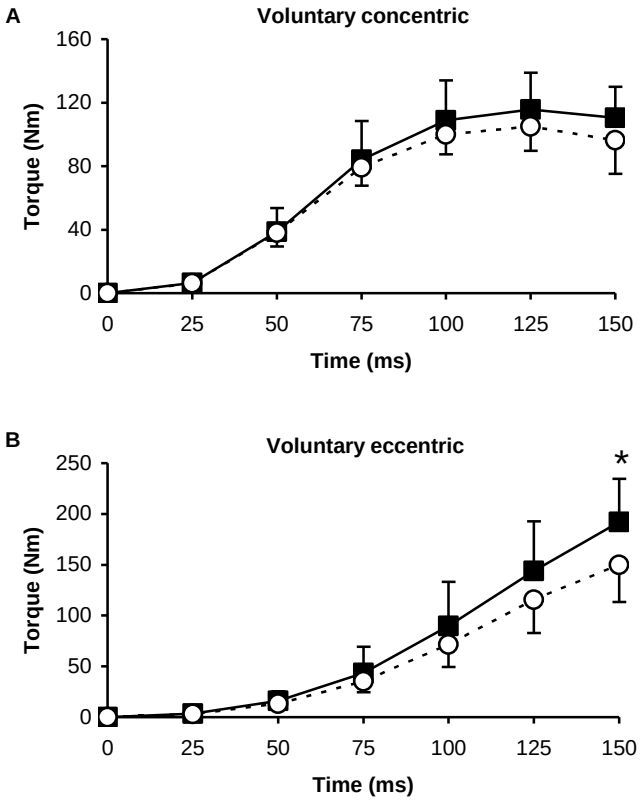

Figure 2: Torqe-time curves of athletes (filled squares) and controls (open circles) achieved during explosive voluntary concentric (A) and eccentric (B) knee extensions. *(P<0.05).

CONCLUSIONS

Discrepancies in dynamic RTD between explosive power athletes and controls are more pronounced in eccentric than concentric contractions. This is the first study to show that initial agonist activation is an important determinant of dynamic RTD, however further analysis is required to establish the contribution of all neural and mechanical factors.

REFERENCES

1.De Ruiter, et al. *J Appl Physiol* **97**, 1693-1701, 2004.
2.Tillin, et al. *Med Sci Sports Exerc* **42**, 781-790, 2010.

ACKNOWLEDGEMENTS

We would like to extend our sincere gratitude to Dr Mickael Begon for his technical assistance.

MECHANICAL MALADAPTATIONS TO ECCENTRIC EXERCISE RESULT IN SUSTAINED HYPERTROPHIC SIGNALING IN SKELETAL MUSCLE CELLS

[1]Sarah M. Abshire, [2] Thomas M. Best, and [1]Timothy A. Butterfield

[1]University of Kentucky, Lexington, KY, USA
[2]The Ohio State University, Columbus, OH, USA
email: tim.butterfield@uky.edu, web: http://www.mc.uky.edu/muscle/

INTRODUCTION

Long term eccentric exercise results in functional, mechanical adaptations including increases in peak isometric force and a rightward shift in the force-length relationship (FLR) [1]. Recently, we have shown that serial sarcomere number adaptations influence the FLR shift following long term eccentric exercise (EEX) [2], and that the magnitude of sarcomere number adaptation relates best to fiber strains during EEX [1]. Although mechanisms of mechanotransduction are beginning to be uncovered, we have shown that stretch activated ion channels (SAC) play an important role in the functional adaptations to EEX [2], whereby SAC blockade abrogated the expected rightward shift of the force-length relationship and isometric force increase during four weeks of EEX. We proposed the role of SAC in EEX-induced adaptation to be the mechanotransduction of fiber strain magnitudes to the activation of the mammalian target of rapamycin (mTOR) pathway [3], which has been established as the major hypertrophic pathway in skeletal muscle [4]. Phosphorylation of $p70^{S6}$kinase ($p70^{s6}k$) at the Threonine 389 (Thr389) site, which is analogous to the Threonine 412 phosphorylation site (Thr412), has been used as an indicator of mTOR pathway activation [5]. Therefore, the purpose of this study was to determine the effect of SAC blockade on the activation of the mTOR pathway following long-term EEX as evidenced by phosphorylation of p70s6k Thr389/412.

METHODS

Dorsiflexor muscles of two groups of New Zealand White (NZW) rabbits were subjected to chronic repetitive EEX (5 sets of 10 repetitions, 95^{o}-145^{o}, 3x/week) for four weeks to produce the expected functional adaptations in FLR and force [1,3]. Group 1 (SAC block) received daily intramuscular injections of streptomyocin (300mg/kg body weight) for the duration of the study. Group 2 (control) received sham injections [3]. After the final exercise bout, animals were allowed to recover for 1 week to allow completion of adaptive responses. One week later, a final EEX bout was performed, and rabbits were immediately euthanized and the tibialis anterior (TA) muscle was excised, separated into medial and lateral portions, frozen and stored at -80^{o}C.

Western blot analyses were performed on homogenized samples of the medial distal (MD) and lateral distal (LD) sections of the TA muscles. Samples were centrifuged and the supernatant proteins (50ug per well) were loaded onto 7.5% Tris-HCl gels. Proteins were then transferred onto PVDF blotting membranes and blocked with Odyssey blocking buffer at room temperature (RT) for 1h. Membranes were then incubated overnight at 4°C in primary antibodies (rabbit anti-$p70^{s6}k$, (1:1000) Santa Cruz Biotechnology, Santa Cruz, CA or mouse anti-$pp70^{s6}k$ Thr389/412, (1:1000) Cell Signal, Danvers, MA). Blots were washed with PBS then incubated in the appropriate secondary antibody (donkey anti-rabbit, (1:10,000) Licor, Lincoln, Nebraska or donkey anti-mouse (1:10,000) Licor, Lincoln, Nebraska) for 1h at RT. Blots were then washed in PBS then scanned on a Licor Odyssey system. Protein bands were quantified using software provided with the Licor Odyssey system.

RESULTS

Following 4 weeks of repetitive EEX, animals in the SAC block group had a trend towards a diminished level of native (non-activated) $p70^{s6}k$ in

the TA (42.3±22.7) when compared to levels in the control (SAC open) group (20.8±8.9, p=0.056) immediately after the final EEX bout. More importantly, the levels of activated (phosphorylated) $p70^{s6}k$ (Thr412) in both the LD and MD portions of the SAC blocked TA muscle were greater when compared to TA muscles in control animals (4.16±0.75 and 4.57±1.41 vs 3.35±0.47 and 3.12±0.69 respectively, $p \leq 0.05$, Figure 1).

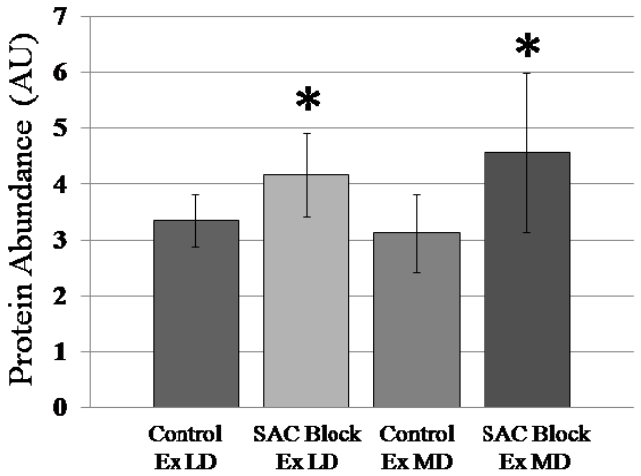

Figure 1: Phosphorylated p70 (Thr412) protein abundance in medial distal and lateral distal portions of the TA muscle. Mean ±SD.

DISCUSSION

Cell signaling through the mTOR pathway is maintained for hours following high force and mechanical loads in muscle [4]. However, the long term regulation and attenuation of the signal after muscle adaptations following weeks of EEX remain unknown. Previously, we reported maladaptations in mechanical function following 4 weeks of EEX in the SAC blocked group [3], including a leftward shift in the FLR with no change in isometric force. Mechanically, these functional maladaptations are in line with a loss of sarcomere number in series concomitant with diminished fiber lengths and no gain myofibril number in parallel.

Here, subjecting these maladapted and shorter muscles to one final EEX bout was a potent activator of the mTOR pathway when compared to control muscles, indicating a strong stimulus for muscle hypertrophy and adaptation even after 4 weeks of EEX. Because mechanical strain is a known stimulus for mTOR pathway activation and protein synthesis [4], it is conceivable that the maladapted fibers experience greater magnitudes of active strain during exercise, resulting in activation the hypertrophic mTOR pathway. Conversely, the control muscles experienced positive adaptations, including a rightward shift of the FLR, an indirect indicator of increased serial sarcomere number and fiber lengths [1]. Thus, during EEX through a given range, the adapted and lengthened fibers experience diminished mechanical strain, and diminished mTOR activation.

CONCLUSIONS

It is expected that the mTOR pathway would be activated following unaccustomed EEX, to increase protein synthesis essential for hypertrophy and exercise-induced adaptations. Here, we demonstrate an attenuated mTOR response following 4 weeks of EEX in muscles that exhibit a rightward shift of the FLR, when compared to muscles that did not adapt through blockade of the SAC channels. We propose that higher mechanical strains in shorter, maladapted fibers result in a sustained mTOR signaling response [6]. The mechanisms whereby SAC blockade abrogates functional adaptations in light of mTOR activation remain to be elucidated.

REFERENCES

1. Butterfield TA and Herzog W. *Pflugers Archiv* **451**, 688-700, 2006.
2. Butterfield et al. *J Appl Physiol* **99**, 1352-1358, 2005.
3. Butterfield TA, Best TM. *Med Sci Sports Exerc*, **41**, 351-6, 2009.
4. Miyazaki M and Esser KA. *J Appl Physiol* **106**, 1367-1373, 2009.
5. Alessandri-HaberN, et al. *J Neurosci*, **29**, 6217-28, 2009.
6. Butterfield TA *Exercise and Sport Sciences Reviews* 2010 (in press)

ACKNOWLEDGEMENTS

This work was funded through the American College of Sports Medicine Research Endowment and The Ohio State University Pomerene Chair in Family Medicine. The authors wish to thank Dr. Karyn Esser and Ms. Amy Ferry for technical assistance.

VARIATION IN MUSCLE MODEL OUTPUT USING CADAVER-SPECIFIC MODEL PARAMETERS

Benjamin W. Infantolino, and John H. Challis

The Pennsylvania State University, University Park, PA, USA
email: bwi100@psu.edu

INTRODUCTION

Musculoskeletal models typically use cadaveric data for the necessary muscle architectural parameters. It has been shown that variability exists in muscle architectural parameters between subjects [1, 2]. This variability may affect model output in particular because it cannot be reduced by normalization with respect to parameters indicative of muscle function [2].

The purpose of this study was to investigate the effect of variations in musculoskeletal architecture on muscle model output. Cadaveric First Dorsal Interosseous (FDI) muscles were fully characterized to produce all the necessary architectural parameters for a muscle model. These muscle parameters were used in a Hill-type muscle model.

METHODS

FDI muscles were removed from eight cadaver hands via blunt dissection. Analysis produced eight complete sets of muscles model parameters. Pennation angle (θ) was measured using a goniometer, muscle mass was measured using an electronic scale, tendon length (*lt*) and fascicle length (*lf*) was measured using a standard rule, and optimal fascicle length was estimated using light microscopy. Physiological cross-sectional area (PCSA) was calculated using muscle mass, optimal fascicle length, pennation angle, and muscle density from Mendez and Keys [3]. Muscle moment arms were determined using the tendon excursion method [4].

The Hill-type muscle model used the measured architectural parameters and a generic force-length curve based [5]. Figure 1 illustrates the model structure. The tendon was allowed to stretch 4% of its length under maximal muscle force. Cadaver-specific architectural muscle properties were used to create eight cadaver specific muscle models (data sets 1-8). In addition, the cadaver architectural parameters were averaged to produce an "average" cadaver (data set 9). Finally, since many muscle models base their parameters on the data of Wickiewicz et al. [6], we used the three muscles from our cadaver set that best exemplified the variability in the muscles in the Wickiewicz et al. set. These muscles were picked based on the coefficient of variation for the estimated optimum fascicle length in the Wickiewicz et al. set, the mean data for these three muscles comprised data set 10.

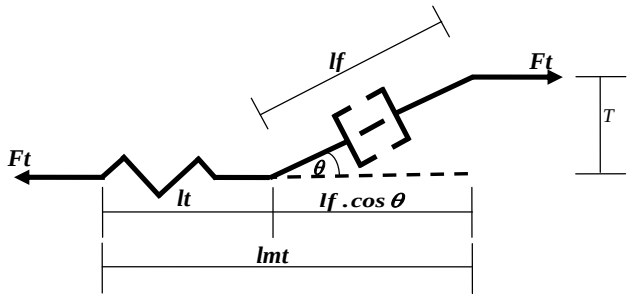

Figure 1: A schematic of the muscle model.

The model's output was the moment-angle curve in the functional range of motion of the muscle. The index finger was moved from 0 to 20^o of abduction in half degree increments. At each position, a maximum isometric muscle contraction was simulated. The model was allowed to come to steady-state before it moved on to the next finger position. From this data, the functional moment-angle curve of each muscle was determined.

Moments (% of maximum) produced at a fixed finger angle (10^o) were compared for each of the 10 data sets. In addition, the fascicle lengths (% of estimated optimal fascicle length) at a fixed finger angle (10^o) were compared across all conditions.

RESULTS AND DISCUSSION

Normalized muscle forces and fascicle lengths for the cadaver-specific models were not in agreement with either the average cadaver model (data set 9) output or data set 10 (Table 1).

In all cases, the models predicted that the FDI muscle would work on the ascending limb of the force-length curve, even when activation was reduced to 50% of maximum. However, none of the models predicted that the muscle would work on the plateau of the force-length curve. This is in contrast to the assumption common in models that muscles generally act at or near the plateau throughout their effective range.

The range of predicted cadaver-specific muscle moment at 10^o was large (12.1 to 44.5%) as was the range of fascicle lengths (27.3 to 55.0% of optimum length). Data set 10 produced values that were larger than those of the average cadaver for the FDI. Both data set 9 (average data) and data set 10 (Wickiewicz et al. based cadaver model) outputs were within the range of the cadaver-specific output. In all cases, the maximum force was predicted at 20^o of abduction.

These results indicate that cadaver-specific model parameters greatly affect model output. This is important as models typically contain cadaveric data and the subject that the model is intended to simulate may not resemble the cadaver. This study highlights the potential need to use subject-specific musculoskeletal parameters in models, to reduce the error that is associated with using data that does not resemble the subject. The other possibility may be to scale the cadaver based musculoskeletal model parameters to the experimental subject, however variability does still appear after scaling [1].

CONCLUSIONS

In this study, a model was constructed that used cadaver-specific inputs for the muscle architecture. Eight fully characterized FDI muscles were used to create eight cadaver-specific musculoskeletal models. In addition to the eight muscles, an average muscle and a muscle based on Wickiewicz et al. were used as model inputs. The cadaver-specific model outputs varied greatly and differed from both the average cadaver output and the Wickiewicz et al. cadaver for the FDI. Based on the evidence from the analysis of the FDI, the differences between data sets suggest that subject-specific musculoskeletal model parameters must be taken into account when creating musculoskeletal models to investigate muscle function.

REFERENCES

1. Duda GN, et al. *J Biomech* **29**, 1185-1190, 1996.
2. Infantolino BW. and Challis JH. *J Anatomy* **216**, 436-469, 2010.
3. Mendez J. and Keys A, *Metabolism* **9**, 184-188, 1960.
4. An KN, et al. *J Biomech* **16**, 419-425, 1983.
5. Hatze H. *Myocybernetic Control Models of Skeletal Muscle*. University of South Africa Press, 1981.
6. Wickiewicz TL, et al. *Clin Orthop Rel Res* **179**, 275-283, 1983.

ACKNOWLEDGEMENTS

We would like to acknowledge Dan Gales for the use of cadavers from Lock Haven University.

Table 1: Model outputs for 10 different sets of cadaver data. (Data sets 1-8 are cadaver-specific, data set 9 is the mean from the cadaver data, and data set 10 matches the variance seen the Wickiewicz et al. data.)

	Muscle									
Parameter	**1**	**2**	**3**	**4**	**5**	**6**	**7**	**8**	**9**	**10**
Muscle Force (% max)	15.3	12.1	41.5	35.6	35.3	17.8	33.6	44.5	26.5	34.7
Fascicle Length (% max)	31.5	27.3	53.1	49.2	49.0	34.3	47.8	55.0	42.2	48.6

TRACKING CONNECTIVE MATERIAL IN MUSCLE

[1]Benjamin W. Infantolino, [1]Jessica N. Hughes, [2]Thomas Neuberger and [1]John H. Challis

[1]Biomechanics Laboratory, The Pennsylvania State University, University Park, PA, USA
[2]Huck Institute of Life Sciences, The Pennsylvania State University, University Park, PA, USA
email: bwi100@psu.edu

INTRODUCTION

Connective tissue in muscle is an important aspect of whole muscle function. It has been proposed that the connective tissue can transmit, to the external tendon, the force produced by the contractile material [1]. The amount of connective tissue has been investigated with various techniques in the literature. Mobley and Eisenberg [2] viewed cross-sections of muscle fibers and estimated the amount of connective tissue to be 17% of the whole muscle volume. Goldspink compressed mouse muscle between plates and measured the amount of fluid compressed from the muscle [3]. In this experiment, the connective tissue was estimated to be 25% of whole muscle volume. In muscle models, the specific tension used is typically based upon isolated muscle fiber preparations because the muscle fibers can be fully activated [4]. This creates problems when using the specific tension values in muscle models as the muscles to be modeled have connective tissue and therefore the cross-sectional area of the muscle will include both contractile and connective tissues. This error will lead to an over estimation of the force generating capabilities in the muscle.

By tracking the connective tissue in muscle the arrangement of the contractile tissue may be assed. This arrangement is typically described in a two-dimensional sense as pennation angle. However, since muscle is three-dimensional, the arrangement of muscle should be described in three-dimensions.

There were two purposes in this study. The first was to track the connective tissue in the First Dorsal Interosseous (FDI) muscle in order to gain a better understanding of the arrangement of contractile tissue in muscle, under the assumption that the muscle fascicles run in the gaps between the connective tissue. The second purpose was to assess the percentage of connective tissue in whole muscle.

METHODS

A singe FDI muscle was removed from an embalmed cadaver using blunt dissection techniques. To reduce the MR scanning time the tissue was immersed in a 1.5% Magnevist (Bayer Health Care, Wayne, NJ) phosphor-buffered solution for 7 days. The achieved short T1 (33 ms) and T2 (7 ms) times allowed for fast imaging with a high contrast-to-noise ratio. To prevent the tissue from drying out and to minimize magnetic susceptibility artifacts during scanning the specimens were surrounded by a flourinert liquid FD-43 (3M, St. Paul, MN). All experiments were conducted on a vertical 14.1 tesla Varian (Varian Inc., Palo Alto, CA) imaging system with direct drive technology. A millipede resonator (Varian) with an inner diameter of 40 mm was used to acquire three-dimensional spin echo images of the muscle tissue. Images up to an isotropic resolution of 50 μm were acquired. A standard imaging experiment with an isotropic resolution of 75 μm comprised a field of view of 45 x 20 x 20 mm^3 and a matrix size of 600 x 268 (75% partial fourier: 201) x 268. With 12 averages and a repetition time of 75 ms (echo time 11.7 ms) the total scan time was 13.5 hours. Matlab (The MathWorks, Inc., Natick, MA) was used for post-processing. By zero-filling each direction with a factor of two the pixel resolution of the standard imaging experiment was 37.5 μm^3.

Mimics (Materialise, Leuven, Belgium) software was used to analyze the MRI images. Connective tissue was identified by a thresholding algorithm in Mimics. The boundaries of whole FDI muscle were identified by one of the authors in the software which allowed the thresholding to be contained to the whole muscle and not any noise on the image

outside of the muscle. Volumes were generated for both the outlined whole muscle and the connective tissue.

RESULTS AND DISCUSSION

The percentage of connective tissue in whole muscle was calculated by dividing the volume of connective tissue by the volume of whole muscle. It was found that the connective tissue accounted for 13.9% of the whole muscle volume.

While tracking the connective tissue, it was found that the contractile tissue was arranged in a manner more complex than the simple two-dimensional arrangement typically presented (Figure 1). The contractile material appeared to be arranged in a spiraling fashion, making approximately a quarter turn along the length of the muscle. In addition, the fascicle did not span the entire length of the muscle belly.

The amount of connective tissue in whole muscle is important in muscle modeling so that corrections can be made when scaling the specific tension measured in isolated muscle preparations to whole muscles. The findings of a complex arrangement of contractile material in whole muscle indicates that perhaps a simple two dimensional description of muscle arrangement is not enough for generating accurate muscle models. However, since the complex arrangement has not been thoroughly quantified, the effect of the arrangement on muscle function cannot be investigated yet.

CONCLUSIONS

Connective tissue in whole muscle has implications for both the specific tension produced by the muscle as well as the functional significance of contractile tissue arrangement in whole muscle. MRI imaging can be used to investigate both of these areas. Currently, the techniques can only be used to investigate cadaveric tissues. However, further investigation of cadaveric tissue may shed light onto the effect connective tissue has on tissue *in vivo*.

This study has shown for the FDI that connective tissue occupies 13.9% of whole muscle volume. The fascicles in the gaps of the connective tissue are arranged in a complex three-dimensional arrangement with fascicle lengths not as great as muscle belly length.

REFERENCES

1. Huijing PA, *J Biomech* **42**, 9-21, 2009.
2. Mobley BA, and Eisenberg BR, *J Gen Physiol* **66**, 31-45, 1975.
3. Goldspink G, *Can J Physiol Pharmacol* **44**, 765-775, 1966.
4. Zajac FE, *Crit Rev Biomed Eng* **17**, 359-411, 1989.

ACKNOWLEDGEMENTS

We would like to acknowledge the use of the Higher Performance Computing Group facilities at Penn State.

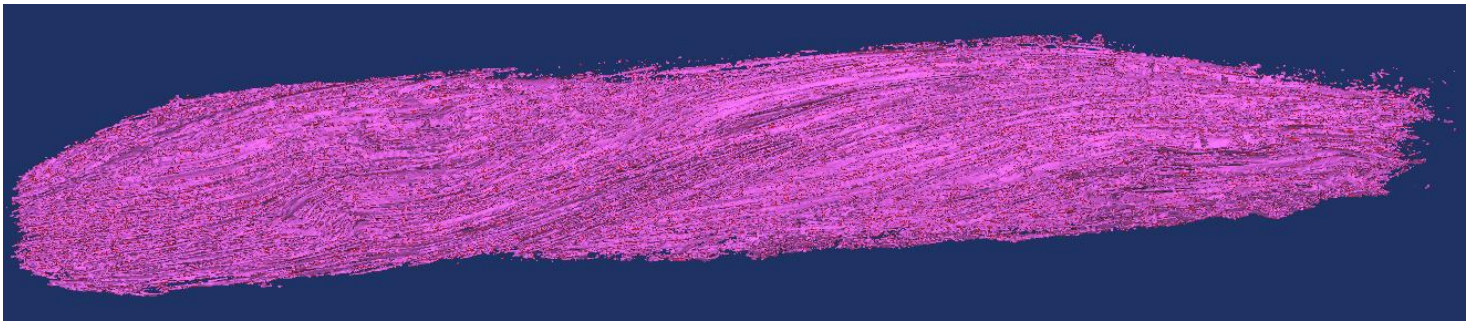

Figure 1: Oblique view of the connective tissue in FDI muscle.

A 3D MODEL DEMONSTRATES THE EFFECTS OF INCREASED ACTIVATION ON NONUNIFORM STRAINS IN MUSCLE

Michael R. Rehorn, Silvia. S. Blemker

University of Virginia, Charlottesville, VA, USA
email: mrr6r@virginia.edu, web: http://mae.virginia.edu/muscle

INTRODUCTION

Muscles are most commonly injured during lengthening contractions [1]. These strain injuries are thought to result from high-localized regions of tissue strain. For example, imaging studies (e.g., [2]) have shown that tissue strains are elevated in the muscle tissue near the proximal aponeurosis of the biceps femoris long head muscle, which is precisely where the muscle is commonly injured. Imaging studies have also shown that increasing activation level increases the magnitude of peak localized strains in muscle [3]. These findings may explain why the degree of fiber damage following lengthening contraction correlates with the overall magnitude of lengthening and activation [4].

The goal of this work was to use three-dimensional (3D) finite-element modeling of muscle to explore the mechanisms by which increasing muscle activation leads to increased strain distributions during lengthening contractions. The results will be used to gain insights into the relationship between whole muscle activation and injury patterns.

METHODS

We created a 3D finite element model (FE) of muscle with dimensions consistent with anatomical measurements of the biceps femoris longhead [5]. This muscle was chosen for analysis because it is a commonly injured hamstrings muscle [6]. The measurements used to describe the model were the aponeurosis lengths, aponeurosis widths, aponeurosis thicknesses, external tendon lengths, and muscle width (Fig. 1). The model was further simplified so that all aponeurosis dimensions were symmetric. Aponeurosis length, width, and thickness were 180*mm*, 40*mm*, and 1*mm*, respectively, while external tendon lengths and muscle widths were adjusted to 5.6*mm* and 35*mm* respectively. This simplification allowed us to isolate the effects of activation without considering geometrical effects.

Muscle and tendon tissue were represented using a transversely isotropic, hyperelastic, quasi-incompressible constitutive model [7]. For muscle, the model includes both active and passive properties that are consistent with the known force-length behavior of skeletal muscle. Fiber maps were defined such that the fiber directions described fibers that extended from the proximal aponeurosis to the distal aponeurosis (Fig. 1).

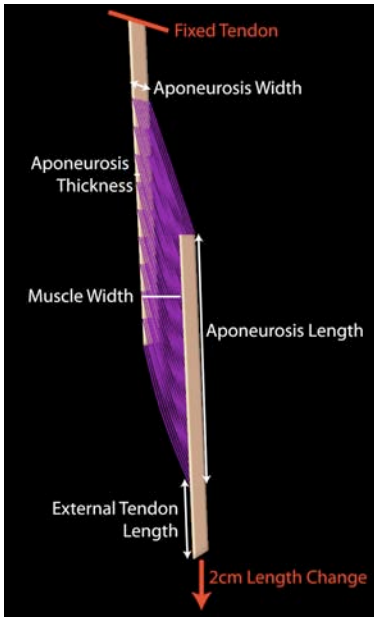

Figure 1. 3D finite-element model. A FE model was constructed with dimensions based on measurements of the BFLH muscle. In all simulations a 2*cm* length change was applied to the distal external tendon.

In order to investigate the effects of activation on the strain distributions within the model, we conducted four separate simulations. In all simulations, a 2*cm* displacement was applied to the end of the distal tendon while the superior region of the proximal tendon was fixed (Fig. 1). The activation profile was different in each case. In the first case, muscle was passively lengthened (the activation level was set to 0%). In the three consecutive tests, the muscle was linearly activated from 0% to 25%, 50%, and 75%, respectively, while lengthening. These loading profiles allowed

us to assess the strain distributions during eccentric contraction. The variation in along-fiber stretch distribution was analyzed in each model. The along-fiber stretch (λ) was defined as $\lambda = \sqrt{\mathbf{a}_o \cdot \mathbf{C} \cdot \mathbf{a}_o}$ where $\mathbf{a}_o$ is fiber direction and $\mathbf{C}$ is the right Cauchy-Green deformation tensor [3]. Furthermore, we sampled the fiber maps in several locations to obtain representative "fibers" that we could track throughout the course of a simulation. Along-fiber stretch values were sampled at fifty evenly distributed points along the length of each representative fiber in order to quantify how along-fiber stretch varied along fibers.

RESULTS AND DISCUSSION

As activation level increased, the strains within the model became more non-uniform (Fig. 2). In the passive case, strains were nearly uniform (Fig. 2B); however, with 75% activation, some regions of the muscle were shortening while others were lengthening (Fig. 2A).

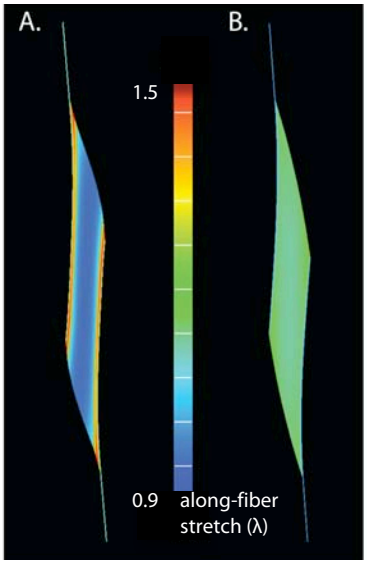

Figure 2. Strain distributions. Along fiber stretches are plotted for the 75% activation case (A) and the passive (0% activation) case (B). Values of along-fiber stretch greater than 1.0 indicate tissue lengthening, while values less than 1.0 indicate tissue shortening.

For all fibers in the model, peak along-fiber stretch within each fiber increased with activation level. By contrast, the total fiber stretch for all fibers decreased with activation level (Fig. 3), which is consistent with the fact that there was more stretch in the aponeuroses and external tendons with increased activation. This analysis shows that, for the same overall musculotendon length changes, the muscle fibers have lower average length changes with activation, put increased peak strains along each fiber. Analysis of the models showed that the increase in peak strains with activation is due to increases in the amount of bulging as activation increases.

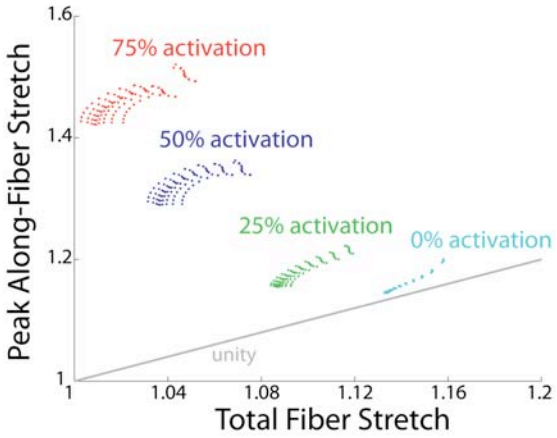

Figure 3. Peak along-fiber stretch vs. total fiber stretch. Peak stretch along each fiber increased with activation while the total fiber stretch decreased with activation.

CONCLUSIONS

These results show that increased activation level within a muscle results in larger localized strains, which is consistent with experimental observations [3]. This nonuniform distribution of strains may explain why muscles are most frequently injured while undergoing active lengthening as opposed to passive lengthening. Future work will explore more complex activation and length change patterns to predict potential injuries during realistic movements.

REFERENCES

1. Noonan, TJ, and Garrett, WE. *Clin Sport Med* **4**, 783-806 1992.
2. Silder et al, Proceedings of ASB, State College, PA, USA, 2009.
3. Fiorentino et al., submitted to *34th Annual ASB Meeting*, 2010.
4. Lieber RL, and Friden J. *J Appl Physiol* **2**, 520-526 1993.
5. Rehorn MR, et al. *J Biomeh* in review.
6. Armfield DR, et al. *Clin Sport Med* **4**, 803-842 2006.
7. Blemker S.,et al. *J Biomech* **38**,657-665, 2005.

AKNOWLEDGEMENTS

We would like to thank Nic Fiorentino and Darryl Thelen. Funding for this work was provided by NIH grant R01 AR 056201.

LIFTING CAPACITY AND FATIGUE RECOVERY IN HEALTHY YOUNG ADULTS AND ELDERLY INDIVIDUALS

[1]Annick Champagne, Annie Nolin and Danik Lafond
[1]Université du Québec à Trois-Rivières, QC, Canada
email: annick.champagne@uqtr.ca

INTRODUCTION

Lifting tasks have been shown to be a risk factor of low back injury in young adults [1]. As ageing is related to loss of muscle strength [2], working elderly subjects exposed to manual handling and lifting tasks may be more prone to develop back pain. Women aged over 65 years having chronic back pain are at least two times more likely to have difficulty with housework mobility tasks such as climbing stairs, walking or lifting [3].

Back and leg extensors strength seems to influence lifting strategies. Strength-impaired elderly individuals used predominantly back strategy and showed increased postural instability during lifting [2]. However, it is unclear if postural instability associated with strength deficit is related to balance problems per se or to age-related modulation of activation patterns of lumbopelvic extensor muscles during lifting. For instance, reduced hip flexibility influences activation patterns of erector spinae in elderly subjects during trunk flexion task [4]. Lumbopelvic extensors strength is associated with muscular endurance in young healthy adults [5]. However, elderly subjects did not show a significant force-endurance relationship of back muscles. One could argue that back muscle fatigue may have less influence on lifting capacity in elderly compare to young adults.

The aim of the study was to investigate the influence of ageing and muscle fatigue on lifting capacity and lumbopelvic extensors activation patterns during a maximal isometric task. It is hypothesized that elderly subjects would produce maximal lifting force and exhibit extensor muscle activation patterns inconsistently. It is also hypothesized that elderly subjects lifting capacity will be less affected by fatigue and show a better capacity to recover from fatigue condition than young healthy subjects.

METHODS

Twenty healthy young adult and 16 healthy community-dwelling elderly male participated in this study. They performed 4 maximum voluntary isometric lifting efforts (T1 to T4) in a semicrouched position, separated by two min of rest. Thereafter, they performed a fatiguing task using a modified Sorensen test on a 45° roman chair. A block of four other isometric lifting trials (T5 to T8) were realized in the same conditions as the first 4-trials. Surface electromyography (EMG) was assessed for paraspinal muscles at T10 and L5 and hip extensor muscles (gluteus maximus: GM, biceps femoris: BF). Dependant variables were maximal lifting force (Newtons/kg), absolute and relative EMG Ratios (EMGRatioA). Ratios were calculated by dividing RMS values between different pairs of lumbopelvic extensor muscles to infer on muscle activation patterns [6]. The EMGRatioA provides the magnitude of the imbalance between muscles while EMGRatioR provides the direction of the imbalance in addition. The decrease of median frequency slope, normalized by the initial MPF value (%MPF/T), was used as an indice of neuromusclar fatigue during the modified Sorensen test. Two-way analysis of variance (ANOVA) with Repeated-measures was applied on each dependant variables and significant p-value was set at < 0.05.

RESULTS AND DISCUSSION

During the first 4-trials of the lifting test, no difference was observed in EMGRatios between young and elderly subjects, although elderly showed lower maximal lift force. Force and EMGRatioA disclosed no difference between trials in both age groups (Figure 1).

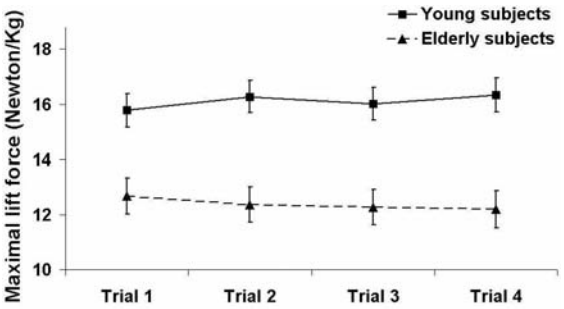

Figure 1: Lifting force across trials (block 1).

Table 1 presents EMGRatioA and force values for pre- (T4) and post-fatigue (T5) conditions. Significant effect of fatigue on force was observed, where both groups showed reduction of force after the fatiguing task. All EMGRatioA implicating L5 and GM/BF showed significant effect of fatigue for both age groups. MPF time-slope during the fatiguing task was significantly higher at L5 level compared to other muscle groups for young subjects (Figure 2). For elderly subjects, no differences were found between muscle groups for MPF time slope.

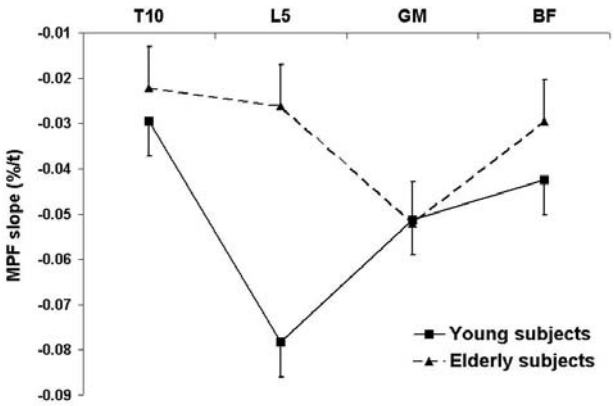

Figure 2: MPF slope during the fatiguing task.

Both young and elderly subjects showed reduction of maximal lift capacity following lumbopelvic muscle fatigue. However, muscle fatigue at L5 was higher in young subject. As the rate of muscle fatigue is predominantly modulated by activation of type II muscle fibers, the predominance of type I muscle fibers previously reported in elderly may explain the lower rate of muscle fatigue at L5 in elderly subjects [5].

One finding of our study is that muscle activation patterns during maximal static lift task are not influenced by the ageing process. The results support the conclusion of Puniello [3] indicating that lifting capacity of elderly subjects may be influenced by postural control deficits.

CONCLUSIONS

Our study showed that ageing process does not alter maximal static lift capacity, with and without lumbopelvic muscle fatigue. Elderly subjects produce lower maximal lifting force but exert muscular efforts with the same activation pattern than young adults.

REFERENCES

1. Adams MA, et al. *Clin Biomech*, **10**, 3-19, 1995.
2. Puniello MS, et al. *Spine*, **26**, 731-737, 2001.
3. Léveillé SG, et al. *J ,Gerontol A Biol Sci Med Sci*, **54**, 487-493, 1999.
4. Brown JMM, et al. *Gerontol*, **40**, 298-306, 1994.
5. Champagne A, et al. *J Manipulative Physiol Ther*, **32**, 521-526, 2009.
6. Edgerton VR, et al. *Theory Pract*, **13**, 179-195, 1997.
7. Merletti R, et al. *Muscle Nerves*, **25**, 65-76, 2002.

Table 1: Pre and post-fatigue values for EMGRatioA and maximal lift force. Data are expressed as mean (SEM).

	Pré-fatigue (T4)		**Post-fatigue (T5)**		***P-Values***	
EMGRatioA	**Young**	**Elderly**	**Young**	**Elderly**	**Fatigue effect**	**Age effect**
T10/L5	1.02 (.29)	1.29 (.33)	1.93 (.38)	2.10 (.43)	**.000**	.649
T10/GM	1.13 (.27)	1.24 (.31)	1.16 (.35)	1.36 (.40)	.808	.692
T10/BF	2.08 (.59)	1.88 (.67)	1.90 (.34)	2.64 (.39)	.510	.652
L5/GM	0.65 (.19)	0.84 (.21)	1.14 (.33)	1.65 (.37)	**.027**	.231
L5/BF	1.29 (.27)	1.07 (.31)	2.63 (.50)	2.76 (.57)	**.000**	.931
GM/BF	1.28 (.37)	0.91 (.42)	1.94 (.48)	1.79 (.54)	**.009**	.661
Maximal lift force	16.34 (0.62)	12.19 (0.68)	13.98 (0.59)	10.53 (0.64)	**.000**	**.000**

SPRING-LOADED ANKLE EXOSKELETONS REDUCE METABOLIC COST AND ALTER GASTROCNEMIUS FASCICLE BEHAVIOUR IN HUMAN HOPPING

Dominic J. Farris and Gregory S. Sawicki

University of North Carolina-Chapel Hill and North Carolina State University, NC, USA
email: djfarris@ncsu.edu

INTRODUCTION

The metabolic cost of hopping is reduced with the assistance of an exoskeleton that places a spring in parallel with the entire leg [1]. Energy stored and returned by the spring replaces work that otherwise would be done by muscle-tendon units (MTU). Similarly, exoskeletons bridging only the ankle joint can replace work from ankle plantar-flexors [2]. Therefore, the first aim of this study was to test if a spring-loaded ankle exoskeleton could reduce the rate of metabolic energy consumption during hopping. It was hypothesized that net metabolic power would be reduced when an ankle exoskeleton with a spring assisting plantar-flexion was used due to less work being done by the plantar-flexor muscles.

However, an alteration in joint level mechanics due to an exoskeleton could affect muscle fascicle and series elastic element (SEE) behavior in the plantar-flexors. The interaction between fascicles and SEE in the gastrocnemius (GM) has been shown, using ultrasound (US) imaging, to result in largely isometric behavior of fascicles during the stance phase of running [3]. This is beneficial for reducing the energetic cost of muscle contraction and promotes storage and return of elastic energy in the SEE. The use of an exoskeleton could perturb this optimal fascicle-SEE interaction. By reducing the required contribution of the plantar-flexors to joint moments, the exoskeleton might lower force across the GM MTU. With less force acting through the SEE, the SEE length change pattern and thus, the fascicle length change pattern, may be altered, resulting in a sub-optimal interaction between the two. Two possible scenarios were considered for reduced force across the SEE: 1) muscle activation is unaltered causing fascicles to shorten and do work 2) Activation is reduced allowing isometric behavior at longer fascicle lengths.

The primary aim of this study was to assess the effects of a spring loaded ankle exoskeleton on gastrocnemius muscle fascicle and SEE behavior during hopping. It was hypothesized that in naïve subjects, muscle activation would not be adjusted, causing fascicles to shorten and do work.

METHODS

At present, preliminary data from one subject (male, age = 32 yrs, height =1.7 m, mass = 63 kg) has been collected. The subject performed bilateral hops at a frequency of 2.2 Hz for four minutes wearing bilateral ankle exoskeletons. In one condition the exoskeletons had a linear spring of stiffness 5.1 $kN \cdot m^{-1}$, fitted in parallel with the ankle plantar-flexors and with a moment arm about the ankle joint of 0.14 m. This produced a torsional stiffness of 1.75 $Nm \cdot deg^{-1}$.

Ground reaction force data were recorded (1080 Hz) from two force platforms (BERTEC, USA) synchronously with kinematic data (120 Hz, VICON, USA) and longitudinal US images (50 Hz) of medial gastrocnemius muscle fascicles [3]. US images were captured using a 128 element linear array probe operating in B-mode at 8.0 MHz (TELEMED, Lithuania).

Inverse dynamic analyses were performed to compute ankle joint moments and powers. The force in the spring was measured with a tension load cell and converted to an ankle moment by multiplication by the moment arm. GM fascicle lengths were determined by manually digitizing the end points of a fascicle in the sequences of US images. Fascicle pennation angle was determined as the angle between the fascicle and the superficial aponeurosis of the GM. Whole GM MTU length was determined from kinematics and the SEE length was then calculated as the MTU length minus the fascicle length after it had been corrected for pennation angle [3].

Oxygen consumption ($\dot{V}O2$) was measured during standing and hopping trials using a portable metabolic system (VIASYS, Germany). $\dot{V}O2$ was averaged over 30 s intervals and net metabolic powers were computed for hopping trials.

RESULTS

These preliminary results indicate that springs in parallel with the ankle joints can reduce the average positive mechanical power output required of the plantar-flexor MTU's by 58%. Also, they reduced net metabolic power by 14% (Figure 1). Figure 2 shows that GM fascicle length change demonstrated isometric behavior without the spring and a pattern of shortening and re-lengthening with the spring. The average fascicle length was 25 mm without the spring and 28 mm with the spring.

DISCUSSION

As hypothesized, there was a reduction in net metabolic power when a spring was added to assist plantar-flexion. This appeared to be a result of the exoskeleton contributing to average power output at the ankle and thus, reducing the contribution of the plantar-flexor muscles.

Furthermore, the addition of the spring altered the length change trajectories of the GM MTU, SEE and fascicles. Shortening and re-lengthening of the fascicles was observed in the spring condition. As hypothesized this could be a result of reduced force across the MTU (due to some of the load being borne by the spring) whilst muscle activation remained unaltered. This situation is undesirable as the muscle fascicles appear to be doing work which is metabolically more expensive and thus the maximum potential benefit of the exoskeleton might not be achieved. However, despite sub-optimal fascicle behavior in the GM there was a large reduction in net metabolic power. Therefore, further analysis will include the knee and hip joint mechanics in an attempt to further explain these results.

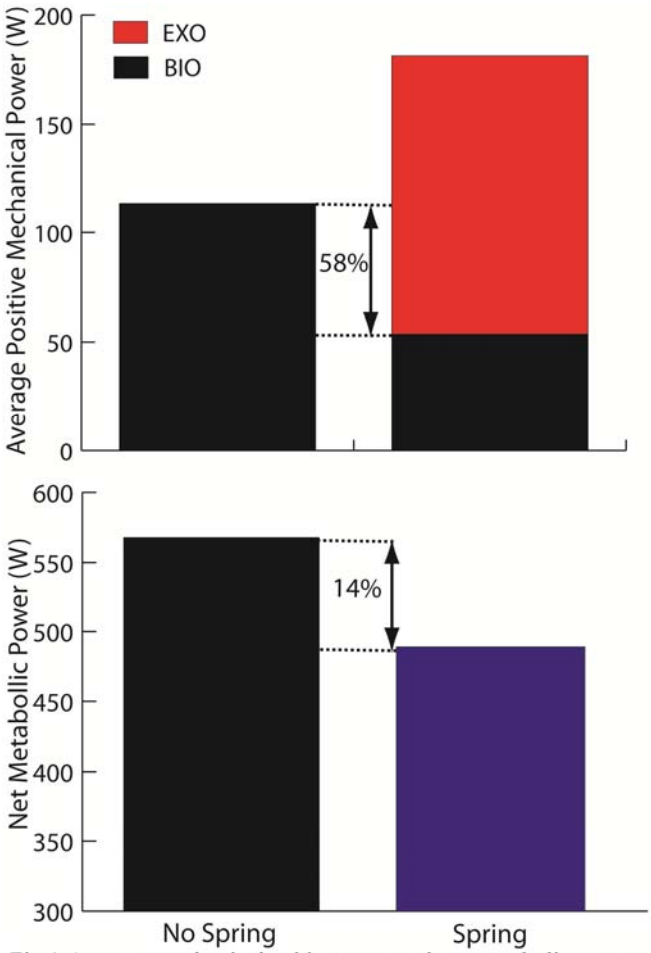

Fig 1.Average mechanical ankle power and net metabolic powers for the two conditions. EXO is the contribution of the spring and BIO shows the biological ankle muscle contribution.

REFERENCES

1. Grabowski, AM & Herr, HM (2009). *J App Physiol*, **107**(3): 670-678.
2. Sawicki, GS & Ferris, DP (2009). *J Exp Biol*, **212**(1): 21-31.
3. Lichtwark, GA et al. (2007). *J Biomech*, **40**(1): 157-164.

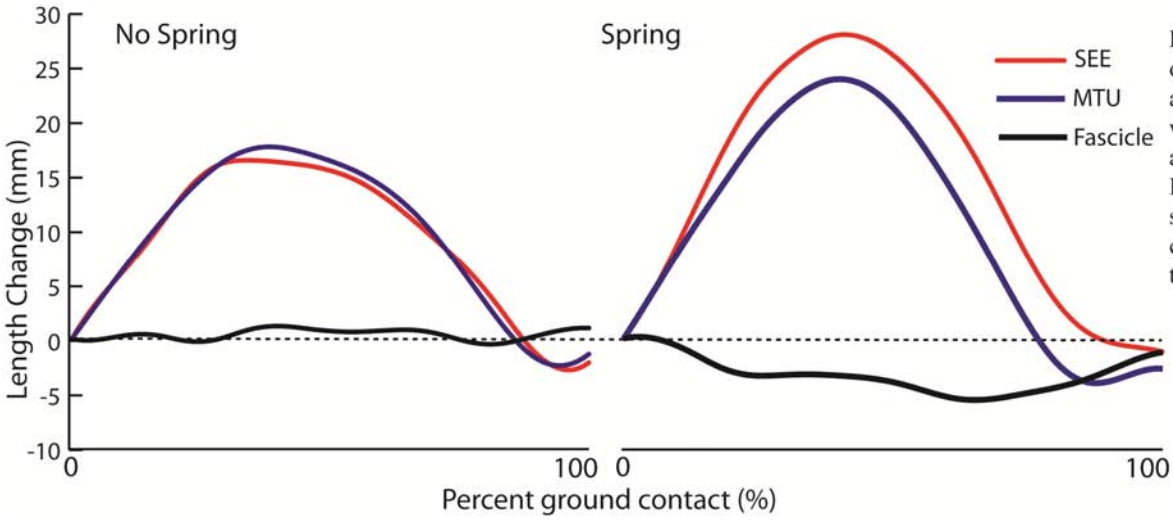

Fig 2. Length changes of the MG MTU, SEE and fascicles with and without a spring to assist plantar-flexion. Length changes are shown over ground contact and are relative to the length at landing.

EVALUATION OF NEUROMUSCULAR DYNAMICS OF HYPERACTIVE REFLEXES AT THE ELBOW POST STROKE

[1,2]Jie Liu, [2]Yupeng Ren, [2,3]Dali Xu, [2,4]Sun G. Chung, [1,2]W. Zev Rymer, and [1,2]Li-Qun Zhang

[1]Northwestern University, Chicago, IL, USA
[2]Rehabilitation Institute of Chicago, Chicago, IL, USA
[3] Western Illinois University, IL, USA
[4]Seoul national University, Seoul, South Korea
email: l-zhang@northwestern.edu, web: http://www.ric.org/reseach/centers/smpp/Staff/index.aspx

INTRODUCTION

Spasticity is a major source of disability in many patients suffering from brain or spinal cord injury of many different etiologies, including stroke, traumatic spinal cord injury, multiple sclerosis, and cerebral palsy. To assess severity of the spastic state and identify its key characteristics post stroke, it is important to evaluated hyperactive reflexes quantitatively in terms of the reflex gain and threshold in stroke. The purpose of this study was to investigate the mechanisms underlying spasticity in stroke and to quantitatively evaluate hyperactive reflexes. The experiment was done isometrically at the elbow joint to minimize nonreflex contributions and thus manifest and characterize hyper-active reflexes accurately.

METHODS

Ten patients post stroke and eleven control subjects participated in the study. All subjects gave informed consent before participating in the study, which was approved by the Institutional Review Board at Northwestern University.

The subject sat upright with the trunk strapped to the backrest and shoulder abducted at 80° and flexed at 10°. The distal forearm, wrist and proximal hand were cast and mounted onto the distal end of an aluminum beam, and the other end of the beam was mounted onto a motor shaft through a torque sensor that measured the elbow extension torque. The elbow flexion- extension axis was aligned with the motor shaft and the motor was locked at a selected elbow flexion angle during tendon tapping, restricting the elbow at an isometric condition.

A hemisphere self-adhesive rubber pad with a diameter of 10 mm was pressed onto the triceps tendon at the most sensitive spot, with the strongest reflex response compared to the neighboring points. An instrumented tendon hammer with a force sensor mounted at its head was used to tap the rubber pad. The flat impact surface of the instrumented tendon hammer hit the dome-shaped rubber pad, which made the tapping force transmission onto the tendon more accurate and consistent, reducing variations of the induced tendon reflexes.

At the beginning, the tapping force was adjusted so that a triceps muscle contraction was clearly evoked. The triceps tendon was then tapped at approximately that level about seven times during a trial, with an interval of about 3 seconds. Three trials were collected at each elbow flexion angle, and the tapping was repeated at 60º, 90º and 120º elbow flexion. The tendon tapping force, triceps EMG signals, and elbow joint extension torque were sampled at 500 Hz after lowpass filtering (8^{th}-order Butterworth filter at 230 Hz cutoff). The sampled EMG signals were full-wave rectified. The tendon tapping force, rectified EMG, and elbow extension torque signals were filtered digitally using a finite impulse response low-pass filter with a cutoff frequency of 150Hz. The signals were then inspected and edited interactively.

Parameters characterizing tendon reflex dynamics include the tendon reflex gain (G_s), the reflex torque varied with the tendon tapping force, the contraction rate (R_c) and the half relaxation rate (R_{hr}). In addition to the above parameters characterizing the system impulse response, the peak tendon tapping force (f_{th}) used to elicit tendon reflexes for each subject was used to characterize the reflex threshold

in tapping force, which characterizes the reflex excitability.

RESULTS AND DISCUSSION

Compared to the controls, stroke survivors showed much different neuromuscular dynamics in tendon reflexes. As shown in the representative cases (Fig. 1), the peak tapping force for the stroke survivor was much lower than that in the control without any neurological disorder. On the other hand, the reflex-mediated EMG response and elbow extension torque in the stroke survivor were much higher and changed much quicker than their counterparts in the control without any neurological disorder.

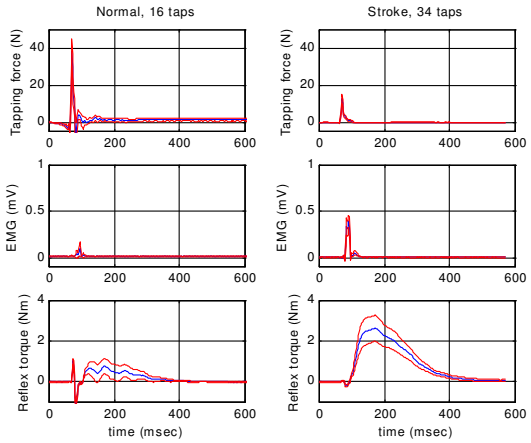

Figure 1. Representative tendon tapping results over multiple taps of the triceps tendon with the elbow joint at 90° flexion. The solid and dashed lines represent mean and standard deviation, respectively.

While the threshold in tapping force in the spastic limbs was significantly lower than that in normal controls across all different elbow joint angles, the tendon reflex gain, the tendon reflex contraction rate and the half relaxation rate in stroke survivors was significantly higher than that of control group ($P<0.05$, Fig. 2).

CONCLUSIONS

This study provides a useful tool to make accurate measurements of both taps to the tendon and the reflex-mediated responses, and characterize their dynamic relationship in terms of tendon reflex gain, contraction rate and half-relaxation rate, and reflex threshold in tapping force. The results showed markedly increased system gain, contraction rate and half-relaxation rate, and decreased reflex threshold in tapping force, provided quantitative measures to characterize hyperactive reflexes post stroke. Practically, the tendon reflex evaluation is easy to do and can potentially provide convenient and quantitative measures in clinical settings.

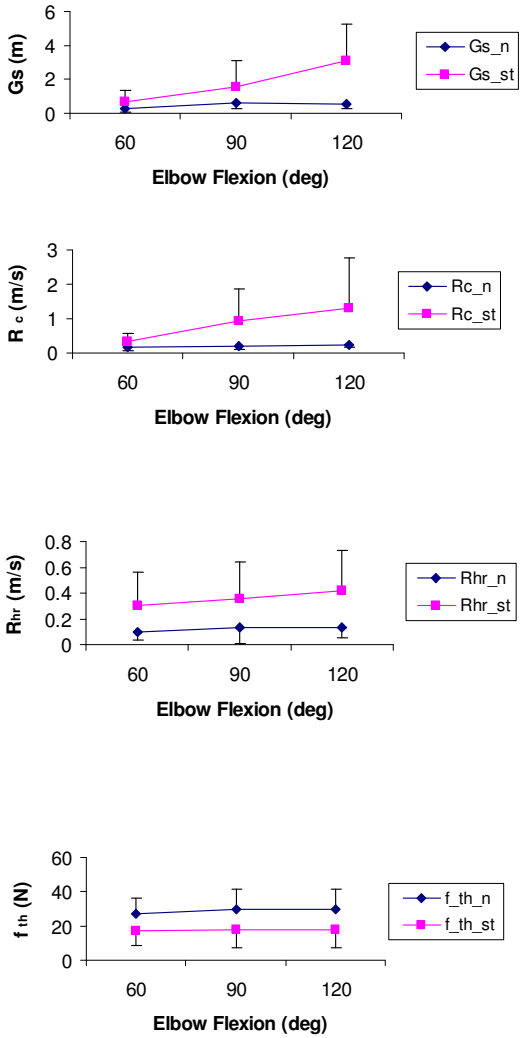

Figure 2. Comparison of the tendon reflex gain (G_s), the contraction rate (R_c) the half relaxation rate (R_{hr}) and the peak tendon tapping force (f_{th}) between the stroke and control groups across three elbow flexion angles. The vertical bars represent the standard deviation across the subjects.

ACKNOWLEDGEMENTS

The authors acknowledge the supports of the National Institutes of Health and National Science Foundation.

PREDICTING THE EFFECT OF PULSE DURATION ON FATIGUE DURING ELECTRICALLY STIMULATED NON-ISOMETRIC CONTRACTIONS

Susan Marion, Maury Hull and Anthony Wexler

University of California, Davis, CA 95616
email: msmarion@ucdavis.edu

INTRODUCTION

Functional electrical stimulation (FES) is increasingly used by individuals with paralysis to regain functional movement, but muscle fatigue can limit the applicability of this technology. Mathematical predictions of power loss during electrically stimulated muscle contractions are essential when trying to not only minimize fatigue, but also determine the relative contributions of force and velocity to fatigue. Our previous mathematical model of non-isometric muscle fatigue for electrical stimulation induced, seated leg extensions accounted for the effect of applied load, but not the effect of pulse duration [1]. Therefore, our objectives were: 1) model muscle fatigue at different pulse durations and 2) experimentally validate the model with new subjects and thus predict the effect of pulse duration on fatigue.

METHODS

Experiments were conducted using a computer-controlled stimulator that sent trains of pulses to surface electrodes on the thighs of 25 able-bodied human subjects. Isometric and non-isometric non-fatiguing and fatiguing leg extension ankle forces and/or knee angles were measured. A 4.5 kg load was applied to the leg during the general non-isometric measurements. Five pulse durations were tested: 600, 400, 250, 200 and 170 μs. Model parameters were identified by minimizing the sum of squares error between the model and observations. Predictive accuracy was determined from linear regression analyses of the maximum angular displacement and angular velocity. Data from approximately half of the subjects and three of the five pulse durations was used to determine which parameters required modification. Data from the remaining half of the subjects, and data from the previous study which predicted the effect of load on fatigue [1], were used to validate the model.

RESULTS AND DISCUSSION

The equation for one of the non-isometric fatigue model parameters required modification. The remaining two non-isometric fatigue model parameters were found to be unnecessary and were removed. The parameter that was modified is a function of other parameters within the model, therefore additional measurements from the subject are not needed to identify this parameter. During validation testing, we predicted the fatigue at the other two pulse durations in the development subjects, at all five pulse durations in the validation subjects from this study, and at one pulse duration but different applied loads in ten subjects from the previous study. More than 63% of the variability in the measurements was explained by the new force-fatigue model (Fig. 1). Day-to-day differences in the number and types of muscle fibers recruited, in the initial conditions, and in the resting position of the free swinging leg before each contraction may have contributed to the random error.

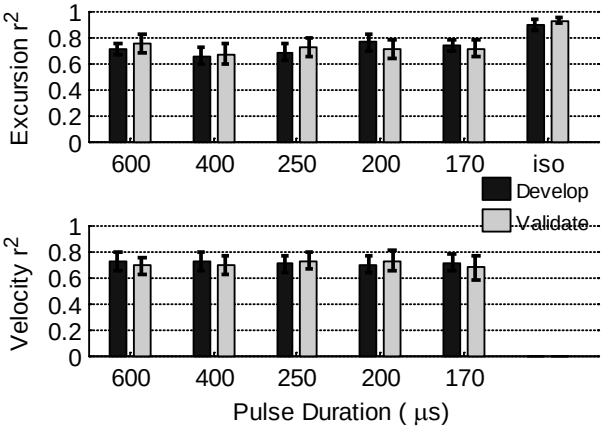

Figure 1: Average linear regression coefficients of determination (r^2; + 95% confidence limit).

CONCLUSIONS

Dynamic fatigue was reasonably well predicted at different pulse durations by the new non-isometric force-fatigue model. This model can help scientists investigate the etiology of non-isometric fatigue and engineers improve the task performance of FES systems.

REFERENCES

1.Marion MS, et al. *Muscle Nerve*, March 2010.

INCORPORATING VELOCITY CHARACTERISTICS INTO COST FUNCTIONS DOES NOT ALTER OPTIMAL MUSCLE FORCES IN NORMAL WALKING

[1]Anantharaman Gopalakrishnan, [1]Nils Hakansson, [1]Jill Higginson
[1]University of Delaware, Newark, DE, USA
email: ananthram.g@gmail.com

INTRODUCTION

The contribution of individual muscle forces to an activity can provide insight into neuromuscular coordination of walking. Optimization techniques are used to distribute forces between synergistic muscles for both static and dynamic tasks. Crowninshield and Brand [1] specified a cost function to maximize endurance in gait of the form $\Sigma(F_i/W_i)^2$, where F_i is the muscle force, W_i is a constant muscle-specific weight factor (physiological cross sectional area) and n is an integer exponent. Variations of this cost function have been used to solve the redundancy problem for close to 30 years despite mounting data from animal models showing that the force distribution model does not reflect experimental observations. Schappacher-Tilp et al. [2] developed a physiologically motivated cost function in which the weight factor (W_i, the maximum isometric force) varied based on the instantaneous force-velocity conditions of the muscle. The muscle forces obtained by minimizing this cost function matched in-vivo muscle force data collected from cats during activities with high muscle velocities such as running and jumping.

The objective of our study was to test whether incorporating muscle contractile conditions in an optimization to solve the redundancy problem would alter the predicted muscle forces in healthy human gait. The computation was treated as a static problem constrained by muscle force-length, force velocity properties and the activation dynamics.

METHODS

Experimental: Three-dimensional kinematic, kinetic and EMG data were collected on one healthy male subject (193 cm, 93 kg) walking on a split-belt treadmill at 1.62 m/s without using handrails.

Simulation: A musculoskeletal model (23 DOF, 54 muscles) was built using OpenSIM [3]. The model parameters were adjusted to minimize inconsistencies between body kinematics and external loads using the residual reduction algorithm [4]. The inverse dynamics was solved in MATLAB (Mathworks, Natick MA). At any time instant, equations of motion for the musculoskeletal model were generated from experimental joint states, velocities and accelerations. The generalized joint forces obtained from this inverse dynamics step served as constraints on muscle forces during optimization.

Initial muscle states (individual fiber lengths and activations) were estimated using the method described in Thelen et al. [4]. Lower and upper bounds on muscle forces at any time instant of the optimization were found by integrating muscle states from the previous time step with input excitations held at 0 and 1 respectively [5] to ensure that muscle forces did not vary arbitrarily. Using the bounds and equality constraints from the equations of motion, the optimizer calculated two individual sets of muscle forces which minimized each cost function respectively. Assuming the input excitation to have been constant over the previous time step ($\Delta t<0.01$), the current muscle states were evaluated by integrating the muscle model over the time gap and repeated for the duration of the gait cycle.

Cost Function: The two cost functions used in this study were of the form $\Sigma(F_i/W_i)^2$. For the constant weight function, $W_i = F_{0i}$, the maximum isometric force [6]. For the variable weight function,

$$W_i = (F_o + a_i)b_i/(v_i+b_i) - a_i, \quad (1)$$

v_i, is the instantaneous shortening velocity, a_i and b_i are Hill's thermodynamic constants, $a_i/F_0 = 0.25$, $b_i/v_0 = 0.25$, and v_0 is the maximum fiber velocity. Simulations were developed using each cost function.

RESULTS AND DISCUSSION

To establish confidence in the method used, the computed muscle excitations were compared with experimental EMG measurements (Figure 1). The excitations matched the EMG well, especially during the peaks. The differences between the EMG and excitations might be due to the choice of muscle model parameters (standardized for all muscles) or the cost functions themselves. High deactivation constants might have caused the computed activations to drop off before the EMG.

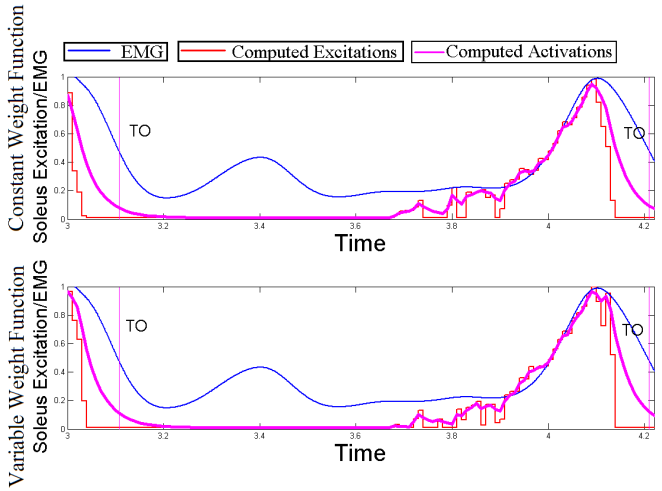

Figure 1: *Matching experimental EMG for the soleus with computed excitation and activation patterns.*

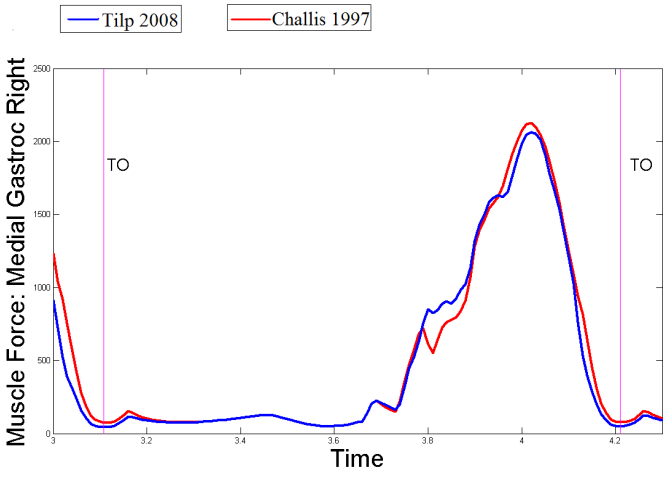

Figure 2: *MGAS muscle forces calculated using the two different cost functions over one gait cycle.*

Muscle forces calculated using both cost functions were largely the same, as demonstrated by the force curves over a gait cycle for the medial gastrocnemius (MGAS) (Figure 2). The similarities in the forces calculated using the two cost functions can be explained by the lower speeds and frequencies of human walking as compared to activities of a cat for which the variable weight function was originally tested [2]. Muscle fiber velocities might not have been high enough to affect the weights in the cost function, resulting in similar force distribution between synergistic muscles for both cost functions.

Based on an observation by Scovil et al. [7], the sensitivity of a forward simulation of walking to the Hill parameters 'a' and 'b' is low. Normalized values of the Hill parameters were assumed to be identical for all muscles in this study. This assumption may have had an effect on the variable weight cost function results because the Hill parameters dictate the shape and intercept of the muscle force-velocity curve.

In summary, we found that the cost functions tested showed little difference in the distribution of muscle forces during healthy gait. Future research will aim to test different sets of cost functions and determine if the choice of the cost function during optimization is critical for accurately predicting muscle activity during normal walking.

REFERENCES

1. Crowninshield and Brand (1981). *J. Biomech.* 14, pp. 793-801.
2. Schappacher-Tilp et al. (2008). *J. Biomech.* 42, pp. 657-660.
3. Delp SL et al. (2007). *IEEE Trans Biomed Eng.* 54, pp. 1940-1950.
4. Thelen et al. (2006) *J. Biomech.* 39, pp. 1107-1115.
5. Thelen et al. (2003) *J. Biomech*. 36, pp. 321-328.
6. Challis (1997) *Med. Eng. Phys*. 19, pp. 253-261.
7. Scovil et al. (2006) *J. Biomech.* 39, pp. 2055-2063.

ACKNOWLEDGEMENTS

The authors are grateful to David Olchowski and Andrew Kubinski, University of Delaware, for their help with data collection and Dr. Walter Herzog, University of Calgary, Canada, for his input on Hill constant values. Funded by NIH R01 HD38582.

JOINT-SPECIFIC POWER PRODUCTION, FATIGUE, AND RECOVERY DURING SUBMAXIMAL EXERCISE

Steven Elmer, Justin Grisham, Sara Hahn, and James Martin
Neuromuscular Function Lab, University of Utah, Salt Lake City, UT, USA
Email: steve.elmer@utah.edu

INTRODUCTION

Fatigue during multi-joint tasks may be due to central and/or peripheral mechanisms and could manifest with equal or differential fatigue at each joint. Martin and Brown [6] evaluated changes in joint-specific powers during 30s of maximal cycling during which overall power decreased by 59% and reported differential joint-specific fatigue. An alternative fatigue model involves maintaining a challenging submaximal power output until volitional failure. Interestingly, submaximal cycling is performed mainly with knee extension actions [5] whereas hip extension dominates maximal cycling [6]. In a time-to-failure model, effort required to maintain constant power is initially submaximal and thus may exhibit similar joint-specific power characteristics to submaximal cycling. However, as such a trial progresses, effort will increase, eventually becoming maximal [2]. Our main purpose for conducting this investigation was to quantify alterations in joint-specific power production during multi-joint exercise in a time-to-failure model. We hypothesized that knee extension power would decrease and hip extension power would increase as the as the effort required to maintain constant power progressed from submaximal to maximal. Our secondary purpose was to determine joint-specific power characteristics following recovery.

METHODS

Nine trained cyclists (31±9y; 73±10kg, 1.76±0.09 m) performed counterweighted single-leg cycling [4] on an isokinetic ergometer (85rpm) at 110% of double-leg lactate threshold power. Participants cycled at this power until volitional failure, after which they rested for 3min and then repeated the effort. Pedal reaction forces were recorded with two 3-component piezoelectric force transducers and pedal and crank position were recorded using digital encoders. Position of the iliac crest was recorded with an instrumented spatial linkage system and limb kinematics were calculated geometrically [7]. Segmental masses, moments of inertia, and locations of centers of mass were estimated using the regression equations reported by de Leva [3]. Sagittal plane joint reaction forces and net joint moments were determined by using inverse dynamic techniques. Joint powers were calculated as the product of net joint moments and joint angular velocities and hip transfer power was calculated as the product of hip joint reaction force and linear velocity. Joint powers were averaged over complete pedal cycles and over extension and flexion phases. Joint powers were analyzed for the initial and final 6s of the first trial and the initial 6s of the second trial. A MANOVA with repeated measures was performed with the measured cycling interval (Trial 1-initial 6s ($T1_i$) vs. Trial 1-final 6s ($T1_f$) vs. Trial 2-inital 6s ($T2_i$)) as the independent variable and ankle plantar flexion, knee extension, knee flexion, and hip extension as dependent variables. If the MANOVA revealed a significant effect of measured interval on joint-specific power values then additional one-way repeated measures ANOVA's with subsequent post-hoc tests were used to identify which measured intervals were performed with different joint-specific power values. Data are presented as mean±standard error of the mean (alpha=0.05).

RESULTS

Mean power delivered to the pedal did not differ (263±12 vs. 257±10 vs. 265±11W for $T1_i$, $T1_f$, $T2_i$, respectively). The MANOVA revealed a significant effect of measured interval on joint-specific powers (Wilk's λ=0.21, $F(8,26)=3.87$, $p<0.01$). The follow-up ANOVA's revealed that the effects of measured interval on knee extension, knee flexion, and hip extension powers were significant ($F(2, 16)=23.02$, $p<0.01$; $F(2, 16)=12.05$, $p<0.01$; $F(2, 16)=11.71$, $p<0.01$; respectively). Compared to $T1_i$, knee extension and knee flexion powers during $T1_f$ were reduced by 32% and 47%, respectively, whereas hip

extension power increased by 28% (Table 1, Figure 1). Power transferred across the hip increased by 227% (11±12 $T1_i$ vs. 25±10W $T1_f$). Joint-specific powers during $T1_i$ and $T2_i$ did not differ.

DISCUSSION AND CONCLUSION

Our primary finding was that knee extension and flexion powers were reduced as the participants approached volitional failure. These reductions were compensated for with increased hip extension power and hip transfer power so that overall power was maintained. Thus, fatigue during constant submaximal cycling resulted in changes in joint-specific power characteristics. The freedom to select among power producing actions at the ankle, knee, and hip is a benefit of this time-to-failure model in which individuals exploit degrees of freedom to accomplish an overall task goal. Our finding of increased hip extension power prior to failure extends upon recent work by Martin and Brown [6], who reported that hip extension was the dominant power producing action during maximal cycling and was more fatigue resistant than knee extension and flexion actions. We interpret this finding to suggest that differential joint-specific fatigue was due to peripheral rather than central mechanisms. Specifically, muscles that span the ankle, knee, and hip could have different metabolic and morphological characteristics [1]. Our design also included a brief rest period and a second trial to help determine if joint-specific power characteristics were restored following recovery. We found that following a 3min recovery period, joint-specific powers reverted to initial characteristics. This suggests that disturbances to the metabolic milieu were small enough that they could be rapidly restored. These findings have implications for multi-joint endurance, strength, power, and rehabilitation exercises that are performed intermittently until partial or complete fatigue.

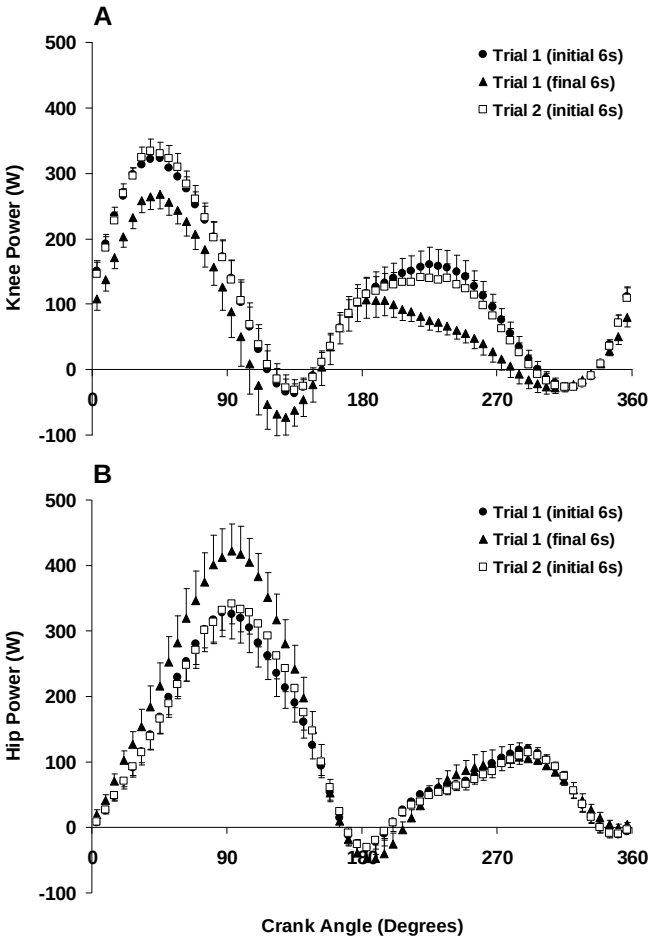

Figure 1: Instantaneous power (Mean±SEM) produced by A) knee and B) hip joint actions during submaximal cycling.

REFERENCES

1. Allen et al. *Physiol Rev*, **88**, 287-332, 2008.
2. Bundle et al. *Am J Physiol*, **291**, R1457-1464, 2006.
3. de Leva, P. *J Biomech*, **29**, 1223-1230, 1996.
4. Elmer, S., Martin, J. *Med Sci Sport Exer*, in press.
5. Ericson, M., *Eur J App Physiol*, **57**, 382-387, 1988.
6. Martin, J., Brown, N. *J Biomech*, **42**, 474-479, 2009.
7. Martin, J. et al. *J App Biomech*, **23**, 224-229, 2007.

ACKNOWLEDGEMENTS

Funded by Peak Graduate Student Research Grant

Table 1: Power produced during submaximal cycling (Mean±SEM)

Cycling Trial	Pedal and Joint-Specific Powers (W)				
	Pedal	Ankle Plantar Flexion	Knee Extension	Knee Flexion	Hip Extension
Trial 1 (initial 6s)	263 ± 12	65 ± 10	146 ± 9	79 ± 14	182 ± 20
Trial 1 (final 6s)	257 ± 10	67 ± 12	100 ± 14[a]	42 ± 7[a]	233 ± 23[a]
Trial 2 (initial 6s)	265 ± 11	66 ± 10	149 ± 11	71 ± 12[a]	188 ± 18

a different than Trial 1 (initial 6s)

AGE-RELATED MODIFICATIONS IN FORWARD REACH MOVEMENT PATTERNS

Sang-I Lin, Chien-Fen Liao

National Cheng Kung University, Tainan, Taiwan
Email: lin31@mail.ncku.edu.tw

INTRODUCTION

Aging is associated with deteriorations in the functions of many systems of the body which could lead to limitations in functional capacity. Modification of movement patterns is a common strategy for older adults to maintain functional independence under their physiological constraints. Forward reaching is a frequently performed activity of daily living. Its performance, typically measured by reach distance, has been found to relate to frailty, higher risk of falling and declined functional capacity in older adults.[1-4] However, it is unclear if older adults adopted different reach movement patterns than young adults and how effective such modifications were. The purpose of this study was to determine the movement patterns used during forward reaching and compare the reach distance between young and older adults.

METHODS

Thirty-three young and 31 older adults participated in this study and were instructed to stand erect, one arm raise to horizontal, and reach forward as far as possible without taking a step for three repetitions. A Vicon motion analysis system was used to record the body kinematics. The kinematic data were then used to calculate the reach distance and joint angular displacement and to estimate the motion of the body's center of mass (COM) in the sagittal plane. Based upon the motion of the hip and ankle joints, a computer algorithm was used to determine the reach movement pattern into hip, ankle or mixed strategy.

RESULTS AND DISCUSSION

For older adults, 80% of the trials showed a hip strategy, with the rest of the trials showing a mixed strategy. For young adults, 20% of the trials showed an ankle strategy, while the rest of the trials showed evenly a hip or mixed strategy. Older adults had significantly greater hip flexion ($p=.002$), and trends of greater hip posterior displacement, and ankle plantarflexion than young adults. The older adults had significantly smaller forward displacement of the COM ($p=.001$), but not reach distance ($p=.093$), than the young adults.

A hip strategy is characterized by greater hip flexion and posterior displacement of the hip. These movements would restrict the forward advancement of the COM while allowing the arm to reach farther forward. Adopting such a movement pattern during forward reaching has been found in young adults to result in significantly greater reach distance but not greater COM displacement, compared to adopting an ankle strategy.[5] Thus, it seems that older adults were capable of adopting a movement pattern that could help to limit balance threat and at the same time maximize task performance.

CONCLUSIONS

Aging was associated with changes in movement strategy that employed more hip motion and resulted in smaller postural disturbance without compromising reach performance. Older clients, especially those with balance impairments, may be encouraged or instructed to adopt a hip strategy to maximize their functional performance during forward reach.

REFERENCES

1. Duncan PW et al. J Gerontol 47, M93-8, 1992
2. Weiner DK et al. J Am Geriatr Soc 40, 203-7, 1992
3. Smith PS et al. Clin Rehab 18, 811-8, 2004
4. Wallmann HW et al. J Gerontol A Biol Sci Med Sci 56, M580-3, 2001

5. Liao CF et al. Gait Posture 28, 16-23, 2008

ACKNOWLEDGEMENTS
The research was supported by a research grant from the National Science Council of Taiwan. (NSC 97-2314-B-006 -003 -MY3)

DO CHILDREN USE A DIFFERENT STRATEGY IN ADAPTING TO A TENDON VIBRATION PERTURBATION DURING STANDING?

Jianhua Wu[1], Sandra McKay[2] and Rosa Angulo-Barroso[3]

[1]Department of Kinesiology and Health, Georgia State University, Atlanta, GA, USA, jwu11@gsu.edu
[2] Research & Program Evaluation, VHA Home Healthcare, Toronto, Canada, smckay@vha.ca
[3]Center for Human Growth & Development, University of Michigan, MI, USA, rangulo@umich.edu

INTRODUCTION

Children quickly develop postural control strategies over the first several years of their lives. Around 7-8 years of age children show more adult-like postural control patterns [1]. Center-of-mass (COM) is usually studied to reveal the whole body control during quiet standing as well as while confronting an external perturbation. This study investigated how children at different ages regulate their COM while adapting to a tendon vibration perturbation during standing. Position of the COM before and during the vibration as well as segmental angles was studied to investigate whether children use an adult-like control strategy.

METHODS

Three groups of healthy people participated in this study: (1) young children (YC) n=8, age 6.3 (SD 0.6) yrs; (2) older children (OC) n=9, age 10.3 (SD 0.9) yrs; (3) young adults (YA) n=10, age 20.5 (SD 1.4) yrs. Reflective markers were placed bilaterally on toe, ankle, knee, hip, shoulder, elbow, wrist, and temple, and one on C7 spine. A six-camera Vicon Peak® motion capture system was used to collect kinematic data. A small wave pulse motor was attached above the right ankle to alter proprio-ceptive information in muscle spindles. When the motor was on, a false impression of ankle plantar-flexion was produced.

Participants stood on a level surface with hands on hips. Two visual conditions were tested: eyes-open (EO) and eyes-closed (EC). Three 40-second trials were collected in each condition. The first 10 seconds of each trial was standing without vibration. Then, vibration (8 seconds) was triggered when the ground reaction force and moment in the sagittal plane were both pointing to the anterior direction. Posterior body sway was elicited during vibration due to the false impression of ankle plantarflexion. Kinematic data were processed to calculate the position of the COM and the segmental angle at the foot, shank, thigh, trunk, and head in the sagittal plane.

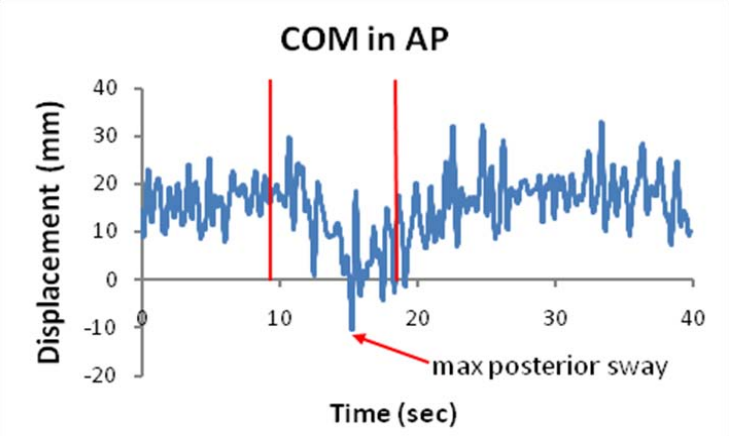

Figure 1: A representative plot of the COM vs. time in the AP direction. Two vertical red lines denote the onset and offset of vibration, respectively. Positive displacement denotes the anterior direction.

Dependent variables include: (1) NpreCOM and NmaxCOM (distance from the COM to the right ankle, normalized by foot length, before the vibration and at the maximal posterior sway during the vibration, respectively), (2) NCOMsway (difference between NpreCOM and NmaxCOM, normalized by foot length), (3) segmental angles with respect to the horizontal for the foot, shank, thigh, trunk, and head.

ANOVAs (3 Group x 2 Visual) with repeated measures on visual condition were conducted on each variable. Post-hoc Tukey analyses were conducted when necessary. Statistical analysis was conducted using SAS® software with an alpha level of $p<0.05$ set for significance.

RESULTS AND DISCUSSION

Before the vibration, all three groups demonstrated similar COM positions in front of the right ankle (NpreCOM in Table 1). There was a visual effect such that the COM was further in front of the right ankle in the EC condition. During the vibration, no difference was found between three groups in the COM at the maximal posterior sway (NmaxCOM in Table 1). Children as young as 6 years old (i.e., YC group) demonstrate similar COM positions with respect to the right ankle before the vibration and at the maximal posterior sway during the vibration.

The magnitude of maximal posterior sway was significantly greater in the YC group compared to the YA group, and all three groups increased the magnitude of posterior sway from EO to EC condition (NCOMsway in Table 1). Even though both YC and OC groups demonstrated similar COM positions with respect to the right ankle when compared to adults, the YC group produced greater posterior sway than adults during vibration.

Table 2 shows the segmental angles at the maximal posterior sway during the perturbation. Significant group difference was found in the thigh, trunk, and head angles between three groups. Specifically, the YC group produced a significantly smaller thigh angle and a greater trunk angle than the YA group in both EO and EC conditions. Also, the OC group produced a significantly smaller head angle than the YA group.

Since all three groups showed similar segmental angles during quiet standing [2], our results indicate that younger children adopt different segmental orientation at the maximal posterior sway when adapting to a tendon vibration perturbation. When responding to a false impression of ankle plantar-flexion, YC group moved the thigh vertical while bending the trunk. In contrast, adults moved the trunk vertical while rotating the thigh forward.

CONCLUSIONS

Children at about 10 years of age demonstrate similar postural control strategy like adults when adapting a tendon vibration perturbation during standing. Children as young as 6 years of age show similar COM positions like adults, but they orient the thigh and trunk differently from adults while adapting to an external perturbation of tendon vibration during standing.

REFERENCES

1.Kirshenbaum N, et al., *Exp Brain Res,* **140**, 420-431, 2001.

2.Wu J, et al. *Exp Brain Res,* **196**, 329-339, 2009.

Table 1: Mean (SD) of normalized COM variables and statistical results.

	EO			EC			Statistical results
	YC	OC	YA	YC	OC	YA	
NpreCOM	0.35 (0.08)	0.34 (0.09)	0.32 (0.10)	0.37 (0.07)	0.34 (0.07)	0.34 (0.10)	V
NmaxCOM	0.27 (0.07)	0.27 (0.08)	0.28 (0.09)	0.26 (0.08)	0.25 (0.06)	0.28 (0.09)	-
NCOMsway	0.08 (0.04)	0.07 (0.03)	0.04 (0.01)	0.12 (0.07)	0.09 (0.03)	0.05 (0.03)	G,V

Note that in statistical results G, V, and G*V denotes a group effect, a visual effect, and a group by visual interaction, respectively.

Table 2: Mean (SD) of segmental angles (unit: degrees) and statistical results.

	EO			EC			Statistical results
	YC	OC	YA	YC	OC	YA	
Foot	172.7 (2.0)	171.7 (3.5)	172.7 (1.8)	172.2 (2.1)	171.4 (3.3)	172.8 (1.8)	-
Shank	87.5 (4.3)	85.0 (4.0)	84.6 (3.2)	85.5 (4.7)	85.2 (3.8)	85.0 (3.1)	G*V
Thigh	90.6 (4.3)	88.2 (4.2)	85.6 (2.5)	90.4 (4.9)	88.1 (4.4)	85.5 (3.0)	G
Trunk	82.9 (5.9)	89.1 (5.1)	92.2 (4.6)	87.1 (6.1)	90.1 (4.7)	91.6 (4.7)	G, V, G*V
Head	21.4 (6.9)	24.7 (5.8)	30.7 (6.3)	25.6 (4.6)	20.5 (12.8)	29.7 (6.5)	G

THE EFFECT OF OBESITY ON BALANCE RECOVERY USING AN ANKLE STRATEGY IS DEPENDENT ON PERTURBATION TYPE

Sara L. Matrangola and Michael L. Madigan

Virginia Polytechnic Institute and State University, Blacksburg, VA, USA
email: smatrang@vt.edu, web: http://www.biomechanics.esm.vt.edu/

INTRODUCTION

More than one-third of adults in the United States (> 72 million) are obese [1]. The prevalence of obesity is not only high, but it continues to increase. For example, the prevalence of obesity among adults more than doubled from 1980 to 2000 [2-3]. One of the concerns with the high and increasing prevalence of obesity is its association with an increased risk of falls. Obese individuals fall twice as often compared to non-obese individuals [4].

The ability to recover balance from a postural perturbation is thought to be related to risk of falls. Therefore, understanding the effects of obesity on balance recovery may improve our understanding as to how obesity contributes to falls. The effect of obesity on balance recovery is not intuitive. Limiting balance to an ankle strategy, obese individuals have increased body weight, which increases the gravitational moment about the ankles. This increased gravitational moment would require larger ankle plantar flexor torque to recover from a perturbation [5], making balance recovery more physically demanding. At the same time, obese individuals have an increased mass moment of inertia about the ankles. Inertia can be defined as the resistance to rate of change in velocity [6]. The increased inertia in the obese may be beneficial in resisting an increase in velocity from a perturbation, making balance recovery less physically demanding. Because of this ambiguity, the purpose of this study was to investigate the effects of obesity on balance recovery using an ankle strategy.

METHODS

Twenty subjects were recruited, including ten normal-weight (age: 21.3 ± 1.1 yrs, BMI: 22.7 ± 0.6 kg/m^2) and ten obese (age: 22.4 ± 3.6 years, BMI: 32.2 ± 2.2 kg/m^2). This study was approved by the Virginia Tech Institutional Review Board, and written consent was obtained from all participants.

Three types of perturbations were used because the effects of obesity may be perturbation dependent. The first type involved releasing subjects from a static forward lean (lean trials) to impose an initial angular displacement from vertical with no initial angular velocity. Body angle relative to vertical (θ) was increased until the subject could no longer recover (return to upright stance). The second type of perturbation involved applying a forward-directed force impulse to the upper back with a ballistic pendulum while subjects stood comfortably (free perturbation trials). This imposed an initial angular velocity at an unconstrained body angle. The third type of perturbation involved applying a forward-directed force impulse to the upper back with a ballistic pendulum, but while subjects leaned against a rigid stop (lean perturbation trials) to impose an initial angular velocity at a controlled body angle. Initial angular velocity was increased until the subject could no longer recover for both free perturbation and lean perturbation trials. During all trials, subjects were harnessed to a backboard to limit balance recovery to an ankle strategy for all trials (contraction of only the muscles spanning the ankle and returning to an upright posture while keeping the body straight and not stepping).

Balance recovery capability was quantified by maximum lean angle (θ_{max}) for lean trials. For free perturbation trials and lean perturbation trials, balance recovery capability was quantified by the maximum angular velocity ($\dot{\theta}_{\max}$) at the body angle at the end of the force perturbation (θ_0).

During all trials, body angle was sampled at 1000 Hz and measured using a linear potentiometer (Unimeasure, Corvallis, OR). Body angle was low-

pass filtered at 20 Hz (eighth order zero-phase-shift Butterworth filter).

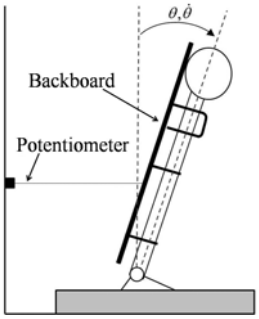

Figure 1. Experimental setup for the three types of perturbations.

A one-way ANOVA was used to investigate the effects of obesity on θ_{max} from lean trials, and $\dot{\theta}_{\max}$ from free and lean perturbation trials. Body angle at the end of the perturbation (θ_0) was included as a covariate. Statistical analysis was performed using JMP v7 (Cary, North Carolina, USA) with a significance level of $p \leq 0.05$.

RESULTS AND DISCUSSION

Obesity impaired balance recovery, but only after certain types of perturbations (Table 1). For the lean trials, θ_{max} was not significantly different between normal-weight and obese subjects ($p=0.497$). In contrast, $\dot{\theta}_{\max}$ was 29.9% ($p=0.008$) and 20.1% ($p=0.035$) lower in obese compared to normal-weight subjects for free and lean perturbations, respectively.

These results indicate that obese subjects had impaired balance recovery when perturbations involved an initial angular velocity, but not when perturbations involved only an initial angular displacement. The differences between perturbation types may be explained by a possible benefit of increased inertia. In particular, increased inertia may be beneficial for recovery after perturbations in which there is limited or no initial velocity because the increased inertia would resist changes in velocity, and therefore would accelerate slower. Theoretically, as initial velocity increases, increased inertia would become detrimental because that increased mass is already moving.

CONCLUSIONS

In conclusion, obese subjects were unable to recover balance using an ankle strategy as well as normal weight subjects when perturbations involved an initial angular velocity. No differences between obese and normal-weight subjects were found when perturbations only involved an initial angular displacement. Future studies should investigate less constrained tasks of balance recovery, such as slipping and tripping, to gain more insight on the source of the increased risk of falls in the obese.

REFERENCES

1. Ogden CL, et al. *NCHS Data Brief*, 1-8, 2007.
2. CDC. *Health, United States. Chartbook Table 75*. 2008.
3. Flegal KM, et al. *Jama*, **288**, 1723-7, 2002.
4. Fjeldstad C, et al. *Dyn Med*, **7**, 4, 2008.
5. Corbeil P, et al. *IEEE Trans Neural Syst Rehabil Eng*, **9**, 126-36, 2001.
6. Meriam JL and LG Kraige, *Engineering Mechanics Dynamics*. 5th ed. ed. Vol. 2. 2002, Hoboken, NJ: John Wiley & Sons.

ACKNOWLEDGEMENTS

SLM was supported by a National Defense Science and Engineering Graduate (NDSEG) Fellowship.

Table 1. Summary of Balance Recovery Measures (Mean ± S.D.)

Perturbation Type	Parameter	Normal-Weight	Obese	
Static Lean	θ_{max}	7.57 ± 1.14	7.18 ± 1.36	
Free Perturbations	θ_0	4.66 ± 0.91	4.83 ± 0.94	*
	$\dot{\theta}_{\max}$	16.53 ± 1.51	11.93 ± 2.72	
Lean Perturbations	θ_0	2.70 ± 0.46	2.65 ± 0.63	*
	$\dot{\theta}_{\max}$	21.06 ± 2.44	17.54 ± 3.92	

*indicates a significant difference between normal-weight and obese subjects ($p<0.05$)

EFFECT OF ARM RESTRICTION ON UPPER BODY RESPONSE TO A SLIP

Aditya Jayadas and Rhonda Boros

Texas Tech University, Lubbock, TX, USA
e-mail: RL.BOROS@TTU.EDU, web: http://www.depts.ttu.edu/hess/biomechanics/

INTRODUCTION

Slip and fall accidents pose a serious threat to individuals, especially the elderly. Several researchers, over the past few decades, have successfully quantified different gait parameters pertaining to the biomechanics of slips and falls in an effort to help reduce the incidence of slip and fall accidents. However, a comprehensive understanding of mechanisms including strategies used by individuals for recovery during a slip perturbation is lacking. Numerous researchers [1, 3, 4] have explored different proactive and reactive strategies that individuals have used to reduce their slip potential when they walk over known and unknown slippery surfaces. Arm reaction has been reported to affect the ability to recover from a slip [2]. Only recently [5] has the upper body response to a slip been explored to any extent, and the effects of load carriage on this response is unknown.

This study investigates upper body response strategies, related to head and arm (hand) motion, in young and elderly subjects during a slip perturbation while carrying a load.

METHODS

This study was conducted at the Ergonomics Laboratory in the Industrial Engineering Department at Texas Tech University. Twenty-eight subjects (14 young, 14 elderly with equal numbers of males and females) participated in the study. All were in good health and passed the screening procedures required for participation. It should be pointed out that data from only four subjects are included in this paper as data analysis is still in its infancy. These four subjects ranged as follows in age (23-78y), height (1.63-1.93m) and mass (51.6-97.1kg).

Gait trials were performed on a circular track equipped with a fall arrest rig system. Subjects walked at their preferred walking pace. Motion data was captured at 120Hz using an 8-camera motion capture system from Motion Analysis Corporation (Santa Rosa, California, USA). Twenty-four (24) reflective markers were used to create a whole body biomechanical model in order to determine the motion of different body segments and the whole body as each subject walked over dry, known and unknown slippery surfaces. The “load” carriage utilized a 0.2kg box (29x23x5cm). The box was carried in front of the body with elbow(s) at approximately 90°, and in the right hand for single arm load. Kinematics data were smoothed using a 6hz Butterworth filter. Resultant velocities for the head and wrist were calculated using 3D positional data. Peak (max) velocities were determined from coordinate data for head, left wrist and right wrist over one stride (heel contact to heel contact of same foot).

RESULTS AND DISCUSSION

Peak linear velocities for the head and hand segments are presented in the figures. “Slip” identifies the slip trial, while “before” and “after” are the adjacent trials to the slip.

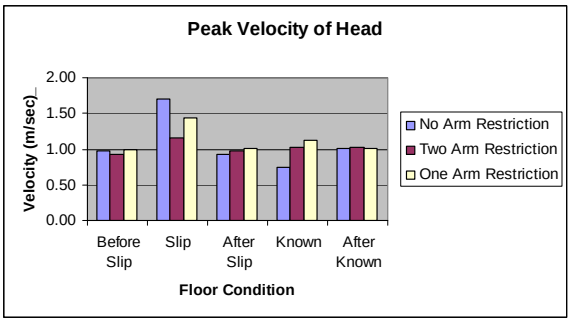

Figure 1: Peak velocity of the head.

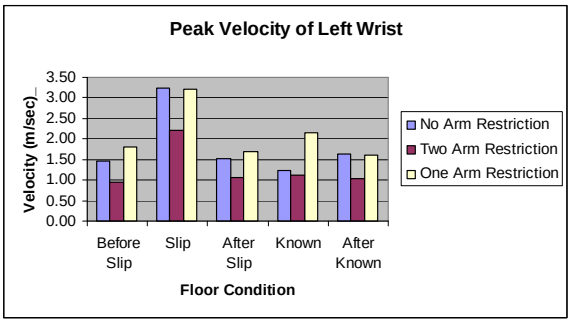

Figure 2. Peak velocity of free hand.

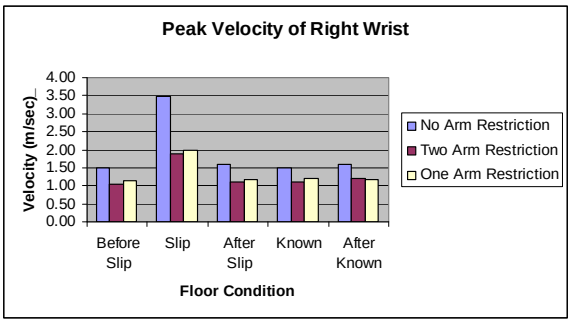

Figure 3. Peak velocity of constrained hand.

Preliminary results demonstrate that upper body strategy is affected by load carriage, and that the method of load carriage (1-hand versus 2) further influences the velocity of head and arm motion in slip recovery. Slip conditions resulted in greater head and arm velocities compared with non-slip, and these velocities tended to be greater in males than females. The 2-handed load carriage resulted in more constrained arm and head velocities compared with the single-hand load-carriage conditions. The no load condition did not consistently produce the highest arm or head velocities as might be expected.

CONCLUSIONS

A successful slip recovery requires either the whole body center of mass (WBCOM) to remain over the base of support (BOS), or that the BOS must accommodate the rapid translation of the WBCOM (i.e., step recovery). The first scenario could likely be accomplished by quick arm and trunk motion and flexibility in the form of range of motion (ROM). The second would likely require upper and lower body coordination, flexibility as well as strength to control WBCOM movement and perform a quick recovery step.

Load carriage appears to hinder the ability of the upper body to respond quickly to an unexpected slip; and suggests when carrying objects, greater reliance is placed on the legs to accommodate the WBCOM acceleration. Examination of the coordinated response of the upper and lower extremities to slip, and the influence of load carriage on this coordinated response is forthcoming.

Considering many people, young and old, carry objects while walking on somewhat unpredictable surfaces (i.e., icy drives, wet floors), identification of successful upper and lower body coordinative response strategies will also help design effective slip and fall recovery training interventions.

References

1. Lockhart, T. E., et al. *Ergonomics*, **46**, 1136-1160, 2003.
2. Marigold, D. S., et al. *J Neurophysiol*, **89**, 1727-1737, 2003.
3. Marigold, D. S. and Patla, A. E. *J Neurophysiol*, **88**, 339-353, 2002.
4. Patla, A. E. *Gait analysis: Theory and Practice.* Mosby-Year books Inc., 1995.
5. Troy, K. L. et al. *J Biomech*, **42**, 1339-1344, 2009.

SENSITIVITY AND SPECIFICITY OF A CLINICAL SCREENING TOOL FOR FALL RISK

Kimberly Edginton Bigelow

University of Dayton, Dayton, OH, USA
email: Kimberly.Bigelow@udayton.edu, web: http://academic.udayton.edu/ewsl

INTRODUCTION

In recent years, a number of fall prevention efforts have emerged to try to prevent the serious and costly problem affecting over 30% of older adults 65 and older each year [1]. Many of these efforts, such as targeted physical therapy and balance retraining, are most effective and feasible when catered to the population at highest risk of falling [1]. One of the risk factors that can help identify these individuals is balance impairment; however, many of the clinical tests used to measure balance are too long to administer or too subjective in scoring to be used as a reliable screening tool [1,2].

Posturography, the use of a force plate to measure center of pressure, has the potential to overcome these limitations. Currently posturography's clinical usefulness is debated, in part because of the lack of standardization in testing methodology and data analysis and presentation [3]. Recently, we presented preliminary results demonstrating the potential of logistic regression modeling to differentiate recurrent fallers from non-recurrent fallers [4]. The current work further develops these findings to demonstrate clinical utility by calculating sensitivity and specificity of the developed models. A secondary aim was to determine future sample size necessary for follow-up work based on these findings.

METHODS

One hundred and fifty subjects participated in this study. Subjects were asked to self-report their fall history for the past year. Subjects were classified as either recurrent or non-recurrent fallers, with recurrent falls being at least two falls in the past year. Twenty-one subjects classified as recurrent fallers (13 females, 8 males; mean age: 83.6 ± 7.6; mean height: 164.3 ± 9.3 cm; mean weight: 72.5 ± 17.5 kg) and 129 subjects classified as non-recurrent fallers (97 females, 32 males; mean age: 81.1 ± 7.9; mean height: 163.2 ± 10.5 cm; mean weight: 72.4 ± 17.4 kg). Exclusion criteria was minimal to represent the diverse population that would need to be screened using this tool. Individuals who could not stand independently, who had undergone physical therapy focused on balance in the last 6 months, or who lived in assisted living or nursing care facilities were excluded.

All subjects performed four quiet-standing tasks while standing on a force-measuring platform (Bertec Corporation, Columbus, OH). These randomized tasks were each 60 seconds long and included: eyes open, comfortable stance; eyes closed, comfortable stance; eyes open, narrow stance (heels and toes touching); and eyes closed, narrow stance. Center of pressure data for the anterior-posterior (A/P) and medial-lateral (M/L) direction was collected at 1000 Hz. For those trials where the subject lost balance, no further analysis was performed on the data for that trial.

From the center of pressure data A/P Sway Range, M/L Sway Range, Mean Sway Velocity, Root Mean Square Displacement, 95% Confidence Ellipse Area, Angular Deviation from A/P, Mean Frequency, and M/L Sway Velocity were calculated. Detrended Fluctuation Analysis was performed and two scaling regions emerged, providing a Short-Term α-Scaling Exponent, a Long-Term α-Scaling Exponent, and a Crossover Point for each the A/P and M/L sway directions.

For each testing condition, stepwise logistic binary regression with forward selection (α=0.15) was performed, considering the parameters above, as well as personal characteristics: Age, Sex, Height, Weight, Body Mass Index (BMI), Shoe Size, and Living Situation (community or retirement home). Nagelkerke R^2 values were calculated for each model to determine goodness of fit. Sensitivity and

specificity were also calculated using PASW (formerly SPSS, Chicago, IL), with a cut value of 0.500.

RESULTS AND DISCUSSION

The logistic regression models developed and presented in this section were based on fall history and were not created to directly predict future falls. A main reason for doing this is that fall history is an important indicator for risk of future falls, but physicians do not often ask about past falls and when they do, patients often give inaccurate responses [1,5]. However, this work also lays the groundwork for an expected large-scale follow-up study using prospective monitoring methods.

In the eyes closed, narrow stance testing condition, 37 subjects (29 non-recurrent fallers) lost balance and could not complete the task. Due to the high prevalence of loss of balance, this testing condition did not seem feasible to perform for general patient screening.

From the remaining three conditions, the eyes closed, comfortable stance condition had the highest Nagelkerke R^2 value (0.411) indicating goodness of fit. The variables entered in this model and their relative significance are shown in Table 1.

Table 1. Logistic Regression Model for Eyes Closed, Comfortable Stance

Parameter	Significance	Exp(B) : Odds Ratio Change
M/L Velocity	0.000	1.227*
M/L Short-Term α-Scaling Exp.	0.052	0.000
BMI	0.055	1.145*
A/P Short-Term α-Scaling Exp.	0.074	2.296e7*
Mean Frequency	0.079	0.020
Age	0.122	1.081*

*Denotes that an *increase* in this parameter's value *increases* the odds of recurrent falling (noted by Exp(B) value greater than 1). For all others a *decrease* in the parameter value would *increase* the odds of recurrent falling

The sensitivity of this model was calculated to be 75%. The specificity of this model was calculated to be 94%. These results suggest that the model does an adequate job of correctly identifying those at high-likelihood of previous fall history. In an ideal screening tool, sensitivity of 100% would ultimately be desirable. However, as a screening tool, sensitivity less than 100% would still likely mean that more individuals would be flagged as at possible high-risk than would be identified without the use of such a tool. A review of the subjects' descriptions of their falls revealed that certain recurrent fallers were falling due to gait-related disorders, such as foot-drop. As such, it would not be expected that this screening tool, focused on identifying postural instability, would identify these individuals. It is hypothesized that the sensitivity of such a tool will never reach 100%, simply because individuals will fall for reasons other than postural instability. However, it is still felt that further development of such a quick screening tool, would ultimately be clinically valuable.

One of the limitations of the current study is sample size. Based on the percent of the current subject who were recurrent fallers, and the number of parameters desired for consideration in the logistic regression model building, it was found that at least 1,491 subjects would be needed to ensure adequate results. Future work will look to expand the subject base and include prospective fall monitoring.

CONCLUSIONS

The proposed clinical screening tool demonstrates merit with a sensitivity of 75% and a specificity of 94%. Future work is needed to develop and validate such a tool further.

REFERENCES

1.AGS, BGS and AAOS. *JAGS* **49**, 664-672, 2001.
2.Cowley A and Kerr K. *Crit Rev Phys Rehabil Med* **15**, 167-205, 2003.
3.Visser J, et al. *Clin Neurophysiol* **119**, 2424-2436.
4. Bigelow K and Berme N. *Proceedings of ASB'09,* State College, PA, 2009.
5. Chou W, et al. *J Gen Int Med* **21**, 117-122, 2006.

ACKNOWLEDGEMENTS

Statistical support by consultant Deanne French was supported by a LEADER Consortium (NSF Advance program) Mini-Grant. Special thanks also to Necip Berme, Haluk Ay, Thomas A. Adams II, and Christopher Bigelow.

POSTURAL STIFFNESS MODEL AND OUTDOOR FALLS IN OLDER ADULTS: THE MOBILIZE BOSTON STUDY

[1] Hyun Gu Kang, [2]Lien Quach, [3] Wenjun Li and [2,4,5] Lewis A. Lipsitz

[1] Kinesiology and Health Promotion, California State Polytechnic University; Pomona, California
[2]Institute for Aging Research, Hebrew SeniorLife, Boston, Massachusetts
[3]Dept of Medicine, University of Massachusetts Medical School, Worcester, Massachusetts;
[4] Harvard Medical School, Boston, Massachusetts;
[5]Division of Gerontology, Beth Israel Deaconess Medical Center, Boston, Massachusetts;

email: hgkang@csupomona.edu www.csupomona.edu/~hgkang

INTRODUCTION

Falls are a serious problem in the health of older adults. Recently, *outdoor* falls have been recognized as a distinct problem occurring even in healthy, middle age and older adults who otherwise don't exhibit typical symptoms of fall risk. Because the outdoors pose greater opportunities for mechanical perturbations on the postural system, the capacity to absorb these perturbations, quantified as mechanical stiffness and damping, may explain outdoor fall risk that other measures of balance function cannot [1]. Cognitive distractions that divert attentional resources seem to impair postural control, and thus may help explain fall risk. Standing posture can be modeled as a inverted pendulum with stiffness and damping, which represent muscle tone, reflexes, and anticipatory control [2]. During dual task, the lack of attentional resources may lead to the inability to maintain adequate muscle tone and thus enough stiffness or damping to maintain upright standing, unable to respond to perturbations.

We tested whether postural stiffness and damping predict the prospective risk of outdoor falls in a representative sample of community-dwelling older adults. We also tested if measuring this during dual task would improve our ability to predict falls in a representative sample of community-dwelling older adults, the MOBILIZE Boston Study cohort.

METHODS

The MOBILIZE Boston Study is a prospective study examining risk factors for falls, including pain, cerebral hypoperfusion, and foot disorders in the older population [3]. The study includes a representative population sample of 765 elderly volunteers age 70 or above from the Boston area. Center of pressure (COP) and falls data with ≥6 months of falls follow-up data were available in 640 participants, who were 77.9±5.3 years old, with height of 1.63±0.10 m and weight of 73.9±15.5 kg. 65% were female.

Subjects stood barefoot with eyes open on a force platform (Kistler 9286AA). The COP data were sampled at 240 Hz in anteroposterior (AP) and mediolateral (ML) directions. Subjects performed two sets of five quiet standing (QS) trials, 30 seconds each. One set included a serial subtractions task (dual task; DT).

Postural stiffness was calculated as previously described [2], where the postural system is modeled as an inverted pendulum with stiffness and damping. Movement of center of mass (COM) was estimated. Fourier transform of the difference between COP and COM was fit to a damped oscillator model to determine K_e (stiffness) and B (damping). K_e, and B values were determined for each trial using MATLAB 7.4, and then scaled to body size [4] and log-transformed.

Falls were reported using a monthly mail-in postcard calendar from each participant, after the COP measurement, with mean follow-up of 17 months (range 6-32 months). The associations between $\boldsymbol{K_e}$ and $\boldsymbol{B}$ values with prospective rate of falls were determined using a negative binomial regression [5] including other covariates associated with falls using SAS 9.1. They include age, sex, race, education, daily alcohol use, gait speed,

executive function, depression, disability, peripheral neuropathy, Berg balance scale, urinary incontinence, and history of falls.

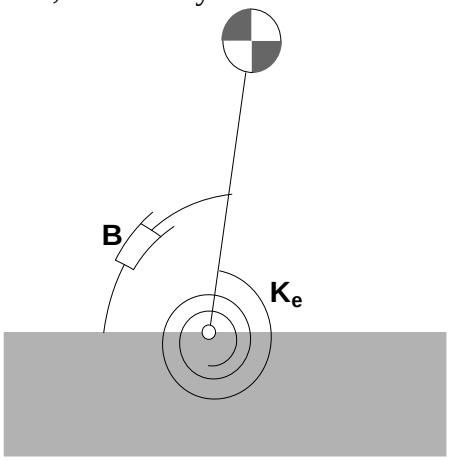

Figure 1. Damped-oscillator inverted pendulum model of quiet standing. Stiffness (***K*****$_e$**) and damping (***B***) describe the resistance to perturbations in the postural system.

RESULTS AND DISCUSSION

Greater postural stiffness (adjusted RR[1]=0.70 ($CI_{95\%}$ 0.50-0.96); p=0.03) and damping (RR=0.49 ($CI_{95\%}$ 0.29-0.82) p=0.007) were associated with lower fall rates outdoors. Results were similar for those measured during dual task. Measurements from AP and ML directions also yielded similar results (Table 1).

The results indicate that the observed stiffness and damping during quiet standing is linked to clinical outcomes of falls. The ability to manage external perturbations may be a key aspect of avoiding falls, particularly outdoors. The decrease in postural stiffness and damping may precede other risk factors for falls. Causes of this decline require further study. Dual tasking did not add to the prediction of falls. The postural system during standing may not be affected by the dual task enough to explain fall risk. A more sophisticated model of postural control that incorporate cognitive function may better explain the role of cognitive distractions on falls. Of note, mechanical stiffness here does not imply osteoarthritic "stiffness" due to joint inflammations or motor rigidity due to Parkinson's disease or other neurologic conditions.

CONCLUSIONS

Greater stiffness and damping in measured during quiet standing was associated with less risk out outdoor falls. Decline in stiffness and damping may be an early marker of fall risk in healthy older adults. Stiffness and damping during dual task were no better at predicting falls than during quiet stance.

REFERENCES

1. Pajala S, et al. *J Geron Med Sci*. **63**:171-8;
2.Winter DA, et al. *J Neurophysiol*. **80**:1211-21, 1998.
3.Leveille SG, et al. *BMC Geriatr*. **8**:16, 2008.
4.Hof AL. *Gait Posture* **4**:223-224, 1996.
5.Leclerc BS et al. *Chronic Dis Can.* **28**:111-120, 2008.

ACKNOWLEDGEMENTS

National Institute on Aging P01AG004390 and T32AG023480

Table 1: Adjusted rate ratios (RR[1]) of the association between stiffness, damping, and outdoor fall rates

Measurement condition		Association of Stiffness K_e with Outdoor Falls			Association of Damping B with Outdoor Falls		
		RR[1]	95% CI[3]	P-value	RR	95% CI	P-value
AP	QS	0.70[2]	0.50 - 0.96	**0.026**	0.64	0.37 - 1.10	0.1
	DT	0.74	0.56 - 1.00	**0.048**	0.61	0.39 - 0.95	**0.027**
ML	QS	0.66	0.46 - 0.93	**0.017**	0.49	0.29 - 0.82	**0.007**
	DT	0.70	0.51 - 0.98	**0.036**	0.56	0.36 - 0.85	**0.007**

AP = anteroposterior values. ML = mediolateral values. QS = quiet stance; DT = dual task. [1]Fall incidence Rate Ratio (RR): increase in fall risk associated with a unit increase in the predictor variable. For example, [2]RR=0.70 indicates that fall rate decreases by a factor of 0.7 (30% reduction) for each unit increase in K_e (after scaling to body size and log-transform). [3]95% CI = 95% confidence interval (CI) of the RR. If the CI includes 1 (i.e., null), the predictor is not significantly associated with fall risk at p = 0.05.

POSTURAL STIFFNESS MODEL AND DUAL TASK IN OLDER ADULTS: THE MOBILIZE BOSTON STUDY

[1] Hyun Gu Kang and [2,3,4] Lewis A. Lipsitz

[1] Kinesiology and Health Promotion, California State Polytechnic University; Pomona, California
[2]Institute for Aging Research, Hebrew SeniorLife, Boston, Massachusetts
[3] Harvard Medical School, Boston, Massachusetts;
[4]Division of Gerontology, Beth Israel Deaconess Medical Center, Boston, Massachusetts;

email: hgkang@csupomona.edu www.csupomona.edu/~hgkang

INTRODUCTION

Cognitive distractions that divert attentional resources seem to impair postural control, and thus may increase fall risk. However, the mechanism by which dual-task affects postural sway or fall risk is not clear, as inconsistent effects have been reported [1]. Standing posture is hypothesized to be controlled through maintaining postural stiffness and damping [2], which represent muscle tone, reflexes, and anticipatory control. During dual task, the lack of attentional resources may lead to the inability to maintain adequate muscle tone to maintain upright standing, reducing postural stiffness, and would increase sway. We tested the effect of dual task on postural stiffness, damping and sway in a representative sample of community-dwelling older adults.

METHODS

The MOBILIZE Boston Study (MBS), which stands for "Maintenance of Balance, Independent Living, Intellect, and Zest in the Elderly of Boston" is a prospective study examining risk factors for falls, including pain, cerebral hypoperfusion, and foot disorders in the older population [3]. The study includes a representative population sample of 765 elderly volunteers age 70 or above from the Boston area. Center of pressure (COP) data were available in 725 participants, who were 77.9±5.3 years old, with height of 1.63±0.10 m and weight of 74.1±19.7 kg. 64% were female.

Subjects stood barefoot with eyes open on a force platform (Kistler 9286AA). The center of pressure (COP) data were sampled at 240 Hz in anteroposterior (AP) and mediolateral (ML) directions. Subjects performed two sets of five quiet standing trials, 30 seconds each. One set included a serial subtractions from 500 by 3 task (S3 task).

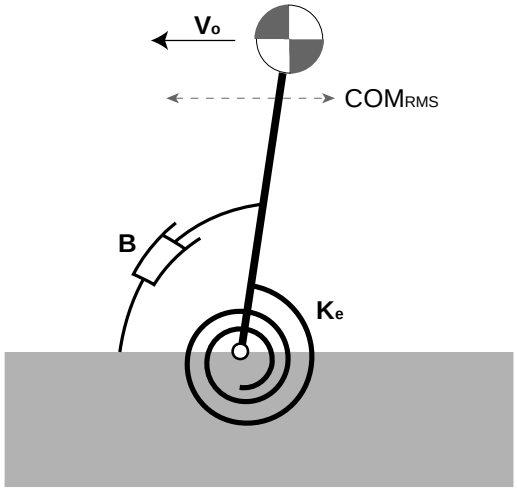

Figure 1. Inverted pendulum model of quiet standing. Its dynamics can be described using stiffness K_e, damping B, RMS amplitude of the COM, and the pendulum velocity at vertical V_o.

Postural stiffness was calculated as previously described [2], where the postural system is modeled as an inverted pendulum with stiffness and damping. Movement of center of mass (COM) was estimated. Fourier transform of the difference between COP and COM was fit to a damped oscillator model to determine K_e (stiffness) and B (damping). Velocity of the inverted pendulum at vertical V_o was also calculated. RMS amplitudes for COP and COM (COP_{rms}, COM_{rms}) K_e, B, and V_o values were determined for each trial using MATLAB 7.4. Because 39% of the subjects had difficulty performing the S3 task (≥5 errors), the subjects were divided into two groups (S3 pass vs. S3 fail groups). The effect of dual task on the parameters was assessed using mixed-model ANOVA (SAS 9.1).

RESULTS AND DISCUSSION

Sway amplitudes and *B* increased with the dual task (Figures 2, 3). V_o increased only in AP direction. K_e decreased only in ML. Yet the S3-fail group increased K_e in AP direction (Figure 2). The S3 task could still independently explain increases in COM_{rms} ($p \leq 0.005$) after including V_o or K_e as a covariate. Thus changes in V_o or K_e did not fully explain increase in sway due to dual task.

Reduction in stiffness in the ML direction may mean a decrease in postural tone. The brain may be prioritizing the maintenance of postural tone in AP direction given the limited attentional resources because the feet may provide "free" stability in ML but not in AP direction. The inverted pendulum model did not fully explain the increase of sway with the dual task. A more sophisticated model of postural control may better explain the role of attention.

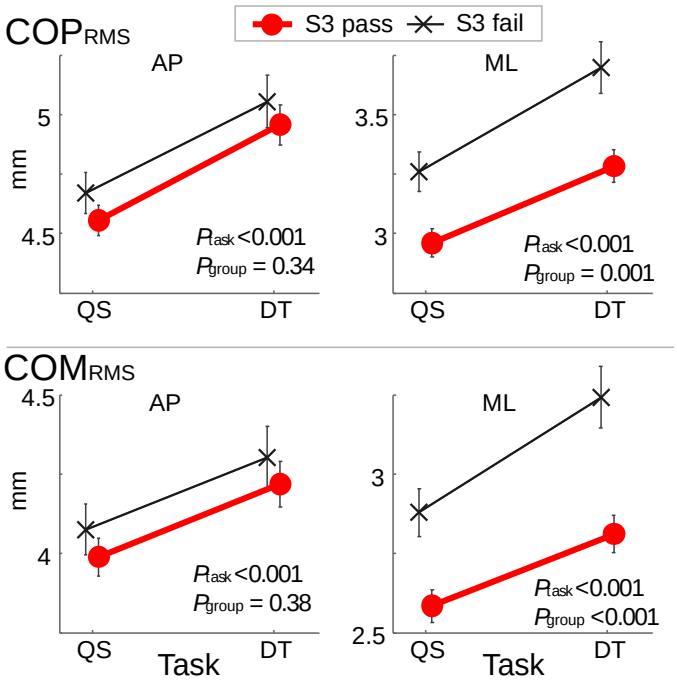

Figure 2: Postural sway (**COP_{RMS}** and **COM_{RMS}**) increased when performing the dual task.

CONCLUSIONS

In community-dwelling older adults, serial subtractions dual-task led to increased sway amplitude and damping. Postural stiffness in the ML direction decreased with dual task, but increased in the AP direction in those who could not perform the S3 task. Changes in stiffness or pendulum velocity did not fully explain the changes in sway. The lumped-parameter model did not fully explain the increase of sway with the dual task.

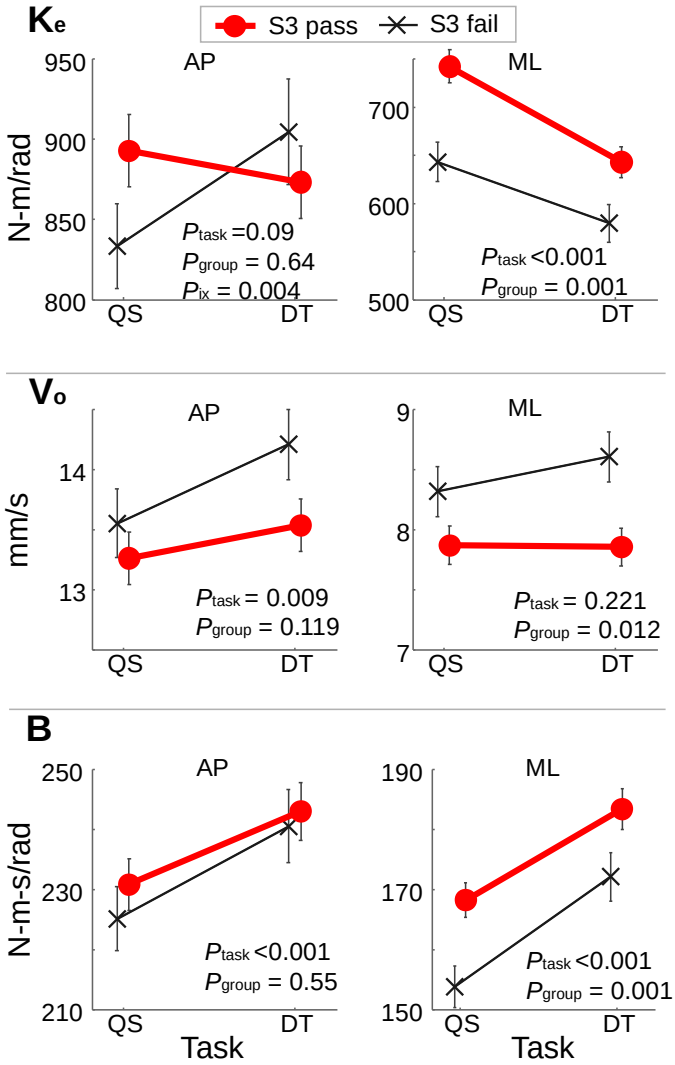

Figure 3. **K_e** increased only in the S3-fail group in AP, and decreased only in ML direction with dual task. **V_o** increased only in the AP direction with dual task. Group differences were found only in ML direction. Damping increased with dual task.

REFERENCES

1. Prado JM et al. *Gerontology*. **53**:274-81, 2007.
2. Winter DA, et al., *J Neurophysiol.* **80**:1211-21, 1998.
3. Leveille SG, et al. *BMC Geriatr*. **8**:16, 2008.

ACKNOWLEDGEMENTS

NIA P01AG 004390 and T32AG023480

AFFECT OF INTENSIVE ENVIRONMENTAL NOISE OF HUMAN POSTURAL CONTROL

Hamid Bateni[1], Anweshana Vaizasatya[1], M. J. Blaschak[1],

[1]Department of Physical Therapy, Northern Illinois University, IL, USA

email: hbateni@niu.edu , web: http://www.chhs.niu.edu

INTRODUCTION

Fall or inability to control posture in a working environment can potentially lead to hazardous conditions and lawsuits [1,2]. One possible factor for disruption of postural control, is environmental noise. Previous studies have shown that loud noise pertains to delayed reading and learning, reduced state of vigilance and task performance and can cause sleep disruption as well as interrupted cognitive processing. However, it is not yet clear how and to what extent environmental noise can affect human performance. The purpose of our study is to determine whether an intermittent white noise of 80 dB could affect the ability to control posture both in terms of the ability to hold the COM static and shifting the COM in a controlled manner.

METHODS

16 healthy young adults (6 Male, 10 female, age range 21-26) were recruited to participate in the study if a) they were healthy, b) right handed and c) had no previous experience of participating in balance studies. Individuals with impaired hearing or vision and those who had a condition that could potentially affect their balance were excluded from the study. Participants stood on the foot platform of Biodex balance system (SD 950 – 320 - Biodex Medical Systems, Shirley, NY, USA) throughout the trials. The display module of Biodex provided a visual picture where it showed a bull's eye and three surrounding rings. A small moving dot at the middle of the screen represented a real-time (20 S/s). The intermittent white noise was played for 30 seconds at 80 dB intensity and was interrupted every second for a period of one second.

The participants were randomly assigned to two different conditions (with and without noise) and four different tests as follows: a) static postural stability tests with eyes open (SEO) participants were asked to stand on the stationary platform and keep their COG as static as possible; b) Static postural stability with eyes closed (SEC); c) dynamic postural stability tests (DYN) where the platform allowed a limited uncontrolled movement around AP and ML axes and d) Limits of Stability tests (LOS) in which participants were presented 9 balls on the display (one central and 8 in surrounding at 50% of BOS) and were challenged to transfer their COP to each of those 8 balls without change in the BOS (Figure 1 A and B).

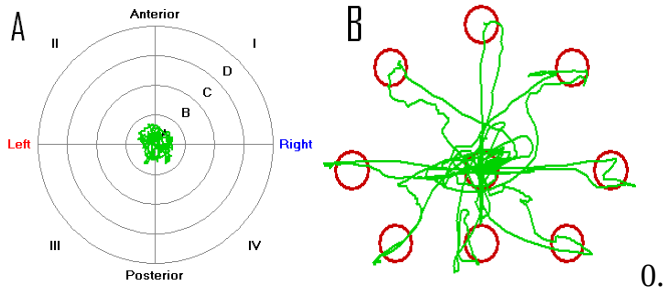

Figure 1: (A) Visual interface during SEO, SEC and DYN tests, where COP is presented to the participant. (B) Visual interface for LOS trials, where subjects attempt to move COP to the eight predefined targets.

3. RESULTS AND DISCUSSION

The difference in the means of the outcome variables between noise and quiet trials for all three conditions of SEO, SEC and DYN were examined. The outcome variables that were considered in analysis where: overall stability index, antero-posterior stability index, medio-lateral stability index, time in zones A, B, C and D and time in quadrants 1, 2, 3 and 4 (please see figure 2). We also examined the difference in means of the noise and quiet trials for the LOS tests for the following outcome variables: overall performance, forward, backward, right, left, forward-right, forward-left, backward-right and backward-left performances.

The results of two way analysis of variance failed to reject the null hypothesis (with $p<.05$) and indicated that there are no significant differences between the noise and the quiet trials. Our results, however, showed significant differences between the conditions when SEO, SEC and DYN trials where being compared ($p=0.0001$).

Although literature consists of conflicting results on whether white noise can facilitate or deteriorate cognitive responses, in general, studies have shown that a background noise impacts attention [3] and cognitive processing [4]. Considering that control of posture is a cognitive demanding task [5], one could expect a change in the performance of individuals when they were exposed to white noise, particularly in LOS trials.

One major difference between our study and most of other studies that may pertain to discrepancies between our results and those of others is the timing of noise exposure. In our study, intermittent white noise was played simultaneous to the measurement, while others have measured cognitive response following exposure to the noise. Therefore, the possibility exists that if an individual worker is exposed to high level of noise, their balance performance will be affected after a period of time.
The second most important difference between our study and those of others is the fact that we were measuring postural control as the outcome variable of our study, while others were focused on cognitive responses. Postural control is a multifactorial complex phenomenon that requires advanced coordination between central nervous system and musculoskeletal system. Previous studies of balance, who have defined a dual task paradigm have shown that if part of the attention are allocated toward additional tasks, lack of enough resources to perform postural control may augment the effect of stimulus [5]. One may speculate that difference in performance between noise and quiet trials could be observed if subjects were exposed to a dual task paradigm.
Our results also reveald that AP stability index was significantly higher than ML stability index, which supports the idea that our participants were having a better level of mediolateral stability (versus antero-posterior stability) during the test. One could speculate that if participants were standing in a less stable posture, the effect of noise on postural sway could be magnified and perhaps significant differences between noise and quiet trials could be observed. To address this issue, we recruited one more subject (Male, 26 years old) to further investigate noise effect in a less stable posture. The subject was instructed to stand in a tandem stance on the platform. SEO, SEC and DYN trials were performed similar to our original data collection. The result of this single subject test was in agreement with the original data, were we did not find any significant effect of noise on postural sway.

CONCLUSION

Our results confirmed that intermittent noise of 80 dB does not have an immediate effect on human postural control. However, our results cannot be generalized to conditions where individuals are exposed to either a higher intensity or longer duration of noise.

References:

1. Bhattacharya, A., Succop, P. A., Kincl, L. D., Lu, M. L., & Bagchee, A. (2002). Postural stability during task performance on elevated and/or inclined surfaces. Occupational Ergonomics, 3(2), 83-97.
2. Chiou S., Bhattacharya, A., & Succop, P. A. (2000). Evaluation of workers' perceived sense of slip and effect of prior knowledge of slipperiness during task performance on slippery surfaces. Aihaj, 61(4), 492-500.
3. Campbell, T., Winkler, I., & Kujala, T. (2005). Disruption of immediate memory and brain processes: an auditory ERP protocol. Brain Res Brain Res Protoc, 14(2), 77-86.
4. Boman, E. (2004). The effects of noise and gender on children's episodic and semantic memory. Scand J Psychol, 45(5), 407-416.
5. Bateni, H., Zecevic, A., McIlroy, W. E., & Maki, B. E. (2004). Resolving conflicts in task demands during balance recovery: does holding an object inhibit compensatory grasping? Exp.Brain Res., 157(1), 49.

WHAT ASPECTS OF POSTURAL TRANSITIONS AFFECT BALANCE CONTROL UPON STANDING?

Angela DiDomenico and Raymond W. McGorry

Liberty Mutual Research Institute for Safety, Hopkinton, MA, USA
email: angela.didomenico@libertymutual.com, web: http://libertymutualgroup.com/researchinstitute

INTRODUCTION

Postural transitions represent self-initiated threats to postural stability [1]. The transition from sitting to standing has received considerable attention in the biomechanical literature, partially due to the musculoskeletal and postural control challenges related to aging that are elucidated during this task [2]. Similar challenges arise during transitions from other postures, although these movements have received minimal attention in the literature. One difficulty in studying such transitions is the variability within the movements, which is generally controlled during sit-to-stand movements. It is uncertain how factors related to the transition from non-seated postures are associated with the resulting imbalance upon standing.

METHODS

Forty-five healthy men aged 18 to 66 years transitioned to standing after maintaining one of three static postures. Static postures included bent at waist, squat, and forward kneel (Figure 1). Nine replications of each condition were analyzed for a total of 27 trials.

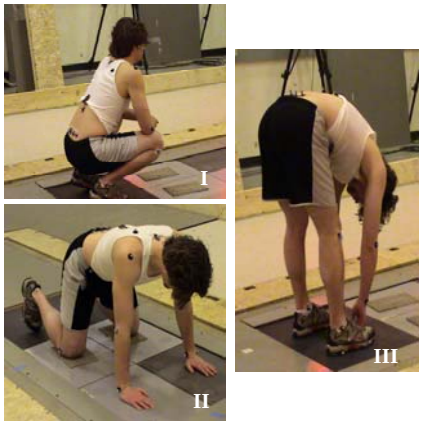

Figure 1. Static postures maintained during the experimental conditions. Squat (I), Forward kneel (II), Bent at waist (III).

Participants transitioned to quiet standing at a self-selected velocity when alerted by an auditory signal. Data was collected for a total of 20s, which included the time to transition (<5s). A minimum rest period of one minute was provided between trials to minimize cumulative fatigue effects.

Whole body motion data was collected at 100Hz and low-pass filtered using a fourth order Butterworth filter, 8Hz cutoff. Whole body center of mass (COM) position data were calculated as the weighted sum of 13 segments. Center of pressure (COP) position data was sampled at 1000Hz from two forceplates prior to low-pass filtering (zero lag fourth-order Butterworth, 5Hz cutoff).

Displacement and velocity of the COM during the transition were calculated for each posture, followed by the area of the base of support upon standing. COP-based balance measures for the period following the transition to standing were calculated to determine the level of balance control. They included COP range AP (antero-posterior), COP range ML (medio-lateral), peak COP velocity AP and peak COP velocity ML. Repeated measures analyses of variance using mixed models were performed to determine the effect of posture (α=0.05).

RESULTS AND DISCUSSION

Postural transitions to standing require substantial movement of the center of mass that is dependent upon the initial position. Three postures were examined that significantly differed in horizontal and vertical displacement of the COM (Figure 2). The peak velocity of the COM during the transition was also significantly affected by the initial posture (Figure 3). The smallest values were associated with bent at waist while the largest values were obtained when transitioning from a forward kneel.

Participants applied motor control strategies when transitioning from bent at waist to prevent excessive movement in the AP direction that could lead to a loss of balance.

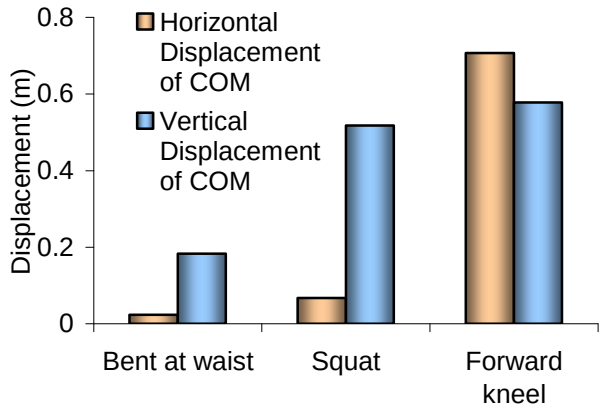

Figure 2. Horizontal and vertical displacement of the COM during postural transitions to standing.

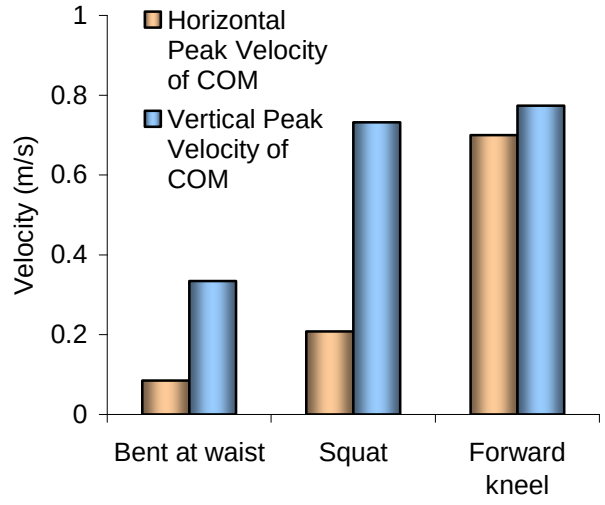

Figure 3. Horizontal and vertical peak velocity of the COM during postural transitions to standing.

The area of the BOS was relatively consistent across posture. The squat resulted in significantly larger areas ($0.14m^2$); mostly due to larger stance widths required to maintain balance during the static squat. There was no significant difference between bent at waist and forward kneel ($0.13m^2$). Since the effect of posture was not significant, the influence of the BOS on the balance control measures was minimal.

Balance measures were generally smaller, reflecting more stability, for bent at waist with increases occurring for the squat and then forward kneel. The trends in the data were similar to those related to the displacement and velocity of the COM. Figure 4 illustrates the effect on COP range ML although the effect was similar for all balance measures, including those related to displacement and velocity of the COP.

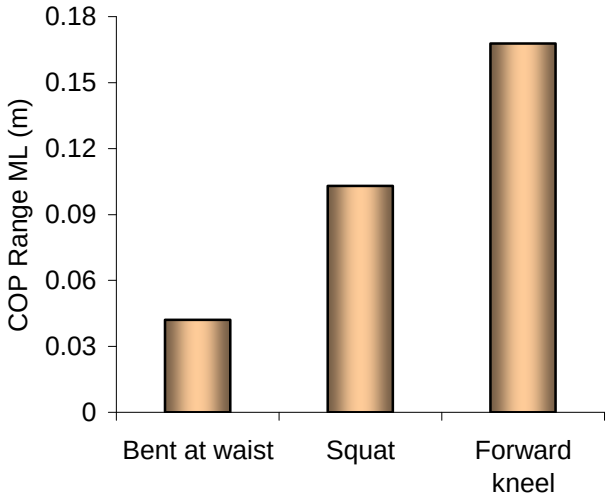

Figure 4. Illustrative example of the effect of posture on the COP-based balance measures.

CONCLUSIONS

The transition from a non-seated posture to standing has been shown to create a perturbation that may be detrimental to balance and increase vulnerability to falls. It is uncertain what aspects of the transitions are responsible for the differences in the imbalances created upon standing but an initial examination of three different non-seated postures indicated that investigations of the movement of the COM might prove more valuable than the area of the BOS established at the end of the transition.

REFERENCES

1. Janssen WGM, et al. *Physical Therapy* **82**, 866-879, 2002.
2. Ikeda ER, et al. *Physical Therapy* **71**, 473-481, 1991.

FOOT PLACEMENT AND SEAT HEIGHT EFFECTS ON SIT-TO-STAND JOINT MOMENTS

[1]Jason Gillette and [2]Catherine Stevermer

[1]Iowa State University, Ames, IA, USA
[2]Des Moines University, Des Moines, IA, USA
email: gillette@iastate.edu

INTRODUCTION

The capability to move from a sitting to a standing position is essential for mobility and is associated with independent living. Altering seat height and foot placement redistributes lower extremity joint moments during a sit-to-stand movement. For example, using a lower seat height increases knee and hip extension moments [1]. From a clinical standpoint, individuals with lower functional status must use compensatory strategies or are unable to complete movements at lower seat heights [2]. More anterior foot placements increase hip extension moments [1], while more posterior foot placements would be expected to increase knee extension and ankle plantarflexion moments. Individuals with end-stage knee osteoarthritis unload their affected leg during sit-to-stand, while improved loading symmetry has been suggested as a positive outcome after total knee arthroplasty [3]. On the other hand, staggered foot placements can be used to promote loading symmetry for hemiparetic patients by placing the affected foot in a more posterior position than the unaffected foot [4].

The purpose of this study was to investigate the effects of changing seat height and foot placement on lower extremity joint moments. It was also of interest to determine whether joint moments for intermediate foot placements could be accurately approximated by averaging the results of bounding foot placements. Consistent with previous studies and biomechanical considerations, it was hypothesized that: 1) knee and hip extension moments would be greater at the low seat height; 2) knee extension moments would be greater in foot-back placement, while hip extension moments would be greater in foot-neutral placement; and 3) knee extension and ankle plantarflexion moments would be greater on the side where the foot is placed in the posterior staggered position.

METHODS

Twenty-one individuals (gender 4/17 M/F, age 22±1 year, height 1.71±0.07 m, mass 68±13 kg) participated in the study. Low (41 cm) and standard (46 cm) seat heights were utilized for sit-to-stand. Three symmetric foot placements were tested: foot-neutral (ankles under knees), foot-back (toes under knees), and foot-intermediate (midfoot under knees). In addition, three asymmetric foot placements were tested: dominant-staggered (dominant toes under knee, nondominant ankle under knee), nondominant-staggered (nondominant toes under knee, dominant ankle under knee), and intermediate staggered (dominant toes under knee, nondominant midfoot under knee). The dominant leg was determined by asking which leg the participant felt more stable on during single leg standing. In total, 2 repetitions of 12 conditions (2 seat heights x 6 foot placements) were completed.

Twenty reflective markers were tracked by an eight-camera system (Vicon). Eight additional markers were recreated using transformations determined from a static standing trial. Participants placed each foot on a separate in-ground force platform (AMTI), and foot placements were indicated on the platforms using colored tape. Sit-to-stand movements were analyzed from seat-off to vertical stabilization as determined from the combined vertical ground reaction forces. Using inverse dynamics, dominant and nondominant maximum ankle plantarflexion, knee extension, and hip extension moments were calculated for each trial, normalized by body mass, and averaged across trials. Multivariate ANOVA was used to test for main effects of seat height and foot placement. When main effects were found for foot placement, post-hoc Scheffe comparisons were utilized for planned comparisons. All significance levels were set to $p < 0.05$.

RESULTS AND DISCUSSION

Maximum joint moments were dependent upon seat height ($p < 0.001$) and foot placement ($p < 0.001$), but not their interaction ($p = 0.998$). The first hypothesis was partially supported in that knee extension and nondominant (but not dominant) hip extension moments were significantly higher at the low seat height (Table 1). The second hypothesis was also partially supported since dominant (but not nondominant) knee extension moments were significantly higher for foot-back, and hip extension moments were significantly higher for foot-neutral. The third hypothesis was fully supported in that dominant knee extension and ankle plantar flexion moments were significantly higher for dominant-staggered, while nondominant knee extension and ankle plantarflexion moments were significantly higher for nondominant-staggered. Thus, knee extension and ankle plantarflexion moments significantly increased in the leg (dominant or nondominant) placed in the posterior position. In addition, knee extension and ankle plantarflexion moments were significantly higher in the leg placed in the posterior position with the intermediate-staggered placement.

Changing seat height had the greatest effect on knee extension moments, where lowering the seat 5 cm increased moments by 11%. Shifting from a foot-back to a foot-neutral placement substantially increased hip extension moments by 49%. Moving a foot from the anterior to the posterior position produced dramatic increases of 81% in ankle plantarflexion and 63% in knee extension moments. Even using an intermediate-staggered position produced an increase of 54% for ankle plantarflexion and 21% for knee extension moments between the anterior and posterior positions. To test predictive accuracy, joint moments for intermediate placements were calculated by averaging the joint moments for bounding placements. These simple approximations were within 10% of actual values for knee extension and hip extension, but less accurate for ankle plantarflexion. Thus, if bounding foot placements are impractical due to pain or range-of-motion limitations, then intermediate placements may be substituted with predictable effects on knee and hip extension moments. Taken together, seat height and foot placement may be manipulated with the goal of reducing targeted joint moments (i.e., post-surgery protection) or to selectively increase joint loading (i.e., post-stroke rehabilitation).

REFERENCES

1. Janssen WGM, et al. *Phys Ther*, **82**, 866-879, 2002.
2. Mazza C, et al. *J Am Geriatr Soc*, **52**, 1750-1754, 2004.
3. Boonstra MC, et al. *Phys Ther*, **90**, 149-156, 2010.
4. Duclos C, et al. *Neurorehabil Neural Repair*, **22**, 715-722, 2008.

Table 1: The effects of seat height and foot placement on lower extremity joint moments.

	Maximum Joint Moments (Nm/kg)					
Foot Placement	**Dominant Ankle Plantarflex.**	**Nondom Ankle Plantarflex.**	**Dominant Knee Extension**	**Nondom. Knee Extension**	**Dominant Hip Extension**	**Nondom. Hip Extension**
Low	0.27 ± 0.12	0.25 ± 0.11	0.90 ± 0.18[a]	0.86 ± 0.18[a]	0.68 ± 0.23	0.70 ± 0.19[a]
Standard	0.25 ± 0.12	0.22 ± 0.11	0.81 ± 0.22	0.78 ± 0.20	0.65 ± 0.24	0.64 ± 0.19
Foot-back	0.28 ± 0.12	0.27 ± 0.11	0.90 ± 0.16[b]	0.87 ± 0.16	0.57 ± 0.20	0.54 ± 0.16
Foot-intermediate	0.22 ± 0.10	0.21 ± 0.09	0.87 ± 0.15	0.85 ± 0.14	0.68 ± 0.21	0.65 ± 0.17
Foot-neutral	0.25 ± 0.12	0.24 ± 0.10	0.78 ± 0.16	0.77 ± 0.14	0.83 ± 0.24[c]	0.83 ± 0.19[c]
Dominant-stagger	0.33 ± 0.11[d]	0.19 ± 0.10	1.01 ± 0.17[d]	0.62 ± 0.18	0.61 ± 0.22	0.73 ± 0.18
Intermed.-stagger	0.30 ± 0.12[d]	0.20 ± 0.10	0.95 ± 0.17[d]	0.78 ± 0.15	0.59 ± 0.21	0.64 ± 0.16
Nondom.-stagger	0.18 ± 0.12	0.32 ± 0.12[e]	0.63 ± 0.17	1.02 ± 0.16[e]	0.72 ± 0.24	0.62 ± 0.16

[a] Low > Standard ($p < 0.05$)
[b] Foot-back > Foot-neutral ($p < 0.05$)
[c] Foot-neutral > Foot-back and Foot-intermediate ($p < 0.05$)
[d] Dominant-staggered and Intermediate-staggered > Nondominant-staggered ($p < 0.05$)
[e] Nondominant-staggered > Dominant-staggered and Intermediate-staggered ($p < 0.05$)

COMPARISON OF ALTERNATE STAIR DESCENT PATTERNS

[1]Catherine A. Stevermer, [2]Michelle Hall and [2]Jason C. Gillette
[1]Post-Professional Doctor of Physical Therapy Program, Des Moines University, Des Moines, Iowa
[2]Department of Kinesiology, Iowa State University, Ames, IA
e-mail: catherine.stevermer@dmu.edu

INTRODUCTION

Self-reported difficulty with stair descent has been correlated with increased fall risk [1]. Individuals with muscle or joint dysfunction may adopt compensatory techniques to negotiate stairs due to muscle weakness, pain, instability or confidence issues. Compensations may include reducing descent speed, using a handrail or descending with a step-by-step (SBS) pattern rather than a step-over-step (SOS) pattern. Researchers reported a slower descent velocity and lower knee extension joint moments with a SBS pattern compared to a SOS pattern [2]. These authors suggested the SBS pattern may also provide additional stability.

There is sparse evidence on center of pressure (COP) measures as an indication of stability during stair negotiation. Researchers have used time-to-boundary (TtB) measures of COP excursions as instability indicators during stance [3,4]. The TtB estimates the time for the COP to reach the border of the base of support based on the instantaneous COP velocity. A lower TtB measure may reveal postural instability and potentially a risk for falls.

The purpose of this project was to determine the effect of alternate stair descent patterns on stability and joint moments. As previously proposed, we expected TtB measures to be higher for a SBS pattern compared to a SOS pattern due to improved stability. In accord with prior research, we also expected knee and hip joint moments to be reduced in a SBS pattern.

METHODS

Eighteen young adults (age 22 ± 2 yrs; height 1.7 ± 0.1 m; mass 69.5 ± 13.0 kg) participated in this project. An eight-camera video system (Vicon, Englewood, CO) was used to track 28 reflective markers placed bilaterally on each subject. Landmarks for tracking included: cervicale, acromion, ASIS, PSIS, sacrum, greater trochanter, mid-femur, lateral femoral condyles, mid-tibia, medial and lateral malleolus, 5th metatarsal head and great toe. Kinematic data were captured at 160 Hz using Vicon Nexus software. A three-step wooden stair module (step height = 19 cm; tread depth = 28 cm) was used for this project. Two portable force platforms (AMTI; Watertown, MA) were placed on the second and third tread to collect ground reaction forces. A third platform was located at the base of the module. Beginning at the top of the staircase, individuals descended three steps to floor level and walked two additional meters. Participants performed stair descent with arms freely moving at their sides at a self-selected pace using two stair descent patterns: SOS and SBS. Each participant completed two trials leading with the right foot and two trials leading with the left foot using each pattern, for a total of eight trials.

Inverse dynamics was used to calculate joint moments, which were normalized by body mass. Time to descend from the second tread to floor contact (2-step descent time) was determined. Medial-lateral TtB calculations were determined using center of pressure variables [4]. The stance (single support) phase of the SOS pattern was determined from initial and final contact with each force platform (detected by a 20% body weight threshold). For the SBS pattern, the single support phase constituted initial contact through the initiation of double support (detected by toe and heel marker positions). For joint moment analysis, the first 50% of the SOS stance phase was compared with the single support phase of SBS. For the TtB comparison, the entire single support phase of the SOS pattern and combined single and double support phases of the SBS pattern were included. For this analysis, only right side leading trials were included. Paired t-tests were conducted on condition differences for 2-step descent time, TtB and lower extremity joint moments. Statistical significance was defined at $p<0.01$.

RESULTS AND DISCUSSION

While descending two steps using the SBS pattern, participants required 46% more time compared to the SOS pattern ($p<0.001$). Participants descended in 3.5 ± 0.5 s using the SBS pattern, while the SOS condition required 1.9 ± 0.3 s. A slower 2-step descent time is consistent with prior work [2].

As expected, the SBS pattern produced a significantly lower knee extension moment ($p<0.001$) than the SOS pattern (Table 1). With an average reduction in knee extension moments of 45% over both steps, individuals with knee joint pain or muscle weakness may adopt the SBS pattern of stair descent as a compensation to reduce joint loading or muscle strength requirements. The hip abduction moment on the second step was also significantly lower with the SBS pattern compared to the SOS pattern ($p<0.001$). The SBS pattern reduces forward momentum when stepping on the second tread before continuing descent. Theoretically, the SBS pattern would require decreased hip abductor activity to control momentum in the frontal plane with increased time in double support. There were no significant differences for knee varus or hip extension moments as a function of stair descent pattern.

There were differences in the hip abduction moments between the two steps (Table 1). Both stair descent patterns required increased hip abduction moments on the second step compared to the first step ($p<0.001$). This may be due to an added stability requirement to control frontal plane momentum. Participants began at a stand-still for both stair descent patterns and there were no differences in hip abduction moment. Consistent with step differences in the frontal plane, knee varus torques also significantly increased ($p<0.001$) from step one (0.19 ± 0.11 Nm/kg) to step two (0.27 ± 0.11 Nm/kg). There were no significant differences in knee extension or hip extension moments as a function of step.

The hypothesis regarding improved stability as measured by the TtB during the SBS pattern was not supported. The peak TtB was reduced by an average of 36% in the SBS pattern compared to the SOS pattern ($p<0.01$) for both measured steps on the staircase (Table 1). Increased hip/pelvic motion in the frontal plane in older adults may contribute to increased fall risk in stair descent [5]. It is possible that the SBS pattern requires additional pelvic movement and more frequent medial-lateral COP shifts for limb advancement, which may contribute to a lower TtB, even in healthy individuals.

CONCLUSIONS

These findings suggest the SBS pattern decreases knee extension and hip abduction joint moments. However, the SBS pattern may not provide extra stability during stair descent. Additional research should expand stability measures relative to compensatory stair technique.

REFERENCES

1. Verghese J, et al. *Arch Phys Med Rehab*, **89(1)**, 100-104, 2008.
2. Ried SM, et al. *Med Sci Sports & Exer*, **39(11)**, 2005-2011, 2007.
3. Slobounov SM, et al. *J Gerontol*, **53A(1)**, B71-B78, 1998.
4. Hertel J, et al. *J Appl Biomech*, **22**, 67-73, 2006.
5. Mian OS, et al. *Gait & Posture*, **25**, 9-17, 2007.

Table 1: **Comparison of Stair Descent Patterns for First and Second Steps**. (*) indicates statistically significant difference in parameter ($p<0.01$) between stair descent patterns; (#) indicates statistically significant difference in parameter ($p<0.01$) between first and second steps.

	First Step			**Second Step**		
Stair Descent Patterns	Time-to-Boundary (s)	Knee Extension (Nm/kg)	Hip Abduction (Nm/kg)	Time-to-Boundary (s)	Knee Extension (Nm/kg)	Hip Abduction (Nm/kg)
Step-Over-Step (SOS)	0.17 ± 0.08*	0.74 ± 0.26*	0.69 ± 0.16#	0.23 ± 0.14*	0.80 ± 0.33*	1.06 ± 0.24*
Step-By-Step (SBS)	0.12 ± 0.02	0.44 ± 0.20	0.63 ± 0.14#	0.13 ± 0.03	0.42 ± 0.26	0.79 ± 0.15

THE EFFECT OF A SUBJECT-SPECIFIC DUAL-TASK ON STANDING BALANCE

[1]Alison L. Sukits, [1]April J. Chambers, [1]Rakié Cham, and [2]Robert D. Nebes

[1]Human Movement and Balance Laboratory, University of Pittsburgh, Pittsburgh, PA, USA
[2]Department of Psychiatry, University of Pittsburgh, Pittsburgh, PA, USA
email: als110@pitt.edu web: http://hmbl.bioe.pitt.edu

INTRODUCTION

Falls are a serious public health concern in older adults, with one in three older adults falling each year [1]. It has been shown that balance impairment is just one of many factors associated with increased fall risk in community-dwelling older adults [2].

Previous research has shown that postural control is negatively compromised when concurrent with a dual-task [3]. However, conflicting research has shown that postural control is enhanced when performed during a dual-task. This inconsistency may be due to the dual-task performed in each study. Dual-task type has been found to impact balance and gait differently [3]. Previous research has suggested that the dual-task should be cognitively challenging as to affect balance but also adjustable in difficulty to match each participant's capacity [4]. Creating a dual-task that is adjustable to each subject may allow for a clearer examination of the impact of dual-task on postural control.

The goal of this preliminary study, part of a larger project, is to identify the effect of a subject-specific, audible, cognitive challenge task on standing balance in older adults.

METHODS

Ten healthy older adults (4 M, 4 F), screened for neurological and orthopedic conditions, participated in this study (Table 1).

Table 1. Participant characteristics. Mean, (SD) and [Range] are shown

Age [years]	Height [m]	Body Mass [kg]
73.5 (3.4) [70.4-79.8]	1.69 (0.066) [1.58-1.79]	73.9 (14.4) [55.6-97.0]

Each participant underwent a series of 12 trials. Each trial lasted 60 seconds and consisted of standing quietly with his or her feet together on a Bertec forceplate (4060A) and performing one of three task conditions.

The task conditions consisted of no task (NT), in which the participant stood quietly without a cognitive challenge, forward (F), in which the participant would repeat a series of numbers in the order it was presented, and backward (B), in which the participant would repeat a series of numbers in the opposite order it was presented. The difficulty of the task was determined for each participant based on individual ability to recall digit spans of two to seven digits backwards [5].

The first block consisted of six trials, in which the participant's eyes were open (EO). The first trial was NT followed by a randomized order of F and B trials. The order of these three trials was then repeated. The second block consisted of repeating the first block; however, the participant's eyes were closed (EC).

Forceplate data, collected at 240 Hz, was filtered using a low-pass Butterworth filter with cut-off frequency of 1.5 Hz and down sampled to 120 Hz [6]. Center of pressure (COP) in millimeters in the anterior-posterior (AP) and medial-lateral (ML) direction were determined. Amount of sway in millimeters was quantified in both AP and ML directions by the root-mean squared (RMS) of the COP using the following [7]:

$$RMS = \sqrt{\frac{1}{n}\sum_{i=1}^{n}(COP_i - \overline{COP})^2}$$

where n is the number of data points. The distance covered by the COP as it oscillated within the base of support in millimeters per second was quantified

as the normalized path length (PL) and found using the following [7]:

$$PL = \left(\sum_{i=1}^{n} \sqrt{(AP_i - AP_{i-1})^2 + (ML_i - ML_{i-1})^2} \right) \times \frac{n}{120}$$

where n is the number of data points and AP and ML are the COP in each direction.

No statistical significance was found between the first and second trial of each task in both EO and EC. These trials were averaged for analysis. As expected, eye condition was significant for RMS and PL, thus the subsequent analyses were performed within eye condition. AP RMS, ML RMS, and PL were entered individually into a within-subject ANOVA. The independent factor was task (NT, F, B) and post-hoc analyses were performed. Statistical significance was set at 0.05.

RESULTS AND DISCUSSION

Task was significant for EC, ML RMS (Fig 1) and EO, PL (Fig 2). For both, NT was different from F and B, but F was not different from B.

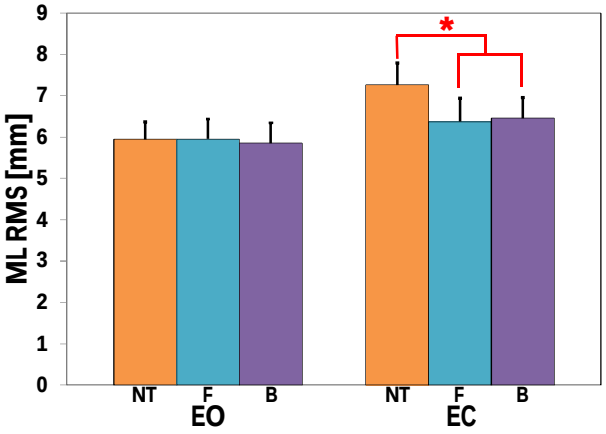

Figure 1. Average ML RMS [mm] for all subjects and each condition. Standard error bars provided.

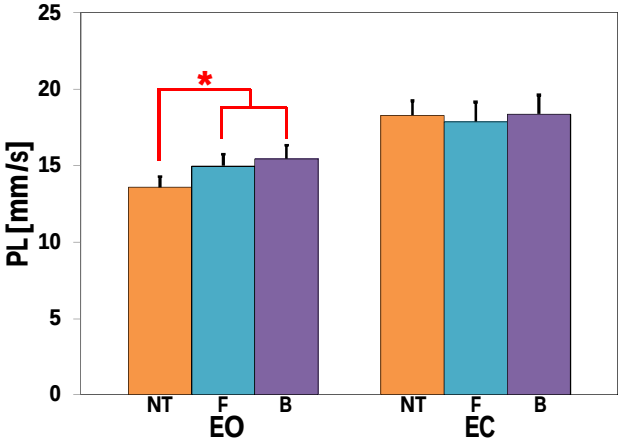

Figure 2. Average PL [mm s^{-1}] for all subjects and each condition. Standard error bars provided.

As shown in Figure 1, when standing with eyes closed and not given a dual-task, there was more sway in the ML direction compared to standing with eyes closed and performing a forward or backwards subject-specific dual-task. This suggests that balance may have improved when the subject-specific dual-task was administered during quiet stance. When given a dual-task to perform, subjects may have been more focused, i.e. less sway, than standing without a task.

However, Figure 2 shows that when standing with eyes open, there was a significant increase in path length when comparing standing without performing a task and performing a forward or backward subject-specific task. These findings may suggest that in the dual-task condition, the postural control system may have been challenged, i.e. "working harder", to maintain balance. Vision also appears to interact with these dual-task effects; however a larger sample size is needed to disentangle this effect.

In summary, this pilot study shows the feasibility of using a dual-task with a difficulty that can be adjusted to the participant's cognitive ability. Further investigations are needed to fully understand the impact of this task on balance.

REFERENCES

1.Talbot LA, et al. *BMC Public Health* **18**, 5-86, 2005.
2.Muir SW, et al. *J Clin Epi* **63**, 389-406, 2010.
3.Huxhold O, et al. *Brain Res Bull* **69**, 294-305, 2006.
4.Salthouse TA, et al. *Mem & Cog* **23**, 59-71, 1995.
5.Nebes B, et al. *Psych Res* **102**, 139-151, 2001.
6.Mahboobin A, et al. *Exp Brain Res* **167**, 260-267, 2005.
7.Kim GT, et al. *J Biomed Sci* **4**, 364-372, 2009.

ACKNOWLEDGEMENTS

Funding Source: NIH/NIA R01 AG030452

LOWER EXTREMITY COORDINATED MOBILIZATION AND STABILIZATION DURING STATIC STANCE: THE UNIQUE ROLE OF THE VASTI MUSCLES

Toran D. MacLeod, Kurt Manal, Lynn Snyder-Mackler and Thomas S. Buchanan

University of Delaware, Newark, DE, USA
email: macleod@udel.edu, web: http://www.cber.udel.edu/

INTRODUCTION

Neuromuscular control strategies have been investigated during a variety of tasks [1,2], and many theories on motor coordination and synergies have been suggested. Different control strategies have been proposed for the limb that mobilizes (e.g., kicks a ball) when compared to the limb that stabilizes (e.g., in stance while the other leg is kicking) [3].

Knee injuries are common during cutting sports, and most often the knee that is injured is the one in stance providing stabilization. We hypothesized that the mobilizing limb would be more specific than the stabilizing limb. The purpose of this study was to investigate if differences in neuromuscular control exist about the knee between the stabilizing and mobilizing limbs during a standing posture.

METHODS

Eleven uninjured athletes (mean age 24.9 ± 2.7 years) volunteered to participate in this study to date. All subjects were regular participants in high level sports. Subjects were positioned standing with their bare feet on a force platform (a separate force platform was used for each foot). Subjects were given visual feedback of their forces on the 6 degree of freedom force platform and were asked to use this information to produce specific static postures. One foot was randomly selected to mobilize the cursor, while the other stabilizing foots' forces did not affect the cursor. The subjects' goal in the experimental protocol was to use their mobilizing foot to position a circular cursor over a narrow target that consisted of two concentric circles. Subjects were instructed to equally divide their body weight between the force plates and simultaneously produce forces tangential to the plane of the force plate. Targets appeared in a random order at one of 18 positions (located at 20° increments of a circle in the forward-backward-medial-lateral plane). Seventy-two trials were performed bilaterally (both feet performed the mobilizing task). A load of 30% of maximum forward-backward force (collected prior to trials) was required to move the cursor in to the target. Subjects were required to hold the cursor within the narrow target for 0.5 seconds before the trial was considered successful.

Electromyography (EMG) activity of 11 muscles, of both legs, was collected from the medial hamstrings (MH), lateral hamstrings (LH), rectus femoris (RF), vastus medialis (VM), vastus lateralis (VL), medial gastrocnemius (MG), lateral gastrocnemius (LG), tibialis anterior (TA), gluteus medius (GM), soleus (SOL), and adductors (ADD) during the final 0.5 second in each target using surface electrodes. The data were full wave rectified, averaged, and normalized using maximum EMG data collected earlier in the session.

Muscle activity at each of the targets was plotted in polar coordinates. The directional EMG data for the stabilizer foot were transposed, so that polar plots represent the muscle activity of both the stabilizer and mobilizer under the same external forces.

The specificity of muscle utilization was analyzed by calculating a specificity index [4] for each muscle. Vector addition was used to calculate the overall magnitude and direction of muscle activity (EMG) based on the polar plots. The specificity index was calculated by dividing the vector sum by the scalar sum, for a value that ranged between zero and one.

RESULTS AND DISCUSSION

The adductors were most active in the medial direction, and gluteus medius was most active in the lateral direction, for both the mobilizing and

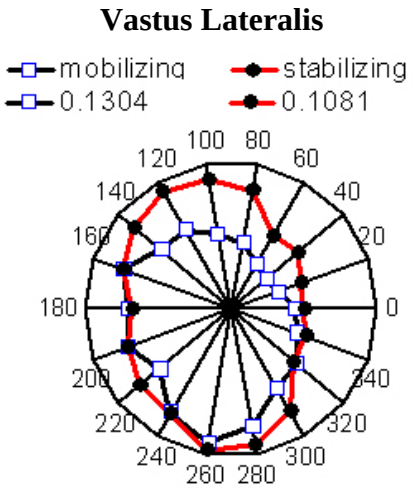

Figure 1: Polar plot of EMG demonstrates the stabilizing VL is more active than the mobilizing VL while pushing forward against the force platform (legend above indicates mobilizing and stabilizing limb and the EMG proportion of MVC).

stabilizing limb. Hamstrings were utilized primarily in the backward direction, for both the mobilizing and stabilizing limb. Rectus femoris was primarily active in the forward direction. These results were not surprising as they correspond to the mechanical moment arms of the muscles.

Interestingly, the vasti of the stabilizing limb contracted differently from the mobilizing limb, and did not always contract in the direction that may be anticipated. For the mobilizing limb, the vasti were active primarily in the backward direction, and were relatively inactive in the forward direction. However, for the stabilizing limb, the vasti were active during both forward and backward directions (Fig. 1). Further, the specificity index for the vasti of the stabilizing limb was smaller than of the mobilizing limb (Fig. 2).

We found a synergistic relationship between the vasti and hamstring muscles of the mobilizing limb. The vasti do not usually act synergistically with the hamstrings except while co-contracting, and the lack of hamstring and vasti muscle activity while pushing forward indicates this was not a typical co-contraction. These results are surprising, and may represent a strategy to stabilize the knee joint with the vasti while the hamstrings mobilize the entire lower extremity.

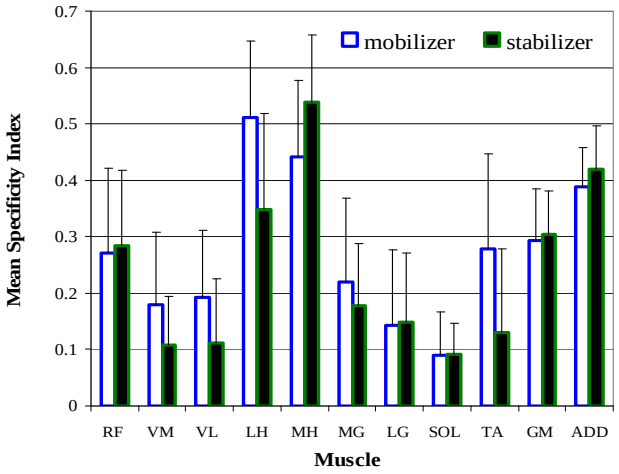

Figure 2: Comparison of mean specificity indices between mobilizing and stabilizing limb indicates differences exist for the vasti muscles.

Knee injury has been found to reduce vasti muscle specificity [4]. Perhaps both the stabilizing and mobilizing limb of ACL deficient subjects would have decreased vasti specificity when compared to healthy individuals. A more global co-contraction of the muscles about the knee could increase joint loading, and explain a portion of the increased incidence of post-traumatic osteoarthritis.

While these data are preliminary, our findings suggest that the vasti of the mobilizing limb have more specific neuromuscular control strategies than the stabilizing limb. Advancing our understanding of the neuromuscular control of the vasti muscles is an important contribution to knee injury prevention and rehabilitation programs.

CONCLUSIONS

We believe the neuromuscular control strategies appear to be less specific for the stabilizing than the mobilizing limb. The vasti muscles play an important role in stabilizing the knee while multi-joint muscles mobilize the limb.

REFERENCES

1. Wang J. *Exp Brain Res*, **178**, 565-570, 2007.
2. Buchanan TS, *J Neurophysiol*, **56**, 1225-1241, 1986.
3. Peters M, *Psychol Bull*, **103,** 179-192, 1988.
4. Williams G, *Med Sci Sports Exerc*, **36**, 1089-1097, 2004.

Supported by NIH R01-AR046386

IS THERE A TRADEOFF BETWEEN STABILIZATION AND MANEUVERABILITY DURING WHOLE-BODY MOVEMENTS?

Helen J. Huang and Alaa A. Ahmed

Neuromechanics Laboratory, University of Colorado, Boulder, CO, USA
email: helen.huang@colorado.edu, http://spot.colorado.edu/~alaa/neuro_lab/

INTRODUCTION

Whole-body movements such as walking and reaching during standing require both stabilization and maneuverability. Currently, there is a dichotomy of balance exercises that focus either on stabilization (ex. balance or "wobble" boards) or maneuverability (ex. video games like Wii Fit's skiing which requires side-to-side shifts in weight). We define stabilization as the static aspect of balance control (restriction of center of pressure excursion), often achieved with muscle coactivation. We define maneuverability as the dynamic aspect of balance control with the ability to make rapid corrective movements (relaxation of center of pressure excursion). These contrasting control strategies suggest that there is a tradeoff between stabilization and maneuverability during whole-body movements. This tradeoff has not been studied in humans to our knowledge [1, 2]. Understanding how humans manage this tradeoff may help identify inappropriate and inefficient biomechanical control strategies that can lead to increased risk for falls or injury.

The purpose of this study was to determine if a tradeoff exists between stabilization and maneuverability in young healthy adults during a goal-directed postural task. We hypothesized that 1) greater stabilization demands will decrease center of pressure excursions and increase muscle activity; 2) greater maneuverability demands will increase center of pressure excursions and decrease muscle activity; and 3) during a condition with high stabilization and high maneuverability demands, subjects will sacrifice stabilization for greater maneuverability and vice versa. This means that the center of pressure excursions and muscle activity values for hypothesis 3 will be in between the values for the high stabilization condition and the high maneuverability condition.

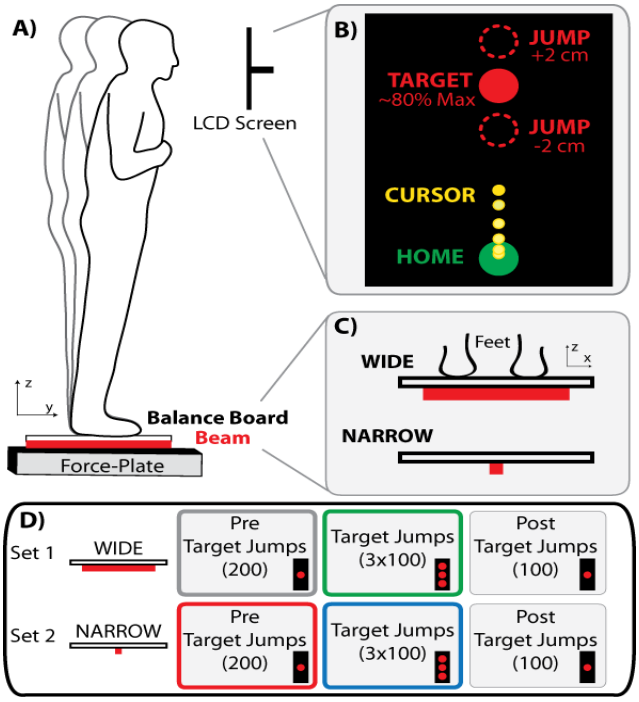

Fig. 1 Experimental setup and protocol

METHODS

Five healthy young adults (age 29±4.2 yrs) used their sense of balance (i.e. center of pressure control) to play a computer game. Subjects shifted their weight forward to move a cursor (0.3cm radius) from a home circle (1.5cm radius) to a target circle (1.5cm radius), located at ~80% of the subject's maximum anterior center of pressure excursion (Fig. 1A&B). Only visual feedback of the sagittal plane center of pressure excursion was provided. To manipulate stabilization demands, subjects stood on a balance board with either a wide (45.7cm) or a narrow (2.5cm) beam of support, which rested on a forceplate (AMTI) (Fig. 1C). To manipulate maneuverability demands, we used target jumps, changing the target location ~500ms after movement initiation. Target jumps were 0, +2, or -2cm in the sagittal plane relative to the original target location (Fig.1B). The experimental protocol

was 200 trials without jumps (Pre Target Jumps), 300 jump trials (Target Jumps), and then 100 trials without jumps (Post Target Jumps) (Fig.1D).

For stabilization, we quantified the center of pressure excursion range in the frontal plane (x-range). For maneuverability, we quantified the maximum center of pressure excursion in the sagittal plane relative to the original target distance (overshoot). We only compared trials to the same (original) target distance and with maximum x-ranges within the narrow beam width so that differences between conditions were not a result of physical constraints. We measured surface electromyography (EMG) (Delsys) of the right and left peroneus longus muscles. We compared performance during different times in the protocol (early and late Pre Target Jumps, early and late Target Jumps, early and late Post Target Jumps). We used a repeated measures ANOVA and post-hoc Tukey Honestly Significantly Difference (THSD) tests to determine statistical significance.

RESULTS AND DISCUSSION

There is a tradeoff between stabilization and maneuverability in young healthy adults in this goal-directed postural task (Fig. 2). Increasing just stabilization demands decreased x-range and overshoot but increased peroneus longus muscle activity (rmANOVA, $p < 0.05$ for all metrics). Increasing just maneuverability demands increased x-range (rmANOVA, $p = 0.06$) and overshoot (*THSD*, $\alpha = 0.05$), but decreased peroneus longus muscle activity slightly. Comparing simultaneous high stabilization and high maneuverability demands to only high stabilization demands, x-range and overshoot (*THSD*, $\alpha = 0.05$) increased. This demonstrates that to gain maneuverability (i.e. greater overshoot), subjects sacrificed stabilization resulting in greater center of pressure excursion in the frontal plane. The peroneus longus muscle activity, however, did not show a decrease, remaining at levels comparable to the stabilization-only condition. Comparing simultaneous high maneuverability and high stabilization demands to only high maneuverability demands, x-range and overshoot decreased. This demonstrates that to satisfy the increased stabilization demands (i.e. restrict frontal plane center of pressure excursion), subjects sacrificed maneuverability resulting in less overshoot.

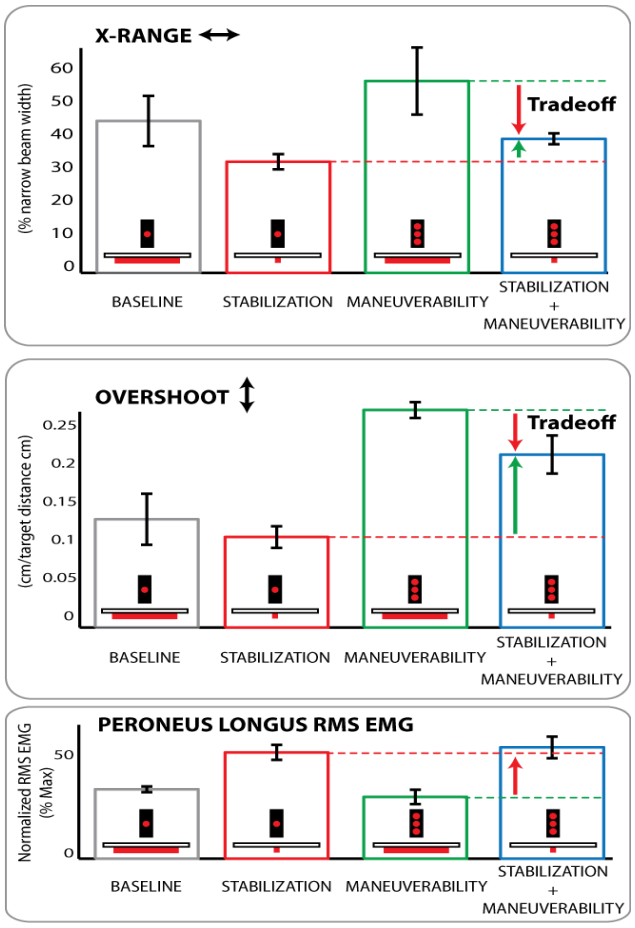

Fig. 2 Frontal plane center of pressure excursion (x-range), sagittal plane overshoot, and left peroneus longus muscle activity for four conditions, mean ± SEM. Baseline: late Pre Target Jumps on the wide beam. Stabilization: late Pre Target Jumps on the narrow beam. Maneuverability: early Target Jumps on the wide beam. Stabilization + Maneuverability: early Target Jumps on the narrow beam. RMS = root mean square.

CONCLUSIONS

Humans must manage a tradeoff between stabilization and maneuverability. Whole-body balance exercises could use this tradeoff to promote maneuverability over stabilization or vice versa. This may be beneficial for older adults, who tend to favor stabilization and muscle coactivation [3].

REFERENCES

1. Hasan, Z. *J. Motor Behav*, **37**(6): 484-493, 2005
2. Jindrich, DL and M. Qiao, *Chaos*, **19**(2), 2009
3. Benjuya et al., *J. Gerontol A Biol Sci Med Sci*, **59**(2): 166-171, 2004

ACKNOWLEDGEMENTS

NIH T32 5AG000279-08 to HJH.

Spinal cord injury and time to instability in seated posture

Sunghoon Shin, Jacob J Sosnoff
University of Illinois, IL, USA
Email: sshin27@uiuc.edu

INTRODUCTION

Spinal cord injury adversely impacts sensory and motor pathways. Depending on the location and severity of injury there is a disruption of efferent and afferent signals below the level of injury. Seated postural control is an essential motor task for individuals with spinal cord injury (SCI) (Gagnon et al., 2005). Although individuals with SCI maintain a seated posture for an extend time during daily physical activities, they have decreased seated postural control compared to healthy counterparts (Seelen et al., 1997).

The majority of research examining seated postural control in SCI has examined traditional parameters of center of pressure motion (e.g. sway path length, area, etc). However, this traditional approach provides minimal information about the stability of seated posture. There are numerous methods to examine postural stability. One method to determine postural stability is by calculating the virtual time to contact (VTC) to the stability boundary (Slobonov et al., 1997). The virtual time provides an estimate of the time required for the center of pressure (COP) to reach the functional stability boundary (see methods). It is calculated at every point in time series of the center of pressure.

Importantly, this method does not measure the relative position of the COP to stability boundary but estimates the time need to reach to the boundary (Slobounov et al., 2006). As such it does not require losses of stability making it ideal for clinical populations.

In the current investigation, we examine VTC in SCI in order to better understand seated postural control of SCI individuals. We expected SCI individuals to have smaller VTC compared to NSCI individuals. Additionally we predict individuals with higher injury level (i.e. lower function) would have smaller VTC compared to those with lower injury levels.

METHODS

16 subjects (mean age 24.6yrs, height 1.71cm, weight 68.2kg, 3 high spinal cord injured (HI), 5 low spinal cord injured (LI) and 8 non-spinal cord injured individuals (NSCI)) participated in this study. Injured level of HI was T10 and above and LI was from T11 to L4. To quantify seated postural control, participants sat on a wooden box placed on force platform (AMTI, Inc.) with their and arms by their side. The platform records three force and three moment components: Fx, Fy, Fz Mx, My, and Mz. The signals were amplified using a six-channel AMTI-Model SGA6-4 amplifier. A maximum gain of 4000 was used and filtered with 4th order low pass Butterworth filter of 10Hz. The data were collected with a sampling frequency of 100 Hz.

In order to calculate virtual time to contact, functional stability boundary was determined by the procedures of Slobounov et al (1997). The “functional stability boundary” of each subject was determined by having them lean forward, backward, laterally and diagonally pivoting at the hip joint, in the circular direction leaning as far as possible without losing balance for one minute (Slobounov et al., 1997). Also, the center of pressure – a reflection of the neuromuscular response to the imbalances of the body's center of gravity was calculated (Winter, 1990).

To examine the effects of the supported and vision on functional boundary and VTC to the stability boundary, subjects did two static postural tasks: sitting still with eyes open (EO) and eyes closed (EC).

RESULTS AND DISCUSSIONS

It is clear in Figure 2, that the HI group has smaller

functional boundary than the NSCI group at both EO and EC (EO: 208.8 vs. 99.4; EC: 195.7 vs.86.1 cm^2, <.05).

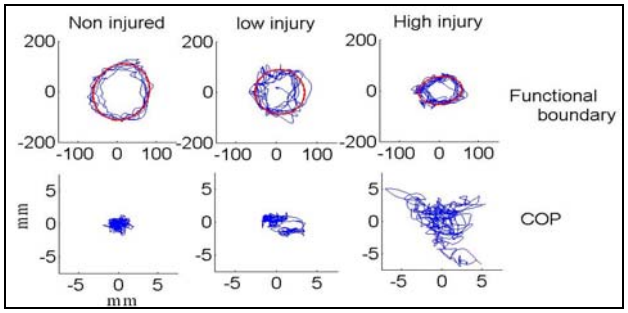

Figure 1. Representative trials of the COP for the boundary trials and EO sitting trials from a subject of each group

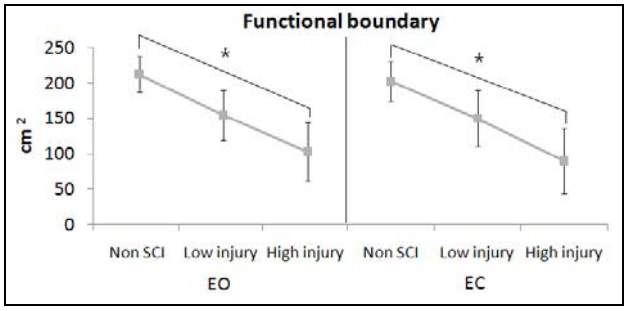

Figure2. Comparisons of mean functional boundaries at EO and EC. *signficnat difference (p<.05).

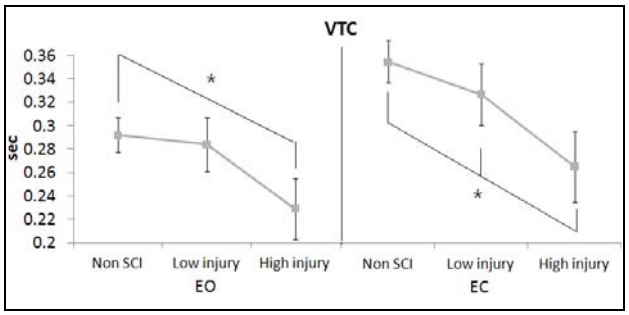

Figure3. Comparisons of mean VTCs to the stability boundary at EO and EC. *significant group difference (p<.05).

Analysis of VTC revealed that HI group had shorter mean VTC than NSCI with EO and HI had shorter VTC to the stability boundary than both other groups with EC (EO: 0.29 vs. 0.23; EC: 0.33 vs. 0.31 vs.0.25, <.05).

Discussion

A novel observation of the current investigation was that only the HI SCI had a smaller stability boundary than the healthy control group. Individuals with spinal cord injury T10 and above lack control of some trunk musculature. The lack of control of the trunk musculature minimizes the amount of sway that they can experience without risking stability. However, individuals with a SCI that does not affect trunk musculature do not demonstrate a limitation in functional stability boundary.

However, the lack of differences in functional stability boundary between the healthy control group and low injury SCI group should not be interpreted as evidence that they do not lack stability in seated postural control. In fact, the examination of virtual time to contact revealed that both the low injury and high injury group had smaller virtual time to contact than the healthy control groups. This was paramount when visual information was not available. This observation implies that individuals with SCI are closer to losing seated postural stability especially when vision is not present.

CONCLUSIONS

The effect of vision on VTC in the HI group implies that when vision is available they can compensate for their lack of proprioceptive input and demonstrate normal seated postural stability. However, when visual feedback is removed they become increasing less stable. More work is necessary to examine whether these stability differences in SCI can be influenced by training or specific rehabilitation regimes.

REFERENCES

1. Gagnon, B., Vincent, C., & Noreau, L. (2005). *Disability and Rehabilitation*, 27(16), 951-960, 2005.

2. Seelen, H. A. M., Potten, Y. J. M., Huson, A., Spaans, F., & Reulen, J. P. H. (1997*) J Electromyography and Kinesiology*, 7(2), 149-160, 1997.

3. Slobounov SM, Slobounova ES, Newell KM (1997). *J Motor Behav*, 1997.

5. Slobounov, S. M., Haibach, P. S., & Newell, K. M. *European Review of Aging and Physical Activity*, 3(2), 55-62, 2006.

6. Winter,D.A. *Biomechanics of Motor Control and Human Movement*, 2nd ed., Wiely, 1990.

FALL RISK DOES NOT DEPEND ON BODY MASS INDEX

[1]Noah J Rosenblatt, [1]David Premier and [1]Mark D. Grabiner
[1]University of Illinois-Chicago, Chicago, IL, USA, email:nrosenbl@uic.edu web

INTRODUCTION

In 2007-2008, 35.5% of adult women in the United States were considered obese [1] and at risk of diminished health-related quality of life [2]. One contributing factor to diminished quality of life associated with obesity is a higher rate of injuries, including fall related injuries [3]. A possible explanation is that obesity increases the risk of falling, although there is limited quantitative support for this.

Increased body mass index (BMI), even in healthy young, is correlated with decreased postural stability during quiet and unipedal stance [4,5]. Accordingly weight loss in younger obese adults improves postural stability and balance [4,6,7]. However, such changes only indirectly link BMI and fall risk, since improved postural stability may not reduce fall risk in obese.

Only one study directly reported a higher prevalence of falls in the obese compared to normal subjects (27% vs. 15%, respectively) [2], and a higher prevalence of stumbles, which have been related to prospective falls in older adults [8]. However, these results relied heavily on retrospective self-report of falls/stumbles over the prior year (i.e. memory).

Therefore, the purpose of this study was to compare the following in obese and normal weight subjects: (1) the number and mechanism of falls during laboratory-induced trips (2) the number of falls recalled over the previous 1 year period (3) the number of falls and stumbles during a 6 month prospective follow-up.

METHODS

Data was extracted from two larger studies which considered the role of training in reducing 1) laboratory induced trips and 2) prospective falls in older adults.

In Study 1, 30 healthy, community-dwelling women age 55+, with no neurological impairments or diabetes, were tripped in the laboratory while walking [9]. Kinematics were extracted using an 8 camera system operating at 120 Hz (Motion Analysis, Santa Rosa, CA). Extracted kinematics include: reaction time (trip onset to recovery foot strike), recovery step length, trunk flexion angle at recovery and trunk flexion angular velocity at recovery, all of which have been associated with falls following laboratory-induced trips [9].

Ninety-nine older women, of similar demographics to those in Study 1, participated in Study 2. The subjects' fall-history during the previous 12 months (termed "retrospective fall") was recorded and the subjects were assigned to a control or training group. Every two weeks, subjects in the control and the trained group reported whether or not they had fallen or stumbled (termed "prospective falls/stumbles"). Since training could influence the relationship between obesity and fall risk, prospective falls by only control subjects 6+ months into the study, are considered (n=30). However, prospective stumbles by control and trained subjects, 6+ months into the study, are considered (n=60).

BMI was calculated for all subjects BMI. The percentage of obese (BMI>30) and normal weight (BMI=18.5-25) subjects who fell after a laboratory-induced trip (termed "laboratory fall"), and those that reported retrospective falls, prospective falls and prospective stumbles was determined. Logistic regressions were run to determine the extent to which BMI could be used to correctly classify stumblers and fallers (SPSS, Chicago, IL).

RESULTS AND DISCUSSION

The incidence of prospective stumbles was greater in normal subjects compared to the obese (42.2% vs. 12.5% respectively; Table 1). This is in contrast to previous findings [2] and may reflect the fact that stumbles were prospectively reported. In addition, stumblers were defined as *anyone* who stumbled, as opposed to someone that "often stumbled" or "felt unsteady when the walked" [2], since even one stumble increase the odds of a fall

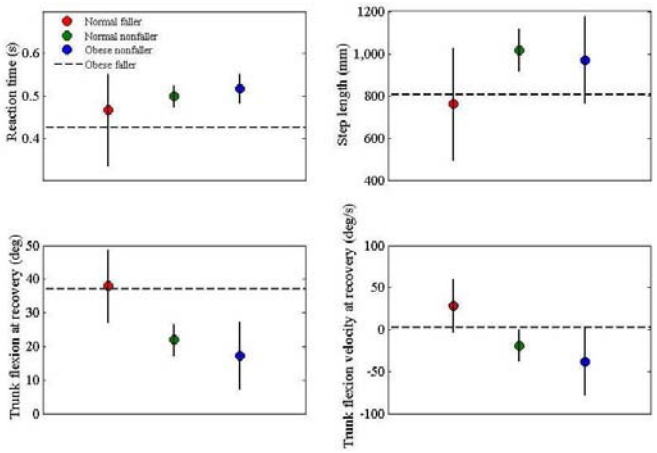

Figure 1: Kinematic variables obtained during laboratory induced trip for obese and normal weight fallers and non-fallers. Mechanisms of both failure and recovery are not different between obese and normal. Bars represent means ± 95% CI. Dotted line represents data from one obese after-step faller.

[8]. Approximately 66% of stumblers were correctly classified using the logistic regression. The logistic function predicted that the odds of stumbling should decrease by 0.85 with a unit increase in BMI (Exp (β), Table 1).

The percent of normal weight retrospective fallers was also greater than that of the obese (Table 1). This may contrast previous findings since we considered all-cause falls without excluding those caused by "overwhelming hazards" that would "result in a fall by most young" [2]. Dissimilar populations may also explain between-study differences. Here only women, age 55+, rather than men and women age 50+, were considered. In addition our subjects were fairly active and healthy, reporting retrospective falls during hikes, biking trips and other similar high-risk activities. While retrospective falls were greater in normal subjects, fallers could not be classified based on BMI.

Sixty percent of obese and 70% of normal weight subjects reported prospective falls. While these percentages are rather high, this may again reflect the physically active population considered. Similar to retrospective fallers, prospective fallers could not be classified based on BMI.

Finally, the incidence of falls in obese versus subjects after a laboratory-induced trip was 28.6% vs 23.1% respectively. While ~25% of all subjects fell, fallers could not be classified based on BMI. The mechanisms of recovery/failure appeared similar between the two groups. Recovery was associated with a longer step length, smaller trunk flexion and larger trunk flexion extension at recovery foot strike in both normal and obese subjects (Fig 1), although the latter may tend to be smaller in the obese. Similarly, failure was associated with large trunk flexion angle and flexion velocity at recovery in both the obese and normal subjects. However, since we had only two obese laboratory fallers, only one of which was an after-step faller, no statistics could be run.

CONCLUSIONS

In conclusion, our results suggest that the middle-aged and older obese women are no more likely to either stumble or fall, than normal weight (or overweight) subjects. Consistent with this idea is the fact that the mechanisms or recovery and failure following a laboratory-induced trip are similar between the two. Although sample sizes were small, the fact that similar results were found for prospective falls, retrospective falls and laboratory-induced trip strongly supports our conclusion. With the limited available information, we do not believe current fall prevention programs should be amended for the obese, though further study is warranted.

REFERENCES

1. Flegal KM, et al. *JAMA* **303**, 235-41, 2010.
2. Fjeldstad C, et al. *Dyn Med* **7**:4, 2008.
3. Finkelstein EA, et al. *Am J Health Promot* **21**, 460-69, 2007.
4. Maffiuletti NA, et al. *J Endocrinol Invest* **28**, 2-7, 2005.
5. Greve J., et al. *Clinics* **62**, 717-20, 2007.
6. Matrangol SL and Madigan ML. *Med Sci Sports Exerc* **41**, 1488-93, 2009.
7. Teasdale N, et al. *Int J Obes* **31**, 153-60, 2007.
8. Srglye JM, et al. *Arch Phys Med Rehab* **90**, 786-91, 2009.
9. Pavol MJ, et al. *J Gerentol* **56**, M428-37, 2001.

Table 1: Percentage of obese and normal weight stumblers/fallers categorized by type of stumble/fall

	Obese (BMI>30)	Normal (BMI=18.5-25)	Predicted by BMI
Prospective Stumbles (N=37*)	12.5% (32%**)	42.2% (14%)	Yes (N=60*, p=0.005)# 68.5% overall classification, Exp(β)=0.847
Laboratory falls (N=20)	28.6%	23.1%	No (N=33, p=0.57)
Retrospective falls (N=62)	34.5% (27%)	42.4% (15%)	No (N=99, p=0.18)
Prospective falls (N=20)	60.0%	70.0%	No (N=30, p=0.63)

* N listed next to stumble/fall type based on total number of subjects used in the regression (predicted by BMI) after removing overweight subjects (BMI = 25-30)
**Percentages in parenthesis based on data reported in [2].
Predicted by BMI – "Yes" if a significant χ^2 distribution ($p<0.05$) from logistic regression based on all available BMI data

MINIMIZING POSTURAL INSTABILITY WHEN CARRYING LOAD: THE EFFECTS OF CARRYING GROCERY BAGS ON THE ELDERLY

Erin Sutton, Danielle Bare, Melissa Taylor, Deborah Kinor, Julia Schaeffer, Alexander Jules, Kimberly Edginton Bigelow

University of Dayton, Dayton, OH, USA
email: bigeloke@notes.udayton.edu, web: http://academic.udayton.edu/ewsl

INTRODUCTION

Each year, approximately one-third of independent adults age 65 years and older experience a fall [1]. Not only do falls reduce physical function; they also yield psychological trauma, including loss of confidence in performing independent physical tasks, feelings of vulnerability, and fear of future falls [2]. Consequently, approximately 40% of nursing home admissions are related to falls or postural instability [2].

Of these falls, many occur when the independent elderly experience postural instability in the form of increased sway during daily activities [1]. To decrease the prevalence of falls, it is imperative that the effects on stability caused by daily activities be assessed.

Because one of the independent activities of daily living is shopping for one's own groceries, this study aimed to determine ways to minimize an elderly person's postural instability while carrying grocery bags [3]. Though research has demonstrated the effect carrying load in a backpack can have on balance [4], the authors could not find any literature examining the effect of carrying groceries.

It was hypothesized that carrying a loaded bag of groceries draped across one's arm, with this arm crossed across the body close to the body (a fall prevention tip recently promoted on a national news program [5]) would not result in reduced sway magnitude as compared to the carrying the same bag traditionally in a single hand by one's side. Whereas, it was hypothesized that carrying equally weighted bags, one in each the right and left hand would reduce medial-lateral sway compared to carrying bags of unequal weights, such as canned goods in the right hand and boxed goods in the left.

METHODS

Twenty-one independent elderly adults participated in this study (9 males, 12 females; mean age: 71.8 ± 5 years; mean height: 171.1 ± 9 cm; mean weight: 78.2 ± 15 kg). They were without recent operations, injuries, or diseases that would prevent them from lifting 4.5 kilograms, and they regularly did their own grocery shopping. They self-reported individual fall history and grocery shopping habits in a questionnaire prior to testing.

Each subject performed the seven randomized tasks shown in Table 1, while standing quietly with eyes open on a force-measuring platform (Model BP5050, Bertec Corporation, Columbus, OH). Two plastic bags holding a combination of six canned goods and three boxed goods (total weight: 4.5 kg) were used, with the distribution of weight changed according to the testing condition. For Tasks C – G the bag(s) held consisted of a mix of canned and box goods. To create an unequal weight distribution for Task B, a bag containing only the canned goods was held in the dominant hand and only the boxed goods in the other. For Tasks D – F the bags were held in or across the dominant arm. Each task lasted for 60 seconds and data was collected at 1000 Hz using Bertec Acquire 4. After the third of seven trials, the subject was given a two-minute break.

From the center of pressure data the Medial-Lateral (M/L) Sway Range and M/L Sway Velocity were calculated. Anterior-Posterior (A/P) Sway Range and Sway Velocity were also calculated for secondary analyses. Paired t-tests using SASS (version 17.0, Chicago, IL), $p < 0.05$, were performed to test the four main hypotheses with a Bonferroni Correction such that $p < 0.0125$ indicated significance.

Table 1. Seven Testing Conditions Performed

Cond.	Description
A	Arms at Side, No Load
B	Two bags (unequal weight) held traditionally hands at side
C	Two bags (equal weight) held traditionally hands at side
D	One bag held traditionally hand at side
E	One bag draped on arm, arm crossed across body
F	Two bags draped on arm, arm crossed across body
G	Two bags (equal weight) carried in backpack

RESULTS AND DISCUSSION

It has been shown that postural instability in the medial-lateral direction is correlated to falls in older adults [6]. As the way that grocery bags are traditionally carried has the potential to increase instability in this direction, the primary analysis of this work centered on the medial-lateral sway parameters. Figure 1 shows the mean M/L Sway Range for each of the testing conditions.

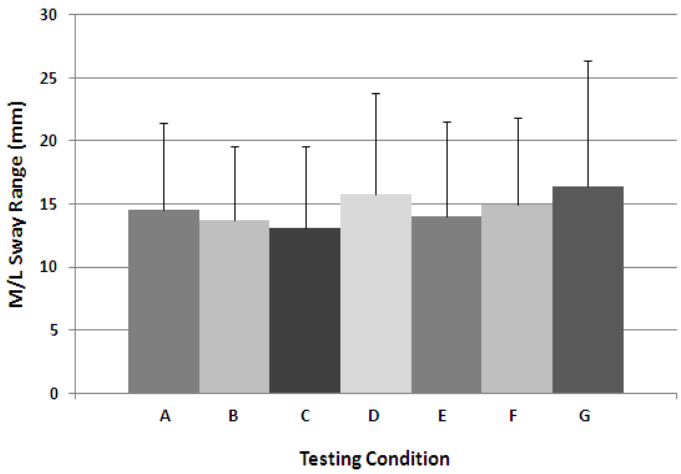

Figure 1. Mean Medial-Lateral Sway Range (mm) and Standard Deviation for the 7 Testing Conditions

Condition E, one grocery bag draped across the subject's arm and the arm crossed across the body, did result in a lower mean M/L Sway Range (14.0 ± 8 mm) compared to Condition D, when the same bag was held traditionally (15.8 ± 8 mm). Condition E had been proposed as a way to prevent falls by bringing the carried load closer to the center of gravity of the individual [5]. Despite this, the difference was not statistically significant ($p = 0.179$), supporting the first hypothesis of this study. Since the bag is placed in front of the body, it was thought that it could increase sway in the Adirection, but this was not observed ($p = 0.282$). As such, this condition does not appear meaningfully better than traditional methods of carrying groceries. Qualitatively, subjects also reported a dislike of carrying groceries this way.

Condition C, two bags of approximately equal weight, held traditionally with one in each hand, caused, on average, the least amount of sway (13.2 ± 6 mm) in the medial-lateral direction. When the bags were held with unequal weight, as in Condition B, the mean sway range increased only slightly (13.8 ± 6 mm). There was no significant difference between the two conditions ($p = 0.604$), proving the second hypothesis of this study wrong. It had been assumed that the weight asymmetry would cause the subject to "wobble" back and forth more than would occur if equal weights were held. These findings suggest that the load distribution for relatively small amounts of groceries is not a meaningful factor for creating postural instability. It is possible that when multiple bags of much heavier weight are carried, a more significant difference would be observed. However, many subjects reported their habits to include frequent trips to the grocery with fewer bags to carry home.

CONCLUSION

The results of this study suggest that the way that groceries are carried does not play a meaningful role in increasing medial-lateral sway while standing. Future work is needed to examine the effect of carrying groceries while walking.

REFERENCES

1.Lehtola H, et al. *Arch Gerontol Geriatr* **42**, 217-224, 2005.
2.Talbot L, et al. *Biol Res Nurs* **1**, 321-331, 2000.
3.Lawton D, Brody E. *Gerontol* **9**, 179-186, 1969.
4.Rodrigues S, et al. *Revista Brasileira de Fisioterapia* **12**, 43-48, 2008.
5. ABC News. Available at: http://abcnews.go.com/GMA/ OnCall/story?id=6173302&page=1
6. Maki BE, et al. *J Gerontol Med Sci* **49**, M72-M84, 1994.

MULTISCALE ENTROPY IDENTIFIES COMPLEXITY CHANGES IN POSTURAL CONTROL OF ADOLESCENT IDOPATHIC SCOLIOSIS

[1]Michael A. Busa, Allison H. Gruber, [2]George E. Gorton III,
[2]Peter D. Masso, [1]Joseph Hamill, [1]Richard E.A. Van Emmerik

[1]University of Massachusetts Amherst, MA, USA
[2]Shriners Hospital, Springfield, MA, USA
email: mbusa@kin.umass.edu, web: http://www.umass.edu/biomechanics/

INTRODUCTION

Adolescent Idiopathic Scoliosis (AIS) is characterized by three-dimensional deformation of the spine resulting in alterations of body posture and segment alignment [1]. Changes in body posture have been found to relate to stability deficits in AIS patients, which may be exacerbated by AIS severity [2]. Previous work has related AIS patients have reduced postural stability characterized by requiring greater neuromuscular control to maintain standing balance in the AP direction [4] and increased lateral sway [5].

Traditional measures used to quantify postural control and stability are derived from the center of mass (COM) or center of pressure (COP). Most measures include discrete summary statistics, such as the range, standard deviation or path length.

Investigation of time series rather than discrete measures such as COM or COP parameters, may be important to identify the complexity of the postural control mechanism. Multiscale entropy (MSE) is a measure that examines patterns in time series data at different scaling factors to gain understanding of the spatio-temporal domain in which phenomena occur [3]. It is based on the Sample Entropy (SampEn)[4] algorithm, which assumes stationarity. A reduction in the entropy is associated with a decrease in the complexity of the system. A decrease of complexity is associated with an increase in constraints on the system and a corresponding reduction in the adaptability to meet possible challenges. Reductions in system complexity have been found as a result of the aging process and in various neurological disorders [5].

The purpose of this study was to examine the MSE of COP in the anterior-posterior (AP) and medio-lateral (ML) directions to determine if a loss of complexity is apparent in postural control in AIS. We hypothesized that MSE values would be reduced in AIS compared to controls. Additionally MSE was examined to determine if it could be used to discriminate between severity levels in AIS.

METHODS

Eighteen AIS patients classified as pre-bracing (PB) (12±2 yrs), 18 AIS patients classified as pre-operative (PO) (13±1 yrs) and ten healthy control (CON) subjects (12±2 yrs) were selected from the Scoliosis Clinic patient database at the Clinical Outcomes Assessment Laboratory at Shriners Hospital, Springfield, MA. All subjects were female.

COP position was measured by a force platform at 1080 Hz and during 5s of bilateral quite stance. Data were filtered with a Butterworth low-pass filter with a cut-off frequency of 50 Hz. MSE was used to analyze the complexity of the COP signal in both the AP and ML directions in accordance with the methods outlined in Costa et al [6]. Parameters for the analysis were set at r=0.001 and m=2 for both directions (r was determined by taking 15% of the standard deviation of the time series data). Scale factors 1 through 12 were examined for changes in the spatio-temporal relationship of the pattern of the COP.

A paired sample T-test was used to detect differences between groups (α=0.05). Effect size was also calculated to determine the biological significance of the differences between groups [7].

RESULTS AND DISCUSSION

Paired sample t-tests revealed significant differences ($p<.05$) between the CON and PO groups in both the AP and ML directions of MSE of COP (Tables 1 and 2). For both directions MSE was reduced in the PO AIS group (Table 3). No significant differences were observed between the CON and PB AIS groups. MSE was reduced as a function of disease severity in AIS (Table 3), but this reduction was only significant for the ML direction (Table 1).

Table 1: Paired sample T-test (p-value)

	CON v. PB	PB v. PO	CON v. PO
AP	0.964	0.151	0.009
ML	0.645	0.048	0.040

Effect sizes in between groups (Table 2) show small to moderate effects between all groups in both postural directions.

Table 2: Effect sizes (Cohen's d)

	CON v. PB	PB v. PO	CON v. PO
AP	0.10	0.21	0.37
ML	0.23	0.41	0.21

The advantage of MSE over SampEn is that insight can be gained into the spatio-temporal scale(s) at which physiological phenomena present themselves. The entropy curve in Figure 1 shows the MSE response over multiple time scales (scale factor 1-12). Taking the integral of each curve shows the differences between three groups, which may be hard to distinguish from examining each scale factor separately.

Table 3: Sum of MSE values for scale factors 1-12

	CON	PB	PO
AP	117.324	115.723	112.161
ML	125.198	127.759	121.816

A possible reason for this reduction in MSE, especially in the more severe AIS group (PO), may be a loss of complexity in the dynamics of postural control in people with AIS. The reduction in complexity could be manifested as patients adopt a more rigid control strategy resulting in a more predictable pattern of COP. An important finding is also that the MSE analysis revealed loss of control complexity in COP in both ML and AP directions when comparing more severe AIS (PO group) to controls. Previous research has only demonstrated reduced postural stability in the lateral direction [7]. The reduced entropy in the COP time series in AIS may affect the control of the COM, as previous work has related greater differences between COM and COP in AIS patients to greater demand of neuromuscular control to maintain standing balance [6].

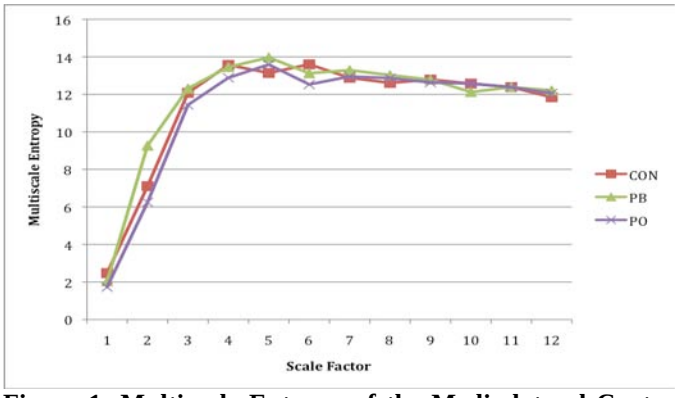

Figure 1: Multiscale Entropy of the Medio-lateral Center of Pressure. Control (CON), Pre-bracing (PB) and Pre-operative (PO)

CONCLUSIONS

MSE analysis revealed decreased entropy in individuals with AIS compared to controls. These decrements were especially present in the more severe AIS group and were observed for both AP and ML postural control. MSE appears to be a powerful tool in distinguishing changes in complexity of the dynamical systems involved in postural control with AIS patients of different severity.

REFERENCES

1. Masso PD & Gorton GE. *Spine* **25**, 457-62, 2000.
2. Gauchard GC, et al. *Spine* **26**, 1052-8, 2001.
3. Nault, M-L et al. *Spine*, 2002. **27**(17): p. 1911-1917
4. Chen, P.-Q., et al. Clinical Biomechanics, 1998. **13**(1, Supplement 1): p. S52-S58.
5. Van Emmerik, R.E.A. & E.E. Van Wegen. *Exerc Sport Sci Rev* **30**, 177-83, 2002.
6. Costa, M. et al *Multiscale entropy analysis of biological signals.* Physical Review, 2005. **71**(021906).
7. Cohen, J (1992). "A power primer". *Psychological Bulletin* **112**: 155–15

TIME-TO-CONTACT IDENTIFIES DIFFERENCES IN POSTURAL CONTROL IN ADOLESCENT IDIOPATHIC SCOLIOSIS

[1]Allison H. Gruber, [1]Michael A. Busa, [2]George E. Gorton III, [1]Richard E.A. Van Emmerik, [2]Peter D. Masso, [1]Joseph Hamill

[1]University of Massachusetts Amherst, MA, USA
[2]Shriners Hospital, Springfield, MA, USA
email: agruber@kin.umass.edu, web: http://www.umass.edu/biomechanics/

INTRODUCTION

Adolescent Idiopathic Scoliosis (AIS) is characterized by 3-D deformations of the spine resulting in geometric and morphological changes of the trunk and rib cage as well as changes in the relationship between body segments [1]. Alterations in body posture are pronounced with increased severity and may be the cause of associated neurological dysfunction [2]. Since neurological functions are involved with balance control, AIS patients are likely to have stability deficits which may be exacerbated by the type and location of the scoliotic curve [3].

Postural stability is commonly quantified by various measures of center of pressure (COP). Smaller values for these parameters are thought to indicate good postural stability [3]. The relationship of head, shoulder and pelvis orientation in AIS patients has previously been shown to contribute to increases in COP sway area thus indicating postural instability [4].

New methods have been developed in the assessment of postural stability that take into account the stability boundaries of the base of support [5,6]. Time-to-contact (TtC) has been developed as a measure taking into account the stability boundary, incorporating both spatial and temporal aspects of COP control. TtC can be viewed as the motor response time available to react to a perturbation or stability loss.

Selection of the appropriate strategy for a given situation is essential to maintaining posture in response to a perturbation. AIS patients may have difficulty selecting the appropriate strategy because of alterations in body posture and compromised sensory systems. Furthermore, severity of specific morphological alterations in the spine may affect the degree of balance dysfunction [3]. Therefore, the purpose of this study was to determine postural stability measured by COP range, COP velocity and TtC between different severities of AIS and healthy controls. We hypothesized TtC will be reduced in patients with AIS and decreases with AIS severity.

METHODS

Eighteen AIS patients classified as pre-bracing (PB), 18 AIS patients classified as pre-operative (PO) and ten healthy control (CON) subjects were selected from the Scoliosis Clinic patient database at the Clinical Outcomes Assessment Lab at Shriners Hospital, Springfield, MA. All subjects were female and there was no significant difference in age between groups (CON= 12 ± 2yrs; PB= 12 ± 2yrs; PO= 13 ± 1yr).

COP position was measured by a force platform at 1080 Hz during 5s of bilateral quite standing. Data was filtered with a Butterworth low-pass filter (cut-off frequency of 50 Hz). COP range (COPr) and COP velocity (COPv) were calculated in the anterioposterior (AP) and mediolateral (ML) directions. TtC was defined as the time it would take the COP to contact a stability boundary given the instantaneous trajectory, velocity and acceleration [7]. For the TtC calculation, a position vector of the COP on a virtual trajectory $\tau_i(t)$ was determined for each moment in time t_i based on the instantaneous COP velocity and acceleration [8]:

$$x, y(\tau) = r_{xi,yi}(t_i) + v_{xi,yi}(t_i)\tau + \left(\frac{a_{xi,yi}(t_i)\tau^2}{2}\right) \quad (1)$$

where $r_{xi,yi}(t_i)$ is the instantaneous position vector, $v_{xi,yi}(t_i)$ is the instantaneous velocity vector and $a_{xi,yi}(t_i)$ is the instantaneous acceleration vector in the x and y directions. The ML stability boundary was

constructed from the ML position of reflective markers placed on the lateral side of each foot and the AP boundary was constructed by reflective markers placed on the toe and heel. The stability boundary was defined by:

$$y - y_b = m(x - x_b) \quad (2)$$

where m is the slope of the line and x_b and y_b are the coordinates of the markers defining the ML and AP boundaries. The time it took for the instantaneous virtual trajectory to cross the stability boundary was determined by substituting Equation 1 into Equation 2 which gives:

$$A\tau^2_b + B\tau_b + C = 0, \quad (3)$$

where $A = [a_y(t_i) - ma_x(t_i)]/2$; $B = V_y(t_i) - mV_x(t_i)$;$C = r_y(t_i) - y_b - m_x[r_x(t_i) - x_b]$. The lowest non-zero value of the time parameter (τ_b) was determined as TtC. Effect sizes (ES) were calculated to determine the differences in COPr, COPv and TtC between groups. Cohen [9] suggested that ES=0.2 indicates a small effect, ES=0.5 a moderate effect and ES=0.8 a large effect.

RESULTS AND DISCUSSION

There was a small effect of AIS severity for COPr and COPv indicating minimal effect of severity between groups (Table 1). However, ML-COPr was greater in PO compared to PB and ML-COPv was greater in CON compared to PB. TtC increased as AIS severity increased, which is contrary to the hypothesis. However, TtC measures showed greater differences between groups than COPr or COPv, suggesting TtC may be a better measure to distinguish balance impairments between healthy controls and AIS patients and between severities of AIS.

The number or locations of spinal curvatures in the AIS patients were not consistent within groups; this may explain similar results in COPr and COPv between PB and PO. Previous studies reported little to no lateral disequilibrium in AIS patients with different severities determined by location and type of curve suggesting double major curves may result in near normal head position because one curve compensated for the other [3]. Taken together with the present study, this finding may partially explain the small effect of AIS between PB and CON for COPr, COPv and TtC because the PB group had double major curves and near normal head position. Although COP measures were similar between PB and PO, TtC may better distinguish the severity effects of AIS, as evidenced by the increased ES.

We hypothesized patients with more severe AIS will have reduced TtC values. Since TtC is the time available to respond to a perturbation, we would expect those with balance impairments to have a more limited time to respond to maintain balance (i.e. lower TtC). Interpretation of TtC calculated with COP can be difficult because there is no clear consequence of the COP falling outside of the base of support [7]. Therefore, increased TtC of the COP in the more severe AIS group may reflect less adaptation or modulation in the control of the COP. The results from the present study suggest that patients with more severe AIS adopt a more rigid control strategy to maintain balance, possible resulting in postural instability.

REFERENCES

1. Masso PD & Gorton GE. *Spine* **25**, 457-62, 2000.
2. Kramers-de Quervain IA, et al. *Eur Spine J* **13**, 449-56, 2004.
3. Gauchard GC, et al. *Spine* **26**, 1052-8, 2001.
4. Nault ML, et al. *Spine* **1**, 293-6, 1997.
5. Van Emmerik, R.E.A. & E.E. Van Wegen. *Exerc Sport Sci Rev* **30**, 177-83, 2002.
6. Haddad JM, et al. Gait Posture, **23**, 429-34, 2006.
7. Haddad JM, et al. *J Appl Biomech* **22**, 155-61, 2006.
8. Slobounov SM, et al. *J mot Behav* **29**, 263-81, 1993.
9. Cohen, J. *Psychological Bulletin* **112**, 155–159, 1992.

Table 1: (Top section) Mean ± SD of TtC, COPr and COPv in the ML and AP direction for each group; (bottom section) ES of AIS severity for TtC, COPr and COPv comparing CON vs. PB, CON vs. PO and PB vs. PO.

	TtC (ms)		COPr (mm)		COPv (mm/s)	
	ML	AP	ML	AP	ML	AP
CON	94.25±26.49	59.33±26.40	12.06±5.62	16.27±9.28	0.28±1.33	0.74±2.26
PB	98.48±18.74	66.97±14.36	11.43±5.74	16.72±9.10	0.11±1.12	0.49±1.68
PO	110.10±19.60	71.92±17.80	14.49±14.99	16.13±8.21	0.49±1.43	0.43±1.85
CON vs. PB	0.20	0.39	0.11	0.05	0.33	0.14
CON vs. PO	0.68	0.58	0.19	0.02	0.54	0.16
PB vs. PO	0.58	0.30	0.27	0.07	0.29	0.03

TRUNK KINEMATICS DISCRIMINATE MULTIDIRECTIONAL FALLS AND RECOVERIES FOLLOWING LARGE POSTURAL DISTURBANCES

[1]Julie B. Cain, [1]Jeremy R. Crenshaw, [2]Kenton R. Kaufman and [1]Mark D. Grabiner

[1]University of Illinois at Chicago, Chicago, IL, USA
[2]Mayo Clinic, Rochester, MN, USA
email: jcain2@uic.edu, web: http://www.uic.edu/ahs/biomechanics/

INTRODUCTION

Over the past twenty years, fall prevention interventions appear to have only incrementally reduced fall-related morbidity and mortality in the United States [2, 5]. This disappointing result may reflect an inherent limitation in the extent to which it is possible to prevent falls by older adults. Technology-based adjunct approaches to limiting the sequela of falls and fall-related injuries includes fall-protection and fall identification. In the former, information regarding an imminent fall is used as a signal event to trigger subsequent processes [1, 4]. In the latter, information regarding an imminent fall can be used to alert appropriate personnel of a falling-event [3]. For both cases, a prerequisite is the ability to sensitively and rapidly use data from the monitored individual to identify an imminent fall.

There have been several efforts to use technology to detect falls by older adults in the laboratory and community. However, the success of these efforts has been limited by an inability to distinguish falls from activities of daily living, the short period of time available between the detection of a loss of balance and impact with the ground, or use of simulated falls that may be inadequate surrogates for actual falls [1, 3, 4, 8].

The purpose of this study was to determine the extent to which trunk kinematics, which discriminate falls from recoveries following laboratory-induced trips [7] and large postural disturbances delivered by a motorized platform [6], could discriminate multi-directional falls from recoveries following delivery of a large postural disturbance that required a compensatory stepping response to avoid falling. We hypothesized that the trunk displacement and acceleration variables during the initial recovery step would distinguish successful from failed recoveries.

METHODS

The data from 15 healthy young adults (age: 22.4±2.8 years, height: 172.9±9.0 cm, mass: 66.3±10.5 kg) and 21 healthy older adults (age: 61.8±6.6 years, height: 164.0±8.64 cm, mass: 74.1±17.1 kg) from previous investigations were re-analyzed in this study. Data collection consisted of a single session for all subjects during which motion capture data were collected at 60 Hz. Standardized postural disturbances were delivered by a microprocessor controlled motorized platform (Active Step™, Simbex, Lebanon, NH). A standardized forward-directed disturbance accelerated the treadmill belt backwards from 0 to 6.5 m/s^2 in 0.5 s. A standardized backward-directed disturbance accelerated the treadmill belt forward from 0 to 10 m/s^2 in 0.14 s (Figure 1). All subjects fell into a safety harness after exposure to the initial standardized disturbance. A brief training protocol, composed of a series of increasingly and then decreasingly challenging postural disturbances was subsequently administered. Following the training protocol, the standardized disturbance was repeated and all subjects successfully recovered.

Anteroposterior (X), mediolateral (Y), and vertical (Z) linear displacements and accelerations of the trunk center of mass (COM) were calculated during the standardized disturbances. From these time series, the displacement and acceleration at 50-350 ms following the postural disturbance were computed at 50 ms intervals. Paired t-tests were used to determine the variables for which between-condition (fall vs. recovery) differences were

significant. Those variables for which between-group differences were significant were entered in a stepwise discriminant analysis in which "fall" or "recovery" represented group membership.

Figure 1: The top left panel shows a young adult subject exposed to a standardized forward-directed disturbance inducing a fall, while the top right panel shows the recovery. The bottom left panel shows an older adult subject exposed to a standardized backward-directed disturbance inducing a fall, while the bottom right panel shows the recovery.

RESULTS AND DISCUSSION

Vertical trunk displacement at 300 and 350 ms after the disturbance, and "sagittal plane" trunk acceleration at 300 ms after the disturbance were included in the final discriminant function (Wilks' Lambda = 0.604, $p < 0.001$). Subjects that fell were characterized by larger vertical displacments of the trunk COM and larger trunk COM accelerations (Table 1). The sensitivity and specificity of the discriminant function was 82%. A cross-validation algorithm classified 82% of all subjects correctly.

CONCLUSIONS

By using technology by which it was possible to cause subjects to safely fall, the results provide preliminary data suggesting that it is sufficient to use biomechanical data to accurately and rapidly distinguish postural disturbances that will result in a fall. Due to the necessity of adhering to safe laboratory conditions, falls were restricted by a safety harness and initiated from a quasi-static standing posture posing a limitation for representing real world falls. However, the present protocol, in which the disturbance magnitudes were sufficient to cause the subjects to irrevocably lose their balance seems to represent an evolution beyond protocols in which falls are initiated voluntarily by the subjects. Further protocol improvements presently allow us to deliver large postural disturbances of specified magnitude and duration while subjects are walking on the platform.

REFERENCES

1. Bourke AK, et al. *Conf Proc IEEE Eng Med Biol Soc*, 2832-5, 2008.
2. CDC and Prevention and the Merck Company Foundation. *The State of Aging and Health in America*, Whitehouse Station, NJ: The Merck Company Foundation, 2007.
3. Estudillo-Valderrama M, et al. *IEEE Trans Inf Technol Biomed*, **13** (6): 874-81, 2009.
4. Kangas M, et al. *Gait Posture*, **29** (4): 571-4, 2009.
5. National Center for Health Statistics, *Healthy People 2000 final review*, Hyattsville, MD, Public Health Service, 2001.
6. Owings TM, et al. *Clin Biomech*, **16** (9): 813-19, 2001.
7. Pavol MJ, et al. *J Gerontology A Biol Sci Med Sci*, **56** (7): M428-37, 2001.
8. Rantz M, et al. *J Nurs Care Qual*, **23** (3): 195-201,2008.

Table 1: Mean ± standard deviations of trunk COM displacement (m) and acceleration (m/s^2) values included in the final discriminant function at two time intervals (ms) following disturbance onset.

Variable	Fall	Recovery
Sagittal plane trunk acceleration at 300ms	-1.00 ± 2.4 m/s^2	0.59 ± 2.2 m/s^2
Vertical trunk displacement at 300ms	0.051 ± 0.15 m	-0.011 ± 0.042 m
Vertical trunk displacement at 350ms	0.035 ± 0.15 m	-0.015 ± 0.042 m

FALL RISK ESTIMATION OF COMMUNITY-DWELLERING ELDERLY USING INVARIANT DENSITY ANALYSIS

Pilwon Hur[1], Hyun Gu Kang[2], Lewis A. Lipsitz[3], and Elizabeth T. Hsiao-Wecksler[1]

[1] Mechanical Science & Engineering, University of Illinois at Urbana-Champaign, Urbana, IL
[2]Kinesiology & Health Promotion, California State Polytechnic University, Pomona, CA
[3]Institute for Aging Research, Hebrew SeniorLife; Harvard Medical School; Beth Israel Deaconess Medical Center, Boston MA

E-mail: phur2@illinois.edu, ethw@illinois.edu Web: www.mechse.uiuc.edu/research/hsiao-wecksler/

INTRODUCTION

Prediction of fall risk of frail and older adults using quiet-stance postural sway data has been the goal of numerous studies [1]. These studies generally used traditional center of pressure (COP) measures (swept area, sway velocity). However, these parameters do not provide insight into the physiological system as a whole. We recently developed invariant density analysis (IDA), which provides new insight into the long-term behavior of COP data [2]. It has been shown to successfully differentiate postural sway behaviors between young, middle, and older adults [2] and recurrent and non-recurrent elderly fallers [3]. We found that 4 out of 5 IDA parameters were significantly different between the faller and non-faller groups [3]. Some traditional measures (TRAD) and stabilogram diffusion analysis (SDA) parameters were found to be significantly different between the two groups [3].

In this study, we examined whether IDA parameters have the ability to better predict fall risk of community-dwelling older adults through a fall-risk prediction model when compared to other metrics of postural sway (TRAD and SDA) and clinical balance measures of Berg and short physical performance battery (SPPB) scores. We also evaluated correlation relationships among these parameters.

METHODS

Experiment

Subject data were obtained from the MOBILIZE Boston Study, a prospective cohort study of 765 community-dwelling elderly [4]. After excluding for insufficient falls follow-up data from 304 non-recurrent fallers (< 2 falls during the first year) and 140 recurrent fallers (≥ 2) were analyzed. Anterior-posterior (AP) and medial-lateral (ML) COP data, Berg and short physical performance battery (SPPB) test scores were collected at baseline. Subjects were asked to stand quietly on a force plate (Kistler, Amherst, NY, sampled at 240 Hz) for five 30s trials with their eyes open. COP data were analyzed using IDA, TRAD, and SDA methods.

IDA analysis

IDA is a stochastic analysis tool for COP data using a Markov-chain model. The invariant density is the eventual probability distribution of finding the COP at any given distance away from the centroid. Five IDA parameters characterize the invariant density. They describe the largest probability of COP staying in a given state (*Ppeak*), how far the COP drifts on average (*MeanDist*), how far the COP reaches out (*D95*), how fast the COP distribution becomes stationary (*EV2*), and how random the COP moves (*Entropy*). In brief, *MeanDist*, and *D95* are related to long-term sway, *Ppeak* and *Entropy* are related to randomness, and *EV2* is related to convergence rate.

Parameters

Postural sway parameters including IDA, TRAD and SDA, and clinical balance measures of Berg and SPPB scores were computed and collected for data analysis.

Fall risk estimation model

Discriminant function analysis (MATLAB) was used to develop fall-risk prediction models to classify recurrent and non-recurrent fallers. Separate models were developed to assess the ability of each type of balance measure - postural sway parameters (IDA, TRAD, and SDA) and clinical balance measures (Berg, SPPB) - for classifying groups of recurrent fallers and non-recurrent fallers. Data were preprocessed such that all parameters had the same variance and were uncorrelated to each other by Mahalanobis transformation. Half of the dataset was chosen randomly for the training set, and the other half for the validation set. Receiver Operating

Characteristic (ROC) analysis was used to compare accuracy and sensitivity of each model.

Correlation analysis

In order to investigate correlation between IDA, TRAD, SDA, and clinical balance measures, Pearson correlation was performed (SPSS Inc). In order to further understand how each parameter affects fall risk, principle component analysis was performed (SPSS Inc). All parameters that showed statistically significant differences between the two groups of recurrent fallers and non-recurrent fallers were used (see [3]). These include *Ppeak*, *MeanDist*, *D95*, *EV2*, *Entropy* from IDA parameters; maximum distance in radial (Rad) direction (*Max_Dist_Rad*), standard deviation in AP direction (*Stdev_AP*), range in AP direction (*Range_AP*), total power in AP direction (*Total_Power_AP*), and area of the stabilogram within a 95% confidence circle (*Area_95%_Circle*) from TRAD parameters; and short-term diffusion coefficient in Rad direction (*DS_Rad*), critical mean square displacement in AP direction (*jc_AP*), from SDA; and Berg and SPPB scores from clinical balance measures.

RESULTS/ DISCUSSION

Accuracies of separate fall risk prediction models based on IDA, TRAD, SDA, or clinical balance measures as determined by ROC analysis are given in Table 1. Accuracy of the IDA model was better by more than 2 % compared to those of other models, suggesting that IDA parameters maybe more sensitive in assessing fall risk.

Accuracies of each model seem relatively low (Table 1). This might suggest that postural sway information itself from quiet stance may not capture the whole spectrum of fall risk. It has been found that factors such as physical strength, mental health, fall history, postural sway in extreme condition can also contribute to fall risk [1].

Correlation analysis (Table 2) found that *Stdev_AP* is highly correlated (0.8 and above) with all TRAD parameters and weakly correlated (0.2 and less) with Berg and SPPB scores. *Entropy* is highly correlated with all IDA parameters except *EV2*, and weakly correlated with Berg and SPPB, and that *EV2* is weakly correlated with Berg, SPPB scores and *DS_Rad*.

Since *Entropy*, *Ppeak*, *MeanDist*, and *D95* were highly correlated among themselves, and based on the interpretation of the IDA parameters, this may imply that long term postural sway and uncertainty (or randomness) of COP motion are highly correlated. All TRAD parameters used in this analysis were highly correlated. This is because all TRAD parameters in Table 2 express measures of the COP fluctuation. Interestingly, Berg and SPPB scores are almost uncorrelated with almost all postural sway parameters, suggesting that these clinical measures provide information that postural sway parameters cannot provide. Principle component analysis showed that there were three main principle components that contribute to fall risk (Table 3). The parameters that correspond to each component imply that fall risk may affect 1) postural sway or fluctuation and randomness, 2) convergence rate of COP to invariant density, and 3) performance on clinical measures (Berg and SPPB scores).

SUMMARY

IDA parameters increased accuracy of a fall-risk prediction model of community-dwelling elderly adults by more than 2 % compared to the accuracy of the other measures. Fall-risk may affect postural sway, randomness, convergence rate and the performance on clinical measures.

FUTURE WORK

Combination of parameters will be used as fall-risk predictors in order to increase model accuracy.

Table 1. Accuracies of separate fall-risk prediction models based on IDA, SDA, TRAD or CLINIC measures

	IDA	SDA	TRAD	CLINIC
Accuracy	72.0%	70.3%	69.0%	68.9%

Table 2. Parameters that showed high and low correlations

	0.8 and above	0.2 and less
Stdev_AP	*Max_Dist_Rad*, *Range_AP*, *Total_Power_AP*, *Area_95%_Circle*	Berg, SPPB
Entropy	*Ppeak*, *MeanDist*, *D95*	Berg, SPPB
EV2		Berg, SPPB, *DS_Rad*

Table 3. Principle components

	Components	Variance
PC1	*Total_Power_AP*, *Range_AP*, *Area_95%_Circle*, *Stdev_AP*, *Max_Dist_Rad*, *MeanDist*, *D95*, *Entropy*	61.3%
PC2	*EV2*, *Berg*, *SPPB*	12.6%
PC3	*Berg*, *SPPB*	7.8%

REFERENCES

1. Campbell AJ et al. *J Gerontol* 44:M112-M117, 1989
2. Hur P et. al. *ASME SBC* Lake Tahoe, CA. August, 2009
3. Hur P et. al. *ASB*, University Park, PA, August, 2009
4. Leveille SG et al. *BMC Geriatr* 8:16, 2008

DYNAMIC BALANCE CONTROL DURING SIT-TO-STAND MOVEMENT: AN EXAMINATION WITH THE CENTER OF MASS ACCELERATION

Masahiro Fujimoto and Li-Shan Chou

Department of Human Physiology, University of Oregon, Eugene, OR, USA
email: chou@uoregon.edu, web: http://biomechanics.uoregon.edu/MAL/

INTRODUCTION

Different movement strategies are used to achieve sit-to-stand (STS) task, depending on balance control ability of the individual. These strategies can be classified by horizontal momentum of the whole body center of mass (COM) and its location relative to the base of support (BOS) [1]. The combinations of COM velocity and position for which loss of balance can be avoided were described as the feasible stability region [2], which would allow us to distinguish the strategy. The COM acceleration also plays an important role. Inability to properly generate COM acceleration would lead to a poor momentum control and result in imbalance. Examining COM acceleration, in addition to its velocity, would provide further insights into balance control during the movement. The purpose of this study was to establish a region of stability using COM acceleration and to characterize age-related differences in the control of COM during the STS movement. Strategies used for the control of COM motion between healthy young and elderly adults were compared using regions of stability derived by COM velocity and acceleration (ROSv and ROSa, respectively).

METHODS

An inverted pendulum model (Fig.1) was used to define ROSv and ROSa. The boundaries of the ROSv were derived using the following equation [3]:

$$-\tilde{X} \le \tilde{\dot{X}} \le 1-\tilde{X} \qquad (1)$$

where $\tilde{X}$ and $\tilde{\dot{X}}$ are normalized COM position and velocity, defined as $\tilde{X} = (X - X_h)/L_f$, $\tilde{\dot{X}} = \dot{X}/(L_f \omega_0)$ ($\omega_0 = \sqrt{g/l}$, $L_f = X_t - X_h$: foot length). The ROSa was defined as the region confined by peak forward COM acceleration needed to be generated prior to the time transferring from the chair (seat-off) for successful termination of the movement within the BOS. COM accelearation profile was modeled as a triangle-shape with the peak in the middle prior to seat-off (Fig.1). The boundaries of the ROSa were derived using the following equation:

$$-\frac{X_h - X}{X - X_i}\tilde{X} \le \tilde{\ddot{X}}_t \le \frac{X_t - X}{X - X_i}(1-\tilde{X}) \qquad (2)$$

where $\tilde{\ddot{X}}_t$ is the normalized peak COM acceleration defined as $\tilde{\ddot{X}}_t = A\ddot{X}_t / L_f$ ($A = l/g$).

Ten healthy young adults [Young (Norm): 6 men, 4 women; mean age 22.2±1.9 years] and ten healthy elderly adults [Elderly: 5 men, 5 women; mean age 70.7±3.3 years] participated in this study. Subjects were asked to stand up from a chair adjusted to their knee height at self-selected natural speed. Data from six trials were collected from each subject. Young subjects were also asked to perform another block of STS trials with purposely bending their trunk prior to seat-off, to make them use a different strategy [Young (Bend)].

Motion data were captured with a motion analysis system (MotionAnalysis, Santa Rosa, CA) at 60 Hz. A total of 29 reflective markers were placed on each subject's bony landmarks. Ground reaction forces (GRFs) were collected by two adjacent AMTI force plates under each foot (AMTI, MA) at 960 Hz. Seat-off was determined as the instant where the vertical GRF reached its peak. One-way ANOVA was used to detect group differences in the normalized COM position, velocity and acceleration. Significance level was set at α=0.05.

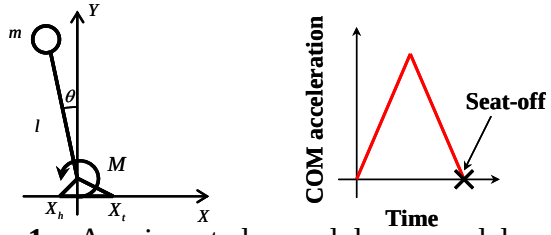

Figure 1: An inverted pendulum model and modeled acceleration profile

RESULTS AND DISCUSSION

Normalized COM velocity at seat-off and peak COM acceleration prior to seat-off with respect to normalized COM position at seat-off for all testing conditions and boundaries of the ROSv and ROSa were plotted in Fig.2 and Fig.3, respectively. Mean values with standard deviations for each group were also indicated.

No significant group differences were detected in mean normalized COM velocity at seat-off (Fig.2). However, mean normalized peak COM acceleration differed significantly among the three groups (Fig.3). This suggests that even though a similar momentum is observed at seat-off to achieve STS task, the momentum is controlled differently prior to seat-off among individuals. Elderly adults demonstrated significantly larger peak COM acceleration than young adults.

Data collected from an elderly subject who complained of difficulty in STS during the experiment were located at or outside the forward boundary of the ROSa (circled in Fig.3). When examined only using COM velocity-position plot, ROSv, the seat-off for this person was initiated with a slower COM velocity with a more anterior position (circled in Fig. 2). This could suggest two possible strategies: this person performed STS 1) with an overall slower COM velocity by generating a smaller acceleration prior to seat-off, or 2) with similar COM acceleration and velocity but initiated seat-off at the time when COM velocity is significantly reduced by a backward acceleration. With the addition of ROSa, we could determine that the latter strategy is what employed by this person, as confirmed with the time-history plots of COM velocity and acceleration (Fig. 4).

CONCLUSIONS

This study demonstrated a potential use of COM acceleration to differentiate individuals with different balance control abilities during STS. The ROSa could serve as a complement to the ROSv, providing insights into how the COM position and motion are controlled prior to seat-off for the execution of STS movement.

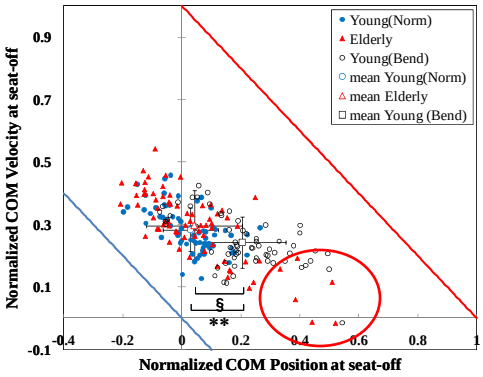

Figure 2: Normalized COM velocity at seat-off vs. normalized COM position (** p=.016, §p=.049.)

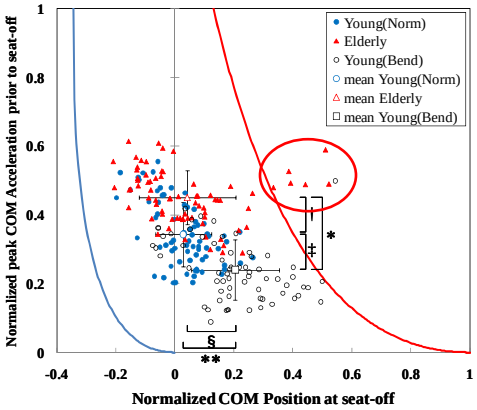

Figure 3: Normalized peak COM acceleration prior to seat-off vs. normalized COM position at seat-off (*p<.001, †p=.016, ‡p=.025, ** p=.016, § p=.049.)

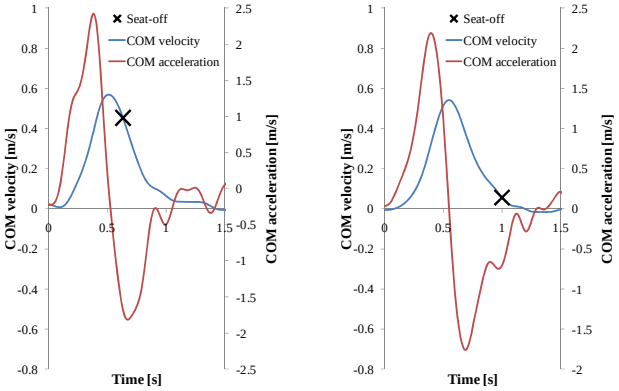

(a) Elderly(Normal) (b) Elderly(with difficulty)

Figure 4: Representative plots of COM velocity and acceleration for (a) normal elderly adults and (b) an elderly who complained of difficulty in STS.

REFERENCES

1.Hughes MA, et al. *Clin. biomech.* **9**(3), 187-192, 1994.

2.Pai YC, & Patton J. *J Biomech* **30**(4), 347-354, 1997.

3.Hof AL, et al. *J Biomech* **38**(1), 1-8, 2005.

APPLICATION OF AUGMENTED REALITY FOR THE ELDERLY FALL RISK PREDICTION

[1]Chih-Hao Chang, [1]Sai-Wei Yang, [1] Yi-Ching TSai, [2] Lin-Fen Hsieh

[1]National Yang-Ming University, Taipei, Taiwan
[2] Shin Kong Wu Ho-Su Memorial Hospital, Taipei, Taiwan
email:swyang@ym.edu.tw, web: http://rehab.ym.edu.tw

INTRODUCTION

Unexpected fall has been a major cause results in bone fracture and further disability for the elderly [1-3]. The elderly fall often combines with varieties of physical and physiological factors such as proprioception, visual, or vestibular dysfunction. The assessment tools of posture balance performance have been developed for years; however, most of studies were focused on the norm establishment.
The purpose of this study was to design an evaluation protocol and measured variables to effectively discriminate the risk factors for the elderly falling prevention.

METHODS

Thirty six subjects were recruited. The control group-No-fall experienced elderly group (NE, n=16, 67.0 ± 3.0); and fall experienced elderly group with at least once fall experience in the past one year prior to this study (FE, n=20, 65.8 ± 1.7 years). All subjects were female with right hand dominated.
Berg Balance Scale and the Functional Reach Test were used to assess the subjects' proprioception and balance ability [3,4].

A Stewart platform integrated with a force platform (AMTI, USA) and a pressure platform (Rsscan, Belgium) was used to produce 10cm/s slip forward, followed by 10^{o} pitch down and up in one second (Fig 1). The virtual reality sense constructed using 3Ds MAX and Virtools was assumed the scenario of the subject sitting on a moving bus encountered an emergency stop (Fig 2).
The measured variables were total CoP traveled distance and bilateral weight bearing ratio. The differences between all of variables of the subjects w/o virtual reality between control and fall experienced group were assessed using two way ANOVA. The level of significance was set at α=0.05 [5~7].

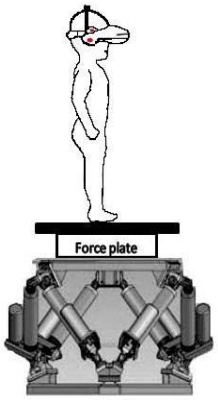

Fig 1: The Dynamic perturbation system
Fig 2: The reality sense of on a moving bus

RESULTS AND DISCUSSION

There were no statistic differences in body weight, height, and BMI among the groups.

The no-fall experienced subjects showed better response to the perturbation (Fig 3). The fall experienced group showed large excursion during the perturbation especially in the period of posture restore. Without augmented reality sense (ARS), there was no significant difference between two groups. With visual input, it induced profound perturbation for the experienced fall subjects (Fig 4, Fig 5).

During the perturbation, both groups had the support leg on left side but the no fall exp. subjects demonstrated even weight support during the recovery period w/o ARS(Fig 6). The uneven

weight support was further augmented with ARS for the fall-experienced subjects.

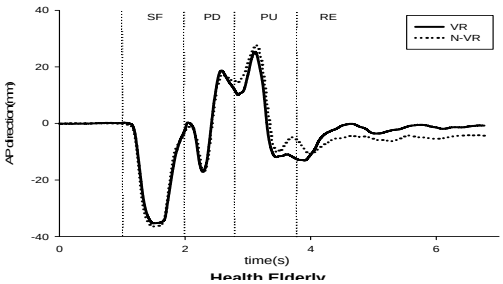

Fig 3: Fore-Aft CoP trajectory for the no-fall experienced elderly

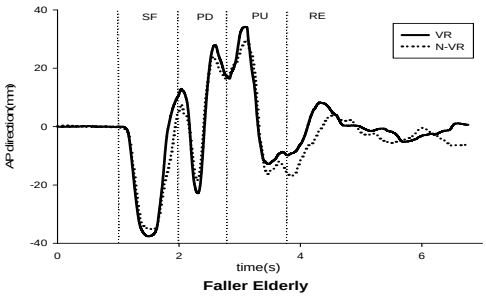

Fig 4: Fore-Aft CoP trajectory for the fall experienced elderly

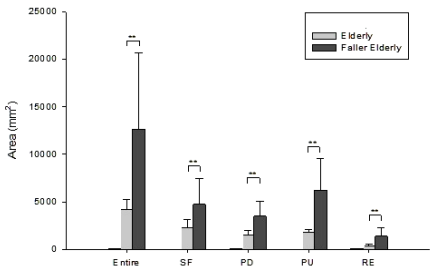

Fig 5: elliptic area of COP in comparison of No fall and fall experienced subjects

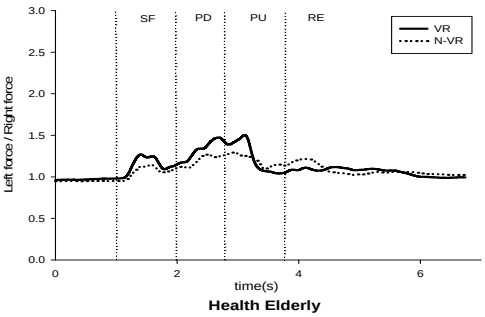

Fig 6: The no-fall experienced subject subjects showed better posture support w/o ARS

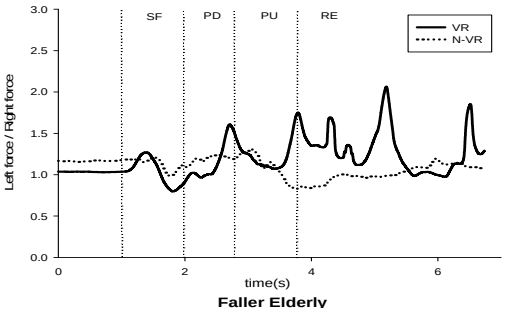

Fig 7: The fall experienced subjects showed uneven body weight support

CONCUSION

The center of pressure and related measured-variables are good means to discriminate the posture control ability. The augmented reality can further enlarge the risk factor.

REFERENCES

1. Buatois S., Gueguen R: *Gerontology*, 52(6): 345-52, 2006
2. Burdea G.Popescu V., *IEEE Trans Rehabil Eng.*430-2, 2000
3. Freitas SMSF., Wieczorek SA., Marchetti PH., Duarte M,*Gait Posture* 22, 322-330 2005
4. Hatzitaki V., Amiridis IG., Arabatzi F. *Gait Posture* 22, 250-257,2005
5. Raymakers JA., Samson MM., Verharr HJ. *Gait & Posture*, 21(1): 48-58, 2005
6. Shaffer SW., Harrison AL. *Physical Therapy*, 87(2): 193, 2007
7. Tossovainen T., Juhola M., J *of Medical Informatics*, 70, 277-283. 2003

ACKNOWLEDGEMENTS

This study was supported by the National Science Council of ROC through grant NSC96-2221-E-010-004-MY3.

AN EXPERIMENTAL STUDY OF POSTURAL CONTROL DURING DOWNWARD REACH AND PICK-UP MOVEMENTS: EFFECTS OF AGE AND LIMITING THE LENGTH OF THE BASE OF SUPPORT

Manuel E. Hernandez MS[1,3], James Ashton-Miller PhD[1,2], and Neil B. Alexander MD[2,3,4]

[1]Biomechanics Research Laboratory, [2]Institute of Gerontology,[3]Mobility Research Center, Division of Geriatric Medicine, Department of Internal Medicine, The University of Michigan, [4]VA Ann Arbor Health Care System Geriatric Research, Education and Clinical Center, Ann Arbor, Michigan.

E-mail: manueleh@umich.edu Web: www.med.umich.edu/geriatrics/moblab/

INTRODUCTION

Difficulty bending down to pick up an object from the floor has been associated with increased fall risk in older adults [1]. Stooping, crouching, or kneeling difficulty is prevalent among older adults but few studies have explored the mechanisms underlying downward reaching and pick-up difficulty [2]. Rapid and accurate control of the center of pressure (COP) is expected for maintaining balance during downward reaching and pick-up movements. Particularly among older adults with stooping, crouching, or kneeling difficulty, as they are associated with decreased lower extremity torque capacity [3].

This study seeks to quantify the effects of body configuration changes in downward reaching and pick-up movements. Limiting the length of the base of support will be used to assess how decreased torque generating capacity affects the balance of healthy older women. Body configuration limitations when reaching down to targets at the reaching envelope are expected to lead to faster and more frequent compensatory COP movements in older women when compared to younger women. Decreasing the length of the base of support at the toe is expected to lead to disproportionate increases in losses of balance during the upward recovery phase of movement.

METHODS

Subjects. Healthy young (mean±SD, age 22±3, Body Mass Index [BMI] 24±5, N = 5) and healthy older women (age 76±7, BMI 25±6, N = 5) were recruited from the local community.

Protocol. To determine whether the effect of age on the COP control of downward reaching movements becomes more pronounced in tasks with a limited base of support, we examined movement time, COP path length, and rate of losses of balance.

Participants performed symmetric two-handed downward reaches to a target placed on the floor while standing with a full or minimal base of support on a platform fixed to a single AMTI force plate (100 Hz sampling rate). Participants were instructed to move the tips of their fingers ‘as fast as possible’ to a pseudo-randomized base of support condition. The minimal base of support was defined as the minimal distance between the toes and the posterior edge of the platform during a successful maximal toe reach (Fig. 1). The target was placed at the participants’ maximal forward reaching distance along the floor. Kinematic data of the entire body were collected using standard motion capture methods (25 Hz sampling rate). Three trials were performed of each foot support condition, but only the

first successful and unsuccessful trials were considered in this analysis.

Analysis of joint motion using optoelectronic cameras provided an assessment of the mean number of losses of balance (LOBs), defined as a stepping response, occurring during 1) the downward reach, or 2) the upward recovery (return-to-stance) movement. Linear mixed models using a restricted maximum likelihood method were used to examine the effect of age, base of support condition, and loss of balance.

RESULTS AND DISCUSSION

Older women had shorter reaching distances and larger minimal bases of support ($p<.05$). Older women tended to have more losses of balance upon return to stance (Table 1). When reaching down, movement time and COP path length were not significantly different between young and older women. However, older women tended to be slower when they lost their balance, while younger women tended to be faster while reaching down when they lost their balance ($p = .063$). COP path length was significantly decreased when performing the downward reaching task on a limited base of support ($p < .005$).

	Young Women (N=5)	**Older Women (N=5)**
Maximal forward reaching distance along floor (cm)*	76.5±5.8	64.6±7.4
Minimal Base of Support (cm)*	8.1±0.7	12.2±1.1
Loss of Balance during upward recovery Phase (%)	20%	40%

Table 1: Characteristics of young and older women (* $p < .05$).

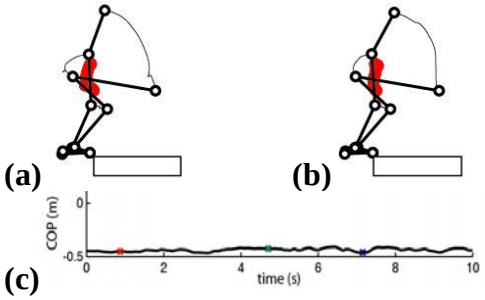

Figure 1: Illustration of movement during successful downward reaching (a) and upward recovery (b) phases with its (c) corresponding COP trajectory.

SUMMARY/CONCLUSIONS

Preliminary findings suggest that when reaching down and picking up an object from the floor, older women, compared to young, may be more likely to lose balance when returning to a stance position. Discrepancies between the downward reaching movement time of successful and unsuccessful movements suggest different mechanisms of losses of balance, which merit further study. The capacity to control excess angular momenta may play a significant role in maintaining balance during downward reaching movements.

REFERENCES

O'Loughlin J.L., Robitaille Y., Boivin J.F., Suissa S. (1993). *Am J Epidemiol*, **137**, 342-354.

Puniello M.S., McGibbon C.A., Krebs D.E. (2000) *J Rehabil Res Dev*, **37**, 341-52.

Hernandez M.E., Ashton-Miller J.A., Alexander N.B. (2010). *Phys Ther*, **90**, 67-74.

ACKNOWLEDGEMENTS

We are grateful to the National Institutes of Health for NRSA Grant Number 1 F31 AG024689-01, which supports this project.

THE EFFECT OF INCREASED INERTIA ON BALANCE USING AN ANKLE STRATEGY

Kerry E. Costello, Sara L. Matrangola and Michael L. Madigan

Virginia Polytechnic Institute and State University, Blacksburg, VA, USA
email: kec@vt.edu, web: http://www.biomechanics.esm.vt.edu/

INTRODUCTION

Obesity is a major medical problem. The prevalence of obesity in the U.S. has doubled since 1980, with one third of the adult population currently considered obese (body mass index > 30 kg/m^2) [1]. Obesity is associated with multiple health conditions, and has also been found to increase risk of falls [2]. Consistent with this, obese individuals exhibit increased postural sway compared to normal weight individuals [3]. Obesity is associated with both increased weight and inertia of the body. When modeling the body as an inverted pendulum, fundamental mechanics suggest that increased inertia may actually be beneficial to balance in some circumstances by decreasing the angular acceleration of the body. In an effort to better understand these and the overall effects of obesity on balance, the goal of the present study was to investigate the effects of increased inertia on balance during quiet standing and balance recovery using an ankle strategy.

METHODS

Twelve normal-weight male subjects participated (age: 22.9 ± 1.9 yrs, BMI: 21.8 ± 2.4 kg/m^2). This study was approved by the Virginia Tech Institutional Review Board and written consent was obtained from all participants.

A customized backboard was designed to constrain balance to an ankle strategy and allow inertia of subjects to be increased without increasing weight (or gravitational torque) (Fig. 1). The backboard that pivoted about an axis aligned with the center of rotation of the ankles. To increase inertia, weights were placed symmetrically on arm pieces extending radially from the axis of rotation. The amount of inertia added to all subjects was I = 22.7 kg*m^2, which was an average of 28.1% of their initial body inertia about the ankles. Balance measurements were taken with and without added inertia to investigate the effects of increased inertia.

Figure 1: Experimental setup showing backboard with weights attached to arm pieces (added inertia condition shown).

Two types of balance measurements were collected: balance during quiet standing, and balance recovery after release from a static forward lean. For the quiet standing measurements, subjects stood as still as possible with eyes closed for 30 seconds while force plate data (Bertec Corp.) and backboard angle data (using a linear potentiometer, Unimeasure, Corvallis, OR.) were sampled at 500 Hz. Four trials were completed with added inertia and four trials were completed without added inertia. The order of presentation of these two conditions was counterbalanced across all subjects. Balance was quantified using 1) the mean center of pressure (COP) speed and 2) width of the 95% confidence interval (CI) of the backboard angle. Values were averaged across all four trials within each condition.

For the balance recovery measurements, subjects were held in a static forward lean, released, and attempted to recover balance using an ankle

strategy. Trials were repeated using progressively larger initial lean angles until subjects could no longer successfully recover. The maximum initial lean angle from which subjects could recover upon release was used to quantify balance recovery. Ankle torque prior to release was maintained at 0.35 body mass * height for all trials. As with the quiet standing measurements, the order of presentation of the two inertia conditions was counterbalanced across all subjects.

A paired t-test was used to determine the effects of added inertia on balance and balance recovery with a significance level of $p \leq 0.05$.

RESULTS AND DISCUSSION

Increased inertia affected balance and balance recovery differently. During quiet standing, mean COP speed tended to increase with inertia, but this difference was not statistically significant (P=0.056) (Fig. 2). The width of the 95% CI of backboard angle during quiet standing showed no significant change in body sway amplitude between conditions (P=0.264) (Fig. 3). Together, these results indicate minimal changes in postural sway during quiet standing with increased inertia.

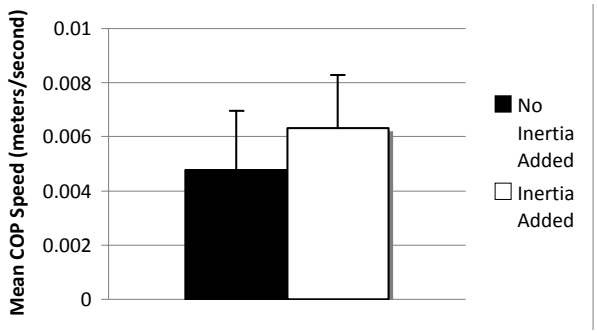

Figure 2: Effect of inertia on mean COP speed. Values reported are mean + standard deviation.

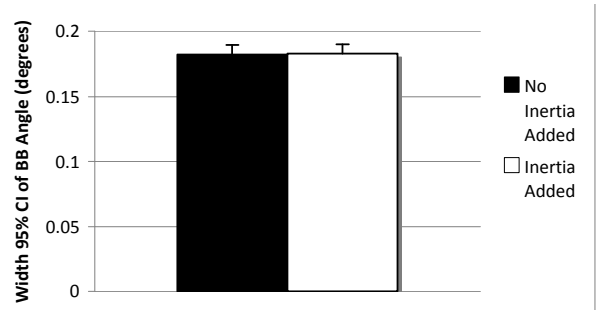

Figure 3: Effect of inertia on width of 95% CI of backboard angle.

During balance recovery measurements, the maximum initial lean angle from which subjects could recover upon release increased with increased inertia (P=0.003) (Fig. 4). This may be a result of the body accelerating less quickly upon release (inertia is in the denominator in the equation for an inverted pendulum below and thus an increase in inertia would decrease the angular acceleration of the body about the ankles).

$$\ddot{\theta}(t) = \frac{mgL_{COM}\sin(\theta(t))}{I}$$

Assuming a consistent reaction time and ankle torque prior to a recovery between the two conditions, this would suggest that the change in angle at which the subjects react to being released will be smaller with increased inertia than without. This may improve their ability to recover, and allow larger angles to be achieved.

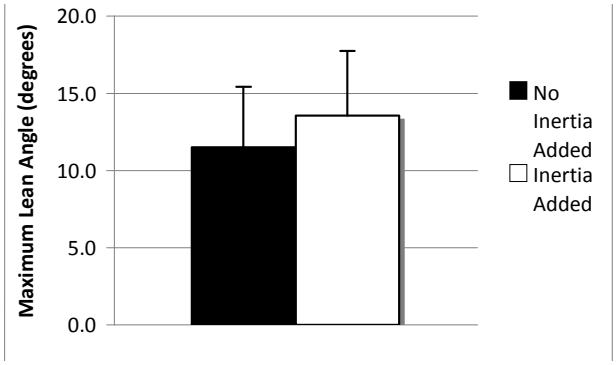

Figure 4: Effect of inertia on maximum lean angle.

CONCLUSIONS

Increased inertia improved the ability to recover balance after release from a static forward lean, but had minimal effect on postural sway during quiet standing. As such, the effects of increased inertia on balance may be dependent on the specific balance task.

REFERENCES

1.Flegal, KM, et al. *JAMA* **288**, 1723-1727, 2002.
2.Fjeldstad, C, et al. *Dyn Med* **7**:4, 2008.
3.Teasdale, N, et al. *Int J Obes (Lond)* **31**, 153-160.

PROACTIVE POSTURAL ADJUSTMENTS DURING MULTIPLE EXPOSURES TO TRIPS

Brooke Coley[1] and Rakié Cham[1]

[1]Human Movement and Balance Laboratory, Department of Bioengineering
University of Pittsburgh, Pittsburgh, PA, USA
Email: bcc4@pitt.edu, web: www.hmbl.bioe.pitt.edu

INTRODUCTION

Balance-challenging environmental hazards can include slipping and tripping, both of which require different postural responses for recovery. It has been reported that trips are more destabilizing for older adults than younger adults, accounting for 25% to over 50% of falls in the elderly [1, 2]. The ability of older adults to exhibit proactive postural adjustments (postural adjustments generated prior to being perturbed in anticipation of the perturbation) comparable to those of young adults during repeated exposure to slipping has been shown [6]. It is apparent that a better understanding is needed to address the differences in postural adjustments adopted by young and older adults in anticipation of a tripping hazard. Studies have used multiple exposures to trips to investigate trip recovery biomechanics [3-5, 8] and the impact of forewarning of the possibility of tripping on changes in the walking pattern. However, limited information exists regarding age-related differences in proactive postural adjustments adopted during multiple exposures to trips when definite knowledge that a trip will occur is provided. The purpose of this study was to investigate proactive postural adjustments in young and older adults measured by the center of mass (COM) state when repeatedly challenged by tripping hazards.

METHODS AND PROCEDURES

Four young (21-35) and six healthy older (65-75) adults, screened for neurological and musculoskeletal abnormalities, were recruited for participation. Subjects were first asked to walk on known dry floors to retrieve baseline gait characteristics. Subjects were then informed that in the next set of trials, at some point they would experience a trip. Subjects had no knowledge of the exact timing at which it would occur nor were they aware that three trips would be randomly inserted into 5 unperturbed trials. All subjects were harnessed to prevent hitting the floor in the case of a loss of balance. Whole body motion data were collected at 120 Hz. The trip was triggered by heel contact of the right foot to catch the left foot midswing. The anterior-posterior (AP) COM position with respect to the ankle of the stance foot was measured 50 milliseconds prior to the

right heel contact triggering the trip. AP-COM position and velocity were the dependent variables in a mixed model ANOVA with subject as a random effect; condition (first trip, walking trial preceding last trip, and last trip), age group (young/old) and the interaction of age group *x* condition as fixed effects. Significance was set at $\alpha = .05$.

RESULTS

AP-COM was significantly correlated with the interaction of age group and condition (p=.0208) (Figure 1). Initially, AP-COM velocity was not different between groups. However, by the walking trial preceding the last trip, older adults (1.25 m/s) had a significantly slower AP-COM velocity than did younger adults (1.5 m/s). No significant differences were observed for AP-COM position.

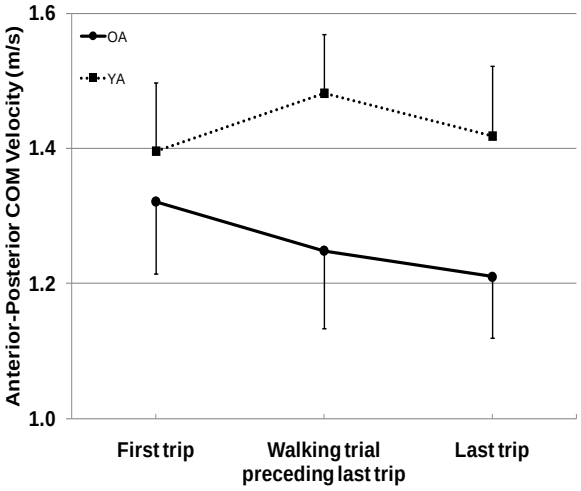

Figure 1. Anterior-posterior COM velocity is significantly affected by age group and condition. Age is denoted by dotted (young) and solid (old) lines. Error bars represent standard error.

DISCUSSION AND SUMMARY

With knowledge that they would experience a trip, young and older adults initially approached the perturbation trials similarly. However, after having experienced a trip, older and younger adults adapted their AP-COM velocity differently. Older adults slowed their AP-COM velocity compared to younger adults who walked faster. These results suggest that the experience rather than knowledge of tripping influences the adoption of proactive strategies in anticipation of a known, upcoming perturbation. Future work will further investigate the effects of having no a priori knowledge of the perturbation on the same group of subjects.

REFERENCES

1. Blake AJ, et al. *Age Ageing* **17**, 365-372, 1988.
2. Campbell et al. *Age Ageing* **19**, 136-141, 1990.
3. Eng JJ et al. *Exp Brain Res* **102**, 339-349, 1994.
4. Grabiner MD et al. *J Gerontol Med Sci* **48,** M97-M102, 1993.
5. Owings TM et al. *Clin Biomech* **16**, 813-819, 2001.
6. Pavol MJ et al. *J Gerontol Med Sci* **59A**, 494-502, 2004.
7. Pijnappels M et al. *Gait Posture* **14**, 11-18, 2001.
8. Schillings AM et al. *J Neurophysiol* **94**, 1158-1168, 2005.

ACKNOWLEDGEMENTS

This study has been supported in part by F31 AG025684-03 NIH Ruth L. Kirschstein Award.

AGE EFFECTS ON LATERAL STABILITY DURING STEPPING

Gregory W. King and Chaitanya K. Akula

University of Missouri – Kansas City, Kansas City, MO, USA
email: kinggr@umkc.edu, web: http://sce.umkc.edu/cme/

INTRODUCTION

Stepping is a common balance recovery strategy that has been studied extensively in the literature. Age-related changes in the stepping strategy have been investigated using a variety of balance perturbation methodologies; however, age effects on lateral stability appear to be consistent across testing paradigms. Specifically, older adults often take steps designed to preserve lateral stability, as evidenced by large components of medial-lateral step length [1,2] and center of mass displacement [3]. Similar results have also been reported during quiet stance and gait activities [4,5]. These studies and others focus on kinematic features of lateral stability; however, there has been little work done to investigate lateral stability from a kinetics perspective, particularly during the strength-intensive landing phase of a protective step. Therefore the purpose of this study was to investigate age effects on kinetic as well as kinematic measures during the landing phase of a balance-restoring step response. We hypothesized that an age-related tendency to use steps more optimized for lateral stability, as quantified by increased peak lateral ground reaction forces and lateral components of step length, would be observed.

METHODS

Participants. Twelve young (YA) and thirteen older (OA) adults participated after providing written informed consent. All participants were free from recent lower extremity fractures, head injury, or neurological disease.

Procedure. All participants performed balance recovery maneuvers facilitated by release from a forward-leaning configuration. The lean magnitude was large enough to ensure all participants required a forward step to regain balance. Participants were instructed to take a single step with the right leg following release. Each participant completed a total of seven trials of the stepping task.

Measurements. Height and weight were recorded for each participant. Foot-floor reactions were captured from the landing location of each stepping trial using a force platform (AMTI, Watertown, MA, USA). Kinematic data was captured from a reflective marker placed on the second metatarsal using a motion capture system (Vicon, Los Angeles, CA, USA). Force and motion data were synchronized and captured at sampling rates of 1000 Hz and 120 Hz, respectively.

Data Analysis. Outcome variables included peak landing phase medial (F_{Medial}) and lateral ($F_{Lateral}$) ground reaction forces; and medial-lateral (L_{ML}) and anterior-posterior (L_{AP}) components of step length. Peak medial and lateral ground reaction forces were defined as the extreme positive and negative values, respectively, of medial-lateral force recorded after the step foot landing event. Step lengths were defined as the net medial-lateral (ML) and anterior-posterior (AP) distances traveled by the step foot metatarsal marker between liftoff and landing events. To correct for differences in participant size, force and step length outcome variables were normalized to participant body weight and height, respectively. All data were processed with MATLAB (The MathWorks, Natick, MA, USA).

Statistical Analysis. Independent samples t-tests were performed on participant aggregates, using a Bonferroni correction to compensate for multiple comparisons. Significant age group

differences were identified by Bonferroni-corrected p-values ≤ 0.05.

RESULTS AND DISCUSSION

Independent samples t-tests revealed significant age-related increases in $F_{Lateral}$ (**Figure 1**; corrected $p<0.05$) and L_{ML} (**Figure 2**; corrected $p<0.05$).

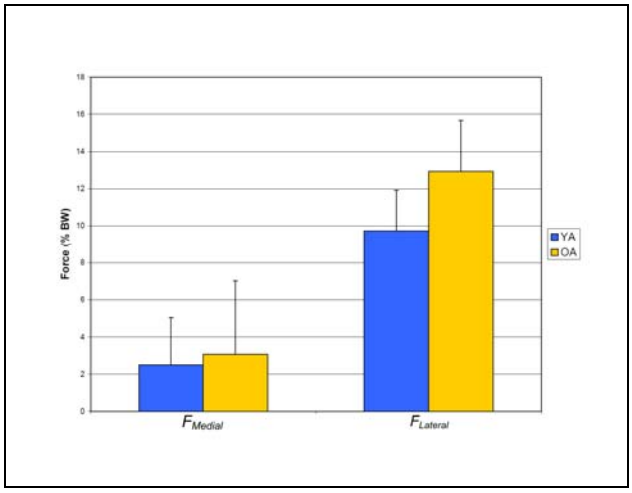

Figure 1: Peak Medial and Lateral landing forces

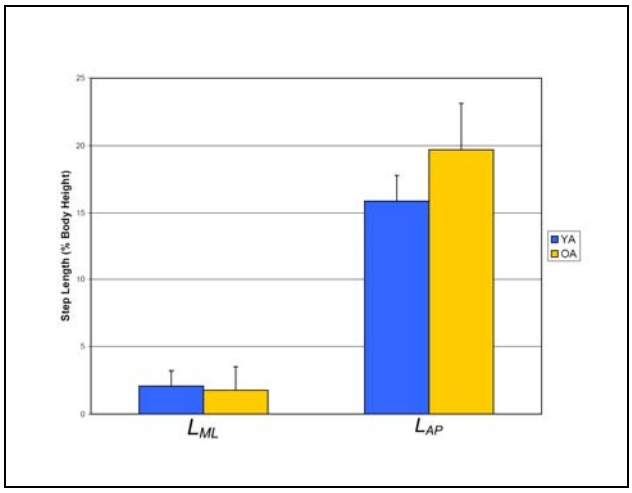

Figure 2: Medial-Lateral and Anterior-Posterior components of step length

Our first result suggests an age-related tendency to use a balance-restoring step response characterized by larger laterally-directed peak ground reaction forces. This finding supports our first hypothesis that older adults would configure their landing phase kinetics for optimal lateral stability. This finding is also consistent with previous studies demonstrating an age-related tendency to preserve lateral stability [2,3]. Our second finding demonstrating an age-related increase in L_{AP}, but not L_{ML}, is inconsistent with our hypothesis and with studies reporting larger lateral step lengths among OA [1,2]. This unexpected finding may be related to our requirement that all participants take single steps to restore balance. Since OA are more likely to use multiple steps [1], they may have used larger-than-natural AP step lengths to ensure successful balance recovery with a single step.

CONCLUSIONS

This study demonstrates an age-related increase in the lateral ground reaction landing force during a balance-restoring step response, suggesting a strategy used by OA to optimize lateral stability. The unexpected absence of age-related differences in ML step lengths is likely related to instructional constraints placed on the number of steps taken.

REFERENCES

1.McIlroy WE, et al. *J Gerontol A Biol Sci Med Sci* **51**, M289-296, 1996.

2.Schulz BW, et al. *Gait Posture* **22**, 198-209, 2005.

3.Rogers MW, et al. *J Gerontol A Biol Sci Med Sci* **56**, M589-594, 2001.

4.Lord SR, et al. *J Am Geriatr Soc* **47**, 1077-1081, 1999.

5.Dean JC, et al. *IEEE Transactions on Biomedical Engineering* **54**, 1919-1926, 2007.

WHOLE-BODY LOCAL DYNAMIC STABILITY DURING WALKING AND RUNNING

Mu Qiao, and Devin, L. Jindrich

Department of Kinesiology and Center for Adaptive Neural Systems
Arizona State University, Tempe, AZ, 85287, USA
email: Mu.Qiao.2@asu.edu, web: http://www.limblab.org/

INTRODUCTION

Highly-simplified models of walking and running can show passive dynamic (i.e. mechanical) stability[1-2]. Although these models capture many important aspects of locomotor dynamics, the extent to which they can describe the stability properties of human locomotion is still unclear. Human locomotion involves coordinating many degrees of freedom (DOFs), which are coupled (mechanically, kinematically, and neutrally) in the control of multi-joint moments. Humans also commonly perform maneuvers (acceleration and deceleration, for example) in addition to constant-velocity locomotion. Several studies have focused on reducing multiple DOFs in a static behavior[3] or on the dynamic behavior of single DOF[4]. However, using individual DOFs to characterize locomotor stability could be incomplete because 1) some DOFs such as joint angles and vertical COM are constrained to limited ranges; 2) individual DOF may only reflect local dynamic behavior, and not the dynamics of the entire system[4]. Moreover, the effects of different maneuvers or gaits on dynamic stability have not been fully characterized. For example, walking might be expected to be more stable than running because there are more opportunities for continuous neural feedback to contribute to stability[5]. This study therefore sought to characterize whole body within-stride stability by analyzing many DOFs. We used Principal Component Analysis (PCA) and calculated Lyapunov exponents on the 1st principal component, which accounts for limb rotation with minor translation[3], to determine the stability among body DOFs within a stride[4]. Specifically, we hypothesized that 1) different joint DOFs do not show differences in stability properties during locomotion; 2) constant speed walking or running is more stable than acceleration or deceleration; 3) walking is more stable than running.

METHODS

We used a VICON® 612 3-D motion tracking system (120Hz), and two force platforms (Bertec) to record kinematics and Ground Reaction Forces (GRFs) (3000Hz). The platforms were obscured by a 120cm × 160cm, 2mm-thick rubber mat. 18 male participants (age = 27.2 ± 4.2yrs; body weight = 70.8 ± 8.3kg; height = 178.9 ± 7.3cm) performed 6 trials in each of 6 locomotion tasks: running and walking at constant velocity, acceleration, and deceleration.

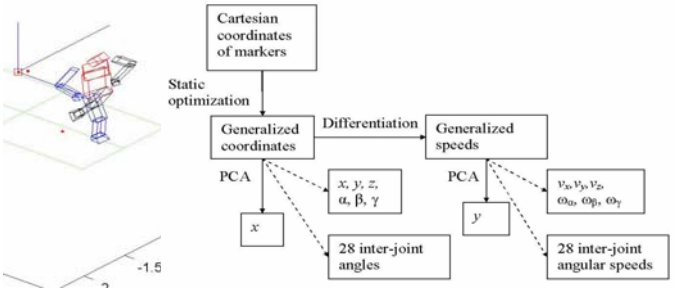

Figure 1: Left, 34-DOF-15-segment human model; Right, progress of processing the data.

RESULTS AND DISCUSSION

Across all trials the 1st principal component of generalized coordinates (x) (R^2 = 0.75±0.1) and corresponding time derivatives (y) (R^2 = 0.65±0.2) accounts for considerable variance. By reconstructing whole-body kinematics using x, motion is constrained to relative limb rotation motion with minor translation[3]. By using x and y together to reconstruct the system's mechanical energy (translational, rotational, and potential energy) and comparing it with original mechanical energy still shows considerable matching (Fig. 2). This again verifies x and y capture fundamental aspects movement dynamics. Fig. 3 shows a representative of $x(t)$ with delays in 3-D space. In each trial Lyapunov exponents were calculated from x, vertical COM, left elbow and left knee. Positive Lyapunov exponents, which indicate an unstable

system, were found for within-stride dynamics during both running and walking.

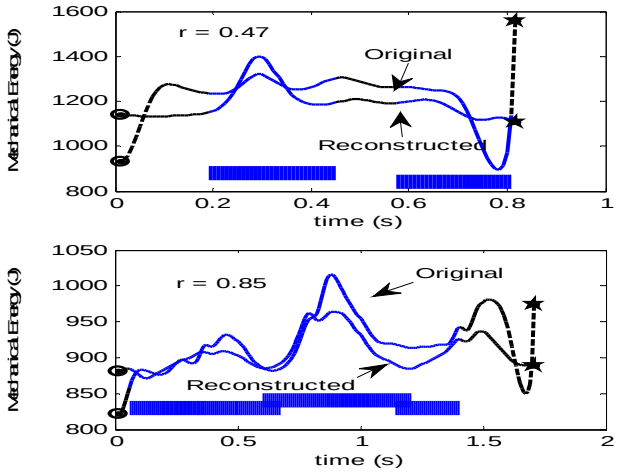

Figure 2: Raw and reconstructed whole body mechanical energy. (Top, running; Bottom, walking, lower bars indicates stance phase)

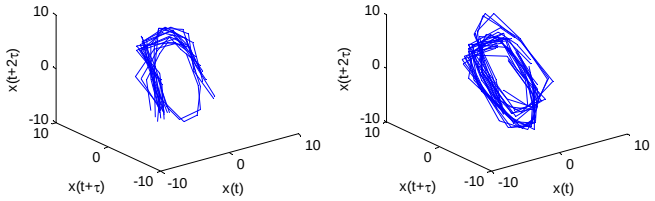

Figure 3: Reconstruction of $x(t)$ in 3D-space using time delayed copies of $x(t)$. (Left constant speed running; Right, constant speed walking)

For x a two-factor (gait; speeding) repeated measure ANOVA showed a significant main effect: running is more unstable than walking ($p < 0.01$) (Fig. 4, UL). Although not significant, all Lyapunov exponents are greater in running than walking. In contrast, if only vertical COM is used (Fig. 4, UR), although running is more unstable than walking manifested by a higher Lyapunov exponent, it is not significant ($p = 0.08$), and speed has main effect ($p < 0.05$). This suggests that using only COM dynamics alone may over-simplify the system's behavior. Similarly, using only data from select DOFs such as individual joint angles (left elbow (Fig. 4, LL, significant interaction, $p < 0.05$), left knee (Fig. 4, LR, no main effect)) can result in conflicting conclusions and may only reflect local dynamic behavior. These conflicts show that individual joints may not effectively represent the whole system's dynamic behavior. Moreover, using x to capture the dynamics of many DOFs shows that movements of the entire body (Fig. 4, UL) may be less stable than individual DOFs such as the vertical COM (Fig. 4 UR).

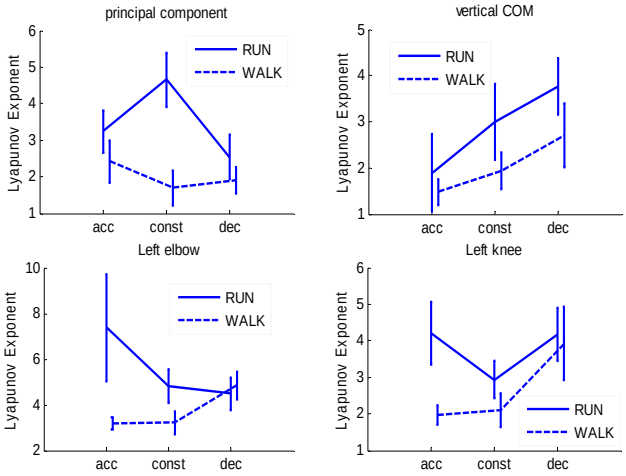

Figure 4: Lyapunov exponent as a function of speeding and gait. (Upper Left (UL), x; Upper Right (UR), vertical COM; Lower Left (LL), left elbow; Lower Right (LR), left knee)

CONCLUSIONS

Our results suggest that stability analysis of individual DOFs may not faithfully capture the dynamics of the entire body during locomotion. The current results focus on within-stride dynamics of the whole body. Humans appear to show less within-stride stability than stability over multiple strides, which has been measured by several studies[4]. Running is more unstable than walking, and maneuvers involve additional decreased stability. These results suggest that considering segmental dynamics and interactions is important for evaluating locomotor stability.

REFERENCES

1. Kuo, A.D., *Stabilization of Lateral Motion in Passive Dynamic Walking.* The International Journal of Robotics Research, 1999. **18**(9): p. 917-930.
2. Seyfarth, A., et al., *Running and walking with compliant legs.* Fast Motions in Biomechanics and Robotics: Optimization and Feedback Control, 2006. **340**: p. 383-401.
3. Ivanenko, Y.P., et al., *Modular Control of Limb Movements during Human Locomotion.* J. Neurosci., 2007. **27**(41): p. 11149-11161.
4. Segal, A.D., et al., *Local dynamic stability in turning and straight-line gait.* Journal of Biomechanics, 2008. **41**(7): p. 1486-1493.
5. Dingwell, J.B. and H.G. Kang, *Differences Between Local and Orbital Dynamic Stability During Human Walking.* Journal of Biomechanical Engineering, 2007. **129**(4): p. 586-593.

DYNAMIC STABILITY DURING SUCCESSFUL AND FAILED COMPENSATORY STEPPING RESPONSES

[1]Jeremy R. Crenshaw, [1]Julie B. Cain, and [1]Mark D. Grabiner

[1]University of Illinois at Chicago, Chicago, IL, USA
email: jcrens2@uic.edu, web: http://www.uic.edu/ahs/biomechanics/

INTRODUCTION

A large postural disturbance may require multiple forward compensatory steps in order to restore dynamic stability. When considered at key events of the compensatory stepping response (CSR), a single measure that considers center of mass of the body (COM) relative to its base of support (BOS) may indicate the current state of dynamic stability and, accordingly, the effectiveness of the CSR. Compared to the distance (*d*) between the COM and BOS, measures that also consider the COM velocity (v_{COM}) better explain the occurrence of a compensatory step [1,2]. Measures that include v_{COM} have shown differences between subjects who restored dynamic stability with one step and those who used multiple steps [3]. Considering v_{COM}, or v_{COM} and the acceleration of the COM (a_{COM}), allows calculation of the time-to-contact that has been used to predict single [4] and multiple [5] compensatory steps. To the best of our knowledge, previous studies have not measured dynamic stability when evaluating falls and recoveries. A useful measure should objectively discriminate these two outcomes, providing insight as to whether and, if so, how unsuccessful CSRs insufficiently maintain dynamic stability. Furthermore, these measures should strongly correlate with trunk and step kinematics, as these variables have been shown to be determinants of successful forward CSRs [6].

The primary purpose of this study was to evaluate the discriminant capability of measures of dynamic stability, and determine the measure with the most accurate classification. We hypothesized that, when evaluated at the completion of the first and second compensatory step, measures that consider the greatest amount of information (v_{COM}, a_{COM}, and/or body size) would have the most accurate classification.

The secondary purpose of this study was to identify kinematic variables that best explain the variance in measures of dynamic stability. We hypothesized that trunk and step kinematics would be strongly ($R^2 > 0.81$) and significantly correlated with measures of dynamic stability.

METHODS

Thirteen healthy, young adults (6 male, age: 22±2.6 years, height: 174.5±10.0 cm, mass: 68.7±11.7 kg) participated in this study. While subjects stood on a custom treadmill (Active StepTM, Simbex, Lebanon, NH), posteriorly-directed treadmill accelerations necessitated multiple forward compensatory steps to avoid a fall. First, subjects were given a standardized postural disturbance (0.5 s acceleration phase of 6.5 m/s^2 followed by a deceleration phase of -0.375 m/s^2). A series of similar postural disturbances (3.0-6.25 m/s^2) was then delivered, sequentially increasing and then decreasing in magnitude. Following this series, subjects were exposed to a second standardized disturbance. Data were considered for this study if subjects failed to recover from the first standardized disturbance, and successfully recovered from the second standardized disturbance. Three dimensional motion capture data were collected at 60 Hz. The following variables were extracted:

- The distance from the BOS (toe marker of the stepping limb) to the COM: $d = BOS - COM$
- The margin of stability [modified from 7]: $MOS = d - \left(v/\sqrt{g/l}\right)$
    - $v = v_{COM} - v_{belt}$; v_{belt} is the velocity of the treadmill belt; g = 9.81 m/s^2; l is the distance in the sagittal plane between the stepping ankle and the COM.
- The temporal stability margin (TTC_{MOS}) [7]: $TTC_{MOS} = MOS/v$

- Time-to-contact considering velocity [modified from 4]: $TTC_{vel} = d/v$
- Time-to-contact considering acceleration [modified from 4]:
  $TTC_{accel} = \left(-v \pm \sqrt{v^2 - 2ad}\right)/a$
  - $a = a_{COM} - a_{belt}$. If d is positive, the smallest positive real solution is chosen. If d is negative, the greatest negative real solution is chosen.

Trunk flexion angle (*TFA*), trunk flexion velocity (*TFV*), time after disturbance onset (*t*), and step length (l_{step}) were also computed.

For all variables, dependent t-tests determined significant differences ($p<0.05$) between falls and recoveries. If significant between-condition differences were found, logistic regressions were used to determine the discriminant capability of included variables. Bivariate correlations were calculated between dynamic stability variables and kinematic variables.

RESULTS AND DISCUSSION

Our first hypothesis was partially supported. TTC_{vel} and TTC_{accel} had the most accurate classification (80.8%, $p \leq 0.001$ for all steps), qualitatively discriminating falls and recoveries more accurately than *d* (76.9%). *MOS* at both steps (step 1 p=0.134; step 2 p=0.612) and TTC_{MOS} at the second step (p=0.267) were not significantly different between falls and recoveries (Table 1).

Aside from the moderate correlation of *d* and l_{step} (R^2 =0.50), the kinematic variables of interest had weak correlations with the dynamic stability variables, suggesting that one kinematic variable is not the key variable in maintaining dynamic stability. At the first step, the greatest amount of variance in *d* and all *TTC* measures was explained by l_{step}. At the second step, the greatest amount of variance in *d*, TTC_{vel}, and TTC_{accel} was explained by *TFA*.

CONCLUSIONS

Of the stability measures investigated, TTC_{vel} and TTC_{accel} at the first and second step were the best predictors of falls and recoveries by young adults. Our results suggest that less *TTC* at the completion of the first compensatory step, possibly due to an inadequate l_{step}, significantly increases the likelihood of a fall. Furthermore, less *TTC* is maintained at the second step, and is associated with a greater *TFA*.

REFERENCES

1.Pai YC, et al. *J Biomech **31**, 1111-1118, 1998.*
2.Pai YC, et al. *J Biomech **33**, 387-392, 2000.*
3.Arampatzis A, et al. *J Biomech **41**, 1754-1761, 2008.*
4.Hasson CJ, et al. *J Biomech **41**, 2121-2129, 2008.*
5.Schulz BW, et al. *J Biomech **39**, 1444-1453, 2006.*
6.Owings TM, et al. *Clin Biomech **16**, 813-819, 2001.*
7.Hof AL, et al. *J Biomech **38**, 1-8, 2005.*

Table 1: Results from the dependent t-tests (fall vs. recovery), logistic regressions (%Class is percent overall correct classification), and bivariate correlations

Variable	Step	Mean ± SD		%Class	R^2			
		Fall	Recovery		*TFA*	*TFV*	*t*	l_{step}
***d* (cm)**	1	16.5 ± 6.9***	26.7 ± 7.1	76.9 ###	0.10	0.12	0.14	0.50 +++
	2	17.6 ± 11.8***	33.5 ± 5.8	76.9 ###	0.29 ++	0.04	0.01	0.04
***TTC*$_{MOS}$ (s)**	1	-0.24 ± 0.02***	-0.22 ± 0.02	73.1 #	0.07	0.06	0.09	0.37 +++
***TTC*$_{vel}$ (s)**	1	0.06 ± 0.02***	0.09 ± 0.02	80.8 ###	0.12	0.18 ++	0.06	0.38 +++
	2	0.05 ± 0.02***	0.10 ± 0.02	80.8 ###	0.27 ++	0.05	0.01	0.03
***TTC*$_{accel}$ (s)**	1	0.05 ± 11.8***	0.09 ± 0.02	80.8 ###	0.11	0.14	0.08	0.40 +++
	2	0.05 ± 0.04***	0.10 ± 0.02	80.8 ###	0.27 ++	0.04	0.01	0.03

Dependent t-tests: ***significance at $p \leq 0.001$; Logistic regression model χ^2 significance: #significance at $p<0.05$, ###significance at $p \leq 0.001$; Bivariate correlation: ++significance at $p<0.01$, +++significance at $p \leq 0.001$

EXPERIMENTAL ANALYSIS OF KINETIC VARIABLES FOR BIOMECHANICAL STS MOVEMENT

[1]Asif Mahmood Mughal and [2]Kamran Iqbal

[1]Center for Advanced Studies in Engineering, Islamabad, Pakistan
[2]University of Arkansas at Little Rock, AR, USA
email: asif@case.edu.pk, kxiqbal@ualr.edu

INTRODUCTION

Sit-to-stand (STS) movement is a common human task which involves combination of a musculoskeletal structure integrated with neural control. Biomechanics researchers and experimentalists have performed variety of experiments for study and analysis of the STS task [1]. The profiles of joint angles have been studied for normal subjects and patients, which helped to synthesize reference system for the joint angles during the movement simulation. Balance of Center of Mass (CoM) and head position (HP) provide mathematical formulation for energy function for gain scheduling for the controlled torques [2]. Other experimental studies in STS show the analysis of Ground reaction forces (GRF) and Center of Pressure [3]. In this study, we used a Bertec Digital Balance Plate for measurement of GRF, moments and CoP during STS maneuver. The major purpose of this study was to develop a procedure to validate biomechanical models for the STS task. We compared the experimental profiles of GRF for STS movement with analytically obtained solutions in [4] and with synthesized data in [5]. We obtained plots of GRF in vertical y-direction and moments along x and z- directions, where distance between the feet represented in x-axis and foot length is in z-axis. These two results validate the modeling scheme which discusses GRF and Moment as variables of interest. Biomechanical models are represented in terms of joint angles and velocities; to validate joint angle profiles of these models directly require expensive mechanism (such as Vicon systems). However, these models can still be validated through indirect means by obtaining results of measureable kinematic and kinetic variables such as GRF and moments. These results shows the applicability of modeling schemes presented in [4-5] for analyses and techniques related to STS movement.

EXPERIMENTAL SETUP

We used a Bertec Digital Balance Plate for measurement of GRF, moments and CoP during STS maneuver. This balance plate senses the data and sends to Bertec Digital Acquire Software for processing via USB cable. This software stores the variables in hard disk as a data file which we further loaded it in MATLAB for analysis and plotting. Further details and technical specification can be seen at bertec.com. There were 13 subjects, 7 male and 6 females, with ages ranging 18-46 yrs and their height ranging from 155-187 cm, and their foot length varies 22.8 – 29.6 cm. There were 10 trails for each subject, first 7 trails were used as training trails and the remaining 3 were for experimental trails. These experiments used a simple chair, with no arm rests and positioned at a place such that it can't move or slip in any direction. The base is fully attached to the ground with a frame of metallic rods which makes it stable against slip and slide. A Bertec Digital Balance Plate placed with the feet frame of the chair and leveled on the ground. Each barefooted subject for each trail sat on a chair with his arm around him and moving from sitting to standing position calmly. A verbal "go" command used to initiate the experiment with data recording started approximately 2 sec prior to the command. We used 500 Hz, and a total of 4 sec data is recorded for each trail, with significant pause time between two trails.

RESULTS AND DISCUSSION

We imported the data files of each trail from each subjects to MATLAB to plot and analyze the experimental results. We rejected data sets of two

female subjects because of recording errors during movement. There GRF results were fine but possibly these subjects were using more pressure to balance during the movements which stand out these results from normal study. Fig 1 shows the ground reaction force (GRF) in vertical direction upward during the movement. These results indicate that initially there is slight decrease in force magnitude, and then further it rises up to its maximum and finally settles at body weight. The difference between lower and higher line is body weight of a subject, as final ground reaction force in this movement is the net body weight. After the maximum peak, the other peaks are due to limb movements which take some time to finally settle; and if a person is moving slightly instead of standing calmly, this also reflects in steady state values.

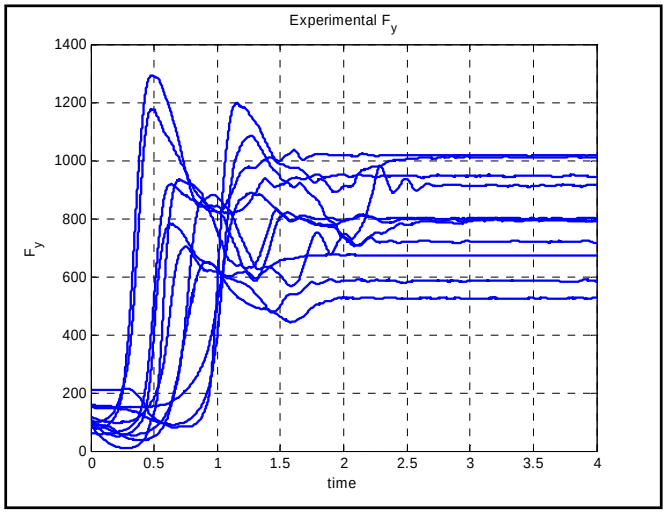

Figure 1 Experimental F_y from 10 subjects on Bertec force plate during STS maneuver

The second plot is to obtain the moment about x and z axis, where distance between the feet represented in x-axis and foot length is in z-axis. Fig 2 shows the moments M_z and M_x, which shows peaks followed by damping or small peaks and finally settling at some specific values. Moments are function of ankle torques in three direction and applied forces from the limbs. In Fig 2, we observe that M_x settles in both positive and negative values, and for four subjects from -10 - -20 N-m. This shows that there is more twist in the movement, which requires control effort to minimize it. It should also be noted that a human foot doesn't have only twist to tilt but combination of both which plays role on balance and maneuver.

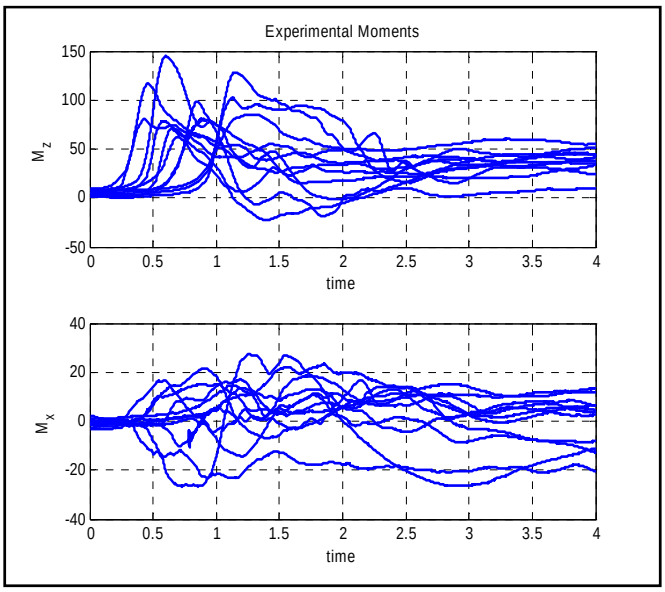

Figure 2 Experimental moments M_z and M_x during the STS maneuver for 10 subjects

REFERENCES

[1] Wim G. M. Janssen, Hans B. J. Bussmann, and Henk J. Stam, "Determinants of sit-to-stand movement: A review", *Physical Therapy*, Vol. 82, No. 9, 2002.

[2] D.S. Resiman, J.P. Scholz and G. Schöner, "Coordination underlying the control of whole body momentum during sit-to-stand", Gait and Posture, Vol. 15, pp45–55, 2002.

[3] Bahrami, F., Riener, R., Jebedar-Maralani, P., and Schmidt, G. "Biomechanical anaylsis of sit-to-stand transfer in healthy and paraplegic subjects". Clinical Biomechanics, Vol. 15, pp123-133 (2000).

[4] Asif Mahmood Mughal and Kamran Iqbal, "Decoupling of 3D Bipedal Model with Holonomic Constrained for Optimal Controller Design of Biomechanical Sit-to-Stand Maneuver," ASME Journal of Biomechanical Engineering, Vol. 132, No. 4, pp1-9, 2010.

[5] Mughal, A. M. and Iqbal, K., "Synthesis of Angular Profiles for Bipedal Sit-to-Stand Movement", 40th Southeastern Symposium on System Theory, 16-18 March, New Orleans, LA, USA, (2008), pp293-297.

KNEE JOINT FORCES AND MOMENTS IN BELOW-KNEE AMPUTEES ACROSS INCREASING STEADY-STATE WALKING SPEEDS

Nicholas P. Fey and Richard R. Neptune

Department of Mechanical Engineering, The University of Texas at Austin, Austin, TX, USA
email: nfey@mail.utexas.edu, web: http://www.me.utexas.edu/~neptune

INTRODUCTION

Unilateral below-knee amputees experience many gait abnormalities relative to non-amputees that often lead to pain and joint disorders [1]. Joint pain is most frequently reported in the intact leg knee, and long term prosthetic use is associated with increased prevalence of developing osteoarthritis [1]. However, the mechanism causing intact knee osteoarthritis in amputees remains unclear. Studies analyzing sagittal plane quantities have identified increased intact leg loading relative to the residual leg, leading some to suggest that the reduced residual leg loads are a protective mechanism against developing residual limb pain. However, protecting the residual leg may lead to long-term detrimental consequences in the intact leg.

Studies analyzing knee joint loading have shown an increased knee abduction (internal) moment is associated with higher medial compartment forces and joint degradation, which is proportional to osteoarthritis severity [2]. But, low severity patients have not shown differences in knee loads compared to control subjects. In amputee gait, research has shown the intact knee abduction moment is greater than the residual leg at self-selected walking speeds and concluded the higher loads may be the cause of joint degradation, although there was no increase in the intact knee abduction moment compared to non-amputee control subjects [3]. Thus, it remains unclear whether the increased intact knee abduction moment causes osteoarthritis in amputees, or if it is an adaptation as a result of the disease.

To date, no study has examined three-dimensional intersegmental joint forces and moments in the intact and residual knees over a range of walking speeds in subjects without a history of osteoarthritis. The influence of walking speed on knee joint forces and moments would be important to investigate since it has been shown to influence muscle activity and joint work in amputees [4]. Thus, the purpose of this study was to examine three-dimensional joint forces and moments across a range of walking speeds to gain insight into potential causes of intact knee osteoarthritis in asymptomatic amputees. We tested four hypotheses at each walking speed: (1) net intersegmental joint forces and (2) moments of the intact knee will be greater than non-amputee control subjects, and (3) net intersegmental joint forces and (4) moments of the intact knee of amputees will be greater than in the residual knee.

METHODS

We tested 14 unilateral, below-knee amputees (11 traumatic, 3 vascular; 45 ± 9 years) and 10 non-amputee control subjects (33 ± 12 years), who were free of any known musculoskeletal disorders and pain. Post-amputation time was 6 ± 3 years. Each amputee used their own prosthesis. Subjects walked along a 10-m walkway at four randomly-ordered, steady-state speeds of 0.6, 0.9, 1.2, and 1.5 (±0.06) m/s, while kinematic data were measured using a motion capture system (Vicon, Oxford Metrics, Inc.) and ground reaction force data were measured using four embedded force plates (Advanced Mechanical Technology, Inc.). Repeated trials were collected until five force plate contacts per foot were measured at each speed.

An inverse dynamics analysis was performed to calculate the intersegmental joint forces and moments using Visual3D (C-Motion, Inc.), which were expressed in the local orthogonal femoral frame. Kinematic and GRF data were low-pass filtered. Joint forces and moments were normalized by the body mass of each subject. A total of nine knee intersegmental moment and force impulses (knee extension, flexion, abduction, internal rotation, and external rotation moment impulses and

lateral, anterior, posterior, and axial force impulses) were computed over stance. For each impulse, two (intact to control knee, intact to residual knee), two-factor, repeated-measures ANOVAs were computed to compare quantities across leg (intact, residual), group (amputee, control) and speed. Pairwise comparisons were made when significant differences were detected using a Bonferroni adjustment ($p \leq 0.05$).

RESULTS AND DISCUSSION

The hypothesis that intact knee moments would be greater than the control subjects was not supported. In fact, knee abduction moment impulse was significantly smaller in the intact knee compared to control subjects at 0.6 and 0.9 m/s ($p \leq 0.031$, Fig. 1). These results are in contrast to previous work that found an increased peak intact knee abduction moment relative to the residual knee [3]. Royer et al. [3] tested patients free from osteoarthritis and of a similar age (42 ± 11 years) to our amputee subjects (45 ± 9 years). However, post-amputation time (17 ± 11) was substantially larger than in our study (6 ± 3 years). Thus, their larger intact knee abduction moment may be an adaptation that occurs with longer prosthesis use or is possibly in response to the initial stages of disease.

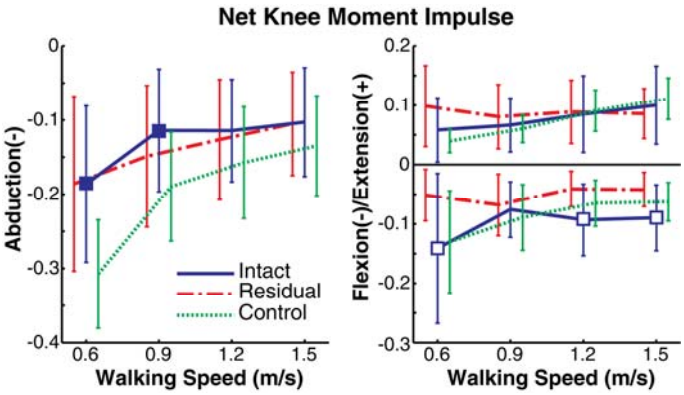

Fig. 1: Mean ± standard deviation moment impulses (N*m*s/kg) of the intact, residual and control knees. Significant intact differences relative to control (■) and residual (□) knees are indicated.

The hypothesis that intact knee moments would be greater than the residual knee was supported with the knee flexion moment impulse at 0.6, 1.2 and 1.5 m/s ($p \leq 0.009$, Fig. 1), and knee external rotation moment impulse at all speeds ($p \leq 0.041$). Also, knee extension moment impulse did not significantly change as speed increased in the residual knee, while it increased in the intact knee ($p \leq 0.043$, Fig. 1). The bilateral asymmetry in these quantities may be a contributing factor to the development of intact knee osteoarthritis.

There were no significant differences found in intersegmental force impulses between legs. The absence of a difference in force impulses does not rule out that amputees do not experience larger intact knee contact forces. Intersegmental joint forces underestimate joint contact forces because they do not account for muscle co-contraction or compressive forces due to ligaments [5]. Modeling studies quantifying the contributions of muscles and external loads to joint contact forces have provided insight into joint loading of non-amputees and future work is needed to analyze amputee gait.

Previous studies have shown amputees experience higher metabolic cost and slower self-selected walking speeds relative to non-amputees. An interesting finding in the present study was that the highest degree of symmetry between residual and intact knee loads occurred at 0.9 m/s. The lower self-selected walking speed by amputees [e.g., 3] may be influenced by the improved load symmetry that occurs at slower speeds.

CONCLUSIONS

Analyzing intersegmental joint forces and moments was inconclusive in identifying potential causes of intact knee osteoarthritis since no intact knee quantities were greater than the control knees. However, bilateral loading asymmetry between intact and residual knees was shown to exist, which may lead to joint degradation over time.

REFERENCES

1. Gailey R, et al. *J Rehabil Res Dev* **45**(1), 15-29, 2008.
2. Sharma L, et al. *Arthritis Rheum* **41**(7), 1233-40, 1998.
3. Royer T and Koenig M. *Clin Biomech* **20**(10), 1119-25, 2005.
4. Silverman AK, et al. *Gait & Posture* **28**(4), 602-609, 2008.
5. Zajac FE, et al. *Gait & Posture* **16**(3), 215-32, 2002.

ACKNOWLEDGEMENTS

This work was supported by NSF Grant 0346514.

BIOMECHANICAL ANALYSIS OF A UNILATERAL TRANSFEMORAL AMPUTEE DURING HILL WALKING TRANSITIONS: A CASE STUDY

Keith A Stern and Jinger S Gottschall

Pennsylvania State University, University Park, PA, USA
email: kas5006@psu.edu

INTRODUCTION

Lower limb muscle imbalances and joint range of motion limitations can often lead to gait disorders due to asymmetric walking patterns. Individuals with unilateral lower limb amputations represent an extreme case of asymmetry, which typically results in decreased anterior-posterior stability during locomotion. An asymmetric gait may not cause an individual to trip or fall during normal level walking, but an asymmetric gait may predispose an individual to trips or falls during challenging tasks such as hill walking or changing surfaces[1]. Understanding the joint kinematics and muscle activities for the successful transition between level and hill surfaces may improve prosthesis design and injury rehabilitation. Younger, healthy individuals navigate hill transitions by reducing speed and step length while modulating muscle activity equally between the two legs[2]. Our goal in the current case study was to evaluate how a unilateral amputee navigates these hill transitions. We hypothesized that range of motion and muscle limitations at the knee and ankle of the injured or prosthetic limb would result in increased range of motion and muscle activity in the healthy or intact limb. Additionally, we hypothesized that a transition step, from a level to a hill surface, initiated with the injured limb would be slower and shorter compared to a transition step initiated with the healthy limb.

METHODS

This case study was an evaluation of a unilateral transfemoral amputee (male, 21 yr, 84.5 kg, 1.8m), a nationally-ranked, Paralympic athlete in throwing events. The prosthetic limb, a C-Leg (Otto Bock, Minneapolis, MN), has an active knee joint controlled by a multiprocessor and hydraulics to continuously adjust knee flexion and extension resistance.

We placed 15 retroreflective markers over the shoes and lower limb joints in order to measure joint angles and temporal spatial gait parameters with a six camera, passive marker system. We also placed electromyography surface electrodes over the lateral gastrocnemius (LG), tibialis anterior (TA), bicep femoris (BF), and vastus lateralis (VL) to record muscle activity during walking. We then compared this muscle activity data to previous data collected within our lab utilizing the same methodology with healthy, young adults[3].

The participant completed randomly assigned overground walking trials on both level and 15-degree ramp surfaces. We focused on 3 separate conditions: level walking, the transition to an uphill ramp (L-UP), and the transition to a downhill ramp (L-DN). Each walking trial was analyzed as one stride from toe off to toe off of the intact limb (IL) or prosthetic limb (PL).

RESULTS AND DISCUSSION

Level walking speed was not different between strides of the IL and PL but step length and stance time were significantly different (Table 1). Walking speed during L-UP was 3% slower during the PL stride but speed during L-DN was 10% faster. Step length of the PL during L-UP was 24% shorter during the first step onto the ramp and 66% shorter during the second step as compared to the step length of the IL. Additionally, step length of the PL during L-DN was 27% greater and time in stance was 18% less as compared to the IL.

All joint angles for each condition show a reduced range of motion and delayed flexion or extension in the PL compared to the IL. Joint angle data verified an asymmetric gait during hill transition strides as there was minimal knee flexion at heel strike in the

PL. Knee flexion was 32 degrees less during the L-UP condition and 5 degrees less during the L-DN condition. Peak hip flexion during terminal swing and early stance was 40 degrees less in the PL during the L-UP condition as compared to the IL and plantar flexion was reduced by 30 degrees (Figure 1).

Figure 1: Hip, knee, and ankle sagittal plane joint angles from toe off to toe off (TO) for IL (solid blue line) and PL (dotted red line).

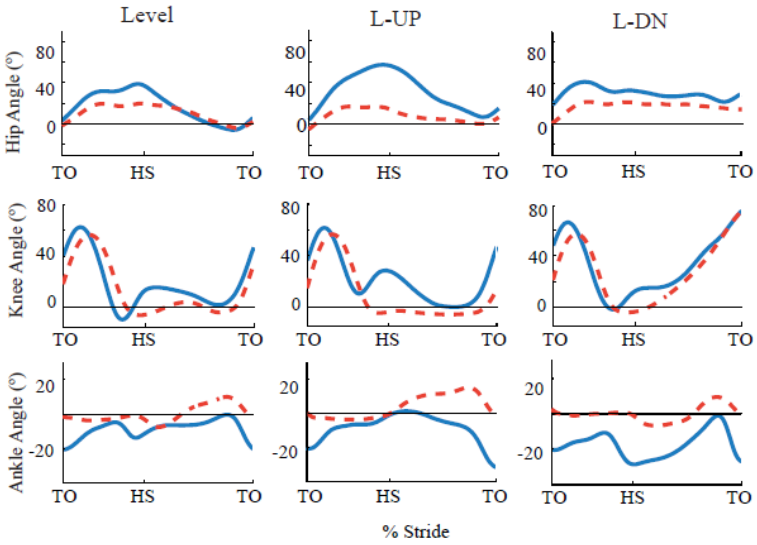

As hypothesized, EMG activity of the LG was significantly greater for the IL as compared to the control group (CL) during both L-UP and L-DN conditions. This is likely due to the increased demand of the IL, which must provide greater propulsion and stability as compared to the CL. Also, during the L-DN condition, BF activity of the IL was 29% greater than the CL during terminal swing. However, VL activity was significantly less during initial stance. Overall, muscle activity in the IL was not consistently greater than the CL, but due to the large hip range of motion it is likely that the muscles of the hip were more active in the IL and PL of the participant.

CONCLUSIONS

Although this case study examined an experienced athlete using an advanced prosthesis, there were still numerous asymmetric gait characteristics. Uphill transitions increased propulsion requirements in the IL as the joint range of motion and step length were greater than the PL. During the downhill transition, there was less anterior-posterior stability as speed and step length decreased in both limbs and there was little co-activation of the thigh muscles in the IL during stance.

REFERENCES

1.Hafner BJ, et al. *Arch Phys Med Rehab* **88**, 207-217, 2007.
2.Gottschall JS, et al. *J Appl Biomech*, submitted.
3.Gottschall JS. *J Neurophys*, submitted

Table 1: Temporal spatial parameters of intact limb (IL) and prosthetic limb (PL), mean (standard deviation). Bold values represent significant differences ($p < 0.05$). *PL two trials only.

	Speed (m/s)		Step Length 1 (m)		Step Length 2 (m)		Stance Time (s)	
	IL	PL	IL	PL	IL	PL	IL	PL
Level	1.36 (0.01)	1.36 (0.03)	**0.71** (0.02)	**0.64** (0.01)	**0.71** (0.03)	**0.64** (0.02)	**0.70** (0.02)	**0.60** (0.02)
L-UP*	1.21 (0.11)	1.18 (0.04)	**0.76** (0.04)	**0.54** (0.06)	0.74 (0.01)	0.35 (0.05)	0.76 (0.06)	0.62 (0.02)
L-DN	**0.086** (0.07)	**1.00** (0.10)	0.55 (0.07)	0.57 (0.08)	0.47 (0.02)	0.43 (0.06)	**0.85** (0.03)	**0.65** (0.01)

Table 2: Muscle activity during the specified phase for the intact limb (IL) of the amputee and the left leg of the control group (CL)[3], mean (standard deviation). All values are a percent difference from level walking of the same limb. Bold values represent significant differences ($p < 0.05$).

	TA initial swing (%)		LG midstance (%)		BF terminal swing (%)		VL initial stance (%)	
	IL	CL	IL	CL	IL	CL	IL	CL
L-UP	126.7 (50.4)	138.9 (75.7)	**205.2 (17.0)**	**150.8 (31.5)**	92.3 (26.0)	124.2 (58.5)	137.4 (18.8)	144.4 (40.1)
L-DN	81.5 (42.3)	109.3 (52.1)	**258.6 (78.4)**	**91.7 (22.1)**	**109.9 (17.2)**	**80.5 (22.7)**	**78.6 (12.8)**	**125.3 (34.5)**

INDIVIDUAL MUSCLE FUNCTION IN BELOW-KNEE AMPUTEE WALKING

Anne K. Silverman and Richard R. Neptune

Department of Mechanical Engineering, The University of Texas at Austin, Austin, TX, USA
email: asilverman@mail.utexas.edu, web: http://www.me.utexas.edu/~neptune

INTRODUCTION

Below-knee amputees lose the functional use of the ankle plantar flexors, which are important for providing body support and forward propulsion in non-amputee walking [1]. In the absence of the ankle-plantar flexors, compensations from other muscle groups are needed to provide these necessary walking subtasks. Experimental studies have shown that a variety of compensatory mechanisms are used in amputee gait, such as increased net joint power and work from the residual hip extensors and the intact ankle plantar flexors [2]. Increased muscle activity has also been observed in the knee extensor and biarticular hamstring muscles [3]. However, the biomechanical function of these compensations is not well-understood. The purpose of this study was to use 3D musculoskeletal modeling and simulations of amputee walking to assess individual muscle contributions to body support and forward propulsion to understand how amputees compensate for the lost ankle plantar flexors.

METHODS

A 3D musculoskeletal model with 14 rigid body segments, 23 degrees of freedom, and 38 Hill-type musculotendon actuators per leg was developed in SIMM (MusculoGraphics, Inc.). Musculoskeletal geometry was based on that of Delp et al. [4]. The ankle muscles on the residual leg were removed and the mass and inertial properties of the residual leg were modified to represent a nominal below knee amputee [5]. The prosthesis stiffness was modeled as a second-order passive spring (Eq.1)

$$\tau = a_0 + a_1\theta + a_2\omega + a_3\theta^2 + a_4\theta\omega \qquad (1)$$

where θ is the ankle angle, ω is the ankle velocity, and τ is the ankle torque. Constants a_0–a_4 (Eq. 1) were determined using a multiple regression analysis of the experimental data (see below).

The excitation of each muscle was defined with a bimodal excitation pattern. A simulated annealing algorithm was used to identify the optimal excitation patterns to emulate the experimental body segment kinematics and ground reaction forces (GRFs). Each muscle had six optimization parameters including onset, offset and amplitude of the two modes. To provide data for the optimization algorithm, kinematic and kinetic data were collected from 14 below-knee amputees walking overground at 1.2 ± 0.06 m/s [2]. The kinematic and GRF data were then averaged across subjects to produce a nominal amputee walking pattern.

Muscle contributions to body support and forward propulsion were quantified by their contributions to the vertical and anterior/posterior (A/P) GRFs, respectively. Individual muscles were then arranged into muscle groups based on anatomical location and muscle function (e.g., three vasti muscles combined into one vasti group). Muscle contributions were analyzed during residual leg stance.

RESULTS AND DISCUSSION

The residual leg vasti, gluteus medius and gluteus maximus muscles were the largest contributors to body support in early and mid-stance (Fig. 1), which was consistent with previous non-amputee simulation studies [6, 7]. The vasti muscles have also been shown to have increased muscle activity in amputee walking [3]. The prosthesis contributed to support throughout stance (Fig. 1), which was consistent with a previous simulation study of 2D symmetric amputee walking showing contributions from the prosthesis to trunk support [8].

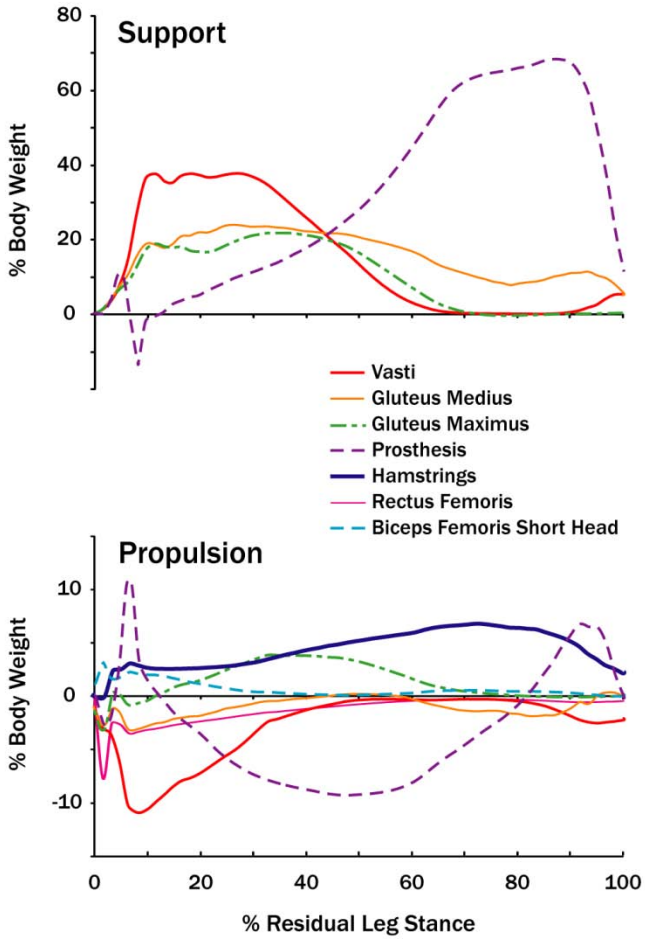

Figure 1: Amputee muscle contributions to body support and forward propulsion over the residual leg stance phase.

The residual leg hamstring muscles were the primary contributors to forward propulsion throughout residual leg stance (Fig. 1). This was consistent with previous non-amputee walking simulation studies that have shown the biarticular hamstrings to contribute positively to the A/P GRF throughout the stance phase [6]. In addition, experimental amputee studies have shown prolonged muscle activity of the hamstrings on the residual leg in early stance [3] and increased hip joint powers and work from the hip extensors to reduce the residual leg braking A/P GRF [2].

In early stance, the biceps femoris short head contributed positively to propulsion, while the rectus femoris, vasti muscles and gluteus medius contributed negatively to propulsion (Fig. 1). In mid-stance, the residual leg gluteus maximus contributed substantially to propulsion (Fig. 1), which has previously been shown in non-amputee walking studies [6]. The prosthesis contributed to propulsion in late stance (Fig. 1) as it returned elastic energy stored in early stance. Previous 2D simulation analyses showed that the prosthesis acts primarily to transfer energy from the leg to the trunk to provide trunk support and forward propulsion in late residual leg stance [8].

CONCLUSIONS

The prosthesis provided considerable propulsion and support in the amputee simulation, but compensations from other muscles were necessary to compensate for the lost ankle muscles. Contributions from the residual leg vasti, gluteus medius and gluteus maximus to support were needed. The amputee simulation also showed contributions of the residual leg hamstrings and gluteus maximus to forward propulsion. Thus, improving the output of these muscles may help improve rehabilitation outcomes and amputee mobility.

REFERENCES

1. Neptune RR, et al. *J Biomech* **34**, 1387-1398, 2001.
2. Silverman AK, et al. *Gait Posture* **28**, 602-609, 2008.
3. Fey NP, et al. *J Electromyogr Kinesiol* **20**, 155-161, 2010.
4. Delp SL, et al. *IEEE Trans Biomed Eng* **37**, 757-767, 1990.
5. Mattes SJ, et al. *Arch Phys Med Rehabil* **81**, 561-568, 2000.
6. Neptune RR, et al. *Gait Posture* **19**, 194-205, 2004.
7. Liu MQ, et al. *J Biomech* **39**, 2623-2630, 2006.
8. Zmitrewicz RJ, et al. *J Biomech* **40**, 1824-1831, 2007.

ACKNOWLEDGEMENTS

This work was supported by National Science Foundation Graduate Research Fellowship and Grant No. 0346514.

FAILED TRIP RECOVERIES OF ABOVE-KNEE AMPUTEES SUGGEST POSSIBLE FALL-PREVENTION INTERVENTIONS

[1] Jeremy R. Crenshaw, [2] Kenton R. Kaufman and [1] Mark D. Grabiner

[1] University of Illinois at Chicago, Chicago, IL , USA
[2] Mayo Clinic, Rochester, MN, USA
email: jcrens2@uic.edu, web: http://www.uic.edu/ahs/biomechanics/

INTRODUCTION

During a one year period, 66% of adults with an above-knee (AK) amputation reported falling [1]. This high incidence of falls necessitates an understanding of fall mechanisms from which rehabilitation and prosthesis design can be amended.

Recovery step length (L_{step}), trunk flexion velocity (*TFV*), and vertical height of the hips (z_{pelvis}) have discriminated trip related falls and recoveries in older, non-amputee adults [2]. The stance limb of the recovery step, i.e., the support limb, provides the initial recovery response that influences these variables. The support limb increases z_{pelvis}, allowing for a long L_{step}, and reduces angular momentum, limiting *TFV* [3]. A prosthetic limb (PL) may not adequately fulfill these roles. Conversely, despite the non-prosthetic limb (NPL) providing adequate support, a recovery step with a PL may be inadequate due to a lack of active control of the PL's knee and ankle.

Previously, we reported that, when the NPL was obstructed during the swing phase, an AK amputee used a "hopping strategy" that relied entirely on the NPL for the recovery step [4]. By avoiding the use of the PL, the available recovery strategies become limited. Further, the hopping strategy may not be viable for all amputees. The purpose of the present study was to further identify recovery strategies and mechanisms that lead to trip-related falls in people with an AK amputation.

METHODS

Three women and two men (age: 43±10.7 years, height: 172±12 cm, mass: 79.7±22.3 kg) with unilateral, AK amputations participated in this study. Four subjects used prostheses with a microcomputer controlled knee (C-Leg®, Otto Bock, Minneapolis, MN), and one subject (subject 5) used a prosthesis with a hydraulic knee (Mauch SNS®, Ossur, Aliso Viejo, CA).

Subjects were tripped as they walked through a motion capture volume by a concealed obstacle that rapidly elevated to 5 cm above the floor. Two trips were attempted for each subject so that the PL and NPL were each obstructed once. Falls were prevented by an instrumented safety harness. Successful trips were classified as a recovery, fall, or rope-assist. Falls corresponded to the subject being unambiguously supported by the safety harness. If more than 10% BW·s was recorded by the safety harness load cell 1 s after the trip the trail was labeled as rope assists.

RESULTS AND DISCUSSION

Seven trip attempts were successful, resulting in 4 trips of the PL and 3 trips of the NPL (Table 1).

1. Obstruction of the prosthetic limb. All trips of the PL were met with a lowering strategy, in which the obstructed limb was lowered to the ground as a support limb. Obstacle contact occurred at or after 50% of the unobstructed swing time, so a lowering strategy, which is appropriate for a trip during late swing, was most likely the correct response [5]. Despite a suitable strategy, the trips resulted in a fall or rope assist. z_{pelvis} of the failed recoveries was lower than when the support limb was the NPL, and similar to values observed in older adult fallers (Table 1). The lower z_{pelvis} coincided with knee flexion of the prosthetic support limb (Figure 1). Conversely, the NPL support limbs elevated the hips by extending the knee and ankle.

2. Obstruction of the non-prosthetic limb. When the NPL was obstructed, subjects demonstrated three recovery strategies (Table 1). Subject 2 fell when attempting a lowering strategy, demonstrating a short L_{step} and large *TFV* (Table 1). When the NPL was obstructed in late swing (64.3%), Subject 3 unsuccessfully attempted an elevating strategy by taking a recovery step with the obstructed limb. A lowering strategy may have been a more appropriate response. Furthermore, the PL as a support limb insufficiently arrested forward momentum, as is evident by a large peak *TFV* (165 deg/s), and shortened L_{step} by providing limited plantarflexion (Table & Figure 1). As previously reported, a hopping strategy was attempted by Subject 1, but resulted in a rope assist, which was associated with a L_{step} and *TFV* similar to that resulting in a fall in older adults (Table 1) [4].

CONCLUSIONS

All subjects fell or used the harness to recover from a trip. When the PL was obstructed, failed lowering strategies were associated with an inappropriate response of the prosthesis marked by knee flexion. When the NPL was obstructed, the subjects either avoided use of the prosthesis, attempted an inappropriate strategy, or responded with a short L_{step} and large *TFV*. These results suggest opportunities for fall prevention through improvements in the prosthetic knee design, as well as rehabilitation to promote reliance on the prosthesis, a longer L_{step}, and less *TFV*.

ACKNOWLEDGEMENTS

Funding by Otto Bock Healthcare, Minneapolis, MN

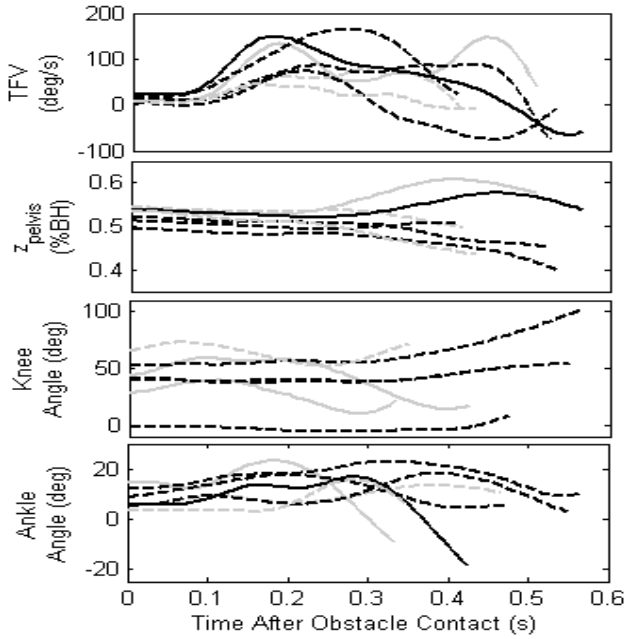

Figure 1: *TFV* & z_{pelvis} from obstacle contact to recovery step completion. Knee & ankle angle from obstacle contact to support limb toe off. An increase in angle represents joint flexion. Black lines represent falls. Grey lines represent rope assists. Dashed lines denote a prosthetic support limb. Solid lines denote a non-prosthetic support limb.

REFERENCES

1. Miller WC, et al. *Arch Phys Med Rehabil* **82**, 1031-1037, 2001.
2. Pavol, MJ, et al. *J Gerontol* **56A**, M428-M437, 2001.
3. Pijnappels M, et al. *J Biomech* **37**, 1811-1818, 2004.
4. Crenshaw JR, et al. *Proceedings of NACOB'08*, Ann Arbor, MI, USA, 2008.
5. Eng, JJ et al. *Exp Brain Res* **102**, 339-349, 1994.

Table 1: Descriptions and kinematic variables at the recovery step of each trip, as well as comparable variables from older adults [2]. Body height = BH; [#]Reported as HipHAT COM velocity.

Obstructed Limb	Strategy	Outcome[subject]	L_{step} (%BH)	*TFV* (deg/s)	z_{pelvis} (%BH)
Prosthetic Limb	Lowering	Rope Assist[1]	33.1	-13.4	49.8
		Rope Assist[5]	47.9	-9.6	43.4
		Fall[3]	36.9	-6.6	40.0
		Fall[4]	52.1	-76.1	45.1
Non-Prosthetic Limb	Lowering	Fall[2]	32.9	-57.4	56.7
	Elevating	Fall[3]	31.9	23.2	50.5
	Hopping	Rope Assist[1]	27.6	37.4	57.7
Older Adults	Lowering	Fall	36.9 ± 8.3	81.6 ± 41.4[#]	47.2 ± 4.5
		Recovery	49.4 ± 5.7	-43.0 ± 52.8[#]	54.5 ± 2.3
	Elevating	Fall	51.8	36.7[#]	51.1
		Recovery	49.8 ± 5.6	26.6 ± 8.3[#]	54.5 ± 1.5

VIRTUAL PROTOTYPING FUNCTIONAL CHARACTERISTICS OF A PASSIVE-DYNAMIC ANKLE FOOT ORTHOSIS

[1]Elisa S. Schrank, [2]John Tierney, [3]Lakisha D. Guinn, [3]Kota Takahashi, [3]Alexander R. Razzook and [1,3,4]Steven J. Stanhope

[1]Department of Mechanical Engineering, University of Delaware, Newark, DE, USA
[2]Center for Composite Materials, University of Delaware, Newark, DE, USA
[3]Biomechanics and Movement Science Program, University of Delaware, Newark, DE, USA
[4]Department of Health, Nutrition and Exercise Sciences, University of Delaware, Newark, DE, USA
email: schranke@udel.edu, web: http://www.udel.edu

INTRODUCTION

Virtual engineering (prototyping) is the integration of geometric models and engineering tools within a computer generated environment [1]. Computer aided design (CAD) enables the virtual modeling and design modification of physical parts. CAD models can be fabricated via selective laser sintering (SLS), a rapid freeform manufacturing technique [2]. Finite element analysis (FEA) tools have been used to explore changes in part geometries to obtain desired functional characteristics of an ankle brace and a prosthetic foot [3,4]. Combining SLS manufacturing with techniques to iteratively optimize fully parameterized virtually prototyped CAD models has the potential to transform the manufacturing of personalized rehabilitation devices.

Passive-dynamic ankle foot orthoses (PD-AFOs) are a class of rehabilitation devices that provide plantar flexion assistance via a spring-like action. We have designed a fully parameterized virtual PD-AFO prototype, which consists of three main components: a footplate, strut and cuff, connected by a set of upper and lower spans (Fig. 1).

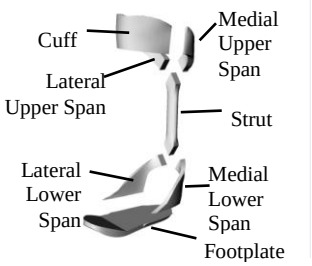

Figure 1: PD-AFO Design.

The CAD prototype is one element of a PD-AFO automated customization and manufacturing framework (Fig. 2) for rapidly customizing and ultimately manufacturing a fit- and function-customized PD-AFO. This paper highlights a sub-method of that framework which uses CAD parameterization and FEA techniques to evaluate and iteratively optimize the PD-AFO's functional characteristics.

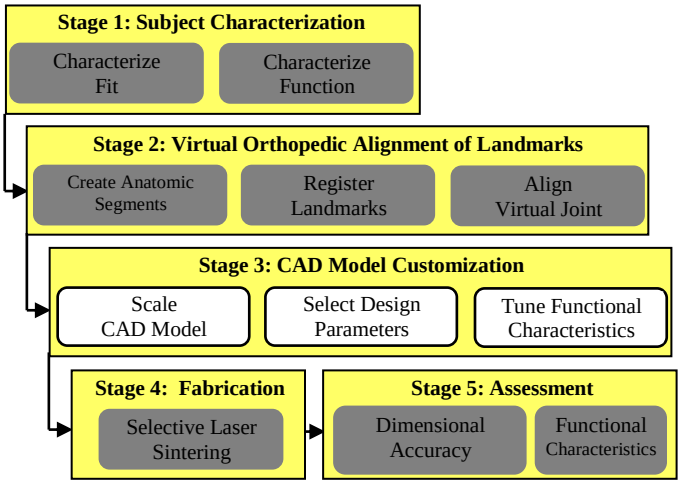

Figure 2: PD-AFO Automated Customization and Manufacturing Framework.

METHODS

CAD Model: The fully parameterized PD-AFO CAD model was constructed in CATIA V5R19 (Dassault Systèmes, Vélizy-Villacoublay, France) and customized for a healthy female (height: 1.62 m; mass: 63.5kg.). 3D locations of orthopedically-aligned landmarks describing the subject's size and shape were obtained via our automated fit customization method [1]. A footplate profile made of a 2D spline that connected the digitized anatomical landmarks on the foot perimeter controlled the footplate shape. The inner cuff surface was formed as a multi-section surface of 4 rows of 3D splines connecting the digitized cuff landmarks. The strut was sized as a function of

shank length and shaped by 11 parallel, joined, 2D profiles. The footplate, cuff, and strut were connected by a set of upper and lower spans constructed as multi-section surfaces. Examples of select parameterized characteristics include footplate and cuff thicknesses, footplate and cuff padding offsets, strut offset and span thicknesses.

A three-component CAD assembly, consisting of the PD-AFO, a cuff insert and a testing rod (Fig. 3a), was constructed so the analytical stiffness conditions mimicked the future experimental stiffness testing setup (Fig. 3b). All three assembly components were meshed with an Octree tetrahedron mesh, and mesh sizes were refined as needed to generate smooth meshes. The testing rod was constrained at the virtual ankle joint center with a frictionless hinge joint, allowing only sagittal plane rotation. The cuff to cuff insert interface was constrained with a fastened connection. The cuff insert to testing rod interface was constrained with a sliding connection, which allowed pistoning. The bottom of the footplate was clamped, and a load normal to the testing rod's longitudinal axis that remained in the sagittal plane was applied to the distal end of the testing rod.

Functional Characteristics Tuning: The functional aspects of the virtual prototype addressed were torsional stiffness, cuff pistoning and the cuff-shank interface (CSI). Torsional stiffness was the ratio between the moment about the testing rod hinge and the angular deformation of the outer center surface of the cuff. The angular deformation was calculated using the translational displacement of the outer center cuff surface in the frontal plane predicted by the FEA. Pistoning was the longitudinal motion of the cuff insert relative to the testing rod during loading. Status of the CSI was determined by the amount of gapping between the testing rod and cuff insert surfaces and the pressure distribution over the inner cuff.

The set of parameters controlling strut cross-sectional area and span thicknesses were iteratively explored to obtain the desired stiffness and minimize pistoning and CSI measures (Fig. 3c).

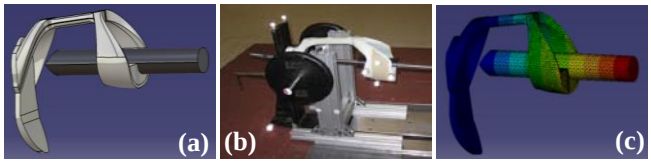

Figure 3: PD-AFO Functional Characteristics Tuning. (a) CAD model assembly with PD-AFO, cuff insert and testing rod. (b) experimental stiffness testing setup. (c) FEA-predicted translational displacement of tuned virtual PD-AFO prototype with applied loads.

RESULTS AND DISCUSSION

Within the virtual environment, a 100N load was applied to the testing rod, initially resulting in a higher-than-targeted stiffness (7.11 Nm/deg), pistoning (2.17 mm/deg), cuff-rod gapping and an uneven pressure distribution at the CSI. Uniformly decreasing the strut cross-sectional area parameter reduced the stiffness to 4.10 Nm/deg. Reducing the lower span thickness parameter decreased pistoning (1.34 mm/deg) and improved CSI indicators (pressure distribution over the cuff), resulting in 13.5° of deformation and a final target stiffness of 3.38 Nm/deg.

Future efforts will automate the optimization process and validate the virtual prototyping process by fabricating the PD-AFO and cuff insert via SLS using DuraForm® EX Natural Plastic (3DSystems, Rock Hill, SC, USA) and experimentally test the functional PD-AFO characteristics.

REFERENCES

1. Wikipedia.com
2. Schrank ES, et al. *Proceedings of ASB'09*, State College, PA, USA, 2009.
3. Faustini MC, et al. *IEEE Trans Biomed Eng*, **55(2)**, 784-90, 2008.
4. South BJ, et al. *J Biomech Eng*, **132(1)**, 1-6, 2010.

ACKNOWLEDGEMENTS

This material is based upon work supported under a National Science Foundation Graduate Research Fellowship and by the University of Delaware.

DIFFERENCES IN SAGITTAL PLANE ANGULAR MOMENTUM BETWEEN BELOW-KNEE AMPUTEES AND NON-AMPUTEES ACROSS A RANGE OF WALKING SPEEDS

Anne K. Silverman and Richard R. Neptune

Department of Mechanical Engineering, The University of Texas at Austin, Austin, TX, USA
email: asilverman@mail.utexas.edu, web: http://www.me.utexas.edu/~neptune

INTRODUCTION

The regulation of whole-body angular momentum is important to prevent falls and recover from trips [1, 2]. Previous studies have shown that the ankle muscles are critical in the regulation of angular momentum. For example, when recovering from a trip, fallers have a reduced peak ankle plantar flexor moment relative to non-fallers [2], which limited their ability to restrain their forward angular momentum. Below-knee amputees have an increased risk and fear of falling relative to non-amputees [3], which may be due to their lack of ankle muscles to help regulate their angular momentum. The purpose of this study was to identify differences in sagittal plane, whole-body angular momentum between below-knee amputees and non-amputees over a wide range of steady-state walking speeds. We analyzed angular momentum across different walking speeds to further highlight differences between amputees and non-amputees, as the regulation of angular momentum has been shown to vary with walking speed [4].

METHODS

Kinematic and kinetic data were collected from twelve amputee and ten control subjects walking at 0.6, 0.9, 1.2, and 1.5 m/s [5]. Kinematic data were collected using an 8-camera motion capture system (Vicon) and a cluster marker set at 120 Hz. Ground reaction force (GRF) data were collected using four AMTI force plates embedded in a 10-m walkway at 1200 Hz. Data were processed in Visual3D (C-Motion). Kinematic and GRF data were low-pass filtered with a cutoff frequency of 6 Hz and 20 Hz, respectively. An inverse dynamics model was used to find the center of mass location and velocity of eight body segments including the left and right thighs, shanks, feet, pelvis and torso. The calculation of whole body angular momentum about the body center of mass was determined as:

$$\vec{H} = \sum_{i=1}^{n}\left[\left(\vec{r}_{CM}^{\,i} - \vec{r}_{CM}\right) \times m_i\left(\vec{v}_{CM}^{\,i} - \vec{v}_{CM}\right) + I^i\vec{\omega}^i\right] \quad (1)$$

where $\vec{r}_{CM}^{\,i}$, $\vec{v}_{CM}^{\,i}$ and $\vec{\omega}^i$ are the position, velocity and angular velocity vectors of the *i*-th segment's center of mass in the laboratory coordinate system, $\vec{r}_{CM}$ and $\vec{v}_{CM}$ are the position and velocity vectors of the total body center of mass in the laboratory coordinate system, and m_i and I_i are the mass and moment of inertia of each body segment.

Angular momentum was normalized by body mass (kg), walking speed (m/s) and body height (m) and then normalized to the intact leg gait cycle for amputees and the right leg gait cycle for non-amputees. Trials were then averaged at each speed for each subject. Sagittal plane angular momentum was defined as positive when directed counterclockwise (torso tilting backward) and negative when directed clockwise (torso tilting forward).

The range of angular momentum, defined as the peak to peak value, in the first and second halves of the gait cycle was compared between groups and across speeds using two, two-factor ANOVAs. The first factor (group) had two levels: amputee and non-amputee. The second factor (speed) had four levels: 0.6, 0.9, 1.2 and 1.5 m/s. When significant differences were found, pair-wise comparisons using a Bonferroni adjustment for multiple comparisons were performed to determine which conditions were significantly different ($\alpha = 0.05$).

RESULTS AND DISCUSSION

There were significant differences in the range of angular momentum between the amputee and non-amputee subjects across speeds (Fig. 1).

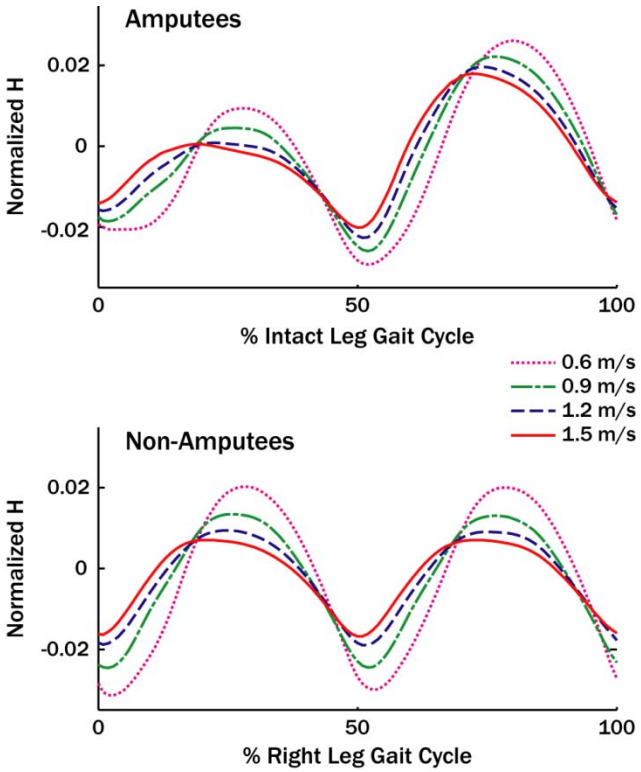

Figure 1: Average sagittal plane angular momentum across walking speeds for amputees and non-amputees.

In the first half of the gait cycle, there were significant group ($p<0.001$), speed ($p<0.001$), and interaction ($p=0.001$) effects on the range of angular momentum. The range was significantly smaller in the amputees compared to non-amputees at all four walking speeds ($p\leq0.039$), resulting in a more negative (forward) angular momentum in amputees (Fig. 1). The range of angular momentum significantly decreased with walking speed for both amputees and non-amputees ($p<0.001$), except with the amputees between 1.2 and 1.5 m/s.

In the second half of the gait cycle, there were also significant group ($p=0.003$), speed ($p<0.001$), and interaction ($p<0.001$) effects on the range of angular momentum. However, in the second half of the gait cycle, the range was significantly larger in the amputees compared to non-amputees at 0.9, 1.2 and 1.5 m/s ($p\leq0.004$). The range significantly decreased with each increase in speed for both groups ($p<0.001$).

Previous studies have shown that there is a smaller propulsive GRF from the residual leg during early intact leg stance (late residual leg stance) compared to non-amputees [5]. A reduced propulsive GRF decreases the positive external moment on the body and corresponding positive rate of change in angular momentum. Similarly, there is a reduced residual leg braking GRF in the second half of the intact leg gait cycle [5] that acts to decrease the negative external moment, which increases the positive rate of change in angular momentum. To assess if the reduced residual leg propulsion is associated with the smaller range in amputee angular momentum in early stance (Fig. 1), a post-hoc Pearson correlation analysis was performed between the peak residual leg propulsive GRF and the range of angular momentum in the first half of the gait cycle at each walking speed. A significant correlation was found at each walking speed ($0.44 \leq r \leq 0.7$, $p\leq0.04$). The analysis was also performed with the peak residual leg braking GRF and the range of angular momentum in the second half of the gait cycle, and a significant correlation was found for 0.9, 1.2 and 1.5 m/s ($0.63 \leq r \leq 0.7$, $p\leq0.002$).

CONCLUSION

These results indicate there are differences in how amputees regulate their angular momentum compared to non-amputees. The lack of residual leg propulsion results in more negative (forward) angular momentum in the first half of the gait cycle. To compensate, reduced residual leg braking in the second half of the gait cycle increases the positive (backward) angular momentum to help restore the momentum balance. Thus, decreased residual leg braking appears to be an important mechanism to regulate angular momentum in amputee walking.

REFERENCES

1. Simoneau GG, et al. *J Appl Biomech* **16**, 1-13, 2000.
2. Pijnappels M, et al. *Gait Posture* **21**, 388-394, 2005.
3. Miller WC, et al. *Arch Phys Med Rehabil* **82**, 1031-1037, 2001.
4. Bennet BC, et al. *Hum Mov Sci* **29**, 114-124, 2010.
5. Silverman AK, et al. *Gait Posture* **28**, 602-609, 2008.

ACKNOWLEDGEMENTS

This work was supported by National Science Foundation Graduate Research Fellowship and Grant No. 0346514.

A PNEUMATICALLY POWERED PORTABLE ANKLE-FOOT ORTHOSIS

[1]K. Alex Shorter, [2]Géza F. Kogler, [3]Eric Loth, [4]William K. Durfee, and [1]Elizabeth T. Hsiao-Wecksler

[1]University of Illinois, Urbana, IL, USA, [2]Georgia Institute of Technology, Atlanta, GA, USA,
[3]University of Virginia, Charlottesville, VA, USA, [4]University of Minnesota, Minneapolis, MN, USA
email: shorter2@illinois.edu, ethw@illinois.edu

INTRODUCTION

Ankle foot orthoses (AFOs) are designed to improve function in individuals with lower limb gait deficiencies. Current powered orthotic technology is used for rehabilitation, diagnostic or training devices to assist walking function, direct measurement of joint motion and force, and to perturb gait in locomotion studies [1]. However, these powered AFOs are tethered to external power supplies and cannot be used outside the laboratory or clinic. Because orthoses are an integral part of rehabilitation, innovative technology, such as portable powered orthotic systems, offer a new treatment modality to improve the functional outcome of rehabilitation. We present a novel portable powered AFO (PPAFO) to provide untethered assistance for in-home rehabilitation of the ankle-foot complex [2].

METHODS

The PPAFO is designed to assist impaired gait by: (1) controlling forefoot velocity at heel strike to prevent foot-slap, i.e., eccentric dorsiflexor assistance, (2) providing modest assistive torque for propulsion and stability at the end of stance, i.e., concentric plantarflexor assistance, (3) supporting the foot in the neutral position during swing to prevent foot-drop, i.e., concentric dorsiflexor assistance, and (4) allowing free range-of-motion during the rest of the gait cycle.

The first generation prototype was made from mostly off-the-shelf components (Fig. 1). A 255 g portable compressed liquid CO_2 bottle and pressure regulator (JacPac, Pipeline Inc., Waterloo) were used to power a dual-vane bidirectional rotary actuator (CRB2BW40; SMC, Noblesville, IN) at the ankle joint. The pressure regulator modulated plantarflexor torque for propulsion assistance. An additional pressure regulator (LRMA-QS-4; Festo, Hauppauge, NY) was used to modulate dorsiflexor torque for foot support during swing. The orthotic tibial and foot piece components are custom fabricated of carbon composite materials and serve as the structural elements of the system. A free motion ankle hinge joint connected the foot piece and tibial section on the medial aspect. Velcro straps secured the PPAFO to the leg and foot.

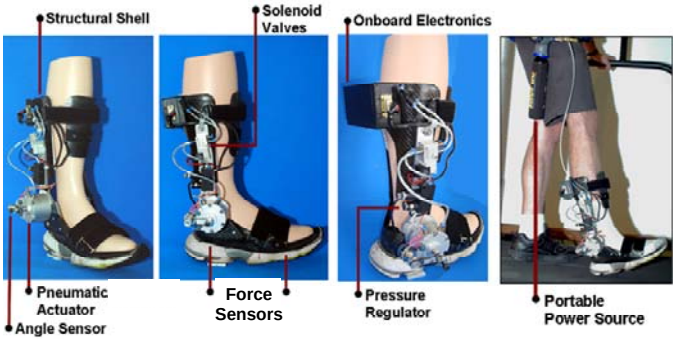

Figure 1: The bidirectional rotary actuator is pneumatically powered using CO_2, which is dispensed from a bottle worn by the subject on the waist (far right).

The direction of the torque could be switched between dorsiflexor and plantarflexor via two solenoid valves (VOVG; Festo, Hauppauge, NY). Switching control of the valves was selected based on specific events during the cycle. Event boundaries for loading response, mid stance, end of stance, and swing were determined using two force sensors (Interlink Electronics, Camarillo, CA) placed on the interface of the foot section under the heel and metatarsal heads. Onboard electronics (eZ430-F2013 microcontroller; Texas Instruments, Dallas, TX) and the portable power source allowed the PPAFO to provide untethered powered assistance. The prototyped weighs 3.2 kg (power supply = 1.2 kg and AFO = 1.9 kg).

The function of the orthosis was demonstrated on healthy individuals during treadmill walking trials. Three experienced treadmill walkers (male, 25±5 yrs) walked at three speeds (self selected, self selected +25%, and self selected -25%) with five footwear conditions (running shoes, PPAFO: no assistance, 30 psi, 50 psi, and 90 psi assistance). Testing found that the 30, 50, and 90 psi pressures corresponded to 2.8 ± 0.02 (SD), 5 ± 0.02, and 9.2 ± 0.05 Nm, respectively. Each subject first walked in their shoes followed by randomized order of the four PPAFO conditions. A trial was 90s in duration. Walking speeds were conducted in the order given above for each footwear condition. To determine the longevity of the system, one subject also walked with a full CO_2 bottle until it was empty. For this test, time and number of steps were recorded while wearing the PPAFO at the 30 psi condition.

Data were collected with a motion capture system at 150 Hz (Vicon, Oxford, UK Model 460), a split belt treadmill with embedded force plates at 1500 Hz (Bertec, Columbus, OH), two pressure transducers at 30 Hz (American Sensor Technology, Mt.Olive, NJ), and the PPAFO force sensors at 30 Hz.

RESULTS

The PPAFO provided functional assistance during the targeted phases of the gait cycle (Fig. 2A) : **(I)** prevention of foot-slap during loading response, **(II)** free range-of-motion early in stance, **(III)** modest plantarflexor assistive torque for propulsion late in stance, and **(IV)** prevention of foot-drop during swing. The sensing capabilities of the PPAFO (Fig. 2B) were successfully used for event detection. The kinematics of the ankle joint were minimally impacted during assisted walking (Fig. 2C). Longevity trials showed that a full CO_2 bottle (255g) lasted 37 min at 30 psi assistance level (~1800 steps).

DISCUSSION AND CONCLUSIONS

Experimental results demonstrated that the PPAFO is capable of providing appropriately timed untethered powered assistance during gait. Unlike other powered orthoses, the untethered nature of the PPAFO would allow for in-home rehabilitation use. The PPAFO provides portability combined with the flexibility to modulate the direction (dorsal or plantar), timing, and magnitude of the assistance. Such diversity allows the orthoses to meet an individual's changing functional requirements, and offers promise as a clinical tool in many arenas of the rehabilitation process.

In the near term tests are planned on subjects with functional needs that would benefit from a powered orthoses. Additionally the performance and efficiency of the device will be improved through development of compact lightweight actuators and enhanced control schemes.

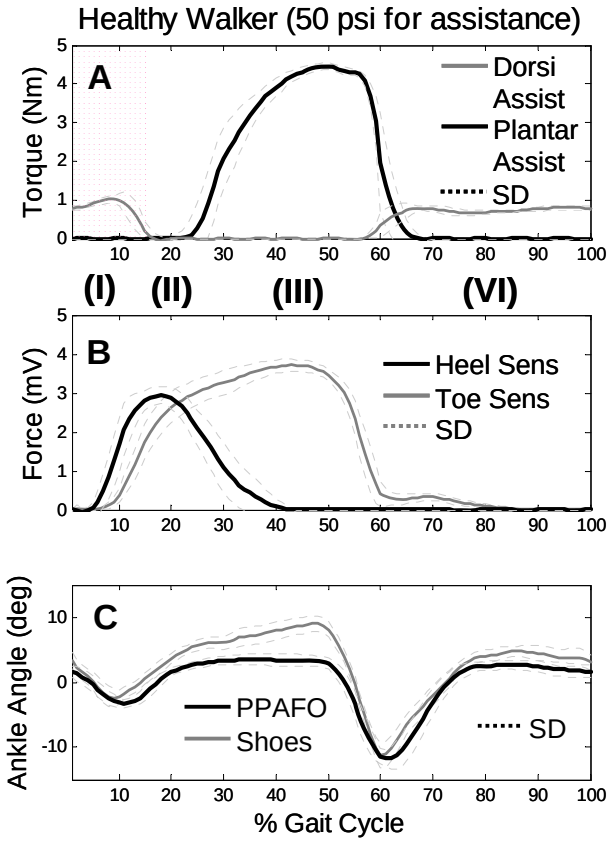

Figure 2: Averaged data (25 gait cycles) from a healthy walker at self-selected walking speed with a peak assistive torque of 4.4 Nm from an operating pressure of 50 psi. The data was normalized to stance and swing with toe off occurring at 60%.

REFERENCES

1. Krebs, H., et al., A paradigm shift for rehabilitation robotics. Eng. Med. Biol. Mag, IEEE, 2008.
2. Hsiao-Wecksler, E.T., et al., Portable powered ankle-foot-orthosis: Provisional Patent, USA.

ACKNOWLEDGEMENTS

This project is part of the Center for Compact and Efficient Fluid Power, an NSF Engineering Research Center (NSF grant #0540834). The authors thank David Li, Emily Morris, Henry Kohring, Joel Gilmer and Jason Thomas for their assistance.

LOWER EXTREMITY MECHANICAL WORK OF DIFFERENT PROSTHETIC FEET: AN IMMEDIATE RESPONSE CASE STUDY

Amanda Allen, Gary D. Heise, and Jeremy D. Smith

School of Sport and Exercise Science, University of Northern Colorado, Greeley, CO, USA, gary.heise@unco.edu

INTRODUCTION

Clinicians and prosthetists often evaluate the introduction of a new prosthesis by observing the gait of a lower limb amputee without the aid of a motion analysis system. Researchers examining differences in prosthetic limbs typically allow for long term adaptation to occur prior to testing (Graham et al., 2007). Limited data exist that focus on immediate kinetic responses to a new prosthetic limb. Noble and Prentice (2006) examined swing leg kinetics in nonamputees during treadmill walking immediately before and after the addition and removal of mass to the left lower limb. They identified immediate changes in mechanics that dissipated after 50 strides, but trial-to-trial changes were not examined because they used averages of 5 trials for analysis. In addition, Linden et al. (1999) introduced an approach that examined the biomechanical response of individual amputees to new prosthetic legs. Because amputees often exhibit unique gait patterns, they justified a statistical approach that tested differences of each subject rather than a group. The goal of the present study was to examine immediate joint kinetic changes during the initial strides of a unilateral, transtibial amputee after he was fitted to different prosthetic feet. Specifically, the mechanical work performed by the lower extremity joints during stance was examined immediately after a new prosthetic foot was introduced.

METHODS

A unilateral, transtibial amputee volunteered for this case study and provided consent in accordance with the local IRB (age = 46 yr, mass = 72.7 kg, height = 170 cm, post-amputation = 18 yr, cause = trauma from work-related accident). A certified prosthetist was present for fit and alignment of different prosthetic feet. After multiple overground walking trials at the participant's preferred speed and with his existing foot (BioQuest model), three additional conditions were examined: C1-True Life 1 (Seattle, low stiffness); C2-True Life 2 (Seattle, high stiffness); and C3-original BioQuest shank/ankle with a new foot plate (10 g less than original). For each new condition, the prosthetist fit and aligned the foot on the participant's endoskeletal prosthetic shank. The participant then completed overground walking trials immediately after the fit and alignment at his preferred speed of walking.

A single video camera recorded a sagittal-plane view of the participant as he contacted an AMTI force platform. Using coordinate data from a motion analysis system, ground reaction force data, and an inverse dynamics analysis, net joint moments were calculated for the ankle, knee, and hip during ground contact of 8 strides among the first 30 strides for each condition (4 strides for each side of the body). Mechanical power was calculated as the product of net joint moment and angular velocity at each joint. Mechanical work during stance was then quantified by integrating the power-time curves. Resulting positive and negative work values at the ankle, knee, and hip were compared across conditions for each limb. Repeated measures ANOVA was used to test for differences in gait speed and mechanical work.

RESULTS AND DISCUSSION

The participant walked slower than the original condition in two of the three foot conditions (see Table 1 below).

Table 1: Preferred walking speed ($m \cdot s^{-1}$) for each foot condition. * slower than Orig ($p < .05$)

	Orig	C1	C2	C3
Means	1.58	1.54	1.52*	1.47*
SDs	0.06	0.05	0.02	0.03

Mean positive and negative mechanical work values at the ankle, knee, and hip joints during stance for each prosthetic foot condition are shown in Figure 1. Compared to group data presented by Silverman et al. (2008), the subject of the present study produced greater positive work at the ankle in both limbs, less positive work at the hip in both limbs, and similar levels of positive work at the knee. The negative work at the hip was drastically different between limbs, which was inconsistent with the results of Silverman et al. (2008). In the intact limb, the greatest amount of negative work was observed at the knee joint which is in agreement with Silverman and colleagues.

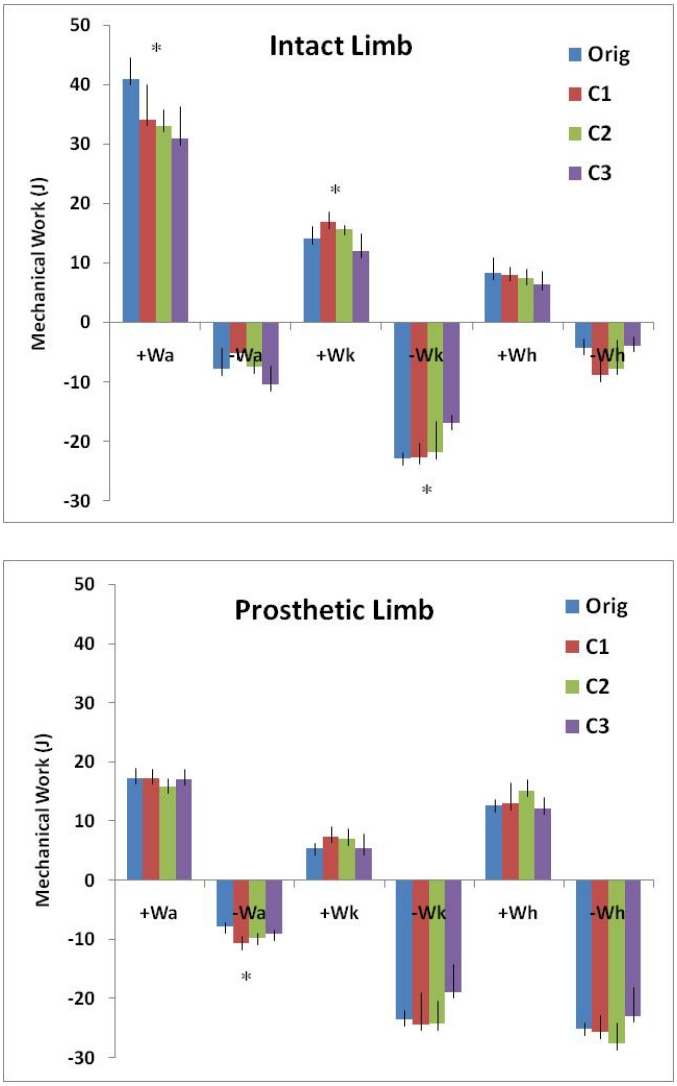

Figure 1: Mean positive and negative mechanical work at the ankle, knee, and hip of the intact limb (top) and prosthetic limb (bottom) for each foot condition. Statistical differences between conditions (*), but within each limb, are shown.

In the intact limb, statistical changes across foot conditions were limited to positive work at the ankle and knee and negative work at the knee. In the prosthetic limb, negative work at the ankle was the only measure that was statistically different across conditions (see Figure 1). Among these changes when comparing the two conditions that were similar in preferred walking speed (Orig & C1) but dissimilar in prosthesis type, the only statistical difference in mechanical work was the increase in negative work at the ankle in the prosthetic limb.

Overall, the gait strategy employed by the single subject of the present investigation relies on greater energy generation at the ankle and knee of the intact limb. In addition, greater energy generation and dissipation were found at the hip on the prosthetic side which is consistent with the results of Silverman et al. (2008). In general, this lower extremity mechanical energy pattern was not disrupted across foot conditions although some minor differences were noted.

CONCLUSIONS

An increase in negative mechanical work at the ankle on the prosthetic side was the only statistical difference between the original prosthetic foot condition and a novel, low stiffness foot condition (C1). Other changes in mechanical work were best explained by the decrease in preferred walking speed from initial to final conditions. Overall, when confronted with different prosthetic feet, more adaptations were made in the intact limb as compared to the prosthetic limb.

REFERENCES

1. Graham LE et al. *Arch Phys Med Rehabil*, **88**, 801-806, 2007.
2. Linden, ML van der et al. *J Biomech*, **32**, 877-889, 1999.
3. Noble JW & Prentice SD. *Exp Brain Res*, **169**, 482-295, 2006.
4. Silverman AK, et al. *Gait Posture* **28**, 602-609, 2008.

ACKNOWLEDGEMENTS

The authors appreciate the help of Ben Struzenburg, of Hanger Prosthetics and Orthotics.

GROUND REACTION FORCE CHARACTERISTICS OF DIFFERENT PROSTHETIC FEET: AN IMMEDIATE RESPONSE CASE STUDY

Gary D. Heise, Amanda Allen, Maryann Hoke, and Jeremy D. Smith

School of Sport and Exercise Science, University of Northern Colorado, Greeley, CO, USA,
gary.heise@unco.edu, jeremy.smith@unco.edu

INTRODUCTION

Adapting to a prosthetic limb is a profound challenge for an amputee regardless of age, overall health, or the reason for amputation. The majority of research that addresses the gait biomechanics of lower limb amputees uses cross-sectional research designs (e.g., Silverman et al., 2008). Prosthetists gain much from these cross-sectional studies and from research that examines the adaptation to new prosthetic limbs (Graham et al., 2007). Researchers examining differences in prosthetic limbs typically allow for long term adaptation to occur prior to testing (Graham et al., 2007). Motivated by the suggestions of clinicians, the present study examined the immediate response of a single, unilateral transtibial amputee to different prosthetic feet. In general, prosthetists do not use the tools of a gait lab to evaluate the fit and alignment of prosthetic legs. In addition, Linden et al. (1999) introduced an approach that examined the biomechanical response of individual subjects to new prosthetic legs. Because amputees often exhibit unique gait patterns, they justified a statistical approach that tested differences of each subject rather than a group. The purpose of the present study was to compare the GRF characteristics of different prosthetic limbs immediately after initial fit and alignment. Multiple trials for each condition were assessed for a single subject so that the mechanics of the initial strides could be assessed.

METHODS

A unilateral, transtibial amputee volunteered for this case study and provided consent (age = 46 yr, mass = 72.7 kg, height = 170 cm, post-amputation = 18 yr, cause = trauma from work-related accident). A certified prosthetist was present for proper fit and alignment of different prosthetic feet. After multiple overground walking trials at the participant's preferred speed and with his existing foot (BioQuest model), three additional conditions were examined: True Life 1 (Seattle, low stiffness); True Life 2 (Seattle, high stiffness); new BioQuest foot (foot plate 10 g less than original). For each new condition, the prosthetist fit and aligned the foot on the participant's endoskeletal prosthetic shank. The participant then completed overground walking trials immediately after the fit and alignment.

GRF data were recorded for four ground contacts for each foot condition and each limb (AMTI force platform, 480 Hz). The following variables were assessed for each trial: 1^{st} peak GRF_v; 2^{nd} peak GRF_v; AP-Braking Impulse; AP-Propulsive Impulse; Lateral Impulse; Vertical Loading Rate over the initial 0.05 s of contact. Repeated measures ANOVA was used to test for differences in gait speed (across conditions) and GRF variables (across limb and conditions). The probability of a Type I error was set at 0.05.

RESULTS AND DISCUSSION

The participant walked slower than the original condition in two of the three foot conditions (see Table 1 below).

Table 1: Preferred walking speed ($m \cdot s^{-1}$) for each foot condition. * slower than Orig ($p < .05$)

	Orig	C1	C2	C3
Means	1.58	1.54	1.52*	1.47*
SDs	0.06	0.05	0.02	0.03

The order presented in Table 1 was the order of testing, and so the decrease in preferred walking speed may be from fatigue. Mean peak GRF values and impulses are shown in Figures 1 and 2

respectively, and mean loading rate values are shown in Table 2.

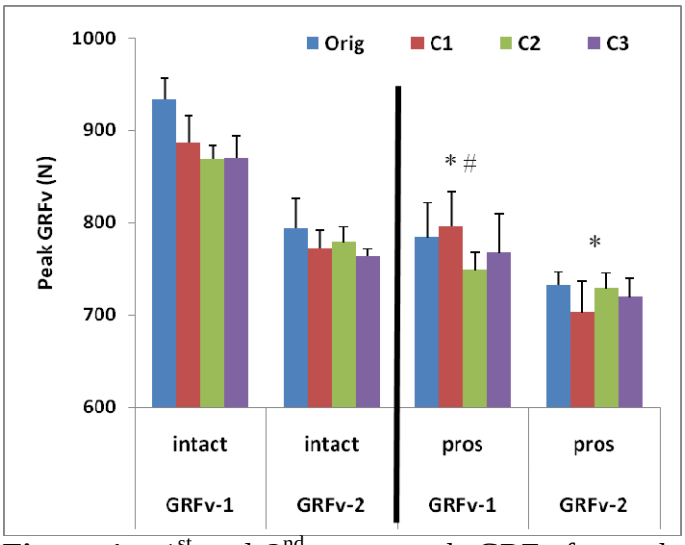

Figure 1: 1st and 2nd mean peak GRF_v for each limb and foot condition. Statistical differences between limbs (*) and conditions (#) are shown on the right side of the figure.

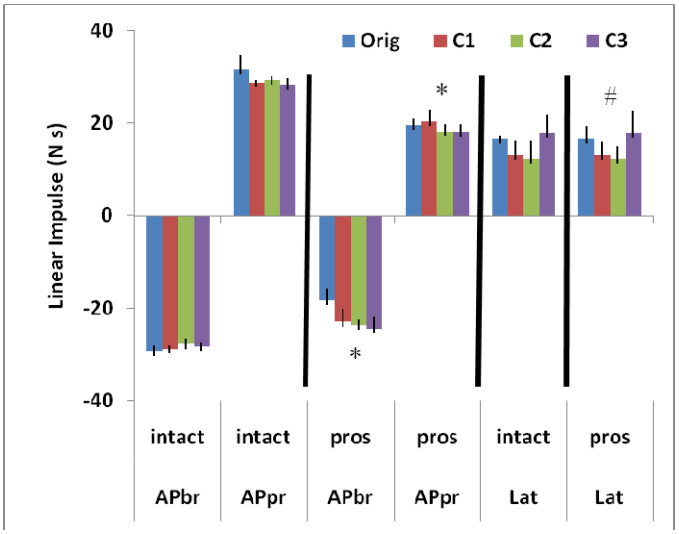

Figure 2: Mean linear impulse associated with AP-braking (APbr), AP-propulsion (APpr), and lateral GRF (Lat) for each limb and foot condition. Statistical differences between limbs (*) and conditions (#) are shown.

Intact limb peak vertical GRFs were greater than prosthetic limb and the initial peak was different across foot conditions (Figure 1). Braking and propulsive impulses also were greater in the intact limb (Figure 2), but no differences across conditions were found in these variables. Limb differences are consistent with previously reported group data (Sanderson & Martin, 1997) and individual data (Linden et al., 1999). Differences across conditions were limited to the initial GRF_v peak and lateral impulse. Loading rate was significantly greater in the intact limb and the Orig condition was greater than other foot conditions (see Table 2).

Table 2: Mean GRF_v loading rate ($kN \cdot s^{-1}$) for each limb and for each foot condition. *Intact > Prosthetic ($p < .001$). **Orig > C1, C2, C3 ($p < .05$)

	Orig**	C1	C2	C3
Intact*	12.5	12.1	11.2	11.1
SD	1.5	0.6	1.1	0.6
Prosthetic	7.5	5.7	6.5	6.9
SD	0.4	0.7	0.5	0.5

Taken collectively, the results presented here are consistent with others who reported higher GRFs in the intact limb compared to the prosthetic limb of unilateral amputees (e.g., Linden et al., 1999). Loading rate was identified as a discriminator between nonamputees who do and do not suffer chronic knee pain (Radin et al., 1991). Radin and colleagues suggested that higher loading rates may be a contributing factor to the development of osteoarthritis. Ironically, a reason given for amputees to increase the overall loading of the intact limb is to reduce, and thus spare, the residual limb from high loads (Sanderson & Martin, 1997).

CONCLUSIONS

The initial GRF_v peak, lateral impulse, and GRF_v loading rate displayed statistical differences across prosthetic foot conditions. The expected differences between intact and prosthetic limbs were not affected by different prosthetic feet.

REFERENCES

1. Graham LE et al.. *Arch Phys Med Rehabil*, **88**, 801-806, 2007.
2. Linden, ML van der et al. *J Biomech*, **32**, 877-889, 1999.
3. Radin EL et al. *J Orthop Research*, **9**, 398-405, 1991.
4. Sanderson DJ & Martin PE. *Gait Posture* **6**, 126-136, 1997.
5. Silverman AK, et al. *Gait Posture* **28**, 602-609, 2008.

ACKNOWLEDGEMENTS

The authors appreciate the help of Ben Struzenburg, of Hanger Prosthetics and Orthotics.

RELATIONSHIPS BETWEEN AMPUTEE INDEPENDENT PROSTHESIS PROPERTIES AND GAIT PERFORMANCE: A PRELIMINARY STUDY

Matthew Major, Martin Twiste, Laurence Kenney and David Howard

University of Salford, Greater Manchester, UK
email: MatthewJ.Major@Gmail.com, web: http://www.healthcare.salford.ac.uk/research

INTRODUCTION

The advancement of trans-tibial prosthetic design in the attempt to improve amputee gait performance has produced a wide range of alternative commercially available modular components. Achieving improved gait performance and prosthetic function depends on: a) the interface between amputee and prosthesis, and b) the mechanical properties of the prosthesis independent of the amputee. Although some previous studies have characterized Amputee Independent Prosthesis Properties (AIPP) [1], the vast majority of studies have only considered the effects of various trans-tibial components on in-vivo amputee performance [2]. However, without also characterizing the AIPP of these components, these studies can only indicate their relative performance, but cannot explain why a particular prosthesis performs better than the next and, hence, cannot directly inform prosthetic design. Furthermore, there exists little quantitative evidence that particular foot properties provide the user with a biomechanical or physiological advantage. Therefore, the aim of this study was to conduct a controlled investigation of the relationships between AIPP and the performance of the amputee during gait.

METHODS

A purpose-built foot-ankle mechanism (Figure 1) was designed for independent control of dorsiflexion (via forefoot spring) and plantar flexion (via rearfoot spring) stiffness properties. This allowed for a systematic investigation of the effects of AIPP on gait, without the problems associated with the use of different commercial products (i.e. inclusion of additional variables as well as stiffness). AIPP was characterized through a modified version of the roll-over shape model [3] and measured with a custom-designed test-rig [4]. Gait kinematics, temporal-spatial parameters, and oxygen consumption of five traumatic amputee subjects were measured. Additionally, the in-vivo roll-over shape and gait kinetics were measured using a 3-axis load cell installed between the pylon and socket. These parameters were observed while the subject walked with each of four combinations of dorsiflexion (DF) and plantar flexion (PF) stiffness of the foot-ankle mechanism (low DF and low PF stiffness (LOLO), low DF and high PF stiffness (LOHI), high DF and low PF stiffness (HILO) and high DF and high PF stiffness (HIHI)), and under the following gait conditions: self-selected and fast (150% of self-selected) walking speeds on a level surface, self-selected speed on 5% grade incline, and self-selected speed on 5% grade decline. The coefficient of variation (CV) was calculated for the swing duration of the prosthetic limb as an indication of relative gait stability. Results were statistically analyzed with the Friedman test for non-parametric repeated measures ANOVA (significance set at $p<=0.05$) and the Nemenyi post-hoc test.

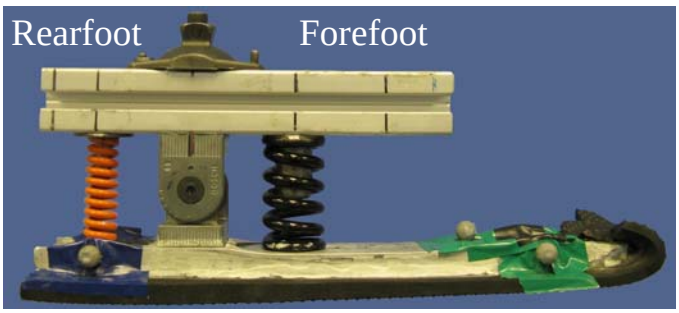

Figure 1: Prosthetic foot-ankle mechanism.

RESULTS AND DISCUSSION

The maximum PF angle observed during stance differed significantly between foot setups ($p<=0.33$ for self-selected and fast walking, $p<=0.77$ for incline and decline walking), with greatest PF associated with low PF stiffness of the foot-ankle

mechanism. Similarly, the maximum DF angle observed during stance differed significantly between foot setups ($p<=0.006$ for all walking conditions), with greatest DF associated with low DF stiffness of the foot-ankle mechanism. There appeared to be no noticeable and consistent difference in flexion of the prosthetic side knee between foot setups for each walking condition. However, averaged across all walking conditions, low DF stiffness produced approximately 4 degrees more flexion of the sound side knee than high DF stiffness during the loading phase of stance ($p<=0.006$ for fast, incline, and decline walking).

Prosthetic limb swing duration CV has previously proven to be a distinguishing factor between trans-tibial amputee fallers and non-fallers (fallers displayed increased CV) [5]. Foot setup LOHI consistently produced lower values of prosthetic limb swing duration CV across all walking conditions. Only for fast walking did the foot setup of HIHI reduce prosthetic limb swing duration CV. This might indicate that a stiffer prosthetic ankle improves stability at higher speeds. Participants consistently rated low DF stiffness as the most stable, and this was consistent with measures of gait symmetry (quantified by the ratio of swing duration time of the sound limb to prosthetic limb) as low DF produced the most symmetric gait.

For each walking condition, noticeable differences were found in metabolic Cost of Transport (ml O_2/kg/m) between some foot-ankle stiffness combinations (Table 1). Generally, low DF stiffness produced lower values of metabolic Cost of Transport (CoT) across all walking conditions. During incline walking, LOLO produced the lowest metabolic CoT, which may be explained by the need for low stiffness to facilitate smooth roll-over during stance when walking uphill. During decline walking, high PF stiffness produced greater metabolic CoT. During level walking at both speeds, the foot setup HIHI produced noticeably greater metabolic CoT. Despite these differences, very few setups were statistically significant from another which could be due to the small number of subjects. For each walking condition, the metabolic energy results were generally consistent with the subjective results of perceived levels of exertion.

This paper discusses the relationships between the amputee independent prosthesis properties and amputee performance. The novelty of this approach is that the methodology provides for a systematic exploration decoupled from the constraints imposed by the use of commercial products. A combination of experiments such as this and amputee gait simulation can be used to identify specific AIPP that optimize particular measures of amputee performance (e.g., stability, metabolic cost, and subjective measures) in order to develop improved prosthetic designs. It is likely that the objectives (underlying such optimisations) would differ between different amputee populations and further work is required to better understand these issues.

REFERENCES

1. van Jaarsveld H, et al. *Prosthet Orthot Int* **14**, 117-124, 1990.
2. Hafner B, et al. *Clin Biomech* **17**, 325-344, 2002.
3. Hansen A, et al. *Prosthet Orthot Int* **24**, 205-215, 2000.
4. Major MJ, et al. *J Biomech* **40**(S2), S595, 2007.
5. Vanicek N, et al. *Gait and Posture* **29**, 415-420, 2009.

Table 1: Metabolic CoT across all conditions. Statistical significance within walking condition is marked with an asterisk (*). SSWS is self-selected walking speed and FWS is fast walking speed.

Metabolic CoT (ml O_2/kg/m) [median (range)]	**Foot-Ankle Mechanism Setup**			
	LOLO	**LOHI**	**HILO**	**HIHI**
SSWS on Level	0.250 (0.019)	0.244 (0.008)*	0.235 (0.026)	0.261 (0.025)*
FWS on Level	0.211 (0.014)	0.208 (0.008)	0.206 (0.028)	0.225 (0.027)
SSWS on Incline	0.292 (0.006)	0.316 (0.012)	0.302 (0.064)	0.299 (0.033)
SSWS on Decline	0.194 (0.033)*	0.204 (0.020)*	0.198 (0.051)	0.204 (0.012)

Roll-Over Shape Dynamics During Stance in Natural Gait

[1]Kota Takahashi, [1]Alexander R. Razzook, [1]LaKisha D. Guinn, [2]Elisa S. Schrank, [1,2,3]Steven J. Stanhope

[1]Biomechanics & Movement Science, University of Delaware, Newark, DE, USA
[2]Department of Mechanical Engineering, University of Delaware, Newark, DE, USA
[3]Department of Health, Nutrition and Exercise Sciences, University of Delaware, Newark, DE, USA
email: ktaka@udel.edu

INTRODUCTION

The ankle joint musculature plays a major role during walking for maintenance of upright support and generation of forward propulsion [1]. In transtibial amputee gait, the effectiveness of a prosthetic foot to achieve optimal gait patterns may be dependent on the extent to which the prosthesis effectively mimics the biomechanical characteristics of a natural ankle. However, traditional biomechanical analysis using inverse dynamics offers limited ability to compare the performance of a prosthesis to a natural ankle due to inadequate assumptions of rigid body segments and a fixed rotational ankle joint axis [2]. Therefore, a universal method for characterizing the dynamics of the combined ankle-foot complex (AFC) is warranted.

Ankle-foot roll-over shape (ROS) has been used as a convenient tool for analyzing the net deformations of an AFC relative to the floor in both natural [3], and amputee [4] subjects. The ROS describes the effective geometrical shape that an AFC conforms to during the stance phase of gait by reporting force platform center-of-pressure locations relative to the non-inertial coordinate system fixed to the shank segment. ROS has been shown to be invariant across walking velocities [3]. However, the dynamics of gait varies with walking velocity [5]. While informative, ROS does not inherently contain information regarding the external loads (ROS-dynamics) associated with the AFC net deformations.

Therefore, the main objective for this study was to examine both ROS and ROS-dynamics of able-bodied subjects during gait.

METHODS

Six able-bodied subjects (4 males and 2 females) underwent instrumented gait analysis. The subjects' age, weight, and height ranged from 21-28 years, 53-132 kg, and 1.62-1.83 meters, respectively. The subjects walked at a scaled velocity of 0.8 statures/second through a calibrated motion capture volume of approximately 4x1.5x2.4 meters containing four staggered strain gauge force platforms. Kinematic data from the motion capture system were sampled at 120 Hz, while the kinetic data from force platforms were sampled at 360 Hz. Kinematic and kinetic data were filtered at 6 Hz and 25 Hz, respectively using a zero-lag low-pass Butterworth filter. Data were processed and analyzed using Visual 3D (C-Motion Inc, Gaithersburg, MD).

ROS data were obtained by transforming stance phase center of pressure (COP) data from the global lab coordinate system (GCS) into the orthogonal shank-based coordinate system (SCS). Likewise, the external loads applied to the AFC at the COP were quantified by transforming the external ground reaction forces (GRF) from the GCS into the SCS. The z axis of the SCS represented the longitudinal axis (created by the vector from ankle joint center to knee joint center), with +z signifying the superior direction. The y axis in SCS represented the anterior-posterior axis with +y signifying the anterior direction. A 20 N vertical ground reaction force threshold defined the stance phase.

RESULTS AND DISCUSSION

The average maximum value of force SCSz across six subjects was 1.2 ($\pm$ .037) body weights (BWs) while the average minimum value of force SCSy was -0.36 ($\pm$ .05) BWs (Table 1). Unlike the anterior-posterior GRF in GCS, the force SCSy was negative during the majority of stance with exception of the first 8.9% (Figure 1). This indicated the external loads were directed

posteriorly relative to the shank through most of stance. The COP SCSy location indicated the anterior progression of the COP relative to the shank during stance, and it's total forward progression averaged 0.12 (± .01) statures. The COP SCSz location described the longitudinal (pseudo deformation) of the AFC during stance, and the total pseudo deformation between heel strike and maximum deformation averaged 0.026 (± .005) statures.

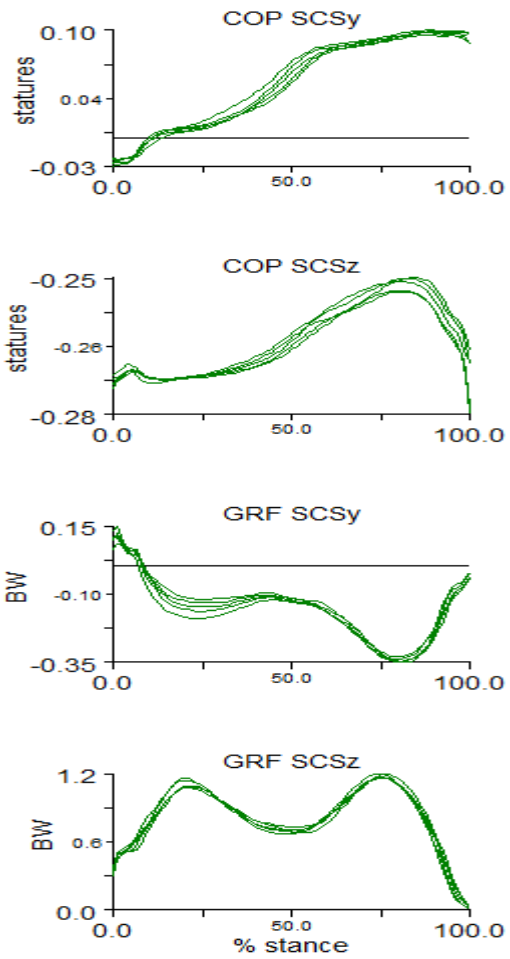

Figure 1: Data of COP and GRF in SCS from the right AFC of a representative subject.

CONCLUSIONS

We have proposed a novel method for characterizing the dynamics of the AFC during stance in gait. The new method combines the shape of the deformation patterns of an AFC, with the forces responsible for the deformation (Figure2). The advantage of this method is that an AFC can be analyzed as one unified shank segment of unknown distal characteristics. We propose this approach will facilitate the direct and objective comparisons of the net dynamics attributed to AFCs having dramatically different structures and functions: such as prosthetic and natural AFCs. Future studies will examine the effects of walking velocities on the external loads applied to the AFC. This new characterization method of AFC dynamics may ultimately assist in fabricating custom prosthetic AFCs having optimal functional characteristics.

REFERENCES

1.Kepple TM et al. *Gait and Posture* **6**, 1-8, 1997.
2.Geil MD et al. *J Biomech* **33**, 1745-1750, 2000.
3.Hansen AH et al. *Clinical Biomechanics* **19**, 407-414, 2004.
4.Curtze C et al. *J Biomech* **42**, 1746-1753, 2009.
5.Winter DA. *Clin Orthop Relat Res* **174**, 147-154, 1983.

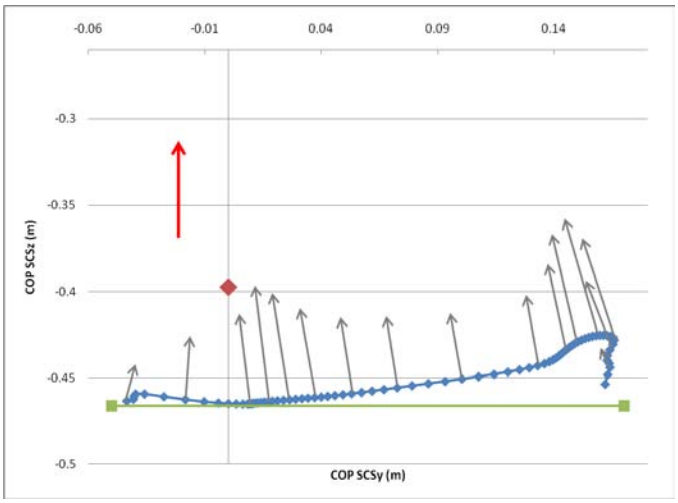

Figure 2: Roll-over shape and net loads applied to the AFC from a representative trial. The blue dots indicate the COP in SCS. Each gray arrow represents the magnitude and direction of the GRF in the SCS. The length of the red arrow is scaled to one body weight. The ankle joint center location in SCS is denoted by the red diamond. The level of the floor during static standing is indicated by the green horizontal line.

	COP SCSy Total Range (statures)	COP SCSy Negative Duration (% stance)	COP SCSz Total Range (statures)	Max GRF SCSy (BW)	Min GRF SCSy (BW)	GRF SCSy Positive Duration (% stance)	Max GRF SCSz (BW)
Mean	**0.122**	**12.2**	**0.026**	**0.125**	**-0.356**	**8.9**	**1.149**
Std	**0.01**	**1.86**	**0.005**	**0.021**	**0.050**	**5.20**	**0.037**

Table 1: Average COP and GRF SCS data from the right AFC of six subjects.

CONTRIBUTION OF TOE- OFF KINEMATICS TO THE PROSTHETIC KNEE FLEXION DURING SWING PHASE OF TRANSFEMORAL AMPUTEE GAIT

[1]Y Dabiri, [2]S Najarian, [3]MR Eslami, [4]S Zahedi, [5]D Moser, [6]E Shirzad, [7]R Moradihaghighat

[1]Amirkabir University of Technology (Tehran Polytechnic), Tehran, Iran
[2]Amirkabir University of Technology (Tehran Polytechnic), Tehran, Iran
[3]Amirkabir University of Technology (Tehran Polytechnic), Tehran, Iran
[4]University of Surrey, Guilford, UK
[5]University of Surrey, Guilford, UK
[6]National Olympic and Paralympics Academy, Tehran, Iran
[7]Amirkabir University of Technology (Tehran Polytechnic), Tehran, Iran
Email: najarian@aut.ac.ir

INTRODUCTION

During normal gait, advancement of the swing limb is enabled by flexion of the swing knee [1]. Anderson et al. [1] examined different parameters that may affect the swing knee flexion of a healthy subject.

In regard to the prosthetic leg, one of the parameters that affect prosthetic knee flexion, is the mass and moment of inertia of the prosthetic leg [2 and 3]. Another parameter that affects prosthetic knee dynamics is the contribution of muscle forces [1, 2]. Toe- off kinematics, as another parameter, affects prosthetic knee flexion. Simulation in the absence of muscular joint torques shows that if the initial joint angular positions and velocities were chosen judiciously, the normal knee kinematics will be approximated [4]. According to Piazza and Delp [5], for normal subject, either increasing hip flexion velocity or decreasing knee flexion velocity at toe-off will decrease knee flexion achieved during swing phase. Anderson et al. [1] found that knee angular velocities at toe-off contribute greatly to swing-phase knee flexion during normal gait. It is expected that this parameter affects prosthetic knee peak flexion angle, too.

A theoretical study that elucidates the importance of the effect of each of aforementioned parameters is needed to provide a basis for design of prosthetic leg that better mimic the behavior of normal one. Therefore, the goal of this paper was to determine the contribution of different forces and toe- off kinematics to the peak knee flexion of transfemoral amputee during swing phase of gait.

METHODS

The lower extremity was modeled as a two-degree of freedom linkage, for which knee and hip were the joints. Only the movements in the sagittal plane were considered to be important. Based on the anatomical data of a transfemoral subject who took part in the study, iliacus, psoas, gastrocnemius, adductor longus, rectus femoris, and hamstrings were included in the model. Assuming a myodesis operation, insertion point of rectus femoris and hamstrings were fixed to the amputated tip of femur [6]. Each muscle was modeled as an ideal force generator [7].

The governing equations of the model were based on the data provided by Piazza and Delp [5]. To separate different forces that influence knee angle, following equation was derived:

$$\theta_K = \theta_K^0 + (t - t_0)\dot{\theta}_K^0$$
$$+ (t - t_0)^2 \left(\iint (M^{-1}C)(2)\begin{bmatrix}\dot{\theta}_H^2 \\ \dot{\theta}_K^2\end{bmatrix}\right.$$

$$+ (M^{-1}V)(2)\begin{bmatrix}-\dot{\theta}_H\dot{\theta}_K \\ 0.0\end{bmatrix}$$

$$\left. + (M^{-1}P)(2)\begin{bmatrix}\ddot{x} \\ \ddot{y}\end{bmatrix} + (M^{-1}G)(2)\right)$$

$$+ M^{-1}(2)\begin{bmatrix} M_H \\ -M_K \end{bmatrix} dtdt) \qquad (1)$$

where $\ddot{\theta}_H$ and $\ddot{\theta}_K$ are hip and shank rotational accelerations, $\ddot{x}$ and $\ddot{y}$ are the acceleration of hip joint in horizontal and vertical directions, respectively. M, C, V, P and G depend upon joint angles and inertial parameters, and "(2)" represents the second row of each matrix. The third and forth right- hand terms are due to Coriolis and centrifugal effects, the fifth right- hand term is due to pelvic motion, the sixth right- hand term is due to gravity effects, and the last right-hand term is due to muscle forces.

The transfemoral amputee who volunteered to take part in the study was asked to walk in his natural cadence along a walkway. The hip and knee joint angles were recorded using a motion analysis system. For further information about experimental data see the report by Dabiri, et al. [6]. Using an inverse dynamics approach the muscle forces were determined to produce recorded hip and knee angles.

RESULTS AND DISCUSSION

Fig. 1 shows the simulated knee angle, and the contribution of different forces and toe- off kinematics in peak knee flexion of a transfemoral amputee. As can be seen in this Figure, the toe- off kinematics has the largest contribution in peak knee flexion.

According to fig. 1, the effect of muscles during swing phase is not noticeable. This is in line with the well- known fact that during swing phase the activity of muscles is not as noticeable as in the stance phase, and that in absence of muscles, if the initial hip and knee angular velocities are selected appropriately, the normal knee kinematics will be approximated, [4].

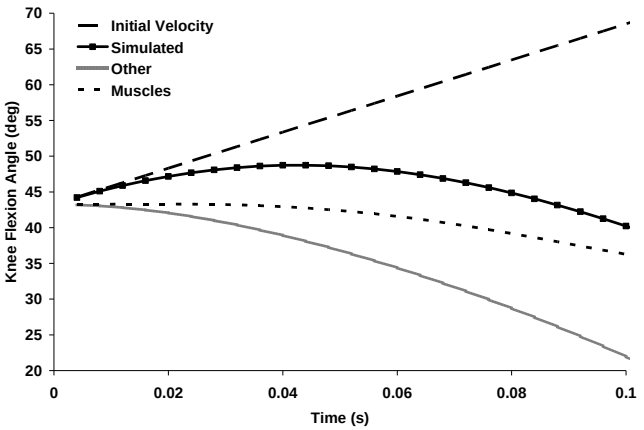

Figure 1: Contribution of the knee initial velocity, Coriolis and centrifugal, pelvic motion, and gravity effects (other), and muscle forces (Muscles) to maximum knee flexion of a transfemoral amputee swing phase of gait. Also, the knee angle resulted from all forces and knee initial velocity (Simulated) is shown.

Our results correspond to the findings of Anderson et al. [1] who reported that the initial knee flexion velocity has the largest effect in peak knee flexion of healthy subjects. However, according to Anderson et al. [1], the effect of muscle forces in peak knee flexion of healthy subjects is -14.5 degree which is larger than those of the transfemoral amputee (7 degree). This is related to the fact that the prosthetic leg has less muscle than the biological one. On the other hand, the effect of other forces in transfemoral amputee model (21 degree) is larger than that of healthy subject (2.5 degree). This may be due to the less control that amputee has over his prosthetic leg.

REFERENCES

1. Anderson FC, *J Biomech* **37,** 731- 737, 2004.
2. Hale SA, *Prosthet Orthot Int* **14**, 125 –135, 1990.
3. Tashman S, et al. *Clin Prosthet Orthot* **9**, 23 - 28, 1985.
4. Mochon S, et al. *J Biomech* **13**, 49–57, 1980.
5. Piazza SJ, et al. *J Biomech* **29**, 723–733, 1996.
6. Dabiri Y, et al. *Research J Biological Sciences* **4**, 1076- 1084, 2009.
7. Anderson FC, et al. *J Biomech* **34**, 153-161, 2001.

ANALYSIS OF ANKLE MUSCLE CO-CONTRACTION IN TRANS-TIBIAL AMPUTEES

[1,2]Mahyo Seyedali, [1,3]David Morgenroth, [1,3]Joseph Czerniecki, and [1,2]Michael Hahn

[1]RR&D Center of Excellence, Department of Veterans Affairs; Departments of [2]Mechanical Engineering and [3]Rehabilitation Medicine, University of Washington, Seattle, WA, USA
email: mehahn@u.washington.edu web: http://www.amputation.research.va.gov/

INTRODUCTION

The human ankle actively controls power absorption, tibial progression and power generation during the stance phase of gait. Prosthetic ankles lack the ability to modulate these functions due to loss of musculoskeletal structures. The commercial prosthesis market is dominated by passive devices that have fixed mechanical properties. Advances have been made in powered prosthesis control for upper extremity devices; however, little has been achieved in creating a powered prosthesis for the lower extremity. Currently available computerized prostheses rely on manual adjustment to change the state of the device [1]. However, new innovations include a device that assists in the transition from level-ground to stair descent and back to level-ground using activation of the Gastrocnemius and Tibialis Anterior as on/off triggers for switching mode [2]. Although this allows for more diverse state control than the traditional passive devices, it is not fluid and may be dangerous in some cases. Several problems in utilizing a powered prosthesis stem from lack of fluid, on-line control.

In an effort to create a powered device that automatically provides damping and varying stiffness, some studies have used electromyographic (EMG) signals as input. Peeraer et al. [3] studied the EMG signals from the hip muscles of one amputee compared to a control group for level-ground walking, in addition to ascending and descending a ramp. Implementing that idea, Huang et al. [4] reported an accurate estimation of locomotive state in mobility tasks using nonstationary EMG signals.

This study sought to determine the residual limb's muscle activation patterns during gait. However, residual limb muscles do not activate as is expected from the natural limb. Centomo et al reported unique co-contraction patterns in amputees compared to able-bodied patients [5]. Little is known about the range of residual limb muscle activation patterns during locomotion. For development of robust state control algorithms it is necessary to quantify the residual limb's co-contraction and general activation patterns. The purpose of this study was to analyze the co-contraction patterns of two residual ankle muscles, Tibialis Anterior (TA) and Medial Gastrocnemius (MG) during three speeds of level-ground walking.

METHODS

Four unilateral trans-tibial amputees participated in this study (56 +/- 14 years; 1.80 +/- 0.12 m; 79.8 +/- 10.6 kg). The protocol was approved by the Institutional Review Board. Written informed consent was obtained prior to each subject's participation. Surface EMG recorded muscle activation at 1200 Hz and foot marker position trajectories were collected at 120 Hz. Signals from the Tibialis Anterior (TA) and Medial Gastrocnemius (MG) for the prosthetic and sound limb were recorded using disposable wet-gel neonatal passive electrodes in a bi-polar single differential configuration. Foot marker trajectories in combination with ground reaction forces were used to determine gait cycle events. All subjects walked on their prescribed prosthetic components for this study. We collected five trials at three different speeds for each subject; self-selected walking speed (SSWS), 10% slower than SSWS, and 10% faster than SSWS.

Initial signal processing involved 1) a band-pass filter from 10-500Hz (manufacturer's settings; Telemyo, Noraxon, Scottsdale, AZ), 2) a high pass 50 Hz 4th order Butterworth filter to remove motion artifact, and 3) a notch 4th order Butterworth filter, from 59.5-60.5Hz to remove ambient power noise

from the signal. The signal was then further processed to calculate linear envelopes for each signal, using the following steps: 1) full-wave rectification, and 2) a low-pass 4th order Butterworth filter with cutoff frequency of 8Hz.

The magnitudes of each muscle's activity were normalized to the patient's maximum contraction that occurred in their fast walking trials. The signals were also time normalized to gait cycle. Co-contraction index (CCI) during the first 10% of gait cycle was quantified by the following equation [6]:

$$CCI = \frac{2 * Antagonist_{max}}{Agonist_{max} + Antagonist_{max}}$$

This early phase of gait was chosen in this exploratory study due to the singular eccentric contraction of the TA controlling the transition from heel-strike to foot-flat in normal gait.

RESULTS AND DISCUSSION

Co-contraction was observed across the different speeds tested in this study. An ensemble average curve of TA and MG activation from a representative subject is presented in Figure 1. Large muscle activation from the MG was observed in early stance, when it would normally be expected to be inactive during normal gait. Limb-specific CCI means are presented in Figure 2. This observation appears to be unique to the residual limb of trans-tibial amputees and independent of walking speed.

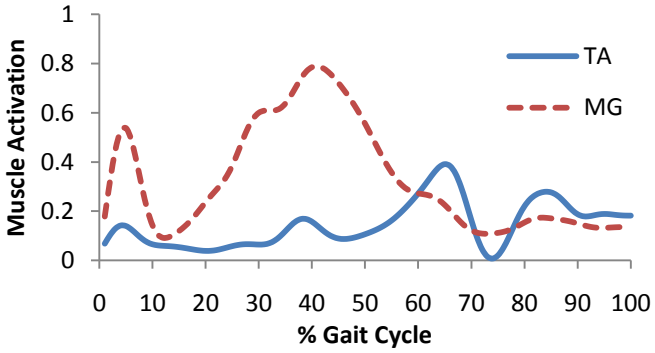

Figure 1: Ensemble average patterns of activation during SSWS for a representative subject.

The preliminary observation of co-contraction between the TA and the MG early in the gait cycle may prove critical to the design and eventual implementation of state control algorithms in novel powered prostheses.

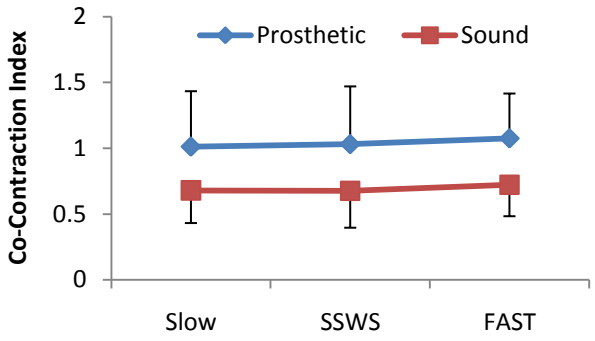

Figure 2: Co-contraction Index means for the first 10% of gait cycle for prosthetic and sound limbs.

Furthermore, the observation that the co-contraction index is relatively independent of walking speed should increase the potential for development of proportional control algorithms based on signal magnitude and phased timing.

CONCLUSIONS

Ongoing work will involve the recruitment of a greater sample of amputee subjects in addition to a control group. Preliminary observations have also revealed an occasional co-contraction pattern during the toe-off stage of the gait cycle (50-70%). This pattern will be explored more thoroughly.

Clinically, there are several factors that should be studied regarding the magnitude and timing of residual limb muscle activation. These include time since amputation, activity level, type of amputation, and age of amputee.

REFERENCES

1. Psonak, R. *Orthotics and Prosthetics in Rehabiliation*, 2000.
2. Au, S., et al. *Neural Networks*, **21**, 654-666, 2008.
3. Peeraer, L., et al. *J Biomed Eng*, **12**(3), 178-182, 1990.
4. Huang, H., et al. *IEEE Biomed Eng* **56**(1), 65-73, 2009.
5. Centomo H., et al. *J Electromyogr and Kinesiol*, **18**(3), 487-494, 2008.
6. Falconer K., et al. *J Electromyogr Clin Neurophysiol*, **25**, 135-149, 1985.

ACKNOWLEDGEMENTS

This study was supported by the VA RR&D service and a grant from the Department of Defense (W81XWH-09-2-0142).

Response to Tripping Perturbations in Transfemoral Amputees

[1]Fabian Sierra, [1]Fan Zhang, [1]He (Helen) Huang and [2,3]Susan E. D'Andrea

[1]University of Rhode Island, Kingston, RI, USA
[2]Brown University, Providence, RI, USA
[3]Center for Restorative and Regenerative Medicine, VA Medical Center, Providence, RI, USA
email: susan.dandrea@gmail.com

INTRODUCTION

Unexpected perturbations during normal gait can lead to falls resulting in serious injuries, especially for the elderly and lower extremity amputees. In the latter, these types of falls may not only cause physical harm, but also can affect their balance confidence and increase fear of falling, resulting in further gait irregularities[3]. If an able bodied person encounters unexpected perturbations during normal walking, it is possible to implement stabilizing strategies to recover from the stumble; however, for lower extremity amputees, the implementation of these strategies can prove difficult. Therefore, the goal of this study is to compare and analyze the reaction strategies of able bodied and lower extremity amputees in an effort to better understand how to assist amputee patients to recover from gait perturbations while maintaining the dynamic walking stability.

METHODS

Ten healthy able bodied (AB) subjects (4 males and 6 females) were recruited for this study. They had no known prior history of neurological or orthopedic abnormalities that would hinder their normal gait during the experiment. Their average age, weight and height were 37 (±16.46) years, 73.90 (±15.93) kg, and 1.70 (±0.10) m. respectively. Five unilateral transfemoral (TF) amputee subjects were recruited for this study (2 males and 3 females). Demographics for these amputee subjects can be found in Table 1. TF subjects were required to wear a Total Knee hydraulic unit as their prosthesis during the experiment.

To simulate gait perturbations (tripping and slipping) in a safe setting, the Symbex ActiveStep® (Lebanon, NH) Fall Prevention Training System, a computer controlled treadmill, was used in this study. Each subject was required to perform 26 trials, two sets of 13 trials (including 5 tripping, 5 slipping, and 3 undisturbed walking tasks). The order of the trials was randomized. Rest periods were allowed to avoid fatigue.

Subjects walked at a self-selected pace. To simulate the perturbation, the treadmill was accelerated 2.2 m/s for 0.16 seconds. Motion capture data were collected at 100 Hz (Qualisys, Gotenburg, Sweden) and synchronized with surface electromyography signals (Delsys, Boston, MA) collected at 1000 Hz from twelve muscles on the hip and the thigh on the dominant/amputated side. A six-degree of freedom load cell was incorporated into the pylon of amputee subjects. Visual 3D (C-Motion, Germantown, MD) was used to model the motion and calculate joint angles.

RESULTS AND DISCUSSION

Response to a gait perturbation induced by a person walking over a platform that is suddenly accelerated can be categorized as mechanical or neurological[1]. The data collected in this experiment are consistent with this hypothesis.

Figure 1 shows a representative response of a TF subject following gait perturbation. When the perturbation is initiated with the foot in contact with the treadmill, the initial response is passive and mechanical as evidenced by the immediate change in the force profile after the trip is initiated. Conversely, when the treadmill belt is accelerated with the limb in swing, the neurological response corresponding to the increase in muscle activation of the thigh muscles is the early response. In both cases, the change in the knee angle pattern aligned with the onset of the increased EMG activity.

a)

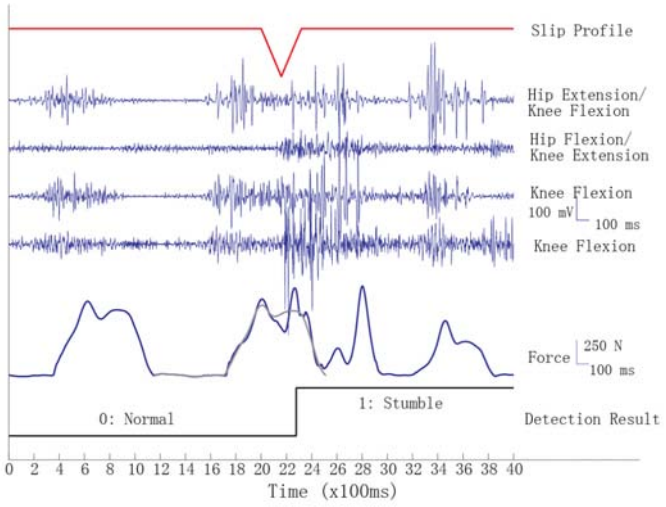

b)

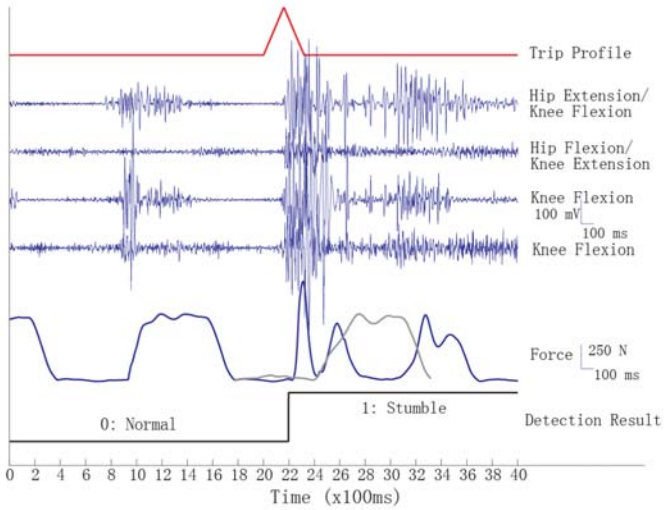

Figure 1: EMG signal, load cell force (along the long axis of the prosthesis) and knee angle for transfemoral subject TF01. (a) Perturbation occurs during the stance phase. (b) Subject is tripped during swing phase. Vertical dashed lines represent significant changes in measured signals affecting the recovery of the individual.

The evaluation of the stability during and the identification of factors compromising balance can be assessed from these results. Our data are consistent with the findings that the activity of the thigh muscles is a key factor in regaining balance after a gait perturbation, controlled largely by the knee motion[2]. These data provide a baseline by which to compare recovery between groups from stumbling. Continuing work will focus on determining the contribution of the individual muscles to the recovery, isolating recovery patterns and using these signals to design a stumble recovery algorithm.

CONCLUSIONS

The long-term goal of this project is the design of stumble detectors and prosthesis control for active stumble recovery, which will improve the safety of lower-limb prosthetic use. Understanding of the mechanisms underlying stumbling and recovery during walking is important for developing these strategies and improving the quality of life for patients with lower-limb amputations.

REFERENCES

1. Cordero AF, et al, *Gait and Posture* **18**:47–59, 2003.
2. Vilensky JA, et al, *Journal of Electromyography and Kinesiology* **9**:161 – 171, 1999.
3. Yang J, et al, *Journal of Electromyography and Kinesiology* **17**:228 – 240, 2007.

ACKNOWLEDGEMENTS

This work was supported by the RI Science and Technology Advisory Council under grant # RIRA 2009-27.

Table 1: Transfemoral subject demographics. Residual Limb Ratio is the ratio between the length of the TF subject's residual limb (measured from the ischial tuberosity to the distal end) to the length of the non-impaired side (measured from the ischial tuberosity to the femoral epicondyle).

Subject	Age (years)	Height (m)	Weight (kg)	Amputation Side	Residual Limb Ratio	Years Post Amputation	Daily Use Prostheses
TF-1	57	1.75	75.8	R	51.40%	31	RHEO
TF-2	46	1.60	97.0	L	92.71%	3	C-Leg
TF-3	38	1.63	65.8	R	67.68%	29	RHEO
TF-4	48	1.66	63.1	R	94.42%	7	C-Leg
TF-5	52	1.54	64.0	L	83.67%	31	RHEO

EFFECTS OF USING HEEL WINDOWS AND SINGLE SUBJECT ANALYSIS TO MEASURE REAR FOOT MOTION DURING RUNNING

[1]James Becker, [1]Louis Osternig, [2]Stanley James, and [1]Li-Shan Chou

[1]Department of Human Physiology, University of Oregon, Eugene, OR, USA
[2]Slocum Center for Orthopedics and Sports Medicine, Eugene, OR, USA
email: chou@uoregon.edu, web: http://biomechanics.uoregon.edu/MAL/index.html

INTRODUCTION

It has been suggested that screening individuals prospectively for injury risk factors may help reduce the number of running related injuries [1]. Since rear foot motion during running is often cited as a contributing factor to overuse injuries, any prospective screening should include a measure of rear foot movement. While tracking markers can be placed directly on the shoe, bone pin studies have indicated that shoe motion is not the same as true rear foot motion [2]. As a solution some authors have advocated the use of windows in the shoe heel counter with markers attached directly to the foot for tracking rear foot motion during running [3]. However, to date, no study has used a three dimensional (3D) analysis to evaluate differences in rear foot motion when measured by placing markers directly on the shoes or by using heel windows.

Additionally, most studies on running injuries use a group design where the average performance of an injured group is compared to the average performance of a non-injured group. However, the performance of any one individual rarely, if ever, matches the average group performance [4]. This is especially true in assessing injury risk, when it is deficits or changes in a single individual that are of concern, not how they compare to an average group performance [4]. In these situations a single subject analysis might yield insights which are masked during a traditional group analysis.

Therefore, the purposes of this study were to use a 3D analysis to compare differences in rear foot motion between markers placed on the shoes and markers placed directly on the rear foot using heel windows. A second purpose was to determine the influence of group verse single subject analysis on any kinematic differences.

METHODS

Thirteen subjects who ran at least 20 miles per week were recruited for this study. Twenty nine reflective markers were attached to the subject's bony landmarks. The shoe markers consisted of two markers along the vertical bisection of the heel counter with a third marker on the lateral side of the shoe. The heel windows markers were placed in the same locations, with marker bases attached directly to the rear foot and extending through holes cut in the heel counter. For each condition, subjects ran approximately 40 laps around a 25 meter track in the laboratory with data being collected over a 5 meter segment of each lap. An 8 camera motion capture system (Motion Analysis Corp) recorded marker position data at 200 Hz while three AMTI (Advanced Mechanical Technology, Inc) force plates recorded ground reaction forces at 1000 Hz.

For the group analysis, 10 trials were used to create an average profile for each subject. Variables of interest included rear foot eversion excursion, percent stance at maximal eversion, maximal instantaneous eversion velocity, and maximal instantaneous vertical loading rate. These were calculated with custom LabView (National Instruments) software. A coefficient of multiple correlation (CMC) was calculated to examine the repeatability of the ankle joint inversion-eversion curve. Each foot was analyzed separately. Significant differences between conditions were evaluated with a dependent observations *t* test, with α set to 0.05.

With the exception of the CMC, the same variables were examined using a single subject analysis. At least 8 trials per condition were used for each subject. Significant differences between trials under both conditions were evaluated on an

individual subject basis with both an independent observations *t* test and a statistical method called Model Statistics [4]. Again, α was set to 0.05.

RESULTS AND DISCUSSION

Due to subject drop out, only 20 feet were included in the final analysis. The results of the group analysis are shown in Table 1. The only significant difference between marker conditions was in the CMC values, with the heel windows markers indicating greater variability in movement patterns. These results suggest placing the markers on the shoe artificially reduces the variability in the measured movement patterns.

Table 1. Results of the group analysis. ***** indicates significant difference between marker conditions.

Parameter	Shoe Markers	Heel Windows
Eversion Excursion (°)	13.66 (± 6.76)	13.83 (± 6.91)
Percent Stance at Max. Eversion (%)	36.76 (± 12.00)	36.77 (± 14.87)
Max. Instant. Eversion Velocity (°/s)	269.50 (± 117.60)	260.60 (± 115.10)
Max. Instant. Vertical Loading Rate (N/Kg BW/s)	84.47 (± 18.47)	82.23 (± 17.16)
CMC Value	**0.92 (± 0.07)**	**0.87 * (± 0.12)**

The lack of significant differences between conditions for the other variables is most likely due to the individualized nature of subject responses, an example of which can be seen in Figure 1. Similar individualized response patterns were observed for the other variables of interest. However, some of the changes were up to 40% in magnitude, suggesting there were differences between conditions; they were just not identified by the group analysis.

Both the *t* test and Model Statistics results indicated that individuals who demonstrated large percent changes in the group analysis did in fact have significant differences between the two marker conditions. Table 2 shows the number of feet with significant differences between conditions under the single subject analysis.

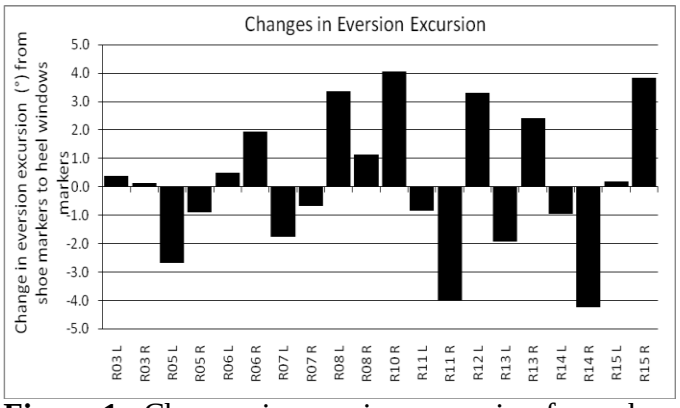

Figure 1. Changes in eversion excursion from shoe markers to heel windows markers

Table 2. Number of feet demonstrating significant differences between marker conditions under the single subject analysis

Parameter	Number of feet with significant differences between marker conditions
Eversion Excursion (°)	10
Percent Stance at Max. Eversion (%)	10
Max. Instant. Eversion Velocity (°/s)	7
Max. Instant. Vertical Loading Rate (N/Kg BW/s)	2

Overall the results of this study suggest joint kinematics and kinetics, as well as the variability in movement patterns of the rear foot, are different when measured with shoe based or heel windows markers. However, given the individualized responses observed in this study, these differences only become evident when the data is analyzed on an individual subject basis, a fact which has important implications for addressing prospective injury risk in runners.

REFERENCES

1. Herljac A. *Phys Med Rehabil Clin N Am*, **16**, 651-667, 2005.
2. Reinschmidt C, et al. *Clin Biomech*, **12**, 8-16, 1997.
3. Butler R, et al. *Am J Sports Med*, **34**, 1998-2005, 1998.
4. Bates B. *Med Sci Sport Exerc*, **28**, 631-638, 1999.

ASSESSMENT OF THE SUPPORT VECTOR MACHINE FOR DETECTING AGE-RELATED CHANGES IN RUNNING KINEMATICS

[1]Reginaldo K Fukuchi, [1]Bjoern M Eskofier, [1]Reed Ferber and [2]Marcos Duarte

[1]Faculty of Kinesiology, University of Calgary, Calgary, AB, Canada
[2]School of Physical Education and Sport, University of São Paulo, Brazil
email: r.fukuchi@ucalgary.ca

INTRODUCTION

There has been an increase in the number of elderly people engaged in recreational and competitive running in order to improve their quality of life. However, there is concern that the incidence of running-related injuries among older adult runners is greater than young adults. Age-related changes in running movement patterns have been suggested as a major cause of running-related injuries [1]. Therefore, the early identification of these changes in running movement patterns in elderly people would collaborate in injury prevention programs. In a previous study we described differences in the lower extremity running kinematic patterns between young and elderly adults [1]. In the present work, we reanalyzed these data to investigate if it is possible to detect gait patterns based on the gait features already assessed. For such, we employed support vector machine (SVM) approach [2,3] to detect changes in lower extremity movement patterns between young adult and elderly runners. We are unaware of any study that has detected running movement patterns in elderly adults using such a statistical learning algorithm approach.

METHODS

Seventeen elderly male adults (age 69±2 yrs) and 17 young male adults (age 31±6 yrs), all regular runners, volunteered to participate in this study. This study was approved by the ethics committee of the University of Sao Paulo, Brazil. Three-dimensional kinematics of the right lower limb was obtained using 4 digital cameras (GRDVL9800U, JVC Inc.). The marker positions were filmed and digitized at 120 Hz using the APAS software (Ariel, Inc) while the subjects were running at 3.1 $m.s^{-1}$. Knee and ankle angles were extracted and analyzed during 5 consecutive stance phases. The procedures adopted in the pre-processing phase were described in more details in our previous study [1]. Twenty-five kinematic features were chosen to train and test the SVM classification algorithm using linear and polynomial kernel function ($d=3$) implemented in Matlab 7.7 (Mathworks, MA, USA). In brief, the idea behind the SVM classifier is to map the features in a high-dimensional space and then define a linear separating hyperplane which is used to assign the features in one of the labeled groups [4]. A 10-fold cross-validation was employed to assess the generalizability of the classifier scheme. In addition, a forward feature selection [2] was used to determine the minimum number of features necessary to achieve the best performance of the classifier.

RESULTS

The performances of the SVM classifier, using linear and polynomial kernel functions [4], were similar and are summarized in Table 1. The polynomial kernel achieved 98.8% accuracy when 12 features were employed for classification while the linear kernel reached the same performance with 17 features. In both conditions, the knee flexion range of motion (KFLXRoM) and the knee frontal plane initial contact angle (ICKABD) were the most important features in providing discriminatory information since they were selected first. The 2D scatter-plot in Figure 1 allows an easy geometric interpretation of the data where we see a line, which represents the hyperplane in a high-dimensional space, separating groups based in these features. The results of the forward feature selection are presented in Figure 2. Using both kernel functions (linear and polynomial) the most accurate method to discriminate between age groups was reached with 17 and 12 kinematics features, respectively. Moreover, it can be observed that adding more than

20 features decreases the performance of the classifier.

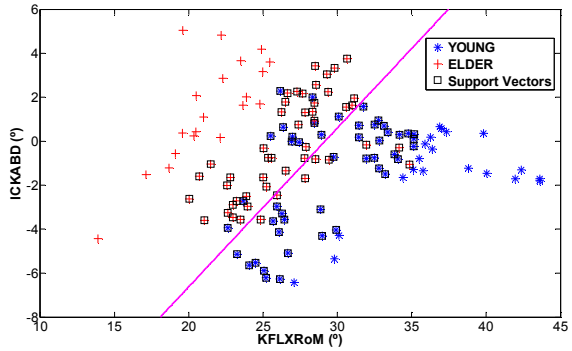

Figure 1: Scatter plot graph showing the distribution of the best two discriminating features (KFLXRoM (horizontal axis) and ICKABD (vertical axis)) and the separating line (hyperplane) and the respective support vectors classified with linear kernel SVM.

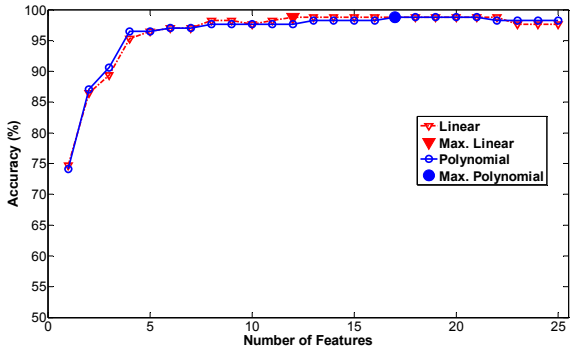

Figure 2: Forward feature selection graph demonstrating the dependence of the classification accuracy on the number of features. Maximum accuracy was achieved requiring 17 (linear) and 12 (polynomial) out of 25 kinematics features.

DISCUSSION

The SVM classifier exhibited the ability to discriminate age-related changes in running kinematic patterns using few variables. In our previous study, we had already presented some differences between groups using inferential statistics [1]. Indeed, the KFLXRoM exhibited the most significant difference ($p<0.001$) when age groups were compared. Although the ICKABD was not significantly different in our previous study, we did point out that on average, the young runners landed in abduction while the elderly landed in knee adduction [1].

The present study also suggests that some features did not contribute positively for the classification algorithm since when more than 22 features in the polynomial kernel and 21 features in the linear kernel were added, the classification performance deteriorated slightly. This characteristic of overfitting has been reported in previous studies and is attributed to the redundancy of information [2,3].

Although further studies are required to investigate the application of SVM to predict changes in movement pattern, the present study showed a promising ability of SVM in discriminating these patterns between age groups using few variables. This promising capability encourages the use of this method in future applications to help understand the causes of running-related injuries among elderly population.

REFERENCES

1. Fukuchi RK. *J Sports Sci* **26**, 1447-1454, 2008.
2. Begg R. *J Biomech* **38**, 401-408, 2005.
3. Wu J. *J Appl Biomech* **24**, 83-87. 2008.
4. Vapnik VN. *Statistical Learning Theory*. John Wiley & Sons, Ltd., 1998

ACKNOWLEDGEMENTS

Reginaldo K Fukuchi wishes to thank The Capes Foundation, Ministry of Education of Brazil for his scholarship.

Table 1: Overall accuracy of detection using two different types of kernel functions in 10-fold experiment.

Kernel function and performance measures	Minimum number of variables	Performance with minimum number of variables	Performance with all variables
Linear	17	0.9882	0.9824
Polynomial *d=3*	12	0.9882	0.9765

FRICTION DEMAND DURING RUNNING AND CUTTING

Mark G Blanchette, Susan M Sigward and Christopher M Powers

University of Southern California, Los Angeles, CA, USA
email: mgblanch@usc.edu, web: **http://pt.usc.edu/labs/mbrl**

INTRODUCTION

Slips occur when the utilized friction (uCOF) of an individual exceeds the available friction provided by the shoe-floor interface.[1] Utilized friction can be influenced by a number of factors including footwear and the nature of the task performed.[2,3] Previous studies have reported that the uCOF during normal speed walking ranges from 0.17 to 0.20,[4] however, no study has examined the friction demands during sport activities. A survey of injuries during netball (a European sport similar to basketball) identified the most severe injuries were the result of slip or fall events.[5] Slip induced injuries in court sports are likely due to greater friction demands associated with sport related tasks.

The purpose of the current study was to examine the uCOF during running and 2 types of cutting maneuvers (side-step cut and V-cut). Knowledge of the uCOF during sport-specific activities is important step in establishing footwear requirements and standards for court surfaces and in order to prevent slip events.

METHODS

Sixteen healthy young men between the ages of 18 and 22 participated in this study. The average age, height and weight of the study participants were 19.7 ± 1.2 yrs, 180.9 ± 8.5 cm, and 77.4 ± 8.3 kg respectively.

To control for the potential influence of varying footwear, subjects were fitted with the same style of cross-training shoe (New Balance Inc., Boston, MA). Practice trials were performed for subjects to become familiar with the instrumentation and procedures. Subjects performed 2 cutting tasks (side-step cut and a V-cut). For the side-step cutting maneuver, subjects ran approximately 5 meters before contacting the foot of their dominant side on a force plate and changed direction to either the right or left at a 35-60° angle from the original direction of motion. For the V-cutting procedure, subjects ran approximately 5 meters before contacting the foot of their dominant side on the force plate, but then backpedaled to either the right or left at a 125-155° angle from the original direction of motion. The speed of each trial was controlled (6.5-8 m/s) using photo electric triggers. To better simulate a real-life athletic condition, the performance of the cutting tasks was unanticipated. A delayed illumination on a board visible to the subjects as they approached the force plate signaled the subjects to either continue running straight ahead or to perform one of the cutting tasks. The order of the tasks performed was randomized for each subject.

Ground reaction forces (GRFs) were recorded using a force platform (Advanced Mechanical Technologies, Inc., Newton, MA) at 1560 Hz. Utilized friction was calculated as the ratio of resultant shear force to vertical force. For each trial, subjects' peak uCOF was determined during the first 50% of the stance phase. To avoid spuriously high uCOF values caused by the division of small GRF values, only data after the first 5% of stance phase was considered. A one-way repeated measures ANOVA was performed to test for differences in peak uCOF among the 3 conditions. Similarly one-way ANOVA's were performed to assess for differences in the vertical force and resultant shear force at the time of peak uCOF. For all ANOVA tests, post-hoc comparisons consisting of paired t-tests were employed using a Fisher's LSD adjustment. All significance levels were set at $p<0.05$.

RESULTS AND DISCUSSION

The ANOVA comparing peak uCOF among the 3 dynamic tasks was significant ($p < 0.001$). Post-hoc testing revealed that uCOF was significantly different among the 3 conditions. On average the uCOF during running had the lowest uCOF while the uCOF during the performance of the V-cut was the highest (Figure 1). With respect to ground reaction forces at the time of peak uCOF, there were no significant differences in the vertical GRF among tasks. However, there was a significant effect of task on the resultant shear GRF ($p < 0.001$). Post-hoc testing revealed that both cutting tasks had significantly greater resultant shear forces compared to running (Figure 2). No difference in the resultant shear force was found between the side-step cut and the V-cut.

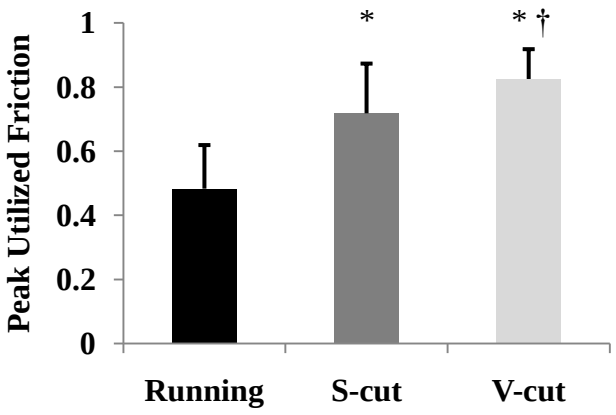

Figure 1. Comparison of peak uCOF across the 3 tasks. * indicates significantly different from running. † indicates significantly different from S-cut.

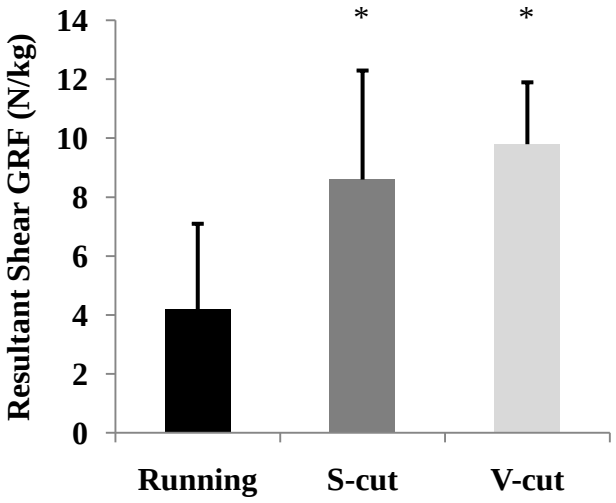

Figure 2. Comparison of Resultant Shear GRF at time of peak utilized friction across the 3 tasks. * indicates significantly different from running.

Our data indicate that uCOF varies significantly based on the task performed. In general, the uCOF for the sport-specific tasks evaluated in the current study far exceeded what has been reported for normal speed walking (0.17-0.20).[3] The increase in uCOF during running and cutting was the result of higher resultant shear forces as no differences in vertical forces were found at the time of peak uCOF.

CONCLUSIONS

The results of our study indicate that the friction demands during various sport-specific tasks are considerable. In particular, cutting tasks were found to require greater friction compared to running. The higher friction demands during cutting were the result of the generation of greater shear forces to facilitate a change in direction. The data obtained from this study can be used to establish available requirements for court surfaces in order to prevent the likelihood of a slip event during athletic competition.

REFERENCES

1. Hanson JP, Redfern MS, Mazumdar M. *Ergonomics*. 1999;**42**(12):1619-33.
2. Burnfield JM, Tsai YJ, Powers CM *Gait & Posture*. 2005;**22**:82-8.
3. Tsai YJ, Powers CM. *Gait & Posture*. 2009;**30**(3):303-6.
4. Redfern et al., *Ergonomics*. 2001;**44**:1138-66.
5. Hopper D. *Australian J Physiol*. 1986;**32**(4):231-39.

JOINT MOMENTS DURING WALKING AND RUNNING AT DIFFERENT SPEEDS

[1]Ana de David, Pro Stergiou[2] and Darren Stefanyshyn[2]

[1]University of Brasilia, Brasilia, DF, Brazil
[2]University of Calgary, Calgary, AB, Canada
email: acdavid@unb.br, web: http://www.unb.br

INTRODUCTION

Walking and running are popular forms of exercise. Fast walking and slow running are recommended as lower loading exercise for overweight people and orthopedic patients. Investigations about joint kinetics during running, compared to walking, at different speeds, are limited. Biomechanical information regarding how lower extremity joint loads change from walking to running as speed increases may be useful for fitness and rehabilitation programs or for sport footwear design. Loads in the lower extremity seem to be speed dependent [1] and kinetic data, in general, have a stronger relationship with speed than kinematic parameters [2]. Therefore, this study compared knee and ankle moments during running, slow running and self-selected comfortable walking and fast walking.

METHODS

Twelve recreational male runners between the age of 20 and 30 years (mean height 1.78 ± 0.06 m and mean mass 74.7 ± 5.7 kg) participated in this study. Right lower limb kinematic data were collected at 240 Hz using an eight-camera motion capture system (Motion Analysis Corp.) and ground reaction forces were measured with a 1200 Hz forceplate (Kistler AG). Subjects were asked to run at 4 m/s ± 10% and at a slow speed that was 30% slower and to walk at self-selected comfortable and fast speeds while wearing control shoes along a 10 m gait laboratory walkway. All subjects performed five trials at each speed. Data reduction was done using Kintrak software (Motion Analysis Corp.). A 4th order Butterworth algorithm was used to filter kinematic data (10 Hz cutoff) and kinetic data (50 Hz cutoff). The analysis involved calculation of sagittal, frontal and transverse moments for the knee and ankle using inverse dynamics. ANOVA with repeated measures was used to compare joint moment peak values among different conditions. The significance level chosen for these tests was $P < 0.05$.

RESULTS AND DISCUSSION

Joint moment curves for running, slow running, comfortable walking and fast walking during stance are shown in Figures 1-5. The ankle moment in the transverse plane showed high variability so it was not included in the analysis

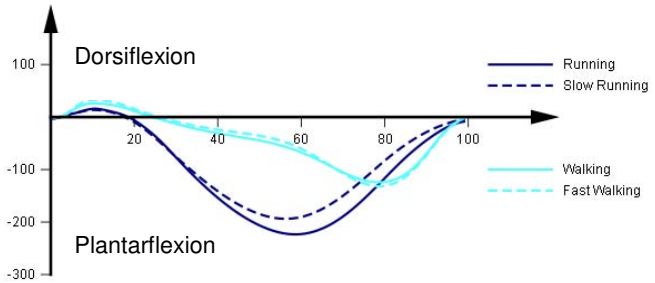

Figure 1: Ankle moment in sagittal plane (Nm).

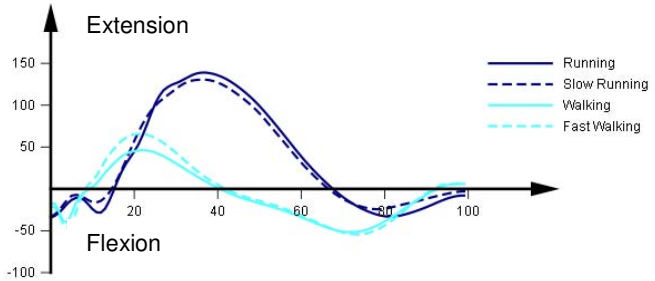

Figure 2: Knee moment in sagittal plane (Nm).

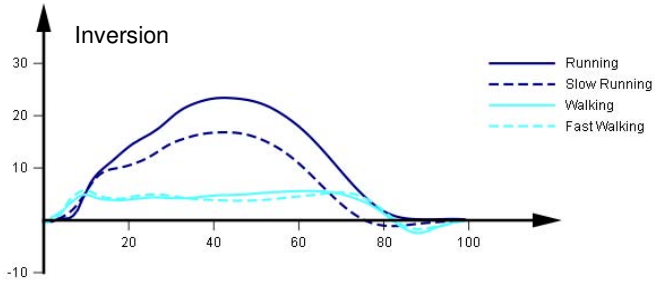

Figure 3: Ankle moment in frontal plane (Nm).

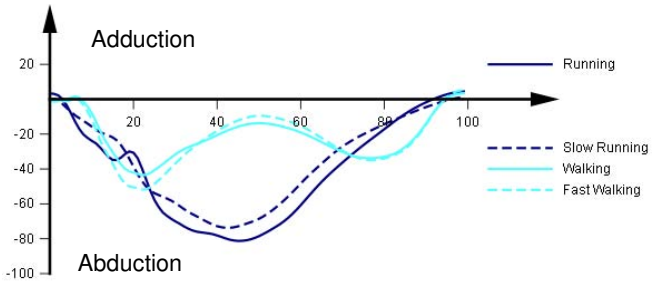

Figure 4: Knee moment in frontal plane (Nm).

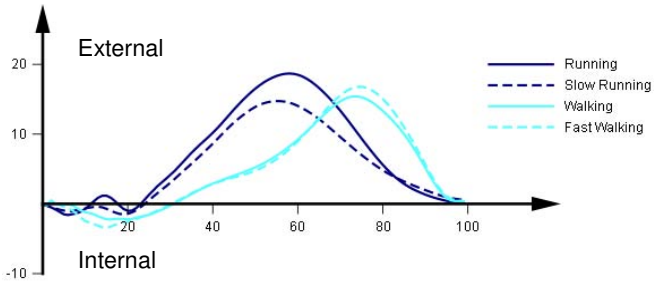

Figure 5: Knee moment in transverse plane (Nm).

Moment patterns are different at the knee and ankle when comparing walking and running movements. The plantarflexion peak occurs later when walking than in running (Fig. 1). Sagittal knee moment presents an extension peak during early stance and a flexion peak at late stance, opposite to running, that presents a predominantly extension peak during the entire stance phase (Fig. 2). The same occurs with the ankle inversion moment while running and slow running (Fig. 3). For comfortable walking and fast walking there are two ankle inversion and knee adduction peaks (Fig. 4). External rotation moment peaks at the knee occur later in comfortable walking and fast walking (Fig. 5). Results showed similar curve patterns when comparing comfortable walking and fast walking or slow running and running. But significantly lower joint loading was found for the ankle in the sagittal and frontal plane and for the knee in the frontal and transverse plane during slow running than running (Table 1). Fast walking showed lower joint loading than slow running in the knee and ankle for the sagittal and frontal plane. When comfortable walking was compared to the other conditions most joint moment peaks were significantly different.

CONCLUSIONS

In the present study data for joint moments at the knee and ankle are provided to compare walking and running loads. Data suggest that when considering reducing joint loading in the lower extremity, walking and fast walking should be recommended. Increasing speed from fast walking to slow running is associated with an increase in the loads in the sagittal and frontal plane. Thus, treatments with orthopedic patients or obese people should take into account the effects of the increase of gait speed in the joint loading.

REFERENCES

1. Stoquart et al. *Clinical Neurophysiology,* **38**, 105-116, 2008.
2. Lelas et al. *Gait and Posture,* **17**, 106-112, 2003.

Table 1: Mean and standard deviation for joint moment peak and speed (n=12).

Joint Moment Peak (Nm)	Running	Slow Running	Fast Walking	Comfortable Walking
Ankle Plantarflexion	224.9 ± 26.5[b,c,d]	195.6 ± 26.0[a,c,d]	133.8 ± 13.9[a,b,d]	124.95 ± 15.9[a,b,c]
Ankle Inversion	27.3 ± 15.8 [b,c,d]	16.9 ± 10.7 [a,c,d]	10.8 ± 5.7 [a,b]	9.44 ± 4.6 [a,b]
Knee Flexion	37.0 ± 21.2 [c,d]	29.6 ± 15.9 [c,d]	57.5 ± 18.1 [a,b,d]	52.34 ± 18.0 [a,b,c]
Knee Extension	143.0 ± 39.3 [c,d]	135.0 ± 38.5 [c,d]	66.8 ± 22.1 [a,b,d]	46.92 ± 24.7 [a,b,c]
Knee Abduction	87.4 ± 37.3 [b,c,d]	75.9± 32.3 [a,c,d]	53.7 ± 14.8 [a,b,d]	43.48 ± 10.3 [a,b,c]
Knee External Rotation	20.1 ± 10.7[b]	15.9 ± 9.3[a]	17.1 ± 3.3[d]	15.53 ± 3.7[c]
Speed (m/s)	4.06 ± 0.13 [b,c,d]	2.91 ± 0.09 [a,c,d]	2.08 ± 0.14 [a,b,d]	1.61 ± 0.10 [a,b,c]

Values are means ± SD.
[a,b,c,d] Condition is significantly different ($P < 0.05$) from running[a], slow running[b], fast walking[c] and comfortable walking[d].

HIGH PLANTAR-FLEXOR PASSIVE STIFFNESS INCREASES ACHILLES TENDON LOADING DURING LANDINGS

John W. Whitting, Julie R. Steele, Deirdre E. McGhee and Bridget J. Munro

Biomechanics Research Laboratory, University of Wollongong, Australia
email: jwhittin@uow.edu.au, web: http://www.uow.edu.au/health/brl

INTRODUCTION

Up to 50% of all sporting injuries are classified as overuse injuries with Achilles and patellar tendinopathies being among the most common, particularly in sports involving repetitive landing [1,2]. During landings, external forces must be absorbed rapidly and eccentrically, which places high loads on extensor mechanisms such as the plantar-flexors and quadriceps. Furthermore, the passive tissues of any musculotendinous complex contribute substantially to the overall forces borne by the entire muscle-tendon unit while actively contracting [3]. As such, it is postulated that limited flexibility through high plantar-flexor passive stiffness or, alternatively, limited dorsiflexion range of motion, may be associated with excessive soft tissue loading and hence, overuse injuries [1]. However, no research has systematically investigated the effects of passive plantar-flexor stiffness on lower limb mechanics during the performance of a dynamic landing task. Therefore, the purpose of this study was to determine how plantar-flexor passive stiffness affected loading at the Achilles and patellar tendons during landings.

METHODS

Passive dorsiflexion range of motion (PROM) and plantar-flexor passive stiffness (PPS; KinCom dynamometer) were quantified for 42 physically active males. The PPS values were obtained by measuring the slope of the torque-angle curve between 15° and 20°, generated while passively stretching the plantar-flexors at $5°.s^{-1}$ [4]. All 42 participants were then ranked from the lowest to highest stiffness ($Nm.°^{-1}$), with the middle 10 PPS values being removed from any further analysis to ensure distinct participant groups; low (LPS) or high (HPS) PPS (see Table 2).

Three-dimensional ankle and knee joint kinematics were then quantified using an Opto*Trak* 3020 motion analysis system while the participants performed 5 single limb drop landings onto a Kistler force platform at a vertical descent velocity of 3.21 ± 0.17 $m.s^{-1}$. Achilles tendon forces during each landing were calculated by dividing the internal plantar-flexor moment by the Achilles tendon moment arm [5]. Similarly, the patellar tendon forces were calculated by dividing the internal quadriceps extensor moment by the patellar tendon moment arm using the equation developed by Herzog and Read [6]. Outcome variables characterizing ankle and knee kinematics and forces generated during landing were then compared between the LPS and HPS groups using a series of independent *t*-tests ($p < 0.05$).

RESULTS AND DISCUSSION

During the single limb drop landings, the LPS group encountered a significantly greater peak vertical ground reaction force, although the peak Achilles and patellar tendon forces were not significantly different between the participant groups (see Table 2). However, the HPS group absorbed their peak Achilles tendon force at a significantly greater percentage of their PROM and displayed significantly more dorsiflexion at the time of their peak eversion angle (see Table 2). Experiencing a peak Achilles tendon strain at approximately half of their PROM (see Table 2), while eccentrically contracting their plantar-flexors during an abrupt landing, would certainly place some of the soft tissues of the HPS group under stress at a substantially more lengthened range than their LPS counterparts. Furthermore, as the functional action of the plantar-flexors is to plantar-flex and invert the foot, excessive dorsiflexion, coupled with a substantially everted foot, would produce even greater tensile loading of the Achilles

tendon and other soft tissues. Therefore, it is reasonable to speculate that the HPS group, already with an inherently high PPS (see Table 2), may have experienced strain of their passive tissues at a more compromised physiological range than their LPS counterparts.

It is also likely that the greater knee flexion angle displayed by the HPS group when landing (see Table 2) contributed to a reduction in the peak vertical ground reaction forces they experienced relative to the LPS group. However, this meant that the HPS group flexed their knees by an excessive 77.5° (see Table 2). Although we found no significant difference for peak knee flexion between the groups, the HPS group flexed their knees by approximately 8° more than the LPS group. From a clinical perspective, the soft tissues of the quadriceps complex, including the patellar tendon, must have been more lengthened in the HPS group. It is reasonable, therefore, to postulate that this additional knee flexion may place the soft tissues of the knee extensor mechanism, under a more compromising physiological load more regularly in the HPS group.

CONCLUSIONS

These results indicate that, when performing single limb drop landings, participants with high passive plantar-flexor stiffness, absorbed external loads through the plantar-flexor and quadriceps complexes at potentially compromising and injurious physiological ranges. The implications of this finding for repetitive sports movements are that high plantar-flexor passive stiffness may cause repetitive overloading of passive structures such as the Achilles and patellar tendons, thereby exposing these athletes to more risk of incurring overuse injuries such as tendinopathies.

REFERENCES

1. Rees JD, et al**.** *Am J Sports Med,* **37(9),** 1855-1867, 2009.
2. Flood L & JE Harrison, *Med J Aust*, **190(2)**, 87-90, 2009.
3. Lieber RL, Skeletal muscle structure, function & plasticity. The physiological basis of rehabilitation. Lippincott, Williams & Wilkins, 2002.
4. Kubo K, et al. *Eur J Appl Physiol*, **85(3-4)**, 226-232, 2001.
5. Self BP & D Paine, *Med Sci Sports Exerc*, **33(8)**, 1338-44, 2001.
6. Herzog W & LJ Read, *J Anat,* **182**, 213-230, 1993.

ACKNOWLEDGEMENTS

This research was funded by the New South Wales Sporting Injuries Committee.

Table 2: Ankle flexibility and landing variables for the low (LPS) & high passive tension (HPS) groups.

	LPS		HPS		
VARIABLE	**N**	**Mean (SD)**	**N**	**Mean (SD)**	***p***
Passive plantar-flexor stiffness (PPS; $Nm.^{\circ-1}$)	16	1.0 (0.2)	16	2.2 (0.4)	0.000
Passive dorsiflexion ROM (PROM; °)	16	28.1 (16.6)	16	27.1 (5.5)	0.823
Peak vertical ground reaction force (N)	16	5272 (1186)	16	4420 (1119)	0.045
Peak vertical ground reaction force ($N.kg^{-1}$)	16	7.1 (1.3)	16	6.2 (1.4)	0.058
Peak dorsiflexion angle (°) *	15	25.9 (4.3)	16	26.7 (4.9)	0.651
Peak ankle eversion angle (°)	16	13.5 (8.8)	16	16.6 (7.0)	0.287
Dorsiflexion % at peak ankle eversion angle #	16	68.5 (18.9)	16	93.2 (24.8)	0.003
Peak Achilles tendon force (N.kg-1)	16	5.5 (0.9)	16	5.7 (0.6)	0.337
Dorsiflexion % at peak Achilles tendon force #	16	29.5 (13.4)	16	49.3 (26.3)	0.012
Peak knee flexion angle (°) *	9	69.5 (10.4)	14	77.5 (12.8)	0.128
Peak patellar tendon force (N.kg-1)	16	6.1 (1.0)	16	6.0 (0.8)	0.389

* Indicates a reduced sample size due to missing data points; # Dorsiflexion % = dorsiflexion angle at event/ PROM

ACCLIMATION TO TREADMILL RUNNING IN MINIMAL FOOTWEAR

[1,2]Trampas TenBroek, [1,2]Pedro Rodrigues, [1]Sean Murphy and [2]Joseph Hamill

[1]New Balance Sports Research Lab, Lawrence, MA, USA
[2]University of Massachusetts Amherst, Amherst, MA, USA
email: trampas.tenbroek@newbalance.com

INTRODUCTION

Barefoot running has received a great deal of attention recently. Proponents claim benefits such as the elimination of impact peaks, greater flexibility and proprioceptual input mitigating potentially detrimental behaviors. However, barefoot running may leave the foot susceptible to a variety of acute environmentally related injuries.

Barefoot inspired footwear has reduced the amount of underfoot material compared to traditional training footwear (TTF). Although many biomechanical comparisons have been conducted on barefoot versus TTF running, biomechanical changes due to running in something in between these extreme conditions are not well understood.

Squadrone and Gallozzi [1] recently reported a more plantar flexed ankle and lower impact force when experienced barefoot runners wore the Vibram Fivefingers. These shoes differ from TTF for several reasons including a thin midsole, a laceless stretch upper, and toes. Therefore, the effect of reducing midsole thickness alone is still not known. Ferris et al [2] reported that runners instantaneously adjusted leg stiffness when taking a single step onto a new material. However, these athletes had ample practice before data were collected and were very aware of the characteristics of the new material. How quickly athletes adjust to different footwear without any a prior knowledge of the shoe characteristics is of particular interest.

The purpose of this study was, therefore, to investigate the impact shock in footwear with different midsole thickness.

METHODS

Ten uninjured, recreational male runners (23-53 years) performed 6 minute runs in 4 footwear conditions (Figure 1) on an aluminum slat treadmill. All shoes had identical uppers with midsoles of different thicknesses. Basic outsole rubber was attached on the lateral heel and medial forefoot of all shoes.

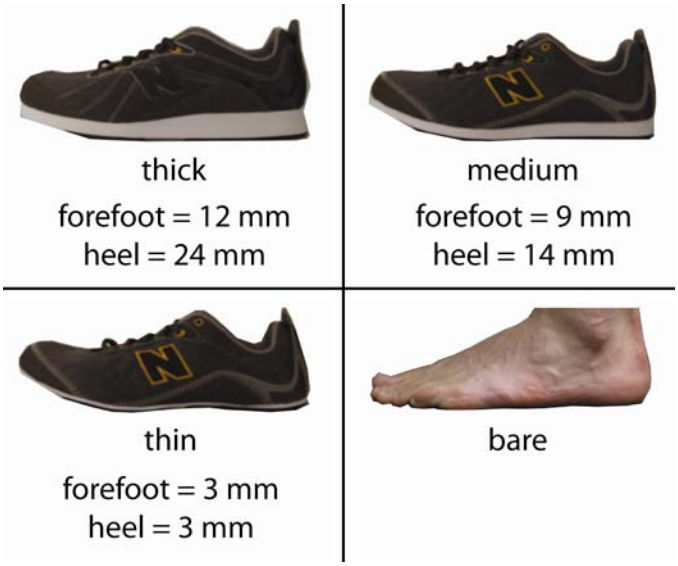

Figure 1: Footwear condition with EVA thickness.

Impact shock was measured at 1000 Hz using two accelerometers attached securely to the distal, antero-medial tibia and the anterior aspect of the forehead. The accelerometers were aligned with the long axis of the tibia and head. The accelerometers were mounted to the skin using 2-sided tape and wrapped with athletic pre-wrap.

To investigate response to each footwear condition, subjects received no information on the footwear. The test administrator put the shoes on while subjects were seated close to the treadmill. Subjects then took one step to straddle the moving treadmill belt. Their next movement was onto the treadmill belt already moving at 3.0 m/s.

Low pass filtered (50 Hz) peak tibial acceleration and peak cranial acceleration values were obtained for steps 1-5, 6-10 and 11-15. Additionally, 5 steps

at 3 minutes and at 6 minutes were analyzed to investigate the effect of time. The four footwear conditions were also compared using ANOVA (criterion alpha level 0.05).

RESULTS AND DISCUSSION

The footwear condition most resembling TTF (thick) resulted in the lowest tibial acceleration (Figure 2) which is consistent with previous findings [3]. These differences are likely a result of effective mass changes made by the athlete.

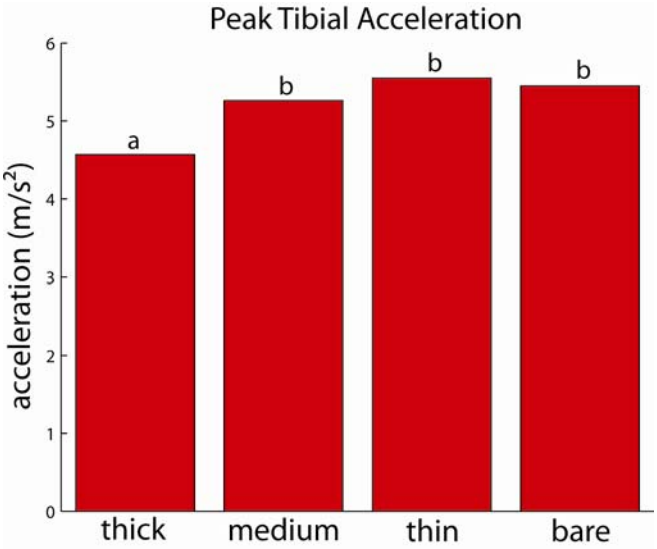

Figure 2: Peak Tibial Acceleration vs. Footwear Condition. Letters distinguish statistical differences.

A trend was found for the thin and medium conditions resulting in greater head accelerations compared to the thick condition, although these differences were not statistically significant (p=0.07 & 0.10 respectively). Conversely, others have shown head accelerations to be quite stable regardless of condition [4,5]. The barefoot and TTF conditions resulted in similar cranial accelerations though their tibial values were quite different. The thin and medium conditions may protect the foot or limit proprioception enough to not elicit kinematic changes equivalent to barefoot. Lack of kinematic adjustment and lack of underfoot dampening material may increase the amount of shock translated to the head. This would align with the findings of Squadrone who found Fivefinger to resemble barefoot running but potentially allow more aggressive running.

Standard deviations of peak accelerations were greater for the 1st five steps in each footwear condition (Figure 3) at the tibia and the head. Although Ferris et al. found instantaneous stiffness alterations to a new surface; it appears that adaptations do not occur instantaneously, but over as few as 5 strides.

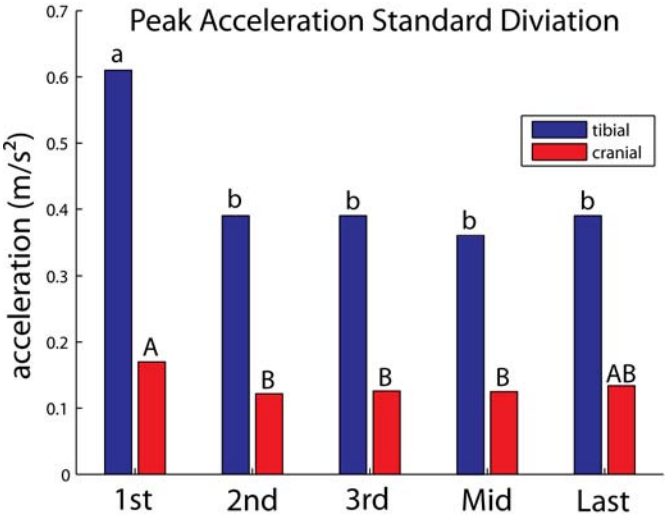

Figure 3: Standard deviations of peak accelerations for the tibia and cranium vs. time. Letters distinguish statistical differences.

CONCLUSIONS

Running in footwear with less material underfoot than TTF results in elevated tibial accelerations likely due to changes in effective mass. Minimal footwear may also result in elevated head accelerations which are normally consistent across many factors. It appears that runners adjust to new, even novel, footwear quickly.

REFERENCES

1. Squadrone, R, et al. *Journal of Sports Medicine and Physical Fitness,* **49**, 6-13.
2. Ferris, DP, et al. *Journal of Biomechanics,* **32**, 787-794.
3. Nigg, BM, et al. *Biomechanics of Running Shoes,* Human Kinetics Books, 1986.
4. Dufek, JS, et al. *Journal of Applied Biomechanics,* **25**, 219-228.
5. Hamill, J, et al. *Human Movement Science,* **14**, 45-60.

THE EFFECT OF FUNCTIONAL FATIGUE AND ANKLE BRACING ON LOWER EXTREMITY RESPONSE TO JUMP LANDING TASKS

Elizabeth D. Stafford and Jason C. Gillette

Iowa State University, Ames IA
email: estaffo1@iastate.edu

INTRODUCTION

Lateral ankle sprains are the most common sports injury. A sprain rate of 79% is reported in basketball and 87% in volleyball [1]. In order to combat this injury, many athletic trainers have used taping and ankle bracing prophylactically. At this institution, the women's volleyball team wear ankle braces at all times for practices and for games. Previous literature has focused on two main areas related to ankle sprain injury prevention: ankle bracing and fatigue. One line of thought is that the presence of tape or a brace at the ankle provides additional proprioceptive feedback and thus improved muscular response to perturbation [2-3]. The opposing argument is that with habitual use, the body adapts to the additional feedback and is more at risk when the supplemental support is removed. Secondly, it is proposed that many of these injuries happen when athletes are tired, and thus the effects of fatigue on muscle response are critical [1,4]. The results have been mixed for both research areas. Previous literature indicates that EMG activity is greater when the ankle is braced than when the ankle is unbraced [2]. Additionally, there are mixed results in time to stabilization and other balance measures when muscles are fatigued [1,4].

The purpose of the current study was to investigate the effect of functional fatigue on lower extremity response to jump landing tasks with and without a semi-rigid ankle brace. The biceps femoris and peroneus brevis muscles are often considered stabilizers in jump landings. Therefore, it was hypothesized that biceps femoris and peroneus brevis muscle activity would increase during landings when fatigued as compared to pre-fatigue. It was also hypothesized that biceps femoris and peroneus brevis muscle activity would be greater with a braced ankle than for an unbraced ankle when fatigued.

METHODS

Eight individuals (2 males/6 females, age 23 ± 2 years, height 1.73 ± 0.11 m, mass 81 ± 29 kg) participated in the study. Breg Ultra FullCourt ankle braces were tested, which are also worn by this institution's volleyball team. Vastus lateralis, biceps femoris, and peroneus brevis EMG signals were measured using a wireless system (Delsys). Maximum voluntary isometric contractions (MVIC) were recorded for each muscle group. For the pre-fatigue tests, participants performed two trials of a backwards jump starting on both feet and landing on the left foot only. An in-ground force platform (AMTI) was used to detect ground contact for the jump landing. After completing this movement with unbraced ankles, participants donned the ankle braces and completed two trials of the same backward jump with the ankles braced.

After finishing the pre-fatigue test, participants completed a fatigue protocol while wearing the ankle braces. The fatigue protocol included the Southeast Missouri agility test (SEMO) and use of a Bosu, cones, and hurdles. Participants averaged a score of 15 on the Borg scale of perceived exertion at the end of the fatigue protocol, indicating that they had worked "hard". As a post-fatigue test, two trials of the backward jump were then performed with the ankles braced, followed by two trials with the ankles unbraced. A linear envelope (10 Hz low-pass filter) was used to determine average muscle activity during the 100 milliseconds prior to landing ("preparation phase"), and 400-500 milliseconds after initial impact of the landing ("stabilization phase"). EMG values were averaged across two trials and normalized to the MVIC. Paired sample t-tests were performed to determine differences in EMG activity between pre-fatigue and post-fatigue and between braced and unbraced jump landings (SPSS). Significance was set at $p < 0.05$.

RESULTS AND DISCUSSION

For the braced condition, the peroneus brevis displayed significantly higher EMG activity ($p=0.033$) during the preparation phase when fatigued as compared to pre-fatigue (Table 1). For the unbraced condition, the increase in peroneus brevis EMG activity approached significance ($p=0.073$) during the landing preparation phase when fatigued as compared to pre-fatigue. When fatigued, biceps femoris EMG activity was significantly higher ($p=0.010$) during the balance stabilization phase for the braced condition as compared to the unbraced condition (Table 2). There were no significant differences in vastus lateralis EMG activity as a function of fatigue or bracing.

It was hypothesized that activity in the stabilizing muscles (biceps femoris and peroneus brevis) would increase when fatigued as compared to pre-fatigue. This hypothesis was not supported for the biceps femoris, which had a nonsignificant 11% increase in activity during landing preparation with fatigue, but actually declined in activity during balance stabilization with fatigue. This hypothesis was partially supported for the peroneus brevis, which displayed a 49% increase in activity during landing preparation with fatigue, resulting in significance differences when braced and approaching significance when unbraced. However, peroneus brevis activity decreased overall during the balance stabilization phase with fatigue. It is of potential interest for ankle sprains that the substantial increase in peroneus brevis activity in landing preparation does not appear to carry over to balance stabilization.

Table 1: EMG activity during landing preparation

		EMG (%MVIC)	
Support	**Muscle**	Pre-Fatigue	Fatigued
Unbraced	PB	0.40 ± 0.18	0.54 ± 0.19[b]
	BF	0.28 ± 0.22	0.32 ± 0.35
	VL	0.76 ± 0.32	0.84 ± 0.36
Braced	PB	0.40 ± 0.20	0.66 ± 0.26[a]
	BF	0.30 ± 0.27	0.32 ± 0.25
	VL	0.72 ± 0.25	0.79 ± 0.40

[a] fatigued > pre-fatigue ($p<0.05$)
[b] fatigued > pre-fatigue ($p<0.10$)
PB – peroneus brevis, BF – biceps femoris
VL – vastus lateralis

Table 2: EMG activity during balance stabilization

		EMG (%MVIC)	
Support	**Muscle**	Pre-Fatigue	Fatigued
Unbraced	PB	0.47 ± 0.27	0.40 ± 0.16
	BF	0.30 ± 0.21	0.23 ± 0.20
	VL	0.67 ± 0.24	0.65 ± 0.28
Braced	PB	0.50 ± 0.27	0.53 ± 0.22
	BF	0.31 ± 0.24	0.30 ± 0.24*
	VL	0.68 ± 0.30	0.76 ± 0.34

* braced > unbraced ($p<0.05$)
PB – peroneus brevis, BF – biceps femoris
VL – vastus lateralis

It was also hypothesized that the activity of the biceps femoris and peroneus brevis would be greater in the braced condition when fatigued than in the unbraced condition. This hypothesis was partially supported by a significant 33% increase in biceps femoris activity during balance stabilization when wearing a brace while fatigued, but there was no difference in landing preparation. The hypothesis was not statistically supported for the peroneus brevis, even though there was a 27% increase in activity with bracing during fatigue. These increases in muscle activity during fatigue may be in response to reduced capability to use ankle strategies for balance stabilization when wearing an ankle brace.

CONCLUSIONS

The results indicate that there is increased peroneus brevis activity during landing preparation when fatigued, particularly when wearing an ankle brace. It is unclear if this is a fatigue induced response to increase stiffness of the ankle prior to landing. In addition, increased peroneus brevis activation may be due to enhanced proprioception provided by the ankle brace. Further analysis of kinematic and kinetic data may provide additional insight into these mechanisms, especially in the landing impact phase where skin movement hinders reliable peroneus brevis EMG measurements.

REFERENCES

1. Shaw MY, et al. *J Athl Train*, **43**, 164-171, 2008
2. Cordova ML, et al. *Br J Sports Med*, **37**, 258-262, 2003.
3. Papadopoulos ES, et al. *BMC Musculoskelet Disord*, **8**, 2007.
4. Vuillerme N, et al. *Gait Posture*, **28**, 521-524, 2008.

MAXIMUM POSSIBLE QUADRICEPS FORCE 50ms AFTER GROUND CONTACT

Zachary Domire, Rhonda Boros and Javad Hashemi

Texas Tech University, Lubbock, TX, USA
email: Zachary.domire@ttu.edu, web: http://www.depts.ttu.edu/hess/research/bio/

INTRODUCTION

Anterior cruciate ligament (ACL) rupture is one of the most common injuries in sport. It is also expensive and requires a lengthy rehabilitation. Furthermore, even when the injured ACL is reconstructed, there is an increased risk of knee osteoarthritis development [1]. Because of these factors, ACL injury prevention is of utmost importance. Determining the mechanism of ACL injury would be exceptionally valuable in developing prevention strategies. DeMorat and colleagues [2] examined aggressive quadriceps loading as a possible mechanism for ACL injury. They found that a quadriceps load of 4500 N applied with the knee in 20º of flexion was sufficient to cause ACL injury in approximately half of the specimens tested. It has been suggested that because of force-length properties [3] or as ACL injuries have been shown to occur within 50ms of landing [4], limited time to develop force [5], 4500N is not an obtainable quadriceps force.

The purpose of this study was to use a simple simulation model to examine the upper bounds of quadriceps force that could contribute to injury during landing.

METHODS

To simulate landing a single muscle-tendon like actuator representing the combined quadriceps muscles was first isometrically activated to allow for pre-activation prior to landing and then stretched for 50ms. The velocity of stretch was ramped from 0-0.61m/s (0-700º/s [6] multiplied by rectus femoris moment arm at 20º [7]).

The base equation for the muscle model [8] is:

$$F=F_{max}.F_L.F_V.q \quad (1)$$

Where, F – muscle force, F_{max} – maximum isometric force, F_L – fraction of force as a result of force-length properties, F_V – fraction of force as a result of force-velocity properties, q – active state.

To simplify the model, the force-length relationship was removed and a maximum isometric force at 20º of flexion was estimated. A parabola was fit to the maximum knee extension strength data reported by Scudder [9] and the torque at 20º was extrapolated. This data was for young healthy men and is considerably higher than values reported elsewhere [10]. The extrapolated torque was then divided by the rectus femoris moment arm at 20º [7]. The force-velocity relationship was modeled using the equations from FitzHugh [11]. Force-velocity parameters were taken from Faulkner and colleagues [12]. This maximum shortening velocity is lower than what is used by many simulations [13]. As the simulated muscle action is eccentric, this will result in higher force production.

A simplified pattern of neural excitation was assumed. A constant pre-activation was applied starting 86ms before landing [14]. This is 70% earlier than what has been reported by others [6]. The activation level of the quadriceps at landing is likely between 15-30% [15]. As this parameter is likely the least certain value, a range of values between 15-100% were examined. At contact maximum activation was assumed. An electro-mechanical delay between initial neural excitation and the development of force was applied. The value used is much lower than what has generally been reported [16]. The relationship between the neural excitation and the active state was represented by a first-order differential equation [17]. To determine the rise time constant for this equation the value was fit to match the rate of force development [18] following a strength training intervention. This resulted in a rate of force development higher than that of elite athletes [16] during the first 50ms of force production. Table 1 summarizes the parameters used in the model.

Table 1: Model parameters.

Maximum Isometric force at 20º	2805N
Moment arm at 20º	0.05m
Tendon strain at max isometric force	4%
Maximum shortening velocity	6fl/s
Force-velocity curvature parameter	4
Rise time constant	10.2s
Electromechanical delay	13.5ms
Pre-activation timing	86ms

RESULTS AND DISCUSSION

When using realistic pre-activation levels, the simulated quadriceps force was under 2000N (Table 2). Even when using maximum pre-activation, the quadriceps force was still far below 4500N.

Table 2: Effect of varying pre-activation levels on quadriceps force 50ms after landing.

Pre-activation level	Force 50ms after landing
15%	1829N
30%	1986N
50%	2231N
100%	3015N

Parameters for the model were chosen to provide a high estimate for possible quadriceps force 50ms after landing. This can be demonstrated by examining each element from equation 1. The maximum isometric force calculated from the knee extension strength data of Scudder [9] is over 8000N. This is substantially higher than values used by DeMorat and colleagues [19] to justify the use of 4500N in their cadaveric testing [2]. The fraction of force as a result of force-length properties comes from the shape of Scudder's torque-angle curve. Studies consistently measure maximum strength at knee flexion angles of at least 60º, noting significant reductions at 20º [10]. The simulation resulted in the fraction of force from the force-velocity relationship 1.5 times the isometric force. This is higher than what has been reported for in vivo studies, even when applying maximal electrical stimulation [20]. The pattern of activation we used was also artificially high. In a realistic activation pattern, pre-activation levels would ramp from 0 to a value of approximately 15-30% at contact and maximum quadriceps activity would not occur until more than 50ms after landing [6,14].

CONCLUSIONS

The results of this study indicate that even in young healthy men, the quadriceps force at the time of ACL injury is likely less than 2000N. Even when maximally activated the quadriceps only produce approximately 3000N. These results suggest that 4500N of quadriceps force is not obtainable within the first 50ms of landing. Furthermore, given that 4500N of quadriceps force was insufficient to rupture nearly half of cadaveric ACL's [2], quadriceps force alone seems to be an unlikely mechanism for ACL injury.

REFERENCES

1.Louboutin, H, et al. *Knee* ***16,*** 239-44. 2009.
2.DeMorat, G, et al. *Am J Sports Med* ***32,*** 477-83, 2004.
3.McLean, SG, et al. *Am J Sports Med* ***33,*** 1106, 2004.
4.Krosshaug, T, et al. *Am J Sports Med* ***35,*** 359-67, 2007.
5.Hashemi, J, et al. *Knee,* epub, 2009.
6.Gehring, D, et al. *Clin Biomech* ***24,*** 82-7, 2009.
7.Visser, JJ, et al. *Eur J Appl Physiol Occup Physiol* ***61,*** 453-60, 1990.
8.Gallucci, JG, and Challis, JH. *J Appl Biomech* ***18,*** 15-27, 2002.
9.Scudder, GN . *Arch Phys Med Rehabil* ***61 ,*** 68-73, 1980.
10.Kulig, K, et al. *Exerc Sport Sci Rev* ***12,*** 417-66, 1984.
11.FitzHugh, R . *J Math Biol* ***4,*** 203-36, 1977.
12.Faulkner, JA, et al. In: *Human Muscle Power*, 81-94, Human Kinetics Publishers Inc., 1986.
13.Domire, ZJ, and Challis, JH . *Comput Methods Biomech Biomed Engin* epub, 2010.
14.Cowling, EJ, et al. *Br J Sports Med* ***37,*** 126-30. 2003.
15.Kellis, E, and Kouvelioti, V. *J Electromyogr Kinesiol* ***19,*** 55-64, 2009.
16.Tillin, NA, et al. *Med Sci Sports Exerc* epub, 2009.
17.Pandy, MG, et al. *J Biomech Eng* ***114,*** 450-60, 1992.
18.Aagaard, P, et al. *J Appl Physiol* ***93,*** 1318-26, 2002.
19.DeMorat, G, et al. *Am J Sports Med* ***33,*** 1106-07, 2004.
20.Dudley, GA, et al. *J Appl Physiol* ***69,*** 2215-21, 1990.

GROUND CONTACT TIME AND RUNNING SPEED IN ELITE CHAMPIONSHIP DISTANCE RACES

Iain Hunter, Ruthann Cunningham, Sarah Ingebretsen, & Doug Butler
Brigham Young University, Provo, UT
E-mail: iain_hunter@byu.edu Web: http://biomech.byu.edu

INTRODUCTION

The goal in distance running is to find a balance between maximum sustainable speed and energy production. This balance plays a vital role in distance running. Throughout the years, athletes have sought for ways to improve performance in this event by balancing the distance of the race with speed.

One way to understand the proper balance of distance and speed is to measure running economy at a given speed. Improvements in running economy increase performance in any distance running event [1].

As a runner increases in speed, changes in movement patterns and forces occur. Specifically, the amount of time the runner spends on the ground decreases [2,3,4]. Faster athletes are able to apply greater ground forces leading to a shorter ground contact time and greater maximum running speeds [2]. While it is known that as running speed increases, ground contact time decreases, there may also be factors other than speed increases that relate to ground contact time. We hypothesized that ground contact time normalized by speed would be correlated with average running speed during an elite 10 km race on the track.

METHODS

A digital camera running at 200 Hz was placed perpendicular to the backstretch of the track at the 2009 USA Track and Field Nationals for the men's 10,000 m final. An 8 m section of the track was visible within the camera view. A 4-m horizontal scaling was completed with adjustments being made according to which lane the runners came through.

The top 13 runners in the race were analyzed. Ground time was determined by initial contact of the left foot until toe-off. Horizontal velocity of the left hip was calculated over the course of one stride from foot contact to the next foot contact of the same foot using Dartfish ProSuite 4.5 (Dartfish Corp, Alpharetta, GA). Lap times were obtained from official meet results.

Ground contact time was normalized by horizontal velocity during the stride of ground time measurement. A simple linear regression using SPSS 18.0 determined the correlation between ground contact time divided by horizontal velocity and average lap speed.

RESULTS AND DISCUSSION

Ground contact time divided by running speed during the measured stride is correlated with average lap running speed for men (Average Race Speed = -58.4 x (GroundTime/Speed) - 0.7, R^2 = 0.545, F= 11.978, p=0.006, Figure 1). One of the runners, Abdi Abdirahmen, was removed from the analysis due to being an outlier (marked in red in Figure 1). The current analysis does not explain why he did not follow the trend of the other athletes, but this runner was well outside the trend

of the other athletes. His leg length relative to body height and, visually, his technique is very unique. In addition to leg length and height, other musculoskeletal structure differences may also be related to his unexpected result.

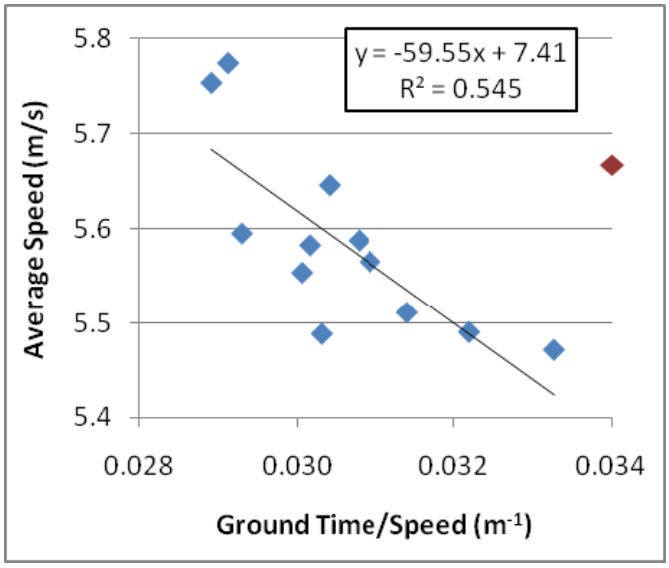

Figure 1: Average speed versus ground time normalized by running speed for the men's 10000 m final at the 2009 US Nationals.

Maximizing running economy during the majority of a 10,000 m race and maximizing running speed during the final stage of the race is critical for maximum performance. There are many runners that can be with the leaders for nearly the entire race, but fall well behind during the last couple of laps. Many authors have considered how ground time is related to maximum sprinting speed which relates nicely to an athlete's ability to finish a race effectively [2, 3, 4]. However, studies are only beginning to focus on the importance of ground time related to running economy.

Over the past few years, improvements in running economy and performance in long distance races have been found through completing plyometric exercises [6, 7]. There may be a connection between plyometric training and leg stiffness through muscular changes that can connect why ground time varies due to factors other than running speed. However, there is much to be learned through further research to determine whether this is true or not.

During distance races it is important to balance running economy with speed. Most laps of a 10,000 m race are run at sub-maximal effort. As the race progresses, the athlete will adjust speeds according to competition and strategy. Often, on the final lap the runner focuses on maximizing effort placing less emphasis on running economy. The plyometric training that is connected with improved running economy may also help in improving final lap finishing speed.

SUMMARY/CONCLUSIONS

This study adds to our knowledge of how ground time is related to running economy. While there is much more to understand, there appears to be something other than running speed that is related to ground time. This other factor or factors may have a connection with running economy. Further laboratory studies will investigate how running economy and ground time are related to factors such as leg stiffness and leg power. As endurance athletes prepare for performances, they should consider training that affects ground time such as plyometrics in ways previously reported [6,7].

REFERENCES

1.Anderson T. *Sports Med* **22**, 76-89, 1996.
2.Weyand PG, et al. *J Appl Physiol* **89**, 1991-1999, 2000.
3.Mann RA, et al. *Am J Sports Med* **14**, 501-510, 1986.
4.Bushnell TD, Hunter I. *Sports Biomechanics* **6**, 261-268, 2007.
5.Rimmer E, Sleivert G. *J Strength Cond Res* **14**, 295-301, 2000.
6.Paavolainen L, et al. *J Appl Physiol* **86**, 1527-1533, 1999.
7.Saunders PU, et al. *J Strength Cond Res* **20**, 947-954, 2006.

ACKNOWLEDGEMENTS

Thank you to USA Track and Field for funding a part of this study.

VARIATIONS IN RUNNING FORM AMONG FEMALE SPRINTERS, MIDDLE, AND DISTANCE RUNNERS

Ruthann Cunningham, Iain Hunter, Matt Seeley, Brent Feland

Brigham Young University, Provo, UT, USA
email: ruthann.cunningham@gmail.com

INTRODUCTION

In the sport of track and field, runners excel at their event due not only to physiological characteristics but also aspects in their form. Characteristics of technique help runners achieve the goal in completing their event with an optimal combination of economy and running speed.

Sprinters move differently than distance runners in their events [1, 4]. This is seen in sprinters displaying a smaller knee range (range of flexion of the knee during the first part of stance, Figure 1a) and shorter ground time (amount of time on the ground during stance) while running at competition speeds. Studies have also found that sprinters have a smaller center of mass separation (horizontal distance from the center of mass to the front of the toe at touchdown, Figure 1b) and longer stride length (horizontal distance divided by time in the air) compared to distance runners while running at speeds specific to their event [1-4]

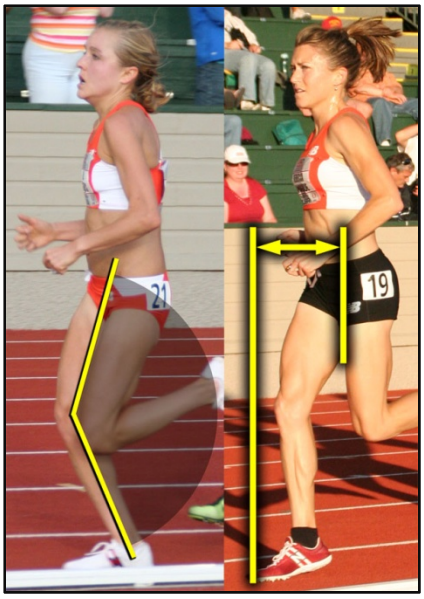

Figure 1: a) Knee range was measured from touchdown to maximum flexion. b) Center of mass separation was measured horizontally from the center of mass to the front of the foot at touchdown.

What lacks in the literature is the comparison of sprinters and distance runners form while they are running at the same speeds. In addition, multiple studies have only compared groups of runners who compete at considerable differences in distance. This study was conducted to determine if sprinters, middle distance, and distance runners running at the same speeds would exhibit different characteristics in their form.

METHODS

Thirty female Division I collegiate runners participated in this study. Runners were separated into categories based on the events they were currently training in: 10 sprinters, 10 middle-distance runners, and 10 distance runners. All participants were asked to run for twenty two steps at 3.17 m/s (8:27 min/mile), 3.58 m/s (7:30 min/mile), 4.11 m/s (6.31 min/mile), 4.87 m/s (5:30 min/mile), and 5.95 m/s (4:30 min/mile) pace. Motion data was captured at each speed with Vicon Nexus 1.4 at 240 Hz. Knee range, ground time, center of mass separation, and stride length were calculated using a customized program created with Visual Basic.NET 2008. Data was then processed using ANOVA and a Tukey post hoc analysis.

RESULTS AND DISCUSSION

Significant differences (p<0.05) occurred between distance runners and the groups of middle distance runners and sprinters in knee range, ground time, center of mass separation, and stride length for all of the five speeds. At all speeds, distance runners displayed a significantly smaller knee range, and stride length compared to middle distance runners and sprinters. In addition, distance runners displayed significantly greater ground time and center of mass separation with all speeds compared

to sprinters and middle distance runners. Results also indicated that as the speed increased, all three groups decreased in knee range measurements and ground time measurements. All three groups increased center of mass separation and stride length as running speed increased. All groups displayed linear slopes as speeds increased with no interactions occurring between groups.

Overall, the distance runners are unique in their technique compared with both other groups. This has some implications for coaches in categorizing someone as a certain type of runner. Sprinters and distance runners have very different VO_2 max, percentage of Type I and II muscle fibers, and body mass indexes. This study shows that sprinters and middle-distance runners are very similar in their running technique. Thus, the main differences between sprinters and middle-distance runners seem to be more physiologically related. However, distance runners have the physiological differences compared with sprinters, but also have different movement patterns. We cannot determine from our results whether the techniques lead to the type of runner, whether the type of training leads to the technique, or if some genetic factors lead to different movements. Future studies may focus on these ideas to help add to the knowledge of selecting people to optimal events.

CONCLUSIONS

While running at the same speeds, runners exhibit characteristics in their form specific to their event. These are even seen in speeds that are faster or slower than what the athletes are used to training or competing at. In addition, middle distance runners display aspects of technique that are in-between distance runners and sprinters in all variables. By understanding these differences, coaches and athletes can analyze current performance and make needed adjustments.

REFERENCES

1.Armstrong, L, et al. *Track Tec* **87**, 2781-2782, 1984.Sawicki GS. *Proceedings of NACOB'08*, Ann Arbor, MI, USA, 2008.
2.Bushnell, T, & Hunter, I. *Sports Biomechanics* **6**(3), 261-268, 2007
3.Mann, R, et al. *Am. J Sports Med* **14**(6), 501-510, 1986.
4.Novacheck, TF. *Gait and Posture* **7**(1), 77-95, 1998.

ACKNOWLEDGEMENTS

Thank you Brigham Young University track and cross country teams.

Table 1: Result of all groups for all conditions. Superscripts (A,B,C) indicate differences between groups at $p<0.05$ in the Tukey post hoc analysis (i.e. a variable with a superscript denotes the variable is significantly different from the other superscripted variables).

	Speed (m/s)	3.17	3.58	4.11	4.87	5.95
Knee Range (deg)	**Sprinter (A)**	25.8 ^{C}	26.2 ^{C}	26.0 ^{C}	23.9 ^{C}	22.8 ^{C}
	Middle (B)	26.8 ^{C}	25.5 ^{C}	25.9 ^{C}	26.2 ^{C}	24.7 ^{C}
	Distance (C)	32.5 ^{AB}	30.8 ^{AB}	32.3 ^{AB}	32.8 ^{AB}	30.9 ^{AB}
Ground Time (s)	**Sprinter (A)**	0.22 ^{C}	0.21 ^{C}	0.18 ^{C}	0.16 ^{C}	0.14 ^{C}
	Middle (B)	0.23 ^{C}	0.21 ^{C}	0.19 ^{C}	0.17 ^{C}	0.14 ^{C}
	Distance (C)	0.25 ^{AB}	0.23 ^{AB}	0.21 ^{AB}	0.19 ^{AB}	0.16 ^{AB}
Center of Mass Separation (m)	**Sprinter (A)**	0.179 ^{C}	0.184 ^{C}	0.189 ^{C}	0.191 ^{C}	0.200 ^{C}
	Middle (B)	0.189 ^{C}	0.188 ^{C}	0.196 ^{C}	0.207 ^{C}	0.214 ^{C}
	Distance (C)	0.207 ^{AB}	0.211 ^{AB}	0.219 ^{AB}	0.230 ^{AB}	0.243 ^{AB}
Stride Length (m)	**Sprinter (A)**	1.305 ^{C}	1.461 ^{C}	1.627 ^{C}	1.819 ^{C}	2.043 ^{C}
	Middle (B)	1.305 ^{C}	1.439 ^{C}	1.605 ^{C}	1.787 ^{C}	2.004 ^{C}
	Distance (C)	1.294 ^{AB}	1.430 ^{AB}	1.589 ^{AB}	1.763 ^{AB}	1.953 ^{AB}

A PROSPECTIVE STUDY OF LOADING VARIABLES IN FEMALE RUNNERS WHO DEVELOP PLANTAR FASCIITIS

Bradley Bowser[1], Joseph Hamill[2] and Irene Davis[1,3]

[1]University of Delaware, Newark, DE, USA
[2]University of Massachusetts, Amherst, MA, USA
[3]Drayer Physical Therapy Institute, Hummelstown, PA, USA
email: bbowser@udel.edu

INTRODUCTION

Plantar fasciitis is reported to be one of the top 3 overuse injuries and one of the top 5 of all injuries sustained by runners [1, 2]. The primary cause of this injury is often attributed to a repetitive stress or overloading of the plantar fascia. Excessive pronation, a flat or cavus foot, and limited dorsiflexion have frequently been cited as predisposers to plantar fasciitis. However, few studies have examined the potential role that loading variables may play in this injury.

The plantar fascia plays an integral role in maintaining the integrity of the longitudinal arch of the foot. Integrity of the arch is maintained by the plantar fascia creating tension between the calcaneous and metatarsal heads. As the foot is loaded in running, this tension increases to maintain stability of the arch. However, runners who have higher than normal external forces, thereby loading the foot more quickly, may be placing greater rates of tension on the plantar fascia. These conditions may place runners at an increased risk for developing plantar fasciitis.

One retrospective analysis has indicated that runners with a history of plantar fasciitis had significantly higher vertical load rates than healthy controls [3]. However, with retrospective analyses, it is difficult to ascertain whether differences between an injured and a control group were a result of the injury or some other unknown factor. It is therefore imperative to look at the prospective nature of this injury.

The purpose of this study was to compare vertical loading rates, vertical impact peak, and peak positive acceleration between female runners who go on to develop plantar fasciitis (PF) and runners who have never reported any running injury (CON). We hypothesized that the PF group would display higher vertical loading rates, vertical impact peaks, and peak positive accelerations of the tibia compared to the CON group.

METHODS

These data are part of a larger study examining prospective running injuries. Female runners between the ages of 18 and 45 years who run a minimum of 20 miles/week were recruited to participate. Participants were required to be injury free for the previous two months before beginning the study. Upon entering the study, ground reaction force and tibial accelerometer data (960 Hz) were collected while participants ran over-ground at 3.7 $m \cdot s^{-1}$ (± 5%). Five acceptable trials were captured.

Each runner's mileage and injuries were then tracked monthly for a 2 year period. During the 2 year follow-up period, 10 participants (age = 28 ± 8 yrs) running 23 ± 8 miles per week, were diagnosed by a clinician with plantar fasciitis. The PF group was compared to a CON group of 10 runners (age 24 ± 8 yrs), running 23 ± 9 miles per week. The CON group was also followed for 2 years and never reported a running injury.

Vertical loading rates (instantaneous (VILR) and average (VALR)), impact peaks (VIP), and peak positive accelerations (PPA) of the tibia were compared across groups. Descriptive statistics including percent difference and effect size (ES) were used to quantify any group differences. ES was calculated as the difference between the two group means divided by the pooled standard deviation. ES was defined as small (d = 0.2), medium (d = 0.4), and large (d = 0.8).

RESULTS AND DISCUSSION

Differences between the PF and CON groups are displayed in Figures 1 and 2. ES was considered large for all variables (VILR, d = 1.20; VALR, d = 1.29; VIP, d = 0.89; PPA, d = 0.98)

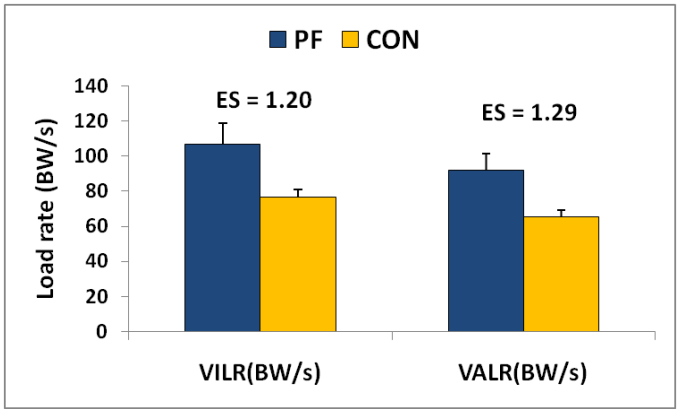

Figure 1. Group differences for instantaneous and average vertical loading rates (VILR and VALR respectively).

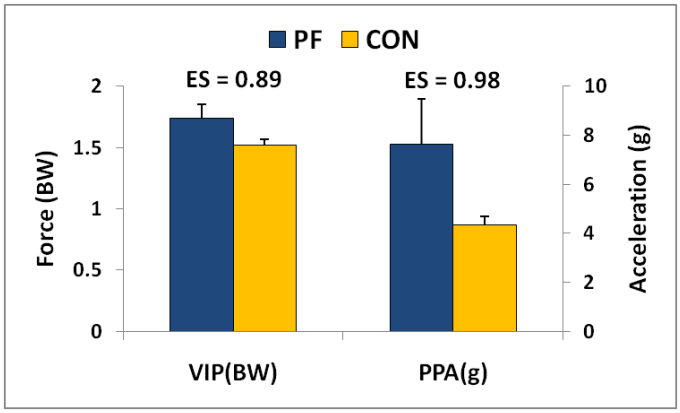

Figure 2. Group differences in peak positive acceleration (PPA) and vertical impact peak (VIP).

The rates at which external forces are applied to the foot and leg during running occur more rapidly in runners who go on to develop plantar fasciitis. This is evidenced by the VILR and VALR being 40% higher in the PF group when compared to the CON group. Additionally, the external load itself is also higher in the control group with VIP and PPA being 15% and 76% higher, respectively, for the PF group.

The increases in external loads and loading rates to the foot while running may be increasing the load and strain rates on the plantar fascia. These mechanical changes to the plantar fascia during running may be associated with the development of plantar fasciitis for those in the PF group.

The results of this study coincide with those found in a retrospective study comparing similar groups. Although the percent differences were not as large as those found in this present study, Pohl et al. reported that runners with a history of plantar fasciitis display higher external loading (8% higher) and loading rates (21% faster) to the foot while running than an uninjured group of runners [3].

High loading rates, impact peaks and PPA of the tibia have all been linked to other running injuries such as stress fractures and patellofemoral pain syndrome [4, 5]. Interventions, such as gait retraining, have been shown to reduce impact loading by teaching runners to land softer [6]. It is possible that decreasing these loading variables may decrease the risk for not only plantar fasciitis, but also other common running injuries.

CONCLUSIONS

The results of this prospective data suggest that runners who have high vertical loading rates, impact peaks, and PPA of the tibia while running may be predisposed to developing plantar fasciitis. Understanding these mechanical differences will aid clinicians in developing optimal treatment plans to help prevent plantar fasciitis. Future studies may include regression models, which include multiple factors, to more accurately predict those who may be at risk for developing plantar fasciitis.

REFERENCES

1. Taunton JE, et al., *Br J Sports Med* **36**, 95-101, 2002.
2. Van Mechelen, W., *Sport Med*, **14**, 320-35, 1992.
3. Pohl MB, et al., *Clin J Sport Med* **19**, 372-6, 2009.
4. Davis IS, et al., *ACSM Annual Meeting*, 2010.
5. Milner CE, et al., *Med Sci Sporst Exerc*, **38,** 323-28, 2006.
6. Crowell et al., JOSPT, in press, 2010

ACKNOWLEDGEMENTS

Supported by Department of Defense grant DAMD17-00-1-5

Step Width and Iliotibial Band Strain during Running

[1]Stacey Meardon, [2]Samuel Campbell and [2]Timothy Derrick

[1]University of Wisconsin – La Crosse, La Crosse, WI, USA
[2]Iowa State University, Ames, IA, USA
email: meardon.stac@uwlax.edu web: http://www.uwlax.edu/pt/lims.htm

INTRODUCTION

Iliotibial band syndrome is a common overuse in runners. The iliotibial band (ITB) is a band of connective tissue that originates at the iliac crest, crosses the hip joint, travels down the lateral portion of the thigh and inserts at Gerdy's Tubercle on the proximal tibia, the distal femur and the patella. Hip adduction and knee internal rotation angles have been positively associated with ITB syndrome in a prospective study [1] and linked with elevated ITB strains and strain rates [2].

Many studies have assessed the effect of stride length manipulations on lower extremity kinematics; however, relatively few published studies have examined the effect of step width on gait mechanics. Studies that have strategically manipulated step width during running report greater pronation, pronation velocity, and tibial excursion with a cross over pattern [3,4]. However, hip and knee kinematics have not been assessed. A narrower step width is likely to increase hip adduction and knee internal rotation as well as result in greater ITB strains and strain rates. Therefore, the purpose of this study was to evaluate the effect of step width on ITB strain and strain rate.

METHODS

Fifteen experienced runners free from injury volunteered for this study (8 males and 7 females, 23.7±5.4 years, 70.3±9.2 kg, 1.7±.08 m). Anthropometric data were collected for later use in a musculoskeletal model.

Subjects ran at their preferred 5k running speed over a force platform (1600 Hz, AMTI, Watertown, MA) until 10 trials of three step width conditions were successfully completed. Motion capture data were concurrently collected with an 8 camera 3D motion capture system (Vicon Nexus, Centennial, CO) at a sampling rate of 160 Hz. Step width was measured as the mediolateral distance between the right and left heel markers during consecutive steps. The mean step width value obtained in the preferred running style condition was then used to calculate minimum target values for the narrow and wide conditions. Minimal acceptable narrow step width was calculated as normal step width minus 5% of leg length; minimal acceptable wide step width was normal step width plus 5% of leg length. The normal step width condition was performed first and order of narrow and wide conditions was balanced to minimize fatigue effects.

Motion capture data and force platform data were exported to MATLAB (The Mathworks, Natick, MA) for signal processing and analysis. Kinematic data were low-pass filtered at 8Hz and imported into a scaled SIMM model [5]. Length of the ITB was calculated by summing the individual segments of the SIMM musculotendonous unit for each frame of data. ITB strains and strain rates were calculated using the equations:

$$Strain = \frac{L_i - L}{L} = \frac{\Delta L}{L} \; x\,100$$

$$Rate\ of\ \ strain = \frac{\Delta Strain}{\Delta Time}$$

where Li is equal to the length of the ITB during time i in the stance phase of the run and L is equal to the resting ITB length calculated during the standing calibration trial [2].

Repeated measures ANOVA was used to evaluate step width effects on the dependent variables of interest. Tukey post-hoc comparisons were performed and Cohen's D effect sizes (ES) were calculated.

RESULTS AND DISCUSSION

Table 1 indicates subjects were able to manipulate their step widths during running while maintaining a consistent running velocity and without changing their heel strike patterns. ITB strain increased as the step width became narrower (Figure 1). Differences were found in ITB peak strain across conditions with the narrow step width condition (3.7±0.5%) having the greatest level of strain compared to normal running (3.1 ± 0.5%) (p<0.01; ES=1.0). Strain during normal step width was also greater than the wide condition (2.7±0.5%) (p<0.01; ES=0.8).

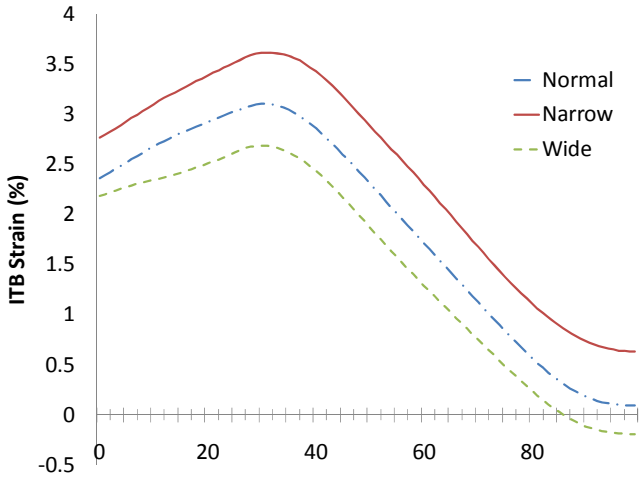

Figure 1: ITB strains across the stance phase of running in three step width conditions.

Strain rates generally increased with the narrowing step width. Minimal differences were found in peak strain rate between the narrow (12.8±8.4%/s) and normal step widths (10.8±10.3%/s) (p=0.22; ES=0.2). Larger differences existed between the narrow and wide step widths (7.4±8.9%/s) (p<0.01; ES=0.5) and the normal and wide step widths (p=0.02; ES=0.3).

ITB impingement occurs at approximately 30° of knee flexion. Greater strain in the ITB was observed at this critical point in the gait cycle with narrower step widths in this study. As expected, hip adduction angle increased with decreasing step length. Knee internal rotation did not differ across conditions. Increased hip adduction, likely the main explanation for the increased strain during narrower step widths, increases the length of the ITB and thus the passive tension. However, activation of the muscles inserting into the ITB can increase active tension. Interestingly, the hip abductor moment was 35% greater in the narrow condition compared to the wide condition (p = 0.07; ES = 0.5) suggesting that increased active tension, in addition to passive tension, occurred during narrower step widths.

CONCLUSIONS

The current study shows that there is an inverse relationship between step width and ITB strain and strain rates. Rate of strain development is a key factor in the development of ITB syndrome [2]. The lower rate strain rates seen in the wider running conditions of this study suggest that a wider step width may be beneficial in the prevention and treatment of ITB syndrome. These findings, in combination with findings from previous studies of injury, suggest that future gait retraining efforts consider step width characteristics, especially if persons demonstrate a crossover pattern. Prior to prescribing step width changes to modulate ITB strain, consideration of the overall coordination and mechanics of the system must be made. Future studies are needed to ascertain the relationship between step width and injury and to identify optimal step characteristics for minimization of tissue loads during running.

REFERENCES

1. Noehren B, et al. *Clin Biomech* **22,** 951-956, 2007.
2. Hamill J, et al. *Clin Biomech* **23**, 1018-1025, 2008.
3. Williams KR, et al. *Int J Sports Biomech* **7**, 76-90, 1991.
4. Pohl MB, et al. *Clin Biomech* **21**, 175-183, 2006.
5. Miller RH et al. *Gait Posture* **26**, 407–413, 2007.

Table 1. Mean values (SD) of study design variables. Superscripts indicate $p \leq 0.05$ for respective comparisons.

Condition	Velocity (m/s)	Step width (cm)	Heel Strike Index (%)
Normal step width	4.04 (0.57)	2.6 (0.04)[2,3]	27.4 (18.2)
Narrow step width	4.04 (0.58)	-6.3 (0.05)[1,3]	31.2 (21.6)
Wide step width	4.03 (0.58)	10.2 (0.04)[1,2]	27.8 (18.2)

[1]normal, [2]narrow, [3]wide step width

VARIATION OF ANATOMICAL PARAMETERS THAT AFFECT ESTIMATED ANTERIOR CRUCIATE LOADING DURING DROP LANDINGS

Chelsey S. Koehler[1,2,3], Timothy R. Lopez[2,3], Thomas W. Kernozek, PhD[1,3], Robert J. Ragan, PhD[2,3]

[1]Department of Health Professions, [2]Department of Physics, [3]La Crosse Institute for Movement Science
University of Wisconsin-La Crosse, La Crosse, WI, USA

email: kernozek.thom@uwlax.edu, web: http://www.uwlax.edu/pt/LIMS.htm

INTRODUCTION

Non-contact anterior cruciate ligament (ACL) injury has been a focus of many investigations in recent decades. Several anatomical and neuromuscular factors have been posed to increase ACL injury risk. Modeling approaches offer a systematic means to examine how these factors manifest in knee loading during high risk movement performance like landing.

Kernozek & Ragan [1] developed a two dimensional model of the knee to estimate anterior cruciate ligament loading during drop landing. This model uses mean values of anatomical parameters obtained from cadaveric and clinical data. However, there are considerable variations in anatomical parameters reported in literature. The purpose of this study was to use this mathematical model to determine how variation in selected anatomical parameters influence estimated ACL tension (*Facl)* and the anterior-posterior (AP) forces on the knee during drop landing performance. Model results can be examined to identify those parameters that influence risk of non-contact ACL injury.

METHODS

Motion analysis, force platform, and EMG data from 21 healthy female students with no history of knee injury or chronic knee pain (age range = 18-24, mean height = 169.46 (SD 6.12) cm, mean weight = 63.83 (SD 8.30) kg) were normalized, averaged, and then used as input to our model. Drop landing data were captured of each subject from 5 performance trials utilizing a toe heel landing pattern from a 40 cm hang bar.

The anatomical parameters chosen for analysis were those that had the greatest potential to affect model predictions (ie. those that appeared in the AP force and moment equations). The anatomical parameters that were examined were the tibial slope, the patellar tendon and hamstring line of force (Fig. 1), the moment arms of the patellar tendon, hamstring, and gastrocnemius at the knee and ankle, ACL stiffness, and nonlinear muscle activation parameters.

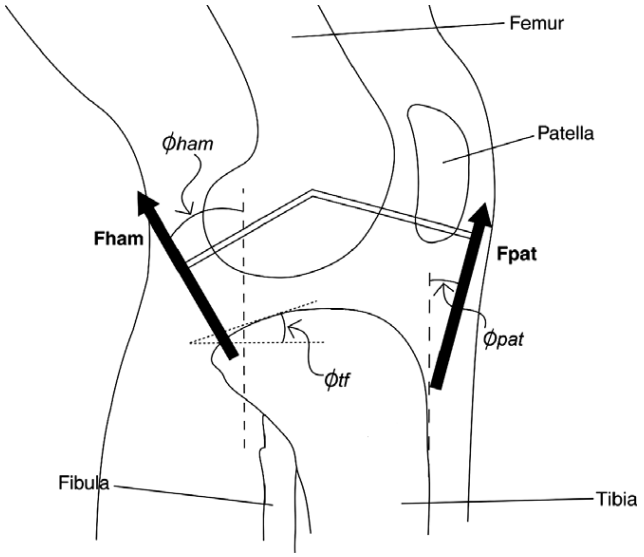

Figure 1: Selected anatomical parameters examined in the model [hamstring line of force (*Φham*), patellar tendon line of force (*Φpat*), and tibial slope (*Φtf*)].

Maximum ACL tension ($Facl_{MAX}$) was the ACL model output examined. Also, the maximum shear component of the forces that directly contribute to $Facl_{MAX}$ (ankle, patellar tendon, hamstring, and tibio-femoral force) were assessed.

Anatomical parameters were varied independently by +/-5% from all control values (those that have been previously published using this model). Parameters yielding the largest percentage change in model outputs were further examined using other published maximum and minimum anatomical data as model inputs.

RESULTS AND DISCUSSION

Model predictions, particularly $Facl_{MAX}$, were most sensitive to change in tibial slope as well as the initial line of force (at full knee extension) of the patellar tendon (Fig. 2). In addition, model outputs of maximum patellar tendon and tibio-femoral shear forces also showed the greatest sensitivity to the tibial slope, affecting their magnitude by 50% and -35%, respectively. Variation in the initial patellar tendon line of force affected maximum patellar tendon shear force by 38%.

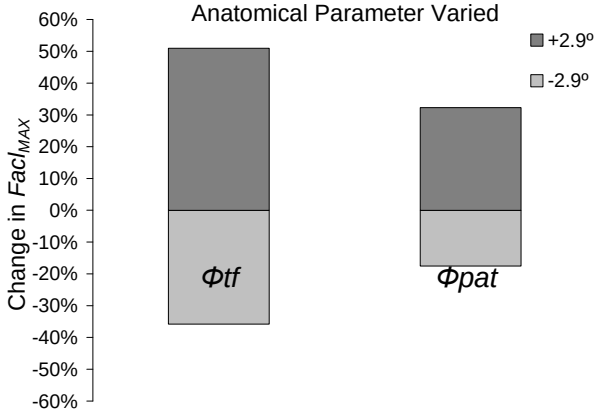

Figure 2: Percent change in $Facl_{MAX}$ due to changing tibial slope (Φtf) and patellar tendon line of force (Φpat) by +/-2.9º (5% in radians).

Todd et al. recently examined radiographic images of 140 patients with non-contact ACL injuries and a control group of 179 subjects with anterior knee pain. Greater tibial slope was reported in subjects with noncontact ACL injuries compared to controls. Similarly, in the present study, tibial slope had a large effect on $Facl_{MAX}$ and AP shear forces during drop landing based on model calculations.

Changes in $Facl_{MAX}$ resulting from variation in the initial patellar tendon line of force reflects previous studies linking this relationship to an increased risk of ACL injury. Anterior tibial translation from the quadriceps force was directly proportional to the patellar tendon line of force. ACL injury has been reported at full knee extension with a greater patellar tendon line of force [3]. Variation in patellar tendon line of force appears to influence $Facl_{MAX}$ during drop landing.

Since the tibial slope and the initial patellar tendon line of force were identified as the parameters most influential to model outputs, extremes from literature were examined using our drop landing data (Table 1).

REFERENCES

1.Kernozek TW, Ragan RJ. *J Clin Biomech* **23**, 1279-1286, 2008.
2.Todd MS, et al. *Am. J. Sports Med.* **38** (1), 63-67, 2010.
3.Herzog W, Read LJ. *J Anat.* **182**, 213-230, 1993.
4.de Boer JJ, et. al. *J Clin Biomech* **24**, 488-492, 2009.

ACKNOWLEDGEMENTS Hi-Tech Funding from the State of Wisconsin.

Table 1: Minimum and maximum anatomical data for the tibial slope (Φtf) [4] and patellar tendon line of force (Φpat) [3] are reported with the corresponding changes in maximum ACL tension ($Facl_{MAX}$) in body weight. Control anatomical and activation parameters values were from Kernozek & Ragan [1].

	Control [1]	**Tibial slope** (Φtf) [4]		**Patellar tendon line of force** (Φpat) [3]	
Anatomical parameter		**Minimum** 1.0°	**Maximum** 15.8°	**Minimum** 10°	**Maximum** 30°
Facl*$_{MAX}$ *(BW)	0.250	0.025	0.707	0.206	0.910
Change in *Facl*$_{MAX}$		-92%	139%	-30%	208%

ANKLE BRACE WITH A HEEL STRAP IS EFFECTIVE IN STABLIZING ANKLE IN FRONTAL PLANE IN WALKING AND RUNNING

Songning Zhang[1], Micheal Wortley[1], Julia Freedman[1] and Daniel Carson[2]
[1] Biomechanics/Sports Medicine Lab, The University of Tennessee, Knoxville, TN, USA
[2] Cincinnati Children's Hospital Research Foundation, Cincinnati, OH, USA
email: szhang@utk.edu, web: web.utk.edu/~sals/resources/biomechanics_laboratory.html

INTRODUCTION

Lateral ankle sprain is the most common injury in all sports [1, 2]. A majority of studies investigating protective effects of ankle braces and lateral ankle sprains have used an inversion drop platform to induce ankle inversion movement in a controlled environment [4]. However, ankle braces are used to treat not only acute and chronic ankle sprains, but also other pathological conditions such as syndesmosis sprain, posterior tibial tendonitis, peroneal tendonitis, and osteoarthritis. Therefore, there is a need to investigate effects of ankle braces in daily activities such as walking and running. A previous study has demonstrated effectiveness of an ankle brace with a heel strapping system (Element™) in an inversion drop and a lateral cutting [4]. The purpose of this study was to examine protective effects of a short version of this brace in walking and running. We hypothesized that greater reduction of eversion range of motion (ROM) and peak eversion velocity would be observed in the brace with the heel strapping system and participants with chronic ankle instability (CAI).

METHODS

Ten subjects (age: 24.1±5.4 yrs, mass: 72.4±12.0 kg & height: 1.74±0.08 m) with no history of previous ankle sprains and ten subjects (age: 24.8±5.7 yrs, mass: 73.0±9.3 kg & height: 1.75±0.09 m) CAI (multiple past ankle sprains and higher scores of the ankle joint functional assessment tool questionnaire (AJFAT) [3]) participated in the study as the control (C) and CAI (U) subjects, respectively. Participants performed five trials in each of six testing conditions: level walking at 1.2 m/s and running at 3.6 m/s wearing no brace (NB), a semi-rigid brace (B1, Element™ - short version of original Element), and a soft lace-up brace (B2, ASO). Three-dimensional kinematic (240 Hz, 7-camera Vicon) and ground reaction force (2400 Hz, AMTI) data were recorded simultaneously. In order to improve tracking of foot movements, holes were cut out in the lab shoes to place markers directly to the foot. Kinematic and kinetic variables were computed and analyzed using Visual 3D (C-Motion, Inc) and customized software (VB_V3D). Selected variables were analyzed using one-way repeated measures analysis of variance ($P < 0.05$).

RESULTS AND DISCUSSION

Due to a lack of group x brace interactions, group data (C and U) were collapsed in the statistical analyses. No significant group or brace effects were found for the 1st (Max1_Fz) or 2nd peak vertical ground reaction force (GRF). The medial-lateral range of the center of pressure (COP_X) showed a significant brace effect in walking ($F = 13.172$, $p < 0.001$). The B1 had significantly less medial COP_X displacement compared to the NB and B2 conditions (Table 1). There was a marginal decrease of medial COP_X in B1 compared to NB in running ($p = 0.066$).

B1 had lower eversion ROM (Ev_ROM) than NB ($p = 0.001$) and B2 ($p = 0.003$) in walking whereas both B1 and B2 had reduced Ev_ROM ($p < 0.001$) than NB ($p < 0.001$) in running. The peak eversion velocity (EV_V) was lower for B1 compared to NB ($p < 0.001$) and B2 ($p = 0.024$) in walking and running, and lower for B2 compared to NB in walking. In addition, the total ankle plantarflexion ROM (PF_ROM) was significantly reduced in B1 ($p < 0.001$) and B2 ($p = 0.014$) compared the no brace, and in B2 ($p < 0.001$) compared to NB in walking (Table 1). In running PF_ROM was significantly reduced for B1 (p 0.001) and ASO ($p < 0.001$) compared to NB.

Although the peak GRFs were not different among the brace conditions, this was expected as the ankle braces are not designed to significantly alter force attenuation capacity but to stabilize foot and ankle complex. This stabilization effect is, however, supported in the reduced COP displacement in walking and running associated with B1. The stabilization effect is mainly evidenced by the frontal-plane ankle kinematic data. The eversion ROM and eversion velocity were both reduced for B1 in walking as well as running compared to NB. The eversion velocity was reduced in walking and running, and the eversion ROM in running for B2. These results also suggested that the B1, the brace with the semi-rigid support and the heel-strapping system, offers better protection compared to the soft-laced ASO brace, B2, mainly in walking.

In addition to the protection effects in the early stance phase of the two gait movements, the braces reduced the total ankle sagittal ROM. This may suggest reduced performance for both braces. However, the past results on B1 and B2 did not show reduced performance in the lateral cutting movement [4]. Further examination of other performance related variables during the movement are warranted.

CONCLUSIONS

This study showed that the short version of Element™ brace offers greater restrictions on ankle eversion and peak eversion velocity as well as COP movement in walking and running. Therefore, the proposed hypotheses were partially supported. ASO brace also offers protection against peak eversion velocity in walking and running and eversion in walking. Whether the protective effects in the early stance hinders performance remains to be examined. The examined variables did not differentiate the participants with chronic ankle instability from the healthy control participants. The lack of the differences may suggest that the method used to define chronic ankle instability warrants further discussions and examinations.

REFERENCES

1. Fong, D. T., et al. (2007). *Sports Med,* **37**, 73-94.
2. Garrick, J. G. (1977). *Am J Sports Med*, **5**, 241-242.
3. Rozzi, S. L., et al. (1999). *J Orthop Sports Phys Ther,* **29**, 478-486.
4. Zhang, S., et al. (2009). *J Orthop Sports Phys Ther,* **39**, 875-883.

ACKNOWLEDGEMENT

Supported by DeRoyal Industries, Inc.

Table 1. Average ground reaction force and ankle kinematic variables: mean ± STD.

	Group	Brace	Max1_Fz (BW)	COP_ X (m)	Ev_ROM (deg)	Ev_V (deg/s)	PF_ROM (deg)
Walk	C	NB	1.06±0.05	-0.064±0.01 [a]	-6.2±2.5 [a]	-112.4±33.2 [a]	-16.9±5.5 [a]
		B1	1.05±0.06	-0.040±0.02 [b]	-1.8±1.5 [b]	-63.3±27.5 [b]	-11.2±5.0 [b]
		B2	1.05±0.06	-0.055±0.02	-3.9±1.9	-74.7±19.0 [c]	-15.6±6.0 [c]
	U	NB	1.03±0.08	-0.074±0.02 [a]	-7.0±5.5 [a]	-128.5±47.7 [a]	-14.7±5.6 [a]
		B1	1.04±0.08	-0.048±0.02 [b]	-3.6±2.0 [b]	-58.9±25.5 [b]	-7.9±3.7 [b]
		B2	1.03±0.08	-0.071±0.01	-5.0±2.2	-76.8±21.5 [c]	-12.5±4.4 [c]
Run	C	NB	1.73±0.18	-0.061±0.02	-8.9±1.4 [a]	-170.1±38.2 [a]	-26.7±4.2 [a]
		B1	1.76±0.16	-0.038±0.02	-5.2±2.6	-88.6±33.1	-20.9±2.5
		B2	1.76±0.25	-0.058±0.01	-5.9±1.6 [c]	-88.9±37.6 [c]	-23.1±5.9 [c]
	U	NB	1.79±0.17	-0.077±0.04	-10.9±4.9 [a]	-179.7±147.5 [a]	-29.9±7.0 [a]
		B1	1.82±0.24	-0.062±0.04	-7.6±3.8	-106.5±56.6	-22.8±8.5
		B2	1.81±0.30	-0.102±0.12	-7.7±3.4 [c]	-108.8±86.7 [c]	-21.6±10.2 [c]

Note: [a] – significant difference between NB and B1, [b] – significant difference between B1 and B2, [c] – significant difference between NB and B2.

METATARSOPHALANGEAL JOINT KINETICS IN RUNNING AND JUMPING

Stephanie E Forrester and Emma Hofmans

Wolfson School of Mechanical and Manufacturing Engineering, Loughborough University, UK;
email: s.forrester@lboro.ac.uk; web: www.sports-technology.com.

INTRODUCTION

Few experimental studies on the kinetics of human motion have considered the contribution of the metatarsophalangeal joint (MPJ). [1,2] investigated the kinetics of the MPJ during running and sprinting using a single force platform and assuming resultant forces and moments at the MPJ were zero until the centre of pressure (COP) acted distal to this joint. The effect of this assumption on the accuracy of the MPJ kinetics is unclear and hence, the contribution of the MPJ to motion remains ambiguous. The purpose of this study was to compare the MPJ kinetics determined using experimental data collected from a single force platform versus two force platforms (one rearfoot and one phalanges) for running and jumping.

METHODS

Eight recreational runners (2 female, 6 male; mean ± SD age 23.5 ± 2.7 years; height 1.79 ± 0.09 m; body mass 73.6 ± 15.4 kg,) gave informed consent. Subjects performed four movements (single leg vertical jump, single leg horizontal jump, heelstrike running and forefoot running) under two footwear conditions (barefoot and shod). These eight conditions were repeated three times on both single and double force platforms giving a total of 48 trials. For the trials using two force platforms the subjects were asked to take-off (jumps) or land (running) with their MPJ aligned with the split between the two platforms. In all trials, a foot outline drawn on the force platform helped subjects judge foot placement and visibly poor trials were repeated. During processing, trials were excluded if the MPJ deviated by > 20 mm from the force platform split. Subjects were asked to run at a self selected steady pace across the force platforms positioned centrally on a 10 m runway and to jump maximally. A number of familiarization trials were completed prior to testing.

Ten retroreflective markers were placed on the greater trochanter, medial and lateral femoral epicondyle, medial and lateral malleolus, heel, first and fifth metatarsal, second phalange and metatarsal head. Synchronous marker trajectories (400 Hz) and ground reaction forces (1200 Hz) were collected using a twelve camera Vicon MX motion capture system (Vicon Motion Systems Ltd., Oxford, UK) and two force platforms (9281CA, Kistler AG, Switzerland). Anthropometric measurements of the shank and foot were taken to determine segmental inertial parameters [3].

The motion capture and force platform data were exported to Matlab (The Mathworks, Natick, MA, USA) for processing. The kinematic data was filtered using a 4th order zero-lag Butterworth filter with a lowpass cut-off of 20 Hz, the force platform data was unfiltered. Three 2D inverse dynamics analyses were performed for each experimental condition based on the following GRF inputs:

[FP1]: single platform assuming no force on the phalanges until COP acted distal to the MPJ;

[FP2]: two platforms with the data from the individual force platforms providing the forces on the rearfoot and phalanges independently; and

[FP3]: two force platforms with the data combined to give a single resultant force platform and assuming no force on the phalanges until COP acted distal to the MPJ.

RESULTS AND DISCUSSION

Barefoot Heelstrike Running: There was no significant difference in running velocity between the single and double force platform trials ([FP1]: 2.67 ± 0.27 $m \cdot s^{-1}$ vs [FP2/3]: 2.65 ± 0.33 $m \cdot s^{-1}$). Similarly, there was no significant difference in the % of stance or GRFz where COP moved distal to the MPJ ([FP1]: 56.0 ± 6.8% & 2.10 ± 0.34 BW vs [FP3]: 49.6 ± 11.6% & 2.09 ± 0.35 BW). [FP2]

indicated that GRF transferred to the phalanges over the stance range 10.3 ± 5.4% to 74.9 ± 12.5%.

There were significant differences ($p < 0.05$) in peak moment, net work done and peak power at the MPJ between the single force platform [FP1] and the two force platform [FP2] and [FP3] trials (Fig. 1a). The results were more consistent at the ankle with significant differences only in net work and peak power between [FP1] and [FP3].

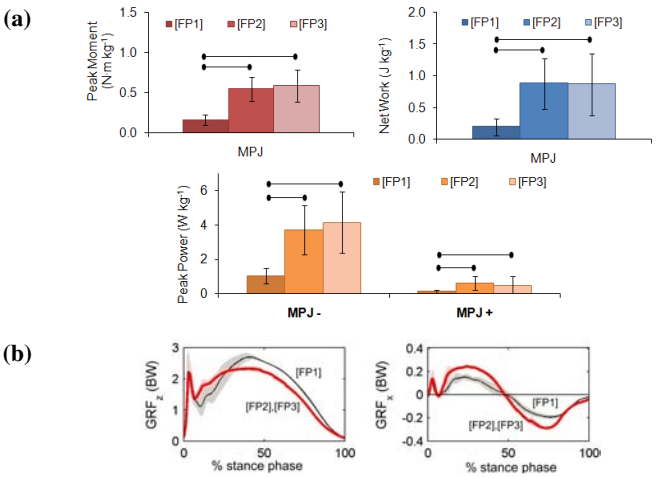

Figure 1: Barefoot heelstrike running. (a) Group mean (± SD) MPJ peak moment, net work and peak power from the three inverse dynamics analyses. Linked black dots indicate significant differences ($p < 0.05$). (b) Representative total GRFs (mean ± SD).

The difference in kinetics between [FP1] and [FP3] was unexpected since both situations were based on the same single force platform assumption. The difference may have arisen from changes in technique necessary to target the double force platform accurately and / or a reduction in accuracy of COP data towards the edge of the platforms. Differences in the GRFs between the single and double force platform trials support changes in technique being a contributing factor (Fig. 1b).

Barefoot Vertical Jump: There was no significant difference in take-off velocity between the single and double force platform trials ([FP1]: 1.11 ± 0.21 $m \cdot s^{-1}$ vs [FP2/3]: 1.03 ± 0.12 $m \cdot s^{-1}$). Similarly, there was no significant difference in the % of stance or GRFz where COP moved distal to the MPJ ([FP1]: 49.8 ± 9.8% & 1.84 ± 0.08 BW vs [FP3]: 54.1 ± 19.1% & 1.72 ± 0.19 BW). [FP2] indicated that GRF transferred to the phalanges over the stance range 0% to 88.5 ± 7.5%.

For jumping, there was no significant difference in peak moment, net work done or peak power at the MPJ between [FP1] and [FP3] (Fig. 2a). However, there were significant differences between both these conditions and [FP2], where the latter gave a higher peak moment, net work done and peak power generated.

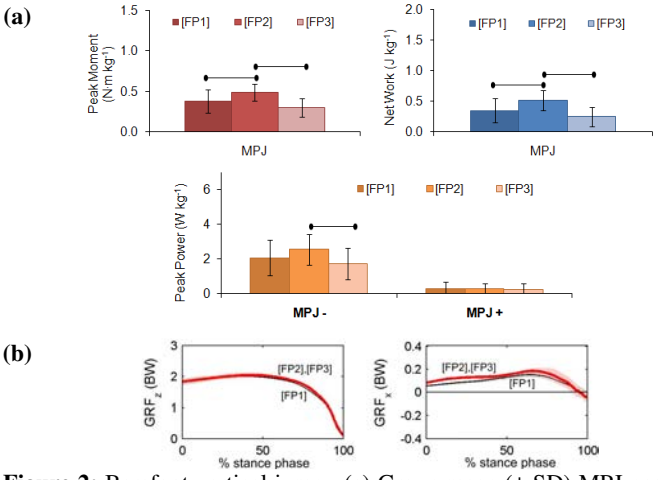

Figure 2: Barefoot vertical jump. (a) Group mean (± SD) MPJ peak moment, net work and peak power from the three inverse dynamics analyses. Linked black dots indicate significant differences ($p < 0.05$). (b) Representative total GRFs (mean ± SD).

Jump technique is expected to have remained consistent between the single and double force platform trials, which is supported by the GRFs (Fig. 2b). The good agreement between [FP1] and [FP3] kinetics suggests that reduced COP accuracy was not a major factor in the experimental methodology. Thus, the differences between the single and double force platforms kinetics are most likely due to the differences in assumptions used in each case.

CONCLUSIONS

Using a single force platform to estimate the kinetic contribution of the MPJ can lead to an underestimate of the peak moment, net work and peak power at this joint. To better quantify the contribution of the MPJ in running would require an experimental set-up that does not compromise technique but does allow forces on the individual foot segments to be measured.

REFERENCES

1. Stefanyshyn DJ and Nigg BM. *J Biomech* **30**, 1081–1085, 1997.
2. Roy JR and Stefanyshyn DJ. *Med Sci Sport Exer* **38**, 562-569, 2006.
3. Yeadon MR. *J Biomech* **23**, 67–74, 1990.

REDUCING ABNORMAL ALIGNMENT IN FEMALE RUNNERS WITH PFPS THROUGH GAIT RETRAINING USING MIRROR FEEDBACK

[1]Richard Willy, [2]Brian Noehren and [1,3]Irene Davis
[1]University of Delaware, Newark, DE, USA [2]University of Kentucky, Lexington, KY, USA
[3]Drayer Physical Therapy Institute, Hummelstown, PA, USA
email: rwilly@udel.edu

INTRODUCTION

Abnormal mechanics, such as hip adduction (HADD), hip internal rotation (HIR), and reduced knee adduction (KADD) during running have been associated with patellofemoral pain syndrome (PFPS) in females. These abnormal movements are thought to increase the dynamic quadriceps angle, resulting in lateral tracking of the patella [1]. Thus, therapies focusing on abnormal hip and knee mechanics have been proposed to treat PFP in females. Addressing these underlying causes of PFP may reduce the risk of developing patellofemoral osteoarthritis (PFOA) later in life [2].

We have shown that gait retraining, using realtime kinematic feedback, significantly improves lower extremity mechanics during running in females with PFPS [3]. These improvements were also associated with significant reductions in pain. However, most clinical settings do not have access to a motion capture system to provide kinematic feedback. More simple methods of feedback are needed to translate this intervention into the clinic.

Therefore, the purpose of this study was to examine the effectiveness of mirror feedback on lower extremity alignment during running in females with PFPS. It was hypothesized that peak HADD and HIR would be reduced, and KADD would be increased during running following this retraining. Pain and function were also expected to improve.

METHODS

This is an ongoing study with 5 subjects (21.2 ±2.5 yrs.) studied, to date. All subjects had anterior knee pain that was ≥3/10 during running for ≥3 months. They were running a minimum of 7 miles per week.

The lower extremity functional index (LEFI), a subjective measure that assesses 20 functional tasks on a scale of 0-4, was first recorded. Running kinematics were then collected as subjects ran down a 25-m runway at 3.35 m/sec (VICON, Oxford, UK). 3-D joint angles were calculated with Visual 3-D software (C-Motion, Bethesda, MD, USA). Subjects with peak hip adduction ≥1 standard deviation above a normative database of uninjured runners were invited to participate in the gait retraining intervention.

Subjects attended 8 retraining sessions over 2 weeks. During each session, subjects viewed themselves in a mirror while running on a treadmill. They were instructed to reduce the inward collapse of their knee by contracting the gluteal musculature. During sessions 5-8, feedback was gradually removed by turning the mirror around. This faded feedback paradigm was used to improve internalization of the new movement pattern. To ensure that only proper running mechanics were reinforced, subjects were not allowed to run on their own while participating in this study. At the conclusion of the retraining phase, all measures from the baseline data collection were repeated.

RESULTS AND DISCUSSION

Mean pain levels were reduced from 4.4/10 ±0.9 at baseline to 0.3/10 ±0.3 at conclusion of the protocol. Similarly, LEFI scores increased from a mean of 63.8/80 ±6.1 to 76.0/80 ±3.5. In addition, peak HADD was reduced (Figure 1) and peak KADD was increased (Figure 3). The changes seen in peak HADD and KADD were associated with large effect sizes (Table 1). In contrast, HIR was not reduced (Figure 2, Table 1).

Changes in pain and LEFS scores exceeded the minimal clinically important difference of 2 and 9, respectively. Improvements in the LEFS indicate that subjects reported a reduction in pain during functional activities other than running. This suggests that changes seen in running mechanics may have transferred to other functional movements.

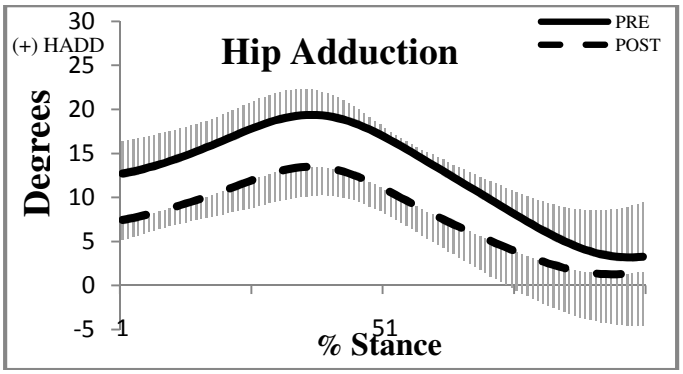

Figure 1: A reduction in HADD was seen throughout stance post training.

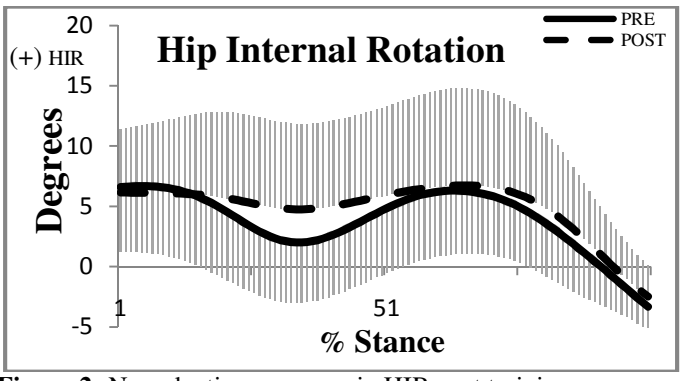

Figure 2: No reduction was seen in HIR post training.

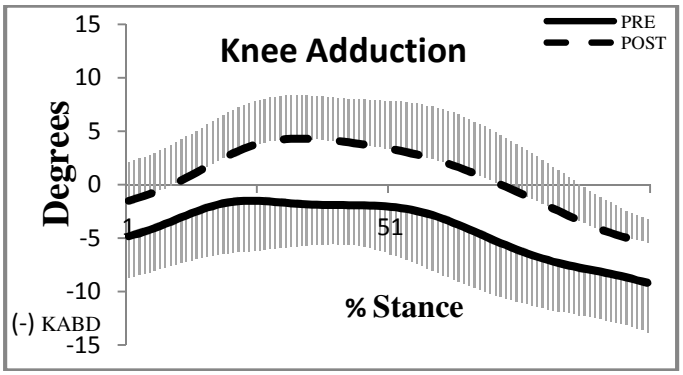

Figure 3: KADD increased to normal values post training

Table 1: Mean (sd) of peak kinematic measures.

Variable	PRE	POST	Effect Size
HADD	19.8º(2.4)	13.7º(2.3)	2.11
HIR	7.8º(4.9)	9.0º(7.6)	0.19
KADD	-0.5º(4.3)	5.1º(4.5)	1.27

The reduction noted in peak HADD may reduce the dynamic Q-angle and resultant lateral tracking of the patella [1]. This change in running mechanics may have contributed to a decrease in knee pain.

Prior to the retraining, the knee was in ABD (valgus) throughout stance, a position associated with lateral maltracking of the patella. Following the intervention, the frontal plane knee mechanics were within the normal range for running.

HIR was not reduced by the retraining. Noehren et al. [3] reported only a small (2.7º) but insignificant reduction in HIR. They attributed this to the fact that their feedback was provided on HADD only. This may also explain the findings of the current study. Frontal plane movements are easily visible to the subjects during the retraining sessions. However, transverse plane movements of the lower extremity may be more difficult to visualize. Further, HIR during running for the subjects enrolled to date fell within a normal range. Therefore, these subjects may have had limited capacity for reducing HIR.

These preliminary results, and those of Noehren et al., suggest that gait retraining can improve mechanics, pain and function in individuals with PFPS. Importantly, these improvements were seen in the absence of strengthening. In fact, it has been shown that hip strengthening, in isolation, does not alter running mechanics [4]. This further underscores the importance of including neuromuscular training in interventions for PFPS.

Based upon these preliminary data, gait retraining with a mirror may transfer readily to the clinical setting. By addressing the underlying mechanics, the chronicity of PFPS may be reduced. This may lead to a decrease in risk of later development of PFOA. This intervention may also be utilized for the treatment of other lower extremity conditions.

CONCLUSIONS

These preliminary data suggest that gait retraining, utilizing a mirror, is effective at improving running mechanics and reducing pain in females with PFPS.

REFERENCES

1. Powers CM, *J. Orthop Sp. Phys. Ther.***40**, 42-51, 2010.
2. Utting M, et al. *Knee.* **5**, 362-365, 2005.
3. Noehren B and Davis IS, *Br J Sports Med.*, **in press**.
4. Willy R, Davis IS, *Proceedings of ASB'09,* State College, PA, USA, 2009.

ACKNOWLEDGEMENTS

Support from the Foundation for Physical Therapy, Drayer Physical Therapy Institute, NIH 1S10 RR022396, DOD W911NF-05-1-0097.

CHANGE IN MEDIAL LONGITUDINAL ARCH STIFFNESS AFTER A PROLONGED RUN

[1]Elizbaeth R. Hageman, [2]Erin D. Ward, and [1]Timothy R. Derrick

[1]Iowa State University, Ames, IA, USA
[2]Central Iowa Foot Clinic, Perry, IA, USA
email: ehageman@iastate.edu, web: http://www.kin.hs.iastate.edu

INTRODUCTION

Little research has quantified medial longitudinal arch (MLA) stiffness during dynamic activity, such as walking and running. While it is commonly believed that pes cavus feet are more rigid and pes planus feet are more mobile, this has not been well supported with research. It has been noted that only 9% of the variance in arch stiffness from sit-to-stand was accounted for by static arch height index, with a higher arch being slightly more rigid [3]. During running the MLA collapses during the initial stages of the stance phase and then reforms during the latter stage. It has been hypothesized that during arch collapse the foot acts as a "mobile adapter" to help absorb some of the energy of the impact. During the propulsive phase the foot acts as a "rigid lever" to efficiently transfer energy generated by the muscles to the ground. If the structures of the arch play a role in this transformation from mobile adapter to rigid lever it would be reasonable to expect a change in the arch stiffness between the collapse and the reformation of the arch. Thus, the purpose of this study was to examine MLA stiffness during these two stages and to note how they change after a prolonged run.

METHODS

Eleven healthy participants (8 males, 3 females; age: 19.8±1.3 yrs; height: 1.73±0.06 m; mass: 69.4±10.0 kg; weekly mileage: 16.9-80.5 km) ran at a comfortable speed (3.28±0.35 m/s) barefoot across a force platform before and after a shod treadmill run (35-45 minutes) at the same speed. All but one subject used a heel-strike pattern. Reflective markers were placed on the right first metatarsal head (2 cm from ground), navicular tuberosity, and medial calcaneus (3 cm (female) or 4 cm (male) from the posterior aspect of foot, 2 cm from ground). An 8 camera motion capture system (200 Hz) and AMTI force platform (1000 Hz) collected marker position and ground reaction forces (GRF). Arch length was defined as the 3-D distance from the medial calcaneus to the first metatarsal head. Navicular height was defined as the 3-D perpendicular distance from that arch length line to the navicular. Changes in arch length and navicular height (displacement) were expressed in relation to a seated trial. Arch stiffness was calculated as the slope of a least-squares regression line fit through the resultant GRF and navicular displacement. Two arch stiffness values were calculated: 1) arch stiffness for the first part of stance (AS_1) and 2) arch stiffness for the second part of stance (AS_2). AS_1 was calculated from 15% of stance to maximum navicular displacement (~55% stance). AS_2 was calculated from maximum navicular displacement to 85% of stance. Mean r^2 values were calculated to determine the linear fit of the regression line for arch stiffness.

RESULTS AND DISCUSSION

A typical deformation by force curve is presented in Figure 1 with the first and last 15% of the stance phase removed. Prior to the run the mean AS_1 arch stiffness was 153.7±56.5 N/mm (r2=0.79) while the mean AS_2 arch stiffness was 241.0±90.5 N/mm (r2=0.95, p=0.01), as shown in Table 1. This 58% increase between the "mobile adapter' arch stiffness and the "rigid lever' arch stiffness implies different or changing mechanisms responsible for maintaining the arch. It has been suggested that midtarsal joint locking or changes in active

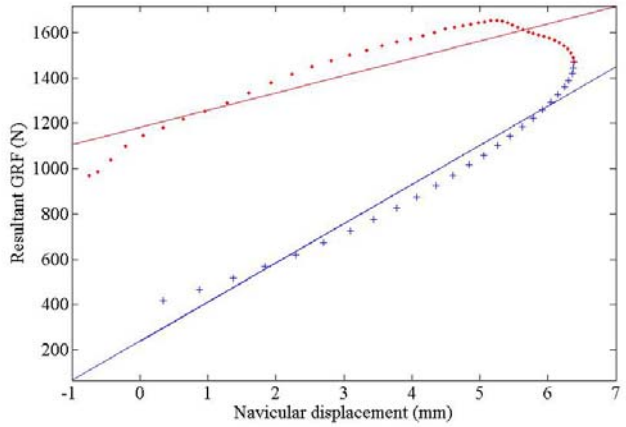

Figure 1: Graph of resultant GRF and navicular displacement during heel-toe running. The least-squares line fitted to the red dots represents arch stiffness during the first part of stance (AS_1) and to the blue crosses represents arch stiffness during the second part of stance (AS_2).

musculature could be responsible for this change. The AS_1 values were similar to plantar fascia stiffness (170±45 N/mm) calculated in vivo using fluoroscopy during the initial tension-elongation curve of slow walking [1]. The large difference between AS_1 and AS_2 also implies that calculating a single value for dynamic arch stiffness may mask some of the physiological processes taking place during running. After the run the mean AS_1 arch stiffness was reduced to 148.2±65.2 N/mm (r2=0.73, p =0.60) and the mean AS_2 arch stiffness was reduced to 228.6±69.7 N/mm (r2=0.96, p=0.18). Because of the large standard deviations, neither difference reached significance but AS_2 showed a trend toward decreased stiffness after the run. If the two arch stiffnesses are controlled by different mechanisms, it might be expected that the stiffness that relies more on active musculature would be more affected by prolonged use. For example, EMG data show posterior tibialis and the triceps surae muscles are more active during the second half of stance phase [2]

Table 1: AS_1 and AS_2 stiffness values before and after a run.

	Before Run	After Run
AS_1 Stiffness (N/mm)	153.7±56.5	148.2±65.2
AS_2 Stiffness (N/mm)	241.0±90.5	228.6±69.7

CONCLUSIONS

The arch of the foot is substantially stiffer during the propulsive phase of the running cycle compared to earlier stages. This lends support to the notion that the foot transforms from a mobile adapter to a rigid lever and thus optimizes its function to the requirements of gait. However, there was no evidence to suggest these functions were impaired after a hard run. Further research will examine the elements responsible for these stiffness values and the role that the shoe plays in maintaining the function of the arch.

REFERENCES

1. Gefen, A. Foot Ankle Int 24, 238-244, 2003.
2. Reber, L et al., Am J Sports Med 21, 805-810, 1993.
3. Zifchock RA et al. Foot Ankle Int 27, 367-372, 2006.

THE EFFECTS OF INDOOR TRACK CURVE RADIUS ON SPRINT SPEED AND GROUND REACTION FORCES

Jesse Tukuafu and Iain Hunter
Brigham Young University, Provo, UT
email: tukuafu22@yahoo.com web: http//biomech.byu.edu

INTRODUCTION

Running on a curved path is an integral part of track and field events. Yet, running on a curved path compared to a straight path has been shown to be significantly slower [1,2]. This decrease in speed may be most apparent when considering indoor track designs. The International Association of Athletic Federations (IAAF) specifies that that a 200 m indoor track can have a radius ranging from 15 m to 19 m with 17.20 m being the "200 m standard indoor track" [3]. In the United States, amateur guidelines for track and field are set forth by the National Collegiate Athletic Association (NCAA). The NCAA specifies for indoor track championships that "the inside radius of the curves on a 200-meter track should be not less than 18 meters and not more than 21 meters" [4]. Depending on the level of competition, a runner could race on a track curve radius ranging from 15 m to 21 m.

Previous studies have attempted to identify the mechanism by which speed is attenuated when running on a curve [1,2]. In order to be continuously changing direction around the curve, medial/lateral (ML) ground reaction forces must be produced.

Decreased vertical ground reaction forces and increased ground contact time are primary components in decreased maximal running speed [5]. As the ML ground reaction forces increase, vertical forces are decreased which results in a loss of running speed.

While speed attenuation on the curve has been researched, previous studies have not focused on how differences in indoor track curve radii can affect sprint performance. In a race, average sprint speed over the length of the race will determine performance. It is unknown how differences in indoor track curve radii will affect sprint speed.

The purpose of this study was to determine the differences in running speeds, ground contact time, and ML impulse that are caused by the range of acceptable indoor track curves.

METHODS

Ten current intercollegiate male sprinters ages 18-25 were recruited as volunteers from the Brigham Young University track team. Subjects performed 45 m maximal sprints under three different conditions. The three sprint conditions were as follows:

- 45 m **straight** sprint
- 45 m sprint with a **21 m track curve** beginning at the 30m mark
- 45 m sprint with a **15 m track curve** beginning at the 30m mark.

Subjects were assigned sprint conditions using a randomized block design performing one condition on each testing day.

All trials were performed at maximal sprint speeds with at least 5 minutes rest between trials to avoid fatigue. The collegiate coach supervised all testing sessions to ensure maximal effort by the subjects.

In order to understand the differences between conditions, ground reaction forces were measured at the 37.5 m mark for each sprint condition using a Kistler force plate (Amherst, New York, USA). Sprinting speed was measured from 30 m to 40 m marks using Brower timing lights (Draper, UT). Mathematically, we rotated the axis of rotation of the force plate to account for the curved paths (Figure 1). Axial rotations for the 21 m and 15 m track curves were 21.6 and 28.6 deg, respectively. Ground contact time was determined from vertical ground reaction forces with a threshold of 100N.

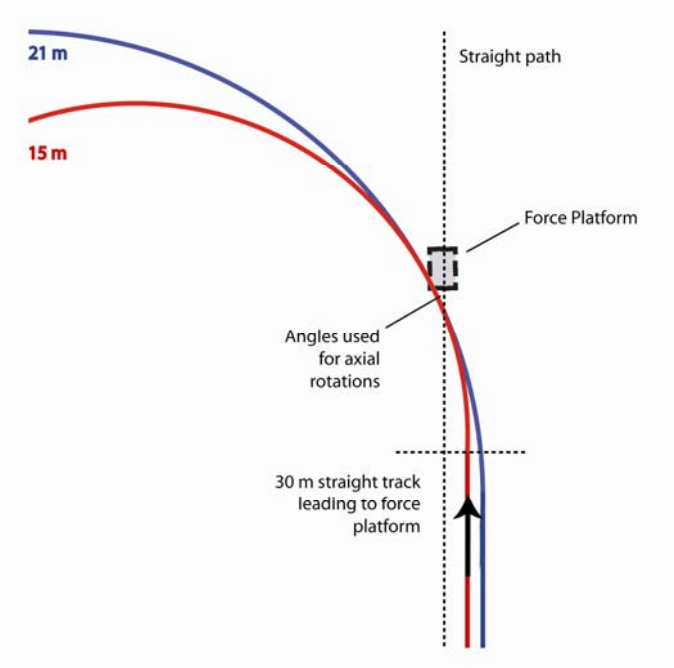

Figure 1: Diagram of the testing setup.

We performed a mixed models analysis of variance blocking on subjects based on sprinting speed, ground contact time, and ML impulse. When we detected a significant effect, we performed a Tukey-adjusted post hoc test (P=.05).

RESULTS AND DISCUSSION

We found that sprinting speed was significantly slower as the radius of the track curve decreased. Runners were 2.6% and 4.7% slower for the 21 m and 15 m track curves respectively compared to straight (Table 1). Interestingly, we found that runners exhibit higher ML impulses and ground contact times on a 21m track curve compared to a 15m track curve. The reasoning for this remains unclear, but there is a difference ground forces between the two curves. This results in a difference in running speed that was expected.

The results of this study may help coaches and athletes to better understand how track conditions will affect sprinting speeds. If the average sprinter from our study were to run 200 m at maximum speed on the 21 m radius curve track in lane 1 the time would be 22.3 s. The same situation on a 15 m radius curve track would take 22.4 s. Sharper track turns result in slower maximum sprint speeds but give sprinters a high percentage of distance spent on straight-aways where maximum speed is higher.

Based on our findings, differences in lane assignment may also play a significant role in race time and progression through heats. Although the difference in times between lanes is likely less than .1 s, this may be enough to affect finishing position.

In races longer than 200m, the different track designs lead to different strategies. Since all competitors runs in lane one after the first lap, tracks with wide turns and short straights make it more difficult to pass other runners effectively. So, while the overall time is not much different between the 15 and 21 m radius curves, the type of track may affect the style and outcome of the race.

REFERENCES

1. Chang Y, & Kram R. *Journal of Experimental Biology*, **210**, 971-982, 2007.
2. Greene PR. *Journal of Biomechanical Engineering*, **107(2)**, 96-103, 1985.
3. Wilson D. *IAAF track and field facilities manual 2008 Edition*. Editions EGC, 2008.
4. Podkaminer B & Danehy L. *2009/2010 NCAA Track and Field and Cross Country Rules*. NCAA, 2008.
5. Weyand PG, et al. *J. Appl. Physiol*. **89**, 1991-1999, 2000.

Table 1: Maximum velocity and corresponding contact times and ML impulses for each condition. Superscripts (A,B,C) indicate differences between groups at $p<0.05$ in the Tukey post hoc analysis (i.e. a variable with a superscript denotes the variable is significantly different from the other superscripted variables).

	Straight (A)	21 m radius (B)	15 m radius (C)
Speed (m/s)	$9.12\pm.066^{BC}$	$8.88\pm.067^{AB}$	$8.69\pm.068^{AC}$
Contact Time (s)	$0.125\pm.003^{BC}$	$0.135\pm.003^{AC}$	$0.131\pm.003^{AB}$
ML Impulse (Ns)	-0.39 ± 2.47^{BC}	52.72 ± 2.51^{AC}	38.40 ± 2.59^{AB}

ARE THE VIBRAM FIVEFINGERS A FUNCTIONAL ALTERNATIVE TO BAREFOOT RUNNING IN *INEXPERIENCED* BAREFOOT RUNNERS?

Max Paquette, Lucas Baumgartner and Songning Zhang
Biomechanics/Sports Medicine Lab, The University of Tennessee, Knoxville, TN, USA
email: mpaquett@utk.edu, web: web.utk.edu/~sals/resources/biomechanics_laboratory.html

INTRODUCTION

Researchers have argued that barefoot running (BF) allows natural foot motions that optimize shock absorption to reduce the risk for running injuries [1,2]. A recent study showed that Vibram FiveFinger (FF) shoes may be effective in imitating BF running mechanics in experienced barefoot runners while providing cutaneous protection from environmental objects [3]. This study investigated two-dimensional kinematic and shoe-ground pressure parameters during treadmill running. To our knowledge, this is the only study that has investigated the biomechanical implications of the Vibram FF shoes. Therefore, the purpose of the current study was to investigate three-dimensional (3D) kinematic and kinetic parameters between FF, BF, and shod running in over-ground running in inexperienced BF runners. We hypothesized that FF condition would yield similar ankle and knee joint angles as well as ground reaction force (GRF) parameters compared to BF and shod conditions but, that significant differences would be observed between BF and shod conditions.

METHODS

Nine male distance runners (age: 28.0 ± 3.5 years, height: 1.80 ± 0.02m, weight: 73.2 ± 5.3kg), who ran at least 20 miles per week, and with minimal previous barefoot running experience, participated in the study. Participants performed five over-ground running trials over a 25 m runway under three different shoe conditions: barefoot, FiveFingers (Vibram) and shod (Adidas)at a running speed of 3.3 ± 0.165 m/s [3] monitored using photocells and an electronic timer. A seven-camera motion analysis system (240Hz, Vicon Motion Analysis) was used to obtain the 3D kinematic data. Reflective anatomical markers were used to define the trunk, pelvis, right thigh, right leg and right foot. Four tracking markers were attached to each segment via a semi-rigid thermoplastic shell. Ground reaction forces were recorded simultaneously with a force platform (1200 Hz, AMTI) during the running trials. The three experimental conditions were counter-balanced and randomized to reduce any condition order effect. Visual3D (C-Motion, Inc.) was used to compute the 3D kinematic and kinetic variables and customized software (VB_V3D) was used to further analyze the variables of interest. Kinematic and kinetic data were filtered using a fourth-order Butterworth low-pass filter with cutoff frequencies of 8 and 50 Hz, respectively. The peak vertical GRF (vGRF, 2nd peak), its time, and sagittal and frontal plane ankle and knee ranges of motion (ROM, from contact to peak) were the variables of interest. Ground reaction forces were normalized to body mass (N/kg). A one-way repeated measures analysis of variance (ANOVA) was performed ($p < 0.05$). Post hoc comparisons were performed with the Bonferonni adjustment on the significant level for multiple comparisons.

RESULTS AND DISCUSSION

No significant differences in the vGRF, passive loading peak and the time to vGRF peak were observed among the shoe conditions. Stance time (ST) was significantly shorter in BF (0.226 s) compared to shod (0.237 s) running ($p=0.004$; Table 1). This finding suggests that our *inexperienced* BF runners reduced ST in BF running to avoid or prevent cutaneous discomfort during the running trials on the hard laboratory floor. Previous research provides support for this result as ST in *experienced* BF runners was not different compared to shod running [3]. No statistical differences were observed between FF (0.229 s) and the other two conditions (BF and shod) indicating that FF shoes may be beneficial in facilitating transition from shod to BF running. Previous research indicates that the foot strike patterns in running dictate the presence or absence of the vGRF transient impact (1st peak) [4]. We identified two out of the nine

subjects as potential fore- or mid-foot strikers. However, no apparent differences in the kinematic and kinetic variables were observed between the potential fore- or mid-foot strikers and heel strikers.

Ankle dorsiflexion range of motion (AROMx) was significantly greater in FF (20.90°) compared to both BF (14.70°, p=0.0001) and shod (16.98°, p=0.040; Figure 1). In addition, AROMx was greater in shod compared to BF (p=0.027). Knee flexion range of motion (KROMx) was greater in shod (25.90°) compared to both BF (21.44°, p=0.0001) and FF (21.60°, p=0.004; Figure 1). The larger AROMx in FF compared to *both* BF and shod could be associated with increased impact attenuation at the ankle, which may indicate the importance of the ankle joint in reducing stresses at the proximal joints. However, ankle dorsiflexion range of motion in *experienced* BF runners has been shown to increase in BF and FF compared to shod running [3]. *Inexperienced* BF runners may benefit from the increased ankle compliance in FF running: an added benefit not present in BF due to their inexperience with BF running. Ankle eversion range of motion (AROMy) was statistically larger in FF (11.19°) compared to BF (9.02°, p=0.045). This reduction in AROMy observed in our *inexperienced* BF runners may, once again, be a strategy used to prevent cutaneous discomfort under the medial arch of the foot during passive loading in stance. Therefore, the small but significant increase in AROMy in FF may further increase lower limb joint impact attenuation observed in the sagittal plane.

CONCLUSION

Our results indicate that greater ankle joint range of motion in FF compared to BF in the sagittal and frontal planes, and to shod in the sagittal plane only, for inexperienced BF runners. Interestingly, the knee range of motion in the sagittal plane was not different between FF and BF, but larger in shod compared to both, which may further support the importance of the ankle in reducing lower limb joint impact stresses. Finally, FF appears to provide biomechanical benefits that could potentially reduce the risk for running injuries. Further and more comprehensive evaluation of the impact related variables are warranted to provide more evidence for the benefits of the barefoot emulating shoes.

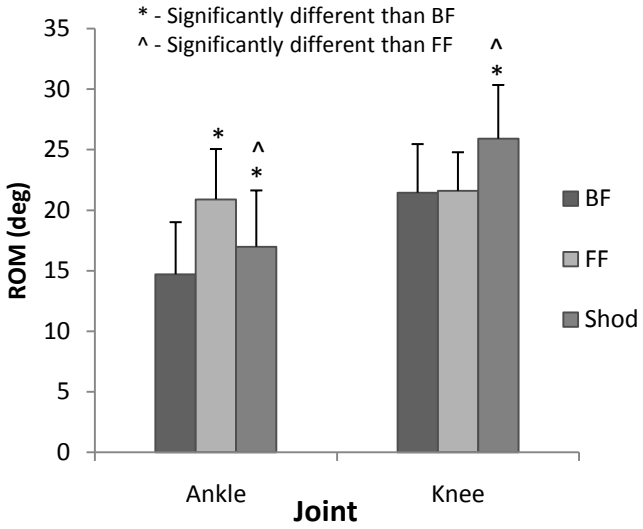

Figure 1: Sagittal Ankle and Knee ROM.

ACKNOWLEDGEMENTS

The Vibram FiveFinger shoes were provided by Vibram USA Inc ®.

REFERENCES

1. Robbins et al. (1987) Med. *Sd.* Sp. Ex. **19**:148-56
2. Hreljac (2004) Med. *Sd.* Sp. Ex. **36**:845-9
3. Squadrone et al.(2009) J Sp. Med. Ph. Fit.**49**:6-13.
4. Liebermann et al. (2010) Nature. **463**:531-536

Table 1. Average vertical GRF and frontal plane ankle and knee ROM variables: mean ± STD.

Condition	vGRF_Max2 (BW)	Time_vGRF (s)	Contact Time (s)	AROMy (deg)
BF	2.57±0.204	0.098±0.010	0.226±0.021	-9.019±3.079
FF	2.62±0.206	0.096±0.006	0.229±0.017	-11.193±2.602*
Shod	2.61±0.196	0.102±0.011	0.237±0.023*	-10.467±3.214

Note: * – significantly different than BF, ^ – significantly different than FF.

NECK MOTION DUE TO THE HALO-VEST IN PRONE AND SUPINE POSITIONS

[1] Paul C. Ivancic and [1] Connor J. Telles
[1] Biomechanics Research Laboratory, Department of Orthopaedics and Rehabilitation, Yale University School of Medicine, New Haven, CT, USA; email: paul.ivancic@yale.edu

INTRODUCTION

The halo-vest orthosis, introduced in 1959 by Perry and Nickel [1] to treat scoliosis or neck muscle paralysis, has been used since then to treat a variety of cervical spine injuries including Jefferson, odontoid, facet, and compression fractures. Previous clinical studies have suggested snaking motion due to the halo-vest during activities of daily living may lead to inadequate healing or nonunion. Snaking motion is defined as rotation in opposing directions throughout the cervical spine.

The objectives of this study were to evaluate motion of the injured cervical spine with normal halo-vest application and vest loose in the prone and supine positions.

Fig. 1. Photograph of the Human Model of the Neck (HUMON) with the halo-vest. Motion tracking flags were fixed to the head, cervical vertebrae, and pelvis.

METHODS

The halo-vest was applied to a Human Model of the Neck (HUMON), which consisted of a cervical spine specimen (n=4) mounted to the torso of an anthropometric test dummy and carrying a surrogate head (**Fig. 1**). HUMON was transitioned from prone, to upright, to supine with the halo-vest applied normally and with the vest loose. Average peak spinal motions were computed in the prone and supine positions and contrasted with the physiologic rotation range, obtained from the intact flexibility test, and statistically compared ($P<0.05$) between normal halo-vest application and vest loose.

RESULTS AND DISCUSSION

Snaking motion of the neck was observed in the prone and supine positions, consisting of extension at head/C1 and C1/2 and flexion at the inferior spinal levels (**Fig. 2**). The largest peak motions were generally observed in the prone position. The intervertebral rotation peaks generally exceeded the physiologic range throughout the cervical spine due to the loose vest in the prone position. Significant increases in the extension peaks at head/C1 (16.9° vs. 5.7°) and flexion peaks at C4/5 (6.9° vs. 3.6°) and C7/T1 (5.2° vs. 0.7°) were observed in the prone position due to the loose vest, as compared to normal halo-vest application. Axial separation was observed at all spinal levels due to the halo-vest, consistent with tensile load that has been observed clinically in halo-vest patients.

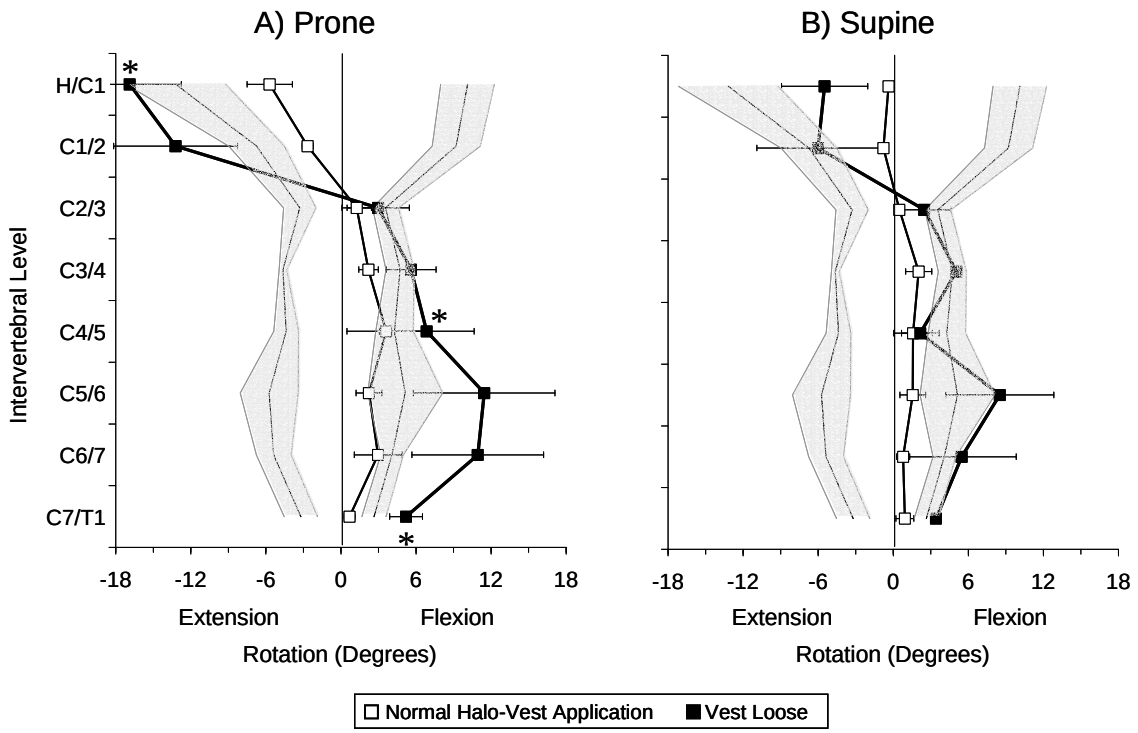

Fig. 2. Average peak rotations of spinal levels head/C1 through C7/T1 in **A**) prone and **B**) supine positions with normal halo-vest application and with the vest loose. The physiologic rotation range (average $\pm$ 1 SD) is indicated in grey shading for flexion and extension. Significant differences ($P<0.05$) in average peak motion between normal halo-vest application and vest loose are indicated with asterisks.

CONCLUSIONS

1. The halo-vest was applied to a Human Model of the Neck, consisting of an injured cervical spine specimen mounted to the torso of an anthropometric test dummy and carrying a surrogate head. The model was used to evaluate neck motion patterns due to the halo-vest in the prone and supine positions and to evaluate the effect of vest loosening.

2. Average peak head/T1 rotation remained within the physiologic limit however the loose vest caused significantly greater head/T1 anterior shear and axial separation in the prone position, as compared to normal halo-vest application.

3. Snaking motion of the neck was observed in the prone and supine positions, consisting of extension at head/C1 and C1/2 and flexion at the inferior spinal levels.

4. In the prone position, the loose vest caused intervertebral rotation peaks which generally exceeded the physiologic range with significantly greater extension at head/C1 and flexion at C4/5 and C7/T1, as compared to normal halo-vest application.

5. The present results underscore the importance of proper vest fit and continued monitoring of strap tightness to reduce snaking motions of the neck in those treated with the halo-vest.

REFERENCES

1. Perry et al. J Bone Joint Surg Am 1959;41-A:37-60.

ACKNOWLEDGEMENTS

We gratefully acknowledge a gift from Ossur Americas, Aliso Viejo, CA, USA, which made this research possible.

MECHANISMS OF WHIPLASH INJURY PREVENTION ATTRIBUTABLE TO ENERGY-ABSORBING SEAT

[1] Paul C. Ivancic and [1] Ming Xiao
[1] Biomechanics Research Laboratory, Department of Orthopaedics and Rehabilitation, Yale University School of Medicine, New Haven, CT, USA; email: paul.ivancic@yale.edu

INTRODUCTION

Motor vehicle crashes remain the leading cause of spinal injury [1]. In attempt to reduce whiplash injuries, manufacturers have incorporated active injury prevention systems in newer automobiles, such as the Whiplash Protection System (WHIPS) introduced by Volvo in 1998. Epidemiological studies have indicated potential benefits of WHIPS in reducing neck injury risk between 21 to 47%, as compared to conventional seats. The majority of previous biomechanical studies were manufacturer-sponsored or contain limited data.

The goals of this study were to investigate whiplash injury prevention mechanisms attributable to WHIPS using simulated rear crashes of a Human Model of the Neck (HUMON).

METHODS

HUMON consisted of a neck specimen (n=6) mounted to the torso of BioRID II and carrying a custom anthropometric head stabilized with muscle force replication (**Fig. 1A**). HUMON was seated and secured in a 2005 Volvo XC90 minivan seat, which included WHIPS and a fixed head restraint. The main components of the WHIPS recliner (**Fig. 1B**) included the energy-absorbing element; return spring; and pivot shaft, guide pin, and window for control of WHIPS motion (**Fig. 1C**). The WHIPS was activated by HUMON's momentum pressing into the seatback during the crash, causing rearward translation and extension of the seatback relative to the seat base and plastic deformation of the energy-absorbing elements. Rear crashes (9.9, 12.0, and 13.3 g) were simulated and motions of the head, neck, torso, pelvis, sled, seatback, and WHIPS were monitored. Significant increases ($P<0.05$) in the spinal motion peaks relative to physiologic limits were determined.

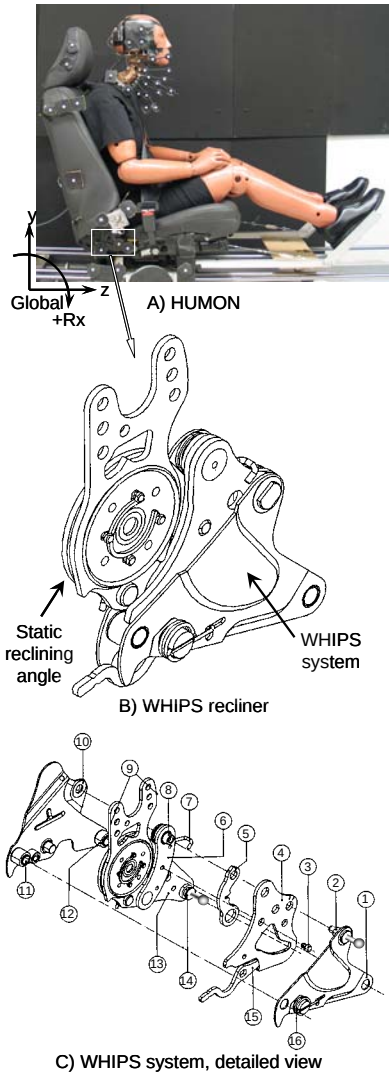

Fig. 1. A) Photograph of the Human Model of the Neck (HUMON) and rear crash apparatus. **B**) The WHIPS recliner. **C**) Detailed view of the WHIPS system including: outer (1) and inner (10) plates with attachment points to the seat base (11,12); indicator (3); folding bracket with WHIPS motion control window (4); energy-absorbing element (5); non-energy-absorbing element (6); pivot shaft (2,8), guide pin (14), and return spring (7) for WHIPS motion; conventional recliner mechanism (9) and bracket (13); latch (15) and spring (16) for folding of backrest. Figures 1B and 1C were adopted from Lundell et al, 1998 [2].

RESULTS AND DISCUSSION

Average WHIPS motions are presented graphically for the 13.3 g crashes (**Fig. 2A**). For all crashes, rearward and upward translations of the WHIPS guide pin within the control window were observed, with peaks reaching 4.1 cm for -Tz and 1.6 cm for +Ty, occurring as early as 76 ms. Motions of the seatback relative to the sled consisted of extension and rearward and downward translations. Peak plastic deformation of the energy-absorbing elements, ranging between 0.6 and 1.2 cm, occurred at 72 ms. The post-crash position of the WHIPS guide pin within the control window (**Fig. 2B**) was consistent with the average computed data.

Average peak C7/T1 rotations significantly exceeded physiologic limits during the 13.3 g crash. The cervical spine maintained its S-shaped curvature throughout the duration of contact of the head with the head restraint. A 42% reduction in peak T1 horizontal acceleration, as compared to sled acceleration, was observed due to WHIPS.

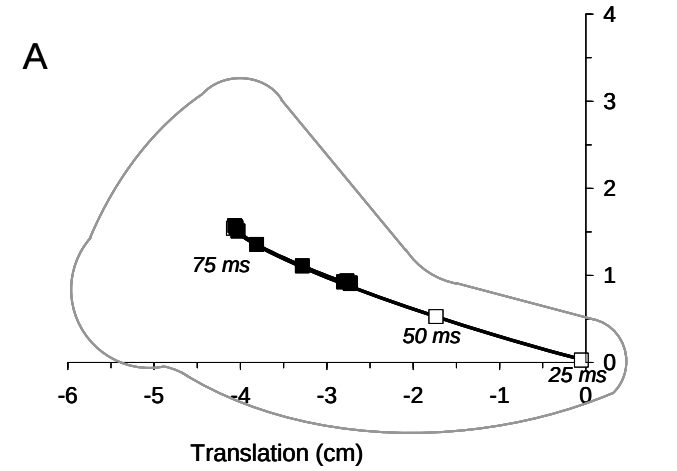

Fig. 2. A) Average motions of the right WHIPS guide pin during the 13.3 g rear crashes. **B**) Representative photograph of the right WHIPS recliner taken after the rear crash.

CONCLUSIONS

1. The present study investigated the whiplash injury prevention mechanisms attributable to the WHIPS energy-absorbing seat using simulated rear crashes of HUMON at 9.9, 12.0 and 13.3 g peak horizontal sled accelerations.

2. A 42% reduction in peak T1 horizontal acceleration, as compared to sled acceleration, demonstrated the energy-absorbing capacity of WHIPS.

3. WHIPS motion included simultaneous: rearward and downward translations and extension of the seatback; deformation of the bi-lateral WHIPS energy-absorbing elements; and reduction in distance between the head and head restraint.

4. Average peak C7/T1 rotations significantly exceeded physiologic limits during the 13.3 g crash. The cervical spine maintained its S-shaped curvature throughout the duration of contact of the head with the head restraint. Lower cervical spine injuries due to excessive motion may occur prior to or during contact of the head with the head restraint, even in the presence of WHIPS.

5. The present study provided insight into the crash-dynamics of the occupant, seatback, and WHIPS. These data may be useful for refining seat design to reduce neck injuries. Future whiplash injury prevention systems will most likely integrate beneficial design features, such as active head restraint and energy-absorbing seat, with more advanced features, such as accident avoidance technology.

REFERENCES

1. National Center for Statistical Analysis. Traffic Safety Facts. Washington, DC: NHTSA, 2008.
2. Lundell et al. SAE Paper No. 980301, 1998.

ACKNOWLEDGEMENTS

This research was supported by grant 5R01CE001257 from the Centers for Disease Control and Prevention (CDC).

DYNAMIC MODELING OF HUMAN LUMBAR SPINE VIA MSC ADAMS®

[1]Majid Tabesh, [2]Mohammad Elahinia

[1,2]Dynamic and Smart Systems Laboratory, University of Toledo, Toledo, Ohio, USA
Email: majid.tabesh.m@gmail.com, web: http://smartsys.eng.utoledo.edu

INTRODUCTION

Spine is a 3D structure responsible for supporting the skeletal body and protecting the spinal cord. The physical state of this supportive structure is vital to the overall health of the body. Due to its supportive role, external loadings and conditions can significantly affect the spinal functionality. For example, the individuals subjected to long-term vibrations in a seated posture, such as truck or tractor drivers, were shown to suffer more frequently from degenerative spinal diseases [1]. This is attributed to compromising effects of the compressive loads in the long run on the flow of nutrients to the intervertebral disks which will lead to the premature deterioration of the disk's annulus tissue.
The spine model in the dynamic analysis software MSC ADAMS® was developed to help evaluate these external loading conditions in various situations such as shocks induced from a bad road setting at the time of driving.

METHOD

In this study only the lumbar region of the spine was considered. The coordinates for the center of mass (CM) of the last thoracic, the five lumbar, and the first sacral vertebrae were derived from the published literature on the morphological and physical balance and alignment of the spine [2]. The inertial mass of each vertebrae in the model were considered as the mass of the vertebrae itself plus the tissues and viscera contained in the area covered by its height (for a typical 80 Kg individual) [3]. Each vertebra was represented as a sphere in ADAMS since only the 3D location of the CMs and their rotations are necessary for dynamic calculations.
The vertebral column has stiffness and damping properties in all the six degrees of freedom. The damping is a result of the viscoelastic properties of bone and intervertebral disks and acts as a kinematic energy absorber in the time of severe dynamic loadings. Several researchers studied such properties of the spinal column from which the translational and rotational stiffness data were elicited [4]. Specifically, the load bearing properties of the spine in flexion-extension, lateral bending, and axial rotation was taken into account as nonlinear equations determined by curve-fitting the moment-rotation experimental data (Figure 1) [4]. The disks were represented as two series *bushing* elements. The rheological model representing the axial mechanical behavior of the spinal motion segment was fitted as two series spring-dashpot blocks (Kelvin model) [5]. An equivalent force-moment was applied to the T12 to account for the weight of the head and the upper torso.
The developed model for the human lumbar spine is shown in Figure 2.

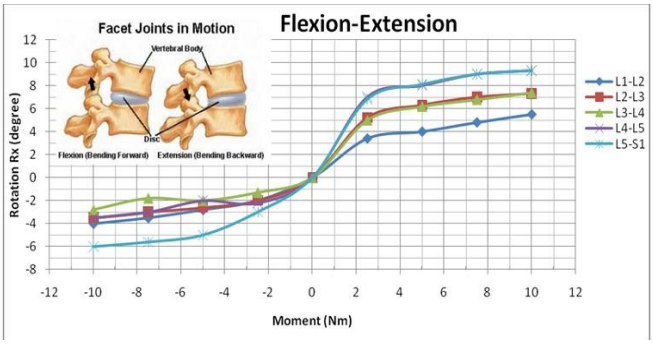

Figure 1 Experimental data representing segment stiffness properties in flexion and extension.

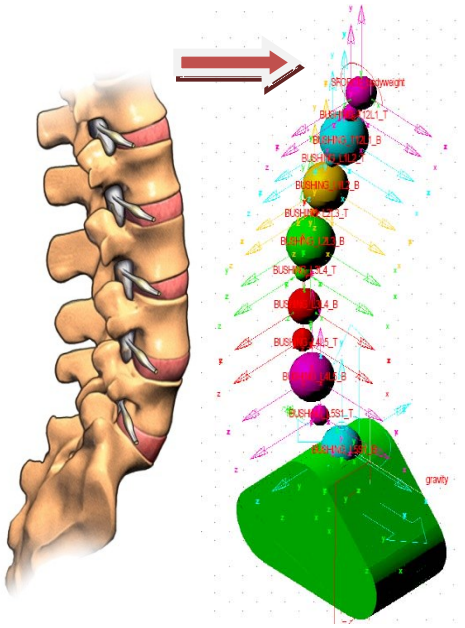

Figure 2 The 3D rigid-body model for the lumbar spine. The vertebral bodies (T12 to S1) are represented as spheres with corresponding inertial properties. Intervertebral disks are represented as two bushing elements in series.

RESULTS AND DISCUSSION

Positive axial shock

This loading case approximated the situation of driving on a bump and attempted to capture the load pattern

exerted on the spinal levels in a sitting posture. An abrupt axial displacement was applied to the seat. Figure 3 demonstrates the various displacements in the lumbar levels with respect to time. It is noticeable that the damping properties of the spine diminished the oscillations immediately. Also, despite the fact that the load was applied in the vertical direction, the vertebral bodies underwent some oscillatory rotations and eventually settled back to their initial condition.

The forces which were transferred through the spine due to this shock are shown in Figure 4. This graph is also oscillatory in trend and illustrates the helpful effect of the damping in intervertebral disks that dissipated the external energy induced to the spine. The loads incurred were not of serious quantities compared to the tolerable loads by the motion segments.

REFERENCES

1. Bonney R.A., et al. *Applied Ergonomics* **34**, 195-200, 2003.
2. Keller T.S., et al. *The Spine J.* **5**, 297–309, 2005.
3. Keller T.S., et al. *J Manipulative and Physiological Therapeutics* 25, 8: 485-496, 2002.
4. Panjabi M.M., et al. *J Bone Joint Surg Am* **76**, 1994, 413-424.
5. Burns M.L., et al. *J. Biomechanics* **17**, 1984, 2:113-130.

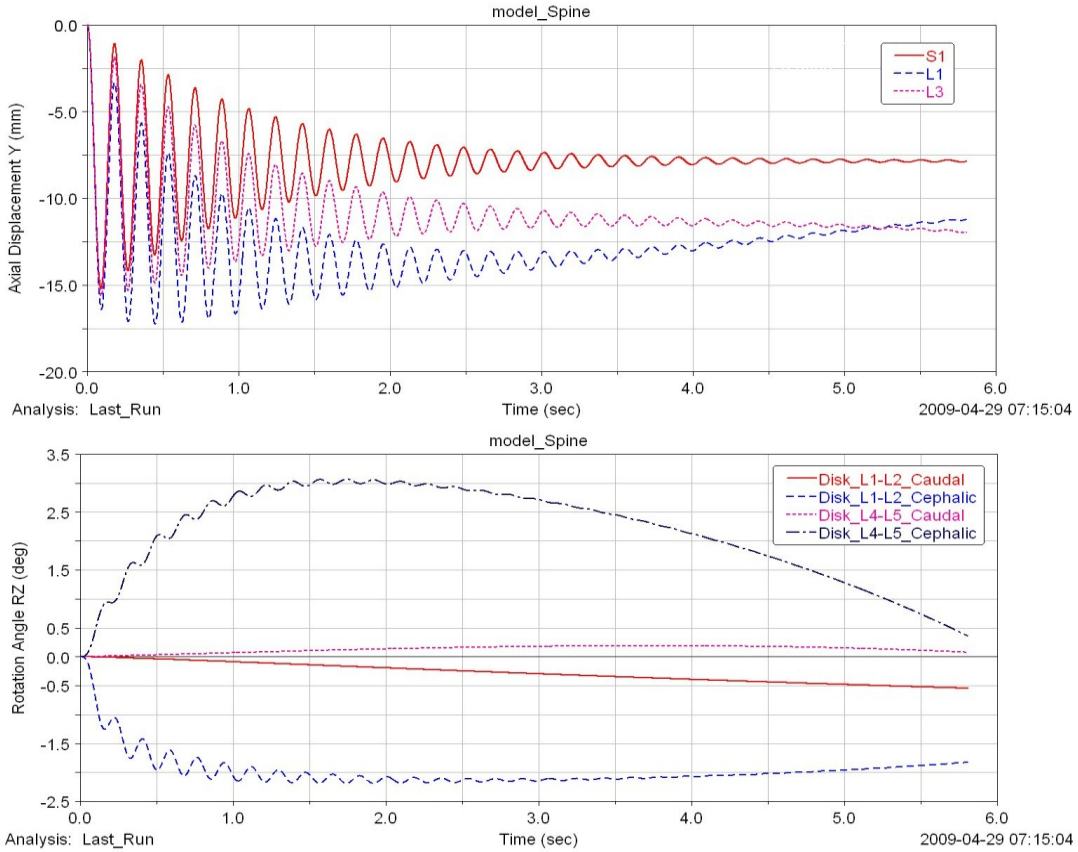

Figure 3 Displacements and rotations in represented vertebral bodies due to a small axial shock applied to the seat.

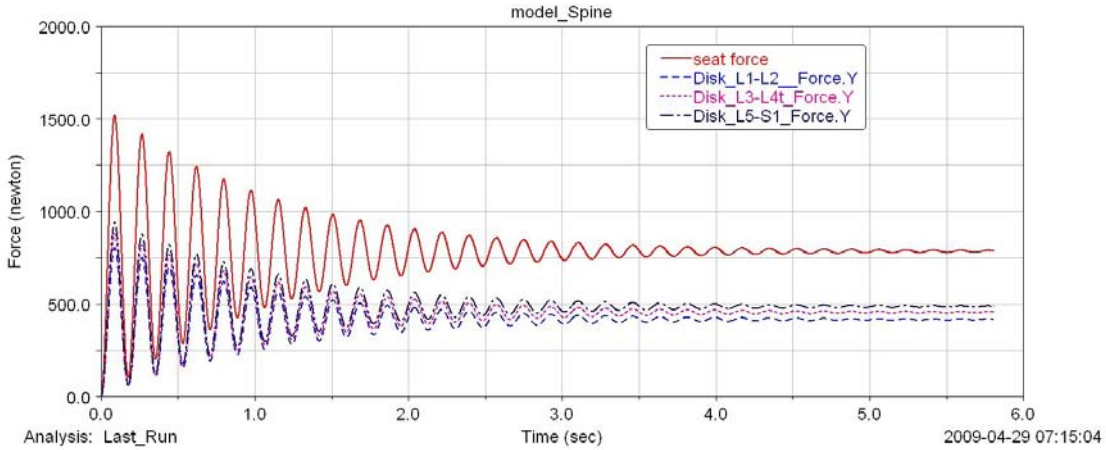

Figure 4 magnitudes of forces transferred in the disks as a result of the axial shock.

IDENTIFICATION OF HYPERELASTIC PROPERTIES OF LUMBAR MULTIFIDUS

[1]Terry K Koo and [2]Yongping Zheng

[1]New York Chiropractic College, Seneca Falls, NY, USA
[2]Hong Kong Polytechnic University, Hong Kong, PRC
email: tkoo@nycc.edu, web: http://www.ultrasonic-solutions.com

INTRODUCTION

Quantitative measurements of elastic properties of lumbar multifidus (LM) may have significant values on low back pain (LBP) diagnosis and prognosis. Attempts have been made to quantify paraspinal soft tissue compliance (deformation per unit load) using instrumented indentation [1]. However, these measures depend not only on the elastic properties of the soft tissues, but also on the shape, thickness, and boundary conditions. Therefore, direct comparison among subjects and sites are difficult. We developed a tissue ultrasound palpation system (TUPS) to make in-vivo elasticity measurements of LM [2,3]. Our previous effort focused on small strains and assumed a linear elastic behavior. The current work extends our previous effort by presenting large strain indentation data on LM to test the feasibility of using TUPS and finite element (FE) modeling to determine non-linear elastic parameters of LM through optimization.

METHODS

Experimental Protocol: Since LM is the only muscle that lies on top of the mamillary process at the lumbar region [4], we located and tested 10 mamillary processes in 3 asymptomatic subjects and 1 right-side affected LBP subject. Subjects were instructed to lie down in a prone position on a treatment table. Each indentation trial involved a ramped load on a marked site to ~25% deformation using the TUPS probe at a rate of ~8%/s. During the indentation trials, each subject was instructed to exhale to a comfortable extent and to suspend breathing. Load-deformation data of 5-7 indentation trials were collected at each site, and curve-fitted with a 3rd order polynomial. A probe alignment arm was used to guide the translation of the TUPS probe during indentation.

Test Apparatus: The TUPS probe has a 5 MHz, 11 mm flat-ended cylindrical ultrasound transducer at its tip mounted in series with a 10 N strain gauge load cell. As an operator manually loads the probe on the tissue surface, the ultrasound module of the TUPS continuously emits ultrasound pulses into the soft tissue. At the interface between the LM and the mamillary process, there is normally an abrupt change of the acoustic impedance, thus producing significant reflections for the incident ultrasonic wave. Hence, thickness and deformation of the LM can be determined from the timing of the echo signals using a cross-correlation procedure, whereas the applied force is measured by the load cell.

Finite element Modeling: The indentation experiment was modeled as a two-dimensional, finite-deformation, axisymmetric problem using Abaqus. The TUPS probe was modeled as a rigid body with a frictionless contact. A vertical displacement that corresponds to 25% tissue deformation was prescribed to the FE model and the corresponding reaction forces were calculated throughout the indentation. The lower surface of the LM was constrained in the vertical direction to account for the fact that the LM lies on top of the mamillary process and assumed a frictionless boundary condition. All soft tissues between the probe and the mamillary process were denoted as LM and modeled as a homogenous layer of hyperelastic material using an order-one Ogden material model. The LM was assumed to be incompressible to simulate the initial apparent incompressibility condition of the soft tissue to indentation. Geometrical nonlinearity was selected within the Abaqus to account for finite-deformation.

Parameter Identification: Two parameters (i.e. an initial shear modulus (μ_1) and a non-dimensional coefficient (α_1)) are required to specify the nonlinear elastic behavior of the LM. Specifically, μ_1 accounts for the linear elastic response of the LM at a small strain and α_1 accounts for the nonlinearity at a larger strain.

A number of steps were carried out to determine the hyperelastic parameters. The technique starts with indentation trials that acquire the force-deformation responses of the LM using TUPS. These responses

were used in a least square minimization algorithm to determine the hyperelastic parameters within the FE model that results in a force-deformation response similar to its measured counterpart. FE meshes were automatically generated using the tissue thickness as an input parameter. Initial guess of μ_1 was based on the analytical solution proposed by Hayes [5] and initial guess of α_1 was arbitrarily set to 15. A Matlab program was developed to carry out an iterative adjustment of material parameters, according to Nelder-Mead simplex method. For each iteration, the Matlab program updates the material parameters and links with the Abaqus to invoke the FE analysis. A Python script extracts the simulation results from the Abaqus to the Matlab after each iteration. This iterative process is repeated until termination criteria meet.

An additional parameter was derived to account for the contribution of all hyperelastic parameters to the LM's overall non-linear elastic behavior. Using the hyperelastic parameters computed at each site, we computed simulated force-deformation (F-D) response of a 40mm thick, hypothetical axisymmetric block induced by an 11 mm flat-ended cylinder and calculated the area under the F-D curve (A_{FD}) from 0 to 10 mm deformation using numerical integration. This approach eliminated the F-D variability due to geometry.

RESULTS AND DISCUSSION

The bilateral force-deformation data at L4 and L5 mamillary processes of the right-side affected LBP subject are plotted in Fig. 1. The small difference among the trials suggests that the TUPS measurements are repeatable.

Our FE optimization approach succeeded in fitting the experimental data accurately for all measurement sites. Table 1 summarizes the Ogden parameter set at each site that produced the best fits. The corresponding A_{FD} is also reported. Symmetry ratios (SR) between the left and right A_{FD} were calculated at each level. Initial shear modulus was also calculated using the linear elastic model proposed by Hayes [5]. It appears that quantification of LM stiffness using linear elastic parameters or models can be misleading. A_{FD} appears to be a more useful parameter for quantifying LM stiffness as it accounts for the overall elastic behavior over a large strain range. Our preliminary results also demonstrated that the LBP subject's LM muscles are not necessary stiffer than the asymptomatic subjects. Hence, the clinical impression of palpable rigidity of LM in subjects with LBP is questionable. However, we noted consistency between clinical symptom and elasticity measurement, that is the right side of the right-affected LBP subject is stiffer than the left side.

Future work will incorporate the FE optimization approach on more LBP and asymptomatic subjects at all lumbar levels to explore the potential use of large strain elasticity measurements on LBP diagnosis and/or prognosis.

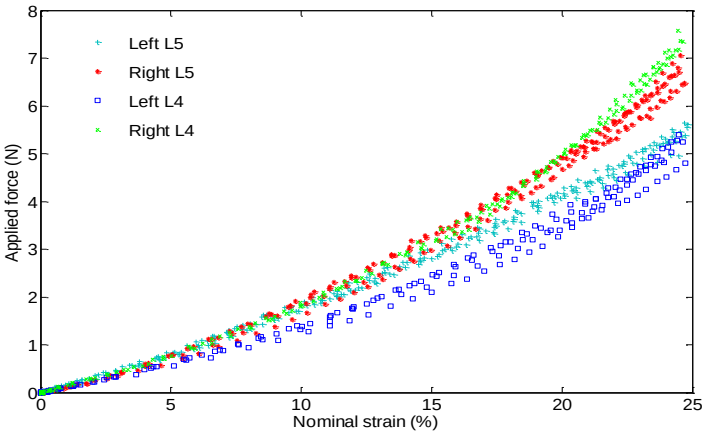

Figure 1: Measured force-deformation data of a right-affected LBP subject at the mamillary processes of the left and right L4 and L5. Data of 5-7 indentation trials are superimposed at each site.

Table 1: Summary of material parameters

Subject#	Site*	Hayes μ_1 (kPa)	Odgen μ_1 (kPa)	Odgen α_1	A_{FD} (Nmm)	SR+
A	L-L4	9.32	10.04	15.77	37.09	
B	L-L3	11.89	10.95	12.95	34.17	
C	L-L4	8.11	8.62	15.81	30.72	0.989
C	R-L4	8.60	9.09	14.93	31.05	
C	L-L5	8.05	8.28	16.36	30.32	0.928
C	R-L5	8.85	8.38	14.58	28.13	
D	L-L4	6.84	7.30	11.15	21.14	0.797
D	R-L4	7.67	8.67	12.48	26.51	
D	L-L5	7.66	9.29	5.730	22.45	0.869
D	R-L5	8.38	9.24	10.25	25.84	

#A, B, C are asymptomatic subjects and D is a right-side affected LBP subject.
*L: left; R: right; +SR: Symmetry ratio between the left and right A_{FD} (≤ 1).

REFERENCES

1. Fischer AA. *Arch Phys Med Rehabil* **68**, 122-125, 1987.
2. Koo TK, et al. *ACC-RAC 2010*, Las Vegas, NV, USA, 2010.
3. Zheng YP, et al. *IEEE Trans Biomed Eng* 43, 912-918, 1996.
4. Macintosh JE, et al. *Spine* **12**, 658-668, 1987.
5. Hayes WC, et al. *J Biomech* **5**, 541-551, 1972.

DISTURBANCES TO INTRINSIC STIFFNESS AND REFLEXIVE MUSCLE RESPONSES FOLLOWING PROLONGED TRUNK FLEXION

Brad Hendershot, B. Bazrgari, K. Muslim, N. Toosizadeh, M.A. Nussbaum and M.L. Madigan

Virginia Tech, Blacksburg, VA, USA
email: nussbaum@vt.edu

INTRODUCTION

Prolonged trunk flexion is associated with an increased risk of low back disorders (LBDs) [1]. Prolonged trunk flexion reduces passive support of the spine due to creep of viscoelastic structures. Ideally, the neuromuscular system detects such alterations and compensates with appropriate and effective muscle activation. Efficient control of muscle activation (i.e., to achieve equilibrium and stability requirements of the trunk) is imperative for avoiding LBDs. Hence, understanding normal and/or disturbed trunk neuromuscular behavior is needed for prevention, treatment, and rehabilitation of LBDs. The goal of this study was to quantify alterations in trunk neuromuscular behaviors induced by prolonged trunk flexion. More specifically, the effects of angle and duration on trunk stiffness and reflex response were investigated.

METHODS

Twelve healthy young adults with no self-reported history of low back pain participated, after completing an informed consent procedure approved by the local IRB. Participants included six males with mean (SD) age = 23(4) yr, stature = 180.3(6.8) cm, and body mass = 75.3(10.8) kg. Respective values for the six females were 22(3) yr, 166.1(7.9) cm, and 60.1(5.5) kg. Trunk posture was monitored using electromagnetic sensors (Xsens, Los Angeles, CA, USA) over the T10 and S1 spinous processes, and muscle activity (EMG) using bipolar surface electrodes over the bilateral erector spinae, internal obliques, external obliques, and rectus abdominis muscles.

Three replications of slow trunk flexion-extension movements were performed to determine the corresponding lumbar flexion angle at which extensor EMG dropped below 5% of maximum (i.e., flexion-relaxation, or FR angle). Each participant completed six experimental sessions involving exposures to 33, 66, and 100% of FR angle for durations of 2 and 16 min. in a counterbalanced order, during which muscle activity (EMG) was minimized. Mean FR angle was 65.2˚, mean treatment levels were 22, 45, and 65˚.

During the experiment, participants stood upright in a structure that restrained the pelvis and lower limbs. Static lumbar flexion was achieved by raising the legs with the torso upright (Fig. 1), thereby minimizing movement, muscle activity, and potential muscle fatigue.

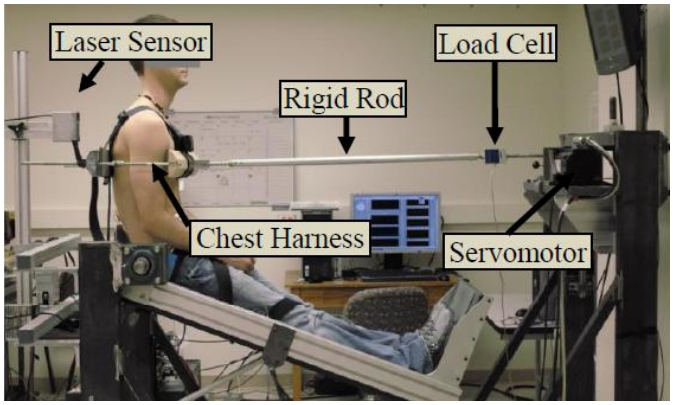

Figure 1: Experimental set-up demonstrating a participant in a 100% (of FR angle) posture.

Prior to and after exposures, a pseudorandom sequence of 12 anterior-posterior position perturbations of ±5mm were applied to the trunk at ~T8 via a servomotor (Kollmorgen, Radford, VA), rigid rod, and chest harness (Fig. 1). During these perturbations, participants maintained an extensor effort of 10% MVC using real-time visual feedback of muscle activity. Trunk displacements (at T8, superior to the chest harness) were measured with a CCD laser displacement sensor (Keyence, Osaka, Japan) and motor encoder. Applied forces were measured using a load cell in-line with the rigid rod (Interface SM2000, Scottsdale, AZ, USA).

Several measures were derived to assess neuromuscular behaviors (during anteriorly-directed perturbations). Reflex response latency was determined as the time delay between displacement onset and the onset of erector spinae muscle reflex response (via EMG) [2]. Intrinsic trunk stiffness was then estimated using a system identification method relating measured trunk kinetics and kinematics during the period prior to reflex response [3]. Reflex response, estimated by subtracting the intrinsic response from measured trunk kinetics, was then related to delayed trunk velocity to estimate reflex gain [4]. Mixed-factor analyses of variance (ANOVA) were used to determine the effects of gender, flexion angle, and duration on these measures ($\alpha = 0.05$).

RESULTS AND DISCUSSION

Mean (SD) muscle reflex delays were similar (p=0.32) for males [62(3) ms] and females [64(5) ms], and were unaffected by trunk flexion (p=0.79). Though not significant (p=0.1), intrinsic trunk stiffness was higher among males than females, at 6075 (1370) and 4916 (1509) N/m, respectively. Intrinsic stiffness decreased significantly (p<0.01 with flexion angle (Fig. 2), but was consistent (p=0.92) between the two exposure durations. The latter was likely a result of relatively quick (2-3 min) exponential decays in passive stiffness at a given strain. Specifically, ~90% of the moment decrement due to relaxation occurred during the first 2 min. of exposure.

Pre-exposure reflex gains tended (p=0.075) to be higher in females [1015(229) Ns/m] than males [926(243) Ns/m]. Trunk reflex gains increased significantly (p<0.01) with flexion angle (Fig. 2), but were unaffected by flexion duration (p=0.41). There was a gender x duration interaction effect (p=0.038) on reflex gain; effects of 2 min. of exposure were similar between genders, though males showed substantially larger increases after 16 min. of exposure. These increased reflex gains are consistent with evidence from animal models in which a hyper-excitable reflex response was found following periods of prolonged ligament stretch [5].

CONCLUSIONS

Despite the roles of intrinsic stiffness and paraspinal reflex responses in spinal stability and neuromuscular control, no prior studies have quantified alterations in these variables following exposure to varying magnitudes and durations of prolonged flexion in humans. Our results (Fig. 2) suggest that increases in trunk reflexive stiffness, at least in healthy individuals, may be a compensation for decreases in passive trunk stiffness (i.e., reflected by predicted intrinsic stiffness) following prolonged trunk flexion.

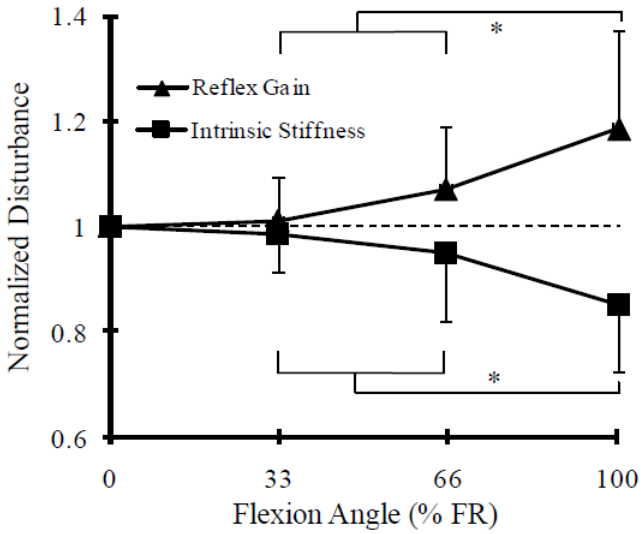

Figure 2: Effects of flexion angle on trunk intrinsic stiffness and reflexive gain (data are normalized to pre-exposure values). Results from post hoc pairwise comparisons are indicated by brackets (* = significant difference).

REFERENCES

1. Kumar S. *Ergonomics* **44**: 17-47, 2001.
2. Granata KP, *et al. J Biomech* **37**: 241-247, 2004.
3. Gardner-Morse MG, et al. *J Biomech* **34**: 457-463, 2001.
4. Moorhouse K, et al. *J Biomech* **40**: 1058-65, 2007.
5. Solomonow M. *J Electromyogr Kinesiol* **14**: 49-60, 2004.

ACKNOWLEDGEMENTS

This publication was supported by Cooperative Agreement Number R01-OH004089 from CDC-NIOSH. Its contents are solely the responsibility of authors and do not necessarily represent the official views of the CDC. The authors dedicate this work to Dr. Kevin P. Granata whose original ideas formed the foundation for the current investigation.

LOAD BEARING CAPABILITY OF ANNULAR FIBERS IS AFFECTED BY THEIR INCOMPLETE LENGTH: A FINITE ELEMENT MODEL ANALYSIS

[1]Mozammil Hussain, [2]Ralph E. Gay and [2]Kai-Nan An

[1]Logan University, Chesterfield, MO, USA
[2]Mayo Clinic, Rochester, MN, USA
email: mozammil.hussain@logan.edu

INTRODUCTION

Collagen fibers within the annulus fibrosus (AF) form concentric layers of mesh that stabilize the disc's mechanical function. These fibers act mainly in tension and regulate disc bulging. Any loss or breakdown of the fibrous tissue architecture may lead to initiation of a degeneration process. Research has shown the presence of interrupted, altered, and incomplete collagen fibers in degenerated discs [1]. These classes of fibers may contribute to the severity of degenerative pathologies in the disc. Little is known about how incomplete fibers may contribute to the mechanisms of disc injury and progressive degeneration.

While discs exposed to repetitive or prolonged compression demonstrate signs of tissue degeneration and decreased signal intensity, distraction of the motion segment has the potential to promote disc regeneration due to re-hydration and up-regulation of collagen, bone morphogenetic proteins and other cellular metabolites [2]. It is not known what biomechanical role incomplete fibers play in governing the mechanics of degenerated discs during distraction.

The objective of the current study was to compare the mechanics of incomplete and complete length of fibers under compression and distraction forces. We hypothesized that incomplete collagen fibers would be subjected to higher stresses than complete fibers in both compression and distraction, but that stresses would be lower in distraction than in compression.

METHODS

This study utilized a finite element (FE) model of a C5-C6 motion segment. The structures included cortical bone, cancellous bone, endplates, AF, and nucleus pulposus (NP). The dimensions of the spinal structures were taken from the anthropometric literature data. Disc structure was assumed to be an elliptical shape. The validation data of the model is documented elsewhere [3].

Due to unavailability of an appropriate technique in the literature, a simple method was employed to subdivide the AF and NP into four quadrants (anterior, posterior, and right and left lateral), as shown in Figure 1. Four arcs were formed where major and minor axes of the elliptical disc intersect with the outer disc perimeter. The mid-points of these four arcs were diagonally connected to form the four disc quadrants. Anisotropy within the AF was simulated by modeling six layers of collagen fibers. These fibers were oriented at an angle of ±70° with respect to the horizontal plane with each layer alternating direction of slant. Four of these six fiber-reinforced layers were embedded in the AF tissue matrix between the outer AF and AF-NP boundaries, thereby subdividing the AF matrix into five regions. A fiber layer was simulated on each of the outer AF and AF-NP boundaries.

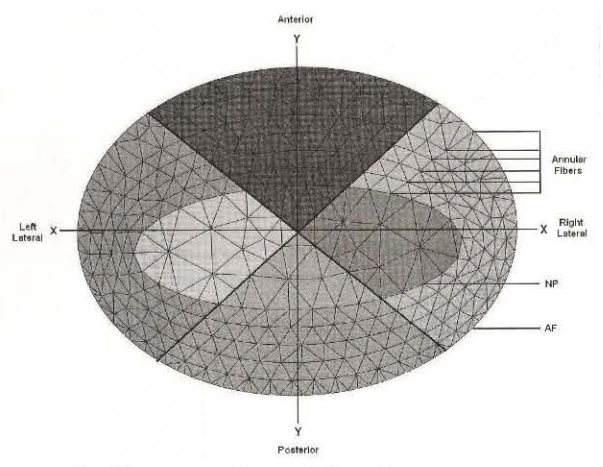

Figure 1: Cross-section of the disc

"Complete" fibers were defined as the fibers running from the superior to the inferior disc

surfaces along the frontal and sagittal planes. This model was referred as a Model M100 in which the complete (100%) lengths of AF fibers were organized in a zigzag alternating fashion.

"Incomplete" fibers ran only 50% of their length compared to the fiber length in Model M100, and were simulated in a wedge (>) fashion originating from superior or inferior disc surfaces up to mid disc space [4]. Five different FE models were developed corresponding to the incomplete fibers in different layers – two inner-most layers of incomplete fibers (Model M50-I), two middle-most layers of incomplete fibers (Model M50-M), two outer-most layers of incomplete fibers (Model M50-O), four inner- and middle-most layers of incomplete fibers (Model M50-IM), and four middle- and outer-most layers of incomplete fibers (Model M50-MO).

Compression (50 N) and distraction (17 N) were applied on the superior surface of the upper vertebra (C5) as a pressure load. The inferior surface of the bottom vertebra (C6) was fixed in the three perpendicular planes. The material properties were adopted from the literature. Regional von-Mises stresses in the four AF quadrants were computed for the six FE models. Commercial FE software, ABAQUS version 6.8.2 (Dassault Systemes Simulia Corp, Providence, Richmond, USA) was used for analysis.

RESULTS AND DISCUSSION

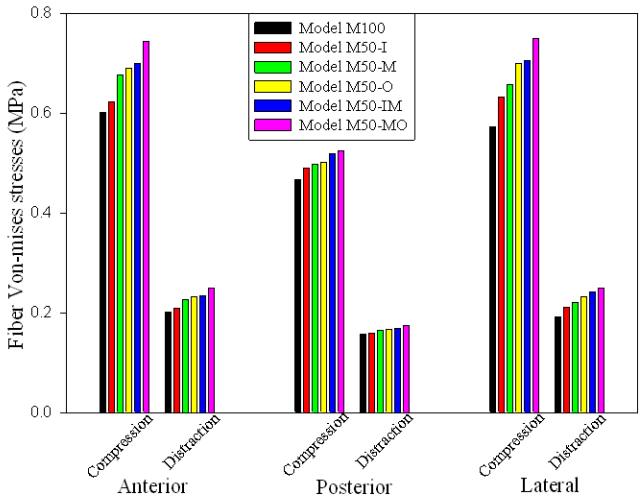

Figure 2: Distribution of von-Mises stresses in complete and incomplete fibers of the AF quadrants

Figure 2 shows the distribution of Von-mises stresses in complete and incomplete fibers in various quadrants of AF. Compared to the complete fiber length, incomplete fibers undergo higher stress. Also, the magnitude of stresses in incomplete fibers further increases due to increasing layers of incomplete fibers. This is because, for a given magnitude of applied load, the reduced length of fibers in various layer(s) resists more load than complete length of fibers.

The model also shows higher fiber stresses in the anterior-lateral AF region than in the posterior AF region. This may be due to increased disc bulging at the anterior-lateral site than at the posterior disc region [5]. A lower AF tissue volume in the posterior cervical disc may be another reason why stress peaks are recorded in the anterior-lateral disc, as a posterior orientation of NP will shield the posterior disc from high stresses [6].

The current results also illustrate that distraction forces lower the stresses in annular fibers compared to compressive forces. Distraction aligns the fibers toward vertical plane while compression aligns them toward horizontal plane. This finding is consistent with a prior study [3] demonstrating that fibers oriented toward vertical plane experience less stress than fibers oriented toward the horizontal plane.

CONCLUSIONS

In conclusion, incomplete AF fibers are subjected to higher stresses than longer, complete fibers that span the complete disc space. The current data supports the hypothesis that incomplete fibers are more stressed than complete fibers, both in compression and distraction. The increased stresses may contribute to fiber breakage and progressive degeneration in the AF. However, distraction lowered the fiber stresses compared to compression. These results should be compared to other biomechanical experiments.

REFERENCES

1. Tsuji H, et al. *Spine* **18,** 204-210, 1993.
2. Guehring T, et al. *Spine* **31,** 1658-1665, 2006.
3. Hussain M, et al. *J Manipulative Physiol Ther* **In Press**.
4. Marchand F, et al. *Spine* **15,** 402-410, 1990.
5. Stokes IA, *J Spinal Disord* **1,** 189-193, 1988.
6. Skrzypiec DM, et al. *Eur Spine J* **16,** 1709-1709, 2007.

A NEW SURROGATE BONE MODEL FOR TESTING INTERVERTEBRAL DEVICES

[1]Anthony G. Au, [1]Ameet K. Aiyangar, [2]Paul Anderson and [1]Heidi-Lynn Ploeg

[1]Department of Mechanical Engineering, University of Wisconsin-Madison, Madison, WI, USA
[2]Department of Orthopaedic Surgery, University of Wisconsin-Madison, Madison, WI, USA
email: aau@cae.wisc.edu

INTRODUCTION

Chronic low back pain is commonly treated by spinal fusion surgery augmented with intervertebral devices. Device subsidence into surrounding vertebrae is a common surgical complication and is often investigated with benchtop tests employing human cadaveric vertebrae. Polyurethane foam is recommended as a bone surrogate for subsidence tests [1], but the absence of a vertebral endplate and cortical shell limits clinical applicability of the conclusions. This can be improved by employing a new surrogate with more representative geometry and material properties, i.e. a polyurethane foam vertebra encased in a fiberglass-reinforced epoxy shell. This study investigated the efficacy of this synthetic vertebra bone surrogate for benchtop subsidence tests of intervertebral devices.

METHODS

Custom-made aluminum-alloy implants were compressed into 10 synthetic L5 vertebrae (Sawbones, Vashon Island, WA) using a materials testing machine (858 Bionix, MTS, Eden Prairie, MN). Implants seated either centrally (smaller diameter implant) or peripherally (larger diameter implant) on the endplate were axially compressed into synthetic vertebrae at a displacement rate of 2.5 mm/min up to a displacement of 5 mm. For comparison, the same implants were similarly compressed into 12 human lumbar vertebrae (T11, L3, L4, and L5) and 12 polyurethane foam blocks. Failure load, subsidence, and failure mode were observed. Subsidence was measured using custom-made extensometers attached between the implant and sample.

RESULTS

Synthetic vertebrae shared several subsidence characteristics with human vertebrae: the implant severely deflected the endplate until the endplate fractured and failed, characterized by a load drop on the force-displacement curve (Fig 1); also, a larger implant seated closer to the periphery of vertebrae required a greater load to fail the endplate than a smaller one seated closer to the center (Fig 2). By contrast, failure load in foam blocks was insensitive to implant placement.

Peripherally seated implants generated less subsidence than centrally placed ones for synthetic vertebrae, human vertebrae, and foam blocks (Table 1). However, significant differences were only found in human vertebrae subsidence levels.

Synthetic vertebrae required the largest forces to fail and also generated the lowest subsidence (Table 1). The synthetic vertebral endplate did not fully fail under loading by the large implant therefore no failure load was recorded.

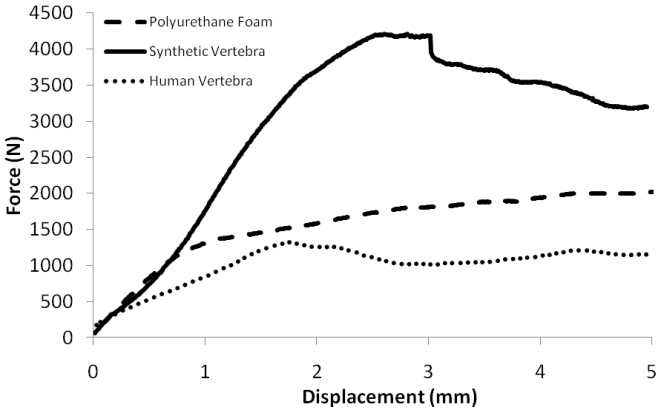

Figure 1: Force-displacement curves from centrally placed implants.

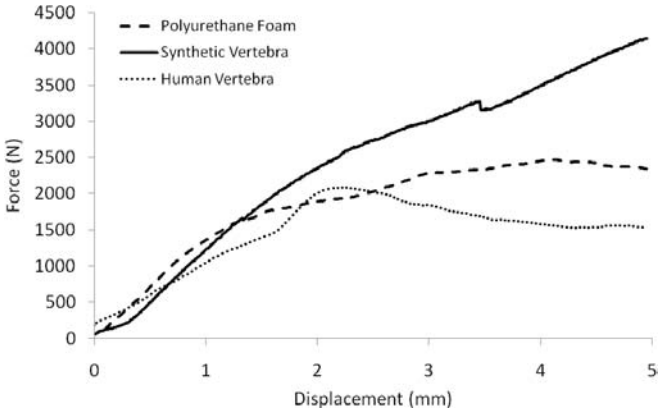

Figure 2: Force-displacement curves from peripherally placed implants.

DISCUSSION AND CONCLUSIONS

Polyurethane foam is a readily available bone surrogate for human vertebrae but its simplicity obviates extrapolation of results to clinical situations. The synthetic vertebrae of this study were more resistant to subsidence than both foam and human vertebrae. However, they replicated some key subsidence aspects observed with human vertebrae, due to the presence of an artificial endplate. The endplate shielded the foam core from localized forces thereby reducing subsidence levels. More importantly, implants seated on the edge of the vertebrae encountered lower subsidence [2].

Understanding the failure mode associated with synthetic vertebrae can foster a better understanding of subsidence. Subsidence in the synthetic vertebra can be modeled as a combination of bending and indentation commonly seen in composite materials [3]. Subsidence of the peripherally placed larger implant was dominated by bending whereas indentation was more influential in subsidence of the centrally placed smaller implant. Endplate fracture generated large subsidence but its absence did not completely eliminate it since the foam core could plastically deform without endplate fracture. This new surrogate is appropriate for benchtop subsidence testing and will help facilitate a more comprehensive understanding of subsidence etiology.

REFERENCES

1. ASTM F 2267-04, 2004.
2. Tan J-S, et al. *Spine* **30**, 638-644, 2005.
3. Shuaeib FM and Soden PD *Composites Science and Technology* **57**, 1249-1259, 1997.

Table 1: Failure force and subsidence generated from centrally and peripherally placed implants (Mean±SD). Matching superscripts indicate significant differences between two groups.

Specimen	Failure Force (N)		Subsidence (mm)	
	Central	Peripheral	Central	Peripheral
Foam Block	1128±144	1169±152	2.72±0.04	2.66±0.04
Synthetic Vertebra	4497±296	N/A	1.01±0.33	0.40±0.30
Human Vertebra	1196±207[a]	1946±487[a]	3.04±0.50[b]	1.95±0.53[b]

ASSESSMENT OF GENDER VARIATIONS IN THE CERVICAL RESPONSE TO REAR IMPACTS

Jessica Fritz and Gerald Harris

Orthopaedic & Rehabilitation Engineering Center (OREC), Marquette University/
Medical College of Wisconsin, Milwaukee, WI, USA
email: jessica.fritz@marquette.edu

INTRODUCTION

Vehicle dynamics including accelerations resulting from changes in velocity (ΔV) are correlated to occupant kinematics in low speed rear impacts [1,2]. The ability to determine cervical Injury Assessment Reference Values (IARVs) results from decades of research examining the mechanics and biomechanics of segmental effects [3]. Gender is a contributing factor to injury risk. Females have a higher incidence of neck injuries than males in similar accident scenarios [4]. Along with vehicle dynamics and gender, head restraints (HRs) affect occupant kinematics in rear impacts. Recently, this has led to an upgrade of the Federal Motor Vehicle Safety Standard (FMVSS) 202 to increase HR height and proximity to the rear of the head [5].

Mathematical Dynamic Modeling (MADYMO, Tass Americas, Livonia, MI), is a commercially available software package used for complex multi-body dynamic modeling. It allows development and analysis of collision simulations and has been widely used in accident reconstruction (vehicle, pedestrian, industrial, etc.). This work used MADYMO simulations to examine the differences in cervical IARVs between male and females in the same rear impact scenarios across a range of ΔVs as well as the biomechanical effects on the neck of HR versus no HR.

METHODS

MADYMO 7.0 (TASS Americas, Livonia, MI) was used to create and analyze output dynamics during rear impacts to an auto seat configuration with restrained Hybrid III 50th percentile male and female dummies. They were seated in the multi-body modeled driver's seat with a defined reference position and an analytical seatbelt. Both genders were modeled in seats with and without HRs. For the simulations with a HR, it was modeled in a high position (Fig. 1). The modeled dummy, HR, steering wheel and/or seat positions were adjusted based on size to maintain consistent relative position. Analyses had a 250 ms duration with a time step of 1 E-05 s. A linear progression of ΔV values ranging from 0-16 kph (0-10 mph) was analyzed. A haversine impulse with a 100 ms duration was applied to the models to simulate a rear impact motor vehicle accident. It was applied as a position versus time pulse and simulated a 1 mph ΔV impact. This replicates the FMVSS 202 pulse for motor vehicle sled tests [6]. The pulse was linearly scaled to reach a ΔV of 16 kph (10 mph).

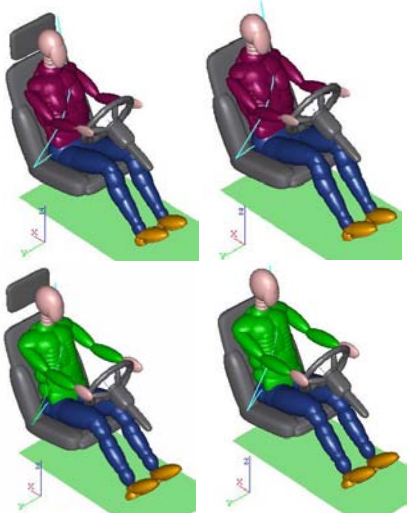

Figure 1: 50th percentile female (top row) and male (bottom row) Hybrid III dummy models seated for rear impact simulations with HR (left) and without HR (right).

The biomechanical Neck Injury Predictor (N_{ij}) for tension-extension (TE), tension-flexion (TF), compression-extension (CE), compression-flexion

(CF) and the overall sum was examined. This IARV was chosen to examine the differences between genders and the effect of headrests on injury prevention. The N_{ij} values were plotted against ΔV to examine the trends with increasing speeds and to determine if any injury thresholds were crossed through the range of 0-16 kph (0-10 mph). N_{ij} has an injury threshold of 1.

RESULTS AND DISCUSSION

The results for N_{ij} TE (NTE) and the sum of the four N_{ij} components are plotted in Figures 2 and 3, respectively. NTE is displayed as a representation of the trend for all N_{ij} components across male versus female and HR versus no HR. NTE is the majority contributor towards the N_{ij} summation.

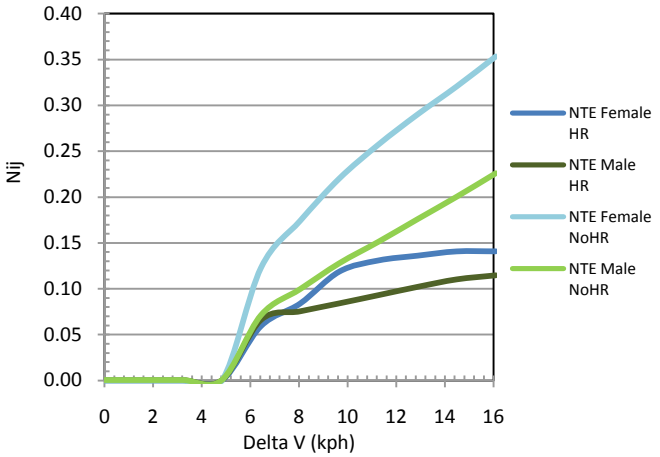

Figure 2: Comparison of NTE values for males and females with and without headrest (HR).

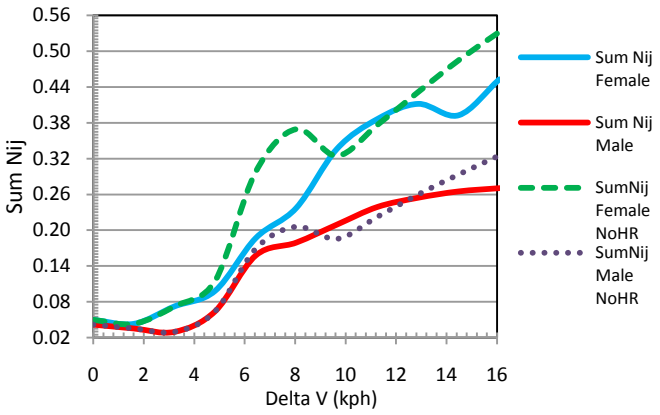

Figure 3: Comparison of N_{ij} sum values for both males and females with and without headrest (HR).

As Figure 2 shows, NTE remains near zero for all four models until approximately 6 kph (4 mph). After this departure from near zero values, each model expresses a near linear positive trend with increasing ΔVs. These results show that the female models have consistently higher values than the male models. More importantly, the models without HR, have much higher slopes and values over twice as high as their gender-matched counterpart at 16 kph (10 mph). The overall sum of N_{ij} exhibits a similar pattern. However, it shows a greater intra-gender difference than inter-gender. At 16 kph (10 mph), the N_{ij} sum is greatest in the female without HR, followed by female with HR, male without HR and male with HR.

CONCLUSIONS

The gender variations seen in this work are consistent with previous studies as well as reports from motor vehicle accidents [4,7]. This points to mechanical and biomechanical differences in the cervical spine between males and females as the seating position and headrest were adjusted for the size of the modeled occupant. As a validity test of the model, the results were compared to a study in which Hybrid III 50th percentile male dummies were subjected to rear impact sled tests using a HR. The NTE results of this work agree with those results in the dummy sled tests [8]. Biomechanical methods of assessment in this study are effective in distinguishing results that differ by gender, i.e. male versus female.

REFERENCES

1. Welcher JB, Szabo TJ & Voss DP. 2001. **SAE**, 2001-01-0899.
2. Szabo TJ, Voss DP & Welcher JB. 2002. **SAE**, 2002-01-0029
3. Meyer AR, Fritz JM & Harris GF. 2009. **Proceedings of the ASME 2009 Summer Bioengineering Conference (SBC2009)**, June 17-21, Lake Tahoe, CA, SBC2009-206177.
4. Ono K, Kaneoka K, Wittik A & Kazjer J. 1997. **SAE**, 973340.
5. National Highway Transportation Safety Administration (NHTSA) FMVSS 202.
6. Kaleto HA & Worthington MJ. 2004. **SAE**, 2004-01-0739.
7. Temming J. 1998. **SAE**, 981191.
8. Voo L, Merkle A, Wright J & Kleinberger M. 2004. **SAE**, 2004-01-0332.

INTER-EXAMINER COMPARISONS OF A HUMAN CLINICAL CERVICAL DIAGNOSIS TECHNIQUE

[1*]B. Rutledge, [1*]T.R. Bush, Ph.D.,
[2]J. Vorro, Ph.D., [3]L. DeStefano, D.O., [3]T. Francisco, D.O., [3]S. Gorbis, D.O., F.A.A.O.

Michigan State University, East Lansing, Michigan, USA
[1]Department of Mechanical Engineering,
[2] Department of Family and Community Medicine, [3]Department of Osteopathic Manipulative Medicine
*email: rutled36@msu.edu, reidtama@msu.edu, web: www.egr.msu.edu/bdrl

INTRODUCTION

Musculoskeletal (MSK) impairments in the human cervical (neck) region are among the highest reported physical disorders, often resulting in intense pain and inhibition of cervical range of motion (ROM). Although many diagnostic techniques to determine cervical dysfunction exist, a clinical assessment technique using palpation is widely practiced by physicians as an indicator of cervical impairment. Palpatory diagnostic techniques can be used to assess varying levels of dysfunction based on numerous factors, including: cervical ROM, tissues textures, quality of motion (smooth, elastic, or bone-on-bone contact) and motion symmetry [1]. However, this diagnosis technique is not taught consistently across medical colleges, and implementation varies between practitioners. Thus, the purpose of this research was to explore the use of three-dimensional kinematics as a potential tool for documenting similarities and differences between clinicians during the diagnoses of cervical function.

METHODS

Prior to testing, all volunteer subjects completed an informed consent, a Visual Analog Pain Scale (VAS) and a Neck Pain and Disability Questionnaire. Three physicians participated in the study; all were blinded to the pain data, blinded to each other's assessments, and had limited verbal communication with the subjects. Upon completion of the consent process, one physician performed a "screening" examination on each subject to establish the test groups (Control and Experimental). The palpatory examination was conducted with the subjects starting from a self-selected neutral seated position, the physician guided subject's heads to the right until an end-range of motion was determined. This was followed by a return to the neutral position, and a guided motion to the left. The physician assessed each subject by evaluating the range and quality of motion during the cervical lateral flexion.

The two test groups had the following criteria:

- Control: Symmetric motion between left and right lateral flexion as determined by the initial screening and a self-selected pain score on the VAS of 0. (n=22, Average Age: 20 years)
- Experimental: Self-selected pain score on the VAS of 3 or greater. (n=18, Average Age: 25 years)

Upon acceptance into one of the test groups, the subjects were escorted into the laboratory where kinematic data were collected. Markers were secured to each temple and above the brow centered on the forehead; also, a triad of markers was attached to the anterior chest, below the sternal notch. Palpatory diagnoses were then conducted in the same manner as the "screening" examination by two different physicians in front of a six-camera motion capture system (Qualisys™, Gothenburg, Sweden).

Following the collection of kinematic data, subjects in the Experimental group immediately received treatment in the form of muscle energy, a standard manual medicine treatment. This treatment was a soft tissue osteopathic manipulation method that involves precisely directed and controlled isometric and/or isotonic muscle contractions to improve MSK function and reduce pain [2]. Upon completion of treatment, the two physicians again conducted post-test palpatory assessments on the

subjects during which kinematic data were recorded. Subjects in the Control group were not treated, and thus dismissed following the kinematic data collection.

Angles for the head relative to the thorax were computed from the three-dimensional position data. Each trial of cervical lateral flexion had three cycles of right to left cervical flexion, resulting in nine end-range values per subject, per assessment. The data were normalized with regard to time, and then the full cervical ranges of motion (maximum flexion left to maximum flexion right) were analyzed, as well as the ranges of motion from neutral to right maximum ROM and neutral to left maximum ROM.

Statistical analyses included two-sample and paired t-tests conducted at a 95% confidence level to determine differences between passive cervical ranges of motion for each examiner.

RESULTS AND DISCUSSION

From kinematic data obtained during the palpatory assessments, comparisons were made to determine inter-examiner reliability of the kinematics. Statistical analyses were conducted on average left and right ROM values, as well as full ROM through two-sample t-tests.

Table 1: Examiner 2 vs. 3 average ROMs (degrees)

Group	Examiner	Left ROM	Right ROM	Full ROM
Control	2	35.50	35.91	71.44
	3	33.43	32.66	66.10
Exp. Pre-Treatment	2	34.12	32.65	66.74
	3	29.93	28.70	58.63
Exp. Post-Treatment	2	34.14	33.47	67.61
	3	30.85	30.58	61.43

Throughout testing, the average ROMs as performed by the physicians were consistently greater for Examiner 2 compared to Examiner 3 (Table 1). This is visually demonstrated through Figure 1, which contains a plot of the kinematic motion for a single trial of a subject in two dimensions. Additionally, the left and right ROM for the subject is documented in Figure 1.

Statistical analysis of the pooled data (both groups, all subjects) showed a significantly greater passive ROM performed by Examiner 2 compared to Examiner 3 for left and right ROM as well as full ROM ($p < 0.001$). Additionally, of the 58 diagnoses documented an agreement on equality of motion was achieved 64% of the time.

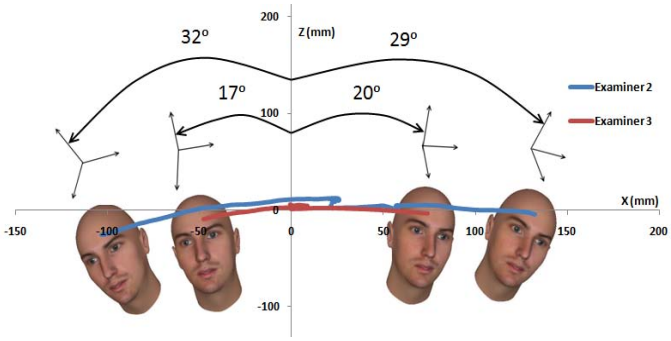

Figure 1: Representation of kinematic motion in 2-D demonstrating differences found between examiners.

No significant differences were observed within trials for a given examiner for both the Control and Experimental groups. This exemplified that, for a given subject, each examiner was *consistent in their own diagnostic motion* process. However, these data also suggest *variations between physicians* with regard to the ROM at the final assessment points. Ultimately, this inconsistency between examiners may be related to the clinical decision processes, i.e. variations between physicians could be attributed to differences in the weighting of the various parameters used to determine the final assessment category.

The methodology and data do indicate, however, that manual medicine diagnostic techniques are amenable to specific kinematic evaluations. This is a positive indication, and permits an optimistic outlook for further objective biomechanical assessments of MSK diagnostic techniques.

REFERENCES

1. Johnston W, et al. *Functional Methods*. Indianapolis: AAO, 2005
2. Chaitow L, *Muscle Energy Techniques*. 2003

ACKNOWLEDGEMENTS

We gratefully thank the American Osteopathic Association for their financial support. We also thank Trevor DeLand and Phil Allore for their help.

COMPARISON OF ENERGY DISSIPATION IN THORACOLUMBAR MOTION SEGMENTS DUE TO LOAD FREQUENCY VARIATION

[1,2] Naira H Campbell-Kyureghyan, [1] Sai Vikas Yalla

[1]University of Wisconsin-Milwaukee, Milwaukee, WI, USA
[2]email: campbeln@uwm.edu

INTRODUCTION

Low back pain is one of the most prevalent problems among the adult population with an annual incidence of 15-20% [1]. One approach to understanding the damage mechanisms of spine components is to determine their behavior under different loading conditions through testing. Since cumulative damage is indicated as associated with low back pain, cyclic testing of motion segments (MS) has been a frequent target of research.

The effect of loading on spinal motion segment damage in previous studies relied on measures such as cycles to failure and accumulated strain to characterize damage, but typically used high loading rates of 15 to 120 cycles per minute [2] and loads, not representative of typical work conditions with cyclic frequencies of 1 to 15 per minute [3]. The current study examines the effects of cyclic loading using energy dissipated per unit volume, energy density (ED), at two typical loading frequencies of 6 and 12 lifts per minute (0.1 and 0.2 Hz) over an eight hour loading period.

METHODS

Human cadaveric thoracolumbar spines, averaging 73.3 (11) years in age, were dissected into 30 motion segments. 10 of the MS were tested for monotonic compressive strength at a quasi-static rate of 4 mm/hr. The remaining 20 MS were randomly assigned to two groups of 10 MS for 8 hour repetitive loading tests at 0.1 and 0.2 Hz. The two frequencies represent 6 and 12 lifts per minute. All MS were positioned at Harrison angles to account for their natural alignment, and preloaded at 350 N for 15 minutes to reduce postmortem effects and simulate torso load.

The load magnitude for repetitive loading was 50% of the monotonic MS failure stress from the same spine. The amount of cumulative energy dissipated (E) from the MS during repetitive loading was determined by the area inside the hysteresis loop of the stress-strain curve as

$$E_n = 0.5*(F_n+F_{n-1})*(\Delta_n-\Delta_{n-1}) + E_{n-1}\ \text{kJ}$$

where E_n (kJ) is the cumulative energy at the n^{th} data point, F is the applied load, and Δ is the deformation of the intervertebral disc (mm). Considering the size and shape variation between MSs, Energy Density (ED) in kJ/mm^3 of the MS was determined by dividing the dissipated energy by the volume of the intervertebral disc.

Regression analysis and goodness of fit tests were used to determine the appropriate model for ED and its variation over time and number of cycles. A special case of the mixed model analysis, a nested design was used at an alpha value of 0.05 to determine the effect of frequency on ED. Cooks distance determined the effective outliers, if any, in the model.

RESULTS

The total energy dissipated by MS tested at 0.1 Hz over 8 hours ranged from 7152 kJ to 1,086,266 kJ. At 0.2 Hz, the cumulative energy ranged from 20,036 kJ to 1,230,750 kJ. On average the total energy dissipated by the end of 8 hour loading period at 0.2 Hz was 42% higher ($p<0.05$) than that at 0.1 Hz.

Cumulative ED displayed a linear relationship ($R^2=0.99$) over the 8-hour time period for both frequencies (Figure 1). ED at the end of the 8-hour loading period was 9.3 (5) kJ/mm^3 for MS tested at 0.2 Hz and 5 (1.5) kJ/mm^3 for MS tested at 0.2 Hz.

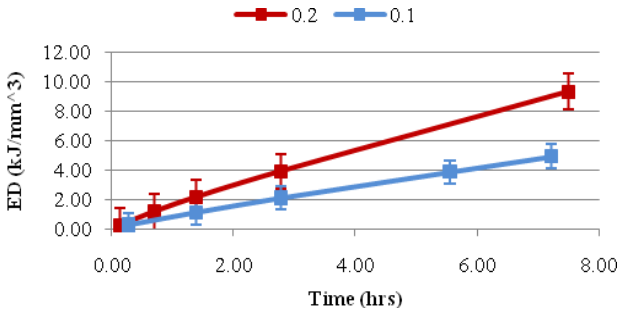

Figure 1. Cumulative ED in MS for the two loading frequencies of 0.1 and 0.2 Hz over and 8-hour period of loading

When frequency was doubled from 0.1 Hz to 0.2 Hz, a significant increase ($p<0.05$) of 91% in ED was observed in the initial 2 hours of loading. The increase remained at an average of 87% (2) for the remainder of the loading period (Figure 2).

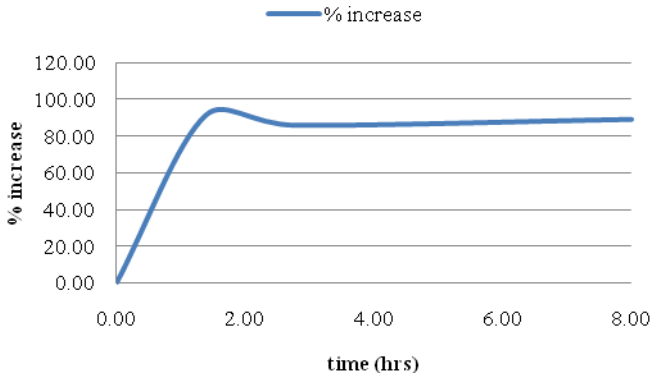

Figure 2. Increase in ED (%) for MS loaded at 0.2 Hz compared to the 0.1 Hz test group

The effect of frequency on ED at 100, 500, 1000, 2000 and 2600 cycles was also compared. At the end of 2600 cycles, the cumulative ED was 4 (2.2) kJ/mm^3 at the 0.1 Hz loading frequency, while at 0.2 Hz ED was 5 (4) kJ/mm^3. The effect of frequency on ED when compared by cycle number did not show any statistical significance ($p>0.05$).

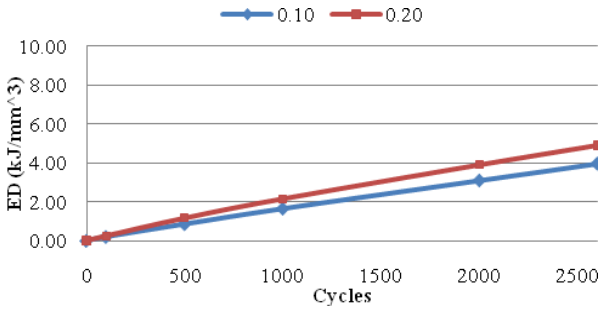

Figure 3. Cumulative ED in MS for the two loading frequencies of 0.1 and 0.2 Hz over the first 2600 cycles

DISCUSSION

As expected, energy density dissipation increased for MS cycled at 0.2 Hz compared to those cycled at 0.1 Hz. When compared versus time, the 0.2 Hz specimens dissipated much more energy, as would be expected due to doubling the number of load cycles over a given time period. When ED is compared to the number of cycles, the 0.2 Hz MS also dissipate more energy, although the observed difference was not found to be statistically significant. The differences in ED for a given number of cycles are due to the viscoelastic nature of the intervertebral discs, which respond differently depending on the deformation velocity.

Importantly, after an initial small number of cycles, the energy density increased linearly for the remainder of the 8-hour test. This is distinct from MS strain and stiffness that both exhibited saturation with cycling [4]. That is, the rate of change of both strain and stiffness slowed considerably after a number of cycles. On the other hand, ED was not subject to saturation (Figure 1).

CONCLUSIONS

ED versus time displayed a significant difference as the frequency was varied, while ED *per cycle* was found to be relatively independent from loading frequency. Importantly, ED did not exhibit saturation and therefore remained a valid measure over the entire loading period. Further research is suggested into the use of ED as damage measure for intervertebral discs subject to repetitive loading.

REFERENCES

1. Sadoughi A. Low back pain. *Seminars in Anesthesia, Perioperative Medicine and Pain* **22**:159-167, 2003.
2. Lotz JC, et al. Intervertebral disc cell death is dependent on the magnitude and duration of spinal loading. *Spine* **25**:1477, 2000.
3 Marras WS, et al. The role of dynamic three-dimensional trunk motion in occupationally-related low back disorders. *Spine* **18**:617-628, 1993.
4. Yalla, SV, et al. Strain in thoracolumbar spine during cyclic loading at two frequencies. *ASB Annual Meeting*, 2009.

A FINITE ELEMENT STUDY OF DUAL BEARING SURFACE SLIDING KINEMATICS AND WEAR IN THE CHARITÉ TOTAL DISC REPLACEMENT

[1]Curtis Goreham-Voss, [1]Thomas Brown

[1]University of Iowa, Iowa City, IA, USA
email: curtis-voss@uiowa.edu

INTRODUCTION

Polyethylene wear in total disc replacements (TDRs) is one of several long-term concerns. In the case of the Charité, the dual bearing surfaces introduce extra complexities in determining how the implant will behave under varying loading and articulation conditions. In this study, a finite element model was used to simulate how wear would change with changes in the centers of rotation for the two articulations. Furthermore, the coefficient of friction for the inferior bearing surface was parametrically altered to evaluate the effect of non-symmetric interface friction.

METHODS

A finite element model of the Charité was created in Abaqus (Figure 1), with the endplates modeled as rigid surfaces and the polyethylene core as a deformable solid with an elastic modulus and Poisson's ratio of 1,400 MPa and 0.3, respectively. Loading and rotations from ISO Standard 18192-1 were applied to reference points attached to the rigid endplates. Rotations were applied to the upper endplate and the axial load was applied to the lower endplate. Initially, the reference points were located at the centers of curvature of the respective endplates. In subsequent trials, these reference points were moved progressively closer to the geometric center of the implant, to study the effect of rotation center position on the resulting wear. In a separate series, the inferior bearing surface friction coefficient (μ_i) was altered, while μ_s (superior) was left at 0.08, to study the effect of non-symmetric friction on wear.

Wear simulation, including cross-shear, was incorporated through Abaqus' adaptive meshing subroutines [1]. At each node, local sliding kinematics and contact pressure were used to calculate cross-shear and a cross-shear dependent wear factor, based on the work of Kang et al [2]. This wear factor was used in the Archard wear formula to calculate the local linear wear at that node. At the end of each motion cycle, the linear wear depths were scaled by an update interval (250,000 cycles) and nodes on the bearing surface were moved accordingly. Abaqus automatically adjusted interior nodes to preserve element quality, and calculated volumetric wear. The volumetric wear was differentiated and multipled by the density of UHMWPE (0.94 mg/mm^3) to determine the wear rate. All simulations were run for 10 million cycles, requiring 40 mesh updates.

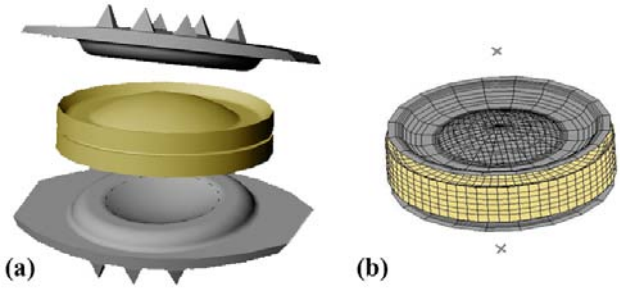

Figure 1. (a) CAD and (b) finite element model of Charité TDR.

RESULTS AND DISCUSSION

Moving the reference points for the implant endpoints had virtually no effect on the resulting wear rate (Figure 2a). Upon closer examination, moving the reference points to the implant center caused shorter travel for the upper endplate and increased travel of the lower endplate, but local sliding kinematics of at the bearing surfaces were unchanged (Figures 2b & 2c).

Perturbations of μ_i also had only minor effects on the overall wear rate. Reducing μ_i from 0.08 to 0.01 resulted in only a 17% reduction in wear (Figure 3a). The maximum linear wear depth on the

superior surface at 10MC decreased only slightly as μ_i was changed, but the inferior linear wear increased substantially, thus resulting in a marked change in the ratio of superior-to-inferior linear wear (Figure 3b). The superior surface continued to have greater wear until μ_i was reduced to less than one-half of μ_s.

CONCLUSIONS

Having two bearing surfaces "in series" can result in very different motion patterns at the respective bearing surfaces, depending on specifics of rotation center position and asymmetry of interface function. However, these very different motion patterns involved only very modest differences in overall implant wear. This finding is encouraging, in terms of technical challenges for wear testing, since wear behavior is more "forgiving" of test protocol variations than the motion patterns would suggest.

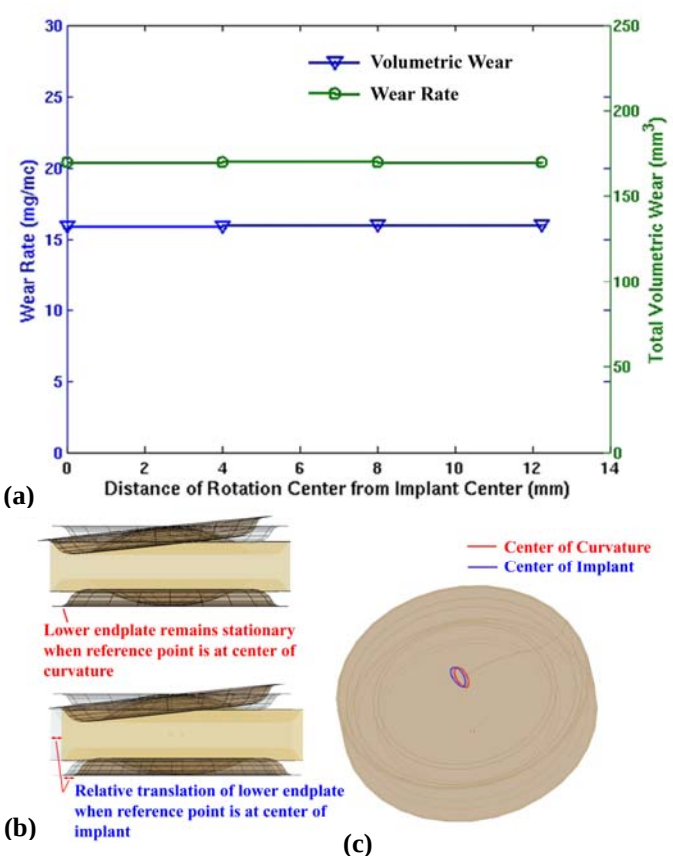

Figure 2. (a) Change in wear and wear rate as the location of the rotation center was changed. (b) Comparison of gross implant movement with center of rotation located at center of implant (top) and superior endplate center of curvature (bottom) and (c) corresponding resulting motion loci.

The predisposition of the Charité to superior-surface wear under the tested conditions is of particular interest, as it is clearly contrary to the intended function of the device. The persistence of this phenomenon raises the concern that laboratory wear simulators may not accurately reproduce *in vivo* kinematics and wear progression. More investigation is needed into the kinematics of the Charité TDR *in vivo* and how that can be most accurately reproduced *ex vivo*.

REFERENCES

1. Goreham-Voss, CM & Brown, TD. NACOB 2008. Abstract #72.
2. Kang et al. 2008. J Biomech. 41(1):340-346.

ACKNOWLEDGEMENTS

This study was supported by a grant from the NIH (AR052653).

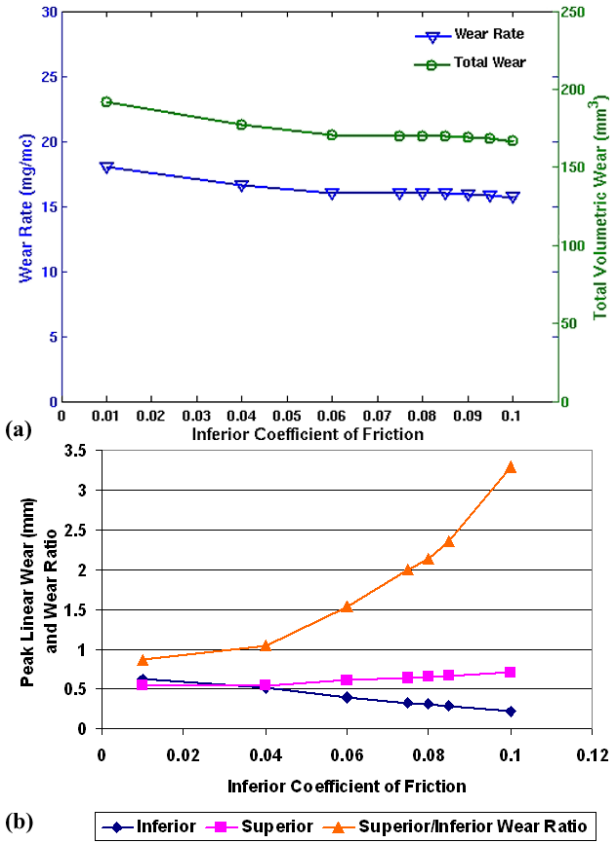

Figure 3. (a) Variation in wear and wear rate as the inferior coefficient of friction is changed. (b) Change in peak linear wear and ration of peak superior to peak inferior linear wear as the inferior coefficient of friction is changed.

EFFECT OF OFF-AXIS FLUOROSCOPY IMAGING ON 2D LUMBAR SPINE KINEMATICS

[1]Ephraim Ben-Abraham, [1]Kristin D. Zhao, [2]Dixon Magnuson, [1]Miranda N. Shaw, [1]Lawrence J. Berglund, [1,3]Ralph E. Gay and [1]Kai-Nan An

[1]Biomechanics Laboratory, Division of Orthopedic Research, Mayo Clinic, Rochester, MN, USA
[2]Department of Radiology, Mayo Clinic, Rochester, MN, USA
[3]Department of Physical Medicine and Rehabilitation, Mayo Clinic, Rochester, MN, USA
email: an.kainan@mayo.edu

INTRODUCTION

Low back pain (LBP) is one of the most prevalent and costly problems facing healthcare systems in North America [1]. Several studies have found lumbar intersegmental motion to be different in patients with LBP compared to asymptomatic persons [2]. This suggests that intersegmental motion parameters or patterns might be used to biomechanically classify LBP. Recent advances in kinematic methods have made the quantification of intersegmental lumbar kinematics possible using fluoroscopy. Due to its availability and reasonable cost, its potential as a diagnostic tool is great. However, it is important to validate and assess the sensitivity of the technique for accurately quantifying the intervertebral rotations in the lumbar spine. Therefore, the purpose of this investigation was to compare fluoroscopic measures of intervertebral rotations with optoelectric measures obtained simultaneously during dynamic flexion-extension movements in vitro. Additionally, the effect of rotations of the fluoroscopic C-arm on the intervertebral kinematics was assessed using the optoelectric data as a gold standard.

METHODS

Six cadaveric lumbar spines (L1-sacrum) were harvested enbloc and non-ligamentous soft tissues were dissected from the spine leaving the vertebral bodies and all ligamentous structures intact. Polymethylmethacrylate (PMMA) orthodontic resin was used to pot the L1 vertebral body in a circular acrylic fixture, and to embed the sacrum. Active optoelectric marker sensors were attached to the bodies of L2-S1 with custom fixtures (Figure 1). These sensors were positioned so that the rotations of each vertebral body could be captured by the Optotrak system. The potted specimen was then secured in a 6-DOF custom dynamic spine testing device, such that the upper most vertebra, L1, was subjected to flexion-extension. Three-axis gimbals and stepper motors are able to generate pure moments and forces in all three planes [3].

Figure 1: Cadaveric spine specimen with optoelectric sensors intact, mounted in 6-DOF dynamic spine testing device in fluoroscope C-arm.

A digital, flat panel, fluoroscopic C-arm was used for the fluoroscopic acquisitions. This fluoroscopic system was selected because of its large free space (distance between the x-ray source housing and detector surface) and large field of view (38 cm) image intensifier. The specimen (mounted in the custom spine simulator) was located near the isocenter of the fluoroscopy unit with the C-arm centered on the lumbar segment to optimally capture sagittal spinal motion. A global coordinate system for the optoelectric system was defined such that it was coincident with the orientation of the fluoroscopic image detector.

Each specimen was pre-conditioned with 5 trials of pure flexion and extension. Flexion-extension movements, starting from a neutral spine

configuration, were induced by applying motion to the uppermost vertebra (L1) using displacement control at a rate of 8 degrees/second. Fluoroscopic sequences were obtained simultaneously with the optoelectric kinematic data. Subsequently, the image detector was rotated about the isocenter in 5 degree increments (posterior oblique angulations) from 5 to 15 degrees, and flexion-extension was simulated at each incremental fluoro position.

The data from the kinematic and fluoroscopy systems were synchronized by aligning the maximum and minimum flexion-extension angles in time. Relative rotation at each motion segment, L2/L3, L3/L4, L4/L5, and L5/S1 were computed from each data set. The optoelectric data was processed using the MotionMonitor software (Innovative Sports Training, Inc.) while the fluoroscopic sequences were processed independently by Medical Metrics (Houston, TX).

To determine the accuracy of the fluoroscopic kinematic measurement techniques, Bland and Altman limits of agreement [4] were determined for each motion segment in each orientation of the C-arm. In addition, the mean absolute differences between the fluoro and optoelectric data were determined for each motion segment and each position of the C-arm. A two-factor ANOVA was performed on the mean differences ($p<0.05$), followed by a Tukey-Kramer post-hoc test.

RESULTS AND DISCUSSION

Based on the results of the two-factor ANOVA performed on the mean differences, there was no significant difference ($p<0.05$) in the mean absolute rotation differences between the optoelectric values and the dynamic fluoroscopic values for the off-axis rotations of the fluoroscope. As shown in Figure 2, the mean absolute differences were less than 0.5 degrees for all motion segments at each off-axis fluoroscopic rotation. The limits of agreement between the Optotrak values and the dynamic fluoroscopic values were relatively consistent for all of the off-axis fluoro rotations, with all conditions having a 95% confidence limit of less than 1.2 degrees.

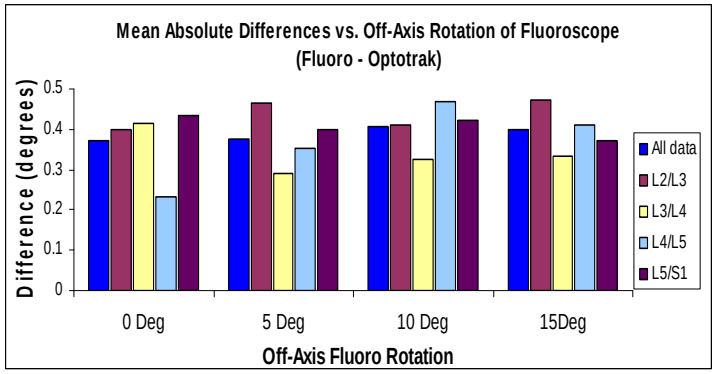

Figure 2: Mean absolute differences (Fluoro-Optotrak) in rotation values for each motion segment as a function of the fluoroscope off-axis rotation.

CONCLUSIONS

The results of this study suggest fluoroscopic measures of intervertebral rotations during dynamic flexion-extension movements can be used to accurately assess spinal motion. Additionally, the effect of rotations of the fluoroscopic C-arm on the intervertebral kinematics was not statistically significant, which implies that using our tracking technique spinal motion may be assessed using fluoroscopic images without perfect alignment (up to 15 degrees off-axis) of the fluoroscope relative to the subject.

REFERENCES

1.Deyo, et al. *Annu Rev Public Health.* 1991.
2.Takayanagi, et al. *Spine.* 2001.
3.Gay, et al. *Clin Biomech*. **21**, 914-919, 2006.
4.Bland and Altman. *J of Biopharmaceutical Statistics*. **17**, 571-582, 2007.

ACKNOWLEDGEMENTS

This research was supported by Grant Number R21AT003957 from the National Center for Complementary & Alternative Medicine. The content is solely the responsibility of the authors and does not necessarily represent the official views of the National Center for Complementary & Alternative Medicine or the National Institutes of Health.

DYNAMIC RESPONSE OF THE TRUNK TO POSITION PERTURBATIONS - EFFECTS OF GENDER, PRELOAD, AND TRUNK ANGLE

Emily Miller, Babak Bazrgari, Brad Hendershot, Maury Nussbaum, and Michael Madigan

Virginia Tech, Blacksburg, VA, USA
email: millerem@vt.edu, web: www.biomechanics.esm.vt.edu

INTRODUCTION

Females are more likely to experience low back pain (LBP) and injury than males.[1] The reasons for this gender difference may relate to factors contributing to the control of spinal stability such as intrinsic muscle stiffness and paraspinal reflexes, i.e. effective trunk stiffness.[2] While no gender differences in effective trunk stiffness have been found following sudden force perturbations[3], this could be due to higher trunk flexion velocity, and thus larger reflexes, observed in females who had smaller trunk mass. In addition, other factors such as trunk extension preload and trunk flexion angle may influence effective trunk stiffness, and therefore spinal stability. In an effort to help understand gender differences in LBP, the goal of this study was to investigate the effects of gender, preload, and trunk angle on the dynamic response of the trunk to small position perturbations.

METHODS

Eight males (21.3±1.4 years, 73.4±6.7 kg) and eight females (23.6±7.3 years, 59.3±5.6 kg) were exposed to sudden anteriorly-directed trunk position perturbations. Participants stood in a custom metal frame (Fig. 1) restraining the pelvis and lower limbs, and were instructed to remain relaxed with their hands at their side and head facing forward. Three force preloads (0, 15, and 30 %effort) based on a maximum extension in upright posture were held, and legs were raised to three angles (0, 20, and 40 degrees) of trunk flexion. During all random conditions, twelve position perturbations were generated by a servomotor (Kollmorgen AKM53K, Radford, VA, USA) and transmitted to the trunk at the T8 level via a rigid harness-rod system (Fig 1). Each perturbation had a target amplitude of 10 mm and a peak velocity of 0.357 m/s.

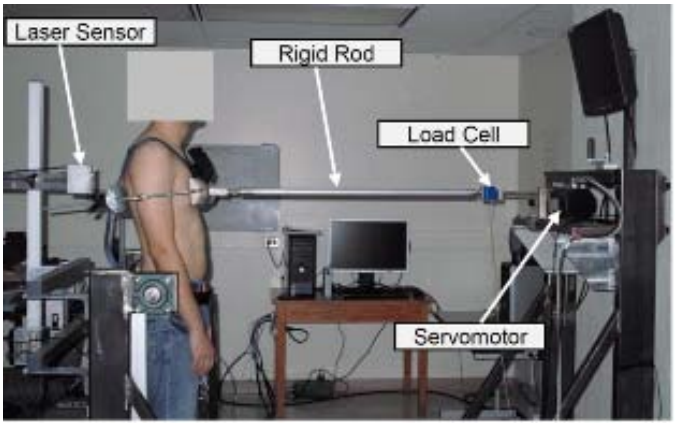

Figure 1. Experimental set-up.

Input motor displacement was measured with a high-accuracy encoder attached to the servomotor shaft, and trunk displacement was measured with a high-accuracy CCD laser displacement sensor (Keyence LK-G 150, Osaka, Japan) aimed at the midline of the dorsal trunk above the harness. Forces during the perturbations were measured using an in-line load cell (Interface SM2000, Scottsdale, AZ, USA) connecting the motor shaft to the harness-rod system. All data were sampled at 1000 Hz and similarly processed with 10 Hz low-pass Butterworth filters to avoid relative phase shifts.

The dynamic response of the trunk that we used as our dependent variable is the measured force when applying a position perturbation to the trunk. It is due to the combined effects of trunk stiffness, damping, and mass. To isolate the intrinsic response that contributes to the stability of the spine, the portion of the response due to accelerating trunk mass was removed, leaving only the measured force response due to stiffness and damping. Trunk stiffness, damping, and mass were estimated with a two degree-of-freedom (2-DOF) linear dynamic model (Fig. 2) representing the trunk and the harness-rod connecting device and using a system of second-order linear differential equations.

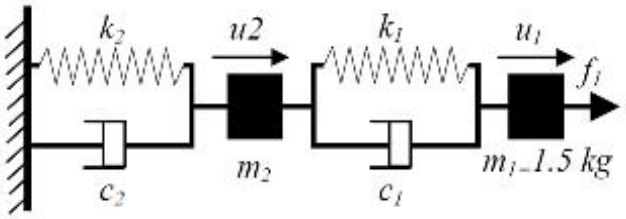

Figure 2. 2-DOF linear dynamic model. Mass (m), damping (c), and stiffness (k) of the harness-rod system and the trunk are represented by systems 1 and 2, respectively, and u and its derivatives represent displacement, velocity, and acceleration. Kinematics from both the motor encoder and laser sensor were model inputs.

Analyses involved the first ~50ms following perturbation onset so any force due to reflexes was not included. Parameter estimation was performed using a least-squares curve fit in MATLAB™ that varied the model parameters to minimize the differences between predicted and experimentally measured forces (MathWorks, Natick, MA, USA).

A 3-way ANOVA was conducted to determine the effects of gender, preload, and trunk angle on the estimated peak dynamic force response.

RESULTS

The model predicted experimentally measured forces with an average correlation of r = 0.996. Main effects indicated that the peak dynamic force response to trunk position perturbations (Figs. 3 and 4) was smaller ($p=0.008$) in females (64.2±5.8 N) than males (91.8±6.3 N), increased with preload ($p<0.001$), and increased with trunk angle ($p<0.001$).

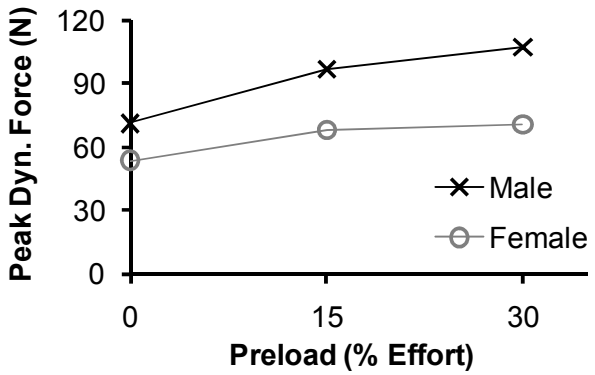

Figure 3. Peak dynamic force response vs. preload.

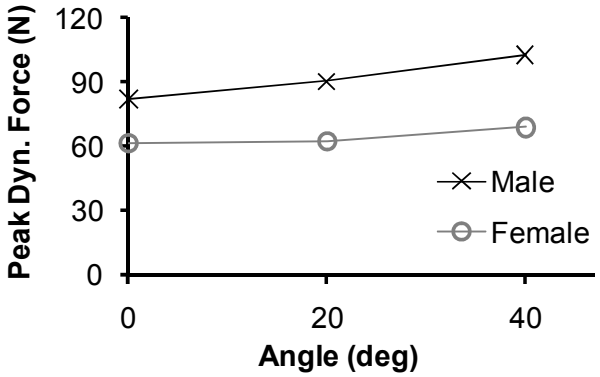

Figure 4. Peak dynamic force response vs. angle.

Interactions indicated that peak dynamic force increased more in males with increasing preload ($p<0.001$) and increasing trunk angle ($p=0.001$), and increased preloads eliminated any effect of trunk angle ($p=0.002$).

DISCUSSION AND CONCLUSIONS

Females exhibited a smaller dynamic force response than males following sudden trunk flexion position perturbations. This smaller response resulting from trunk stiffness and damping may be related to the increased rate of LBP and injury in females.[1] The dynamic response was also seen to increase with preload and trunk angle, and even more so in males than females. This gender difference could be because males have decreased joint laxity, as is seen in the knee,[4] or because they can achieve greater stiffness with their ability for active muscle contribution (strength). Therefore, the gender risk of LBP in females could be further pronounced in the workplace where tasks involve various carrying loads and postures.

REFERENCES

1.Macfarlane GJ, et al. *Spine* **22**, 1143-1149, 1997.
2.Kearney IE and Hunter IW, *Crit Rev Biomed Eng* **18**, 55-87, 1990.
3.Moorehouse KM and Granata KP. *JBiomech* **38**, 2000-2007, 2005.
4.Park HS et al. *J Orthop Res* **26**, 937-944.

ACKNOWLEDGEMENTS

This research was funded by NIAMS/NIH grant number 2 RO1 AR046111.

The quantitative assessment of contribution of risk factors to overstress at adjacent segments after lumbar fusion: removal of posterior ligaments, pedicle screws

[1]Kyoung-Tak Kang, [2]Hwa-Yong Lee, [2]Ka-Yeon Kim, [2]Ho-Joong Kim and [1]Ju-Woong Jang

[1]Korea Bone Bank, Seoul, Korea
[2]Yonsei University, Seoul, Korea
email: tagi1024@gmail.com

INTRODUCTION

Adjacent segment deterioration (ASD) is a serious sequela of spinal fusion surgery that has recently become much more widespread due to an increasing number of spinal fusions performed [1]. Moreover, previous studies [2] of potential risk factors for ASD have found that instrumentation, posterior lumbar interbody fusion, injury to the facet joint of the adjacent segment, fusion length, age, and sagittal alignment, are all risk factors for ASD. However, the actual significance of these risk factors remains controversial, possibly due to differing patient populations and methodologies [2]. Even though fusion probably affects motion and causes stress to adjacent segments, the following questions remain: to what extent does each risk factor impact ASD? What is the most decisive factor among the many risk factors for ASD? And, are there interactions between risk factors for ASD? In order to search for the answers to these questions, we planned to investigate the stress and the range of motion (ROM) at adjacent segments after fusion, using finite element (FE) model of lumbar spine. Two important risk factors were chosen such as instrumentation (pedicle screws) or the ablation of continuity of proximal ligament complex (PLC) among many risk factors. Therefore, the purpose of this study is to investigate changes of the range of motion (ROM) at adjacent segments after lumbar fusion according to whether or not pedicle screws is removed and whether or not the continuity of proximal ligament complex (PLC) is preserved.

MATERIALS AND METHODS

A three-dimensional, non-linear finite element model of the lumbar spine that consisted of three lumbar vertebrae, intervertebral discs and associated spinal ligaments have been developed. Geometrical details of the human lumboscral spine (L2-L5) were obtained form high-resolution computed tomography CT images of a 46-years old male subject who had no spine deformities. Digital CT data were imported to softwares (Mimics, Materialise Inc., Leuven, Belgium), and three-dimensional geometrical surface of the lumbosacral spine was generated. The FE method was analyzed with commercial software (ABAQUS 6.6-1; Hibbitt, Karlsson and Sorenson, Inc.; Providence, RI). Material properties were validated in our laboratory, as reported in our prior publications [3]. In order to simulate the decompression state, a supraspinous ligament and interspinous ligament between L3 and L4 spinous processes were removed along with partial removal of L3 and L4 spinous processes. Furthermore, the inferior portion of L3 lamina, and ligamentum flavum of L3-4 were removed. Pp model has the continuity of PLC between L2 spinous process and remained L3 spinous process, while the L3 spinous process and PLC between L2 and L3 were totally removed in the Sp model. This model simulated the scenario of the instrumented PLF. First, PLF was represented as bilateral rectangular columns of fusion mass between the posterior surfaces of the transverse processes of L3 and L4. The screws were inserted into the pedicles of L3 and L4. This model simulated the scenario of PLF state with removal of pedicle screws. Therefore, this model was made by removal of pedicle screws in the WiP model. Combined with each models, 4 scenarios were simulated, that is, the preservation of the continuity of PLC with pedicle screws (Pp WiP), the preservation of continuity of PLC without pedicle screws (Pp WoP), the sacrifice of PLC with pedicle screws (Sp WiP), the sacrifice of PLC without pedicle screws (Sp WoP) Fig.1. To validate the model, the same loading conditions used in Yamamoto et al's study were applied [4]. Therefore, 10 Nm flexion, 10 Nm extension, 10 Nm torsion, and 10 Nm lateral bending moment under the 150 N preload were imposed on the L2 vertebral body, respectively. To reach 10 Nm moments, the five load steps were applied to four models.

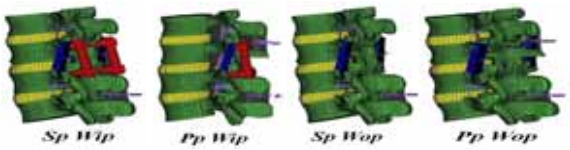

Figure 1: The four FE models in the current study

RESULTS & DISCUSSINON

The intact L3-L5 model was validated in our laboratory, as reported in our prior publications [3].

3.1 Comparison of range of motion between models

The range of motion at each corresponding level was compared among three models (the intact and four models) under each moment (Fig. 2). Under flexion moment, the largest difference of motion at the L2-3 segment (proximal adjacent segment) was observed between Sp WiP model and Pp WoP model (7.6° and 6.4°, respectively), and the range of motion at distal adjacent segment (L4-L5 segment) was less influenced by the variance of fusion models than at proximal adjacent segment (Fig. 2). Relatively larger motion at fusion segment was shown in Sp WoP and Pp WoP models, which lead to less increased motion at the superior adjacent segment (L2-3), compared to the WiP models, and vice versa, in the WiP model (Fig. 2). L3-4 fusion also produced increased motion at both adjacent segments under extension moment. Changes of proximal adjacent segment motion model became most pronounced in the Sp WiP (4.8°), and least changes was noted in Wop models (4.3°), which is similar trend to flexion moment applied. However, compared to flexion moment, distal adjacent segments (L4-5) had similar differences of motion to proximal adjacent segment (L2-3). Fusion segment (L3-4) of the WiP models, on the contrary, had less motion than the WoP models (Fig. 2).

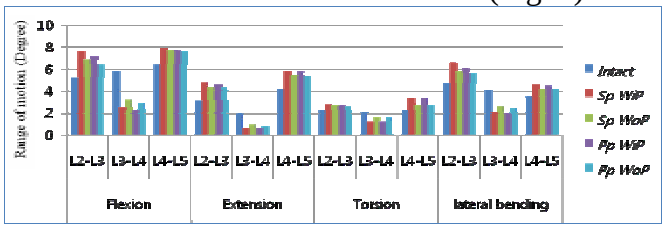

Figure 2: The comparison of the range of motion at each corresponding segment between intact models and four fusion models

Similar patterns of changes of motion were also shown under torsion (axial rotation) and lateral bending moment. The changes became more prominent in the Sp WiP model (Fig. 2). As expected, the ablation of PLC with disruption of continuity of proximal segment in both Sp WiP and Sp WoP models caused increase of range of motion at proximal adjacent segments, compared to each corresponding Pp model. This study also demonstrated that the pedicle screw augmented more mechanical stress at adjacent segments after fusion. Conversely, in the Pp WoP and Sp WoP models, which simulated the scenario of removal of pedicle screws, relatively more motion was allowed at the fusion segment (L3-4) under 4 pure moments, and simultaneously compensatory motion at the adjacent segments reduced compared to each corresponding WiP model. This phenomenon became especially more pronounced at the superior adjacent segment under flexion moment. This is explained by the decrease of stiffness of fusion segments resulting from the removal of pedicle screws. Accordingly, Sp WiP shown the most increase of range of motion at proximal adjacent segments, and Pp WoP exhibited the least increase of range of motion at proximal adjacent segments among current FE models

CONCLUSIONS

From many previous studies, fusion itself seems to lead to increased stress at adjacent segments, and be a main factor of ASD. However, the current study suggest that only fusion does not cause ASD, but decompression procedure, that is removal of PLC, is also a significant factor leading to increased stress at a proximal adjacent segment, and the combined effect of these risk factors would make the adjacent segments overstressed significantly

REFERENCES

1.Lee CK. *Spine* **13**, 375-377,1988.
2.Park P, et al. *Spine* **29**, 1938-1944, 2004.
3.HJ Kim, et al. *Medical & Biological Engineering & Computing* **47**, 599–605, 2009.
4.Yamamoto I, et al, *Spine* **14**, 1256-1270, 1989

OPTIMIZING POSITION OF THE HORIZONTAL BENCH PRESS USING SURFACE ELECTROMYOGRAPHY

Miguel Jagessar

The University of Trinidad and Tobago, Trinidad, West Indies
email: miguel.jagessar@gmail.com

INTRODUCTION

Poor technique of the horizontal bench press (HBP) can lead to under developed pectoral muscles and chronic shoulder pain. Not controlling the weight during the eccentric and concentric phases of the lift and bouncing the bar off the chest is common poor practice. Many bench pressers use a variety of hand and body positions in hope that muscle fibers of the pectoralis major will be maximally recruited. Some of these positions have resulted in muscle imbalance and injuries.

An examination into the effect of glenohumeral (GH) joint angle, scapula and lower-back position on electromyographic (EMG) activity of the prime movers (upper clavicular and lower sternocostal heads of the pectoralis major (UCPM and LSPM), anterior deltoid (AD) and the long head of the triceps brachii (TB)) of the HBP can give insight into maximizing pectoral development and minimizing injuries. The optimum range of width of grip (WG) that produced maximum EMG activity in both the upper clavicular and lower sternocostal heads of the pectoralis major expressed as a percentage of biacromial width (BW) was found to be from 165 -190% for the HBP [1].

This study seeks to determine the optimum hand and body position for maximizing recruitment of the pectoralis major muscle using surface EMG (SEMG). It was hypothesized that a specific glenohumeral (GH) joint angle, scapula and lower back position would yield maximum EMG activity in the pectoralis major during the concentric phase of the HBP.

METHODS

Nine experienced (minimum of 2 yrs) male weight trainers were recruited and all signed consent forms prior to testing. EMG activity was recorded from the UCPM, LSPM, AD and the TB for six predetermined positions. Three GH joint angles (GHJAs) of 50º, 70º, and 90º with lower back naturally arched (LBNA) and scapula rotated (SR), one GHJA of 70º with scapula neutral (SN) and LBNA, and two positions of lower back arched (LBA) and flat (LBF) with 50º GHJA and SR. GHJA was kept consistent by use of two vertical wooden poles placed medially of the upper arm. Rolled towels maintained the SR and LBA positions. Feet were placed on a high box to produce the flat back position. On the day of testing subjects easily grasped the form for each position. Subjects produced maximum voluntary isometric contractions (MVICs) of the UCPM, LSPM, AD and TB by lying supine on the bench, holding an un-weighted bar stationary in their customary bench press position at approximately mid length of ascent while a spotter gradually applied increasing downward force symmetrically on the bar until the subject indicated that the contraction was maximum and the force maintained then EMG activity was recorded for 3 secs. Three trials for each position were then performed with 3 minutes rest intervals. WG was standardized to165% BW.

EMG activity was detected by pairs of 1cm disc Ag/AgCl electrodes with inter-electrode distance of 2cm. Bipolar centers were placed on the surface of the skin over the muscle bellies offset 2cm from the mid-length of the muscles to avoid innervation zones. Two ML865 Power Lab 4/25T, data acquisition systems coupled by a common trigger recorded EMG activity. Signals were sampled at 1000 Hz, filtered at 10 Hz (high pass) and 500 Hz (low pass), full-wave rectified, integrated, time normalized, found as %MVIC and expressed as a percentage of maximum %MVIC for each muscle. Recordings were processed for the concentric phase (from the lowest position to soft elbow lock out)

and represented total energy of the lift. Processing EMG activity for the whole concentric phase helped to eliminate variance in readings by containing overall change in EMG activity, due to movement of electrodes for individual trials, constant.

RESULTS AND DISCUSSION

Effect of GH Joint Angle: Tukey post-hoc test showed that there was no significant difference in mean %MVIC for the UCPM, LSPM and TB muscles for changes in GHJA. However, direct comparisons showed that for the UCPM the 50º and 70º GHJAs produced greater mean %MVIC than the 90º GHJA (Fig. 1). There was significant difference in mean %MVIC of the AD between the 50º and 90º GHJAs.

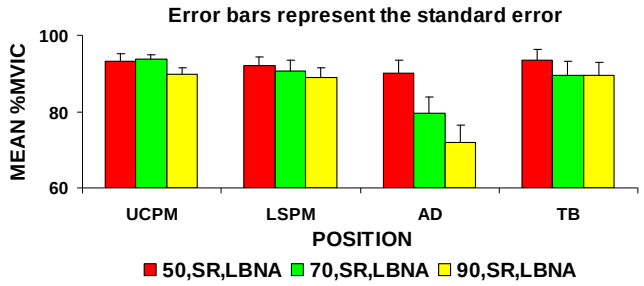

Figure 1: Mean %MVIC in UCPM, LCPM, AD and TB for the 50º, 70º and 90º GHJAs.

It is common belief that to target the pectoral muscles, the HBP should be performed with a close to 90º GHJA. The results show that this is not the case and that the 50º or 70º GHJA can be used to work the pectoral muscles effectively. Furthermore the 90º JA has been shown to increase the risk of shoulder injury, instability, atraumatic osteolysis of distal clavicle and pectoralis major rupture [2].

Effect of Scapula Position: The correct anatomical position for the scapula is back and rotated downwards. In this position greater stability of the GH joint is achieved. During the eccentric and concentric phases of the HBP the scapulae retracts and protracts however, a flat bench surface does not allow free movement of the scapulae and increases risk of shoulder injury. For this reason the rolled towel was used to create space between the scapulae and bench surface to allow free retraction and protraction. Independent samples t-test revealed that there was no significant difference in mean %MVIC in the UCPM, LCPM, AD and TB between rotated and neutral scapula positions. Therefore muscle recruitment would not be compromised when the technique of rotating the scapula backwards is utilized during the HBP. More importantly the GH joint would be less prone to injury.

Effecct of Lower back Position: Some bench pressers experience discomfort in the lower back during the HBP due to excessive curvature of the lower lumbar region. To relieve stress, the flat back position can be used without affecting the benefits of the horizontal bench press. There was significant difference in mean %MVIC for the AD and TB between the LBA and LBF position. Direct comparisons of mean %MVIC for the UCPM, LSPM, AD and TB showed greatest EMG activity for the LBF position (Fig. 2).

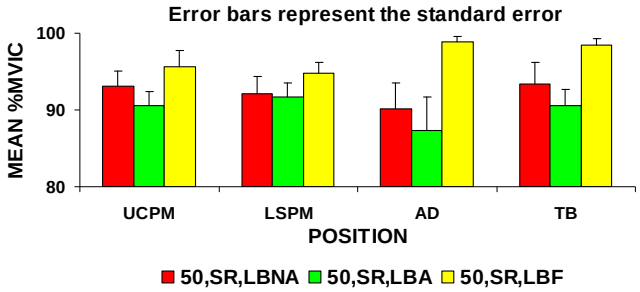

Figure 2: Mean %MVIC in UCPM, LCPM, AD and TB for LBNA, LBA and LBF positions.

Recommendations: To minimize shoulder injury and maintain recruitment of the UCPM, LSPM, AD and TB muscles, the HBP should be performed with a 50-70º GHJA with SR for free movement and either the LBF or LBNA position. Bench design can help maintain optimum position. We can be 95% assured that a specific body position does not yield maximum EMG activity in the pectoralis major.

REFERENCES

1.Clemons J, and C Aaron. *J. Strength Cond. Res* **11**, 82-87, 1997.
2.Green CM, and P Comfort. *Strength and Conditioning Journal*. **5**, 10-14, 2007.

ACKNOWLEDGEMENT

Special thanks to Prof. David Sanderson, School of Human Kinetics. University of British Columbia.

QUANTATIVE ANALYSIS of sEMG of the UPPER EXTREMITY MUSCULATURE WHILE CUTTING COMMON PADDLE SPORT ENTANGLEMENT MATERIALS USING TWO DIFFERENT TOOLS

Gretchen D Oliver, Tina Aldrich and Merry Moiseichik

University of Arkansas, Fayetteville, AR, USA
email: goliver@uark.edu

INTRODUCTION

The element of safety equipment has been stressed in the paddle sport community. However, the equipment recommendations for entanglement situations in paddle sports have been vague. Not only has the general safety equipment suggested been ambiguous, but the effectiveness of the equipment has been scarce in the literature. Paddlers often choose to carry some type of cutting device in case they become entangled. Traditionally, the cutting device of choice is a knife, not to exclude other tools such as shears/scissors. There are no data available that precludes the use of one cutting device over another. However, it would be assumed that the cutting device of choice would be one that was most effective and efficient.

There have been few studies examining muscle activations while using a knife in culinary environments [1,2] however, there has yet to be an investigation examining muscle activations between two different cutting tools possibly used in the paddle sport community. It was therefore the purpose of the current investigation to quantify muscle activations of the upper extremity musculature while performing cutting maneuvers of two different common entanglement materials using two different cutting devices, a knife and shears/scissors.

METHODS

Twenty-nine right handed adults (mean age: 26 $\pm$ 4.76 years, height: 175.5 $\pm$ 10.3 cm, mass: 80.5 $\pm$ 20.5 kg) volunteered to participate. All participants were deemed injury free and had no bias for cutting instrument. Data collection sessions were conducted indoors at the University's Health, Physical Education, and Recreation building. All testing protocols were approved by the University's Review Board.

Surface electromyographic (sEMG) data were collected on the participant's dominate arm biceps, triceps, wrist extensors and wrist flexors. A Noraxon Myopac 1400L 8-channel amplifier was used to record and analyze sEMG. The signal was full wave rectified and smoothed based on the smoothing algorithms of root mean squared at windows of 100 ms. Throughout all testing, sEMG data were sampled at a rate 1000 Hz.

Participants performed maximum isometric voluntary contractions (MVICs) for each muscle to establish baseline measures. After MVICs were performed, participants sat in a sit-on-top kayak on the lab floor and cut two different ropes (NRS kayak tow bag and NRS throw bag ropes) using two different tools (Kretzer wire scissors and NRS River Shorty knife). Order of tool used for cutting was randomized for each participant. Each participant was timed and given a maximum of 10 seconds to cut through each material. A rest period of one minute was given between cuts to eliminate fatigue.

Muscle activation data were analyzed using repeated measures MANOVA and speed of cut data were analyzed using repeated measures ANOVA, to determine differences at the .05 level. Cut success was analyzed using a frequency distribution.

RESULTS AND DISCUSSION

Overall there were significant differences in muscle activation by tool ($p = .000$) as well as material ($p = .001$). The knife required significantly greater muscle activation to cut both materials than the shears. There were significant differences in cutting time by tool ($p=.000$) and material ($p = .000$). The

knife took significantly longer to cut both materials than did the shears/scissors. The knife and shears/scissors cut the tow rope successfully in the time allotted for all 29 participants. The shears/scissors had the same success for the throw rope. The knives' cut success on the throw rope was 28 of 29. Means and standard deviations of average %MVIC for the muscles analyzed are presented in Figures 1 and 2.

The results of this study support the notion of shears/scissors being more effective than a knife in cutting tow and throw ropes. Using the shears or scissors versus a knife may be more appealing to individuals because of the decreased muscle activation. Decreased muscle activation does not necessarily mean that a weaker individual would be more successful with the shears/scissors but instead means that shears/scissors would be an attractive option if one were fatigued from the paddling sport. Essentially the individual would want to choose an implement that would require less muscle activation.

CONCLUSIONS

The results of this study support that shears/scissors are significantly faster and require less muscle activation of the upper arm and forearm musculature than a knife at cutting tow and throw rope. With the inability of humans to breathe underwater, a faster cutting tool is advantageous in water sport entanglement emergencies. However, current recommendations of the American Canoe Association for entanglement safety only suggest carrying a knife.

Based on the results of this study it is evident that the shears/scissors are more efficient and effective at cutting materials that would typically have one entangled. Further studies are warranted comparing the cutting devices. It is advised that further studies include both right and left handed participants, wet materials (versus the dry materials used in the current study) as well as have the participant not only in the kayak but in the water in the kayak.

REFERENCES

1.Claudon L. *Int J Indust Ergo* **36**, 239-246, 2006.
2.Bao S. *Int J Indust Ergo* **27**, 375-385, 2001.

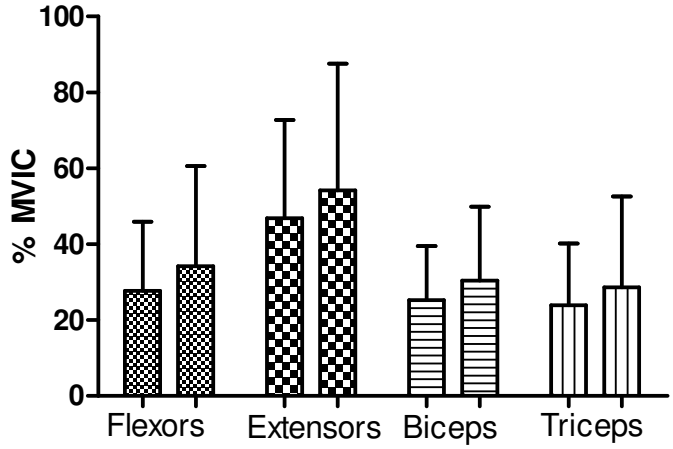

Figure 1. Means %MVIC using knife on materials 1 and 2.

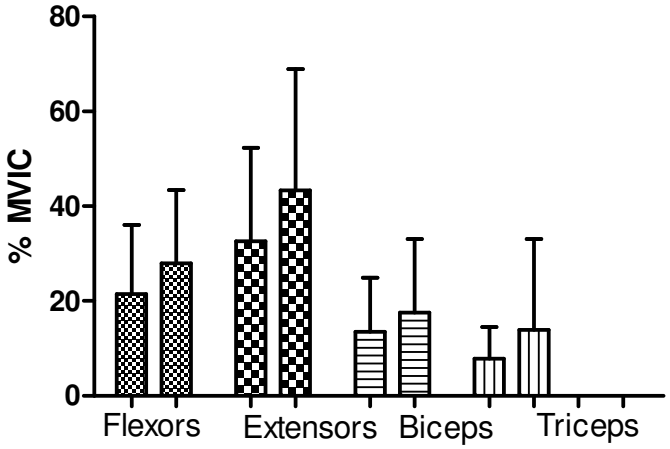

Figure 2. Means of %MVIC using shears on materials 1 and 2.

WINDMILL PITCHING KINETICS: INJURY IMPLICATIONS IN HIGH SCHOOL SOFTBALL PITCHERS

Hillary A. Plummer, David W. Keeley, Gretchen D. Oliver
University of Arkansas, Fayetteville, AR, USA
email: goliver@uark.edu

INTRODUCTION

Fast-pitch softball has become a year round sport for many female athletes. The Amateur Softball Association has reported that 2.5 million fast-pitch players were registered to play in 2008 [1]. Of those, 1.3 million were between the ages of 12 and 18. Despite the recent increased popularity of fast-pitch softball, there are few quantitative studies assessing upper extremity kinetics and injury implications during the windmill softball pitch. With an increased number of females participating in softball, there is an augmented need to further explore the pitching motion. It has been observed that similar torques are produced in both softball and baseball pitchers [2]. Therefore with the risk of injuries in windmill softball pitchers becoming as paramount as those in baseball, understanding the mechanics of the pitching motion is imperative [2]. Thus, it was the purpose of this study to quantify upper extremity kinetics during the windmill softball delivery in high school softball pitchers.

METHODS

A randomized control trial was implemented in a controlled laboratory setting. High school softball pitchers (n=7; 17.7$\pm$2.6 years; 169$\pm$5 cm; 69.1$\pm$5.4 kg) reported for testing prior to engaging in resistance training or any vigorous activity. Kinematic and kinetic data were collected using The MotionMonitor^{TM} motion capture system (Innovative Sports Training, Chicago IL) at a rate of 1000Hz. Prior to completing test trials, participants had a series of ten electromagnetic sensors attached at the following locations: (1) the medial aspect of the torso at C7 [3]; (2) medial aspect of the pelvis at S1 [3]; (3) the distal/posterior aspect of the throwing humerus; (4) the distal/posterior aspect of the throwing forearm; (5) the distal/posterior aspect of the non-throwing humerus; (6) the distal/posterior aspect of the non-throwing forearm; (7) distal/posterior aspect of stride leg femur; (8) distal/posterior aspect of stride leg fibula; (9) distal/posterior aspect of non stride leg femur; and (10) distal/posterior aspect of non stride leg fibula. Sensors were affixed to the skin using double sided tape and secured using flexible hypoallergenic athletic tape. An eleventh sensor was attached to a wooden stylus and used to digitize the palpated position of the bony landmarks. Standard inverse dynamics were used to calculate throwing kinetics from the fastest pitch deemed a strike. Kinetic parameters calculated included forces along and torques about the anterior/posterior, medial/lateral, and longitudinal axes of the shoulder and elbow. Means and standard deviations were calculated at three instances during the pitch (6 o'clock, 12 o'clock, and release).

Following all set-up and pre-testing protocols, participants were allotted an unlimited time to perform their own specified pre-competition warm-up routine. After completing their warm-up and gaining familiarity with the pitching surface, each participant threw a series of maximal effort fastballs for strikes toward a catcher located at the regulation distance (12.2 m). The pitching surface was positioned so that the participants stride foot would land on top of the 40 x 60 cm Bertec force plate (Bertec Corp, Columbus, Ohio) which was anchored into the floor.

RESULTS AND DISCUSSION

Compressive forces within the shoulder and elbow joints increased steadily throughout the movement, peaking near ball release. A compressive force equal to 56% $\pm$ 32% body weight (BW) was observed at the shoulder at the point of release. Additionally, a compressive force equal to 48% $\pm$ 17% BW was observed at the elbow at release. An increase in internal rotation torque was seen after 6 o'clock. This torque changed direction prior to

release, reaching a maximum external rotation torque of 1% ± 1% BW near release. Elbow extension torque, acting to resist elbow flexion torque, reached a maximum value of 11% ± 5% BW at release.

The kinetics observed in the current study are similar to those reported in previous examinations. The excessive compressive forces that occur at both the shoulder and elbow, at the time of ball release, act to prevent distraction of the humerus/forearm. It is not uncommon for softball pitchers to pitch multiple games in a day on consecutive days. The repetitive motion of the windmill softball pitch and the forces acting on the shoulder and elbow during each pitch may lead to overuse injuries of the upper extremity. These overuse injuries are possibly related to the repeated exposures of high magnitude compressive forces. Functionally the biceps brachii and flexor/pronator muscle groups act to eccentrically contract in attempt to decelerate maximum elbow extension as well as provide active stability of the elbow in attempt to prevent further shoulder distraction at ball release [1,4].

Additionally, the current study identified an elbow extension torque equal to 11% BW*H at ball release. At this instant the elbow is in a position of full extension. To counteract this torque, and prevent possible hyperextension of the elbow, the biceps must contract eccentrically in attempt to control the elbow extension.

CONCLUSIONS

During the windmill pitching motion, peak distraction forces are experienced at both the elbow and shoulder near the time of ball release. We propose that the repeated occurrence of distraction forces of this magnitude could be an implication of greater incidence of biceps-labral overuse injuries in softball pitchers. Previous studies have shown that the biceps is more active in the windmill softball pitch near the point of release than the muscle activity throughout the overhand pitching motion in baseball [1]. With the knowledge of the current study's kinetic magnitudes we may be able to provide a premise for rehabilitative and preventative programs regarding overuse injuries in the upper extremity of windmill softball pitchers. These results must be interpreted with caution as more studies need to be conducted to see if a relationship exists between biceps activity and increased elbow and shoulder kinetics.

REFERENCES

1.Rojas IL, et al. *Am J Sports Med* **37**: 558-565, 2009.
2.Barrentine SW, et al. *J Orthop Sports Phys Ther* **28**: 405-414, 1998.
3.Myers, JB, et al. *Am J Sports Med* **33**: 263-271, 2005.
4.Udall JH, et al. *J Shoulder Elbow Surg* **18**:773-778, 2009.

Table 1: Mean (± SD) for selected kinetic parameters. Forces are reported as percent bodyweight (%BW) and torques are reported as percent body weight times height (%BW*H).

Parameter	6 o'clock	12 o'clock	release
Shoulder Compressive Force	2 (+ 1)	7 (± 3)	56 (± 32)
Shoulder Internal Rotation Torque	-4 (± 1)	-1 (± 1)	1 (± 1)
Shoulder Flexion Torque	3 (± 2)	-1 (± 1)	18 (± 10)
Elbow Compressive Force	4 (± 2)	6 (± 3)	48 (± 17)
Elbow Extension Torque	2 (± 1)	3 (± 1)	11 (± 5)
Elbow Valgus Torque	1(±2)	-2 (± 3)	-2 (± 4)

ASSOCIATION BETWEEN ATTRIBUTES OF A CYCLIST AND BICYCLE SEAT PRESSURE

Dustin Nash, Eadric Bressel, and Dennis Dolny
Biomechanics Laboratory, Utah State University, Logan UT, USA
email: eadric.bressel@usu.edu

INTRODUCTION

Bicycle seat pressure is thought to be the principal risk factor for bicycle seat injuries, however there is a lack of understanding regarding the characteristics of a cyclist that predict bicycle seat pressure. Body weight is a potential factor as it represents the sum of pressure distributed to a surface [1] however, the relationship may depend on whether the criterion measure is mean or peak pressure [2]. Another potential predictor of bicycle seat pressure may be the structure and position of the pelvis during bicycling [3]. For instance, if there is an ergonomic mismatch between the pelvis and bicycle seat, body weight distribution may increase interface pressure. Other factors, such as flexibility or experience level of the bicyclist may also influence seat pressure [4,5] but have not been fully tested. The lack of a comprehensive seat model that predicts seat pressure limits the ability to develop effective strategies to treat and prevent bicycle seat related injuries. The purpose of this study was to determine if select attributes of a cyclist were associated with mean and peak seat pressures during stationary cycling and to determine which of the associated variables were the best predictors of seat pressure.

METHODS

There were two data collection phases to this correlational study in which forty males between the ages 20-50 years volunteered. For the first phase, attributes of the participant (age, weight, flexibility, experience level and ischial tuberosity width) were measured. Ischial tuberosity width was determined from pressure peaks in isobar plots (Fig. 1) that were recorded while participants sat on a flat solid table in a pelvic neutral posture. Interface pressures were collected using a pressure-sensing array system (pressure mat; FSA system, Vista Medical Ltd; Fig. 1). From the known sensor area (63 mm^2) and inter-sensor distance (2.9 mm) of the pressure mat, the rectilinear distance between peaks was calculated (Fig. 1).

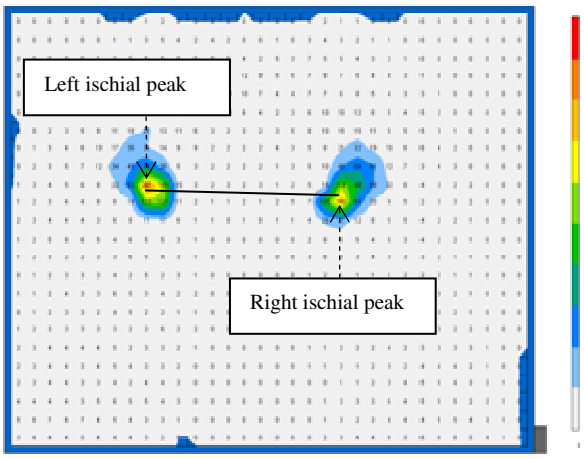

Figure. 1. Pressure map with isobar lines of a participant sitting on a solid table surface. Ischial tuberosity width was the rectilinear distance between peaks (solid black line).

The second phase required participants to ride a stationary cycle ergometer while pelvic tilt angles and seat pressure were measured on two different traditional seats (fi'zi:k Arione and Bontrager inform RL). Pelvic tilt angles were collected using a motion analysis system (Vicon MX system) that tracked retro-reflective markers placed on the cycle ergometer and on the skin over bony landmarks of the pelvis. Pelvic tilt angles were computed from filtered coordinate data using the pelvis CODA model in Visual3D (C-motion Inc.). Mean and peak bicycle seat interface pressures were collected simultaneously with pelvic angle assessments using the FSA pressure-sensing array system

Statistical relationships among attributes of participants and seat pressures were assessed with correlation coefficients (r) and those variables identified as being significantly related to seat pressure served as predictor variables in a sequential linear regression model: Alpha = 0.05.

RESULTS AND DISCUSSION

From the correlational analysis for the fi'zi:k seat (Table 1), it may be observed that weight and ischial tuberosity width were significantly related to mean seat pressure (P = 0.001, 0.02). Regarding peak pressure for the fi'zi:k seat, flexibility was negatively related (P = 0.01) and experience level was positively related to peak pressure (P = 0.01, 0.03). The correlational results for the Bontrager seat also revealed that weight was significantly related to mean pressure (P = 0.001), however, anterior pelvic tilt was inversely related to peak pressure (P = 0.01; Table 1).

Results of the linear regression for the fi'zi:k seat revealed that 50% of the variance in mean pressure was accounted for by body weight. By adding ischial tuberosity width to the model, the amount of variance explained increased (R^2 = 0.52) but ischial tuberosity width was not a significant contributor to the model (P = 0.33). When peak pressure was the criterion measure for the fi'zi:k seat, 17% of the variance was accounted for by sit-and-reach scores alone. Adding experience level to this model marginally improved it (R^2 = 0.23) but the additional variance added was not significantly unique (P = 0.10). Finally, for the Bontrager seat, weight was the only predictor of mean pressure and accounted for 43% of the variance. Regarding peak pressure for the Bontrager seat, anterior pelvic tilt accounted for 43% of the variance explained.

These results indicate that predictors of seat pressure are likely seat design specific and will vary depending on whether the criterion is mean or peak pressure. This observation is clinically relevant as peak pressure may be most related to injury from loads [2]. The results also indicate that a comprehensive seat pressure model will be challenging to build given the numerous seat designs available.

In conclusion, body weight alone accounted for the most variance in mean pressure whereas pelvic tilt and flexibility accounted for the most variance in peak pressure. These variables, related to seat pressure, may give some guidance to cyclists and clinicians who intend to prevent or alleviate the symptoms associated with bicycle seat injuries.

REFERENCES

1. Forner Cordero A. et al. *J Biomech* **37**, 1427-32, 2004.
2. Kernozek TW. et al. A*rch Phys Med Rehabil* **83**, 868-71, 2002.
3. Potter JJ. et al. *Med Sci Sports Exerc* **40**, 1126-34, 2008.
4. Sauer JL. et al. *Med Sci Sports Exerc* **39**, 2204-11, 2007.
5. Bressel E. et al. *Med Sci Sports Exerc* **35**, 327-32, 2003.

Table 1: Correlation coefficients (r) for all variables examined (n = 40)

Variable	Age	Weight	Flexibility	Exp. level	IT width	Anterior pelvic tilt
Age	1.00					
Weight	0.13	1.00				
Flexibility	-0.41[a]	-0.01	1.00			
Exp. level	0.23	-0.11	-0.28	1.00		
IT width	0.18	0.39[b]	-0.33[b]	0.13	1.00	
Anterior Pelvic tilt	0.48	-0.14	-0.51[b]	0.39	-0.01	1.00
Mean pressure (fi'zi:k)	0.09	0.71[a]	0.11	-0.09	0.44[b]	-0.39
Mean pressure (Bontrager)	0.02	0.66[a]	0.18	-0.09	0.30[c]	-0.33
Peak pressure (fi'zi:k)	-0.17	-0.08	-0.41[a]	-0.35[a]	-0.06	-0.49[c]
Peak pressure (Bontrager)	0.02	0.11	0.14	-0.29[c]	0.03	-0.66[a]

Note: IT = ischial tuberosity and Exp. = experience. [a]P = < 0.01 ; [b]P = 0.01-0.05; and [c]P = 0.06-0.10

APPLICATION OF SPACESUIT GLOVE PERFORMANCE TESTS TO ATHLETIC AND PERSONAL PROTECTIVE EQUIPMENT

[1]Scott England, [1]Elizabeth Benson, [2]Miranda Mesloh, [2]Shelby Thompson and [3]Sudhakar Rajulu

[1]MEI Technologies, Inc, Anthropometry & Biomechanics Facility, National Aeronautics and Space Administration (NASA), Houston, TX, USA
[2]Lockheed Martin, Anthropometry & Biomechanics Facility, National Aeronautics and Space Administration (NASA), Houston, TX, USA
[3]Anthropometry & Biomechanics Facility, National Aeronautics and Space Administration (NASA), Houston, TX, USA
email: scott.a.england@nasa.gov, web: http://hefd.jsc.nasa.gov/abf.htm

INTRODUCTION

Despite decades of continuous improvement, astronauts must still struggle with inhibited dexterity and accelerated fatigue due to the necessity of wearing a pressurized extra-vehicular activity (EVA) glove [1]. Recent research in the Anthropometry and Biomechanics Facility at NASA's Johnson Space Center has focused on developing requirements for improvements in the design of the next generation of EVA glove. In the course of this research, it was decided to expand the scope of the testing to include a variety of commercially available athletic and consumer gloves in an attempt to provide a more recognizable comparison against which investigators and designers may evaluate the current state of EVA glove mobility and strength. This comparison is being provided with the hope that innovative methods may foster commercial development of gloves for various athletic and personal protective endeavors.

METHODS

For this investigation, three subjects completed hand strength and fingertip mobility tests under seven gloved conditions. Gloves to be evaluated were drawn from various athletic and personal protective equipment fields, and included a ski glove, hockey glove, baseball mitt, latex glove, leather work glove, and 4000-series EVA glove. To minimize variability due to fit, subjects were selected who could fit well into a typical large glove, and had approximately 70th- to 90th-percentile hand length and middle finger length.

Mobility

To evaluate the mobility of the gloves, retroreflective markers were attached to the tips of the index and middle fingers and in an array to the back of the subject's dominant hand in a method inspired by Kuo et al. [2]. Each subject then traced their index and middle fingers through three planar sweeps of their maximum range of motion (Fig. 1) while kinematic data was collected at 100 Hz with a Vicon Motion Capture System (Oxford Metrics, Oxford, UK). The areas enclosed by the trajectories swept by the fingertips were calculated using a custom-written MATLAB script. The ratio of the ungloved fingertip area to the area in each gloved state provided a metric of degraded mobility attributable to the presence of the glove.

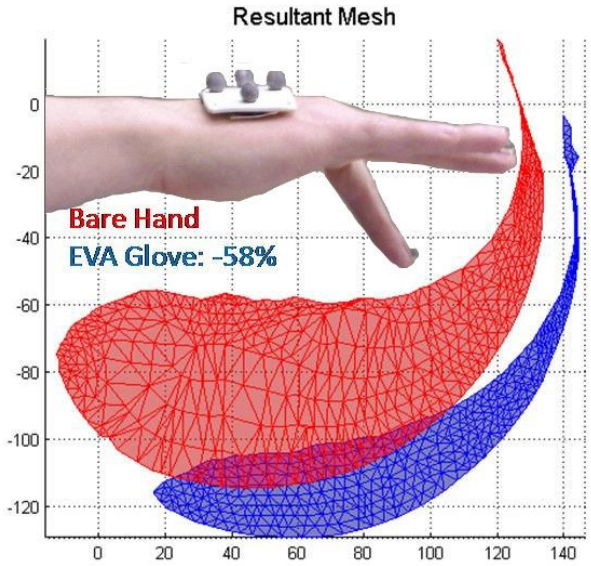

Figure 1: Areas swept by the index finger while barehanded (red/above) and while wearing the 4000 series EVA glove (blue/below).

Strength

To evaluate the influence of gloved state on strength, the subjects exerted and sustained a maximal grip or pinch force for 3 seconds as force data was recorded at 1000 Hz. Subjects were given a 2-minute period to rest to avoid fatigue effects and then the measure was repeated three total times or until three consecutive maximum exertions fell within 10% of each other. Grip strength was recorded using a Jamar hand dynamometer (Sammons Preston, Bolingbrook, IL). Pinch strength was recorded using a calibrated force transducer in both a lateral pinch and pulp-2 pinch grip. The lateral pinch represents the posture one would use to hold a key, whereas the pulp-2 pinch is formed by pressing the pads of the thumb and index finger together while they are fully extended.

RESULTS AND DISCUSSION

Individual subject data was averaged to provide the relative performance of each glove. As expected, maximal fingertip mobility was observed with very thin or no gloves present. The latex glove provided nearly identical mobility to barehanded, 102% and 98% of the area swept by the barehanded index finger and middle finger respectively. The worst performing glove for mobility was the baseball mitt, permitting just 10% and 11% of the barehanded mobility. Average mobility results for all gloves are shown in Table 1.

Table 1: Mean mobility (n = 3) in gloved states.

Glove Type	Area in mm^2 (% of Barehand)	
	Index Finger	Middle Finger
Barehand	7778 (100%)	8415 (100%)
Ski	5228 (67%)	5935 (71%)
**Hockey*	4083 (47%)	5094 (54%)
Baseball	798 (10%)	910 (11%)
Latex	7956 (102%)	8258 (98%)
Leather	5294 (68%)	5311 (63%)
EVA	3235 (42%)	3350 (40%)
**n = 1 for Hockey glove*		

Changes in strength as a function of gloved state revealed some interesting fluctuations. It was expected that thinner gloves would minimally alter strength and bulkier gloves like the 4000-series EVA glove and baseball mitt would produce drastic reductions in strength. That was generally true for grip strength: the latex glove allowed 91% of the barehanded grip strength and the 4000-series EVA glove and baseball mitt reduced grip strength to 53% and 28% of the barehanded grip strength respectively. For lateral pinch and pulp-2 pinch strength, generally small reductions and in some cases increases in strength were observed (Table 2). The key pinch produced varied results depending on the purpose of the glove. Slight increases may be attributable to extra grip and padding on the bracing index finger. The lack of large reductions in pulp-2 pinch strength from the barehanded condition was surprising and may result from the gloves giving subjects a mechanical advantage by bending the index finger and thumb.

Table 2: Mean strength (n = 3) in gloved states.

Glove Type	Magnitude in lbf (% of Barehand)		
	Grip	Lateral Pinch	Pulp Pinch
Barehand	123.5 (100%)	27.4 (100%)	11.5 (100%)
Ski	97.3 (79%)	24.1 (88%)	11.9 (105%)
**Hockey*	86.1 (67%)	24.9 (89%)	11.5 (113%)
Baseball	33.9 (28%)	13.7 (50%)	9.4 (86%)
Latex	113.7 (91%)	26 (95%)	11.7 (100%)
Leather	100.8 (82%)	24.6 (90%)	12.2 (107%)
EVA	66.7 (53%)	24.8 (90%)	14.2 (126%)
**n = 1 for Hockey Glove*			

These combined findings and methods may be useful in making future design decisions for gloves depending on their purpose and duration of use, be it a 1-hour game, an 8-hour EVA, or a 10-hour shift. Efforts to maximize functionality will benefit from refined methods to minimize degradation of mobility and strength.

CONCLUSIONS

The strength and mobility data showed interesting trends in the relative performance of gloves designed for very different purposes. These methods may be modified and applied to improve the capabilities of additional gloves, be they for athletic or protective purposes.

REFERENCES

1. Cadogan D and Graziozi D. *Proceedings of ICES* '96, Monterey, CA, USA, 1996.
2. Kuo LC, et al. *J Electromyography & Kines.* **19**, 829 – 839, 2009.

ACKNOWLEDGEMENTS

The authors wish to thank the Constellation EVA Project Office for funding this work.

ARCHERY BIOMECHANICS: A KINEMATICAL APPROACH

[1]Hayri Ertan, [2]Rafet Irmak

[1] Anadolu University, School of Physical Education and Sport, Eskişehir/TURKEY
[2] University of Dokuz Eylul, School of Physical Therapy and Rehabilitation, Izmir/TURKEY
email: hayriertan@gmail.com

INTRODUCTION

Archery can be described as static sport, which involves stable sequence of performed movement patterns. Researches in which archery shooting movement was analysed stated that M. Deltoideus contracted higher than that of M. Biceps Brachii (Nishizono, 1987). Carlsöö (1975) founded that M. Deltoideus had a major role in arrow shot movements (drawing, aiming, and release). The amount of load on muscle and bone component of both shoulders was found to be one of the basic elements of movements in archery.

METHODS

Williams (1962) has calculated the force distributions on gleno-humeral joints. He has set a fixed drawing weight as 30 lbs and calculated the weights on bowstring, drawing and bow arms horizontal abductor muscles (M) and joints (J) during shooting an arrow. He has calculated the force in the bowstring as 34.2 lbs when the archer pulls back the string with a force of 30 lbs., and the included angle between the two portions of the string is 128 degrees. The direction of the muscle force, M, and joint force, J was estimated from photograph as intersection of M, J and the applied load. M and J forces were calculated as 115 lbs and 139 lbs respectively for drawing arm. The same procedure was applied for bow arm and forces have been calculated as 114 and 142 lbs. But Williams (1962) did not mention the effect of angular changes affect by the technical and anatomical specifications of the archer. So, The purpose of the current study to describe the load distribution during archery shooting on horizontal abductor muscles and in gleno-humeral joints when the angles change between the applied load and their intersection with M and J forces.

RESULTS AND DISCUSSION

We have found that when the angles between the muscular force-load and the joint-load increase the load on muscular components of shoulders and gleno-humeral joints also increase. On the contrary, when the angles decrease on the mentioned structures, the proportion of the load that is carried by bony parts increases (Degrees 40 and 32: 114 (M) and 139 (J) lbs; degrees 39 and 31: 111 (M) and 141 (J) lbs; degrees 38 and 30: 107 (M) and 146 (J) etc.).

CONCLUSIONS

It can be concluded that the current findings may be used as one of the talent identification criteria. Besides, archers and their coaches should add some training methodologies as a precaution to decrease the weight that is carried by shoulder musculature.

REFERENCES

1.Williams N. *Biomechanics of Human Motion*, WB. Sounders Company, London, 1962.
2.Ertan H, et al. *Human Movement Science* **22**, 37-45, 2003.
3.Ertan H, et al. *J of Electromyography and Kinesiology* **15**, 222-227, 2005.

THE INFLUENCE OF SEX AND MATURATION ON KNEE VALGUS MOMENTS DURING CUTTING: IMPLICATIONS FOR ACL INJURY

[1]Christopher M. Powers, [2]Christine D. Pollard, [1]Szu-Ping Lee, [1]Guilherme Cesar, [1]Susan M. Sigward
[1]University of Southern California, Los Angeles, CA, USA
[2]California State University Long Beach, Long Beach, CA, USA
email: powers@usc.edu, web: http://pt.usc.edu/labs/mbrl

INTRODUCTION

Non-contact anterior cruciate ligament (ACL) injury rates are 3-8 times greater for female athletes when compared to their male counterparts.[1] To better understand the biomechanical and neuromuscular risk factors associated with ACL injuries in females, numerous studies have examined sex differences in lower extremity biomechanics during athletic tasks. Studies in this area consistently have reported that females perform athletic maneuvers with decreased knee and hip flexion, increased knee extensor moments and quadriceps activation and greater knee valgus moments when compared to males.[2,3] Taken together, this biomechanical profile is thought to put females at an increased risk for ACL injury.

With respect to injury risk, the greater knee valgus moments observed in females are thought to be most problematic as it has been reported that this variable is a predictor of ACL injury.[4] Although females have been shown to exhibit higher knee valgus moments when compared to males, it is not known at what age this gender difference emerges. The purpose of this study was to examine sex differences in knee valgus moments during cutting and to determine if differences exist across various stages of maturation. We hypothesized that sex differences in frontal plane knee loading would emerge post-puberty as this coincides with the time in which there is the greatest disparity in ACL injuries between males and females.[6]

METHODS

Subjects consisted of 153 soccer athletes (76 males and 77 females) between the ages of 9 and 22. Subjects were divided into groups based on maturation: pre-pubertal (n=35), pubertal (n=40), post-pubertal (n=38) and young adult (n=40). Classification was based on the Pubertal Maturation Observational Scale[7] and a self-report of Tanner stages for pubic hair development.

Each subject performed a side-step cutting maneuver by pivoting off their dominant foot (i.e. the foot used to kick a ball) and changing direction to the opposite side at a 45° angle. The speed of the task was controlled to fall between 5.5-7.0 m/s. Kinematic data were obtained using an 8-camera motion analysis system (Vicon, Oxford Metrics Ltd). Ground reaction forces were recorded using a force platform (AMTI, Inc). Visual3D software (C-Motion, Inc.) was used to quantify lower limb kinematics and kinetics (inverse dynamics equations). The dependent variable of interest was the average knee valgus moment during weight acceptance (the time between heel strike and the first trough in the resultant ground reaction force).[7] Moment data were normalized to body mass and height.

To assess differences in the average knee valgus moment between the sexes and across maturation levels, a 2 x 4 (group x maturation level) ANCOVA was performed. Cutting speed was used as the co-variate. In the event of a significant main effect for maturation, LSD post-hoc testing was performed. Statistical analyses were performed using SPSS software. Significance levels were set at $P \leq 0.05$.

RESULTS

Significant main effects for sex and maturation were found (Figure 1). There was no sex x maturation interaction. When collapsed across stages of maturation, females had higher average knee valgus moments compared to males (0.74 vs. 0.61 Nm/kg*ht). The largest sex difference occurred in the pre-pubertal group (1.04 vs. 0.72 Nm/kg*ht).

When collapsed across gender, the highest average knee valgus moments were observed in the pre-pubertal athletes followed by the pubertal, post-pubertal and young adult groups. Post-hoc testing revealed significant differences between all groups with the exception of the post-pubertal and young adults.

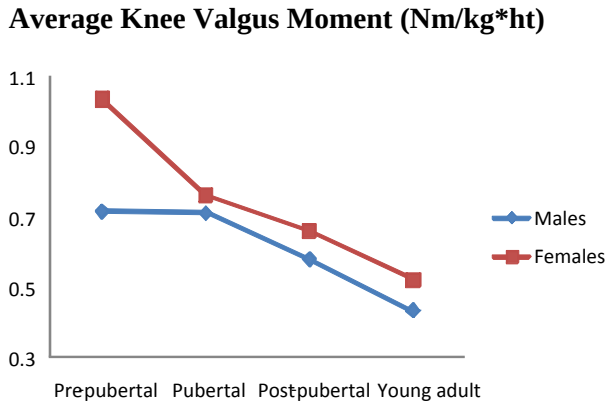

Figure 1. Comparison of the average knee valgus moment between gender across maturation levels.

DISCUSSION

Consistent with previous literature, our study revealed that female athletes had higher knee valgus moments compared to males. This gender difference was consistent across all maturational levels. Contrary to our hypothesis however, the higher knee valgus moments observed in female athletes did not emerge post-puberty as no interaction between level of maturation and sex were noted. In fact, sex differences in frontal plane cutting biomechanics already were present in the pre-pubertal group. This finding is in contrast to previous studies that have suggested that gender differences in lower extremity biomechanics appear following puberty.[8]

Our findings have implications with respect to the implementation of ACL injury prevention training programs that aim to improve lower extremity biomechanics in order to reduce injury risk. Given that sex differences in cutting were evident pre-puberty, the implementation of injury prevention programs should be considered at this stage of maturational development.

CONCLUSIONS

The higher knee valgus moments observed in females during cutting reflects a biomechanical pattern that places greater mechanical loads on the knee joint and perhaps the ACL. Interestingly, the tendency of females to exhibit a higher knee valgus moment compared to males did not emerge post-puberty and was most pronounced in pre-pubertal athletes.

REFERENCES

1. Agel et al. *J Ath Train.* 42:270-277, 2005.
2. Sigward et al. *Clin Biomech.* 21:41-48, 2006.
3. Pollard et al. *Clin J Sports Med.* 17:38-42, 2007.
4. Hewett et al. *Am J Sports Med.* 33:492-501, 2005.
5. Shea et al. *J Pediatr Orthop.* 24:623-628, 2004.
6. Davies et al. *Occup Ther Pediatr.* 20:19-24, 2000.
7. Besier et al. Med Sci Sports Exerc. 33:1168-1175, 2001.
8. Hewett et al. *Am J Sports Med.* 33:492-501, 2005.

ACKNOWLEDGEMENTS

This study was funded by the National Institutes of Health (R01 AR053073-02).

THE INFLUENCE OF GLOVE AND HAND POSITION ON PRESSURE OVER THE ULNAR NERVE DURING CYCLING

Josh Slane, Mark Timmerman, Heidi Ploeg and Darryl Thelen

University of Wisconsin-Madison, Madison, WI, USA
email: jaslane@wisc.edu, web: http://www.engr.wisc.edu/groups/nmbl/

INTRODUCTION

Sensory and motor impairments of the hand are common among both amateur and experienced bicyclists [1,2]. This condition, termed Cyclist's Palsy, most often presents as paresthesia in the fifth and ulnar aspect of the fourth finger, sometimes accompanied with weakness in the abductors or adductors [3]. Chronic ulnar nerve compression is believed to be the primary cause of Cyclist's Palsy. Guyon's Canal, the location where the ulnar nerve enters the hand, is located relatively superficially, making the ulnar nerve susceptible to compression when pressure is placed over the hypothenar region of the hand [1]. Suggestions for preventing Cyclist's Palsy include wearing padded gloves, frequently changing hand positions and riding a properly fit bicycle. However, the relative effectiveness of these interventions has yet to be substantiated [3].

The purpose of this study was to evaluate the effects of hand position and glove padding on pressure over the ulnar nerve. Specifically, we considered three different hand positions typically used on road bicycles and one position used on mountain/hybrid bicycles. We also compared gloves that were padded with either gel or foam materials located over the hypothenar eminence, thenar eminence and/or metacarpals. We hypothesized that (1) the greatest pressure over the hypothenar region would be found with the hands in the drops position; (2) the largest pressure reduction would be achieved using compliant padding over the hypothenar eminence.

METHODS

Thirty-six healthy adults (18 male, 18 female) were tested (38.9±13 yrs, 74.2±13.9 kg and 174±9 cm). An adjustable stationary cycle was adjusted to match the dimensions of each subject's personal

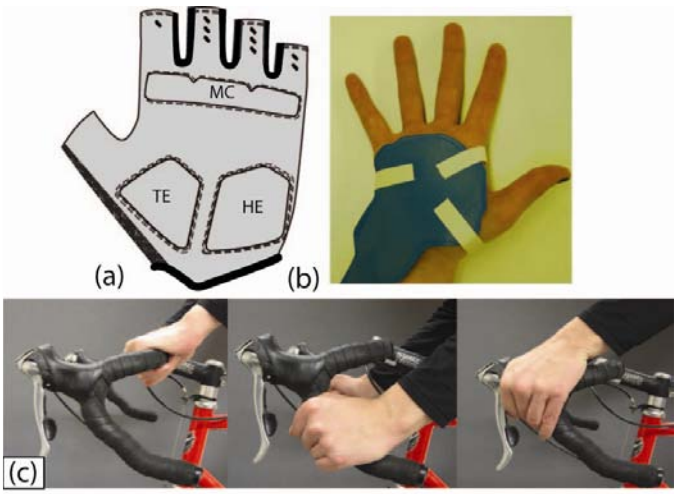

Figure 1: a) For test gloves, padding was varied over the hypothenar eminence (HE), thenar eminence (TE) and metacarpal heads (MC). b) Attachment of pressure mat to hand. c) Tops, drops and hoods hand positions, respectively.

road bicycle. Subjects performed a series of trials in which glove padding (Fig. 1a) and hand position (Fig. 1c) were randomly varied while power and cadence levels were kept consistent. A pressure sensitive mat (229 sensors, 4.4 mm per side, Novel gmbh) was used to record pressure distribution over the hypothenar region of the subject's dominant hand (Fig. 1b), while a motion capture system (PhoeniX Technologies Inc.) was used to record upper extremity kinematics. Data collected from each pressure sensor were interpolated at 100 evenly spaced intervals over full pedal strokes using piecewise cubic splines. Cyclic pressure curves from twelve consecutive pedal strokes were then averaged together. We then quantified both the pressure distributions and peak pressure over the hypothenar eminence for each condition.

Three-dimensional images of the subject's hand with and without the pressure mat attached were obtained using a laser scanner (Shape-Grabber Inc). These laser scans allowed for the creation of

subject-specific pressure images that related pressure distribution to the underlying anatomy (Fig. 2). The compressive stiffness of the gel and foam padding inserts were measured separately with a materials testing machine (Instron 1000, 100-lb capacity load cell, 15 mm circular indenter).

RESULTS AND DISCUSSION

Analysis of the pressure distributions revealed that the most substantial pressure concentrations nearest Guyon's Canal were observed with the hands in the drops and hoods positions (Fig. 2). Pressure magnitudes were greatest with the hands in the drops and straight bar positions (Table 1), which were each significantly higher than that seen in the tops and hoods positions ($p < 0.05$). Hypothenar pressure did not significantly vary between male and female cyclists.

Padding in the hypothenar region of the glove reduced peak pressures seen in the no glove condition from 21-28%, with the highest pressure reduction achieved using foam. There was no significant pressure reduction achieved when using 5 mm padding over 3 mm. The foam padding/glove system was found to be ~50% less stiff than the gel, suggesting that pressure reduction was achieved using a more compliant interface. The drops hand position induced the greatest amount of wrist extension (~54°), which could exacerbate nerve compression [2].

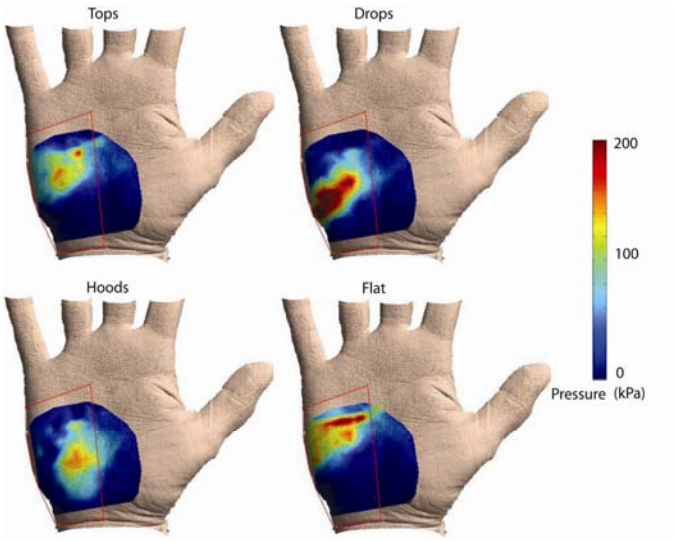

Figure 2: Peak hypothenar pressure for the 4 tested hand positions

CONCLUSIONS

The results demonstrate that pressure over the ulnar nerve can be reduced with cycling gloves that include relatively thin, compliant padding in the hypothenar region. Pressure distributions varied substantially between hand positions, such that appropriate pad placement is dependent on riding style. Further research is needed to quantitatively relate hypothenar pressure magnitudes and durations to risk for ulnar nerve damage.

REFERENCES

1.Black S, et al. *Am J Orthop* **36**, 377-379, 2007.
2.Capitani D, et al. *J Neurol* **249**, 1441-1445, 2002.
3.Kennedy J. *Neurol Clin* **26**, 271-279, 2008.

ACKNOWLEDGEMENTS

Trek Bicycle Corporation, Waterloo, WI.

Table 1: Average (SD) peak pressure (kPa) for all combinations of glove and hand positions

Glove	Padding	Thickness (mm) HE-TE-MC	Stiffness (kN/m)	Tops[1, 2]	Drops[1,3]	Hoods[1,3]	Straight Bar[1]
None	None	---	---	137 (12)	165 (12)	134 (12)	152 (12)
1	None	---	---	129 (11)	160 (13)	125 (11)	155 (15)
2	Gel	3-3-3	22	123 (11)	147 (13)	114 10)	123 (12)
3	Gel	5-5-3	17	113 (11)	142 (13)	103 (8)	127 (13)
4	Foam	3-3-3	10	108 (9)	133 (11)	104 (8)	121 (10)
5	Foam	5-5-3	8	113 (9)	128 (10)	96(8)	116 (10)

[1]No Glove vs. Padded Glove, $p < 0.05$ [2]Glove 4 vs. Glove 2, $p < 0.05$ [3]Glove 5 vs. Glove 2, $p < 0.05$

A MODEL PREDICTING ANTERIOR SHEAR STRESS IN THE SHOULDER DURING THE SLIDE STEP DELIVERY IN HIGH SCHOOL BASEBALL PITCHERS

[1]David W. Keeley, [1]Gretchen D. Oliver [2]Tom Hackett and [3]Michael R. Torry

[1]University of Arkansas, Fayetteville AR, USA
[2]Steadman Clinic, Vail, CO, USA
[3]Steadman Philippon Research Institute, Vail, CO, USA
email: dwk0611@msn.com, web: http://coehp.uark.edu

INTRODUCTION

Baseball pitching is one of the most dynamic overhand movements in sports and repeatedly subjects the shoulder to high magnitudes shear stress [1]. Shoulder injury, and in particular injury to the labral complex in high school baseball pitchers is often attributed to this stress [2]. Thus, the purpose of this study was to identify those pitching kinematics associated with anterior/posterior forces (sheer stress) in the shoulder at maximum external rotation (MER) and use those parameters to develop a model predicting the anterior component of the sheer stress. It was hypothesized that the anterior component of the sheer stress in the shoulder would be correlated to multiple kinematics parameters and could ultimately be predicted from a linear combination of these variables.

METHODS

Thirty-four healthy high school baseball pitchers participated in this study. All kinematic data were collected and processed using The MotionMonitor™ electromagnetic tracking system (Innovative Sports Training, Chicago IL). Electromagnetic sensors were attached to the upper body as shown in Figure 1. Following sensor attachment, the positions of various bony landmarks were palpated and digitized using an additional sensor.

After digitization, participants were allotted unlimited time for warm-up before test trails. Test trails consisted of maximal effort fastball pitches thrown toward a catcher located 18.44m from an indoor pitching mound. All pitches were delivered from the stretch position using the slide step delivery. Only those data from the fastest pitch passing through the strike-zone were selected for detailed analysis.

Data describing the position and orientation of electromagnetic sensors were collected at 1000 Hz and filtered using a 4th order Butterworth filter with a cutoff frequency of 13.4 Hz. Throwing kinematics were calculated using the standards and conventions recommended by the International Shoulder Group of the International Society of Biomechanics (ISB) [6,7].

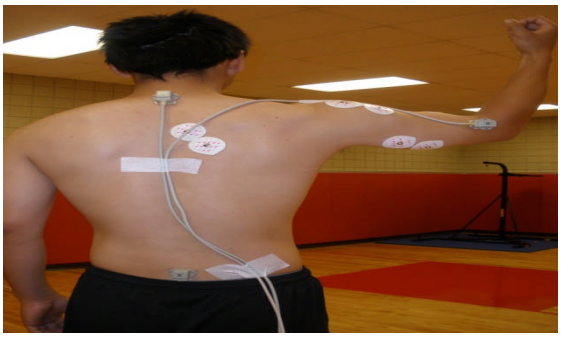

Figure 1. Sensor attachment for the humerus and trunk in the current study.

Throwing kinetics were calculated using standard inverse dynamics techniques with the torso and arm modeled as four rigid links in series and connected by ball-and-socket joints [5]. For the shoulder joint, resultant forces for the torso were calculated in the global inertial reference frame and local segment-based reference frames were establish for the throwing humerus and forearm using the ISB standards [6,7]. Anterior sheer stress was defined as the component of the resultant force acting along the anterior/posterior axis of the shoulder in the positive direction. This force was normalized to percent body weight.

Following the determination of a normally distributed sample, Pearson correlation coefficients were calculated to identify those parameters significantly related to anterior shoulder force at MER. Following the correlation analysis, multiple regression techniques were used to develop the model that best predicted anterior force at MER.

For all models, anterior force at MER was the dependent variable while those variables significantly related to this force were the independent variables.

RESULTS and DISCUSSION

In the current study, anterior sheer stress at MER averaged 25 ± 14% BW (194 ± 108N). For the correlation analyses, a total of 47 parameters were analyzed from foot contact (FC) thru release (REL) for their relationship with the sheer force. The results of these analyses indicated that 3 parameters (pelvis axial rotation velocity at FC, torso axial rotation velocity at both FC and MER) were related to the anterior component of sheer forces in the shoulder ($r^2 = 0.24$; $p = 0.003$).

The results of overall model using these parameters showed that each of the multiple regression models accounted for a significant amount of variability in anterior sheer stress. However; further analysis of regression coefficients (Table 1) indicated that only the rate of pelvis axial rotation at FC should be retained in the final model. In this final model, 24% ($r^2 = 0.24$; $p = 0.003$) of the variability in the anterior force in the shoulder could be explained using the rate of axial pelvis rotation at FC.

It has been shown that the repeated loading of the shoulder can be detrimental to the joint [3]. As a result of this loading, anterior laxity of the glenohumeral joint can result [1]. As a product of this dysfunction, both subacromial and internal impingement have been reported [4]. At MER, an increase in the magnitude of anterior stress within the shoulder, coupled with amplified anterior laxity may result in increased tightness of the posterior aspect of the joint [4].

CONCLUSIONS

Although the magnitude of anterior stress explained by the model is somewhat small, it may be attributed to the fact that the final model included only 1 of the 47 parameters. This might be the result of the strong correlation between the pelvis and torso parameters. It appears that there may be a moderator effect occurring between the significantly correlated independent variables. Thus, in a situation such as this, pitchers may be able to decrease anterior sheer stress in the shoulder substantially more than the magnitude suggested by the final model by decreasing the rate of axial pelvis rotation at FC.

REFERENCES

1. Adams, JS. *Clin Sports Med* **10**, 839-861, 2008.
2. Fleisig, GS, et al. *Sports Biomech* **8**, 10-21, 2009.
3. Fleisig, GS, et al. *Am J Sports Med* **23**, 233-239, 1995.
4. Ramappa, AJ, et al. *J Ped Orthop* **30**, 1-7, 2010.
5. Sabick, MB, et al. *J Shoulder Elbow Surg* **13**, 349-355, 2004.
6. Wu, G, et al. *J Biomech* **35**, 543-548, 2002.
7. Wu, G, et al. *J Biomech* **38**, 981-992, 2005.

Table 1. Results of regression coefficient analysis all models with anterior sheer stress as dependent variable.

		Unstandardized Coefficients		Standardized Coefficients			Correlations			Collinearity Statistics	
	Model	B	Std. Error	Beta	t	Sig	Zero-order	Partial	Part	Tolerance	VIF
1	(Constant)	300.09	39.9		8.112	0.000					
	Pelvis Axial Rotation Velocity @ FC	-0.24	0.076	-0.490	-3.176	0.003	-0.490	-0.490	-0490	1.000	1.000
2	(Constant)	309.82	39.2		7.907	0.000					
	Pelvis Axial Rotation Velocity @ FC	-0.02	0.092	-0.405	-2.148	0.040	-0.497	-0.360	-0.333	0.677	1.476
	Torso Axial Rotation Velocity @ FC	-0.05	0.063	-0.149	-0.792	0.434	-0.379	-0.141	-0.123	0.677	1.476
3	(Constant)	412.08	81.3		5.067	0.000					
	Pelvis Axial Rotation Velocity @ FC	-0.17	0.094	-0.448	-1.771	0.087	-0.490	-0.308	-0.270	0.637	1.569
	Torso Axial Rotation Velocity @ FC	-0.03	0.064	-0.076	-0.395	0.696	-0.379	-0.072	-0.060	0.629	1.590
	Torso Axial Rotation Velocity @ MER	-0.172	0.120	-0.25	-1.428	0.164	-0.430	-0.252	-0.218	0.756	1.323

IDENTIFYING DIFFERENT BIOMECHANICAL 'TECHNIQUES' - TECHNIQUE TAXONOMY APPLIED TO GOLF PUTTING.

Pat McLaughlin and Russell Best

[1]Institute of Sport, Exercise and Active Living, Victoria University, Melbourne, Australia
email: patrick.mclaughlin@vu.edu.au

INTRODUCTION

Biomechanical analysis of golf putting has focused almost exclusively on separating players into groups based on handicap or putt result. Study designs are then based on assumptions on the relationship between handicap, putt result and putting technique. These studies then test for statistically significant differences between groups split on handicap or putting performance. In simple terms, the assumptions used in previous studies are:
Handicap assumption: The putting technique of low handicap players is different to that of middle handicap players, and high handicap players.
Accuracy assumption: The putting technique of accurate putters is different to less accurate putters.

McLaughlin, Best and Carlson (2008) divided 38 players into handicap groups (low=0-9, middle=10-18, high=18-27). ANOVAs showed no significant differences ($F(2,107)=1.65$, $p=.2$) in putt result data (low 33±33cm, middle 34±24cm, high 45±32cm) and effect size was small ($\eta^2=.03$) for a 4m putting task. The question of technique was ignored.

McCarty (2002) divided less accurate from accurate players based on ball finishing position. Groups were not significantly different on handicap ($p=0.98$ at 2m, $p=0.06$ at 4m). McCarty showed groups were very inconsistent; ie. a large variation in how an accurate (and less accurate) putt was achieved. Putt result data was not related to putting technique.

Another method for finding different techniques within one sporting activity is cluster analysis. Cluster analysis is the grouping of like items based on defined parameters from the movement of interest. Like patterns are grouped together and, if more than one pattern/techniquue exists, each pattern is shown to be statistically distinct from the other. Cluster analysis has been used in many areas (eg. biology/taxonomy). In biomechanics its use is less common but it has been used infrequently for over 25 years (eg. Wilson and Howard, 1983).

The aim of this paper is to present cluster analysis as a more appropriate tool for the identification of different techniques in a sporting activity. The study will present data from one study in three different ways and the types of errors produced when not using cluster analysis will be discussed.

METHODS

Putting testing was conducted on the practice putting green at a private golf club in Melbourne. Thirty eight players (handicap 15.3 ±6.9; age 55.3 ±17.8) participated in the study. Each player completed five putts at a hole 4m away.

Players putted while standing on a pliance pressure mat (capacitance sensor mat, 16 x 16 sensor matrix, 50Hz; novel gmbh, Germany) and moved off the mat after each putt. 2D video (50Hz) was recorded perpendicular to the putt direction and synchronized with the pliance mat. The pliance mat was validated against an AMTI platform for measurement of centre of pressure (COP). The result of each putt was noted (holed out OR left/right, long/short, distance from hole). The putting stroke was broken down into backswing (BS), downswing (DS), ball contact (BC) and follow through (FT).

Data were analysed in three ways, each based on dividing players into groups: 1) handicap; 2) putt result (accuracy); 3) cluster analysis. Non-parametric tests were used to determine significant differences between groups within each analysis method.

Putts that contained incomplete data were excluded, thus 108 putts were assessed. Each individual putt

was treated as a separate item in the analysis. A total of 62 parameters were available for assessment. For cluster analysis, the most influential parameters related to medio-lateral centre of pressure movement (COPx). These parameters form the basis of the results and discussion section.

RESULTS AND DISCUSSION

Table 1 reveals that two distinct techniques were established using cluster analysis. The three methods show inconsistent results with no parameter providing a significant difference between groups for all three methods. Of the three methods, only the cluster analysis groups have scientific validity.

The data clearly shows that the assumption of different techniques based on handicap or accuracy leads to Type I (as depicted in Table 1) and Type II errors (most likely to occur in regressions if the two techniques are not dealt with separately).

Cluster analysis data shows that although there is a significant difference between the two clusters/techniques for handicap, there is a wider range of handicaps in each group (meaning the split isn't as simple as high vs low handicaps). These two clusters, or techniques, are defined by parameters related to execution of the skill, rather than the result or the players' overall golf performance.

This study also found that players can appear in both clusters; ie. use both techniques. The inconsistency of technique within accuracy groups that McCarty (2002) alluded to is further complicated when two techniques are used within the same player. This technique 'change' within an individual could arise as a response to the previous trial's result, or for many other reasons.

CONCLUSIONS

This study's findings add weight to the argument that, for scientific studies, players should not be classified based on pre-existing (handicap) or result-based (accuracy) measures. Cluster analysis is the best way to search for different 'techniques' within the same activity. Also, it should not be assumed that one player uses only one of the techniques.

Searching for and choosing the correct method for distinguishing biomechanical 'techniques' is a critical aspect of biomechanical analysis (for all skills) but is rarely carried out. Type I and II errors can be avoided if no a priori assumptions are made. Cluster analysis is a robust technique that searches for techniques based on execution of the skill.

REFERENCES

1. McCarty, J. D. (2002). MSc thesis, Purdue University, USA.
2. McLaughlin, P, Best, R. & Carlson, J. (2008) World Scientific Congress of Golf V,USA.
3. Wilson, B.D. & Howard, A. 1983 J Hum Mvt Stud 9: 71-80.

Table 1: Mean and SD for COPx parameters by group and by study design.

Method	BS Range COPx (mm)	DS Range COPx (mm)	DS COPx Max. vel. (cm/s)	BC COPx Vel. (cm/s)	Absolute Putt Result (cm from hole)	Handicap
Handicap						
Low (n=30)	4.6±2.9	4.5±4.1*	29.9±24.6*	7.7±24.5*	35.3±34.6	5.9±2.0*
Middle (n=53)	6.5±4.8	5.2±3.6	36.3±26.0	23.0±28.9	34.1±24.1	13.7±2.3
High (n=25)	7.8±6.3	8.7±5.6	55.0±34.3	30.3±36.3	47.5±32.2	22.3±3.4
Cluster						
1 (n= 77)	4.9±2.7*	3.9±2.6*	25.5±15.7*	5.2±16.9*	36.8±28.5	12.4±5.9*
2 (n=31)	9.6±7.0	10.6±4.8	71.8±28.3	58.4±22.9	39.5±32.3	16.4±6.6
Accuracy						
More (n=54)	5.8±3.7	5.5±4.4	37.1±26.9	21.2±27.3	15.8±11.5*	12.0±5.8*
Less (n=54)	6.8±5.7	6.1±4.7	40.5±31.2	19.6±33.8	59.3±25.6	15.0±6.6
Total (n=108)	**6.3±4.8**	**5.8±4.5**	**38.8±29.0**	**20.5±30.6**	**37.6±29.5**	**13.5±6.4**

*Significant differences between groups within study design

TWO-DIMENSIONAL SEQUENTIAL ANALYSIS OF THE FRONT SNAP KICK

[1]Wendi H. Weimar, [1]Nels H. Madsen, [2]John C. Garner and [3]Yong T. Wang

[1]Auburn University, Auburn, Al, USA
[2]University of Mississippi, University, MS, USA
3Georgia State University, Atlanta, GA, USA
email: weimawh@auburn.edu, web: http://www.auburn.edu

INTRODUCTION

Proximal to distal sequencing is a process characterized by the summation of speed from the more proximal segments to the more distal segments in an attempt to reach maximum velocity of the distal segment [1]. While this premise is well accepted, the method by which this is achieved requires further investigation [2]. Therefore, the purpose of this research was to determine if the lower extremity exhibits the criteria of proximal to distal sequencing during the front snap kick and if so, the method by which this sequenced is achieved through kinematic and kinetic analysis.

METHODS

Fifteen people with experience commensurate with obtaining a black belt (avg ht: 1.77 m, avg mass: 68.82 kg, avg time training = 10.7 yrs) were asked to perform a front snap kick at chin height. The motions of the lower extremity were captured using an integrated Motion Reality Inc. (Marietta, GA) motion capture system (60Hz). Further mathematical analysis allowed for a description of moments at the joints of interest [2].

RESULTS AND DISCUSSION

The graphical relationship of the linear velocity of the adjacent segments of the lower extremity reveal that the front snap kick follows the proximal to distal sequence as expected (Fig 1). Notice how the segments begin with similar velocity until the proximal segment reaches maximum velocity, at this point the distal segment separates from the proximal segment and reaches a maximum velocity at the point where the proximal segment reaches a minimum. This pattern clearly demonstrates the summation of speed.

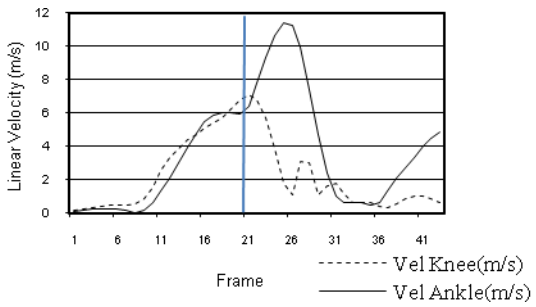

Figure 1. Linear velocity of upper and lower leg. Vertical line indicates initiation of knee extension.

The study of proximal to distal sequencing has given rise to two proposed mechanisms by which this is achieved. Table 1 presents a comparison of the two contrasting methods by which proximal to distal sequencing occurs. Method 1 suggests that a muscle action, considered to be outside the defined system, provides a negative acceleration of the proximal segment, which allows the inertia of the distal segment to whip or snap the distal segment in the direction of the original motion. This can be thought of as analogous to snapping a towel, where the towel is the segment, and your hand provides the external moment in the opposite direction of the original movement. The movement of the towel begins with upward motion, then the hand pulls rapidly downward and the towel continues forward due to its inertia. When applied to the lower extremity during a kicking motion, initially the hip is flexing. Just prior to peak angular velocity of the lower leg, the moment about the hip changes direction from a flexion moment to an extension moment and the inertia of the lower leg causes the lower leg to continue forward and for the knee to proceed into extension.

Method 2 suggests that an internal source, such as a muscle action at the common joint is responsible for the acceleration of the distal segment forward and that an example of Newton's third law is the reason for the slowing of the more proximal segment. When applied to the lower extremity during a kicking motion, the hip is initially flexing and when the thigh reaches peak speed, the knee extensors would accelerate the lower leg forward and the force causing the acceleration of the lower leg, would cause acceleration in the opposite direction on the upper leg.

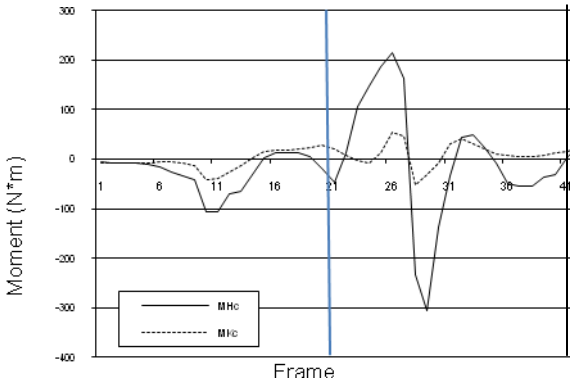

Figure 3. Moment about the hip and knee. Vertical line indicates initiation of knee extension.

Figure 3 presents the moment about the hip and knee and provide insight into which method is being employed to produce the proximal to distal sequence. Interestingly, it appears that this motion utilizes both methods. Notice that at the initiation of knee extension there is an extension moment about the hip *and* an extension moment about the knee. Presumably, both of these moments would contribute to the slowing the proximal segment as well as to the dramatic increase in the angular velocity of the distal segment. Of course, the extension moment at the hip could be the result of posterior pelvic girdle rotation, which would imply the extension moment without movement of the thigh. However, in this case, it appears that knee extension is the result of both hip and knee extension moments and the more dramatic flexion moments that occur at frame 26 are utilized to "freeze" the whole leg at its highest point.

Previously, proximal to distal movements have fit neatly into one method or the other. In addition, it has been suggested that neither method indicated here is the most efficient [3]. Therefore, these results suggest that a more complete explanation still exists to explain the mechanism behind proximal to distal sequencing and why the body adopts this procedure.

REFERENCES

1.Bunn JW. *Scientific Principles of Coaching (2nd Ed.)*, Toronto: Prentice Hall, 1972.

2.Sorensen H, et al. *J Sport Sciences* **14**, 483-495, 1996.

3.Putnam CA. *J Biomechanics* **26**, 125-135, 1993.

Table 1: Methods of proximal to distal sequencing.

	Method 1	Method 2
Source of moment that accelerates distal segment	External	Internal
Cause of motion of the distal segment	Inertial whip action	Muscle action at common joint
Source of moment that slows proximal segment	Muscle action at proximal joint	Action/reaction at common joint

THE INFLUENCE OF TISSUE MASSES ON LOWER EXTREMITY INJURIES AND REPORTED PAIN IN VARSITY SOCCER PLAYERS

Alison Schinkel-Ivy, Timothy A. Burkhart and David M. Andrews

University of Windsor, Windsor, ON, Canada
email: schinke@uwindsor.ca, web: www.uwindsor.ca/kinesiology

INTRODUCTION

The individual tissues of the shank (soft tissues such as lean and fat mass, and rigid tissue (bone)) have been shown to influence the propagation of the shock wave through the leg following impact [1]. Additionally, the ratios of these tissues (eg. lean: bone mass, lean:fat mass) may also affect the response of the tibia following impact. This suggests that how the shock wave propagates may differ based on the tissue composition of the leg.

Impacts to the lower extremities are experienced in a repetitive fashion during many sports, such as track and field, basketball, soccer, and volleyball, due to the running and jumping requirements characteristic of each. Numerous risk factors, such as the magnitude of tibial shock experienced on impact [2], have been identified for lower extremity injuries in athletes. Other factors associated with local leg tissue composition have been identified as potential influences on injury [1]; however, the relationships between the magnitudes and ratios of leg tissue masses and lower extremity injury and pain have yet to be examined. Therefore, the purpose of this study was to determine the effects of leg tissue composition on lower extremity injury and pain in varsity soccer players. Magnitudes and ratios of leg tissue masses were quantified over the course of the season in order to evaluate any changes that might occur due to extended exposure.

METHODS

Thirty-six male (n=29) and female (n=7) varsity soccer players participated in the study. The athletes were asked to complete questionnaires which provided information on their training habits, health, medical, and injury history, and physical activity history. The questionnaire also asked athletes to provide, for both the left and right lower extremities, ratings for different types of pain (for example, throbbing, stabbing, aching, heavy, or tender) on a four-point scale ranging from none (0) to severe (3) (15 pain descriptors x 3 possible points for each = 45 possible points for each extremity). Surface anthropometric measurements (lengths, breadths, circumferences, and skinfolds) were taken for the left and right lower extremities for all athletes [3,4]. Questionnaires and measurements were completed at the beginning, middle, and end of the soccer season, which ran from September through to November 2009.

The anthropometric measurements were used as inputs into regression equations in order to predict fat mass (FM), lean mass (LM), wobbling mass (WM=FM+LM) and bone mineral content (BMC) of the segments of the lower extremity (leg and leg+foot) [3]. Tissue mass ratios were calculated for both the leg and leg+foot segments. Additionally, any lower extremity injuries experienced by the athletes (bilaterally) were evaluated and reported to the investigators by two certified athletic therapists working with the teams.

RESULTS AND DISCUSSION

Compared to the uninjured athletes, those who were assessed with an injury had greater mean leg WM (4%) and LM (6%) and less mean leg FM (10%), while mean leg BMC was comparable. Further, over the course of the season, those that reported an injury showed a greater decrease in leg+foot WM, compared to the uninjured athletes (150 g decrease compared to 90 g decrease, respectively). The mean ratios of LM to BMC in the right leg (13.25 vs. 11.63 for injured and non-injured, respectively), and LM to FM in the right leg+foot (7.89 and 6.17), were significantly greater for the injured athletes in both cases. Finally, significant negative relationships were found between the mean reported

pain and the magnitude of BMC (r=-0.34), WM (r=-0.383), and LM (r=-0.373), such that, as the magnitude of these tissues increased, the amount of pain reported decreased (Fig. 1 and 2).

The results of the present study imply that injured athletes have greater LM:BMC and LM:FM ratios in the leg than uninjured athletes. It is possible that there is an optimal relationship between the masses of LM, BMC, and FM within the leg, involving smaller amounts of LM relative to BMC and FM, that allows for maximal attenuation of shock following impact. However, the quantification of the effects of each of these tissues, as well as the identification of the optimal ratios required to minimize injury, warrants further investigation.

In the present study, it was found that as BMC, WM, and LM increased, the amount of pain reported by the athletes decreased. Schinkel et al. [1] reported that decreased tissue masses within the shank tended to be associated with increased acceleration responses at the tibia following simulated running impacts, while Milner et al. [2] found that a group of runners with stress fractures experienced greater tibial accelerations than their uninjured counterparts. These associations may assist in explaining the negative relationship between pain and leg tissue masses. These findings agree with previous work in which athletes with pain from medial tibial stress syndrome were found to have a lower tibial bone mineral density (BMD) than a control group [5]. Additionally, Bennell et al. [6] found that stress fracture cases had less LM in the lower extremity, which parallels the negative relationship between leg LM and pain observed in the present study.

CONCLUSIONS

The results of this study provide insight into the relationships between leg tissue masses and lower extremity pain and injuries in varsity soccer players. A better understanding of the tissue composition of individuals prior to engaging in sport and physical activity and the relationships that may exist between tissue composition and injury and pain reporting, may allow for preventative measures to be taken that will reduce the risk of injury and discomfort throughout their athletic season.

REFERENCES

1. Schinkel, A et al. *Proceedings of ISB'09,* Cape Town, South Africa, 2009.
2. Milner, CE et al. *Med Sci Sports Exerc 38*, 323-8, 2006.
3. Holmes, J et al. *J Appl Biomech 21*, 371-82, 2005.
4. Burkhart, TA et al. *J Biomech 41*, 1604-10, 2008.
5. Magnusson, HI et al. *Am J Sports Med 29*, 712-5, 2001.
6. Bennell, KL et al. *Am J Sports Med 24*, 810-8, 1996.

ACKNOWLEDGEMENTS

Thanks to NSERC for funding and to Robyn Bertram, Kathy Harvie, and David Stoute for their help with data collection.

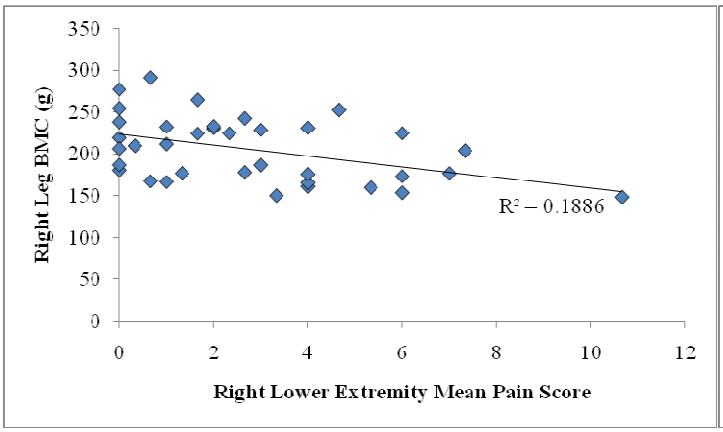

Figure 1: Relationship between the mean pain scores in the right lower extremity and the mean right leg BMC across the three testing sessions (r=0.434; p<0.05).

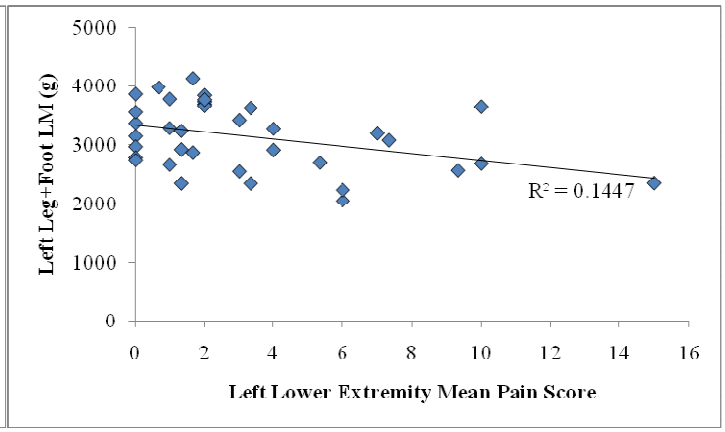

Figure 2: Relationship between the mean pain scores in the left lower extremity and the mean left leg+foot LM across the three testing sessions (r=0.380; p<0.05).

FREQUENCY RESPONSE OF THE WRIST AND ELBOW FOLLOWING IMPACTS WITH AND WITHOUT WRIST GUARDS

Timothy A. Burkhart and David M. Andrews

University of Windsor, Windsor, ON, Canada
email: burkha3@uwindsor.ca, web: http://www.uwindsor.ca/hk/biomechanics-and-ergonomics

INTRODUCTION

Despite their potential as an injury prevention mechanism, there is little agreement as to the efficacy of wrist guards in preventing injuries to the forearm. For a wrist guard to be effective at preventing impact-related injuries, it must be able to delay the peak force and be a source of energy storage and redirection [1], most commonly through a rigid volar structure.

To date, studies on wrist protective devices have generally included an analysis of the initial impact forces only and have ignored the effect of the shock wave on more proximal anatomical structures. Furthermore, quantification of the frequency response of the upper extremity to impact has also been limited to the impact forces or has focused on the soft tissues only; little is known regarding the response of the underlying bone.

Therefore, the purpose of this study was to quantify the frequency response of the radius (at the wrist) and ulna (at the elbow) following impacts simulating forward falls, with and without wrist guards in place.

METHODS

A seated human pendulum apparatus [2] was used to simulate the flight and impact phases of a forward fall such that the extended upper extremities of 28 healthy university aged subjects (15 male, 13 female) impacted two vertically mounted force plates. Impacts were executed while wearing an off-the-shelf wrist guard (Firefly Sport Line, model number: 065627) at a velocity of approximately 1 m/s and a force of 0.5 BW.

A skin-mounted accelerometer (MMA1213D and MMA3201D, Freescale Semiconductor, Inc, Ottawa ON, Canada) was firmly attached to the radial styloid process (representative of the wrist) and the olecranon process (representative of the elbow), to measure the effects of the impact force as it traveled through the forearm. Accelerations were measured in the axial (parallel with the long axis of the forearm) and off-axis (normal to the long axis of the forearm in the sagital plane) directions.

The force and acceleration signals were subjected to a Fast Fourier Transform (FFT) to determine the power spectrum of the respective signals. The mean power frequency (MnPF) and the peak frequency (PF) between 10-30 Hz were calculated. All signals were sampled at 4096 Hz and filtered with a 4^{th} order low pass Butterworth filter with a 100 Hz cut-off. All data collection and signal processing were performed with a custom LabView program.

RESULTS and DISCUSSION

The mean MnPF and PF of the axial acceleration responses following impact ranged from approximately 25 Hz to 28Hz for the elbow and wrist, respectively, and between 14Hz and 15Hz for the wrist and elbow (Table 1). The frequency response at the wrist was greater in the off-axis direction with mean MnPF and PF values of approximately 31Hz and 18Hz, respectively. However, at the elbow, the mean MnPF in the off-axis direction was nearly 20% less than the axial response. The mean PF values in the axial and off-axis directions were comparable (Table 1).

The MnPF of the input force decreased by 33% between the unguarded and guarded conditions, while the PF increased significantly from 11.3Hz to 12.5Hz. Similarly, the MnPF of the wrist axial, wrist off-axis and elbow off-axis acceleration

responses also decreased significantly during the wrist guard conditions.

The use of a wrist guard lead to an increase in the axial PF at the wrist and elbow; only significantly at the elbow (Figure 1). Conversely, the PF in the off-axis direction decreased significantly at both the wrist and elbow when the wrist guard was worn (Figure 1).

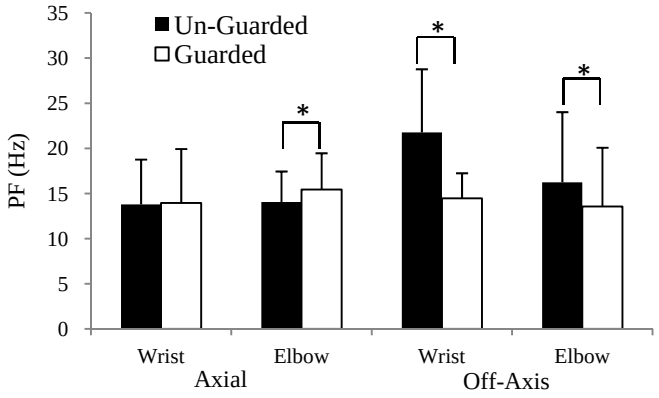

Figure 1: Comparison of PF in the axial and off-axis direction at the wrist and elbow (*p<0.05).

The PFs measured in this study correspond well with values from soft tissue vibrations determined by accelerometers in the lower extremity [3]. However, the MnPFs reported here are higher than the 15Hz found for the lower extremity [4], with respect to bone vibrations.

As a protective mechanism, wrist guards should adequately decrease the magnitude of the forces experienced at the susceptible structures (i.e. dissipation of energy) and increase the time to peak loads applied through the wrist. This, theoretically, should be indicated in the frequency spectrum as a decrease in the MnPF and a shift in the PF to lower frequencies. The results suggest that the wrist guard tested in this study was capable of effectively attenuating the off-axis forces only, as both the MnPF and the PF decreased in the off-axis direction at the wrist and elbow.

The mechanism behind the off-axis decreases may be a result of the shunting of the forces along the rigid volar splint, or as a result of changes in wrist angle at impact when the wrist guard is worn (i.e. eliminating excessive wrist extension).

The results presented here suggest that the design of the wrist guard tested may be effective in attenuating the higher frequency response of the bone in the off-axis direction only. Modifications to the current design of, and materials used in, the volar splints need to be made in order to provide a better attenuating effect along the length of the forearm.

REFERENCES

1. Hwang IK. et al. *J Biomech Eng* **128,** 229-234, 2006.
2. Burkhart TA and Andrews DM. *J Appl Biomech* in press
3. Pain MTG and Challis JH. *J Appl Biomech* **18,** 231-242, 2002.
4. Lafortune MA et al. *J Biomech* **28**, 989-993, 1995.

ACKNOWLEDGEMENTS

Thanks to NSERC for funding this project and Don Clarke for his technical assistance.

Table 1: Overall means and SDs of the MnPF and PF for the force, and acceleration responses.

		Axial Acceleration		Off-Axis Acceleration	
	Impact Force	Wrist	Elbow	Wrist	Elbow
MnPF (Hz)					
Mean	7.66	28.18	24.85	31.89	20.02
SD	2.85	5.46	3.7	4.89	7.13
PF (Hz)					
Mean	11.88	13.87	14.75	18.11	14.90
SD	1.53	2.17	2.11	2.94	2.43

EFFECTS OF EQUINE RACETRACK SURFACE TYPE, DEPTH, AND CONFINING AREA ON FORCE AND DISPLACEMENT MEASUREMENTS USING A TRACK-TESTING DEVICE

[1]Jacob J. Setterbo, [2]Akihiro Yamaguchi, [1]Mont Hubbard, [1]Shrinivasa K. Upadhyaya and [1]Susan M. Stover

[1]University of California, Davis, CA, USA
[2]Tokyo University of Agriculture and Technology, Tokyo, Japan
email: jjsetterbo@ucdavis.edu, web: http://biosport.ucdavis.edu/research-projects/biomechanical-evaluation-of-thoroughbred-racehorse-track-surfaces/setterbo-homepage

INTRODUCTION

Injuries and fatalities are a major problem in the Thoroughbred racehorse industry. Although racetrack surface is considered one of the risk factors, epidemiological results have been mixed [1]. In an attempt to improve the safety of racehorses in the US, several traditional dirt surfaces have been replaced with multimillion dollar synthetic, or all-weather, track surfaces. These synthetic surfaces are purported to be "kinder" to the horses, but because they are relatively new, their dynamic properties are not fully understood.

Recently there have been studies comparing dirt and synthetic surfaces with instrumented horses [2,3], and track-testing devices have been used to examine dirt surfaces [4,5], but to date there are no published studies comparing the dynamic properties of dirt and synthetic surfaces with a repeatable impact device. A laboratory system consisting of a track-testing device and a large laboratory box to contain track surfaces has been developed. The purpose of this study was to assess the effects of equine racetrack surface type, depth, and confining area on force and displacement measurements using a track-testing device in a controlled laboratory environment.

METHODS

A modified track-testing device (TTD) [4] was used to measure the forces and displacement during impact into a dirt and synthetic surface contained within the laboratory box. The TTD consisted of a 27.8 kg mass with a 5" diameter impacting piece which was dropped 12" to impact the surface below. The laboratory box had inner dimensions of 42"x42"x30". The bottom 20" of the box was constructed to replicate the subsurface of a synthetic surface. Combinations of 2 types of racetrack surface (dirt and synthetic), 3 depths (approximately 3.7", 5.4" and 7.2") and 3 rigid confining areas (12"x12", 32"x32", and 42"x42") were tested in a completely randomized order. The depths were constructed within each confining area using a consistent compaction method. A total of 36 trials were performed. The peak force, load rate, force duration, maximum deformation, and percent of energy returned were extracted from the data using custom software (MATLAB, The MathWorks Inc, Natick, Mass.). The effects of surface type, depth, and confining area on measured impact values were compared using analysis of variance (α=0.05).

RESULTS AND DISCUSSION

Surface type, depth and confining area all had a significant effect ($p<0.05$) on the measured impact values. The moisture content (% by mass) of the dirt and synthetic surface was 9.2 ± 0.2% and 5.7 ± 0.3%, respectively. Surface type greatly influenced the results; the dirt and synthetic surface were significantly different for all impact values considered ($p<0.05$) Similar to instrumented horse studies [2,3], the peak force and load rate for the synthetic surface were smaller than that for the dirt surface: the synthetic surface peak force (4,575 ± 873 N) and load rate (372,615 ± 111,749 N/s) were only 55% and 29%, respectively, of the dirt surface peak force (8,271 ± 1,708 N) and load rate (1,276,173 ± 366,226 N/s). These lower peak forces and load rates may be safer for the horse, as one study showed a positive correlation between the occurrence of lameness and peak forces measured

by an impact device [6]. The force duration and maximum deformation for the synthetic surface were each nearly twice as large as that for the dirt surface. The longer force duration and larger deformation suggest that the synthetic surface is more pliable than the dirt surface at this compaction level. The percent of energy returned for the synthetic surface (3.5 ± 0.6%) was more than 180% greater than that for the dirt surface (1.9 ± 0.5%). This result suggests the synthetic surface is more elastic than the dirt surface and likely returns more energy to the hoof.

Depth and confining area also significantly affected the results. For all impact values considered, the 3.7" depth was significantly different than the 7.2" depth, but the 5.4" depth was not always significantly different than the other two. These results suggest that the 5.4" depth is not yet deep enough to eliminate the effects of the subsurface. For all impact values considered, the 12"x12" confining area was significantly different from both the 32"x32" and 42"x42" confining areas, which were not significantly different from each other. Thus, the 42"x42" laboratory box is sufficiently large to not affect impact values for this type of impact testing.

CONCLUSIONS

The results of this study suggest the synthetic surface has mostly favorable characteristics compared to the dirt surface for this compaction level. These favorable characteristics for the synthetic surface include a much lower peak force and load rate as well as a longer force duration, a larger maximum deformation, and a larger percent of energy returned. The depth and confining area results provide information on the effects of the laboratory box boundaries, and specifically indicate the box is sufficiently wide enough for similar impact testing. However, note that the compaction levels in this study do not quite simulate the compaction conditions of the tracks, and only one synthetic surface and one dirt surface were considered.

REFERENCES

1. Stover, S. M. (2003). *Clin Tech Equine Pract*, **2**(4), 312-322.
2. Setterbo, J. J. et al. (2009). *Am J Vet Res*, **70**(10), 1220-1229.
3. Robin, D. et al. (2009). *Equine Vet J*, **41**(3), 253-256.
4. Ratzlaff, M. H. et al. (1997). *J Equine Vet Sci*, **17**(1), 35-42.
5. Peterson, M. L., & McIlwraith, C. W. (2008). *Equine Vet J*, **40**(6), 602-605.
6. Cheney, J. A. et al. (1973). *Am J Vet Res*, **34**(10), 1285-1289.

ACKNOWLEDGEMENTS

Supported by grants from the Grayson-Jockey Club Research Foundation, the Southern California Equine Foundation, and the Center for Equine Health with funds provided by the State of California pari-mutuel fund and contributions by private donors.

CONTRIBUTION OF TRUNK AND PELVIS ROTATION TO PUNCHING IN BOXING

[1]Silvia Cabral, [1]Filipa João, [1] Sandra Amado, [1]António Veloso

[1]Neuromechanics of the Human Movement Group
[1]Faculty of Human Kinetics, Technical University of Lisbon, Lisbon, Portugal
email: scabral@fmh.utl.pt, web: http://www.fmh.utl.pt

INTRODUCTION

Sports involving throwing, striking and kicking activities, such as tennis, squash, baseball, football, among others, demand the production of maximum speed at the end of the distal segment in a kinematic chain. Research done on the biomechanics of these various, yet somehow similar sporting techniques, suggests that athletes generate large hand and foot speeds as a result of a proximal-to-distal sequencing motion. In other words, motion initiates in the larger, heavier proximal body segments and, as the energy increases, proceeds outward to the smaller, lighter distal segments (1). The way in which these mechanics are associated with distal end maximal speeds can be explained by Bunn's "summation of speed principle" (3). As the name suggests, this principal states that each succeeding segment initiates motion at the time of maximum speed of its proximal segment, generating higher distal end-point speeds than the latter.

Proximal-to-distal sequences have been reported in several sports. Woo and Chapman (2) found a proximal to distal sequence of peak linear and angular velocities from the trunk to the wrist, in a squash forehand stroke. The authors observed that these velocities increased progressively throughout the kinematic chain.

The kinematics of a squash forehand are fairly similar to those of a forehand in tennis, baseball pitching, and even to those of an uppercut punch in boxing. However, to the authors' knowledge, the existence of a proximal to distal sequencing in boxing has not been reported in literature. Furthermore, the few studies performed on the biomechanics of boxing are focused on the quantitative analysis of punching (force and speed generated) and its relation to head injuries, rather than the punching technique.

With this in mind, the purpose of this study is to investigate the existence of a proximal to distal sequence in boxing, through the 3D kinematic analysis of the uppercut. The author hypothesises that boxers also produce a proximal to distal sequencing motion in order to generate large hand speeds.

METHODS

This investigation represents a case study of a European champion in full contact boxing (26 yrs, 1.67m, 64Kg). The athlete performed 6 uppercut punches in total, 3 with each arm, all in the same stance (right leg leading). The motion was captured with a system of 9 infrared cameras (Qualisys Oqus 300, Qualisys AB, Gothenburg, Sweden), at a frequency of 200Hz, using Qualisys Track Manager (Version 2.2, Qualisys AB, Gothenburg, Sweden). Kinematic data, particularly the absolute angular velocities of the trunk, pelvis, and punching upperarm as well as the angle formed between the first two segments were computed in Visual 3D (Version 4.75.13, C-Motion, Inc, Rockville, USA), following an x-y-z Cardan sequence.

RESULTS AND DISCUSSION

The kinematic analysis of the uppercut technique showed that the proximal to distal sequencing, characteristic from kicking, throwing and striking activities is also used in boxing, to generate high hand speeds. As will be explained, this motion is highlighted in the acceleration phase of the uppercut, which comprises the acceleration of the segments towards the target, up to the instant of impact. During this phase, considering the segments' kinematics, there seems to be a temporal dissociation of the active muscles – the muscles of the distal segments act after those of the respective

proximal segments – which causes the body to accelerate towards the target in a twisting motion, that starts in the lower limbs and proceeds distally, through the pelvis, trunk and arms, similarly to what has been reported in literature (1). This proximal to distal twisting motion can be observed in Fig 1, in terms of the axial rotation, as the pelvis begins to rotate towards the target ($11.59^{o}.s^{-1} \pm 50.88$), while the trunk is still rotating in the opposite direction ($-125.09^{o}.s^{-1} \pm 49.16$), forming a maximum intersegmental angle of $41.42^{o} \pm 2.16$, in the right uppercut, and $23.80^{o} \pm 1.48$, in the left. The difference in angles is due to the athlete's stance, as he performed both punches with the right leg leading.

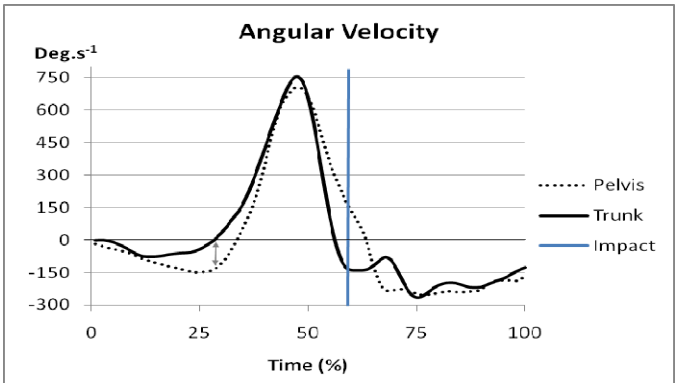

Figure 1: Axial angular rotation of the pelvis and trunk during a right uppercut. This graph represents the mean values of 3 right uppercuts, normalized in time.

As a result of the twisting motion, the trunk and shoulder muscles are forced to stretch just before they contract, thus generating elastic energy that will potentiate the contraction. Furthermore, by stretching immediately before contracting, the muscle contraction could greatly benefit from the stretch reflex. In addition, during the acceleration phase, the trunk not only rotates around the longitudinal axis, but also rotates around the antero-posterior and medio-lateral axes, producing a combination of extension and lateral flexion towards the side of the punch. This motion possibly induces the trunk muscles to stretch even more, thus further increasing their contribution to the punching force/velocity.

In line with Bunn's "summation of speed principle", this proximal to distal twisting motion is a major contributing factor in the production of high hand speeds, as can be observed in fig. 2 with the subsequent, increasing peaks in the angular velocities of the pelvis ($765.19^{o}.s^{-1} \pm 29.49$), trunk ($866.69^{o}.s^{-1} \pm 42.54$) and arm ($1404.58^{o}.s^{-1} \pm 102.23$ for the right arm), respectively.

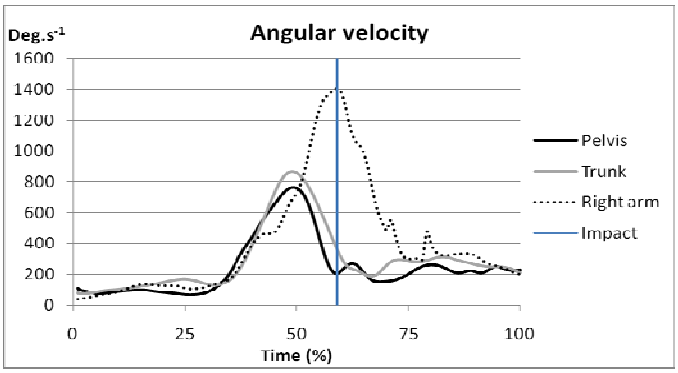

Figure 2: Pelvis, trunk and right arm angular velocities during the right uppercut. This graph represents the mean values of 3 right uppercuts, normalized in time.

CONCLUSIONS

As the authors hypothesised, the proximal to distal sequencing characteristic of striking and throwing activities, such as tennis, squash and baseball, among others, is also present in boxing.

In the particular case of an uppercut, the proximal to distal twisting motion contributed to the subsequent increase in the angular velocity of the pelvis, trunk and arm, as previously suggested by the summation of speed principle. Future research should focus in the development of a biomechanical model that includes the trunk and shoulder muscles, and in the analysis of the electromyographic activity of these muscles, in order to validate the model and provide a better understanding of the use of elastic energy and stretch reflex in this proximal to distal sequence.

REFERENCES

1.Marshal RM and Elliott BC. *J Sports Sciences* **18**, 247-254, 1999.

2.Woo H and Chapman AE. *Proceedings of the 8th Biennial Conference*, Canadian Society of Biomechanics, 1994.

3.Bunn J. *Scientific Principles of Coaching*, Englewood Cliffs, NJ: Prentice-Hall, 1972.

REGULATION OF ANGULAR IMPULSE DURING GOLF SWINGS WITH DIFFERENT CLUBS

J. L. McNitt-Gray [1,2,3], P. S. Requejo[5,2], and H. Flashner [4],
[1]Department of Biomedical Engineering, [2]Kinesiology, [3]Biological Sciences
[4]Aerospace and Mechanical Engineering, University of Southern California, Los Angeles, CA
[5]Rehabilitation Engineering, Rancho Los Amigos National Rehabilitation Center, Downey, CA
E-mail: mcnitt@usc.edu

INTRODUCTION

Regulation of linear and angular momentum during well-practiced goal-directed movements involves control of the total body center of mass trajectory (CM) in relation to the reaction forces generated during contact with the environment[1]. During the golf swing, the resultant horizontal component of the reaction force (RFh) at each foot creates a moment about a vertical axis passing through the CM that accelerates rotation of the body toward the target. Prior to the initiation of the down swing, this force couple applied to the body is created by the posterior directed RFh applied to the target foot (left foot in right handed players) and the anterior directed RFh applied to the rear foot (right foot)[2]. Generation of linear momentum in the direction of the target has been associated with the "shift in weight" from the rear leg to the target leg during the downswing[3,4], all while maintaining the CM trajectory within the base of support. Temporal sequencing of RFs generated by the same player using different clubs (driver vs irons) has been reported to be consistent within player[2]; However, magnitudes of the vertical and anterior posterior components of the target leg RF were reported to be higher than when using a driver as compared to an iron [2].

During competition, players are permitted to use a limited number of clubs that vary in mechanical properties (e.g. shaft stiffness, club length, clubface angle, mass distribution etc.). Sometimes, a player needs to place a ball at a distance that falls into the gap between two clubs and must decide whether to push the distance on one club (e.g. 7 iron) or reduce distance on the other (e.g. 6 iron). In this study, we used a within-subject design to determine if the target and rear foot RFhs and moments are modified when attempting to regulate ball distance using the We hypothesized that the target and rear foot RFh magnitudes and corresponding moments about the CM orientation would differ when attempting to vary ball distance and that the orientation of the RFh in relation to pin at the time of force modulation would remain the same.

METHODS

Skilled golfers (n=12; handicap < 5) were asked to participate in accordance with the institutional review board for human subjects. Reaction forces at the artificial turf-plate interface were quantified during each swing using dual force plates (Kistler, 1200 HZ). Kinematics of the body during the golf swing was captured at 110 Hz using reflective markers (MATT, Motion Reality, Inc.). Ball contact was synchronized at the time of ball contact using a microphone signal sampled along with the force-time data. Each player performed the golf swing by placing one foot on each plate using their normal address and hit a golf ball toward a target ("pin") located behind a net. Each player repeated the swing four times as they would normally (N) and then four times as if attempting to either increase (+) (driver, 6 iron; TaylorMade-adidas Golf) or decrease (-) the distance (6 iron) to "fill the gap" between their clubs. Moments generated by the target and rear leg RFs about the CM were calculated from the cross product of the position vector from the CM to the center of pressure of the rear and the target legs and the resultant horizontal reaction force (RFh) measured for each foot. Moments generated by each foot were used to determine within player differences in kinematics, RF and moment generation between clubs and across attempted distances (-,N,+).

RESULTS AND DISCUSSION

As expected, moments created about the anterior-posterior and mediolateral axes passing through the CM acted in opposition to each other; Whereas, the moments created by the RFh about the vertical axis summed together to create a resultant moment toward target (Figures 1, 2).

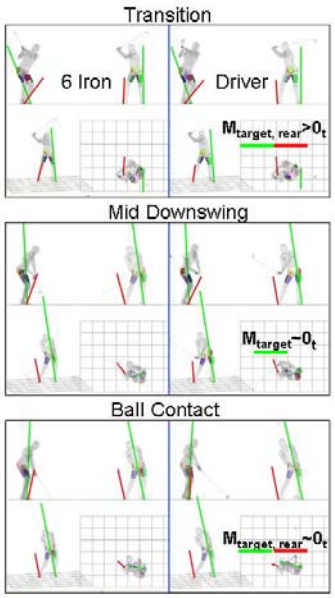

Figure 1. Target (green) and rear (red) foot reaction forces during the downswing for an exemplar player using a 6 Iron and a Driver.

Regulation of the moment generated by RFh about the CM was modulated primarily by increasing or decreasing the magnitude of the resultant horizontal reaction force (Figure 2). Each player elected to modify the reaction force between club and distance conditions, keeping the orientation of the RFh in during the period of force modulation the same within player (Figure 3).

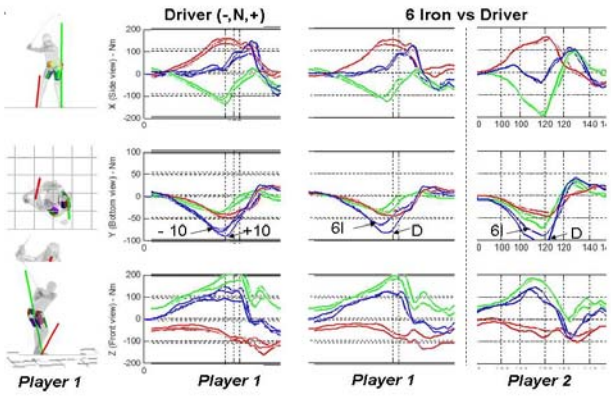

Figure 2. Comparison of moments about the mediolateral (bottom), anterior posterior (top), and vertical axis (middle) axes within and between clubs for two players. Moment-time characteristics are player specific, modulation of the net moment (blue) magnitude occurs during the same interval and may involve contributions from both feet.

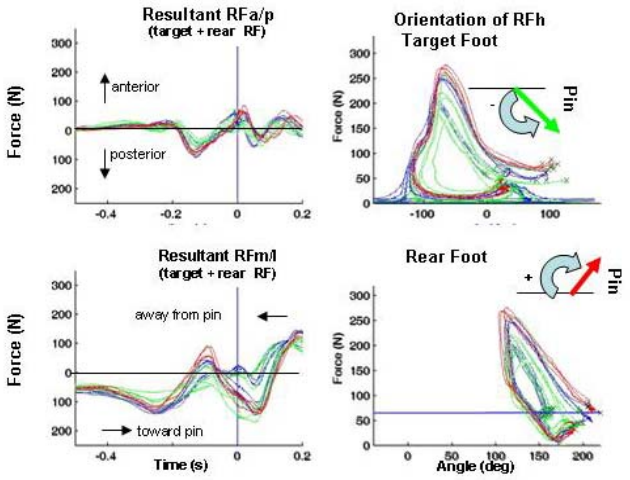

Figure 3. Modulation of resultant reaction forces acting on both feet when using the driver (- (green), Normal (blue), + (red) distances) was greater in the mediolateral component of the RFh (toward (+)/away from target) than the RFha/p. The modulation in RFh magnitude for each foot also occurred over the same range of angles across distances (-, N,+). Comparison of the blue curves indicates larger RFh forces were greater for the driver as compared to the 6-iron under normal (blue) conditions.

CONCLUSIONS

Subtle yet consistent regulation of angular impulse was observed within player across clubs and distances. These changes in control between task conditions were observed as deviations from the remarkably consistent [2] force-time characteristics of each foot under normal conditions. Regulation of angular impulse by amplification of the reaction force while maintaining player-specific orientation of the reaction force relative to the pin may prove advantageous from both a muscle coordination and performance point of view.

REFERENCES

1. Mathiyakom W, et al. *J. Biomech*, **39**, 990-1000, 2006.
2. Williams, K. & Cavanagh, P.R. *MSSE* 15(3), 247-255, 1983.
3. Ball, KA & Best, RJ. *J Sports Sci* 25(7), 757-779, 2007.
4. Hellstrom, J. (Review; 2009), *Sports Medicine* 39(9), 723-741, 2009.

ACKNOWLEDGEMENTS partial funding for this research was provided by TaylorMade-adidas Golf. The authors thank David Anderson and Ian Wright for discussions and suggestions during this project.

A FRAMEWORK FOR MEASUREMENT AND MODELING OF HUMAN CLIMBING

Shawn D. Russell, Chris A. Zirker, and Silvia S. Blemker

Multiscale Muscle Mechanics Lab
Department of Mechanical and Aerospace Engineering
University of Virginia, Charlottesville, VA, USA
email: sdr2n@virginia.edu, web: http://www.mae.virginia.edu/muscle/

INTRODUCTION

The human musculoskeletal system is configured primarily for stable and efficient locomotion based on bipedal gait patterns. However we are often tasked with motion or postures for which the body is not optimized, such as climbing. Human climbing is a task that requires vertical motion and incorporates all four limbs in coordinated trajectories.

Rock climbing is a popular sport that clearly benefits from expertise and ability; however, there is limited knowledge of the kinematics and kinetics of climbing. For example, how much work must be done by muscles to propel the body upward? How is this work distributed between the upper and lower extremities? How do differing climbing strategies (i.e. varying grip width, step height, and hand posture) and climbing experience affect work done? The goal of this project was to create an experimental and inverse dynamics modeling paradigm to analyze human climbing and answer these questions.

METHODS

Three experienced (Yosemite decimal system grade 5.12+) and three inexperienced climbers were asked to climb a wall instrumented with six force plates (Fig. 1). Three climbing strategies were investigated, varying: grip width, step height, and hand/forearm posture. Climbers were directed to climb up and down a minimum of three times per trial. During each trial kinematics, force plate (wall reactions), and electromyography (EMG muscle activation) data were collected. Analysis focused on quantifying the effects of each climbing strategy on, developed forces at the wall, joint torques, and work done per distance traveled.

For each climbing subject a 19 segment 18 joint 44 degree of freedom patient specific model (Fig. 1) was created in MSC.Adams, using the LifeMod plug-in (Biomechanics Research Group San Clemente, CA), from individual anthropometric data (age, weight, height, and gender) using the Generator of Body Data (GeBOD) database [1].

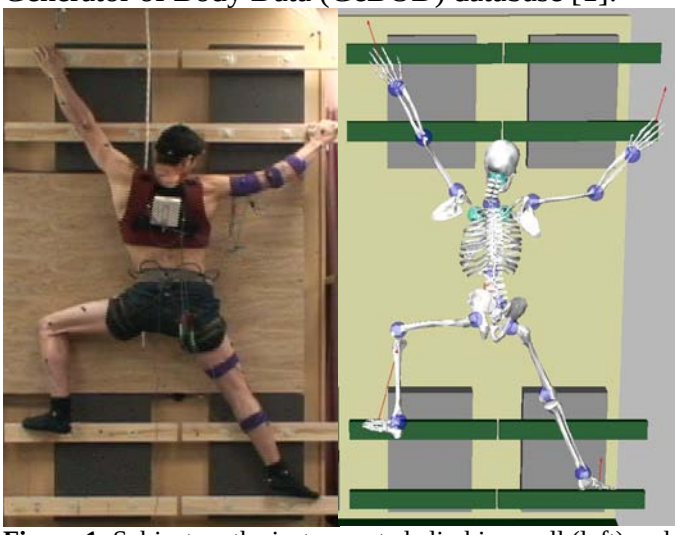

Figure 1: Subject on the instrumented climbing wall (left) and model representation (right) of climbing trial (wide grip width trial).

Inverse dynamic analyses were conducted for each trial. Collected motion data was used to drive the model motion for kinematic analysis, and force plate data were then included for full dynamic analysis of the climbing motions. Verification of the model joint torque predictions was performed through the comparison with experimentally collected EMG.

Total body work was calculated as the sum of the work done by each joint over one ascent-descent motion. Work done by each joint was calculated as the sum of the absolute value of the dot product of the joint torque and the incremental rotational displacement over the motion. Similarly external work, defined as the work to move the body center

of mass (CoM), was calculated as the sum of the absolute value of the dot product of the composite wall reaction force and the incremental center of mass displacement over one ascent-descent motion [2].

RESULTS AND DISCUSSION

Comparison of simulated joint torques and collected EMG data confirmed that model predictions were similar to the experimental motion (Fig. 2).

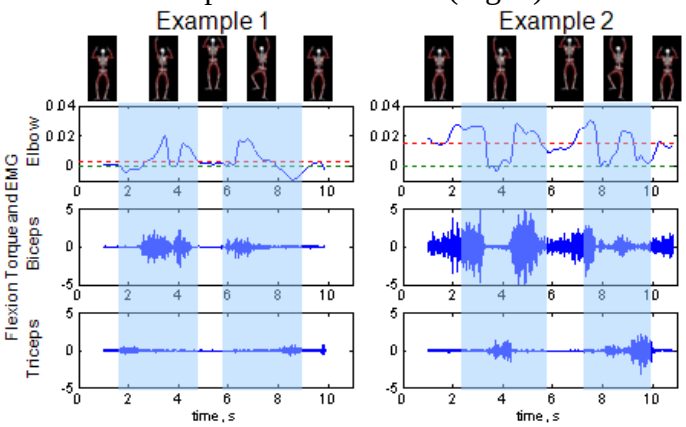

Figure 2: Normalized elbow flexion torque compared with activation levels of the biceps and triceps muscle groups.

In normal climbing subjects when required to step up from a low step to a higher one and back down did 19.7 J/kg-m of total work, more than 10 times more work than required for normal walking 1.5 J/kg-m. Of the total work used in climbing, only 11.1 J/kg-m or 56% is done to move the CoM (external work) with the balance representing work done to move the body segments about the CoM, this is similar to walking where only 52% of the total work contributes to CoM motion.

Varying climbing strategy affected the work done while climbing (Fig. 3). Typically as climbing strategies deviated from a climber's natural climbing technique the work per distance traveled increased. This is seen when varying grip width where increasing the grip width from shoulder width (narrow) to 200% (mid) and 300% shoulder width (wide) resulted in a 32% increase in the work done per climb. Hand posture had a similar effect, straight neutral and externally rotated hand positions had little effect on work done while climbing, internal rotation of the hands however resulted in increased work done in climbing. Surprisingly, a low step height (22.5cm) required more normalized work than either the normal (35cm) or high (45cm) step heights. This is likely due to the normalization with respect to distance traveled. Limb movements for each step height were similar with the short step resulting in the smallest change in center of mass position. Future experiments will add more height variation in an attempt to determine the optimum step height for efficient climbing.

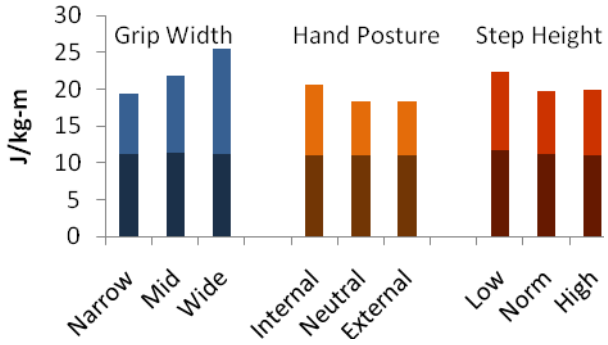

Figure 3: Average normalized work done while using various climbing strategies, shaded region represents contribution of external work.

Comparison of climbing between experienced and inexperienced subjects revealed little difference in the total work done by each group, 20.2 J/kg-m and 19.6 J/kg-m respectively. However the experienced climbers did 22% more work in the lower body joints as compared to the upper body joints. In contrast inexperienced climbers only did 14% more work with their lower body as compared to the upper body. An in depth investigation of these differences has been submitted in Zirker et al [3].

CONCLUSIONS

Climbing represents an abnormal form of locomotion for humans requiring coordinated motion of all four limbs. The framework for measurement and modeling of human climbing presented here provides a unique platform for exploring control strategies of both the upper and lower extremities and their interaction.

REFERENCES

1. Cheng H, et al. *Generator of Body Data (GEBOD) Manual.* Sys Res Lab Inc, Dayton, OH. 1994.
2. Willems P, et al. *J Exp Bio*, **198**, 379-393, 1995.
3. Zirker C, et al. *34th Annual ASB Meeting (Submitted)*, 2010.

ACKNOWLEDGEMENTS

This work was funded by the DARPA (Defense Advanced Research Project Agency) Z-Man project

A KINEMATIC COMPARISON OF THREE DIFFERENT VOLLEYBALL BLOCKING TECHNIQUES

[1, 2]Taubi Neves, [2]Matt Seeley, [2]A. Wayne Johnson and [2]J. William Myrer

[1]Utah State University, Logan, UT, USA; [2]Brigham Young University, Provo, UT, USA
email: wayne_johnson@byu.edu

INTRODUCTION

Effective blocking is strongly correlated to team success in volleyball [1]. The identification of techniques that increase blocking effectiveness is important. Effective blockers are able to quickly: move laterally to prepare for the jump, jump high, and raise their hands high above and over the net [2]. Currently, three common arm swing techniques are used in volleyball blocking: traditional, swing, and chicken wing (Figure 1). Presently, it is not clear what arm swing results in the most effective block. The purpose of this study was to discover which arm swing is most likely to result in the most effective block. Related to this question, we asked four research questions: Which arm swing most effectively minimizes the time that is required to (1) move laterally in preparation for the block, and (2) raise both hands above the net? Also, which arm swing best facilitates the (3) highest vertical jump and (4) greatest magnitude of net penetration? In this context, net penetration was quantified as the distance that the athlete was able to reach above (vertical) and over (anterior-posterior) the net. We hypothesized that: (1) the traditional arm swing would allow the athletes to get off the ground faster and get their hands above the net quicker, followed by the chicken wing and swing technique, and (2) the swing technique would maximize jump height and net penetration, followed by the chicken wing and traditional techniques.

METHODS

Thirteen female collegiate volleyball players gave informed consent and participated in this study (age = 19 ± 1 yrs, height = 182 ± 8 cm, mass = 70.6 ± 8.0 kg). Subjects regularly practiced each technique, in combination with the running step footwork pattern, for 2 weeks until they: (1) were comfortable with each swing, and (2) met an acceptable performance level, as evaluated by the principle investigator. One 14-mm reflective marker was applied to each subject over the distal second metatarsal (outside of the shoe), the sacrum, and the dorsal side of the third proximal phalanx of each hand. Also, one reflective marker was placed on top of each side of a volleyball net set at regulation height. Following a standardized warm-up, high-speed video (250 Hz) was used to track the spatial trajectories of the reflective markers while subjects performed three successful trials using each arm swing in a randomized order. For each trial, subjects lined up in their starting position, facing the net. Upon a signal given by the primary researcher, subjects performed a maximum effort block jump to

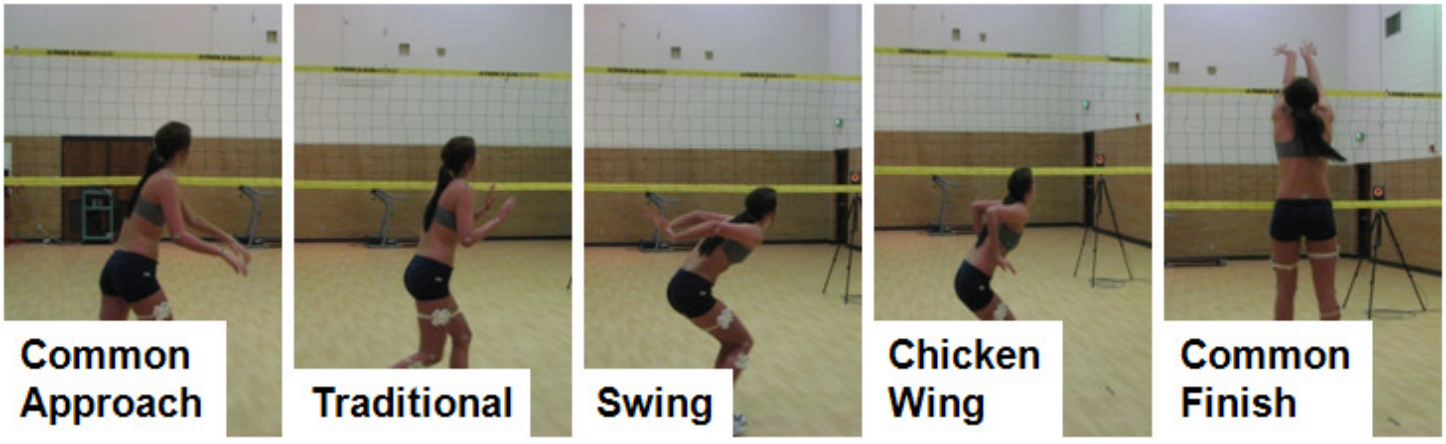

Figure 1. The traditional arm swing involves a relatively stationary arm position. The swing technique involves a typical counterjump motion. The chicken wing technique is a compromise between the other two.

their right using the running step footwork pattern and appropriate arm swing (Figure 1). The spatial coordinates for each marker for each trial were calculated using VICON Nexus. All remaining calculations were performed using custom written algorithms in MatLab. Coordinate data were smoothed using a 4^{th} order Butterworth low-pass filter (10 Hz). The four dependent variables were then calculated: (1) Time to takeoff: duration between initial motion and the instant the subject left the ground; (2) Time to hands above the net: duration between initial motion and the instant that the finger marker was higher than the net markers; (3) Jump height: maximal height of the sacral marker during the jump; and (4) Maximal net penetration, as described in the introduction. Repeated measures ANOVA and Sidaks *post-hoc* comparisons determined the effect of arm swing technique on the dependent variables ($\alpha = 0.05$).

RESULTS AND DISCUSSION

Means and standard deviations for the dependent variables are presented in Table 1. The chicken wing technique resulted in the fastest time to takeoff and time to hands above the net; this technique also resulted in the second largest net penetration and jump height. The swing arm technique resulted in the second fastest time to takeoff and time to hands above the net, as well as the greatest jump height and net penetration. The traditional arm swing resulted in the slowest time to takeoff speed and time to hands above the net, and smallest jump height and net penetration.

The results of this study could help coaches choose the most appropriate arm swing for teams and individual blockers. It appears that the chicken wing is the fastest of the three blocking techniques. The swing technique, however, results in the highest jump height and greatest net penetration. Interestingly, and contrary to our hypothesis, the traditional technique was the least effective as indicated by the results related to every dependent variable. Volleyball players, especially middle blockers, will likely benefit by learning both the swing and chicken wing techniques. If ample time is available, the swing technique would be recommended. If the blocker had to make a quick move, however, the chicken wing technique may be most beneficial.

REFERENCES

1.Lenberg KS. *Coaching Volleyball: Defensive Fundamentals and Techniques* (2 ed.). Coaches Choice, 2004.
2.Buekers MJ. *Res Q Exerc Sport,* **62(2)**, 232-235, 2004.

ACKNOWLEDGEMENTS

The authors acknowledge Eadric Bressel and Gerald Smith for their contributions to the data collection process.

Table 1. Means, standard deviations, and *p* values related to post hoc comparisons made between time to takeoff, time to hands above the net for each hand, jump height, and net penetration for each hand. The independent variables were the three arm swing techniques: traditional (T), swing, (S), and chicken wing (CW).

	T	S	CW	T vs S	T vs CW	S vs CW
Time to Takeoff (s)	1.37 ± 0.12	1.37 ± 0.12	1.37 ± 0.12	0.167	0.054	0.497
Time to Hands Above Net (s)						
Left Hand	1.39± 0.11	1.33 ± 0.11	1.31 ± 0.10	0.005	0.007	0.843
Right Hand	1.38 ± 0.11	1.33 ± 0.11	1.31 ± 0.10	0.02	0.03	0.894
Jump Height (cm)	152.2 ± 5.6	157.3 ± 6.2	155.2 ± 5.9	<0.001	<0.001	<0.001
Net Penetration (cm)						
Left Hand	29.0 ± 6.0	33.8 ± 7.3	30.5 ± 7.2	0.001	0.265	0.069
Right Hand	29.4 ± 5.9	34.5 ± 6.8	31.6 ± 6.8	0.001	0.025	0.045

BIOMECHANICS OF THE CROSS-COUNTRY SIT-SKIER AND IMPACT ON SIT-SKI DESIGN
A TOP SECRET 2010 PROJECT

[1,2,3]Marie-Pierre Leblanc-Lebeau, [1,2]Denis Rancourt, [1,2]Eve Langelier,
[1,2,3]Marc-André Cyr, [1,2]Jean-Luc Lessard and [1,2,3]Cécile Smeesters
[1]Human Performance and Safety Research Group (PERSÉUS), Sherbrooke QC, Canada
[2]Department of Mechanical Engineering, Université de Sherbrooke, Sherbrooke QC, Canada
[3]Research Center on Aging, Sherbrooke QC, Canada
e-mail: Cecile.Smeesters@USherbrooke.ca web: http://eureka.gme.usherb.ca/perseus/

INTRODUCTION

In paralympic cross-country skiing, athletes compete in one of three categories: visually impaired athletes compete with an able-bodied guide and use 2 skis and 2 poles; standing athletes compete using 2 skis and 0, 1 or 2 poles; and sitting athletes compete on a sit-ski with 2 skis and use 2 poles. Even within each category there is a wide range of disabilities, for example, from complete impairment of the lower limbs and minimal trunk muscle activity for LW10 sitting athletes, to only partial impairment of the lower limbs and normal trunk muscle activity for LW12 sitting athletes. Actual race time is thus multiplied by a percentage factor dependent on disability and the skier with the lowest calculated race time within each category is the winner.

Furthermore, disability obviously affects the muscle power produced by the athlete to increase and maintain speed, but for sit-skiers it also uniquely affects their ability to negotiate turns. An LW12 sit-skier can lean toward the inside of a turn to increase the centripetal force and thus avoid tipping over toward the outside of a turn. However, an LW10 sit-skier is physically unable to lean into a turn and can only avoid tipping over toward the outside of a turn by using his outside pole to push himself toward the inside of a turn. Their only other option is to slow down to negotiate turns, which is not the best strategy if they want to win a race.

The completely rigid structure of current sit-ski designs makes negotiating turns especially difficult. Indeed, whether it is because they under-compensated or over-compensated for a turn, sit-skiers will often find themselves precariously balancing on only one ski during turns, narrowly avoiding tipping over toward the outside or the inside of the turn. The purpose of this project was thus to improve sit-ski design to make it more stable and more agile during turns. To do so we studied the effect of adding a tilting mechanism to the sit-ski on maximum allowable turning velocities.

METHODS

So as to better understand the biomechanics of a cross-country skier negotiating a turn on a tilting sit-ski, a simple dynamic model was elaborated (Figure 1). We then determined the effect of centre of mass (h) and center of rotation (h_r) heights, turn radius (r) and lean angle of skier and sit-ski (φ) on the maximum allowable turning velocities (v_{max}).

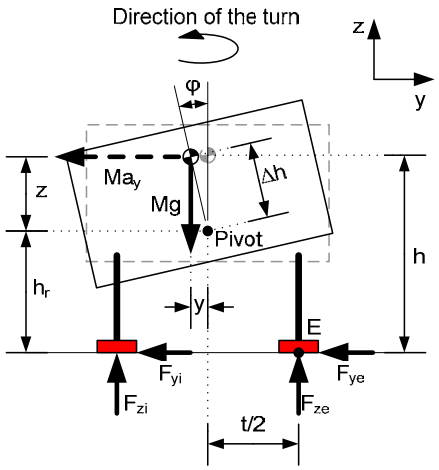

Figure 1: Free body diagram of a cross-country skier negotiating a turn on a tilting sit-ski. Internal (F_{zi} and F_{yi}) and external (F_{ze} and F_{ye}) ski forces, mass of skier and sit-ski (M), gravitational (g) and centripetal (a_y) accelerations, center of mass (h) and center of rotation (h_r) heights, distances between centre of mass and centre of rotation (z, y and Δh), distance between skis (t) and lean angle of skier and sit-ski (φ).

RESULTS

At the limit of stability, the internal ski forces (F_{zi} and F_{yi}) tend to zero and the cross-country skier is about to tip over toward the outside of the turn. Our model then showed that the maximum allowable turning velocity is given by:

$$v_{\max} = \sqrt{rg\,\frac{t/2 + (h - h_r)\sin\phi}{h_r + (h - h_r)\cos\phi}}$$

Our model results showed that:

- Maximum allowable turning velocity (v_{max}) increased if centre of mass height (h) decreased (Figure 2).
- Maximum allowable turning velocity (v_{max}) increased if center of rotation height (h_r) decreased (Figure 3).
- Maximum allowable turning velocity (v_{max}) increased if turn radius (r) increased (Figure 4).
- Maximum allowable turning velocity (v_{max}) increased if lean angle of skier and sit-ski (φ) increased (Figures 2, 3 and 4).

DISCUSSION AND CONCLUSIONS

Therefore, to increase the maximum allowable turning velocity (v_{max}) a sit-ski with a tilting mechanism should have low centre of mass (h) and center of rotation (h_r) heights. This is especially important for tight turns, since the maximum allowable turning velocity (v_{max}) decreases if turn radius (r) decreases (Figure 4).

A tilting sit-ski design would thus allow both skis to remain in contact with the ground when negotiating turns and could allow even LW10 athletes to lean toward the inside of a turn to go faster. In fact, for the tightest turns (r=15m), a lean angle of skier and sit-skier (φ) of only 5 to 10deg could increase maximum allowable turning velocity (v_{max}) by 0.68 to 1.31m/s (Figure 4).

These results were experimentally validated in the field and, to date, have resulted in one silver and one bronze medal at the 2010 Paralympic Games in Vancouver.

ACKNOWLEDGEMENTS

This work was funded by the Own the Podium – Top Secret 2010 program from the Canadian Olympic Committee. We also thank the Canadian paralympic cross-country ski team.

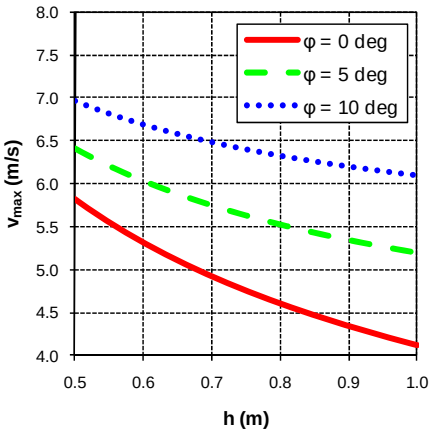

Figure 2: Maximum allowable turning velocity (v_{max}) as a function of center of mass height (h) and lean angle of skier and sit-skier (φ) with r=15m, g=9.81m/s^2, t=0.23m, h_r=0.222m.

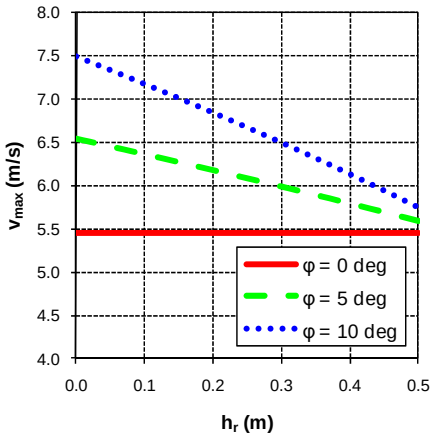

Figure 3: Maximum allowable turning velocity (v_{max}) as a function of center of rotation height (h_r) and lean angle of skier and sit-skier (φ) with r=15m, g=9.81m/s^2, t=0.23m, h=0.569m.

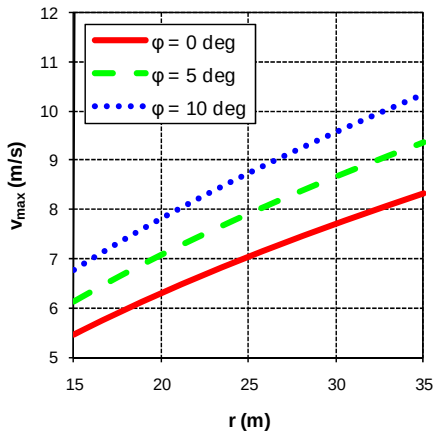

Figure 4: Maximum allowable turning velocity (v_{max}) as a function of turn radius (r) and lean angle of skier and sit-skier (φ) with g=9.81m/s^2, t=0.23m, h=0.569m, h_r=0.222m.

STEADY-STATE HANDLING CHARACTERISITICS OF A BICYCLE

Stephen M. Cain and Noel C. Perkins

University of Michigan, Ann Arbor, MI, USA
email: smcain@umich.edu

INTRODUCTION

Bicycling is a complex task. A bicycle must be stabilized by the human rider for most speeds, and is only self-stable within a limited speed range [1]. Bicycles are designed for both stability and maneuverability and these are competing goals. Extensive research reveals how bicycle parameters affect stability [2] whereas little research has focused on bicycle maneuverability.

To examine maneuverability, we start with the steady-state handling of a vehicle [3]. In particular, one can deduce how the gain or sensitivity of a vehicle output (lateral acceleration) to a vehicle input (steering torque) is affected by vehicle geometry, which has important implications for human control [4,5]. The goal of this study is to develop a parallel steady-state handling model of a bicycle and rider and an instrumented bicycle to test model fidelity.

METHODS

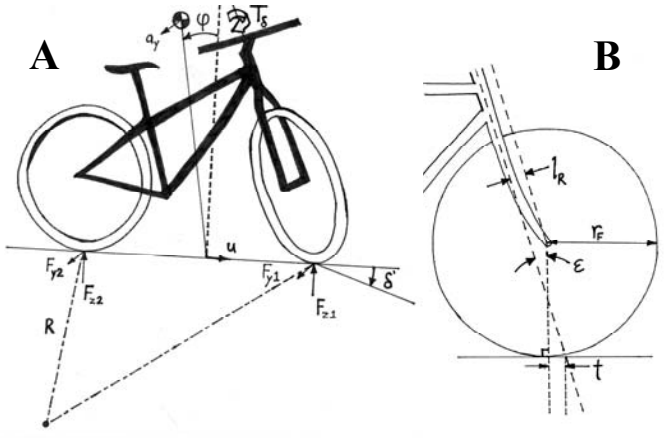

Figure 1: *The bicycle model*. **(A)** A bicycle in steady turning; important parameters are noted and are positive in the direction of the arrows. **(B)** Front end of the bicycle showing geometric dimensions and the relationship between rake (l_R), trail (t), steer axis tilt (ε), and front wheel radius (r_F)

Steady-state handling bicycle model

We develop a steady-state handling model for a bicycle making a turn of constant radius with constant speed. Relative to the dominant forces (lateral tire forces and weight), we neglect air drag, longitudinal tire forces and vertical tire moments. We assume that the turn radius is much larger than the bicycle wheelbase and assume small steer and roll angles. We use the benchmark bicycle parameters [1]. The equations governing steady-state handling are derived from Newton's law in the lateral direction and moment equilibrium about the vertical axis. The tires obey a linear elastic tire model. The relevant results are as follows:

(1) $a_y = \varphi g$

(2) $\zeta = 1 + \frac{C_{F\gamma 1}}{C_{F\alpha 1}} \tan\varepsilon$

(3) $\eta = \frac{F_{z1}}{C_{F\alpha 1}} - \frac{F_{z2}}{C_{F\alpha 2}}$

(4) $R = \frac{1}{\left(\zeta\delta' - \eta\frac{a_y}{g}\right)}$

(5) $u = R\sqrt{\frac{a_y}{R}}$

(6) $t = \frac{(r_F \cos(90° - \varepsilon) - l_R)}{\sin(90° - \varepsilon)}$

(7) $T_\delta = (t\cos\varepsilon)F_{y1} - (t\cos\varepsilon)F_{z1}(\varphi + \delta' \tan\varepsilon)$

a_y = lateral acceleration of COM
φ = roll angle
g = acceleration of gravity
ζ = steer angle coefficient
$C_{F\gamma 1}$ = front tire roll stiffness
$C_{F\alpha 1,2}$ = tire side-slip stiffness
ε = steer axis tilt
η = understeer coefficient
$F_{z1,2}$ = vertical force on tire
R = turn radius
δ' = ground steer angle
u = forward speed
t = trail
r_F = front wheel radius
l_R = rake
T_δ = steering torque

Solutions are found by specifying the lean angle and steer angle and then solving for the resulting lateral acceleration and steer torque. We evaluate results for both idealized (rigid) tire behavior and elastic tire behavior drawing on experimental results [6].

To explore the effects of bicycle geometry, we alter the fork rake as this parameter can also be altered easily on a physical bicycle (Figure 1B). Rake, which determines the location of the front wheel relative to the rest of the bicycle, alters the trail, which has a major effect on both stability [2] and

the maneuverability of the bicycle (equation 7). The fork rake, wheel radius, and steer axis tilt all affect the trail of the bicycle (Figure 1B and equation 6).

Instrumented bicycle

We are nearing the completion of a novel instrumented bicycle. Once complete, the bicycle will be used to validate our steady-state handling model. The instrumented bicycle will allow us to measure steering torque (load cell), steering angle (optical encoder), bicycle lean angle and rider lean angle (3-axis accelerometers), and bicycle speed (magnetic pick-up). At this time, all sensors are functional; only the accelerometers and the speed sensor need to be integrated into the data acquisition system of the instrumented bicycle.

RESULTS AND DISCUSSION

We found that fork rake (through its relationship to trail) has a significant effect on the steady-state turning characteristics of a bicycle. The model predicts that a change in sign of the trail will cause a change in sign of the ratio of lateral acceleration to steer torque (Figure 2). If trail is positive, as on a traditional bicycle, the ratio is negative; this means that during a steady turn, a rider must apply counterclockwise steer torque when negotiating a clockwise turn. If trail is negative, then the ratio is positive; this means that a rider must apply a clockwise steer torque to negotiate a clockwise turn. This has extremely important implications for the control strategy that the human rider must use. Not only can changes in trail be used to change the stability of a bicycle [2], but changes in trail can be used to completely reverse the control strategy that must be used by the rider.

We found that the magnitude of the sensitivity of lateral acceleration to steer torque increases with an increase in bicycle speed and with a decrease in the magnitude of the trail. The inclusion of a linear elastic tire model increases the sensitivity of lateral acceleration to steer torque for a given bicycle geometry.

CONCLUSIONS

Via a simple model for steady-state handling of a bicycle, we show that fork rake (through its relationship to trail) has a pronounced influence on bicycle maneuverability and likely the control strategy that must be employed by the human rider. The influence of fork rake on maneuverability is captured by bicycle models employing either rigid or elastic tire approximation. Future work will focus on using the new instrumented bicycle to validate the above predictions of steady-state turning.

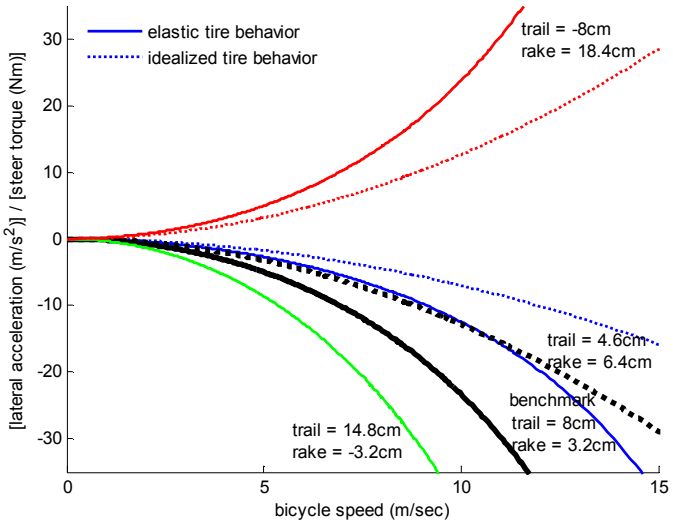

Figure 2: *Sensitivity (ratio of lateral acceleration over steer torque) as a function of speed for different values of rake (and therefore trail).* The results for the benchmark bicycle parameters [1] are noted and shown by the thicker black curve. For reference, most bicyclists travel at speeds between 2.8 m/sec (6.2mph) and 7.8 m/sec (17.4mph) [7].

REFERENCES

1. Meijaard JP, et al. *Proc. R. Soc. A.* **463**, 1955-1982, 2007.
2. Moore J and Hubbard M. *The Engineering of Sport 7* **2**, 311-318, 2008.
3. Cossalter V, et al. *Vehicle System Dynamics* **31**, 157-181, 1999.
4. Weir, DH. PhD thesis. UCLA, 1972.
5. Doyle AJR. *Training, Human Decision Making and Control*, 351-370. Elsevier Science Publishers, 1988.
6. Roland RD. *Mechanics and Sport* ed JL Bleustein, 35-83. ASME, 1973.
7. Allen DP, et al. *Transporation Research Record* **1636**, 29-36, 1998.

ACKNOWLEDGEMENTS

We would like to thank Dexter Bike and Sport for donated and highly discounted parts needed to construct the instrumented bicycle.

VARIATIONS IN CLIMBING STRATEGIES BETWEEN EXPERIENECED AND INEXPERIENCED ROCK CLIMBERS

Christopher A. Zirker, Shawn D. Russell, Silvia S. Blemker

Multiscale Muscle Mechanics Lab
University of Virginia, Charlottesville, VA, USA
email: chriszirker@virginia.edu, web: http://www.mae.virginia.edu/muscle/

INTRODUCTION

Rock climbing has rapidly grown in popularity in recent years and presents unique locomotive challenges not found in other sports. Unlike bipedal walking, the upper extremities contribute to both balance and propulsion during climbing thus increasing the variability in gait patterns. This study compares the vertical gait characteristics of experienced and inexperienced climbers to examine variations in climbing strategy which result in an optimized climbing gait.

Experienced climbers have been shown to perform similar magnitudes of total work as inexperienced climbers during identical climbing tasks [1] but were visibly less fatigued by the same climbing tasks as compared to inexperienced climbers. Experienced climbers were shown to perform a higher percentage of the total work with the lower extremities, suggesting differences exist in locomotive strategies between the groups. The goal of this study was to examine differences in joint angle trajectories and the resulting passive moment-generating characteristics between experienced and inexperienced climbers. We hypothesize that experienced climbers utilize joint angle trajectories that take advantage of passive moments, thus requiring less effort to perform the given climbing task.

METHODS

Three experienced (Yosemite Decimal System grade 5.12+) and three inexperienced healthy adult volunteers climbed on an 8'x8' climbing wall instrumented with force plates. Kinematic data was recorded using motion capture system. A full-body 37-point Vicon Plug-in-Gait marker set was used although the clavicle and sternum markers were obscured. Each subject climbed up and down a minimum of three times.

A full-body musculoskeletal model was used which combines validated upper extremity [2] and lower extremity models [3] incorporating properties of individual muscles, joints and bones (Fig.1). OpenSim [4] was used to scale the model to each subject's anthropometry and perform inverse kinematics using experimentally collected data. These kinematics were then applied to the unscaled model and used to calculate passive muscle moments as described below.

Figure 1: Full-body musculoskeletal model used for calculating muscle lengths and moment generating potential. Experienced climbers (left) maintained a more relaxed posture as compared to inexperienced climbers (right).

Reported joint kinematics and total work were calculated via the LifeMod climbing model [1]; kinematics were similar to OpenSim climbing kinematics. Passive muscle moments as a function of each climbing motion for the medial gastrocnemius, biceps femoris long head and biceps were calculated based on the OpenSim model.

RESULTS AND DISCUSSION

Experienced rock climbers demonstrated decreased elbow flexion, external hip rotation, and plantar flexion compared to inexperienced climbers (Fig.2). Inexperienced climbers tended to keep the torso

close to the wall throughout each climbing gait cycle by externally rotating at the hip, bending at the elbows, and standing on the inside edge of the foot. In contrast, experienced climbers leaned back away from the wall, maintained a slight bend at the elbow, and stood on forefoot (Figs.1 and 2).

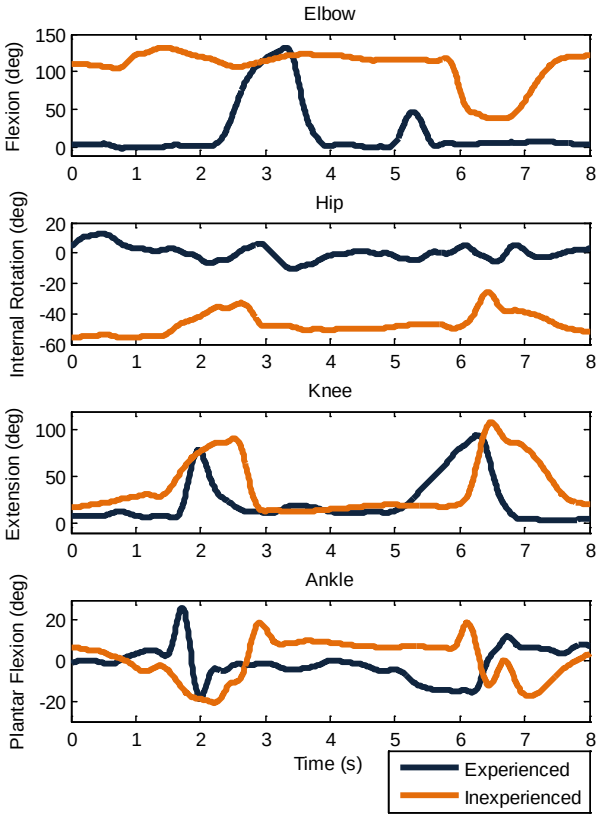

Figure 2: Example of variation in joint kinematics between an experienced and inexperienced climber.

When compared to inexperienced climbers, experienced climbers performed a greater percentage of the total work at the ankle, knee and hip while reducing the work performed at the elbow (Fig.3).

While experienced climbers perform more work with the lower extremities, this work is done more efficiently than by inexperienced climbers. The kinematic climbing model predicted that the experienced climbers would have higher passive muscle moments by 56% at the ankle and 64% at the knee by the gastrocnemius and 96% at the elbow by the biceps (Fig.3). These data support our hypothesis that experienced climbers used body positions that maximized passive moments, which would thus would reduce the effort required for vertical locomotion.

CONCLUSIONS

While experienced climbers have been shown to perform similar total work to inexperienced climbers, experienced subjects demonstrated a climbing strategy which led to increased passive muscle moment generation at joints where greater work was performed. Future work should include analysis of EMG data to estimate active muscle force characteristics and compare co-contraction between muscle groups.

REFERENCES

1.)Russell SD et al., submitted to *34th Annual ASB Meeting*, 2010.

2.)Holzbaur KR et al., *Ann Biomed Eng*. 2005 Jun;33(6):829-40.

3.)Delp SL et al., IEEE *Trans Biomed Eng*. 1990 Aug;37(8):757-67.

4.)Delp SL et al., *IEEE Trans Biomed Eng*. 2007 Nov;54(11):1940-50.

ACKNOWLEDGEMENTS

This work was funded by DARPA (Defense Advanced Research Project Agency).

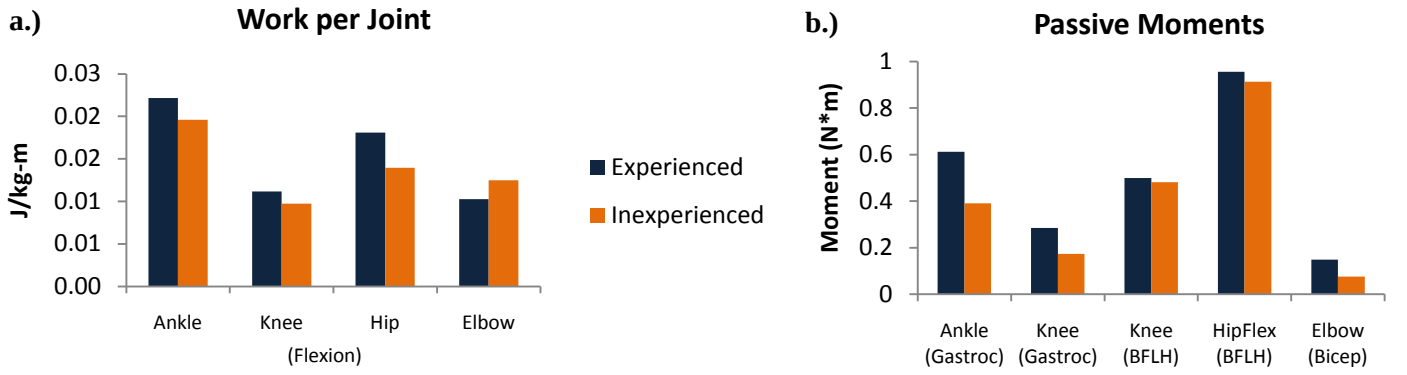

Figure 3: a.) Experienced climbers performed more work at lower extremity joints and less at the elbow when compared to inexperienced climbers. **b.)** Increased passive fiber forces led to higher passive joint moments.

VELOCITY OF THE TAEKWONDO AXE KICK AND RESULTANT LINEAR ACCELERATION OF AN INSTRUMENTED HEAD FORM

[1]Gabriel P. Fife, [1]Thomas W. Kaminski, [2]David O'Sullivan, [3]Willy Pieter, [4]Isshin Shin, [5]Taehee Lim

[1]University of Delaware, Newark, Delaware USA
[2]Seoul National University, Seoul, South Korea
[3]University of Asia and the Pacific, Pasig, Philippines
[4]Seoul National University, Seoul, South Korea
[5]Yongin University, Yongin, South Korea
email: fifeg@udel.edu

INTRODUCTION

The Centers for Disease Control and Prevention refer to concussion as a "silent epidemic" (300,000/year) [1]. In Taekwondo (TKD), concussion incidence is three times greater than in American football [2,5]. To this date a biomechanical analysis of TKD head kicks and head injury outcomes does not exist. The purpose of this investigation was to assess the effect of various kicks on resultant head linear acceleration (RLA), change in head velocity and peak foot velocity of kicks.

METHODS

Two males (22.00±0.0 years, 184±0.0cm, 81.30±1.8 kg) and two females 20.00±2.8 years, 171.0±1.4 cm, 63.00±5.2 kg) elite TKD athletes were recruited for this pilot study. Resultant linear head acceleration (RLA) data were collected from five the axe kick (FA) and clench axe kick (JH) randomly performed five times. A Hybrid II Crash Dummy head (H2D) and neck were instrumented with a tri-axial piezoelectric accelerometer, PCB Piezotronics 356A66 (Depew, New York) mounted at the head center of gravity. The change in head velocity was observed by placing a reflective marker at the apex of the H2D head. The H2D was fixed to a height adjustable frame and fitted with a protective TKD helmet (LeCAF - Seoul, South Korea). Acceleration data were captured at 10,000 Hz using Qualisys Track Manager (Gothenburg, Sweden) and processed in accordance with SAE J211-1. Each subjects' foot was marked with reflective markers at the heel and between the first and second metatarsals to allow for determining peak foot velocities. A Mann-Whitney U test was used to compare the linear velocities of the axe kicks and RLA within men and women. The level of significance was set to 0.05.

RESULTS AND DISCUSSION

Table 1 displays the descriptive statistics of peak foot velocity by type of axe kick as well as RLA. In the men, there was a significant difference in RLA as a result of the kick with the clench axe kick scoring higher ($p = 0.016$, ES = 1.70). In the women, the foot velocity was higher for the clench axe kick ($p = 0.025$, ES = 1.58).

A previous investigation by Viano [4] report kinematics of a Hybrid III Crash Test Dumy head and RLA with a high average head RLA of 71.2g with the hook and a low of 24.1g with the uppercut punch. These values were averaged across all participating weight divisions and only observed head injury characteristics as produced by Olympic male boxers. Our results indicate a mean RLA produced by elite TKD athletes of the head comparable to that of the boxing uppercut. A Previous live competition analysis [3] conclude the axe kick variations are high culprits for concussion in TKD although other kicks are used but not always resulting in concussion.

CONCLUSIONS

As our initial pilot study is the first of its kind to observe head RLA on an instrumented head form and peak foot velocities of kicks it is recommended that future studies include analysis of a larger

subject pool including other kick techniques commonly reported to cause concussion in taekwondo.

REFERENCES

1. Atlanta, GA: Centers for Disease Control and Prevention; 2003.
2. Delaney JS. *Clin J Sports Med.* **12**, 80-70, 2004.
3. Koh JO. Cassidy JD. *Clin J Sports Med.* **14(2)**, 72-79, 2004.
4. Pieter, W. The 2nd International Symposium for Taekwondo Studies, Seoul: Daekyung Books, pp. 110-117.
5. Viano et al. *Neurosurgery*. **57**, 1154-1172, 2005.

ACKNOWLEDGEMENTS

We would like to thank Mike Gratopp of Denton ATD Inc. (Rochester Hills, MI USA) for their contribution in donating the H2D device

Table 1: Linear velocity ($m*s^{-1}$) and magnitude as a function of axe kick in elite taekwondo athletes

Clench axe kick	**Men**	**Women**
Foot velocity ($m*s^{-1}$)	9.70 ± 2.16	9.10 ± 2.33
Head velocity ($m*s^{-1}$)	3.90 ± 1.33	2.93 ± 0.55
Resultant Head Linear Acceleration (g)	33.28 ± 11.09	18.22 ± 4.84
Front axe kick		
Foot velocity ($m*s^{-1}$)	8.48 ± 1.86	6.21 ± 0.98
Head velocity ($m*s^{-1}$)	3.63 ± 1.10	3.11 ± 0.50
Resultant Head Linear Acceleration (g) (g)	20.66 ± 7.03	18.48 ± 7.20

BIOMECHANICAL ENERGETIC ANALYSIS OF PITCHING MOTION OF PROFESSIONAL JAPANESE BASEBALL PITCHERS

[1]Kei Aoki, [1]Masaaki Mochimaru and [2]Ryutaro Himeno

[1]National Institute of Advanced Industrial Science and Technology (AIST), Koto-ku, Tokyo, Japan
[2]Riken, Wako, Saitama, JAPAN
email: aoki-kei@aist.go.jp, web: http://www.dh.aist.go.jp/

INTRODUCTION

Baseball is one of the most popular sports in Japan. According to the census of 2005, the players are more than 9.7 million persons, including about 3 million student players. If these young players keep playing baseball for a long time in their lives, the profitable and long tail effects are expected as follows; (1) healthcare of the players themselves, (2) stimulation of the community to which the players belong, (3) economic boost for the increasing supply of the baseball equipments. These effects also contribute the prosperity of the professional baseball league. For this issue, the players need not only to prevent injury but also to progress or maintain their ability. Especially, a lot of pitchers tend to have a frequent occurrence of injury to throwing arm. Therefore, it is important to clarify the mechanism of the pitching motion of the baseball player who keeps playing baseball for a long time at the forefront of the professional baseball league and has little injury.

Our purpose is to examine the characteristics of pitching motion of a veteran professional Japanese pitcher. The pitching motion was evaluated quantitatively using energy consumption calculated from joint power, and 2 quantitative indices were defined, called "distribution ratio of joint concentric energy" and "pitching efficiency."

METHODS

Two Japanese subjects were examined. One was a 46-year-old veteran pitcher (Subject A, 1.76m, 84.6 kg, left-hander). He had his 28-year professional career and was still an active player. Another pitcher for comparison was a 24-year-old rookie player and had his 2-year professional career (Subject B, 1.82 m, 84.1 kg, right-hander).

Fig. 1 shows our measurement condition. Fifty seven markers were attached on each subject. Pitching motion was measured using motion capture system (VICON Nexus, VICON) including 16 cameras and floor force plates (BP400-600-1000PT, AMTI). Measurement frequency was 250 Hz. A pitcher's mound was flat and a catcher took a catching posture 18.44 m from the pitcher's mound. Subjects pitched a fastball to the catcher just like their usual practices. The velocity of the ball was measured using high-speed camera (MEMRECAM GX-1, NAC Image Technology). The proposal for this study was approved by the Institutional Review Board on ergonomic research, AIST.

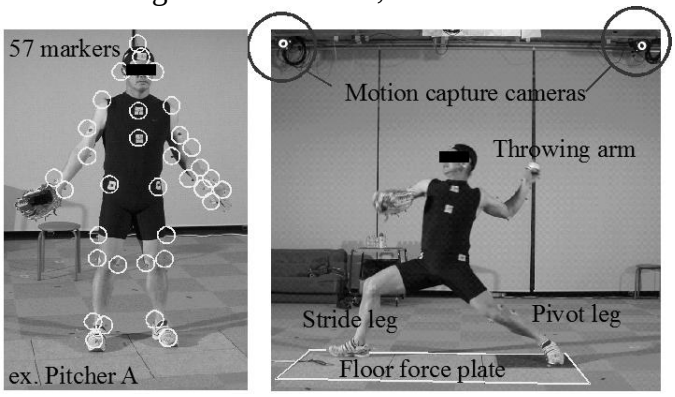

Figure 1: Measurement condition (ex. Subject A).

Measured motion data were analyzed using a 3-D biomechanical rigid segment model (Visual3D, C-Motion). The whole body of the model was divided into head and neck, upper torso, lower torso, right and left upper arms, right and left forearms, right and left hands, right and left thighs, right and left shanks, and right and left feet. Analyzed results were calculated as time-series data of joint angle, joint moment, and joint power. This joint power was integrated into energy consumption. The time-series data were divided into windup phase (WU), early cocking phase (EC), late cocking phase (LC), acceleration phase (AC), and follow-through phase (FT) as shown in Fig. 2. Refer the details to [1].

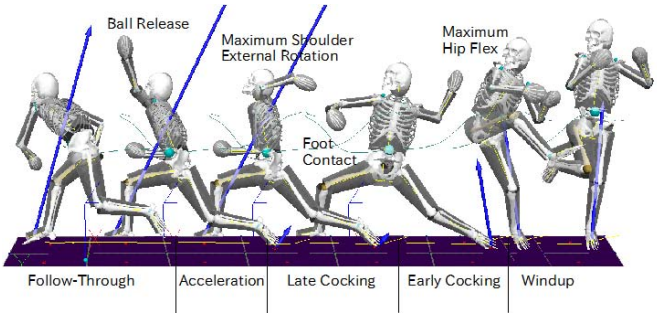

Figure 2: Definition of pitching phase.

In order to analyze the pitching motion using biomechanical energetics, concentric joint energy consumption during EC phase, LC phase and AC phase were calculated, respectively. The concentric joint energy consumption was added up at pivot leg, torso, and throwing arm. Each consumption rate of the sum of the concentric joint energy consumption in the whole body was defined as "distribution ratio of joint concentric energy" (DRE). This ratio means degrees of contribution of each part and/or each phase to acceleration of a ball in the direction of home plate. Furthermore, "pitching efficiency" (PE) was defined as the kinetic energy of a ball per the joint energy consumption of the whole body from EC phase to AC phase. If the ball velocity is larger or the joint energy consumption is lower, the PE is larger. This value means the endurance of pitching.

RESULTS AND DISCUSSION

Fig. 3 shows the representative DRE of subject A and B. The DREs of the pivot leg during EC and LC phase of subject A were higher than those of subject B. Plus, the DRE of the torso during AC phase of subject A was also higher than that of subject B. Reversely, the DRE of the throwing arm during AC phase of subject A was lower than that of subject B. These results indicate that subject A pitches using his whole body better and makes the load of his throwing arm smaller than subject B.

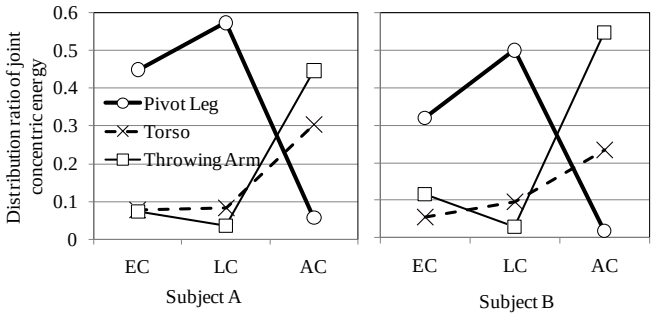

Figure 3: Distribution ratio of joint concentric energy

Table 1 shows the representative PE of both subjects. The PE of the subject A was larger than subject B in spite of his slower ball velocity. This result shows that subject A pitches more efficient than subject B. Fig. 4 shows the breakdown of the energy consumption of the whole body. In Fig. 4, the whole body eccentric joint energy consumption during EC phase of subject A is especially smaller than that of subject B. Reversely, the pivot leg concentric joint energy consumption during EC phase of subject A is larger than that of subject B. These results mean that the body of subject A is pushed out actively with his pivot leg on the pitcher's mound. This action seems to contribute the reduction of the pivot leg concentric joint energy consumption during the next LC phase.

Table 1: Pitching efficiency.

	Subject A	Subject B
Ball velocity [m/s]	33.6	36.9
Ball kinetic energy [J]	79.0	95.3
Whole body energy [J]	918.0	1237.1
Pitching efficiency	0.0861	0.0770

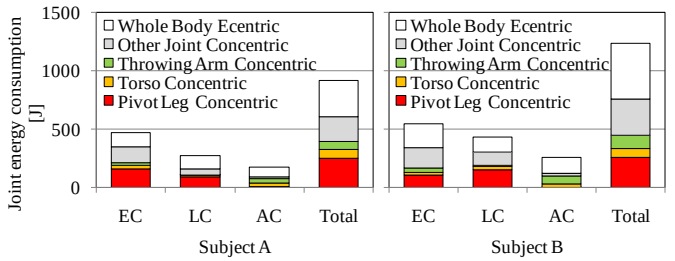

Figure 4: Breakdown of the whole body energy consumption.

CONCLUSIONS

We analyzed pitching motion of a veteran professional Japanese pitcher (subject A) from a viewpoint of biomechanical energetics. As a result, subject A pitches efficiently using his whole body, especially his pivot leg during EC phase well. This motion strategy also seems effective for the prevention of injury to throwing arm. Our future work will be to verify the effect of the strategy, increasing subjects and trials.

REFERENCES

1.Lin HT, et al. *J Chinese Institute of Engineers* **26**, 861-868, 2003.

RELATIONSHIP BETWEEN SACRAL SKIN BLOOD FLOW OSCILLATIONS AND VASODILATORY FUNCTIONS IN PEOPLE AT RISK FOR PRESSURE ULCERS

Yih-Kuen Jan, Fuyuan Liao, David W. Garrison, and Mark A. Anderson
University of Oklahoma Health Sciences Center, Oklahoma City, OK, USA
email: yjan@ouhsc.edu (Dr. Jan), web: http://www.ah.ouhsc.edu/rehab/yih_kuen.asp

INTRODUCTION

The role of microvascular function in the risk for pressure ulcers can be assessed by studying the changes of skin blood flow oscillations (BFO) in response to causative factors of pressure ulcers such as local heating [1]. Previous studies, using either Fourier- or wavelet-based spectral analysis, provide essential contributions to the understanding of the control mechanisms of BFO [2]. Wavelet analysis of skin BFO reveals five characteristic frequencies, associated with endothelial metabolic activities, sympathovagal neurogenic activities, vascular myogenic activities, breathing movements, and heart beats. This method allows clinicians and researchers to non-invasively assess microvascular dysfunction in various pathological populations. However, wavelet analysis is a linear method and cannot characterize the nonlinear properties embedded in BFO of the cardiovascular system. The cardiovascular system is a complex, nonlinear dynamical system, and skin blood flow regulation is therefore a nonlinear process [3].

Nonlinear analyses are currently widely used to evaluate variability and rhythms in physiological signals (e.g. heart rate variability and gait variability) in order to understand the underlying structure of these variations [4]. To date, a decrease of nonlinear behavior of physiological rhythms is considered to be associated with diseases and aging. At this stage, these few studies using some nonlinear analysis of BFO have not established a guideline indicating which analysis methods are appropriate to analyze nonlinear properties of BFO. The purposes of this study were to systemically quantify the nonlinear properties of sacral skin BFO and to explore their relationships with impaired vasodilatory function in people at risk for pressure ulcers.

METHODS

A total of 25 participants were studied. The participant were divided into 3 groups: ten people aged 65-75 years with normal vasodilation (Biphasic Thermal Index (BTI) (5.5, 4.5, 10.1)), ten people aged 75-85 years with slight impaired vasodilation (BTI (3.7, 3.2, 6.7)), and five people with impaired vasodilation (BTI (2.4, 1.7, 4.5)). The degree of microvascular impairment was quantified by the Biphasic Thermal Index (BTI) [2]. The Biphasic Thermal Index is defined as ratios of first peak, nadir, and second peak to baseline blood flow during the biphasic vasodilation.

The laser Doppler flowmetry (LDF) (BMP main unit and P-435 probe, Vasamedics, Eden Prairie, MN) was used to measure sacral skin blood flow oscillations. Skin blood flow was recorded on a computer via an analog-to-digital converter with a sample frequency of 20Hz. The temperature of the heater probe (TCO, Vasamedics, Eden Prairie, MN) was set to 42˚C to heat the sacral skin. This heating protocol was designed to differentiate between axon reflex mediated vasodilation and nitric oxide mediated vasodilation [5].

Nonlinear indexes were calculated during the pre-heating (1-10 min) and maximal vasodilation (51-60 min) periods. We chose the most commonly used nonlinear indexes that have proven useful in the quantification of nonlinear properties of heart rate variability (HRV), to include Hurst exponent (HE), detrended fluctuation analysis (DFA), sample entropy (SampEn), correlation dimension (CD), and largest Lyapunov exponent (LLE) [6]. The Wilcoxon signed rank tests were used for between-subject comparisons. The level of significance was set at 0.05. Matlab (R2008b, MathWorks, Natick, MA) were used to implement nonlinear analysis and statistical testing.

RESULTS AND DISCUSSION

Hurst exponent (short-term self similarity) showed a decrease in nonlinear properties of BFO under local heating as compared with baseline BFO in both the 65-75 years group (p<0.01) and the 75-85 years group (p<0.05). People with impaired vasodilatory function did not show a significant decrease in Hurst exponent in response to local heating (p>0.05).

The scaling exponents obtained from the detrended fluctuation analysis (long-term self-similarity) were calculated in terms of three scaling regions: short-term α_1, intermediate-term α_2, and long-term α_3. For the three groups, the intermediate-term scaling exponent α_2 changed significantly in response to local heating (p<0.01), but the short-term and long-term scaling exponents did not have a significant difference (p>0.05). Moreover, compared with the 75-85 years group, the changes in α_2 for the 65-75 years group were more prominent (p=0.076). The short-term scaling exponent α_1 and long-term scaling exponent α_3 didn't show significant changes in response to local heating in all three groups.

The sample entropy index did not show any significant difference in three groups during pre-heating and maximal vasodilation periods.

Similar findings were observed in the correlation dimension index with the Hurst exponent. Correlation dimension (complexity of the dynamic system) showed a decrease in nonlinear properties of BFO under local heating as compared with baseline BFO in both the 65-75 years group (p<0.01) and the 75-85 years group (p<0.05), but not in the impaired group (p>0.05).

The largest Lyapunov exponent (chaotic behavior) showed a decrease in nonlinear properties of BFO under local heating as compared with baseline BFO in all three groups (p<0.05).

CONCLUSIONS

Our results indicate that nonlinear properties of BFO can be used to predict impaired vasodilatory function based on laser Doppler time series. Laser Doppler flowmetry has been established as a useful tool to assess microvascular function; however, the variations of blood flow limit its use as a direct measurement. Analysis of nonlinear properties embedded in BFO can overcome temporal variations of laser Doppler measurements. Further, nonlinear analysis of BFO can complement current linear spectral (wavelet) analysis used to characterize blood flow control mechanisms. With a better understanding of linear and nonlinear properties of microvascular function, the role of microvascular dysfunction in pressure ulcer development can be better defined.

REFERENCES

1. Geyer, M.J., et al., *Using wavelet analysis to characterize the thermoregulatory mechanisms of sacral skin blood flow.* Journal of Rehabilitation Research & Development, 2004. **41**(6): p. 797-806.
2. Jan, Y.K., et al., *Wavelet analysis of sacral skin blood flow oscillations to assess soft tissue viability in older adults.* Microvascular Research, 2009. **78**(2): p. 162-168.
3. Stefanovska, A. and Bracic, M., *Physics of the human cardiovascular system.* Contemporary Physics, 1999. **40**(1): p. 31-55.
4. Harbourne, R.T. and Stergiou, N., *Movement Variability and the Use of Nonlinear Tools: Principles to Guide Physical Therapist Practice.* Physical Therapy, 2009. **89**(3): p. 267-282.
5. Minson, C.T., et al., *Nitric oxide and neurally mediated regulation of skin blood flow during local heating.* Journal of Applied Physiology, 2001. **91**(4): p. 1619-26.
6. Beckers, F., et al., *Aging and nonlinear heart rate control in a healthy population.* American Journal of Physiology-Heart and Circulatory Physiology, 2006. **290**(6): p. H2560-H2570.

ACKNOWLEDGEMENTS

This work was supported by the Christopher and Dana Reeve Foundation (JA2-0701-2) and Switzer Fellowship, National Institute on Disability and Rehabilitation Research (H133F060025).

FREQUENCY CONTENT OF CARTILAGE IMPACT SIGNAL REFLECTS ACUTE HISTOLOGIC STRUCTURAL DAMAGE

Anneliese Heiner, James Martin, Todd McKinley, Jessica Goetz, Daniel Thedens and Thomas Brown

University of Iowa, Iowa City, IA, USA
email: anneliese-heiner@uiowa.edu web: http://poppy.obrl.uiowa.edu/

INTRODUCTION

Controlled impaction of articular cartilage provides a model for studying cartilage injury associated with post-traumatic osteoarthritis. Typically, cartilage explant specimens are struck with an impactor, and the resulting chondrocyte viability, chondrocyte metabolism, or structural damage is compared to nonimpacted controls. Mechanical measures from the impact itself, such as cartilage loading rate and peak impact force, are also frequently measured.

Determining cartilage impact damage histologically requires appreciable time and expense for specimen preparation. In contrast, mechanical measures from the impact can be quickly determined from the impact force trace.

The purpose of this study was to determine if a relationship could be detected between a new mechanical outcome measure and histologically-apparent cartilage structural damage. The new mechanical measure was a quantification of the frequency response of the impact force trace, namely, the percent of the total signal with high-frequency content. Histologically-apparent cartilage structural damage was evaluated with a histologic scale designed to quantify acute damage.

METHODS

Osteochondral specimens excised from bovine lateral tibial plateaus were each impacted once using a drop tower. The impactor tip was a flat-ended, 5.5 mm diameter brass cylinder with a rounded edge. One of six impact energies was delivered with one of two masses (0.59 or 1.04 kg). An accelerometer measured impact force (Fig. 1a). Each impact force trace underwent frequency analysis by Fast Fourier Transform (Fig. 1b), with a resonant peak at around 5 KHz being digitally filtered out. The amount of high-frequency content in each impact trace was then calculated as the percent of the total signal that was greater than 2 KHz. Two KHz was chosen because the most regular impact traces (such as the impact trace designated as “4%” in Fig. 1) had minimal signal content above that frequency.

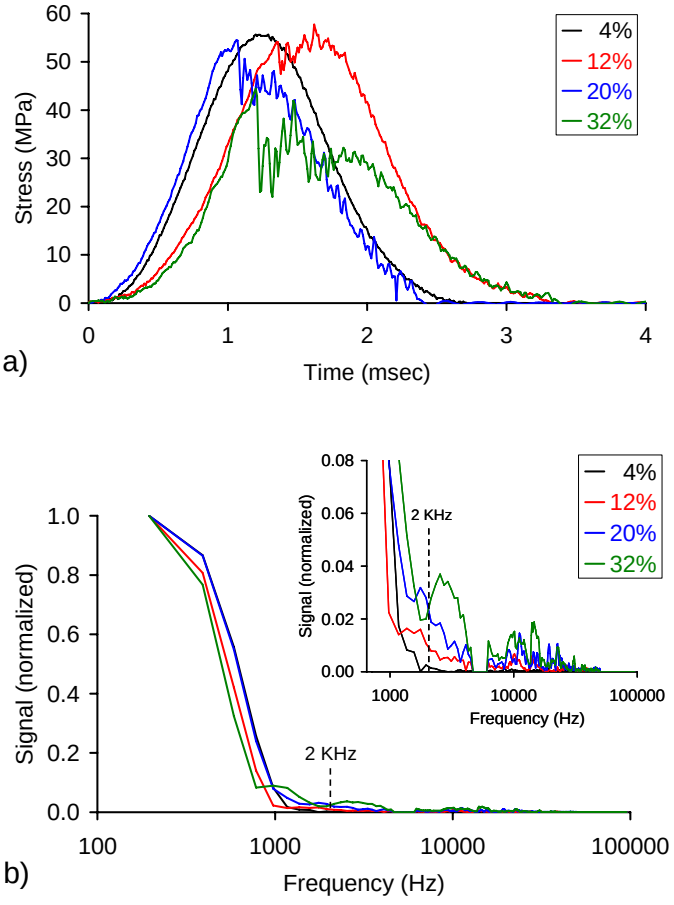

Figure 1: Impact traces from bovine osteochondral specimens – a) stress versus time and b) signal versus frequency (inset shows higher-frequency components in more detail). The impact traces shown demonstrate a range of the percent total signal greater than 2 KHz.

Specimens underwent histologic analysis to quantify acute structural damage resulting from the impact. OARSI guidelines for histological preparation were followed. Five-micron-thick sections were selected from the center of the impact site, stained with Safranin-O, digitized on a stepper-motor-driven microscope stage, and reconstructed into high-resolution JPEG images.

Each digitized section was evaluated on a new eight-point scale developed to quantify acute structural damage in terms of articular surface cracking and cartilage crushing (Fig. 2). Articular surface crack damage was given a score of 0, 1, or 2. Cartilage crush scores were assigned independently of, and weighted greater than, the articular surface damage score. Sections were given crush scores of 0, 3, 4, or 5. The articular surface crack score was added to the cartilage crush score to get a total specimen damage score ranging from 0 to 7. Three experienced observers applied the scoring scale to the histological sections on two separate occasions, yielding six separate observations for each specimen. The six scores were averaged to yield a mean value for each specimen.

Kendall's coefficient of concordance (W) was calculated between the frequency content measure and the specimen-averaged histologic damage score for all data, and for each impact mass separately.

RESULTS AND DISCUSSION

The histologic structural damage score increased with the proportion of high-frequency content in the impact trace (Fig. 3). The coefficients of concordance were 0.864 ($p = 0.005$) for all data, 0.851 ($p = 0.035$) for the lower-mass impacts, and 0.927 ($p = 0.017$) for the higher-mass impacts. The frequency content measure and the cartilage structural damage score had good concordance, for the data as a whole and for each separate impact mass. This suggests that the frequency content of a cartilage impact signal, specifically the proportion of high-frequency force components, could be used as a surrogate measure of acute cartilage injury. Taking advantage of this relationship could reduce the time and expense of histological processing needed to morphologically assess cartilage damage, for purposes of initial screening when evaluating new impaction protocols.

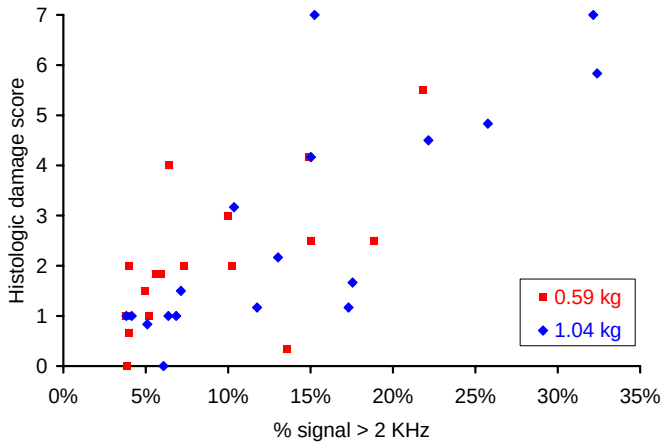

Figure 3: A higher percent of cartilage impact force signal in the higher frequencies (> 2 KHz) was related to a higher cartilage histologic structural damage score (W = 0.854).

ACKNOWLEDGEMENTS

This research was funded by NIH P50 AR055533. The authors also thank Dr. Steve Hillis, Ms. Gail Kurriger, Ms. Abigail Lehman, Dr. M. James Rudert, and Ms. Sarah A. Wiechert.

Figure 2: Examples of cartilage histologic structural damage scores. The articular surface crack score was added to the cartilage crush score to get a total specimen damage score ranging from 0 to 7.

Evaluation of Frost's 3-way rule equation for bone adaptation to mechanical stimulation

[1]Mobin Rastgar Agah and [1]Vanessa Yingling

[1]Temple University, Philadelphia, PA
email: mobin.rastgar.agah@temple.edu, http://www.temple.edu/chp/departments/kinesiology/SkAD_Lab.htm

INTRODUCTION

A classic equation for bone modeling called the "3-way" rule was presented by H.M Frost in 1990 [1,2]. Two advantages of the 3-way rule are the introduction of woven bone formation and the inclusion of a proportioning coefficient that can be used to incorporate the effects of factors other than mechanical loading in the equation. The purpose of this work was to use the 3-way rule to predict changes in femur histomorphometry using available experimental data from growing rats with the intent to develop a model of suppressed estradiol during growth.

METHODS

The governing equation in Frost's 3-way rule for bone formation and resorption is

$$\mathrm{f(M)} = \Gamma\,(\epsilon + P)\dot{k}$$

In this equation Γ is the modeling operator defining the areas of bone formation/resorption and $\dot{k}$ is the maximum rate of it. $\epsilon + P$ can vary between 0 and 1. P is the proportioning coefficient to adjust the calculated drift rate to experimental data and ϵ is the mechanical usage coefficient and can be calculated by

$$\varepsilon = \left|\frac{|E_{obs}| - |MES|}{|E_{sat}| - |MES|}\right| \; if \; |MES| < |E_{obs}| < |E_{sat}|$$

In this equation $|E_{obs}|$ is the observed strain history on bone perioseal and endocortical surfaces. $|MES|$ is the modeling stimulation strain history and $|E_{sat}|$ is the strain history that stimulate anarchic bone resorption or woven bone formation.

In order to evaluate the accuracy of the three-way rule equation for rat femur, the initial cortical area was modeled by 2 concentric ellipses. The average geometrical data derived from a previously published article [3] and incorporated into the model. The area was split into an array of small squares to estimate geometrical changes during simulation. This method can be developed further for the simulation on actual bone images using the pixels of image in the same way.

Based on the available published data 400 μstrain and 750 μstrain were selected as $|MES|$ and $|E_{sat}|$ and 25 GPa as Young's modulus for rat femur [4,5,6].

The elastic beam theory was used to calculate the strain distribution on the rat femur diaphysis under an eccentric longitudinal load. The normal load assumed to be 5 mm and 3.8 mm out of center respectively in medial and posterior direction throughout the simulation. The normal force assumed to be 3.2 times average body weight that was recorded weekly from 6 weeks to 24 weeks of age. Bone formation rate was assumed to be 3 mm/mm^2/year. The strain stimulus was calculated as the time average of strain resulting from loading and was controlled during simulation to remain below overload limit. The histomorphometric result of simulation was compared to the experimental data.

The simulation was run several times with the loading on the cross section kept constant and the formation/resorption threshold on the endocortical surface assumed to be 70% of its value on periosteal surface. The effect of following parameters were studied after a simulation of 5 week formation and resorption: (1) Overload threshold, changed from 600 to 1000 μstrain and (2) Maximum bone formation rate, changed from 1 to 4 mm/mm^2/year

RESULTS AND DISCUSSION

The result shows respectively 4.9%, 4.2% and 9.8% error in cortical area, ML 2nd moment of inertia and product moment of inertia. Figure 2 and 3 show the

effect of overload threshold on the change in cortical area after 5 weeks.

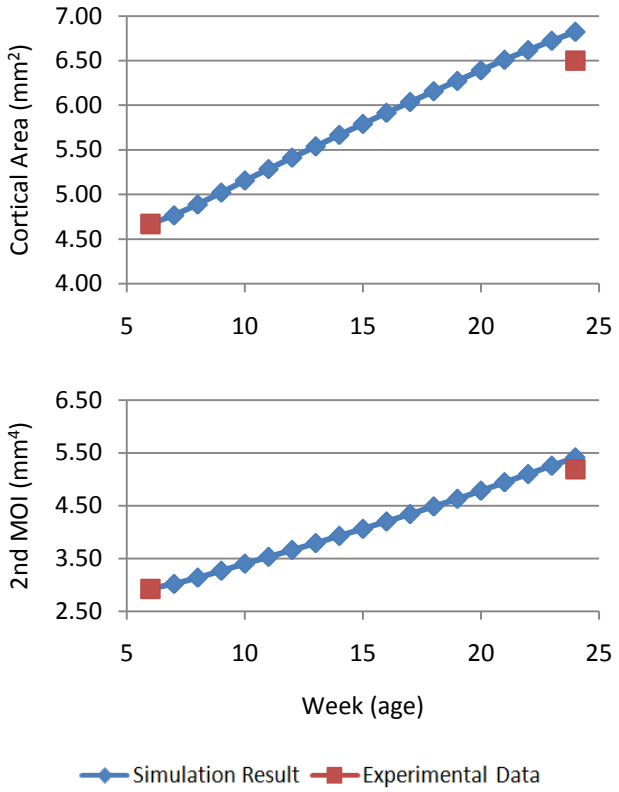

Figure1: Comparison of simulation result with experimental data. Top: cortical area, Bottom: 2nd moment of inertia

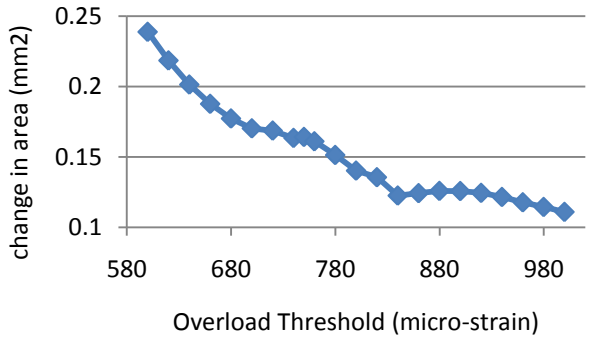

Figure 2: Change in difference in cortical area before and after simulation as a function of shift in the overload (woven bone formation) threshold.

3-way rule may be used as modeling equation in rat femur. Overload threshold and bone formation rate parameters are characteristics of bone that can be functions of other variables like age, hormonal level and gender and need to be determined by experiment for different conditions. Changes in these variables can have meaningful effects on net bone formation.

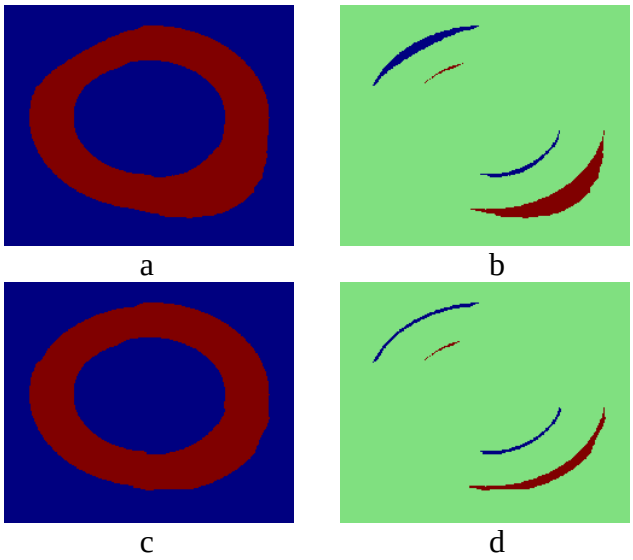

Figure 3: Sample cortical area predicted by simulation with 600 (a,b) and 1000 (c,d) µstrain overload threshold. left (a,c): cortical area after simulation. right (c,d): formation (red) and resorption (blue) areas.

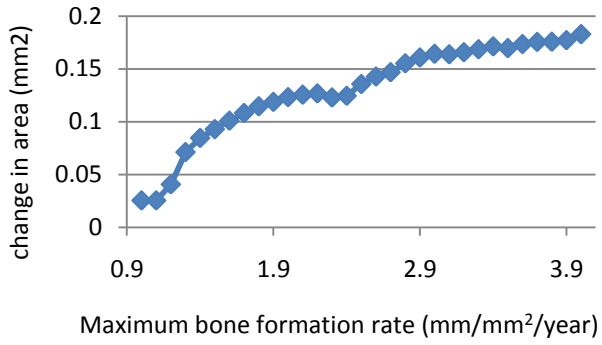

Figure 4: Change in difference in cortical area before and after simulation as a function of maximum formation rate

REFERENCES

1- Frost HM, *Anat Rec* **226**(4), 403-413, 1990
2- Frost HM, *Bone Miner* **22**(2), 117-127, 1993.
3- Yingling VR, et al. *Bone*, **38**, 67-73, 2006
4- Keller TS, et al. *J Biomech* **22**(11/12), 1115-1127, 1989
5- Turner CH, et al. *J Bone Miner Res*, **9**(1), 87-97, 1994
6- Turner CH, et al. *J Bone Miner Res*, **10**(10), 1544-1549, 1995

LOCALIZED MEASURES OF TENDON IMPINGEMENT ON THE MEDIAN NERVE WITHIN THE CARPAL TUNNEL

[1]Nicole M Kunze, [1]Jessica E Goetz, [2]Daniel R Thedens,
[1]Thomas E Baer, [1]Ericka A Lawler, and [1]Thomas D Brown
[1] Department of Orthopaedics & Rehabilitation University of Iowa, Iowa City IA,
[2] Department of Radiology, University of Iowa, Iowa City IA
email: jessica-goetz@uiowa.edu web: http://poppy.obrl.uiowa.edu/

INTRODUCTION

There is increasing evidence that carpal tunnel syndrome (CTS) may be caused at least in part by impingement on the median nerve by the digital flexor tendons. Impingement of the median nerve typically results in a change of nerve shape which is visible on MR images. However, the most commonly applied measure of median nerve shape is a general measure typically termed a flattening ratio. Flattening ratios assume that the median nerve can be approximated as an ellipse, and that the overall structure shape can be quantified as a ratio of the major axis to the minor axis [1]. The closer this value is to 1, the rounder the structure. However, while an ellipse is a good approximation of median nerve shape, flattening ratio provides no indication of localized deformations. To overcome this limitation, we have developed a new method for quantifying MRI-apparent local deformations of the median nerve resulting from interactions with specific tendons within the carpal tunnel.

METHODS

MRI scans of five individuals were obtained with the hand and wrist in a variety of poses using a 3D DESS pulse sequence on a Siemens 3T MRI scanner. Hands were positioned either in 0 or 35 degrees of wrist flexion, and images were acquired with the hand relaxed, or while performing one of three isometric loading activities (flat press, squeeze grip, index pinch) [2]. The acquired image resolution was 0.2 mm x 0.2 mm x 1.0 mm.

The tendons and the median nerve were semi-automatically segmented on axial images within the bounds of the carpal tunnel. Next, a computational region-growing technique was employed to perform a slice-by-slice proximal-ward propagation of the known tendon identities from the mid-hand to the completed carpal tunnel segmentations [3].

An anatomic coordinate system was defined for each individual using the distal forearm bones. This system was centered at the middle of the radial plateau with the x-axis directed towards the ulnar styloid, the y-axis directed volarly, and the z-axis directed distally along the shaft of the radius. All identified segmentations were rotated into this anatomic coordinate system (Figure 1). Referencing to this radius/ulna-based coordinate system afforded registration of carpal tunnel structure geometries collected with the subjects' arms in various orientations within the scanner, which was necessary to accommodate the different wrist angulations and functional activities that were imaged.

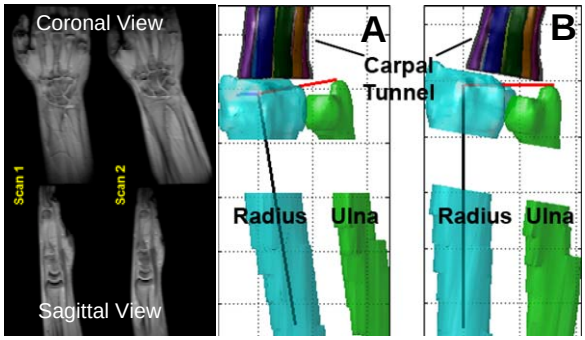

Figure 1: MR scout images (left) of one subject's varied wrist position for two different neutral scans. The neutral wrist model is shown in the MRI-based coordinate system (A) and rotated into the anatomic system (B).

2D cross sections at the levels of the pisiform and the hook of the hamate were isolated from the registered 3D carpal tunnel models. Structures immediately adjacent to the nerve in these locations were registered in 5 degree increments around the nerve boundary. A structure was considered adjacent if its edge was within 1 mm of the nerve boundary. Median nerve "crowding" was indexed in terms of the fraction of the nerve perimeter experiencing thus-defined adjacency.

To quantify localized deformation of the median nerve boundary, chains of shape numbers were computed. Interior angles were computed between adjacent 0.5 mm line segments defining the nerve boundary. Shape numbers were assigned to each local angle by binning into 20-degree slope change increments (Figure 2). Negative values represented the boundary being pushed into the nerve center, and positive values indicated areas of localized outward pinch. Values of 0 and 1 represented little/no change in the boundary, whereas values closer to 8 (for positive angles) or -8 (for negative angles) represented steeper changes in direction between line segments. Shape chains corresponding to the boundary of the nerve were assembled by compiling associated shape numbers.

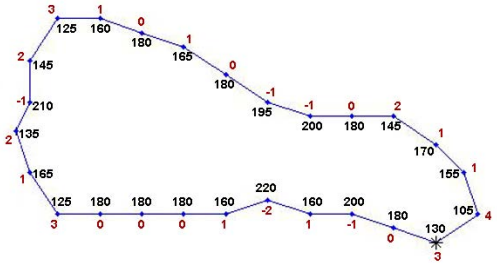

Figure 2: Shape number example with interior angles shown in black, and corresponding shape numbers shown in red outside the boundary.

RESULTS AND DISCUSSION

Comparing shape chains and percentages of nerve adjacency provided an objective measure of nerve deformation by adjacent structures. Shape chains (Figure 3) associated with unloaded scans typically

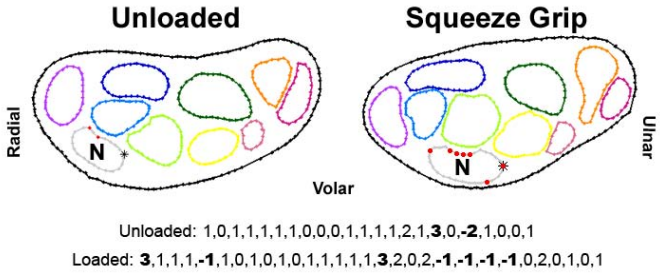

Figure 3: Comparison of shape chains at the level of the pisiform for a hand in zero degrees of wrist flexion with an unloaded hand (left) and performing a squeeze grip activity (right). N represents the nerve. Nerve chain values begin from the black asterisk and continue clockwise around the boundary. Shape number values in bold correspond to points plotted in red. The string of -1's in the loaded activity (right) indicates a local impingement on the median nerve from the adjacent tendon.

contained few shape numbers greater than 2 or any long series of shape numbers less than zero. This indicated a smooth, mostly convex nerve boundary when the hand was unloaded. However, when the hand was functionally loaded, there were more high shape numbers (>2), and there were more chains of negative numbers. This indicated an increased incidence of nerve pinch around the boundary (large positive numbers) or localized nerve impingement (strings of negative numbers).

The adjacency measure (Figure 4), showed that loading of the hand, as well as flexion of the wrist, typically increased the percentage of the nerve that was adjacent to a neighboring tissue structure.

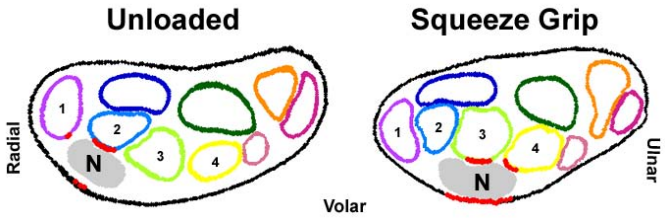

Figure 4: Comparison of adjacency for the hand position described in Figure 3. Red points indicate locations where a given structure is within 1 mm of the nerve (N). Labeled tendons are: 1- flexor pollicis longus (thumb), 2 - superficial index, 3 - superficial long, and 4 - superficial ring finger. Total percent adjacency of the unloaded nerve is 24% and of the loaded nerve is 57%.

CONCLUSIONS

Registering the carpal tunnel models to an anatomic coordinate system eliminated variation in tissue shapes associated with variations in wrist orientation relative to the scanner axis. Comparing shape chains and percentage of nerve adjacency allows investigation of specific tendon/nerve interactions which cause nerve deformation that may potentially be associated with CTS.

REFERENCES

1. Monagle K, et al. *AJR Am J Roentgenol* 172(6): 1581-1586, 1999.
2. Goetz JE, et al. 33rd Annual Meeting of the ASB, State College, PA, 2009; 891.
3. Kunze N, et al. *Orthop Res and Rev*, 1: 1-12, 2009.

ACKNOWLEDGEMENTS

Funding was provided by NIH AR 053899.

RELATIONSHIPS BETWEEN DUAL ENERGY X-RAY ABSORPTIOMETRY (DXA) AND COMPUTED TOMOGRAPHY (CT) MEASURES OF BONE AND THEIR ABILITY TO PREDICT FRACTURE LOAD

Karen L. Troy and W. Brent Edwards

Department of Kinesiology and Nutrition, University of Illinois at Chicago, Chicago, IL, USA
E-mail: klreed@uic.edu, Web: www.uic.edu/ahs/biomechanics

INTRODUCTION

Targeted mechanical loading may be a means to improve bone strength in high-risk populations. However, optimal implementation of such a program requires knowledge of how human bone changes in strength over time in response to novel mechanical stimulations. We have developed a human model of bone adaptation in which subjects apply a compressive load to their distal radius by leaning onto their palm to achieve a load of 300 N for 50 cycles per day, 3 days per week.

Changes to bone density and mass, as a result of this loading, were initially quantified using dual energy x-ray abosorptiometry (DXA). Although DXA data have been shown to correlate with fracture strength of vertebral bodies [1], approximately 52% of the variance in fracture load remains unexplained by DXA measures. DXA does not allow for the detection of changes in bone mineral distribution within the region of interest, or changes in cross-sectional shape and moment of inertia, all of which may heavily influence bone fracture load and may change as a result of targeted mechanical loading. Therefore, in addition to DXA, we have begun to acquire computed tomography (CT) data for subjects in our loading protocol.

Theoretically, DXA and CT measures of bone mineral density and content should be related both to one another and to fracture strength, with CT potentially providing higher spatial resolution and a true volumetric bone density. Our purpose was to determine the relationships between CT and DXA measures used to describe bone, and to determine which measures, if any, were the best predictors of fracture load in the distal radius.

METHODS

A total of 25 matched DXA and CT data sets were analyzed in this study. Five sets came from right female cadaver upper extremities obtained as anatomic gifts. The other twenty data sets were pre/post data collections from right/left pairs of five young women (age 22.2 ± 2.7 yrs; height 167.5 ± 7.3 cm; mass 67 ± 2.9 kg) who participated in the previously described mechanical loading intervention. All protocols were institutionally approved and living subjects gave written informed consent before any data were collected.

DXA were acquired and analyzed by a single operator on a Hologic QDR-4500 scanner using standard protocols. CT data were acquired on a GE Brightspeed CT scanner at a resolution of 0.234 x 0.234 mm in-plane, 0.625 mm slice thickness. CT data were reconstructed using a high spatial frequency ("bone") algorithm. For each subject and specimen, CT and DXA data were acquired on the same day on the same scanner. A calibration phantom was included in the CT scans. For both DXA and CT the analyzed region of interest was the ultra-distal radius. This is the 15-mm transverse section of the radius immediately proximal to the subchondral plate.

DXA can be used to quantify bone mineral content (BMC, g) and bone mineral density (BMD, g/cm^2), BMD is equal to BMC (g) divided by the projected area of the bone (cm^2) on the detector. As such, BMC and BMD from DXA are often described as areal BMC and BMD, or aBMC and aBMD.

CT data were thresholded to capture those voxels that contained mineralized bone tissue (cut-off value: 226 Hounsfield Units, HU; Fig 1). The mean HU of this volume was converted to density (ρ, g/cm^3) using data from the calibration phantom. The total thresholded volume was considered the (mineralized) bone volume (BV, mm3), having density ρ. These values were used to calculate the volumetric BMC (vBMC=ρ*BV, g). The distal-most 5 mm set of slices were used to calculate the minimum areal moment of inertia (I_{min}, mm^4) of the

radius. Validated subject-specific finite element models based on CT data were used to predict fracture load in an axial compression scenario.

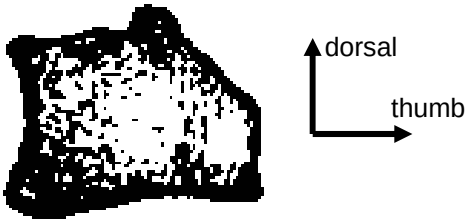

Figure 1 Thresholded transverse cross-section of the distal radius, located 2 mm proximal to subchondral plate. Black regions indicate mineralized bone.

All DXA, CT, and model-derived variables were tested for significant Pearson's correlations (r) with each other and with fracture load. Those variables that were significantly correlated with fracture load were entered into a stepwise linear regression.

RESULTS AND DISCUSSION

For a given specimen vBMC was consistently larger than aBMC, but both measures were highly correlated (Fig 2; r=0.962, p<0.001) and were each related to fracture load (vBMC r=0.714 p<0.001, aBMC r=0.688 p=0.001). In contrast, aBMD and ρ were not correlated with each other (Fig 3), even though they were both related to fracture load (r=0.631, p=0.002, aBMD r=0.610, p=0.003).

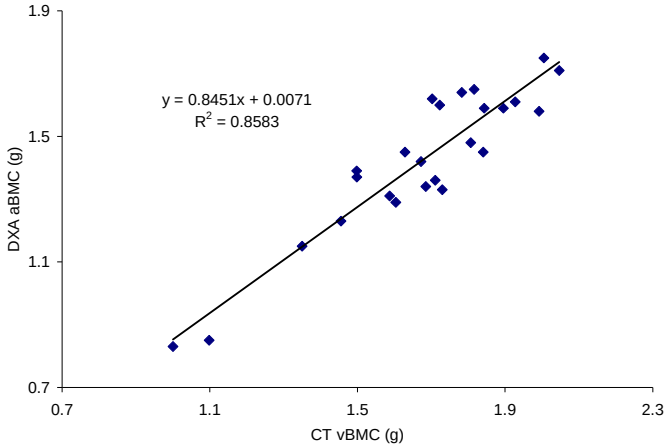

Figure 2 aBMC versus vBMC

These four variables were the only variables that correlated with fracture load, and all four were included as candidate variables for stepwise linear regression. The final model included only CT data:

fracture load (N) =-6014 + 2013*vBMC (g)
+9564*ρ (g/cm^3).

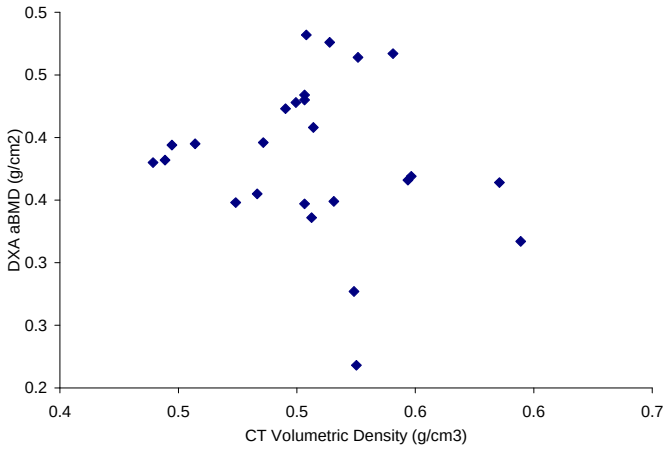

Figure 3 Areal BMD versus volumetric density, ρ. These two measures are analagous for CT and DXA, respectively.

This model was able to closely predict fracture load (R^2=0.778), however the error (±9.9%) was of similar magnitude to the changes we expect as a result of our mechanical loading intervention. Thus, we conclude that simple DXA or CT measures, as well as regression models based on these measures, may not be sufficiently sensitive to quantify changes in bone strength following a mechanical loading intervention in humans.

CONCLUSIONS

Our purpose was to compare DXA and CT measures of bone quality and to determine which measures best predicted fracture load. CT and DXA measures of BMC were closely related to each other, with CT measures providing more accurate predictions of fracture strength. During a mechanical loading intervention bone may change in structure to become significantly stronger without large increases in BMC or BMD. For example, rats ulnae exposed to mechanical loading showed a 8.6% increase in BMD but a 64-165% increase in energy to failure [2]. This highlights the importance of accurate methods for evaluating the response of bone to a given stimulus. Our current data suggest that subject-specific model-based estimates of fracture strength may be an important outcome measure to examine intervention efficacy.

REFERENCES

[1] Tabensky AD et al. *J Bone Miner Res* 11, 1981-8 (1996).
[2] Robling AG et al. *J Bone Miner Res* 17, 1545–1554(2002).

ACKNOWLEDGEMENTS

Funding provided by the Department of Kinesiology and Nutrition. Dr. Mary Lou Bareither assisted by acquiring and analyzing all DXA data.

TEMPERATURE DEPENDENCE ON PORCINE INTERNAL CAROTID ARTERY VASCULAR MECHANICS

John C. Fitzpatrick, Franco M. Capaldi

Drexel University, Philadelphia, PA, USA

email: capaldi@coe.drexel.edu

INTRODUCTION

In the United States, over 500,000 arterial bypass operations are performed each year [1]. If a healthy length of autologous artery is not available, saphenous vein or engineered grafts may be used. Mechanical differences existing between the graft and native vasculature may cause local flow disturbances and ultimately lead to the progressive development of intimal hyperplasia, the main mode of occlusive graft failure and primary reason for low long-term patency rates in small-diameter arterial grafts [2-4]. The role of mechanics in the context of arterial grafting has included compliance mismatch, vessel hemodynamics, and biological remodeling. There are few studies that test and model vascular mechanics with a three-dimensional approach permitting simulation of physiological processes, therefore limiting the applicability of results. Though some investigators [5-8] have applied a three-dimensional strain energy function (SEF) to describe arterial mechanics, the source data was collected from vessels maintained in water baths at room temperature, rather than heated, conditions. This may introduce considerable error if the resulting constitutive parameters are used to model arterial mechanics at physiological conditions, since residual strain and internal forces in the vessel change between room temperature (20.5°C) and body temperature (37°C).

METHODS

Fresh porcine carotid arteries were obtained from an abbatoir (Kolb Brothers, Spring City, PA) and transported on ice. Intact vessel segments (3-4 cm length) were dissected of connective tissue and 2 mm vessel rings were cut from each end for cross-sectional area and opening angle image analysis, as described by Chuong and Fung [9]. The intact vessel was bound to nylon tubing plugs with 4-0 silk sutures and mechanically tested.

The mechanical testing protocol consisted of axial preconditioning at constant pressure followed by inflation at fixed axial stretch ratios. Vessel gage length was measured as the distance between inner sutures when the vessel was pressurized at 80 mmHg. Five axial preconditioning cycles were carried out, during which the vessel was stretched axially with a linear actuator (Ultra Motion, Cutchogue, NY) under stepper motor control (Advanced Micro Systems, NH) between axial stretch ratios of 1.40 and 1.60, maintaining 80 mmHg (10.66 kPa) internal pressure with an inline hydrostatic column of isotonic saline.

After axial preconditioning, the vessel was measured again to account for length increase [8] and held at axial stretch ratios between 1.40 and 1.60, in 0.05 increments, during five inflation cycles between 80mmHg (10.66 kPa) and 190 mmHg (25.33 kPa). The closed system was pressurized through a syringe injection port. For these loading cycles, line pressure and axial force are measured by a pressure transducer (Omega, CT), and load cell (Transducer Techniques, CA), respectively. A high-resolution CCD camera recorded the vessel's outer diameter at the midpoint of its length (PixeLINK, ON) and an MgO thermocouple was used to monitor water bath temperature (Gordo Sales, UT). The pressure transducer, thermocouple, and load cell interfaced with a signal conditioning controller (SC-2350; National Instruments, Austin, TX). All data values were recorded simultaneously from these sources in a LabVIEW routine.

The preconditioning and inflation protocols described above were performed at 22°C and 37°C. Following the final room-temperature inflation

cycle (λ_z=1.60), the response of the vessel was monitored for approximately 2.5 hours as the water bath heated from 23.9°C to 37°C. Heat was applied after a 25-minute vessel relaxation period at room temperature. Similarly, each opening angle image was captured after a 5-minute equilibrium hold period as temperature ramped from 22°C to 42°C.

RESULTS AND DISCUSSION

While the vessel was held at constant axial stretch ratio (λ_z=1.6), pressure of 90 mmHg (12 kPa), and temperature of 20.5°C, the axial tension within the artery relaxed by ~0.2 N, decreasing from 7.39 N to 7.20 N (Figure 1, on left).

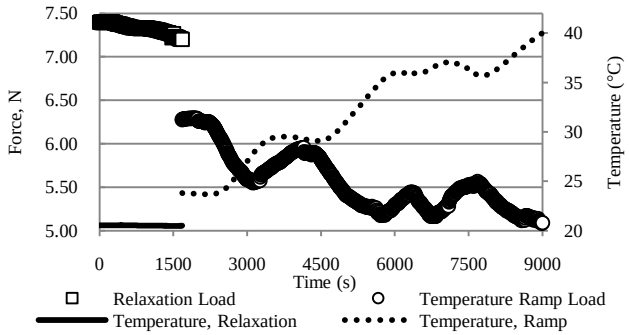

Figure 1: Observed vessel tension with water bath temperature constant (left) and during temperature ramp (right).

As the water bath heated, axial tension within the vessel decreased, fluctuating only when the heating element turned off. Temperature ramp data (on right in Figure 1) reflects an initial axial force of 6.27 N at 23.8°C due to an equilibrated temperature fluctuation between data sets. The observed axial loads at 37°C during the heating and equilibrating periods average to 5.30 N. This represents a decrease of 1.90 N between the stress states of a relaxed internal carotid artery at room and physiological temperatures. The effect of heating on the opening angle (θ_0) and corresponding inner radius (R_i) of the same vessel, averaged from both ring segments at the vessel's ends, indicate increases in residual stress (Figure 2).

Relations for principal stretches in the loaded state,

$$\lambda_r = \frac{R(\pi-\theta_0)}{\lambda_z r\pi}, \quad \lambda_\theta = \frac{\pi r}{(\pi-\theta_0)R},$$

are based on deformations in the unloaded and zero-stress states and have been used in previous studies modeling arterial mechanics [5-9]. As we may infer from our own study, physiological models based on room-temperature experimental data may be subject to a high degree of error from multiple sources. For the internal carotid artery tested in this study, axial load decreased by approximately 26.3% between 20.5°C and 37°C. Likewise, error would be expected to range between 12.8% and 16.6% for both λ_r and λ_θ, which are computed based on opening angle measurements (θ_0 and R_i).

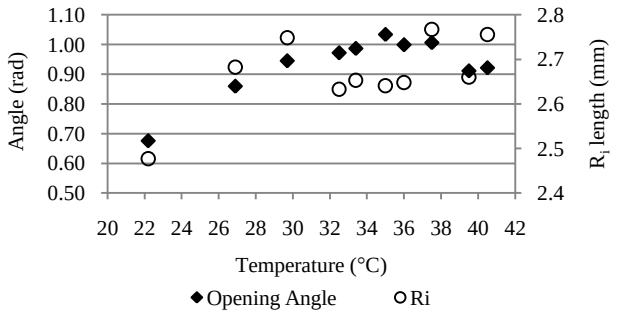

Figure 2: Opening angle and opening angle inner radius increase between room temperature (22°C) and 37°C.

CONCLUSIONS

Though blood vessels are known to be temperature-dependent materials, temperature dependency is not modeled in constitutive relations for mechanical behavior used recently [5-8]. Therefore, in order to appropriately model a physiologically relevant blood vessel, the mechanical data fit to a SEF must be collected at the relevant temperature(s). Our experimental results indicate large errors may result if room-temperature data is used to parameterize equations that are later used to simulate physiological vessel mechanics. Noting these possible errors, we aim to model data obtained at 37°C with a 3-D SEF and incorporate these parameters into future multiphysics simulations.

REFERENCES

1.MacNeill, B.D., et al. *Vasc Med*, **7**, 241-246, 2002.
2.Ballyk, P., et al. *J Biomech* **31**, 229-237, 1998.
3.Bassiouny, H.S., et al. *J Vasc Surg* **15**, 708-717, 1992.
4. Weston, M.W., et al. *J Biomech* **29**, 187-198, 1996.
5.Takamizawa, K., et al. *J Biomech* **20**, 7-17, 1987.
6.Vaishnav, R.N., et al. *Circ Res* **32**, 577-583, 1973.
7.Vonmaltzahn, W.W., et al. *J Biomech* **17**,839-847, 1984.
8.Wang, C., et al. *Am J Physiol-Heart C* **291**, H1200-H1209, 2006.
9.Chuong, C.J., et al. *J Biomech Eng-T ASME* **108**, 189-192, 1986.

EFFECTS OF POSTERIOR CAPSULE ATTACHMENT STATUS ON FLEXION MOMENT RESISTANCE IN THE HIP

Nick Stroud, James Rudert, Thomas Baer, and Thomas Brown
University of Iowa, Iowa City, IA, USA
email: nstroud@engineering.uiowa.edu

INTRODUCTION

Native hip femoroacetabular impingement (FAI) and total hip arthroplasty (THA) impingement/dislocation are issues of great interest and concern in contemporary hip joint biomechanics. Due to the complex three-dimensional (3D) kinematic/kinetic relationships that are involved in both circumstances, it is desirable to have experimental capabilities for producing and measuring impingement events in a controlled laboratory environment. The capsule of the hip joint is left to provide important contribution to stability, both pre- and post-impingement, but direct physical data are lacking. In response to this need, a novel methodological advancement is reported involving a method to measure the 3D reaction forces and moments of a cadaveric hip joint during impingement events. This advancement is implemented in a 4 channel servohydraulic system designed for simulating realistic hip joint motion.

METHODS

The servohydraulic simulator was designed and fabricated to interface with the load frame of an MTS 858 Bionix testing machine (Figure 1). The simulator consists of 2 concentric yokes mounted to the Bionix's axial-rotary actuator. The outer yoke controls specimen abduction-adduction (±20º), while the inner yoke controls flexion-extension (±115º). The Bionix's rotary channel controls specimen endorotation-exorotation (±25º), and its axial channel controls resultant contact force magnitude. The pelvis of the specimen is affixed to a 6 degree of freedom (DOF) load cell attached to the inner yoke, while the femur is mounted to a 2 DOF translational stage that permits subluxation or dislocation if conditions so dictate. The specimen is positioned within the servohydraulic simulator with concentricity between anatomic joint members and the servohydraulic testing system. The joint rotational center is found by iteratively solving a cost function where motion capture data of the femur was best fit to a sphere. Optimally the center of the fitted sphere coincides with the center of the joint. A Qualisys© motion capture system was used to record position data of visual markers fixed to the femur as it was moved throughout its range of motion at a rate of 100Hz.

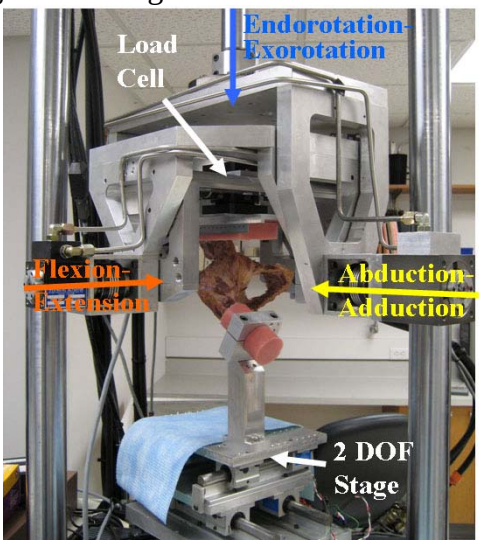

Figure 1. Photograph of the hip simulator. The axial translation is shown along the axis of endorotation-exorotation (blue). The other joint rotational axes are flexion-extension (orange), and abduction-adduction (yellow). A cadaveric hemi-pelvis is shown potted in polymethyl-methacrylate and fixed to the innermost yoke via the 6 DOF load cell (top white). The stationary femoral component is fixed to the translational stage (bottom white).

The resisting moments and contact forces are computed using a custom MATLAB program. The load/moment data stream provided by the 6 DOF load cell during testing is spatially transformed, to obtain forces and moments with respect to the hip joint center. The resulting numerical data provide a 3D assessment of contact force and resisting moment of the specimen in motion at every 0.01 second increment.

Illustrative data were captured for a cadaveric specimen undergoing a joint motion simulation reproducing a 0º to 90º flexion under a constant contact force of 300N. The intention of the experimental set was to observe the effects of various hip joint posterior capsule modifications often resulting from THA surgery. First a native hip with all soft tissue removed and having an intact joint capsule was tested. In subsequent trials the posterior portion of the hip capsule was tightly sutured to the posterior femoral neck at flexion angles 45º and 0º. In the last two trials, the sutures were removed and the posterior portion of the joint capsule was released from its bony attachment around 3/8 the circumference, and then around ½ of the circumference.

RESULTS AND DISCUSSION

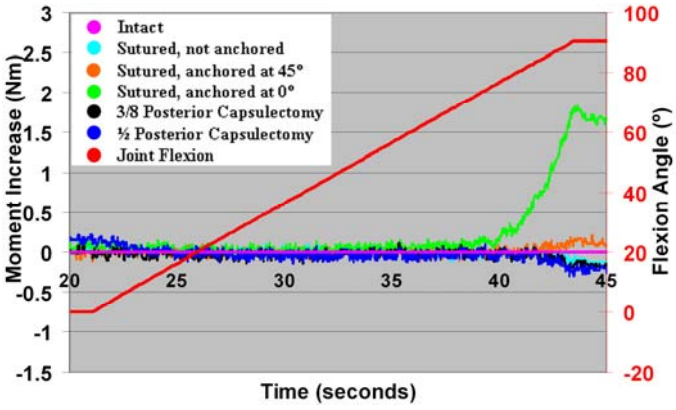

Figure 2. Joint resisting moments for six different capsule attachment conditions for a native hip. The resisting moment from the intact trial was subtracted from subsequent trials, to identify the effect of each capsule perturbation. It was observed that when the posterior portion of the capsule was tightly sutured to the femur (green), an elevated resisting moment was seen compared to the normal anatomic state, beginning at apparently 75º of flexion.

The trial with the rigid posterior joint capsule sutured at 0º flexion achieved the highest resisting moment (Figure 2), with the trial sutured at 45º flexion having the next highest resisting moment. The partial capsulectomy cases did not behave significantly differently from the intact case. However, a complete capsulectomy trial underwent frank dislocation.

Fully three-dimensional studies of impingement of implant/bone constructs or of native hip joints are difficult to perform, as detection of abrupt loading transients, and delineation of desired joint force and moment data through geometric transformations can be challenging to implement. The advancements reported here constitute a viable solution for these difficult measurement challenges.

ACKNOWLEDGEMENTS

Financial support was provided by the Department of Veterans Affairs and by NIH AR053553. The assistance of Dr. Yuki Tochigi is appreciated.

A 3-D BREAST SOFTWARE PHANTOM TO INVESTIGATE BREAST BIOMECHANICS DURING ULTRASOUND STRAIN IMAGING USING FINITE ELEMENT MODELING

Syeda Naema Hashmi and Mallika Keralapura

Biomedical Systems Laboratory, San Jose State University, San Jose, CA, USA
Email: mallika.keralapura@sjsu.edu, Web: http://www.engr.sjsu.edu/mkeralapura/

INTRODUCTION

Ultrasound based strain imaging is becoming popular for breast tumor differentiation on the basis that malignant cancers are stiff [1]. One implementation of this technique is to apply a small free-hand compression to the breast during which ultrasound radio-frequency (RF) data is recorded. RF data is processed to estimate spatial deformation, strain and sometimes modulus using a linear elasticity framework [2]. Generally, no particular strategy is used for maximizing ultrasound strain contrast given that the technique works quite well for larger stiff carcinomas that exhibit *desmoplasia* [3]. Difficulties have been noted with obtaining contrast for small and non-palpable tumors [1]. Developing a novel technology like strain imaging to image cancer involves significant in-lab science commonly done with tissue mimicking phantoms. These are generally rectangular blocks of gelatin mixed with other materials to resemble breast tissue's mechanical properties [4]. These types of phantoms simulate ideal boundary conditions quite different from what is seen in-vivo. Hence the problems faced in-vivo may be difficult to recreate or analyze.

In this project, our goal is to develop a platform – a 3-D software breast phantom to investigate breast ultrasound strain imaging settings using Finite Element Modeling (FEM) of breast biomechanics. We propose that the described tool can not only be used in ultrasound strain investigation but also in developing newer techniques to image cancer without real access of patient MRI or CT images. Others have modeled the breast by building patient specific breast FEM models based on the patient's Magnetic Resonance (MR) or Computer Tomography (CT) images for modeling and interpreting of Mammography, MR Elastography and non-linear elastography to improve elastic modulus reconstruction or to provide information of soft tissue mechanics [5-6]. These models are very application specific given the magnitude of the deformation encountered and the required accuracy of prediction. To our knowledge, no biomechanical models have been reported that investigate ultrasound strain imaging settings in 3-D. Here, we report the most commonly used stimuli in ultrasound strain imaging: static-compression and estimate tumor strain and stress for different scenarios to understand clinical implications.

METHODS

As a first step, we developed a 3-D anatomical model of a female breast in standing position using Solidworks software using anatomical resources. We setup the breast model to consist of 6 macroscopic layers: Areola, Skin, Fat, Glandular, Muscle and Chest wall. We imported this structural geometry into COMSOL v3.5a for FEM analysis using the structural mechanics module to relate applied stress and measured strain. In particular, we compensated for external forces like gravity and internal forces due to the ribs, pectoralis fascia and the cooper's ligaments in the FEM models using equations developed in [7], making the models applicable to different patient positions. Other groups that have modeled patient specific biomechanical models [5-6] have also modeled these large layers, display the glandular regions to be diffuse and naturally compensate body forces. Here we use a lumped glandular region for simplicity of the phantom.

We define the FEM sub-domain setting as Elastic Moduli (KPa) for the different layers (skin: 200, muscle: 26, fat: 18, glandular: 28, tumor: 106) with all Bulk Moduli: 1.5MPa, Poisson's Ratio: 0.49 [9]. Boundary constraints were defined as: lower muscle fixed to chest wall, stimulus applied on contact between breast and transducer, all other boundaries are free to move constrained by body forces. Mesh was Lagrange-Quadratic, tetrahedral and solver was elastic direct pardiso. We next simulated

experiments by modeling tumors of different sizes and stiffness positioned within the breast phantom at different depths. A transducer in contact with the skin directly above the tumor applied the stress locally to the breast. We measured local stresses and strains and quantified contrast transfer efficiency [8].

RESULTS AND DISCUSSION

Fig 1a shows the breast simulation phantom and its layers. Fig 1b shows the change in shape when the breast was positioned as supine from standing. Fig1c-e shows displacement, normal strain and normal stress due to an external compression of 4N by the transducer to breast tumor tissue. Tumor displayed low strain when compared to the background with significant stress concentration effects due to the complicated stress field (Fig 1e) consistent with what has been seen with other standard phantoms [8] and in-vivo [1]. Fig 1f shows a contrast transfer efficiency curve. Deeper regions have worse efficiency than shallow regions using this phantom indicating that a strain image of a stiff tumor located deep in the tissue may not portray stiffness information adequately when compared to when the tumor is located in a shallow region. These results are encouraging as they point toward current clinical problems but further investigation is needed before conclusions can be made. We also compared the efficiency with previously reported rectangular phantom data [8]. Their results do not show significant depth dependence but values are similar for the shallow case.

CONCLUSIONS

We have developed a simple 3D breast software phantom to investigate ultrasound strain imaging settings for improving contrast in clinical scenarios for difficult acquisitions. We have demonstrated the strain imaging experiment for an external force applied by a transducer to a tumor. We also demonstrate the use of this phantom in assessing a clinical relevant problem of imaging deep tumors.

REFERENCES

1. Nariya, C et. al. *J. Ultrasound Med.* **29**:1-7, 2010.
2. Egorov, V *Br. Cancer Treat* **118**:67–80, 2009.
3. Hall TJ et. al. *Ultr. Med. Biol.* **29**:427–435, 2003.
4. Hall, TJ et. al. *IEEE UFFC* **44**, 1355–1365, 1997.
5. Bliznakova, *Phys.Med.Biol.* **48**:3699–3719, 2003.
6. Whiteley,*Math Med and Biol* **24**: 327−345, 2007.
7. Gefen A, *Tech. Health Care.* **15**: 259-271, 2007.
8. Ponnekanti, H, *Ult. Med. Biol.* **4**:533-543, 1995.
9. Krouskop, TA, *Ultr. Imaging*. **20**: 260-274, 1998.

Fig 1: (a) Breast software phantom (b) supine position model (c) Displacement map (d) strain map and (e) stress map due to 4N force applied by the transducer on the skin above a 10cm deep tumor of stiffness 105KPa (f) contrast efficiency curve combining tumor stiffness and position

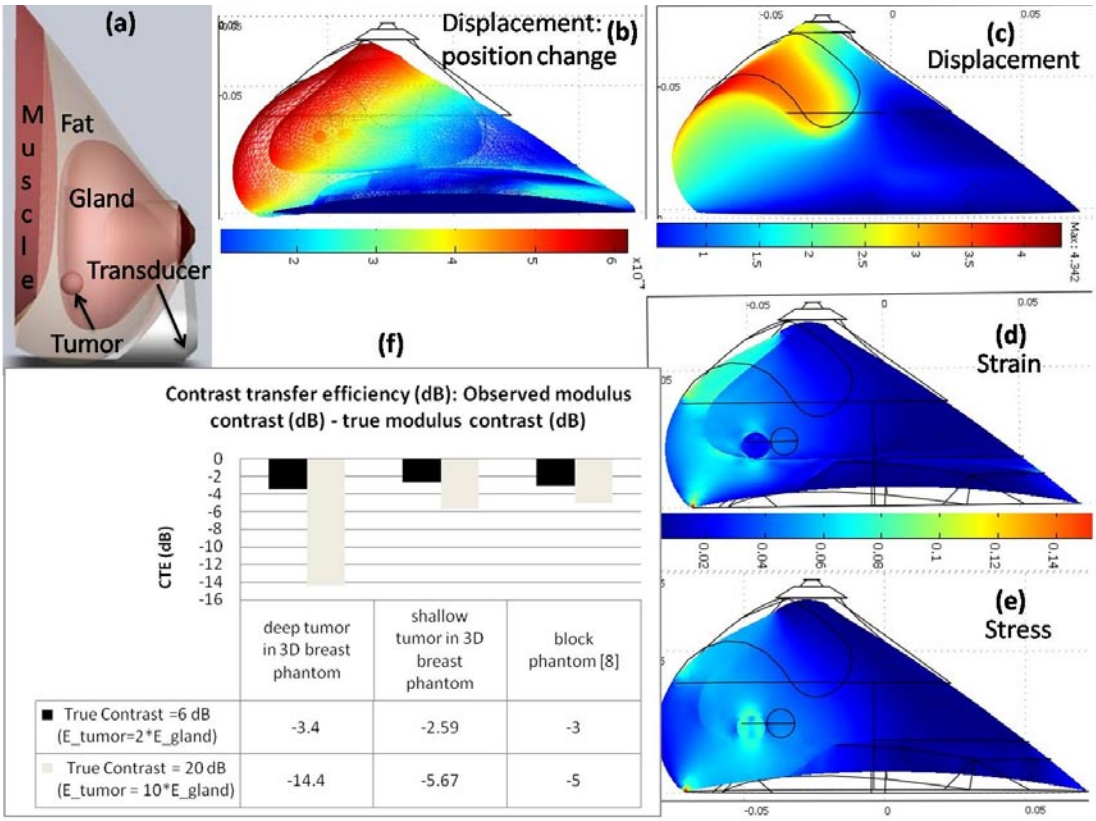

EFFECTS OF NORMAL AND SHEAR LOADS ON BLOOD PERFUSION AND REACTIVE HYPEREMIA IN THE SKIN

Abinand Anbazhagan Manorama, Tamara Reid Bush and Seungik Baek

Michigan State University, East Lansing, MI, USA
email: anbazhag@msu.edu, reidtama@msu.edu, web: www.egr.msu.edu/~reidtama

INTRODUCTION

Aging of the human body causes significant changes in the integumentary system (skin), such as a thinning epidermis and dermis, and increased time for skin repairs. Many older individuals have limited mobility and are confined to chairs or beds. Elderly individuals in these situations are highly prone to pressure ulcers, also known as bed sores. These wounds are breakdowns in the skin and develop in regions where tissues are subject to pressure between bony regions and the bed or chair. Though it is well documented that mechanical loading is a major factor leading to an increased incidence of pressure ulcers [1], it is still unclear how external loading conditions, in particular, combined normal and shear loads affect regional blood perfusion (PU) and transcutaneous oxygen levels (tcpO2) in human skin. Both PU and tcpO2 levels are related to the health of the skin.

The goal of this work was to:

- Document the subject acceptable ranges of normal and shear loads on the forearm.
- Determine if the addition of shear load to an existing normal load produced changes in PU or tcpO2 levels in the forearm skin.
- Determine if changes in PU and tcpO2 occurred during the resting times over the duration of the test session.

METHODS

Fifteen subjects, (7 males and 8 females) with an average age of 23 years and a standard deviation of 2.4 years voluntarily participated in the research. Seven conditions with various loadings on the forearm were tested (Table 1). These conditions were repeated on the same subjects in an identical manner one week after the initial test session. Following each of the conditions, a two minute rest period occurred during which data were collected.

Table 1: Description of the series of test conditions

	Description of test condition
1	Arm resting on a support. No contact with load cell.
2	Normal load of forearm
3	Normal (weight of forearm) + shear force
4	Normal load of forearm + 1 rice bag (8.9 N)
5	Normal (weight of forearm + 8.9 N) + shear force
6	Normal load of forearm + 2 rice bags (17.8 N)
7	Maximum normal and a shear forces applied by subject

An AMTI (Watertown, MA) multi-axis load cell was used to collect the force data, while the PU and tcpO2 data were collected using a Perimed (Stockholm, Sweden) Laser Doppler system. The temperature under the blood perfusion probe was maintained at 37° C.

During the test conditions, normal loads were applied by placing rice bags of known weight on the forearm, in addition to the weight of the forearm itself. Shear loads were induced by the subject; the subject shifted his or her forearm forward on the load cell. Subjects were instructed to apply the shear load and to make sure slippage did not occur.

For the analysis, the mean values of PU and tcpO2 were selected for a 20 second interval, during which the fluctuations of forces were less than 1.5 N. For the resting times, the analysis corresponded to 20-40 seconds of the second minute of the resting time. A paired t-test, conducted at a 95% confidence level ($p<0.05$) was performed to compare the effects of normal and shear load on PU and tcpO2.

RESULTS AND DISCUSSION

It was found that the average normal and shear loads applied by the subjects were highly

individualized. The normal load for the relaxed resting arm ranged from 12 N to 32 N. The conditions where the subjects applied shear load to the base of the forearm recorded shear loads ranging from 2 N to 25 N across the subject pool. For the final condition where the subjects leaned on the forearm and applied the maximum comfortable load, normal loads ranged from 28 N to 103 N, and shear loads ranged from 5 N to 49 N.

Comparisons between trials with normal load and those with combined (normal and shear) loads were conducted. Analyses showed that blood flow and transcutaneous oxygen decreased when a shear load was applied in addition to normal load. Though a significant statistical difference was not obtained in all of the cases (at 95% confidence interval), 'medium' effect sizes (> 0.5) were noted in majority of cases, thus showing that significant statistical differences would be obtained, with a larger sample size. The p-values and the effect sizes are listed in Table 2.

The PU level increased as soon as each loading condition was released, possibly due to reactive hyperemia. Reactive hyperemia is a large increase in blood flow following temporary occlusion [2] and it has been suggested in animal models that repetition of ischemia-reperfusion can damage the microcirculation. In addition, when the PU levels during the various recovery periods were compared, a trend of increasing PU from one resting time (RT) to the subsequent resting time was noted (Figure 1).

It is possible that the gradual increase in PU during resting times may have been simply due to the repetition of forces in our study design and the fact that not all PU values reached the resting values by the end of the two minute rest period.

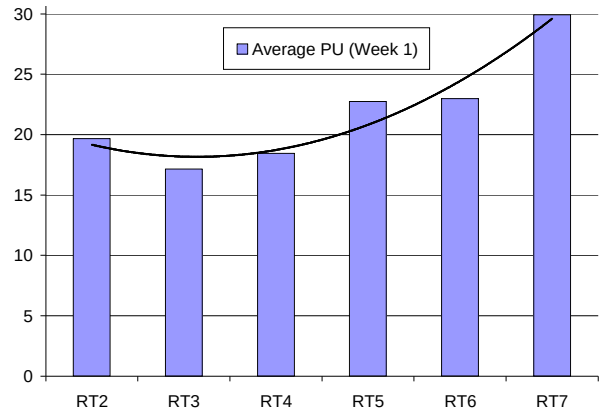

Figure 1: Average PU values obtained during the recovery periods for all subjects, with a polynomial best-fit line (Week 1).

CONCLUSIONS

These data support the finding that combined (normal and shear) loading resulted in additional reduction in PU and tcpO2 levels in human skin as compared to normal loading alone. Several researchers discuss shear force as a factor linked to pressure ulcer generation [3,4]. However, a void in the research exists as past studies have not provided quantification of forces, particularly shear values on human skin. The research presented here, which relates shear loading to PU and tcpO2 levels in human skin, begins to address this void.

REFERENCES

1. Bouten C.V, et al. *Arch. Phys. Med. Rehab.* **84**, 616-619, 2003.
2. Addor G, et al. *Physiol. Res.* **57**, 685-692, 2008.
3. Goossens R, et al. *J. Biomech.* **28**, 225-230, 1995.
4. Van Geffen P, et al. *J. Biomech.* **41**, 2237–2245, 2008.

Table 2: Results of statistical comparisons. PU is perfusion level, tcpO2 is oxygen level

Conditions compared		Week	P value (PU)	P value (tcpO2)	Effect size (PU)	Effect size (tcpO2)
Normal load of forearm	Normal load of forearm + shear	Week 1	0.023	< 0.001	0.555	0.701
		Week 2	0.108	< 0.001	0.750	0.596
Normal load of forearm + 8.9 N	Normal load of forearm + 8.9 N + shear	Week 1	0.136	0.455	0.510	-0.129
		Week 2	0.524	< 0.001	0.277	0.451

TESTING FOR MATERIAL PROPERTIES OF THE HUMAN ANTERIOR CRUCIATE LIGAMENT

[1]Yupeng Ren, [1]Chulhyun Ahn, [1,2]Hyung Soon Park, [4]David T. Fung and [1-4]Li-Qun Zhang
[1]Rehabilitation Institute of Chicago, Chicago, IL.
[2]Departmet of Physical Medicine and Rehabilitation, [3]Department of Orthopaedic Surgery.
[4]Department of Biomedical Engineering, Northwestern University, Chicago, IL.
e-mail: l-zhang@northwestern.edu

INTRODUCTION

Anterior cruciate ligament (ACL) is the most commonly injured human knee ligament and extensive research have been conducted on experimental and computational aspects of ACL injury. However, there is still a lack of information on the anisotropic properties of the human ACL. ACL is often modeled as isotropic and homogenous materials or modeled as transversely isotropic but using estimated material properties [1-2].

The purpose of this study was to perform material testing experiments of human ACL and determine the values of material coefficients in the chosen constitutive relations that give adequate approximation of the mechanical behavior of the ACL.

METHODS

In the transversely isotropic constitutive relations used in the literature [1-3], there are two terms, one describing the isotropic portion of the ligament and the other describing the property along the long axis of the material. Thus, at least two tests, with loads parallel and perpendicular to the material axis, are needed to determine the material coefficients. For these experiments, samples of human ACL were harvested from fresh-frozen cadaveric knees. The ligaments were immersed in normal saline solution and frozen at -70^{o} C. The ACL was then cut into 2mm thick slices using a slicer along the ACL fiber direction (Figure 1a). The test specimen was then obtained by punching a slice using a custom cutter with two parallel blades of fixed distance in between (Figure 1b).

For the material testing, one piece of specimen was cut along the fiber orientation (longitudinal), and another transverse to the fiber orientation. Tissues were kept moist with 0.9% normal saline during the testing.

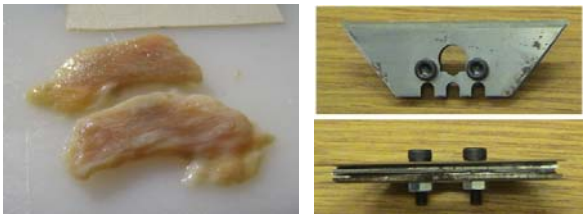

(a) (b)

Figure 1. ACL testing specimen preparation: (a) 2mm thick slices using a slicer along the ACL fiber orientation, (b) A custom cutter with two parallel blades.

The ends of the test samples were mounted in a custom set of clamps for materials testing. Two small dark markers were affixed to the sample and formed a gauge length for strain measurement using a motion analysis system. The zero-load length of each sample was determined by consecutively applying and removing a load up to 0.5N. The sample was cycled 10 times between 0.0mm and 1.0mm elongation, at a rate of 0.02mm/s. This yielded a strain rate of approximately 2%/s. The zero-load length was reestablished and the sample was then immediately loaded to failure at the same rate. All tests were videotaped, and load and crosshead position were digitally acquired at 30Hz. Figure 2 shows the experimental setup for this test.

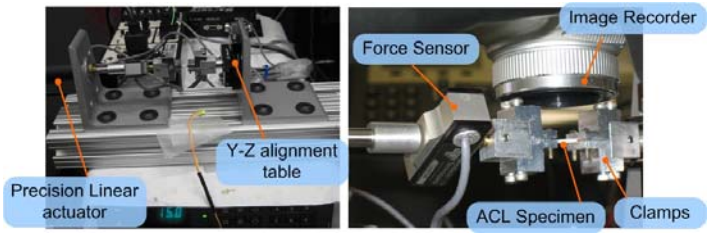

Figure 2. Experimental setup for uniaxial tension test of the human ACL.

RESULTS AND DISCUSSION

The test data were used to determine the coefficients appearing in relevant material equations

[1-3]. For the case of this experimental setting, the stress-stretch relationship was derived from the general constitutive relation as follows:
For the transverse specimen:

$$\sigma = C_1\left(\lambda^2 - \frac{1}{\lambda}\right) + C_2\left(\lambda - \frac{1}{\lambda^2}\right) \quad (1)$$

where σ was the tensile stress transverse to the fiber orientation, λ the stretch transverse to the fiber, and C_1 and C_2 material constants to be determined from the experiment.

For the longitudinal specimen:

$$\sigma = C_1\left(\lambda^2 - \frac{1}{\lambda}\right) + C_2\left(\lambda - \frac{1}{\lambda^2}\right) + \lambda\frac{\partial F_2}{\partial \lambda} \quad (2)$$

$$\lambda\frac{\partial F_2}{\partial \lambda} = \begin{cases} 0, & \lambda < 1, \\ C_3\left(e^{C_4(\lambda-1)} - 1\right), & 1 \le \lambda < \lambda^*, \\ C_5\lambda + C_6, & \lambda \ge \lambda^*, \end{cases} \quad (3)$$

where σ was the tensile stress along the fiber orientation (longitudinal), λ the stretch along the fiber, λ^* the stretch at which all collagen fibers were straightened, and C_3 through C_6 material constants.

Data from stretching the ligament transverse to the fiber orientation was curve-fitted using equation (1) and values of coefficients C_1 and C_2 were estimated. The values thus obtained were fed into the Equations (2) and (3). With the use of experimental curve from stretching along the fiber directions, the values of C_1 through C_6 and λ^* were determined using Matlab Curve Fitting Toolbox.

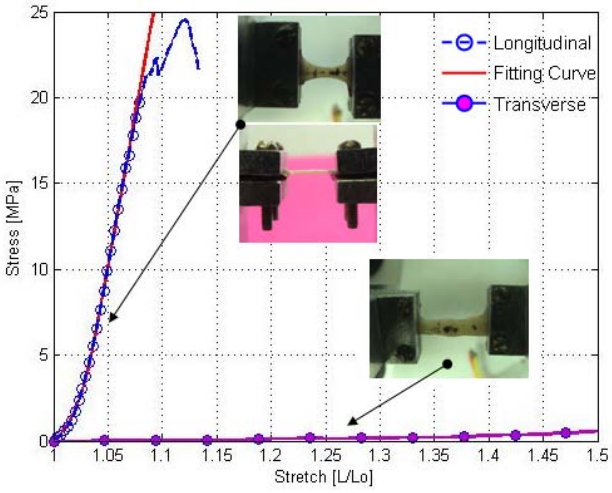

(a)

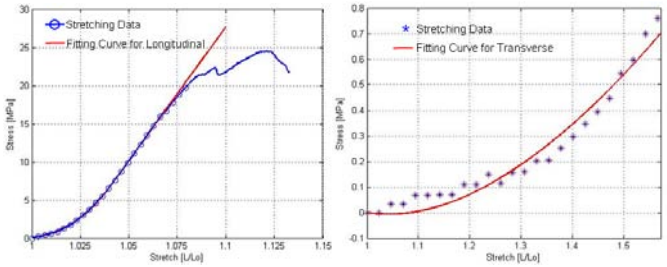

(b) (c)

Fig. 2. Cauchy stress vs. stretch in the ACL specimen (circle: experimental data points used for curve fitting, red solid line: curve-fitting). (a) stretch parallel and transverse to the fibers, (b) stretch along the fibers, (c) stretch transverse to the fibers.

Figure 2 shows the experimental data along the fibers (b) and transverse to the fibers (c), and the curve fitting results. The estimated values of coefficients are as follows: C_1=1.236 MPa, C_2=-1.342 MPa, C_3=1.163 MPa, C_4=47.75, C_5=349.8 MPa, λ^*=1.039.

CONCLUSIONS

In this work, bi-directional ACL mechanical properties parallel to the fiber orientation (longitudinal) and perpendicular to the fiber orientation (transverse) were determined by harvesting regular shaped tissue samples in the corresponding longitudinal and transverse directions. Novel information regarding the mechanical properties of the ACL in relation to the different modes of deformation was determined, which may be directly useful in various forms of constitutive models of the ACL.

The proposed work is our preliminary study about the material property of human ACL. Further study is needed to implement this testing protocol on larger samples with statistical results.

REFERENCES

1. Limbert, G. et al. 2004. *J. Biomech*. **37**, 1723-1731.
2. Weiss, J. A. et al.1996. *Computer Methods in Appl Mechanics Eng*. **135**, 107-128.
3. Park, H. et al. 2010. *J. Biomech*. **43**, in press.

ACKNOWLEDGEMENTS

We acknowledge the support of the NIH.

VISCOELASTIC PROPERTIES OF DIABETIC & NON-DIABETIC PLANTAR SOFT TISSUE

[1,2]Shruti Pai and [1,2,3]William R. Ledoux

[1]VA RR&D Center of Excellence for Limb Loss Prevention and Prosthetic Engineering, Seattle, WA 98108, and Departments of [2]Mechanical Engineering and [3]Orthopaedics and Sports Medicine, University of Washington, Seattle, WA 98195
email: wrledoux@u.washington.edu, web: www.amputation.research.va.gov

INTRODUCTION

A serious complication of diabetes is plantar ulceration, which can often lead to amputation of the affected limb [1]. Approximately 24 million Americans were estimated to have diabetes in 2007 [2]. Development of improved treatments that can reduce plantar ulceration requires understanding the tissue property changes that occur with disease progression. Stress relaxation tests provide a means of quantifying and comparing the time-dependent behavior of tissues by fitting the relaxation data to an appropriate viscoelastic model. Thus, the purpose of this study was to characterize the viscoelastic behavior of both diabetic and non-diabetic plantar tissue.

METHODS

Plantar tissue specimens were obtained from eight fresh frozen cadaveric feet, four diabetic (20.3±8.1 yrs post-diagnosis) and four non-diabetic, from age and weight-matched donors. All feet were harvested within 24hrs post-mortem, and kept frozen until thawing overnight for testing. Two specimens were obtained from each foot at locations subject to loading and ulceration, namely the hallux and calcaneus (Fig. 1A). The plantar soft tissue was dissected free from the underlying muscle and bone, cut into cylindrical specimens using a 1.905cm diameter punch, and further dissected from the skin to maintain *in vivo* thickness (~3 to 11mm depending on location). Specimens were stored on ice until immediately prior to testing. One foot was tested per day and specimen testing order was randomized to minimize any effect due to time between dissection and testing. Since tissue properties are most meaningful under biomechanically realistic loading that is experimentally repeatable, uniaxial unconfined compression tests were modified to constrain the tissue specimens at both ends to emulate the *in vivo* bone and skin boundary conditions. Each specimen was placed between two platens covered with 220 grit sandpaper in an environmental chamber near 100% humidity and at 35°C attached to a materials testing machine. A biomechanically realistic target load, based on specimen area, donor weight, and normative ground reaction force and contact area [3], was applied to the specimens in a load control test of ten 1Hz sine waves to determine the target displacement. Specimens were then tested in displacement control by preconditioning with ten 1Hz sine waves to the target displacement followed by a ramp and hold stress relaxation test to the target displacement (Fig. 1B). Ramp and hold times were 0.1s and 300s respectively.

The resulting force data were normalized by peak force and fit to the viscoelastic model using least squares regression. Fung's quasi-linear viscoelastic (QLV) theory [4] was chosen to model the data as it provides meaningful fit coefficients and has previously been applied to the plantar soft tissue [5]. A direct-fit approach was used whereby the stress-strain data from the ramp portion of the test were first fit to an exponential equation to determine the elastic coefficients A and B. The hold data was then used to simultaneously determine the time constants τ_1 and τ_2 and viscous parameter C.

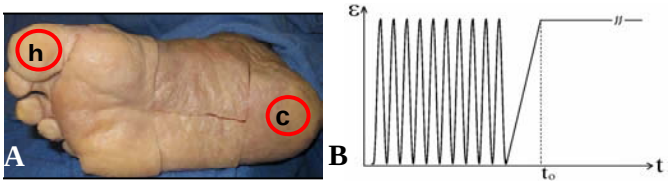

Figure 1: Specimen (A) locations at the hallux (h) and calcaneus (c) and (B) applied strain history.

RESULTS AND DISCUSSION

The relaxation curves obtained from the diabetic and non-diabetic plantar soft tissue varied considerably. In the case of tissue at the hallux (Fig. 2), the diabetic tissue accounted for both the most viscous (D4) and least viscous (D2) behavior. Conversely, the non-diabetic tissue at the calcaneus accounted for both the most viscous (N1) and least viscous (N4) behavior.

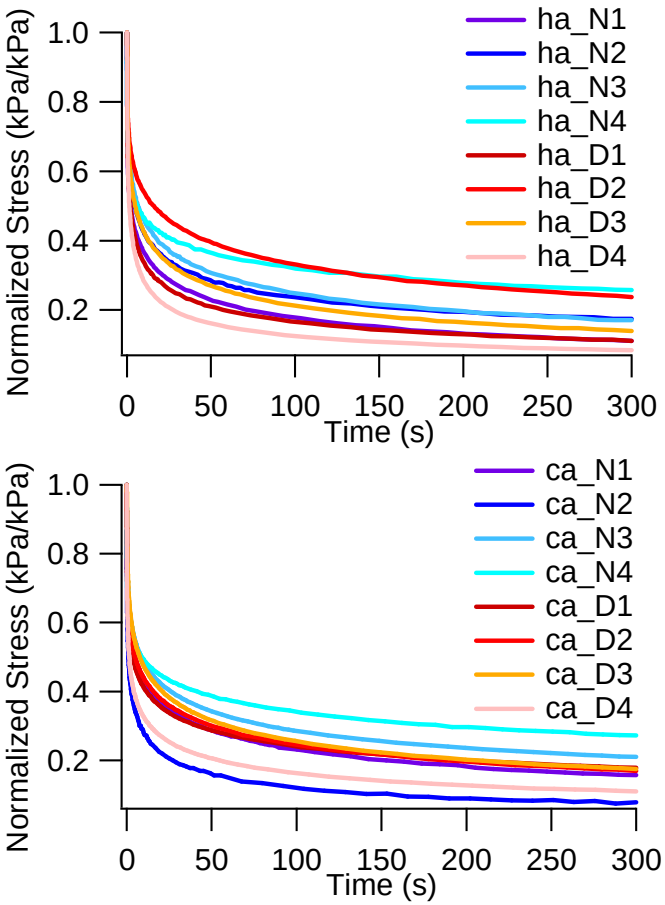

Figure 2: Relaxation curves for diabetic (D) and non-diabetic (N) specimens at the hallux (ha) and calcaneus (ca).

Based on the observed variability in the relaxation curves, it is not surprising that the QLV fit coefficients also varied considerably (Table 1). Although a smaller difference in τ_2 was anticipated as the specimens appeared to reach steady state at similar rates, this discrepancy is partially an artifact of the higher distribution of data points at the beginning of the curve that were required to capture the initial relaxation. More importantly, the model's tendency towards non-unique solutions (i.e., several acceptable combinations of coefficient values) was reduced by using a direct fit approach, making the curve fitting algorithm more robust and much less sensitive to supplied initial guesses for coefficients.

Tests are ongoing to increase the number of specimens and to look at other relevant specimen locations (e.g., the metatarsal heads). While statistical tests are yet to be conducted due to the small variable set of data, the current findings suggest that there are few changes in the viscoelastic behavior of the plantar tissue in the presence of diabetes or due to location.

Table 1: Fit coefficients at both locations tested for both diabetic (D) and non-diabetic (N) specimens.

	A (Pa)	B	C	τ_1 (s)	τ_2 (s)
			hallux		
N1	0.72	26.4	0.863	0.008	244
N2	0.93	24.8	0.591	0.025	288
N3	5.57	22.1	1.986	0.034	1602
N4	8.14	21.5	0.287	0.000	219
D1	0.65	28.3	0.841	0.031	91
D2	1.27	22.2	4.962	0.041	9103
D3	1.26	26.8	0.900	0.056	332
D4	0.68	27.0	1.140	0.034	57
			calcaneus		
N1	0.72	20.6	6.837	0.010	2495
N2	0.84	30.5	1.045	0.010	66
N3	2.62	20.5	0.729	0.025	1294
N4	2.21	17.9	0.268	0.002	251
D1	1.93	20.8	0.506	0.012	223
D2	0.46	23.0	0.631	0.017	468
D3	0.89	22.6	1.246	0.051	1135
D4	0.11	24.6	0.812	0.011	108

REFERENCES

1. Van Schie CH, *Int J LE Wnds* **4**(3), 160-70, 2005.
2. CDCP, *Nat Diab Fact Sheet* Atlanta, GA: 2007.
3. Ledoux WR, *Gait Posture* **15**, 1-9, 2002.
4. Fung YC, *Biomechanics* Springer-Verlag, 1993.
5. Ledoux WR, *J Biomech* **40**(13), 2975-81, 2007.

ACKNOWLEDGEMENTS

This work is being supported by NIH grant 1R01 DK75633 and the VA RR&D Service.

CHANGES IN CROSS SECTIONAL STRESS AT THE DISTAL RADIUS FOLLOWING SHORT TERM MECHANICAL LOADING

W. Brent Edwards and Karen L. Troy

[1]University of Illinois at Chicago, Chicago, IL, USA
email: edwardsb@uic.edu, web: http://www.uic.edu/ahs/biomechanics

INTRODUCTION

As the benefits of physical activity and exercise on bone quality continues to gain acceptance, mechanical loading based interventions are becoming more common. Most of this work has focused on strengthening bones of the lower extremity, despite the fact that nearly 40% of all dollars spent on physical therapy following osteoporotic fractures are to treat the distal forearm [1]. Moderate improvements in bone mineral content are known to occur following 9-12 months of weight-bearing exercise. However, our recent work suggests that in the short-term (i.e., 7-14 weeks), mechanical loading causes an acute and reversible reduction in bone mineral content [2]. It remains unclear if this initial reduction in bone mineral content is associated with an increase in fracture risk during this time period. The purpose of this study was to evaluate changes in fracture risk by quantifying cross sectional mechanical properties of the distal radius after seven weeks of mechanical loading.

METHODS

Five young females (age 22.2 ± 2.7 yrs; height 167.5 ± 7.3 cm; mass 67 ± 2.9 kg) were recruited for this institutionally approved study. Following written informed consent, subjects participated in a voluntary mechanical loading intervention targeting the distal radius of the non-dominant forearm. The dominant side served as a within-subject control. The loading program required subjects to lean onto their palm, thereby applying a compressive force, for 50 cycles per day, 3 days per week, for 7 weeks (Fig 1). A load cell device and oscilloscope provided real-time visual feedback of the applied load so that subjects could achieve a target load of 300 N (≈ ½ bodyweight) every 2 sec (Fig 1). Subject-specific finite element models estimated this force to cause a peak compressive strain of 1,803 ± 659 με on the periosteal surface of the distal radius (mean strain over the entire periosteal surface: 349 ± 146 με). Power spectral analysis revealed the frequency of the loading waveform to have major components at 1 and 2 Hz.

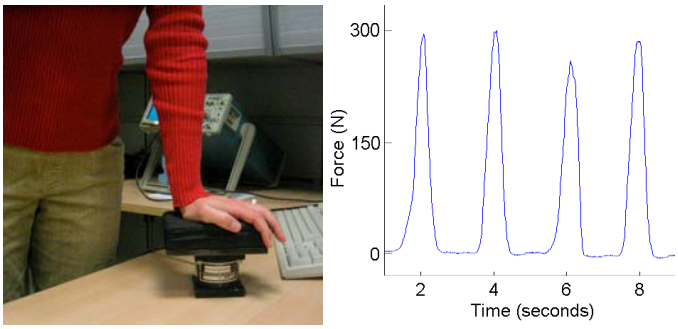

Figure 1: Experimental set-up and force recording.

High resolution computed tomography (CT) data were acquired pre- and post-intervention for both dominant and non-dominant forearms (voxel size: 625 x 234 x 234 μm). A calibration phantom was included to establish relationships between Hounsfield units and apparent density. The CT data were resliced based on bony landmarks to ensure similar coordinate systems between pre- and post-intervention CT scans. A single transverse cross section, 7.5 mm proximal to the subchondral plate, was extracted for data analysis.

Changes in cross sectional properties were quantified using VA-BATTS software [3]. VA-BATTS is an open-source software that calculates cross sectional properties and out-of-plane stresses for cross sections having inhomogeneous material properties. Four stress analyses were run for each cross section to examine pre/post differences in stress due to 1) axial compression, 2) bending about a coronal axis (dorsal/palmer bending), 3) bending about a sagittal axis (medial/lateral bending), and 4) torsion. The applied axial compressive (500 N), bending (10 Nm), and torsional load magnitudes (angle of twist 0.005 rad/mm) were arbitrarily chosen to produce physiological stresses between 10 and 30 MPa.

Dependent variables of interest included cross sectional area, modulus weighted principal moments of inertia, modulus weighted polar moment of inertia, maximum compressive stress due to axial loading (σ_a), maximum compressive (σ_{bc}) and tensile stresses (σ_{bt}) due to coronal and sagittal bending, and maximum shear stress due to torsion (τ). Changes in pre- and post-intervention dependent variables, for both loaded and unloaded radii, were compared using paired Student's t-tests with the criterion alpha level set to 0.05. Cohen's *d* effect sizes were used to help guide the interpretation of meaningful findings.

RESULTS AND DISCUSSION

No significant pre/post changes in cross sectional area or moments of inertia were observed in either the loaded or control radii. A significant increase and large effect size was observed for coronal σ_{bc} (Fig 2; Table 1), indicating that the bone was weaker in coronal bending after seven weeks of loading. Although, increases in τ were similar between loaded and control radii, the pre/post increase was only significant for the control (also indicating a weaker bone for torsional loading).

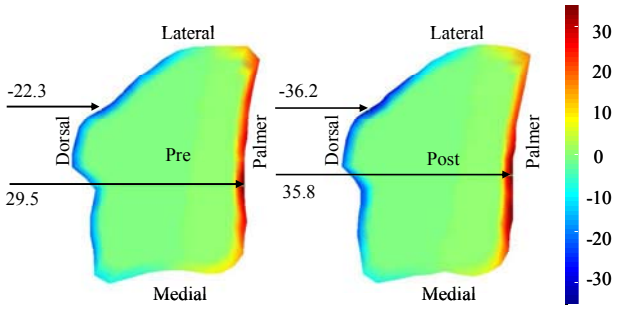

Figure 2: Representative pre- and post-intervention CT slices illustrating coronal σ_{bc} and σ_{bt}.

In general, stresses were higher post-loading in both the loaded and control radii, indicating an overall decrease in mechanical properties. This raises questions about the reliability in comparing longitudinally collected CT data. We attempted to control for this by using the same scanner with identical scanning protocols for both pre- and post-intervention data. However, arguments pertaining to reliability cannot explain the much larger change and effect sizes for bending stresses in the loaded radius (Table 1). Neither can they explain the observed discrepancy in change and effect size for axial stress in the control radii (Table 1). Thus, the observed increases in stress for the control radii may be explained by a systemic bone remodeling response, since presumably the radii of the subjects were at stasis prior to the loading intervention.

The observed increases in maximum bending stress could not be explained by changes in cross sectional properties. This suggests, perhaps, that changes in stress arose from an increase in the heterogeneity of bone density distribution. We believe this may be a result of increased remodeling space and/or trabecular surface resorption that reflects osteoclastic activity prior to any significant bone apposition.

CONCLUSIONS

Short-term mechanical loading of the distal radius caused a reduction in bending resistance as indicated by increased stress concentrations for inhomogeneous beam theory analysis. These results suggest that the radius may be at increased risk for fracture, should a fall occur during the initial stages of a mechanical loading intervention. More work is needed to determine the relationship between single CT slice stress analysis and whole bone failure, and how this short-term response is related to long-term changes in bone strength.

REFERENCES

1.Melton LJ. *J Bone Miner Res* **18**, 1139-1141, 2003.
2.Troy KL & Edwards WB. *Proceedings of ORS*, New Orleans, LA, USA, 2010.
3.Kourtis, LC, et al. *Comput Methods Biomech Biomed Engin* **11**, 463-476, 2008.

Table 1: % Change and Effect Sizes (ES) for loaded and control radii. Positive values represent an increase in stress for axial compression σ_a, bending compression σ_{bc} and tension σ_{bt}, and torsion τ. * = $p<0.05$

	σ_a	Coronal σ_{bt}	Coronal σ_{bc}	Sagittal σ_{bt}	Sagittal σ_{bc}	τ
%Change Loaded	-0.50	16.66	51.36*	22.99	42.99	17.37
%Change Control	15.36	13.35	16.42	12.54	3.77	18.20*
ES Loaded	-0.04	0.39	1.21	0.36	0.82	0.41
ES Control	1.53	0.32	0.39	0.28	0.06	0.59

ACL LENGTH CHANGES DURING ROBOTIC SIMULATION OF KNEE LAXITY TESTS

Andy Dong-Gil Lee, Jennifer E. Hagen, Christopher J. Wahl, Paul. A. Manner, and Peter R. Cavanagh

University of Washington, Seattle, WA, USA
email: cavanagh@uw.edu

INTRODUCTION

Knee laxity tests are performed to assess the integrity of the anterior cruciate ligament (ACL) and other structures of the knee joint. In order to understand the mechanical behavior of the ACL, *in vivo* strain measurements during a Lachman test have been made using a Differential Variable Reluctance Transducer (DVRT) (peak strain 3.7% under a 150N anterior shear load) [1]. In addition, robotic systems have been used to assess the *ex vivo* kinematics of the knee and forces in the ACL by comparing resultant forces among intact, ACL-deficient, and ACL-reconstructed knees during simulated laxity tests (a 134 N anterior tibial load, or a combined 10 Nm of valgus torque and 5 Nm of internal and external tibial torques) [2]. The purpose of this study was to develop a method using a seven degree of freedom (7-DOF) robotic system to combine a simulated robotic laxity test with direct measurement of ACL length change.

METHODS

The main components of the 7-DOF robotic system are listed in **Table 1**. Since the R2000 robotic system (Parallel Robotic System, Hampton, NH) has limited rotational motions in raw and pitch axes (± 15 degrees), a rotary stage fixation system (Cleveland Clinic, Cleveland, OH) was built to simulate the full knee flexion motion. This robotic system uses the joint coordinate system as defined by Grood and Suntay [3]. A microscribe was used to measure coordinates of the robot and anatomical landmarks of the knee. A 6-DOF load cell (ATI, Apex, NC) was used to acquire three forces and three moments in a tibial reference frame. A micro-miniature DVRT (M-DVRT) (Microstrain, Williston, VT) was implemented to measure ACL length change directly. A dynamic three-dimensional position measurement sensor (Polaris, NDI, Waterloo, ON) was installed to compute kinematic data. Custom position and force control software was used (LabVIEW, National Instruments, Austin, TX).

Table 1: The main components of the current 7-DOF robotic system.

Component	Function
R2000 robot	6-DOF robotic system
Rotary stage	7^{th} DOF rotary fixation system
Microscribe	Coordinate measurement
Load cell	6-DOF force and torque measurement
M-DVRT	Strain measurement sensor
Polaris system	Dynamic 3-D position measurement
LabVIEW software	Position and force controller

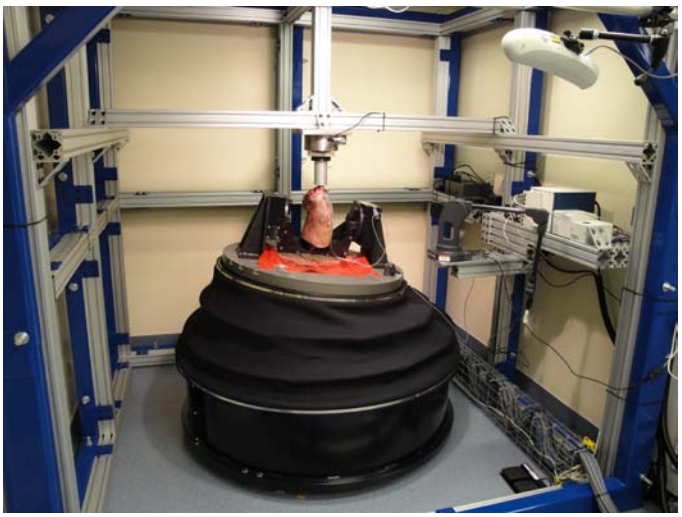

Figure 1: The 7-DOF robotic system. A human cadaveric knee specimen is shown mounted for the testing.

A left human cadaveric knee (32 year-old male) from the mid femur to the mid tibia was used to demonstrate the procedure (**Figure 1**). The specimen was stored at -20°C before testing. It was

then thawed at room temperature and denuded of soft tissue 4 inches proximal and distal to the knee joint line to expose the femur and the tibia which were then potted using body filler (Bondo, 3M, Maplewood, MN) in aluminum tubes. The distal end of the tibia was mounted on the 6-DOF load cell and the proximal end of the femur was mounted on the rotary stage using custom clamps. The specimen was neutrally mounted on the robotic system at 0° of flexion. An incision was made along the medial margin of the patella and the patella tendon to gain access to ACL. The initial neutral distance between the two insertion barbs of the M-DVRT was 5mm. The M-DVRT was attached to the mid-section of the anteromedial (AM) bundle of ACL at 30° of knee flexion (**Figure 2**). A cyclic load with 150N of anterior tibial load at 30° of flexion was applied to the specimen to simulate a Lachman test. Resultant forces from the tibia and local length changes of ACL were simultaneously acquired during the simulated Lachman testing.

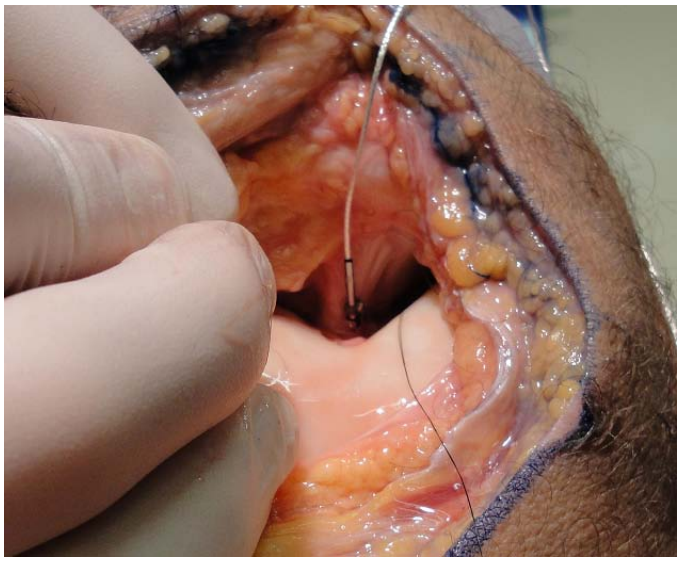

Figure 2: The M-DVRT attached to the mid-section of the AM bundle of ACL at 30° of flexion.

RESULTS AND DISCUSSION

The actual loading profiles tracked the desired loading profiles reasonably well after the first loading cycle (**Figure 3**), although there was a time lag in return to baseline after loading.

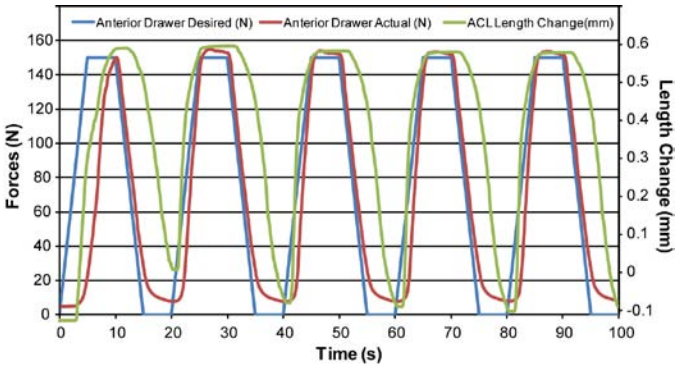

Figure 3: Results from simulated Lachman test showing the desired and actual loads together with the change in gauge length. Distance between the 2 M-DVRT insertion barbs changed a total of 0.7mm from the initial neutral distance of 5mm.

The limitations of the M-DVRT in measuring ACL characteristics include the fact that only local length changes in the surface fibers of the ligament are evaluated. There is also a possibility for bony impingement of the sensor or mechanical interference from the lead wires that could affect sensor outputs. The slack-taut characteristics of ACL and the actual length of the ligament will need to be evaluated in order to estimate true ACL strain.

CONCLUSIONS

This robotic system performed well during a simulated Lachman test. Future work will concentrate on the development of a method to calculate actual strain in the ligament during a variety of motions.

REFERENCES

1. Beynnon BD, et al. *J Biomech* **31**, 519-525, 1998.
2. Woo SL, et al. *J Bone Joint Surg Am* **91**, 78-84, 2009.
3. Grood ES, et al. *J Biomech Eng* **105**, 136-144, 1983.

ACKNOWLEDGEMENTS

The contributions of Nicholas M. Kramer, Robb W. Colbrunn, and Antonie J. van den Bogert are gratefully acknowledged.

UNDERSTANDING THE EFFECTS OF LIGAMENT SECTIONING ON THE STABILITY OF THE ANKLE AND SUBTALAR JOINT USING EULER ANGLES AND THE ROTATION ABOUT A HELICAL AXIS

[1]Julie Choisne, [1]Stacie I. Ringleb , [1]Michael Samaan, [1]Sebastian Bawab and [2]Dayanand Naik

[1]Mechanical Engineering, Old Dominion University, Norfolk, VA, USA
[2]Math and Statistics Old Dominion University, Norfolk, VA, USA
email: SRingleb@odu.edu

INTRODUCTION

It is critical to understand the kinematics of the intact and unstable hindfoot in order to prevent abnormal joint mechanics that can impair the function of the foot and lower extremity and may lead to a breakdown in foot structure and pain. One example of a pathology that can lead to long-term complications is subtalar joint instability, as this instability is most often diagnosed as ankle instabilities [1].

The effects of ligament sectioning on ankle and subtalar joint kinematics in all planes of motion using Euler angles analysis was previously studied [2]. The Euler angle method decomposes the motion onto three anatomic planes that is convenient to describe each individual motion. Another method that could be used to assess joint kinematics is to examine the helical axis data. The helical axis is a screw axis that can describe the motion between two bones by considering the angle of rotation around this axis and the amount of translation along this same axis. This method may be most appropriate for the subtalar joint, as the subtalar joint axis has been described to be the helical axis between the talus and the calcaneus. The purpose of this study was to calculate the helical axis at the ankle and subtalar joint and to examine the differences between the Euler angles method and the helical axis analysis.

METHODS

Seven fresh-frozen cadaveric lower extremities were obtained sectioned at the midpoint of the shank (5 left, 3 right; mean age 74.3 years; 6 female, one male, one unspecified). Each specimen was placed into a custom six degree-of-freedom positioning and loading device [2]. Kinematic data were collected from the tibia, talus and calcaneus with a Polhemus Liberty (Polhemus, Colchester, VT) and The MotionMonitor (Innovative Sports Training, Chicago, IL).

Data were collected by applying inversion/eversion, internal/external rotation plantar/dorsiflexion, supination/pronation and inversion/eversion when the foot was dorsiflexed. Data from the aforementioned motions were collected on an intact hindfoot and after sequentially sectioning the anterior talofibular ligament (ATFL), the calcaneofibular ligament (CFL), the cervical ligament and the interosseus ligament.

Euler angles were exported directly from the MotionMonitor and analyzed with a custom program written in Matlab (The Mathworks, Natick, MA). Helical axes were calculated using Spoor & Veldpaus [3] method for each frame with reference to the previous frame using a custom Matlab program. The angles of interest for each kinematic method (i.e., intact vs. ATFL cut, etc.) were calculated. A repeated measure ANOVA (α=0.05) with a modified Hochberg's correction was used to analyze the data using SASS.

RESULTS AND DISCUSSION

Results using the helical axis representation are presented as a net rotation about the helical axis. The Euler angle methods calculated rotations about three axes of rotation (inversion/eversion, internal/external rotation and plantarflexion/ dorsiflexion). Only rotations that were both statistically and clinically significant (i.e., at least a 3º difference) are discussed here.

Significant differences were found at the subtalar joint during inversion after the interosseus ligament was cut for the helical axis method (8.7º±5.5º to 16.1º±10º, p<.0001) and the Euler angle method (7.0º±2.0º to 20.4º±9.5º, p<.0001). When internal rotation was applied, a significant difference was observed using the helical axis method between the CFL cut and cervical ligament cut conditions (3.9º±3.4º to 6.4º±6.6º, p=.0441), but not using the Euler method. During supination (Figure 1), when the interosseus ligament was sectioned, there was a significant difference for the helical axis (8.4º±6.3º to 15.1º±10.98º, p=0.0039). Additionally, Euler angles showed significance in the inversion direction (8.4º±7.4º to 17.8º±9.5º, p<.0001) and in internal rotation (13.1º±5.9 to 18.7º±11.3º, p=0.0038) when supination was applied.

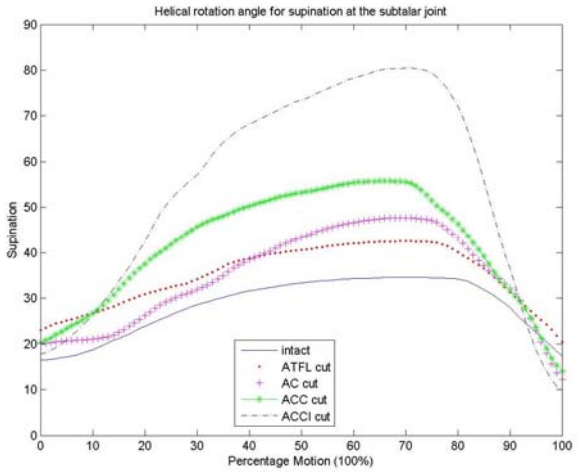

Figure 1. Rotation About the Helical Axis when Supination (i.e., combined inversion, internal rotation and plantarflexion) was applied

At the ankle joint, during internal rotation, there was a significant increase in the Euler angle after the ATFL was sectioned (6.1º±3.5º to 14.9º±5.0º, p<.0001), where no significance was observed when using the helical axis rotation.

Because the helical axis method quantifies the net rotation about the axis of rotation of the joint, while the Euler method calculated rotations about three axes, the helical method may be a better alternative to identifying subtalar joint instability. However, it is important to continue to consider Euler angles, as they may also detect instabilities that are not detected.

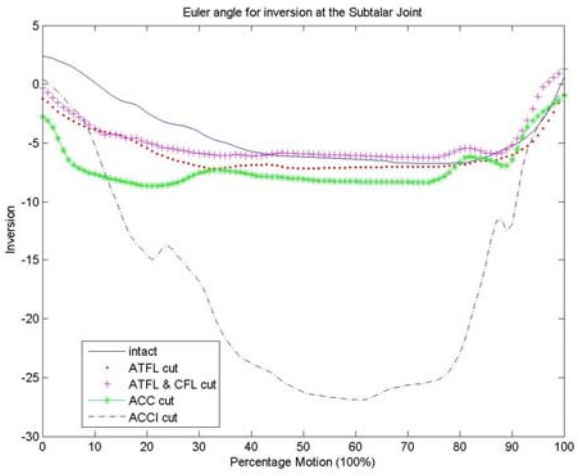

Figure 2. Rotation About the Inversion Axis During Supination using the Euler Method (note inversion is negative).

CONCLUSIONS

When inversion and supination were applied to the hindfoot between the cervical ligament cut condition and interosseous ligament cut condition, significance was found using both techniques. Additionally, the helical axis method found additional significant differences at the subtalar joint during inversion between the CFL and cervical ligament cut condition, when the Euler method did not. This suggests that the helical axis method may able to detect subtalar joint instability before the Euler method can because it considers a net rotation about the joint axis of rotation, instead of individual rotations about three axes.

REFERENCES

1.Thomas O. Clanton. *Orthopedic Clinics of North America* **20**, 583-592, 1989.
2.Ringleb SI, et al. The effects of lateral ligament sectioning on the stability of the ankle and the subtalar joint, *ASB abstract*, 2009.
3.Spoor CW, et al. *J. Biomechanics* **13**, 391-393, 1980.

ACKNOWLEDGEMENTS

This study was partially funded by the American Orthopaedic Foot and Ankle Society.

A NEW INSTRUMENT FOR ASSESSING HEEL PAD MECHANICAL PROPERTIES

[1,2]Daniel J. Gales and [1]John H. Challis

[1]Pennsylvania State University, University Park, PA, USA
[2]Lock Haven University, Lock Haven, PA, USA
email: djg153@psu.edu

INTRODUCTION

It has been shown that heel pad mechanical properties can change under certain conditions: for example, injury [1], due to aging [2], and due to different exercise regimes [3]. In clinical settings the measurement of heel pad stiffness is typically accomplished through manual palpation.

Different methods for measuring heel pad properties in vivo have been reported including ultrasound based techniques [4], pendulum techniques [5], and indentation techniques [6]. Rome and Webb [7] developed a hand-held indentation device for measuring heel pad properties in vivo. In this device, a 6 mm diameter probe was attached to a strain-gauge load cell. The probe passed through a Perspex indentation plate. To measure displacement, the actuator of a linear variable differential transformer was attached to the Perspex plate. Displacement and force were manually controlled.

Although the manual testing device of Rome and Webb [7] has many desirable qualities it relies on the operator to produce consistent displacement rates to heel pads across a range of subjects. Therefore the purpose of this study was to develop a reliable and accurate tool to assess the mechanical properties of the human heel pad, where the displacement rate is computer controlled.

METHODS

For device development and validation a surrogate for a human heel pad was used – an open-celled foam blank with similar properties to the human heel pad. Its mechanical properties were tested using both the new device and a dynamic testing system. With both systems force and displacement data were collected. For each protocol, the open-celled foam was indented 5 mm at 2.5 mm/s for 10 compressions.

The first protocol utilized a custom indenter with a force sensor attached to a stepper motor (Fig. 1). A piezoelectric uniaxial force transducer (Kistler 9212) was attached to an Exonic Systems stepper motor (IAI Incorporated). Displacement and rate of displacement of the stepper motor were computer controlled. Attached to the load cell was a 6 mm diameter aluminum, flat-tipped probe. Displacement of the force transducer was measured using a linear variable differential transformer (LVDT). Force and displacement data were collected using a custom Labview program collecting data at 1,000 Hz.

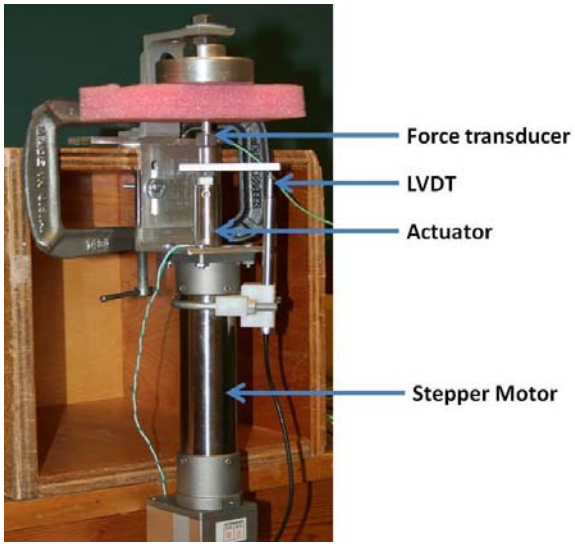

Figure 1: Custom Heel Pad Indenter with 6 mm probe.

The second protocol utilized a dynamic material testing system (MTS) (Instron 8031) to assess the force and displacement properties of the foam blank (Fig. 2). A 6 mm diameter, aluminum, flat-tipped probe was attached to the force sensor of the MTS. The open-celled, foam blank was secured to the

linear actuator of the MTS. The MTS was operated in displacement mode and displacement and force data were collected at 10,000 Hz.

To compare the two systems the Bland and Altman [8] method of differences was used. The MTS results were considered the criterion against which the custom indenter was compared.

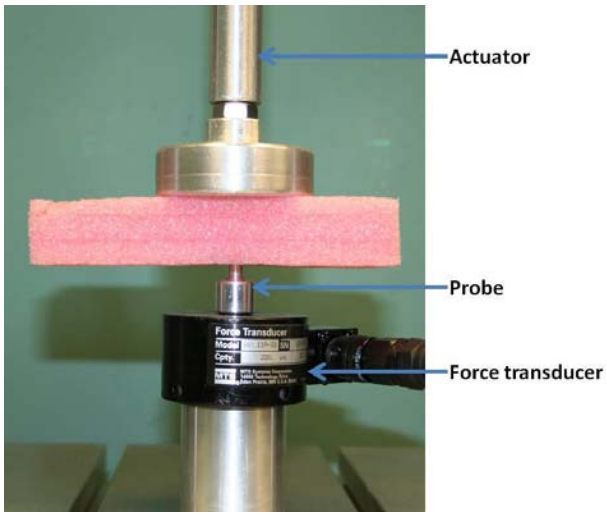

Figure 2: MTS with 6 mm probe

RESULTS AND DISCUSSION

The Bland and Altman [8] method of differences was used to compare the two methods for determining peak force. Results for the first 10 force peaks are found in Figure 3.

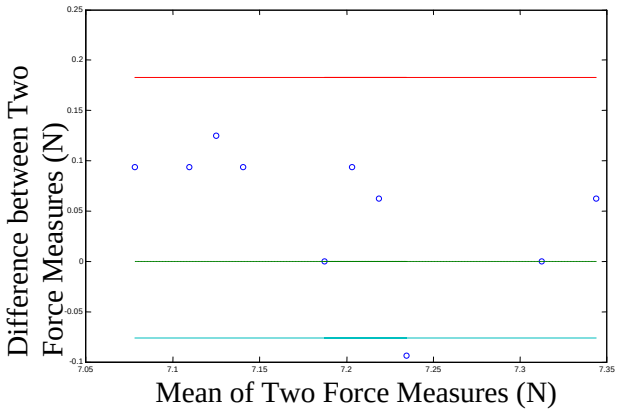

Figure 3: Bland and Altman (1986) results for MTS versus heel pad indenter forces.

The 95% confidence intervals indicate good agreement between the MTS force output and the custom heel pad indenter output. Regression analysis of the pairs of differences versus the means of the pairs of measures produced a gradient line that was not statistically different from zero; indicating no proportional bias in these measures. The differences between the pairs of measures were statistically different from zero indicating a relative bias. Similar results for displacement measures between these two devices were found.

The custom heel pad indenter is a computer controlled, motorized device designed for measuring heel pad properties in vivo. Data obtained using a foam blank indicate that this device is valid to measure mechanical properties. The presence of no proportional bias in the force measures indicates that this device operates well. The presence of a relative bias indicates a systematic offset in the device which can be adjusted for in future data collection with the heel pad indenter.

CONCLUSIONS

The results of this study indicate that this heel pad indenter is an accurate tool for measuring force and displacement properties of human heel pad-like materials. With further research, this device may be used in clinical settings to assess the heel pad properties of normal subjects and those in unique populations including diabetic patients and those with chronic heel pain.

REFERENCES

1.Rome K, et al. *Clin Biomech*, **16**, 901-905, 2001.
2.Kinoshita H, et al. *Eur J Appl Physiol*, **73**, 404-409, 1996.
3.Challis JH, et al. *J App Biomech*, **24**, 377-381, 2008.
4.Morag E. and Cavanagh P. *J. Biomech* **32**, 359-370, 1999.
5.Kinoshita H, et al. *Int J Sports Med* **14**, 312-319, 1993.
6.Wang CL, et al. *J. Formos Med Assoc* **97**, 850-854, 1998.
7.Rome K. and Webb P. *Clin Biomech*, **15**, 298-300, 2000.
8.Bland JM and Altman DG. *Lancet*, **1**, 307-310, 1986.

FATIGUE PROPERTIES OF PROXIMAL HUMERAL FRACTURES FIXED WITH LOCKED PLATE SYSTEM

Jihui Li, Ph.D; Robert Hymes, MD; Jeff Schulman, MD; Mark Theiss, MD

Inova Fairfax Hospital, Falls Church, Virginia, USA
email: jihui.li@inova.org

INTRODUCTION

Locked plate system is a relatively new technique to fix displaced proximal humeral fractures. It was believed to have better initial stability and fixation strength over non-locked plate in elderly patients with poor bone quality [1]. However, its fatigue properties were not well known in previous research because: 1. The relationship between bone mineral density (BMD) and the mechanical strength of the locked plate fixation was conflicting [2, 3]; 2. Fatigue induced damage could not be monitored in real time to demonstrate the damage progression during the entire fatigue process.

The purpose of this research was to develop a new method to study the fatigue properties of proximal humeral fractures fixed with locked plate system. Quantitative CT (QCT) was used to determine the depths and apparent density of local cancellous and cortical bones penetrated by screws. The hypothesis was that the mechanical strength of the fixation is influenced by local bone quality (cortical density and cancellous density) and depth of screw penetration (cortical depth and cancellous depth). Acoustic emission (AE) technique was used to real timely monitor the fatigue induced microcracks.

METHODS

Five pairs of cadaveric humeri were harvested and scanned using QCT with a K_2HPO_4 calibration phantom included in each scan. A proximal humeral fracture was created and stabilized with a PERI-LOC® locked plate system (Smith & Nephew Inc.). Post-op QCT were taken and registered onto pre-op QCT in Mimics (Materialise Inc.) to determine the path of each screw. The sum of the penetration depth of all the screws in the cortical bone was defined as cortical depth (T_{cor}), and that in the cancellous bone was cancellous depth (T_{can}). BMD (equivalent to K_2HPO_4) of local bone along screw path was measured and converted to apparent density [4]. Averaged apparent density of all the screws of the local cortical bone was defined as cortical density (D_{cor}), and that of cancellous bone was cancellous density (D_{can}).

The specimens were mounted onto a Bionix system (MTS Inc.) and subjected to a cyclic compressive load of 500±100 N at 2 Hz for 15,000 cycles, or until gross failure [5] (Fig.1). The load was applied 30° posteromedially to the anteroposterior plane to simulate a force at the glenohumeral joint in 0° of abduction. The failure was defined as bone fracture or 20 mm of vertical displacement of the actuator. A nonlinear regression model was proposed to study the influences of T_{cor}, T_{can}, D_{cor} and D_{can} to the failure cycle number N:

$$\ln N = a \cdot T_{cor} + b \cdot D_{cor} + c \cdot T_{can} + d \cdot D_{can} + e \cdot T_{cor}^2 + f \cdot D_{cor}^2 + g \cdot T_{can}^2 + h \cdot D_{can}^2 + i \quad (1)$$

Where a to h are coefficients and i is the intercept. Statistical analysis was performed using SAS.

Seven AE sensors (PAC Inc.) were glued onto the specimen surface to detect AE microcracks occurred during fatigue test. A signal captured by four or more sensors was locatable in 3D, and defined as a Type I microcrack. Otherwise, the signal was unlocatable and defined as a Type II microcrack. The locations of Type I microcracks were calculated and overlaid onto X-ray images of the specimen to demonstrate the real time damage progression along the fatigue procedure [6]. The amplitude range of each microcrack was used to indicate the damage severity.

Fig.1. Test setup with AE sensors attached.

RESULTS

Based on the failure cycles (Table 1), the specimens could be divided into three groups: the first group included 3L and 3R, failed in less than 1,000 cycles. The second group had 1L, 2L, 1R, 2R and 4R, failed in less than 6,000 cycles. The third group had 4L, 5L and 5R, survived or failed around 15,000 cycles. Most of the failures were because the actuator displacement reached the 20 mm limit. Statistical analysis showed that the failure cycle number of the humeral fracture fixation was mainly influenced by D_{cor}, D_{can}, T_{can} and T_{can}^2. D_{can}'s influence is much more than D_{cor}. No significant influences were found for T_{cor} and three quadratic items. The resulted nonlinear model was:

$$\ln N = 6.1064D_{cor} + 0.5157T_{can} + 56.0885D_{can} - 0.0011T_{can}^2 - 67.2296 \quad (2)$$

The residual (σ^2) of the model was 0.6411.

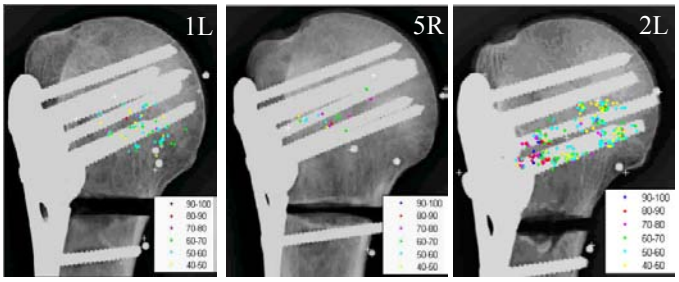

Fig. 2: Calculated locations of Type I microcracks in 1L, 5R and 2L. Color legend showed amplitude range of the microcracks.

Based on the location and amplitude of Type I microcracks occurred during fatigue tests, the specimens could be divided into three groups as well: 1L and 1R had low amplitude microcracks accumulating around the middle and tip area of the screws until failure (Fig.2). Damage was found jumping among screws in a spread pattern. 2R, 3L, 4R, 5L, 5R had few microcracks randomly distributing at the middle area. 2L, 3R and 4L at first had high amplitude microcracks accumulating at the plate-screw interface area and finally lower amplitude microcracks at the middle and tip area.

DISCUSSION AND CONCLUSIONS

This study demonstrated that the screw penetration depth in cancellous bone, quality of local cancellous and cortical bones are important biomechanical factors that may determine the success of the humeral fracture fixation surgery using locked plate system. Meanwhile, AE technique provided unique information for us to understand the progression of the fatigue induced damage. It was found that in some failed specimens the damage started from the screw-plate interface area, indicating the nearby cortical bones may be the first barrier to resist fatigue loading. During the final failure period of most specimens, microcracks occurred mainly at the middle and tip area of the screws, suggested that the screw-cancellous bone interfaces is the final barrier. These implied screws should go through bone areas that can provide stronger resistance to fatigue load.

The limitation of this study was that the calculated locations of Type I AE microcracks are not very accurate due to the small size of the specimen and high velocity of AE signals. As a result we were unable to correlate a Type I microcrack to a specific screw-bone interface and identify its role in the fatigue failure of the humeral fracture fixation.

REFERENCES

1. Smith et al., JBJS, 2007.
2. Siffri et al., J Orthop Trauma, 2006.
3. Weinstein et al., J Shoulder Elbow Surg., 2006.
4. Lotz et al., J Comput Assist Tomogr., 1990.
5. Sanders et al., J Shoulder Elbow Surg., 006.
6. Li et al., JNE, 2009.

ACKNOWLEDGEMENTS

This study was funded by Inova Executive Grant #150061. The authors acknowledged Smith & Nephew Inc. for providing the implants.

Table 1: Mechanical and AE test results. Disp. is actuator displacement; Cycle No. is failure cycle number.

Specimen	1L	2L	3L	4L	5L	1R	2R	3R	4R	5R
Cycle No.	3118	5740	815	14514	15000	3687	2914	166	3356	15000
Disp. (mm)	20	20	20	20	5.41	20	15.3	20	13.2	7.63
Type I No.	99	313	15	67	1	51	9	108	4	17
Type II No.	2010	1817	213	398	65	1066	83	1150	101	104

THE USE OF ULTRASOUND ELASTOGRAPHY TO ASSESS LONG-TERM TENDON REMODELING AND MECHANICS FOLLOWING MUSCULOTENDON INJURY

Laura Chernak, Amy Silder, Kenneth Lee and Darryl Thelen

University of Wisconsin-Madison, Madison, WI, USA
email: lchernak@wisc.edu, web: http://www.engr.wisc.edu/groups/nmbl/

INTRODUCTION

Acute musculotendon strain injuries are challenging to treat clinically, with athletes being at a high risk of reinjury when returning to sport [1]. Long-term changes in musculotendon morphology may contribute to reinjury risk. In particular, previously injured muscles often exhibit evidence of residual scar tissue at the musculotendon junction [2], which has inferior structural organization of collagen fibers [3]. We recently showed using dynamic MR imaging study that such morphological changes are linked to alterations in muscle tissue deformation patterns near the site of prior injury [4]. However, the fast relaxation time of collagenous tissue limits the use of MRI to conduct similar analysis on tendon. An alternative approach is to use ultrasound (US) elastography [5], which is a speckle tracking approach to measuring *in vivo* tissue deformation patterns [6]. Our objective was to assess the potential for using US elastography to quantify tendon mechanics in normal and previously injured hamstrings undergoing passive stretch.

METHODS

Pilot data were obtained from a single adult male (28y) with a history of left biceps femoris injuries, including the most recent injury 5y prior to testing. A series of six passive knee extension trials were conducted for each limb with the subject supine on an examination table and the hip fixed to 90deg. The ultrasound transducer (10MHz, 38mm wide) was positioned over the biceps femoris proximal tendon/aponeurosis and aligned with the underlying fiber direction of the tendon. Radio frequency (RF) and B-Mode images were then simultraneously collected using a SonixTOUCH Research scanner (Ultrasonix Medical Corporation, Richmond, BC, Canada) as a therapist slowly extended the knee from 90deg to maximum extension. The force required to extend the knee was measured using a hand-held load cell, and an electronic goniometer was used to monitor the knee flexion angle (Fig. 1). Internal knee flexion moments throughout the trials were then computed from the collected data.

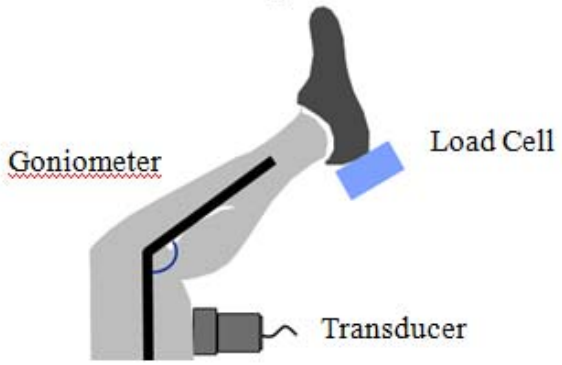

Figure 1. Experimental setup.

A statistical correlation approach was used to compute the cumulative two-dimensional motion of a region of interest containing the tendon. We did this by first defining a rectangular kernel around each pixel, and then cross-correlating the (0.4x0.2mm) RF signals within the kernel with candidate positions of the kernel in a subsequent frame [5,6]. The kernel translations that maximized the cross-correlation were then determined. Sub-pixel displacements were estimated using a 2D quadratic fit of the correlation function. After computing pixel displacements, a region of interest over the tendon was then identified and meshed via triangular elements with ~2mm edge lengths [4]. Linear least squares were used to compute the nodal displacements that best agreed with the computed pixel displacements at each frame. Frame-to-frame nodal displacements were accumulated over time to estimate the cumulative motion of the tendon. In this study, we report the tendon motion along the transducer beam direction, which is known to track approximately one order of magnitude better than transverse to the beam, due to the phase information inherent in the RF data [6].

RESULTS AND DISCUSSION

Passive moment-angle data demonstrated a high repeatability between trials for each limb (Fig. 2). The similarity between the slopes of the moment angle curves between limbs suggests that injury-related changes to muscle-tendon mechanics may did not seem to be detectable at the joint level for this subject.

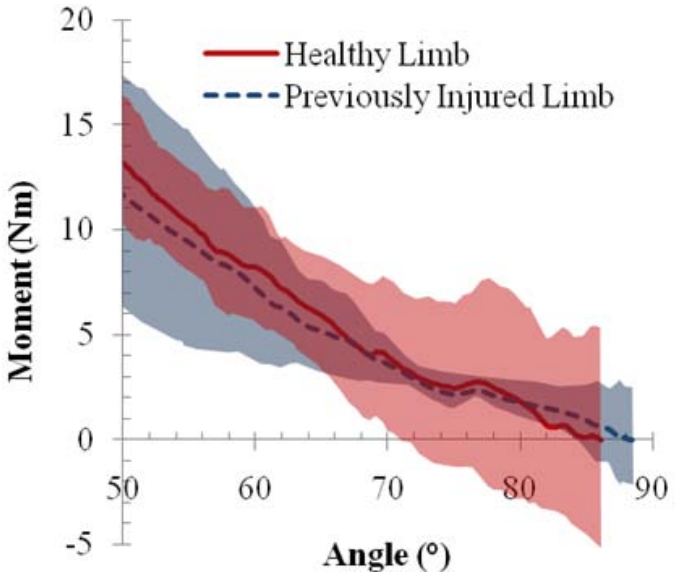

Figure 2. Passive knee flexion moment-angle relationships (mean±1sd) for the healthy and previously injury limb across four passive stretch trials.

The injured conjoint tendon was diffusely enlarged and heterogenously hypoechoic with loss of the normal parallel fibrillar pattern (Fig. 3). Computed displacement patterns were consistent between repeated trials for each respective limb, with ~1-4 mm of motion along the beam direction and ~5 mm of motion in the direction transverse to the beam. The previously injured tendon exhibited larger net motion and greater variability in motion across the tendon width, when compared with the tendon on the uninjured limb (Fig. 3). These dissimilarities suggest that mechanical differences between healthy and previously injured tendinous tissue are likely present, and may be detectable using ultrasound elastography.

CONCLUSIONS

Ultrasound elastography shows promise as a quantitative tool to characterize injury-induced changes in tendon morphology and mechanics.

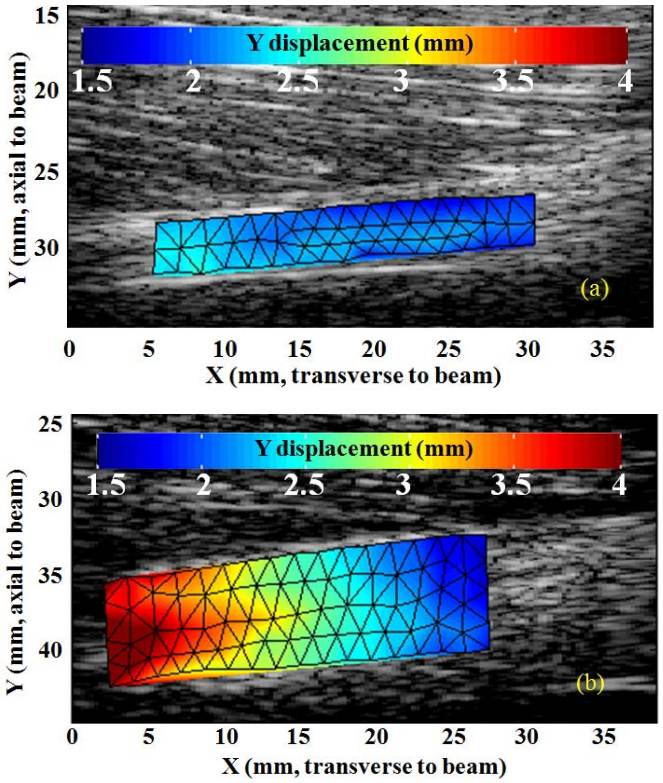

Figure 3. Along-beam displacement patterns in the proximal conjoint tendon for the (a) healthy and (b) previously injured limb

REFERENCES

1. Orchard J, et al. *Br J Sports Med* **36** 39–44, 2002.
2. Silder A, et al. *Skeletal Radiol* **37**, 1101-09, 2008.
3. Lin TW, et al., *J Biomech* **37**, 865-77, 2004.
4. Silder A, et al. *J Biomech*, in press.
5. Farron J, et al. *IEEE Trans Ultrason Ferroelectr Freq Control*, **56**, 27-35, 2009.
6. Ophir J, et al., *Proc. Inst. Mech. Eng.* **213**, 203-233, 1999.

ACKNOWLEDGEMENTS

NIH AR056201, Tomy Varghese, Amy Hauri, Bryan Heiderscheit, Ryan DeWall, Kate Ludwig.

SIMULATION OF A PERCUTANEOUS AORTIC VALVE DEPLOYMENT INTO A PATIENT-SPECIFIC AORTIC ROOT

[1,2]Eric Sirois, [2]Qian Wang and [1,2]Wei Sun

[1]Biomedical Engineering Program and [2]Mechanical Engineering Department
University of Connecticut, Storrs, CT
email: weisun@engr.uconn.edu

INTRODUCTION

For patients with severe aortic valve disease, valve replacement via open-chest surgery has long been then the preferred method of treatment. For patients with comorbidities or advanced age, the risk of intraprocedural mortality can outweigh the potential benefit of valve replacement and these patients are often denied surgery [1]. Recently, minimally-invasive percutaneous aortic valve (PAV) replacement has emerged as a viable alternative for these patients. Although significant experience with PAV procedures has been gained through multicenter clinical trials, various adverse effects have been detected after device implantation [2]. This study documents an investigation of the hemodynamic environment changes that occur following PAV intervention using a combination of finite element analysis (FEA) and computational fluid dynamics (CFD).

METHODS

PAV-aortic root model. The PAV leaflet geometries used in this study were detailed in a previous study [3]. A 13 mm high rigid stent was added around the valve leaflets, having a stent thickness of 0.5 mm, resulting in a size 23 PAV. The geometry of an aortic root was obtained using ECG-gaited clinical cardiac 64-slice multidetector row CT scans collected at Hartford Hospital, CT, with IRB approval. A 68 year old male with no known comorbidities was selected for this study. The patient's aortic annulus size was determined from image analysis to be 21 mm. The patient's aortic valve and root geometries were digitized and reconstructed using custom in-house software.

Finite element simulation of PAV deployment. The geometries developed above were imported into the finite element analysis software ABAQUS (DSS Simulia, Warwick, RI). Aortic root, aortic valve leaflet, and ascending aorta material properties were assigned using linear elastic models with Young's moduli of 1200-1500kPa and Poisson ratio of 0.45. Note that since the final deformed aortic root and leaflet geometries were determined by the stent expansion, using either linear elastic or nonlinear hyperelastic tissue material properties for the root and leaflet would not have had a significant impact on their final geometries. The loading condition was assigned to expand the aortic annulus region to its full diameter of 23 mm, designed to mimic the clinical practice of over-sizing [4]. The stent was deployed such that approximately one third of the stent was below the aortic annulus. Contact modeling was accomplished using master-slave pairs of the PAV stent and the aortic root wall.

CFD physics modeling. A shear-rate dependant non-Newtonian fluid with a constant density of 1056 kg/m3 was used. To implement the non-Newtonian model, a power-law shear-rate dependant relationship was used [5]. The solution was obtained using the *k-epsilon* turbulence model, solved by the commercial CFD package Star-CCM+ (CD-Adapco, Plymouth, MI). The velocity-pressure coupling method was the SIMPLE algorithm. A second order differencing scheme was chosen for resolving velocity and turbulence quantities. The unsteady solution was discretized into 1 ms intervals and solved using the Unsteady Reynolds-Averaged Navier-Stokes model.

Implementation of boundary conditions. The initial boundary conditions for this patient were physiologically appropriate velocity inlet (at the aortic annulus) and pressure outlets (at the ascending aorta and coronary arteries) [6, 7]. To develop accurate boundary conditions following

PAV intervention, the pre-interventional aortic annulus velocity profile (u) was scaled in accordance with an annulus diameter increase from 21 mm to 23 mm and a heart rate (HR) increase from 73 bpm to 91 bpm [8]. This scaling was accomplished by setting the net volume change over one cardiac cycle (ΔV), i.e. the stroke volume, to be the volumetric flow rate (Q) integrated over time:

$$\Delta V_1 = \int Q_1 \, \delta t_1 = \Delta V_2 = \int Q_2 \, \delta t_2 \qquad (1)$$

By continuity, the post-intervention velocity (upost) at any time increment was calculated by:

$$u_{post} = \frac{u_{pre} A_{pre} (HR)_{post}}{A_{post} (HR)_{pre}} \qquad (2)$$

The aortic pressure outlet was converted into a three-element Windkessel model, containing two resistor elements (Rp and Rc) and one capacitor element (C). Windkessel in the time domain was accomplished for each time (t) by [9]:

$$\frac{dP_{ao}}{dt} = \frac{(R_p + R_c) Q_{ao}}{R_p C} + R_c \frac{dQ_{ao}}{dt} - \frac{P_{t-1}}{R_p C} \qquad (3)$$

The coronary artery boundary conditions were replaced with unique time-varying resistive elements for each outlet. These resistances were used to prescribe each coronary flowrate (Q) as a function of its corresponding reservoir pressure (P_{res}) and resistance (R) such that $Q = -P_{res}/R$. Reservoir pressure was calculated for each coronary branch as a function of observed pressure (P) and velocity. At any time, P_{res} was given as [7]:

$$P_{res} = \left(\int_0^t P(t) + P_{t=0} \right) e^{-(a+b)t} \qquad (4)$$

The values a and b are constants obtained from continuity requirements and direct curve fitting.

RESULTS AND DISCUSSION

Model validation. The model was validated where possible by comparison with data reported from clinical use of PAVs. Pre-operatively, we observed from the CFD simulation a max transvalvular pressure gradient of 77.9 mmHg and a mean systolic ejection period transvalvular pressure of 45.8 mmHg, which compare favorably with the 78+/-19 and 45+/-12 mmHg observed by Bauer *et al*. [8]. We also observed a simulated EOA of 0.696 cm^2. These values also compare favorably with PAV replacement candidate hemodynamic data reported by Clavel *et al*. of 47+/-17 mmHg mean pressure gradient and 0.6+/-0.14 cm^2 EOA [10] and by Ben-Dor *et al*. of 43+/-13 mmHg mean pressure gradient and 0.63+/-0.14 cm^2 EOA [11]. Thus, the patient examined here was hemodynamically equivalent to other PAV replacement candidates.

Post deployment, we obtained the peak transvalvular pressure gradient of 22.63 mmHg which compared favorably with the 20+/-7 mmHg observed by Bauer *et al*. [8]. The mean transvalvular pressure gradient observed of 11.52 mmHg was slightly higher than the 8+/-2 mmHg from Bauer *et al*. [8], well higher than the 3.88+/-1.62 mmHg from Ben-Dor *et al*. [11], and within the 10+/-4 mmHg from Clavel *et al*. [10]. Also, we observed a post-deployment EOA of 1.56 cm^2, compared with 1.69+/-0.11 cm^2 from Bauer *et al*. [8], 1.97+/-0.41 cm^2 from Ben-Dor *et al*. [11], and 1.61+/-0.40 cm^2 from Clavel *et al*. [10]. These comparisons indicated that the simulated post-deployment hemodynamics were similar to those observed clinically following PAV intervention.

Flow analysis. Flow conditions were examined before and after the simulated PAV intervention (Fig.1). Although peak velocity values were similar, the magnitude and length of the central jet were significantly reduced by PAV intervention. Additionally, the displaced native leaflets appear to cause a low pressure region that resulted in virtually no change in coronary artery flow despite a 25% increase in cardiac output following intervention.

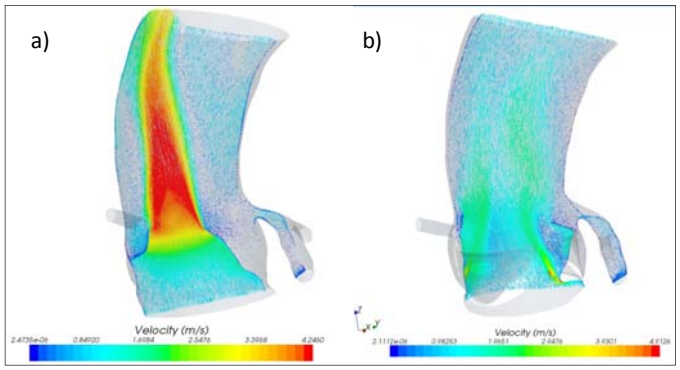

Figure 1 – Velocity vector profile of the aortic root at peak systole, for a) pre-intervention and b) post-intervention.

REFERENCES 1. Iung, B., et al., Eur Heart J., 2003. **24**(13): p. 1231-43; 2. Grube, E., et al., J Am Coll Cardiol. , 2007. **1**(50): p. 69-76. 3. Li and Sun, Annals of Biomed Eng. 2010 in-press; 4. Webb, J., et al., Catheter Cardiovasc Interv, 2004. **63**(1): p. 89-93; 5. Merrill, E., et al., J, 1963. **3**: p. 199-213; 6. Olufsen, M., Am J Physiol., 1999. **276**(1 Pt 2): p. H257-68; 7. Aguado-Sierra, J., et al., in *Conf Proc IEEE Eng Med Biol Soc*. 2007. p. 2693-6; 8. Bauer, F., et al., Circulation, 2004. **110**(11): p. 1473-6; 9. Stergiopulos, N., J. Meister, and N. Westerhof, Am J Physiol., 1995. **268**(4 Pt. 2): p. H1540-8; 10. Clavel, M., et al., J Am Coll Cardiol, 2009. **53**(20): p. 1892-3;11. Ben-Dor, I., et al., Am J Cardiol, 2009. **104**(6): p. 850-5.
ACKNOWLEDGEMENT: Dr. Primiano and Dr. McKay at the Hartford Hospital for providing the CT scans, and CT DPH 2010-0085 and GAANN Pre-doctoral fellowship.

HIGH COEFFICIENT OF FRICTION AT THE HAND-OBJECT INTERFACE CONTRIBUTES TO INCREASED MAXIMUM GRIP FORCE BY THE PHALANXES DURING POWER GRIP

Leah R. Enders, Alexander K.J. Engel and Na Jin Seo

University of Wisconsin-Milwaukee, Milwaukee, WI, USA

email: lrenders@uwm.com, web: http://pantherfile.uwm.edu/seon/www

INTRODUCTION

Power grip is commonly used in everyday activities such as holding a bottle or cup. During power grip, a person generates hand forces that are normal (perpendicular) and shear (parallel) relative to the surface of the gripped object [1]. A person may adopt different grip strategies depending on the coefficient of friction (COF) between the hand and handle for the following reasons. First, a high friction surface may reduce the need for precise coordination of hand muscles to direct digit force [2-3]. Secondly, both normal and shear forces produced by phalanxes can induce reaction force on the palm, which contributes to overall power grip force generation [4-5]. Thus, if the COF between the hand and handle is high, people may increase shear force at the phalanges to maximize overall grip force. It is important to investigate how persons compensate for different frictional surfaces during power grip in order to understand the biomechanical mechanisms that underlie a person's grip strategy and strength.

The goal of this study was to examine the effect of friction between hand and grip surface on a person's grip strategy. The hypothesis of this study was that during maximum power grip, normal force will be greater when the grip object provides a high COF with the skin compared to a low COF. Also hypothesized is that the increase in normal force will be accompanied by an increased shear to normal force ratio for the rubber surface compared to the paper surface.

METHODS

Thirteen young healthy individuals (ages 19-30 years) were seated with the forearm horizontal on an arm rest. Using the non-dominant hand, subjects were instructed to perform a 5 second maximum power grip on a custom-made grip dynamometer (Fig. 1). Each phalanx's normal force and shear force (in the proximal-distal direction of the finger) were recorded at 50 Hz. The grip dynamometer had two surface coverings: paper and rubber with COF with the finger skin of 0.3 [6] and 0.9 [7], respectively. The grip dynamometer's diameter was 26.6 mm for both coverings.

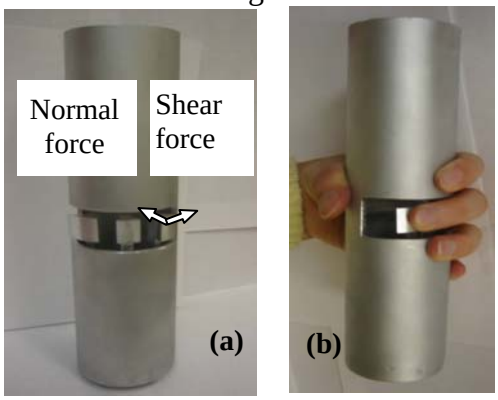

Figure 1: A custom-made grip dynamometer measuring shear and normal forces on three contact pads (a) that align with each phalanx of a single finger during power grip (b).

Maximum power grip was repeated three times for each finger and surface condition (for a total of 30 trials). Two minute breaks were allowed between consecutive grips to minimize muscle fatigue. For each grip trial, normal and shear forces were averaged over the two second period in which the mean normal force was the greatest. In addition, the mean ratio of shear force to normal force was computed for that period. ANOVA was performed to determine if the maximum normal force and the shear to normal force ratio observed for the phalanxes of the five fingers significantly varied with grip surface.

RESULTS AND DISCUSSION

Mean normal force for the phalanxes during maximum power grip was significantly higher for the rubber surface, 23.2 N, than for the paper surface, 22.5 N (Fig. 2; p=.012). The mean shear to normal force ratio produced with the rubber surface, 0.23, was significantly higher than that for the paper surface, 0.19 (Fig. 3, p<.01).

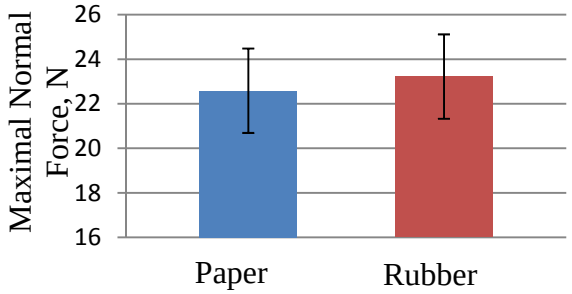

Figure 2: Mean ± SE normal force produced by the fingers during maximum power grip for the two grip surfaces (p=0.012), averaged across repetitions, phalanxes, fingers, and subjects.

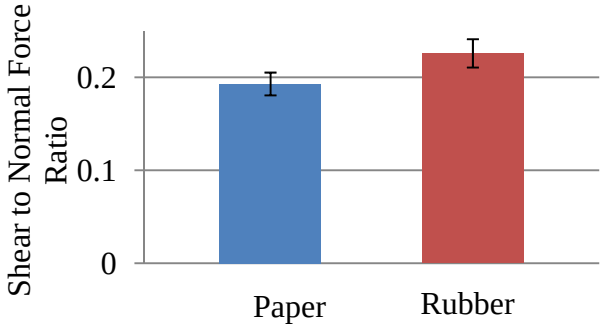

Figure 3: Mean ± SE shear to normal force ratios observed during maximum power grip for the two grip surfaces (p<.01), averaged across repetitions, phalanxes, fingers, and subjects.

The higher shear and normal forces for the rubber surface may be attributable to alleviated muscle coordination requirement. To achieve a stable grip, force vectors applied to the surface must fall within a specific angle range with respect to the object surface [3]. The angle range is dependent on COF. The higher the COF, the larger the angle range in which a person could apply a force and still maintain a stable grip [3]. Increase in the angle range may require less muscle coordination and precision [2], thereby allowing a person to exert greater normal and shear forces. In addition, the subjects may have generated greater shear force for the rubber surface to increase the reaction force against the palm and maximize overall grip force applied to the handle [4].

Wimer et al. [1] found little evidence of shear force contribution to grip force. The difference between the present study and the previous study could be due to study design. The latex gloves used in the previous study may have decreased sensory feedback for subjects and consequently decreased the effect of COF on the subjects' grip strategy.

CONCLUSIONS

The biomechanical investigation of the digit force generated during power grip is important in order to better understand people's grip strategy in completing everyday tasks. It was found that people generated shear force (approximately 19% to 23% of the normal force) in addition to grip force (normal to object surface) during maximum power grip. Furthermore, people produced greater grip force and greater shear force for a rubber surface compared to a paper surface. Increasing frictional coupling between hand and grip objects may assist people in generating greater grip force, thereby aiding in completing everyday tasks.

REFERENCES

1.Wimer B, et. al. *Med Engineering and Physics* **31**, 695-704, 2009.
2.Cole KJ. *Exp Brain Res* **175,** 285-291, 2006.
3.MacKenzie CL, Iberall T. *The grasping hand*. 1994.
4.Seo NJ, et al. *J. of Biomech* **40**, 3236-3243, 2007.
5.Edgren CS, et al. *Human Factors* **46**, 244-251, 2004.
6.Buchholz B, et al. *Ergonomics* **31**, 317-325, 1988.
7.Seo NJ, Armstrong TJ. *Ergonomics* **52**, 609-616, 2009.

ACKNOWLEDGEMENTS

This study was funded by the University of Wisconsin-Milwaukee College of Engineering and Applied Sciences Fostering Undergraduate Research Program and by the University of Wisconsin System Administration. The authors thank Armstrong TJ and Woolley CB for the custom-made grip dynamometer.

ELBOW AND WRIST MUSCLE FIBER OPERATING RANGES THROUGHOUT THE RANGE OF MOTION FOR FLEXION-EXTENSION AND PRONATION-SUPINATION

Dan Dorman, Rena Warren and Roger Gonzalez

LeTourneau University, Longview, TX, USA
email: rogergonzalez@letu.edu,

INTRODUCTION

Musculoskeletal models of the human arm and forearm have been developed as useful tools for understanding biomechanics of the elbow and wrist and they can answer questions that are difficult to answer experimentally [1,2]. We have developed a model to quantify individual muscle force and moment contributions to net joint moments and to estimate muscle fiber operating ranges of individual muscles over the full range of motion for elbow flexion-extension (EFE) and forearm pronation-supination (PS). A previous model [1] verified moment arms for the following 16 muscles crossing the elbow and wrist in EFE and PS: triceps brachii (TRI), biceps brachii (BIC), brachialis (BRA), brachioradialis (BRD), supinator (SUP), pronator teres (PRO), extensor carpi radialis longus (ECRL), extensor carpi radialis brevis (ECRB), extensor carpi ulnaris (ECU), extensor digiti minimi (EDM), extensor digitorum communis (EDC), flexor carpi radialis (FCR), flexor carpi ulnaris (FCU), flexor digitorum superficialis (FDS), abductor pollicis longus (APL), and palmaris longus (PL). Our aim was to build on this model to verify force generating properties (peak isometric muscle force, optimal fiber length, pennation angle, and tendon slack length) of our Hill-type muscle model.

METHODS

Peak isometric muscle force (the product of physiological cross sectional area [PCSA] and muscle specific tension), optimal fiber length (l_O^M), pennation angle (α), and tendon slack length (l_S^T) values were obtained or determined for each of the 16 muscles.

Values for l_O^M, α, and PCSA were obtained directly from a literature survey [3,4]. Values for l_O^M and α were weighted based on the number of subjects, and l_O^M values were normalized as necessary to an optimal fiber length of 2.7 µm. PCSA values were obtained from an MRI study of healthy subjects [5].

Since values for l_S^T cannot be measured precisely, values for the model were estimated such that the shape of the summed isometric moment vs. joint angle curves (both active and passive) of the model approximated the isometric moments from an experiment with a Biodex isometric dynamometer.

Specific tension values reported in the literature vary, from 35 to 148 N/cm^2 according to one source [6]. We used one specific tension value, 58 N/cm^2, for all muscles in the model to scale the model's moments to the experimental moments.

Muscle fiber operating ranges were estimated by dividing the model's fiber length values of each muscle over the range of motion of EFE and PS by each muscle's optimal fiber length.

RESULTS AND DISCUSSION

Net EFE and PS moments from our model approximated, within one standard deviation, experimentally measured moments (Fig. 1). General trends and magnitudes were reproduced by the model and were within the range of the experimental moments except for the extremes of the range of motion of pronation and supination. While the model moment's do not exactly replicate the mean experimental moments, they do represent the net moment variations in the experimental data, and differences can be accounted for by the variation of strength and muscle architecture in the subjects and specimens from which experimental moments and model parameters are based, as well as limitations of the model. These limitations include the assumption that all fibers in a muscle have the same optimal fiber length (resulting in a

narrower operating range), the use of wrap objects to model muscle pathways, and singular points, rather than areas, of origin and insertion.

One strength of our model versus previous models is that it is based on PCSA estimates from younger, healthy subjects rather than cadaver specimens. Models based on cadaver PCSAs have used more than one specific tension for various muscle groups, whereas our model needed just one specific tension for all muscles.

The majority of the muscle fiber operating ranges from our model were on the ascending limb and/or plateau region of the force-length curve, while the BRD, PRO, SUP, and EDM operated on the plateau and descending limb. As expected, muscles have a greater operating range over EFE than PS. Our findings that some muscles likely operate on the descending limb are supported by *in vivo* studies that have shown that various muscles can operate on either the ascending limb, plateau, or descending limb of the force-length curve [7].

CONCLUSIONS

Our aim was to determine force and moment contributions of individual muscles of the arm and forearm based on a validated model. This has been achieved by considering the operating ranges of muscle fibers and the breakdown of net EFE and PS joint moments into muscle moments, forces, and moment arms. We believe these results can be used as a resource to further study the forces and moments of the muscles of the arm and forearm, especially as they may affect elbow and wrist intersegmental loading conditions.

REFERENCES

1.Ramsay JW, et al. *J Biomech* **42**, 463-473, 2009.
2.Gonzalez RV, et al. *J Biomech* **30**, 705-712, 1997.
3.Murray WM, et al. *J Biomech* **33**, 943-952, 2000.
4.Lieber RL, et al. *J Hand Surgery* **17A**, 787-798, 1992.
5.Holzbaur KR, et al. *J Biomech* **40**, 742-749, 2007.
6.Buchanan TS. *Med Eng Phys* **17**, 529-536, 1995.
7.Loren GJ, et al. *J Biomech* **29**, 331-342, 1996.

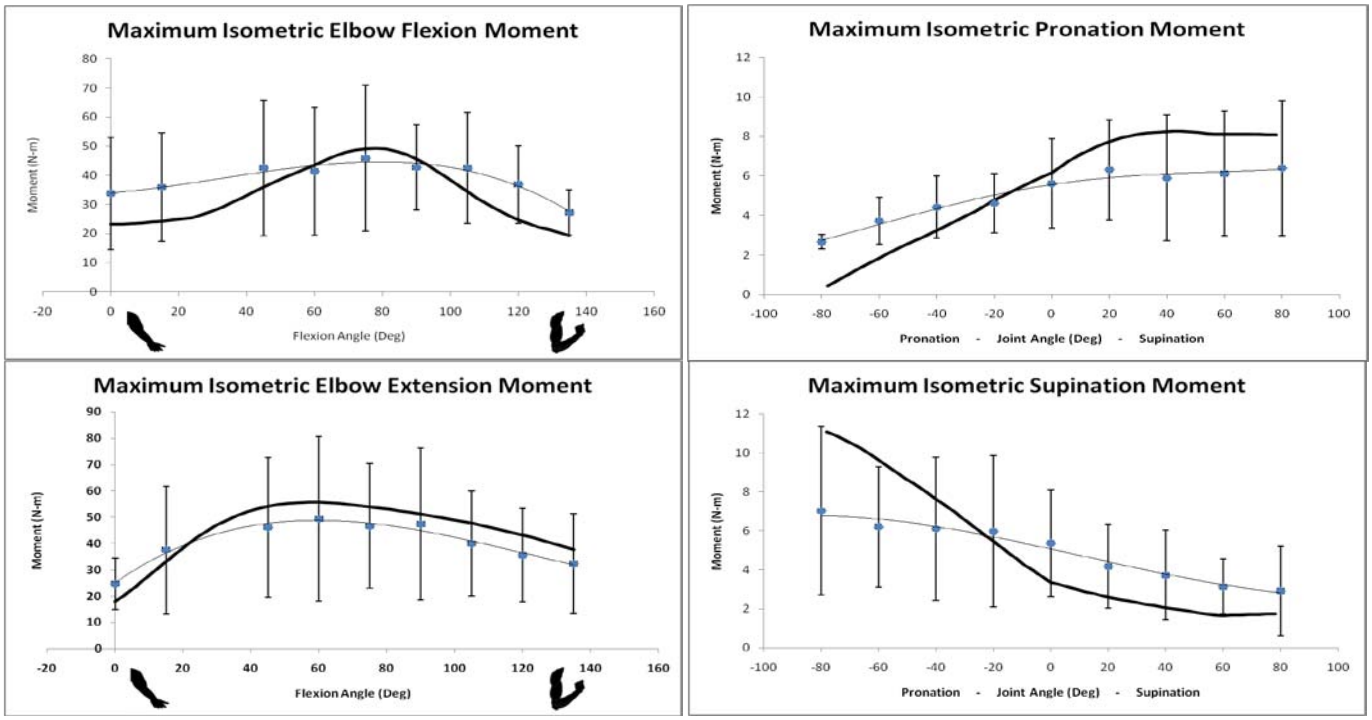

Figure 1: Comparison of experimental (dotted line with standard deviation bars) and model (thick line) maximum isometric moments versus joint angle.

THE INFLUENCE OF ALTERING PUSH FORCE EFFECTIVENESS ON INDIVIDUAL MUSCLE DEMAND DURING WHEELCHAIR PROPULSION

[1]Jeffery W. Rankin, [2]Andrew M. Kwarciak, [2]W. Mark Richter and [1]Richard R. Neptune

[1]Department of Mechanical Engineering, The University of Texas at Austin, Austin, TX, USA
[2]Max Mobility LLC, Antioch, TN, USA
email: jwr383@mail.utexas.edu, web: http://www.me.utexas.edu/~neptune

INTRODUCTION

Up to 70% of the 1.5 million manual wheelchair users in the United States will eventually develop upper extremity overuse injuries and/or pain [e.g., 1], which is in part due to the high load requirements and low mechanical efficiency of wheelchair propulsion. The shoulder is of particular interest, as injuries at this joint are common and greatly affect user mobility and overall quality of life. The low mechanical efficiency of wheelchair propulsion is partially related to users applying non-tangential handrim forces, which do not propel the wheelchair and therefore create an ineffective use of generated muscle force. As a result, previous studies have used various measures of handrim force effectiveness (e.g. fraction effective force, FEF) as a guide for developing rehabilitation programs, comparing propulsion techniques or modifying wheelchair geometry in an effort to reduce muscle demand [e.g., 2].

However, the relationship between FEF and muscle demand is not well understood. Experimental studies have found inconsistent correlations between FEF and mechanical efficiency [3, 4]. Modeling studies have found increasing FEF results in higher shoulder moments and total muscle mechanical work estimates [5], suggesting that increasing FEF increases upper extremity demand. However, no study has identified individual muscle contributions to the handrim forces, which can provide insight into how changing FEF influences muscle demand. Therefore, the purpose of this study was to use forward dynamics simulations of the wheelchair propulsion push phase to identify individual muscle contributions to the handrim forces and assess the influence of increasing FEF on muscle demand.

METHODS

An upper extremity musculoskeletal model based on the work of Holzbaur et al. [6] was used to generate forward dynamics simulations of wheelchair propulsion. The model consisted of six rotational degrees of freedom representing the joints of the upper extremity and trunk lean, and 26 Hill-type musculotendon actuators representing the major muscle groups crossing the elbow and shoulder joints. A dynamic optimization algorithm was used to identify the muscle excitation patterns to produce two different simulations: one that emulated normal wheelchair mechanics of a representative subject and another that maximized FEF. In both simulations, the optimization minimized differences between the simulation and experimentally collected joint kinematics and handrim forces. The second simulation added average FEF to the cost function to be maximized.

To determine individual muscle contributions to the tangential, radial and lateral handrim forces, muscle forces were independently applied to the model at each time step and the resultant handrim forces were calculated by solving the system equations of motion. In addition, the capacity of each muscle to contribute to the handrim forces was assessed by applying a constant 100 N force for each muscle during the push phase. In both analyses, the push phase was divided into three equal regions and the average handrim force contributions by each muscle were determined within each region.

RESULTS AND DISCUSSION

The analysis of largest muscle contributions to the handrim forces showed that most muscles contribute to both the tangential and ineffective (i.e. vector sum of radial and lateral) forces

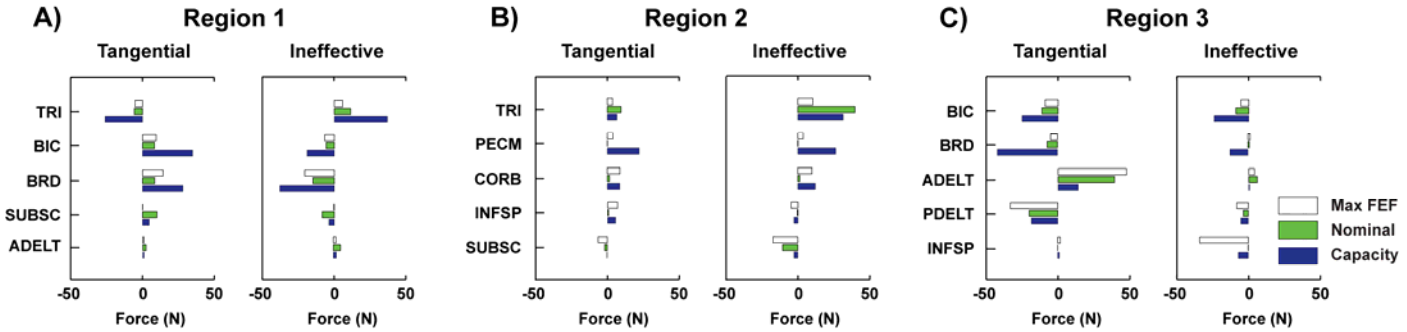

Figure 1: Positive and negative handrim force contributions by each muscle during the push phase.

simultaneously during the push phase (Fig. 1). Thus, the constrained circular motion created by the handrim during the push phase is not necessarily optimal for converting muscle force into external power.

There were several differences in individual muscle handrim force contributions between the nominal and maximal FEF simulations. In Region 1, the elbow flexors (BIC, BRD) are ideally suited for simultaneously providing tangential and reducing ineffective handrim forces (Fig. 1A, see muscle capacity), which resulted in these muscles being recruited during the maximal FEF simulation (Fig. 1A). However, in order to maintain the required net tangential force, the tangential contribution from the subscapularis (SUBSC) had to be reduced.

In Region 2, the maximal FEF simulation increased handrim force contributions from muscles with lower relative contributions to the ineffective force (i.e., decreasing TRI and increasing shoulder flexor (PECM, CORB) contributions, Fig. 1B). The maximal simulation also increased SUBSC and infraspinatus (INFSP) contributions, resulting in a reduction in the ineffective force with minimal effect on the tangential force. The switch in muscle force contributions from muscles crossing the elbow to those crossing the shoulder during the maximal FEF simulation was consistent with previous inverse dynamics studies showing net shoulder joint moments are higher when increasing FEF [7].

In Region 3, the infraspinatus (INFSP), posterior deltoid (PDELT) and elbow flexors (BIC, BRD) were the only muscles that had the capacity to reduce the ineffective handrim force (Fig. 1C, see muscle capacity). As a result, the maximal FEF simulation greatly increased INFSP activity to reduce the ineffective force without changing the tangential force. The simulation also increased co-contraction of ADELT and PDELT to further reduce the ineffective force, while maintaining the required net tangential force.

CONCLUSIONS

A detailed understanding of how individual muscles contribute to the handrim forces during wheelchair propulsion can assist in assessing how changing FEF affects muscle recruitment and overall demand. These results can help guide current rehabilitation methods to target specific muscle groups and improve rehabilitation outcomes. The analysis showed that a circular motion may not be optimal for converting muscle force into external power, as most muscles simultaneously contribute to both tangential and ineffective handrim forces. Further, care should be taken when using increasing FEF as a rehabilitation goal, as higher FEF values shift handrim force contributions from muscles crossing the elbow to those crossing the shoulder, which are already susceptible to overuse injuries.

REFERENCES

1. Finley, MA, et al., *J Rehabil Res Dev* **41,** 395-402, 2004.
2. Kotajarvi, BR, et al., *Arch Phys Med Rehabil* **87,** 510-515, 2006.
3. Dallmeijer, AJ, et al., *Am J Phys Med Rehabil* **77,** 213-221, 1998.
4. de Groot, S, et al., *Clin Biomech* **17,** 219-226, 2002.
5. Bregman, DJ, et al., *Clin Biomech* **24,** 13-19, 2009.
6. Holzbaur, KR, et al., *Ann Biomed Eng* **33,** 829-840, 2005.
7. Desroches, G, et al., *Arch Phys Med Rehabil* **89,** 1155-1161, 2008.

ACKNOWLEDGEMENTS

This work was supported by NIH grant R01HD53732.

Shoulder Kinematics and Kinetics during Wheelchair Propulsion in Persons with Tetraplegia

[1]Mat Yarossi, [1,2]Trevor Dyson-Hudson, [1,2]Gail Forrest, [3]Andrew Kwarciak, [4]Sue Ann Sisto

[1]Kessler Foundation Research Center, West Orange, NJ; [2] Department of Physical Medicine and Rehabilitation, University of Medicine and Dentistry of New Jersey - New Jersey Medical School, Newark, NJ; [3]MAX mobility, LLC, Antioch, TN; [4]Division of Rehabilitation Sciences, Stony Brook University, Stony Brook, NY

email: myarossi@kesslerfoundation.org, web: http://www.kesslerfoundation.org

INTRODUCTION

Shoulder pain is common in persons with spinal cord injury (SCI), with a reported prevalence of 30% to 73% [1]. Shoulder pain in persons with SCI represents a form of repetitive strain injury resulting, in part, from an increased reliance on the upper limbs for mobility. Manual wheelchair propulsion is a highly repetitive, weight-bearing activity that imposes considerable demand on the shoulder complex [1,2]. These demands may be even greater in persons with tetraplegia who may have only partial innervation of the shoulder complex muscles as a result of their injury [2]. Although numerous studies have been carried out documenting shoulder biomechanics during wheelchair propulsion in persons with SCI, most have focused primarily on persons with paraplegia [3,4]. The purpose of this investigation, therefore, was to quantify shoulder kinetics and kinematics during manual wheelchair propulsion in persons with tetraplegia.

METHODS

Twenty-one men (mean age, 36.3±11.9y) with chronic tetraplegia (duration of wheelchair use, 11.2±8.2y) who used a manual wheelchair as their primary means of mobility (≥40h/week) were enrolled in this study. All participants provided informed consent prior to testing procedures.

Data collection included anthropometric and wheelchair measurements. The experimental setup and data collection methods are described in detail elsewhere [5] and are presented briefly here. Kinetic data were collected at 240 Hz from instrumented wheelchair wheels capable of measuring three-dimensional forces and moments occurring at the pushrim (SmartWheel, Three Rivers Holdings, LLC, Mesa, AZ). SmartWheel devices were placed on both sides of the subject's wheelchair. The wheelchair was then secured to a dynamometer consisting of two independent steel tubular rollers – one for each wheel – using a 4-belt tie-down system. Subjects were instructed to propel their wheelchair on the dynamometer at a self-selected speed to acclimate themselves to the experimental setup. Subjects were then instructed to propel their wheelchair at 0.9m/s. Real-time speed feedback was presented on a monitor in front of the roller system. Data collection was initiated when the subject was able to maintain a speed between 0.67 m/s and 1.12 m/s and continued for 20 seconds.

Kinetic data collection was synchronized with the kinematic data collection using an external trigger. Three-dimensional kinematic data were collected at 120 Hz using a passive marker motion capture system (Vicon Motion Systems, Oxford, UK). Reflective markers were placed on each wheel and on the bony landmarks on the upper limbs and trunk in accordance with International Society of Biomechanics (ISB) recommendations [6].

Data from 5 consecutive right-sided push strokes were selected for analysis. Each stroke cycle was defined as the push phase followed by the recovery phase [7]. All data were normalized to 100% of the stroke cycle.

The upper limb was modeled as three connected rigid body segments to represent the hand, forearm, and upper arm. Each segment was described using the ISB recommended local coordinate system. The distal segment was rotated to the proximal segment

(humerus to the trunk) using a Z-X-Y order Euler rotation to represent the anatomical angles for the shoulder, elbow, and wrist. The trunk was rotated into the global reference frame of the lab. Three motions of the upper limb were analyzed: shoulder flexion-extension, shoulder abduction-adduction, and shoulder internal-external rotation. All joint angles were equal to zero at neutral seated position. The forearm and upper arm were modeled as truncated circular cones and the hand was modeled as a semi-ellipsoid. Mass, center of mass, and moment of inertia were determined using the body segment parameter equations [8].

Three-dimensional forces obtained from the SmartWheel were projected onto the hand. The point of force application was defined as halfway between the wrist center and the hand center of mass, placing it at the base of the palm. Inverse dynamic equations [9] were used to find forces and moments at the shoulder. The moments about the joints produced by these calculations represent the net joint moments.

RESULTS AND DISCUSSION

Compared to persons with paraplegia propelling on a similar roller system at the same target speed [3], persons with tetraplegia showed less maximal shoulder flexion, abduction, and shoulder internal rotation (Table 1). In addition, maximum shoulder flexion, adduction, and internal rotation moments were three to four times less in subjects with tetraplegia (Table 2). Reduced range of motion and decreased shoulder moments during the propulsion phase of wheelchair propulsion in the tetraplegic group is likely due to impairment of the muscles of the upper limb. Limited muscle innervation in the tetraplegic group decreases the functional workspace of the limb and may reduce the capacity to produce force. This could lead to an increase in push frequency and greater muscular effort, which can increase the risk and/or exacerbate symptoms of a repetitive strain-type injury [1]. Although others have investigated various aspects of propulsion biomechanics in persons with tetraplegia [2], their results are based on data from subjects propelling an "experimental wheelchair" - not their own personal wheelchair. Wheelchair type and set-up can have a significant impact on propulsion biomechanics [1]. Therefore, it is also important to test subjects in their own wheelchairs if one is to get an accurate assessment of shoulder kinetics and kinematics during wheelchair propulsion in persons with SCI.

Table 1: Tri-planar shoulder kinematics.

	Yarossi 2010	Koontz 2002
Shoulder Angle	Angle (°)	Angle (°)
Maximum Flexion	3.7 (10.6)	19.1 (6.6)
Maximum Extention	36.9 (7.8)	43.2 (5.7)
Maximum Abduction	24.2 (8.5)	42.0 (6.7)
Minimum Abduction	16.1 (5.6)	26.0 (4.1)
Maximum Internal Rotation	21.9 (10.4)	52.1 (11.3)
Minimum Internal Rotation	2.6 (11.1)	24.5 (11.0)

Table 2: Tri-planar shoulder moments.

	Yarossi 2010	Koontz 2002
Shoulder Moment	Moment (N.m)	Moment (N.m)
Maximum Flexion	8.91 (5.92)	28.6 (8.6)
Maximum Extention	3.92 (1.87)	3.9 (2.6)
Maximum Adduction	6.04 (4.41)	21.3 (12.0)
Maximum Abduction	5.31 (1.43)	2.2 (2.5)
Maximum Internal Rotation	4.97 (2.03)	21.6 (5.9)
Maximum External Rotation	3.20 (1.91)	2.3 (1.5)

CONCLUSIONS

Results from this study show marked differences in shoulder biomechanics between persons with tetraplegia compared to persons with paraplegia [3]. Further research is needed to address the shoulder health and wheelchair seating issues associated with specific kinematic and kinetic patterns exhibited by persons with tetraplegia.

REFERENCES

1. Preservation of upper limb function following SCI. *J Spinal Cord Med*, **28**, 434-70, 2005.
2. Kulig K et al. *Clin Biomech*, **16**, 744-751, 2001.
3. Koontz AM, et al. *J Rehab Res Dev*, **39**, 635-49, 2002.
4. Boninger ML et al. *Spinal Cord*, **36**, 418-426, 1998.
5. Boninger ML et al. *Arch Phys Med Rehabil* 84, 1615-1620, 2003.
6. Wu G. *J Biomech*, **38**, 98 1-92, 2005.
7. Kwarciak AM et al. *Arch Phys Med Rehab*, **90**, 20-6, 2009.
8. Yeadon MR et al. *J Biomech*, **23**, 67-74, 1990.
9. Requejo PS et al. *Med Eng Phys*, **27**, 19-29, 2005.

ACKNOWLEDGEMENTS

Funding for this study was provided by the New Jersey Commission on Spinal Cord Injury.

Correlation between Wrist Biomechanics and Median Nerve Health Parameters in Manual Wheelchair Users

Kevin Toosi, MD, MS; Bradley Impink, BS; Jennifer Collinger, PhD;
Jennifer Yang, MD; Alicia Koontz, PhD; Michael Boninger, MD

Human Engineering Research Laboratories
Department of Veterans Affairs & University of Pittsburgh
Pittsburgh, PA, 15206

INTRODUCTION

Carpal tunnel syndrome (CTS) is a major public health problem in the United States, with as many as 3 million individuals suffering from its symptoms and complications [1], such as pain, tingling, numbness, and weakness in the hands and wrists. One population struck particularly hard by CTS is manual wheelchair users (MWUs). The prevalence of CTS in this population is between 49% and 73% [2-5]. CTS is poorly tolerated by this population because they rely on their arms for mobility, transfers and activities of daily living. Multiple cross-sectional studies have investigated CTS prevalence in MWUs and very few have looked at the relationship between wrist biomechanics and CTS [6]. The results have implicated that the prevalence of CTS increased with the duration of paralysis and certain biomechanical parameters; however, long-term studies have yet to be conducted. The objective of the present study was to investigate wrist biomechanical variables, to compare the changes in these variables along with quantified changes in median nerve health at two time-points, and to examine any possible correlation at each time point.

METHODS

33 manual wheelchair users with a spinal cord injury (SCI) were recruited and tested at two visits. Visits ranged from a minimum of 23 months to 101 months apart; mean time between visits was 53.8±24.9 months. During each visit, the subjects underwent bilateral nerve conduction studies (NCS) on the median and ulnar nerves [7]. Wrist kinematics variables were measured in manual wheelchair users during wheelchair propulsion [8]. An Optotrak motion analysis system was used to track the position of infrared markers placed on bony landmarks of the upper extremity. Kinetics data was also recorded using Smart^{Wheel} as the subjects propelled their wheelchairs at two speeds. Upper extremity joint angles and wrist joint forces and moments during wheelchair propulsion were calculated using inverse dynamic methods [9].

RESULTS

The changes in NCS parameters from visit 1 to visit 2 were not statistically significant; however, trends which may represent deteriorating median nerve health were noted in our analysis. Mean median nerve sensory and motor latencies increased from the first visit to the second one; likewise, mean median motor amplitude decreased during the same period of time. Particularly, between visits 1 and 2, women demonstrated significant median nerve deterioration in their dominant hands when compared to men, including significant increases in motor latency and sensory latency. The results of the correlational analyses demonstrated that maximum radial deviation had a significant negative correlation with the median sensory amplitude and a significant positive correlation with the median motor latency at the 2nd visit (Figure 1).

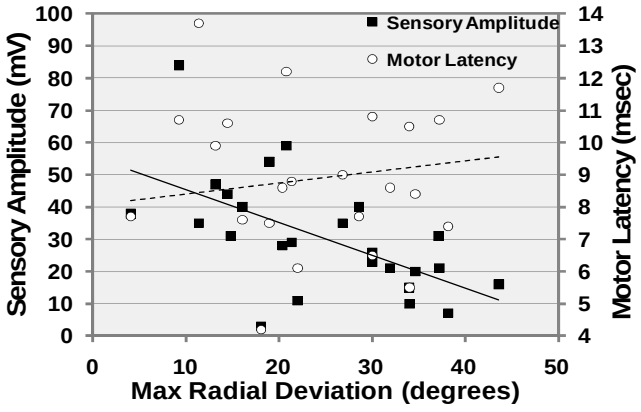

Figure 1: The correlations between maximum radial deviation and the median sensory amplitude and motor latency in the follow-up visit.

Significant differences were also found between maximum forces and maximum moments in dominant hands of female subjects who previously showed significant median nerve deterioration [8]. Our analyses also showed that maximum abduction force had a significant positive correlation with the median motor latency and maximum flexion moment had a significant positive correlation with the median sensory latency (Figure 2).

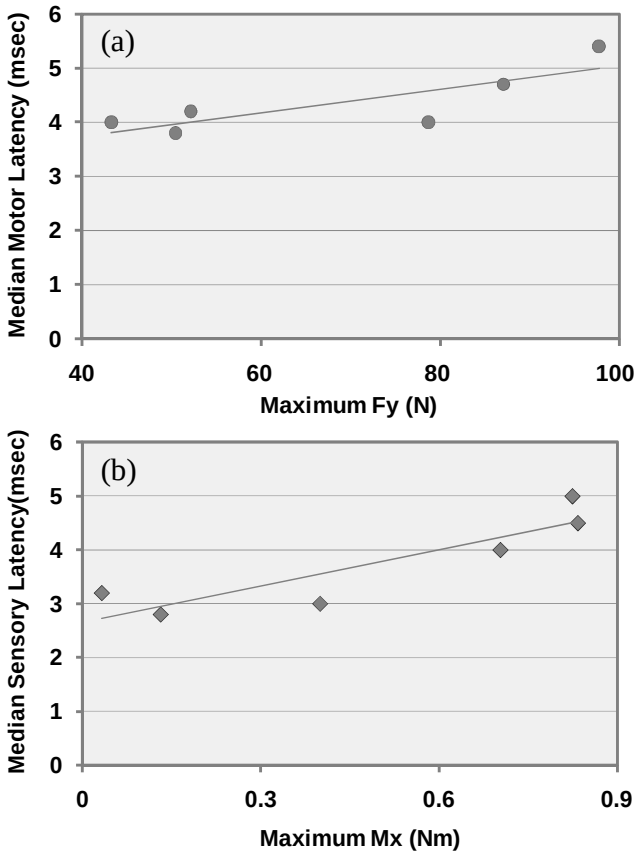

Figure 2: The positive correlations between (a) maximum abduction force and median motor latency, and (b) maximum flexion moment and median sensory latency in dominant hands of female subjects at the second visit.

CONCLUSIONS

By performing nerve conduction studies and biomechanical testing at two time-points, we attempted to link subject NCS findings and biomechanics variables at baseline and follow-up visits. Radial deviation's negative correlation with sensory amplitude and positive correlation with motor latency suggested that greater radial deviation during wheelchair propulsion could be associated with higher risk of median nerve injury. In addition, positive correlation between wrist forces and moments and median nerve health parameters indicates a need to modify force required to propel a wheelchair in order to preserve upper limb integrity. This information can provide insight into the cause of median nerve injury and possible development of carpal tunnel syndrome in manual wheelchair users.

ACKNOWLEDGMENTS

This research was funded by the Department of Veterans Affairs, grant numbers: B869RA, B2290T and B3057R, OAA01 (VA Office of Academic Affiliations), the National Institutes of Health Training Rehabilitation Clinicians for Research Careers, and NIDRR grant#H133A011107. The contents of this paper do not represent the views of the Department of Veterans Affairs or the US Government.

REFERENCES

1. Tanaka, S., Wild, D. K., Seligman, P. J., Behrens, V., Cameron, L., & Putz-Anderson, V. (1998) The US prevalence of self-reported carpal tunnel syndrome: 1988 National Health Interview Survey data. American Journal of Public Health, 84,1846-1848.

2. Aljure, J., Eltorai, I., Bradley, W. E., Lin, J. E., & Johnson, B. (1985) Carpal tunnel syndrome in paraplegic patients. PARAPLEGIA, 23,182-186.

3. Gellman, H., Chandler, D. R., Petrasek, J., Sie, I., Adkins, R., & Waters, R. L. (1988) Carpal tunnel syndrome in paraplegic patients. Journal of Bone and Joint Surgery [Am], 70, 517-519.

4. Tun, C. G., & Upton, J. (1988) The paraplegic hand: Electrodiagnostic studies and clinical findings. Journal of Hand Surgery [Am],13, 716-719.

5. Davidoff, G., Werner, R., & Waring, W. (1991) Compressive mononeuropathies of the upper extremity in chronic paraplegia. PARAPLEGIA, 29,17-24.

6. Baldwin, M. A., Boninger, M. L., Shimada, S. D., Cooper, R. A., & O'Connor, T. J. (1998) A Relationship between pushrim kinetics and median nerve dysfunction. Proceedings 21st Annual RESNA Conference, St. Paul, MN. 6-26-1998.

7. Yang, J., Boninger, M. L., Koontz, A. M., Cowan, R. E., Helkowski, W. M., Impink, B. G. (2009) Longitudinal Median Nerve Health in Wheelchair Users with Paraplegia. Journal of Spinal Cord Medicine.

8. Mercer, J. L., Boninger, M. L., Koontz, A. M., Ren, D., Dyson-Hudson, T, & Cooper, R. A. (2006) Shoulder joint kinetics and pathology in manual wheelchair users. Clinical Biomechanics, 21, 781–789.

9. Cooper, R. A., Robertson, R. N., VanSickle, D. P., Boninger, M. L., Shimada, S. D. (1997). Methods for determining three-dimensional wheelchair pushrim forces and moments— a technical note. Journal of Rehabilitation Research and Development, 34(2), 162–170.

Effect of Concomitant Latissimus Dorsi Transfer on Joint Reaction Force for Reverse Total Shoulder Arthroplasty

[1] Matthew Hansen, [2]James Otis, [1] William Ciccone, [1]Marc Jacofsky, [2]Andrew Jaczynski, [3]Aaron Boyles,

[1]The CORE Institute, Sun City West, AZ, USA
[2] SHRI-CORE Research Labs, Sun City West, AZ, USA
[3] Midwestern University Arizona College of Osteopathic Medicine, Glendale, AZ
email: james_c_otis@sbcglobal.net

INTRODUCTION

Although reverse total shoulder arthroplasty (TSA) may restore shoulder abduction and forward flexion in the setting of a massive rotator cuff tear, the ability to use the extremity for ADLs is often limited by external rotation weakness. Even though the reverse TSA restores abduction, the patient may be unable to bring the hand to his or her mouth because with the elbow flexed the weight of the hand causes the shoulder to fall into internal rotation. Concomitant transfer of the latissimus dorsi to the posterior greater tuberosity is a solution advocated by some surgeons. Gerber et al [1] reported significant improvement in abduction, forward flexion and external rotation in patients receiving concomitant latissimus dorsi transfer (LDT). While clinical results are promising, there is a need to document the effect of the inferiorly-directed force contributed by the LTD on the joint reaction force (JRF) because of its importance to fixation and stability. Therefore, it is hypothesized that this inferiorly-directed force partially counteracts the superiorly-directed force of the deltoid, resulting in decreased shear forces on the glenoid baseplate-bone interface.

METHODS

Three cadaver shoulder specimens were dissected and reverse TSA was performed. The rotator cuff was completely released to simulate a massive rotator cuff tear. Each shoulder was mounted in a shoulder controller [2] that simulates neuromuscular control and replicates in vivo glenohumeral kinematics. The controller utilizes an optical, three dimensional tracking system (Optotrak, Northern Digital Inc., Waterloo, ON). The humerus was weighted to simulate the full mass of the upper extremity and stepper motors (Industrial Devices Corp, Salem, NH) were connected to the insertion points of the anterior, middle and posterior divisions of the deltoid by Spectra® cord. Simulated active abduction in the scapular plane was performed using position closed-loop feedback control. The joint reaction force at the glenosphere was measured at 5° intervals from 30°-70°. A fourth stepper motor was then connected to the greater tuberosity with 2.73kg applied to simulate a LDT and the test was repeated. Five trials were performed under each condition. Four-factor ANOVA statistical analysis with Bonferroni correction and $\alpha = 0.05$ was performed.

RESULTS AND DISCUSSION

After simulated LDT the JRF demonstrated an increase in magnitude at abduction angles between 30° and 65° inclusive ($p=0.033$). The superiorly-directed shear force was significantly decreased as a result of the LDT for angles between 45° and 70° ($p<0.0001$). The compressive component of the JRF was increased for all abduction angles ($p=0.025$).

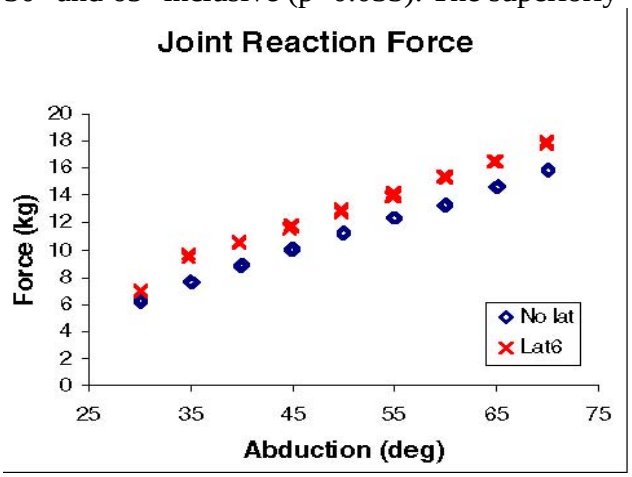

Figure 1: JRF magnitudes for the reverse TSA condition (No lat) and the concomitant LTD (Lat6) condition for one specimen.

The force required to achieve abduction increased for the middle deltoid (p=0.035) and anterior deltoid (p=0.036) for the simulated LDT condition at all abduction angles. The posterior deltoid force required for abduction decreased at all abduction angles (p=0.031).

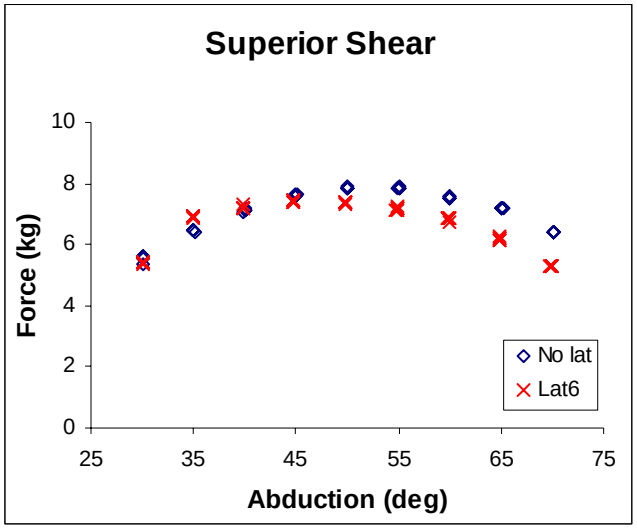

Figure 2: Magnitude of the superiorly-directed shear force for the reverse TSA (No lat) and the concomitant LTD (Lat6) conditions for one specimen.

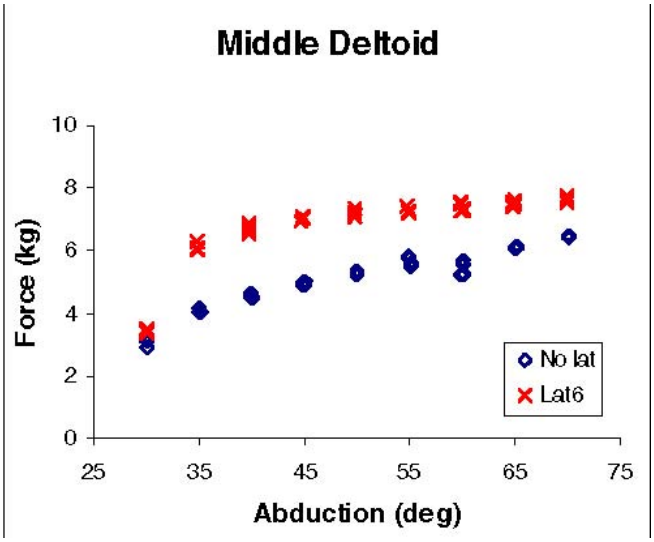

Figure 3: Magnitude of the middle deltoid force for the reverse TSA (No lat) and the concomitant LTD (Lat6) conditions for one specimen.

CONCLUSIONS

In this model of reverse total shoulder arthroplasty concomitant transfer of the latissimus dorsi decreased the superiorly-directed shear force. In addition to providing improved external rotation strength, these lower shear forces may have a protective effect on baseplate fixation by reducing the risk of failure in shear. This may provide additional justification for the transfer. Although superior shear was decreased, total JRF was increased as a result of an increase in the compressive component. Further investigation is needed to determine the potential gain in joint stability and whether the glenoid bone can support such elevated compressive forces.

Additionally, the force required in the anterior and middle deltoid was increased after the LDT. This indicates the need for sufficient deltoid strength and rehabilitation.

REFERENCES

1. Gerber, C, et al.: Reverse Delta-III Total Shoulder Replacement Combined with Latissimus Dorsi Transfer. *JBJS-A*, **89**:940-947, 2007.
2. Hansen, ML, et al.: Biomechanics of Massive Rotator Cuff Tears: Implications for Treatment. *JBJS-A*, **90**:316-325, 2008.

ACKNOWLEDGEMENTS

Support was provided by Equinoxe Reverse, Exactech Inc., Gainesville, FL. Institutional support has been provided by Stryker Corp.

SHOULDER KINEMATIC PATTERNS DURING EXECUTION OF CIRCUIT RESISTANCE TRAINING IN INDIVIDUALS WITH PARAPLEGIA: A CASE SERIES

[1,3]Linda M. Riek, [2]Paula M. Ludewig and [3]Deborah A. Nawoczenski

[1]University of Rochester, Rochester, NY, USA
[2]University of Minnesota, Minneapolis, MN, USA
[3]Ithaca College, Rochester, NY, USA

email: lmriek@rochester.rr.com

INTRODUCTION

Following spinal cord injury (SCI), shoulder demands are radically altered as usage and upper extremity weight-bearing increase. Consequently, shoulder pain associated with impingement is common in persons with paraplegia (40% prevalence). Although little is known regarding shoulder health and injury prevention following SCI, exercise including circuit-resistance training (CRT) is encouraged in rehabilitation and community settings to promote shoulder health. Ironically, positions inherent to CRT programs may increase shoulder impingement risk, either subacromial or internal. In the able-bodied, impingement is associated with altered shoulder kinematics, including increased scapular anterior tilt (AT), downward rotation (DR), internal rotation (IR), and glenohumeral (GH) IR[1]. Previous literature supports scapular AT and GHIR as key detrimental motions for shoulder impingement [1]. These same potentially detrimental kinematic patterns may be present during the execution of CRT exercises from a wheelchair level.

The purpose of this study was twofold: 1) to critically evaluate three-dimensional (3-D) scapular and GH kinematic patterns among wheelchair-based upper extremity CRT exercises in order to determine which exercises place the shoulder at greater impingement risk and 2) to evaluate whether specific humeral modifications during execution of upper extremity CRT exercises will alter 3-D scapular and GH kinematic patterns such that shoulder impingement risk can be minimized.

METHODS

In this case-series design, three subjects with SCI at the second thoracic (T2) level or below and without shoulder pain participated. During the first session, the one repetition maximum (1-RM) was determined for five Cybex Total Access™ exercises (chest press, seated row, lat pulldown, overhead press, cabled rickshaw). During the second session, 3-D shoulder kinematic data were collected using the Flock of Birds™ electromagnetic tracking system. At each station, the subject performed one paced set of ten repetitions at 50% 1-RM in both a traditional position and a modified arm position.

Exercises were rank-ordered based on the magnitude of deviation from previously established normative data for scapular anterior tilt, internal rotation, downward rotation, and GH internal rotation [3]. Based on the magnitude of deviation at specific humerothoracic (HT) elevation angles of 45º and 60º (subacromial impingement risk) and 105º and 120º (internal impingement risk), values for each kinematic variable within one standard deviation (sd) from normative values were assigned one point, between one and two sd were assigned two points and beyond two sd were assigned three points. Comparisons between traditional and modified positions for each exercise were also assessed at selected positions of HT elevation. Differences exceeding five degrees or more of scapular or GHIR angles at these selected angles were considered a modifiable change.

RESULTS AND DISCUSSION

Three subjects (50 $\pm$ 13 years and neurologic level ranging from the fourth to twelfth thoracic level) participated. At less than 60 degrees, the risk of subacromial impingement (combined patterns of scapular AT, IR, DR, and GHIR) was greatest for

rickshaw, row or chest press, and lat pulldown. At greater than 105 degrees, the risk of internal impingement was greatest for overhead press followed by lat pulldown (Figure 1). Findings also suggest that modified arm positions can result in more favorable kinematics during the execution of CRT as demonstrated by a maximum decrease in scapular AT of 22 degrees during row and 12 degrees during chest press at 60 degrees HT elevation (Figure 2). At 105 degrees HT elevation, GHIR demonstrated a maximum decrease of 7 degrees during overhead press (Figure 2).

This study is limited to three participants. Ongoing studies include an expanded sample size and simultaneous collection of kinematic and muscle activation data during execution of CRT. Initial findings are promising that impingement risk during the execution of CRT can be reduced by modifying arm positions.

REFERENCES

1.Ludewig PM, et al. *Physical Therapy* **80**, 276-291, 2000.
2.Bey MJ, et al. *Clinical Biomechanics* **22**, 767-773, 2007.
3.Ludewig PM, et al. *The Journal of Bone and Joint Surgery* **91**, 378-389, 2009.

ACKNOWLEDGEMENTS

We acknowledge the National Spinal Injury Association, Rochester Chapter and the Pieters Family Life Center.

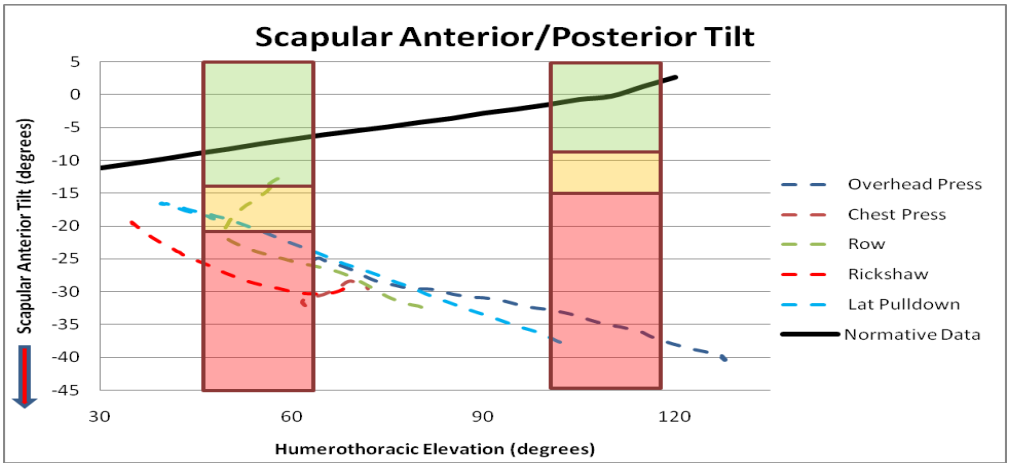

Figure 1: **S**capular anterior tilt (one of four kinematic patterns) for subject one during five CRT exercises. Green boxes are ± 1sd, orange are between 1-2sd, and red are greater than 2 sd from normative data reflecting scapular positions considered least to most risk, for subacromial (45-60 degrees) or internal (105-120 degrees) impingement.

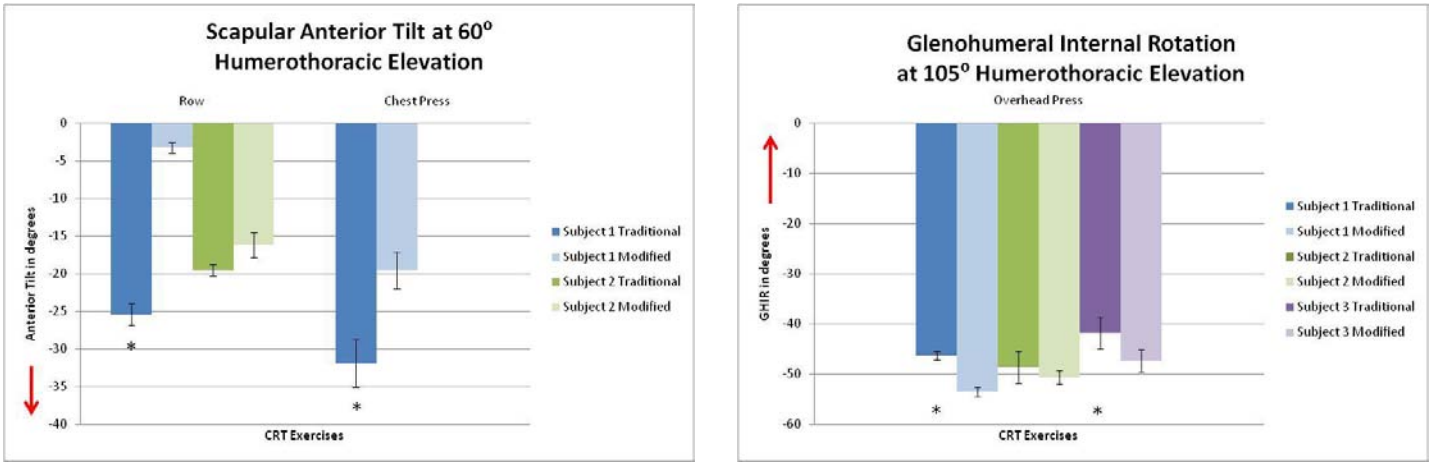

a **b**

Figure 2: a) Scapular anterior tilt at 60 degrees HT Elevation and b) GH internal rotation at 105 degrees HT elevation. Asterisks indicate greater than 5 degree differences between traditional and modified positions.

ALTERATIONS IN SHOULDER JOINT PERCEPTION PRE AND POST WORKDAY

[1]Luke Ettinger, [2] Laurel Kincl, [1]Andrew Karduna
University of Oregon [1]Department of Human Physiology, [2] Labor Education and Research Center
email: lettinge@uoregon.edu, web: http://biomechanics.uoregon.edu/obl/

INTRODUCTION

Dental hygienists have a high incidence of shoulder pain and pathology, which may be associated with the demands of the workplace environment and or work related responsibilities. In dental hygienists, injuries to the upper extremity are believed to be the result of low level static loads placed on the shoulder, awkward and constrained posture and fatigue inducing repetitive arm motions (1, 4). The sensation of joint position is believed to help maintain posture and joint stability during motor tasks (3). Joint Position Sense (JPS) tasks are an established method for accessing proprioceptive responses to limb movement (2). The current study attempts to measure shoulder proprioception in dental hygienist using JPS before and after a typical workday. It is hypothesized that repetitive arm usage in the workplace will result in decrements in shoulder JPS in dental hygienists. It is conceivable that proprioceptive errors could affect the fine motor skills needed to perform dental hygiene, and could thus place patients and hygienists at a higher risk of injury. To date, there have been no published studies comparing unconstrained JPS tasks between pre and post workdays in any population. Additionally, no studies of this nature have been conducted within the workspace of any population.

METHODS

Twenty four female dental hygienists participated in this study (mean age, 43 years). All subjects worked more than 40 hours per week and all data were collected before and after an 8 hour or longer workday. All data were collected at the dental hygienists' place of employment. Kinematic data were collected via the Polhemus Fastrack magnetic tracking system with two receivers: thorax and humerus (Figure 1). The thoracic receiver was attached using double sided adhesive tape to the manubrium, inferior to the jugular notch. The humeral receiver was placed over the deltoid tuberosity using a molded cuff. Bony landmarks were digitized using the stylus during the calibration phase of our experimental protocol. For all trials, data were collected at a rate of 40 Hz.

Figure 1: Experimental setup, attachment of sensors and head mounted display.

During calibration and data collection trials, subjects were in a standing position. The arbitrary coordinate systems defined by the Polhemus were converted to anatomically appropriate coordinate systems based on the recommendations of the International Society of Biomechanics Committee for Standardization and Terminology (6). Subjects were fit with a head mounted display (Cybermind Hi-Res) that removed visual input of their arm in space. During the active positioning phase, target positions for humeral plane and elevation were presented to the subject digitally using a custom program written in LabView (Figure 2). Subjects preformed 5 active positioning and repositioning tasks to previously established coordinates in a random order. Target positions were [45°, 75°] [40°. 70°], [35°,70°], [40°, 75°], [45°, 65°] for plane and elevation respectively. Once the subject had actively positioned their arm in the target, they were asked to try and remember where there hand was in space. Then the subjects were instructed to relax their arm at their side for several seconds. The

subject was asked to reposition their arm to the perceived target location; no visual information was presented to the subject during reposition of the arm. When the subject perceived that they had successfully repositioned their arm to the positioned coordinates, they clicked a button with their non-dominant hand which automatically ended the trial.

For statistical analysis a 2-way repeated measure ANOVA was run where vector error was the dependent variable. Both trial number and pre – post workday conditions were the independent variables. Vector error is defined as the angle between the positioned vector, located between the center of the humeral head and the elbow center and the repositioned vector, located again between the center of the humeral head and elbow center (5). The α level was set at 0.05 for all statistical analysis.

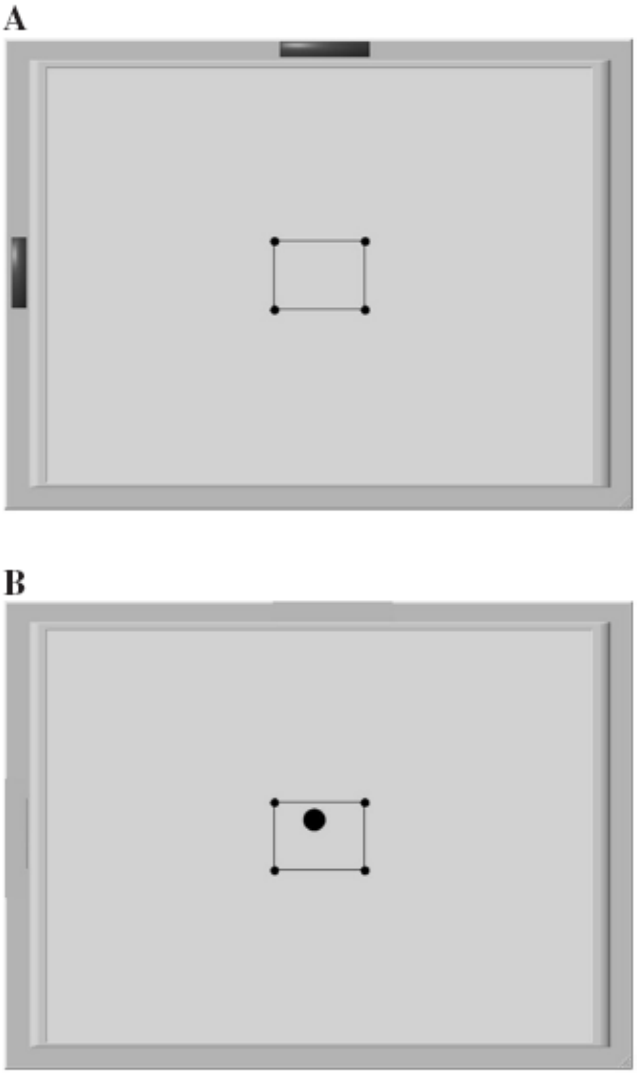

Figure 2: Computer output as seen in the head mounted display (**A**) guiding the subject to the target position and (**B**) with the shoulder in the target position.

RESULTS AND DISCUSSION

The results of the ANOVA indicate that there were no significant differences for vector error ($p = 0.13$) between the pre and post workday conditions. Additionally, there were no significant differences in repositioning error based on target location.

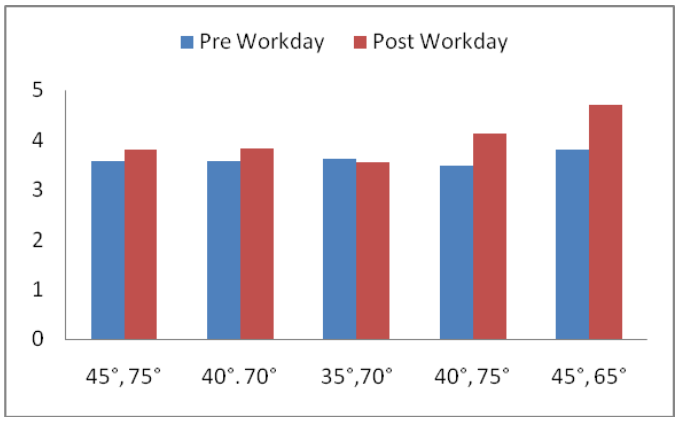

Figure 3: Vector error for pre and post workday JPS.

Fatigue mechanisms have been related to alterations in proprioceptive tasks such as JPS (2). Our study design accesses JPS immediately before and after a full workday in order to accurately identify any changes in proprioception that might result from workday fatigue. Although there were no significant changes in proprioception post workday in dental hygienists, it is possible that proprioceptive changes occur in other populations with high incidences of work related injury. Further analysis might separate dental hygienists into groups based on duration of employment as hygienist injury rates are correlated to job longevity (1).

ACKNOWLEDGEMENTS

This work was funded in part by a NIOSH grant - 5R01OH008288.

REFERENCES

1. Akesson I, et al. *Int Arch Occ Env Hea* **72**: 395-403 1999.
2. Hung-Maan, et al. E*Clinical Biomechanics* **18**: 843-847, 2003.
3. Madhavan S, et al. *Experimental Brain Research* **164**: 18-28, 2005.
4. Ohlsson K, et al. *Occupational and Environmental Medicine* **51**: 826, 1995.
5. Suprak D, et al. *J Orthop Res* **24**: 559-568, 2006.
6. Wu G, et al. *J Biomech* **38**: 981-992, 2005.

THE EFFECTS OF NOISE AND INERTIA DISTRIBUTION DURING A PLANAR REACHING TASK

[1]Hung Nguyen, [2]Jonathan Dingwell

[1]Department of Mechanical Engineering, University of Texas, Austin, TX, USA
[2]Nonlinear Biodynamics Lab, Dept. of Kinesiology, University of Texas, Austin, TX, USA
Email: hpnguyen@mail.utexas.edu, Web: http://www.edb.utexas.edu/faculty/dingwell/

INTRODUCTION

While reaching is a very elementary task, it requires a high level of control to overcome one fundamental challenge during movement: noise. One strategy the nervous system could use to minimize the effect of noise is to implement proximal and distal control over the multi-segment body. Preliminary work demonstrated that during a reaching task, endpoint accuracy was more sensitive to perturbations of the proximal joints than distal joints and implementing distal control yielded the best performance in minimizing the noise [1]. The results closely agreed with experimental findings by [2]. In the present paper we are interested in whether the same strategy is still viable when the inertial properties of the upper extremity are manipulated. Do the inertial properties of the upper arm and/or forearm significantly affect the endpoint performance and energetic cost of reaching? Using a 2dof arm model, we demonstrated that there is a trade-off between endpoint accuracy and energetic cost for different inertia distributions of the upper extremity.

METHODS

A 2-dof torque-driven arm model was simulated. For each movement, the arm performed a straight-line outward reaching movement from point A to point B (Fig. 1a). The feedforward movement trajectory of the endpoint was generated using Minimum Jerk motion. Once this endpoint trajectory was defined, the joint angular position, velocity, and acceleration were calculated using inverse kinematics. Corresponding joint torques were then calculated by inverse dynamics. These baseline torques were then subjected to perturbation by signal-dependent noise [3].

Proportional-Derivative (PD) controllers (Fig.1b) were implemented at the shoulder and elbow joints to determine the effects of these controllers on the endpoint accuracy and mechanical energy. Eight different combinations of noise and controller were simulated (Figs. 2 & 3). The two dependent measures in the simulation were endpoint error and mechanical energy. The endpoint error was defined as the magnitude distance from desired endpoint position (x_d, y_d). Energy was calculated by integrated the power curve of each movement.

To investigate the effect of inertial distribution in the upper extremity, we manipulated the mass of the upper and forearm to generate different inertia ratios while keeping the total mass and length of the arm constant. The inertia ratio (IR) was defined as

$$IR = \frac{inertia\ of\ upper\ arm}{inertia\ of\ forearm}.$$

Simulations were implemented in Matlab (MathWorks Inc., Natick, MA). Each condition was simulated for 60 trials and the average values were recorded. Anthropometric data were obtained from Winter [4] assuming H=1.75 m and M=75.0 kg. One-factor ANOVAs were performed to determine statistical significance. Standard anthropomorphic values for the arm yielded an IR of 1.07.

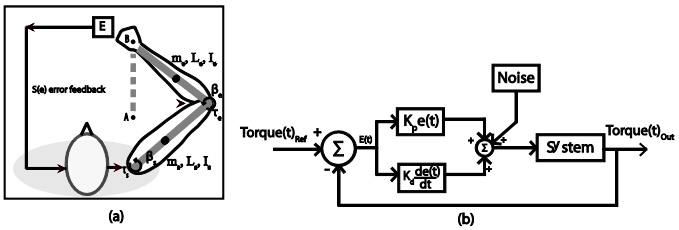

Figure 1: (a) Schematic of the reaching model and **(b)** Proportional-Derivative controllers which applied torques at the elbow and shoulder.

RESULTS AND DISCUSSION

Endpoint Error

Endpoint performance was more sensitive to distal (elbow) noise than to proximal (shoulder) noise during pure feedforward (No Cntrl) reaching (0.53 vs. 1.81 cm, $p<0.001$). When IR was increased from 1.07 to 4.0 (i.e. larger upper arm), endpoint errors increased significantly during distal perturbations (from 1.81 to 2.49 cm, $p<0.001$). When IR was decreased from 1.07 to 0.25 (i.e. larger forearm), endpoint errors were significantly smaller for both distal and proximal perturbations.

When noise was present at both the distal and proximal joints, using a distal controller significantly reduced endpoint error over proximal control for all inertia ratios. For all inertia ratios, the PD controller eliminated all residual noise in the system (Fig. 2).

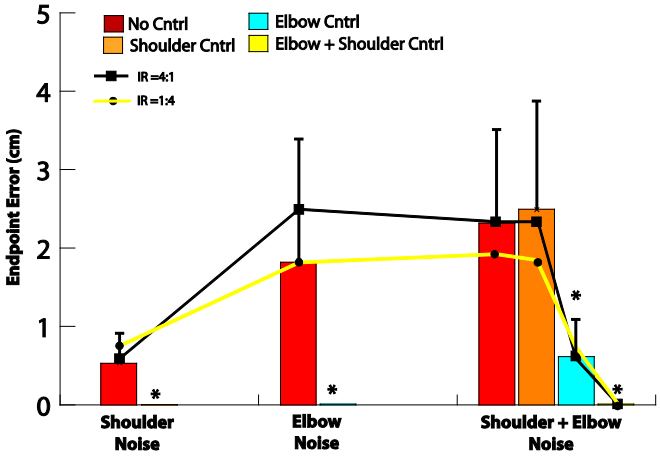

Figure 2: Endpoint error performance and control for different inertia ratios.

Energetic Cost

For an anthropometric arm (Fig. 3-bar), there were statistical significant differences in energetic cost for proximal and distal control; however the difference in the raw values were small. When noise was added to both joints, implementing distal control resulted in significantly lower energy expenditure.

Different IR's yielded very large differences in energetic cost (Fig. 3). Mechanical energy increased dramatically as more mass was shifted toward the forearm. When IR was increased from 1.07 to 4.0, average energetic cost decreased significantly (from 2.47 to 1.33 J, $p<0.001$). When IR was decreased from 1.07 to 0.25, the average energetic cost increased significantly (from 2.47 to 4.21 J, $p<0.001$). Thus, when the forearm is *large* relative to the upper arm, more energy is required to compensate for distal and proximal noise, even when total arm mass is held constant. The arm is more sensitive to noise when the forearm is relatively larger than the upper arm.

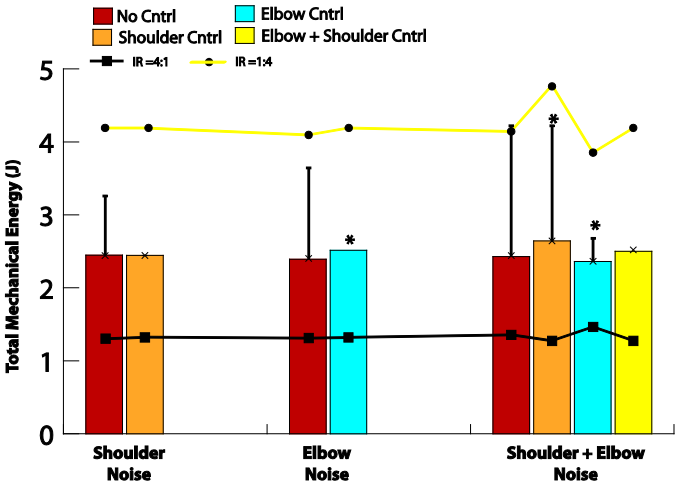

Figure 3: Energetic cost and control for different inertia ratio

CONCLUSIONS

Optimization of inertia distribution has been used as a tool to design robotic manipulators [5]. These optimization methods are necessary to find the trade-off between energetic cost and endpoint accuracy. While higher IR generally produces better endpoint performance, it is energetically more costly. Human inertia ratios appear to find a balance between energetic cost and endpoint performance. However, we also rely heavily on feedback control to improve performance.

REFERENCES

1. Nguyen HP & Dingwell JB, *Proceedings of ASB '09*, State College, PA, USA, 2009.
2. Cusumano JP, et al. *Bio Cybern* **94**, 369-79, 2006.
3. Hamilton AF, *Exp Brain Res*, **157**(4): 416-30, 2004
4. Winter DA, *Biomechanics and Motor Control of Human Movement*, Wiley & Sons, Ontario, CA.
5. Yang DCH, *Int J Robotics Res* ***5,*** *120-128, 1986.*

EFFECT OF PLICATION ON GLENO-HUMERAL TRANSLATION – A PRELIMINARY IN VITRO STUDY

[1,2]Rao, S; [1,3]Miana, A; [1]Lenhoff, M; [1] Backus, S; [1,5]Vanadurongwan, B; [1]Chen, N; [1]Brown, A; [1]Coleman, S; [1]Cordasco, F; [1]Altchek, D; [1]S Fealy, [1]C Imhauser, [4]A Karduna,[1]R Warren, [1]T Wright, [1]R Zifchock, [1]H Hillstrom

[1]Hospital for Special Surgery, [2]New York University, NY, [3]Instituto Vita, Sao Paulo, Brazil; [4]University of Oregon, Eugene, USA; [5]Siriraj Hospital, Mahidol University, Bangkok, Thailand. email: smita.rao@nyu.edu

INTRODUCTION

Increasing clinical evidence suggests that capsular plication may be a means to surgically correct anterior instability of the shoulder. Previous studies have demonstrated reduced humeral head translation, reflecting increased glenohumeral stability, following thermal or arthroscopic capsulorrhaphy (suture plication). However, these studies tested humeral head translation using a mechanized jig [1] or simulated clinical testing. [2] Previously tested activities may not represent humeral head translation seen during open chain functional activities. These findings are important because open chain functional activities, such as the pitching and throwing, are frequently used by individuals reporting anterior shoulder instability.

The effect of suture plication on humeral head translation during functional open chain activities (flexion, abduction and external rotation) is not known. The purpose of our study was to assess the effect of plication on humeral head translation during three functional open chain activities; flexion, abduction and external rotation.

METHODS

One cadaver (two upper limbs) with no known musculoskeletal pathology was mechanically grounded to a vertical steel stanchion, allowing unrestrained motion of the upper extremities. The scapula and humerus were instrumented with one Steinmann pin and four reflective markers each.

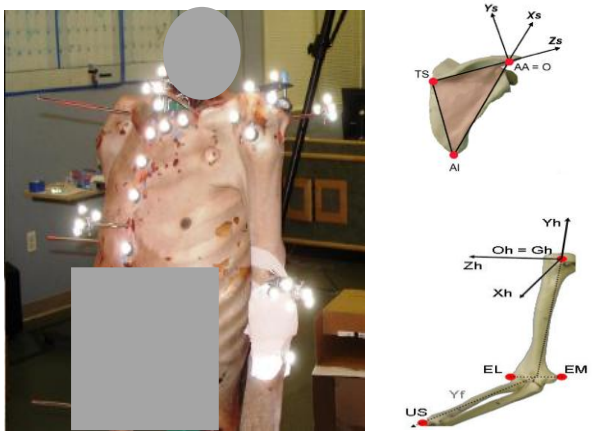

Fig 1. Instrumentation and co-ordinate systems

Anatomical coordinate systems were defined, according to ISB recommendations, [3] for the scapula and humerus with a digitizer. (Coordinate systems depicted in Fig. 1) Kinematic data were collected at 100 Hz using a 10-camera system. (Motion Analysis Inc) A single tester (AM) applied markers, performed all digitizing and moved the upper limb through three tasks (glenohumeral flexion, abduction and external rotation) before and after open suture plication. Peak motion (glenohumeral flexion, abduction and external rotation) before and after plication was repeatable to within 3 degrees. Open suture plication surgery was performed by an orthopedic surgeon (NC).

Data were analyzed using Visual 3D (C-motion Inc, MD). Glenohumeral motion was defined using using a y-z'-y" Euler sequence of rotations, where y is the supero-inferior axis, and z is the medial-lateral axis.[3] The location of the humeral head was modeled as the center of the glenohumeral joint, estimated using the functional joint center.

RESULTS

Modest reduction in antero-posterior (AP) and supero-inferior (SI) translation was noted following plication (Fig 2) during external rotation. No differences in humeral head translation were found during flexion or abduction.

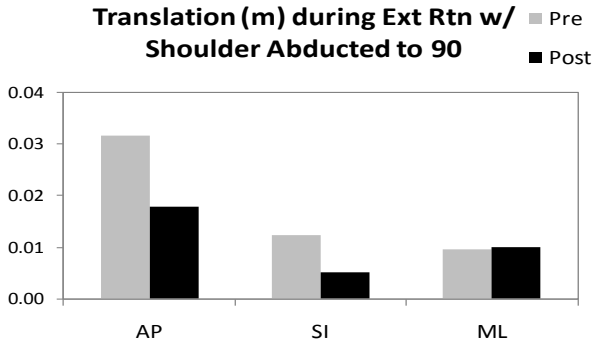

Fig 2. Reduction in range of humeral head translation during external rotation (units: m) before and after plication.

DISCUSSION:

We developed a novel cadaveric model with which to study the passive motion characteristics of the glenohumeral joint, before and after open suture plication. These findings may be important because they help define mechanisms by which open suture plication may affect shoulder mechanics.

The findings of our preliminary study indicate that suture plication is accompanied by reduction in anterior-posterior translation of the humeral head during open chain external rotation. Our results demonstrating a 43% decrease in anterior-posterior translation following plication are consistent with previous findings demonstrating 45-60% change in humeral head translation following surgery [1, 2].

These results are consistent with previous reports and indicate that suture plication affords improved glenohumeral stability without loss of functional range of motion. The difference in magnitude of translation may also be explained by extent of shoulder loading during activity and by differences in surgical technique.

The current study used an *in vitro* model and focused on passive motion characteristics to understand the role of the passive constraints in stabilizing and controlling bone motions. Future studies will extend this approach to *in vivo* models and include the contribution of shoulder musculature to glenohumeral motion.

ACKNOWLEDGEMENTS: David Adar from the Psychomotor Skill Laboratory at Hospital for Special Surgery for assistance with the cadaveric specimen.

REFERENCES

1. Alberta, F.G., et al., J Bone Joint Surg Am, 2006. 88(1): p. 179-87.
2. Magit, D.P., J.E. Tibone, and T.Q. Lee, Am J Sports Med, 2008. 36(7): p. 1389-96.
3. Wu, G., et al. J Biomech, 2005. 38(5): p. 981-992.

The Effect of Biceps Reattachment Site on Moment Arm

[1,2]David Weir, [2]Christopher Schmidt, [2]Andrew Wong, [2]Michael Howard and [1,2]Mark Miller

[1]University of Pittsburgh, Pittsburgh, PA, USA
[2]Allegheny General Hospital, Pittsburgh, PA, USA
email: dweir@wpahs.org

INTRODUCTION

Avulsion of the distal biceps tendon from the tuberosity occurs mostly in middle-aged males resulting from eccentric loading of the flexed, supinated forearm [1]. When non-operative treatment is chosen, supination strength decreases by 50% and flexion strength is reduced by 35-40% [2]. Surgical repair has been shown to be a better alternative than non-operative treatments for restoration of strength and endurance [2, 3].

Current surgical methods include one and two incision repair techniques in which the tendon is reattached to the anterior or posterior aspect of the tuberosity respectively. Methods of attachment of the tendon include using sutures, suture anchors and cortical buttons. Although studies have examined the fixation strength of these types of repairs, little has been done to examine the effect that attachment location has on functional outcome of the repair [4].

The objective of this project is to determine the impact that the reattachment location has on torque generating ability of the forearm described as its moment arm. The results of this study can help surgeons gain a better understanding of how to optimize the repair and thereby improve the expected outcome of patients with distal biceps injuries.

METHODS

A total of 6 frozen upper extremity cadaveric specimens (5 male), with an average age of 60 (36-83) years, were used. The specimens included the full forearm from the hand to the mid-humerus proximally. Specimens with medical histories of rheumatoid arthritis, degenerative joint disease or any orthopaedic anomaly were excluded. Prior to the day of testing, each specimen was allowed to thaw overnight at room temperature and kept moist with normal saline.

An elbow simulator, that includes computer controlled actuators to exert known loads on the forearm applied through the biceps tendon, was adapted to a device capable of measuring isometric forearm torque generated by cadaveric elbows [5]. The device has an adjustable shaft that attaches to a plate mounted on the distal radius. The other end of the shaft transmits load to a torque sensor (Transducer Techniques, Temecula, CA) which is wired into a computer data acquisition system.

Each specimen was mounted in the elbow simulator with the humerus and ulna fixed firmly to the frame at 90° of flexion. The proximal end of the distal biceps tendon was attached to an actuator using 80lb test line. The adjustable shaft was attached to the distal radius plate. The forearm was then rotated and locked into three positions: 60° supination, neutral and 60° pronation. The biceps tendon was loaded to 15 lbs, and the torque was measured for the native tendon attachment. Then the biceps tendon was detached and attached at four different locations. For each forearm position, each test was repeated three times.

With the arm fully supinated, the borders of the radial tuberosity were identified and marked as shown in Figure 1. A line connecting the two midpoints of the borders was used to define the center axis line. The highest point (apex) on the tuberosity at the tendon-bone interface was identified using calipers. A medial to lateral line, parallel to the tuberosity border lines, was drawn to define the apex diameter line. Using these markings as a guide, four reattachment points were systematically placed in the radius as shown in Figure 1.

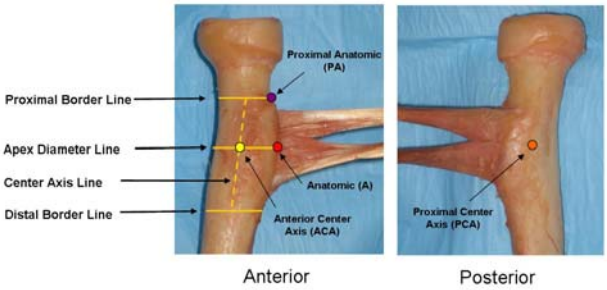

Figure 1: Diagram of distal biceps tendon reattachment locations.

A regression line was fitted to the torque vs. load data for each test. The moment arm for each tendon attachment was defined as the slope of the regression line. A positive moment arm value indicated that the biceps generated a supination torque.

Statistical analysis consisted of two-way repeated measures analysis of variance with Tukey's post-hoc testing to compare the means of individual treatment groups with one another.

RESULTS AND DISCUSSION

Tendon location and forearm position significantly affected the moment arm of the biceps ($p<0.05$). The native tendon had a mean moment arm of 5.67 ±2.86 and 10.44 ±1.45 (mm) in 60° supination and neutral respectively. Reattachment to Location (A) in all forearm positions showed no significant difference from the native. Location (ACA) was significantly lower in supination (0.15 ±3.48) and neutral (7.65 ±1.95), while Location (PCA) was significantly higher in supination (7.21± 3.02) compared to the native. Location (PA) (4.69 ±2.75) was significantly higher than (ACA) in supination. No difference was observed between all tendon locations in pronation. Figure 2 summarizes the results.

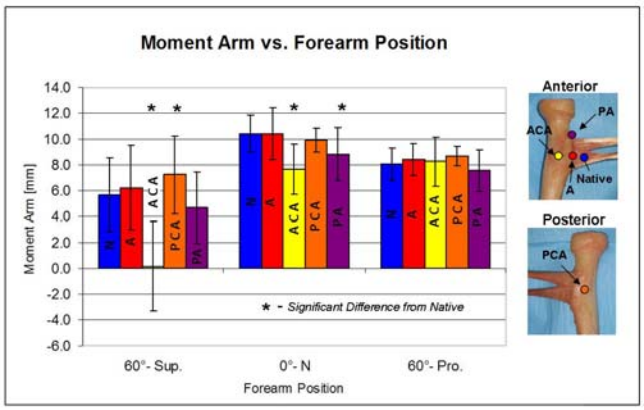

Figure 2: Summary of results for moment arm vs. forearm position

Reattachment of the distal bicep tendon to its anatomic position showed no difference in moment arm to the native. A more central attachment on the anterior radius resulted in a significantly lower moment arm than the native in neutral and supinated positions. We believe this observation is due to less wrapping of the tendon around the tuberosity with an anterior position. Further, this finding is supported by an increase in moment arm at a posterior attachment with the arm in a supinated position.

A proximal anatomic location trended to have a lower moment arm than the native in all forearm positions, but was only significantly different in neutral. Clinically these findings would suggest that if the muscle was contracted and the tendon could not be inserted to its native position then a proximal ulnar position would be better than a more central anterior one.

CONCLUSIONS

This biomechanical study provides support for the importance of anatomic restoration of the native tendon moment arm during the repair of ruptured distal biceps tendons. The surgeon needs to pay particular attention to the geometry of the tuberosity and be mindful of the location of tendon reattachment as it could play a critical role in maximizing the functional outcomes of patients.

REFERENCES

1. Chillemi, C., et al. (2007). *Arch Orthop Trauma Surg* **127**(8): 705-8.
2. Hetsroni, I., et al. (2008). Injury **39**(7): 753-60.
3. Baker, B. E. and D. Bierwagen (1985). *J Bone Joint Surg Am* **67**(3): 414-7.
4. Kettler, M., et al. (2007). *Am J Sports Med*. 35(9): 1544-8.
5. Kuxhaus, L. (2009) *ASME J Medical Devices*

SHOULDER EXTERNAL ROTATION DURING PHYSICAL ASSESSMENT AND THROWING ACTIVITY

[1]Nigel Zheng and [2]Koco Eaton

[1]University of North Carolina at Charlotte, NC, USA
[2]University of South Florida, Tampa Rays, FL, USA

Email: nzheng@uncc.edu

INTRODUCTION

Throwing arm injuries are common and often related to shoulder external and internal rotational laxity. Both shoulder external and internal rotational laxity are often checked in a physical assessment. The shoulder external rotation of the throwing arm during physical assessment is reported to be about 10 degree greater than the non-throwing arm [1]. Throwing arm injuries often occur during throwing activities. Extremely high shoulder external rotation (about 180^o) and high internal rotation velocity (over 7000 ^{o}/s) during baseball pitching are reported [2]. High forces and torques were generated during throwing activity.

Physical assessment is often performed for diagnosis of throwing arm injuries. Quantitative assessment of shoulder rotational flexibility may provide new insights to physical assessment and options for treatment. It is not sure whether it may provide any signs for prevention of throwing arm injuries. It is hypothesized that the shoulder external rotation during physical assessment is related to the shoulder maximum external rotation during baseball pitching. The objective of this study is to establish a relationship between the shoulder rotational laxity during physical assessment and during baseball pitching. Strong relationship may allow us to predict injury risks for throwing arm injuries from physical assessment.

METHODS

One hundred collegiate baseball pitchers (mass 87.0 ± 8.0 kg, height 1.86 ± 0.06 m) who were healthy at the time of test were recruited. After signing consent forms they filled a self-report questionnaire of throwing arm injuries. They were then examined on both shoulders using a custom-made wireless device (Fig. 1). The resistance onset angle (ROA) at 2 N force applied at the wrist, end-point angle (EPA) at 40 N force applied at the wrist, shoulder rotational flexibility (SRF) in both external and internal rotations, free range of motion (fROM, sum of the internal ROA and external ROA) and end range of motion (eROM, sum of the internal EPA and external EPA) of both shoulders were determined (Fig. 2).

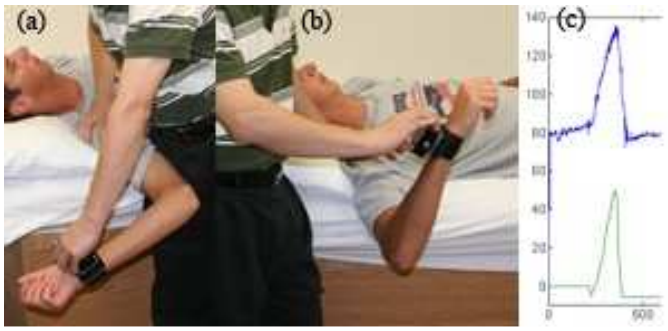

Figure 1: Shoulder rotational testing (a) external rotation, (b) internal rotation, and (c) shoulder rotational angle and force applied during test.

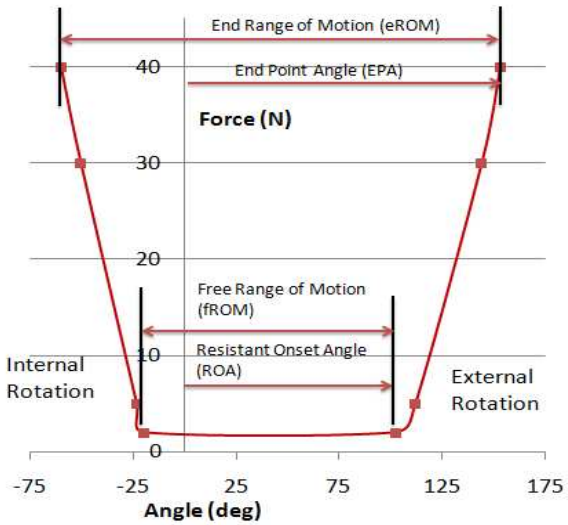

Figure 2: Definitions of the Resistant Onset Angle (ROA), the End Point Angle (EPA), the free Range of Motion (fROM), and the end Range of Motion (eROM).

Seventeen reflective markers were attached to major bone landmarks of a subject and 10 fastball pitching motions were collected at 240 Hz using a 10-camera motion capture system (FX40, VICON, UK). The maximum shoulder external rotation (MER) was determined according to previously reported method [3] and normalized from the leading foot contact to the ball release. Pearson correlation coefficients were determined (SPSS, Chicago, IL). Significances were tested at the 0.01 level.

RESULTS

Among 100 subjects, 27 had experiences of throwing arm injuries in the past year and 11 had throwing arm surgery history (9 on the elbow and 2 on the shoulder). Table 1 lists the shoulder external rotation angle and shoulder rotational flexibility during physical assessment, and the maximum external rotation and gun speed during pitching. There were no significant differences among three groups with no injury, with injury in the past year, and with surgery history.

Table 1: Shoulder External Rotation (EPA) and Shoulder Rotational Flexibility (SRF) during physical assessment and the Maximum External Rotation (MER) and ball gun speed during pitching for three groups with no injury (H), injury in the past year (I) and with surgery (S).

	EPA (^{o})	SRF (^{o}/Nm)	MER (^{o})	GunSpeed (mph)
H	75 ± 12	3.16 ± 0.8	174 ± 10	77.5 ± 4.6
I	81 ± 16	3.31 ± 0.9	171 ± 12	77.4 ± 5.8
S	79 ± 8	3.18 ± 1.0	171 ± 11	79.0 ± 4.3

Table 2 lists the Pearson correlation coefficients and significance p values. There were significant correlations between the maximum shoulder external rotation and ball gun speed, and between the shoulder external rotation and shoulder rotational flexibility.

Table 2: Pearson Correlation Coefficient

	MER	EPA	SRF	GunSpeed
MER		-0.027	0.018	0.416**
EPA			0.365**	-0.058
SRF				-0.124

** $p<0.000$

DISCUSSION

From 100 collegiate baseball pitchers, no significant correlation between the shoulder external rotation during physical assessment and the maximum shoulder external rotation was found. Our hypothesis was disproved. Both the shoulder external rotation and shoulder rotational flexibility had very low Pearson correlation coefficient with the maximum shoulder external rotation and ball gun speed (Table 1). During the physical assessment, the scapular was stabilized manually. During the throwing activity, the scapular was free to move and made significant contribution to the shoulder external rotation. The shoulder external rotation during physical assessment was mainly from the glenohumeral joint, whereas during the throwing activity, both the glenohumeral joint and the scapulothoracic articulation made contribution to the shoulder external rotation measured.

Shoulder physical assessment is often performed in diagnosis of throwing arm injuries. It may have limited application in predicting risks for throwing arm injuries. More complex evaluation, such as motion analysis, may be needed to develop preventive measures to throwing arm injuries. Future research should focus on the role of the scapula in throwing activities, and evaluation of the glenohumeral joint and the scapulothoracic articulation in throwing activities.

REFERENCES

1. Borsa PA et al, *Med Sci Sports Exerc.* Jan 2006 38(1):21-26.
2. Zheng, N et al, *Athletic Therapy Today*, July 1999
3. Zheng N et al, Biomechanics of Pitching, George Hung (ed) *Biomedical Engineering Principles in Sports* Kluwer Academic/Plenum Publishers 2004

ACKNOWLEDGEMENTS

This study was funded by a clinical research grant from the Major League Baseball. Authors also would like to thank Bryan Conrad, Bo Gao, Hernando Pacheco, Hongsheng Wang and Bing Xiao for their assistance in data collection and reduction.

A DYNAMIC CT TECHNIQUE FOR ASSESSMENT OF WRIST JOINT INSTABILITY

[1]Kristin Zhao, M.A., [2]Shuai Leng, Ph.D., [2]Mingliang Qu, M.D., [2]Cynthia McCollough, Ph.D., [1]Kai-Nan An, Ph.D.
[1]Biomechanics Laboratory, Division of Orthopedic Research; [2]Department of Radiology
Mayo Clinic, Rochester, MN 55905 USA
email: zhao.kristin@mayo.edu

INTRODUCTION

The wrist is one of the most intricate articulations of the musculoskeletal system, in which the delicate balance is maintained by a complex set of intrinsic and extrinsic ligamentous connections between seven carpal bones. Injuries to the bones and ligaments in the wrist may potentially irreversibly disrupt this balance and initiate progressive degenerative disease and osteoarthritis (OA). Muscle forces across the hand and wrist, as well as the numerous and complex articulations, pose significant challenges for diagnosis and treatment.

Researchers and clinicians are fortunate to utilize biplanar fluoroscopy methods to accurately determine the arthrokinematics of articulations in real time for joints such as the hip, shoulder, and knee, where limited superposition of bone geometry occurs within the 2D fluoro images. Our 4D CT method will complement biplanar fluoroscopy because, as a tomographic imaging modality, its strength lies in imaging joints with complicated, multi-articulated structures (such as the wrist) that are problematic for the biplanar approach. 4D CT provides a widely available, high spatial and temporal resolution, geometrically precise method to *dynamically* image the complicated multi-articulated joints of the wrist. This technique was demonstrated in a cadaveric forearm/hand specimen.

METHODS

A custom motion simulator was fabricated to simulate radial-ulnar deviation at the wrist joint. We exposed the proximal ends of the radius and ulna bones in the cadaveric forearm, and firmly mounted them to the device (Fig. 1). The hand was attached to an acrylic paddle via a single plastic screw through the second intermetacarpal space, just proximal to the deep intermetacarpal ligament. Two linear slides under the paddle provided composite motions in the x and z-axes. A programmable stepper motor (connected to a laptop) produced belt-driven motion of the paddle in the x-axis, with free motion of the paddle in the z-axis, allowing the hand to perform periodic radioulnar motion through a maximum arc of 30° (10° of radial deviation and 20° of ulnar deviation). The wrist was programmed to move at 30 cpm, representing a typical wrist motion speed.

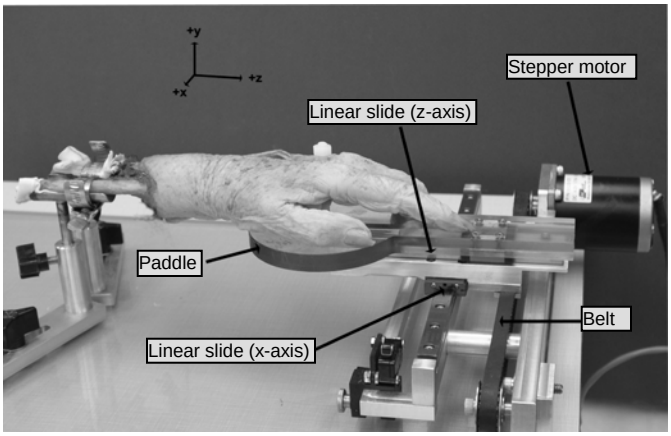

Figure 1: Cadaveric wrist in custom simulator.

The 4D CT technique consists of a non-gated sequential scanning mode in which periodicity of wrist motion is not required. The cadaveric wrist was imaged using a Siemens Definition FLASH dual-source scanner (Siemens Healthcare, Forchheim, Germany). In this mode, there was no table translation between successive scans. Two seconds of data were acquired (one motion cycle). Scan parameters were 0.28 second gantry rotation, 2 x 64 x 0.6 mm detector collimation (38.4 mm z-axis coverage), 140 kVp, and 200 mAs per rotation. Twenty images were reconstructed over the 2 second cycle using the commercially implemented dual-source cardiac reconstruction algorithm. 3D images at each of 20 time points in the motion cycle

were generated using volume rendering techniques (VRT) on the scanner's image processing workstation. Dose values were assessed for the 4D scanning technique by scanning the cadaveric wrist at different dose levels. Image quality was evaluated at each dose level to determine the minimal dose at which the scans still had sufficient diagnostic image quality.

RESULTS AND DISCUSSION

The carpal bones, distal radius, ulna, and joint spaces were clearly delineated in the rendered images (Fig. 2), without motion blurring or banding artifacts, in all motion phases. 4D image sequences were generated from the 3D images to visualize the motion of each carpal bone and the change in joint spaces throughout the motion cycle. The estimated skin dose in this preliminary study, with scanning parameters of 140 kVp, 200 mAs per rotation, and a 2 second scan time, was about 55 mGy, which is a factor of 40 lower than the minimum threshold for skin effects (2 Gy) [1]. Thus, no deterministic skin injury is possible. Potential cancer risk is similarly negligible because of the small exposure volume and insensitivity of the exposed tissues to radiation.

The 4D CT technique provides dynamic, high spatial and temporal resolution, and geometrically precise *dynamic* images of the complex wrist joint. Future work aimed at assessing the arthrokinematics and joint contact characteristics during dynamic wrist joint movements in vivo will provide valuable clinical information for assessing dynamic joint instabilities before they progress to static deformities and OA.

ACKNOWLEDGEMENTS

The authors would like to thank Lawrence Berglund for fabrication of the motion simulator. This work was partially supported by Mayo Novel Methodology DA Award 1 UL1 RR024150-01.

REFERENCES

[1]. Stecker MS, Balter S, Towbin RB, et al. Guidelines for patient radiation dose management. J Vasc Interv Radiol 2009; 20:S263-273.

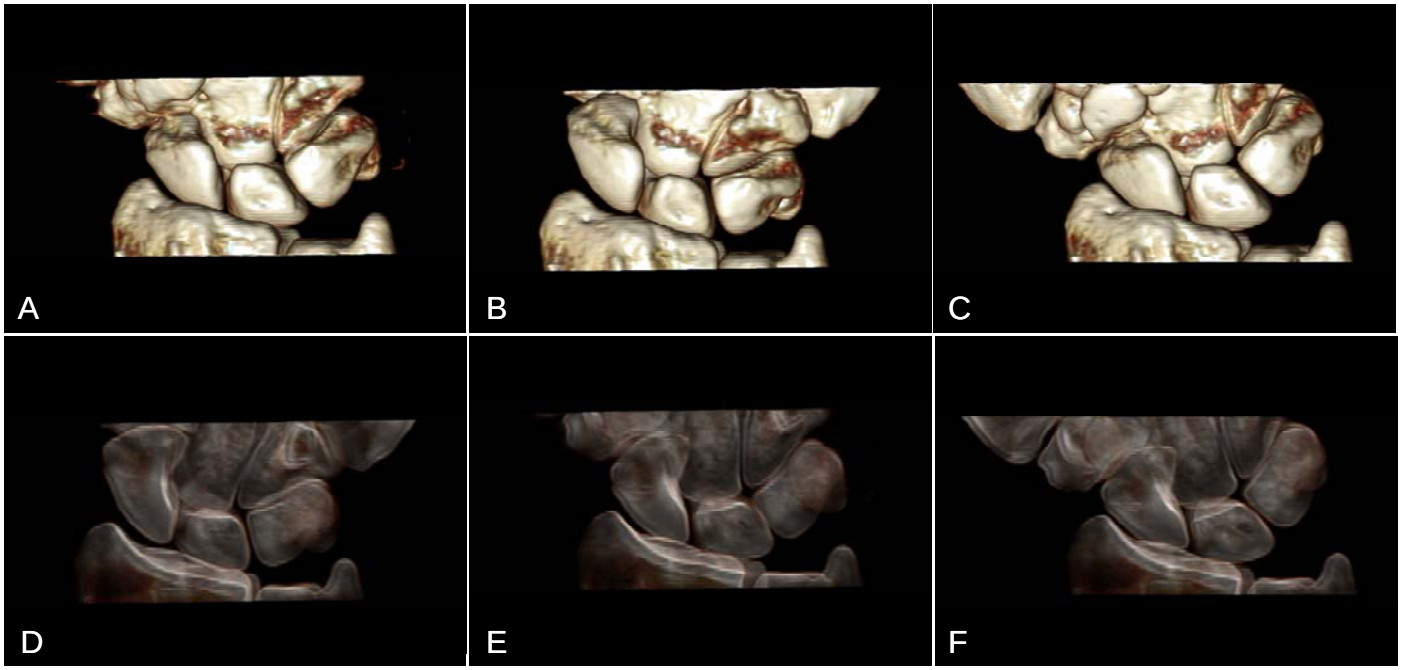

Figure 2: Three volumes from the dynamic 4D CT imaging sequence, volume rendered (top row, dorsal view) and virtual radiography images (bottom row) in radial deviation (A, D), neutral (B, E), and ulnar deviation positions (C, F).

A METHOD OF GEOMETRIC DESCRIPTION OF THE GLENOID FOSSA

Krystyna Gielo-Perczak

Worcester Polytechnic Institute, Worcester, MA, USA
email: gieloperczak@wpi.edu

INTRODUCTION

Recent analyses of the glenohumeral joint have not focused on the contribution of geometric parameters like the shape of the glenoid fossa, radius of the humerus, the attachment of the deltoideus lateral part in relation to the glenoid fossa and the angular measure of the articular surface of the humerus head. The glenoid concavity is irregular and less marked than the convexity of the humeral head, thus it needs adequate radiographic data and analysis. There are two major controversies relating to the shape of the glenoid which is considered with or without the cartilage surfaces of the glenohumeral joint. One represents the concept that the glenoid is flatter or apparently shallow if taking into account the bone surfaces beneath the articulating surfaces as determined from a plain radiograph.
Gielo-Perczak [1] confirmed in experimental studies the influence of the variance in the glenoid concavity on physical capabilities. These observations suggest that there exist more geometric details which never were considered but should be taken into strength analysis of glenohumeral joint.

METHODS

The purpose of the current study was to propose a method of geometrical description of the glenoid fossa and formulate a necessary number of segments tangent to the glenoid, which can be used to determine the planar shape of the glenoid fossa.
The problem of defining the smallest number of tangents which can be used to determine the planar shape of the glenoid fossa was resolved. Assuming that a glenoid fossa can be described as a convex function and defined as a polyhedral model, the mathematical task was formulated [2]. Reference axes Y-Z were fixed in the scapula at the center of the lateral margin of the acromion (the middle deltoid attachment), where the Y-axis was parallel to the longitudinal axis of the thorax. The concavity of the glenoid fossa, as a convex function, was considered as a polyhedral model of f based on linearizations f_i, $i=1,...,k$ with an error of

$$\varepsilon_i(z) = f(z) - f_i(z) = f(z) - \langle g_i, z - z_i \rangle - f(z_i) \qquad \text{[Eq.1]}$$

where g_i is a subgradient of f in the point z_i (if f is differentiable). The nodes $z_i,...,z_k$ on the curve of the glenoid in the frontal plane were determined when the maximal linearization error $\varepsilon(z)$ was minimal. The tangents to a given glenoid fossa in the frontal plane $f(z_i)$ are the straight lines at the points $(z_i, f(z_i))$ which cross Z-axis at the angles $\phi_1,\ldots, \phi_i$. Applying the smallest error of the polyhedral model of a convex function [3], it was found that the minimum number of tangents necessary to approximate a glenoid shape is

$$k = \frac{c}{2\sqrt{2}\cdot e}\ , \qquad \text{[Eq. 2]}$$

where c is the height of glenoid fossa measured along Y-axis; e is the tolerance of measurement. Both terms are expressed in [mm]. For example, if the height of glenoid fossa c was 39.1 mm and the humerus MRI slices were 2 mm in thickness, then the number of tangents was seven (Fig. 1). For thinner MRI slices, the minimum number of tangents needed to fit the glenoid fossa geometric surface would be larger.
Magnetic resonance images were taken at the same arm positions for all 12 male participants. Data were recorded by using the 1,5-T Sigma system (GE Medical Systems, Milwaukee, WI). The method of geometrical description of the glenoid fossa concavity in a frontal plane, for a cross section thorough the acromion, has been applied for 12 subjects participating in an experiment to determine their glenoid geometries. The participants' mean age was 40.5±8 years, with an average height of 178 ±7.09 cm and body weight of 81.54±15.60kg. The geometric data of the glenoid concavity means

the tangents' inclination ϕ_i at the seven nodes (i=7) on the curve of the glenoid and the distances z_i between the middle deltoid attachment and a point at which each tangent to the glenoid fossa crosses the Z-axis were collected (Table 1).

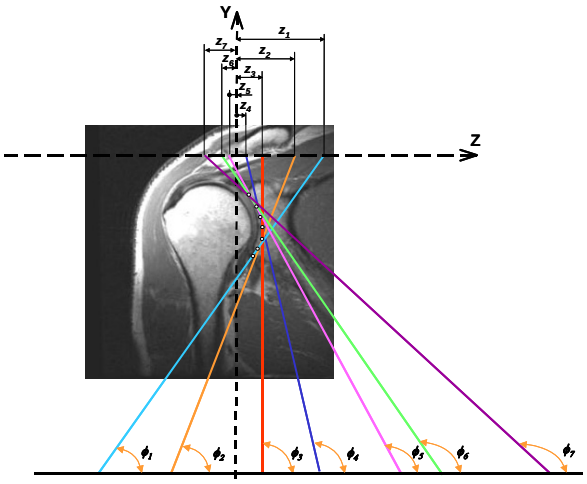

Figure 1: The group of seven tangents approximated the bone surface data that fit to the glenoid fossa geometric surface from MRI slice of 2 mm in thickness.

RESULTS

The MRI results for12 subjects confirm variability in tangent inclinations and distances of tangents from the lateral deltoid attachment. Considering and measuring the angles of tangents as the parameters of the glenoid fossa will provide new information on the interface shape sensitivity of glenohumeral joint stability. These analytical mechanical considerations may provide a better biomechanical basis for joint modeling and lead to consideration of articular geometry. The study responds to the recent studies confirming an emerging need to include glenoid inclination, mechanics of the deltoid muscle, and glenoid labrum concavity into stability analyses of the glenohumeral joint.

CONCLUSIONS

The current method of geometrical description of concavity of the glenoid fossa will help to analyze analytically relationship between glenoid concavity and muscle/s (i.e. deltoid) attachment on the glenohumeral head position as a meaningful geometric component of the glenohumeral joint and its influence on joint strength.

REFERENCES

1.Gielo-Perczak K. et al. *Ergonomics* **50**:11, 1856-1870, 2007.
2.Fletcher R. *Practical Methods of Optimization*, John Wiley & Sons, Chichester, 1987
3.Bertsekas DP, *Nonlinear Programming*, Athena Scientific, Belmont, MA, 1995

Table 1: Geometric parameters of the glenoid fossa shapes at the seven nodes (i =7) for 12 subjects.

		1	2	3	4	5	6	7	8	9	10	11	12
z_1	mm	67.2	14.2	30.8	28.6	27.8	34.3	10.6	37.9	49.4	8.2	67.1	20.8
z_2	mm	56.4	11.8	24.1	30.1	33.1	23.7	16	23.7	38.3	26.5	37.3	13.4
z_3	mm	38.2	8	18.9	14.4	30.5	14.2	7.7	10.1	30.4	15.1	17.6	12.3
z_4	mm	30.3	1.1	8.9	9.4	16.5	4.7	4.6	8.3	22.4	34	11.5	10.1
z_5	mm	16.3	-1.2	2.6	5.6	8.8	-1.2	-0.7	1.7	15.1	0.9	5.3	8.8
z_6	mm	8.4	2.2	-3.4	-4	0.7	-5.6	-2.8	-5.8	5.4	-1.9	-7.2	3
z_7	mm	5.7	6	-8	-3.7	1.7	-14.6	-5.5	-12.5	-11.4	2.8	-20	-6.5
ϕ_1	°	50.2	78.5	70	72.8	69.1	63.3	75	66	58	93.3	53	57
ϕ_2	°	56.4	81.7	76	71.5	64.7	73	64	78	66	74	73	72
ϕ_3	°	70.7	87.3	81	87.1	67	83.5	84	95	73	87.5	92	74
ϕ_4	°	78.7	98.5	93	92.9	82.4	95.7	93	97	81	103.6	98	81
ϕ_5	°	95.4	102.7	101	97.8	92.2	103.9	109	106	90	107.5	105	85
ϕ_6	°	105.8	95.9	109	110.9	104.4	110.5	116	116	103	112.1	120	109
ϕ_7	°	109.6	87.3	116	110.4	102.5	123.6	125	124	124	102.4	132	136

Effects of Midcarpal Arthrodesis on Wrist Coupling and Performance

Garg, R[1]; Kraszewski, A[1]; Stoecklein, H. [1]; Backus, S. [1]; Lenhoff, M. [1]; Wolff, A. [1]; Hillstrom, H[1]; Wolfe, S.W[1, 2]

[1]Hospital for Special Surgery, NY, USA
[2]Weill Cornell Medical College, NY, USA
email: gargr@hss.edu

INTRODUCTION

A composite wrist motion of radial deviation/extension to ulnar deviation/flexion has been termed the "dart thrower's motion" and is thought to be important to many activities requiring force and accuracy [1,2]. There is little information concerning the relationship between functional performance and wrist "coupling [3]," the amount of flexion-extension per degree of radial-ulnar deviation. The purpose of our study is to compare wrist coupling and functional performance between healthy subjects, healthy splinted subjects, and those who have undergone midcarpal arthrodesis. We hypothesize that altered wrist coupling will result in diminished performance.

METHODS

Eighteen reflective markers were fixed to the upper extremity, trunk, and pelvis of ten healthy males and ten males who had undergone midcarpal arthrodesis of their dominant wrist. Each healthy subject performed 15 dart, basketball and football throws, and hammered 15 nails with and without a hinged splint that constrained radial-ulnar deviation (RUD). Each arthrodesis subject performed these tasks without a splint. Three-dimensional angular excursions of the wrist were acquired at 200Hz with a 12-camera Motion Analysis system (Santa Rosa, CA). The wrist joint coordinate system was implemented in Visual3D (Germantown, MD) to calculate angles. Dart and football throwing performance was measured as the distance to the target's center. A graduated scoring system was used for basketball accuracy. Hammering performance was measured by time taken to drive a nail flush, total number of strikes, and ratio of missed strikes to total number of strikes. Coupling was expressed as angles using the arctangent2 function (e.g. -45° indicates 1:1 coupled FE and RUD). Paired and unpaired t-tests were used to compare coupling values and performance for healthy, splinted and arthrodesis subjects.

RESULTS AND DISCUSSION (Table 1)

Wrist coupling and performance were significantly reduced by splinting in dart throwing, basketball throwing and hammering for healthy subjects. Wrist coupling was also reduced for football throws, however, no difference was found in performance by splinting. Performance was significantly different between healthy (free condition) and midcarpal arthrodesis subjects for all the tasks, except football. Wrist coupling was also reduced for all tasks in arthrodesis subjects, however, it reached statistical significance only for basketball throwing.

CONCLUSIONS

Constraining radial-ulnar deviation results in diminished wrist coupling during functional tasks. Diminished wrist coupling can result in reduced functional performance in several tasks that require both accuracy and force. Surgical and rehabilitative efforts should be focused on the restoration of wrist coupling following injury.

REFERENCES

1. Palmer AK, Werner FW, Murphy D, Glisson R. Functional wrist motion: a biomechanical study. *J Hand Surg [Am]*. 1985 Jan; 10(1): 39-46..
2. Werner FW, Green JK, Short WH, Masaoka S. Scaphoid and lunate motion during a wrist dart throw motion. *J Hand Surg [Am]*. 2004 May; 29(3): 418-22

3. Li ZM, Kuxhaus L, Fisk JA, Christophel TH. Coupling between wrist flexion-extension and radial-ulnar deviation. *Clin Biomech (Bristol, Avon)*. 2005 Feb; 20(2): 177-83.

Table 1. Performance and coupling measures for dart throwing, hammering, basketball and football throwing tasks averaged across ten healthy (free and splinted) and ten midcarpal arthrodesis subjects.

	Dart Throwing		**Hammering**				**Basketball Throwing**		**Football Throwing**	
	Coupling (°)	Perf (mm)	Coupling (°)	Time (sec)	# of strikes	% missed	Coupling (°)	Perf (0-5)	Coupling (°)	Perf (mm)
Free(F)	-64.3°	69	-59.7°	2.4	4.8	5%	-73.0°	3.9	-80.7°	155
Splinted(S)	-78.3°	103	-75.9°	3.5	6.3	9%	-85.0°	3.5	-89.3°	159
Midcarpal Arthrodesis (MA)	-74.5°	133	-63.8°	9.0	17.2	6%	-80.5°	2.8	-98.2°	166
F vs. S *p*	**0.0001**	**0.012**	**0.0001**	0.137	0.119	**0.044**	**0.001**	**0.029**	**0.013**	0.722
F vs. MA *p*	0.081	**0.0001**	0.314	**0.0001**	**0.0001**	0.593	**0.046**	**0.042**	0.129	0.622

Note that a coupling value closer to -45° indicates a more coupled motion.

Performance (Perf): **Dart Throwing**: Distance (mm) of dart from the target center
Hammering: Time (sec) taken per nail # of strikes to drive the nail flush. Ratio of missed to the total no of strikes per nail.
Basketball Throwing: 5 points for every ball sunk, 2 points for hitting either front or back of the rim, 1 point for hitting the side of the rim, and 0 for missing the rim altogether
Football Throwing: Distance (mm) from the center of impact to the center of the target

TOPOLOGY OF SUBCHONDRAL SURFACES IN THE FIRST TRAPEZIOMETACARPAL JOINT AS A FUNCTION OF GENDER AND BONE

[1]Eni Halilaj, [1]Michael Rainbow, [2]Nilay Patel, [2]Douglas Moore, and [2]Joseph Crisco
[1]Brown University and [2]Department of Orthopaedics, Alpert Medical School of Brown University and Rhode Island Hospital, Providence, RI, USA
email: ehalilaj@cs.brown.edu, web: http://www.brownbiomechanics.org

INTRODUCTION

Osteoarthritis (OA) of the saddle-shaped trapezio-metacarpal (thumb CMC) joint affects 15% of adults over thirty and two-thirds of women over 55[1]. The geometry of articulating surfaces is thought to play an important role in the etiology of OA, as it influences load distribution in the joint. Previous *in vitro* stereophotogrammetric studies have shown that the thumb CMC joint is smaller women than in men[2].

Our long-term goal is to document the progression of bony changes in CMC OA using clinical computed tomography (CT) scans. We have confirmed our ability to generate (and parameterize) accurate subchondral surfaces from clinical CT images[3]. The purpose of this study was to extend the validation of that work by analyzing bones from a larger series of *in vivo* CT images. Specifically we wanted to evaluate subchondral surface as a function of gender and bone, in the thumb CMC.

METHODS

CT volumes of the dominant wrist of 14 volunteers, 7 males (age 25 +/- 3 yr.) and 7 females (age 24 +/- 3 yr.), were generated as part of an unrelated study. The images were generated using a 16-slice clinical CT scanner (General Electric, Milwaukee, WI) at tube settings of 80kVp and 80mA, slice thickness of 0.625mm, and in-plane resolution of 0.3mm x 0.3mm. The first metacarpal (MC1) and trapezium (TPM) were segmented from each volume with commercial software (Materialise, Ann Arbor, MI), yielding 3-D bone models comprised of polygon meshes. The mating subchondral surfaces on the TPM and MC1 were manually selected and used for our surface analysis (Fig.1); a fifth-order polynomial was fit to the point cloud for each region of interest; principal curvatures (k_{min}, k_{max}) and k_{rms}[4] were calculated at each point on the surface (Fig. 2). K_{min}, k_{max} and k_{rms} were averaged across each surface and the average values were used for comparisons of inter-subject variability. A two-way repeated measures analysis of variance (ANOVA) was used to evaluate the differences between men and women, as well as the differences between the MC1 and TPM articulating surfaces.

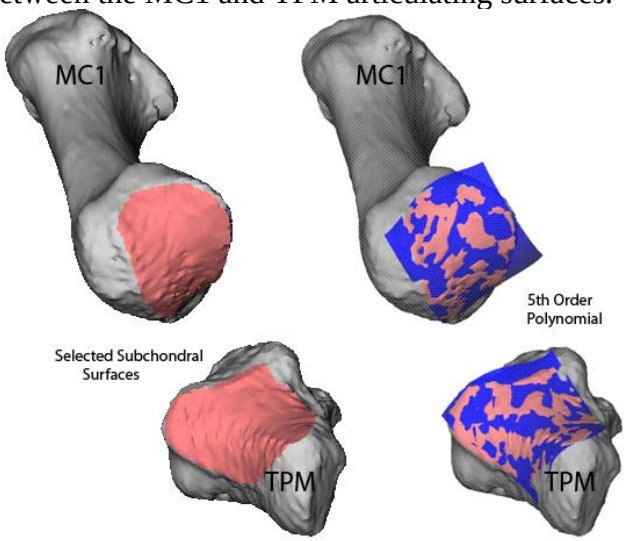

Figure1. Selected subchondral surfaces for the first metacarpal and the trapezium, and respective polynomial fits**.**

RESULTS AND DISCUSSION

The average articulating surface areas for both the trapezium and the metacarpal were significantly smaller in females than in males (24% and 25%, respectively, Table 1). Fifth-order polynomials accurately modeled the articular surfaces for both the TPM (R^2=0.99; RMS error=0.10 mm) and MC1 (R^2=0.96; RMS error=0.31mm).

K_{min}, k_{max}, and k_{rms} of MC1 were significantly lower (in magnitude) in men than in women, suggesting that men have a flatter metacarpal surface than women (Table 1). K_{rms} and k_{min} for the trapezial surface were also lower (in magnitude) in men, but these results were not statistically significant (Table 1).

Comparison of the principal curvatures within the ANOVA revealed that the the trapezium had a significantly higher k_{min}, higher k_{rms}, and lower k_{max} (all magnitudes) than the metacarpal (Table 2). This suggests that, in general, the curvature geometry differs significantly between the two bones and that this joint is not a perfect saddle.

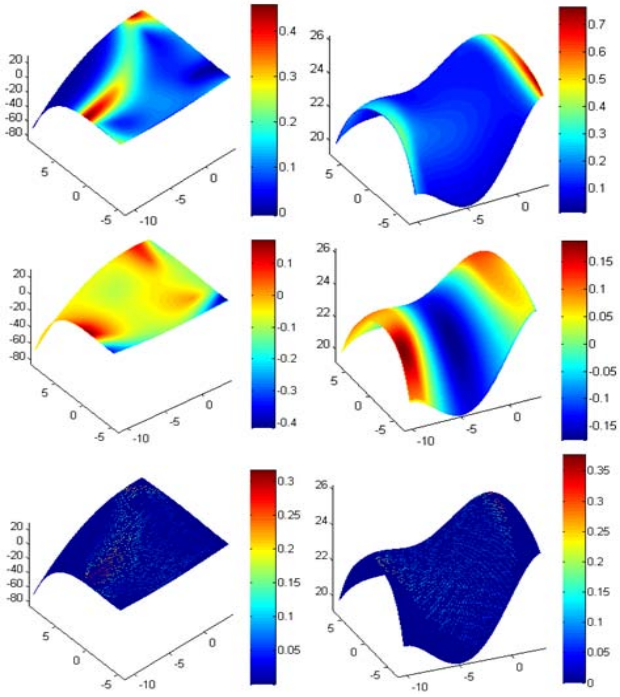

Figure 2. Curvature (kmin, kmax, krms) maps for the trapezial (left) and the metacarpal (right) surfaces

CONCLUSIONS

In this study we present principal curvature data generated from CT scans of young (~25 yr.) volunteers. We found significant gender-related differences in the first metacarpal, but not in the trapezial subchondral surfaces. We also found significant changes between bones. These results are consistent with existing *in vitro* data generated via stereophotogrammetric analysis of explanted trapeziae and metacarpal bones[1]. Therefore, our findings provide further confidence in the utility of clinical CT images for studying topology of the first CMC joint *in vivo* and identifying changes that develop with OA progression (if any).

We have evidence to support current theories that variations in subchondral bone topology, and therefore deviation from a perfect saddle shape, may be an important etiologic factor in the development of OA. Further investigation is needed, however, to document changes as disease progresses.

REFERENCES

1.Haara et al., *J. of Bone and Joint Surgery*, 2004
2.Xu, L. et al., *J. of Hand Surgery*, 1998.
3.Patel, N. et al., *ORS* 2010
4.Ateshian GA, et al. *J. Biomech*, 1992.

Table 1. Gender differences in curvature and articular surface area of the first metacarpal (MC1) and trapezium (TPM)

	MC1			TPM		
	Male	**Female**	**p-value**	**Male**	**Female**	**p-value**
Surface Area (mm^2)	173.7±8.3	131.4± 11.6	p<0.001	184.5±25.0	140.0±15.2	p=0.004
Kmin (mm^{-1})	-0.114±.063	-0.032±.068	p =0.010	-0.167±.013	-0.184±.016	p =0.069
Kmax (mm^{-1})	0.056±.067	0.153±.078	p =0.0073	0.048±.011	0.042±.022	p =0.541
Krms (mm^{-1})	0.129±.006	0.148±.016	p=0.037	0.143±.011	0.152±.018	p =0.364

Table 2. Bone differences in curvature and articular surface area

	MC1	TPM	p-value
Surface Area (mm^2)	150.9±23.4	160.5±30.1	p=0.39
Kmin (mm^{-1})	-0.070±.078	-0.176±.017	p <0.001
Kmax (mm^{-1})	0.108±.088	0.045±.018	p =0.032
Krms (mm^{-1})	0.139±.016	0.148±.016	p =0.017